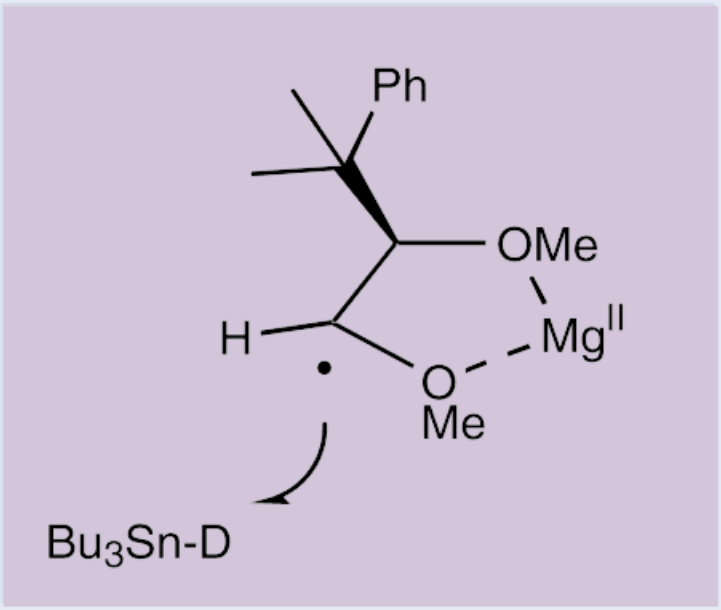
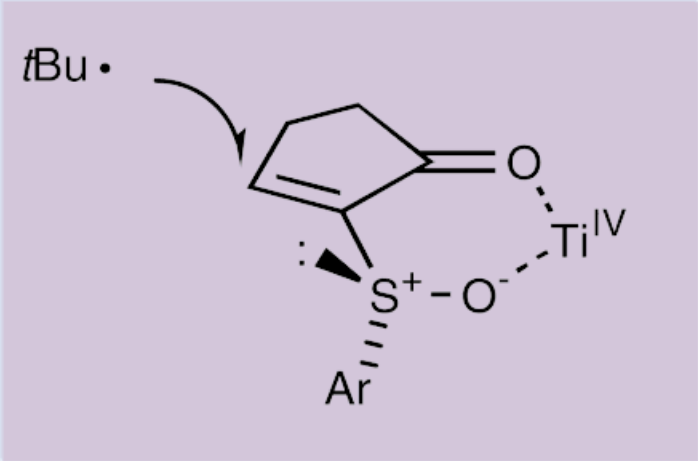
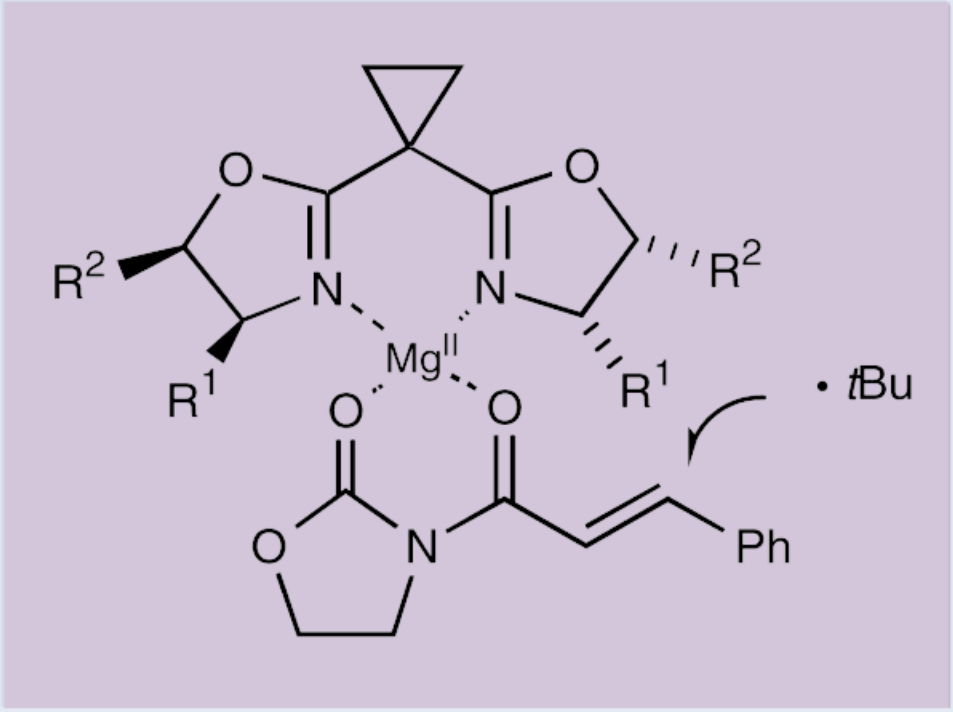


Free Radical Reactions - Lewis Acids

Complexation
Chelation
Catalysis





ANGEWANDTE CHEMIE ©WILEY-VCH

Use of Lewis Acids in Free Radical Reactions

Philippe Renaud* and Michèle Gerster

After a long period of neglect, radical chemistry has been investigated seriously, and exciting new developments have been reported. Radical steps are now incorporated in an increasing number of total syntheses. The stereochemical aspect of these reactions has been particularly studied during the last decade. While diastereoselective reactions in cyclic systems as well as cyclization reactions are well established, the possibility of performing diastereoselective reactions in acyclic systems is more recent. However, progress has been extremely rapid in this field. A new dimension was opened wp by the use of Lewis acids, which have been employed first in polymerization reactions and later for controlling reactivity and diastereoselectivity. Enantioselective reactions are being investigated intensively and initial results show great promise. Recently, the first success in enantioselective catalysis of radical reactions was reported. This review gives an overview of the development of radical reactions controlled by Lewis acids. Polymerization reactions, stereoselective reactions based on substrate control, and chiral auxiliary control, as well as enantioselective radical reactions will be discussed. The different roles of the metal center (monocomplexation, chelation, template effect, etc.) will be used to rationalize the results.

Keywords: asymmetric synthesis · chelates · Lewis acids · radical reactions · radicals

1. Introduction

The general feeling of synthetic chemists about free radicals has dramatically changed during the last 15 years. Before that time free radicals were considered mainly as interesting reaction intermediates with very limited synthetic potential, and the few known clean radical reactions were considered as exceptions. However, the 1980s have seen an emergence of new free radical synthetic methods largely based on organomercury and organotin compounds. More recently, atom- and group-transfer reactions, as well as reductive and oxidative single-electron transfer (SET) processes have become very popular.[1]

Parallel to this development, the stereochemistry of radical reactions has been investigated, and results exceeding the initial expectation have been obtained.[2] Interestingly, the rules developed to rationalize the stereochemical outcome of radical reactions are very similar to the ones formerly developed for ionic and concerted reactions. However, because of the neutral nature of radicals, the effect of solvent and other possible complexing agents that are crucial for ionic and concerted reactions were not investigated until very recently. It has been well established that radical reactions can be rationalized by applying the frontier molecular orbital theory. The electronic character of the radical determines whether SOMO–LUMO or SOMO–HOMO interactions are predominating.[3] By analogy to pericyclic reactions it is expected that Lewis acids will strongly influence the outcome of radical reactions and will play a crucial role, similar to the one they play in cycloaddition reactions. Reactivity, as well as regio- and stereoselectivity, should be influenced by the presence of Lewis acidic additives.

Recently, most of these expectations were confirmed and exceptional effects have been obtained on the stereochemical outcome of radical reactions by using complexing agents, mainly Lewis acids. Effects on the reaction rates have also been observed, thus opening the way to catalysis of radical reactions. Since these effects are of great importance for future synthetic applications, we wish to summarize in this account the results concerning the use of Lewis acids in radical reactions with particular emphasis on the stereochemical control.

[*] Prof. P. Renaud, Dr. M. Gerster
Université de Fribourg
Institut de Chimie Organique
Pérolles, CH-1700 Fribourg (Switzerland)
Fax: (+41) 26-300-97-39
E-mail: philippe.renaud@unifr.ch

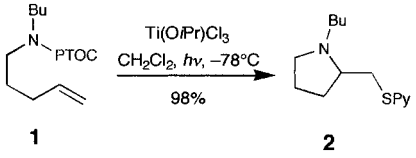
2. Reactivity and Regioselectivity Control

The first application of Lewis acids in radical reactions concerned polymerization reactions.[4] For example, it has been observed that homopolymerization of acrylonitrile and methyl methacrylate could be enhanced by the addition of $ZnCl_2$ and very important effects have been observed in

 © WILEY-VCH Verlag GmbH, D-69451 Weinheim, 1998 1433-7851/98/3719-2563 $ 17.50+.50/0

copolymerization:[5] Without Lewis acids regular alternating copolymers are only formed from monomer pairs consisting of one strong electron acceptor and one strong electron donor, but with monomers less differentiated in their electronic character, the alternation was poor. A major breakthrough resulted from the work of Bamford[6] and Hirooka[7] when they described the formation of regular 1:1 copolymers from propylene and acrylonitrile in the presence of $EtAlCl_2$. Following this work, different Lewis acids have been used, and of them zinc, aluminum, boron, and tin derivatives gave the best results. For example, it was found that allylboron halides can be used in a catalytic amount to control the alternation of the monomers.[8] Polymerization of alkyl methacrylates that are initiated by aluminum porphyrins are greatly accelerated in the presence of sterically hindered Lewis acids such as methylaluminum di(2,6-di-*tert*-butyl-4-methylphenoxide) (MAD)[9] and aluminum tris(2,6-diphenylphenoxide) (ATPH).[10]

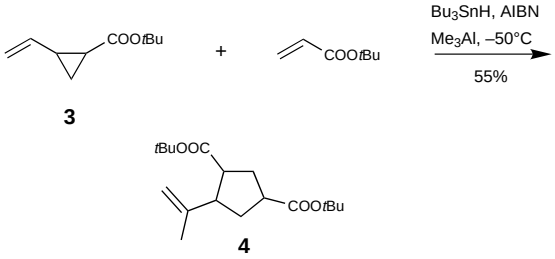
The work on polymerization reactions proves that Lewis acids can be used to control the reactivity of radicals. This possibility has not been used in traditional synthesis until very recently. An early example concerns aminyl radicals that are known to be activated by protonation.[11] It was then demonstrated that Lewis acids could induce the same effects.[12, 13] For example, the PTOC-carbamate **1** cyclizes in almost quantitative yield (GC analysis) to give the pyrrolidine **2** in the presence of $Ti(OiPr)Cl_3$ [Eq. (1); PTOC = pyridine-2-



1 2 (1)

thion-*N*-oxycarbonyl].[12] Under strictly neutral conditions (no Lewis and no Brønsted acid) the cyclic product is not formed. The yield of cyclized product **2** exceeds the amount of Lewis acid employed. This suggests that the Lewis acid is acting as a catalyst.[14]

Complexation of the alkene partner is also expected to lead to enhancement of the radical addition rate with complexed alkenes being more reactive towards alkyl radicals that possess a well established nucleophilic character. This was confirmed by ab initio calculations[15] and by some early observations. For instance, radical alkenylation of vinylcyclopropyl ester **3** with acrylate gives the cyclopentane derivative **4** in high yield in the presence of Me_3Al at low temperature [Eq. (2); AIBN = azobisisobutyronitrile].[16] In the absence of



3 4 (2)

Me_3Al the reaction does not proceed at all at $-50\,^{\circ}C$. This result is attributed to complexation of the ester functionality in either the cyclopropyl or the acrylate moiety.

A more convincing demonstration of this effect was given by Sato et al. who examined the relative reactivity of *tert*-butyl acrylate **5** and *N*,*N*-dimethyl acrylamide **6** toward the *n*-butyl radical addition [Eq. (3)].[17] In the absence of a Lewis acid the ester reacts more rapidly and **7** is formed preferentially (**7**:**8** = 68:32). The presence of one equivalent of di(2,4,6-trimethylphenoxy)aluminum chloride increases the yield of the addition to the acrylamide and **8** becomes the major product of the reaction (**7**:**8** = 24:76). This result arises from the fact that the amide is a stronger base and is preferentially

Philippe Renaud was born in Neuchâtel in 1959. After undergraduate study at the University of Neuchâtel he continued his education at the ETH Zürich through a Ph. D. in 1986 under the supervision of Dieter Seebach. From October 1986 to December 1987 he was a postdoctoral associate of M. A. Fox at the University of Texas at Austin. In 1988 he started an independent research program at the University of Lausanne. From 1992 to 1993 he was supported by the Alfred Werner Fellowship. In October 1993 he moved to the University of Fribourg as an associate professor. His group is active in the field of synthetic organic chemistry based on the use of free radical intermediates, with emphasis on stereochemical aspects.

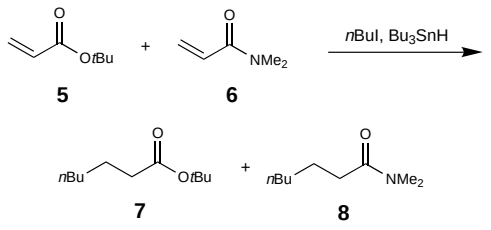


P. Renaud



M. Gerster

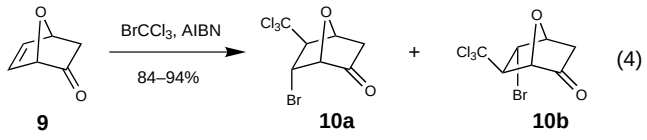
Michele Gerster was born in 1969 in Sion, Switzerland. She studied chemistry at the University of Lausanne. Before starting her Ph. D., she worked for four months with R. K. Haynes in Sydney on the total synthesis of antimalarial compounds. She received her Ph. D. in 1997 under the direction of Professor Renaud at the University of Fribourg with a dissertation entitled: "Study of the Influence of Lewis Acids on the Stereoselectivity of Radical Reactions". She is currently carrying out postdoctoral research in Cambridge, England, in the group of Steven V. Ley where she is involved in the total synthesis of biologically active compounds.



(3)

complexed by the Lewis acid. Interestingly, the activating effect of the Lewis acid has also a positive effect on the overall yield of the reaction (41 →78 %), which confirms the excellent compatibility of Lewis acids and radical chain reactions.

The regioselectivity of the radical addition to 7-oxabicyclo[2.2.1]hept-5-en-2-one (**9**) is influenced by the presence of Lewis acids [Eq. (4)).[18] Kharasch-type addition of bromotrichloromethane to **9** gives **10a** preferentially, which results



(4)

from the addition at C5 (**10a**:**10b** = 74:26). In the presence of Lewis acids such as $Ti(OiPr)_2Cl_2$ the regioselectivity is inverted and **10b** is the major product of the reaction (**10b**:**10a** = 26:74). This inversion can be explained from the HOMO coefficients of alkene **5**. Indeed, it was calculated that protonation of the carbonyl group makes the coefficient at C6 larger than the coefficient at C5.[18]

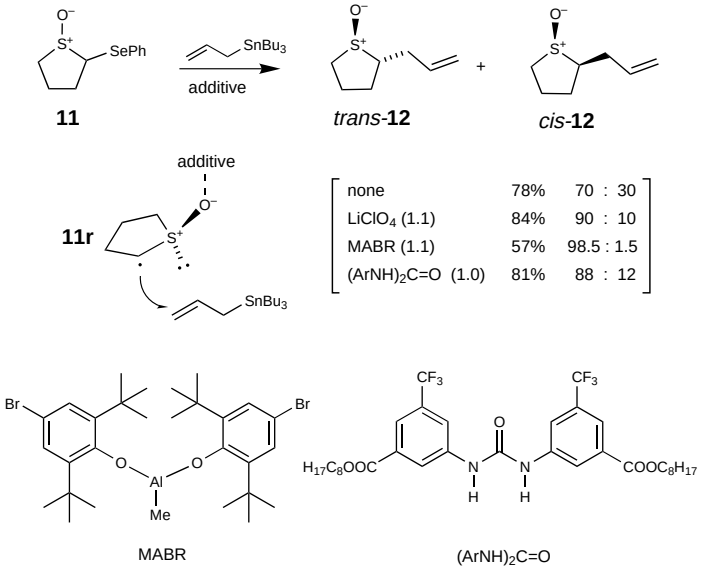
3. Control of Diastereoselectivity

Particular attention has been devoted to the control of the diastereoselectivity but, despite impressive progress, the control of the stereochemistry of radical reactions still represents a barrier for their application in organic synthesis. For the purpose of clarity, we have divided this part of the review between complex formation with monodentate ligands (monocomplexation) and with polydentate ligands (chelation), the ligands being either the radicals or the radical traps. These two approaches lead to remarkable stereoselectivity enhancement and control.

3.1. Monocomplexation

3.1.1. Cyclic Radicals

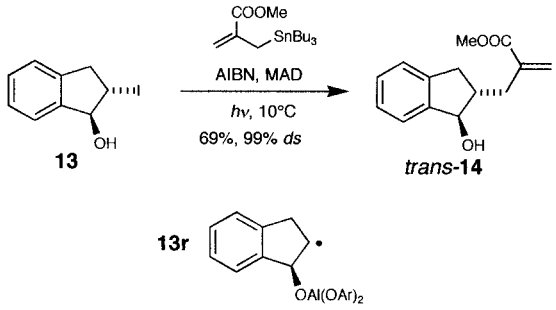
Investigation of 1,2-asymmetric induction in the presence of an additive is reported for radicals derived from cyclic sulfoxides and alcohols. For example, a study of cyclic sulfinamides[19] and sulfoxides[20, 21] shows an interesting solvent effect attributed to hydrogen bonding.[22] The use of oxophilic Lewis acids give even more impressive results: excellent stereoselectivity enhancement is obtained for the allylation of **11** in the presence of lithium perchlorate (Scheme 1).[20, 21] The use of very bulky Lewis acids also



Scheme 1. Allylation of **11** (see text for explanation).

proved to be possible without detrimental effect on yields. With methylaluminum di(4-bromo-2,6-di-*tert*-butylphenoxide (MABR) for example, the *trans* isomer of **12** is formed in 98.5 % *ds*.[21] Good levels of stereoselectivity (up to 90 % *ds*) are still observed when 10 mol % of MABR is used. A similar approach was developed by running the reactions in the presence of diarylureas that form bis-hydrogen-bonded complexes.[23] In all of these systems the additives complex the oxygen atom of the sulfinyl groups and therefore allow a good steric differentiation of the two faces.

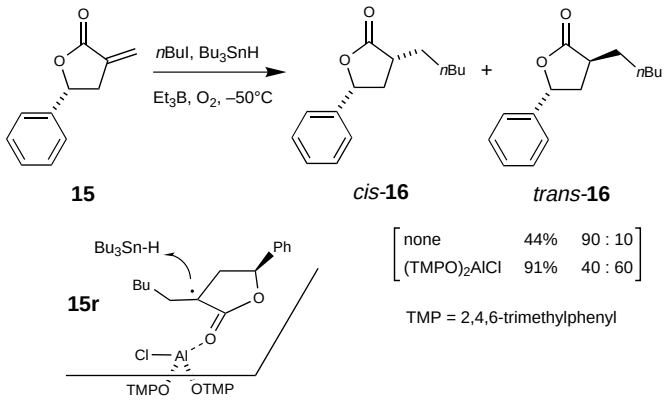
Very bulky methylaluminum diphenoxides also promote selective radical deuteration and allylation of iodohydrin **13** in over 99 % *ds* [Eq. (5)]. Formation of an aluminum alkoxide



(5)

derivative was achieved by treatment of the alcohol with MAD prior to the radical reaction.[24, 25] The extreme bulkiness of the aluminum derivative cannot be rivaled by bulky protective groups. For example, the corresponding *tert*-butyldiphenylsilyl ether is deuterated in only 89 % *ds*.

A single example of 1,3-asymmetric induction controlled by Lewis acids has been reported.[26] Radical addition to the α-methylenebutyrolactone **15** gives *cis*-**16** as the major product (90 % *ds*) in the absence of a Lewis acid (Scheme 2). In the presence of bis(2,4,6-trimethylphenoxy)aluminum chloride, the stereoselectivity is reversed and *trans*-**16** is isolated with a moderate stereoselectivity (60 % *ds*). This difference is ex-

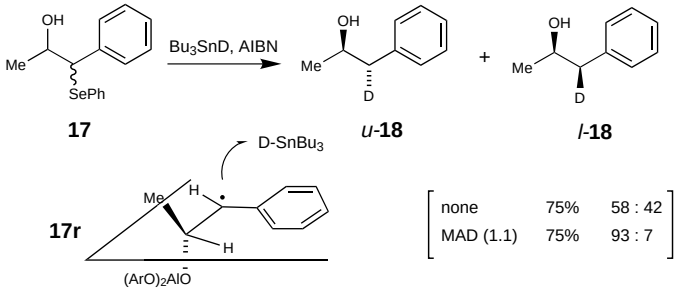


Scheme 2. The influence of a Lewis acid on the yield and product ratio on the radical addition to **15**.

plained by complexation of the carbonyl group of the lactone radical **15r** as shown in Scheme 2.

3.1.2. Acyclic Radicals

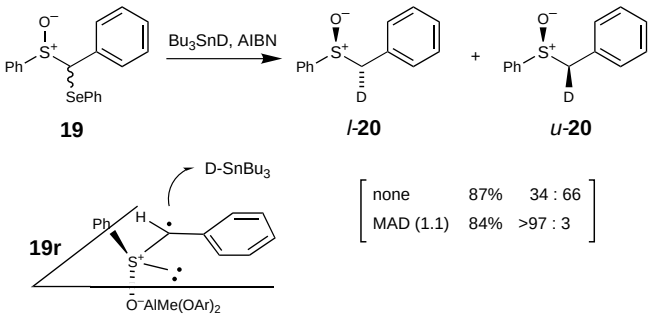
Control of the diastereoselectivity in the acyclic series has been a long standing concern and still remains a formidable challenge for organic chemists. The use of Lewis acids to solve this problem is very promising. Indeed, it has been shown in many examples that radical reactions are characterized by early transition states and therefore the radical conformation is of crucial importance. Chelation is an effective way to fix the conformation of radicals (see Section 3.2). Monocomplexation may also be very efficient to control the conformation and to allow the differentiation between the diastereotopic faces of a radical. However, with this approach a second factor, such as the presence of $A^{1,3}$ strain, is required to control the radical conformation.[27] Benzyl radicals that possess an adjacent chiral center belong to this class with their conformation being controlled by the $A^{1,3}$ strain and excellent levels of stereoselectivity are obtained when the size of the groups at the stereogenic center is well differentiated. For example, the 2-hydroxy-1-phenylpropyl radical generated from **17** is deuterated with Bu_3SnD with low selectivity (*u*-**18**:*l*-**18** = 58:42, Scheme 3).[28] In the presence of MAD (1.1



Scheme 3. Influence of Lewis acids on the radical deuteration of **17**.

equivalents), a *u*-**18**:*l*-**18** = 93:7 ratio is obtained as a result of the formation of the aluminum alcoholate **17r**, in which the three substituents at the stereogenic center are of very different sizes. The model based on minimization of the $A^{1,3}$ strain is depicted in Scheme 3. This example, as well as the reaction of iodohydrin **13** [Eq. (5)], does not involve the formation of a complex, but rather the formation of a covalent O – Al bond.

A second similar example is based on complex formation between sulfoxide and Lewis acids. The sulfoxide **19** gives *u*-**20** as the major isomer upon deuteration in the absence of a Lewis acid (Scheme 4). In the presence of 1.1 equivalents of

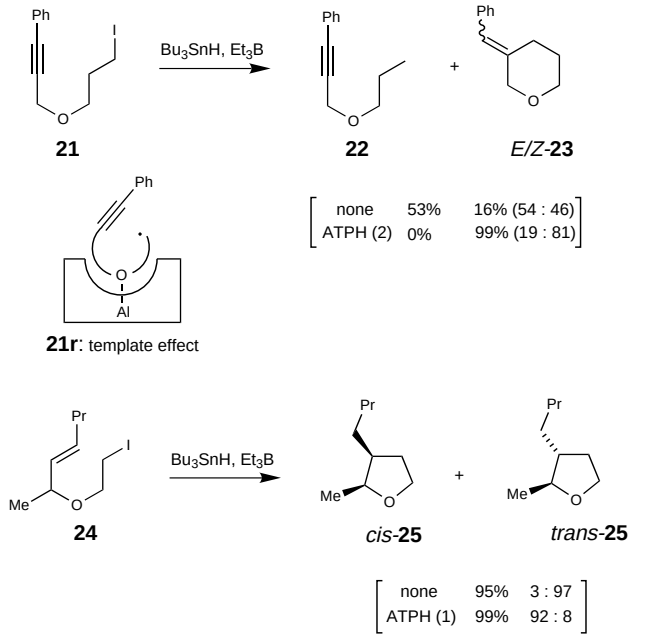


Scheme 4. Influence of Lewis acids on the radical deuteration of **19**.

bulky Lewis acids such as MAD and MABR a reversal of the stereoselectivity is observed and *l*-**20** is formed in over 97% *ds*. The model **19r**, based on the minimization of $A^{1,3}$ strain, was proposed to rationalize this result.[29] Interestingly, the monocomplexation has two consequences: it strongly favors the radical conformation where the pair of electrons are coplanar to the aryl group relative to the conformation having the oxygen atom and the aryl group in the same plane. Secondly, because of its exceptional size, it completely shields one face of the radical. A similar effect, although much more modest, has been observed during the radical reductive alkylation of enamines which is also controlled by $A^{1,3}$ strain. In this case, lithium perchlorate was used to complex a sulfonyl group.[30]

3.1.3. Cyclization Reactions

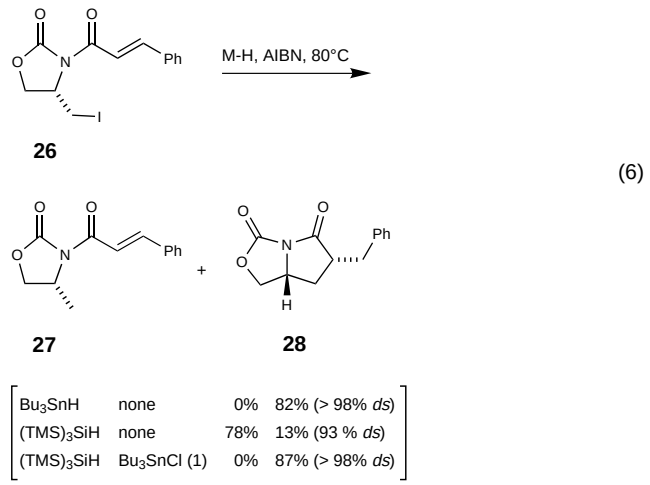
A remarkable template effect is reported by Maruoka and co-workers during the cyclization of substituted propargyl and allyl ethers. Aluminum tris(2,6-diphenylphenoxide) (ATPH) has a dramatic influence on the rate of cyclization.[31] For instance, treatment of **21** with Bu_3SnH/Et_3B under neutral conditions gives mainly the reduced product **22** along with a small amount of the cyclized product **23** (Scheme 5). In the presence of ATPH an almost quantitative yield of **23** is obtained together with good *E/Z* stereocontrol. This result is explained by a template effect, with the complexation enhancing the proximity between the radical center and the alkyne moiety. The same strategy applied to precursor **24** allows not only an enhancement in the yield of cyclized product, but also the complete inversion of the stereochemical outcome. In the absence of a Lewis acid *trans*-**25** (97% *ds*) is produced as the major isomer, which is in good agreement with the Beckwith – Houk rules.[32] In the presence of two equivalents of ATPH, *cis*-**25** becomes the major isomer



Scheme 5. Template effect in the cyclization of a substituted propargyl and allyl ether.

(92% *ds*). Such an inversion of selectivity is unattainable under ordinary radical reaction conditions.

Another example of the influence of Lewis acids upon radical cyclization is depicted in Equation (6).[33] Iodide **26** gives, upon treatment with Bu_3SnH (slow addition technique)



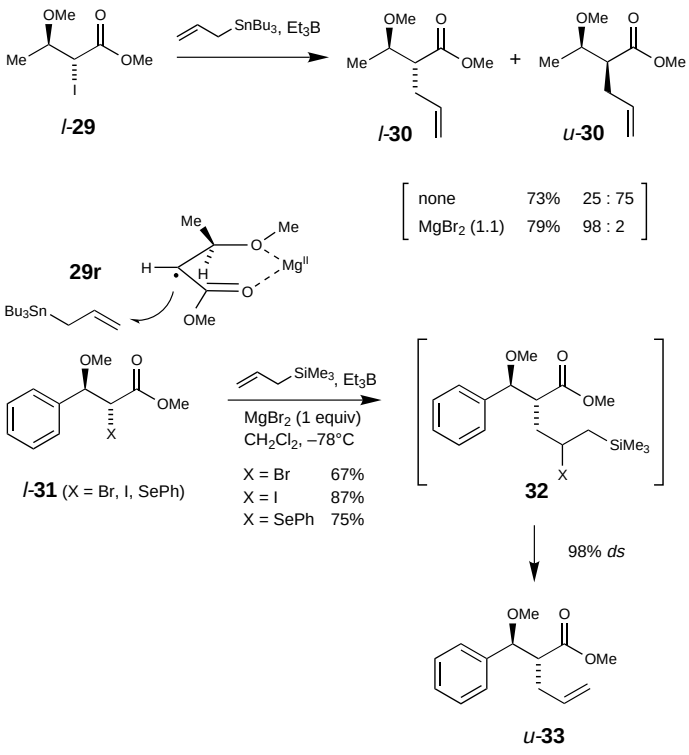
(6)

at 80 °C, the cyclization product **28**. Under analogous conditions, $(TMS)_3SiH$ furnished mainly the product of direct reduction **27** (TMS = trimethylsilyl). This unexpected difference ($(TMS)_3SiH$ is known to reduce primary alkyl radicals slower than Bu_3SnH by one order of magnitude) is caused by the presence of Bu_3SnI, which acts as a Lewis acid. Indeed, the reaction with $(TMS)_3SiH$ in the presence of one equivalent of Bu_3SnCl gave a result very similar to the one obtained when Bu_3SnH was used as the reducing agent. The role of the Lewis acid is to control the rotamer population so that the *N*-enoyloxazolidinone can attain a conformation that favors cyclization. The nature of the Lewis acid (Bu_3SnCl versus Bu_3SnBr) is also of importance for the diastereochemical outcome of the reaction, but the reasons for this are still unclear.

3.2. Chelation

3.2.1. Complexed Radicals

The study of β-hydroxy and β-alkoxy ester enolate radicals has attracted a great deal of attention since the first example of a stereoselective reaction mediated by an acyclic radical discovered by Hart and Huang.[34] In the absence of Lewis acids the stereochemical outcome is controlled by the conformation of the starting radicals, and a model based on the minimization of $A^{1,3}$ and $A^{1,2}$ strains has been proposed.[27, 35] Following this work, Guindon et al. reported the first example of a chelation-controlled radical reaction.[36] A complete reversal of the stereoselectivity is observed when radical reduction of methyl 2-iodo-3-methoxy-2-methylbutyrate is conducted in the presence of MgI_2.[37] Similar results are obtained for the allylation of methyl 3-methoxy-2-iodobutyrate *l*-**29**: in the absence of a Lewis acid, *u*-**30** is formed preferentially (Scheme 6); however, in the presence

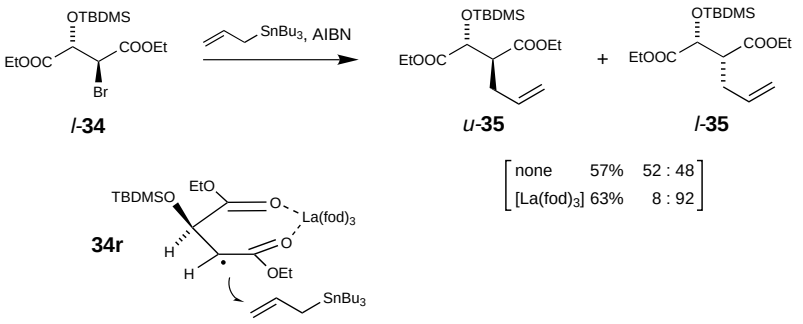


Scheme 6. Chelate-controlled radical reaction.

of three equivalents of $MgBr_2$ the *like* isomer *l*-**30** is produced with an excellent diastereoselectivity.[37] Chelation control (see **29r**) is at the origin of the stereochemical outcome. Interestingly, chelation also has an effect on the efficiency of the process: in the presence of Lewis acids, the reactions proceed more readily even at low temperature (−78 °C) than in their absence. This effect was nicely used to perform

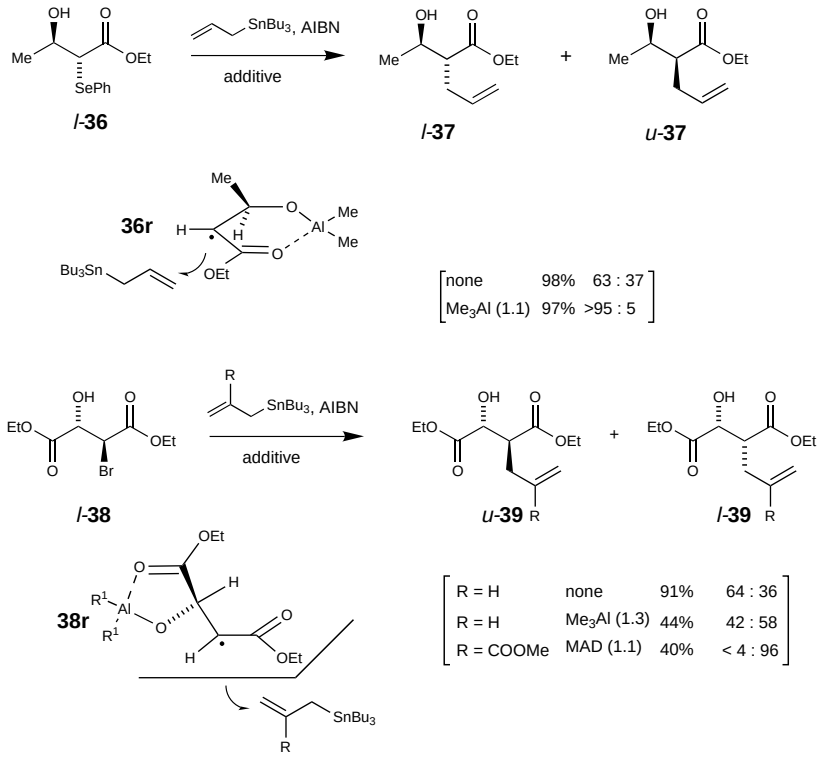
allylation of substrates such as *l*-**31** with allyltrimethylsilane in the presence of triethylborane as the radical initiator.[38] The reaction proceeds through the intermediate **32**, which decomposes readily to give *u*-**33**. The key step of the reaction is an atom (Br/I) or a group (PhSe) transfer, which is promoted by the chelation.

The stereochemical control of the allylation of 3-bromo-2-oxysuccinate has also been investigated.[39] Moderate to good results have been observed with silylethers such as *l*-**34**. The allylation is not stereoselective in the absence of Lewis acids. However, in the presence of lanthanum tris(6,6,7,7,8,8,8-heptafluoro-2,2-dimethyloctane-3,5-dione) [La(fod)$_3$], the diester *l*-**35** is obtained in 92% *ds* (Scheme 7). The formation of the 7-membered ring chelate **34r** is proposed to account for the observed stereoselectivity. The bulkyness of the *tert*-butyldimethylsilyl protecting group disfavors the five- and six-membered ring chelates involving the ether oxygen atom.



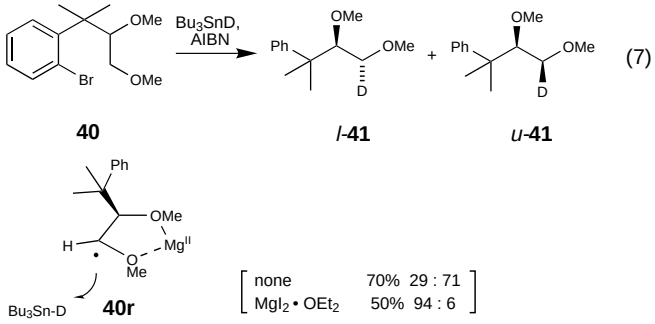
Scheme 7. Increase in the stereoselctivity during the allylation of *l*-**34**.

An excellent level of stereocontrol is obtained when starting directly from the unprotected β-hydroxyesters (Scheme 8). Ethyl 3-hydroxy-2-phenylselanylbutyrate *l*-**36** is allylated to *l*-**37** in the presence of 1.1 equivalents of Me_3Al in over 95% *ds* via the cylic radical **36r**.[40] In the absence of an additive *l*-**37** is also formed preferentially, but the stereoselectivity is much lower (61% *ds*), presumably as a consequence of intramolecular hydrogen bonding.[41] Interestingly, this approach is also successful with the malic acid derivative *l*-**38**. Low levels of stereocontrol are obtained in the absence of an additive and in the presence of Me_3Al. An excellent stereoselectivity (> 96% *ds*) was observed with MAD in favor of the *like* isomer *l*-**39**. This outcome results from the formation of the five-membered ring chelate **38r**, which minimizes $A^{1,3}$ strain. These observations are complementary to the work reported by Nagano et al. in Scheme 7; the absence of the OH protecting group allows for a complete change in the nature of the chelate.



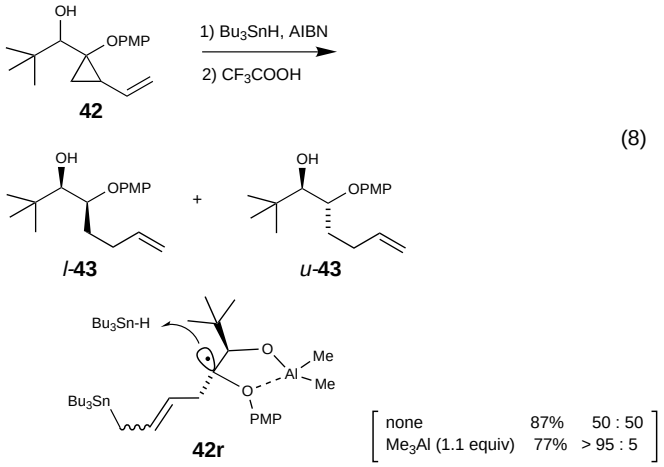
Scheme 8. Increase in the stereoselctivity during the allylation of unprotected β-hydroxy ester.

Another class of synthetically useful intermediates are 1-oxy substituted radicals. In the presence of an adjacent chiral center good levels of 1,2-asymmetric induction are observed. Giese et al. and Curran et al. have rationalized these results by a model very similar to the classical Felkin – Anh model developed for nucleophilic additions to carbonyl compounds.[42] The presence of a heteroatom at the stereogenic center enables chelation control. The first example of such a system is shown in Equation (7).[43] Under neutral conditions *u*-**41** is obtained in



71% *ds* according to the Felkin – Anh model. In the presence of $MgI_2 \cdot OEt_2$ a chelation-controlled reaction occurs and *l*-**41** is obtained in 94% *ds* (50% yield). The proposed model for this reaction **40r** is a radical analogue of the Cram cyclic model for nucleophilic additions.

A surprising result is obtained during the radical opening of the vinylcyclopropane **42**. After protodestannylation of the intermediate allylstannane, the monoprotected diol *l*-**43** is formed with a high (>95% *ds*) and unexpected stereoselectivity when Me_3Al is used as the additive [Eq. (8); PMP = p-methoxyphenol].[44] This major product formation cannot

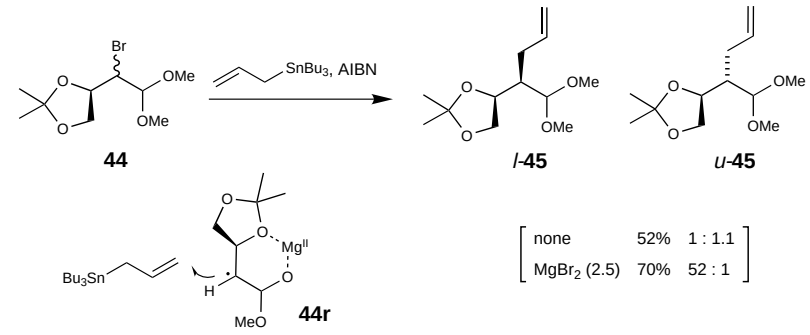


(8)

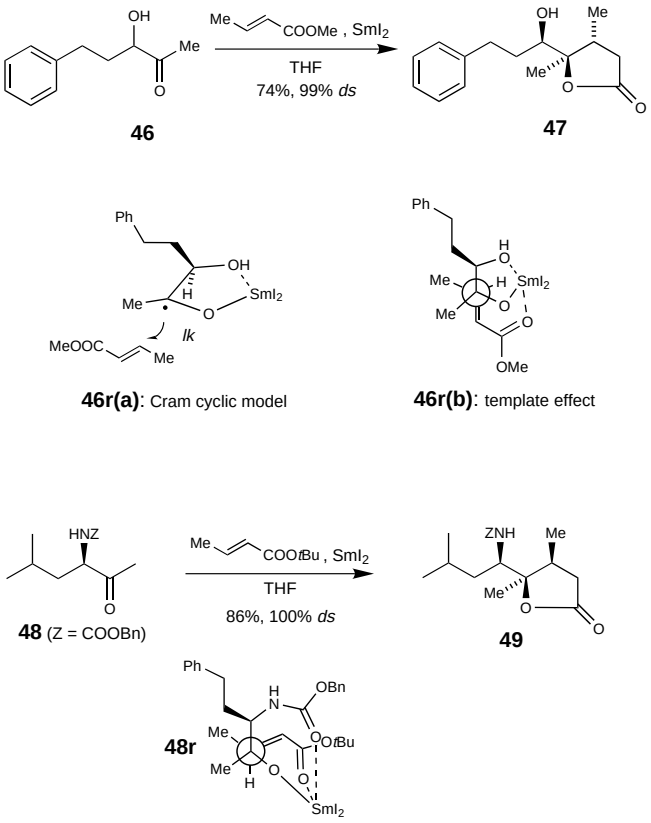
be rationalized by the Cram cyclic model. This result is best explained by invoking pyramidalization of the radical **42r** and attack from the more crowded face *syn* to the *tert*-butyl group (this may be called the "*anti* Cram cyclic model"). Indeed, steric interactions between the two vicinal alkyl groups are critical and dominate the interactions between the *tert*-butyl group and the incoming tin hydride.

Nagano and co-workers have reported highly stereoselective chelation-controlled allylation and deuteration of 2,2′-dialkoxy-substituted radicals.[45] The radical allylation of the bromoacetal **44** in the presence of 2.5 equivalents of $MgBr_2 \cdot OEt_2$ gives *l*-**45** (>98% *ds*; Scheme 9). The stereochemical outcome is best explained by the formation of the six-membered ring chelate **44r**.

Several chelation-controlled radical reactions of ketyl radicals generated by single electron reduction of ketones with samarium iodide are reported and included in recent reviews.[46] Only selected examples will be presented here. Two typical examples of 1,2-asymmetric induction are described in Scheme 10. Reduction of the α-hydroxy ketone **46**



Scheme 9. Chelate-controlled allylation of **44**.



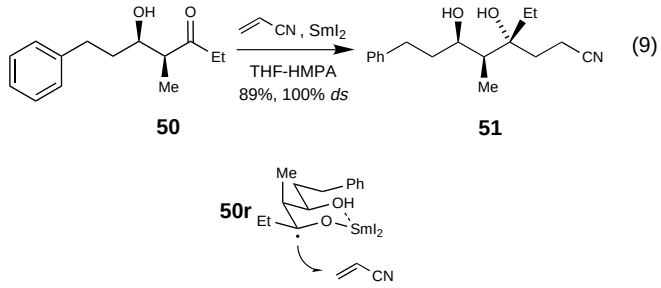
Scheme 10. Example of a 1,2-asymmetric induction.

with SmI_2 in the presence of methyl crotonate gave the lactone **47** with excellent stereocontrol.[47, 48] Formation of a five-membered ring by chelation of the samarium(III) ion explains the *like* topicity (*lk*) for the formation of the first new stereogenic center (see **46r(a)**, Cram cyclic model). The control of the second center occurs via coordination of the ester group of methyl crotonate with the samarium(III) cation as shown in **46r(b)**. The samarium not only controls the conformation of the radical, it also brings the radical trap into the proximity of the radical center (template effect). Similar chelation control coupled with template effects are also observed with 1-aminoketones derivatives. Treatment of **48** with SmI_2 in the presence of *tert*-butyl crotonate gives the lactone **49** as one of the four possible isomers.[48] The stereoselectivity is best explained by chelation and complexation of the radical trap to the samarium cation as shown in **48r**.[49].

Six-membered ring chelates are also proposed when β-hydroxyketones are employed. A typical example is reported in Equation (9) (HMPA = hexamethylphosphoramide). The β-hydroxyketone **50** is coupled to acrylonitrile under SmI_2 reductive conditions to give **51** with complete stereocontrol via the cyclic intermediate **50r**.[50]

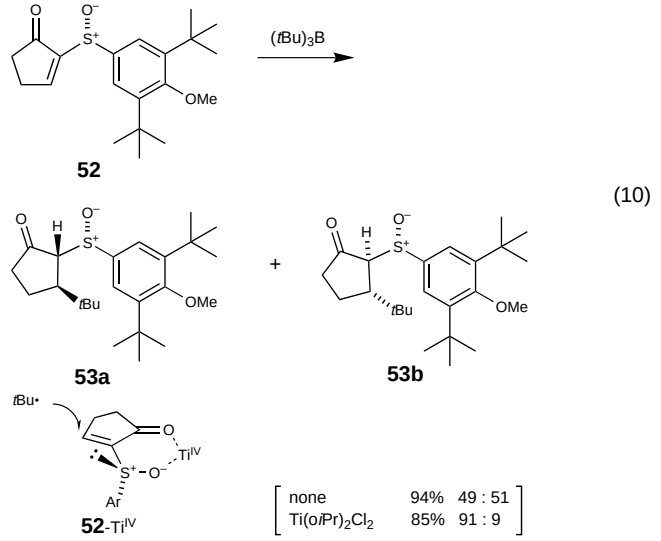
3.2.2. Complexed Olefins

Chelation control during radical addition to chiral olefins has also been investigated. Toru and co-workers have reported high β-stereo-



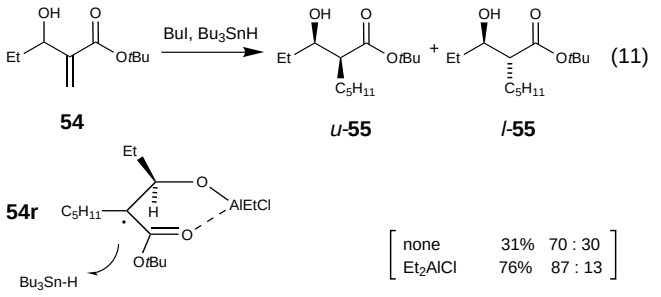
(9)

selectivity in the radical addition to 2-arylsulfinylcyclopentenone **52** in the presence of Lewis acids such as $TiCl_2(OiPr)_2$ (92% ds), ZnBr2, $MgCl_2$, and $ZrCl_4$ [Eq. (10)].[51] The α-diastereoselectivity of radical addition to a α,β-unsaturated



(10)

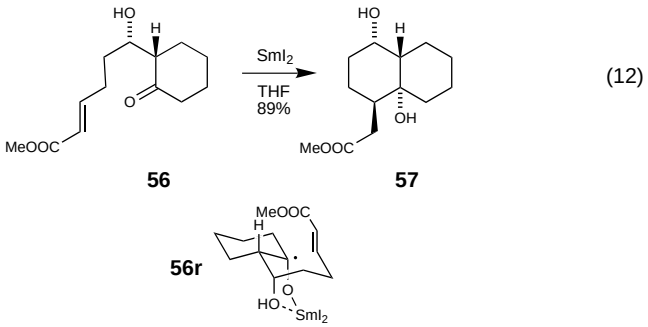
ester such as **54** can also be controlled by Lewis acids [Eq. (11)]. For example, the use of Et_2AlCl provides the *unlike* isomer *u*-**55** as the major product (70 →87% *ds*) via the cyclic radical **54r**.[17] Again, the complexation is beneficial for the yield of the reaction (31 →76%).



(11)

3.2.3. Cyclization Reactions

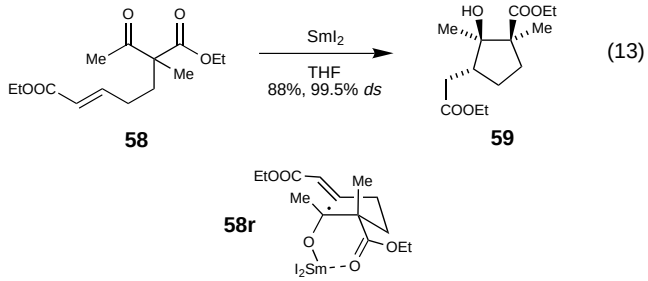
The only examples reported in this area concern the SmI_2-promoted cyclization of ketyl radicals. The recent review of Molander et al.[1h] treats this point in detail and only selected examples will be presented here. Three important reaction classes will be discussed. The first class is the hydroxy-directed intramolecular ketone – olefin coupling.[52–54] One typical example is reported in Equation (12). Treatment of ketone



(12)

56 with SmI_2 affords the *trans* bicyclic compound **57** in 89% yield.[52] The stereochemistry is best explained by the six-membered ring chelate **56r**.

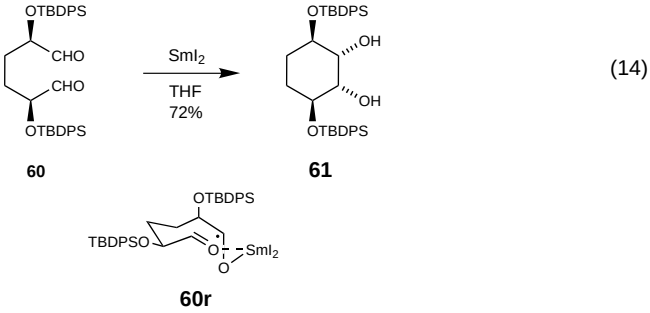
The cyclization of β-dicarbonyl substrates is a second example where chelation is used to achieve excellent yields and control of the stereochemistry. Molander et al. have for example reported the highly stereocontrolled cyclization of β-ketoester **58** to the polysusbtituted cyclopentane **59** [Eq. (13)].[55] Chelation of the samarium(III) ion produces



(13)

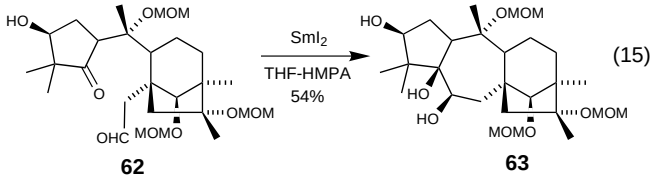
the six-membered ring ketyl intermediate which cyclizes via the chairlike transition state **58r** according to the well established Beckwith – Houk model.[32]

A third class of radical reactions which can be run under chelation control is the pinacolic coupling. For instance, the intramolecular McMurry-type pinacol coupling gives stereoselectivities that arise from chelation control.[56] Samarium iodide offers a very attractive alternative to the McMurry procedure.[57] Coupling of dialdehydes such as **60** yields the *cis*-diol **61** in good yield and excellent stereoselectivity [Eq. (14);



(14)

TBDPS = *tert*-butyldiphenylsilyl] via the 9-membered ring ketyl radical **60r**.[58] Matsuda et al. used a samarium mediated pinacol coupling as a key step in the synthesis of (−)-grayanotoxin III. For this purpose the ketoaldehyde **62** is treated with SmI_2 to afford the *cis*-diol **63** [Eq. (15); MOM = methoxymethyl].[59]

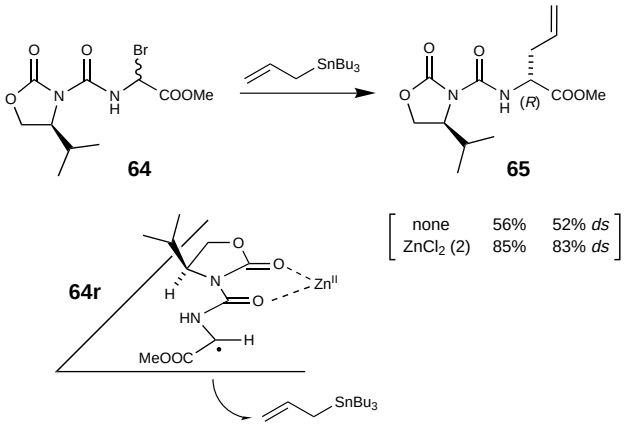


62 63 (15)

3.3. Chiral Auxiliaries

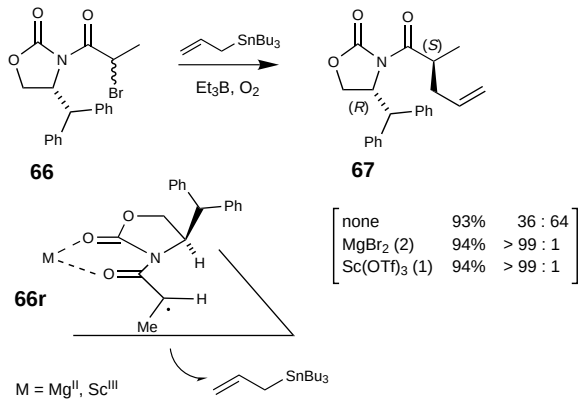
3.3.1. Intermolecular Reactions

The use of chiral auxiliaries proved to be particularly efficient for the preparation of enantiopure materials via radical reactions.[60] When the auxiliary is attached at the radical center excellent levels of stereocontrol have been obtained in conformationally restricted systems such as C_2-symmetric amides, sterically congested systems, and sulfonamides. Complexation with Lewis acids is a promising alternative for controlling radical conformation. Yamamoto et al. have shown that the allylation of the chiral glycine derivative **64** is stereoselective when run in the presence of zinc chloride (Scheme 11).[61] It is noted that zinc chloride also plays the role of a radical initiator.



Scheme 11. Increase in the stereoselctivity during the allylation of **64**.

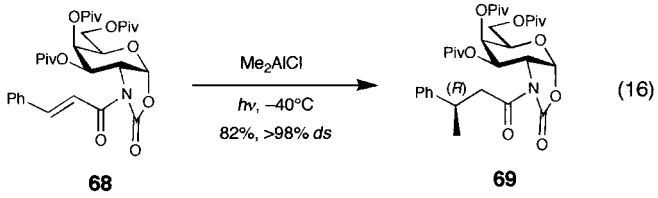
The use of oxazolidinone chiral auxiliaries in radical reactions in the presence of Lewis acids is very promising. Sibi and Ji have reported extraordinary high levels of stereoselectivity with an oxazolidinone derived from diphenylalaninol.[62] The allylation of **66** is not stereoselective in the absence of Lewis acids because of the existence of at least four rotamers of the radical intermediate (Scheme 12). In the presence of two equivalents of magnesium bromide or one equivalent of scandium triflate an excellent stereocontrol is reached and (*R,S*)-**67** is formed preferentially in over 99% *ds*.



Scheme 12. Increase in the stereoselctivity during the allylation of **66**.

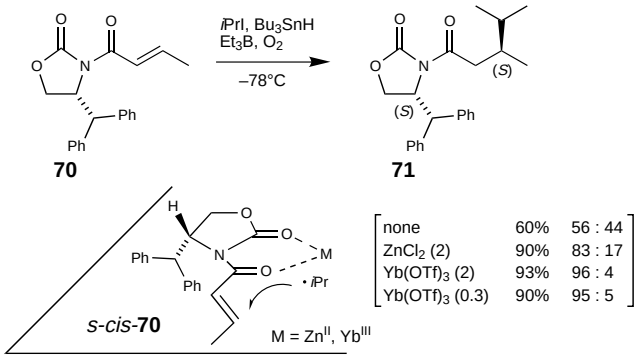
This result is explained by chelation of the Lewis acid with the bidentate radical ligand (see **66r**).

The chiral auxiliary can also be attached to the olefin moiety. This strategy offers several advantages and was investigated thoroughly for cycloaddition reactions. This work has provided important information on the conformation and the reactivity of activated alkenes in the presence of Lewis acids. Moreover, the enhanced basicity of unsaturated systems relative to saturated ones offers a possibility of catalysis.[63] Kunz and Rück have reported early examples of methyl radical additions to chiral oxazolidinones in the presence of Me_2AlCl.[64] Me_2AlCl is used in large excess and acts as a radical source and as a Lewis acid. Excellent diastereoselectivity has been obtained with the bicyclic carbohydrate oxazolidinone **68** [Eq. (16)].

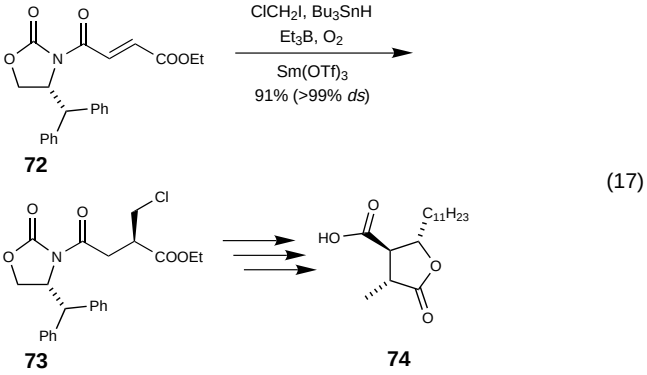


68 69 (16)

Sibi and Ji reported good α-stereoselectivity in radical additions to *N*-propenoyloxazolidinone; the stereocontrol is achieved via chelation control similar to the one described in Scheme 12.[65] The β-stereoselectivity can also be controlled in such systems. Radical addition to *N*-butenoyloxazolidinone **70** gives preferentially (*S,S*)-**71** in the presence of Lewis acids such as zinc chloride (83% *ds*) and ytterbium triflate (96% *ds*) (Scheme 13).[66] In this last case the use of only 0.3 equivalent of the Lewis acid leads to practically no drop in the stereoselectivity and yield. A further advantage of ytterbium triflate is its compatibility with small amounts of water, which is an important practical problem with classical Lewis acids, particularly for catalytic uses. The stereochemical outcome is best explained by the *Si*-face addition of the radical onto **70** lying preferentially in a s-*cis* conformation as a result of the complexation. This strategy was applied for the synthesis of (−)-nephrosteranic acid **74** from **72** [Eq. (17)].[67]

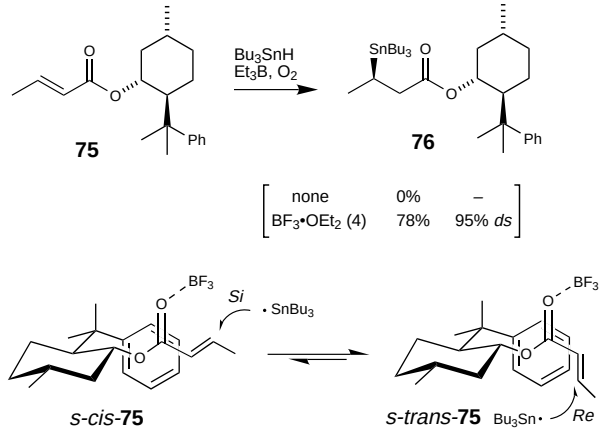


Scheme 13. Increase in the yield and stereoselctivity during the radical addition to **70**.



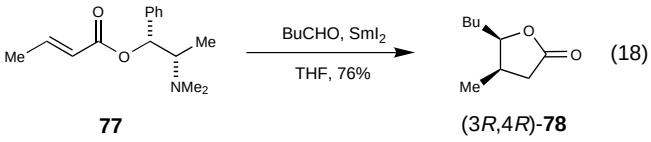
(17)

The use of ester-bound chiral auxiliaries in radical reactions is scarce because of the difficulties in controlling the conformation (*E*/*Z* and s-*cis*/s-*trans*). Nishida et al. reported a solution to this problem for the radical hydrostannylation of 8-phenylmenthyl crotonate **75**.[68] The use of $BF_3 \cdot Et_2O$ favors the s-*trans* conformation, and attack from the *Re* face is preferred (Scheme 14). A highly enantioselective γ-butyrolactone synthesis was developed by Fukuzawa et al. based on



Scheme 14. Example of the use of a chiral ester auxillary.

the samarium iodide promoted coupling of aldehydes and ketones with acrylate and crotonate esters derived from *N*-methylephedrine.[69] A typical example is presented in Equation (18). Addition of the ketyl radical derived from pentanal

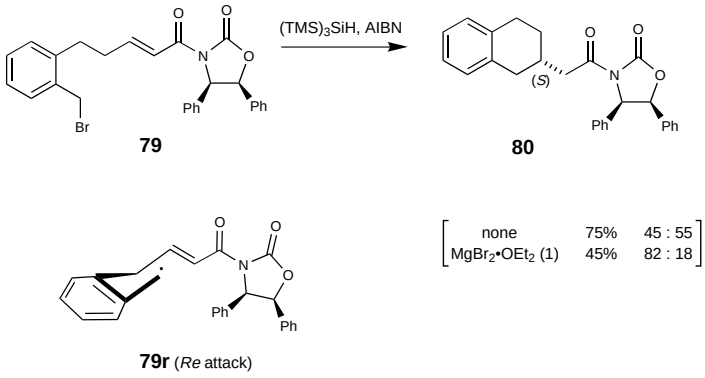


(18)

to crotonate **77** gives the disubstituted γ-butyrolactone **78** in a *cis*:*trans* ratio of 97:3 and with a 94% *ee* for the *cis* isomer. This represents a case where the face selectivity is very high, as well as the coupling of the two prochiral centers. It is worth noticing that the chiral auxiliary is cleaved cleanly during the lactonization step. The importance of samarium chelation in this process is demonstrated by the absence of selectivity when the reaction is run with HMPA as a cosolvent.

3.3.2. Cyclization Reactions

Radical cyclization of *N*-enoyloxazolidinone **79** has been examined by Badone et al. (Scheme 15).[70] The presence of $MgBr_2$ is necessary to obtain a moderate stereoselectivity and

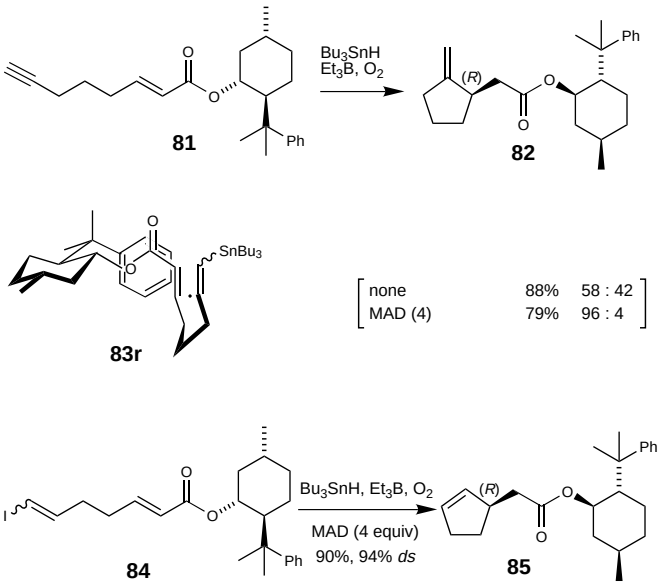


Scheme 15. Radical cyclization of **79**.

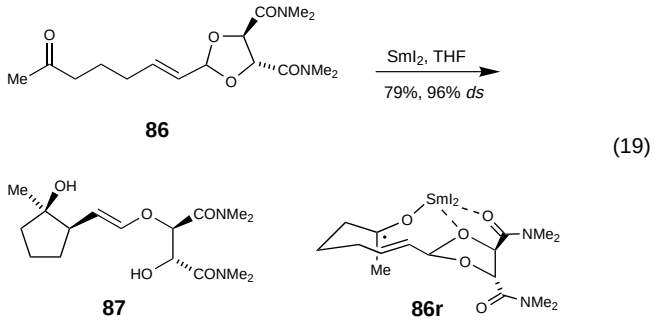
the stereochemical outcome of this reaction is rather surprising. Calculations have indicated that a chelated s-*cis* transition state is preferentially attacked from the *Re* face, presumably because of attractive van der Waals interactions between the arene groups.

Nishida and co-workers have also extended the use of unsaturated phenylmenthyl esters (see Scheme 14 for intermolecular reactions) to cyclization reactions. Good to excellent stereoselectivities are observed during cyclizations of vinyl radicals derived from **81** and **84** (Scheme 16).[71–73] The model is essentially similar to the one reported for intermolecular reactions, with the radical **83r** lying in a *Z* and s-*trans* conformation.

A unique reaction with tartramide acetals as chiral auxiliaries is reported by Molander et al.[74] Treatment of the keto acetal **86** with samarium iodide furnished the cyclopentanol derivative **87** in good yield and with excellent stereocontrol [Eq. (19); *cis*:*trans* = 99:1, 99% *ds* for the *cis* isomer]. The selectivity is rationalized by a highly ordered, tricyclic transition structure **86r** that is made possible by the tridentate nature of the ketyl intermediate.



Scheme 16. Radical cyclization of **81** and **84**.



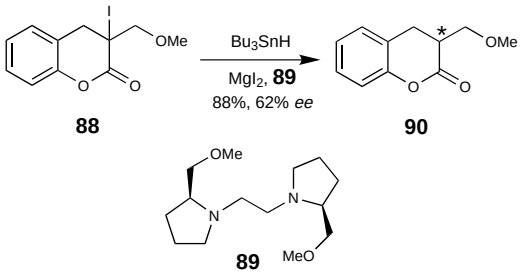
(19)

4. Enantioselective Reactions

Lewis acids have been widely used for highly enantioselective ionic and concerted reactions such as Diels–Alder reactions.[75] The development of enantioselective radical reactions mediated or eventually catalyzed by chiral Lewis acids represents a formidable challenge and preliminary experiments from several research groups have already been reported.

4.1. Complexed Radicals Generated by Homolysis of C–X Bonds

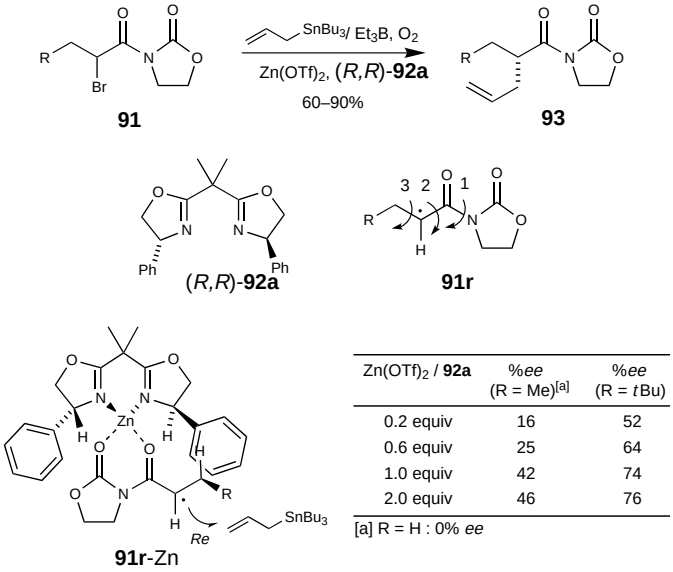
Hoshino and co-workers have reported the enantioselective reduction of the α-iodolactone **88** with tin hydride in the presence of one equivalent of MgI_2 and the diamine ligand **89** [Eq. (20)].[76] Lactone **90** is formed in 88% yield and 62% *ee*. This system offers several important features for enantioselective reactions: first, the cyclic nature of the substrate restricts the number of possible radical conformations. Second, the methoxy group is expected to allow chelation of the Lewis acid and result in a very well defined radical



(20)

conformation. Interestingly, a substoichiometric amount of MgI_2/**89** (0.5 equivalent) leads to a substantial enantioselectivity (52% *ee*).

In a recent paper Porter et al. have described the enantioselective allylation of *N*-(α-bromoalkanoyl) oxazolidinones of type **91** in the presence of zinc triflate and bisoxazoline ligands (*R,R*)-**92a** (Scheme 17).[77] The enantioselectivity depends on

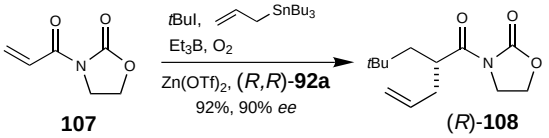


$Zn(OTf)_2$ / **92a**	%*ee* (R = Me)[a]	%*ee* (R = *t*Bu)
0.2 equiv	16	52
0.6 equiv	25	64
1.0 equiv	42	74
2.0 equiv	46	76

[a] R = H : 0% *ee*

Scheme 17. Enantioselective radical allylation.

the size of the R group and on the quantity of chiral Lewis acid, thus suggesting that an equilibrium between the bromide **91** and the Lewis acid precedes the formation of the radical **91r**. The moderate enantioselectivity is explained by a nonselective background reaction involving noncomplexed **91** competing with the Lewis acid promoted reaction. Better enantioselectivities are obtained when the same radicals are formed by radical addition to acryloyloxazolidinone [Eq. (21)]. Chelation of the zinc atom allows rotation 1

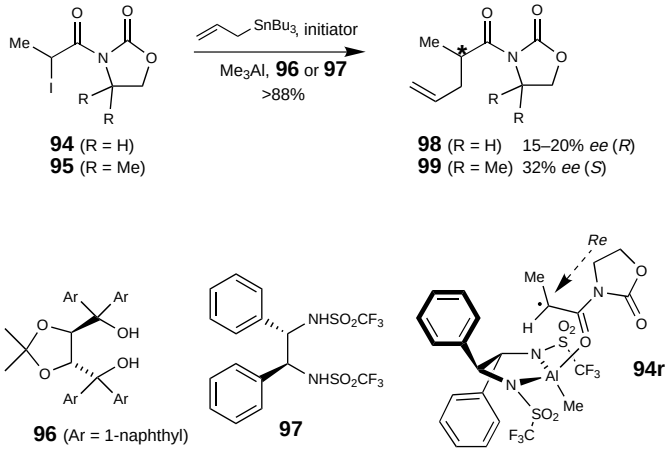


(21)

around the N–C(O) bond of radical **91r** to be controlled. Interestingly, the rotation 2 around the C(O)–C(2) bond is also controlled by the complexation, and the s-*cis* conformer

is favored (this phenomenon is well documented for the complexation of unsaturated esters and amides.[78, 79]) Rotation 3 around the C(2)–C(3) bond is controlled by allylic 1,3-strain. Based on these considerations, the model **91r**–Zn model complex is proposed to account for the preferential *Re*-face allylation.

The allylation of *N*-(α-iodopropionyl)oxazolidinones **94** and **95** was investigated by us (Scheme 18).[80] The resulting radicals **94r** and **95r** were allylated with low enantioselectivities (up to 34% *ee*). An analogy can be drawn between the



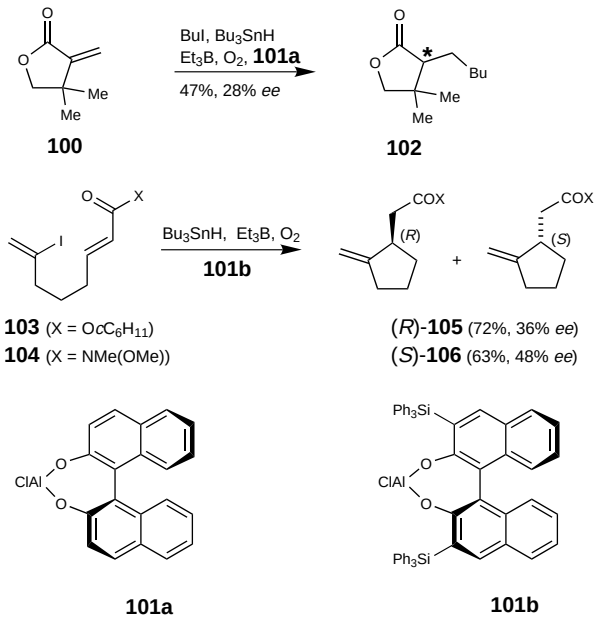
Scheme 18. Allylation of **94** and **95**.

reaction with the Corey (*S*,*S*)-bistriflamide **97** as ligand and the Diels–Alder reaction.[81] A similar model based on the monocomplexation of the radical at the exocyclic carbonyl group and the radical lying in a s-*trans* conformation is proposed. The reactions with TADDOL **96** as the ligand are more difficult to rationalize at the moment.

4.2 Radical Additions to Complexed Olefins

Sato et al. have reported the radical addition to methylene lactone **100** in the presence of aluminum binolate **101a**.[17] α-Alkylated lactone **102** is obtained in a 28% *ee* (Scheme 19). Nishida et al. has reported an intramolecular addition in the presence of four equivalents of aluminum binolate **101b** to the α,β-unsaturated ester **103** with a 36% *ee*.[82] The Weinreb amide **104** gives a similar enantioselectivity (48% *ee*) under identical conditions, but the sense of induction is opposite. These results were rationalized by assuming s-*trans* and s-*cis* conformations of the ester and amide radicals, respectively.

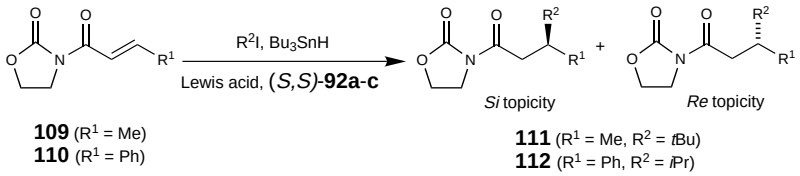
Addition of the *tert*-butyl radical to acrylamide **107** followed by allylation in the presence of bisoxazoline **92a** furnished the amide **108** in excellent

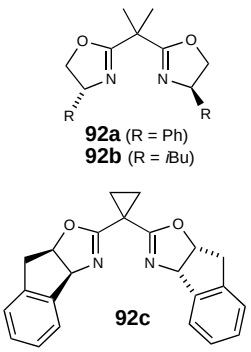


Scheme 19. Additions to a complexed olefin.

yield and enantioselectivity (90% *ee*) [Eq. (21)].[83] Interestingly, this reaction gives much higher selectivities than the allylation of the corresponding bromide **91** described in Scheme 17.[77, 83] This observation is explained by the stronger basicity of enoyloxazolidinone relative to alkanoyloxazolidinone, and by the enhanced reactivity of complexed enoyl systems towards radicals relative to the noncomplexed forms. This reactivity enhancement is certainly less pronounced or even nonexistent for the bromine atom abstraction step when **91** is used as the radical precursor.

The first example of β-enantioselectivity was reported by Sibi and Porter et al.[84] Addition of alkyl radicals to **109** and **110** gives promising *ee* values of up to 82% in the presence of bisoxazolines **92a** and **92b** (Scheme 20). Substoichiometric quantities of Lewis acids (down to 0.05 equivalent) still give a





Substrate / product	Topicity	Lewis acid	Ligand	T [°C]	% Yield	%*ee*
109 / **111**	*Re*	$Zn(OTf)_2$ (1.0)	**92a**	–78	90	82
109 / **111**	*Re*	$Zn(OTf)_2$ (0.2)	**92a**	–78	71	70
109 / **111**	*Re*	$MgBr_2$(1.0)	**92a**	–78	78	82
110 / **112**	*Re*	MgI_2(1.0)	**92a**	–78	88	47
110 / **112**	*Si*	MgI_2(1.0)	**92b**	–78	88	74
110 / **112**	*Si*	MgI_2(0.05)	**92b**	–78	57	40
110 / **112**	*Re*	MgI_2(0.30)	**92c**	–78	91	97
110 / **112**	*Re*	MgI_2(0.05)	**92c**	–78	92	90
110 / **112**	*Re*	MgI_2(0.30)	**92c**	25	87	93

Scheme 20. β-Enantioselective radical addition.

40 % *ee*. Zinc and magnesium are the best metals for this reaction. The rationalization of the results is complicated by the fact that homochiral bisoxazolines bearing aryl (**92a**) and alkyl (**92b**) substituents give opposite reaction topicities. More recently, Sibi and Ji have optimized the reactions.[85] An excellent enantioselectivity of 97 % *ee* is obtained with the ligand **92c** and MgI_2 at $-78\,^{\circ}C$ with 30 mol % of catalyst. The reaction is truly catalytic since an *ee* of 90 % is reached with only 5 mol % of catalyst. Moreover, an enantioselectivity of 93 % *ee* is still obtained with 30 mol % of catalyst at room temperature. A model is proposed where the ligand–MgI_2 complex adopts an octahedral geometry.[86]

5. Summary and Outlook

The use of Lewis acids in radical reactions is opening new applications for this type of chemistry in general organic synthesis and particularly in asymmetric synthesis. The growth of this strategy has developed quickly, particularly if we consider the number of parameters which have to be fulfilled. Radical chain reactions are complex from a kinetic point of view and electron transfer reactions between radicals and the Lewis acid metal centers have to be avoided. Fortunately, several different kinds of Lewis acids based on main group, lanthanides, and other transition metals have proved to be compatible with radical reactions. In numerous examples yield enhancement is observed and highly efficient radical additions to olefins are reported at low temperatures ($-78\,^{\circ}C$ or lower). Moreover, several preliminary results indicate that catalysis of radical reactions is possible. Up to now this point was mainly demonstrated for the radical addition to complexed olefins. However, the possibility of the catalysis of atom abstraction reactions also exists. These catalytic effects are of considerable importance for the development of enantioselective radical reactions.

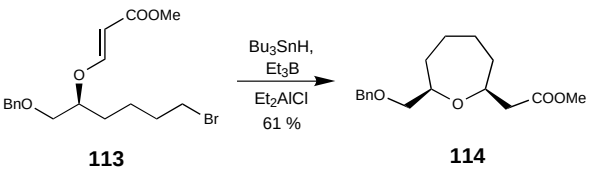
Another noteworthy point for future applications of radical reactions controlled by Lewis acids is their incorporation into reaction cascades. Indeed, formation of several bonds in a one-pot procedure is typical of radical chemistry, and highly attractive from a synthetic point of view. Lewis acids may be used to control the chemo- regio- and stereoselectivity of such processes.

Addendum

During the edition of this manuscript several examples of radical reactions that are controlled by Lewis acids have been reported. These new results are described below following the organization of the main part of the review.

Addendum to Section 2

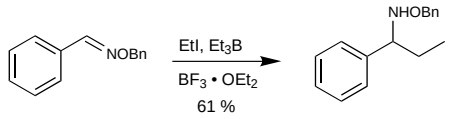
Rate enhancement of intramolecular additions to α,β-unsaturated esters have been reported.[86] For example, starting from the β-alkoxyacrylate **113** the oxepane **114** is obtained in 61 % in the presence of Et_2AlCl at $0\,^{\circ}C$ [Eq. (22); no product is observed at this temperature in the absence of the Lewis acid]. Several reports of intermolecular radical additions to imines and oxime ethers have appeared. Efficient



(22)

113 **114**

rate enhancements are obtained with simple aldoxime ethers;[87] treatment of the aldoxime ether **115** with Et_3B/EtI proceeds smoothly in the presence of $BF_3 \cdot OEt_2$ to give **116** in 61 % yield while in the absence of a Lewis acid it is formed in only 19 % [Eq. (23)]. This reaction compares favorably with

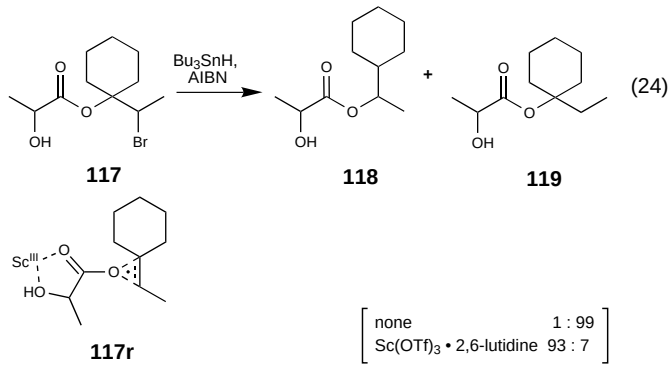


(23)

115 **116**

anionic reactions based on traditional organometallic reagents, particularly when the tolerance of functional groups is considered. Interestingly, this reaction does not require the use of tin hydride when ethyl radicals are added. A similar effect has been reported recently by Bertrand et al. and a chain mechanism involving the formation of ethyl radicals directly from Et_3B and the intermediate nitrogen-centered radical is proposed.[88] Lewis acids have only a marginal effect on the rate and stereoselectivity of radical additions to imines and oxime ethers derived from glyoxylic acid.[88, 89]

The results of reactivity enhancement are best rationalized by the enhancement of the eletrophilic character of the complexed radical or the complexed radical trap. Stabilization of a polarized transition state of a radical reaction represents an alternative explanation that has been examined recently. Lewis acids can enhance efficiently the rate of the 1,2-acyloxy shift of β-(alkoxy)alkyl radicals (Surzur–Tanner rearrangement). Rate enhancement of up to three orders of magnitude have been observed.[90] A typical example is reported in Equation (24). The lactate **117** gives upon reduction with tin



(24)

117 **118** **119**

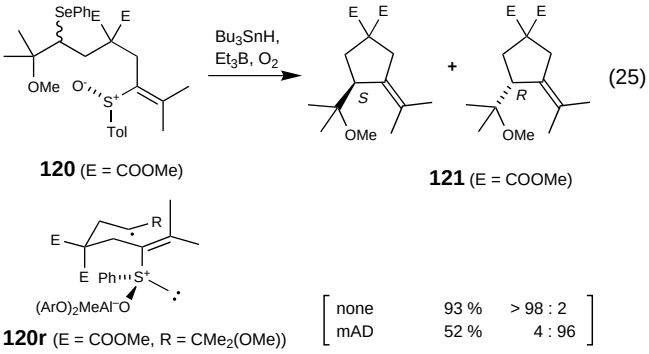
117r

hydride, **118** (rearranged product) and **119** (product of direct reduction) in a 1:99 ratio. In the presence of scandium(III) triflate the rearranged product **118** predominates (**118**:**119** = 93:7). Since the synthetic applications of the Surzur–Tanner rearrangement is severely limited by its slowness, the use of Lewis acids are expected to broaden its scope. Interestingly,

calculations predict that a three-center mechanism (**117r**) is favored by protonation of the ester carbonyl group.[91] This may have some interesting consequences on the stereochemistry of this rearrangement.

Addendum to Section 3.1.3

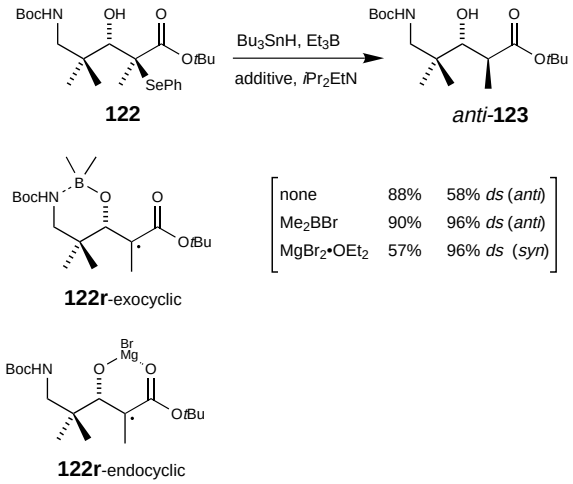
Malacria et al. have reported a radical cyclization–β-elimination tandem process leading to optically active methylenecyclopentane derivatives.[92] The stereochemical outcome of the reaction can be nicely reversed by the use of monocomplexation with the bulky Lewis acid MAD [Eq. (25)]: Cyclization of the alkenyl sulfoxide **120** gives (*S*)-**121** (96% *ee*) in the absence of a Lewis acid while in the



presence of MAD (*R*)-**121** is obtained in a 92% *ee* with a moderate yield. Monocomplexation of the sulfoxides according to **120r** rationalizes this result.

Addendum to Section 3.2.1

An elegant control of the configuration of β-hydroxy-γ-amino ester enolate radicals was reported by Guindon et al.[93] the proper choice of the Lewis acid allows the switch from an endocyclic radical to an exocyclic radical (Scheme 21). For example, reduction of the selenoester **122** in the absence of Lewis acid gives *anti*-**123** with a low diastereoselectivity (58% *ds*), while in the presence of Me_2BBr the *anti* isomer is



Scheme 21. The change from an endocyclic to an exocyclic radical by changing the Lewis acid.

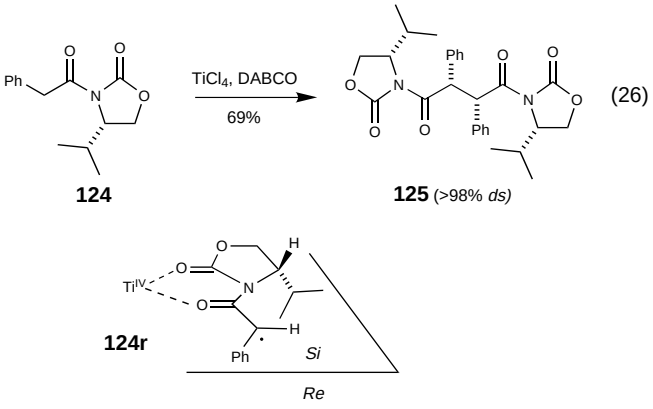
strongly favored (96% *ds*) as a consequence of the formation of an exocyclic radical (**122r**-exocyclic). A reversal of the stereoselectivity is observed with the more oxophilic $MgBr_2 \cdot OEt_2$ (*syn*-**123**, 96% *ds*). This can be explained by the formation of an endocyclic intermediate radical (**122r**-endocyclic).

Addendum to Section 3.2.2

Toru and co-workers have reported full details of this work on cyclic 2-(arylsulfinyl)-2-cycloalkenones[94] [Eq. (10)] as well as related reactions in acyclic systems where hydrogen bonds are playing a key role.[95]

Addendum to Section 3.3

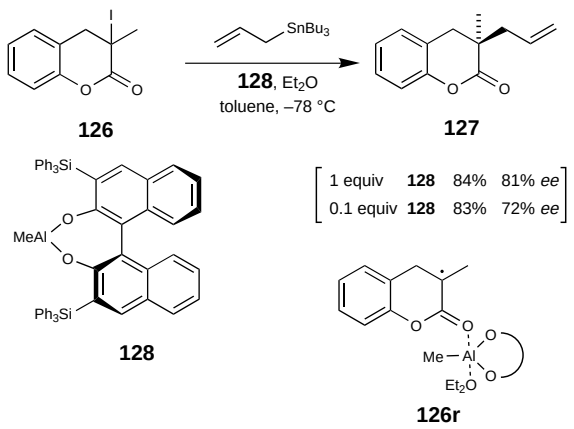
A highly stereoselective oxidative dimerization of in situ generated titanium enolate bearing an oxazolidine chiral auxiliary has been described by Kise et al.[96] Treatment of the *N*-(phenylacetyl)oxazolidinone **124** with $TiCl_4$ gives the dimer (*S,S*)-**125** as a single diastereomer [Eq. (26); DABCO = 1,4-diazabicyclooctane]. The stereochemical outcome is best



rationalized by reaction of the chelate radical **124r** from the less hindered *Si* face. Further investigation of the use of chiral esters have been published,[97, 98] and these results confirm the conclusions from the work of Nishida et al. (Schemes 14 and 16).

Addendum to Section 4

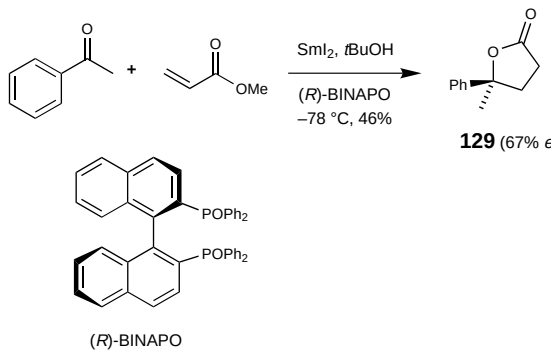
Hoshino et al. have reported an extension of his previous work [Eq. (20)] by performing allylation reactions in the presence of Me_3Al/3,3′-bis(triphenylsilyl)binaphthol **128**.[99] Enantiomeric excesses of up to 91% are obtained. As a typical example, the α-iodolactone **126** is allylated to **127** in 84% yield and 81% *ee* in the presence of one equivalent of **128** (Scheme 22). The degree of asymmetric induction depends dramatically on the presence of one equivalent of Et_2O as additive. Therefore, formation of an unusual five-coordinate aluminum complex was postulated (**126r**), which contrasts with the well-known tendency of aluminum to form four-coordinate complexes. Another interesting aspect of this work is that less than stoichiometric amounts of Lewis acid are able to induce a fair level of induction: **127** is obtained in 72% *ee* when only 0.1 equivalent of the Lewis acid **128** is used.



Scheme 22. Et_2O-dependent allylation of the iodolactones.

Porter et al. have further developed the reaction depicted in Scheme 17. They observed that allylsilanes give higher enantioselectivities than allylstannanes for the allylation of oxazolidinone derivatives.[100] The Lewis acid character of the stannyl bromide byproduct is detrimental to the transformation. This undesired effect can be efficiently suppressed by using the iodide as the starting material. Sibi et al. have investigated the use of pyrazole templates instead of oxazolidinone for β-enantioselectivity.[101] However, the observed enantioselectivities are inferior (and inverse) to those observed with oxazolidinone (Scheme 20).

The first example of an enantioselective samarium diiodide mediated ketyl radical addition to an olefin has been reported by Mikami and Yamakoa.[102] Addition of acetophenone to methyl acrylate furnishes the lactone **129** in 46% yield and 67% *ee* [Eq. (27)]. Two equivalents of the chiral ligand (*R*)-BINAPO are necessary to reach this enantioselectivity.



(27)

The authors thank the Swiss National Science Foundation who supported their work within the Project 20-45'755.95 and the CHiral2 project 20-48'164.96. M.G is very grateful to the Stipendienfonds der Chemischen Industrie Basel for financial support. We are also indebted to Prof. K. Maruoka, Prof. M. Malacria, and Prof. M. P. Sibi for allowing us to cite some of their works not yet published when this manucript was written.

Received: July 7, 1997
Addendum: July 24, 1998 [A240IE]
German version: *Angew. Chem.* **1998**, *110*, 2704 – 2722

[1] Recent review articles: a) B. Giese, *Radicals in Organic Synthesis: Formation of Carbon – Carbon Bonds*, Pergamon, Oxford, **1986**; b) G. Pattenden, *Chem. Soc. Rev.* **1988**, *17*, 361 – 382; c) D. P. Curran in *Comprehensive Organic Synthesis*, *Vol. 4* (Eds.: B. M. Trost, I. Fleming, M. F. Semmelhock), Pergamon, Oxford, **1991**, p. 715; d) C. P. Jasperse, D. P. Curran, T. L. Fevig, *Chem. Rev.* **1991**, *91*, 1237 – 1286; e) W. B. Motherwell, D. Crich, *Free-Radical Reactions in Organic Synthesis*, Academic Press, London, **1992**; f) A. L. J. Beckwith, *Chem. Soc. Rev.* **1993**, 143 – 151; g) G. G. Melikyan, *Synthesis* **1993**, 833 – 850; h) G. A. Molander, C. R. Harris, *Chem. Rev.* **1996**, *96*, 307 – 338; i) B. B. Snider, *Chem. Rev.* **1996**, *96*, 339 – 363; j) S. Z. Zard, *Angew. Chem.* **1997**, *109*, 723 – 737; *Angew. Chem. Int. Ed. Engl.* **1997**, *36*, 673 – 685.

[2] a) B. Giese, *Angew. Chem.* **1989**, *101*, 993 – 1104; *Angew. Chem. Int. Ed. Engl.* **1989**, *28*, 969 – 1146; b) N. A. Porter, B. Giese, D. P. Curran, *Acc. Chem. Res.* **1991**, *24*, 296 – 304; c) T. V. RajanBabu, *Acc. Chem. Res.* **1991**, *24*, 139 – 145; d) W. Smadja, *Synlett* **1994**, 1 – 26; e) D. P. Curran, N. A. Porter, B. Giese, *Stereochemistry of Radical Reactions*, VCH, Weinheim, **1996**.

[3] B. Giese, *Angew. Chem.* **1983**, *95*, 771 – 782; *Angew. Chem. Int. Ed. Engl.* **1983**, *22*, 753 – 764.

[4] J. Penelle, A. B. Padias, J. H. K. Hall, H. Tanaka, *Adv. Polym. Sci.* **1992**, *102*, 73 – 103.

[5] *Alternating Copolymers* (Eds.: J. M. G. Cowie), Plenum, New York, **1985**.

[6] C. H. Bamford, S. Brumby, R. P. Wayne, *Nature* **1966**, *209*, 292 – 294; C. H. Bamford in ref. [5], pp. 75 – 152.

[7] M. Hirooka, H. Yabuuchi, S. Morita, S. Kawasumi, K. Nakaguchi, *J. Polym. Sci. Part B* **1967**, *5*, 47 – 55.

[8] M. Hirooka, K. Mashita, T. Kato, T. Kondo, S. Yasui, S. Morita, *ACS Polymer Preprints* **1978**, *19*, 3.

[9] M. Kuroki, T. Watanabe, T. Aida, S. Inoue, *J. Am. Chem. Soc.* **1991**, *113*, 5903 – 5904.

[10] K. Maruoka, M. Akakura, H. Yamamoto, *Synlett* **1995**, 81 – 82.

[11] M. B. Gasc, A. Lattes, J. J. Perie, *Tetrahedron* **1983**, *39*, 703 – 731; M. Newcomb, T. M. Deeb, *J. Am. Chem. Soc.* **1987**, *109*, 3163 – 3165; M. Newcomb, M. U. Kumar, *Tetrahedron Lett.* **1990**, *31*, 1675 – 1678; M. Newcomb, T. M. Deeb, D. J. Marquardt, *Tetrahedron* **1990**, *46*, 2317 – 2328; M. Newcomb, D. J. Marquardt, T. M. Deeb, *Tetrahedron* **1990**, *46*, 2329 – 2344; M. Newcomb, D. J. Marquardt, M. U. Kumar, *Tetrahedron* **1990**, *46*, 2345 – 2352; B. J. Maxwell, C. H. Schiesser, B. A. Smart, J. Tsanaktsidis, *J. Chem. Soc. Perkin Trans. 2* **1994**, 2385 – 2387.

[12] M. Newcomb, C. Ha, *Tetrahedron Lett.* **1991**, *32*, 6493 – 6496.

[13] B. J. Maxwell, J. Tsanaktsidis, *J. Chem. Soc. Chem. Commun.* **1994**, 533 – 534; W. R. Bowman, P. T. Stephenson, A. R. Young, *Tetrahedron* **1996**, *52*, 11 445 – 11 462. See also the reaction in the presence of redox systems: F. Minisci, *Acc. Chem. Res.* **1975**, *8*, 165 – 171; J.-L. Bourgeois, L. Stella, J.-M. Surzur, *Tetrahedron Lett.* **1981**, *22*, 61 – 64; L. Stella, *Angew. Chem.* **1983**, *95*, 368 – 80; *Angew. Chem. Int. Ed. Engl.* **1983**, *22*, 337 – 349.

[14] A detailed discussion of the Lewis acid activation of dialkylaminyl radical reactions appeared after the writing of our manuscript: C. Hau, O. M. Musa, F. N. Martinez, M. Newcomb, *J. Org. Chem.* **1997**, *62*, 2704 – 2710.

[15] T. Clark, *J. Chem. Soc. Chem. Commun.* **1986**, 1774 – 1776.

[16] K. S. Feldman, A. L. Romanelle, J. R. E. Ruckle, G. Jean, *J. Org. Chem.* **1992**, *57*, 100 – 110.

[17] H. Urabe, K. Yamashita, K. Suzuki, K. Kobayashi, F. Sato, *J. Org. Chem.* **1995**, *60*, 3576 – 3577.

[18] J.-P. Vionnet, K. Schenk, P. Renaud, *Helv. Chim. Acta* **1993**, *76*, 2490 – 2499.

[19] A. Waldner, A. De Mesmaeker, P. Hoffmann, T. Mindt, T. Winkler, *Synlett* **1991**, 101 – 104.

[20] P. Renaud, M. Ribezzo, *J. Am. Chem. Soc.* **1991**, *113*, 7803 – 7805.

[21] P. Renaud, N. Moufid, L. H. Kuo, D. P. Curran, *J. Org. Chem.* **1994**, *59*, 3547 – 3552.

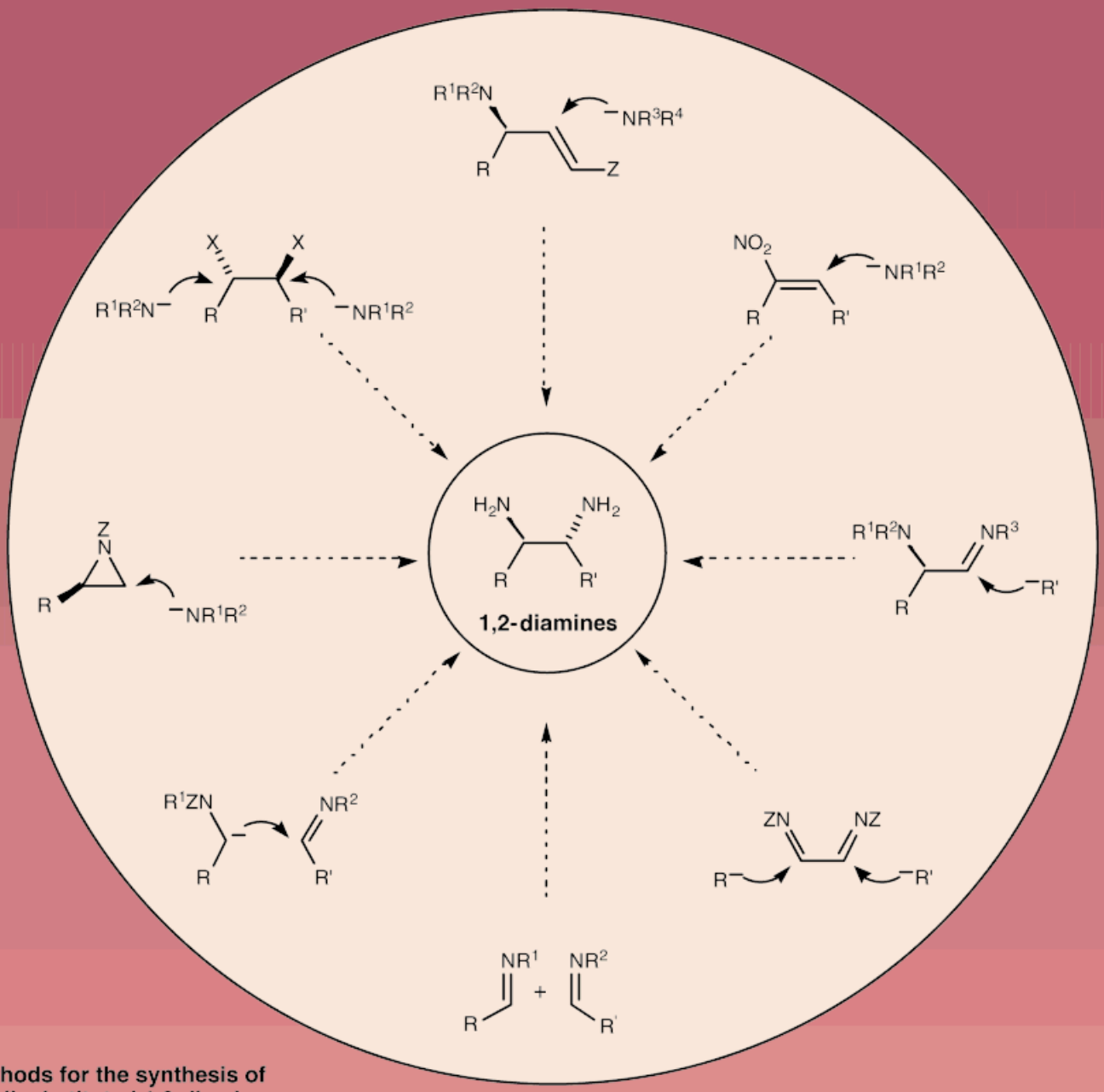
[22] Giese has reported early examples of solvation effects in reactions of 2-ethoxy- und 2-hydroxy substituted cyclic Radicals.[2a]

[23] D. P. Curran, L. H. Kuo, *J. Org. Chem.* **1994**, *59*, 3259 – 3261.

[24] N. Moufid, P. Renaud, *Helv. Chim. Acta* **1995**, *78*, 1001 – 1005.

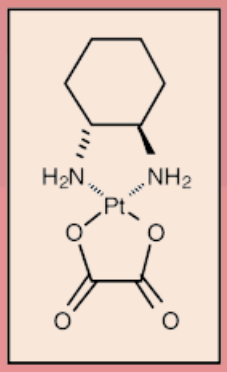
[25] For a related early example involving lithium alcoholate see ref. [1a], p. 63.
[26] H. Urabe, K. Kobayashi, F. Sato, *J. Chem. Soc. Chem. Commun.* **1995**, 1043 – 1044.
[27] B. Giese, W. Damm, R. Batra, *Chemtracts: Org. Chem.* **1994**, *7*, 355 – 370.
[28] N. Moufid, P. Renaud, C. Hassler, B. Giese, *Helv. Chim. Acta* **1995**, *78*, 1006 – 1012.
[29] P. Renaud, T. Bourquard, M. Gerster, N. Moufid, *Angew. Chem.* **1994**, *106*, 1680 – 1682; *Angew. Chem. Int. Ed. Engl.* **1994**, *33*, 1601 – 1603; P. Renaud, T. Bourquard, P. A. Carrupt, M. Gerster, *Helv. Chim. Acta* **1998**, *81*, 1048 – 1063; P. Renaud, *Chimia* **1997**, *51*, 236 – 238.
[30] P. Renaud, P. Björup, P.-A. Carrupt, K. Schenk, S. Schubert, *Synlett*, **1992**, 211 – 213; S. Schubert, P. Renaud, P.-A. Carrupt, K. Schenk, *Helv. Chim. Acta* **1993**, *76*, 2473 – 2489.
[31] T. Ooi, Y. Hokke, K. Maruoka, *Angew. Chem.* **1997**, *109*, 1230 – 1231; *Angew. Chem. Int. Ed. Engl.* **1997**, *36*, 1183 – 1185.
[32] A. L. J. Beckwith, C. H. Schiesser, *Tetrahedron* **1985**, *41*, 3925 – 3941; D. C. Spellmeyer, K. N. Houk, *J. Org. Chem.* **1987**, *52*, 959 – 974.
[33] M. P. Sibi, J. G. Ji, *J. Am. Chem. Soc.* **1996**, *118*, 3063 – 3064.
[34] D. J. Hart, H.-C. Huang, *Tetrahedron Lett.* **1985**, *26*, 3749 – 3752; D. J. Hart, H.-C. Huang, R. Krishnamurthy, T. Schwarz, *J. Am. Chem. Soc.* **1989**, *111*, 7507 – 7519.
[35] D. J. Hart, R. Krishnamurthy, *J. Org. Chem.* **1992**, *57*, 4457 – 4470.
[36] Y. Guindon, J.-F. Lavallée, M. Llinas-Brunet, G. Horner, J. Rancourt, *J. Am. Chem. Soc.* **1991**, *113*, 9701 – 9702.
[37] Y. Guindon, B. Guerin, C. Chabot, N. Mackintosh, W. W. Ogilvie, *Synlett* **1995**, 449 – 451.
[38] Y. Guindon, B. Guérin, C. Chabot, W. Ogilvie, *J. Am. Chem. Soc.* **1996**, *118*, 12528 – 12535.
[39] H. Nagano, Y. Kuno, *J. Chem. Soc. Chem. Commun.* **1994**, 987 – 988; H. Nagano, Y. Kuno, Y. Omori, M. Iguchi, *J. Chem. Soc. Perkin Trans. 1* **1995**, 389 – 394.
[40] M. Gerster, L. Audergon, N. Moufid, P. Renaud, *Tetrahedron Lett.* **1996**, *37*, 6335 – 6338.
[41] Examples of hydrogen bonding in similar systems: D. P. Curran, A. C. Abraham, *Tetrahedron* **1993**, *49*, 4821 – 4840; D. P. Curran, P. S. Ramamoorthy, *Tetrahedron* **1993**, *49*, 4841 – 4858; S. Hanessian, H. Yang, R. Schaum, *J. Am. Chem. Soc.* **1996**, *118*, 2507 – 2508; E. P. Kündig, L. H. Xu, P. Romanens, *Tetrahedron Lett.* **1995**, *36*, 4047 – 4050.
[42] M. Chérest, H. Felkin, N. Prudent, *Tetrahedron Lett.* **1968**, 2199 – 2204; B. Giese, W. Damm, J. Dickhaut, F. Wetterich, S. Sun, D. P. Curran, *Tetrahedron Lett.* **1991**, *32*, 6097 – 6100; Y.-D. Wu, K. N. Houk, *J. Am. Chem. Soc.* **1992**, *114*, 1656 – 1661; J. E. Eksterowicz, K. N. Houk, *Tetrahedron Lett.* **1993**, *34*, 427 – 430; W. Damm, J. Dickhaut, F. Wetterich, B. Giese, *Tetrahedron Lett.* **1993**, *34*, 431 – 434.
[43] P. Renaud, M. Gerster, *J. Am. Chem. Soc.* **1995**, *117*, 6607 – 6608.
[44] M. Gerster, K. Schenk, P. Renaud, *Angew. Chem.* **1996**, *108*, 2523 – 2525; *Angew. Chem. Int. Ed. Engl.* **1996**, *35*, 2396 – 2399.
[45] H. Nagano, Y. Azuma, *Chem. Lett.* **1996**, 845 – 846.
[46] a) Reference [1h]; b) F. Matsuda, *J. Synth. Org. Chem. Jpn.* **1995**, *53*, 987 – 998.
[47] M. Kawatsura, F. Matsuda, H. Shirahama, *J. Org. Chem.* **1994**, *59*, 6900 – 6901.
[48] M. Kawatsura, F. Deckura, H. Shirahama, F. Matsuda, *Synlett* **1996**, 373 – 376.
[49] See also: C. Alvarez-Ibarra, A. G. Csakÿ, I. Lopez de Silanes, M. L. Guiroga, *J. Org. Chem.* **1997**, *62*, 479 – 484.
[50] M. Kawatsura, K. Hosaka, F. Matsuda, H. Shirahama, *Synlett* **1995**, 729 – 732.
[51] T. Toru, Y. Watanabe, M. Tsusaka, Y. Ueno, *J. Am. Chem. Soc.* **1993**, *115*, 10464 – 10465; T. Toru, Y. Watanabe, N. Mase, M. Tsusaka, T. Hayakawa, Y. Ueno, *Pure Appl. Chem.* **1996**, *68*, 711 – 714.
[52] M. Kito, T. Sakai, K. Yamada, F. Matsuda, H. Shirahama, *Synlett* **1993**, 158 – 162.
[53] M. Kito, N. Haruta, H. Shirahama, F. Matsuda, *Synlett* **1996**, 1057 – 1060.
[54] G. A. Molander, J. A. McKie, *J. Org. Chem.* **1995**, *60*, 872 – 882.
[55] G. A. Molander, C. Kenny, *Tetrahedron Lett.* **1987**, *28*, 4367 – 4370; G. A. Molander, C. Kenny, *J. Am. Chem. Soc.* **1989**, *111*, 8236 – 8246.
[56] J. E. McMurry, *Chem. Rev.* **1989**, *89*, 1513 – 1524.
[57] J. L. Namy, J. Souppe, H. N. Kagan, *Tetrahedron Lett.* **1983**, *24*, 765 – 766; G. A. Molander, C. Kenny, *J. Org. Chem.* **1987**, *53*, 2132 – 2134.
[58] J. L. Chiara, W. Cabri, S. Hanessian, *Tetrahedron Lett.* **1991**, *32*, 1125 – 1128.
[59] T. Kan, F. Matsuda, M. Yanagiya, H. Shirahama, *Synlett* **1991**, 391 – 392; T. Kan, S. Hosokawa, S. Nara, M. Oikawa, S. Ito, F. Matsuda, H. Shirahama, *J. Org. Chem.* **1994**, *59*, 5532 – 5534.
[60] See ref. [2e], chap. 5.
[61] Y. Yamamoto, S. Onuki, M. Yumoto, N. Asao, *J. Am. Chem. Soc.* **1994**, *116*, 421 – 422.
[62] M. P. Sibi, J. Ji, *Angew. Chem.* **1996**, *108*, 198 – 200; *Angew. Chem. Int. Ed. Engl.* **1996**, *35*, 190 – 192.
[63] I. R. Hunt, C. Rogers, S. Woo, A. Rauk, B. A. Keay, *J. Am. Chem. Soc.* **1995**, *117*, 1049 – 1056.
[64] K. Rück, H. Kunz, *Synthesis* **1993**, 1018 – 1028.
[65] M. P. Sibi, J. Ji, *J. Org. Chem.* **1996**, *61*, 6090 – 6091.
[66] M. P. Sibi, C. P. Jasperse, J. Ji, *J. Am. Chem. Soc.* **1995**, *117*, 10779 – 10780.
[67] M. P. Sibi, J. Ji, *Angew. Chem.* **1997**, *109*, 266 – 268; *Angew. Chem. Int. Ed. Engl.* **1997**, *36*, 274 – 276.
[68] M. Nishida, A. Nishida, N. Kawahara, *J. Org. Chem.* **1996**, *61*, 3574 – 3575.
[69] S.-I. Fukuzawa, K. Seki, M. Tatsuzawa, K. Mutoh, *J. Am. Chem. Soc.* **1997**, *119*, 1482 – 1483.
[70] D. Badone, J. M. Bernassau, R. Cardamone, U. Guzzi, *Angew. Chem.* **1996**, *108*, 575 – 578; *Angew. Chem. Int. Ed. Engl.* **1996**, *35*, 535 – 538.
[71] M. Nishida, E. Ueyama, H. Hayashi, Y. Ohtake, Y. Yamaura, E. Yanaginuma, O. Yonemitsu, A. Nishida, N. Kawahara, *J. Am. Chem. Soc.* **1994**, *116*, 6455 – 6456.
[72] M. Nishida, H. Hayashi, O. Yonemitsu, A. Nishida, N. Kawahara, *Synlett* **1995**, 1045 – 1046.
[73] M. Nishida, H. Hayashi, Y. Yamaura, E. Yanaginuma, O. Yonemitsu, A. Nishida, N. Kawahara, *Tetrahedron Lett.* **1995**, *36*, 269 – 272.
[74] G. A. Molander, J. C. McWilliams, B. C. Noll, *J. Am. Chem. Soc.* **1997**, *119*, 1265 – 1276.
[75] I. Ojima, *Catalytic Asymmetric Synthesis*, VCH, Weinheim, **1993**; R. Noyori, *Asymmetric Catalysis in Organic Synthesis*, Wiley, New York, **1994**.
[76] M. Murakata, H. Tsutsui, O. Hoshino, *J. Chem. Soc. Chem. Commun.* **1995**, 481 – 482.
[77] J. H. Wu, G. Zhang, N. A. Porter, *Tetrahedron Lett.* **1997**, *38*, 2067 – 2070. An extension of this work was published after writing this review: N. A. Porter, J. H. Wu, G. Zhang, A. D. Reed, *J. Org. Chem.* **1997**, *62*, 6702 – 6703; J. H. Wu, G. Zhang, N. A. Porter, *Tetrahedron Lett.* **1997**, *38*, 2067 – 2070.
[78] C. Chapuis, J. Jurczak, *Helv. Chim. Acta* **1987**, *70*, 436 – 444.
[79] W. Oppolzer, C. Chapuis, G. Bernardinelli, *Helv. Chim. Acta* **1984**, *67*, 1397 – 1401.
[80] A.-R. Fhal, P. Renaud, *Tetrahedron Lett.* **1997**, *38*, 2661 – 2664.
[81] E. J. Corey, S. Sarshar, J. Bordner, *J. Am. Chem. Soc.* **1992**, *114*, 7938 – 7939.
[82] M. Nishida, H. Hayashi, A. Nishida, N. Kamahara, *Chem. Commun.* **1996**, 579 – 580.
[83] J. H. Wu, R. Radinov, N. A. Porter, *J. Am. Chem. Soc.* **1995**, *117*, 11029 – 11030.
[84] M. P. Sibi, J. Ji, J. H. Wu, S. Gürtler, N. A. Porter, *J. Am. Chem. Soc.* **1996**, *118*, 9200 – 9201.
[85] M. P. Sibi, J. Ji, *J. Org. Chem.* **1997**, *62*, 3800 – 3801.
[86] Y. Yuasa, W. Sato, S. Shibuya, *Synth. Commun.* **1997**, *27*, 573 – 585.
[87] H. Miyabe, R. Shibata, C. Ushiro, T. Naito, *Tetrahedron Lett.* **1998**, *39*, 631 – 634.
[88] M. P. Bertrand, L. Feray, R. Nouguier, L. Stella, *Synlett* **1998**, 780 – 782.
[89] H. Miyabe, C. Ushiro, T. Naito, *Chem. Commun.* **1997**, 1789 – 1790.

[90] E. Lacôte, P. Renaud, *Angew. Chem.* **1998**, *110*, 2369 – 2371; *Angew. Chem. Int. Ed.* **1998**, *37*, 2259 – 2262.
[91] H. Zipse, *J. Am. Chem. Soc.* **1997**, *119*, 1087 – 1093.
[92] E. Lacôte, B. Delouvrié, L. Fensterbank, M. Malacria, *Angew. Chem.* **1998**, *110*, 2219 – 2221; *Angew. Chem. Int. Ed.* **1998**, *37*, 2116 – 2118.
[93] Y. Guindon, Z. Liu, G. Jung, *J. Am. Chem. Soc.* **1997**, *119*, 9289 – 9290.
[94] N. Mase, Y. Watanabe, Y. Ueno, T. Toru, *J. Org. Chem.* **1997**, *62*, 7794 – 7800.
[95] N. Mase, S. Wake, Y. Watanabe, T. Toru, *Tetrahedron Lett.* **1998**, *39*, 5553 – 5556.
[96] N. Kise, K. Kumada, Y. Terao, N. Ueda, *Tetrahedron* **1998**, *54*, 2697 – 2708.
[97] A. Katsumata, T. Iwaki, K. Fukumoto, M. Ihara, *Heterocycles* **1997**, *46*, 605 – 616.
[98] E. Lee, J.-W. Jeong, Y. Yu, *Tetrahedron Lett* **1997**, *38*, 7765 – 7768.
[99] M. Murakata, T. Jono, Y. Mizuno, O. Hoshino, *J. Am. Chem. Soc.* **1997**, *119*, 11713 – 11714.
[100] N. A. Porter, J. H. L. Wu, G. Zhang, A. D. Reed, *J. Org. Chem.* **1997**, *62*, 6702 – 6703.
[101] M. P. Sibi, J. J. Shay, J. Ji, *Tetrahedron Lett.* **1997**, *38*, 5955 – 5958.
[102] K. Mikami, M. Yamakoa, *Tetrahedron Lett.* **1998**, *39*, 4501 – 4504.

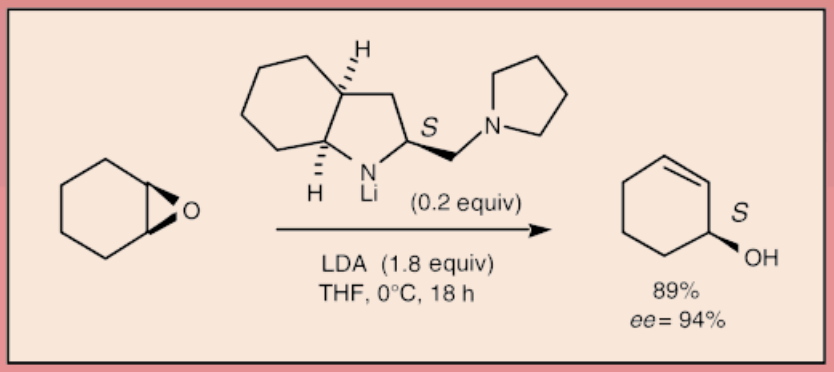


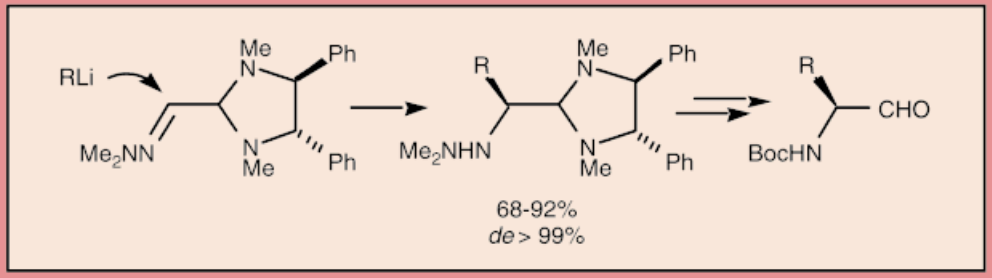
methods for the synthesis of 1,2-disubstituted 1,2-diamines

applications in stereoselective organic synthesis



antitumor agents





ANGEWANDTE CHEMIE
© WILEY-VCH

The Chemistry of Vicinal Diamines

Denis Lucet, Thierry Le Gall,* and Charles Mioskowski*

Compounds incorporating the 1,2-diamine functionality are currently the topic of studies conducted in several fields. For instance, in chemotherapy, various platinum 1,2-diamino complexes are evaluated as antitumor agents that could be employed as substitutes for cisplatin to reduce toxicity and to circumvent drug resistance. Chiral, enantiomerically pure 1,2-diamines (or vicinal diamines) and their derivatives are also used increasingly in stereoselective organic synthesis, for example as chiral auxiliaries, or as metal ligands in catalytic asymmetric synthesis. These utilizations brought about the development of synthetic methods for the preparation of aliphatic 1,2-diamines in diastereomerically and enantiomerically pure form. The problem of stereochemical control encountered in their synthesis depends on the number of substituents on the carbon chain. Thus, it is necessary to control two stereogenic centers when the target compound is disubstituted at the C1 and C2 positions. Numerous strategies have been developed to meet this need. Among relevant methods that have been applied, the diastereoselective introduction of a nitrogen atom in an enantiomerically pure molecule containing another nitrogen atom, and the diastereo- and enantioselective coupling of bisimines, are particularly effective. In the first sections of this account, the occurrence of 1,2-diamines in biologically active compounds—including natural products—and in the field of organic synthesis will be highlighted. In the next section an overview of the methods for preparation of vicinal diamines will be presented.

Keywords: chiral auxiliaries · diamines · N ligands · synthetic methods

1. Introduction

Many natural products that have valuable biological properties contain a 1,2-diamino moiety. In recent years several synthetic diamine derivatives have also been employed as medicinal agents, in particular in chemotherapy. Their use in organic synthesis has also increased considerably recently, especially in the field of catalytic asymmetric synthesis. Hence, interest in these compounds brought about numerous studies aimed at the design of efficient diastereo- and enantioselective routes to 1,2-diamines. This review article firstly presents, briefly, the occurrence of products containing the 1,2-diamine functionality, as well as their biological and therapeutic properties, then the applications of vicinal diamines and their derivatives as tools in organic synthesis, and lastly the methods of preparation of these compounds, essentially covering the literature until October 1997. The review deals only with aliphatic 1,2-diamines, not with aromatic ones.

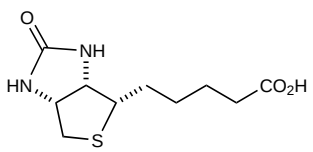
[*] Dr. T. Le Gall, Dr. C. Mioskowski,[+] Dr. D. Lucet
CEA-Saclay, Service des Molécules Marquées, Bât. 547
Département de Biologie Cellulaire et Moléculaire
F-91191 Gif-sur-Yvette (France)
Fax: (+33) 1-69-08-79-91
E-mail: legall@dsvidf.cea.fr
mioskow@aspirine.u-strasbg.fr

[+] Université Louis Pasteur
Laboratoire de Synthèse Bio-Organique associé au CNRS
Faculté de Pharmacie
74 route du Rhin, BP 24, F-67401 Illkirch (France)

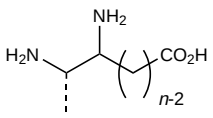
2. Biological Properties and Medicinal Interest of Vicinal Diamines

2.1. Vicinal Diamines in Natural Products

Biotin (or vitamin H, **1**), which is an essential cofactor to carboxylase-catalyzed reactions, is one of the compounds found in nature that contain the 1,2-diamino moiety in their skeleton, in this case included in an imidazolidinone ring.[1] A large number of natural products, especially peptides, contain a *n*,*n*+1-diamino carboxylic acid substructure such as **2**. 2,3-Diaminopropanoic acid is a constituent of several peptidic



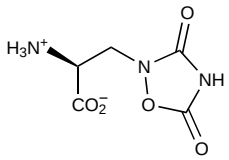
biotin **1**



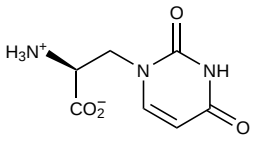
n,*n*+1-diaminocarboxylic acid **2**

 © WILEY-VCH Verlag GmbH, D-69451 Weinheim, 1998 1433-7851/98/3719-2581 $ 17.50+.50/0

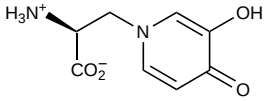
antibiotics such as edeines[2a] and tuberactomycin[2b] derivatives. The bleomycins, first isolated in 1966,[2c] are a family of glycopeptides containing the 2,3-diaminopropanamide moiety; they are chemotherapeutic agents used for the clinical treatment of malignant lymphomas and squamous cell carcinomas.[2d–f] β-(Methylamino)-L-alanine is a neurotoxin that has been linked to the so-called Guam disease.[2g] Neuroexcitatory quisqualic acid (**3**)[2h] and the nonproteinic amino acids willardiine (**4**),[2i] mimosine (or leucenol, **5**)[2j–l] and the isoxazolinone alanine derivative **6**[2m] also all include the 2,3-diaminopropanoic residue. Amphomycin,[3a,b] aspartocin,[3c] lavendomycin,[3d] glumamycin,[3e] antrimycin,[3f] and cirratiomycin,[3g] are potent antibacterial peptides incorporating the 2,3-diaminobutanoic acid residue. Compounds belonging to the emeriamine and emericedines families (**7**, and **8**, respectively) inhibit the oxidation of long-chain fatty acids.[3h]



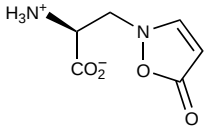
L-quisqualic acid **3**



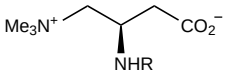
willardiine **4**



mimosine **5**



6



R=H: emeriamines **7**
R=acyl: emericedines **8**

The well known antibiotics penicillins (**9**) and cephalosporins (**10**) also contain a 2,3-diamino carboxylic acid unit, incorporated into the penam and cephem structures, respectively. Nocardicines (**11**) are also 3-amino-β-lactam antibiotics. In several other natural products, one of the two nitrogen atoms is included in an heterocycle. Two significant examples are the indolizidine alkaloid slaframine (**12**),[4a] and the recently isolated balanol (**13**), a potent inhibitor of protein kinase C.[4b]

2.2. Applications in Medicinal Chemistry

The 1,2-diamine functionality can be found in various compounds displaying a broad spectrum of biological activity. In 1989 Michalson and Szmuszkovicz reviewed medicinal agents incorporating the 1,2-diamine unit.[5] Among them we can cite, for instance, antiarrhythmics,[6] antidepressant agents,[7] antihypertensives, antipsychotics, analgesics, anti-



D. Lucet



T. Le Gall

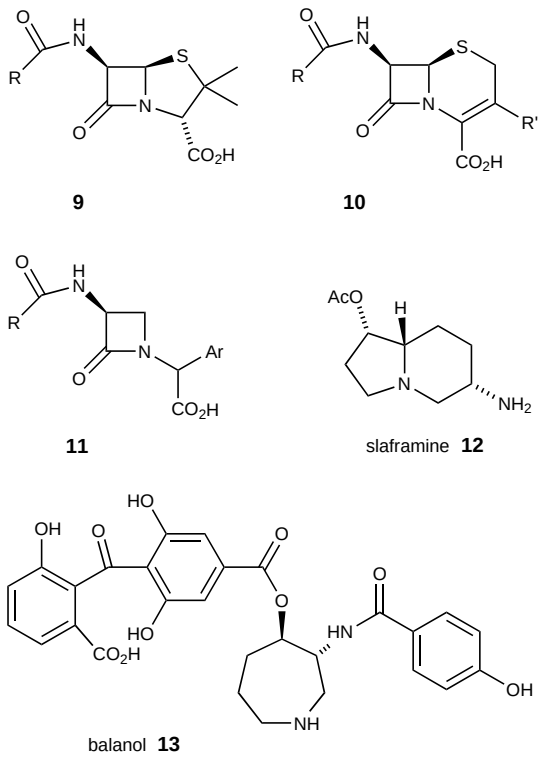


C. Mioskowski

Denis Lucet was born in 1968 near Paris. In 1992 he graduated from the École Supérieure de Physique et de Chimie Industrielles (ESPCI) in Paris. After having spent a one year undergraduate research time at the École Polytechnique with Professor J.-Y. Lallemand, he recently completed his doctoral thesis under the supervision of Drs. C. Mioskowski and T. Le Gall at the Commissariat à l'Énergie Atomique (CEA) in Saclay. He spent a two-month post-doctoral time in the group of Professor P. Vogel at the University of Lausanne, and is now working as a development chemist in the Synthetic Chemistry Department of Kodak, in Chalon-sur-Saône (France).

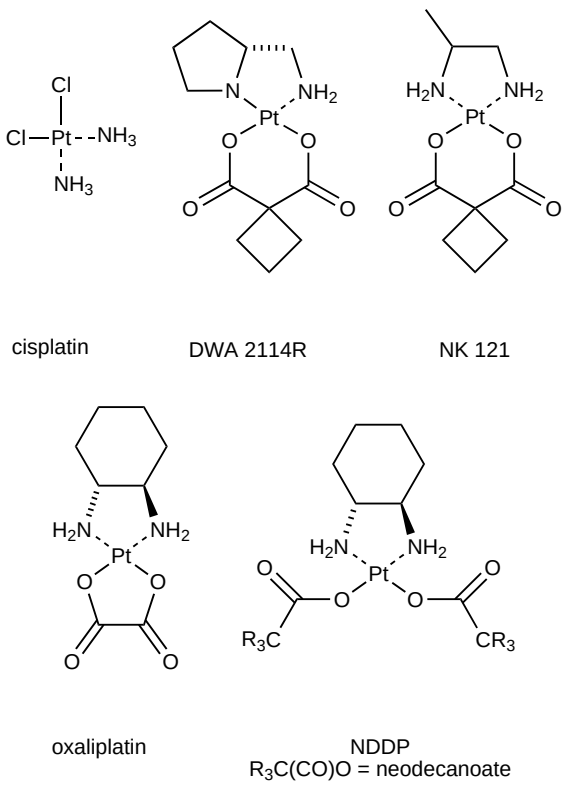
Thierry Le Gall was born in 1959 in Cléden-Poher, Brittany. He studied at the Université de Bretagne Occidentale in Brest, then at the École Nationale Supérieure de Chimie de Rennes (ENSCR). He got a Ph. D. in 1986 on the synthesis of analogues of arachidonic acid metabolites, under the direction of Dr. R. Grée, at the Université de Rennes 1. He spent one year as a post-doctoral researcher under the direction of Professor R. H. Schlessinger at the University of Rochester, NY. He has been working since 1988 in the Service des Molécules Marquées (CEA, Saclay). In recent years, he has been involved in the stereoselective synthesis of myo-inositol analogues and α-amino acids.

Charles Mioskowski was born in 1946 in Falck, Lorraine. He studied at the École Nationale Supérieure de Chimie de Strasbourg (ENSCS). He received a Ph. D. at the Université Louis Pasteur de Strasbourg in 1978 on asymmetric synthesis with chiral sulfoxides. He then joined the group of E. J. Corey at Harvard University as a post-doctoral fellow (1978–1979). He has been Director of Research at the CNRS since 1984, in the Laboratoire de Synthèse Bioorganique at the Faculté de Pharmacie de Strasbourg, and since 1991 he is head of the Service des Molécules Marquées at the CEA, in Saclay. His research interests are organic and bioorganic chemistry.



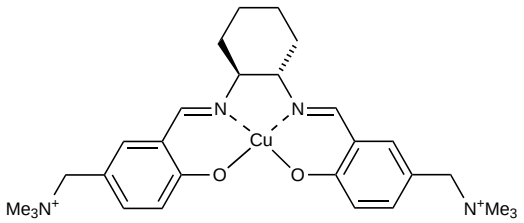
anxiety agents, anticancer drugs, and antiparasitic agents. Some important and illustrative examples will be described in this section.

Antitumoral properties of cisplatin (*cis*-diamminedichloroplatinum(II)) were serendipitously discovered by Rosenberg in the mid 1960s.[8a] Its success in antitumor chemotherapy brought about the synthesis of many diamine–platinum complexes in a search for drugs having greater activity, less toxicity, and to circumvent drug resistance that may develop in certain tumors.[8b] Among the 1,2-diaminoplatinum complexes described, several possess higher antitumoral activity than cisplatin.[8c–h] Some 1,2-diaminoplatinum compounds, either used clinically or at an advanced stage of testing, are depicted in Scheme 1.[8i]



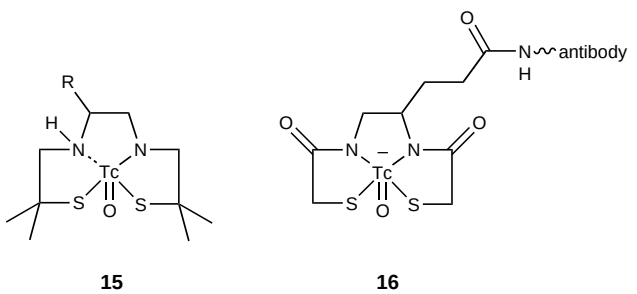
Scheme 1. Cisplatin and some 1,2-diaminoplatinum compounds currently used or evaluated as anticancer drugs.

In recent years, metal complexes of salen Schiff bases such as **14**, were reported to bind selectively with DNA.[9] In the presence of a cooxidant or under aerobic conditions a cleavage of the DNA was observed in several cases. These studies could lead to the development of artificial restriction enzymes or antitumor drugs.

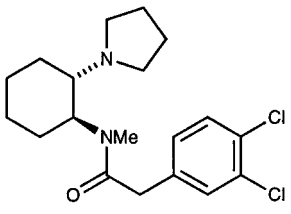


Several compounds that incorporate the 1,2-diamine moiety, such as EDTA (see the Appendix for a list of abbreviations), can strongly chelate metal ions, to form stable complexes. This property has been employed in particular in the field of nuclear medicine, since the complexes of metallic radioactive isotopes can be used as imaging agents.

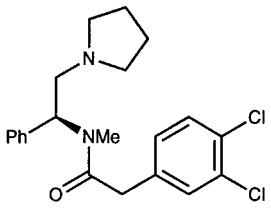
Bleomycin–A_2DM is known to accumulate in the cells of some cancer tumors; the coupling of the Co^{III} complex of this antibiotic with an EDTA-containing derivative led to a compound that could then be labeled by a radioactive metal ion. The ^{111}In-radiolabeled adduct proved to be a useful diagnostic tool for determining both the size and the location of malignancies in cancer patients.[10a] Complexes of technetium-99m (^{99m}Tc) with diamide dithiolate ligand systems have also been used as radiopharmaceuticals for the detection and the evaluation of renal diseases,[10b] or as brain perfusion imaging agents (for example **15**).[10c] When labeled with ^{99m}Tc complexes, antibodies such as **16** can become useful agents for the targeted delivery of radioactivity for diagnostic imaging, as well as for the delivery of therapeutic radionucleides to tumors.[10d,e]



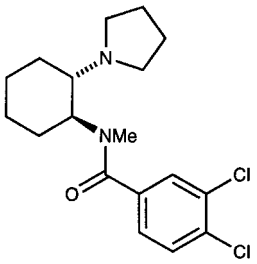
Pharmaceutical studies have disclosed the existence of three major opioid receptor types, namely, μ, δ, and κ.[11a, b] Since the discovery of the opioid properties of the 1,2-diaminocyclohexane derivative U-50,488 (**17**) as a highly selective κ agonist,[11c] many structural analogues (cyclic and acyclic ones) of improved affinity and selectivity for the κ receptor have been reported (for example ICI-199,441 (**18**)).[11d] Highly selective κ-opioid agonists may provide useful analgesics, free from the potential for abuse and the adverse side effects of μ agonists like morphine.[11e, f] Interestingly, benzamide derivatives such as **19** are morphine-like analgesics with affinity for the μ-opioid receptor.[11g] 1,2-Diaminocyclohexane derivatives have again received increasing attention because of the discovery of the selective action of their diastereomers at κ or σ receptor sites. Indeed, compound **20**, which is the *cis* stereoisomer of U-50,488, has practically no affinity for κ receptors, whereas its affinity for non-opioid σ receptors is high.[11h–l]



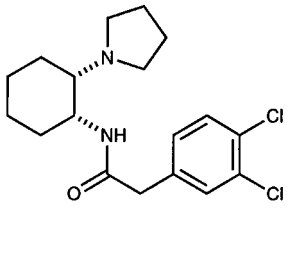
U-50,488 **17**
κ agonist



ICI-199,441 **18**
κ agonist



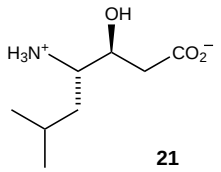
19
μ agonist



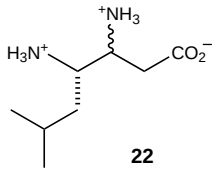
20
σ agonist

Analogues of acyclic derivatives such as ICI-199,441 have been modified into affinity labels that are useful pharmacological or biochemical tools to investigate κ opioid receptors.[11l]

Ethylenediamine and *cis*-1,2-diaminocyclohexane are potent irreversible inhibitors of lysyl oxidase, an enzyme involved in the formation of covalent cross-linkage in elastin and collagen. The central role of lysyl oxidase in connective tissue fiber formation has suggested that potent inhibitors of this enzyme may have chemotherapeutic potential as antifibrotic agents.[12a] Peptides that contain amino analogues of statine (**21**), such as **22**, may be potent renine inhibitors and could provide agents for control of cases of renin-associated hypertension.[12b,c]



21



22

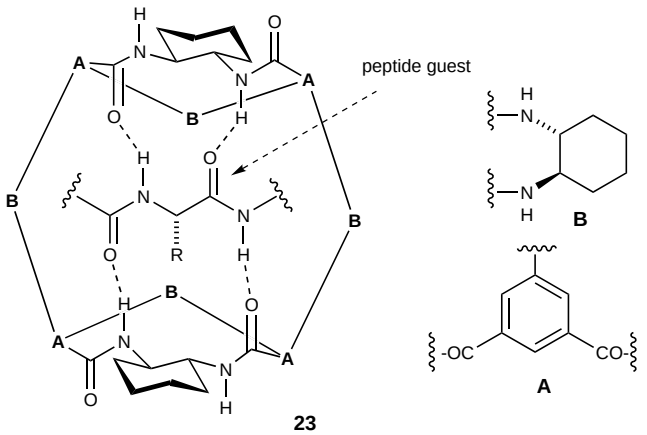
3. Vicinal Diamines in Organic Synthesis

The next sections will highlight the importance of 1,2-diamines in organic synthesis, and of compounds that are easily prepared from 1,2-diamines, such as 1,2-bisimines and 1,2-diamides.

1,2-Diamino compounds are valuable synthetic intermediates for the preparation of heterocycles.[13a] Diamines such as TMEDA are widely used as additives to stabilize and activate organometallic reagents and inorganic salts.[13b]

Vicinal diamines have also found application in cryptand chemistry.[14] Indeed, they are interesting building blocks for the construction of nitrogen-containing macrocycles, for instance diazacrown ether analogues, which could find use in asymmetric synthesis as chiral ligands.

In the field of supramolecular and host–guest chemistry, the synthetic macrocycle **23**, built up from (*R*,*R*)-1,2-diaminocyclohexane, was shown by Still et al. to bind to amino acid residues in peptide chains with very high selectivities for chirality and side-chain identity.[15a] "Two-armed" synthetic receptors that bind peptides in water were more recently described; they are also derived from C_2-symmetric 1,2-diamines (Scheme 2).[15b]



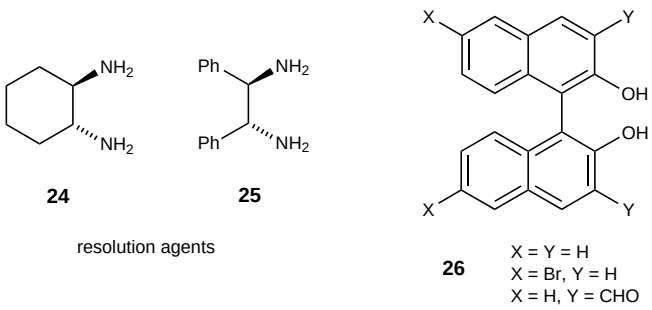
23

Scheme 2. Schematic representation of **23**, a synthetic receptor for peptides.

Chiral non-racemic vicinal diamines have received increasing attention during the last decades. Indeed, enantiomerically pure 1,2-diamines and their derivatives are particularly useful as chiral auxiliaries or ligands, and they have found tremendous application in stereoselective synthesis. In this field, chiral, C_2-symmetric 1,2-diamines[16] and their various derivatives offer especially great promise as new reagents for enantioselective synthesis.

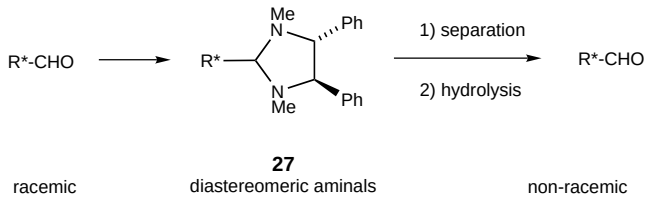
3.1. Resolution of Racemates and Determination of Enantiomeric Excess

Symmetrical vicinal diamines have been used for racemate resolution. For example, (*R*,*R*)-1,2-diaminocyclohexane (**24**) and (*R*,*R*)-1,2-diphenylethylenediamine (**25**, also called stilbenediamine, or stien) were used to resolve atropisomeric binaphthols **26** (Scheme 3).[17]



Scheme 3. 1,2-Diamines used to resolve binaphthol atropisomers.

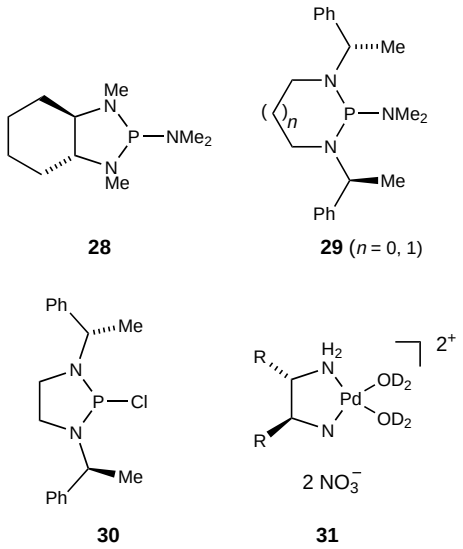
Mangeney and Alexakis et al. showed that symmetrical vicinal diamines are interesting compounds as resolving agents for chiral aldehydes.[18] Thus, the reaction of a racemic aldehyde with an enantiopure symmetrical 1,2-diamine affords diastereoisomeric imidazolidines (aminals) **27** that can be separated into each enantiomer of the aldehyde after acidic hydrolysis (Scheme 4).



Scheme 4. Resolution of aldehydes with a chiral vicinal diamine.

Diastereomeric aminals also allow the determination of the enantiomeric composition of chiral aldehydes and substituted cycloalkanones, either by NMR spectroscopy or by a chromatographic technique (HPLC or GC).[19a, b] Alexakis et al. then introduced phosphorus derivatives such as **28**, which were obtained from C_2-symmetric diamines, for the determination of the enantiomeric composition of chiral alcohols, thiols, and amines by ^{31}P, ^{1}H, ^{13}C and ^{19}F NMR spectroscopy (Scheme 5).[19c,d] Phosphorus compounds **29**[19e] and **30**[19f] were also employed for such a purpose by other authors.

(*R*,*R*)-1,2-Diphenylethylenediamine has been used as a chiral solvating agent for the determination of the enantiomeric purity of chiral carboxylic acids by NMR spectroscopy.[20a] Recently, the enantiomeric ratio of unprotected amino acids was analyzed with the help of palladium complexes **31**.[20b]



Scheme 5. 1,2-Diamine derivatives employed to determine the enantiomeric composition of chiral compounds.

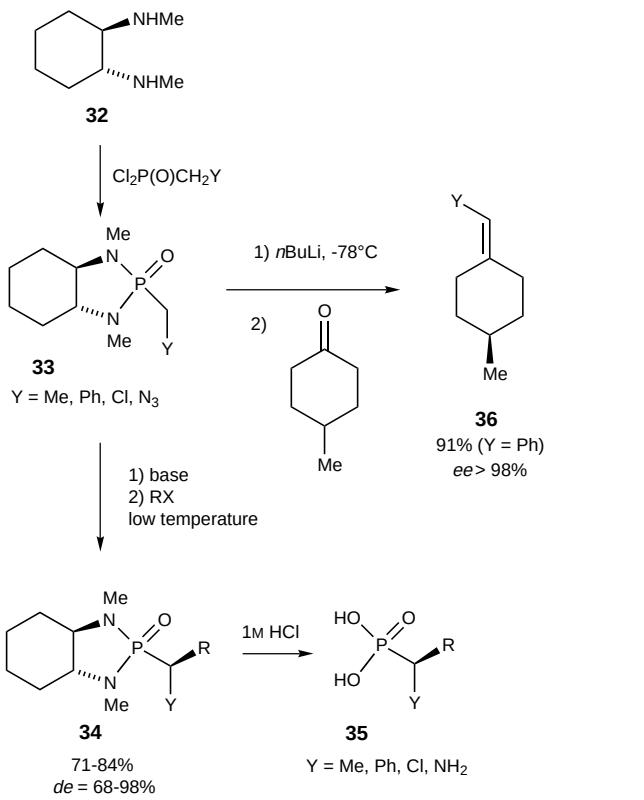
3.2. Vicinal Diamines and Their Derivatives as Chiral Auxiliaries in Diastereoselective Synthesis

Several chiral auxiliaries derived from 1,2-diamines have been employed in highly stereoselective reactions. They often have C_2 symmetry, although early examples described by Mukaiyama involve unsymmetrical auxiliaries.[21] In this section, we will deal successively with bicyclic phosphonamides, imidazolidin-2-ones, diazaborolidines, and aminals as chiral auxiliaries in diastereoselective synthesis.

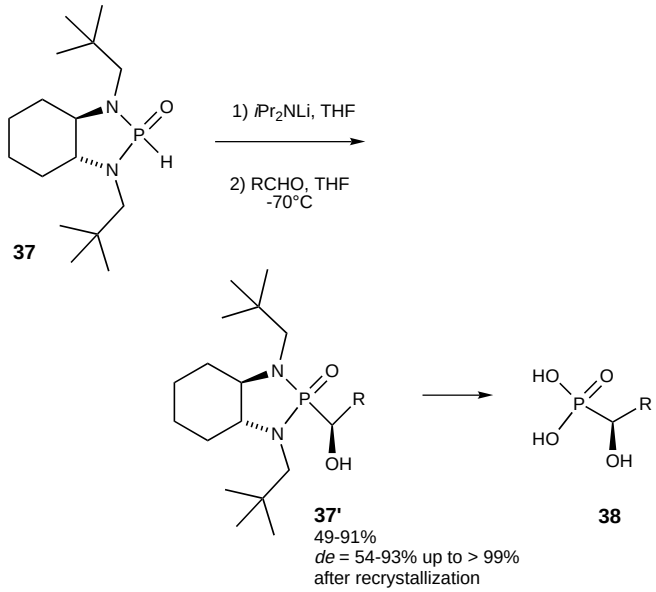
Hanessian[22a–e] and others[22f] have demonstrated the usefulness of chiral bicyclic phosphonamides **33** as chiral auxiliaries in organic synthesis. Reactions of such systems proceed in good yields and with high diastereoselectivities (Scheme 6). Anions derived from **33** can be trapped by an alkyl halide[22a–d] and after hydrolysis of the adducts **34** optically active α-substituted α-alkyl phosphonic acids **35** can be obtained, which are important surrogates for carboxylic acids. Asymmetric olefination through the Wittig reaction on phosphoramides **33** is also possible; alkylidenecyclohexanes **36** were obtained from substituted 2-methylcyclohexanone with very good enantiomeric excesses.[22e]

Spilling et al. have recently described the stereoselective synthesis of α-hydroxyphosphonic acids **38** from the chiral bicyclic phosphinamide **37** (Scheme 7).[22f] The rigidity of these bicyclic systems is probably important in dictating the levels of asymmetric induction observed.

Imidazolidin-2-ones derived from (*S*)- or (*R*)-ephedrine have been employed as chiral auxiliaries in highly diastereoselective reactions[23] (Scheme 8). Helmchen et al.[23a] described the homoaldol addition of the titanium compound obtained from *N*-alkylurea **39** with aldehydes or ketones. This reaction afforded alcohols **39′** ($de = 88-96\,\%$, $de > 98\,\%$ after recrystallization), which were then converted to γ-lactones **40**. Cardillo et al.[23b–g] studied various diastereoselective processes by utilizing 3-acyl-imidazolin-2-ones derived from



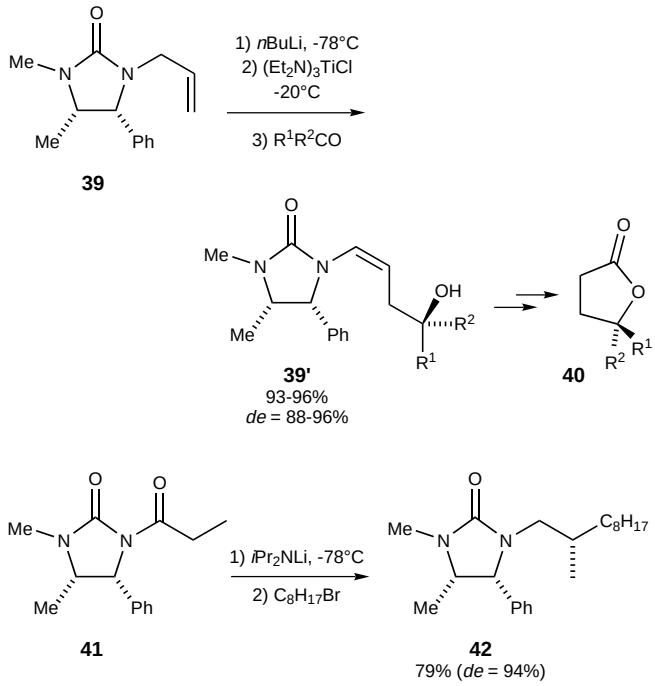
Scheme 6. Chiral bicyclic phosphonamides, derived from a 1,2-diamine, as chiral auxiliaries.



Scheme 7. Use of a chiral bicyclic phosphonamide in the synthesis of α-hydroxyphosphonic acids.

ephedrine, such as the alkylation of compound **41**.[23b] The alkylation of 3-acyl-imidazolin-2-ones derived from several α-amino acids was also reported recently.[24]

Davies et al.[25] utilized imidazolidin-2-ones derived from C_2-symmetric 1,2-diamines as chiral auxiliaries. Dibutylboron enolates of 1,3-diacylimidazolin-2-ones **42** react with aldehydes in a *syn*-stereoselective aldol reaction[25a] (Scheme 9), while the corresponding potassium enolates react stereoselectively with alkyl halides.[25b] After cleavage of the chiral auxiliary and reduction, enantiomerically enriched diols **45** and alcohols **47** are then obtained, respectively.

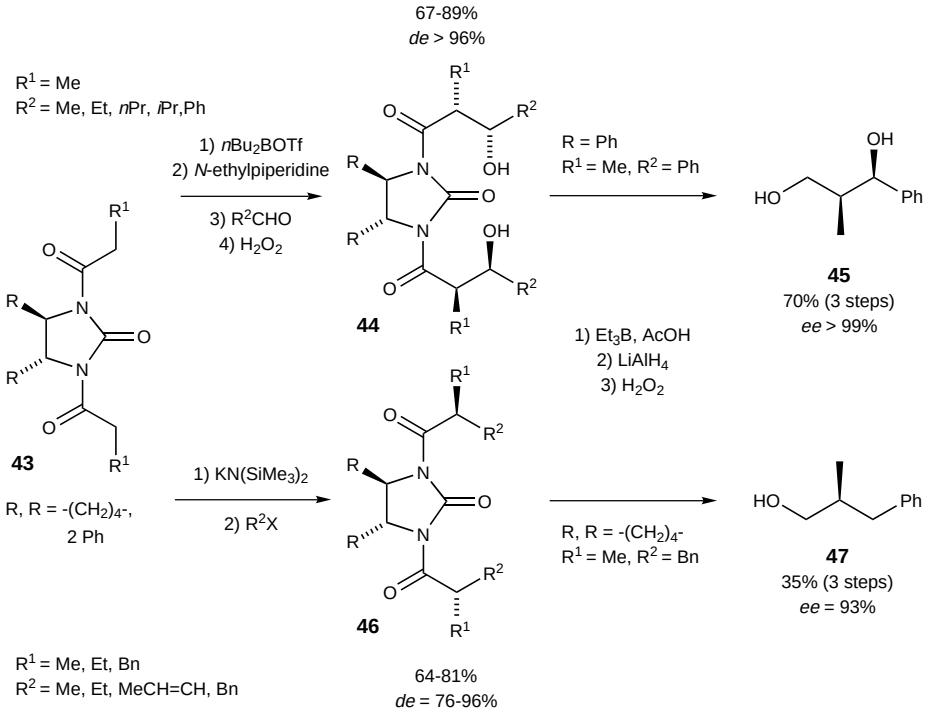


Scheme 8. Diastereoselective syntheses with imidazolidin-2-ones derived from ephedrine.

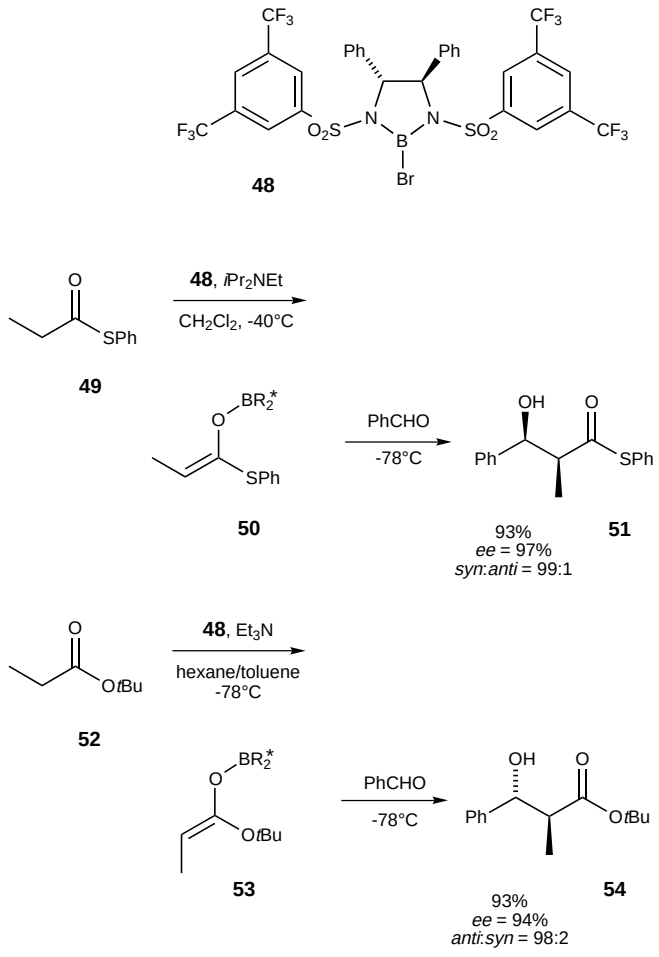
Corey et al. have developed enantioselective processes that make use of chiral, boron-containing chiral auxiliaries derived from 1,2-diphenylethylenediamine.[26] For example, the enantioselective synthesis of either *syn*- or *anti*-aldol products by using the diazaborolidine **48** was described (Scheme 10). Thus, in aldol reactions of benzaldehyde mediated by **48**, *S*-phenyl thiopropionate (**49**) was converted into the *syn*-aldol product **51** ($ee = 97\,\%$, *syn*:*anti* = 99:1, yield = 93 %), while *tert*-butyl propionate (**52**) afforded the *anti*-aldol product **54** ($ee = 94\,\%$, *anti*:*syn* = 98:2, yield = 93 %).[27] The divergence in stereochemistry was attributed to the intermediacy of boron enolates of either *E* or *Z* configuration, depending of the ester structure.

The same diazaborolidine **48** was used to promote other diastereo- and enantioselective processes, such as the reaction of a thiopropionate ester with aldimines, to afford *anti*-β-amino thioesters,[28] a Darzens reaction that led mainly to *anti*-α-bromo β-hydroxy esters,[29] and an Ireland–Claisen rearrangement of achiral allylic esters.[30] In the latter process, either *erythro* or *threo* adducts could be obtained selectively, depending on the conditions used for the enolate formation. As shown in Scheme 11, *syn*-aldol products (**57**) were also obtained with high diastereomeric and enantiomeric excesses from diethyl ketone (**55**), in reactions mediated by the boron reagent **56**.[31]

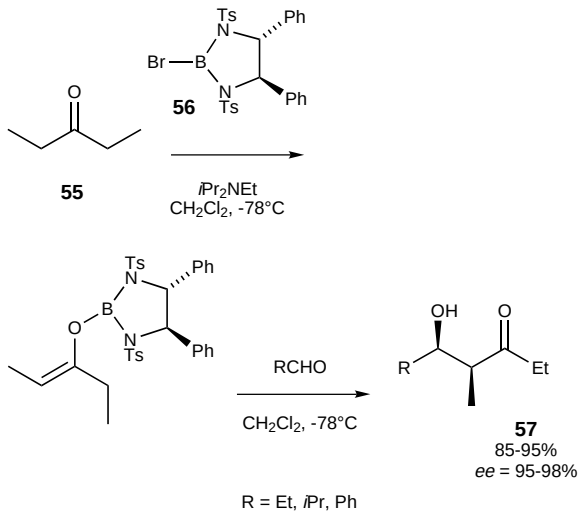
The allylborane derivative **58** (Scheme 12) was shown to be an excellent reagent for the enantioselective allylation of aldehydes ($ee = 95-98\,\%$). The adducts **59** are useful pre-



Scheme 9. C_2-symmetric imidazolidin-2-ones as chiral auxiliaries.



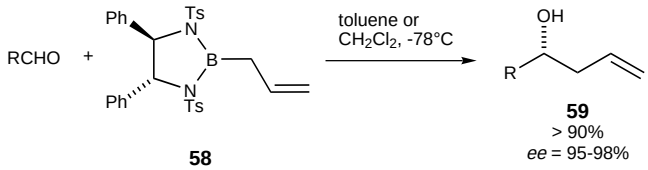
Scheme 10. Diastereo- and enantioselective aldolization reactions of boron enolates derived from a C_2-symmetric diazaborolidine (**48** = R_2^*BBr).



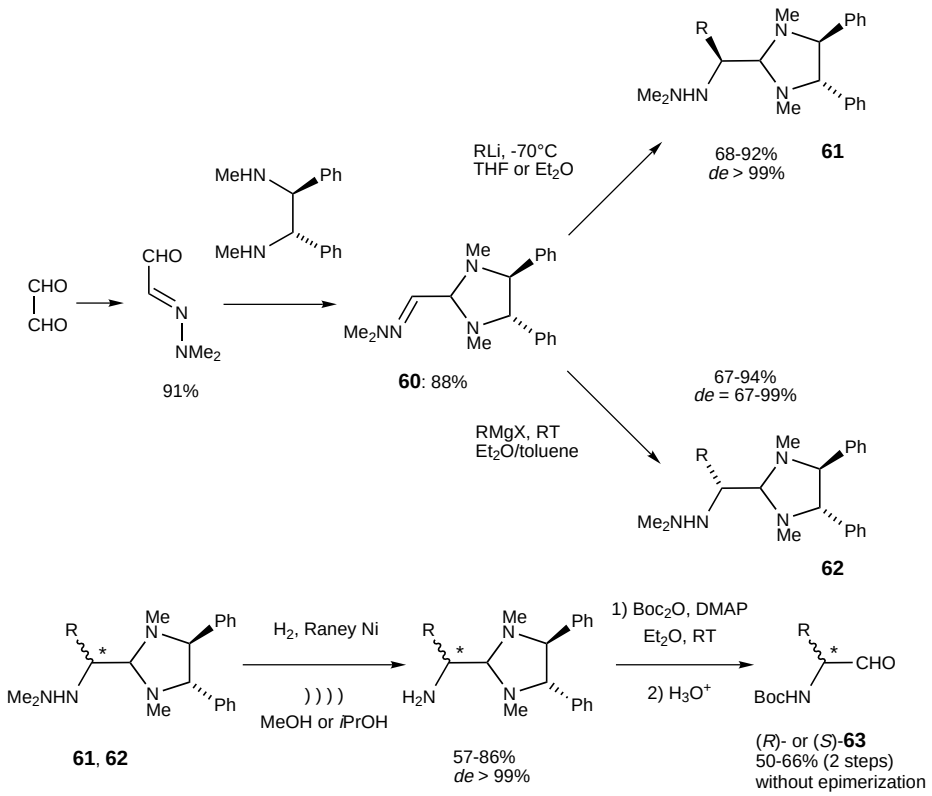
Scheme 11. Use of a C_2-symmetric diazaborolidine in aldolization reactions of diethyl ketone.

cursors of β-hydroxy- and γ-hydroxycarboxylic acid derivatives.[32]

Alexakis and Mangeney et al. utilized chiral aminals obtained from aldehydes and C_2-symmetric 1,2-diamines as chiral auxiliaries,[18c, 33a] and showed that these compounds can



Scheme 12. Enantioselective allylation of an aldehyde with a chiral 1,2-diamine-based allylborane reagent.



Scheme 13. Chiral aminal template in the diastereoselective synthesis of α-amino aldehydes.

exert impressive stereocontrol (Scheme 13). Glyoxal monohydrazone-derived chiron (**60**) gave a single diastereomer upon reaction with an organolithium reagent in THF, through steric control.[33b,c] By contrast, **60** underwent a stereoreverse, chelation-controlled reaction with a Grignard reagent in toluene (to afford the adduct of opposite configuration after removal of the chiral auxiliary). N–N bond cleavage, followed by protection of the amino group, and acidic aminal hydrolysis afforded the corresponding Boc-protected α-amino aldehydes **63** without epimerization.

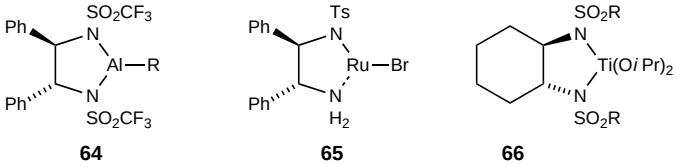
Such chiral C_2-symmetric aminals have also been used as chiral controllers in various reactions,[34, 35] such as the enantioselective *ortho*-lithiation of a tricarbonylchromium complex,[34a] and the 1,3-dipolar cycloaddition of azomethine ylides to α,β-unsaturated carbonyl compounds.[35]

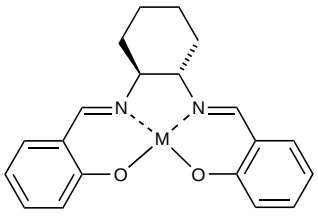
3.3. Vicinal Diamines and Their Derivatives as Chiral Ligands in Asymmetric Synthesis

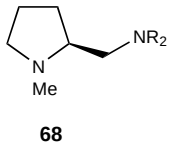
In this section most significant or recent examples of the use of chiral 1,2-diamine ligands (or reagents noncovalently bound to the substrate) in the field of asymmetric synthesis will be presented.[36, 37] In some types of reactions these external ligands are to be used in stoichiometric amount, but in many cases a catalytic amount is sufficient to obtain very good results.

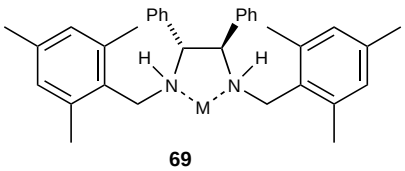
The most widely used ligands incorporating a vicinal diamine moiety are derivatives of 1,2-diphenylethylenediamine and of 1,2-diaminocyclohexane. These chiral derivatives may be mainly divided into three families:

- Lewis acid derivatives, and more generally 1,2-diamines substituted by electron-withdrawing groups (for example the ligands in **64**–**66**);
- ligands obtained from aromatic aldehydes and 1,2-diamines, such as the salen-type ligand (**67**);
- other more simple 1,2-diamine derivatives such as **68** and **69**.







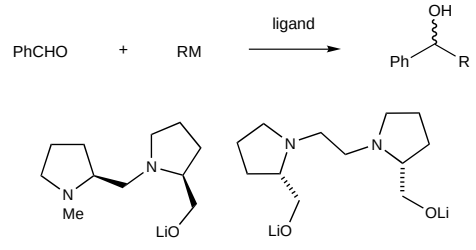


All these chiral compounds are used increasingly in various reactions. Such applications are presented in the following paragraphs.

3.3.1. Alkylation of Aldehydes

Enantioface differentiating addition of organometallic reagents to carbonyl compounds is an important reaction to establish a C–C bond with concomitant control of a stereogenic center. Numerous enantioselective reactions have been performed with the help of external, chiral 1,2-diamine ligands. The approaches listed in Table 1 require very low temperatures and the use of a stoichiometric amount or more of the chiral ligand.

Table 1. Enantioselective addition of organometallic reagents to benzaldehyde in the presence of a 1,2-diamine ligand.



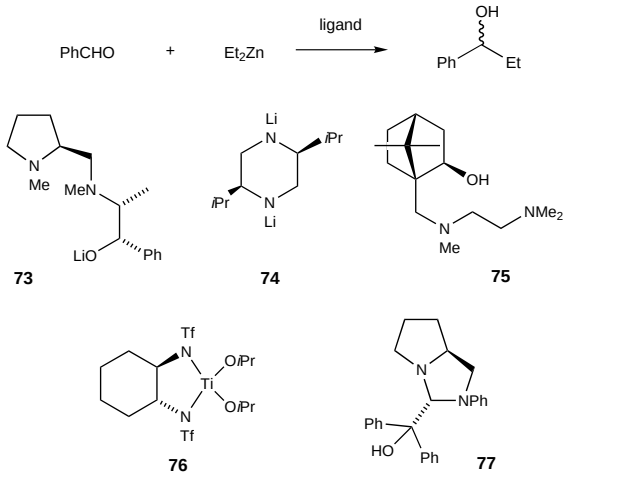
Entry	RM	*T* [°C]	Ligand	*ee* [%]	*R*,*S*	Ref.
1	BuLi	– 123	**70**	95	*S*	[38a]
2	BuLi	– 85	**71**	30	*R*	[38b]
3	1-naphthylMgBr	– 100	**72**	75	*S*	[38c]

The enantioselective nucleophilic addition of dialkyzinc reagents to aldehydes in the presence of a catalytic amount (0.01 to 10 mol %) of a chiral ligand has been studied extensively by several groups.[38] Results obtained in the addition of diethylzinc to benzaldehyde in the presence of 1,2-diamine ligands are depicted in Table 2. In recent years Knochel et al. have extended the scope of this reaction by using aliphatic aldehydes and zinc organometallic reagents.[39] The asymmetric trimethylsilylcyanation of aldehydes catalyzed by chiral (salen)titanium(IV) complexes has also been described.[40]

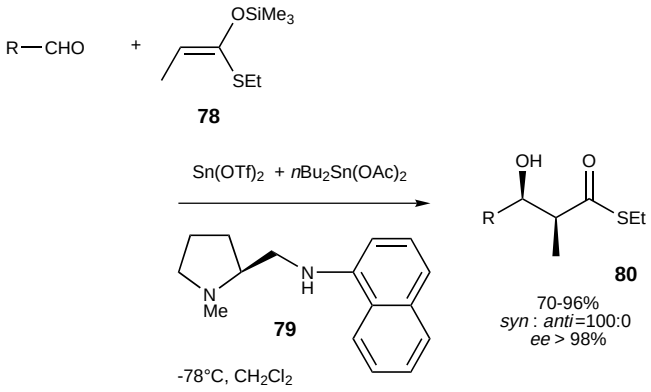
3.3.2. Aldol Reactions

Kobayashi and Mukaiyama et al. have shown that asymmetric aldol reactions of achiral silylenol ethers can be performed with excellent stereochemical control by the combined use of tin(II) triflate, dibutyltin diacetate, and a chiral 1,2-diamine (Scheme 14).[41a] Thus, when vicinal diamine **79** was used in a stoichiometric fashion in the reaction-

Table 2. Enantioselective alkylation of benzaldehyde by diethylzinc in the presence of various 1,2-diamine-based complexes.

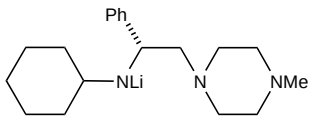


Entry	Ligand	*ee* [%]	*R*,*S*	Ref.
1	**73**	95	*S*	[38d]
2	**74**	90	*R*	[38e]
3	**75**	87	*S*	[38f]
4	**76**	98 – 99	*S*	[38g – i]
5	**77**	96	*S*	[38j]



Scheme 14. Enantioselective Mukaiyama aldolizations in the presence of a chiral vicinal diamine.

of the silylenol ether **78** with various aldehydes the *syn*-aldol products **80** were formed exclusively (*ee* > 98 %). Excellent results were also obtained with tin(II) oxide instead of dibutyltin diacetate.[41b] Very good enantioselectivity (*ee* up to 86 %) was also obtained in aldol reactions that utilized lithium amide **81** as the base.[41c]

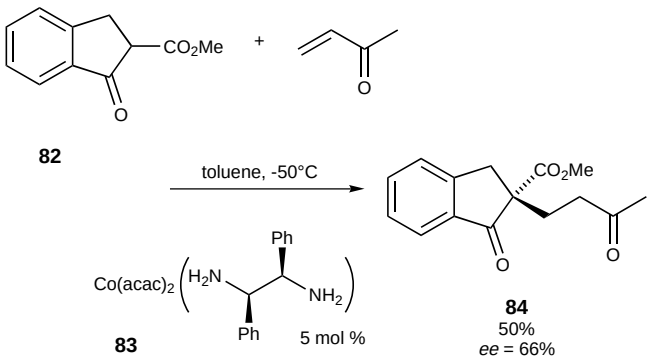


81

3.3.3. Conjugate Addition of Organometallic Reagents to α,β-Unsaturated Carbonyl Compounds

Asymmetric conjugate addition to α,β-unsaturated carbonyl compounds in the presence of a chiral additive has received

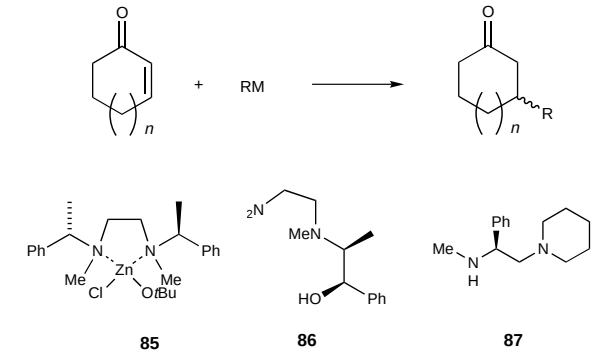
much attention in the last few decades. One of the first studies, carried out by Brunner et al., was a cobalt-catalyzed 1,4-addition:[42] enantiomeric excesses of up to 66% were obtained by using stien as the chiral ligand in complex **83** (Scheme 15).



Scheme 15. Enantioselective conjugate addition in the presence of a 1,2-diaminocobalt complex.

The conjugate addition of Grignard reagents to α,β-unsaturated ketones catalyzed by diaminezinc(II) complexes has been reported.[43a] The reaction of isopropylmagnesium bromide with 2-cyclohexenone in the presence of catalyst **85** proceeded with 8% enantiomeric excess. Much better enantioselectivities were obtained on the addition of chirally modified heterocuprates to cycloalkenones (Table 3).[43b–d]

Table 3. Enantioselective conjugate addition of chirally modified heterocuprates to cycloalkenones.



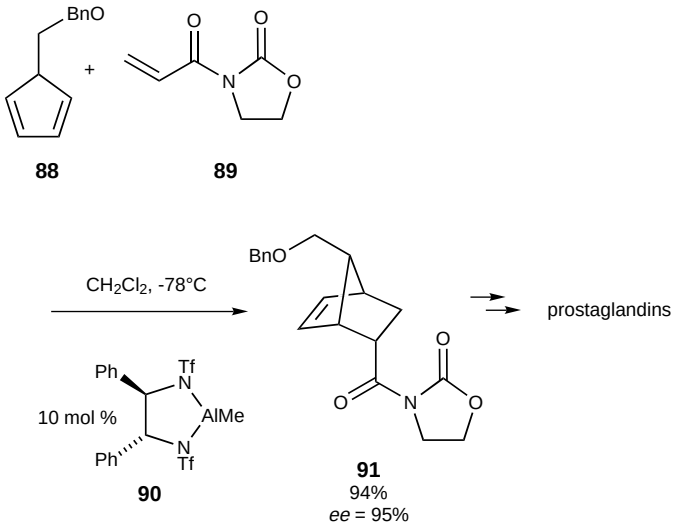
Entry	RM	*n*	Ligand (L*H)	*ee* [%]	Adduct config.	Ref.
1	EtL*CuLi	1	**86**	92	*R*	[43b]
2	MeL*CuLi	0	**87**	32	*R*	[43c]
3	*n*BuL*CuLi	0	**87**	45	*S*	[43c]
4	MeL*CuLi	1	**87**	58	*S*	[43c]
5	*n*BuL*CuLi	1	**87**	83	*S*	[43c]
6	MeL*CuLi	2	**87**	75	*S*	[43c]
7	*n*BuL*CuLi	2	**87**	96	–[a]	[43c]
8	MeL*CuLi	3	**87**	67	–[a]	[43c]
9	*n*BuL*CuLi	3	**87**	86	–[a]	[43c]

[a] The configuration of the adduct was not determined.

Mukaiyama et al.also showed that a chiral diamine derived from hydroxyproline is a good catalyst for the high enantioselective 1,4-addition of thiols to cyclohexen-2-one.[21, 44]

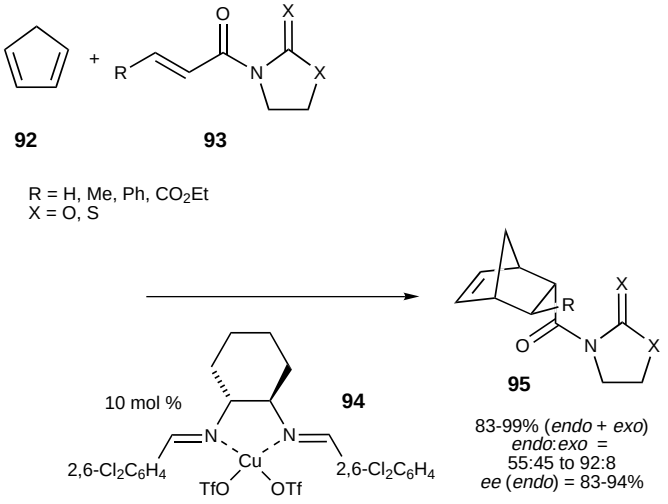
3.3.4. Diels–Alder Reactions

Corey et al. have demonstrated that diazaaluminolidine **90** is an effective Lewis acidic catalyst for the cycloaddition ;of cyclopentadiene derivatives to activated dienophiles (Scheme 16).[31, 45a, b] The cycloadduct **91** is a valuable intermediate for prostaglandins synthesis.[26]



Scheme 16. Use of a 1,2-diaminoaluminum additive in an enantioselctive Diels–Alder addition.

More recently, Evans et al. reported that bisiminecopper(II) complexes of type **94** are also effective chiral catalysts for Diels–Alder reactions and afford cycloadducts **95** with 83–94% enantiomeric excess (Scheme 17).[45c] The use of more

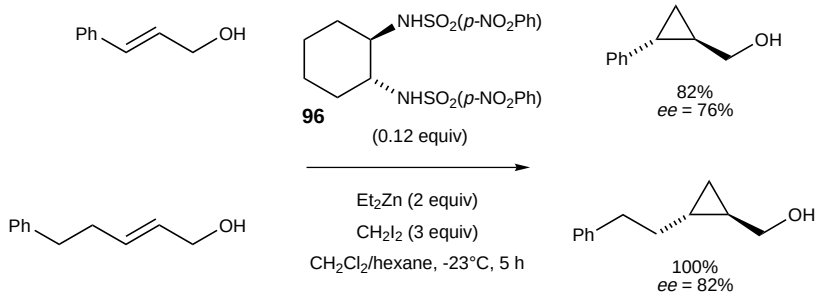


Scheme 17. Enantioselective Diels–Alder addition in the presence of a [Cu^{II}(salen)] complex.

reactive sulfur-containing dienophiles enhanced the *endo*/*exo* diastereoselectivity of the reactions.

3.3.5. Cyclopropanation

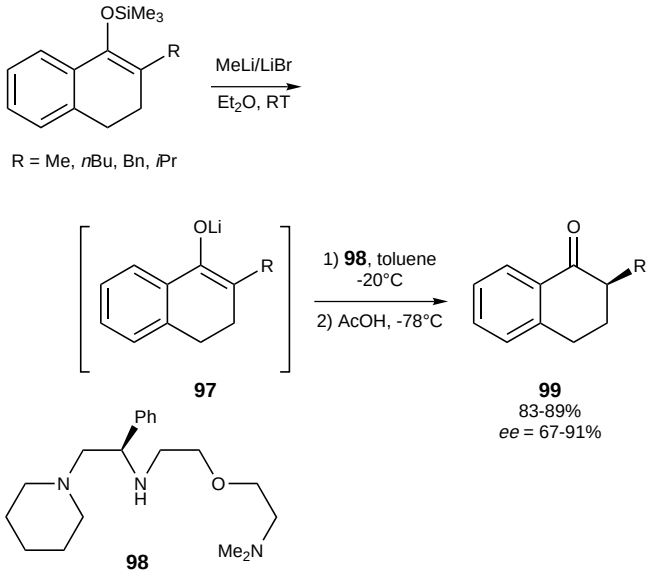
Kobayashi et al. developed a catalytic, enantioselective Simmons–Smith cyclopropanation of allylic alcohols by the $Et_2Zn-CH_2I_2$ system in the presence of a catalytic amount of a chiral sulfonamide, with **96** being the most efficient one (Scheme 18).[46] Other catalysts derived from 1,2-diamines have also been studied.[47]



Scheme 18. Enantioselective cyclopropanation reactions in the presence of the bissulfonamide **96**.

3.3.6. Enantioselective Protonation of Enolates

There are several examples of the use of 1,2-diamino compounds in the enantioselective protonation of enolates. For instance, Yasukata and Koga[48] reported the very efficient protonation with AcOH of complexes formed between cyclic achiral lithium enolates **97**, the chiral vicinal diamine **98**, and LiBr (Scheme 19). The asymmetric induction was much better in toluene than in polar solvents.



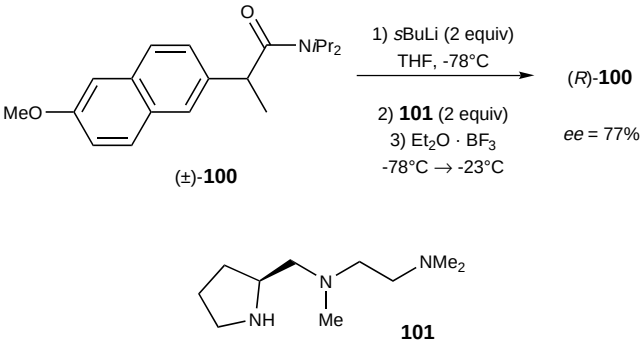
Scheme 19. Enantioselective protonation of cyclic enolates with a chiral 1,2-diamine.

Vedejs et al. have also investigated the use of 1,2-diamines in the enantioselective protonation of amide enolates.[49] As an example, treatment of racemic naproxen amide (**100**) with *s*BuLi, then with triamine **101**, followed by boron trifluoride-diethyl etherate afforded (*R*)-**100** with 77% *ee* (Scheme 20). Slightly lower enantiomeric excesses were obtained with diamines, while monoamines were much less efficient.

3.3.7. Deprotonation With Chiral Lithium Amides

In recent years enantioselective deprotonation of ketones or epoxides with chiral lithium amide bases, often derived from 1,2-diamines, has received much attention and several reviews on the subject have been published.[50]

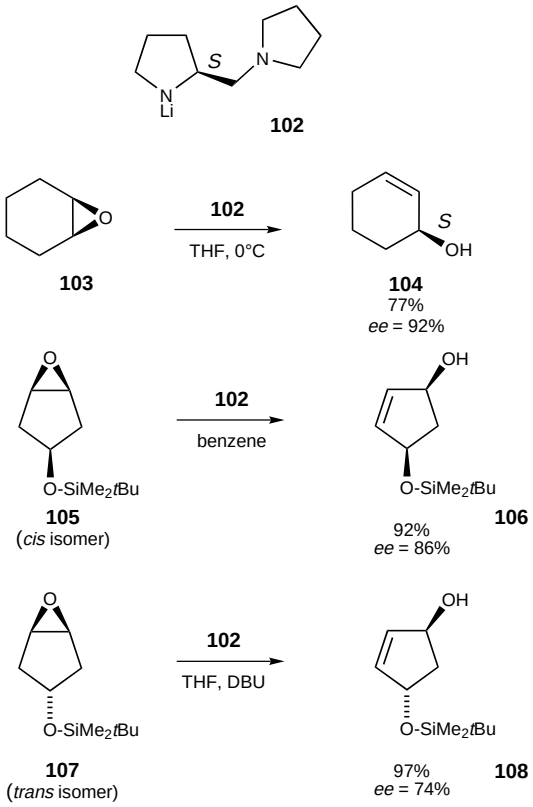
Asami showed that the enantioselective-opening of cyclohexene oxide (**103**) with lithium pyrrolidide (**102**) led to (*S*)-2-cyclohexen-1-ol (**104**) in 92% enantiomeric excess (Scheme 21).[51a–c] Similar results were obtained in the preparation of chiral monoprotected cyclopent-2-en-1,4-diols **106** and **108**, which are useful chiral building blocks.[51d] Other chiral bases derived from 1,2-diamines have been used by Singh et al.[52]



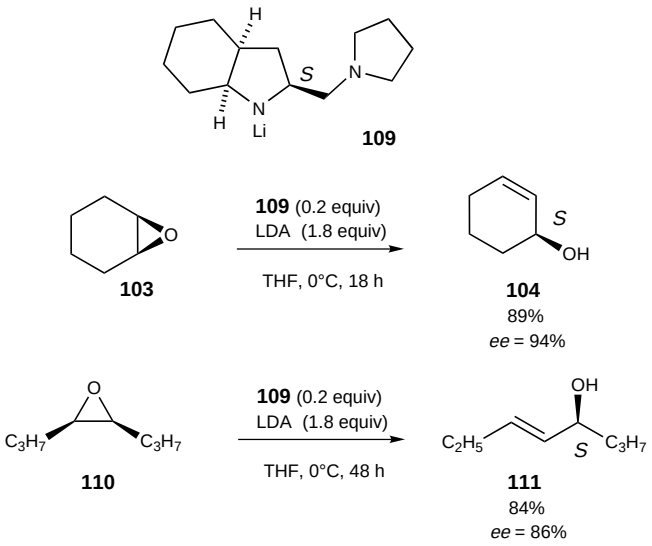
Scheme 20. Enantioselective protonation of an amide enolate with a chiral 1,2-diamine.

Catalytic enantioselective deprotonation of *meso*-epoxides and ketones, which use only a catalytic amount of the chiral lithium base plus a stoichiometric amount of a non-chiral base has also been reported by the groups of Asami,[53a, b] Koga,[53c] and Alexakis.[53d] In a recent example,[53b] (*S*)-2-cyclohexen-1-ol (**104**) was obtained from **103** in 94% *ee* with 20 mol% of the bulky chiral lithium amide **109**, in the presence of 180 mol% of LDA (Scheme 22). A high enantioselectivity was also shown to occur in the reaction of the epoxide **110** derived from an acyclic olefin.

Recently, Simpkins et al.[54] described the enantioselective conversion of episulfoxides that contain prostereogenic centers, such as **112**, into alkenyl sulfoxides by treatment with chiral lithium amides (Scheme 23). The C_2-symmetric bislithium amide **113** was found to effect the rearrangement with up to 88% *ee*.



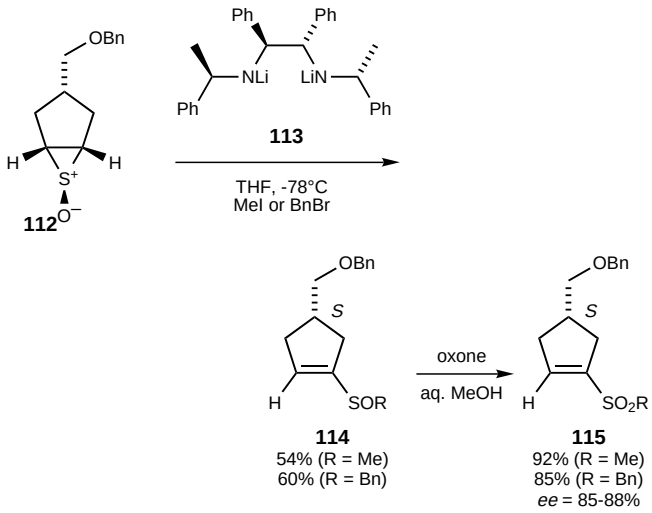
Scheme 21. Enantioselective deprotonation of *meso*-epoxides with the chiral lithium amide **102**.



Scheme 22. Catalytic enantioselective deprotonation of *meso*-epoxides with the chiral lithium amide **109**.

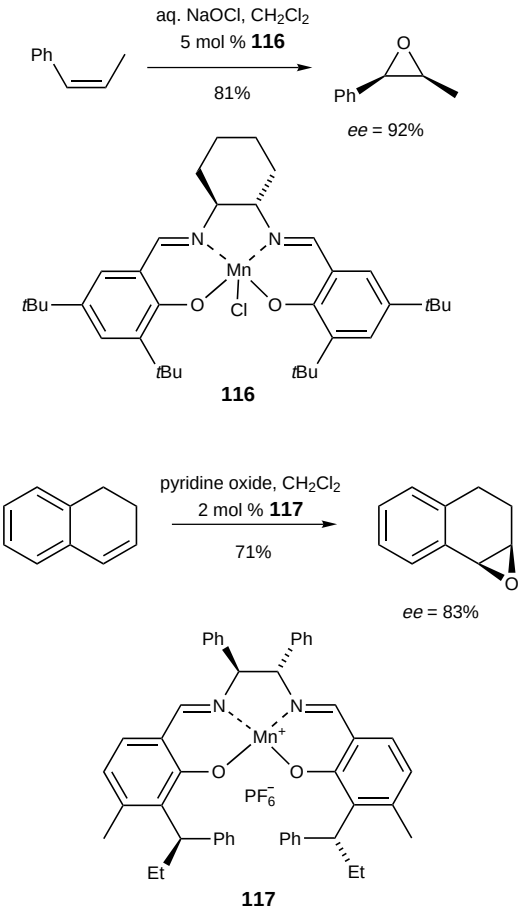
3.3.8. Epoxidation, Dihydroxylation, and Aziridination

Kochi et al. have demonstrated that achiral metal complexes containing salen-type ligands are active catalysts for the epoxidation of nonfunctionalized olefins, with the cationic manganese(III) complexes being the most efficient.[55] Jacobsen et al.[56a–c] and, independently, Katsuki et al.[56d–h] then prepared chiral derivatives of [Mn(salen)] complexes such as **116** and **117** and, by using oxidants such as PhIO or



Scheme 23. Enantioselective conversion of episulfoxides into alkenyl sulfoxides with a bislithium amide.

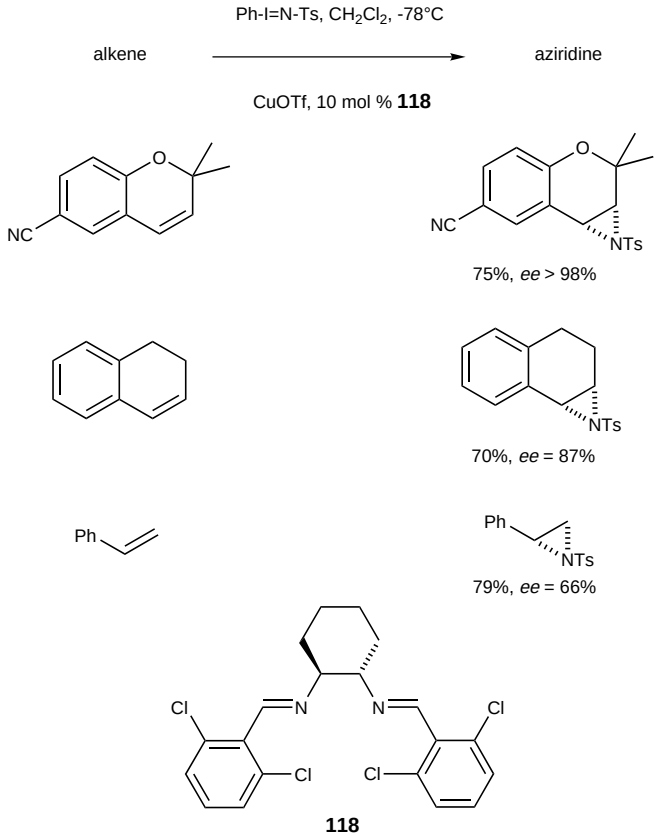
commercial bleach (aqueous solution of NaOCl), achieved the catalytic epoxidation of simple olefins under phase-transfer conditions, with enantiomeric excesses exceeding 90%. The efficient enantioselective epoxidation of dienyl sulfones was also described recently.[56i] Some illustrative examples are shown in Scheme 24. The epoxidation of several



Scheme 24. Enantioselective epoxidation reaction with [Mn(salen)] complexes.

olefins with the Jacobsen catalyst occluded in a polydimethylsiloxane membrane was reported recently by Vankelecom et al. to proceed with enantioselectivities similar to those obtained with the homogeneous catalyst. The catalytic membrane is regenerable by a simple washing procedure.[57]

A reaction closely related to epoxidation is aziridination. Jacobsen et al. have reported that the chiral ligand **118** is quite efficient in the enantioselective Cu^{I}-catalyzed aziridination of unfunctionalized alkenes (Scheme 25).[58]

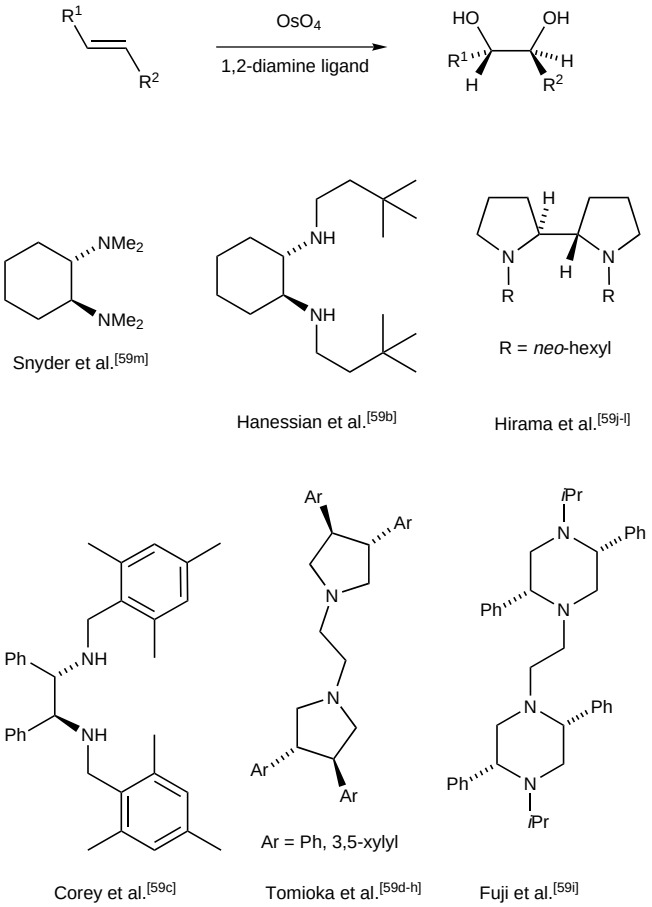


Scheme 25. Enantioselective aziridination reactions in the presence of a salen ligand **118**.

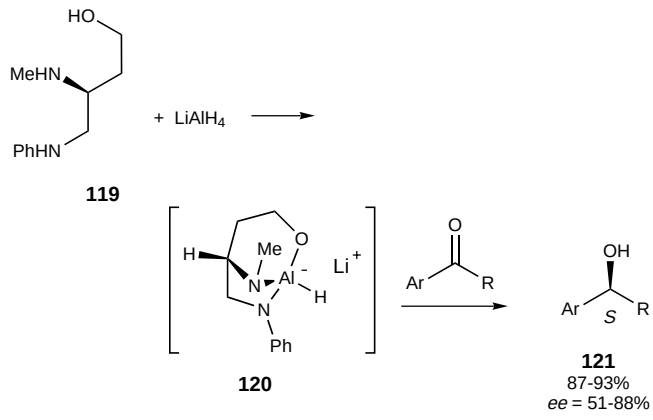
Apart from the outstandingly successful development of OsO_4-catalyzed dihydroxylation of olefins according to the Sharpless procedure, a number of recent methods employ chiral 1,2-diamines as ligands in this reaction (Scheme 26).[38c, 26, 59] Despite the good to excellent enantioselectivities that can be obtained, the reactions are stoichiometric in both OsO_4 and the chiral ligand: in situ recycling is prevented by the formation of very stable chelate complexes between the ligand and osmium(VI) glycolate intermediates.

3.3.9. Reduction of Prochiral Carbonyl Compounds

In 1982 Fujisawa et al.[60] described the enantioselective reduction of alkyl phenyl ketones by using the chiral hydride reagent **120**, prepared from lithium aluminium hydride and (*S*)-4-anilino-3-methylamino-1-butanol (**119**, Scheme 27). The corresponding *S*-configured alcohols **121** were obtained in 51 – 88 % *ee*.



Scheme 26. Chiral 1,2-diamino ligands for asymmetric dihydroxylation under stoichiometric conditions.

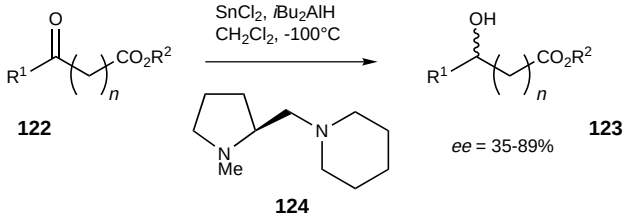


Scheme 27. Enantioselective reduction of alkyl phenyl ketones with a 1,2-diamine-derived chiral hydride reagent.

The asymmetric reduction of prochiral keto esters **122** by a chiral complex derived from **124**, tin(II) chloride, and diisobutylaluminium hydride has been realized by Mukaiyama et al. (Scheme 28).[61]

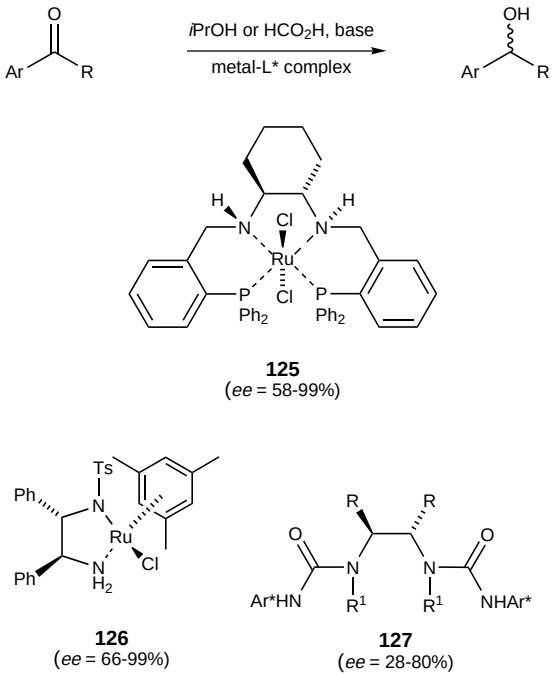
More recently Mukaiyama et al. reported the enantioselective reduction of aromatic, cyclic ketones and imines with sodium borohydride, catalyzed by [Co^{II}(salen)] complexes.[62] Very good enantiomeric excesses (up to 97 %) were obtained.

The reduction of aromatic ketones was also carried out successfully by asymmetric hydrogen transfer (with *i*PrOH or



Scheme 28. Enantioselective reduction of a prochiral ketone in the presence of a chiral 1,2-diamine-based ligand.

HCO_2H used as a hydrogen donor)[63] with ruthenium complexes such as **125**[64a] and **126** (Scheme 29).[64b, c, d] Several recent studies make use of other metal complexes, by using various diamine-derived ligands such as diureas **127**.[64b, e, f, g]



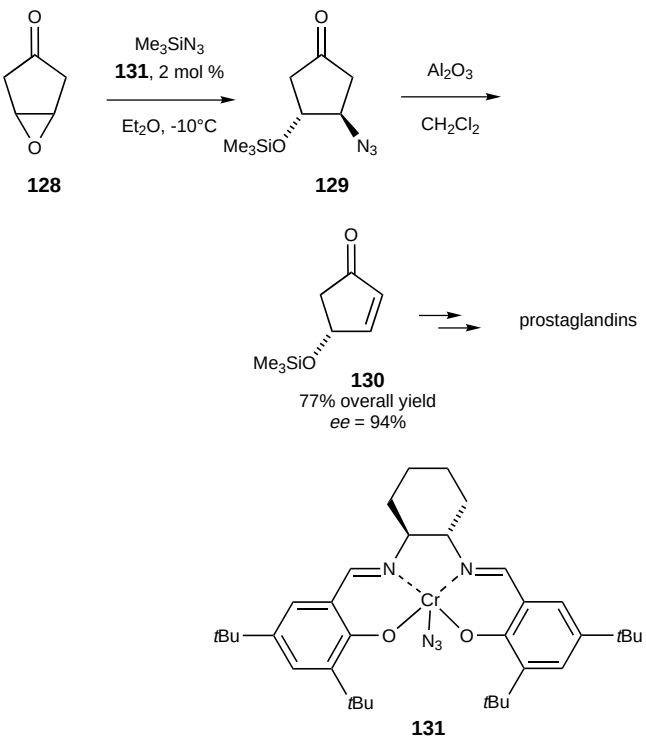
Scheme 29. 1,2-Diamino ligands and metal complexes used in prochiral ketone enantioselective reductions. The enantiomeric excesses obtained are given in parentheses.

Efficient asymmetric-transfer hydrogenation of α,β-acetylenic ketones mediated by **126** and other Ru^{II} catalysts was also reported recently by Noyori et al.[64h]

3.3.10. Miscellaneous Applications

Other recent synthetic applications include the enantioselective *ortho*-lithiation of substituted ferrocenes mediated by (*R*,*R*)-1,2-bis(dimethylamino)cyclohexane.[65] Trost et al. have developed palladium-catalyzed enantioselective allylic alkylations with either carbon or nitrogen nucleophiles that make use of chiral amide ligands derived from 1,2-diamines.[66a–f] Chiral thioarylimidazolines[67a] and diazaphospholidines[67b] derived from C_2-symmetric vicinal diamines were also employed recently as ligands for enantioselective palladium-catalyzed asymmetric allylation.

Jacobsen et al. reported the enantioselective nucleophilic ring opening of epoxides catalyzed by [Cr^{III}(salen)] complexes such as **131** (Scheme 30).[68] By using trimethylsilyl azide as the nucleophile, epoxide **128** was selectively converted into compound **129**; after basic alumina-promoted azide elimination enone **130**, a useful precursor in prostaglandins synthesis, was obtained (*ee* = 94%).



Scheme 30. Enantioselective opening of an epoxide in the presence of a [Cr^{III}(salen)] complex.

Metal complexes containing salen-type ligands were also employed as catalysts in the enantioselective oxidation of sulfides.[69]

Recently Noyori et al. reported that efficient kinetic resolution of racemic alcohols could be achieved by hydrogen transfer catalyzed by a diamine–Ru^{II} complex,[70] and Jacobsen et al. described the kinetic resolution of racemic, terminal epoxides by means of a hydrolysis catalyzed by chiral (salen)–cobalt complexes, which afforded both the unreacted substrates and the products (1,2-diols) in high enantiomeric excess.[71]

3.4. Conclusion

This section has highlighted the growing utility of enantiomerically pure vicinal diamines and their derivatives as chiral auxiliaries and ligands in asymmetric synthesis. Optically active pyrrolidine-containing molecules, 1,2-diphenylethylenediamine, and 1,2-diaminocyclohexane derivatives, more readily available than other ones, are mainly the most widely used. However, the ubiquitous character of the 1,2-diamino moiety and the increasing interest in vicinal diamines brought about the search for new methods for their preparation, especially stereoselective ones. The next section will present the major ways of preparation of such compounds.

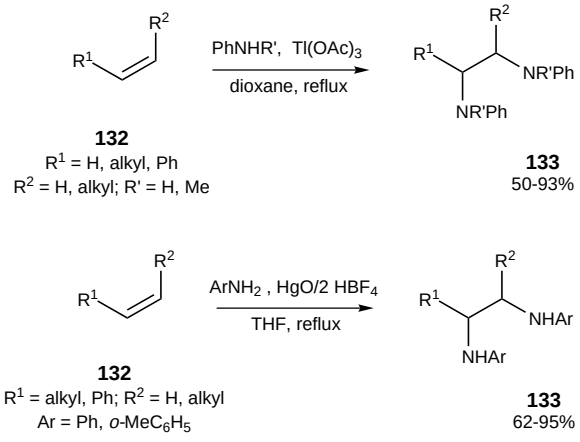
4. Vicinal Diamines: Methods of Preparation

Conceptually, the simplest procedure for the generation of the 1,2-diamino unit is the ammonolysis of the corresponding vicinal dihalide. However, this method, which was applied at the beginning of this century for the preparation of ethylenediamine, mainly yields elimination products in more complex systems.[72a] Although enantiopure 1,2-disubstituted 1,2-diamines have frequently been obtained through resolution[72b–g] diastereo- and enantioselective methods are employed increasingly in their synthesis. In the following paragraphs we will give an overview of the many reported syntheses of 1,2-diamines, with emphasis on the stereoselective ones. The methods will be arranged in the following manner: we will discuss first the ones in which the two nitrogen atoms are introduced concomitantly on the carbon skeleton, then the methods that utilize a compound already containing one of the two final nitrogen atoms of the target 1,2-diamine as the substrate, then the preparation of 1,2-diamines from compounds that already contain both nitrogen atoms, and lastly the syntheses starting from two nitrogen-containing substrates and involves the formation of the C1 – C2 bond.

4.1. Vicinal Diamines from Alkenes by Direct Introduction of Two Nitrogen Atoms

Although several methods are known for the oxidative transformation of alkenes into 1,2-diols (for instance, the dihydroxylation with $KMnO_4$ or OsO_4), the analogous strategy for vicinal diamines has been less developed.[73] Nevertheless, there are some methods that allow such olefin "diamination", which mainly use organometallic reagents.

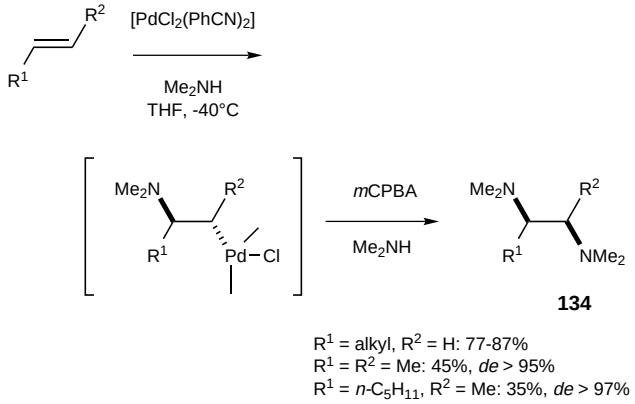
Barluenga et al. have reported a convenient preparation of aromatic vicinal diamines **133** from olefins in the presence of thallium[74] or mercury salts (Scheme 31).[75] The yields are



Scheme 31. Direct diamination of alkenes with thallium or mercury salts.

generally good, but the addition of aliphatic primary amines does not occur in the presence of thallium acetate and has not been reported for the mercury method. This procedure is thus limited to aromatic vicinal diamines.

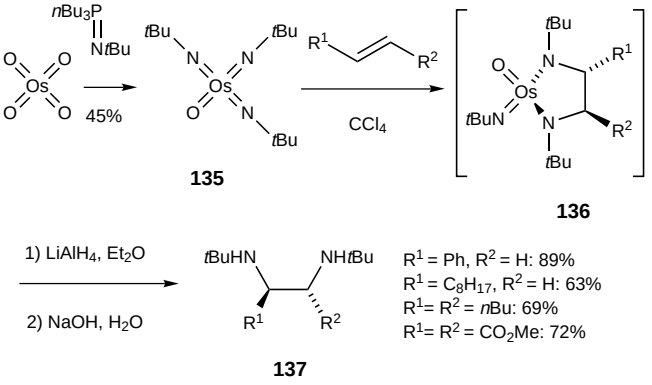
At the same time, Bäckvall showed that the aminopalladation of *E* alkenes, followed by oxidation in the presence of an excess of amine afforded the corresponding vicinal diamines **134** (Scheme 32).[76] Terminal olefins were diaminated in good



Scheme 32. Direct diamination of alkenes via an aminopalladatio compound.

yields (77 – 87 %) and the diamination was overall *cis* stereospecific. No results were reported for *Z* olefins, and only dimethylamine was used. Thus, the procedure has been applied only to the preparation of tertiary (*N,N,N′,N′*-tetramethyl)-*syn*-1,2-diamines.

In 1977 Sharpless et al.[77] showed that the triimidoosmium complex **135** reacted with monosubstituted and disubstituted *E*-olefins through a stereospecific *cis* addition to give vicinal diamines **137** (Scheme 33). However, this method has several

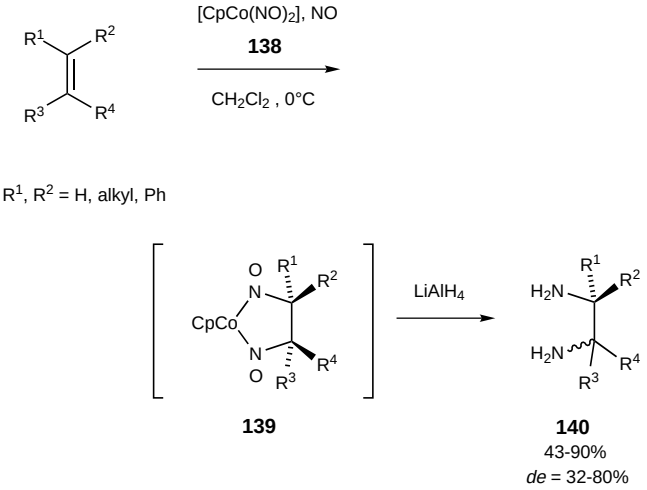


Scheme 33. Direct diamination of alkenes with a diimidoosmium complex.

drawbacks. The complex **135** must be prepared beforehand from OsO_4, which is a costly reagent, and must be used in stoichiometric amounts. Moreover, this complex is unreactive toward disubstituted *Z* olefins, thus the method only allows the preparation of secondary *N*-*tert*-butyl-substituted *syn*-1,2-diamines.

In 1980 Bergman et al. reported a more general 1,2-diamination of alkenes with nitric oxide and a cobalt complex.[78] Indeed, this procedure works satisfactorily for terminal, *E* and *Z*, di-, tri-, and at least some tetra-substituted alkenes and leads to various aliphatic primary 1,2-diamines. It

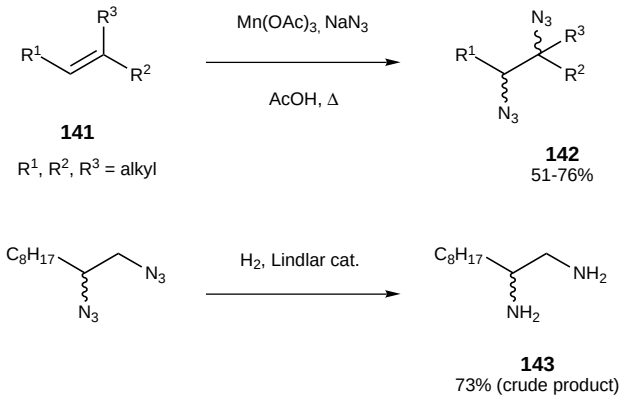
utilizes the cobalt-based reagent **138** and nitric oxide (Scheme 34). Primary vicinal diamines are obtained in moderate to excellent yield. Despite the complete stereospecificity (*cis* addition) of the first step (some 1,2-dinitrosoalkane – Co complexes **139** were isolated), the production of



Scheme 34. Diamination of alkenes with a nitrosylcobalt complex.

diastereomeric diamines arises from epimerization during the $LiAlH_4$ reduction. No examples are given of non-racemic series.

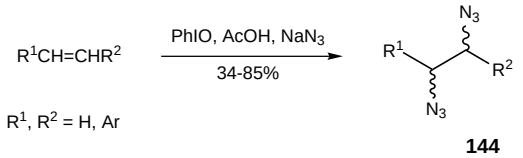
In 1985 Fristad et al. reported a Mn^{III}-catalyzed direct conversion of alkenes **141** into 1,2-diazides **142** (Scheme 35).[79] $Mn^{III}-N_3$ species formed in situ are capable of oxidatively transferring a $N_3^{\bullet}$ radical to alkenes. Yields were moderate to



Scheme 35. Preparation of 1,2-diamines through diazidation of alkenes with a diazide-manganese complex.

good and stereoselectivity was fair (4:1 to 6:1) in cyclic series. The diazidation, coupled with the reduction of the 1,2-diazides, constitutes a simple two-step route to 1,2-diamines such as **143**. Such a reduction step can be performed by hydrogenation over Lindlar's catalyst. However, care should be exercised with azides and oxidizing agents: a case of explosion was reported by the authors!

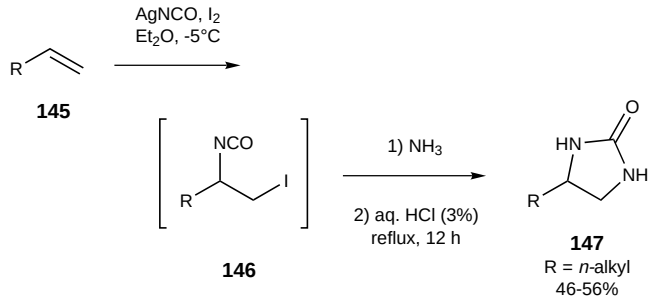
The conversion of alkenes into 1,2-diamines has also been realized from direct diamination procedures not involving organometallic species. For instance, a method for the preparation of vicinal diazides **144** has also been described by Moriarty et al. (Scheme 36).[80] This strategy no longer uses



Scheme 36. Synthesis of vicinal diazides by using hypervalent iodine.

metal complexes as did Fristad's method, but a hypervalent iodine oxidation in the presence of sodium azide. Although this method is direct and quite simple, it lacks stereoselectivity and its scope has been explored mainly with aryl-substituted alkenes.

Substituted imidazolidin-2-ones can be considered as a protected form of 1,2-diamines. In 1983 Ghomi and Orr published a simple preparation of 4-substituted imidazolidin-2-ones **147** (Scheme 37).[81] The first step is analogous to the



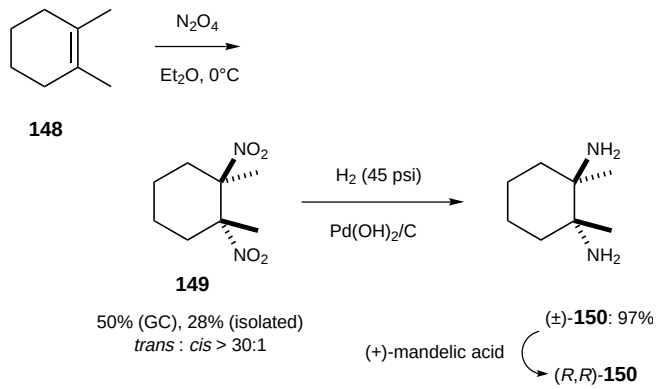
Scheme 37. Preparation of 4-substituted imidazolidin-2-ones from alkenes.

methodology of Swift and Swern (Section 4.5; Scheme 57). Freshly prepared silver isocyanate and iodine are added to a terminal alkene **145** to afford a β-iodoalkyl isocyanate **146**. After treatment with ammonia and dilution with HCl, the corresponding 4-alkylimidazolidin-2-one **147** was obtained (overall yield: 46 – 56 %). No examples concerning polysubstituted alkenes were given.

In the course of the investigation of C_2-symmetric 1,2-diamines as chiral ligands in asymmetric catalysis, Jacobsen and Zhang reported the preparation of *trans*-1,2-diamino-1,2-dimethylcyclohexane (**150**) by the highly diastereoselective oxidation of olefin **148** by dinitrogen tetroxide (Scheme 38).[82] This methodology is mainly suited for the synthesis of vicinal diamines adjacent to tertiary centers because primary and secondary dinitro intermediates would be prone to epimerization.

4.2. Vicinal Diamines from Dienes and Heterodiimides

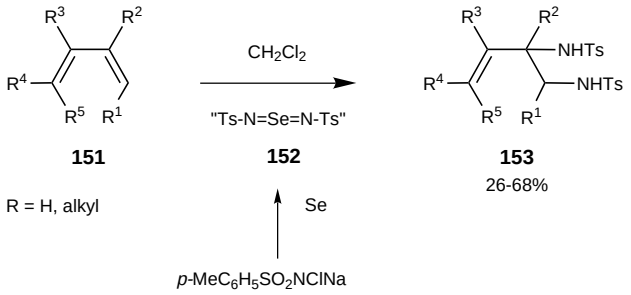
Indirect diamination of double bond containing compounds can also be used to prepare vicinal diamines. Thus, the Diels – Alder adducts of 1,3-dienes and selenium- or sulfur-contain-



Scheme 38. Preparation of cyclic 1,2-diamine by N_2O_4 addition to a cycloalkene.

ing dimides have been shown to undergo rearrangements that lead to unsaturated 1,2-diamines.

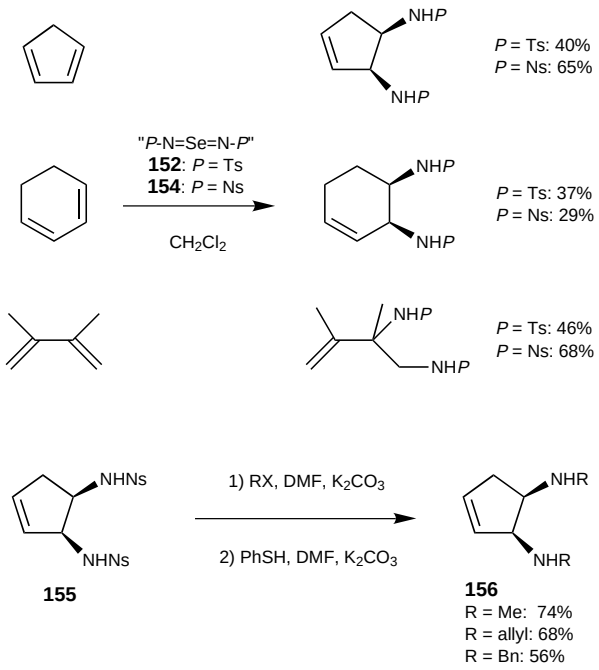
In 1976 Sharpless and Singer reported that the reaction of 1,3-dienes **151** with the diimidoselenium compound **152** afforded 1,2-disulfonamidoalkenes **153**, by a Diels–Alder reaction followed by a [2,3]-sigmatropic rearrangement (Scheme 39).[83a]



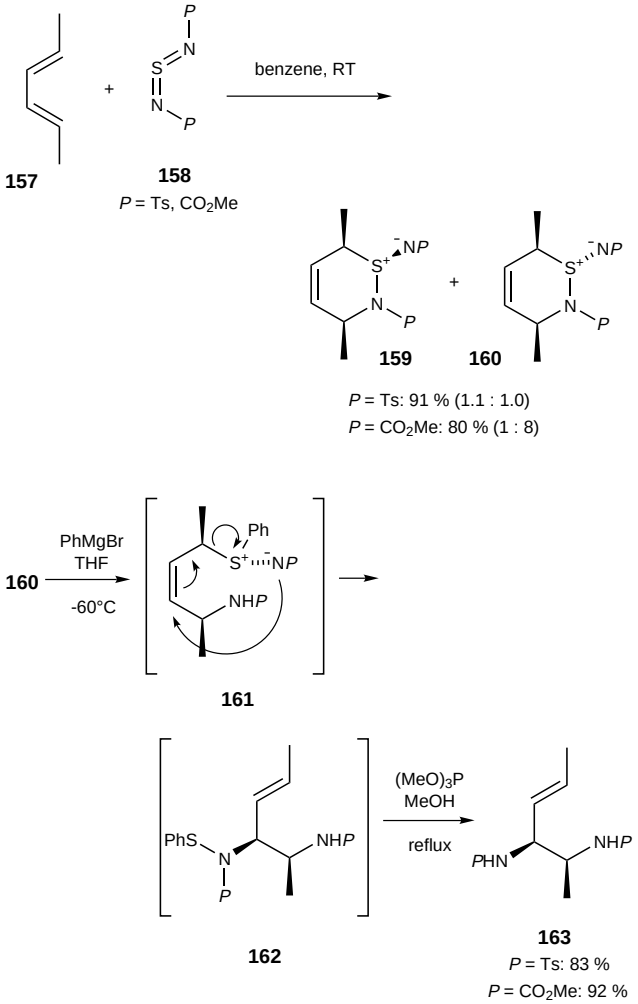
Scheme 39. Diamination of 1,3-dienes with a diimidoselenium species.

The yields were poor to fair (26–68%) and the removal of the *para*-toluenesulfonyl groups required harsh conditions that are incompatible with many other functional groups. More recently, following the publication of a simple method for the deprotection of nitro-substituted benzenesulfonamides,[83b] Sharpless et al. reinvestigated their method by using a modified diimidoselenium reagent **154** that has *ortho*-nitrobenzenesulfonyl residues (Scheme 40).[83c] The yields of the allylic aminations were not improved, but the deprotection of the amine functions were much easier. Dimethyl-, diallyl-, and dibenzyldiamines **156** were thus prepared in good yields.

Weinreb et al. designed a related stereocontrolled synthesis of unsaturated vicinal diamines from the Diels–Alder adducts of sulfur dioxide diimides **158** and 1,3-dienes (Scheme 41).[84] Treatment of adduct **160**, obtained from 2,4-hexadiene (**157**) with phenylmagnesium bromide, and then with trimethylphosphite yielded the *syn*-diamine derivative **163**. The first step is a ring opening mediated by the Grignard reagent, which leads to an allylic sulfinimine **161** that undergoes a [2,3]sigmatropic rearrangement to a sulfenamide **162**. Desulfurization of the sulfenamide with trimethylphosphite afforded the *syn*-diamine derivative. From *E*,*E*- and *E*,*Z*-



Scheme 40. Diamination of 1,3-dienes with a modified diimidoselenium species.

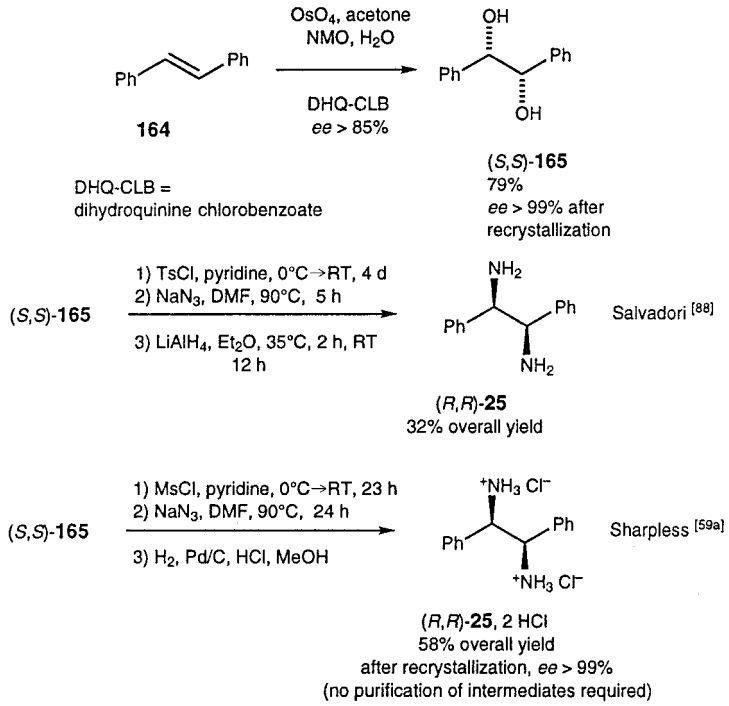


Scheme 41. Stereocontrolled synthesis of unsaturated 1,2-diamine derivatives from Diels–Alder adducts of sulfur dioxide diimides and 1,3-dienes.

1,3-dienes, *syn* and *anti* adducts were obtained, respectively. These adducts contain a double bond that may be used for further functionalization.

4.3. Vicinal Diamines from 1,2-Diols or 1,2-Dihalides

Taking into account the recent developments of catalytic asymmetric epoxidation,[85] of catalytic asymmetric dihydroxylation,[59a, 86] and of catalytic asymmetric aminohydroxylation,[87] a "catalytic asymmetic diamination" may appear in the near future. However, the efficiency and scope of osmium-catalyzed asymmetric dihydroxylation allows access to various enantiomerically pure 1,2-diols that can be converted by several methods into enantiopure vicinal diamines, for instance through double displacement by nitrogen nucleophiles. Such a procedure is illustrated by the syntheses of (*R*,*R*)-stilbenediamine **25** reported by Salvadori et al.[88] and Sharpless et al.[59a] (Scheme 42). This method may be adapted for the preparation of other enantiomerically pure diamines, provided the corresponding alkenes contain no functional groups that are incompatible with osmium tetroxide.



Scheme 42. Syntheses of (*R*,*R*)-stilbenediamine from the 1,2-diol (*R*,*R*)-**165** (≡ (*S*,*S*)-**165**), prepared by catalytic asymmetric dihydroxylation of stilbene.

Since the catalytic asymmetric dihydroxylation developed by Sharpless provides a convenient access to optically active diols **166**, and since cyclic derivatives such as sulfites **167**[89a] or sulfates **168**[89b, c] show a good electrophilic behavior toward various nitrogen nucleophiles, the coupling of these two efficient procedures can be used for the synthesis of optically active vicinal diamines (Scheme 43). 1,2-Dihalides were used as substrates in the synthesis of racemic *n*,*n*+1-diamino carboxylic acid derivatives.[10b] Enantiomerically pure C_2-symmetric 1,2-diamines were also prepared from tartaric acid, either by a twofold Mitsunobu reaction of a diol intermediate with hydrazoic acid[90a] or by displacement of a bismesylate with sodium azide.[90b] The preparation of (2*S*,3*S*)-diaminobutane from the corresponding racemic bismesylate involved a resolution.[90c]

4.4. Vicinal Diamines from β-Amino Alcohols or β-Halogenoalkylamines

There are several methods for the preparation of 1,2-diamines that actually consist of the introduction of a second amino group into compounds already containing a nitrogen functionality. Amines substituted at the β position by an hydroxyl group or by an halide are widely used as such starting materials.

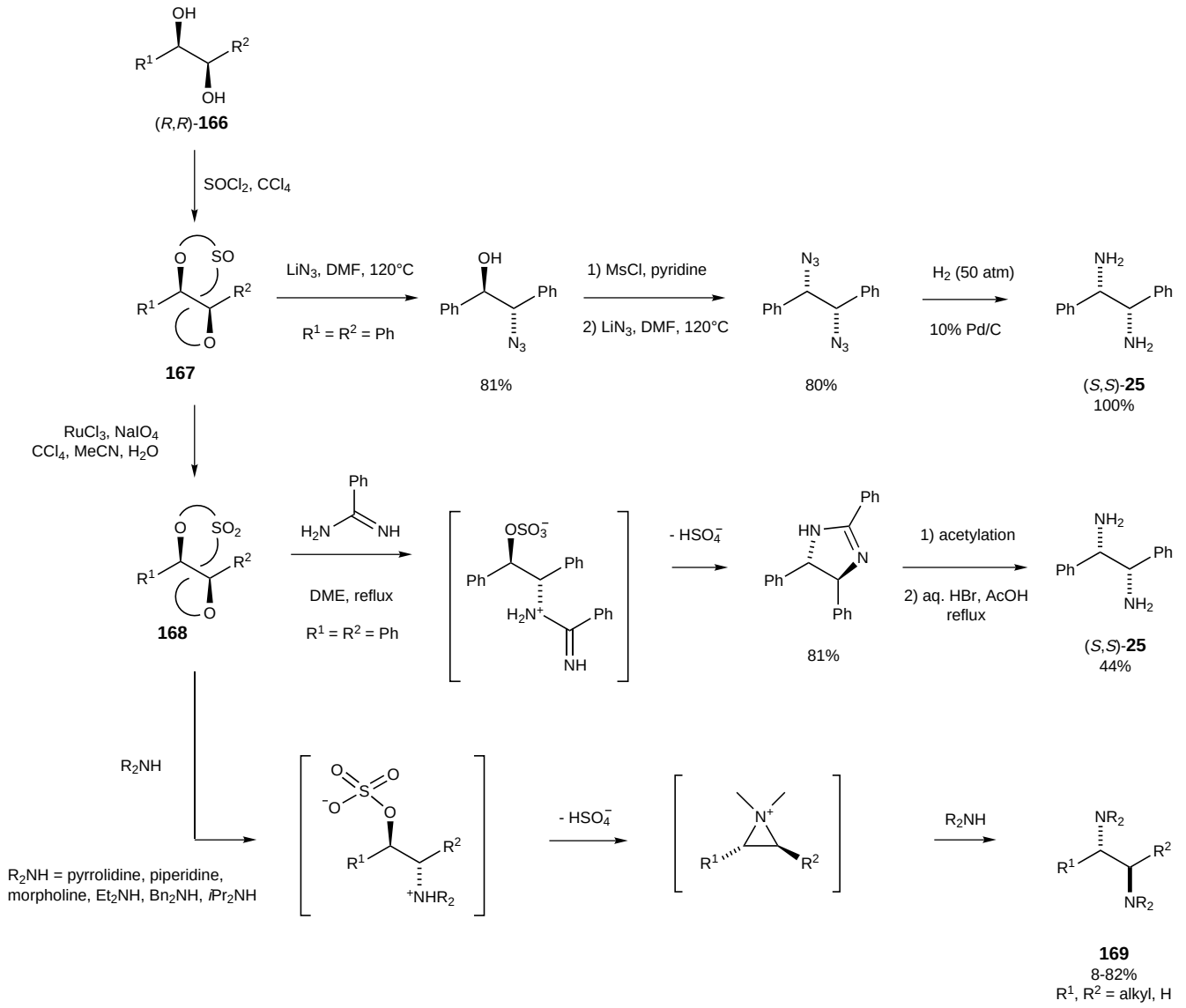
4.4.1. Vicinal Diamines from β-Amino Alcohols

After transformation of the hydroxyl group of a β-amino alcohol into a leaving group, substitution by a nitrogen nucleophile then affords a diamine precursor. Several optically active β-amino alcohols can be found in nature, they can also be prepared, for example, from α-amino acids through alkylation or reduction.

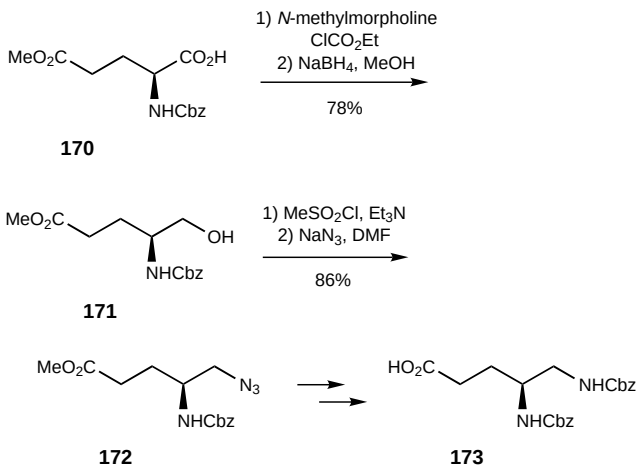
A Mitsunobu reaction may be used to introduce the nitrogen nucleophile (an azide[91a–d] or a phthalimide.[91e–g]) A synthesis of statine analogues involved an intramolecular Mitsunobu reaction.[12c] Nucleophilic displacements of tosylates or mesylates are also frequently employed, as in the synthesis of (−)-slaframine,[92] in the synthesis of (*R*)- and (*S*)-2,3-diaminopropanol from L- and D-serine,[93] or in the synthesis of (3*R*,4*R*)- and (3*R*,4*S*)-β,γ-diamino acids from D-phenylalanine.[94] Several protected, chiral triamines and diamines were synthesized by Kokotos et al.[95] For example, the Cbz-protected 4,5-diaminopentanoic acid **173** was prepared from the glutamic acid derivative **170** through a sequence involving the nucleophilic displacement of a mesyl group by sodium azide (Scheme 44).

A Walden inversion does not always occur during such displacements; for example, Rossi et al. observed a retention of configuration in the reaction of potassium phthalimide with the mesylate **174** as a consequence of the participation of the oxazolidinone nitrogen atom in the displacement mechanism (Scheme 45).[96] However, this effect was completely suppressed by the treatment of **174** with chlorotrimethylsilane and then with sodium azide. Thus, the two diastereomeric amines **176** and **178** could be prepared from a common precursor. The taxol side chain analogue **179** was then synthesized in a few steps from **178**.

A stereo- and regioselective route to chiral diamines, which were required for use as ligands in organocopper conjugate additions, was developed by Dieter et al. from (−)-ephedrine and (−)-pseudoephedrine.[97] Their strategy (Scheme 46) relied on the transformation of a chiral 1,2-amino alcohol



Scheme 43. Preparation of enantiopure 1,2-diamines from cyclic sulfites and sulfates.

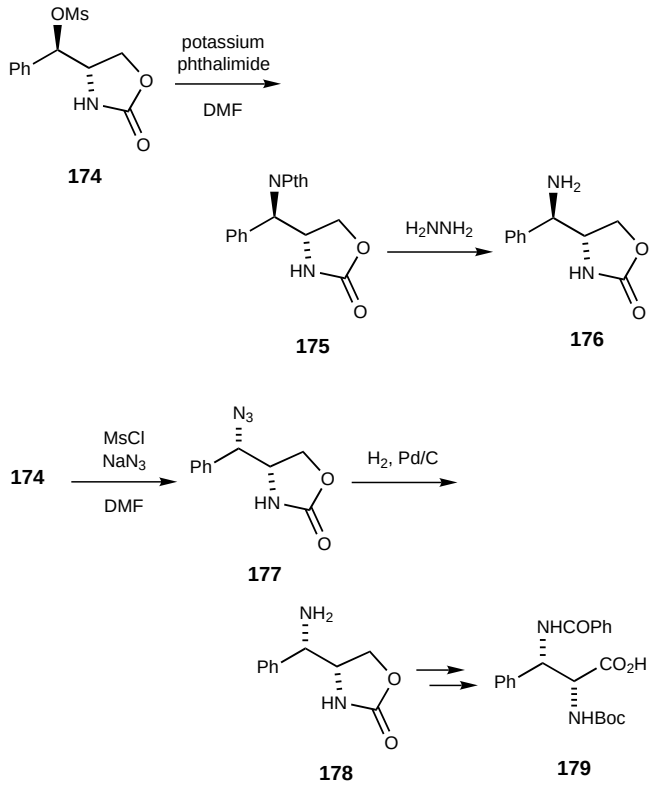


Scheme 44. Synthesis of 4,5-diaminopentanoic acid in the form of its bis(benzyloxycarbamate).

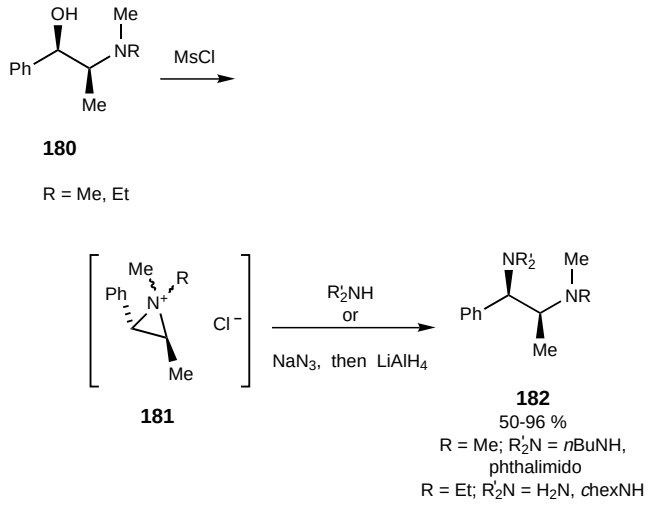
180 into an aziridinium **181** (by intramolecular displacement of a mesylate group), which was then treated with various nitrogen nucleophiles to afford the corresponding diamines or diamine precursors **182**.

Rossiter et al.[98] have described a related method relying on the opening of aziridiniums **187** generated from 1,2-amino alcohols **186** (Scheme 47). These alcohols were prepared from alkenes **183**, by Sharpless asymmetric dihydroxylation, conversion of diols **184** into epoxides **185**, and nucleophilic opening of **185** by piperidine. The reaction of aziridiniums **187** with methylamine afforded single regioisomers **188** (*ee* > 95%). The diamines were employed as ligands for chiral amidocuprates that were used in enantioselective conjugate addition to cyclic enones.

O'Brien et al. then reported a one-pot method to convert (*R*)-styrene oxide (**189**) into 1,2-diamines **191** (Scheme 48).[99a] However, only diamines derived from reactive amines such as



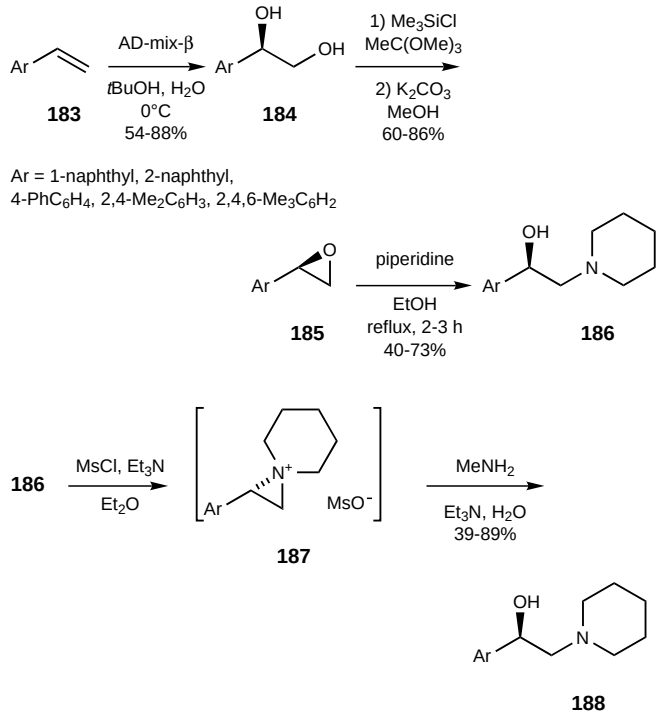
Scheme 45. Synthesis of *syn*- and *anti*-1,2-diamine derivatives from a common mesylate precursor.



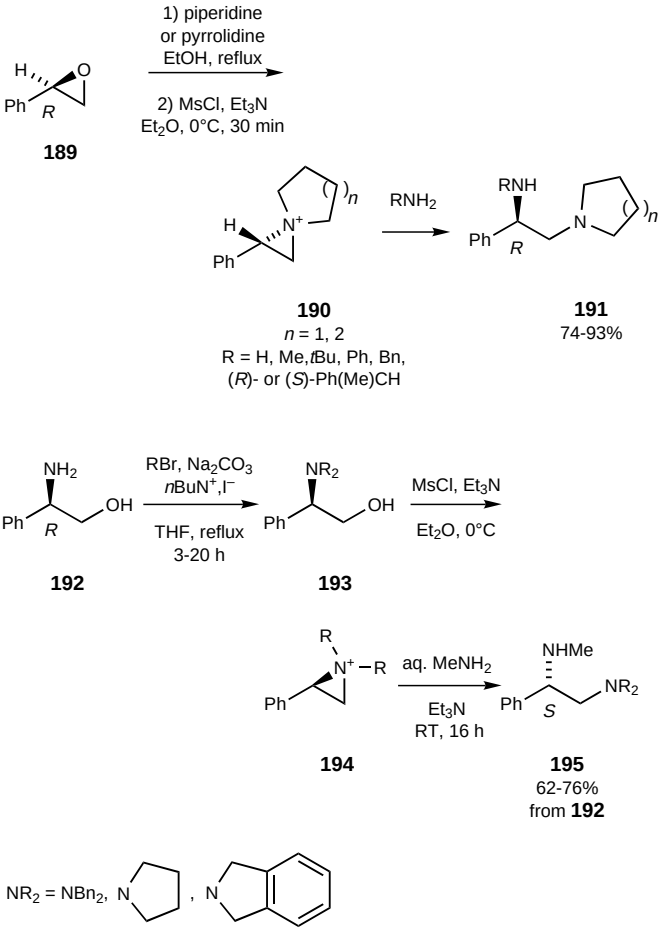
Scheme 46. Synthesis of vicinal diamines from (−)-ephedrine.

piperidine or pyrrolidine were available in this way. In a further improvement they showed that phenylglycinol (**192**), commercially available in both enantiomeric forms, can be used as a precursor to diamines **195** that contain other susbtituents; in this case, a N-dialkylation step is needed prior to the generation of aziridiniums **194**.[99]

Rayner et al. demonstrated recently that 2,3-epoxy amines **196** can also be used as substrates for the generation of aziridinium intermediates **197** (Scheme 49).[100] Addition of nitrogen nucleophiles onto these species proceeded regioselectively, to give 1,2-diamines **198**. Homochiral epoxides **196**

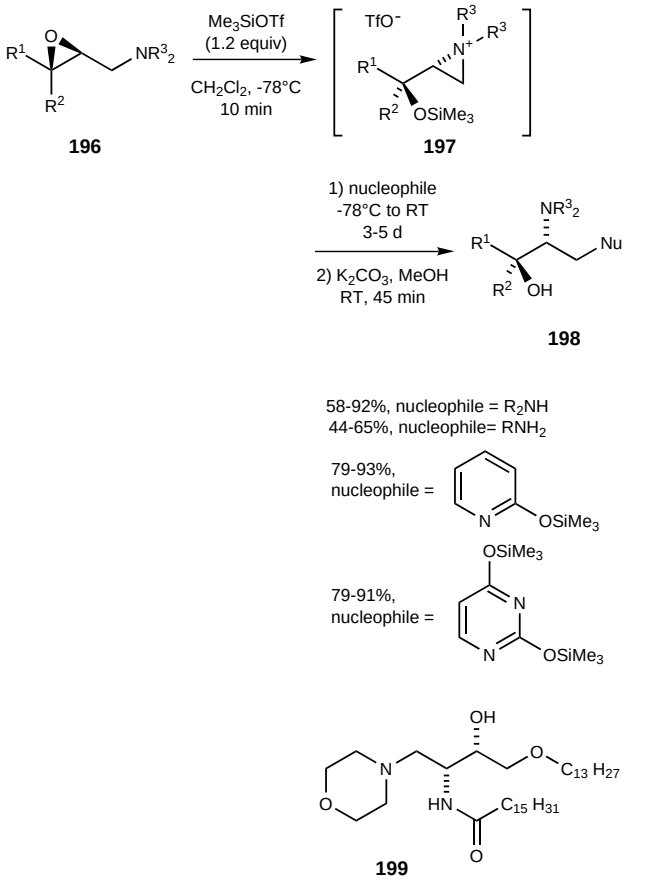


Scheme 47. Synthesis of vicinal diamines from enantiomerically pure aryl epoxides.



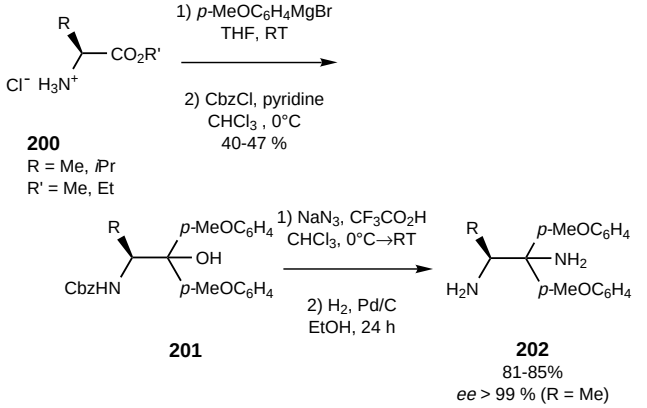
Scheme 48. Synthesis of vicinal diamines from (*R*)-styrene oxide or (*R*)-phenylglycinol.

can be obtained from the corresponding epoxy alcohols prepared by Sharpless asymmetric epoxidation. This methodology was used to synthesize compound **199**, a potential inhibitor of glucosylceramide synthase.



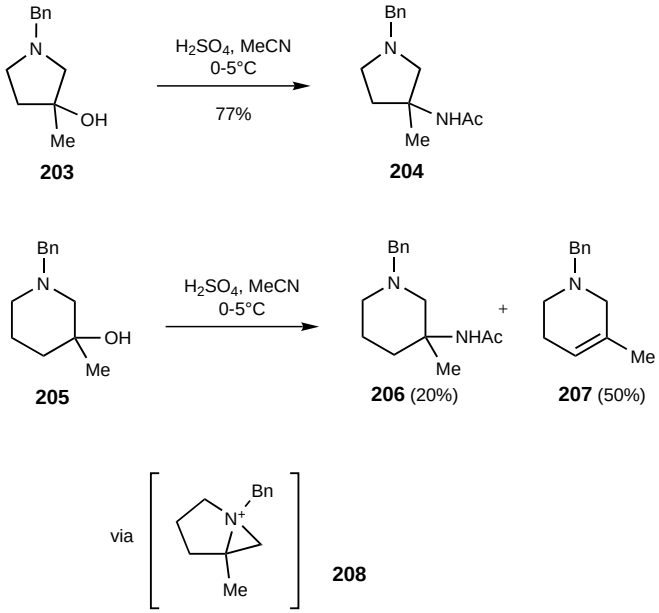
Scheme 49. Synthesis of vicinal diamines from 2,3-epoxy amines via aziridinium salts.

In their reported synthetic route to trisubstituted diamines, Burrows et al. made use of the bisalkylation of α-amino esters **200** (Scheme 50).[101] After substitution of the hydroxyl group with azide under acidic conditions and hydrogenolysis, diamines **202** having the same substituent twice on a carbon atom were obtained. Their incorporation in salen–nickel complexes was then studied.



Scheme 50. Synthesis of vicinal diamines by the bisalkylation of α-amino esters.

The Ritter reaction of several cyclic hydroxyamines was recently studied by Taylor et al. (Scheme 51).[102] While the treatment of the pyrrolidine **203** with acetonitrile and sulfuric acid afforded the expected acetamide **204** in 77% yield, under the same conditions, **205** gave only 20% of acetamide **206**, along with alkene **207**. In the latter case it was suggested that a stable aziridinium compound **208** formed, which would not react easily with acetonitrile because of steric congestion.



Scheme 51. The Ritter reaction of several cyclic β-hydroxyamines.

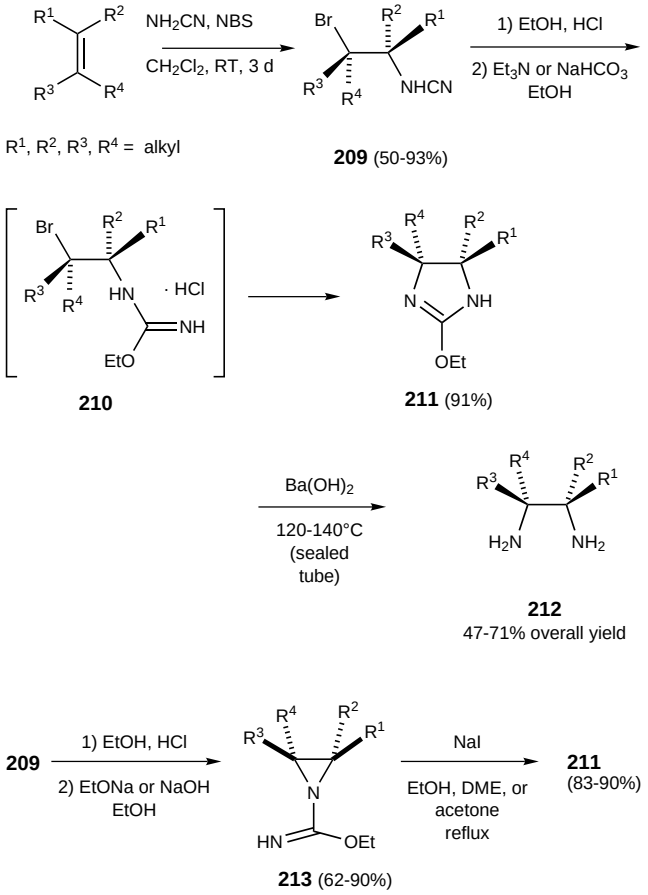
The opening of 2-oxazolines[103] or of serine-derived β-lactones[104] by amines has also been used to prepare 1,2-diamine derivatives.

4.4.2. Vicinal Diamines from β-Halogenoalkylamines

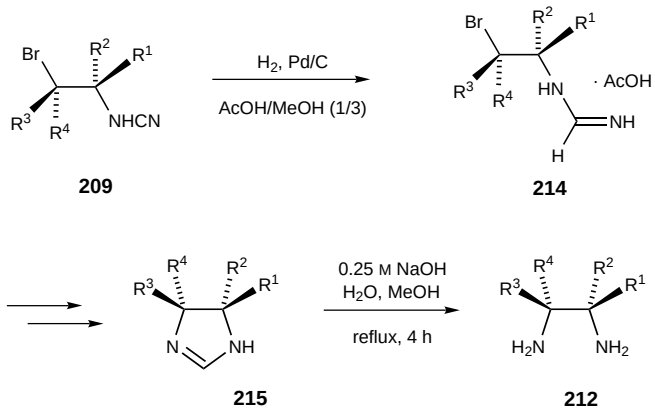
Several conditions can be employed to obtain β-halogenoalkylamines from alkenes; substitution of the halide by a nitrogen nucleophile then affords 1,2-diamine derivatives.

In 1983, Kohn and Jung described a method for the stereospecific preparation of nitrogen-unsubstituted vicinal diamines **212** as outlined in Scheme 52.[105] The first step was the addition of *N*-bromosuccinimide and cyanamide to an unactivated alkene to give a β-bromoalkyl cyanamide **209**. This adduct gave in situ the corresponding isourea **210** in an acidic ethanolic medium. Treatment of this compound with a mild base produced the 2-ethoxyimidazoline **211** directly. Basic hydrolysis in the last step then yielded the vicinal diamine **212** (overall yield: 47% to 71%). More basic conditions must be used to obtain compounds **211** from *Z* alkenes; in this case, aziridine **213** was isolated, and then rearranged to **211** in the presence of sodium iodide.

Less stringent conditions for both the cyclization and the final ring-cleavage steps were also developed by the use of formamidine **214** instead of isourea **210** (Scheme 53).[105] Amidine **214** was obtained without hydrogenolysis of the C–Br bond by catalytic hydrogenation of cyanamide **209**



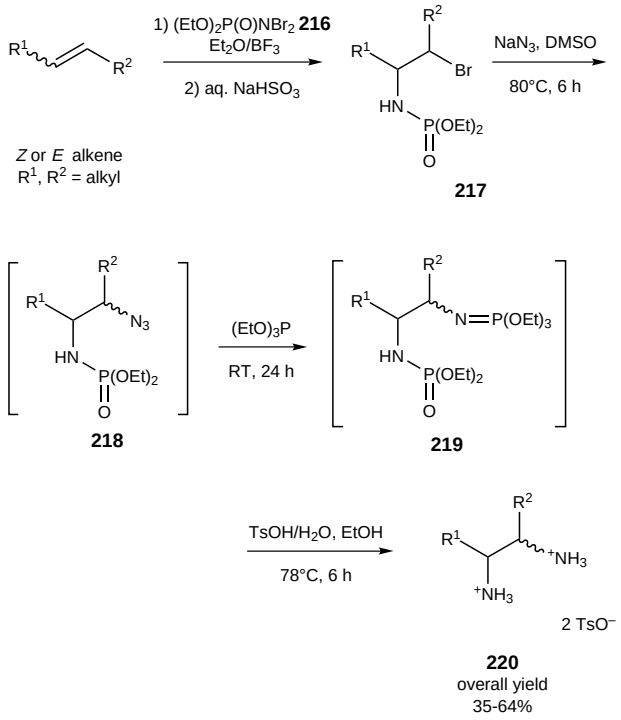
Scheme 52. Synthesis of vicinal diamines from alkenes and cyanamide.



Scheme 53. Modified procedure for the preparation of vicinal diamines from alkenes and cyanamide.

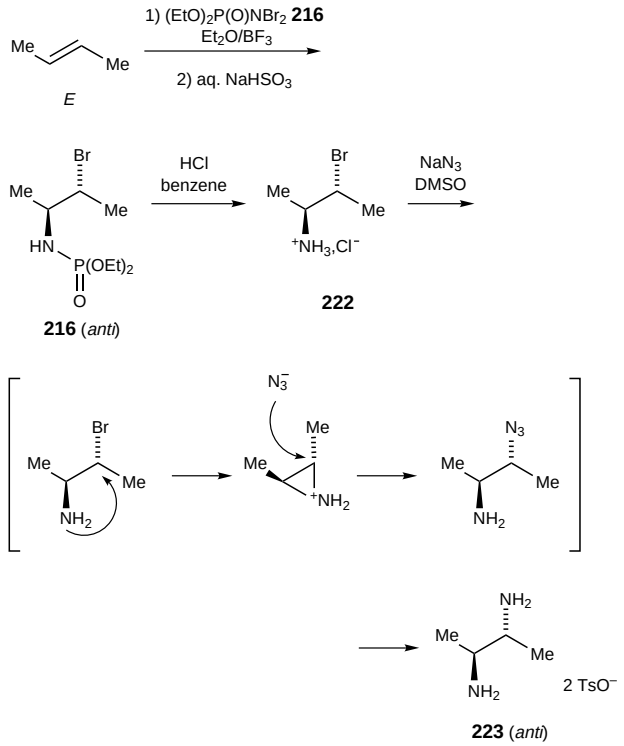
under acidic conditions with palladium on charcoal. Ring cleavage of the imidazoline **215** was then accomplished with diluted NaOH.

More recently, Zwierzak et al. reported an expedient synthesis of vicinal diamines from the bromophosphoramidates **217**, obtained by the reaction of alkenes and diethyl *N*,*N*-dibromophosphoramidate (**216**, Scheme 54).[106] Compounds **217** were converted to vicinal diamines by a one-pot procedure that involved the displacement of the bromide ion by sodium azide and the reduction of the azide in a Staudinger reaction.



Scheme 54. Synthesis of vicinal diamines from alkenes and a dibromophosphoramidate.

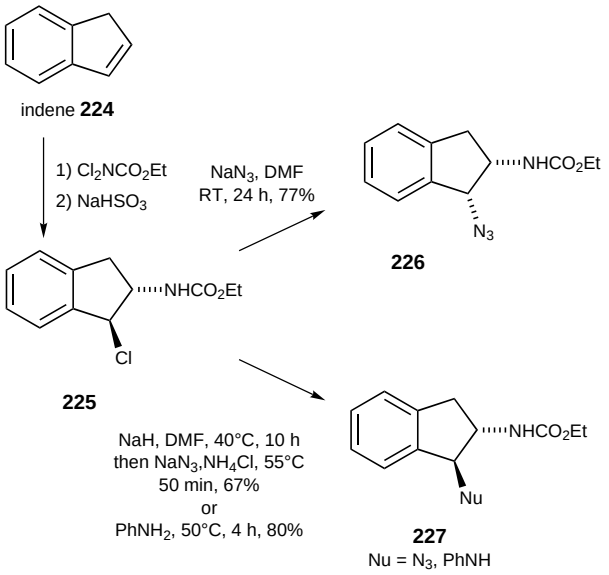
Diamination proceeded stereospecifically only with cyclic alkenes, to give *cis*-1,2-diamines. In the case of acyclic olefins, epimerization occurred, presumably in the azidation step with participation of the amidophosphoryl group. A modification consisting of the cleavage of the N–P bond prior to the azidation, as depicted in Scheme 55,[106] then led to a new



Scheme 55. Stereospecific synthesis of an acyclic *anti*-1,2-diamine from an *E* alkene

stereospecific diamination of open-chain olefins, with *syn*- and *anti*-1,2-diamines being obtained from *Z* and *E* alkenes, respectively. However, this strategy cannot be used in the case of sterically congested alkenes, which cannot undergo aminobromination.

Orlek reported an approach to the preparation of either *cis*- or *trans*-1,2-diamino derivatives of benzobicyclic compounds.[107] An example is described in the Scheme 56. The



Scheme 56. Diastereoselective synthesis of cyclic diamine derivatives.

trans-chloro carbamate **225** was obtained by the reaction of indene (**224**) with ethyl *N*,*N*-dichlorocarbamate, followed by cleavage of the N – Cl bond. The reaction of **225** with nitrogen nucleophiles then led to either *cis* adducts **226** or *trans* adducts **227**, depending on the conditions used.

Other selective syntheses of 1,2-diamines from β-halogenoamine derivatives have been described.[108]

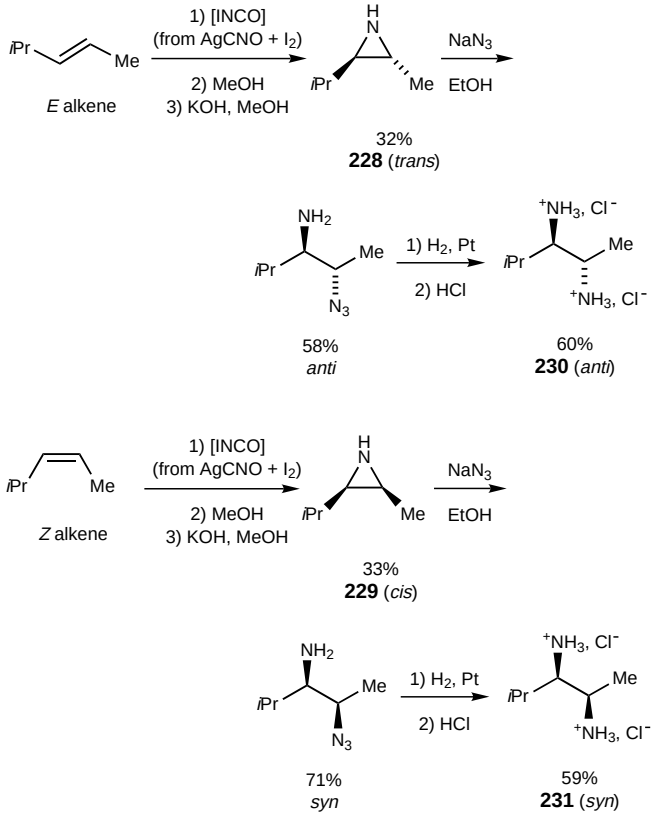
4.5. Vicinal Diamines from the Opening of Aziridines by Nitrogen Nucleophiles

Numerous methods have been reported for the preparation of aziridines.[109] Therefore, it is not surprising that many studies describe the stereoselective synthesis of vicinal diamines by the opening of aziridines by nitrogen nucleophiles. Some features must be kept in mind regarding this method:

1) N-unprotected aziridines can themselves act as nucleophiles and thus lead to the formation of oligomers or polymers.[110] Hence, it is necessary to protect them first, and two types of protected aziridines may be distinguished:
   - "nonactivated" aziridines, the nitrogen atom of which retains basic properties; their opening usually proceeds only after protonation, or quaternarization, or activation by a Lewis acid.
   - "activated" aziridines, in which the nitrogen atom is substituted by an electron-withdrawing group that can stabilize a negative charge, thus facilitating a nucleophilic opening.
2) The regioselectivity observed in the opening of a disubstituted aziridine may not be good, especially when the substituents are structurally close.

It must also be pointed out that although ways to obtain chiral, non-racemic aziridines have been described[109b, c] (from chiral epoxides,[111a, b] from chiral diols,[111c] or by using catalytic asymmetric aziridination of alkenes[58, 112]), none as yet are very general. Of the numerous examples described in the literature, only some significant ones will be detailed here.

In 1967, Swift and Swern[113] disclosed a strategy that provides access to either *syn*- or *anti*-1,2-diamines, and involves the aziridines, obtained from olefins, being opened by the azide ion (Scheme 57). Iodine isocyanate, generated in

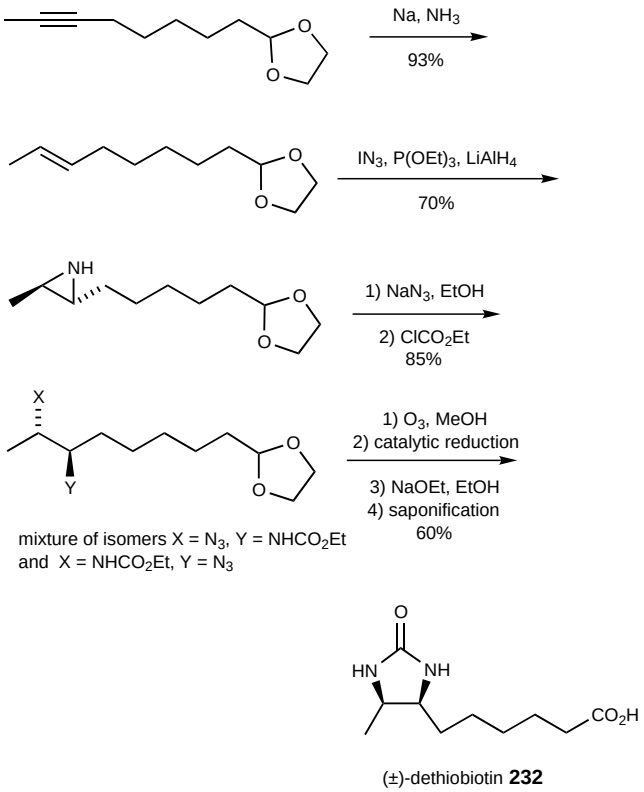


Scheme 57. Stereoselective synthesis of either *syn*- or *anti*-1,2-diamines from *Z* or *E* alkenes through aziridine opening.

situ from silver isocyanate and iodine, added stereospecifically to *Z*- or *E*-4-methyl-2-pentene, to yield *cis*-aziridine **228** and *trans*-aziridine **229**, respectively, after basic treatment. These were then converted into the corresponding diamine hydrochloride salts **230** and **231** by ring opening with the azide ion, followed by catalytic hydrogenation. Although the sequence is stereospecific, the overall yields are quite low: a ketone by-product may be formed during the reaction with iodine isocyanate by an elimination – hydrolysis mechanism.[114] Loss of product can also occur because of the volatility of aziridines and their solubility in water. A related method was applied successfully by Parry et al. to the

synthesis of racemic dethiobiotin **232**, the biological precursor of the vitamin biotin[115] (Scheme 58).

Several other nitrogen nucleophiles have been used instead of sodium azide (Scheme 59).[116] Thus, the opening of *N*-phthalimido-aziridines **233** by aniline,[117] and the ytterbium



Scheme 58. Diastereoselective synthesis of racemic dethiobiotin.

triflate catalyzed opening of N-protected aziridines **236** by amines[118] have been reported. Imidazole was recently shown to add to *N*-acylaziridines **238** under pressure, but modest yields of recovered products were obtained.[119] Aziridine-2-carboxylic esters **240** reacted regioselectively with azidotrimethylsilane, and also with acetonitrile, in the presence of BF_3;[120] in this case, imidazolines **242** were obtained as intermediates, and were then readily hydrolyzed. The reaction of azidotrimethylsilane with *N*-tosylaziridines **244**, catalyzed by an imidochromium species, has also been reported.[121]

The synthesis of a new chiral auxiliary, (1*R*,2*R*,3*R*,6*R*)-3,6-dimethylcyclohexane-1,2-diamine, involved the opening of a *N*-tosylaziridine with sodium azide.[122] Duréault et al.[123] had previously studied the reaction of the diaziridine **249** derived from D-mannitol with four equivalents of sodium azide (Scheme 60). In the absence of BF_3 the nucleophilic opening of one aziridine ring was followed by the intramolecular opening of the second ring, to yield the piperidine **248**. On the other hand, two intermolecular openings by sodium azide occurred in the presence of BF_3, probably because the negative charge of the intermediate amide that results from the first nucleophilic attack is partially masked. The bisazide **250** thus obtained was considered a precursor of *Nα*,*Nβ*-chemodifferentiated *α*,*β*-L-diaminopropionic acids such as **251**.

In 1990 Tanner et al.[124] performed the opening of the non-racemic aziridine **252**, derived from tartaric acid, with various nucleophiles, including sodium azide (Scheme 61). In the latter case, a direct precursor of vicinal diamines was thus obtained as a single adduct **253**, as a consequence of the C_2 symmetry of the substrate. As expected, the two ester groups and the tosyl moiety activate the aziridine.

The optically active aziridine **254** obtained by enzymatic transesterification was used by Fuji et al.[125] as the starting material in their study of both the intramolecular and the intermolecular opening of aziridines (Scheme 62). Treatment of the benzylcarbamate **255** by potassium *tert*-butylate led regioselectively to the corresponding 5-membered cyclic carbamate **256**. However, both regioisomers were formed from intermolecular opening of **257** by using various nucleophiles (Table 4). Lithium anilide gave the best regioselectivity although the chemical yield was not satisfactory in that case.

Table 4. Regioselective outcome in the opening of aziridine **257** with various nucleophiles.

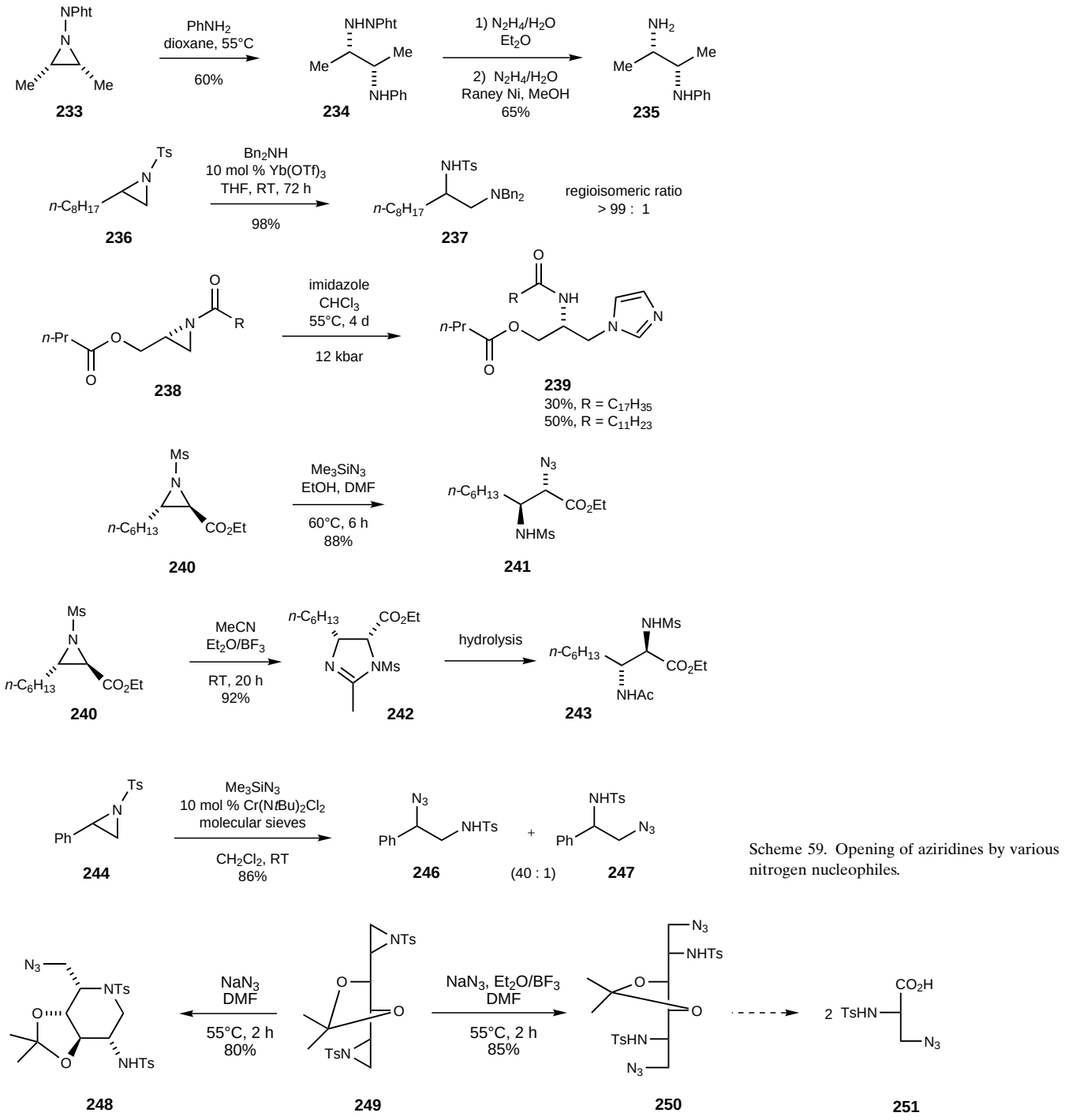
Entry	Nucleophile	Conditions			Yield (**258**) [%]	Yield (**259**) [%]
		solvent	*T*	*t*		
1	$PhNH_2$	–	rt	4 d	54	23
2	PhNHLi	THF	rt	12 h	43	7
3	NaN_3	DMF	50 °C	2 h	60	27
4	Me_3SiN_3	EtOH, DMF	80 °C	6 h	45	22

N-Nosylaziridines such as **260** were recently introduced as activated aziridine electrophiles by Maligres et al.[126] (Scheme 63). They were shown to be 50–60 times more reactive than *N*-tosylaziridines. The reaction of primary and secondary amines with a 2-phenyl-substituted aziridine was not regioselective, while only one regioisomer was obtained from 2-methyl-substituted aziridine **260**. Moreover, the deprotection of the *N*-nosyl group of adducts **261** was performed under mild conditions.

4.6. Vicinal Diamines from Electrophilic Amination

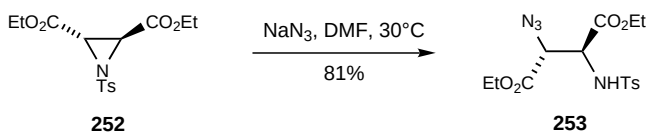
Electrophilic amination of *β*-amino enolates has been used for the preparation of several vicinal diamines. For instance, the C_2-symmetric (*R*,*R*)-2,3-diaminotetraline (**268**) was prepared by Gmeiner and Hummel[127] by the amination of a chiral *β*-amino ketone **265** with dibenzyl azodicarboxylate, which afforded the *trans* adduct **267** exclusively after reduction (Scheme 64). This compound was then transformed in a few steps into the target diamine. It remains to be seen if such selectivity can also be obtained when a similar reaction is performed with acyclic substrates.

Recently, Davies et al. described the preparation of (2*S*,3*S*)-2,3-diaminobutanoic acid by using the diastereoselective conjugate addition of lithium (*α*-methylbenzyl)benzylamide (**270**) to *tert*-butyl crotonate (**269**) as the first step (Scheme 65).[128] The direct trapping of the intermediate enolate by an electrophilic nitrogen source was not possible, so it was carried out in two steps. Thus, the enolate generated from **271** was treated with trisyl azide, to afford **273** as a single diastereomer, although with a low yield (32%). Reduction of



Scheme 59. Opening of aziridines by various nitrogen nucleophiles.

Scheme 60. Influence of $BF_3 \cdot OEt_2$ on the outcome of the opening of a bisaziridine derived from D-mannitol by sodium azide.



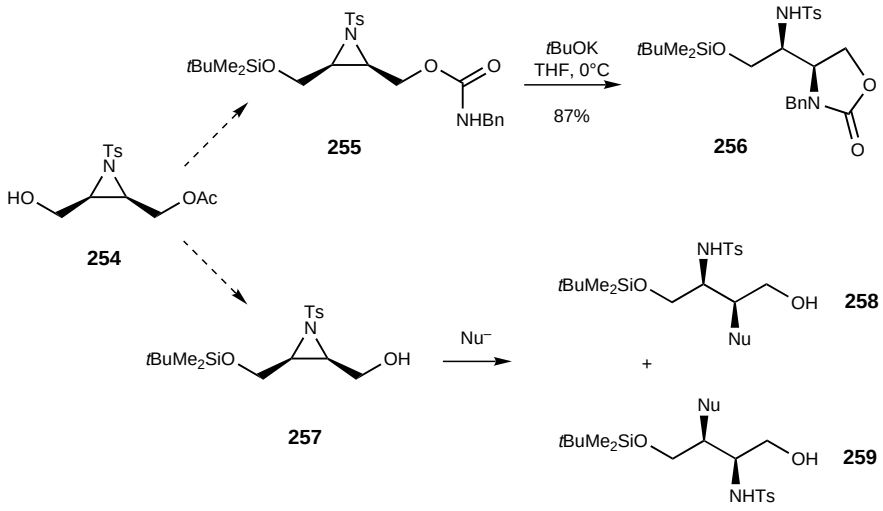
Scheme 61. Opening of an aziridine derived from tartaric acid by sodium azide.

the azide functional group, followed by several deprotections, led to (2*S*,3*S*)-**275**.

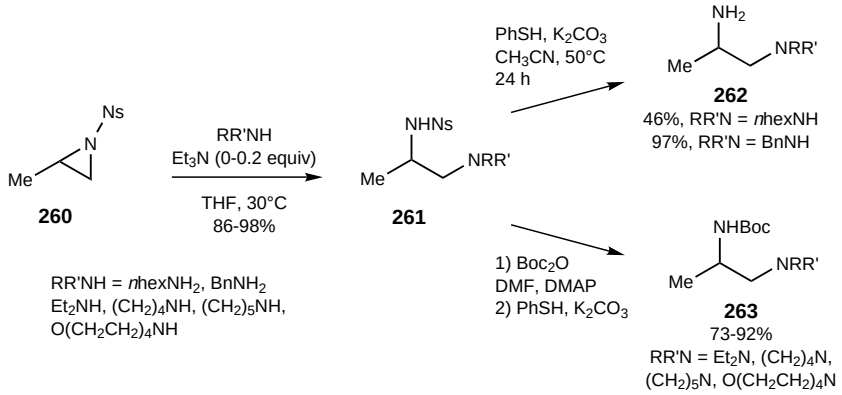
The reaction of *N*-(9-phenylfluoren-9-yl)aspartate enolates with electrophilic aminating agents was studied by Sardina et al.[129] This reaction allowed access to both *syn*- and *anti*-2,3-diaminosuccinic acid derivatives. It was not possible to prepare selectively the *syn* adducts, but highly *anti*-selective conditions were obtained by using either di-*tert*-butyl or dibenzyl azodicarboxylate as the electrophile.

4.7. Vicinal Diamines from Carbon – Carbon Bond Cleavage

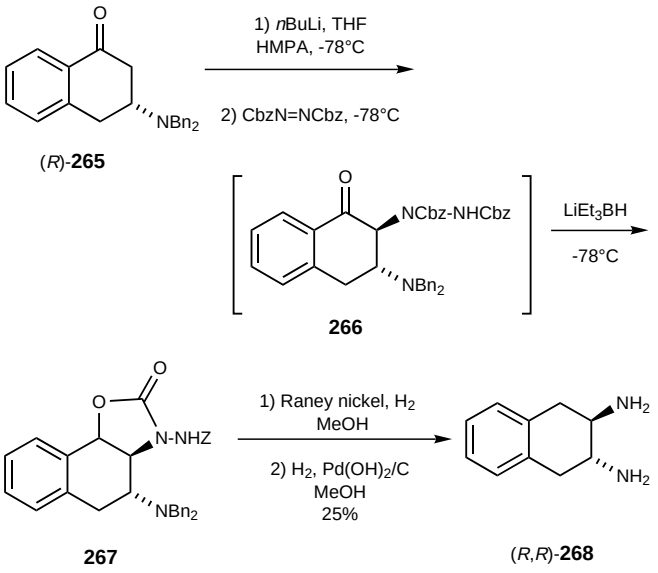
Several degradative rearrangements involve the breaking of a carbon – carbon bond and the formation of a carbon – nitrogen bond; when applied to compounds already having



Scheme 62. Intramolecular versus intermolecular opening of chiral aziridines: influence on the regioselectivity of the opening.



Scheme 63. Synthesis of 1,2-diamines from an *N*-nosylaziridine.



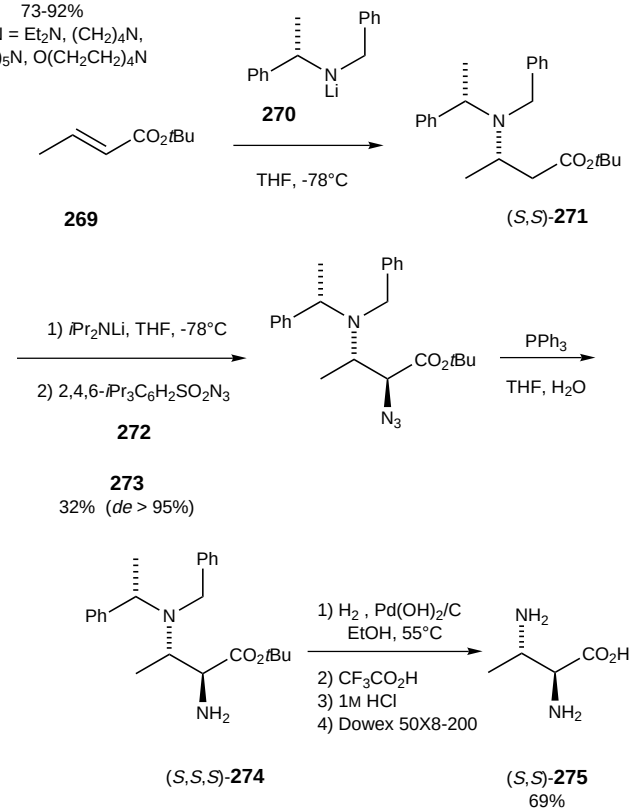
Scheme 64. Synthesis of (*R*,*R*)-2,3-diaminotetraline by the electrophilic amination of a chiral β-amino ketone.

a nitrogen function they lead to 1,2-diamine derivatives. Indeed, such products have been prepared by the Curtius,[130] Hofmann,[104, 131a] Schmidt,[131a, b] and Beckmann[131c–e] rearrangements (Scheme 66). Shioiri et al.[130g] synthesized L-diaminopropanoic acid derivative **277** by using a modified Curtius reaction of acid **276** with diphenyl phosphorazidate, followed by deprotection and protection steps. The compound **277** was then utilized in a synthesis of cyclotheonamide B, a macrocyclic thrombin inhibitor. Stetter et al.[131a] synthesized 1,2-adamantanediamine (**279**) by a Hofmann rearrangement and 1,2-noradamantanediamine (**281**) by a Schmidt rearrangement.

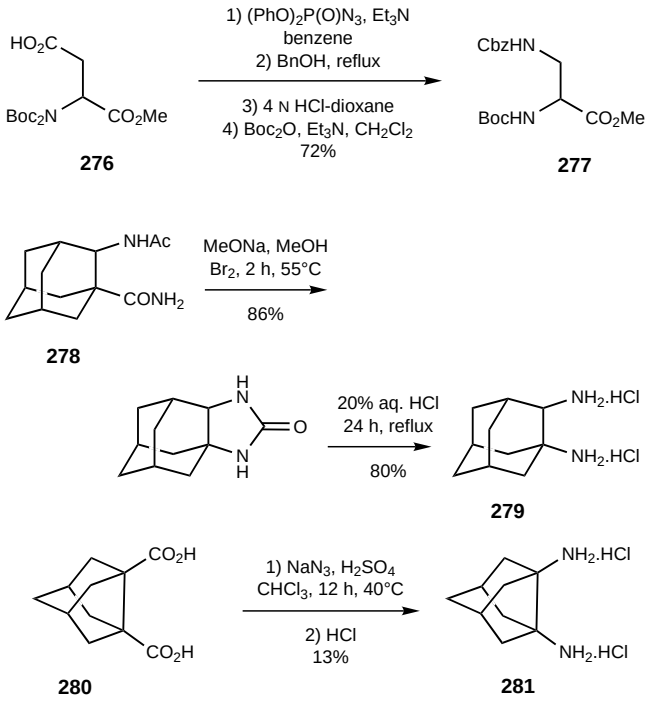
4.8. Vicinal Diamines from Activated β,γ-Unsaturated Amines

The double bond of β,γ-unsaturated amines may be activated by palladium or iodine to undergo the nucleophile additon of a nitrogen group.

For instance, Cardillo et al.[132] described the preparation of monosub-

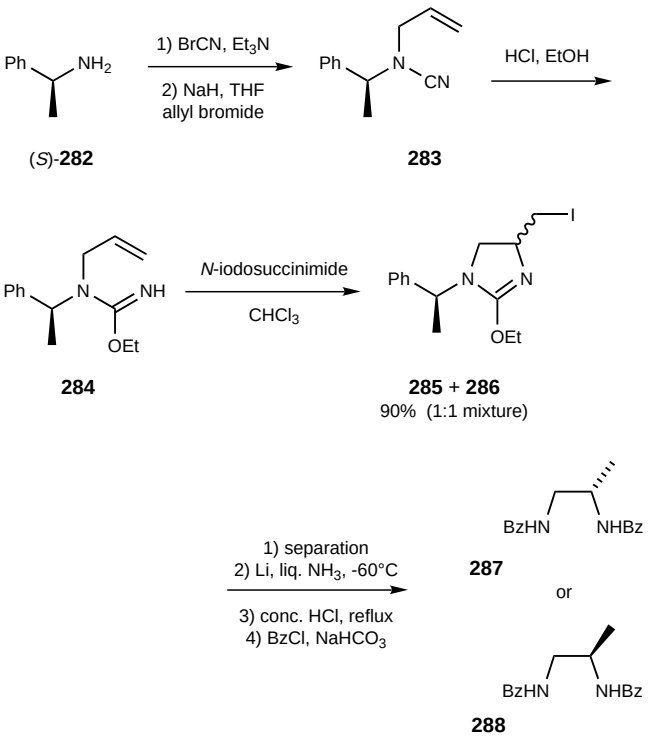


Scheme 65. Preparation of a 2,3-diaminocarboxylic acid through a diastereoselective conjugate addition.



Scheme 66. Examples of rearrangements used in the synthesis of 1,2-diamines.

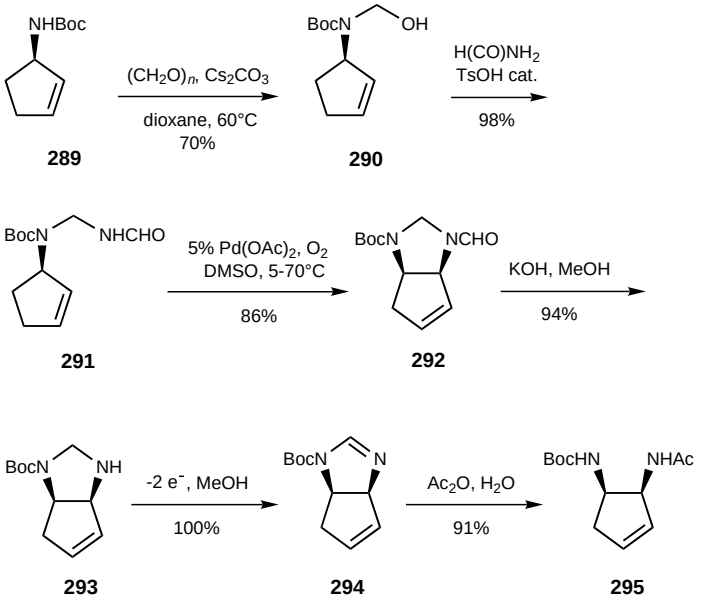
stituted, chiral 1,2-diamines that used the iodofunctionalization of isourea **284** derived from (*S*)-1-phenylethylamine (**282**) as the key step (Scheme 67). The cyclization was not stereoselective, but the two imidazolines **285** and **286** obtained were then separated easily by chromatography. After reduction of the chiral auxiliary with metallic lithium and hydrolysis



Scheme 67. Imidazolines as intermediates in the synthesis of monosubstituted vicinal diamines.

of the imidazolines, the corresponding enantiomeric diamines were obtained, which were isolated as benzamides **287** and **288**.

The palladium(II) catalyzed oxidative cyclization of various allylic aminals to imidazolidines was also reported recently by Hiemstra, Speckamp et al.[133] It was shown that aminals derived from formamide were the most successful nucleophiles. In acyclic compounds, a moderate stereoselectivity was observed, while only *cis*-substituted heterocycles were obtained from cyclopentenylamine-derived aminals such as **291** (Scheme 68). The conversion of the imidazolidine **292** into the



Scheme 68. Synthesis of a cyclic vicinal diamine from an imidazolidine obtained by oxidative cyclization of an allylic aminal.

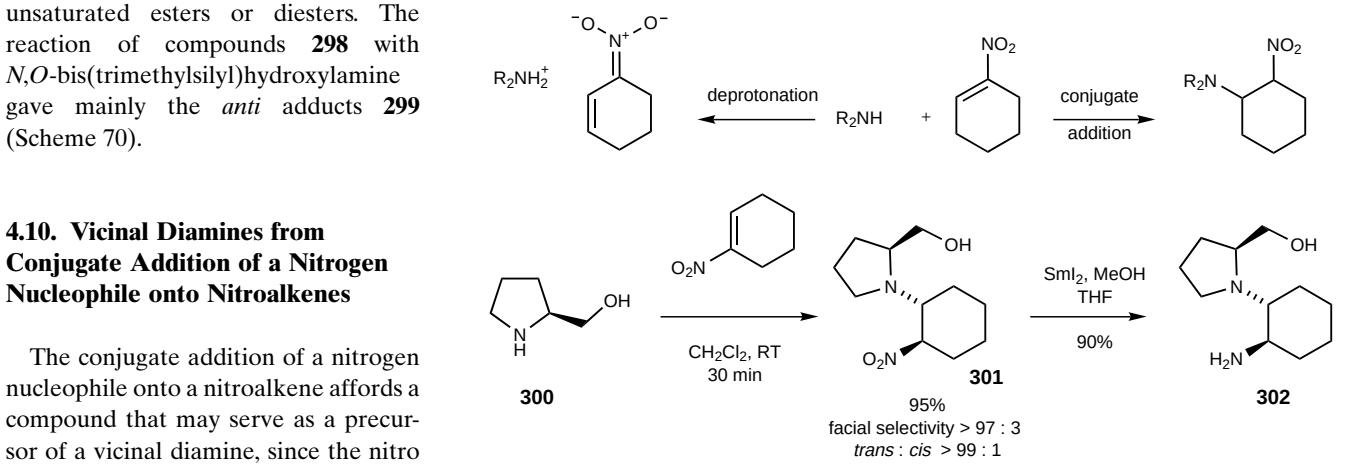
protected vicinal diamine **295**, which included the deformylation of **292**, the electrochemical oxidation of the obtained imidazolidine **293** to imidazoline **294**, and the hydrolytic cleavage of the latter, was described.

In 1993 Ernst and Bellus et al.[134a] reported an elegant way to prepare 1,2-diamines, based on the [3,3]sigmatropic rearrangement of allylic trichloroacetamidates **296** derived from α-amino acids. Under palladium(II)-catalyzed conditions, the aza–Claisen type rearrangement proceeded with a complete chirality transfer, to afford only the corresponding *anti* diastereomer (Scheme 69). Although the yields of adducts **297** were only moderate (43–62%), the excellent diastereoselectivity observed makes this method very attractive and was applied to the synthesis of (2*S*,3*S*)-diaminobutanoic acid. A similar rearrangement was described in the same year by Doherty et al.[134b]

4.9. Vicinal Diamines from β,γ-Unsaturated Amines Activated by an Electron-Withdrawing Group

Aminodeoxystatine was prepared by the nonstereoselective conjugate addition of ammonia to an α,β-unsaturated ester that is γ-substituted by a protected amino group.[12b] More recently, it has been shown by Reetz et al.[135] that nitrogen nucleophiles with a N–O bond add stereoselectively to α,β-

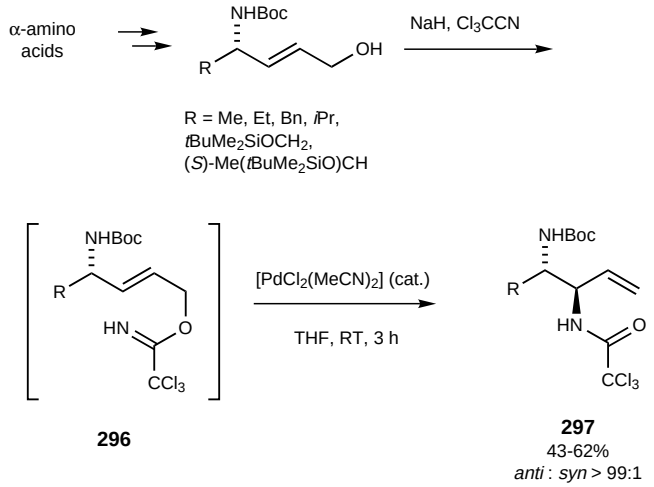
unsaturated esters or diesters. The reaction of compounds **298** with *N,O*-bis(trimethylsilyl)hydroxylamine gave mainly the *anti* adducts **299** (Scheme 70).



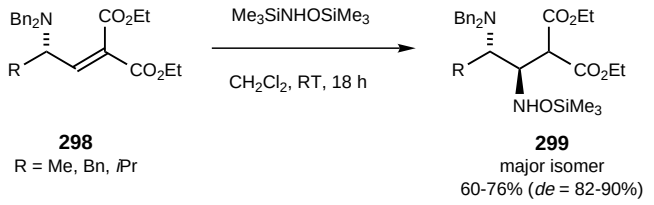
Scheme 71. Diastereoselective addition of (*S*)-2-pyrrolidinemethanol to 1-nitrocyclohexene.

4.10. Vicinal Diamines from Conjugate Addition of a Nitrogen Nucleophile onto Nitroalkenes

The conjugate addition of a nitrogen nucleophile onto a nitroalkene affords a compound that may serve as a precursor of a vicinal diamine, since the nitro group can be reduced to an amine by a variety of reagents. The stereochemical outcome of the addition of amines to (2-nitropropenyl)benzene was studied by Southwick and Anderson,[136] who reported that the *syn* adducts were formed predominantly under thermodynamic conditions. In recent years, several groups used chiral nitrogen nucleophiles, with the aim to design a synthetic route to diastereo- and enantiomerically pure vicinal diamines.



Scheme 69. *Anti*-selective [3,3]sigmatropic rearrangement of allylic trichloroacetamidates derived from α-amino acids.

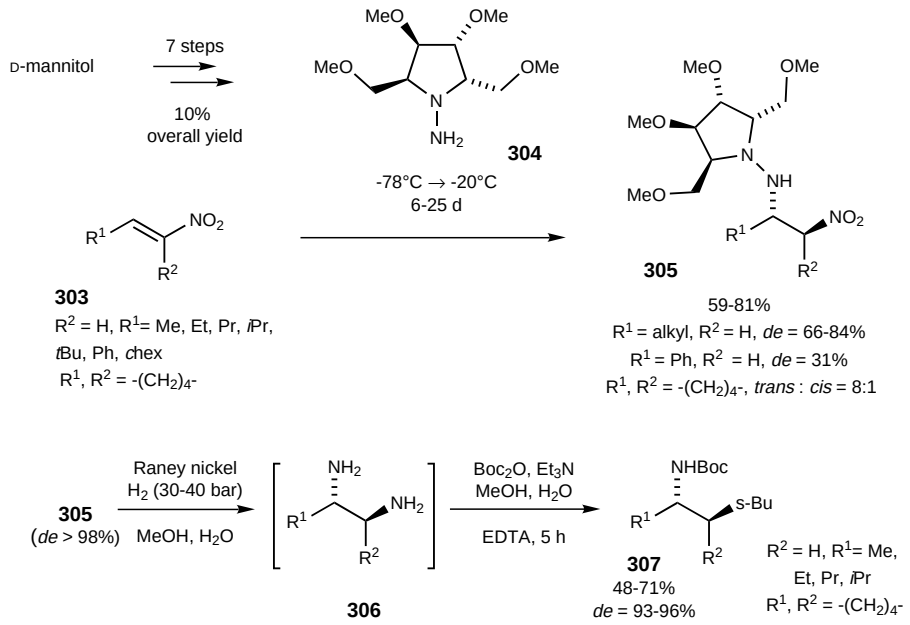


Scheme 70. Diastereoselective conjugate addition of *N,O*-bis-(trimethylsilyl)hydroxylamine on α,β-unsaturated diesters derived from α-amino acids.

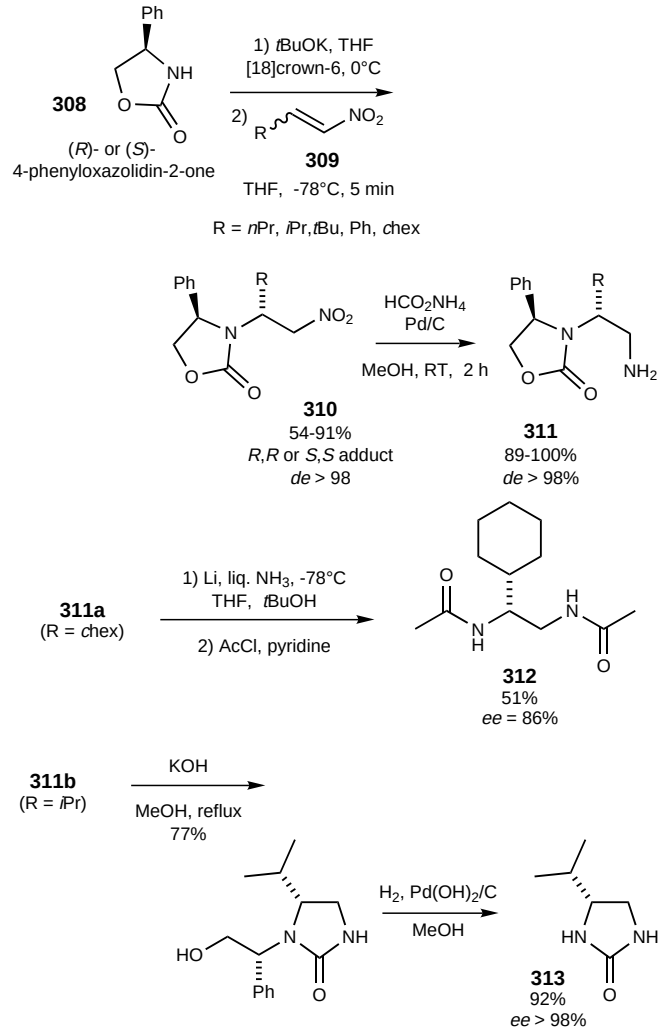
The reaction of various chiral amines with nitroalkenes was evaluated by Sturgess et al., who showed that β-amino alcohols reacted faster than monofunctional amines.[137a] Depending on the nucleophile used, either conjugate addition or deprotonation was observed (Scheme 71). The addition products were often found to be unstable, since they slowly underwent retroaddition at room temperature. However, the reaction of (*S*)-2-pyrrolidinylmethanol (**300**) with 1-nitrocyclohexene afforded a single adduct **301** in both excellent stereoselectivity and yield; its nitro group was then reduced with samarium diiodide in methanol, under conditions that prevent epimerization.[137b]

A related approach was recently published by Enders et al. (Scheme 72).[138] The chiral, C_2-symmetric *N*-aminopyrrolidine **304** derived from D-mannitol was used as the nitrogen nucleophile. It reacted slowly with nitroalkenes at $-20\,^{\circ}C$ in diethyl ether to afford the corresponding adducts **305** with good stereoselectivity ($de = 66-84\,\%$), except in the case of β-nitrostyrene ($de = 31\,\%$). The *trans* adduct was obtained preponderantly from 1-nitrocyclohexene. In most cases, the major isomers were isolated by column chromatography, which had to be performed on deactivated silica gel in order to avoid a degradation of the products by a retro-Michael addition. The adducts **305** were then transformed into the corresponding vicinal diamines **306** in a single step by treatment with hydrogen in the presence of Raney nickel, which reduced the nitro group and cleaved the N–N bond. The Boc-protected diamines **307** were eventually obtained with enantiomeric excesses ranging from 93 to 96 % and with good overall yields (48–71 %). Thus, diastereo- as well as enantioselective access to vicinal diamines is made possible by this method. It still suffers from several drawbacks: the chiral auxiliary is available only as one optical form and its synthesis is lengthy (seven steps from D-mannitol); also, 6 to 25 days are necessary to get the addition to completion.

We recently reported a study on the conjugate addition of the potassium salt of 4-phenyl-2-oxazolidinone (**308**) to monosubstituted nitroalkenes (Scheme 73).[139] This nucleophile was chosen for the following reasons: it is commercially available in both enantiomeric forms, or can be synthesized easily; the adducts were expected to be less prone to β-elimination than β-aminonitroalkanes, since the nitrogen atom would not be basic; the heterocycle could be cleaved easily to generate the amino group; furthermore, we thought that it could give high levels of asymmetric induction. We found that the potassium salt of (*R*)- or (*S*)-**308** added very rapidly to nitroalkenes at $-78\,^{\circ}C$. In all cases, the adducts **311**



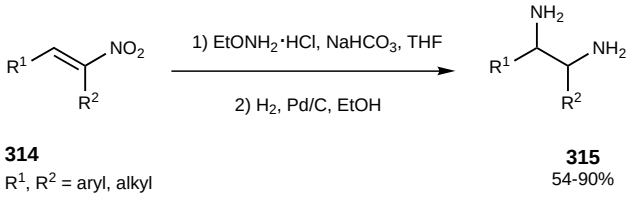
Scheme 72. Diastereoselective conjugate addition of a chiral aminopyrrolidine derived from D-mannitol to various nitroalkenes; enantioselective synthesis of vicinal diamines.



Scheme 73. Diastereoselective addition of (*R*)- or (*S*)-4-phenyl-2-oxazolidinone to monosubstituted nitroalkenes; enantioselective syntheses of protected vicinal diamines.

were obtained with excellent diastereoselectivity, only one isomer being observed in the ^{1}H and ^{13}C NMR spectra. The first examples were carried out in the presence of [18]crown-6; we have recently shown that, while the crown ether accelerates the reaction, it has no effect on the stereochemical outcome. Two of these stable adducts were converted into amines **311**, which are protected forms of vicinal diamines, by using a catalytic hydrogen-transfer reduction of the nitro group. The oxazolidinone moiety of **311a** was cleaved by reduction with lithium in liquid ammonia, to form an acyclic diamine which was isolated as the bisacetamide **312** (*ee* = 86%). In an other example, the basic treatment of **311b** followed by hydrogenolysis afforded the optically pure imidazolidinone **313**.

A one-pot preparation of racemic 1,2-diamines from nitroalkenes recently reported by Mukaiyama et al.[140] is also worthy of note. The adducts obtained from the addition of *O*-ethylhydroxylamine to nitroolefins **314** were reduced directly under hydrogen in the presence of palladium on carbon (Scheme 74). The yields of the diamines **315** ranged from 54 to 90%; *cis-trans* mixtures were obtained from cyclic substrates.



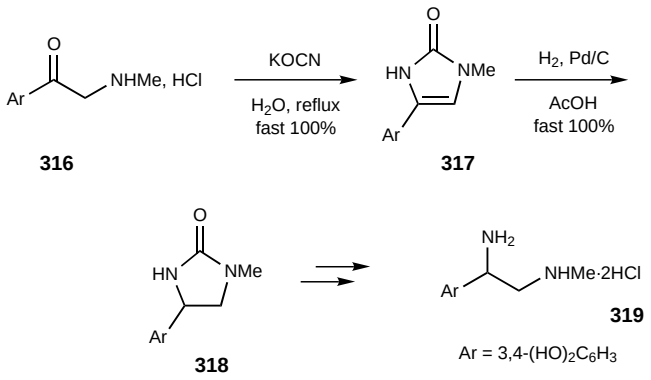
Scheme 74. One-pot preparation of 1,2-diamines from nitroalkenes.

4.11. Vicinal Diamines from α-Amino Ketones or α-Amino Aldehydes

Two widely used methods, the reductive amination and the Strecker condensation, allow the amine groups to be obtained from aldehydes or ketones. When applying these methods to α-amino ketones, products having a 1,2-diamine moiety are thus obtained.

4.11.1. Reductive Amination

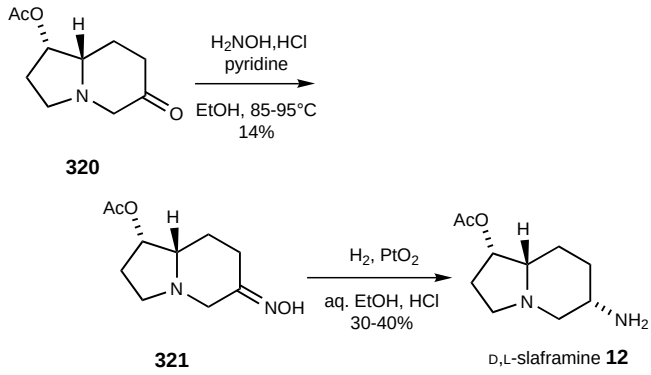
In 1947 Duschinsky et al.[141] described the synthesis of amino analogues of adrenaline, arterenol, and ephedrine from α-amino ketones (Scheme 75). For example, the reaction of potassium cyanate with adrenalone hydrochloride (**316**) in water afforded the imidazolinone **317**, which was then reduced



Scheme 75. Synthesis of an amino analogue of adrenaline.

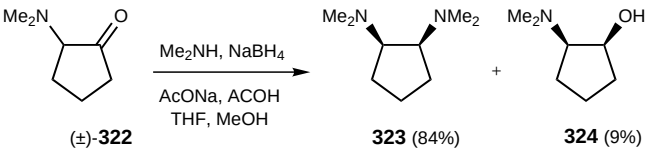
to the corresponding imidazolidinone **318**. The later was then transformed in a few steps into the vicinal diamine **319**.

In the last step of their synthesis of the alkaloid D,L-slaframine, Gensler and Hu[142] utilized the hydrogenation of the oxime **321**, derived from the corresponding ketone **320**, to introduce the amino group stereoselectively, although in low yield (Scheme 76).



Scheme 76. Synthesis of D,L-slaframine by the catalytic hydrogenation of an oxime.

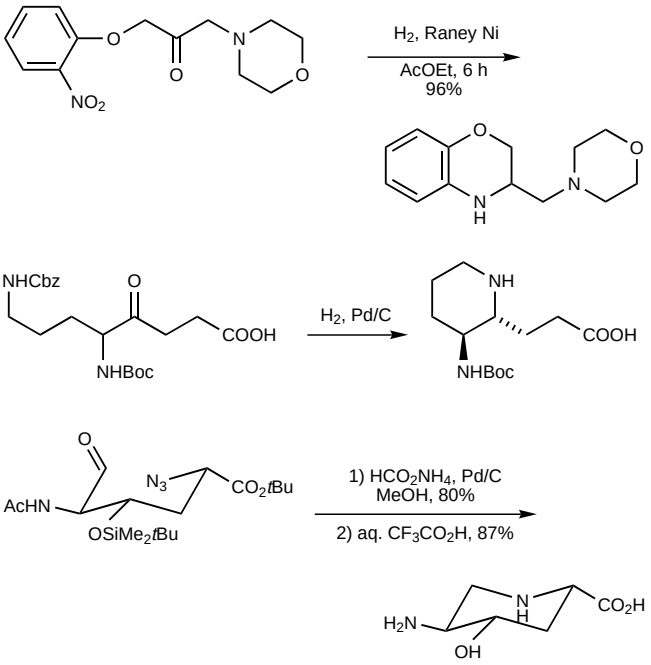
The reductive amination of 2-(dimethylamino)cyclopentanone (**322**) with dimethylamine and sodium borohydride was shown by Fraenkel and Pramanik[143] to give the *cis*-1,2-diamine **323** selectively (Scheme 77). Some amino alcohol



Scheme 77. Stereoselective synthesis of 1,2-bis(dimethylamino)-cyclopentane by reductive amination.

324, which results from the reduction of the ketone, was also obtained in this reaction. The amount of this by-product was lowered by employing a slow addition of the reducing agent.

Several intramolecular reductive aminations that lead to various nitrogen-containing heterocycles have also been reported. In these methods, the amino group that condenses with the carbonyl function may be generated by reduction of a nitro group[144] by reductive cleavage of a protecting group,[145] or by reduction of an azido group[146] (Scheme 78); the other



Scheme 78. Synthesis of 1,2-diamines by intramolecular reductive amination.

amino function must be either substituted or masked by a protecting group stable under these conditions.

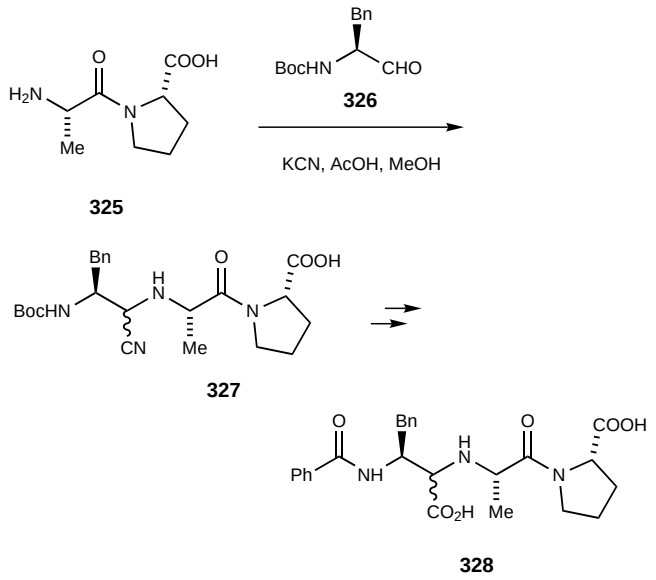
An enantioselective access to 1,2-diaminocyclohexanes was also reported by Schlichter and Frahm,[11k] who used (*S*)-α-methylbenzylamine in the reductive amination step.

4.11.2. Strecker Condensations

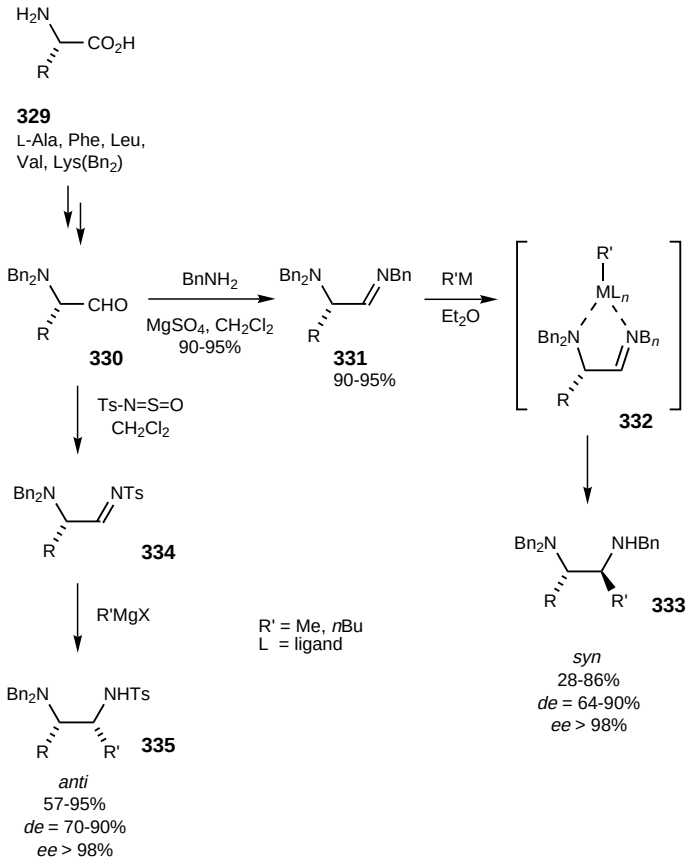
To introduce a carbon atom and a nitrogen atom simultaneously from a carbonyl compound, one can use the Strecker condensation or the related Bucherer–Berg reaction; in the latter case an hydantoin is formed. Both reactions have been applied to the synthesis of products containing nitrogen functionalities on vicinal carbon atoms of α-amino ketones.[147] Greenlee et al.[148] prepared several analogues of the angiotensin-converting enzyme inhibitor enalapril, such as **328**, by a Strecker reaction. The condensation of dipeptide **325** with the porotected α-amino aldehyde **326** afforded compound **327** as a mixture of two epimers (Scheme 79).

4.12. Vicinal Diamines from α-Amino Imines, α-Amino Oximes, or α-Amino Hydrazones

Reetz et al.[149] have developed an approach to the synthesis of vicinal diamines based on the stereoselective alkylation of imines derived from *N*,*N*-dibenzylamino aldehydes **330**, which were obtained from α-amino acids **329** (Scheme 80). A survey of the addition of various organometallic reagents to *N*-benzylimines **331** in diethyl ether showed that the combinations

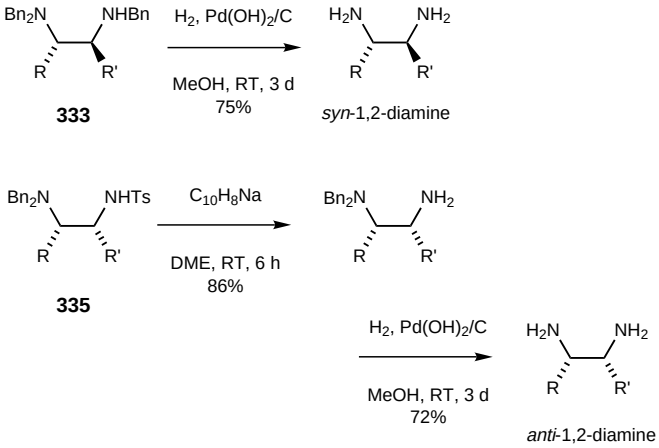


Scheme 79. Synthesis of a 1,2-diamino compound through a Strecker condensation.



Scheme 80. Synthesis of either *syn*- or *anti*-1,2-diamines by alkylation of chiral imines derived from α-amino acids.

*n*BuLi/$CeCl_3$ and 3 MeLi/$CeCl_3$ were the most effective, in terms of both yield and selectivity. Moreover, the addition proceeded without any racemization. To explain the observed *syn* selectivity, the authors postulated the intermediacy of chelates **332**, which would be attacked preferentially from the less hindered face, to give the *syn* adducts **333**. With the aim to reverse the diastereoselectivity, other substrates such as **334** that have a tosyl group instead of the benzyl group were alkylated with Grignard reagents. The electron-withdrawing substituent was expected to reduce the donor strength of the aldimine nitrogen atom and prevent chelation from occurring. Indeed, *anti* adducts **335** were then obtained selectively. The pure diamines were then recovered under conditions that prevented any racemization from occurring (Scheme 81). This

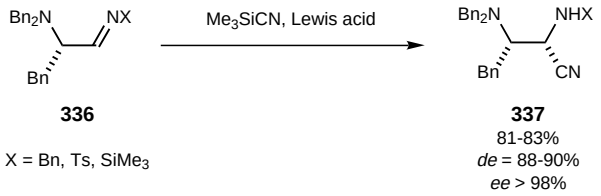


Scheme 81. Preparation of unprotected *syn*- or *anti*-1,2-diamines; cleavage of protecting groups.

method allows the preparation of either (*S*,*R*)- or (*S*,*S*)-diamines from a (*S*)-α-amino acid. While the diastereoselectivity of the alkylations is not complete (> 90 %), this strategy is still very efficient when the target diamine can derive from a natural α-amino acid.

Alkylation of imines derived from α-amino acids has been performed by Laschat et al. by using an hetero–ene reaction.[150]

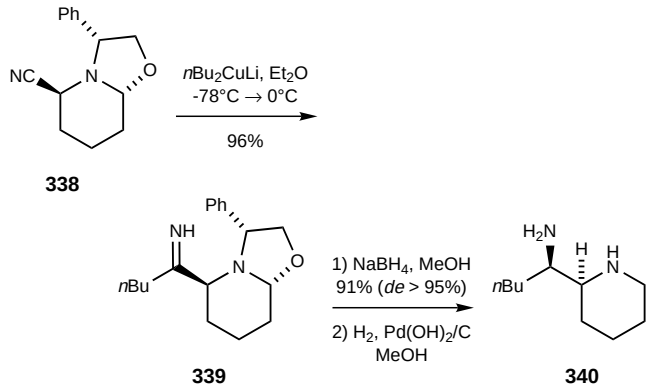
The Lewis acid promoted addition of trimethylsilylcyanide to *N*-benzyl, *N*-tosyl, and *N*-silyl aldimines **336** was also studied by Reetz et al. (Scheme 82).[151] Conditions were



Scheme 82. Addition of trimethylsilylcyanide to chiral imines derived from an α-amino acid.

found that yield selectively the nonchelation-controlled adducts **337**, but an optimization had to be carried out for each substrate.

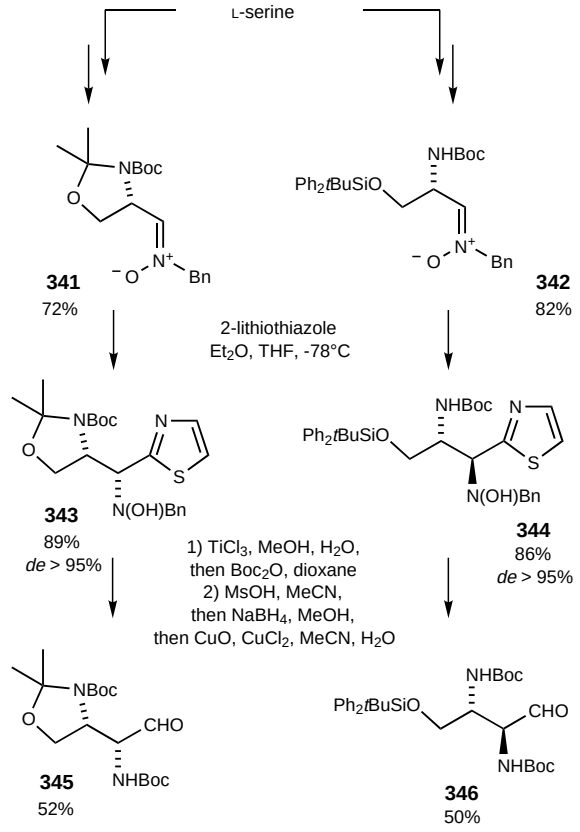
The reduction of imines, which are formed from the alkylation of α-amino nitriles, can be employed to prepare 1,2-diamines. An example of such process has been reported by Husson et al. (Scheme 83).[152a] Imine **339**, obtained from the versatile synthon **338**,[152b] was reduced with high stereoselectivity by sodium borohydride. After cleavage of the



Scheme 83. Preparation of a 1,2-diamine by reduction of an α-amino imine.

chiral auxiliary the 1,2-diamine **340** was obtained. The diamine was then used to prepare an analogue of the alkaloid tetraponerine.

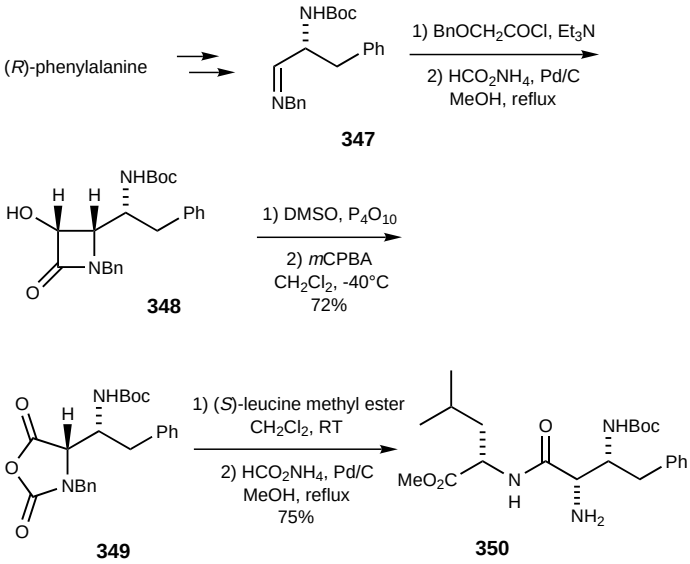
Nitrones derived from α-amino acids can also be used as diamine precursors, as demonstrated by Dondoni, Merino et al.,[153a] who designed a route to both C2 diastereomers of 2,3-diamino-4-hydroxybutanals. Their strategy was based on the addition of 2-lithiothiazole, a nucleophilic aldehyde synthetic equivalent, on differently protected L-serine-derived nitrones **341** and **342** (Scheme 84). While an *anti* selectivity was observed in the addition to the straight chain substrate, to give **343**, the opposite selectivity resulted from the addition to the cyclic substrate **342**. The difference in selectivity was explained by different reactive conformations of the nitrones in the postulated modified Felkin–Anh transition state model. Conversion of the adducts into either protected *syn*- or *anti*-diamino aldehydes **345** and **346**, which are useful synthetic chirons, included $TiCl_3$-mediated hydroxylamine cleavage and a standard sequence to generate the aldehyde function from the thiazolyl group.



Scheme 84. Synthesis of either *syn*- or *anti*-1,2-diamines from L-serine through the addition of 2-lithiothiazole to differently protected nitrones.

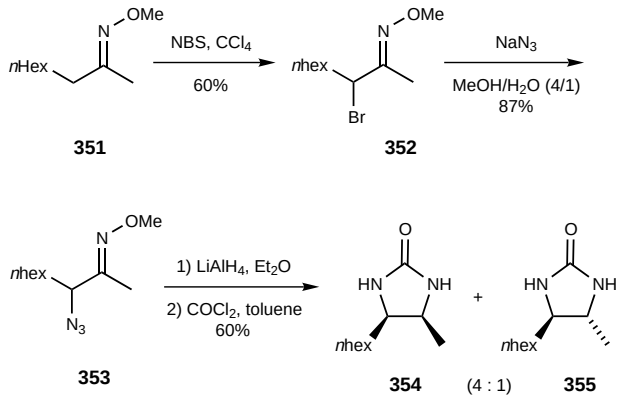
Other nucleophiles, such as Grignard reagents[153b–d] or lithium acetylides,[153e] have been added to α-amino nitrones. Merino et al. described the synthesis of (2*S*,3*R*)- and (2*S*,3*S*)-2,3-diaminobutanoic acids from nitrones **341** and **342**, respectively,[153b] and the synthesis of several vicinal diamines, with *syn* selectivity, with nitrones derived from L-alanine, L-valine, and L-phenylalanine.[153d]

Another use of imines derived from α-amino acids in the synthesis of diamines (Scheme 85) was reported by Palomo et al.[154] The cycloaddition of the imine **347**, obtained from (*R*)-phenylalanine methyl ester, with the ketene, generated from benzyloxyacetyl chloride, proceeded with complete stereoselectivity. After cleavage of the C2–C3 bond of the β-lactam **348**, achieved through an efficient oxidative sequence, the treatment of the obtained *N*-carboxyanhydride **349** with (*S*)-leucine methyl ester, followed by removal of the *N*-benzyl group, afforded **350**, a protected form of amino-deoxybestatine.



Scheme 85. Stereoselective synthesis of a 1,2-diamine derivative from an imine by stereoselective β-lactam formation.

Shatzmiller and Bercovici[155] used the displacement of α-bromo oxime ethers **352** by sodium azide, followed by exhaustive reduction of the adducts **353** by lithium aluminium hydride to selectively prepare *anti* diamines, which were then separated as their imidazolidinones **354** (Scheme 86). The intermediacy of a 5-membered complex formed at first between aluminum and the amino oxime was proposed to account for the *anti* selectivity of the reduction. A similar approach has recently been described by De Kimpe and D'Hondt.[156]

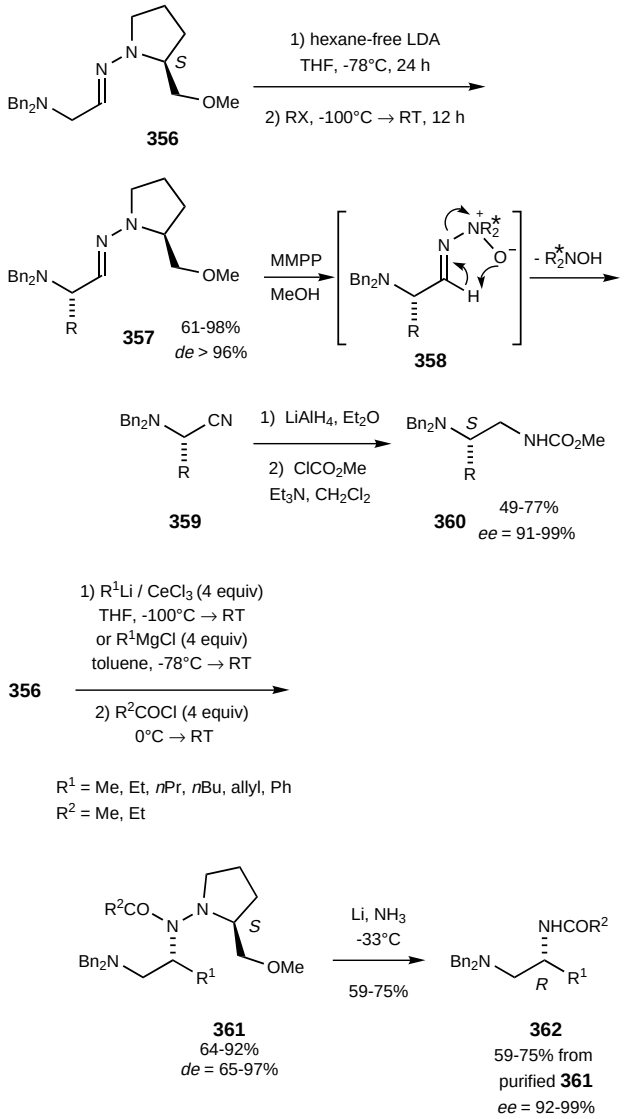


Scheme 86. Synthesis of *cis*- and *trans*-imidazolidin-2-ones, precursors of 1,2-diamines, from an oxime ether.

Two methods for the enantioselective synthesis of monosubstituted vicinal diamines that make use of dibenzylaminoacetaldehyde SAMP-hydrazone (**356**) were recently reported by Enders et al.[157] (Scheme 87). Thus, in the first method,[157a] the anion generated from the chiral hydrazone was treated with various alkyl, allyl, or benzyl halides to afford the corresponding adducts **357**, essentially as one diastereomer ($de > 96\,\%$). To get complete deprotonation of the hydrazone, hexane-free LDA must be used, and the reaction mixture must be kept at $-78\,^{\circ}C$ for 24 hours. Also, purification of the adducts must be performed on a deactivated silica gel to avoid epimerization. After a short reaction sequence, that involved the conversion of the hydrazone into a nitrile **359** by an aza–Cope elimination, differently protected diamines **360** were then obtained ($ee = 91-99\,\%$).

The second method[157b] is based on the 1,2-addition of alkyl cerium compounds or Grignard reagents to the hydrazone **356**, which led selectively, after reaction with an acyl chloride, to the N-protected hydrazines **361** ($de = 65-97\,\%$). It is presumed that one equivalent of the organometallic reagent coordinates both the methoxy group and the nitrogen atom of the auxiliary, and that excess reagent then adds to the *re* face. Reductive cleavage of the N–N bond of the purified major isomers afforded, without much racemization, the differently protected vicinal diamines **362** ($ee = 92-99\,\%$).

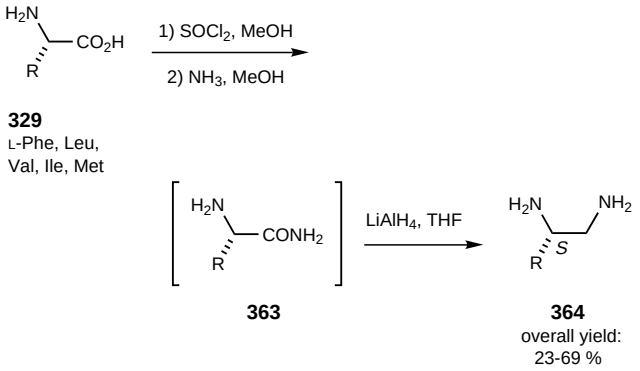
The combination of these two methods could result in the design of a quite general stereoselective access to 1,2-disubstituted 1,2-diamines.



Scheme 87. Enantioselective synthesis of monosubstituted 1,2-diamines from a chiral amino hydrazone.

4.13. Vicinal Diamines by Reduction of α-Amino Amides or α-Amino Nitriles

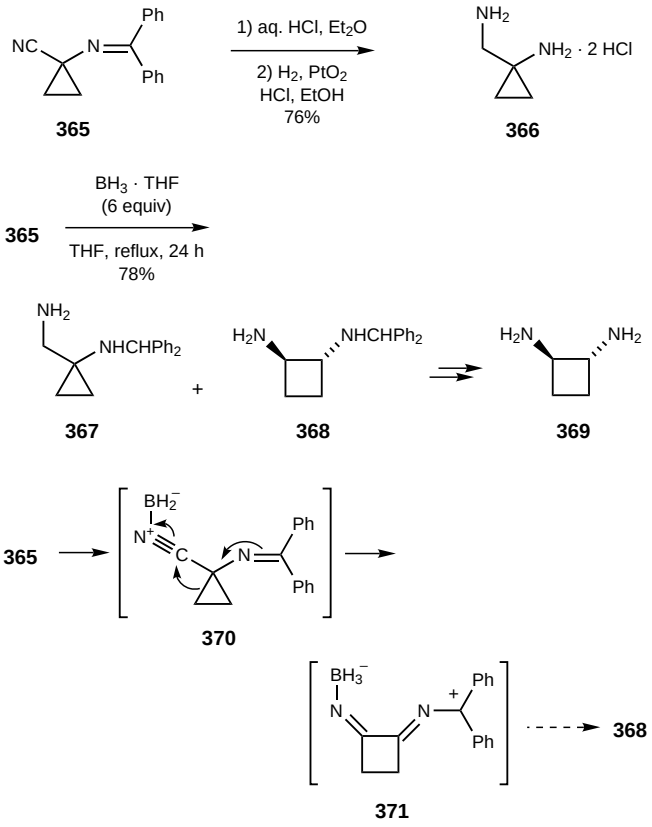
The reduction of amides derived from natural α-amino acids is a convenient way to obtain monosubstituted, vicinal diamines.[158, 43d] For example, Brunner et al. synthesized diamines **364** in this manner with high enantiomeric purity (Scheme 88).[158b] They were then used as ligands in platinum complexes that caused inhibition of DNA synthesis in tumor cells.



Scheme 88. Preparation of monosubstituted vicinal diamines from α-amino acids.

A recently reported synthesis of ^{15}N-labeled ethylenediamine and diethylenediamine made use of the reduction of [^{15}N]tritylglycinamide.[159]

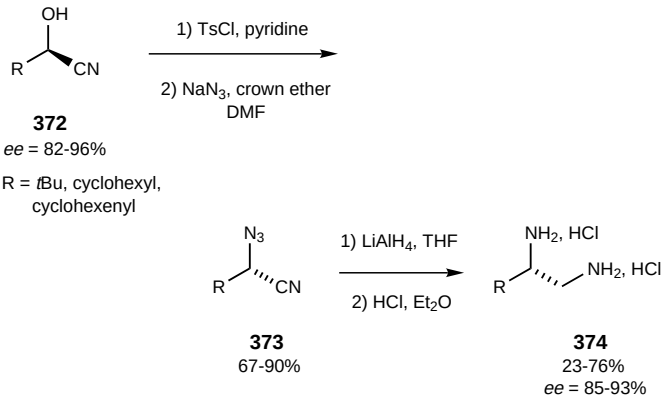
Husson et al. prepared 1-amino-1-(aminomethyl)cyclopropane (**366**) by hydrolysis of imine **365** followed by reduction of the nitrile functionality (Scheme 89).[160] The direct reduc-



Scheme 89. Synthesis of 1-amino-1-(aminomethyl)cyclopropane and *trans*-1,2-diaminocyclobutane.

tion of **365** by a borane – THF complex produced a mixture of diamines **367** and **368**, the latter arising from a ring-expansion reaction of **365**. Compound **368** was then converted into *trans*-1,2-diaminocyclobutane (**369**).

Effenberger et al.[161] took advantage of the ready access to optically active cyanohydrines **372** in their synthesis of monosubstituted 1,2-diamines **374**, which also made use of a nucleophilic substitution by sodium azide (Scheme 90).



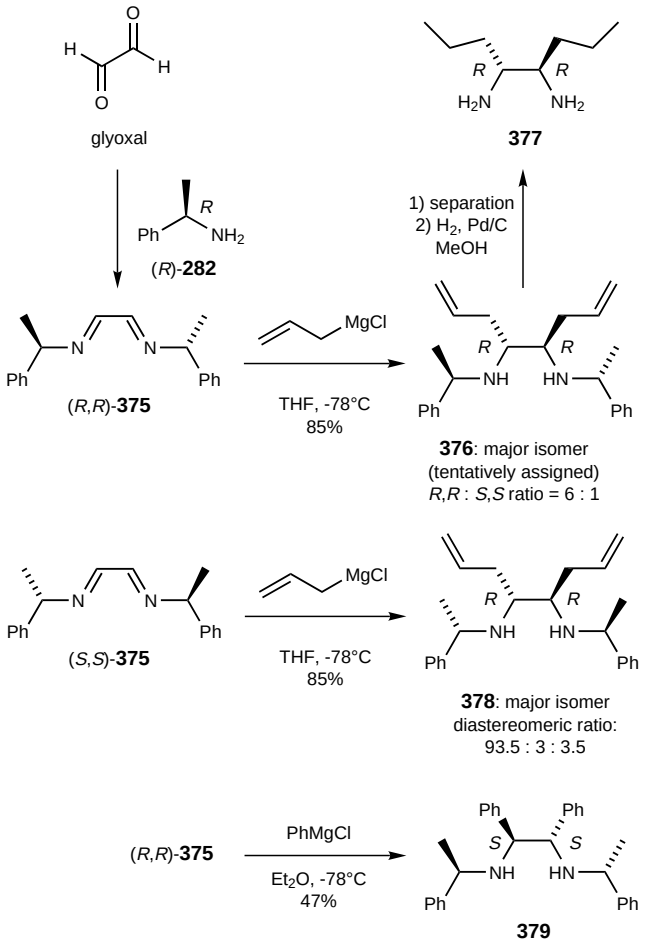
Scheme 90. Synthesis of monosubstituted 1,2-diamines from chiral, non-racemic cyanohydrines.

1,2-Diamines have also been prepared by reduction of optically active α-amino nitriles obtained from asymmetric Strecker reaction.[162]

4.14. Vicinal Diamines by Alkylation of Glyoxal Bisimines

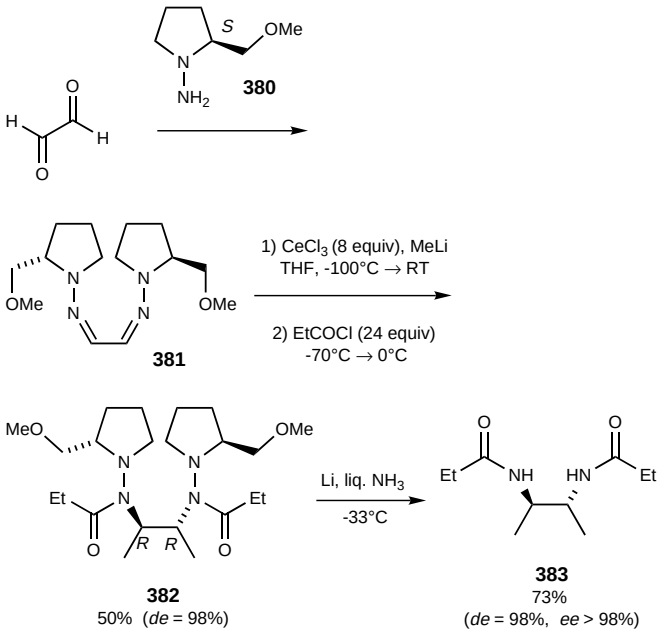
In 1991 Neumann et al. showed that the nucleophilic addition in THF of allylmagnesium chloride to bisimines derived from glyoxal afforded essentially the corresponding *syn*-1,2-diamines. The high *syn* stereoselectivity was presumed to arise from a Cram chelation control. By employing the bisimine (*R*,*R*)-**375**, prepared from commercially available (*R*)-α-methylbenzylamine (**282**), a 6:1 ratio of the two *syn* diastereomers was obtained, the major isomer being tentatively assigned as **376**, which was then converted into enantiomerically pure C_2-symmetric diamine **377** (Scheme 91).[163] Reactions of the same bisimine (or its enantiomer) with other organometallic reagents have since been reported; they also proceed with *syn* selectivity, but with opposite stereochemical outcomes. Savoia et al.[164] obtained the diamine **378** as the major isomer from the reaction of (*S*,*S*)-**375** with allylzinc bromide in THF, and adduct **379** was mainly obtained by Simpkins et al.[165] from the reaction of (*R*,*R*)-**375** with phenylmagnesium chloride in diethyl ether (Scheme 91). In both cases, the configuration of the major isomer was established by X-ray structure analysis.

Enders et al. described the diastereo- and enantioselective synthesis of various C_2-symmetric, protected 1,*n*-diamines from dialdehydes by the alkylation, with organocerium



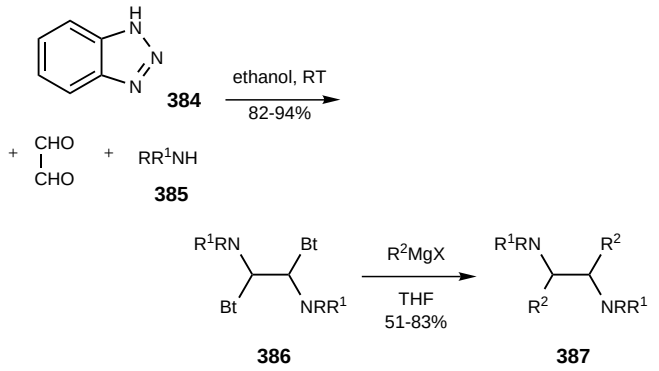
Scheme 91. Addition of Grignard reagents to the bisimine derived from glyoxal and either (*S*)- or (*R*)-α-methylbenzylamine.

compounds, of the bishydrazones derived from the chiral hydrazines SAMP or RAMP.[166] In one example, bishydrazone **381** derived from glyoxal was used as the substrate; while the yield of the addition was moderate, the enantiomeric excess of the final protected C_2-symmetric vicinal diamine **383**, recovered after N–N cleavage, was excellent (Scheme 92).



Scheme 92. Diastereo- and enantioselective bisaddition of an organocerium reagent to a SAMP-derived bishydrazone.

In 1990 Katritzky et al.[167] also employed glyoxal as the starting material in a synthetic route to tertiary and secondary, symmetrical, racemic, vicinal diamines (Scheme 93). Double condensations between benzotriazole (**384**), glyoxal, and either aromatic or secondary aliphatic amines afforded stable adducts **386**; aliphatic primary amines led to oligomers or polymers. Displacement of the benzotriazolyl moieties were then realized by treatment with Grignard reagents, to give the diamines **387** as *syn*–*anti* mixtures.



RR^{1}NH = piperidine, morpholine, nBu$_2$NH, Bn$_2$NH, PhNH$_2$, p-MeC$_6$H$_5$NH$_2$, m-MeC$_6$H$_5$NH$_2$

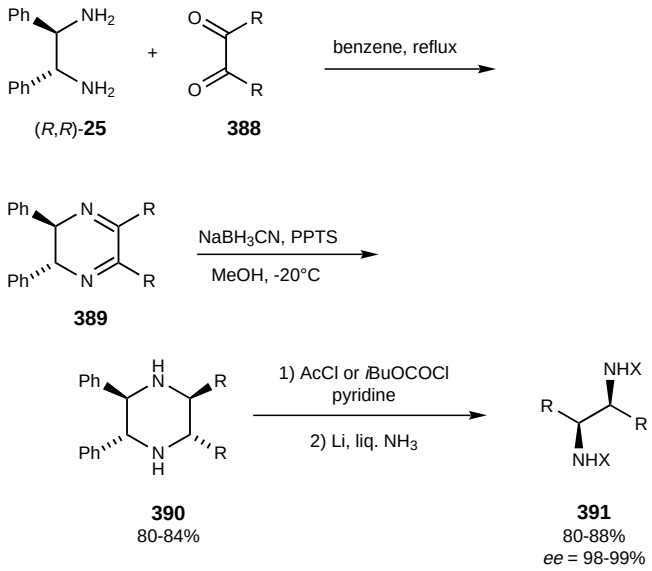
Bt = benzotriazol-1-yl, benzotriazol-2-yl

R^2 = Me, nBu, Bn, Ph

Scheme 93. Synthesis of symmetrical, racemic, vicinal diamines by alkylation of the products of double condensation between benzotriazole, glyoxal, and amines.

4.15. Vicinal Diamines by Reduction of Diketone Bisimines or Bisoximes

An elegant, efficient route to enantiomerically pure C_2-symmetric vicinal diamines that used another such diamine, (*R*,*R*)-1,2-diphenylethylenediamine, as the source of chirality was devised by Nantz et al.[168] (Scheme 94). The reduction of



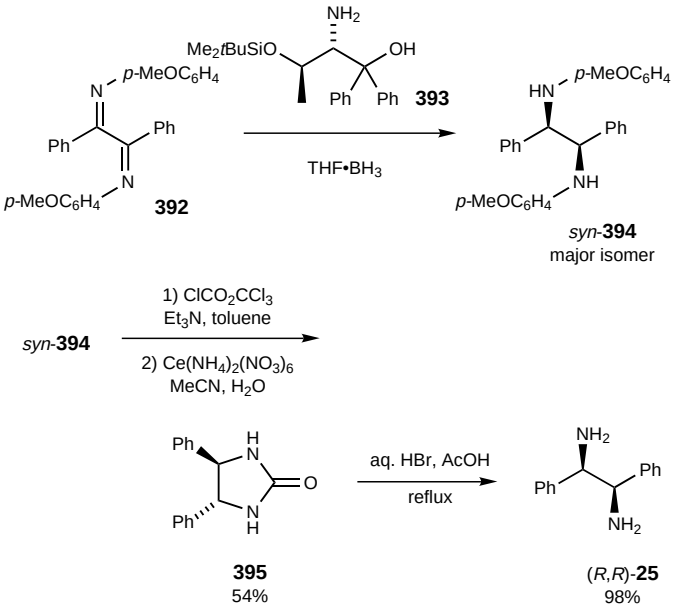
R = alkyl
X = *t*Boc, Ac

Scheme 94. Enantioselective synthesis of C_2-symmetric vicinal diamines by reduction of a chiral dihydropyrazine.

the dihydropyrazine **389** (R = Me), formed from this diamine and 2,3-butanedione, to piperazine **390** (R = Me) by several reagents was studied. Acid-catalyzed sodium cyanoborohydride reduction at $-20\,^{\circ}C$ was found to be the most selective. Various diketones **389** were then reduced under similar conditions. After separation of the minor isomer by chromatography, a short sequence that involved a dissolving metal C–N cleavage provided the protected diamines efficiently **391**. Both enantiomers of stilbenediamine have been prepared by a related strategy involving the reduction of a 2,2-disubstituted 4,5-diphenyl-2*H*-imidazole and a resolution step.[72d]

The catalytic asymmetric reduction of 1,2-bis(*para*-methoxyphenylimino)-1,2-diphenylethane (**392**) was recently reported by Fujisawa et al.[169] (Scheme 95). An oxazaborolidine, obtained from L-threonine derivative **393**, served as the catalyst in a process that afforded selectively the *syn*-diamine **394** in excellent yield. The enantiomeric purity of **394** was excellent (99% *ee*), even when a small amount of catalyst was used (Table 5). No *meso* isomer formed when one equivalent of the ligand was used. Complete deprotection of the amine groups was then carried out, to give the enantiomerically pure (*R*,*R*)-diamine **25**.

1,2-Diamines have also been prepared by reduction of 1,2-bisoximes[131a, 170] or 1,2-bisoxime ethers.[171]



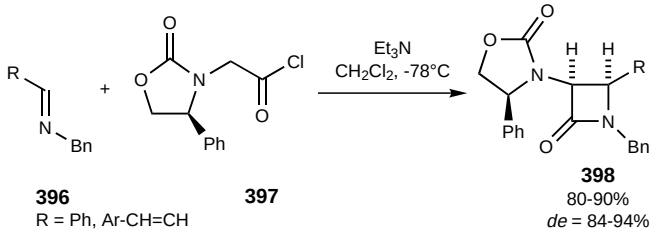
Scheme 95. Enantioselective reduction of a bisimine by using an oxazaborolidine obtained from L-threonine derivative **393**.

Table 5. Diastereo- and enantioselectivity in the reduction of bisimine **392** in the presence of various amounts of **393**.

Entry	Ligand **393** [mol%]	Yield (**394**) (*syn* + *anti*) [%]	*syn*:*anti*	*syn ee* [%]
1	0.5	90	95:5	99
2	50	96	96:4	99
3	100	90	>99:1	99

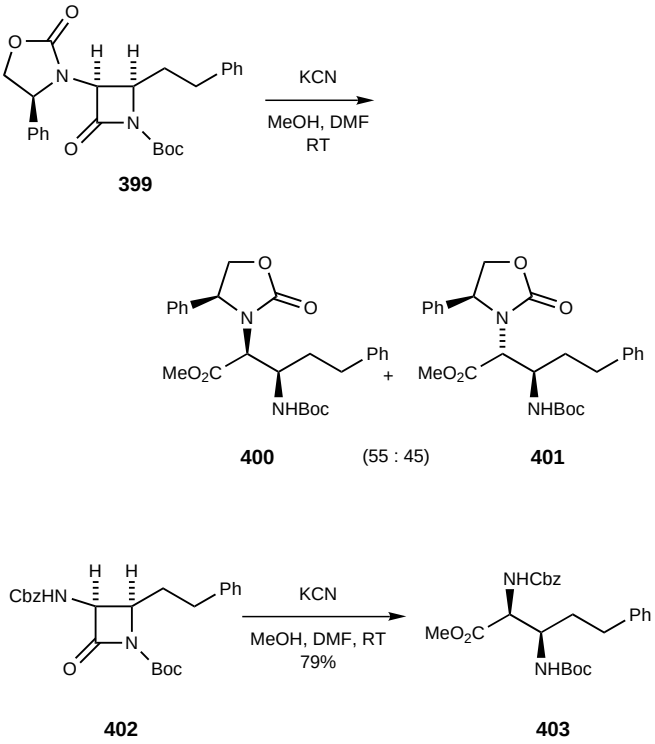
4.16. Vicinal Diamines from 3-Amino-β-lactams

Several approaches to the synthesis of β-lactams with a nitrogen function on the C3 position have been described.[172, 173] A significant example has been reported by Evans and Sjogren (Scheme 96):[174] the Staudinger reaction of



Scheme 96. Diastereoselective synthesis of an 3-oxazolidyl-β-lactam by a Staudinger reaction.

the ketene derived from a chiral, enantiomerically pure oxazolidylacetyl chloride **397** with imines **396** led with very good diastereoselection to the corresponding *cis*-β-lactams **398**. The oxazolidinone ring can then be cleaved to generate an amino group. The diamines can in principle be obtained through opening of the ring of these β-lactams. Such a process has recently been performed by Palomo et al.[175] (Scheme 97). While the methanolysis of β-lactam **399**, substituted with an

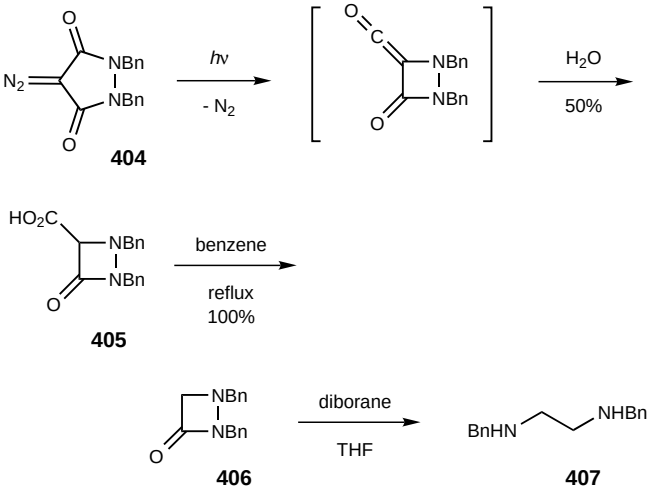


Scheme 97. Ring opening of 3-amino-β-lactams.

oxazolidyl group, afforded a mixture of the *syn* adduct **400** and *anti* adduct **401**, a single protected diamine **403** was obtained from **402** under similar conditions.

4.17. Vicinal Diamines from 1,2-Diazetidinones

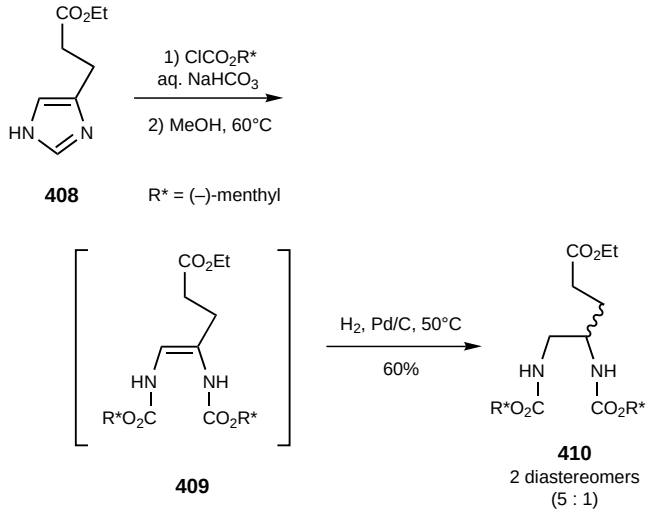
The cleavage of the N–N bond of a 1,2-diazetidine should lead to the corresponding 1,2-diamine. However, since there are no general synthesis of such heterocyclic compounds, this method has not been greatly employed. In one example Moody et al. obtained 1,2-di(benzylamino)ethane (**407**) from the reduction of diazetidinone **406** with diborane in THF (Scheme 98).[176] The diazetidinone itself had been prepared from the photochemical ring contraction of 4-diazopyrazolidine-3,5-dione **404**.



Scheme 98. Synthesis of 1,2-(dibenzylamino)ethane from a diazetidinone.

4.18. Vicinal Diamines from Imidazoles

The Bamberger ring cleavage of imidazoles with an acylating agent leads to ene–diacylamines, which may be reduced to diacylamines. This approach was applied by Altman et al.[177] for the synthesis of enantiomerically enriched diacylamines (Scheme 99). They employed (−)-menthyl chloroformate as the acylating agent; after ring cleavage of

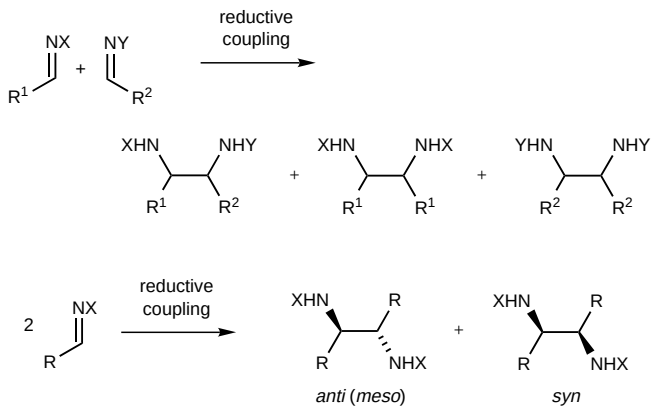


Scheme 99. Diastereoselective reduction of a chiral ene–diacylamine obtained from the Bamberger ring cleavage of an imidazole by using (−)-menthyl chloroformate as the acylating agent.

the imidazole **408**, the catalytic hydrogenation of ene-diacylamine **409** with palladium on carbon afforded a 5/1 mixture of the corresponding diastereomeric vicinal biscarbamates **410**.

4.19. Vicinal Diamines by Reductive Coupling of Imines

In principle, the reductive coupling of imines (with the help of a metal or of a metallic complex) seems a simple way to prepare vicinal diamines; in fact, it is usually applied only to the synthesis of symmetrical diamines, since one can expect to obtain a mixture of products from the coupling of two different imines (Scheme 100).



Scheme 100. Reductive coupling of imines.

Various conditions have been utilized to couple imines, which lead to variable proportions of *anti*- (*meso*-) and *syn*-diamines; some examples follow.

Reductive coupling of aryl *N*-alkylimines can be performed in good yields by photoreduction[178a] or by electrolysis.[178b] Low-valent titanium reagents were employed by Seebach et al.[179a, b] in the reductive coupling of aryl *N*-alkylimines. Similar species, generated from titanium tetrachloride and magnesium amalgam, allowed Mangeney et al.[179c] to obtain symmetrical vicinal diamines with good *anti* selectivity, along with the amine from imine reduction. Periasamy et al. showed that 2-methylimidazolidines are obtained when *N*-alkylimines are coupled with the $TiCl_4/Mg/BrCH_2CH_2Br$ combination in THF.[179d]

The reductive dimerization of *N*-benzylidene aniline with alkali metals was performed by Smith et al., who found conditions that allowed the stereoselective formation of the *syn* or *anti* adducts.[180a] Roskamp and Petersen[180c] prepared unsubstituted vicinal diamines, with moderate to good *anti* selectivity, by coupling *N*-trimethylsilylimines with the d^1 niobium reagent, $[NbCl_4(THF)_2]$. They also developed a method of using nitriles as substrates in conjunction with tributyltin hydride.

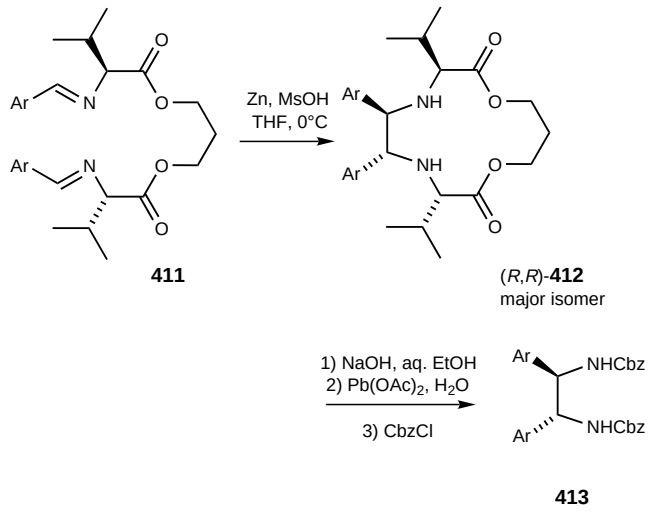
More recently, reductive couplings that used samarium diiodide,[180d, e, i] indium,[180f] and ytterbium[180j] were reported and Pansare et al. described the intramolecular coupling of unsymmetrical dibenzylidene sulfamides mediated either by zinc activated by chlorotrimethylsilane or by samarium diiodide; the cyclic sulfamides obtained were easily converted into the corresponding unsymmetrical 1,2-diaryl-1,2-diamines.[180k] Aluminum, an inexpensive, stable, easy to handle, nontoxic material was used in conjunction with potassium hydroxide.[180b, g] A lead/aluminium bimetallic redox system gave good yields of the adducts, but with poor selectivity.[180h]

Imwinkelried and Seebach also showed that it was possible to prepare 1,2-bis(dialkylamino)-1,2-diaryl ethylene directly from aromatic aldehydes by using an aminative reductive coupling mediated by tris(dialkylamino)methylvanadium (IV).[181]

It is worthy of note that none of these methods allows the direct preparation of enantiomerically pure compounds, which are usually only obtained after an optical resolution.[72] However, reports on the coupling of chiral, non-racemic imines have recently appeared:

Shono et al.[182a] described a stereoselective synthesis of (*R*,*R*)-1,2-diarylethylenediamines **413** by the reductive, intramolecular coupling of chiral, aromatic bisimines **411,** derived from (*S*)-valine methyl ester in the presence of zinc (Scheme 101). A three-carbon chain linkage between the two valine moieties afforded the best selectivity. The selectivity also improved for substrates having a *para*-electron-donating substituent on the aryl group (Table 6). Other macrocycles containing a vicinal diamine moiety have been prepared accordingly, the intramolecular coupling being performed with either electroreduction or zinc powder.[182b]

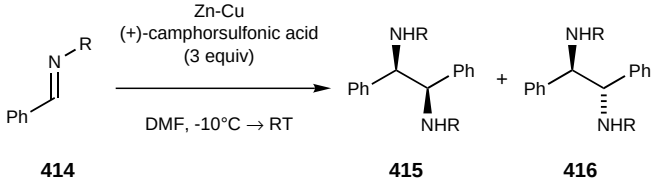
In 1995 Fujisawa et al.[183] reported the enantioselective pinacol coupling of benzaldimine **414**, promoted by the use of a zinc–copper couple, in the presence of three equivalents of (+)-camphorsulfonic acid (Scheme 102). The best results were obtained starting from *N*-*para*-methoxyphenylbenzaldimine, with the *R*,*R* adduct **415** formed with good diaste-



Scheme 101. Intramolecular reductive coupling of chiral, non-racemic bisimines.

Table 6. Diastereoselectivity in the intramolecular reductive coupling of chiral, non-racemic bisimines.

Entry	Ar	Yield (**412**) [%]	*R*,*R*:*R*,*S* (**412**)	Yield (**413**) (two diastereomers)
1	C_6H_5	68	91:9	72
2	*p*-$MeOC_6H_4$	68	97:3	71
3	*p*-ClC_6H_4	63	89:11	73
4	*p*-NCC_6H_4	59	72:28	57



Scheme 102. Enantioselective coupling of imines mediated by a zinc–copper couple in the presence of (+)-camphorsulfonic acid.

reoselectivity and an excellent enantiomeric excess (Table 7). It is presumed that the reaction involves the reductive coupling of a chiral iminium salt formed from the imine and (+)-camphorsulfonic acid.

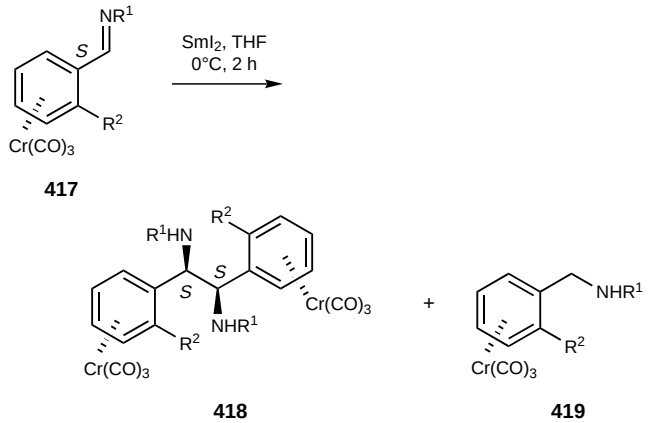
Table 7. Diastereo- and enantioselectivity in the reductive coupling of benzaldimines **414** mediated by a zinc–copper couple in the presence of (+)-camphorsulfonic acid.

Entry	R	Yield (**415**+**416**) [%]	*syn*:*anti*	*ee* (**415**) [%]
1	*p*-$MeOC_6H_4$	88	70:30	97
2	C_6H_5	64	50:50	52
3	$C_6H_5CH_2$	54	53:47	34
4	$(p\text{-}MeOC_6H_4)_2CH$	64	50:50	0

Very recently, Uemura et al.[184] demonstrated that no *anti*, only *syn*-diamines **418** were formed during the samarium diiodide-mediated coupling of enantiomerically pure tricarbonyl(benzaldimine)chromium complexes **417**, along with variable amounts of amines **419** (Scheme 103; Table 8).

Table 8. Reductive coupling of differently substituted chiral tricarbonyl-(benzaldimine)chromium complexes **417** with samarium diiodide.

Entry	R^1	R^2	Yield [**418**] [%]	Yield [**419**] [%]
1	Me	Me	65	25
2	Me	OMe	67	10
3	Me	Br	45	41
4	Me	Cl	48	46
5	$PhCH_2$	Me	54	38
6	$PhCH_2$	*i*Pr	51	29

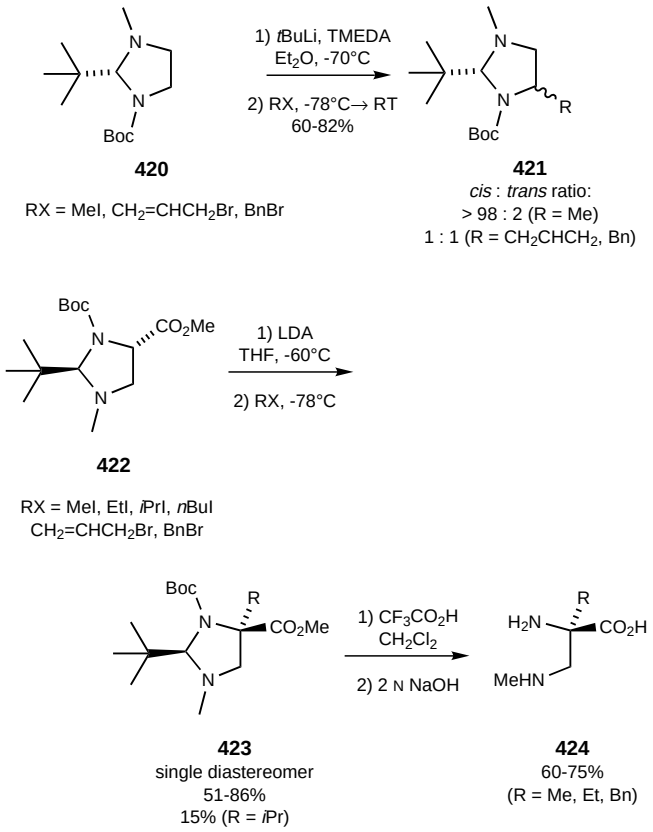


Scheme 103. SmI_2-mediated reductive coupling of chiral tricarbonyl-(benzaldimine)chromium complexes.

4.20. Vicinal Diamines from Other Compounds Containing a 1,2-Diamino Moiety

As seen throughout the preceding sections, the last step of a vicinal diamine synthesis often includes the transformation of a compound already containing a masked 1,2-diamine moiety. For example, the hydrolysis of an imidazolidinone is used in many syntheses. In this section, we will not describe other such transformations in detail. However, the utilization of imidazolines as chiral templates for the preparation of enantiomerically enriched vicinal diamines is worthy of note.

Pfammatter and Seebach[185] reported the reaction of the anion generated from the enantiopure *N*-Boc-imidazolidine **420** with various electrophiles (Scheme 104). While *trans* adducts were usually obtained, as in the reaction with methyl iodide, a 1/1 mixture of diastereomers was obtained with either allyl or benzyl bromide. The cleavage of the heterocycles **421** was not described. The ester **422** was prepared selectively from **420**, and was then used as a precursor to various 2,3-diaminoalkanoic acids. Treatment of **422** with LDA, followed by an alkyl halide, yielded the corresponding α-alkylated ester **423** as a single diastereomer. Even 2-iodopropane could be used as the electrophile, although in this case, a low yield of adduct was obtained. Several adducts **423** were then hydrolyzed to give the free α,β-diamino acids **424**. The conditions used in this two-step procedure cannot be applied conveniently to unbranched substrates (which have an exchangeable proton in the position α to the ester function), since racemization occurs in these cases.

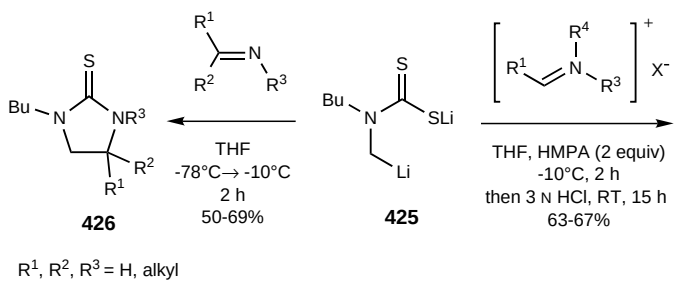


Scheme 104. Stereoselective synthesis of 1,2-diamine derivatives from enantiopure, chiral imidazolidines.

Fraenkel et al.[186] prepared diastereomerically pure *meso*-2,3-bis(methylamino)butane and *cis*-1,2-bis(methylamino)cycloalkanes by the hydrogenation of 1,3-dimethylimidazolin-2-one derivatives. The opening of 2-(aminomethyl)aziridine derivatives by carbon nucleophiles was also used to synthesize vicinal diamines.[187]

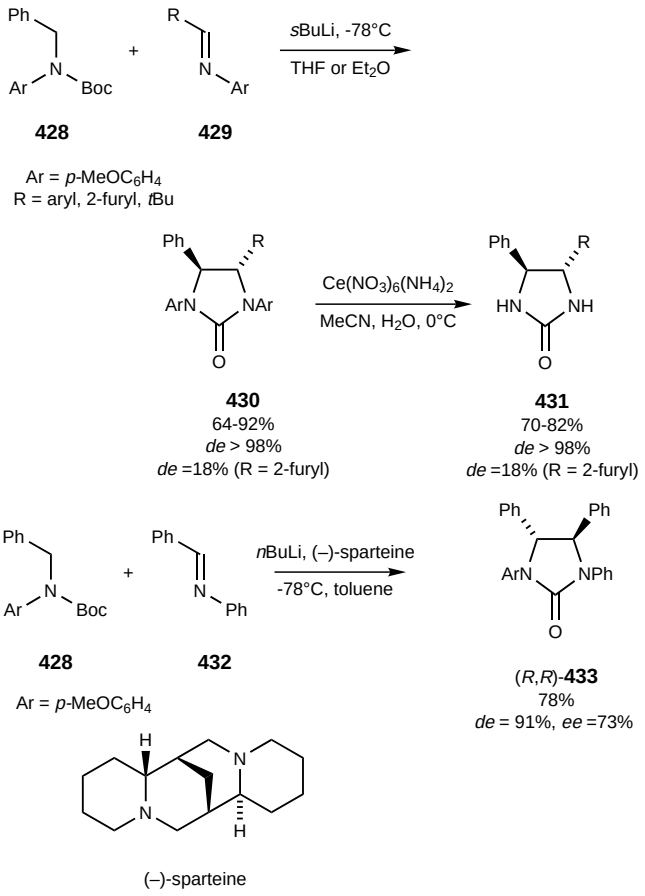
4.21. Vicinal Diamines from Addition of an α-Nitrogen Anion onto Imines or Iminiums

Several authors have recognized that the reaction of an α-nitrogen anion with an imine could yield a 1,2-diamine precursor. For example, Ahlbrecht and Schmitt[188] described a) the reaction of lithium *N*-butyl-*N*-lithiomethyldithiocarbamate (**425**) with imines to give imidazolidine-2-thiones **426**, and b) the reaction with iminium salts to give diamines **427** (Scheme 105).



Scheme 105. Preparation of 1,2-diamine derivatives by reaction of an α-nitrogen anion with imines or iminium salts.

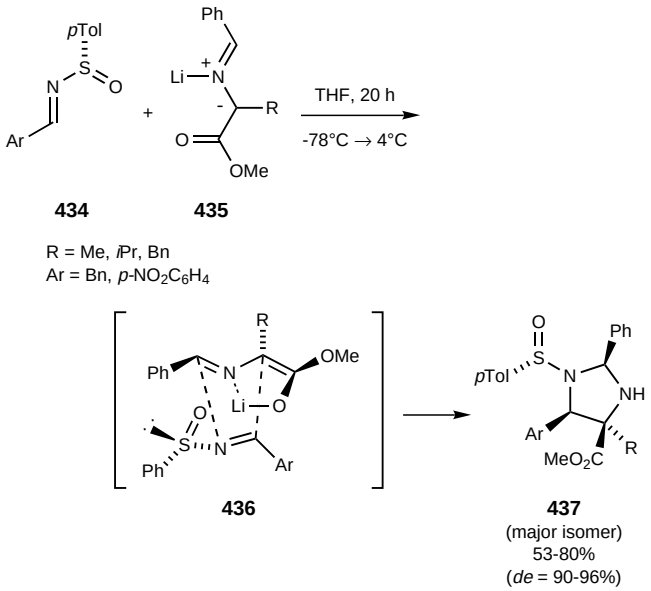
In 1996 Kise, Yoshida et al. reported the stereoselective synthesis of *trans*-imidazolidin-2-ones by the reaction of the carbanion of *N*-benzyl-*N*-Boc-*para*-anisidine (**428**) with imines **429**, which are derived from *para*-anisidine and do not have an exchangeable proton (Scheme 106).[189] Very good stereoselectivities were obtained, either in diethyl ether or in THF, depending on the substrate. Treatment of the adducts **430** with ceric ammonium nitrate afforded in good yields the unprotected *trans*-imidazolidinones **431**, which are precursors of 1,2-diamines. The method was limited to the preparation of adducts substituted only by aryl or *tert*-butyl groups, and also only in racemic form. However, an enantioselective version of this process was soon reported by Beak et al. (Scheme 106).[190] They showed that the reaction of **428** with *n*-butyllithium in toluene, in the presence of (−)-sparteine, followed by addition to *N*-benzylideneaniline (**432**) yielded *trans*-imidazolidinone (*R*,*R*)-**433** as the major adduct with a 73% enantiomeric excess.



Scheme 106. Stereoselective synthesis of *trans*-imidazolidin-2-ones, precursors of 1,2-diamines, by reaction of an α-nitrogen anion with imines.

4.22. Vicinal Diamines by 1,3-Dipolar Cycloaddition of Azomethine Ylides with Imines

1,3-Dipolar cycloaddition of an azomethine ylide with an imine results in the formation of an imidazolidine, which can then be converted into a 1,2-diamine. Only few reports on this reaction have been made, but it was recently applied by Viso, Fernández de la Pradilla et al.[191] to the synthesis of enantiopure *N*-sulfinyl imidazolidines (Scheme 107). The reaction of

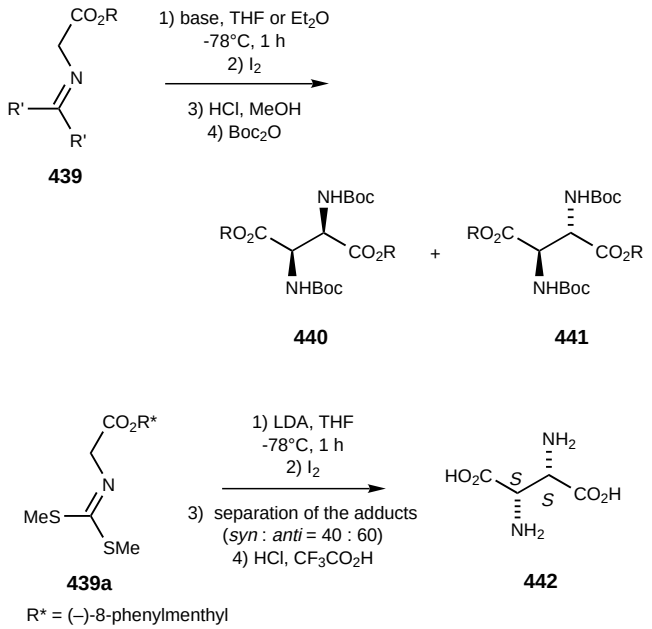


Scheme 107. 1,3-Dipolar cycloaddition of azomethine ylides with enantiopure sulfinimines.

ylides **435,** derived from *N*-benzylidene α-amino esters, with enantiopure sulfinimines **434** afforded the cycloadducts **437** with high diastereoselectivity. A predominant *endo* approach of the ylide to the less hindered β face of the sulfinimine (**436**) was suggested. Diamine **438** was then prepared in two steps from one of these adducts.

4.23. Vicinal Diamines from Oxidative Dimerization of Glycinates

Alvarez-Ibarra et al.[192] recently reported the oxidative dimerization of enolates derived from glycine derivatives **439** in the presence of iodine (Scheme 108). The products were converted into 3-aminoaspartates **440** and **441**. The stereochemical outcome of the reaction depends strongly under the conditions used for the generation of the enolates, which suggests that it is a function of the *E* or *Z* geometry of the



Scheme 108. Synthesis of 3-aminoaspartates by the oxidative dimerization of enolates of glycine esters.

enolates. Excellent *syn* selectivity was obtained when lithium bases were used (Table 9). The dimerization of 8-phenylmenthyl glycinate **439a** proceeded with low diastereoselectivity, but allowed the preparation of C_2-symmetric (2*S*,3*S*)-3-aminoaspartic acid (**442**).

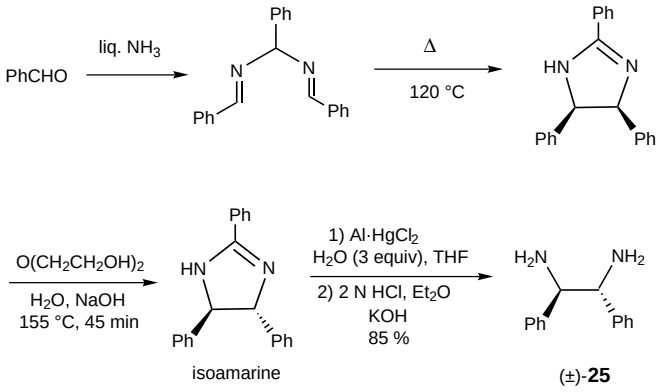
Table 9. Diastereoselectivity in the oxidative dimerization of glycinates.

Entry	R	R′	Base	Solvent	**440**:**441**	Yield [%]
1	Et	SMe	*t*BuLi	THF	55:45	80
2	Et	SMe	*t*BuLi	Et_2O	45:55	60
3	*t*Bu	SMe	*t*BuLi	THF	98:02[a]	80
4	*t*Bu	SMe	LDA	THF	98:02[a]	80
5	*t*Bu	SMe	KO*t*Bu	THF	50:50	80
6	Et	Ph	*t*BuLi	THF	98:02[a]	80
7	Et	Ph	LDA	THF	90:10	90
8	Et	Ph	*t*BuLi	Et_2O	98:02[a]	95
9	Et	Ph	LDA	Et_2O	95:05	85
10	Et	Ph	KO*t*Bu	Et_2O	50:50	60

[a] Only one diastereomer was observed in the 300-MHz ^{1}H NMR spectrum of the crude product.

4.24. Recent Preparations of Vicinal Diamines

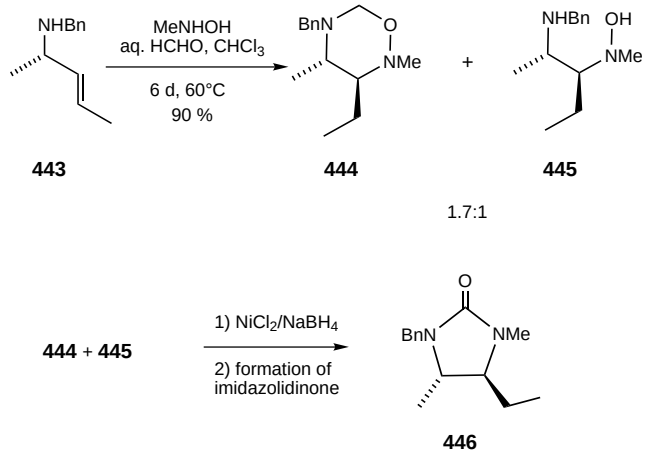
Several recent new relevant syntheses of diamines have appeared since the completion of this review. Saravanan and Singh synthesized various chiral, non-racemic diamines from (*S*)-*O*-acetylmandelic acid, a cheap starting material.[193] A route to the four enantiomers of 2,3-diaminobutanoic acid from *tert*-butyl crotonate, which makes use of the asymmetric aminohydroxylation of Sharpless, was reported by Han et al.[194] An improvement in a previously reported preparation of (±)-1,2-diphenylethylenediamine **25** from isoamarine, which is available from benzaldehyde and ammonia, was described by Corey and Kühnle[195] (Scheme 109).



Scheme 109. Preparation of (±)-1,2-diphenylethylenediamine from benzaldehyde and ammonia.

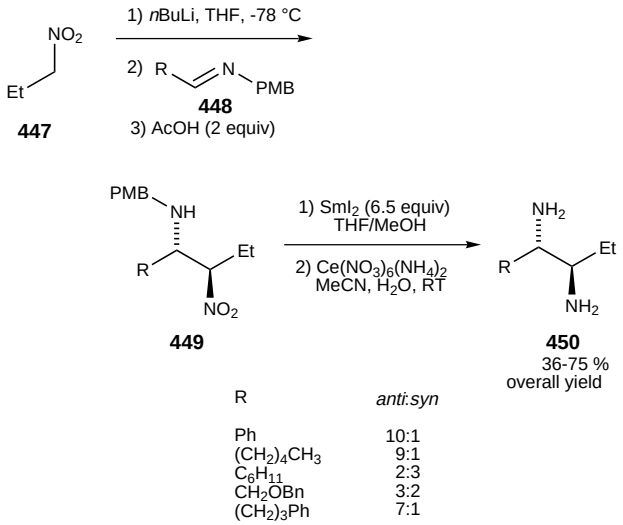
The combined use of samarium diiodide and ytterbium triflate in the reductive coupling of *N*-benzylbenzaldimine under mild conditions was reported by Annunziata et al.[196a] A very good *syn*:*anti* ratio (>98:2) was obtained at room temperature. Lower levels of stereocontrol were observed in the coupling of homochiral imines. A similar coupling was also recently described by Benenji et al.[196b]

Knight et al.[197a] reported the formation of 1,2,5-oxadiazinanes from allylamines and nitrones through a reverse-Cope elimination and a Meisenheimer rearrangement. The conversion of such a compound **444** (obtained from **443** together with amino hydroxylamine **445**) into the corresponding diamine, characterized as the *trans*-imidazolidinone **446** (single diastereomer), was recently published[197b] (Scheme 110).



Scheme 110. Preparation of a *trans*-imidazolidinone from an allylamine and a nitrone.

The nitro–Mannich reaction was employed as the key step in a stereoselective route to 1,2-diamines by Anderson et al.[198] (Scheme 111). Deprotonation of the nitro compound **447** at −78 °C, followed by addition of imine **448** and then of acetic acid, led to *β*-nitro amine **449**. This compound was converted in two steps to the corresponding diamine **450**. Both the nitro compound and the imine tolerate either alkyl or phenyl substituents. *Anti* selectivity was observed in most cases, but the *syn* adduct was obtained from phenylnitromethane and benzaldimine (*anti*:*syn* = 1:15). Treatment of

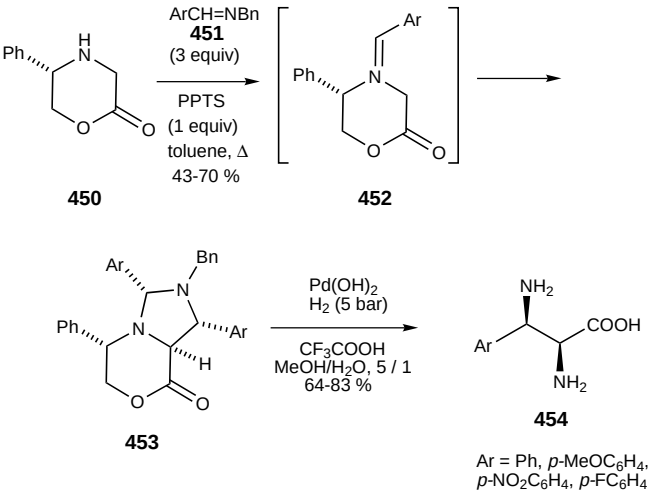


R	*anti*:*syn*
Ph	10:1
$(CH_2)_4CH_3$	9:1
C_6H_{11}	2:3
CH_2OBn	3:2
$(CH_2)_3Ph$	7:1

Scheme 111. Stereoselective synthesis of 1,2-diamines with the ;nitro–Mannich reaction.

propyl nitronate with (*S*)-PhCH(Me)N=CHPh led essentially to one *anti*-*β*-nitro amine; access to homochiral 1,2-diamines by using this method may thus be envisioned.

The cycloaddition of aromatic imines **451** to enantiomerically pure azomethine ylides derived from (5*S*)-phenylmorpholin-2-one **450**, as described by Harwood et al.,[199] was completely diastereoselective (Scheme 112). Hydroge-



Scheme 112. Two-step synthesis of *syn*-(2*S*,3*R*)-3-aryl-2,3-diamino acids by cycloaddition of chiral azomethine ylides with aromatic imines.

nolysis of the cycloadducts **453** under acidic conditions afforded the corresponding *syn*-(2*S*,3*R*)-3-aryl-2,3-diamino acids **454**, which were thus prepared in a straightforward two-step sequence.

Bennani and Hanessian[200] published a review dealing with the use of *trans*-1,2-diaminocyclohexane derivatives as chiral reagents. A review by O'Brien detailed the recent uses of chiral lithium amide bases, including those derived from 1,2-diamines, in asymmetric synthesis.[201] Other recent papers reporting utilizations of vicinal diamines or their derivatives in organic synthesis are noted in the references.[202–212]

5. Summary and Outlook

In this review article, we saw that various compounds incorporating the 1,2-diamino functionality have important biological properties. These compounds may be natural products or synthetic compounds and some of them are useful medicinal agents. Vicinal diamine derivatives also find increasing utilization in organic synthesis, either as chiral auxiliaries or as metallic ligands, especially in the field of catalytic asymmetric synthesis. The importance of the vicinal diamine moiety has brought about numerous methods of preparation. However, few of them are of broad scope. Most of them are only well suited for the preparation of specific classes of 1,2-diamines such as primary, secondary, or tertiary diamines, or only *syn* or *anti* compounds. Other ones only allow the formation of symmetrical 1,2-diamines.

A more general way to prepare vicinal diamines selectively is thus still sought after. Considering the topical development of catalytic enantioselective synthesis, one can envision that asymmetric diamination of alkenes might be a convenient response to this problem. Other solutions will probably then be designed, since, as can be seen from the many examples of syntheses summarized in this review, one thing organic chemists certainly do not lack is imagination.

Appendix: Abbreviations

acac	acetylacetonate
aq.	aqueous
Boc	*tert*-butyloxycarbonyl
Bt	benzotriazolyl
Cbz	benzyloxycarbonyl
Cp	cyclopentadienyl
DMAP	4-dimethylaminopyridine
DME	1,2-dimethoxyethane
DMF	dimethylformamide
DMSO	dimethylsulfoxide
EDTA	ethylenediaminetetraacetic acid
hex	hexyl
*c*hex	cyclohexyl
HMPA	hexamethylphosphorotriamide
L	ligand
LDA	lithium diisopropylamide
liq.	liquid
*m*CPBA	*meta*-chloroperbenzoic acid
MMPP	magnesium monoperoxyphthalate
Ms	methanesulfonyl
Mt	mesityl
NBS	*N*-bromosuccinimide
NMO	*N*-methylmorpholine
Ns	4-nitrobenzenesulfonyl
PPTS	pyridinium *para*-toluenesulfonate
RAMP	(*R*)-1-amino-2-(methoxymethyl)pyrrolidine
salen	*N,N′*-bis(salicylidene)ethylenediamine
SAMP	(*S*)-1-amino-2-(methoxymethyl)pyrrolidine
stien	stilbenediamine
Tf	trifluoromethanesulfonyl
THF	tetrahydrofuran
TMEDA	*N,N,N′,N′*-tetramethylethylenediamine
tosyl	*para*-toluenesulfonyl
trisyl	2,4,6-triisopropylbenzenesulfonyl
trityl	triphenylmethyl
Ts	*para*-toluenesulfonyl

One of us (D.L.) gratefully thanks the financial support of Rhône-Poulenc Agro during his Ph. D. training.

Received: July 1, 1997 [A 237 IE]
German version: *Angew. Chem.* **1998**, *110*, 2724 – 2772

[1] a) M. A. Eisenberg in *Escherichia coli and Salmonella typhimurium*, *Vol. 1* (Ed.: F. C. Neidhardt), American Society for Microbiology, Washington DC, **1987**, pp. 544 – 550; b) A. Marquet, *Pure Appl. Chem.* **1993**, *65*, 1249 – 1252.

[2] a) T. P. Hettinger, L. C. Craig, *Biochemistry* **1970**, *9*, 1224 – 1232; b) H. Yoshioka, T. Aoki, H. Goko, K. Nakatsu, T. Noda, H. Sakakibara, T. Take, A. Nagata, J. Abe, T. Wakamiya, T. Shiba, T. Kaneko, *Tetrahedron Lett.* **1971**, *23*, 2043 – 2046; c) H. Umezawa, K. Maeda, T. Takeuchi, Y. Okami, *J. Antibiot. Ser. A* **1966**, *19*, 200 – 209; d) M. Otsuka, T. Masuda, A. Haupt, M. Ohno, T. Shiraki, Y. Sugiura, K. Maeda, *J. Am. Chem. Soc.* **1990**, *112*, 838 – 845; e) S. M. Hecht, *Acc. Chem. Res.* **1986**, *19*, 383 – 391; f) J. Stubbe, J. W. Kozarich, *Chem. Rev.* **1987**, *87*, 1107 – 1136; g) P. S. Spencer, P. B. Nunn, J. Hugon, A. C. Ludolph, S. M. Ross, D. N. Roy, R. C. Roberston, *Science* **1987**, *237*, 517 – 522; h) J. E. Baldwin, R. M. Adlington, D. J. Birch, *J. Chem. soc. Chem. Commun.* **1985**, 256 – 257 and references cited therein; i) J. H. Dewar, G. Shaw, *J. Chem. Soc.* **1962**, 583 – 585; j) A. F. Bickel, *J. Am. Chem. Soc.* **1947**, *65*, 1801 – 1803; k) R. Adams, V. V. Jones, *J. Am. Chem. Soc.* **1947**, *65*, 1803 – 1805; l) A. F. Bickel, *J. Am. Chem. Soc.* **1947**, *65*, 1805 – 1806; m) F. Lambein, N. Schamp, L. Vandendriessche, R. Van Parijs, *Biochem. Biophys. Res. Commun.* **1969**, *37*, 375 – 382.

[3] a) M. Bodanszky, N. C. Chaturvedi, J. A. Scozzie, R. K. Griffith, A. Bodanszky, *Antimicrob. Agents Chemother.* **1969**, 135 – 138; b) A. Bodanszky, M. Bodanszky, *J. Antibiot. Ser. A* **1970**, *23*, 149 – 154; c) W. K. Hausmann, D. B. Borders, J. E. Lancaster, *J. Antibiot. Ser. A* **1969**, *22*, 207 – 210; d) I. Uchida, N. Shigematsu, M. Ezaki, M. Hashimoto, *Chem. Pharm. Bull.* **1985**, *33*, 3053 – 3056; e) M. Fujino, M. Inoue, J. Ueyanagi, A. Miyake, *Bull. Chem. Soc. Jpn.* **1965**, *38*, 515 – 517; f) K. Morimoto, N. Shimada, H. Naganawa, T. Takita, H. Umezawa, *J. Antibiot.* **1981**, *34*, 1615 – 1618; g) T. Shiroza, N. Ebisawa, K. Furihata, T. Endo, H. Seto, N. Otake, *Agric. Biol. Chem.* **1982**, *46*, 865 – 867; h) S. Shinagawa, T. Kanamaru, S. Harada, M. Asai, H. Okazaki, *J. Med. Chem.* **1987**, *30*, 1458 – 1463.

[4] a) R. A. Gardiner, K. L. Rinehart, Jr., J. J. Snyder, H. P. Broquist, *J. Am. Chem. Soc.* **1968**, *90*, 5639 – 5640; b) P. Kulanthaivel, Y. F. Hallock, C. Boros, S. M. Hamilton, W. P. Janzen, L. M. Ballas, C. R. Loomis, J. B. Jiang, B. Katz, J. R. Steiner, J. Clardy, *J. Am. Chem. Soc.* **1993**, *115*, 6452 – 6453.

[5] E. T. Michalson, J. Szmuszkovicz, *Prog. Drug. Res.* **1989**, *33*, 135 – 149.

[6] Z. Zubovics, L. Toldy, A. Varró, G. Rabloczky, M. Kürthy, P. Dvortsák, G. Jerkovich, E. Tomori, *Eur. J. Med. Chem. Chim. Ther.* **1986**, *21*, 370 – 378.

[7] J. Szmuszkovicz, P. F. Von Voigtlander, M. P. Kane, *J. Med. Chem.* **1981**, *24*, 1230 – 1236.

[8] a) B. Rosenberg, L. VanCamp, J. E. Trosko, V. H. Mansour, *Nature* **1969**, *222*, 385 – 386; b) A. Pasini, F. Zunino, *Angew. Chem.* **1987**, *99*, 632; *Angew. Chem. Int. Ed. Engl.* **1987**, *26*, 615 – 624; c) H. Brunner, P. Hankofer, U. Holzinger, B. Treittinger, H. Schönenberger, *Eur. J. Med. Chem.* **1990**, *25*, 35 – 44; d) H. Brunner, P. Hankofer, U. Holzinger, B. Treittinger, *Chem. Ber.* **1990**, *123*, 1029 – 1038; e) R. Gust, T. Burgemeister, A. Mannschreck, H. Schönenberger, *J. Med. Chem.* **1990**, *33*, 2535 – 2544; f) L. R. Kelland, G. Abel, M. J. McKeage, M. Jones, P. M. Goddard, M. Valenti, B. A. Murrer, K. R. Harrap, *Cancer Res.* **1993**, *53*, 2581 – 2586; g) D.-K. Kim, Y.-W. Kim, H.-T. Kim, K. H. Kim, *Bioorg. Med. Chem. Lett.* **1996**, *6*, 643 – 646; h) A. R. Khokhar, S. Al-Baker, S. Shamsuddin, Z. H. Siddik, *Bioorg. Med. Chem. Lett.* **1997**, *40*, 112 – 116; i) J. Reedijk, *Chem. Commun.* **1996**, 801 – 806.

[9] a) D. J. Gravert, J. H. Griffin, *J. Org. Chem.* **1993**, *58*, 820 – 822; b) K. Sato, M. Chikira, Y. Fujii, A. Komatsu, *J. Chem. Soc. Chem. Commun.* **1994**, 625 – 626; c) C. J. Burrows, S. E. Rokita, *Acc. Chem. Res.* **1994**, *27*, 295 – 301; d) S. Bhattacharya, S. S. Mandal, *J. Chem. Soc. Chem. Commun.* **1995**, 2489 – 2490; e) D. J. Gravert, J. H. Griffin, *Inorg. Chem.* **1996**, *35*, 4837 – 4847; f) S. Routier, J.-L. Bernier, M. J. Waring, P. Colson, C. Houssier, C. Bailly, *J. Org. Chem.* **1996**, *61*, 2326 – 2331; g) T. Tanaka, K. Tsurutani, A. Komatsu, T. Ito, K. Iida, Y. Fujii, Y. Nakana, Y. Usui, Y. Fukuda, M. Chikira, *Bull. Chem. Soc. Jpn.* **1997**, *70*, 615 – 629.

[10] a) L. H. DeRiemer, C. F. Meares, D. A. Goodwin, C. I. Diamanti, *J. Lab. Comp. Radiopharm.* **1981**, *18*, 1517 – 1534; b) S. Kasina, A. R. Fritzberg, D. L. Johnson, D. Eshima, *J. Med. Chem.* **1986**, *29*, 1933 – 1940; c) H. F. Kung, Y.-Z. Guo, C.-C. Yu, J. Billings, V. Subramanyam, J. C. Calabrese, *J. Med. Chem.* **1989**, *32*, 433 – 437; d) A. R. Fritzberg, P. G. Abrams, P. L. Beaumier, S. Kasina, A. C. Morgan, T. N. Rao, J. M. Reno, J. A. Sanderson, A. Srinivasan, D. S. Wilbur, J.-L. Vanderheyden, *Proc. Natl. Acad. Sci. USA* **1988**, *85*, 4025 – 4029; e) L. M. Gustavson, T. N. Rao, D. S. Jones, A. R. Fritzberg, A. Srinivasan, *Tetrahedron Lett.* **1991**, *32*, 5485 – 5488.

[11] a) J. A. Lord, A. A. Waterfield, J. Hughes, H. W. Kosterlitz, *Nature* **1977**, *267*, 495 – 499; b) S. J. Paterson, L. E. Robson, H. W. Kosterlitz, *Br. Med. Bull.* **1983**, *39*, 31 – 36; c) J. Szmuszkovicz, P. F. Von Voigtlander, *J. Med. Chem.* **1982**, *25*, 1125 – 1126; d) G. F. Costello, R. James, J. S. Shaw, A. M. Slater, N. C. J. Stutchbury, *J. Med. Chem.* **1991**, *34*, 181 – 189; e) A. Cowan, D. E. Gmerek, *Trends Pharmacol. Sci.* **1986**, *7*, 69 – 72; f) M. J. Millan, *Trends Pharmacol. Sci.* **1990**, *11*, 70 – 76; g) B. V. Cheney, J. Szmuszkovicz, R. A. Lahti, D. A. Zichi, *J. Med. Chem.* **1985**, *28*, 1853 – 1864; h) B. R. de Costa, W. D. Bowen, S. B. Hellewell, C. George, R. B. Rothman, A. A. Reid, J. M. Walker, A. E. Jacobson, K. C. Rice, *J. Med. Chem.* **1989**, *32*, 1996 – 2002; i) B. R. de Costa, K. C. Rice, W. D. Bowen, A. Thurkauf, R. B. Rothman, L. Band, A. E. Jacobson, L. Radesca, P. C. Contreras, N. M. Gray, I. Daly, S. Iyengar, D. T. Finn, S. Vazirani, J. M. Walker, *J. Med. Chem.* **1990**, *33*, 3100 – 3110; j) L. Radesca, W. D. Bowen, L. Di Paolo, B. R. de Costa, *J. Med. Chem.* **1991**, *34*, 3058 – 3065; k) W. H. Schlichter, A. W. Frahm, *Tetrahedron: Asymmetry* **1992**, *3*, 329 – 332; l) A.-C. Chang, A. E. Takemori, W. H. Ojala, W. B. Gleason, P. S. Portoghese, *J. Med. Chem.* **1994**, *37*, 4490 – 4498.

[12] a) S. N. Gacheru, P. C. Trackman, S. D. Calaman, F. T. Greenaway, H. M. Kagan, *J. Biol. Chem.* **1989**, *264*, 12963 – 12969; b) R. C. Arrowsmith, K. Carter, J. G. Dann, D. E. Davies, C. J. Harris, J. A. Morton, P. Lister, J. A. Robinson, D. J. Williams, *J. Chem. Soc. Chem. Commun.* **1986**, 755 – 757; c) S. Thaisrivongs, H. Schostarez, D. T. Pals, S. R. Turner, *J. Med. Chem.* **1987**, *30*, 1837 – 1842.

[13] a) A. E. A. Popter in *Comprehensive Heterocyclic Chemistry, Vol. 3* (Eds.: A. R. Katritzky, C. W. Rees), Pergamon, Oxford, **1984**, p. 179; b) R. K. Haynes, S. C. Vonwiller, in *Encyclopedia of Reagents for Organic Synthesis, Vol. 7* (Ed.: L. A. Paquette), Wiley, New York, **1995**, pp. 4811 – 4815.

[14] J.-M. Lehn, *Acc. Chem. Res.* **1978**, *11*, 49 – 57.

[15] a) S. S. Yoon, W. C. Still, *J. Am. Chem. Soc.* **1993**, *115*, 823 – 824; b) M. Torneiro, W. C. Still, *Tetrahedron* **1997**, *53*, 8739 – 8750.

[16] J. K. Whitesell, *Chem. Rev.* **1989**, *89*, 1581 – 1590.

[17] a) M. Kawashima, R. Hirata, *Bull. Chem. Soc. Jpn.* **1993**, *66*, 2002 – 2005; b) H. Brunner, H. Schiessling, *Angew. Chem.* **1994**, *106*, 130; *Angew. Chem. Int. Ed. Engl.* **1994**, *33*, 125 – 126.

[18] a) P. Mangeney, A. Alexakis, J. F. Normant, *Tetrahedron Lett.* **1988**, *29*, 2677 – 2680; b) A. Alexakis, P. Mangeney, I. Marek, F. Rose-Munch, E. Rose, A. Semra, F. Robert *J. Am. Chem. Soc.* **1992**, *114*, 8288 – 8290; c) A. Alexakis, P. Mangeney, N. Lensen, J.-P. Tranchier, R. Gosmini, S. Raussou, *Pure Appl. Chem.* **1996**, *68*, 531 – 534.

[19] a) D. Cuvinot, P. Mangeney, A. Alexakis, J.-F. Normant, J.-P. Lellouche, *J. Org. Chem.* **1989**, *54*, 2420 – 2425; b) A. Alexakis, J. C. Frutos, P. Mangeney, *Tetrahedron: Asymmetry* **1993**, *4*, 2431 – 2434; c) A. Alexakis, S. Mutti, P. Mangeney, *J. Org. Chem.* **1992**, *57*, 1224 – 1237; d) A. Alexakis, J. C. Frutos, S. Mutti, P. Mangeney, *J. Org. Chem.* **1994**, *59*, 3326 – 3334; e) R. Hulst, N. Koen de Vries, B. L. Feringa, *Tetrahedron: Asymmetry* **1994**, *5*, 699 – 708; f) P. G. Devitt, M. C. Mitchell, J. M. Weetman, R. J. Taylor, T. P. Kee, *Tetrahedron: Asymmetry.* **1995**, *6*, 2039 – 2044.

[20] a) R. Fulwood, D. Parker, *J. Chem. Soc. Perkin Trans. 2* **1994**, 57 – 64; b) B. Staubach, J. Buddrus, *Angew. Chem.* **1996**, *108*, 1443 – 1445; *Angew. Chem. Int. Ed. Engl.* **1996**, *35*, 1344 – 1346.

[21] T. Mukaiyama, *Tetrahedron* **1981**, *37*, 4111 – 4119.

[22] a) S. Hanessian, D. Delorme, S. Beaudoin, Y. Leblanc, *J. Org. Chem.* **1984**, *106*, 5754 – 5756; b) Y. L. Bennani, S. Hanessian, *Tetrahedron* **1996**, *52*, 13837 – 13866; c) S. Hanessian, Y. L. Bennani, D. Delorme, *Tetrahedron Lett.* **1990**, *31*, 6461 – 6464; d) S. Hanessian, Y. L. Bennani, *Tetrahedron Lett.* **1990**, *31*, 6465 – 6468; e) S. Hanessian, S. Beaudoin, *Tetrahedron Lett.* **1992**, *33*, 7655 – 7658; f) V. J. Blazis, K. J. Koeller, C. D. Spilling, *Tetrahedron: Asymmetry* **1994**, *5*, 499 – 502.

[23] a) H. Roder, G. Helmchen, E.-M. Peters, K. Peters, H.-G. von Schnering, *Angew. Chem.* **1984**, *96*, 895; *Angew. Chem. Int. Ed. Engl.* **1984**, *23*, 898 – 899; b) G. Cardillo, A. D'Amico, M. Orena, S. Sandri, *J. Org. Chem.* **1988**, *53*, 2354 – 2356; c) R. Amoroso, G. Cardillo, P. Sabatino, C. Tomasini, A. Trerè, *J. Org. Chem.* **1993**, *58*, 5615 – 5619; d) G. Cardillo, A. De Simone, L. Gentilucci, P. Sabatino, C. Tomasini, *Tetrahedron Lett.* **1994**, *35*, 5051 – 5054; e) G. Cardillo, S. Casolari, L. Gentilucci, C. Tomasini, *Angew. Chem.* **1996**, *108*, 1939 – 1941; *Angew. Chem. Int. Ed. Engl.* **1996**, *35*, 1848 – 1849; f) G. Cardillo, L. Gentilucci, C. Tomasini, M. P. V. Castejon-Bordas, *Tetrahedron: Asymmetry* **1996**, *7*, 755 – 762; g) G. Cardillo, L. Gentilucci, A. Tolomelli, C. Tomasini, *Tetrahedron Lett.* **1997**, *38*, 6953 – 6956; h) B. M. Trost, M. A. Ceshi, B. König, *Angew. Chem.* **1997**, *109*, 1562 – 1564; *Angew. Chem. Int. Ed. Engl.* **1997**, *36*, 1486 – 1489.

[24] K. Königsberg, K. Prasad, O. Repic, T. J. Blacklock, *Tetrahedron: Asymmetry* **1997**, *8*, 2347 – 2354.

[25] a) S. G. Davies, A. A. Mortlock, *Tetrahedron: Asymmetry.* **1991**, *2*, 1001 – 1004; b) S. G. Davies, A. A. Mortlock, *Tetrahedron Lett.* **1992**, *33*, 1117 – 1120.

[26] E. J. Corey, *Pure Appl. Chem.* **1990**, *62*, 1209 – 1216.

[27] E. J. Corey, S. S. Kim, *J. Am. Chem. Soc.* **1990**, *112*, 4976 – 4977.

[28] E. J. Corey, C. P. Decicco, R. C. Newbold, *Tetrahedron Lett.* **1991**, *32*, 5287 – 5290.

[29] E. J. Corey, S. Choi, *Tetrahedron Lett.* **1991**, *32*, 2857 – 2860.

[30] E. J. Corey, D.-H. Lee, *J. Am. Chem. Soc.* **1991**, *113*, 4026 – 4028.

[31] E. J. Corey, R. Imwinkelried, S. Pikul, Y. B. Xiang, *J. Am. Chem. Soc.* **1989**, *111*, 5493 – 5495.

[32] E. J. Corey, C.-M. Yu, S. S. Kim, *J. Am. Chem. Soc.* **1989**, *111*, 5495 – 5496.

[33] a) A. Alexakis, N. Lensen, J.-P. Tranchier, P. Mangeney, J. Feneau-Dupont, J. P. Declercq, *Synthesis* **1995**, 1038 – 1050; b) A. Alexakis, N. Lensen, P. Mangeney, *Tetrahedron Lett.* **1991**, *32*, 1171 – 1174; c) A. Alexakis, N. Lensen, J.-P. Tranchier, P. Mangeney, *J. Org. Chem.* **1992**, *57*, 4563 – 4565.

[34] a) A. Alexakis, T. Kanger, P. Mangeney, F. Rose-Munch, A. Perrotey, E. Rose, *Tetrahedron: Asymmetry* **1995**, *6*, 47 – 50; b) P. Mangeney, R. Gosmini, S. Raussou, M. Commerçon, A. Alexakis, *J. Org. Chem.* **1994**, *59*, 1877 – 1888; c) A. Alexakis, R. Sedrani, J.-F. Normant, P. Mangeney, *Tetrahedron: Asymmetry* **1990**, *1*, 283 – 286; d) M. Commerçon, P. Mangeney, T. Tejero, A. Alexakis, *Tetrahedron: Asymmetry* **1990**, *1*, 287 – 290; e) A. Alexakis, R. Sedrani, P. Mangeney, *Tetrahedron Lett.* **1990**, *31*, 345 – 348.

[35] S. Kanemasa, T. Hayashi, J. Tanaka, H. Yamamoto, T. Sakurai, *J. Org. Chem.* **1991**, *56*, 4473 – 4481.

[36] A. Togni, L. M. Venanzi, *Angew. Chem.* **1994**, *106*, 517; *Angew. Chem. Int. Ed. Engl.* **1994**, *33*, 497 – 526.

[37] K. Tomioka, *Synthesis* **1990**, 541 – 549.

[38] a) T. Mukaiyama, K. Soai, T. Sato, H. Shimizu, K. Suzuki, *J. Am. Chem. Soc.* **1979**, *101*, 1455 – 1460; b) L. Colombo, C. Gennari, G. Poli, C. Scolastico, *Tetrahedron* **1982**, *38*, 2725 – 2727; c) K. Tomioka, M. Nakajima, K. Koga *Chem. Lett.* **1987**, 65 – 68; d) E. J. Corey, F. J. Hannon, *Tetrahedron Lett.* **1987**, *28*, 5233 – 5236; e) K. Soai, S. Niwa, M. Watanabe, *Tetrahedron Lett.* **1987**, *41*, 4841 – 4842; f) W. Oppolzer, R. N. Radinov, *Tetrahedron Lett.* **1988**, *29*, 5645 – 5648; g) M. Yoshioka, T. Kawakita, M. Ohno, *Tetrahedron Lett.* **1989**, *30*, 1657 – 1660; h) H. Takahashi, T. Kawakita, M. Yoshioka, S. Kobayashi, M. Ohno, *Tetrahedron Lett.* **1989**, *30*, 7095 – 7098; i) H. Takahashi, T. Kawakita, M. Ohno, M. Yoshioka, S. Kobayashi, *Tetrahedron* **1992**, *48*, 5691 – 5700; j) M. Asami, S. Inoue, *Chem. Lett.* **1991**, 685 – 688.

[39] a) M. J. Rozema, S. AchyuthaRao, P. Knochel, *J. Org. Chem.* **1992**, *57*, 1956 – 1958; b) P. Knochel, W. Brieden, M. J. Rozema, C. Eisenberg,

Tetrahedron Lett. **1993**, *34*, 5881 – 5884; c) S. Berger, F. Langer, C. Lutz, P. Knochel, T. A. Mobley, C. K. Reddy, *Angew. Chem.* **1997**, *109*, 1603 – 1605; *Angew. Chem. Int. Ed. Engl.* **1997**, *36*, 1496 – 1498.

[40] a) Y. Belokon, N. Ikonnikov, M. Moscalenko, M. North, S. Orlova, V. Tararov, L. Yashkina, *Tetrahedron: Asymmetry* **1996**, *7*, 851 – 855; b) Y. Jiang, L. Gong, X. Feng, W. Hu, W. Pan, Z. Li, A. Mi, *Tetrahedron* **1997**, *53*, 14327 – 14338.

[41] a) S. Kobayashi, H. Uchiro, Y. Fujishita, I. Shiina, T. Mukaiyama, *J. Am. Chem. Soc.* **1991**, *113*, 4247 – 4252; b) S. Kobayashi, T. Kawasuji, N. Mori, *Chem. Lett.* **1994**, 217 – 220; c) M. Muraoka, H. Kawasaki, K. Koga, *Tetrahedron Lett.* **1988**, *29*, 337 – 338.

[42] H. Brunner, B. Hammer, *Angew. Chem.* **1984**, *96*, 305 – 306; *Angew. Chem. Int. Ed. Engl.* **1984**, *23*, 312 – 313.

[43] a) J. F. G. A. Jansen, B. L. Feringa, *J. Chem. Soc. Chem. Commun.* **1989**, 741 – 742; b) E. J. Corey, R. Naef, F. J. Hannon, *J. Am. Chem. Soc.* **1986**, *108*, 7114 – 7116; c) B. E. Rossiter, M. Eguchi, A. E. Hernández, D. Vickers, J. Medich, J. Marr, D. Heinis, *Tetrahedron Lett.* **1991**, *32*, 3973 – 3976; d) B. E. Rossiter, M. Eguchi, G. Miao, N. M. Swingle, A. E. Hernández, D. Vickers, E. Fluckiger, R. G. Patterson, K. V. Reddy, *Tetrahedron* **1993**, *49*, 965 – 986.

[44] T. Mukaiyama, A. Ikegawa, K. Suzuki, *Chem. Lett.* **1981**, 165 – 168.

[45] a) E. J. Corey, S. Sarshar, J. Bordner, *J. Am. Chem. Soc.* **1992**, *114*, 7938 – 7939; b) S. Pikul, E. J. Corey, *Org. Synth.* **1992**, *71*, 30 – 37; c) D. A. Evans, T. Lectka, S. J. Miller, *Tetrahedron Lett.* **1993**, *34*, 7027 – 7030.

[46] a) H. Takahashi, M. Yoshioka, M. Ohno, S. Kobayashi, *Tetrahedron Lett.* **1992**, *33*, 2575 – 2578; b) H. Takahashi, M. Yoshioka, M. Shibasaki, M. Ohno, N. Imai, S. Kobayashi, *Tetrahedron* **1995**, *51*, 12013 – 12026; c) N. Imai, K. Sakamoto, H. Takahashi, S. Kobayashi, *Tetrahedron Lett.* **1994**, *35*, 7045 – 7048.

[47] a) N. Imai, K. Sakamoto, M. Maeda, K. Kouge, K. Yoshizane, J. Nokami, *Tetrahedron Lett.* **1997**, *38*, 1423 – 1426; b) S. E. Denmark, B. L. Christenson, D. M. Coe, S. P. O'Connor, *Tetrahedron Lett.* **1995**, *36*, 2215 – 2218; c) S. E. Denmark, B. L. Christenson, S. P. O'Connor, *Tetrahedron Lett.* **1995**, *36*, 2219 – 2222.

[48] T. Yasukata, K. Koga, *Tetrahedron: Asymmetry* **1993**, *4*, 35 – 38.

[49] a) E. Vedejs, N. Lee, *J. Am. Chem. Soc.* **1991**, *113*, 5483 – 5485; b) E. Vedejs, N. Lee, *J. Am. Chem. Soc.* **1995**, *117*, 891 – 900.

[50] a) P. J. Cox, N. S. Simpkins, *Tetrahedron: Asymmetry* **1991**, *2*, 1 – 26; b) K. Koga, *Pure Appl. Chem.* **1994**, *66*, 1487 – 1492; c) N. S. Simpkins, *Pure Appl. Chem.* **1996**, *68*, 691 – 694.

[51] a) M. Asami, *Chem. Lett.* **1984**, 829 – 832; b) M. Asami, *Tetrahedron Lett.* **1985**, 5803 – 5806; c) M. Asami, H. Kirihara, *Chem. Lett.* **1987**, 389 – 392; d) M. Asami, *Bull. Chem. Soc. Jpn.* **1990**, *63*, 1402 – 1408.

[52] a) D. Bhuniya, V. K. Singh, *Synth. Commun.* **1994**, *24*, 375 – 385; b) D. Bhuniya, A. DattaGupta, V. K. Singh, *Tetrahedron Lett.* **1995**, *36*, 2847 – 2850; c) D. Bhuniya, A. DattaGupta, V. K. Singh, *J. Org. Chem.* **1996**, *61*, 6108 – 6113.

[53] a) M. Asami, T. Ishizaki, S. Inoue, *Tetrahedron: Asymmetry* **1994**, *5*, 793 – 796; b) M. Asami, T. Suga, K. Honda, S. Inoue, *Tetrahedron Lett.* **1997**, *38*, 6425 – 6428; c) T. Yamashita, D. Sato, T. Kiyoto, A. Kumar, K. Koga, *Tetrahedron Lett.* **1996**, *37*, 8195 – 8198; d) J. P. Tierney, A. Alexakis, P. Mangeney, *Tetrahedron: Asymmetry* **1997**, *8*, 1019 – 1022.

[54] A. J. Blake, S. M. Westaway, N. S. Simpkins, *Synlett* **1997**, 919 – 920.

[55] a) K. Srinivasan, P. Michaud, J. K. Kochi, *J. Am. Chem. Soc.* **1986**, *108*, 2309 – 2320; b) recent review: T. Katsuki, *Coord. Chem. Rev.* **1995**, *140*, 189 – 214.

[56] a) W. Zhang, J. L. Loebach, S. R. Wilson, E. N. Jacobsen, *J. Am. Chem. Soc.* **1990**, *112*, 2801 – 2803; b) E. N. Jacobsen, W. Zhang, A. R. Muci, J. R. Ecker, L. Deng, *J. Am. Chem. Soc.* **1991**, *113*, 7063 – 7064; c) L. Deng, E. N. Jacobsen, *J. Org. Chem.* **1992**, *57*, 4320 – 4323; d) R. Irie, K. Noda, Y. Ito, N. Matsumoto, T. Katsuki, *Tetrahedron Lett.* **1990**, *31*, 7345 – 7348; e) R. Irie, K. Noda, Y. Ito, T. Katsuki, *Tetrahedron Lett.* **1991**, *32*, 1055 – 1058; f) R. Irie, Y. Ito, T. Katsuki, *Synlett* **1991**, 265 – 266; g) R. Irie, K. Noda, Y. Ito, N. Matsumoto, T. Katsuki, *Tetrahedron: Asymmetry* **1991**, *2*, 481 – 494; h) T. Kuroki, T. Hamada, T. Katsuki, *Chem. Lett.* **1995**, 339 – 340; i) M. F. Hentemann, P. L. Fuchs, *Tetrahedron Lett.* **1997**, *38*, 5615 – 5618.

[57] I. F. J. Vankelecom, D. Tas, R. F. Parton, V. Van de Vyver, P. A. Jacobs, *Angew. Chem.* **1996**, *108*, 1445 – 1447; *Angew. Chem. Int. Ed. Engl.* **1996**, *35*, 1346 – 1348.

[58] Z. Li, K. R. Conser, E. N. Jacobsen, *J. Am. Chem. Soc.* **1993**, *115*, 5326 – 5327.

[59] a) H. C. Kolb, M. S. VanNieuwenhze, K. B. Sharpless, *Chem. Rev.* **1994**, *94*, 2483 – 2547; b) S. Hanessian, P. Meffre, M. Girard, S. Beaudoin, J.-Y. Sancéau, Y. Bennani, *J. Org. Chem.* **1993**, *58*, 1991 – 1993; c) E. J. Corey, P. DaSilva Jardine, S. Vigil, P.-W. Yuen, R. D. Connel, *J. Am. Chem. Soc.* **1989**, *111*, 9243 – 9244; d) K. Tomioka, M. Nakajima, K. Koga, *J. Am. Chem. Soc.* **1987**, *109*, 6213 – 6215; e) K. Tomioka, M. Nakajima, Y. IItaka, K. Koga, *Tetrahedron Lett.* **1988**, *29*, 573 – 576; f) K. Tomioka, M. Nakajima, K. Koga, *Tetrahedron Lett.* **1990**, *31*, 1741 – 1744; g) M. Nakajima, K. Tomioka, K. IItaka, K. Koga, *Tetrahedron* **1993**, *49*, 10793 – 10806; h) M. Nakajima, K. Tomioka, K. Koga, *Tetrahedron.* **1993**, *49*, 10807 – 10816; i) K. Fuji, K. Tanaka, H. Miyamoto, *Tetrahedron Lett.* **1992**, *33*, 4021 – 4024; j) M. Hirama, T. Oishi, S. Ito, *J. Chem. Soc. Chem. Commun.* **1989**, 665 – 666.; k) T. Oishi, M. Hirama, *J. Org. Chem.* **1989**, *54*, 5834 – 5835; l) T. Oishi, K.-I. Iida, M. Hirama, *Tetrahedron Lett.* **1993**, *34*, 3573 – 3576; m) M. Tokles, J. K. Snyder, *Tetrahedron Lett.* **1986**, *27*, 3951 – 3954.

[60] T. Sato, Y. Goto, T. Fujisawa, *Tetrahedron Lett.* **1982**, *23*, 4111 – 4112.

[61] T. Mukaiyama, K. Tomimori, T. Oriyama, *Chem. Lett.* **1985**, 813 – 816.

[62] a) T. Nagata, K. Yorozu, T. Yamada, T. Mukaiyama, *Angew. Chem.* **1995**, *107*, 2309 – 2311; *Angew. Chem. Int. Ed. Engl.* **1995**, *34*, 2145 – 2147; b) K. D. Sugi, T. Nagata, T. Yamada, T. Mukaiyama, *Chem. Lett.* **1996**, 737 – 738; c) K. D. Sugi, T. Nagata, T. Yamada, T. Mukaiyama, *Chem. Lett.* **1996**, 1081 – 1082; d) K. D. Sugi, T. Nagata, T. Yamada, T. Mukaiyama, *Chem. Lett.* **1997**, 493 – 494.

[63] Recent review: R. Noyori, S. Hashigushi, *Acc. Chem. Res.* **1997**, *30*, 97 – 102.

[64] a) J.-X. Gao, T. Ikariya, R. Noyori, *Organometallics* **1996**, *15*, 1087 – 1089; b) A. Fujii, S. Hashiguchi, N. Uematsu, T. Ikariya, R. Noyori, *J. Am. Chem. Soc.* **1996**, *118*, 2521 – 2522; c) K.-J. Haack, S. Hashigushi, A. Fujii, T. Ikariya, R. Noyori, *Angew. Chem.* **1997**, *109*, 297 – 300; *Angew. Chem. Int. Ed. Engl.* **1997**, *36*, 285 – 288; d) S. Hashiguchi, A. Fujii, J. Takehara, T. Ikariya, R. Noyori, *J. Am. Chem. Soc.* **1995**, *117*, 7562 – 7563; e) P. Gamez, B. Dunjic, M. Lemaire, *J. Org. Chem.* **1996**, *61*, 5196 – 5197; f) R. ter Halle, A. Bréheret, E. Schulz, C. Pinel, M. Lemaire, *Tetrahedron: Asymmetry* **1997**, *8*, 2101 – 2108; g) P. Krasik, H. Alper, *Tetrahedron* **1994**, *50*, 4347 – 4354; h) K. Matsumura, S. Hashiguchi, T. Ikariya, R. Noyori, *J. Am. Chem. Soc.* **1997**, *119*, 8738 – 8739.

[65] Y. Nishibayashi, Y. Arikawa, K. Ohe, S. Uemura, *J. Org. Chem.* **1996**, *61*, 1172 – 1174.

[66] a) B. M. Trost, R. C. Bunt, *Angew. Chem.* **1996**, *108*, 70 – 73; *Angew. Chem. Int. Ed. Engl.* **1996**, *35*, 99 – 102; b) B. M. Trost, S. Tanimori, P. T. Dunn, *J. Am. Chem. Soc.* **1997**, *119*, 2735 – 2736; c) B. M. Trost, Z. Shi, *J. Am. Chem. Soc.* **1996**, *118*, 3037 – 3038; d) B. M. Trost, L. Li, S. D. Guile, *J. Am. Chem. Soc.* **1992**, *114*, 8745 – 8747; e) B. M. Trost, D. L. Van Vranken, *J. Am. Chem. Soc.* **1992**, *114*, 9327 – 9343; f) B. M. Trost, *Isr. J. Chem.* **1997**, *37*, 109 – 118.

[67] a) T. Morimoto, K. Tachibana, K. Achiwa, *Synlett* **1997**, 783 – 785; b) H. Tye, D. Smyth, C. Eldred, M. Wills, *Chem. Commun.* **1997**, 1053 – 1054.

[68] a) L. E. Martínez, J. L. Leighton, D. H. Carsten, E. N. Jacobsen, *J. Am. Chem. Soc.* **1995**, *117*, 5897 – 5898; b) J. L. Leighton, E. N. Jacobsen, *J. Org. Chem.* **1996**, *61*, 389 – 390; c) K. B. Hansen, J. L. Leighton, E. N. Jacobsen, *J. Am. Chem. Soc.* **1996**, *118*, 10924 – 10925.

[69] a) K. Nakajima, M. Kojima, J. Fujita, *Chem. Lett.* **1986**, 1483 – 1486; b) M. Palucki, P. Hanson, E. N. Jacobsen, *Tetrahedron Lett.* **1992**, *33*, 7111 – 7114; c) K. Noda, N. Hosoya, K. Yanai, R. Irie, T. Katsuki, *Tetrahedron Lett.* **1994**, *35*, 1887 – 1890; d) K. Imagawa, T. Nagata, T. Yamada, T. Mukaiyama, *Chem. Lett.* **1995**, 335 – 336.

[70] S. Hashiguchi, A. Fujii, K.-J. Haack, K. Matsumura, T. Ikariya, R. Noyori, *Angew. Chem.* **1997**, *109*, 300 – 303; *Angew. Chem. Int. Ed. Engl.* **1997**, *36*, 288 – 290.

[71] M. Tokunaga, J. F. Larrow, F. Kakiuchi, E. N. Jacobsen, *Science* **1997**, *277*, 936 – 938.

[72] a) G. T. Morgan, W. J. Hickinbottom, *J. Soc. Chem. Ind. London* **1924**, *43*, 307 – 310; b) F. P. Dwyer, F. L. Garvan, A. Shulman, *J. Am. Chem. Soc.* **1959**, *81*, 290 – 294; c) R. G. Asperger, C. F. Liu, *Inorg. Chem.* **1965**, *4*, 1492 – 1494; d) S. Pikul, E. J. Corey, *Org. Synth.* **1992**, *71*, 22 – 29; e) K. Saigo, N. Kubota, S. Takebayashi, M. Hasegawa, *Bull. Chem. Soc. Jpn.* **1986**, *59*, 931 – 932; f) E. J. Corey, D.-H. Lee, S. Sarshar,

Tetrahedron: Asymmetry **1995**, *6*, 3 – 6; g) I. Alfonso, C. Astorga, F. Rebolledo, V. Gotor, *Chem. Commun.* **1996**, 2471 – 2472.
[73] M. B. Gasc, A. Lattes, J. J. Perie, *Tetrahedron* **1983**, *39*, 703 – 731.
[74] V. G. Aranda, J. Barluenga, F. Aznar, *Synthesis* **1974**, 504 – 505.
[75] a) J. Barluenga, L. Alonso-Cires, G. Asensio, *Synthesis.* **1979**, 962 – 964; b) J. Barluenga, F. Aznar, M. C. S. de Mattos, W. B. Kover, S. Garcia-Granda, E. Pérez-Carreño, *J. Org. Chem.* **1991**, *56*, 2930 – 2932.
[76] a) J.-E. Bäckvall, *Tetrahedron Lett.* **1975**, 2225 – 2228; b) J.-E. Bäckvall, *Tetrahedron Lett.* **1978**, 163 – 166.
[77] A. Chong, K. Oshima, K. B. Sharpless, *J. Am. Chem. Soc.* **1977**, *99*, 3420 – 3426.
[78] a) P. N. Becker, M. A. White, R. G. Bergman, *J. Am. Chem. Soc.* **1980**, *102*, 5676 – 5677; b) P. N. Becker, R. G. Bergman, *Organometallics* **1983**, *2*, 787 – 796.
[79] W. E. Fristad, T. A. Brandvold, J. R. Peterson, S. R. Thompson, *J. Org. Chem.* **1985**, *50*, 3647 – 3649.
[80] R. M. Moriarty, J. S. Khosrowshahi, *Tetrahedron Lett.* **1986**, *27*, 2809 – 2812.
[81] S. Ghomi, D. E. Orr, *Chem. Ind.* **1983**, 928.
[82] W. Zhang, E. N. Jacobsen, *Tetrahedron Lett.* **1991**, *32*, 1711 – 1714.
[83] a) K. B. Sharpless, S. P. Singer, *J. Org. Chem.* **1976**, *41*, 2504 – 2506; b) T. Fukuyama, C.-K. Jow, M. Cheung, *Tetrahedron Lett.* **1995**, *36*, 6373 – 6374; c) M. Bruncko, T.-A. V. Khuong, K. B. Sharpless, *Angew. Chem.* **1996**, *108*, 453 – 455; *Angew. Chem. Int. Ed. Engl.* **1996**, *35*, 454 – 456.
[84] a) H. Natsugari, R. R. Whittle, S. M. Weinreb, *J. Am. Chem. Soc.* **1984**, *106*, 7867 – 7872; b) H. Natsugari, E. Turos, S. M. Weinreb, R. J. Cvetovich, *Heterocycles* **1987**, *25*, 19 – 24.
[85] a) T. Katsuki, K. B. Sharpless, *J. Am. Chem. Soc.* **1980**, *102*, 5974 – 5976; b) Y. Gao, R. M. Hanson, J. M. Klunder, S. Y. Ko, S. Masamune, K. B. Sharpless, *J. Am. Chem. Soc.* **1987**, *109*, 5765 – 5780.
[86] E. N. Jacobsen, I. Marko, W. S. Mungall, G. Schröder, K. B. Sharpless *J. Am. Chem. Soc.* **1988**, *110*, 1968 – 1970.
[87] a) G. Li, H. T. Chang, K. B. Sharpless, *Angew. Chem.* **1996**, *108*, 449 – 452; *Angew. Chem. Int. Ed. Engl.* **1996**, *35*, 451 – 453; b) O. Reiser, *Angew. Chem.* **1996**, *108*, 1406 – 1408; *Angew. Chem. Int. Ed. Engl.* **1996**, *35*, 1308 – 1309.
[88] D. Pini, A. Iuliano, C. Rosini, P. Salvadori, *Synthesis* **1990**, 1023 – 1024.
[89] a) B. B. Lohray, J. R. Ahuja, *J. Chem. Soc. Chem. Commun.* **1991**, 95 – 97; b) R. Oi, K. B. Sharpless, *Tetrahedron Lett.* **1991**, *32*, 999 – 1002; c) P. F. Richardson, L. T. J. Nelson, K. B. Sharpless, *Tetrahedron Lett.* **1995**, *36*, 9241 – 9244.
[90] a) J. Skarzewski, A. Gupta, *Tetrahedron: Asymmetry* **1997**, *8*, 1861 – 1867; b) C.-C. Lim, K. F. Mok, K. Y. Sim, P.-H. Leung, *Tetrahedron: Asymmetry.* **1997**, *8*, 2045 – 2050; c) M. G. Scaros, P. K. Yonan, S. A. Laneman, P. N. Fernando, *Tetrahedron: Asymmetry.* **1997**, *8*, 1501 – 1506.
[91] a) J. Altman, D. Ben-Ishai, *Tetrahedron: Asymmetry.* **1993**, *4*, 91 – 100; b) J. Altman, D. Ben-Ishai, W. Beck, *Tetrahedron: Asymmetry.* **1994**, *5*, 887 – 894; c) T. Oishi, M. Hirama, L. R. Sita, S. Masamune, *Synthesis* **1991**, 789 – 792; d) U. Schmidt, K. Mundinger, B. Riedl, G. Haas, R. Lau, *Synthesis.* **1992**, 1201 – 1202; e) K. Burgess, D. S. Linthicum, H. Shin, *Angew. Chem.* **1995**, *107*, 975; *Angew. Chem. Int. Ed. Engl.* **1995**, *34*, 907 – 909; f) K. Burgess, J. Ibarzo, D. S. Linthicum, D. H. Russell, H. Shin, A. Shitangkoon, R. Totani, A. J. Zhang, *J. Am. Chem. Soc.* **1997**, *119*, 1556 – 1564; g) Q. Li, D. T. W. Chu, K. Raye, A. Claiborne, L. Seif, B. Macri, J. J. Plattner, *Tetrahedron Lett.* **1995**, *36*, 8391 – 8394.
[92] J.-R. Choi, S. Han, J. K. Cha, *Tetrahedron Lett.* **1991**, *32*, 6469 – 6472.
[93] F. Demirci, A. H. Haines, C. Jia, D. Wu, *Synthesis* **1996**, 189 – 191.
[94] S. Kano, T. Yokomatsu, H. Iwasawa, S. Shibuya, *Chem. Pharm. Bull.* **1988**, *36*, 3341 – 3347.
[95] a) G. Kokotos, T. Markidis, V. Constantinou-Kokotou, *Synthesis* **1996**, 1223 – 1226; b) G. Kokotos, V. Constantinou-Kokotou, E. del Olmo - Fernandez, I. Toth, W. A. Gibbons, *Liebigs Ann. Chem.* **1992**, 961 – 964.
[96] F. M. Rossi, E. T. Powers, R. Yoon, L. Rosenberg, J. Meinwald, *Tetrahedron* **1996**, *52*, 10279 – 10286.
[97] R. K. Dieter, N. Deo, B. Lagu, J. W. Dieter, *J. Org. Chem.* **1992**, *57*, 1663 – 1671.
[98] G. Miao, B. E. Rossiter, *J. Org. Chem.* **1995**, *60*, 8424 – 8427.
[99] a) P. O'Brien, P. Poumellec, *Tetrahedron Lett.* **1996**, *37*, 5619 – 5622; b) S. E. de Sousa, P. O'Brien, *Tetrahedron Lett.* **1997**, *38*, 4885 – 4888; c) S. E. de Sousa, P. O'Brien, P. Poumellec, *Tetrahedron: Asymmetry* **1997**, *8*, 2613 – 2618; d) S. E. de Sousa, P. O'Brien, P. Poumellec, *J. Chem. Soc. Perkin Trans. 1* **1998**, 1483 – 1492.
[100] Q. Liu, A. P. Marchington, N. Boden, C. M. Rayner, *J. Chem. Soc. Perkin Trans. 1* **1997**, 511 – 525.
[101] S.-J. Wey, K. J. O'Connor, C. J. Burrows, *Tetrahedron Lett.* **1993**, *34*, 1905 – 1908.
[102] G. M. Taylor, S. J. Baker, A. Gedney, D. J. Pearson, G. E. M. Sibley, *Tetrahedron Lett.* **1996**, *37*, 1297 – 1300.
[103] M. J. Fazio, *J. Org. Chem.* **1984**, *49*, 4889 – 4893.
[104] a) A. M. Warshawsky, M. V. Patel, T.-M. Chen, *J. Org. Chem.* **1997**, *62*, 6439 – 6440; b) L. D. Arnold, T. H. Kalantar, J. C. Vederas, *J. Am. Chem. Soc.* **1985**, *107*, 7105 – 7109.
[105] a) H. Kohn, S.-H. Jung, *J. Am. Chem. Soc.* **1983**, *105*, 4106 – 4108; b) S.-H. Jung, H. Kohn, *J. Am. Chem. Soc.* **1985**, *107*, 2931 – 2943; c) S.-H. Jung, H. Kohn, *Tetrahedron Lett.* **1984**, *25*, 399 – 402.
[106] a) K. Osowska-Pacewicka, A. Zwierzak, *Synthesis* **1990**, 505 – 508; b) K. Osowska-Pacewicka, A. Zwierzak, *Tetrahedron* **1985**, *41*, 4717 – 4725.
[107] a) B. S. Orlek, *Tetrahedron Lett.* **1986**, *27*, 1699 – 1702; b) B. S. Orlek, G. Stemp, *Tetrahedron Lett.* **1991**, *32*, 4045 – 4048.
[108] a) K. Stingl, J. Martens, *Liebigs Ann. Chem.* **1994**, 243 – 250; b) A. Benalil, B. Carboni, M. Vaultier, *Tetrahedron* **1991**, *47*, 8177 – 8194; c) A. Valasinas, B. Frydman, H. C. Friedmann *J. Org. Chem.* **1992**, *57*, 2158 – 2160; d) P. N. Confalone, G. Pizzolato, E. G. Baggiolini, D. Lollar, M. R. Uskokovic, *J. Am. Chem. Soc.* **1975**, *97*, 5936 – 5938.
[109] a) E. G. Kemp in *Comprehensive Organic Synthesis, Vol. 7* (Eds.: B. M. Trost, I. Fleming), Pergamon, Oxford, **1991**, pp. 469 – 513; b) D. Tanner, *Angew. Chem.* **1994**, *106*, 625; *Angew. Chem. Int. Ed. Engl.* **1994**, *33*, 599 – 619; c) H. M. I. Osborn, J. Sweeney, *Tetrahedron: Asymmetry* **1997**, *11*, 1693 – 1715.
[110] H. Bestian, *Methoden Org. Chem. (Houben-Weyl) 4th ed.* Vol. E11/2, **1958,** pp. 250 – 251.
[111] a) D. Tanner, P. Somfai, *Tetrahedron Lett.* **1987**, *28*, 1211 – 1214; b) J. Legters, L. Thijs, B. Zwanenburg, *Tetrahedron Lett.* **1989**, *30*, 4881 – 4884; c) B. B. Lohray, Y. Gao, K. B. Sharpless, *Tetrahedron Lett.* **1989**, *30*, 2623 – 2626.
[112] D. A. Evans, M. M. Faul, M. T. Bilodeau, B. A. Anderson, D. M. Barnes, *J. Am. Chem. Soc.* **1993**, *115*, 5328 – 5329.
[113] G. Swift, D. Swern, *J. Org. Chem.* **1967**, *32*, 511 – 517.
[114] A. Hassner, C. Heathcock, *Tetrahedron* **1964**, *20*, 1037 – 1042.
[115] R. J. Parry, M. G. Kunitani, O. I. Viele, *J. Chem. Soc. Chem. Commun.* **1975**, 321 – 322.
[116] a) K. Nakajima, T. Tanaka, K. Morita, K. Okawa, *Bull. Chem. Soc. Jpn.* **1980**, *53*, 283 – 284; b) H. Stamm, P. Assithianakis, B. Buchholz, R. Weiß, *Tetrahedron Lett.* **1982**, *23*, 5021 – 5024; c) W. Chamchaang, A. R. Pinhas, *J. Org. Chem.* **1990**, *55*, 2531 – 2533.
[117] M. Egli, L. Hoesch, A. S. Dreiding, *Helv. Chim. Acta* **1985**, *68*, 220 – 230.
[118] M. Meguro, N. Asao, Y. Yamamoto, *Tetrahedron Lett.* **1994**, *35*, 7395 – 7398.
[119] N. A. J. M. Sommerdijk, P. J. J. A. Buynsters, H. Akdemir, D. G. Geurts, R. J. M. Nolte, B. Zwanenburg, *J. Org. Chem.* **1997**, *62*, 4955 – 4960.
[120] J. Legters, J. G. H. Willems, L. Thijs, B. Zwanenburg, *Recl. Trav. Chim. Pays-Bas* **1992**, *111*, 59 – 68.
[121] W.-H. Leung, M.-T. Yu, M.-C. Wu, L.-L. Yeung, *Tetrahedron Lett.* **1996**, *37*, 891 – 892.
[122] T. Kuroki, T. Katsuki, *Chem. Lett.* **1995**, 337 – 338.
[123] a) A. Duréault, I. Tranchepain, C. Greck, J.-C. Depezay, *Tetrahedron Lett.* **1987**, *28*, 3341 – 3344; b) A. Duréault, I. Tranchepain, J.-C. Depezay, *J. Org. Chem.* **1989**, *54*, 5324 – 5330.
[124] D. Tanner, C. Birgersson, H. K. Dhaliwal, *Tetrahedron Lett.* **1990**, *31*, 1903 – 1906.
[125] K. Fuji, T. Kawabata, Y. Kiryu, Y. Sugiura, *Heterocycles* **1996**, *42*, 701 – 722.
[126] P. E. Maligres, M. M. See, D. Askin, P. J. Reider, *Tetrahedron Lett.* **1997**, *38*, 5253 – 5256.
[127] P. Gmeiner, E. Hummel, *Synthesis* **1994**, 1026 – 1028.
[128] A. J. Burke, S. G. Davies, C. J. R. Hedgecock, *Synlett* **1996**, 621 – 622.

[129] a) E. Fernández-Megía, M. M. Paz, F. J. Sardina, *J. Org. Chem.* **1994**, *59*, 7643 – 7652; b) E. Fernández-Megía, F. J. Sardina, *Tetrahedron Lett.* **1997**, *38*, 673 – 676.
[130] a) B. R. Baker, M. V. Querry, S. F. Safir, S. Bernstein, *J. Org. Chem.* **1947**, *12*, 138 – 154; b) B. R. Baker, M. V. Querry, W. L. McEwen, S. Bernstein, S. R. Safir, L. Dorfman, Y. Subbarow, *J. Org. Chem.* **1947**, *12*, 186 – 198; c) E. J. Moriconi, W. C. Crawford, *J. Org. Chem.* **1968**, *33*, 370 – 378; d) P. N. Confalone, G. Pizzolato, M. R. Uskokovic, *J. Org. Chem.* **1977**, *42*, 135 – 139; e) A. Fliri, K. Hohenlohe-Oehringen, *Chem. Ber.* **1980**, *113*, 607 – 613; f) P. J. Dunn, R. Häner, H. Rapoport, *J. Org. Chem.* **1990**, *55*, 5017 – 5025; g) J. Deng, Y. Hamada, T. Shioiri, *Tetrahedron Lett.* **1996**, *37*, 2261 – 2264; h) R. K. Olsen, W. J. Hennen, R. B. Wardle *J. Org. Chem.* **1982**, *47*, 4605 – 4611.
[131] a) H. Stetter, V. Löhr, A. Simos, *Liebigs Ann. Chem.* **1977**, 999 – 1004; b) L. A. Paquette, L. D. Wise, *J. Am. Chem. Soc.* **1965**, *87*, 1561 – 1566; c) P. Dallemagne, O. Tembo, S. Rault, M. Robba, *Bull. Soc. Chim. Fr.* **1989**, 98 – 103; d) P. Dallemagne, S. Rault, M. Cugnon de Sévricourt, M. Robba, *Heterocycles* **1988**, *27*, 1637 – 1642; e) M. H. Wu, E. N. Jacobsen, *Tetrahedron Lett.* **1997**, *38*, 1693 – 1696.
[132] E. Bruni, G. Cardillo, M. Orena, S. Sandri, C. Tomasini, *Tetrahedron Lett.* **1989**, *30*, 1679 – 1682.
[133] R. A. T. M. van Benthem, H. Hiemstra, G. R. Longarela, W. N. Speckamp, *Tetrahedron Lett.* **1994**, *35*, 9281 – 9284.
[134] a) J. Gonda, A.-C. Helland, B. Ernst, D. Bellus, *Synthesis* **1993**, 729 – 733; b) A. M. Doherty, B. E. Kornberg, M. D. Reily, *J. Org. Chem.* **1993**, *58*, 795 – 798.
[135] M. T. Reetz, D. Röhrig, K. Harms, G. Frenkling, *Tetrahedron Lett.* **1994**, *35*, 8765 – 8768.
[136] P. L. Southwick, J. E. Anderson, *J. Am. Chem. Soc.* **1957**, *79*, 6222 – 6230.
[137] a) M. L. Morris, M. A. Sturgess, *Tetrahedron Lett.* **1993**, *34*, 43 – 46; b) M. A. Sturgess, D. J. Yarberry, *Tetrahedron Lett.* **1993**, *34*, 4743 – 4746.
[138] D. Enders, J. Wiedemann, *Synthesis* **1996**, 1443 – 1450.
[139] D. Lucet, L. Toupet, T. Le Gall, C. Mioskowski, *J. Org. Chem.* **1997**, *62*, 2682 – 2683.
[140] K. Imagawa, E. Hata, T. Yamada, T. Mukaiyama, *Chem. Lett.* **1996**, 291 – 292.
[141] R. Duschinsky, L. A. Dolan, L. O. Randall, G. Lehmann, *J. Am. Chem. Soc.* **1947**, *69*, 3150.
[142] W. J. Gensler, M. W. Hu, *J. Org. Chem.* **1973**, *38*, 3848 – 3853.
[143] G. Fraenkel, P. Pramanik, *J. Org. Chem.* **1984**, *49*, 1314 – 1316.
[144] a) S. P. Gupta, S. S. Chatterjee, P. C. Jain, N. Anand, *Synthesis* **1974**, 660 – 661; b) T. E. D'Ambra, K. G. Estep, M. R. Bell, M. A. Eissenstat, K. A. Joseph, S. J. Ward, D. A. Haycock, E. R. Baizman, F. M. Casiano, N. C. Beglin, S. M. Chippari, J. D. Grego, R. K. Kullnig, G. T. Daley, *J. Med. Chem.* **1992**, *35*, 124 – 135.
[145] a) I. Gómez-Monterrey, M. J. Domínguez, R. González-Muñiz, J. R. Harto, M. T. García-López, *Tetrahedron Lett.* **1991**, *32*, 1089 – 1092; b) M. Martín-Martinez, M. T. García-López, R. González-Muñiz, *Tetrahedron Lett.* **1992**, *33*, 2187 – 2190.
[146] B. I. Glänzer, Z. Györgydeák, B. Bernet, A. Vasella, *Helv. Chim. Acta* **1991**, *74*, 343 – 369.
[147] a) G. F. Hennion, J. E. Reardon, *J. Org. Chem.* **1967**, *32*, 2819 – 2822; b) M. Villacampa, M. Martínez, G. González-Trigo, M. M. Söllhuber, *Heterocycles* **1992**, *34*, 1885 – 1895.
[148] W. J. Greenlee, P. L. Allibone, D. S. Perlow, A. A. Patchett, E. H. Ulm, T. C. Vassil, *J. Med. Chem.* **1985**, *28*, 434 – 442.
[149] M. T. Reetz, R. Jaeger, R. Drewlies, M. Hübel, *Angew. Chem.* **1991**, *103*, 109; *Angew. Chem. Int. Ed. Engl.* **1991**, *30*, 103 – 106.
[150] a) S. Laschat, R. Fröhlich, B. Wibbeling, *J. Org. Chem.* **1996**, *61*, 2829 – 2838; b) S. Laschat, *Liebigs Ann. Chem.* **1997**, 1 – 11.
[151] M. T. Reetz, M. Hübel, R. Jaeger, R. Schwickardi, R. Goddard, *Synthesis* **1994**, 733 – 738.
[152] a) J. Zhu, J.-C. Quirion, H.-P. Husson, *Tetrahedron Lett.* **1989**, *30*, 5137 – 5140; b) J. Royer, H.-P. Husson, *Janssen Chim. Acta* **1993**, *11*, 3 – 8.
[153] a) A. Dondoni, F. L. Merchan, P. Merino, T. Tejero, V. Bertolasi, *J. Chem. Soc. Chem. Commun.* **1994**, 1731 – 1733; b) P. Merino, A. Lanaspa, F. L. Merchan, T. Tejero, *Tetrahedron Lett.* **1997**, *38*, 1813 – 1816; c) P. Merino, A. Lanaspa, F. L. Merchan, T. Tejero, *Tetrahedron: Asymmetry* **1998**, *9*, 629 – 646; d) P. Merino, A. Lanaspa, F. L. Merchan, T. Tejero, *Tetrahedron: Asymmetry.* **1997**, *8*, 2381 – 2401; e) J.-N. Denis, S. Tchertchian, A. Tomassini, Y. Vallée, *Tetrahedron Lett.* **1997**, *38*, 5503 – 5506.
[154] a) C. Palomo, J. M. Aizpurua, F. Cabré, C. Cuevas, S. Munt, J. M. Odriozola, *Tetrahedron Lett.* **1994**, *35*, 2725 – 2728; b) C. Palomo, F. P. Cossío, C. Cuevas, B. Lecea, A. Mielgo, P. Román, A. Luque, M. Martinez-Ripoll, *J. Am. Chem. Soc.* **1992**, *114*, 9360 – 9369.
[155] S. Shatzmiller, S. Bercovici, *Liebigs Ann. Chem.* **1992**, 1005 – 1009.
[156] N. De Kimpe, L. D'Hondt, *Synthesis* **1993**, 1013 – 1017.
[157] a) D. Enders, R. Schiffers, *Synthesis* **1996**, 53 – 58; b) D. Enders, E. Chelain, G. Raabe, *Bull. Soc. Chim. Fr.* **1997**, *134*, 299 – 306; c) Recent review on the use of SAMP and RAMP: D. Enders, M. Klatt in *Encyclopedia of Reagents for Organic Synthesis, Vol. 1* (Ed.: L. A. Paquette), Wiley, New York, **1995**, pp. 178 – 182.
[158] a) G. Buono, C. Triantaphylides, G. Peiffer, F. Petit, *Synthesis* **1982**, 1030 – 1033; b) H. Brunner, M. Schmidt, G. Unger, H. Schönenberger, *Eur. J. Med. Chem. Chim. Ther.* **1985**, *20*, 509 – 512.
[159] E. Zang, P. J. Sadler, *Synthesis* **1997**, 410 – 412.
[160] a) F. Vergne, D. J. Aitken, H.-P. Husson, *J. Org. Chem.* **1992**, *57*, 6071 – 6075; b) F. Vergne, K. Partogyan, D. J. Aitken, H.-P. Husson, *Tetrahedron* **1996**, *52*, 2421 – 2428.
[161] F. Effenberger, A. Kremser, U. Stelzer, *Tetrahedron: Asymmetry* **1996**, *7*, 607 – 618.
[162] D. M. Stout, L. A. Black, W. L. Matier, *J. Org. Chem.* **1983**, *48*, 5369 – 5373.
[163] W. L. Neumann, M. M. Rogic, T. J. Dunn, *Tetrahedron Lett.* **1991**, *32*, 5865 – 5868.
[164] G. Alvaro, F. Grepioni, D. Savoia, *J. Org. Chem.* **1997**, *62*, 4180 – 4182.
[165] K. Bambridge, M. J. Begley, N. S. Simpkins, *Tetrahedron Lett.* **1994**, *35*, 3391 – 3394.
[166] D. Enders, M. Meiers, *Angew. Chem.* **1996**, *108*, 2391 – 2393; *Angew. Chem. Int. Ed. Engl.* **1996**, *35*, 2261 – 2263.
[167] A. R. Katritzky, W.-Q. Fan, C. Fu, *J. Org. Chem.* **1990**, *55*, 3209 – 3213.
[168] M. H. Nantz, D. A. Lee, D. M. Bender, A. H. Roohi, *J. Org. Chem.* **1992**, *57*, 6653 – 6657.
[169] M. Shimizu, M. Kamei, T. Fujisawa, *Tetrahedron Lett.* **1995**, *36*, 8607 – 8610.
[170] a) A. Dornow, K. J. Fust, H. D. Jordan, *Chem. Ber.* **1957**, *90*, 2124 – 2137; b) H. S. Broadbent, E. L. Allred, L. Pendleton, C. W. Whittle, *J. Am. Chem. Soc.* **1960**, *82*, 189 – 193.
[171] a) C. Dell'Erba, A. Mele, M. Novi, G. Petrillo, P. Stagnaro, *Tetrahedron* **1992**, *48*, 4407 – 4418; b) C. Dell'Erba, M. Novi, G. Petrillo, D. Spinelli, C. Tavani, *Tetrahedron.* **1996**, *52*, 3313 – 3326.
[172] Recent reviews: a) F. H. van der Steen, G. van Koten, *Tetrahedron.* **1991**, *47*, 7503 – 7524; b) J. Backes, *Methoden Org. Chem. (Houben-Weyl) 4th ed.*, *Vol. E16b* **1991**, pp. 31 – 288.
[173] J. R. Belletini, M. J. Miller, *J. Org. Chem.* **1996**, *61*, 7959 – 7962.
[174] D. A. Evans, E. B. Sjogren, *Tetrahedron Lett.* **1985**, *26*, 3787 – 3790.
[175] a) C. Palomo, J. M. Aizpurua, C. Cuevas, A. Mielgo, R. Galarza *Tetrahedron Lett.* **1995**, *36*, 9027 – 9030; b) C. Palomo, J. M. Aizpurua, R. Galarza, A. Mielgo, *Chem. Commun.* **1996**, 633 – 634.
[176] G. Lawton, C. J. Moody, C. J. Pearson, *J. Chem. Soc. Chem. Commun.* **1984**, 754 – 756.
[177] J. Altman, M. Grinberg, M. Wilchek, *Liebigs Ann. Chem.* **1990**, 339 – 343.
[178] a); A. Padwa, W. Bergmark, D. Pashayan, *J. Am. Chem. Soc.* **1969**, *91*, 2653 – 2660; b) H. Tanaka, T. Nakahara, H. Dhimane, S. Torii, *Synlett* **1989**, 51 – 52.
[179] a) C. Betschart, D. Seebach, *Helv. Chim. Acta* **1987**, *70*, 2215 – 2231; b) C. Betschart, B. Schmidt, D. Seebach, *Helv. Chim. Acta.* **1988**, *71*, 1999 – 2021; c) P. Mangeney, T. Tejero, A. Alexakis, F. Grosjean, J. Normant, *Synthesis* **1988**, 255 – 257; d) M. Periasamy, M. R. Reddy, J. V. B. Kanth, *Tetrahedron Lett.* **1996**, *37*, 4767 – 4770.
[180] a) J. G. Smith, I. Ho, *J. Org. Chem.* **1972**, *37*, 653 – 656; b) E. von Angerer, G. Egginger, G. Kranzfelder, H. Bernhauer, H. Schönenberger, *J. Med. Chem.* **1982**, *25*, 832 – 837; c) E. J. Roskamp, S. F. Pedersen, *J. Am. Chem. Soc.* **1987**, *109*, 3152 – 3154; d) E. J. Enholm, D. C. Forbes, D. P. Holub, *Synth. Commun.* **1990**, *20*, 981 – 987; e) T. Imamoto, S. Nishimura, *Chem. Lett.* **1990**, 1141 – 1142; f) N. Kalyanam, G. Venkateswara Rao, *Tetrahedron Lett.* **1993**, *34*, 1647 – 1648; g) B. Baruah, D. Prajapati, J. S. Sandhu, *Tetrahedron Lett.* **1995**,

36, 6747 – 6750; h) H. Tanaka, H. Dhimane, H. Fujita, Y. Ikemoto, S. Torii, *Tetrahedron Lett.* **1988**, *29*, 3811 – 3814; i) J. M. Aurrecoechea, A. Fernandez-Acebes, *Tetrahedron Lett.* **1992**, *33*, 4763 – 4766; j) K. Takaki, Y. Tsubaki, S. Tanaka, F. Beppu, Y. Fujiwara, *Chem. Lett.* **1990**, 203 – 204; k) S. V. Pansare, M. G. Malusare, *Tetrahedron Lett.* **1996**, *37*, 2859 – 2862.

[181] R. Imwinkelried, D. Seebach, *Helv. Chim. Acta* **1984,** *67*, 1496 – 1502.

[182] a) T. Shono, N. Kise, H. Oike, M. Yoshimoto, E. Okazaki, *Tetrahedron Lett.* **1992**, *38*, 5559 – 5562; b) N. Kise, H. Oike, E. Okazaki, M. Yoshimoto, T. Shono, *J. Org. Chem.* **1995**, *60*, 3980 – 3992.

[183] M. Shimizu, T. Iida, T. Fujisawa, *Chem. Lett.* **1995**, 609 – 610.

[184] N. Taniguchi, M. Uemura, *Synlett* **1997**, 51 – 53.

[185] E. Pfammatter, D. Seebach, *Liebigs Ann. Chem* **1991**, 1323 – 1336.

[186] J. Akester, J. Cui, G. Fraenkel, *J. Org. Chem.* **1997**, *62*, 431 – 434.

[187] D. S. Jones, A. Srinivasan, S. Kasina, A. R. Fritzberg, D. W. Wilkening *J. Org. Chem.* **1989**, *54*, 1940 – 1943.

[188] H. Ahlbrecht, C. Schmitt, *Synthesis* **1994**, 719 – 722.

[189] N. Kise, K. Kashiwagi, M. Watanabe, J. Yoshida, *J. Org. Chem.* **1996**, *61*, 428 – 429.

[190] Y. S. Park, M. L. Boys, P. Beak, *J. Am. Chem. Soc.* **1996**, *118*, 3757 – 3758.

[191] A. Viso, R. Fernández de la Pradilla, C. Guerrero-Strachan, M. Alonso, M. Martínez-Ripoll, I. André, *J. Org. Chem.* **1997**, *62*, 2316 – 2317.

[192] C. Alvarez-Ibarra, A. G. Csákÿ, B. Colmenero, M. L. Quiroga, *J. Org. Chem.* **1997**, *62*, 2478 – 2482.

[193] P. Saranavan, V. K. Singh, *Tetrahedron Lett.* **1998**, *39*, 167 – 170.

[194] H. Han, J. Yoon, K. D. Janda, *J. Org. Chem.* **1998**, *63*, 2045 – 2048.

[195] E. J. Corey, F. N. M. Kühnle, *Tetrahedron Lett.* **1997**, *38*, 8631 – 8634.

[196] a) R. Annunziata, M. Benaglia, M. Cinquini, F. Cozzi, L. Raimondi, *Tetrahedron Lett.* **1998**, *39*, 3333 – 3336; b) S. Talukdax, A. Benenji, *J. Org. Chem.* **1998**, *63*, 3468 – 3470.

[197] a) M. B. Gravestock, D. W. Knight, S. R. Thornton, *J. Chem. Soc. Chem. Commun.* **1993**, 169; b) K. E. Bell, M. P. Coogan, M. B. Gravestock, D. W. Knight, S. R. Thornton, *Tetrahedron Lett.* **1997**, *38*, 8545 – 8548.

[198] H. Adams, J. C. Anderson, S. Peace, A. M. K. Pennell, *J. Org. Chem.*, submitted.

[199] D. Alker, L. M. Harwood, C. E. Williams, *Tetrahedron Lett.* **1998**, *39*, 475 – 478.

[200] Y. Bennani, S. Hanessian, *Chem. Rev.* **1997**, *97*, 3161 – 3195.

[201] P. O'Brien *J. Chem. Soc. Perkin Trans. 1* **1998**, 1439 – 1457.

[202] Use of chiral aminals derived from C_2-symmetric 1,2-diamines in the stereoselective conjugate addition of aryllithium reagents: L. F. Frey, R. D. Tillyer, A.-S. Caille, D. M. Tschaen, U.-H. Dolling, E. J. J. Grabowski, P. J. Reider *J. Org. Chem.* **1998**, *63*, 3120 – 3124.

[203] Enantioselective alkylation of aldehydes or imines in the presence of 1,2-diamine-derived ligands: a) T. Suzuki, Y. Hirokawa, K. Ohtake, T. Shibata, K. Soai *Tetrahedron: Asymmetry* **1997**, *8*, 4033 – 4040; b) A. Corruble, J.-Y. Valnot, J. Maddaluno, Y. Prigent, D. Davoust, P. Duhamel *J. Am. Chem. Soc.* **1997**, *119*, 10042 – 10048; c) C. Lutz, V. Lutz, P. Knochel *Tetrahedron* **1998**, *54*, 6385 – 6402.

[204] Enantioselective deprotonation of epoxides or ketones: a) A. Z.-Q. Khan, R. W. de Groot, P. I. Arvidsson, Ö. Davidsson *Tetrahedron: Asymmetry* **1998**, *9*, 1223 – 1229; b) M. Toriyama, K. Sugasawa, M. Shindo, N. Tokutake, K. Koga *Tetrahedron Lett.* **1997**, *38*, 567 – 570.

[205] Use of 1,2-diamine-derived ligands in asymmetric transfer hydrogenation: a) S. Inoue, K. Nomura, S. Hashiguchi, R. Noyori, Y. Izawa *Chem. Lett.* **1997**, 957 – 958; b) M. Bernard, V. Guiral, F. Delbecq, F. Fache, P. Sautet, M. Lemaire *J. Am. Chem. Soc.* **1998**, *120*, 1441 – 1446; c) E. Breysse, C. Pinel, M. Lemaire *Tetrahedron: Asymmetry* **1998**, *9*, 897 – 900; d) R. ter Halle, E. Schulz, M. Lemaire *Synlett* **1997**,1257 – 1258.

[206] Evaluation of chiral phosphinamides, some of them prepared from 1,2-diamines, as catalysts in the asymmetric reduction of ketones by borane: B. Burns, N. P. King, H. Tye, J. R. Studley, M. Gamble, M. Wills *J. Chem. Soc. Perkin Trans. 1* **1998**, 1027 – 1038.

[207] Asymmetric acylation of *meso*-diols in the presence of a chiral 1,2-diamine: T. Oriyama, K. Imai, T. Hosoya, T. Sano *Tetrahedron Lett.* **1998**, *39*, 397 – 400.

[208] Palladium-catalyzed asymmetric allylic alkylations: a) B. M. Trost, X. Ariza *Angew. Chem.* **1997**, *109*, 2749 – 2751; *Angew. Chem. Int. Ed. Engl.* **1997**, *36*, 2635 – 2637; b) T. Constantieux, J.-M. Brunel, A. Labande, G. Buono *Synlett* **1998**, 49 – 50; c) I. C. F. Vasconcelos, G. K. Anderson, N. P. Rath, C. D. Spilling *Tetrahedron: Asymmetry* **1998**, *9*, 927 – 935.

[209] Kinetic resolution of racemic allenes with [Mn^{III}(salen)] complex as catalyst: Y. Noguchi, H. Takiyama, T. Katsuki *Synlett* **1998**, 543 – 545.

[210] Enantioselective rearrangement mediated by a C_2-symmetric bislithium amide: S. E. Gibson (née Thomas), P. Ham, G. R. Jefferson *Chem. Commun.* **1998**, 123 – 124.

[211] Asymmetric synthesis of cyclic ethers by rearrangement of oxonium ylides in the presence of a chiral bisimine: J. S. Clark, M. Fretwell, G. A. Whitlock, C. J. Burns, D. N. A. Fox *Tetrahedron Lett.* **1998**, *39*, 97 – 100.

[212] Asymmetric catalyzed metallo – ene reactions in the presence of chiral ligands, including diamine-derived bisamides: W. Oppolzer, D. L. Kuo, M. W. Hutzinger, R. Léger, J.-O. Durand, C. Leslie *Tetrahedron Lett.* **1998**, *38*, 6213 – 6216.

Spongistatins, Cynachyrolides, or Altohyrtins? Marine Macrolides in Cancer Therapy

Jörg Pietruszka*

Isolation and Structure Determination

Marine organisms have been a rich source for new drugs during the last decades. Though only an infinitely small fraction of all marine species has been explored, a plethora of new and diverse structures and structural features with, in some cases, fascinating physiological properties could be isolated.[1, 2] Cytotoxic, antineoplastic compounds are of special interest; this field of research has been followed systematically with great commitment and success—also thanks to the intensive efforts of the American National Cancer Institute (NCI)—for over 30 years.[2] The bioactive macrolides are particularly promising.[3]

In 1993 three independant research groups reported a new class of remarkably cytotoxic marine macrolides, the spongipyrans, from marine sponges for the first time (see Table 1).[4] The research was guided by bioassays and led to the identification and structure determination of spongistatins 1–9 (Pettit et al.[4a, 5]) from *Spongia sp.* and *Spirastrella spinispirulifera*, cinachyrolide A (Fusetani et al.[4b]) from *Cinachyra*, and altohyrtins A–C as well as 5-desacetylaltohyrtin A (Kitagawa et al.[4c, 6]) from *Hyrtios* (Figure 1). The achievement of the three groups is especially noteworthy, since only trace amounts (0.5–13.8 mg) of these extremely potent, physiologically active compounds could be isolated for extensive NMR experiments after laborious extractions and multiple chromatographic purifications. The relationship of all substances is clear: Apart from the 42-membered macrolactone ring (longest carbon chain) there are two spiroketals (*AB* and *CD* rings) and one bis(tetrahydropyran) fragment (*EF* rings) as prominent structural features. Variations (spongistatins 5, 7–9) exhibit an additional five-membered ring (*G* ring). However, there are evidently differences; the proposed relative configurations of the spiroketal units (*AB*/*CD*), the (*E*)-tetrahydropyran ring as well as the stereogenic centers C14–16 and C47 diverge from each other. The absolute configurations were only determined for the altohyrtins, whose structures were postulated by Kitagawa et al.[6b, c] It was tempting to think that all macrolides, apart from the substituents at C50, only differ in their degree of acetylation. First total syntheses from Evans et al. (altohyrtin C)[7] and Kishi et al. (altohyrtin A)[8]—both from Harvard University—confirmed this. In the following these syntheses and different synthetic approaches from Heathcock,[9] Paquette,[10] Paterson,[11] and Smith[12] will be presented.

Studies Towards the Total Synthesis

There are strategic features that all approaches to the total synthesis have in common, namely, the late macrolactonization—in all reported cases Yamaguchi conditions (2,4,6-trichlorobenzoyl chloride, trialkylamine, then 4-dimethylaminopyridine) were applied—and a proposed coupling of the "northern hemisphere" **1** to the "southern hemisphere" of the spongipyrans by a Wittig reaction (aldehyde C28) to furnish double bond C28–C29 (Scheme 1). The side chain (C44–C51) can be incorporated before the lactonization either completely (Kishi et al.[8b]), partly (Smith et al.[12a] and Paterson et al.[11b]), or not at all (Evans et al.[7c]) in the southern hemisphere. However, because of the different substituents at C50 of the various altohyrtins, an introduction at the latest possible moment seems to be advantageous. In both total syntheses allylstannanes were used for a ring opening of an epoxypyran to join the resulting chain with the *EF* ring system. The strategy for the bis(tetrahydropyran) unit was similar (the numbering of the carbons atoms in the synthetic building blocks is already based on the final molecule): After separate synthesis of the *E* and *F* rings, a coupling of a C37-lithiated species to an aldehyde (C38) was anticipated. Evans et al. applied an anomeric sulfone (C37) as carbanion-stabilizing group, whereas Kishi et al. utilized an 1-iodo enolether. For the northern hemisphere different approaches were followed. While the Evans group made use of a selective aldol addition (aldehyde C15 and (*E*)-boron enolate C16) as the key step for the coupling of the spiroketal units, the Kishi group carried out the formation of a C17–C18 bond by the Ni^{2+}/Cr^{2+}-mediated addition of a vinyl iodide (C18) to an aldehyde (C17). After oxidation to a ketone (C17) the reaction sequence was completed with an intramolecular hetero-Michael cyclization to form the *C* ring with concomitant formation of the *CD* spiroketal unit.

The synthesis (Evans) of spiroketals *AB* and *CD* including the coupling to compound **1** is outlined in Scheme 2. Starting

[*] Dr. J. Pietruszka
Institut für Organische Chemie der Universität
Pfaffenwaldring 55, D-70569 Stuttgart (Germany)
Fax: (+49) 711-685-4269
E-mail: joerg.pietruszka@po.uni-stuttgart.de

 © WILEY-VCH Verlag GmbH, D-69451 Weinheim, 1998 1433-7851/98/03719-2629 $ 17.50+.50/0

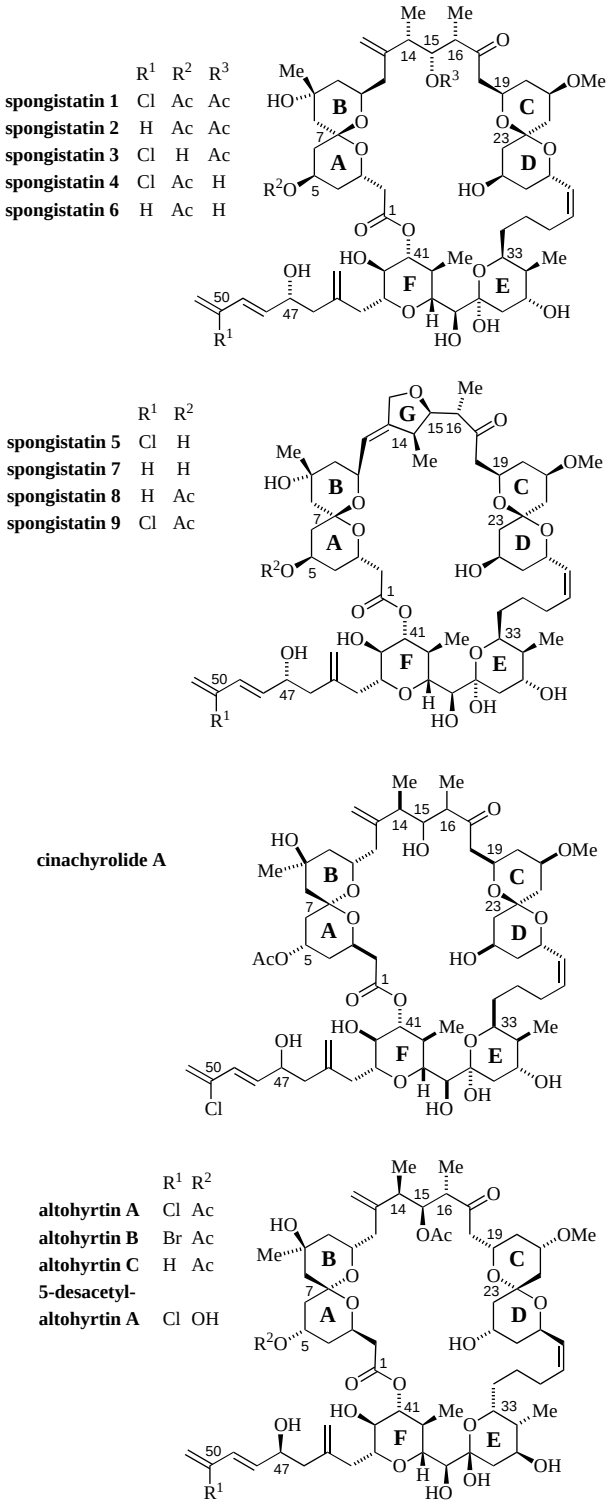
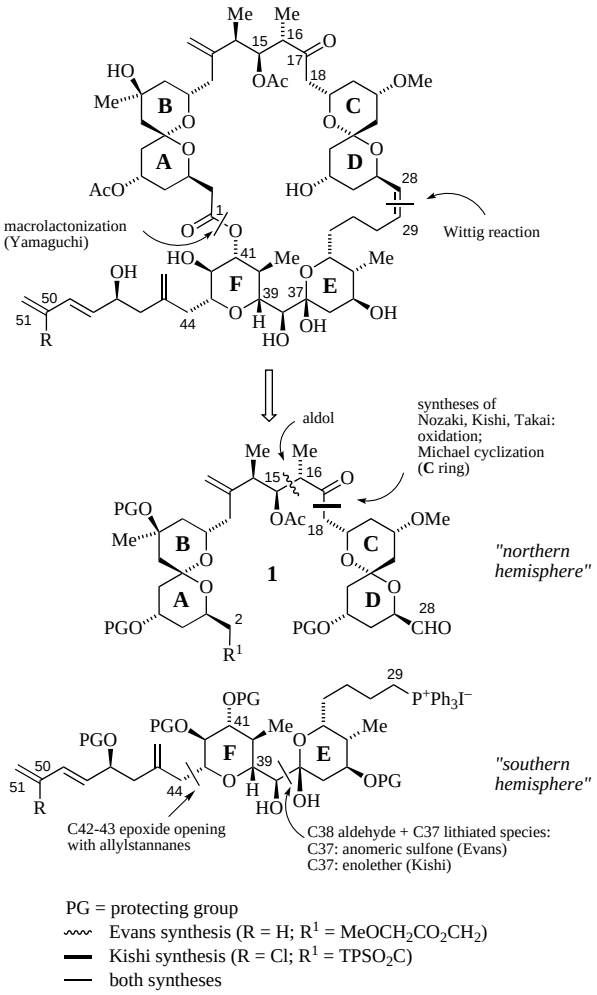


Figure 1. Structures originally proposed for the marine macrolides spongistatin 1 – 9,[4a, 5] cinachyrolide A,[4b] altohyrtin A – C, and 5-desacetylaltohyrtin A.[4c, 6]

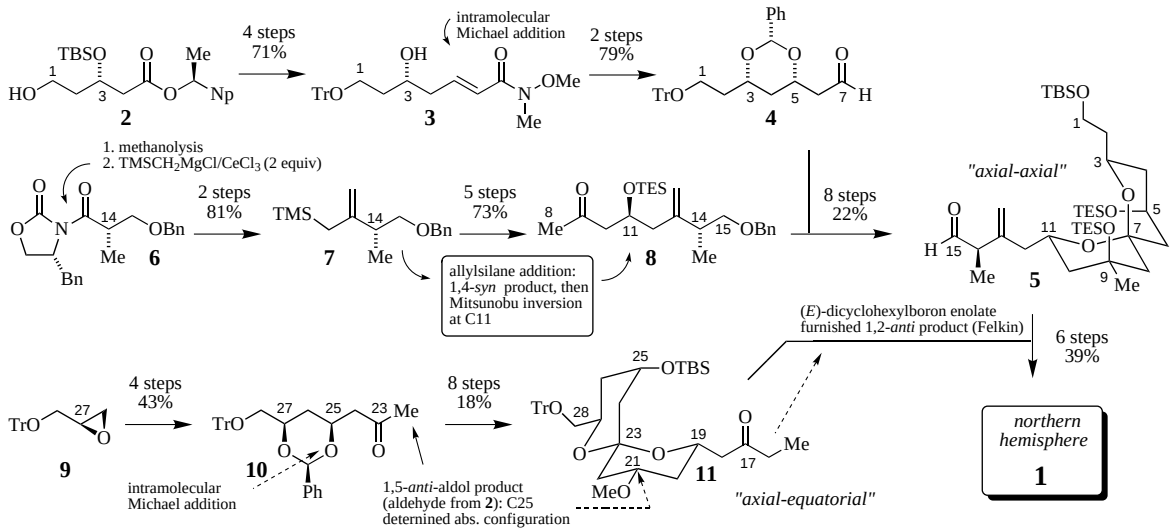


Scheme 1. Retrosynthesis of altohyrtin A and C. TPS = *tert*-butyldiphenylsilyl.

from chiral building block **2**—which is readily available by selective opening of a protected 3-hydroxyglutamic acid anhydride with a chiral alcohol (1-(2-naphthyl)ethanol)—the convergent construction of the carbon skeleton C1 – C15 began. Reduction and Wittig reaction yielded the hydroxamic acid derivative **3**. The newly formed stereogenic center at C5 was then introduced with a highly diastereoselective, intramolecular Michael addition (1,3-*syn*) of a hemiacetal (from **3**, PhCHO, KO*t*Bu) to the α,β-unsaturated carbonyl compound. Reduction with diisobutylaluminium hydride (DIBALH) furnished aldehyde **4** in a high overall yield. The second building block (C8 – C15) was synthesized from oxazolidinone **6**. Through a nice sequence first the allylsilane **7** was formed, which in turn was selectively (1,4-*syn*) added to the suitably protected aldehyde. The right configuration at C11 was obtained after Mitsunobu inversion. Aldol addition of a boron enolate obtained from ketone **8** to aldehyde **4** gave the *AB* fragment in the open-chain form; after oxidation of the alcohol (C7) and acidic liberation of the hydroxyl groups at C1, C3, C5, and C11, a spontaneous spiroketalization occured. In this case the thermodynamically favored "axial – axial" anomer was isolated (anomeric stabilization; equatorial substituents at C3 and C11; the axial hydroxyl groups at C5 can further stabilize this product through formation of hydrogen bonds to ring oxygen atoms).

Only at this stage was the tertiary center C9 formed; the nucleophilic attack (with methyllithium/cerium trichloride) occurred diastereoselectively from the lower face. For the synthesis of the *CD* spiroketal very similar building blocks

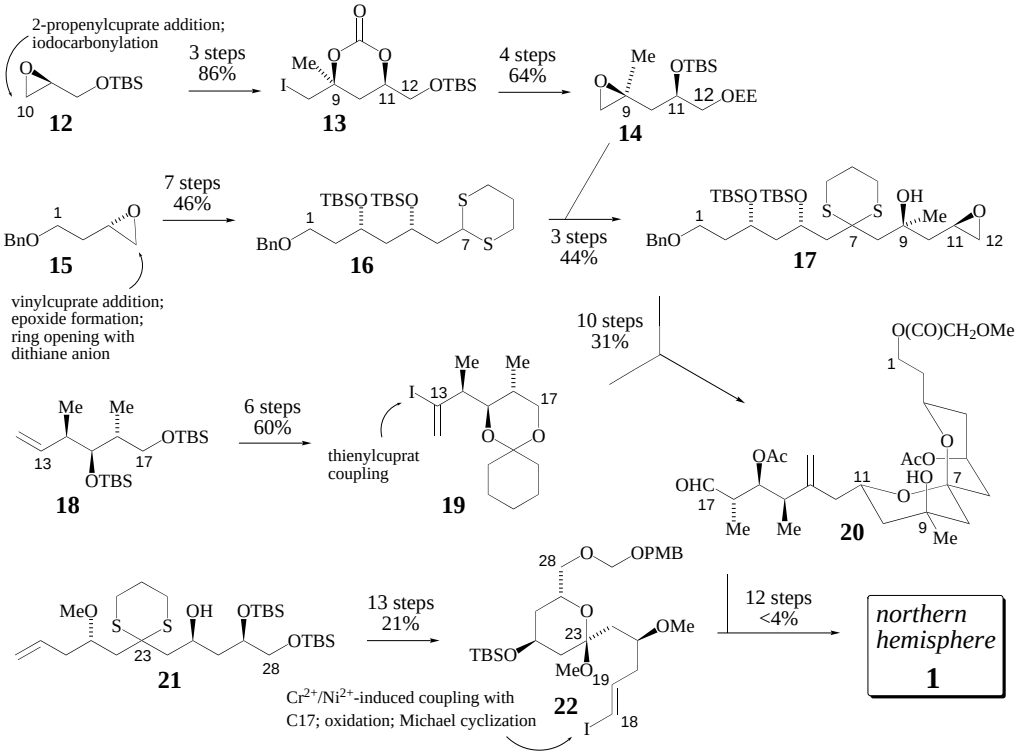
 © WILEY-VCH Verlag GmbH, D-69451 Weinheim, 1998 1433-7851/98/03719-2630 $ 17.50+.50/0



Scheme 2. Synthesis of the northern hemisphere of altohyrtin C according to Evans et al.[7a, c] Bn = benzyl, Np = 2-naphthyl, TBS = *tert*-butyldimethylsilyl, TES = triethylsilyl, TMS = trimethylsilyl, Tr = trityl = triphenylmethyl.

and concepts were used. Again, key steps were the well-established intramolecular Michael addition (chain extension of epoxide **9**, then 1,3-*syn* addition of a hemiacetal to the α,β-unsaturated compound) and a 1,5-*anti* aldol addition of ketone **10** to an aldehyde, which is, for instance, available from **2** through oxidation. The configuration at C21 was exclusively determined by the configuration at C25; that at C19 had no influence at all. The spiroketalization proved problematic since in this case the axial – equatorial product **11** was needed. After equilibration with $Mg(O_2CCF_3)_2$ in CF_3CO_2H/CH_2Cl_2 the desired spiro product could be obtained in a 2.2:1 ratio. The synthesis of the northern hemisphere **1** was completed after the selective aldol addition of the (*E*)-dicyclohexylboron enolate derived from keton **11** to the C1 – C15 fragment **5**. Ingenious manipulations of the protecting groups enabled, among others, the acetylation of the hydroxyl group at C5.

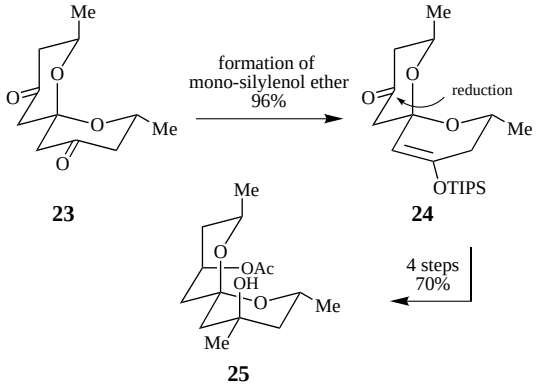
The Kishi group followed a different approach (Scheme 3). Starting from epoxides **12** and **15** the carbon skeleton C1 – C12 was obtained after repeated dithiane coupling. In the second step the dithiane adduct **16** was added to epoxide **14**. With this, oxirane **17** was synthesized, and the C1 – C17 fragment was furnished after a cuprate coupling with vinyl iodide **19** (obtained from alkene **18**). Manipulation of the protecting groups and spiroketalization (*N*-iodosuccinimide-induced dithiane cleavage) to the *AB* spiroketal proved unproblematic. Finally, Dess – Martin periodinane oxidation led to aldehyde **20**. For the synthesis of the C18 – C28 fragment, the group again relied on the dithiane method. Compound **21** is readily available from the corresponding enantiomerically pure epoxides. However, the spiroketal was not directly synthesized from this intermediate; instead only



Scheme 3. Synthesis the northern hemisphere of altohyrtin A according to Kishi et al.[8a] EE = ethoxyethyl, PMB = *p*-methoxybenzyl.

the *D* ring of altohyrtin A with a suitable vinyl iodide grouping in the side chain (**22**) was formed. As described above, an interesting sequence followed, starting with the transition metal induced coupling of vinyl iodide **22** to aldehyde **20**. Oxidation to the ketone (C17) and intramolecular Michael cyclization yielded only one of the four possible diastereomers. Whereas the configuration at C19 proved to be correct, the spiro center was wrongly configured. After epimerization the desired spiroketal was obtained in 50% yield. Further manipulation of the protecting group and selective oxidations of the side-chains provided the suitably protected northern hemisphere **1**.

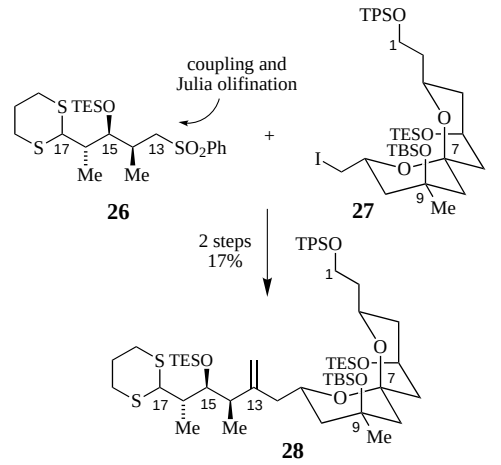
Similar strategies for the formation of the spiroketals were followed by other groups as well.[9, 10, 11a, c, d, 12b, c] In a model study Heathcock and co-workers[9a] have established an efficient entry to the *AB* ring system (Scheme 4). Startin



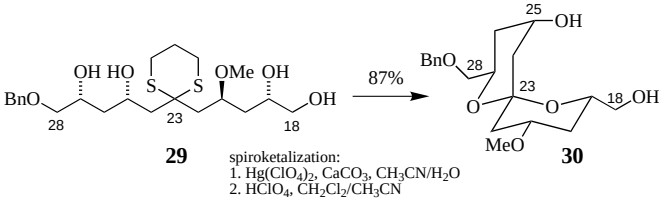
Scheme 4. Synthesis of the *AB* model spiroketal **25** according to Heathcock et al.[9a] TIPS = triisopropyl.

gfrom the readily available C_2-symmetric spiro diketone **23** a diastereoselective functionalization via the monosilyl enolether **24** to product **25** could be achieved. The one-pot dithiane method for the synthesis of acyclic precursors of the spiroketals has been intensively used by the Smith group. To introduce the C13–C17 side chain, this research group proposed a nice variation that unfortunately led to product formation in relatively unsatisfactory yield:[12c] Alkylation of sulfone **26** (C13) with iodide **27** was followed by a Julia olefination and thus the formation of the exocyclic double bond at C13 (**28**, Scheme 5). One problem for both reported total syntheses is the unusual configuration at C23 of the *CD* spiroketal. Smith and co-workers showed that the presence of calcium ions can play a critical, constructive role. Presumably, they promote the selective, acid-catalyzed spiroketalization of dithiane **29** to the desired product **30** (Scheme 6).[12b] Surprisingly, Paquette et al. observed no complications with this reaction. Silylation of alcohol **31** and deprotection of the hydroxyl groups at C19 and C27 were reported to spontaneously yield spiroketal **32** (Scheme 7).[10b]

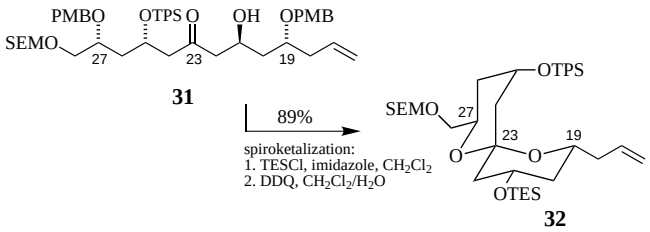
The synthesis of the southern hemisphere from Evans et al. is summarized in Scheme 8.[7b] The *E* ring was synthesized from the readily available hydroxamic acid derivative **33**. The stereogenic center at C35 of thioester **34** was formed by a Felkin-selective aldol addition of a thioketene acetal to an



Scheme 5. Sulfone strategy for the coupling of the side chain to the *AB* ring system according to Smith et al.[12c]



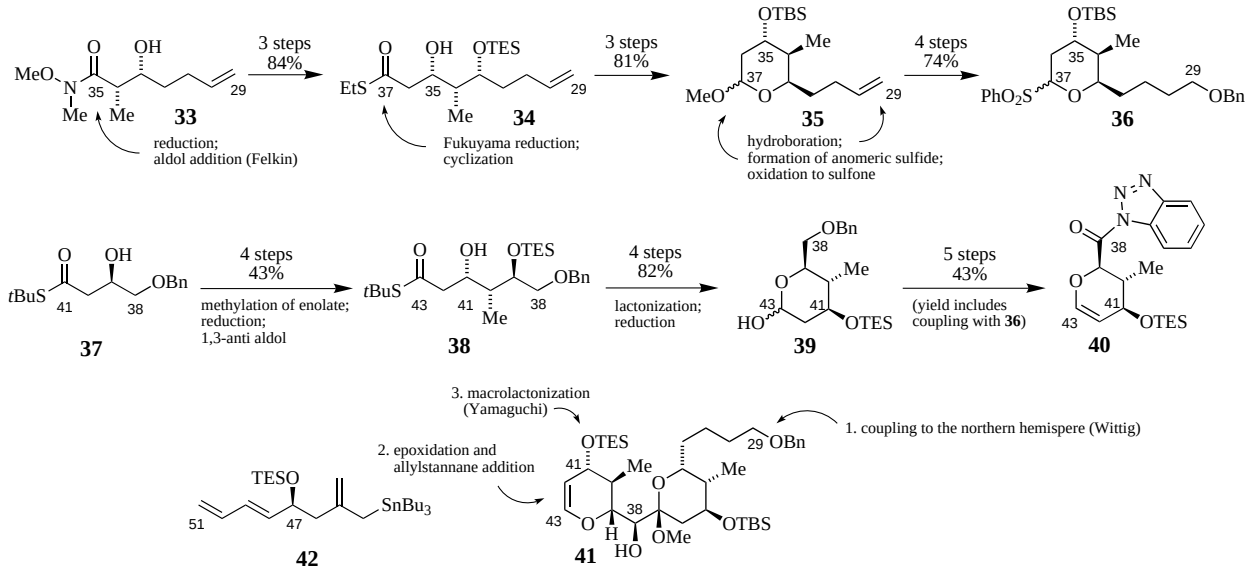
Scheme 6. Calcium ion induced selective spiroketalization according to Smith et al.[12b]



Scheme 7. Selective formation of the *CD* spiroketal **32** according to Paquette et al.[10b] SEM = 2-(trimethylsilyl)ethoxymethyl.

aldehyde, which had been synthesized by reduction of **33** with DIBALH. Mild reduction utilizing Fukuyama conditions (Lindlar catalyst, Et_3SiH, 1-hexene, acetone) followed by acidic hydrolysis of the silyl protecting group and concomitant cyclization furnished, after silylation, the methyl pyranoside **35**. The anomeric sulfone **36** was synthesized in four steps from **35**. A similar route was possible for synthesizing the *F* ring (**37** → **38**). The hemiacetal **39** was formed after desilylation, Ag^I mediated lactonization, DIBALH reduction, and silylation. Elimination to form the enolether and oxidation at C38 furnished, after debenzylation, an aldehyde that should have been a suitable coupling partner for sulfone **36**. However, all attempts failed, and the desired product was obtained only after use of the activated benzotriazolylamide **40**. The sulfone group was then transformed to the methyl pyranoside and, after reduction ($KBHEt_3$) to the alcohol (C38), building block **41** was isolated. This compound was successfully coupled with the northern hemisphere by a Wittig reaction (C29); diastereoselective epoxidation with dimethyl dioxirane

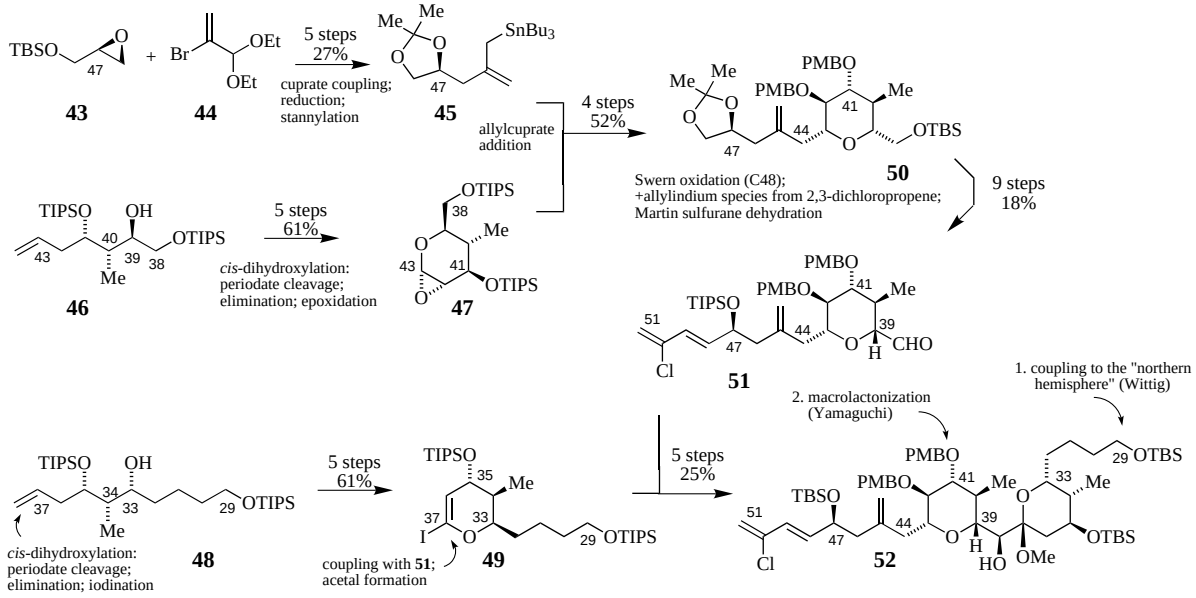
 © WILEY-VCH Verlag GmbH, D-69451 Weinheim, 1998 1433-7851/98/03719-2632 $ 17.50+.50/0



Scheme 8. First total synthesis of altohyrtin C according to Evans et al.[7b, c]

(C42 – C43) and Lewis acid catalyzed ring opening with allylstannane **42** introduced the C44 – C51 side chain. The Yamaguchi macrolactonization was surprisingly very selective: Although both the hydroxyl groups at C41 and C42 were not protected, this reaction gave a single product in high yield (86 %). Final manipulation of the protecting groups led to the isolation of altohyrtin C, a compound that, after comparison of all spectral data, proved to be identical with spongistatin 2.[7c]

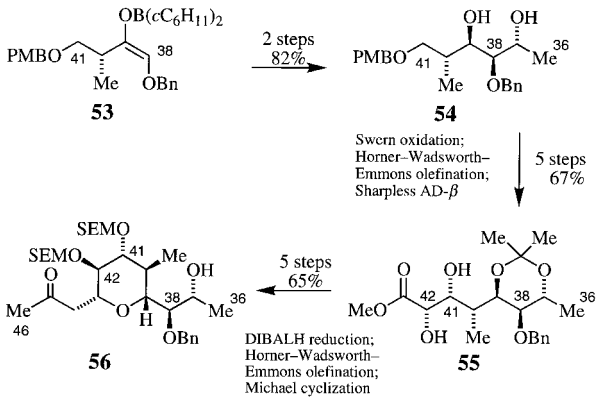
The alternative approach to the southern hemisphere from Kishi and co-workers is described in Scheme 9.[8b] As mentioned above, the side chain C44 – C51 was brought in at an early stage; the stereogenic center at C47 was already present in the starting oxirane **43**, which was obtained by Sharpless epoxidation. Cuprate coupling with vinyl bromide **44** and introduction of the tributylstannyl group yielded intermediate **45**. The *F* ring was formed starting from protected triol **46**. A typical sequence consists of a *cis*-dihydroxylation of the alkene and periodate cleavage to the aldehyde with spontaneous formation of the hemiacetal. After elimination and treatment of the enolether with dimethyl dioxirane, epoxide **47** was obtained. A similar sequence was used for the *E* ring fragment (**48** →**49**). The starting materials **46** and **48** were also accessible by reliable methods: In each case addition of Brown crotylboranes to the appropriate achiral aldehydes (C39 or C33) resulted in the formation of two new stereogenic centers (C39, C40 and C33, C34, respectively), and the corresponding enantiomerically pure alkenes were isolated. Degradation of the double bonds to the aldehydes and repeated addition of allylborane furnished **46** and **48**. After coupling of the allyl compound **45** (transmetalation to the



Scheme 9. First total synthesis of altohyrtin A according to Kishi et al.[8b]

cuprate) with epoxide **47**, the synthesis of the side chain was completed in nine steps (**50** →**51**). The aldehyde obtained was directly suitable for the finishing synthesis of the southern hemisphere. It must be pointed out that at this stage, with the addition of the allylindium species derived from 2,3-dichloropropene, the decision for the synthesis of either altohyrtin A, B, or C was made. The final steps to the C29 – C51 building block **52** were initiated by direct reaction of the C37-lithiated species **49** ($MgBr_2$ additive) with aldehyde **51**; the detour via the activated ester was in this case not necessary. The formation of the methyl pyranoside (C37) was accomplished by iodomethanolysis and reductive dehalogenation in the presence of bromobenzene (to prevent reaction of the vinyl chloride). After preparation of the Wittig salt (C29) and coupling with the northern hemisphere the synthesis was successfully completed by the macrolactonization. Spectroscopic analysis proved that the compound formed, altohyrtin A, and spongistatin 1 were identical.

Further synthetic work on the southern hemisphere was reported by Smith and co-workers[12a]—who very effectively used dithiane methodology and Julia olefination (methylenation at C45) to synthesize the entire building block—and Paterson et al. (Scheme 10).[11b] The latter group approached



Scheme 10. Synthesis of the *F* ring of the southern hemisphere according to Paterson et al.[11b]

the synthesis of the *EF* ring in a completely different way. Whereas all the other groups coupled the rings to form the C37 – C38 bond, Paterson and co-workers synthesized the carbon chain C36 – C41 at an early stage by aldol addition of boron enolate **53** to acetaldehyde (→**54**). Two more stereogenic centers (C41 and C42) were introduced by selective asymmetric Sharpless dihydroxylation after chain extension (Swern oxidation, Horner – Wadsworth – Emmons olefination). The ester **55** was subsequently transformed to the substituted *F* Ring **56**. It might be advantageous that the stereochemistry at C38 was determined at an early step, whereas the side chain C47 – C51 could be coupled at a later stage and with high flexibility. The future will show whether this synthetic plan is effective.

Biological Aspects

To sum up the first two successful total syntheses by the research groups of Evans and Kishi, it should be noted that the spectial merit of the approach of Evans et al. lies not only in the efficient application of methods developed in the group, but also in the convergence and flexibility (longest linear chain: 32 steps starting from **6**, ≈0.7% yield; synthesis by Kishi: 37 steps, ≈0.01% total yield starting from **12**). In the future the physiological activity and the potential application in cancer therapy will be at the center of interest. The outstanding GI values (Table 1) are certainly impressive, but reports on the selectivity for tumor cells and other cells are still lacking. In vitro tests proved that spongistatins efficiently inhibit mitosis by binding to tubilin and blocking microtubule assembly. It was found that at least three different, characteristic binding sites to the tubulin dimer must be present.[5f] First investigations of structure – activity relationships by Hamel

Table 1. Data of the macrolides spongistatin 1 – 9,[a] cinachyrolide A, altohyrtin A – C, and 5-desacetylaltohyrtin A

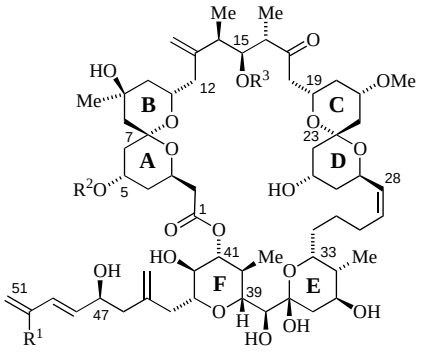
Compound	Yield (isolated prod.)	Bioassay (cel line)	Cytotoxicity
spongistatin 1[a]	3.5×10^{-6} % 13.8 mg[b]	P388	GI_{50} $2.5-3.5\times10^{-11}$ M[f] GI_{50} 1.3×10^{-10} M[g] IC_{50} 5.3×10^{-6} M[h] IC_{50} 3×10^{-11} M[i],[5f]
spongistatin 2[a]	1×10^{-6} % 4.34 mg[b]	P388	GI_{50} 8.51×10^{-10} M[g] IC_{50} 4.6×10^{-6} M[h] IC_{50} 2×10^{-9} M[i],[5f]
spongistatin 3	6.7×10^{-7} % 2.69 mg[b]	P388	GI_{50} 8.32×10^{-10} M[g] IC_{50} 1.3×10^{-5} M[h] IC_{50} 1×10^{-9} M[i],[5f]
spongistatin 4	4.4×10^{-7} % 10.7 mg[c]	P388	GI_{50} 1.0×10^{-10} M[g] IC_{50} 5.1×10^{-6} M[h] IC_{50} 1×10^{-10} M[i],[5f]
spongistatin 5	5.4×10^{-7} % 12.9 mg[c]	P388	GI_{50} 1.2×10^{-10} M[g] IC_{50} 6.7×10^{-6} M[h] IC_{50} 2×10^{-10} M[i],[5f]
spongistatin 6	3.5×10^{-7} % 8.4 mg[c]	P388	GI_{50} 1.1×10^{-9} M[g] IC_{50} 4.4×10^{-6} M[h] IC_{50} 8×10^{-10} M[i],[5f]
spongistatin 7	2.2×10^{-7} % 5.4 mg[c]	P388	GI_{50} 1.0×10^{-9} M[g] IC_{50} 5.3×10^{-6} M[h] IC_{50} 2×10^{-9} M[i],[5f]
spongistatin 8	7.5×10^{-8} % 1.8 mg[c]	P388	GI_{50} 2.3×10^{-10} M[g] IC_{50} 5.5×10^{-6} M[h] IC_{50} 3×10^{-9} M[i],[5f]
spongistatin 9	2.2×10^{-7} % 5.4 mg[c]	P388	GI_{50} 4.0×10^{-11} M[g] IC_{50} 4.2×10^{-6} M[h] IC_{50} 3×10^{-10} M[i],[5f]
cinachyrolide A	1.7×10^{-5} % 1.1 mg[d]	L1210	IC_{50} $<6\times10^{-10}$ g mL^{-1}[i],[4b]
altohyrtin A[a]	6.9×10^{-6} % 7.6 mg[e]	L1210 KB	IC_{50} 3×10^{-11} g mL^{-1}[i] IC_{50} 1×10^{-11} g mL^{-1}[j],[4c]
altohyrtin B	4×10^{-7} % 0.5 mg[e]	L1210 KB	IC_{50} 3×10^{-11} g mL^{-1}[i] IC_{50} 2×10^{-11} g mL^{-1}[j],[6a]
altohyrtin C[a]	4×10^{-7} % 0.5 mg[e]	L1210 KB	IC_{50} 1.3×10^{-9} g mL^{-1}[i] IC_{50} 4×10^{-10} g mL^{-1}[j],[6a]
5-desacetyl altohyrtin A	4.2×10^{-6} % 4.7 mg[e]	L1210 KB	IC_{50} 3.3×10^{-9} g mL^{-1}[i] IC_{50} 3×10^{-10} g mL^{-1}[j],[6a]

[a] Spongistatin 1 and altohyrtin A as well as spongistatin 2 and altohyrtin C are identical.[8b, 7c] [b] From 400 kg (wet weight) of *Spongia sp*.[5a] [c] From 2409 kg (wet weight) of *Spirastella spinispirulifera*.[5b–d] [d] From 6.6 kg (wet eight) of *Cinachyra sp*.[4b] [e] From 112 kg (wet weight) of *Hyrtios altum*.[4c, 6] [f] Typical values for a subgroup of especially chemoresistent tumor types in the NCI test.[4a] [g] All 60 cancer cell lines of the standard screen of the NCI were considered.[5f] [h] Inhibition of the glutamate-induced polymerization of tubuline.[5f] [i] Inhibition of the L1210 cell growth. [j] Inhibition of the KB cell growth.

 © WILEY-VCH Verlag GmbH, D-69451 Weinheim, 1998 1433-7851/98/03719-2634 $ 17.50+.50/0

et al. with the different spongistatins provided no evidence of crucial functionalities.[5f] This result fits very well to the observation made by Kishi et al., namely, that C23-*epi*-altohyrtin A is highly cytotoxic as well.[8b] To obtain more detailed information, especially in view of in vivo tests and possible medical applications, larger quantities of these compounds are a prerequisite. This is certainly a dilemma in the case of active substances of marine origin; the isolation from tons of sponges is only partly justifiable for ecological reasons, a large-scale cultivation does not seem to be possible at present. As long as the isolation of the genes is still wishful thinking, total synthesis remains the only possibility for obtaining sufficient amounts of the desired compound for further systematic investigations—for the reported cytotoxicity a few grams should be more then enough for a start. This still remains the aim of different research groups. A comparison of the altohyrtins and spongistatins with other natural antineoplastics indicates that there is strong competition. Commercially available drugs such as taxol or taxotere are established;[13] other compounds, for example, the epothilones, are impressive not only because of their excellent cytotoxicity test results, but especially because of their very economic accessability through the cultivation of myxobacteria.[14] The bryostatins, a relatively new class of marine macrolides, are in a way the competition in the own backyard, since the first clinical tests are already underway.[2, 15] A long list of further potential candidates could be easily made (see, for instance, ref. [2, 3]).

With the first total syntheses—and only these could at this stage prove it—the structures of the spongipyranes have been unequivocally established. The new proposed structures are summarized in Figure 2. The structures published by Kitagawa et al. have been confirmed, and the relationship to the spongistatins 1 and 2 was established. Inevitably, this leads to the (corrected) structures for the spongistatins 3, 4, and 6 and possibly for cinachyrolide A as well as spongistatins 5, and 7–9. Further total syntheses must and will follow to provide larger quantities of these fascinating substances in order to gain more insight into the clinical potential of these macrolides. Only then can the ultimate question of which route leads to sufficient amounts of a possible drug be answered.



	R^1	R^2	R^3
altohyrtin A, spongistatin 1	Cl	Ac	Ac
altohyrtin B	Br	Ac	Ac
altohyrtin C, spongistatin 2	H	Ac	Ac
5-desacetylaltohyrtin A, spongistatin 3	Cl	H	Ac
spongistatin 4, cinachyrolide A	Cl	Ac	H
spongistatin 6	H	Ac	H

Figure 2. Proposal for the new classification of the marine macrolides spongistatin 1–4, and 6, cinachyrolide A, altohyrtin A–C, and 5-desacetylaltohyrtin A.

German version: *Angew. Chem.* **1998**, *110*, 2773–2780

Keywords: altohyrtins · antitumor agents · natural products · spongistatins · total syntheses

[1] A collection of reviews is dedicated to marine natural products: *Chem. Rev.* **1993**, *93*, 1671–1944; D. J. Faulkner, *Nat. Prod. Rep.* **1997**, *14*, 259–302 (annual review), and references therein.

[2] G. R. Pettit, *Pure Appl. Chem.* **1994**, *66*, 2271–2281.

[3] R. D. Norcross, I. Paterson, *Chem. Rev.* **1995**, *95*, 2041–2114.

[4] a) G. R. Pettit, Z. A. Cichacz, F. Gao, C. L. Herald, M. R. Boyd, J. M. Schmidt, J. N. A. Hooper, *J. Org. Chem.* **1993**, *58*, 1302–1304; b) N. Fusetani, K. Shinoda, S. Matsunaga, *J. Am. Chem. Soc.* **1993**, *115*, 3977–3981; c) M. Kobayashi, S. Aoki, H. Sakai, K. Kawazoe, N. Kihara, T. Sasaki, I. Kitagawa, *Tetrahedron Lett.* **1993**, *34*, 2795–2798.

[5] a) G. R. Pettit, Z. A. Cichacz, F. Gao, C. L. Herald, M. R. Boyd, *J. Chem. Soc. Chem. Commun.* **1993**, 1166–1168; b) G. R. Pettit, C. L. Herald, Z. A. Cichacz, F. Gao, J. M. Schmidt, M. R. Boyd, N. D. Christie, F. E. Boettner, *J. Chem. Soc. Chem. Commun.* **1993**, 1805–1807; c) G. R. Pettit, C. L. Herald, Z. A. Cichacz, F. Gao, M. R. Boyd, N. D. Christie, J. M. Schmidt, *Nat. Prod. Lett.* **1993**, *3*, 239–244; d) G. R. Pettit, Z. A. Cichacz, C. L. Herald, F. Gao, M. R. Boyd, J. M. Schmidt, E. Hamel, R. Bai, *J. Chem. Soc. Chem. Commun.* **1994**, 1605–1606; e) R. Bai, Z. A. Cichacz, C. L. Herald, G. R. Pettit, E. Hamel, *Mol. Pharmacol.* **1993**, *44*, 757–766; f) R. Bai, G. F. Taylor, Z. A. Cichacz, C. L. Herald, J. A. Kepler, G. R. Pettit, E. Hamel, *Biochemistry* **1995**, *34*, 9714–9721.

[6] a) M. Kobayashi, S. Aoki, H. Sakai, N. Kihara, T. Sasaki, I. Kitagawa, *Chem. Pharm. Bull.* **1993**, *41*, 989–991; b) M. Kobayashi, S. Aoki, I. Kitagawa, *Tetrahedron Lett.* **1994**, *35*, 1243–1246; c) M. Kobayashi, S. Aoki, K. Gato, I. Kitagawa, *Chem. Pharm. Bull.* **1996**, *44*, 2142–2149.

[7] a) D. A. Evans, P. J. Coleman, L. C. Diaz, *Angew. Chem.* **1997**, *109*, 2951–2954; *Angew. Chem. Int. Ed. Engl.* **1997**, *36*, 2737–2741; b) D. A. Evans, B. W. Trotter, B. Côté, P. J. Coleman, *Angew. Chem.* **1997**, *109*, 2954–2957; *Angew. Chem. Int. Ed. Engl.* **1997**, *36*, 2741–2744; c) D. A. Evans, B. W. Trotter, B. Côté, P. J. Coleman, L. C. Dias, A. N. Tyler, *Angew. Chem.* **1997**, *109*, 2957–2961; *Angew. Chem. Int. Ed. Engl.* **1997**, *36*, 2744–2747.

[8] a) J. Guo, K. J. Duffy, K. L. Stevens, P. I. Dalko, R. M. Roth, M. M. Hayward, Y. Kishi, *Angew. Chem.* **1998**, *110*, 198–202; *Angew. Chem. Int. Ed.* **1998**, *37*, 187–190; b) M. M. Hayward, R. M. Roth, K. J. Duffy, P. I. Dalko, K. L. Stevens, J. Guo, Y. Kishi, *Angew. Chem.* **1998**, *110*, 202–206; *Angew. Chem. Int. Ed.* **1998**, *37*, 190–196.

[9] a) M. M. Claffey, C. H. Heathcock, *J. Org. Chem.* **1996**, *61*, 7646–7647; b) C. J. Hayes, C. H. Heathcock, *J. Org. Chem.* **1997**, *62*, 2678–2679.

[10] a) L. A. Paquette, D. Zuev, *Tetrahedron Lett.* **1997**, *38*, 5115–5118; b) L. A. Paquette, A. Braun, *Tetrahedron Lett.* **1997**, *38*, 5119–5122.

[11] a) I. Paterson, R. M. Oballa, R. D. Norcross, *Tetrahedron Lett.* **1996**, *37*, 8581–8584; b) I. Paterson, L. E. Keown, *Tetrahedron Lett.* **1997**, *38*, 5727–5730; c) I. Paterson, R. M. Oballa, *Tetrahedron Lett.* **1997**, *38*, 8241–8244; d) I. Paterson, D. J. Wallace, K. R. Gibson, *Tetrahedron Lett.* **1997**, *38*, 8911–8914; e) a synthesis of the C1–28 segment has been finished recently: I. Paterson, personal communication.

[12] a) A. B. Smith III, L. Zhuang, C. S. Brook, A. M. Boldi, M. D. McBriar, W. H. Moser, N. Murase, K. Nakayama, P. R. Verhoest, Q. Lin, *Tetrahedron Lett.* **1997**, *38*, 8667–8670; b) A. B. Smith III, L.

 © WILEY-VCH Verlag GmbH, D-69451 Weinheim, 1998 1433-7851/98/03719-2635 $ 17.50+.50/0

Zhuang, C. S. Brook, Q. Lin, W. H. Moser, R. E. Lee Trout, A. M. Boldi, *Tetrahedron Lett.* **1997**, *38*, 8671–8674; c) A. B. Smith III, Q. Lin, K. Nakayama, A. M. Boldi, C. S. Brook, M. D. McBriar, W. H. Moser, M. Sobukawa, L. Zhuang, *Tetrahedron Lett.* **1997**, *38*, 8675–8678; d) the synthesis of a C39–C51 model compound and the corresponding cytotoxicities were recently reported: A. B. Smith III, Q. Lin, G. R. Pettit, J.-C. Chapuis, J. M. Schmidt, *Bioorg. Med. Chem. Lett.* **1998**, *8*, 567–568.

[13] K. C. Nicolaou, W.-M. Dai, R. K. Guy, *Angew. Chem.* **1994**, *106*, 38–69; *Angew. Chem. Int. Ed. Engl.* **1994**, *33*, 15–44, and references therein.

[14] a) G. Höfle, N. Bedorf, H. Steinmetz, D. Schomburg, K. Gerth, H. Reichenbach, *Angew. Chem.* **1996**, *108*, 1671–1673; *Angew. Chem. Int. Ed. Engl.* **1996**, *35*, 1567–1569; b) L. Wessjohann, *Angew. Chem.* **1997**, *109*, 739–742; *Angew. Chem. Int. Ed. Engl.* **1997**, *36*, 739–742, and references therein.

[15] G. R. Pettit, *Prog. Chem. Org. Nat. Prod.* **1991**, *57*, 153–195, and references therein.

New Developments in Nitrogen Fixation

Felix Tuczek* and Nicolai Lehnert

The prospect of producing ammonia from dinitrogen at room temperature and ambient pressure in analogy to nature has fascinated coordination chemists for a long time. Modeling the conditions present in the enzyme with low-molecular weight compounds, however, is extremely difficult in this case. So far, the iron–molybdenum cofactor (FeMoco), which is the center of bonding and reduction of dinitrogen in the enzyme nitrogenase,[1] has not been synthesized.[2] Furthermore, this cofactor does not bind N_2 in isolated form. It therefore appears more promising to realize a catalytic cycle based on the mono- and binuclear transition metal N_2 compounds that give NH_3 or N_2H_4 upon protonation. On the other hand, a "biomimetic" approach is important for understanding aspects of the function of the enzyme on a molecular level.[3] The results of these two different research directions, however, have always been considered as closely related.

Through coordination to one or more metal centers, the dinitrogen ligand, which is extremely inert in free form, acquires a different degree of "activation" (Figure 1).[4] In principle, systems suitable for protonation reactions are those with "moderate" to "strong" activation as well as compounds which cleave the N_2 molecule upon coordination. However, if the aim is to achieve relevance to the biological process, "mild" conditions are important. "Nonactivated" systems, although not protonable, may also provide information fundamental to an understanding of the metal–N_2 bond. Besides the two mentioned, central problems, "nitrogen fixation" also involves reactions of the dinitrogen ligand or its partly reduced, complex-bound derivatives leading to the incorporation of nitrogen from N_2 into (mostly organic) compounds. Recently, there has been important progress in each of these areas, which will be reported here in the order of increasing activation of N_2.

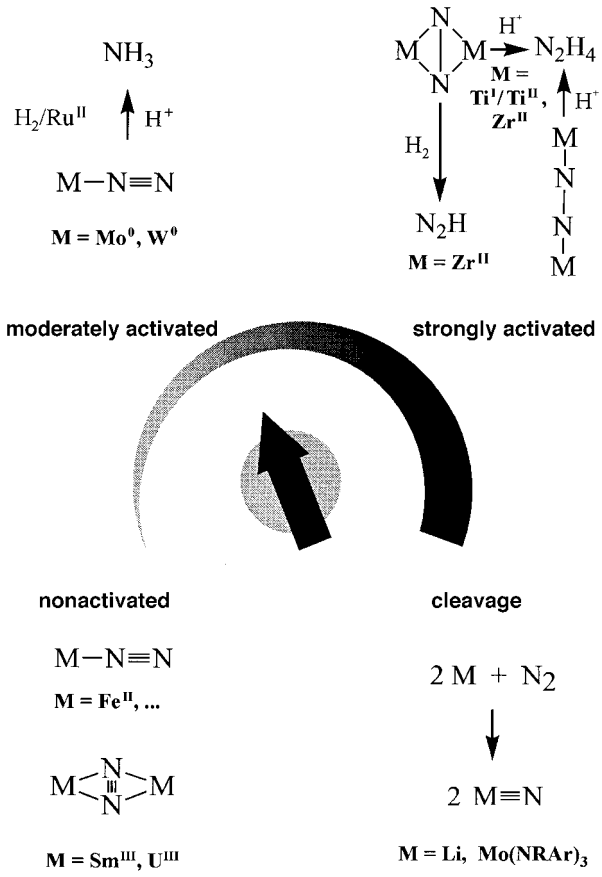


Figure 1. "Tuning" the activation of the N_2 ligand by the choice of the coordinating metal. The activation scale may be divided into four regimes; typical representatives mentioned in the text are indicated. The arrow points to the minimal degree of activation necessary for protonation.

N_2-containing systems in which the N–N distances are similar to that in free dinitrogen are termed "nonactivated" and are found among compounds exhibiting an *end-on* coordination of N_2 to transition metals, for example Fe^{II}. It appears that there is now a further bonding mode possible in this category: the nonactivating *side-on* coordination to lanthanide and actinide centers. Up to now, this bonding mode had been known only for a Sm^{III} complex.[5] The recent isolation and structural characterization of the *side-on* N_2-bridged complex $[\{U(NN_3')\}_2(\mu\text{-}\eta^2\text{:}\eta^2\text{-}N_2)]$ ($NN_3' = N(CH_2$

[*] Dr. habil. F. Tuczek, Dipl.-Chem. N. Lehnert
Institut für Anorganische und Analytische Chemie der Universität
Staudingerweg 9, D-55099 Mainz (Germany)
Fax: (+49) 6131-39-2990
E-mail: Tuczek@iacgu7.chemie.uni-mainz.de

 © WILEY-VCH Verlag GmbH, D-69451 Weinheim, 1998 1433-7851/98/03719-2636 $ 17.50+.50/0

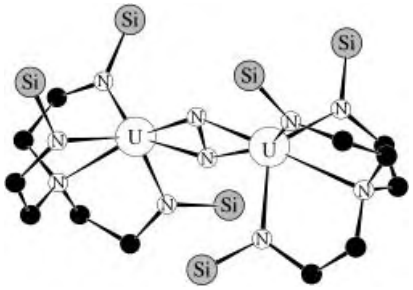


Figure 2. The complex $[\{U(NN'_3)\}_2(\mu\text{-}\eta^2\text{:}\eta^2\text{-}N_2)]$ ($NN'_3 = N(CH_2CH_2NSiBu^tMe_2)_3$); the terminal residues on the silyl groups are omitted for clarity.

$CH_2NSiBu^tMe_2)_3$; Figure 2), however, proved that actinides are also able to bind dinitrogen in this geometry.[6] The N–N distance of 1.109(7) Å is comparable to that in free N_2 (1.0975 Å). This is in sharp contrast to the *side-on*- or *edge-on*-bridged complexes of the early transition metals such as titanium and zirconium which belong to the most highly activated N_2 compounds (see below). While the reduction of N_2 in these systems is caused by electron donation from the metals into the *antibonding* π^* orbitals of this ligand (Figure 3), the *side-on* coordination in the lanthanide and actinide systems is probably due to a σ-donor interaction of the *bonding* π^b orbital. The exact nature of this bond,

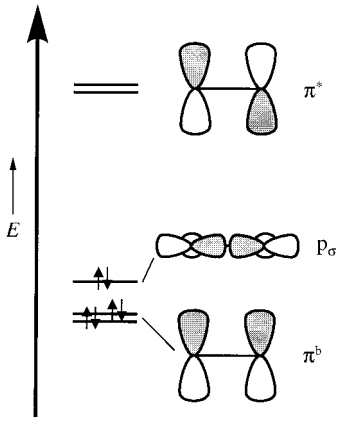
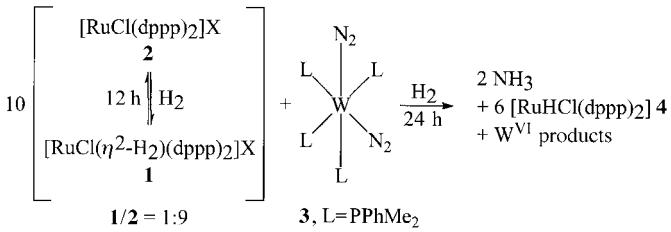


Figure 3. Frontier orbitals of the N_2 molecule.

however, is as yet not entirely understood. As the *side-on* mode is preferred over the much more common *end-on* coordination, the σ-donor interaction of p_σ with the metal must be energetically less favorable than the *side-on* coordination through π^b (Figure 3). Possibly this is a consequence of the extremely weak σ-donor capability of the N_2 ligand through p_σ which is also known from the complexes of the d-block metals.

"Moderately activated" systems are those which are protonable, but do not exhibit drastically increased N–N bond lengths (or lowered N–N stretching frequencies) over free N_2. Among this category are the *trans* and *cis*-dinitrogenmolybdenum and -tungsten complexes, some of which give NH_3 with mineral acids. In other cases, well-defined, complex-bound intermediates N_2H_x ($x = 1-3$) of the protonation to NH_3 can be isolated.[7–9] This chemistry, which is probably most relevant to nitrogenase, has now been extended by Hidai and co-workers who effected the protonation of the complex-bound N_2 not with mineral acids but with a H_2 complex, *trans*-$[RuCl(\eta^2\text{-}H_2)(dppp)_2]X$ (**1**) (dppp = 1,2-bis(diphenylphosphanyl)propane; X = PF_6, BF_4, OTf (OSO_2CF_3), BPh_4).[10] The H_2 complex **1** is slowly generated in situ from $[RuCl(dppp)_2]X$ (**2**) under H_2 (1 atm); compounds **1** and **2** are present under equilibrium conditions in the ratio 1:9 (Scheme 1). The N_2



Scheme 1. Synthesis of **1** (from **2**) and its reaction with **3** to give **4** and NH_3.

complex *cis*-$[W(N_2)_2(PMe_2Ph)_4]$ (**3**) reacts with a ninefold excess of this mixture under H_2 to give two equivalents of NH_3. In the most favorable case a 55% yield with respect to tungsten is achieved. The reaction mixture also contains $[RuHCl(dppp)_2]$ (**4**) as well as free PMe_2Ph-ligand. Since **4** does not bind H_2, however, the reaction cannot be made cyclic with respect to hydrogen.

Of particular interest with regard to this reaction is the problem of how the formation of the N–H bond proceeds: does the ruthenium–H_2 complex act as a metal acid; that is, is the N_2 ligand protonated in analogy to the reactions with mineral acids, or is there an initial, direct interaction between N_2 and H_2 mediated by the metal? The first possibility is supported by the fact that the H_2 complex **1** is markedly acidic ($pK_a = 4.4$). With a similar compound, protonation of the N_2 ligand in *trans*-$[W(N_2)_2(dppe)_2]$ (**5**) to the "hydrazido(2–)" stage had been evidenced before (dppe = 1,2-bis(diphenylphosphanyl)ethane).[11] This reaction as well as further reduction of "hydrazido(2–)" to NH_3 can likewise be achieved with the mixture of **1** and **2**. Also in favor of a close mechanistic relationship between the protonation with mineral acids and the Ru^{II}-mediated reaction with H_2 is the observation that the nature of the counterion X strongly influences the yield of NH_3. Finally, the presence of free phosphane in the reaction mixture indicates that in the later stages of the protonation reaction phosphane ligands are lost as well. The alternative mechanism, N–H bond formation through interaction between N_2 and H_2, has recently been demonstrated by Fryzuk et al. for a Zr^{II} $\mu\text{-}\eta^2\text{:}\eta^2\text{-}N_2$ complex.[12] In contrast to the reaction system of Nishibayashi et al., which requires *two* different metal centers for bonding and activation of N_2 and H_2, both molecules are bound to *one* complex in this case. However, the N_2 *side-on*- or *edge-on*-coordinating Zr^{II} and Ti^{I}/Ti^{II} complexes belong to the "strongly activated" systems (Figure 1);[13] besides the arrangement of both molecules in one ligand sphere, this high degree of activation certainly contributes to facilitating the reaction between N_2 and H_2.

If the reaction of the *cis* tungsten complex **3** with the mixture of **1** and **2** under H_2 (1 atm) is carried out in the presence of acetone, acetone-azine $Me_2C{=}N{-}N{=}CMe_2$ is

 © WILEY-VCH Verlag GmbH, D-69451 Weinheim, 1998 1433-7851/98/03719-2637 $ 17.50+.50/0

formed. It also should be possible to initiate other reactions of the Mo/W–N_2H_x complexes by protonation of the N_2 precursors with the H_2/Ru^{II} system. Recently, Mori et al. reported an alternative to incorporate nitrogen into organic substrates.[14] A solution of a Ti^{IV} compound TiX_4 (X = Cl, O*i*Pr) in THF was stirred with an excess of trimethylsilyl chloride (TMSCl) and Li under dry air for 24 h, hydrolyzed with 10% HCl, and made basic with K_2CO_3. If, for example, PhCOCl was added to this mixture, $PhCONH_2$ was obtained in 88% yield. N-heterocycles can also be synthesized in this way. The authors assume that intermediates of the type $[TiX_m\{N(TMS)_n\}_o]$ are formed. Thus, the catalytic function of titanium would not be involved in a fixation or activation of N_2, but rather in a bonding of amide which results from an initial cleavage of N_2 by lithium. Interestingly, the related formation of nitride from N_2 by transition metal complexes has been evidenced only recently.[15] These N_2-cleaving systems mark the upper end of the activation scale (Figure 1).

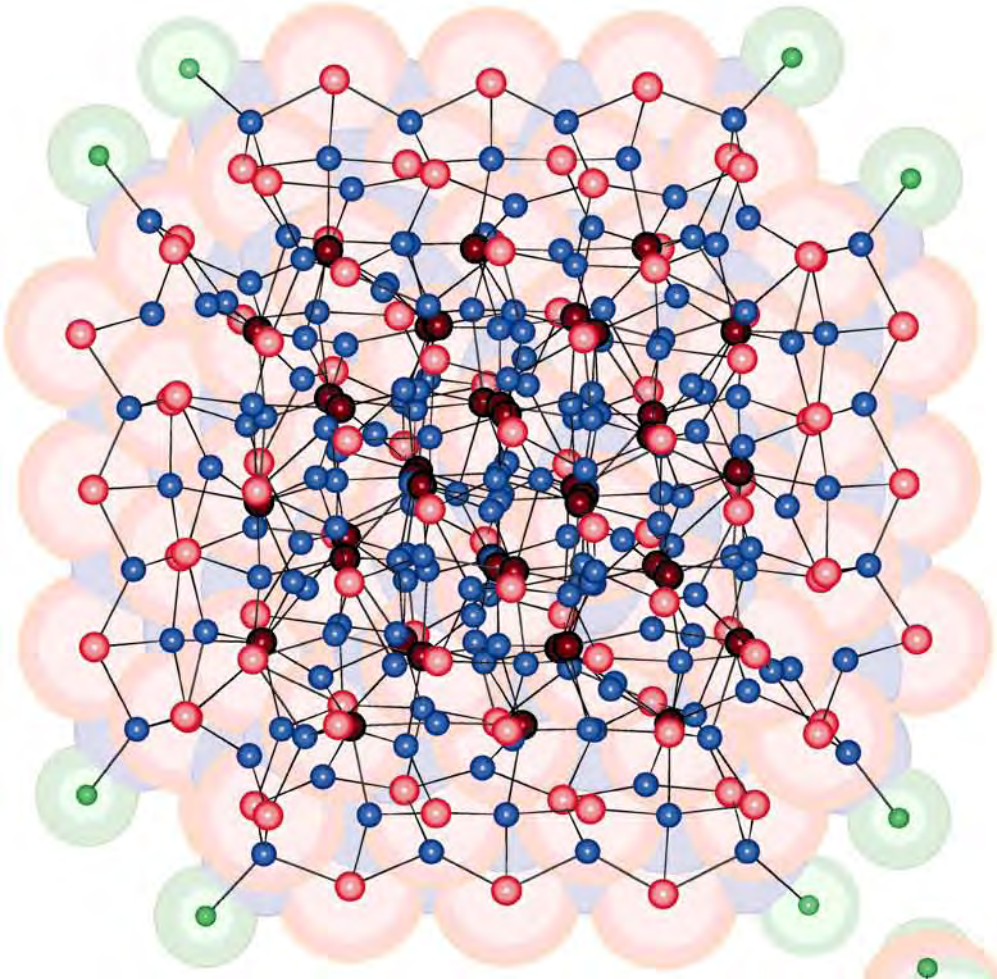
What is the significance of the reported studies with respect to the two goals mentioned initially, the understanding of nitrogenase activity and the realization of a corresponding catalytic cycle in vitro? First these results deepen our knowledge about the metal–N_2 bond and its reactivity as a function of the metal center. Both *side-on* and *end-on* coordination, which are both candidates for the bonding of N_2 to FeMoco, may lead to very strong or no activation at all depending on the coordinating metal center. The reaction of the complex-bound N_2 molecule with H_2 is novel and this molecule may also be activated by coordination to a transition metal center. Finally, further progress has been made to understand the reactivity of the complex-bound N_2 molecule beyond protonation. All of these findings are relevant to the investigation of the nitrogenase function. In terms of the goal of transforming one of the most inert molecules at ambient conditions in chemical reactions, nitrogen fixation continues to play a pioneering role. The vision remains of integrating in particular the protonation to NH_3 into a catalytic cycle.

German version: *Angew. Chem.* **1998**, *110*, 2780–2782

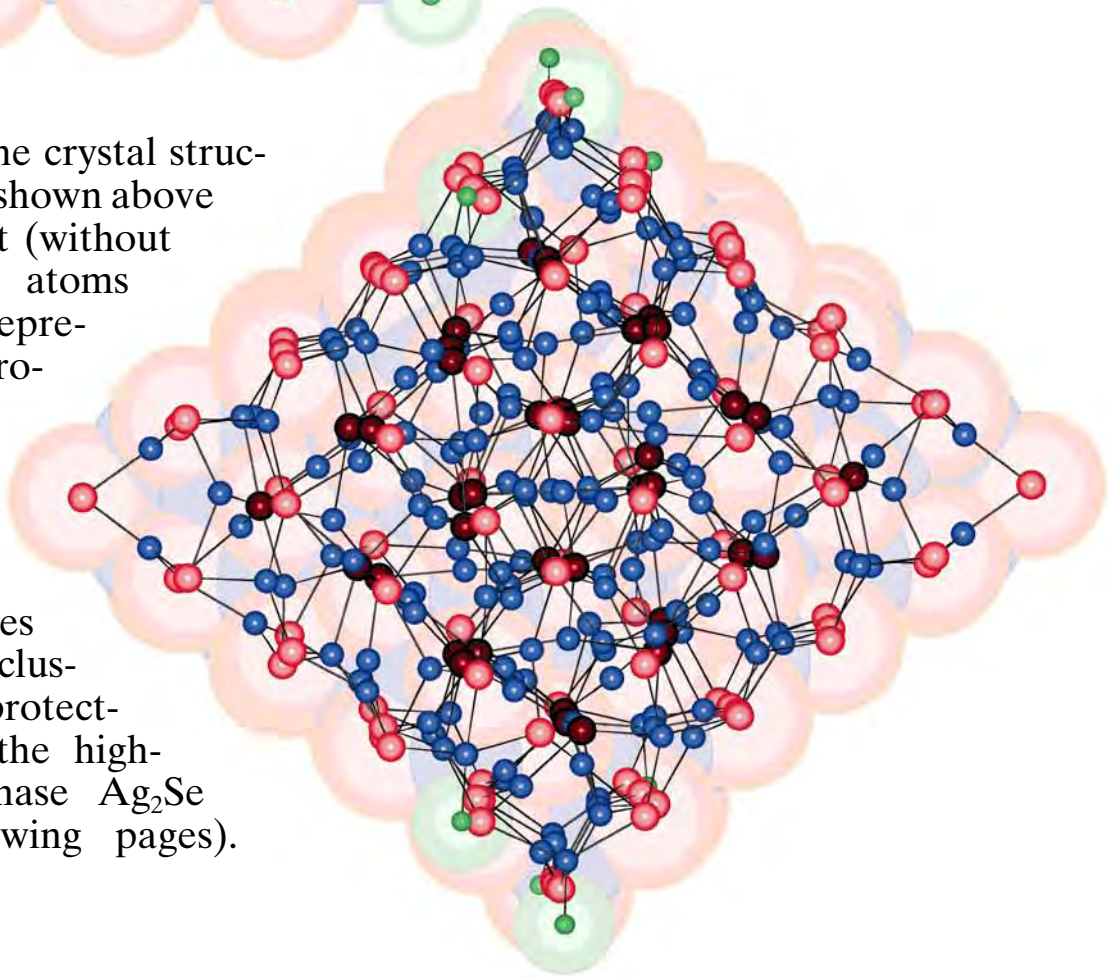
Keywords: bioinorganic chemistry · metalloenzymes · nitrogen fixation · nitrogenases · protonations

[1] See, for example: J. B. Howard, D. C. Rees, *Chem. Rev.* **1996**, *96*, 2965; B. K. Burgess, D. J. Lowe, *Chem. Rev.* **1996**, *96*, 2983; R. R. Eady, *Chem. Rev.* **1996**, *96*, 3013.
[2] A. Müller, E. Krahn, *Angew. Chem.* **1995**, *107*, 1172; *Angew. Chem. Int. Ed. Engl.* **1995**, *34*, 1071.
[3] See, for example: a) *Molybdenum Enzymes, Cofactors and Model Systems* (Eds.: E. Stiefel, D. Coucouvanis, W. E. Newton), American Chemical Society, Washington, DC, **1993**, chapters 20–23; b) R. N. F. Thorneley, D. J. Lowe, *J. Biol. Inorg. Chem.* **1996**, *1*, 576; D. Sellmann, J. Sutter, *Acc. Chem. Res.* **1997**, *30*, 460; D. Coucouvanis, *J. Biol. Inorg. Chem.* **1996**, *1*, 594; c) R. L. Richards, *Coord. Chem. Rev.* **1996**, *154*, 83; R. L. Richards, *Pure Appl. Chem.* **1996**, *68*, 1521.
[4] This term is generally understood with respect to protonation or other reactions involving electrophilic attack to the N_2 unit.
[5] W. J. Evans, T. A. Ulibarri, J. W. Ziller, *J. Am. Chem. Soc.* **1988**, *110*, 6877.
[6] P. Roussel, P. Scott, *J. Am. Chem. Soc.* **1998**, *120*, 1070.
[7] M. Hidai, Y. Mizobe, *Chem. Rev.* **1995**, *95*, 1115.
[8] G. J. Leigh, *Acc. Chem. Res.* **1992**, *25*, 177.
[9] R. A. Henderson, G. J. Leigh, C. J. Pickett, *Adv. Inorg. Chem. Radiochem.* **1983**, *27*, 197.
[10] Y. Nishibayashi, S. Iwai, M. Hidai, *Science* **1998**, *279*, 540
[11] G. Jia, R. H. Morris, C. T. Schweitzer, *Inorg. Chem.* **1991**, *30*, 594.
[12] M. D. Fryzuk, J. B. Love, S. J. Rettig, V. G. Young, *Science* **1997**, *275*, 1445.
[13] See also: R. Duchateau, S. Gambarotta, N. Beydoun, C. Bensimon, *J. Am. Chem. Soc.* **1991**, *113*, 8986.
[14] M. Mori, K. Hori, M. Akashi, M. Hori, Y. Sato, M. Nishida, *Angew. Chem.* **1998**, *110*, 659; *Angew. Chem. Int. Ed.* **1998**, *37*, 636.
[15] C. E. Laplaza, C. C. Cummins, *Science* **1995**, *268*, 861.

 © WILEY-VCH Verlag GmbH, D-69451 Weinheim, 1998 1433-7851/98/03719-2638 $ 17.50+.50/0



A distorted cube-like cluster with edges of about 2.3 nm in length are formed by the Ag atoms (blue), Se^{2-} ligands (dark red), and Se atoms (light red) of the Se*n*Bu groups in $Ag_{172}Se_{40}(Se\textit{n}Bu)_{92}(dppp)_4]$ (dppp = bis-(diphenylphosphanyl)-propane).



The result of the crystal structure analyses is shown above and to the right (without C atoms, P atoms green); the representations are rotated by 90° with respect to each other. The topology of the Se atoms indicates that the Ag–Se cluster is a ligand-protected section of the high-temperature phase Ag_2Se (see the following pages).

 © WILEY-VCH Verlag GmbH, D-69451 Weinheim, 1998 1433-7851/98/3719-2639 $ 17.50+.50/0

Synthesis and Structure of New Ag–Se Clusters: $[Ag_{30}Se_8(SetBu)_{14}(PnPr_3)_8]$, $[Ag_{90}Se_{38}(SetBu)_{14}(PEt_3)_{22}]$, $[Ag_{114}Se_{34}(SenBu)_{46}(PtBu_3)_{14}]$, $[Ag_{112}Se_{32}(SenBu)_{48}(PtBu_3)_{12}]$, and $[Ag_{172}Se_{40}(SenBu)_{92}(dppp)_4]$**

Dieter Fenske,* Nianyong Zhu, and Timo Langetepe

Dedicated to Professor Hans Bock on the occasion of his 70th birthday

The synthesis, structure, and physical properties of large metal clusters are being investigated in many research groups.[1] A part of this interest lies in the metal chalcogenide clusters. Although a remarkably large number of transition metal sulfur clusters have been reported, there are significantly fewer selenium and tellurium analogues known, or even clusters with selenato and tellurato ligands.[2, 3] In the last few years interest in this class of compounds has increased dramatically, in that one can use them, for example, as precursors in the production of semiconducting metal selenides and tellurides. In the meantime a considerable number of multinuclear metal selenide cluster complexes are known which are protected by a ligand shell from further reaction to stable binary selenides. Examples for this are $[Ni_{34}Se_{22}(PPh_3)_{10}]$, $[Cu_{70}Se_{35}(PEt_3)_{22}]$, and $[Cu_{146}Se_{72}(PPh_3)_{30}]$.[4–6] These compounds are formed from the reaction of PR_3 complexes (R = organic group) with metal halides and $Se(SiMe_3)_2$. Very often though the thermodynamically stable metal selenides are formed. Calculations have shown that the PR_3-stabilized cluster complexes are metastable.[7, 8] With the above method it is possible, for example, to obtain copper chalcogenide clusters which can be described as a section of the structure of the binary Cu_2E phase (E = S, Se, Te) surrounded by PR_3 ligands.

In contrast, the synthesis of analogous silver clusters is considerably more difficult. The reaction of AgCl with, for example, $Se(SiMe_3)_2$ in the presence of PR_3 normally affords insoluble Ag_2Se. On the other hand, the reaction of AgCl, PR_3, and $RTeSiMe_3$ preferably provides silver clusters with Te^{2-} and TeR^- ligands. The structure of the cluster complexes formed depends very much upon the tertiary phosphane used and also on the organic group bound to tellurium. Some examples of compounds with known structures are:[9] $[Ag_6(TenBu)_6(PEt_3)_4]$, $[Ag_{10}(TePh)_{10}(PMe_3)_2]_\infty$, $[Ag_{30}(TePh)_{12}Te_9(PEt_3)_{12}]$, $[Ag_{32}(TenBu)_{18}Te_7(PEt_3)_6]$, $[Ag_{46}(TeMes)_{12}Te_{17}(PEt_3)_{16}]$, and $[Ag_{48}(TenBu)_{24}Te_{12}(PEt_3)_{14}]$. We report herein on further Ag clusters which can be isolated from the reaction of silver carboxylates with $RSeSiMe_3$ and PR_3 or bidentate phosphanes.

The reaction of $PnPr_3$, tBuSeSiMe$_3$, and silver benzoate in pentane at −40 °C affords $[Ag_{30}Se_8(SetBu)_{14}(PnPR_3)_8]$ (**1**) in the form of light-senstitive orange crystals [Eq. (1)]. At

$$PhCO_2Ag \xrightarrow[PnPr_3]{tBuSeSiMe_3} [Ag_{30}Se_8(SetBu)_{14}(PnPr_3)_8] \quad \mathbf{1} \qquad (1)$$

higher temperatures only Ag_2Se can be isolated. Compound **1** crystallizes in the space group $P\bar{1}$ and possesses an inversion center. The structure of **1** is shown in Figure 1 and consists of

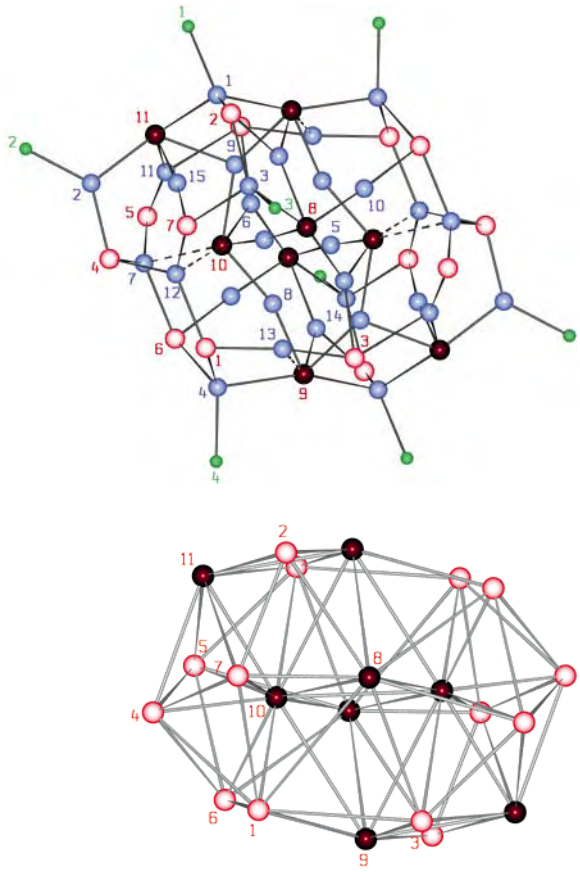


Figure 1. Top: molecular structure of **1** (without C atoms).[12] The P and Ag atoms are depicted in green and blue, respectively, Se^{2-} ligands are dark red, and Se atoms from the SetBu ligands are light red. For the sake of clarity only the atom number is given and the corresponding atom type can be deduced from the color. Bottom: Se atom skelteton. Selected bond lengths (±0.2 pm) and angles (±0.1°): Ag1–P1 247.3, Ag1–Se2 270.5, Ag1–Se9 285.5, Ag1–Se11 288.5, Ag5–Se8 251.5, Ag5–Se10 250.7, Ag7–Se4 260.6, Ag7–Se5 258.2, Ag7–Se6 269.4, Ag7–Se10 299.9, Ag9–Se9 261.8, Ag9–Se10 270.3, Ag9–Se11 280.5; Se8-Ag5-Se10 174.8, Se9-Ag9-Se10 143.1, Se9-Ag9-Se11 113.6, Se10-Ag9-Se11 102.3.

an $Ag_{30}Se_{22}$ cluster, in which the Ag atoms are coordinated in different ways and the Se atoms exist as Se^{2-} ligands and SetBu$^-$ groups. The Se^{2-} ligands are bound in different ways: the atoms Se8–Se10 act as μ_6-bridging ligands, whereas Se11 is μ_5-bridging ligand. They exhibit both short (249.8–270.2(2) pm) and long (276.2–305.0(2) pm) bond lengths to the silver atoms. The selenium atoms of the SetBu groups act as μ_2- and μ_3-bridging ligands (μ_2-Se: Se3, Se5; Ag–Se: 252.1–262.0 pm; μ_3-Se: Se1, Se2, Se4, Se6, Se7; Ag–Se: 251.5–276.4(2) pm).

Ten silver atoms (Ag5, Ag8, Ag10, Ag11, Ag15, and their symmetry equivalents) are almost linearly coordinated by two Se atoms (Se-Ag-Se: 157.2–176.7°). These Ag atoms are bound to both Se^{2-} and SetBu$^-$ ligands (Ag–Se: 249.8–255.9(2) pm). The eight Ag atoms bound to the P atoms of

[*] Prof. Dr. D. Fenske, Dr. N. Zhu, T. Langetepe
Institut für Anorganische Chemie der Universität
Engesserstrasse, Geb. 30.45, D-76128 Karlsruhe (Germany)
Fax: (+49) 721-661921

[**] This work was supported by the Deutsche Forschungsgemeinschaft (SFB 195).

 © WILEY-VCH Verlag GmbH, D-69451 Weinheim, 1998 1433-7851/98/3719-2640 $ 17.50+.50/0

the phosphane ligands (Ag1 – Ag4 and symmetry equivalents) have different coordination modes. Atom Ag2 has a distorted trigonal-planar environment, coordinated by P2, an Se*t*Bu$^-$, and an Se^{2-} ligand. In contrast, Ag1 is bound to one Se*t*Bu$^-$ (Se2) and two Se^{2-} (Se9, Se11) ligands, and to P1 in a distorted tetrahedral environment. Atoms Ag3 and Ag4 have likewise distorted tetrahedral coordination, but are each bound to a P atom from a P*n*Pr group, one Se^{2-}, and two Se*t*Bu$^-$ ligands. Of the other twelve silver atoms, eight have distorted trigonal coordination (Ag6, Ag9, Ag13, Ag14) and Ag7 and Ag12 are bound to Se*t*Bu$^-$ and Se^{2-} ligands in distorted tetrahedral environment. Figure 1 (bottom) shows that the Se atoms form a layered structure in which the first and third layers contain six Se atoms. The remaining ten Se atoms form the middle layer. Within the Se polyhedron, all the Se–Se distances are larger than 386 pm.

The reaction of silver benzoate, PEt_3, and *t*BuSeSiMe$_3$ in THF affords cluster **2** in a yield of 60 % [Eq. (2)]. The reaction temperature must not exceed $-20\,^{\circ}C$, otherwise only an

$$PhCO_2Ag \xrightarrow[PEt_3]{t\text{BuSeSiMe}_3} [Ag_{90}Se_{38}(Set\text{Bu})_{14}(PEt_3)_{22}] \quad \mathbf{2} \qquad (2)$$

amorphous product is isolated along with Ag_2Se. Cluster **2** possesses an inversion center and crystallizes in the form of black platelets in the space group $P\bar{1}$. The structure of **2** is shown in Figure 2. The organic groups bound to phosphorus and selenium are omitted for the sake of clarity. Compound **2** contains 90 Ag and 38 Se^{2-} centers, as well as 14 Se*t*Bu$^-$ and 22 PEt_3 ligands. The Se atoms form a torus-shaped polyhedron, which is made up of Se_3 faces (Figure 3); however, there are no bonding interactions between the Se atoms. The light red Se atoms of the Se*t*Bu$^-$ groups are found at the surface of the polyhedron, which has approximately D_{6h} symmetry.

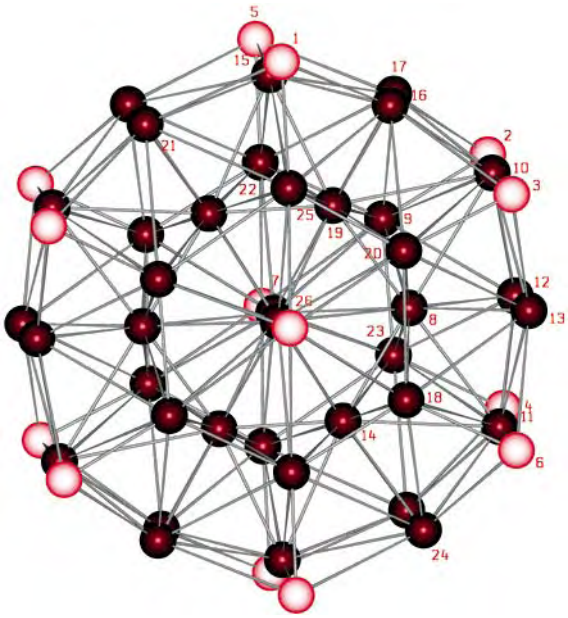


Figure 3. Part of the Se skeleton in **2**. The Se^{2-} atoms are shown in dark red, and Se atoms from the Se*t*Bu ligands in light red.

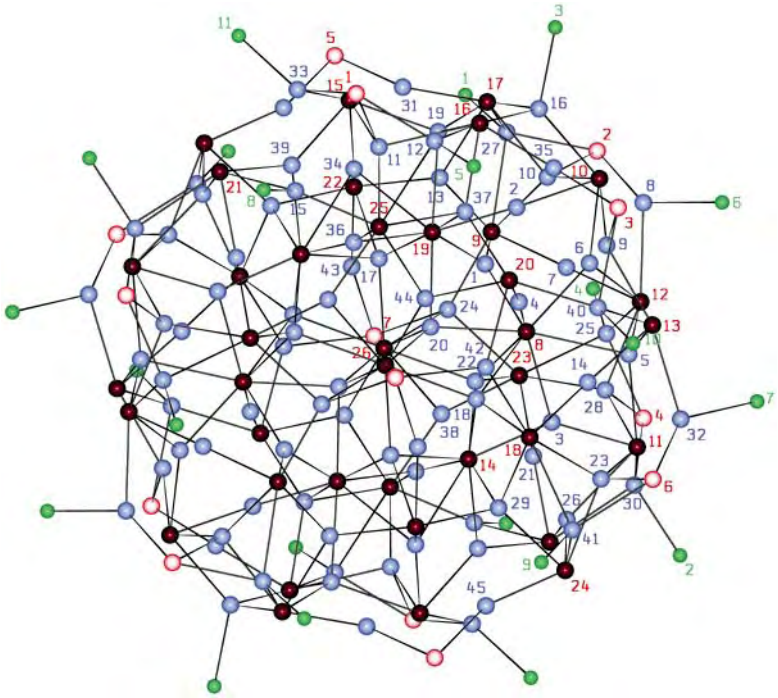


Figure 2. Molecular structure of **2** (without C atoms).[12] The P atoms are colored green, Se atoms from the Se*t*Bu ligands light red, Se^{2-} ligands dark red, and the Ag atoms blue. The atom number is given and the corresponding atom type can be deduced from the color. Selected bond lengths (±0.4 pm) and angles (±0.1°): Ag7–Se9 249.3, Ag7–Se12 250.2, Ag1–Se8 271.7, Ag1–Se9 261.9, Ag1–Se19 280.1, Ag19–Se15 274.8, Ag19–Se16 276.9, Ag19–Se17 272.2, Ag19–Se19 292.5; Se9-Ag7-Se12 176.7, Se8-Ag1-Se19 94.0, Se8-Ag1-Se9 136.4, Se9-Ag1-Se19 129.5, Se15-Ag19-Se16 106.1, Se15-Ag19-Se17 118.3, Se15-Ag19-Se19 106.3, Se16-Ag19-Se17 117.1, Se17-Ag19-Se19 108.2, Se16-Ag19-Se19 98.8.

Atoms Se7 and Se26 are found on the sixfold axis. The remaining Se atoms form two shells: the first inner sphere contains only Se^{2-} centers, while the second outer sphere contains both Se^{2-} and Se$^-$ centers from the Se*t*Bu groups. The Se atoms of the 14 Se*t*Bu groups act as μ_2 (Se5, Ag–Se5: 250.4 – 252(2) pm) and μ_3 bridges (Se1 – Se4, Se6, Se7; Ag–Se: 251.5 – 297.8(2) pm). The Se^{2-} atoms also have different coordination modes. The Se^{2-} atoms in the outer shell act either as μ_4 or μ_5 bridges (Se10 – Se13, Se15 – Se17, Se21, Se24; Ag–Se: 250.2 – 305.6(2) pm). In contrast, the remaining Se^{2-} centers each form five to eight bonds to silver atoms.

A description of the coordination relationships is difficult as the Ag–Se bond lengths vary over a large range. For the Ag atoms one can recognize different distorted coordination polyhedra. The Ag atoms that are bound to PEt_3 groups are coordinated either in trigonal-planar (Ag8, Ag15, Ag32, Ag33) or in distorted tetrahedral fashion (Ag12, Ag16, Ag25, Ag27, Ag30, Ag40, Ag41) to the Se atoms of the Se*t*Bu groups, the remaining 68 Ag atoms are bound only to Se^{2-} centers. Of the 68 Ag atoms, 20 are bound in a distorted linear fashion to two Se^{2-} neighbors (Ag2, Ag4, Ag7, Ag9, Ag14, Ag21, Ag31, Ag35, Ag38, Ag43, Ag45; Ag–Se 249.3 – 259.1(4) pm; Se-Ag-Se: 147.5 – 176.7(3)°). A further 28 Ag atoms have distorted trigonal-planar environments (Ag1,

Ag3, Ag6, Ag10, Ag13, Ag17, Ag23, Ag26, Ag34, Ag36, Ag39, Ag42, Ag44, Ag–Se: 255.9 – 293.2(4) pm). The remaining 20 silver atoms are bound to Se^{2-} atoms in a distorted tetrahedral manner (Ag5, Ag11, Ag18, Ag19, Ag20, Ag22, Ag24, Ag28, Ag29, Ag37; Ag–Se: 258.6 – 305.6(49) pm).

The reaction of silver laurate, P*t*Bu$_3$, and *n*BuSeSiMe$_3$ leads to the formation of $[Ag_{114}Se_{34}(Se\mathit{n}Bu)_{46}(P\mathit{t}Bu_3)_{14}]$ (**3**; Figure 4). If the monodentate phosphane ligand is replaced by

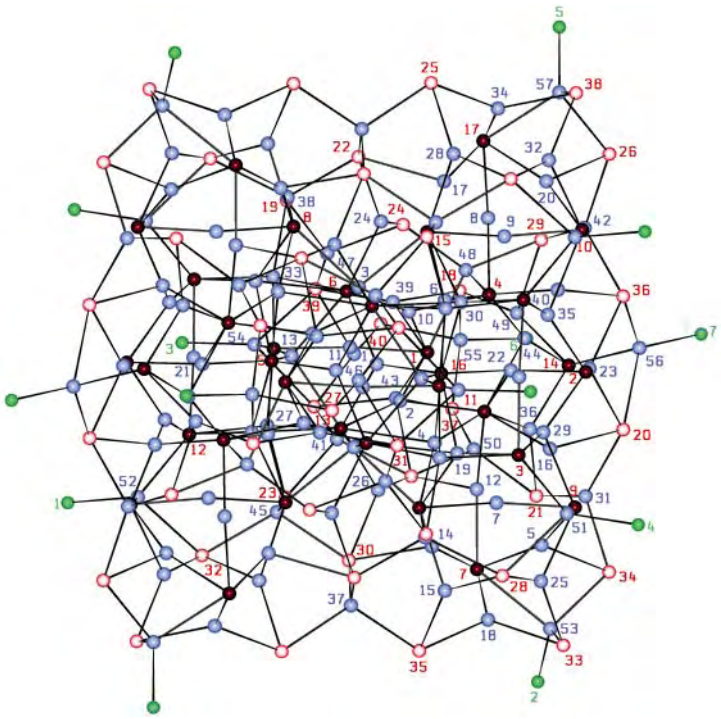


Figure 4. Molecular structure of **3**.[12] For the sake of clarity the atoms of the P*t*Bu$_3$ and Se*n*Bu ligands are not shown. (P atoms are green, Ag atoms blue, Se^{2-} ligands dark red, and the Se atoms of the Se*n*Bu light red.) The atom number is given and the corresponding atom type can be deduced from the color. Selected bond lengths (±0.4 pm) and angles (±0.1°): Ag11–Se1 250.3, Ag11–Se5 247.2; Ag1–Se6 272.3, Ag1–Se13 269.4, Ag1–Se16 262.6; Ag3–Se6 262.9, Ag3–Se8 285.5, Ag3–Se13 264.1, Ag3–Se15 282.8, Se1-Ag11-Se5 175.1; Se6-Ag1-Se13 108.9, Se6-Ag1-Se16 127.3, Se13-Ag1-Se16 122.6, Se6-Ag3-Se8 86.2, Se6-Ag3-Se13 163.9, Se6-Ag3-Se15 103.1, Se8-Ag3-Se13 105.4, Se8-Ag3-Se15 98.3, Se13-Ag3-Se15 86.6.

bis(diphenylphosphanyl)propane (dppp) under the same reaction conditions (−30 °C), the largest Ag cluster known up till now is formed, $[Ag_{172}Se_{40}(Se\mathit{n}Bu)_{92}(dppp)_4]$ (**4**) [Eq. (3)].

$$[Ag_{114}Se_{34}(Se\mathit{n}Bu)_{46}(P\mathit{t}Bu_3)_{14}]\ \ \mathbf{3}$$
$$\uparrow P\mathit{t}Bu_3$$
$$C_{11}H_{23}CO_2Ag + \mathit{n}BuSeSiMe_3 \qquad (3)$$
$$\downarrow dppp$$
$$[Ag_{172}Se_{40}(Se\mathit{n}Bu)_{92}(dppp)_4]\ \ \mathbf{4}$$

Clusters **1** and **2** are spherical and show no similarity to the bulk material structures of Ag_2Se and Ag_2S.[10] In contrast there is a remarkable agreement with respect to the topology of the Se centers between clusters **3** and **4**, and Ag_2E (E = S, Se). The selenium skeletons of **3** and **4** (Figure 5) correspond to a distorted cubic-centered structure that is also found in Ag_2Se. Therefore, the cluster structures of **3** and **4** can be described as different sizes of cross sections of Ag_2Se.

We have already observed similar size-dependent structural changes in the PR_3-stabilized Cu_2E clusters (E = S, Se),[4–6, 11] though the transition to cross sections from the structure of the binary Cu_2E phase already occurs with 70 Cu atoms. It is not surprising that the dependence of the structures of ionic clusters in the gas phase is likewise controlled by the number of ions. Examples for this are $(MgCl_2)_n$, $(KCl)_n$, and $(LiF)_n$[13] as well as Cu_2E clusters in the gas phase.[14]

As already described in the structures of **1** and **2**, the Se^{2-} and Se*n*Bu$^-$ ligands act as bridges between the Ag atoms in both **3** (Figure 4) and **4** (Figure 6). The Se*n*Bu groups act as either μ_3- or μ_4-bridging ligands (**3**: Ag–Se: 249.8 – 306.4(3) pm; **4**: Ag–Se: 241.3 – 306.5(3) pm). The Se^{2-} centers in **3** function as μ_4-, μ_5-, μ_6-, and μ_7-bridging ligands, and the Ag–Se distances lie in the range of 247 – 309 pm. In **4** the coordination relationships are significantly more complex. Within Ag–Se distances of 244 – 303 pm the Se^{2-} centers act as μ_5, μ_6, μ_7, and μ_8 bridges.

In Ag_2Se the Ag atoms have trigonal and tetrahedral coordination. In agreement with this, the Ag atoms in **3** and **4** are also coordinated by Se atoms in trigonal and tetrahedral environments. There are 14 P*t*Bu$_3$ ligands (P1 – P7) bound to the cluster surface of **3**, and four dppp ligands to the surface of **4**. The silver atoms bound to these P atoms have distorted tetrahedral coordination.

With increasing cluster size, the distribution of the Ag atoms in the molecular structure becomes more chaotic. As a result, problems emerged in the refinement of **4**. However, this shows that one can assume that in compounds **1** – **4** one has in reality ligand-protected sections of the Ag_2Se structure, because in the solid bulk material of Ag_2Se the Ag^+ anions are disordered.[9] This is probably also the reason for the fact that in the analogous reaction to Equation (3) of silver acetate, P*t*Bu$_3$, and *n*BuSeSiMe$_3$, cluster **5** is formed [Eq. (4)]. The structure of

$$CH_3CO_2Ag \xrightarrow[P\mathit{t}Bu_3]{\mathit{n}BuSeSiMe_3} [Ag_{112}Se_{32}(Se\mathit{n}Bu)_{48}(P\mathit{t}Bu_3)_{12}]\ \ \mathbf{5} \qquad (4)$$

5 is almost identical to that of **3**. The difference to **3** lies in the number of phosphane ligands coordinated to the cluster surface; this is why **5** has two Ag atoms less than **3**. The number of Se atoms and their structure are identical in **3** and **5**; however, the ratio of Se^{2-} to Se*n*Bu$^-$ ligands is different.

The silver clusters **1** – **5** are formed in part from breaking the Se–C bond in *t*BuSeSiMe$_3$ and *n*BuSeSiMe$_3$. As a result of a redox reaction complexes are produced with Se^{2-} and SeR^- ligands, whose cluster surface is covered with phosphane ligands and the organic groups bound to selenium. The influence of the phosphane ligands on the structure of the silver – selenium core is made clearer, in that they evidently are able to intervene in the formation of stable Ag_2Se and AgSeR at specific steps. However, it is still unclear why this should lead to the formation of defined structures that are reproducible under the given experimental conditions. It may be possible that this is determined by the surface energy of the cluster molecule. Calculations for this are currently being carried out. On the assumption that in **1** – **5** Se^{2-} and SeR^- ligands exist, all the Ag atoms must possess a formal charge of

 © WILEY-VCH Verlag GmbH, D-69451 Weinheim, 1998 1433-7851/98/3719-2642 $ 17.50+.50/0

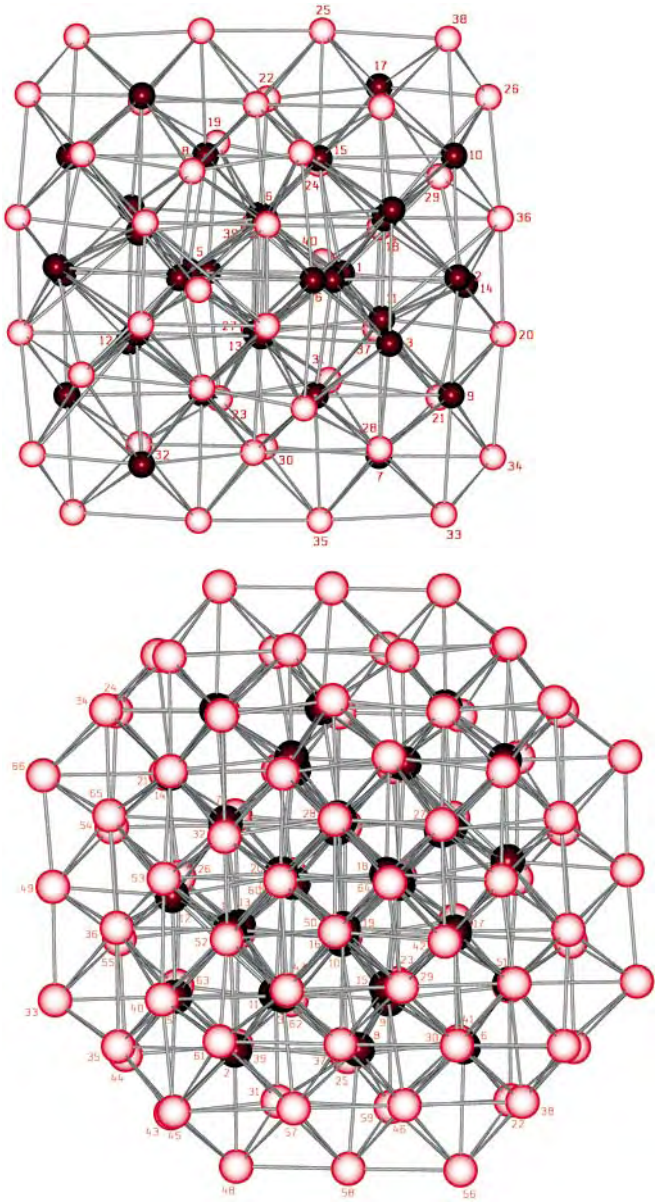


Figure 5. Skeleton structure of the Se atoms in **3** (above) and **4** (below). The Se^{2-} ligands are shown in dark red, and the Se atoms from the Se*n*Bu groups in light red.

1 + (d^{10} configuration). Correspondingly there is no evidence of Ag–Ag interactions; all Ag–Ag distances are greater than 290 pm.

Experimental Section

1: P*n*Pr$_3$ (0.26 mL, 1.31 mmol) was added to a solution pfPhCO$_2$Ag (0.15 g, 0.65 mmol) in pentane (10 mL) at −40 °C. Then *t*BuSeSiMe$_3$ (0.20 mL, 0.86 mmol) was added. After a short time a clear solution was formed. Within 2 d the solution turned dark green from which orange crystals of **1** were formed (yield: 60 %).

2: In an analogous way to **1** PhCO$_2$Ag (0.15 g, 0.65 mmol) in THF (10 mL) was treated at −40 °C with PEt$_3$ (0.10 mL, 0.64 mmol) and *t*BuSeSiMe$_3$ (0.20 mL, 0.86 mmol). After a few minutes a dark brown solution was formed. After a further 2 d black platelets of **2** crystallized (yield: 60 %).

3: $C_{11}H_{23}CO_2Ag$ (0.10 g, 0.33 mmol) in pentane (10 mL) was treated with P*t*Bu$_3$ (0.30 mL, 1.26 mmol) and *n*BuSeSiMe$_3$ (0.10 mL, 0.43 mmol) at −30 °C. Black crystals of **3** were formed after about 14 d from the deeply colored solution (yield: 30 %).

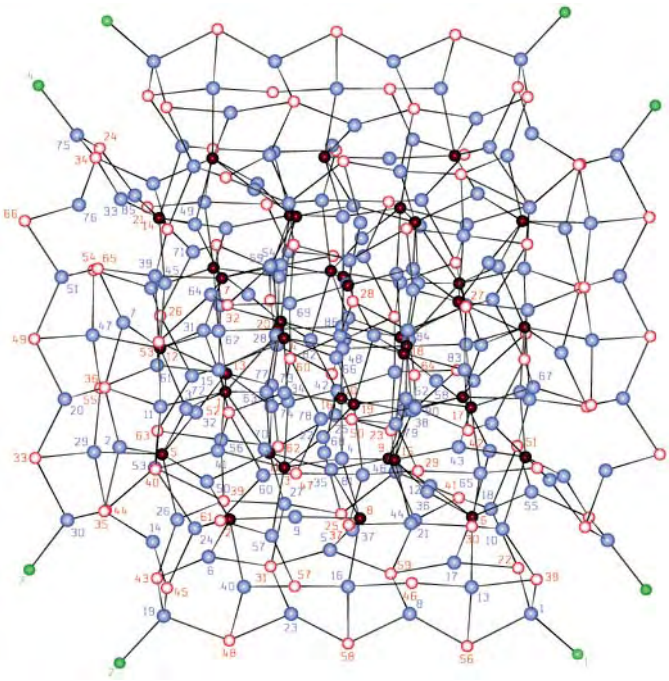


Figure 6. Molecular structure of **4** (without C atoms).[12] The P atoms are colored green, Se^{2-} ligands red, Se atoms from the Se*n*Bu-ligands light red, and Ag atoms blue. The atom number is given and the corresponding atom type can be deduced from the color. Selected bond lengths (±0.7 pm) and angles (±0.2°): Ag9–Se2 254.4(6), Ag9–Se8 255.0(6), Ag2–Se5 272.6, Ag2–Se5 2585, Ag2–Se36 257.2, Ag4–Se3 279.9, Ag4–Se8 278.1, Ag4–Se15 278.4, Ag4–Se16 267.1; Se2-Ag9-Se8 176.2, Se5-Ag2-Se35 92.3, Se5-Ag2-Se36 121.9, Se35-Ag2-Se36 145.3, Se3-Ag4-Se8 112.6, Se3-Ag4-Se15 101.1, Se3-Ag4-Se16 112.4, Se8-Ag4-Se15 97.2, Se8-Ag4-Se16 120.4, Se15-Ag4-Se16 110.2.

4: $C_{11}H_{23}CO_2Ag$ (0.32 g, 1.04 mmol) in CHCl3/toluene (1/3, 10 mL) was treated with dppp (0.11 g, 0.26 mmol) and *n*BuSeSiMe$_3$ (0.25 mL, 0.05 mmol) at −20 °C. After 2 d reaction time the solution was allowed to slowly warm up to room temperature. Within 14 d black crystals of **4** were formed from the dark brown solution together with Ag_2Se (yield: 20 %)

5: AgAc (0.10 g, 0.60 mmol) in pentane/THF (1/1, 10 mL) was treated with P*t*Bu$_3$ (0.25 mL, 1.05 mmol) and P*n*Bu$_3$ (0.20 mL, 0.86 mmol) at −30 °C. After 28 d black crystals of **5** were formed (yield: 60 %).

The results of the elemental analyses of **1**–**5** (Ag, P, Se) agree with the given empirical formulae.

Received: May 15, 1998 [Z11863IE]
German version: *Angew. Chem.* **1998**, *110*, 2783–2788

Keywords: clusters · selenium · silver · structure elucidation

[1] *Clusters and Colloids. From Theory to Applications* (Ed.: G. Schmid), VCH, Weinheim, **1994**; *Physics and Chemistry of Metal Cluster Compounds* (Ed.: L. J. de Jongh), Kluwer, Dordrecht, **1994**.

[2] I. Dance, K. Fisher, *Prog. Inorg. Chem.* **1994**, *41*, 637; L. C. Roof, J. W. Kolis, *Chem. Rev.* **1993**, *93*, 1037; J. Arnold, *Prog. Inorg. Chem.* **1995**, *43*, 353.

[3] D. Ohlmann, H. Pritzkow, H. Grützmacher, M. Anthamatten, R. Glaser, *J. Chem. Soc. Chem. Commun*. **1995**, 1011; B. J. Bonasis, G. P. Mitchell, F. J. Hollander, J. Arnold, *Inorg. Chem*. **1994**, *33*, 1797; J. Zhao, D. Adcock, W. T. Pennington, J. W. Kolis, *Inorg. Chem*. **1990**, *29*, 4358; I. Dance, G. Lee, *Spec. Publ. R. Soc. Chem.* **1993**, 131; J. G. Brennan, T. Siegrist, P. J. Carrol, S. H. Stuczynski, P. Reynders, L. E. Brus, M. L. Steigerwald, *Chem. Mater*. **1990**, *2*, 403.

[4] D. Fenske, J. Ohmer, J. Hachgenei, *Angew. Chem.* **1985**, *97*, 993; *Angew. Chem. Int. Ed. Engl.* **1985**, *24*, 993; D. Fenske, J. Ohmer, J.

 © WILEY-VCH Verlag GmbH, D-69451 Weinheim, 1998 1433-7851/98/3719-2643 $ 17.50+.50/0

Hachgenei, K. Merzweiler, *Angew. Chem.* **1988**, *100*, 1300; *Angew. Chem. Int. Ed. Engl.* **1988**, *27*, 1277.
[5] H. Krautscheid, D. Fenske, G. Baum, M. Semmelmann, *Angew. Chem.* **1993**, *105*, 1364; *Angew. Chem. Int. Ed. Engl.* **1993**, *32*, 1303.
[6] D. Fenske, H. Krautscheid, *Angew. Chem.* **1990**, *102*, 799; *Angew. Chem. Int. Ed. Engl.* **1990**, *29*, 796.
[7] S. Dehnen, A. Schäfer, R. Ahlrichs, D. Fenske, *Chem. Eur. J.* **1996**, *2*, 429; S. Dehnen, A. Schäfer, D. Fenske, R. Ahlrichs, Angew. *Chem.* **1994**, *106*, 786; *Angew. Chem. Int. Ed. Engl.* **1994**, *33*, 746.
[8] D. van der Putten, D. Olevano, R. Zanoni, H. Krautscheid, D. Fenske, *J. Electron Spectrosc.* **1995**, *76*, 207.
[9] J. F. Corrigan, D. Fenske, *Chem. Commun.* **1996**, 943; J. F. Corrigan, D. Fenske, *Chem. Commun.* **1997**, 1837; J. F. Corrigan, D. Fenske, W. P. Power, *Angew. Chem.* **1997**, *109*, 1224; *Angew. Chem. Int. Ed. Engl.* **1997**, *36*, 1176.
[10] G. A. Wiegers, *Am. Mineral.* **1971**, *56*, 1882; Z. G. Pinsker, C. Chiangliang, R. M. Imamov, E. L. Lapidus, *Sov. Phys. Crystallogr. (Engl. Transl.)* **1965**, *7*, 225.
[11] S. Dehnen, D. Fenske, *Angew. Chem.* **1994**, *106*, 2369; *Angew. Chem. Int. Ed. Engl.* **1994**, *33*, 2287; S. Dehnen, D. Fenske, *Chem. Eur. J.* **1996**, *2*, 1407; S. Dehnen, D. Fenske, A. C. Deveson, *J. Cluster Sci.* **1996**, *3*, 351; A. C. Deveson, S. Dehnen, D. Fenske, *J. Chem. Soc. Dalton Trans.* **1997**, 4491.
[12] Crystal structure analysis: STOE-IPDS ($Mo_{K\alpha}$ radiation); Data collection and refinement (SHELXS-86, SHELXL-93); empirical corrections (habit). **1**: triclinic, space group $P\bar{1}$ (no. 2), $Z=1$, lattice constants (190 K): $a=1770.4(4)$, $b=1849.1(4)$, $c=1856.1(4)$ pm, $\alpha=96.21(3)$, $\beta=101.49(3)$, $\gamma=93.34(3)^\circ$, $V=5900\times10^6$ pm^3, $\mu(Mo_{K\alpha})=5.901$ mm^{-1}, $2\Theta_{max.}=50^\circ$; of 22182 reflections measured, 16085 were independent ($R_{int}=0.082$) and 11914 observed with $I>2\sigma(I)$; 667 parameters (Ag, Se, P, anisotropic and C isotropic); max. residual electron density: 2.7 e Å^3; $R_1=0.070$; $wR_2=0.18$. **2**: triclinic, space group $P\bar{1}$ (no. 2), $Z=1$, lattice constants (170 K): $a=2025.0(4)$, $b=2521.2(5)$ $c=2643.1(5)$ pm, $\alpha=61.15(2)$, $\beta=80.10(3)$, $\gamma=67.36(3)^\circ$, $V=11629\times10^6$ pm^3, $\mu(Mo_{K\alpha})=7.85$ mm^{-1}, $2\Theta_{max.}=52^\circ$; of 64995 reflections measured, 41759 were independent ($R_{int}=0.10$) and 21790 observed with $I>2\sigma(I)$; 1110 parameters (Ag, Se, P, anisotropic, C isotropic); max. residual electron density 2.8 e Å^{-3}; $R_1=0.098$; $wR_2=0.28$. **3**: triclinic, space group $P\bar{1}$ (no. 2), $Z=1$, lattice constants (170 K): $a=2619.4(5)$, $b=2765.9(6)$ $c=2815.7(6)$ pm, $\alpha=116.39(3)$, $\beta=91.46(3)$, $\gamma=100.30(3)^\circ$, $V=17851.0\times10^6$ pm^3, $\mu(Mo_{K\alpha})=7.18$ mm^{-1}, $2\Theta_{max.}=50^\circ$; of 56227 reflections measured, 43345 were independent ($R_{int}=0.10$) and 20294 observed with $I>2\sigma(I)$; 1330 parameters (Ag, Se anisotropic, P, C isotropic); max. residual electron density 2.7 e Å^{-3}; $R_1=0.089$; $wR_2=0.22$. **4**: triclinic, space group $P\bar{1}$ (no. 2), $Z=1$, lattice constants (170 K): $a=2824.0(6)$, $b=2980.0(6)$ $c=3225.0(6)$ pm, $\alpha=67.14(3)$, $\beta=68.02(3)$, $\gamma=67.94(3)^\circ$, $V=22333\times10^6$ pm^3, $\mu(Mo_{K\alpha})=9.09$ mm^{-1}, $2\Theta_{max.}=48^\circ$; of 99240 reflections measured, 64156 were independent and 22753 observed with $I>2\sigma(I)$; 1933 parameters (Ag, Se, P, anisotropic, C isotropic); max. residual electron density 4.8 e Å^{-3}; $R_1=0.12$; $wR_2=0.35$. The high R value is partly a result of the fact that a portion of the C atoms on the *n*Bu groups could not be localized. Apart from that it was not possible to distinguish the disordered solvent molecules. **5**: **5**·2THF; triclinic, space group $P\bar{1}$ (no. 2), $Z=1$, lattice constants (170 K): $a=2598.3(5)$, $b=2626.1(8)$ $c=2952.9(6)$ pm, $\alpha=112.85(3)$, $\beta=112.11(3)$, $\gamma=90.61(3)^\circ$, $V=16911\times10^6$ pm^3, $\mu(Mo_{K\alpha})=7.52$ mm^{-1}, $2\Theta_{max.}=50^\circ$; of 70408 relections measured, 49109 were independent and 35916 observed with $I>2\sigma(I)$; 1623 parameters (Ag, Se, P, anisotropic, C isotropic); max. residual electron density 3.1 e Å^{-3}; $R_1=0.065$; $wR_2=0.18$. Further details on the crystal structure investigation may be obtained from the Fachinformationszentrum Karlsruhe, D-76344 Eggenstein-Leopoldshafen, Germany (fax: (+49) 7247-808-666; e-mail: crysdata@fiz-karlsruhe.de), on quoting the depository numbers CSD-408688 to CSD-408692.
[13] K. Eichkorn, U. Schneider, R. Ahlrichs, *J. Chem. Phys.* **102**, *19*, 7557; C. Ochsenfeld, R. Ahlrichs, *Ber. Bunsen-Ges. Phys. Chem.* **1994**, *98*, 34; C. Ochsenfeld, J. Gauss, R. Ahlrichs, *J. Chem. Phys.* **1995**, *103*, 7401; C. Ochsenfeld, R. Ahlrichs, *J. Chem. Phys.* **1994**, *101*, 5977; C. Ochsenfeld, R. Ahlrichs, *Ber. Bunsen-Ges. Phys. Chem.* **1995**, *99*, 1191.
[14] I. G. Dance, K. J. Fisher, *J. Chem. Soc. Dalton Trans.* **1997**, 2563.

Detection of Catalytic Activity in Combinatorial Libraries of Heterogeneous Catalysts by IR Thermography

Arnold Holzwarth, Hans-Werner Schmidt, and Wilhelm F. Maier*

The ever increasing need for more selective heterogeneous catalysts in chemical processing cannot be satisfied by conventional catalyst development and, therefore, combinatorial approaches should be considered. The combinatorial synthesis and screening of large numbers of organic compounds is already an established tool for the development of new pharmaceuticals,[1] while the combinatorial approach to the development of new solid materials has just started. In 1995 the first combinatorial developments of new materials, like new magnetoresists[2] and new superconductors[3] were reported. In 1997 libraries produced efficiently by wet-chemical syntheses with the help of ink-jet technology were created for the development of new luminescent materials.[4] New blue photoluminescent materials followed in 1998.[5] The true potential of the combinatorial approach to materials development becomes apparent by reports on thin film libraries of 25000 different materials on 7.5-cm diameter substrates. These libraries were prepared by thin film technologies using physical evaporation techniques.[6] To apply such techniques to the development of new heterogeneous catalyst materials an efficient method for the reliable spatially resolved detection of catalytic activities is required. Promising recent developments are the use of spatially resolved ionization techniques.[7] In the above-mentioned development of photoluminescent materials charge-coupled detector (CCD) cameras were applied which have excellent spatial resolution.[4–6] For the simultaneous display of catalytic activities on a catalyst library an IR-video camera appears attractive.

The applicability of IR thermography in heterogeneous catalysis was demonstrated already in 1987, where oscillations in a catalytic reaction of hydrogen with oxygen across a 4 cm^2 catalyst wafer could be monitored.[8a] Since this is a very exothermic reaction (241 kJ mol^{-1}), the temperature variations were as large as 70 °C. In the same year temperature differences smaller than 5 °C were measured for the hydrogenation of cyclohexene on Pt/SiO_2 catalysts with IR thermography.[8b] This technique was later applied to the screening of heterogeneous catalysts for hydrogen oxidation on 16 free-standing catalyst pellets.[9] Since the size of the catalyst pellets (4×3 mm) and the temperature differences observed (80 °C) limit both the spatial and the thermal resolution of these experiments, there is little prospect for application of such thermographic methods for the reliable detection of catalytic activity on large catalyst libraries with its microscopic amounts of catalysts. More promising is a recent report on the application of IR-thermographic methods for the combinatorial selection of small encoded polymer bead catalysts in

[*] Prof. Dr. W. F. Maier, Dr. A. Holzwarth, H.-W. Schmidt
Max-Planck-Institut für Kohlenforschung
Kaiser-Wilhelm-Platz 1, D-45470 Mülheim an der Ruhr (Germany)
Fax: (+49) 208-306-2987
E-mail: maier@mpi-muelheim.mpg.de

 © WILEY-VCH Verlag GmbH, D-69451 Weinheim, 1998 1433-7851/98/3719-2644 $ 17.50+.50/0

solution phase.[10] Here we report the detection of catalytic activities for heterogeneous reactions of small catalyst amounts (less than 200 μg) on a model library by IR thermography.

Visible light images mainly result from reflection and therefore require an external light source. In contrast, IR radiation is actively emitted from all objects and no external light source is required for imaging—even gases emit IR radiation. The IR image of an object is composed of emitted and reflected radiation; the relative ratio is different for each surface. The different colors on these images visualize different photon intensities of detected IR radiation. From these photon intensities blackbody temperatures can be calculated by Planck's law. These blackbody temperatures can be converted to the actual surface temperature of the object only if no reflection occurs or becomes insignificant and its emissivity is known.

Local differences in emissivity and reflectivity on a library surface and its individual catalyst spots do appear as different photon intensities, which can be misinterpreted as different temperatures, although the true surface temperatures are identical. Only at large temperature differences, like the 80 K reported,[8, 9] small differences in emissivity become negligible. When small temperature differences of a few K or smaller are to be identified, emissivity differences have to be corrected. A closely related problem is the rate of heat dissipation from tiny amounts of catalysts on the solid library. The temperature difference at the catalyst surface relative to the library surface decreases with decreasing catalyst mass. One also has to be aware that IR emission from reactants and products increases with temperature. These emissions can be reflected on the library surface causing undesired changes to the image. Therefore, IR emitters like the hydrocarbons used in our experiments can strongly affect the IR image. Our experimental design as well as our choice of IR camera were selected to reduce the effect of the above-mentioned IR-imaging problems.

Common high-sensitivity focal plane array (FPA) IR cameras are based on one of three detector materials, the semiconductors indium–antimonide (InSb), cadmium–mercury–telluride (CMT), or platinum–silicide (PtSi). InSb or CMT detector based cameras are very sensitive, but suffer from nonlinear response and a lack of long-term signal stability, which requires frequent correction and calibration of signals. The correctability and stability of the photoresponse of the PtSi-FPA detector is superior to that of the other FPA detectors.[11] We have therefore selected a PtSi-based camera, the AEGAIS from AIM equipped with a 256 × 256 PtSi-array detector and a lens with 50 mm focal length.

The primary interest of this study was to display temperature differences due to catalytic activity on a library of heterogeneous catalysts. This was achieved by applying a linear correction to the detector response and subtracting the IR image of the library just before the start of the reaction (Figure 1 a) as background (offset) from the images during an isothermal catalytic experiment. Figure 1 a shows the wells in the library surface as well as the catalyst spots due to local emissivity differences. After emissivity correction and image subtraction Figure 1 b results. The local emissivity differences of the library are no longer visible. The heat evolution due to

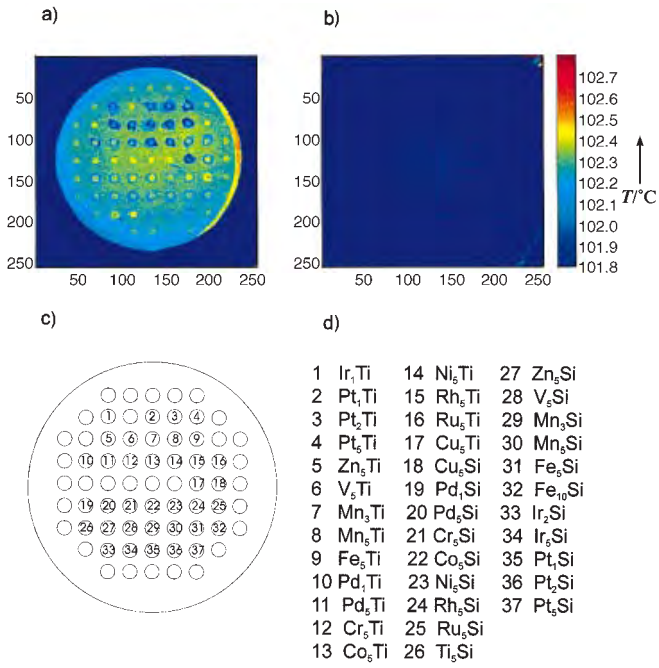


Figure 1. a) IR image of the catalyst library without emissivity correction. b) Emissivity-corrected IR-thermographic image of the catalyst library prior to the start of catalytic reactions. The bar on the right gives the temperature/color key of the temperature window [°C]. c) Deposition pattern of the library. d) Composition of the oxide catalyst spots of the library according to the AMM notation (the molar percentages of active metal and base metal oxide are given, that is AMM-Ti_3Si stands for 3 mol % titania in 97 mol % silica).

catalytic activity can now be reliably detected since only temperature changes will be visible.

To avoid reflections at the catalyst library, a slate plate of low reflectivity was chosen as substrate. The effects of thermal IR emission from hydrocarbon reactants and products in the gas phase were reduced by the use of a 3.6-μm cut-on IR filter.

Owing to the rapid development of combinatorial chemistry the principal preparation of large libraries by evaporation techniques[2, 3, 5, 6] or wet-chemical deposition [4] even at higher pressures[12] is already state of the art. Our model library of new catalyst materials was based on the sol–gel procedure for the preparation of amorphous microporous mixed oxides (AMM). AMM materials show a monomodal narrow micropore size distribution, a large surface area, high porosity, and a homogeneous dispersion of the catalytically active centers in the materials (no domains). Thus a large variety of catalytically active elements can be atomically dispersed in the shape-selective environment of micropores. These materials have already shown unusual properties as powder catalysts or as catalytic membranes in selective oxidations, hydrocracking, hydrogenations, etherifications, and esterifications.[13] The vast number of AMM materials preparable makes this class of materials a promising target for combinatorial searches of catalytic activities. The individual sols identified in Figure 1 d were deposited in amounts of 1.5–5 μL corresponding to less than 200 μg of final catalyst spots in the small wells on the surface of the slate substrate, followed by controlled drying, and calcination of the library. Figure 1 c and 1 d show the library and its chemical composition. The

 © WILEY-VCH Verlag GmbH, D-69451 Weinheim, 1998 1433-7851/98/3719-2645 $ 17.50+.50/0

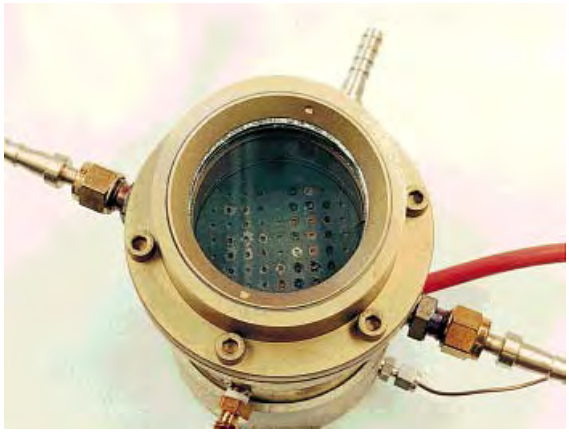


Figure 2. Photograph of the reactor with a mounted library.

reactor has been equipped with a large IR-transparent BaF_2 window (Figure 2). The calcined library was placed in the reactor and reduced at 300 °C for 3 h under a constant flow of hydrogen prior to the experiments. As test reactions the hydrogenation of 1-hexyne at 100 °C and the oxidation of isooctane and toluene at 350 °C were chosen.

Figure 3 shows the corrected IR image of the library surface during the hydrogenation of 1-hexyne at 100 °C. Of the 37 catalysts only four appear catalytically active, that is the

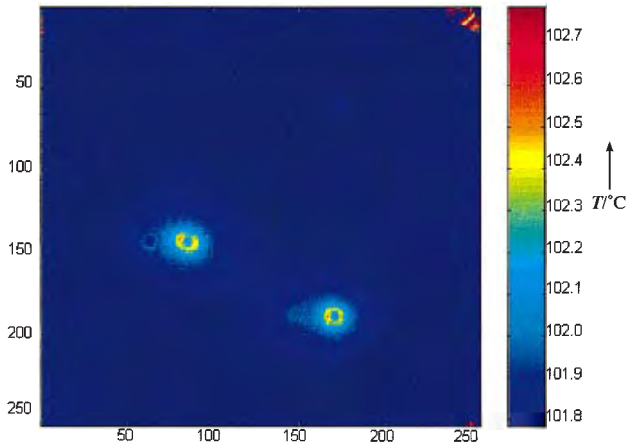


Figure 3. Emissivity corrected IR-thermographic image of the catalyst library during 1-hexyne hydrogenation in the gas phase at 100 °C. According to IR-thermographic measurements the temperature of the library was 101.8 °C.

AMM-Pd_1Si, and AMM-Pd_5Si on the left as well as AMM-Pt_2Si and AMM-Pt_5Si on the right. The clean image obtained is remarkable, since it results from 2 – 20 μg Pd or Pt in the AMM matrix. Temperature differences of 0.1 K are clearly resolved, while the highest temperature difference obtained does not exceed 0.7 °C.

On the same library by increasing the temperature to 350 °C and switching the gas-phase flow to Ar and then to air and isooctane, catalytic oxidation properties were examined. Figure 4a shows the results. Now the AMM-Ti materials were more active than the AMM-Si based catalysts. For the catalytic isooctane oxidation (Figure 4a) the catalyst samples AMM-Pt_1Ti, -Pt_2Ti, -V_5Ti, -Pd_1Ti, -Ru_5Ti, and -Cu_5Ti show activity. Since aromatic compounds usually show a different

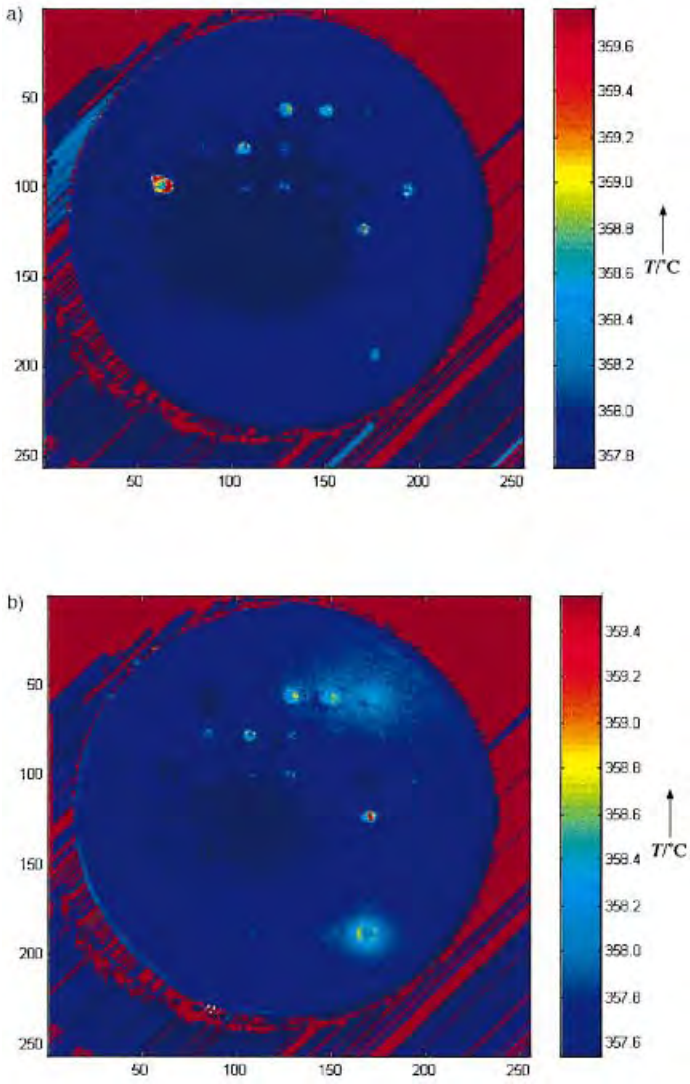


Figure 4. Emissivity-corrected IR-thermographic images of the catalyst library during isooctane oxidation in the gas phase at 350 °C (a) and of the catalyst library during toluene oxidation in the gas phase at 350 °C (b). According to IR-thermographic measurements the temperature of the library was 357.7 °C.

behavior towards catalytic oxidation, the oxidation of toluene was examined (Figure 4b). The difference observed relative to the isooctane oxidation was larger than expected. Figure 4b shows that AMM-Pd_1Ti, which was very active in isooctane oxidation, is now inactive, while the AMM-Pt_5Si, inactive in the oxidation of isooctane, is now one of the most active materials. AMM-Pt_5Ti, while active in the toluene oxidation, shows low activity for isooctane oxidation. Like in the isooctane oxidation AMM-Pt_1Ti, -Pt_2Ti, -V_5Ti, and -Cu_5Ti are active catalysts. For both oxidation experiments the actual temperature difference detected by the camera was 1 to 2 °C. This is significantly larger than the temperature difference in the hydrogenation reaction, which reflects the higher exothermicity of these reactions.

We have demonstrated that, after careful removal of artefacts, IR imaging is a very powerful tool for the detection of catalytic activities on combinatorial libraries. Temperature differences down to 0.1 K can reliably be detected and the heat evolution of catalyzed gas-phase reactions on small

 © WILEY-VCH Verlag GmbH, D-69451 Weinheim, 1998 1433-7851/98/3719-2646 $ 17.50+.50/0

catalyst amounts (< 200 μg) identified. Reactions have been observed at temperatures up to 350 °C, indicating that the method can be applied over a wide temperature range. The method has also been applied successfully to the detection and screening of enantioselectivity in liquid-phase reactions (see the following communication),[14] stressing its general usefulness.

Clearly, high-throughput screening of larger libraries could now be achieved with IR imaging of catalyst activity. We are presently engaged in the adjustment of a robotic system for automated library preparation, automated quantification of the heat response of the individual samples on the library with the help of software, and improvement of the signal sensitivity of the camera setup. Detection of catalytic activity in combinatorial libraries reduces the time necessary to find new potential catalysts. The development of the most promising candidates into useful new catalyst materials still requires more conventional laboratory techniques.

Experimental Section

For the sol preparations tetraethoxysilane (TEOS) was used as the silica precursor and tetraisopropoxytitanium as titania percursor. The following precursors were used for the other elements: $PdCl_2$, Na_2PtCl_6, $IrCl_4 \cdot x H_2O$, $RuCl_3 \cdot x H_2O$, $CoCl_2 \cdot 6 H_2O$, $[Fe(acac)_3]$, $[Mn(acac)_3]$, $(i\mathrm{PrO})_3VO$, $CrCl_3 \cdot 6 H_2O$, $[Cu(acac)_2]$, $[Ni(acac)_2]$, $ZnCl_2$, $[Pd(acac)_2]$.

Preparation of sols: The silica sols were prepared according to the standard procedure by Klein et al.[12] The compounds were used in the molar ratios for the sol preparation as indicated by the AMM notation.

The titania sols were prepared by dissolving titanium isopropoxide (3.36 mmol, 1 mL) in dry ethanol (3.33 mL) while stirring. After the mixture had been stirred for 30 min, 8 N HCl (8.33 μL) was added. After 5 min, concentrated HCl (46.7 μmol) was slowly added over about 20 min, then ethanol (833 μL), and finally an ethanolic solution (833 μL) of the metal precursor.

Preparation of the catalyst library: The catalyst library was prepared by pipetting μL amounts of titania or silica sols into the wells (diameter 1.5 mm, depth 0.6 mm) of the slate library substrate. In the case of the silica sols 1.5 μL (equivalent to 192 μg silica catalyst) and in the case of the titania sols 5 μL (equivalent to 182 μg of titania catalyst) were deposited. After evaporation of the solvent the library was heated to 65 °C with a heating rate of 1 °C min^{-1} and kept at that temperature for 30 min. Then the temperature was increased to 250 °C (heating rate of 1 °C min^{-1}) where it was kept for 180 min. The library was then allowed to cool down to room temperature at a rate of about 1 °C min^{-1}.

Correction and calibration procedure of the IR-camera system: The detector response was corrected prior to the catalytic reaction by a two-point correction taking images of the library at temperatures 5 °C above and below the desired reaction temperature (hydrogenation: 100 °C, oxidation: 350 °C). Before the organic reactant was evaporated into the feed flow of hydrogen or synthetic air, an IR image of the library was taken and subtracted as background. To assign a temperature scale to the IR images six calibration measurements were performed for each experiment taking images of the library at six different temperatures. By fitting a quadratic polynome to the pixels of the calibration images temperature values were assigned to the different colors of all corrected images.

Received: May 19, 1998 [Z11883IE]
German version: *Angew. Chem.* **1998**, *110*, 2788 – 2792

Keywords: combinatorial chemistry · heterogeneous catalysis · IR thermography

[1] a) S. R. Wilson, A. W. Czarnik, *Combinatorial Chemistry—Synthesis and Application*, Wiley, **1997**; b) Sonderausgabe: Combinatorial Chemistry, *Acc. Chem. Res.* **1996**, *29*; c) F. Balkenhohl, C. von dem Bussche-Hünnefeldt, A. Lansky, C. Zechel, *Angew. Chem.* **1996**, *108*, 2436 – 2488; *Angew. Chem. Int. Ed. Engl.* **1996**, *35*, 2289 – 2337.
[2] B. Gabriel, H. Chang, X. Sun, P. G. Schultz, X.-D. Xiang, *Science* **1995**, *270*, 273 – 275.
[3] X.-D. Xiang, X. Sun, G. Briceno, Y. Lou, K.-A. Wang, H. Chang, W. G. Wallace-Freedman, S.-W. Chen, P. G. Schultz, *Science* **1995**, *268*, 1738 – 1740.
[4] X.-D. Sun, K.-A. Wang, Y. Yoo, W. G. Wallace-Freedman, C. Gao, X.-D. Xiang, P. G. Schultz, *Adv. Mater.* **1997**, *9*, 1046 – 1049.
[5] J. Wang, Y. Yoo, C. Gao, I. Takeuchi, X. Sun, H. Chang, X.-D. Xiang, P. G. Schultz, *Science* **1998**, *279*, 1712 – 1714.
[6] a) E. Danielson, J. H. Golden, E. W. McFarland, C. M. Reaves, W. H. Weinberg, X.-D. Wu, *Nature* **1997**, *389*, 944 – 948; b) E. Danielson, M. Devenney, D. M. Giaquinta, J. H. Golden, R. C. Haushalter, E. W. McFarland, D. M. Poojary, C. M. Reaves, W. H. Weinberg, X.-D. Wu, *Science* **1998**, *279*, 837 – 839.
[7] W. H. Weinberg, B. Jandeleit, K. Self, H. Turner, *Curr. Opin. Solid State Mater. Sci.* **1998**, *3*, 104 – 110; S. M. Sankan, *Nature* **1998**, *394*, 350 – 353.
[8] a) P. C. Pawlicki, R. A. Schmitz, *Chem. Eng. Prog.* **1987**, *2*, 40 – 45; b) G. Georgiades, V. A. Self, P. A. Sermon, *Angew. Chem.* **1987**, *99*, 1050 – 1052; *Angew. Chem. Int. Ed. Engl.* **1987**, *26*, 1042 – 1044.
[9] a) F. C. Moates, M. Somani, J. Annamalai, J. T. Richardson, D. Luss, R. C. Willson, *Ind. Eng. Chem. Res.* **1996**, *35*, 4801 – 4803, b) R. C. Willson (Technology Licensing Co.), US-A 02756, **1997**, WO-A 97 32208 [*Chem. Abstr.* **1997**, *127*, 230453].
[10] S. J. Taylor, J. P. Morken, Science **1998**, *280*, 267 – 270.
[11] W. Gross, T. Hierl, M. Schulz, SPIE's International Symposium on Optical Science, Engineering and Instrumentation, San Diego, **1998**.
[12] J. Klein, H.-W. Schmidt, W. F. Maier, *Angew. Chem.*, in press.
[13] a) S. Klein, S. Thorimbert, W. F. Maier, *J. Catal.* **1996**, *163*, 476 – 488; b) S. Bukeikhanova, H. Orzesek, U. Kolb, K. Kühlein, W. F. Maier, *Catal. Lett.* **1998**, *50*, 93 – 105; c) S. Storck, W. F. Maier, I. M. Miranda Salvado, J. M. F. Ferreira, D. Guhl, W. Souverijns, J. A. Martens, *J. Catal.* **1997**, *172*, 414 – 426.
[14] M. T. Reetz, M. H. Becker, K. M. Kühling, A. Holzwarth, *Angew. Chem.* **1998**, *110*, 2792 – 2795; *Angew. Chem. Int. Ed.* **1998**, *37*, 2647 – 2650.

Time-Resolved IR-Thermographic Detection and Screening of Enantioselectivity in Catalytic Reactions

Manfred T. Reetz,* Michael H. Becker, Klaus M. Kühling, and Arnold Holzwarth

Dedicated to Professor Gernot Boche on the occasion of his 60th birthday

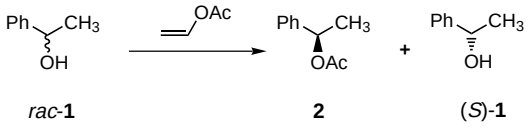
The development of chiral homogeneous metal catalysts and biocatalysts for the enantioselective synthesis of optically active compounds is of considerable academic and industrial interest.[1] Traditionally such catalysts have been prepared and studied one by one, which is extremely time-consuming. Following the advent of combinatorial methods in pharmaceutical research,[2] a few attempts have been made to apply certain aspects of combinatorial chemistry to asymmetric catalysis.[3] So far success has been limited, one reason being the lack of efficient methods for rapid screening of enantioselective reactions. Recently we showed how in-vitro evolu-

[*] Prof. M. T. Reetz, Dipl.-Chem. M. H. Becker, Dipl.-Chem. K. M. Kühling, Dr. A. Holzwarth
Max-Planck-Institut für Kohlenforschung
Kaiser-Wilhelm-Platz 1, D-45470 Mülheim an der Ruhr (Germany)
Fax: (+49) 208-306-2985
E-mail: reetz@mpi-muelheim.mpg.de

 © WILEY-VCH Verlag GmbH, D-69451 Weinheim, 1998 1433-7851/98/3719-2647 $ 17.50+.50/0

tion can be used to create libraries of mutant lipases for the catalytic enantioselective hydrolysis of chiral esters; the underlying principle is based on the combination of proper methods of random mutagenesis, gene expression, and screening.[4] Accordingly, a rapid photometer test for enantioselectivity was developed, which however is restricted to chiral esters and cannot be adapted to include such substrates as chiral alcohols, diols, amines, amino alcohols, or epoxides.[4, 5] Herein we demonstrate for the first time the use of an infrared camera[6] as a tool in the thermographic screening of enantioselective reactions mediated by biocatalysts or chiral transition metal catalysts.

In all experiments the same instrument[7] and method were employed as described in the preceding publication concerning the detection of the heterogeneous catalysts in gas-phase reactions.[8] In our system we used a modified microtiter plate for carrying out the reactions.[9] As a model reaction we first chose the enantioselective acylation of 1-phenylethanol (**1**) with vinyl acetate, which results in the formation of ester **2**. This transformation is known to occur with 99% enantioselectivity in favor of the (*R*)-ester **2** in the presence of catalytic amounts of immobilized lipase from *Candida antarctica* (Novo SP 435; Scheme 1).[10]



rac-**1** **2** (*S*)-**1**

Scheme 1. Lipase-catalyzed enantioselective synthesis of **2** from *rac*-**1**.

In the present system we prepared separate solutions of vinyl acetate with (*R*)-**1**, (*S*)-**1**, and *rac*-**1** in the wells of a modified microtiter plate.[11] Prior to the initiation of the reaction by addition of the enzyme, the temperature was calibrated in the range of 25–35 °C. Figure 1a shows the respective arrangement of the reaction vessels containing the different solutions at various concentrations at 30 °C. Then the immobilized enzyme (5 mg) was added and the plate shaken (5 s). Temperature changes in the reaction wells were monitored periodically, shaking being interrupted for the measurements. Detection of the reactions was performed for 5 s, resulting in 250 recordings which were averaged and reproduced visually in Figures 1a–c. Although the samples in Figure 1a do not yet contain the biocatalyst, several of them show semicircle-like thermographic emissions of weak intensities. These effects originate from the top part of the walls of the glass vessels and are typical of the setup. The exact position of each vessel changes slightly upon shaking. It is the IR emission stemming from the center of the reaction vessel which is of actual interest and which is not influenced by the effect described above. Figure 1b clearly shows that (*R*)-**1** reacts preferentially with respect to (*S*)-**1**, as seen by the appearance of red spots corresponding to a significant rise in temperature. Under the same conditions the well containing (*S*)-**1** remains cool, whereas *rac*-**1** leads to a moderate rise in temperature. The major part of the reaction is over after 3.5 minutes (Figure 1c). The lowest horizontal row constitutes the control experiment in the absence of enzyme.

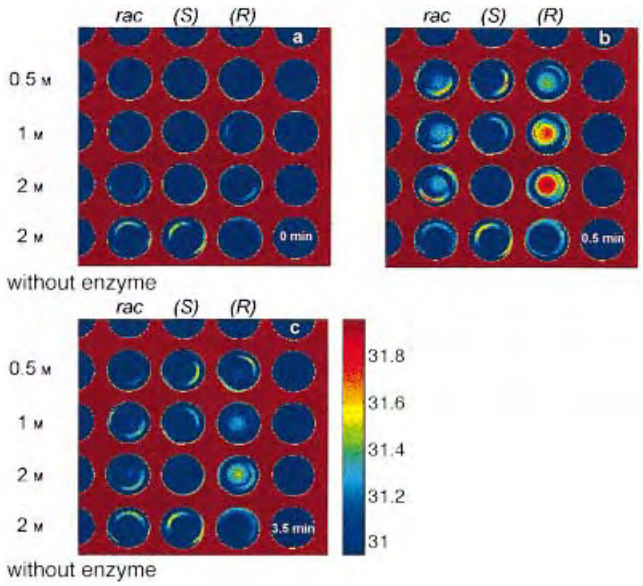
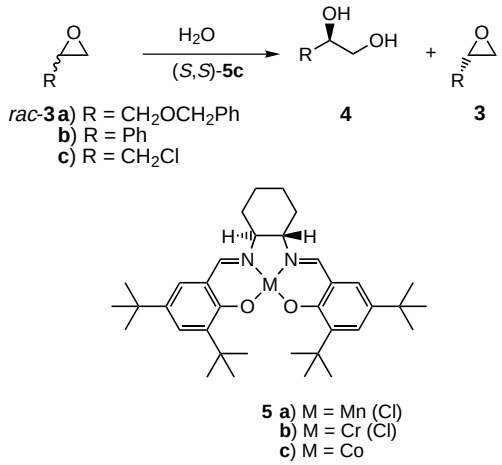


Figure 1. Time-resolved IR-thermographic imaging of the lipase-catalyzed enantioselective acylation of **1** after a) 0, b) 0.5, and c) 3.5 min. The control experiment without enzyme is given in the bottom row in each case. The bar on the far right is the temperature/color key of the temperature window used [°C].

We then turned to enantioselective transition metal catalysis and chose the ring-opening hydrolysis of epoxides **3** with formation of diols **4** as a model reaction under homogeneous conditions (Scheme 2). Jacobsen et al. have described manganese-, chromium-, and cobalt-containing salen catalysts



rac-**3a**) R = CH_2OCH_2Ph **4** **3**
b) R = Ph
c) R = CH_2Cl

5a) M = Mn (Cl)
b) M = Cr (Cl)
c) M = Co

Scheme 2. Transition metal catalyzed enantioselective synthesis of **4.** See text for more details on the substrates **3** and the catalysts **5**.

5a–c (salen = *N*,*N*′-bis(salicylidene)ethylenediamine dianion), respectively, which induce the kinetic resolution of racemic epoxides by enantioselective ring-opening reactions.[12] In the case of water as the nucleophile, the cobalt catalyst **5c** was reported to be the most active and selective.[13] Accordingly, the (*S*,*S*)-configurated catalyst **5c** reacts completely selectively with (*R*)-**3b** or (*S*)-**3c** in respective racemic mixtures (note change in descriptors due to the CIP-convention), whereas the (*R*,*R*)-catalyst induces the opposite stereoselectivity.

In order to demonstrate the screening capability of the IR camera under these homogeneous conditions, the activity and

 © WILEY-VCH Verlag GmbH, D-69451 Weinheim, 1998 1433-7851/98/3719-2648 $ 17.50+.50/0

selectivity of the three metal catalysts (*S*,*S*)-**5a**–**c** were tested thermographically in the hydrolysis of epichlorohydrin **3c**.[14] The corresponding time-resolved temperature changes are recorded in Figure 2. The cobalt complex (*S*,*S*)-**5c** is found to be the most active catalyst; it reacts selectively with the epoxide (*S*)-**3c**. The Cr catalyst (*S*,*S*)-**5b** is also selective, although less active, whereas the Mn complex (*S*,*S*)-**5a** displays no significant activity. This is in line with results obtained by Jacobsen et al. using benzoic acid as the nucleophile.[12] It can also be seen that in the case of the Co complex heat generation after seven minutes is so pronounced for the reaction of (*S*)-**3c** and *rac*-**3c** that no significant difference in visualization using the applied temperature window (1 °C range) can be detected. Therefore, the temperature scale covered by the window was increased to a total of 10 °C, resulting in the clear identification of the "hottest" reaction (cf. Figure 2e with 2f).

Finally, relative substrate activity was screened by studying the hydrolysis of three different chiral epoxides **3a**–**c** with the cobalt catalyst (*S*,*S*)-**5c**.[15] Figures 3a–c clearly demonstrate that (*S*)-**3a**[16] is the most reactive substrate followed by (*S*)-**3c** and (*R*)-**3b**. The same relative reactivity of (*R*)-**3b** and (*S*)-**3c** has previously been reported by Jacobsen et al. in laboratory-scale reactions.[13]

In conclusion, we have demonstrated that time-resolved IR-thermographic screening of enantioselectivity in catalytic reactions is feasible. Since spacial resolution is no problem, the screening of large libraries of asymmetric catalysts should be possible. The method should also be amenable to the study of other chemical and biochemical processes in solution such as molecular recognition in host–guest chemistry or antibody–antigen interactions. We are currently attempting to refine our approach to include quantitative analyses of catalyst activity and (enantio)selectivity.

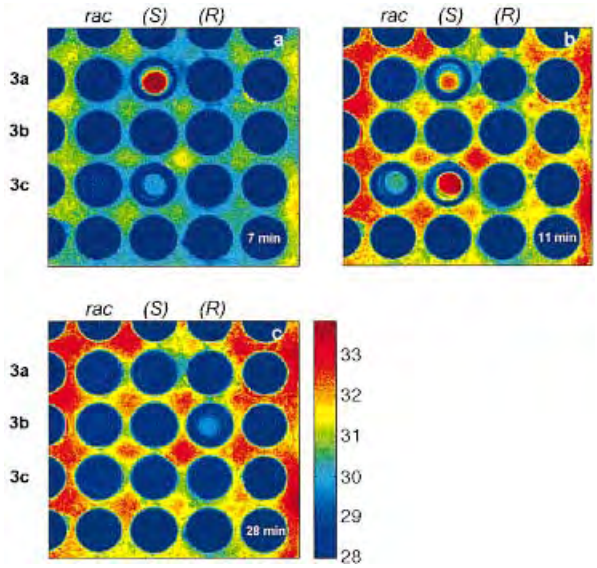


Figure 3. Time-resolved IR-thermographic imaging of the hydrolysis of epoxides **3a**–**c** catalyzed by (*S*,*S*)-**5c** after a) 7, b) 11, and c) 28 min. The bar on the far right is the temperature/color key of the temperature window used [°C].

Received: May 19, 1997 [Z11882IE]
German version: *Angew. Chem.* **1998**, *110*, 2792–2795

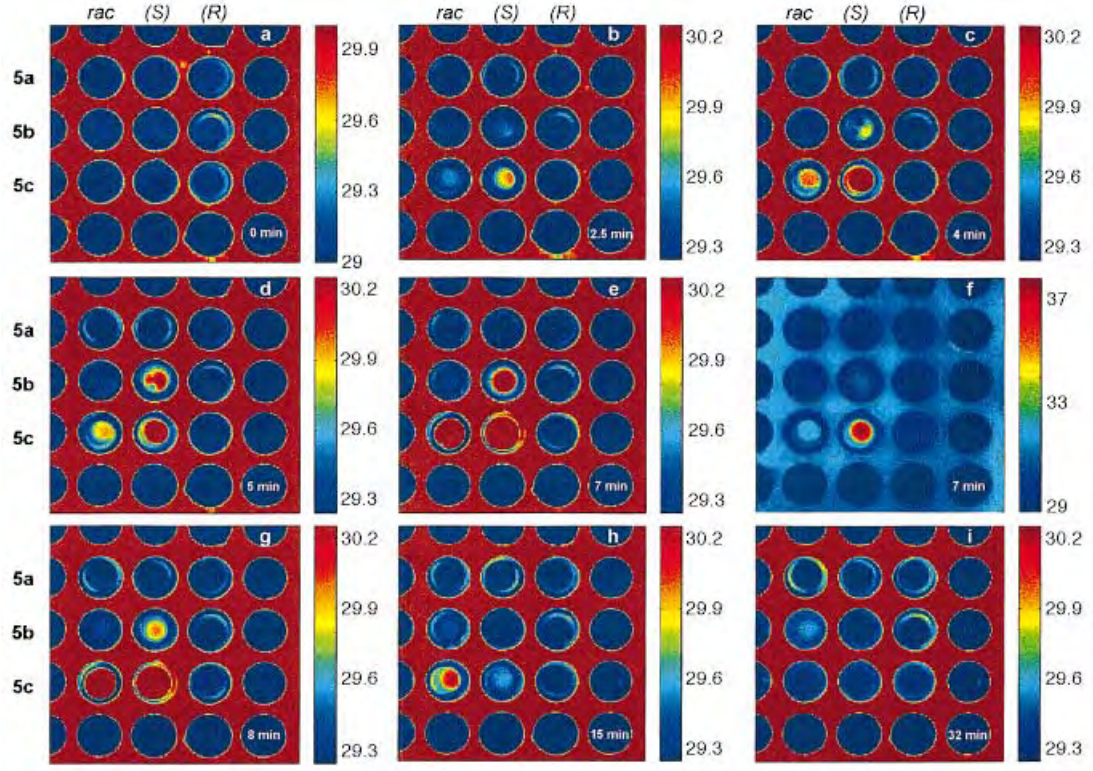


Figure 2. Time-resolved IR-thermographic imaging of the hydrolysis of **3c** catalyzed by metal complexes (*S*,*S*)-**5a**–**c** after a) 0, b) 2.5, c) 4, d) 5, e) 7, g) 8, h) 15, and i) 32 min. In (f) the same figure is shown as in (e), however, the temperature scale ranges over 10 K. The bar on the far right of each figure is the temperature/color key of the temperature window used [°C].

 © WILEY-VCH Verlag GmbH, D-69451 Weinheim, 1998 1433-7851/98/3719-2649 $ 17.50+.50/0

Keywords: asymmetric catalysis · biocatalysts · combinatorial chemistry · homogeneous catalysis · IR-thermographic screening

[1] a) D. J. Berrisford, C. Bolm, K. B. Sharpless, *Angew. Chem.* **1995**, *107*, 1159 – 1171; *Angew. Chem. Int. Ed. Engl.* **1995**, *34*, 1059 – 1070; b) R. Noyori, *Asymmetric Catalysis in Organic Synthesis*, Wiley, New York, **1994**; c) A. Pfaltz, *Acc. Chem. Res.* **1993**, *26*, 339 – 345; d) *Chirality in Industry: The Commercial Manufacture and Applications of Optically Active Compounds* (Eds.: A. N. Collins, G. N. Sheldrake, J. Crosby), Wiley, Chichester, **1992**; e) *Chirality in Industry II: Developments in the Commercial Manufacture and Applications of Optically Active Compounds* (Eds.: A. N. Collins, G. N. Sheldrake, J. Crosby), Wiley, Chichester, **1997**; f) A. Persidis, *Nat. Biotechnol.* **1997**, *15*, 594 – 595; g) R. A. Sheldon, *Chirotechnology: Industrial Synthesis of Optically Active Compounds*, Dekker, New York, **1993**; h) *Industrial Enzymology* (Eds.: T. Godfrey, S. West), 2nd ed., Macmillan, London, **1996**.

[2] a) F. Balkenhohl, C. von dem Bussche-Hünnefeld, A. Lansky, C. Zechel, *Angew. Chem.* **1996**, *108*, 2436 – 2488; *Angew. Chem. Int. Ed. Engl.* **1996**, *35*, 2288 – 2337; b) J. S. Früchtel, G. Jung, *Angew. Chem.* **1996**, *108*, 19 – 46; *Angew. Chem. Int. Ed. Engl.* **1996**, *35*, 17 – 42; c) *Chem. Rev.* **1997**, *97* (2), 347 – 510 (Special Issue on Combinatorial Chemistry); d) S. R. Wilson, A. W. Czarnick, *Combinatorial Chemistry: Synthesis and Application*, Wiley, New York, **1997**.

[3] a) G. Liu, J. A. Ellman, *J. Org. Chem.* **1995**, *60*, 7712 – 7713; b) K. Burgess, H.-J. Lim, A. M. Porte, G. A. Sulikowski, *Angew. Chem.* **1996**, *108*, 192 – 194; *Angew. Chem. Int. Ed. Engl.* **1996**, *35*, 220 – 222; c) B. M. Cole, K. D. Shimizu, C. A. Krueger, J. P. A. Harrity, M. L. Snapper, A. H. Hoveyda, *Angew. Chem.* **1996**, *108*, 1776 – 1779 *Angew. Chem. Int. Ed. Engl.* **1996**, *35*, 1668 – 1671; d) C. Gennari, H. P. Nestler, U. Piarulli, B. Salom, *Liebigs Ann.* **1997**, 637 – 647.

[4] M. T. Reetz, A. Zonta, K. Schimossek, K. Liebeton, K.-E. Jaeger, *Angew. Chem.* **1997**, *109*, 2961 – 2963; *Angew. Chem. Int. Ed. Engl.* **1997**, *36*, 2830.

[5] For an alternative quick photometer test of ester hydrolysis see: L. E. Janes, R. J. Kazlauskas, *J. Org. Chem.* **1997**, *62*, 4560 – 4561.

[6] Application of IR cameras in the thermographic detection of chemical processes based on heterogeneous catalysis: a) G. Georgiades, V. A. Self, P. A. Sermon, *Angew. Chem.* **1987**, *99*, 1050 – 1052; *Angew. Chem. Int. Ed. Engl.* **1987**, *26*, 1042 – 1043; b) P. C. Pawlicki, R. A. Schmitz, *Chem. Eng. Prog.* **1987**, *83* (2), 40 – 45; c) L. Lobban, G. Philippou, D. Luss, *J. Phys. Chem.* **1989**, *93*, 733 – 736; d) F. C. Moates, M. Somani, J. Annamalai, J. T. Richardson, D. Luss, R. C. Willson, *Ind. Eng. Chem. Res.* **1996**, *35*, 4801 – 4803; e) D. E. Bergbreiter, *Chemtracts: Org. Chem.* **1997**, *10*, 683 – 686; f) S. J. Taylor, J. P. Morken, *Science* **1998**, *280*, 267 – 270.

[7] In our system we used an AIM-256[2] IR camera (AIM, Heilbronn, Germany) with a PtSi-FPA detector and a germanium lens. This detection system is sensitive to IR radiation in the wavelength range 3 – 5 μm and to temperature changes of 10 – 100 mK, depending upon the conditions.

[8] A. Holzwarth, H. W. Schmidt, W. F. Maier, *Angew. Chem.* **1998**, *110*, 2788 – 2792; *Angew. Chem. Int. Ed.* **1998**, *37*, 2644 – 2647.

[9] A commercially available Eppendorf-Thermomixer was modified such that the top was replaced by an aluminum plate. Holes were drilled into the plate and cylindrical glass reaction vessels about 8 mm in diameter and 35 mm in height placed therein.

[10] a) A. L. E. Larsson, B. A. Persson, J.-E. Bäckvall, *Angew. Chem.* **1997**, *109*, 1256 – 1258; *Angew. Chem. Int. Ed. Engl.* **1997**, *36*, 1211 – 1212; b) M. T. Reetz, A. Zonta, J. Simpelkamp, *Angew. Chem.* **1995**, *107*, 373 – 376 *Angew. Chem. Int. Ed. Engl.* **1995**, *34*, 301 – 303.

[11] In the experiment equimolar solutions of 100 μL of (*R*)-**1**, (*S*)-**1** and *rac*-**1** in toluene were mixed correspondingly with 100 μL vinyl acetate in toluene. Three different concentrations were used: 0.5 M, 1 M and 2 M.

[12] a) J. F. Larrow, S. E. Schaus, E. N. Jacobsen, *J. Am. Chem. Soc.* **1996**, *118*, 7420 – 7421; b) S. E. Schaus, E. N. Jacobsen, *Tetrahedron Lett.* **1996**, *37*, 7937 – 7940; c) E. N. Jacobsen, F. Kakiuchi, R. G. Konsler, J. F. Larrow, M. Tokunaga, *Tetrahedron Lett.* **1997**, *38*, 773 – 776.

[13] M. Tokunaga, J. F. Larrow, F. Kakiuchi, E. N. Jacobsen, *Science* **1997**, *277*, 936 – 938.

[14] For the catalyst screening in the hydrolysis of epichlorohydrin **3c** a mixture of (*S*,*S*)-**5a**, (*S*,*S*)-**5b**, and (*S*,*S*)-**5c** (each 60.0 μmol) in toluene (1.00 mL) and acetic acid (120 μmol, 7.21 mg, 6.86 mL) was stirred in an open flask for 1 h. After removal of the solvent the three residues were dried in vacuum. Each of these activated catalysts (*S*,*S*)-**5a – c** was dissolved in toluene (300 μL) and distributed in three reaction vessels. Epichlorohydrin **3c** (1.00 mmol, 92.5 mg, 78.4 mL) was added. As described before the temperature was calibrated in the range of 24 – 39 °C. The reaction was initiated by the addition of water (0.55 equiv, 0.55 mmol, 9.9 μL) at 27 °C. Screening was performed similar to the first experiments, except that the detection time was prolonged, averaging 500 recordings in 10 s.

[15] For the substrate activity screening the cobalt catalyst (*S*,*S*)-**5c** was activated as described before. Nine aliquots each containing 2.00 μmol of the catalyst in toluene (100 μL) were distributed in the wells of the microtiter plate. The three different epoxides **3a – c** in the (*R*)-, (*S*)-, and *rac*-form were added to the catalyst, resulting in the arrangement shown in Figure 3. The reaction mixtures contained the epoxides at a concentration of 3.95 M in toluene and a final volume of 253 μL. Detection of the reactions was performed for 10 s, resulting in 500 recordings which were averaged.

[16] Substrate **3a** was not included in the studies carried out by Jacobsen et al.[12, 13]

Molecular Model for Aluminophosphates Containing Fluoride as a Structure-Directing and Mineralizing Agent**

Yu Yang, Jiri Pinkas, Martina Schäfer, and Herbert W. Roesky*

Dedicated to Professor Ernst Otto Fischer on the occasion of his 80th birthday

Microporous materials such as zeolites, alumino- and gallophosphates, and their transition metal substituted analogues are currently targets of a very active research effort. Their traditional uses as size- and shape-selective catalysts,[1] molecular sieves, adsorbents, and ion exchangers are complemented by new applications as reaction vessels of molecular dimensions,[2] highly ordered matrices for fabrication of optoelectronic nanodevices[3] and sensors,[4] and molds for the preparation of carbon molecular sieves.[5] Their syntheses rely mainly on hydrothermal methods in aqueous and recently also in nonaqueous media.[6, 7] Important developments in the synthetic methodology were achieved by introduction of HF in the reaction mixture. Fluoride acts as a mineralizer and a structure-directing agent,[8] and its presence promotes growth of large crystals of molecular sieves.[9] Fluoride itself is in many cases not retained in the resulting structure. However, in some frameworks fluoride ions coordinate to the metal center, as has been reported for aluminophosphates (AFI,[8]

[*] Prof. Dr. H. W. Roesky, Y. Yang, Dr. J. Pinkas, Dr. M. Schäfer
Institut für Anorganische Chemie der Universität
Tammannstrasse 4, D-37077 Göttingen (Germany)
Fax: (+49) 551-393373
E-mail: hroesky@gwdg.de

[**] This work was supported by the Deutsche Forschungsgemeinschaft. J.P. thanks the Alexander von Humboldt-Stiftung for a research fellowship.

 © WILEY-VCH Verlag GmbH, D-69451 Weinheim, 1998 1433-7851/98/3719-2650 $ 17.50+.50/0

LTA,[10] AST,[11] GIS,[12] and CHA[13]), for gallophosphates (LTA,[8] CLO,[14] CHA,[15] and ULM-*n* compounds[16]), and recently also for indium phosphates.[17] Other such examples include transition metal doped aluminophosphates (CrAPO-5,[18] CoAPO-34[19]) as well as microporous oxyfluorinated metallophosphates of vanadium[20] and iron.[21] Interestingly, fluoride can also coordinate to the phosphorus center and form fluorophosphate (Zn[22]).

There has been increasing interest in developing rational syntheses of alumino- and gallophosphates. To reach this goal, we and others followed the building-block strategy in which preformed clusters of alumino- or gallophosphate that possess reactive groups and are soluble in organic solvents are expected to condense and form extended three-dimensional structures. Pore size, shape, and dimensionality would be governed by the characteristics of the building blocks. We extended the "library" of known molecular models of alumino- and gallophosphate secondary building units (SBUs) found in extended three-dimensional structures of these materials.[23] To the previously known model compounds, mimicking a single four-ring[24–28] (4R or 4) and a double four-ring[28–31] (D4R or 4–4), we added a double six-ring[32] (D6R or 6–6) and a single six-ring[33] (6R or 6). Herein we report on the synthesis and the structural and spectroscopic characterization of aluminophosphonate cluster **1**, which contains two tricyclic capped six-ring moieties (C6R or $6 \equiv 1$) and a central cube-like unit (D4R) incorporating terminal and bridging fluoride ions (FAl(μ-F)$_2$AlF).

$[Cs_3(thf)_3F(i\text{BuAl})_3(t\text{BuPO}_3)_4]_2[(i\text{BuAl})_2Al_2(\mu\text{-F})_2(t\text{BuPO}_3)_4]$ **1**

Reaction of equimolar amounts of Cs(*i*Bu$_3$AlF)[34] and *tert*-butylphosphonic acid in THF provides **1** as colorless block crystals in 25% yield. The reaction solution contains several other by-products, one of which was identified by ^{31}P NMR spectra as cubic [*i*BuAlO$_3$P*t*Bu]$_4$ (**2**).[29] The molecular structure of **1** in the solid state was established by single-crystal X-ray crystallography (Figure 1).[35] The cluster consists of a central cube-like $Al_4P_4O_{12}(\mu\text{-F})_2F_2$ core and two peripheral tricyclic $Al_3P_4O_{12}$ units. These two capped six-rings are related by a crystallographically imposed C_2 axis passing through the bridging F1 and F2 atoms; **1** possesses pseudo-C_{2v} symmetry. The capped six-rings are isoelectronic with the $[Al_3P_4O_{16}]^{3-}$ structural motif found in a host of layered aluminophosphates,[7b] and the C6R building unit was also found in three-dimensional frameworks of BPH[36] and AFS[23] types. The central cube is connected to the two capped six-rings through "sandwiched" triangles of cesium atoms. These cesium atoms interact with the three terminal phosphonate oxygen atoms of the C6R units along with the terminal fluorine atoms F3 and four bridging oxygen atoms of the central core. Recently, we reported similar interactions of gallophosphonates with Li, Na, and K ions.[37] The coordination sphere of each cesium center is completed by one oxygen atom of a THF molecule. There are two additional THF half-molecules of crystallization in the asymmetric unit. Compound **1** contains Al atoms in two different coordination environments: two octahedral *mer*-Al1O$_3$F$_3$ and eight tetrahedral AlO$_3$C units. A prominent feature of **1** is the FAl(μ-F)$_2$AlF unit formed from two edge-sharing octahedra. This unit can serve as a molecular model for analogous units observed in GIS- and CHA-type AlPO$_4$ phases. The Al1–F1 and Al1–F2 bridging distances (1.863(3) and 1.909(3) Å, respectively) closely match the corresponding distances in AlPO$_4$-CHA (1.854(2) and 1.894(2) Å).[13b] The short Al1–F3 distance (1.724(3) Å) is the same as in bioctahedral $[Al_2F_8(H_2O)_2]^{2-}$ (1.729(2) Å).[38] The F3 atoms are four-coordinated and reside 0.95 Å above the triangle of the three cesium atoms (Cs–F3 2.835(3)–2.970(4) Å).

The ^{13}C DEPT NMR spectra display two singlets (ratio ca. 3:1) for *i*BuAl methyl groups and four doublets (3:2:2:2) for *t*BuP methyl groups, which is in agreement with the solid-state structure. Furthermore, four signals in the ^{31}P NMR spectrum of **1** suggest that the structure is retained in solution. A single resonance at $\delta = 14.7$ for the three crystallographically inequivalent phosphorus atoms P3, P4, and P5 hints at a rotation of the capped six-ring units about the Al1-F1-P6 axes that is fast on the NMR time scale. In fact, on lowering the temperature below $-20\,^{\circ}$C, this signal decoalesces to two peaks ($\delta = 14.3$, 13.8 at $-60\,^{\circ}$C). This attests to the slow rotation of the C6R units. Owing to its lower intensity, the high-field signal is assigned to P4, and the stronger signal at low field to P3 and P5. These two phosphorus centers are rendered equivalent in a racemization process by which **1** is interconverted between left- and right-handed C_2-symmetric propellerlike enantiomeric forms via a C_{2v}-symmetric transition state. A signal at $\delta = 16.5$ is very close to the ^{31}P NMR chemical shift of **2** ($\delta = 16.9$), and it was assigned to P6 of the capping phosphonate groups. The remaining two signals of equal intensity show coupling to fluorine and must therefore belong to the central D4R unit. A triplet ($\delta = 18.8$) and a broad quartet ($\delta = 30.3$) were assigned to P2 and P1, respectively; there is a correlation between the ^{31}P NMR shift and the mean P-O-Al bond angle in AlPO$_4$ polymorphs.[39] The phosphorus center is more strongly shielded as the average P-O-Al angle widens. We found that this correlation is also valid for the phosphonate groups in **1** and **2** ($r = 0.9902$) as well as [MeAlO$_3$P*t*Bu]$_6$ (**3**)[32] (Table 1). The ^{19}F NMR spectrum

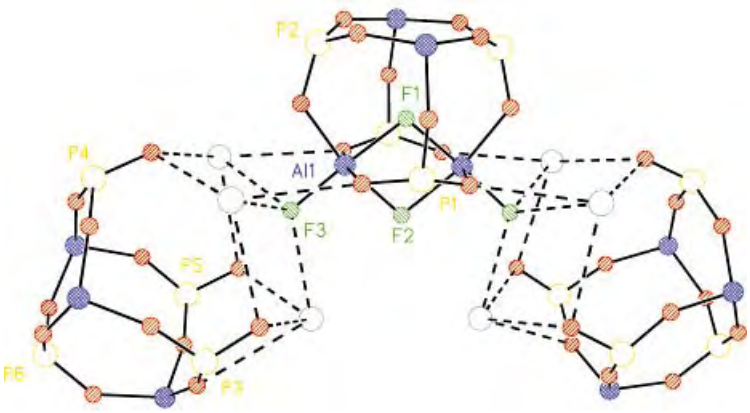


Figure 1. Molecular structure of **1**. The carbon atoms of all *i*BuAl and *t*BuP groups and THF molecules are omitted for clarity; Al: blue, P: yellow, O: red, F: green, Cs: gray. Selected bond distances [Å] and angles [°]: Al1–F1 1.863(3), Al1–F2 1.909(3), Al1–F3 1.724(3); Al1-F1-Al1′ 101.9(2), Al1-F2-Al1′ 98.5(2).

 © WILEY-VCH Verlag GmbH, D-69451 Weinheim, 1998 1433-7851/98/3719-2651 $ 17.50+.50/0

Table 1. Correlation between the ^{31}P NMR chemical shift and the mean P-O-Al bond angle in **1**, **2**, and **3**.

Compd, atom	$\delta(^{31}P)$[a]	P-O-Al [°]
1, P1	30.2	128.7
1, P2	19.0	143.6
1, P6	17.2	147.5
2	16.9	150.5
3	13.4	154.6

[a] In C_6D_6.

features two broad singlets of equal intensity ($\delta = -96.8$ and -131.5). We assigned them to the bridging and terminal fluorine atoms, respectively, in analogy to $AlPO_4$-CJ2[40] and in accord with an empirical rule that higher coordination causes higher shielding.[20b]

Compound **1** features several interesting structural motifs that are closely related to those of zeolitic frameworks. Moreover, the strong Al–F bonds in the starting material are retained in the product, which provides a lead for the investigation of the mineralizing action and structure-directing role of fluoride in the microporous materials by ^{19}F NMR spectroscopy. Most importantly, this molecule contains several reactive centers, which may be employed in the transformation of this precursor to porous materials.

Experimental Section

1: A solution of *tert*-butylphosphonic acid (0.23 g, 1.7 mmol) in THF (20 mL) was added dropwise to an equimolar solution of Cs(*i*Bu$_3$AlF) in THF (5 mL) at 0 °C. The resulting solution was stirred overnight at room temperature and then concentrated to 15 mL. A white precipitate was removed by filtration, and the clear solution was allowed to stand at room temperature for 10 d. Colorless block crystals of **1** (0.13 g) formed in 25% yield; m.p. > 350 °C. ^1H NMR (250 MHz, [D$_8$]THF): $\delta = -0.18$ (d, J = 6.9 Hz, 4H; Al(D4R)CH$_2$), -0.09 (d, J = 7.0 Hz, 12H; Al(C6R)CH$_2$), 0.91–1.29 (m, 156H; CH$_3$), 1.77 (m; THF), 1.89 (sept, J = 6.6 Hz, 8H; CH), 3.64 (m; THF); ^{13}C DEPT NMR (100 MHz, [D$_8$]THF): $\delta = 68.2$ (s; CH_2O, THF), 28.8 (s; Al(C6R)CH$_2$CH(*C*H$_3$)$_2$), 28.5 (s; Al(D4R)CH$_2$CH(*C*H$_3$)$_2$), 27.0 (s; Al(D4R)CH$_2$*C*H(CH$_3$)$_2$), 26.9 (s; Al(C6R)CH$_2$*C*H(CH$_3$)$_2$), 26.4 (s; *C*H$_2$, THF), 26.1 (d, J = 1.5 Hz; P(3, 4, 5)C(*C*H$_3$)$_3$), 26.0 (d, J = 1.8 Hz; PC(*C*H$_3$)$_3$), 25.9 (d, J = 2.1 Hz; PC(*C*H$_3$)$_3$), 24.9 (d, J = 1.7 Hz; P(1)C(*C*H$_3$)$_3$); ^{19}F NMR (188 MHz, [D$_8$]THF): $\delta = -96.8$ (s, $\Delta\tilde{\nu}_{1/2}$ = 100 Hz; F1, F2), -131.5 (s, $\Delta\tilde{\nu}_{1/2}$ = 100 Hz; 2F3); ^{31}P NMR (162 MHz, [D$_8$]THF): $\delta = 30.3$ (br q, J(PF) = 9 Hz, 2P; P1), 18.8 (t, J(PF) = 11.5 Hz, 2P; P2), 16.5 (s, 2P; P6), 14.7 (s, 6P; P3, P4, P5); IR (KBr): $\tilde{\nu}$ = 2952, 2926, 2871, 1481, 1464, 1425, 1363, 1263, 1187, 1148, 1047, 946, 878, 836, 813, 698, 671, 541, 504, 466 cm^{-1}; MS (EI): *m/z* (%): 832 (87) [Bu$_6$P$_4$Al$_4$O$_{12}$F$_3$], 785 (100) [Bu$_6$P$_4$Al$_4$O$_{12}$F]; elemental analyses (THF removed by drying under vacuum) calcd for $C_{80}H_{180}Al_{10}Cs_6F_4O_{36}P_{12}$ (3233.48): C 29.72, H 5.61; found: C 29.8, H 6.1.

Received: April 14, 1998 [Z11729IE]
German version: *Angew. Chem.* **1998**, *110*, 2795–2798

Keywords: aluminum · cage compounds · fluorine · phosphonate complexes · zeolite analogues

[1] a) J. M. Thomas, *Angew. Chem.* **1994**, *106*, 963; *Angew. Chem. Int. Ed. Engl.* **1994**, *33*, 913; b) N. Herron, W. E. Farneth, *Adv. Mater.* **1996**, *8*, 959; c) I. W. C. E. Arends, R. A. Sheldon, M. Wallau, U. Schuchardt, *Angew. Chem.* **1997**, *109*, 1190; *Angew. Chem. Int. Ed. Engl.* **1997**, *36*, 1144; d) M. E. Davis, *Chem. Eur. J.* **1997**, *3*, 1745.

[2] a) G. A. Ozin, C. Gil, *Chem. Rev.* **1989**, *89*, 1749; b) *Inclusion Chemistry with Zeolites: Nanoscale Materials by Design* (Eds.: N. Herron, D. R. Corbin), Kluwer, Dodrecht, **1995**; c) G. Sundararabu, M. Leibovitch, D. R. Corbin, J. R. Scheffer, V. Ramamurthy, *Chem. Commun.* **1996**, 2159; d) S. B. Ogunwumi, T. Bein, *Chem. Commun.* **1997**, 901; e) M. J. Sabater, A. Corma, A. Domenech, V. Fornes, H. Garcia, *Chem. Commun.* **1997**, 1285; f) B.-Z. Zhang, X.-Y. Li, *Chem. Commun.* **1998**, 349.

[3] a) G. A. Ozin, A. Kuperman, A. Stein, *Angew. Chem.* **1989**, *101*, 373; *Angew. Chem. Int. Ed. Engl.* **1989**, *28*, 359; b) G. A. Ozin, *Adv. Mater.* **1992**, *4*, 612; c) G. A. Ozin, S. Ozkar, *Adv. Mater.* **1992**, *4*, 11.

[4] a) K. J. Balkus, L. J. Ball, B. E. Gnade, J. M. Anthony, *Chem. Mater.* **1997**, *9*, 380. b) T. Bein, *Chem. Mater.* **1996**, *8*, 1636.

[5] J. Rodriguez-Mirasol, T. Cordero, L. R. Radovic, J. J. Rodriguez, *Chem. Mater.* **1998**, *10*, 550.

[6] a) Q. Huo, R. Xu, *J. Chem. Soc. Chem. Commun.* **1990**, 783; b) R. H. Jones, J. M. Thomas, R. Xu, Q. Huo, Y. Xu, A. K. Cheetham, D. Bieber, *J. Chem. Soc. Chem. Commun.* **1990**, 1170.

[7] a) R. E. Morris, S. J. Weigel, *Chem. Soc. Rev.* **1997**, 309; b) S. Oliver, A. Kuperman, G. A. Ozin, *Angew. Chem.* **1998**, *110*, 48; *Angew. Chem. Int. Ed*. **1998**, *37*, 46.

[8] H. Kessler, J. Patarin, C. Schott-Darie in *Advanced Zeolite Science and Application*, (Eds.: J. C. Jansen, M. Stöcker, H. G. Krage, J. Weitkamp), Elsevier, Amsterdam (*Stud. Surf. Sci. Catal.* **1994**, *85*, 75).

[9] a) A. Kuperman, S. Nadimi, S. Oliver, G. A. Ozin, J. M. Garces, M. M. Olken, *Nature* **1993**, *365*, 239; b) S. Nadimi, S. Oliver, A. Kuperman, A. Lough, G. A. Ozin, J. M. Garcés, M. M. Olken, P. Rudolf in *Zeolites and Related Microporous Materials: State of the Art 1994* (Eds.: J. Weitkamp, H. G. Karge, H. Pfeifer, W. Hölderich), Elsevier, Amsterdam (*Stud. Surf. Sci. Catal.* **1994**, *84*, 93).

[10] a) L. Sierra, C. Deroche, H. Gies, J. L. Guth, *Microporous Mater.* **1994**, *3*, 29; b) L. Schreyeck, F. D'agosto, J. Stumbe, P. Caullet, J. C. Mougenel, *Chem. Commun.* **1997**, 1241.

[11] C. Schott-Darie, J. Patarin, P. Y. Le Goff, H. Kessler, E. Benazzi, *Microporous Mater.* **1994**, *3*, 123.

[12] J.-L. Paillaud, B. Marler, H. Kessler, *Chem. Commun.* **1996**, 1293.

[13] a) M. M. Harding, B. M. Kariuki, *Acta Crystallogr. Sect. C* **1994**, *50*, 852; b) S. Oliver, A. Kuperman, A. Lough, G. A. Ozin, *J. Mater. Chem.* **1997**, *7*, 807.

[14] M. Estermann, L. B. McCusker, C. Baerlocher, A. Merrouche, H. Kessler, *Nature* **1991**, *352*, 320.

[15] C. Schott-Darie, H. Kessler, M. Soulard, V. Gramlich, E. Benazzi in *Zeolites and Related Microporous Materials: State of the Art 1994* (Eds.: J. Weitkamp, H. G. Karge, H. Pfeifer, W. Hölderich), Elsevier, Amsterdam (*Stud. Surf. Sci. Catal.* **1994**, *84*, 101).

[16] a) G. Ferey, *J. Fluorine Chem.* **1995**, *72*, 187; b) T. Loiseau, G. Ferey, *J. Mater. Chem.* **1996**, *6*, 1073; c) S. J. Weigel, S. C. Weston, A. K. Cheetham, G. D. Stucky, *Chem. Mater.* **1997**, *9*, 1293.

[17] H. Du, J. Chen, W. Pang, J. Yu, I. D. Williams, *Chem. Commun.* **1997**, 781.

[18] S. F. Radaev, W. Joswig, W. H. Baur, *J. Mater. Chem.* **1996**, *6*, 1413.

[19] N. Rajic, A. Ristic, A. Tuel, V. Kaucic, *Zeolites* **1997**, *18*, 115.

[20] a) D. Riou, G. Ferey, *J. Solid State Chem.* **1994**, *111*, 422; b) D. Riou, F. Taulelle, G. Ferey, *Inorg. Chem.* **1996**, *35*, 6392.

[21] a) M. Cavellec, D. Riou, J.-M. Greneche, G. Ferey, *Inorg. Chem.* **1997**, *36*, 2187. b) M. Cavellec, C. Egger, J. Linares, M. Nogues, F. Varret, G. Ferey, *J. Solid State Chem.* **1997**, *134*, 349.

[22] P. S. Halasyamani, M. J. Drewitt, D. O'Hare, *Chem. Commun.* **1997**, 867.

[23] W. M. Meier, D. H. Olson, *Atlas of Zeolite Structure Types*, 3rd revised ed., Butterworth-Heinemann, London, **1992**.

[24] S. A. Sangokoya, W. T. Pennington, G. H. Robinson, D. C. Hrncir, *J. Organomet. Chem.* **1990**, *385*, 23.

[25] F. E. Hahn, B. Schneider, F.-W. Reier, *Z. Naturforsch. B* **1990**, *45*, 134.

[26] a) C. C. Landry, A. Hynes, A. R. Barron, I. Haiduc, C. Silvestru, *Polyhedron* **1996**, *15*, 391; b) A. Keys, S. Bott, A. R. Barron, *Chem. Commun.* **1996**, 2339.

[27] a) D. J. Browning, J. M. Corker, M. Webster, *Acta Crystallogr. Sect. C* **1996**, *52*, 882; b) J. M. Corker, D. J. Browning, M. Webster, *Acta Crystallogr. Sect. C* **1996**, *52*, 583.

[28] a) M. R. Mason, R. M. Matthews, M. S. Mashuta, J. F. Richardson, *Inorg. Chem.* **1996**, *35*, 5756; b) M. R. Mason, M. S. Mashuta, J. F. Richardson, *Angew. Chem.* **1997**, *109*, 249; *Angew. Chem. Int. Ed. Engl.* **1997**, *36*, 239.

 © WILEY-VCH Verlag GmbH, D-69451 Weinheim, 1998 1433-7851/98/3719-2652 $ 17.50+.50/0

[29] a) Y. Yang, H.-G. Schmidt, M. Noltemeyer, J. Pinkas, H. W. Roesky, *J. Chem. Soc. Dalton Trans.* **1996**, 3609.
[30] J. E. Cassidy, J. A. Jarvis, R. N. Rothon, *J. Chem. Soc. Dalton Trans.* **1975**, 1497.
[31] M. G. Walawalkar, R. Murugavel, H. W. Roesky, H.-G. Schmidt, *Inorg. Chem.* **1997**, *36*, 4202.
[32] Y. Yang, M. G. Walawalkar, J. Pinkas, H. W. Roesky, H.-G. Schmidt, *Angew. Chem.* **1998**, *110*, 101; *Angew. Chem. Int. Ed.* **1998**, *37*, 96.
[33] Y. Yang, J. Pinkas, M. Noltemeyer, M. Schäfer, H. W. Roesky, *Inorg. Chem.*, submitted.
[34] Cs(*i*Bu$_3$AlF) was prepared according to a modified procedure of B. Werner, B. Neumüller, *Chem. Ber.* **1996**, *129*, 355.
[35] Crystal data for **1**: $C_{104}H_{228}Al_{10}Cs_6F_4O_{42}P_{12}+2\times1/2\,C_4H_8O$, $M_r=3738.23$, monoclinic, space group $C2/c$, $a=28.890(4)$, $b=27.177(3)$, $c=25.096(4)$ Å, $\beta=117.17(1)^\circ$, $V=17530(4)$ Å^3, $Z=4$, $\rho_{calcd}=1.441$ g cm^{-3}, $F(000)=7776$, $\lambda=0.71073$ Å, $T=133$ K, $\mu(Mo_{K\alpha})=14.63$ cm^{-1}, min./max. transmission: 0.6284/0.6679, crystal size $0.35\times0.30\times0.30$ mm, $2.18^\circ\le2\Theta\le48.00^\circ$; of 196896 data collected, 13762 were independent ($R_{int}=0.0802$). For the final refinement of the 1114 parameters, 2190 restraints were used. $R1=\Sigma|F_o-F_c|/\Sigma F_o=0.0464$ for $I>2\sigma(I)$ and $wR2=[\Sigma w(F_o^2-F_c^2)^2/\Sigma wF_o^4]^{1/2}=0.1198$ for all data; min./max. residual electron density: $-0.599/0.896$ e · Å^{-3}. One of the cesium atoms is disordered over two positions (occupancies 0.9:0.1). One *i*Bu group is disordered over two (occupancies 0.35:0.65), and one *t*Bu group over three positions (occupancies 0.5:0.25:0.25). In one of the THF molecules, one carbon atom is disordered over two positions (occupancies 0.2:0.8), whereas the carbon atoms of another THF molecule are disordered over three positions (occupancies 0.45:0.35:0.20). The two THF half-molecules of crystallization in the asymmetric unit are disordered over the two different inversion centers in space group $C2/c$. The data were collected on a Stoe-Siemens-Huber four-circle diffractometer with a Siemens CCD area detector using φ scans. The crystal was transferred in an inert oil and then flash-cooled in a nitrogen stream.[41] For the integration of intensities, the program SAINT[42] was used. A semiempirical absorption correction was employed for all data. The structure was solved with direct methods (SHELXS-96)[43] and refined against F^2.[44] All non hydrogen atoms were refined anisotropically. For the hydrogen atoms, the riding model was used. Crystallographic data (excluding structure factors) for the structure reported in this paper have been deposited with the Cambridge Crystallographic Data Centre as supplementary publication no. CCDC-101366. Copies of the data can be obtained free of charge on application to CCDC, 12 Union Road, Cambridge CB21EZ, UK (fax: (+44) 1223-336-033; e-mail: deposit@ccdc.cam.ac.uk).
[36] G. Harvey, C. Baerlocher, T. Wroblewski, *Z. Kristall.* **1992**, *201*, 113.
[37] a) M. G. Walawalkar, R. Murugavel, A. Voigt, H. W. Roesky, H.-G. Schmidt, *J. Am. Chem. Soc.* **1997**, *119*, 4656; b) M. G. Walawalkar, R. Murugavel, H. W. Roesky, I. Uson, R. Kraetzner, *Inorg. Chem.* **1998**, *37*, 473.
[38] N. Herron, R. L. Harlow, D. L. Thorn, *Inorg. Chem.* **1993**, *32*, 2985.
[39] D. Müller, E. Jahn, G. Ladwig, U. Haubenreisser, *Chem. Phys. Lett.* **1984**, *109*, 332.
[40] F. Taulelle, T. Loiseau, J. Maquet, J. Livage, G. Ferey, *J. Solid State Chem.* **1993**, *105*, 191.
[41] T. Kottke, D. Stalke, *J. Appl. Crystallogr.* **1993**, *26*, 615.
[42] SAINT, *Program for Reduction and Integration of Diffraction Data*, V.4.050, AXS, **1997**.
[43] G. M. Sheldrick, SHELXS-96, *Program for Structure Solution*, *Acta Crystallogr. Sect. A* **1990**, *46*, 467.
[44] G. M. Sheldrick, SHELXL-96, *Program for Structure Refinement*, Universität Göttingen, **1996**.

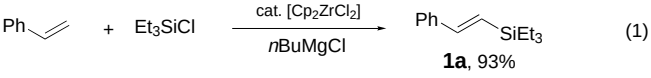
Zirconocene-Catalyzed Silylation of Alkenes with Chlorosilanes**

Jun Terao, Kazushi Torii, Koyu Saito, Nobuaki Kambe,* Akio Baba, and Noboru Sonoda

Organosilanes play an important role in organic synthesis as useful intermediates in a number of synthetic transformations.[1] To date, a variety of procedures have been developed for the introduction of silyl functionalities into organic molecules. The most straightforward and practical methodology for C–Si bond formation involves electrophilic trapping of the corresponding organometallic reagents of main group metals with chlorosilanes. An attractive alternative is the transition metal catalyzed silylation of unsaturated compounds,[1, 2] as exemplified by the hydrosilylation of alkenes and alkynes.[2a, 3] The reactions in this category proceed not only with silanes containing one or more hydrogen atoms, but also with various silylating reagents such as disilanes,[2c, d] silacyclobutanes or silacyclopropanes,[4] silyl cyanides,[5] silylgermanes,[6] silylstannanes,[7] silylselenides,[6] and iodosilanes.[8]

Although chlorosilanes are the most readily available silylating reagents, their use in catalytic silylation has not yet been achieved. This is probably due to the difficulty of the oxidative addition of the Si–Cl bonds to transition metal centers.[9] We report herein the first example of the transition metal catalyzed silylation of alkenes with chlorosilanes as well as silylsulfides, silylselenides, and silyltellurides. This reaction proceeds under mild conditions with a catalytic amount of a zirconocene complex[10] in the presence of a Grignard reagent to give alkenylsilanes and/or allylsilanes.

For example, styrene reacted with chlorotriethylsilane in refluxing THF in the presence of *n*BuMgCl and a catalytic amount of zirconocene dichloride (conditions A) to give the *E* isomer of alkenylsilane **1a** in 93% yield and with greater than 99% regio- and stereoselectivities [Eq. (1)]. In this reaction,



(1)

only a trace amount of Et_3Si*n*Bu (< 5%) was formed as a by-product, probably through the direct reaction of Et_3SiCl with *n*BuMgCl.

Table 1 summarizes the results of the silylation of styrene using different reagents and catalysts. When [Cp_2TiCl_2] was

[*] Prof. Dr. N. Kambe, J. Terao, K. Torii, K. Saito, Prof. Dr. A. Baba, Prof. Dr. N. Sonoda[†]
Department of Applied Chemistry, Faculty of Engineering
Osaka University
Suita, Osaka 565-0871 (Japan)
Fax: (+81) 6-879-7390
E-mail: kambe@ap.chem.eng.osaka-u.ac.jp
[†] Current address:
Department of Applied Chemistry, Faculty of Engineering
Kansai University, Suita, Osaka 564-8680 (Japan)

[**] This work was supported in part by a Grant-in-Aid from the Ministry of Education, Science, Sports and Culture, Japan. Thanks are due to the Instrumental Analysis Center, Faculty of Engineering, Osaka University, for MS and HR-MS measurements as well as elemental analyses. J.T. is grateful to the JSPS for the Research Fellowship Program for Young Scientists.

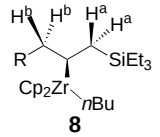
Table 1. Silylation of styrene with R_3SiX in the presence of R′MgX′ and a catalytic amount of $[Cp_2MCl_2]$.[a]

Entry	R_3SiX	R′MgX′	M	Product	Yield [%][b]
1	Et_3SiCl	*n*BuMgCl	Zr	**1a**	93 (84)
2	Et_3SiCl	*n*BuMgCl	Ti	**1a**	21
3	Et_3SiCl	*n*BuMgCl	Hf	**1a**	0[c]
4	Et_3SiCl	*s*BuMgCl	Zr	**1a**	78
5	Et_3SiCl	EtMgBr	Zr	**1a**	57
6	Me_3SiCl	*n*BuMgCl	Zr	**1b**	48
7	Me_3SiSPh	*n*BuMgCl	Zr	**1b**	92 (86)
8	$Me_3SiSePh$	*n*BuMgCl	Zr	**1b**	89
9	$Me_3SiTePh$	*n*BuMgCl	Zr	**1b**	48

[a] Conditions: styrene (1.0 mmol), R_3SiX (2.0 mmol), R′MgX′ (1.5 mmol), $[Cp_2MCl_2]$ (0.05 mmol), THF (1.7 mL), reflux, 40 min. [b] Yield according to NMR spectroscopy. The yield of the isolated product is given in parentheses. [c] No reaction.

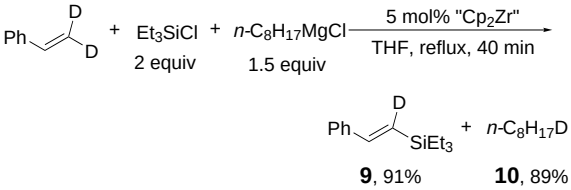
used instead of $[Cp_2ZrCl_2]$, **1a** was obtained in only 21% yield (entry 2). Under the same conditions, $[Cp_2HfCl_2]$ was ineffective (entry 3). The use of *s*BuMgCl and EtMgBr in place of *n*BuMgCl afforded **1a** in yields of 78 and 57%, respectively (entries 4 and 5), but no reaction took place with MeMgCl and *t*BuMgCl. When Me_3SiCl was used as the silylating reagent, (*E*)-2-phenyl-1-(trimethylsilyl)ethylene (**1b**) was obtained in only a moderate yield along with unchanged styrene, probably because of the low boiling point of Me_3SiCl (entry 6). This problem was solved by employing Me_3SiSPh, which afforded **1b** in an excellent yield (entry 7). The reaction also proceeded when $Me_3SiSePh$ and $Me_3SiTePh$ were used as the silylating reagents (entries 8 and 9).

Results from reactions with some other representative alkenes are shown in Table 2. Use of 4-methylstyrene yielded the corresponding alkenylsilane **2** in 91% yield (entry 1; *p*-Tol = 4-MeC_6H_4). A reaction at 80 °C with ethylene (1 atm at 20 °C in an autoclave, conditions B) gave **3** in 75% yield based on nPr_3SiCl (entry 2). Interestingly, when β-methylstyrene was employed as an internal alkene, allylsilane **4a** was obtained in 22% yield as the sole product rather than the corresponding alkenylsilane (entry 3). This result can be explained by assuming that in the reaction medium β-methylstyrene isomerized to allylbenzene, which then underwent silylation to give **4a**. Indeed, when allylbenzene was employed **4a** was obtained in 46% yield under the same conditions (entry 4, conditions A). It is noteworthy that under conditions C the reaction proceeded smoothly at room temperature to yield **4a** in 87% yield (entry 4). A trimethylsilyl group could be introduced efficiently by the use of either Me_3SiCl or Me_3SiSPh (entries 5 and 6). A similar reaction of allyltrimethylsilane with Me_3SiCl afforded 1,3-bis(trimethylsilyl)propene (**5**) in 73% yield as a 1:1 mixture of stereoisomers (entry 7). Alkenes having a simple alkyl substituent also afforded the corresponding alkenylsilane **6** and **7** in 74 and 70% yields, respectively (entries 8 and 9), along with byproducts which may involve stereoisomers of the corresponding allylsilanes. The product selectivities—that is, alkenylsilanes versus allylsilanes—can be rationalized by assuming the common intermediate **8**. Alkenylsilanes and/or allylsilanes result from β-elimination with abstraction of H^a or H^b with concomitant formation of butane and "Cp_2Zr". This mechanism accounts for the selective formation of allylsilanes **4** from allylbenzene; that is, the β-elimination from **8** proceeds exclusively at the benzylic side when R = Ph in favor of conjugated double bond formation by abstraction of H^b. In the cases of 1-butene and 1-octene (R = Me, n-C_5H_{11}), H^a was abstracted predominantly, giving rise to **6** and **7**.



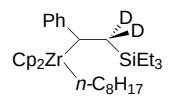
8

To prove the β-elimination mechanism the following labeling experiment was performed. The reaction of $PhCH{=}CD_2$ with Et_3SiCl (2 equiv) and n-$C_8H_{17}MgCl$ (1.5 equiv) in the presence of "Cp_2Zr" (5 mol%), prepared in situ from $[Cp_2ZrCl_2]$ and *n*BuMgCl (2 equiv),[11] was conducted under reflux for 40 min [Eq. (2)]. Addition of benzaldehyde in order to trap



9, 91% **10**, 89% (2)

the remaining n-$C_8H_{17}MgCl$ followed by quenching with aqueous 0.1N HCl gave nearly equal amounts of monodeuterated products **9** (deuterium content >98%) and **10** (deuterium content >95%).[12] This result supports that one of the deuterium atoms of $PhCH{=}CD_2$ was transferred to the terminal carbon atom of the octyl group by β-elimination from **11**.



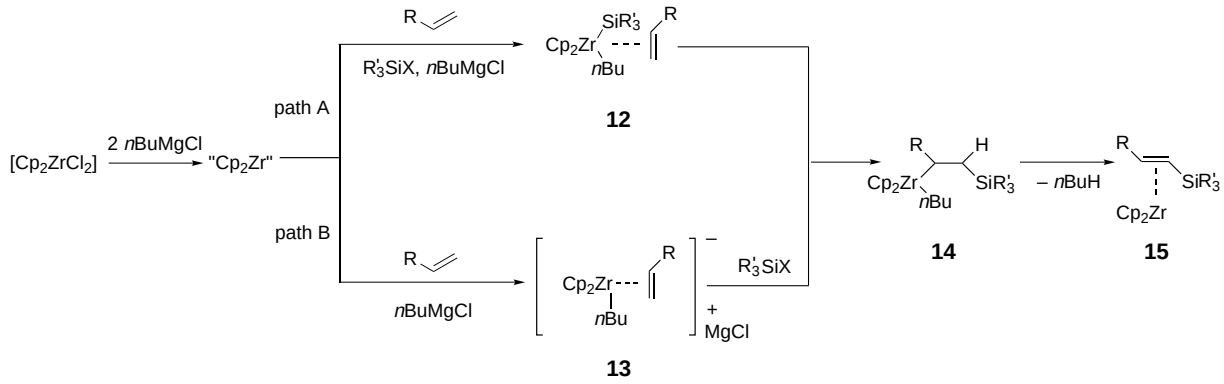
11

Table 2. Silylation of alkenes with R_3SiX in the presence of *n*BuMgCl and a catalytic amount of $[Cp_2ZrCl_2]$.

Entry	Alkene	R_3SiX	Conditions[a]	*T* [°C]	Product	Yield [%][b]
1	*p*-Tol	Et_3SiCl	A	66	*p*-Tol, $SiEt_3$ **2**	91 (90)
2	$CH_2{=}CH_2$	nPr_3SiCl	B	80	$SinPr_3$ **3**	75[c]
3	Ph	Et_3SiCl	A	66	Ph, $SiEt_3$ **4a**	22[d]
4	Ph	Et_3SiCl	A	66	**4a**	46
			C	20		87 (82)
5	Ph	Me_3SiCl	C	20	Ph, $SiMe_3$ **4b**	82 (73)
6	Ph	Me_3SiSPh	C	20	**4b**	69
7	$SiMe_3$	Me_3SiCl	C	20	Me_3Si, $SiMe_3$ **5** (*E*:*Z*=52:48)	73 (69)
8	Et	Et_3SiCl	D	20	Et, $SiEt_3$ **6** (*E*:*Z*=74:26)	74
9	n-C_6H_{13}	Et_3SiCl	C	20	n-C_6H_{13}, $SiEt_3$ **7** (*E*:*Z*=27:73)	70

[a] For details of conditions A – D, see the Experimental Section. [b] Yield according to NMR spectroscopy. The yield of the isolated product is given in parentheses. [c] Based on nPr_3SiCl. [d] Unchanged alkene was recovered (67%).

 © WILEY-VCH Verlag GmbH, D-69451 Weinheim, 1998 1433-7851/98/3719-2654 $ 17.50+.50/0 *Angew. Chem. Int. Ed.* **1998**, *37*, No. 19



Scheme 1. Plausible pathways for the zirconocene-catalyzed silylation reaction. R = alkyl, aryl, H; R″ = Me, Et, *n*Pr; X = Cl, SPh, SePh, TePh.

We also conducted several control experiments in order to elucidate the reaction pathway leading to dialkylzirconocene intermediates such as **8** or **11**. Since a small amount of the corresponding silane R_3SiH is formed as a by-product (< 5 %) in the present silylation reaction and since it is known that zirconocene complexes catalyze the addition of R_3SiH to alkenes,[13] we first examined whether hydrosilylation is involved. When a reaction similar to that in entry 5 of Table 2 was carried out in the presence of Et_3SiH, only **4b** was obtained as the silylated product in 86 % yield, and unchanged Et_3SiH was recovered. This result rules out the intermediacy of R_3SiH. We then examined the role of Grignard reagents. The reaction of a stoichiometric amount of "Cp_2Zr", generated in situ as described above, with allylbenzene (1 equiv) and Et_3SiCl (1 equiv) failed to give **4a** or saturated silylation product $PhCH_2CH_2CH_2SiEt_3$, even after quenching the resulting mixture with aqeous HCl. However, a similar reaction in the presence of one equivalent of *n*BuMgCl afforded **4a** in 72 % yield. These results indicate that *n*BuMgCl does in fact promote the C – Si bond formation.

Although the detailed mechanism of this silylation reaction has not been clarified yet, it is possible that **12** or **13** (Scheme 1) serves as the key intermediate leading to the dialkylzirconocene complex **14**. The former has a Zr – Si bond which undergoes alkene insertion (path A).[14] In path B a zirconate complex **13** directly reacts with chlorosilanes at the olefinic terminal carbon atom to give **14**.[15] The resulting dialkyl complex **14** undergoes β-elimination to afford **15**, which acts as a source of "Cp_2Zr" to complete the catalytic cycle.

In conclusion, a novel silylation reaction of alkenes with chlorosilanes and related silylating reagents has been developed by the use of a zirconocene catalyst. This reaction is promoted by Grignard reagents, giving rise to alkenylsilanes and/or allylsilanes under mild conditions. It is suggested that the product selectivities are determined at the β-elimination step from the dialkylzirconocene intermediates.

Experimental Section

Conditions A**:** (*E*)-1-Phenyl-2-(triethylsilyl)ethylene (**1a**): *n*BuMgCl (0.90 M in THF, 2.30 mL, 2.07 mmol) was added to a mixture of styrene (145 mg, 1.39 mmol), Et_3SiCl (420 mg, 2.79 mmol) and [Cp_2ZrCl_2] (20.0 mg, 0.07 mmol) at 20 °C under nitrogen. After the mixture was heated at reflux for 40 min, aqueous 1N HCl (2 mL) was added at 0 °C, and the mixture was again warmed to 20 °C. A saturated solution of aqueous NH_4Cl (50 mL) was added, and the product was extracted with diethyl ether (50 mL). The organic phase was dried over $MgSO_4$ and evaporated to give a yellow crude product (93 % yield according to NMR spectroscopy). Purification by column chromatography on silica gel with hexane as the eluent afforded 255 mg (84 %) of **1**.

Conditions B: Ethenyltripropylsilane (**3**): A magnetic stirring bar, nPr_3SiCl (257 mg, 1.33 mmol), and [Cp_2ZrCl_2] (15.0 mg, 0.05 mmol) were placed in a 50-mL stainless steel autoclave equipped with a pyrex glass insert. *n*BuMgCl (0.90 M in THF, 3.00 mL, 2.70 mmol) was added at 20 °C under nitrogen, and the autoclave was purged with ethylene several times and then charged with ethylene (about 2 mmol) at 1 atm and 20 °C. After the mixture was heated at 80 °C for 40 min, the autoclave was opened and aqueous 1N HCl (3 mL) was added at 0 °C. A workup similar to that for **1a** afforded **3** in 75 % yield (according to NMR spectroscopy) based on nPr_3SiCl.

Conditions C: (*E*)-1-Phenyl-3-(triethylsilyl)-1-propene (**4a**): *n*BuMgCl (0.90 M in THF, 3.90 mL, 3.51 mmol) was added to a mixture of allylbenzene (137.5 mg, 1.16 mmol), Et_3SiCl (438 mg, 2.91 mmol), and [Cp_2ZrCl_2] (34.0 mg, 0.12 mmol) at 20 °C under nitrogen. Stirring of the solution for 4 h at 20 °C followed by workup similar to that for **1a** gave a yellow crude product (87 % yield according to NMR spcetroscopy). Purification by column chromatography on silica gel with hexane as the eluent afforded 226 mg (82 %) of **4a**.

Conditions D: 1-(Triethylsilyl)-1-butene (**6**): A 50-mL pyrex glass vessel containing a magnetic stirring bar, Et_3SiCl (750 mg, 4.98 mmol), and [Cp_2ZrCl_2] (58.0 mg, 0.20 mmol) was cooled at – 78 °C. The gas was then evaculated under reduced pressure, and 1-butene (2.01 mmol, 45 mL, 1 atm and 20 °C) was introduced. Afterwards *n*BuMgCl (0.9 M in THF, 6.60 mL, 5.94 mmol) was added at the same temperature, the vessel was sealed, and the solution was stirred for 24 h at 20 °C. Workup similar to that for **1a** gave **6** as a pale yellow crude product (*E*/*Z* = 74/26) in 74 % yield (according to NMR spectroscopy) based on 1-butene.

Received: April 9, 1998 [Z 11714 IE]
German version: *Angew. Chem.* **1998**, *110*, 2798 – 2801

Keywords: alkenes · silanes · silylations · zirconium

[1] a) *The Chemistry of Organic Silicon Compounds* (Eds.: S. Patai, Z. Rappoport), Wiley, Chichester, **1989**; b) L. Hevesi in *Comprehensive Organic Functional Group Transformations*, *Vol. 2* (Ed.: S. V. Ley), Elsevier, Oxford, **1995**, pp. 899 – 950; c) D. A. Armitage in *Comprehensive Organometallic Chemistry II, Vol. 2* (Ed.: A. G. Davies), Elsevier, Oxford, **1995**, pp. 1 – 44.

[2] Recent reviews of transition metal catalyzed reactions of organosilanes: a) T. Hiyama, T. Kusumoto in *Comprehensive Organic Synthesis*, *Vol. 8* (Ed.: I. Fleming), Pergamon, Oxford, **1991**, pp. 763 – 792; b) S. Murai, N. Chatani, *J. Synth. Org. Chem. Jpn.* **1993**, *51*, 421 – 433; c) C. A. Recatto, *Aldrichimica Acta* **1995**, *28*, 85 – 92; d) K. A. Horn, *Chem. Rev.* **1995**, *95*, 1317 – 1350.

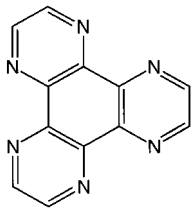
 © WILEY-VCH Verlag GmbH, D-69451 Weinheim, 1998 1433-7851/98/3719-2655 $ 17.50+.50/0

[3] A. M. LaPointe, F. C. Rix, M. Brookhart, *J. Am. Chem. Soc.* **1997**, *119*, 906 – 917, and references therein.
[4] a) H. Saso, W. Ando, *Chem. Lett.* **1988**, 1567 – 1570; b) H. Sakurai, T. Imai, *Chem. Lett.* **1975**, 891 – 894.
[5] N. Chatani, T. Hanafusa, *J. Chem. Soc. Chem. Commun.* **1985**, 838 – 839.
[6] A. Ogawa, H. Kuniyasu, M. Takeba, T. Ikeda, N. Sonoda, T. Hirao, *J. Organomet. Chem.*, in press.
[7] M. Hada, Y. Tanaka, M. Ito, M. Murakami, H. Amii, Y. Ito, H. Nakatsuji, *J. Am. Chem. Soc.* **1994**, *116*, 8754 – 8765, and references therein.
[8] a) H. Yamashita, T. Kobayashi, T. Hayashi, M. Tanaka, *Chem. Lett.* **1991**, 761 – 762; b) N. Chatani, N. Amishiro, S. Murai, *J. Am. Chem. Soc.* **1991**, *113*, 7778 – 7780; c) N. Chatani, N. Amishiro, T. Morii, T. Yamashita, S. Murai, *J. Org. Chem.* **1995**, *60*, 1834 – 1840.
[9] H. Yamashita, M. Tanaka, M. Goto, *Organometallics* **1997**, *16*, 4696 – 4704, and references therein.
[10] Recent reviews on the application of zirconocene complexes in syntheses: a) R. F. Jordan, *Adv. Organomet. Chem.* **1991**, *32*, 325 – 387; b) E. Negishi in *Comprehensive Organic Synthesis Vol. 5*, (Ed.: L. A. Paquette), Pergamon, Oxford, **1991**, pp. 1163 – 1184; c) E. Negishi, T. Takahashi, *Acc. Chem. Res.* **1994**, *27*, 124 – 130.
[11] It has been proposed that $[Cp_2ZrCl_2]$ reacts with two equivalents of *n*BuMgCl to yield the $[Cp_2Zr(butene)]$ complex, which serves as an equivalent of "Cp_2Zr"; a) E. Negishi, F. E. Cederbaum, T. Takahashi, *Tetrahedron Lett.* **1986**, *27*, 2829 – 2832; see also references [10b, c]; for recent studies on the mechanism of $[Cp_2Zr(butene)]$ formation, see b) V. K. Dioumaev, J. F. Harrod, *Organometallics* **1997**, *16*, 1452 – 1464; c) F. Soleil, R. Choukroun, *J. Am. Chem. Soc.* **1997**, *119*, 2938 – 2939.
[12] The content and position of deuterium in **9** was determined by ^1H NMR spectroscopy. The deuterium content of **10** was determined by a comparison of the mass spectrum of **10** (EI, 70 eV) with that of octane. Incorporation of a deuterium at the terminal carbon atom of **10** was confirmed by ^{13}C NMR spectroscopy (100 MHz, $CDCl_3$): A signal for a terminal carbon atom at $\delta = 13.9$ that appears as a triplet due to coupling with D ($J = 1.9$ Hz) is observed in addition to a singlet at $\delta = 14.2$ for the other terminal carbon atom.
[13] T. Takahashi, M. Hasegawa, N. Suzuki, M. Saburi, C. J. Rousset, P. E. Fanwick, E. Negishi, *J. Am. Chem. Soc.* **1991**, *113*, 8564 – 8566; M. R. Kesti, M. Abdulrahman, R. M. Waymouth, *J. Organomet. Chem.* **1991**, *417*, C12 – C15; J. Y. Corey, X.-H. Zhu, *Organometallics* **1992**, *11*, 672 – 683; M. R. Kesti, R. M. Waymouth, *Organometallics* **1992**, *11*, 1095 – 1103.
[14] $[Cp_2Zr(SiMe_3)Cl]$ does not react with ethylene (6 atm, Et_2O, 2 d); a) T. D. Tilley, *J. Am. Chem. Soc.* **1985**, *107*, 4084 – 4085; however, insertion of ethylene into Zr – Si bonds of $[Cp^*ZrCl_2Si(SiMe_3)_3]$ and $[CpCp^*ZrCl\{Si(SiMe_3)_3\}]$ ($Cp^* = C_5Me_5$) has been reported; b) J. Arnold, M. P. Engeler, F. H. Elsner, R. H. Heyn, T. D. Tilley, *Organometallics* **1989**, *8*, 2284 – 2286.
[15] As the pathway leading to **13** is similar, it has been proposed that zirconate complexes $[Cp_2ZrEt(CH_2{=}CH_2)MgBr]$ and $[Cp_2ZrPh(CH_2{=}CH_2)MgBr]$ are formed by the reaction of $[Cp_2ZrCl_2]$ with three equivalents of EtMgBr or by the reaction of $[Cp_2ZrPh_2]$ with one equivalent of EtMgBr: T. Takahashi, N. Suzuki, M. Kageyama, Y. Nitto, M. Saburi, E. Negishi, *Chem. Lett.* **1991**, 1579 – 1582.

A Robust (10,3)-a Network Containing Chiral Micropores in the Ag^I Coordination Polymer of a Bridging Ligand that Provides Three Bidentate Metal-Binding Sites**

Brendan F. Abrahams, Patricia A. Jackson, and Richard Robson*

A major goal in the crystal engineering of coordination polymers is the design and synthesis of microporous networks that maintain structural integrity upon exchange or loss of channel guest molecules. One strategy to achieve more robust framework structures that we have been developing is to harness the powerful chelate effect by employing bridging ligands that bind metal centers strongly at chelating sites. The planar ligand 1,4,5,8,9,12-hexaazatriphenylene (hat, **1**) provides a pleasingly symmetrical array of three bidentate sites at which metal centers can realistically be expected to be strongly and predictably bound, each site closely resembling those in the classical chelating agents 2,2′-bipyridine and 1,10-phenanthroline. The ligand hat has already been put to use to bind trios of metal ions in discrete molecular species,[1] but our interest is to generate infinite networks.



1

A particularly appealing aspect of connecting ligands providing two or more bidentate sites is that when a metal center takes on three of them the metal itself adopts the role of three-connecting node. Ligands such as hat, therefore, in combination with appropriate metal centers provide access, in principle, to a range of intriguing and little known three-connected nets whose topologies have been catalogued by Wells.[2]

One feature of hat of potentially great interest and usefulness is its delocalized π-electron system which may provide facile electronic communication between attached metal centers; such communication throughout an extended 3D network could lead to unusual properties. Intense interest has been focussed on the photophysical properties associated with the metal-to-ligand charge transfer chromophores in complexes of 2,2′-bipyridine and related ligands and upon binuclear and oligonuclear mixed-valence complexes of bridging ligands containing pyridine and pyrazine residues,[3] including hat itself.[4] We believe that mixed-valence 3D coordination polymers of planar bridging ligands with delocalized π-electron systems, of which hat is only one example, may provide unique physical properties; the generation of such systems is one of our long-term objectives. The results reported here are part of an initial exploratory study of the

[*] Dr. R. Robson, Dr. B. F. Abrahams, Dr. P. A. Jackson,
School of Chemistry, University of Melbourne
Parkville, Victoria 3052 (Australia)
Fax: (+61) 3-9347-5180
E-mail: r.robson@chemistry.unimelb.edu.au

[**] The authors thank Dr. B. F. Hoskins of the University of Melbourne for helpful discussions and advice and gratefully acknowledge support from the Australian Research Council and the American Chemical Society Petroleum Research Fund.

 © WILEY-VCH Verlag GmbH, D-69451 Weinheim, 1998 1433-7851/98/3719-2656 $ 17.50+.50/0

potential of hat to generate well-defined coordination polymer networks in the form of single crystals. We start here with the monopositive and relatively "innocent" metal center Ag^{I} and hope by studies of "simple" systems of this type to build up a foundation of knowledge and experience from which the more ambitious assault on mixed valence structures can be launched. The system described below is the first structurally characterized coordination polymer of hat[5] or, for that matter, of any bridging ligand that provides three bidentate sites with strong metal-binding properties. It has the (10,3)-a topology[2] and provides micropores that are chiral. Furthermore, as described below, the retention of framework integrity upon exchange of the solvent housed in its chiral channels indicates an encouraging network resilience.

Slow intermixing of solutions of hat in nitromethane and $AgClO_4$ in acetonitrile by diffusion gave orange crystals of composition $[Ag(hat)ClO_4]\cdot 2\,CH_3NO_2$ which were studied by single-crystal X-ray diffraction. The unit cell is tetragonal but almost equidimensional ($a = 12.652(1)$, $c = 12.362(1)$ Å). Individual crystals are enantiomorphic as indicated by the chiral space group of the one selected for study. Presumably enantiomorphic crystals of both hands are formed. All silver centers are equivalent, being chelated by three hat ligands which provide an N_6 coordination environment intermediate between octahedral and trigonal prismatic. The ligands are also all equivalent, each chelating three metal centers. Some essential features of the structure are shown in Figure 1 which

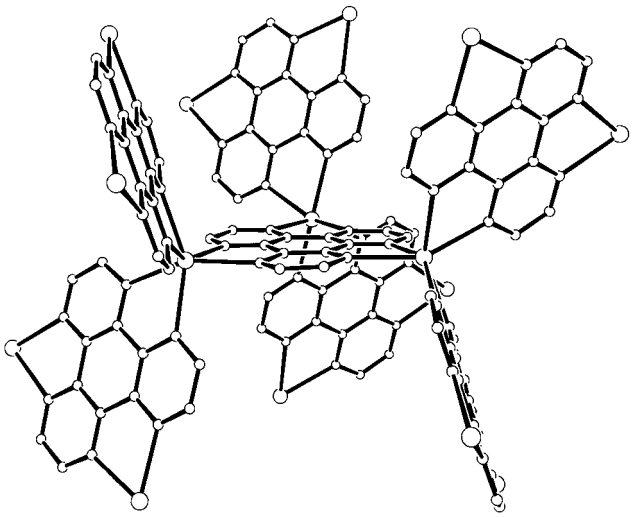


Figure 1. A segment of the Ag/hat framework in $[Ag(hat)ClO_4]\cdot 2\,CH_3NO_2$. Larger circles represent the Ag and smaller circles the C/N atoms.

focusses on a central (horizontal) hat ligand bound by three silver atoms each in turn bearing two other hat ligands. The extended 3D network therefore is three-connected with two types of essentially trigonal node, one located at the metal and the other at the midpoint of the ligand. The topology is that of the (10,3)-a net, the most symmetrical of all the three-connected nets, which in its geometrically most regular form is cubic with strictly trigonal planar nodes and exactly 120° angles.[2] Figure 2 shows two versions of the structure seen from the same angle slightly displaced from the tetragonal axis.

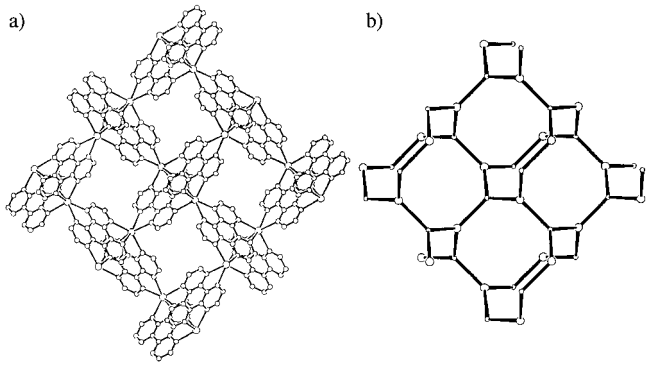


Figure 2. Representation of the Ag/hat framework topology viewed from a direction slightly displaced from the tetragonal axis. In a) Ag atoms (larger circles) and the C/N atoms of hat (smaller circles) are shown, whilst in b) the (10,3)-a connectivity is revealed more clearly by replacing each ligand by a single trigonal node (smaller circles).

The three planar ligands around each silver atom produce three "bays". The perchlorate ions, which are positionally ordered but orientationally disordered, are found in one of these three bays and it is this positional ordering that reduces the overall symmetry from cubic to tetragonal. The Ag/hat framework nevertheless shows only very minor deviations from the most regular form possible for the (10,3)-a net. The framework was estimated to occupy about 48 % of the crystal volume by using the PLATON program.[6]

The nitromethane molecules, which are unusually well ordered relative to the solvent molecules in many other solvated coordination polymers, are located in the large micropores clearly apparent in Figure 2. Each nitromethane molecule associates with two neighbors, making very close $N^{\delta+}\cdots O^{\delta-}$ contacts of 3.02 Å,and thereby generates fourfold helices (Figure 3). The nitromethane helices have the same left-handed character as the internal surfaces of the chiral framework micropores by which they are surrounded and templated. Similarly short $N\cdots O$ contacts (3.00 – 3.07 Å) are observed in the crystal structure of nitromethane itself.[7]

After the data collection had been completed the crystal was removed from its Lindemann tube and allowed to equilibrate with the atmosphere. Remarkably, the same crystal still displayed X-ray diffraction, which now revealed a cubic structure with a cell volume of 1935.6(2) $Å^3$, significantly smaller than that of the original tetragonal cell of 1978.9(3) $Å^3$. A structural determination for the cubic daughter crystal indicated retention of an almost unchanged Ag/hat framework. The solvent molecules however were now unresolved and the perchlorate anions, which were clearly defined, were disordered over three crystallographically equivalent sites. These sites were located within the bays between ligands referred to above at positions similar to that of the ordered perchlorate in the tetragonal nitromethane-containing parent. Infra-red analysis of other crystals obtained from the same reaction mixture indicated replacement of nitromethane by H_2O upon exposure to the atmosphere. Estimation of the nonframework volume and the electron densities in the intraframework regions by using the PLATON program suggested the composition had changed to $[Ag(hat)ClO_4]\cdot 4\,H_2O$,[8] in good agreement with the composition indicated

 © WILEY-VCH Verlag GmbH, D-69451 Weinheim, 1998 1433-7851/98/3719-2657 $ 17.50+.50/0

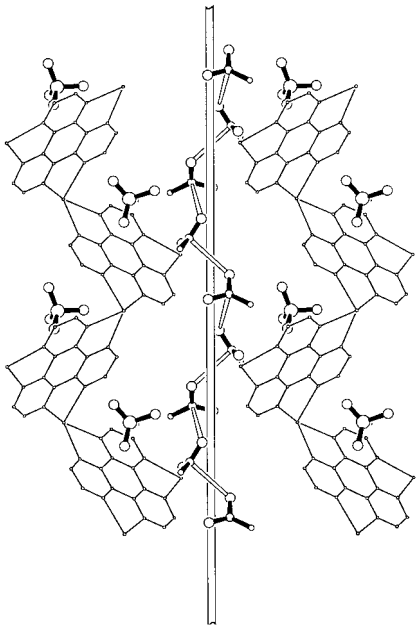


Figure 3. The disposition of the anions and the fourfold helical arrangement of the nitromethane molecules in $[Ag(hat)ClO_4]\cdot 2CH_3NO_2$. Circles in order of decreasing size represent Cl, O, N, and C, respectively. For ease of visualization the $(CH_3NO_2)_n$ helix is shown wrapped around an imaginary central "pole". The "open" connections represent close $N^{\delta+}\cdots O^{\delta-}$ intermolecular contacts (3.02 Å). For clarity only part of the Ag/hat helical channel (very small circles) which surrounds the nitromethane helix is shown; those parts behind and in front are omitted as are the perchlorate anions associated with them.

by the elemental analysis of a sample exposed to the atmosphere ($[Ag(hat)ClO_4]\cdot 3.5H_2O$). Following this second data collection, the *same* crystal was further immersed in nitromethane and resealed in a Lindemann tube. This granddaughter crystal still diffracted and now showed a cubic unit cell of volume of 1987(2) Å^3—essentially the same as the volume of the tetragonal cell of the original grandparent crystal. It appears that, in the second exchange of solvent, the crystal is unable to regain the grandparent's regular ordering of the anion. Upon reexposure of the *same* crystal to the atmosphere it reverts once again to the smaller cubic cell (1929.1(8) Å^3). Despite the changes in crystal symmetry and in unit cell volume, it is clear that the Ag/hat framework persists from generation to generation in these successive solvent exchanges.

Treatment of $AgBF_4$ with hat under identical reaction conditions to those used above for the perchlorate salt gave tetragonal crystals with the essentially identical dimensions $a = 12.647(2)$, $c = 12.347(3)$ Å.

A number of coordination polymers with the (10,3)-a topology have been discovered in recent times.[9] We suspect that as the rapidly expanding field of coordination polymers continues to evolve, more and more examples of this net, referred to by Wells as the three-connected analogue of diamond, will emerge and that it may come to dominate three-connected 3D structures in the same way diamond is presently the dominant structure for four-connected 3D coordination polymers.

The preliminary results presented in this report bode well for the future generation of a range of crystalline coordination polymers of hat (and related ligands) with a wide variety of metal centers, in some cases with chiral channels, with real prospects of unusual properties and robust enough for practical applications.

Experimental Section

A solution of $AgClO_4$ (23 mg) in CH_3NO_2 (3 mL) was added to a suspension of hat (15 mg) in CH_3NO_2 and the mixture was heated in a sealed vessel on the steam bath for three days. The bright yellow suspended solid was collected by filtration, washed with CH_3NO_2, then equilibrated with the atmosphere for several days. Yield, 18 mg. IR (KBr): $\tilde{\nu} = 437$m, 629s, 637s, 1087vs, 1100vs, 1114vs, 1233s, 1343w, 1385vs, 1473s, 1543w cm^{-1}; elemental analysis calcd. for $C_{12}H_{13}AgClN_6O_{7.5}$ ($[Ag(hat)ClO_4]\cdot 3.5H_2O$): C 28.6, H 2.6, N 16.6; found: C 28.9, H 1.3, N 16.5. Powder XRD indicated this material had the same cubic unit cell as the daughter crystal. The best single crystals for crystallographic study were obtained as follows: CH_3NO_2 (8 mL) was added to hat (5 mg) in a long 8 mm diameter tube; not all the hat dissolved. A solution of $AgClO_4$ (7 mg) in CH_3CN (4 mL) was carefully layered on top of the hat/CH_3NO_2 mixture followed by benzene (6 mL). The tube was stoppered and light was excluded. After three weeks large, bright orange multifaceted crystals suitable for X-ray crystallography were obtained. A selected crystal was sealed with mother liquor in a Lindemann glass capillary tube for diffraction measurements and then exposed to the atmosphere, after which diffraction experiments on the cubic hydrated form were performed. Crystal data for $[Ag(hat)ClO_4]\cdot 2CH_3NO_2$ (and for $[Ag(hat)ClO_4]\cdot 4H_2O$ in parentheses): $M_r = 563.64$ (513.61), tetragonal (cubic), space group $P4_32_12$ ($P2_13$), $a = 12.652(1)$ (12.463(1)), $c = 12.362(1)$ Å, $V = 1978.9(3)$ (1935.6(3)) Å^3, $Z = 4$ (4), $\rho_{calcd} = 1.872$ (1.762) g cm^{-3}, $\mu(Mo_{K\alpha}) = 1.218$ (1.232) mm^{-1}, $F(000) = 1096$ (1024). Intensity data for 4570 (4490) reflections ($2\theta_{max} = 50$ (50)°), yielding 1739 (1145) independent reflections were measured at 295(2) K with $Mo_{K\alpha}$ radiation (graphite monochromator) using an Enraf-Nonius CAD-4 MachS diffractometer employing ω ($\omega/2\theta$) scans. Data were corrected for Lorentz, polarization and absorption[10] effects, min./max. transmission factors = 0.7868/0.8502 (0.7835/0.8721). The structures were solved by using the Patterson method[11] (direct methods[12]). Full-matrix least-squares refinement[13] based on F^2 converged with $R1 = 0.0554$ (0.1576), $wR2 = 0.1523$ (0.4499); 125 (22) parameters. Max. residual electron density 0.52 (0.87) e Å^{-3}. Crystallographic data (excluding structure factors) for the structures reported in this paper have been deposited with the Cambridge Crystallographic Data Center as supplementary publication no. CCDC-101558 (CCDC-101559). Copies of the data can be obtained free of charge on application to CCDC, 12 Union Road, Cambridge CB2 1EZ, UK (fax: (+44) 1223-336-033; e-mail: deposit@ccdc.cam.ac.uk).

Received: May 12, 1998 [Z11847IE]
German version: *Angew. Chem.* **1998**, *110*, 2801 – 2804

Keywords: channel structures · chirality · coordination polymer · microporosity · silver

[1] a) R. Nasielski-Hinkens, M. Benedek-Vamos, D. Maetens, J. Nasielski, *J. Organomet. Chem.* **1981**, *217*, 178; b) A. Masschelein, A. Kirsch-De Mesmaeker, C. Verhoeven, R. Nasielski-Hinkens, *Inorg. Chim. Acta* **1987**, *129*, L13; c) P. Baxter, J.-M. Lehn, A. DeCian, J. Fischer, *Angew. Chem.* **1993**, *105*, 92; *Angew. Chem. Int. Ed. Engl.* **1993**, *32*, 69.

[2] A. F. Wells, *Three-Dimensional Nets and Polyhedra*, Wiley, New York, **1977**, chap. 5.

[3] P. Bonhote, A. Lecas, E. Amouyal, *Chem. Commun.* **1998**, 885, and references therein; V. Balzani, F. Scandola, *Supramolecular Photochemistry*, Ellis Horwood, Chichester, **1991**.

[4] K. Warnmark, O. Heyke, J. A. Thomas, J.-M. Lehn, *Chem. Commun.* **1996**, 2603; T. J. Rutherford, O. Van Gijte, Kirsch-De Mesmaeker, F. R. Keene, *Inorg. Chem.* **1997**, *36*, 4465; T. J. Rutherford, F. R. Keene, *Inorg. Chem.* **1997**, *36*, 3580.

[5] Lehn and co-workers[1c] have speculated on the possibility of forming oligomers and polymers with the hexaphenyl derivative of hat.

[6] Platon Program: A. L. Spek, *Acta Crystallogr. Sect. A* **1990**, *46*, C34.

[7] I. Y. Bagryanskaya, Y. V. Gatilov, *Zh. Strukt. Khim.* **1983**, *24*, 158.

 © WILEY-VCH Verlag GmbH, D-69451 Weinheim, 1998 1433-7851/98/3719-2658 $ 17.50+.50/0

[8] The number of nitromethane molecules and perchlorate anions per unit cell in the tetragonal $[Ag(hat)ClO_4]\cdot 2CH_3NO_2$ crystal indicated by the crystallography showed excellent agreement with the number calculated with the PLATON Program[6] on the basis of the electron density in the framework voids. This agreement affords confidence in the number of water molecules ($4H_2O$ per $[Ag(hat)]ClO_4$) present in the cubic hydrated crystal calculated in the same way by using the PLATON program, which in addition accorded well with the $3.5H_2O$ indicated by elemental analysis.
[9] S. Decurtins, H. W. Schmalle, P. Schneuwly, H. R. Oswald, *Inorg. Chem.* **1993**, *32*, 1888; S. Decurtins, H. W. Schmalle, P. Schneuwly, J. Ensling, P. Gutlich, *J. Am. Chem. Soc.* **1994**, *116*, 9521; S. Decurtins, H. W. Schmalle, R. Pellaux, P. Schneuwly, A. Hauser, *Inorg. Chem.* **1996**, *35*, 1451; Carlucci, G. Ciani, D. M. Proserpio, A. Sironi, *J. Am. Chem. Soc*. **1995**, *117*, 12861; B. F. Abrahams, S. R. Batten, H. Hamit, B. F. Hoskins, R. Robson, *Chem. Commun*. **1996**, 1313; L. Carlucci, G. Ciani, D. M. Proserpio, A. Sironi, *Chem. Commun*. **1996**, 1393; C. J. Kepert, M. J. Rosseinsky, *Chem. Commun*. **1998**, 31.
[10] G. M. Sheldrick, SHELX-76, Program for Crystal Structure Determination, University of Cambridge, U. K., **1976**.
[11] G. M. Sheldrick, SHELXS-86, Program for Crystal Structure Solution, Universität Göttingen, **1986**.
[12] G. M. Sheldrick, SHELXS-97, Program for Crystal Structure Solution, Universität Göttingen, **1997**.
[13] G. M. Sheldrick, SHELXL-97, Program for Crystal Structure Refinement, Universität Göttingen, **1997**.

Efficient Palladium-Catalyzed Cyclotrimerization of Arynes: Synthesis of Triphenylenes**

Diego Peña, Sonia Escudero, Dolores Pérez,*
Enrique Guitián,* and Luis Castedo

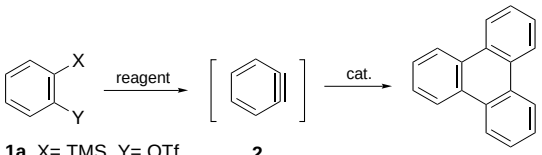
Over the last 15 years much effort has been devoted to the preparation and characterization of transition metal complexes of arynes.[1] Parallel studies on the reactivity of these complexes—particularly those of Ti, Zr,[2] and Ni[3]—have shown that characteristic reactions involve insertion of molecules containing multiple bonds (e.g. alkenes, alkynes, CO) into the metal–aryne bond, which in a way is reminiscent of the chemistry of alkyne complexes. However, while alkynes participate in a number of synthetically useful metal-catalyzed transformations,[4] the synthetic applications of metal–aryne complexes are limited owing to the lack of a general and mild method for their generation and the need for stoichiometric amounts of metal in their reactions.

As part of a project aimed at the development of new reactions of arynes promoted by metal complexes, here we report on the metal-mediated cyclotrimerization of arynes. These preliminary results show that the reaction proceeds in the presence of catalytic amounts of metal and that it has great potential for the preparation of triphenylenes, which are found at the core of many discotic liquid crystals[5] and have therefore been the target of many synthetic studies.[6]

There are many precedents of triphenylene formation under conditions that lead to arynes, especially when arynes are generated from an organometallic system.[7] For example, triphenylene was obtained in 85% yield from the decomposition of 2-fluorophenylmagnesium bromide in THF.[8] Closer to our results, triphenylene was isolated in 30% yield during attempts at obtaining a platinum complex of benzyne (1,2-didehydrobenzene).[9] An example of the formation of triphenylene as side product of a palladium-catalyzed domino reaction has also been reported.[10] However, to the best of our knowledge, efficient preparation of triphenylenes by metal-catalyzed reaction of arynes is without precedent.

Development of a catalytic procedure for the trimerization of arynes requires careful selection of the catalyst and the method for generation of the aryne. The catalyst was chosen from among the various metal systems used for trimerization of alkynes; suitable candidates contained metals such as Ni, Co, Pd, and Pt. We decided to carry out the first trials with palladium complexes because they are easy to handle and in general stable. Among the many procedures available for the generation of arynes[11] we sought one that could be used under mild reaction conditions and did not involve strong bases or oxidants. The method of choice was the fluoride-induced elimination of Me_3Si and TfO groups (Tf = trifluoromethanesulfonyl), which proceeds at room temperature.[12]

Early in our study we found that when 2-trimethylsilylphenyl trifluoromethanesulfonate (**1a**) was treated with CsF and a catalytic amount (3 mol%) of $[Pd(PPh_3)_4]$ in acetonitrile, the only low-polarity product detected was triphenylene (**3**), which was isolated in 52% yield [Eq. (1)]. To optimize the



1a, X= TMS, Y= OTf
1b, X=Y=Br
2
3

(1)

reaction conditions, exhaustive experimentation was carried out; some significant results are given in Table 1. The best results were obtained using 10 mol% of $[Pd(PPh_3)_4]$[13] and 2 equivalents of anhydrous CsF in acetonitrile at room temperature (entry 1), which afforded triphenylene in 83% yield. Use of other sources of Pd^0 (entries 2 and 3) or fluoride (entry 4) gave slightly lower yields. Likewise, alternative methods to generate benzyne, such as reaction of 1,2-dibromobenzene (**1b**) with *n*BuLi, in the presence of $[Pd(PPh_3)_4]$ (entry 5) also gave poorer results. It is noteworthy that triphenylene was not detected in the reaction mixture when **1a** was treated with CsF in the absence of a Pd catalyst (entry 6), and that when **1a** was treated with $[Pd(PPh_3)_4]$ in the absence of fluoride, the starting material was untouched (entry 7). In our opinion, these two control experiments provide good evidence of the intermediacy of benzyne as the

[*] Dr. D. Pérez, Prof. E. Guitián, D. Peña, S. Escudero, Prof. L. Castedo
Departamento de Química Orgánica
Universidad de Santiago de Compostela and
Unidad Asociada al CSIC
E-15706 Santiago (Spain)
Fax: (+34) 9-81-595012
E-mail: qoenrgui@usc.es

[**] This work was supported by the DGES (PB96-0967). D.P. and S.E. thank the Spanish Ministry of Education (MEC) for the award of research grants.

 © WILEY-VCH Verlag GmbH, D-69451 Weinheim, 1998 1433-7851/98/3719-2659 $ 17.50+.50/0

Table 1. Metal-catalyzed synthesis of triphenylene [**3**, see Eq. (1)].[a]

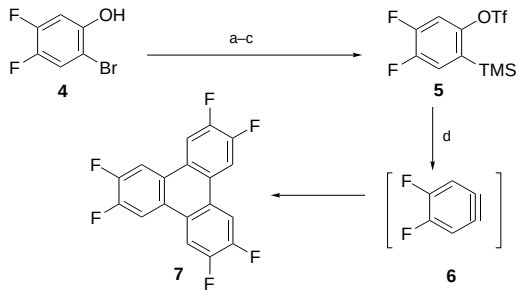
Entry	Starting material	Reagent	Catalyst (0.1 equiv)	Additives	Yield [%][b]
1	**1a**	CsF	$[Pd(PPh_3)_4]$	–	83
2	**1a**	CsF	$[Pd_2(dba)_3]$	dppe	70
3	**1a**	CsF	$[Pd_2(dba)_3]$	$P(o\text{-tol})_3$	60
4	**1a**	Bu_4NF	$[Pd(PPh_3)_4]$	–	71
5	**1b**	BuLi	$[Pd(PPh_3)_4]$	–	40
6	**1a**	CsF	–	–	–
7	**1a**	–	$[Pd(PPh_3)_4]$	–	–

[a] Reaction conditions: MeCN, RT, 12 h (entries 1–3, 6, 7); THF, 0 °C, 12 h (entries 4, 5). [b] Yield of isolated product. dba = *trans,trans*-dibenzylideneacetone, dppe = 1,2-bis(diphenylphosphanyl)ethane, tol = C_6H_4Me.

reactive species, and suggest that the metal promotes the reaction by acting as a template.

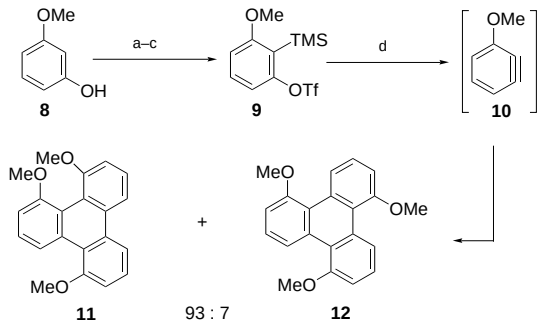
Next, we applied the optimized cyclotrimerization procedure developed for benzyne to the substituted arynes **6** and **10**, to see if it was compatible with donor and acceptor substituents on the aryne and to determine the regiochemistry of the reaction. Furthermore, we were interested to know if the reaction is of general utility for the synthesis of functionalized triphenylenes.

The precursor of 4,5-difluorobenzyne (**6**) was 4,5-difluoro-2-trimethylsilylphenyl triflate (**5**), which was prepared from commercially available 2-bromo-4,5-difluorophenol (**4**) in three steps. Treatment of **5** with CsF in the presence of 10 mol % of $[Pd(PPh_3)_4]$ afforded 2,3,6,7,10,11-hexafluorotriphenylene (**7**) in 52 % yield (Scheme 1).



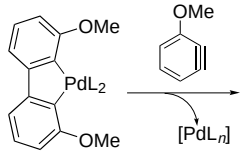
Scheme 1. Synthesis of **7** via intermediate **6**. a) HMDS. b) 1. *n*BuLi; 2. TMSCl, THF, −78 °C. c) 1. *n*BuLi; 2. Tf_2O, 0 °C. d) $[Pd(PPh_3)_4]$ (0.1 equiv), CsF, CH_3CN, RT. HMDS = 1,1,1,3,3,3-hexamethyldisilazane, TMS = trimethylsilyl.

Generation of 3-methoxybenzyne (**10**) from triflate **9** under the same conditions afforded a mixture of 1,5,12- and 1,5,9-trimethoxytriphenylenes (**11** and **12**, respectively) in 93:7 ratio and 81 % overall yield (Scheme 2).



Scheme 2. Synthesis of **11** and **12** via intermediate **10**. a) HMDS. b) 1. LDA; 2. TMSCl. c) 1. *n*BuLi; 2. Tf_2O. d) $[Pd(PPh_3)_4]$ (0.1 equiv), CsF, CH_3CN, RT. LDA = lithium diisopropylamide.

Similarly high regioselectivity has been reported in metal-catalyzed alkyne cyclotrimerizations,[14] suggesting that alkyne and aryne cyclotrimerizations have similar mechanisms. If this is the case, isolation of the asymmetrically substituted isomer **11** as major product is explained by selective formation of the metallacyclic intermediate **13** as a result of C–C bond formation between the carbon atoms with less steric hindrance [Eq. (2)]. Our approach thus allows efficient prepa-



(2)

ration of 1,12-substituted triphenylenes, which are currently of interest owing to their potential application as chiral cores for liquid crystals.[15]

Experimental Section

A solution of the aryne precursor (**1**, **5**, or **9**; 1 mmol) in CH_3CN (2 mL) was added to a suspension of finely powdered anhydrous CsF (2 mmol) and $[Pd(PPh_3)_4]$ (0.1 mmol) in CH_3CN (1 mL), and the mixture was stirred under argon at room temperature for 12 h. The solvent was evaporated, and the residue was purified by column chromatography (silica gel) to isolate the trimers.[16]

Received: March 31, 1998 [Z11669IE]
German version: *Angew. Chem.* **1998**, *110*, 2804–2806

Keywords: arynes · cyclotrimerizations · palladium · triphenylenes

[1] a) S. J. McLain, R. R. Schrock, P. R. Sharp, M. R. Churchill, W. J. Youngs, *J. Am. Chem. Soc.* **1979**, *101*, 263–265; b) M. A. Bennett, T. W. Hambley, N. K. Roberts, G. B. Robertson, *Organometallics* **1985**, *4*, 1992–2000; c) S. L. Buchwald, B. T. Watson, *J. Am. Chem. Soc.* **1986**, *108*, 7411–7414; d) M. A. Bennett, H. P. Schwemlein, *Angew. Chem.* **1989**, *101*, 1349; *Angew. Chem. Int. Ed. Engl.* **1989**, *28*, 1296–1320; e) J. F. Hartwig, R. G. Bergman, R. A. Andersen, *J. Am. Chem. Soc.* **1991**, *113*, 3404–3418; f) J. Cámpora, S. L. Buchwald, *Organometallics* **1993**, *12*, 4182–4187; g) K. Mashima, Y. Tanaka, A. Nakamura, *Organometallics* **1995**, *14*, 5642–5651.

[2] "Transition Metal Alkyne Complexes: Zirconium–Benzyne Complexes": S. L. Buchwald, R. D. Broene in *Comprehensive Organometallic Chemistry II, Vol. 12* (Eds.: E. W. Abel, F. G. A. Stone, G. Wilkinson), Pergamon, Oxford, **1995**, pp. 771–784, and references therein.

[3] M. A. Bennett, E. Wenger, *Chem. Ber.* **1997**, *130*, 1029–1042, and references therein.

[4] a) "Transition Metal Alkyne Complexes: Transition Metal-Catalyzed Cyclotrimerization": D. B. Grotjahn in *Comprehensive Organometallic Chemistry II, Vol. 12* (Eds.: E. W. Abel, F. G. A. Stone, G. Wilkinson), Pergamon, Oxford, **1995**, pp. 741–770; b) N. E. Schore, *Chem. Rev.* **1988**, *88*, 1081–1119, c) K. P. C. Vollhardt, *Angew. Chem.* **1984**, *96*, 525; *Angew. Chem. Int. Ed. Engl.* **1984**, *23*, 539–556.

[5] a) S. Chandrasekhar, *Liq. Cryst.* **1993**, *14*, 3–14; b) N. Boden, R. S. Bushby, J. Clements, *J. Chem. Phys.* **1993**, *98*, 5920–5931.

[6] a) P. T. Wright, I. Gillies, J. D. Kilburn, *Synthesis* **1997**, 1007–1009; b) S. Kumar, M. Manickam, *Chem. Commun.* **1997**, 1615–1616.

[7] a) C. M. Buess, D. D. Lawson, *Chem. Rev.* **1960**, *60*, 313–330; b) K. D. Bartle, H. Heaney, D. W. Jones, P. Lees, *Tetrahedron* **1965**, *21*, 3289–3296.

[8] H. Heaney, P. Lees, *Tetrahedron Lett.* **1964**, 3049–3052.

[9] T. L. Gilchrist, F. J. Graveling, C. W. Rees, *J. Chem. Soc.* **1971**, 977–980.

 © WILEY-VCH Verlag GmbH, D-69451 Weinheim, 1998 1433-7851/98/3719-2660 $ 17.50+.50/0

[10] G. Dyker, *Angew. Chem.* **1994**, *106*, 117; *Angew. Chem. Int. Ed. Engl.* **1994**, *33*, 103 – 105.
[11] a) R. W. Hoffmann, *Dehydrobenzene and Cycloalkynes*, Academic Press, New York, **1967**; b) H. Hart in *The Chemistry of Functional Groups, Suppl. C2: The Chemistry of Triple-Bonded Functional Groups* (Ed.: S. Patai), Wiley, Chichester, **1994**, pp. 1017 – 1134.
[12] Y. Himeshima, T. Sonoda, H. Kobayashi, *Chem. Lett.* **1983**, 1211 – 1214.
[13] Prepared in our laboratory by a published procedure: "Palladium in Organic Synthesis": L. S. Hegedus in *Organometallics in Synthesis: A Manual* (Ed.: M. Schlosser), Wiley, **1994**. Commercially available material gave poorer yields.
[14] a) L. S. Meriwether, E. C. Colthup, G. W. Kinnerly, R. N. Reusch, *J. Org. Chem.* **1961**, *26*, 5155 – 5163; b) Y. Wakatsuki, O. Nomura, K. Kitaura, K. Morokuma, H. Yamazaki, *J. Am. Chem. Soc.* **1983**, *105*, 1907 – 1912.
[15] a) N. Boden, R. J. Bushby, A. N. Cammidge, S. Duckworth, G. Headdock, *J. Mater. Chem.* **1997**, *7*, 601 – 605; b) K. Praefcke, A. Eckert, D. Blunk, *Liq. Cryst.* **1997**, *22*, 113 – 119.
[16] Triphenylene and the substituted derivatives gave correct analytical and spectroscopic data. **3**: M.p. 194 °C (literature value[6a] 198 °C). **7**: ^{1}H NMR ([D$_8$]THF) $\delta = 8.42$ (t, $J = 10.3$ Hz, 6H); MS: *m*/*z* (%): 336 (100), 168 (16); HR-MS: calcd for $C_{18}H_6F_6$: 336.0374, found: 336.0364. **11**: M.p. 188 °C; ^{1}H NMR ($CDCl_3$) $\delta = 9.04$ (dd, $J = 8.5$, 0.8 Hz, 1H), 8.10 (d, $J = 8.1$ Hz, 1H), 8.00 (d, $J = 8.1$ Hz, 1H), 7.48 (m, 3H), 4.04 (s, 3H), 3.97 (s, 6H); ^{13}C NMR ($CDCl_3$) $\delta = 158.2$, 157.9, 157.0, 133.0, 132.6, 131.9, 127.3, 127.0, 126.8, 121.1, 118.8, 118.4, 118.1, 115.9, 115.0, 110.4, 108.7, 108.5, 56.1, 55.8, 55.7; MS: *m*/*z* (%): 318 (100), 303 (25), 288 (15); HR-MS: calcd for $C_{21}H_{18}O_3$: 318.1256, found: 318.1268. **12**: ^{1}H NMR ($CDCl_3$) $\delta = 9.00$ (dd, $J = 8.5$, 1.2 Hz, 3H), 7.48 (t, $J = 8.2$ Hz, 3H), 7.14 (dd, $J = 8.1$, 1.0 Hz, 3H), 4.02 (s, 9H); MS: *m*/*z* (%): 318 (100), 303 (22), 288 (30).

Investigations into the Manzamine Alkaloid Biosynthetic Hypothesis**

Jack E. Baldwin,* Timothy D. W. Claridge, Andrew J. Culshaw, Florian A. Heupel, Victor Lee, David R. Spring, Roger C. Whitehead, Robert J. Boughtflower, Ian M. Mutton, and Richard J. Upton

Over the past decade there has been an upsurge in the discovery of biologically active natural products from marine sponges.[1] In comparison to terrestrial plant and microbial systems, little is known about the biosynthesis of sponge metabolites.[2] One class of cytotoxic sponge metabolites which have recently fascinated organic chemists are the manzamine alkaloids. The first member of this class, manzamine A (**1**, Figure 1), was isolated in 1986 by Higa et al.[3]

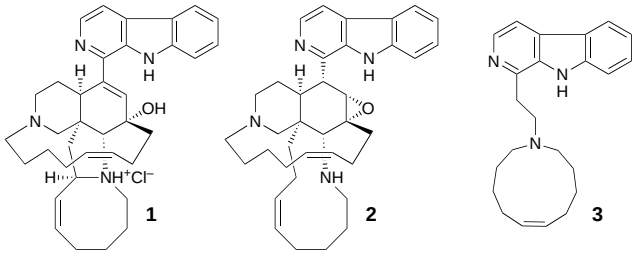


Figure 1. Manzamine A (**1**), B (**2**), and C (**3**).

and recently synthesized.[12] The unprecedented structure led the authors to the conclusion that "no obvious biogenetic path" could be envisaged leading to **1**. Manzamines B (**2**) and C (**3**) were subsequently isolated from the same sponge.[4]

In 1992, we put forward a biogenetic hypothesis for the formation of the manzamines.[5] We proposed that each structure could be reduced into four building blocks: ammonia, a C_{10} unit (a symmetrical dialdehyde), tryptophan, and a C_3 unit (an acrolein equivalent), shown in Scheme 1 for manzamine B (**2**). The key step in the proposal is the intramolecular *endo* Diels – Alder cycloaddition of the bis-dihydropyridine **4**.[6] To date it is not known whether a "Diels – Alderase" exists.[7]

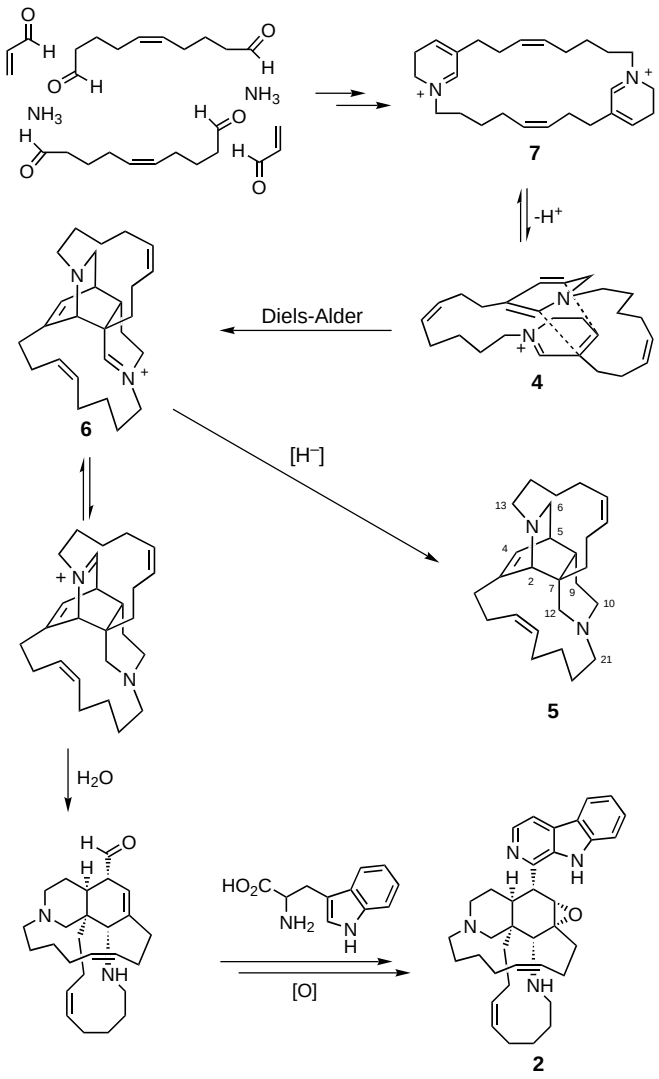
Since the publication of the hypothesis a large number of manzamine and related alkaloids have been isolated from various species of sponge worldwide.[8] Despite the lack of experimental evidence, the proposal has been applied repeatedly to explain the biogenetic origin of the manzamine and related alkaloids. One related alkaloid is keramaphidin B (**5**, Scheme 1), which was isolated independently by both the Kobayashi and Andersen groups.[9] Structurally **5** is simply the reduced form of the proposed cycloadduct **6** (Scheme 1). Herein, we report the biomimetic synthesis of **5**, the first in vitro chemical evidence for this proposal.

The synthesis of **7** was first communicated in 1996,[6e] but we found the route unsatisfactory because of moderate yields (7% overall) and the instability of one intermediate. Since then we have modified the synthesis (Scheme 2) with significant improvements (37% overall yield). Hydroxyphosphonium salt **8** was masked as its tetrahydropyranyl (THP) derivative **9** (93%). Olefin **10** was obtained from the ylide generated from **9** and 3-(3-pyridyl)propanal in 83% yield. Acid-mediated deprotection gave the alcohol **11** (94%), which was treated with *p*-toluenesulfonyl chloride to give **12** (95%). A one-pot Finkelstein reaction, dimerization and macrocyclization was effected by the slow addition of **12** into a mixture of NaI in 2-butanone under reflux. The crude product was reduced to give bis-tetrahydropyridine **13** in 56% yield over the two steps. Oxidation of **13** with 3-chloroperbenzoic acid (*m*CPBA) furnished diastereomeric N-oxides (98%), which could be treated with trifluoroacetic anhydride to give bis-dihydropyridine **7** (100%).

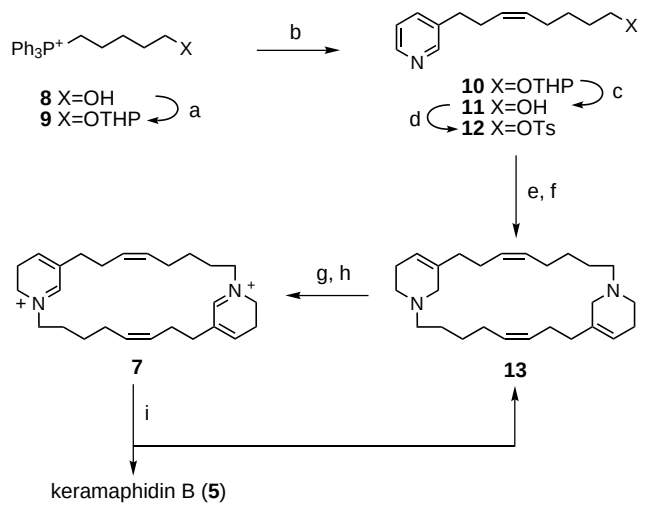
[*] Prof. J. E. Baldwin, Dr. T. D. W. Claridge, Dr. A. J. Culshaw, Dr. F. A. Heupel, Dr. V. Lee, D. R. Spring, Dr. R. C. Whitehead
The Dyson Perrins Laboratory
University of Oxford
South Parks Road, Oxford OX1 3QY (UK)
Fax: (+44) 1865-275-632
E-mail: jack.baldwin@chem.ox.ac.uk
R. J. Boughtflower, I. M. Mutton, Dr. R. J. Upton
Glaxo Wellcome Research and Development
Gunnels Wood Road, Stevenage, Hertfordshire SG1 2NY (UK)

[**] This work was supported financially by the EPSRC (A.J.C and D.R.S) and the Rhodes Trust (F.A.H). We are indebted to Prof. Raymond J. Andersen (Department of Chemistry, University of British Columbia, Canada) and Prof. Jun'ichi Kobayashi (Faculty of Pharmaceutical Sciences, Hokkaido University, Japan), for their generous gifts of keramaphidin B. We also thank the EPSRC mass spectrometry service (Swansea) for high resolution mass measurements.

 © WILEY-VCH Verlag GmbH, D-69451 Weinheim, 1998 1433-7851/98/3719-2661 $ 17.50+.50/0



Scheme 1. A hypothesis for the biosynthesis of the manzamine alkaloids.[5]



Scheme 2. Synthesis of bis-dihydropyridine **7**. Reagents and conditions: a) 1.5 equiv 3,4-dihydro-2*H*-pyran, 0.01 equiv pyridinium *p*-toluenesulfonate, CH_2Cl_2, 15 h, 93%; b) 1.2 equiv potassium hexamethyldisilazide, THF, −78°C to RT, 1 h, then 3-(3-pyridyl)propanal, −78°C to RT, 2 h, 83% (Z:$E \approx 99$:1); c) 3M HCl, MeOH, 3 h, 94%; d) 1.5 equiv *p*-toluenesulfonyl chloride, 2 equiv Et_3N, CH_2Cl_2, 0°C, 3 h, 95%; e) 1.2 equiv NaI, 2-butanone, △, 192 h; f) 3 equiv $NaBH_4$, MeOH, −78°C to RT, 0.5 h, 56% over 2 steps; g) 2 equiv *m*CPBA, CH_2Cl_2, 0°C, 98%; h) 4 equiv trifluoroacetic anhydride, CH_2Cl_2, 100%; i) MeOH/1M aqueous TRIS buffer (1/1; pH 7.3; TRIS = tris(hydroxymethyl)aminomethane), 1 h; then 3 equiv $NaBH_4$, MeOH, −78°C to RT, 0.5 h, 0.2–0.3%.

It was eventually discovered that dissolution of **7** in an aqueous methanol buffer, followed by reduction, yielded a small but detectable amount of keramaphidin B (**5**) within a complex mixture of products. After extensive chromatographic purification of this mixture, **5** was isolated in 0.2–0.3% yield.[10] The synthetic material was identified by NMR spectroscopy, LC-MS, and by doping the synthetic sample with authentic material (Figure 2). The major product (60–85%) was the recyclable bis-tetrahydropyridine **13**. This compound originated from disproportionation of **4** giving a mixture of tetrahydropyridine and the pyridinium salt, which was subsequently reduced to afford **13**.[11]

In conclusion, we have demonstrated the chemical feasibility of our theoretical proposal for the biosynthesis of the manzamine alkaloids. The low yield of keramaphidin B (**5**) reflects the preference of **4** to disproportionate and the difficulty of purification. A "Diels–Alderase" that limited the conformational mobility of the substrate would not only decrease the change in entropy towards the transition state, but could also exclude the disproportionation.

Received: April 28, 1998 [Z11786IE]
German version: *Angew. Chem.* **1998**, *110*, 2806–2808

Keywords: alkaloids · biomimetic synthesis · biosynthesis · Diels–Alder reactions · manzamine

[1] D. J. Faulkner, *Nat. Prod. Rep.* **1997**, *14*, 259–302, and references therein; C. A. Bewley and D. J. Faulkner, *Angew. Chem.* **1998**, *110*, 2280–2297; *Angew. Chem. Int. Ed.* **1998**, *37*, 2162–2178.

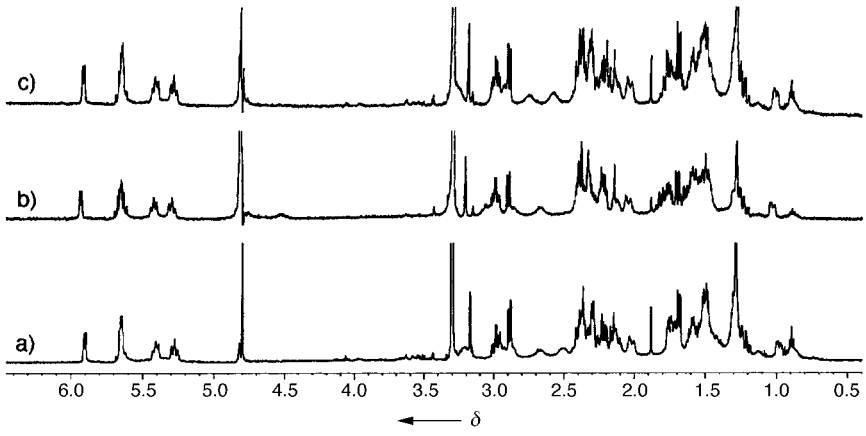


Figure 2. ^1H NMR doping experiment of **5** (500 MHz, CD_3OD): a) synthetic material; b) authentic material of similar concentration; c) 1:1 mixture of (a) and (b).

 © WILEY-VCH Verlag GmbH, D-69451 Weinheim, 1998 1433-7851/98/3719-2662 $ 17.50+.50/0

[2] M. J. Garson, *Nat. Prod. Rep.* **1989**, *6*, 143 – 170.

[3] R. Sakai, T. Higa, C. W. Jefford, G. Bernardinelli, *J. Am. Chem. Soc.* **1986**, *108*, 6404 – 6405.

[4] R. Sakai, S. Kohmoto, T. Higa, C. W. Jefford, G. Bernardinelli, *Tetrahedron Lett.* **1987**, *28*, 5493 – 5496.

[5] J. E. Baldwin, R. C. Whitehead, *Tetrahedron Lett.* **1992**, *33*, 2059 – 2062.

[6] For previous model studies, see a) J. E. Baldwin, T. D. W. Claridge, F. A. Heupel, R. C. Whitehead, *Tetrahedron Lett.* **1994**, *35*, 7829 – 7832; b) L. Gil, A. Gateau-Olesker, C. Marazano, B. C. Das, *Tetrahedron Lett.* **1995**, *36*, 707 – 710; c) L. Gil, A. Gateau-Olesker, Y.-S. Wong, L. Chernatova, C. Marazano, B. C. Das, *Tetrahedron Lett.* **1995**, *36*, 2059 – 2062; d) L. Gil, X. Baucherel, M.-T. Martin, C. Marazano, B. C. Das, *Tetrahedron Lett.* **1995**, *36*, 6231 – 6234; e) J. E. Baldwin, T. D. W. Claridge, A. J. Culshaw, F. A. Heupel, S. Smrcková, R. C. Whitehead, *Tetrahedron Lett.* **1996**, *37*, 6919 – 6922; f) J. E. Baldwin, L. Bischoff, T. D. W. Claridge, F. A. Heupel, D. R. Spring, R. C. Whitehead, *Tetrahedron* **1997**, *53*, 2271 – 2290.

[7] S. Laschat, *Angew. Chem.* **1996**, *108*, 313 – 315; *Angew. Chem. Int. Ed. Engl.* **1996**, *35*, 289 – 291.

[8] Reviews: a) R. J. Andersen, R. W. M. Van Soest, F. Kong in *Alkaloids: Chemical and Biological Perspectives, Vol. 10* (Ed.: S. W. Pelliter), Pergamon, London, **1996**, pp. 302 – 352; b) M. Tsuda, J. Kobayashi, *Heterocycles* **1997**, *46*, 765 – 794; c) N. Matzanke, R. J. Gregg, S. M. Weinreb, *Org. Prep. Proced. Int.* **1998**, *30*, 1 – 51; more recent examples: d) J. Kobayashi, D. Watanabe, N. Kawasaki, M. Tsuda, *J. Org. Chem.* **1997**, *62*, 9236 – 9239; e) Y. Guo, E. Trivellone, G. Scognamiglio, G. Cimino, *Tetrahedron* **1998**, *54*, 541 – 550; f) F. Kong, E. I. Graziani, R. J. Andersen, *J. Nat. Prod.* **1998**, *61*, 267 – 271; g) M. Tsuda, D. Watanabe, J. Kobayashi, *Tetrahedron Lett.* **1998**, *39*, 1207 – 1210; h) D. Watanabe, M. Tsuda, J. Kobayashi, *J. Nat. Prod.* **1998**, *61*, 689 – 692; i) R. J. Clark, K. L. Field, R. D. Charan, M. J. Gibson, I. M. Brereton, A. C. Willis, *Tetrahedron* **1998**, *54*, 8811 – 8826; for a recent review on the total synthesis of manzamine alkaloids see: j) E. Magnier, Y. Langlois, *Tetrahedron* **1998**, *54*, 6201 – 6258.

[9] a) J. Kobayashi, M. Tsuda, N. Kawasaki, K. Matsumoto, T. Adachi, *Tetrahedron Lett.* **1994**, *35*, 4383 – 4386; b) F. Kong, R. J. Andersen, *Tetrahedron* **1995**, *51*, 2895 – 2906.

[10] ^{1}H NMR (750 MHz, CD_3OD, 50 °C): $\delta = 0.93$ (1H, ddd, $J = 12$, 4.5, 1.5 Hz; C(8)H), 1.21 (1H, qd, $J = 14$, 4 Hz; C(9)H), 1.36 – 1.40 (1H, m; C(14)H), 1.42 – 1.63 (8H, m; C(14)H′, C(15)H_2, C(16)H, C(22)H, C(23)H_2, and C(9)H′), 1.67 (1H, dd, $J = 9$, 2.5 Hz; C(6)H), 1.69 – 1.76 (4H, m; C(20)H_2, C(19)H, and C(22)H′), 1.99 (1H, br d, $J = 13$ Hz; C(24)H), 2.08 (1H, d, $J = 11.5$ Hz; C(12)H), 2.09 – 2.12 (1H, m; C(27)H), 2.20 (1H, ddd, $J = 12.5$, 5.5, 1.5 Hz; C(13)H), 2.20 – 2.28 (2H, m; C(5)H and C(24)H′), 2.30 – 2.42 (7H, m; C(28)H_2, C(27)H′, C(19)H′, C(16)H′, C(21)H, and C(12)H′), 2.69 – 2.71 (1H, m; C(10)H), 2.78 (1H, br t, $J = 13$ Hz, C(10)H′), 2.87 (1H, dd, $J = 9$, 2 Hz; C(6)H′), 2.95 (1H, td, $J = 12.5$, 5 Hz; C(13)H′), 3.03 – 3.06 (1H, m; C(21)H′), 3.11 (1H, s; C(2)H), 5.25 (1H, pseudo t, $J = 10.5$ Hz; C(25)H), 5.38 (1H, pseudo t, $J = 10$ Hz, C(26)H), 5.60 – 5.66 (2H, m; C(17)H and C(18)H), 5.86 (1H, d, $J = 6$ Hz; C(4)H); diastereotopic protons are assigned as X and X′, where the ′ indicates the lower field proton; ^{13}C NMR (188.7 MHz, CD_3OD) $\delta = 21.32$ (C22), 21.68 (C19), 23.80 (C16), 26.10 (C24), 26.53 (C27), 27.12 (C9), 27.50 (C14, C15 and C23), 37.81 (C28), 38.99 (C5), 42.10 (C20), 44.62 (C8), 48.77 (C10), 50.94 (C12), 54.48 (C6), 55.15 (C13), 57.04 (C21), 65.04 (C2), 124.52 (C4), 131.27 (C18), 132.59 (C25), 132.60 (C17), 133.33 (C26), 142.94 (C3); only signals which can be clearly observed above the noise or which can be traced back through HMQC experiments are reported; *m*/*z* (APCI) 381 (MH^+, 100%); HRMS found: 381.3270; calcd for $C_{26}H_{41}N_2$ (MH^+): 381.3270.

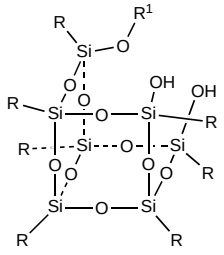
[11] The reaction of **7** in buffer was monitored by ^{1}H NMR spectroscopy. By the time the reaction was quenched with $NaBH_4$, all the signals arising from **7** had virtually disappeared. Therefore, the majority of **13** was not derived from the reduction of **7**.

[12] J. D. Winkler, J. M. Axten, *J. Am. Chem. Soc.* **1998**, *120*, 6425 – 6426.

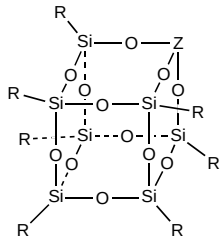
A New Route to Heterosilsesquioxane Frameworks**

Frank J. Feher,* Daravong Soulivong, Frank Nguyen, and Joseph W. Ziller

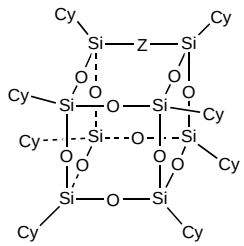
Incompletely condensed silsesquioxanes such as **1** and **2**[1, 2] are versatile precursors to a diverse range of Si/O and Si/O/M frameworks, and a wide variety of heterosilsesquioxanes can be prepared by reactions that transform Si – OH groups into new siloxane (i.e., Si-O-Si) or heterosiloxane (i.e., Si-O-M) linkages.[3–11] In virtually all cases, the resulting products are formally derived from the substitution of heteroatoms for Si atoms in a silsesquioxane framework (e.g., **3**). In this paper we report a new method for preparing discrete heterosilsesquioxane frameworks. This method introduces heteroatoms and heteroatom-containing groups by nucleophilic substitution reactions at framework Si atoms and affords products derived from the formal replacement of a framework oxygen atom in **4** by a heteroatom or other divalent bridging group (e.g., **5**).



1, R^1 = H
2, R^1 = $SiMe_3$



3, Z = heteroatom and any ligands



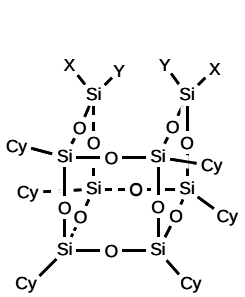
4, Z = O; Cy = *c*-C_6H_{11}
5, Z = heteroatom or other bridging group

The key to our approach is ditriflate **6**, which can be prepared in high yield by the reaction of $Cy_8Si_8O_{12}$ (**4**) with triflic acid (TfOH) in noncoordinating solvents such as CH_2Cl_2 or C_6H_6.[12] The triflate groups from **6** are rapidly displaced by many nucleophiles with complete stereochemical inversion at both Si centers. With difunctional nucleophiles (e.g., H_2O), there are two possible products: difunctional derivatives resulting from two sequential bimolecular displacement reactions (e.g., **7**) or "edge-capped" products resulting from intramolecular cyclization of the monosubstituted (e.g., **4**).[12] Cyclization is usually favored when reactions are performed in dilute solutions with stoichiometric quantities of reagents.

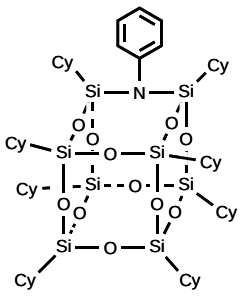
The reaction of **6** with aniline produces **8** and/or **9** in high yield. When the reaction is performed in toluene/Et_3N with an excess of aniline (> 4 equiv), **8** is obtained in > 95% NMR yield. The structure of **8**, which was assigned on the basis of

[*] Prof. F. J. Feher, Dr. D. Soulivong, Dr. F. Nguyen, Dr. J. W. Ziller
Department of Chemistry, University of California at Irvine
Irvine, CA 92697 (USA)
Fax: (+1) 714-824-2657
E-mail: fjfeher@uci.edu

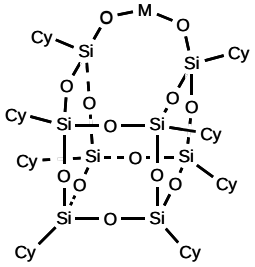
[**] These studies were supported by the National Science Foundation (USA) and Phillips Laboratory (Edwards AFB), and Los Alamos National Laboratory.



6, X = OTf, Y = Cy
7, X = Cy, Y = OH
8, X = Cy, Y = NHPh



9



10, M = SO_2
11, M = B*n*Bu
12, M = CrO_2

compelling multinuclear NMR data, a mass spectrum, and combustion analysis, was confirmed by a single-crystal X-ray diffraction study.[13] As illustrated in Figure 1, the placement

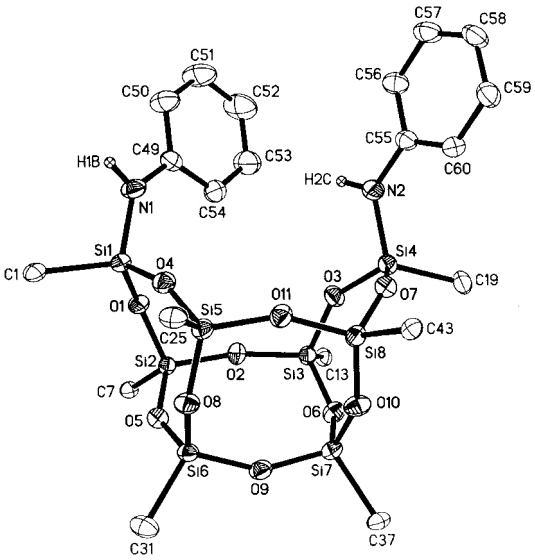


Figure 1. ORTEP plot of **8**. For clarity, thermal ellipsoids are plotted at 50% probability level and only C attached to Si are shown. Selected bond lengths [Å] and angles [°]: Si1 – N1 1.714(3), Si1 – O4 1.629(2), Si1 – O1 1.625(2), Si4 – N2 1.708(3), Si4 – O3 1.625(2), Si4 – O7 1.630 (2), other Si – O 1.609 – 1.630; N1-Si1-O4 110.76(13), N1-Si1-O1 109.06(13), O1-Si1-O4 109.47(12), O1-Si1-O4 109.47(12), N2-Si4-O3 105.01(13), N2-Si4-O7 110.73(13), O3-Si4-O7 109.04(12).

of two C_6H_5NH groups in nominally "endo" positions induces conformational changes within the Si/O framework of **8** that lead to a more open structure. All of the bond lengths and interbond angles are normal, but torsional rotation about the Si – O bonds involving Si1 and Si4 increases the Si1 – Si4 distance to approximately 5.8 Å. This is almost twice the Si – Si separation typically observed for Si-O-Si linkages in polyhedral silsesquioxanes ($\sim$3.1 Å).[14]

When the reaction of **6** with aniline is performed with only a slight excess of aniline (1.1 equiv), the product obtained in high yield is **9**, which was assigned on the basis of multinuclear NMR data, a mass spectrum, and combustion analysis. To the best of our knowledge, **9** is the first polyhedral heterosilsesquioxane to contain nitrogen within the framework. As a solid, **9** is relatively air stable, and its thermal stability appears to rival **4**. However, solutions of **9** react slowly with water to afford a number of products derived from the hydrolysis of Si – N bonds.

Ditriflate **6** also reacts rapidly with $(n\text{Bu})_4\text{NHSO}_4$ to produce **10** in high yield. The reaction can be accomplished with 1.1 equiv of the HSO_4^- salt in the presence of Et_3N or by reacting **6** with slightly more than two equivalents of $(n\text{Bu})_4\text{NHSO}_4$. In the latter reaction, the second equivalent of HSO_4^- appears to act as a base for deprotonation and cyclization of the monosubstituted intermediate rather than a second nucleophile. This reaction is surprising at first because it produces strongly acidic H_2SO_4 in a noncoordinating solvent, but it is undoubtedly preferable to the formation of two bisulfate groups containing a strongly electron-withdrawing silsesquioxane framework. Compound **10** reacts quickly with traces of water to produce disilanol **7** and sulfuric acid.

The structure of **10** was assigned on the basis of multinuclear NMR data and the fact that only one equivalent of HSO_4^- is required for the reaction; this assignment was confirmed by a single-crystal X-ray diffraction study.[13] As illustrated in Figure 2, the formal substitution of a large SO_4

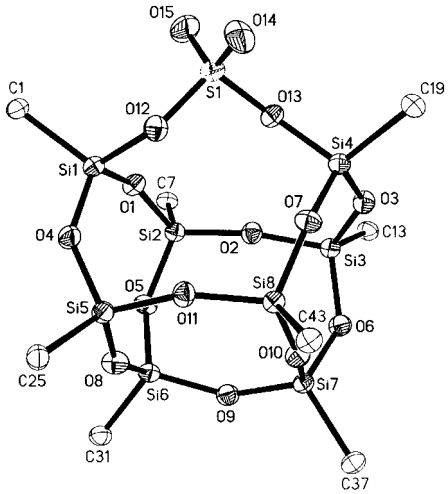


Figure 2. ORTEP plot of **10**. For clarity, thermal ellipsoids are plotted at 50% probability level and only C attached to Si are shown. Selected bond lengths [Å] and angles [°]: S1 – O14 1.417(2), S1 – O15 1.418(2), S1 – O12 1.549(2), S1 – O13 1.548(2), Si1 – O12 1.693(2), Si4 – O13 1.686 (2), other Si – O 1.610 – 1.629; O14-S1-O15 120.21(14), O14-S1-O12 107.18(11), O14-S1-O13 109.17(11), O15-S1-O12 109.34(11), O15-S1-O13 107.28(11), O12-S1-O13 102.19(10), S1-O12-Si1 129.63, S1-O13-Si4 131.87(11).

group for a single bridging siloxane oxygen requires many conformational changes. None of these changes are energetically costly because the bending potential of Si-O-Si is very broad and shallow,[15] but the cumulative effect of these changes is a highly distorted structure for **10**.

It is likely that many structurally similar heterosilsesquioxanes and metallasilsesquioxanes can be prepared by reactions of **6** with reagents capable of delivering divalent O-M-O

 © WILEY-VCH Verlag GmbH, D-69451 Weinheim, 1998 1433-7851/98/3719-2664 $ 17.50+.50/0

groups. We have only begun to explore these possibilities, but our preliminary work with nBuB(OH)$_2$ and K_2CrO_4/[18]crown-6 is very encouraging. In the case of nBuB(OH)$_2$, the addition of freshly purified nBuB(OH)$_2$ to a solution of **6** in C_6H_6/Et_3N produces **11** and variable amounts of **4**. We suspect that **4** is formed by the reaction of **6** with water rather than a direct reaction of **6** with the boronic acid because nBuB(OH)$_2$ is extremely difficult to dry without effecting its cyclotrimerization[16] and because the reaction of **6** with traces of water is known to produce **4**.[12] In the case of K_2CrO_4/[18]crown-6, extensive decomposition of the chromium reagent is observed during the reaction, but multinuclear NMR spectra clearly indicate that **12** is produced in approximately 20% yield. Authentic **12** can be prepared in high yield by the reaction of **7** with CrO_3/$MgSO_4$ in CCl_4.[17]

In summary, we have developed a new and potentially general method for synthesizing discrete heterosilsesquioxane frameworks. This method, which introduces heteroatoms by nucleophilic substitution on framework Si atoms rather than electrophilic substitution on framework O atoms, provides access to a wide range of new compounds, including polyhedral clusters that are formally derived from replacement of a framework oxygen atom in **4** by a heteroatom or other divalent bridging group.

Experimental Section

8: A solution of aniline (98 mg, 1.1 mmol) in benzene (1 mL) was added dropwise to a solution of **6** (308 mg, 0.23 mmol) and triethylamine (45 mg, 0.45 mmol) in benzene (2 mL). After stirring the resulting emulsion for 1 h at 25 °C, the benzene layer was decanted from the ammonium triflate. The oily ammonium triflate was rinsed twice with benzene (0.5 mL). The combined benzene fractions were evaporated to dryness under reduced pressure to afford **8** as a microcrystalline white solid (201 mg, 71%). The product obtained in this manner is spectroscopically pure (^{1}H, ^{13}C, ^{29}Si NMR); colorless crystals were obtained by recrystallization from hexanes. ^{1}H NMR (500 MHz, $CDCl_3$, 25 °C): $\delta = 7.20$ (t, $J = 7.7$ Hz, 4H), 6.79 (t, $J = 7.8$ Hz, 2H), 6.68 (d, $J = 7.3$ Hz, 4H), 3.73 (br s, 2H), 1.86 (br m, 40H), 1.34 (br m, 40H), 1.00 (br m, 2H), 0.89 (br m, 6H); ^{13}C{^{1}H} NMR (125 MHz, $CDCl_3$, 25 °C): $\delta = 145.68$, 128.82, 118.16, 117.41, 27.635, 27.508, 26.937, 26.902, 26.867, 26.826, 26.632, 26.546 (CH_2), 24.75, 24.14, 23.06 (1:2:1 for CH); ^{29}Si{^{1}H} NMR (99 MHz, $CDCl_3$, 25 °C): $\delta = -51.91$, -67.41, -69.77 (1:1:2); elemental analysis calcd for $C_{60}H_{100}N_2O_{11}Si_8$ (found): C 57.65 (57.81), H 8.06 (7.87), N 2.24 (2.63); m.p. 164.7 °C (by differential scanning calorimetry).

9: A solution of aniline (11.9 mg, 0.128 mmol) in benzene (0.5 mL) was added dropwise to a solution of **6** (159.0 mg, 0.117 mmol) and triethylamine (34.1 mg, 0.337 mmol) in benzene (2 mL). Workup as described above for **8** and precipitation from $CHCl_3$/CH_3CN affords **9** as an analytically pure white powder (115 mg, 85%). ^{1}H NMR (500 MHz, $CDCl_3$, 25 °C): $\delta = 7.13$ (m, 4H), 7.05 (m, 1H), 1.69–1.58 (br s, 35H), 1.47–1.39 (br m, 10H), 1.20–1.12 (br s, 35H), 0.95–0.82 (br s, 10H), 0.70–0.65 (br s, 6H), 0.22 (m, 2H); ^{13}C{^{1}H} NMR (125 MHz, $CDCl_3$, 25 °C): $\delta = 142.66$, 130.94, 128.56, 125.20 (s for C's aromatic), 27.60, 27.55, 26.92, 26.87, 26.75, 26.71, 26.68, 26.55 (CH_2), 23.48, 23.21, 23.11 (s for CH, 2:1:1); ^{29}Si{^{1}H} NMR (99 MHz, $CDCl_3$, 25 °C): $\delta = -55.52$, -67.81, -68.26 (1:2:1); MS (70 eV, 200 °C, relative intensity): m/z: 1156 ([M+H]$^+$, 35%), 1072 ([M − Cy]$^+$, 100%); elemental analysis calcd for $C_{54}H_{93}NO_{11}Si_8$ (found): C 56.06 (55.43), H 8.10 (8.12), N 1.21 (1.41); m.p. 358.7 °C (by differential scanning calorimetry).

10: A solution of **6** (295.4 mg, 0.217 mmol) in benzene (3 mL) was added to a solution Bu_4NHSO_4 (162.3 mg, 0.478 mmol) in benzene (3 mL) and stirred for 1 h. The colorless benzene solution was decanted and evaporated to dryness (25 °C, 0.01 Torr) to afford a white solid, which was washed with CH_3CN and dried in vacuo to afford spectroscopically pure **10** (196 mg, 90%). Analytically pure, colorless crystals were obtained by crystallization from benzene/CH_3CN. ^{1}H NMR (500 MHz, $CDCl_3$, 25 °C): $\delta = 1.74$ (br s, 40H), 1.23 (br s, 40H), 1.02 (br m, 2H), 0.80 (br m, 6H); ^{13}C{^{1}H} NMR (125 MHz, $CDCl_3$, 25 °C): $\delta = 27.32$, 27.30, 27.04, 26.73, 26.70, 26.41, 25.61 (CH_2), 23.20, 22.87, 22.84 (2:1:1 for CH); ^{29}Si{^{1}H} NMR (99 MHz, $CDCl_3$, 25 °C): $\delta = -67.38$, -67.76, -69.34 (1:1:2); MS (70 eV, 200 °C, relative intensity): m/z: 1077.7 ([M − Cy]$^+$, 100); elemental analyis calcd for $C_{48}H_{88}O_{15}SSi_8$ (found): C 49.62 (49.45), H 7.63 (7.67).

11: A solution of nBuB(OH)$_2$ (27.9 mg, 0.274 mmol) in benzene (0.5 mL) was added to a solution of **6** (152.6 mg, 0.112 mmol) and Et_3N (60.8 mg, 0.601 mmol) in benzene (3 mL) and stirred for 0.5 h at 25 °C. Evaporation of the solvent, extraction with benzene (10 mL), concentration to ≈1 mL and addition of CH_3CN (10 mL) afforded 127 mg of a white powder containing **11** and **4** in a ratio of 81:19. Attempts to separate **11** and **4** by extraction or fractional crystallization were unsuccessful. For **11**: ^{1}H NMR (500 MHz, $CDCl_3$, 25 °C): $\delta = 1.74$ (br s, 40H), 1.36 (m, 2H), 1.23 (44H), 0.88 (t, 3H), 0.74 (br s, 8H); ^{13}C{^{1}H} NMR (125 MHz, $CDCl_3$, 25 °C): $\delta =$ 27.57, 27.55, 27.51, 26.91, 26.76, 26.56, 25.23, 17.36, 16.63 (s for CH_2), 24.00, 23.66, 23.12 (s for CH, 1:2:1), 14.07 (CH_3); ^{29}Si{^{1}H} NMR (99 MHz, $CDCl_3$, 25 °C): $\delta = -67.39$, -69.58, -69.94 (1:2:1); MS (70 eV, 200 °C, relative intensity): m/z: 1107 ([M − Bu]$^+$, 20%), 1081 ([M − Cy]$^+$, 100%).

12 was prepared as a bright orange solid in 55% yield (87 mg) from **7** (148 mg, 0.135 mmol), CrO_3 (133 mg, 1.330 mmol), and $MgSO_4$ (371 mg) in CCl_4 (4 mL) according to the procedure described in ref. [17]. ^{1}H NMR (500 MHz, $CDCl_3$, 25 °C): $\delta = 1.75$ (br m, 40H), 1.24 (br m, 40H), 0.87 (br m, 2H), 0.78 (br m, 6H); ^{13}C{^{1}H} NMR (125 MHz, $CDCl_3$, 25 °C): $\delta = 27.54$, 27.49, 27.46, 27.40, 26.83, 26.69, 26.66, 26.54, 26.51 (s for CH_2), 23.76, 23.68, 23.02 (s for CH, 1:2:1); ^{29}Si{^{1}H} NMR (99 MHz, $CDCl_3$, 25 °C): $\delta = -62.19$, -67.14, -69.68 (1:1:2).

Received: April 22, 1998 [Z11767IE]
German version: *Angew. Chem.* **1998**, *110*, 2808–2811

Keywords: cage compounds · silicon

[1] J. F. Brown, L. H. Vogt, *J. Am. Chem. Soc.* **1965**, *87*, 4313–4317.
[2] F. J. Feher, D. A. Newman, J. F. Walzer, *J. Am. Chem. Soc.* **1989**, 111, 1741–1748.
[3] F. J. Feher, T. A. Budzichowski, *Polyhedron* **1995**, *14*, 3239–3253.
[4] R. Murugavel, V. Chandrasekhar, H. W. Roesky, *Acc. Chem. Res.* **1996**, *29*, 183–189.
[5] J. D. Lichtenhan, *Comments Inorg. Chem.* **1995**, *17*, 115–130.
[6] P. G. Harrison, *J. Organometal. Chem.* **1997**, *542*, 141–183.
[7] W. A. Herrmann, R. Anwander, V. Dufaud, W. Scherer, *Angew. Chem.* **1994**, *106*, 1338–1340; *Angew. Chem. Int. Ed. Engl.* **1994**, *33*, 1285–1286.
[8] M. Crocker, R. H. M. Herold, A. G. Orpen, *Chem. Commun.* **1997**, 2411–2412.
[9] T. Maschmeyer, M. C. Klunduk, C. M. Martin, D. S. Shepard, J. M. Thomas, B. F. G. Johnson, *Chem. Commun.* **1997**, 1847–1848.
[10] V. Ruffieux, G. Schmid, P. Braunstein, J. Rose, *Chem. Eur. J.* **1997**, *3*, 900–903.
[11] H. C. L. Abbenhuis, S. Krijnen, R. A. van Santen, *Chem. Commun.* **1997**, 331–332.
[12] F. J. Feher, D. Soulivong, A. E. Eklund, *Chem. Commun.* **1998**, 399–400.
[13] Crystal data for **8**: $M = 1250.14$, monoclinic, space group $P2_1/c$, $a =$ 1023.02(5), $b = 2610.18(13)$, $c = 2519.10(12)$ pm, $\beta = 97.538(1)°$, $V =$ 6.6685(6) nm^3, $Z = 4$, $\rho_{calcd} = 1.245$ Mg m^{-3}, $F(000) = 2696$, $\lambda =$ 71.073 pm, $T = 158$ K, $\mu(Mo_{K\alpha}) = 0.218$ mm^{-1}, crystal dimensions: $0.09 \times 0.23 \times 0.30$ mm, $2.26° \le 2\theta \le 56.6°$; of the 40533 collected reflections, 15573 are independent, and these were used for the refinement of 786 parameters; maximal residual electron density: 539 e nm^{-3}, $R1(F > 4\sigma(F)) = 0.068$ and $wR2 = 0.147$ (all data) with $R1 = \Sigma||F_o| - |F_c||/\Sigma|F_o|$ and $wR2 = (\Sigma w(F_o^2 - F_c^2)^2/\Sigma w(F_o^2)^2)^{0.5}$. Crystal data for **10**: $M = 1161.96$, monoclinic, space group $P2_1/n$, $a =$ 1558.20(7), $b = 1847.80(9)$, $c = 2093.07(10)$ pm, $\beta = 100.106(1)°$, $V =$ 5.9330(5) nm^3, $Z = 4$, $\rho_{calcd} = 1.301$ Mg m^{-3}, $F(000) = 2496$, $\lambda =$ 71.073 pm, $T = 158$ K, $\mu(Mo_{K\alpha}) = 0.277$ mm^{-1}, crystal dimensions: $0.13 \times 0.21 \times 0.22$ mm, $2.96° \le 2\theta \le 56.6°$; of the 37062 collected

 © WILEY-VCH Verlag GmbH, D-69451 Weinheim, 1998 1433-7851/98/3719-2665 $ 17.50+.50/0

reflections, 14141 are independent, and these were used for the refinement of 650 parameters; maximal residual electron density: 402 e nm^{-3}, $R1(F>4\sigma(F))=0.054$ and $wR2=0.113$ (all data) with $R1=\Sigma||F_o|-|F_c||/\Sigma|F_o|$ and $wR2=(\Sigma w(F_o^2-F_c^2)^2/\Sigma w(F_o^2)^2)^{0.5}$. Data were collected on a Siemens CCD platform diffractometer. The SMART program package was used for data collection. Raw frame data was processed by using SAINT and SADABS to yield the reflection data file. All subsequent calculations were performed using the SHELXTL program. The structure was solved by direct methods and refined on F^2 by full-matrix least-squares techniques. The analytical scattering factors for neutral atoms were used throughout the analysis and hydrogen atoms were included by using a riding model. Crystallographic data (excluding structure factors) for the structures reported in this paper have been deposited with the Cambridge Crystallographic Data Center as supplementary publication no. CCDC-101403. Copies of the data can be obtained free of charge on application to CCDC, 12 Union Road, Cambridge CB2 1EZ, UK (fax: (+44) 1223-336-033; e-mail: deposit@ccdc.cam.ac.uk).

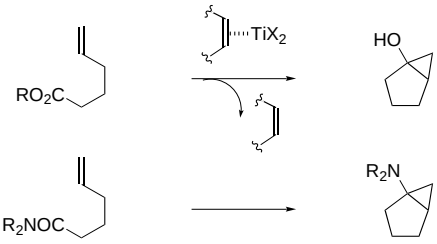
[14] M. G. Voronkov, V. Lavrent'ev, *Top. Curr. Chem.* **1982**, *102*, 199–236.
[15] J. A. Tossell, G. V. Gibbs, *Acta Crystallogr. Sect. A* **1978**, *34*, 463–472.
[16] K. Torssell in *Progress in Boron Chemistry, Vol. 1* (Eds.: H. Steinberg, A. L. McCloskey), Pergamon, Oxford, **1964**.
[17] F. J. Feher, R. L. Blanski, *J. Chem. Soc. Chem. Commun.* **1990**, 1614–1616.

Highly Enantio- and Diastereoselective Synthesis of 2-Substituted 1-Bicyclo[3.1.0]hexanols**

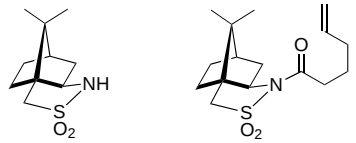
Ryo Mizojiri, Hirokazu Urabe, and Fumie Sato*

Bicyclic cyclopropanols and their derivatives, such as the trimethylsilyl ethers, have been utilized as useful intermediates in organic synthesis by the manipulation of their reactive cyclopropanol moiety.[1] However, the asymmetric preparation of these compounds has been quite limited so far,[2, 3] even though current developments in enantioselective synthesis should call for the use of optically active cyclopropanols as starting materials.

The reaction of unsaturated esters,[4] amides,[5] imides,[6] and related compounds[7] with an alkene–titanium complex[8] is a very convenient method to prepare bicyclic cyclopropanols[4] and cyclopropylamines[5] in one step [Eqs. (1) and (2); X = R′O, Cl, Br]. Extension of this transformation to an asymmetric version would clearly serve as a simple route to optically active cyclopropanols (or cyclopropylamines). To this end, the use of a chiral titanium complex was successful.[9] An alternative approach is to incorporate a chiral auxiliary in



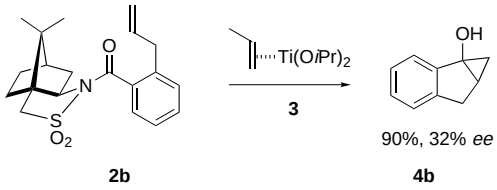
the substrate. Thus, an unsaturated carboxylic acid derivative having a chiral leaving group on its acyl group would afford the corresponding optically active bicyclic cyclopropanol; surprisingly, this method has not been reported yet. We chose Oppolzer's camphorsultam **1**[10] as the leaving group, because



1 **2a**

the known enantioselective α-alkylation of the *N*-acyl derivative **2a**[11] could be performed not only with activated halides (i.e., allyl or benzyl halides) but also with nonactivated counterparts (i.e., primary alkyl halides).[11] As we show here, this allowed the preparation of a variety of substituted bicyclic cyclopropanols.

The ability of acylsulfonamides to act as esters in reaction (1) to give cyclopropanols (rather than as amides in reaction (2) to yield cyclopropylamines) has not been demonstrated. This issue as well as the asymmetric induction in the nucleophilic addition to *N*-acylcamphorsultams[12] is addressed in the reaction of **2b** with [Ti(O*i*Pr)$_2$(η^2-propene)] (**3**) as shown in Equation (3).[4a] To our satisfaction, optically



2b **4b**

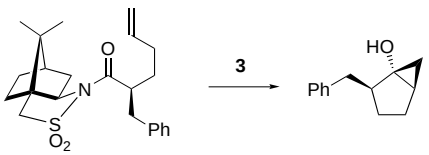
active cyclopropanol **4b** was obtained, while the possible byproduct, a *N*-cyclopropylsulfonamide, was not detected at all. Unfortunately, the enantiopurity of the product does not reach a satisfactory level.

Nonetheless, the α-branched acylsultams, readily prepared by diastereoselective alkylation of the *N*-acylcamphorsultam **2a** according to the literature method,[11] showed nearly complete stereocontrol in the cyclopropanol cyclization. Thus, treatment of **2c** with **3** afforded **4c** virtually as a single product and in high yield [Eq. (4)]. The diastereoselectivity was determined by ^{1}H NMR spectroscopy in comparison with an authentic mixture of the diastereoisomers, and the relative configuration shown for **4c** was established by NOE experi-

[*] Prof. Dr. F. Sato, R. Mizojiri, Dr. H. Urabe
Department of Biomolecular Engineering
Tokyo Institute of Technology
4259 Nagatsuta-cho, Midori-ku, Yokohama, Kanagawa 226-8501 (Japan)
Fax: (+81) 45-924-5826
E-mail: fsato@bio.titech.ac.jp

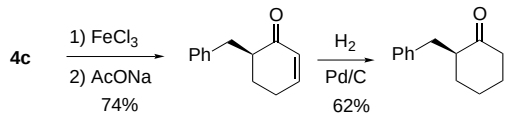
[**] We thank the Ministry of Education, Science, Sports and Culture (Japan) for financial support.

 © WILEY-VCH Verlag GmbH, D-69451 Weinheim, 1998 1433-7851/98/3719-2666 $ 17.50+.50/0



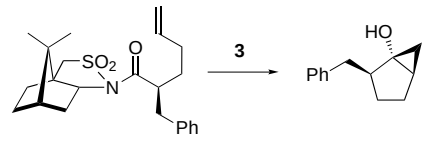
2c *ds* > 99: 1 **4c** 86% *ds* > 99: 1 >98% *ee* (4)

ments. That the enatiopurity of **4c** maintains the original value of **2c** was verified by a ^{1}H NMR chiral shift study ([Eu(hfc)$_3$], hfc = 3-(heptafluoropropylhydroxymethylene)-D-camphorate). The absolute structure of **4c** was determined by derivatization to the known (−)-2-(phenylmethyl)cyclohexanone[13] through ring expansion with $FeCl_3$[14] followed by hydrogenation of the resultant cyclohexenone [Eq. (5)].

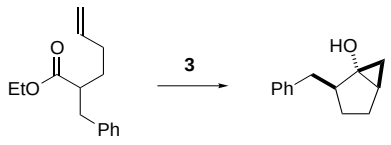


(5)

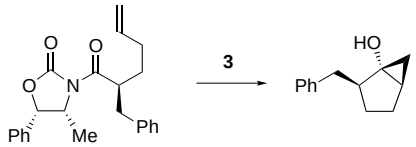
The highly stereoselective construction of the bicyclic cyclopropanol moiety (which, at the same time, leads to the high diastereoselectivity) seems to arise from a cooperative effect of the chiral auxiliary used and the neighboring alkyl substituent that results in the second chiral center (R in Table 1). If instead of the acylsultam **2c**, its diastereoisomer **2j** [Eq. (6)], a simple ethyl ester **5** [Eq. (7)],[4b] or the *N*-acyloxazolidinone **7** from Evans et al.[15] [Eq. (8)] is used, there is a considerable decrease in the diastereoselectivity. This supports the above rationalization.



2j *ds* > 99:1 **6** 78% *ds* = 92: 8 (6)



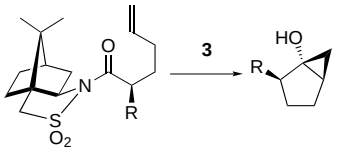
5 **6** 77% *ds* = 66:34 (7)



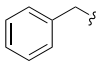
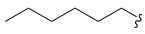
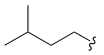
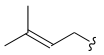
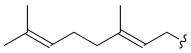
7 **6** 38% *ds* = 74:26 (8)

Table 1 shows that a variety of bicyclic cyclopropanols can be obtained in good yields and with high diastereoselectivities. Another important feature of this reaction is the compatibility of a variety of functional groups. For instance, the reaction of **2f** and **2g** afforded the desired products with their internal olefins intact. In addition, oxygen functionalities such as a silyl ether and even a *tert*-butyl ester group in substrates **2h** and **2i** survived the reaction conditions. The parent camphorsultam **1** was recovered after the reaction (80–90% for entries 1 and 2) and could be recycled for other runs.

Table 1. Diastereoselective synthesis of optically active cyclopropanols by the following reaction:[a]



2 *ds* > 99: 1 **4** >98% *ee*

Entry	R	Derivative	Yield of **4** [%][b]	*ds*[c]
1		**c**	86	> 99:1[d]
2		**d**	58	> 95:5
3		**e**	80	> 95:5
4		**f**	87	> 95:5
5		**g**	74	> 95:5
6	*t*BuMe$_2$SiO 	**h**	84	> 95:5
7	*t*BuO$_2$C	**i**	56	92:8[d]

[a] For details, see the Experimental Section. [b] Yield of isolated product. [c] Determined by ^{1}H and ^{13}C NMR spectroscopy of the crude and purified samples, unless otherwise noted. [d] Determined by ^{1}H NMR spectroscopy in comparison with an authentic mixture of the diastereomers.

In summary, the cyclization of unsaturated acylsulfonamides derived from Oppolzer's camphorsultam with low-valent titanium complex **3** affords optically active bicyclic cyclopropanols, which are difficult to prepare by existing methods. The synthetic utility of the products **4**, an example for which is illustrated by the preparation of an optically active 6-substituted-2-cyclohexenone [Eq. (5)], will be reported in due course.

Experimental Section

The following procedure for the preparation of **4c** is representative: To a solution of **2c** (80 mg, 0.20 mmol) and Ti(O*i*Pr)$_4$ (0.12 mL, 0.40 mmol) in Et$_2$O (2.0 mL) was added *i*PrMgCl (0.57 mL of a 1.40 M solution in Et$_2$O, 0.80 mmol) at −50 °C under argon. After the reaction mixture was stirred

 © WILEY-VCH Verlag GmbH, D-69451 Weinheim, 1998 1433-7851/98/3719-2667 $ 17.50+.50/0

at low temperature (ca. −45 to −40 °C) for 1 h, it was stirred at 0 °C for another hour. After the addition of water (0.20 mL) in THF (0.40 mL), the solution was stirred for 0.5 h at room temperature. The resultant suspension was filtered through celite, which was subsequently washed with Et_2O. The filtrate and Et_2O fractions were concentrated in vacuo to afford a crude oil. Purification by column chromatography (silica gel, hexane/ether 5/1) afforded **4c** (32 mg, 86 % yield) as a colorless oil. $[\alpha]_D^{27} = -0.65$ ($c = 0.46$ in $CHCl_3$); IR (neat): $\tilde{\nu} = 3404, 3062, 2929, 1948, 1876, 1602, 1495, 1452, 976, 756, 701\ cm^{-1}$; ^1H NMR (300 MHz, $CDCl_3$): $\delta = 7.15-7.32$ (m, 5H), 2.87 (dd, $J = 6.0$, 13 Hz, 1H), 2.43–2.66 (m, 2H), 1.82 (ddt, $J = 4.2$, 7.8, 12 Hz, 1H), 1.61–1.70 (m, 1H), 1.69 (s, 1H), 1.48 (dd, $J = 7.8$, 12 Hz, 1H), 1.37 (dt, $J = 9.0$, 4.2 Hz, 1H), 0.86–0.91 (m, 1H), 0.76 (dd, $J = 5.4$, 9.0 Hz, 1H), 0.67 (t, $J = 5.4$ Hz, 1H); ^{13}C NMR (75 MHz, $CDCl_3$): $\delta = 12.8$, 24.3, 25.3, 28.3, 37.9, 46.8, 67.1, 126.1, 128.6, 128.9, 141.7.

Received: April 7, 1998 [Z11699IE]
German version: *Angew. Chem.* **1998**, *110*, 2811–2814

Keywords: asymmetric synthesis · chiral auxiliaries · cyclizations · cyclopropanols · titanium

[1] Reviews: S. Murai, I. Ryu, N. Sonoda, *J. Organometal. Chem.* **1983**, *250*, 121–133; I. Kuwajima, E. Nakamura, *Top. Curr. Chem.* **1990**, *155*, 1–39; I. Kuwajima, E. Nakamura in *Comprehensive Organic Synthesis*, *Vol. 7* (Eds.: B. M. Trost, I. Fleming), Pergamon, Oxford, **1991**, pp. 441–454; T. Hirao, *Top. Curr. Chem.* **1996**, *178*, 99–147; other reports: I. Ryu, K. Matsumoto, Y. Kameyama, M. Ando, N. Kusumoto, A. Ogawa, N. Kambe, S. Murai, N. Sonoda, *J. Am. Chem. Soc.* **1993**, *115*, 12330–12339; M. Kirihara, S. Yokoyama, H. Kakuda, T. Momose, *Tetrahedron Lett.* **1995**, *36*, 6907–6910, and references therein.

[2] For the preparation of optically active, bicyclic cyclopropanols, see T. Sugimura, T. Futagawa, A. Tai, *Tetrahedron Lett.* **1988**, *29*, 5775–5778; T. Sugimura, T. Futagawa, M. Yoshikawa, A. Tai, *Tetrahedron Lett.* **1989**, *30*, 3807–3810.

[3] For the preparation of other types of optically active cyclopropanols, see T. Kunz, H.-U. Reissing, *Tetrehedron Lett.* **1989**, *30*, 2079–2082; T. Imai, H. Mineta, S. Nishida, *J. Org. Chem.* **1990**, *55*, 4986–4988; J. Pietruszka, M. Widenmeyer, *Synlett* **1997**, 977–979.

[4] a) A. Kasatkin, F. Sato, *Tetrahedron Lett.* **1995**, *36*, 6079–6082; b) A. Kasatkin, K. Kobayashi, S. Okamoto, F. Sato, *Tetrahedron Lett*. **1996**, *37*, 1849–1852; c) J. Lee, H. Kim, J. K. Cha, *J. Am. Chem. Soc*. **1996**, *118*, 4198–4199; d) J. Lee, Y. G. Kim, J. G. Bae, J. K. Cha, *J. Org. Chem.* **1996**, *61*, 4878–4879; e) S. Okamoto, M. Iwakubo, K. Kobayashi, F. Sato. *J. Am. Chem. Soc.* **1997**, *119*, 6984–6990; f) J. S. U, J. Lee, J. K. Cha, *Tetrahedron Lett*. **1997**, *38*, 5233–5236; g) S. Hikichi, G. P.-J. Hareau, F. Sato, *Tetrahedron Lett*. **1997**, *38*, 8299–8302.

[5] V. Chaplinski, A. de Meijere, *Angew. Chem.* **1996**, *108*, 491–492; *Angew. Chem. Int. Ed. Engl.* **1996**, *35*, 413–414; J. Lee, J. K. Cha, *J. Org. Chem.* **1997**, *62*, 1584–1585; V. Chaplinski, H. Winsel, M. Kordes, A. de Meijere, *Synlett* **1997**, 111–114; J. Lee, J. S. U, S. C. Blackstock, J. K. Cha, *J. Am. Chem. Soc*. **1997**, *119*, 10241–10242.

[6] J. Lee, J. D. Ha, J. K. Cha, *J. Am. Chem. Soc*. **1997**, *119*, 8127–8128.

[7] S. Y. Cho, J. Lee, R. K. Rammi, J. K. Cha, *J. Org. Chem.* **1997**, *62*, 8235–8236.

[8] O. G. Kulinkovich, S. V. Sviridov, D. A. Vasilevski, *Synthesis* **1991**, 234.

[9] E. J. Corey, A. Rao, M. C. Noe, *J. Am. Chem. Soc.* **1994**, *116*, 9345–9346.

[10] Reviews: W. Oppolzer, *Pure Appl. Chem.* **1990**, *62*, 1241–1250; B. H. Kim, D. P. Curran, *Tetrahedron* **1993**, *49*, 293–318.

[11] W. Oppolzer, R. Moretti, S. Thomi, *Tetrahedron Lett.* **1989**, *30*, 5603–5606; W. Oppolzer, J. Blagg, I. Rodriguez, E. Walter, *J. Am. Chem. Soc.* **1990**, *112*, 2767–2772.

[12] To the best of our knowledge, asymmetric induction by nucleophilic addition to the carbonyl group of the acylcamphorsultams has not been reported.

[13] A. I. Meyers, D. R. Williams, M. Druelinger, *J. Am. Chem. Soc.* **1976**, *98*, 3032–3033; K. Saigo, A. Kasahara, S. Ogawa, H. Nohira, *Tetrahedron Lett.* **1983**, *24*, 511–512.

[14] Y. Ito, S. Fujii, M. Nakatsuka, F. Kawamoto, T. Saegusa in *Organic Syntheses*, *Coll. Vol. 6* (Ed.: W. E. Noland), Wiley, New York, **1988**, pp. 327–333.

[15] D. J. Ager, I. Prakash, D. R. Schaad, *Chem. Rev.* **1996**, *96*, 835–875; D. A. Evans, E. Vogel, J. V. Nelson, *J. Am. Chem. Soc.* **1979**, *101*, 6120–6123; D. A. Evans, M. D. Ennis, D. J. Mathre, *J. Am. Chem. Soc.* **1982**, *104*, 1737–1739; D. A. Evans, A. E. Weber, *J. Am. Chem. Soc.* **1987**, *109*, 7151–7157.

Two New Isopolyoxotungstates(VI) with the Empirical Composition $Cs_2W_2O_7 \cdot 2H_2O$ and $Na_2W_2O_7 \cdot H_2O$: An Icosatetratungstate and a Polymeric Compound**

Irene Brüdgam, Joachim Fuchs, Hans Hartl,* and Rosemarie Palm

Dedicated to Professor Hartmut Bärnighausen on the occasion of his 65th birthday

Owing to their structural and electronic diversity, iso- and heteropolyoxometalates with different metal centers and varying oxidation states undergo an exceptionally wide variety of reactions, which have applications in many fields of chemistry (synthesis, analytical chemistry, catalysis, biochemistry).[1] The number of dissimilar polyoxometalates is enormous; however, certain structural units appear repeatedly, depending on the metal counterion and the synthesis conditions. These can serve as structural components of large, in some cases huge, polyoxometalates formed by conservative self-organizing processes.[2, 3] Examples of isopolytungstates (VI) include the dodecatungstates $H_2W_{12}O_{40}^{6-}$ (Keggin-type)[4] and $H_2W_{12}O_{42}^{10-}$ (paratungstate-Z),[5] the heptatungstate $W_7O_{24}^{6-}$,[6] and the hexatungstate $W_6O_{19}^{2-}$[7] as well as fragments of these anions, which act as isolated units or as components of high molecular aggregates. These groups are linked to each other either directly or through cations and heteroatoms.

Isopolyoxotungstates are produced in a similar manner as other polyoxometalates by acidification of aqueous solutions of monotungstates. In the present case, we used the oxide WO_3, which reacts in water like the hypothetical diprotic acid H_2WO_4, for the acidification. The molar ratio of H^+ introduced to WO_4^{2-} is defined as the degree of acidification of the metalate solution, the molar ratio of H^+ that reacted per WO_4^{2-} is the degree of protonation.[8] The title compounds $Cs_2W_2O_7 \cdot 2H_2O$ (**1**) and $Na_2W_2O_7 \cdot H_2O$ (**2**), which are formally prepared according to Equation (1), display a degree

$$2\,WO_4^{2-} + 2\,H^+ \rightleftharpoons W_2O_7^{2-} + H_2O \qquad (1)$$

[*] Prof. Dr. H. Hartl, I. Brüdgam, Prof. Dr. J. Fuchs, R. Palm
Institut für Anorganische und Analytische Chemie
der Freien Universität
Fabeckstrasse 34–36, D-14195 Berlin (Germany)
Fax: (+49) 30-838-3310
E-mail: hartl@chemie.fu-berlin.de

[**] This work was supported by the Fonds der Chemischen Industrie.

 © WILEY-VCH Verlag GmbH, D-69451 Weinheim, 1998 1433-7851/98/3719-2668 $ 17.50+.50/0

of protonation of 1. The degree of acidification of a tungstate solution is one of the most important factors in determining which polyoxometalate is formed. Other conditions, especially the type of cation present, also play a role. Alkali metal cations, for example, show a gradual change in coordination behavior dependent on the ion radius. When crystallized from the aqueous solution, the cations are normally coordinated by oxygen atoms of the polyoxometalate anions as well as by water molecules. In contrast to the Na^+ ion, the larger and softer Cs^+ ion prefers the polyanion ligands to the aqua ligands.[9] This difference in coordination behavior is expected to influence the condensation and crystallization processes through the formation of different cation–anion pairs in solution.

Recently we reported two new isopolytungstates $Na_5H_3W_6O_{22}\cdot 18H_2O$ (**3**)[10] and $K_7HW_5O_{19}\cdot 10H_2O$ (**4**);[11] both were synthesized from weakly alkaline solutions under the same conditions. The only difference between the two was that in the first case we used Na^+, and in the second K^+, as cation. Compounds **3** and **4** display certain structural similarities in that their anions represent fragments of the heptatungstate ion $W_7O_{24}^{6-}$ (Figure 1).[6] In the course of isolating

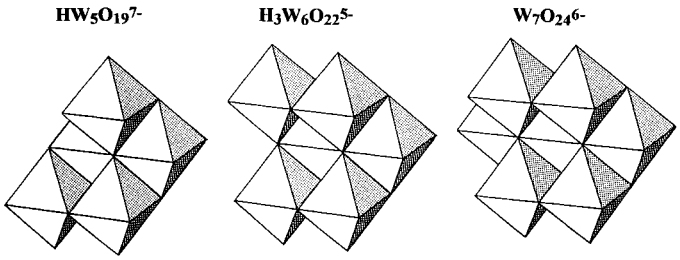


Figure 1. Polyhedra representation of the anions $HW_5O_{19}^{7-}$, $H_3W_6O_{22}^{5-}$, and $W_7O_{24}^{6-}$.

3,[10] a colorless microcrystalline substance could be separated from the filtrate after the solution was left standing for months. The use of IR and Raman spectroscopy enabled us to identify the compound as $Na_2W_2O_7\cdot 4H_2O$. A sodium ditungstate that contains water has recently been described by Simons[12]; however, this was a pentahydrate. The tetrahydrate can be obtained in higher yields by starting with a solution of $WO_3\cdot H_2O$ and $Na_2WO_4\cdot 2H_2O$ in a ratio of 1:3 instead of 1:7. After thermal degradation, the monohydrate **2** is produced in microcrystalline form. Single crystals of **2** were obtained from the solution in a hydrolysis autoclave at 150–180 °C. The identity of these two substances, synthesized by different methods, was determined by IR and Raman spectroscopy. The nearly water insoluble **2** is the first known structure of a high polymeric oxotungstate to contain water.[13]

The basic structural components of **2** are planar W_4O_{16} units, which consist of edge-sharing WO_6 octahedra in a rhomboidal arrangement (Figure 2). The W_4O_{16} units are linked to the anions $H_3W_6O_{22}^{5-}$ and $HW_5O_{19}^{7-}$ since they are fragments of these anions (as well as of the heptatungstate $W_7O_{24}^{6-}$).[5] In **2**, the $W_4O_{16}^{8-}$ units share common vertices, leading to $^1_\infty[W_4O_{14}^{4-}]$ chains. The Na^+ ions bridge the chains of polytungstates, which are arranged in a rod packing parallel to

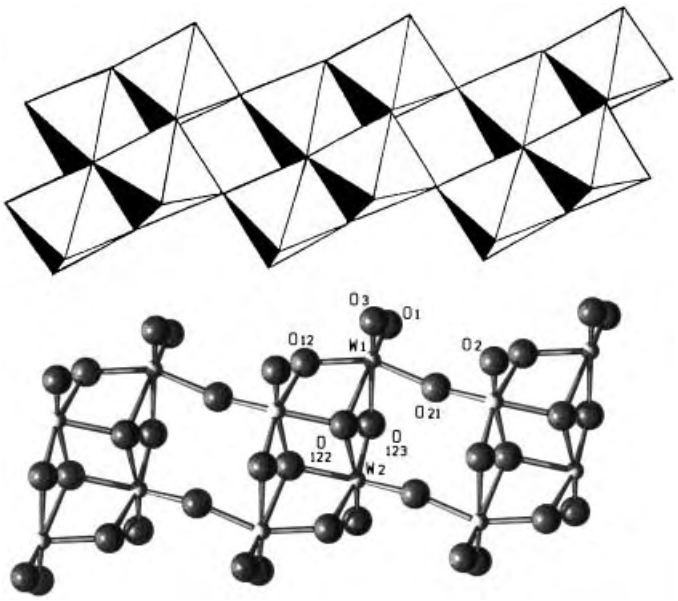


Figure 2. Polyhedra and ball-and-stick representation of the anion $^1_\infty[W_4O_{14}^{4-}]$. Selected bond lengths [Å]: W–$O_{term.}$ 1.71–1.75, W–μ_2-O 1.78–2.24, W–μ_3-O 2.23–2.27.

the *b* axis. The molecule of crystal water is shared by the two crystallographically independent Na^+ ions, which are coordinated by five (Na1) and six oxygen atoms (Na2, Figure 3). The octahedral NaO_6 groups are linked through diagonally arranged edges, forming an isometric chain structure parallel to the polytungstate chains. The resulting gaps are filled with

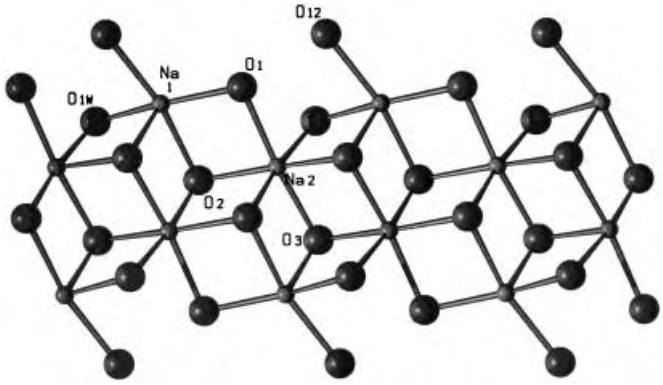


Figure 3. Ball-and-stick representation of the sodium–oxygen polyhedra chain of **2**.

quadratic NaO_5 pyramids, which share common edges with three NaO_6 octahedra. The $W_4O_{16}^{8-}$ structural unit is already known as a component of $Li_2WO_4\cdot 4/7\,H_2O$.[14] However, the four WO_6 octahedra are not connected in a rhombic planar fashion in this compound, but compactly as tetrahedra.

An even better example, which demonstrates clearly how the type of cation present influences polyoxotungstate formation, is the cesium compound **1**, which was synthesized in the same manner as **3** and **4**. A crystal structure analysis[15] shows that the actual compound hiding behind the given empirical formula in the title has the formula $Cs_{24}W_{24}O_{84}\cdot 24H_2O$. The anion $W_{24}O_{84}^{24-}$ present in **1** (symmetry C_i) is the

largest discrete isopolyoxotungstate known to date. It does not have any structural similarities to **2**–**4**. Not only is it made up of WO_6 octahedra, but it also contains WO_5 units, which are very rare. Six vertice-sharing WO_6 octahedra form an inner ring. Six W_3O_{13} groups are condensed to this ring, again through common octahedra vertices. The W_3O_{13} groups are made up of two vertice-sharing octahedra WO_6 and one quadratic pyramid WO_5, which is distorted in the direction of a trigonal bipyramid (Figures 4 and 5, top). The

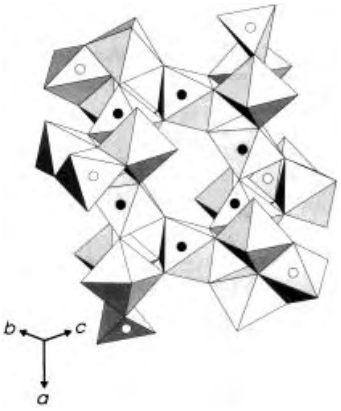


Figure 4. Polyhedra representation of the anion $W_{24}O_{84}^{24-}$. Black dots: inner ring of vertice-sharing WO_6 octahedra; white dots: WO_5 units, which together with two WO_6 octahedra make up the W_3O_{13} structural fragments. Selected bond lengths [Å]: W–O_{ring} 1.75–2.13; WO_6 octahedra: W–$O_{term.}$ 1.71–1.78, W–μ_2-O 1.78–2.32, W–μ_3-O 2.03–2.14; WO_5 units: W–$O_{term.}$ 1.73–1.81, W–μ_2-O 1.88–1.97, W–μ_3-O 2.01–2.04.

WO_5 pyramid shares two neighboring edges of its base (two μ_2-O atom and one μ_3-O atom) with the two WO_6 octahedra; one of the two terminal oxygen atoms is axial. All of the oxygen atoms of the six inner octahedra are involved in cross-linking, whereas the outer WO_6 octahedra and the WO_5 groups each bear two terminal oxygen atoms. The bond lengths between W and the asymmetrically bridging μ_2-O atoms alternate between short and long, a result of the distortion of the WO_6 octahedra commonly observed in polytungstates.[7b]

Of the twelve cesium cations in the asymmetrical unit, one is situated above and one below the center of symmetry in the middle of the anion. These fit perfectly into the cavities formed by the oxygen atoms of the anion and have an unusually high coordination number of 15, if one takes into account Cs–O distances up to 3.6 Å; only oxygen atoms of the anion are in the sphere of coordination. The other cesium atoms have a seven- to elevenfold coordination by oxygen atoms of the polyanion and crystal water molecules. The anion and all of the cesium atoms (minus the water molecules) are shown in a space-filling model in the bottom part of Figure 5. The fit of the cesium atoms in the oxygen atom packing, and the fact that this bulky anion could not be isolated with other alkaline cations, suggests that the large cesium cations promote its formation through a type of template effect.

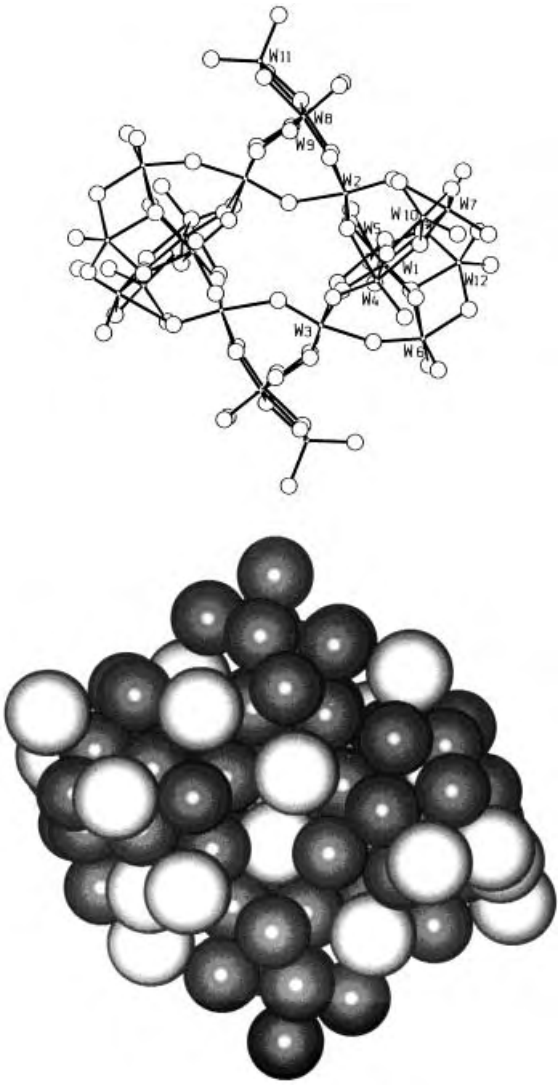


Figure 5. Ball-and-stick (top) and space-filling representation (bottom) of the anion $W_{24}O_{84}^{24-}$. The light balls in the bottom part represent the Cs^+ ions built in to the oxygen packing.

Experimental Section

1: Cs_2WO_4 (1 g, 1.9 mmol), synthesized by melting $WO_3 \cdot H_2O$ (pure, Merck) and Cs_2CO_3 (Fluka) at 1000 °C in a porcelain crucible, is stirred under argon (CO_2 exclusion) in a Cautex beaker with $WO_3 \cdot H_2O$ (0.07 g, 0.28 mmol) in 1.5 mL of H_2O at 20 °C for 2 h (degree of acidification: 0.294 based on $WO_3 \cdot H_2O/Cs_2WO_4$). The solution is separated from a very fine solid substance by filtration (possibly more than once). After letting the solution stand for several hours (pH ≈ 8), **1** crystallizes in the form of flat, trapezoidal columns. The compound is soluble in water, but cannot be recrystallized in aqueous solution.

2: An aqueous solution of 1M sodium monotungstate (10 mL) is heated to 150–180 °C with tungstic acid (0.7 g, 2.8 mmol) in a hydrolysis autoclave (pressure hydrolysis system II, Berghof) in a PTFE insert (degree of acidification: 0.56 based on $WO_3 \cdot H_2O/Na_2WO_4$). Compound **2** crystallizes along with a white powder after about three weeks. The powder can be separated from the product by repeatedly decanting in water in a ultrasound bath. The purity of the product can be verified with IR and Raman spectroscopy. Data on the yields of **1** and **2** is difficult to obtain because of a fluctuation in yields depending on the quality of the mechanical separation process (filtering, decanting) of the solid-state products, which all precipitate out of the solution simultaneously.

Received: January 19, 1998
Revised version: June 25, 1998 [Z11374IE]
German version: *Angew. Chem.* **1998**, *110*, 2814–2817

Keywords: isopolymetalates · structure elucidation · tungsten

 © WILEY-VCH Verlag GmbH, D-69451 Weinheim, 1998 1433-7851/98/3719-2670 $ 17.50+.50/0

[1] a) M. T. Pope, *Heteropoly and Isopoly Oxometalates*, Springer, Berlin, **1983**; b) M. T. Pope, A. Müller, *Angew. Chem.* **1991**, *103*, 56; *Angew. Chem. Int. Ed. Engl.* **1991**, *30*, 34; c) "Polyoxometalates": *Platonic Solids to Anti-Retroviral Activity* (Eds.: M. T. Pope, A. Müller), Kluwer, Dordrecht, **1994**; d) D. E. Katsoulis, *Chem. Rev.* **1998**, *98*, 359.

[2] A. Müller, E. Krickemeyer, H. Bögge, M. Schmidtmann, C. Beugholt, P. Körgeler, C. Lu, *Angew. Chem.* **1998**, *110*, 1278; *Angew. Chem. Int. Ed.* **1998**, *37*, 1220;

[3] a) A. Müller, E. Krickemeyer, J. Meyer, H. Bögge, F. Peters, W. Plass, E. Diemann, S. Dillinger, F. Nonnenbruch, M. Randerath, C. Menke, *Angew. Chem.* **1995**, *107*, 2293; *Angew. Chem. Int. Ed. Engl.* **1995**, *34*, 2122; b) K. Wassermann, M. H. Dickmann, M. T. Pope, *Angew. Chem.* **1997**, *109*, 1513; *Angew. Chem. Int. Ed. Engl.* **1997**, *36*, 1445; c) A. Müller, F. Peters, M. T. Pope, D. Gatteschi, *Chem. Rev.* **1998**, *98*, 239.

[4] a) J. F. Keggin, *Nature* **1933**, *131*, 908; b) J. F. Keggin, *Proc. R. Soc. A* **1934**, *144*, 75.

[5] a) R. Allmann, *Acta Crystallogr. Sect. B* **1971**, *27*, 1393; b) A. Chrissafidou, J. Fuchs, H. Hartl, R. Palm, *Z. Naturforsch. B* **1995**, *50*, 217.

[6] a) J. Fuchs, E. P. Flindt, *Z. Naturforsch. B* **1979**, *34*, 1393; b) K. G. Burtseva, T. S. Chernaya, M. I. Sirota, *Sov. Phys. Dokl. (Engl. Transl.)* **1978**, *23*, 784.

[7] a) G. Henning, A. Hüllen, *Z. Kristallogr.* **1969**, *130*, 162; b) J. Fuchs, W. Freiwald, H. Hartl, *Acta Crystallogr. Sect. B* **1978**, *34*, 1764.

[8] a) K. H. Tytko, O. Glemser, *Adv. Inorg. Chem. Radiochem.* **1976**, *19*, 239; b) *Gmelin Handbook of Inorganic Chemistry*, *Molybdenum*, Suppl. Vol. B, **1987**, *3a*, 77.

[9] a) V. Hubert, H. Hartl, *Z. Naturforsch. B* **1996**, *51*, 969; b) H. Hartl, V. Hubert, *Acta Crystallogr. Sect. C* **1996**, *52*, 757.

[10] H. Hartl, R. Palm, J. Fuchs, *Angew. Chem.* **1993**, *105*, 1545; *Angew. Chem. Int. Ed. Engl.* **1993**, *32*, 1492.

[11] J. Fuchs, R. Palm, H. Hartl, *Angew. Chem.* **1996**, *108*, 2820; *Angew. Chem. Int. Ed. Engl.* **1996**, *35*, 2651.

[12] E. L. Simons, *Inorg. Chem.* **1964**, *3*, 1079.

[13] Crystal structure analysis of **2**:[16] $M_r = 543.6$, triclinic, space group $P\bar{1}$, $a = 6.0101(11)$, $b = 7.1801(7)$, $c = 8.6447(9)$ Å, $\alpha = 108.04(1)$, $\beta = 96.10(1)$, $\gamma = 104.12(1)^\circ$, $V = 337.25(9)$ Å^3, $\rho_{calcd} = 5.4$ g cm^{-3}, $\mu_{Mo} = 362.4$ cm^{-1}, crystal size $0.3 \times 0.1 \times 0.5$ mm^3, $2\theta_{max} = 60^\circ$, STOE four-circle diffractometer, $Mo_{K\alpha}$ radiation, graphite monochromator, ω scanning, $T = 293$ K, 2144 measured reflections, 1969 symmetry-independent reflections, 1912 reflections $> 2\sigma(I)$, absorption correction (DIFABS), 109 refined parameters (W, Na, O anisotropic; no H atoms), structure solution with direct methods (SHELXS-86) and difference Fourier techniques (XTAL 3.5), weighting $1/\sigma^2(F)$, residual electron density < 2.2 e Å^{-3}, $R = 0.05$ ($I > 2.8\sigma I$), $Rw = 0.073$.

[14] A. Hüllen, *Naturwissenschaften* **1964**, *51*, 508.

[15] Crystal structure analysis of **1**:[16] $M_r = 9378.9$, monoclinic, space group $P2_1/n$, $Z = 2$, $a = 17.548(3)$, $b = 20.351(3)$, $c = 19.401(3)$ Å, $\beta = 90.98(2)$, $V = 6927.42$ Å^3, $\rho_{calcd} = 4.49$ g cm^{-3}, $\mu_{Mo} = 274.2$ cm^{-1}, crystal size $0.3 \times 0.3 \times 0.2$ mm^3, $2\theta_{max} = 50^\circ$, $Mo_{K\alpha}$ radiation, Nonius-CAD4 four-circle diffractometer, graphite monochromator, $\omega/2\theta$ scanning, $T = 293$ K, 15367 measured reflections, 12030 symmetry-independent reflections, 8358 reflections $> 2\sigma(I)$, absorption correction (psi scan, max./min. transmission 99.9/53.9%), isotropic extinction correction, 437 refined parameters (W, Cs anisotropic; O isotropic; no H atoms), residual electron density < 6.9 e Å^{-3}, structure solution with direct methods (SHELXS-86) and difference Fourier techniques (XTAL 3.5), weighting $1/\sigma^2(F)$, $R = 0.076$ ($I > 2\sigma I$), $Rw = 0.05$.

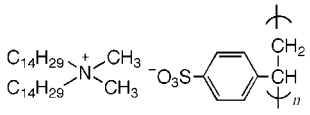
[16] Further details on the crystal structure investigation may be obtained from the Fachinformationszentrum Karlsruhe, D-76344 Eggenstein-Leopoldshafen, Germany (fax: (+49) 7247-808-666; e-mail: crysdata@fiz-karlsruhe.de), on quoting the depository numbers CSD-408188 (**1**) and CSD-408189 (**2**).

A Fullerene/Lipid Electrode Device: Reversible Electron Transfer Reaction of C_{60} Embedded in a Cast Film of an Artificial Ammonium Lipid on an Electrode in Aqueous Solution**

Naotoshi Nakashima,* Takeshi Tokunaga, Yuko Nonaka, Takashi Nakanishi, Hiroto Murakami, and Takamasa Sagara

The development of lipid bilayer modified electrodes whose structures mimic those of biomembranes is highly attractive, because such a study would produce a methodology for novel surface modification and functionalization. We and other have focused on the combination of fullerene chemistry and the chemistry of lipid bilayer membranes.[1] The goal in this study is to design and construct a system showing fast electron transfer reactions of fullerenes using lipid films as an electrode modifier. Fullerenes form multiply charged anions because of their high degrees of degeneracy of the LUMO, which lead to a variety of unique properties;[2, 3] however, the electrochemistry of fullerene thin films is rather complicated.[3, 4]

We describe here for the first time the discovery that C_{60} embedded in a cast film of an artificial lipid with multiple ion pair interactions (poly(ion-complexed) lipid)—namely, dimethylditetradecylammonium poly(styrene sulfonate) (**1**)—on an electrode undergoes two reversible electron transfer reactions with the underlying electrode in an aqueous solution. Furthermore, the generated radical monoanion and the dianion are very stable. To our knowledge, no report has been published thus far describing reversible electron transfer reactions of fullerene thin films on electrodes in an aqueous solution.[5] The poly(ion-complexed) lipid **1** used in this study is insoluble in water, but possesses fundamental characteristics of dispersed lipid bilayer membranes in an aqueous solution.[6] We also used cast films of the biological lipid dimyristoylphosphatidyl choline (**2**) as matrix films for comparison with **1**.



1

Compound **1** was synthesized according to the previously described method[7] and analyzed by IR and NMR spectroscopy as well as elemental analysis. This compound is readily soluble in benzene and can be used to form, by the conventional solvent evaporation method, multibilayer films. Lipid **2** was purchased from Sigma and used as received. Production

[*] Prof. N. Nakashima, T. Tokunaga, Y. Nonaka, T. Nakanishi, Dr. H. Murakami, Dr. T. Sagara
Department of Applied Chemistry, Faculty of Engineering
Nagasaki University
Bunkyo-cho, Nagasaki 852-8521 (Japan)
Fax: (+81) 95-847-9896
E-mail: nakasima@net.nagasaki-u.ac.jp

[**] This work was supported in part by the Grant-in-Aids from the Ministry of Education, Science, Sports, and Culture, Japan; the Ogasawara Science and Technology Foundation; and the Iketani Science and Technology Foundation.

and stability of the multiply charged anions of C_{60} (Bucky USA, 99.995%) were examined with the electrochemical method. Modified electrodes were prepared by the following procedure: A portion (10 μL) of C_{60}/**1** or C_{60}/**2** in benzene ([**1**] = [**2**] = 15.2 mM, [C_{60}] = 0.80 mM) was placed on a homemade basal plane pyrolytic graphite (BPG) disk electrode[6] (area 0.20 cm^2) and then dried under air. The electrochemical properties of the cast films on the BPG electrode was examined at 25 °C with cyclic voltammetry (BAS-100BW Electrochemical Analyzer, Bioanalytical Systems) under an argon atmosphere. A Ag/AgCl/saturated KCl electrode and a Pt plate electrode were used as the reference and the counter electrodes, respectively.

The electrogenerated C_{60} radical monoanion at the electrode modified with C_{60} alone in the aqueous system has been reported to be unstable; that is, the voltammetric response disappears after several cyclic potential scans.[8] Szucs and coworkers[9] observed a reduction current for fullerene films on an electrode in an alkaline aqueous solution, but the electrochemistry was completely irreversible. The fullerene C_{60} incorporated in a cast film of the biological lipid **2** on an electrode did not communicate with the underlying electrode; that is, no faradaic current was observed for a C_{60}/**2**-modified electrode (data not shown). In contrast, C_{60}/**1**-modified electrodes gave quite different results. Figure 1 shows typical cyclic voltammograms (CVs) for a cast film of C_{60}/**1** on BPG. There are two reversible redox couples at formal potentials of −290 and −910 mV. The behavior of both couples did not change even after 50 cycles. The cathodic and anodic peak currents for C_{60} increased in proportion to the square root of the scan rates in the range of 5 – 500 mV s^{-1} (data not shown), indicating that the electrochemistry is diffusion-controlled.[10]

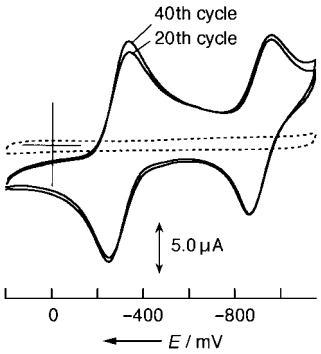


Figure 1. Cyclic voltammograms for cast films of **1** (dotted line) and C_{60}/**1** (solid lines) on electrodes in water. Supporting electrolyte: 0.5 M tetraethylammonium chloride, reference electrode: Ag/AgCl/saturated KCl, scan rate: 100 mV s^{-1}.

The amount of C_{60} that has reacted, as calculated from the CV of the C_{60}/**1**-modified electrode at a very low scan rate (2 mV s^{-1}), was 2.6×10^{-9} mol cm^{-2} [11] (average for four films). This corresponds to a coverage of about 17 monolayers of C_{60} or about 180 monolayers of C_{60}/**1** (assuming cross-sectional areas of 1.0 and 0.5 nm^2 for C_{60}[12] and **1**, respectively). This result indicates that the fullerene in the film is disposed in such a way that it can communicate electrochemically with the underlying electrode.

The further stability of the electrogenerated radical monoanion and the dianion of C_{60} in this system was examined by the potential hold experiment. As shown in Figure 2, the radical monoanion is unusually stable; that is, virtually no change in the CVs for the first redox wave was observed even after holding the potential for 90 min at −600 mV. A hold of several minutes at −1150 mV, where the fullerene is present as a dianion, did not affect the CVs, but longer holds caused a gradual decrease in the current. This suggests irreversible decomposition of the C_{60} dianion and/or dissolution of the C_{60} dianion into the bulk solution.

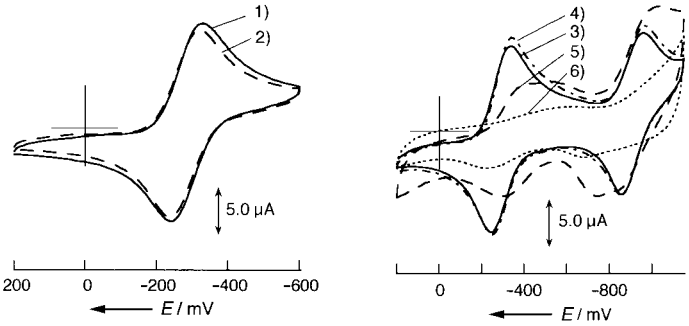


Figure 2. Effect of holding the potential for various lengths of time in the measurement of the cyclic voltammograms for a cast film of C_{60}/**1**. Hold time: 1) and 3): 0 min; 2) 90 min at −600 mV; 4) 1.5 min at −1150 mV; 5) 16.5 min at −1150 mV; 6) 61.5 min at −1150 mV. Supporting electrolyte, 0.5 M tetraethylammonium chloride, reference electrode: Ag/AgCl/saturated KCl, scan rate: 100 mV s^{-1}.

Since the electrochemical reduction of cast films of C_{60} involves incorporation of cations, supporting electrolytes are known to influence the voltammograms.[13, 14] In our system, however, the CVs for cast films of C_{60}/**1** on BPG were essentially the same in 0.5 M aqueous solutions of NaCl, KCl, and $CaCl_2$ (data not shown). Taken together with the result for the C_{60}/**2**-modified electrode, this indicates that these electrolyte cations are not major counterions of the fullerene radical monoanion and of the fullerene dianion. Instead, the dimethylditetradecylammonium cation in **1** may act as the counterion during the reduction of the fullerenes.[15]

In conclusion, we have designed and constructed a fullerene/lipid device which shows stable and reversible electron transfer reactions of C_{60} with the electrode. Our finding would be applicable to a variety of fullerene derivatives, higher fullerenes, and metallofullerenes.

Received: March 17, 1998 [Z11598IE]
German version: *Angew. Chem.* **1998**, *110*, 2817 – 2818

Keywords: cyclic voltammetry · fullerenes · electron transfer · lipids

[1] a) H. Hungerbühler, D. M. Guldi, K.-D. Asmus, *J. Am. Chem. Soc.* **1993**, *115*, 3386 – 3387; b) S. Niu, D. Mauzerall, *J. Am. Chem. Soc.* **1996**, *118*, 5791 – 5795; c) J. M. Janot, P. Seta, R. V. Bensasson, S. Leach, *Synth. Met.* **1996**, *77*, 103 – 106; d) H. Murakami, Y. Watanabe, N. Nakashima, *J. Am. Chem. Soc.* **1996**, *118*, 4484 – 4485; e) M. Hetzer, S. Bayerl, X. Camps, O. Vostrowsky, A. Hirch, T. M. Bayerl, *Adv. Mater.* **1997**, *9*, 913 – 917.

[2] a) *Buckminsterfullerenes* (Eds.: W. E. Billups, M. A. Ciufolini), VCH, New York, **1993**; b) *Physics and Chemistry of the Fullerenes* (Ed.: K. Prassides), Kluwer, Dordrecht, **1993**; c) *Chemistry and Physics of Fullerenes and Related Materials*, *Vol. 5* (Eds.: K. M. Kadish, R. S. Ruoff), The Electrochemical Society, Pennington, **1997**.

[3] a) J. Chlistunoff, A. J. Bard in *Handbook of Organic Conductive Molecules and Polymers* (Ed.: H. S. Nalwa), Wiley, Chichester, **1997**; b) see reference [3a], pp. 333 – 412.

 © WILEY-VCH Verlag GmbH, D-69451 Weinheim, 1998 1433-7851/98/3719-2672 $ 17.50+.50/0

[4] a) J. Chlistunoff, D. Cliffel, A. J. Bard, *Thin Solid Films* **1995**, *257*, 166 – 184; b) see reference [3a], pp. 390 – 394, 406 – 408; c) A. Deronzier, J.-C. Moutet, P. Seta, *J. Am. Chem. Soc.* **1994**, *116*, 5019 – 5020.
[5] For reversible electron transfer reactions of a C_{60}/γ-cyclodextrin complex dissolved in an aqueous solution, see P. Boulas, W. Kutner, M. T. Jones, K. M. Kadish, *J. Phys. Chem.* **1994**, *98*, 1282 – 1287.
[6] A.-E. F. Nassar, Y. Narikiyo, T. Sagara, N. Nakashima, J. F. Rusling, *J. Chem. Soc. Faraday Trans.* **1995**, *91*, 1775 – 1782, and references therein.
[7] N. Nakashima, Y. Yamaguchi, H. Eda, M. Kunitake, O. Manabe, *J. Phys. Chem. B* **1997**, *101*, 215 – 220.
[8] J. J. Davis, H. A. O. Hill, A. Kurz, A. D. Leighton, A. Y. Safronov, *J. Electroanal. Chem.* **1997**, *429*, 7 – 11.
[9] A. Szucs, A. Loix, J. B. Nagy, L. Lamberts, *J. Electroanal. Chem.* **1995**, *397*, 191 – 203.
[10] The peak separations between the cathodic and the anodic waves were 62 ± 3 mV. The electrochemistry of our system is governed by the diffusion of C_{60} and/or the electrolytes, and/or by electron hopping (self-exchange electron transfer between C_{60} molecules in the film).
[11] The total amount of electroactive C_{60} in the film should be greater than this because the redox reaction at a scan rate of 2 mV s^{-1} still involves diffusing species.
[12] C. Jehoulet, Y. S. Obeng, Y.-T. Kim, F. Zhou, A. J. Bard, *J. Am. Chem. Soc.* **1992**, *114*, 4237 – 4247.
[13] See reference [3a], pp. 386 – 390.
[14] A. Szucs, A. Loix, J. B. Nagy, L. Lamberts, *J. Electroanal. Chem.* **1996**, *402*, 137 – 148.
[15] The charge balance is maintained by incorporation of cations from the bulk solution.

Direct NMR Spectroscopic Observation of a Lanthanide-Coordinated Water Molecule whose Exchange Rate Is Dependent on the Conformation of the Complexes

Silvio Aime,* Alessandro Barge, Mauro Botta, Alvaro S. De Sousa, and David Parker

The development of magnetic resonance imaging (MRI) techniques for medical diagnosis has been accompanied by an explosive growth of interest in the study of water-soluble, paramagnetic metal complexes as contrast agents.[1] The contrast agents markedly improve the image contrast by enhancing the nuclear magnetic relaxation rates of the water protons in the tissues where they are distributed. The agents currently used in clinical practice are chelates of the Gd^{III} ion, which is particularly suitable because of its high magnetic moment and long electronic relaxation time (T_{1e}). The mechanism of the relaxation enhancement involves the modulation of the dipolar interaction between the magnetic moment of the electrons in Gd^{III} ions and the nuclear spins of the water protons in the inner and outer coordination sphere of the complex.[1, 2] The efficiency of the process depends primarily on the number q of water molecules bound to the metal ion, their exchange rate (k_{ex}) with the bulk water, and the rate of molecular reorientation. The residence lifetime τ_M ($\tau_M = 1/k_{ex}$) plays a particularly important role since it contributes directly to the modulation of the electron – nucleus dipolar interaction, and it controls the efficiency of the transfer of the paramagnetic effect to the bulk water. Thus, the issue of the water exchange rate in lanthanide(III) complexes is of paramount importance in the development of novel contrast agents for MRI. In fact, in a number of Gd^{III} chelates with $q = 1$ τ_M is much longer than that found for Ln^{III} aquo ions, which is of the order of nanoseconds,[3] and it may limit the relaxation efficiency of the contrast agents.[4]

Among the different complexes used as contrast agents for MRI, $[Gd(dota)]^-$ (dota = 1,4,7,10-tetraazacyclododecane-1,4,7,10-tetraacetic acid) should be the candidate of choice because of its high thermodynamic and kinetic stability. The long electronic relaxation time of the Gd^{III} ion prevents the observation of the NMR spectra of its complexes, and its solution structure had to be inferred from the ^1H and ^{13}C NMR spectra of the related complex $[Eu(dota)]^-$. As previously reported, $[Eu(dota)]^-$ consists of a pair of isomers, namely, **M** and **m**, endowed with the same square [3333] conformation of the macrocyclic ring, but with a different layout of the acetate arms. This difference results in a square antiprismatic and a twisted antiprismatic geometry for **M** and **m**, respectively (see Scheme 1).[5] The two isomers are in slow exchange near room temperature and yield two distinct sets of six resonances in the ^1H NMR spectrum for the C_4-symmetric ring and the diastereotopic CH_2CO protons. The resonance of the coordinated water molecule has not been observed (nor in other $[Ln(dota)]^-$ chelates) because its exchange rate is too fast on the NMR time scale ($k_{ex} = 4.1 \times 10^6$ s^{-1} at 298 K, as inferred from ^{17}O NMR data on $[Gd(dota)]^-$).[6] Recently, we reported that a Gd^{III} complex with a dota-like ligand containing four *N*-methylcarboxamide groups in place of the four carboxylate groups displays a large increase in the residence lifetime of the coordinated water molecule.[7] The slow exchange rate is a consequence of the stronger $Gd-OH_2$ interaction and a stabilizing hydrogen-bonding interaction to the proximate anions. The slow exchange of the coordinated water in this type of complex may give further insight into the relationship between the solution structure of the Ln^{III} chelate complex and the water exchange rate.

Here we have considered the Eu^{III} complex with the macrocyclic ligand dotam (dotam = 1,4,7,10-tetrakis(carbamoylmethyl)-1,4,7,10-tetraazacyclododecane). Figure 1 shows the ^1H NMR spectrum of $[Eu(dotam)]^{3+}$ in CD_3CN at 232 K. The compound is present as a mixture of **M** and **m** isomers whose ^1H chemical shifts are similar to those reported for the parent complex $[Eu(dota)]^-$ (Scheme 1). A 2D-EXSY NMR experiment carried out at 274 K in D_2O confirmed this analogy, and enabled the resonances to be assigned.[5b] In addition to the expected set of ligand resonances, an extra resonance for each isomer (of relative intensity two) is found at $\delta = 84.11$ (**M** isomer) and $\delta = 19.03$ (**m** isomer), respectively, which are assigned to the water molecules coordinated to

[*] Prof. S. Aime, Dr. A. Barge, Dr. M. Botta
Dipartimento di Chimica I.F.M., Università di Torino
Via P. Giuria 7, I-10125 Torino (Italy)
Fax: (+390) 11-670-7524
E-mail: aime@ch.unito.it
Dr. A. S. De Sousa, Prof. D. Parker
Department of Chemistry, Durham University
South Road, DH1 3LE Durham (UK)

 © WILEY-VCH Verlag GmbH, D-69451 Weinheim, 1998 1433-7851/98/3719-2673 $ 17.50+.50/0

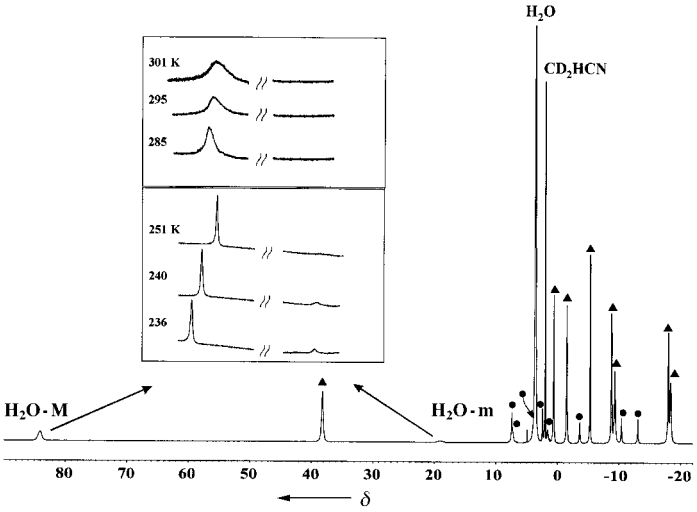
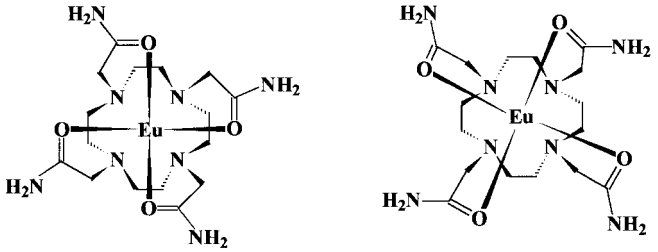


Figure 1. ^{1}H NMR spectrum (400 MHz) of [Eu(dotam)]$(SO_3CF_3)_3$ in CD_3CN at 232 K. The inset shows the expanded regions containing the bound water peaks for the two isomeric forms of the complex recorded at various temperatures. The symbols ▲ and ● indicate the ligand resonances of **M** and **m** isomers, respectively.



Scheme 1. Schematic representation of the two diastereoisomers of $[Eu(dotam)]^{3+}$. The water molecule, coordinated in the apical position above the plane of the four oxygen atoms, has been omitted for clarity.

the Eu^{III} ion. This assignment has been checked by measuring the ^{2}H NMR spectrum, in CH_3CN at 232 K, of a sample of $[Eu(dotam)]^{3+}$ that had undergone H/D exchange with D_2O. The ^{2}H resonances of free and **M**- and **m**-coordinated water molecules are observed at the same positions as in the ^{1}H NMR spectrum. In addition to the water signals, the ^{2}H NMR spectrum shows the resonances of the ^{2}H-exchanged $C(O)NH_2$ groups at $\delta = -5.6$ and 1.4, respectively.

A progressive broadening of the water resonance in the proton spectrum of the **m** isomer is observed upon increasing the temperature, which disappears at 243 K (see inset to Figure 1). The corresponding signal of the **M** isomer starts to broaden only at a temperature above 273 K. In the temperature range from 223 to 303 K the resonance of free water ($\delta_H = 3.57$) first broadens (maximum broadening at 248 K) then sharpens up and broadens again from 283 K. Selective irradiation of the free water resonance at 232 K results in the saturation of the **m** water signal only, whereas the same experiment carried out at 283 K caused the saturation of the corresponding **M** water peak. This behavior is consistent with the occurrence of a chemical exchange between free and bound water, which takes place at a rather different rate in the two isomers. Bandshape analysis has allowed the exchange rates at the various temperatures to be assessed and the following kinetic activation parameters to be determined: **M** isomer: $\Delta H^{\#} = 79.0(\pm 1.9)$ kJ mol^{-1}, $\Delta S^{\#} = 65.7(\pm 6.5)$ J mol^{-1} K^{-1}); **m** isomer: $\Delta H^{\#} = 79.0(\pm 2.5)$ kJ mol^{-1}, $\Delta S^{\#} = 110.8(\pm 10.4)$ J mol^{-} K^{-1}.

Under the assumption that the water exchange occurs through a dissociative mechanism, as is commonplace for nine-coordinate Ln^{III} complexes,[6] the observed behavior highlights the view that the release of water is much easier in the **m** isomer than in the **M** isomer (at 298 K τ_M is 1.88×10^{-5} s in **m** and 4.16×10^{-3} s in **M**). These results allows us to detect for the first time a dependence of the rate of water exchange on minor structural changes and are of relevance to the design of more efficent contrast agents for MRI. Indeed, until now the modulation of the exchange rate of the coordinated water, a crucial point for attaining an optimum relaxation efficiency, appeared possible only through variation of the overall residual charge of the complexes. It follows that the search for contrast agents of improved efficacy based on a dota-like coordination polyhedron may be addressed to systems endowed with a **m**-type structure. We have recently found that a shift towards this structural form occurs by introducing bulky substituents at the methylenic carbon atom of the acetate arms of $[Ln(dota)]^-$ complexes.[8]

Experimental Section

The ligand dotam was prepared by an established procedure.[9] Eu$(SO_3CF_3)_3$ was obtained by refluxing a stoichiometric amount of trifluoromethanesulfonic acid and Eu_2O_3 in water for 0.5 h.[10] Eu$(SO_3CF_3)_3$ (0.37 mmol) in dry acetonitrile (50 mL) was refluxed for 30 min under N_2 and then treated with a solution of dotam (0.37 mmol) in dry methanol (25 mL). The mixture was refluxed for 1.5 h, cooled to room temperature, and concentrated in vacuo. Addition of dichloromethane resulted in precipitation of the complex. Yield: 61 %. ^{1}H NMR (400 MHz, CD_3CN (500 μL) and H_2O (5 μL), 232 K, TMS): **M** isomer: $\delta = -18.37$ (CH_2CONH_2), -18.00 (CH_2CONH_2), -9.31 (ring CH_2, equatorial), -8.78 (ring CH_2, axial), -5.31 (CH_2CONH_2), -1.52 (CH_2CONH_2), 0.61 (ring CH_2, equatorial), 38.16 (ring CH_2, axial); ***m*** isomer: $\delta = -13.10$ (ring CH_2, equatorial), -10.41 (CH_2CONH_2), -3.64 (CH_2CONH_2), -1.52 (ring CH_2, axial), 2.43 (CH_2CONH_2), 3.57 (CH_2CONH_2), 7.40 (ring CH_2, axial), 7.41 (ring CH_2, equatorial).

The k_{ex} values were obtained by fitting the experimental spectra with the lineshape routine DNMR-SIM simulation program for dynamic NMR spectra (version 1.00, 1994) developed by G. Haegele and R. Fuhler, Institut für Anorganische and Strukturchemie I, Universität Düsseldorf. This program is available on the Internet.

Received: March 2,1998
Revised version: May 14, 1998 [Z11544IE]
German version: *Angew. Chem.* **1998**, *110*, 2819 – 2820

Keywords: lanthanides · macrocyclic ligands · NMR spectroscopy · water exchange

[1] a) R. B. Lauffer, *Chem Rev.* **1987**, *87*, 901 – 927; b) J. A. Peters, J. Huskens, D. J. Raber, *Prog. Nucl. Magn. Reson. Spectrosc.* **1996**, *28*, 283 – 350; c) S. Aime, M. Botta, M. Fasano, E. Terreno, *Chem. Soc. Rev.* **1998**, *27*, 19 – 29.

[2] a) I. Bertini, C. Luchinat, *NMR of Paramagnetic Molecules in Biological Systems*, Benjamin/Cummings, Menlo Park, **1996**; b) S. H. Koenig, R. D. Brown III, *Prog. Nucl. Magn. Reson. Spectrosc.* **1990**, *22*, 487 – 567.

 © WILEY-VCH Verlag GmbH, D-69451 Weinheim, 1998 1433-7851/98/3719-2674 $ 17.50+.50/0

[3] a) R. V. Southwood-Jones, W. L. Earl, K. E. Newman, A. E. Merbach, *J. Chem. Phys.* **1980**, *73*, 5909 – 5917; b) C. Cossy, L. Helm, A. E. Merbach, *Inorg. Chem.* **1988**, *27*, 1973 – 1979.
[4] a) S. Aime, M. Botta, M. Fasano, S. Paoletti, P. L. Anelli, F. Uggeri, M. Virtuani, *Inorg. Chem.* **1994**, *33*, 4707 – 4711; b) G. Gonzalez, D. H. Powell, V. Tissières, A. E. Merbach, *J. Phys. Chem.* **1994**, *98*, 53 – 59; c) S. Aime, M. Botta, M. Fasano, S. Geninatti Crich, E. Terreno, *J. Biol. Inorg. Chem.* **1997**, *2*, 470 – 479.
[5] (a) S. Aime, M. Botta, G. Ermondi, *Inorg. Chem.* **1992**, *31*, 4291 – 4299; (b) S. Hoeft, K. Roth, *Chem. Ber.* **1993**, *126*, 869 – 873.
[6] D. H. Powell, O. M. Ni Dhubhghaill, D. Pubanz, L. Helm, Y. S. Lebedev, W. Schlaepfer, A. E. Merbach, *J. Am. Chem. Soc.* **1996**, *118*, 9333 – 9346.
[7] S. Aime, A. Barge, M. Botta, A. De Sousa, D. Parker, *J. Am. Chem. Soc.* **1997**, *119*, 4767 – 4768.
[8] S. Aime, M. Botta, E. Terreno, unpublished results.
[9] S. Amin, J. R. Morrow, C. H. Lake, M. R. Churchill, *Angew. Chem.* **1994**, *106*, 824 – 826; *Angew. Chem. Int. Ed. Engl.* **1994**, *33*, 773 – 775.
[10] P. H. Smith, K. N. Raymond, *Inorg. Chem.* **1985**, *24*, 3469 – 3477.

A Novel Aldol Condensation with 2-Methyl-4-pentenal and Its Application to an Improved Total Synthesis of Epothilone B**

Aaron Balog, Christina Harris, Kenneth Savin, Xiu-Guo Zhang, Ting Chao Chou, and Samuel J. Danishefsky*

Dedicated to Professor Ryoji Noyori

The recognition that the fermentation metabolites epothilones A and B (**1** and **2**, respectively) have potent in vitro antitumor properties and function through a paclitaxel-like (taxol-like) mechanism as inhibitors of microtubule disassembly has spurred a great deal of multidisciplinary research.[1, 2] Included in the pursuits which have followed in the wake of the exciting biology of the epothilones is the goal of total synthesis. Indeed, for those research groups (such as ours) for whom fermentation-derived epothilones are not available, chemical synthesis provides the only recourse to gain access to this series.

The total syntheses of epothilones A and B were accomplished by our group[3] and, shortly thereafter, by groups directed by Nicolaou[4a–e] and Schinzer.[5] A collection of fully synthetic epothilones from our laboratory,[6] as well as an even more extensive compendium from Nicolaou and co-workers,[7] were used to identify the zones of the epothilones that could undergo molecular modification with maintenance of biological function, at least at the in vitro level. The mapping exercises on structure – activity relationships performed by both groups provided very similar conclusions. An interesting finding first reported by our group,[6] and shortly thereafter by Nicolaou et al.,[7] was that the 12,13-deoxy versions of epothilones A and B (**3** and **4**, respectively) were quite active in in vitro assays. This discovery suggested the possibility that the epoxide linkages of the epothilones, which might be detrimental from the standpoint of peripheral toxicity, may not be crucial for eventual clinical function.

Our original synthesis of the epothilones, though quite long, had the feature of high stereoselectivity in each of the coupling steps.[3] While a disadvantage in enhancing access to multicomponent libraries,[4d,e, 7a] stereoselectivity allowed for accumulation of substantial quantities of fully synthetic key epothilones. Comparable harvesting of required amounts of material through the stereorandom olefin metathesis route, practiced by others[4, 5] as well as ourselves,[6a] would be virtually prohibitive. Its overall length notwithstanding, our first-generation total synthesis, which features the highly stereoselective LACDAC (*L*ewis *a*cid *c*atalyzed *d*iene – *a*ldehyde *c*yclocondensation) and *B*-alkyl Suzuki coupling steps, produced substantial quantities of epothilones. In fact, the only published in vivo data on epothilones available when this manuscript was submitted were obtained with our fully synthetic materials.[6c] These early findings in xenograft mice identified some significant toxicity problems with the highly potent epothilone B (**2**). Remarkably, in vivo studies in the interperitoneal mode of injection demonstrate that the less potent 12,13-deoxyepothilone B (**4**) is well tolerated and is virtually curative against human mammary tumor xenografts.[8] The lead compound **4** has many significant and clear advantages over paclitaxel in terms of efficacy against multiple drug resistent (MDR) tumors when administered intraperitoneally. We shall return to issues of bioactivity shortly.

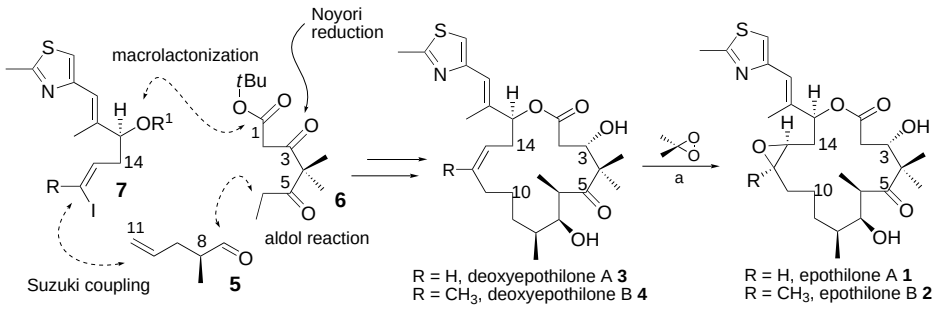
These exciting early results[8] underscored the need for a greatly improved total synthesis which can sustain a serious and substantial discovery research program for assaying candidate structures in rodents as well as in higher animals. We now report major progress in this regard. Our new route, which retains the advantages of high stereoselectivity throughout, is totally reworked in the treatment of the once difficult C1 – C11 domain. Scheme 1 provides an overview of the problem.

The new route is based on four findings, each of which has implications well beyond epothilone. The first is the ease of formation and the synthetic utility of the (*Z*)-lithium enolate **10**, which is readily prepared from **8** (Scheme 2). The ethyl ketone unit, from which the critical enolate is formed, is part

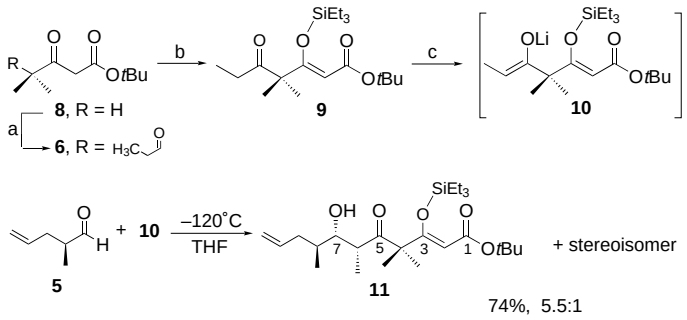
[*] Prof. S. J. Danishefsky,[+] Dr. A. Balog, Dr. C. Harris, Dr. K. Savin
Laboratory for Bioorganic Chemistry
Sloan-Kettering Institute for Cancer Research
1275 York Avenue, Box 106, New York, NY 10021 (USA)
X.-G. Zhang, Dr. T.-C. Chou
Laboratory for Molecular Pharmacology and Therapeutics Program
Sloan-Kettering Institute for Cancer Research
[+] Further address:
Havemeyer Hall, Department of Chemistry, Columbia University
New York, NY 10027 (USA)

[**] This research was supported by the National Institutes of Health (NIH, grants CA-28824 and CA-08748). Postdoctoral Fellowship support is gratefully acknowledged by A.B. (NIH, CA-GM 72231), C.H. (American Cancer Society, PF-98 – 173 – 001), and K.S. (NIH, GM-18248). We gratefully acknowledge Dr. George Sukenick (NMR Core Facility, Sloan-Kettering Institute) for NMR and mass spectral analyses. Professor Dr. G. Höfle of the Gesellschaft für Biotechnologische Forschung is gratefully acknowledged for providing natural epothilones A and B for comparative analysis. We also thank Professor Gunda Georg of the University of Kansas for bringing the epothilone problem to our attention. We dedicate this paper to Professor Ryoji Noyori, whose accomplishments were critical to this work.

 © WILEY-VCH Verlag GmbH, D-69451 Weinheim, 1998 1433-7851/98/3719-2675 $ 17.50+.50/0



Scheme 1. Overview of the new synthetic route to epothilones A and B (**1** and **2**, respectively). a) See references [3a–c].



Scheme 2. Synthesis of **10** and its aldol condensation with **5**. a) NaH, THF, 25 °C, then *n*BuLi, 0 °C, then propionyl chloride, −50 °C, 71%; b) NaH, THF, 0 °C, then TESOTf, −50 °C, 78%; c) LDA, THF, −33 °C, 5 min. LDA = lithium diisopropylamide, TES = triethylsilyl, Tf = trifluoromethanesulfonyl.

of a β,δ-diketoester ensemble embracing carbon atoms 1–6 of the target compound (see **6**).

The second and perhaps most surprising finding is that the sense of addition of enolate **10** to the readily available (*S*)-aldehyde **5**[9] provides the desired C7–C8 *anti* relationship with good diastereoface selectivity in conjunction with the expected C6–C7 *syn* relationship (by lk-addition)[10] (see compound **11** and its stereoisomer).[11] The 5.5:1 outcome for the diastereoface selectivity of this aldol reaction is counter to expectations arising from the traditional models first advanced by Cram and then by Felkin.[12] These extensively invoked formulations, which differ widely in their underlying conformational assumptions and stereochemical treatments, usually converge in terms of their predicted outcome.

The high diastereoface selectivity arises from a peculiarity of aldehyde **5** and reflects, somehow, the relationship of its vinyl and formyl groups. It is not, to a first approximation, the result of a gross property of the novel enolate **10**. Indeed, the same enolate, upon addition of phenylpropanal (**12a**), performs in the expected fashion,[10] yielding an 11:1 ratio of **13a** and **14a** (Table 1). Furthermore, with aldehyde **12b**, the dihydro derivative of **5**, the ratio of *syn* to *anti* diastereomers (with respect to the groups on C7 and C8; **13b**:**14b**) drops to 1:1.3. Moreover, when the distance between the vinyl and formyl groups is extended, as in **12c**, selectivity is also compromised. By contrast the phenyl and dimethylallyl analogues of **5** (**12d** and **12e**), *bearing the same relationship of unsaturated groups* as in **5**, exhibit good *anti* selectivity (see products **13d** and **13e** as well as **14d** and **14e**). Also, aldehyde **12f**, a substrate that on the basis of chelation control tends to favor the *anti*-diastereoface product,[13] performs normally with enolate **10** to afford a 1:4 ratio of **13f** and **14f**. We shall return to a consideration of these interesting data. First, we deal with the impact of the strong diastereoface selectivity (*anti* > *syn*) in the aldol reaction of **5** and **10** for achieving a dramatically improved total synthesis of epothilone B.[11]

The rather favorable result in establishing the C7–C8 bond allowed us to explore the possibility that the C1–C7 fragment could be incorporated as an achiral block. For this hope to become a real option, it would be necessary to gain control over the eventual stereochemistry at C3. This was to be accomplished by the implementation of an asymmetric, reagent-controlled Noyori reduction (see below).[14]

The third critical element was the finding that the key *B*-alkyl Suzuki coupling, which controls the geometry of the trisubstituted double bond, can be conducted successfully even on the elaborate substrate **15**, obtained from **11**. The cognate substrate for the Suzuki reaction was the previously described[3b] vinyl iodide **16**. The remarkable coupling step afforded the (*Z*)-olefin **17** and thence **18** after removal of the silyl protecting group on C15 (Scheme 3). The β,δ-diketo ester

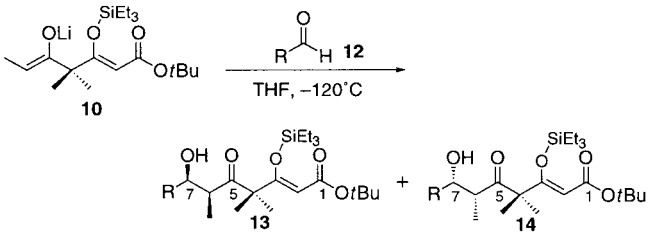
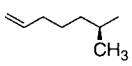
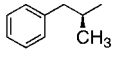
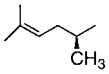
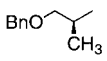
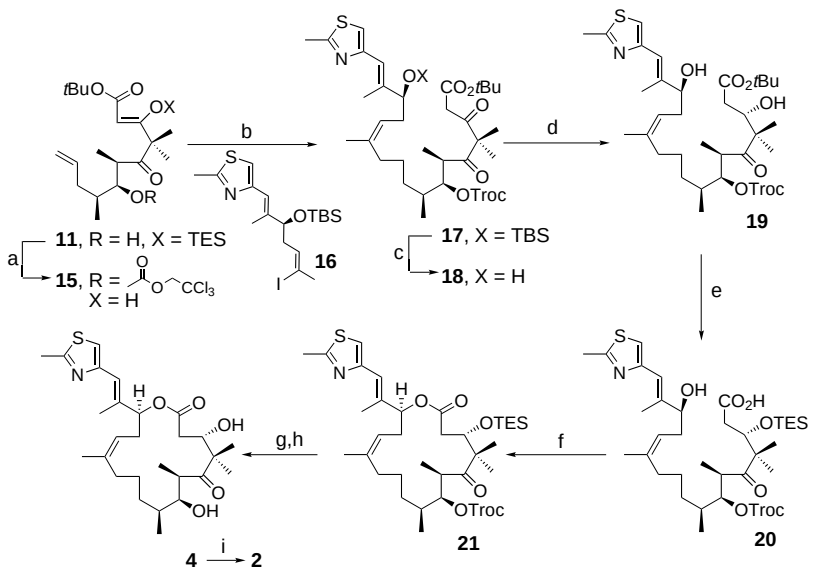


Table 1. Aldol reaction of enolate **10** with different aldehydes **12**.

12	R	Yield. [%]	**13**:**14**
a		64	11:1.0
b		80	1:1.3
c		68	1:2.0
d		63	1:5.0
e		71	1:4.5
f		61	1:4.0

 © WILEY-VCH Verlag GmbH, D-69451 Weinheim, 1998 1433-7851/98/3719-2676 $ 17.50+.50/0



Scheme 3. Synthesis of deoxyepothilon B (**4**) and epothilone B (**2**) from the product of the aldol reaction (**11**). a) TrocCl, pyridine, CH_2Cl_2, 0 →25 °C, then 0.5 N HCl in MeOH, 0 °C, 87 %; b) 9-BBN, THF, **15**, then **16**, $[Pd(dppf)Cl_2]$, Ph_3As, Cs_2CO_3, H_2O, DMF; c) 0.4 N HCl in MeOH, 50 % (over two steps); d) [(*R*)-(binap)$RuCl_2$], H_2 (83 bar), MeOH, HCl, 25 °C, 7 h, 88 % (d.r. > 95:5); e) TESOTf, 2,6-lutidine, CH_2Cl_2, −78 →25 °C, then HCl/MeOH, 77 %; f) 2,4,6-trichlorobenzoyl chloride, TEA, 4-DMAP, $PhCH_3$, 78 %; g) SmI_2, cat. NiI_2, THF, −78 °C, 95 %; h) HF · pyridine, THF, 98 %; i) 2,2-dimethyldioxirane, CH_2Cl_2, −50 °C, 98 % (d.r. > 20:1). 9-BBN = 9-borabicyclo[3.3.1]nonane, binap = 2,2′-bis(diphenylphosphanyl)-1,1′-binaphthyl, 4-DMAP = 4-dimethylaminopyridine, dppf = 1,1′-bis(diphenylphosphanyl)ferrocene, TBS = *tert*-butyldimethylsilyl, TEA = triethylamine, Troc = trichloroethoxycarbonyl.

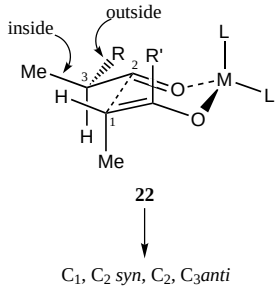
array in **18** responded well to asymmetric catalytic reduction under modified Noyori conditions[14b] to give the diol **19** (88 %, *d.r.* > 95:5). The ability to maintain strict regiochemical and diastereoface control in the Noyori reduction arose only after extensive developmental studies, which will be described elsewhere.[15] With this reduction achieved, no significant obstacles remained in the total synthesis. The conversion of **19** into deoxyepothilone B (**4**) and then epothilone B (**2**) was accomplished by methodologies worked out in our previous syntheses[3] as well as the syntheses of Nicolaou et al.[4]

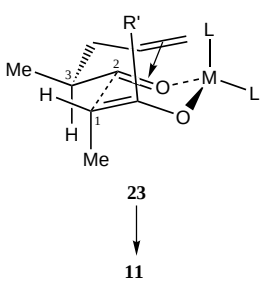
The matter of explaining the results of the key aldol coupling of **5** and **10** is best approached through earlier arguments of Roush on the diastereoface selectivity of reactions of (*Z*)-enolates.[16b] Roush postulated that with an enolate such as **10**, the conformer that reacts according to the Curtin–Hammett principle[17] would be one in which the R group of the aldehyde is distanced from the methyl and the R′ group of the enolate.[16b] The methyl group of the "α-methylaldehyde" rather than the R group is placed on the inside face of the transition state complex **22**. The aldol reaction will lead to the *anti* product. Of course, if R is approximately equal to methyl with respect to the effective A value (conformation energy), the selectivity for *anti* product correspondingly must deteriorate. To rationalize why maximal *anti* selectivity was obtained from aldehyde **5** or related systems **12d** and **12e**, it can be argued that the presence of unsaturation at C4–C5 in the aldehyde moiety provides a favorable nonbonding interaction between the double bond in the aldehyde and the carbonyl group of the enolate. This interaction tends to stabilize the transition state leading to the observed stereoisomer (see **23**). Tthe possibility of fine-tuning the structure of Curtin–Hammett conformers in C–C bond forming reactions through subtle secondary interactions has significant implications for the enhancement of stereoselectivity.

Quite aside from identifying a potentially important principle governing diastereoface selection, the total synthesis we present herein enables a serious and focused drug-discovery program in the epothilone area directed toward obtaining analogues in useful amounts for in vivo examination. The opportunities for preclinical biological exploration opened up by this greatly improved access to the epothilones are being pursued in a resolute way. For instance, we have recently found using fully synthetic material that compound **4** has a far superior efficacy and a much more exploitable maximum tolerable dose (MTD) than paclitaxel, adriamycin, camptothecin, or epothilone B when administered intraperitoneally.[8] Of course, the optimal administration of paclitaxel is intravenous. Therefore, we recently compared **4** with paclitaxel for intravenous administration in xeongraft mice. Our previously reported toxicity[8] in the intravenous administration of **4** has now been overcome by using a slow infusion protocol (over 4 h). This has allowed us to compare the therapeutic profiles of **4** and paclitaxel in the intravenous modality. Our comparisons were conducted in nude mice bearing the MX-1 xenograft. Even under the formulation conditions for paclitaxel (Cremophor–EtOH), **4** is equally effective (**4**: ca. 99 % tumor reduction for a dose of 30 mg kg^{-1}; paclitaxel: ca. 99 % tumor reduction for a dose of 24 mg kg^{-1}).

Received: June 15, 1998 [Z11982IE]
German version: *Angew. Chem.* **1998**, *110*, 2821–2824

Keywords: aldol reactions · epothilones · natural products · Suzuki coupling · total synthesis





[1] a) D. M. Bollag, P. A. McQuency, J. Zhu, O. Hensens, L. Koupal, J. Liesch, M. Goetz, E. Lazarides, C. M. Woods, *Cancer Res.* **1995**, *55*, 2325; b) G. Höfle, N. Bedorf, H. Steinmetz, D. Schomburg, K. Gerth, H. Reichenbach, *Angew. Chem.* **1996**, *108*, 1671; *Angew. Chem. Int. Ed. Engl.* **1996**, *35*, 1567; c) K. Gerth, N. Bedorf, G. Höfle, H. Irschik, H. Reichenbach, *J. Antibiot.* **1996**, *49*, 560.
[2] P. B. Schiff, J. Fant, S. B. Horwitz, *Nature* **1979**, *277*, 665.

[3] a) A. Balog, D. Meng, T. Kamenecka, P. Bertinato, D.-S. Su, E. J. Sorensen, S. J. Danishefsky, *Angew. Chem.* **1996**, *108*, 2976; *Angew. Chem. Int. Ed. Engl.* **1996**, *35*, 2801; b) D.-S. Su, D. Meng, P. Bertinato, A. Balog, E. J. Sorensen, S. J. Danishefsky, Y.-H. Zheng, T.-C. Chou, L. He, S. B. Horwitz, *Angew. Chem.* **1997**, *109*, 775; *Angew. Chem. Int. Ed. Engl.* **1997**, *36*, 757; c) D. Meng, P. Bertinato, A. Balog, D.-S. Su, T. Kamenecka, E. J. Sorensen, S. J. Danishefsky, *J. Am. Chem. Soc.* **1997**, *119*, 10073.

[4] a) Z. Yang, Y. He, D. Vourloumis, H. Vallberg, K. C. Nicolaou, *Angew. Chem.* **1997**, *109*, 170; *Angew. Chem. Int. Ed. Engl.* **1997**, *36*, 166; b) K. C. Nicolaou, F. Sarabia, S. Ninkovic, Z. Yang, *Angew. Chem.* **1997**, *109*, 539; *Angew. Chem. Int. Ed. Engl.* **1997**, *36*, 525; c) K. C. Nicolaou, N. Winssinger, J. A. Pastor, S. Ninkovic, F. Sarabia, Y. He, D. Vourloumis, Z. Yang, T. Li, P. Giannakakou, E. Hamel, *Nature* **1997**, *387*, 268; d) K. C. Nicolaou, Y. He, D. Vourloumis, H. Vallberg, F. Roschangar, F. Sarabia, S. Ninkovic, Z. Yang, J. I. Trujillo, *J. Am. Chem. Soc.* **1997**, *119*, 7960; e) K. C. Nicolaou, S. Ninkovic, F. Sarabia, D. Vourloumis, Y. He, H. Vallberg, M. R. V. Finlay, Z. Yang, *J. Am. Chem. Soc.* **1997**, *119*, 7974; f) K. C. Nicoloau, Y. He, D. Vourloumis, H. Vallberg, Z. Yang, *Angew. Chem.* **1996**, *108*, 2554; *Angew. Chem. Int. Ed. Engl.* **1996**, *35*, 2399.

[5] D. Schinzer, A. Limberg, A. Bauer, O. M. Böhm, M. Cordes, *Angew. Chem.* **1997**, *109*, 543; *Angew. Chem. Int. Ed. Engl.* **1997**, *36*, 523.

[6] a) D. Meng, D.-S. Su, A. Balog, P. Bertinato, E. J. Sorensen, S. J. Danishefsky, Y.-H. Zheng, T.-C. Chou, L. He, S. B. Horwitz, *J. Am. Chem. Soc.* **1997**, *119*, 2733; b) A. Balog, P. Bertinato, D.-S. Su, D. Meng, S. J. Danishefsky, Y.-H. Zheng, T.-C. Chou, L. He, S. B. Horwitz, *Tetrahedron Lett.* **1997**, *38*, 4529; c) D.-S. Su, A. Balog, D. Meng, P. Bertinato, S. J. Danishefsky, Y.-H. Zheng, T.-C. Chou, L. He, S. B. Horwitz, *Angew. Chem.* **1997**, *109*, 2178; *Angew. Chem. Int. Ed. Engl.* **1997**, *36*, 2093.

[7] a) K. C. Nicolaou, D. Vourloumis, T. Li, J. Pastor, N. Winssinger, Y. He, S. Ninkovic, F. Sarabia, H. Vallberg, F. Roschangar, N. P. King, M. R. V. Finlay, P. Giannakakou, P. V. Pinard, E. Hamel, *Angew. Chem.* **1997**, *109*, 2181; *Angew. Chem. Int. Ed. Engl.* **1997**, *36*, 2097; b) K. C. Nicolaou, F. Sarabia, S. Ninkovic, M. R. V. Finlay, C. N. C. Boddy, *Angew. Chem.* **1998**, *110*, 85; *Angew. Chem. Int. Ed.* **1998**, *37*, 81; c) K. C. Nicolaou, S. Ninkovic, M. R. V. Finlay, F. Sarabia, T. Li, *Chem. Commun.* **1997**, 2343; d) K. C. Nicolaou, H. Vallberg, N. P. King, F. Roschangar, Y. He, D. Vourloumis, C. G. Nicolaou, *Chem. Eur. J.* **1997**, *3*, 1957; e) K. C. Nicolaou, M. R. V. Finlay, S. Ninkovic, N. P. King, D. Vourloumis, Y. He, *Chem. Eur. J.* **1997**, *3*, 1971.

[8] T.-C. Chou, Z.-G. Zhang, A. Balog, D.-S. Su, D. Meng, K. Savin, J. R. Bertino, S. J. Danishefsky, *Proc. Natl. Acad. Sci. USA* **1998**, *95*, 9642.

[9] The aldehyde **5** was readily available by the preparation given in N.-H. Lin, L. E. Overman, M. H. Rabinowitz, L. A. Robinson, M. J. Sharp, J. Zablocki *J. Am. Chem. Soc.* **1996**, *118*, 9062. The alcohol precursor to this aldehyde could also be accessed by yeast reduction of the corresponding allylic alcohol, thereby shortening the synthetic pathway (24 steps) by three steps.

[10] C. H. Heathcock in *Asymmetric Synthesis*, *Vol. 3* (Ed.: J. D. Morrison), Academic Press, New York, **1984**, p. 111.

[11] The stereochemistry of the minor diastereomer with respect to the groups on C7 and C8 was presumed to be *syn*, but was not rigorously proven. This was based on precedent,[16a] assuming that this isomer arises from facial selectivity in the aldol reaction and not as a consequence of the *E* configuration of the enolate group of **10**. Similarly, the stereochemistry assigned as the *syn*,*syn* products **14** was not proven in each case. Those assignments also rely to varying extents on the examples given in ref. [16a].

[12] For transition state models for diastereomeric additions on carbonyl groups, see a) D. J. Cram, F. A. Elhafez, *J. Am. Chem. Soc.* **1952**, *74*, 5828; b) D. J. Cram, K. R. Kopecky, *J. Am. Chem. Soc.* **1959**, *81*, 2748; c) J. W. Cornforth, R. H. Cornforth, K. K. Mathew, *J. Am. Chem. Soc.* **1959**, *81*, 112; d) G. J. Karabatsos, *J. Am. Chem. Soc.* **1967**, *89*, 1367; e) M. Cherest, H. Felkin, N. Prudent, *Tetrahedron Lett.* **1968**, 2199; f) N. T. Ahn, O. Eisenstein, *Nouv. J. Chem.* **1977**, *1*, 61; g) A. S. Cieplak, *J. Am. Chem. Soc.* **1981**, *103*, 4540, h) E. P. Lodge, C. H. Heathcock, *J. Am. Chem. Soc.* **1987**, *109*, 2819.

[13] M. T. Reetz, *Angew. Chem.* **1984**, *96*, 542; *Angew. Chem. Int. Ed. Engl.* **1984**, *23*, 556.

[14] a) R. Noyori, T. Ohkuma, M. Kitamura, *J. Am. Chem. Soc.* **1987**, *109*, 5856; b) D. F. Taber, L. J. Silverberg, *Tetrahedron Lett.* **1991**, *32*, 4227; c) review: D. J. Ager, S. A. Laneman, *Tetrahedron Asymmetry* **1997**, *8*, 3327.

[15] The Noyori reduction of various diketo esters was very dependent on the amount of acid in the reaction mixture. Without the presence of stoichiometric acid, the rate of reduction and the selectivity dropped in the reduction. At higher pressures, the chemoselectivity of the reduction was poor resulting in reduction of both of the alkene groups. Furthermore, the carbonyl group at C5 was never reduced under these conditions, but was absolutely necessary for the reduction of the carbonyl group at C3. When an alcohol functionality was at C5, no reduction was seen. A. Balog, unpublished results.

[16] a) I. Mori, K. Ishihara, C. H. Heathcock, *J. Org. Chem.* **1990**, *55*, 1114; b) W. R. Roush, *J. Org. Chem.* **1991**, *56*, 4151.

[17] For a statement of the Curtin–Hammet principle in predicting and rationalizing stereoselection, see E. Eliel, S. H. Wilen, *Stereochemistry of Organic Compounds*, Wiley, New York, **1994**, p. 649.

Structures of Solvent-Free, Monomeric LiCCH, NaCCH, and KCCH**

Douglas B. Grotjahn,* Aldo J. Apponi, Matthew A. Brewster, Ju Xin, Lucy M. Ziurys*

Organoalkali metal compounds are important reagents for introducing organic groups into organic and organometallic compounds in substitution or addition reactions.[1] For example, active ingredients in widely used oral contraceptives contain alkynyl groups that are introduced by the addition of alkali metal acetylides to steroidal ketones.[2] Organoalkali metal compounds show a pronounced tendency toward aggregation,[3] and alkali metal acetylides are no exception.[4, 5] The organic portion and co-ligand(s) (including solvent) influence reactivity and structure of the organoalkali metal compound dramatically, both in solution and in the solid state. An example of the structural changes induced by subtle variation of coligands is that whereas the crystallization of PhCCLi in the presence of tetramethylpropylenediamine gives dimeric units,[5e] similar treatment with the homologous tetramethylhexylenediamine gives tetrameric units.[5d] Such aggregated structures have provided the only experimental information about alkynyl–alkali metal bond lengths to date, but with one recent exception,[4d] the alkali metal acetylides

[*] Prof. D. B. Grotjahn
Department of Chemistry, San Diego State University
5500 Campanile Drive, San Diego, CA 92182-1030 (USA)
Fax: (+1) 619-594-4634
E-mail: grotjahn@chemistry.sdsu.edu
Prof. L. M. Ziurys, Dr. A. J. Apponi, M. A. Brewster, Dr. J. Xin
Department of Chemistry, Department of Astronomy
Steward Observatory, University of Arizona
Tucson, AZ 85721 (USA)
Fax: (+1) 520-621-1532
E-mail: lziurys@as.arizona.edu

[**] This research was supported by the U.S. National Science Foundation grants CHE 9531244 (to D.B.G. and L.M.Z.), AST 95-03274, and NASA grant NAGW 2989 (to L.M.Z.).

Supporting information for this article is available on the WWW under http://www.wiley-vch.de/home/angewandte/ or from the author.

 © WILEY-VCH Verlag GmbH, D-69451 Weinheim, 1998 1433-7851/98/3719-2678 $ 17.50+.50/0

treated by theory have been in a monomeric, solvent-free state.[6] There is a clear trend toward longer metal–carbon bond lengths on increased solvation or oligomerization,[3] so direct comparison of experimental and theoretical data on alkynyl alkali metal compounds has been impossible. Notable approaches to monomeric alkyl or aryllithium compounds[7] have relied on large alkyl or aryl groups; such a strategy will probably not work for alkynyl compounds because the R group of RCCM is so far removed from the metal center M.

Here we report the first structural characterization of alkynyl alkali metal compounds in a monomeric state. The title molecules MCCH (M = Li, Na, K) are the simplest alkynyl derivatives of each metal, and thus are ideally suited for a direct comparison of experiment and theory. Each was made in a monomeric form in the absence of other ligands in the gas phase, and each structure was determined by millimeter/submillimeter spectroscopy, as was recently done for MCH_3 (M = Li, Na).[8] The experimental data[9] should allow further improvements in theoretical calculations, which in the case of the predicted values for the Li–C bond in LiCCH spread over the range 1.842 to 1.931 Å[6]

A direct absorption spectrometer in continuous-wave mode[10] was used to observe isotopomers of MCCH. Phase-locked Gunn oscillators with frequencies in the range 65–140 GHz were used as the radiation source. Schottky-barrier diode multipliers were used to double, triple, or quadruple the frequency to obtain an overall frequency range of 65–560 GHz. The reaction chamber was a double-pass cell with a length of 0.5 m. In the cell HCCH (30 mTorr) was treated with metal vapor ($\leq$ 1 mTorr) to produce MCCH (M = Li, Na, K). Argon (30–50 mTorr) was used as a carrier gas for the metal and a direct current discharge (about 0.5 A at 200 V) was used to facilitate the reaction. The deuterium isotopomers MCCD for all three metals were studied by using DCCD.

The use of BrCCH[11] with Li gave such intense signals for the product that the two ^{13}C isotopomers $LiC^{13}CH$ and $Li^{13}CCH$ were observed. No discharge was required with BrCCH, and typically only a few mTorr of this precursor was required. Finally, ^{6}LiCCH was also measured by using Li enriched in ^{6}Li. To carry out a frequency measurement scans with a width of 5 MHz were made, both in decreasing and increasing frequency, and one to four pairs of such scans were then averaged. Linewidths varied from 200–1500 kHz in the frequency range 100–530 GHz, primarily because of modulation broadening, and typically 20–40 data points were taken over an absorption line. Gaussian functions were used to fit the data. Experimental accuracy of the frequencies is estimated to be $\pm$ 50 kHz.

The alkali metal acetylides are linear molecules with $^1\Sigma$ ground electronic states, and the rotational quantum number is, therefore, *J*. No fine or magnetic hyperfine structure was observed, which is not unexpected because the alkali metal acetylides are closed-shell species. Nuclear-quadrupole interactions involving the metal nuclei were also not seen. However, the $J = 0 \rightarrow 1$ transitions, where this splitting is most likely to be resolved, were below the frequency range of the spectrometer.

A typical spectrum of LiCCH is shown in Figure 1, which presents the $J = 22 \rightarrow 23$ transition of this species. The top part

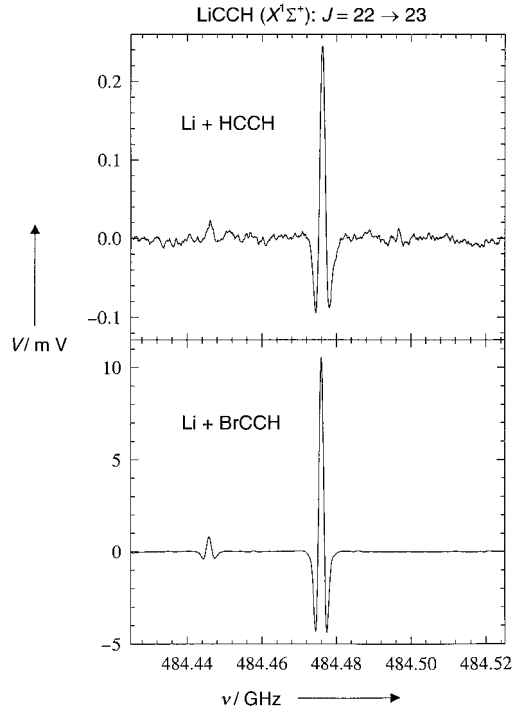


Figure 1. Top: Typical spectrum ($J = 22 \rightarrow 23$) for LiCCH made from Li and HCCH with a direct current discharge. Bottom: The same transition observed for LiCCH from the reaction of Li and BrCCH. The signal-to-noise ratio is much lower using BrCCH, and no discharge was necessary.

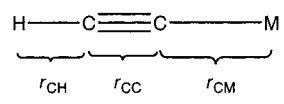
of the figure shows the spectrum of LiCCH made from HCCH, whereas the lower part shows that of LiCCH made from BrCCH, which clearly produced much stronger signals. The molecular constants shown in Table 1 were derived by using a $^1\Sigma$ Hamiltonian. To fit the data within experimental uncertainty,[12] the rotational constant B_o, the first-order centrifugal distortion constant D_o, and second order distortion parameter H_o were needed for each isotopomer. However, only B_o was needed to determine the moment of inertia and hence the structure. From the structure the bond lengths r_{CM}, r_{CC}, and r_{CH} were calculated, and the values are listed in Table 2.

Table 1. Molecular constants (in MHz) for MCCH isotopomers.[a]

Species	B_o	D_o	$10^7 H_o$
LiCCH	10544.0909(45)	0.011373(14)	0.27(12)
^{6}LiCCH	11545.322(12)	0.013054(13)	–
$LiC^{13}CH$	10287.534(33)	0.010714(72)	–
$Li^{13}CCH$	10539.046(12)	0.011241(11)	–
LiCCD	9622.8736(92)	0.0086047(69)	–
NaCCH	4510.116(10)	0.0028240(46)	0.0363(70)
NaCCD	4181.180(84)	0.002282(25)	0.025(25)
KCCH	2970.8168(31)	0.0017560(13)	0.1310(22)
KCCD	2764.999(14)	0.0013966(21)	0.0497(11)

[a] The errors quoted in parentheses are based only on the errors in the statistical analysis (3σ).

The C–H bond lengths for NaCCH and KCCH were assumed to be 1.06 Å and the other two lengths were deter-



 © WILEY-VCH Verlag GmbH, D-69451 Weinheim, 1998 1433-7851/98/3719-2679 $ 17.50+.50/0

Table 2. Comparison of experimental and calculated bond lengths (in Å) in MCCH (M = Li, Na, K).

Molecule	Source	M–C	C–C	C–H	Ref.
LiCCH	exp.[a]	1.888	1.226	1.061	this work
LiCCH	exp.[b]	1.888	1.227	1.062	this work
LiCCH	STO-4G	1.862	1.213	1.070	[6b]
LiCCH	SS[c]	1.921	1.219	1.056	[6b]
LiCCH	SS+d[c]	1.931	1.208	1.056	[6b]
LiCCH	INDO	1.842	1.220[d]	1.099[d]	[6c]
NaCCH	exp.[a]	2.221	1.217	1.06[d]	this work
NaCCH	RCCSD(T)	2.23	1.23	1.07	[6e]
KCCH	exp.[a]	2.540	1.233	1.06[d]	this work

[a] Millimeter spectroscopy; r_o structure (see text). [b] Millimeter spectroscopy; r_s structure (see text). [c] SS = Gaussian split-shell basis set, SS+d = same with carbon 3d orbitals. [d] Assumed value.

mined directly from the moments of inertia I_o of the two isotopomers studied, MCCH and MCCD, that is, from the r_o structure. For the lithium analogue, every atom was substituted. Unfortunately, the ^{13}C atom nearest the lithium atom in LiCCH was found to be very close to the center of mass, and, therefore, Li^{13}CCH was not used in the calculations. However, sufficient substitutions were still available for LiCCH that both r_s and r_o structures could be determined. The r_s structures are thought to result in better estimates of the true bond lengths because effects of zero-point vibrations largely cancel in this method.[13] In fact, the estimated accuracies for r_s bond lengths are ± 0.0005 Å, as opposed to ± 0.005 Å for r_o bond lengths.[13] On the other hand, the effects of vibration are not too critical if the molecules are fairly rigid, as the acetylides certainly are. Experimental verification comes from the similar values of r_o and r_s bond lengths for LiCCH shown in Table 2.

The carbon–metal bond lengths appear to be the shortest ones known for organoalkali metal compounds of each metal. The three main factors responsible for this are probably the small size and the sp hybridization of the organic portion, and the solvent-free, monomeric nature of each species. The closest precedents among organolithium compounds would be the following three monomers: gas-phase CH_3Li (C–Li distance 1.959 Å),[8] gas-phase $LiCH(SiMe_3)_2$ (2.03(6) Å),[4b] and a solid-phase aryllithium featuring an ether ligand (2.017(7) Å).[4a] Our experimental results for the C–C and C–H bond lengths compare well with those predicted from ab initio calculations. However, for the relatively well-studied LiCCH the predicted Li–C bond lengths ranged from 1.842 to 1.931 Å,[6] whereas our results set this length at 1.888 Å. On the other hand, our experimental value for the Na–C length in NaCCH is only 0.01 Å shorter than an ab initio result.[6e] Differences in bond lengths in experimental or theoretical r_e and experimental r_o structures such as ours are typically on the order of 0.01 Å or less,[14] and as discussed above, r_s structures are even better. Thus, the differences between our experimental data and calculated values should allow refinement of calculations involving the highly electropositive alkali metals in MCCH and other organoalkali compounds.[15]

Received: April 6, 1998 [Z11688IE]
German version: *Angew. Chem.* **1998**, *110*, 2824–2827

Keywords: alkali metals · alkynes · gas-phase chemistry · rotational spectroscopy

[1] *Methoden Org. Chem. (Houben-Weyl), Carbanionen, Band E19d* (Ed.: M. Hanack), Thieme, Stuttgart, **1993**; M. Gray, M. Tinkl, V. Snieckus in *Comprehensive Organometallic Chemistry II, Vol. 11* (Eds.: E. W. Abel, F. G. A. Stone, G. Wilkinson), Pergamon, New York, **1995**, Chap. 1; A. Mordini in *Comprehensive Organometallic Chemistry II, Vol. 11* (Eds.: E. W. Abel, F. G. A. Stone, G. Wilkinson), Pergamon, New York, **1995**, Chap. 2.

[2] D. Lednicer, L. A. Mitscher, *The Organic Chemistry of Drug Synthesis*, Wiley, New York, **1977**, Chap. 10, especially pp. 162–165; H. H. Inhofen, W. Logemann, A. Hohlweg, A. Serini, *Chem. Ber.* **1938**, *71*, 1024–1032; C. Djerassi, L. Miramontes, G. Rosenkranz, F. Sondheimer, *J. Am. Chem. Soc.* **1954**, *76*, 4092–4094.

[3] Reviews: a) J. L. Wardell in *Comprensive Organometallic Chemistry, Vol. 1* (Eds.: E. W. Abel, F. G. A. Stone, G. Wilkinson), Pergamon, Oxford, **1982**, Chap. 2, pp. 43–120; b) W. N. Setzer, P. von R. Schleyer, *Adv. Organomet. Chem.* **1985**, *24*, 353–451; c) C. Schade, P. von R. Schleyer, *Adv. Organomet. Chem.* **1987**, *27*, 169–278; d) E. Weiss, *Angew. Chem.* **1993**, *105*, 1565–1587; *Angew. Chem. Int. Ed. Engl.* **1993**, *32*, 1501–1523; e) P. G. Willard in *Comprehensive Organic Synthesis, Vol. 1* (Eds.: B. M. Trost, I. Fleming), Pergamon, Oxford, **1991**, pp. 1–47; f) M. A. Beswick, D. S. Wright in *Comprehensive Organometallic Chemistry II, Vol. 1* (Eds.: E. W. Abel, F. G. A. Stone, G. Wilkinson), Pergamon, New York, **1995**, Chap. 1.

[4] Solution studies: a) G. Fraenkel, P. Pramanik, *J. Chem. Soc. Chem. Commun.* **1983**, 1527–1529; b) R. Hässig, D. Seebach, *Helv. Chim. Acta* **1983**, *66*, 2269–2273; c) W. Bauer, D. Seebach, *Helv. Chim. Acta* **1984**, *67*, 1972–1988 d) R. Gareyev, A. Streitwieser, *J. Org. Chem.* **1996**, *61*, 1742–1747.

[5] Solid-state structures: a) H. Föppl, *Angew. Chem.* **1958**, *70*, 401; b) E. Weiss, H. Plass, *Chem. Ber.* **1968**, *101*, 2947–2955; c) M. Atoji, *J. Chem. Phys.* **1972**, *56*, 4947–4951; d) B. Schubert, E. Weiss, *Angew. Chem.* **1983**, *95*, 499–500; *Angew. Chem. Int. Ed. Engl.* **1983**, *22*, 496–497; e) B. Schubert, E. Weiss, *Chem. Ber.* **1983**, *116*, 3212–3215; f) M. Geissler, J. Kopf, B. Schubert, E. Weiss, W. Neugebauer, P. von R. Schleyer, *Angew. Chem.* **1987**, *99*, 569–570; *Angew. Chem. Int. Ed. Engl.* **1987**, *26*, 587–588; g) B. Goldfuss, P. von R. Schleyer, F. Hampel, *J. Am. Chem. Soc.* **1997**, *119*, 1072–1080.

[6] a) A. Veillard, *J. Chem. Phys.* **1968**, *48*, 2012–2016; b) A. Streitweiser, Jr., J. E. Williams, Jr., S. Alexandratos, J. M. McKelvey, *J. Am. Chem. Soc.* **1976**, *98*, 4778–4784; c) A. Hinchliffe, *J. Mol. Struct.* **1977**, *37*, 145–152; d) S. Bachrach, A. Streitweiser, Jr. *J. Am. Chem. Soc.* **1984**, *106*, 2283–2287; e) D. Woon, personal communication; f) reference [5g] reports a study of π interactions in metal acetylides.

[7] a) K. Ruhlandt-Senge, J. J. Ellison, R. J. Wehmschulte, F. Pauer, P. P. Power, *J. Am. Chem. Soc.* **1993**, *115*, 11353–11357; B. Schiemenz, P. Power, *Angew. Chem.* **1996**, *108*, 2288–2290; *Angew. Chem. Int. Ed. Engl.* **1996**, *35*, 2150–2152. B. Schiemenz, P. Power, *Organometallics* **1996**, *15*, 958–964; b) J. L. Atwood, T. Fjeldberg, M. F. Lappert, N. T. Luong-Thi, R. Shakir, A. J. Thorne, *J. Chem. Soc. Chem. Commun.* **1984**, 1163–1165.

[8] D. B. Grotjahn, T. C. Pesch, J. Xin, L. M. Ziurys, *J. Am. Chem. Soc.* **1997**, *119*, 12368–12369.

[9] a) Spectroscopic details for NaCCH have been reported in reference [9b]. Here we report corrected data, which properly assign the ground vibrational state. In addition, excited-state data for LiCCH have been obtained and will be reported separately; b) B.-Z. Li, L. M. Ziurys, *Astrophys. J.* **1997**, *482*, L215–L217.

[10] L. M. Ziurys, W. L. Barclay, Jr., M. A. Anderson, D. A. Fletcher, J. W. Lamb, *Rev. Sci. Instrum.* **1994**, *65*, 1517–1522.

[11] V. Sawitsch, *Ann. Chem. Pharm.* **1861**, *119*, 182–185.

[12] The errors quoted in Table 1 are based only on errors in the statistical analysis (3σ). The deviations $\nu_{obs} - \nu_{calcd}$ in the five parameters were typically less than 75 kHz.

[13] W. Gordy, R. L. Cook, *Molecular Spectra*, Wiley, New York, **1984**, p. 691.

[14] a) Experimental values: M. D. Harmony, V. W. Laurie, R. L. Kuczkowski, R. H. Schwendeman, D. A. Ramsay, F. J. Lovas, W. J. Lafferty,

 © WILEY-VCH Verlag GmbH, D-69451 Weinheim, 1998 1433-7851/98/3719-2680 $ 17.50+.50/0

A. G. Maki, *J. Phys. Chem. Ref. Data* **1979**, *8*, 619 – 721; b) discussion of theory and experiment: R. D. Topsom, *Prog. Phys. Org. Chem.* **1987**, *16*, 85 – 124.

[15] D. J. DeFrees, B. A. Levi, S. K. Pollack, W. J. Hehre, J. S. Binkley, J. A. Pople, *J. Am. Chem. Soc.* **1979**, *101*, 4085 – 4089.

A Coordination-Induced 1,4 → 1,2-Quinonediimine Isomerization**

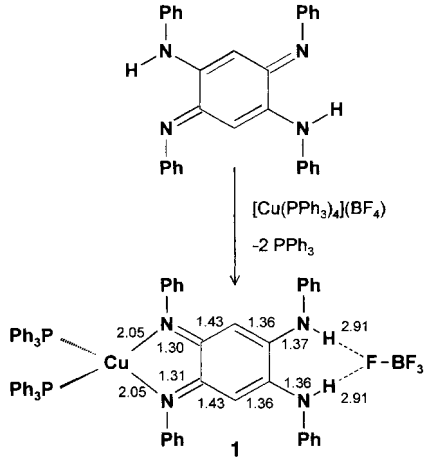
Jochen Rall, Andreas F. Stange, Klaus Hübler, and Wolfgang Kaim*

Dedicated to Professor Bernt Krebs on the occasion of his 60th birthday

Azophenine (2,5-diamino-1,4-benzoquinonediimine, ap) is a long known *para*-quinonoid compound, which can be obtained in various ways from aniline.[1] Although azophenine bears a close similarity to the increasingly used bis-chelate ligand family derived from 2,5-dihydroxy-1,4-benzoquinone[2] its coordination chemistry has hitherto remained unexplored.[3] This is all the more surprising since metal complexes of quinonoid compounds with O and N donor functionalities have been much studied recently for reasons of their unusual electronic structures (with sometimes ambiguous oxidation state formulations),[4] their potential uses in molecular biology,[5] and their possible occurrence in enzymes.[6] In particular, copper-dependent amine oxidases show an interaction between the redox-active metal center and a functionalized "topaquinone" ligand present as a modified tyrosine side chain.[7–9] Since this topaquinone ligand reacts with amine substrates to form quinoneimine intermediates,[6, 8, 9] we set out to treat copper compounds with the bifunctional azophenine ligand.

Treatment of azophenine with $[Cu(PPh_3)_4](BF_4)$ in acetone (or dichloromethane) results in the spontaneous formation of the copper(I) complex $[Cu(PPh_3)_2(ap)](BF_4)$ (**1**, Scheme 1).[10] The complex is highly soluble in acetone, dichloromethane, and alcohols, but insoluble in hydrocarbons. Any remaining azophenine could be removed by column chromatography. Treatment of ap with two equivalents of $[Cu(PPh_3)_4](BF_4)$ also yielded the mononuclear complex and not a dinuclear compound.

Single crystals of **1** were obtained from a solution of acetone/pentane and were analyzed by crystallography.[11] They were found to contain three equivalents of acetone as supported by elemental analysis and ^{1}H NMR spectroscopy. Refinement of the molecular structure (Figure 1) revealed two quite remarkable structural features of **1**:



Scheme 1. Synthesis of **1** from ap. The general bond pattern in **1** and selected bond lengths [Å] are shown.

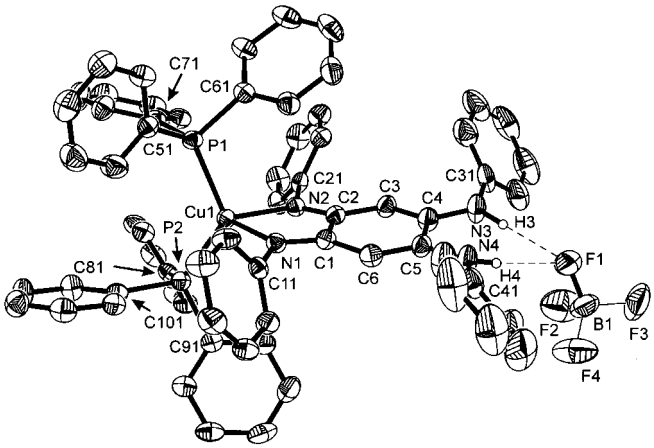


Figure 1. View of the structure of **1** in the crystal. Selected bond lengths [Å] and bond angles [°]: Cu1 – N1 2.052(4), Cu1 – N2 2.054(4), Cu1 – P2 2.2439(13), Cu1 – P1 2.2571(13), N1 – C1 1.307(5), N2 – C2 1.300(5), N3 – C4 1.368(6), N4 – C5 1.364(6), C1 – C6 1.430(6), C1 – C2 1.483(6), C2 – C3 1.426(6), C3 – C4 1.357(6), C4 – C5 1.486(6), C5 – C6 1.360(6); N1-Cu1-N2 79.18(14), N2-Cu1-P2 115.90(11), N2-Cu1-P1 104.88(11), C1-N1-Cu1 114.5(3), N1-Cu1-P2 111.57(11), N1-Cu1-P1 114.42(11), P2-Cu1-P1 122.62(5), C2-N2-Cu1 114.5(3).

1) The tetracoordinate copper(I) center is bound in a chelate fashion by two *o*-quinonediimine N-donor centers; the C=N bond lengths (standard deviation ≤ 0.006 Å) and the general bond pattern within the six-membered ring are summarized in Scheme 1. Clearly, there has been an isomerization from the usually more stable *para*-quinonediimine state[12] to the higher energy *ortho* form to allow the formation of a chelate complex between the π electron-rich metal and a strongly π-accepting[4b,c, 13] *o*-quinonediimine ligand.[14] This situation results in the occurrence of a metal-to-ligand charge transfer (MLCT) absorption of the complex at 525 nm (Figure 2); the long-wavelength intraquinone transition of the free ligand at 390 nm is slightly shifted to 395 nm in the complex.

[*] Prof. Dr. W. Kaim, Dr. J. Rall, Dr. A. F. Stange, Dr. K. Hübler
Institut für Anorganische Chemie der Universität
Pfaffenwaldring 55, D-70550 Stuttgart (Germany)
Fax: (+49) 711-685-4170
E-mail: kaim@iac.uni-stuttgart.de

[**] This work was supported by the Deutsche Forschungsgemeinschaft, the Volkswagen Foundation, and the Fonds der Chemischen Industrie. We thank Dr. K.-W. Klinkhammer for helpful suggestions, and T. Sixt and T. Scheiring for assistance.

 © WILEY-VCH Verlag GmbH, D-69451 Weinheim, 1998 1433-7851/98/3719-2681 $ 17.50+.50/0

2) The secondary amine functionalities in the 4,5-positions engage in N–H···F···H–N "chelate" hydrogen bonding[15] to one flourine center of the tetrafluoroborate anion (Scheme 1, Figure 1). The three remaining fluorine atoms are disordered.[11]

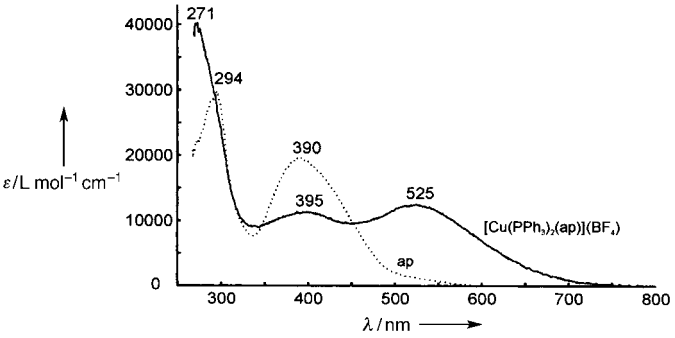


Figure 2. UV/Vis absorption spectrum of azophenine (ap) and **1** in dichloromethane.

Effects 1) and 2), therefore, both contribute to the stabilization of the *ortho*-quinonoid over the usually lower energy *para*-quinonoid form,[12] thus illustrating a further aspect to be considered in the intriguing coordination chemistry[2, 4, 13] of quinonoid ligands.

Received: May 4, 1998 [Z11808IE]
German version: *Angew. Chem.* **1998**, *110*, 2827–2829

Keywords: copper · hydrogen bonding · isomerizations · N ligands · quinones

[1] a) C. Kimich, *Ber. Dtsch. Chem. Ges.* **1875**, *8*, 1026; *b)* O. Fischer, E. Hepp, *Ber. Dtsch. Chem. Ges.* **1888**, 21, 676; c) P. Grünanger, *Methoden Org. Chem. (Houben-Weyl) 4th ed.,* Vol. VII/3b, **1979**, p. 244; d) P. Ruggli, F. Buchmeier, *Helv. Chim. Acta* **1945**, *28*, 850.

[2] a) C. G. Pierpont, L. C. Francesconi, N. D. Hendrickson, *Inorg. Chem.* **1977**, *16*, 2367; b) J. T. Wroblewski, D. B. Brown, *Inorg. Chem.* **1979**, *18*, 498; c) F. Tinti, M. Verdaguer, O. Kahn, J.-M. Savariault, *Inorg. Chem.* **1987**, *26*, 2380; d) M. A. Calvo, A. M. M. Lanfredi, L. A. Oro, M. T. Pinillos, C. Tejel, A. Tiripicchio, F. Ugozzoli, *Inorg. Chem.* **1993**, *32,* 1147.

[3] For related compounds, see a) M. L. Hsieh, M. L., M. C. Cheng, S. M. Peng, *Inorg. Chim. Acta* **1988**, *145*, 1; b) J. V. Folgado, R. Ibanez, D. Beltran, J. M. Savariault, J. Galy, *Inorg. Chem.* **1988**, *27*, 19; c) H.-Y. Cheng, G.-H. Lee, S.-M. Peng, *Inorg. Chim. Acta* **1992**, *191*, 25.

[4] a) C. G. Pierpont, C. W. Lange, *Prog. Inorg. Chem.* **1994**, *41*, 331; b) R. A. Metcalfe, A. B. P. Lever, *Inorg. Chem.* **1997**, *36*, 4762; c) T. Jüstel, J. Bendix, N. Metzler-Nolte, T. Weyhermüller, B. Nuber, K. Wieghardt, *Inorg. Chem.* **1998**, *37*, 35.

[5] D. B. Hall, R. E. Holmlin, J. K. Barton, *Nature* **1996**, *382*, 731, and references therein.

[6] W. Kaim, J. Rall, *Angew. Chem.* **1996**, *108*, 47; *Angew. Chem. Int. Ed. Engl.* **1996**, *35*, 43.

[7] S. M. Janes, D. Mu, D. Wemmer, A. J. Smith, S. Kaur, D. Maltby, A. L. Burlingame, J. P. Klinmann, *Science* **1990**, *248*, 981.

[8] a) P. F. Knowles, D. M. Dooley in *Metal Ions in Biological Systems, Vol. 30* (Eds.: H. Sigel, A. Sigel), Dekker, New York, **1994**, p. 361; b) W. S. McIntire, C. Hartmann in *Principles and Application of Quinoproteins* (Ed.: V. L. Davison), Dekker, New York, **1993**, p. 97.

[9] J. P. Klinmann, D. Mu, *Annu. Rev. Biochem.* **1994**, *63*, 299.

[10] Synthesis of **1**: A solution of $[Cu(PPh_3)_4](BF_4)$ (600 mg, 0.50 mmol) in acetone (10 mL) was added to a stirred suspension of azophenine[1d] (220 mg, 0.50 mmol) in acetone (20 mL). A rapid change from orange to deep purple was observed. After one hour the solution was filtered and subjected to column chomatography on silica gel. Elution with acetone/pentane (9/1) yielded first some azophenine and then the purple complex $[Cu(PPh_3)_2(ap)](BF_4)$ (**1**) (415 mg, 66%). Single crystals suitable for X-ray diffraction were grown at 4 °C from a solution of acetone/pentane (1/1) and were identified from crystallography as the solvate $[Cu(PPh_3)_2(ap)](BF_4)\cdot 3$ acetone. Correct C,H,N analysis; UV/Vis (CH_2Cl_2): $\lambda_{max}(\varepsilon) = 525$ (12500), 395 (11400 M^{-1} cm^{-1}) nm; ^1H NMR ($CDCl_3$): $\delta = 7.96$ (s, 2H, N-*H*), 6.7–7.4 (m, 50H, Ph), 6.21 (s, 2H, C3-*H*, C6-*H*), 2.15 (s, 18H, acetone solvate).

[11] a) Crystals of $[Cu(PPh_3)_2(ap)](BF_4)\cdot 3C_3H_6O$ were immersed in Nujol. One well-shaped crystal of dimensions $0.4 \times 0.3 \times 0.3$ mm^3 was transferred into a capillary and mounted on a Syntex P3 diffractometer. Data were collected at −90 °C with $Mo_{K\alpha}$ radiation (0.71069 Å, ω-scan): 12346 collected, 11541 unique, and 10929 observed reflections; 932 parameters and 84 restraints; $2\theta_{max} = 50°$. $C_{66}H_{54}BCuF_4N_2P_2\cdot 3C_3H_6O$, $M_r = 1289.66$ g mol^{-1}, monoclinic, space group $P2_1/c$ (No. 14), $a = 16.971(5)$, $b = 17.848(4)$, $c = 23.346(5)$ Å, $\beta = 107.36(2)°$, $V = 6749(3)$ $Å^3$, $Z = 4$, $\rho_{calcd} = 1.269$ g cm^{-3}, $\mu = 4.32$ cm^{-1}, $wR2 = 0.194$ ($R1 = 0.070$ based on 8244 reflections with $F_0 > 4\sigma(F_0)$). Largest difference peak/hole: +0.94/−0.59 e $Å^{-3}$. The structure was solved by direct methods by using the SHELXTL-PLUS package.[11b] Refinement was achieved with the same program employing full matrix least-squares methods on $|F^2|$. Except for the three disordered fluorine atoms and the solvent molecules, all non-hydrogen atoms were refined anisotropically. The hydrogen atoms were refined without geometrical constraints by adjusting their isotropic displacement parameters to 1.2 times the value for the corresponding carbon and nitrogen atoms. The BF_4^- ion showed disorder in terms of rotation around the B1–F1 axis in two orientations (50% occupation each). Acetone solvent molecules were found on three different sites in the asymmetric unit. Crystallographic data (excluding structure factors) for the structure reported in this paper have been deposited with the Cambridge Crystallographic Data Centre as supplementary publication no. CCDC-101396. Copies of the data can be obtained free of charge on application to CCDC, 12 Union Road, Cambridge CB2 1EZ, UK (fax (+44) 1223-336–033; e-mail: deposit@ccdc.cam.ac.uk); b) G. M. Sheldrick, SHELXTL-PLUS An Integrated System for Solving, Refining and Displaying Structures from Diffraction Data, Rel. 5.03, Siemens Analytical X-Ray Instruments Inc., **1994**.

[12] H. Rumpel, H.-H. Limbach, *J. Am. Chem. Soc.* **1989**, *111*, 5429.

[13] H. Masui, A. B. P. Lever, E. S. Dodsworth, *Inorg. Chem.* **1993**, *32*, 258, and references therein.

[14] A similar 1,4→1,2 (*para*→*ortho*) quinone isomerization had been deduced from EPR results of a ruthenium(II) complex with the deprotonated and partially oxidized 2,4,5-trihydroxytoluene ligand: E. Waldhör, B. Schwederski, W. Kaim, *J. Chem. Soc. Perkin Trans 2* **1993**, 2109.

[15] For examples of N–H···F hydrogen bonding, see a) F. S. Stephens, *J. Chem. Soc. Dalton Trans.* **1972**, 1350; b) A. S. Batsanov, P. Hubberstey, and C. E. Russell, *J. Chem. Soc. Dalton Trans.* **1994**, 3189.

 © WILEY-VCH Verlag GmbH, D-69451 Weinheim, 1998 1433-7851/98/3719-2682 $ 17.50+.50/0

Alkylation of Porous Silicon by Direct Reaction with Alkenes and Alkynes**

James E. Bateman, Robert D. Eagling, David R. Worrall, Benjamin R. Horrocks,* and Andrew Houlton*

Methods for the derivatization of silicon surfaces have generally relied upon reactions with the native oxide.[1] Recently, however, synthetic strategies for the fabrication of covalently bound monolayers have been developed which exploit the inherent reactivity of the hydrogen-terminated surface formed on fluoride etching.[2–9] Such a layer is also known to terminate the surface of photoluminescent porous silicon (PS), and associated molecular functionalization routes have also been reported for this material.[3] Cases of PS derivatization methods have, until recently, been limited to modification of the surface through the formation of Si–O-bonded films by reactions with, for example, alcohols and carboxylic acids.[4, 5] Methods for direct alkylation of silicon surfaces through Si–C bonds have now been reported by several workers,[2, 6–8] with one of these being for PS;[8a] such films have been shown to be very stable. To date these reactions with alkenes have generally relied upon catalysis (e.g. radical initiators, Pt complexes, $EtAlCl_2$) for reaction.[2, 6, 8a] Here we present the covalent modification of PS by direct reaction with unsaturated hydrocarbons *in the absence of catalyst.* The reaction, with alkenes or alkynes, can be carried out with either neat reagent or in dilute solution.

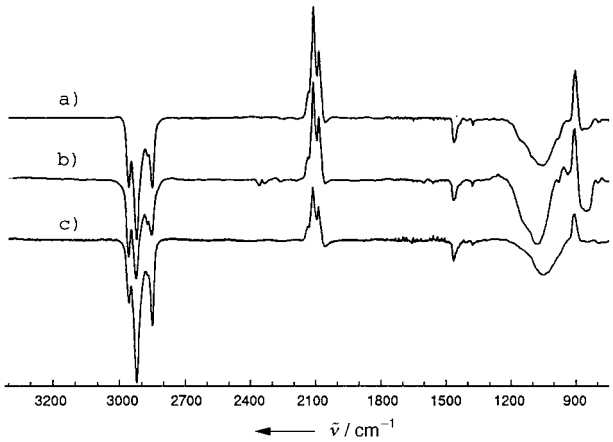


Figure 1. Transmission IR spectra of porous silicon after reaction with a) 1-octene (5 d), b) 1-octyne (1 d), and c) 1-undecene (5 d); 200 scans at a resolution of 4 cm^{-1}. All spectra were recorded relative to unmodified porous silicon.

[*] Dr. B. R. Horrocks, Dr. A. Houlton, Dr. J. E. Bateman, R. D. Eagling
Department of Chemistry
University of Newcastle-upon-Tyne
Newcastle-upon-Tyne, NE1 7RU (UK)
Fax: (+44) 191-222-6929
E-mail: andrew.houlton@ncl.ac.uk
b.r.horrocks@ncl.ac.uk
Dr. D. R. Worrall
Department of Chemistry, University of Loughborough
Loughborough, Leicestershire, LE11 3TU (UK)

Table 1. Assignment of the IR bands for modified PS (n.o. = not observed).

Assignment	Hexene/PS [cm^{-1}]	Octene/PS [cm^{-1}]	Undecene/PS [cm^{-1}]	Vinylferrocene/PS [cm^{-1}]	Octyne/PS [cm^{-1}]
$\nu(C{\equiv}CH)$	–	–	–	–	n.o.
$\nu_{Cp}(CH)$	–	–	–	3098	–
$\nu(C{=}CH_2)$	n.o.	n.o.	n.o.	n.o.	–
$\nu_a(CH_3)$	2961	2961	2961	n.o.	2961
$\nu_a(CH_2)$	2924	2924	2924	2920	2927
$\nu_s(CH_3)$	2878	2878	2878	n.o.	2878
$\nu_s(CH_2)$	2856	2854	2854	2850	2856
$\nu(C{\equiv}C)$	–	–	–	–	n.o.
$\nu(C{=}C)$	n.o.	n.o.	n.o.	n.o.	–
$\delta_a(CH)$	1466	1464	1464	–	1458
$\delta_s(CH_3)$	1381	1380	1380	–	1382
$\nu(CC)$	–	–	–	1107	–
$\delta(CH)$	–	–	–	1000	–
$\pi(CH)$	–	–	–	815	–

FT-IR spectra (Figure 1, Table 1) of PS samples after reaction with alkene or alkyne show bands for C–H stretching modes around 2900 cm^{-1} and C–H deformation modes at 1465 and 1380 cm^{-1} of alkyl chains attached to the silicon surface. The use of relatively volatile adsorbates minimized the possibility of physisorbed hydrocarbon remaining within the porous structure. In addition, strong bands due to the olefinic (or acetylenic) C–C stretch and C–H stretch and C–H deformation modes, present in the IR spectrum of the starting molecules, are absent in the spectra of the modified PS, indicating that rehybridization of the terminal alkene (alkyne) group from sp^2 (sp) to sp^3 has taken place. No intermediate olefinic species was observed, in contrast with the reported catalytic hydrosilylation route.[8] Loss of the major part of the hydrogen termination of the PS is evident from the negative bands for the $Si-H_x$ stretch modes around 2100 cm^{-1} and the $Si-H_2$ scissors mode at 915 cm^{-1}. This suggests that the reaction proceeds by abstraction of surface hydrogen rather than attack at Si–Si back bonds, which is in contrast to reported mechanisms for the reaction of PS with alcohols.[3, 4] Even after five days of reaction, the band for the $Si-H_x$ stretch retains up to 30% of its original intensity, indicating incomplete modification of the surface. This may be due to microporous regions of the PS which are inaccessible to hydrocarbon molecules of chain length C_6-C_{11}. Preferential loss of particular hydride species was not observed, which is in agreement with previous studies on PS modification.[4, 8, 10] The peak at 1050 cm^{-1} is assigned to the Si-O-Si asymmetric stretch. Earlier work has shown PS to be highly sensitive to oxidation under typical preparative conditions[3, 11] using normal Schlenk line procedures. Oxidation of the PS is therefore seen to compete with alkylation.[12]

To demonstrate that functional molecules can be attached to the surfaces vinylferrocene was used. Figure 2 shows a typical cyclic voltammogram (CV) of the ferrocenyl-modified porous silicon, and Figure 3 shows the dependence of the anodic peak current i_{pa} on the scan rate. The large anodic peak current is due to oxidation of ferrocene (Fc) moieties attached to the porous structure, and the relatively small cathodic peak current results from the reduction of Fc^+.[13] The latter is not simply due to the rectifying properties of the *p*-type semi-

 © WILEY-VCH Verlag GmbH, D-69451 Weinheim, 1998 1433-7851/98/3719-2683 $ 17.50+.50/0

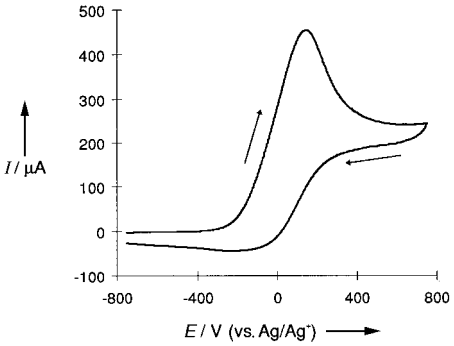


Figure 2. Cyclic voltammogram under ambient illumination of porous silicon (0.38 cm^2) after modification with vinylferrocene. The scan rate was 2 $mV s^{-1}$, the electrolyte was 0.1 M nBu_4NPF_6 in MeCN, and the reference electrode was Ag/0.01 M Ag^+.

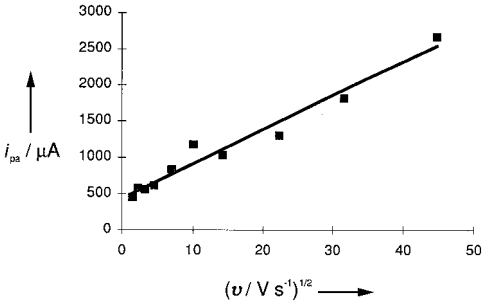


Figure 3. Dependence of the anodic peak current i_{pa} on $v^{1/2}$ for a ferrocenyl-modified PS layer. The electrolyte was 0.1 M nBu_4NPF_6.

conductor–electrolyte interface since illumination (100-W tungsten–halogen lamp) produced no change in the CV. In addition, our previous work[9] has shown that nearly symmetrical surface waves for tethered ferrocenes are observed on silicon electrodes under ambient illumination. An alternative, loss of Fc^+ to the external solution, was not observed and is also inconsistent with the lack of a large decrease in i_{pa} with cycle number. Based on prior reports that Fc^+ has a redox potential sufficient to inject holes into single-crystal silicon,[14] we propose that the oxidized ferrocenes inject holes into silicon crystallites that are electrically isolated from the bulk of the semiconductor. The reaction scheme is then that described by Equations (1) and (2); Si_n represents a silicon crystallite.

at the silicon substrate: $Fc \rightarrow Fc^+ + e^-$ (1)

in the porous film: $Fc^+ + Si_n^0 \rightarrow Fc + Si_n^+$ (2)

A linear dependence of i_{pa} on the square root of the scan rate, $v^{1/2}$ typical of a diffusional process was observed rather than the direct proportionality between i_{pa} and v expected for surface-confined electrochemistry.[13] However, such behavior is frequently observed in polymer-coated electrodes[15] when complete oxidation of all the redox centers (Fc groups) is not achieved due to slow charge/mass transport. This interpretation of the data in Figure 3 is also consistent with the high resistivity of porous silicon.[16]

Photoluminescence (PL) measurements showed that the PL of the PS samples was significantly quenched on alkylation with no shift in wavelength being observed. A decrease in PL emission intensity after modification is well documented and can be explained as being due to adsorbed surface species acting as nonradiative recombination centers.[3]

Stability tests on the 1-octene-modified PS (reaction time of five days) showed it to be significantly more robust than unmodified PS. No change in the IR spectra was observed after boiling in water and KOH solution (pH 12) for one hour. Unmodified PS has been shown to undergo substantial oxidation and degradation after such treatment.[8, 17] The use of ethanolic KOH solution (75 % KOH, 25 % ethanol, pH 12), however, led to stripping of the porous layer after one hour at room temperature due to increased pore wetting.[8a, 11] The linear n-octyl chain does not, therefore, provide the same degree of protection to the PS surface as does the more bulky *tert*-butyl group examined by Buriak and Allen.[8a]

In conclusion, porous silicon can be alkylated by direct reaction with unsaturated hydrocarbons and no catalyst. The Si–C-bound layers produced are significantly more robust than the Si–O-bound layers obtained by reaction of PS with alcohols, etc. This method also allows the attachment of chemically reactive groups such as redox agents onto the surface.

Experimental Section

Porous silicon was formed by galvanostatic anodization for 4 min of a p-doped Si(100) wafer (1–10 Ω cm) in a solution of 48 % aqueous HF and ethanol (50/50) in a Teflon cell with a current density of 19 $mA cm^{-2}$. The PS was then rinsed in deionized water (Millipore, 18 MΩ) to remove ethanol, immersed in 48 % aqueous HF to ensure removal of any remaining oxide, and finally rinsed in deionized water (20 s) and dried in a N_2 stream. A transmission FT-IR spectrum indicated that samples so prepared were hydrogen-terminated with little or no oxide present. These samples were then immersed in 1 M solutions of 1-octene, 1-octyne, and 1-undecene (Aldrich, > 97 %) in toluene and heated at reflux (110–180 °C) typically for 18–20 h before analysis by FT-IR spectroscopy (Biorad FTS-60 spectrometer fitted with a narrow-band MCT detector). After reaction the samples were rinsed in toluene and dried under vacuum. Some hydrogen termination was still observed after reaction times of up to five days.

Ferrocenyl-derivatized porous silicon was also prepared by direct reaction of vinylferrocene (0.5 M solution in toluene) with porous silicon. After washing with toluene and acetone to remove physisorbed material, the ferrocenyl-modified porous silicon was examined by CV (electrolyte: 0.1 M nBu_4NPF_6 in MeCN). The reference electrode Ag/0.01 M $AgNO_3$ was separated from the working electrode by a fine glass frit.

Received: April 14, 1998 [Z11716IE]
German version: *Angew. Chem.* **1998**, *110*, 2829–2831

Keywords: alkylations · hydrosilylations · silicon · surface chemistry

[1] J. Sagiv, *J. Am. Chem. Soc.* **1980**, *102*, 92–98; R. Maoz, J. Sagiv, *J. Colloid Interface Sci.* **1984**, *100*, 465–496.
[2] a) M. R. Linford, C. E. D. Chidsey, *J. Am. Chem. Soc.* **1993**, *115*, 12631–12632; b) M. R. Linford, P. Fenter, P. M. Eisenberger, C. E. D. Chidsey, *J. Am. Chem. Soc.* **1995**, *117*, 3145–3155; c) A. Bansal, X. Li, I. Lauermann, N. S. Lewis, W. H. Weinberg, *J. Am. Chem. Soc.* **1996**, *118*, 7225–7226.
[3] M. J. Sailor, E. J. Lee, *Adv. Mater.* **1997**, *9*, 783–793.
[4] N. Y. Kim, P. E. Laibinis, *J. Am. Chem. Soc.* **1997**, *119*, 2297–2298.

 © WILEY-VCH Verlag GmbH, D-69451 Weinheim, 1998 1433-7851/98/3719-2684 $ 17.50+.50/0

[5] E. J. Lee, T. W. Bitner, J. S. Ha, M. J. Shane, M. J. Sailor, *J. Am. Chem. Soc.* **1996**, *118*, 5375 – 5382.
[6] L. A. Zazzera, J. F. Evans, M. Deruelle. M. Tirrell, C. R. Kessel, P. McKeown, *J. Electrochem. Soc.* **1997**, *144*, 2184 – 2189.
[7] M. M. Sung, G. J. Kluth, O. W. Yauw, R. Maboudian, *Langmuir* **1997**, *13*, 6164 – 6168.
[8] a) J. M. Buriak, M. J. Allen, *J. Am. Chem. Soc.* **1998**, *120*, 1339 – 1340; b) J. H. Song, M. J. Sailor, *J. Am. Chem. Soc.* **1998**, *120*, 2376 – 2381; c) N. Y. Kim, P. E. Laibinis, *J. Am. Chem. Soc.* **1998**, *120*, 4516 – 4517.
[9] G. C. Cleland, B. R. Horrocks, A. Houlton, *J. Chem. Soc. Faraday Trans.* **1995**, *91*, 4001 – 4003; R. D. Eagling, J. E. Bateman, N. J. Goodwin, W. Henderson, B. R. Horrocks, A. Houlton, *J. Chem. Soc. Dalton Trans.* **1998**, 1273.
[10] The positive "tail" on the low-frequency side of the $Si-H_x$ stretching band below 2100 cm^{-1} may, however, indicate the formation of a less tightly bound surface hydride species in which the silicon atom is also bonded to an alkyl group [Eq. (3)]. Such a decrease in the Si – H

$$>SiH_2 + RCH{=}CH_2 \rightarrow >SiH(CH_2)_2R \quad (3)$$

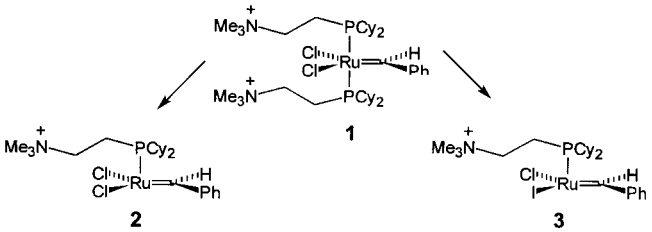
stretching frequency, with increasing alkyl substitution, has been observed previously for alkylsilanes; see, for example, G. Lucovsky, *Solid State Comm.* **1979**, *29*, 571 – 576.
[11] J. E. Bateman, R. D. Eagling, B. R. Horrocks, A. Houlton, D. R. Worrall, *Chem. Commun.* **1997**, 2275 – 2276.
[12] Based on the results of experiments on the oxidation of PS, it is estimated that approximately 30% of the loss of $Si-H_x$ groups is attributable to oxidation, the remaining 70% is due to reaction with hydrocarbon.[10]
[13] A. J. Bard, L. R. Faulkner, *Electrochemical Methods*, Wiley, New York, **1970**.
[14] P. E. Laibinis, C. E. Stanton, N. S. Lewis, *J. Phys. Chem.* **1994**, *98*, 8765 – 8774.
[15] R. H. Terrill, R. W. Murray, *Molecular Electronics* (Eds.: J. Jortner, M. Ratner), Blackwell Science, Oxford, **1997**, chap. 6, pp. 215 – 240.
[16] M. I. J. Beale, J. D. Benjamin, M. J. Uren, N. G. Chew, A. G. Cullis, *J. Cryst. Growth* **1985**, *73*, 622 – 636.
[17] K.-H. Li, C. Tsai, S. Shih, T. Hsui, D. L. Kwong, J. C. Campbell, *J. Appl. Phys.* **1992**, *72*, 3816 – 3817.

Olefin Metathesis of a Ruthenium Carbene Complex by Electrospray Ionization in the Gas Phase**

Christian Hinderling, Christian Adlhart, and Peter Chen*

We report the direct mass spectrometric observation of an olefin metathesis reaction[1] of an acyclic alkene and the ring-opening metathesis (ROM) of cycloalkenes in the gas phase by the water-soluble ruthenium benzylidene complex **1** developed by Grubbs et al.[2] Besides constituting the first observation of olefin metathesis in the gas phase by a complex that performs the same reaction in solution, the mass spectrometric study finds and quantifies intramolecular π complexation of the penultimate double bond in the growing oligomeric chain to the metal center, and provides surprising evidence that, except for a large increase in the absolute rates, the gas phase reactions of a $[RuCl_2(=CHPh)(PR_2R')_2]$ complex closely parallel the corresponding reactions in solution.

The electrospray ionization[3, 4] tandem mass spectrometric (ESI-MS/MS) experiment was performed in a modified TSQ-7000 mass spectrometer (Finnigan MAT) as described in our reports on gas-phase C – H activation[5] by $[CpIr(PMe_3)(CH_3)]^+$, oxo-transfer reactions[6] by $[O{=}Mn^V(salen)]^+$ (salen = *N,N'*-bis(salicylidene)ethylenediamine dianion), the Ziegler – Natta polymerization[7] of α-olefins by $[Cp_2ZrR]^+$, and reversible hydrogenation of olefins[8] by $[Rh(PMe_3)_2]^+$. Complex **1** was synthesized as described by Grubbs et al.[2] A 10^{-5} M solution of the diiodide salt of **1** in CH_2Cl_2 was then electrosprayed. Ions were thermalized with about 10 mTorr inert gas in the first octopole region (Scheme 1).



Scheme 1. Reactions of **1** in the mass spectrometer. Cy = cyclohexyl.

Under relatively mild desolvation conditions, that is with a tube lens potential of 44 V in front of the first octopole, the mass spectrum consisted of signals due to the dication **1**, the monocation **2**, which was formed by the loss of one phosphane ligand from **1**, and a second monocation **3** with a mass that indicated that one of the chloride ligands in **2** had been replaced with an iodide. The use of the dichloride salt of **1** instead of the diiodide eliminated **3**. As the tube lens potential was increased stepwise to 150 V, first the intensity of the peak due to **2** increased at the expense of that for **1**, and then decreased with the loss of the second phosphane (the phosphane appears in the mass spectrum because it carries the charge on its side chain), loss of trimethylamine, and loss of HCl. These fragments are consistent with the assumed structure. When 1-butene was used as the thermalization gas, a new signal with the mass corresponding to the ruthenium propylidene product **4** (loss of styrene) appeared in the spectrum as a result of an olefin metathesis reaction. Moreover, when either **1** or **2** was mass-selected in the first quadrupole, and then allowed to react with 1-butene in the second octopole, the only metathesis product we obtained in both cases was **4** (Figure 1). Complex **3** exhibited considerably lower reactivity with alkenes in comparable experiments.[9]

With cyclobutene[10] or norbornene, the new complexes **5a** ($n=1$) and **6** ($n=1$) were formed predominately. Their masses correspond to the adducts of **2** with the cycloalkenes, as expected for ROM products. Collision-induced dissociation (CID) of **5a** ($n=1$) or **6** ($n=1$) led to loss of the cycloalkene mass,[11] presumably reforming **2** (Scheme 2). Closer exami-

[*] Prof. Dr. P. Chen, C. Hinderling, C. Adelhart
Laboratorium für Organische Chemie
Eidgenössische Technische Hochschule
Universitätstrasse 16, CH-8092 Zürich (Switzerland)
Fax: (+41) 1-632-1280
E-mail: chen@org.chem.ethz.ch

[**] This work was supported by the Schweizerischen Nationalfonds zur Förderung der wissenschaftlichen Forschung and the ETH Zürich. A graduate fellowship for C.H. from the Stipendienfonds der Basler Chemischen Industrie is gratefully acknowledged.

 © WILEY-VCH Verlag GmbH, D-69451 Weinheim, 1998 1433-7851/98/3719-2685 $ 17.50+.50/0

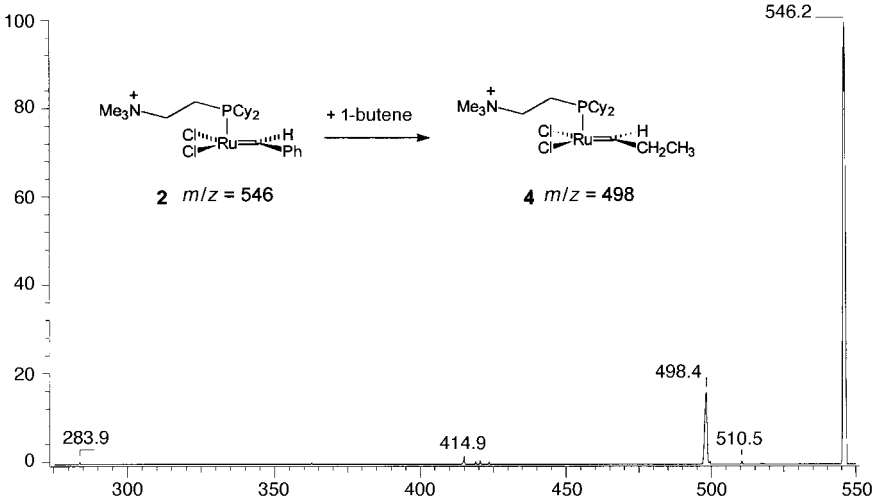
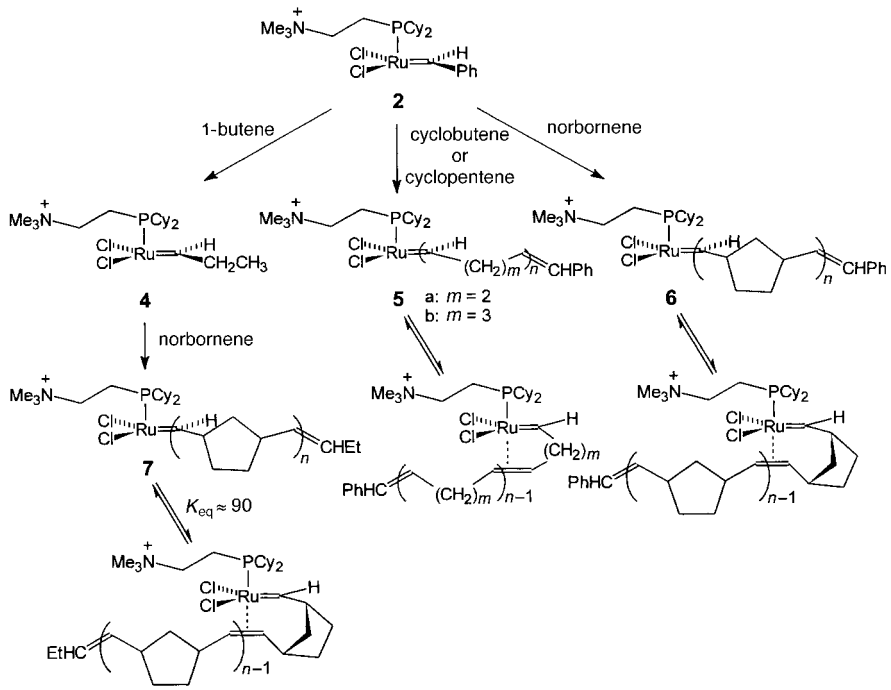


Figure 1. Daughter-ion spectrum of a dilute solution of **1** in CH_2Cl_2: Electrospray ionization was followed by desolvation, collisional removal of one phosphane ligand, and thermalization in octopole 1, mass-selection of the ion at $m/z = 546$ in quadrupole 1, reaction with 1-butene in octopole 2, and mass analysis in quadrupole 2.



Scheme 2. Reactions of **2** in the mass spectrometer.

nation of the mass spectrum produced when **2** was allowed to react with cyclobutene in the first octopole revealed a smaller peak at the mass expected for **5a** ($n = 2$), thus indicating that a second molecule of cyclobutene had added. This prompted a comparison of 1-butene with cyclobutene, cyclopentene, and norbornene, in which **2** was mass-selected in the first quadrupole and then collided with the alkenes (10 mTorr) in the octopole collision cell. These experiments gave product distributions from which the relative rates (Table 1) were extracted by kinetic modeling of the multiple additions of the cycloalkenes.[12] Addition of up to three cycloolefin units was established; the last adducts were observed in a segmented-scan mode. In order to probe the electronic influence of an alkyl versus aryl residue on the ROM reaction, **4**, generated in the first octopole by reaction of **2** and 1-butene, was mass-selected and then collided with norbornene in the collision cell under the same conditions.

Several mechanistic points can be made from the data, even without the more thorough thermochemical measurements (by CID reaction thresholds[13]) that are possible with the present instrument.[5] Electrospray ionization of medium-to-large organometallic complexes has been reported,[14, 15] but has not been combined systematically[16] with the broad range of ion–molecule reaction techniques available for mechanistic work on small gas phase organometallic ions.[17] Other workers investigating ion–molecule reactions have observed olefin metathesis with several simple metal carbenes,[18] for example $[Mn{=}CH_2]^+$, $[Fe{=}CH_2]^+$, and $[Co{=}CH_2]^+$. Most of the metatheses have been observed with deuterated ethylene. The present result constitutes, however, the first instance in which a solution-phase olefin metathesis catalyst has been shown to effect the same reaction in the gas phase.

Absolutely critical to the significance of the experiment is the extent to which the gas-phase and solution-phase reactions resemble each other: many features that appear in solution-phase metathesis reactions (or at least the trends) also appear in the gas-phase reactions. Dissociation of one phosphane ligand from complex **1** is a prerequisite for metathesis

Table 1. Relative rate constants, normalized to the **2** → **4** reaction.[a]

Reaction	Relative rates (relative intensities)		
	$k_{0\rightarrow1,\,rel}$	$k_{1\rightarrow2,\,rel}$	$k_{2\rightarrow3,\,rel}$
2 + 1-butene → **4**	1.0 (0.150)	NA	NA
2 + cyclopentene → **5b**	0.01 (0.0015)	–	–
2 + cyclobutene → **5a**	13 (4.86)	0.03 (0.0151)	–
2 + norbornene → **6**	15 (7.32)	0.01 (0.00678)	–
4 + norbornene → **7**	9 (2.53)	0.1 (0.0238)	0.1 (0.000154)

[a] Extracted by kinetic modeling of the peak intensities for the addition of the first, second, and third alkene units to either **2** or **4** to form **4**–**7**. The peak intensities, given in parentheses, are relative to the intensity of either **2** or **4** in the respective daughter-ion spectrum. (NA = not applicable; – indicates not observed).

 © WILEY-VCH Verlag GmbH, D-69451 Weinheim, 1998 1433-7851/98/3719-2686 $ 17.50+.50/0

reactions both in the gas phase and in solution,[19] as evidenced by the presence of products like **4** and the complete absence of metathesis products containing two of the phosphane ligands. The gas-phase ion **2** shows no metathesis reactivity with carbonyl compounds, which agrees with the behavior observed in solution.[20] The metathesis product of the reaction of **2** with 1-butene is the ruthenium–propylidene complex **4**, and not the alternative ruthenium–methylene complex. Within the signal-to-noise ratio of about 100:1 in a normal scan spectrum (10000:1 can be achieved in segmented-scan mode), the other possible product is absent. We believe that this represents a kinetic preference in the metathesis reaction which becomes evident because of reaction under nonequilibrating conditions. Precisely the same kinetic preference was reported by Grubbs et al.[21] in the reaction of $[RuCl_2(=CHPh)(PCy_3)_2]$ with 1-butene in solution; studies showed that this initially forms the propylidene complex before equilibrating to the thermodynamically favored methylene complex. As is evident in Table 1, ROM of the first cycloalkene unit is much easier than subsequent additions, which is entirely consistent with the observation by Grubbs et al.[21] that the ruthenium–benzylidene complexes in ROMP reactions in solution showed rates of initiation much greater than the subsequent rates of propagation (the ratio k_i/k_p is 9 for norbornene at 17 °C.)

The gross trends in the relative rates in the present work are rationalized by invoking an intramolecular π complex between the metal center and the penultimate double bond, once at least one cycloalkene unit has added to either **2** or **4**. Exactly this type of π complex[22] has been observed for ruthenium[23] and tungsten[24] carbene complexes by X-ray crystallography, and, furthermore, has been proposed to explain the *cis* selectivity[25] in ROMP as well as relative rates in both ROMP[26]and ADMET[27] reactions. We can interpret the reactivity pattern of **2** with 1-butene, cyclobutene, cyclopentene, and norbornene by assuming that addition of further cycloalkene units to the uncomplexed metal center is in competition with intramolecular π complexation. Patton and McCarthy[26] have suggested that this π complex precedes the metallocyclobutane on the reaction coordinate for the reverse reaction (loss of cycloolefin with regeneration of **2**). We propose that cyclobutene and norbornene exhibit the highest rates because the short and/or rigid spacer in **5a** or **6** disfavors π complexation. The longer, more flexible methylene chain in **5b**, on the other hand, favors intramolecular π complexation; it inhibits further addition and facilitates the loss of cyclopentene. In this picture, the apparent rate for the reaction **2**→**5b** is so low because the ROM of cyclopentene is easily reversible, not because it is intrinsically slow. The second and subsequent ROM additions are always slower than the first because the reactions going from $n=0$ to $n=1$ for all of the entries in Table 1 lack the preequilibria that slow the subsequent additions. The benzylidene complex **2** is more reactive, presumably on electronic grounds, than the propylidene complex **4** in the addition of the first norbornene unit. However, in the next addition, **6** ($n=1$) is slower than **7** ($n=1$) even though the only structural difference (an aryl versus an alkyl residue at the end of the chain) is remote from the metal center. The reduced reactivity of **6** ($n=1$) versus **7** ($n=1$) most likely stems from the better donor properties of a styryl group relative to a simple olefin. This property facilitates π complexation and thus adds a less favorable preequilibrium to the overall rate of the next addition. Lastly, we can take the reduction in the rate for adding one more norbornene unit between **4** and **7**, as the equilibrium constant for intramolecular complexation ($K_{eq}\sim 90$ or $\Delta G_{diss.}\approx 3\,kcal\,mol^{-1}$ at 70 °C). This is possible because the electronic influence of the alkylidene ligands in **4** and **7** should be comparable. We are currently working on generalizing this kinetic method for determining the equilibrium constant so that we can explore systematically the steric and electronic effects on the complexation.

The absolute rate is the exception to the overall similarity of the gas phase and solution-phase reactions. As in the case of the Ziegler–Natta polymerization by unsolvated metallocene cations,[7] the olefin metathesis and ROM reactions reported here are accelerated by up to a factor of about 10^4 relative to the reactions in solution described by Grubbs and co-workers.[21] The gas-phase second-order rate constant was estimated by comparing measured product yields for reaction in the second octopole to the computed number of total collisions (reactive and nonreactive). These values were obtained from a Monte–Carlo simulation of ion transmission through a "high-pressure" octopole.[7] The model was validated by comparison of the computed versus measured ion residence time in the octopole collision cell.[28] While the absence of any external preequilibria[29] with solvent molecules or free phosphane, as well as the absence of ion-pairing effects, certainly contribute, the rate acceleration can be attributed at least in part to the ion dipole or ion-induced dipole interaction common to all ion–molecule reactions. These interactions can provide up to $10\,kcal\,mol^{-1}$ towards passage over an activation barrier for a bimolecular reaction.[30] The rate increase is not large enough to render the metathesis reactions of **2** diffusion-controlled as evidenced by the solution-phase reactivity differences which are still displayed in the gas-phase reactions. An increase in absolute rates that nevertheless preserves relative rates, as observed for the metathesis reaction, differs from the result in the typical organic ion–molecule reactions,[30] for example S_N2 or proton-transfer reactions. This result occurs presumably because of the absence of large changes in charge distribution along the metathesis reaction coordinate, despite the fact that the molecule is charged.

Lastly, in the ROM reaction of **2** and **4** with the cycloalkenes, one could have been worried that the complexes with masses corresponding to **5a**–**7** might be *intermolecular* π complexes rather than ROM products. Two lines of argument indicate, however, that they are in fact ROM products: a) The reaction of **2** and an acyclic olefin, 1-butene, in the mass spectrometer clearly involves an olefin metathesis. It would be curious, then, if ROM did not occur for cycloalkenes whose metathesis rates are typically not too dissimilar from those for acyclic alkenes.[31] b) The relative rates in Table 1 are consistent with a ROM reaction. Moreover, Patton and McCarthy[26] state that norbornene is more readily lost from an intermolecular π complex than is cyclopentene, which is precisely the opposite from the ordering in the present work.

 © WILEY-VCH Verlag GmbH, D-69451 Weinheim, 1998 1433-7851/98/3719-2687 $ 17.50+.50/0

Further investigations on the selectivity and thermochemistry of the reaction are planned. Applications of this method to anionic molybdenum and tungsten carbene ROMP catalysts,[32] for which the catalytically active species are not well-characterized, will also be explored.

Received: April 22, 1998 [Z11765IE]
German version: *Angew. Chem.* **1998**, *110*, 2831 – 2835

Keywords: carbene complexes · gas-phase chemistry · mass spectrometry · metathesis · ruthenium

[1] The homogeneous olefin metathesis reaction, was first recognized as such by: a) N. Calderon, H. Y. Chen, K. W. Scott, *Tetrahedron Lett.* **1967**, 3327; it is reviewed thoroughly in a recent monograph: b) *Olefin Metathesis and Metathesis Polymerization*, K. J. Ivin, J. C. Mol, Academic Press, New York, **1997**.

[2] B. Mohr, D. M.Lynn, R. H. Grubbs, *Organometallics* **1996**, *15*, 4317.

[3] The basic electrospray source for mass spectrometry is described by: C. M. Whitehouse, R. N. Dreyer, M. Yamashita, J. B. Fenn, *Anal. Chem.* **1985**, *57*, 675.

[4] A complete monograph on the technique is: *Electrospray Ionization Mass Spectrometry* (Ed.: R. D. Cole), Wiley, New York, **1997**.

[5] a) C. Hinderling, D. A. Plattner, P. Chen, *Angew. Chem.* **1997**, *109*, 272; *Angew. Chem. Int. Ed. Engl.* **1997**, *36*, 243; b) C. Hinderling, D. Feichtinger, D. A. Plattner, P. Chen, *J. Am. Chem. Soc.* **1997**, *119*, 10793.

[6] D. Feichtinger, D. A. Plattner, *Angew. Chem.* **1997**, *109*, 1796; *Angew. Chem. Int. Ed. Engl.* **1997**, *36*, 1718.

[7] D. Feichtinger, D. A. Plattner, P. Chen, *J. Am. Chem. Soc.* **1998**, *120*, 7125.

[8] Y. M. Kim, P. Chen, *Int. J. Mass Spectrom.*, submitted.

[9] Much lower reactivity of ruthenium carbenes with iodide, relative to chloride ligands was also reported by: E. L. Dias, S. T. Nguyen, R. H. Grubbs, *J. Am. Chem. Soc.* **1997**, *119*, 3887.

[10] Cyclobutene was prepared by E_2-elimination from cyclobutyl mesitylate. The material was checked by ^{1}H NMR spectroscopy to ensure that none of the isomeric 1,3-butadiene formed.

[11] Selection of one isotopomer of **6** ($n=1$), followed by CID with 1.4 mTorr argon in the collision cell at a collision energy of approximately 50 eV (laboratory system) leads to the following masses (relative intensity) in the daughter spectrum: 225 (0.38), 284 (0.69), 546 (1.0), 640 (0.86). The first two masses appear as daughter ions in the CID of **2**.

[12] The simplest possible kinetic model was used in which up to four sequential pseudo-first order differential rate expressions were numerically integrated with the POWERSIM (Modelldata AS) computational package. Because of the finite transit time through the collision cell, the integration was carried out to a fixed (arbitrary) time. The absolute rates are therefore also arbitrary, but the relative rates are physically meaningful.

[13] a) L. F. Halle, P. B. Armentrout, J. L. Beauchamp, *Organometallics* **1982**, *1*, 963; b) P. B. Armentrout, L. F. Halle, J. L. Beauchamp, *J. Am. Chem. Soc.* **1981**, *103*, 6501; c) P. B. Armentrout, J. L. Beauchamp, *J. Am. Chem. Soc.* **1981**, *103*, 784. For some more recent work on small complexes, see d) L. S. Sunderlin, D. Wang, R. R. Squires, *J. Am. Chem. Soc.* **1993**, *115*, 12060; e) L. S. Sunderlin, R. R. Squires, *J. Am. Chem. Soc.* **1993**, *115*, 337.

[14] a) R. Colton, J. C. Traeger, *Inorg. Chim. Acta* **1992**, *201*, 153; b) A. J. Canty, P. R. Traill, R. Colton, I. M. Thomas, *Inorg. Chim. Acta* **1993**, *210*, 91; c) R. Colton, A. D'Agostino, J. C. Traeger, *Mass Spec. Rev.* **1995**, *14*, 79; and references therein; d) L. P. Kane-Maguire, R. Kanitz, M. M. Sheil, *J. Organomet. Chem.* **1995**, *486*, 243; e) B. H. Lipshutz, K. L. Stevens, B. James, J. G. Pavlovich, J. P. Snyder, *J. Am. Chem. Soc.* **1996**, *118*, 6796; f) C. Q. Jiao, B. S. Freiser, S. R. Carr, C. J. Cassidy, *J. Am. Soc. Mass Spectrom.* **1995**, *6*, 521; g) C. L. Gatlin, F. Turecek, in Ref. [4], Chap. 15.

[15] Some analytical applications of electrospray MS to catalytic reactions have appeared: a) Z. M. Dzhabieva, V. P. Kozlovskii, Yu. M. Shul'ga, A. F. Dodonov, G. P. Belov, *Russ. Chem. Bull.* **1996**, *45*, 474; b) R. Saf, R. Schitter, C. Mirtl, F. Stelzer, K. Hummel, *Macromol.* **1996**, *29*, 7651; c) A. O. Aliprantis, J. W. Canary, *J. Am. Chem. Soc.* **1994**, *116*, 6985; d) S. R. Wilson, Y. Wu, *Organometallics* **1993**, *12*, 1478; e) R. T. Alpin, J. E. Baldwin, C. J. Schofield, S. G. Waley, *FEBS Lett.* **1990**, *277*, 212.

[16] For a recent exception, see T. G. Spence, T. D. Burns, L. A. Posey, *J. Phys. Chem. A* **1997**, *101*, 139.

[17] For a recent monograph: *Organometallic Ion Chemistry* (Ed.: B. S. Freiser), Kluwer: Dordrecht, **1996**. For other recent work, see, for example: a) M. Dieterle, J. N. Harvey, C. Heinemann, J. Schwarz, D. Schröder, H. Schwarz, *Chem. Phys. Lett.* **1997**, *277*, 399; b) G. Hornung, D. Schröder, H. Schwarz, *J. Am. Chem. Soc.* **1997**, *119*, 2273; c) R. Wesendrup, H. Schwarz, *Organomet.* **1997**, *16*, 461; d) G. Hornung, D. Schröder, H. Schwarz, *J. Am. Chem. Soc.* **1995**, *117*, 8192;e)D. Schröder, W. Zummack, H. Schwarz, *J. Am. Chem. Soc.* **1994**, *116*, 5857; f) K. K. Irikura, J. L. Beauchamp, *J. Phys. Chem.* **1991**, *95*, 8344; g) K. K. Irikura, J. L. Beauchamp, *J. Am. Chem. Soc.* **1991**, *113*, 2769; h) K. K. Irikura, J. L. Beauchamp, *J. Am. Chem. Soc.* **1989**, *111*, 75; i) P. B. Armentrout, *Acc. Chem. Res.* **1995**, *28*, 430; j) B. S. Freiser, *Acc. Chem. Res.* **1994**, *27*, 353.

[18] a) A. E. Stevens, J. L. Beauchamp, *J. Am. Chem. Soc.* **1979**, *101*, 6449; b) D. B. Jacobson, B. S. Freiser, *J. Am. Chem. Soc.* **1985**, *107*, 67; c) D. B. Jacobson, B. S. Freiser, *J. Am. Chem. Soc.* **1985**, *107*, 2605; d) D. Stöckigt, H. Schwarz, *Chem. Ber.* **1992**, *125*, 2817.

[19] D. M. Lynn, B. Mohr, R. H. Grubbs, *J. Am. Chem. Soc.* **1998**, *120*, 1627.

[20] S. T. Nguyen, L. K. Johnson, R. H. Grubbs, R. H. Ziller, *J. Am. Chem. Soc.* **1992**, *114*, 3974.

[21] P. Schwab, R. H. Grubbs, J. W. Ziller, *J. Am. Chem. Soc.* **1996**, *118*, 100.

[22] An intramolecular π complex was hypothesized for $[RuCl_2(=CHR)(PCy_3)]$ when R contains a double bond (Z. Wu, A. D. Benedicto, R. H. Grubbs, *Macromolecules* **1993**, *26*, 4975) and is assumed in the mechanistic schemes in Ref. [9].

[23] J. Tallarico, P. J. Bonitatebus, M. L. Snapper, *J. Am. Chem. Soc.* **1997**, *119*, 7157.

[24] a) C. A. Toledano, H. Rudler, J.-C. Daran, Y. Jeannin, *J. Chem. Soc. Chem. Comm.* **1984**, 574; b) C. A. Toledano, A. Parlier, H. Rudler, J.-C. Daran, Y. Jeannin, *J. Chem. Soc. Chem. Comm.* **1984**, 576.

[25] a) E. A. Ofstead, J. P. Lawrence, M. L. Senyek, N. Calderon, *J. Mol. Cat.* **1980**, *8*, 227; b) K. J. Ivin, G. Lapienis, J. J. Rooney, *Makromol. Chem.* **1982**, *183*, 9.

[26] a) P. A. Patton, T. J. McCarthy, *Macromolecules* **1984**, *17*, 2939; b) P. A. Patton, T. J. McCarthy, *Polym. Prepr.* **1985**, *26*, 66; c) P. A. Patton, T. J. McCarthy, *Macromolecules* **1987**, *20*, 778.

[27] ADMET = *A*cyclic *d*iene *met*athesis. A rate decrease was observed in ADMET polymerization by: K. Brzezinska, P. S. Wolfe, M. D. Watson, K. B. Wagener, *Macromol. Chem. Phys.* **1996**, *197*, 2065.

[28] The ion residence time can be measured by simultaneous scanning of the quadrupoles before and after the octopole collision cell and monitoring the ion current at a given mass as a function of time delay between the two quadrupoles. The measured residence times are on the order of several milliseconds for collision gas pressures of several millitorrs. The results agree very well with the model, indicating that the reaction in the collision cell can be considered as a thermal reaction at the manifold temperature of 70 °C.

[29] In reference [19], a tenfold rate acceleration is reported under conditions where protonation had shifted the preequilibrium such that the ratio of monophosphane to bisphosphane complex was 1:2, as determined by NMR spectroscopy. This indicates that the preequilibrium for phosphane dissociation cannot account for the major part of the rate difference between solution and gas phase.

[30] a) W. E. Farneth, J. I. Brauman, *J. Am. Chem. Soc.* **1976**, *98*, 7891; b) W. N. Olmstead, J. I. Brauman, *J. Am. Chem. Soc.* **1977**, *99*, 4219; c) O. I. Asubiojo, J. I. Brauman, *J. Am. Chem. Soc.* **1979**, *101*, 3715; d) M. J. Pellerite, J. I. Brauman, *J. Am. Chem. Soc.* **1980**, *102*, 5993; e) S. Sharma, P. Kebarle, *J. Am. Chem. Soc.* **1982**, *104*, 19; f) G. Caldwell, T. F. Magnera, P. Kebarle, *J. Am. Chem. Soc.* **1984**, *106*, 959; g) T. B. McMahon, T. Heinis, G. Nicol, J. K. Hovey, P. Kebarle, *J. Am. Chem. Soc.* **1988**, *110*, 7591.

[31] a)W. J. Kelly, N. Calderon, *J. Macromol. Sci. Chem.* **1975**, *A9*, 911; b) T. J. Katz, J. McGinnis, *J. Am. Chem. Soc.* **1975**, *97*, 1592; c) R. H. Grubbs, P. L. Burk, D. D. Carr, *J. Am. Chem. Soc.* **1975**, *97*, 3265; d) T. J. Katz, R. Rothschild, *J. Am. Chem. Soc.* **1976**, *98*, 2519; e) T. J. Katz, J. McGinnis, *J. Am. Chem. Soc.* **1977**, *99*, 1903.

 © WILEY-VCH Verlag GmbH, D-69451 Weinheim, 1998 1433-7851/98/3719-2688 $ 17.50+.50/0

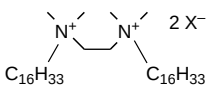
[32] a) B. L. Goodall, W. J. Kroenke, R. J. Minchak, L. F. Rhodes, *J. Appl. Polym. Sci.* **1993**, *47*, 607; b) M. McCann, D. McDonnell, B. L. Goodall, *J. Mol. Catal. A* **1995**, *96*, 31; c) L. F. Rhodes (B. F. Goodrich, USA), EP-B 0435146 A2, **1990** [*Chem. Abstr.* **1991**, *115*, 184150]; d) A. M. Mazany (B. F. Goodrich, USA), EP-B 0755938 A1, **1995** [*Chem. Abstr.* **1997**, *126*, 200209].

Gemini Surfactants as New, Low Molecular Weight Gelators of Organic Solvents and Water**

Reiko Oda, Ivan Huc,* and Sauveur J. Candau

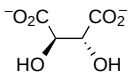
During the last decade a number of reports have described the solution-state self-assembly of small molecules into elongated aggregates such as rods, ribbons, helices, or tubules. When these structures are sufficiently long and entangled they may entrap the solvent molecules in a network and lead to the formation of gels.[1] Although the organization of the aggregates has rarely been elucidated at the molecular level,[2] it is generally agreed that the process of aggregate elongation in water or in organic solvents arises from one or more of several factors: the presence of chiral centers often induces helicity and decreases the crystallinity observed for racemates;[1] directional attractive interactions such as hydrogen bonding[3] or face-to-face $\pi-\pi$ aromatic stacking[4] help generate linear arrays of molecules. In gemini[5] (dimeric) surfactants, covalent connections between charged head groups were also shown to promote the formation of wormlike micelles and tubules in water.[6, 7] Herein we show that head-group connection also allows gemini surfactants to gel organic solvents upon their assembly into aggregates similar to those formed in water.

Compounds **1**–**5** consist of dimers of cetyltrimethylammonium ions (CTA) with various counterions. Compounds **1** and **2** form gels in chlorinated solvents (CH_2Cl_2, $CHCl_3$, $Cl_2CHCHCl_2$) that remain unchanged after several months. At temperatures above 40 °C the solutions are completely transparent and fluid. They become translucent and viscous upon standing for several hours at 25 °C. The solvent thickening is so efficient that a gel as dilute as 10 mM (gel point for $CHCl_3$) in a 1 cm diameter test tube can be turned upside down without any flow. This means that one molecule of **1** entraps about 1200 molecules of $CHCl_3$. At concentrations lower than the gel point a gel phase separates, and leaves a layer of free solvent.

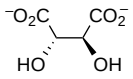


1–**5**

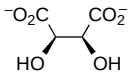
1: 2X⁻ = L-tartrate
2: 2X⁻ = D-tartrate
3: 2X⁻ = *meso*-tartrate
4: 2X⁻ = L-malate
5: 2X⁻ = 2 Br⁻



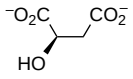
L-tartrate



D-tartrate



meso-tartrate



L-malate

When warm solutions of **1** and **2** are mixed in equimolar proportions no gel forms, and the racemate partially precipitates. The *meso* derivative **3** is poorly soluble in chlorinated solvents, and does not form gels either. Thus, for this system, chirality seems essential for gel formation. The gels are easily disrupted upon the addition of alcohols (5–10% volume%) which suggests that hydrogen bonding also plays a role in gel cohesion. The importance of hydrogen bonds is supported further by the fact that **4**, which lacks one of the hydroxyl groups of **1**, does not form gels with organic solvents. Nevertheless, the residual quantities of water[8] contained in a freshly opened bottle of solvent are necessary to partially solvate the polar groups. In anhydrous solvents **1** and **2** tend to crystallize instead of forming gels.

The most probable structure for these gels is thus an entangled network of long fibers with polar groups at the core of the aggregate, and nonpolar hydrocarbon chains in contact with the solvent, like in an inverted long micelle, or in an inverted ribbon.[9] Yet, hydrogen bonding and chirality are not sufficient to explain the formation of the fibers, and head-group connection between the ammonium ions also plays a critical role. Indeed, the monomeric form $(CTA)_2$-L-tartrate is freely soluble in chlorinated solvents, and does not form gels. In water, hydrophobic effects dominate the process of surfactant aggregation. Short and rigid covalent connections enforce proximity between charged head groups that would otherwise repulse each other. The result is a change in the spontaneous curvature of the water–surfactant interface, as under the screening effect of salt[10] or of a hydrophobic counterion.[11] In nonpolar media the aggregation is directed by electrostatic forces. A possible effect of head-group connections is the reciprocal bridging of bisanions and biscations, a prerequisite to the assembly of a noncovalent polymeric material.[12]

The texture of the gels were examined with transmission electron microscopy (TEM). The images revealed very regular and long helical fibers (Figure 1A). The pitch is 130 nm for a fiber with a width of 20 nm and a length exceeding one micron. The L-tartrate **1** gives exclusively right-handed helices, and its enantiomer **2** gives left-handed helices. These helices are strongly entangled, and sometimes pack into parallel domains. Although the TEM images do not show the inner structure of the helices, their thickness indicate that they are superstructures, probably consisting of stacked rods or ribbons.

[*] Dr. I. Huc
Laboratoire de Chimie Supramoléculaire
Université Louis Pasteur
4 rue Blaise Pascal, F-67000 Strasbourg (France)
Fax: (+33) 388-35-80-99
E-mail: ihuc@chimie.u-strasbg.fr

Dr. R. Oda, Dr. S. J. Candau
Laboratoire de Dynamique des Fluides Complexes
Université Louis Pasteur, Strasbourg (France)

[**] This work was supported by Rhône-Poulenc and the Centre National de la Recherche Scientifique. We thank M. Schmutz for helping with the electron microscopy.

 © WILEY-VCH Verlag GmbH, D-69451 Weinheim, 1998 1433-7851/98/3719-2689 $ 17.50+.50/0

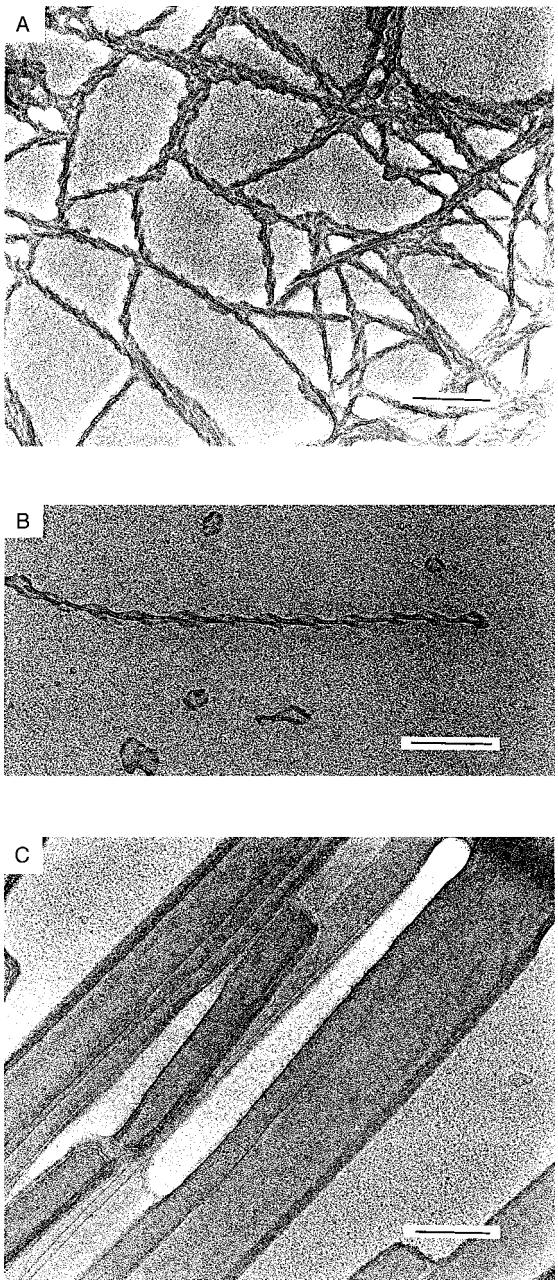


Figure 1. TEM image of the gel formed by **1** in $CHCl_3$ (A); an individual helix of **1** in water (B); the gel formed by **1**+**2** in water (C). The scale bar represents 200 nm.

Besides the chlorinated solvents mentioned above, **1** and **2** also form gels with other polarizable solvents such as CCl_4, toluene, xylenes, chlorobenzene, or pyridine, but the gels thicken at slightly higher concentrations (ca. 20–30 mM). Compounds **1** and **2** are not soluble in hydrocarbons, Et_2O, EtOAc, or acetone. No gels are formed in alcohols. However, we found that **1** and **2** are among the rare compounds having the ambidextrous ability to gel water as well as organic solvents.[9a, 13] This could in fact be expected on the basis that the dibromide **5** also forms long tubules in water.[6] For this system, chirality is not required for gelation in aqueous media, and the racemic mixture **1**+**2** consistently gels water without crystallizing. However, the observation that **3** and **4** are not gelators shows that even in water the number and the orientation of the hydroxyl groups of the tartrate molecules are critical.

No phase separation (gel point) was observed upon dilution of the gels in water. Even at concentrations below 1 mM, the gels were always formed across the entire sample, and simply became more easily and irreversibly disrupted under mechanical stress. Interestingly, the gels formed by **1**+**2** proved more viscous and less fragile than the gels formed by **1** or **2** alone. With TEM we observed multilayered platelets that are several μm long and 0.1–0.3 μm wide for **1**+**2** (Figure 1C) and right-handed and left-handed helical multilayered ribbons for **1** and **2**, respectively (Figure 1B). The pitch of the helices is 250 nm; approximately twice the pitch of the helices observed in chloroform. Overall, the structures observed in water very closely resemble those in chloroform. In particular, one enantiomer generates a helix with the same chirality in both water and chloroform.

In view of the data presented here, we propose that the aggregates in water and in organic solvents both have the multilayered structure shown in Figure 2. The cationic headgroup layers are held in close contact by bridging bisanions and a network of hydrogen bonds, which involves some water molecules. In water the external layers of the stack expose their polar heads to the solvent, whereas in organic solvents only hydrophobic chains are exposed to the solvent. As a consequence of the similarity of the inner structure of the aggregates in different solvents, a given chiral anion induces similar helicities regardless of the media.

In conclusion, we have described new low molecular weight gelators based on gemini surfactants.[1a] Covalent connections

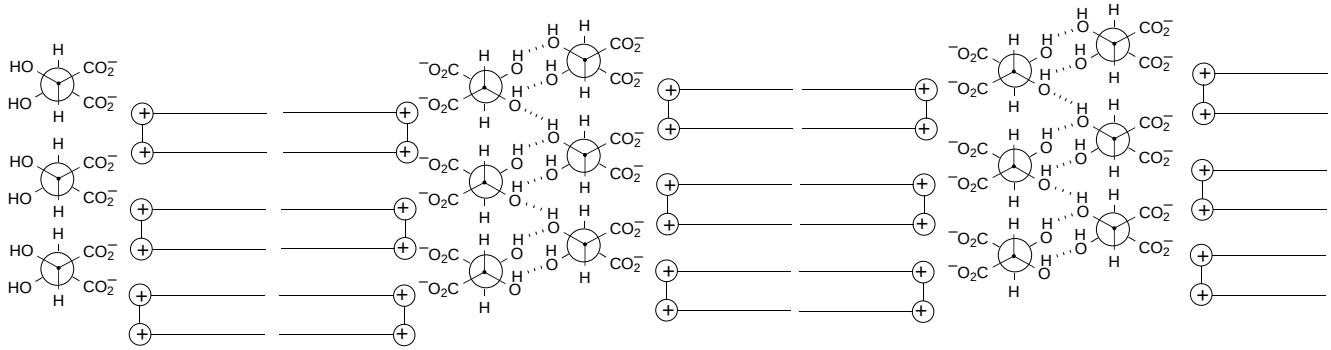


Figure 2. Proposed structure for the aggregates of **2** in water and in organic solvents. The dimeric cations are shown schematically, and the D-tartrate molecules are shown as Newman projections. Other conformers of the tartrate molecules cannot be ruled out, neither can anion bridges across the gap between two cationic layers.

 © WILEY-VCH Verlag GmbH, D-69451 Weinheim, 1998 1433-7851/98/3719-2690 $ 17.50+.50/0

between the charged head groups as well as chiral centers in the counterions are critical factors for determining the morphologies of the aggregates and their ability to gel various solvents.

Experimental Section

Compound **5** was synthesized as described before.[6] Compounds **1**–**4** and the CTA tartrates were prepared from **5** (dissolved in a water/methanol mixture) or cetyltrimethylammonium bromide by elution with water on a strongly basic anion exchange resin (Dowex 1×8, 50–100 mesh, 10 equivalents). The ammonium hydroxides were mixed with an equivalent amount of a tartaric acid, and the solution was lyophilized. The products were recrystallized from $CHCl_3/Et_2O$ (1/9, v/v) or $EtOH/Et_2O$ (1/9, v/v).

Received: April 9, 1998 [Z11713IE]
German version: *Angew. Chem.* **1998**, *110*, 2835–2838

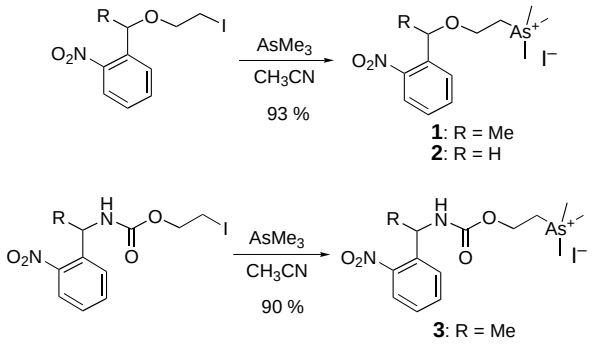
Keywords: amphiphiles · electron microscopy · gels · surfactants · self-organization

[1] a) P. Terech, R. G. Weiss, *Chem. Rev.* **1997**, *97*, 3133–3159; b) J.-H. Fuhrhop, W. Helfrich, *Chem. Rev.* **1993**, *93*, 1565–1582; c) J. M. Schnur, *Science* **1993**, *262*, 1669; d) A. E. Rowan, R. J. M. Nolte, *Angew. Chem.* **1998**, *110*, 65–71; *Angew. Chem. Int. Ed.* **1998**, *37*, 63–68.
[2] F. M. Menger, Y. Yamasaki, K. K. Catlin, T. Nishimi, *Angew. Chem.* **1995**, *107*, 616–617; *Angew. Chem. Int. Ed. Engl.* **1995**, *34*, 585–586.
[3] a) K. Hanabusa, M. Yamada, M. Kimura, H. Shirai, *Angew. Chem.* **1996**, *108*, 2086–2088; *Angew. Chem. Int. Ed. Engl.* **1996**, *35*, 1949–1951; b) J.-H. Fuhrhop, C. Boettcher, *J. Am. Chem. Soc.* **1990**, *112*, 1768–1776.
[4] a) F. Placin, M. Colomès, J.-P. Desvergne, *Tetrahedron Lett.* **1997**, *38*, 2665–2668; b) C. S. Snijder, J. C. de Jong, A. Meetsma, F. van Bolhuis, B. L. Feringa, *Chem. Eur. J.* **1995**, *1*, 594–597.
[5] F. M. Menger, C. A. Littau, *J. Am. Chem. Soc.* **1993**, *115*, 10083–10090; R. Zana, M. Benrraou, R. Rueff, *Langmuir* **1991**, *7*, 1072–1075.
[6] R. Oda, I. Huc, S. J. Candau, *Chem. Commun.* **1997**, 2105–2106, and references therein.
[7] R. Zana, Y. Talmon, *Nature* **1993**, *362*, 228–230.
[8] Addition of excess water to the organogel causes demixing and precipitation.
[9] a) N. Yamada, E. Koyama, T. Imai, K. Matsubara, S. Ishida, *Chem. Commun.* **1996**, 2297–2298; b) M. Tata, V. T. John, Y. Y. Waguespack, G. L. McPherson, *J. Am. Chem. Soc.* **1994**, *116*, 9464–9470; c) K. Hanabusa, H. Kobayashi, M. Suzuki, M. Kimura, H. Shirai, *Colloid Polym. Sci.* **1998**, *276*, 252–259.
[10] M. Sasaki, T. Imae, S. Ikeda, *Langmuir* **1989**, *5*, 211–215.
[11] a) S. Gravsholt, *J. Colloid Interface Sci.* **1976**, *57*, 575–577; b) K. Bijma, J. B. F. N. Engberts, *Langmuir* **1997**, *13*, 4843–4849.
[12] J.-M. Lehn, *Makromol. Chem. Macromol. Symp.* **1993**, *69*, 1–17.
[13] M. Jokić, J. Makarević, M. Žinić, *J. Chem. Soc. Chem. Commun.* **1995**, 1723–1724.

2-Nitrobenzylarsonium Compounds That Photorelease Heavy-Atom Cholinergic Ligands for Time-Resolved Crystallographic Studies on Cholinesterases**

Ling Peng, Florian Nachon, Jakob Wirz, and Maurice Goeldner*

Heavy-atom derivatives have found widespread use in macromolecular crystallography, because they are essential in obtaining correct diffraction phases which are required for solving the three-dimensional structure of proteins.[1] Photolabile precursors of biologically interesting molecules, which can be converted rapidly from an inactive form to an active form by light (caged compounds), can provide temporally and spatially controlled release of enzyme substrates or receptor ligands by rapid photolysis,[2] and are thus important tools in the time-resolved crystallographic studies[3] of structural changes at the atomic level during an enzymatic reaction. Here we present 2-nitrobenzylarsonium compounds **1**–**3** (Scheme 1) as photolabile precursors of cholinergic ligands



Scheme 1. Synthesis of **1**–**3**.

that contain arsenic as a heavy-atom. They were prepared to facilitate an investigation of the catalytic process of cholinesterases by time-resolved crystallography.

Both acetylcholinesterase (AChE) and butyrylcholinesterase (BuChE) hydrolyze the neurotransmitter acetylcholine very rapidly to acetate and choline.[4] Although the three-dimensional structures of AChE[5] and of several AChE-inhibitor complexes[6] have been solved, questions concerning the traffic of substrate and products to and from the active

[*] Prof. Dr. M. Goeldner, Dr. L. Peng, F. Nachon
Laboratoire de Chimie Bio-organique
UMR 7514 CNRS – Faculté de Pharmacie
Université Louis Pasteur de Strasbourg
BP 24, F-67401 Illkirch cedex (France)
Fax: (+33) 3-88-67-88-91
E-mail: goeldner@bioorga.u-strasbg.fr
Prof. Dr. J. Wirz
Institut für Physikalische Chemie der Universität
Klingelbergstrasse 80, CH-4056 Basel (Switzerland)
E-mail: wirz2@ubaclu.unibas.ch

[**] This work was supported by the European Community Biotechnology Programme No. 960081, the Association Française contre les Myopathies, the Centre National de la Recherche Scientifique, and the Swiss National Science Foundation.

 © WILEY-VCH Verlag GmbH, D-69451 Weinheim, 1998 1433-7851/98/3719-2691 $ 17.50+.50/0

site, raised in view of the high turnover rate ($20\,000\ s^{-1}$), remain unanswered.[7] An ideal approach to investigating these issues is the emergent time-resolved Laue crystallography[3] using caged cholinergic ligands.[8–11] These ligands are able to photorelease either choline (enzyme product) or carbamylcholine (enzyme substrate), allowing the initiation and control of the catalytic process of AChE at different stages.[11] The three-dimensional structure of the AChE complex obtained by the Laue method with a data collection time of 1 ms[12] is comparable to that obtained by conventional monochromatic crystallography. However, it can be difficult to locate choline in the electron density maps during time-resolved crystallographic studies, because the enzyme active site is filled with a number of water molecules[5, 6] whose electron density signals would, very likely, blend with those of choline. The use of heavy-atom derivatives of choline, such as arsenocholine, should help to overcome this problem since they should display stronger peaks in the electron density maps. Thus, arsenic has been incorporated as a heavy-atom substitute for nitrogen in the choline moiety of the caged cholinergic ligands **1**–**3**. Probes **1** and **2** are potential photolabile precursors of arsenocholine for the time-resolved crystallographic studies on cholinesterases, and probe **3** is one of arsenocarbamylcholine, provided they retain the required biochemical and photochemical properties. Here we report their syntheses, photochemical and biochemical characterizations, as well as the X-ray structures of **2** and its N-homologue.

The arsonium compounds **1**–**3** (Scheme 1) were synthesized almost quantitatively by substitution of the corresponding iodo precursors with trimethylarsane. The X-ray structure of **2** (Figure 1a) shows that the geometry about the arsenic atom is perfectly tetrahedral, similar to that found in arsenobetaine[13] and acetylarsenocholine.[14] Furthermore, the 2-nitrobenzyl and choline moieties of **2** are isostructural with those of its N-homologue (Figure 1b). As expected, the arsenic atom in **2** gave a much stronger diffraction signal than the corresponding nitrogen atom in the homologue (Figure 2).

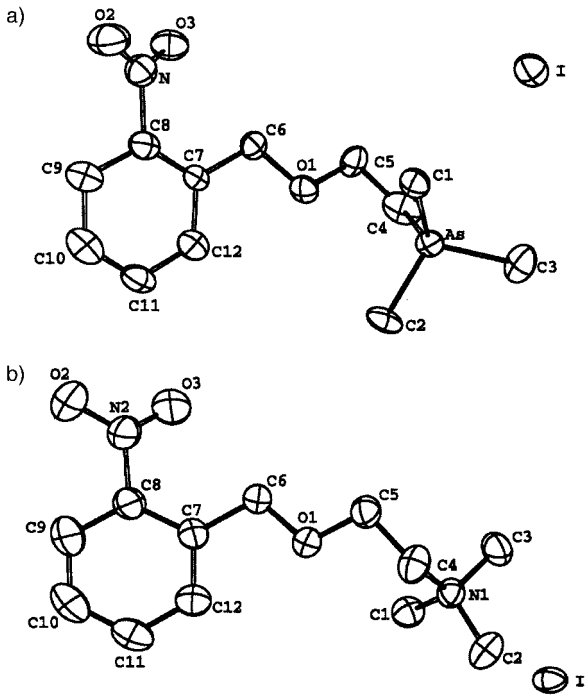


Figure 1. Crystal structures of **2** (a) and its N-homologue (b).

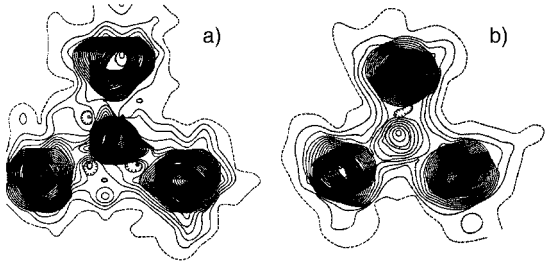


Figure 2. Electron density maps of the trimethylarsonium moiety (a) in **2** and the trimethylammonium moiety (b) in the N-homologue. The plane containing the three methyl groups was chosen for the calculation. The central spheroid in (a) is the As atom of **2**, while that in (b) is the corresponding N atom of the N-homologue.

The arsonium compounds **1**–**3** showed inhibitory properties on both purified *Torpedo* AChE and human serum BuChE (Table 1). The inhibition on BuChE is purely competitive, while that on AChE is of mixed competitive/noncompetitive type. The values of the inhibition constants (Table 1) are very similar to those obtained with the N-homologues,[8, 11] showing that quaternary arsonium salts are indeed satisfactory substitutes for ammonium salts with these cholinergic enzymes. These results support earlier findings,[15] where acetylarsenocholine was described as a cholinergic agonist for the nicotinic and muscarinic receptors as well as a substrate for AChE.

Table 1. Photofragmentation parameters and inhibition constants on cholinesterases of **1**–**3**.

Compd	k [s^{-1}][a]	Φ[b]	$K_{i(A)}$ [μM][c]	$K_{i(B)}$[μM][d]
1	9.1×10^4	0.26	17	18
2	2.2×10^2	0.17	4	11
3	5.1×10^4	0.33	63	29

[a] Rate constant of photofragmentation in 0.1M phosphate buffer, pH 6.45. [b] Quantum yield determined for 365 nm irradiation. [c] Inhibition constant on acetylcholinesterase (AChE). [d] Inhibition constant on butyrylcholinesterase (BuChE).

The use of **1**–**3** for time-resolved crystallographic studies depends critically on the rate and the quantum yield of their photofragmentation to give the desired products. The kinetics of the photochemical fragmentation were investigated by flash laser photolysis at 308 nm. The transient product, detected around 400 nm (Figure 3), is characteristic of an *aci*-nitro intermediate,[16] similar to what was observed for the N-homologue.[8, 9] The kinetics of photofragmentation (Figure 3) depend upon the nature of the released molecule, the substituent at the α-benzylic position (Table 1), and the pH value (data not shown); all of these parameters are in agreement with the currently favored fragmentation mechanism.[16] Most importantly, the half-times of the *aci*-nitro intermediates of **1** and **3** were around 10 μs, which is compatible with the enzyme turnover rate. Furthermore, the quantum yields (Table 1) of **1**–**3**, determined by comparing the extent of their photoconversion

 © WILEY-VCH Verlag GmbH, D-69451 Weinheim, 1998 1433-7851/98/3719-2692 $ 17.50+.50/0

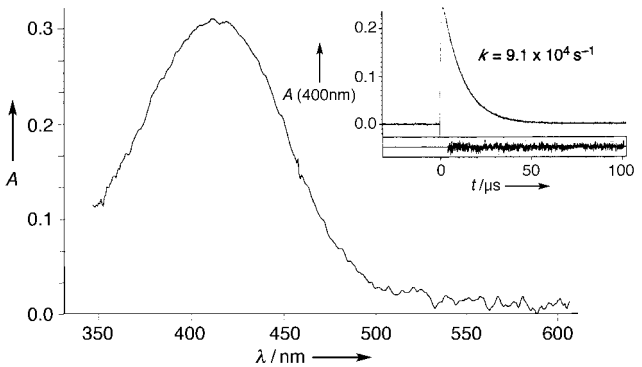


Figure 3. Spectrographic trace of the transient absorption (1 μs delay) after 308 nm laser flash photolysis of **1** (0.3 mM **1** in 0.1 mM phosphate buffer, pH 6.45, 20 °C). Insert: Kinetic trace of the transient absorbance changes at 400 nm.

at 365 nm with that of 1-(2-nitrophenyl)ethyl carbamylcholine ($\Phi = 0.29$),[9] are sufficient for the envisioned applications.

Thus, the arsonium compounds **1**–**3** are heavy-atom analogues of caged cholinergic ligands, and they possess biochemical and photochemical properties very similar to those of their N-homologues. The structural similarities between **2** and its N-homologue, and the strong X-ray diffracting effect of arsenic, confer to the As probes the desired properties for crystallographic studies on cholinesterases. Most importantly, **1** and **3** show excellent kinetic properties and quantum yields for the photorelease of arsenocholine and arsenocarbamylcholine, respectively. Thus they hold much promise in providing a decisive contribution to future time-resolved crystallographic studies on the catalytic mechanism of cholinesterases, and they might also be applicable to other systems.

Experimental Section

All the details for the photochemical reactions and the inhibition of ligands on cholinesterases can be found in references [8,10]. Crystallographic data (excluding structure factors) for the structures (**2** ($C_{12}H_{19}NO_3AsI$) and its *N*-homologue ($C_{12}H_{19}N_2O_3I$)) reported in this paper have been deposited with the Cambridge Crystallographic Data Center as supplementary publication nos CCDC-102120 and CCDC-102121, respectively. Copies of the data can be obtained free of charge on application to CCDC, 12 Union Road, Cambridge CB2 1EZ, UK (fax: (+44) 1223-336-033; e-mail: deposit@ccdc.cam.ac.uk).

1: White powder; ^{1}H NMR (200 MHz, $CDCl_3$): $\delta = 1.56$ (d, 3H, $J = 6.2$ Hz), 2.26 (s, 9H), 3.09–3.17 (m, 2H), 3.70–3.86 (m, 2H), 5.06 (q, 1H, $J =$ 6.3 Hz), 7.44–7.52 (m, 1H), 7.60–7.76 (m, 2H), 7.79 (dd, 1H, $J = 1.1$, 8.0 Hz); MS (positive-ion FAB): *m/z* (%): 313.8 (100) [$C_{13}H_{21}NO_3As$]; elemental analysis calcd for $C_{13}H_{21}NO_3AsI$: C 35.40, H 4.80, N 3.18, As 16.99; found: C 35.47, H 4.76, N 3.09, As 17.03.

2: White crystals; ^{1}H NMR (200 MHz, $CDCl_3$): $\delta = 2.19$ (s, 9H), 3.22 (t, 2H, $J = 5.8$ Hz), 4.05 (t, 2H, $J = 5.8$ Hz), 4.90 (s, 2H), 7.52–7.69 (m, 3H), 8.00 (dd, 1H, $J = 1.3$, 7.8 Hz); MS (positive-ion FAB): *m/z* (%): 299.8 (100) [$C_{12}H_{19}NO_3As$].

3: Very hygroscopic white powders; ^{1}H NMR (200 MHz, CD_3CN): $\delta = 1.56$ (d, 3H, $J = 6.9$ Hz), 1.91 (s, 9H), 2.67 (t, 2H, $J = 5.8$ Hz), 4.33 (t, 2H, $J =$ 5.8 Hz), 5.10–5.21 (m, 1H), 6.77 (s br, 1H), 7.44–7.53 (m, 1H), 7.71–7.76 (m, 2H), 7.85 (d, 1H, $J = 8.8$ Hz); MS (positive-ion FAB): *m/z* (%): 356.8 (100) [$C_{14}H_{22}N_2O_4As$]; elemental analysis calcd for $C_{14}H_{22}N_2O_4AsI$: C 34.73, H 4.58, N 5.79, As 15.48; found: C 34.86, H 4.62, N 5.88, As 15.45.

Received: April 27, 1998 [Z 11782 IE]
German version: *Angew. Chem.* **1998**, *110*, 2838–2840

Keywords: arsenic · bioorganic chemistry · enzyme inhibitors · photochemistry

[1] T. L. Blundell, L. N. Johnson, *Protein Crystallography*, Academic Press, London, **1976**.
[2] S. R. Adams, R. Y. Tsien, *Annu. Rev. Physiol.* **1993**, *55*, 755–784; G. P. Hess, *Biochemistry* **1993**, *32*, 989–1000.
[3] D. W. J. Cruickshank, J. R. Helliwell, L. N. Johnson, *Time-Resolved Macromolecular Crystallography*, Oxford University Press, Oxford, **1992**, and references therein.
[4] A. Chatonnet, O. Lockridge, *Biochem. J.* **1989**, *260*, 625–634.
[5] J. L. Sussman, M. Harel, F. Frolow, C. Oefner, A. Goldman, L. Toker, I. Silman, *Science* **1991**, *253*, 872–879.
[6] M. Harel, I. Schalk, L. Ehret-Sabatier, F. Bouet, M. Goeldner, C. Hirth, P. H. Axelsen, I. Silman, J. L. Sussman, *Proc. Natl. Acad. Sci. USA* **1993**, *90*, 9031–9035; M. Harel, G. J. Kleywegt, R. B. G. Ravelli, I. Silman, J. L. Sussmann, *Structure* **1995**, *3*, 1355–1366; Y. Bourne, P. Taylor, P. Marchot, *Cell* **1995**, *83*, 503–512; M. Harel, D. M. Quinn, H. K. Nair, I. Silman, J. L. Sussmann, *J. Am. Chem. Soc.* **1996**, *118*, 2340–2346; M. L. Raves, M. Harel, Y.-P. Pang, I. Silman, A. P. Kozikowski, J. L. Sussmann, *Nature Struct. Biol.* **1997**, *4*, 57–63.
[7] D. R. Ripoll, C. H. Faerman, P. H. Axelsen, I. Silman, J. L. Sussman, *Proc. Natl. Acad. Sci. USA* **1993**, *90*, 5128–5132; M. K. Gilson, T. P. Straatsma, J. A. McCammon, D. R. Ripoll, C. H. Faerman, P. H. Axelsen, I. Silman, J. L. Sussman, *Science* **1994**, *263*, 1276–1278; A. Shafferman, A. Ordentlich, D. Barak, C. Kronman, R. Ber, T. Bino, N. Ariel, R. Osman, B. Velan, *EMBO J.* **1994**, *13*, 3448–3455.
[8] L. Peng, M. Goeldner, *J. Org. Chem.* **1996**, *61*, 185–191.
[9] a) T. Milburn, N. Matsubara, A. P. Billington, J. B. Udgaonkar, J. W. Walker, B. K. Carpenter, W. W. Webb, J. Marque, W. Denk, J. A. McCray, G. P. Hess, *Biochemistry* **1989**, *28*, 49–55; b) J. W. Walker, J. A. McCray, G. P. Hess, *Biochemistry* **1986**, *25*, 1799–1805.
[10] L. Peng, J. Wirz, M. Goeldner, *Angew. Chem.* **1997**, *109*, 420–422; *Angew. Chem. Int. Ed. Engl.* **1997**, *36*, 398–400; L. Peng, J. Wirz, M. Goeldner, *Tetrahedron Lett.* **1997**, *38*, 2961–2964.
[11] L. Peng, M. Goeldner, *Methods Enzymol.* **1998**, *291*, 265–278; L. Peng, I. Silman, J. L. Sussman, M. Goeldner, *Biochemistry* **1996**, *35*, 10854–10861.
[12] R. B. G. Ravelli, M. L. Raves, Z. Ren, D. Bourgeois, M. Roth, J. Kroon, I. Silman, J. L. Sussman, *Acta Crystallogr. Sect. D* **1998**, in press.
[13] J. R. Cannon, J. S. Edmonds, K. A. Francesconi, C. L. Raston, J. B. Saunders, B. W. Skelton, A. H. White, *Aust. J. Chem.* **1981**, *34*, 787–798, and references therein.
[14] A. Kostick, A. S. Secco, M. Billinghurst, D. Abrams, S. Cantor, *Acta Crystallogr. Sect. C* **1989**, *45*, 1306–1309.
[15] B. Hedlund, H. Norin, A. Christakopoulos, P. Alberts, T. Bartfai, *J. Neurochem.* **1982**, *39*, 871–873.
[16] J. W. Walker, G. P. Reid, J. A. McCray, D. R. Trentham, *J. Am. Chem. Soc.* **1988**, *110*, 7170–7177; A. Barth, K. Hauser, W. Mäntele, J. E. T. Corrie, D. R. Trentham, *J. Am. Chem. Soc.* **1995**, *117*, 10311–10316.

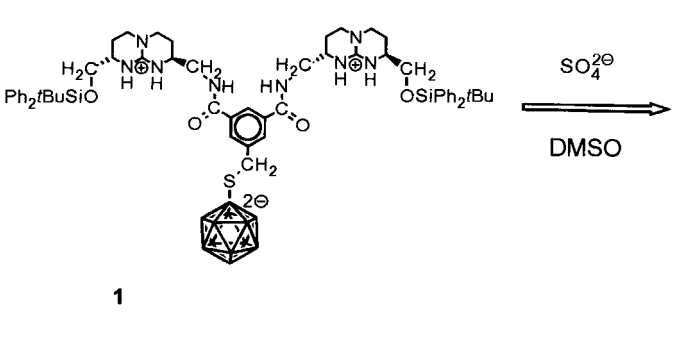
 © WILEY-VCH Verlag GmbH, D-69451 Weinheim, 1998 1433-7851/98/3719-2693 $ 17.50+.50/0

The Binding of Sulfate Anions by Guanidinium Receptors is Entropy-Driven**

Michael Berger and Franz P. Schmidtchen*

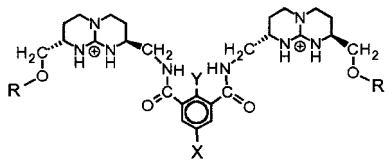
There is good reason to attribute the binding of guests by host molecules to functional and geometrical complementarity, and to the preorganization of binding substructures in the artificial receptor.[1] This assumption emphasizes the importance of mutual enthalpic interactions, but disregards entropic contributions that have been found in many cases to govern the host–guest binding event in solution.[2–4] The rational design of abiotic host compounds must therefore address the fundamental contributions to the association free energy separately, and requires in the first place the dissection of its constituent enthalpy and entropy parts by experimentation in order to learn about the options available to avoid total enthalpy–entropy compensation.[5] This phenomenon often disguises and eventually prevents any visible progress in host design.

A study of the binding of the sulfate anion to abiotic guanidinium receptors could provide a good starting point. The ditopic host **1** binds sulfate anions even in DMSO,[6] and congener **2** was able to extract this guest from very dilute (10^{-4} M) aqueous solutions into chloroform with unprecedented efficiency [99.8%; Eq. (1)].[7] An NMR titration study that



1

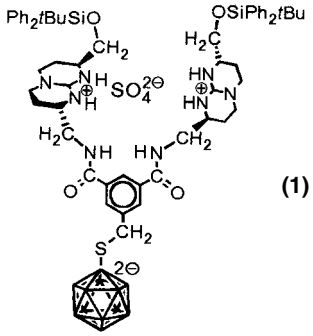
employed the analogous host **2** only gave a lower limit for the association constant (K_a for **2** in $CD_3OD > 10^6\,M^{-1}$), while host **4** in a similar investigation in aqueous DMSO (DMSO/H_2O, 1/1) revealed complexation of sulfate ions with $K_a = 290\,M^{-1}$. In both cases the complexation-induced shifts (CIS) of the aromatic ^1H signals were monitored by NMR spectroscopy, since the more sensitive NH signals experienced sulfate-catalyzed proton exchange that rendered them invisible on the NMR time scale. The splitting of the K_a-related free energies of association $\Delta G_a^\ominus$ into its components $\Delta H_a^\ominus$ and $\Delta S_a^\ominus$ by NMR methods requires rather laborious and imprecise van't Hoff analysis of the binding data. A much more



	X	Y	R	counter-ion
1	$CH_2SB_{12}H_{11}^{2\ominus}$	H	$SitBuPh_2$	—
2	$OC_{16}H_{33}$	H	$SitBuPh_2$	$Cl^\ominus$
3	$OCH_2C_6H_5$	H	$SitBuPh_2$	$Cl^\ominus$
4	CH_2OH	H	H	$Cl^\ominus$
5	OH	H	$SitBuPh_2$	$Cl^\ominus$
6	Br	F	H	$ClO_4^\ominus$

accurate and faster method is isothermal titration calorimetry (ITC),[8] which gives $\Delta H_a^\ominus$ directly as a primary parameter of measurement; $\Delta G_a^\ominus$ and the host–guest stoichiometry n are estimated from titration curve fitting. The reaction entropy $\Delta S_a^\ominus$ may then be readily calculated from the Gibbs–Helmholtz equation.

A typical example of the quality of the data obtained is shown in Figure 1 for the primary heat pulse for the binding of sulfate ions by host **3** in methanol.[9] By integration of each pulse at each titration step the titration curve can be derived and analyzed through curve-fitting methods.[10]



(1)

Guest complexation is strongly endothermic and gives $\Delta H_a^\ominus = +7.7$ kcal mol^{-1}. The fitting process, however, reveals $K_a = 6.8 \times 10^6\,M^{-1}$ and $n = 1.03$ as an independent fit parameter. Thus, at room temperature associa-

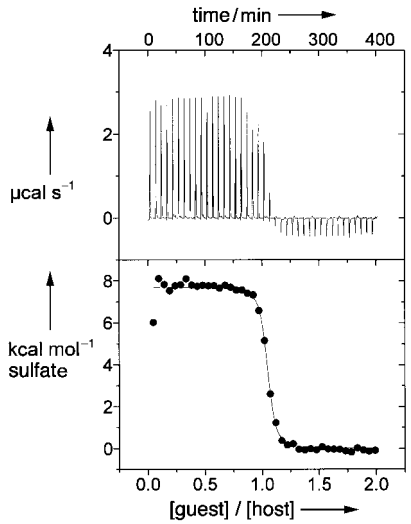


Figure 1. ITC titration of host **3** (0.137 mM) with tetramethylammonium sulfate (2.865 mM) in methanol at 303 K. $\Delta H^\ominus = +7.7$ kcal mol^{-1}; $K_a = 6.8 \cdot 10^6\,M^{-1}$; $n = 1.03$;

[*] Prof. Dr. F. P. Schmidtchen, Dipl.-Chem. M. Berger
Institut für Organische Chemie und Biochemie
der Technische Universität München
Lichtenbergstrasse 4, D-85747 Garching (Germany)
Fax: (+49) 89-289-13345
E-mail: fpschmid@nucleus.org.chemie.tu-muenchen.de

[**] This work was supported by the Deutsche Forschungsgemeinschaft and the Fonds der Chemischen Industrie.

 © WILEY-VCH Verlag GmbH, D-69451 Weinheim, 1998 1433-7851/98/3719-2694 $ 17.50+.50/0

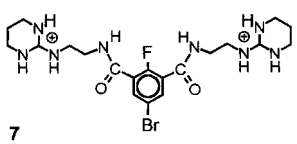
tion is strongly entropy-driven with $T\Delta S^{\circ}_{a}$ by far outweighing the unfavorable ΔH°_{a} value (Table 1). Host **5**, which lacks the benzyl ether functionality of **3**, shows a very similar enthalpy and entropy of association, which indicates that the third aromatic substituent is not involved in guest binding. The

Table 1. Binding of sulfate ions with guanidinium hosts at 303 K.[a]

Host	n	ΔH°_{a} [kcal mol^{-1}]	K_a [M^{-1}]	ΔG°_{a} [kcal mol^{-1}]	$T\Delta S^{\circ}_{a}$ [kcal mol^{-1}]
1[b]	0.47	+1.50	284	−3.40	+4.90
3	1.03	+7.71	6.8×10^{6}	−9.47	+17.18
5	0.95	+7.07	4.9×10^{6}	−9.27	+16.34
6	1.12	+7.28	4.4×10^{5}	−7.82	+15.10
7	0.94	+5.46	2.7×10^{6}	−8.91	+14.37
9	0.54	+3.76	313	−3.43	+7.22
10	0.46	+2.76	553	−3.80	+6.56

[a] Sulfate: bis(tetramethylammonium) sulfate, solvent: methanol, unless otherwise stated. [b] Bis(tetraethylammonium) sulfate, DMSO.

introduction of a fluorine substituent in the 2-position of the aromatic core together with the removal of the silyl ether functionalities to give the free hydroxyl groups in **6** yields an inferior host for sulfate binding. Though enthalpy appears unaffected, which suggests an almost identical guest-binding mode in the receptors discussed so far, the entropy is diminished. This reflects some solvophobic interactions between the silyl moieties in hosts **2**, **3**, and **5** on binding, which is not available in **6**. The hydroxyl groups apparently do not participate in the complexation of sulfate ions in methanol. The relief of some of the folding strain on going from **6** to the monocyclic guanidinium receptor **7** seemingly allows a better mutual fit, which is expressed as a more negative (less positive) ΔH°_{a} value, whereas ΔS°_{a} is hardly affected. The quite respectable association constant in methanol (K_a (**7** in CH_3OH) $= 2.7\cdot10^{6}$ M^{-1}) was initially believed to also allow the complexation of sulfate ions with this host in water. However, the heat effects turned out to be vanishingly small, and we could not derive a titration curve. ^{19}F NMR spectroscopy proved helpful, and the titration of **7** with sulfate ions in D_2O gave $K_a = 84$ M^{-1} at 298 K.

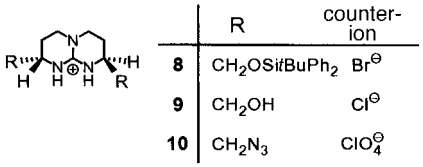


7

Since both the guanidinium group and the sulfate anions are solvated very effectively in protic solvents, the positive ΔH°_{a} value observed reflects the endothermic reorganization of the solvent shell upon complexation. The complex is less solvated than the sum of its free components, and the release of solvent molecules thus leads to the entropic overcompensation of the unfavorable positive ΔH°_{a} of desolvation. This effect is smaller in the more hydrophilic host **6** and results in a smaller entropy contribution and weaker binding.

The low solubility of the electroneutral zwitterionic host **1** in protic solvents thwarted the direct comparison to the cationic guanidinium receptors. Titration in DMSO, however, uncovered the unexpected host–guest stoichiometry of 0.5. As host **1** dimerizes under these conditions[6] this result is compatible with the sulfate ions binding to the host dimer without disrupting its aggregate structure.[11] Because this binding event most likely displaces one weekly bound anionic borane cluster rather than strongly bound solvent molecules from the first guanidinium binding site in the yin–yang dimer,[6] the enthalpy and entropy of guest association are more negative than found with cationic hosts. Nevertheless, complex formation remains entropy-driven even in this case.

In an effort to compare and quantify the virtue of combining two guanidinium groups in a ditopic host, the monotopic parent bicyclic guanidines **8** and **9** were tested in



DMSO. Neither produced a heat effect on titration with sulfate ions, which suggested a total lack of complexation and underlined the benefit of the covalent linkage in the ditopic hosts. In water the bishydroxyl anchor group **9** does not show any enthalpic interaction with sulfate ions either, but in methanol some endothermic association is observed ($\Delta H^{\circ}_{a} = +3.76$ kcal mol^{-1}) with $K_a = 313$ M^{-1}. The replacement of the hydroxyl groups by non-hydrogen-bonding azido substituents roughly doubles K_a (553 M^{-1}), primarily because of a favorable enthalpic effect. However, the binding affinity of the monotopic guanidinium anchor groups are still four orders of magnitude lower than that of their ditopic counterparts. The calorimetric results of the binding of sulfate ions to guanidinium hosts attest to the dominating role of solvation and calls for solvation design as a profitable way to improve guest-binding affinity and selectivity.

Received: May 6, 1998 [Z11824IE]
German version: *Angew. Chem.* **1998**, *110*, 2840–2842

Keywords: calorimetry · guanidine · host–guest chemistry · thermodynamics

[1] a) D. J. Cram, *Angew.Chem.* **1988**, *100*, 1041–1052; *Angew. Chem. Int. Engl.* **1988**, *27*, 1009–1020; b) F. P. Schmidtchen, M. Berger, *Chem. Rev.* **1997**, *97*, 1609–1646.
[2] R. Meissner, X. Garcias, S. Mecozzi, J. Rebek, Jr., *J. Am. Chem. Soc.* **1997**, *119*, 77–85.
[3] W. Peschke, F. P. Schmidtchen, *Tetrahedron Lett.* **1995**, *36*, 5155–5158.
[4] D. J. Cram, H.-J. Choi, J. A. Bryant, C. B. Knobler, *J. Am. Chem. Soc.***1992**, *114*, 7748–7765.
[5] D. H. Williams, M. S. Westwell, *Chem. Soc. Rev.* **1998**, 57–63.
[6] M. Berger, F. P. Schmidtchen, *J. Am. Chem. Soc.* **1996**, *118*, 8947–8948.
[7] H. Stephan, K. Gloe, P. Schiessl, F. P. Schmidtchen, *Supramolec. Chem.* **1995**, *5*, 273–280.
[8] a) I. Wadsö, *Chem. Soc. Rev.* **1997**, 79–86; b) J. E. Ladbury, B. Z. Chowdhry, *Chem. Biol.* **1996**, *3*, 791–801.
[9] Details about the syntheses of the hosts will be published in a full paper.
[10] The measurements were performed with a MCS-ITC instrument (MicroCal). In all cases, the sulfate solution was injected into the cell containing the host. The heat of dilution was corrected for by injecting

 © WILEY-VCH Verlag GmbH, D-69451 Weinheim, 1998 1433-7851/98/3719-2695 $ 17.50+.50/0

the sulfate solution into neat solvent and subtracting this data from that of the host–guest titration. The data was analyzed and fit by the Origin software (MicroCal).[12]

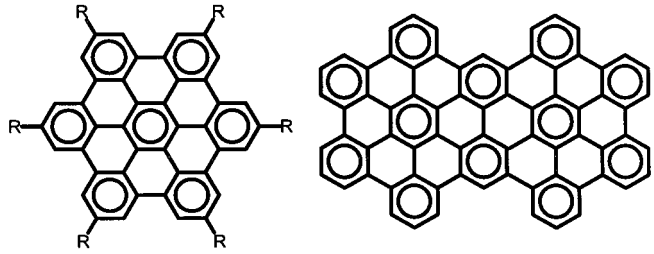
[11] Close inspection of the multidimensional error hypersurface of the NMR binding data in the reaction of **1** and sulfate ions revealed no minimum that would justify accounting for a 1:2 host–guest complex.[6] Recalculation of the primary data with host dimerization and 1:1 host–guest complexation incorporated gave $K_a = 680\ M^{-1}$, which is in reasonable agreement with the present determination conducted at a slightly higher temperature.

[12] T. Wiseman, S. Williston, L.-N. Lin, *Anal. Biochem.* **1989**, *179*, 131–137.

A Soluble C_{60} Graphite Segment**

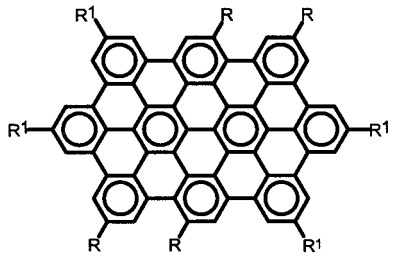
Vivekanantan S. Iyer, Kimihiro Yoshimura, Volker Enkelmann, Rebekka Epsch, Jürgen P. Rabe, and Klaus Müllen*

We recently described an efficient cycloaddition-cyclodehydrogenation route to obtain very large polycyclic aromatic hydrocarbons (PAHs) such as **1a** (C_{42}) and **2** (C_{72}).[1–3] Owing to the extremely low solubility of the parent compounds, the soluble hexa-*n*-alkyl derivatives **1b** were synthesized in order to perform complete spectroscopic characterization of these compounds. Discotic meso phases with stacked discs were thereby observed. Physisorption of **1b** onto substrate surfaces gave rise to the formation of monomolecular adsorbate layers, which were characterized by scanning tunneling microscopy (STM).[1–3]



1a: R = H
1b: R = *n*-alkyl

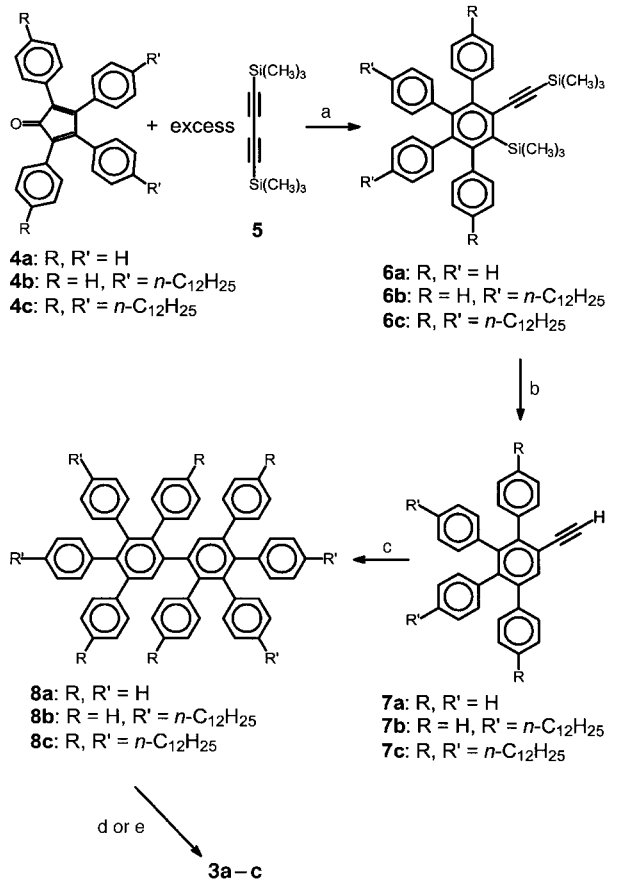
2



3a: R, R^1 = H
3b: R = H, R^1 = *n*-$C_{12}H_{25}$
3c: R, R^1 = *n*-$C_{12}H_{25}$

A comparable protocol is impossible with larger discs (e.g. C_{72}, C_{78}, C_{96}, C_{132}) since the synthetic strategies are not readily transferable to the respective *n*-alkyl derivatives. We describe here the remarkable C_{60} hydrocarbon **3a**,[4, 5] which, as a homologue of **1a**, is predicted to be the most thermodynamically stable of the $C_{60}H_{22}$ PAH isomers.[6] The synthesis of **3a** in gram or even decagram quantities is surprisingly straightforward. More importantly, however, soluble tetra- and octa-*n*-alkyl derivatives (**3b** and **3c**, respectively) of this large disk can be prepared, and the formation of monolayers from solution is possible even with discs of that size. This could prove to be a central step for the electronic characterization of molecular graphite models.

Following the construction principle reported by our group for larger PAHs, an oligophenyl precursor of **3** is available by a twofold Diels–Alder reaction between butadiyne and tetraphenylcyclopentadienone (**4a**, Scheme 1). The reaction



Scheme 1. a) **4a**, **4b**, or **4c** (1 equiv), 250 °C, Ph_2O, 3–6 h, ca. 100%; b) $nBu_4N^+F^-$ (10 equiv), THF, **6a**: 85%, **6b**: 86%, **6c**: 88%; c) **4a**, **4b**, or **4c** (1.1 equiv), 250 °C, Ph_2O, 3–6 h, ca. 100%; d) $Cu(OSO_2CF_3)_2$ (60 equiv), $AlCl_3$ (60 equiv), 25 °C, CS_2, **3a**: >90%; e) $FeCl_3$, CH_3NO_2, CH_2Cl_2, Ar, 15–30 min, **1a**: >80%, **3b**: 75%.

of **4a** with a large excess of 1,4 bis(trimethylsilyl)butadiyne (**5**)—both starting materials are commercially available—resulted in the formation of **6a** in nearly quantitative yield.

[*] Prof. Dr. K. Müllen, Dr. V. S. Iyer, K. Yoshimura, Priv.-Doz. Dr. V. Enkelmann
Max-Planck-Institut für Polymerforschung
Ackermannweg 10, D-55128 Mainz (Germany)
Fax: (+49) 6131-379-350
E-mail: muellen@mpip-mainz.mpg.de
R. Epsch, Prof. Dr. J. P. Rabe
Institut für Physik der Humboldt-Universität, Berlin (Germany)

[**] This work was supported by the Volkswagen-Stiftung, the Bundesministerium für Bildung, Wissenschaft, Forschung und Technologie, and the Commission of the European Union. V.S.I. thanks the Max-Planck-Gesellschaft for a scholarship, and K.Y. thanks Canon Inc., Tokyo, for the sabbatical and the financial support of his stay.

 © WILEY-VCH Verlag GmbH, D-69451 Weinheim, 1998 1433-7851/98/3719-2696 $ 17.50+.50/0

Monoadduct **6a** was desilylated with an excess of tetrabutylammonium fluoride to afford **7a** (85%), which subsequently underwent another Diels–Alder reaction with **4a** followed by loss of the CO group to give **8a** (99%). The tetra-*n*-dodecyl (**8b**) and octa-*n*-dodecyl derivatives (**8c**) were prepared analogously from **8a** and the corresponding substituted cyclopentadienones[7] **4b** and **4c** (Scheme 1 and Table 1). All

Table 1. Selected spectroscopic data[a] of **3a**, **3c**, and **8a**.

3a: MS (LD-TOF): *m*/*z* (%): 746 (0.6), 745 (5), 744 (20), 743 (65), 742 (100) [M^+] (calcd for $C_{60}H_{22}$: 746.0 (0.7), 745.18 (4.7), 744.17 (22), 743.17 (67), 742.17 (100)); UV/Vis (1,1,2,2-tetrachloroethane): $\lambda_{max} = 290$, 425, 450 (shoulder), 550, 590 (shoulder)

3c: MS (MALDI-TOF): *m*/*z* (%): 2095 (0.5), 2094 (2), 2093 (8), 2092 (22), 2091 (50), 2090 (88), 2089 (100), 2088 (55) [M^+] (calcd for $C_{156}H_{214}$: 2094.69 (0.5), 2093.69 (2.2), 2092.69 (7.6), 2091.68 (22.2), 2090.68 (51.1), 2089.68 (87.8), 2088.67 (100), 2087.67 (56.6)); ^{1}H NMR (500 MHz, [D$_4$]1,2-dichlorobenzene, 170 °C): $\delta = 9.84$ (s, 2H), 9.55 (s, 2H), 9.42 (m_c, 10H), 4.44 (m_c, 4H), 3.75 (m_c, 12H), 2.73 (m_c, 4H), 2.57 (m_c, 12H), 2.12–1.10 (m, 168H); UV/Vis ($CHCl_3$): λ_{max} (ε) = 276 (50800), 290 (45600, shoulder), 410 (67700), 450 (28200, shoulder), 482 (12900), 510 (6700)

8a: MS (FD, 8 kV): *m*/*z* (%): 762.1 (100) [M^+] (calcd for $C_{60}H_{42}$: 762.3); ^{13}C NMR (125 MHz, [D$_2$]1,1,2,2-tetrachloroethane, 140 °C): $\delta = 142.28$, 141.57, 140.79, 140.42, 140.16, 140.03, 139.74, 139.17, 132.88, 131.77, 130.12, 127.44, 126.77, 126.52, 126.08, 125.61, 125.46, 125.19

[a] All LD-TOF and MALDI-TOF mass spectra were calibrated with samples of C_{60} and C_{70} fullerenes. The matrix for the MALDI-TOF measurements was 9-nitroanthracene. FD = field desorption, MALDI = matrix-assisted laser desorption/ionization.

oligophenyls **8** are readily soluble in organic solvents. The crystal structure of **8a** (Figure 1) clearly shows that the phenyl substituents are strongly twisted with respect to the central biphenyl unit (twisting angle = 61°). Furthermore, the outer phenyl rings are in close proximity, which is necessary for the cyclodehydrogenation leading to the planar structure **3a**.[8]

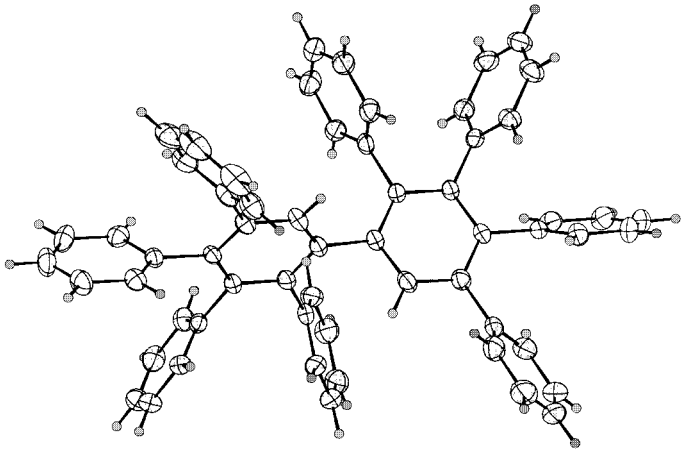


Figure 1. Crystal structure of **8a**.

The cyclodehydrogenation of **8a** with copper(II) trifluoromethanesulfonate and aluminum(III) chloride in carbon disulfide proceeded smoothly and led to **3a** (>90%). High-resolution laser desorption time-of-flight mass spectrometry (LD-TOF) of **3a** (*m*/*z* = 742, see Table 1 for isotope distribution) was performed and proved the loss of exactly 20 hydrogen atoms. Similar to other large PAHs, the crude burgundy sample of **3a** does not yield a defined X-ray powder diffractogram, which suggests the amorphous character of the solid. Quick sublimation of the crude product under ultrahigh vacuum at 680 °C yielded pure **3a** as a light orange powder[9] which was sufficiently soluble in 1,1,2,2-tetrachloroethane, and a UV/Vis spectrum was obtained (Table 1).

Mass spectrometric studies of **3a** at higher laser intensities revealed a fragment ion of the formula $C_{54}H_{22}^+$ with a relative intensity (based on [**3a**]$^+$) of up to 45%. The fact that no charged C_6 or C_3 fragments could be observed suggests that **3a** or [**3a**]$^+$ photodegraded to $C_{54}H_{22}^+$ and neutral fragments.[10]

Attempts to perform the analogous cyclodehydrogenation of **8b** resulted in unidentified product mixtures because of the inherently high acidity of the reaction mixture. The use of iron(III) chloride allowed the cyclodehydrogenation to occur under significantly milder conditions and without side reactions (such as alkyl group migrations or chlorinations). Hydrogen chloride was continuously removed from the reaction mixture by a steady flow of argon. Under these conditions, **3b** was obtained from **8b** in 75% yield. The high-resolution mass spectrum of **3b** is shown in Figure 2.

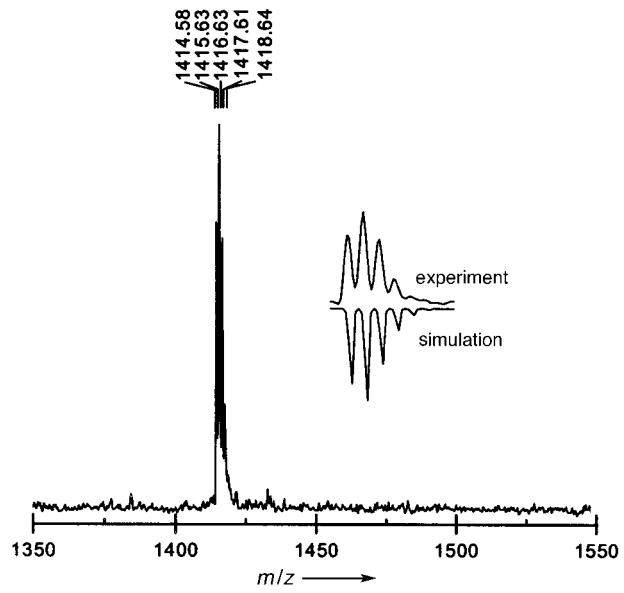


Figure 2. MALDI-TOF mass spectrum of **3b** (molecular-ion area). The insert compares the experimental and the calculated M^+ signal of **3b**.

To further enhance the solubility of **3**, it was intended to synthesize the octa-*n*-alkyl compound **3c**. However, the method successful for the synthesis of **3b** yielded only partially cyclodehydrogenated as well as partially cyclized, chlorinated products rather than **3c**.[11] To our surprise, experiments to dehalogenate the product mixture with potassium in tetrahydrofuran led to completely cyclized octa-*n*-alkyl C_{60} compound **3c** (60%). UV/Vis, mass, and ^{1}H NMR spectra were obtained for the highly soluble **3c** (Table 1, Figure 3a, b). The spatially most confined aryl protons (H_a) in the bay region show a singlet at $\delta = 9$, and the H_b protons show a singlet at $\delta = 9.55$. The broadening of

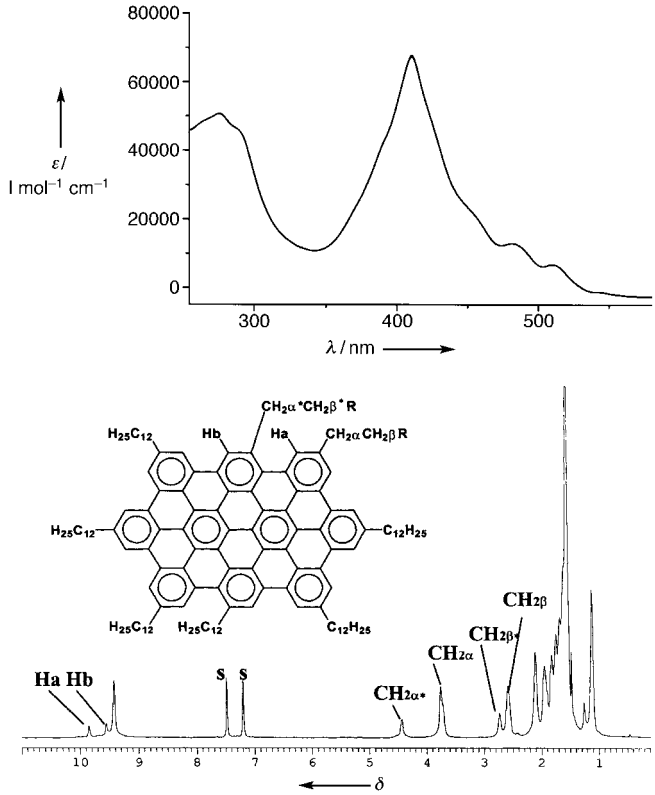


Figure 3. a) UV/Vis spectrum of a solution (1.4×10^{-5} M) of **3c** in chloroform. b) ^{1}H NMR spectrum of **3c** (2 mg) in [D_4]1,2-dichlorobenzene (1.5 mL) at 170 °C.

the signal presumably arises from aggregates of the large molecular discs that may exist even at the high temperatures used to record the spectrum. This clearly demonstrates that the characterization of very large PAHs (size in the nanometer range) reaches the limits of the standard methods in organic chemistry.

As a result of the improved solubility of **3b** and **3c**, it was possible for the first time to prepare highly ordered monolayers (2D crystal) of PAHs larger than **1**. Figures 4a and 5a show STM images of monolayers from **3b** and **3c** which were obtained in situ at the interface between solutions in 1,2,4-trichlorobenzene and the basal surface of graphite. The positions of the aromatic discs correspond to areas of high tunneling currents.[12, 13] The alkyl chains could not be resolved, which is an indication of high conformational mobility of the side chains at room temperature. Both **3b** and **3c** show a double-row structure; however, the orientation of the discs of **3b** alternates from row to row (fishbone pattern), whereas the orientation of **3c** is maintained within the rows and only the distances between them alternate.[14] The parameters of the unit cell of **3b**[15] correspond to a surface area which is in close agreement to the value calculated from the van der Waals circumference of two flat molecules per unit cell. In contrast, the experimentally determined value for the surface area of **3c** is larger than that theoretically calculated, which means that the molecular packing also contains free surface areas. Figures 4b and 5b illustrate packing models, for which only one of the many comparable conformations for the alkyl chains is shown.

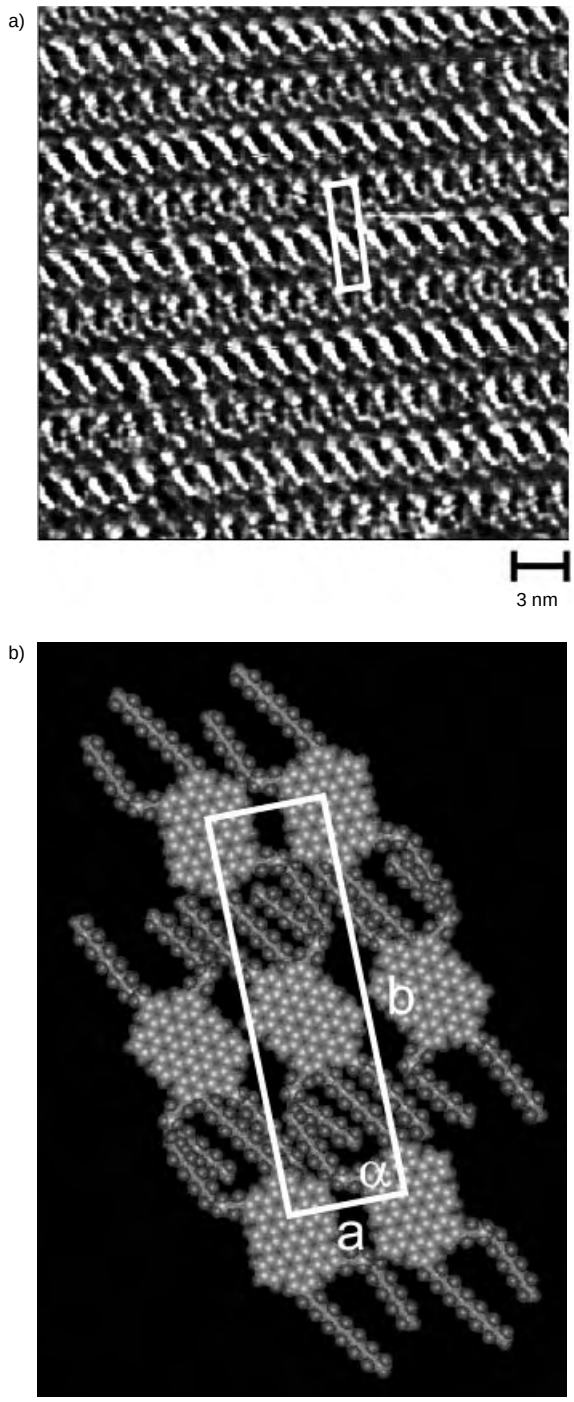


Figure 4. STM image (a) and model (b) of **3b** on the basal surface of graphite.

It is remarkable that the submolecularly resolved pictures of **3c** show three similarly directed strips with a distance of 0.4 ± 0.02 nm over each molecule. The latter do not result from the graphite lattice of the support layer since they are seen only over the aromatic discs and not in the entire picture. Furthermore, the distance of 0.246 nm[16] between equivalent graphite atoms is significantly lower than the distance between the individual strips. This value, however, is in good agreement with the distance between the benzene subunits of

 © WILEY-VCH Verlag GmbH, D-69451 Weinheim, 1998 1433-7851/98/3719-2698 $ 17.50+.50/0

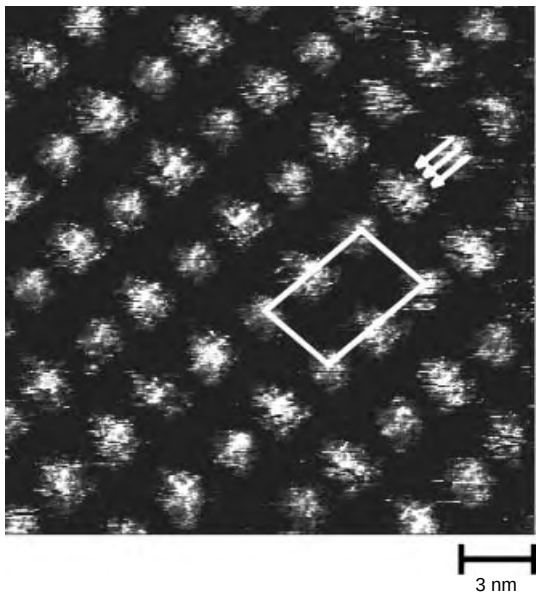


Figure 5. STM image (a) and model (b) of **3c** on the basal surface of graphite.

the aromatic discs (0.38 nm). In addition, this distance also occurs in the pattern of the electronic state density of the frontier orbitals of the free molecules, which are believed to create the contrast between molecular adsorbates on graphite.[13, 17] Therefore, one can assign the submolecular contrast to the local electronic state densities of the conjugated systems. Based upon this, it is possible to determine the orientation of the aromatic discs on the substrate.

To date, it is unclear whether a transition to a graphite-like electronic behavior can be observed with increasing size of the PAH discs.

Received: April 21, 1998 [Z 11760 IE]
German version: *Angew. Chem.* **1998**, *110*, 2843 – 2846

Keywords: cyclodehydrogenations · graphite segments · nanostructures · polycycles · scanning tunneling microscopy

[1] V. S. Iyer, M. Wehmeier, J. D. Brand, M. A. Keegstra, K. Müllen, *Angew. Chem.* **1997**, *109*, 1675 – 1679; *Angew. Chem. Int. Ed. Engl.* **1997**, *36*, 1604 – 1607.

[2] M. Müller, V. S. Iyer, C. Kübel, V. Enkelmann, K. Müllen, *Angew. Chem.* **1997**, *109*, 1679 – 1682; *Angew. Chem. Int. Ed. Engl.* **1997**, *36*, 1607 – 1610.

[3] A. Stabel, P. Herwig, K. Müllen, J. P. Rabe, *Angew. Chem.* **1995**, *107*, 1768 – 1770; *Angew. Chem. Int. Ed. Engl.* **1995**, *34*, 1609 – 1611.

[4] E. Clar, *The Aromatic Sextet*, Wiley, London, **1972**.

[5] A graphite disc was originally believed to be a plausible structure of [60]fullerene. According to this model, it was calculated that such a stable structure would require 20 or more hydrogen atoms in the periphery: H. Kroto, *Angew. Chem.* **1997**, *109*, 1648 – 1664; *Angew. Chem. Int. Ed. Engl.* **1997**, *36*, 1578 – 1593.

[6] J. R. Dias, *J. Chem. Inf. Comput. Sci.* **1991**, *31*, 89 – 96.

[7] A general procedure for the synthesis of substituted cyclopentadienone derivatives has been reported.[1]

[8] The crystal structure analysis was performed on a Nonius-CAD4 diffractometer with graphite-monochromated $Cu_{K\alpha}$ radiation ($\lambda = 1.5418$ Å) at room temperature. The lattice parameters were determined by least-squares analysis from the angles of 25 reflections ($\theta >$ 20 °C). The intensities were measured with $\theta/2\theta$ scans. The structures were solved with direct methods, and the C atoms were refined with anisotropic directional parameters, the H atoms were considered to be in a riding model. Empirical absorption correction; programs used: Molen, SIR92, and CRYSTALS. **6**: orthorhombic, *Fdd*2, $a = 6.5306(4)$, $b = 30.765(2)$, $c = 42.623(1)$ Å, $V = 8563.4(9)$ Å^3, $Z = 8$, $\rho_{calcd} = 1.183$ g cm^{-3}, $\mu = 4.74$ cm^{-1}; of 2079 reflections, 1579 were observed ($I > 3\sigma(I)$), $R = 0.042$, $R_w = 0.047$. Further details on the crystal structure analysis can be obtained from the Fachinformationszentrum Karlsruhe, D-76344 Eggenstein-Leopoldshafen, Germany (fax: (+49) 7247-808-666; e-mail: crysdata@fiz-karlsruhe.de), on quoting the depository number CSD-391072.

[9] We thank Professor Dr. N. Karl (Universität Stuttgart) for the sublimation experiments.

[10] The time delay between laser desorption and detection is on the order of microseconds. For structure elucidation of small carbon clusters, see for example H. J. Hwang, A. Van Orden, K. Tanaka, E. W. Kuo, J. R. Heath, R. J. Saykally, *Mol. Phys.* **1993**, *79*, 769 – 776, and references therein.

[11] The partial cyclodehydrogenation could be a result of the strain caused by the alkyl substituents in the bay region. We have observed this phenomenon in previous cyclodehydrogenations.[2]

[12] D. P. E. Smith, H. Hörber, C. Gerber, G. Binnig, *Science* **1989**, *245*, 43 – 45.

[13] R. Lazzaroni, A. Calderone, J. L. Brédas, J. P. Rabe, *J. Chem. Phys*, **1997**, *107*, 99 – 105.

[14] According to Figure 4a, the tunnel current through the aromatic discs of **3b**, the longer axis of which is tilted with respect to the *b* axis of the unit cell, is higher than that through the molecules, which are oriented almost parallel to the *b* axis. To explain the differing contrasts, it is assumed that the aromatic discs opposite to the graphite substrate which are tilted against the *b* axis, are like an additional graphite layer, whereas the molecules in the other rows are rotated relative to the graphite lattice.

[15] **3b**: Unit cell: $a = (1.71 \pm 0.15)$ nm, $b = (5.69 \pm 0.17)$ nm, $\alpha = 87 \pm 2°$; surface demand $A = (9.72 \pm 1.15)$ nm^2 (experimental) and $A =$ 9.86 nm^2 (calculated from van der Waals circumferences); **3c**: unit cell: $a = (3.41 \pm 0.20)$ nm, $b = (5.45 \pm 0.32)$ nm, $\alpha = 79 \pm 2°$; surface demand $A = (18.24 \pm 2.26)$ nm^2 and $A = 15.26$ nm^2 (calculated from van der Waals circumferences).

[16] D. Tománek, S. G. Louie, H. J. Mamin, D. W. Abraham, R. E. Thomson, E. Ganz, J. Clarke, *Phys. Rev. B* **1987**, 35, 7790 – 7793.

[17] Individual benzene units along the long axis of the aromatic discs could not be resolved, which is probably due to a (albeit small) molecular mobility.

 © WILEY-VCH Verlag GmbH, D-69451 Weinheim, 1998 1433-7851/98/3719-2699 $ 17.50+.50/0

Total Syntheses of Vancomycin and Eremomycin Aglycons**

David A. Evans,* Michael R. Wood, B. Wesley Trotter, Timothy I. Richardson, James C. Barrow, and Jeffrey L. Katz

Vancomycin, isolated in 1956 from *Streptomyces orientalis*,[1] is the prototypical member of a large family of antibiotics whose structures consist of an arylglycine-rich heptapeptide aglycon to which are appended an array of sugar residues. Structural diversity within this family of natural products is created by variation in the aglycon amino acid constituents and in the nature, position, and number of incorporated sugar residues.[2] Clinical applications of vancomycin to the treatment of Gram-positive bacterial infections and its efficacy against methicillin-resistant *Staphylococcus aureus* have established vancomycin as the antibiotic of last resort against infections by this deadly pathogen.[3] Recently, emergence of bacterial strains resistant to treatment by this family of antibiotics[4] has provided the stimulus for us and others[5] to develop reaction methodology and strategies relevant to the synthesis of the individual members of this family of natural products. In this communication we report the first syntheses of the vancomycin aglycon (**1**) and the eremomycin aglycon (**2**).[6]

The initial phase of our synthesis program in this area focused on the development of reactions critical to the synthesis of this family of target structures. Relevant methodology includes new asymmetric amino acid syntheses[7] and new macrocyclization reactions amenable to the construction of macrocyclic diaryl ether[8] and biaryl-containing[9] tripeptides. Application of this methodology to the synthesis of bis-dechlorovancomycin (orienticin C) aglycon has recently been reported.[10]

The most formidable synthesis challenges that the vancomycin skeleton presents are the three stereochemical elements of atropisomerism present in the structure as a consequence of hindered rotation in each of the cyclic tripeptide subunits. Our recent efforts have been directed toward the development of strategies for controlling these architectural features during the assemblage of the vancomycin skeleton. A detailed account of studies that have culminated in the current vancomycin synthesis is presented in the following communication.[11] These investigations have dictated both the general synthesis plan (Figure 1) and the strategy for controlling atropselectivity in each of the cyclic tripeptide subunits designated as M(2–4), M(4–6), and M(5–7).[12]

The amino acids required for the (4–7)-tetrapeptide were synthesized by our chiral auxiliary-based methodology.[7, 13] We envisioned two potential analogues of amino acid 6 (Figure 1, X = H, X = Cl) that could afford the desired M(4–6) chlorine atropisomer from either stereochemical outcome of an S_NAr-based macrocyclization given the versatility of the Sandmeyer reaction ($NO_2 \rightarrow H$, or $NO_2 \rightarrow Cl$). Preparation of the amino acids 6 commenced with (isothiocyanoacetyl)-oxazolidinone **3** (Scheme 1).[7c] Stannous triflate mediated aldol reaction of **3** with aldehyde **4a** or **4b**[14] proceeded with good diastereoselection (dr = 95:5) to afford the derived *syn* aldol adducts **5a** and **5b**. In subsequent manipulations of these adducts, the presence of the electrophilic halogen-containing nitroaromatic nucleus, particularly in the chlorinated series **4b**–**14b**, necessitated careful optimization of reaction parameters in order to minimize undesirable S_NAr-based fluoride displacement reactions. After Boc protection and transformation to the oxazolidinone in a one-pot sequence, selective removal of the chiral auxiliary was effected under carefully controlled conditions[15] to afford carboxylic acids **6a** and **6b**.

Peptide coupling of **6a** and **6b** with amino acid 7 (EDCI·HCl, HOBt, 4/1 CH_2Cl_2/DMF) provided dipeptides **7a** and **7b**. While endocyclic oxazolidinone cleavage of **7a** could be accomplished with LiOH (MeOH/H_2O), the corresponding transformation of chloro-containing **7b** was hampered by competing S_NAr-based displacement of the highly reactive aromatic fluoride on ring 6. Use of Li_2CO_3 in MeOH minimized this side reaction and provided **8b**, which was used in unpurified form after aqueous workup. Following Boc cleavage, coupling of **8a** and **8b** to amino acid 5 and subsequent protecting group exchange afforded tripeptides

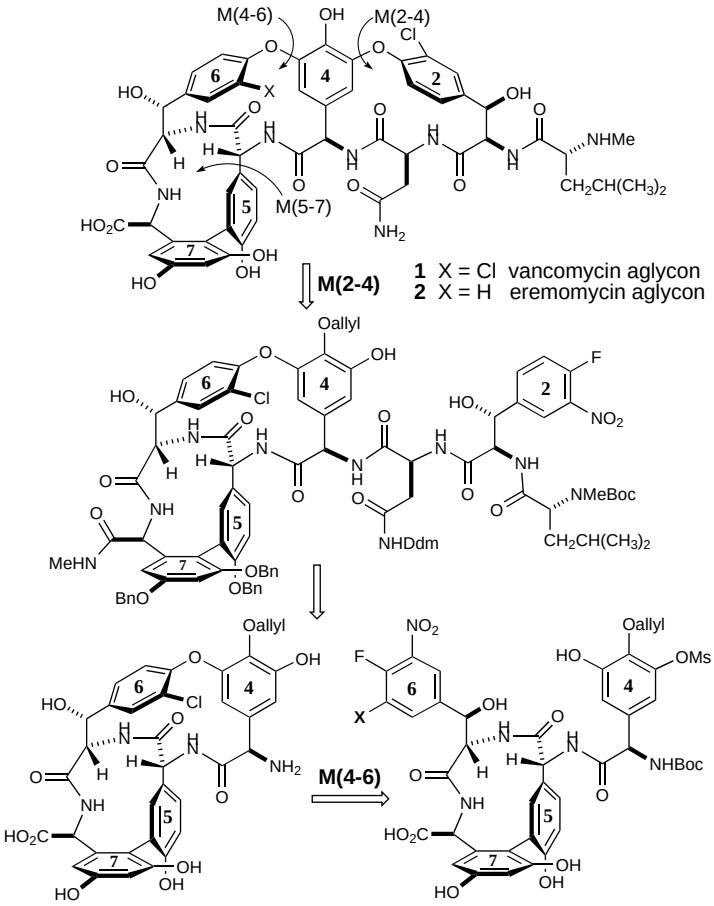


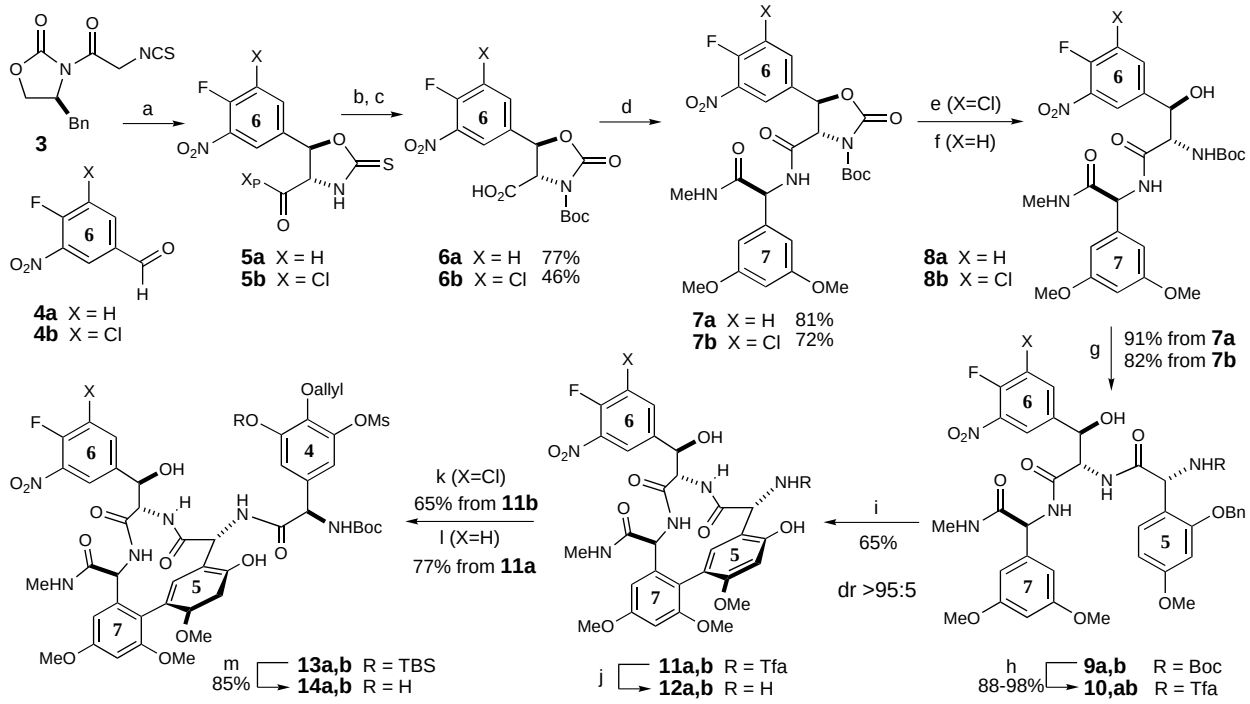
Figure 1. Assemblage strategy for vancomycin and eremomycin aglycons. See ref. [6] for abbreviations.

[*] Prof. D. A. Evans, M. R. Wood, B. W. Trotter, T. I. Richardson, J. C. Barrow, J. L. Katz
Department of Chemistry & Chemical Biology, Harvard University
Cambridge, MA 02138 (USA)
Fax: (+1) 617-495-1460
E-mail: evans@chemistry.harvard.edu

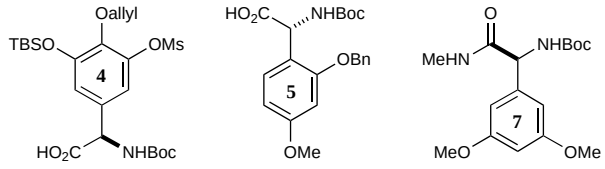
[**] Financial support has been provided by the National Institutes of Health (NIH).

Supporting information for this article is available on the WWW under http://www.wiley-vch.de/home/angewandte/ or from the author.

 © WILEY-VCH Verlag GmbH, D-69451 Weinheim, 1998 1433-7851/98/3719-2700 $ 17.50+.50/0



Scheme 1. Synthesis of the M(5–7)-tetrapeptide. a) $Sn(OTf)_2$, *N*-ethylpiperidine, THF, −78 °C, then **4**; b) Boc_2O, DMAP, CH_2Cl_2, then 1:1 HCO_2H/30 % H_2O_2; c) 3.1 equiv LiOOH, −5 °C (X = Cl), 1.2 equiv LiOOH, −10 °C (X = H); d) amino acid 7, TFA, DMS, CH_2Cl_2, 0 °C, then **6**, EDCI · HCl, HOBt, CH_2Cl_2/DMF (X = Cl), THF (X = H), 0 °C; e) Li_2CO_3, MeOH, room temperature; f) LiOH, MeOH/H_2O; g) TFA, DMS, CH_2Cl_2, 0 °C, then amino acid 5, EDCI · HCl, HOBt, THF, 0 °C; h) TFA, DMS, CH_2Cl_2, 0 °C, then TFAA, 2,6-lutidine, CH_2Cl_2, room temperature; i) VOF_3, $BF_3 \cdot Et_2O$, $AgBF_4$, TFA/CH_2Cl_2, 0 °C, then $NaHB(OAc)_3$; j) $NaHCO_3$, MeOH, H_2O, room temperature, 6 d (X = Cl), 9–14 d (X = H); k) amino acid 4, HATU, HOAt, collidine, CH_2Cl_2/DMF, −20 °C, 16 h; l) isobutyl chloroformate, *N*-methylmorpholine, EtOAc, −10 → −5 °C, 30 min, then amino acid 4 in EtOAc/DMF, −20 °C → rt, 2 h; m) HF · pyridine, THF, room temperature, 1 h (X = Cl), TBAF, CH_2Cl_2, 0 °C, 15 min (X = H). See ref. [6] for abbreviations.

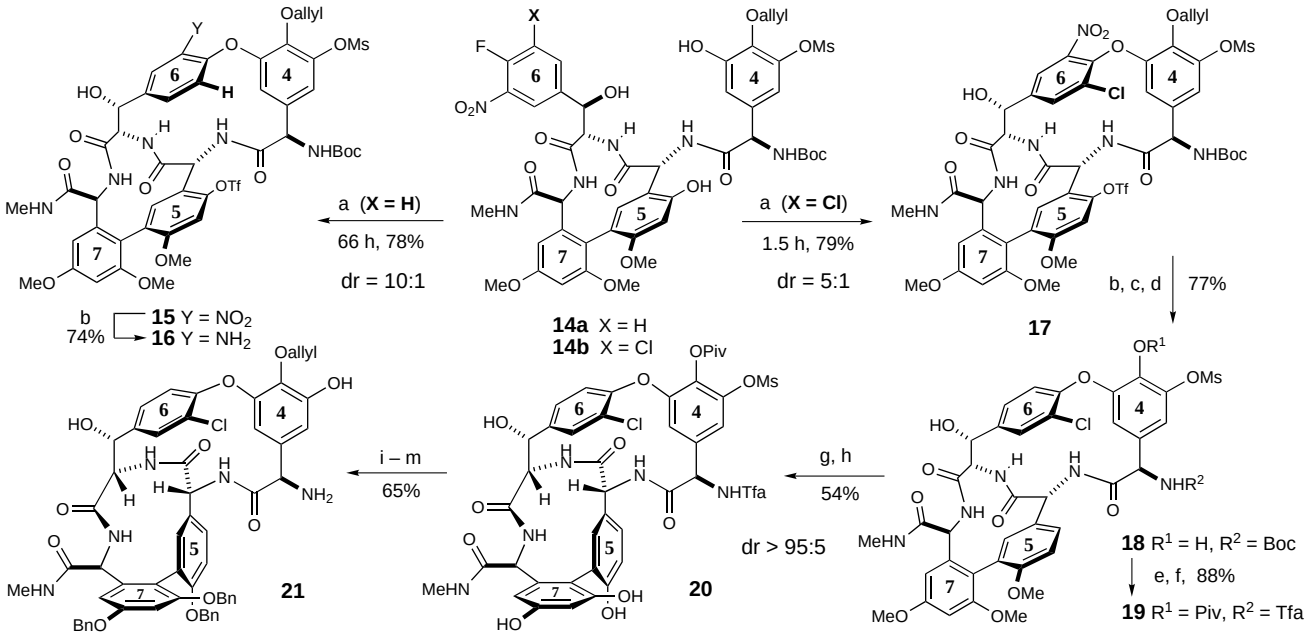


10a and **10b** in excellent overall yield for the hydrolysis and coupling events (see Scheme 1).

Oxidative cyclization of **10a** and **10b** according to our previously reported conditions (VOF_3)[9, 10] provided the M(5–7) cyclic tripeptides **11a** and **11b** as their unnatural *R* atropisomers (dr > 95:5). The reductive quench for this oxidation was modified to employ $NaBH(OAc)_3$ in place of zinc dust to avoid the unwanted reduction of the nitro group in ring 6. As noted previously, the desired cleavage of the aryl benzyl ether in ring 5 was also observed under the reaction conditions.[9, 10] We also investigated the analogous oxidative cyclizations of more conventional amino acid 7 ester analogues of tripeptide **10**. However, these substrates exhibited significant levels of epimerization of the C-terminal amino acid residue during the cyclization process, a side reaction that was suppressed through use of the illustrated *N*-methyl amides.

In preparation for incorporating amino acid 4 into the M(5–7) tripeptide **12**, removal of the trifluoroacetamide protecting group in **11** was accomplished by treatment with $NaHCO_3$ in MeOH/H_2O. These conditions effected conversion into amines **12** with no detectable aromatic fluoride displacement for either **12a** or **12b** by HPLC. Coupling[16] of **12** and amino acid 4 provided tetrapeptides **13**. As a prelude to M(4–6) macrocyclization, silyl deprotection of the phenolic hydroxyl in ring 4 was accomplished for **13a** under basic conditions (TBAF, THF), while acidic deprotection conditions (HF · pyridine) proved necessary for substrate **13b**.[17]

Atropisomer control during the construction of the M(4–6) macrocycle has posed a major challenge to the development of a successful vancomycin synthesis. In conjunction with evaluating potential strategies for achieving the proper disposition of the chloro substituent in ring 6, substrates **14a** and **14b** were examined with respect to the diastereoselectivity of their individual cyclization processes (Scheme 2). Optimal conditions for intramolecular S_NAr cyclization (Na_2CO_3, DMSO, room temperature),[18] when applied in the dechloro series starting from **14a**, provided the *undesired* nitro atropisomer (dr = 10:1); in situ derivatization of the phenolic hyxdoxy group in ring 5 afforded **15**. Reduction of the nitro group in **15** provided the major atropisomer **16** as a crystalline aniline whose structure was established by X-ray analysis.[19, 20] These results led to the speculation that the analogue **14b** with a chloro substituent in ring 6 might also cyclize with the same stereochemical outcome (**14b** → **17**) if the stereochemical bias for the nitro group were maintained. In the event, cyclization of **14b** afforded the desired atropisomer **17** as a 5:1 mixture of atropdiastereomers in 79 % yield (Scheme 2). The enhanced electrophilicity of **14b** was evident in the striking rate difference for the two cyclizations (**14a**: 66 h; **14b**: 1.5 h). More remarkable was the fact that **14b**



Scheme 2. Synthesis of the M(4–6)(5–7) bicyclic tetrapeptide. a) Na_2CO_3, DMSO, room temperature, 66 h (X = H), 1.5 h (X = Cl), then Tf_2NPh, 1 h; b) Zn^0, HOAc, EtOH, 40 °C; c) $NaNO_2$, H_3PO_2, cat. Cu_2O, THF/H_2O, 0 °C, 1 h; d) [Pd(dppf)Cl_2]·CH_2Cl_2, Et_3N, HCO_2H, DMF, 75 °C; e) PivCl, Et_3N, THF, room temperature; f) TFA, DMS, CH_2Cl_2, 0 °C, then TFAA, 2,6-lutidine, CH_2Cl_2, 0 °C to room temperature; g) $AlBr_3$, then EtSH, 0 °C; h) MeOH, 55 °C; i) BnBr, Cs_2CO_3, Bu_4NI, DMF, 0 °C; j) LiSEt, THF, 0 °C; k) allyl-Br, Cs_2CO_3, DMF, 0 °C; l) LDA, THF, −78 °C; m) LiOH, THF/H_2O/MeOH, 0 °C. See ref. [6] for abbreviations.

cyclized at an appreciable rate upon dissolution in DMSO and other polar, aprotic solvents *without added base*. Bicyclic peptide **17** was submitted to reduction (Zn, HOAc, EtOH, 40 °C) and diazotization/reduction ($NaNO_2$, H_3PO_2, Cu_2O, THF/H_2O, 0 °C),[21] to give the desired monochloride in 88% yield. NOE experiments confirmed that the major atropisomer possessed the desired *R* configuration.[22] Palladium-catalyzed reduction of **17** removed both the extraneous aryl triflate on ring 5 and the phenolic allyl protecting group on ring 4 (Scheme 2),[23] affording phenol **18** in 87% yield.[24] Protecting group adjustment (**18** → **19**) and cleavage of the phenolic methyl ethers ($AlBr_3$/CH_2Cl_2, EtSH, 0 °C) was followed by M(5–7) atropisomerization (MeOH, 55 °C, 24 h) to give the bicyclic peptide **20**, which possesses the desired *S* biaryl configuration (dr > 95:5). It is noteworthy that **20** and its analogue without a chloro substitutent in ring 6, which comprise the M(5–7) aglycon subunits common to every member of the vancomycin family, contain the 5–6 *cis*-amide found in vancomycin.[25] In preparation for the final peptide coupling, the triphenol was benzylated, the phenolic hydroxy group in ring 4 was transformed to its allyl ether, and the mesylate and trifluoroacetamide protecting groups were removed to provide free amine **21**.

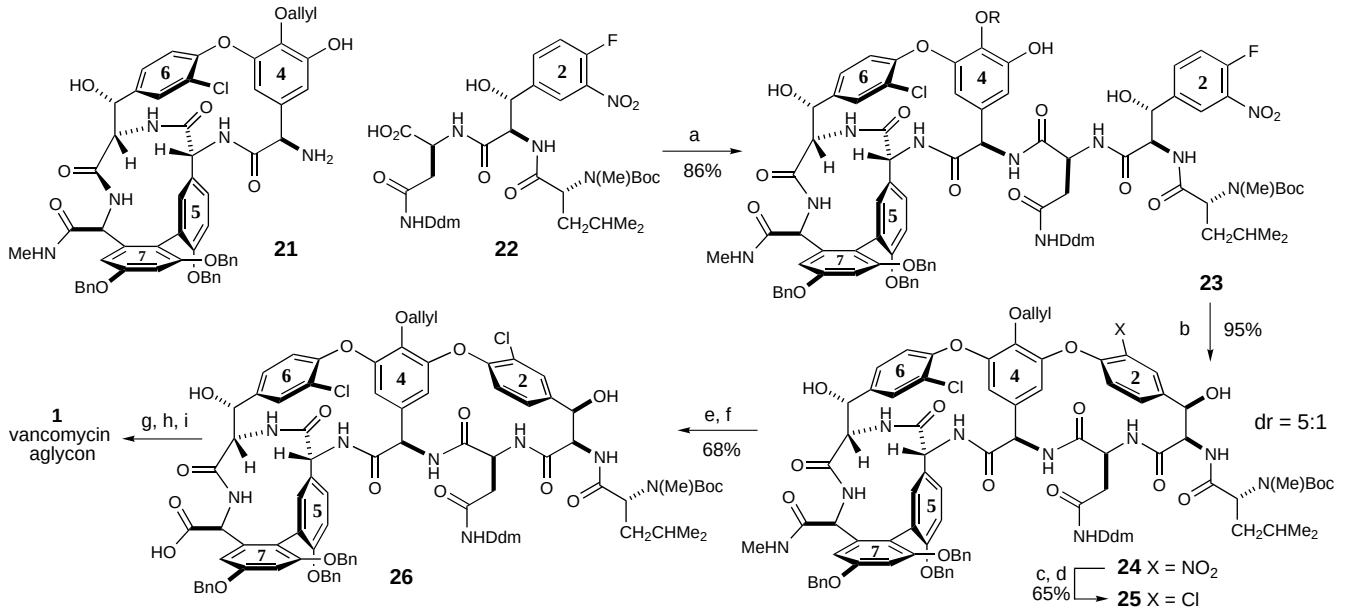
The completion of the aglycon synthesis is summarized in Scheme 3. Coupling of **21** and tripeptide **22**[10b] (EDCI·HCl, HOAt, THF, 0 °C) afforded heptapeptide **23** in 86% yield with no detectable epimerization (Scheme 3). Under optimal conditions (CsF, DMSO, room temperature, 5 h), intramolecular S_NAr cyclization provided the fully assembled tricyclic core of vancomycin as a 5:1 mixture of M(2–4) atropisomers favoring the desired *R* configuration **24** (95% yield). The mixture of nitro atropisomers was reduced (Zn, AcOH, EtOH, 40 °C) to provide two diastereomeric anilines which were separated by silica gel chromatography, affording a single atropisomer in 80% yield. Sandmeyer transformation[26] to the protected vancomycin aglycon **25** proceeded in 81% yield.

Deprotection of **25** to vancomycin aglycon (**1**) followed the sequence developed for the synthesis of orienticin C.[10b] The *N*-methyl amide moiety at the carboxyl terminus was removed by selective nitrosation in the presence of seven other amidic functional groups (N_2O_4, NaOAc, CH_2Cl_2, MeCN, 0 °C) followed by treatment with lithium hydrogen peroxide to give **26** in 68% yield.[27] Superficially, this transformation appears improbable in view of the other competing nitrosation sites; however, the steric effects associated with amide nitrosation have been documented.[28] Subsequent deprotection of allyl ether **26** ([$Pd(PPh_3)_4$], morpholine, THF, 0 °C) proceeded in 62% yield. Benzyl deprotection in the presence of the aryl chlorides was achieved using transfer hydrogenation conditions (Pd/C, 1,4-cyclohexadiene, EtOH, room temperature, 70% yield).[29] Final deprotection of the acid-labile nitrogen-protecting groups (Boc, Ddm) was effected through prolonged exposure to trifluroacetic acid (TFA/CH_2Cl_2, 3/1, DMS, 83% yield) to afford vancomycin aglycon (**1**), which proved identical (^{1}H NMR, COSY, HPLC, MS, [α]) to a natural sample.[30, 31]

The route detailed here provides vancomycin aglycon (**1**) in 40 steps (longest linear sequence) from 3,5-dimethoxybenzyl alcohol (amino acid 7). Eremomycin aglycon (**2**)[32] was also successfully synthesized through an identical strategy. These syntheses provide diastereoselective solutions to each of the biaryl ether and biaryl macrocycles and define a convergent assemblage process which can be extended to a variety of natural and unnatural analogues in the vancomycin series.

Received: August 17, 1998 [Z12295IE]
German version: *Angew. Chem.* **1998**, *110*, 2864–2868

 © WILEY-VCH Verlag GmbH, D-69451 Weinheim, 1998 1433-7851/98/3719-2702 $ 17.50+.50/0



Scheme 3. Assemblage of the vancomycin aglycon. a) EDCI, HOAt, THF, 0 °C; b) CsF, DMSO, room temperature; c) Zn^0, HOAc, EtOH, 40 °C; d) HBF_4, *t*BuONO, MeCN, then CuCl, $CuCl_2$, H_2O; e) N_2O_4, NaOAc, CH_2Cl_2/CH_3CN, 0 °C; f) H_2O_2, LiOH, THF/H_2O; g) $[Pd(PPh_3)_4]$, morpholine, THF; h) 10 % Pd/C, 1,4-cyclohexadiene, EtOH, room temperature; i) TFA, DMS, CH_2Cl_2, 0 °C to room temperature. See ref. [6] for abbreviations.

Keywords: antibiotics · eremomycin · natural products · total synthesis · vancomycin

[1] M. H. McCormick, W. M. Stark, G. E. Pittenger, R. C. Pittenger, G. M. McGuire, *Antibiot. Annu.* **1955 – 56**, 606 – 611.

[2] For a comprehensive discussion of the vancomycin antibiotics see: *Glycopeptide Antibiotics* (Ed.: R. Nagarajan), Marcel Dekker, New York, **1994**.

[3] a) D. H. Williams, *Natl. Prod. Reports* **1996**, 469 – 477; b) M. Foldes, R. Munro, T. C. Sorrell, S. Shankar, M. Toohey, *J. Antimicrob. Chemother.* **1983**, *11*, 21 – 26.

[4] a) S. Tabaqchali, *Lancet*, **1997**, *350*, 1644 – 1645; b) R. C. Moellering, *Clinical Infectious Diseases* **1998**, *26*, 1196 – 1199; c) C. T. Walsh, S. L. Fisher, I.-S. Park, M. Prahalad, Z. Wu, *Chem. Biol.* **1996**, *3*, 21 – 28, and references therein.

[5] For reviews on methodology relevant to the synthesis of the vancomycin aglycon structure see: a) D. A. Evans, K. D. DeVries in ref. [2], pp. 63 – 103; b) A. V. Rama Rao, M. K. Gurjar, K. L. Reddy, A. S. Rao, *Chem. Rev.* **1995**, *95*, 2135 – 2168; c) J. Zhu, *Synlett*. **1997**, 133 – 144; d) R. M. Williams, J. A. Hendrix, *Chem. Rev.* **1992**, *92*, 889 – 917.

[6] Abbreviations: dr: diastereomer ratio; X_p: (4*S*)-4-(phenylmethyl)-2-oxazolidinone; Tfa: trifluoroacetyl TFA: trifluoroacetic acid; Boc: *tert*-butoxycarbonyl; NOE: nuclear Overhauser effect; Tf: trifluoromethanesulfonyl; Ms: methanesulfonyl; Bn: benzyl; Piv: pivaloyl; Ddm: 4,4′dimethoxydiphenylmethyl; EDCI · HCl: 1-(3-(dimethylamino)propyl)-3-ethylcarbodiimide hydrochloride; HOBt: 1-hydroxybenzotriazole; DMAP: 4-dimethylaminopyridine; DMS: dimethylsulfide; TFAA: trifluoroacetic anhydride; HATU: *O*-(7-azabenzotriazol-1-yl)-1,1,3,3-tetramethyluronium hexafluorophosphate; HOAt: 7-aza-1-hydroxybenzotriazole; LDA: lithium diisopropylamide; dppf: 1,1′-bis(diphenylphosphanyl)ferrocene.

[7] a) D. A. Evans, D. A. Evrard, S. D. Rychnovsky, T. Früh, W. G. Wittingham, K. M. DeVries, *Tetrahedron Lett.* **1992**, *33*, 1189 – 1192; b) D. A. Evans, T. C. Britton, J. A. Ellman, R. L. Dorow, *J. Am. Chem. Soc.* **1990**, *112*, 4011 – 4030; c) D. A. Evans, A. E. Weber, *J. Am. Chem. Soc.* **1987**, *109*, 7151 – 7157.

[8] a) D. A. Evans, J. A. Ellman, K. M. DeVries, *J. Am. Chem. Soc.* **1989**, *111*, 8912 – 8914; b) D. A. Evans, C. J. Dinsmore, A. M. Ratz,*Tetrahedron Lett.* **1997**, *38*, 3189 – 3192; c) D. A. Evans, P. S. Watson, *Tetrahedron Lett.* **1996**, *37*, 3251 – 3254.

[9] a) D. A. Evans, C. J. Dinsmore, D. A. Evrard, K. M. DeVries, *J. Am. Chem. Soc.* **1993**, *115*, 6426 – 6427; b) D. A. Evans, C. J. Dinsmore, *Tetrahedron Lett.* **1993**, *34*, 6029 – 6032.

[10] For the synthesis of orienticin C aglycon see: a) D. A. Evans, C. J. Dinsmore, A. M. Ratz, D. A. Evrard, J. C. Barrow, *J. Am. Chem. Soc.* **1997**, *119*, 3417 – 3418; b) D. A. Evans, J. C. Barrow, P. S. Watson, A. M. Ratz, C. J. Dinsmore, D. A. Evrard, K. M. DeVries, J. A. Ellman, S. D. Rychnovsky, J. Lacour, *J. Am. Chem. Soc.* **1997**, *119*, 3419 – 3420.

[11] D. A. Evans, C. J. Dinsmore, P. S. Watson, M. R. Wood, T. I. Richardson, B. W. Trotter, J. L. Katz, *Angew. Chem.* **1998**, *111*, 2868 – 2872; *Angew. Chem. Int. Ed.* **1998**, *37*, 2704 – 2708.

[12] The seven amino acid residues are numbered consecutively starting from the amino terminus. The M(X – Y) nomenclature refers to the macrocycle containing an oxidative cross-link between aryl groups of residues X and Y. Bicyclic moieties will be identified as M(W – Y)(X – Z).

[13] Amino acid 4 was derived from (*R*)-*para*-hydroxy-phenylglycine.

[14] Compound **4b** was prepared by the chlorination of **4a**: F. D. March, W. B. Farnham, D. J. Sam, B. E. Smart, *J. Am. Chem. Soc.* **1982**, *104*, 4680 – 4682. 4-Fluoro-3-nitrobenzaldehyde (**4a**) was prepared from 4-fluorobenzaldehyde: F. Michael, D. Noffz, *Chem. Ber.* **1957**, *90*, 1586 – 1589. Dr. S. Rubenstein is acknowledged for the preparation of this material.

[15] Alternate conditions and reagents were plagued by competitive endocyclic oxazolidinone hydrolysis and/or undesired nucleophilic displacement of the fluoride. D. A. Evans, T. C. Britton, J. A. Ellman, *Tetrahedron Lett.* **1987**, *28*, 6141 – 6144.

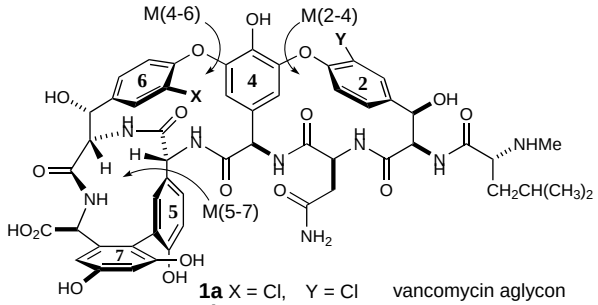
[16] HATU-mediated peptide coupling: L. A. Carpino, A. El-Fahan, C. A. Minor, F Albericio, *J. Chem. Soc. Chem. Commun.* **1994**, 201 – 203.

[17] The removal of the TBS protecting group highlighted the significant reactivity difference between the chloro and des-chloro substrates. Treatment of **13b** with TBAF resulted in immediate M(4 – 6) cyclization with reduced diastereoselection. See also ref. [24].

[18] Studies of the cyclization of **14a** revealed that the observed atropselectivity depended significantly on the base used, varying from 4:1 (KF) to 10:1 (Na_2CO_3) in favor of the unnatural atropisomer. It was further observed that cyclization of substrates in which the *meta*-phenols of amino acid 4 were *both* unmasked proceeded with negligible selectivity under a variety of conditions, necessitating the synthesis of a fully differentiated triphenol.

[19] Following diazotization/reduction of aniline **16**, eremomycin aglycon (**2**) was synthesized by a route analogous to that presented for

vancomycin. Synthetic **2** gave ^{1}H NMR, HPLC, and mass spectral data identical to a natural comparison sample (refs. [23] and [27]).
[20] We thank Mr. Kevin Campos for determining the X-ray structure of this intermediate.
[21] H. J. Shine, S. E. Rhee, *J. Am. Chem. Soc.* **1986**, *108*, 1000 – 1006.
[22] This assignment was confirmed by chemical correlation to a minor atropisomer corresponding to **16**.
[23] S. Cacci, P. G. Ciattini, E. Morera, G. Ortar, *Tetrahedron Lett.* **1986**, *27*, 5541 – 5544.
[24] Separation of the undesired M(4 – 6) atropisomer was most conveniently achieved at this stage; the desired isomer was isolated in 69% yield.
[25] The stereochemistry of **20** was confirmed by ROESY analysis (500 MHz).
[26] D. L. Boger, R. M. Borzilleri, S. Nukui, R. T. Beresis, *J. Org. Chem.* **1997**, *62*, 4721 – 4736.
[27] D. A. Evans, P. H. Carter, C. J. Dinsmore, J. C. Barrow, J. L. Katz, D. W. Kung, *Tetrahedron Lett.* **1997**, *38*, 4535 – 4538.
[28] J. Garcia, J. Gonzalez, R. Segura, J. Vilarrasa, *Tetrahedron* **1984**, *40*, 3121 – 3127.
[29] A. M. Felix, E. P. Heimer, T. J. Lambros, C. Tzougraki, J. Meienhofer, *J. Org. Chem.* **1978**, *43*, 4194 – 4196.
[30] We thank Dr. Bret Huff of Eli Lilly & Company for generous samples of vancomycin · HCl and eremomcyin · HOAc.
[31] Vancomycin aglycon was prepared from vancomycin · HCl according to: R. Nagarajan, A. A. Schabel, *J. Chem. Soc. Chem. Comm.* **1988**, 1306 – 1307; see also F. J. Marshall, *J. Med. Chem.* **1965**, *8*, 18 – 24.
[32] Eremomycin aglycon was prepared from eremomycin · HOAc according to: G. F. Gause, M. G. Brazhnikova, N. N. Lomakina, T. F. Berdnikova, G. B. Fedorova, N. L. Tokareva, V. N. Borisova, G. Y. Batta, *J. Antibiotics* **1989**, *42*, 1790 – 1799.



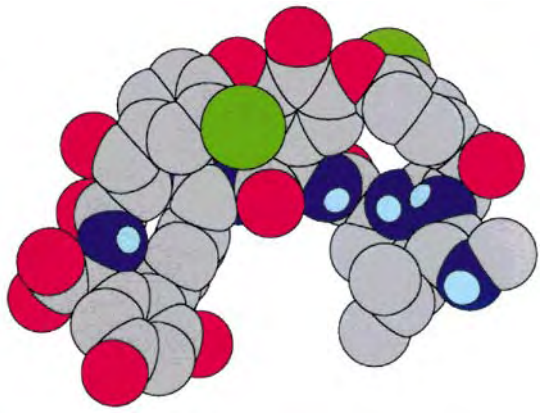


Figure 1. Space-filling representation of the vancomycin aglycon.[3b]

Nonconventional Stereochemical Issues in the Design of the Synthesis of the Vancomycin Antibiotics: Challenges Imposed by Axial and Nonplanar Chiral Elements in the Heptapeptide Aglycons**

David A. Evans,* Christopher J. Dinsmore, Paul S. Watson, Michael R. Wood, Timothy I. Richardson, B. Wesley Trotter, and Jeffrey L. Katz

In the preceding communication, we described the first syntheses of the heptapeptide aglycons of vancomycin (**1a**) and eremomycin (**1b**).[1] This contribution focuses on the development of stereoselective methods for the synthesis of the three stereochemical elements of atropisomerism present in vancomycin.[2] The development of a strategy for controlling these architectural features is one of the principal challenges presented by this family of natural products. As an aid in the ensuing discussion, a space-filling representation of the vancomycin aglycon, taken from the X-ray structure by Sheldrick et al.,[3] is provided (Figure 1).

[*] Prof. D. A. Evans, C. J. Dinsmore, P. S. Watson, M. R. Wood, T. I. Richardson, B. W. Trotter, J. L. Katz
Department of Chemistry & Chemical Biology, Harvard University
Cambridge, MA 02138 (USA)
Fax: (+1) 617-495-1460
E-mail: evans@chemistry.harvard.edu

[**] Financial support has been provided by the National Institutes of Health (NIH).

The high barrier to rotation about the biaryl bond[4] in vancomycin introduces an element of axial chirality into the structure, while hindered rotation about the axes defined by the *para*-oriented CH(OH) and *O*-aryl substituents in ring 2 and ring 6 incorporates two examples of planar chirality. Collectively, these three features of the aglycon architecture present the significant challenge of controlling atropisomerism in the construction of each of the three macrocyclic tripeptide subunits designated as M(2 – 4), M(4 – 6), and M(5 – 7).[5] Hence, even with asymmetric syntheses of the amino acid constituents[6] and an assemblage strategy in hand,[7] one is still faced with the problem of producing the vancomycin aglycon skeleton as only one of eight possible atropdiastereomers.

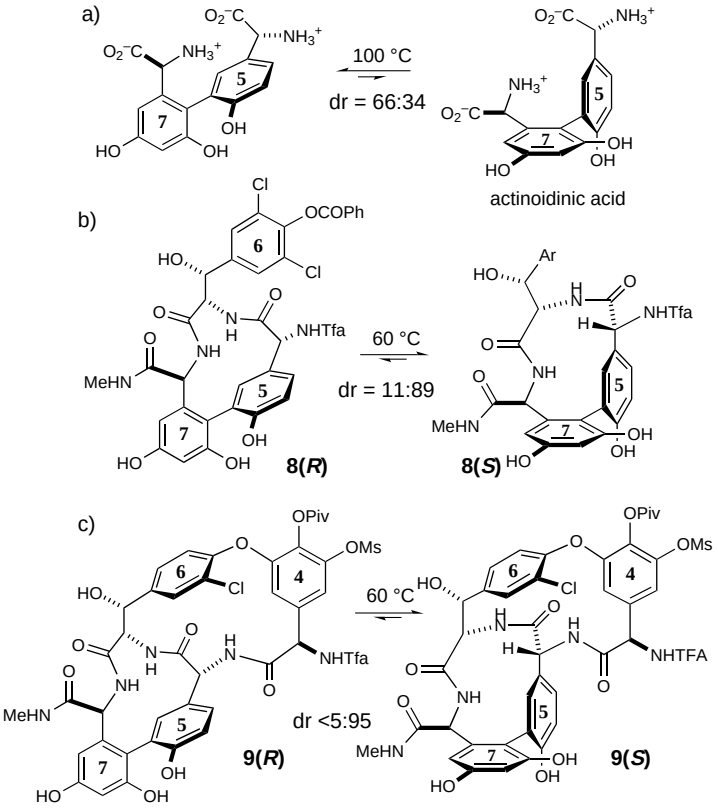
The vancomycin aglycon skeleton (**1a**) consists of three interlocking cyclic tripeptides that collectively afford a conformationally rigid cup-shaped structure (Figure 1).[3] It is evident that the biaryl bond connecting amino acids 5 and 7 is the pivotal rigidifying amino acid crosslink. We therefore adopted the premise that macrocyclization model studies for the individual rings lacking the M(5 – 7) tripeptide subunit, while informative in identifying the local contributions to atropdiastereoselection, could prove unreliable stereochemical predictors for more complex cyclization substrates containing the M(5 – 7) fragment.

The construction of the M(5 – 7) biaryl subunit[8] forms the basis of the synthesis plan. After the incorporation of an additional *ortho* benzyloxy substituent on ring 5, high levels of kinetic atropdiastereoselection for the unnatural atropisomeric product **3(*R*)** were observed in the oxidative cyclization

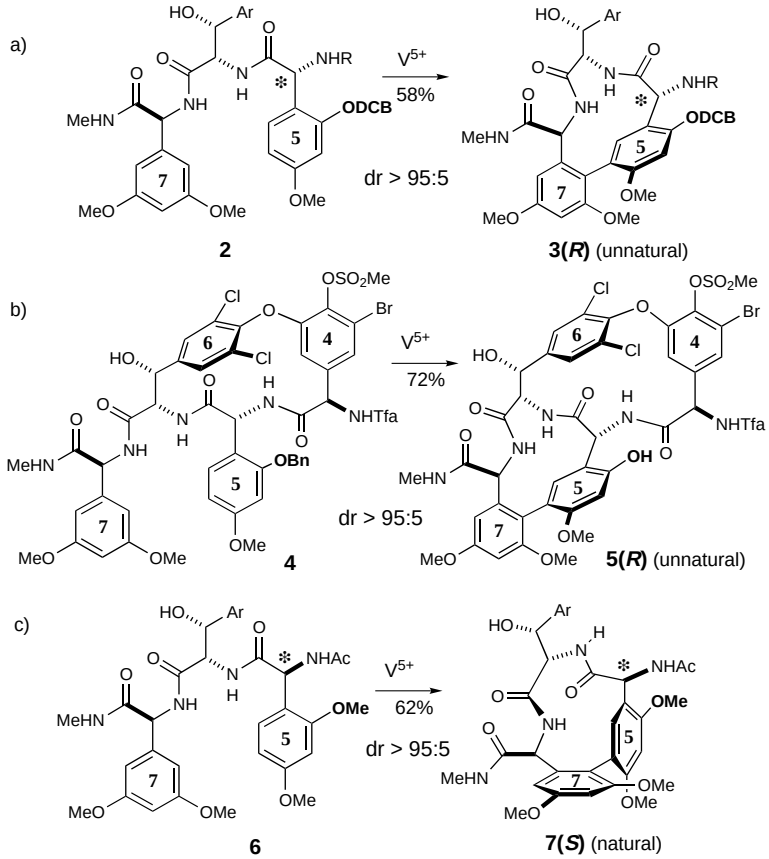
 © WILEY-VCH Verlag GmbH, D-69451 Weinheim, 1998 1433-7851/98/3719-2704 $ 17.50+.50/0

of tripeptides such as **2** (Scheme 1a).[9, 10] This stereochemical bias also extends to the more complex oxidative cyclization found in the orienticin C synthesis (Scheme 1b).[7] A(1,3) strain[11] was implicated as the stereochemical control element in these cyclizations when it was found that the diastereomeric tripeptide **6**, containing the epimeric arylglycine in position 5, underwent a highly diastereoselective oxidative ring closure to the natural atropisomeric product **7** with *S* configuration.[10b] These observations reveal that the absolute stereochemistry of the substituent benzylic to ring 5 may be employed to control the absolute stereochemistry of the M(5–7) ring closure.

The thermodynamic biaryl atropisomer bias in vancomycin is dictated by the global structure rather than by stereochemical relationships proximal to the biaryl linkage (Scheme 2). For example, Jeffs et al. has isolated amino acid components from the controlled hydrolysis of vancomycin and aridicin.[12] Both atropisomers of the biaryl-containing diamino diacid, referred to as actinoidinic acid, have been isolated in pure form and individually equilibrated at 100 °C to afford a 2:1 equilibrium ratio of atropisomers where the *R* (unnatural) isomer is favored (Scheme 2a). This result can be contrasted with the equilibration of the M(5–7) cyclic tripeptide **8(*R*)** which now favors (dr = 89:11) the natural atropisomer **8(*S*)** (Scheme 2b).[10] The bias for the natural *S* atropdiastereomer found in the natural product is further enhanced (dr > 95:5) in the M(5–7) (4–6) bicyclic tetrapeptide (Scheme 2c).[1]

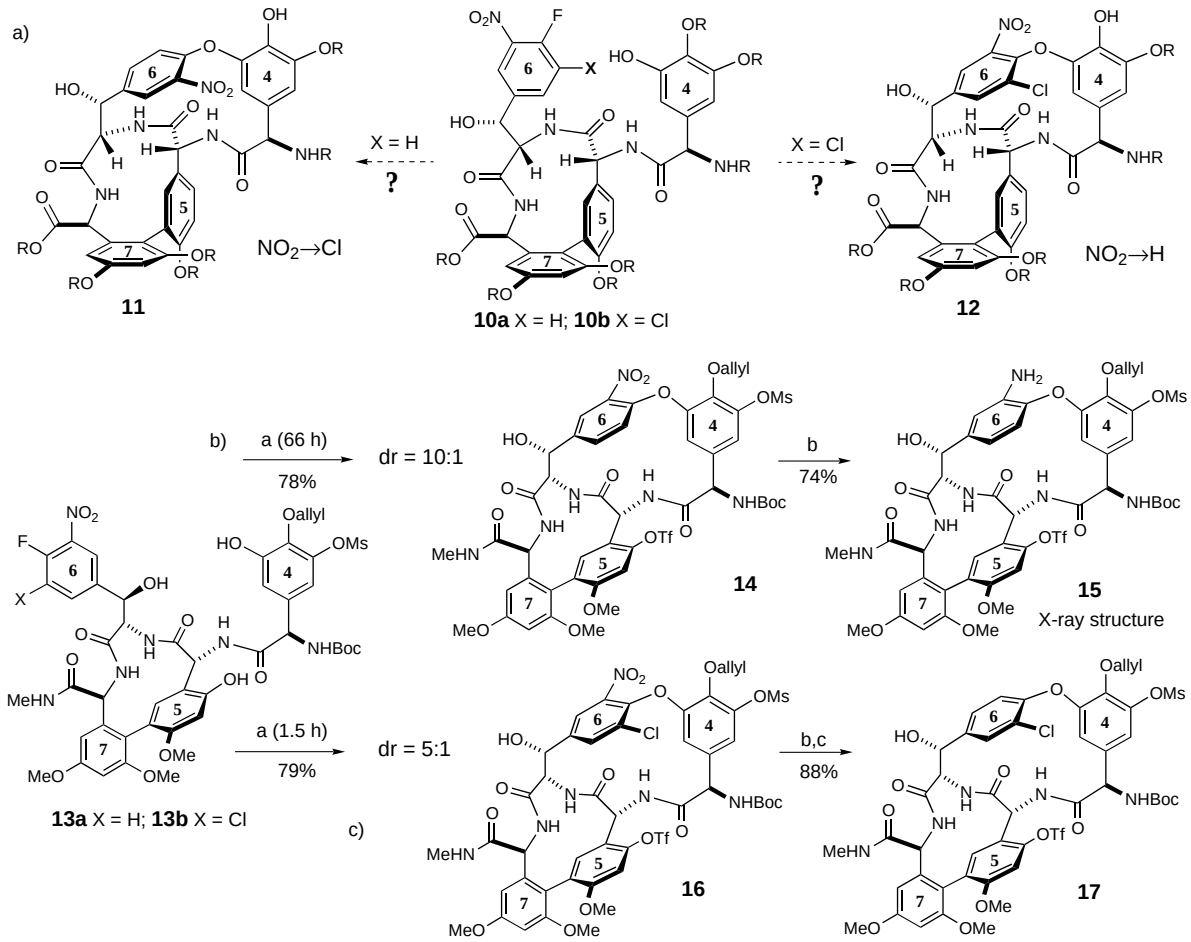


Scheme 2. Biaryl equilibration of the M(5–7) macrocycle. See ref. [9] for abbreviations.



Scheme 1. Diastereoselective oxidative M(5–7) macrocyclizations. See ref. [9] for abbreviations.

S_NAr macrocyclizations of phenolic substrates now constitute a reliable method for the construction of macrocyclic diaryl ether containing tripeptides.[13] This reaction has recently been employed in the construction of the M(2–4) subunit in our synthesis of orienticin C.[7] Our plan to implement a diastereoselective variant of this process for the construction of the M(4–6) subunit of vancomycin is shown in Scheme 3a. Either illustrated stereochemical outcome (**10a** → **11** or **10b** → **12**) would provide access to the proper atropisomer with a chloro substituent in ring 6 given the versatility of the Sandmeyer reaction ($NO_2 \rightarrow H$ or $NO_2 \rightarrow Cl$). This cyclization strategy was evaluated on tetrapeptides **13a** and **13b** (Scheme 3).[1] Macrocyclization of **13a** with Na_2CO_3 (DMSO, room temperature, 66 h) afforded the *undesired* M(4–6) atropisomer **14** with 10:1 stereoselectivity (Scheme 3b). NOE experiments established that the predominant product was the unnatural *S* isomer.[14] X-ray crystallographic analysis of the major atropisomeric aniline **15** verified this stereochemical assignment. The cyclization of chlorinated analogue **13b** retained the stereochemical bias for the nitro substituent, forming the desired biaryl ether **16** with 5:1 atropdiastereoselection (Scheme 3c). Transformation of **16** to the derived aniline, followed by diazotization and



Scheme 3. Diastereoselective S_NAr-based M(4–6) macrocyclizations. a) Na_2CO_3, DMSO, room temperature, then Tf_2NPh, 1 h; b) Zn°, HOAc, EtOH, 40 °C; c) $NaNO_2$, H_3PO_2, cat. Cu_2O, THF/H_2O, 0 °C, 1 h. See ref. [9] for abbreviations.

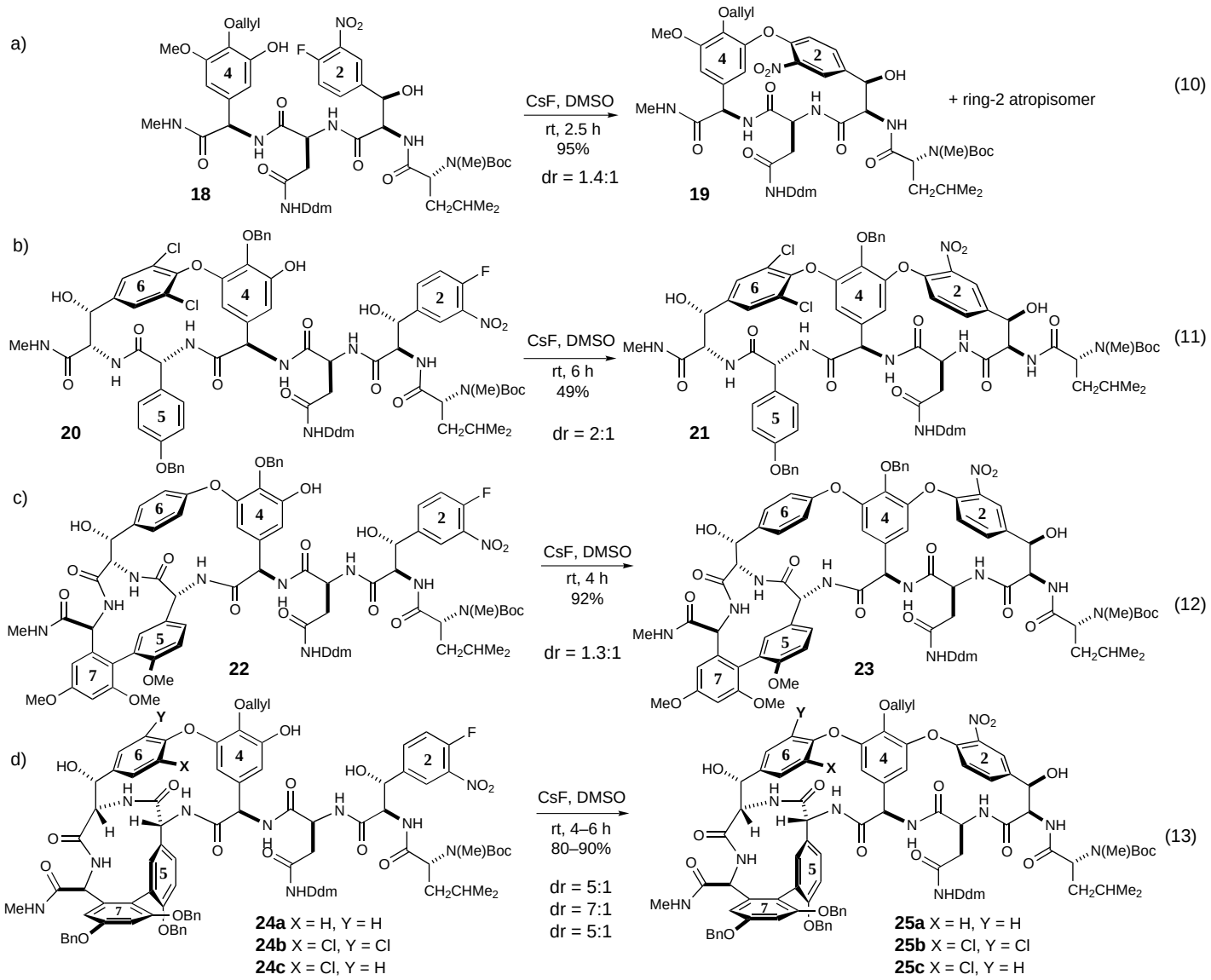
reduction, afforded the M(4–6)(5–7) bicyclic monochloride **17,** a pivotal intermediate for the synthesis of vancomycin.[1]

The last phase of the synthesis required the successful incorporation of the M(2–4) macrocycle into M(4–6)(5–7) bicyclic tetrapeptide intermediates. Accordingly, a detailed study of the stereochemical control elements that might influence the atropdiastereoselection of the chloro substituent on ring 2 was undertaken in the S_NAr cyclizations illustrated in Scheme 4. In simple tetrapeptides such as **18**, macrocyclization (CsF, DMSO, 25 °C, 2.5 h) proceeds with low stereoselectivity (dr = 1.4:1) (Scheme 4a). Variation of solvent (DMSO or DMF) and cyclization promoters failed to significantly improve these results. It is evident from this and related investigations that there is a negligible stereochemical bias imparted by the amide backbone from amino acids 1–3 to the cyclization process.[15, 16]

At the next level of architectural complexity, M(2–4) cyclizations on hexapeptide substrates containing the M(4–6) subunit were investigated. Cyclization (CsF, DMSO, 25 °C, 6 h) of **20** was weakly diastereoselective (dr = 2:1), favoring the desired *R* atropisomer (Scheme 4b).[14, 17] A modest reduction in rate, relative to that of **18**, was also observed. Conformational effects imposed by the M(4–6)(5–7) bicyclic tetrapeptide were then evaluated (Scheme 4c, d). Substrate **22**, containing the unnatural M(5–7) configuration, cyclized with poor atropdiastereoselection (dr = 1.3:1). This selectivity is in fact similar to that observed in the cyclization of **20**. In both **20** and **22**, the 5–6 amide bonds adopt a *trans* rather than the *cis* configuration found in vancomycin.

We next investigated the impact of the natural M(5–7) biaryl atropisomer, which contains the *cis* 5–6 amide bond (substrates **24a–c**, (Scheme 4d)). Cyclizations of **24a–c** gave the desired M(2–4) atropisomer with good selectivity. It is noteworthy that the cyclization stereoselectivity of chlorine-containing **24b** (dr = 7:1) is only marginally greater than that observed for its dechloro counterpart **24a** (dr = 5:1). This observation establishes that the chloro substituent in ring 6 is not a dominant stereochemical determinant in the cyclization process. This point is confirmed in the cyclization of the monochloro atropisomer **24c** that contains two of the three atropisomeric relationships required for vancomycin (Scheme 4d). This cyclization, as predicted by the preceding analogies, also affords the desired disposition of the chloro substituent in ring 2, thus establishing all of the atropdiastereomeric relationships found in vancomycin. The natural M(5–7) biaryl configuration evidently imparts subtle steric and electronic effects which provide a kinetic bias for the desired M(2–4) cyclization.[18]

 © WILEY-VCH Verlag GmbH, D-69451 Weinheim, 1998 1433-7851/98/3719-2706 $ 17.50+.50/0



Scheme 4. Diastereoselective S_NAr-based M(2–4) macrocyclizations. See ref. [9] for abbreviations.

Collectively, the observations recorded herein have dictated the direction of the syntheses of both eremomycin and vancomycin that are described in the preceding communication.[1]

Received: August 17, 1998 [Z12296IE]
German version: *Angew. Chem.* **1998**, *110*, 2868–2872

Keywords: antibiotics · atropisomerism · chirality · nucleophilic aromatic substitutions · vancomycin

[1] D. A. Evans, M. R. Wood, B. W. Trotter, T. I. Richardson, J. C. Barrow, J. L. Katz, *Angew. Chem.* **1998**, *110*, 2864–2868; *Angew. Chem. Int. Ed.* **1998**, *37*, 2700–2704.

[2] For a general discussion of chirality in structures devoid of chiral centers see: E. L. Eliel, S. H. Wilen, *Stereochemistry of Carbon Compounds*, Wiley, New York, **1994**, Chapter 14, pp. 1119–1190. See p 1193 for the definition of atropisomerism.

[3] a) Ureido-balhimycin structure: G. M. Sheldrick, E. Paulus, L. Vertesy, F. Hahn, *Acta Crystallogr. Sect. B* **1995**, *51*, 89–98; b) Vancomycin structure: M. Schäfer, T. R. Schneider, G. M. Sheldrick, *Structure*, **1996**, *4*, 1509–1515.

[4] a) F. H. Westheimer, J. E. Mayer, *J. Chem. Phys.* **1946**, *14*, 733–738; b) F. H. Westheimer, *J. Chem. Phys.* **1947**, *15*, 252–260; c) M. Rieger, F. H. Westheimer, *J. Am. Chem. Soc.* **1950**, *72*, 19–28.

[5] The seven amino acid residues are numbered consecutively, starting from the amino terminus. The M(X–Y) nomenclature refers to the macrocycle containing an oxidative crosslink between aryl groups of residues X and Y. Bicyclic moieties will be identified as M(X–Y)(Y–Z).

[6] a) D. A. Evans, D. A. Evrard, S. D. Rychnovsky, T. Früh, W. G. Wittingham, K. M. D eVries, *Tetrahedron Lett.* **1992**, *33*, 1189–1192; b) D. A. Evans, T. C. Britton, J. A. Ellman, R. L. Dorow, *J. Am. Chem. Soc.* **1990**, *112*, 4011–4030; c) D. A. Evans, A. E. Weber, *J. Am. Chem. Soc.* **1987**, *109*, 7151–7157.

[7] For the synthesis of orienticin C aglycon see: a) D. A. Evans, C. J. Dinsmore, A. M. Ratz, D. A. Evrard, J. C. Barrow, *J. Am. Chem. Soc.* **1997**, *119*, 3417–3418; b) D. A. Evans, J. C. Barrow, P. S. Watson, A. M. Ratz, C. J. Dinsmore, D. A. Evrard, K. M. DeVries, J. A. Ellman, S. D. Rychnovsky, J. Lacour, *J. Am. Chem. Soc.* **1997**, *119*, 3419–3420.

[8] For model studies directed toward the construction of the M(5–7) biaryl linkage see: a) K. C. Nicolaou, X.-J. Chu, J. M. Ramanjulu, S. Natarajan, S. Bräse, F. Rübsam, C. N. C. Boddy, *Angew. Chem.* **1997**, *109*, 1551–1552; *Angew. Chem. Int. Ed. Engl.* **1997**, *36*, 1539–1540; b) K. C. Nicolaou, J. M. Ramanjulu, S. Natarajan, S. Bräse, H. Li, C. N. C. Boddy, *Chem. Commun*. **1997**, 1899–1900.

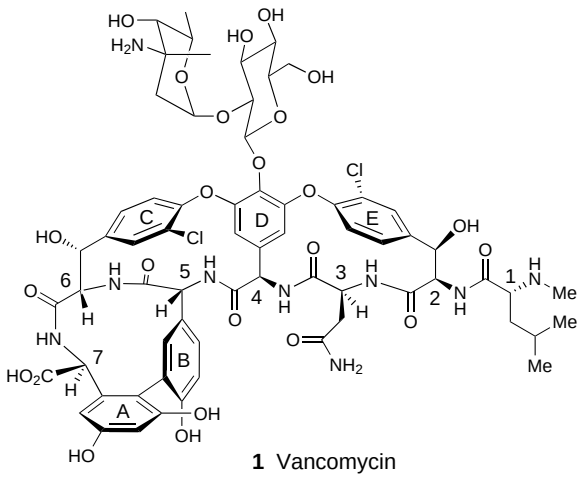
 © WILEY-VCH Verlag GmbH, D-69451 Weinheim, 1998 1433-7851/98/3719-2707 $ 17.50+.50/0

[9] Abbreviations: Tfa: trifluoroacetyl; TFA: trifluoroacetic acid; DMSO: dimethyl sulfoxide; Boc: *tert*-butoxycarbonyl; NOE: nuclear Overhauser effect; Tf: trifluoromethanesulfonyl; Ms: methanesulfonyl; Ac:acetyl; Ddm: 4,4Ödimethoxydiphenylmethyl; Bn: benzyl; DCB: 3,4-dichlorobenzyl; Piv: pivaloyl.
[10] a) D. A. Evans, C. J. Dinsmore, D. A. Evrard, K. M. DeVries, *J. Am. Chem. Soc.* **1993**, *115*, 6426 – 6427; b) D. A. Evans, C. J. Dinsmore, *Tetrahedron Lett.* **1993**, *34*, 6029 – 6032.
[11] R. W. Hoffmann, *Chem. Rev.* **1989**, *89*, 1841 – 1860.
[12] P. W. Jeffs, G. Chan, L. Mueller, C. DeBrosse, L. Webb, R. Sitrin, *J. Org. Chem.* **1986**, *51*, 4272 – 4278.
[13] a) A. V. Rama Rao, M. K. Gurjar, K. L. Reddy, A. S. Rao, *Chem. Rev.* **1995**, *95*, 2135 – 2168; b) J. Zhu, *Synlett*. **1997**, 133 – 144.
[14] The configuration of the M(4 – 6) and M(2 – 4) macrocycles could be ascertained from ^{1}H NOE data for protons on the nitro-containing aromatic ring; their positions may be established relative to the benzylic hydroxyl-bearing stereocenters *para* to the diaryl ether linkage.
[15] D. A. Evans, P. S. Watson, *Tetrahedron Lett.* **1996**, *37*, 3251 – 3254.
[16] Similar observations have been made in monocyclic model systems. a) D. L. Boger, R. M. Borzilleri, S. Nukui, *Bioorg. Med. Chem. Lett.* **1995**, *5*, 3091 – 3096; b) D. L. Boger, R. M. Borzilleri, S. Nukui, R. T. Beresis, *J. Org. Chem.* **1997**, *62*, 4721 – 4736.
[17] A related cyclization (K_2CO_3/$CaCO_3$, DMF, 45 °C) proceeding with negligible atropselectivity has recently been reported: D. L. Boger, R. T. Beresis, O. Loiseleur, J. H. Wu, S. L. Castle, *Bioorg. Med. Chem. Lett.* **1998**, *8*, 721 – 724.
[18] The option of thermal atropisomer equilibration of the M(2 – 4) and M(4 – 6) rings is also possible. Boger et al. have begun to explore these processes: D. L. Boger, O. Loiseleur, S. L. Castle, R. T. Beresis, J. H. Wu, , *Bioorg. Med. Chem. Lett.* **1997**, *7*, 3199 – 3202. See also ref. [16b].

Total Synthesis of Vancomycin Aglycon—Part 1: Synthesis of Amino Acids 4 – 7 and Construction of the AB-COD Ring Skeleton

K. C. Nicolaou,* Swaminathan Natarajan, Hui Li, Nareshkumar F. Jain, Robert Hughes, Michael E. Solomon, Joshi M. Ramanjulu, Christopher N. C. Boddy, and Masaru Takayanagi

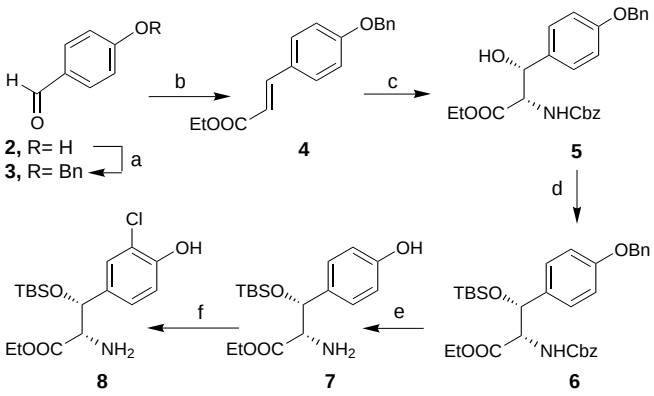
Vancomycin (**1**, Figure 1) is a clinically effective antibiotic used in cases of severe bacterial infections caused by several drug resistant pathogens.[1] Its medical importance and intriguing mode of action[2] coupled with its unusual molecular architecture[3] has fascinated synthetic chemists for some time.[4] Having established a number of new synthetic technologies and strategies aimed at this structural type,[5] we have recently focused our efforts on the total synthesis of **1**.[6] In this and the following communication,[7] we wish to report our progress and findings in the field, beginning with the stereoselective synthesis of amino acids 4 – 7 (compounds **8**, **22**, **27**, and **32**), the biaryl ring system (**35**), and the construction of the AB-COD skeleton (**46a**) of vancomycin.



1 Vancomycin

Figure 1. Molecular structure of vancomycin (**1**). The amino acids are labeled with numbers, and the aromatic rings with capital letters.

Scheme 1 outlines the synthesis of amino acid 6 in its protected form **8**. Thus, benzylation of 4-hydroxybenzaldehyde (**2**) with BnBr under basic conditions (98% yield),



Scheme 1. Reagents and conditions: a) K_2CO_3 (1.5 equiv), BnBr (1.0 equiv), KI (0.1 equiv), DMF, 25 °C, 12 h, 98%; b) $(EtO)_2(O)PCH_2COOEt$ (1.1 equiv), KOH (1.5 equiv), THF, 25 °C, 12 h, 95%; c) NaOH (3.0 equiv), $BnOCONH_2$ (3.1 equiv), *t*BuOCl (3.0 equiv), $(DHQD)_2AQN$ (0.05 equiv), $K_2[OsO_2(OH)_4]$ (0.04 equiv), *n*PrOH:H_2O (1:1), 25 °C, 12 h, 45% (87% *ee*); d) TBSOTf (1.1 equiv), 2,6-lutidine (1.5 equiv), CH_2Cl_2, 0 °C, 0.5 h, 98%; e) H_2, $Pd(OH)_2$/C (0.01 equiv), MeOH, 0.5 h, 95%; f) SO_2Cl_2 (1.0 equiv), Et_2O (3.0 equiv), CH_2Cl_2, 0 °C, 1 h, 80%. Bn = benzyl; Cbz = benzyloxycarbonyl; TBS = *tert*-butyldimethylsilyl. TBSOTf = *tert*-butyldimethylsilyltrifluoromethanesulfonate.

followed by olefination with the anion of $(EtO)_2(O)PCH_2COOEt$, furnished α,β-unsaturated ethyl ester **4** (95% yield) via compound **3**. Asymmetric aminohydroxylation (AA) according to the Sharpless protocol[8] gave directly the Cbz derivative (**5**) of the desired amino alcohol in 45% yield and

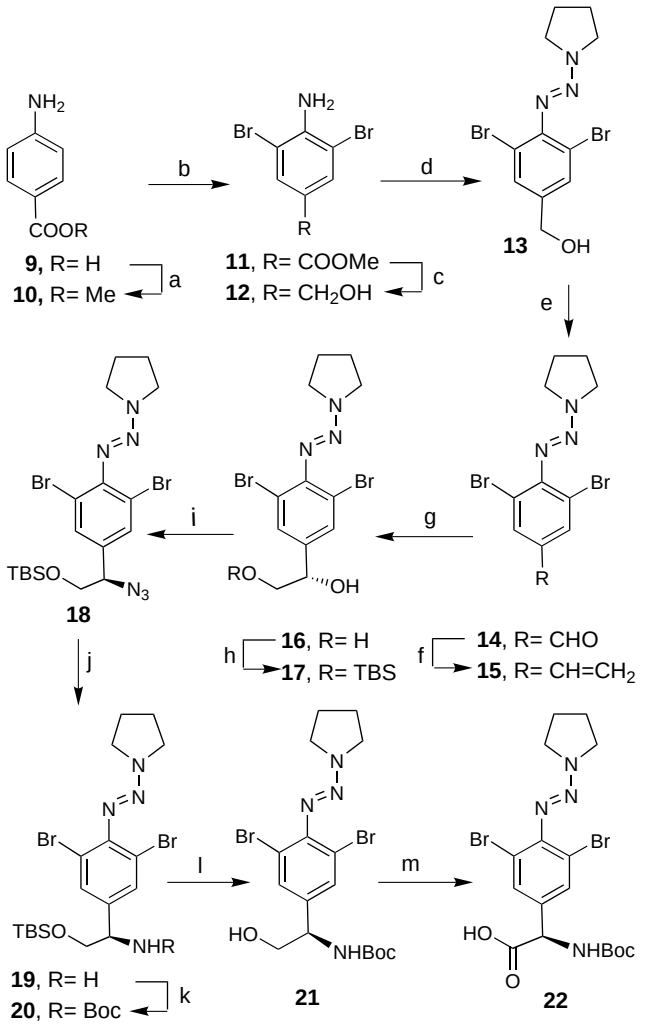
[*] Prof. Dr. K. C. Nicolaou, Dr. S. Natarajan, H. Li, Dr. N. F. Jain, R. Hughes, Dr. M. E. Solomon, Dr. J. M. Ramanjulu, C. N. C. Boddy, Dr. M. Takayanagi
Department of Chemistry and
The Skaggs Institute for Chemical Biology
The Scripps Research Institute
10550 North Torrey Pines Road, La Jolla, California 92037 (USA)
Fax: (+1) 619-784-2469
E-mail: kcn@scripps.edu
and
Department of Chemistry and Biochemistry
University of California, San Diego
9500 Gilman Drive, La Jolla, California 92093 (USA)

[**] We thank Dr. D. H. Huang and Dr. G. Siuzdak for assistance with the NMR spectroscopy and mass spectrometry, respectively. Financial support for this work was provided by the National Institutes of Health (USA), The Skaggs Institute for Chemical Biology, postdoctoral fellowships from the National Institutes of Health (to J.M.R.) and the George E. Hewitt Foundation (to M.S.), and grants from Pfizer, Schering Plough, Hoffmann La Roche, Merck, and Dupont Merck.

 © WILEY-VCH Verlag GmbH, D-69451 Weinheim, 1998 1433-7851/98/3719-2708 $ 17.50+.50/0

87% *ee*. The hydroxy group in **5** was then protected by exposure to TBSOTf and 2,6-lutidine (98% yield), and the resulting compound **6** was subjected to hydrogenolysis (H_2, 10% $Pd(OH)_2/C$), which caused cleavage of both the benzyl and Cbz groups, affording phenol **7** (95% yield). Finally, chlorination of **7** with SO_2Cl_2[9] resulted in the formation of the targeted intermediate **8** in 80% yield. This enantiomerically enriched fragment was coupled with pure fragment **35** and the diastereoisomers were separated (see Scheme 4).

The synthesis of the central amino acid (amino acid 4) equivalent **22** was carried out as shown in Scheme 2. Thus, 4-aminobenzoic acid (**9**) was methylated and thence brominated to afford dibromide **11** (98% overall yield) via methyl ester **10**. The ester group in **11** was reduced with $LiAlH_4$ to afford alcohol **12** (95% yield) and the amino group of the latter was diazotized ($NaNO_2$/HCl). The formed diazonium salt was then intercepted with pyrrolidine to afford triazene **13** in 75% overall yield. Oxidation of the hydroxy group in **13** with PCC led to the corresponding aldehyde (**14**, 88% yield), which was converted by Wittig reaction into terminal olefin **15** (92% yield). Asymmetric dihydroxylation (AD) with AD-α according to the Sharpless procedure[10] then furnished diol **16** (95% yield, 95% *ee*) which was selectively silylated with TBSCl/imidazole to afford monosilylated compound **17** (88% yield). Reaction of **17** with DPPA in the presence of Ph_3P and DEAD afforded, with inversion of configuration,[11] azide **18** in 79% yield, while reduction of the latter with Ph_3P and H_2O at 65 °C led to the desired amine **19** (78% yield). Finally, formation of the Boc derivative **20** ($(Boc)_2O$, Et_3N, 95% yield) followed by desilylation (TBAF, 93% yield) and oxidation with TEMPO/NaOCl (75% yield) led to triazene carboxylic acid **22** via compound **21**.

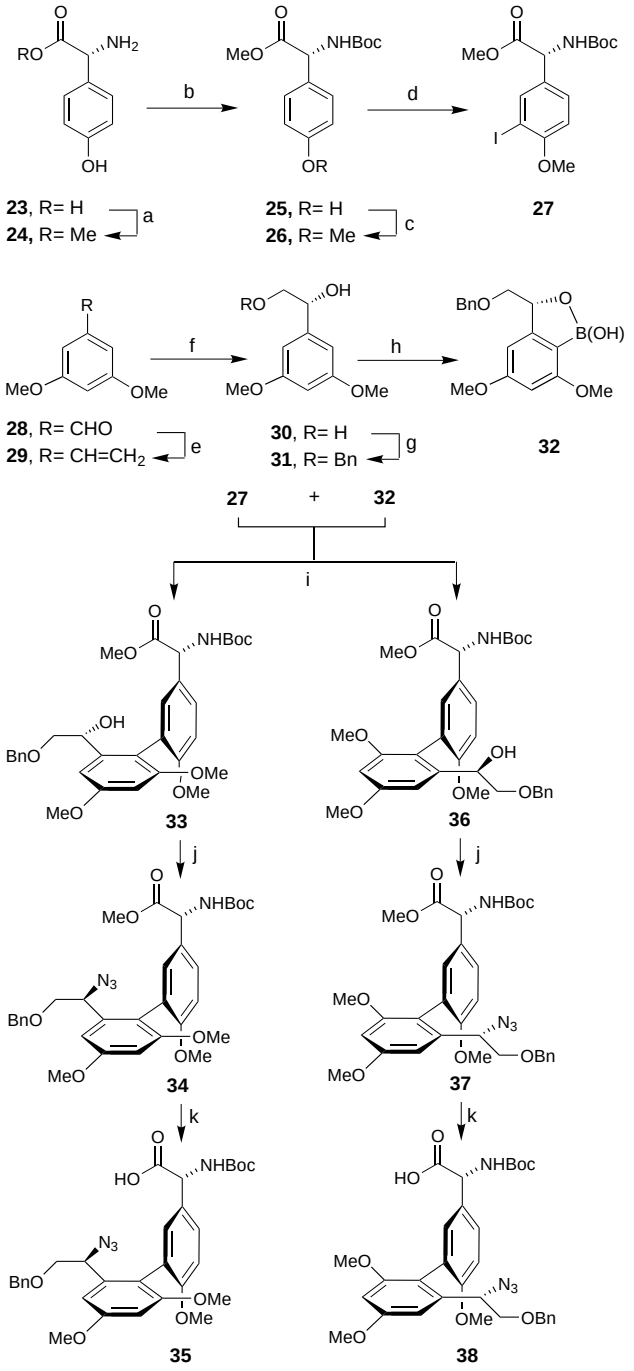


Scheme 2. Reagents and conditions: a) $SOCl_2$ (1.0 equiv), MeOH, reflux, 2 h, 100%; b) Br_2 (2.0 equiv), AcOH, 25 °C, 0.5 h, 98%; c) $LiAlH_4$ (1.5 equiv), THF, 0 °C, 2 h, 95%; d) 6 M HCl (5.0 equiv), $NaNO_2$ (1.2 equiv), AcOH:H_2O (1:2), 0 °C, 0.5 h, then KOH (8.0 equiv), pyrrolidine (1.5 equiv), 0 °C, 0.5 h, 75%; e) PCC (1.5 equiv), CH_2Cl_2, 25 °C, 2 h, 88%; f) *n*BuLi (1.4 equiv), CH_3PPh_3Br (1.5 equiv), THF, −20 °C, 2 h, 92%; g) AD-α (1.4 g mmol^{-1}), *t*BuOH/H_2O (1:1), 6 h, 95%, (95% *ee*); h) TBSCl (1.1 equiv), imidazole (1.5 equiv), DMF, 0 °C, 5 h, 88%; i) Ph_3P (2.5 equiv), DEAD (2.5 equiv), DPPA (2.5 equiv), THF, 0 °C, 2 h, 79%; j) Ph_3P (3.0 equiv), H_2O (10.0 equiv), THF, 60 °C, 3 h, 78%; k) $(Boc)_2O$, Et_3N, CH_2Cl_2, 25 °C, 4 h, 95%; l) TBAF (1.2 equiv), THF, 0 °C, 2 h, 93%; m) TEMPO (1.0 equiv), 5% aq. NaOCl (3.0 equiv), 5% $NaHCO_3$, KBr (0.05 equiv), Me_2CO, 0 °C, 1 h, 75%. Boc = *tert*-butoxycarbonyl; DEAD = diethyl azodicaboxylate; DPPA = diphenylphosphoryl azide; PCC = pyridinium chlorochromate; TBAF = tetra-*n*-butylammonium fluoride; TEMPO = 2,2,6,6-tetramethyl-1-piperidinyloxy, free radical.

The more challenging AB biaryl system of vancomycin,[4a, 5b,c] which contains the amino acids 5 and 7, was constructed in the form of its azide equivalent **35** from its components **27** and **32**, as summarized in Scheme 3. Fragment **27** was synthesized in a straightforward manner from 4-hydroxyphenylglycine (**23**) by esterification (**23** → **24**, 98%), Boc derivative formation (**24** → **25**, 95%), methylation (**25** → **26**, 93%), and iodination (**26** → **27**, 90%). The boronic acid derivative **32** corresponding to amino acid 7 was constructed from 3,5-dimethoxybenzaldehyde (**28**) by a sequence requiring Wittig olefination (**28** → **29**, 91%), Sharpless asymmetric dihydroxylation (**29** → **30**, AD-β, 92% yield, 96% *ee*), selective monobenzylation with $n(Bu_2SnO)$/BnBr (**30** → **31**, 89%),[12] and boronation (**31** → **32**, 55%). The latter operation was effected by the action of *n*BuLi (2.2 equiv) on benzylic alcohol **31**,[13] followed by quenching with $B(OMe)_3$ and acidic hydrolysis.

Coupling of fragments **27** and **32** proceeded smoothly under Suzuki conditions[14] ($[Pd(Ph_3P)_4]$ cat., Na_2CO_3) furnishing the two atropisomers **33** and **36** in 84% yield and about 2:1 ratio. The major compound was proven to be the desired natural atropisomer **33** by incorporating it into the AB-COD ring system of vancomycin (see compound **46a** in Scheme 5) and establishing its stereochemistry by NOE studies (Table 2). Both atropisomers **33** and **36** were taken through the sequence shown in Scheme 3 to the desired biaryl fragments **35** and **38**, respectively. Thus, introduction of an azido group (DPPA, Ph_3P, DEAD)[11] accompanied by inversion of stereochemistry (**33** → **34**, 95% and **36** → **37**, 90%) was followed by ester hydrolysis with LiOH in aqueous THF (**34** → **35**, 99% and **37** → **38**, 99%).

Having constructed these appropriate functionalized fragments, we were in a position to address their assembly into more advanced systems. Below, we describe the coupling of these intermediates and the assembly of the AB-COD framework of vancomycin with the correct stereochemistry and functionality for further elaboration, as well as work on related isomers.[4a, b] These studies also allowed the identification of the proper atropisomer of the AB biaryl system and



Scheme 3. Reagents and conditions: a) TMSCl (2.1 equiv), MeOH, 25 °C, 15 h, 98 %; b) $(Boc)_2O$ (1.1 equiv), K_2CO_3 (4.0 equiv), dioxane:H_2O (1:1), 25 °C, 4 h, 95 %; c) MeI (2.0 equiv), K_2CO_3 (4.0 equiv), DMF, 25 °C, 6 h, 93 %; d) I_2 (1.2 equiv), CF_3COOAg (2.2 equiv), $CHCl_3$, 25 °C, 12 h, 90 %; e) *n*BuLi (1.3 equiv), CH_3PPh_3Br (1.5 equiv), THF, −20 °C, 10 h, 91 %; f) AD-β (1.4 g mmol^{-1}), *t*BuOH/H_2O (1:1), 25 °C, 8 h, 92 % (96 % *ee*); g) nBu_2SnO (1.0 equiv), toluene, reflux, 1 h, then BnBr (1.5 equiv), nBu_4NI (0.5 equiv), 70 °C, 2 h, 89 %; h) *n*BuLi (2.2 equiv), benzene, 0 → 25 °C, 2 h, then $B(OMe)_3$, THF, −78 °C → 25 °C, 6 h, dilute HCl, 55 %, i) $[Pd(Ph_3P)_4]$ (0.2 equiv), Na_2CO_3 (1.2 equiv), $PhCH_3$/MeOH/H_2O (10:1:0.5), 90 °C, 4 h, about 2:1 (**33**:**36**) ratio of atropisomers, 84 % combined yield; j) DPPA (2.5 equiv), DEAD (2.5 equiv), Ph_3P (2.5 equiv), THF, −20 °C, 2 h, 95 % of **34**, 90 % of **37**; k) LiOH (1.5 equiv), THF/H_2O (1:1), 0 °C, 0.5 h, 99 % of **35**, 99 % of **38**. TMS = trimethylsilyl.

of the COD ring framework through NMR spectroscopic techniques (see structures **46a** and **46b** and Tables 1 and 2).

Table 1. Selected physical properties of compounds **8**, **22, 34**, **42a**, and **46a**.

8: $R_f = 0.24$ [silica gel, 5 % methanol in chloroform]; $[\alpha]_D^{25} = -11.5$ ($c = 0.85$ $CHCl_3$); IR (film): $\tilde{\nu}_{max} = 3366, 2943, 2849, 2555, 1737, 1602, 1502, 1467, 1290, 1255, 1079\ cm^{-1}$; ^1H NMR (500 MHz, CD_3OD): $\delta = 7.19$ (d, $J = 2.0$ Hz, 1H), 6.99 (dd, $J = 8.5$, 2.0 Hz, 1H), 6.78 (d, $J = 8.5$ Hz, 1H), 4.89 (d, $J = 3.5$ Hz, 1H), 4.06 (m, 1H), 3.98 (m, 1H), 3.37 (bs, 1H), 1.12 (t, J = 5.0 Hz, 3H), 0.80 (s, 9H), −0.08 (s, 3H), −0.26 (s, 3H); ^{13}C NMR (125 MHz, CD_3OD): $\delta = 173.8, 154.1, 134.5, 129.3, 127.1, 121.5, 117.3, 76.7, 62.8, 62.3, 26.2, 19.0, 14.4, -4.4, -5.1$; HRMS (FAB): calcd for $C_{17}H_{29}ClNO_4Si$ [M+H$^+$]: 374.1554; found: 374.1549.

22: $R_f = 0.18$ [silica gel, 10 % methanol in chloroform]; $[\alpha]_D^{25} = -97.4$ ($c =$ 0.98 MeOH); IR (film): $\tilde{\nu}_{max} = 3344, 2976, 2872, 1711, 1415, 1367, 1313, 1223, 1162, 1052, 1020\ cm^{-1}$; ^1H NMR (500 MHz, CD_3OD): $\delta = 7.53$ (s, 2H), 4.89 (bs, 1H), 3.81 (bs, 2H), 3.54 (bs, 2H), 1.99 (bs, 2H), 1.95 (bs, 2H), 1.33 (s, 9H); ^{13}C NMR (125 MHz, CD_3OD): $\delta = 157.2, 148.7, 139.7, 132.2, 118.7, 112.0, 80.8, 52.3, 47.9, 28.7, 28.6, 24.9, 24.6$; HRMS (FAB): calcd for $C_{17}H_{22}Br_2N_4O_4Cs$ [M+Cs$^+$]: 636.9062; found: 636.9087.

34: $R_f = 0.22$ [silica gel, 30 % ethyl acetate in hexanes]; $[\alpha]_D^{25} = -18.1$($c =$ 0.25 $CHCl_3$); IR (film): $\tilde{\nu}_{max} = 3359, 2936, 2838, 2092, 1744, 1713, 1603, 1488, 1459, 1343, 1255, 1201, 1159, 1056\ cm^{-1}$; ^1H NMR (500 MHz, [D_6]acetone): $\delta = 7.43$ (dd, $J = 8.5$, 2.0 Hz, 1H), 7.32 – 7.21 (m, 5H), 7.16 (d, $J = 2.0$ Hz, 1H), 7.01 (d, $J = 8.5$ Hz, 1H), 6.67 (d, $J = 6.0$ Hz, 1H), 6.63 (d, $J = 2.5$ Hz, 1H), 6.58 (d, $J = 2.5$ Hz, 1H), 5.29 (d, $J = 8.0$ Hz, 1H), 4.62 (dd, $J = 9.2$, 3.0 Hz, 1H), 4.35 (s, 2H), 3.84 (s, 3H), 3.65 (s, 3H), 3.65 (s, 3H), 3.59 (s, 3H), 3.60 – 3.56 (m, 1H), 3.50 – 3.49 (m, 1H), 1.39 (s, 9H); ^{13}C NMR (100 MHz, [D_6]acetone): $\delta = 172.5, 161.4, 161.2, 160.8, 159.3, 158.6, 154.9, 131.8, 129.9, 129.1, 128.9, 128.2, 128.2, 125.8, 119.8, 112.0, 103.8, 98.9, 79.1, 74.4, 73.0, 62.9, 58.0, 56.1, 55.6, 55.6, 52.5, 28.5$; HRMS (FAB): calcd for $C_{32}H_{38}N_4O_8Cs$ [M+Cs$^+$]: 739.1744; found: 739.1718.

42a: $R_f = 0.58$ [silica gel, 50 % acetone in hexanes]; $[\alpha]_D^{25} = +85.8$ ($c = 1.94$ $CHCl_3$); IR (film): $\tilde{\nu}_{max} = 3418, 3365, 2955, 2932, 2859, 2099, 1720, 1675, 1605, 1503, 1409, 1341, 1259, 1201, 1158, 1098, 1027\ cm^{-1}$; ^1H NMR (500 MHz, $CDCl_3$): $\delta = 7.47$ (br s, 1H), 7.30 (d, $J = 2.0$ Hz, 1H), 7.28 – 7.17 (m, 10H), 6.83 (d, $J = 8.5$ Hz, 1H), 6.71 (m, 2H), 6.66 (d, $J = 2.0$ Hz, 1H), 6.39 (d, $J = 2.0$ Hz, 1H), 6.10 (d, $J = 8.5$ Hz, 1H), 5.18 (m, 1H), 4.91 (m, 1H), 4.72 (d, $J = 9.0$ Hz, 1H), 4.57 (dd, $J = 8.5$, 3.0 Hz, 1H), 4.46 – 4.38 (m, 2H), 4.32 – 4.26 (m, 1H), 4.16 (m, 1H), 4.09 (m, 1H), 3.96 (br s, 2H), 3.86 (s, 3H), 3.71 (br s, 2H), 3.60 (s, 3H), 3.51 (s, 3H), 3.39 (dd, $J = 11.0$, 9.0 Hz, 1H), 3.30 (m, 1H), 2.06 (m, 4H), 1.40 (s, 9H), 1.32 (dd, $J = 7.5$, 7.0 Hz, 3H), 0.75 (s, 9H), −0.06 (s, 3H), −0.23 (s, 3H); ^{13}C NMR (125 MHz, $CDCl_3$): $\delta = 168.5, 168.4, 168.2, 160.2, 157.8, 157.5, 154.5, 152.1, 141.9, 138.3, 137.5, 136.5, 134.2, 132.2, 129.3, 128.3, 128.1, 127.7, 127.6, 127.5, 127.2, 126.7, 126.6, 125.5, 125.2, 122.5, 119.6, 117.6, 117.5, 111.1, 102.5, 98.6, 80.3, 73.6, 73.3, 71.9, 62.0, 60.3, 59.8, 57.5, 55.6, 55.3, 55.1, 53.3, 51.0, 46.2, 28.2, 25.6, 24.0, 23.6, 17.8, 14.1, -4.4, -5.8$; HRMS (FAB): calcd for $C_{60}H_{73}BrClN_9O_{12}SiCs$ [M+Cs$^+$]: 1386.3074; found: 1386.3160.

46a: $R_f = 0.11$ [silica gel, 50 % acetone in hexanes]; $[\alpha]_D^{25} = -20.8$ ($c = 0.48$ $CHCl_3$); IR (film): $\tilde{\nu}_{max} = 3273, 2930, 1651, 1488, 1416, 1318, 1249, 1159, 1097, 1058, 1029\ cm^{-1}$; ^1H NMR (600 MHz, [D_6]acetone): $\delta = 8.14$ (s, 1H), 7.64 (d, $J = 1.9$ Hz, 1H), 7.49 (dd, $J = 8.4$, 1.9 Hz, 1H), 7.37 – 7.32 (m, 6H), 7.26 (m, 1H), 7.14 (d, $J = 2.3$ Hz, 1H), 7.06 (m, 1H), 7.03 (d, $J = 8.4$ Hz, 1H), 6.93 (d, $J = 8.6$ Hz, 1H), 6.88 (d, $J = 2.1$ Hz, 1H), 6.62 (d, $J = 2.1$ Hz, 1H), 6.22 (d, $J = 10.9$ Hz, 1H), 6.06 (d, $J = 8.5$ Hz, 1H), 5.90 (s, 1H), 5.63 (d, $J = 8.5$ Hz, 1H), 5.41 (d, $J = 3.8$ Hz, 1H), 5.18 (d, $J = 4.5$ Hz, 1H), 4.75 (d, $J = 5.8$ Hz, 1H), 4.57 (m, 2H), 4.40 – 4.37 (m, 2H), 3.96 – 3.93 (m, 1H), 3.89 (br s, 2H), 3.83 (s, 3H), 3.82 – 3.79 (m, 1H), 3.64 (s, 3H), 3.62 (s, 3H), 3.69 – 3.62 (br s, 2H), 2.06 (m, 4H), 1.38 (s, 9H); ^{13}C NMR (100 MHz, [D_6]acetone): $\delta = 170.8, 170.6, 168.4, 162.7, 161.0, 159.5, 158.1, 156.0, 152.5, 152.2, 142.2, 140.5, 139.5, 139.5, 138.7, 136.1, 129.1, 128.7, 128.6, 128.3, 128.0, 127.9, 127.4, 127.0, 125.0, 124.2, 122.3, 119.4, 114.4, 113.2, 106.1, 98.4, 79.6, 73.6, 72.9, 70.2, 63.9, 56.6, 56.0, 55.6, 55.0, 52.7, 51.6, 47.0, 36.1, 28.5, 24.5, 24.1$; HRMS (FAB): calcd for $C_{52}H_{55}BrClN_7O_{11}Cs$ [M+Cs$^+$]: 1200.1886; found: 1200.1965.

In retrospect, we now know that the major atropisomer of the biaryl system described above possesses the correct stereochemical arrangement (**35**, Scheme 3) for the vancomycin molecule. The coupling of this biaryl fragment with

 © WILEY-VCH Verlag GmbH, D-69451 Weinheim, 1998 1433-7851/98/3719-2710 $ 17.50+.50/0

Table 2. Diagnostic NOEs for structural determination of selected atropisomers.[a]

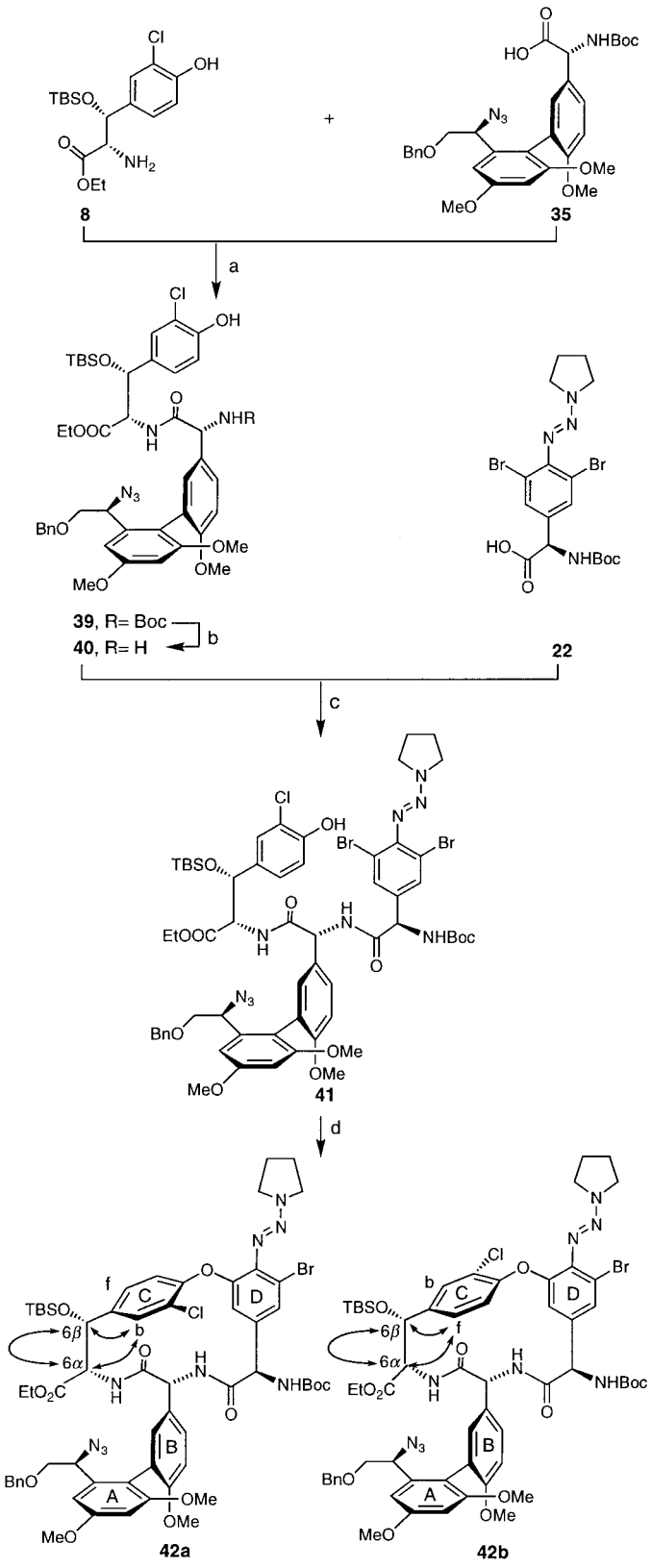
Compound	Solvent	(^{1}H – ^{1}H) NOE[b]
42a	$CDCl_3$	$6\alpha \leftrightarrow 6\beta$; $6\alpha \leftrightarrow$ Cb; $6\beta \leftrightarrow$ Cb
42b	$CDCl_3$	$6\alpha \leftrightarrow 6\beta$; $6\alpha \leftrightarrow$ Cf; $6\beta \leftrightarrow$ Cf
46a	[D_6]acetone	$6\alpha \leftrightarrow 6\beta$; $6\alpha \leftrightarrow$ Cb; $6\beta \leftrightarrow$ Cb; $5\alpha \leftrightarrow$ Bb; $6\alpha \leftrightarrow 5\alpha$
46b	[D_6]acetone	$6\alpha \leftrightarrow 6\beta$; $6\alpha \leftrightarrow$ Cf; $6\beta \leftrightarrow$ Cf; $5\alpha \leftrightarrow$ Bb; $6\alpha \leftrightarrow 5\alpha$
50a	[D_6]acetone	$6\alpha \leftrightarrow 6\beta$; $6\alpha \leftrightarrow$ Cb; $6\beta \leftrightarrow$ Cb
50b	[D_6]acetone	$6\alpha \leftrightarrow 6\beta$; $6\alpha \leftrightarrow$ Cf; $6\beta \leftrightarrow$ Cf
54a	[D_6]acetone	$6\alpha \leftrightarrow$ Cf; $6\beta \leftrightarrow$ Cb; $5\alpha \leftrightarrow$ Bf
54b	[D_6]acetone	$6\alpha \leftrightarrow$ Cb; $6\beta \leftrightarrow$ Cf; $5\alpha \leftrightarrow$ Bf

[a] ^{1}H-^{1}H NOESY, 600 MHz, 300 K. [b] For the atom labeling in **42a** and **42b** see formula of compounds **46a** and **46b** in Scheme 5.

amino acid 6 in the form of derivative **8** (EDC/HOAt, 85% yield, de ca. 13:1), and the elaboration of the resulting dipeptide **39** (chromatographically separated from the minor diastereoisomer) to the desired COD ring system **42a** and its atropisomer **42b** is shown in Scheme 4. Thus, cleavage of the Boc group from **39** by the action of TMSOTf and 2,6-lutidine (90% yield), followed by EDC/HOAt induced coupling of the resulting amine **40** with the derivative of the central amino acid, **22**, furnished tripeptide **41** in 76% yield. Exposure of **41** to $CuBr \cdot SMe_2$, K_2CO_3, and pyridine in CH_3CN at reflux[5a] resulted in the formation of the two atropisomers of the COD ring **42a** and **42b** in 60% combined yield (ca. 1:1 ratio). NMR (e.g. COSY and NOESY) analysis of **42a** and **42b** established the identity of these two atropisomers by revealing the expected NOE data for each compound (see Scheme 4 and Tables 1 and 2).

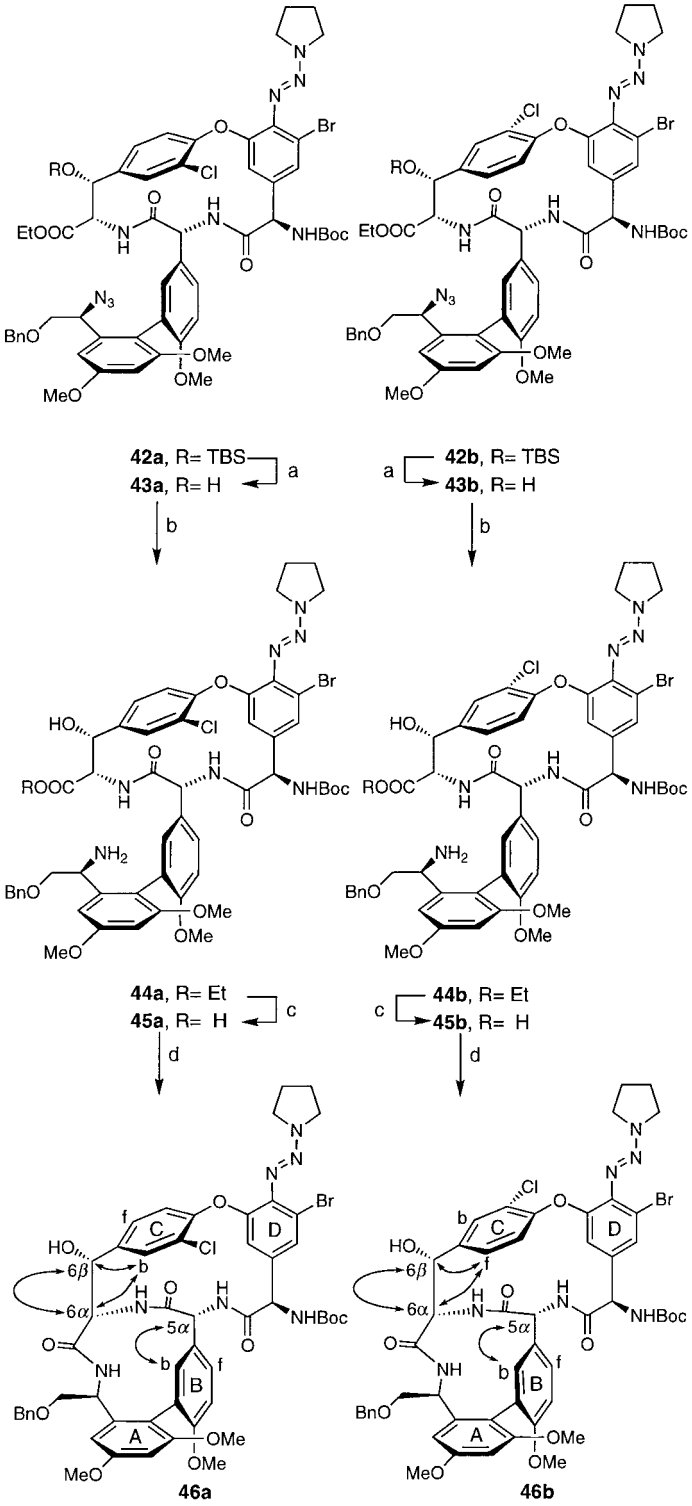
The elaboration of both atropisomers **42a** and **42b** to the respective AB-COD ring frameworks (**46a** and **46b**) is shown in Scheme 5. It was indeed pleasing to observe that the second ring closure could be effected smoothly by a lactamization protocol as we demonstrated recently in model systems.[5c] Thus, the correct atropisomer **42a** was desilylated with TBAF, furnishing hydroxy ester **43a** (80% yield). This deprotection was necessary to facilitate, in a subsequent step, the basic hydrolysis of the ethyl ester which proved, otherwise, robust. The azido group in **43a** was then reduced to an amino group by the action of Et_3P in the presence of H_2O at 25 °C, furnishing amino ester **44a** (71% yield), which was hydrolyzed easily with LiOH in THF/H_2O (1:1) at 0 °C to afford amino acid **45a** (68% yield). Finally, exposure of **45a** to FDPP[15] in the presence of iPr$_2$NEt in DMF at 25 °C resulted in the formation of the AB-COD ring framework **46a** in 71% yield. A similar sequence allowed the preparation of **46b** from **42b** via intermediates **43b** – **45b**. Again NMR spectroscopy (COSY and NOESY) proved instrumental in establishing the stereochemical arrangement within these unusual frameworks and the arrangement of the AB ring system. Thus, the observed NOEs (see Scheme 5 and Table 2) for **46a** and **46b** were consistent with those observed for **42a** and **42b** with regards to the COD ring stereochemistry and also established the stereochemical identity of the original biaryl system **35** as being natural.

In order to learn more about the properties of the various atropisomers of the AB-COD ring systems, we undertook the

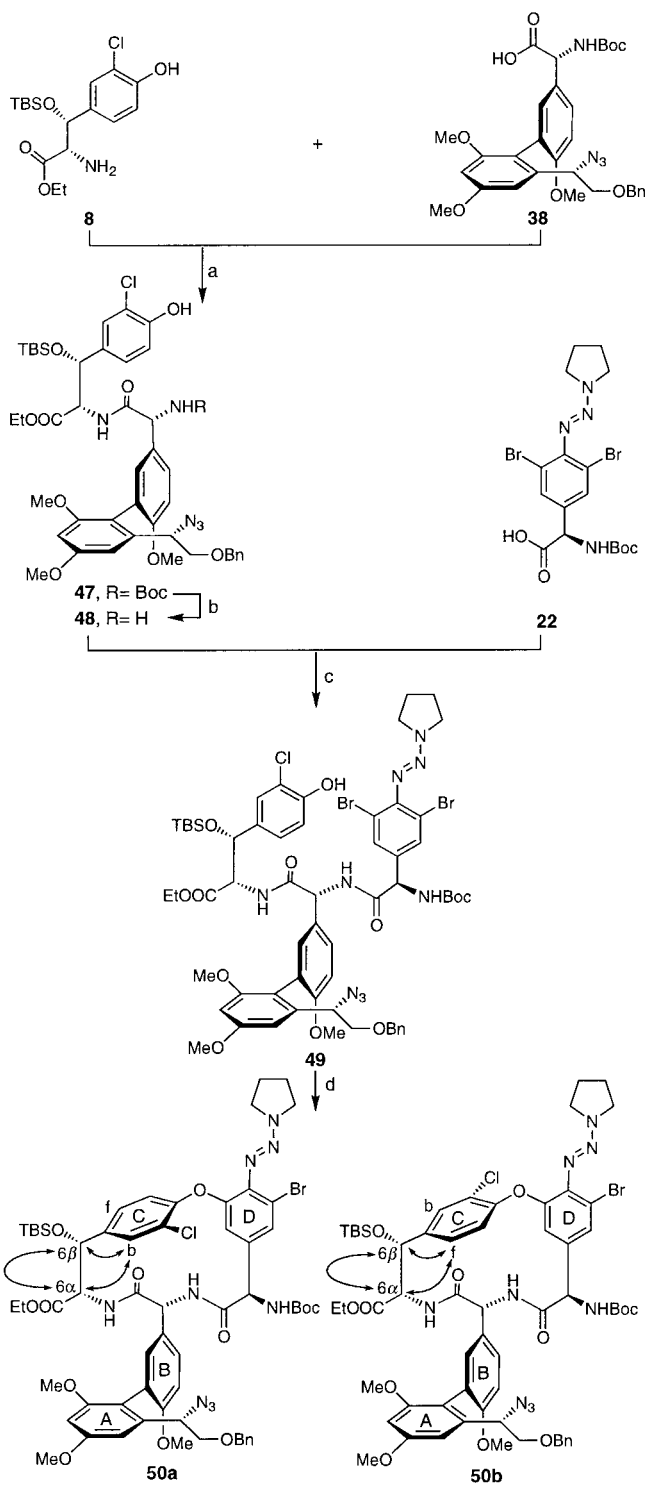


Scheme 4. Reagents and conditions: a) EDC (3.0 equiv), HOBt (3.3 equiv), THF, 0 °C, 12 h, 85%; b) TMSOTf (3.4 equiv), 2,6-lutidine (3.0 equiv), CH_2Cl_2, 0 °C, 3 h, 90%; c) EDC (3.0 equiv), HOAt (3.3 equiv), THF, −5 °C, 12 h, 76%; d) $CuBr \cdot SMe_2$ (3.0 equiv), K_2CO_3 (3.0 equiv), pyridine (3.0 equiv), MeCN, reflux, 20 min, ca. 1:1 ratio of atropisomers, 60% combined yield. EDC = 1-ethyl-3-(3-dimethylamino)propylcarbodiimide hydrochloride; HOAt = 1-hydroxy-7-azabenzotriazole; HOBt = 1-hydroxybenzotriazole.

 © WILEY-VCH Verlag GmbH, D-69451 Weinheim, 1998 1433-7851/98/3719-2711 $ 17.50+.50/0



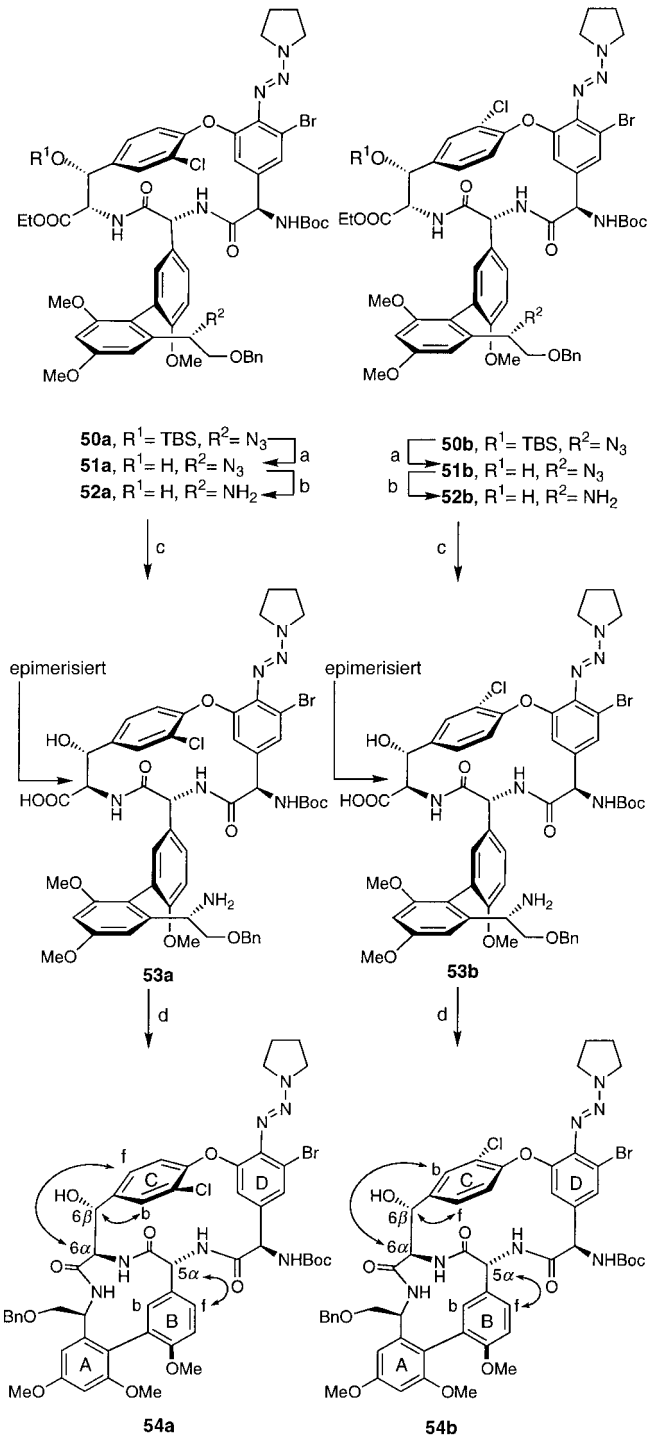
Scheme 5. Reagents and conditions: a) TBAF (1.5 equiv), THF, 0 °C, 2 h, 80% of **43a**, 100% of **43b**; b) Et_3P (2.0 equiv), H_2O (10.0 equiv), CH_3CN, 25 °C, 12 h, 71% of **44a**, 79% of **44b**; c) LiOH (5.0 equiv), THF/H_2O (1:1), 0 °C, 20 min, 68% of **45a**, 62% of **45b**; d) FDPP (3.0 equiv), iPr_2NEt (5.0 equiv), DMF, 25 °C, 12 h, 71% of **46a**, 52% of **46b**. FDPP = pentafluorophenyl diphenylphosphinate.



Scheme 6. Reagents and conditions: a) EDC (3.0 equiv), HOAt (3.3 equiv), THF, 0 °C, 10 h, 83%; b) TMSOTf (3.4 equiv), 2,6-lutidine (3.0 equiv), CH_2Cl_2, 0 °C, 3 h, 91%; c) EDC (3.0 equiv), HOAt (3.3 equiv), THF, 0 °C, 10 h, 70%; d) $CuBr \cdot SMe_2$ (3.0 equiv), K_2CO_3 (3.0 equiv), pyridine (3.0 equiv), MeCN, reflux, 20 min, about 1:1 ratio of atropisomers, 60% combined yield.

incorporation of the atropisomer of the biaryl system **35**, compound **38**, into the AB-COD framework. As outlined in Scheme 6, the coupling of **38** with fragments **8** and **22** and the further elaboration proceeded in a similar fashion as for its isomer **35**, furnishing the two atropisomers **50a** and **50b** via intermediates **47**–**49**. However, it was interesting to observe facile epimerization at the indicated positions (see structures **53** and **54**, Scheme 7) on attempted elaboration of **50a** and

 © WILEY-VCH Verlag GmbH, D-69451 Weinheim, 1998 1433-7851/98/3719-2712 $ 17.50+.50/0



Scheme 7. Reagents and conditions: a) TBAF (1.5 equiv), THF, 0 °C, 2 h, 90% of **51a**, 95% of **51b**; b) Ph_3P (3.0 equiv), THF, H_2O (10.0 equiv), 60 °C, 3 h, 82% of **52a**, 71% of **52b**; c) LiOH (1.5 equiv), MeOH:H_2O (10:1), 0 °C, 2 h, 92% of **53a**, 90% of **53b**; d) HATU (1.5 equiv), iPr$_2$NEt (3.0 equiv), DMF, 25 °C, 8 h, 50% of **54a**, 51% of **54b**. HATU = *N*-[(dimethylamino)-1*H*-1,2,3-triazole[4,5-*b*]-pyridin-1-ylmethylene]-*N*-methylmethanaminium hexafluorophosphate.

50b to the corresponding AB-COD ring frameworks. Thus, while desilylation of **50a** and **50b** and subsequent reduction of the azido group proceeded smoothly to afford amino esters **52a** and **52b** via **51a** and **51b**, respectively, attempted LiOH saponification of the ethyl ester in aqueous MeOH/H_2O (10:1) at 0 °C resulted in essentially complete epimerization of the adjacent stereocenters to furnish **53a** and **53b**. Lactamization of the amino acids **53a** and **53b** in the presence of HATU[16] and iPr$_2$NEt resulted in the formation of the respective AB-COD ring frameworks **54a** and **54b**. The stereochemical assignments were based on experiments with both sets of compounds **53a**/**53b** and **54a**/**54b** which revealed the appropriate coupling constants ($J_{6\alpha,6\beta} = 9.8$ Hz for **54a** and **54b**) and NOEs (see structures **54a** and **54b**, Scheme 7 and Table 2). While it was possible to arrest the epimerization process during the saponification of **52a** and **52b** by changing the hydrolysis conditions (THF/H_2O, 1:1), the ring-closure reactions with the non-epimerized amino acids proceeded with lower yields and, most significantly, with epimerization at the indicated positions,[4e] leading to the same products **54a** and **54b** as before. Thus, it appears that, with the unnatural AB atropisomers in place, the AB-COD ring frameworks prefer to reside in the epimeric form shown, irrespective of the atropisomeric position of the chlorine atom.

Further elaboration of the natural AB-COD framework (**46a**) to the vancomycin AB-COD-DOE tricyclic framework and its conversion into the aglycon of vancomycin are reported in the following communications.[7]

Received: April 14, 1998
Revised version: June 5, 1998 [Z11733/Z11734IE]
German version: *Angew. Chem.* **1998**, *110*, 2872 – 2878

Keywords: amino acids · antibiotics · natural products · synthetic methods · vancomycin

[1] *Glycopeptide Antibiotics* (Ed.: R. Nagarajan), Dekker, New York, **1994**.
[2] D. H. Williams, *Nat. Prod. Rep.* **1996**, *13*, 469.
[3] a) G. M. Sheldrick, P. G. Jones, O. Kennard, D. H. Williams, G. A. Smith, *Nature* **1978**, *271*, 223 – 225; b) P. J. Loll, A. E. Bevivino, B. D. Korty, P. H. Axelson, *J. Am. Chem. Soc.* **1997**, *119*, 1516 – 1522; c) M. H. McCormick, W. M. Stark, R. C. Pittenger, G. M. McGuire, *Antibiot. Annu.* **1955 – 1956**, 606 – 611; d) C. M. Harris, T. M. Harris, *J. Am. Chem. Soc.* **1982**, *104*, 4293 – 4295; e) C. M. Harris, H. Kopecka, T. M. Harris, *J. Am. Chem. Soc.* **1983**, *105*, 6915 – 6922.
[4] a) D. A. Evans, C. J. Dinsmore, *Tetrahedron Lett.* **1993**, 34, 6029; D. A. Evans, C. J. Dinsmore, A. M. Ratz, D. A. Evrard, J. C. Barrow, *J. Am. Chem. Soc.* **1997**, *119*, 3417; b) D. A. Evans, J. A. Ellman, K. M. DeVries, *J. Am. Chem. Soc.* **1989**, *111*, 8912; D. A. Evans, C. J. Dinsmore, D. A. Evrard, K. M. DeVries, *J. Am. Chem. Soc.* **1993**, *115*, 6426; D. A. Evans, P. S. Watson, *Tetrahedron Lett.* **1996**, *37*, 3251; D. A. Evans, J. C. Barrow, P. S. Watson, A. M. Ratz, C. J. Dinsmore, D. A. Evrard, K. M. DeVries, J. A. Ellman, S. D. Rychnovsky, J. J. Lacour, *J. Am. Chem. Soc.* **1997**, *119*, 3419; D. A. Evans, C. J. Dinsmore, A. M. Ratz, *Tetrahedron Lett.* **1997**, *38*, 3189; c) D. L. Boger, O. Loiseleur, S. L. Castle, R. T. Beresis, J. H. Wu, *Bioorg. Med. Chem. Lett.* **1997**, *7*, 3199; D. L. Boger, R. M. Borzilleri, S. Nukui, R. T. Beresis, *J. Org. Chem.* **1997**, *62*, 4721; D. L. Boger, R. M. Borzilleri, S. Nukui, *J. Org. Chem.* **1996**, *61*, 3561; D. L. Boger, R. M. Borzilleri, S. Nukui, *Bioorg. Med. Chem. Lett.* **1995**, *5*, 3091; D. L. Boger, Y. Nomoto, B. R. Teegarden, *J. Org. Chem.* **1993**, *58*, 1425, and references therein; d) R. Beugelmans, G. P. Singh, M. Bois-Choussy, J. Chastanet, J. Zhu, *J. Org. Chem.* **1994**, *59*, 5535; R. Beugelmans, J. Zhu, N. Husson, M. Bois-Choussy, G. P. Singh, *J. Chem. Soc. Chem. Commun.* **1994**, 439; R. Beugelmans, S. Bourdet, J. Zhu, *Tetrahedron Lett.* **1995,** *36*, 1279; J. Zhu, R. Beugelmans, S. Bourdet, J. Chastanet, G. Roussi, *J. Org. Chem.* **1995**, *60*, 6389; M. Bois-Choussy, R. Beugelmans, J.-P. Bouillon, J. Zhu, *Tetrahedron Lett.* **1995**, *36*, 4781; J. Zhu, J.-P. Bouillon, G. P. Singh, J. Chastanet, R. Beugelmans, *Tetrahedron Lett.* **1995**, *36*, 7081;

 © WILEY-VCH Verlag GmbH, D-69451 Weinheim, 1998 1433-7851/98/3719-2713 $ 17.50+.50/0

R. Beugelmans, L. Neuville, M. Bois-Choussy, J. Zhu, *Tetrahedron Lett*. **1995**, *36*, 8787; R. Beugelmans, M. Bois-Choussy, C. Vergne, J.-P. Bouillon, J. Zhu, *Chem. Commun*. **1996**, 1029; M. Bois-Choussy, L. Neuville, R. Beugelmans, J. Zhu, *J. Org. Chem*. **1996**, *61*, 9309; C. Vergne, M. Bois-Choussy, R. Beugelmans, J. Zhu, *Tetrahedron Lett*. **1997**, *38*, 1403; e) A. J. Pearson, J. G. Park, *J. Org. Chem*. **1992**, *57*, 1744; A. J. Pearson, J. G. Park, P. Y. Zhu, *J. Org. Chem*. **1992**, *57*, 3583; A. J. Pearson, H. Shin, *Tetrahedron* **1992**, *48*, 7527; A. J. Pearson, K. Lee, *J. Org. Chem*. **1994**, *59*, 2304; A. J. Pearson, H. Shin, *Tetrahedron* **1994**, 59, 2314; A. J. Pearson, K. Lee, *Tetrahedron* **1995,** *60*, 7153; A. J. Pearson, G. Bignan, *Tetrahedron Lett*. **1996**, *37*, 735; A. J. Pearson, G. Bignan, P. Zhang, M. Chelliah, *J. Org. Chem*. **1996**, *61*, 3940; A. J. Pearson, P. Zhang, G. Bignan, *J. Org. Chem*. **1997**, *62*, 4536; f) A. V. R. Rao, T. K. Chakraborty, S. P. Joshi, *Tetrahedron Lett*. **1992**, *33*, 4045; A. V. R. Rao, T. K. Chakraborty, K. L. Reddy, A. S. Rao, *Tetrahedron Lett*. **1992**, *33*, 4799; A. V. R. Rao, M. K. Gurjar, V. Kaiwar, V. B. Khare, *Tetrahedron Lett*. **1993**, *34*, 1661; A. V. R. Rao, K. L. Reddy, M. M. Reddy, *Tetrahedron Lett*. **1994**, *35*, 5039; A. V. R. Rao, T. K. Chakraborty, K. L. Reddy, A. S. Rao, *Tetrahedron Lett*. **1994**, *35*, 5043; A. V. R. Rao, K. L. Reddy, A. S. Rao, *Tetrahedron Lett*. **1994**, *35*, 5047; A. V. R. Rao, K. L. Reddy, A. S. Rao, *Tetrahedron Lett*. **1994**, *35*, 8465; A. V. R. Rao, K. L. Reddy, A. S. Rao, T. V. S. K. Vittal, M. M. Reddy, P. L. Pathi, *Tetrahedron Lett*. **1996**, *37*, 3023; A. V. R. Rao, M. K. Gurjar, P. Lakshmipathi, M. M. Reddy, M. Nagarajan, S. Shashwati, B. V. N. B. S. Sarma, N. K. Tripathy, *Tetrahedron Lett*. **1997**, *38*, 7433; g) N. Pant, A. D. Hamilton, *J. Am. Chem. Soc*. **1988**, *110*, 2002; M. J. Stone, M. S. Van Dyk, P. M. Booth, D. H. Williams, *J. Chem. Soc. Perkin Trans. 1* **1991**, 1629; K. Nakamura, S. Nishiyama, S. Yamamura, *Tetrahedron Lett*. **1996**, *37*, 191; H. Konishi, T. Okuno, S. Nishiyama, S. Yamamura, K. Koyasu, Y. Terada, *Tetrahedron Lett*. **1996**, *37*, 8791; A. G. Brown, M. J. Crimmin, P. D. Edwards, *J. Chem. Soc. Perkin Trans. 1* **1992**, 123; R. B. Lamont, D. G. Allen, I. R. Clemens, C. E. Newall, M. V. J. Ramsay, M. Rose, S. Fortt, T. Gallagher, *J. Chem. Soc. Chem. Commun.* **1992**, 1693; R. G. Dushin, S. J. Danishefsky, *J. Am. Chem. Soc*. **1992**, *114*, 3471; D. W. Hobbs, W. C. Still, *Tetrahedron Lett*. **1987**, *28*, 2805.

[5] a) K. C. Nicolaou, C. N. C. Boddy, S. Natarajan, T. Y. Yue, H. Li, S. Bräse, J. M. Ramanjulu, *J. Am. Chem. Soc.* **1997**, *119*, 3421; b) K. C. Nicolaou, X.-J. Chu, J. M. Ramanjulu, S. Natarajan, S. Bräse, F. Rübsam, C. N. C. Boddy, *Angew. Chem*. **1997**, *109*, 1518; *Angew. Chem. Int. Ed. Engl*. **1997**, *36*, 1539; c) K. C. Nicolaou, J. M. Ramanjulu, S. Natarajan, S. Bräse, H. Li, C. N. C. Boddy, F. Rübsam, *Chem. Commun*. **1997**, 1899; d) K. C. Nicolaou, H. J. Mitchell, F. L. van Delft, F. Rübsam, R. M. Rodriguez, *Angew. Chem*. **1998**, *110*, 1972 – 1974; *Angew. Chem. Int. Ed.* **1998**, *37*, 1871 – 1874.

[6] For recent reviews, see: a) A. V. R. Rao, M. K. Gurjar, K. L. Reddy, A. S. Rao, *Chem. Rev.* **1995**, *95*, 2135; b) K. Burgess, D. Lim, C. I. Martinez, *Angew. Chem*. **1996**, *108*, 1162; *Angew. Chem. Int. Ed. Engl*. **1996**, *35*, 1077; c) J. P. Zhu, *Synlett* **1997**, 133, and references therein.

[7] a) K. C. Nicolaou, N. F. Jain, S. Natarajan, R. Hughes, M. Solomon, H. Li, J. M. Ramanjulu, M. Takayanagi, A. E. Koumbis, T. Bando, *Angew. Chem*. **1998**, *110*, 2879 – 2881; *Angew. Chem. Int. Ed*. **1998**, *37*, 2714 – 2716; b) K. C. Nicolaou, M. Takayanagi, N. F. Jain, S. Natarajan, A. E. Koumbis, T. Bando, J. M. Ramanjulu, *Angew. Chem.* **1998**, *110*, 2881 – 2883; *Angew. Chem. Int. Ed.* **1998**, *37*, 2717 – 2719.

[8] B. Tao, G. Schlingloff, K. B. Sharpless, *Tetrahedron Lett*. **1998**, *39*, 2507. We thank Professor Sharpless for information on this asymmetric aminohydroxylation procedure.

[9] D. Masilamani, M. M. Rogic, *J. Org. Chem*. **1981**, *46*, 4486.

[10] H. C. Kolb, M. S. VanNieuwenhze, K. B. Sharpless, *Chem. Rev.* **1994**, *94*, 2484.

[11] B. Lal, B. Pramanik, M. S. Manha, A. K. Bose, *Tetrahedron Lett*. **1977**, 1977.

[12] S. David, S. Hanessian, *Tetrahedron* **1985**, *41*, 643.

[13] For a review on directed orthometalation, see: V. Snieckus, *Chem. Rev.* **1990**, *90*, 879.

[14] N. Miyaura, A. Suzuki, *Chem. Rev.* **1995**, *95*, 2483.

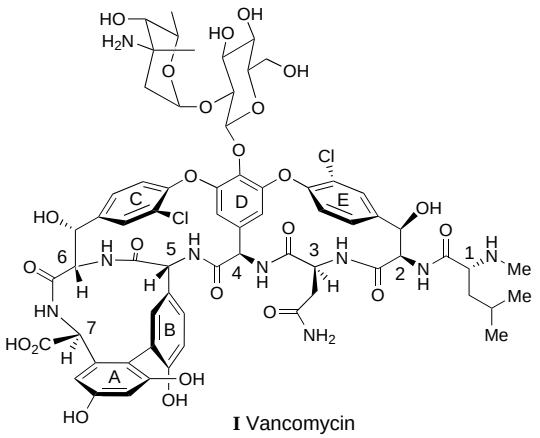
[15] S. Chen, J. Xu, *Tetrahedron Lett*. **1991**, *32*, 6711 – 6714.

[16] A. Ehrlich, H.-U. Heyne, R. Winter, M. Beyermann, H. Haber, L. A. Carpino, M. Bienert, *J. Org. Chem*. **1996**, *61*, 8831 – 8838.

Total Synthesis of Vancomycin Aglycon—Part 2: Synthesis of Amino Acids 1 – 3 and Construction of the AB-COD-DOE Ring Skeleton

K. C. Nicolaou,* Nareshkumar F. Jain, Swaminathan Natarajan, Robert Hughes, Michael E. Solomon, Hui Li, Joshi M. Ramanjulu, Masaru Takayanagi, Alexandros E. Koumbis, and Toshikazu Bando

In the preceding communication,[1] we reported the synthesis of the AB-COD ring system of vancomycin (**I**, Figure 1). Herein, we describe conversion of this intermediate (**16**, see



I Vancomycin

Figure 1. Molecular structure of vancomycin **I**.

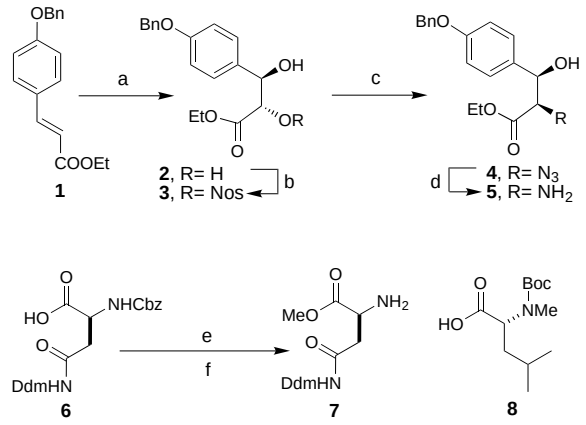
Scheme 3) into the AB-COD-DOE framework (**20a**, see Scheme 3) of vancomycin (**I**) by assembling and attaching the required tripeptide **15**, followed by triazene-driven ring closure.

Scheme 1 presents the three amino acid derivatives [compounds **8** (amino acid 1), **5** (amino acid 2), and **7** (amino acid 3)] required for the completion of the AB-COD-DOE ring framework, and their construction from readily available substrates. Thus, the derivative of amino acid 2, **5,** was reached from aryl ester **1** by the following four-step sequence:[2] 1) Sharpless asymmetric dihyroxylation (AD) to give **2** (79% yield, 92% *ee*); 2) regioselective nosylation (nosyl = Nos = 4-nitrobenzenesulfonyl), to give **3** (60% yield);

[*] Prof. Dr. K. C. Nicolaou, Dr. N. F. Jain, Dr. S. Natarajan, R. Hughes, Dr. M. E. Solomon, H. Li, Dr. J. M. Ramanjulu, Dr. M. Takayanagi, Dr. A. E. Koumbis, Dr. T. Bando
Department of Chemistry and
The Skaggs Institute for Chemical Biology
The Scripps Research Institute
10550 North Torrey Pines Road, La Jolla, California 92037 (USA)
Fax: (+1) 619-784-2469
E-mail: kcn@scripps.edu
and
Department of Chemistry and Biochemistry, University of California, San Diego, 9500 Gilman Drive, La Jolla, California 92093 (USA)

[**] We thank Dr. D. H. Huang and Dr. G. Suizdak for assistance with the NMR spectroscopy and mass spectrometry, respectively. This work was financially supported by the National Institutes of Health (USA), The Skaggs Institute for Chemical Biology, postdoctoral fellowships from the National Institutes of Health (to J. M. R.) and the George E. Hewitt Foundation (to M. S.), and grants from Pfizer, Schering Plough, Hoffmann La Roche, Merck, and Dupont Merck.

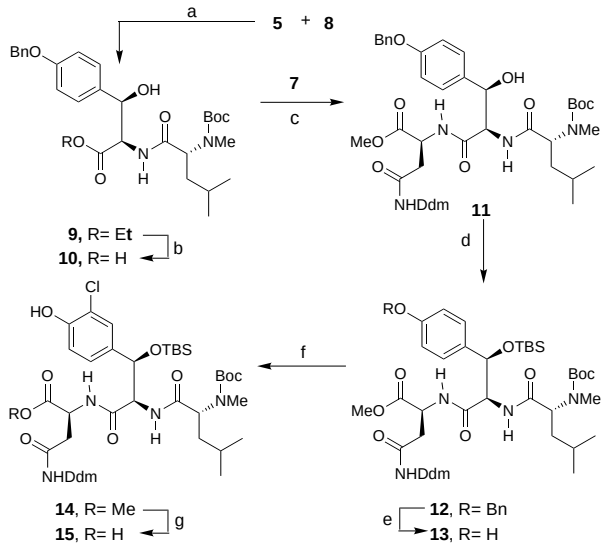
 © WILEY-VCH Verlag GmbH, D-69451 Weinheim, 1998 1433-7851/98/3719-2714 $ 17.50+.50/0



Scheme 1. Reagents and conditions: a) AD-β,[7] (1.4 g mmol^{-1}), Me-SO_2NH_2 (1.0 equiv), *t*BuOH/H_2O (1:1), 25 °C, 12 h, 79 % (92 % *ee*); b) NosCl (1.0 equiv), Et_3N (2.0 equiv), DMF, 0 °C, 5 h, 60 %; c) NaN_3 (1.5 equiv), DMF, 55 °C, 12 h, 90 %; d) $SnCl_2 \cdot H_2O$ (2.0 equiv), MeOH, 25 °C, 2 h, 90 %; e) MeI (2.0 equiv), K_2CO_3 (2.0 equiv), DMF, 25 °C, 12 h, 70 %; f) H_2, 20 wt % $Pd(OH)_2$/C, MeOH, 25 °C, 1 h, 99 %. Boc = *tert*-butoxycarbonyl; Bn = benzyl; Cbz = carbobenzyloxy; Ddm = 4,4′-dimethoxy diphenylmethyl; DMF = dimethylformamide; NosCl = 4-nitrobenzenesulfonyl chloride.

3) displacement with NaN_3 to afford **4** (90 % yield); and 4) reduction with $SnCl_2$ (90 % yield). The derivative of amino acid 3, **7**, was prepared from the known compound **6** simply by methylation to afford the corresponding methyl ester (70 % yield) followed by hydrogenolysis of the Cbz group (99 % yield).

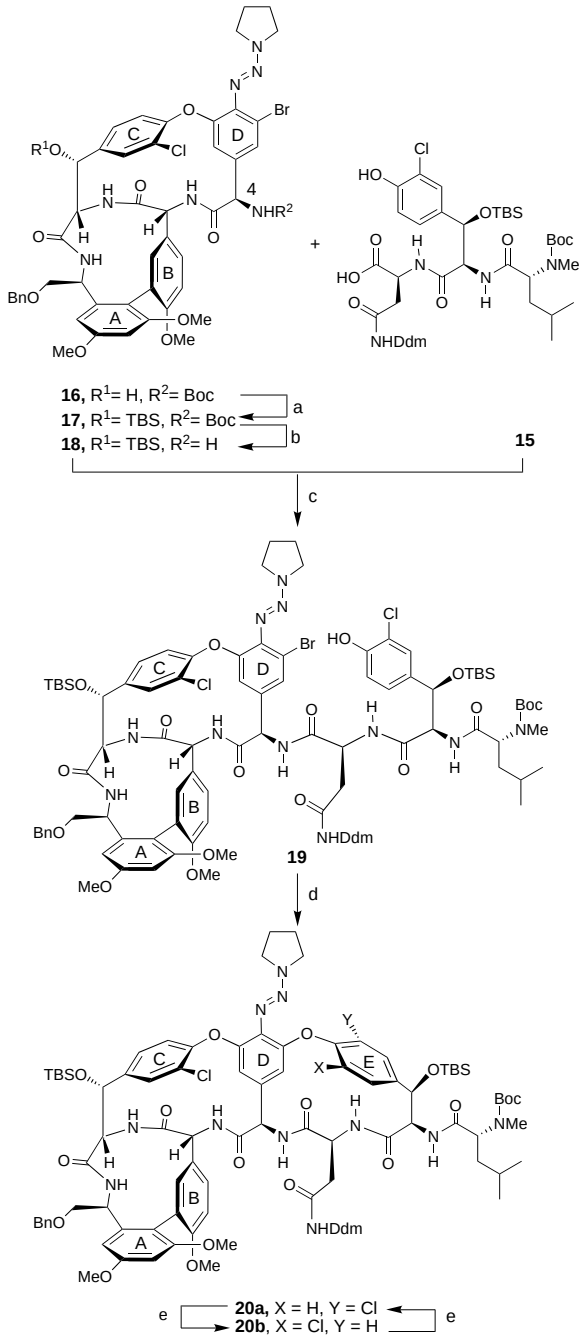
Tripeptide **15** was assembled as summarized in Scheme 2. Thus, coupling of fragments **5** and **8** proceeded smoothly under EDC/HOBt to give **9** (93 % yield), whereas attachment of fragment **7** onto the carboxylic acid group of dipeptide **10**, obtained from basic hydroylsis (LiOH, THF:H_2O, 99 % yield) of **9**, required the action of EDC/HOAt (82 % yield). Protection of the hydroxy group of **11** was then carried out



Scheme 2. Reagents and conditions: a) EDC (3.0 equiv), HOBt (3.3 equiv), THF, 0 °C, 12 h, 93 %; b) LiOH (2.0 equiv), THF/H_2O (1:1), 0 °C, 1 h, 99 %; c) EDC (3.0 equiv), HOAt (3.3 equiv), THF, 0 °C, 12 h, 82 %; d) TBSOTf (1.3 equiv), 2,6-lutidine (2.2 equiv), CH_2Cl_2, 0 °C, 2 h, 81 %; e) H_2, 20 wt % $Pd(OH)_2$/C, MeOH, 25 °C, 1 h, 99 %; f) SO_2Cl_2, Et_2O, 25 °C, 75 %; g) LiOH (4.0 equiv), *t*BuOH/H_2O (2:1), 0 °C, 0.5 h, 75 %. EDC = 1-ethyl-3-(3-dimethylamino)propylcarbodiimide hydrochloride; HOAt = 1-hydroxy-7-azobenzotriazole; HOBt = 1-hydroxy-1*H*-benzotriazole; TBS = *tert*-butyldimethylsilyl; Tf = trifluoromethanesulfonate.

with TBSOTf in the presence of 2,6-lutidine to afford silyl ether **12**, from which the benzyl group was cleaved by hydrogenolysis (H_2, 20 % $Pd(OH)_2$/C, 99 %). Finally, chlorination of **13** (SO_2Cl_2, 75 % yield), followed by mild saponification (LiOH, *t*BuOH/H_2O, 75 % yield), furnished the desired tripeptide fragment **15**.

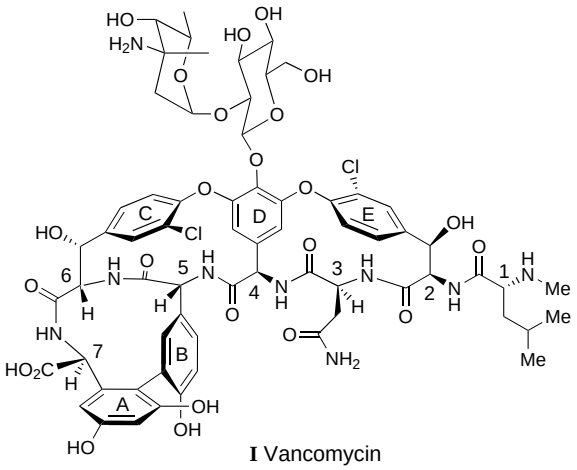
With the two segments **15** and **16** in hand, the task of joining them together and effecting the final ring closure came within reach (Scheme 3). In preparation for this union, the free



Scheme 3. Reagents and conditions: a) TBSOTf (10.0 equiv), 2,6-lutidine (20.0 equiv), CH_2Cl_2, −10 °C, 3.5 h, 83 % ; b) TMSOTf (3.0 equiv), 2,6-lutidine (1.2 equiv) , CH_2Cl_2, 0 °C, 2 h, 84 %; c) EDC (3.0 equiv), HOAt (10.0 equiv), −5 °C, 12 h, 81 %; d) $CuBr \cdot SMe_2$ (3.0 equiv), K_2CO_3 (3.0 equiv), pyridine (3.0 equiv), MeCN, reflux, 2 h, 72 %, **20a: 20b** about 1:3; e) 1,2-dichlorobenzene, 140 °C, 4 h, > 90 %, **20a:20b** about 1:1. TMS = trimethylsilyl.

 © WILEY-VCH Verlag GmbH, D-69451 Weinheim, 1998 1433-7851/98/3719-2715 $ 17.50+.50/0

hydroxyl group of **16** was silylated with TBSOTf/2,6-lutidine to afford the corresponding silyl ether (**17**, 83 % yield), and the free amine at C-4 was released by removing the Boc group (TMSOTf, 2,6-lutidine, 84 % yield) to furnish compound **18**. The coupling of **18** and **15** was carried out smoothly in the presence of EDC/HOAt (81 % yield) leading to the cyclization precursor **19**. Ring closure of **19** was then achieved by subjecting it to the previously developed conditions ($CuBr \cdot SMe_2$, K_2CO_3, pyr. CH_3CN, $\triangle$),[3] furnishing the targeted polycyclic intermediate[4] in 72 % yield as a mixture of the two atropisomers **20a** and **20b** (ca. 1:3 ratio). COSY and ROESY NMR experiments facilitated the stereochemical assignment of the two atropisomers **20a** and **20b** (Figure 2). Selected



I Vancomycin

Figure 2. Stereochemical assignments of atropisomers **20a** and **20b** based on NOE measurements (COSY and ROESY, 600 MHz, CD_3OD, 323 K).

physical data for **20a**, **20b**, and their precursor compound **19** are listed in Table 1. Chromatographic separation followed by heating either atropisomer in 1,2-dichlorobenzene[5] at 140 °C for 4 h resulted in the formation of a mixture of the two atropisomers **20a** and **20b**, in a ratio of approximately 1:1 (> 90 % recovered yield).[6]

Culminating in the construction of a highly functionalized vancomycin scaffold, the chemistry described herein brings the total synthesis of this antibiotic and its aglycon within striking distance. The attainment of the latter goal is described in the following communication.[8]

Received: April 30, 1998 [Z 11807 IE]
German version: *Angew. Chem.* **1998**, *110*, 2879 – 2881

Keywords: amino acids · antibiotics · natural products · synthetic methods · vancomycin

Table 1. Selected physical properties of compounds **19**, **20a** and **20b**.

19: $R_f = 0.29$ [silica gel, 1:2:7 acetone: ethyl acetate: benzene]; $[\alpha]_D^{25} = +21.3$ ($c = 0.52$, CH_3OH); IR (film): $\tilde{\nu}_{max}$ 3334, 2944, 2924, 2847, 2360, 1659, 1606, 1508, 1484, 1464, 1250, 1202, 1172, 1148, 1109, 1031 cm^{-1}; ^1H NMR (600 MHz, [D$_6$]acetone): $\delta = 8.18$ (br s, 2H), 7.78 (d, $J = 8.0$ Hz, 1H), 7.73 (d, $J = 8.2$ Hz, 1H), 7.68 (d, $J = 1.9$ Hz, 1H), 7.58 (d, $J = 7.3$ Hz, 1H), 7.49 (dd, $J = 8.5$, 1.6 Hz, 1H), 7.40 – 7.33 (m, 6H), 7.28 (m, 1H), 7.16 – 7.07 (m, 6H), 7.04 (m, 1H), 6.95 (d, $J = 2.1$ Hz, 1H), 6.89 (d, $J = 9.1$ Hz, 1H), 6.87 – 6.81 (m, 5H), 6.89(d, $J = 5.4$ Hz, 1H), 6.62 (d, $J = 2.0$ Hz, 1H), 6.19 (br s, 1H), 6.11 (d, $J = 8.2$ Hz, 1H), 5.95 (br s, 2H), 5.48 (s, 1H), 5.10(d, $J = 5.8$ Hz, 1H), 4.83 (m, 1H), 4.73 (d, $J = 6.3$ Hz, 1H), 4.68 (dd, $J = 8.1$, 5.8 Hz, 1H), 4.61 – 4.58 (br, 1H), 4.58 (s, 2H), 4.44 (br s, 1H), 4.35 (d, $J = 11.9$ Hz, 1H), 3.96 (m, 1H), 3.89 (dd, $J = 9.9$, 3.5 Hz, 1H), 3.83 (s, 3H), 3.78 (s, 3H), 3.85 – 3.60 (m, 5H), 3.74 (s, 3H), 3.65 (s, 3H), 3.63 (s, 3H), 2.86 (dd, $J = 15.5$, 4.7 Hz, 1H), 2.71 (m, 1H), 2.56 (s, 3H), 2.03 (m, 4H), 1.71 – 1.32 (m, 12H), 0.90 (s, 9H), 0.82 (s, 9H), 0.88 – 0.84 (m, 6H), 0.084 (s, 3H), 0.044 (s, 3H), 0.020 (s, 3H), – 0.13 (s, 3H); ^{13}C NMR (150 MHz, [D$_6$]acetone): $\delta = 171.5$, 171.0, 170.1, 169.9, 169.8, 169.6, 167.8, 161.1, 159.7, 159.6, 158.2, 153.3, 153.1, 152.3, 147.0, 141.6, 140.8, 139.8, 139.4, 138.0, 136.1, 135.5, 134.1, 131.5, 130.2, 129.6, 129.4, 129.3, 129.0, 128.9, 128.7, 128.3, 128.1, 127.9, 127.6, 127.3, 126.1, 125.3, 124.3, 122.5, 121.0, 119.7, 117.5, 114.6, 114.6, 113.6, 98.8, 98.3, 93.8, 93.7, 92.0, 80.1, 74.7, 74.4, 73.7, 70.6, 70.5, 64.2, 60.5, 60.4, 56.4, 56.2, 56.0, 55.7, 55.6, 55.5, 55.4, 52.7, 51.0, 38.8, 37.5, 37.4, 28.6, 26.2, 26.1, 25.4, 24.2, 23.5, 22.0, 18.8, 18.6, 14.4, – 4.6, – 4.7, – 4.8, – 4.9; HRMS (FAB): calcd for $C_{99}H_{124}BrCl_2N_{11}O_{19}Si_2Cs$ [M+Cs$^+$]: 2110.6208; found: 2110.6354.

20a: $R_f = 0.45$ [silica gel, 60 % ethyl acetate in benzene]; $[\alpha]_D^{25} = +20.0$ ($c = 0.11$, CH_3OH); IR (film): $\tilde{\nu}_{max}$ 3353, 2925, 2857, 2341, 2340, 1966, 1878, 1654, 1640, 1606, 1586, 1566, 1503, 1484, 1401, 1387, 1323, 1245, 1202, 1109, 1065, 1031 cm^{-1}; ^1H NMR (600 MHz, CD_3OD, 323 K): $\delta = 7.59$ (br s, 1H), 7.48 (d, $J = 6.7$ Hz, 1H), 7.36 – 7.26 (m, 8H), 7.21 (bd, $J = 8.0$ Hz, 1H), 7.16 (m, 1H), 7.08 – 6.97 (m, 9H), 6.72 (d, $J = 8.2$ Hz, 2H), 6.56 (d, $J = 2.5$ Hz, 1H), 5.86 (s, 1H), 5.78 (s, 1H), 5.72 (s, 1H), 5.48 (d, $J = 4.5$ Hz, 1H), 5.43 (br s, 1H), 5.29 (s, 1H), 4.90 (br s, 1H), 4.85 (br s, 1H), 4.77 (br s, 1H), 5.56 (m, 2H), 4.38 (br s, 1H), 4.09 (br s, 1H), 3.85 – 3.60 (m, 7H), 3.80 (s, 3H), 3.75 (s, 3H), 3.70 (s, 3H), 3.67 (s, 3H), 3.42 (s, 3H), 2.78 (br s, 3H), 2.64 – 2.55 (m, 2H), 2.07 (m, 4H), 1.80 – 1.30 (m, 12H), 1.11 – 0.7 (m, 24H), 0.1 (s, 3H), 0.65 (s, 3H), 0.03 (s, 3H), 0.02 (s, 3H); HRMS (FAB): calcd for $C_{99}H_{123}Cl_2N_{11}O_{19}Si_2Cs$ [M+Cs$^+$]: 2028.6967; found: 2028.6820.

20b: $R_f = 0.29$ [silica gel, 60 % ethyl acetate in benzene]; $[\alpha]_D^{25} = -7.27$ ($c = 0.11$, CH_3OH); IR (film): $\tilde{\nu}_{max}$ 2358, 2337, 2062, 2015, 1868, 1844, 1828, 1791, 1770, 1681, 1667, 1652, 1607, 1578, 1509, 1458, 1464, 1417, 1391, 1362, 1322, 1251 cm^{-1}; ^1H NMR (600 MHz, [D$_6$]acetone, 323 K): $\delta = 8.27$ (br s, 1H), 7.68 – 7.54 (m, 5H),7.43 – 7.41 (m, 3H), 7.38 – 7.35 (m, 3H), 7.31 – 7.29 (m, 4H), 7.26 – 7.22 (m, 3H), 7.14 – 7.11 (m, 6H), 7.00 – 6.98 (m, 2H), 6.98 (d, $J = 2.1$ Hz, 1H), 6.92 (d, $J = 8.7$ Hz, 1H), 6.86 – 6.82 (m, 5H), 6.77 (d, $J = 8.0$ Hz, 1H), 6.62 (d, $J = 2.3$ Hz, 1H), 6.31 (d, $J = 8.3$ Hz, 1H), 6.01 (d, $J = 8.1$ Hz, 1H), 5.90(s, 1H), 5.84 (br s, 1H), 5.48 (s, 1H), 5.50 (d, $J = 3.3$ Hz, 2H), 5.09 (br s, 1H), 4.70 (m, 2H), 4.46 (br s, 1H), 4.39 (d, $J = 12.0$ Hz, 1H), 3.99 (t, $J = 9.9$, 9.6 Hz, 1H), 3.92 (dd, $J = 9.9$, 3.4 Hz, 1H), 3.85 (s, 3H), 3.84 – 3.79 (m, 4H), 3.78 (s, 3H), 3.75 (s, 3H), 3.67 (s, 3H), 3.55 (s, 3H), 2.84 (s, 3H), 2.09 – 2.05 (m, 4H), 1.71 (br s, 1H), 1.62 – 1.60 (m, 1H), 1.52 (s, 9H), 0.95 (s, 9H), 0.93 (s, 9H), 0.93 – 0.90 (m, 6H), 0.16 (s, 3H), 0.11 (s, 3H), 0.10 (s, 3H), 0.08 (s, 3H); HRMS (FAB): calcd for $C_{99}H_{123}Cl_2N_{11}O_{19}Si_2Cs$ (M+Cs$^+$): 2028.6967; found: 2028.6832.

[1] Preceding communication: K. C. Nicolaou, S. Natarajan, H. Li, N. F. Jain, R. Hughes, M. Solomon, J. Ramanjulu, C. N. C. Boddy, M. Takayanagi, *Angew. Chem.* **1998**, *109*, 2872 – 2878; *Angew. Chem. Int. Ed.* **1998**, *37*, 2708 – 2714.

[2] For a similar procedure, see: A. V. R. Rao, T. K. Chakraborty, K. L. Reddy, A. S. Rao, *Tetrahedron Lett.* **1994**, *35*, 5043 – 5046.

[3] K. C. Nicolaou, C. N. C. Boddy, S. Natarajan, T. Y. Yue, H. Li, S. Bräse, J. M. Ramanjulu, *J. Am. Chem. Soc.* **1997**, *119*, 3421 – 3422.

[4] For a previous synthesis of an AB-COD-DOE ring framework related to vancomycin, see: D. A. Evans, J. C. Barrow, P. S. Watson, A. M. Ratz, C. J. Dinsmore, D. A. Evrard, K. M. D eVries, J. A. Ellman, S. D. Rychnovsky, J. Lacour, *J. Am. Chem. Soc.* **1997**, *119*, 3419 – 3420.

[5] D. L. Boger, R. T. Beresis, O. Loiseleur, J. H. Wu, S. L. Castle, *Bioorg. Med. Chem. Lett.* **1998**, *8*, 721 – 724.

[6] For selected references relating to the chemistry, biology and medicine of vancomycin, see references [1 – 4] in the preceeding paper.[1]

[7] H. C. Kolb, M. S. VanNieuwenhze, K. B. Sharpless, *Chem. Rev.* **1994**, *94*, 2484.

[8] K. C. Nicolaou, M. Takayanagi, N. F. Jain, S. Natarajan, A. E. Koumbis, T. Bando, J. M. Ramanjulu, *Angew. Chem.* **1998**, *110*, 2881 – 2883; *Angew. Chem. Int. Ed.* **1998**, *37*, 2717 – 2719.

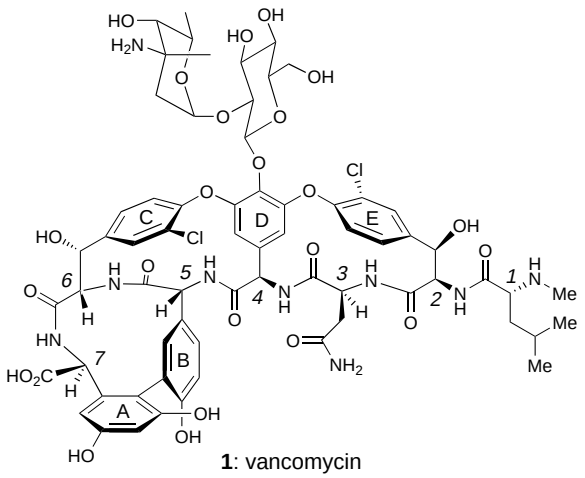
 © WILEY-VCH Verlag GmbH, D-69451 Weinheim, 1998 1433-7851/98/3719-2716 $ 17.50+.50/0

Total Synthesis of Vancomycin Aglycon—Part 3: Final Stages

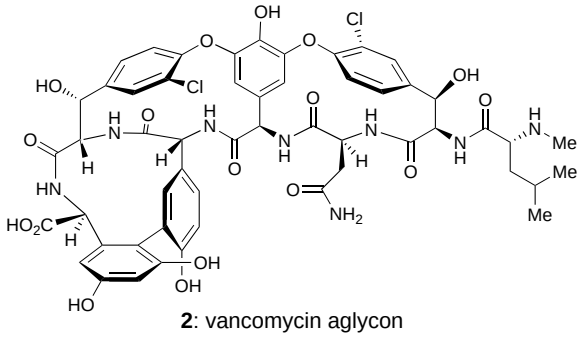
K. C. Nicolaou,* Masaru Takayanagi, Nareshkumar F. Jain, Swaminathan Natarajan, Alexandros E. Koumbis, Toshikazu Bando, Joshi M. Ramanjulu

In the two preceding communications,[1, 2] we described the construction of the vancomycin (**1**) key amino acid building blocks and their assembly to the skeletal framework (**3**) of this naturally occurring antibiotic. For completion of the total synthesis of the vancomycin aglycon (**2**), the following tasks remained: a) conversion of the triazene moiety into a phenol group; b) oxidation of the homobenzylic alcohol to a carboxyl group; and c) removal of all the protecting groups. Herein we report the accomplishments of these tasks which culminated in the total synthesis of the aglycon (**2**) of vancomycin (**1**).

The substitution of the triazene moiety with a hydroxyl group in the advanced vancomycin precursor **3**[2] (Scheme 1) proved more challenging than anticipated. Thus, initial attempts to effect this transformation by using standard methods (for example, aqueous acidic conditions,[3] diazotization followed by treatment with $Cu_2O/Cu_3(NO_3)_2 \cdot 2.5\,H_2O$[4]) failed to produce significant amounts of the desired phenolic compound, leading instead to the corresponding reduction product **8**. It was after considerable experimentation that the following sequence was devised and proved successful in delivering the targeted vancomycin aglycon (**2**). Thus, the triazene functionality in **3** was reduced with Raney Ni[5] in an efficient reaction that also caused partial debenzylation, producing a mixture of aniline derivatives **4** and **5** (ca. 1:1 ratio). Further hydrogenolysis of this mixture (H_2, 10% $Pd(OH)_2$/C) resulted in clean formation of the aniline derivative **5** (85% yield from **3**). Diazotization of the amino group in compound **5** by the action of HBF_4 and isoamyl nitrite at $-20\,^{\circ}C$ furnished diazonium salt **6** which was treated in situ with saturated aqueous potassium iodide solution to afford iodide **7**. The latter compound (**7**) was found to be contaminated with the corresponding reduced product **8** (ca. 6:4 ratio in favor of **7**, inseparable mixture). This mixture was converted into the desired phenol (**10**) via its boronate (**9**), at which stage the reduced product was easily removed by silica gel chromatography. Thus, deprotonation of all the NH groups in **7** and halogen–metal exchange at $-40\,^{\circ}C$ with excess MeMgBr and *i*PrMgBr,[6] followed by quenching of the resulting aryl Grignard species with excess $B(OMe)_3$, resulted in the formation of the aryl boronate[7, 8] derivative **9**. This compound (**9**) was then oxidized in situ with basic H_2O_2, leading to a mixture of phenol **10** and reduced product **8**. Preparative layer silica gel chromatography gave pure **10** in 50% overall yield (from **5**). It is worth noting that no significant stereochemical changes were observed during these transformations. Prior to oxidation of the primary hydroxyl group to the desired carboxylic acid moiety, it was considered prudent to protect the phenolic group. This objective was achieved by exposure of **10** to excess of MeI in the presence of Cs_2CO_3, leading to methoxy derivative **11** in 95% yield.



1: vancomycin



2: vancomycin aglycon

The oxidation of the primary hydroxyl group in **11** was smoothly effected by sequential treatment with Dess–Martin reagent[9] and potassium permanganate,[10] furnishing, after treatment with diazomethane, methyl ester **12** via the corresponding aldehyde and carboxylic acid (90% overall yield). Finally, all protecting groups were removed from **12** by exposure to $AlBr_3$ and EtSH,[11] furnishing vancomycin aglycon (**2**) in 50% yield. Synthetic aglycon **2**[12, 13] and derivative **12**[14] revealed identical physical properties (HPLC, ^{13}C NMR, IR, $[\alpha]_D^{25}$, MS) to those exhibited by samples derived from natural vancomycin (**1**)[15] (see Table 1 for selected physical data).

The chemistry described in this series of papers paves the way for the total synthesis of vancomycin (**1**) itself and other

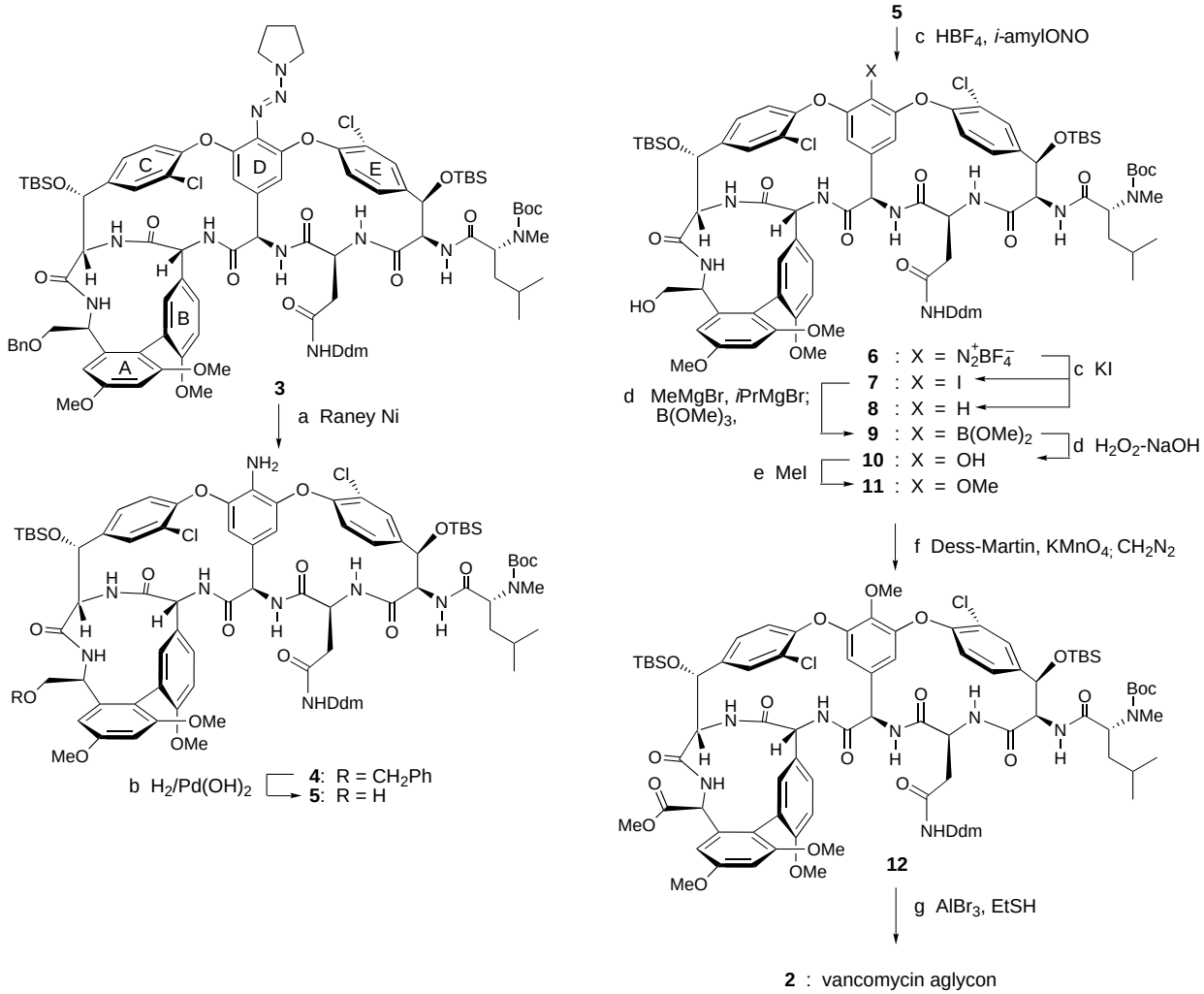
[*] Prof. Dr. K. C. Nicolaou, Dr. M. Takayanagi, Dr. N. F. Jain, Dr. S. Natarajan, Dr. A. E. Koumbis, Dr. T. Bando, Dr. J. M. Ramanjulu
Department of Chemistry and
The Skaggs Institute for Chemical Biology
The Scripps Research Institute
10550 North Torrey Pines Road, La Jolla, California 92037 (USA)
Fax: (+1) 619-784-2469
E-mail: kcn@scripps.edu
and
Department of Chemistry and Biochemistry
University of California, San Diego
9500 Gilman Drive, La Jolla, California 92093 (USA)

[**] We thank Dr. D. H. Huang and Dr. G. Siuzdak for assistance with the NMR spectroscopy and mass spectrometry, respectively. This work was financially supported by the National Institutes of Health (USA), The Skaggs Institute for Chemical Biology, postdoctoral fellowships from the National Institutes of Health USA (to J.M.R.) and the George E. Hewitt Foundation, and grants from Pfizer, Schering Plough, Hoffmann La Roche, and Dupont Merck.

Table 1. Selected physical and spectroscopic data of compounds **2** and **12**.

2 (trifluoroacetate salt): $[\alpha]_D^{25} = +80.63$ ($c = 0.4$, CH_3OH); IR (KBr): $\tilde{\nu}_{max} =$ 3398, 3010, 2918, 2846, 1717, 1671, 1589, 1513, 1431, 1262, 1206, 1175, 1139, 1057, 1032 cm^{-1}; ^1H NMR (600 MHz, CD_3OD, 330 K): $\delta = 7.73$ (br. d, $J =$ 7.8 Hz, 1H), 7.68 (bs, 1H), 7.64 (d, $J = 2$ Hz, 1H), 7.54 (dd, $J = 8.3$, 1.6 Hz, 1H), 7.5 (br. d, $J = 7.9$ Hz, 1H), 7.16 (d, $J = 8.4$ Hz, 1H), 7.06 (d, $J = 2$ Hz, 1H), 6.95 (m, 2H), 6.45 (d, $J = 2.2$ Hz, 1H), 6.42 (d, $J = 2.2$ Hz, 1H), 5.95 (br. s, 1H), 5.91 (br. s, 1H), 5.78 (br. s, 1H), 5.34 (br. s, 2H), 5.26 (d, $J =$ 3.6 Hz, 1H), 4.79 (s, 1H), 4.75 (s, 1H), 4.68 (d, $J = 5.7$ Hz, 1H), 4.24 (br. d, $J = 8.3$ Hz, 1H), 4.16 (s, 1H), 3.99 (dd, $J = 7.2$, 7.0 Hz, 1H), 2.96 (br. d, 1H), 2.75 (s, 3H), 2.0–1.8 (m, 2H), 1.75–1.57 (m, 2H), 0.89 (d, $J = 6.4$ Hz, 3H), 0.88 (d, $J = 6.3$ Hz, 3H); for signal assignments see ref. [18]; ^{13}C NMR (150 MHz, CD_3OD, 330 K): $\delta = 175.5$, 172.5, 171.8, 170.4, 170.1, 169.4, 168.9, 159.3, 158.0, 156.6, 153.5, 151.7, 149.9, 148.5, 142.4, 141.0, 137.6, 136.1, 131.8, 130.2, 129.2, 128.8, 128.5, 128.1, 127.3, 126.5, 125.3, 122.3, 119.0, 118.6, 110.3, 108.2, 106.7, 104.3, 74.3, 73.4, 64.1, 62.2, 59.8, 58.8, 57.5, 56.6, 55.3, 52.9, 40.3, 36.5, 33.1, 25.6, 23.0, 22.8, 17.2; MALDI MS: calcd for $C_{52}H_{53}Cl_2N_8O_{17}$ [$M+H^+$]: 1143, found 1143.

12: $R_f = 0.40$ (silica gel, 5% MeOH in CH_2Cl_2); IR (KBr): $\tilde{\nu}_{max} = 2930$, 2855, 2338, 1741, 1675, 1647, 1610, 1577, 1506, 1487, 1664, 1417, 1318, 1238, 1173, 1107, 1022, 830 cm^{-1}; ^1H NMR (600 MHz, CD_3OD, 330 K): $\delta = 7.62$ (m, 2H), 7.55 (dd, $J = 1.84$ Hz, 1H), 7.35 (br. s, 1H), 7.21 (d, $J = 12.6$ Hz, 1H), 7.07 (m, 1H), 6.98 (m, 3H), 6.91 (d, $J = 9$ Hz, 1H), 6.87 (d, $J = 9.6$ Hz, 1H), 6.80 (d, $J = 11.4$ Hz, 2H), 6.72 (m, 2H), 6.63 (d, $J = 2.7$ Hz, 1H), 6.35 (d, $J =$ 2.28 Hz, 1H), 5.85 (s, 1H), 5.71 (m, 1H), 5.70 (s, 1H), 5.51 (d, $J = 4.8$ Hz, 1H), 5.41 (s, 1H), 4.91 (m, 1H), 4.85 (m, 1H), 4.75 (m, 1H), 4.19 (br. s, 1H), 4.14 (s, 3H), 4.07 (br. s, 1H), 3.83 (s, 3H), 3.79 (s, 3H), 3.75 (s, 3H), 3.71 (s, 3H), 3.71 (s, 3H), 3.44 (s, 3H), 2.78 (s, 3H), 2.54 (m, 2H), 2.31 (m, 1H), 2.21 (m, 1H), 1.41 (br. s, 9H), 0.90 (s, 9H), 0.89 (s, 9H), 0.84 (d, $J = 6.24$ Hz, 3H), 0.79 (d, $J = 6.24$ Hz, 3H), 0.13 (s, 3H), 0.1 (s, 3H), 0.09 (s, 3H), 0.08 (s, 3H); ^{13}C NMR (150 MHz, CD_3OD, 330 K): $\delta = 175.6$, 174.4, 173.5, 172.4, 172.1, 171.3, 169.6, 168.6, 161.3, 160.1, 160.0, 159.9, 159.7, 159.6, 158.6, 158.3, 154.1, 152.4, 151.3, 141.5, 139.4, 138.3, 136.5, 136.3, 135.0, 134.6, 130.7, 129.7, 129.5, 129.0, 128.9, 128.7, 128.0, 127.8, 125.0, 124.6, 124.5, 122.8, 114.6, 114.4, 113.0, 107.1, 106.1, 105.8, 99.1, 74.2, 73.5, 64.3, 61.6, 60.9, 60.5, 57.5, 56.5, 56.1, 55.7, 55.6, 55.4, 52.2, 36.4, 30.0, 28.4, 27.3, 24.9, 24.2, 23.1, 20.3, 18.7, 13.9, -5.0, -5.1, -5.4; FAB HRMS: calcd for $C_{90}H_{112}Cl_2N_8O_{21}Si_2Cs$ [$M+Cs^+$]: 1899.5912, found 1899.6060.



Scheme 1. Reagents and conditions: a) Raney Ni, MeOH, 25 °C, 10 h; b) H_2, $Pd(OH)_2$/C, 25 °C, 1 h, 85% overall from **3**; c) HBF_4 (20 equiv), isoamyl nitrite (20 equiv), MeCN, −20 °C, 0.5 h; then saturated aqueous KI, −20 → 25 °C, 2 h; d) MeMgBr (30 equiv), −40 → −20 °C, 1 h; then *i*PrMgBr (30 equiv), −40 °C, 2 h; $B(OMe)_3$ (100 equiv), −40 → 0 °C, 1 h; 1:1 mixture of 30% aqueous H_2O_2 and 10% aqueous NaOH solution, −20 → 0 °C, 0.5 h, overall 50% **10** and 40% **8** from **5**; e) Cs_2CO_3 (5 equiv), MeI (10 equiv), DMF (0.01 M), 0 °C, 1 h, 95%; f) Dess–Martin periodinane (3.0 equiv), CH_2Cl_2, 0.5 h; $KMnO_4$ (1 M aqueous solution, 10 equiv), *t*BuOH/5% aqueous Na_2HPO_4, 0.5 h; CH_2N_2, Et_2O, 25 °C, 5 min, 90%; g) $AlBr_3$ (20 equiv), EtSH:CH_2Cl_2 (1:1), 25 °C, 2.5 h, 50%. Boc = *tert*-butoxycarbonyl; Bn = benzyl; Ddm = 4,4-dimethoxydiphenylmethyl; DMF = dimethylformamide; TBS = *tert*-butyldimethylsilyl.

 © WILEY-VCH Verlag GmbH, D-69451 Weinheim, 1998 1433-7851/98/3719-2718 $ 17.50+.50/0 *Angew. Chem. Int. Ed.* **1998**, *37*, No. 19

naturally occurring glycopeptide antibiotics and sets the stage for the design and synthesis of combinatorial libraries of these important structures for chemical biology studies. Particularly rewarding in this venture were the development and utilization of the triazene-based synthetic technology for the construction of complex biaryl ethers[16] and the adoption of the Suzuki coupling reaction in the strategy[1] for the synthesis of the AB ring system of the target molecule.[17,19]

Received: August 21, 1998 [Z12317IE]
German version: *Angew. Chem.* **1998**, *110*, 2881 – 2883
Keywords: amino acids · antibiotics · natural products · total synthesis · vancomycin

[1] K. C. Nicolaou, S. Natarajan, H. Li, N. F. Jain, R. Hughes, M. Solomon, J. Ramanjulu, C. N. C. Boddy, M. Takayanagi, *Angew. Chem.* **1998**, *109*, 2872 – 2878; *Angew. Chem. Int. Ed.* **1998**, *37*, 2708 – 2714.
[2] K. C. Nicolaou, N. F. Jain, S. Natarajan, R. Hughes, M. E. Solomon, H. Li, J. M. Ramanjulu, M. Takayanagi, A. E. Koumbis, T. Bando, *Angew. Chem.* **1998**, *109*, 2879 – 2881; *Angew. Chem. Int. Ed.* **1998**, *37*, 2714 – 2716.
[3] a) M. L. Gross, D. h. Blank, W. M. Welch, *J. Org. Chem.* **1993**, *58*, 2104 – 2109; b) N. Satyamurthy, J. B. Bario, G. T. Bida, M. E. Phelps, *Tetrahedron Lett*. **1990**, *31*, 4409 – 4412.
[4] T. Cohen, A. G. Dietz, Jr., J. R. Misor, *J. Org. Chem*. **1977**, *42*, 2053 – 2058; b) A. T Lewin, R. J. Michl, *J. Org. Chem.* **1974**, *39*, 2261 – 2264; c) A. T. Lewin, *J. Org. Chem.* **1967**, *32*, 3844 – 3850.
[5] A. Alexakis, N. Lensen, P. Mangeney, *Tetrahedron Lett*. **1991**, *32*, 1171 – 1174
[6] L. Boymond, M. Rottlander, G. Cahiez, P. Knochel, *Angew. Chem.* **1998**, *110*, 1801 – 1804; *Angew. Chem. Int. Ed.* **1998**, *37*, 1701 – 1703.
[7] S. W. Breur, J. A. Broster, *J. Organomet. Chem.* **1972**, *35*, C5.
[8] D. A. Evans, J. C. Barrow, P. S. Watson, A. M. Ratz, C. J. Dinsmore, D. A. Evrard, K. M. D eVries, J. A. Ellman, S. D. Rychnovsky, J. Lacour, *J. Am. Chem. Soc.* **1997**, *119*, 3419 – 3420.
[9] a) D. B. Dess, J. C Martin, *J. Org. Chem*. **1983**, *48*, 4155 – 4156; b) D. B. Dess, J. C Martin, *J. Am. Chem. Soc.* **1991**, *113*, 7277 – 7287.
[10] A. Abiko, J. C. Roberts, T. Takemasa, S. Masamune, *Tetrahedron Lett*. **1986**, *27*, 4537 – 4540.
[11] M. Node, K. Nishide, K. Fuji, E. Fujita, *J. Org. Chem.* **1980**, *45*, 4275 – 4277.
[12] a) F. J. Marshall, *J. Med. Chem.* **1965**, *8*, 18 – 22; b) R. Nagarajan, A. A. Schabel, *J. Chem. Soc. Chem. Commun*. **1988**, 1306 – 1307.
[13] HPLC conditions for vancomycin aglycon (**2**): C18 reverse-phase column (Vydac), gradient solvent system containing 0.05 % TFA (H_2O:CH_3CN, 95:5 → 70:30, 0 → 20 min), flow rate 1.0 mL min^{-1}, 25 °C, retention time 17.2 min.
[14] Authentic compound **12** was obtained from natural vancomycin hydrochloride by the following sequence: 1) introduction of the benzyloxycarbonyl (Cbz) group at the N atom (Cbz-Cl, NaOH, MeOH/H_2O); 2) methylation of the three phenolic hydroxy groups and the carboxyl moiety (Cs_2CO_3, MeI, DMF); 3) sugar hydrolysis (TFA, CH_2Cl_2[12]); 4) methylation of the newly liberated phenolic hydroxy group (Cs_2CO_3, MeI, DMF); 5) silylation of the benzylic hydroxy group (TBSOTf, 2,6-lutidine); 6) protection of the primary amide with a Ddm groups (Ddm-OH, AcOH, H_2SO_4 cat.); and 7) Cbz → Boc exchange (H_2, 10 % $Pd(OH)_2$/C; then Boc_2O, Et_3N). (TBSOTf = *tert*-butyldimethylsilyltrifluoromethanesulfonate).
[15] We thank Dr. L. Homer Pearce of Lilly Research Laboratories for a generous gift of naturally occurring vancomycin.
[16] K. C. Nicolaou, C. N. C. Boddy, S. Natarajan, T. Y. Yue, H. Li, S. Bräse, J. M. Ramanjulu, *J. Am. Chem. Chem.* **1997**, *119*, 3421 – 3422.
[17] For selected references relating to the chemistry, biology and medicine of vancomycin, see references [1 – 4] in the first paper[1] of this series.
[18] D. H. Williams, M. P. Williamson, *J. Am. Chem. Soc.* **1981**, *103*, 6580 – 6585; D. H. Williams, J. R. Kalman, *J. Am. Chem. Soc.* **1977**, *99*, 2768 – 2774.
[19] Note added in proof (Sept. 3, 1998): Direct conversion of triazene **3** into the corresponding aryl iodide was achieved by treatment with TMSCl)NaI in acetonitrile at 0 °C: H. Ku, J. R. Barrio, *J. Org. Chem.* **1981**, *46*, 5239 – 5241.

Site-Directed Surface Derivatization of MCM-41: Use of High-Resolution Transmission Electron Microscopy and Molecular Recognition for Determining the Position of Functionality within Mesoporous Materials**

Douglas S. Shephard,* Wuzong Zhou,*
Thomas Maschmeyer, Justin M. Matters,
Caroline L. Roper, Simon Parsons,
Brian F. G. Johnson, and Melinda J. Duer

Dedicated to Professor Sir John M. Thomas on the occasion of his 65th birthday

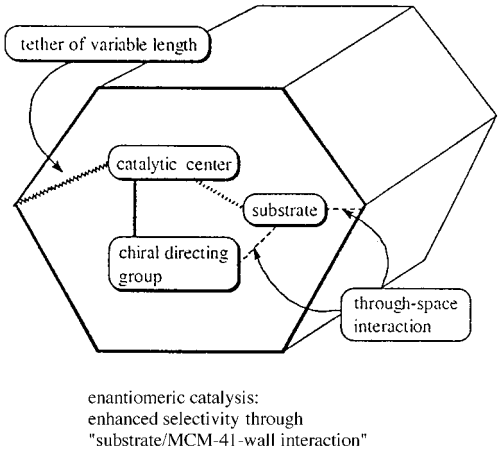
There is considerable commercial interest in the immobilization of catalysts on solid oxide supports, since the active materials thus prepared are considerably easier to handle, retrieve, and recycle than their homogeneous counterparts.[1] They may also exhibit improved activities and selectivities over those found for the homogeneous analogues. An approach used frequently in the heterogenization of homogeneous catalysts onto siliceous materials is the covalent linking of the active moiety to the surface through a surface-bound tether containing a functional group (for example $(MeO)_3Si$-$CH_2CH_2CH_2NH_2$).[2, 3] This methodology has been employed successfully in the functionalization of various traditional types of silica support, and with the advent of mesoporous silicas, in particular MCM-41,[4] it has been utilized extensively in the development of the surface chemistry of these materials.

The two key features of mesoporous silicas are their highly regular structure composed of channels in a hexagonal arrangement with diameters of 20 to 100 Å and their large surface areas ($\geq 750\ m^2 g^{-1}$). The large pore sizes offer the possibility to tether sizeable and complex catalytically active sites within the silica framework. The topological restraints produced by the confinement of solvent, substrate, and reactant may be expected to give a greater efficiency and selectivity in the catalytic process (Figure 1 a).

MCM-41 is composed of particles that usually range in size from 0.5 to 5 μm. Both the internal and external surfaces terminate in a layer of silanol groups (Si – OH), which are the reactive handle by which any derivatization/anchoring of catalytic centers may take place. Hence, derivatization of the surface of freshly calcined MCM-41 with an appropriately functionalized tether for anchoring a given catalyst will take

[*] Dr. D. S. Shephard, Dr. W. Zhou, Dr. T. Maschmeyer, Dr. J. M. Matters, C. L. Roper, Prof. B. F. G. Johnson, Dr. M. L. Duer
The University Chemical Laboratories
Lensfield Road, Cambridge, CB2 1EW (UK)
Fax: (+44) 1223-336-343
E-mail: dss1001@cus.cam.ac.uk (D.S.S.)
wz10001@cus.cam.ac.uk (W.Z.)
Dr. S. Parsons
Department of Chemistry
The University of Edinburgh
Edinburgh (UK)

[**] This work was supported by a Smithson Research Fellowship (The Royal Society/Peterhouse) to D.S.S, an EPSRC post-doctoral research award to B.F.G.J and an EU Fellowship (TMR) to T.M.



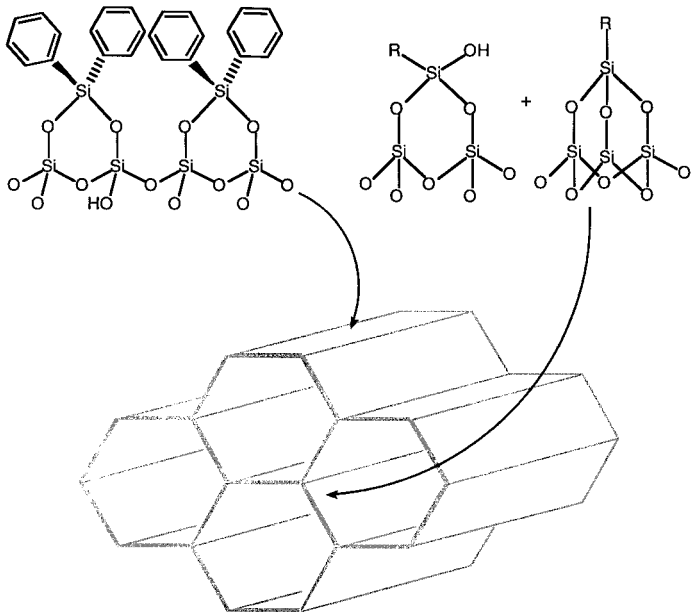


Figure 1. a) Conceptual representation of a catalyst encapsulated within a single MCM-41 pore to illustrate the substrate–wall interactions. b) A schematic representation of the passivation of the external surface with R_2SiCl_2 and the subsequent derivatization of the internal surface. R = $(CH_2)_3NH_2$.

place predominantly on the external surfaces of the particles because of their greater accessibility. Subsequent coupling of the catalytically active species to the support will hence take place at the most accessible tethers, thus giving heterogenized catalysts covering predominantly the outer surface of the MCM-41 particles. Furthermore, it should be possible to increase the dispersion and maximize performance per active site by using low loadings of the catalyst, so that the catalytic entities will bond almost exclusively to the external surface. This situation would be similar to that when amorphous silica is used as the support.

As part of our ongoing program to construct enantioselective catalysts[4] that are located within the channels of MCM-41 (so as to elucidate confinement effects on their turnover frequency (TOF) and selectivity) we have developed the first technique to determine directly the position of tethers bearing functional groups within a mesoporous matrix. Herein we report: 1) a method for the synthesis and characterization of selectively functionalized mesoporous silica (MCM-41) from a combination of Ph_2SiCl_2 and $(MeO)_3SiCH_2CH_2CH_2NH_2$ (Figure 1b); b) the synthesis and structural characterization of a model compound $[Ru_6C(CO)_{14}(\eta^6\text{-}C_6H_4C_{10}H_{20}O_6)\cdot NH_4PF_6]$ (**2**), which exhibits the ammonium–cluster-crown interaction that must correspond to the binding interaction between $[Ru_6C(CO)_{14}(\eta^6\text{-}C_6H_4C_{10}H_{20}O_6]$ (**1**) and a mesoporous silica surface derivatized with the ammonium functionality; 3) the host–guest-type binding of **1** onto the walls of mesoporous silica (MCM-41)[5] functionalized with $(-O)_3SiCH_2CH_2CH_2NH_3^+BF_4^-$ (Figure 2), and with a pore

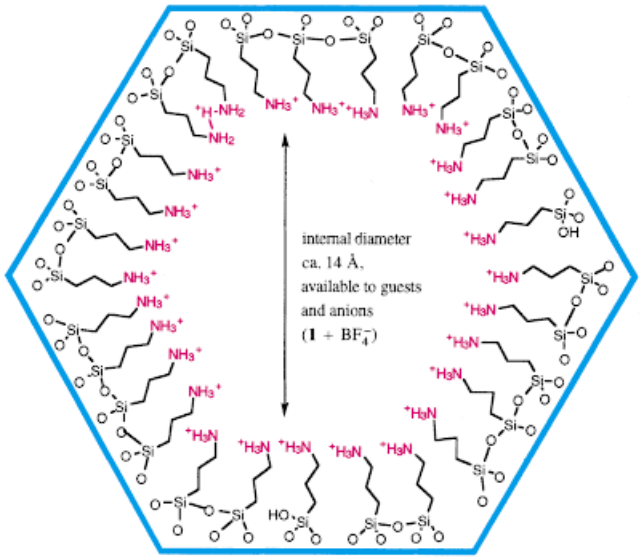


Figure 2. An MCM-41 pore fully derivatized with $(-O)_3SiCH_2CH_2CH_2NH_3^+BF_4^-$.

diameter of approximately 30 Å, together with spectroscopic proof of the retention of the integrity of the cluster probe (FT-IR spectroscopy and ^{13}C magic-angle spinning (MAS) NMR spectroscopy); and 4) determination of the positions of the cluster–tether ensemble inside and outside the siliceous mesopores by bright-field high-resolution transmission electron microscopy.

The surface of the mesoporous silica (MCM-41) was derivatized by the well-established method of condensation of one or several Si–OMe bonds with the surface silanol groups.[6] The first sample A was treated with $(MeO)_3SiCH_2CH_2CH_2NH_2$ (twofold excess) in THF for 12 h at ambient temperature. The second sample B was first treated with Ph_2SiCl_2 (0.01 equiv) on the assumption that the most kinetically available Si–OH groups were those on the outside surfaces of the silica particles (ca. 1 μm in diameter) and hence, these would be silylated and deactivated to further reaction. By this method the amine tether is expected to be located predominantly inside the channels.[7] The sample was then treated with $(MeO)_3SiCH_2CH_2CH_2NH_2$ as for A. Both samples were washed with copious amounts of THF and dried under vacuum (10^{-3} mmHg) at 348 K. Acidification by the

 © WILEY-VCH Verlag GmbH, D-69451 Weinheim, 1998 1433-7851/98/3719-2720 $ 17.50+.50/0

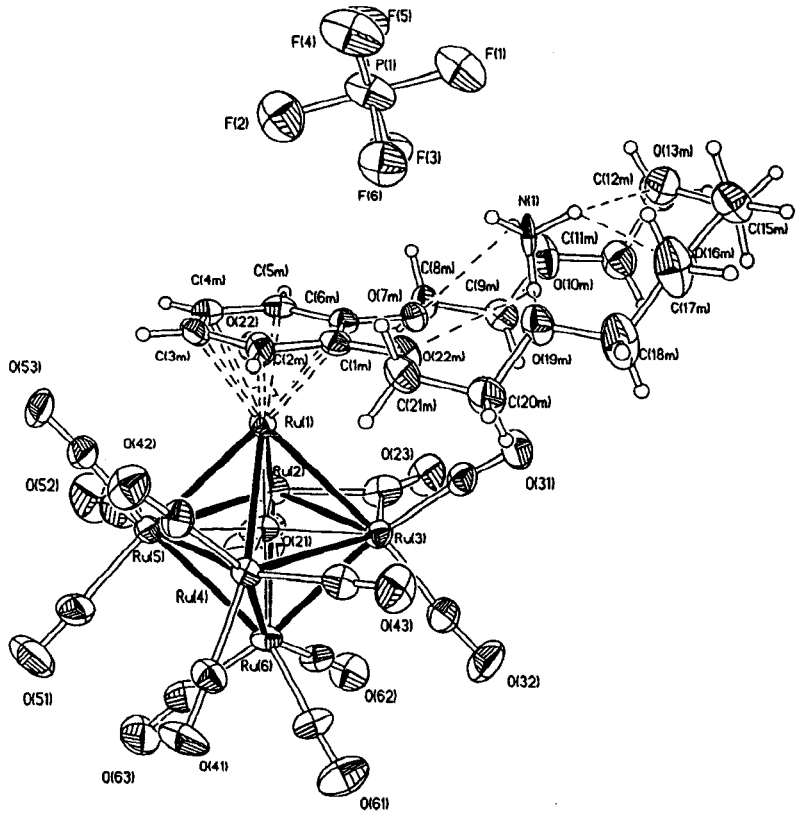


Figure 3. The crystal structure of **2**. Bond lengths [Å]: Ru(1)–C(1m) 2.288(9), O(7m)–N(1) 2.94(2), Ru(1)–C(2m) 2.246(9), O(10m)–N(1) 2.84(2), Ru(1)–C(3m) 2.216(10), O(13m)–N(1) 2.80(2), Ru(1)–C(4m) 2.203(10), O(16m)–N(1) 2.79(2), Ru(1)–C(5m) 2.255(9), O(19m)–N(1) 2.87(2), Ru(1)–C(6m) 2.291(9), O(22m)–N(1) 3.02(2), C(1m)–C(2m) 1.397(13), N(1)–F(1) 3.05(2), C(2m)–C(3m) 1.420(12), N(1)–F(3) 3.07(2), C(3m)–C(4m) 1.416(14), N(1)–F(6) 2.96(2), C(4m)–C(5m) 1.388(14), C(5m)–C(6m) 1.390(14), C(6m)–C(1m) 1.417(13).

addition of about one equivalent of HBF_4 (with respect to NH_2 groups) in diethyl ether/THF (1/1) yielded the ammonium head groups. Again the samples were washed, dried, and stored under an inert atmosphere.

As part of the continued development of the chemistry of the areneruthenium clusters based on the Ru_6C unit,[8] we have examined ways to incorporate these redox active units[9] into supramolecular assemblies. Given the wealth of host–guest chemistry of crown compounds[10] we concentrated our initial investigations in this area with a view to examine the molecular recognition behavior of the new receptor clusters. The cluster compound **1** was synthesized by direct reaction of the arylcrown ether with the hexaruthenium carbido cluster $[Ru_6C(CO)_{17}]$, and displays host–guest type behavior with Na^+ and NH_4^+ ions (shown both spectroscopically and electrochemically).[11] Furthermore, incorporation of such recognition characteristics (e.g for RNH_3^+) in the cluster unit has led to several possible applications, wherein these metal-rich domains may, with appropriate functionality, be directed onto surfaces or large (nanoscale) biomolecules (see Figure 4). This paper describes one such application. To verify the host–guest interaction between **1** and ammonium guests, the model host–guest complex **2** was crystallized from a stochiometric mixture of **1** and NH_4PF_6 in CH_2Cl_2/toluene by layering with diethyl ether.

The crystal structure of **2**, a model for the surface binding, shows the arene ring is η^6-coordinated to a single ruthenium atom (Figure 3). The oxygen atoms in the macrocyclic ring remain approximately planar, with a mean deviation of 0.186 Å. This plane lies at an angle of 27.2° to the arene ring that bonds the macrocycle to the cluster. The ammonium ion can be clearly seen to act as a guest within the macrocyclic cavity. The nitrogen atom lies 0.805(16) Å above the average plane of the oxygen atoms, with three of the hydrogen atoms[12] interacting with two oxygen atoms each, and with the remaining hydrogen atom directed towards the counterion.

Binding, and hence staining, of the the ammonium-functionalized surface to the cluster–crown compound **1** was achieved by the addition of the functionalized MCM-41 samples A and B to a solution of the cluster–crown compound **1** in dichloromethane to form a slurry**.** The dark red solutions grew paler whilst the previously white MCM-41 became brown/black, which indicated the uptake of **1.** After several hours the solution was filtered off, and the now dark solid was washed thoroughly with dichloromethane and dried under vacuum. When this methodology is employed with non-functionalized MCM-41 no detectable loading of the "staining" cluster **1** could be observed. The ^{13}C MAS NMR spectra for samples A and B further established the presence of the cluster–tether ensemble (Figure 4), with the chemical

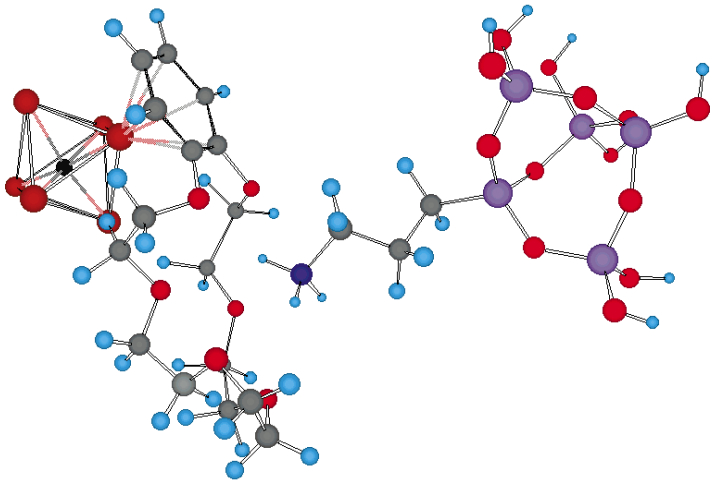


Figure 4. A Chem 3D model of the interaction of **1** with $H_3N^+CH_2CH_2CH_2Si{\equiv}$MCM-41. Modified MM2 parameters (less metal carbonyl groups) have been used.

shifts observed being consistent with those of their solution analogues.[10] The CO absorption band in the IR spectra (Nujol mull) showed that **1** was present in both samples, although the main absorptions were shifted by about 10 cm^{-1} to lower energy, which possibly indicates the existence a

 © WILEY-VCH Verlag GmbH, D-69451 Weinheim, 1998 1433-7851/98/3719-2721 $ 17.50+.50/0

secondary C=O ··· H–X-type interaction (where X is N^+ or to a lesser extent OSi). The main absorption in sample A was shifted the most. This may arise from a greater contribution from the secondary interaction (see above) and possibly indicates how a greater surface density of functionalized tethers may be produced on the outer surface of MCM-41. The spectral profiles for both samples were essentially identical.

Both samples and also a calcined sample of MCM-41 were then imaged by high-resolution transmission electron microscopy (HR-TEM) (Figure 5a–c). The micrographs show representative examples of the materials produced, with all being essentially homogeneous. Figure 5a reveals the regular nature of the mesopores of the MCM-41 silica (the inset shows a Fourier transform with spots in the 100 direction); the absence of 001 spots in the Fourier transform shows that there is no crystallographic order in the direction of the pore axis. Inspection of the micrographs of A·**1** and B·**1** (Figures 5b and c, respectively) revealed dramatic differences were produced by the two different synthetic procedures. The dark surfaces of MCM-41 in A indicate that **1** is present predominantly at the external surfaces of this sample, adhered by the host–guest interaction (Figure 4). This indicates that the majority of the ammonium tethers are bound to the outer surface of MCM-41. In stark contrast, the electron micrograph of B has essentially "clean" exterior surfaces but retains strong image contrast of the clusters inside the mesopores (compare with Figure 5a). Thus, in sample B the tethers have been forced to bind almost entirely to the internal surface of MCM-41. Since the available internal volume[13] of the siliceous host is several orders of magnitude greater than that occupied by the introduced "staining agent" **1** (taking into account the reduction in pore volume because of the internally bound tethers) the distribution of **1** across the internal surface will be dictated by the position of the grafted ammonium tethers. The distribution of "staining agent" within the pores, as indicated by Figure 5c, is uniform and reflects an even circumfusion of the alkylammonium tethers.

We have presented the first method for directly imaging the position of functional tethers grafted onto the surface of a mesoporous material and, at the same time, have validated a simple method by which one may direct the location of the grafted functionality within mesoporous solids. This has been made possible by a strong partnership between supramolecular, organometallic, and solid-state chemistry. The results presented herein provide a foundation for the future examination of the effects of mesopore confinement on catalysis.

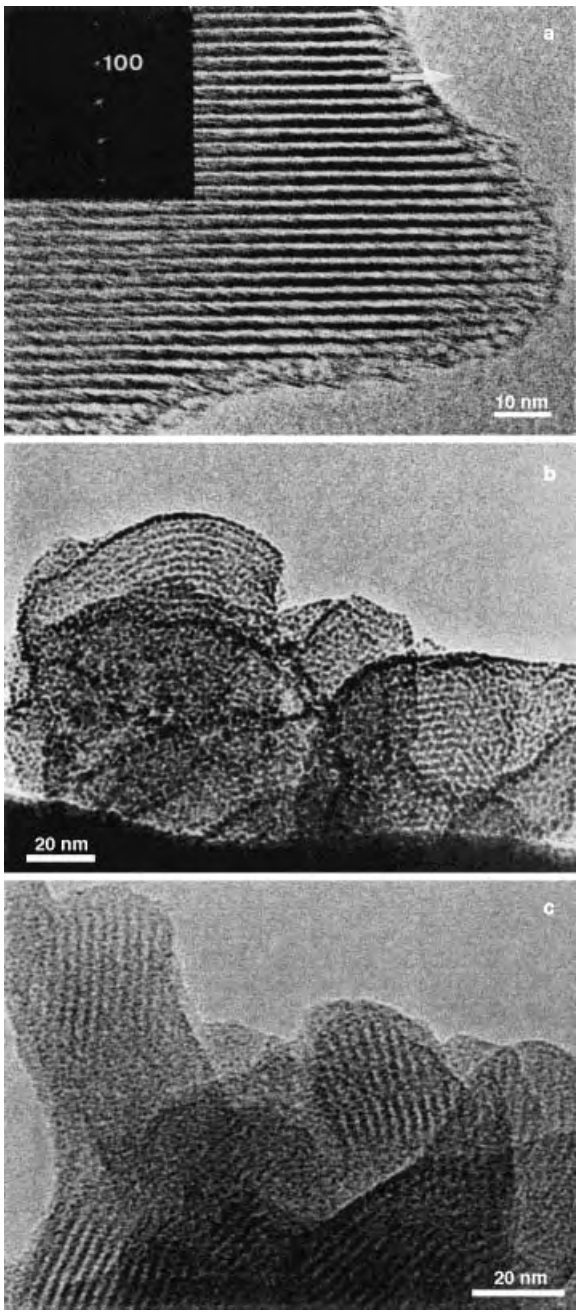


Figure 5. a) A HR-TEM micrograph of calcined MCM-41. The inset shows the Fourier transform with data in the 100 direction. b) A HR-TEM micrograph of sample A "stained" with **1** that shows strong contrast on the surface of the particles, which indicates the clusters are bound predominently to the outer surface of the derivatized MCM-41 particles. c) A HR-TEM micrograph of sample B "stained" with **1** that shows the presence of clusters within the MCM-41 channels (dark spots) and little or no contrast at the surface of the particles over and above that of calcined MCM-41.

Experimental Section

All reactions were carried out with the exclusion of air and with solvents freshly distilled in an atmosphere of nitrogen. FT-IR spectra were recorded on a Perkin-Elmer 1600 series FT-IR spectrometer in CH_2Cl_2 with NaCl cells or a Nujol mull. Positive-ion fast atom bombardment (FAB) mass spectra were obtained on a Kratos MS50TC spectrometer, with CsI as a calibrant. Separation of products was accomplished by thin layer chromatography on plates supplied by Merck (Kieselgel-60 F_{254}, 0.25 mm).

Preparation of propylammonium-functionalized MCM-41 samples A and B: MCM-41 (1 g) was dehydrated under vacuum at 200 °C for 2 h and was then slurried in THF (30 mL). Ph_2SiCl_2 (0.02 mL) was added, and the suspension was stired for one hour. The reaction mixture was cooled to 195 K, and $(MeO)_3Si(CH_2)_3NH_2$ (1.0 mL) added. The slurry was stirred for 3 h, slowly warmed to ambient temperature, and then left for a further 20 h at 50 °C. After this time the mixture was filtered and washed with copious amounts of THF (100 mL) and diethyl ether (50 mL), and dried under high vacuum. The ammonium functionality was obtained through acidification by the addition of a solution of $HBF_4 \cdot OEt_2$ (85%) in diethyl ether diluted in diethyl ether (30 mL) to the now dry white solid and stirred for 30 min. The resulting slurry was then filtered and washed with diethyl ether (100 mL), and dried under vacuum.

1: In a typical reaction $[Ru_6C(CO)_{17}]$ (200 mg, 0.18 mmol) and benzo[18]-crown-6 (130 mg, 0.42 mmol) were dissolved in dibutyl ether (25 ml) and

 © WILEY-VCH Verlag GmbH, D-69451 Weinheim, 1998 1433-7851/98/3719-2722 $ 17.50+.50/0 *Angew. Chem. Int. Ed.* **1998**, *37*, No. 19

refluxed under N_2 for 16 h. The resulting products were eluted on a silica column, first with pure dichloromethane, to yield $[Ru_6C(CO)_{17}]$ starting material (ca. 20 mg). Further elution with dichloromethane/methanol (99/1) gave a brown solution of **1**. This was recrystallized from dichloromethane by layering with hexane to give pure **1** (107 mg, 44 %). IR (cm^{-1}): 2074m, 2023vs, 1980w, 1967sh, 1808vw; positive-ion MS (FAB): *m/z*: 1324, 1294, 1267, 1237, 1209, 1182, 1153, 1125, 1096, 1067, 1039, 1011, 981, 952, 925 (calcd for $[M^+]$: 1324); ^{1}H NMR: $\delta = 6.14$ (dd, $J = 3$, 5 Hz, 2H), 5.47 (dd, $J = 3$, 5 Hz, 2H), 4.33 (m, 2H), 4.04 (m, 2H), 3.85 (m, 4H), 3.59 (m, 12H); ^{13}C NMR: $\delta = 197.6$, 126.5, 83.7, 77.7, 71.1, 70.7 (overlapped), 70.5, 68.9; elemental analysis: found: C 27.9, H 1.9, N 0.0; calcd: C 28.1, H 1.8, N 0.0. A crystal structure of this compound has been obtained.[14]

Cocrystallization of **1** with NH_4PF_6: A solution of **1** was stirred with a slight excess (1.1 equiv) of NH_4PF_6 in methanol (30 mL) for an hour. The product $\mathbf{1}\cdot NH_4^+PF_6^-$ was crystallized by layering a solution in CH_2Cl_2/toluene with diethyl ether (94 % yield). IR: $\tilde{\nu}_{co} = 2074$m, 2023vs, 1984w, 1964w, 1805vw (cm^{-1}); ^{1}H NMR: $\delta = 7.04$ (s, 4H), 5.70 (dd, $J = 3$, 6 Hz, 2H), 5.09 (dd, $J = 3$, 6 Hz, 2H), 4.21 (m, 2H), 3.90 (m, 2H), 3.70 (m, 16H); positive-ion MS (FAB): *m/z*: 1340 (calcd: 1338).

Crystal structure of **2:** $C_{34.5}H_{32}F_6NO_{20}Ru_6$, $M_r = 1532.00$, monoclinic, space group $P2_1/c$, a = 9.6080(16), $b = 17.071(2)$, c = 28.633(4) Å, $\beta = 95.806(14)^\circ$, $V = 4672.2(12)$ Å^3, $\rho = 2.178$ g cm^{-3}, $Z = 4$, $Mo_{K\alpha}$ radiation, $\lambda = 0.71073$ Å, $\mu = 2.024$ mm^{-1}, $T = 220(2)$ K. The data were collected on a Stoe Stadi four-circle diffractometer equipped with a cooling device (Oxford Cryosystems) from a rapidly cooled crystal (red needle, mounted axially, dimensions: $0.58 \times 0.12 \times 0.12$ mm^3), over the range $5.20 < 2\theta < 50.06^\circ$. Absorption correction was achieved by ψ scans (max./min. transmission 0.322/0.286). Of a total of 10316 reflections collected, 8243 were independent ($R_{int} = 0.0872$). The structure was solved by Patterson methods (DIRDIF program)[15] and refined against F^2 with the SHELXTL program[16] with $R_1 = 0.0545$ (for 5460 data with $F > 4\sigma(F)$) and $wR_2 = 0.1223$ (all data). Hydrogen atoms were placed in calculated positions and allowed to refine riding on their carbon atoms. The lattice contains a disordered toluene solvate molecule centered about an inversion center (one half per asymmetric unit in two orientations with equal occupancy). Max./min. residual electron density 1.484/ − 0.813 e Å^{-3}.

A · **1** and B · **1:** A solution of **1** (0.04 g) in CH_2Cl_2 (20 mL) was added to a slurry composed of A or B (0.2 g) in diethyl ether (10 mL), and the mixture stirred for 20 h under ambient conditions. The brown solid was then filtered off and washed with CH_2Cl_2 (20 mL) and diethyl ether (50 mL), and dried under high vacuum (0.5 h).

MASNMR spectroscopy: The spectra were recorded on a Chemagnetics CMX 400 NMR spectrometer at a spectral frequency of 100.56 MHz. Pulses at 399.98 MHz for ^{1}H were used for the cross polarization (CP) and decoupling experiments. ^{13}C excitation pulse (90°) = 3.6 μs. The ^{1}H 90° pulse length was 3.6 μs, and a contact time of 2 ms was used for the proton CP experiments. Recycle delays of 5 s were left between scans for the CP experiments, and for the proton decoupling experiments. A decoupling field strength of 62.5 kHz was used during the acquisition. All spectra are referenced to TMS at $\delta = 0$, with the alkyl resonance of hexamethylbenzene at $\delta = 17.35$ used as a secondary external reference. The temperature used in the experiments was 298 ± 0.5 K. The sample spinning speed was 6 MHz and was controlled to within ± 5 Hz. Of the order of 5000 scans and 1024 data points per scan were collected.

HR-TEM of activated A · **1** and B · **1**: The sample was ground in air. The dry powder was then deposited on a copper grid with a holey carbon film, transferred to a Jeol TEM-200CX electron microscope (operating at 200 kV), and kept in the microscope vacuum overnight. The images were recorded at magnifications of 49 000 ×.

Received: March 30, 1998 [Z11653IE]
German version: *Angew. Chem.* **1998**, *110*, 2847 – 2851

Keywords: clusters · crown compounds · electron microscopy · mesoporosity · molecular recognition

[1] *Applied Homogeneous Catalysis with Organometallic Compounds*, *Vol. 2* (Eds.: B. Cornils, W. A. Herrmann), VCH, New York, **1997**, pp. 605 – 23; J. H. Clark, D. K. Macquarrie, *Chem. Soc. Rev.* **1996**, *25*, 303.

[2] J. F. Dias, K. J. Balkus, F. Bedioui, V. Kurshev, L. Kevan, *Chem. Mater.* **1997**, *9*, 61; D. J. Macquarrie, D. B. Jackson, *Chem. Comm.* **1997**, 1781; A. Cauvel, G. Renard, D. Brunek, *J. Org. Chem.* **1997**, *62*, 749; L. Chun-Jing, L. Shou-Gui, P. Wen-Qin, C. Chi-Ming, *Chem. Comm.* **1997**, 65; P. Sutra, D. Brunel, *Chem. Comm.* **1996**, 2485.

[3] T. Maschmeyer, R. D. Oldroyd, G. Sankar, J. M. Thomas, I. J. Shannon, J. A. Klepetko, A. F. Masters, J. K. Beattie, C. R. A. Catlow, *Angew. Chem.* **1997**, *109*, 1713; *Angew. Chem. Int. Ed. Engl.* **1997**, *36*, 1639.

[4] J. M. Thomas, T. Maschmeyer, B. F. G. Johnson, D. S. Shephard, *J. Mol. Catal.* **1998**, in press.

[5] J. S. Beck, J. C. Vartuli, *Curr. Opin. Solid State Mater. Sci.* **1996**, *1*, 76; D. A. Antonelli, J. Y. Ying, *Curr. Opin. Colloid Sci.* **1996**, *1*, 523; D. Ozkaya, J. M. Thomas, W. Zhou, unpublished results.

[6] J. Liu, X. Feng, G. E. Fryxell, L.-Q. Wang, A. Y. Kim, M. Gong, *Adv. Mater.* **1998**, *10*, 161.

[7] This general methodology has been employed in a previous study,[3] although then unvalidated.

[8] D. Braga, P. J. Dyson, F. Grepioni, B. F. G. Johnson, *Chem. Rev.* **1994**, *6*, 1585.

[9] S. R. Drake, B. F. G. Johnson, J. Lewis, *J. Chem. Soc. Dalton. Trans.* **1989**, 243; A. J. Blake, A. Harrison, B. F. G. Johnson, E. J. L. McInnes, S. Parsons, D. S. Shephard, L. J. Yellowlees, *Organometallics* **1995**, *14*, 3160; S. R. Drake, *Polyhedron*, **1990**, *9*, 455.

[10] J. M. Lehn, *Supramolecular Chemistry Concepts and perspectives*, VCH, New York, **1995**; R. M. Izatt, J. S. Bradshaw, K. Paulak, *Chem. Rev.* **1991**, *91*, 1721; B. P. Hay, J. R. Rustad, *J. Am. Chem. Soc.* **1994**, *116*, 6316; F. C. J. M. van Veggel, W. Verboom, D. N. Reinhoudt, *Chem. Rev.* **1994**, *94*, 1279; *Biosensors: a Practical Approach* (Ed.: A. E. G. Cass), IRL Press, Oxford, **1990**; P. D. Beer, *Chem. Soc. Rev.* **1989**, *18*, 409; P. D. Beer, H. Sikanyika, C. Blackburn, J. F. McAleer, M. G. B. Drew, *J. Organomet. Chem.* **1988**, *356*, C19; K. H. Pannell, D. C. Hambrick, G. S. Lewandos, *J. Organomet. Chem.* **1975**, *99*, C19; K. J. Odell, E. M. Hyde, B. L. Shaw, I. Shephard, *J. Organomet. Chem.* **1979**, *168*, 103.

[11] D. Shephard, B. F. G. Johnson, J. Matters, S. Parsons, *J. Chem. Soc. Dalton Trans.* **1998**, 2289.

[12] The hydrogen atoms were placed in calculated postions and allowed to refine riding on their respective atoms.

[13] This is estimated by using an internal surface area of about 600 m^2g^{-1} and an internal pore diameter of 30 Å.

[14] J. M. Matters, Ph. D. Thesis, University of Cambridge (UK) **1997**.

[15] P. T. Beurskens, G. Beurskens, W. P. Bosman, R. de Gelder, S. Garcia-Granda, R. O. Gould, R. Isra'l, J. M. M. Smits, DIRDIF, Crystallography Laboratory, University of Nijmegen, The Netherlands, **1993**.

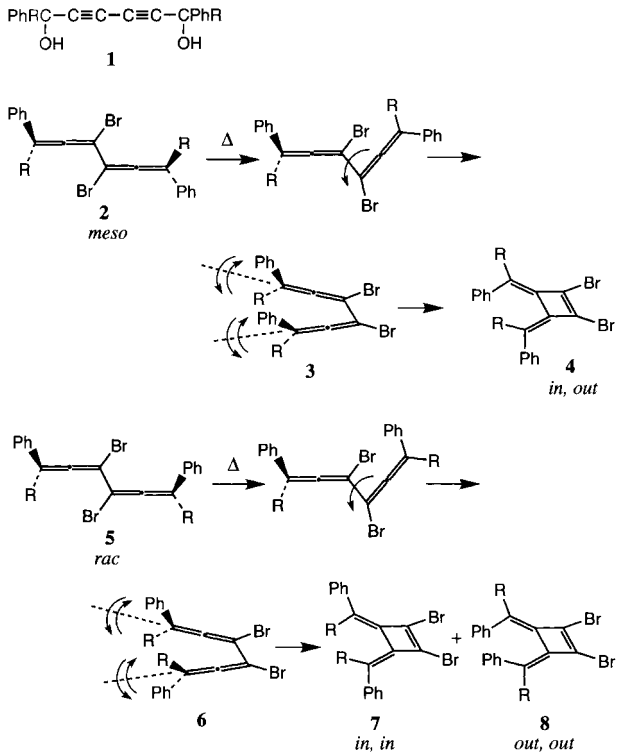
[16] G. M. Sheldrick, SHELXTL version 5, Siemens Analytical X-ray, Instruments, Madison, WI. **1995.**

 © WILEY-VCH Verlag GmbH, D-69451 Weinheim, 1998 1433-7851/98/3719-2723 $ 17.50+.50/0

Stereoselective Thermal Conversion of s-*trans*-Diallene into Dimethylenecyclobutene via s-*cis*-Diallene in the Crystalline State

Fumio Toda,* Koichi Tanaka, Tomoyuki Tamashima, and Masako Kato

It has been well established that thermal bimolecular organic reactions proceed efficiently in the solid state by mixing the powdered substrate and reagent.[1] However, no thermally irreversible unimolecular reaction from crystal to crystal has been reported, although reversible reactions such as thermochromism and single crystal to single crystal thermal conversion of a cyclic photodimer of a styrylpyrylium derivative to its monomer[2] are known. We report the thermal crystal-to-crystal conversion of s-*trans*-1,1,6,6-tetraaryl-3,4-dibromo-1,2,4,5-hexatetraenes (**2a**, **2b**, and **5b**) into the corresponding 3,4-bis(diarylmethylene)-1,2-dibromocyclobutenes (**4a**, **4b**, and **7b** and **8b**) via s-*cis*-diallenes (**3a**, **3b**, and **6b**). These thermal conversions involve two crystal-to-crystal reactions. First the s-*trans* configuration of **2a** (**2b** or **5b**) is rearranged to the s-*cis* conformer in the crystal to give **3a** (**3b** and **6b**, respectively; Scheme 1). In the second step the cyclization of **3a** occurs in the crystal to give **4a**. This cyclization proceeds stereoselectively; compound **2b** gave **4b**, and **5b** gave a 1:1 mixture of **7b** and **8b**, through a [2+2] conrotatory cyclization. It is surprising that the thermal rearrangement and stereoselective cyclization occur so readily despite the necessary movement of a sterically bulky group in the crystal, although single crystal to single crystal photodimerization of a styrylpyrylium derivative[2] and of cinnamic acid[3] to the corresponding dimer is known.



Scheme 1. Thermal conversion of s-*trans*-diallenes into dimethylenecyclobutenes via s-*cis*-diallenes. **a**: R = Ph; **b**: R = *p*-MeC_6H_4.

Heating the colorless crystals of s-*trans*-1,1,6,6-tetraphenyl-3,4-dibromohexa-1,2,4,5-tetraene (**2a**) at 150 °C, prepared from 1,1,6,6-tetraphenylhexa-2,4-diyne-1,6-diol (**1a**) and aqueous HBr according to the reported method,[4] gave 3,4-bis(diphenylmethylene)-1,2-dibromocyclobutene (**4a**) (m.p. 199 °C) in quantitative yield. The differential scanning calorimetry (DSC) measurement of the crystal of **2a** showed a peak for an exothermic process at around 156 °C and one for an endothermic process at 198 °C. The cyclization to **4a** occurs at around 156 °C. Thermal cyclizations of **2a** to **4a**,[5] and of unsubstituted and alkyl-substituted diallenes to the corresponding dimethylenecyclobutenes[6] in solution have been described. However, the cyclization of diallene in the solid state has never been reported. Since no liquid state was observed during the conversion of **2a** to **4a**, the reaction in the crystal is a real solid-state reaction. The s-*trans* conformation of **2a** was elucidated by an X-ray structural analysis. The structure is not unreasonable because even 1,2,4,5-hexatetraene exists in a s-*trans* form both in the gas phase[7] and in solution.[8] In order to cyclize to **4a**, **2a** should first isomerize to its s-*cis* isomer (**3a**) in the crystal. The conformational change of **2a** to **3a** requires a rotation of the sterically bulky 1,1-diphenylallene moiety around the single bond connecting the two allene groups in the crystalline state (see Scheme 1). A similar conformational change of s-*trans*-diallene to s-*cis*-diallene in solution, followed by the addition of SO_2 to give a cyclic sulfone derivative has been discussed.[9] Furthermore, thermal conversion of the s-*cis*-diallene **3a** to **4a** should also be accompanied by a molecular motion of the 1,1-diphenylmethylene groups. This dynamic behavior of the molecules in the crystalline state is very interesting. To verify whether the rearrangement of s-*strans*-diallene to s-*cis*-diallene and the cyclization of the latter to dimethylenecyclobutene proceed stereoselectively, the thermal reactions of *meso*- (**2b**) and *rac*-s-*trans*-1,6-diphenyl-1,6-di(*p*-tolyl)-3,4-dibromohexa-1,2,4,5-tetraene (**5b**) were studied.

The reaction of a mixture of *meso*- and *rac*-1,6-diphenyl-1,6-di(*p*-tolyl)hexa-2,4-diyne-1,6-diol (**1b**) with aqueous HBr gave a mixture of **2b** and **5b**, which upon fractional recrystallization gave pure **2b** and **5b** as colorless crystals (see Experimental Section). The structures of these were elucidated by X-ray analyses (Figure 1).[10] Heating crystals of **2b** at 135 °C gave the *in,out* isomer **4b**, while heating **5b** at 145 °C gave a 1:1 mixture of the *in,in* isomer **7b** and the *out,out*-3,4-bis(phenyl-*p*-tolylmethylene)-1,2-dibromocyclobutene (**8b**) in quantitative yields. Although the structures of all the products were elucidated by X-ray analyses, only the representative structure of **8b** is shown in Figure 2.[11] The structures of the products can also be determined easily from their ^{1}H NMR spectra: although the spectrum for **4b** shows

[*] Prof. Dr. F. Toda, Dr. K. Tanaka, T. Tamashima
Department of Applied Chemistry
Faculty of Engineering, Ehime University
Matsuyama, Ehime 790 (Japan)
Fax: (+81) 899-927-9923
E-mail: toda@en3.ehime-u.ac.jp
Dr. M. Kato
Department of Chemistry
Faculty of Science, Nara Women's University
Kita Wuoya Higashi-machi, Nara 630 (Japan)

 © WILEY-VCH Verlag GmbH, D-69451 Weinheim, 1998 1433-7851/98/3719-2724 $ 17.50+.50/0

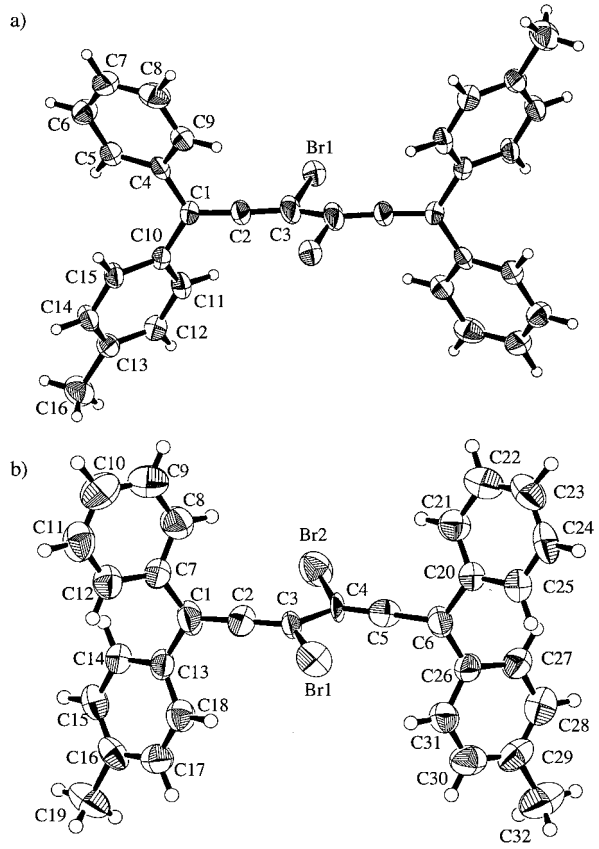


Figure 1. Crystal structure of (a) **2b** and (b) **5b**. Selected bond lengths [Å] and angles [°]: for **2b**: Br1 – C3 2.16(2), C1 – C2 1.30(1), C1 – C4 1.49(1), C1 – C10 1.47(1), C2 – C3 1.28(1), C3 – C3′ 1.21(2); C2-C1-C4 119.9(8), C2-C1-C10 119.3(8), C4-C1-C10 120.8(7), C1-C2-C3 175(1), Br1-C3-C2 111(1), Br1-C3-C3′ 98(1), C2-C3-C3′ 149(2); for **5b**: Br1 – C3 1.94(2), Br2 – C4 1.87(2), C1 – C2 1.33(5), C1 – C7 1.48(1), C1 – C13 1.49(1), C2 – C3 1.26(6), C3 – C4 1.51(3) C4 – C5 1.19(4), C5 – C6 1.42(4), C6 – C20 1.506(9), C6 – C26 1.465(9); C2-C1-C7 118(2), C2-C1-C13 120(2), C7-C1-C13 119.9(6), C1-C2-C3 172(3), Br1-C3-C2 115(2), Br1-C3-C4 113(1), C2-C3-C4 131(2), Br2-C4-C3 113(1), Br2-C4-C5 116(1), C3-C4-C5 130(2), C4-C5-C6 176(2), C5-C6-C20 117(1), C5-C6-C26 120(1), C20-C6-C26 120.2(6).

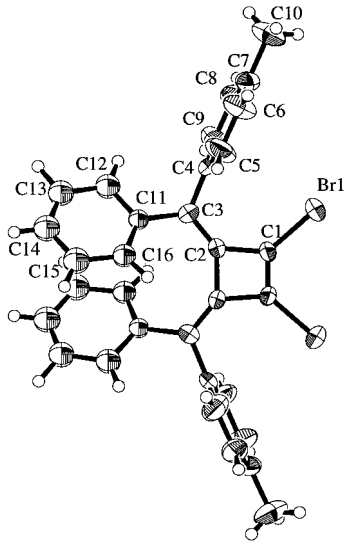


Figure 2. Crystal structure of **8b**. Selected bond lengths [Å] and angles [°]: Br1 – C1 1.858(8), C1 – C1′ 1.30(2), C1 – C2 1.48(1), C2 – C2′ 1.52(2), C2 – C3 1.32(1), C3 – C4 1.50(1), C3 – C11 1.58(2); Br1-C1-C1′ 131.7(3), Br1-C1-C2 134.0(6), C1′-C1-C2 94.2(5), C1-C2-C2′ 85.8(5), C1-C2-C3 132.7(8), C2′-C2-C3 141.5(6), C2-C3-C4 119.6(9), C2-C3-C11 120.1(10).

both the shielded and normal methyl signals at $\delta = 2.07$ and 2.39, respectively, whereas those of **7b** and **8b** show only a signal for a shielded methyl group at $\delta = 2.10$ and a normal methyl signalat $\delta = 2.39$, respectively.

The thermal reaction of **2b** and **5b** in boiling xylene gave the same products. The steric course of the solid-state reaction is shown in Scheme 1. Compounds, **2b** and **5b** rearrange first to **3b** and **6b**, respectively, and their conrotatory [2+2] ring closure gives **4b** and a 1:1 mixture of **7b** and **8b**, respectively. Mechanistic studies of the thermal conversion of diallene to dimethylenecyclobutene in solution and in the gas phase have revealed that it is an electrocyclic conrotatory process has been established.[12]

To verify that these reactions really occur in the solid state and not in the liquid state, the thermal reaction of **5b** in the crystal was studied by taking DSC measurements and recording IR spectra, and by monitoring the course of the reaction through a microscope. In the DSC diagram of **5b** revealed an peak for an exothermic reaction at around 150 °C which is attributable to the rearrangement of **5b** to **6b** followed by cyclization to a mixture of **7b** and **8b** and a peak for an endothermic conversion at around 193 °C, which is attributable to the melting point of the product (Figure 3). This

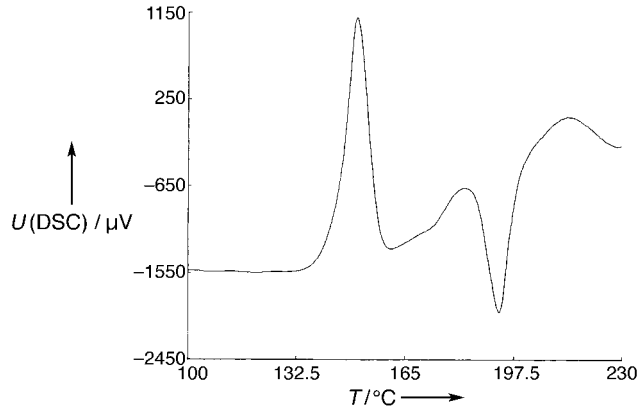


Figure 3. DSC diagram of **5b**.

assignment is resonable, since a 1:1 mixture of **7b** and **8b** showed a peak for an endothermic process at 194 °C in the DSC measurement. On the other hand, **2b** showed a peak for an exothermic conversion at around 178 °C and one for an endothermic one at 216 °C that is attributable to the melting point of **4b** (m.p. 214 – 215 °C). When the IR spectrum of a single crystal of **5b** was measured continuously every minute for 50 min at 125 °C, the signal at $\tilde{\nu} = 1927\ cm^{-1}$ (C=C=C) gradually decreased and finally disappeared (Figure 4). By heating **5b** in the crystalline state at 135 °C on a hot plate for 80 min, it was completely converted to **7b** and **8b** without melting. This conversion from crystal-to-crystal was monitored through a microscope, and a molten state was not observed throughout the reaction, although the reaction product was no longer a single crystal (Figure 5). These findings clearly support that the conversion of s-*trans*-diallene into dimethylenecyclobutene via s-*cis*-diallene really occurs in the crystalline state and not in the molten state. They also

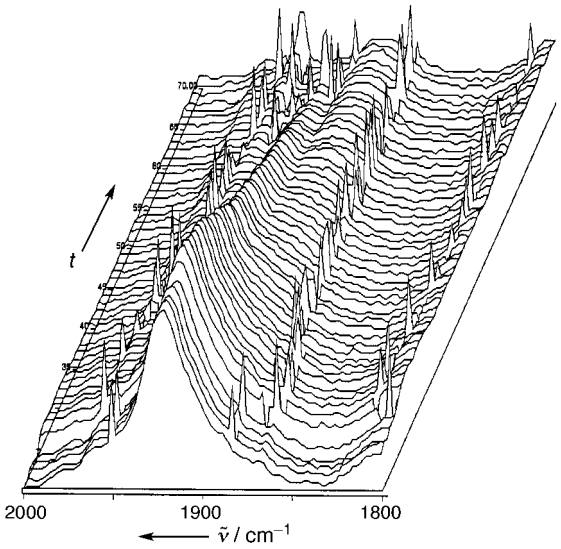


Figure 4. IR spectra showing the thermal reaction of **5b** in the crystalline state at 125 °C. The spectrum was measured every minute for 50 min.

verify that the molecular motion of the sterically bulky 1,1-diarylallene group in the rearrangement of s-*trans*-diallene to its s-*cis* isomer and that of the 1,1-diarylmethylene group in the cyclization of s-*cis*-diallene to dimethylenecyclobutene occur in the crystal.

Experimental Section

2b and **5b**: Aqueous HBr was added to a solution of **1b** (10 g) in AcOH (200 mL) at room temperature to give crystalline material. The crystals formed were filtered, washed with water, and air dried. The dried crystals were suspended in diethyl ether and filtered to give insoluble **2b** and an solution of **5b** in diethyl ether. Recrystallization of **2b** and **5b** from AcOEt gave pure **2b** as colorless needles (4 g, 30% yield) and **5b** as colorless prisms (4 g, 30% yield). **2b**: IR: $\tilde{\nu}$ = 1929 cm^{-1} (C=C=C); ^{1}H NMR: δ = 2.40 (s, 6H, Me), 7.20–7.48 (m, 18H, Ar); elemental analysis calcd for $C_{32}H_{28}Br_2$: C 67.63, H 4.26; found: C 67.84, H 4.13. **5b**: IR: $\tilde{\nu}$ = 1927 cm^{-1} (C=C=C); ^{1}H NMR: δ = 2.40 (s, 6H, Me), 7.20–7.48 (m, 18H, Ar); elemental analysis calcd for $C_{32}H_{28}Br_2$: C 67.63, H 4.26; found: C 67.70, H 7.24.

4b: Compound **2b** (0.2 g) was heated in the crystalline state at 135 °C for 1.5 h to give **4b** (0.2 g, 100% yield) as colorless needles after recrystallization from AcOEt. M.p. 214–215 °C; ^{1}H NMR: δ = 2.07 (s, 3H, Me), 2.39 (s, 3H, Me), 6.45–6.85 (m, 9H, Ar), 7.13–7.35 (m, 9H, Ar); elemental analysis calcd for $C_{32}H_{24}Br_2$: C 67.63, H 4.26; found: C 67.89, H 4.13.

7b and **8b**: Compound **5b** (0.4 g) was heated in the crystalline state at 125 °C for 1.5 h to give a 1:1 mixture (by ^{1}H NMR spectroscopy) of **7b** and **8b** (0.4 g, 100% yield). Fractional recrystallization of the mixture gave pure **7b** as colorless needles (m.p. 180–183 °C) and pure **8b** as colorless needles (m.p. 215–218 °C). **7b**: ^{1}H NMR: δ = 2.10 (s, 6H, Me), 6.48–6.52 (d, 4H, Ar), 6.70–6.74 (d, 4H, Ar), 7.23–7.26 (m, 10H, Ar); elemental analysis calcd for $C_{32}H_{24}Br_2$: C 67.63, H 4.26; found: C 67.46, H 3.97. **8b**: ^{1}H NMR: δ = 2.39 (s, 6H, Me), 6.66–6.87 (m, 10H, Ar), 7.10–7.25 (m, 8H, Ar); elemental analysis calcd for $C_{32}H_{24}Br_2$: C 67.63, H 4.26; found: C 67.66, H 4.13.

Received: April 20, 1998
Revised version: June 16, 1998 [Z 11756 IE]
German version: *Angew. Chem.* **1998**, *110*, 2852–2855

Keywords: allenes · cyclobutenes · electrocyclic reactions · solid-state chemistry

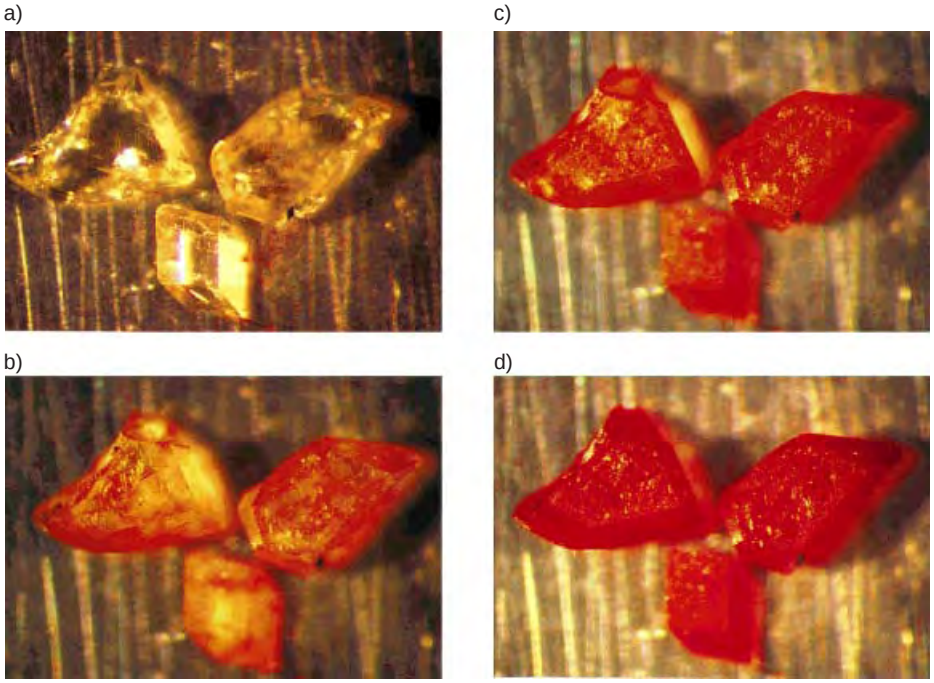


Figure 5. The thermal reaction of a crystal of **5b** to a crystal of a 1:1 mixture of **7b** and **8b** as observed through a microscope. The photos show the crystal before heating (a), as well as after 15 (b), 40 (c), and 80 min at 135 °C (d).

[1] F. Toda, *Synlett* **1993**, 303; F. Toda, *Acc. Chem. Res.* **1995**, *28*, 480.
[2] V. Enkelmann, G. Wegner, K. B. Wagener, *Angew. Chem.* **1993**, *105*, 1678; *Angew. Chem. Int. Ed. Engl.* **1993**, *32*, 1653
[3] V. Enkelmann, G. Wegner, K. Novak, K. B. Wagener, *J. Am. Chem. Soc.* **1993**, *115*, 10390.
[4] M. Higashi, F. Toda, K. Akagi, *Chem. Ind.* **1969**, 491.
[5] F. Toda, H. Ishihara, K. Akagi, *Tetrahedron Lett.* **1969**, 2531; F. Toda, K. Kumada, N. Ishiguro, K. Akagi, *Bull. Chem. Soc. Jpn.* **1970**, *43*, 3535.
[6] H. Hopf, *Angew. Chem.* **1970**, *82*, 703; *Angew. Chem. Int. Ed. Engl.* **1970**, *9*, 732; H. Hopf, F. Lenich, *Chem. Ber.* **1973**, *106*, 3461; L. Skattebol, S. Solomon, *J. Am. Chem. Soc.* **1965**, *87*, 732; W. D. Huntsman, H. Wristers, *J. Am. Chem. Soc.* **1963**, *85*, 3308; W. D. Huntsman, H. Wristers, *J. Am. Chem. Soc.* **1967**, *89*, 342; B. A. Coller, M. L. Heffernan, A. J. Jones, *Aust. J. Chem.* **1968**, *21*, 1807.
[7] M. Traetteberg, G. Paulen, H. Hopf, *Acta Chem. Scand.* **1973**, *27*, 2227.
[8] B. Pedersen, J. Schaug, H. Hopf, *Acta Chem. Scand. A* **1974**, *28*, 864.
[9] G. Schoen, H. Hopf, *Liebig Ann. Chem.* **1981**, 165.
[10] a) Crystal data for **2b**: $C_{32}H_{24}Br_2$, M_r = 568.35, triclinic, space group $P\bar{1}$ (No. 2), a = 8.547(3), b = 13.633(5), c = 6.049(2) Å, α = 102.34(3), β = 104.80(3), γ = 96.10(3)°, V = 656.0(5) Å^3, Z = 1, ρ_{calcd} = 1.439 g cm^{-3}, crystal dimensions 0.50 × 0.10 × 0.02 mm, μ = 31.16 cm^{-1}, T = 293 K, R = 0.050, wR = 0.065, and S = 1.43 for 154 parameters and 1174 unique observed reflections with $I > 3\sigma(I)$, $\Delta\rho_{max}$ = 0.68 e Å^{-3}. **5b**: $C_{32}H_{24}Br_2$, M_r = 568.35, monoclinic, space group

 © WILEY-VCH Verlag GmbH, D-69451 Weinheim, 1998 1433-7851/98/3719-2726 $ 17.50+.50/0

$P2_1/n$ (No. 14), $a = 10.979(6)$, $b = 14.897(5)$, $c = 16.606(4)$ Å, $\beta = 101.28(3)^\circ$, $V = 2663(1)$ Å^3, $Z = 4$, $\rho_{calcd} = 1.417$ g cm^{-3}, crystal dimensions $0.36 \times 0.32 \times 0.18$ mm, $\mu = 30.70$ cm^{-1}, $T = 293$ K, final $R = 0.048$, $wR = 0.062$, and $S = 1.45$ for 307 parameters and 2158 unique observed reflections with $I > 3\sigma(I)$, $\Delta\rho_{max} = 0.58$ e Å^{-3}. Diffraction data for **2b** and **5b** were collected on a Rigaku AFC-7R diffractometer with graphite-monochromated $Mo_{K\alpha}$ radiation ($\lambda = 0.71073$ Å) to $2\theta_{max} = 55^\circ$. The structures of **2b** and **5b** were solved by direct methods and heavy-atom Patterson methods, respectively, and expanded with Fourier techniques. The diallene moiety of **5b** was found to be disordered. All calculations were carried out with the teXsan crystallographic software package from the Molecular Structure Corporation. b) Crystallographic data for the structures reported in this paper have been deposited with the Cambridge Crystallographic Data Centre as supplementary publication no. CCDC-101408. Copies of the data can be obtained free of charge on application to CCDC, 12 Union Road, Cambridge CB21EZ, UK (fax: (+44) 1223-336-033; e-mail: deposit@ccdc.cam.ac.uk).

[11] Crystal data for **8b**: $C_{32}H_{24}Br_2$, $M_r = 568.35$, monoclinic, space group $C2/c$ (No. 15), $a = 6.641(7)$, $b = 28.502(4)$, $c = 13.773(5)$ Å, $\beta = 96.66(5)^\circ$, $V = 2589(2)$ Å3, $Z = 4$, $\rho_{calcd} = 1.458$ g cm^{-3}, crystal dimensions $0.34 \times 0.06 \times 0.04$ mm, $\mu(Mo_{K\alpha}) = 31.58$ cm^{-1}, $T = 295$ K, $R = 0.057$, $wR = 0.075$, and $S = 1.67$ for 145 parameters and 969 unique observed reflections with $I > 3\sigma(I)$, $\Delta\rho_{max} = 0.68$ e Å^{-3}. Data collection and analysis were carried out in a similar way to those for **5b**. The phenyl groups were refined with two disordered positions.[10b]

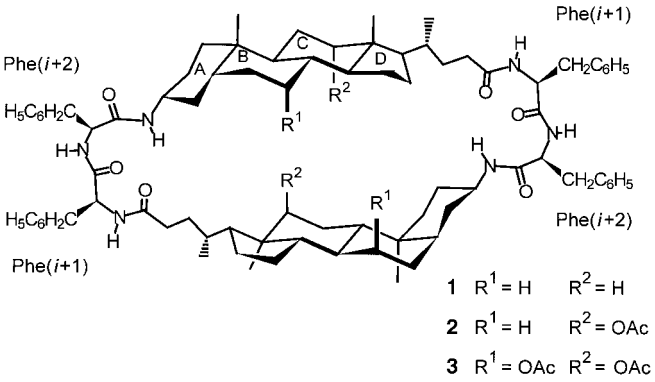
[12] K. Kleveland, L. Skattebol, *J. Chem. Soc. Chem. Commun.* **1973**, 433; D. J. Pasto, S. H. Yang, *J. Org. Chem.* **1989**, *54*, 3544; D. J. Pasto, W. Kong, *J. Org. Chem.* **1989**, *54*, 4028.

Crystal Structure of a Peptide–Steroid Macrocycle—Intramolecular Attraction between Steroids and Peptidic β(I) Turns**

Dieter Albert, Martin Feigel,* Jordi Benet-Buchholz, and Roland Boese

The concave surface of cholanic acids seems to be preorganized to bind molecular guests through weak interactions. Examples are the cholaphanes—synthesized by Davis, Bonar-Law, and co-workers from cholanic acid derivatives and aromatic spacers—which encapsulate carbohydrates and anions in solution.[1] Other researchers have used the hydroxyl groups on the α side of the steran residue to position covalently attached units such as peptides, carbohydrates, or polycyclic arenes.[2]

We intend to develop molecular hosts of designed characteristics by combining the rigid, concave surface of cholanic acids with the flexibility and functionality of amino acids.[3, 4] Analyzing the NMR spectra of compounds **1**–**3**, we found



1 $R^1 = H$ $R^2 = H$
2 $R^1 = H$ $R^2 = OAc$
3 $R^1 = OAc$ $R^2 = OAc$

that substitution of the cholanic surfaces by acetoxy groups influences the conformation of the peptide part.[4] The present work describes for the first time the solid-state structure of such a macrocycle (**1**) containing a steroid (lithocholic acid) and a dipeptide (Phe-Phe). The structure demonstrates that an optimal approach between the two steroidal surfaces in the molecule is achieved when the peptide parts fold to form two β(I) turns.

Compound **1** was obtained by cyclodimerization of the pentafluorophenol ester of bis(phenylalaninyl)-3-amidolithocholic acid.[4] Crystallization of **1** from chloroform yielded prisms which were suitable for X-ray diffraction. The structure was solved using the Patterson search method of Egert and Sheldrick;[5] the steran residue of lithocholic acid was used as a structural fragment. The macrocycle **1** adopts a compressed form of C_2 symmetry in the crystal. The two lithocholic acid units of the molecule are in van der Waals contact (Figure 1). The close contact between the α surface of

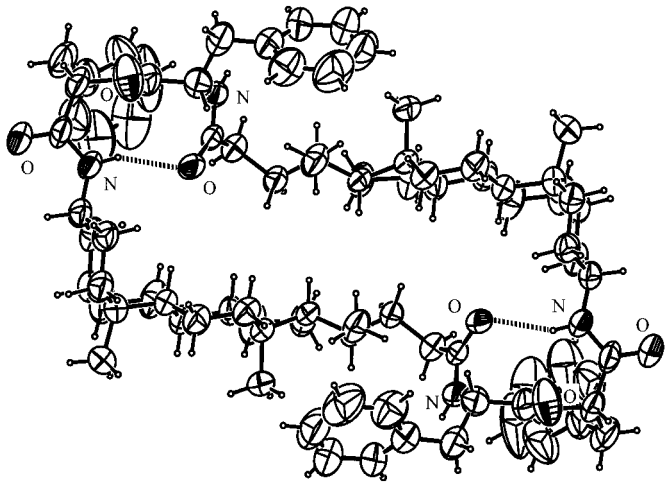


Figure 1. Structure of **1** in the crystal.

rings C and D and the branched side chain of the opposite lithocholic acid is particularly visible in Figure 1. The approach is achieved since the peptide parts of the molecule fold into β loops. The dihedral angles ϕ and ψ of the peptide parts (Phe$(i+1)$: $\phi/\psi = -75.7/-12.2$; Phe$(i+2)$: $\phi/\psi = -81.2/-3.5$) correspond to those found in a β(I) turn (residue$(i+1)$: $\phi/\psi = -60/-30$; residue$(i+2)$: $\phi/\psi = -90/0$).[6]

[*] Prof. Dr. M. Feigel, Dr. D. Albert
Fakultät für Chemie der Universität
Universitätsstrasse 150, D-44780 Bochum (Germany)
Fax: (+49) 234-709-4497
E-mail: feigel@indi-f.orch.ruhr-uni-bochum.de
Dipl.-Chem. J. Benet-Buchholz, Prof. Dr. R. Boese
Institut für Anorganische Chemie der Universität-Gesamthochschule Essen (Germany)

[**] This work has been supported by the Fonds der Chemischen Industrie. D.A. thanks the Studienstiftung des Deutschen Volkes for a grant.

The occurrence of phenylalanine in the $i+1$ and $i+2$ positions of the β turn is rather unusual.[7] The lipophilicity of the lithocholic acid residues apparently determines the geometry in the peptide part of **1**.

The crystal packing is influenced by an intermolecular van der Waals attraction between the lipophilic outer β surface of the lithocholic acids. They stack to form layers of steroids perpendicular to the crystallographic c axis. Three of the layers can be seen in Figure 2; the orientations of the

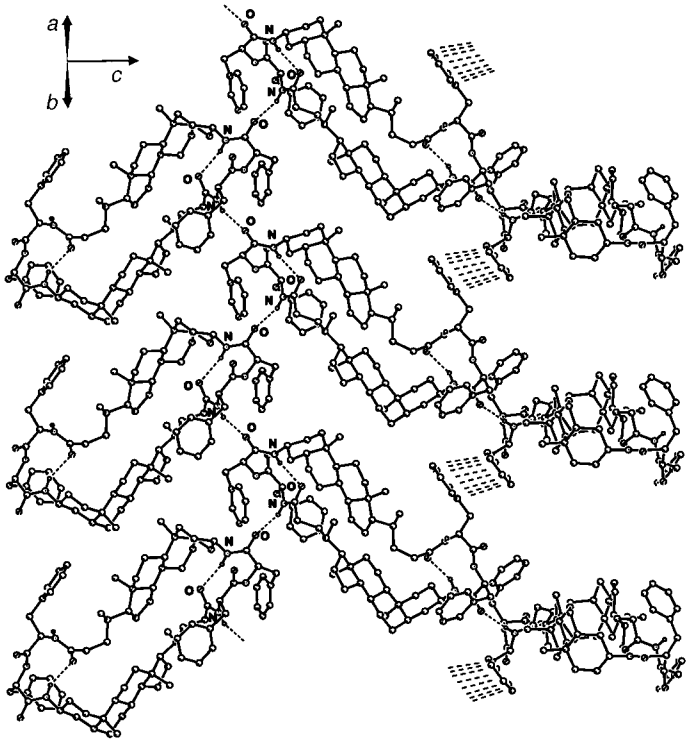


Figure 2. Formation of helical chains of hydrogen bonds between steroid layers in the crystal structure of **1**. The nitrogen and oxygen atoms within the chain of hydrogen bonds are marked. The π stacking between the aromatic side chains of Phe($i+1$) is indicated by dashed lines.

macrocycles in each layer differ by 120°, corresponding to the trigonal space group $P3_221$ of the crystal. The orientation is stabilized by hydrogen bonding between the NH protons of Phe($i+1$) in one layer and the carbonyl oxygen atoms of Phe($i+2$) in the adjacent layer (Table 1). The intermolecular hydrogen bonds together with the intramolecular hydrogen bonds of the β turns build helical chains of hydrogen bonds in which both types of interactions presumably stabilize each other (Figure 2).

The remaining free space in the crystal is occupied by chloroform and ethyl acetate molecules. Chloroform is found at two different positions. One of the molecules is relatively fixed and orientated so that its CH group comes in close contact to the carbonyl oxygen

Table 1. Geometrical parameters of the intra- and intermolecular hydrogen bonds.

Atoms	Distance [pm]		Angle [°]
	H···O	C/N···O	C/N-H···O
NH(lithochol) O=C(lithochol)	203	303	155.6
NH(Phe($i+1$)) O=C(Phe($i+2$))	185	288	157.5
CH($CHCl_3$) O=C(Phe($i+1$))	234	328	145.0

atom of Phe($i+1$), which is not involved in other hydrogen bonds (Table 1). The NH proton of the corresponding amide bond (NH–Phe($i+2$)) does not contribute to any hydrogen bonding and is shielded from further contacts by the phenyl ring of Phe($i+2$). The second molecule of chloroform has two different orientations with occupation factors 0.5/0.5. Additional electron density is found in the crystal which can be explained by the presence of ethyl acetate with an occupation factor of 0.5. Four molecules of chloroform and one molecule of ethyl acetate per macrocycle **1** result as the total composition based on the symmetry of the crystal.

The chloroform and ethyl acetate molecules together with the phenyl groups of Phe($i+1$) are assembled in channels along the c axis of the crystal (Figure 3). High displacement factors of these structural elements indicate flexibility and perhaps mobility in the channels. The structure is also stabilized by π interaction between the aromatic side chains of the residues Phe($i+1$);[8] the phenyl rings of neighboring macrocycles are grouped "face to face" (see Figure 2).

Artificial β turns are normally synthesized to induce the conformation of an antiparallel β sheet in peptides or to orient side chains of amino acids within the loop region.[9] The system described here is structurally able to do both functions. We look forward to seeing whether similar macrocycles with longer peptide chains, with other amino acids, or even open chain compounds will adopt the β-turn structure observed in **1**. Furthermore, the combination of a strong lipophilic steroid with polar peptides will open up biochemical applications, for example the fixation of peptides in lipid membranes.

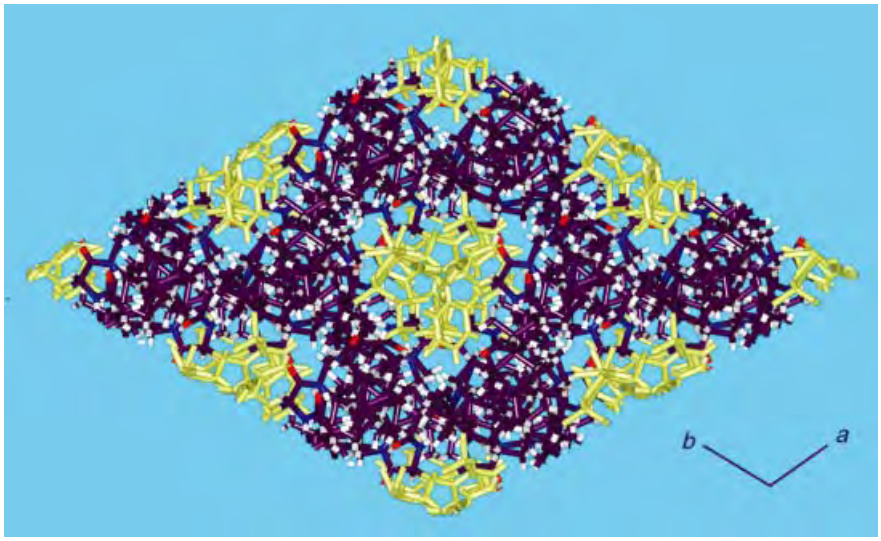


Figure 3. View along the crystallographic c axis onto four unit cells of the structure of **1**. The included solvent chloroform and ethyl acetate molecules as well as the aromatic side chains of Phe($i+1$) are colored yellow; they fill channels along the c axis.

 © WILEY-VCH Verlag GmbH, D-69451 Weinheim, 1998 1433-7851/98/3719-2728 $ 17.50+.50/0

Experimental Section

X-ray structure determination of **1** ($C_{84}H_{114}N_6O_6$) at 220 K: The crystal contains chloroform and ethyl acetate and is stable at room temperature. Crystal size $0.24 \times 0.18 \times 0.17$ mm, Siemens SMART CCD area detector on a free axis platform, $Mo_{K\alpha}$ radiation, graphite monochromator. Cell dimensions from the positions of 5466 reflections: $a = 14.1464(1)$, $c = 42.8884(2)$ Å, $V = 7432.97(21)$ Å^3; trigonal, space group $P3_221$ (no. 154), $Z = 3$, $\rho_{calcd} = 1.062$ Mg m^{-3}, $\mu = 0.22$ mm^{-1}, empirical absorption correction based on redundant data (SADABS program, Siemens), max./min. transmission 1.000/0.816, R(merg) before/after correction 0.0633/0.0519, data collection $\Theta_{max} = 22.46^\circ$, detector distance 4.457 cm, half-sphere scan in ω with 0.3° spacing and four data sets of 636, 465, 636, and 465 pictures with $\phi = 0$, 88, and 180°, where more than 97% of the data are nominally recorded (data reduction with SAINT Program, V4.028, Siemens), decay correction (< 2%) by repetition of the measurements of the first 50 pictures at the end of the data sampling; of 49471 refections measured, 6471 were independent and 4174 observed ($I > 2\sigma(I)$); $R_{merg} = 0.0874$ (F^2). Structure solution with PATSEE[5] (no solution with direct methods) and refinement to F^2 (SHELXTL-Plus Ver. 97-1/Iris), 591 parameters, hydrogen atoms as riding groups with 1.2 or (for methyl groups) 1.5 times the isotropic displacement parameter of the corresponding carbon atom. $R = 0.0872$ ($I > 2\sigma(I)$), $wR2 = 0.2385$, GOF(F^2) = 1.068, $w^{-1} = \sigma^2(F_o^2) + (0.1074P)^2 + 4.41P$ with $P = [(\text{max. } F_o^2, 0) + 2F_c^2)]/3$, largest residual electron density 0.32 e Å^{-1}. Further details on the crystal structure investigation may be obtained from the Fachinformationszentrum Karlsruhe, D-76344 Eggenstein-Leopoldshafen, Germany (fax: (+49) 7247-808-666; e-mail: crysdata@fiz-karlsruhe.de), on quoting the depository number CSD-408718.

Received: May 18, 1998 [Z11868IE]
German version: *Angew. Chem.* **1998**, *110*, 2855 – 2857

Keywords: β turns · hydrogen bonds · peptides · steroids · structure elucidation

[1] a) R. P. Bonar-Law, A. P. Davis, B. A. Murray, *Angew. Chem.* **1990**, *102*, 1497 – 1499; *Angew. Chem. Int. Ed. Engl.* **1990**, *29*, 1407 – 1409; b) A. P. Davis, *Chem. Soc. Rev.* **1993**, 243 – 253; R. P. Bonar-Law, L. G. Mackay, C. J. Walter, V. Marvaud, J. K. M. Sanders, *Pure Appl. Chem.* **1994**, *66*, 803 – 810; c) A. P. Davis, J. F. Gilmer, J. J. Perry, *Angew. Chem.* **1996**, *108*, 1410 – 1413; *Angew. Chem. Int. Ed. Engl.* **1996**, 35, 1312 – 1315; d) K. Lappalainen, E. Kolehmainen, *Liebigs Ann.* **1997**, 1965 – 1968.

[2] a) U. Maitra, B. G. Bag, *J. Org. Chem.* **1994**, *59*, 6114 – 6115; b) U. Maitra, B. G. Bag, *J. Org. Chem.* **1992**, *57*, 6979 – 6981; c) R. Boyce, G. Li, P. Nestler, T. Suenaga, W. C. Still, *J. Am. Chem. Soc.* **1994**, *116*, 7955 – 7956; d) Y. Cheng, T. Suenaga, W. C. Still, *J. Am. Chem. Soc.* **1996**, *118*, 1813 – 1814; e) G. Wess, K. Bock, H. Kleine, M. Kurz, W. Guba, H. Hemmerle, E. Lopez-Calle, K. H. Baringhaus, H. Glombik, A. Enhsen, W. Kramer, *Angew. Chem.* **1996**, *108*, 2363 – 2366; *Angew. Chem. Int. Ed. Engl.* **1996**, 35, 2222 – 2224; f) M. J. Sofia, R. Kakarla, N. Kogan, R. Dulina, Y. W. Hui, N. T. Hatzenbuhler, D. Liu, A. Chen, T. Wagler, *Bioorg. Med. Chem. Lett.* **1997**, *7*, 2251 – 2254.

[3] D. Albert, M. Feigel, *Tetrahedron Lett.* **1994**, *35*, 565 – 568.

[4] D. Albert, M. Feigel, *Helv. Chim. Acta* **1997**, *80*, 2168 – 2181.

[5] E. Egert, G. M. Sheldrick, *Acta Crystallogr. Sect. A* **1985**, *41*, 262 – 268.

[6] See: K. Wüthrich, M. Billeter, W. Braun, *J. Mol. Biol.* **1984**, *180*, 715.

[7] E. G. Hutchinson, J. M. Thornton, *Protein Sci.* **1994**, *3*, 2207 – 2216.

[8] C. A. Hunter, *Chem. Soc. Rev.* **1994**, 101 – 109.

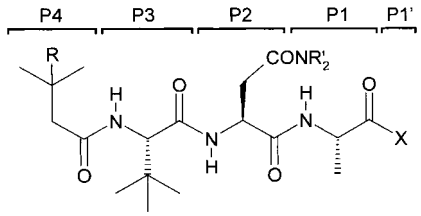
[9] See D. S. Kemp, P. E. McNamara, *J. Org. Chem.* **1985**, *50*, 5834 – 5838; U. Nagai, K. Sato, *Tetrahedron Lett.* **1985**, *26*, 647 – 650; M. Feigel, *J. Am. Chem. Soc.* **1986**, *108*, 181 – 182; R. Hirschmann, *Angew. Chem.* **1991**, *103*, 1305 – 1330; *Angew. Chem. Int. Ed. Engl.* **1991**, *30*, 1278 – 1301; M. Kahn, *Synlett* **1993**, 821 – 826; E. G. von Roederen, H. Kessler, *Angew. Chem.* **1994**, *106*, 684 – 686; *Angew. Chem. Int. Ed. Engl.* **1994**, *33*, 1745 – 1747; P. Schneider, J. W. Kelly, *Chem. Rev.* **1995**, *95*, 2169 – 2187; R. R. Gardner, G.-B. Liang, S. H. Gellmann, *J. Am. Chem. Soc.* **1995**, *117*, 3280 – 3281; U. Schopfer, M. Stahl, T. Brandl, R. W. Hoffmann, *Angew. Chem.* **1997**, *109*, 1805 – 1807; *Angew. Chem. Int. Ed. Engl.* **1997**, *36*, 1745 – 1747.

The Conformation of a Peptidyl Methyl Ketone Inhibitor Bound to the Human Cytomegalovirus Protease**

Steven R. LaPlante, Dale R. Cameron, Norman Aubry, Pierre R. Bonneau, Robert Déziel, Chantal Grand-Maître, William W. Ogilvie, and Stephen H. Kawai*

The transferred nuclear Overhauser effect (TRNOE) experiment represents a powerful NMR tool for the study of protein – ligand interactions.[1] Aided by computational chemistry, the method can provide valuable structural information concerning the conformation of a ligand when bound to a macromolecule. A key condition of the TRNOE method, however, is that the exchange between the free and complexed forms of the molecule to be investigated is rapid (faster than its spin-lattice relaxation rate) and reversible. In the present work, we provide the first structure of a peptidyl inhibitor bound to the human cytomegalovirus (HCMV) protease.[2] The use of the peptidyl methyl ketones MK1 and MK2 represents a novel approach to probing the structure of classical activated carbonyl inhibitors of serine proteases, which are themselves incompatible with the TRNOE method (Scheme 1). To date, such investigations of inhibitors of these enzymes have utilized, almost exclusively, peptide cleavage products or slowly cleaved substrates.[3]

There presently exists considerable interest in HCMV protease as a target for therapeutic agents against HCMV infection, which remains a serious clinical problem.[4] More-



MK1:	R = CH_3	R' = CH_3	X=CH_3
MK2:	R = H	R' = CH_3	X=CH_3
TFMK3:	R = CH_3	R' = CH_3	X=CF_3
PFEK4:	R = CH_3	R' = CH_3	X=CF_2F_3
AKA5:	R = CH_3	R'$_2$ = -$(CH_2)_4$-	X=C(O)N(H)CH_2(*p*-IC_6H_4)

Scheme 1. Various peptidyl inhibitors of HCMV protease. The numbers over the individual amino acids correspond to the notation of Schechter and Berger[10] for which a natural peptide substrate is cleaved between P1 and P1′.

[*] Dr. S. H. Kawai, Dr. S. R. LaPlante, Dr. D. R. Cameron, N. Aubry, Dr. P. R. Bonneau, Dr. R. Déziel, C. Grand-Maître, Dr. W. W. Ogilvie
Departments of Chemistry and Biological Sciences
Bio-Méga Research Division
Boehringer Ingelheim (Canada) Ltd.
2100 Cunard St., Laval, Québec, H7S2G5 (Canada)
Fax: (+1) 514-682-8434

[**] Dr. L. Lagacé and M.-J. Massariol are gratefully acknowledged for providing the enzyme used in the present studies, as are G. Fazal, J. A. O'Meara, and C. Chabot for the synthesis of activated carbonyl inhibitors. We are grateful to Prof. L. Tong for providing the X-ray structure. We also thank Dr. F. Ni, Dr. Z. Chen, and Dr. P. Xu for valuable discussions and technical support.

over, the highly novel nature of this serine protease, as evidenced in its recently elucidated X-ray crystallographic structure,[5] has also fueled its investigation. Our efforts with respect to medicinal chemistry[6] have led to an array of activated peptidyl–carbonyl compounds such as trifluoromethyl ketone TFMK3 and pentafluoroethyl ketone PFEK4. Such molecules are classical serine protease inhibitors which act by reversibly forming stable covalent adducts with the serine residue at the active site.[7] However, the possibility of clarifying the protease-bound conformation of these types of inhibitors by TRNOE techniques is precluded by their very slow rates of exchange. Methyl ketones MK1 and MK2 were designed to circumvent this problem since, although they very closely mimic their potent activated carbonyl analogues, the exchange between the free and bound states is very rapid due to their inability to form covalent hemiketal adducts with the protease.[8] Another key feature of MK1 and MK2 is the presence of the ketonic CH_3 group, which is positionally equivalent to the P1′ amido NH group[10] and whose NMR resonance may provide information on the conformation in the P1–P1′ region of bound peptides.

Initial 1D NMR experiments[11] led to the observation of HCMV protease induced line broadening of the proton signals of MK1. Consistent with specific complexation by the enzyme, the ^{1}H NMR spectrum of the inhibitor upon titration with enzyme presented a nearly uniform broadening as compared to the resonances of the ligand in the uncomplexed state. The enzyme-dependent changes in the methyl signal of the alanine moiety at P1 shown in Figure 1 A are representative of the observed spectral changes as a whole. Upon subsequent addition of PFEK4 to the sample, the peak heights for the proton signals of unbound MK1 were restored as a consequence of the displacement of MK1 from the active site by its much more potent activated carbonyl analogue (Figure 1 B).

Transferred NOE studies were undertaken to obtain detailed structural information concerning the binding of the present inhibitors. Owing to the unfortuitous superposition of the resonances for *tert*-butyl groups at P3 and P4 of MK1 in 1D studies, TRNOE experiments were carried out with the isopropyl analogue MK2, whose side-chain signals were conveniently separated. The ^{1}H NOESY spectrum of MK2 in the presence of HCMV protease (selected regions of which are shown in Figure 2) presented negative NOE crosspeaks resulting from interproton cross-relaxation of the enzyme-bound inhibitor. Figure 2 A, which shows the NH-aliphatic

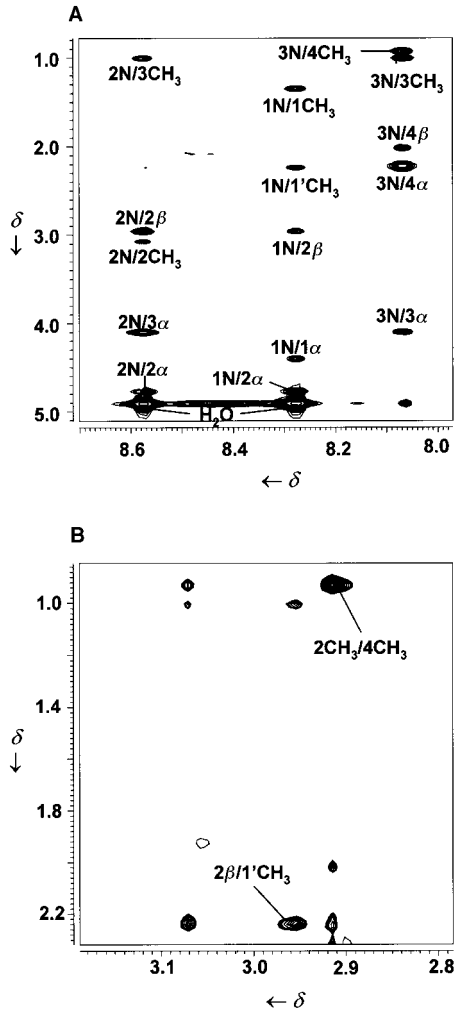


Figure 2. Selected regions of the 2D NOESY spectrum of 3.1 mM MK2 in the presence of 0.26 mM HCMV protease, recorded using a mixing time of 150 ms. A) The NH-aliphatic region. B) The aliphatic region with key interresidue side-chain correlations.

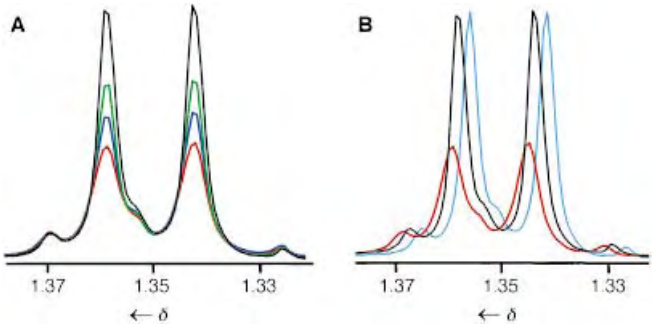


Figure 1. A) HCMV protease induced changes in the ^{1}H NMR signal of the P1-α-methyl group of MK1: MK1 alone (black) and in the presence of enzyme with molar excesses of inhibitor of 30-fold (green), 15-fold (blue), and 7-fold (red). B) The effect of PFEK4 on the protease-induced changes in the P1-α-methyl signal of MK1: inhibitor alone (black), a 7-fold excess in the presence of HCMV protease (red), and following subsequent addition of PFEK4 (cyan). (Signals have been skewed for the sake of clarity.)

region of the spectrum, presents a pattern of interresidue amide–C$^\alpha$H correlations between C$^\alpha$H(i) and NH($i+1$) of strong intensity alternating with weak intraresidue crosspeaks between C$^\alpha$H(i) and NH(i), which is characteristic of an extended peptide conformation.[12] This is corroborated by other key NOEs, indicated in Figure 2 B, including that between the methyl groups at P2 and P4. Also of importance is a crosspeak between one of the side-chain methyl groups at P2 and the ketonic methyl group, which indicates the presence of a "kink" at the C-terminal end of the chain.

The volumes of the NOE crosspeaks were subsequently scaled and converted[13] into interproton distance restraints for molecular modeling of enzyme-complexed MK2 using the method of restrained simulated annealing. These calculations[14] afforded a single family of structures, for which a final representative example consistent with the NMR data is

 © WILEY-VCH Verlag GmbH, D-69451 Weinheim, 1998 1433-7851/98/3719-2730 $ 17.50+.50/0

presented in Figure 3. Both the extended backbone conformation and the kink between positions P1 and P1′ are clearly evident.

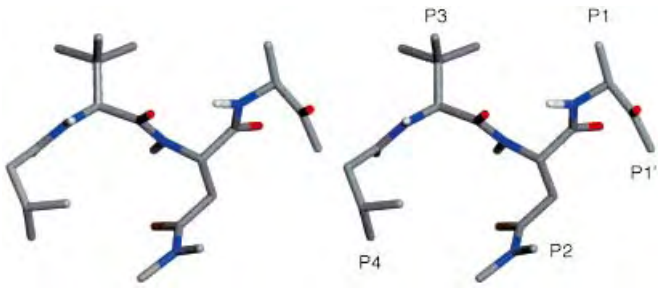


Figure 3. Stereoview of a representative structure derived from NMR data of MK2 when bound to HCMV protease, generated by restrained simulated annealing.

Finally, the subsequent elucidation of the crystal structure of the covalent complex of HCMV protease and the peptidyl α-ketoamide inhibitor AKA5[15] allows us to compare the conformations of bound inhibitors derived separately by NMR and crystallographic methods. As is evident in Figure 4,

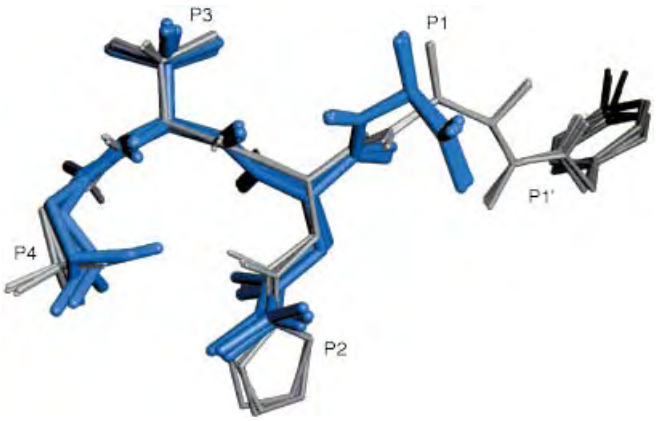


Figure 4. Comparison of the structures of HCMV protease bound inhibitors MK2 (blue, 29 low-energy conformers) obtained through transferred NOE methods and AKA5 (gray, four crystallographically unique conformers) derived from the X-ray crystallographic structure of the enzyme–inhibitor complex[15].

the four structures derived crystallographically and the superimposition of 29 structures determined from NMR experiments are in very good agreement.

The results described herein serve to underline the utility of peptidyl methyl ketones to probe the structure of activated carbonyl inhibitors of a serine protease using TRNOE methods. The bound conformation of MK2 will invariably aid in the rational design of inhibitors of HCMV protease and, potentially, the development of agents against HCMV disease.

Received: May 8, 1998 [Z11833IE]
German version: *Angew. Chem.* **1998**, *110*, 2858–2860

Keywords: conformation analysis · molecular modeling · NMR spectroscopy · peptidomimetics

[1] Review: F. Ni, *Prog. Nucl. Magn. Res.* **1994**, *26*, 517–590.
[2] All of the present studies employed the HCMV protease mutant Ala143 →Gln to overcome the problem of self-cleavage: C. Pinko, S. A. Margosiak, D. Vanderpool, J. C. Gutowski, B. Condon, C.-C. Kan, *J. Biol. Chem.* **1995**, *270*, 23634–23640. A detailed description of the preparation of recombinant enzyme has been published.[9]
[3] a) F. Ni, Y. Zhu, H. A. Scheraga, *J. Mol. Biol.* **1995**, *252*, 657–671, and references therein; b) E. F. Meyer, Jr., G. M. Clore, A. M. Gronenborn, H. A. S. Hansen, *Biochemistry* **1988**, *27*, 725–730; c) S. R. LaPlante, N. Aubry, P. R. Bonneau, D. R. Cameron, L. Lagacé, M.-J. Massariol, H. Montpetit, C. Plouffe, S. H. Kawai, B. D. Fulton, Z. Chen, F. Ni, *Biochemistry* **1998**, *37*, 9793–9801.
[4] E. S. Mocarski, Jr. in *Virology, Vol. 2* (Ed.: B. N. Fields) Lippincott-Raven, Philadelphia, PA, **1995**, pp. 2447–2492; W. J. Britt, C. A. Alford in *Virology, Vol. 2* (Ed.: B. N. Fields), Lippincott-Raven, Philadelphia, PA, **1995**, pp. 2493–2525.
[5] X-ray crystallographic structures of apoenzyme: a) L. Tong, C. Qian, M.-J. Massariol, P. R. Bonneau, M. G. Cordingley, L. Lagacé, *Nature* **1996**, *383*, 272–275; b) X. Qiu, J. S. Culp, A. G. DiLella, B. Hellmig, S. S. Hoog, C. A. Janson, W. W. Smith, S. S. Abdel-Meguid, *Nature* **1996**, *383*, 275–279; c) H.-S. Shieh, R. G. Kurumball, A. M. Stevens, R. A. Stegeman, E. J. Sturman, J. Y. Pak, A. J. Wittwer, M. O. Palmier, R. C. Wiegand, B. C. Holwerda, W. C. Stallings, *Nature* **1996**, *383*, 279–282; d) P. Chen, H. Tsuge, R. J. Almassy, C. L. Gribskov, S. Katoh, D. L. Vanderpool, S. A. Margosiak, C. Pinko, D. A. Matthews, C.-C. Kan, *Cell* **1996**, *86*, 835–843.
[6] W. W. Ogilvie, M. Bailey, M.-A. Poupart, A. Abraham, A. Bhavsar, P. R. Bonneau, J. Bordeleau, Y. Bousquet, C. Chabot, J.-S. Duceppe, G. Fazal, S. Goulet, C. Grand-Maître, I. Guse, T. Halmos, P. Lavallée, M. Leach, E. Malenfant, J. A. O'Meara, R. Plante, C. Plouffe, M. Poirier, F. Soucy, C. Yoakim, R. Déziel., *J. Med. Chem.* **1997**, *40*, 4113–4135. The IC_{50} values of the present inhibitors provided therein were determined using the described method.[9]
[7] a) B. Imperiali, R. H. Abeles, *Biochemistry* **1986**, *25*, 3760–3767; b) T.-C. Liang, R. H. Abeles, *Biochemistry* **1987**, *26*, 7603–7608; c) C. V. Xeï, *Biochemistry* **1997**, *36*, 1308–1313.
[8] The lack of reactivity of MK1 towards attack by the serine residue at the active site has been verified by ^{13}C NMR studies with carbonyl-labeled samples of MK1 and PFEK4.[9]
[9] P. R. Bonneau, C. Grand-Maître, D. J. Greenwood, L. Lagacé, S. R. LaPlante, M.-J. Massariol, W. W. Ogilvie, J. A. O'Meara, S. H. Kawai, *Biochemistry* **1997**, *36*, 12644–12652.
[10] Amino acid residue notation of I. Schechter, A. Berger, *Philos. Trans. R. Soc. London Ser. B* **1970**, *257*, 249–264.
[11] The 1D NMR spectra were acquired on a Bruker AMX spectrometer (500 MHz). Samples were prepared by addition of concentrated solutions of MK1 in [D_6]DMSO (and of HCMV protease in standard buffer) to an aqueous buffer composed of 500 mM Na_2SO_4, 50 mM NaCl, 1 mM EDTA, 50 mM [D_{11}]tris(hydroxymethyl)aminomethane (Tris), and 5 mM [D_{10}]dithiothreotol containing 10 % D_2O (spiked with [2,2,3,3-D_4]TSP) followed by adjustment of the pH to 7. Stock solutions were added successively such that samples consisted of protease:MK1 ratios of 0:1, 1:30, 1:15, and 1:7. The spectra were acquired at 20 °C, and suppression of the water signal was achieved by continuous low-power irradiation during the relaxation delay with the transmitter set on the H_2O resonance. The 2D NOESY experiments (J. Jeener, B. H. Meier, P. Bachmann, R. R. Ernst, *J. Chem. Phys.* **1979**, *64*, 4546–4553; S. Macura, R. R. Ernst, *Mol. Phys.* **1980**, *41*, 95–117) were carried out on a Varian UNITY instrument (750 MHz) equipped with pulse field gradient accessories. Samples consisted of 3.1 mM MK2 and 0.26 mM protease in the standard buffer at pH 7. Phase-sensitive spectra were acquired at 10 °C using the time proportional phase incrementation (TPPI) method (D. Marion, K. Wüthrich, *Biochem. Biophys. Res. Commun.* **1983**, *113*, 967–974; A. G. Redfield, S. D. Kuntz, *J. Magn. Res.* **1975**, *19*, 250–254). Water suppression was achieved by inserting a 3-9-19 WATERGATE module prior to acquisition (M. Piotto, V. Saudek, V. Sklenar, *J. Biolmol. NMR* **1992**, *2*, 661–665; V. Sklenar, M. Piotto, R. Lippek, V. Saudek, *J. Magn. Reson. A* **1993**, *102*, 241–245). The NOESY spectra were acquired using mixing times of 50, 100, 150, and 250 ms, and a selective flip-back pulse was employed just prior to the readout pulse to maintain the water magnetization along the positive z axis during

 © WILEY-VCH Verlag GmbH, D-69451 Weinheim, 1998 1433-7851/98/3719-2731 $ 17.50+.50/0

acquisition and relaxation delay (G. Lippens, C. Dhalluin, C. Wieruszeski, *J. Biomol. NMR* **1995**, *5*, 327–331).
[12] K. Wüthrich, *NMR of Proteins and Nucleic Acids*, Wiley, New York, **1986**, p. 162, and references therein.
[13] J. D. Baleja, J. Moult, B. D. Sykes, *J. Magn. Res.* **1990**, *87*, 375–384.
[14] The modeling of MK2 was carried out with the program Discover 95.0 and the CFF95 force field (Molecular Simulations Inc. San Diego, CA, USA). All calculations were performed without nonbonded or coulombic cutoffs and a dielectric constant of 1.0. Twenty-five NMR-derived distance restraints were generated from the NMR data using a method similar to that of Sykes et al.[13] The restraints were applied as strong (1.8–2.7 Å), medium (1.8–3.5 Å), or weak (1.8–5.0 Å) flat-bottomed potentials. A single, high-temperature unrestrained dynamics run was performed at 1000 K using a timestep of 1 fs, with 40 structures collected at intervals of 10 ps to generate a starting set of conformations. Each structure was cooled and minimized using the following simulated annealing protocol: The temperature was lowered to 500 K at a rate of 50 K ps^{-1}, where strong restraints were applied, and then to 250 K (5 K ps^{-1}). The remaining restraints were added, and cooling to 50 K (0.5 K ps^{-1}) was performed followed by restrained minimization to a final gradient of 0.01 kcal mol^{-1} Å^{-1}. Twenty-nine low-energy structures were isolated (average total restraint violation: 0.11 kcal mol^{-1}; root mean square deviation for all heavy atoms: 0.241), and a representative consistent with the NMR data was selected.
[15] L. Tong, C. Qian, M.-J. Massariol, R. Déziel, C. Yoakim, L. Lagacé, *Nature Struct. Biol.*, in press.

Calixarene-Based Copper(I) Complexes as Models for Monocopper Sites in Enzymes**

Sébastien Blanchard, Loïc Le Clainche, Marie-Noëlle Rager, Benoît Chansou, Jean-Pierre Tuchagues, Arthur F. Duprat, Yves Le Mest, and Olivia Reinaud*

Metalloenzymes are fascinating natural "factories" adept at transforming organic molecules with high efficiency and selectivity.[1] A good chemical model for metalloenzymes is a key to the understanding of the fundamental mechanisms of the chemistry involved in the catalytic cycles and to the design of efficient and selective new tools for the synthetic chemist. Although mononuclear copper enzymes constitute an important class of proteins,[2] few, if any, chemical systems allow the specific chemistry at a monocopper site to be modeled. The first step for the elaboration of a biomimetic system is the conception of a synthetic model for the active copper(I) center (since the copper center in this oxidation state is the active form for the activation of small molecules).[2] For this purpose, three important elements are required:

- A polydentate ligand to coordinate to the cuprous ion and reproduce the geometry and the chemical properties of the amino acid residues involved in the coordination sphere of the metal.
- An appropriate environment to prevent the formation of binuclear species.
- A vacant site to allow the coordination and exchange of an external ligand.

The classic strategy to protect a redox metal center, is based on tuning the sterical environment provided by a tripodal ligand. This approach presents a dilemma: high steric hindrance will prevent the cuprous ion from reacting with an external substrate molecule; but on the other hand, a decrease in the steric bulk will drive the reaction with O_2 (or any other oxidant) to produce binuclear copper(II) complexes.[3]

Here we describe a new supramolecular model of the mononuclear cuprous sites, which takes advantage of the conic shape of a calix[6]arene that is appropriately functionalized with three pyridine (Py) moieties. The role of the pyridine groups is to provide an N_3 donor set for the copper ion, thereby mimicking the imidazole residues which coordinate the type II cuprous ion in enzymes such as dopamine β-hydroxylase, peptidylglycine α-amidating monooxygenase, copper amine oxidases, as well as nitrate reductases.[2] The geometry of the system is designed to orient the fourth coordination site toward the inside of the conic cavity provided by the calixarene skeleton. The role of the calixarene is thus to protect the metal center from any undesired interaction with another metal center, to facilitate the approach of an organic molecule, and finally to operate a means of selection based on its size and nature.

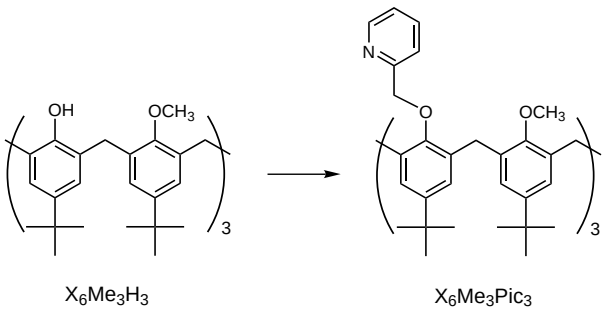
The new tridentate N-ligand $X_6Me_3Pic_3$ was synthesized in two steps from *p-tert*-butylcalix[6]arene (X_6H_6). The first step involved the alternate protection of three out of the six phenolic OH functions of the calixarene by a known selective methylation procedure.[4] Treatment of this key intermediate $X_6Me_3H_3$ with picolyl chloride in the presence of K_2CO_3 in DMF provided the desired tripod $X_6Me_3Pic_3$ in 87% yield (Scheme 1). The ^{1}H NMR spectrum of this ligand recorded at 297 K is characteristic of a major flattened *cone* conformation with C_3 symmetry. The methoxy groups are projected toward the inside of the cavity as indicated by the high field shift of the methyl protons in the spectrum. However, a low-temperature study revealed the presence of a minor conformer of lower symmetry, which is in equilibrium with the conic conformation.[5]

The addition of 1.1 equivalents of $[Cu(MeCN)_4]PF_6$ to a solution of $X_6Me_3Pic_3$ in $CDCl_3$ resulted in the formation of a

[*] Dr. O. Reinaud, S. Blanchard, L. Le Clainche, M.-N. Rager
Laboratoire de Structure et Réactivité des Complexes Moléculaires, U.M.R. CNRS 7576
Ecole Nationale Supérieure de Chimie de Paris
11 rue Pierre et Marie Curie, F-75231 Paris Cedex 05 (France)
Fax: (+33) 1-43-26-07-70
E-mail: reinaud@ext.jussieu.fr
Dr. B. Chansou, Prof. J. P. Tuchagues
Laboratoire de Chimie de Coordination du CNRS
205 route de Narbonne, F-31077 Toulouse cedex (France)
Dr. A. F. Duprat
Laboratoire de Recherches Organiques associé au CNRS
Ecole Supérieure de Physique et Chimie Industrielles
10 rue Vauquelin, F-75231 Paris Cedex 05 (France)
Dr. Y. Le Mest
Laboratoire de Chimie, Electrochimie Moléculaires et Chimie Analytique, U.M.R. CNRS 6521
Département de Chimie, Université de Bretagne Occidentale U.F.R. Sciences, B.P. 809
6 Avenue Le Gorgeu, F-29285 Brest Cedex (France)

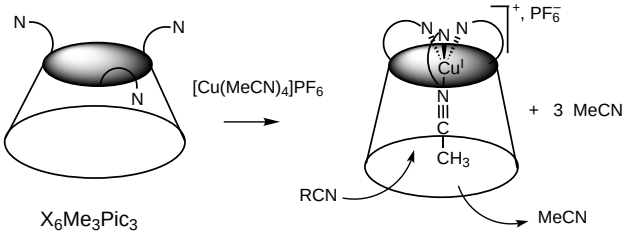
[**] We thank Dr. A. van Dorsselaer and H. Nierengarten (LSMBO, Strasbourg, France) for the mass spectra of our complex.

 © WILEY-VCH Verlag GmbH, D-69451 Weinheim, 1998 1433-7851/98/3719-2732 $ 17.50+.50/0



Scheme 1. Synthesis of $X_6Me_3Pic_3$. Conditions: $PyCH_2Cl \cdot HCl$, K_2CO_3, DMF, reflux 3 h; 87%.

new compound as shown by ^1H NMR spectroscopy. The simplicity of the overall profile excludes the presence of oligomeric species and is in good agreement with a mononuclear complex with C_3 symmetry. The large chemical shifts observed for the protons on the pyridine ring, together with the IR stretches of the corresponding C_5N skeleton attest to the coordination of the copper(I) ion to the nitrogen atoms on the pyridine rings. The ^1H NMR signal for the methoxy protons now appears at a lower field in the spectrum, thus indicating that the calixarene conformation has changed upon complexation. There is also a new broad resonance at $\delta = -1.2$ that does not belong to the calixarene-based ligand and vanished upon addition of deuterated acetonitrile. All these observations strongly suggest that the cuprous ion is four coordinate surrounded by: a) three pyridine groups, which are projected toward the inside of the cone of the calixarene, thus pushing out the methoxy groups, and b) an acetonitrile molecule, which sits inside the π-basic conic cavity as a consequence of the steric hindrance induced by the capping at the lower rim of the calixarene (Scheme 2).



Scheme 2. Synthesis and ligand exchange of cuprous $X_6Me_3Pic_3$ complexes.

The acetonitrile ligand was easily exchanged by the addition of 20 molar equivalents of propionitrile as shown in the ^1H NMR spectrum by the appearance of two new signals at $\delta = -0.7$ (q, 2H) and -1.7 (t, 3H). Under the same experimental conditions, allyl nitrile was also effective for this substitution process, whereas neither benzonitrile nor benzylnitrile were effective, even after two days. These observations may be attributed to steric crowding, which causes unfavorable interactions between these large molecules and the calixarene cavity.

Single crystals of the cuprous complex were obtained from a $CHCl_3$ solution containing 25 molar equivalents of propionitrile. The structure of $[Cu(X_6Me_3Pic_3)(NCEt)]PF_6$ was established by X-ray crystallographic analysis (Figure 1).[6] The Cu^I center resides in a regular tetrahedral N_4 ligand environment, with close to C_{3v} symmetry, provided by the three pyridine groups and the propionitrile ligand. The

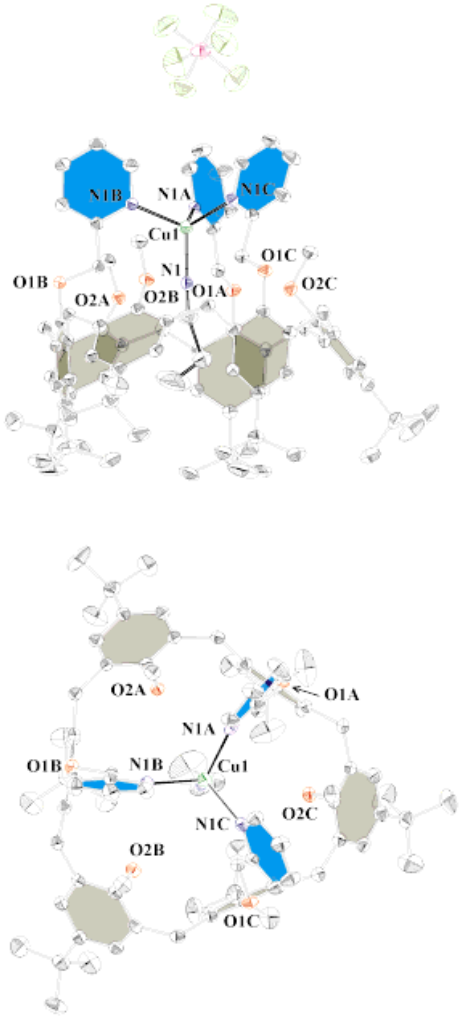


Figure 1. Crystal structure of $[Cu(X_6Me_3Pic_3)(NCEt)]PF_6$. Top: side view; bottom: plan view. The aromatic rings of the calixarene macrocycle and pyridine ligands are shaded in light gray and blue, respectively. Selected bond lengths [Å] and angles [°]: Cu–N1 1.949(7), Cu–N1A 2.090(7), Cu–N1B 2.097(7), Cu–N1C 2.127(6); N1-Cu-N1A 115.0(3), N1-Cu-N1B 111.6(3), N1A-Cu-N(1B) 107.3(2), N1-Cu-N1C 111.8(2), N1A-Cu-N1C 102.6(2), N1B-Cu-N1C 108.1(2).

average value for the three $Cu-N_{Py}$ distances of 2.105 Å is similar to those for four-coordinate Cu^I compounds with aromatic N-donor ligands.[7] The propionitrile ligand (Cu–N 1.949(7) Å) is buried deep inside the cavity of the *tert*-butylcalix[6]arene macrocycle in a *cone* conformation. The diameters of the openings at the two ends of the cavity can be estimated by the distances between two opposite O atoms (7.91 Å) and C_{tBu} atoms (11.28 Å). The unit cell includes two enantiomeric molecules: the metal-centered chirality results from the helical shape provided by the three pyridine groups wrapping around the metal ion. In solution, conformational exchange occurs between the two enantiomeric forms.

 © WILEY-VCH Verlag GmbH, D-69451 Weinheim, 1998 1433-7851/98/3719-2733 $ 17.50+.50/0

The complex is surprisingly stable: it was not oxidized under an atmosphere of O_2 in most common solvents and the acetonitrile remained coordinated to the cuprous ion after chromatography on silica gel in air. This lack of reactivity towards O_2 contrasts the facile exchange of the acetonitrile ligand with molecules as large as allyl nitrile. These observations can be explained by either the intrinsic instability of the CuO_2 adduct or by the metal center having a high redox potential.[8] Indeed, preliminary cyclic voltammetric experiments in CH_2Cl_2 revealed essentially an irreversible oxidation of Cu^{I} to Cu^{II}, at $E_p(ox) = +1.05$ V (versus ferrocene/ferrocenium), associated with a very broad and cathodically shifted reduction peak ($\Delta E_p = E_p(ox) - E_p(red) = 1.0$ V). The particularly high value of this oxidation potential is best explained by the tetrahedral environment in which the copper ion is constrained, which strongly stabilizes Cu^{I} relative to oxidation to Cu^{II}.[7]

Although calix[6]arenes have long been utilized for the construction of supramolecular assemblies, their ability to accommodate a transition metal has scarcely been explored.[10] The work herein demonstrates that although it is very flexible,[5, 10] a calix[6]arene can participate both in the formation of a stable mononuclear transition metal complex and in the construction of a receptacle which interacts with an external molecule. Indeed, the novel ligand $X_6Me_3Pic_3$ appears to fulfill three essential requirements for playing the role of a metalloenzyme active site pocket by providing: a) a N_3 donor set that allows the formation of a stable cuprous complex upon coordination of a fourth ligand at the remaining binding site, b) a cavity that acts not only as protection for the metal center but also as a funnel for external organic molecules that compete for binding to the metal center, and c) a geometrical constrain that confers to the Cu^{+} ion an unusually high oxidation potential. We are currently investigating the catalytic properties of these copper(I) complexes as well as developing the synthesis of complexes with divalent transition metal ions and other tridentate calix[6]arene-based ligands.

Experimental Section

$X_6Me_3Pic_3$: Under an argon atmosphere, dry K_2CO_3 (2.86 g, 20.7 mmol, 15 equiv), X_6Me_3 (1.40 g, 1.38 mmol), and 2-chloromethylpyridine chlorohydrate (1.36 g, 8.28 mmol, 6 equiv) were suspended in dry DMF (70 mL). The reaction mixture was heated to reflux for 3 h. Water (350 mL) was poured into the warm light orange solution and then stored for 12 h at 4 °C. The resulting white precipitate was collected by filtration over a glass frit, washed with water, dried under vacuum over KOH, recrystallized from $MeCN/CH_2Cl_2$, and finally dried under vacuum overnight at 40 °C. Yield: 1.65 g (87 %). M.p. 270 °C (loss of solvent molecules at 191 °C); ^{1}H NMR (250 MHz, $CDCl_3$): $\delta = 0.83$ (s, 27 H; *t*Bu), 1.37 (s, 27 H; *t*Bu), 2.33 (s, 9 H; OCH_3), 3.43 (d, $J = 15$ Hz, 6 H; Ar-αCH_{eq}), 4.61 (d, $J = 15$ Hz, 6 H; Ar-αCH_{ax}), 5.1 (s, 6 H; Py-αCH_2), 6.72 (s, 6 H; *Ar*-H), 7.25 (t, $J = 4.8$ Hz, 3 H; *Py*-H), 7.26 (s, 6 H; *Ar*-H), 7.80 (t, $J = 3$ Hz, 3 H; *Py*-H), 7.91 (d, $J = 3$ Hz, 3 H; *Py*-H), 8.56 (d, $J = 4.8$ Hz, 3 H; *Py*-H); IR (KBr): $\tilde{\nu} = 1595$ (m), 1575 (w), 1480 (s), 1460 (sh), 1430 (s) cm^{-1}: (C=N, C=C (Py)); elemental analysis calcd for $C_{87}H_{105}N_3O_6 \cdot 1.5\,H_2O \cdot DMF$: C 77.85, H 8.31, N 4.09; found: C 77.82, H 8.33, N 3.96.

$[Cu(X_6Me_3Pic_3)(NCMe)]PF_6$: Dioxygen-free $CDCl_3$ (1 mL) was added to a schlenk flask containing $X_6Me_3Pic_3$ (200 mg, 0.155 mmol) and $[Cu(NCMe)_4]PF_6$ (64 mg, 0.17 mmol, 1.1 equiv) under an argon atmosphere. The mixture was stirred for 4 h, filtered over celite, and an aliquot (0.1 mL) of the resulting homogeneous tan solution was diluted in an NMR tube with $CDCl_3$ (0.4 mL). ^{1}H NMR (250 MHz, $CDCl_3$): $\delta = -1.2$ (br s, 3 H; coordinated CH_3CN); 0.81 (s, 27 H; *t*Bu), 1.41 (s, 27 H; *t*Bu), 2.0 (br s, 9 H, free CH_3CN); 3.01 (s, 9 H; OCH_3), 3.37 (d, $J = 15$ Hz, 6 H; Ar-αCH_{eq}), 4.32 (d, $J = 15$ Hz, 6 H; Ar-αCH_{ax}), 5.54 (s, 6 H; Py-αCH_2), 6.76 (s, 6 H; *Ar*-H), 7.30 (s, 6 H; *Ar*-H), 7.67 (t, $J = 5$ Hz, 3 H; *Py*-H), 7.96 (t, $J = 7$ Hz, 3 H; *Py*-H), 8.06 (d, $J = 7$ Hz, 3 H; *Py*-H), 8.94 (d, $J = 5$ Hz, 3 H; *Py*-H). Exchange of the acetonitrile ligand was accomplished through the addition of 20 equivalents of another nitrile RCN to the NMR tube. The rest of the solution was chromatographed directly on silica gel (THF/CH_2Cl_2 (2.5/97.5) as eluent) to give $[Cu(X_6Me_3Pic_3)(NCMe)]PF_6$ as a white solid ($R_f = 0.4$) which was dried under vacuum for 24 h at room temperature. M.p. > 280 °C (decomp); IR (KBr) $\tilde{\nu} = 1610$ (m), 1575 (w), 1485 (s), 1465 (sh), 1490 (s) cm^{-1} (C=N, C=C (Py)); elemental analysis calcd for $C_{89}H_{108}N_4O_6CuPF_6 \cdot THF \cdot 0.5\,CH_2Cl_2$: C 67.93, H 7.13, N 3.38, Cu 3.84; found: C 68.01, H 7.06, N 3.07, Cu 3.60; (the presence of solvent molecules was confirmed by NMR spectroscopy); ESI-MS (CH_2Cl_2): 1392.4 ($[Cu(X_6Me_3Pic_3)(NCCH_3)]^+$. This peak was isolated and fragmented (MS–MS) and shown to lose a mass of 43 Da (CH_3CN).

Received: March 10, 1998 [Z11569IE]
German version: *Angew. Chem.* **1998**, *110*, 2861 – 2864

Keywords: bioinorganic chemistry · calixarenes · coordination chemistry · copper · N ligands

[1] Reviews of bioinorganic enzymology: *Chem. Rev.* **1996**, *96*, 2237 – 3042.
[2] a) J. P. Klinman, in ref. [1], 2541 – 2561; b) W. Kaim, J. Rall, *Angew. Chem.* **1996**, *108*, 47 – 64 ; *Angew. Chem. Int. Ed. Engl.* **1996**, *35*, 43 – 60.
[3] a) N. Kitajima, Y. Moro-oka, *Chem. Rev.* **1994**, *94*, 737 – 757; b) W. B. Tolman, *Acc. Chem. Res.* **1997**, *30*, 227 – 237; c) K. D. Karlin, S. Kaderli, A. D. Zuberbühler, *Acc. Chem. Res.* **1997**, *30*, 139 – 147.
[4] R. G. Janssen, W. Verboom, D. N. Reinhoudt, A. Casnati, M. Freriks, A. Pochini, F. Ugozzoli, R. Ungaro, P. M. Nieto, M. Carramolino, F. Cuevas, P. Prados, J. de Mendoza, *Synthesis*, **1993**, 380 – 386.
[5] Such a conformational behaviour has already been described in detail for some closely related $X_6Me_3Bn_3$ calixarenes: a) S. Kanamathareddy, C. D. Gutsche, *J. Org. Chem.* **1994**, *59*, 3871 – 3879; b) J. P. M. van Duynhoven, R. G. Janssen, W. Verboom, S. M. Franken, A. Casnati, A. Pochini, R. Ungaro, J. de Mendoza, P. M. Nieto, P. Prados, D. N. Reinhoudt, *J. Am. Chem. Soc.* **1994**, *116*, 5814 – 5822.
[6] Crystal structure analysis: $[C_{90}H_{110}N_4O_6Cu]PF_6 \cdot 7\,CHCl_3$, $M_r = 2387.9$, colorless crystal ($0.6 \times 0.6 \times 0.4$ mm), triclinic, space group $P\bar{1}$, $a = 16.195(2)$, $b = 18.249(3)$, $c = 22.435(3)$ Å, $\alpha = 108.20(2)$, $\beta = 110.88(2)$, $\gamma = 93.57(2)^\circ$, $V = 5771.5(2)$ Å^3, $Z = 2$, $\rho_{calcd} = 1.374$ g cm^{-3}, $\mu(Mo_{K\alpha}) = 7.48$ cm^{-1}. Of the 39919 reflections collected at 160 K (STOE-IPDS diffractometer) in the $\theta = 1.85 - 22.72^\circ$ range, 14724 were unique; 1468 parameters were refined on F^2 with all data [SHELX-97][11] to give the final R indices: $R1$ [$I > 2\sigma(I)$] = 0.0916 and $wR2$ (all data) = 0.2321. The crystals were poorly shaped and weakly diffracting, thus giving low-resolution data and relatively high R values. One reason for these effects is the high amount of disorder in the crystal structure. The *t*Bu groups of the calixarene ligand and the CH_2 group of the propionitrile are disordered and could be refined onto two positions using distance and ADP restraints. In addition, the lattice bound $CHCl_3$ molecules are disordered. Crystallographic data (excluding structure factors) for the structure reported in this paper have been deposited with the Cambridge Crystallographic Data Centre as supplementary publication no. CCDC-101179. Copies of the data can be obtained free of charge on application to CCDC, 12 Union Road, Cambridge CB2 1EZ, UK (fax: (+44) 1223-336-033; e-mail: deposit@ccdc.cam.ac.uk).
[7] S. M. Carrier, C. E. Ruggiero, R. P. Houser, W. B. Tolman, *Inorg. Chem.* **1993**, *32*, 4889 – 4899, and references therein.
[8] Although several superoxo Cu^{II} complexes have been characterized at low temperature[3] (for an X-ray structure, see K. Fujisawa, M. Tanaka, Y. Moro-oka, N. Kitajima, *J. Am. Chem. Soc.* **1994**, *116*, 12079 – 12800), their room temperature stability seems to be precluded for entropic reasons. In the specific case of a neutral N_3 ligand, these species have been proposed as transient intermediate in the

 © WILEY-VCH Verlag GmbH, D-69451 Weinheim, 1998 1433-7851/98/3719-2734 $ 17.50+.50/0

formation of binuclear peroxo adducts but never observed.[3, 9] Hence, the possibility of a thermodynamically unfavored equilibrium with $[Cu(X_6Me_3Pic_3)(O_2)]^+$ cannot be ruled out, even if it has not yet been observed under these experimental conditions.

[9] A. D. Zuberbühler in *Bioinorganic Chemistry of Copper*, (Eds.: K. D. Karlin, Z. Tyeklár), Chapman & Hall, New York, **1993**, pp. 264 – 276, and references therein.

[10] a) C. D. Gutsche, *Calixarenes*, *Monographs in Supramolecular Chemistry*, (Ed.: J. F. Stoddart), The Royal Society of Chemistry, Cambridge, **1989**; b) *Calixarenes. A Versatile Class of Macrocyclic Compounds,* (Eds.: J. Vicens, V. Böhmer), Kluwer Academic Publishers, Dordrecht **1991**; c) V. Böhmer, *Angew. Chem.* **1995**, *107*, 785 – 818 ; *Angew. Chem. Int. Ed. Engl.* **1995**, *34*, 713 – 745; d) C. Wieser, C. B. Dieleman, D. Matt, *Coord. Chem. Rev.* **1997**, *165*, 93 – 161; e) A. Ikeda, S. Shinkai, *Chem. Rev.* **1997**, *97*, 1713 – 1734.

[11] G. M. Sheldrick, SHELX-97, Program for X-ray structure analysis, Universität Göttingen, **1997**.

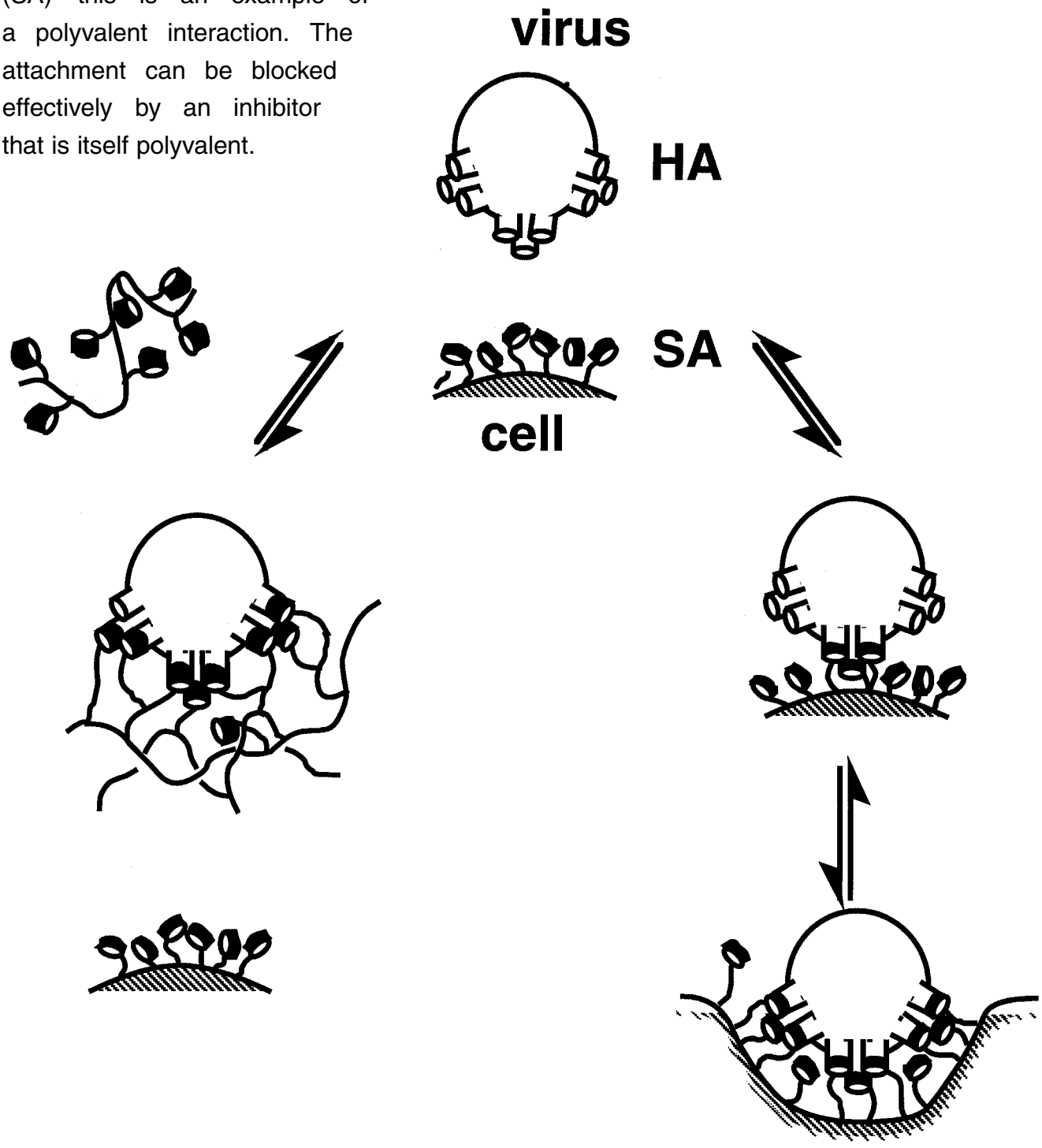
Deposition of Data from X-Ray Structure Analyses

In order to make life easier for authors and referees the Cambridge Crystallographic Data Centre (CCDC) and the Fachinformationszentrum Karlsruhe (FIZ) have unified their procedures for the depostion of data from single-crystal X-ray structure analyses.

Prior to submitting a manuscript please deposit the data for your compound(s) **electronically** at the appropriate date base, that is, at the CCDC for organic and organometallic compounds and at the FIZ for inorganic compounds. Both data bases will be pleased to provide help (see our *Notice to Authors* in the first issue of this year). In general, you will receive a depository number from the data base within two working days after electronic deposition; please include this number with the appropriate standard text (see our Notice to Authors) in your manuscript. This will enable the referees to retrieve the structure data quickly and efficiently if they need this information to reach their decision.

This is now the uniform procedure for manuscripts submitted to the journals *Advanced Materials, Angewandte Chemie, Chemistry–A European Journal, the European Journal of Inorganic Chemistry, and the European Journal of Organic Chemistry.*

The attachment of an influenza virus to a target cell occurs through multiple simultaneous interactions between hemagglutinin (HA) and sialic acid (SA)—this is an example of a polyvalent interaction. The attachment can be blocked effectively by an inhibitor that is itself polyvalent.



ANGEWANDTE CHEMIE ©WILEY-VCH

Polyvalent Interactions in Biological Systems: Implications for Design and Use of Multivalent Ligands and Inhibitors**

Mathai Mammen, Seok-Ki Choi, and George M. Whitesides*

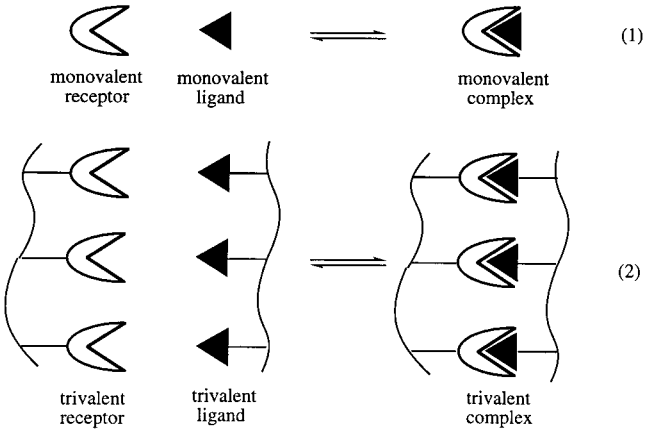
Polyvalent interactions are characterized by the simultaneous binding of multiple ligands on one biological entity (a molecule, a surface) to multiple receptors on another. These interactions occur throughout biology, and have a number of characteristics that monovalent interactions do not. In particular, polyvalent interactions can be collectively much stronger than corresponding monovalent interactions, and they can provide the basis for mechanisms of both agonizing and antagonizing biological interactions that are fundamentally different from those available in monovalent systems. The first part of this review examines the theoretical framework for polyvalency, describes a consistent nomenclature for polyvalent interactions, and discusses the central role of entropy in polyvalency. This examination is qualitative, and selectively highlights the most important characteristics of polyvalency. The second part surveys a number of biological processes that involve polyvalent interactions, with detailed discussion of examples that help to illustrate the many settings for polyvalent systems. This systematic survey suggests new targets and new strategies for the design of pharmaceutical agents based on polyvalency. The third part discusses principles of design, synthesis, and assay of synthetic polyvalent ligands, using the attachment of the influenza virus to an erythrocyte as a prototypical polyvalent system. This discussion of the activities of polyvalent, polymeric inhibitors of the hemagglutination induced by this virus indicates that there are multiple modes of interaction in this representative and particularly well studied polyvalent interaction; the two most important are entropically enhanced binding and steric stabilization.

Keywords: cooperative effects · molecular recognition · noncovalent interactions · polyvalency · receptors

1. Polyvalent Interactions Occur Throughout Biology

The valency of a particle—a small molecule, oligosaccharide, protein, nucleic acid, lipid or aggregate of these molecules; a membrane or organelle; a virus, bacterium, or cell—is the number of separate connections of the same kind that it can form with other particles through ligand–receptor interactions [Eqs. (1), (2)]. This review examines systems in which two biological entities interact oligovalently or polyvalently, that is, through simultaneous, specific association of two or more ligands and receptors.

The idea that many biological systems interact through multiple simultaneous molecular contacts is familiar; it has, however, become a new focus of inquiry in molecular biochemistry as the importance of interactions involving multiple proteins and ligands has begun to be unraveled. The possibility that multiple simultaneous interactions have unique collective properties that are qualitatively different from properties displayed by their constituents, which interact monovalently, suggests new strategies for the design of drugs and research reagents for biochemistry and biology. Enhancing or blocking collective or polyvalent interactions may benefit from (or require) strategies fundamentally different from those used in monovalent molecular interactions.



[*] Prof. G. M. Whitesides, Dr. M. Mammen, Dr. S.-K. Choi
Department of Chemistry and Chemical Biology
Harvard University
12 Oxford Street, Cambridge, MA 02138 (USA)
Fax: (+1) 617-495-9857
E-mail: gwhitesides@gmwgroup.harvard.edu

[**] A list of the abbreviations used is provided in the Appendix.

 © WILEY-VCH Verlag GmbH, D-69451 Weinheim, 1998 1433-7851/98/3720-2755 $ 17.50+.50/0

Few biological interactions have so far been established unambiguously to be polyvalent. Thus, here we hypothesize that interactions between biological entities that present multiple ligands and receptors commonly involve polyvalency. This review both summarizes and projects: Its objective is to hypothesize that polyvalency is an important type of interaction in biological systems, and to organize and review experimental information that supports or is relevant to this hypothesis. It also outlines some of the thermodynamic principles that distinguish polyvalent from monovalent interactions, and suggests strategies that are designed specifically to interfere with or promote interactions that are polyvalent.

In Section 3 we discuss the thermodynamics of polyvalent interactions as well as the concepts of cooperativity (using the familiar cooperativity parameter α) and polyvalent enhancement in binding (using β, a new parameter that we believe will be more useful than α for the evaluation of polyvalent inhibitors). In the subsequent sections, we detail interactions in biology that have been well studied and that are certainly or plausibly polyvalent; these interactions serve to illustrate some of the distinct and interesting properties of polyvalent systems. Finally, we discuss the principles and practice of the design of polyvalent ligands, and describe methods of assaying and quantifying the effectiveness of these ligands.

2. Examples of Polyvalent Interactions Relevant to Human Biology

The following examples of polyvalency are drawn from interactions relevant to human biology. The order of categories reflects both the present depth of understanding of these types of interactions and the intensities of the research activities focused on them.

2.1. Adhesion of a Virus to the Surface of a Cell: Influenza and Bronchial Epithelial Cells

In the first step of infection, the influenza virus attaches to the surface of a bronchial epithelial cell (Figure 1).[1, 2] The attachment occurs by interaction between multiple trimers of the hemagglutinin (HA, a lectin that is densely packed on the surface of the virus, about 2–4 per 100 nm^2 or 600–1200 per virus particle) and multiple moieties of *N*-acetylneuraminic acid (=sialic acid (SA), the terminal sugar on many glycoproteins and one that is also arranged densely on the surface of the target cell, about 50–200 per 100 nm^2). Table 1 provides other examples of cell–virus interactions. A growing



G. M. Whitesides



M. Mammen



S.-K. Choi

George M. Whitesides was born in 1939 in Louiseville, KY. He received his A.B. degree from Harvard College in 1960, and his Ph.D. from the California Institute of Technology with J. D. Roberts in 1964. He was a member of the faculty of the Massachusetts Institute of Technology from 1963 to 1982. He joined the Department of Chemistry at Harvard University in 1982, and was Department Chairman from 1986 to 1989. He is now Mallinckrodt Professor of Chemistry at Harvard University. He has served on many government and industrial councils and advisory boards, is a member of the editorial board for 17 scientific journals, and has received numerous awards including the Arthur C. Cope Award from the American Chemical Society. He is the author of over 600 publications, and his present research interests include biochemistry, surface chemistry, materials science, molecular virology, optics, self-assembly, and organic synthesis.

Mathai Mammen was born in Vellore, India, and raised in Halifax, Nova Scotia. He obtained his B.Sc. Honours in Chemistry from Dalhousie University, and his Ph.D. with G. M. Whitesides from Harvard in 1996. Working in both theory and experiment, he examined aspects of the influence of both entropy and electrostatics on the interaction of systems of molecules. He received his M.D. from Harvard, and was a member of the Harvard Medical School–Massachusetts Institute of Technology Division of Health Sciences and Technology. His research interests include the application of synthetic and biophysical chemistry to the solution of biologically and medically relevant problems (new tools for research, new pharmaceutical constructs, and new medical devices). He co-founded Advanced Medicine, Inc. in South San Francisco, CA and joined in July 1998.

Seok-Ki Choi was born in Puan, South Korea. He received his B.S. degree in Chemistry in 1986 from Seoul National University, where he then obtained his M.S. degree in Organic Chemistry in 1988 with S.-H. Chang. In July 1994, he received his Ph.D. degree in Organic Chemistry under K. Nakanishi at Columbia University in New York. His doctorate research examined the molecular mechanism of action of wasp neurotoxins. Following postdoctoral studies with G. M. Whitesides at Harvard, he joined Advanced Medicine, Inc. in South San Francisco, CA in April 1997. His areas of interest are biological and physical–organic chemistry of natural products and biologically relevant macromolecules.

Table 1. Examples of ligands and receptors[a] on the surfaces of virus and host cells.[3–5]

DNA viruses	Disease/application	Molecule on virus	Molecule on host
Papovaviridae *Polyomavirus* Polyomavirus	DNA-containing tumor virus	VP1[6]	**S**: NeuAc(α2,3)Gal(β1,3)GalNAc[6, 7] **S**: sialyloligosaccharides
Adenovirus *Mastadenovirus* Human adenovirus	acute respiratory disease, pneumonia, gastroenteritis (also a useful vector for gene therapy)	**P**: residues 1–141 of E3gp (fiber knob protein)[8] **P**: RGD base of the penton base protein (different from fiber protein)	**P**: class I MHC[9] **P**: penton base interacts with β_2 integrins[10]
Herpesviridae-alpha *Herpes simplex virus* type 1	herpes simplex	**P**: glycoprotein E and D[11–20]	**P**: gD, gH (proposed two-step attachment)
Varicella–Zoster virus	chicken pox, shingles	**P**: glycoprotein I (gE)[21, 22] (gE dimer resembles Fc receptor)	
Herpesviridae-beta *Cytomegalovirus* Human cytomegalovirus	major cause of infant blindness and retardation; implicated in AIDS and cancer (Kaposi sarcoma)	**P**: gC-11, gp residues 204–297 (86 kDa) of the gene of the H301 α-domain resembling class I MHC α3[23, 24]	**S**: heparan sulfate **P**: class I HLA MHC through β_2-microglobulin[25]
Lymphocryptovirus Epstein–Barr virus	mononucleosis	**P**: gp350[26] **P**: gp3[26]	**P**: C3d receptor CR2 (CD21) of B-lymphocytes; resembling C3 complement fragment C3d[27]
Poxviridae *Orthopoxvirus* Vaccina virus	used for small pox vaccination; similar antigenic patterns to variola virus	**P**: residues 71–80 of the VGF protein; resembling EGF α	**P**: receptor of the epidermal growth factor[27] (there is some evidence to the contrary, however[28]).
Parvoviridae *Parvovirus* Canine Parvovirus	this virus is a model for the human strain, which causes erythema infectiosum ("fifth disease"); the human form may cause hydrops fetalis or fetal death if contracted during pregnancy	**P**: GP1-anchored protein[29]	**P**: 3201 T-cells **P**: surface of precursors of erythrocytes in the bone marrow (infection can cause anemia)
Hepadnavirus Human hepatitis B virus *Hepatitis type B*	serum hepatitis, a chronic infection that results in liver failure and death in 1–2% of cases	**P**: pre-S portion of the Env protein **P**: residues 21–47 of the preS portion of the Env protein **P**: pre-S1 sequence of large S protein[30, 31];	**P**: IL-6 receptor, pre-S1 binding protein **P**: hepatocyte receptor for polymerized serum albumin **P**: hepatocyte receptor for polymeric IgA **P**: sialoglycoprotein **P**: mediated attachment through soluble IL6, gaining entry into nonliver cells indirectly **S**: asialoglycoprotein receptor[32]
Avian hepatitis B virus	serum hepatitis in birds		**P**: glycoprotein 180[33]
RNA viruses	**Disease**	**Molecule on virus**	**Molecule on host**
Picornaviridae *Enterovirus* Poliovirus	polio	**P**: residues 95–105 of the VP1 capsid protein[34]	**P**: member of the immunoglobulin superfamily,[35] not CD44 as previously reported.[36]
Rhinovirus Human rhinovirus	common cold	**P**: residues of VP1 and VP3 major capsid proteins lining a canyon on the virus surface[37–39]	**P**: ICAM-1[40]
Cardiovirus Encephalomyocarditis virus	mengo fever, rarely fatal; pathogenic for many animals (has caused outbreak of fatal myocarditis in pigs, for instance)	**P**: residues of VP1 and VP3 major capsid[41]	**P**: sialoglycoprotein **P**: VCAM-1[42]
Aphthovirus Foot and mouth disease virus	highly infectious disease of cattle, sheep, pigs, and goats (10–70% mortality); usually nonfatal in humans, but readily contracted from animals (causes high fevers)	**P**: NS28 glycoprotein **P**: residues 145–147 (RGD) and 203–213 of VP1 protein **P**: residues 133–158 and C-terminal region of the VP1 protein[37, 38, 43]	**P**: integrins
Reoviridae *Rotavirus* Human rotavirus	single most important cause of gastroenteritis and diarrhea in human infants worldwide: more than 500 million cases annually, resulting in 5 million deaths	**P**: C-terminal portion of hemagglutinin[44–46]	1. **P**: K562 erythroleukemia cells? 2. **P**: β-adrenergic receptor? 3. **P**: sialoglycoproteins in the vili of cells in the small intestine 4. **S**: sialic acids[47, 48]
Togaviridae *Alphavirus* Semliki forest virus	fever, encephalitis	**P**: nucleocapsid	**P**: class I HLA and H-2 MHC molecules[49–51]
Lactate dehydrogenase-elevating virus	fever, encephalitis	**P**: envelope glycoprotein (VP-3P)[52]	**P**: class II 1a MHC molecule of macrophage[53]

Table 1. (cont.)

RNA viruses	Disease/application	Molecule on virus	Molecule on host
Sindbis	related to the western equine encephalitis virus, ca. 5% mortality	**P**: E1-E2[54]	**P**: high-affinity laminin receptor[55, 56]
Rubivirus Rubella	rubella (German measles)		**S**: unidentified glycolipid[57, 58]
Orthomyxoviridae *Influenzavirus* Influenza virus	major cause of various forms of human respiratory disease, including fatal pneumonia	**P**: hemagglutinin protein (HN or H protein)[59–61]	**P**: HN protein, liver cell **S**: sialyloligosaccharides influenza A:[62] **S**: NeuAc(α2,6)Gal(β1,4)GlcNAc, **S**: NeuAc(α2,3)Gal(β1,3)GalNAc, **S**: NeuAc(α2,3)Gal(β1,4)GlcNAc influenza C:[63] **S**: 9-*O*-AcNeuAc
Paramyxoviridae *Paramyxovirus* Sendai virus	as a genus, *Paramyxovirus* is second only to respiratory syncitial virus in causing lower respiratory tract infections in young children	**P**: hemagglutinin protein[64–66]	**S**: sialyloligosaccharides **S**: NeuAc(α2,3)Gal(β1,3)GalNAc **S**: NeuAc(α2,8)NeuAc(α2,3)Gal-(β1,3)GalNAc, **S**: ganglioside GD1a
Newcastle disease virus	lower respiratory tract infections	**P**: hemagglutinin neuraminidase[67]	**S**: sialyloligosaccharides **S**: NeuAc(α2,3)Gal(β1,3)GalNAc[68]
Morbillivirus Measles virus	measles	**P**: measles virus hemagglutinin[69]	**P**: CD46[70]
Pneumovirus Respiratory syncytial virus	leading cause of lower respiratory tract infections (bronchiolitis and pneumonia), possible role in sudden infant death syndrome, major cause of middle-ear infections	**P**: fusion protein; nucleocapsid[71]	
Coronavirus, OC43	common cold, pharyngitis		**S**: $Neu5,9Ac_2$[72]
Rhabdoviridae *Vesiculovirus* Vesicular stomatitis virus		**P**: glycoprotein[73]	**S**: phosphatidylserine **S**: Phosphatidyl inositol **S**: GM_3 ganglioside[74]
Lyssavirus Rabies virus	rabies	**P**: residues 151–238 of G protein, resembling Curare-mimetic neurotoxins[75, 76]	**P**: BHK-21 cells **P**: acetylcholine receptor (residues 173–204 of the α subunit) **S**: sialylated gangliosides
Retroviridae[4, 77] *Oncovirus C—human* Human T-cell leukemia virus (HTLV-1)	cancer—leukemia	**P**: residues 246–253 of the envelope glycoprotein, resembling both the extracellular portion of HLA-B MHC molecule and IL2[78]	**P**: class I HLA MHC molecule **P**: Interleukin-2 receptor
Radiation leukemia virus	cancer—leukemia		**P**: T-cell receptor:L3T4 molecule complex[79]
Amphotrophic retrovirus	cancer—leukemia		**P**: CD34 on marrow progenitor cells[80]
Oncovirus C—Avian Avian leukosis virus	cancer		**P**: low-density lipoprotein receptor[81, 82]
Oncovirus C—Mammalian Murine leukemia virus (Moloney)	cancer—leukemia	**P**: envelope gp71[83]	**P**: lymphoma cell surface IgM **P**: hydrophobic protein (622 amino acids) of unknown function
Ecotropic murine retrovirus	cancer	**P**: envelope glycoprotein[84]	**P**: basic amino acid transporter[85]
Nonecotropic murine leukemia virus	leukemia	**P**: gp70 (surface)[86]	
HIV-1	AIDS	**P**: gp120-resembling Ig heavy-chain regions	**P**: CD4 of T-cell
		P: gp120-resembling neuroleukin	**P**: CD4 molecule interacting with class II HLA-DR MHC molecule
		P: gp120-resembling vasoactive intestinal peptide[87, 88]	**S**: galactosyl ceramide (or closely related molecule on human colon epithelial HT29 cells) **P**: CR2, especially in EBV infected cells **P**: chemokine receptors CXCR-4 (T-cell trophic) and CCR-5 (macrophage trophic; both are seven-transmembrane G-protein coupled receptors[89])
HIV-2	AIDS		**P**: CD4[90]
Simian immunodeficiency virus	immunodeficiency syndrome analogous to AIDS in simians	**P**: SIV mac239[91]	**P**: CD4
African swine virus		**P**: p12, p72[92, 93]	

[a] **P** = protein; **S** = sugar (glycoprotein or glycolipid).

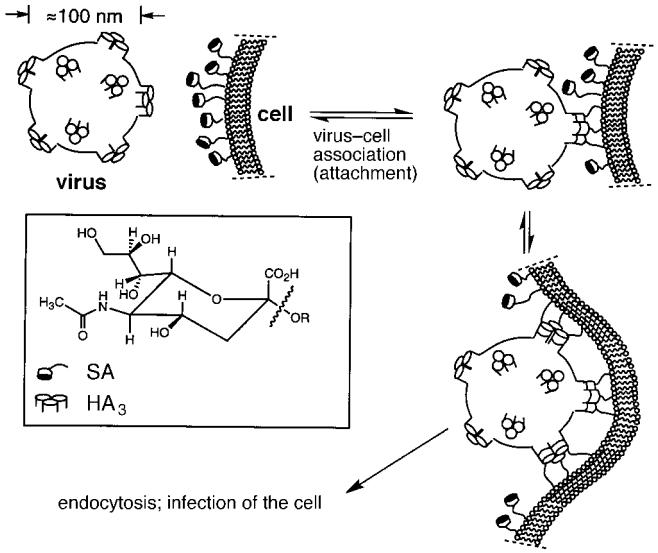


Figure 1. The influenza virus attaches to cells by interaction of trimeric hemagglutinin (HA_3, shown as protruding cylinders on the virus) with sialic acid (SA, shown as caps on the cell). Only a few of the hemagglutinin trimers and SA groups are represented; neither is to scale.

number of viruses are found to use more than one type of interaction for attachment to the target cell.

2.2. Adhesion of a Bacterium to the Surface of a Cell: *E. coli* and Urethral Endothelial Cells

Uropathogenic strains of the bacterium *E. coli* attach both directly and indirectly to the surface of epithelial cells in the urethra and bladder through polyvalent interactions (Figure 2). Several bacterial proteins have been identified that confer this tissue preference. Two examples are P-fimbrae (containing protein G) and type I fimbrae (containing the FimH adhesin), and both are located on the surface of *E. coli*.[94]

We illustrate polyvalency in this system using P-fimbrae as an example. First, these uropathogenic bacteria can use the lectin-like protein G located on the tips of their P-fimbrial filaments to adhere strongly and specifically to multiple copies of the Gal(α1,4)Gal (P_K antigen)[95] portion of a glycolipid present on the surface of the epithelial cells in the urinary tract, especially the kidney. Second, multiple copies of F-protein on the surface of the *E. coli* attach polyvalently to fibronectin, a soluble glycoprotein. The fibronectin, in turn, binds polyvalently to the surface of the epithelial cell. The *E. coli* collect in these tissues of the urinary tract, multiply there, and may cause disease (especially pyelonephritis). In general, bacteria bind either directly to a cellular surface, or to molecules in the extracellular matrix of preferred tissues. Bacteria bind both to sugars and proteins; examples are listed in Tables 2–4.

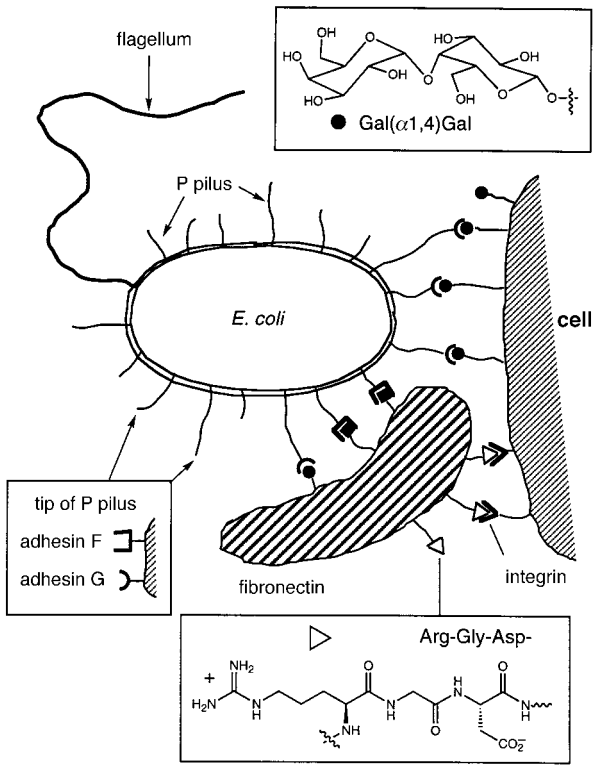


Figure 2. Attachment of uropathogenic *E. coli* bacteria to endothelial urethral cells. This attachment is mediated either by type I fimbrae or by P-fimbrae on the surface of the bacterium. In this example, the bacteria use lectin-like adhesin G located on the tips of their fimbrial filaments (P-fimbrae) to adhere specifically to multiple copies of Gal(α1,4)Gal (P_K antigen) expressed on the surface of the epithelial cells. In addition, multiple copies of adhesin F on the surface of the *E. coli* attach to fibronectin; fibronectin presents multiple copies of Arg-Gly-Asp (RGD) residue to bind tightly to epithelial cell by use of multivalent interactions of RGD and an integrin class of receptor. The illustration (especially, adhesins G and F) is not to scale.

2.3. Binding of Cells to Other Cells: Neutrophil and Arterial Endothelial Cells

The attachment of a neutrophil initially suspended in rapidly flowing blood to the endothelial cells closest to a site of inflammation occurs through polyvalent interactions.[188–190] Signaled by nearby inflammation, this initially rapidly transported neutrophil adheres to the surface of the endothelial cells, and then rolls slowly (10–20 μm min^{-1}); endothelial cells are those that line the interior of the blood vessels (Figure 3). This rolling is mediated by interactions between multiple E- and P-selectins on the surface of the endothelial cell (these selectins are not normally present on the surface of these cells, and are induced by cytokines during inflammation) and multiple glycoproteins displaying sialyl Lewis^X (sLe^X, a tetrasaccharide) on the surface of the neutrophil.[190] In addition, L-selectin, present on the surface of the neutrophil, interacts with sialyl Lewis^X, present on the endothelial cell. The valency of this set of interactions may significantly influence the kinetics, dynamics, and specificity of neutrophil recruitment.[191] Table 5 (page 2763) provides other examples of cell–cell interactions.

2.4. Binding of Cells to Polyvalent Molecules: Bacteria, Antibodies, and Macrophages

All classes of antibodies—one of the key groups of proteins making up the immune system—have multiple equivalent

Table 2. Examples of bacteria that bind sugars (**S**) and proteins (**P**) on the surfaces of host cells.

Bacterium	Disease	Molecule on bacterium	Molecule on host
Actinomyces naeslundii 12104 and A. viscosus LY7	chronic oral disease		**S**: GalNAcβ-containing glycosphingolipids (GSLs), e.g. GalNAc(β1,3)Gal(α)-*O*-ethyl[96, 97]
Candida albicans	part of normal flora of the oral and (female) genital tract, causes disease secondary to a predisposing condition (e.g. diabetes mellitus, immunodeficiency, long-dwelling catheters, antimicrobials that eliminate normal bacterial flora)	**P**: laminin receptor (37 kDa) **P**: fibrinogen-binding mannoprotein (58 kDa) **P**: C3d receptor **P**: Ubiquitin[98]	**S**: fucose-containing glycosides[99] on epithelial surface
Chlamydia trachomatis	chronic keratoconjunctivitis that can proceed to scarring and blindness, sexually transmitted diseases, respiratory infections	**S**: polysaccharide containing 7–9 mannose residues[100]	**P**: mannose-binding proteins[100]
Enteroaggregative *E. coli* (*EAggEC*)	food poisoning	**P**: hemagglutinins[101]	**S**: sialic acid
Uropathogenic *E. coli*	urinary tract infection	**P**: PapG adhesin[102] **P**: FimH adhesin[103]	**S**: Gal(α1,4)Gal on glycolipid **P?**: uroplakins Ia and Ib
S-fimbriated *E. coli*	cerebral vascular complications of meningitis		**S**: NeuGc(α2,3)Gal and NeuAc(α2,8)NeuAc[104] **S**: NeuGc(α2,3)Gal and NeuAc(α2,8)NeuAc[105] (found on endothelial cells of brain microvasculature)
Helicobacter pylori	gastroduodenal ulcers, gastric cancers	**P**: hemagglutinin **P**: laminin-binding protein	**S**: Lewis(b) blood group antigen[106] **S**: Neu5Ac(α2,3)Gal (SA-dependent strains)[107, 108]
Mycoplasma pneumoniae	Pneumonia	**P**: protein (40 and 90 kDa) on the tips of the pili[109]	**S**: long-chain sialo-oligosaccharides[110, 111]
Mycoplasma bovis	pneumonia, genital and urinary tract infection	**P**: protein (26 kDa)[112]	**S**: sialic acid residues and probably also sulfatide groups
Neisseria menigitidis Meningococcus	meningitis, acute adrenal insufficiency	**P**: pili (unusual in that pili contain digalactosyl-2,4-diacetamido-2,4,6-trideoxyhexose)[113]	**P**: CD66 on epithelial cells and neutrophils[114] **P**: glycoprotein G of RSV on the surface of the target cell (coinfection)[115]
Porphyromonas (Bacteroides) gingivalis	gingivitis		**S**: D-GalNAc[116]
Pseudomonas aeruginosa	colonizes regions devoid of natural defenses (catheters), and causes disease in immunodeficient hosts	**P**: pilus adhesin	**S**: GalNAc(β1,4) in asialo-GM1 and asialo-GM2 or GM1[117] **S**: salivary mucin glycopeptides (sialic acid)[118] **S**: lactose of glycolipids[119]
Rhizobium lupini		**P**: L-fucose-binding protein	**S**: L-fucose[120]
Staphylococcus saprophyticus	urinary tract infection	**P**: surface lectins	**S**: blood group A (terminal GalNAc)[121]
Streptococcus suis	meningitis		**S**: Gal(α1,4)Gal present in the P1 and Pk blood group antigen[122] **S**: N-Ac(α2 $\rightarrow$3poly-NAc-lactosamine glycans; NeuNAc(α2,3)Gal(β1,4)GlcNAc[123]
Streptococci (M+ group A)	nasopharyngitis; release of erythrogenic toxins can cause scarlet fever; can occur as secondary infection to influenza virus, and ultimate cause of fatal pneumonias in these cases		**P**: C3, mainly C3b and iC3b on PMN[124]
Streptococcus sanguis, *Streptococcus sobrinus* (oral cavity)	part of normal flora in the upper respiratory tract: *deficiency* can cause disease		**S**: sialic acid of salivary glycoproteins[125]
Yersinia enterocolitica	severe abdominal pain and diarrhea; can cause fatal sepsis in some cases		**S**: Gal, GalNAc, Lac in intestinal mucin[126]

receptor sites: two (IgD, IgE, IgG, IgA), four (IgA), six (IgA), or ten (IgM). Polyvalent binding to the structures that these antibodies recognize—antigens or other ligands present on the surfaces of bacteria, viruses, parasites, drugs, "nonself" cells, or other structures including noncovalent complexes not usually present in the blood circulation—seems to be an ubiquitous characteristic of immune recognition. These interactions may both inhibit processes important to infection (e.g., attachment of a foreign organism to target cells) and promote clearance (removal of the foreign particles either by

Table 3. Examples of bacteria that bind to the derivatives of the glycolipid lactosylceramide.[119, 122, 127–133]

Bacterium	Target tissue
Bacteroides fragilis	large intestine
Bacteroides ovatus	large intestine
Bacteroides vulgatus	large intestine
Bacteroides distasonis	large intestine
Bacteroides thetaiotamicron	large intestine
Lactobacillus fermentum	large intestine
Lactobacillus acidophilus	various places
Fusobacterium necrioohorus	large intestine
Fusobacterium varium	large intestine
Clostridium difficile	large intestine
Clostridium botulinum	large intestine
Propionibacterium granulosum	skin, large intestine
Propionibacterium acne	skin
Propionibacterium freudenreichii	milk products
Actinomyces viscosus	mouth
Actinomyces naeslundii	mouth
Shigella dysenteriae	large intestine
Shigella flexnerii	large intestine
Shigella sonnei	large intestine
Salmonella typhimurium	large intestine
E. coli	intestine
Vibrio cholerae	small intestine, large intestine
Campylobacter jejunii	intestine
Hemophilus influenzae	respiratory tract
Yersinia pseudotuberculosis	intestine
Yersinia pestis	intestine
Neisseria gonorrhoeae	genital tract
Pseudomonas aeruginosa	respiratory tract

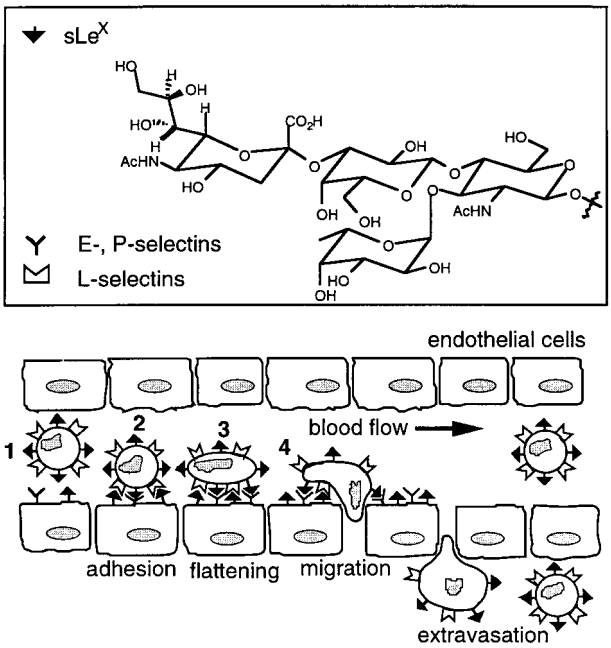


Figure 3. Injury results in expression and display of E- and P-selectins on the surface of nearby endothelial cells. Neutrophils (**1**) are attracted to this site (**2**). The neutrophil interacts polyvalently (through sLe^X moieties) with E- and P-selectins. In addition, L-selectins, expressed on the surface of the neutrophil, interact with sLe^X moieties present on the endothelial cell. Neutrophils change their shape upon attachment (**3**). Further adhesion mediated by integrins leads to extravasation (**4**).

Table 4. Examples of bacteria that bind sugars (**S**) and proteins (**P**) in the extracellular matrix.

Bacterium	Disease	Ligand (receptor) on the bacterium	Ligand (receptor) on the host matrix
Aspergillus fumigatus conidia	various localized fungal infections		**P**: D domains of the fibrinogen molecule[134]
Borrelia burgdorferi	lyme disease		**P**: integrin αIIbβ3 (glycoprotein IIb-IIIa) (RGD)[135]
Bordetella pertussis	whooping cough (pertussis)	**P**: pertactin and filamentous hemagglutinin (FHA); cell-binding sequence (RGD)[136]	
Candida albicans	part of normal flora of the oral and (female) genital tract, causes disease secondary to a predisposing condition (e.g. diabetes mellitus, immunodeficiency, long-dwelling catheters, antimicrobials that eliminate normal bacterial flora)	**P**: 37-kDa laminin receptor **P**: fibrinogen-binding mannoprotein (58 kDa) **P**: C3d receptor **P**: ubiquitin[98]	**S**: cell-wall polysaccharide of *Streptococcus gordonii* during coinfection[137] **S**: various oligosaccharides containing both β-1,2 and α-1,2 linkages[138–140]
Chlamydia trachomatis	chronic keratoconjunctivitis that can proceed to scarring and blindness, sexually transmitted diseases, respiratory infections	**P**: heparin-binding protein[141]	**S**: heparan sulfate-like GAG[141, 142] with a decasaccharide of minimum chain length[143]
Enterococcus faecalis	diarrhea		**S**: galactose, fucose, and mannosamine, but not mannose[144]
E. coli with S fimbriae	gastrointestinal infections	**P**: S-fimbriae protein SfaA	**S**: inhibited by NeuAc(α2,3)lactose[145] **S**: glycolipids containing terminal Gal($3SO_4$)β-1 residues[132]
Haemophilus influenzae	upper respiratory infections, often secondary to influenza virus	**P**: proteins of high molecular weight (HMW-1 and HMW-2)[146]	
Leishmania donovani	protozoan parasite causing kala-azar (visceral leishmaniasis)	**P**: heparin-binding protein	**S**: heparin[147]
Mycobacterium paratuberculosis	not a major human pathogen		**P**: fibronectin[148, 149]
Mycobacterium bovis	chronic granulomatous infections, especially in the lung	**P**: protein 85B and p55 protein	**P**: collagen-binding domain of fibronectin, glycoprotein present in plasma[150]

Table 4. (cont.)

Bacterium	Disease	Ligand (receptor) on the bacterium	Ligand (receptor) on the host matrix
Mycobacterium avium-intracellulare (MAI)	a common pathogen in AIDS patients		**P**: laminin, collagen I, and fibronectin[151]
Prevotella intermedia	periodontal infection	**P**: lactoferrin-binding protein (lactoferrin inhibits the binding)	**P**: fibronectin, collagen of type I and type IV, and laminin[152]
Salmonella enteritidis	severe diarrhea (common food poison from chicken and chicken eggs)		**P**: fibronectin[153]
Staphylococcus aureus	major human pathogen responsible for wide range of infections, can proceed to meningitis, endocarditis, and osteomyelitis	**P**: three repeats of a 38-residue D motif **P**: fibronectin-binding proteins (galel A and ZZ-FnBP B) **P**: protein (60 kDa) **P**: collagen-binding domain (CBD) of collagen adhesin **P**: collagen receptor containing either two or three copies of a repeat motif with 187 amino acids	**P**: N-terminal fragment (29 kDa) of fibronectin (Fn29 K)[154] **P**: fibronectin[155] **P**: bone sialoprotein (BSP) (small, ca. 80 kDa) integrin-binding, RGD-containing bone matrix glycoprotein[156, 157] **P**: collagen of cartilage[158] **P**: collagen[159, 160] **P**: N-terminal region (heparin-binding domain) of fibronectin[161]
Staphylococcus aureus	osteomyelitis and infectious arthritis	**P**: collagen adhesin **P**: fibrinogen receptor (clumping factor) fibronectin-binding protein (FnBP) **P**: unknown protein (60 kDa)	**P**: collagen (high degree of specificity and affinity)[162] **P**: fibrinogen[163, 164] **P**: laminin (the pepsin-derived (P1) fragment)[165, 166] **P**: vitronectin[167]
Staphylococcus saprophyticus	urinary tract infections		**S**: adherence is partially inhibited by mannose[168]
Streptococcus	wide range of gastrointestinal and respiratory infections		**P**: collagen type I[160]
Group A streptococci	infective endocarditis, glomerulonephritis, and rheumatic fever	**P**: lipoteichoic acid (LTA) and M protein (binding is inhibited by LTA)[169, 170] **P**: glyceraldehyde-3-phosphate dehydrogenase (GAPDH)[171, 172] **P**: protein F[173] **P**: PAM (related to the M proteins) **P**: M3 protein[174]	**P**: fibronectin **P**: human plasminogen and plasmin **P**: multiple binding to plasma fibrinogen, albumin and fibronectin
Nephritis(+) and nephritis(-) group A streptococci	glomerulonephritis	**P**: nephritis plasmin binding protein (NPBP)[175]	**P**: human plasmin (the binding is blocked by ε-aminocaproic acid)
Streptococcus bovis	urinary tract infections, endocarditis	**S**: lipoteichoic acid derivative[176]	
Streptococcus defectivus	not a human pathogen	**P**: surface protein (ca. 200 kDa)	**S**: cell-secreted extracellular matrix (ECM)[177]
Streptococcus dysgalactiae	neonatal sepsis and meningitis	**P**: fibronectin (Fn) receptors FnBA and FnBB	**P**: fibronectin[156, 157]
Streptococcus pneumoniae	pneumonia		**P**: laminin; collagen types I, II, and IV; fibronectin; and vitronectin[178]
Streptococcus pyogenes	major pathogen responsible for a wide range of systemic and local infections, and associated with post-streptococcal immunological disorders	**P**: protein F (X-ray structure known) **P**: streptococcal fibronectin-binding protein (Sfb protein, sequence of 37 amino acids)[179, 180] **P**: glycosaminoglycan-binding protein (GAG-BP; 9 kDa)[181] **P**: M protein[182, 183]	**P**: fibronectin[148, 184] **P**: basal laminae of human cardiac muscle
Veillonella atypica PK1910 (oral bacterium)	oral infections		**S**: co-aggregations with certain human oral streptococci (both lactose-inhibitable and lactose-non-inhibitable)[185]
Yersinia enterocolitica	abdominal pain and diarrhea	**P**: membrane protein YadA	**P**: cartilage-derived human cellular fibronectin and human plasma fibronectin[186]
Yersinia pseudotuberculosis	abdominal pain and diarrhea	**P**: adhesin YadA	**P**: β1 integrins[187]

degradation by macrophages and other components of the immune system, or by filtration by the kidney).[207] Polyvalency is used here for high-affinity binding to surfaces that have repeated epitopes, a defining characteristic of the surfaces of almost all invading pathogens.

Mannose residues on the tail (the Fc portion) of the antibody interact with mannose receptors (the Fc receptor) on the surface of a macrophage (a type of white blood cell important for clearing infectious particles). The interaction of a *single* Fc portion with its receptor seems to be too weak to

Table 5. Examples of polyvalent cell–cell interactions.

Cell 1	Molecule on cell 1	Cell 2	Molecule on cell 2
neutrophil	L-selectin, P-selectin[192–194]	endothelial cell	sulfated sLe^X[193, 195]
neutrophil	sulfated sLe^X[196]	endothelial cell	E-selectin[196]
neutrophil	E-selectin,[193] cadherins[198]	neutrophil	sulfated sLe^X[193]
neuron	neural-cell-adhesion molecule (NCAM) such as L1, NCAM-H, CD24, and α_6-integrin[192, 197]	endothelial cell	E-selectin[196]
T-cell	T-cell receptor[199]	antigen-presenting cells	MHC[199]
T-cell	CD3[200]	antigen-presenting cells	MHC
T-cell	CD28[201]	antigen-presenting cells	MHC
platelet	Ia/IIa	endothelial cell	collagen[202]
platelet	IIb/IIIa[203]	platelet	IIb/IIIa
tumor cell	GalTase[204]	endothelial cell	GlcNAc
sperm	GalTase[204]	egg	GlcNAc
aging red blood cell	desialylated glycoproteins[205, 206]	hepatocyte	C-type lectin

induce a response by the macrophage; that is, free (uncomplexed) antibody in solution does not activate macrophages, nor does a single antibody bound to a degraded piece of foreign pathogen. However, *multiple* antibodies bound to the surface of an infecting particle do interact strongly with multiple receptors on the surface of the macrophage, and give a three-layered structure stabilized at both interfaces through polyvalent interactions (Figure 4).[208–210]

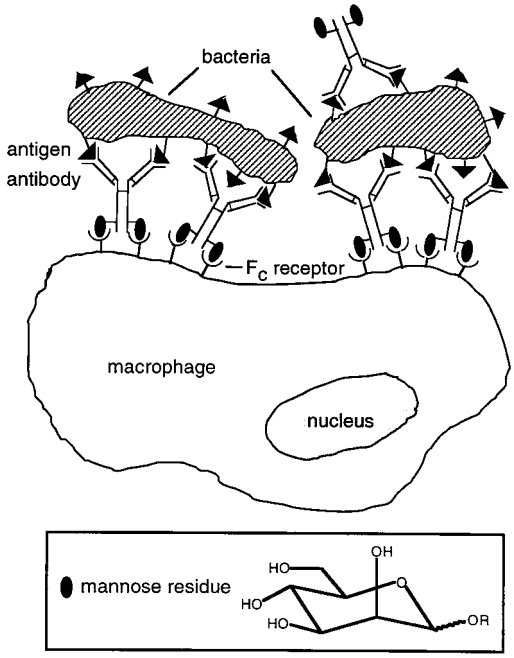


Figure 4. Layered polyvalent binding of a macrophage to bacterium (or other pathogens) through antibodies. The antibody recognizes a surface ligand (usually a protein) on the surface of bacterium, and can bind bivalently. The macrophage recognizes (with Fc receptors) the mannose residues on the constant region "tail" of the antibody, and also binds multivalently to the antibody-decorated pathogen.

Furthermore, not only does polyvalency in this system permit stability and specificity in the recognition of a bacterium by a macrophage, but subsequent action by the macrophage is also critically dependent on polyvalent interactions. Multiple interactions between the macrophage and the antibody-coated bacterium lead to a cross-linking of the surface receptors on the macrophage, triggering an internal signal in the macrophage to ingest (phagocytose) the bacterium which then leads to its degradation.[211] In Section 4.3.1, we discuss a general mechanism for this sort of polyvalent signal transduction. Other examples of polyvalent molecules that attach to the surfaces of cells are given in Tables 6 and 7.

2.5. Binding of Polyvalent Molecules to Polyvalent Molecules: Binding of Transcription Factors to Multiple Sites on DNA

An example of molecules that interact polyvalently is taken from the biology of gene regulation by oligomeric transcription factors (Figure 5). The retinoid X receptor (RXR) functions as a transcription factor in the presence of its ligand.[258] Each RXR–ligand complex (RXR-L) binds a DNA single strand called the cellular retinol-binding protein II element (CRBP-II element). The intrinsic affinity of one unit of RXR-L for one CRBP-II element is low; that of a dimer $(RXR\text{-}L)_2$ for two adjacent elements $(CRBP\text{-}II)_2$ is higher, but still low; that of a tetramer $(RXR\text{-}L)_4$ for four adjacent elements $(CRBP\text{-}II)_4$ is moderate; and that of a pentamer $(RXR\text{-}L)_5$ for five adjacent elements $(CRBP\text{-}II)_5$ is high, and significantly higher than that of the tetramer. In this example, the transcription factor is functioning as a polyvalent aggregate of ligands, and the DNA containing multiple binding sites is a polyvalent receptor (examples are given in Table 8). Polyvalency of this sort creates a transcriptive response that is highly sensitive to the concentration of the transcription factor: The rate of transcription is proportional to $\Sigma_n C_n[\text{CRBP-II}]^n$, where C_n are constants.

Since the rate of transcription is mostly likely highest with the pentamer, the rate is approximately proportional to $[\text{CRBP-II}]^5$; this dependence on concentration is much higher than is possible with monovalent interactions (for which the

Table 6. Receptors for bacterial toxins.[127, 129, 212, 213]

Bacterium	Toxin	Ligand[a]
Vibrio cholerae	cholera toxin[214]	**S**: GM_1: Gal(β1,3)GalNAc(β1,4)(NeuAc(α2,3))Gal(β1,4)Glc(β)-ceramide[215, 216] **S**: isoligands:[216] NeuAc(α2,3)Gal(β1,3)GalNAc(β)(NeuAc(α2,3)Gal(β1,4)Glc(β)-ceramide, Gal(β)GalNAc(β1,4)(NeuAc(α2,8)NeuAc(α2,3)Gal(β1,4)Glc(β)-ceramide, GalNAc(β1,4)-Gal(β1,3)GalNAc(β1,4)((NeuAc(α2,3))Gal(β1,4)Glc(β)-ceramide, Fuc(α1,2)Gal(β1,3)-GalNAc(β1,4)((NeuAc(α2,3))Gal(β1,4)Glc(β)-ceramide, Gal(β1,3)GalNAc(β1,4)-(R-NeuAc(α2,3)Gal(β1,4)Glc(β)-ceramide (R = Lucifer yellow CH, rhodamine, or DNP)
E. coli	heat-labile toxin[217]	**S**: GM1[145]
Clostridium tetani	tetanus toxin	**S**: Gal(β1,3)GalNAc(β1,4)((NeuAc(α2,8))NeuAc(2,3)Gal(β1,4)Glc(β)-ceramide[218] **S**: isoligands: NeuAc(α2,3)Gal(β1,3)GalNAc(β1,4)((NeuAc(α2,8))NeuAc(α2,3)-Gal(β1,4)Glc(β)-ceramide, NeuAc(α2,8)NeuAc(α2,3)Gal(β1,3)GalNAc(β1,4)(NeuAc(α2,8)-NeuAc(α2,3)Gal(β1,4)Glc(β)-ceramide
Clostridium botulinum	botulinum toxin A and E[219]	**S**: NeuAc(α2,8)NeuAc(α2,3)Gal(β1,3)GalNAc(β1,4)(NeuAc(α2,8))NeuAc(α2,3)-Gal(β1,4)Glc(β)-ceramide
Clostridium botulinum	botulinum toxin B, C, and F[219]	**S**: NeuAc(α2,3)Gal(β1,3)GalNAc(β1,4)(NeuAc(α2,8))NeuAc(α2,3)Gal(β1,4)Glc(β)-ceramide
Clostridium botulinum	botulinum toxin B[220]	**S**: Gal(β)-ceramide
Clostridium perfringens	delta toxin[213]	**S**: GalNAc(β1,4)(NeuAc(α2,3))Gal(β1,4)Glc(β)-ceramide
Clostridium difficile	toxin A[221]	**S**: Gal(α1,3)Gal(β1,4)GlcNAc(β1,3)Gal(β1,4)Glc(β)-ceramide
Clostridium difficile	shiga-like toxin (SLT)-I and SLT-II/IIc[222]	**S**: Gal(α1,4)Gal(β) (P1 disaccharide), Gal(α1,4)Gal(β1,4)GlcNAc(β) (P1 trisaccharide), or Gal(α1,4)Gal(β1,4)Glc(β) (Pk trisaccharide)
Shigella dysenteriae or *E. coli*	shiga toxin[213, 222]	**S**: Gal(α1,4)Gal(β)-ceramide
Shigella dysenteriae or *E. coli*	vero toxin[223]	**S**: Gal(α1,4)Gal(β1,4)Glc(β)-ceramide
Bordella pertussis	pertussis toxin[224, 225]	**S**: NeuAc(α2,6)Gal[224, 225]
S. Dysenteriae I	dysenteriae toxin[128]	**S**: GlcNAc(β1)

[a] **S** = sugar.

Table 7. Examples of cross-linking of surface receptors as a mechanism of signal transduction.[a]

Process	Receptor – ligand
degranulation of mast cells (allergy)	allergens oligomerize IgE on the surface of the mast cell (P, N:N)[226–230]
cellular differentiation and growth (developmental biology: differentiation, migration, apoptosis)	fibroblast growth factor (FGF) dimerizes FGF receptor; a role for heparin in forming a polyvalent template for FGF and other heparin-binding growth factors is emerging (P, N:N)[231–235] epidermal growth factor (EGF) dimerizes EGF receptor (NP)[236] cytokine stem cell factor (SCF) dimerizes kit receptor on the surface of the stem cell (P, 1:2)[237] transforming growth factor (TGF) dimerizes TGF receptor (NP)[238] platelet-derived growth factor (PDGF) dimerizes PDGF receptor (P, 1:2)[239] a single human growth hormone (hGH) dimerizes hGH receptor (P, 1:2)[240–242] hepatocyte growth factor (HGF) dimerizes c-Met receptor; heparin may provide a polyvalent template for HGF (see FGF above; P, N:N)[243] EPO dimerizes EPO receptor on erythrocyte precursor cell (P, N:N)[244] vascular endothelial growth factor (VEGF) binds to VEGF Receptor Flt-1 (NP)[245] IL6 hexamerizes IL6 receptor (P)[246] IL4 dimerizes its receptor (P, 1:2)[247] human macrophage colony stimulating factor (M-CSF) dimerizes M-CSF receptor (P, 1:2)[248] lactogenic hormone can dimerize prolactin receptors (PRLR) (P, 1:2)[249] two monovalent granulocyte colony stimulating factors (G-CSF) stimulate the dimerization of two G-CSF receptors (NP)[250]
compaction during early embryogenesis	receptor for X hapten and multivalent X hapten (free multivalent versions of X hapten decompact; monovalent X haptens have no effect; P, N:N)[251]
parasympathetic response (autonomic nervous system)	acetylcholine receptor undergoes heterodimerization by unknown mechanism (NP?)[252]
acrosomal reaction in the interaction of sperm with egg (reproductive biology)	GalTase on sperm, GlcNAc on the exterior of the egg (P, N:N)[253]
peptide-independent clonal expansion of B-cells (immunology)	antibody on the surface of a B-cell; polysaccharide coats on the surface of microorganisms (P, N:N)[254]
interferon actions	interferon-alpha (IFN-alpha) dimerizes its receptor (P, N:N)[255]
T-cell clonal expansion	T-lymphocyte receptors CD28 and CTLA-4 bind and are oligomerized by co-stimulatory molecules CD80 (B7 – 1) and CD86 (B7 – 2) on antigen presenting cells (P, N:N)[256]
bacterial chemotaxis	aspartate dimerizes bacterial receptor Tar (NP)[257]

[a] P, 1:2 = Heterobivalent ligand dimerizes two surface receptors; P, N:N = *N*-valent ligand oligomerizes *N* surface receptors; P = probably polyvalent, but with unknown ligand – receptor stoichiometry; NP = possibly a non-polyvalent mechanism.

Table 8. Examples of transcription factors that bind polyvalently to DNA.[259–261]

Transcription factor	Number of sites that recognize DNA
BZip-type transcription factors	2 (noncovalent, homodimers)[262]
lambda repressor	2 (noncovalent, homodimers)[263]
p53	4 (noncovalent, homotetramers)[264]
RXR to CRBP-II	4–5 (noncovalent, oligomers)[265]
estrogen receptor	2 (noncovalent, homodimers; the dimer is induced by estradiol and binds DNA 50 times more rapidly than the monomer)[266]
thyroid hormone receptor	2 (noncovalent, homodimers or noncovalent heterodimer with 9-*cis*-retinoic acid receptor; the dimer is induced by binding to thyroid hormone)[267]
Zn fingers	1–3 (covalent, heterooligomers)[268, 269]

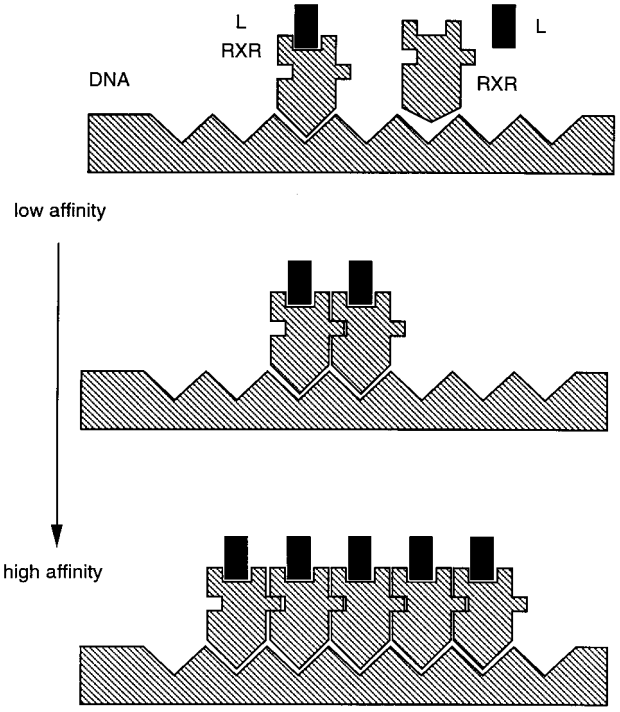


Figure 5. Binding of transcription factors to multiple sites on DNA. Top: The complex of monomeric retinoid X receptor (RXR) and ligand (L), RXR-L, binds with low affinity to the cellular retinol-binding protein II element (CRBP-II) on DNA. Middle: The dimeric complex $(RXR\text{-}L)_2$ has higher affinity than the monomeric complex. Bottom: The pentameric complex $(RXR\text{-}L)_5$ has very high affinity for DNA.

rate of transcription would be proportional to the concentration of the monovalent transcription factor, [CRBP-II]).

3. Nomenclature and Thermodynamics

3.1. Free Energy and Binding Constants in *N*th Order Polyvalent Interactions

We start with nomenclature. In chemistry, it is universal to think of molecular recognition in terms of two components: a protein receptor and a species recognized by the receptor (a ligand, inhibitor, substrate, epitope, or some other molecule or portion of molecule, depending on the context); here we will use the word ligand for this second species. In chemical nomenclature, the receptor is a protein with a declivity or pocket on its surface; the ligand is the molecular entity that fits into that pocket [see Eq. (1) on page 2755]. The receptor is the lock; the ligand is the key. In the literature of cell-surface biology, usage has not been consistent, and both the receptor and the ligand have been called the receptor, with the convention that the receptor was the species on the surface of the target cell. Wherever possible, we will use the chemical system of nomenclature: In this review, the receptor is the protein with a surface declivity that participates in specific recognition.

For polyvalent interactions as a class, there is no accepted nomenclature. Because there are a number of different ways in which N receptor sites can interact with N ligands, and because the free energy of binding of an interaction depends strongly on its details, there is probably no simple general nomenclature. We will use the least complex system of nomenclature that we can. We will call an interaction between N ligands and N receptors distributed on two entities an Nth-order polyvalent interaction that occurs with free energy of association ΔG_N^{poly}. Equation (2) illustrates a third-order polyvalent interaction that occurs with free energy of association ΔG_3^{tri}. The proposed nomenclature for polyvalent interactions is summarized in Figure 6.

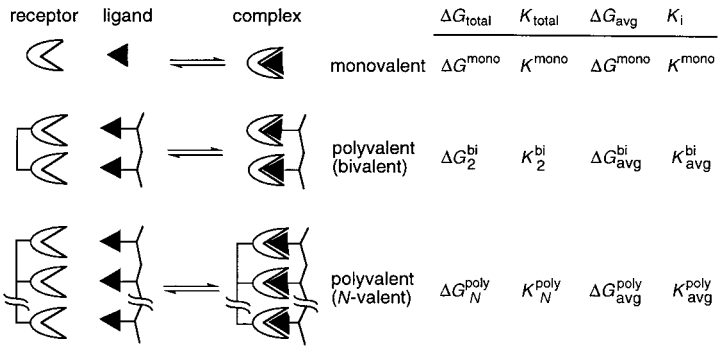


Figure 6. Proposed nomenclature for the polyvalent interactions; relationships between free energies of binding (ΔG) and inhibition constants (K_i) for both monovalent and polyvalent systems.

The average free energy of interaction, ΔG_{avg}^{poly}, between a single ligand moiety and a single receptor moiety in the polyvalent interaction shown in Figure 6 is equal to $\Delta G_N^{poly}/N$ [Eq. (3)]. A monovalent ligand–receptor interaction occurs

$$\Delta G_{avg}^{poly} = \Delta G_N^{poly}/N \quad (3)$$

$$\Delta G = -RT\ln(K) \quad (4)$$

$$K_N^{poly} = (K_{avg}^{poly})^N \quad (5)$$

with free energy change ΔG^{mono}; N monovalent, independent receptors interact with N monovalent, independent ligands

with a free energy change of $N\Delta G^{mono}$. The most useful comparisons of free energies of association involve the same numbers of ligands and receptors, and must be considered thoughtfully if different numbers of ligands and receptors (and different units for equilibrium constants) are involved. Equations (3) – (5) give the values of the corresponding association constants K.

Other terms have been used in the literature to refer (often imprecisely and inconsistently) to the thermodynamics of polyvalent interactions. It may be useful to review these terms briefly, and to incorporate them into the nomenclature we introduce in this manuscript.

"Affinity" is a qualitative term, and "affinity constant" its quantitative associate used correctly to mean association constant K. "Avidity" is a term whose origin is unclear, but refers to the association constant of a polyvalent interaction. We would precisely define avidity as the quantity given by Equation (5), K_N^{poly}. As an example, a Fab fragment (the portion of one arm of an antibody that contains the ligand binding site) binds a ligand with a certain affinity K. The intact antibody is a covalent collection of more than one Fab fragment (IgG, for example, has two Fab fragments). The binding of bivalent IgG to a dense surface of ligand can be imagined conceptually as the binding of one monovalent entity to the same surface, and described by a different association constant. That association constant, K_2^{bi} in this review, is referred to as the avidity of the bivalent antibody. In many instances, the avidity is found to be greater than the affinity K of the component monovalent interactions (Fab fragment). The extent to which K_2^{bi} is greater than K depends sensitively on both the structure and geometry of the antibody and the precise arrangement of the ligands on the surface. Since avidity has traditionally only been used to refer to polyvalent interactions where $N \approx 2-10$, and not for $N \approx 10^5$, we will not use this term in this manuscript because we do not want to conplicate further an already confusing system of nomenclature. We will use the terms defined by Equations (3) – (5) consistently.

The "chelate effect" had its origin in chemistry, and is often used in organometallic chemistry to refer qualitatively to the enhanced binding of electron donor groups (like an amine) for a metal (like iron) when the donor groups are joined covalently by some linking group. Again in this review, the chelate effect refers to those instances when K_N^{poly} is greater than K of any of the component interactions in the analogous fully monovalent binding event. As an example, K would refer to the association constant K for the interaction of methylamine with iron, and K_2^{bi} is the association constant of ethylenediamine with iron. The chelate effect refers to the observation that K_2^{bi} is often greater than K. The degree to which K_2^{bi} is larger than K is highly dependent on the structure and geometry of the linking group.

3.2. Cooperativity: The Magnitude of α

The average free energy of interaction between a ligand moiety and receptor moiety in a polyvalent interaction (ΔG_{avg}^{poly}) can be greater than, equal to, or less than the free energy in the analogous monovalent interaction [ΔG^{mono}; Eqs. (6) – (8)]. Following accepted nomenclature in biochem-

$$\Delta G_{avg}^{poly} = \alpha \Delta G^{mono} \quad (6)$$

$$N\Delta G_{avg}^{poly} = \Delta G_N^{poly} = \alpha N \Delta G^{mono} \quad (7)$$

$$K_N^{poly} = (K_{avg}^{poly})^N = (K^{mono})^{\alpha N} \quad (8a)$$

$$\alpha = \frac{\lg(K_N^{poly})}{\lg(K^{mono})^N} \quad (8b)$$

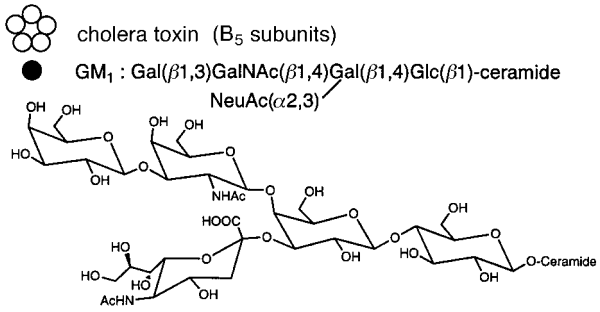
istry, we call these classes of polyvalent interactions positively cooperative (synergistic), noncooperative (additive), or negatively cooperative (interfering), respectively. We follow the convention of defining α as the degree of cooperativity.[270] The units of α depend on the order of the polyvalent interaction.

Cooperativity in biology has been rigorously defined and reviewed previously.[271, 272] The best studied positively cooperative systems in biology do not involve polyvalency. For example, the binding of four O_2 molecules to tetrameric hemoglobin occurs with cooperativity; that is, the free energy of binding of the second oxygen molecule to hemoglobin is more favorable than the binding of the first, and $-\Delta G_{avg}^{poly} > -\Delta G_{(first)}^{mono}$. The degree of cooperativity, α, in such non-polyvalent systems is greater than one and unitless.

There are presently no convincingly characterized examples of positive cooperativity for *polyvalent* systems in the literature. As a class, to our knowledge, polyvalent interactions have not been quantified sufficiently frequently or carefully for positive cooperativity to be inferred unambiguously in even one system.[273]

One example of a positively cooperative polyvalent interaction ($\alpha > 1$) *may* be the association of pentameric cholera toxin with GM_1, an oligosaccharide portion of the GM_1 ganglioside (Figure 7). Cholera toxin consists of five subunits (AB_5). The binding of the toxin to *monomeric* GM_1 (GM_1 that has been cleaved from the ceramidyl moieties on the cellular surface) provides a well-studied example of positive cooperativity through purely enthalpically enhanced binding. As will be discussed shortly, the entropy of the first binding event of a monomeric GM_1 derivative to pentameric cholera toxin is equal to the entropy of each subsequent binding event. All differences in the free energies of binding (Figure 7) of monomeric GM_1 to the toxin are therefore due to differences in enthalpy. Schoen et al. performed calorimetric studies of the binding of pentameric B_5 to five independent GM_1 oligosaccharide units in solution.[274] They found that the binding constant of the first ligand was *lower* than the binding constant of the second by a factor of 4. Calculated purely statistically, the binding constant of the first ligand would be expected to be *greater* by a factor of 5/2 than the second binding constant.[275] We conclude that the binding was enhanced enthalpically.

Schoen et al. also report that the binding of pentavalent B_5 to the surface of a cell that is densely covered with GM_1 moieties occurs essentially irreversibly and with greater ΔG of association than the binding of pentameric cholera toxin to five monomeric units of GM_1. Since the enthalpy of interaction is approximately the same for single (monovalent) GM_1 and for GM_1 immobilized on a surface, this difference in



State	No. of ligands (l)	Configuration	$l\Delta G - j\Delta q$
1	0		0
2	1		ΔG
3	2		$2\,\Delta G$
4	2		$2\,\Delta G - \Delta q$
5	3		$3\,\Delta G - \Delta q$
6	3		$3\,\Delta G - 2\,\Delta q$
7	4		$4\,\Delta G - 3\,\Delta q$
8	5		$5\,\Delta G - 5\,\Delta q$

Figure 7. The binding of five molecules of GM_1 oligosaccharide to pentavalent cholera toxin occurs with enthalpically enhanced binding; that is, the binding of one GM_1 oligosaccharide increases the favorable enthalpy of binding of the next GM_1 oligosaccharide.[268] Since the individual molecules of GM_1 oligosaccharide translate and rotate independently, the binding in this system is entropically neutral. l = number of ligands, j = number of contacts between GM_1 units, q = interaction energy (enthalpy) of two GM_1 units in contact.

the ΔG of association can be attributed to differences in entropy between these two types of association: The affinity of a polyvalent receptor can be greatly enhanced through multipoint attachment. Because the affinity of the pentamer for the polyvalent surface was not quantified, the extent of cooperativity, if any, is unknown.

The following are two examples of interactions that are probably negatively cooperative (interfering; $\alpha < 1$); that is, unlike the case of positive cooperativity (hemoglobin and O_2), the binding of the second ligand to the second receptor occurs with a less favorable free energy than the binding of the first ligand to the first receptor. The first example is the binding of a bivalent antibody to ligands that are densely packed on a biological surface—such as a mammalian cell, a virus, or a solid support for an enzyme-linked immunosorbant assay (ELISA)—or immobilized in a polymeric matrix (Figure 8).[276] In general, monovalent binding constants of antibodies for small organic ligands vary significantly, but are in the range of $10^5 - 10^8\,\text{M}^{-1}$. For non- or positively cooperative systems, we expect $K_2^{bi} \geq (K^{mono})^2 \approx (10^5 - 10^8)^2\,\text{M}^{-1}$. Karush et al. found that a bivalent antibody for a surface antigen on *Bacillus sp.* bound with 30-fold higher affinity than did the corresponding monovalent antibody (a monovalent antibody is one in which the two or more binding sites present in the native protein

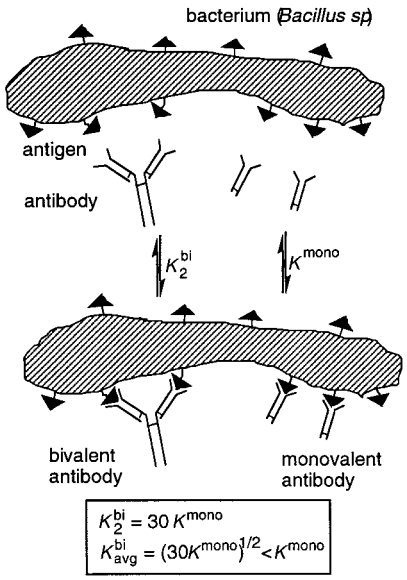


Figure 8. The binding of a bivalent antibody to ligands packed on the surface of a bacterium is negatively cooperative.[270]

have been disconnected chemically or enzymatically); that is, $K_2^{bi} = 30\,K^{mono} < (K^{mono})^2\,\text{M}^{-1}$.[277] The binding here is therefore negatively cooperative.

In a second example (Figure 9) Lee et al. studied the binding of di- and trivalent galactose-containing ligands which bind C-type lectins on the surface of hepatocytes;[206] the

Oligosaccharide	K for complex of lectin/Gal-oligosaccharide (M^{-1})
Gal(β1)OMe	$K^{mono} = 7 \times 10^4$
Gal(β1,4)GlcNAc(β1,2) Gal(β1,4)GlcNAc(β1,4) Man	$K_2^{bi} = 3 \times 10^7$
Gal(β1,4)GlcNAc(β1,2)Man(α1,6) Gal(β1,4)GlcNAc(β1,2)Man(α1,3) Man Gal(β1,4)GlcNAc(β1,4)	$K_3^{tri} = 2 \times 10^8$

Figure 9. Binding of mono-, bi-, and trivalent Gal-terminated oligosaccharides to C-type mammalian hepatic lectins.[201]

density of these receptors is unknown. Where $K^{mono} = 7 \times 10^4\,\text{M}^{-1}$, $K_2^{bi} = 3 \times 10^7\,\text{M}^{-1} = 420\,K^{mono}$, and $K_3^{tri} = 2 \times 10^8 = 2800\,K^{mono}$. Since $K_2^{bi} < (K^{mono})^2$ and $K_3^{tri} < (K^{mono})^3$, these di- and trivalent ligands also bind with negative cooperativity.

These examples illustrate an important characteristic of polyvalent interactions: Even though bivalent binding in these cases was negatively cooperative ($\alpha > 1$), the measured affinity for a bivalent molecule was much higher than for the monovalent molecule. Tight binding does not require positive cooperativity in the sense that this phrase is traditionally used. In the classic study of hemoglobin binding four molecules of oxygen, for example, the free energy of binding of oxygen to tetrameric hemoglobin correlates positively with the number of oxygen molecules bound (see above). In polyvalent bind-

ing, the free energy of binding of each ligand in a polyvalent complex does not have to correlate positively with the number of ligand molecules bound.

Thus, cooperativity, as defined in the traditional biochemical sense, is neither as useful nor as descriptive a parameter for polyvalent systems as it is for monovalent ones. We therefore introduce here a new, empirical metric describing the enhancement of binding of polyvalent systems. By extension from the cooperativity parameter α, we call this new metric β. Thus, although a polyvalent interaction may be qualitatively much stronger than any one of the monomeric interactions contributing to it, these monomeric interactions may still be interfering with,[1] or indifferent to, one another (the "sticking" of polyvalent ligands to affinity gels during affinity chromatography probably represents such a case). Only by a quantitative comparison of polyvalent and monovalent interactions is it possible to establish the nature of cooperativity.

3.3. Enhanced Affinity in Polyvalent Interactions: The Magnitude of β

In many polyvalent systems, the number N of ligand–receptor interactions is unknown. For example, we recently synthesized polymeric, polyvalent inhibitors of agglutination of erythrocytes by influenza virus. These inhibitors were composed of a polyacrylamide backbone, and a certain fraction of the side chains terminated in sialic acid (SA) groups.[2] The SA moieties on this polymer interact specifically with multiple hemagglutinin (HA) receptor sites on the surface of the influenza virus (see Section 2.1) and consequently prevent the interaction of influenza with its target cell. Using a polymer whose side chains present both SA groups and a small number of biotin groups (as a ligand for attachment of enzyme-conjugated streptavidin in a subsequent step in the assay), we measured the binding of this polymeric polyvalent inhibitor to the surface of the virus using an ELISA-like assay (Figure 10).[278] The surface-bound virus was incubated with varying concentrations of polymer containing SA, and the amount of bound polymer was measured indirectly through an enzyme-linked streptavidin–biotin interaction. The measurable quantities in constructing a binding isotherm were the amount of SA contained on polymer bound to the surface of the virus, the concentration of SA [SA], and the corresponding concentration of polymer [P]. The latter was derived by dividing [SA] by the average number Q of SA groups per polymer chain (which was a known quantity in our experiments, and could be calculated from the known degree of polymerization and the experimentally fixed mole fraction of side chains containing SA). Neither the number of polymers bound to the virus nor the number N of SA groups on each polymer that were bound to HA receptor sites were measured. We analyzed this interaction between polymer and virus by determining the amount of bound polymer as a function of [SA]. At half-maximal binding $1/K^{\mathrm{ELISA}} \equiv [\mathrm{SA}] \equiv Q[\mathrm{P}]$, where K^{ELISA} is equivalent to an association constant [Eq. (9), Figure 10]. Since the value of N in this polyvalent interaction is unknown here, no statement

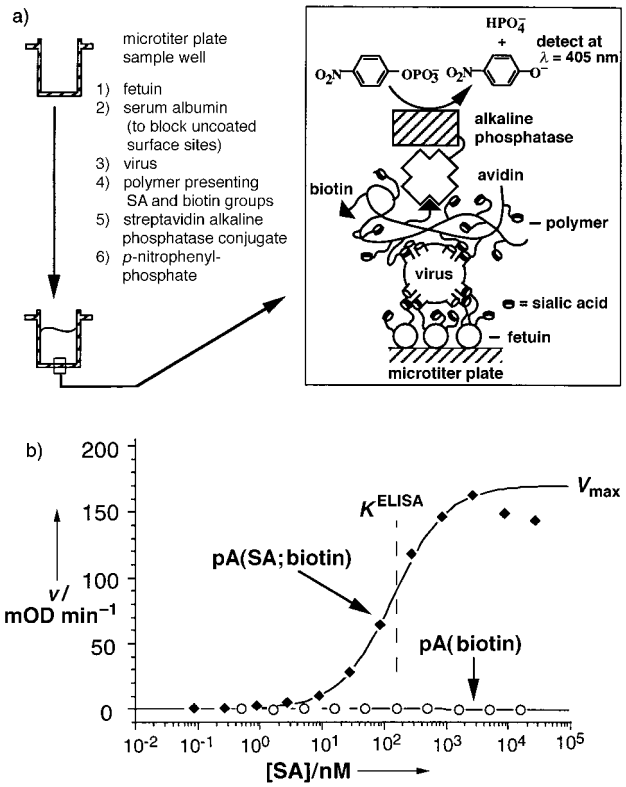


Figure 10. ELISA-type assay for measuring the binding of a biotin-labeled polyacrylamide bearing sialic acid groups (pA(SA; biotin)) to influenza virus. a) Schematic representation of the important binding events occurring during the assay. The influenza virus was immobilized on a fetuin-coated surface from a suspension containing 50 $\mu g\,mL^{-1}$ of viral protein. The polymer (pA(SA; biotin)) was adsorbed to the immobilized virus through SA–HA interactions. The amount of adsorbed polymer was determined by use of a streptavidin–alkaline phosphatase conjugate binding tightly to biotin groups of the polymer: The quantitation was based on measurement of the rate of enzymatic hydrolysis of *p*-nitrophenyl phosphate (given as the rate of change of absorbance at 405 nm). b) A plot showing the binding of pA(SA; biotin) to immobilized influenza virus. The rate of enzymatic hydrolysis was measured as a function of the concentration of polymer-linked SA groups in solution: pA(SA; biotin) The pA(biotin) indicates a polyacrylamide presenting biotin as a side chain: The polymer was tested as a negative control to verify the need for SA groups for binding. The curve superimposed over the data shows a nonlinear fit of the data to a Langmuir isotherm. The constants K^{ELISA} and $v_{\max}$ are shown; $K^{\mathrm{ELISA}} = [\mathrm{SA}]$ at $0.5v_{\max}$. To be consistent in the text, however, we converted K^{ELISA} from [SA] into the equivalent concentration of polymer simply by dividing by the average number of SA moieties on the polymer chain (200). Thus, the converted K^{ELISA} is equal to K_N^{poly}.

regarding cooperativity (α) is possible. The value of K^{mono} in this example is $5 \times 10^2\,\mathrm{M}^{-1}$; the value of K^{ELISA} for our best inhibitor is $10^8\,\mathrm{M}^{-1}$ based on SA; this means $10^{10}\,\mathrm{M}^{-1}$ based on the polymer.[278] That is, monomeric SA binds half-maximally at $[\mathrm{SA}] = 2 \times 10^{-3}\,\mathrm{M}$, whereas the polymer containing SA binds half-maximally to the surface of the virus at $[\mathrm{SA}] = 10^{-8}\,\mathrm{M}$. The polyvalent inhibitor may be therefore useful regardless of its value of α.

We propose an enhancement factor β, which we define as the ratio of the two association constants K^{ELISA} (with respect to the polymer P, and equal to 10^{10} in the example above) and K^{mono} [Eq. (9)], which we prefer to cooperativity (α) in

$$K^{\mathrm{ELISA}} = \beta K^{\mathrm{mono}} \qquad (9)$$

discussion of enhanced affinity of polyvalent systems: Molecules that have high values of β are useful, regardless of whether the interactions that generate them are cooperative or not. In any system where N is unknown, but the total quantity of bound polyvalent molecule is known, β will be a useful parameter. Only if the value of N is known can the precise relationship known between ΔG_N^{poly}, K_N^{poly}, α, and β be calculated [Eqs. (10), (11)]. The quantity β is, using a language familiar to some, the ratio of avidity and the component affinity of the monovalent equivalent to the interaction.

$$\Delta G_N^{poly} = \Delta G^{mono} - RT\ln(\beta) \quad (10)$$

$$\beta = K_N^{poly}/K^{mono} \quad (11)$$

3.4. Enthalpy of a Polyvalent Interaction

The parameter ΔG_N^{poly} is made up of enthalpic (ΔH_N^{poly}) and entropic (ΔS_N^{poly}) components [Eq. (12)]. As a first approximation, the value of ΔH_N^{poly} is the sum of the enthalpies of N mono-

$$\Delta G_N^{poly} = \Delta H_N^{poly} - T\Delta S_N^{poly} \quad (12)$$

valent interactions, $N\Delta H^{mono}$. This value may be made either larger or smaller by other interactions around the active site.

Enthalpically enhanced binding: In some circumstances, the binding of one ligand to a receptor with a given enthalpy may cause the next ligand to bind to its receptor with greater enthalpy; that is, the value of ΔH_{avg}^{poly} is in this case more negative (more favorable) than the value of ΔH^{mono}. Such binding is enthalpically enhanced: One well-studied example (albeit non-polyvalent) is the binding of four molecules of oxygen to hemoglobin. A less well studied (polyvalent) example of enthalpically enhanced binding is pentameric cholera toxin binding to five GM_1 moieties on the surface of a cell (see Section 3.2).

Enthalpically diminished binding: If the binding of one ligand to its receptor interferes with the next binding event, the enthalpy of the polyvalent interaction is less favorable than that expected for N equivalent monovalent interactions. Such binding is enthalpically diminished, and can occur when formation of multiple ligand–receptor interactions between two polyvalent entities requires energetically unfavorable molecular conformations. As a rule of thumb, the more conformationally rigid the polyvalent entity is, the more likely it is that even small spatial mismatches between the ligand and its receptor will result in enthalpically diminished binding (unless the geometric fit between ligand and receptor is accurate at a picometer scale, which is exceedingly rare).

The enthalpy of binding for polyvalent interactions is easy to describe qualitatively, but difficult to estimate quantitatively, either experimentally or theoretically. Consider a bivalent receptor (**1**, Figure 11 a). If the two receptor sites are independent and noninterfering, the binding of two monovalent ligands (**2**) to **1** occurs with twice the enthalpy of binding one ligand ($2\Delta H^{mono}$). For dimeric ligand **3**, in which the two ligands are joined by a rigid group R and fixed

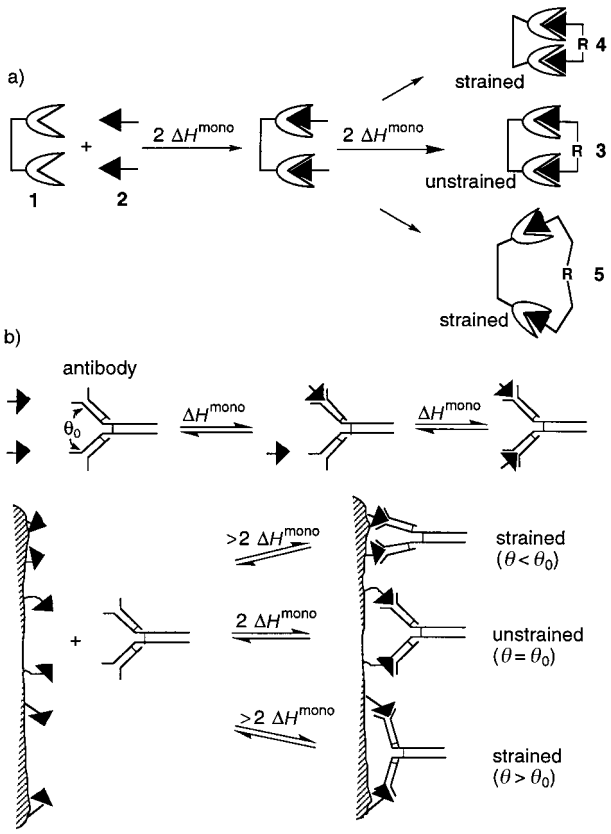


Figure 11. Enthalpy of binding for polyvalent interactions. a) Possible binding modes of monovalent and divalent ligands to a divalent receptor. b) The binding of a divalent antibody to ligand present at variable densities on the surface may be enthalpically diminished due to strain induced by distortion of the antibody from its most stable conformation (θ_0).

at exactly the same geometry as **2**, the enthalpy of binding is twice that of the equivalent monovalent analogue: $\Delta H_2^{bi} = 2\,\Delta H^{mono}$. If the geometry of **3** does not fit the spacing of **1**, the two ligands can still bind, but the aggregate must distort either by displacing the receptors from their equilibrium position to fit the geometry of L-R-L, or by distorting L-R-L from *its* equilibrium position to fit the receptors, or both. Since the average spacing between receptors in proteins is large relative to most organic molecules (for example, the two binding sites in an antibody are approximately 100 Å apart), the most common situation is usually that R is too short (**4**) to allow a good fit of both ligand–receptor pairs. Although it may be possible, using molecular mechanics, to estimate the enthalpic strain introduced in compressing R to fit when it is too long (**5**), it is difficult to estimate the enthalpy of distorting the receptor protein, or of noncovalent interactions between the group R and the protein, or between the subunits of the protein dimer. Figure 11 b illustrates these considerations of enthalpy with an example using the binding of bivalent antibodies to ligands immobilized randomly on a surface.

3.5. Entropy of Interaction

Understanding the entropy of polyvalent interactions is, we believe, essential to understanding the relationship of mono-

valent to polyvalent binding. Incomplete understanding of entropy in the design of polyvalent inhibitors has resulted in many synthetic polyvalent molecules that are less effective or only marginally more effective than their monovalent counterparts. The many bivalent systems joined by flexible linkers (e.g. oligo(ethylene glycol) or polymethylene) provide examples of systems that can almost be guaranteed to fail for entropic reasons.[279, 280]

We can consider the total entropy of a polyvalent interaction ΔS_N^{poly} in terms of contributions from changes in translational ($\Delta S_{trans,N}^{poly}$), rotational ($\Delta S_{rot,N}^{poly}$), and conformational entropies ($\Delta S_{conf,N}^{poly}$) of the receptors and ligands on association, and a contribution accounting for changes in the entropy of the surrounding water ($\Delta S_{H_2O,N}^{poly}$). The latter is often largely due to the entropy of hydrophobic interactions [Eq. (13)].

$$\Delta S_N^{poly} = \Delta S_{trans,N}^{poly} + \Delta S_{rot,N}^{poly} + \Delta S_{conf,N}^{poly} + \Delta S_{H_2O,N}^{poly} \quad (13)$$

3.5.1. Translational and Rotational Entropies

The translational entropy of a molecule arises from its freedom to translate independently through space; the value of ΔS_{trans} is related to the logarithm of its mass M ($\Delta S_{trans} \propto \ln(M)$), and inversely to the logarithm of its concentration ($\Delta S_{trans} \propto \ln([L])^{-1}$). The rotational entropy, ΔS_{rot}, arises from the freedom of the particle to rotate around all three of its principle axes, and is related logarithmically to the product of its three principle moments of inertia I_x, I_y, and I_z ($\Delta S_{rot} \propto \ln(I_x I_y I_z)$). The values of ΔS_{trans} and ΔS_{rot} for a particle are, therefore, only weakly (logarithmically) dependent on its mass and dimensions. To a first approximation, the translational and rotational entropies of *all* particles— ligands, receptors, ligand–receptor aggregates—are equal. When two particles associate, a total of three translational and three rotational degrees of freedom are lost. If the differences in the masses of the particles are ignored (often, the masses of particles are within a factor of 10; almost always, they are within a factor of 100), then the total translational and rotational entropic cost of associating the two particles, whether they be monovalent or polyvalent, is approximately the same provided they are at the same concentration. In biology, concentrations of molecules can vary over more than twelve orders of magnitude (mM to fM). Even though the translational entropy is only logarithmically dependent on concentration, such a wide range makes knowledge of the concentration of interacting particles essential to estimating the importance of translational entropy: This cost increases with decreasing concentration.

3.5.2. Conformational Entropy

Case I: $\Delta S_{conf} = 0$

We discuss the role of entropy in polyvalent interactions using a simple bivalent interaction as a model. The total entropic cost of association of two monovalent receptors with two monovalent ligands is $2\,\Delta S_{trans} + 2\,\Delta S_{rot}$ (Figure 12a). If the two ligands and two receptors are connected by a rigid linking group (that is, one in which no torsional rotation around bonds is possible) having precisely the correct spacing to match the two receptor and ligand sites, then the total entropic cost of assembling these two bivalent species is approximately $\Delta S_{trans} + \Delta S_{rot}$ (half the entropic cost of association of two independent pairs of molecules, and the same as that of one monovalent interaction; Figure 12b). Once a single ligand–receptor interaction occurs between these two rigid bivalent species, subsequent *intra*molecular interactions between the second ligand moiety on the rigid bivalent species and the second receptor site can occur without additional translational and rotational entropic cost, and at no cost in conformational entropy. If there are no additional enthalpic costs, the binding of the second ligand to the second receptor (intramolecularly) occurs with a greater change in free energy ($\Delta H \approx \Delta H^{mono}$, $\Delta S \approx 0$; therefore $\Delta G \approx \Delta H^{mono}$) than does the first. Such binding is entropically enhanced.

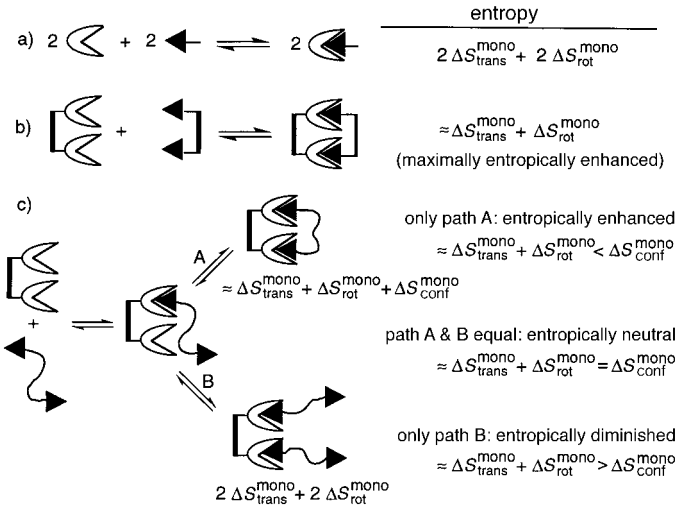


Figure 12. Relationships among translational, rotational, and conformational entropies for a divalent system with a rigid and flexible linking groups.

We have ignored the entropy of hydration thus far, but discuss it in Section 3.5.3. In brief, however, the entropic changes of hydration/dehydration that accompany most biological interactions do not change the spirit of these arguments, and simply add a constant to the value of each entropy discussed.

Case II: $\Delta S_{conf} \neq 0$

Case I is, in general, unrealistic: All linking groups are somewhat flexible, and ΔS_{conf} is almost always less than zero (unfavorable) on complexation; that is, the number of conformations available to the bivalent ligand before complexation is greater than that following complexation. If this conformational cost is less than the total translational and rotational cost, then the total entropic cost of bivalent association is still less than for the monovalent case, and binding is still entropically enhanced (Figure 12c, path A). In the case where this conformational cost equals the translational and rotational cost (Figure 12c, paths A and B), the binding is entropically neutral and the total energetic cost of complexing the second ligand on the dimeric species is the same as the entropic cost of complexing a second dimeric

species. In principle, the conformational entropic cost of complexing the second ligand of the dimeric species can exceed the translational and rotational entropic cost. In that case, the second ligand of the dimeric species will never outdo the binding of a second dimeric species (Figure 12c, path B), and the binding is entropically diminished.

Interestingly, entropy and enthalpy can have partly compensating effects on the affinity of polyvalent interactions: Whereas conformational flexibility increases the conformational entropic cost of association, the same flexibility increases the likelihood that all ligand–receptor interactions can occur without energetic strain. This loss in conformational entropy on association of a polyvalent ligand with a polyvalent receptor has been notoriously difficult to quantitate. The change in entropy on freezing a single, rotating carbon–carbon bond is approximately 0.5 kcal mol^{-1}. The range of values for other single bonds is 0.1–1.0 kcal mol^{-1}.[281, 282] The maximum loss in conformational entropy would occur if all bonds that were initially rotating freely lost all degrees of torsional freedom on complexation. The upper estimate for this loss in ΔS_{conf} is then approximately $0.5\,N$ kcal mol^{-1}, where N is the number of single bonds in the tether linking two ligands or receptors. For a long flexible chain, this number can be large: For a triethyleneglycol spacer, it can be unfavorable to the extent of as much as 10 kcal mol^{-1}.[281, 282]

3.5.3. Entropy of Solvation

A final contribution to the total entropy of association in aqueous systems is the change in the entropy of the surrounding molecules of water, ΔS_{H_2O}. The major contributor to interactions in water (both hydrophobic interactions and those involving polar groups) is the release of organized water from exposed faces of the biological molecules and the resulting increase in entropy. Quantitative measurements and predictions of hydrophobic interactions have been reviewed extensively.[283] These terms will usually have similar values per ligand in monovalent and polyvalent systems (unless the linker changes conformation or associates with the surface of the receptor, and as a result, changes its association with solvent on complexation), and therefore changes none of the arguments presented in the preceding sections. In general, a negative value of ΔS is added to the total ΔS for each ligand–receptor interaction that occurs, irrespective of whether in the context of a monovalent or polyvalent interaction.

There are a number of classes of polyvalent interactions whose entropic characteristics differ markedly. Interactions can occur when both species are initially freely diffusing in solution (the initial six degrees of translational freedom for two such particles are reduced to three degrees following complexation), and we classify these interactions as three-dimensional. When one or both species are restricted to diffusion in a plane or in a line, the interactions are classified as two- and one-dimensional, respectively. The translational and rotational entropic costs of association depend on the number of translational and rotational degrees of freedom lost on complexation. The cost (the combined values of ΔS_{trans} and ΔS_{rot}) is greatest for particles associating in three dimensions, less in two dimensions, and least in one dimension. That is, the entropic cost of association between N ligands freely diffusing in two dimensions (such as ligands tethered to the surface of a cell) with N receptors also freely diffusing in two dimensions (such as trans-membrane proteins on the surface of another cell) is less than for the interaction of these species diffusing independently in three dimensions. We will discuss these issues of dimensionality in Section 4.4, which describes signal transduction by cross-linking of receptors on a surface.

3.6. Kinetics and Enhanced Affinity

Studies of the kinetics for high-affinity polyvalent interactions suggest that the enhancement is mostly due to decreases in the rate of dissociation (k_{off}) of the two polyvalent entities, rather than to increases in the rate of association. Binding of anti-DNP antibodies to DNP-lys, relative to the binding of the same antibody to the DNP-covered surface of ΦX174, established that the values of k_{on} for binding to the surface differed by only a factor of 2 (k_{on}(surface) $\approx 3.7 \times 10^7\,\text{M}^{-1}\,\text{s}^{-1}$, k_{on}(DNP-lys) $\approx 8 \times 10^7\,\text{M}^{-1}\,\text{s}^{-1}$), whereas the values of k_{off} differed by a factor of 10^4 (k_{off}(surface) $\approx 3.3 \times 10^{-4}\,\text{s}^{-1}$, k_{off}(DNP-lys) $\approx 1.0\,\text{s}^{-1}$).[284] Since the rate of a process is related qualitatively (and often quantitatively) to its thermodynamics,[285] these measurements are intuitively consistent with polyvalency: The thermodynamic cost of the first ligand–receptor interaction between two polyvalent entities is approximately the same as the thermodynamic cost of the analogous monovalent interaction; it is therefore plausible that the rates of association might be similar. Dissociation of species interacting polyvalently requires breaking N ligand–receptor interactions; it is therefore plausible that dissociation occurs more slowly in the polyvalent interaction than in the corresponding monovalent one.

4. Characteristics of Polyvalent Interactions in Biology

4.1. Functional advantages of Polyvalent Interactions

In many cases, biological systems seem to use polyvalent interactions rather than an equivalent number of monovalent ones, or one very strong monovalent one, because of certain functional advantages. Examples of functional advantages are discussed in the following.

4.1.1. Achieving Very Tight Binding from Ligands with Modest or Low Surface Area

The magnitude of the total free energy of polyvalent interaction, ΔG_N^{poly}, can be high, and the resulting binding affinities, K_N^{poly}, can be very favorable. In principle, the strength of polyvalent interactions can be much stronger than can be reached by a single interaction between a ligand of low molecular weight and a protein, regardless of cooperativity. The tightest known association for a single interaction between a receptor and a small organic ligand is that between

biotin and streptavidin ($K^{mono} \approx 10^{15}\,M^{-1}$).[286, 287] The polyvalent binding of the most potent, trivalent, naturally occurring oligosaccharides presenting three GalNAc groups to the C-lectin asialoglycoprotein receptor on the surface of hepatocytes occurs with $K_{avg}^{poly} = 10^{8}\,M^{-1}$, even though for simple galactose $K_{mono} = 10^{3}\,M^{-1}$.[206] Interactions with much tighter association constants ($> 10^{15}\,M^{-1}$) have also been claimed.[288] The accuracy in association constants of such magnitude is uncertain as measurement is quite difficult in practice.

4.1.2. Grading Biological Responses or Signaling

In a polyvalent system the strength of a signal can vary greatly, depending on the number of ligand–receptor pairs that participate; to a first approximation, strength might correlate with *N*. This capability to generate a broad range of signal strengths (much broader than the binary "on" and "off" of a single ligand occupying a single receptor site) might, in principle, provide a capability to generate a graded (or graduated) response to a biological signal.

One example of this type of graded response might be the clearance of pathogens by antibody-mediated attachment to macrophages (Figure 13). Where a single antibody is unable to cause a macrophage to ingest a pathogen (macrophages do not bind effectively to a single antibody), two antibodies can lead to ingestion. More antibodies should further strengthen the degree of polyvalency between pathogen and macrophage, and subsequently increase the likelihood that the pathogen will be recognized and cleared. In this case, polyvalency provides a mechanism for recognition: Most pathogens have surfaces that present multiple copies of an epitope. Thus nonspecific adhesion of one receptor on the antibody to a non-polyvalent target on a native (self) surface would not lead to tight, polyvalent adhesion to that surface. Furthermore, macrophages fail to recognize pieces of pathogen if they bind to only a single antibody, but do recognize whole pathogen when it binds to multiple antibodies.[211]

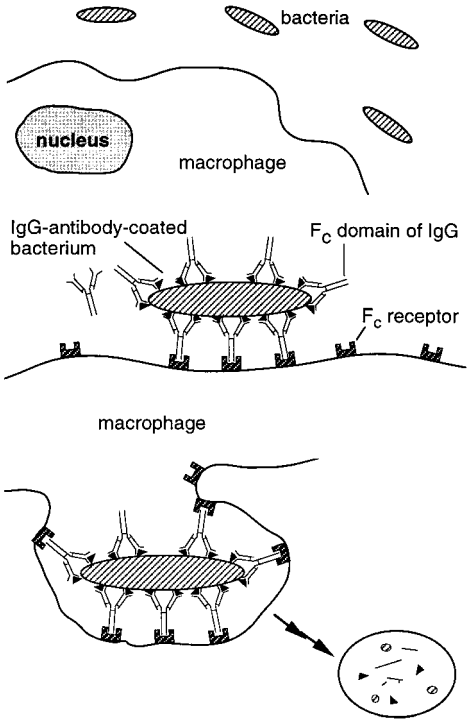


Figure 13. Clearance of pathogens by antibody-mediated attachment to macrophages. An bacterium coated with IgG antibodies is eliminated from the circulation ("cleared") through phagocytosis by a macrophage or neutrophil: The surface of the macrophage has Fc receptors that recognize the Fc region of IgG molecules. The multivalent binding of the antibody-coated bacterium (or virus) to multiple Fc receptors of a macrophage activates the phagocytotic process. Unbound IgG does not bind effectively to the Fc receptors on the macrophage. The representations are not drawn to scale.

Another mechanism by which antibodies lead to the elimination of a pathogen is to trigger the complement cascade (described in more detail in Section 4.1.7; see Figure 16). The constant region on the tail of the antibody, the Fc portion, interacts with one of five clefts on the soluble C1, a pentavalent protein that initiates the complement cascade on binding.[289, 290] Protein C1 is not activated by antibody alone, or by a single antibody–antigen complex. The more densely clustered the antibodies are on a surface (of, for example, a pathogen), the more likely it is that C1 will bind and be activated, and the more likely it is that the pathogen will be destroyed.

4.1.3. Evolutionary Efficiency: Multiplying an Existing Interaction versus Constructing a New One

Biological evolution of new interacting entities may require interactions between new molecules or sets of molecules. Intuitively, there lies evolutionary advantage in borrowing from an existing pool of interactions rather than building new ones. On occasion, environmental forces may confer some evolutionary advantage to an organism that replaces an existing low-affinity interaction with a high-affinity one. Simply increasing the number of individual weak interactions to yield a collectively stronger one replaces the need for evolving a new molecule for a new interaction.

4.1.4. Increasing Strength and Specificity of Binding Through Heteromeric Polyvalency

A polyvalent interaction may involve a mixture of ligand–receptor pairs (more than one type of ligand interacting with more than one type of receptor; we call this type of interaction "heteromeric polyvalency"), and may result in both greater strength and specificity than equivalent monovalent interactions. If, by involving an additional class of ligand, the total number of interactions is increased, then the total strength of the interaction may also increase. The specificity ($A_{N-1}B$ relative to A_N) can increase by differentially regulating the expression of A and B in or on a cell; that is, a cell may bind to another cell expressing only a certain mole fraction of A and B on its surface. Two examples detailed in Section 2 (*E. coli* adhesion and neutrophil adhesion) illustrate heteromeric polyvalency.

4.1.5. Creating Conformal Contact Between Large Biological Surfaces

Figure 14 illustrates an instance where many weak interactions (K_N^{poly}) confer a biological advantage over a single one of equal strength ($K^{mono} = K_N^{poly}$): conformal contact. Such

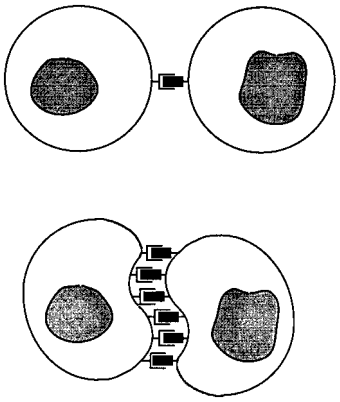


Figure 14. Conformal contact of large biological surfaces (see text for further details).

intimate contact may confer a number of advantages on a pair of cells. For example, the communication between two cells in such intimate contact might be more efficient and more rapid than between cells touching in only one small area. A single strong interaction would not promote intimate, conformal contact between the two surfaces.

4.1.6. Induction of Specific Geometric Shapes and Molecular Distributions

Polyvalent interactions can lead to macroscopic reorganizations and redistributions of molecules. One example of a large change in shape is the conversion of a spherically shaped neutrophil into a flattened one on adhesion to a surface composed of endothelial cells. This occurs after specific interactions between the surfaces of the two cells (Figure 3). An example of a change in molecular distribution is the clustering of receptors in a clathrin-coated pit (Figure 15).

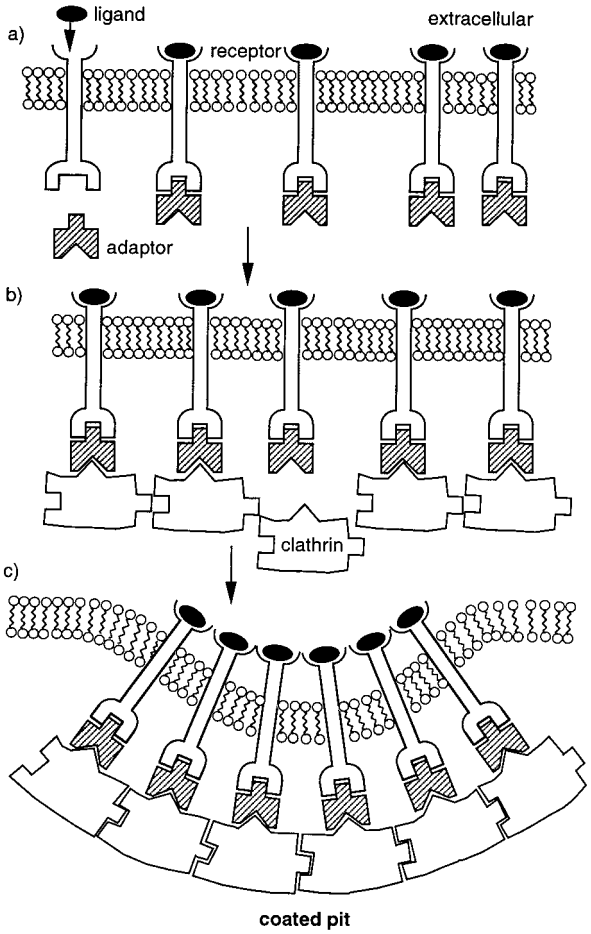


Figure 15. Induction of specific geometric shapes and molecular distributions: clustering of receptors in a clathrin-coated pit. One example is receptor-mediated endocytosis of low-density lipoproteins (LDL). The ligand (LDL) binds to a LDL receptor in the plasma membrane of a cell. Monovalent binding of the ligand to the receptor allows binding of the resulting complex to an adaptor molecule in the cytoplasm, which can induce formation of the clathrin-coated pit by multivalent association of clathrin and other coat-associated proteins.

4.1.7. Signaling by Induction of Large Conformational Changes

In some polyvalent systems, interaction induces a large change in the conformation of one or both of the interacting species. For example, DNA is efficiently stored in a specifically coiled conformation by making multiple, repeated (polyvalent) contacts with a polymeric histone. A remarkable example is that of IgM binding polyvalently to the polyvalent surface of an invading pathogen. Here, a conformation of the IgM that is induced by the polyvalent association serves as a signal. IgM is a class of antibody with five bivalent structures (that is, ten binding sites) extending randomly from a central ring. On binding decavalently to the surface, all five bivalent structures point in a common direction, and portions of the central ring are then more exposed than prior to binding and differently organized. These portions initiate the chain of reactions that constitute the complement cascade (Figure 16) by interaction with soluble pentavalent protein C1 in the blood. This cascade concludes in the assembly of proteins C5b – C9 (the membrane attack complex) in the membrane of the microorganism; this structure causes wide channels (holes) to form in the membrane and results in the death of the microorganism. Binding of IgM to monovalent ligands in the blood does not result in such conformational changes, and does not induce the complement cascade. Polyvalency is necessary in this instance not for tight binding, but for signaling and activation through conformational change.

4.1.8. Preventing Undesired Interaction: Natural Polyvalent Inhibitors

Whereas polyvalency can strongly promote desired interactions, it can also be a useful strategy in preventing certain undesired biological interactions, especially those that are themselves polyvalent (here, polyvalency is used against polyvalency). For example, the fluid coating the interior of the lungs of most mammals contains several mucins (proteins presenting oligosaccharides terminated in sialic acid). These mucins, especially α_2-macroglobulin, can bind to influenza and other SA-binding viruses, and thereby inhibit their attachment to target cells (Figure 17). As we discuss in some detail in Section 5.2, polyvalency may be used here both for

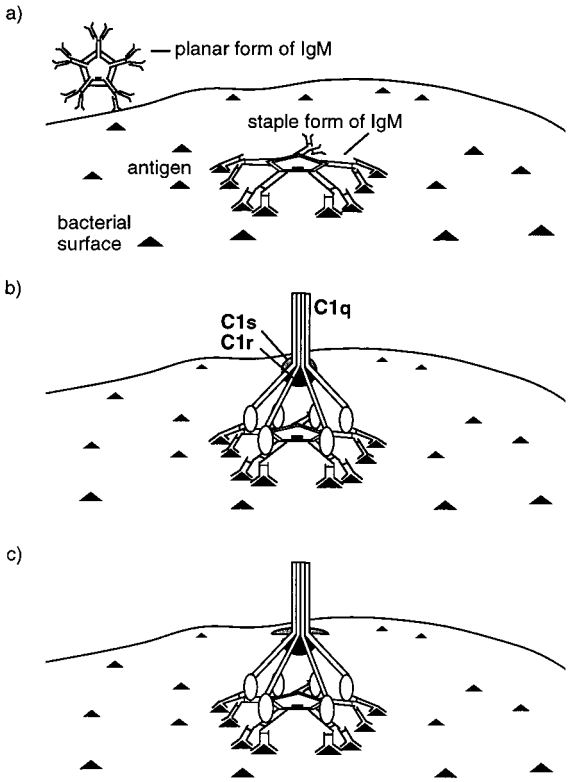


Figure 16. Signaling by induction of large conformational changes. Conformational change of a pentameric immunoglobulin IgM upon multivalent binding to antigens on bacterial surface activates the complement cascade. a) A pentavalent IgM molecule binds to antigens on the surface of the bacterium and adopts a "staple" form. b) C1q (three pairs of Y shape) of the C1 complex (C1q, C1r, C1s) binds directly to a conformationally modified IgM. c) Binding of C1q to IgM leads to activation of the C1 complex (the activation of C1r/C1s—shown as the change in the orientation): C1 is activated only when at least two C1q heads bind simultaneously to antibodies. Such activation of the C1 – IgM complex initiates the complement pathway, leading eventually to the death of a bacterium.

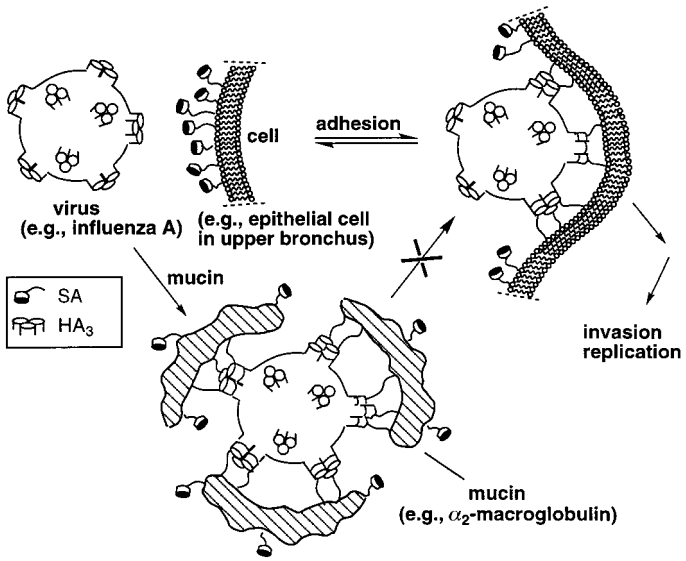


Figure 17. Prevention of the attachment of influenza virus to the surface of a cell. Mucin, a natural glycoprotein with high surface densities of sialic acid groups, is a potent inhibitor of the adhesion of virus by competitive, multivalent binding of the sialyl groups to hemagglutinins on the surface of virus.

tight binding to the pathogen and for steric stabilization of the pathogen surface (a mechanism characteristic of this class of polyvalent interaction).

By rigorously understanding the various systems in which biological organisms use polyvalent interactions at the molecular level, we can begin to see new classes of strategies for pharmaceutical intervention. In the following sections, we discuss well-studied classes of polyvalency, and attempt to illustrate some of the unusual characteristics of polyvalent interactions.

4.2. Attachment of Viruses to Host Cells

Some examples of ligand – receptor interactions important in the attachment of a virus to host cells are given in Table 1.[75] Attachment of a virus to its host is the first step to viral infection, and involves the simultaneous association of multiple molecules on the surface of the virus with multiple molecules on the surface of its host cell (Figure 18).[291] The recognition event between virus and its host cell has been reviewed previously.[75]

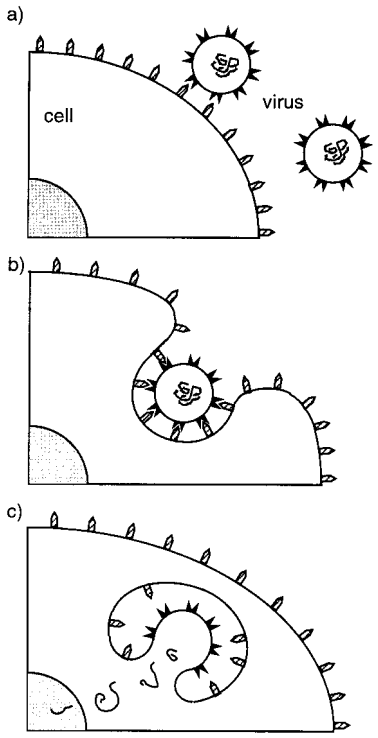


Figure 18. Schematic representation of the entry of viruses into cellular hosts. a) A virus attaches to the surface of a cell through polyvalent interactions of viral receptors and cellular ligands. b) The cell endocytoses the virus. c) Acidification of virus-containing vesicles after endocytosis triggers fusion of the vesicle with cell and exposure of viral DNA.

The molecules involved on the surfaces of the virus and cell that mediate attachment are most directly identified when this attachment is inhibited by either a high concentration of corresponding free monomer of that molecule, or by monoclonal antibodies against that molecule. Such a strategy is used often when the ligand is a sugar or small molecule. A less direct characterization of the molecules involved in attach-

ment comes from correlations of mutations (either man-made or natural) that are unable to bind successfully to the target cell; that is, if a mutation of a particular protein eliminates the ability of the virus to attach, it is involved in the attachment either directly or indirectly. This second strategy is often used for receptors or ligands that are proteins. Although a growing number of molecules on surfaces have been implicated in virus–cell recognition, there are often ambiguities. Because viral particles adhere to many substances nonspecifically, it is often difficult to distinguish nonbiospecific from biospecific binding. Some viral particles may enter a host cell by nonspecific transport (the same mechanism that a cell uses to internalize small molecules). Some proteins on the surface of a virus can recognize more than one type of ligand on the cellular surface. Finally, certain viral particles may associate with a protein freely diffusing in solution, which in turn recognizes molecules on the surface of a cell (mediated attachment). Viruses bind to almost all classes of molecules on cellular surfaces: sugars[292] (for example, polyoma[7] and orthomyxoviruses[293] recognize sialyloligosaccharides), phosphatidyl lipids (for example, vesicular stomatitis virus (VSV) recognizes phosphatidylserine and phosphatidylinositol[58]), and proteins (for example, HIV recognizes CD4,[294] human rhinovirus recognizes intercellular adhesion molecule-1, ICAM-1[295]).

The system for viral attachment and inhibition that has been most extensively studied in the context of polyvalency is the orthomyxovirus A(X-31) (an engineered strain of influenza) attaching to the surface of erythrocytes (Figure 1).[1, 2] This attachment occurs through multiple simultaneous interactions between viral HA and cellular SA. Accurate measurements of the affinity between influenza virus and erythrocyte have not been performed so far. The lower limit for K_N^{poly} is, however, estimated to be $10^{13}\,M^{-1}$. Since the association constant between a single molecule of SA and a single HA receptor is $K^{mono} \approx 10^3\,M^{-1}$, the interaction between cell and virus is clearly polyvalent ($\beta \approx 10^8 > 1$). Since the value of N is unknown, we can make no statement regarding cooperativity (α).

Another extensively studied virus–cell interaction is that between the protein gp120 on the human immunodeficiency virus (HIV) and the 60 K glycoprotein CD4 on the surface of the T-cell (Figure 19). High concentrations of solubilized CD4 (CD4 that has been chemically cleaved from the surface of a cell) inhibits attachment. HIV is an example of a virus that can use alternate molecules on the surface of cells: HIV can infect glioma and rhabdosarcoma cells, both of which lack CD4. Solubilized CD4 does not block attachment and subsequent infection of these cell types.[296]

There are many examples of mediated binding of virus to cells. One example involves the hepatitis B virus, which in some cases binds to aggregates of serum albu min; these aggregates in turn bind to receptors for albumin on the surface of hepatocytes.[297] A second well-studied example begins with the bivalent attachment of antivirus antibodies to the surface of the virus (examples include Dengue virus, West Nile virus, and HIV).[298] Fc receptors on the surface of the target cell then interact polyvalently with multiple Fc tails. This mechanism of attachment is the same as that used by macrophages in recognition of foreign pathogens: interestingly, whereas the former leads to infection, the latter leads to clearance.

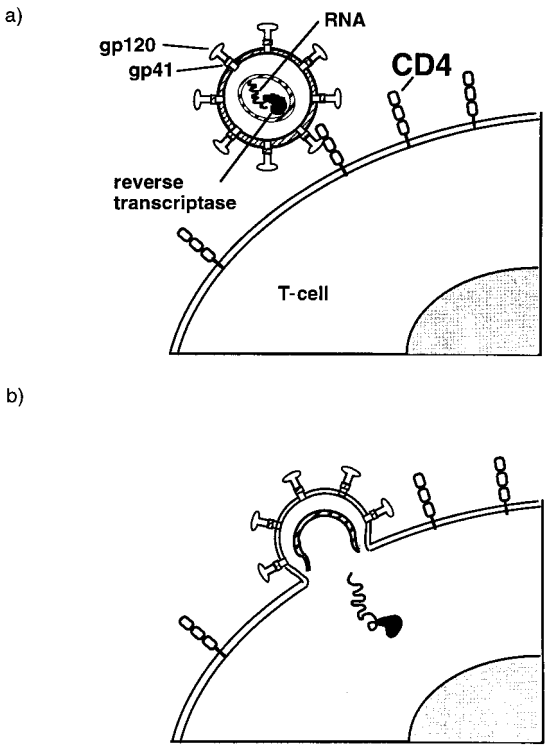


Figure 19. Adhesion of HIV to the target T-cell. a) Binding of gp120 on the surface of the virus to CD4 on the surface of the T-cell. b) Fusion of the virus envelope with the cell membrane and entry of viral RNA genome into the cell.

4.3. Attachment of Bacteria to Host Tissues: Tissue Tropism

Bacterial pathogens can be divided into two classes: intracellular (those that enter a cell and multiply there) and extracellular (those that live among cells, but not inside them). The mechanism of infection by those that are intracellular is similar to that of viruses: Infection is initiated by attachment of the pathogen to the host cell (Tables 2–4). Bacteria that are extracellular often migrate to and collect in particular tissues. Concentration of bacteria in specific tissues (tissue tropism) can occur by specific interactions between molecules on the surface of the bacteria and either molecules on the surfaces of cells in the preferred tissue, or components of the extracellular matrix characteristic of that tissue. Many specific interactions between bacteria and either host cell or extracellular matrix have been reviewed previously.[299, 300] As with viruses, the specificity of the interaction is usually defined by the molecule that is the best inhibitor of an adhesion or agglutination assay. These assays are most often used when the interaction is between a lectin on the bacterial surface and a sugar on either the host cell or the extracellular matrix (Table 2). At present, bacterial interactions appear more likely than viral ones to involve proteins as both ligand and receptor (Tables 3 and 4). These protein–protein interactions are more difficult to study, mainly because the "monomer" is either not known, not available, or loses its "shape" when removed from the the membrane. As a result, most of the detailed studies of bacterial and viral interactions to date involve lectin–sugar interactions, and not protein–protein ones.

Many examples of bacterial interactions with host cells come from the pioneering work of Duguid et al., who were the first to study the agglutination properties of enteric bacteria systematically.[301] Enteric bacteria are those that take up residence in the gastrointestinal tract of mammals. In most cases, the enteric bacteria express fimbriae of type 1, which bind to mannose on the surface of epithelial cells in the gut (for example, enteric *E. coli*, *Klebsiella pneumonia*, and *Salmonella*). This interaction can be assayed by agglutination of guinea pig erythrocytes (the surface of which is densely coated with mannose residues). A well-studied example is that of the uropathogenic *E. coli* described in Section 1.

Certain other enteric *E. coli* bacteria contain fimbrial hemagglutinins on their surface that bind specifically on the surface of the epithelial cell of various glycoproteins containing sialic acid. A well-studied example of sialic acid recognition occurs on an *E. coli* containing the K99 fimbrial lectin,[302] which recognizes *N*-glycolylneuraminic acid located specifically on NeuAc(α2,3)Gal(β1,4)Glc(β1)-ceramide. Enteric strains of *Vibrio cholera* produce a variety of hemagglutinins.[303] The most prevalent of these hemagglutinins binds to fucose derivatives on the epithelial surface.

The host organism often mounts a relatively nonspecific defense that is also polyvalent against these polyvalent pathogens. One example is the Tamm–Horsfall glycoprotein, the most abundant glycoprotein in human urine. This glycoprotein contains a variable number of N-linked oligomannose units, and binds a wide range of bacteria.[304]

4.4. Attachment of Polyvalent Molecules to Cells

Polyvalent molecules can interact with cells and bacteria and cause responses ranging from growth and differentiation to clearance and death. Some of these responses are only possible if the molecule is polyvalent, and would not occur with even a very tightly binding monovalent molecule. We provide examples for antibody–cell interactions, the attachment of toxins to their target cells, and signal transduction through association of polyvalent molecules (hormones, growth regulators).

Immunoglobulins bind polyvalently to the surfaces of cells. As described earlier, the groundbreaking work of Karush et al. showed that the bivalent form of an antibody binds to biological surfaces more tightly than does the equivalent monovalent form.[305] Karush et al. studied the adhesion of both IgG and IgM to a DNP-derivatized surface of the bacteriophage ΦX174, which is specific for *E. coli*. Using a peptic digest, they converted the bivalent IgG and decavalent IgM into monovalent forms, and compared the association constants with those of the unmodified antibodies. They found a 10^3- and 10^6-fold difference for IgG and IgM ($\beta = 5 \times 10^2$ and 10^5, respectively). Moreover, the measured association constant of decavalent IgM, K_{10}^{deca}, was greater than $10^{11}\,M^{-1}$.

More recently, Karush et al. examined the adhesion of a polyclonal mixture of IgG isolated from the serum of a mouse innoculated with a gram positive bacteria *Bacillus sp*.[277] The surface of *Bacillus sp.* presents a peptidoglycan called murein,[306] which exhibits a high degree of periodicity. The association constant for the bivalent IgG was 30-fold higher ($\beta = 30$) than for the monovalent form derived by reduction with 2-sulfanylethylamine. Examining the kinetics of this interaction, Karush et al. also concluded that the rates of association for the bivalent and monovalent forms were almost the same, but that the rate of dissociation for the bivalent species was 30-fold lower than that of the monovalent one.

Two important advantages of a bivalent antibody over a monovalent one are high affinity (β>1) and recognition. The latter is due to a weak affinity of the bivalent antibody for fragments of bacteria floating free in solution and for non-bacterial surfaces that may have epitopes similar to that on the bacterial surface (it is unlikely that the similar epitope occurs at high density on a non-bacterial surface).

A second example is the binding of the human growth hormone (hGH) to receptors on its target cell (Figure 20). This hormone presents two different protein domains held

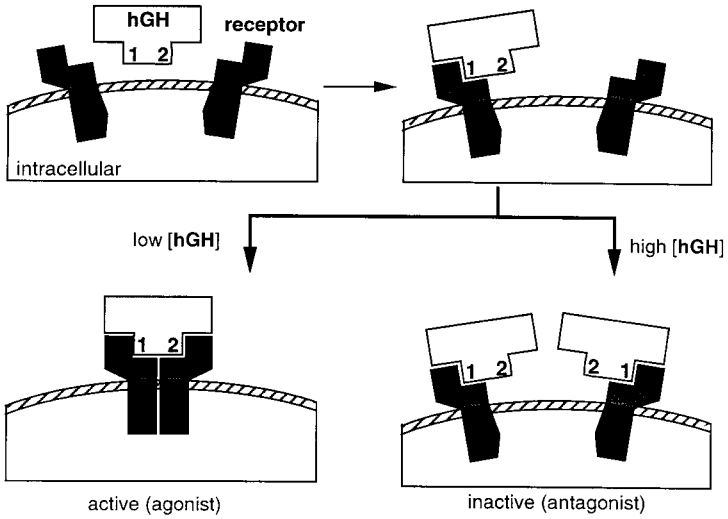


Figure 20. Heteromeric polyvalency. Sequential dimerization model for activation of the human growth hormone (hGH) receptor.

apart by a rigid protein spacer. Although these domains are different, they both recognize the same receptor on the surfaces, but with different affinities. This is another example that falls into the class we previously called heteromeric polyvalency.[307]

4.4.1. Signal Transduction by Cross-Linking of Receptors on a Cellular Surface

Cell growth, differentiation, migration and apoptosis are regulated in part by polypeptide growth factors or cytokines.[308, 309] As these factors are unable to pass the hydrophobic cell membrane, a fundamental question is how they transduce their signal into the cell. A number of ligand–receptor interactions have been identified that involve surface receptor dimerization. Many growth factors and cytokines are polyvalent, and exert their effects through binding and dimerizing (or oligomerizing) cell-surface receptors: Evidence of such a mechanism has been accumulating over the past few years (Table 7), and this area has been reviewed.[308]

Association of a polyvalent ligand to multiple diffusing receptors in a cellular membrane is often involved. In some cases, a single signaling molecule may present two parts, each of which binds a surface receptor (as with human growth hormone, discussed in the preceding section). In this case, the ligand is heterovalent/bivalent. However, polyvalency (as we define it) is not always involved in the mechanism of receptor dimerization. It is entirely possible that in some cases, two ligand-occupied receptors may interact with a favorable energy of dimerization relative to two unoccupied receptors.[257] Dimerization has been observed after binding of a number of cytokines and growth factors: protein–tyrosine kinase receptors, cytokine receptors, antigen receptors, receptors for the tumor necrosis factor (TNF) and related factors, and serine–threonine kinase receptors.[308]

The interaction between an allergen and the surface of a mast cell illustrates some of the unusual properties of systems that use cross-linking of receptors. The mast cell presents multiple copies of the bivalent antibody IgE, and can degranulate (release histamine, which promotes local inflammation) in response to a wide range of allergens. Monovalent ligands for IgE do not trigger degranulation; polyvalent ligands do (Figure 21). The polyvalent binding to the surface of the mast cell can lead to the cross-linking of two molecules of IgE. The cross-linked surface-bound IgE binds (through a transmembrane portion) to an unidentified intracellular protein, and this interaction, in turn, initiates a signal cascade that ends in degranulation. For mast cells, the minimum cross-linking unit needed for release of histamine is two linked IgE molecules,[230, 310] and thus degranulation requires that antigens have $N \geq 2$.[311] Interactions of symmetric and asymmetric bivalent ligands with bivalent antibodies on the surface of the mast cell have been correlated with histamine release.[312, 313]

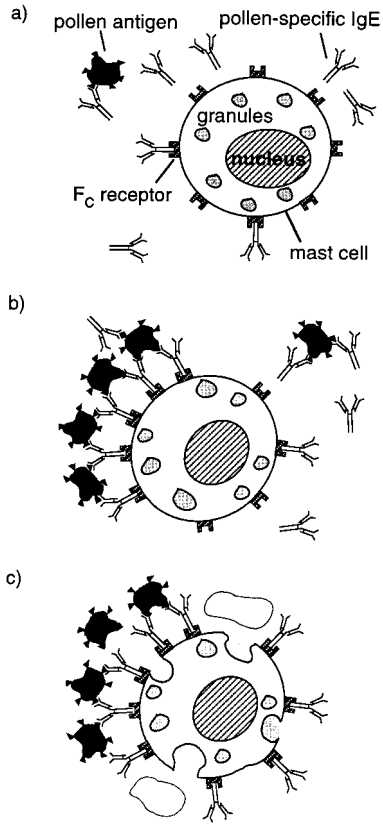


Figure 21. Degranulation of mast cells after binding of a polyvalent allergen. a) After the first exposure to pollen, IL-4 drives B-cells to produce IgE in response to pollen antigens; pollen-specific IgE binds to Fc receptors on the surface of a mast cell. b) The second exposure to pollen leads to the activation of a mast cell by multivalent binding and cross-linking of IgE molecules and antigens. c) An activated mast cell releases its contents by exocytosis of granules containing histamine and heparin, causing allergic rhinitis (hay fever).

Degranulation illustrates an important property of polyvalent interactions in membranes: the receptors in membrane sometimes act polyvalently (for example, by binding polyvalently to the polyvalent allergen) and sometimes not (without the allergen, the receptors do not bind polyvalently to the intracellular protein(s) in the signal transduction cascade). Whether or not receptors bind polyvalently to a polyvalent ligand depends on the detailed balance of three thermodynamic parameters: 1) the enthalpy of complexation; 2) the conformational entropic cost to the ligand on complexation; and 3) the concentration of the receptor in the membrane (which is related to the translational entropic cost of complexation). We have already discussed the first two factors.

The concentration of the receptor in the membrane partly determines the likelihood of signal transduction. The mechanisms by which a cross-linked state of a receptor induces a response in the cell fall conceptually into two classes:

1) An intracellular protein (often a kinase, as for signal transduction following recognition of polyvalent antigen by T-cell receptors[314]) may bind tightly to an intracellular portion made up of portions of both species in the dimer, but not bind, or weakly bind, individual receptors.
2) The two receptors that make up the dimer may chemically modify one another. An example of this is autophosphorylation,[315] in which each receptor phosphorylates the other at specific positions. The phosphorylated species is then recognized by an intracellular protein, such as proteins containing a Src-homology 2 (SH2) domain.[315]

With either mechanism, the step that limits the rate of signal transduction is the ligand-mediated receptor dimerization, and the rate of this step is inversely dependent on the concentration of receptor in the membrane. The translational entropy of a molecule (receptor) in a membrane (two-dimensional) is less than the translational entropy of that molecule in solution (three-dimensional). The binding of a polyvalent molecule to N receptors on a cellular surface can, therefore, be more favorable than the corresponding N monovalent interactions in solution ($-\Delta G_N^{\mathrm{poly}} > -N\Delta G^{\mathrm{mono}}$). The translational entropy of a molecule both in solution and in a membrane is inversely dependent on the concentration of that molecule: the greater the concentration of the receptor in the membrane, the less the entropic cost of complexing a polyvalent ligand. The sensitivity of the cross-linking reaction to the concentration of a ligand is important to both the character and sensitivity of the biological response. The likelihood of a biological response may be regulated by controlling the concentration of receptor or ligand in a membrane, and is the consequence of a balance of two effects:

1) *False signaling*: A spontaneous (unsignaled) cross-link corresponds to false signaling; that is, signaling in the absence of a bivalent ligand. The likelihood of a sponta-

neously formed cross-linked dimer is proportional to the square of the concentration of the receptor in the membrane. The concentration in the membrane must therefore be sufficiently low that the probability of spontaneous cross-linking is acceptably low.

2) *Sensitivity to true signaling*: The translational entropic cost of cross-linking increases with the logarithm of the concentration of receptor in the membrane. The concentration in the membrane must be sufficiently high that the polyvalent allergen is able to cross-link the receptors. An excellent example of the sensitivity of the likelihood of signaling to the concentration of receptor in the membrane is provided by Shur et al.:[253] Sperm expresses molecules of galactosyltransferase (GalTase) receptor on its surface, and these interact specifically with *N*-acetylglucosamine (GlcNAc) groups on the glycoprotein ZP3 on the surface of an egg. Upon productive interaction between sperm and egg, the sperm undergoes a violent morphological change called the acrosomal reaction; this reaction releases enzymes involved in penetration of the protective coating of the egg. Increasing the expression of GalTase on sperm head increases the sensitivity to the ZP3-induced acrosomal reaction.[253]

We put forward the hypothesis that the concentration of receptors that are involved in signal transduction through cross-linking must be under tight control: Raising the concentration would increase the sensitivity of the cell to polyvalent signal, and would also increase the chances of spontaneous, or false, signal transduction; decreasing the concentration would decrease the sensitivity of the cell, and increase the chances of not transducing a signal even in the presence of physiologically effective concentrations of polyvalent ligand.

The dimer that is formed through interaction with a polyvalent molecule in solution may be a homodimer or a heterodimer. The qualitative arguments made above apply in either case. An example of heterodimerization is the binding of the platelet-derived growth factor (PDGF) to the cell surface. The PDGF-A chain binds only α receptors, while the PDGF-B chain binds both α and β receptors. PDGF is a dimer joined covalently through a disulfide linkage. The AA dimer induces the $\alpha\alpha$ receptor homodimer, the AB dimer induces the $\alpha\beta$ receptor heterodimer, and the BB dimer induces all three combinations of receptor dimer.[316]

In some cases, the degree of polyvalency of the ligand determines the fate of the cell with which it interacts. One example is the "positive versus negative selection" of T-cells in the thymus during early maturation of these cells.[317] Direct cross-linking of the TCR by antibodies against CD3 induces conversion of immature CD4+:CD8+ cells into mature CD4+ cells, even in the absence of MHC. In the thymus, peptides that have a high affinity for the MHC sites on the endothelial cells bind to a large number of MHC receptors, and, together with the MHC, present a high-valency surface that interacts with passing immature CD4+:CD8+ T-cells. Peptides that have low affinity for the MHC, however, present a low valency surface for the passing T-cells. Low-valency aggregation appears to be a critical parameter in positive selection leading to mature T-cells. High-valency aggregation appears to be important in negative selection, and leads to T-cell death due to extensive aggregation of T-cell receptors at the interface between the surfaces of the T-cell and the thymic endothelial cell.

Many ligand–receptor interactions are not polyvalent and do not involve receptor dimerization. For such receptors, occupation of the binding cleft by the ligand may induce a specific conformational change that transduces a signal into the cellular interior. One example that involves the integrin family of receptors illustrates the efficiency and versatility of biological systems: Both receptor occupancy and receptor dimerization are important mechanisms on the same receptor.[318] Integrin receptors mediate cell adhesion, signal transduction, and cytoskeletal organization. In one study, receptor occupancy by a monovalent ligand induced receptor redistribution, but minimal signaling through tyrosine phosphorylation. Aggregation by a bivalent noninhibitory antibody (antibody that does not block the cleft on the integrin receptor that binds its ligand) immobilized on the surface of beads induced intracellular accumulation of $pp125^{FAK}$ and tensin, but no accumulation of other cytoskeletal proteins such as talin. Combining monovalent ligand with the antibody induced accumulation of seven cytoskeletal proteins—including α-actinin, talin, and F-actin—thereby mimicking multivalent interactions with fibronectin or polyvalent peptide (natural, polyvalent ligands for this integrin). Integrins therefore mediate a complex repertoire of functions through distinct effects on receptor occupancy or aggregation, or both.

4.5. Attachment of Polyvalent Molecules to Other Polyvalent Molecules: The Control of Transcription

Gene expression is often regulated at the level of transcription. Genes are transcribed when the necessary protein machinery is recruited (that is, associates in a functional conformation) to a region of the DNA near the beginning of the gene. Such recruitment must be sequence-specific. In most organisms, RNA polymerase is recruited by a protein or proteins, transcription factor(s), that bind both to a specific site on DNA and to the RNA polymerase. Very often, the site on the DNA that recognizes the transcription factor is found in multiple copies (from pairs to octets). Also very often, the transcription factors are themselves polyvalent. Bivalent transcription factors (for example a leucine zipper, Figure 22) are found in many forms: Some are homodimers, and others are heterodimers; some are joined covalently, and others are joined noncovalently. In almost all cases, transcription factors that bind to the DNA as dimers or multimers do not bind as monomers: polyvalency is used in transcription to increase both the strength and the specificity of attachment; note, for example, the interaction of DNA with retinoid X receptor (RXR) transcription factor (see Section 2). In this example, small changes in concentration of a transcription factor lead to large, nonlinear increases in the rate of transcription through a polyvalent mechanism (the rate of transcription is approximately proportional to the $[RXR]^5$). The presence of more than two half-sites in one hormone response element is not unique to RXR response elements (Table 7).[319]

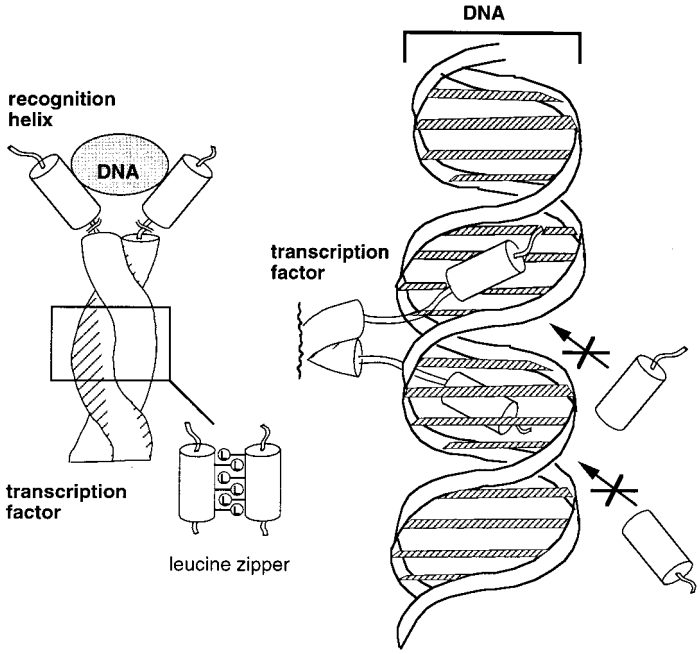


Figure 22. Dimeric transcription factors. A coiled coil of α helices from two separate polypeptide subunits, stabilized by a leucine zipper, holds two recognition helices in a position to bind sequences in the major groove of DNA.

4.6. Attachment of Cells to Other Cells

A number of other cell–cell interactions may occur polyvalently (Table 5). One example described in Section 2.3 is neutrophil attachment to endothelial cells near a site of tissue injury. A second example may be the clearance of non-sialylated cells from the blood by the liver (Figure 23). Lee

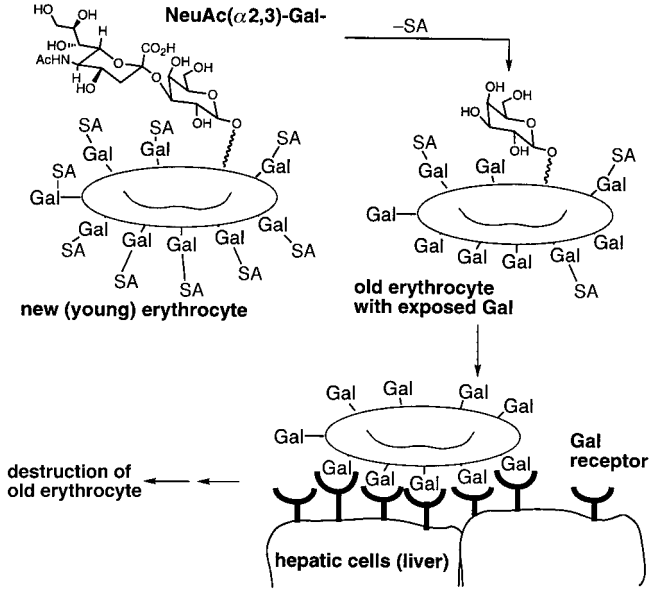


Figure 23. Clearance of non-sialylated erythrocytes from the blood by liver.

et al. have examined extensively the role of polyvalency in the association of synthetic di- and trivalent galactose-containing ligands to C-type lectins on the surface of hepatocytes.[206] An example of a cell that becomes progressively desialylated, as a reflection of age, is the red blood cell (erythrocyte). Desialylation exposes a galactosyl group, and occurs as a consequence of the hydrolytic action of different neuraminidases, both free in the blood and bound to endothelial cells that line the interior of the blood vessels. The probability of hepatic clearance may be correlated with the interaction energy between the surfaces of the hepatic cell and the erythrocyte. As the density of galactosyl ligands on the surface of the erythrocyte increase, the interaction energy also increases. Thus as red blood cells age, the density of the "clearance signal" on their surface increases until the interaction energy between its surface and that of the hepatocyte is sufficiently high that it promotes adhesion and clearance. The resulting lifetime of a typical red blood cell in human blood circulation is 120 days. We suggest that polyvalency may, in this instance, be used as part of a timer that enables the body to judge the age of erythrocytes and select those that are old enough to be removed from circulation and destroyed.

A third example of cell–cell interactions is that between a class I MHC-bearing antigen-presenting cell and a CD8+ T-cell; both are essential components of the immune system (Figure 24). The cell presenting antigen may, for example, be a

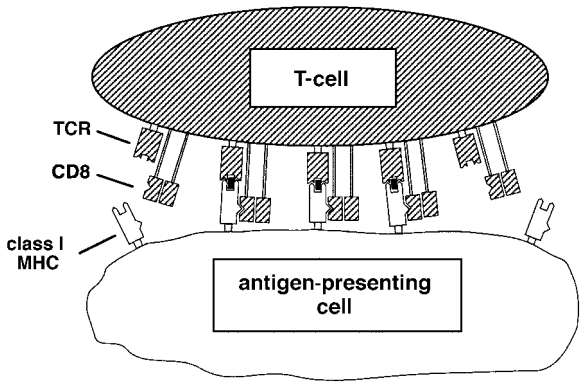


Figure 24. Interactions between a cell (bearing class I MHC and presenting antigen) and a T-cell (expressing T-cell receptor and CD8). Class I MHC interacts with both CD8 and the TCR.

cell infected by a virus: Some small but finite portion of the proteinaceous components of the virus produced by the cell are degraded intracellularly into small peptides composed of nine amino acids. These nonapeptides are then presented on the surface of the infected cell as an extracellular binding cleft of a class of transmembrane protein called the class I major histocompatibility complex (MHC).[320] This complex is recognized by a complementary T-cell receptor on the surface of a CD8-bearing (cytotoxic) T-cell. The consequence of one such recognition event is unclear. The consequence of several such events is the transduction of a signal into the interior of the T-cell that induces it to kill the cell that is presenting the antigens. The requirement for a large number of discrete recognition events prevents excessive destruction of cells that are not infected; that is, a high interaction energy distributed across multiple interactions corresponds to a high level of certainty that the cell harbors a virus inside.

A fourth example of cell–cell interactions is that involved in cell migration. A well-studied interaction that may be important in cell migration is that between the galactosyltransferase (GalTase) protein on one cell and the GlcNAc-terminated glycoproteins and glycolipids on another cell. Cells express different densities of both GlcNAc and GalTase. The levels of expression may vary with time and biological environment. The strength of adhesion between the cells is related to the number of contacts between the two surfaces, and therefore to the densities of both GlcNAc and GalTase. In a classic experiment, Schnaar et al. showed that a malignant cell expressing GalTase on its surface will migrate along a concentration gradient of immobilized GlcNAc, whereas the same cell not expressing GalTase will not.[341] Shur et al. have demonstrated that cells expressing GlcNAc will migrate along a concentration gradient of immobilized GalTase.[204] This interaction between GalTase and GlcNAc may be important in a range of cell–cell interactions—including those necessary for a metastatic tumor to attach to, or migrate to, a remote site (Figure 25)—and for productive interaction of a sperm with an unfertilized egg.[318]

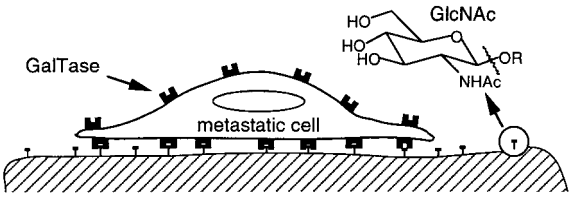


Figure 25. Adhesion of a metastatic cell to laminin. GalTase is expressed on the edges of migrating cells, where it is associated with the cytoskeleton and mediates cell migration by binding to oligosaccharides terminated with *N*-acetylglucosamine (GlcNAc).

5. Implications for Medicinal Chemistry: Polyvalent Pharmaceuticals

Polyvalency is ubiquitous in biology. An understanding on the molecular level of biological systems that are polyvalent suggests strategies for the design of drugs. In principle, polyvalent molecules might both agonize and antagonize; experiments to date have been designed to inhibit undesired biological processes (antagonize) rather than to promote desired ones (agonize).

5.1. Polyvalent Inhibition

A polyvalent inhibitor has two or more linked ligands that act simultaneously at two or more linked receptors. The collection of ligands can be joined covalently (joined through a defined linker,[311, 313, 321–328] tethered to the backbone of a polymer,[2, 329, 330] tethered to the head groups of a dendrimer,[331] or tethered to the surface of a small protein), or noncovalently (tethered to the head groups of molecules in liposomes, membranes, or surfaces[194, 332, 333]). Examples of the various backbones that have been successfully used to construct polymeric inhibitors are given in Table 9. Each has a different advantage and disadvantage with respect to ease of synthesis, flexibility with which it can be modified synthetically, biodegradability, bioavailability, and toxicity. As an example of an advantage, polyacrylamides of high molecular weight are more effective inhibitors of hemagglutination induced by influenza virus than are polyacrylamides of low molecular weight;[278] as examples of disadvantages, these polyacrylamides of high molecular weight are also toxic, less easily cleared by the kidney, and more difficult to synthesize.

One issue that may limit the use of certain polymers of extremely high molecular weight, including polyacrylamides, is that molecules of size greater than that of a protein of 60–70 kDa cannot be filtered effectively by the kidney (mainly because such molecules are too large to pass through the pores in the glomeruli of the kidney). Such large molecules must be degraded enzymatically in the liver (degradative clearance), and can thereby produce a wide range of metabolites that are potentially toxic. One strategy would be to join small polyvalent inhibitors through biodegradable linkages. The rate of hydrolysis of these linkages must be greater than the rate of uptake of these polymers into the liver. There are expected to be, however, certain polymeric structures of high molecular weight that are effectively benign in vivo.

Polyvalent inhibitors that bind the pathogenic particle have advantages over inhibitors that bind the host. One may, in principle, use either partner of a ligand–receptor pair as the basis for a polyvalent drug to inhibit their interaction. Generally, we expect that a strategy that involves the binding of pathogen will cause fewer side effects than the binding of the molecules characteristic of the host. The choice in the cases of non-infectious diseases may be less clear because both partners in the ligand–receptor pair may be natural to the patient.

5.2. Mechanism of Polyvalent Inhibition

5.2.1. Inhibiting Attachment of a Virus to a Host Cell

We[1, 2] and others (Matrosovich et al.,[329, 356] Roy et al.,[357, 358] Gamian et al.,[359] and Sabesan et al.[360]) have constructed a wide range of polymers that inhibit the attachment of influenza virus to erythrocytes (which serve as surrogate target cells). This system is currently the most extensively studied of all polyvalent interactions, and serves as the prototypical system on which many of our conclusions are based. The most effective class of inhibitors to date is the linear polymer polyacrylamide presenting multiple copies of the C-glycoside of sialic acid (SA) as side chains (Figure 26): The most effective of this class prevents hemagglutination (the cross-linking of erythrocytes by virus) at concentrations of 35 pM, whereas the monomeric α-methylsialoside inhibits hemagglutination at concentrations of greater than 2 mM (for details of this SA–HA interaction, see Section 4.2).[2, 335] This 10^8-fold enhancement in ability to hemagglutinate erythrocytes is the largest known increase in activity for any synthetic polyvalent system known to us. Since we do not know the number (N) of attachment points between the polymer and the viral surface, we can make no statement regarding the degree of cooperativity (α) of binding [Eq. (8)]. Regardless of the extent of cooperativity, however, the polyvalent inhibitors are remarkably effective and may illus-

Table 9. Examples of synthetic multivalent ligands.

Multivalent ligand	Multivalent receptor	Assay	Enhancement of binding (β)
polyacrylamide with SA-containing side chains prepared by copolymerization[334]	HA on the surface of influenza virus X31	HAI[a]	$10^3 - 10^4$
polyacrylamide with SA-containing side chains prepared from pNAS[2, 335]	HA on the surface of influenza virus X31	HAI, OPTCOL	$10^5 - 10^8$
polyacrylamide with SA-containing side chains prepared from pNAS[278]	HA on the surface of influenza virus X31	ELISA-binding assay	$10^4 - 10^5$
poly(7-oxanorbornene) containing α-mannose as side chains,[336] prepared by ROMP[b]	concanavalin A	cell agglutination assay mediated by concanavalin A	5×10^4 based on α-mannose
poly(7-oxanorbornene) containing β-glucose as side chains,[330] prepared by ROMP[b]	concanavalin A	cell agglutination assay mediated by concanavalin A	2×10^3 based on β-glucose
dendrimers containing SA[331, 337]	HA on the surface of influenza virus X31	inhibition of horse radish peroxidase	10^2
dendrimer (Man-α)$_{16}$[337]	concanavalin A	inhibition of binding of concanavalin A to yeast mannan	4
dendrimer (NeuAc-α)$_{15}$[338]	lectin (*L. flavus*)	inhibition of lectin to orosomucoid	12
dendrimer (*N*-acetyllactosamine)$_{2-8}$[339]	erythrina cristagalli lectin	inhibition of the interaction between lectin and porcine from stomach mucin (IC50)	1 – 10
dendrimer (GlcNAc)$_{2-8}$[339]	wheat germ agglutinin	inhibition of the interaction between lectin and porcine from stomach mucin (IC50)	1 – 10
liposomes containing SA[332, 333]	HA on the surface of influenza virus X31	HAI	$10^4 - 10^6$
liposomes containing 332 antibodies (664 binding sites)[340]	modified red blood cells	fluorescence quenching	2 – 10
liposomes containing sLe^X mimetics[194]	P-selectin IgG conjugate	inhibition of binding of P-selectin IgG to HL-60 cell	2×10^6
GalNAc linked to BSA[c] (BSA(GalNAc)$_{39}$)[341]	amebic surface lectin	inhibition of human red cell mediated by *E. histolytica* lectin	1.4×10^5
T-10 fragments (glycopeptide) were polymerized	*M. Prolifera* cells	competition assay using radioactive monomer and cold polymer	1
α-melanotropin (MSH) linked to TMV[d][342]	Cloudman S-91 melanoma cell	agonist activity for tyrosinase stimulation	6
dimeric α-MSH[343]	melanocytes	functional melanocyte dispersion assay	7
liposomes containing enkephalin[344]	bovine brain homogenates	displacement of radioactive (^{3}H-labeled) enkephalin	13
α_2-macroglobulin (4-*O*-Ac-Neu5Ac)[345, 346]	HA on the surface of influenza virus X31	HAI	10^5
mono-, di-, tri-, and tetraantennary galactose derivatives[347]	rabbit hepatocytes[348]	inhibition of radioactive glycopeptides	10^5 (triantennary)
triantennary galactoside[349]	hepatic asialoglycoprotein receptor	in vivo	2×10^3
bivalent SA[279, 280]	influenza virus (hemagglutinin)	binding assay (^{1}H NMR)	10^2
bivalent sLe^X[196]	E-selectin	inhibition of adherence of E-selectin to HL-60 cells	5
bivalent sLe^X *O*-glycan[350]	lymphocyte	inhibition of adherence of lymphocyte to endothelial cell	> 50
bivalent cyclosporin[351]	cyclophilin (Cyp) A	fluorescence titration assay	≈ 1 for monomeric Cyp, > 1 for membrane-bound Cyp
bivalent indole linked by variable length alkanes[352]	serotonin receptors: 5HT$_{1A}$, 5HT$_{1D}$, 5HT-UT, and 5HT$_{1E}$	radioligand displacement assay	4×10^2
bivalent L-Lys-D-Ala- D -Ala linked by a rigid 10-Å linker[353, 354]	synthetically bivalent vancomycin linked by a succinyl linker	competition assay with the monomer using capillary electrophoresis, fluorescence, and surface plasmon resonance assays	10^3
bivalent opiods[355]	guinea pig brain membranes	inhibition of radioactive ethylketazorine	20

[a] Hemagglutination inhibition assay. [b] Ring-opening metathesis polymerization. [c] Bovine serum albumin. [d] Tobacco mosaic virus.

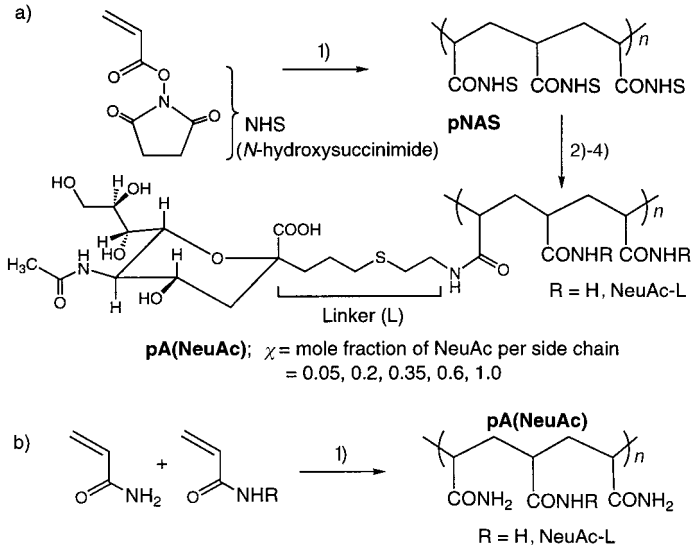


Figure 26. Synthesis of polyacrylamides with side chains containing multiple copies of α-C-sialosides, pA(NeuAc). a) Derivatization of an activated ester of poly(*N*-acryloyloxysuccinimide) (pNAS): 1) radical-catalyzed polymerization; 2,2′-azobisisobutyronitrile (AIBN), tetrahydrofuran (THF), 60 °C; 2) χ molar equivalents of NeuAc-L-NH_2 (per mole of activated ester on the polymer), triethylamine, *N*,*N*-dimethylformamide (DMF), room temperature; 3) excess ammonia; 4) dialysis against distilled water. By varying the number of equivalents of NeuAc-L-NH_2 (χ equiv), five types of pA(NeuAc, $\chi = 0.05$, 0.2, 0.35, 0.6, 1.0) were prepared; χ denotes the mole fraction of NeuAc in the polymers and is defined as the number of side chains containing NeuAc divided by the total number of side chains. b) Direct radical-catalyzed copolymerization of a mixture of two or more monomeric acrylamides.

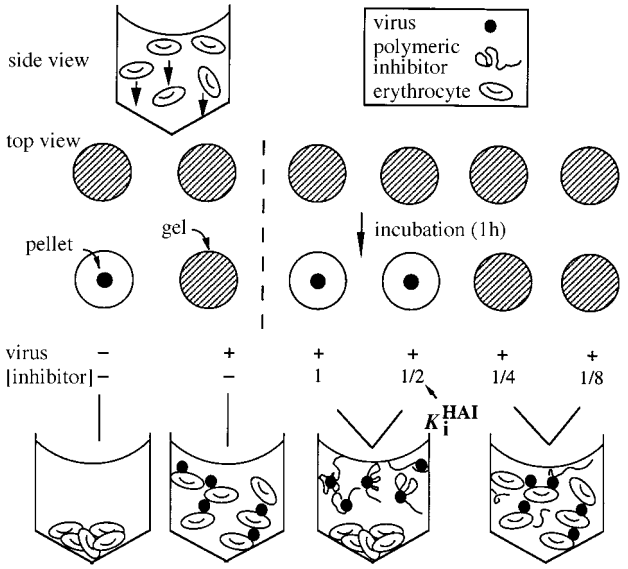


Figure 27. Schematic representation of the hemagglutination inhibition (HAI) assay. The assay requires a sequential mixing of three components in a microtiter well; 1) incubation (30 min) of virus and inhibitor (at various concentrations); 2) addition of erythrocytes to the mixture followed by incubation for about one hour. The 250-μL microtiter well is viewed both from the side and the top. Hemagglutination (formation of a gel) is represented by hashed marks; a pellet of erythrocytes is shown as a dark spot. The concentration of the inhibitor is one unit in the third well from the left, and is sequentially lowered by a factor of two in the wells to the right of the third well. The value for the lowest concentration of inhibitor that inhibits hemagglutination is, in this case, 0.5 units.

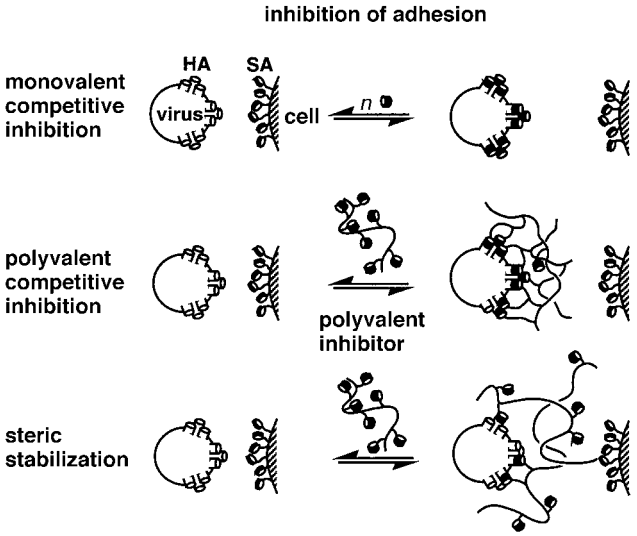


Figure 28. An example of inhibition of an unwanted polyvalent interaction using polyvalent molecules. Influenza virus attaches to its host cell through polyvalent interaction of HA with SA. Monomeric molecules containing SA units inhibit attachment by competitive inhibition, whereas polymeric molecules inhibit attachment by a combination of two conceptually independent, limiting mechanisms: 1) high-affinity binding through polyvalency (polyvalent competitive inhibition) and/or 2) steric stabilization of a surface (steric inhibition).

trate a general strategy for inhibition of interactions between two polyvalent surfaces; the values of β for a number of polymeric inhibitors are much greater than 1, and these classes of inhibitors are therefore potentially very useful.

This system is the one that has been explored in greatest detail to date with respect to mechanism of action of polyvalent inhibitors, and has had the structural determinants of effectiveness most clearly defined. The hemagglutination inhibition (HAI) assay has mainly been used to evaluate polyvalent, polymeric inhibitors of influenza viral attachment. This assay measures the lowest concentration of inhibitor (in terms of sialic acid groups, whether free in solution or bound to a polyvalent carrier) that is able to inhibit the virally mediated cross-linking of erythrocytes (Figure 27).

There are, in principle, two different limiting mechanisms of action for polyvalent inhibition of influenza virus to erythrocytes, the sum of which contribute to the observed inhibition constant K_i^{HAI} (Figure 28): 1) entropically enhanced competitive inhibition and 2) steric stabilization. We have performed experiments that have deconvoluted the results from hemagglutination inhibition into contributions from entropic enhancement of inhibition and steric stabilization, and showed that both mechanisms of action are significant.

5.2.2. Competitive Inhibition

We define this mechanism as that acting through binding of the inhibitor (a structural analogue of sialic acid, SA) at HA, and therefore competitively preventing the binding of cellular SA to the same HA. The ability of an inhibitor containing SA to inhibit an interaction competitively is related directly to its dissociation constant with the viral surface. Figure 29 illustrates three related equilibria and their corresponding association constants: The association constant between mono-

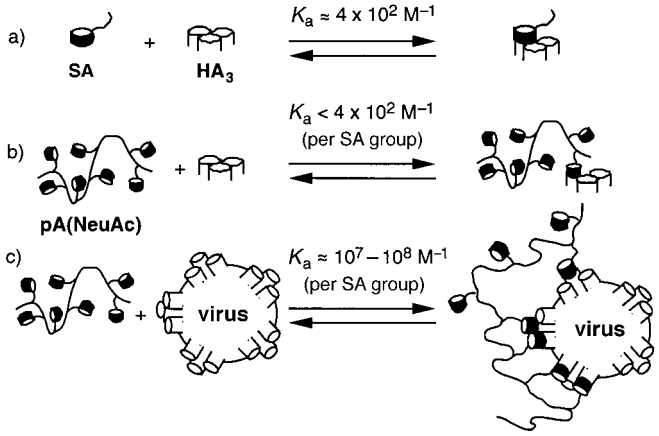


Figure 29. Association constants (K_a) for the association of sialic acid (SA, NeuAc) and hemagglutinin (HA): a) monomeric SA and HA from HA_3; b) SA from polyvalent polyacrylamide, pA(NeuAc), and HA from HA_3; c) SA from polyvalent polyacrylamide, pA(NeuAc), and HA on the surface of virus.

meric SA and trimeric hemagglutinin (HA_3) is $4 \times 10^2\,M^{-1}$ in terms of SA; that between polyacrylamide presenting multiple copies of SA and HA_3 is less than $10^2\,M^{-1}$ (unmeasurably small with NMR and fluorescence assays);[1] and that between SA on a polymer and HA on the viral surface is 10^7–$10^8\,M^{-1}$.[278] A comparison of the magnitudes of these equilibria is useful: The polymer appears to bind more poorly to HA_3 ($N=3$) than does the monomeric SA ($N=1$), in spite of a greater degree of polyvalency. This lower affinity of the polymer for HA_3 may be due to steric interference of the large, water-swollen polymer backbone on the interaction between each SA group and its binding cleft on HA_3. The binding of the polyvalent SA to the polyvalent surface (expressing multiple HA_3 receptors) is, however, much more effective than the binding of polyvalent SA to HA_3. That is, by increasing the degree of polyvalency from $N=3$ to $N \approx 10-10^2$ (the number of HA receptors bound to one polymer molecule), any steric interference in binding has been overwhelmed.

Since the association constant K_a is a direct measure of the ability of an inhibitor to inhibit competitively, a comparison of the values of K_a and $1/K_i^{HAI}$ (K_i^{HAI} has units of a dissociation constant, and $1/K_i^{HAI}$ has units of an association constant) provides a measure of the importance of competitive inhibition in preventing hemagglutination. We have examined the binding of virus to a polyacrylamide in which 20% of the side chains were derivatized with SA; this mixture of polymers were fractionated into portions that varied in molecular mass.[278] We have shown that the values of K_a for these polymers ranged between $10^6-10^8\,M^{-1}$. The values of $1/K_i^{HAI}$, on the other hand, varied between 10^7 and $10^9\,M^{-1}$. That is, the ability of the polyvalent inhibitor to bind tightly to the viral surface accounts for much, but not all, of its enhanced effectiveness over monovalent inhibitors.

5.2.3. Steric Stabilization

This mechanism involves inhibiting the interaction of the viral surface with the cellular surface by a means other than competitively occupying the binding clefts on HA. We envision the polymer forming a loose, water-swollen, gellike layer on the viral surface. This layer sterically prevents the close approach of the cellular surface. An analogous mechanism may play an important role in keeping microparticles stable in suspension (as is often used in the food industry) by the addition of hydrophilic polymers such as poly(ethylene glycol) and poly(acrylic acid). In a limiting case, the polymer presenting SA may bind with very poor affinity, but a single binding event brings the large, water-swollen polymer to the viral surface.

We have performed two sorts of experiments that demonstrate that steric stabilization may be important in inhibiting virus–cell interaction by polymeric polyvalent molecules: The first experiment is indirect, and we describe it below. We concluded that even though the polymer examined was $1/K_i^{HAI} \approx 10^7$ times more effective at preventing hemagglutination than an analogous monomer, the affinity of the polymer for the viral surface was only 10^6 times higher; that is, the additional factor of 10 was likely due to a mechanism other than affinity, and we hypothesize that this additional enhancement is due to steric stabilization.

The second experiment is more direct than the first: We attempted to increase the ability of a given polymer to stabilize the virus sterically, and simultaneously to decrease the affinity of this polymer for the surface of the virus.[361] We first describe the experiment and the results, then we rationalize these results in terms of mechanism. The SA groups on the polymer bind to two sites on the surface of the virus: HA and NA (neuraminidase, a second protein on the surface of the virus that is less abundant than HA). Binding of SA to both sites may be important in determining the affinity of the polymer for the surface of the virus. We synthesized three different monomeric inhibitors of NA that do not bind significantly to HA, and do not inhibit agglutination by itself even at concentrations as high as 40 mM. We found that addition of any of these NA inhibitors augmented the effectiveness of the polymer in inhibiting viral hemagglutination in a concentration-dependent manner (Figure 30) that depended on the affinity of the NA inhibitor for NA. For polymers bearing a high mole fraction of sialic acid, the enhancement was 20-fold in the presence of NA inhibitor; for polymers bearing low mole fractions, the enhancement was twofold or less.

Displacement of a sialic acid on the polymer from a NA site by the NA inhibitor would have two effects (Figure 31): It would lower the affinity of the polymer for the surface of the virus (that is, it would lower the total number of ligand–receptor interactions), and it would increase the size of the loops that extend from the surface of the virus and thereby increase the ability of the polymer to inhibit the approach of another surface (steric stabilization). The NA molecules rise only 50 Å from the viral surface, while the HA molecules rise 100 Å. Release from low-lying NA sites may create a more effective barrier between the surface of the erythrocyte and the SA-binding sites on the tips of the HA. This example demonstrates that steric stabilization is not only an important mechanism of action of polyvalent inhibitors, but also that it can be modulated.

The mechanism of polyvalent inhibition will certainly be dependent on the system, but we have shown through a

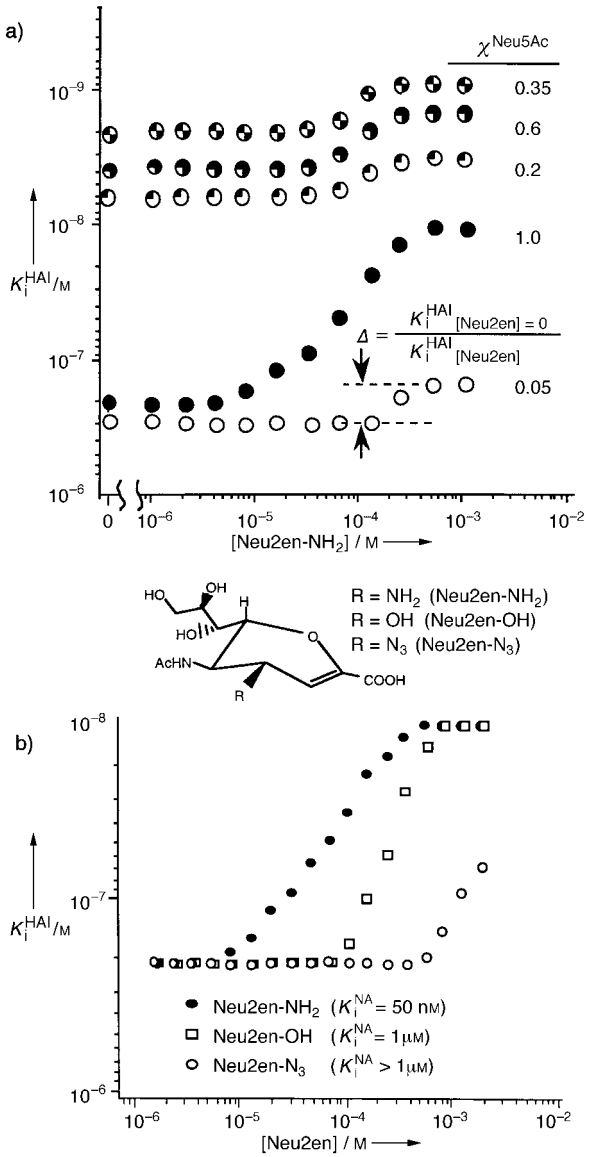


Figure 30. Augmentation of the effectiveness of the polymeric sialic acid inhibitor by monomeric neuraminidase (NA) inhibitors (Neu2en). a) The values of pA(NeuAc) ($\chi^{NeuAc} = 0.05$, 0.2, 0.35, 0.6, 1.0) are shown as a function of the concentration of Neu2en–NH_2 (50 nM – 50 mM). The presence of Neu2en–NH_2 in the system, at concentrations greater than about 0.5 mM, increased the effectiveness of pA(NeuAc) in inhibiting hemagglutination by 2- to 20-fold (enhancement is defined as $\Delta = (K_i^{HAI}{}_{[Neu2en]} = 0)/(K_i^{HAI}{}_{[Neu2en]})$. The enhancement of the polymer pA(NeuAc, $\chi^{NeuAc} = 1.0$) was greatest (ca. 20-fold) among tested polymers. b) The values for pA(NeuAc, $\chi^{NeuAc} = 1.0$) were measured as a function of the concentrations of three different Neu2en (Neu2en–NH_2, –OH, and –N_3). The concentrations of Neu2en required for half-maximal enhancement, $[Neu2en]_{1/2\Delta}$, were 70 μM, 300 μM, and ≥2 mM for Neu2en–NH_2, Neu2en–OH, and Neu2en–N_3, respectively. Although the data are limited, there seems to be a correlation between $[Neu2en]_{1/2\Delta}$ and values of K_i^{HAI}.

collection of experiments that both high affinity and a high degree of conformational flexibility are desirable properties of these polyvalent inhibitors. Steric stabilization may be a new strategy in the design of effective pharmaceutical agents. In the case of infectious agents, for example, we may, in principle, build polyvalent inhibitors of attachment that involve any molecule that binds tightly to the surface of the infectious agent. We are, remarkably, not limited to the

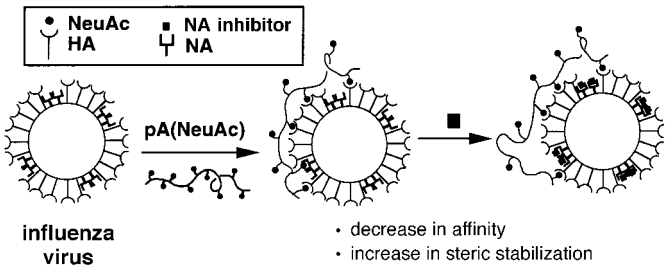


Figure 31. The hypothetical mechanism describing the modes of action of pA(NeuAc) in inhibition of influenza-mediated hemagglutination, and the effect of NA inhibitors on HAI activities of the pA(NeuAc). The presence of NA inhibitor is believed to release NeuAc from active sites of NA and/or HA sites, which may subsequently lead to expansion of gel layers.

polymers that present molecules that are directly involved in attachment. As an example, monomeric inhibitors of the surface enzyme neuraminidase, which is not involved in the attachment of influenza to cell, could nevertheless be presented on polymers to prevent attachment sterically.[362, 363] These polymers may function by binding to and establishing a hydrated gel layer on the surface of the virus or bacterium. Thus, polymers of a drug may change the original mechanism of action for that drug. Although there are currently no examples of such drugs, we have recently obtained some promising results using polymers of NA inhibitors that do not bind HA, but nevertheless inhibit hemagglutination effectively.[363]

We have described experiments with influenza virus whose results imply that steric stabilization may be an important mechanistic component of the anti-adhesive properties of large polymeric constructs targeting influenza virus. Given what we feel are the most likely of the possible biochemical mechanisms for steric stabilization, however, we believe that is it less likely that smaller constructs (such as Lee's glycoclusters[205]) exhibit significant steric stabilization of their targets. These constructs are comparable in size to antibodies (actually smaller than them), and the importance of steric inhibition in both remains to be established.

5.3. Polyvalent Promotion

In Section 5.2 synthetic agents that *inhibited* an undesired adhesion of two surfaces interacting polyvalently was described. There are few examples to date, however, of synthetic polyvalent molecules that trigger a signal upon binding, and thereby *promote* a desired interaction. Four examples are as follows:

1) Gong et al. described a polymer presenting multiple copies of GlcNAc that upon interaction with the surface of sperm triggered the acrosomal reaction (see Secion 4.4.1).[253]
2) Carrithers et al. described bivalent peptides targeted to G-protein-coupled receptors.[343] The ligand domain was either alpha-melanocyte stimulating hormone, an alpha-MSH receptor antagonist (alpha-MSH-ANT), or bombesin. These ligands were characterized in a functional melanocyte dispersion assay.
3) As described in Section 4.4.1, Dembo et al. described a series of bivalent antigen molecules that interacted with IgE molecules on the surface of a mast cell and thereby triggered degranulation.[226, 227, 324]

4) Multiple insulin molecules were attached to poly(acrylic acid) through an amide linkage.[364] This polyvalent insulin was more active (as a mitogen) on a per ligand basis than monovalent (natural) insulin.

5.4. Assaying the Polyvalent Interaction

There exist a number of methods for probing, assessing, and quantifying polyvalent interactions. Some assays may be direct measures of affinity; from these affinities, one may, in principle, extract free energies of interaction. Other assays may measure a complex aggregate of characteristics, only one of which is free energy of interaction: These other characteristics may include extent of hydration, ability to stabilize a molecule or surface sterically, and/or ability to cross-link multivalent receptors. We will not discuss here assays of polyvalent materials that go beyond examining their local effectiveness (i.e., assays that probe the often special pharmacodynamics and pharmacokinetics of large polyvalent materials relative to small monovalent ones, and even relative to large globular ones such as proteins).

5.4.1. Assays that Yield the Free Energy of Interaction of a Polyvalent System

To quantify a binding constant thermodynamically (i.e., to obtain a binding constant), the relative proportions of uncomplexed and complexed ligand or receptor must be directly or indirectly measured. Depending on the stability of the complex (related to its lifetime), different techniques can be used. Table 10 gives examples of a variety of techniques that have been used to measure polyvalent interactions.

Table 10. Techniques available to quantitate polyvalent interactions.

Technique	Example of an application	Enables measurement of			Comments
		affinity	inhibition[a]	kinetics	
hemagglutination inhibition assay[2]	1. inhibitors of the influenza–erythrocyte interactions, 2. antibody interactions with the surface of wide range of bacteria	no	yes	no	widely used; easily performed; in general, limited to inhibition constants greater than 1 nM
ELISA assay[278]	inhibitors of the influenza–erythrocyte interaction	yes	no	no	requires synthetic labeling of the polyvalent species; in general limited to dissociation constants greater than 10–50 nM
fluorescence-activated cell sorter[365]	antibody interactions with the surface of a cell	yes	yes, in principle	no	requires covalent modification of the antibody; based on the separation and subsequent quantification of bound and unbound forms
OPTCOL assay[335]	inhibitors of the influenza–erythrocyte interaction	no	yes	no	enables measurement under physiologically relevant conditions (collision velocity of cells, relative orientation, and other factors are controlled by the user); measurement involves a single cell and a single microsphere coated with viral particles, and the lower limit of measurable inhibition constants is less than 10^{-18} M.
affinity capillary electrophoresis[353]	dimers of vancomycin interacting with dimers of D-Ala-D-Ala	yes	no	no	this technique has much promise, and many extensions to other systems are possible and underway
surface plasmon resonance	antibody binding to synthetic surfaces presenting different densities of antigen (DNP, anti-DNP system);[366] influenza binding to immobilized hemagglutinin[367]	yes	no	yes	requires milligrams of the polyvalent material (other techniques in this table require 100 less in general); other related techniques include acoustic plate mode and surface acoustic wave, and are all based on the detection of small changes in dielectric constant near an interface
pipette suction	1. two erythrocytes bound by various agglutinins,[368] 2. CD2-containing jurkat cells adhering to LFA-3 in a planar membrane[369]	yes, in principle	yes, in principle	no	based on the quantification of the energy required to deform complementary cell surfaces during adhesion and separation; may be difficult to perform, or on the integrated forces required to separate two biological surfaces.
shear flow[370–372]	neutrophil interaction with surfaces derivatized noncovalently with different selectins	yes	yes, in principle	no	based on counting large number of events (stuck, non-stuck) under an optical microscope; probability of adhesion is measured as a function of flow rate of solution past surface
dissociation under influence of gravity[373, 374]	adhesion of vero green monkey kidney cells to growth surface	yes	no	no	time required to fall off surface is measured and correlated with strength of adhesion; centrifugal forces are almost always applied to hasten assay
optical microscopy counting aggregates[375]	sperm–egg interactions, and inhibition of these interactions	yes, in principle	yes	no	based on counting a large number of events (bound, unbound) following agitation; probability of adhesion can be measured as a function of concentration of inhibitor; difficult to perform
atomic force microscopy[376]	surfaces containing streptavidin interacting with surfaces containing biotin	yes	yes, in principle	no	highly sensitive (a single molecule–molecule interaction can be measured); expensive equipment required; covalent derivatization of small objects required
light scattering[377]	none to our knowledge	yes	yes, in principle	no	

[a] Inhibition of surface–surface interactions. The effectiveness of the assay is a result of both steric stabilization and enhanced affinity.

5.4.2. More Complex Assays of Polyvalency

In Vitro Aggregation

Some assays are available that can be used to measure the ability of a polyvalent ligand to aggregate a polyvalent receptor (precipitation, gel formation, aggregation). For example, a bivalent antibody can precipitate polyvalent proteins in immunoprecipitation assays (Figure 32). Although

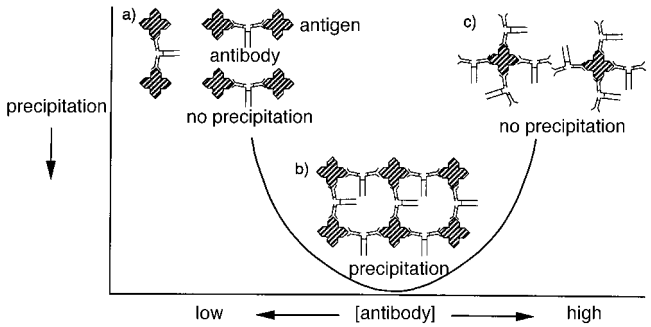


Figure 32. Influence of concentration of antigen in an immunoprecipitation assay. a) Formation of soluble antigen–antibody complexes in the presence of excess antigens. b) Formation of insoluble complexes (extensive lattice) near the equivalence point. c) Formation of soluble complexes in the presence of excess antibodies.

the affinity of the bivalent entity is important in determining the ability of the bivalent antibody to precipitate, other characteristics can be as, or even more, important: At low concentrations, the antibody fails to bind to the polyreceptor; at a certain concentration, precipitation occurs; at higher concentrations, each polyreceptor is surrounded by the antibody and precipitation again does not occur. In this example, affinity alone does not determine the pattern of precipitation.

In Vitro Inhibition of Aggregation

An example of an assay that measures the ability of a molecule to prevent two surfaces from interacting is the hemagglutination inhibition (HAI) assay (Figure 27). If the mechanism of inhibiting interaction was strictly based on competitive inhibition of all ligand–receptor pairs, the assay would only depend on the average affinity of each ligand–receptor pair in the polyvalent molecule (K_{avg}^{poly}). In such a case, an identical monovalent ligand (L) at a concentration $[L]^{mono} = K_{avg}^{poly}/K^{mono}$ should be equally effective in preventing two surfaces from interacting. As we have shown, the ability of a polyvalent inhibitor to prevent two biological surfaces from interacting may, however, involve steric stabilization, in which case molecular characteristics such as size, degree of hydration, and conformational flexibility play a role. Therefore, in cases where steric stabilization plays an important mechanistic role in inhibition, the concentration of the monovalent analogue of the ligand must be higher than the effective concentration of ligand in the polyvalent molecule ($[L]^{mono} > K_{avg}^{poly}/K^{mono}$) to be equally effective.

A limitation of the HAI assay stems from the minimum concentration of virus required to agglutinate erythrocytes.[2] This minimum concentration corresponds to approximately 1 nM of hemagglutinin protein in the assay vessel. The maximum value of K_i^{HAI} that can then be estimated reliably is therefore approximately 1 nM. We have recently described an assay in which two mesoscale particles (particles whose dimensions are approximately 0.1–100 μm) undergo a collision under the precise control of two independently controlled optical tweezers (optically controlled collision, OPTCOL; Figures 33–35).[335] This assay enables precise examination of the probability of adhesion under biologically relevant conditions. The biochemical and biomechanical

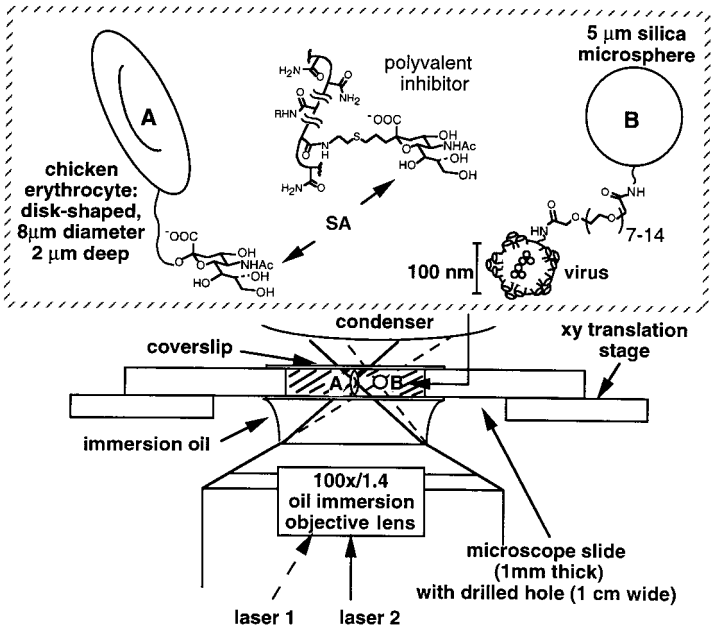


Figure 33. Schematic representation of the setup for the OPTCOL experiment, which uses lasers to quantitate the interaction between an erythrocyte ("A") and a microsphere covalently coated with influenza virus ("B"). A 1-cm hole is drilled in a microscope slide, and a "floor" is created with a coverslip. Particles A and B along with an inhibitor of the A–B interaction are added in buffer to this 100-μL "vessel". A second coverslip is placed to close the vessel, and the slide is placed under an inverted microscope. Two lasers are fed into the microscope. Each laser is focused through a lens. Particles A and B are "trapped" optically at the foci of the two lasers, and can be moved precisely and rapidly in three dimensions by manual or computerized translation of the foci. Shown are schematic drawings of the erythrocyte "A" (with SA covalently bound to various proteins and lipids embedded in the surface of the cell), the microsphere "B" (with virus tethered covalently to its surface), and the polymeric inhibitor (see also Figure 34).

determinants of adhesion between two biological objects following a collision are complex, and may vary from one system to another. The components of the solution, the relative orientation, the impact parameter, and the relative collision velocity are all under the user's control. These are precisely the variables that influence the probability of adhesion in vivo. We have illustrated the utility of the OPTCOL assay by evaluating the probability of adhesion of a single erythrocyte to a single virus-coated microsphere, both in the absence and presence of an inhibitor bearing sialic acid (Figure 34). The OPTCOL assay requires, in principle, only a single virus-coated microsphere and a single erythrocyte, and therefore the theoretical limit for association constants is as high as $10^{15}\,M^{-1}$. We assayed inhibitors using OPTCOL whose

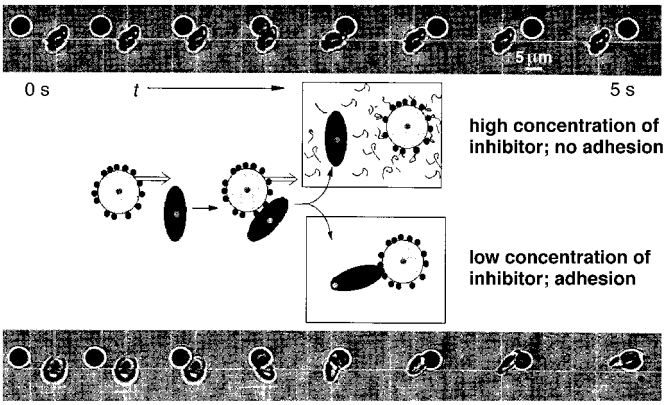


Figure 34. Schematic representation of the OPTCOL assay[328]. The virus-coated microsphere (in the mobile trap) is translated using one point of laser trap at a constant velocity and collides with the erythrocyte (in the stationary trap) above its center of mass; during this collision, the erythrocyte rotates. The erythrocyte remains in the stationary trap (the center of the right-hand crosshair) as the microsphere collides with it. The microsphere continues to translate linearly at constant velocity until it reaches a point approximately 20 μm from the original position of the erythrocyte. If the concentration of inhibitor is sufficiently high, the cell loses its initial contact with the microsphere and remains in the stationary trap as the microsphere translates past it. When no inhibitor, or too little inhibitor, is present, the cell adheres tightly to the passing microsphere, moves out of the stationary trap, and is "captured." Examination of the probability of adhesion as a function of concentrations of the inhibitor's sialic acid groups yielded an inhibition constant. We performed multiple repetitions of collisions for multiple pairs of microsphere and erythrocyte. Micrographs of the virus-coated microsphere before and after collision with the erythrocyte are shown.

values of $1/K_{avg}^{poly}$ varied from 1 nM to 10 mM. Four inhibitors all gave $K_{avg}^{poly} = 1$ nM, and were indistinguishable using HAI. We distinguished these four inhibitors easily using OPTCOL, and the best inhibitor prevented attachment 50% of the time at a sialic acid concentration of 35 pmol L^{-1}; it is the most potent known inhibitor of attachment of influenza virus to erythrocytes. We emphasize that this assay is empirical: It works because it can be calibrated by data measured in other ways.

OPTCOL is a versatile new bioassay for studying dynamic interactions in biochemistry. It offers an approach to investigating interactions between moving biological objects that is both quantitative and interpretable. The simplicity of the OPTCOL technique suggests broad applicability to the study of adhesion of mesoscale objects using relevant parameters in the areas of cell biology, microbiology, medicinal chemistry, and biophysics.

In Vivo Assays

In vivo assays measure the overall success of the inhibitor in protecting animals against infection; these assays include, but are not limited to, a measure of the inhibitor to prevent polyvalent interaction. The molecule may, for example, not only slow the rate of infection by blocking attachment to host receptors, but may slow the rate of clearance by blocking the clearance mechanisms. In the latter case, the polyvalent inhibitor might even increase overall infection! Overall success depends on these and other complex criteria such as toxicity, and often require that whole organisms be used for assays.

5.5. Future Prospects for Polyvalent Inhibitors

Polyvalent ligands directed at many of the naturally occurring polyvalent targets will undoubtedly be designed and synthesized. The mechanisms that are dominant for the success of monovalent agents are still important for poly-

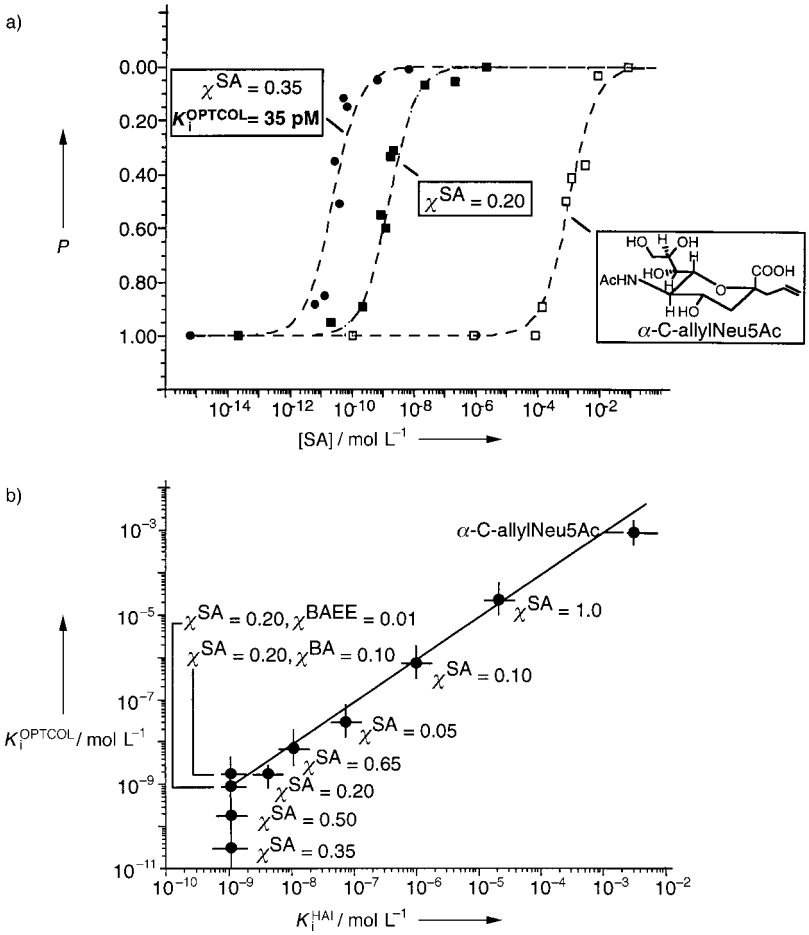


Figure 35. a) Typical inhibition curves obtained from OPTCOL experiments showing the probability of adhesion P as a function of the concentration of inhibitor (expressed as the concentration of SA groups).[328] The curves are fits of a binding isotherm (no cooperativity terms) with K_i as an adjustable parameter. We conservatively estimate the uncertainty in our measurements by fitting the data with two limiting values of K_i that exclude most (90%) of the data points. Probabilities were determined from at least 20 independent trials using 4–6 pairs of microsphere and erythrocyte. The values of K_i^{OPTCOL} were defined to be the value of [SA] for 50% probability of adhesion. b) The plot of measured values of K_i^{OPTCOL} against K_i^{HAI} show good agreement for $K_i^{OPTCOL} > 1$ nmol L^{-1}. BA = benzylamine, BAEE = bis(aminoethyl) ether. The error bars corresponding to a factor of ±2; the values of K_i^{HAI} were obtained from the literature.[5] For all inhibitors with $K_i^{OPTCOL} < 1$ nmol L^{-1}, K_i^{HAI} is approximately 1 nmol L^{-1}. For the solid line, $K_i^{HAI} = K_i^{OPTCOL}$ is valid.

valent ones, but at least one other mechanism not relevant to monovalent agents may also play a role: steric stabilization. Many issues must be clarified before polyvalency can be used for the design of and the prediction of outcomes of polyvalent inhibitors. Central questions include the following:

1) What is the best scaffold on which to present multiple copies of a ligand? The possibilities include both covalent frameworks (linear and branched polymers, dendrimers, proteins, and biodegradable beads) and noncovalent frameworks (liposomes). The "best" choice may be a function of the application. The conformational flexibility of the scaffold plays an important role, for example, in the ability of the polyvalent species to stabilize its target sterically, and in the value of B.
2) What are the chemical determinants of affinity for its target? What are the chemical determinants of the ability of the polyvalent species to stabilize its target sterically? These two questions relate to the best ways to design the spacing, rigidity, and hydrophilicity of the macromolecule. Despite extensive work, the precise rules that govern the specific (ligand–receptor) attachment of a polymer to a surface are not yet clear. The physical structure and arrangement of the group of "attached" polymers on the receptor-laden surface is also not clear from either a theoretical perspective, or an experimental one.
3) What are the chemical determinants of the toxicity of polyvalent inhibitors? These determinants may not be related in a simple way to those known to influence the toxicity of small molecules. The reason may be that small molecules are often designed, for a number of reasons, to be relatively hydrophobic, for example, to increase lifetimes in circulation by associating nonspecifically to proteins and thereby avoiding rapid filtration by the kidney. These small molecules are therefore often cleared predominantly by the liver. Polyvalent ligands can be hydrophilic and remain in circulation for prolonged periods because of their size. By varying the sizes of these polyvalent species, perhaps by varying the biodegradability of the linkages connecting its different segments, these molecules can be designed to be cleared by the liver, spleen, or kidney. The chemical determinants of toxicity will depend, in part, on the route of clearance.
4) What are the best ways to deliver polyvalent ligands? Because these polyvalent species are often large, they may not pass passively and rapidly through hydrophobic membranes; injection may be more appropriate than ingestion or transdermal delivery for applications within the vascular space, for instance. These issues of delivery are related to those for protein-based drugs. We are just beginning to understand some of these issues, while others remain completely unexplored. The kinetics and biophysical mechanisms of passage of polymeric molecules across porous membranes is also relevant here, and remains an area of exploration in biophysics and statistical mechanics. The same challenges that are faced in the delivery of polyvalent materials, however, serve as advantages from a pharmacokinetic perspective. That is, once a polyvalent molecule of sufficient size is delivered to the vascular compartment, the biological lifetime is expected to be greater than that of the monovalent analogue. Lengthening lifetimes has several advantages including reduced dosing frequency (and therefore increased compliance) and the ability to use materials that have intrinsically lower therapeutic indices (with the same dosing frequency, the difference between peak and trough concentrations of the active agent will be less than that for agents cleared more quickly).

Applications of polyvalent molecules as pharmaceuticals should be possible, and should open new doors in the industry. Although this review is not the forum for exhaustively presenting new areas of application, describing two such areas may be illustrative of the potential of polyvalency.

Any biological surface that interacts with another biological surface through multiple attachment points can, in principle, be a target for polyvalent drug design. That is, naturally polyvalent interactions can be antagonized with synthetic polyvalent molecules. One example may be that molecules that are composed of repeating units of small moieties essential for viral attachment and entry may provide a general strategy for the inhibition of viral infection. Since steric stabilization is expected to play a role in the mechanism, inhibitors presenting multiple copies of a single ligand may be active even against virus particles that may use more than one, or alternative, receptors for primary viral attachment (e.g. HIV). A second example may be that the interactions between platelets, or between denuded endothelia and platelets, may be inhibited using a polyvalent inhibitor of integrin binding. These agents might be particularly useful if more than one type of ligand is incorporated into the backbone such that only regions expressing more than one type of receptor (i.e., sites of pathology) are targets of this highly specific polyvalent agent. Such agents may find uses in the treatment of pathological clotting (e.g. deep-vein thrombosis, arterial thrombosis in a coronary artery leading to myocardial infarction, formation of a clot in a fibrillating atrium leading to myocardial infarction or stroke).

A second type of application is in agonizing interactions that are not naturally polyvalent with synthetic polyvalent molecules. For example, one may design a molecule that presents multiple copies of acetyl choline or epinephrine that binds very tightly to cholinergic and adrenergic receptors, respectively. These polyvalent materials may be useful agonists of the parasympathetic and sympathetic nervous system. Since the affinity of these agents will most likely be a function of the density and accessibility of receptors on a surface, there is a likelihood of designing molecules that are targeted to cells not according to whether or not they express these particular classes of receptors, but rather according to the concentration at which they are expressed. This strategy may then allow specificity to be built into a pharmaceutical agent that is physically independent of the details of the individual ligand–receptor interaction.

6. Conclusions

Polyvalency occurs broadly in biological systems, but remains largely unappreciated by those who study either biology or design and synthesize chemical agents intended to

interact with biological processes. Polyvalent interactions in biology suggest new targets for interaction using pharmaceuticals that are themselves polyvalent. The greatest barriers to the design of effective polyvalent pharmaceuticals may be a deficiency in the tools to assay polyvalent interactions, and an incomplete understanding of the theoretical framework underlying it. Successful design of synthetic polyvalent systems requires a detailed understanding of the delicate balance between entropy and enthalpy. Chemists and biochemists understand enthalpy well; they do not understand entropy, especially conformational entropy, as well.

Polyvalency confers characteristics on a system that are not present in monovalent interactions. For example, the following are possible with polyvalency: achieving very tight binding from ligands with modest or low surface area; grading (graduating) biological responses, possibly with nonlinear dependence on the strength of the signal; creating new interactions by mixing, matching, and multiplying existing ones; achieving large conformal contact between biological surfaces, such as those on cells, and enabling efficient communication; inducing changes in the morphologies of large structures such as cells; signaling by the induction of large conformational changes of molecules; inducing changes in the distribution of molecules in a membrane; signaling through oligomerization or dimerization; and inhibiting undesired interactions, such as those between invading pathogens (which are themselves polyvalent) and their targets.

The study of polyvalency may provide new targets and new strategies for the design of pharmaceutical agents. Although the detailed examination of the active site of receptors as an aid in the design and synthesis of tightly binding monomers will continue, new strategies will have to be developed to design scaffolds that hold multiple designed ligands together. The degree of flexibility, the extent of hydration, and the size of the scaffold will play important roles in the design of successful polyvalent pharmaceuticals. In fitting with the strategy most commonly used with small pharmaceuticals, the first polyvalent ligands will probably be designed to be inhibitors of some undesirable process. The first areas of application will probably be in the design of inhibitors of attachment of both viruses and bacteria. Other applications, such as those in cancer (e.g. inhibition of metastasis), are more speculative. Eventually, as with the current wave of protein-based drugs, polyvalent ligands may be designed that promote desired effects, such as modulating the immune system to promote the clonal expansion of specific cellular components.

Assaying a polyvalent interaction remains a fundamental challenge. Functional assays may be more important for polyvalent interactions than for monovalent ones. That is, assays that measure only the affinity of a polyvalent molecule for its target may not be optimally useful in predicting the biological effect. Useful assays should weigh the characteristics of the polyvalent ligand that are important for achieving the desired goal. For example, an effective bivalent molecule for the purpose of aggregating a polyvalent receptor (such as for purification of cells on a large scale by immunoprecipitation, where antibodies are prohibitively expensive) might be composed of two ligands linked through a long flexible linker. An effective bivalent molecule for the purpose of bivalent binding to a single polyvalent receptor (for example, for tight binding to the surface of a pathogen) might be two ligands spaced by a rigid linker of a length that approximates the spacing of receptor sites on the surface of the polyvalent receptor. In this example, both purposes involve the design of a bivalent ligand; the principles of design depend on the purpose. The assay, therefore, must reflect the characteristics important in the use of the polyvalent species.

The inhibition of adhesion of influenza virus A (X-31) to erythrocytes by polyacrylamide presenting multiple sialic acid groups is currently the most extensively studied system of polyvalent inhibition. The most important conclusion that we reach through this set of studies is that the polyvalent, polymeric inhibitors function through at least two distinct, limiting mechanisms: high-affinity, entropically enhanced binding and steric stabilization (defined as the "blocking" of a surface through the development of a large, hydrated "gel" layer). Our most effective inhibitors in studies of the model system involving influenza are effective at inhibiting the interaction between influenza virus and erythrocytes at approximately $10^7 - 10^8$ times lower concentration than the corresponding monomer. In one detailed study in this series of polymers, approximately 10^6 of the total enhancement was due to increased affinity of the polymer for the surface of the virus, and 10^2 was due to steric stabilization.[378]

Appendix: Abbreviations Used in the Text

α	cooperativity constant, defined by Equations (7) and (8b)
β	cooperativity constant appropriate for polyvalent interactions, defined by Equations (9) – (11)
CD4	protein found on the surface of helper T-cells
CD8	protein found on the surface of cytotoxic T-cells
CRBP	cellular retinol binding protein
DNP	dinitrophenol
ELISA	enzyme-linked immunosorbant assay
Fab	monovalent, antigen-binding arm of an antibody
Fc	portion of antibody that is structurally different from the Fab and relatively constant in sequence within an antibody class; the "tail" of an antibody
Gal	galactose
GalTase	galactosyltransferase
GlcNAc	*N*-acetylglucosamine
HA	hemagglutinin
HAI	hemagglutination inhibition assay
hGH	human growth hormone
HIV	human immunodeficiency virus
ICAM	intercellular adhesion molecule
IgE	immunoglobulin class E
IgG	immunoglobulin class G
IgM	immunoglobulin class M
MHC	major histocompatibility complex
MSH	melanocyte stimulating hormone
NA	neuraminidase
Neu5Ac	5-acetylneuraminic acid
OPTCOL	optical collision assay
PDGF	platelet derived growth factor

RXR	retinoid X receptor
SA	sialic acid
sLe^X	sialyl $Lewis^X$
SH2	Src homology 2 protein
TCR	T-cell receptor
TNF	tumor necrosis factor
VSV	vesicular stomatitis virus

Our work in this area was generously supported by the National Institutes of Health (NIH, grants GM30367 and GM 39589). The NMR facilities at Harvard were supported by the NIH (grant 1-S10-RR04870-01) and the National Science Foundation (grant CHE88-14019). M.M. was supported by Eli Lilly and Johnson & Johnson predoctoral fellowships. We would like to thank Eric E. Simanek for numerous invaluable discussions, Anna Poon for her help in preparing the manuscript, and Valeri Martichonok for his help in designing figures and collecting important sets of data.

Received: August 14, 1997 [A 249 IE]
German version: *Angew. Chem.* **1998**, *110*, 2908 – 2953

[1] W. J. Lees, A. Spaltenstein, W. J. E. Kingery, G. M. Whitesides, *J. Med. Chem.* **1994**, *37*, 3419 – 3433.
[2] M. Mammen, G. Dahmann, G. M. Whitesides, *J. Med. Chem.* **1995**, *38*, 4179 – 4190.
[3] L. C. Norkin, *Clin. Microbiol. Rev.* **1995**, *8*, 293 – 315.
[4] A. D. Miller, *Proc. Natl. Acad. Sci. USA* **1996**, *93*, 11 407 – 11 413.
[5] J. M. Bergelson, R. W. Finberg, *Trends Microbiol.* **1993**, *1*, 287 – 288.
[6] T. Stehle, S. C. Harrison, *Structure* **1996**, *4*, 183 – 194.
[7] H. Fried, L. D. Cahan, J. C. Paulson, *Virology* **1981**, *109*, 188 – 192.
[8] H. Liebermann, R. Mentel, L. Dohner, S. Modrow, W. Seidel, *Virus Res.* **1996**, *45*, 111 – 122.
[9] D. Chatterjee, J. V. Maizel, Jr., *Proc. Natl. Acad. Sci. USA* **1984**, *81*, 6039 – 6043.
[10] M. Goldman, Q. Su, J. M. Wilson, *Gene Therapy* **1996**, *3*, 811 – 818.
[11] D. WuDunn, P. G. Spear, *J. Virol.* **1989**, *63*, 52 – 58.
[12] G. Dubin, S. Basu, D. L. P. Mallory, M. Basu, S. R. Tal, H. M. Friedman, *J. Virol.* **1994**, *68*, 2478 – 2486.
[13] D. C. Johnson, R. L. Burke, T. Gregory, *J. Virol.* **1990**, *64*, 2569 – 2576.
[14] R. Kumarasamy, H. A. Blough, *Arch. Biochem. Biophys.* **1985**, *236*, 593 – 602.
[15] W. C. Lee, A. O. Fuller, *J. Virol.* **1993**, *67*, 5088 – 5097.
[16] K. S. Rosenthal, M. D. Leuther, B. G. Barisas, *J. Virol.* **1984**, *49*, 980 – 983.
[17] M. T. Shieh, P. G. Spear, *J. Virol.* **1994**, *68*, 1224 – 1228.
[18] E. Trybala, T. Bergstroem, B. O. Svennerholm, S. Jeansson, J. C. Glorioso, S. Olofsson, *J. Gen. Virol.* **1994**, *75*, 743 – 752.
[19] E. Trybala, B. O. Svennerholm, T. Bergstroem, S. Olofsson, S. Jeansson, J. L. Goodman, *J. Virol.* **1993**, *67*, 1278 – 1285.
[20] P. G. Spear, M. T. Shieh, B. C. Herold, D. WuDunn, T. I. Koshy, *Adv. Exp. Med. Biol.* **1992**, *313*, 341 – 353.
[21] V. Litwin, M. Sandor, C. Grose, *Virology* **1990**, *178*, 263 – 272.
[22] Z. Zhu, Y. Hao, M. D. Gershon, R. T. Ambron, A. A. Gershon, *J. Virol.* **1996**, *70*, 6563 – 6575.
[23] J. F. Wright, A. Kurosky, S. Wasi, *Biochem. Biophys. Res. Commun.* **1994**, *198*, 983 – 989.
[24] C. S. Wright, J. Jaeger, *J. Mol. Biol.* **1993**, *232*, 620 – 638.
[25] J. E. Grundy, J. A. McKeating, P. J. Ward, A. R. Sanderson, P. D. Griffiths, *J. Gen. Virol.* **1987**, *68*, 793 – 803.
[26] G. R. Nemerow, M. D. Moore, N. R. Cooper, *Adv. Cancer Res.* **1990**, *54*, 273 – 300.
[27] G. R. Nemerow, R. A. Houghten, M. D. Moore, N. R. Cooper, *Cell* **1989**, *46*, 429 – 436.
[28] A. W. Hugin, C. Hauser, *J. Virol.* **1994**, *68*, 8409 – 8412.
[29] D. P. Barbis, C. R. Parrish, *Braz. J. Med. Biol. Res.* **1994**, *27*, 401 – 407.
[30] Y. Itoh, S. Kuroda, T. Miyazaki, S. Otaka, Y. Fujisawa, *J. Biotechnol.* **1992**, *23*, 71 – 82.
[31] A. R. Neurath, N. Strick, P. Sproul, *J. Exp. Med.* **1992**, *175*, 461 – 469.
[32] U. Treichel, B. K. H. Meyer, R. J. Stockert, T. Poralla, G. Gerken, *J. Gen. Virol.* **1994**, *75*, 3021 – 3029.
[33] K. Kuroki, R. Cheung, P. L. Marion, D. Ganem, *J. Virol.* **1994**, *68*, 2091 – 2096.
[34] J. A. Bibb, G. Witherell, G. Bernhardt, E. Wimmer, *Virol.* **1994**, *201*, 107 – 115.
[35] M. Gromeier, H. H. Lu, G. Bernhardt, J. J. Harber, J. A. Bibb, E. Wimmer, *Ann. N. Y. Acad. Sci.* **1995**, *753*, 19 – 36.
[36] M. J. Bouchard, V. R. Racaniello, *J. Virol.* **1997**, *71*, 2793 – 2798.
[37] K. S. Au, N. M. Mattion, M. K. Estes, *Virology* **1993**, *194*, 665 – 673.
[38] P. W. Mason, E. Rieder, B. Baxt, *Proc. Natl. Acad. Sci. USA* **1994**, *91*, 1932 – 1936.
[39] R. Zhao, D. C. Pevear, M. J. Kremer, V. L. Giranda, J. A. Kofron, R. J. Kuhn, M. G. Rossmann, *Structure* **1996**, *4*, 1205 – 1220.
[40] N. H. Olson, P. R. Kolatkar, M. A. Oliveira, R. H. Cheng, J. M. Greve, A. McClelland, T. S. Baker, M. G. Rossmann, *Proc. Natl. Acad. Sci. USA* **1993**, *90*, 507 – 511.
[41] D. G. Scraba, *J. Struct. Biol.* **1990**, *104*, 52 – 62.
[42] S. A. Huber, *J. Virol.* **1994**, *68*, 3453 – 3458.
[43] M. D. Rolsma, H. B. Gelberg, M. S. Kuhlenschmidt, *J. Virol.* **1994**, *68*, 258 – 268.
[44] A. H. Choi, *Virology* **1994**, *200*, 301 – 306.
[45] J. E. Strong, D. Tang, P. W. K. Lee, *Virology* **1993**, *197*, 405 – 411.
[46] D. Tang, J. E. Strong, P. W. K. Lee, *Virology* **1993**, *197*, 412 – 414.
[47] F. Superti, G. Donelli, *J. Med. Virol.* **1995**, *47*, 421 – 428.
[48] E. Mendez, C. F. Arias, S. Lopez, *J. Virol.* **1996**, *70*, 1218 – 1222.
[49] J. M. Wahlberg, H. Garoff, *J. Cell Biol.* **1992**, *116*, 339 – 348.
[50] M. Suomalainen, H. Garoff, *J. Gen. Virol.* **1992**, *66*, 5106 – 5109.
[51] D. L. Huso, O. Narayan, G. W. Hart, *J. Virol.* **1988**, *62*, 1974 – 1980.
[52] K. S. Faaberg, G. A. Palmer, C. Even, G. W. Anderson, P. G. Plagemann, *Virus Res.* **1995**, *39*, 331 – 340.
[53] C. Even, R. R. Rowland, P. G. Plagemann, *Virus Res.* **1995**, *39*, 355 – 364.
[54] M. Carleton, H. Lee, M. Mulvey, D. T. Brown, *J. Virol.* **1997**, *71*, 1558 – 1566.
[55] K. S. Wang, R. J. Kuhn, E. G. Strauss, S. Ou, J. H. Strauss, *J. Virol.* **1992**, *66*, 4992 – 5001.
[56] J. A. Maassen, C. Terhorst, *Eur. J. Biochem.* **1981**, *115*, 153 – 158.
[57] P. Mastromarino, L. Cioe, S. Rieti, N. Orsi, *Med. Microbiol. Immunol.* **1990**, *179*, 105 – 114.
[58] P. Mastromarino, C. Conti, P. Goldoni, B. Hauttecoeur, N. Orsi, *J. Gen. Virol.* **1987**, *68*, 2359 – 2369.
[59] P. Bullough, F. Hughson, J. J. Skehel, D. C. Wiley, *Nature* **1994**, *371*, 37 – 43.
[60] S. J. Watowich, J. J. Skehel, D. C. Wiley, *Structure* **1994**, *2*, 719 – 731.
[61] M. N. Matrosovich, A. S. Gambaryan, A. B. Tuzikov, N. E. Byramova, L. V. Mochalova, A. A. Golbraikh, M. D. Shenderovich, J. Finne, N. V. Bovin, *Virology* **1993**, *196*, 111 – 121.
[62] I. Gunther, B. Glatthaar, G. Doller, W. Garten, *Virus Res.* **1993**, *27*, 147 – 160.
[63] W. Fitz, P. B. Rosenthal, C. H. Wong, *Bioorg. Med. Chem. Lett.* **1996**, *4*, 1349 – 1353.
[64] S. Bagai, D. P. Sarkar, *Biochim. Biophys. Acta* **1993**, *1152*, 15 – 25.
[65] C. M. Sanderson, H. H. Wu, D. P. Nayak, *J. Virol.* **1994**, *68*, 69 – 76.
[66] R. M. Epand, S. Nir, M. Parolin, T. D. Flanagan, *Biochemistry* **1995**, *34*, 1084 – 1089.
[67] R. Heckert, J. Riva, S. Cook, J. McMillen, R. D. Schwartz, *Avian Dis.* **1996**, *40*, 770 – 777.
[68] A. Chiba, K. Matsumura, H. Yamada, T. Inazu, T. Shimizu, S. Kusunoki, I. Kanazawa, A. Kobata, T. Endo, *J. Biol. Chem.* **1997**, *272*, 2156 – 2162.
[69] D. Naniche, T. F. Wild, C. C. Rabourdin, D. Gerlier, *J. Gen. Virol.* **1993**, *74*, 1073 – 1091.
[70] D. Naniche, G. Varior-Krishnan, F. Cervoni, T. F. Wild, B. Rossi, C. Rabourdin-Combe, D. Gerlier, *J. Virol.* **1993**, *67*, 6025 – 6032.
[71] J. Li, R. Ling, J. S. Randhawa, K. Shaw, P. J. Davis, K. Juhasz, C. R. Pringle, A. J. Easton, D. Cavanagh, *Virus Res.* **1996**, *41*, 185 – 191.
[72] C. Krempl, B. Schultze, G. Herrler, *Adv. Exp. Med. Biol.* **1995**, *380*, 371 – 374.

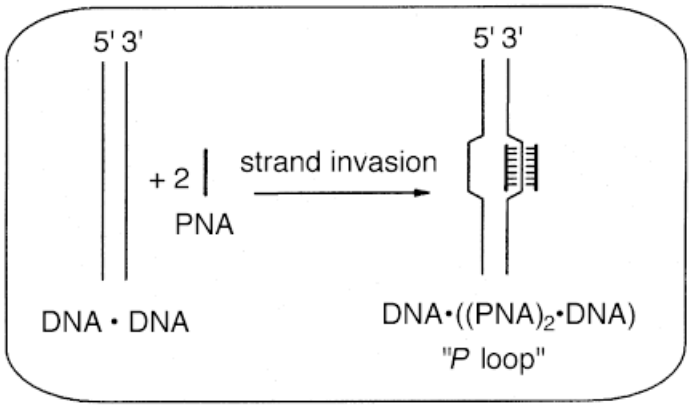
[73] R. L. Thimmig, J. V. Hughes, R. J. Kinders, A. G. Milenkovic, T. C. Johnson, *J. Gen. Virol.* **1980**, *50*, 279 – 291.
[74] J. M. Coll, *Arch. Virol.* **1995**, *140*, 827 – 851.
[75] T. L. Lentz, *J. Gen. Virol.* **1990**, *71*, 751 – 766.
[76] F. P. Hanssens, H. J. Nauwynck, M. B. Pensaert, *J. Virol.* **1993**, *67*, 4492 – 4496.
[77] R. A. Weiss, C. S. Tailor, *Cell* **1995**, *82*, 531 – 533.
[78] J. Gavalchin, N. Fan, M. J. Lane, L. Papsidero, B. J. Poiesz, *Virology* **1993**, *194*, 1 – 9.
[79] N. Hiraiwa, M. Hiraiwa, R. Kannagi, *Biochem. Biophys. Res. Commun.* **1997**, *231*, 183 – 186.
[80] G. M. Crooks, D. B. Kohn, *Blood* **1993**, *82*, 3290 – 3297.
[81] L. Connolly, K. Zingler, J. A. T. Young, *J. Virol.* **1994**, *68*, 2760 – 2764.
[82] P. Bates, J. A. Young, H. E. Varmus, *Cell* **1993**, *74*, 1043 – 1051.
[83] J. Choppin, D. L. Schaffar, P. Debre, J. P. Levy, *J. Immunol.* **1981**, *126*, 2347 – 2351.
[84] D. Kabat, *Virology* **1989**, *171*, 467 – 474.
[85] H. Wang, M. P. Kavanaugh, R. A. North, D. Kabat, *Nature* **1991**, *352*, 729 – 731.
[86] D. Ott, A. Rein, *J. Virol.* **1992**, *66*, 4632 – 4638.
[87] J. A. Smythe, B. Nardelli, P. Chatterjee, R. C. Gallo, J. M. Gershoni, *Protein Eng.* **1994**, *7*, 145 – 147.
[88] P. M. Cereda, G. Palu, M. Rassu, M. Toni, W. Malwood, M. Dettin, B. C. Di, *Antiviral Chem. Chemother.* **1991**, *2*, 157 – 161.
[89] T. N. Wells, A. E. Proudfoot, C. A. Power, M. Marsh, *Chem. Biol.* **1996**, *3*, 603 – 609.
[90] P. R. Clapham, A. McKnight, R. A. Weiss, *J. Virol.* **1992**, *66*, 3531 – 3537.
[91] L. Marcon, H. Choe, K. A. Martin, M. Farzan, P. D. Ponath, L. Wu, W. Newman, N. Gerard, C. Gerard, J. Sodroski, *J. Virol.* **1997**, *71*, 2522 – 2527.
[92] A. Angulo, A. Alcami, E. Vinuela, *Arch. Virol. Suppl.* **1993**, *7*, 169 – 183.
[93] M. V. Borca, P. Irusta, C. Carrillo, C. L. Afonso, T. Burrage, D. L. Rock, *Virology* **1994**, *201*, 413 – 418.
[94] I. Connell, W. Agace, P. Klemm, M. Schembri, S. Marild, C. Svanborg, *Proc. Natl. Acad. Sci. USA* **1996**, *93*, 9827 – 9832.
[95] B. Westerlund, T. K. Korhonen, *Mol. Microbiol.* **1993**, *9*, 687 – 694.
[96] N. Stromberg, T. Boren, *Infect. Immun.* **1992**, *60*, 3268 – 3277.
[97] N. Stromberg, T. Boren, A. Carlen, J. Olsson, *Infect. Immun.* **1992**, *60*, 3278 – 3286.
[98] P. Sepulveda, J. L. Lopez, D. Gozalbo, A. Cervera, J. P. Martinez, W. L. Chaffin, *Infect. Immun.* **1996**, *64*, 4406 – 4408.
[99] F. D. Tosh, L. J. Douglas, *Infect. Immun.* **1992**, *60*, 4734 – 4739.
[100] C. Kuo, N. Takahashi, A. F. Swanson, Y. Ozeki, S. Hakomori, *J. Clin. Invest.* **1996**, *98*, 2813 – 2818.
[101] F. Qadri, A. Haque, S. M. Faruque, K. A. Bettelheim, R. Robins-Browne, M. J. Albert, *J. Clin. Microbiol.* **1994**, *32*, 510 – 514.
[102] M. J. Kuehn, J. Heuser, S. Normark, S. J. Hultgren, *Nature* **1992**, *356*, 252 – 255.
[103] X. R. Wu, T. T. Sun, J. J. Medina, *Proc. Natl. Acad. Sci. USA* **1996**, *93*, 9630 – 9635.
[104] H. Schroten, F. G. Hanisch, R. Plogmann, J. Hacker, G. Uhlenbruck, R. Nobis-Bosch, V. Wahn, *Infect. Immun.* **1992**, *60*, 2893 – 2899.
[105] F. G. Hanisch, J. Hacker, H. Schroten, *Infect. Immun.* **1993**, *61*, 2108 – 2115.
[106] T. Boren, P. Falk, K. A. Roth, G. Larson, S. Normark, *Science* **1993**, *262*, 1892 – 1895.
[107] S. Hirmo, S. Kelm, R. Schauer, B. Nilsson, T. Wadstrom, *Glycoconjugate J.* **1996**, *13*, 1005 – 1011.
[108] P. M. Simon, P. L. Goode, A. Mobasseri, D. Zopf, *Infect. Immun.* **1997**, *65*, 750 – 757.
[109] G. Franzoso, P. C. Hu, G. A. Meloni, M. F. Barile, *Infect. Immun.* **1993**, *61*, 1523 – 1530.
[110] T. Feizi, *Trends Biochem. Sci.* **1994**, *19*, 233 – 234.
[111] T. Feizi, *Clin. Infect. Dis.* **1993**, *17*, 63 – 65.
[112] K. Sachse, H. Pfutzner, M. Heller, I. Hanel, *Vet. Microbiol.* **1993**, *36*, 307 – 316.
[113] E. Stimson, M. Virji, K. Makepeace, A. Dell, H. R. Morris, G. Payne, J. R. Saunders, M. P. Jennings, S. Barker, M. Panico, *Mol. Microbiol.* **1995**, *17*, 1201 – 1214.
[114] M. Virji, K. Makepeace, D. J. Ferguson, S. M. Watt, *Mol. Microbiol.* **1996**, *22*, 941 – 950.
[115] M. W. Raza, C. C. Blackwell, M. M. Ogilvie, A. T. Saadi, J. Stewart, R. A. Elton, *FEMS Immunol. Med. Microbiol.* **1994**, *10*, 25 – 30.
[116] Y. Murakami, S. Hanazawa, K. Nishida, H. Iwasaka, S. Kitano, *Biochem. Biophys. Res. Commun.* **1993**, *192*, 826 – 832.
[117] H. B. Sheth, K. K. Lee, W. Y. Wong, G. Srivastava, O. Hindsgaul, R. S. Hodges, W. Paranchych, R. T. Irvin, *Mol. Microbiol.* **1994**, *11*, 715 – 723.
[118] C. Carnoy, R. Ramphal, A. Scharfman, J. M. Lo-Guidice, N. Houdret, A. Klein, C. Galabert, G. Lamblin, P. Roussel, *Am. J. Respir. Cell. Mol. Biol.* **1993**, *9*, 323 – 334.
[119] I. J. Rosenstein, C. T. Yuen, M. S. Stoll, T. Feizi, *Infect. Immun.* **1992**, *60*, 5078 – 5084.
[120] J. P. Wisniewski, M. Monsigny, F. M. Delmotte, *Biochimie* **1994**, *76*, 121 – 128.
[121] J. Beuth, H. L. Ko, L. Tunggal, G. Pulverer, *Dtsch. Med. Wochenschr.* **1992**, *117*, 687 – 691.
[122] S. Haataja, K. Tikkanen, J. Liukkonen, C. Francois-Gerard, J. Finne, *J. Biol. Chem.* **1993**, *268*, 4311 – 4317.
[123] J. Liukkonen, S. Haataja, K. Tikkanen, S. Kelm, J. Finne, *J. Biol. Chem.* **1992**, *267*, 21 105 – 21 111.
[124] K. Hong, T. Harada, T. Nishimura, K. Inoue, *Immunology* **1993**, *80*, 640 – 644.
[125] P. A. Murray, A. Prakobphol, T. Lee, C. I. Hoover, S. J. Fisher, *Infect. Immun.* **1992**, *60*, 31 – 38.
[126] M. Mantle, S. D. Husar, *Infect. Immun.* **1993**, *61*, 2340 – 2346.
[127] K. Bock, K.-A. Karlsson, N. Stromberg, S. Teneberg, *Adv. Exp. Med. Biol.* **1988**, *228*, 153 – 186.
[128] M. J. Farthing, *Trans. R. Soc. Trop. Med. Hyg.* **1985**, *79*, 569 – 576.
[129] K.-A. Karlsson, *Annu. Rev. Biochem.* **1989**, *58*, 309 – 350.
[130] K. K. Lee, H. B. Sheth, W. Y. Wong, R. Sherburne, W. Paranchych, R. S. Hodges, C. A. Lingwood, H. Krivan, R. T. Irvin, *Mol. Microbiol.* **1994**, *11*, 705 – 713.
[131] T. Masuzawa, R. Suzuki, Y. Yanagihara, *Microbiol. Immunol.* **1991**, *35*, 199 – 208.
[132] N. V. Prasadarao, C. A. Wass, J. Hacker, K. Jann, K. S. Kim, *J. Biol. Chem.* **1993**, *268*, 10 356 – 10 363.
[133] L. Saiman, A. Prince, *J. Clin. Invest.* **1993**, *92*, 1875 – 1880.
[134] V. Annaix, J. P. Bouchara, G. Larcher, D. Chabasse, G. Tronchin, *Infect. Immun.* **1992**, *60*, 1747 – 1755.
[135] J. Coburn, J. M. Leong, J. K. Erban, *Proc. Natl. Acad. Sci. USA* **1993**, *90*, 7059 – 7063.
[136] E. Leininger, C. A. Ewanowich, A. Bhargava, M. S. Peppler, J. G. Kenimer, M. J. Brennan, *Infect. Immun.* **1992**, *60*, 2380 – 2385.
[137] A. R. Holmes, R. McNab, H. F. Jenkinson, *Infect. Immun.* **1996**, *64*, 4680 – 4685.
[138] H. Kobayashi, N. Shibata, S. Suzuki, *Infect. Immun.* **1992**, *60*, 2106 – 2109.
[139] N. Shibata, K. Hisamichi, T. Kikuchi, H. Kobayashi, Y. Okawa, S. Suzuki, *Biochemistry* **1992**, *31*, 5680 – 5686.
[140] K. Shibata, T. Mita, H. Nakamura, K. Yamashiro, S. Gotoh, K. Hiranuma, K. Higashi, H. Hirano, *Biochimie* **1993**, *75*, 459 – 465.
[141] H. Su, L. Raymond, D. D. Rockey, E. Fischer, T. Hackstadt, H. D. Caldwell, *Proc. Natl. Acad. Sci. USA* **1996**, *93*, 11 143 – 11 148.
[142] J. P. Zhang, R. S. Stephens, *Cell* **1992**, *69*, 861 – 869.
[143] J. C. Chen, J. P. Zhang, R. S. Stephens, *J. Biol. Chem.* **1996**, *271*, 11 134 – 11 140.
[144] C. Pascu, W. Hryniewicz, T. Wadstrom, T. W. Zareba, *Curr. Microbiol.* **1997**, *34*, 6 – 11.
[145] R. Virkola, J. Parkkinen, J. Hacker, T. K. Korhonen, *Infect. Immun.* **1993**, *61*, 4480 – 4484.
[146] J. W. St. Geme III, S. Falkow, S. J. Barenkamp, *Proc. Natl. Acad. Sci. USA* **1993**, *90*, 2875 – 2879.
[147] B. A. Butcher, L. A. Sklar, L. C. Seamer, R. H. Glew, *J. Immunol.* **1992**, *148*, 2879 – 2886.
[148] P. Valentin-Weigand, S. R. Talay, K. N. Timmis, G. S. Chhatwal, *Int. J. Med. Microbiol. Virol. Parasit. Infect. Dis.* **1993**, *278*, 238 – 245.
[149] P. Valentin-Weigand, K. M. Moriarty, *Res. Microbiol.* **1992**, *143*, 75 – 79.
[150] P. Peake, A. Gooley, W. J. Britton, *Infect. Immun.* **1993**, *61*, 4828 – 4834.
[151] S. P. Rao, K. R. Gehlsen, A. Catanzaro, *Infect. Immun.* **1992**, *60*, 3652 – 3657.

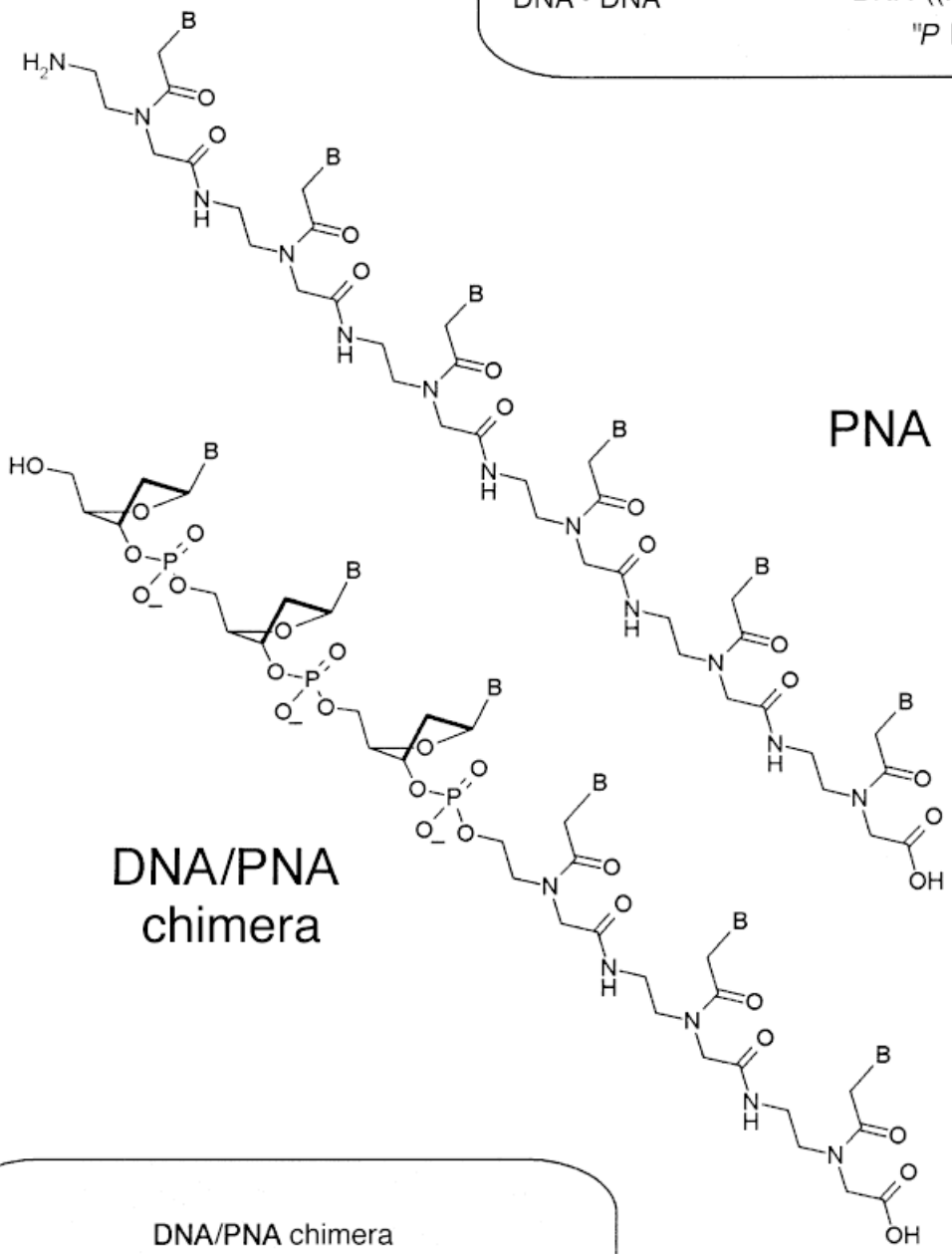
[152] K. R. Alugupalli, S. Kalfas, S. Edwardsson, A. Forsgren, R. R. Arnold, A. S. Naidu, *Oral Microbiol. Immunol.* **1994**, *9*, 174 – 179.
[153] S. K. Collinson, P. C. Doig, J. L. Doran, S. Clouthier, T. J. Trust, W. W. Kay, *J. Bacteriol.* **1993**, *175*, 12 – 18.
[154] S. Huff, Y. V. Matsuka, M. J. Mcgavin, K. C. Ingham, *J. Biol. Chem.* **1994**, *269*, 15563 – 15570.
[155] B. Rozalska, T. Wadstrom, *Scand. J. Immunol.* **1993**, *37*, 575 – 580.
[156] M. J. McGavin, S. Gurusiddappa, P. E. Lindgren, M. Lindberg, G. Raucci, M. Hook, *J. Biol. Chem.* **1993**, *268*, 23946 – 23953.
[157] M. H. McGavin, D. Krajewska-Pietrasik, C. Ryden, M. Hook, *Infect. Immun.* **1993**, *61*, 2479 – 2485.
[158] J. M. Patti, J. O. Boles, M. Hook, *Biochemistry* **1993**, *32*, 11428 – 11435.
[159] L. M. Switalski, W. G. Butcher, P. C. Caufield, M. S. Lantz, *Infect. Immun.* **1993**, *61*, 4119 – 4125.
[160] L. M. Switalski, J. M. Patti, W. Butcher, A. G. Gristina, P. Speziale, M. Hook, *Mol. Microbiol.* **1993**, *7*, 99 – 107.
[161] S. Bozzini, L. Visai, P. Pignatti, T. E. Petersen, P. Speziale, *Eur. J. Biochem.* **1992**, *207*, 327 – 333.
[162] J. M. Patti, H. Jonsson, B. Guss, L. M. Switalski, K. Wiberg, M. Lindberg, M. Hook, *J. Biol. Chem.* **1992**, *267*, 4766 – 4772.
[163] P. Ciborowski, J. I. Flock, T. Wadstrom, *J. Med. Microbiol.* **1992**, *37*, 376 – 381.
[164] D. Mcdevitt, P. Francois, P. Vaudaux, T. J. Foster, *Mol. Microbiol.* **1994**, *11*, 237 – 248.
[165] C. R. Carneiro, E. Postol, C. Boilesen, R. R. Brentani, *Braz. J. Med. Biol. Res.* **1993**, *26*, 689 – 697.
[166] J. D. Lopes, M. dos Reis, R. R. Brentani, *Science* **1985**, *229*, 275 – 277.
[167] O. D. Liang, M. Maccarana, J. I. Flock, M. Paulsson, K. T. Preissner, T. Wadstrom, *Biochim. Biophys. Acta* **1993**, *1225*, 57 – 63.
[168] L. G. Milagres, C. E. Melles, *Rev. Inst. Med. Trop. Sao Paulo* **1992**, *34*, 315 – 321.
[169] H. S. Courtney, C. von Hunolstein, J. B. Dale, M. S. Bronze, E. H. Beachey, D. L. Hasty, *Microb. Pathog.* **1992**, *12*, 199 – 208.
[170] J. B. Dale, R. W. Baird, H. S. Courtney, D. L. Hasty, M. S. Bronze, *J. Infect. Dis.* **1994**, *169*, 319 – 323.
[171] E. Hanski, P. A. Horwitz, M. G. Caparon, *Infect. Immun.* **1992**, *60*, 5119 – 5125.
[172] E. Hanski, M. Caparon, *Proc. Natl. Acad. Sci. USA* **1992**, *89*, 6172 – 6176.
[173] A. Berge, U. Sjobring, *J. Biol. Chem.* **1993**, *268*, 25417 – 25424.
[174] K. H. Schmidt, K. Mann, J. Cooney, W. Kohler, *FEMS Immunol. Med. Microbiol.* **1993**, *7*, 135 – 143.
[175] R. Poon-King, J. Bannan, A. Viteri, G. Cu, J. B. Zabriskie, *J. Exp. Med.* **1993**, *178*, 759 – 763.
[176] C. Von Hunolstein, M. L. Ricci, G. Orefici, *J. Med. Microbiol.* **1993**, *39*, 53 – 57.
[177] R. C. Tart, I. van de Rijn, *Infect. Immun.* **1993**, *61*, 4994 – 5000.
[178] M. Kostrzynska, T. Wadstrom, *Int. J. Med. Microbiol. Virol. Parasit. Infect. Dis.* **1992**, *277*, 80 – 83.
[179] G. C. Fogg, C. M. Gibson, M. G. Caparon, *Mol. Microbiol.* **1994**, *11*, 671 – 684.
[180] S. R. Talay, P. Valentin-Weigand, P. G. Jerlstrom, K. N. Timmis, G. S. Chhatwal, *Infect. Immun.* **1992**, *60*, 3837 – 3844.
[181] B. D. Winters, N. Ramasubbu, M. W. Stinson, *Infect. Immun.* **1993**, *61*, 3259 – 3264.
[182] J. R. Wang, M. W. Stinson, *Infect. Immun.* **1994**, *62*, 442 – 448.
[183] R. Watanabe-Ohnishi, J. Aelion, L. LeGros, M. A. Tomai, E. V. Sokurenko, D. Newton, J. Takahara, S. Irino, S. Rashed, M. Kotb, *J. Immunol.* **1994**, *152*, 2066 – 2073.
[184] S. Sela, A. Aviv, A. Tovi, I. Burstein, M. G. Caparon, E. Hanski, *Mol. Microbiol.* **1993**, *10*, 1049 – 1055.
[185] C. V. Hughes, R. N. Andersen, P. E. Kolenbrander, *Infect. Immun.* **1992**, *60*, 1178 – 1186.
[186] H. Schulze-Koops, H. Burkhardt, J. Heesemann, T. Kirsch, B. Swoboda, C. Bull, S. Goodman, F. Emmrich, *Infect. Immun.* **1993**, *61*, 2513 – 2519.
[187] J. B. Bliska, M. C. Copass, S. Falkow, *Infect. Immun.* **1993**, *61*, 3914 – 3921.
[188] A. Varki, *J. Clin. Invest.* **1997**, *99*, 158 – 162.
[189] J. B. Lowe, P. A. Ward, *J. Clin. Invest.* **1997**, *99*, 822 – 826.
[190] M. A. Gimbrone, T. Nagel, J. N. Topper, *J. Clin. Invest.* **1997**, *99*, 2062 – 2070.
[191] L. L. Kiessling, N. L. Pohl, *Chem. Biol.* **1996**, *3*, 71 – 77.
[192] S. M. Albelda, C. W. Smith, P. A. Ward, *FASEB J.* **1994**, *8*, 504 – 512.
[193] S. D. Rossen, C. R. Bertozzi, *Curr. Opin. Cell Biol.* **1994**, *6*, 663 – 673.
[194] W. Spevak, C. Foxall, D. H. Charych, F. Dasgupta, J. O. Nagy, *J. Med. Chem.* **1996**, *39*, 1018 – 1020.
[195] L. A. Lasky, *Annu. Rev. Physiol.* **1995**, *57*, 827 – 872.
[196] S. A. DeFrees, F. C. A. Gaeta, Y. C. Lin, Y. Ichikawa, C.-H. Wong, *J. Am. Chem. Soc.* **1993**, *115*, 7549 – 7550.
[197] G. Kadmon, B. Imhof, P. Altevogt, M. Schachner, *Biochem. Biophys. Res. Commun.* **1995**, *214*, 94 – 101.
[198] L. Shapiro, A. M. Fannon, P. D. Kwong, A. Thompson, M. S. Lehmann, G. Gruebel, J. Legrand, J. Als-Nielsen, D. R. Colman, W. A. Hendrickson, *Nature* **1995**, *374*, 327 – 337.
[199] J. McCluskey, L. F. Boyd, P. F. Highet, J. Inman, D. H. Margulies, *J. Immunol.* **1988**, *141*, 1451 – 1455.
[200] M. D. Kazatchkine, D. T. Fearon, *Immunodeficiency* **1990**, *2*, 17 – 41.
[201] P. P. Firpo, I. Axberg, M. Scheibel, E. A. Clark, *AIDS Res. Hum. Retroviruses* **1992**, *8*, 357 – 366.
[202] S. A. Santoro, L. W. Cunningham, *J. Clin. Invest.* **1977**, *60*, 1054 – 1060.
[203] M. Kamiyama, Y. S. Arkel, K. Chen, K. Shido, *J. Lab. Clin. Med.* **1991**, *117*, 209 – 217.
[204] B. D. Shur, *Curr. Opin. Cell Biol.* **1993**, *5*, 854 – 863.
[205] R. T. Lee, Y. C. Lee, *Neoglycoconjugates: Preparation and Applications* (Eds: Y. C. Lee, R. T. Lee), Academic Press, San Diego, **1994**, pp. 23 – 50.
[206] Y. Lee, R. Lee, *Acc. Chem. Res.* **1995**, *28*, 321 – 327.
[207] N. J. Dimmock, *Trends Biochem. Sci.* **1987**, *12*, 70 – 74.
[208] N. W. Boyce, S. R. Holdsworth, *Kidney Int.* **1989**, *36*, 537 – 544.
[209] S. K. Dower, C. DeLisi, J. A. Titus, D. M. Segal, *Biochemistry* **1981**, *20*, 6326 – 6334.
[210] W. Engelhardt, H. Gorczytza, A. Butterweck, H. Moenkemann, J. Frey, *Eur. J. Immunol.* **1991**, *21*, 2227 – 2238.
[211] Z. K. Indik, J. G. Park, S. Hunter, A. D. Schreiber, *Blood* **1995**, *86*, 4389 – 4399.
[212] K. A. Karlsson, *Trends Biochem. Sci.* **1991**, *12*, 265 – 272.
[213] K.-A. Karlsson, *Curr. Opin. Struct. Biol.* **1995**, *5*, 622 – 635.
[214] B. Goins, E. Freire, *Biochemistry* **1988**, *27*, 2046 – 2052.
[215] V. Bhakuni, D. Xie, E. Freire, *Biochemistry* **1991**, *30*, 5055 – 5060.
[216] S. Kabir, *J. Med. Microbiol.* **1987**, *23*, 9 – 18.
[217] A. Abe, K. Komase, A. Bangtrakulnonth, O. A. Ratchtrachenchat, K. Kawahara, H. Danbara, *J. Clin. Microbiol.* **1990**, *28*, 2616 – 2620.
[218] L. Paoletti, M. R. Wessels, A. K. Rodewald, A. A. Shroff, H. J. Jennings, D. L. Kasper, *Infect. Immun.* **1994**, *62*, 3236 – 3243.
[219] C. Montecucco, E. Papini, G. Schiavo, *Experientia* **1996**, *52*, 1026 – 1032.
[220] C. C. Blackwell, A. T. Saadi, M. W. Raza, J. Stewart, D. M. Weir, *J. Clin. Pathol.* **1992**, *45*, 20 – 24.
[221] M. J. H. M. Wolfhagen, R. Torensma, A. C. Fluit, C. J. M. Aarsman, M. Jansze, J. Verhoef, *Toxicon* **1994**, *32*, 129 – 132.
[222] G. D. Armstrong, E. Fodor, R. Vanmaele, *J. Infect. Dis.* **1991**, *164*, 1160 – 1167.
[223] J. M. Richardson, P. D. Evans, S. W. Homans, A. Donohue-Rolfe, *Nature Struct. Biol.* **1997**, *4*, 190 – 193.
[224] L. D. Heerze, G. D. Armstrong, *Biochem. Biophys. Res. Commun.* **1990**, *172*, 1224 – 1229.
[225] P. E. Stein, A. Boodhoo, G. D. Armstrong, L. D. Heerze, S. A. Cockle, M. H. Klein, R. J. Read, *Nature Struct. Biol.* **1994**, *1*, 591 – 596.
[226] M. Dembo, B. Goldstein, A. K. Sobotka, L. M. Lichtenstein, *J. Immunol.* **1979**, *123*, 1864 – 1872.
[227] M. Dembo, B. Goldstein, A. K. Sobotka, L. M. Lichtenstein, *J. Immunol.* **1978**, *121*, 354 – 358.
[228] M. Dembo, B. Goldstein, *J. Immunol.* **1978**, *121*, 345 – 353.
[229] P. Kane, J. Erickson, C. Fewtrell, B. Baird, D. Holowka, *Mol. Immunol.* **1986**, *23*, 783 – 790.
[230] D. M. Sigal, J. D. Taurog, H. Metzger, *Proc. Natl. Acad. Sci. USA* **1977**, *74*, 2993 – 2995.
[231] M. W. Pantoliano, R. A. Horlick, B. A. Springer, D. D. E. Van, T. Tobery, D. R. Wetmore, J. D. Lear, A. T. Nahapetian, J. D. Bradley, W. P. Sisk, *Biochemistry* **1994**, *33*, 10229 – 10248.

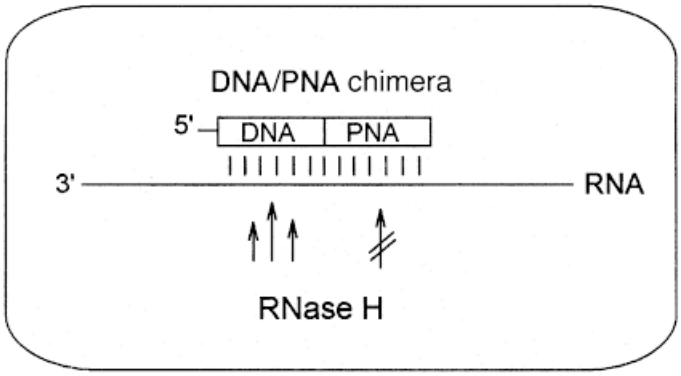
[232] M. A. Lemmon, J. Schlessinger, *Trends Biochem. Sci.* **1994**, *19*, 459 – 463.
[233] T. F. Deuel, *Annu. Rev. Cell Biol.* **1987**, *3*, 443 – 492.
[234] H. Geyer, K. Himmelspach, B. Kwiatkowski, S. Schlecht, S. Stirm, *Pure Appl. Chem.* **1983**, *55*, 637 – 653.
[235] H. Q. Miao, D. M. Ornitz, E. Aingorn, S. A. Bensasson, I. Vlodavsky, *J. Clin. Invest.* **1997**, *99*, 1565 – 1575.
[236] M. A. Lemmon, Z. M. Bu, J. E. Ladbury, M. Zhou, D. Pinchasi, I. Lax, D. M. Engelman, J. Schlessinger, *EMBO J.* **1997**, *16*, 281 – 294.
[237] M. A. Lemmon, D. Pinchasi, M. Zhou, I. Lax, J. Schlessinger, *J. Biol. Chem.* **1997**, *272*, 6311 – 6317.
[238] O. Letourneur, J. F. Goetschy, M. Horisberger, M. G. Grutter, *Biochem. Biophys. Res. Commun.* **1996**, *224*, 709 – 716.
[239] D. L. Hynds, M. Summers, J. Vanbrocklyn, M. S. Odorisio, A. J. Yates, *J. Neurochem.* **1995**, *65*, 2251 – 2258.
[240] M. Mellado, J. M. Rodriguezfrade, L. Kremer, C. Vonkobbe, A. M. Deana, I. Merida, C. Martineza, *J. Biol. Chem.* **1997**, *272*, 9189 – 9196.
[241] J. A. Wells, *Proc. Natl. Acad. Sci. USA* **1996**, *93*, 1 – 6.
[242] M. Sundstrom, T. Lundqvist, J. Rodin, L. B. Giebel, D. Milligan, G. Norstedt, *J. Biol. Chem.* **1996**, *271*, 32197 – 32203.
[243] T. F. Zioncheck, L. Richardson, J. Liu, L. Chang, K. L. King, G. L. Bennett, P. Fugedi, S. M. Chamow, R. H. Schwall, R. J. Stack, *J. Biol. Chem.* **1995**, *270*, 16871 – 16878.
[244] O. Livnah, E. A. Stura, D. L. Johnson, S. A. Middleton, L. S. Mulcahy, N. C. Wrighton, W. J. Dower, L. K. Jolliffe, I. A. Wilson, *Science* **1996**, *273*, 464 – 471.
[245] B. Barleon, F. Totzke, C. Herzog, S. Blanke, E. Kremmer, G. Siemeister, D. Marme, G. Martinybaron, *J. Biol. Chem.* **1997**, *272*, 10382 – 10388.
[246] W. Somers, M. Stahl, J. S. Seehra, *EMBO J.* **1997**, *16*, 989 – 997.
[247] A. Duschl, W. Sebald, *Eur. Cytokine Network* **1996**, *7*, 37 – 49.
[248] K. Koths, *Mol. Reprod. Dev.* **1997**, *46*, 31 – 38.
[249] A. Gertler, J. Grosclaude, C. J. Strasburger, S. Nir, J. Djiane, *J. Biol. Chem.* **1996**, *271*, 24482 – 24491.
[250] T. Horan, J. Wen, L. Narhi, V. Parker, A. Garcia, T. Arakawa, J. Philo, *Biochemistry* **1996**, *35*, 4886 – 4896.
[251] B. G. Barisas, S. J. Singer, J. M. Sturtevant, *Immunochemistry* **1977**, *14*, 247 – 252.
[252] R. Maggio, P. Barbier, F. Fornai, G. U. Corsini, *J. Biol. Chem.* **1996**, *271*, 31055 – 31060.
[253] X. Gong, D. H. Dubois, D. J. Miller, B. D. Shur, *Science* **1995**, *269*, 1718 – 1721.
[254] E. Baba, M. Nakamura, Y. Tanaka, M. Kuroki, Y. Itoyama, S. Nakano, Y. Niho, *J. Immunol.* **1993**, *151*, 1013 – 1024.
[255] V. C. Gibbs, M. Takahashi, M. Aguet, A. Chuntharapai, *J. Biol. Chem.* **1996**, *271*, 28710 – 28716.
[256] J. A. L. Greene, G. M. Leytze, J. Emswiler, R. Peach, J. Bajorath, W. Cosand, P. S. Linsley, *J. Biol. Chem.* **1996**, *271*, 26762 – 26771.
[257] M. G. Surette, J. B. Stock, *J. Biol. Chem.* **1996**, *271*, 17966 – 17973.
[258] H. Chen, M. L. Privalsky, *Proc. Natl. Acad. Sci. USA* **1995**, *92*, 422 – 426.
[259] B. C. Cunningham, M. Ultsch, A. M. De Vos, M. G. Mulkerrin, K. R. Clausner, J. A. Wells, *Science* **1991**, *254*, 821 – 825.
[260] N. Jones, *Cell* **1990**, *61*, 9 – 11.
[261] R. P. Lawther, G. W. Hatfield, *Proc. Natl. Acad. Sci. USA* **1980**, *77*, 1862 – 1866.
[262] T. E. Ellenberger, C. J. Brandl, K. Struhl, S. C. Harrison, *Cell* **1992**, *71*, 1223 – 1237.
[263] N. Benson, C. Adams, P. Youderian, *Mol. Microbiol.* **1994**, *11*, 567 – 579.
[264] R. Li, M. R. Botchan, *Cell* **1993**, *73*, 1207 – 1221.
[265] J. A. Ladias, *J. Biol. Chem.* **1994**, *269*, 5944 – 5951.
[266] B. J. Cheskis, S. Karathanasis, C. R. Lyttle, *J. Biol. Chem.* **1997**, *272*, 11384 – 11391.
[267] Y. Nomura, T. Nagaya, H. Tsukaguchi, J. Takamatsu, H. Seo, *Endocrinology* **1996**, *137*, 4082 – 4086.
[268] R. C. Hoffman, S. J. Horvath, R. E. Klevit, *Protein Sci.* **1993**, *2*, 951 – 965.
[269] A. C. Jamieson, H. Wang, S. H. Kim, *Proc. Natl. Acad. Sci. USA* **1996**, *93*, 12834 – 12839.
[270] K. A. Connors, *Binding Constants: The Measurement of Molecular Complex Stability*, Wiley, New York, **1987**.
[271] D. E. Koshland, K. Neet, *Annu. Rev. Biochem.* **1968**, *37*, 359 – 410.
[272] B. Perlmutter-Hayman, *Acc. Chem. Res.* **1986**, *19*, 90 – 96.
[273] E. N. Kaufman, R. K. Jain, *Cancer Res.* **1992**, *52*, 4157 – 4167.
[274] A. Schoen, E. Freire, *Biochemistry* **1989**, *28*, 5019 – 5024.
[275] For an Nth order polyvalent interaction, K_i, the ith binding constant, equals $(N+1-i)/i$. Therefore for $N=5$, $K_2/K_1=(5/1)/(4/2)=5/2$.
[276] T. Tanaka, R. Suzuno, K. Nakamura, A. Kuwahara, K. Takeo, *Electrophoresis* **1986**, *7*, 204 – 209.
[277] A. Y. Karush, B. Dzantiev, *Mol. Immunol.* **1990**, *27*, 965 – 971.
[278] G. B. Sigal, M. Mammen, G. Dahmann, G. M. Whitesides, *J. Am. Chem. Soc.* **1996**, *118*, 3789 – 3800.
[279] G. Glick, J. R. Knowles, *J. Am. Chem. Soc.* **1991**, *113*, 4701 – 4703.
[280] G. D. Glick, P. L. Toogood, D. C. Wiley, J. J. Skehel, J. R. Knowles, *J. Biol. Chem.* **1991**, *266*, 23660 – 23669.
[281] M. Mammen, E. I. Shakhnovich, J. M. Deutch, G. M. Whitesides, *J. Org. Chem.* **1998**, *63*, 3821 – 3830.
[282] M. Mammen, E. Shakhnovich, G. M. Whitesides, *J. Org. Chem.* **1998**, *63*, 3168 – 3175.
[283] W. Blokzijl, J. B. F. N. Engberts, *Angew. Chem.* **1993**, *105*, 1610 – 1648; *Angew. Chem. Int. Ed. Engl.* **1993**, *32*, 1545 – 1579.
[284] F. Karush, *Compr. Immunol.* **1978**, *5*, 85 – 116.
[285] N. Agmon, R. D. Levine, *Chem. Phys. Lett.* **1977**, *52*, 197 – 201.
[286] G. Weber, *Adv. Protein Chem.* **1975**, *29*, 1 – 83.
[287] N. M. Green, *Adv. Protein Chem.* **1975**, *29*, 85 – 133.
[288] D. Spillmann, M. M. Burger, *J. Cell. Biochem.* **1996**, *61*, 562 – 568.
[289] G. J. Arlaud, M. G. Colomb, J. Gagnon, *Immunol. Today* **1987**, *8*, 1076 – 1077.
[290] L. Stryer, *Biochemistry*, 4th ed., Freeman, New York, **1995**.
[291] M. Tardieu, R. L. Epstein, H. L. Weiner, *Int. Rev. Cytol.* **1982**, *80*, 27 – 61.
[292] A. Varki, *Glycobiology* **1993**, *3*, 97 – 130.
[293] J. C. Paulson, J. E. Sadler, R. L. Hill, *J. Biol. Chem.* **1979**, *254*, 2120 – 2124.
[294] A. G. Dalgleish, P. C. L. Beverley, P. R. Clapham, D. H. Crawford, M. F. Greaves, R. A. Weiss, *Nature* **1984**, *312*, 763 – 767.
[295] J. M. Greve, G. Davis, A. M. Meyer, C. P. Forte, S. C. Yost, C. W. Marlor, M. E. Kamarck, A. McClelland, *Cell* **1989**, *56*, 839 – 847.
[296] P. R. Clapham, J. N. Weber, D. Whitby, K. McIntosh, A. G. Dalgleish, P. J. Maddon, K. C. Deen, R. W. Sweet, R. A. Weiss, *Nature* **1989**, *305*, 60 – 62.
[297] P. Pontisso, M. A. Petit, M. J. Bankowski, M. E. Peeples, *J. Virol.* **1989**, *63*, 1981 – 1988.
[298] R. M. H. V. Van, G. Hardie, *Immunochemistry* **1976**, *13*, 503 – 507.
[299] I. Ofek, N. Sharon, *Curr. Top. Microbiol. Immunol.* **1990**, *151*, 90 – 113.
[300] I. Ofek, N. Sharon, *Infect. Immun.* **1988**, *56*, 539 – 547.
[301] J. P. Duguid, D. C. Old in *Bacterial Adherance*, *Vol. 6* (Ed.: E. H. Beachey), Chapman & Hall, London, **1980**, pp. 185 – 217.
[302] M. Lindahl, R. Brossmer, T. Wadstrom, *Glycoconjugate J.* **1987**, *4*, 51 – 58.
[303] R. A. Finkelstein, L. F. Hanne, *Infect. Immun.* **1982**, *36*, 1199 – 1208.
[304] F. DellOlio, F. J. J. de Kanter, D. H. van den Eijnden, F. Serafini-Cessi, *Carbohyd. Res.* **1988**, *178*, 327 – 332.
[305] C. L. Hornick, F. Karush, *Immunochemistry* **1972**, *9*, 325 – 340.
[306] K. H. Schleifer, *Methods Mircobiol.* **1985**, *18*, 125 – 156.
[307] J. A. Wells, *Proc. Natl. Acad. Sci. USA* **1996**, *93*, 1 – 6.
[308] C. H. Heldin, *Cell* **1995**, *80*, 213 – 223.
[309] C. F. Ware, S. Vanarsdale, T. L. Vanarsdale, *J. Cell. Biochem.* **1996**, *60*, 47 – 55.
[310] K. E. Becker, T. Ishizaka, H. Metzger, K. Ishizaka, P. M. Grimley, *J. Exp. Med.* **1973**, *138*, 394 – 399.
[311] R. P. Siraganian, W. A. Hook, B. B. Levin, *Immunochemistry* **1975**, *12*, 149 – 155.
[312] M. Dembo, B. Goldstein, *Immunochemistry* **1978**, *15*, 307 – 313.
[313] C. Wofsy, B. Goldstein, M. Dembo, *J. Immunol.* **1978**, *121*, 593 – 601.
[314] J. C. Cambier, W. A. Jensen, *Curr. Opin. Genet. Dev.* **1994**, *4*, 55 – 63.
[315] L. Naldini, E. Vigna, R. Ferracini, P. Longati, L. Gandino, M. Prat, P. M. Comoglio, *Mol. Cell. Biol.* **1991**, *11*, 1793 – 1803.
[316] P. Kanakaraj, S. Raj, S. A. Khan, S. Bishayee, *Biochemistry* **1991**, *30*, 1761 – 1767.
[317] Y. Takahama, H. Suzuki, K. S. Katz, M. J. Grusby, A. Singer, *Nature* **1994**, *371*, 67 – 70.

[318] S. Miyamoto, K. M. Yamada, *Science* **1995**, *267*, 883 – 885.
[319] G. A. Brent, J. W. Harney, Y. Chen, R. L. Warne, D. D. Moore, P. R. Larsen, *Mol. Endocrin.* **1989**, *3*, 1996 – 2005.
[320] A. K. Abbas, A. H. Lichtman, J. S. Pober, *Cellular and Molecular Immunology*, Saunders, Philidelphia, **1997**.
[321] D. Barlocco, P. Fadda, W. Fratta, *Farmaco* **1993**, *48*, 387 – 396.
[322] H. E. Castagnino, J. Milei, F. A. Toranzos, V. Weiss, R. Beigelman, *Jpn. Heart J.* **1990**, *31*, 845 – 855.
[323] T. Costa, M. Wuster, A. Herz, Y. Shimohigashi, H. C. Chen, D. Rodbard, *Biochem. Pharmacol.* **1985**, *34*, 25 – 30.
[324] M. Dembo, B. Goldstein, A. K. Sobotka, L. M. Lichtenstein, *J. Immunol.* **1979**, *122*, 518 – 528.
[325] P. Holliger, T. Prospero, G. Winter, *Proc. Natl. Acad. Sci. USA* **1993**, *90*, 6444 – 6448.
[326] A. Piergentili, W. Quaglia, S. K. Tayebati, F. Paparelli, L. Malmusi, L. Brasili, *Farmaco* **1994**, *49*, 83 – 87.
[327] P. S. Portoghese, A. A. Garzon, H. Nagase, C. E. Lin, A. E. Takemori, *J. Med. Chem.* **1991**, *34*, 1292 – 1296.
[328] H. Kizuka, R. N. Hanson, *J. Am. Chem. Soc.* **1987**, *30*, 722 – 726.
[329] L. V. Mochalova, A. B. Tuzikov, V. P. Marinina, A. S. Gambaryan, N. E. Byramova, N. V. Bovin, M. N. Matrosovich, *Antiviral. Res.* **1994**, *23*, 179 – 190.
[330] K. H. Mortell, R. V. Weatherman, L. L. Kiessling, *J. Am. Chem. Soc.* **1996**, *118*, 2297 – 2298.
[331] "Synthesis and Antigenic Properties of Sialic Acid-Based Dendrimers": R. Roy, D. Zanini, S. J. Meunier, A. Romanowska, *ACS Symp. Ser.* **1994**, *560*, 104 – 119.
[332] J. E. Kingery-Wood, K. W. Williams, G. B. Sigal, G. M. Whitesides, *J. Am. Chem. Soc.* **1992**, *114*, 7303 – 7305.
[333] W. Spevak, J. O. Nagy, D. H. Charych, M. E. Schaefer, J. H. Gilbert, *J. Am. Chem. Soc.* **1993**, *115*, 1146 – 1147.
[334] A. Spaltenstein, G. M. Whitesides, *J. Am. Chem. Soc.* **1991**, *113*, 686 – 687.
[335] M. Mammen, K. Helmerson, R. Kishore, S.-K. Choi, W. D. Phillips, G. M. Whitesides, *Chem. Biol.* **1996**, *3*, 757 – 763.
[336] K. H. Mortell, M. Gingras, L. L. Kiessling, *J. Am. Chem. Soc.* **1994**, *116*, 12053 – 12054.
[337] R. Roy, *Curr. Opin. Struct. Biol.* **1996**, *6*, 692 – 702.
[338] D. Zanini, R. Roy, *J. Am. Chem. Soc.* **1996**, *119*, 2088 – 2095.
[339] D. Zanini, R. Roy, *Bioconjugate Chem.* **1997**, *8*, 187 – 192.
[340] T. D. Heath, R. T. Fraley, J. Bentz, E. W. Voss, J. N. Herron, D. Papahadjopoulos, *Biochim. Biophys. Acta* **1984**, *770*, 148 – 158.
[341] P. Adler, S. J. Wood, Y. C. Lee, R. T. Lee, J. W. A. Petri, R. L. Schnaar, *J. Biol. Chem.* **1995**, *270*, 5164 – 5171.
[342] R. Wunderlin, S. D. Sharma, P. Minakakis, R. Schwyzer, *Helv. Chim. Acta* **1985**, *68*, 12 – 22.
[343] M. D. Carrithers, M. R. Lerner, *Chem. Biol.* **1996**, *3*, 537 – 542.
[344] S. Tetsui, J. Zhao, S. Kimura, Y. Imanishi, *Int. J. Pept. Protein Res.* **1996**, *48*, 95 – 101.
[345] K. Hanaoka, T. J. Pritchett, S. Takasaki, N. Kochibe, S. Sabeson, J. C. Paulson, *J. Biol. Chem.* **1989**, *264*, 9842 – 9849.
[346] T. J. Pritchett, J. C. Paulson, *J. Biol. Chem.* **1989**, *264*, 9850 – 9858.
[347] Y. C. Lee, R. R. Townsend, M. R. Hardy, J. Lönngren, J. Arnarp, M. Haraldsson, H. Lönn, *J. Biol. Chem.* **1983**, *258*, 199 – 202.
[348] R. T. Lee, Y. C. Lee, *Biochem. Biophys. Res. Commun.* **1988**, *155*, 1444 – 1451.
[349] E. A. L. Biessen, H. Broxterman, J. H. VanBoom, T. J. C. VanBerkel, *J. Med. Chem.* **1995**, *38*, 1846 – 1852.
[350] H. Maaheimo, R. Renkonen, J. P. Turunen, L. Penttilä, O. Renkonen, *Eur. J. Biochem.* **1995**, *234*, 616 – 625.
[351] P. J. Belshaw, D. M. Spencer, G. R. Crabtree, S. L. Schreiber, *Chem. Biol.* **1996**, *3*, 731 – 738.
[352] K. L. LeBoulluec, R. J. Mattson, C. D. Mahle, R. T. McGovern, H. P. Nowak, A. J. Gentile, *Bioorg. Med. Chem. Lett.* **1995**, *5*, 123 – 126.
[353] a) J. Rao, G. M. Whitesides, *J. Am. Chem. Soc.* **1997**, *119*, 10286 – 10290; b) J. Rao, J. Lahiri, L. Isaacs, R. M. Weis, G. M. Whitesides, *Science* **1998**, *280*, 708 – 711.
[354] L. Yan, J. Rao, G. M. Whitesides, *J. Am. Chem. Soc.* **1998**, in press.
[355] E. F. Hahn, S. Nishimura, R. R. Goodman, G. W. Pasternak, *J. Pharmacol. Exp. Ther.* **1985**, *235*, 839 – 845.
[356] M. N. Matrosovich, L. V. Mochalova, V. P. Marinina, N. E. Byramova, N. V. Bovin, *FEBS Lett.* **1990**, *272*, 209 – 212.
[357] R. Roy, D. Zanini, S. J. Meunier, A. Romanowska, *J. Chem. Soc. Chem. Commun.* **1993**, 213 – 217.
[358] R. Roy, C. A. Laferriere, *Carbohyd. Res.* **1988**, *177*, C1 – C4.
[359] A. Gamian, H. J. Jennings, C. A. Laferriere, R. Roy, *J. Carbohydr. Chem.* **1987**, *6*, 161 – 165.
[360] S. Sabesan, J. O. Duus, S. Neira, P. Domaille, S. Kelm, J. C. Paulson, K. Bock, *J. Am. Chem. Soc.* **1992**, *114*, 8363 – 8375.
[361] S.-K. Choi, M. Mammen, G. M. Whitesides, *Chem. Biol.* **1996**, *3*, 97 – 104.
[362] S.-K. Choi, G. M. Whitesides, unpublished results.
[363] S.-K. Choi, M. Mammen, G. M. Whitesides, *J. Am. Chem. Soc.* **1997**, *119*, 4103 – 4111.
[364] G. P. Chen, Y. Ito, Y. Imanishi, *Bioconjugates Chem.* **1997**, *8*, 106 – 110.
[365] P. Metezeau, *Biol. Cell* **1993**, *78*, 129 – 134.
[366] P. A. van der Merwe, A. N. Barclay, *Curr. Opin. Immunol.* **1996**, *8*, 257 – 261.
[367] D. K. Takemoto, J. J. Skehel, D. C. Wiley, *Virology* **1996**, *217*, 452 – 458.
[368] E. Evans, K. Ritchie, R. Merkel, *Biophys. J.* **1995**, *68*, 2580 – 2587.
[369] A. Tozeren, K. L. Sung, L. A. Sung, M. L. Dustin, P. Y. Chan, T. A. Springer, S. Chien, *J. Cell Biol.* **1992**, *116*, 997 – 1006.
[370] E. B. Finger, K. D. Puri, R. Alon, M. B. Lawrence, U. H. von Andrian, T. A. Springer, *Nature* **1996**, *379*, 266 – 269.
[371] R. Alon, R. C. Fuhlbrigge, E. B. Finger, T. A. Springer, *J. Cell Biol.* **1996**, *135*, 849 – 865.
[372] P. K. Gopalan, C. W. Smith, H. Lu, E. L. Berg, L. V. McIntire, S. I. Simon, *J. Immunol.* **1997**, *158*, 367 – 375.
[373] W. Hertl, W. S. Ramsey, E. D. Nowlan, *In Vitro* **1984**, *20*, 796 – 801.
[374] H. Ernst, M. K. Zanin, D. Everman, S. Hoffman, *J. Cell Sci.* **1995**, *108*, 3807 – 3816.
[375] M. B. Macek, L. C. Lopez, B. D. Shur, *Dev. Biol.* **1991**, *147*, 440 – 444.
[376] E. L. Florin, V. T. Moy, H. E. Gaub, *Science* **1994**, *264*, 415 – 417.
[377] N. C. Santos, M. A. Castanho, *Biophys. J.* **1996**, *71*, 1641 – 1650.
[378] Note added in proof: "A Lysoganglioside/Poly-L-glutamic Acid Conjugate as a Picomolar Inhibitor of Influenza Hemagglutinin": H. Kamitakahara, T. Suzuki, N. Nishigori, Y. Suzuki, O. Kanie, C.-H. Wong, *Angew. Chem.* **1998**, *110*, 1607 – 1611; *Angew. Chem. Int. Ed.* **1998**, *37*, 1524 – 1528.

Polyamide or peptide nucleic acids (PNAs) bind with higher affinity to complementary nucleic acids than their natural congeners.







DNA/PNA chimeras can assume biological functions, such as the activation of ribonuclease H for the cleavage of RNA.

ANGEWANDTE CHEMIE © WILEY-VCH

PNA: Synthetic Polyamide Nucleic Acids with Unusual Binding Properties**

Eugen Uhlmann,* Anusch Peyman, Gerhard Breipohl, and David W. Will

Dedicated to Professor Wolfgang Pfleiderer on the occasion of his 70th Birthday

Since the investigation of oligonucleotides as potential therapeutics that target nucleic acids was initiated, the search for nucleic acid mimetics with improved properties, such as strengthened binding-affinity to complementary nucleic acids, increased biological stability, and improved cellular uptake, has accelerated rapidly. In 1991 Nielsen et al. first described what is undoubtedly one of the most interesting of the new derivatives, the polyamide or peptide nucleic acids (PNAs), in which the entire sugar–phoshate backbone is replaced by an *N*-(2-aminoethyl)glycine polyamide structure. Since even minor structural changes in oligonucleotides, such as the replacement of an oxygen atom by sulfur (phosphorothioates), or by a neutral methyl group (methyl phosphonates), result in a decrease in binding affinity, it was even more astonishing to find that the drastic structural changes in PNAs result in nucleic acid mimetics with higher binding-affinity to complementary DNA and RNA than unmodified oligonucleotides. The remarkable binding properties of PNAs have spawned a rapidly expanding new field of research, where the targets are the synthesis of PNAs and PNA analogues, and their application as therapeutics, DNA diagnostics, and tools in biotechnology. In addition, investigation of PNAs and PNA/DNA chimeras can be used to generate information on the structural and biological properties of DNA and RNA themselves. Furthermore, they may trigger the generation of new ideas on models for alternative living systems and potential transitions between different genetic systems.

Keywords: antisense agents · DNA recognition · gene technology · molecular recognition · peptide nucleic acids

1. Introduction

The most important molecular recognition event in nature is the base-pairing of nucleic acids, which guarantees the storage, transfer, and expression of genetic information in living systems. The highly specific recognition through the natural pairing of the nucleobases has become increasingly important for the development of DNA diagnostics and for oligonucleotide therapeutics in the form of antisense and antigene oligonucleotides.[1–4] In the last few years, attempts to optimize the properties of oligonucleotides have resulted in the synthesis and analysis of a huge variety of new oligonucleotide derivatives[5] with modifications to the phosphate group, the ribose, or the nucleobase. The most radical change to the natural structure, however, was made by the Danish group of Buchardt, Nielsen, Egholm, and Berg[6–9], who replaced the entire sugar–phosphate backbone by an *N*-(2-aminoethyl)glycine-based polyamide structure (Figure 1). The astonishing discovery that these polyamide or peptide nucleic acids (PNAs) bind with higher affinity to complementary nucleic acids than their natural counterparts,[10] and obey the Watson–Crick base-pairing rules resulted in the rapid establishment of a new branch of research focussed on diagnostic and therapeutic applications of this highly interesting compound class.[11–14] Soon after, the ability of PNAs to displace one strand of a DNA double-helix, an inefficient process with natural oligonucleotides, was reported.[15] The combination of PNA and DNA to form

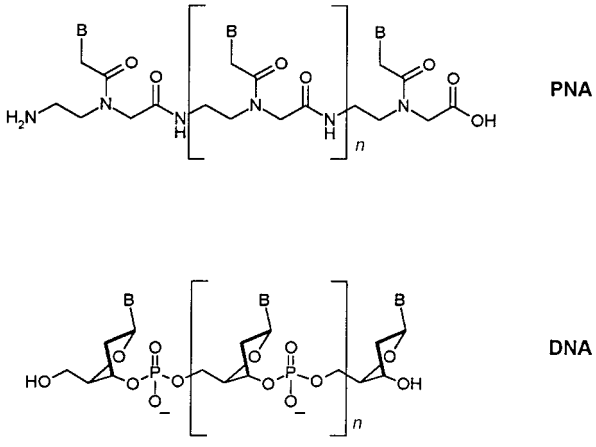


Figure 1. Structures of PNA and DNA. B = nucleobase.

[*] Dr. E. Uhlmann, Dr. A. Peyman, Dr. G. Breipohl, Dr. D. W. Will
Hoechst Marion Roussel Deutschland GmbH, G 838
D-65926 Frankfurt am Main (Germany)
Fax: (+49) 69-305-89713
E-mail: eugen.uhlmann@hmrag.com

[**] A list of abbreviations used is provided in the Appendix.

 © WILEY-VCH Verlag GmbH, D-69451 Weinheim, 1998 1433-7851/98/3720-2797 $ 17.50+.50/0

PNA/DNA chimeras results in new structures, which, in addition to excellent binding, can also assume biological functions, such as a primer function for DNA polymerases.[16] Furthermore, as self-organising structures PNAs are of fundamental interest in material sciences, as well as in the study of evolution of potential alternative life-forms.[16–18] In the following sections the synthesis, properties, and possible applications of PNAs and PNA/DNA chimeras are described.

2. Monomeric Building Blocks for the Synthesis of PNAs

A variety of different monomeric building blocks have been used for the synthesis of PNAs and their structural analogues. These differ from each other in the type of protecting group (PG) for the amino function of the backbone and/or for the nucleobase, and also in the structure of the backbone. Other achiral and chiral backbone building blocks have been employed in addition to *N*-(2-aminoethyl)glycine. The structures of the most important of the monomeric building blocks and their synthesis are described below. The selection is limited to monomers where a detailed description of the synthetic route has been reported, and to those monomers that have been employed for the synthesis of oligomers.

2.1. PNA Monomeric Building Blocks with an Aminoethylglycine Backbone

The "classical" PNA backbone consists of the amino acid *N*-(2-aminoethyl)glycine, where the secondary amino func-

Eugen Uhlmann was born in Bad Schussenried (Germany) in 1953 and studied chemistry at the University of Konstanz where he worked under the supervision of Professor W. Pfleiderer on the development of new protecting groups for oligonucleotide synthesis. After receiving his Ph.D in organic chemistry in 1981, he joined Hoechst AG in Frankfurt and established a laboratory for nucleotide synthesis. In 1984/1985 he spent one year in the Department of Molecular Biology and Genetics at the Massachusetts General Hospital and Harvard Medical School in Boston. Since 1986 he has been employed in the pharmaceutical division of Hoechst AG (now Hoechst Marion Roussel) where he works on the synthesis of new nucleic acid derivatives and their therapeutic use as antisense agents.


E. Uhlmann


A. Peyman

Anusch Peyman was born in Freiburg (Germany) in 1958, he studied chemistry at the University of Freiburg and completed his Ph.D. on the stereoselective dimerization of free radicals under the supervision of C. Rüchardt. From 1987–1988 he carried out postdoctoral research with J. R. Knowles at Harvard University on the reaction mechanism of triosephosphate-isomerase. In 1988 he joined the Peptide/Nucleotide group of Hoechst AG pharmaceutical division, and in 1991 spent one year working on ribozymes with J. Szostak at Harvard Medical School. In 1992 he returned to the medicinal chemistry division of Hoechst (now Hoechst Marion Roussel) and carries out research on antisense oligonucleotides and peptidomimetics.


G. Breipohl


D. W. Will

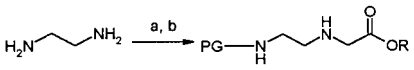
Gerhard Breipohl was born in Bielefeld in 1951 and studied chemistry at the Westfälische-Wilhelms University in Münster where he worked under the supervision of Professor B. Franck on the biosynthesis of mycotoxins. After receiving his Ph.D. in 1982 he worked for one year as a postdoctoral fellow at the Massachusetts Institute of Technology with G. Buechi. In 1983 he joined the peptide/nucleotide group of pharmaceutical research at Hoechst (now Hoechst Marion Roussel). There his research areas were the synthesis of enzyme inhibitors, hormone analogues, receptor antagonists, non-natural amino acids, peptide mimetics, PNAs and also the development of linkers and coupling methods for solid phase synthesis. In 1996 he moved to Chemical Development at HMR and works on developing and optimizing synthetic procedures for drug candidates.

David William Will was born in Bathgate (Scotland) in 1967, studied chemistry at the University of Edinburgh and completed his Ph. D. on the synthesis of modified oligonucleotides under the supervision of Professor Tom Brown in 1992. From 1992–1993 he carried out postdoctoral research on oligonucleotide mimetics and antisense therapeutics with Dr. Eugen Uhlmann in the Peptide/Nucleotide group of Hoechst AG pharmaceuticals division in Frankfurt. In 1994 he moved to the European Molecular Biology Laboratory in Heidelberg and worked on the synthesis of modified ribozymes with Dr. Brian Sproat. He continued this work at Ribonetics GmbH in Göttingen. In late 1994 he returned to Hoechst AG and continued his research on antisense therapeutics. In 1997 he joined the Automated Synthesis and New Technologies team of Hoechst Marion Roussel in Frankfurt.

tion is acylated with a nucleobase acetic acid derivative. Acid- or base-labile protecting groups are normally used for temporary protection of the primary amino function. The preparation of the monomers can be divided into the synthesis of a suitably protected *N*-aminoethylglycine, and the nucleobase acetic acid derivatives. Their syntheses are described in the following sections.

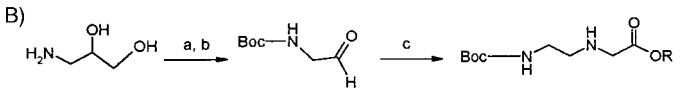
Figure 2 shows the three most important synthetic routes to aminoethylglycine: alkylation of 1,2-diaminoethane with halogenoacetic acid derivatives[19–22] (Figure 2A), reductive

A)



PG	R	a	b	Ref.
Boc	Me	1. $ClCH_2COOH$ 2. MeOH/HCl	$(Boc)_2O$, dioxane/H_2O	[19]
Boc	*t*Bu	$(Boc)_2O$, NEt_3, CH_2Cl_2	$ClCH_2COOtBu$, NEt_3, CH_2Cl_2	[22]
Fmoc	*t*Bu	$BrCH_2COOtBu$, CH_2Cl_2	Fmoc-ONSu, DIEA	[20]
Mmt	Et	1. $ClCH_2COOH$ 2. EtOH/HCl	Mmt-Cl, NEt_3, CH_2Cl_2	[21]

B)



R	a	b	c	Ref.
Me	$(Boc)_2O$, NaOH, H_2O	KIO_4, H_2O	$H_2NCH_2COOMe{\cdot}HCl$, NaOAc, H_2, Pd/C	[23]
Et	$(Boc)_2O$, NaOH, H_2O	KIO_4, H_2O	$H_2NCH_2COOEt{\cdot}HCl$, NaOAc, H_2, Pd/C	[23]
Et	$(Boc)_2O$, NaOH, H_2O	$NaIO_4$, H_2O	$H_2NCH_2COOEt{\cdot}HCl$, $NaBH_3CN$, MeOH	[24]

C)

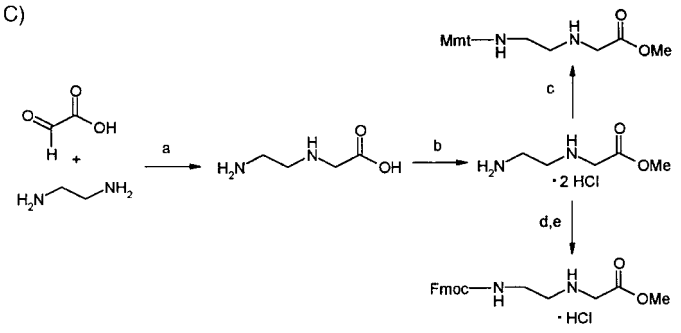


Figure 2. A) Synthesis of Aeg derivates by alkylation of 1,2-diaminoethane. B) Synthesis of Boc–Aeg derivates by reductive amination from Boc-aminoacetaldehyde and glycine esters. C) Synthesis of Aeg derivates by reductive amination from 1,2-diaminoethane and glyoxylic acid:[25,26] a) H_2/Pd/C, H_2O; b) MeOH/HCl; c) Mmt-Cl, DMF, NEt_3; d) Fmoc-(ONSu), dioxane/H_2O; e) MeOH/HCl.

amination with glycine esters and protected aminoacetaldehyde[23, 24] (Figure 2B), and reductive amination using 1,2-diaminoethane and glyoxylic acid[25, 26] (Figure 2C). Further reaction steps lead to protected aminoethylglycine derivatives with unprotected secondary amino groups to which the nucleobase acetic acid derivatives can be coupled.

The synthesis of nucleobase acetic acid derivatives is shown in Figures 3–6. Thyminyl acetic acid, which does not require an additional base protecting group, can be prepared either by alkylation of thymine with halogenoacetic acid esters[6, 27] followed by saponification, or by direct alkylation with bromoacetic acid[28] (Figure 3). We prefer the latter method because of its simplicity.

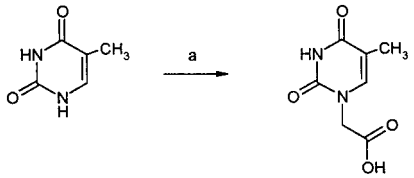
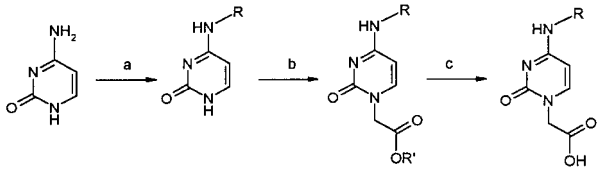


Figure 3. Synthesis of thyminyl acetic acid. Method 1:[27] a) 1. $BrCH_2COOMe$, K_2CO_3, DMF; 2. NaOH, H_2O. Method 2:[28] a) $BrCH_2COOH$, KOH, H_2O.

A common feature in the synthesis of cytosyl acetic acid derivatives (Figure 4) is that the protecting group on the exocyclic 4-amino function of cytosine is introduced in

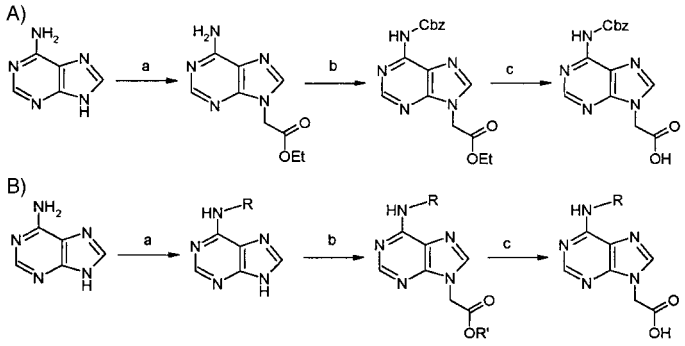


R	R'	a	b	c	Ref.
Cbz	Me	Cbz-Cl/ pyridine	$BrCH_2COOMe$, K_2CO_3, DMF	NaOH (aq.)	[27]
Cbz	*t*Bu	Cbz-Cl, DMAP, pyridine	$BrCH_2COOtBu$, K_2CO_3, Cs_2CO_3, DMF	HCl/dioxane, CH_2Cl_2	[20]
Mmt	Me	Mmt-Cl, pyridine, NEM	$BrCH_2COOMe$, NaH/ DMF	NaOH, H_2O/dioxane,	[25]
*t*BuBz	Me	*t*BuBz-Cl/ pyridine	$BrCH_2COOMe$, NaH/ DMF	NaOH, H_2O/ dioxane	[26]
An	Me	anisoyl chloride/ pyridine	$BrCH_2COOMe$, NaH/ DMF	NaOH, H_2O/ dioxane	[36]

Figure 4. Synthesis of cytosyl acetic acid derivatives.

the first step by using the appropriate acid chloride or Mmt chloride in pyridine. The resulting benzyloxycarbonyl,[9, 20, 27] 4-*tert*-butylbenzoyl, anisoyl,[22, 26] and Mmt derivatives[25] are then N^1-alkylated with methyl bromoacetate[25–27] or *tert*-butyl bromoacetate[20]. Finally, cleavage of the ester group under basic or acidic conditions gives the corresponding cytosyl acetic acid derivative.

The synthesis of the adenyl acetic acid derivatives is shown in Figure 5. The first synthetic route (Figure 5a)[27] involves N^9 alkylation of adenine by ethyl bromoacetate. Attempts to protect the exocyclic 6-amino functionality with Cbz-Cl resulted in a complex mixture of products. However, the use of *N*-(benzyloxycarbonyl)-*N'*-ethylimidazolium tetrafluoroborate (Rapoport's reagent)[29] proceeds smoothly to give the desired product. The other synthetic routes (Figure 5b) involve the initial protection of the 6-amino group of adenine. In this case, the reaction with Cbz-Cl is unproblematic.[20] Introduction of the Mmt[25] or anisoyl groups[26] in pyridine



R	R'	a	b	c	Ref.
Cbz	*t*Bu	NaH, Cbz-Cl, DMF	$BrCH_2COOtBu$, K_2CO_3, Cs_2CO_3, DMF	TFA, CH_2Cl_2, Et_3SiH	[20]
Mmt	Me	Mmt-Cl, pyridine, NEM	$BrCH_2COOMe$, NaH/ DMF	NaOH, H_2O/dioxane	[25]
An	Me	anisoyl chloride/ pyridine	$BrCH_2COOMe$, NaH/ DMF	NaOH, H_2O/ dioxane	[26]

Figure 5. A) Synthesis of Cbz-protected adenyl acetic acid according to Dueholm et al.:[27] a) $BrCH_2COOEt$, NaH, DMF; b) *N*-(benzyloxycarbonyl)-*N*′-ethylimidazolium tetrafluoroborate, DMF, CH_2Cl_2; c) NaOH (aq.). B) Synthesis of adenyl acetic acid via the N^6-protected adenine.[20, 25, 26]

also proceeds smoothly. The resulting protected adenine derivatives are then N^9-alkylated with methyl or *tert*-butyl bromoacetate. The desired protected adenyl acetic acid derivatives are obtained by alkaline saponification, or by ester hydrolysis under acidic conditions, with the addition of triethylsilane to prevent partial loss of the Cbz group.

The preparation of the guanyl acetic acid derivatives (Figure 6) presents the greatest synthetic challenge. The difficulty of obtaining selective N^9 alkylation while avoiding N^7 alkylation is well known in nucleoside chemistry. This selectivity problem can often be diminished by the use of 2-amino-6-chloropurine in alkylation reactions. Figure 6a shows the synthesis of the first protected guanyl acetic acid derivative to be used in PNA monomer synthesis.[27] 2-Amino-6-chloropurine is alkylated in moderate yield with bromoacetic acid. The desired O^6-benzylguanyl acetic acid is then obtained by exchange of the chlorine atom with sodium benzyloxide. However, this derivative is no longer in use because of solubility and stability problems under the conditions necessary for Boc cleavage.[27]

N^2-Cbz guanyl acetic acid is obtained by the procedure described in Figure 6b.[20] Reaction of 2-amino-6-chloro purine with allyl bromide results in a 3:1 ratio of N^9/N^7-alkylated products, which gives 9-allyl guanine after chromatographic separation and acid hydrolysis. The N^2 amino functionality of this compound is then protected by reaction with Cbz-imidazolide and KH in the presence of [18]crown-6 as a phase transfer catalyst. After ozonolysis of the allyl function and oxidative work-up the desired N^2-Cbz-guanyl acetic acid is obtained.

The synthesis of guanyl acetic acid protected on N^2 by the Mmt group, which can be cleaved under weakly acidic conditions, is depicted in Figure 6c.[25] Again, 2-amino-6-chloropurine is used for the synthesis. The Mmt group is introduced on N^2 after alkylation with methyl bromoacetate. Under the conditions of the subsequent alkaline saponification of the methyl ester the chlorine in position 6 is also exchanged, and the desired guanyl acetic acid is obtained.

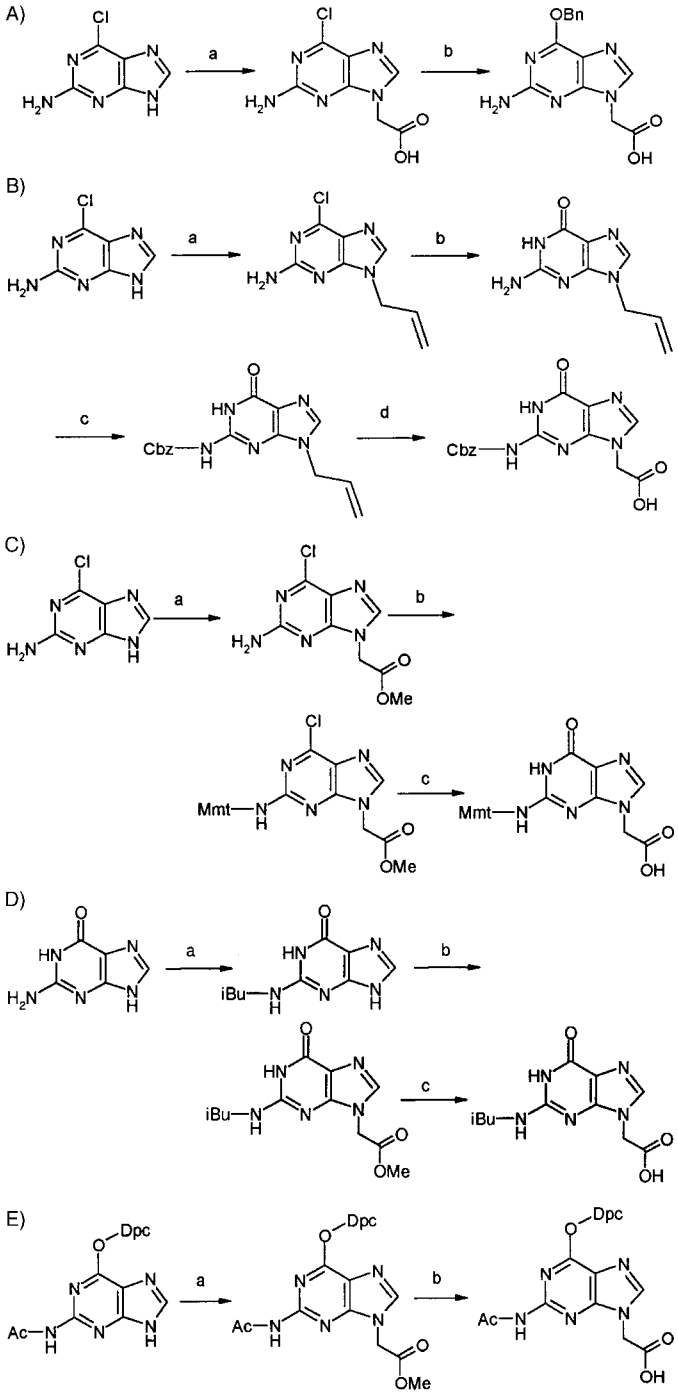


Figure 6. A) Synthesis of O^6-benzylguanyl acetic acid:[27] a) $BrCH_2COOH$; b) $PhCH_2ONa$, DMF. B) Synthesis of N^2-Cbz-guanyl acetic acid:[20] a) $BrCH_2CH{=}CH_2$, K_2CO_3, DMF; b) 1N HCl, reflux; c) Cbz-imidazole, [18]crown-6, KH, THF; d) 1. O_3, CH_2Cl_2, MeOH; 2. Me_2S; 3. $NaClO_2$, NaH_2PO_4, H_2O, THF, *t*BuOH, 2-methyl-2-butene. C) Synthesis of N^2-Mmt-guanyl acetic acid:[25] a) $BrCH_2COOMe$, NaH/DMF; b) Mmt-Cl, pyridine, NEt_3; c) 10% NaOH (aq), reflux. D) Synthesis of N^2-iBu-guanyl acetic acid:[26] a) Isobutyryl chloride, NEt_3/ DMF; b) $BrCH_2COOMe$, NaH/DMF; c) NaOH, H_2O/dioxane. E) Synthesis of N^2-Ac-O^6-Dpc-guanyl acetic acid:[22] a) $BrCH_2COOMe$, DMF, DIEA; (b) NaOH/ MeOH/ dioxane/ H_2O.

Figure 6d shows the synthesis of guanyl acetic acid carrying a base-labile isobutyryl protecting group on the 2-amino

function.[26]. N^2-Isobutyrylguanine is readily obtained by acylation of guanine with isobutyryl chloride in triethylamine/DMF or pyridine. This compound can then be alkylated with methyl bromoacetate under standard conditions to give a mixture of N^7/N^9-alkylated products. After chromatographic separation and alkaline saponification of the methyl ester the desired N^2-Ibu-guanyl acetic acid is obtained.

A useful alternative method to prevent N^7 alkylation is the use of N^2-acetyl-O^6-(diphenylcarbamoyl)purine[30] (Figure 6e). Alkylation of this compound with methyl bromoacetate in DIEA/DMF, and subsequent precipitation gives exclusively the N^9-alkylated product.[22] Subsequent alkaline saponification gives N^2-Ac-O^6-Dpc-guanyl acetic acid in good yield.

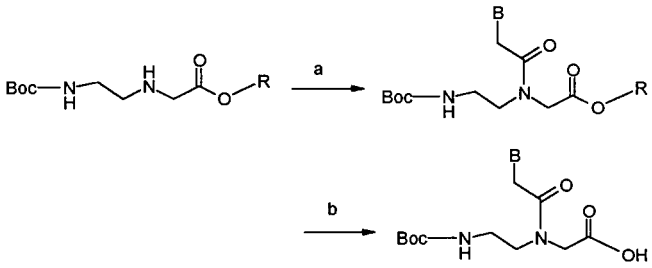
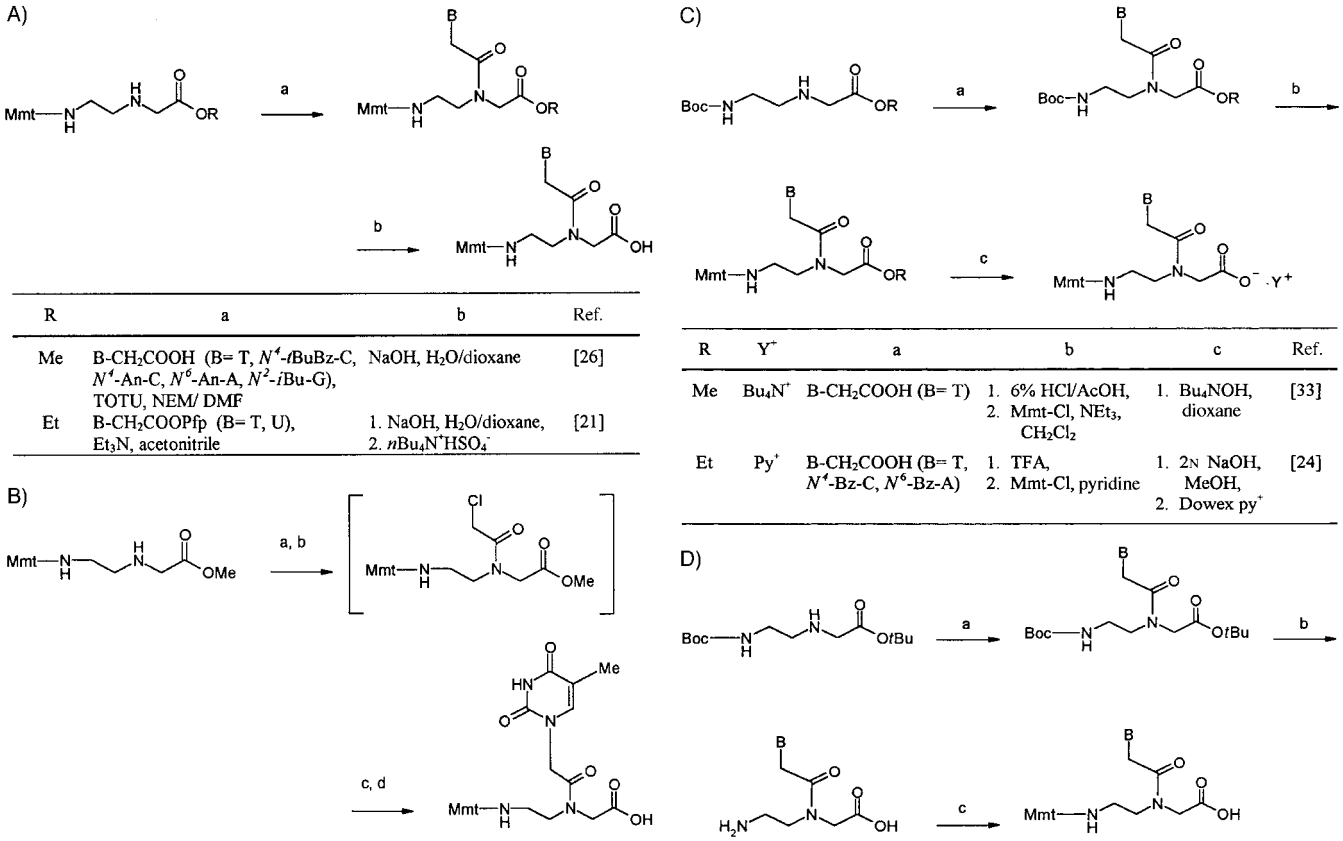


Figure 7. Synthesis of Boc–PNA monomers:[27] a) B-CH_2COOH (B = T, N^4-Cbz-C, N^6-Cbz-A, O^6-Bn-G, N^2-Cbz-G), DCC/HOObt[160] or PyBrop/DIEA; b) LiOH/THF/H_2O or NaOH/MeOH/H_2O

2.1.1. Monomers with Acid-labile N-Protecting Groups

The first reported syntheses of PNA[6] used monomers with the trifluoroacetic acid-labile Boc group for N-terminal temporary protection[8, 9, 27]. The exocyclic functional groups of the nucleobases are protected with Cbz and/or benzyl groups, which can be cleaved with liquid hydrofluoric acid or trifluoromethanesulfonic acid. The synthesis of PNA monomers with this protecting group combination and the building blocks described above is shown in Figure 7. Standard peptide coupling reagents, such as DCC/HOBt[31] or PyBrop,[32] are used to attach the nucleobase acetic acid derivatives to the secondary amino function of the Boc-protected aminoethylglycine ester.

These Boc-monomers are unsuitable for the synthesis of PNA/DNA chimeras, as the strongly acidic conditions (TFA/HF) necessary for deprotection would lead to depurination of the DNA-part of the oligomers. The Mmt-protected monomers described by us,[26] and others[21, 24, 33, 34] (Figure 8) can be deprotected under much milder conditions (trichloroacetic acid), and thus do not have this disadvantage. In particular, the combination with base-labile protecting groups for the exocyclic amino functionalities of the nucleobases cytosine, adenine, and guanine allows deprotection conditions that are compatible with standard oligonucleotide synthesis. Protect-



R	a	b	Ref.
Me	B-CH_2COOH (B= T, N^4-*t*BuBz-C, N^4-An-C, N^6-An-A, N^2-*i*Bu-G), TOTU, NEM/ DMF	NaOH, H_2O/dioxane	[26]
Et	B-$CH_2COOPfp$ (B= T, U), Et_3N, acetonitrile	1. NaOH, H_2O/dioxane, 2. $nBu_4N^+HSO_4^-$	[21]

R	Y^+	a	b	c	Ref.
Me	Bu_4N^+	B-CH_2COOH (B= T)	1. 6% HCl/AcOH, 2. Mmt-Cl, NEt_3, CH_2Cl_2	1. Bu_4NOH, dioxane	[33]
Et	Py^+	B-CH_2COOH (B= T, N^4-Bz-C, N^6-Bz-A)	1. TFA, 2. Mmt-Cl, pyridine	1. 2N NaOH, MeOH, 2. Dowex py^+	[24]

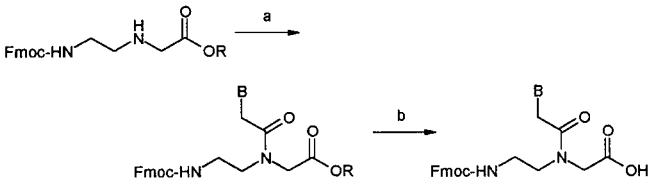
Figure 8. A) Two routes for the synthesis of Mmt monomers.[21, 26] B) Alternative synthesis of Mmt monomers:[36] a) $ClCH_2COCl$, NEt_3, THF; b) DMF, THF ↑ ; c) thymine, K_2CO_3, DMF; d) NaOH, H_2O/dioxane. C) Synthesis of Mmt monomers from the corresponding Boc monomers.[24, 33, 34] D) Synthesis of Mmt monomers via intermediates which can be precipitated:[22] a) B-CH_2COOH (B = T, N^4-An-C, N^6-An-A, N^2-*i*Bu-G, N^2-Ac-O^6-Dpc-G), TOTU, NEM/DMF or propylphosphonic anhydride, EtOAc, NEt_3; b) 95% TFA, c) Mmt-Cl, NEt_3, DMF.

ing groups established in oligonucleotide synthesis, such as the benzoyl-, anisoyl-, and *tert*-butyl benzoyl-groups for cytosine and adenine, or the isobutyryl- and acetyl-groups for guanine, are especially suitable in this context. The synthesis of these monomers, which are universally applicable for the synthesis of PNAs and PNA/DNA chimeras, is shown in Figures 8 A – C. The synthetic route[26] we follow utilizes TOTU[35] to couple the nucleobase acetic acids to Mmt-Aeg-OMe. The monomer synthesis is concluded by saponification of the methyl ester with sodium hydroxide in water/dioxane and subsequent purification by chromatography on silica gel with an eluent that contains triethylamine. Stetsenko et al.[21] coupled thyminyl and uracil acetic acids, as their pentafluorophenyl active esters, to Mmt-Aeg-OEt. After saponification of the ethyl ester with sodium hydroxide the monomers are converted into their tetrabutylammonium salts. Figure 8 B shows an attractive alternative method[36] employed by us for the synthesis of the thymine derivative. Acylation of Mmt-Aeg-OMe with chloroacetyl chloride in THF, gives a chloroacetyl derivative that can be used, after solvent exchange from THF to DMF, to alkylate thymine directly. A further synthetic route (Figure 8 C), reported by van der Laan et al.[33, 34] and Finn et al.[24], gives the Mmt-Aeg-esters by a Boc to Mmt "protecting group exchange", starting from the Boc-Aeg-esters. After saponification the monomers are converted into their tetrabutylammonium or pyridinium salts.

The route shown in Figure 8 D is used by us[22] for the large-scale synthesis of monomers. It avoids the need for chromatographic purification steps, as the fully protected intermediates that result from the coupling reaction are readily purified by precipitation.

2.1.2. Monomers with Base-labile N-Protecting Groups

So far, only Aeg monomers incorporating the base-labile Fmoc protecting group have been described. The synthesis of these monomeric building blocks is shown in Figure 9.



	a	b	Ref.
*t*Bu	B-CH_2COOH (B= T, N^4-Cbz-C, N^6-Cbz-A, N^2-Cbz-G), EDC, DMF or BOP, HOBt, DMF	HCl/dioxane or TFA, CH_2Cl_2, Et_3SiH	[20]
Me	B-CH_2COOH (B= T, N^4-Mmt-C, N^6-Mmt-A, N^2-Mmt-G), TOTU or PyBOP/ DMF /NEt_3	NaOH/dioxane/H_2O	[25]

Figure 9. Synthesis of Fmoc monomers.

Thomson et al.[20] combined the Fmoc group with the Cbz-nucleobase protection strategy of Nielsen et al.[6, 27] The monomers are obtained by the coupling of the nucleobase acetic acid derivatives to Fmoc-Aeg-OtBu, using for example BOP[37] as the activator. Treatment with HCl/dioxane or TFA results in cleavage of the *tert*-butyl ester. The addition of triethylsilane in this step is necessary to prevent partial Cbz cleavage in the adenine building block. The problem remains, however, that strongly acidic conditions (HF, TFMSA) are required to cleave the Cbz-protecting groups employed in these monomers.

A combination of the Fmoc group with the Mmt group, which can be cleaved under mildly acid conditions, gives monomers that allow deprotection under substantially milder conditions (Figure 9).[25] Although synthesis of these monomers, by the coupling of the nucleobase acetic acid derivatives with TOTU[35] or PyBOP[38], is unproblematic, the subsequent cleavage of the methyl ester in the presence of the Fmoc group is rather more challenging. The partial Fmoc-cleavage observed during this procedure can be readily reversed by the addition of a small quantity of Fmoc(ONSu) before work up.

2.2. Monomeric PNA Building-blocks with Modified Backbones

Structures that are either homologues or other modifications of the *N*-aminoethylglycine backbone have also been synthesized. In addition, monomers that incorporate chiral building blocks have been described and used for oligomer synthesis either in combination with aminoethylglycine monomers, or for the synthesis of homo-oligomers.

2.2.1. Monomers with Achiral Backbones

Phosphonic ester nucleic acids (PHONAs)[39] are PNA analogues with an *N*-(2-hydroxyethyl)aminomethylphosphonic acid backbone. PHONA monomer synthesis (Figure 10) involves reaction of O-Mmt protected aminoethanol with

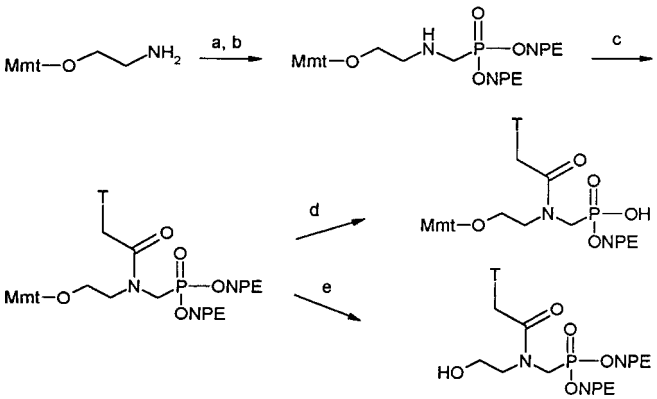


Figure 10. Synthesis of PHONA monomers:[39a] a) CH_2O, MeOH; b) $H(O)P(ONPE)_2$, 100 °C; c) thyminyl acetic acid, HOBt, NEM, DIC, DMF; d) 0.1 M DBU, pyridine; e) 80 % AcOH.

formaldehyde and phosphonic acid-bis[ethyl (4-nitrophenyl) ester]. The protected aminomethylphosphonic acid backbone unit is then coupled with thyminyl acetic acid. Subsequent selective cleavage of one of the NPE protecting groups with DBU[40] gives the desired thymine monomer that is employed

for the synthesis of PHONA homo-oligomers, and for incorporation into PNA and DNA oligomers.

Hyrup et al.[41–43] described monomers (Figure 11) based on homologues of aminoethylglycine: aminoethyl-β-alanine (**A**), aminopropylglycine (**B**) and aminopropyl-β-alanine (**C**).

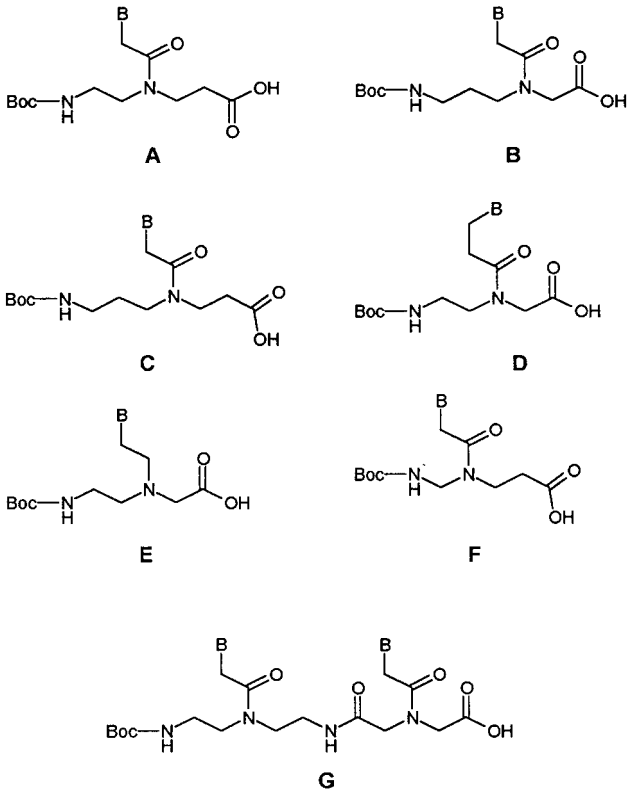


Figure 11. Monomers with modified backbone structures (**A**–**E**)[41–43] and special PNA building blocks for "retro-inverse"-PNAs (**F**[44] and **G**[45]).

Variation in the spacing (**D**) and type of attachment (**E**) of the nucleobase to the Aeg backbone were also described. These compounds are synthesized in an analogous manner to the procedures described for the Aeg derivatives.

Special monomers that are used to prepare "retro-inverse" PNAs[44] are shown in Figure 11 (**F**). Heterodimers of *N*-(2-aminoethyl)ethylenediamine and iminodiacetic acid (**G**)[45] are also used for this purpose.

2.2.2. Monomers with Chiral or Olefinic Backbones

Monomers with a chiral center in the backbone (Figure 12) have been described by several research groups. The amino acid derivatives that constitute the backbone are assembled through reductive amination of Boc-alaninal with glycine methyl ester[28] (**H**) or of Boc-glycinal with amino acid esters[46, 47] (**I**), followed by coupling of the nucleobase acetic acid derivatives to give the desired monomeric building blocks.

Further backbone variations based on ornithine (**J**)[48, 49], proline (**K**, **L**),[50–53] the conformationally constrained diaminocyclohexane (**M**),[54, 55] and the phophoramidite of 2-aminopropanediol (**N**)[56] have recently been described, as well as monomers for olefinic PNAs (**O**),[57] in which the central amide bond is replaced by a configurationally defined C–C double bond.

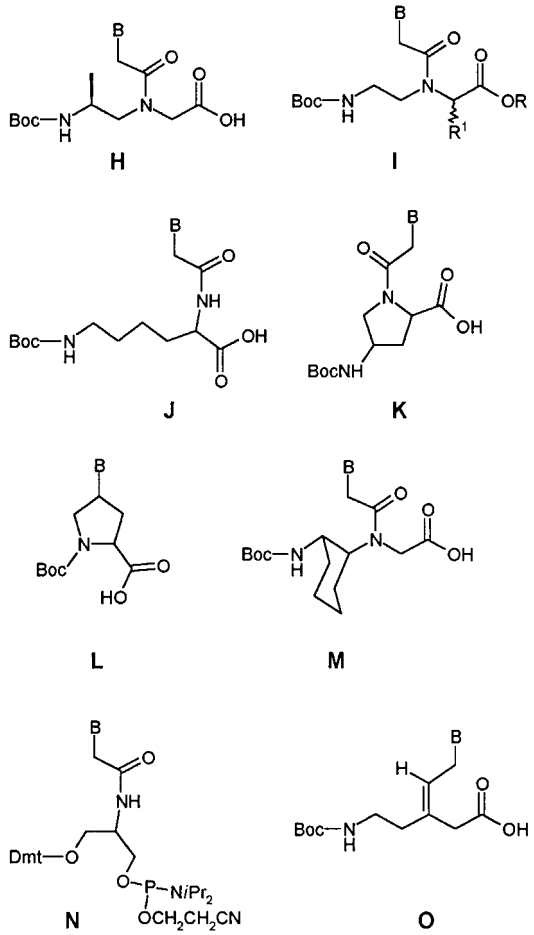


Figure 12. Monomers **H**,[28] **I** (example of R_1: CH_3, $CH_3CH_2CH(CH_3)$, CH_2OH, $CH_2CH_2CO_2H$, $(CH_2)_4NH_2$)[46, 47], **J** (based on ornithine),[48, 49] **K, L** (based on proline),[50–53] **M** (based on diaminocyclohexane)[54, 55] and **N** (based on 2-aminopropan-1,3-diol)[56] with chiral backbones and monomers based on a Z-olefinic structure (**O**).[57]

3. PNA Oligomer Synthesis

The following possibilities for preparing PNAs are summarized in Table 1.

3.1. PNAs with the Aminoethylglycine Backbone

3.1.1. The tert-Butyloxycarbonyl/Benzyloxycarbonyl (Boc/Cbz) Protecting Group Strategy

The earliest PNAs to be synthesized were homopolymers of thymine.[6, 8] They were prepared by Merrifield solid-phase synthesis on a Boc-L-lysine-derivatized MBHA polystyrene resin (Figure 13a) and were thus obtained as C-terminal lysine amides. The positive charge on the lysine side-chain helps to suppress the undesirable tendency of PNAs to self-aggregate, and simplifies their purification and characterization. The monomers described in Section 2.1.1 were used for PNA synthesis as preformed pentafluorophenyl active esters. The synthesis cycle consisted of cleavage of the N-terminal Boc temporary protecting group with TFA, followed by monomer coupling to the N terminus, which

Table 1. Summary of selected PNA synthesis methods.

Ref.	N-terminal protecting group	Base and protecting group	Solid support type	Coupling method (yield)	Capping	Cleavage and deprotection
[58]	Boc	T: none, C: N^4-Cbz, A: N^6-Cbz, G: N^2-Cbz	MBHA-polystyrene (Fig. 13a)	HBTU, diethylcyclohexylamine in DMF/pyridine (97%)	N^1-benzyloxycarbonyl-N^3-methylimidazole triflate	TFA/TFMSA
[59]	Boc	T: none, C: N^4-Cbz, A: N^6-Cbz, G: N^2-Cbz	MBHA-polystyrene	HATU, DIPEA in NMP/pyridine (99%)	acetic anhydride/NMP/pyridine, piperidine	TFA/TFMSA
[20]	Fmoc	T: none, C: N^4-Cbz, A: N^6-Cbz, G: N^2-Cbz	MBHA- or Rink-resin	pentafluorophenyl active ester (95–99%)	acetic anhydride/DIEA in NMP	HF/anisole
[25]	Fmoc	T: none, C: N^4-Mmt, A: N^6-Mmt, G: N^2-Mmt	Breipohl linker-polystyrene (Fig. 13d) or aminohexyl-succinyl-CPG	PyBOP, NEM in DMF (94%)	–	95% TFA or NH_3/H_2O
[68]	Fmoc	T: none, C: N^4-Bz, A: N^6-Bz, G: N^2-*i*Bu	hydroxydodecanoic acid-CPG (Fig. 13b)	HATU, DIPEA in DMF (not reported)	acetic anhydride in DMF	NH_3/EtOH
[26]	Mmt	T: none, C: N^4-*t*BuBz, A: N^6-An, G: N^2-*i*Bu	aminohexylsuccinyl-CPG or -Tentagel (Fig. 13c)	HATU or PyBOP, NEM or DIEA in DMF (95–99%)	acetic anhydride/lutidine/*N*-methylimidazole in THF	NH_3/H_2O

[a] The abbreviations are shown in the appendix.

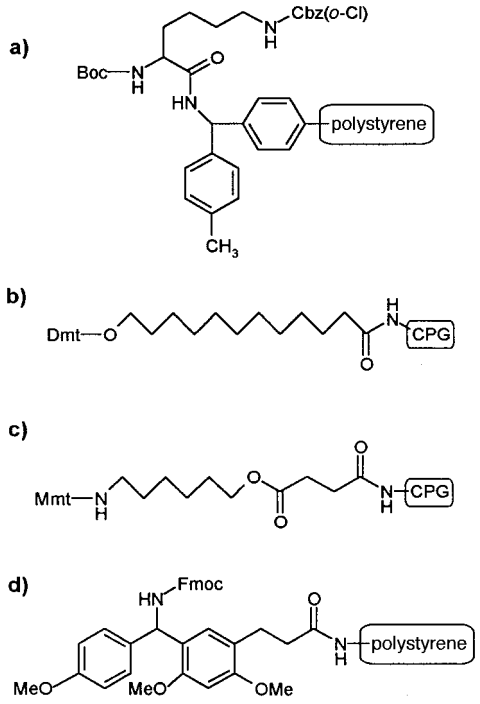


Figure 13. Supports for the solid-phase synthesis of PNA and PNA/DNA chimeras: a) Boc-Lys(Cl-Cbz)-MBHA-polystyrene;[6, 8, 27] b) dimethoxytrityl-12-hydroxydodecanoic acid-CPG;[68] c) monomethoxytrityl aminohexylsuccinate-CPG;[25, 26] d) Breipohl linker.[25]

proceeded in 94–99% yield. On completion of chain elongation the PNA oligomer was cleaved from the support with HF. Remarkably, even in these early reports PNA-nitrobenzylamido-acridinium conjugates[6, 8] were synthesized as photonuclease/intercalator ligands to provide evidence for binding.

The use of monomeric building blocks based on Boc-protected thymine, (N^4-benzyloxycarbonyl)cytosine,[7] (N^6-benzyloxycarbonyl)adenine, and (O^6-benzyl)guanine[9] in combination with in situ activation by DCC in 50% DMF/dichloromethane was reported to give coupling efficiencies of 98–100% per cycle. In 1994 the first detailed description of the preparation of these monomers and their use in PNA synthesis was published.[27] Highly efficient coupling, measured by a quantitative ninhydrin test, was achieved for all four monomers by in situ activation with DIC. Cleavage of the N-terminal Boc-group was carried out with 50% TFA in dichloromethane and, after coupling, any unreacted amino functionalities were capped with acetic anhydride in pyridine/dichloromethane. Cleavage of these mixed sequence PNA oligomers from the solid support was carried out with HF/2.5% thioanisole, and the products were purified by reversed-phase HPLC.

A systematic investigation to find the optimal synthesis conditions for a 17mer model PNA sequence, using in this case an N^2-Cbz-protected guanine monomer, was carried out by Christensen et al.[58] who found that the highest coupling efficiencies were obtained with HBTU. They also found that the use of N^1-benzyloxycarbonyl-N^3-methylimidazolium triflate instead of acetic anhydride in the capping reaction generated fewer undesirable side products. The most important side-reaction, however, was found to be the migration of the nucleobase acetic acid from the secondary amino function to the free N-terminal amino function of the aminoethylglycine backbone under basic or neutral conditions (Figure 14a). In a subsequent study the synthesis of the same PNA

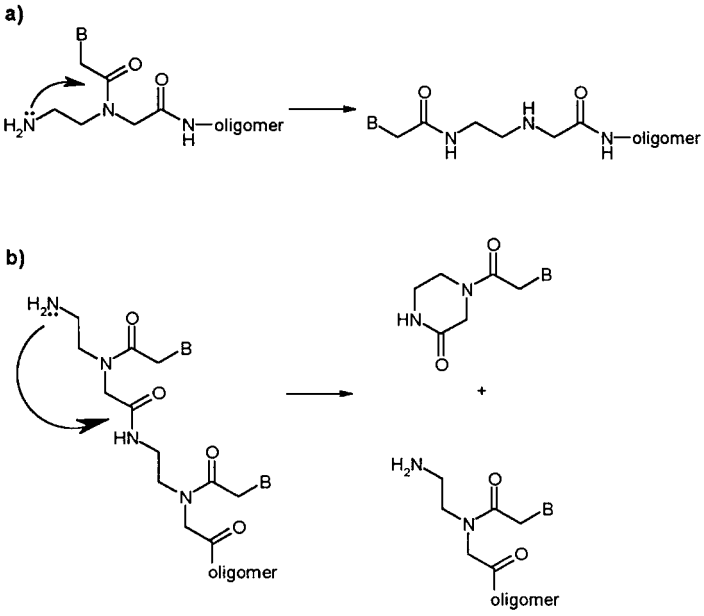


Figure 14. a) *N*-Acyl transfer reaction;[58] b) N-terminal deletion reaction.[20]

heptadecamer[59] was found to be even more efficient by using Boc/Cbz-protected monomers and HATU as the coupling reagent. Average coupling efficiencies of 99.4% per cycle were achieved on a commercial peptide synthesizer (5 μmol scale). The coupling step used a sevenfold monomer excess and a short preactivation with HATU/DIEA. Capping was carried out with acetic anhydride/NMP/pyridine, followed by a piperidine wash step to destroy any highly reactive acetylated nucleobase derivatives that can be formed in the capping step.[59]

The Boc/Cbz protected PNA monomers can also be used in conjunction with HATU activation for the synthesis of PNAs on a polyethylene glycol-polystyrene graft copolymer[60] and on polystyrene-grafted polyethylene films. [61]

The incorporation of various nonstandard nucleobases in PNAs has also been reported (Figure 15). Pseudoisocytosine[62] has been incorporated into PNAs to investigate the

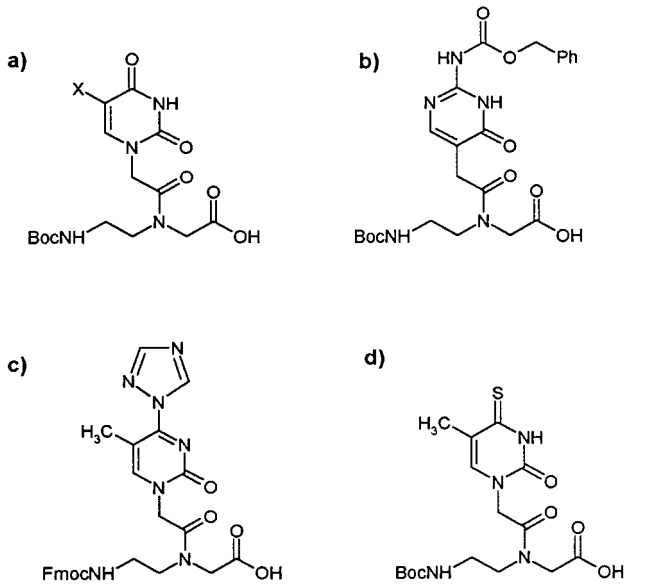


Figure 15. PNA monomeric building blocks with modified nucleobases. a) 5-Bromo- (X = Br) or 5-Iodo-uracil (X = I); b) pseudoisocytosine; c) triazolothymine; d) 4-thiothymine.

binding properties of bis(PNAs) (see Section 4.3.2), in which two different PNA sequences are linked "head-to-tail" by a flexible 8-amino-3,6-dioxaoctanoic acid linker.[63] A second nonstandard nucleobase, 5-iodouracil, has been incorporated into a bis(PNA)/peptide chimera.[64] The iodine atom was used to provide phase information for the X-ray crystal structure determination of a bis(PNA)/oligonucleotide complex. Similarly, the incorporation of 5-bromouracil[65] facilitated the structure determination of PNA · PNA duplexes. Structural investigations using photochemical reactions can be carried out on PNAs containing 4-thiothymine.[66] By using the Fmoc strategy we incorporated 5-methyl-4-(*3H*-(1,2,4)triazol-1-yl)-3,4-dihydro-*1H*-pyrimidin-2-one into PNAs.[25] This nucleobase should have served as an intermediate for the synthesis of 5-methylcytosine or thymine derivatives, however, in contrast to the analogous reaction in oligonucleotides,[67] attempts to exchange the triazolyl function in N-terminal deprotected PNAs by ammonia, ethylenediamine, or sodium hydroxide were unsuccessful.

3.1.2. The 9-Fluorenylmethyloxycarbonyl (Fmoc) Protecting Group Strategy

PNA monomers that utilize the Fmoc group for the temporary protection of the N-terminal in combination with the protection of the benzyloxycarbonyl nucleobase have been synthesized and used for PNA oligomer synthesis.[20] PNAs were obtained as their C-terminal amides or C-terminal acids when MBHA/MBHA-Rink or chlorotrityl polystyrene supports were used, respectively, for solid phase PNA synthesis. Cleavage of the N-terminal Fmoc group was carried out with 30% piperidine in 20% DMSO/NMP. The monomers, as their pentafluorophenyl active esters, were used in twofold excess in the coupling step. The synthesis cycle was completed with a capping step that used acetic anhydride/DIEA in NMP. Yields of 95 to 99% per cycle were obtained. A comparison of the pentafluorophenyl coupling method with HBTU/HOBt activation of the free acids of the monomers demonstrated the superiority of the former method.[20]

On completion of the oligomer synthesis the final N-terminal Fmoc group was retained, and the PNA was cleaved from the support with HF/anisole. The intact terminal Fmoc group could be used as a lipophilic handle to facilitate separation of the full-length PNA from failure sequences by reversed-phase HPLC, and could be removed after purification by treatment with piperidine. However, cleavage of the N-terminal PNA unit (Figure 14b) was observed as a new side-reaction on longer treatment with piperidine. On the other hand the N-acyl transfer reaction (Figure 14a) that had been reported previously[58] was not detected under these conditions.

Although the Fmoc strategy is undoubtedly milder than the Boc/Cbz strategy, its combination with the MBHA-solid phase linker and the benzyloxycarbonyl group for nucleobase protection still necessitates the use of harsh acidic conditions for the cleavage and deprotection of the PNA oligomer. Use of the Fmoc group as the temporary protecting group in combination with the Mmt group for protection of the exocyclic amino functions of the nucleobases[25] is more advantageous. The Mmt group gives the monomeric building blocks excellent solubility in organic solvents, and can be removed by treatment with 80% acetic acid on completion of the PNA oligomer synthesis. Oligomer synthesis can be carried out with our amide linker (Figure 13d), which allows simultaneous cleavage of the PNA amide from the solid support and deprotection of the Mmt groups with trifluoroacetic acid. Alternatively, the use of strongly acidic conditions can be avoided completely by the use of our base-labile aminohexylsuccinyl linker,[26] which allows cleavage of the deprotected PNA-hydroxyhexylamide from the support with concentrated aqueous ammonia.

A further variation of the Fmoc PNA synthesis strategy has been described by Bergmann et al.[68] for the synthesis of PNA/DNA chimeras. An Fmoc/acyl protecting group strategy was proposed for the N^4-benzoylcytosine-, N^6-benzoyladenine- and N^2-isobutyrylguanine-derivatized monomeric building blocks. Coupling was carried out with HATU/DIEA in DMF, and capping with acetic anhydride in DMF. The use of a 12-hydroxydodecanoic acid-derivatized aminoalkyl-CPG support (Figure 13b) allowed the attachment of the first PNA

unit through an ester group. The synthesized oligomer was cleaved, together with the acyl protecting groups of the nucleobase, by treatment with a solution of anhydrous ethanolic ammonia.

3.1.3. The 4-Methoxyphenyldiphenylmethyl/Acyl (Mmt/Acyl) Protecting Group Strategy

In an effort to find a milder method for PNA synthesis that would be compatible with conditions for DNA synthesis, we developed a new synthesis strategy that used the Mmt group for the temporary protection of the N-terminus and acyl protecting groups for the nucleobases.[26] The Mmt/acyl monomeric building blocks were described in section 2.1.1 (Figure 8). The lipophilic Mmt group improves the solubility of the monomers in polar organic solvents, such as DMF or acetonitrile. The solubility of the monomers could be further improved by the use of the *tert*-butylbenzoyl or anisoyl groups instead of the more commonly used unsubstituted benzoyl protecting group.

The synthesis cycle for the Mmt/acyl strategy is shown in Figure 16. The temporary protecting group Mmt can be cleaved under very mild conditions (3% trichloroacetic acid in dichloromethane), and the coupling efficiency can be determined very easily by measurement of the coloured Mmt cations released. The coupling step itself was carried out in DMF by using a short preactivation with HATU or PyBOP in the presence of DIEA. Capping, in an analogous manner to DNA synthesis, was carried out with acetic anhydride/lutidine/N-methylimidazole in THF. The use of a base-labile aminohexylsuccinyl linker between the CPG- or Tentagel solid-support and the PNA (Figure 13c) allowed the simultaneous cleavage of the desired PNA oligomer from the support and deprotection of its nucleobases with concentrated aqueous ammonia. To avoid potential side reactions (Figure 14) the final N-terminal Mmt protecting group was left intact during the ammonia treatment and subsequently removed by treatment with 80% acetic acid. Alternatively, the PNA strand could be converted into its base-stable N-terminal acetyl form by cleavage of the final Mmt group and subsequent capping.

The PNAs were thus obtained in the form of their C-terminal hydroxyhexylamides. The N-terminal Mmt group can be used as a lipophilic handle, in an analogous manner to the Dmt group in oligonucleotide purification, for so called "Trityl-on" reversed-phase HPLC purification. We also found that analysis and purification of N-terminal acetylated PNAs that contained more than three thymine or guanine residues can be carried out by ion-exchange HPLC or FPLC at pH 12, since at this high pH both guanine and thymine nucleobases are deprotonated. HPLC under alkaline conditions, which is especially useful for self-aggregating guanine-rich PNA sequences, has also been described by Bohler et al.[18] and Schmidt et al.[69] Similarly to oligonucleotides, PNA/DNA

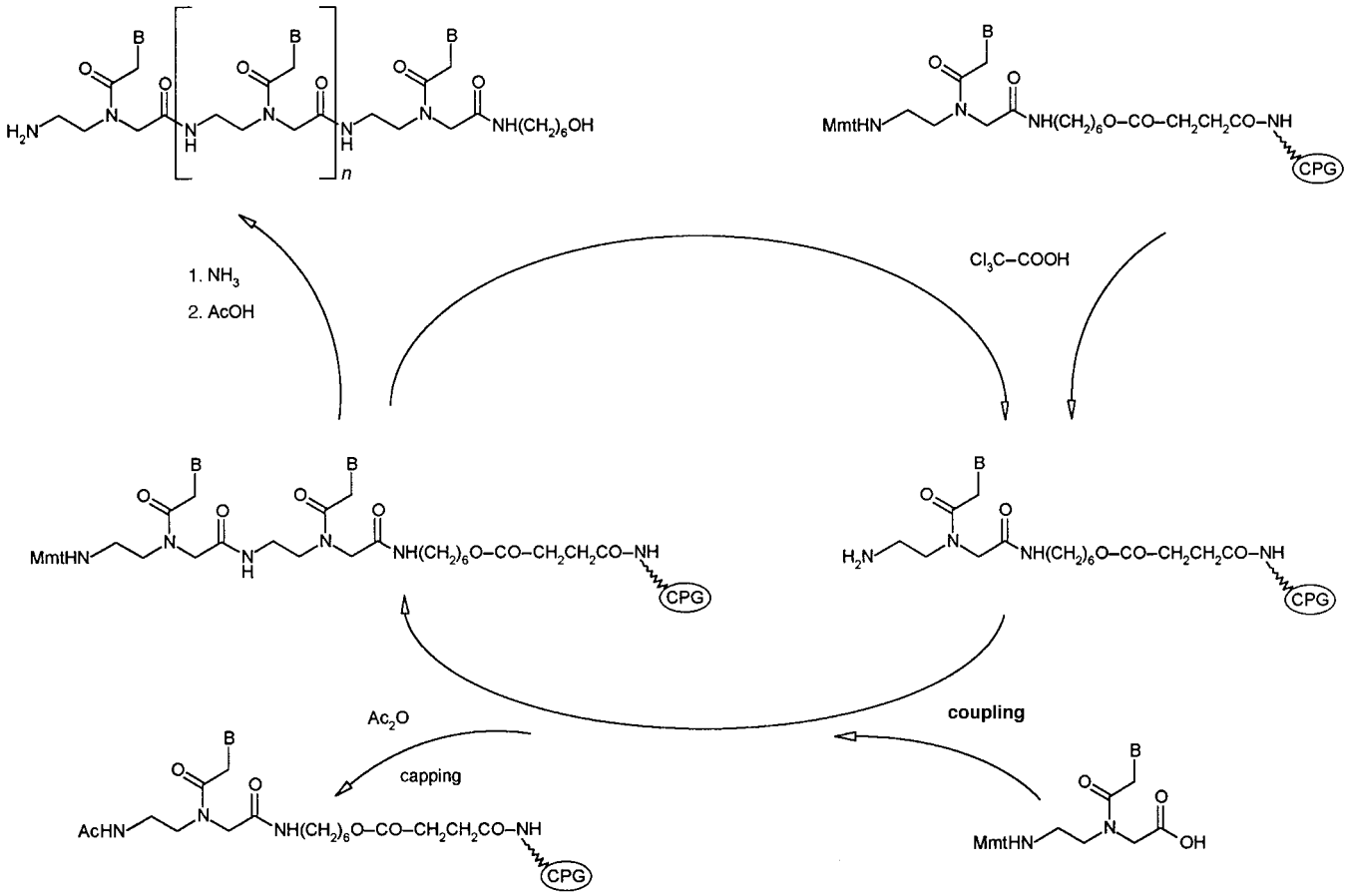


Figure 16. PNA synthesis cycle for the Mmt/Acyl-protecting group strategy.[26] Favored PNA coupling reagents are HATU, HBTU, and PyBOP.

chimeras have a multiple negative charge, (see Section 3.3) and can be analysed and purified by polyacrylamide gel electrophoresis.[70]

We use the Mmt/Acyl strategy routinely for the synthesis of PNAs and PNA/DNA chimeras on a 3 to 5 μmol scale on a modified Eppendorf Biotronik Ecosyn D300 DNA synthesizer[71] or in one to two μmol scale on an ABI (Applied Biosystems) DNA synthesizer similarly to van der Laan et al.[34]

3.1.4 Other Strategies

There is one preliminary report of the synthesis of H-ttttt-Gly-NH_2 that uses a PNA monomer with the thiol-labile dithiasuccinate (Dts) group for N-terminal temporary protection.[72]

A more exotic method for the synthesis of PNAs, which uses submonomers that do not contain the nucleobase,[73a] is outlined in Figure 17. The strategy involves the stepwise assembly of the aminoethylglycine PNA backbone units by solid-phase synthesis and acylation of the secondary amino functionality with nucleobase acetic acids. This strategy, which is reminiscent of peptoid synthesis,[73b] was applied to the synthesis of Ac-$(t)_8$-NH_2. It remains to be seen if this method in which, apart from the nucleobase acetic acid derivatives, only one monomeric building block must be synthesized, can be more generally applied to the synthesis of mixed-sequence PNAs.

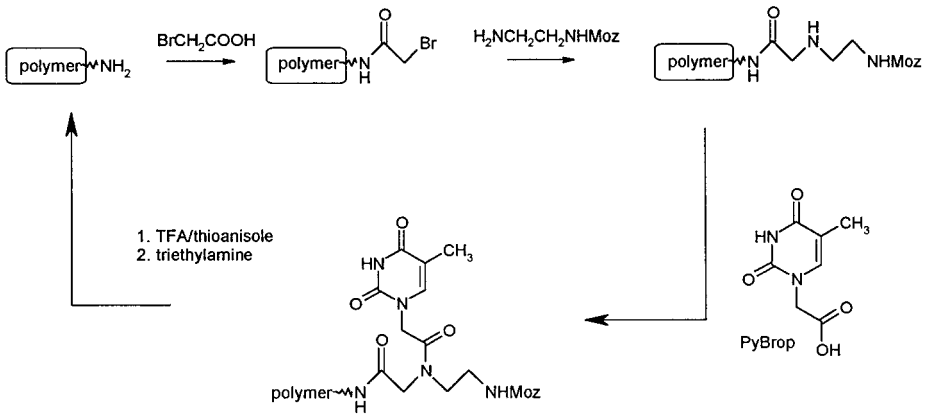


Figure 17. PNA synthesis cycle using submonomers.[73a] (Moz = 4-methoxybenzyloxycarbonyl).

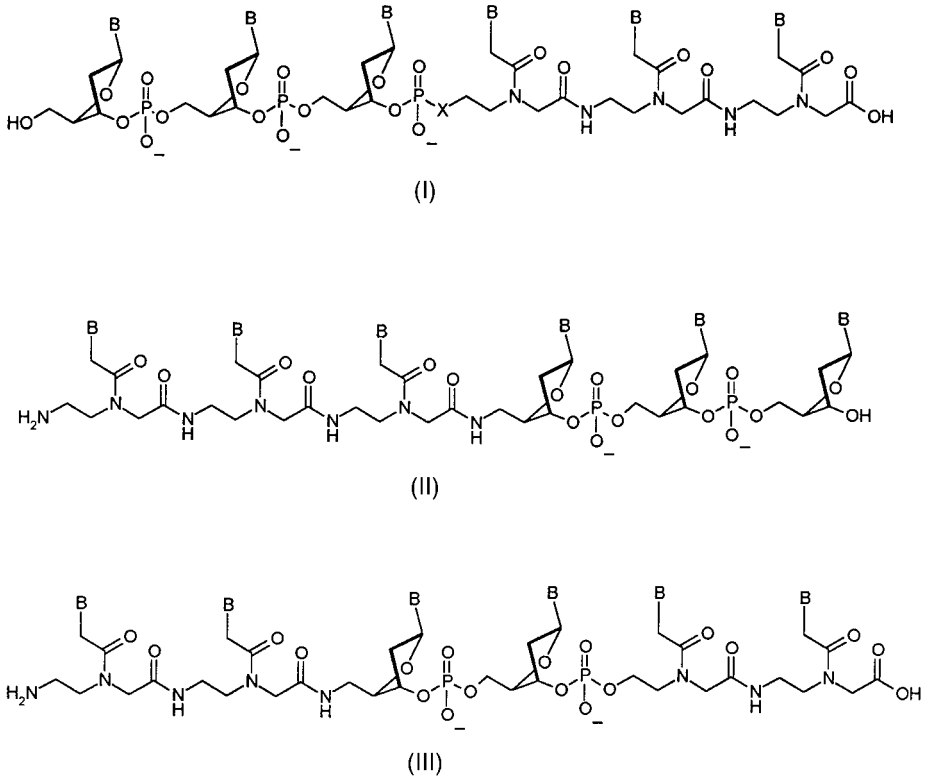


Figure 18. PNA/DNA chimeras: (I) 5′-DNA-(linker)-PNA-(*pseudo*-3′), X = NH or O; (II) (*pseudo*-5′)-PNA-(linker)-DNA-3′; (III) (*pseudo*-5′)-PNA-(linker)-DNA-(linker)-PNA-(*pseudo*-3′).

3.2. PNAs with Modified Backbones

The synthesis of backbone-modified PNAs is, in most cases, carried out in analogous ways to the methods described above. For instance, hetero-oligomeric PNAs composed of normal aminoethylglycine and aminoproline building blocks were assembled using the Boc strategy.[51, 74] This is not the case, however, for PNA derivatives that deviate strongly from the basic aminoethylglycine structure, such as the PHONAs where special synthetic methods had to be developed.[39, 75, 76]

3.3. Synthesis of PNA/DNA Chimeras

Although pure PNAs have truly remarkable binding properties, their handling during work-up, analysis, and purification is often difficult because of their tendency to self-aggregate. The synthesis of chimeric molecules composed of PNA and DNA (Figure 18) is one possible approach to addressing this problem, and would simultaneously improve the cellular uptake and the RNase H activation properties of PNAs (see Section 5).

The two principle strategies for the synthesis of PNA/DNA chimeras are "block condensation" of presynthesized PNA and DNA oligomers in solution, and stepwise "on-line" solid-phase synthesis with suitably protected

monomeric building blocks. The successful synthesis of PNA/DNA chimeras by the block condensation approach is fraught with difficulties, which include insufficient solubility and low yields,[77] and has not been realized so far. The on-line solid-phase synthesis strategy has proven to be the most successful and flexible method for the synthesis of PNA/DNA chimeras. However, to ensure full compatibility of the conditions for PNA and DNA synthesis, this method entails the development of special protecting group strategies. It also entails the synthesis of linker molecules (Figure 19) to connect PNA to DNA and vice versa.

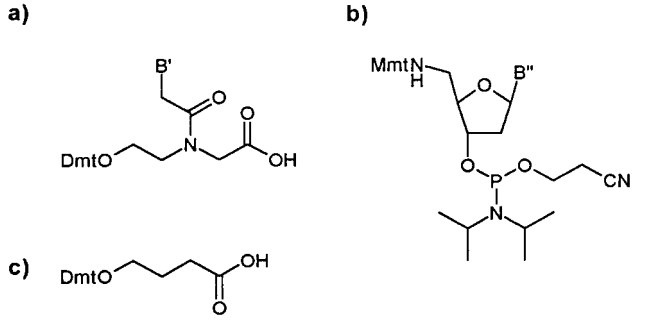


Figure 19. Types of linker molecules:[81] a) *N*-(2-hydroxyethyl)glycine PNA – DNA linker (B′ = T, N^4-An-C, N^6-An-A, N^2-iBu-G); b) 5′-amino-2′,5′-dideoxynucleoside-DNA-PNA linker (B″ = T, N^4-Bz-C, N^6-Bz-A, N^2-iBu-G); c) simple, nonhybridizing PNA – DNA linker.

So far the synthesis of three different structural classes of PNA/DNA chimeras have been described (Figure 18): (I) 5′-DNA-(linker)-PNA-(*pseudo*-3′); (II) (*pseudo*-5′)-PNA-(linker)-DNA-3′; and (III) PNA-DNA-PNA chimeras, which are a combination of (I) and (II). To avoid confusion we use lower-case letters for PNA units, and upper-case letters for DNA units when writing the sequences of PNA/DNA chimeras.

The synthesis of the homothymine oligomer (*pseudo*-5′)-(acetyl)-tttt-TTTT-3′ (T: 5′-amino-5′-deoxythymidine) of structure type (II) was carried out by van der Laan et al.[33] through on-line solid-phase synthesis on CPG. The 3′-DNA part was synthesized by standard DNA synthesis methods[78] on a 10-μmol-scale. The 3′-phosphoramidite of 5′-*N*-(4-monomethoxytrityl)amino-5′-deoxythymidine (Figure 19b), described by Bannwarth[79] and Mag et al.,[80] was used as the linker between the DNA and PNA, and was coupled to the 5′-end of the thymidylate trimer through the standard DNA synthesis cycle. Cleavage of the terminal Mmt protecting group with 2% trichloroacetic acid in dichloromethane was followed by the stepwise assembly of the PNA tetramer part in over 85% yield per cycle by using an Mmt-protected thymine PNA monomer and HBTU/DIEA activation. The terminal Mmt group was removed after the final synthetic cycle and the amino terminus was capped with acetic anhydride. Finally, treatment with ammonia removed the β-cyanoethyl protecting groups from the internucleotide bridges and cleaved the oligomer from the solid support. Unfortunately, no binding data were reported for the purified and characterized chimera.

Three PNA/DNA chimeras of structure type (I) have been synthesized by Petersen et al.[77] After initial unsuccessful attempts to couple nucleoside 3′-phosphoramidites to a hydroxyl-modified PNA oligomer in solution, they too changed to the on-line solid-phase synthesis strategy. The PNA – DNA linker utilized was *N*-(2-hydroxyethyl)-*N*-(thymin-1-ylacetyl)glycine (Figure 19a, B′ = T). Although the use of the Boc-protected thymine PNA monomer is possible for homopyrimidine chimeric sequences, it is unsuitable for chimeras containing purine bases in the DNA part; the use of HF to cleave the benzyloxycarbonyl protecting groups of cytosine, guanine, and adenine would lead to depurination in the DNA part. For this reason only homopyrimidine chimeras could be synthesized with this protecting group strategy. Synthesis was performed on a CPG solid support derivatized with a glycine linked to 4-(hydroxymethyl)benzoic acid. The PNA part was assembled from Boc/Cbz protected monomers.[58] The Dmt-protected hydroxyethylglycine – thymine linker building block was then attached, which after detritylation facilitated the assembly of the DNA part of the chimera according to standard DNA synthesis methods.[78] The resulting chimeras were linked in a "head-to-tail" manner, that is with the 3′-end of the DNA part attached to the N-terminus of the PNA part. Conversely, the use of nucleoside-5′-phosphoramidites allowed the synthesis of "head-to-head"-linked chimeras, in which the 5′-end of the DNA part is attached to the N-terminus of the PNA part. Since the amino terminus of PNAs corresponds to the 5′-end of DNA, a change of orientation takes place at the PNA – DNA junction in this type of chimera. After solid-phase synthesis the chimeras that bore a C-terminal glycine unit were cleaved with 0.1M aqueous sodium hydroxide. The benzoyl protecting groups of deoxycytidine-containing chimeras were removed by treatment with concentrated ammonia at 55°C overnight.

Bergmann et al.[68] synthesized PNA/DNA chimeras of types (I) and (III). A sarcosine-linked CPG solid support was used for the synthesis of homopyrimidine (*pseudo*-5′)-PNA-(linker)-DNA-3′ chimeras. Interestingly, the DNA part was assembled from special nucleoside 3′-phosphoramidites containing palladium-, or base-labile allyl protection, instead of the more usual cyanoethyl phosphate protection. Synthesis of the DNA strand was terminated with an Mmt-protected 5′-amino-5′-deoxynucleoside-3′-phosphoramidite[79] (Figure 19b), which serves as the DNA – PNA linker. The PNA part of the homopyrimidine chimeras was then synthesized from Boc/Cbz-protected PNA monomers. The oligopyrimidine DNA part is stable enough to survive the strongly acidic conditions required for deprotection of the PNA part. The chimeras were completely deprotected by treatment with concentrated ammonia. The use of Fmoc/acyl-protected PNA building blocks for the synthesis of mixed sequences with acid-sensitive purine nucleosides in the DNA part was suggested.[68] However, neither the preparation of these monomeric building blocks, nor their use in the synthesis of purine-containing mixed sequences have been described in detail.

The synthesis of chimeras of the type (I) starts by preparation of an alkylamino-CPG support derivatized with Dmt-protected 12-hydroxydodecanoic acid (Figure 13b).[68]

The first PNA unit was coupled to the unmasked hydroxyl function to give an ester linkage, which could be cleaved on completion of the chimera synthesis by treatment with anhydrous ethanolic ammonia. The PNA chain was extended with Fmoc/acyl-protected monomers. The DNA part of the chimera was then assembled by the coupling of standard cyanoethyl-protected DNA monomers directly onto the N-terminus of the PNA part, to give a phosphoramidate PNA – DNA linkage. The negatively charged chimeras were purified by preparative polyacrylamide gel electrophoresis, and characterized by mass spectrometry. Their nuclease stability (Section 5.1) and binding properties (Section 4.3) were then investigated.

Finn et al.[24] described the synthesis of two PNA/DNA chimeras of type (II) by using an approach based on the chimera synthesis strategy of van der Laan et al.[33] and the Mmt PNA synthesis strategy of Will et al.[26] The DNA – PNA linker employed was a 5′-amino-5′-deoxynucleotide, as described by Bergmann et al.[68] Unfortunately only the synthesis of homopyrimidine sequences was reported. The strong tendency of such sequences to form triple helices, however, complicates the study of their duplex formation with complementary nucleic acids (see Section 4.3).

The first synthesis of uracil-containing PNA/DNA chimeras was reported by Stetsenko et al.[21] An Mmt protected uracil PNA monomer was used to assemble oligomers of type (II), again by using 5′-amino-5′-deoxythymidine as the DNA – PNA linker. T_m measurements of these chimeras indicated that the DNA part was involved in cooperative binding to the complementary nucleic acid.

We recently reported the synthesis of PNA/DNA chimeras of all three structural types, which contained all four nucleobases in both the PNA and the DNA parts.[81] The previous year we introduced the Mmt/acyl protected PNA monomers, whose protecting group combination was chosen with the aim of synthesizing PNA/DNA chimeras.[26] It was of critical importance to us that the assembly of the DNA part could be carried out with commercially available standard DNA monomers. Chimeras of type (I) were synthesized on a CPG solid support derivatized with a 6-aminohexylsuccinate linker (Figure 13c), and were thus obtained as C-terminal hydroxyhexylamides. The PNA – DNA linkers employed were Dmt-protected, nucleobase-derivatized hydroxyethylglycine derivatives (Figure 19a). Alternatively, linkers that do not interact with complementary nucleic acids, such as Dmt-protected 4-hydroxybutyric acid (Figure 19c), could be used. After cleavage of the Dmt protecting group by 3 % trichloroacetic acid in dichloromethane, the DNA part was assembled by standard DNA synthesis methods.[78] Chimeras of type (II) were synthesized on a CPG solid support by utilizing 5′-amino-2′,5′-dideoxynucleoside-3′-phosphoramidites as DNA – PNA linkers (Figure 19b). The synthesis of chimeras of structure type (III), in which two structural transitions occur in a single sequence, were also reported for the first time. The enormously strong binding of these PNA-DNA-PNA chimeras to complementary DNA is especially interesting, and occurs when one PNA part binds through Watson – Crick and the other PNA part through Hoogsteen base-pairing (see Section 4.3.2).

3.4. Synthesis of PNA/Peptide Chimeras

The synthetic methods reported so far for PNA synthesis are mostly modifications and extensions of "standard" peptide synthesis strategies. It is thus no surprise that chimeras of PNA and peptides can be synthesized "on-line" by, for example, the Boc and Fmoc methods. Koch et al.[82] synthesized a PNA pentadecamer with a heptapeptide attached to the N-terminus through a tris(8-amino-3,6-dioxaoctanoic acid) by using the Boc/Cbz PNA synthesis strategy combined with Boc peptide synthesis. The chimera was found to have a slightly higher T_m on hybridization with an overhanging DNA template, which was attributed to the presence of two positively charged arginine units in the peptide. Circular dichroism (CD) experiments showed that the presence of the peptide did not significantly affect the structure of the PNA – DNA duplex. As the peptide was a substrate for protein kinase A the chimera could be enzymatically labelled with a radioactive phosphate group by kinazing the serine side-chain residue.

A PNA/peptide/PNA chimera that consisted of two oligopyrimidine PNA nonamers linked by a -His-Gly-Ser-Ser-Gly-His- peptide was synthesized by Betts et al.[64] The structure of the stable triple-helical complex formed by this chimera with an oligopurine-DNA strand was solved by X-ray crystallography. The synthesis of similar bis(PNA) structures that utilize a positively charged lysine hairpin has been described by Griffith et al.[83] PNAs with N-terminal oligohistidine peptides have been prepared by Boc/Cbz PNA synthesis followed by Fmoc peptide synthesis.[84] The resulting $(His)_6$-linker-PNA-chimeras could be bound to a nickel-derivatized column material and the capture of specific DNA and RNA sequences on the immobilized PNA was demonstrated.

4. Chemical and Physical Properties of PNAs and Chimeras

4.1. Chemical Stability

With the exception of the nucleobases, PNAs and DNA have no functional groups in common. As a result of this the chemical stability of the two compound classes is completely different. In contrast to DNA, which depurinates on treatment with strong acids, PNAs are completely acid stable. It is thus possible to synthesize PNAs by using standard protecting groups from peptide chemistry that require cleavage with trifluoromethanesulfonic acid or anhydrous HF.[27] PNAs are also sufficiently stable to weak bases that the classical, ammonia-cleavable nucleobase protecting groups, or the piperidine-labile Fmoc amino protecting group can be applied in PNA synthesis.[20, 25] The only noteworthy chemical instability of PNAs is caused by the free amino functionality at the N-terminus. A slow N-acyl transfer of the nucleobase acetic acid, or a cleavage of the N-terminal PNA unit by ring closure can occur[58] (see Figure 14), predominantly under basic conditions. This side-reaction can be suppressed by capping the final N-terminal amino function, for example with an

acetyl group. Acid-labile amino protecting groups are thus more suitable for PNA synthesis.[26]

The chemical stability of PNA/DNA chimeras is determined by the stability of the individual parts of the molecule, for example by the acid-lability of the DNA part. On the other hand, there are cooperative stabilization effects; the DNA part of 5′-DNA-PNA chimeras protects the PNA part from the deletion reaction shown in Figure 14b.

4.2. Solubility

Pure PNAs are neutral compounds with a tendency for self-aggregation and limited water solubility. However, the introduction of charged groups, for instance a C-terminal lysine amide, greatly improves their properties. For example H-$(t)_{10}$-Lys-NH_2 is water soluble at concentrations in excess of 1.5 mM.[8] PNA solubility drops with increasing length and purine:pyrimidine ratio.[13] Surprisingly, however, we found a homoadenine PNA polymer to be highly water soluble. Positive charges can also be introduced by modification of the PNA backbone, for instance by replacement of the glycine by a lysine unit.[47] The incorporation of only two such groups greatly increases the solubility of the oligomers. Alternatively, negative charges can be introduced, such as in the PNA–DNA chimeras, which show enhanced water solubility.[81]

4.3 Binding Affinity

PNAs bind superbly well to complementary DNA and even better to complementary RNA. The strongest binding affinity is to PNA itself. As PNAs are uncharged they appear to be predestined to form triple helical structures. The original design of PNAs[6] was based on a computer model of a DNA triple helix, in which the sugar–phosphate backbone of the third strand was replaced by the PNA scaffold. In spite of this, these PNA · $(DNA)_2$ triple helices are only observed for certain sequences (see Section 4.3.2). The formation of $(PNA)_2$ · DNA hybrids is favored, sometimes under strand displacement in double-stranded DNA. If the sequence is inappropriate for the formation of triple helices, then PNA · DNA, PNA · RNA or, if applicable, PNA · PNA duplexes are formed.

4.3.1. Duplex Formation with Complementary DNA and RNA

PNAs obey the Watson–Crick rules on hybridization with complementary DNA and RNA. In contrast to DNA they can, however, bind in both the parallel and antiparallel orientation,[10, 81] whereby the PNA C-terminus corresponds to the 3′ end, and the N-terminus to the 5′ end of normal oligonucleotides. As shown in Table 2, the antiparallel orientation is favored. Antiparallel PNA · DNA hybrids are considerably more stable than the corresponding DNA · DNA complexes. The increased stability results in an increase in T_m of approximately 1 K/base. Antiparallel PNA · RNA duplexes are even more stable, with a T_m increase of about 1.5 K/base relative to DNA · RNA hybrids. Consequently, PNA · RNA duplexes are on average 0.2–0.5 K/base more stable than the corresponding PNA · DNA duplexes.[85] The stability of parallel PNA · DNA and PNA · RNA duplexes is almost exactly the same as that of (antiparallel) DNA · DNA and DNA · RNA duplexes, respectively. There are dramatic differences in the kinetics of formation of duplexes of differing orientation. A kinetic study of PNA complex formation, carried out by Rose[86] using capillary electrophoresis, showed that the antiparallel complex was formed immediately (< 30 s), whereas the formation of the parallel complex required several hours.

Table 2. Melting temperatures of PNA and PNA/DNA-chimeras with complementary DNA or RNA in parallel (p) and antiparallel orientation (ap). The amino (H)-terminus of PNA corresponds to the 5′-terminus of DNA.

Sequence	T_m [°C]				Buffer[d]	Ref.
	DNA^{ap}	DNA^{p}	RNA^{ap}	RNA^{p}		
H-tgt acg tca caa cta[a]	69.5	56.1	72.3	51.2	A	[10]
5′-TGT ACG TCA CAA CTA	53.3	–	50.6	–	A	[10]
H-aca tca tgg tcg[b]	58.7	47.6	62.3	43.5	B	[81]
5′-ACA TCA TGG TCG	47.9	–	44.5	–	B	[81]
5′-ACA TCA t̲gg tcg[b, c]	52.6	< 25	52.1	< 25	B	[81]

[a] Terminal carboxamide. [b] Terminal 6-(hydroxyhexyl)carboxamide. [c] t̲: T-hydroxyethylglycine as PNA–DNA linker. [d] Buffer A: 100 mM NaCl, 10 mM NaH_2PO_4, 0.1 M EDTA, pH 7.0; buffer B: 140 mM KCl, 10 mM NaH_2PO_4, 0.1 M EDTA, pH 7.4.

An especially interesting aspect of PNA · DNA duplex formation is its dependence on ionic strength. In a careful study by Tomac et al.,[87] the T_m of DNA · DNA hybrids was shown to increase considerably (more than 20 K for a 10-mer) with increasing salt concentration (0.01 to 0.5 M NaCl), whereas the T_m of PNA · DNA duplexes decreases (ca. 8 K), so that duplex stability is almost identical at 0.5 M NaCl. Increasing in the salt concentration even further has only a weak destabilizing effect on both PNA · DNA and DNA · DNA duplexes. The contrasting effect of ionic strength on duplex formation can be explained by the association of counterions in the case of DNA · DNA duplex formation, and by displacement of counterions in the case of PNA · DNA duplex formation.

Base-pair mismatches result in a reduction of the T_m value of 8–20 K.[10] This discrimination is, in some cases, approximately double that observed for DNA · DNA duplexes.

PNA/DNA chimeras also obey the Watson–Crick rules on hybridization with complementary DNA and RNA[34, 81] (Table 2). The T_m value of chimera · DNA duplexes usually lies between that of the corresponding PNA · DNA and DNA · DNA duplexes. In detail, the T_m value is strongly dependent upon the PNA:DNA ratio in the chimera, the sequence, and also the nature and position of the linker molecule between DNA and PNA. Exclusively antiparallel-oriented complexes are formed between 5′-DNA–PNA chimeras with an hydroxyethylglycine-type linker and DNA and RNA under physiological conditions. Base-pairing mismatches in either the PNA or the DNA part result in a similar reduction in the melting temperature, whereas a base-pairing mismatch at the PNA–DNA linker results in a somewhat smaller drop in the T_m value,[34, 81] which suggests that the

duplex is slightly destabilized at the DNA – PNA transition. A stronger structural perturbation occurs at the PNA – DNA junction of duplexes with chimeras of type (II). In this case, the transition consists of an amide bond between the PNA carboxy group and the 5′-amino function of the terminal nucleotide. Interestingly, the reduction in the T_m value of the duplex with RNA is much smaller than that of the duplex with DNA. The fact that PNA · RNA duplexes are structurally more similar to DNA · RNA duplexes than PNA · DNA duplexes are to DNA · DNA duplexes may explain the improved tolerance of the perturbation caused by the transition in duplexes with RNA. The introduction of a PNA unit at the ends of a chimera perturbs the duplex structure much less than its introduction in the middle of the sequence.[68, 88] In this context, self-complementary DNA/PNA chimeras, such as the Dickerson-type oligomer 5′-CGCGAAttcgcg, are noteworthy. In the very stable duplexes formed by these chimeras each PNA unit is paired with a DNA unit, which apparently results in a relatively uniform duplex structure.[81]

Great caution is required in the interpretation of binding studies of PNA/DNA chimeras that contain a homothymine – PNA part, as these compounds have a tendency to form at least partial triple-helical structures. For example, Finn et al.[24] reported that the introduction of a mismatch in the PNA part of the PNA – DNA chimera Ac-tttcttTGCCAT-3′ resulted in a dramatic reduction of 37.3 K in the T_m value, whereas a mismatch in the DNA part resulted in a reduction of only 1.9 K. In our opinion, the only explanation for this large difference in destabilization is the formation of a partial triple-helical structure in the PNA part (Figure 20), since it is

```
      1      2
      ↓      ↓
         tttcttTGCCAT-3' Hs (p)
5'-ATGGCAAAGAAA-3'
3'-TACCGTttcttt-5'      WC (ap)

1: G --> C ⇒ ΔTm 1.9 K
2: G --> A ⇒ ΔTm 37.3 K
```

Figure 20. Partial triple-helix structure (Upper case: DNA, lower case: PNA; T: 5′-amino-5′-deoxythymidine). Hs = Hoogsteen base-pairing, WC = Watson – Crick base-pairing.

well known that a $(t)_n \cdot (dA)_n$ duplex is an exceptionally good acceptor for an additional PNA strand and forms a $(t)_n \cdot (dA)_n \cdot (t)_n$ triple helix. The binding data for a (homopyrimidine PNA)/DNA chimera reported by Petersen et al.[77] cannot be unambiguously interpreted, presumably for the same reasons. The T_m data of Stetsenko et al.,[21] on the other hand, show unambiguously that the DNA part of uracil-containing PNA/DNA chimeras participates in binding to complementary DNA.

The replacement of the glycine unit in PNA building blocks by other amino acids has various effects on duplex stability that depend upon the amino acid side-chain.[46, 47] In all cases the D-configuration is most favored. Small, uncharged side-chains, such as those of D-alanine and D-serine, do not influence duplex stability. Positively charged side-chains, such as in D-lysine, have a stabilizing effect of approximately 1 K/unit, whereas negatively charged side-chains, such as in D-glutamic acid, have a destabilizing effect.

4.3.2. Triple Helix Formation

(Homopyrimidine PNA) oligomers and PNA oligomers with a high pyrimidine:purine ratio bind to complementary DNA normally by formation of unusually stable $(PNA)_2 \cdot$ DNA triple helices.[6] However, in the case of C-rich PNAs and GC-rich DNA duplexes, PNA · $(DNA)_2$ triple helices are observed. The T_m value of H-$(t)_{10} \cdot (dA)_{10}$ is 73 °C, whereas that of the corresponding $(dT)_{10} \cdot (dA)_{10}$ hybrid lies below 23 °C.[6] However, it should be borne in mind that the PNA decamer forms a triple-helical structure, while the DNA forms a duplex. As a rule of thumb the T_m value is increased by approximately 10 K per base pair in $((t)_n)_2 \cdot (dA)_n$ complexes.[8] A very strong hysteresis, of up to 30 K,[62, 83] in the UV – melting curves of $(PNA)_2 \cdot$ DNA triple helices is an indication of the rather slow kinetics of triple-helix formation under these conditions.[89] Base-pairing mismatches result in a drop in melting temperature of 14 – 25 K.[7] Demidov et al.[90] concluded from a detailed kinetic investigation that both the binding efficiency and the sequence specificity are kinetically controlled. The sequence specificity of triple-helix formation is based on the selectivity of formation of the intermediate PNA · DNA duplex, whereas binding of the third strand contributes only slightly to selectivity.

The melting temperature of triplexes containing cytosine in their sequences is, as expected, pH-dependent (Table 3).[7]

Table 3. pH-dependence of the melting temperature of $(PNA)_2 \cdot$ DNA triple helices.

PNA[a]	DNA	T_m [°C]		
		pH 5.0	pH 7.2	pH 9.0
H-ttt tct ttt t	5′-d(AAA AGA AAA A)	80	74	71
H-ttt ttt ttt t	5′-d(AAA AAA AAA A)	71	73	71

[a] Terminal carboxamide.

The triple helix is most stable at pH 5 (C^+GC). Surprisingly the CGC base arrangement still contributes to the stability of the complex even at pH 9, where protonation of cytosine is no longer expected. A possible explanation for this behavior is a local increase in the pKa of cytosine in the triple-helical structure, or Hoogsteen base pairing through only one hydrogen bond. The pH-dependence can be eliminated in "bis(PNAs)" (see below) by the introduction of pseudoisocytosine in the Hoogsteen strand (Figure 21),[62] as has been demonstrated previously for DNA triple helices.[91, 92]

If only one PNA sequence is used to form a $(PNA)_2 \cdot$ DNA triple helix then both strands are necessarily either parallel or antiparallel to the DNA strand. Although the literature describes both orientations as being equally stable,[62, 93] we found for the sequence (*pseudo*-5′)-tctctt-(*pseudo*-3′) that the antiparallel orientation (T_m: 30 °C) was more stable than the parallel orientation (T_m: 22 °C) at pH 5. The antiparallel duplex formed initially is both kinetically and thermodynamically favored and hence determines the orientation of the strands in the triple helix. When two different homopyrimidine PNA sequences are used, the most stable complex is formed when the Watson – Crick PNA strand is oriented antiparallel and the Hoogsteen strand is parallel to the purine strand of the DNA.[62]

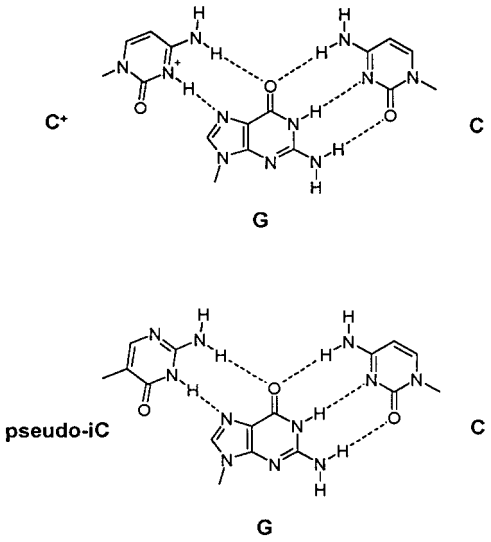


Figure 21. Hoogsteen binding with protonated cytosine (top) and with pseudoisocytosine (bottom).[62]

DNA triple helices can also be formed with the base motifs A*AT and G*GT (* represents Hoogsteen base-pairing), whereby the homopurine Hoogsteen strand is antiparallel to the Watson–Crick homopurine strand.[94] In contrast, the analogous $(PNA)_2 \cdot DNA$ triple helices are not formed by homopurine PNA.[95]

PNAs also form stable $(PNA)_2 \cdot RNA$ triple helices with RNA.[96–98] Although this type of hybrid is less-well investigated than that with DNA, the T_m values appear to be similar to those of $(PNA)_2 \cdot DNA$ triple helices. The PNA decamer H-ttcttctttt-Lys-NH_2 was found to bind to complementary RNA with a T_m of 69 °C.[98] So far, proof of triple-helix formation has mostly been provided by indirect methods, such as biological experiments. For example, the translation of CAT–mRNA was successfully inhibited by the triple helix forming PNA described above, whereas a different duplex-forming PNA had no inhibitory activity, in spite of its higher T_m value.[98]

In "bis(PNAs)" the Watson–Crick PNA strand, which binds antiparallel to DNA, and the parallel Hoogsteen strand are joined by a linker to form a single molecule (Figure 22a).[62, 64, 83]

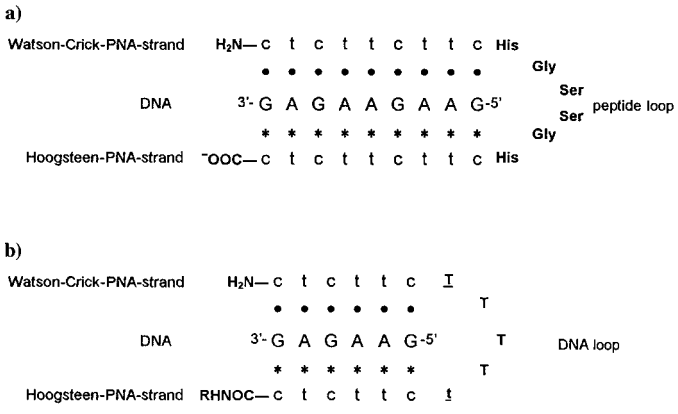
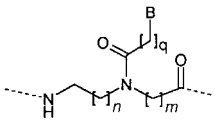


Figure 22. a) Peptide-[64] and b) DNA-bridged[81] bis(PNAs). Watson–Crick base-pairing: ●; Hoogsteen base-pairing: *; t: hydroxyethylglycine intermediate building block; T: 5′-amino-5′-deoxythymidine intermediate building block.

This leads to a small increase in the melting temperature, which presumably arises from a slight reduction in the entropy loss on triple-helix formation. The T_m value of the hybrid formed with H-tctcttt-(*eg*-1)$_3$-tttctct-Lys-NH_2 and 5′-d(CGCAGAGAAACGC) is 49 °C, where (*eg*-1) is the linker 8-amino-3,6-dioxaoctanoic acid. The corresponding triple helix formed by H-tctcttt-Lys-NH_2 and H-tttctct-Lys-NH_2 with the same DNA sequence melts at 45 °C. The hysteresis in the UV–melting curve, which is always observed for $(PNA)_2 \cdot DNA$ triple helices, is in this case largely suppressed, amounting to only 2–3 K. The high local concentration of the third strand presumably leads to much more rapid triple helix formation.[62] Sequence discrimination in bis(PNAs) is extremely high. Base mismatches result in a reduction of the melting temperature of, in some cases, over 30 K, which Egholm et al.[62] interpreted as evidence for the double-recognition process (by both PNA strands). The pH-dependence of bis(PNA) triple helix formation could be eliminated by the incorporation of pseudoisocytosine in place of cytosine in the Hoogsteen strand, but was unaffected by the same substitution in the Watson–Crick strand,[62] which confirms the proposed mode of binding (Figure 21). Variation of the linker molecule indicates that bis(PNAs) with a positively charged lysine–aminohexyl linker bind considerably better than those with a neutral (*eg*-1) linker (see above),[83] possibly as a consequence of electrostatic interactions with the negatively charged DNA. Yet another example of a bis(PNA) is the PNA/DNA chimera (*pseudo*-5′)-ctcttcTTTTtcttctc-(*pseudo*-3′) shown in Figure 22b. This molecule is so designed that the amino terminal PNA part binds through a Watson–Crick base pairing to a complementary hexamer 3′-GA-GAAG-5′, while the DNA part serves as a loop to allow the carboxy terminal PNA part to fold back and bind through Hoogsteen base-pairing.[81] The resulting triple helix formed under acidic conditions melts at 65 °C, while the DNA analogue melts at a mere 27 °C.

The binding behaviour of alternating PNA–PHONA oligomers is similar to that of PNAs. An alternating thymine 12-mer of this type binds to $d(A)_{12}$ to form a triple helix with a melting temperature of 62.6 °C.[39b] This is somewhat lower than that of the corresponding $(PNA)_2 \cdot DNA$ triple helix and can be explained by the charge repulsion between the phosphate and phosphonate groups, but is nonetheless much higher than that of the corresponding DNA triple helix. Very little is known about the binding properties of pure PHONAs.[39a] Although a PHONA-$(t)_{10}$/$(dA)_{10}$ complex has a similar T_m value to the corresponding $(T)_{10} \cdot (dA)_{10}$ duplex, it probably also forms a triple-helical structure.

PNA oligomers that contain a monomer unit with a backbone extended by one methylene group, or with a lengthened linker to the nucleobase (Figure 23), maintain the basic ability to form triple helices. Although this modification is combined with a considerable drop (approximately 13–18 K) in triple-helix stability,[41, 42] analysis of the sequence-specificity of binding nevertheless indicates that the nucleobases of these units apparently contribute to binding: base-pair mismatches result in a T_m drop of 6–21 K. The incorporation of *pa*–PNA units (Figure 23) results in the smallest loss of triple-helix stability in this series. Homo-



n	m	q	Backbone / Linker	Abbreviation
1	2	1	*N*-(2-aminoethyl)-β-alanine	β-PNA
2	1	1	*N*-(3-aminopropyl)glycine	*apg*-PNA
1	1	2	propionic acid	*pa*-PNA

Figure 23. PNA units with extended backbones or extended spacing of the nucleobase from the backbone.

oligomers of *pa*–PNA monomers bind to complementary DNA, although with a very low melting temperature. Homo-oligomers of β-PNA and *apg*-PNA monomers do not bind to complementary DNA. This is to be expected as only *pa*–PNA building blocks maintain the correct nucleobase spacing in the corresponding oligomers, whereas the incorporation of several β-PNA or *apg*-PNA building blocks forces the nucleobase spacing "out-of-phase" relative to natural nucleic acids.

A $(t)_{10}$ homo-oligomer of *orn*–PNA, a PNA analogue based on the amino acid ornithine, does not bind to complementary DNA. It does bind, however, to the oligoribonucleotide $r(A)_{10}$ to form a triple helix, $(orn\text{-}PNA)_2\cdot$RNA, with a T_m of 21 °C.[48] The replacement of the acetyl linker that connects the nucleobase to the Aeg backbone, by an ethylene group also compromises the stability of $(PNA)_2\cdot$DNA triple helices (and PNA·DNA duplexes), with a reduction in T_m of approximately 17 K.[43] The substitution of a t–t unit by the heterodimer shown in Figure 11 (Structure **G**) has little effect on the triple helix binding properties of PNAs.[45]

4.3.3. Strand Displacement

The propensity of homopyrimidine-PNAs to form $(PNA)_2\cdot$DNA triple helices is so strong that under certain conditions they can bind as a triple helix to one strand of double-stranded DNA (ds-DNA), while the second DNA strand is displaced[6, 15, 90, 99–101] and forms a single-stranded loop structure (P loop[90]). This loop structure is equivalent to the D-loop structure (displacement loop) formed under RecA-protein-mediated recombination. Prerequisites for strand displacement by PNA are: a DNA duplex that is not too stable, such as in A–T-rich regions, and, most importantly, a low salt concentration (< 50 mM NaCl).[15, 101]

Even in their original work on PNAs, Nielsen et al.[6] applied various techniques to demonstrate strand displacement between a PNA H-$(t)_{10}$-Lys-NH_2 and a DNA fragment that contained the $(dA)_{10}\cdot(T)_{10}$ target sequence: photofootprinting experiments with an acridine derivative showed protection of $(dA)_{10}$, whereas $(T)_{10}$ was not protected. In addition, incubation with staphylococcal nuclease resulted in increased cleavage of $(T)_{10}$, whereas the cleavage of $(dA)_{10}$ was unaffected. The $(T)_{10}\cdot P$-loop structure can also be cleaved by the single-strand-specific reagents $KMnO_4$ and nuclease S1. In another experiment the displaced single strand was even recognized by RNA-polymerase, such that the PNA-(ds-DNA) complex was an efficient transcription promoter for RNA-polymerases.[102] Evidence for the formation of a triple helix came from treatment of the complex (PNA: H-ttcttctttt-Lys-NH_2; ds-DNA: 5′-AAGAAGAAAA·3′-TTCTTCTTTT) with dimethyl sulfate. In this experiment the N^7 residues of the guanines were not methylated because of their involvement in Hoogsteen base pairs with a further PNA strand.[99] The pH dependence of strand displacement (SD) ($SD_{pH5.5} > SD_{pH6.5} > SD_{pH7.5}$) is also good evidence for triple helix formation,[99] as is the binding of two streptavidin molecules per complex when biotinylated PNAs are used.[103] This last experiment was carried out using electron microscopy, which allowed direct visualization of strand displacement.[103] Strand displacement is, as already discussed for triple-helix formation, largely independent of the orientation (parallel or antiparallel) of the pyrimidine PNA strand in relation to the purine strand of the complementary DNA.[93] An especially interesting aspect of strand displacement is its dependence on salt concentration. In a detailed kinetic study, Wittung et al.[100] showed that the activation energy required for strand displacement increases considerably with increasing salt concentration (Table 4). This is clearly a kinetic,

Table 4. Activation energies E_a for the binding of PNA to a poly(dA)·poly(dT) by strand replacement.[100]

PNA[a]	*c*(NaCl) [mM]	E_a [kJ mol^{-1}]
t_{10}	50	58.4 ± 3
t_{10}	150	68.8 ± 4
t_5ct_4	50	79 ± 4

[a] Carboxy terminal lysine amide.

rather than a thermodynamic effect: whereas strand displacement no longer occurs at salt concentrations as low as 80–100 mM,[101] the PNA complex can be preformed without difficulty at lower salt concentrations and then resists even higher salt concentrations of up to 500 mM.[15]

Strand displacement is highly sequence specific. In the example shown in Table 4 for a 10-mer, the activation energy increases by 20 kJ mol^{-1} for one base mismatch,[100] and strand displacement is no longer observed at 20 °C when two mismatches are present. Nielsen et al.[101] reached the same conclusion in studies of the inhibition of the cleavage of double-stranded DNA by restriction enzymes. The cleavage was completely inhibited by the complementary PNA oligomer; was reduced in the presence of a single mismatch; and was not inhibited at all when two mismatches were present. This was in spite of a reduction in the T_m value from 73 to 59 °C and 46 °C for a single and double mismatch, respectively, which, in an assay carried out at 37 °C, should still have allowed complex formation. This can be explained by the slow kinetics of strand displacement (60 to 100 times slower) when a base mismatch is present.[90, 100] The sequence specificity in this case can be described as being kinetically controlled.

Peffer et al.[93] used a transcription assay to show that although strand displacement normally occurs very rapidly (50% in 4 min), the dissociation of PNAs from these complexes is very slow (around 50% in 5–20 h). Detailed kinetic studies of strand displacement have been carried out by Demidov et al.[90] with gel shift and nuclease S1 assays, and by Wittung et al.[100] with CD spectroscopy, which allows real-time observation of strand displacement. The striking result from these studies is that the reaction kinetics are approximately second or third order with respect to the PNA

concentration, which suggests that two or more PNA molecules are involved in the rate-determining step. The activation energy of the reaction is around that required for the opening of several base pairs in double-stranded DNA. The salt concentration dependence also indicates that this is an essential part of the "activated state." Furthermore, at high PNA concentrations an intermediate can be observed at the beginning of the reaction, which may be a complex that is locally overloaded with PNA. On the basis of these results several suggestions for reaction pathways and intermediates were made, however none could fully account for all the experimental findings.[100] One variant is reversible strand displacement by formation of a PNA·DNA double helix of the Watson–Crick type, followed by the very rapid and irreversible formation of a triple helix to give the stable product[90, 100] (see Section 5.3.2 and Figure 26).

4.3.4. Binding of PNA to PNA

PNAs form extremely stable duplexes with complementary PNA sequences.[104] For example, the duplex formed by the PNA decamer H-gtagatcact-(L)-Lys-NH_2 and the complementary antiparallel sequence H-agtgatctac-(L)-Lys-NH_2 melts at 67 °C. The corresponding antiparallel DNA·PNA duplex melts at 51 °C and the DNA·DNA duplex at 33.5 °C. The antiparallel strand orientation is characteristically more stable. The corresponding parallel duplex melts at 45.5 °C, which, although 20 °C lower, is still considerably higher than the T_m of the corresponding DNA·DNA duplex. The kinetics of PNA·PNA duplex formation has been investigated by Wittung et al.[104] with CD spectroscopy. Carboxy terminal L- and D-lysine amides induce the formation of helices with opposite chirality. The spectrum of the duplex with L-lysine amide is comparable to that of the DNA·DNA double helix. A CD spectrum could not be obtained in the absence of an amino acid, presumably because of the formation of a racemate of duplexes with opposite helicity. Duplex formation occurs in seconds, and is followed by a reorganization process that is ascribed to inversion of the duplex to give the favored chiral form. Furthermore, the existence of PNA·PNA·PNA triple-helical structures has been proposed based on studies by CD spectroscopy.[54]

It should be mentioned that other self-pairing PNA derivatives exist, which are not based on the aminoethyl glycine backbone, for example the alternating alanyl/homoalanyl oligomers.[105, 106] Obviously, the nucleobase spacing in these artificial polyamide nucleic acid analogues is different from that in natural nucleic acids.

4.4. The Structure of PNA/DNA and PNA/RNA Complexes

4.4.1. The Structure of PNA·DNA Duplexes

Reasonably detailed structural information has been obtained from the NMR spectroscopic study of two antiparallel PNA·DNA duplexes (8-mer and 10-mer).[107] The DNA strand is in a conformation similar to the *B* form, with a glycosidic anti-conformation, and the deoxyribose in the C2′-endo form. The chemical shift of the imino protons of the PNA nucleobases is shifted slightly upfield relative to those of the DNA, and the NOESY cross peaks indicate Watson–Crick base-pairing.

A more recent NMR study[108] showed that an octameric antiparallel PNA·DNA duplex contained elements of both *A*-form (lateral positioning of the base pairs) and *B*-form DNA (backbone curvature, base pair inclination, helical rise). The right-handed helix contains approximately 13 base-pairs per turn compared to 10 base pairs for B-form DNA. The major groove is widened, and the minor groove is correspondingly shallow and narrow. The base stacking varies considerably within the sequence. The primary amide bonds of the PNA backbone are, without exception, in the *trans* conformation. The carbonyl oxygen atoms of the backbone–nucleobase linker point towards the carboxy terminus of the PNA strand, while the amide carbonyl groups of the backbone are, with a few exceptions, directed towards the solvent. As with PNA·RNA duplexes (see Section 4.4.2) there is no evidence for the formation of hydrogen bonds between the amide and carbonyl groups in the backbone.

The CD spectra of antiparallel PNA·DNA duplexes are similar to DNA·DNA spectra and indicate the formation of a right-handed helix.[10, 107] The CD spectra of parallel PNA·DNA duplexes, however, indicate a structure that differs considerably from that of either the *B* and *A* form.[10] Although crystals of a 10-mer PNA·DNA duplex have been obtained,[109] no results from the X-ray structure analysis were obtained because of insufficient resolution. The reduced affinity of minor groove binders and the inability of intercalators to bind to PNA·DNA duplexes[110] make it difficult to draw conclusions concerning structural changes, as these results are additionally complicated by the "missing" charges on the backbone.

4.4.2. The Structure of PNA·RNA Duplexes

Detailed structural information for PNA·RNA duplexes has also been obtained from a ^1H NMR spectroscopic study.[111] In this case the backbone of the PNA strand was enriched to greater than 98% with ^{13}C and ^{15}N to simplify the assignment of the ^1H signals. All bases form Watson–Crick base pairs, the glycosidic torsion angle in the RNA strand indicates an anti-conformation, and the ribose sugars are in the 3′-*endo* form. The RNA strand thus resembles an *A*-form structure. The tertiary amide bonds are all in the *cis* conformation, and the secondary amide protons of the backbone do not participate in any form of hydrogen bonding, which contradicts predictions from molecular modelling.[112, 113] NMR spectroscopy has also ruled out the existence of such hydrogen bonds in single-stranded PNAs.[114] The carbonyl group of the tertiary amide in the PNA backbone is isosteric to the C2′-hydroxyl group, which increases the solvent contact of the carbonyl oxygen atom.

The CD spectra of antiparallel PNA·RNA duplexes are also in agreement with this structure, and indicate the formation of a right-handed helix with a geometry similar to the *A* or *B* form.[10]

4.4.3. The Structure of $(PNA)_2 \cdot DNA$ Triple Helices

Important information on the structure of $(PNA)_2 \cdot DNA$ triple helices was obtained from a 1995 publication by Betts et al.,[64] who carried out an X-ray crystal structure analysis of the complex formed by a bis(PNA) and its complementary antiparallel DNA (see Figure 22). The nucleobases of the PNA strand bind to the DNA by Watson–Crick and Hoogsteen base pairing. The structure is different, however, from both *A*-form and *B*-form DNA, and forms a "*P* helix" with 16 bases per turn. The DNA phosphate groups are hydrogen bonded to the PNA backbone amide protons of the Hoogsteen strand. These hydrogen bonds, together with additional van der Waals contacts and the lack of electrostatic repulsion, are the main factors responsible for the enormous stability of the triple helix. The helix is considerably widened, with an average base displacement of 6.8 Å, compared to 4.5 Å in *A*-form DNA. The deoxyribose of the DNA strand is, as in *A*-form DNA, in the C3′-*endo* conformation. The bases, however, lie almost perpendicular to the helix axis, which is characteristic of *B*-form DNA. The Watson–Crick PNA–DNA interaction is further stabilized by hydrogen bonding to the solvent in the minor groove.

The crystal structure is in agreement with the CD spectra of $(PNA)_2 \cdot DNA$ triple helices measured in solution.[115] These indicate the presence of a right-handed helix and a geometry similar to that of the pure DNA triple helix.

The first evidence for the structure of *P* loops (see Section 4.3.3), which are formed on strand displacement in double-stranded DNA by bis(PNA) to produce a $(PNA)_2 \cdot$ DNA triple helix,[116] are also of interest. The introduction of a DNA-cleaving group (Gly-Gly-His, Ni^{2+}-cleavage) onto the 5′- or 3′-end of the bis(PNA) results in cleavage of not only the hybridizing DNA strand, but also of the *P* loop at specific positions. This is evidence for a close spatial arrangement of all four strands, and perhaps even for the existence of a quadruple-stranded bis(PNA) $\cdot$ $(DNA)_2$ complex.

4.4.4. The Structure of PNA · PNA Duplexes

In a recent article Rasmussen and Sandholm[65] reported the X-ray crystal structure analysis of a self-complementary PNA · PNA duplex (H-cgtacg-NH_2). This duplex exists as both right- and left-handed helices, which are stacked coaxially and alternately in the crystal, and thus form a continuous pseudohelix. As expected the base-pairing is of Watson–Crick-type, whereby the bases lie almost perpendicular to the helix axis, with a propeller twist of only about 5–9°. The base pairs are displaced by 8.3 Å relative to the helix axis, which gives a wide helix (28 Å) with 18 bases per turn (compare with the 11 and 10 bases per turn in A- and B-form DNA, respectively). Since both strands lie rather close to each other the helix has a very wide and deep major groove, and a narrow and shallow minor groove. The amide groups of the backbone are in the *trans* conformation and the carbonyl groups of the linkers point towards the carboxy terminus. Thus, the structure bears a strong similarity to the *P* form of $(PNA)_2 \cdot DNA$ helices described above.[64]

5. Biological Properties of PNAs and Chimeras

5.1. Stability in Biological Systems

The use of PNAs as antisense or antigene therapeutics requires that they show sufficiently high biological stability in serum and in cells. While unmodified oligonucleotides are digested relatively rapidly by nucleases in serum,[1] the peptide-like structure of PNAs makes their potential degradation by peptidases or proteases a possibility. However, PNAs have a remarkably high biostability in both human serum and in cell extracts.[117] For example, after a two hour incubation of the homopolymer H-$(t)_{10}$-Lys-NH_2 in human serum, or in cytoplasmic, or nuclear fractions of mouse tumour cells no significant degradation could be detected by HPLC. The PNA homopolymer was also stable to proteinase K and porcine intestinal mucosa peptidase, whereas the control peptide ACTH(4–10) was degraded rapidly under the same conditions.[117]

Figure 24 shows the stability of the PNA oligomer H-$(t)_8$-Lys-NH_2 compared to the unmodified oligonucleotide $(T)_8$ on incubation with fresh guinea pig serum. The HPLC analysis

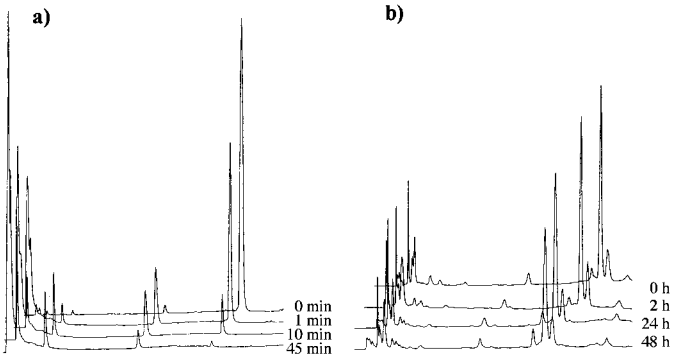


Figure 24. Comparison of the stability of unmodified DNA and PNA in fresh guinea pig serum: a) Ion exchange HPLC after incubation of $(T)_8$; b) reversed-phase HPLC after incubation of H-$(t)_8$-Lys-NH_2.

shows that the natural oligonucleotide has a very short half-life of only a few minutes, whereas around 50% of the PNA is still intact after two days. In contrast to the oligonucleotide, where distinct cleavage intermediates can be observed, the PNA oligomer produces no detectable degradation intermediates. It is thus probable that the disappearance of the PNA from the guinea pig serum is not because of its degradation, but rather that its detection is concealed by slow association with components of the serum.

DNA/PNA chimeras in which the PNA part is connected to the 3′-end of the DNA part[81] are approximately 50 times more stable in foetal calf serum than the corresponding unmodified oligonucleotides. PNA/DNA chimeras with only one PNA unit at the 5′- and 3′-ends are still 25 times more stable in human serum than the corresponding unmodified oligodeoxynucleotides.[68] The explanation for this behaviour is that the major nuclease activity in serum is caused by 3′-exonucleases. However, oligonucleotides are additionally subject to slow degradation by endonucleases, which cleave predominantly at pyrimidine nucleotides.[118, 119] Therefore, mod-

ification of the DNA part of the PNA/DNA chimera, by for example the introduction of phosphorothioate internucleoside bridges, can contribute considerably to its stabilization.

5.2. Cellular Uptake of PNAs and Chimeras

The cellular uptake of PNAs is extremely low.[11, 13, 120] It is thus not surprising that so far there are no reports of antisense activity of pure PNAs in cell culture without the use of techniques that help to bypass the membrane barrier. The antisense and antigene activity of PNAs has been studied by direct intracellular microinjection of the PNAs.[96, 97, 121] Alternatively, permeabilization of the cell membrane by lysolecitin[122] or detergents like Tween 20[123] allows the entry of PNAs into cells. In the case of transient transfection assays the PNA can be transfected in the form of a plasmid/PNA complex by using LipofectAmine in the absence of serum.[124] Covalent attachment of PNA to peptides that bind selectively to cell surface receptors can increase their cellular uptake into specific cell types.[125]

There are two reports which contradict these and our own studies and show that PNAs are taken up in rat embryo fibroblasts[121] and human myoblasts.[126] However, PNAs were applied at the high concentration (20 μM) in these studies. A punctate intracellular distribution was observed, which suggests a localization of the PNA in vesicles. However, neither of these reports demonstrated biological activity of the PNAs on incubation with these cells.

DNA/PNA chimeras, on the other hand, are taken up by Vero cells or NIH3T3 cells even at the low extracellular concentration (1 μM). The degree and kinetics of uptake are similar to those observed for an oligonucleotide of the same sequence.[81] The intracellular distribution of fluorescently labelled DNA/PNA chimeras is also similar to that of pure oligonucleotides. In our studies, pure PNAs, such as H-$(t)_8$-Lys-NH_2, could only be detected in cells at high concentrations (> 50 μM), where cytotoxic effects could also be observed.

5.3. Inhibition of Gene Expression

5.3.1. Inhibition of Translation

The sequence-specific inhibition of replication, transcription, and translation by PNAs could potentially be exploited for therapeutic applications (Figure 25). Although in the meantime numerous publications have appeared on translation inhibition by antisense oligonucleotides, there are remarkably few studies of PNA oligomers as antisense agents. Most reports so far have been on translation inhibition by PNAs in cell-free systems. For instance, the in vitro translation of an SV40-T-antigen-mRNA containing a sequence complementary to H-$(t)_3ac(t)_2c(t)_2$ could be inhibited sequence specifically at a PNA concentration of 1 to 2 μM.[97] The mechanism of inhibition was very probably steric blocking and not an RNase H-mediated mRNA degradation (see Section 5.6.1). A specific reduction in SV40-T-antigen expression was obtained at an intracellular PNA concentration of 1 μM by microinjection of PNA into cells. The expression of the *β-gal* control was not affected under these conditions. The therapeutic window was very narrow, however, as at a PNA concentration of only 5 μM, unspecific inhibition of *β-gal* expression was found, whereas at PNA concentrations lower than 0.5 μM no translation inhibition was detectable.[96] Interestingly, the antisense activity of PNAs after microinjection is less than that of the analogous propynyl–pyrimidine phosphorothioate sequences. Possible reasons are the slower kinetics of association of PNAs with the complementary RNA, or the inability of PNAs to stimulate RNase H (see Section 5.6.1). PNAs in these studies offer the advantage over other steric blockers, such as 2′-O-alkyl oligoribonucleotides, that their antisense activity is not limited to sequences targeted to the 5′-untranslated region.[96] It must be borne in mind, however, that homopyrimidine PNAs, such as H-$(t)_5(ct)_5$, were used in these studies, which in our experience tend to form partial triple-helical structures even under neutral conditions.

In vitro translation inhibition is also possible with PNAs containing all four bases at concentrations as low as 100 nM.[127] An 80% inhibition in the translation of PML/RAR (promyelocytic leukemia/retinoic acid receptor-α) was achieved with a PNA pentadecamer targeted against the translational start region at a concentration of 200 nM. A 40-fold higher concentration of an unmodified oligonucleotide was necessary to reach the same level of inhibition. However, the use of PNA concentrations of greater than 300 nM again led to unspecific inhibition of translation. A different PNA oligomer targeted against the PML/RAR fusion region was inactive under the same conditions. This is in agreement with the results of Knudsen and Nielsen,[98] which show that PNAs targeted against the 5′-proximal region to the AUG start codon can cause specific inhibition, whereas PNAs targeted to the coding region are inactive.

The behavior of triple helix forming PNAs is different, as is that of bis(PNAs) or clamp-PNAs which form at least partial triple-helical structures. Such $(PNA)_2 \cdot$ RNA triple-helix forming derivatives cause a stop in translation even when they are targeted against the coding region of mRNA. This can be confirmed by the detection of a truncated protein.[98] However, since the efficiency of translation inhibition does not correlate simply to the binding affinity, sequence optimization has to be carried out for each new target.

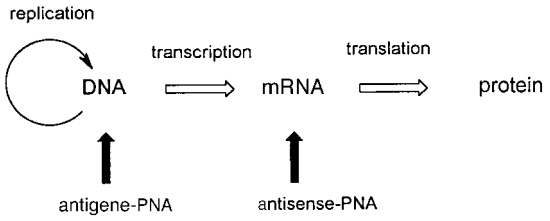


Figure 25. Potential applications of PNAs in therapeutics: inhibition of replication and transcription of DNA by antigene PNAs, and inhibition of the translation of mRNA by antisense PNAs.

5.3.2. Inhibition of Transcription

Transcription inhibition by PNAs can occur either by triple-helix formation, or by a strand invasion or strand displace-

ment process (Figure 26). Strand invasion, in which the PNA displaces one DNA strand in a DNA duplex, is especially attractive as the PNA · DNA duplex formed initially obeys the Watson – Crick base pairing rules. Consequently all four bases

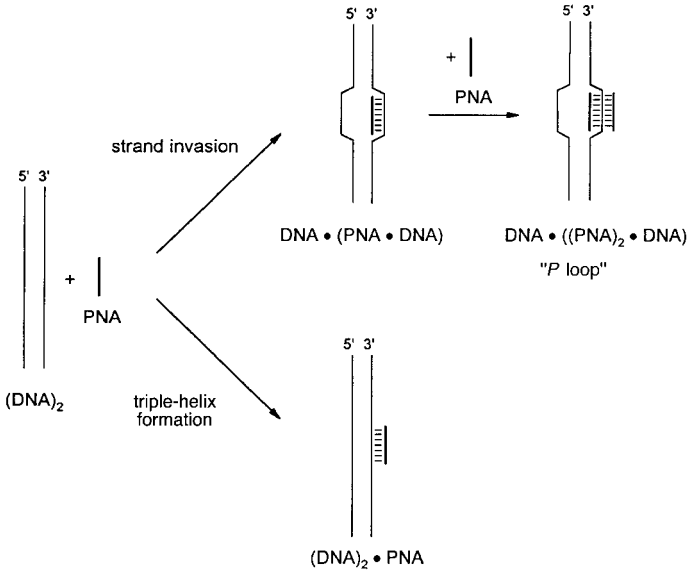


Figure 26. Strand invasion and triple-helix formation by PNAs.

in the double-stranded DNA can, in principle, be recognized. The locally formed PNA · DNA duplex can then, when appropriate, bind to a further PNA molecule to form a local $(PNA)_2 \cdot DNA$ triple helix. In contrast, direct formation of $(DNA)_2 \cdot PNA$ triple helices is at present only efficient for homopurine · homopyrimidine double strands and C-rich homopyrimidine PNAs.[128] For example, the thymine of a T · A base pair in a DNA duplex cannot be specifically recognized on triple-helix formation by any of the four natural bases. The manner in which PNAs interact with double-stranded DNA receptors, is therefore highly dependent upon the base composition of the sequence employed.

The original studies of strand invasion were carried out on homopyrimidine PNAs at low salt concentrations.[12, 97, 129] The binding of a homopyrimidine PNA oligomer to the homopurine sequence of the template strand results in an efficient blockade of transcription (Figure 27a). The binding of the PNA oligomer to the nontemplate strand, however, has little effect on the RNA polymerase reaction in vitro. The length of the transcript formed depends upon both the sequence and the polymerase employed. A high thymine content in the pyrimidine PNA gives shorter transcripts, which is equivalent to more efficient blocking of the RNA polymerase. This may be a consequence of retarded protonation of the cytosine, or with the tendency of thymine-rich PNAs to form at least partial triple-helical structures. The displacement of the nontemplate strand by homopyrimidine PNA, with the subsequent formation of a P loop,[90] which is stabilized by a $(PNA)_2 \cdot DNA$ complex, can be demonstrated by DNase footprinting.[130] This displacement leads to efficient inhibition of T7-DNA-polymerase in cell-free systems. However, this inhibition could not be reproduced in living cells, as the

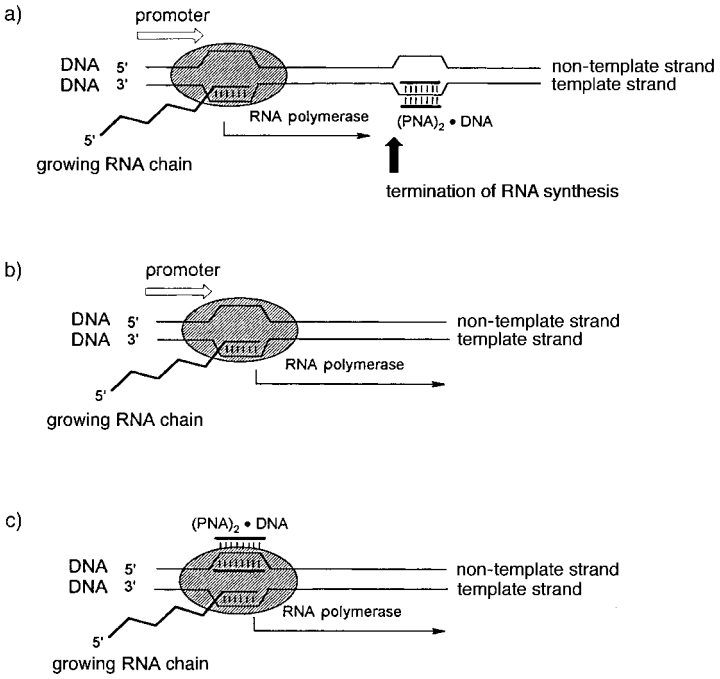


Figure 27. a) Inhibition of transcription by PNAs through strand invasion and triple helix formation on the single strand; b) open promoter complex; c) activation of transcription by PNAs.

$(PNA)_2 \cdot DNA$ complex is probably not formed at physiological salt concentrations.

We know of only one study so far in which PNAs that contain all four bases inhibited transcription in a cell-based assay successfully.[122] The PNAs, targeted against CAG triplet repeats, were originally used for the selective isolation of transcriptionally active chromatin fragments by strand displacement.[131] The cells had to be permeabilized by treatment with lysolecitin before a sequence specific and dose dependent inhibition of the transcription of the genes for the androgen receptor (AR) and the TATA binding protein (TBP) could be obtained. The transcription of the c-myc gene was not inhibited by the AR/TBP-specific PNAs, and conversely a c-myc-specific PNA oligomer inhibited c-myc transcription, but not that of AR/TBP.

The main obstacle to therapeutic use of the strand displacement principle is the stability of the natural DNA double strand, especially GC-rich sequences, under physiological salt conditions (see Section 4.3.3). A possible explanation for the surprisingly positive findings of Boffa et al.[122] may be that the PNA oligomer was targeted against a transcriptionally active DNA fragment. This supposition is supported by the dramatically increased kinetics of strand invasion during the active transcription process.[132]

5.4. Activation of Transcription

The initiation of transcription of double stranded DNA into RNA by RNA polymerases/transcription factors involves the formation of an "open" complex, in which about 12 base pairs are exposed as a single strand such that they can base-pair with the synthesized RNA (Figure 27b). This open complex is

equivalent to the P-loop structure[90] formed when two PNA strands form a triple helix with the nontemplate strand. In fact, a DNA · ((PNA)$_2$ · DNA) complex is recognized by RNA polymerases, and RNA transcription is initiated at the P loop (Figure 27c).[102] It is thus possible to view such PNA target structures as artificial promoters, in which an appropriate PNA oligomer can act, in a broader sense, as a transcription factor to control transcription.

5.5. Inhibition of Replication

The elongation of DNA primers by DNA polymerases can be inhibited by PNAs in cell free systems (see Section 5.6.3). Consequently the inhibition of DNA replication by PNAs should be possible if the DNA duplex is susceptible to strand invasion under physiological salt conditions, or if the DNA is single-stranded during the replication process. In fact, in the case of extrachromosomal mitochondrial DNA, which is largely single-stranded during replication, efficient inhibition of replication by PNAs is possible.[126]

5.6. Interactions with Enzymes

5.6.1. Ribonuclease H (RNase H)

RNA becomes a substrate for cleavage by the ubiquitous intracellular enzyme RNase H when it forms a double strand with unmodified oligodeoxyribonucleotides. The ability of oligonucleotides to stimulate RNA cleavage by RNase H is largely dependent upon their chemical structure. It is well known that antisense oligonucleotides with the ability to activate RNase H (phosphodiester and phosphorothioate oligonucleotides) are generally much better antisense inhibitors than those without this ability (e.g. methylphosphonates, 2′-O-alkyl oligoribonucleotides, α-oligonucleotides, and hexitol nucleic acids). PNAs also belong to the group of nucleic acid analogues that do not stimulate RNase H on duplex formation with RNA. It is thus hardly surprising that, in spite of their excellent binding properties, PNAs have been reported to be less effective as antisense agents than the RNase H-stimulating propynyl pyrimidine phosphorothioates.[96]

We have found, however, that DNA/PNA chimeras are able to stimulate RNA cleavage by RNase H on formation of a chimera · RNA double strand. RNA cleavage occurs at the ribonucleotides which base-pair with the DNA part of the chimera (Figure 28). The cleavage is sequence specific, as random sequence DNA/PNA chimeras do not cleave the RNA under the same conditions.[133]

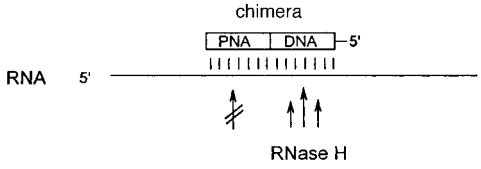


Figure 28. Schematic diagram of RNase H-mediated cleavage of RNA in a duplex with a PNA/DNA chimera.

5.6.2. Telomerase

Telomerase is a ribonucleoprotein composed of a protein component with DNA polymerase activity, and an RNA component that acts as a primer binding site. Human telomerase synthesizes long (TTAGGG)$_n$ repeats at the 3′-end of DNA strands. PNA sequences that are complementary to the RNA-primer binding site inhibit telomerase activity better than the corresponding phosphorothioate oligonucleotides because of their higher binding affinity.[123] IC_{50} values as low as 1 nM were measured for human telomerase inhibition by PNAs.[134] The activity is dependent upon the binding site and base composition of the PNA oligomer.

5.6.3. DNA Polymerases and Reverse Transcriptases

PNAs do not normally interact directly with DNA polymerases and reverse transcriptases. They can, however, terminate the elongation of oligonucleotide primers by binding to the template strand, or even compete directly with the oligonucleotide primer for binding to the template. For example, primer extension catalysed by *Taq*-polymerase can be terminated by using the PNA H-(t)$_{10}$ that binds to a (dA)$_{10}$ sequence in the template.[12] Similarly, primer extension by MMLV reverse transcriptase can be inhibited by an appropriate PNA oligomer.[97]

PNAs themselves cannot act as primers in polymerase reactions because of their structure. However, we recently demonstrated[16] that uncharged PNA primers with only a single 5′-amino-2′,5′-dideoxynucleoside at the *C*-terminus (Figure 29) are recognized by a variety of polymerases, such

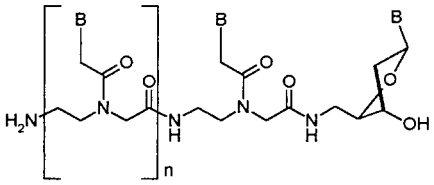


Figure 29. Structure of a PNA primer, which contains only a 5′-amino-2′,5′-dideoxynucleoside at the carboxy terminus.[16]

as the Klenow fragment of DNA polymerase I (*Escherichia coli*) and *Vent*DNA-polymerase (*Thermococcus litoralis*). This observation is made even more remarkable by crystallographic and biochemical investigations that suggest that the polymerases bind to the negative charges of the phosphate backbone through conserved amino acids in their sequences. A linear amplification is possible with the use of thermostable polymerases and an excess of PNA–DNA primer.[16] Wenninger and Seliger found that DNA templates with a PNA unit in the middle are accepted, in principle, as polymerization templates by the Klenow fragment of DNA-polymerase I. However, a partial termination of polymerization in the neighborhood of the modification takes place, which is dependent upon the structure of the incorporated PNA unit.[135] Interestingly the chemical polymerization of both PNA units and ribonucleotides on PNA templates is possible.[18] It is also worth mentioning that PNA-analogue triphosphates can be incorporated by DNA polymerases and lead to chain termination.[136] They may, therefore, be of interest principally for use in Sanger sequencing.

6. Potential Applications

6.1. Therapeutics

Potential therapeutic applications for PNAs arise from their biological properties described in Section 5. The use of PNAs for translation inhibition (antisense agents), transcription and replication modulation (antigene agents), and ribonucleoprotein interactions (inhibitors of enzymes such as telomerase) are, in principle, potential therapeutic strategies. Although the results with PNAs in cell-free systems are very encouraging, their poor cellular uptake is, at present, the main obstacle to their effective therapeutic use. The inability of antisense PNAs[96–98, 121, 137] to stimulate cellular RNase H is a further limitation.

The most promising candidates for antisense PNA constructs are, at present, the DNA/PNA chimeras, as they are taken-up by cells to a similar extent as oligonucleotides, bind to complementary RNA exclusively in the antiparallel orientation, and stimulate the sequence specific cleavage of RNA by RNase H on duplex formation.[81, 133] In addition, they have improved aqueous solubility relative to pure PNAs because of their partially negatively charged structure. The DNA part of these chimeras can be stabilized against endonuclease degradation by, for example, the introduction of phosphorothioate internucleotide bridges.[1] Preliminary investigations in cell culture indicate that three to five nucleotides in DNA/PNA chimeras are sufficient to generate antisense effects that are superior in terms of efficacy and specificity to those generated by uniformly modified phosphorothioate oligonucleotides.

In theory, antigene agents (strand invaders and triple-helix formers) should be extremely useful in therapeutic applications as a consequence of the high dose effect (one or two copies of the DNA target per cell). The first studies aimed at the use of PNA strand invasion for therapeutic purposes are: the specific inhibition of interaction of the transcription factor NF-κB with an IL2-Rα-binding site by PNA strand invasion;[124] the invasion of CAG triplet repeats resulting in inhibition of the transcription of the androgen receptor in human prostate cancer cells;[122] and transcription inhibition of a PML/RAR hybrid gene that is involved in acute promyelocytic leukemia.[127] Although PNAs associate with double-stranded DNA more than 500 times faster than normal oligonucleotides,[138] the strand invasion process in vitro is only really efficient at salt concentrations of less than 50 mM,[129] whereas the physiological salt concentration is greater than 100 mM. This should not, however, discourage investigation of this process at the cellular level, since under in vivo conditions additional effects, such as binding stabilization by cellular proteins, may play a role. For example, Boffa et al.[122] were able to inhibit specifically the transcription of the androgen receptor and TATA binding protein genes, as well as the c-myc gene in lysolecitin permeabilized cells with PNAs. It should be mentioned here that although the antigene PNA was targeted against the sense strand of the DNA, it inhibited transcription from both strands of the DNA template equally well. This contradicts the results of studies in cell-free systems, and may result, for example, from the RNA polymerase II elongation complex in vivo being much larger than the pol II complex in reconstituted systems, or to the additional influence exerted by the nucleosomal structures of the chromatin template used.[122] Strand invasion by PNAs also appears to be favored by an active transcription process ("suicide transcription").[132]

The reverse transcription of the *gag* gene of HIV-1 can be inhibited by PNAs in vitro.[139] In this case the inhibition obtained with a bis(PNA) oligomer, which recognizes the 10 nucleobase RNA target through 20 PNA nucleobases, is more efficient than that obtained with the corresponding antisense PNA decamer. Nevertheless, the reverse transcription can be completely inhibited by a pentadecameric antisense PNA at a molar ratio of 10:1 (PNA/RNA), whereby no RNase H cleavage of the RNA is detected.

The inhibition of the replication of mutant human mitochondrial DNA (*mt*DNA) by PNAs[126] is a potential approach to the treatment of patients with diseases caused by heteroplasmy of the *mt*DNA (see Section 5.5). In heteroplasmy the mutated and wild-type DNA are both present in the same cells. It has been shown that the use of PNAs under physiological conditions can inhibit the replication of the mutated mtDNA without affecting the wild-type *mt*DNA. The potential use of PNAs to inhibit human telomerase,[123] which is found in approximately 90% of all human tumours, has already been discussed (see Section 5.6.2). Finally it should be pointed out that PNAs can also be used to stimulate transcription.[102] This principle (see Section 5.4) should also be therapeutically applicable in place of a protein substitution therapy, provided that the appropriate gene, which is not, or only weakly, expressed, is not defective in the coding region.

6.2. Diagnostics

The following properties of PNAs can be exploited in the use of PNAs in DNA diagnostics: 1) PNAs have better sequence discrimination, and form more stable hybrids than oligonucleotides (see Section 4.3.1). 2) In contrast to oligonucleotides, PNAs can cause strand invasion in double-stranded DNA. 3) PNAs alter the electrophoretic mobility of complementary nucleic acids considerably on binding on account of their neutral character. It is thus advantageous to use PNAs for screening for genetic mutations, such as the detection of the CFTR gene in cystic fibrosis.[140] The procedure is based on the ability of PNA·DNA hybrids to form stable complexes at low ionic strengths and increased temperature (70 °C). These complexes can be detected rapidly by capillary electrophoresis. As an alternative to the Southern hybridization technique, labeled PNAs can be used as probes in pre-gel hybridization experiments.[141] Since PNA binding, in contrast to DNA binding, is largely independent of the ionic strength, it is possible to dissociate double-stranded DNA at low salt concentrations and hybridize it with PNA before gel electrophoresis.

The "PCR clamping" method for the detection of point mutations[142] is based on the ability of PNAs to bind more strongly to complementary nucleic acids than oligonucleotides, combined with their inability to function as primers in

the polymerase chain reaction (PCR). Targeting of the PNA oligomer, even partially, against the primer binding site can block the formation of the PCR product. Skilful choice of the length of the primer can even allow discrimination of alleles, which differ only in one base pair. Discrimination of point mutations in the Ki-*ras* gene has been carried out by PCR clamping.[143] A PNA oligomer complementary to wild-type Ki-*ras* DNA strongly inhibits amplification of the wild-type gene, relative to the mutated gene, to which it binds with lower affinity (Figure 30).

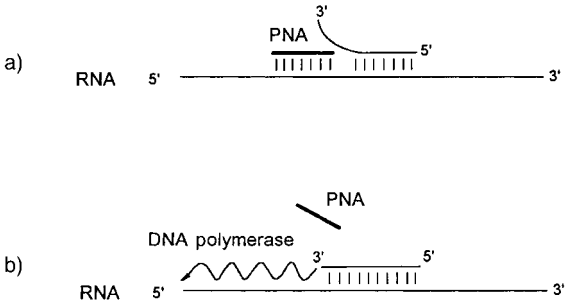


Figure 30. Schematic diagram of the "PCR clamping" technique: a) Blockade of the PCR reaction by strong binding of the PNA to the wild-type gene; b) positive PCR caused by weaker PNA binding to the mutated gene.

Demers et al. have used PNAs to suppress the preferential amplification of small allelic PCR products during copying of VNTR loci (variable number of tandem repeats), which leads to false genotypic patterns.[144] mRNA can be detected rapidly and with high sensitivity in paraffin slices with PNAs in an in situ hybridization technique.[145] The quantitation of telomeric repeats is also possible with PNAs.[146] The use of PNAs immobilized on surfaces as sequence specific DNA biosensors,[147–149] whereby hybridization can be detected electrochemically,[147] is especially interesting. However, the detection of PNA · DNA hybrids is also possible by using antibody Fab fragments.[150]

6.3. PNAs as Tools in Biotechnology

In addition to the applications for PNAs already described, such as PCR clamping and strand displacement, they can also be used for the modulation of enzymatic cleavage. For example, after strand displacement by PNA in a DNA duplex, the displaced DNA strand can be selectively cleaved by nuclease S1.[151] The single-strand-specific nuclease S1 can, in combination with two PNAs, be transformed into an "artificial restriction enzyme" that cleaves both DNA strands, and whose recognition sequence is determined by the PNA sequences employed (Figure 31). Conversely, PNAs can also be used to block DNA cleavage by restriction enzymes.[101] Furthermore, PNAs can be used to prevent the methylation of DNA sequence-specifically. On dissociation of the PNA · DNA complex only the unmethylated recognition sequence can be cleaved by the appropriate methylase-sensitive restriction enzymes.[152, 153] This principle of "rare genome-cutters" has been exploited in a similar way with triple-helix forming oligonucleotides.[154] PNAs can be used as facilitators to increase ribozyme activity in long RNA substrates that are only inadequately cleaved by Hammerhead ribozymes.[155] Modified PNAs are also useful for the sequence-specific purification of nucleic acids,[84] and for the isolation of active genes.[131] Finally it should be mentioned that, similar to oligonucleotides, PNAs can be used to generate chemical compound libraries,[156] from which, analogously to the aptamer principle,[157] molecules with defined properties can be selected.

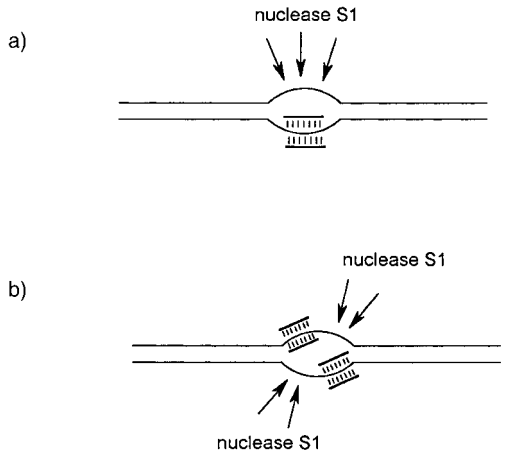


Figure 31. Artificial restriction enzymes: a) Single-strand cleavage by PNA; b) double-strand cleavage by double PNA clamping.

7. Conclusions and Future Prospects

In the last several years, efficient methods for the synthesis of both PNAs and PNA/DNA chimeras have been developed. The initial enthusiasm for this substance class, because of high binding-affinity and specificity, has, in practice, been somewhat dampened by their relatively poor solubility and the tendency for self-aggregation. However, targeted structural modifications, such as the introduction of positive or negative charges, can suppress these problems, so that, at least for in vitro experiments, PNAs are highly valuable. In specialized applications, such as PCR clamping and strand invasion, PNAs have clear advantages over their natural counterparts, and extend the arsenal of biotechnological and diagnostic tools.

The therapeutic utilization of PNAs as antisene agents is, given their nuclease stability, largely dependent upon the intracellular availability of the oligomers. Although the uptake of pure PNAs by cells in culture is poor, the use of PNA/DNA chimeras to inhibit gene expression in cell culture is possible. Unfortunately no data on the pharmacology and toxicity of PNA derivatives has yet been published. Information on this aspect of PNAs is expected to emerge in the next years, especially when the considerable growth in the number of publications in the PNA area is considered. At present, around fifteen first-generation oligonucleotides, phosphorothioates are in clinical development, many with promising results.[158, 159] In 1997 the first of the second-generation oligonucleotides, chemical chimeras of oligodeoxynucleotide

phosphorothioates and 2′-O-substituted oligoribonucleotides, was brought into clinical development. The investigations of the next years will show if PNA-based oligomers also have the potential to become a new generation of drugs. However, even if the therapeutic development of PNAs should fail, PNAs will remain valuable tools for the analysis of the function of new genes which emerge from the sequencing of the human genome ("functional genomics").

It is apparent that the combination of PNA with natural nucleic acid structures in the form of chimeras leads to extraordinarily interesting molecules, which can be recognized by certain enzymes, such as DNA polymerases or RNase H. In addition to their potential diagnostic and therapeutic applications, these PNA/DNA chimeras are of particular interest in mechanistic studies of biological processes.

PNA is also an extraordinarily interesting molecule from a structural point of view. Numerous studies of the structure of PNA complexes with itself and with natural nucleic acids have been published already. Not only do these studies improve our understanding of PNA structure, but they also supply new information on the structural and biological properties of DNA and RNA themselves. Consequently, studies on PNAs and PNA/DNA chimeras should provide valuable insights into the possibility of the evolution of alternative forms of life, and on potential transitions between different genetic systems. This in turn may give rise to new ideas on so far unexplored methods of storing and transmitting genetic information.

Appendix: List of Abbreviations

Aeg	*N*-(2-aminoethyl)glycyl
An	anisoyl
Bn	benzyl
Boc	*tert*-butyloxycarbonyl
BOP	benzotriazolyl-1-oxytris(dimethylamino)phosphonium hexafluorophosphate
t-BuBz	4-*tert*-butylbenzoyl
Bz	benzoyl
Cbz	benzyloxycarbonyl
CPG	controlled pore glass
DBU	1,8-diazabicyclo[5.4.0]undec-7-ene
DCC	dicyclohexylcarbodiimide
DIC	*N,N*′-diisopropylcarbodiimide
DIEA	ethyl diisopropylamine
Dmt	bis(4-methoxyphenyl)phenylmethyl
Dpc	diphenylcarbamoyl
Dts	dithiasuccinyl
Fmoc(ONSu)	9-fluorenylmethyloxycarbonyl (*N*-hydroxysuccimide)
HATU	*O*-(7-azabenzotriazol-1-yl)-1,1,3,3-tetramethyluronium hexafluorophosphate
HBTU	*O*-(benzotriazol-1-yl)-1,1,3,3-tetramethyluronium hexafluorophosphate
HOBt	1-hydroxybenzotriazole
HOObt	3-hydroxy-4-oxo-3,4-dihydro-1,2,3-benzotriazine
MBHA	(4-methylbenzhydryl)amine
iBu	isobutyry
Mmt	4-methoxyphenyldiphenylmethyl
NEM	*N*-ethylmorpholine
NMP	*N*-methylpyrrolidone
NPE	(4-nitrophenyl)ethyl
Pfp	pentafluorophenyl
PG	protecting group
PyBOP	benzotriazolyl-1-oxy-trispyrrolidinophosphonium hexafluorophosphate
PyBrop	bromo tris(pyrrolidino)phosphonium hexafluorophosphate
TFA	trifluoroacetic acid
TFMSA	trifluoromethanesulfonic acid
THF	tetrahydrofuran
TOTU	*O*-[(cyano(ethoxycarbonyl)methylene)amino]-1,1,3,3-tetramethyluronium tetrafluoroborate

Received: July 16, 1997
Revised version: October 20, 1997 [A 243 IE]
German version: *Angew. Chem.* 1998, *110*, 2954 – 2983

[1] E. Uhlmann, A. Peyman, *Chem. Rev.* **1990**, *90*, 543 – 584.
[2] U. Englisch, D. H. Gauss, *Angew. Chem.* **1991**, *103*, 629 – 646; *Angew. Chem. Int. Ed. Engl.* **1991**, *30*, 613 – 630.
[3] N. T. Thuong, C. Helene, *Angew. Chem.* **1993**, *105*, 697 – 723; *Angew. Chem. Int. Ed. Engl.* **1993**, *32*, 666 – 690.
[4] S. T. Crooke, C. F. Bennett, *Annu. Rev. Pharmacol. Toxicol.* **1996**, *36*, 107 – 129.
[5] E. Uhlmann, A. Peyman, D. W. Will, *Encyclopedia of Cancer*, *Vol. 1* (Ed.: J. R. Bertino), Academic Press, San Diego, CA, **1997**, pp. 64 – 81.
[6] P. E. Nielsen, M. Egholm, R. H. Berg, O. Buchardt, *Science* **1991**, *254*, 1497 – 1500.
[7] M. Egholm, P. E. Nielsen, O. Buchardt, R. H. Berg, *J. Am. Chem. Soc.* **1992**, *114*, 9677 – 9678.
[8] M. Egholm, O. Buchardt, P. E. Nielsen, R. H. Berg, *J. Am. Chem. Soc.* **1992**, *114*, 1895 – 1897.
[9] M. Egholm, C. Behrens, L. Christensen, R. H. Berg, P. E. Nielsen, O. Buchardt, *J. Chem. Soc. Chem. Commun.* **1993**, 800 – 801.
[10] M. Egholm, O. Buchardt, L. Christensen, C. Behrens, S. M. Freier, D. A. Driver, R. H. Berg, S. K. Kim, B. Norden, P. E. Nielsen, *Nature* **1993**, *365*, 566 – 568.
[11] O. Buchardt, M. Egholm, R. H. Berg, P. E. Nielsen, *Trends Biotechnol.* **1993**, *11*, 384 – 386.
[12] P. E. Nielsen, M. Egholm, R. H. Berg, O. Buchardt, *Anti-Cancer Drug Des.* **1993**, *8*, 53 – 63.
[13] B. Hyrup, P. E. Nielsen, *Bioorg. Med. Chem.* **1996**, *4*, 5 – 23.
[14] C. Meier, J. W. Engels, *Angew. Chem.* **1992**, *104*, 1039 – 1041; *Angew. Chem. Int. Ed. Engl.* **1992**, *31*, 1008 – 1010.
[15] D. Y. Cherny, B. P. Belotserkovskii, K. M. D. Frank, M. Egholm, O. Buchardt, R. H. Berg, P. E. Nielsen, *Proc. Natl. Acad. Sci. USA* **1993**, *90*, 1667 – 1670.
[16] M. J. Lutz, S. A. Benner, S. Hein, G. Breipohl, E. Uhlmann, *J. Am. Chem. Soc.* **1997**, *119*, 3177 – 3178.
[17] P. E. Nielsen, *Origins Life Evol. Biosphere* **1993**, *23*, 323 – 327.
[18] C. Bohler, P. E. Nielsen, L. E. Orgel, *Nature* **1995**, *376*, 578 – 581.
[19] E. P. Heimer, H. E. Gallo-Torres, A. M. Felix, M. Ahmad, T. J. Lambros, F. Scheidl, J. Meienhofer, *Int. J. Pept. Protein Res.* **1984**, *23*, 203 – 211.
[20] S. A. Thomson, J. A. Josey, R. Cadilla, M. D. Gaul, C. F. Hassman, M. J. Luzzio, A. J. Pipe, K. L. Reed, D. J. Ricca, R. W. Wiethe, S. A. Noble, *Tetrahedron* **1995**, *51*, 6179 – 6194.
[21] D. A. Stetsenko, E. N. Lubyako, V. K. Potapov, T. L. Azhikina, E. D. Sverdlov, *Tetrahedron Lett.* **1996**, *37*, 3571 – 3574.
[22] G. Breipohl, D. W. Will, A. Peyman, E. Uhlmann, *Tetrahedron* **1997**, *53*, 14671 – 14686.
[23] K. L. Dueholm, M. Egholm, O. Buchardt, *Org. Prep. Proced. Int.* **1993**, *25*, 457 – 461.

[24] P. J. Finn, N. J. Gibson, R. Fallon, A. Hamilton, T. Brown, *Nucleic Acids Res.* **1996**, *24*, 3357 – 3363.
[25] G. Breipohl, J. Knolle, D. Langner, G. O'Malley, E. Uhlmann, *Bioorg. Med. Chem. Lett.* **1996**, *6*, 665 – 670.
[26] D. W. Will, G. Breipohl, D. Langner, J. Knolle, E. Uhlmann, *Tetrahedron* **1995**, *51*, 12069 – 12082.
[27] K. L. Dueholm, M. Egholm, C. Behrens, L. Christensen, H. F. Hansen, T. Vulpius, K. H. Petersen, R. H. Berg, P. E. Nielsen, O. Buchardt, *J. Org. Chem.* **1994**, *59*, 5767 – 5773.
[28] L. Kosynkina, W. Wang, T. C. Liang, *Tetrahedron Lett.* **1994**, *35*, 5173 – 5176.
[29] B. E. Watkins, J. S. Kiely, H. Rapoport, *J. Am. Chem. Soc.* **1982**, *104*, 5702.
[30] R. Zou, M. J. Robins, *Can. J. Chem.* **1987**, *65*, 1436 – 1437.
[31] W. König, R. Geiger, *Chem. Ber.* **1970**, *103*, 788 – 798.
[32] B. Castro, J. Coste, M. N. Dufour, A. Pantaloni, *Pept. Chem. Struct. Biol. Proc. Am. Pept. Symp.* **1990**, *11*, 900 – 901.
[33] A. C. van der Laan, N. J. Meeuwenoord, E. Kuyl-Yeheskiely, R. S. Oosting, R. Brands, J. H. van Boom, *Recl. Trav. Chim. Pays-Bas* **1995**, *114*, 295 – 297.
[34] A. C. van der Laan, R. Brill, R. Kuimelis, E. Kuyl-Yeheskiely, J. H. van Boom, A. Andrus, R. Vinayak, *Tetrahedron Lett.* **1997**, *38*, 2249 – 2252.
[35] W. König, G. Breipohl, P. Pokorny, M. Birkner, *Pept. Proc. Eur. Pept. Symp.* **1991**, *21*, 143 – 145.
[36] G. Breipohl, D. W. Will, D. Langner, J. Knolle, E. Uhlmann, *Innovation and Perspectives in Solid Phase Synthesis* (Ed.: R. Epton), Mayflower, Birmingham, UK, **1996**, S. 61 – 64.
[37] D. Le-Nguyen, B. Castro, *Pept. Chem.* **1988**, 231 – 238.
[38] J. Coste, D. Le-Nguyen, B. Castro, *Tetrahedron Lett.* **1990**, *31*, 205 – 208.
[39] a) A. Peyman, E. Uhlmann, K. Wagner, S. Augustin, G. Breipohl, D. W. Will, A. Schaefer, H. Wallmeier, *Angew. Chem.* **1996**, *108*, 2797 – 2800; *Angew. Chem. Int. Ed. Engl.* **1996**, *35*, 2636 – 2638; b) A. Peyman, E. Uhlmann, K. Wagner, S. Augustin, C. Weiser, D. W. Will, G. Breipohl, *Angew. Chem.* **1997**, *109*, 2919 – 2922; *Angew. Chem. Int. Ed. Engl.* **1997**, *36*, 2809 – 2812.
[40] E. Uhlmann, W. Pfleiderer, *Helv. Chim. Acta* **1981**, *64*, 1688 – 1703.
[41] B. Hyrup, M. Egholm, M. Rolland, P. E. Nielsen, R. H. Berg, O. Buchardt, *J. Chem. Soc. Chem. Commun.* **1993**, 518 – 519.
[42] B. Hyrup, M. Egholm, P. E. Nielsen, P. Wittung, B. Norden, O. Buchardt, *J. Am. Chem. Soc.* **1994**, *116*, 7964 – 7970.
[43] B. Hyrup, M. Egholm, O. Buchardt, P. E. Nielsen, *Bioorg. Med. Chem. Lett.* **1996**, *6*, 1083 – 1088.
[44] A. H. Krotz, O. Buchardt, P. E. Nielsen, *Tetrahedron Lett.* **1995**, *36*, 6937 – 6940.
[45] P. H. Lagriffoul, M. Egholm, P. E. Nielsen, R. H. Berg, O. Buchardt, *Bioorg. Med. Chem. Lett.* **1994**, *4*, 1081 – 1082.
[46] K. L. Dueholm, K. H. Petersen, D. K. Jensen, M. Egholm, P. E. Nielsen, O. Buchardt, *Bioorg. Med. Chem. Lett.* **1994**, *4*, 1077 – 1080.
[47] G. Haaima, A. Lohse, O. Buchardt, P. E. Nielsen, *Angew. Chem.* **1996**, *108*, 2068 – 2070; *Angew. Chem. Int. Ed. Engl.* **1996**, *35*, 1939 – 1941.
[48] K. H. Petersen, O. Buchardt, P. E. Nielsen, *Bioorg. Med. Chem. Lett.* **1996**, *6*, 793 – 796.
[49] E. Lioy, H. Kessler, *Liebigs Ann.* **1996**, 201 – 204.
[50] B. P. Gangamani, V. A. Kumar, *Tetrahedron* **1996**, *52*, 15017 – 15030.
[51] S. Jordan, C. Schwemler, W. Kosch, A. Kretschmer, E. Schwenner, U. Stropp, B. Mielke, *Bioorg. Med. Chem. Lett.* **1997**, *7*, 681 – 686.
[52] G. Lowe, T. Vilaivan, *J. Chem. Soc. Perkin Trans. 1* **1997**, 547 – 554.
[53] G. Lowe, T. Vilaivan, *J. Chem. Soc. Perkin Trans. 1* **1997**, 539 – 546.
[54] P. Wittung, P. Nielsen, B. Norden, *J. Am. Chem. Soc.* **1997**, *119*, 3189 – 3190.
[55] P. Lagriffoule, P. Wittung, M. Eriksson, K. K. Jensen, B. Norden, O. Buchardt, P. E. Nielsen, *Chem. Eur. J.* **1997**, *3*, 912 – 919.
[56] K. S. Ramasamy, W. Seifert, *Bioorg. Med. Chem. Lett.* **1996**, *6*, 1799 – 1804.
[57] M. Cantin, R. Schütz, C. J. Leumann, *Tetrahedron Lett.* **1997**, *38*, 4211 – 4214.
[58] L. Christensen, R. Fitzpatrick, B. Gildea, K. H. Petersen, H. F. Hansen, T. Koch, M. Egholm, O. Buchardt, P. E. Nielsen, J. Coull, R. H. Berg, *J. Pept. Sci.* **1995**, *1*, 175 – 183.
[59] T. Koch, H. F. Hansen, P. Andersen, T. Larsen, H. G. Batz, K. Otteson, H. Örum, *J. Pept. Res.* **1997**, *49*, 80 – 88.
[60] F. Albericio, J. Barcardit, G. Barany, J. M. Coull, M. Egholm, E. Giralt, G. W. Griffin, S. A. Kates, E. Nicolas, N. A. Sole, *Pept. Proc. Eur. Pept. Symp.* **1994**, *23*, 271 – 272.
[61] L. Christensen, P. E. Nielsen, O. Buchardt, M. Egholm, R. H. Berg, *Pept. Proc. Eur. Pept. Symp.* **1994**, *23*, 283 – 284.
[62] M. Egholm, L. Christensen, K. L. Dueholm, O. Buchardt, J. Coull, P. E. Nielsen, *Nucleic Acids Res.* **1995**, *23*, 217 – 222.
[63] R. M. Cook, J. H. Adams, D. Hudson, *Tetrahedron Lett.* **1994**, *35*, 6777 – 6780.
[64] L. Betts, J. A. Josey, J. M. Veal, S. R. Jordan, *Science* **1995**, *270*, 1838 – 1841.
[65] H. Rasmussen, J. S. Kastrup, J. N. Nielsen, J. M. Nielsen, P. E. Nielsen, *Nature Struct. Biol.* **1997**, *4*, 98 – 101.
[66] P. Clivio, D. Guillaume, M.-T. Adeline, J.-L. Fourrey, *J. Am. Chem. Soc.* **1997**, *119*, 5255 – 5256.
[67] Y. Z. Xu, Q. Zheng, P. F. Swann, *J. Org. Chem.* **1992**, *57*, 3839 – 3845.
[68] F. Bergmann, W. Bannwarth, S. Tam, *Tetrahedron Lett.* **1995**, *36*, 6823 – 6826.
[69] J. G. Schmidt, P. E. Nielsen, L. E. Orgel, *Anal. Biochem.* **1996**, *235*, 239 – 241.
[70] D. W. Will, G. Breipohl, D. Langner, E. Uhlmann, *Innovation and Perspectives in Solid Phase Synthesis* (Ed.: R. Epton), Mayflower, Birmingham, UK, **1996**, pp. 65 – 68.
[71] E. Uhlmann, D. W. Will, G. Breipohl, A. Peyman, D. Langner, J. Knolle, G. J. O'Malley, *Nucleosides Nucleotides* **1997**, *16*, 603 – 608.
[72] K. J. Jensen, E. Bardaji, F. Albericio, J. M. Coull, G. Barany, *Pept. Proc. Eur. Pept. Symp.* **1994**, *23*, 757 – 758.
[73] a) L. S. Richter, R. N. Zuckermann, *Bioorg. Med. Chem. Lett.* **1995**, *5*, 1159 – 1162; b) R. N. Zuckermann, J. M. Kerr, S. B. Kent, W. H. Moos, *J. Am. Chem. Soc.* **1992**, *114*, 10646 – 10647.
[74] S. Jordan, C. Schwemler, W. Kosch, A. Kretschmer, U. Stropp, E. Schwenner, B. Mielke, *Bioorg. Med. Chem. Lett.* **1997**, *7*, 687 – 690.
[75] V. A. Efimov, M. V. Choob, A. L. Kalinkina, O. G. Chakhmakhcheva, R. Stromberg, A. C. van der Laan, N. J. Meeuwenoord, E. Kuyl-Yeheskiely, J. H. van Boom, *Collect. Czech. Chem. Commun.* **1996**, *61*, S262-S264.
[76] A. C. van der Laan, R. Stromberg, J. H. van Boom, E. Kuyl-Yeheskiely, V. A. Efimov, O. G. Chakhmakhcheva, *Tetrahedron Lett.* **1996**, *37*, 7857 – 7860.
[77] K. H. Petersen, D. K. Jensen, M. Egholm, P. E. Nielsen, O. Buchardt, *Bioorg. Med. Chem. Lett.* **1995**, *5*, 1119 – 1124.
[78] M. D. Matteucci, M. H. Caruthers, *J. Am. Chem. Soc.* **1981**, *103*, 3185 – 3191.
[79] W. Bannwarth, *Helv. Chim. Acta* **1988**, *71*, 1517 – 1527.
[80] M. Mag, J. W. Engels, *Nucleic Acids Res.* **1989**, *17*, 5973 – 5988.
[81] E. Uhlmann, D. W. Will, G. Breipohl, D. Langner, A. Ryte, *Angew. Chem.* **1996**, *108*, 2793 – 2797; *Angew. Chem. Int. Ed. Engl.* **1996**, *35*, 2632 – 2635.
[82] T. Koch, M. Naesby, P. Wittung, M. Joergensen, C. Larsson, O. Buchardt, C. J. Stanley, B. Norden, P. E. Nielsen, H. Oerum, *Tetrahedron Lett.* **1995**, *36*, 6933 – 6936.
[83] M. C. Griffith, L. M. Risen, M. J. Greig, E. A. Lesnik, K. G. Sprankle, R. H. Griffey, J. S. Kiely, S. M. Freier, *J. Am. Chem. Soc.* **1995**, *117*, 831 – 832.
[84] H. Oerum, P. E. Nielsen, M. Joergensen, C. Larsson, C. Stanley, T. Koch, *BioTechniques* **1995**, *19*, 472 – 480.
[85] K. K. Jensen, H. Oerum, P. E. Nielsen, B. Norden, *Biochemistry* **1997**, *36*, 5072 – 5077.
[86] D. J. Rose, *Anal. Chem.* **1993**, *65*, 3545 – 3549.
[87] S. Tomac, M. Sarkar, T. Ratilainen, P. Wittung, P. E. Nielsen, B. Norden, A. Graeslund, *J. Am. Chem. Soc.* **1996**, *118*, 5544 – 5552.
[88] D. Wenninger, H. Seliger, *Nucleosides Nucleotides* **1997**, *16*, 977 – 980.
[89] E. A. Lesnik, L. M. Risen, D. A. Driver, M. C. Griffith, K. Sprankle, S. M. Freier, *Nucleic Acids Res.* **1997**, *25*, 568 – 574.
[90] V. V. Demidov, M. V. Yavnilovich, B. P. Belotserkovskii, M. D. Frank-Kamenetskii, P. E. Nielsen, *Proc. Natl. Acad. Sci. USA* **1995**, *92*, 2637 – 2641.
[91] A. Ono, P. O. P. Ts'O, L.-S. Kan, *J. Am. Chem. Soc.* **1991**, *113*, 4032 – 4033.
[92] A. Ono, P. O. P. Ts'O, L.-S. Kan, *J. Org. Chem.* **1991**, *57*, 3225 – 3230.
[93] N. J. Peffer, J. C. Hanvey, J. E. Bisi, S. A. Thomson, C. F. Hassman, S. A. Noble, L. E. Babiss, *Proc. Natl. Acad. Sci. USA* **1993**, *90*, 10648 – 10652.
[94] C. Helene, *Curr. Opin. Biotechnol.* **1993**, *4*, 29 – 36.

[95] P. E. Nielsen, L. Christensen, *J. Am. Chem. Soc.* **1996**, *118*, 2287 – 2288.
[96] M. A. Bonham, S. Brown, A. L. Boyd, P. H. Brown, D. A. Bruckenstein, J. C. Hanvey, S. A. Thomson, A. Pipe, F. Hassman, J. E. Bisi, B. C. Froehler, M. D. Matteucci, R. W. Wagner, S. A. Noble, L. E. Babiss, *Nucleic Acids Res.* **1995**, *23*, 1197 – 1203.
[97] J. C. Hanvey, N. J. Peffer, J. E. Bisi, S. A. Thomson, R. Cadilla, J. A. Josey, D. J. Ricca, C. F. Hassman, M. A. Bonham, K. G, Au, S. G. Carter, D. A. Bruckenstein, A. L. Boyd, S. A. Noble, L. E. Babiss, *Science* **1992**, *258*, 1481 – 1485.
[98] H. Knudsen, P. E. Nielsen, *Nucleic Acids Res.* **1996**, *24*, 494 – 500.
[99] P. E. Nielsen, M. Egholm, O. Buchardt, *J. Mol. Recognit.* **1994**, *7*, 165 – 170.
[100] P. Wittung, P. E. Nielsen, B. Norden, *J. Am. Chem. Soc.* **1996**, *118*, 7049 – 7054.
[101] P. E. Nielsen, M. Egholm, R. H. Berg, O. Buchardt, *Nucleic Acids Res.* **1993**, *21*, 197 – 200.
[102] N. E. Mollegaard, O. Buchardt, M. Egholm, P. E. Nielsen, *Proc. Natl. Acad. Sci. USA* **1994**, *91*, 3892 – 3895.
[103] V. V. Demidov, D. I. Cherny, A. V. Kurakin, M. V. Yavnilovich, V. A. Malkov, M. D. Frank-Kamenetskii, S. H. Soennichsen, P. Nielsen, *Nucleic Acids Res.* **1994**, *22*, 5218 – 5222.
[104] P. Wittung, P. E. Nielsen, O. Buchardt, M. Egholm, B. Norden, *Nature* **1994**, *368*, 561 – 563.
[105] U. Diederichsen, *Angew. Chem.* **1996**, *108*, 458 – 461; *Angew. Chem. Int. Ed. Engl.* **1996**, *35*, 445 – 448.
[106] U. Diederichsen, H. W. Schmitt, *Tetrahedron Lett.* **1996**, *37*, 475 – 478.
[107] M. Leijon, A. Graeslund, P. E. Nielsen, O. Buchardt, B. Norden, S. M. Kristensen, M. Eriksson, *Biochemistry* **1994**, *33*, 9820 – 9825.
[108] M. Eriksson, P. E. Nielsen, *Nature Struct. Biol.* **1996**, *3*, 410 – 413.
[109] J. S. Kastrup, M. Pilgaard, F. S. Jorgensen, P. E. Nielsen, H. Rasmussen, *FEBS Lett.* **1995**, *363*, 115 – 117.
[110] P. Wittung, S. K. Kim, O. Buchardt, P. Nielsen, B. Norden, *Nucleic Acids Res.* **1994**, *22*, 5371 – 5377.
[111] S. C. Brown, S. A. Thomson, J. M. Veal, D. G. Davis, *Science* **1994**, *265*, 777 – 777.
[112] O. Almarsson, T. C. Bruice, J. Kerr, R. N. Zuckermann, *Proc. Natl. Acad. Sci. USA* **1993**, *90*, 7518 – 7522.
[113] O. Almarsson, T. C. Bruice, *Proc. Natl. Acad. Sci. USA* **1993**, *90*, 9542 – 9546.
[114] S. M. Chen, V. Mohan, J. S. Kiely, M. C. Griffith, R. H. Griffey, *Tetrahedron Lett.* **1994**, *35*, 5105 – 5108.
[115] S. K. Kim, P. E. Nielsen, M. Egholm, O. Buchardt, R. H. Berg, B. Norden, *J. Am. Chem. Soc.* **1993**, *115*, 6477 – 6481.
[116] M. Footer, M. Egholm, S. Kron, J. M. Coull, P. Matsudaira, *Biochemistry* **1996**, *35*, 10673 – 10679.
[117] V. Demidov, V. N. Potaman, M. D. Frank-Kamenetskii, M. Egholm, O. Buchard, S. H. Sonnichsen, P. E. Nielsen, *Biochem. Pharmacol.* **1994**, *48*, 1310 – 1313.
[118] A. Peyman, E. Uhlmann, *Biol. Chem. Hoppe-Seyler* **1996**, *377*, 67 – 70.
[119] A. Peyman, M. Helsberg, G. Kretzschmar, M. Mag, A. Ryte, E. Uhlmann, *Antiviral Res.* **1997**, *33*, 135 – 139.
[120] P. Wittung, J. Kajanus, K. Edwards, P. Nielsen, B. Norden, B. G. Malmstroem, *FEBS Lett.* **1995**, *365*, 27 – 29.
[121] S. A. Noble, M. A. Bonham, J. E. Bisi, D. A. Bruckenstein, P. H. Brown, S. C. Brown, R. Cadilla, M. D. Gaul, J. C. Hanvey, C. F. Hassman, J. A. Josey, M. J. Luzzio, P. M. Myers, A. J. Pipe, D. J. Ricca, C. W. Su, C. L. Steveson, S. A. Thomson, R. W. Wiethe, L. E. Babiss, *Drug Dev. Res.* **1995**, *34*, 184 – 195.
[122] L. C. Boffa, P. L. Morris, E. M. Carpaneto, M. Louissaint, V. G. Allfrey, *J. Biol. Chem.* **1996**, *271*, 13228 – 13233.
[123] J. C. Norton, M. A. Piatyszek, W. E. Wright, J. W. Shay, D. R. Corey, *Nature Biotechnol.* **1996**, *14*, 615 – 619.
[124] T. A. Vickers, M. C. Griffity, K. Ramasamy, L. M. Risen, S. M. Freier, *Nucleic Acids Res.* **1995**, *23*, 3003 – 3008.
[125] S. Basu, E. Wickstrom, *Bioconjugate Chem.* **1997**, *8*, 481 – 488.
[126] R. W. Taylor, P. F. Chinnery, D. M. Turnbull, R. N. Lightowlers, *Nature Genet.* **1997**, *15*, 212 – 215.
[127] C. Gambacorti-Passerini, L. Mologni, C. Bertazzoli, P. le Coutre, E. Marchesi, F. Grignani, P. E. Nielsen, *Blood* **1996**, *88*, 1411 – 1417.
[128] P. Wittung, P. Nielsen, B. Norden, *Biochemistry* **1997**, *36*, 7973 – 7979.
[129] P. E. Nielsen, M. Egholm, O. Buchardt, *Gene* **1994**, *149*, 139 – 145.
[130] D. Praseuth, M. Grigoriev, A.-L. Guieysse, L. L. Pritchard, A. Harel-Bellan, P. E. Nielsen, C. Helene, *Biochim. Biophys. Acta* **1996**, *1309*, 226 – 238.
[131] L. C. Boffa, E. M. Carpaneto, V. G. Allfrey, *Proc. Natl. Acad. Sci. USA* **1995**, *92*, 1901 – 1905.
[132] H. J. Larsen, P. E. Nielsen, *Nucleic Acids Res.* **1996**, *24*, 458 – 463.
[133] M. Reiter, D. W. Will, S. Hein, G. Breipohl, J. W. Engels, E. Uhlmann, unpublished results.
[134] S. E. Hamilton, A. E. Pitts, R. R. Katipally, X. Jia, J. P. Rutter, B. A. Davies, J. W. Shay, W. E. Wright, D. R. Corey, *Biochemistry* **1997**, *36*, 11873 – 11880.
[135] D. Wenninger, H. Seliger, *Nucleosides Nucleotides* **1997**, *16*, 761 – 768.
[136] C. I. Martinez, K. Burgess, *Abstr. Pap. 213rd ACS National Meeting* (San Francisco, CA) **1997**, CARB-095.
[137] A. De Mesmaeker, K.-H. Altmann, A. Waldner, S. Wendeborn, *Curr. Opin. Struct. Biol.* **1995**, *5*, 343 – 355.
[138] M. Iyer, J. C. Norton, D. R. Corey, *J. Biol. Chem.* **1995**, *270*, 14712 – 14717.
[139] U. Koppelhus, V. Zachar, P. E. Nielsen, X. Liu, J. Eugen-Olsen, P. Ebbesen, *Nucleic Acids Res.* **1997**, *25*, 2167 – 2173.
[140] C. Carlsson, M. Jonsson, B. Norden, M. T. Dulay, R. N. Zare, J. Noolandi, P. E. Nielsen, L.-C. Tsui, J. Zielenski, *Nature* **1996**, *380*, 207.
[141] H. Perry-O'Keefe, X.-W. Yao, J. M. Coull, M. Fuchs, M. Egholm, *Proc. Natl. Acad. Sci. USA* **1996**, *93*, 14670 – 14675.
[142] H. Oerum, P. E. Nielsen, M. Egholm, R. H. Berg, O. Buchardt, C. Stanley, *Nucleic Acids Res.* **1993**, *21*, 5332 – 5336.
[143] C. Thiede, E. Bayerdoerffer, R. Blasczyk, B. Wittig, A. Neubauer, *Nucleic Acids Res.* **1996**, *24*, 983 – 984.
[144] D. B. Demers, E. T. Curry, M. Egholm, A. C. Sozer, *Nucleic Acids Res.* **1995**, *23*, 3050 – 3055.
[145] M. Thisted, T. Just, K.-J. Pluzek, K. H. Petersen, J. J. Hyldig-Nielsen, S. E. Godtfredsen, *Cell Vision* **1996**, *3*, 358 – 363.
[146] P. M. Lansdorp, N. P. Verwoerd, F. M. van de Rijke, V. Dragowska, M.-T. Little, R. W. Dirks, A. K. Raap, H. J. Tanke, *Hum. Mol. Genet.* **1996**, *5*, 685 – 691.
[147] J. Wang, E. Palecek, P. E. Nielsen, G. Rivas, X. Cai, H. Shiraishi, N. Dontha, D. Luo, P. A. M. Farias, *J. Am. Chem. Soc.* **1996**, *118*, 7667 – 7670.
[148] H. F. Arlinghaus, M. N. Kwoka, K. B. Jacobson, *Anal. Chem.* **1997**, *69*, 3747 – 3753.
[149] J. Weiler, H. Gausepohl, N. Hauser, O. N. Jensen, J. D. Hoheisel, *Nucleic Acids Res.* **1997**, *25*, 2792 – 2799.
[150] M. H. Hansen, L. L. Sode, J. J. Hyldig-Nielsen, J. Engberg, *J. Immunol. Methods* **1997**, *203*, 199 – 207.
[151] V. Demidov, M. D. Frank-Kamenetskii, M. Egholm, O. Buchardt, P. E. Nielsen, *Nucleic Acids Res.* **1993**, *21*, 2103 – 2107.
[152] A. G. Veselkov, V. V. Demidov, P. E. Nielsen, M. D. Frank-Kamenetskii, *Nucleic Acids Res.* **1996**, *24*, 2483 – 2487.
[153] A. G. Veselkov, V. V. Demidov, M. D. Frank-Kamenetskii, P. E. Nielsen, *Nature* **1996**, *379*, 214.
[154] S. A. Strobel, P. B. Dervan, *Nature* **1991**, *350*, 172 – 174.
[155] E. Jankowsky, G. Strunk, B. Schwenzer, *Nucleic Acids Res.* **1997**, *25*, 2690 – 2693.
[156] P. E. Nielsen, *Methods Enzymol.* **1996**, *267*, 426 – 433.
[157] M. Famulok, J. W. Szostak, *Angew. Chem.* **1992**, *104*, 1001 – 1011; *Angew. Chem. Int. Ed. Engl.* **1992**, *31*, 979 – 988.
[158] W. Roush, *Science* **1997**, *276*, 1192 – 1193.
[159] S. Akhtar, S. Agrawal, *Trends Pharm. Sci.* **1997**, *18*, 12 – 18.
[160] W. König, R. Geiger, *Chem. Ber.* **1970**, *103*, 2034 – 2040.

Explosions as a Synthetic Tool? Cycloalkynes as Precursors to Fullerenes, Buckytubes, and Buckyonions

Rüdiger Faust*

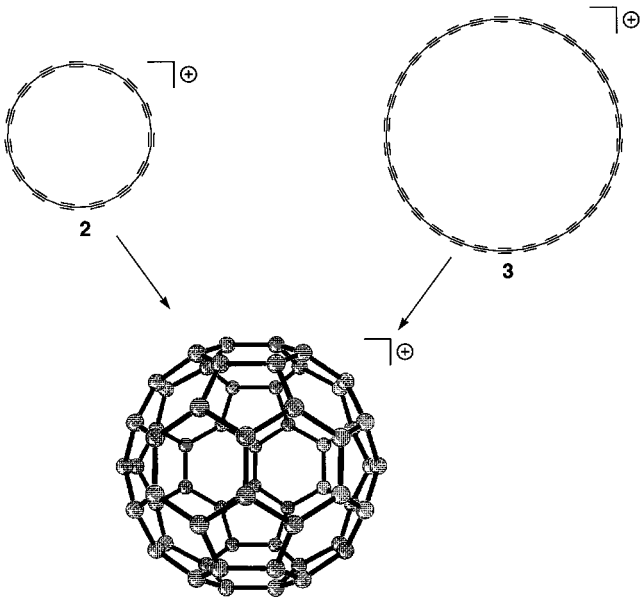
Why would anyone attempt to synthesize fullerenes from elaborate precursors if all it takes is graphite and a suitable energy source such as a strong electric field or laser power? One of the answers to this somewhat unfair question bears a certain philosophical charm reminiscent of the motto that the way is the goal. Of course, the benefit of the synthetic methodology developed to obtain carbon-rich materials in a rational fashion is multitudinous and undisputed.[1] But there is more. Firstly, research on endohedral fullerene complexes, in many ways the most exciting and the most unprecedented aspect of fullerene chemistry and physics, is severely limited because of the very low yields encountered in their preparation. A promising approach to improve the current situation lies in the development of synthetic strategies towards these molecules, and first steps in this direction have been made.[2] Secondly, knowledge about crucial stages of the fullerene formation process and about the rules that govern the observed product distribution remains rather sketchy. The design of more sophisticated fullerene precursors may allow the investigation of this process under conditions that are more controllable than the chaotic plasma of carbon atoms at around 3000 K.

Strained cycloalkynes are attractive starting materials for the energy-induced transformation of carbon-rich materials to fullerenes or related structured forms of carbon. In ideal cases, the high-energy content of a given cycloalkyne can lead to the coalescence of the cyclic structure to a thermodynamically more stable carbon sphere. Furthermore, incorporation of benzenoid or cyclopentadienyl substructures into cycloalkynes offers the opportunity to coordinate metal fragments, thereby providing a synthetic entry to endohedral fullerene complexes. Significant progress towards these goals has recently been made, and a selection of the (thermo)chemistry of new dehydrobenzoannulenes and alkyne-based cyclophanes is highlighted here.

[*] Dr. R. Faust[+]
Pharmazeutisch-Chemisches Institut der Universität
Im Neuenheimer Feld 364, D-69120 Heidelberg (Germany)

[+] New address:
University College London
Department of Chemistry, Christopher Ingold Laboratories
20 Gordon Street, London WC1H 0AJ (UK)
Fax: (+44) 171-380-7463
E-mail: r.faust@ucl.ac.uk

The first evidence for the feasibility of a cycloalkyne →fullerene conversion was produced by Diederich et al.[3] shortly before macroscopic quantities of buckminsterfullerene C_{60} (**1**) were available.[4] In Fourier transform laser desorption (FT-LD) mass spectrometric experiments they observed that cations of cyclo-C_{30} (**2**) undergo an efficient ion–molecule coalescence to give fullerene ions such as $\mathbf{1}^+$ (Scheme 1). In a related series of experiments, cyclic cationic

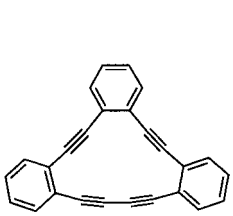


Scheme 1. Transformation of cationic carbon rings to C_{60}^+.

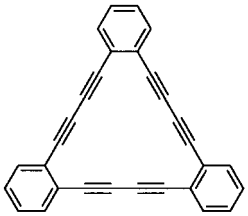
carbon structures such as **3** (depicted in D_{30h} symmetry) were also shown to rearrange to spherical C_{60} ions.[5] However, the preparation of bulk quantities of the neutral cyclocarbons and hence of the fullerenes from these precursors remains elusive.[6]

More recent developments exploit the energy content of readily accessible cycloalkynes based on phenyl–alkynyl structural motives, albeit not always with fullerene formation in mind. For example, the strained dehydrobenzoannulene **4**[7] could be converted by light, heat (145 °C), or pressure

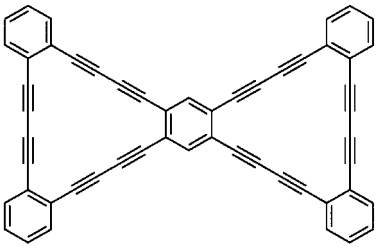
 © WILEY-VCH Verlag GmbH, D-69451 Weinheim, 1998 1433-7851/98/3720-2825 $ 17.50+.50/0



4



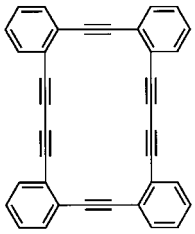
5

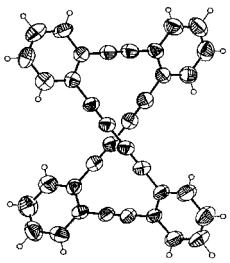


6

(1380 bar) in a topochemical polymerization reaction that is typical for butadiynes into a deeply colored polymer. A similar thermochemical behavior (strongly exothermic transformation around 200 °C) was observed for compounds **5** and **6**.[8] However, none of the systems **4** – **6** shows any tendency to produce spherical forms of carbon under the conditions investigated.

The situation is drastically different when the thermochemistry of cycloalkyne **7**[9] is considered (Figure 1). The high energy content of **7** becomes apparent when the compound is



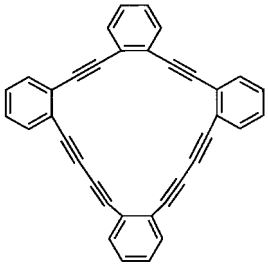


7

Figure 1. The structure of **7** in the crystal deviates considerably from that suggested by the structural formula.

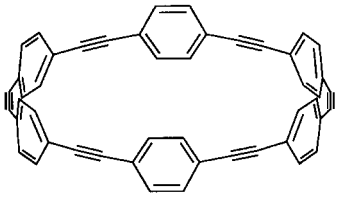
heated to 245 °C. At this temperature **7** "explodes violently with a flash of orange light".[9] An investigation of the black, carbonaceous residue by transmission electron microscopy revealed the presence of not only amorphous carbon and graphite, but also of closed-shell carbon particles, namely, buckytubes and buckyonions.[10] It is not unlikely that the molecular structure of **7** observed in the crystal (Figure 1) supports its explosive transformation to these fullerenoid carbon allotropes. While **7** is commonly, and deceivingly, depicted as a planar rectangle, the X-ray structural analysis reveals that **7** adopts a nonplanar, twisted D_2-symmetric conformation in the crystal in which the two butadiynyl linkages are crossing on top of each other.

The thermal decomposition of **7** into fullerenic substructures is a milestone in fullerene formation and represents the first example of a macroscopic preparation of closed-shell carbon particles from acetylenic precursors. However, molecular allotropes of carbon, such as C_{60} or higher fullerenes, were not found among the decomposition products. It is interesting to note in this context that **8**,[11] a structural isomer of **7** with a saddle-shaped solid-state conformation, also shows thermal transformations, but in this case they occur at temperatures of around 50 °C lower than those of **7** and are accompanied by a release of 50 kJ mol^{-1} more energy. Although an insoluble carbonaceous material is formed during this process, further details of its nature are currently not known.

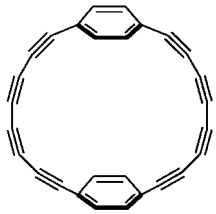


8

Cyclophanes have previously been envisioned as precursors to the fullerenes,[12] and alkynyl-based cyclophanes ("cyclophynes") are beginning to play an eminent role in this field. Two experimental results may serve to demonstrate the substantial energy content of these molecules. Firstly, belt-shaped [6]paraphenylacetylene **9**[13] explodes when heated to



9

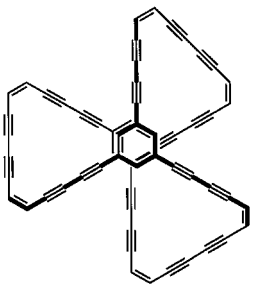


10

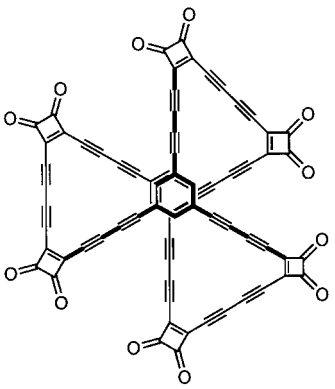
80 °C in the presence of oxygen. Under inert gas, temperatures of about 240 °C are needed to induce decomposition. No attempts have been made to characterize the decomposition products that are described as a brown, polymeric mixture. Secondly, [8.8]paracyclophaneoctayne **10**[14] could only be prepared in a protected form in which four of the eight alkynyl units are complexed by μ-acetylene(hexacarbonyl)dicobalt moieties. Efforts to release the highly strained hydrocarbon from its octacobalt complex resulted in large amounts of insoluble material.

Major steps towards the transformation of acetylenic cyclophanes into fullerenes have recently been made by Rubin et al. At the center of their promising approach[15] lies a preformed sixty-carbon cyclophyne cage, which is meant to be brought by appropriate activation techniques to coalesce to buckminsterfullerene C_{60}. The prototypical cyclophyne **11**[16] ($C_{60}H_{18}$), skillfully assembled in only four steps from 1,3,5-triethynylbenzene, is stable for weeks in dilute solutions in the dark. The cyclophyne **11** adopts a chiral, helical D_3 conformation in the solid state, and according to calculations racemizes rapidly even at low temperatures. Disappointingly, **11** was very reluctant to loose hydrogen in matrix-assisted

 © WILEY-VCH Verlag GmbH, D-69451 Weinheim, 1998 1433-7851/98/3720-2826 $ 17.50+.50/0



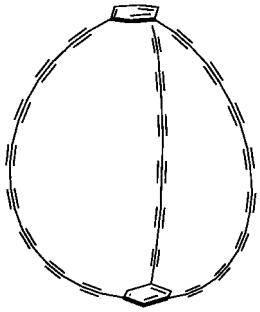
11
($C_{60}H_{18}$)



12
[$C_{60}H_6(CO)_{12}$]

LD-MS experiments and does not collapse under dehydrogenation to fullerene C_{60}. The most abundant ion (negative-ion mode) corresponds to the parent ion of **11** and only partial dehydrogenation to $C_{60}H_{14}^-$ is observed. The authors speculate that the reasons for the failure of **11** to produce fullerenes are the pronounced flexibility of the system and, more importantly, the remaining hydrogens of the $C_{60}H_{18}$ hydrocarbon are poor leaving groups.

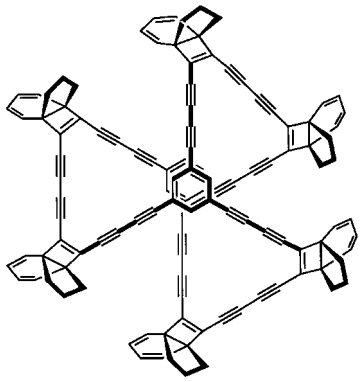
In a straightforward refinement of their concept Rubin et al. have turned to cyclophyne **12,**[17] in which the vinylic hydrogen atoms of **11** are replaced by 1,2-dioxocyclobuteno groups. This cyclic diketone moiety has been used previously[6, 18] as a synthetic equivalent for alkynyl groups, which can be generated from the dione by thermally or photochemically induced CO expulsion. Successive decarbonylation of **12** should ultimately lead to cyclophyne **13** with the composition $C_{60}H_6$. In contrast to the synthesis of cyclophyne **11**, the preparation of **12** is a more tedious, multistep (eight synthetic steps) procedure that furnished a sensitive material that is stable in CH_2Cl_2 solution for only two hours. The instability of **12** notwithstanding, the mass spectrometric behavior of the compound proved to be intriguing. The parent ion of **12**, $C_{60}H_6(CO)_{12}$, can neither be observed in the positive- nor in the negative-ion mode, but fragments thereof resulting from the loss of eight to eleven CO groups are detectable. The most abundant ions observed in the negative ion mode are $C_{60}^{\bullet-}$ and $C_{60}H_6^{\bullet-}$. The anion of the carbon cluster C_{60} was unambiguously identified as a fullerene, since its fragmentation pattern shows the successive loss of C_2 units that is typical for spherical carbon particles. $C_{60}H_6^{\bullet-}$ on the other hand does not lose C_2 fragments, which suggests that it does not have a fullerene structure.



13
($C_{60}H_6$)

It may be speculated that $C_{60}H_6^{\bullet-}$ is best represented by structure **13**. It is noteworthy that the formation of fullerene ions from acetylenic **12** is observed in the negative-ion mode, which is considered to be "milder" than the positive-ion mode, which was previously used to detect ionized carbon spheres. It thus appears that **12** is structurally predisposed for fullerene formation. However, attempts to perform the exhaustive decarbonylation on a macroscopic scale by irradiating dilute solutions of **12** in THF with pulsed laser light did not lead to the formation of buckminsterfullerene C_{60}.

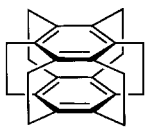
An alternative strategy for fullerene production through the intermediacy of **13** was adopted (and pursued independently and simultaneously to the work described above) by Tobe et al.[19] Their attempt to overcome the difficulties encountered in the exhaustive dehydrogenation of **11** led to the design of a similar cyclophyne **14**, in which six alkynyl



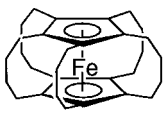
14

groups are masked by so-called [4.3.2]propellatrienes. Laser-induced [2+2] cycloreversion[20] cleave the bicyclic substructures to generate six equivalents of indane, thereby furnishing cyclophyne **13**. Consequently, the LD mass spectra (positive-ion mode) of **14** feature an intense signal for C_{60} cations with a C_2-fragmentation pattern. In the negative-ion mode, C_{60} anions are formed only to a minor extent, and the spectrum is dominated by $C_{60}H_6^{\bullet-}$ ions. Again, upon photolyzing solutions of **14** no indication for the macroscopic formation of fullerenes was observed, despite the promising fact that indane had been produced.

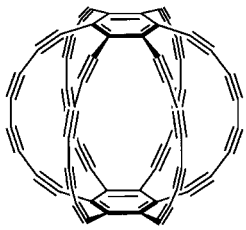
In light of the mass spectrometric results described above, a rational fullerene synthesis from cyclophyne precursors appears to be within reach. With superphane **15**[21] and superferrocenophane **16**[22] as established structural precedences, it may well be that reports about a successful synthesis



15



16



17

of "superphyne" **17**, an acetylenic isomer of buckminsterfullerene, or even a corresponding "supermetallophyne" will appear in the near future.

German version: *Angew. Chem.* **1998**, *110*, 2985 – 2988

 © WILEY-VCH Verlag GmbH, D-69451 Weinheim, 1998 1433-7851/98/3720-2827 $ 17.50+.50/0

Keywords: alkynes · cyclophanes · fullerenes · mass spectrometry

[1] F. Diederich, Y. Rubin, *Angew. Chem.* **1992**, *104*, 1123 – 1146; *Angew. Chem. Int. Ed. Engl.* **1992**, *31*, 1101 – 1123; F. Diederich, *Nature (London)* **1994**, *369*, 199 – 207.
[2] F. T. Edelmann, *Angew. Chem.* **1995**, *107*, 1071 – 1075; *Angew. Chem. Int. Ed. Engl.* **1995**, *34*, 981 – 985; S. Nagase, K. Kobayashi, T. Akasaka, *Bull. Chem. Soc. Jpn.* **1996**, *69*, 2131 – 2142.
[3] Y. Rubin, M. Kahr, C. B. Knobler, F. Diederich, C. L. Wilkins, *J. Am. Chem. Soc.* **1991**, *113*, 495 – 500; S. W. McElvany, M. M. Ross, N. S. Goroff, F. Diederich, *Science* **1993**, *259*, 1594 – 1596; N. S. Goroff, *Acc. Chem. Res.* **1996**, *29*, 77 – 83.
[4] For an account of the developments leading to the isolation of C_{60}, see H. W. Kroto, *Angew. Chem.* **1992**, *104*, 113 – 133; *Angew. Chem. Int. Ed. Engl.* **1992**, *31*, 111 – 129. See also R. F. Curl, *Angew. Chem.* **1997**, *109*, 1636 – 1647; *Angew. Chem. Int. Ed. Engl.* **1997**, *36*, 1566 – 1577; H. W. Kroto, *Angew. Chem.* **1997**, *109*, 1648 – 1664; *Angew. Chem. Int. Ed. Engl.* **1997**, *36*, 1578 – 1593; R. E. Smalley, *Angew. Chem.* **1997**, *109*, 1666 – 1673; *Angew. Chem. Int. Ed. Engl.* **1997**, *36*, 1594 – 1603.
[5] J. Hunter, J. Fye, M. F. Jarrold, *Science* **1993**, *260*, 784 – 786; D. E. Clemmer, M. F. Jarrold, *J. Am. Chem. Soc.* **1995**, *117*, 8841 – 8850; G. von Helden, N. G. Gotts, M. T. Bowers, *Nature (London)* **1993**, *363*, 60 – 63.
[6] F. Diederich, Y. Rubin, O. Chapman, N. S. Goroff, *Helv. Chim. Acta* **1994**, *77*, 1441 – 1457.
[7] K. P. Baldwin, A. J. Matzger, D. A. Scheiman, C. A. Tessier, K. P. Vollhardt, W. J. Youngs, *Synlett* **1995**, 1215 – 1218.
[8] M. M. Haley, S. C. Brand, J. J. Pak, *Angew. Chem.* **1997**, *109*, 864 – 866; *Angew. Chem. Int. Ed. Engl.* **1997**, *36*, 836 – 838.
[9] R. Boese, A. J. Matzger, K. P. C. Vollhardt, *J. Am. Chem. Soc.* **1997**, *119*, 2052 – 2053.
[10] M. S. Dresselhaus, G. Dresselhaus, P. C. Eklund, *Science of Fullerenes and Carbon Nanotubes,* Academic Press, San Diego, USA, **1996**.
[11] M. M. Haley, M. L. Bell, J. J. English, C. A. Johnson, T. J. R. Weakley, *J. Am. Chem. Soc.* **1997**, *119*, 2956 – 2957.
[12] R. Faust, *Angew. Chem.* **1995**, *107*, 1559 – 1562; *Angew. Chem. Int. Ed. Engl.* **1995**, *34*, 1429 – 1432, and references therein.
[13] T. Kawase, H. R. Darabi, M. Oda, *Angew. Chem.* **1996**, *108*, 2803 – 2805; *Angew. Chem. Int. Ed. Engl.* **1996**, *35*, 2664 – 2666.
[14] M. M. Haley, B. L. Langsdorf, *Chem. Commun.* **1997**, 1121 – 1122.
[15] Y. Rubin, *Chem. Eur. J.* **1997**, *3*, 1009 – 1016; Y. Rubin, *Chimia* **1998**, *52*, 118 – 126.
[16] Y. Rubin, T. C. Parker, S. I. Khan, C. L. Holliman, S. W. McElvany, *J. Am. Chem. Soc.* **1996**, *118*, 5308 – 5309.
[17] Y. Rubin, T. C. Parker, S. J. Pastor, S. Jalisatgi, C. Boulle, C. L. Wilkins, *Angew. Chem.* **1998**, *110*, 1353 – 1356; *Angew. Chem. Int. Ed.* **1998**, *37*, 1226 – 1229.
[18] Y. Rubin, C. B. Knobler, F. Diederich, *J. Am. Chem. Soc.* **1990**, *112*, 1607 – 1617; Y. Rubin, S. S. Lin, C. B. Knobler, J. Anthony, A. M. Boldi, F. Diederich, *Angew. Chem.* **1991**, *103*, 6943 – 6949; *Angew. Chem. Int. Ed. Engl.* **1991**, *30*, 698 – 700.
[19] Y. Tobe, N. Nakagawa, K. Naemura, T. Wakabayashi, T. Shida, Y. Achiba, *J. Am. Chem. Soc.* **1998**, *120*, 4544 – 4545.
[20] Y. Tobe, T. Fujii, H. Matsumoto, K. Naemura, Y. Achiba, T. Wakabayashi, *J. Am. Chem. Soc.* **1996**, *118*, 2758 – 2759; Y. Tobe, H. Matsumoto, K. Naemura, Y. Achiba, T. Wakabayashi, *Angew. Chem.* **1996**, *108*, 1924 – 1926; *Angew. Chem. Int. Ed. Engl.* **1996**, *35*, 1800 – 1802.
[21] Y. Sekine, M. Brown, V. Boekelheide, *J. Am. Chem. Soc.* **1979**, *101*, 3126 – 3127.
[22] M. Hisatome, J. Watanabe, K. Yamakawa, Y. Iitaka, *J. Am. Chem. Soc.* **1986**, *108*, 1333 – 1334.

Strategies for the Dynamic Integration of Combinatorial Synthesis and Screening**

Arasu Ganesan*

The generation and screening of large populations is a familiar concept in biology. It is central to recombinant DNA techniques and occurs in nature during evolution. Such approaches are only now being truly appreciated by chemists. Combinatorial organic synthesis, linked to high-throughput screening, has become an important part of the drug discovery process.[1] Areas such as materials science, catalysis, and engineered biosynthesis are also increasingly influenced by combinatorial ways of thinking.[2] Traditionally, library synthesis and screening are two separate activities which are performed sequentially. Here, recent examples are highlighted where the composition of a library undergoes fluid and dynamic change during selection for a desired property.[3]

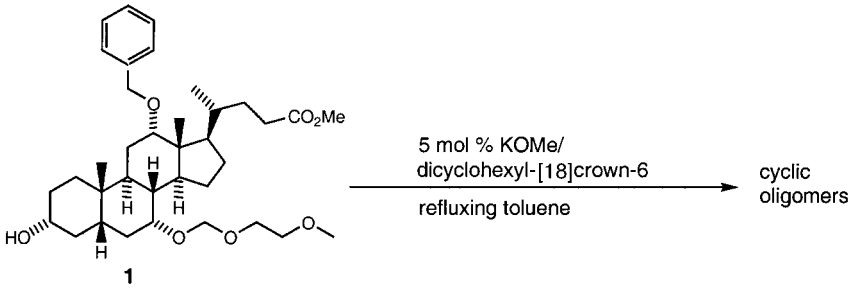
This idea originated in the field of molecular recognition. When a metal cation is mixed with a set of ligands, a large number of complexes is possible. However, under equilibrating conditions, the actual composition is dictated by thermodynamic stability.[4] The best binder can be identified simply by determination of the predominant component without the need to test each ligand individually. Lehn et al.[5] have described this approach as a virtual combinatorial library.[6]

The Sanders group has used transesterification as a route to combinatorial libraries. For example, the steroidal hydroxy ester **1** (Scheme 1) was mainly converted into the macrocyclic trimer, tetramer, and pentamer (83:12:5 respectively, by mass percentage) upon heating.[7] When the experiment was repeated with an equimolar amount of NaI, the equilibrium

[*] Dr. A. Ganesan
Institute of Molecular and Cell Biology
National University of Singapore
30 Medical Drive, Singapore 117609 (Singapore)
Fax: (+65) 779-1117
E-mail: mcbgane@imcb.nus.edu.sg

[**] The author thanks Dr. Chris Larson (Salk Institute, San Diego), Dr. David Oare (Advanced Medicine Inc., South San Francisco), and Dr. Paramjeet Singh (Institute of Molecular and Cell Biology, Singapore) for helpful comments on the manuscript.

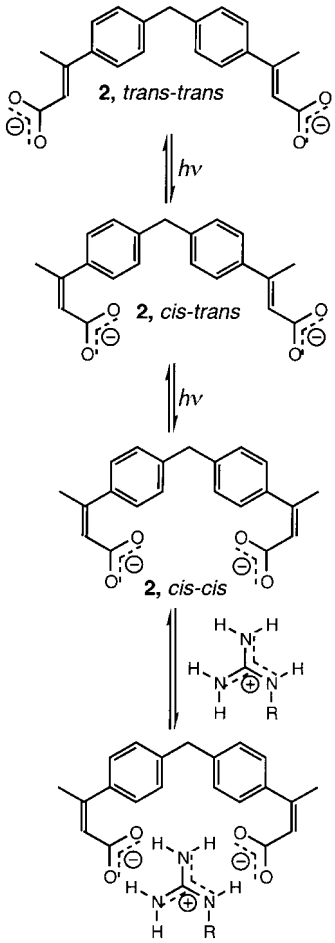
 © WILEY-VCH Verlag GmbH, D-69451 Weinheim, 1998 1433-7851/98/3720-2828 $ 17.50+.50/0



Scheme 1. Thermodynamically controlled transesterification.

shifted towards the higher oligomers (61:24:14), probably due to a template effect by the polyether substituent. Mixed macrocycles have also been obtained by the combination of two hydroxyester monomers.[8]

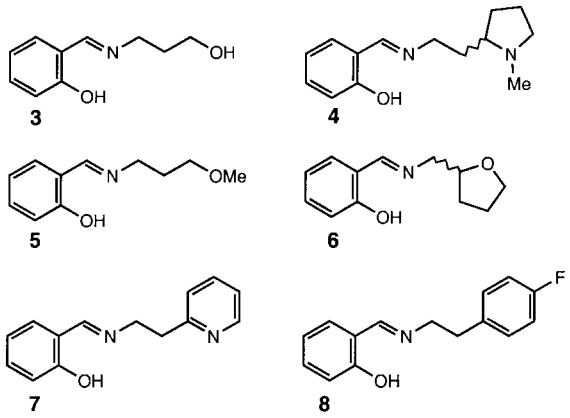
Photochemically induced *cis*–*trans* isomerization of the dicarboxylate **2** (Scheme 2) was used by Eilseev and Nelen to drive the equilibration reaction.[9] Of the three geometrical



Scheme 2. Amplification of a guanidine receptor by *cis*–*trans* isomerization.

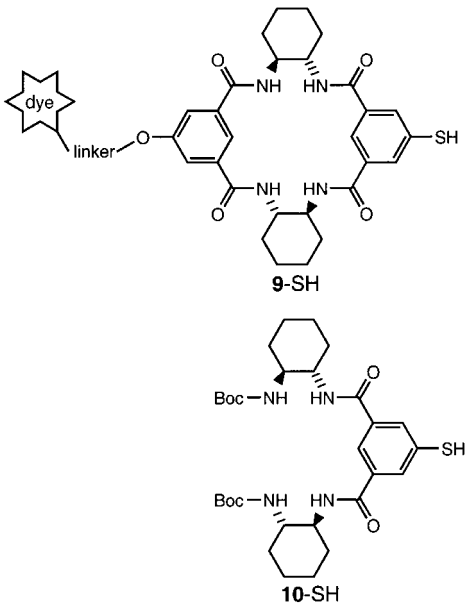
isomers, the *cis,cis* form has an optimal structure for guanidine binding through salt bridges. Approximately 30 cycles of irradiation and passage over an immobilized arginine column altered the proportion of *cis,cis*, *cis,trans*, and *trans,trans* isomers in solution from 3:28:69 to 48:29:23, while **2** retained by the column had the ratio 85:13:2.

In the above examples, the number of components that undergo selection is very small. A system with more practical potential was reported by Klekota et al.[10] The aldimines **3**–**8** (Scheme 3) can form a total of 36 unique bis(salicylaldiminato) complexes with divalent cations. In the presence of excess zinc, the amount of **4** eluted from an affinity column of double-stranded poly-d(AT) DNA was significantly decreased. The complex $Zn^{2+}(\mathbf{4})_2$ was independently shown to bind DNA with an apparent equilibrium constant K_d of 1.1 μM.



Scheme 3. Salicylaldimines tested for DNA binding in the presence of zinc cations.

Equilibration by reversible disulfide bond formation was demonstrated by Hioki and Still.[11] Screening of a tripeptide library immobilized on beads identified a number of ligands for the fluorescent disulfide **9**-SS-**9**, including Ac-D-Pro-L-Val-D-Val-polystyrene (Scheme 4). Incubation of the disulfide



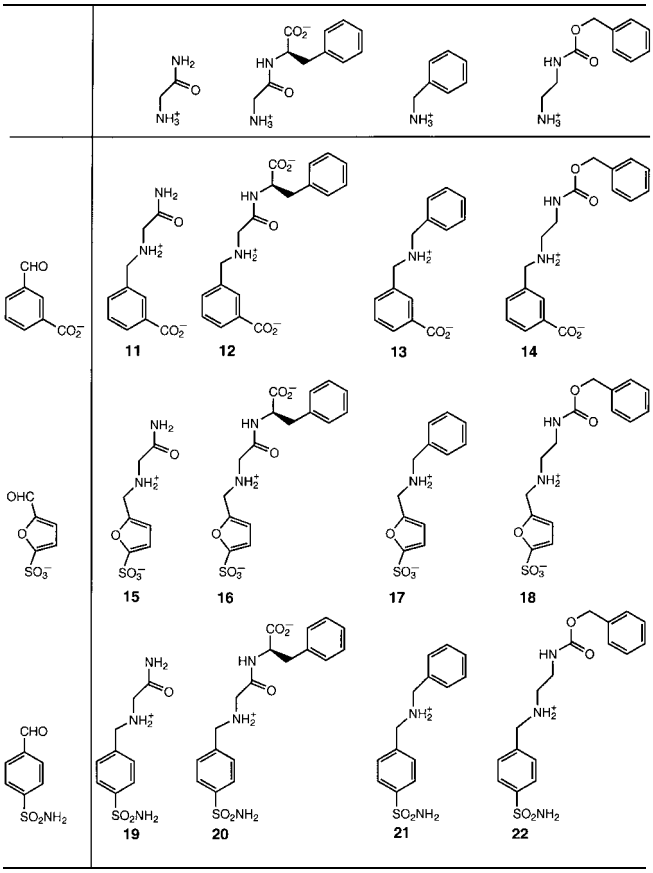
Scheme 4. Tripeptide receptors used in disulfide equilibration reactions; Boc = butoxycarbonyl.

 © WILEY-VCH Verlag GmbH, D-69451 Weinheim, 1998 1433-7851/98/3720-2829 $ 17.50+.50/0

with thiophenol resulted in an equilibrium mixture of 65% of **9**-SS-**9** and Ph-SS-Ph as well as 35% of **9**-SS-Ph. When the reaction was carried out in the presence of immobilized tripeptide ligand (3.7 equiv), the composition shifted to 95% of **9**-SS-**9** and Ph-SS-Ph. Virtually all the Ph-SS-Ph was in solution, while the beads to which **9**-SS-**9** was bound could be readily identified by the fluorescent tag. The disulfide was subsequently released in high purity. In a separate experiment, the mixed disulfide **9**-SS-**10** was equilibrated with **10**-SH. Once again, the peptide ligand biased the population towards **9**-SS-**9** and **10**-SS-**10**, with the equilibrium constant changing from 1.8 to 32 in favor of the symmetrical disulfides.

Dynamic equilibration as a route to the identification of enzyme inhibitors was explored by Huc and Lehn.[12] When a set of four amines and three aldehydes are mixed, twelve imines are generated reversibly, which can be trapped by reduction to give the mixture **11**–**22** (Table 1). When the

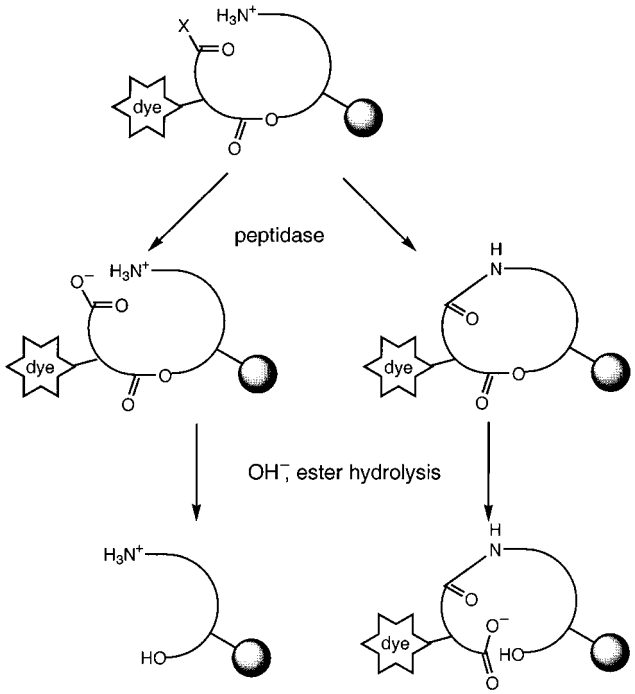
Table 1. A set of three aldehydes and four amines used to generate potential carbonic anhydrase inhibitors.



reaction was carried out in the presence of carbonic anhydrase (one equivalent based on the aldehyde; a 15-fold excess of amines was used to compensate for reactions with the lysine side chains of the enzyme), HPLC analysis revealed that the enzyme almost doubled the relative proportion of **21.** *para*-Substituted sulfonamides are known to be carbonic anyhdrase inhibitors, and the selection of **21** over **19**, **20**, and **22** is consistent with the steric requirements of the enzyme.

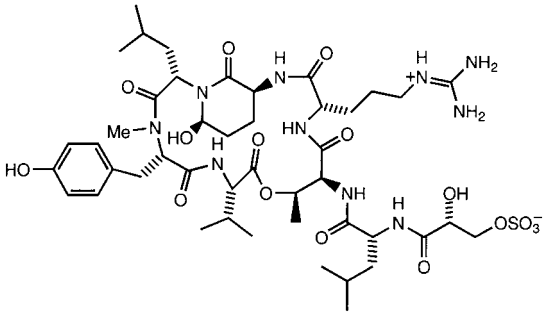
Swann et al.[13] used a nonspecific protease to catalyze both peptide bond formation and hydrolysis. Incubation of the peptides Tyr-Gly-Gly and Phe-Leu with thermolysin resulted in at least fifteen products, as observed by HPLC. The reaction was then repeated by placing thermolysin and the peptides in one half of a dialyzer, while the other half contained a monoclonal antibody ($c = 1\ \mu g\,mL^{-1}$) able to recognize the N terminus of β-endorphin (Tyr-Gly-Gly-Phe-Leu, $K_d = 7.1$ nM). Amplification of this pentapeptide could not be proven directly, but the mixture modestly inhibited radiolabeled β-endorphin binding to the antibody. Similarly, trypsin hydrolysates of bovine serum albumin and the peptide Gly-Pro-Arg (a known fibrinogen binder) were incubated with thermolysin in the presence of fibrinogen. Two tetrapeptides, Gly-Pro-Arg-Leu and Gly-Pro-Arg-Phe, were identified that were weakly bound ($K_d = 100\ \mu M$) to fibrinogen. If the considerable practical problems related to efficient peptide–peptide equilibration are overcome, this method could become an alternative to phage peptide display.

Although equilibration is not involved, Burger and Bartlett[14] have recently reported a creative example of the preselection of suitable library members by the target. Since both peptide bond formation and hydrolysis proceed via the same transition state, linear peptides that are cyclized by a peptidase would also be good templates for inhibitors. A strategy was devised (Scheme 5) which enabled bead-bound substrates that undergo cyclization to be picked out of a library. The synthetic peptide **23** (Scheme 6) is based on the blue-green algal trypsin inhibitor A90720A (equilibrium constant $K_i = 10$ nM against bovine trypsin). The peptide

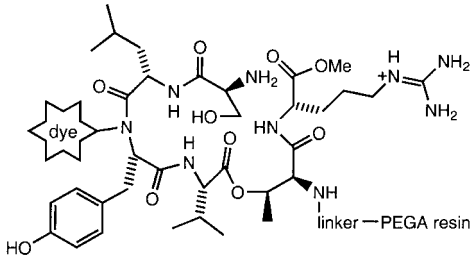


Scheme 5. A strategy for the identification of macrocyclic substrates and inhibitors of proteases: The unfavorable substrate (left) does not cyclize in the presence of the peptidase, but the favorable substrate (right) does. The product obtained after ester hydrolysis (right) is fluorescent in contrast to the dye-free product on the left (the circles represent the resin beads).

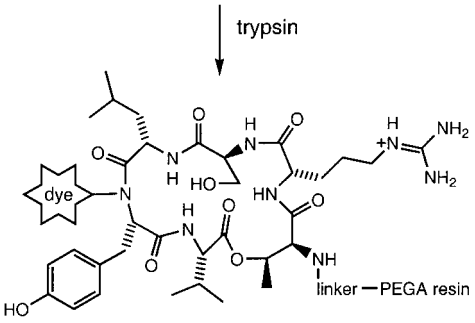
 © WILEY-VCH Verlag GmbH, D-69451 Weinheim, 1998 1433-7851/98/3720-2830 $ 17.50+.50/0 *Angew. Chem. Int. Ed.* **1998**, *37*, No. 20



A90720A, a natural trypsin inhibitor



23, a resin-bound synthetic analogue



24

Scheme 6. Design of a trypsin inhibitor. PEGA = poly(ethylene glycolamide).

was cyclized by trypsin in a mixed aqueous-organic solvent to form the macrocycle **24**. As expected, **24** is a substrate for trypsin in aqueous solution, and slow turnover at low enzyme concentrations enabled an apparent K_i of 230 nM to be calculated. Presumably, replacement of the scissile bond by a transition-state analogue would result in a true inhibitor. As in the example from Still et al., selection of components immobilized on beads should enable the rapid screening of large libraries.

The concept of dynamically tailoring library composition is still in its infancy. The examples so far have concentrated on proof of principle in situations where the selected component could be predicted beforehand (with the exception of DNA-binding $Zn^{2+}(\mathbf{4})_2$). A number of issues have to be addressed before the full potential of this approach can be realized:

1. The need for reversibility severely limits the types of chemical reaction suitable for equilibration. Even with fully reversible reactions, kinetic barriers are likely to arise with complex systems, which prevent complete exploration of all possible components within a reasonable timeframe.

2. Selection of a biological target, such as a protein, would impose further restrictions (e.g. aqueous media, physiologically compatible temperatures, and pH value). The target would also have to be present in equimolar quantities or in excess. For these reasons, applications related to materials science rather than drug discovery may be easier to achieve.

3. Unless the amplification is dramatic, careful analysis of library composition with and without selection is necessary. This places practical limits on the library size.

German version: *Angew. Chem.* **1998**, *110*, 2989 – 2992

Keywords: combinatorial chemistry · molecular evolution · molecular recognition

[1] For recent overviews on combinatorial chemistry, see a) *Chem. Rev.* **1997**, *97*(2); b) *Curr. Opin. Chem. Biol.* **1997**, *1*(1); *Curr. Opin. Chem. Biol.* **1998**, *2*(3); N. K. Terrett, Combinatorial Chemistry, Oxford University Press, Oxford, **1998**; for a comprehensive, regularly updated Internet database, visit http://www.5z.com/divinfo.

[2] The precise boundaries of "combinatorial chemistry" have been debated, see K. Burgess, *Chem. Eng. News* **1997**, *75*(6), 4; D. P. Curran, P. Wipf, *Chem. Eng. News* **1997**, *75*(11), 6.

[3] For a review of selection techniques, see P. A. Brady, J. K. M. Sanders, *Chem. Soc. Rev.* **1997**, *26*, 327 – 336.

[4] For some recent examples of self-assembly, see a) S. J. Rowan, D. G. Hamilton, P. A. Brady, J. K. M. Sanders, *J. Am. Chem. Soc.* **1997**, *119*, 2578 – 2579; b) B. Hasenknopf, J.-M. Lehn, N. Boumediene, A. Dupont-Gervais, A. Van Dorsselaer, B. Kniesel, D. Fenske, *J. Am. Chem. Soc.* **1997**, *119*, 10956 – 10962; c) D. L. Caulder, K. N. Raymond, *Angew. Chem.* **1997**, *109*, 1508 – 1510; *Angew. Chem. Int. Ed. Engl.* **1997**, *36*, 1440 – 1442; d) S. Sakai, Y. Shigemasa, T. Sasaki, *Tetrahedron Lett.* **1997**, *38*, 8145 – 8148; e) for a self-assembling catalyst, see C. L. Hill, X. Zhang, *Nature* **1995**, *373*, 324 – 326.

[5] B. Hasenknopf, J.-M. Lehn, B. O. Kneisel, G. Baum, D. Fenske, *Angew. Chem.* **1996**, *108*, 1987 – 1990; *Angew. Chem. Int. Ed. Engl.* **1996**, *35*, 1838 – 1840.

[6] This terminology can be confusing, as it was previously used to describe libraries which are computationally modeled prior to synthesis; for a review, see J. H. Van Drie, M. S. Lajiness, *Drug Discovery Today* **1998**, *3*, 274 – 283.

[7] P. A. Brady, J. K. M. Sanders, *J. Chem. Soc. Perkin Trans. 1*, **1997**, 3237 – 3253.

[8] S. J. Rowan, J. K. M. Sanders, *J. Org. Chem.* **1998**, *63*, 1536 – 1546.

[9] a) A. V. Eliseev, M. I. Nelen, *J. Am. Chem. Soc.* **1997**, *119*, 1147 – 1148; b) A. V. Eliseev, M. I. Nelen, *Chem. Eur. J.* **1998**, *4*, 825 – 834.

[10] B. Klekota, M. H. Hammond, B. L. Miller, *Tetrahedron Lett.* **1997**, *38*, 8639 – 8642.

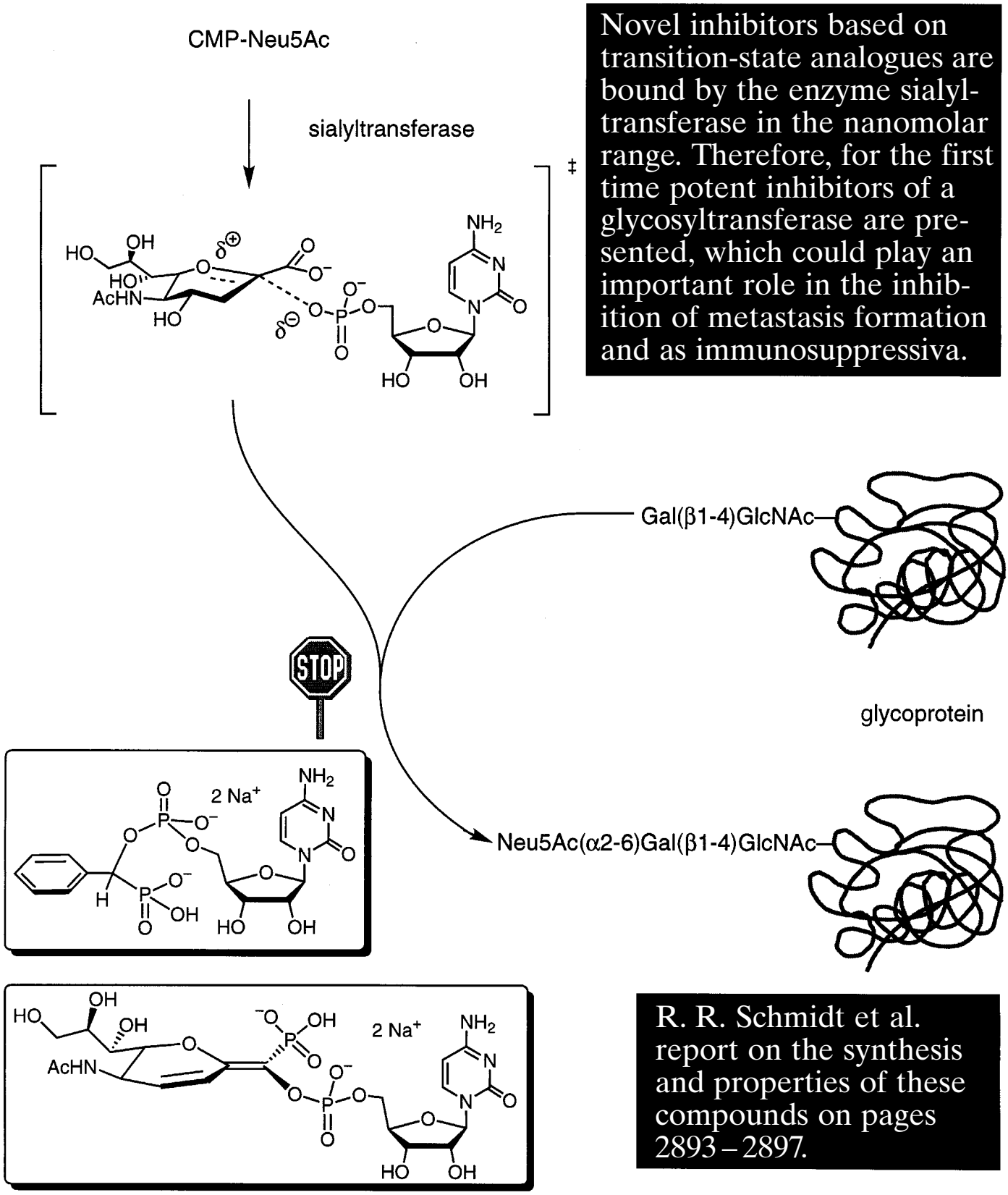
[11] H. Hioki, W. C. Still, *J. Org. Chem.* **1998**, *63*, 904 – 905.

[12] I. Huc, J.-M. Lehn, *Proc. Natl. Acad. Sci. USA* **1997**, *94*, 2106 – 2110.

[13] P. G. Swann, R. A. Casanova, A. Desai, M. M. Frauenhoff, M. Urbancic, U. Slomczynska, A. J. Hopfinger, G. C. Le Breton, D. L. Venton, *Biopolymers* **1996**, *40*, 617 – 625.

[14] M. T. Burger, P. A. Bartlett, *J. Am. Chem. Soc.* **1997**, *119*, 12697 – 12698.

 © WILEY-VCH Verlag GmbH, D-69451 Weinheim, 1998 1433-7851/98/3720-2831 $ 17.50+.50/0



Novel inhibitors based on transition-state analogues are bound by the enzyme sialyltransferase in the nanomolar range. Therefore, for the first time potent inhibitors of a glycosyltransferase are presented, which could play an important role in the inhibition of metastasis formation and as immunosuppressiva.

R. R. Schmidt et al. report on the synthesis and properties of these compounds on pages 2893 – 2897.

Determination of End-to-End Distances in a Series of TEMPO Diradicals of up to 2.8 nm Length with a New Four-Pulse Double Electron Electron Resonance Experiment**

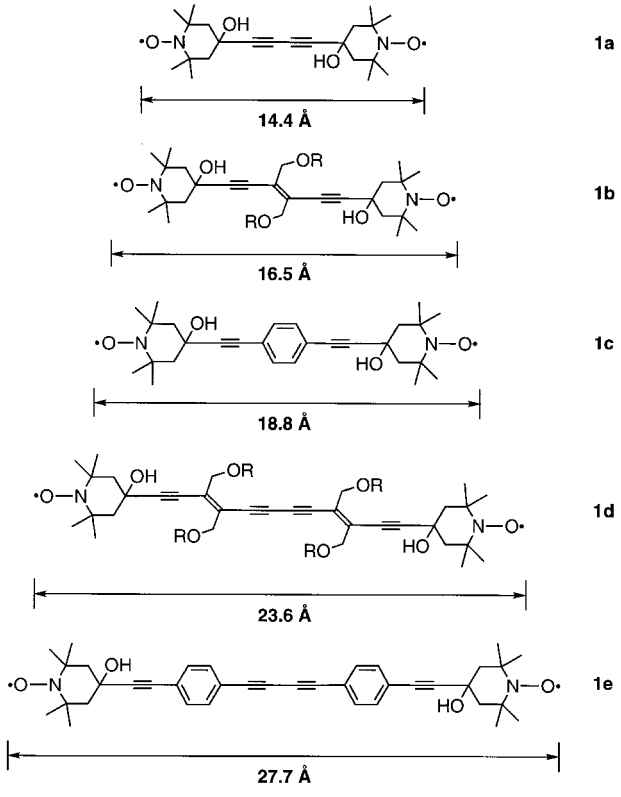
Rainer E. Martin, Matthias Pannier, François Diederich,* Volker Gramlich, Michael Hubrich, and Hans W. Spiess*

Organic di- and polyradicals with two or more weakly interacting unpaired electrons have received considerable attention in recent years as a result of their promising materials properties for use as organic molecular ferromagnets or superconductors.[1] Sterically shielded nitroxide radicals often exhibit a chemical inertness quite uncharacteristic of other free radicals, thus making them the subject of intense theoretical and experimental investigations. The use of such free radicals as reporter groups has rapidly evolved into one of the most powerful and versatile tools in biophysics for the study of biological systems.[2–4] In particular, the determination of distances between functional groups and the resulting topologies in biological systems[5] and amorphous solids, or the size and shape of ionic multiplets in ionomers,[6–8] is of fundamental interest and continues to attract attention as a challenging yet rewarding field of research. Unfortunately, the lack of periodic structures often severely restricts or simply prohibits the application of classical scattering techniques in such systems.

Free radicals can, however, be studied conveniently by electron paramagnetic resonance (EPR) spectroscopy.[9] This technique allows for the determination of interatomic distances of dipolar coupled electrons of up to several nanometers by making use of the dipolar coupling between the spin probes. The coupling leads to shorter longitudinal relaxation times (T_1) and phase memory times (T_m), which have been used for estimating distances in spin-labeled iron porphyrins.[10] Quantitative determination of distances, however, requires more sophisticated techniques, such as pulsed double electron electron resonance (DEER) spectroscopy, which was pioneered by Milov and Tsvetkov[11] and Larsen and Singel.[12]

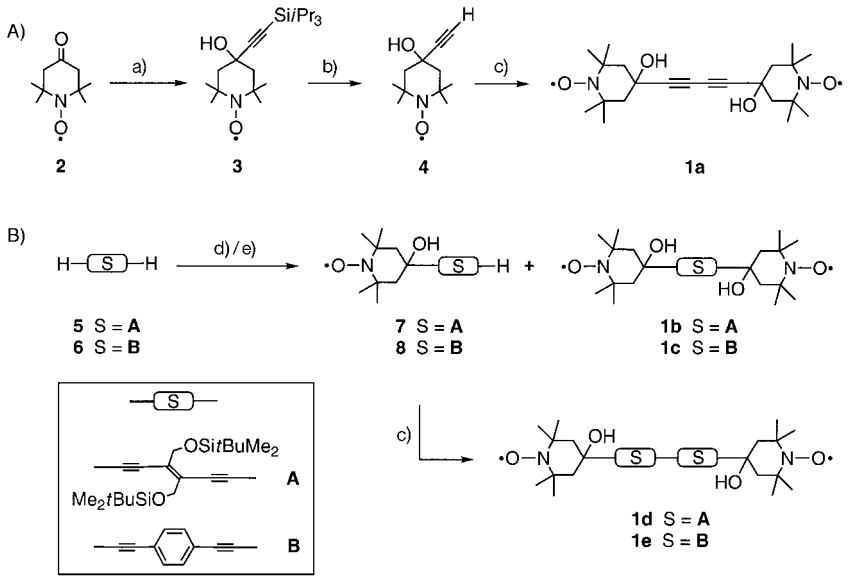
To the best of our knowledge, this technique has so far not been applied for the quantitative determination of unknown structures. Only first attempts to study end-to-end distances in a series of aliphatic hydrocarbons have been reported.[13] This situation is partly a consequence of technical limitations of pulsed EPR (dead time),[14] but also because of the lack of such measurements for a series of compounds with well-defined end-to-end distances ranging up to several nanometers. Here we provide such a data set by extending the three-pulse DEER sequence[13] to a four-pulse sequence that generates an echo and therefore, overcomes the dead-time problem. The systems studied are the TEMPO diradicals **1a**–**e** (R = Si*t*BuMe$_2$) in which the two TEMPO moieties are linked by rigid, conjugated spacers with large, well-defined end-to-end distances. Such compounds are of particular interest as precursors (models) for highly conjugated polymers for electronic, photonic, and optical applications.[15]

4,4′-(Butadiyne-1,4-diyl)bis(4-hydroxy-2,2,6,6-tetramethylpiperidine-*N*-oxyl) (BIPO, **1a**)[16] was synthesized by a new, simple, and short route (Scheme 1a). The slow addition of a solution of lithiated triisopropylsilylacetylene in THF by syringe pump to a solution of 2,2,6,6-tetramethyl-4-oxopiperidine-*N*-oxyl (**2**)[17] in THF at 0 °C gave **3** in 64% yield. Interestingly, the X-ray crystal structure analysis of **3** disclosed that the triisopropylsilylacetylene residue, rather than the hydroxyl group, adopts the axial position (Figure 1).[18] The analysis of the crystal lattice showed that intermolecular hydrogen bonding is not at the origin of the observed conformational preference, since the nitroxyl oxygen atom and the hydrogen atom of the hydroxyl group of neighboring molecules are at a distance of 4.57 Å. Subsequent removal of the silyl protecting group of **3** with *n*Bu$_4$NF in wet THF afforded the free acetylene derivative **4** (96% yield), which was oxidatively dimerized under Hay conditions[19] to give **1a**[16a] in 79% yield. In the synthesis of diradicals **1b**–**e** (Scheme 1B), addition of dilithiated (*E*)-3,4-bis[(*tert*-butyldimethylsilyloxy)methyl]hex-3-ene-1,5-diyne (**5**)[20] or *p*-diethynylbenzene (**6**)[21] to a solution of **2** (2 equiv) in THF in the presence of high concentrations of LiBr (up to 10 equiv)[22] afforded both mono- and bis-coupled products (**7**: 28%, **1b**:



[*] Prof. Dr. F. Diederich, Dipl.-Chem. R. E. Martin
Laboratorium für Organische Chemie, ETH Zentrum
Universitätstrasse 16, CH-8092 Zurich (Switzerland)
Fax: (+41) 1-632-1109
E-mail: diederich@org.chem.ethz.ch
Prof. Dr. H. W. Spiess, Dipl.-Phys. M. Pannier, Dr. M. Hubrich
Max-Planck-Institut für Polymerforschung
Postfach 3148, D-55021 Mainz (Germany)
Fax: (+49) 6131-379-100
E-mail: spiess@mpip-mainz.mpg.de
[**] Prof. Dr. V. Gramlich
Laboratorium für Kristallographie, ETH Zentrum
Sonneggstrasse 5, CH-8092 Zürich (Switzerland)

 © WILEY-VCH Verlag GmbH, D-69451 Weinheim, 1998 1433-7851/98/3720-2834 $ 17.50+.50/0



Scheme 1. Preparation of TEMPO diradicals **1a**–**e**. Reagents and conditions: a) iPr$_3$C≡CH, nBuLi, THF, 0 °C, 1 h, then 20 °C, 2 h, 64 %; b) nBu$_4$NF, wet THF, 96 %; c) CuCl, *N*,*N*,*N*′,*N*′-tetramethylethylenediamine (TMEDA), O_2, CH_2Cl_2, 4-Å molecular sieves, 3 h, **1a**: 79 %, **1d**: 55 %, **1e**: 86 %; d) **5**, nBuLi (2 equiv), anhydrous LiBr (10 equiv), **2**, THF, 0 °C, 1 h then 20 °C, 2 h, **7**: 28 %, **1b**: 39 %; e) **6**, nBuLi (2 equiv), anhydrous LiBr (1 equiv), **2**, THF, 0 °C, 1 h, then 20 °C, 2 h, **8**: 25 %, **1c**: 9 %.

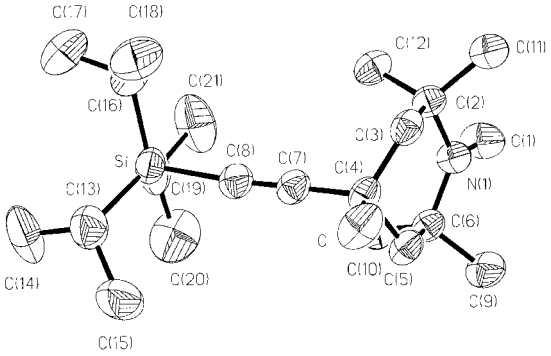


Figure 1. Molecular structure of TEMPO radical **3**. The ORTEP drawing depicts thermal ellipsoids at the 30 % probability level. Selected bond lengths [Å] and angles [°]: O(1)–N(1) 1.283(4), N(1)–C(2) 1.494(5), C(2)–C(3) 1.520(6), C(3)–C(4) 1.516(6), C(4)–C(7) 1.465(7), C(7)–C(8) 1.208(6); O(1)-N(1)-C(2) 115.5(3), N(1)-C(2)-C(3) 109.6(3), C(2)-C(3)-C(4) 117.9(3), C(3)-C(4)-C(7) 113.9(3), C(4)-C(7)-C(8) 176.5(4).

39 %, and **8**: 25 %, **1c**: 9 %). Oxidative Hay coupling of **7** and **8** led to the diradicals **1d** and **1e**, respectively (Table 1).

The analysis of the DEER signals closely follows that of the conventional three-pulse DEER experiment, as described by the groups of Tsvetkov[11] and Singel.[12] The time-domain signal I_{4p}(DEER) consists of two exponentials that lie back to back and are superimposed by a modulation [Eqs. (1)–(4)],

$$I_{4p}(\mathrm{DEER})(\Delta t) = \cos(\omega_{AB}\Delta t)\exp(kCF_B\Delta t) \quad (1)$$

$$\omega_{AB} = \omega_{DD}(3\cos^2\theta_{AB} - 1) \quad (2)$$

$$k = \frac{8\pi^2\mu_B^2 g_A g_B}{9\hbar\sqrt{3}} \qquad \omega_{DD} = \frac{\mu_B^2 g_A g_B}{\hbar}\frac{1}{r_{AB}^3} \quad (3, 4)$$

where C is the concentration of the unpaired electron spins, F_B the fraction of electron spins excited by the microwave pulse at frequency ν_2 (Figure 2), μ_B the Bohr magneton, g_A and g_B the g factors of the respective electron, and r_{AB} the electron–electron distance. Furthermore, $\Delta t = t_B - 2\tau$ (Figure 2), θ_{AB} is the angle between the magnetic field B_0 and the dipolar axis that connects the two electrons, and ω_{DD} is the dipolar coupling constant in angular frequency units. Equation (1) describes an oscillation with frequency $\nu_{AB} = \omega_{AB}/2\pi$ which arises from the superimposition of the dipolar coupling between the two unpaired electrons within the diradical on an exponential decay, and reflects the much weaker dipole–dipole coupling between different diradicals.[23, 24]

The information about the end-to-end distance r_{AB} is encoded in ω_{AB}. For a powder an average value over the different orientations of end-to-end vectors has to be taken, which results in a spectrum with two singularities that correspond to $\theta_{AB} = 90°$, resembling the well-known Pake spectrum of a spin pair in nuclear magnetic resonance.[25]

The symmetric four-pulse DEER time-domain signal of the longest diradical (**1e**)

Table 1. Selected physical data of **1b**-**e**.[a]

1b: M.p. 124–125 °C; UV/Vis (EtOH): λ_{max} (ε) = 270 (25400), 277 nm (22600, sh); FT-IR ($CHCl_3$): $\tilde{\nu}$ = 3689m, 3589m, 3300m, 3000m, 2958s, 2933s, 2856s, 2356m, 2332m, 1600m, 1494w, 1472m, 1463m, 1433w, 1421w, 1379w, 1361m, 1343m (N-O•), 1261m, 1237w, 1183m, 1100s, 1006m, 939w, 915w, 891w, 839s cm^{-1}; FAB-MS: m/z: 707.5 (100, [MH$_3^+$]), 706.4 (90, [MH$_2^+$]), 705.4 (37, [MH$^+$]), 704.4 (33, [M^+]), 692.4 (16, [MH$_3$ – CH$_3$]$^+$), 691.4 (36, [MH$_2$ – CH$_3$]$^+$), 690.4 (53, [MH – CH$_3$]$^+$), 689.4 (84, [M – CH$_3$]$^+$); elemental analysis calcd for $C_{38}H_{68}N_2O_6Si_2$ (705.15): C 64.73, H 9.72, N 3.97; found: C 64.73, H 9.50, N 3.74.

1c: M.p. 182–183 °C; UV/Vis (EtOH): λ_{max} (ε) = 212 (18400), 217 (18100), 270 (42100), 282 nm (41700); FT-IR ($CHCl_3$): $\tilde{\nu}$ = 3622s, 3467m, 3011s, 2978s, 2889m, 2467w, 1600w, 1483w, 1444w, 1396w, 1373w, 1342w (N–O•), 1250w, 1044s, 878m cm^{-1}; FAB-MS: m/z: 469.3 (100, [MH$_3$]$^+$), 468.3 (28, [MH$_2$]$^+$), 467.3 (10, [MH]$^+$), 466.3 (5, [M]$^+$); HR-FAB-MS: m/z: found: 469.3077 ([MH$_3$]$^+$, $^{12}C_{28}H_{41}N_2O_4^+$); calcd: 469.3066; elemental analysis calcd for $C_{28}H_{38}N_2O_4 \cdot 0.5\,H_2O$ (475.63): C 70.71, H 8.26, N 5.89; found: C 70.30, H 8.04, N 5.70.

1d: M.p. 114 °C (decomp); UV/Vis (EtOH): λ_{max} (ε) = 267 (26600), 280 (27200), 294 (25600), 314 (21600), 343 (25800), 367 nm (22700); FT-IR ($CHCl_3$): $\tilde{\nu}$ = 3689w, 3589m, 3360w, 3000m, 2959s, 2933s, 2856s, 2356m, 2332m, 1600m, 1472m, 1463m, 1379w, 1361m, 1343w (N–O•), 1256m, 1237w, 1100s, 1042w, 1020w, 1006w, 939w, 916w, 891w, 839s cm^{-1}; FAB-MS: m/z: 1053.4 (16, [MH$_3$ – O]$^+$), 1052.4 (31, [MH$_2$ – O]$^+$), 1051.4 (38, [MH – O]$^+$), 1050.4 (29, [M – O]$^+$), 632.2 (100); HR-FAB-MS: m/z: found: 1051.6842 ([MH – O]$^+$, $^{12}C_{58}H_{103}N_2O_7{}^{28}Si_4$), calcd: 1051.6842.

1e: m.p. 169–170 °C (decomp); UV/Vis (EtOH): λ_{max} (ε) = 224 (17100), 233 (15100), 261 (17000), 277 (18400), 292 (24600), 310 (33400), 332 (41000), 356 nm (35000); FT-IR ($CHCl_3$): $\tilde{\nu}$ = 3622s, 3467m, 3022s, 2974s, 2889m, 1444w, 1389w, 1342w (N–O•), 1250m, 1044s, 878m cm^{-1}; EI-MS: m/z: 593.2 (3, [MH$_3$]$^+$), 592.2 (6, [MH$_2$]$^+$), 591.1 (10, [MH]$^+$), 590.2 (3, [M]$^+$), 559.2 (92, [M – HNO]$^+$), 140.0 (100); HR-EI-MS: m/z: found: 590.3136 (M^+, $^{12}C_{38}H_{42}N_2O_4^+$), calcd: 590.3144.

[a] All new compounds described were fully characterized by melting point, FT-IR and UV/VIS spectroscopy, EI or FAB mass spectrometry, and high-resolution mass spectrometry and/or correct elemental analysis.

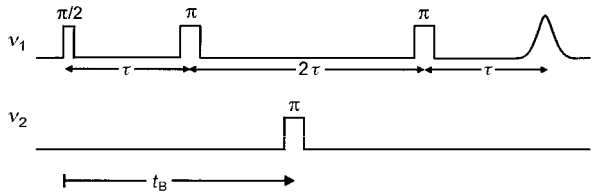


Figure 2. The newly developed four-pulse DEER sequence consists of a refocused echo at microwave frequency ν_1 and a π pulse at ν_2, which is incremented in time. The time t_B is the incrementation time which starts at $t_B = \tau$ and ends at $t_B = 3\tau$. τ is the fixed evolution time of the refocused Hahn echo pulse sequence. All microwave pulses utilized were of a duration of 32 ns and had a frequency difference of $\Delta\nu = 60$ MHz.

of the series recorded at 15 K in a polystyrene matrix is shown in Figure 3a. The exponentials and the superimposed modulation are clearly visible. After subtraction of the exponential decay and Fourier transformation a Pake-type spectrum is obtained (Figure 3b). In contrast to the conventional DEER experiment where only singularities can be observed, broad contributions to the line shape are observable with the four-pulse DEER sequence.[12, 13] This substantial advantage and improvement is a consequence of the absence of dead time in the four-pulse DEER experiment and allows for the first time to measure broad distributions of dipolar couplings.

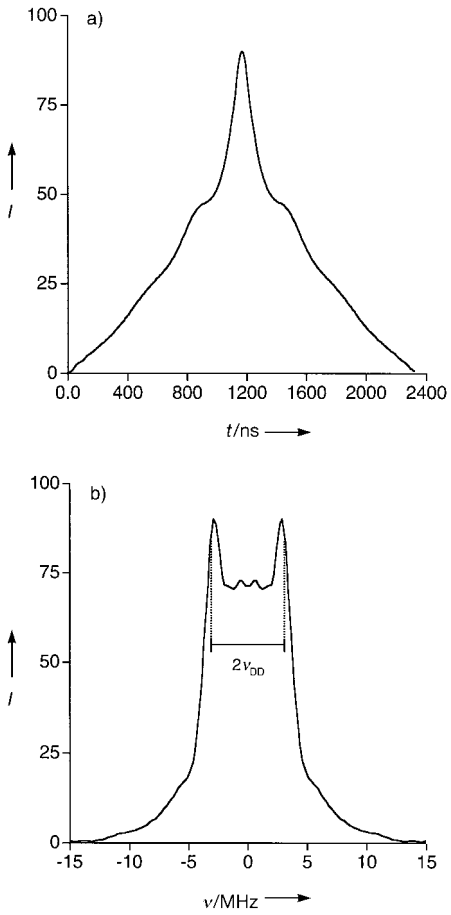


Figure 3. a) Four-pulse DEER time-domain signal of diradical **1e** mixed into polystyrene at 15 K. All pulses had a length of $t_P = 32$ ns and the evolution time τ had a duration of 1200 ns. b) Four-pulse DEER spectrum of **1e** as obtained by Fourier transformation of the time-domain data in a) after subtracting two exponentials and zero filling. The bar indicates the distance $2\nu_{DD}$ between the two singularities of an unbroadened Pake pattern that fits the experimental spectrum.

In the present study, the singularities that define the dipolar coupling constant and thus the electron–electron distance are very narrow and clearly recognizable. Only the "foot" of the Pake spectrum is not visible, as would be expected from orientation selection owing to only partial excitation of the inhomogenously broadened EPR spectrum of ^{14}N-labeled nitroxide.[12] The measured coupling constants and calculated electron–electron distances for the series **1a–e** are given in Table 2, together with results of molecular dynamics simulations, which revealed averaged end-to-end distances from 1.5 nm (**1a**) to 2.8 nm (**1e**).[26]

Table 2. Dipolar coupling constants ν_{DD} and interradical distances r_{AB} obtained for **1a–e** by molecular dynamics simulations and experimentally measured data.

Compd	ν_{DD} [MHz]	$\Delta\nu_{DD}$[a] [MHz]	r_{AB}^{th}[b] [Å]	r_{AB}^{exp}[c] [Å]
1a	–	–	14.4 ± 1.0	–
1b	14.16	0.49	16.5 ± 1.0	15.4 ± 0.2
1c	10.25	0.49	18.8 ± 1.0	17.2 ± 0.3
1d	4.88	0.49	23.6 ± 1.0	22.0 ± 0.7
1e	3.05	0.49	27.7 ± 1.0	25.7 ± 1.4

[a] Experimental error of the dipolar coupling constant. [b] Averaged distances estimated from molecular dynamics simulations, measured from oxygen to oxygen of the terminal N–OH groups.[26] [c] Experimentally obtained distances.

The uncertainty of about ± 1 Å is not from spectroscopic limitations, but reflects the conformational freedom of the nitroxide spin labels, which result from the axial/equatorial positions of the alkyne substituents on the six-membered rings as well as from rotations about the C(sp)–C(sp^3) bonds. For the shortest diradical **1a**, no experimental coupling constant could be obtained, since it was not possible to apply microwave π pulses shorter than 32 ns, as would be necessary to excite the dipolar subspectra. This bandwidth problem leads to a lower interradical distance limit for the present method of approximately 1.5 nm. On the other hand, at least five full oscillations with the frequency corresponding to the singularities in the Pake pattern should be observable in an interval of length τ for a precise distance determination (see Figure 3b). The length of the whole sequence (4τ) should not exceed the phase memory time T_m considerably for sensitivity reasons. Both requirements combined let us expect an upper distance limit of about 8 nm for the method to be applicable. Experimental and estimated distances are in good agreement, considering the fact that the DEER experiments were performed in a matrix at 15 K, while molecular dynamics simulations were done in the gas phase at ambient temperature. The experimental distances appear to be systematically shorter than the calculated ones by about 8%, but we refrain from drawing any conclusions from that.

With the diradical series **1a–e**, we have demonstrated the amenability of advanced Fourier transformation electron electron double resonance spectroscopy for measuring electron–electron distances in the range of 1.6 to 2.8 nm. This provides a base for applying this technique to more complex

 © WILEY-VCH Verlag GmbH, D-69451 Weinheim, 1998 1433-7851/98/3720-2836 $ 17.50+.50/0

systems, where intergroup distances might not be so well defined. We are currently exploring the practical limits of the four-pulse DEER experiment for the determination of distance distributions up to the theoretical limit which is expected to be about 8 nm.

Experimental Section

Typical procedure for the coupling of lithiated acetylenes and TEMPO radical **2**. Compounds **1b** and **7**: A solution of *n*BuLi (0.17 mL, 0.28 mmol, 1.6 M solution in *n*-hexane) was added slowly to a solution of **5** (0.050 g, 0.138 mmol) and anhydrous LiBr (0.12 g, 1.38 mmol) in dry THF (30 mL) under N_2 at 0 °C, and the mixture was stirred for 30 min. Subsequently, a solution of **2** (0.12 g, 0.69 mmol) in dry THF (4 mL, over 4-Å molecular sieves) was introduced by syringe pump within 1 h, and the solution stirred for an additional 2 h at 20 °C. The mixture was diluted with a saturated solution of aquous NH_4Cl (100 mL) and extracted with CH_2Cl_2, and the organic phase was dried ($MgSO_4$). Separation by flash chromatography (SiO_2, *n*-hexane/AcOEt 5/1) furnished **7** (0.021 g, 28 %) as a slightly orange solid, and purification of the residue by preparative thin layer chromatography (SiO_2, *n*-hexane/AcOEt 1/1) yielded **1b** (0.038 g, 39 %) as an orange solid.

Typical procedure for oxidative Hay couplings. Compound **1d**: TMEDA (0.016 mL, 0.11 mmol) and CuCl (0.003 g, 0.03 mmol) were added over 5 min to a solution of **7** (0.042 g, 0.079 mmol) in dry CH_2Cl_2 (5 mL) over 4-Å molecular sieves at 20 °C. After the mixture had been stirred in air for 3 h, a solution of EDTA (EDTA = ethylenediaminetetraacetic acid, pH 8) was added, and the mixture extracted with CH_2Cl_2 until the washings remained colorless. The organic phase was washed with a saturated aqueous solution of NaCl and dried ($MgSO_4$). Purification by flash chromatography (SiO_2, *n*-hexane/AcOEt 3/1) afforded **1d** (0.023 g, 55 %) as an orange solid.

Distance determination. The four-pulse DEER measurements were performed on a modified Bruker ESP380E X-band Fourier transformation spectrometer. One channel of the microwave pulse-forming unit was used for a second microwave frequency. An HP-86290B RF plug-in module in an HP-8350B sweep oscillator was employed as the source for the second frequency. The output microwave of the HP-86290B RF plug-in module was increased by an amplifier from Miteq (AMF-5S-8012-18). The probehead used was a commercial electron nuclear double resonance (ENDOR) resonator from Bruker (EN4118X-MD4), which was overcoupled for obtaining a broad resonator resonance line. The resolution of four-pulse DEER experiments depends on the length of the constant time interval 2τ. For the precise determination of long distances we used $\tau =$ 1200 ns. This in turn necessitated a measurement temperature of 15 K to ensure that enough signal was left despite phase relaxation for a period of 4.8 μs. The choice of a difference of 60 MHz between the two microwave frequencies enabled us to work with a single-mode resonator yet still excite transitions of the two nitroxide moieties selectively.

Received: April 21, 1998 [Z11762IE]
German version: *Angew. Chem.* **1998**, *110*, 2994 – 2998

Keywords: diradicals · double electron electron resonance spectroscopy · EPR spectroscopy

[1] a) A. Rajca, *Chem. Rev.* **1994**, *94*, 871 – 893; b) J. S. Miller, A. J. Epstein, *Angew. Chem.* **1994**, *106*, 399 – 432; *Angew. Chem. Int. Ed. Engl.* **1994**, *33*, 385 – 415; c) J. S. Miller, *Adv. Mater.* **1992**, *4*, 435 – 438; d) J. H. Zhang, A. J. Epstein, J. S. Miller, C. J. O'Connor, *Mol. Cryst. Liq. Cryst.* **1989**, *176*, 271 – 276; e) D. W. Wiley, J. C. Calabrese, J. S. Miller, *Mol. Cryst. Liq. Cryst.* **1989**, *176*, 277 – 288.

[2] J. F. W. Keana, *Chem. Rev.* **1978**, *78*, 37 – 64.

[3] *Spin Labeling-Theory and Applications* (Ed.: L. J. Berliner), Academic Press, London, **1976**.

[4] "Resolved Electron-Electron Spin-Spin Splittings in EPR Spectra": G. R. Eaton, S. S. Eaton in *Biological Magnetic Resonance*, *Vol. 8* (Eds.: L. J. Berliner, J. Reuben), Plenum, New York, **1989**, pp. 339 – 398.

[5] Y.-K. Shin, C. Levinthal, F. Levinthal, W. L. Hubbel, *Science* **1993**, *259*, 960 – 963.

[6] *Ionomers*, *Characterization*, *Theory*, *and Applications* (Ed.: S. Schlick), CRC, New York, **1996**.

[7] V. Schädler, A. Franck, U. Wiesner, H. W. Spiess, *Macromolecules* **1997**, *30*, 3832 – 3838.

[8] V. Schädler, V. Kniese, T. Thurn-Albrecht, U. Wiesner, H. W. Spiess, *Macromolecules* **1998**, submitted.

[9] J. E. Wertz, J. R. Bolton, *Electron Spin Resonance*, McGraw-Hill, New York, **1972**.

[10] M. H. Rakowsky, K. M. More, A. V. Kulikov, G. R. Eaton, S. S. Eaton, *J. Am. Chem. Soc.* **1995**, *117*, 2049 – 2057.

[11] a) A. D. Milov, K. M. Salikhov, M. D. Shirov, *Fiz. Tverd. Tela* **1981**, *23*, 975 – 982; b) A. D. Milov, A. B. Ponomarev, Y. D. Tsvetkov, *Chem. Phys. Lett.* **1984**, *110*, 67 – 72.

[12] R. G. Larsen, D. J. Singel, *J. Chem. Phys.* **1993**, *98*, 5134 – 5146.

[13] V. Pfannebecker, H. Klos, M. Hubrich, T. Volkmer, A. Heuer, U. Wiesner, H. W. Spiess, *J. Phys. Chem.* **1996**, *100*, 13428 – 13432.

[14] *Modern Pulsed and Continuous-Wave Electron Spin Resonance* (Eds.: L. Kevan, M. K. Bowman), Wiley, New York, **1990**.

[15] *Electronic Materials: The Oligomer Approach* (Eds.: K. Müllen, G. Wegner), Wiley-VCH, Weinheim, **1997**.

[16] a) P. G. Hamill, A. E. Yost, J. D. Sandman, *Mol. Cryst. Liq. Cryst. Sci. Technol. Sect. A* **1992**, *211*, 339 – 346; b) J. S. Miller, D. T. Glatzhofer, J. C. Calabrese, A. J. Epstein, *J. Chem. Soc. Chem. Commun.* **1988**, 322 – 323; c) Yu. V. Korshak, T. V. Medvedeva, A. A. Ovchinnikov, V. N. Spector, *Nature (London)* **1987**, *326*, 370 – 372.

[17] a) M. B. Neiman, E. G. Rozantzev, Yu. G. Mamedova, *Nature (London)* **1962**, *196*, 472 – 474; b) G. Sosnovsky, M. Konieczny, *Synthesis* **1976**, 735 – 736; c) for a review on the chemistry of hindered piperidines, see M. Dagonneau, E. S. Kagan, V. I. Mikhailov, E. G. Rozantsev, V. D. Sholle, *Synthesis* **1984**, 895 – 916.

[18] X-ray crystal structure of **3** at 293 K: $C_{20}H_{38}NO_2Si$, $M_r = 352.6$, triclinic space group $P\bar{1}$, $\rho_{calcd} = 1.056$ g cm^3, $Z = 4$, $a = 7.741(9)$, $b = 8.516(10)$, $c = 33.80(3)$ Å, $\alpha = 91.84(8)$, $\beta = 92.46(8)$, $\gamma = 94.41(9)^\circ$, $V = 2218(4)$ Å^3. Data were measured on an Syntex P21 diffractometer with $Mo_{K\alpha}$ radiation ($\lambda = 0.71073$ Å) with ω scans. The structure was solved by direct methods and refined by full-matrix least-squares analysis (SHELXTL PLUS; heavy atoms anisotropic, H atoms fixed, whereby H positions are based on stereochemical considerations) to give $R1 = 0.0663$, $wR2 = 0.1711$ for 4142 independent observed reflections and 570 variables [$I \geq 2.0\sigma(I)$, $2.4 \leq \theta \leq 20.0^\circ$]. Crystallographic data (excluding structure factors) for the structure reported in this paper have been deposited with the Cambridge Crystallographic Data Centre as supplementary publication no. CCDC-101294. Copies of the data can be obtained free of charge on application to CCDC, 12 Union Road, Cambridge CB2 1EZ, UK (fax: (+44) 1223-336-033; e-mail: deposit@ccdc.cam.ac.uk).

[19] A. S. Hay, *J. Org. Chem.* **1962**, *27*, 3320 – 3321.

[20] R. R. Tykwinski, M. Schreiber, R. Pérez Carlón, F. Diederich, V. Gramlich, *Helv. Chim. Acta* **1996**, *79*, 2249 – 2281.

[21] S. Takahashi, Y. Kuroyama, K. Sonogashira, N. Hagihara, *Synthesis* **1980**, 627 – 630.

[22] P. E. van Rijn, S. Mommers, R. G. Visser, H. D. Verkruijsse, L. Brandsma, *Synthesis* **1981**, *116*, 459 – 460.

[23] K. M. Salikhov, S. A. Dzuba, A. M. Raitsimring, *J. Magn. Reson.* **1981**, *42*, 255 – 276.

[24] V. V. Kurshev, A. M. Raitsimring, Y. D. Tsvetkov, *J. Magn. Reson.* **1989**, *81*, 441 – 454.

[25] A. Abragam, *The Principles of Nuclear Magnetism*, Clarendon, Oxford, **1983**.

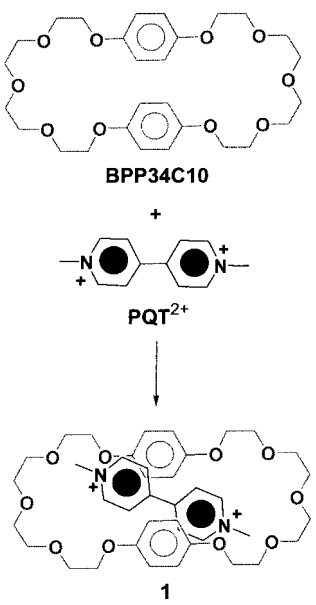
[26] CVFF force field, Insight II (Version 95.0), Biosym Technologies, San Diego, **1995**. Instead of N–O$^\bullet$, the parameter set for the N – OH group was used for the simulations. Hartman et al. recommended the use of a C=O group as a surrogate for the nitroxyl N – O$^\bullet$ moiety in performing simulations (D. Hartmann, R. Philipp, K. Schmadel, J. J. Birktoft, L. J. Banaszak, W. E. Trommer, *Biochemistry* **1991**, *30*, 2782 – 2790). However, the error introduced in the end-to-end distance measurements by using N–OH instead of C=O and performing the simulations in the absence of solvent molecules is more than outweighted by the conformational freedom of the nitroxide spin labels arising from the axial/equatorial positions of the alkyne substituents on the six-membered rings and the rotations about the C(sp) – C(sp^3) bonds.

 © WILEY-VCH Verlag GmbH, D-69451 Weinheim, 1998 1433-7851/98/3720-2837 $ 17.50+.50/0

A New Motif for the Self-Assembly of [2]Pseudorotaxanes; 1,2-Bis(pyridinium)ethane Axles and [24]Crown-8 Ether Wheels**

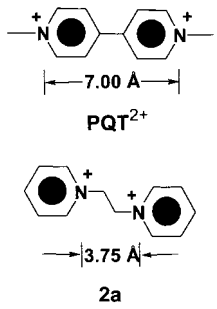
Stephen J. Loeb* and James A. Wisner

The threading of the paraquat dication PQT^{2+} through the cavity of bis(paraphenylene)[34]crown-10 (BPP34C10) to form the [2]pseudorotaxane $[(BPP34C10)(PQT)]^{2+}$ (**1**) was the genesis of a diverse range of molecules that contain mechanical linkages (rotaxanes, catenanes, molecular shuttles, and switches) derived from this basic interaction, and stands as a landmark discovery in the area of supramolecular chemistry (Scheme 1).[1] Many examples of rotaxanes have



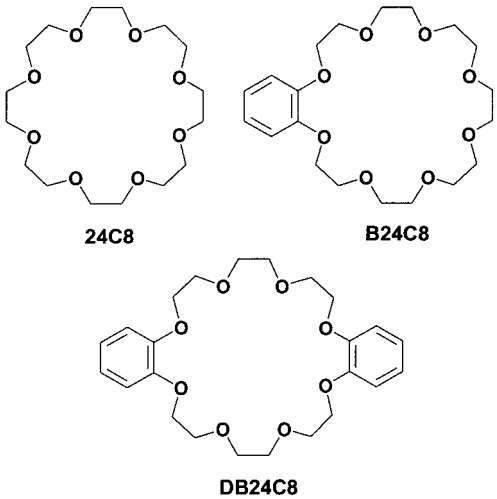
Scheme 1. Formation of the [2]pseudorotaxane **1** by insertion of the linear dicationic axle PQT^{2+} through the cavity of the neutral crown ether wheel BPP34C10.

now been reported involving π stacking between electron-rich and electron-poor aromatic rings,[2] hydrogen bonding between secondary dialkylammonium ions and crown ethers[3] or between amides and large ring lactams,[4] hydrophobic interactions within the cavity of a cyclodextrin,[5, 6] and metal–ligand interactions between transition metal ions and cyclic ligands.[7–9] In many of these systems the ion–dipole interaction between positively charged atoms of one component and the Lewis basic atoms of the other component makes a significant contribution to the binding. Although these electrostatic interactions are not directional and predictable in the same manner as hydrogen bonds or metal–ligand bonds, they are nonetheless extremely important. For example, the PQT^{2+} ion in **1** is tilted away from perpendicular by 62° so as to maximize the $N^+\cdots O$ interactions and also form weak $CH\cdots O$ hydrogen bonds along with the major π-stacking components.[1]



Scheme 2. Comparison of the intramolecular N^+-N^+ distances in the isomeric pyridinium ions PQT^{2+} and $[pyCH_2CH_2py]^{2+}$ (**2a**).

Herein, we present a new motif for the design of [2]pseudorotaxanes based on the simple concept of optimizing $N^+\cdots O$ interactions between pyridinium ions and simple crown ethers.[10] The N^+-N^+ distance in PQT^{2+} is about 7.00 Å while in the isomeric 1,2-bis(pyridinium)ethane dication **2a** it is only about 3.75 Å (Scheme 2). Although Stoddart et al. have reported that the interaction between dibenzylparaquat and DB24C8 is negligible,[11, 12] an examination of CPK and computer models suggested a good match between **2a** (the "axle") and the 24-membered crown ethers (wheels) 24C8, B24C8, and DB24C8 (Scheme 3) that should



Scheme 3. Formation of [2]pseudorotaxanes from 24C8, B24C8, and DB24C8.

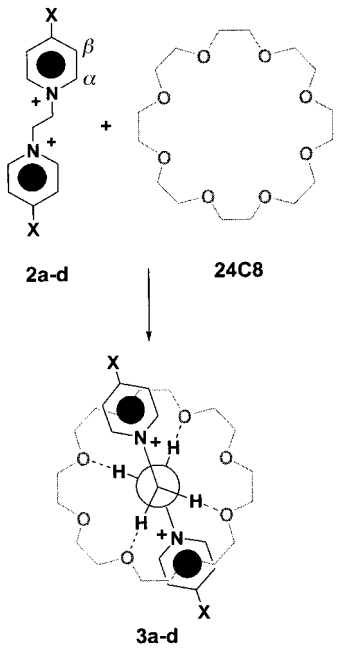
optimize the $N^+\cdots O$ interactions. Scheme 4 shows how two sets of $N^+\cdots O$ interactions might be accompanied by a series of four $C-H\cdots O$ hydrogen bonds that are formed with alternate oxygen atoms in the crown ether. The question remains as to whether these interactions are sufficient to produce a stable [2]pseudorotaxane in the absence of the π-stacking interactions found in **1** and related molecules.

The addition of one equivalent of 24C8 to a solution of one equivalent of $\mathbf{2a}(BF_4)_2$ in MeCN gave the [2]pseudorotaxane **5a**. An association constant K_a of 165 M^{-1} was measured for this interaction by ^1H NMR titration in MeCN at 298 K. By variation of the substitutuent X on the pyridinium ring other axles can be incorporated and a more detailed understanding of the overall interaction can be obtained. The strength of the interaction can be controlled by varying X as shown in Table 1. In particular, the introduction of the electron-with-

[*] Prof. Dr. S. J. Loeb, J. A. Wisner
Department of Chemistry and Biochemistry
University of Windsor
Windsor, ON, N9B 3P4 (Canada)
Fax: (+1) 519-973-7098
E-mail: loeb@uwindsor.ca

[**] Financial support for this work was provided by the Natural Sciences and Engineering Research Council of Canada.

 © WILEY-VCH Verlag GmbH, D-69451 Weinheim, 1998 1433-7851/98/3720-2838 $ 17.50+.50/0



Scheme 4. Newman projection along the C–C vector of the $N^+CH_2CH_2N^+$ portion of the dication $[XpyCH_2CH_2pyX]^{2+}$, **2a–d**, (X = H, Me, Ph, CO_2Et,). This combination of $N^+\cdots O$ ion–dipole interactions and C–H···O hydrogen bonds might stabilize the formation of [2]pseudorotaxanes with 24C8.

drawing group CO_2Et results in the largest association constant for the interactions with each of the three crown ethers.

Incorporation of aromatic groups into the crown ether provides the possibility of π stacking between the pyridinium rings and the catechol rings of the crown ether. In the ^1H NMR spectra of the two pseudorotaxanes derived from **2a** (X = CO_2Et) with B24C8 (**4d**) and DB24C8 (**5d**) π stacking in solution is clearly evident: the signals for the β protons of the pyridine group shift upfield (δ = 8.56, 8.36, and 8.14 for the pseudorotaxanes with 24C8, B24C8, and DB24C8, respectively). This trend is mirrored by a uniform increase in K_a from 320 to 740 to 1200 M^{-1} and an increase in the intensity of a charge transfer absorption band at about 370 nm (Figure 1). In addition, **3d–5d** show significant downfield shifts (δ = 0.20–0.31)for the α and NCH_2 protons, which is indicative of the formation of C–H···O hydrogen bonds to the oxygen atoms of the crown ether.

These results and the threading conformation proposed in Scheme 4 are supported by the solid-state structure of $[(Et O_2CpyCH_2CH_2pyCO_2Et)(DB24C8)]^{2+}$ (**5d**; py = $C_5H_4N^+$).[13] Figures 2 and 3 show different views of the threading of the dicationic axle through the cavity of the DB24C8 macrocycle. The [2]pseudorotaxane is stabilized by 1) eight $N^+\cdots O$ interactions (N–O 3.76–4.88 Å), 2) eight C–H···O hydrogen bonds (the four predicted ones between the bridging ethane unit and alternate ether oxygen atoms as well as four others between α-pyridinium hydrogen atoms and symmetry related O5 atoms

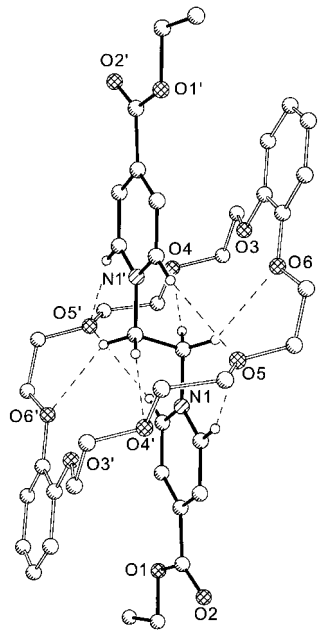


Figure 2. A ball-and-stick representation of the crystal structure of **5d**, formed from $[EtO_2CpyCH_2CH_2pyCO_2Et]^{2+}$ (**2d**) and DB24C8.

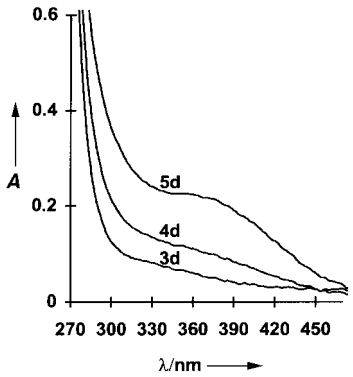


Figure 1. UV absorption spectra of **3d, 4d,** and **5d**. The intensity of the charge-transfer band in the region 270–470 nm increases with increased capacity for π-stacking interactions.

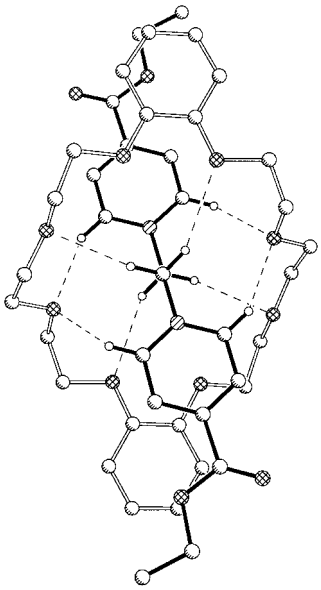


Figure 3. A ball-and-stick representation of the crystal structure of **5d**, shown along the C9–C9′ bond. This view corresponds to the Newman projection show schematically in Scheme 4. N^+–O distances: $N1^+$–O3 4.88, $N1^+$–O4 4.43, $N1^+$–O5 3.76, $N1^+$–O6 4.66 Å. C–H···O hydrogen bonds (lengths [Å] and angles [°]): H9A–O4′ 2.54, H9B–O6′ 2.66, H6A–O5 2.36, H7A–O5′ 2.54; C9-H9A-O4′ 165.0, C7-H7A-O5′ 141.0, C6-H6A-O5 154.2, C9-H9B-O6′ 150.0.

Table 1. Association constants (K_a) and free energies of complexation (ΔG) for **3a–d**, **4a–d**, and **5a–d** formed from $[X\text{-}pyCH_2CH_2py\text{-}X]^{2+}$, **2a–d**, and 24C8, B24C8, or DB24C8 in MeCN at 298 K.[a]

	24C8		B24C8		DB24C8	
X	K_a [M^{-1}]	$-\Delta G$ [kJ mol^{-1}]	K_a [M^{-1}]	$-\Delta G$ [kJ mol^{-1}]	K_a [M^{-1}]	$-\Delta G$ [kJ mol^{-1}]
H (**a**)	165	12.7	195	13.1	180	12.9
Me (**b**)	105	11.6	205	13.2	230	13.5
Ph[b] (**c**)	160	12.6	300	14.2	320	14.3
CO_2Et[b] (**d**)	320	14.3	740	16.4	1200	17.6

[a] Sample concentrations 2.0×10^{-3}–5.0×10^{-3} M. [b] Chemical exchange was slow on the NMR time scale and peaks were observed for both complexed and uncomplexed species. K_a was determined by integration from a 1:1 mixture. All other K_a values were determined by NMR titration experiments by using the program EQNMR.[16] Estimated errors: < 10% for $K_a > 100$.

 © WILEY-VCH Verlag GmbH, D-69451 Weinheim, 1998 1433-7851/98/3720-2839 $ 17.50+.50/0

(C – O 2.36 – 2.66 Å), and 3) π-stacking interactions between the electron-rich catechol rings of the crown ether and the electron-poor aromatic rings and ester group of the pyridinium salt.

The new binding motif for the formation of [2]pseudorotaxanes presented herein demonstrates for the first time that simple crown ethers can be used to form [2]pseudorotaxanes. The ability to easily tune the interaction strength and the availability of these simple components bodes well for the extension of this motif to more complex supramolecular systems with interlocked [*n*]rotaxanes and [*n*]catenanes.

Experimental Section

All pyridinium bromide salts were prepared by the literature method.[14] The BF_4^- salts were precipitated from water by the addition of $NaBF_4$ or NH_4BF_4 and recrystallized before use. DB24C8 was purchased from Aldrich and used as received. B24C8 and 24C8 were prepared by literature methods.[15] In a typical experiment, [2]pseudorotaxanes were formed in solution by mixing equimolar solutions of **2a**$(BF_4)_2$ – **d**$(BF_4)_2$ and crown ether in MeCN. Typical data for [2]pseudorotaxanes in which X = CO_2Et: **3d**: ^{1}H NMR (300 MHz, CD_3CN, 298 K): $\delta = 9.27$ (d, 4H, $J = 5.3$ Hz; α-pyH), 8.56 (d, 4H, $J = 5.3$ Hz; β-pyH), 5.40 (s, 4H; NCH_2), 4.50 (q, 4H, $J = 7.1$ Hz; C(O)OCH_2), 3.50 (s, 32H; OCH_2), 1.44 (t, 6H, $J = 7.1$ Hz; CH_3); ES-MS *m*/*z* (%): 770 (5) $[M - BF_4]^+$, 341 (100) $[M - 2BF_4]^{2+}$. **4d**: ^{1}H NMR (300 MHz, CD_3CN, 298 K): $\delta = 9.24$ (d, 4H, $J = 6.4$ Hz; α-pyH), 8.36 (d, 4H, $J = 6.4$ Hz; β-pyH), 6.80 (m, 4H; Ar), 5.46 (s, 4H; NCH_2), 4.47 (q, 4H, $J = 7.1$ Hz; C(O)OCH_2), 4.02 (m, 4H; ArOCH_2), 3.94 (m, 4H; OCH_2), 4.83 (m, 8H; OCH_2), 3.63 (m, 4H; OCH_2), 3.43 (m, 4H; OCH_2), 3.18 (m, 4H; OCH_2), 1.44 (t, 6H, $J = 7.1$ Hz; CH_3); ES-MS *m*/*z* (%): 818 (7) $[M - BF_4]^+$, 365 (100) $[M - 2BF_4]^{2+}$. **5d**: ^{1}H NMR (300 MHz, CD_3CN, 298 K): $\delta = 9.24$ (d, 4H, $J = 6.7$ Hz; α-pyH), 8.14 (d, 4H, $J = 6.7$ Hz; β-pyH), 6.74 (m, 8H; Ar), 5.58 (s, 4H; NCH_2), 4.40 (q, 4H, $J = 7.1$ Hz; C(O)OCH_2), 4.00 (m, 24H; OCH_2) 1.44 (t, 6H, $J = 7.1$ Hz; CH_3); ES-MS *m*/*z* (%): 865 (12) $[M - BF_4]^+$, 389 (100) $[M - 2BF_4]^{2+}$.

Received: April 28, 1998 [Z 11791 IE]
German version: *Angew. Chem.* **1998**, *110*, 3010 – 3013

Keywords: crown compounds · rotaxanes · self-assembly · supramolecular chemistry

[1] B. L. Allwood, N. Spencer, H. Shahriari-Zavareh, J. F. Stoddart, D. J. Williams, *J. Chem. Soc. Chem. Commun.* **1987,** 1064 – 1066;
[2] D. Philp, J. F. Stoddart, *Angew. Chem.* **1996,** *108,* 1242 – 1286; *Angew. Chem. Int. Ed. Engl.* **1996,** *35,* 1154 – 1196, and references therein.
[3] P. R. Ashton, P. T. Glink, J. F. Stoddart, P. A. Tasker, A. J. P. White, D. J. Williams, *Chem. Eur. J.* **1996,** *2,* 729 – 736.
[4] R. Jäger, F. Vögtle, *Angew. Chem.* **1997**, *109,* 966 – 980; *Angew. Chem. Int. Ed. Engl.* **1997,** *36,* 930 – 944, and references therein.
[5] A. P. Lyon, D. H. Macartney, *Inorg. Chem.* **1997,** *36,* 729 – 736, and references therein.
[6] D. B. Amabilino, P. R. Ashton, S. E. Boyd, M. Gómez-López, W. Hayes, J. F. Stoddart, *J. Org. Chem.* **1997,** *62,* 3062 – 3075.
[7] H. Sleiman, P. N. W. Baxter, J.-M. Lehn, K. Airola, K. Rissanen, *Inorg. Chem.* **1997,** *36,* 4734 – 4742.
[8] P. Gaviña, J.-P. Sauvage, *Tetrahedron Lett.* **1997,** *38,* 3521 – 3524.
[9] M. Fujita, F. Ibukuro, H. Seki, O. Kamo, M. Imanari, K. Ogura, *J. Am. Chem. Soc.* **1996,** *118,* 899 – 900, and references therein.
[10] For a recent example of host – guest interactions between crown ethers and pyridinium compounds, see M. Lämsä, J. Huuskonen, K. Rissanen, J. Pursiainen, *Chem. Eur. J.* **1998**, *4*, 84 – 92.
[11] M.-V. Martínez-Díaz, N. Spencer, J. F. Stoddart, *Angew. Chem.* **1997,** *109,* 1991 – 1994; *Angew. Chem. Int. Ed. Engl.* **1997,** *36,* 1904 – 1907.
[12] For an example of a pseudorotaxane involving DB24C8 and a paraquat type molecule, see P. R. Ashton, S. J. Langford, N. Spencer, J. F. Stoddart, A. J. P. White, D. J. Williams, *Chem. Commun.* **1996,** 1387 – 1388.
[13] Crystal structure data for **5d**$(BF_4)_2$: monoclinic, space group $P2_1/c$, $a = 13.2421(4)$, $b = 15.7037(5)$, $c = 12.1739(4)$ Å, $\beta = 94.909(1)^\circ$, $V = 2522.3(1)$ Å^3, $Z = 2$, $\rho_{calcd} = 1.308$ g cm^{-3}, $2\theta_{max} = 45.0^\circ$, $Mo_{K\alpha}$ radiation ($\lambda = 0.71073$ Å), $T = 296$ K. A pale yellow crystal with dimensions $0.2 \times 0.2 \times 0.3$ mm was grown by vapor diffusion of isopropyl ether into a solution of **5d** in MeCN and mounted on a fibre. The 3280 unique reflections ($R_{int} = 0.0715$) were integrated from frame data obtained from programmed hemisphere scan routine on a Siemens SMART CCD diffractometer. Decay (< 1%) was monitored by 50 standard data frames measured at the beginning and end of data collection. Systematic absences in the diffraction data and determined unit-cell parameters were consistent with the space group $P2_1/c$. Lorentzian-polarization correction and semi-empirical absorption correction, based on redundant data at varying effective azimuthal angles, were applied to the data ($\mu = 0.112$ cm^{-1}, min./max. transmission = 0.221/0.492). The structure was solved by direct methods, with Fourier syntheses, and refined with full-matrix least-squares methods against $|F^2|$ data to give $R(F) = 0.0815$, $wR(F^2) = 0.2271$, GOF = 1.033, $N_o/N_v = 3275/354$. All non-hydrogen atoms were refined anisotropically. Hydrogen atoms were treated as idealized contributions. Scattering factors and anomalous dispersion coefficients are contained in the SHELXTL 5.03 program library (Sheldrick, G. M., Madison, WI). Crystallographic data (excluding structure factors) for the structure reported in this paper have been deposited with the Cambridge Crystallographic Data Centre as supplementary publication no. CCDC-101459. Copies of the data can be obtained free of charge on application to CCDC, 12 Union Road, Cambridge CB2 1EZ, UK (fax: (+44) 1223-336-033; e-mail: deposit@ccdc.cam.ac.uk).
[14] M. I. Attalla, N. S. McAlpine, L. A. Summers, *Z. Naturforsch. B* **1984,** *39,* 74 – 78.
[15] C. J. Pedersen, *J. Am. Chem. Soc.* **1967,** *89,* 7017 – 7036.
[16] J. Hynes, *J. Chem. Soc. Dalton Trans.* **1993,** 311 – 312.

$[Te_6N_8(TeCl_4)_4]$—Tellurium Nitride Stabilized by Tellurium Tetrachloride

Werner Massa, Carsten Lau, Michael Möhlen, Bernhard Neumüller, and Kurt Dehnicke*

Exactly 100 years ago tellurium nitride was first obtained by the reaction of tellurium tetrabromide with liquid ammonia.[1] The composition TeN was ascribed to this yellow, extremely poorly soluble, and highly exlosive substance. Considering the analogy to the crystallographically well characterized homologues S_4N_4[2] and Se_4N_4,[3] this assignment has not been entirely ruled out to this day.[4] However, later analytical work made the composition Te_3N_4 with tetravalent tellurium probable.[5–7] The tellurium compounds with nitride functionalities which were characterized in recent years also derive from tellurium(+IV). Among these are the complexes of type **1** with X = Cl[8] and F,[9] which correspond to the structure motif **A** with pyramidal nitride functionality, and the nitride

[*] Prof. Dr. K. Dehnicke, Prof. Dr. W. Massa, Dr. C. Lau, Dr. M. Möhlen, Priv.-Doz. Dr. B. Neumüller
Fachbereich Chemie der Universität
Hans-Meerwein-Strasse, D-35032 Marburg (Germany)
Fax: (+49) 6421-28-8917

 © WILEY-VCH Verlag GmbH, D-69451 Weinheim, 1998 1433-7851/98/3720-2840 $ 17.50+.50/0

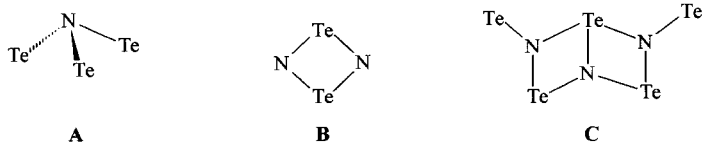
halides **2**[10] and **3**[11] with the structure motif **B** and trigonal-planar nitride functionality, which is also realized in **4** with the structure motif **C**.

$N[Te(NSN)X]_3$ **1** ($X = F, Cl$)

$[Te_4N_2Cl_8](AsF_6)_2$ **2**

$[Te_3N_2Cl_5(SbCl_5)]SbCl_6$ **3**

$Te_{11}N_6Cl_{26}$ **4**



A **B** **C**

We now found a method of approach to tellurium nitride stabilized by $TeCl_4$ molecules in the reaction of tellurium tetrachloride with tris(trimethylsilyl)amine in THF [Eq. (1)]. This tellurium nitride can be obtained in more than 80% yield.

$$10\,TeCl_4 + 8\,N(SiMe_3)_3 \xrightarrow{THF} \underset{\mathbf{5}}{[Te_6N_8(\mathbf{TeCl_4})_4]} + 24\,ClSiMe_3 \qquad (1)$$

Compound **5** forms pale yellow, moisture-sensitive, non-explosive crystals. According to the crystal structure analysis[13] these crystals still contain 7.5 equivalents of THF per formula unit, four of which enter into weak bonding interactions with the atoms Te1 and Te2. With 271.3 pm their Te–O distances agree with the Te–O bond lengths of 273.1 pm in $[TeCl_4(OPCl_3)]_2$.[16] The core of the structure of $[\mathbf{5}\cdot 4\,THF]\cdot 3.5\,THF$ consists of the rhombic dodecahedral unit Te_6N_8, in which the tellurium atoms form the corners of a distorted octahedron and the nitrogen atoms occupy the faces of the octahedron as μ_3 ligands (Figure 1). Four of these

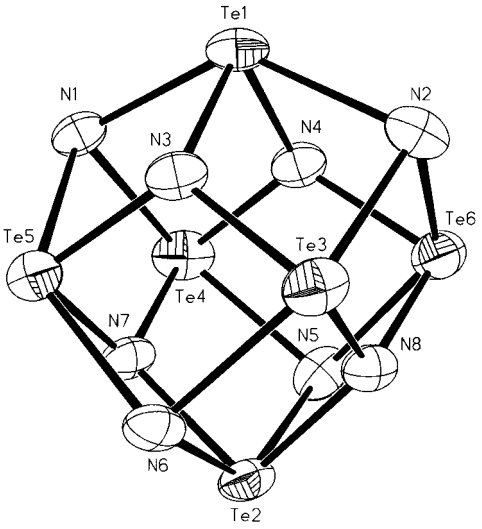


Figure 1. View of the Te_6N_8 core in the structure of $[\mathbf{5}\cdot 4\,THF]\cdot 3.5\,THF$. Displacement ellipsoids are at the 30% probability level at 223 K.

nitrogen atoms are coordinated with $TeCl_4$ molecules, the chlorine atoms of which adjust themselves well to the shape of the Te_6N_8 core due to the steric effect of the free electron pair at the tellurium atom (Figure 2). At the same time, with 304–331 pm the distances of the chlorine ligands of the $TeCl_4$ molecules to the Te atoms of the core which are not

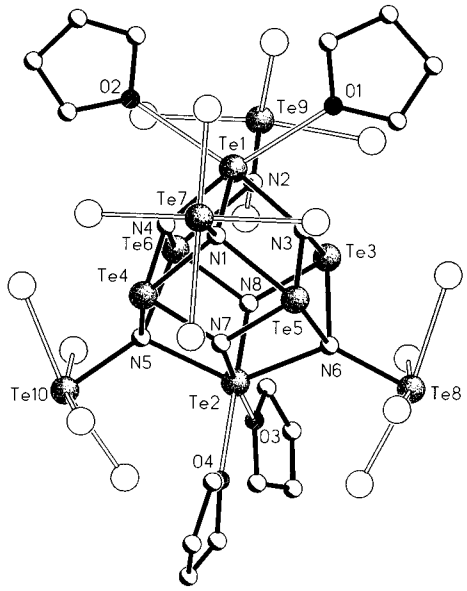


Figure 2. Molecular structure of $[\mathbf{5}\cdot 4\,THF]$ in the crystal. In the disordered $TeCl_4$ groups at Te(8–10) only the more strongly occupied orientations are shown. Selected average bond lengths [pm] and angles [°] (standard deviations taken from the mean of the single values): Te(1–6)–N(1,2,5,6) 228.5(6), Te(7–10)–N(1,2,5,6) 204.0(6), Te(1–6)–N(3,4,7,8) 201.3(6), Te(1,2)–O(1–4) 271.3(8), Te–Cl 251.6(4); Te-N(1,2,5,6)-Te 95.5(2), Te-N(3,4,7,8)-Te 114.4(2), Te-N(1,2,5,6)-Te(7–10) 121.0(2).

coordinated with THF are clearly below the van der Waals sum of radii (381 pm). Since the shielding of the Te_6N_8 core obtained thereby is not yet perfect, the tellurium atoms Te1 and Te2 which are facing each other are solvated by THF molecules. This results in Te_6N_8 molecules which are isolated from one another in the crystal lattice because of their jacket and thus lose their explosive character. Upon heating under argon $\mathbf{5}\cdot 7.5\,THF$ loses tetrahydrofuran at 83 °C. From 141 °C onwards **5** is intrinsically unstable with dinitrogen evolution and blackening under separation of tellurium beginning. At 168 °C, finally, $TeCl_4$ can be observed as yellow sublimate.

The $TeCl_4$ molecules bonded to the nitrogen atoms N(1,2,5,6) cause not only a restriction of the Te-N-Te bond angles of the Te_6N_8 skeleton from 114.4° to 95.5° at N(3,4,7,8), but also a stretching of the affected Te–N bonds of the Te_6N_8 core to 228.5 pm on average; all the other Te–N distances are only 201.3 pm. As a result, the latter are only a bit shorter than the Te–N bonds of the nitride functionality in the molecular complex **1** with 203.1 pm for X = F[9] and 206.1 pm for X = Cl.[8] Almost the same length is also shown by the Te–N bonds of the $TeCl_4$ molecules which are connected to the Te_6N_8 skeleton (av 204.0 pm). Te–N bonds which are a little shorter with an approximate length of 198 pm were observed in the cationic complexes **2** and **3**.[10, 11] In all cases these distances approximately meet the value of 199 pm for Te–N single bonds.[17] An approximately planar surrounding of the tellurium atoms by the four chlorine atoms as given in **5** is also observed in the polymeric structure of phenyltellurium trichloride.[18]

In THF **5** shows dynamic behavior in the ^{125}Te NMR spectrum. Only two signals of different intensities are observed at $\delta = 716$ for the coordinated $TeCl_4$ molecules

and at $\delta = 567$ for the tellurium atoms of the Te_6N_8 core. This is in accord with the idea of a synchronized change of location for the four $TeCl_4$ molecules on the Te_6N_8 surface. Detachment of the $TeCl_4$ molecules does not take place in this process; the ^{125}Te NMR signal of $TeCl_4$ in THF is at $\delta =$ 1036.[19] Because of their disorder behavior the change of location of the $TeCl_4$ molecules is also indicated in the crystalline state, even at 223 K. In contrast, the THF molecules which are only loosely bonded are subject to quick exchange according to the ^{1}H NMR spectrum.

Received: May 20, 1998 [Z11886IE]
German version: *Angew. Chem.* **1998**, *110*, 3008 – 3010

Keywords: nitride · nitrogen · tellurium

[1] R. Metzner, *Ann. Chim. Phys.* **1898**, *15*, 250.
[2] B. D. Sharma, J. Donohue, *Acta Crystallogr*. **1963**, *16*, 891; M. L. DeLucia, P. Coppens, *Inorg. Chem.* **1978**, *17*, 2336.
[3] H. Bärnighausen, T. von Volkmann, J. Jander, *Acta Crystallogr.* **1966**, *21*, 571; H. Folkerts, B. Neumüller, K. Dehnicke, *Z. Anorg. Allg. Chem.* **1994**, *620*, 1011.
[4] H. Garcia-Fernandez, *Bull. Soc. Chim. Fr.* **1973**, 1210; see also N. Wiberg, Holleman-Wiberg, *Lehrbuch der Anorganischen Chemie*, 101st ed., de Gruyter, Berlin, **1995**.
[5] W. Strecker, W. Ebert, *Chem. Ber.* **1925**, *58*, 2527.
[6] C. Mahr, Dissertation, Universität Marburg, **1928**.
[7] O. Schmitz-DuMont, B. Ross, *Angew. Chem.* **1967**, *79*, 1061; *Angew. Chem. Int. Ed. Engl.* **1967**, *6*, 1071.
[8] H. W. Roesky, J. Münzenberg, M. Noltemeyer, *Angew. Chem.* **1990**, *102*, 73; *Angew. Chem. Int. Ed. Engl*. **1990**, *29*, 61.
[9] J. Münzenberg, H. W. Roesky, S. Besser, R. Herbst-Irmer, G. M. Sheldrick, *Inorg. Chem.* **1992**, *31*, 2986.
[10] J. Passmore, G. Schatte, T. S. Cameron, *J. Chem. Soc. Chem. Commun.* **1995**, 2311.
[11] C. Lau, H. Krautscheid, B. Neumüller, K. Dehnicke, *Z. Anorg. Allg. Chem.* **1997**, *623*, 1375.
[12] C. Lau, B. Neumüller, K. Dehnicke *Z. Anorg. Allg. Chem.* **1996**, *622*, 739.
[13] Crystal structure determination of $[\mathbf{5}\cdot 4\,THF]\cdot 3.5\,THF$ ($C_{30}H_{60}Cl_{16}N_8O_{7.5}Te_{10}$, $M_r = 2496.06$): A colorless crystal (ca. $0.54 \times 0.54 \times 0.45$ mm) was analyzed with an area detector system (IPDS, Stoe) at $-50\,^\circ$C with $Mo_{K\alpha}$ radiation ($\lambda = 71.069$ pm, graphite monochromator). Unit cell monoclinic, $a = 2291.7(2)$, $b = 1222.7(1)$, $c =$ 5356.0(5) pm, $\beta = 101.74(1)^\circ$; $V = 14694 \times 10^{-30}$ m^3, space group $I2/a$, $Z = 8$, $\rho_{calcd} = 2.257$ Mg m^{-3}, $\mu(Mo_{K\alpha}) = 4.53$ mm^{-1}, $F(000) = 9184$. Because of a rapid decline in intensity at increasing diffraction angle, data were only collected up to $\theta = 24^\circ$, $\Phi = 0 - 250^\circ$, $\Delta\Phi = 1^\circ$, $t = 1$ min per record. Of 55355 reflections collected, 11290 were independent ($R_{int} =$ 0.060) and 7648 observed ($I \geq 2\sigma(I)$). Measurement at even lower temperature was not possible, since a phase transition apparently occurs at approximately 220 K. Below this temperature diffuse streaks occur along the nevertheless very long c axis with maxima corresponding to a double superstructure. Semiempirical absorption corrections (from equivalent reflections) were carried out, and the structure was solved by direct methods and refined against all F^2 data[14] by full matrix. The $TeCl_4$ molecules bonded to the Te_6N_8 core showed strong disorder. Three of them had to be described by split atom models, which in two cases showed also a shift component in addition to a rotational component. All atoms, just as those of the core, could be refined with individual anisotropic displacement parameters. The four THF molecules coordinated at the core could be refined without using split positions, but with large anisotropic displacement parameters. The 3.5 THF molecules per molecule additionally fitted into gaps of the packing, one of which was situated on a twofold axis, and showed very strong motion and/or disorder. A model refined with split positions for two THF molecules converged at $wR_2 = 0.1182$ (all reflections) and $R = 0.0404$ (observed reflections). Because of the less than satisfactory possibility of describing the electron density blurred over this solvent range, its contribution to the structure factors was calculated by way of Back-Fourier transformation[15] and subtracted from the data set. Thereafter, the main structure $[\mathbf{5}\cdot 4\,THF]$ could be refined with clearly improved accuracy ($wR_2 =$ 0.0901, $R = 0.0348$, residual electron density 0.95/ – 0.79 e Å^{-3}). The geometrical details documented here refer to this refinement. The structure determined at 223 K has the character of a high-temperature form in which the solvate molecules and $TeCl_4$ groups show high mobility or disorder. As documented in the quite physically meaningful shapes of displacement ellipsoids ($U_{eq} = 0.054 - 0.083$ Å^2) of all atoms of the Te_6N_8 core, its orientation is not noticeably involved. Thus, no significant influence on the geometry is expected. Crystallographic data (excluding structure factors) for the structure reported in this paper (those obtained by Back-Fourier transformation as well as those obtained according to the disorder model) have been deposited with the Cambridge Crystallographic Data Centre as supplementary publication no. CCDC-101663 and CCDC-101664. Copies of the data can be obtained free of charge on application to CCDC, 12 Union Road, Cambridge CB2 1EZ, UK (fax: (+44) 1223-336-033; e-mail: deposit@ccdc.cam.ac.uk).
[14] G. M. Sheldrick, *SHELXTL 5.03*, Siemens Analytical X-ray Instruments, Inc., Madison, WI (USA), **1996**.
[15] P. van der Sluis, A. L. Spek, *Acta Crystallogr. Sect. A* **1990,** *46,* 194 – 201.
[16] K. Gretenkord, E. Lührs, B. Krebs, zitiert in B. Krebs, F.-P. Ahlers, *Adv. Inorg. Chem.* **1990**, *35*, 235.
[17] J. P. Johnson, G. K. McLean, J. Passmore, P. S. White, *Can. J. Chem.* **1989**, *67*, 1687.
[18] F. W. B. Einstein, T. Jones, *Acta Crystallogr. Sect. B* **1982**, *38*, 617.
[19] C. Lau, Dissertation, Universität Marburg, **1997**.

Langmuir – Blodgett Films of Single-Molecule Nanomagnets**

Miguel Clemente-León, Hélène Soyer, Eugenio Coronado,* Christophe Mingotaud,* Carlos J. Gómez-García, and Pierre Delhaès

The discovery that individual molecules can act as magnets of nanometer size is a very recent one.[1, 2] The most thoroughly studied single-molecule magnets are the mixed-valence manganese clusters $[Mn_{12}O_{12}(carboxylate)_{16}]$ (carboxylate = acetate,[1, 3] propionate,[4] benzoate,[5] and 4-methylbenzoate[6]), referred to here as Mn_{12}. The current excitement for this kind of magnetic cluster is primarily due to

[*] Prof. Dr. E. Coronado, M. Clemente-León, Dr. C. J. Gómez-García
Dept. Quimica Inorganica. Univ. de Valencia
Dr. Moliner 50, E-46100 Burjasot (Spain)
Fax: (+34) 96-3864322
E-mail: eugenio.coronado@uv.es
Dr. C. Mingotaud, H. Soyer, Dr. P. Delhaès
Centre de Recherche Paul Pascal – CNRS
Avenue A. Schweitzer, F-33600 Pessac (France)
Fax: (+33) 556845600
E-mail: mingotaud@axpp.crpp.u-bordeaux.fr

[**] This work was supported by the Ministeno de Educación y Cultura (Grant No. MAT98-0880) and the EU. M.C.-L. thanks the Generalitat Valenciana for a predoctoral fellowship. We thank the Spanish CICYT and the Generalitat Valenciana for the financial support to purchase the SQUID magnetometer.

 © WILEY-VCH Verlag GmbH, D-69451 Weinheim, 1998 1433-7851/98/3720-2842 $ 17.50+.50/0

the presence of a large magnetic hysteresis comparable to that observed in hard magnets.[1b] This provides the possibility of molecular bistability, opening the way to store information at the molecular level. On the other hand, these nanomagnets provide unique examples for observing the tunneling of an electron through a potential barrier from one orientation to another, which is a fundamental question in physics.[7–9] An elegant approach to arranging molecules into well-organized multilayered films is to use the Langmuir–Blodgett (LB) technique.[10] Although for the most part this method has been used to arrange organic molecules, it was shown very recently that inorganic clusters[11] or even extended layered solids[12] can also be organized as LB films. Here we report the first LB films based on the single-molecule magnets Mn_{12}. These materials contain well-organized magnetic monolayers formed by Mn_{12} clusters that, as expected, exhibit a marked magnetic hysteresis.

In the Mn_{12} clusters the metallic core is formed by an internal tetrahedron of four manganese(IV) ions, each of spin $S = 3/2$, surrounded by eight manganese(III) ions of spin $S = 2$ (Figure 1).[1a] In the crystalline state these neutral clusters



Figure 1. Schematic view of the $[Mn_{12}O_{12}(benzoate)_{16}]$ cluster from the axial viewpoint showing the equatorial phenyl rings. The four water molecules and the eight axial phenyl groups have been omitted for clarity. The larger dark circles represent the manganese ions, the light gray circles the oxygen atoms, and the small black circles the carbon atoms.

exhibit hysteresis with coercive fields as large as 1.5 T at 2 K.[1b] This hysteresis has a molecular origin. It is due to the magnetic relaxation properties of the cluster. In fact, exchange interactions within the cluster results in a ground state with large spin ($S = 10$) that encounters a thermal barrier for reversal of the direction of magnetization along the uniaxial magnetic axis. This leads to extremely slow relaxation times at very low temperature.

In view of the interesting results obtained in the building-up of LB films of molecular metal oxide clusters (i.e., polyoxometalates),[11] extension of the LB technique to the Mn_{12} clusters appears very desirable for fabricating organized films of the aforementioned single-molecule magnets. Two Mn_{12} clusters were used: the acetate and the benzoate derivatives. Upon spreading pure sample at the gas–water interface, the two manganese clusters do not form a stable Langmuir film. Therefore, a mixture of these complexes and a lipid is needed to obtain a monolayer. Behenic acid $CH_3(CH_2)_{20}COOH$ or behenic alcohol $CH_3(CH_2)_{20}CH_2OH$ was used as matrix. In the case of behenic alcohol, Brewster angle microscopy reveals that Mn_{12} clusters form crystallites on the top of the organic layer. In contrast, this optical technique suggests that an homogeneous monolayer is formed upon use of behenic acid as matrix. The resulting molecular system is clearly two-dimensional at the gas–water interface. Furthermore, the Langmuir film is stable over time if the lipid:cluster ratio is high enough (typically 5 or higher). When behenic acid is used as matrix, transfer of the monolayer onto a solid hydrophobic substrate is easily achieved at a surface pressure of 30 $mN\,m^{-1}$. A Y-type LB film is then obtained with a transfer ratio close to 0.90–0.95.

The structure of these brown LB films was investigated by IR spectroscopy and X-ray diffraction. Besides the bands at 2920, 2851, 1472, and 1463 cm^{-1} assigned to the stretching and scissoring modes of the C–H bonds, the IR spectra present a small broad band at about 1550 cm^{-1} which becomes clearly detectable when the concentration of clusters is high enough in the monolayer. This band comes from the carboxylate group and demonstrates that the cluster is indeed diluted within the multilayers. Whatever the complex concentration may be, this band presents no clear dichroism. Such a result is not surprising in view of the quasi-isotropic distribution of the carboxylate groups around the Mn_{12} core. In contrast, the IR bands associated with the alkyl chains are dichroic. The tilt angle of the hydrophobic tails is then easily evaluated: It is close to 22–24° for both the pure matrix and the organic/inorganic mixtures. As a result, the manganese cluster does not strongly modify the matrix organization.

X-ray diffraction shows a continuous evolution as a function of the concentration of the complex within the pristine layer. One to three Bragg peaks are observed for low concentrations of the benzoate cluster (lipid:cluster ratio higher than 20). In this case, the Bragg peaks have the same position as those for the LB films of pure behenic acid and corresponds to a periodicity of about 53.5 Å. However, the intensity of each peak is lower and its width is much larger than in the pristine film. This indicates that the organic layer structure is still maintained, but the coherence length has decreased in the material due to the insertion of the inorganic cluster.[13] Interestingly, when the concentration of the complex is large enough (typically for a lipid:cluster ratio that is lower than or equal to 10), the Bragg peaks associated to the behenic acid periodicity are very weak, but a new peak is clearly observed which corresponds to a new periodicity of 72 ± 2 Å. Taking into account that the disk shape of the benzoate cluster has a van der Waals diameter of about 22.5 Å and a thickness of about 18 Å,[5] such a distance corresponds to the intercalation of a monolayer of clusters in between a bilayer of behenic acid. In view of these distances the clusters should be preferably oriented with the axial direction perpendicular to the plane of the layer. We can conclude that the degree of organization of the clusters within the films is strongly dependent on the lipid:cluster ratio. For the higher ratios isolated clusters or partial monolayers of clusters are

obtained, while for ratios in the range of 10:1 to 5:1 lamellar structures with the clusters organized in well-defined monolayers are observed (Figure 2).

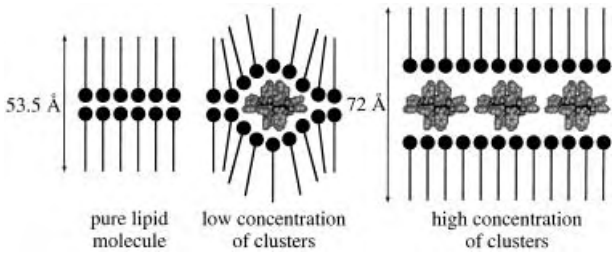


Figure 2. Schemes of the Y-type Langmuir–Blodgett films formed when the lipid:cluster ratio is varied.

The magnetic properties of the LB films were measured after deposition of about 300 layers onto a diamagnetic mylar substrate. Magnetic susceptibility data have provided information on the composition of the LB films. By comparison with the parent crystalline salt, one can calculate how many Mn_{12} clusters are trapped within the LB film. As the area of the substrate and the number of deposited layers is known, it is straightforward to estimate the density of clusters within a layer and the effective diameter per cluster. Thus, in the 10:1 and 5:1 films the estimated size of the benzoate cluster within the layer gives an effective diameter of about 22 ± 2 Å, which closely fits to the real value (see above), indicating that these clusters are close packed. For films with lower concentrations of clusters (ratio 20:1), the effective diameters are larger than 80 Å, which is in agreement with the dispersion of the clusters in between the organic layers, as suggested from X-ray data.

The most remarkable magnetic result comes from the magnetization data obtained as a function of the applied magnetic field below and above the blocking temperature (the temperature below which hysteretic behavior is observed) of the cluster (4 K). As for the parent crystalline salt, the benzoate film shows at 2 K a marked hysteresis loop (Figure 3) with a coercive field of about 0.1 T (0.06 T for the acetate film), which vanishes as the temperature is increased to 4 K (see inset). However, in contrast with the crystals, the magnetization at 5 T is far from saturation. This result is general for all the investigated films. We also observe that the shape of the loop depends on the orientation of the film with respect to the applied magnetic field H (Figure 3). Thus, when H is parallel to the plane of the magnetic monolayer, the loop is softer than when H is perpendicular. Such anisotropy constitutes further support of the preferential orientation of the clusters within the layers (with the uniaxial magnetic axis of the cluster perpendicular to the monolayer). On the other hand, the magnetic features remain completely unchanged when the film is cooled in the presence of a polarizing field of 5 T. This indicates that, in contrast to what has been observed for crystalline powders and frozen glasses,[3] in the LB films the field is completely unable to orient the clusters. Finally, the coercive field at 2 K is reduced by an order of magnitude when we pass from the crystal to the film. Such a difference is surely related to the different spin dynamics of the Mn_{12} cluster in these two media, as it is submitted to different

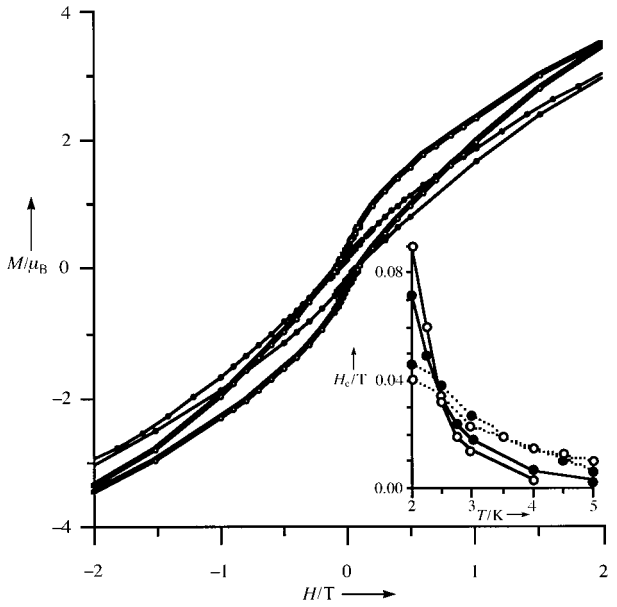


Figure 3. Hysteresis loops at 2 K of the Langmuir–Blodgett film prepared with the $[Mn_{12}O_{12}(benzoate)_{16}]$ cluster and behenic acid with a lipid:cluster ratio of 10:1; magnetic field H perpendicular (thick lines) and parallel (thin lines) to the film layer. Inset: Temperature dependence of the coercive field for the LB films of benzoate (solid lines) and acetate clusters (dotted lines). Filled and open circles refer to the orientation of the LB film with respect the applied field (parallel and perpendicular, respectively).

environments and packings. In fact, the magnetic relaxation in the Mn_{12} cluster can be strongly affected by its surroundings. For example, the presence of paramagnetic species around the cluster leads to an enhancement of the relaxation of the magnetization.[14]

A precedent for a magnetic LB film showing a weak hysteresis with a coercive field of 0.02 T was recently reported.[12] However, in that case the hysteresis has a cooperative origin. It is a consequence of the magnetic ordering established in a polymeric manganese phosphonate layer, which in the solid state is a weak ferromagnet. Such an approach to magnetic LB films involves the difficult formation in solution of structurally ordered polymeric layers in order to construct films with a "magnetic memory". The molecular origin of the hysteresis in the LB films of single-molecule magnets reported here avoids these difficulties and opens a very efficient and simple way to design well-organized molecular multilayers with useful magnetic properties or combination of properties.

Experimental Section

The manganese complexes were synthesized following the published procedure.[5] Chemical analysis and magnetic measurements confirmed the identity and purity of the manganese complexes. Behenic acid and behenic alcohol were obtained from Fluka (purity > 99%). Chlorofrom (HPLC grade, Prolabo) was used as spreading solvent. Solutions of the manganese complexes (concentration ca. 10^{-4}–10^{-5} M) and the lipids (concentration ca. 10^{-3} M) were kept at $-18\,^{\circ}C$ during the experiments in order to limit solvent evaporation. Built-up films were obtained by the vertical lifting method using an ATEMETA trough working at room temperature under a continuous flow of dried nitrogen. A stepwise compression of the monolayer was performed. After each increase of the surface pressure, a

 © WILEY-VCH Verlag GmbH, D-69451 Weinheim, 1998 1433-7851/98/3720-2844 $ 17.50+.50/0

waiting time (10 to 30 minutes) allowed the system to reach equilibrium. Steps of 2 mN m^{-1} were usually chosen. The subphase was water (Q grade, Millipore) with a resistivity higher than 18 MΩ cm. The dipping speed was generally set to 0.5 cm min^{-1}. Films were transferred onto optically polished calcium fluoride (precoated with three monolayers of behenic acid) for IR measurements, onto optically polished and silanized glass substrate for low-angle X-ray experiments, and onto a diamagnetic mylar sheet for magnetic SQUID measurements.

IR spectra were recorded on a FTIR 750 Nicolet spectrometer. To determine the orientation of the lipid molecules in the LB films, the linear dichroism in the IR region was used. In a first spectrum, the incident light was set perpendicular to the substrate normal; in a second, the incident IR beam formed an angle of 60° with the substrate normal. The out-of-plane dichroic ratio β for each band is then defined as the ratio of the IR absorption in both spectra. The angle between the substrate normal and the transition dipole moment can then be evaluated from β using a model already described.[15]

X-ray diffraction patterns were obtained using a conventional generator (Kristalloflex Siemens Ltd) delivering non-monochromatized line-focused $Cu_{K\alpha}$ radiation. This beam passes through the sample, which is mounted vertically and oscillated during exposure. The integrated intensities of the Bragg reflections were collected by an INEL CPS 120 curved position-sensitive detector (with a resolution of 0.1° in 2θ) associated with an IBM computer for peak assignments.

The magnetic measurements were performed with a Quantum Design MPMS-XL SQUID magnetometer between 2 and 300 K. For such experiments, about 300 layers were deposited on a diamagnetic mylar sheet ($0.075 \times 5 \times 15$ mm). The procedure followed for the magnetic susceptibility measurement is described elsewhere.[11] For the magnetization measurements the hysteresis loops were recorded in about 5 hours. Each loop contains 180 points. To stabilize each data point a time of about 2 minutes was required. The errors in the magnetization data are in the range of 1 – 5 %.

Received: May 13, 1998 [Z11851IE]
German version: *Angew. Chem.* **1998**, *110*, 3053 – 3056

Keywords: clusters · magnetic properties · monolayers · single-molecule magnets · thin films

[1] a) D. Gatteschi, A. Caneschi, L. Pardi, R. Sessoli, *Science* **1994**, *265*, 1054 – 1058; b) R. Sessoli, D. Gatteschi, A. Caneschi, M. A. Novak, *Nature* **1993**, *365*, 141 – 143.
[2] a) D. N. Hendrickson, D. M. Adams, C.-C. Wu, S. M. J. Aubin in *Magnetism: A supramolecular function* (Ed.: O. Kahn), *NATO ASI Ser. Ser. C 484* **1996**, pp. 357 – 382; b) see G. Christou in ref. [2a] pp. 383 – 409; c) S. M. J. Aubin, M. W. Wemple, D. M. Adams, H. L. Tsai, G. Christou, D. N. Hendrickson, *J. Am. Chem. Soc.* **1996**, *118*, 7746 – 7754; d) Z. Sun, C. M. Grant, S. L. Castro, D. N. Hendrickson, G. Christou, *Chem. Commun.* **1998**, 721.
[3] M. R. Cheesman, V. S. Oganesyan, R. Sessoli, D. Gatteschi, A. J. Thomson, *Chem. Commun.* **1997**, 1677 – 1678.
[4] H. J. Eppley, H. L. Tsai, N. de Vries, K. Folting, G. Christou, D. N. Hendrickson, *J. Am. Chem. Soc.* **1995**, *117*, 301 – 317.
[5] R. Sessoli, H. L. Tsai, A. R. Schake, S. Wang, J. B. Vincent, K. Folting, D. Gatteschi, G. Christou, D. N. Hendrickson, *J. Am. Chem. Soc.* **1993**, *115*, 1804 – 1816.
[6] S. M. J. Aubin, Z. Sun, I. A. Guzei, A. L. Rheingold, G. Christou, D. N. Hendrickson, *Chem. Commun.* **1997**, 2239 – 2240.
[7] J. Friedman, M. P. Sarachik, J. Tejada, R. Ziolo, *Phys. Rev. Lett.* **1996**, *76*, 3830 – 3833.
[8] L. Thomas, F. Lionti, R. Ballou, D. Gatteschi, R. Sessoli, B. Barbara, *Nature* **1996**, *383*, 145 – 147.
[9] B. Schwarzschild, *Phys. Today* **1997**, 17 – 19.
[10] A. Ulman, *An Introduction to Ultrathin Organic Films: From Langmuir-Blodgett to Self-Assembly*, Academic Press, Boston, **1991**.
[11] M. Clemente-León, C. Mingotaud, B. Agricole, C. Gómez-Garcia, E. Coronado, P. Delhaes, *Angew. Chem.* **1997**, *109*, 1143 – 1145; *Angew. Chem. Int. Ed. Engl.* **1997**, *36*, 1114 – 1116.
[12] C. T. Seip, G. E. Granroth, M. W. Meisel, D. R. Talham, *J. Am. Chem. Soc.* **1997**, *119*, 7084 – 7094.
[13] J. Reiche, U. Pietsch, H.-P. Fink, H. Lemmetuinen, *Acta Polymer.* **1992**, *43*, 206.
[14] K. Takeda, K. Awaga, *Phys. Rev. B* **1997**, *56*, 14560 – 14565.
[15] M. Vandevyver, A. Barraud, A. Ruaudel-Teixier, P. Maillard, C. Gianotti, *J. Colloid Interface Sci.* **1982**, *85*, 571.

Efficient Suzuki-Type Cross-Coupling of Enantiomerically Pure Cyclopropylboronic Acids**

Shao-Man Zhou, Min-Zhi Deng,* Li-Jun Xia, and Ming-Hua Tang

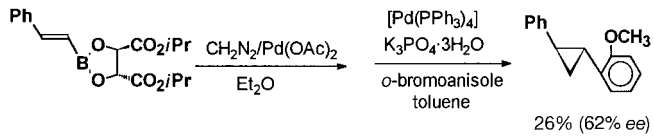
Transition metal catalyzed Suzuki-type cross-coupling reactions are versatile and powerful methods for the formation of carbon – carbon bonds, because most of these reactions are stereospecific and offer many other advantages.[1] The proposed mechanism of the palladium-catalyzed cross-coupling[1a] contains a transmetalation reaction between organoboron compounds and palladium halide complexes as well as subsequent reductive elimination steps. Undoubtedly, understanding the change in stereochemistry of the chiral carbon atom upon use of a chiral alkylboron compound as reagent is of interest for organic chemists. Bäckvall and Åkermark reported that the configuration of the chiral carbon atom of the alkyl group was retained upon transmetalation from mercury to palladium.[2] Stille found that the transmetalation reaction of a chiral benzyltin compound with a palladium complex in hexamethyl phosporamide (HMPA) proceeded with inversion.[3] Hiyama and co-workers investigated the palladium-catalyzed cross-coupling reaction of chiral alkylsilanes with aryl triflates (triflate = trifluoromethanesulfonate). They determined that the stereochemistry is affected by both the reaction temperature and the nature of the solvent and could be controlled from almost complete retention to inversion by tuning these factors.[4] Recently, we prepared racemic cyclopropylboronic acids and subjected them to Suzuki-type coupling reactions with bromoarenes[5] or bromoacrylates.[6] Herein we report the palladium-catalyzed cross-coupling of optically active cyclopropylboron compounds.

[*] Prof. M.-Z. Deng, Dr. S.-M. Zhou
Laboratory of Organometallic Chemistry
Prof. L.-J. Xia, M.-H. Tang
Analytical Chemistry Department
Shanghai Institute of Organic Chemistry
Chinese Academy of Sciences
354 Fenglin Lu, Shanghai 200032 (China)
Fax: (+86) 21-64166128
E-mail: dengmz@pub.sioc.ac.cn

[**] We are grateful to the Natural Science Foundation of China for financial support.

Supporting information for this article is available on the WWW under http://www.wiley-vch.de/home/angewandte/ or from the author.

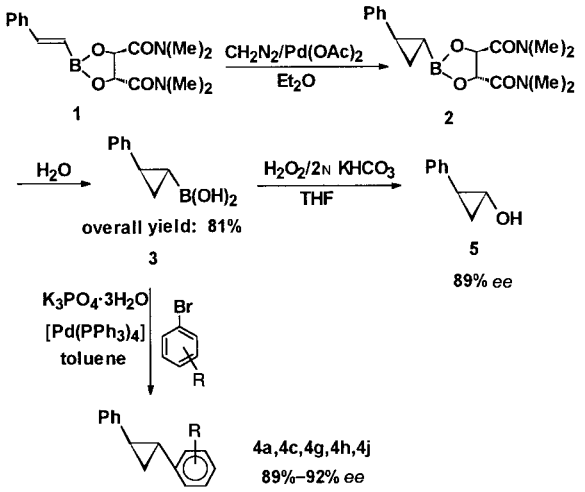
In the initial investigation, (*E*)-styrylboronic acid was esterified by (+)-diisopropyl tartrate (DIPT), and subsequent asymmetric cyclopropanation of the styrylboronic ester gave 2-phenylcyclopropylboronic ester. Afterwards, palladium-catalyzed cross-coupling with *o*-bromoanisole was conducted at 100 °C with toluene as solvent to afford optically active cyclopropyl-substituted anisol (62 % *ee*) in 26 % overall yield (Scheme 1).



Scheme 1. Synthesis of optically active cyclopropyl-substituted anisol by palladium-catalyzed cross-coupling.

The result was unsatisfactory, in particular the yield of coupling product was poor. Pietruszka et al. also investigated the cyclopropanation of alkenylboronic esters derived from (+)-DIPT and alkenyl boronic acids and the subsequent cross-coupling of the cyclopropanation product with iodobenzene; they obtained similar results.[7] The Suzuki-type cross-coupling of cyclopropylboronic esters with aryl halides was also reported by Marsden et al.,[8] but the yields of coupling products were lower. We recently showed that the yields of coupling products upon use of cyclopropylboronic acids[5, 6] as starting materials were higher than with cyclopropylboronic esters.[8] Therefore, we attempted to hydrolyze the cyclopropylboronic ester of DIPT with many reagents ($BF_3 \cdot Et_2O$, $TiCl_4$, $AlCl_3$, 2N HCl, 2N H_2SO_4, etc.) to afford the corresponding cyclopropylboronic acid, but the efforts failed. Fortunately, in numerous experiments on different derivatives of tartaric acid, it was found that in the asymmetrically induced cyclopropanation of (*E*)-1-alkenylboronic ester[9] (+)-*N*,*N*,*N*′*N*′-tetramethyltartaric acid diamide (TMTA)[10] is a better chiral auxiliary than (+)-DIPT. The optically active cyclopropylboronic ester of (+)-TMTA obtained in situ was readily hydrolyzed by water to give the corresponding optically active cyclopropylboronic acid in good yield (Scheme 2).

Under our previous conditions[5, 6] the optically active cyclopropylboronic acid could easily enter the cross-coupling reaction with bromobenzene to afford the optically active cyclopropyl-substituted benzene (Scheme 2). The absolute configuration of the product was determined by comparison of the specific rotation. For example, the (*E*)-styrylboronic ester of (+)-TMTA (**1**) was cyclopropanated to give, after hydrolysis, (1*R*,2*R*)-2-phenylcyclopropylboronic acid (**3**). This species underwent oxidation to (1*R*,2*S*)-(−)-2-phenyl-1-cyclopropanol (**5**), for which the sign of the specific rotation agreed with that reported[11] (Scheme 2). The sense of the specific rotation of product **4a** obtained by coupling of **3** with bromobenzene was also the same as that of (1*R*,2*R*)-(−)-1,2-diphenylcyclopropane[12] (Table 1), and the *ee* value of the oxidation product **5** was similar to that of **4a** (Scheme 2). In addition, the reactions of cyclopropylboronic acid of the same optical purity with different electrophiles gave the corresponding cross-coupling products with similar optical purities (Table 1). These results suggest that the absolute configuration of the center of chirality, on which the coupling reaction occurred, was retained in the coupling process.



Scheme 2. Synthetic route to optically active cyclopropyl-substituted benzene derivatives. See Table 1 for the substituent R.

Of course also *S*,*S* isomers (**4b, 4d**, **4e, 4f, 4i, 4k, 4m**) could be obtained by using (−)-TMTA as auxiliary. The results of the coupling reaction between optically active cyclopropylboronic acids and various electrophiles are shown in Table 1. The enantiomeric excesses of all products were determined by HPLC on appropriate chiral columns. Table 1 demonstrates that the chemical yields and optical purities of the coupling products thus obtained were higher than with previously reported methods.

We have presented the first detailed investigations of palladium-catalyzed Suzuki-type cross-coupling reactions with chiral organoboron coumpounds. The results indicate that the absolute configuration of the chiral carbon atom was retained in the cross-coupling process. The optical purities and yields of the coupling products are satisfactory. This method opens the door for the synthesis of other optical active cyclopropyl derivatives by the preparation and subsequent cross-coupling of optically active cyclopropylboronic acids with electrophiles.

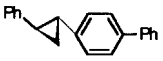
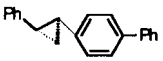
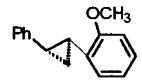
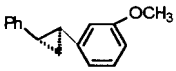
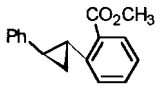
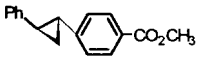
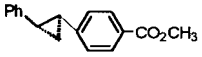
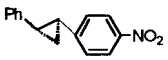
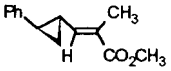
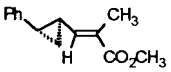
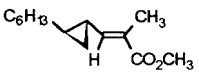
Received: May 11, 1998 [Z11839IE]
German version: *Angew. Chem.* **1998**, *110*, 3061 – 3063

Keywords: boron · chiral auxiliaries · cross-coupling · palladium

[1] a) N. Miyaura, A. Suzuki, *Chem. Rev.* **1995**, *95*, 2457 – 2483; b) T. Ishiyama, M. Yamamoto, N. Miyaura, *Chem. Lett.* **1996**, *12*, 1117; c) T. Ishiyama, T. Ahiko, N. Miyaura, *Tetrahedron Lett.* **1996**, *37*, 6889; d) S.-B. Jang, *Tetrahedron Lett.* **1997**, *38*, 1793; e) W. Shen, *Tetrahedron Lett.* **1997**, *38*, 5575; f) M. Larhed, A. Hallberg, *J. Org. Chem.* **1996**, *61*, 9582.
[2] J. E. Bäckvall, B. J. Åkermark, *J. Chem. Soc. Chem. Commun.* **1975**, 82.
[3] a) J. W. Labadie, J. K. Stille, *J. Am. Chem. Soc.* **1983,** *105*, 669; b) J. W. Labadie, J. K. Stille, *J. Am. Chem. Soc.* **1983**, *105*, 6129.
[4] Y. Hatanaka, T. Hiyama, *J. Am. Chem. Soc.* **1990,** *112*, 7793.

 © WILEY-VCH Verlag GmbH, D-69451 Weinheim, 1998 1433-7851/98/3720-2846 $ 17.50+.50/0

Table 1. Coupling reactions of various chiral cyclopropylboronic acids with electrophiles.[a]

Chiral auxiliary	Product		$[\alpha]_D^T$ [°] (c in $CHCl_3$)	Config.	Yield [%][b]	*ee* [%]
(+)-TMTA		**4a**	$[\alpha]_D^{17}$ −379.0 (0.496)[c]	(1*R*,2*R*)	77	91[d]
(−)-TMTA		**4b**	$[\alpha]_D^{16}$ 388.2 (1.003)[c]	(1*S*,2*S*)	81	91[d]
(+)-TMTA		**4c**	$[\alpha]_D^{16}$ −425.3 (1.123)	(1*R*,2*R*)	90	91[d]
(−)-TMTA		**4d**	$[\alpha]_D^{16}$ 421.8 (1.103)	(1*S*,2*S*)	88	90[d]
(−)-TMTA		**4e**	$[\alpha]_D^{16}$ 250.8 (1.250)	(1*S*,2*S*)	78	91[d]
(−)-TMTA		**4f**	$[\alpha]_D^{16}$ 343.6 (1.164)	(1*S*,2*S*)	73	90[e]
(+)-TMTA		**4g**	$[\alpha]_D^{16}$ −159.5 (0.981)	(1*R*,2*R*)	83	91[f]
(+)-TMTA		**4h**	$[\alpha]_D^{16}$ −450 (0.322)	(1*R*,2*R*)	79	92[d]
(−)-TMTA		**4i**	$[\alpha]_D^{12}$ 426.8 (0.963)	(1*S*,2*S*)-	84	90[d]
(+)-TMTA		**4j**	$[\alpha]_D^{16}$ −519.0 (0.973)	(1*R*,2*R*)	87	89[d]
(−)-TMTA		**4k**	$[\alpha_D^{12}$ 511.0 (1.000)	(1*S*,2*S*)	86	89[d]
(+)-TMTA		**4l**	$[\alpha]_D^{16}$ −377.3 (0.275)	(1*R*,2*R*)	80	92[d]
(−)-TMTA		**4m**	$[\alpha]_D^{17}$ 358.1 (0.296)	(1*S*,2*S*)	81	90[d]
(+)-TMTA		**4n**	$[\alpha]_D^{20}$ −40.1 (0.412)	(1*R*,2*R*)	76	82[d]

[a] Coupling reactions were conducted at 100 °C in toluene with the chiral cyclopropylboronic acids (1.1 equiv), the bromoarenes or bromoacrylates (1.0 equiv), $K_3PO_4 \cdot 3H_2O$ (3.3 equiv), and $[Pd(PPh_3)_4]$ (0.03 equiv). [b] Yields of isolated product based on the bromoarene or bromoacrylate. [c] (1*R*,2*R*)-1,2-Diphenylcyclopropane (**4a**): $[\alpha]_D^{20} = -418°$ ($c = 0.96$ in $CHCl_3$),[12b] 100 % *ee*; (1*S*,2*S*)-1,2-diphenylcyclopropane (**4b**): $[\alpha]_D^{22} = 362°$ ($c = 0.038$ in $CHCl_3$),[12a] 86 % *ee*. [d] Determined by HPLC (Chiralcel OD). [e] Determined by HPLC (Chiralcel OJ). [f] Determined by HPLC (Chiralcel AD).

[5] X.-Z. Wang, M.-Z. Deng, *J. Chem. Soc. Perkin Trans 1* **1996**, 2663 – 2664.
[6] S.-M. Zhou, Y.-L. Yan, M.-Z. Deng, *Synlett* **1998**, 198 – 200.
[7] J. Pietruszka, M. Widenmeyer, *Synlett* **1997**, 977 – 979.
[8] J. P.Hildebrand, S. P. Marsden, *Synlett* **1996**, 893 – 894.
[9] a) P. Fontani, B. Carboni, M. Vaultier, R. Carrie, *Tetrahedron Lett.* **1989**, *30*, 4814; b) P. Fontani, B. Carboni, M. Vaultier, G. Maas, *Synthesis.* **1991**, 605.
[10] Both enantiomers of the tartramide can easily be prepared by Seebach's procedure: D. Seebach, H.-O. Kalinowski, W. Langer, G. Crass, E.-M. Wilka, *Organic Syntheses, Collect. Vol. VII*, Wiley, New York, **1990,** pp. 41 – 50.
[11] T. Imai, H. Maineta, S. Nishida, *J. Org. Chem*. **1990**, *55*, 4986.
[12] a) M. Mintas, A. Mannschreck, *J. Chem. Soc. Chem. Commun*. **1979**,602; b) M. P. Wachter, T. M. Harris, *Tetrahedron* **1970**, 26, 1685.

Nanomolar Inhibitors for Two Distinct Biological Target Families from a Single Synthetic Sequence: A Next Step in Combinatorial Library Design?**

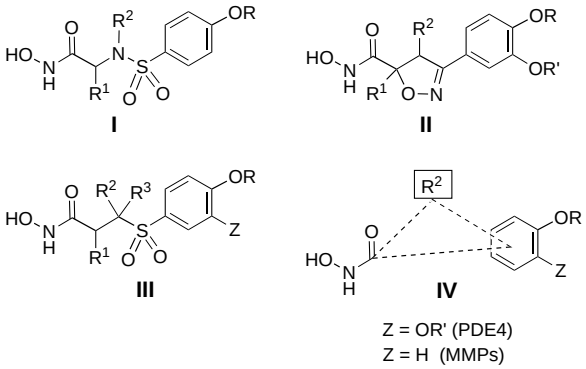
Christopher J. Burns,* Robert D. Groneberg, Joseph M. Salvino, Gerard McGeehan, Stephen M. Condon, Robert Morris, Matthew Morrissette, Rose Mathew, Shelley Darnbrough, Kent Neuenschwander, Anthony Scotese, Stevan W. Djuric, John Ullrich, and Richard Labaudiniere

The application of combinatorial chemistry and parallel synthesis tools to drug discovery has significantly increased the chemist's ability to prepare large sets or libraries of pharmacologically relevant compounds.[1] The design of small molecule libraries has traditionally been directed at either general lead generation[2] or more focused lead optimization libraries.[1] Recent empirical evidence suggests that certain minimum pharmacophore patterns[3] present within small-molecule lead structures can result in recognition by more than one member of a specified target family of interest (e.g. G-protein-coupled receptors).[4] Consequently a third class of combinatorial library has emerged: the target family directed library.[5] A key element in the design of such libraries is the inclusion of specific pharmacophore patterns or pharmacophoric points (e.g. hydroxamic acids or thiols for metalloenzymes) considered to be "privileged" for recognition of a target class of interest. Target family directed libraries offer the possibility of rapidly furnishing new lead structures for novel biomolecular targets as they arise within each family from molecular biology and genome research.[6]

Ideally, a target family directed library should incorporate the appropriate privileged pharmacophore pattern(s), and should also introduce sufficient diversity to ensure a range of pharmacological, pharmacokinetic, and physicochemical properties for the library members. Screening of a target family library may thereby not only provide lead structures for biological targets within a specific family, but initial structure – activity relationships (SAR) and selectivity data as well. It is therefore important to identify combinatorial-based synthetic approaches that allow rapid, efficient entry into such compound libraries.

Here we report a specific embodiment of the combinatorial chemistry paradigm that may have more general implications: the generation of multiple libraries—from a single synthetic sequence—that have been constructed to recognize members of two unrelated biological target families. Central to this approach was our identification of a novel structural template (**III**) that, with only a small but important change in functional decoration, could independently display the necessary pharmacophore patterns for inhibition of members of either of two different biomolecular target families (matrix metalloproteinases (MMPs) or phosphodiesterases (PDEs)). This recognition has permitted the pursuit of a straightforward synthetic route that efficiently generates a variety of combinatorially diversified α,β-unsaturated ester intermediates ($\mathbf{I}_{m-n}$, see Scheme 1). These intermediates can then be directed—depending upon the choice of the pharmacophoric characteristics chosen for the chemical input used in the divergent step—toward two structurally related but functionally distinct β-sulfonyl hydroxamic acid libraries.

Inhibition of the MMP collagenase-1 (MMP-1, EC3.4.24.7), the 72-kDa gelatinase (MMP-2, EC3.4.24.24), and the enzyme stromelysin-1 (MMP-3, EC3.4.24.17), and inhibition of the cAMP-specific phosphodiesterases (e.g. PDE4) has formed the basis for considerable research into therapies for oncology, asthma, and rheumatoid arthritis.[7] Within both of these target families, small-molecule inhibitors have been identified and are presently in clinical development.[7] Although there is little structural similarity between the natural substrates of these two distinct enzyme families (a peptide sequence for the MMPs and a cyclic nucleotide monophosphate for the PDEs), we have noted an apparent convergence of pharmacophore patterns (**IV**) for two independent series of hydroxamate-based MMP and PDE4 inhibitors (**I**[8] and **II**,[9] respectively). This convergence was consistent with the readily accessible structural template **III** designed in our lab. Contingent upon aryl substituent Z, structure type **III** can



display key pharmacophoric elements for recognition of either the MMP or the PDE target families, and therefore was used as the basis for construction of our first multiple target family directed libraries.

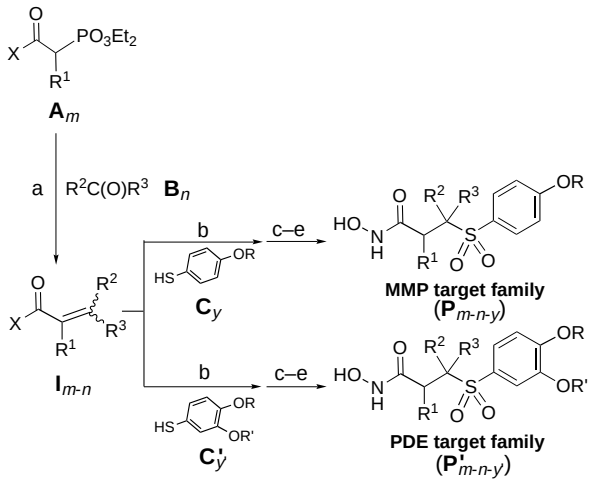
Synthetic routes were designed to allow the construction and subsequent elaboration of the diversified intermediate esters ($\mathbf{I}_{m-n}$) in both solution and the solid phase (Scheme 1).[10] The solution-phase synthesis (method A) served to explore the requisite chemical transformations, to perform the reactions on millimole scale, and to incorporate functional groups deemed incompatible with the solid-phase route. The solid-phase methodology (method B) rapidly provided micromole quantities of material for in vitro screening.[11]

[*] Dr. C. J. Burns, Dr. R. D. Groneberg, Dr. J. M. Salvino, Dr. G. McGeehan, Dr. S. M. Condon, R. Morris, M. Morrissette, R. Mathew, S. Darnbrough, Dr. K. Neuenschwander, A. Scotese, Dr. S. W. Djuric, Dr. J. Ullrich, Dr. R. Labaudiniere
Rhône-Poulenc Rorer
500 Arcola Rd., Collegeville, PA 19426 (USA)
Fax: (+1) 610-454-3311
E-mail: christopher.burns@rp-rorer.com

[**] We thank Dr. R. Harrison, Dr. J. Souness, Dr. J. Uhl, and J. Kline for the pharmacological data.

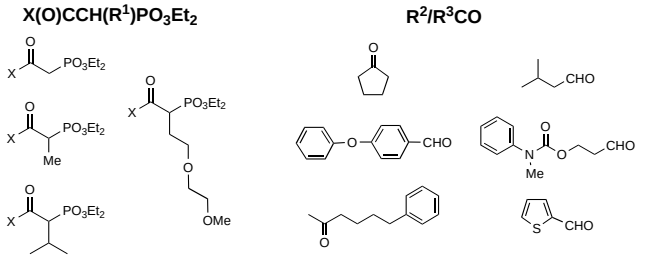
Supporting information for this article is available on the WWW under http://www.wiley-vch.de/home/angewandte/ or from the author.

 © WILEY-VCH Verlag GmbH, D-69451 Weinheim, 1998 1433-7851/98/3720-2848 $ 17.50+.50/0



Scheme 1. Single synthetic route to multiple target family directed libraries. Method A (solution-phase synthesis): a) NaH (1 equiv), THF, $-40\,^{\circ}C \rightarrow RT$, then $R^2C(O)R^3$ (1 equiv); b) *n*BuLi (0.1 equiv), ArSH (1.5 equiv), THF, $0\,^{\circ}C \rightarrow RT$; c) TFA/$CH_2Cl_2$, 1:5 (v/v); d) $(COCl)_2$ (2 equiv), CH_2Cl_2, DMF, then TMS-ONH_2 (5 equiv), CH_2Cl_2; e) oxone (1.5 equiv), MeOH/water, 1/1 (v/v), $0\,^{\circ}C \rightarrow RT$. Method B (solid-phase synthesis): a) KHMDS or LiHMDS (4 equiv), THF, $0\,^{\circ}C \rightarrow RT$, 0.5 h, filter, then $R^2C(O)R^3$ (5 equiv), THF/cyclohexane, 72 h; b) *n*BuLi (4 equiv), ArSH (20 equiv), THF, 100 h; c) *m*-CPBA (13 equiv), 1,4-dioxane, 16 h; d) TFA/CH_2Cl_2 1/1 (v/v), 2 h; e) EDCI (4 equiv), hydroxylamine-based Wang resin, 20 h, then TFA/CH_2Cl_2, 1/1 (v/v), 1.5 h. TFA = trifluoroacetic acid; TMS = trimethylsilyl; HMDS = bis(trimethylsilyl)amide; X = O*t*Bu, Wang resin.

The five-step synthesis permits independent variation at three regions of template **III** (R^1, R^2/R^3, and SAr(OR)(Z)). Diversification at R^1 and R^2/R^3 is achieved early in the synthetic route by Wadsworth–Horner–Emmons olefination of selected aldehydes and ketones. Selection of the substituents at these positions was based on several parameters including size, shape, and hydrophobicity/hydrophilicity (Scheme 2). The key chemical transformation that directs

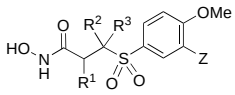


Scheme 2. Sampling of inputs used in the construction of diversified intermediates $\mathbf{I}_{m-n}$.

the olefinic ester intermediates $\mathbf{I}_{m-n}$ away from one target family and toward another (i.e., the divergent step) is the conjugate addition of aromatic thiols that are appropriately functionalized to complete the desired pharmacophore patterns.

As exemplified in Table 1, the choice of the appropriate arylthiolate ($\mathbf{C}_y$ or $\mathbf{C}'_{y'}$) in the divergent step of Scheme 1 defines the final products as either metalloproteinase or phosphodiesterase inhibitors. Use of *p*-alkoxythiophenols

Table 1. Enzyme inhibitory activity for examples from multiple target family directed libraries.[a]



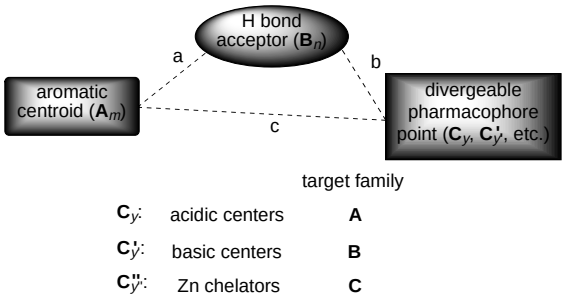
Compd[d]	K_i [μM][b]			IC_{50} [μM][c]
	MMP-1	MMP-2	MMP-3	PDE4
1	0.2	0.01	0.05	> 1
2	7	0.02	9	> 1
3	> 10	> 10	> 10	0.001

[a] K_i and IC_{50} are mean values from two or more determinations of purified compounds (see the supporting information). [b] Ref. [12]. [c] Ref. [13]. [d] Compound **1** (RPR 121683): $R^1 = H$; $R^2/R^3 = (-CH_2CH_2CH_2CH_2-)$; Z = H; **2**: (RPR 123303): $R^1 = H$; R^2 = 4-phenylbenzyl; $R^3 = Z = H$; **3** (RPR 123145): $R^1 = H$; $R^2 = Ph(CH_2)_4$; $R^3 = H$; Z = OMe.

such as 4-methoxythiophenol afforded potent inhibitors of MMP-1, MMP-2, and MMP-3.[14a] Selectivity among the MMPs varied according to the substituents R^1 and R^2/R^3 incorporated during the initial diversification steps. In fact, both broad-spectrum (**1**) and selective (**2**) MMP inhibitors were revealed during the screening process, thus demonstrating the versatility of this combinatorial approach. Alternatively, addition of discrete 3,4-dialkoxyphenyl thiolates to $\mathbf{I}_{m-n}$ elicited a switch in target family, and provided inhibitors of PDE4 effective at nanomolar concentrations while suppressing activity against the MMPs (e.g. **3**).[14b]

The application of combinatorial chemistry to drug discovery can result in structurally similar inhibitors for multiple targets (including members of multiple target families) as a natural consequence of general library screening.[15] It is the lure of adding front-end design elements to expedite such events that holds particular appeal. The advantages of combinatorial chemistry "directed" toward multiple target classes by a single synthetic sequence are the potential for higher hit rates during screening of the resulting libraries against biochemical targets within the targeted families, and the diminished need to develop two different routes (to two different libraries) to accomplish the same end.

We speculate that such a method of focusing combinatorial design could have applications beyond the example cited here, and could represent a logical evolutionary step from libraries directed at targets within a single target family.[5] Computational analysis of empirical structure–activity data has begun to permit the explicit identification of key pharmacophore points and complete pharmacophore patterns that are common (or similar yet distinct) to more than one target family (for a simplified hypothetical example, see Scheme 3). The identification of these privileged pharmacophore patterns can be used to drive the design of structure types and synthetic routes that are amenable to combinatorial or parallel diversification. Optimally, the synthetic design would incorporate a divergent step that can direct the library members toward one pharmacophore pattern and away from another. Such a divergent step can impart a high level of selectivity for one target family over another despite the partial pharmacophore pattern commonalities that they share (as was observed in the MMP/PDE example presented here).



Scheme 3. Similarities and differences for the hypothetical pharmacophore pattern of three distinct target families, which have been superposed to aid in the design of multiple target family libraries. Design of the corresponding library structure types and synthetic route would optimally include diversification of the conserved pharmacophore points $\mathbf{A}_m$ and $\mathbf{B}_n$ (various aromatic rings and H-bond acceptors separated by a distance of *a* in this example) followed by divergence of the resulting combinations (upon incorporation of the input bearing the distinguishing pharmacophore points $\mathbf{C}_y$, $\mathbf{C}_{y'}$, or $\mathbf{C}_{y''}$) toward product libraries with different final pharmacophore patterns, therein biased to recognize different biological target families.

In summary, we have exemplified a method by which the convergence of template design and combinatorial principles can be exploited to maximize the impact of a single synthetic route. The approach allowed for the efficient creation of two functionally distinct target family directed small-molecule libraries from this route. In applying this methodology, we have rapidly discovered novel, potent, and selective inhibitors within two therapeutically important biomolecular target families: the matrix metalloproteinases and the phosphodiesterases. We propose that the incorporation of multiple target family directed front-end design elements into combinatorial library design could ultimately expedite the pharmaceutical lead discovery process.

Received: May 11, 1998 [Z 11843 IE]
German version: *Angew. Chem.* **1998**, *110*, 3044 – 3047

Keywords: combinatorial chemistry · drug design · enzyme inhibitors · metalloenzymes · phosphodiesterases

[1] For recent reviews, see a) F. Balkenhohl, C. von dem Bussche-Hünnefeld, A. Lansky, C. Zechel, *Angew. Chem.* **1996**, *108*, 2436 – 2487; *Angew. Chem. Int. Ed. Engl.* **1996**, *35*, 2288 – 2337; b) E. M. Gordon, M. A. Gallop, D. V. Patel, *Acc. Chem. Res.* **1996**, *29*, 144 – 154; c) D. V. Patel, E. M. Gordon, *Drug Discovery Today* **1996**, *1*, 134 – 144.

[2] General compound libraries for lead generation are often constructed around maximized pharmacophoric diversity and novelty. In some cases, a bias is incorporated toward discrete molecular recognition motifs (e.g. β-turn motifs) and/or inclusion of substructural elements with historically attractive pharmacokinetic (or other "druglike") characteristics. Such libraries are not normally directed at a particular target or class of targets. For a recent overview, see R. A. Fecik, K. E. Frank, E. J. Gentry, S. R. Menon, L. A. Mitscher, H. Telikepalli, *Med. Res. Rev.* **1998**, *18*, 149 – 185.

[3] P. Gund, *Annu. Rep. Med. Chem.* **1979**, *14*, 299 – 308.

[4] See, for example: T. W. Schwartz, U. Gether, H. T. Schambye, S. A. Hjorth, *Curr. Pharm. Design* **1995**, *1*, 325 – 342.

[5] For an introduction, see J. C. Hogan, *Nature* **1996**, *384 (Suppl.)*, 17 – 19. Examples of libraries implicitly or explicitly constructed to interact with multiple members of a particular target family: 1) Seven-transmembrane G-protein-coupled receptors: a) R. N. Zuckermann, E. J. Martin, D. C. Spellmeyer, G. B. Stauber, K. R. Shoemaker, J. M. Kerr, G. M. Figliozzi, D. A. Goff, M. A. Siani, R. J. Simon, S. C. Banville, E. G. Brown, L. Wang, L. S. Richter, W. H. Moos, *J. Med. Chem.* **1994**, *37*, 2678 – 2685; b) R. Hirschmann, W. Yao, M. A. Cascieri, C. D. Strader, L. Maechler, M. A. Cichy-Knight, J. Hynes Jr., R. D. van Rijn, P. A. Sprengeler, A. B. Smith III, *J. Med. Chem.* **1996**, *39*, 2441 – 2448, and references therein; 2) aspartyl proteases: E. K. Kick, J. A. Ellman, *J. Med. Chem.* **1995**, *38*, 1427 – 1430; 3) kinases: a) J. K. Chen, S. L. Schreiber, *Angew. Chem.* **1995**, *107*, 1041 – 1058; *Angew. Chem. Int. Ed. Engl.* **1995**, *34*, 953 – 969; b) T. C. Norman, N. S. Gray, J. T. Koh, P. G. Schultz, *J. Am. Chem. Soc.* **1996**, *118*, 7430 – 7431; 4) matrix metalloproteinases: D. A. Campbell, J. C. Bernak, *J. Am. Chem. Soc.* **1994**, *116*, 6039 – 6040.

[6] L. J. Beeley, D. M. Duckworth, *Drug Discovery Today* **1996**, *1*, 474 – 480.

[7] Matrix metalloproteinases: R. P. Beckett, M. Whittaker, *Exp. Opin. Ther. Patents* **1998**, *8*, 259 – 282. Phosphodiesterases: J. A. Karlsson, D. Aldous, *Exp. Opin. Ther. Patents* **1997**, *7*, 989 – 1003.

[8] L. J. MacPherson, D. T. Parker (Ciba-Geigy), EP-B 606046 A1, **1994**; recent detailed report: L. J. MacPherson, E K. Bayburt, M. P. Capparelli, B. J. Carroll, R. Goldstein, M. R. Justice, L. Zhu, S. Hu, R. A. Melton, L. Fryer, R. L. Goldberg, J. R. Doughty, S. Spirito, V. Blancuzzi, D. Wilson, E. M. O'Byrne, V. Ganu, D. T. Parker, *J. Med. Chem.* **1997**, *40*, 2525 – 2532.

[9] E. F. Kleinman (Pfizer), WO-A 95/14681, **1995;** recent detailed report: E. F. Kleinman, E. Campbell, L. A. Giordano, V. L. Cohan, T. H. Jenkinson, J. B. Cheng, J. T. Shirley, E. R. Pettipher, E. D. Salter, T. A. Hibbs, F. M. DiCapua, J. Bordner, *J. Med. Chem.* **1998**, *41*, 266 – 270.

[10] Quality and purity for all library members was tested by HPLC/MS, with further characterization (NMR spectroscopy, elemental analysis) of all final products from method A. Note that when ketones are used as $\mathbf{B}_n$ in method A, steps b and c are reversed, with the thiol addition typically performed in pyridine with heating. The final steps d and e remain the same. In examples where R^1 and either R^2 or R^3 are not hydrogen, both the solution and solid-phase methods give principally the *E* olefin (for $\mathbf{I}_{m-n}$) and stereospecific *anti*-thiol addition ("erythro" product) consistent with a recent study in solution by Naito and co-workers: O. Miyata, T. Shinada, I. Ninomiya, T. Naito, T. Date, K. Okamura, S. Inagaki, *J. Org. Chem.* **1991**, *56*, 6556 – 6564. Levels of the "*threo*" epimer were typically below 15%, but did reach as high as 40 – 50% in method B when R^1 was large (e.g. CH_2CH_2SPh).

[11] For our first libraries, almost 300 compounds (more than 200 from method B) were prepared and screened as singles using these routes (see ref. [14]). In general, yields from method A were greater than 30% overall, with an average yield of more than 80% for each step. For method B, overall yields were typically 5 – 25% (see the supporting information).

[12] Inhibitory activity on recombinant human MMP-1, MMP-2, and MMP-3 (biogenesis) is measured according to the methods of C. G. Knight, F. Willenbrock, G. Murphy, *FEBS Lett.* **1992**, *296*, 263 – 266.

[13] Inhibitory activity against guinea pig macrophage homogenate PDE4 was performed according to a two-step radioisotopic method: W. J. Thompson, W. L. Terasaki, P. M. Epstein, S. J. Strada, *Adv. Cyclic Nucl. Res.* **1979**, *10*, 69 – 92.

[14] a) In total, 73% of compounds prepared with the MMP pharmacophore pattern (Scheme 1, $\mathbf{P}_{m-n-y}$) gave greater than 90% inhibition when screened at a concentration of 10 μM for at least one MMP, which typically resulted in K_i values of 1 μM or less; b) 33% of compounds prepared with the PDE motif ($\mathbf{P}^-_{m-n-y}$) afforded $IC_{50} < 100$ nM in the PDE4 assay.

[15] Consider, for example, compounds based on the 1,4-benzodiazepine (BZD) scaffold, which are rigid β-turn peptide mimics with known biopharmaceutical pedigree. Such features, combined with the plausibility of introducing three to four points of diversity onto the scaffold during its construction, have made BZD an appealing substructure for combinatorial library synthesis (for reviews, see S. H. DeWitt, A. W. Czarnik, *Acc. Chem. Res.* **1996**, *29*, 114 – 122 and J. A. Ellman, *Acc. Chem. Res.* **1996**, *29*, 132 – 143) and a prolific source of hits and leads against targets ranging across a number of biological target classes (CCK-A, FTase, gpIIb/IIIa, etc.). In such cases, the desired end—hits and leads against multiple target families using a single synthetic route (or at least similar synthetic routes)—is ultimately achieved without the need for explicit pharmacophore pattern comparison across the target types to be screened.

 © WILEY-VCH Verlag GmbH, D-69451 Weinheim, 1998 1433-7851/98/3720-2850 $ 17.50+.50/0

Synthesis of Optically Active α-Aminophosphinic Acids by Catalytic Asymmetric Hydrogenation in Organic Solvents and Aqueous Micellar Media**

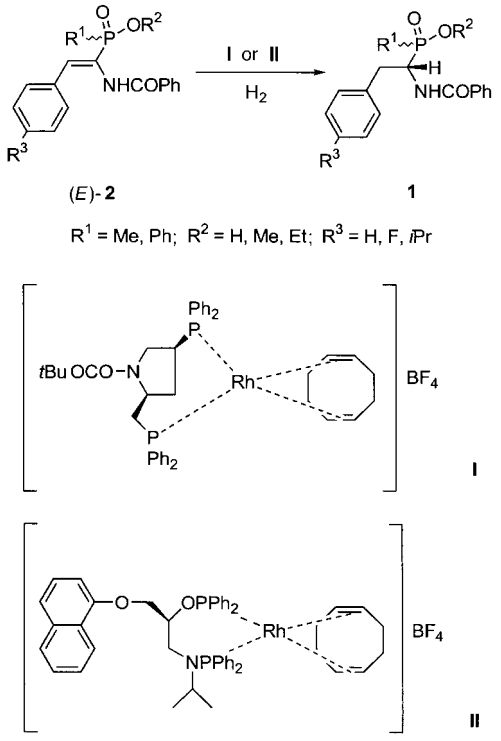
Torsten Dwars, Ute Schmidt, Christine Fischer, Ingrid Grassert, Rhett Kempe, Roland Fröhlich, Karlheinz Drauz,* and Günther Oehme*

Dedicated to Professor Hanswalter Krause on the occasion of his 70th birthday

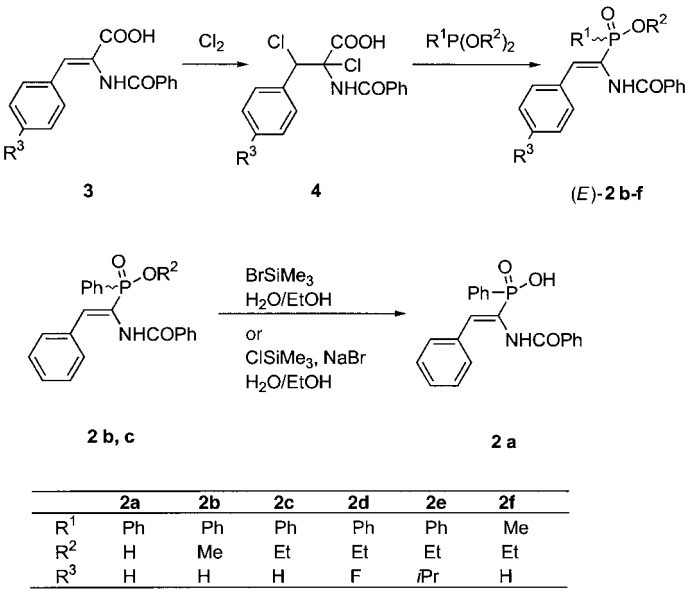
As structural analogues of α-aminocarboxylic acids, α-aminophosphinic acids can have interesting biological properties and serve as active substances in herbicides, bactericides, and antibiotics.[1] The synthesis of optically active α-aminophosphinic acids and their derivatives by means of catalytic asymmetric reactions is hitherto unknown. Only the diastereoselective addition of phosphonites to imines to form chiral α-aminophosphinic esters was described by Afarinkia et al.[2] Martin et al.[3] obtained an optically pure acylated α-aminophosphinic acid by resolution of racemic 1-*N*-carbobenzoxyamino-2-phenylethylphosphonous acid with α-phenylethylamine according to Baylis et al.[4] and subsequent alkylation. We were now able for the first time to synthesize optically active α-aminophosphinic acid derivatives **1** from the unsaturated precursors **2** with high enantioselectivities by catalytic asymmetric hydrogenations with rhodium(I) complexes **I**[5] and **II**[6] (Scheme 1). The reactants **2** can be obtained in two steps from the dehydroamino acids **3** according to the method of Brovarets et al.[7] (Scheme 2).

The ^{1}H NMR spectrum (^3J(P,CH) ≈ 20 Hz) shows that the substrates thus synthesized possess an *E* configuration. According to HPLC analyses of the α-benzamidodehydrophosphinic acid esters **2**, two enantiomers are present in which the phosphorus atoms are the centers of chirality. In contrast, acid **2a** is a racemate owing to the tautomerism of the POOH structure.

As shown in Table 1, optically active acylated α-aminophosphinic acid derivatives are available from suitable precursors by means of catalytic hydrogenations under varying conditions with cationic, optically active rhodium complexes such as **I** and **II** containing a seven-membered chelating ring. The activities of **I** and **II** (represented here by the reaction half-time $t_{1/2}$) are lower than for the hydrogenations of amino acid[8] and aminophosphonic acid precursors,[9] and decrease as expected when the ratio of substrate to catalyst is increased (Table 1, entries 3 and 4). Greater enantiomeric excesses are obtained with **I** (79–98% *ee*) than with **II** (31–79% *ee*). The hydrogenation of **2a** in methanol is less enantioselective than that of esters **2b** and **2c**. The methyl ester **2b** is hydrogenated at a higher reaction rate than the ethyl ester **2c**, but the enantioselectivities are almost identical. In contrast to **I**, hydrogenations with **II**, which contains the ligand PROPRAPHOS (see Scheme 1 for the structure), are more strongly dependent on changes in the reaction condi-



Scheme 1. Catalytic asymmetric hydrogenation of the α-benzamidodehydrophosphinic acids **2** to **1** with the catalysts **I** and **II**.



	2a	2b	2c	2d	2e	2f
R^1	Ph	Ph	Ph	Ph	Ph	Me
R^2	H	Me	Et	Et	Et	Et
R^3	H	H	H	F	*i*Pr	H

Scheme 2. Syntheses of the substrates **2**.

[*] Prof. Dr. K. Drauz
Degussa AG, C+D Fine Chemicals
Rodenbacher Chaussee 4, D-63403 Hanau (Germany)
Fax: (+49) 6181-59-4318
E-mail: prof.karlheinz.drauz@degussa.de
Prof. Dr. G. Oehme, T. Dwars, U. Schmidt, Dr. C. Fischer, Dr. I. Grassert, Dr. R. Kempe
Institut für Organische Katalyseforschung an der Universität Rostock e.V.
Buchbinderstrasse 5-6, D-18055 Rostock (Germany)
Fax: (+49) 381-46693-24
E-mail: goehme@chemie1.uni-rostock.de
Dr. R. Fröhlich
Institut für Organische Chemie der Universität Münster (Germany)

[**] This work was supported by Degussa AG and by the BMBF. We wish to thank Dr. Michalik for recording the NMR spectra.

Table 1. Results of the asymmetric hydrogenation of the substrates **2a–f**.

Entry	Substrate				Catalyst[a]				Remarks
					I		II		
	R^1	R^2	R^3		$t_{1/2}$[b] [min]	ee_C [%]	$t_{1/2}$[b] [min]	ee_C [%]	
1	Ph	H	H	**2a**	16	81	14	56	
2	Ph	Me	H	**2b**	8	86	38	76	
3	Ph	Et	H	**2c**	15	87	70	75	
4	Ph	Et	H	**2c**	95	86	131	71	C:S = 1:100[d]
5	Ph	Et	F	**2d**	20	87	60	64	
6	Ph	Et	*i*Pr	**2e**	20	87	141	60	
7	Ph	Et	H	**2c**	30	91	40	31	in benzene
8	Ph	Et	H	**2c**	16	79	40	79	in CH_2Cl_2
9	Ph	Et	H	**2c**	13	96	–	–	in water[c]
10	Me	Et	H	**2f**	8	93	20	77	
11	Me	Et	H	**2f**	6	98	–	–	in water[c]

[a] Reaction conditions: 0.5 mmol of substrate, 0.01 mmol of catalyst, 7.5 ml of methanol, 25 °C, 0.1 MPa of hydrogen. [b] Reaction half-time. [c] Catalyst:substrate:SDS = 1:50:100. [d] C = catalyst, S = substrate.

tions. An influence of the substituents at the β phenyl ring (**2d**, **2e**) on the rate of hydrogenation ($t_{1/2} = 60$, 70, 141 min for entries 5, 3, 6) as well as a strong solvent dependence of the enantioselectivities (MeOH: 75% *ee*, C_6H_6: 31% *ee*, CH_2Cl_2: 79% *ee* for entries 3, 7, 8) are clear. The highest enantioselectivity was obtained in water with added sodium dodecyl sulfate (SDS; Table 1, entries 9, 11) with 96 and 98% *ee*, respectively. In addition, the aqueous micellar system is extremely efficient because of the high activities. The substituents at the phosphorus atom seem to have an influence on the rates of the reaction with the two catalysts (**2c** (R^1 = Ph): 15 and 70 min, respectively; **2f** (R^1 = Me): 8 and 20 min, respectively), but only to a much lesser degree on the selectivities (**2c**: 87 and 75% *ee*, respectively; **2f**: 93 and 77% *ee*, respectively), which we currently ascribe to steric effects. The *ee* values with respect to the α-C atom (ee_C) can be determined from the enantiomeric excesses of the diastereomer pairs of the ester.[10]

After the hydrogenation (Table 1, entry 9), the diastereomeric ester **1c** was hydrolyzed with hydrochloric acid, and the phosphinic acid formed thereby was recrystallized from 50% acetic acid. The optical purity of the α-*N*-benzoylamino-β-phenylethylphenylphosphinic acid **1a** was 99% *ee* according to a capillary electrophoretic analysis. X-ray structure analysis revealed an *S* configuration for the new center of asymmetry[11] (Figure 1). With the catalytic synthetic pathway described here, these enantiomerically pure α-aminophosphinic acids can now be synthesized in a novel way.

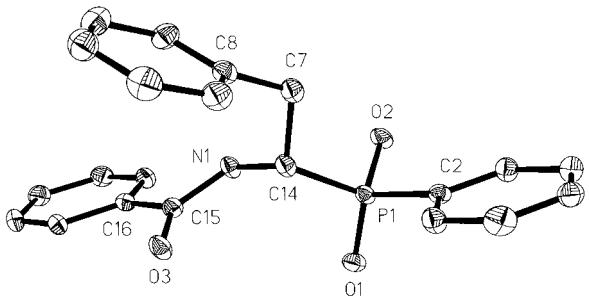


Figure 1. View of the structure of **1a** in the crystal.

Experimental Section

The (*E*)-α-*N*-benzoylamino-β-phenylethenephosphinic acid esters **2b–f** were prepared according to reference [7].

2a: **2b** or **2c** (10 mmol) was stirred with bromotrimethylsilane (20 mmol) in 20 ml of $CHCl_3$ (10 mmol) or with chlorotrimethylsilane (10 mmol) and NaBr (10 mmol) in 20 ml of acetonitrile for 30 min at room temperature. The solution was then concentrated in vacuo, mixed with EtOH/water, and stirred for 5 min. Upon evaporation of the solvent, the acid precipitated in the form of colorless crystals (74% yield).

1a–f: In the presence of catalyst **I** or **II** (0.01 mol) and in the strict absence of oxygen, compounds **2** (0.5 mmol) in 7.5 ml of methanol (or in water with 1 mmol of SDS, see Table 1) were hydrogenated at 25 °C and a hydrogen pressure of 0.1 MPa up to the theoretical hydrogen uptake.[12] Then the solvent was removed in vacuo, and the residue was dissolved in a little CH_2Cl_2/MeOH (29/1) and filtered through a 3-cm plug of silica gel in order to remove the rhodium complex quantitatively. After concentration of the filtrate, the product was obtained in 96% yield. The enantiomeric excess with respect to the center of chirality formed was determined with HPLC (chiral stationary phase: Chiralpak AD (column: 250×4.6 mm^2, DAICEL), eluent: hexane/ethanol (9/1), Liquid Chromatograph 1090, Hewlett-Packard) and, in the case of (S_C)-α *N*-benzoylamino-β-phenylethylphosphinic acid, capillary electrophoretically (boric acid buffer, 10 mM β-cyclodextrin, 0.05% polyvinyl alcohol, pH 9.6, $U = 15$ kV, capillary: 30 cm $\times$ 50 μm, BioFocus 3000 Capillary Electrophoresis system, BIO-RAD).

All isolated compounds were characterized with elemental analysis, NMR and IR spectroscopy, and mass spectrometry.

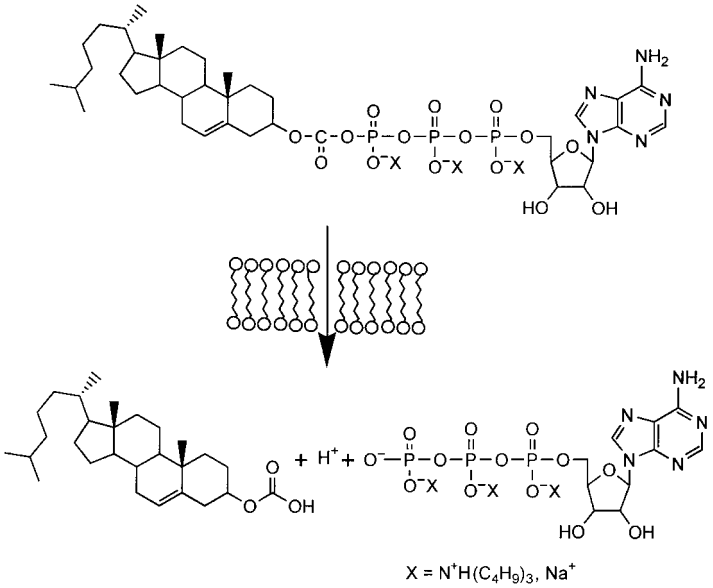
Received: May 29, 1998 [Z11916IE]
German version: *Angew. Chem.* **1998**, *110*, 3033–3035

Keywords: aminophosphinic acids · asymmetric catalysis · hydrogenations · rhodium

[1] L. Maier, P. J. Diel, *Phosphorus Sulfur Silicon* **1994**, *90*, 259–279; "Aminophosphonates: Natural Occurrence, Biochemistry and Properties": P. Kafarski, P. Mastalerz in *Beiträge zur Wirkstofforschung, Akademie Industrie Komplex Arzneimittelforschung* (Eds.: P. Oehme, H. Löwe, E. Göres), Berlin, **1984**.
[2] K. Afarinkia, J. I. G. Cadogan, C. W. Rees, *Synlett* **1992**, 124–125.
[3] M. T. Martin, T. S. Angeles, R. Sugasawara, N. I. Aman, A. D. Napper, M. J.Darsley, R. S. Sanchez, P. Booth, R. C. Titmas, *J. Am. Chem. Soc.* **1994**, *116*, 6508–6512.
[4] E. K. Baylis, C. D. Campbell, J. G. Dingwall, *J. Chem. Soc. Perkin Trans. 1* **1984**, 2845–2853.
[5] K. Achiwa, *J. Am. Chem. Soc.* **1976**, *98*, 8265–8266.
[6] H. W. Krause, H. Foken, H. Pracejus, *New J. Chem.* **1989**, *13*, 615–620.
[7] V. S. Brovarets, K. V. Zyuz, L. N. Budnik, V. A. Solodenko, B. S. Dratsch, *Zh. Obsh. Khim.* **1993**, *63*, 1259–1265.
[8] H. J. Kreuzfeld, C. Döbler, H. W. Krause, C. Facklam, *Tetrahedron: Asymmetry* **1993**, *4*, 2047–2051.
[9] U. Schmidt, G. Oehme, H. W. Krause, *Synth. Commun.* **1996**, *26*, 777–781.
[10] HPLC analyses of the dehydroaminophosphinic esters (enantiomeric ratio 1:1) and the diastereomeric pairs of enantiomers (ee_1 und ee_2) lead to a system of equations for the proportions of the four isomers obtained after hydrogenation (A: (S_C,S_P); B: (R_C,R_P); C: (S_C,R_P); D: (R_C,S_P)): A+D = 50, B+C = 50, A/B = (100+ee_1)/(100 – ee_1) and C/D = (100 + ee_2)/(100 – ee_2). Solving this system of equations and combining the calculated values with identical C configurations provides the desired ee_C value after subtraction.
[11] Crystal structure analysis of **1a**: CAD4 diffractometer, graphite-monochromatized Cu $_{K\alpha}$ radiation, $\lambda = 1.54178$ Å, structure solution with direct methods (SHELXS-86: G. M. Sheldrick, *Acta Crystallogr. Sect. A* **1990**, *46*, 467.), full-matrix least-squares refinement against F^2 (SHELXL-97: G. M. Sheldrick, not yet published), structure representation: XP (Siemens); crystal dimensions: $1.10 \times 0.25 \times 0.20$ mm^3, colorless prisms, space group $P2_1$, monoclinic, $a = 12.850(5)$, $b =$

5.293(1), $c = 13.741(3)$ Å, $\beta = 108.69(4)^\circ$, $V = 885.3(5)$ Å^3, $Z = 2$, $\rho_{calcd} = 1.371$ g cm^{-3}, 4036 measured reflections, 2022 symmetry-independent reflections, of which 1858 were observed ($I = 2\sigma(I)$), $R = 0.046$, wR^2 (all data) $= 0.096$, 239 parameters, Flack parameter 0.01(3). Crystallographic data (excluding structure factors) for the structure reported in this paper have been deposited with the Cambridge Crystallographic Data Centre as supplementary publication no. CCDC-101627. Copies of the data can be obtained free of charge on application to CCDC, 12 Union Road, Cambridge CB2 1EZ, UK (fax: (+44) 1223-336033; e-mail: deposit@ccdc.cam.ac.uk).

[12] I. Grassert, V. Vill, G. Oehme, *J. Mol. Catal. A* **1997**, *116*, 231–236.



Scheme 1. Schematic representation of the transfer of Chol-ATP across the membrane and the release of ATP by hydrolysis.

Transmembrane Transport of Adenosine 5′-Triphosphate Using a Lipophilic Cholesteryl Derivative**

Annett Kreimeyer, François André, Catherine Gouyette, and Tam Huynh-Dinh*

Numerous studies to find prodrugs of nucleoside 5′-monophosphates have been reported.[1] However, little work has been described on synthetic carrier systems for nucleoside 5′-triphosphates.[2] To our knowledge no nucleotide derivatives currently exist that are capable of effecting the transfer across membranes with subsequent release of the parent nucleoside 5′-triphosphate. For instance a phospholipid ester of 3′-azido-3′-deoxythymidine (AZT) 5′-triphosphate has been shown to be an effective anti-HIV agent in vitro, but required liposomal formulation; its intracellular hydrolysis led to AZT 5′-monophosphate instead of AZT 5′-triphosphate.[3]

We have recently described the synthesis of acyl nucleoside 5′-di- and 5′-triphosphates as potential membrane-permeable prodrugs.[4, 5] Further development of this work led us to synthesize derivatives of adenosine 5′-triphosphate (ATP). Herein, we present the results of a ^{31}P NMR based study of the transfer of cholesteryloxycarbonyl-ATP (Chol-ATP) (Scheme 1) as a model of a lipophilic nucleotide.

Chol-ATP was synthesized in one step from ATP and cholesteryl chloroformate.[5] A suitable method to investigate the transmembrane transport of liponucleotide conjugates is ^{31}P NMR spectroscopy since it allows both the monitoring of ATP release after internalization of Chol-ATP into liposomes and the distinction between external and internal species in a well-compartmented system.[6, 7] Moreover, ^{31}P NMR resonances are highly sensitive probes of local pH changes.[8] Our approach consists of recording ^{31}P NMR spectra of Chol-ATP in the presence of small unilamellar vesicles (SUV) in a phosphate-buffered system using a pH gradient to distinguish between resonances of ATP molecules located inside and/or outside the liposomes.

Essential requirements of such an experiment are that the compound of interest does not act as a detergent damaging the liposomal structure, and that its hydrolysis kinetic is compatible with the incubation time in the presence of the vesicles.[9] In order to observe the resonances of ATP at different pH values, the liposomes must be able to maintain the proton gradient (ΔpH) across the membrane within the required acquisition time of the ^{31}P NMR spectrum (one hour). To monitor Chol-ATP transport through membranes and the subsequent ATP release, the specific pattern of a ^{31}P NMR spectrum of ATP entrapped in liposomes was first characterized. For this purpose, we prepared vesicles containing ATP. Figure 1 shows ^{31}P NMR spectra of ATP (internal concentration 50 mM) entrapped in liposomes prepared in a phosphate-buffered medium recorded at different times. The comparison of these spectra provided three important pieces of information: a) The appearance of an inorganic phosphate peak, at a resonance frequency identical to the initial step before the pH jump, indicates the preservation of the pH 5 in the inner volume of the liposomes during the acquisition time. This, and the fact that no extravesicular ATP resonances occurred, demonstrates the integrity of the vesicles (Figure 1b). b) After the pH jump the integral value for the two inorganic phosphate resonances gives an accurate determination of the distribution between the inner (6%) and outer volume (94%). As a result, the concentration of internal ATP was equivalent to 3 mM with respect to the total volume. c) A direct comparison of the lineshapes of intra- and extravesicular ATP resonances, while

[*] Dr. T. Huynh-Dinh, Dr. A. Kreimeyer, C. Gouyette
Unité de Chimie Organique
URA CNRS 487, Département de BGM, Institut Pasteur
28, rue du Docteur Roux, F-75724 Paris Cedex 15 (France)
Fax: (+33) 1-45-68-84-04
E-mail: hdt@pasteur.fr
Dr. F. André
Section de Bioénergétique, DBCM
CEA-Saclay, F-91191 Gif-sur-Yvette (France)

[**] The authors are indebted to Aline Bluzat for her excellent technical help in the preparation of SUV and in the integration of ATP into liposomes. They are also grateful to Francis Haraux and Jean-Michel Neumann for fruitful discussions.

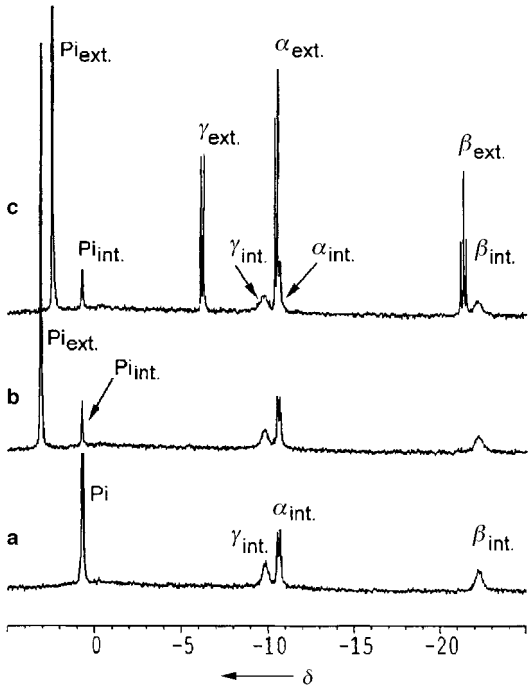


Figure 1. ^{31}P NMR spectra (121.49 MHz) of free ATP, entrapped in liposomes in a phosphate-buffered solution at 25 °C: a) Equilibrated at pH 5; b) after addition of aqueous NaOH, external pH set at pH 8—no phosphorus lines of external ATP were detected; c) after addition of 3 mM ATP extravesicular. The addition of stock ATP modified the extravesicular pH, responsible for a slight shift of the corresponding inorganic phosphate resonance. int. = intravesicular; ext. = extravesicular; Pi = inorganic phosphate.

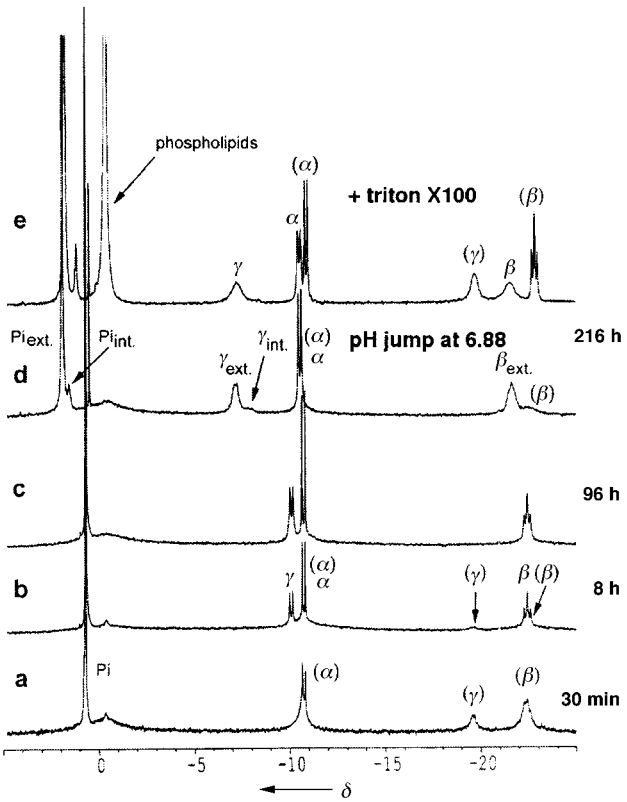


Figure 2. ^{31}P NMR spectra (121.49 MHz) of Chol-ATP incubating in a phosphate-buffered solution containing the liposomes (lipid content 32 mg mL^{-1}) recorded after a) 30 min incubation time at pH 5, b) 8 h at pH 5, c) 96 h at pH 5, d) pH jump to pH 6.88 after addition of aqueous NaOH at 216 h incubation time, and e) addition of Triton X100. Chol-ATP signals are quoted in parentheses; int. = intravesicular; ext. = extravesicular.

both species have been set at equivalent concentrations, revealed that the internal ATP phosphorus resonances were considerably broadened (Figure 1c). Moreover, the broadening was much more marked for β- and γ-phosphate resonances than for α ones. It is expected that the observation of free ATP internalized in liposomes will be very difficult.

To study the transmembrane transport of Chol-ATP the compound was incubated for nine days with SUV, which did not contain entrapped Chol-ATP, and monitored by ^{31}P NMR spectroscopy (Figure 2). The lifetime of the compound was also controlled by ^{31}P NMR spectroscopy in the same buffered medium (pH 5) in the absence of liposomes ($t_{1/2} = 69$ h). The total disappearence of the γ-phosphate signal of Chol-ATP after 96 h can be explained by an association of the molecule in the water–membrane interface. Moreover the absence of any sharp resonance of phospholipids provided evidence that there was no destruction of the liposomal structure due to Chol-ATP. When aqueous NaOH was added in the NMR tube the resonances of ATP, as well as of inorganic phosphate (both extravesicular), were shifted (Figure 2d). During the required acquisition time of the ^{31}P NMR spectrum the adjustment of the pH between the different compartments started. This induced a pH-dependent shift of the resonances of ATP and consequently they were broadened. Considering the typical large pattern of entrapped ATP, one can assume that under these conditions the corresponding signals could be broadened beyond detection. Despite these shortcomings, a weak signal centered at $\delta = -8.2$ was observed (Figure 2d). This resonance was in agreement with the predicted chemical shift of the γ-phosphorus of entrapped ATP, calculated through the pH value which was indicated by the resonance of the internal inorganic phosphate peak. Thus, the release of ATP from Chol-ATP, inside the liposomes, can be assumed. To confirm this result, we added the detergent Triton X100 to the solution to break the liposomal structure. Consequently, the signals of the phospholipids appeared, indicating their micellization. Hence, the ΔpH was neutralized and the resonances of extra- and intravesicular phosphorus coalesced. The areas of the signals of the β- and γ-phosphate groups of the total free ATP (Figure 2e) increased by 10% after the detergent addition, when compared to the area of the signal for free external ATP (Figure 2d); this increase can be considered as the amount of entrapped ATP. Concomitantly, the signal of the γ-phosphate of residual intact Chol-ATP (Figure 2e) reappeared.

As a further proof, we checked the evolution of the ΔpH between the compartments during Chol-ATP internalization. It is indeed expected that the hydrolysis of Chol-ATP leads to the release of protons (Scheme 1). In a control experiment, a pH jump in the same phosphate-buffered system containing only liposomes was applied and the development of the proton gradient was monitored by ^{31}P NMR spectroscopy over a long period (Figure 3A). In contrast to the decreasing ΔpH value in the control experiment, an initial increase of the

 © WILEY-VCH Verlag GmbH, D-69451 Weinheim, 1998 1433-7851/98/3720-2854 $ 17.50+.50/0

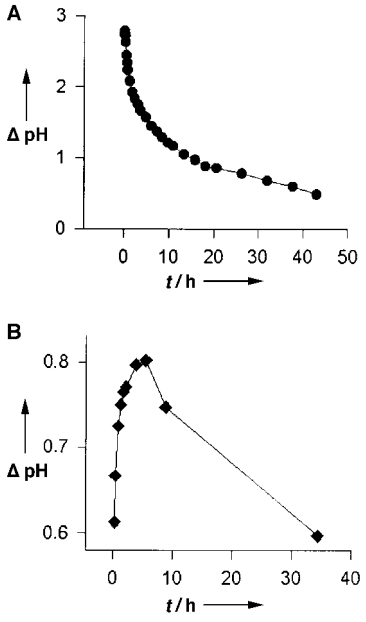


Figure 3. Evolution of the proton gradient between the two compartments after a pH jump in solutions (A) containing only liposomes and (B) containing liposomes and Chol-ATP.

proton gradient in the presence of Chol-ATP was observed, reflecting the hydrolysis of Chol-ATP and thus the release of the intravesicular ATP (Figure 3B).

In summary, we have demonstrated that ATP bearing a cholesteryl moiety at the γ-phosphate group can be transported across the membrane bilayer. It is now of interest to evaluate these model drug carriers of adenosine and various therapeutic nucleosides in integrated systems or living cells.

Experimental Section

Cholesteryloxycarbonyl-adenosine 5′-triphosphate: White powder. The ^{1}H NMR spectrum (D_2O) showed the characteristic signals of adenosine; protons of the cholesteryl moiety were observed between $\delta = 2.05$ and 0.57. ^{31}P NMR (D_2O, proton-decoupled, pH 7.1): $\delta = -10.35$ (d, α-P, $J_{PP} = 19.8$ Hz), -18.82 (br, γ-P), -21.51 (br, β-P). Mass spectrum (electrospray): calcd for $C_{38}H_{60}N_5O_{15}P_3(NBu_3)_3$: 919.33; found 919.4. HPLC (gradient: 5–70% acetonitrile in 0.01M triethylammonium acetate, pH 7): t_{ret} 17.04 min. Chol-ATP ($HNBu_3$ or Na salt) is freely soluble in water and organic solvents (dichloromethane, acetonitrile, alcohols).

Vesicles preparation: SUV of defined size were prepared by reverse-phase evaporation using a mixture of egg phosphatidylcholine and phosphatidic acid (mole ratio 9:1) according to Rigaud and Pitard.[10] The phosphate-buffered solution referred to in the text contained KH_2PO_4 (20mM), K_2SO_4 (15mM), and Na_2SO_4 (15mM) at pH 5.0 (90% H_2O/10% D_2O). After extrusion through 200-nm nucleopore membranes, the final lipid concentration was about 30 mg mL^{-1}. For the preparation of liposomes with entrapped ATP, the same procedure was applied in the presence of ATP 50mM, and external ATP was finally thoroughly removed by filtration of the SUV through pD 10 columns (Pharmacia).

^{31}P NMR experiments: ^{31}P NMR spectra were recorded on a Bruker DMX-300 operating at 121.49 MHz, and referenced relative to external H_3PO_4 85%. Two levels of broad band proton decoupling were applied for all the experiments. Samples were prepared immediately prior to use. In a glass vial, Chol-ATP (9 mg) was directly dissolved in the SUV preparation (550 µL, lipid concentration 30 mg mL^{-1}, phosphate-buffered solution pH 5.0, 90% H_2O/10% D_2O). After quick introduction into the spectrometer, an initial ^{31}P NMR spectrum ($t = 0$) was recorded (90° pulse 6 µs, relaxation delay 5 s, 16 scans). In general, successive short spectra (16 to 64 scans) were acquired at the beginning of the incubation to monitor the pH gradient development. Better signal-to-noise spectra (512 scans) were then recorded to monitor the slow kinetics of internalization and hydrolysis of Chol-ATP. The pH jump was performed by injection of a few microliters of NaOH 1N into the NMR tube.

Received: April 14, 1998 [Z11718IE]
German version: *Angew. Chem.* **1998**, *110*, 3013–3016

Keywords: drug design · liposomes · membranes · NMR spectroscopy · nucleotides

[1] For reviews, see: T. Huynh-Dinh, *Curr. Opin. Invest. Drugs* **1993**, *2*, 905–915; R.-J. Jones, N. Bischofberger, *Antiviral Res.* **1995**, *27*, 1–17.
[2] T. Li, S. J. Krasne, B. Persson, H. R. Kaback, F. Diederich, *J. Org. Chem.* **1993**, *58*, 380–384; A. O. Goldring, I. H. Gilbert, N. Mahmood, J. Balzarini, *Bioorg. Med. Chem. Lett.* **1996**, *6*, 2411–2416; I. Tabushi, Y. Kobuke, J. Imuta, *J. Am. Chem. Soc.* **1981**, *103*, 6152–6157.
[3] G. M. T. van Wijk, K. Y. Hostetler, E. Kroneman, D. D. Richman, C. N. Sridhar, R. Kumar, H. van den Bosch, *Chem. Phys. Lipids* **1994**, *70*, 213–222.
[4] D. Bonnaffé, B. Dupraz, J. Ughetto-Monfrin, A. Namane, Y. Henin, T. Huynh-Dinh, *J. Org. Chem.* **1996**, *61*, 895–902.
[5] A. Kreimeyer, J. Ughetto-Monfrin, A. Namane, T. Huynh-Dinh, *Tetrahedron Lett.* **1996**, *37*, 8739–8742.
[6] J.-M. Neumann, M. Hervé, J.-C. Debouzy, F. I. Guerra, C. Gouyette, B. Dupraz, T. Huynh-Dinh, *J. Am. Chem. Soc.* **1989**, *111*, 4270–4277; Y. Henin, C. Gouyette, O. Schwartz, J.-C. Debouzy, J.-M. Neumann, T. Huynh-Dinh, *J. Med. Chem.* **1991**, *34*, 1830–1837.
[7] J. M. K. Roberts, O. Jardetzky, *Biochim. Biophys. Acta* **1981**, *639*, 53–76; A. Kurkdjian, J. Guern, *Annu. Rev. Plant Physiol. Plant Mol. Biol.* **1989**, *40*, 271–303.
[8] K. J. Hellingwerf, W. N. Konings, K. Nicolay, R. Kaptein, *Photobiochem. Photophys.* **1981**, *2*, 311–319. H. Akutsu, H. Utsumi, Y. Koyama, Y. Kyogoku, *Photobiochem. Photophys.* **1986**, *11*, 227–236.
[9] Hydrolysis of Chol-ATP in aqueous solution showed a selective cleavage at the mixed anhydride bond with a half-life time (63 h) large enough to allow diffusion of Chol-ATP molecules into the liposomes before their hydrolysis.
[10] "Liposomes as Tools for the Reconstitution of Biological Systems": J.-L. Rigaud, B. Pitard in *Liposomes as Tools in Basic Research and Industry* (Eds.: J. R. Philippot, F. Schuber), CRC Press, Boca Raton, **1995**, pp. 71–88.

Ca_2AuN: A Nitride Containing Infinite Zigzag Gold Chains**

Paul F. Henry and Mark T. Weller*

Previous investigation of the calcium–gold–nitrogen ternary phase field[1] resulted in the characterization of Ca_3AuN,[2] which crystallizes with the cubic perovskite structure. This structural type is well represented in nitride chemistry, for example Ca_3XN (X = P, As, Sb, Bi, Ge, Sn, and Pb).[3] The nitrogen atom in these compounds is surrounded

[*] Prof. M. T. Weller, Dr. P. F. Henry
Department of Chemistry, University of Southampton
Highfield, Southampton, SO17 1BJ (UK).
Fax: (+44) 1703-593592
E-mail: mtw@soton.ac.uk

[**] This research was supported by the EPSRC (GR/J27059) and we thank S. Hull of the Rutherford Appleton Laboratories for assistance with the collection of the powder neutron diffraction data. We also thank Dr. M. Webster for help with generation of the Patterson maps.

 © WILEY-VCH Verlag GmbH, D-69451 Weinheim, 1998 1433-7851/98/3720-2855 $ 17.50+.50/0

by an octahedron of calcium atoms; the octahedra share corners and are linked into a three-dimensional framework. Here we report the synthesis of a new ternary calcium auride nitride with the formula $(Ca^{2+})_2Au^-N^{3-}$ by using high-pressure techniques, and its structural characterization from Rietveld refinement of powder neutron and X-ray diffraction data. Full details of the structural determination will be presented elsewhere.[4]

Atomic data and thermal displacement parameters are given in Tables 1 and 2, respectively. The most distinctive

Table 1. Refined atomic data for Ca_2AuN. Space group *Cmcm*; $a = 3.58139(4)$, $b = 18.06421(19)$, $c = 4.91905(5)$ Å.

Atom	Wyckoff site	x	y	z	$(U_i/U_{eq}) \times 100$ [Å^2]
Au	4*c*	0	0.04026(6)	¼	2.06
Ca1	4*c*	0	0.39767(9)	¼	1.36
Ca2	4*c*	0	0.21499(8)	¼	0.95
N	4*c*	0	−0.19337(4)	¼	0.84

Table 2. Anisotropic displacement parameters [Å$^2 \times 100$].[a]

Atom	U_{11}	U_{22}	U_{33}	U_{12}	U_{13}	U_{23}
Au	3.96(7)	1.26(5)	0.96(5)	0	0	0
Ca1	1.39(7)	1.10(7)	1.59(8)	0	0	0
Ca2	0.90(7)	0.99(8)	0.96(7)	0	0	0
N	0.86(4)	0.66(4)	1.00(4)	0	0	0

[a] The anisotropic displacement factor exponent takes the form: $[h^2a^{*2}U_{11} + \ldots + 2hka^*b^*U_{12} + \ldots]$.

feature of the refined structure is the presence of infinite, planar zigzag gold chains parallel to the crystallographic *c* axis (Figure 1). However, the anisotropic thermal component U_{11} of the gold atom is relatively large (0.0396(7) Å^2), possibly

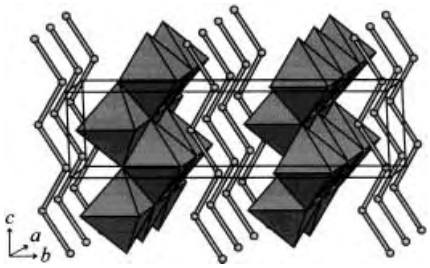


Figure 1. View of the refined structure of Ca_2AuN illustrating the zigzag gold chains parallel to the *c* axis, and the edge-sharing Ca_6N octahedra.

reflecting minor buckling of the chains, but attempts to disorder the gold sites gave unstable refinements. The chains are regular with inter-gold bond lengths of 2.857(1) Å, slightly shorter than those found in metallic gold (2.884 Å). The Au-Au-Au bond angle is 118.80(7)°. The coordination sphere of gold is completed by seven contacts to calcium in the range 3.137(2) – 3.242(7) Å (Figure 2). Within each gold layer the successive gold chains are stacked in phase separated by the atomic distance *a*; the gold chains within successive layers are related by a translation of ½*a*+½*b*. The Ca – N contacts of 2.431(1) – 2.490(1) Å are very close to those found in α-Ca_3N_2 (2.451(2) – 2.482(2) Å).[5]

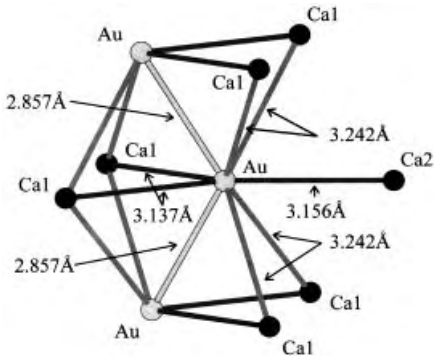


Figure 2. Environment of a gold atom in Ca_2AuN showing the ninefold coordination: two contacts to gold and seven contacts to calcium.

In solid-state materials containing gold – gold bonding, the known structural motifs are: linear chains (e.g., $KAuO_2$[6]), two-dimensional planes (e.g., Au_2Th[7]), dimeric species (e.g., EuAuGe[8]), and complex three-dimensional frameworks (e.g., corner-sharing double tetrahedra in $K_4Au_7Ge_2$).[9] Zigzag chains have been reported in the binary alloy CaAu,[10] although it has not been fully structurally characterized. Some materials containing Au^- ions have been shown to behave as pseudo-halides (e.g., Cs_3AuO[11] and CsAu[12]) and, therefore, it was thought that Ca_2AuN would be isotypic with Ca_2NCl.[13] However, the refined structure of Ca_2AuN is more closely related to that of CaAu as the gold environment in each material is almost identical. Ca_2AuN is best described as CaN zigzag chains inserted into the CaAu structure. Thus, Ca_2AuN is the first example of a ternary material containing zigzag gold chains and is only the second example of a gold nitride.

It was also found that the known cubic perovskite material, Ca_3AuN, could not be synthesized by the high-pressure route. Attempts led to the formation of Ca_2AuN, Ca_3N_2, and a small amount of a cubic phase related to Ca_3AuN by a doubling of *a*.

Experimental Section

A polycrystalline sample of Ca_2AuN was prepared by reaction of Ca_3N_2 powder (Aldrich, 99 + %) and gold foil (99.99 + %) in the correct stoichiometric ratio under high-pressure dry nitrogen (BOC, 99.999%). Due to the air and moisture sensitivity of nitrides all materials were handled in a dry nitrogen atmosphere glovebox. Ca_3N_2 and small pieces of gold foil were mixed intimately, loaded into an alumina crucible, which was then placed in a Nimonic pressure vessel,[14] and sealed. The bomb was attached to a high-pressure nitrogen supply, flushed, and then filled with the required pressure of dry nitrogen, ranging from 100 bar to 200 bar. The sample end of the bomb was heated in a tube furnace at 820 °C for 3 days then cooled to room temperature and the sample reground; at the reaction temperature the pressure in the system was approximately double the initial pressure. A second heat treatment was applied, under the same conditions as before, for a further 16 h followed by cooling to room temperature at a rate of 3 °C min^{-1}. No reaction of the product with the alumina crucible was apparent and the resultant powder was dark gray in color. The series of experiments at various initial pressures of 100 – 200 bar produced identical products.

Powder X-ray diffraction data were collected by using a Siemens D5000 diffractometer ($Cu_{K\alpha 1}$ radiation). Lattice parameters were obtained by indexing with the PC software program TREOR90.[15] Powder neutron diffraction data were collected on the POLARIS diffractometer at the ISIS spallation neutron source, Rutherford Appleton Laboratory, at room temperature. Rietveld refinement was carried out on the data collected in

 © WILEY-VCH Verlag GmbH, D-69451 Weinheim, 1998 1433-7851/98/3720-2856 $ 17.50+.50/0

the high-resolution 145° detector bank, by using the GSAS suite of programs.[16] Nitrogen content, measured from C,H,N analysis, showed the nitrogen stoichiometry to be 1.01(3), assuming a Ca:Au ratio of 2:1.

Received: April 20, 1998 [Z 11753 IE]
German version: *Angew. Chem.* **1998**, *110*, 3040 – 3041

Keywords: calcium · gold · neutron diffraction · nitrides · solid-state structures

[1] "Nitride und Nitridoverbindungen in Systemen Li – (Ca, Sr, Ba) – (Cu, Ag, Au) – N": J. Jäger, PhD Thesis, Technische Hochschule Darmstadt, **1995**.
[2] J. Jäger, D. Stahl, P. C. Schmidt, R. Kniep, *Angew. Chem. Int. Ed. Engl.* **1993**, *32*, 709 – 710; *Angew. Chem.* **1993**, 105, 738 – 739.
[3] M. Y. Chern, D. A. Vennos, F. J. DiSalvo, *J. Solid State Chem.* **1992**, *96*, 415 – 425.
[4] P. F. Henry, M. T. Weller, unpublished results.
[5] Y. Laurent, J. Lang, M. T. Le Bihan, *Acta. Crystallogr. Sect. B* **1968**, *24*, 494 – 499.
[6] H.-D. Wasel-Nielen, R. Hoppe, *Z. Anorg. Allg. Chem.* **1970**, *375*, 43 – 54.
[7] A. Brown, *Acta. Crystallogr.* **1961**, *14*, 860 – 865.
[8] R. Pöttgen, *J. Mater. Chem.* **1995**, *5*, 505 – 508.
[9] U. Zachwieja, *Z. Anorg. Allg. Chem.* **1995**, *621*, 975 – 978.
[10] F. Merlo, *J. Less Common Met.* **1982**, *86*, 241 – 246.
[11] C. Feldmann, M. Jansen, *Z. Anorg. Allg. Chem.* **1995**, *621*, 201 – 206.
[12] G. A. Tinelli, D. F. Holcomb, *J. Solid State Chem.* **1978**, 25, 157 – 160.
[13] C. Hadenfeldt, H. Herdejürgen, *Z. Anorg. Allg. Chem.* **1987**, *545*, 177 – 183.
[14] D. B. Currie, S. E. Dann, P. F. Henry, M. T. Weller, *J. Mater. Chem.* **1998**, in press.
[15] P. E. Werner, L. Eriksson, M. Westdahl, *J. Appl. Crystallogr.* **1985**, *18*, 367 – 370.
[16] A. C. Larson, R. B. von Dreele, General Structural Analysis System, Los Alamos National Laboratory, **1994**, LAUR 86 – 748.

Proof of Potassium Ions by Luminescence Signaling Based on Weak Gold – Gold Interactions in Dinuclear Gold(I) Complexes**

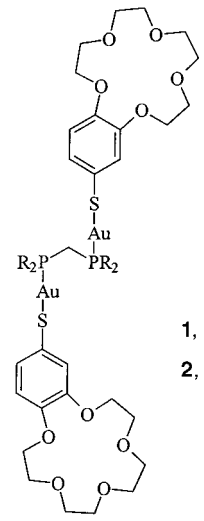
Vivian Wing-Wah Yam,* Chi-Kwan Li, and Chui-Ling Chan

The search for host molecules that can selectively recognize specific guest molecules at their receptor site and produce a measurable physical change is currently of immense interest. Spectroscopic detection of metal ions or anions is of great importance both in classical analytical chemistry and in the molecular design of ion sensors that involve optical signal transformation. The utilization of sensitive luminescence signaling has always been an attractive and popular option, particularly when combined with a selective and specific complexing process involving the target species. Ion-controlled luminescence probes are of interest for ion sensing as well as for the construction of molecular optoelectronic switches.[1–3] A number of ion-binding organic receptors have been studied, most of which were based on polyaromatic luminophores[2a, c, 4] and the exploitation of photoinduced electron transfer (PET) processes.[1–3] Although there has been increased attention given to the design of metalloreceptors in recent years, most of it has focused on systems with metal-to-ligand charge-transfer (MLCT) excited states,[5] with relatively few studies of other systems.[5a, b, 6]

In recent years there has been a growing interest in the study of polynuclear gold(I) complexes, in particular with regard to the phenomenon of aurophilicity associated with these complexes, which results from weak gold – gold interactions.[7] Recent studies by us[8] and others[9] have shown that the presence of weak gold – gold interactions in a number of di- and polynuclear gold(I) complexes gives rise to unique electronic spectroscopic features; in particular many of them exhibit intense yellowish green to orange-red phosphorescence. In general, we and others observed that an increase in gold – gold interactions leads to a lower energy emission.

Herein, we describe a versatile luminescence ion probe for potassium ions based on the switching on and off of the gold – gold interactions. The present system not only serves as a molecular phosphorescent ion sensor and a molecular optoelectronic switch, but also provides spectroscopic evidence for potassium ion induced gold – gold interactions.

The complexes $[Au_2(dppm)(S\text{-benzo[15]crown-5})_2]$ (**1**) and $[Au_2(dcpm)(S\text{-benzo[15]crown-5})_2]$ (**2**) were synthesized by the reaction of $[Au_2(dppm)Cl_2]$ and $[Au_2(dcpm)Cl_2]$, respectively, with two equivalents of 4′-sulfanylmonobenzo[15]-crown-5 in the presence of triethylamine in dichloromethane under an inert atmosphere of nitrogen (dppm = bis(diphenylphosphanyl)methane; dcpm = bis(dicyclohexylphosphanyl)methane). The identities of **1** and **2** were confirmed by ^{1}H NMR spectroscopy, positive-ion FAB-mass spectrometry, and satisfactory elemental analyses,[10] and the structure of **2** was confirmed by an X-ray crystal structure determination; the Au – Au separation is 3.28 Å.[11]



1, R = phenyl
2, R = cyclohexyl

The electronic spectra of **1** and **2** in dichloromethane/methanol (1/1) containing 0.1 M tetra-*n*-butylammonium hexafluorophosphate as supporting electrolyte show spectral changes upon addition of K^+ ions (Figure 1). Isosbestic points were observed at 266, 335, and 390 nm for **1** and at 235 and 352 nm for **2**, which are indicative of a clean reaction. Control experiments with the crown-free analogues $[Au_2(dppm)\{S\text{-}3,4\text{-}(OMe)_2C_6H_4\}_2]$ (**3**) and $[Au_2(dcpm)\{S\text{-}3,4\text{-}(OMe)_2C_6H_4\}_2]$ (**4**) showed no UV/Vis spectral changes upon addition of K^+ ions under the

[*] Prof. V. W.-W. Yam, C.-K. Li, C.-L. Chan
Department of Chemistry, The University of Hong Kong
Pokfulam Road, Hong Kong (P.R. China)
Fax: (+852) 28571586
E-mail: wwyam@hkucc.hku.hk

[**] V.W.W.Y thanks the Research Grants Council, the Croucher Foundation, and The University of Hong Kong for financial support. C.L.C acknowledges the the Croucher Foundation and the Sir Edward Youde Memorial Fund Council for scholarships.

 © WILEY-VCH Verlag GmbH, D-69451 Weinheim, 1998 1433-7851/98/3720-2857 $ 17.50+.50/0

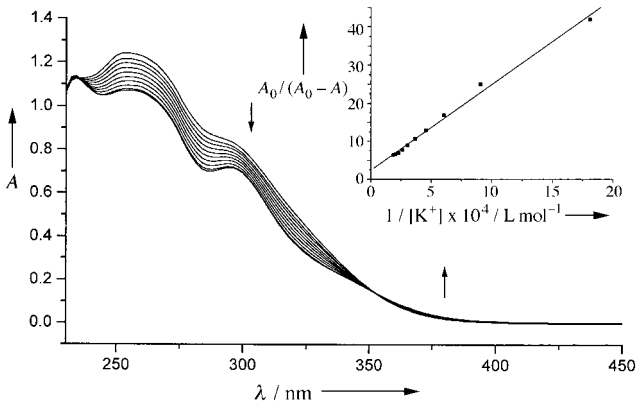


Figure 1. UV/Vis spectral changes of **2** (5.3×10^{-5} mol L^{-1}) upon addition of various concentrations of potassium ions in CH_2Cl_2/MeOH (1/1; 0.1 M nBu_4NPF_6). The insert shows the plot of $A_o/(A_o - A)$ versus $1/[K^+]$ at 290 nm

same conditions. This observation is supportive of the importance of the crown moieties in the specific association of **1** and **2** with K^+ ions rather than resulting from changes in the solvent polarity. A plot of $A_0/(A_0 - A)$ versus $[K^+]^{-1}$ yielded a satisfactory straight line, which indicated that the complexation of a K^+ ion to the dinuclear Au^I complex was in a 1:1 ratio (A and A_0 refer to the absorbance at 290 nm with and without K^+ ions, respectively). Since the ionic radius of the K^+ ion is too large to fit into the cavity of a benzo[15]-crown-5, the 1:1 complexation ratio indicates that the K^+ ions are sandwiched between two benzo[15]crown-5 units within the dinuclear Au^I complex. The lg K values for the binding of K^+ ions to **1** and **2** were 3.4 and 4.0, respectively.

The changes in the luminescence response of **1** and **2** towards K^+ ion binding were found to be more pronounced. The emission spectra of **1** (Figure 2) with excitation at 390 nm, the isosbestic wavelength, showed a drop in intensity at approximately 502 nm with the concomitant formation of a new long-lived, low-energy emission band at 720 nm upon addition of K^+ ions. An isoemissive point was obtained at about 600 nm. The lifetime of the excited state for the emission band at 720 nm was determined as 0.2 μs. Interestingly, in the absence of K^+ ions, the emissive lifetime of the

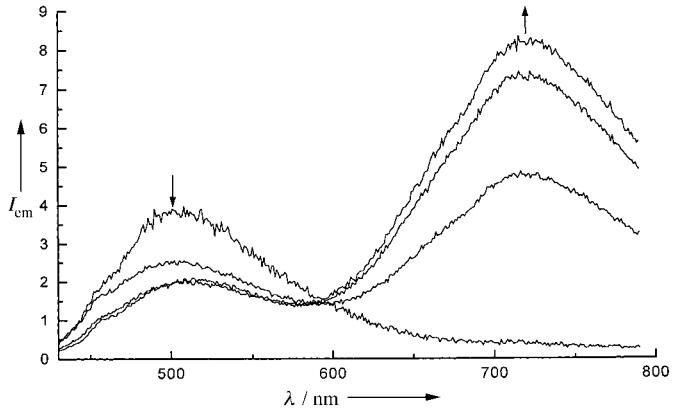


Figure 2. Emission spectra of **1** (1.7×10^{-3} mol L^{-1}) upon addition of various concentrations of potassium ions in CH_2Cl_2/MeOH (1/1; 0.1 M nBu_4NPF_6).

band at 520 nm was less than 0.1 μs. Successive addition of free benzo[15]crown-5 to the mixture of **1** and K^+ led to the observation of a reverse trend, in which the low-energy emission at 720 nm dropped in intensity with a concomitant rise in the high-energy emission at 502 nm. This result is indicative of the reversible nature of the ion-binding process. A plot of $I_0/(I - I_0)$ versus $[K^+]^{-1}$ for **1** yielded a satisfactory straight line, which further confirmed that the complexation of K^+ ion to the dinuclear Au^I complex was in a 1:1 ratio; thedetermined lg K value of 3.2 is in close agreement with that obtained from absorption measurements (I_0 and I refer to the emission intensity at 720 nm in the absence and in the presence of K^+ ions, respectively). The identity of the $\{\mathbf{1} \cdot K^+\}$ adduct was confirmed by electrospray-ionization mass spectrometry (ESI-MS). Similar to the absorption studies, control experiments with the crown-free analogues **3** and **4** under the same conditions showed no changes in the emission characteristics upon addition of K^+ ions, supportive of the importance of the crown moieties in the specific association of **1** and **2** with K^+ ions.

Despite the well known high affinity of benzo[15]crown-5 for sodium ions, addition of Na^+ ions to **1** did not give rise to the growth of a new emission band at 720 nm. This is consistent with our rationale for the design of complexes **1** and **2** as a photoswitch. In solution the Au – Au separation in **1** and **2** is large as a result of the floppy nature of their structures. Thus, an emission typical of monomeric Au^I – phosphane was observed at around 502 nm. Upon addition of K^+ ions, which have ionic radii too large to fit into the cavity size of benzo[15]crown-5, the K^+ ions would tend to sandwich between two crown ethers, thereby bringing the two Au^I centers into close proximity. Such Au – Au interactions that involve the overlap of the 5d, 6s, and $6p_z$ orbitals on each Au atom with those of the other Au atom would give rise to bonding and antibonding combinations of dσ, dσ*, dπ, dπ*, dδ, dδ*, sσ, sσ*, pσ, and pσ* character (the z axis is taken to be the Au – Au bond axis). A net stabilization of the dinuclear Au acceptor orbitals sσ or pσ would result. Thus a red emission characteristic of the ligand-to-metal – metal bond charge transfer (LMMCT; from the thiolate ligand to the gold – gold bond)[12] is observed. Addition of an excess of free benzo[15]crown-5 to the mixture of **1** and K^+ ions extracted the sandwiched K^+ ions from **1**, with a breaking of the short Au – Au contact and a reversal of the emission trend. Similarly, addition of Na^+ ions to a mixture of **1** and K^+ ions also caused a drop in the intensity of the emission band at 720 nm, probably as a result of the high affinity of the benzo[15]crown-5 unit for Na^+ ions, which displace the K^+ ions. Similar findings were also observed for complex **2**. Although one cannot eliminate the possibility that the generation of the low-energy emission band at 720 nm in **1** and at 713 nm in **2** upon addition of K^+ ions is a result of the slowing down of the rate of nonradiative decay that arises from the interlocking of the two crown units by K^+ ions to render the complexes more rigid, we favor the assignment of the low energy emission band as derived from a LMMCT state resulting from the formation of a weak Au – Au interaction.

Received: April 7, 1998 [Z11697IE]
German version: *Angew. Chem.* **1998**, *110*, 3041 – 3044

 © WILEY-VCH Verlag GmbH, D-69451 Weinheim, 1998 1433-7851/98/3720-2858 $ 17.50+.50/0

Keywords: crown compounds · gold · luminescence · molecular switches · S ligands

[1] For example, see a) F. L. Carter, R. E. Scatkowski, H. Wohltzened, *Molecular Electronic Devices*, North Holland, Amsterdam, **1988**; b) V. Balzani, F. Scandola, *Supramolecular Photochemistry*, Ellis Horwood, London, **1991**; c) H. J. Schneider, H. Durr, *Frontiers in Supramolecular Organic Chemistry and Photochemistry*, VCH, Weinheim, **1991**.

[2] a) J. P. Konopelski, F. Kotzyba-Hibert, J. M. Lehn, J. P. Desvergne, F. Fages, A. Castellan, H. Bouas-Laurent, *J. Chem. Soc. Chem. Commun.* **1985**, 433; b) J. M. Lehn, *Angew. Chem.* **1988**, *100*, 91; *Angew. Chem. Int. Ed. Engl.* **1988**, *27*, 89; c) F. Fages, J. P. Desvergne, H. Bouas-Laurent, P. Marsau, J. M. Lehn, F. Kotzyba-Hibert, A. Albrecht-Gary, M. Al-Joubbeh, *J. Am. Chem. Soc.* **1989**, *111*, 8672; d) J. M. Lehn, *Angew. Chem.* **1990**, *102*, 1347; *Angew. Chem. Int. Ed. Engl.* **1990**, *29*, 1304; e) D. J. Cram, *Angew. Chem.* **1988**, *100*, 1041; *Angew. Chem. Int. Ed. Engl.* **1988**, *27*, 1009.

[3] a) A. W. Czarnik, *Acc. Chem. Res.* **1994**, *27*, 302; b) A. W. Czarnik in *Fluorescent Chemosensors for Ion and Molecule Recognition*, American Chemical Society, Washington, DC, **1993**; c) "Chemosensors of Ion and Molecular Recognition": A. W. Czarnik, J.-P. Desvergne, *NATO ASI Ser. Ser. C 492*, **1997**; d) A. P. de Silva, H. Q. N. Gunaratne, C. P. McCoy, *Nature* **1993**, *364*, 42; e) A. P. de Silva, H. Q. N. Gunaratne, T. Gunnlaugsson, A. J. M. Huxley, C. P. McCoy, J. T. Rademacher, T. E. Rice, *Chem. Rev.* **1997**, *97*, 1515.

[4] F. Fages, J. P. Desvergne, H. Bouas-Laurent, *J. Am. Chem. Soc.* **1989**, *111*, 96.

[5] a) P. D. Beer, *Adv. Inorg. Chem*, **1992**, *39*, 79; b) P. D. Beer, *Chem. Commun.* **1996**, 689; c) S. C. Rawle, P. Moore, N. W. Alcock, *J. Chem. Soc. Chem. Commun.* **1992**, 684; d) D. B. MacQueen, K. S. Schanze, *J. Am. Chem. Soc.* **1991**, *113*, 6108; e) D. I. Yoon, C. A. Berg-Brennan, H. Lu, J. T. Hupp, *Inorg. Chem.* **1992**, *31*, 3192; f) Y. Shen, B. P. Sullivan, *Inorg. Chem.* **1995**, *34*, 6235; g) S. Watanabe, O. Onogawa, Y. Komatsu, K. Yoshida, *J. Am. Chem. Soc.* **1998**, *120*, 229; h) R. Grigg, W. D. J. A. Norbert, *J. Chem. Soc. Chem. Commun.* **1992**, 1300; i) V. W. W. Yam, K. M. C. Wong, V. W. M. Lee, K. K. W. Lo, K. K. Cheung, *Organometallics* **1995**, *14*, 4034; j) V. W. W. Yam, K. K. W. Lo, K. K. Cheung, *Inorg. Chem.* **1995**, *34*, 4013; k) V. W. W. Yam, V. W. M. Lee, K. K. Cheung, F. Ke, K. W. M. Siu, *Inorg. Chem.* **1997**, *36*, 2124; l) V. W. W. Yam, V. W. M. Lee, *J. Chem. Soc. Dalton Trans.* **1997**, 3005; m) V. W. W. Yam, A. S. F. Kai, *Chem. Commun.* **1998**, 1091.

[6] a) A. L. Balch, V. J. Catalano, M. A. Chatfield, J. K. Nagle, M. M. Olmstead, P. E. Reedy, *J. Am. Chem. Soc.* **1991**, *113*, 1252; b) A. L. Balch, F. Neve, M. M. Olmstead, *Inorg. Chem.* **1991**, *30*, 3395; c) L. Fabbrizzi, G. D. Santis, M. Licchelli, P. Pallavicini, A. Perotti, *J. Chem. Soc. Dalton Trans.* **1992**, 3283; d) L. Fabbrizzi, G. Francese, M. Licchelli, A. Perotti, A. Taglietti, *Chem. Commun.* **1997**, 581; e) R. Grigg, W. D. J. A. Norbert, *J. Chem. Soc. Chem. Commun.* **1992**, 1298; f) P. Ghosh, P. K. Bharadwaj, J. Roy, S. Ghosh, *J. Am. Chem. Soc.* **1997**, *119*, 11903.

[7] a) H. Schmidbaur, *Gold Bull.* **1990**, *23*, 11; b) F. Scherbaum, A. Grohmann, B. Huber, C. Krüger, H. Schmidbaur, *Angew. Chem.* **1988**, *100*, 1602; *Angew. Chem. Int. Ed. Engl.* **1988**, *27*, 1544; c) P. Pyykkö, *Chem. Rev.* **1997**, *97*, 597; d) Y. Jiang, S. Alvarez, R. Hoffmann, *Inorg. Chem.* **1985**, *24*, 749; e) D. M. P. Mingos, *J. Chem. Soc. Dalton Trans.* **1976**, 1163; f) D. E. Harwell, M. D. Mortimer, C. B. Knobler, F. A. L. Anet, M. F. Hawthorne, *J. Am. Chem. Soc.* **1996**, *118*, 2679; g) R. Narayanaswamy, M. A. Young, E. Parkhurst, M. Ouellette, M. E. Kerr, D. M. Ho, R. C. Elder, A. E. Bruce, M. R. M. Bruce, *Inorg. Chem.* **1993**, *32*, 2506.

[8] a) C. M. Che, H. L. Kwong, V. W. W. Yam, K. C. Cho, *J. Chem. Soc. Chem. Commun.* **1989**, 885; b) C. M. Che, H. L. Kwong, C. K. Poon, V. W. W. Yam, *J. Chem. Soc. Dalton Trans.* **1990**, 3215; c) V. W. W. Yam, T. F. Lai, C. M. Che, *J. Chem. Soc. Dalton Trans.* **1990**, 3747; d) C. M. Che, H. K. Yip, V. W. W. Yam, P. Y. Cheung, T. F. Lai, S. J. Shieh, S. M. Peng, *J. Chem. Soc. Dalton Trans.* **1992**, 427; e) V. W. W. Yam, S. W. K. Choi, *J. Chem. Soc. Dalton Trans.* **1993**, 2057; f) V. W. W. Yam, W. K. Lee, *J. Chem. Soc. Dalton Trans.* **1993**, 2097; g) V. W. W. Yam, C. L. Chan, K. K. Cheung, *J. Chem. Soc. Dalton Trans.* **1996**, 4019.

[9] a) T. M. McCleskey, H. B. Gray, *Inorg. Chem.* **1992**, *31*, 1733; b) C. King, J. C. Wang, N. I. Md. Khan, J. P. Fackler, Jr., *Inorg. Chem.* **1989**, *28*, 2145; c) N. I. Md. Khan, C. King, D. D. Heinrich, J. P. Fackler, Jr., L. C. Porter, *Inorg. Chem.* **1989**, *28*, 2150; d) H. R. C. Jaw, M. M. Savas, R. D. Rogers, W. R. Mason, *Inorg. Chem.* **1989**, *28*, 1028; e) H. R. C. Jaw, M. M. Savas, W. R. Mason, *Inorg. Chem.* **1989**, *28*, 4366; f) A. Vogler, H. Kunkely, *Chem. Phys. Lett.* **1988**, *150*, 135; g) W. B. Jones, J. Yuan, R. Narayanaswamy, M. A. Young, R. C. Elder, A. E. Bruce, M. R. M. Bruce, *Inorg. Chem.* **1995**, *34*, 1996; h) S. D. Hanna, J. I. Zink, *Inorg. Chem.* **1996**, *35*, 297; i) S. D. Hanna, S. I. Khan, J. I. Zink, *Inorg. Chem.* **1996**, *35*, 5813; j) D. V. Toronto, B. Weissbart, D. S. Tinti, A. L. Balch, *Inorg. Chem.* **1996**, *35*, 2484; k) J. C. Vickery, M. M. Olmstead, E. Y. Fung, A. L. Balch, *Angew. Chem.* **1997**, *109*, 1227; *Angew. Chem. Int. Ed. Engl.* **1997**, *36*, 1179; l) D. Li, C. M. Che, S. M. Peng, S. T. Liu, Z. Y. Zhou, T. C. W. Mak, *J. Chem. Soc. Dalton Trans.* **1993**, 189.

[10] **1:** ^{1}H NMR ($CDCl_3$): $\delta = 3.7-4.1$ (m, 34H, CH_2 (crown ether) and PCH_2P); 6.6, 7.0–7.1 (m, 6H, Ar-*H*); 7.2–7.4, 7.6–7.7 (m, 20H, P*Ph*$_2$); positive-ion FAB-MS: *m*/*z*: 1077 [*M* − S-benzo[15]crown-5$^+$]; elemental analysis calcd for **1** · 2CH_2Cl_2: C 42.71, H 4.14; found: C 42.89, H 3.91. **2:** ^{1}H NMR ($CDCl_3$): $\delta = 1.1-2.2$ (m, 46H, dcpm); 3.7–4.1 (m, 32H, CH_2 (crown ether)); 6.6, 7.0–7.1 (m, 6H, Ar-*H*); positive-ion FAB-MS: *m*/*z*: 1101 [M^+ − S-benzo[15]crown-5]; elemental analysis calcd for **2** · 1/2CH_2Cl_2: C 44.53, H 5.89; found: C 44.28, H 5.88. **3:** ^{1}H NMR ($CDCl_3$): $\delta = 3.7-3.8$ (m, 14H, OCH_3 and PCH_2P); 6.6, 7.0–7.1 (m, 6H, Ar-*H*), 7.2–7.4, 7.6–7.7 (m, 20H, P*Ph*$_2$); positive-ion FAB-MS: *m*/*z*: 947 [$M^+ - SC_6H_4(OMe)_2$; elemental analysis calcd for **3**: C 44.11, H 3.58; found: C 43.94, H 3.67. **4**: ^{1}H NMR ($CDCl_3$): $\delta = 1.1-2.2$ (m, 46H, dcpm), 3.8 (d, 12H, OCH_3), 6.6, 7.0–7.1 (m, 6H, Ar-*H*); positive-ion FAB-MS: *m*/*z* = 971 [$M - SC_6H_4(OMe)_2^+$]; elemental analysis calcd for **4** · $CH_2Cl_2 \cdot H_2O$: C 40.57, H 5.47; found: C 40.21, H 5.21.

[11] V. W. W. Yam, K. K. Cheung, unpublished results.

[12] J. M. Forward, D. Bohmann, J. P. Fackler, Jr., R. J. Staples, *Inorg. Chem.* **1995**, *34*, 6330.

Sensitivity Enhancement in Transverse Relaxation Optimized NMR Spectroscopy**

Guang Zhu,* Xiangming Kong, Xianzhong Yan, and Konghong Sze

Continuing efforts to study ever larger biologically relevant proteins by NMR spectroscopy have resulted in many advances over the past 10 years; one notable development is the introduction of multidimensional heteronuclear techniques for proteins labeled with ^{13}C and ^{15}N. These techniques have greatly facilitated NMR studies of the structure and function of proteins with molecular weights up to 30 kD. However, their application to larger proteins is hampered by the decrease in the molecular tumbling rate.[1] This shortens the transverse relaxation time of the protein, which in turn

[*] Dr. G. Zhu, M.Sc. X. Kong, M.Sc. X. Yan, Dr. K. Sze
Department of Biochemistry
Hong Kong University of Science and Technology
Clear Water Bay, Kowloon (Hong Kong)
Fax: (+852) 2358-1552
E-mail: gzhu@ust.hk

[**] The authors thank Dr. David Smith for helpful discussions and Dr. Mingjie Zhang for a sample of ^{15}N-labeled calmodulin. This work was supported by grants from the Research Grant Council of Hong Kong (HKUST 563/95M, 6197/97M, and 6038/98M), and the Hong Kong Biotechnology Research Institute is acknowledged for the purchase of the spectrometer.

leads to larger spectral line widths and lower sensitivity. In a high magnetic field, dipole–dipole interactions and chemical shift anisotropy are the dominant factors in the relaxation of ^{1}H, ^{13}C, and ^{15}N. These two relaxation mechanisms can significantly interfere with one another,[2] a fact that must be taken into account in more precise measurements of protein dynamics[3] by NMR spectroscopy. Recently, a major advance in the study of large proteins (>30 kD) was made with the discovery that the interference between dipole–dipole interaction and chemical shift anisotropy can greatly reduce the transverse relaxation rates of ^{1}H and ^{15}N, and thus make the study of very large biomolecules possible.[4] This line-narrowing effect is utilized in transverse relaxation optimized spectroscopy (TROSY), in which only one component ($\omega_N+\pi^1J_{NH}$, $\omega_H-\pi^1J_{NH}$) of the four multiplets ($\omega_N\pm\pi^1J_{NH}$, $\omega_H\pm\pi^1J_{NH}$) of a ^{15}N–^{1}H moiety is observed. Theoretical calculations indicate that almost complete cancellation of the transverse relaxation of this component can be realized at a ^{1}H frequency near 1 GHz. The experimental results demonstrated a dramatic reduction in spectral line widths in a TROSY ^{15}N–^{1}H spectrum compared to those of an HSQC spectrum at 750 MHz.[4] Since only one component of the four multiplets is observed in the 2D ^{15}N–^{1}H TROSY experiment, the total intensity of the signal is reduced by 75%. However, the much narrower line widths in both dimensions make this experiment especially attractive compared to the traditional HSQC experiment for NMR studies of larger biomolecules.

We observed that the sensitivity of the TROSY experiment could be improved by a factor of $\sqrt{2}$ by simply changing the original phase cycles and the data-processing procedure. This method is similar to that applied in the sensitivity-enhanced HSQC, HMQC, and TOCSY experiments.[5] The pulse sequence of the sensitivity-enhanced TROSY experiment is shown in Figure 1. For each t_1 value, two transients are recorded with different radio frequency (rf) pulses and receiver phase cycles and are stored separately. The coherence transfer and evolution in the pulse sequence can be evaluated on the basis of the product operator formalism and the single-transition base operators[6] $S^{\pm}_{12}=\frac{1}{2}S^{\pm}+I_zS^{\pm}$ and $S^{\pm}_{34}=\frac{1}{2}S^{\pm}-I_zS^{\pm}$. The relaxation formalism is given in reference [4].

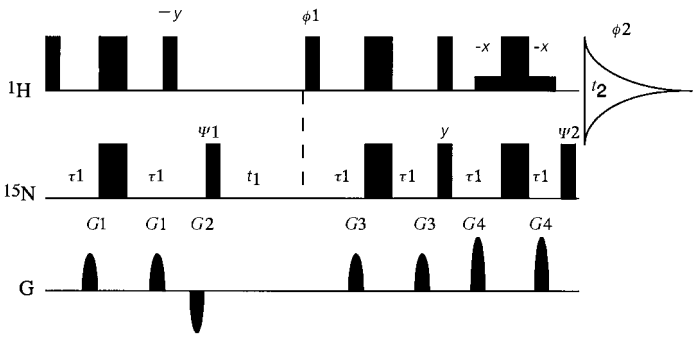


Figure 1. Pulse scheme of the sensitivity-enhanced ^{15}N–^{1}H TROSY correlation experiment. The narrow and wide bars represent nonselective 90° and 180° pulses, respectively. Pulses are applied along the x direction unless indicated otherwise. Because the water signal cannot be suppressed by presaturation owing to strong radiation damping at high magnetic field, solvent suppression was performed by the watergate scheme with an rf pulse of 2.1 ms at 110 Hz. The delay τ_1 corresponds to $1/(4\,^1J_{NH})=2.7$ ms. All gradients are applied along the z axis. The magnitudes of $G1$, $G2$, $G3$ and $G4$ are 12, 19, 14 and 21 G/cm with durations of 0.4, 1.0, 0.4, and 0.5 ms, respectively. Two transients were acquired and stored separately for each increment of t_1. The final absorption spectrum is obtained by the method described in the text. The first transient is obtained by using of the phase cycle $\psi1=y,\ x,\ -y,\ -x;\ \phi1=y;\ \psi2=x;\ \mathrm{rec}\,\phi2=x,\ -y,\ -x,\ y$. For the second transient, the phase cycle $\psi1=y,\ x,\ -y,\ -x;\ \phi1=-y;\ \psi2=-x;\ \mathrm{rec}\,\phi2=x,\ y,\ -x,\ -y$ is used. Note that the sign convention for the receiver phase may differ among the spectrometer manufacturers.[8]

For the first transient in the first step of the phase cycle (where $\psi1=y$, $\phi1=y$, $\psi2=x$, and $\mathrm{rec}\,\phi2=x$) the magnetization σ_1 before acquisition can be expressed by Equation (a).

$$\begin{aligned}\sigma_1=&\tfrac{1}{2}I^-[i\cos(\omega_s^{12}t_1)-\sin(\omega_s^{12}t_1)]\exp(-R_{12}t_1)\\&+\tfrac{1}{2}I^-[i\cos(\omega_s^{34}t_1)+\sin(\omega_s^{34}t_1)]\exp(-R_{34}t_1)\\&+I^-S_z[-i\cos(\omega_s^{12}t_1)+\sin(\omega_s^{12}t_1)]\exp(-R_{12}t_1)\\&+I^-S_z[i\cos(\omega_s^{34}t_1)+\sin(\omega_s^{34}t_1)]\exp(-R_{34}t_1)\end{aligned}\qquad(a)$$

Here R_{12} and R_{34} are the relaxation rates of the individual components of the S spin,[4] and ω_s^{12} and ω_s^{34} are $\omega_N+\pi^1J_{NH}$ and $\omega_N-\pi^1J_{NH}$, respectively. In the second step of the phase cycle (where $\psi1=x$, $\phi1=y$, $\psi2=x$, and $\mathrm{rec}\,\phi2=-y$) the magnetization σ_2 before detection is given by Equation (b).

$$\begin{aligned}\sigma_2=&\tfrac{1}{2}I^-[-\cos(\omega_s^{12}t_1)-i\sin(\omega_s^{12}t_1)]\exp(-R_{12}t_1)\\&+\tfrac{1}{2}I^-[\cos(\omega_s^{34}t_1)-i\sin(\omega_s^{34}t_1)]\exp(-R_{34}t_1)\\&+I^-S_z[\cos(\omega_s^{12}t_1)+i\sin(\omega_s^{12}t_1)]\exp(-R_{12}t_1)\\&+I^-S_z[\cos(\omega_s^{34}t_1)-i\sin(\omega_s^{34}t_1)]\exp(-R_{34}t_1)\end{aligned}\qquad(b)$$

The magnetization of the first transient in a four-step phase cycle is given by Equation (c). Similarly, the magnetization of the second transient can be expressed by Equation (d).

$$\begin{aligned}M_1=&2[\sigma_1(d)-i\sigma_2(d)]\\=&-2I^-[-i\cos(\omega_s^{12}t_1)+\sin(\omega_s^{12}t_1)]\exp(-R_{12}t_1)\\&+4I^-S_z[-i\cos(\omega_s^{12}t_1)+\sin(\omega_s^{12}t_1)]\exp(-R_{12}t_1)\end{aligned}\qquad(c)$$

$$\begin{aligned}M_2=&-2I^-[i\cos(\omega_s^{12}t_1)+\sin(\omega_s^{12}t_1)]\exp(-R_{12}t_1)\\&+4I^-S_z[i\cos(\omega_s^{12}t_1)+\sin(\omega_s^{12}t_1)]\exp(-R_{12}t_1)\end{aligned}\qquad(d)$$

During the acquisition period, no decoupling is applied, and the detectable magnetization relaxes in a manner similar to that of ^{15}N in the t_1 domain. The detectable magnetization can be expressed by Equations (e) and (f).[4] Here R_{13} and R_{24} are the relaxation rates of the individual components of the I spin,[4] and ω_I^{13} and ω_I^{24} are $\omega_H+\pi^1J_{NH}$ and $\omega_H-\pi^1J_{NH}$, respectively. The signal intensities of the detectable magnetization of the two transients are given by Equations (g) and (h).

$$I^-\rightarrow A(\exp[i\omega_I^{13}-R_{13}]t_2+\exp[i\omega_I^{24}-R_{24}]t_2)\qquad(e)\text{-}$$

$$2I^-S_z\rightarrow A(\exp[i\omega_I^{13}-R_{13}]t_2-\exp[i\omega_I^{24}-R_{24}]t_2)\qquad(f)$$

$$M_1=-4[-i\cos(\omega_s^{12}t_1)+\sin(\omega_s^{12}t_1)]\exp(-R_{12}t_1)\exp(i\omega_I^{24}t_2-R_{24}t_2)\qquad(g)$$

$$M_2=-4[i\cos(\omega_s^{12}t_1)+\sin(\omega_s^{12}t_1)]\exp(-R_{12}t_1)\exp(i\omega_I^{24}t_2-R_{24}t_2)\qquad(h)$$

After data acquisition, the two transients for each t_1 value are added and subtracted, respectively, to form corresponding real and imaginary FIDs with a 90° shift added to one of the two resulting FIDs. The final pure absorption spectrum can be obtained by data processing according to the method of States et al.[7]

The effectiveness of the sensitivity-enhanced TROSY (enTROSY) experiment is demonstrated by ^{15}N–^{1}H correlation

 © WILEY-VCH Verlag GmbH, D-69451 Weinheim, 1998 1433-7851/98/3720-2860 $ 17.50+.50/0

spectroscopy of ^{15}N-labeled calmodulin. Measurements were made at 15 °C on a Varian Inova 500 MHz NMR spectrometer, and the protein concentration was 1 mM in H_2O/D_2O (9/1) at pH 6.8. Figure 2 displays a small region of $^{15}N-^{1}H$ correlation spectra of calmodulin. Figure 2a shows the conventional HSQC spectrum obtained without the use of

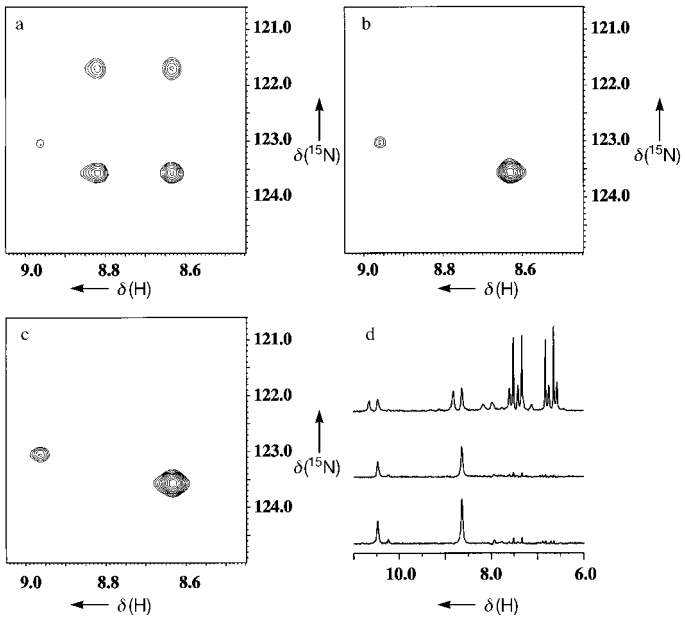


Figure 2. Contour plots of $^{15}N-^{1}H$ correlation spectra of ^{15}N-labeled calmodulin. a) Conventional HSQC spectrum, obtained without decoupling during the t_1 and t_2 periods. b) Spectrum recorded in a conventional TROSY experiment.[4] c) Spectrum recorded in a sensitivity-enhanced TROSY experiment (see text). d) One-dimensional cross sections from the spectra a–c at $\delta(^{15}N) = 123.6$ (from top to bottom). The peaks between 6 and 8 ppm in the HSQC cross section correspond to the cross-peak multiplets at the ^{15}N frequency ($\omega_N - \pi^1 J_{NH}$), which is not observed by TROSY experiments. Spectra b and c, which were recorded and processed with the same parameters, have been scaled to the same noise level. The spacing factor between two consecutive contour lines is 1.2.

decoupling during the t_1 and t_2 periods. It is notable that even at 500 MHz there are significant differences in line width between the four individual multiplets. Figures 2b and 2c are taken from spectra recorded in conventional and sensitivity-enhanced TROSY experiments, respectively. Comparison of Figures 2b and 2c, as well as all other correlation peaks (not shown here), shows that a uniform enhancement in sensitivity of all peaks by a factor of $\sqrt{2}$ was achieved without introducing any artifacts.

The introduction of the TROSY experiment makes NMR spectroscopy a promising technique for studying the structure and function of larger biomolecules. We have improved the sensitivity of the original 2D TROSY experiment by a factor of $\sqrt{2}$ by using different phase cycling and data-processing schemes. This improvement will doubtless have widespread practical application in high-field NMR studies of large proteins.

Received: June 19, 1998 [Z 12014 IE]
German version: *Angew. Chem.* **1998**, *110*, 3019–3021

Keywords: NMR spectroscopy · proteins

[1] a) G. Wagner, *J. Biomol. NMR* **1993**, *3*, 375–385; b) D. Nietlispach, R. T. Clower, R. W. Broadhurst, Y. Ito, J. Keller, M. Kelly, J. Ashurst, H. Oschkinat, P. J. Domaille, E. D. Laue, *J. Am. Chem. Soc.* **1996**, *118*, 407–415.

[2] a) H. M. McConnell, *J. Chem. Phys.* **1956**, *25*, 709–715; b) R. R. Vold, R. L. Vold, *Prog. NMR Spectrosc.* **1978**, *12*, 79–133; c) M. Goldman, *J. Magn. Reson.* **1984**, *60*, 437–452; d) S. Wimperis, G. Bodenhausen, *Mol. Phys.* **1989**, *66*, 897–919; e) J. Boyd, U. Hommel, I. D. Campbell, *Chem. Phys. Lett.* **1990**, *175*, 477–482.

[3] a) L. E. Kay, L. K. Nicholson, F. Delaglio, A. Bax, D. A. Torchia, *J. Magn. Reson.* **1992**, *97*, 359–375; b) A. G. Palmer, N. J. Skelton, W. J. Chazin, P. E. Wright, M. Rance, *Mol. Phys.* **1992**, *75*, 699–711; c) N. Tjandra, A. Szabo, A. Bax, *J. Am. Chem. Soc.* **1996**, *118*, 6986–6991.

[4] K. Pervushin, R. Riek, G. Wider, K. Wuthrich, *Proc. Natl. Acad. Sci. USA* **1997**, *94*, 12366–12371.

[5] a) A. G. Palmer III, J. Cavanagh, P. E.Wright, M. Rance, *J. Magn. Reson.* **1991**, *93*, 151–170; b) J. Cavanagh, M. Rance, *J. Magn. Reson.* **1990**, *88*, 72–85; c) L. E. Kay, P. Keifer, T. Saarinen, *J. Am. Chem. Soc.* **1992**, *114*, 10663–10665; d) J. Schleucher, M. Sattler, C. Griesinger, *Angew. Chem.* **1993**, *105*, 1518–1521; *Angew. Chem. Int. Ed. Engl.* **1993**, *32*, 1489–1491.

[6] a) R. R. Ernst, G. Bodenhausen, A. Wokaun, *The Principles of Nuclear Magnetic Resonance in One and Two Dimensions*, Clarendon, Oxford, **1987**; b) O. W. Sorensen, G. W. Eich, M. H. Levitt, G. Bodenhausen, R. R. Ernst, *Prog. NMR Spectrosc.* **1983**, *16*, 163–192.

[7] D. I. States, R. A. Haberkorn, D. J. Buben, *J. Magn. Reson.* **1982**, *93*, 151.

[8] Note added in proof: A reviewer's comments alerted us to a difference between Varian and Bruker spectrometers, which requires that the *y*-axis receiver phases be inverted. It is also necessary to invert the *y*-axis pulse phases. In the pulse sequence of Figure 1, the particular phase cycling means that only the phase of the second 90° ^{1}H pulse needs to be considered. For optimal sensitivity, the phase of this pulse should be $-y$ for Varian and $+y$ for Bruker. If this phase is inverted then the "steady-state" enhancement, described by Pervushin et al. (*J. Am. Chem. Soc.* **1998**, *120*, 6394–6400) after this manuscript was submitted, will be lost. The sensitivity enhancement presented in this work is independent of the phase of this pulse and a $\sqrt{2}$ enhancement is gained over the corresponding TROSY experiment that has the same phase for this pulse.

Directed Positioning of Organometallic Fragments Inside a Calix[4]arene Cavity

Catherine Wieser-Jeunesse, Dominique Matt,* and André De Cian

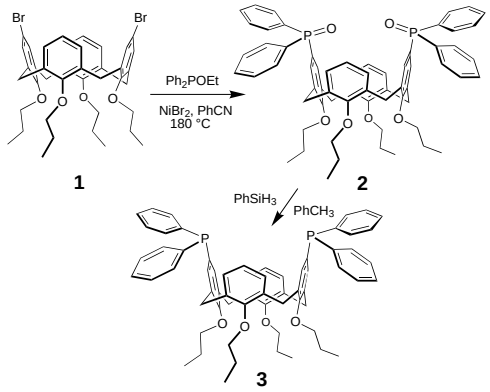
A major attraction of cone-shaped calix[4]arenes concerns the presence of a macrocyclic cavity defined by four symmetrically sited phenoxy rings.[1] To date, exploitation of such organized structures has mostly relied on converging π systems on the inner side that facilitate weak binding of various substrates,[2] including certain metal cations.[3] Surprisingly, despite increasing interest in the application of calixarenes as ligands in transition metal chemistry,[4] the

[*] Dr. D. Matt, Dr. C. Wieser-Jeunesse
Université Louis Pasteur, UMR 7513 CNRS
Groupe de Chimie Inorganique Moléculaire
1 rue Blaise Pascal, F-67008 Strasbourg Cedex (France)
Fax: (+33) 3-88-617852
E-mail: dmatt@chimie.u-strasbg.fr
Dr. A. De Cian
Université Louis Pasteur, UMR 7513 CNRS
Laboratoire de Cristallochimie et Chimie Structurale
4 rue Blaise Pascal, F-67008 Strasbourg Cedex (France)

 © WILEY-VCH Verlag GmbH, D-69451 Weinheim, 1998 1433-7851/98/3720-2861 $ 17.50+.50/0

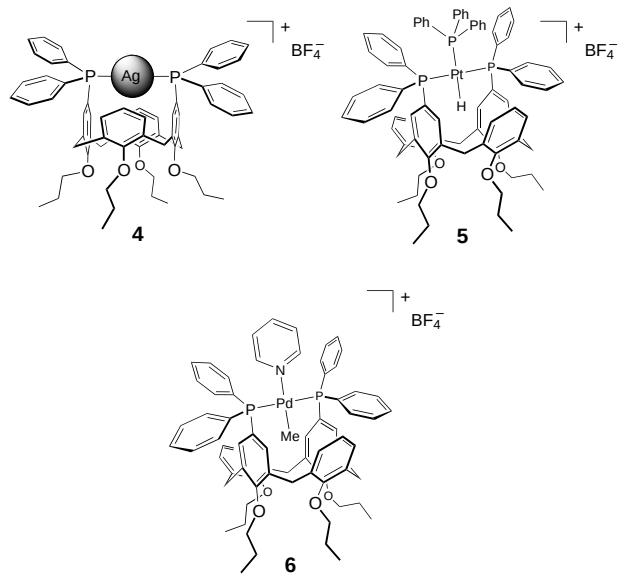
interior of the cavity has not been used to entrap or confine reactive fragments bound to transition metal ions.[5] Such architectures could possess the capability to promote metal-centered reactions that are sterically constrained, thereby allowing combined shape control and regioselectivity.[6] Furthermore, it is likely that the cavity walls will afford protection of highly reactive "M–R" units against undesired side reactions. We now report the first calix[4]arenes with organometallic fragments positioned inside the larger opening of the cavity.

Our approach to the construction of such systems exploits the coordinative properties of the hemispherical ligand **3**, a calix[4]arene bearing two P^{III} centers located on distal *p*-carbon atoms of the upper rim. Diphosphane **3** was conveniently prepared in two steps from **1**[7] by using well-established procedures:[8] diphosphorylation of **1** with $Ph_2POEt/NiBr_2$ resulted in formation of the di(phosphane oxide) **2**, which was then quantitatively reduced with $PhSiH_3$ to afford **3** (Scheme 1).



Scheme 1. Synthesis of the hemispherical ligand **3** in two steps.

Diphosphane **3** seems to be an ideal scaffold on which to assemble *trans*-chelate complexes: for example it reacts with one equivalent of $AgBF_4$ to form complex **4**. The FAB mass spectrum of **4** exhibits an intense signal at *m*/*z* 1069.6 with the appropriate isotopic profile for the $(\mathbf{4}-BF_4)^+$ ion. NMR data collected for **4** show the molecule to possesses C_2 symmetry,



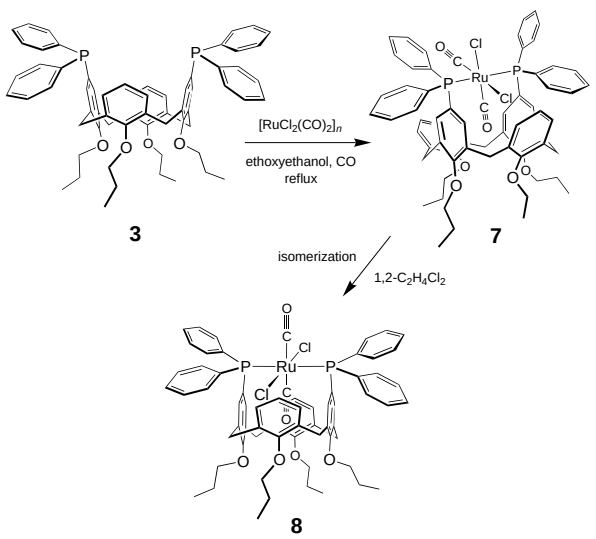
with the chemical shift found for the ^{31}P NMR signal being exactly as expected for the assigned structure.[9]

The above studies serve to indicate, not unsurprisingly, that the phosphane groups remain readily accessible for complexation with Ag^+ ions; more challenging targets were then sought. Treatment of **3** with $[PtH(thf)(PPh_3)_2]^+$ in refluxing THF afforded the platinum(II) complex **5** quantitatively. As for **4**, the ^1H and ^{13}C NMR data indicate an apparent C_2-symmetry for the calixarene skeleton. Furthermore, the ^{31}P NMR spectrum unambigously establishes the *trans*-spanning behavior of the diphosphane as well as the presence of two types of phosphorus atoms (the phosphorus atoms on the calixarene appear as a doublet with ^{195}Pt satellites at $\delta = 15.0$; $J(P,P') = 20$ Hz, $J(P,Pt) = 2706$ Hz). The bulky PPh_3 ligand, positioned *trans* to the hydride ligand, forces the Pt–H bond to point inside the calixarene cavity. The signal for the hydride atoms appears approximately 1.3 ppm upfield with respect to the related $[PtH(PPh_3)_3]^+$ ion,[10] thus reflecting the high shielding effect of the two phenoxy rings that border the hydride atom. In contrast to other complexes of the type $[PtH(PPh_3)(\widehat{P\,P})]^+$ that contain a *trans*-spanning diphosphane,[11] complex **5** is inert towards *cis*/*trans* isomerization in solution. Since only the *trans* isomer has the necessary stereochemical features to position the hydride atom group inside the cavity, the reluctance to isomerize attests to the stability of the inclusion complex.

With the aim to entrap larger metallo-fragments inside the cavity, a solution of **3** in THF was treated with the cationic alkylpalladium complex $[PdMe(cod)(thf)]BF_4$ (cod = cyclooctadiene). Subsequent addition of pyridine resulted in the quantitative formation of complex **6**. Characteristic features of the ^1H NMR spectrum are the presence of a triplet for the methyl group at $\delta = -0.79$, a solitary AB quartet for the $ArCH_2Ar$ bridges, and a virtual triplet for four (*o*-*P*)–Ar*H* hydrogen atoms ($|{}^3J(PH)+{}^5J(PH)| = 9$ Hz). In the ^{31}P NMR spectrum the phosphorus atoms appear as a singlet at $\delta = 27.0$. Two-dimensional NOESY spectra (500 MHz) indicate that the methyl hydrogen atoms lie in close proximity to the phenolic CH bonds of the two phosphorus-substituted phenoxy rings. Taking into account that the bulky pyridine ligand does not allow gyroscopic spinning of the pyridine-Pd-Me fragment around the P–P axis, these findings clearly establish that the methyl group is locked inside the cavity.

A further illustration of the unique complexing properties of calixarene **3** concerns the positioning of octahedral metal centers at the entrance of the cavity. Treatment of commercial ruthenium trichloride with carbon monoxide in boiling ethoxyethanol followed by the addition of **3** afforded the Ru^{II} complex **7** in high yield (Scheme 2). The *cis* arrangement of the two carbonyl units was inferred from the infrared spectrum, which showed two absorption bands in the CO region ($\tilde{\nu} = 2072$(s) and 1995(s) cm^{-1}). Complex **7** slowly isomerizes in 1,2-dichloroethane into the *trans,trans,trans* isomer **8** ($\tilde{\nu}(C{\equiv}O) = 1924$(s) cm^{-1}). The *trans*-spanning behavior of the diphosphane was confirmed by an X-ray diffraction study (Figure 1). The most remarkable feature of this structure is the entrapment of one metal carbonyl unit inside the calixarene cavity, the CO ligand being exactly intercalated

 © WILEY-VCH Verlag GmbH, D-69451 Weinheim, 1998 1433-7851/98/3720-2862 $ 17.50+.50/0 *Angew. Chem. Int. Ed.* **1998**, *37*, No. 20



Scheme 2. Positioning of octahedral ruthenium units at the mouth of calixarene **3**.

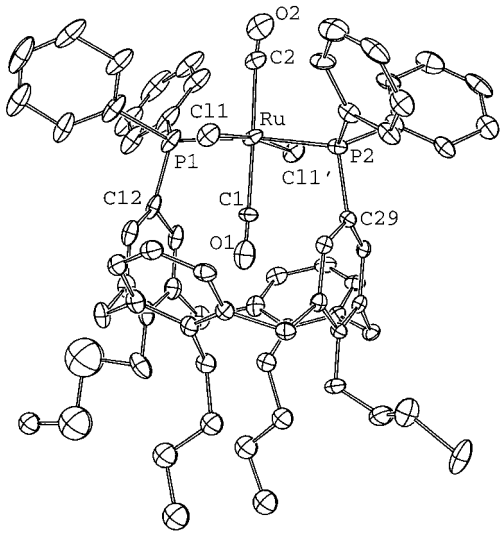


Figure 1. Structure of complex **8** (ORTEP). Selected bond lengths [pm] and angles [°]: Ru – P1 240.9(5), Ru – P2 240.3(5), Ru – C1 196(2), Ru – C2 188(2), Ru – Cl 241.0(3), P1 – C12 182(2), P2 – C29 184(1); P1-Ru-P2 172.2(3), Cl-Ru-Cl 171.9(2), Ru-P(1)-C(12) 106.6(5), Ru-P(2)-C(29) 107.2(5). The molecule possesses a mirror plane containing the phosphorus and ruthenium atoms. Each carbon atom of the propyl groups that are linked to the OArP rings are disordered over two positions.

between the two bordering P-substituted phenyl rings. The distance between these planes and the CO ligand axis is rather short (about 2.75 Å), thus suggesting a bonding interaction between the sandwiched CO and the two PPh rings. The relatively low $\tilde{\nu}$(CO) frequency (1924(s) cm^{-1} compared with 1998 cm^{-1} for *trans,trans,trans*-$[RuCl_2(CO)_2(PPh_3)_2]$[12]) supports this assumption.

Experimental Section

All reactions were carried out in dry solvents under purified nitrogen.

2: Yield: 82 %; m.p. > 280 °C; ^{1}H NMR (300 MHz, $CDCl_3$, 25 °C): δ = 7.76 – 7.69 and 7.54 – 7.48 (20 H, PPh_2), 7.40 (d, 4 H, *m*-H of OArP, ^3J(P,H) = 12 Hz), 6.24 and 6.02 (AB_2 spin system, 6 H, *m*- and *p*-H of OAr, ^3J = 7.5 Hz), 4.42 and 3.12 (AB spin sytem, 8 H, ArCH_2Ar, ^2J(A,B) = 13 Hz), 4.08 (pseudo t, 4 H, OCH_2, $^3J \approx 8$ Hz), 3.60 (t, 4 H, OCH_2, ^3J = 8 Hz), 1.94 (m, 4 H, OCH_2CH_2), 1.82 (m, 4 H, OCH_2CH_2), 1.06 (t, CH_3, ^3J = 8 Hz), 0.90 (t, CH_3, ^3J = 8 Hz); ^{13}C{^{1}H} NMR (50 MHz, $CDCl_3$, 25 °C): δ = 161.52 and 155.12 (2s, arom. C_q – O), 137.67 – 122.31 (arom. C atoms), 77.14 and 76.74 (2s, OCH_2), 30.96 (s, ArCH_2), 23.51 and 23.17 (2s, CH_2CH_3), 10.84 and 9.86 (2s, CH_3); ^{31}P{^{1}H} NMR (121 MHz, $CDCl_3$, 25 °C): δ = 29.4 (s, PPh_2); elemental analyses calcd for $C_{64}H_{66}O_6P_2 \cdot 0.5\,CHCl_3$ (993.18 + 59.69): C 73.58, H 6.37; found: C 74.00, H 6.37.

3: Yield: 75 %; m.p. 230 – 233 °C; ^{1}H NMR (300 MHz, $CDCl_3$, 25 °C): δ = 7.37 – 7.33 (20 H, PPh_2), 7.06 (d, 4 H, *m*-H of OArP, ^3J(P,H) = 8 Hz), 6.29 and 6.11 (AB_2 spin system, 6 H, *m* and *p*-H of OAr, ^3J = 8 Hz), 4.41 and 3.06 (AB spin sytem, 8 H, ArCH_2Ar, ^2J(A,B) = 13 Hz), 4.03 (pseudo t, 4 H, OCH_2, $^3J \approx 8$ Hz), 3.63 (t, 4 H, OCH_2, ^3J = 8 Hz), 2.00 (m, 4 H, OCH_2CH_2), 1.81 (m, 4 H, OCH_2CH_2), 1.06 (t, CH_3, ^3J = 7.5 Hz), 0.91 (t, CH_3, ^3J = 7.5 Hz); ^{13}C{^{1}H} NMR (50 MHz, $CDCl_3$, 25 °C): δ = 159.80 and 155.10 (2s, arom. C_q – O), 137.25-122.02 (arom. C atoms), 77.00 and 76.60 (2s, OCH_2), 30.94 (s, ArCH_2Ar), 23.51 and 23.15 (2s, CH_2CH_3), 10.82 and 9.93 (2s, CH_3); ^{31}P{^{1}H} NMR (121 MHz, $CDCl_3$, 25 °C): δ = – 6.4 (s, PPh_2); elemental analyses calcd for $C_{64}H_{66}O_4P_2$ (961.18): C 79.98, H 6.92; found: C 80.18, H 6.74.

4: Yield: 80 %; m.p. 187 – 190 °C (decomp); ^{1}H NMR (300 MHz, $CDCl_3$, 25 °C): δ = 7.43-7.37 (24 H, arom. H), 6.82 (s, 4 H, *m*-H of OArP), 6.18 (t of B_2A spin system, 2 H, *p*-H of OAr, ^3J = 8 Hz), 4.40 and 3.05 (AB spin system, 8 H, ArCH_2Ar, ^2J(A,B) = 13 Hz), 4.01 (pseudo t, 4 H, OCH_2, $^3J \approx$ 8 Hz), 3.70 (t, 4 H, OCH_2, ^3J = 8 Hz), 1.98 (m, 4 H, OCH_2CH_2), 1.89 (m, 4 H, OCH_2CH_2), 1.09 (t, CH_3, ^3J = 7.5 Hz), 0.83 (t, CH_3, ^3J = 7.5 Hz); ^{13}C{^{1}H} NMR (50 MHz, $CDCl_3$, 25 °C): δ = 157.18 and 156.85 (2s, arom. C_q – O), 136.09-123.02 (arom. C atoms), 77.64 and 76.59 (2s, OCH_2), 30.85 (s, ArCH_2Ar), 23.91 and 23.57 (2s, CH_2CH_3), 10.79 and 9.80 (2s, CH_3); ^{31}P{^{1}H} NMR (121 MHz, $CDCl_3$, 25 °C): δ = 10.4 (two d, PPh_2, $J(^{107}Ag,P)$ = 503 Hz, $J(^{109}Ag,P)$ = 580 Hz); MS (FAB): *m/z* calcd for $C_{64}H_{66}O_4P_2Ag$ [*M* – BF_4]: 1069; found 1069.6; elemental analyses calcd for $C_{64}H_{66}BF_4O_4P_2Ag$ (1155.86): C 66.51, H 5.76; found: C 66.66, H 5.43.

5: Yield: 73 %; m.p. 226 – 230 °C; ^{1}H NMR (300 MHz, $CDCl_3$, 25 °C): δ = 7.42 – 7.02 and 6.87 (43 H, arom. H), 6.24 (t of B_2A spin system, 2 H, *p*-H of OAr, ^3J(A,B) = 6 Hz), 4.44 and 3.09 (AB spin sytem, 8 H, ArCH_2Ar, ^2J(A,B) = 13 Hz), 4.04 (pseudo t, 4 H, OCH_2, $^3J \approx 6$ Hz), 3.69 (t, 4 H, OCH_2, ^3J = 7 Hz), 1.97 (m, 4 H, OCH_2CH_2), 1.89 (m, 4 H, OCH_2CH_2), 1.10 (t, CH_3, ^3J = 9 Hz), 0.92 (t, CH_3, ^3J = 7 Hz), – 6.93 (dt with Pt satellites, 1 H, PtH, $^2J(H,P_{cis})$ = 17 Hz, $^2J(H,P_{trans})$ = 167 Hz); ^{13}C{^{1}H} NMR (50 MHz, $CDCl_3$, 25 °C): δ = 157.39 and 156.70 (2s, arom.C_q – O), 136.40 – 122.43 (arom. C atoms), 77.90 and 76.65 (2s, OCH_2), 30.93 (s, ArCH_2), 23.51 and 22.94 (2s, CH_2CH_3), 10.74 and 9.77 (2s, CH_2CH_3); ^{31}P{^{1}H} NMR (121 MHz, $CDCl_3$, 25 °C): δ = 24.2 (t with Pt satellites, PPh_3, ^2J(P,P′) = 20 Hz, J(P,Pt) = 2120 Hz), 15.0 (d, PPh_2, ^2J(P,P′) = 20, J(P,Pt) = 2706 Hz). MS (FAB): *m/z* calcd for $C_{82}H_{82}O_4P_3Pt$ [*M* – BF_4]: 1418.5; found: 1418.8 (expected isotopic profile); elemental analyses calcd for $C_{82}H_{82}BF_4O_4P_3Pt$ (1506.38): C 65.38, H 5.49; found: C 65.18, H 5.43.

6 : Yield: 81 %; m.p. 163 – 166 °C (decomp); ^{1}H NMR (300 MHz, CD_2Cl_2, 25 °C): δ = 7.79 (d, 2 H, *o*-H of pyridine), 7.52 (t, 1 H, *p*-H of pyridine, ^3J = 5 Hz), 7.32 – 7.24 (20 H, PPh_2), 7.06 – 7.00 (m, 6 H, *m*- and *p*-H of OAr), 6.79 (m br, 2 H, *m*-H of pyridine), 6.62 (virtual t, 4 H, AA′XX′A″A‴ spin system (X = P), 4 H, *m*-H of OArP, $|^3J$(P,H)+^5J(P′,H)$|$ = 9 Hz), 4.56 and 3.24 (AB spin sytem, 8 H, ArCH_2Ar, ^2J(A,B) = 13 Hz), 4.15 (pseudo t, 4 H, OCH_2, $^3J \approx 8$ Hz), 3.81 (t, 4 H, OCH_2, ^3J = 7 Hz), 2.06 (m, 4 H, OCH_2CH_2), 1.97 (m, 4 H, OCH_2CH_2), 1.15 (t, CH_3, ^3J = 7 Hz), 0.96 (t, CH_3, ^3J = 7 Hz), – 0.79 (t, 3 H, Pd-CH_3, J(P,H) = 6 Hz); ^{13}C{^{1}H} NMR (CD_2Cl_2, 50 MHz, 25 °C): δ = 157.95 and 157.59 (2s, arom. C_q – O), 151.66 – 121.56 (arom. C atoms), 78.32 and 77.08 (2s, OCH_2), 31.32 (s, ArCH_2Ar), 23.98 (s, CH_2CH_3), 11.00 and 9.98 (2s, CH_3); ^{31}P{^{1}H} NMR (CD_2Cl_2, 121 MHz, 25 °C): δ = 27.0 (s, PPh_2) MS (FAB): *m/z* calcd for $C_{65}H_{69}O_4P_2Pd$ [*M* – pyridine – BF_4]: 1081; found: 1081.1 (expected isotopic profile); elemental analyses calcd for $C_{70}H_{74}BF_4NO_4P_2Pd$ (1248.53): C 67.34, H 5.95, N 1.12; found: C 67.41, H 6.10, N 0.93.

7 : Yield: 84 %; m.p. > 280 °C; IR (KBr): $\tilde{\nu}$(C≡O) = 2072(s) and 1995(s) cm^{-1}; ^{1}H NMR (500 MHz, CD_2Cl_2, 25 °C): δ = 8.31 – 8.28 and 7.36 – 7.34 (20 H, PPh_2), 6.82 (virtual t, 4 H, *m*-H of OArP), 6.81 and 6.65 (B_2A spin system, 6 H, *m*- and *p*-H of OAr, ^3J(A,B) = 6 Hz), 4.47 and 3.19 (AB spin sytem, 8 H, ArCH_2Ar, ^2J(A,B) = 13 Hz), 3.99 (pseudo t, 4 H,

OCH_2, $^3J \approx 8$ Hz), 3.78 (t, 4H, OCH_2, $^3J = 7$ Hz), 2.02 (m, 4H, OCH_2CH_2), 1.94 (m, 4H, OCH_2CH_2), 1.11 (t, CH_3, $^3J = 7.5$ Hz), 0.91 (t, CH_3, $^3J = 9$ Hz); $^{13}C\{^1H\}$ NMR (75 MHz, CD_2Cl_2, 25 °C): $\delta = 158.48$ and 157.75 (2s, arom.C_q–O), 135.02–123.95 (arom. C atoms), 78.47 and 76.79 (2s, OCH_2), 31.09 (s, ArCH_2), 23.95 and 23.51 (2s, CH_2CH_3), 11.05 and 10.01 (2s, CH_2CH_3), C≡O not detected; $^{31}P\{^1H\}$ NMR (121 MHz, CD_2Cl_2, 25 °C): $\delta = 12.9$ (s, PPh_2); MS (FAB): *m/z* calcd for $C_{65}H_{66}ClO_5P_2Ru$ [M – Cl – (CO)]: 1125; found: 1125.5 (expected isotopic profile); elemental analyses calcd for $C_{66}H_{66}Cl_2O_6P_2Ru$ (1189.18): C 66.66, H 5.59; found: C 66.54, H 5.63.

8: Yield: 95%; IR (KBr): $\tilde{\nu}$(C≡O) = 1924(s) cm^{-1}; ^1H NMR (500 MHz, CD_2Cl_2, 25 °C): $\delta = 7.91$–7.89 and 7.37–7.35 (20H, PPh_2), 6.86 and 6.67 (B_2A spin system, 6H, *m*- and *p*-H of OAr, $^3J(A,B) = 7.5$ Hz), 6.75 (virtual t ABXX′A′B′ spin system, 4H, *m*-H of OArP, $^3J(A,X) \approx {}^3J(B,X) \approx 5$ Hz), 4.51 and 3.22 (AB spin sytem, 8H, ArCH_2Ar, $^2J(A,B) = 13$ Hz), 4.14 (pseudo t, 4H, OCH_2, $^3J \approx 8$ Hz), 3.79 (t, 4H, OCH_2, $^3J = 7$ Hz), 2.01 (m, 4H, OCH_2CH_2), 1.95 (m, 4H, OCH_2CH_2), 1.13 (t, CH_3, $^3J = 7.5$ Hz), 0.90 (t, CH_3, $^3J = 9$ Hz); $^{31}P\{^1H\}$ NMR (121 MHz, CD_2Cl_2, 25 °C): $\delta = 42.4$ (s, PPh_2). Crystal data for $\mathbf{8} \cdot C_2H_4Cl_2$: $M_r = 1288.14$, orthorombic, space group *Pbcm*, $a = 19.4779(6)$, $b = 17.7412(3)$, $c = 17.2124(5)$ Å, $V = 5947.5(5)$ Å^3, $Z = 4$, $\rho_{calcd} = 1.44$ g cm^{-3}, $Mo_{K\alpha}$ radiation ($\lambda = 0.71073$ Å), $\mu = 0.544$ mm^{-1}. Data were collected on a Kappa CCD Enraf Nonius system at 173 K. The structure was solved by direct methods and refined on F_o^2 by full-matrix least squares. All non-hydrogen atoms were refined anisotropically. $R1 = 0.089$ and $wR2 = 0.117$ for 3296 data with $I > 3\sigma(I)$. Crystallographic data (excluding structure factors) for the structure reported in this paper have been deposited with the Cambridge Crystallographic Data Centre as supplementary publication no. CCDC-101566. Copies of the data can be obtained free of charge on application to CCDC, 12 Union Road, Cambridge CB2 1EZ, UK (fax: (+44) 1223-336-033; e-mail: deposit@ccdc.cam.ac.uk).

Received: May 8, 1998 [Z11832IE]
German version: *Angew. Chem.* **1998**, *110*, 3027–3030

Keywords: calixarenes · intercalation · phosphanes · supramolecular chemistry

[1] For example, see "Calixarenes": C. D. Gutsche in *Monographs in Supramolecular Chemistry, Vol. 1* (Ed.: J. F. Stoddart), Royal Society of Chemistry, Cambridge, **1989**; V. Böhmer, *Angew. Chem.* **1995**, *107*, 785–818; *Angew. Chem. Int. Ed. Engl.* **1995**, *34*, 713–745; M. A. van Wageningen, E. Snip, W. Verboom, D. N. Reinhoudt, H. Boerrigter, *Liebigs Ann.* **1997**, 2235–2245.

[2] For example, see R. Ungaro, A. Pochini, G. Andreeti, P. Domiano, *J. Chem. Soc. Perkin Trans. 2* **1985**, 197–201; W. Xu, R. J. Puddephatt, L. Manojlovic-Muir, K. W. Muir, C. S. Frampton, *J. Incl. Phenom.* **1994**, *19*, 277–290; V. C. Gibson, C. Redshaw, W. Clegg, M. R. J. Elsegood, *J. Chem. Soc. Chem. Commun.* **1995**, 2371–2372; J. L. Atwood, K. T. Holman, J. W. Steed, *Chem. Commun.* **1996**, 1401–1407; P. D. Beer, M. G. B. Drew, P. B. Leeson, M. I. Ogden, *Inorg. Chim. Acta* **1996**, *246*, 133–141; C. L. Raston, J. L. Atwood, P. J. Nichols, I. B. N. Sudria, *Chem. Commun.* **1996**, 2615–2616; R. Abidi, M. V. Baker, J. M. Harrowfield, D. S.-C. Ho, W. R. Richmond, B. W. Skelton, A. H. White, A. Varnek, G. Wipff, *Inorg. Chim. Acta* **1996**, *246*, 275–286; A. Ikeda, Y. Suzuki, M. Yoshimura, S. Shinkai, *Tetrahedron* **1998**, *54*, 2497–2508.

[3] A. Ikeda, S. Shinkai, *J. Am. Chem. Soc.* **1994**, *116*, 3102–3110.

[4] D. V. Khasnis, J. M. Burton, J. D. McNeil, H. Zhang, M. Lattman, *Phosphorus Sulfur Silicon* **1993**, *75*, 253–256; C. Dieleman, C. Loeber, D. Matt, A. De Cian, J. Fischer, *J. Chem. Soc. Dalton Trans.* **1995**, 3097–3100; D. M. Roundhill, *Progr. Inorg. Chem.* **1995**, *43*, 533–592; I. Neda, H.-J. Plinta, R. Sonnenburg, A. Fischer, P. G. Jones, R. Schmutzler, *Chem. Ber.* **1995**, *128*, 267–273; B. R. Cameron, S. J. Loeb, *Chem. Commun.* **1996**, 2003–2004; C. Loeber, D. Matt, P. Briard, D. Grandjean, *J. Chem. Soc. Dalton Trans.* **1996**, 513–524; C. Wieser, D. Matt, J. Fischer, A. Harriman, *J. Chem. Soc. Dalton Trans.* **1997**, 2391–2402; M. Giusti, E. Solari, L. Giannini, C. Floriani, A. Chiesi-Villa, C. Rizzoli, *Organometallics* **1997**, *16*, 5610–5612; A. Zanotti-Gerosa, E. Solari, L. Giannini, C. Floriani, A. Chiesi-Villa, C. Rizzoli, *Chem. Commun.* **1997**, 183–184; C. Wieser, C. B. Dieleman, D. Matt, *Coord. Chem. Rev.* **1997**, *165*, 93–161.

[5] A homooxacalix[4]arene-Eu complex containing a coordinated acetone molecule that is located inside the cavity has been reported: Z. Asfari, J. M. Harrowfield, M. I. Ogden, J. Vicens, A. H. White, *Angew. Chem.* **1991**, *103*, 887–889; *Angew. Chem. Int. Ed. Engl.* **1991**, *30*, 854–856.

[6] H. K. A. C. Coolen, P. W. N. M. van Leeuwen, R. J. M. Nolte, *Angew. Chem.* **1992**, *104*, 906–909; *Angew. Chem. Int. Ed. Engl.* **1992**, *31*, 905–907; M. T. Reetz, S. R. Waldvogel, *Angew. Chem.* **1997**, *109*, 870–873; *Angew. Chem. Int. Ed. Engl.* **1997**, *36*, 865–867; K. Goto, R. Okazaki, *Liebigs Ann.* **1997**, 2393–2407.

[7] M. Larsen, M. Jørgensen, *J. Org. Chem.* **1996**, *61*, 6651–6655.

[8] V. I. Kalchenko, L. I. Atamas, V. V. Pirozhenko, L. N. Markovsky, *Zh. Obshch. Khim.* **1992**, *62*, 2623–2625; S. Ozegowski, B. Costisella, J. Gloede, *Phosphorus Sulfur Silicon.* **1996**, *119*, 209–223; C. Loeber, C. Wieser, D. Matt, A. De Cian, J. Fischer, L. Toupet, *Bull. Soc. Chim. Fr.* **1995**, *132*, 166–177.

[9] M. Camalli, F. Caruso, S. Chaloupka, P. N. Kapoor, P. S. Pregosin, L. M. Venanzi, *Helv. Chim. Acta* **1984**, *67*, 1603–1611.

[10] K. Thomas, J. T. Dumler, B. W. Renoe, C. J. Nyman, D. M. Roundhill, *Inorg. Chem.* **1972**, *11*, 1795–1799.

[11] G. Bracher, D. M. Grove, L. M. Venanzi, F. Bachechi, P. Mura, L. Zambonelli, *Helv. Chim. Acta* **1980**, *63*, 2519–2530.

[12] R. Vac, J. H. Nelson, E. B. Milosavljević, L. Solujić, *Inorg. Chem.* **1989**, *28*, 3831–3836.

A New Radical Allylation Reaction of Dithiocarbonates**

Béatrice Sire, Stéphanie Seguin, and Samir Z. Zard*

In contrast to radical cyclizations, which have practically revolutionized the construction of polycyclic systems, intermolecular radical additions to olefins have had a comparatively limited impact on organic synthesis.[1] This is chiefly because of the difficulty in avoiding competing bimolecular side reactions which, in the case of intramolecular processes, can usually be controlled by the use of high dilution techniques (e.g. slow, syringe pump addition of one of the reagents). With stannane-based reactions, for example, the difficulty lies in preventing premature hydrogen atom transfer to the radical before it adds to the olefin. One special exception is the allylation reaction with allyltriorganotin.[2] In this case, the allyl transfer step is the one that regenerates the stannyl radical to propagate the chain and, even if this step is not very fast by radical reaction standards,[3] there are no other major competing pathways. This fairly general and quite useful intermolecular C–C bond forming procedure unfortunately uses tin and therefore suffers from the same drawbacks as other tin-based systems: high cost and difficulty in removing toxic organotin contaminants.[4] These are serious

[*] Dr. S. Z. Zard,[+] Dr B. Quiclet-Sire, S. Seguin
Institut de Chimie des Substances Naturelles
91198 Gif-Sur-Yvette (France)
Fax: (+33) 1-69-07-72-47

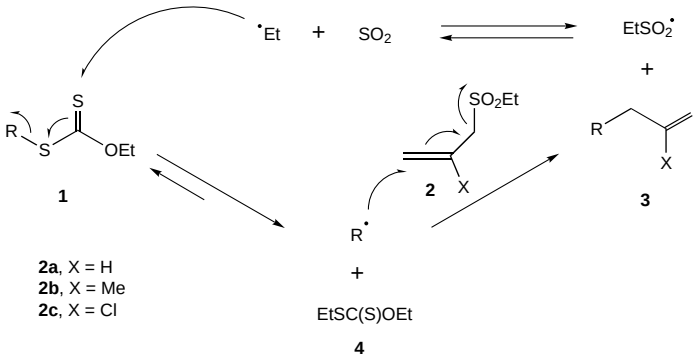
[+] Further address:
Laboratoire de Synthèse Organique associé au CNRS
Ecole Polytechnique, 91128 Palaiseau Cedex (France)
Fax: (+33) 1-69-33-30-10

[**] We wish to thank Thi-My Ly for preparing compound **1e**.

 © WILEY-VCH Verlag GmbH, D-69451 Weinheim, 1998 1433-7851/98/3720-2864 $ 17.50+.50/0

limiting factors for the large-scale application of stannane chemistry in the pharmaceutical industry. The corresponding organosilane or organogermane analogues[5] are not only more expensive, but are also less reactive. The β cleavage of the C–Si and C–Ge bond in the radical adduct is considerably slower than that of a C–Sn linkage. More recently, allyl aryl sulfones or sulfides have been examined as allylating agents, but the process still requires stoichiometric amounts of an organostannane or a distannane to generate the radical from the substrate.[6]

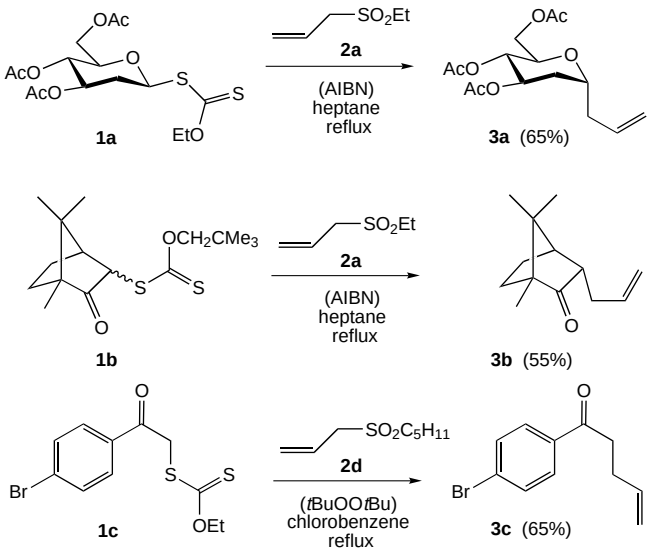
We have recently shown that it is possible to accomplish a radical allylation starting from aliphatic iodides by using allyl ethyl sulfone, without the intervention of tin or any other heavy metal.[7] Aliphatic iodides, however, are in many cases fragile and sensitive substances (e.g. anomeric iodides in sugars) that are readily degraded by a variety of ionic substitution and elimination reactions.[8] Bromides or chlorides are more robust, but react too sluggishly with ethyl radicals to propagate the chain cleanly. It seemed to us that this difficulty could perhaps be circumvented by replacing the iodide by a dithiocarbonate group (xanthate), which exhibits sufficient affinity to radicals but is less subject to ionic degradation.[9] The projected allylation sequence is summarized in Scheme 1.



Scheme 1. Radical allylation of an aliphatic xanthate with allyl ethyl sulfone.

The ethanesulfonyl radical generated in the allyl transfer step can extrude sulfur dioxide to give an ethyl radical, which is reactive enough to abstract the xanthate group from the starting material **1**. The problem of producing a carbon-centered radical is thus solved in a simple manner without using any tin-containing additives. Allyl aryl sulfones, which have previously been used as radical allylating agents,[6] produce arenesulfonyl radicals, $ArSO_2^{\bullet}$; these do not fragment to give aryl radicals and therefore cannot propagate the chain.[10]

Xanthate **1a** was easily prepared by treating the corresponding bromide with commercially available potassium *O*-ethyl xanthate. In contrast to its iodo analogue, this nicely crystalline compound can be handled and stored without any difficulty. We were pleased to find that, upon heating with a threefold excess of allyl ethyl sulfone in refluxing heptane using azoisobutyronitrile (AIBN) as initiator, the expected, and previously known,[11] 1α-allyl 2-deoxyglucose derivative **3a** was smoothly produced in 65% yield. The stereochemistry is in line with earlier observations on the addition of radicals at the anomeric position.[12] In the same way, neopentyl xanthate **1b** derived from camphor afforded the corresponding allylated product (Scheme 2).

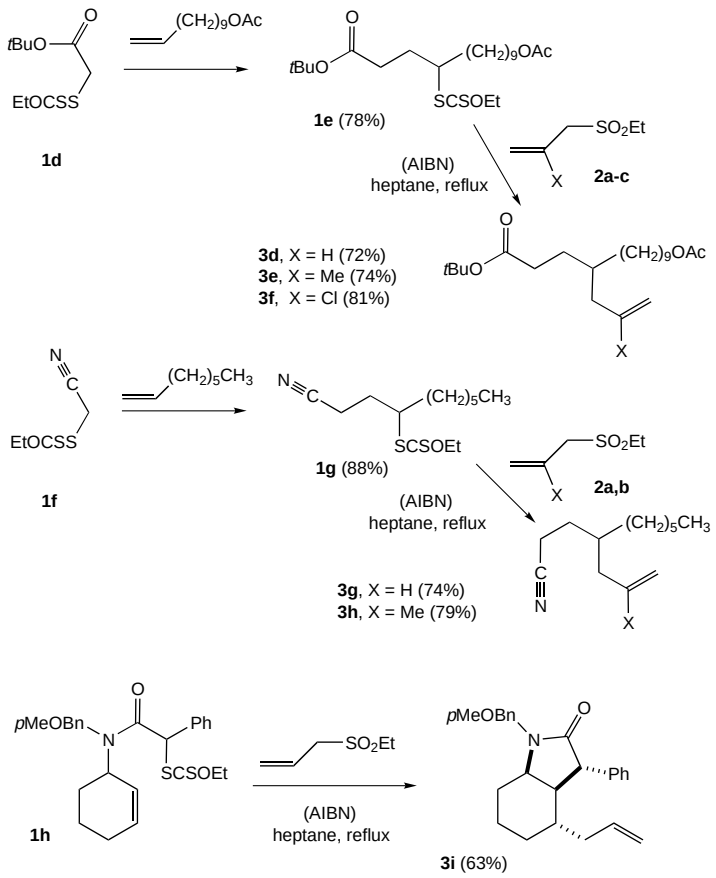


Scheme 2. Examples of radical allylation of xanthates with allyl ethyl and allyl pentyl sulfone.

If needed, a few drops of chlorobenzene may be added to the heptane to improve solubility; alternatively, chlorobenzene alone may be used in conjunction with di-*tert*-butyl peroxide as the initiator because of its longer lifetime at the higher reflux temperature. The latter conditions are illustrated by the conversion of *p*-bromophenacyl xanthate **1c** into the allylated product **3c** with use of allyl *n*-pentyl sulfone (**2d**). Even though this allylating reagent proved equally efficient in terms of yield (a pentyl radical now replaces the ethyl radical in Scheme 1), it is less volatile than **2a** and therefore less easily removed from the reaction mixture.

Another important advantage of using a xanthate precursor is that it is possible to combine the radical allylation with a xanthate transfer to introduce two new C–C bonds across an unactivated olefinic bond.[9] For example, radical addition of xanthate **1d** to 10-undecylenyl acetate gave **1e** (78%), which was readily converted into **3d** in 72% yield with allyl ethyl sulfone. It is worth stressing that such a transformation would be difficult to accomplish through the corresponding iodides. Kharasch-type additions of iodoacetates are capricious and often require the presence of hexabutyldistannane to ensure reproducibility.[1c, 13c] Moreover, the reaction frequently leads to γ-lactones by ionic ring closure through substitution of the iodine in the adduct by the carbonyl oxygen atom of the ester.[13] The conversion of octene into **1g** by addition of xanthate **1f** (derived from chloroacetonitrile) followed by allylation is another example.

The reactions in Scheme 3 show that this new allylation procedure can be extended to include allyl groups substituted in the 2-position by chlorine or a methyl group (**3e**, **3f**, and **3h**) and presumably a variety of other substituents. This opens



Scheme 3. Xanthate transfer followed by radical allylation with allyl ethyl sulfone.

up many opportunities for further modifications. The 2-chloroallyl group (in **3f**) is especially interesting in this respect since it can be converted into an acetylene by simple treatment with base.[14] Finally, the allylation may be preceded by a cyclization step as shown by the direct transformation of xanthate **1h** into **3i** (63%). Only one diasteriomer is obtained for which the stereochemistry shown is tentatively assigned on the basis of its NMR spectrum. Unlike the intermolecular examples discussed above, there is no need in this case to isolate the intermediate xanthate.

We have described here a new, flexible radical process for grafting various allyl appendages without recourse to toxic or expensive reagents. The starting xanthates are readily available either by traditional nucleophilic substitutions with xanthate salts or by a radical xanthate transfer reaction. The latter approach is especially appealing because it allows the expedient construction of complex frameworks from simple unactivated olefins.

Experimental Section

Typical experimental procedure: Under an inert atmosphere AIBN is added portionwise over several hours to a refluxing solution of the xanthate (1 mmol) and the appropriate allyl sulfone (3 mmol) in degassed heptane (4 mL; a few drops of chlorobenzene may be added to aid solubility if necessary). The reaction mixture is concentrated under vacuum, and excess allyl ethyl sulfone removed by passing a stream of dry air over the warmed (50–60 °C) residue. This treatment also eliminates the relatively volatile diethyl xanthate coproduct **4**. Finally, chromatography on silica furnishes the desired product. If chlorobenzene alone is used as the solvent, then di-*tert*-butyl peroxide is the preferred initiator.

Received: May 11, 1998 [Z11841IE]
German version: *Angew. Chem.* **1998**, *110*, 3056–3058

Keywords: allylations · allyl sulfones · C–C coupling · radical reactions · xanthate

[1] a) B. Giese, *Radicals in Organic Synthesis: Formation of Carbon–Carbon Bonds*, Pergamon, Oxford, **1986**; b) B. Giese, B. Kopping, B. T. Göbel, J. Dickhaut, G. Thoma, K. J. Kulicke, F. Trach, *Org. React.* **1996**, *48*, 301–856; c) D. P. Curran in *Comprehensive Organic Synthesis*, Vol. 4 (Eds.: B. M. Trost, I. Fleming), Pergamon, Oxford, **1991**, pp. 715–831; D. P. Curran, *Synthesis* **1988**, 417–439, 489–513.

[2] a) C. Servens, M. Pereyre, *J. Organomet. Chem.* **1971**, *26*, C4–C6; b) J. Grignon, M. Pereyre, *J. Organomet. Chem.* **1973**, *61*, C33–C35; c) J. Grignon, C. Servens, M. Pereyre, *J. Organomet. Chem.* **1975**, *96*, 225–235; d) M. Kosugi, K. Kurino, K. Takayama, T. Migita, *J. Organomet. Chem.* **1973**, *56*, C11–C13; e) G. E. Keck, J. B. Yates, *J. Org. Chem.* **1982**, *47*, 3590–3591; f) G. E. Keck, E. J. Enholm, J. B. Yates, M. R. Wiley, *Tetrahedron* **1985**, *41*, 4079–4094; g) G. E. Keck, J. H. Byers, *J. Org. Chem.* **1985**, *50*, 5442–5444; h) J. E. Baldwin, R. M. Adlington, C. Lowe, I. A. O'Neil, G. L. Sanders, C. J. Schofield, J. B. Sweeney, *J. Chem. Soc. Chem. Commun.* **1988**, 1030–1031; i) J. E. Baldwin, R. M. Adlington, D. J. Birch, C. J. A. Crawford, J. B. Sweeney, *J. Chem. Soc. Chem. Commun.* **1986**, 1339–1340; j) G. A. Russell, L. L. Herold, *J. Org. Chem.* **1985**, *50*, 1037–1040; k) K. Mizuno, M. Ikeda, S. Toda, Y. Otsuji, *J. Am. Chem. Soc.* **1988**, *110*, 1288–1290; l) H. Fliri, C.-P. Mak, *J. Org. Chem.* **1985**, *50*, 3438–3442; m) M.-Y. Chen, J.-M. Fang, Y.-M. Tsai, R.-L. Yeh, *J. Chem. Soc. Chem. Commun.* **1991**, 1603–1604; n) D. L. J. Clive, C. Chua Paul, Z. Wang, *J. Org. Chem.* **1997**, *62*, 7028–7032.

[3] D. P. Curran, P. A. van Elburg, B. Giese, S. Giliges, *Tetrahedron Lett.* **1990**, *31*, 2861–2864.

[4] a) M. Pereyre, J.-P. Quintard, A. Rahm, *Tin in Organic Synthesis*, Butterworths, London, **1987**; b) W. P. Neumann, *The Organic Chemistry of Tin*, Wiley, London, **1970**.

[5] a) J. P. Light, M. Ridenour, L. Beard, J. W. Hershberger, *J. Organomet. Chem.* **1987**, *326*, 17–24; b) M. Kosugi, H. Kurata, K. Kawata, T. Migita, *Chem. Lett.* **1991**, 1327–1328; c) C. Chatgilialoglu, C. Ferreri, M. Ballestri, D. P. Curran, *Tetrahedron Lett.* **1992**, *32*, 6387–6390.

[6] a) F. Pontén, G. Magnusson, *J. Org. Chem.* **1996**, *61*, 7463–7466; b) D. P. Curran, B. Yoo, *Tetrahedron Lett.* **1992**, *33*, 6931–6934; c) C. Chatgilialoglu, A. Alberti, M. Ballestri, D. Macciantelli, D. P. Curran, *Tetrahedron Lett.* **1996**, *37*, 6391–6394.

[7] F. Le Guyader, B. Quiclet-Sire, S. Seguin, S. Z. Zard, *J. Am. Chem. Soc.* **1997**, *119*, 7410–7411.

[8] R. D. Chambers, S. R. James in *Comprehensive Organic Chemistry, Vol. 1* (Eds.: D. H. R. Barton, W. D. Ollis), Pergamon, Oxford, **1979**, pp. 493–575.

[9] S. Z. Zard, *Angew. Chem.* **1997**, *109*, 724–737; *Angew. Chem. Int. Ed. Engl.* **1997**, *36*, 672–685.

[10] a) C. Chatgilialoglu in *The Chemistry of Sulfones and Sulfoxides* (Eds.: S. Patai, Z. Rappoport, C. J. M. Stirling) Wiley, Chichester, **1988**, pp. 1089–1113; b) M. Bertrand, *Org. Prep. Proc. Int.* **1994**, *26*, 257–290.

[11] S. Danishefsky, J. K. Kerwin Jr., *J. Org. Chem.* **1982**, *47*, 3803–3805.

[12] B. Giese, J. Dupuis, *Angew. Chem.* **1983**, *95*, 633; *Angew. Chem. Int. Ed. Engl.* **1983**, *22*, 622–623.

[13] a) M. S. Kharasch, P. S. Skell, P. Fischer, *J. Am. Chem. Soc.* **1948**, *70*, 1055–1059; b) G. A. Kraus, K. Landgrebe, *Tetrahedron* **1985**, *41*, 4039–4046; c) M. Degueil-Castaing, B. DeJeso, G. A. Kraus, K. Landgrebe, B. Maillard, *Tetrahedron Lett.* **1986**, *27*, 5927–5930; d) D. P. Curran, C.-T. Chang, *J. Org. Chem.* **1989**, *54*, 3140–3157.

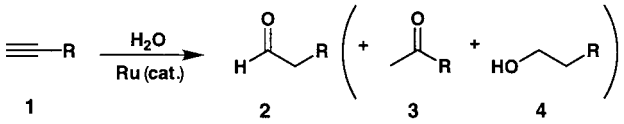
[14] For a recent example, see H.-J. Liu, D. Sun, *Tetrahedron Lett.* **1997**, *38*, 6159–6162.

 © WILEY-VCH Verlag GmbH, D-69451 Weinheim, 1998 1433-7851/98/3720-2866 $ 17.50+.50/0

The First Anti-Markovnikov Hydration of Terminal Alkynes: Formation of Aldehydes Catalyzed by a Ruthenium(II)/Phosphane Mixture

Makoto Tokunaga and Yasuo Wakatsuki*

The use of water as a reagent in organic synthesis is an important topic from the viewpoint of economics, safety, and the environment.[1] For example, metal-catalyzed hydration of alkynes provides an important route to carbonyl compounds. Since all known additions of water to terminal alkynes follow Markovnikov's rule, the hydration of 1-alkynes with Hg^{II}/acid,[2] Au^{III},[3] Ru^{III},[4] $RhCl_3$,[5] Pt^{II},[6] or other metal catalysts[7] leads exclusively to ketones.[2] We report herein a novel hydration of terminal alkynes catalyzed by Ru^{II} complexes, which in the presence of appropriate auxiliary phosphane ligands leads to predominantly anti-Markovnikov addition of water and yields aldehydes with only a small amount of ketones (Scheme 1).



a, R = *n*-C_4H_9 **e**, R = Ph
b, R = *n*-C_6H_{13} **f**, R = CH_2Ph
c, R = *n*-$C_{10}H_{21}$ **g**, R = $(CH_2)_3Cl$
d, R = *t*-C_4H_9 **h**, R = $(CH_2)_2OCH_2Ph$

Scheme 1. Ru-catalyzed anti-Markovnikov hydration of terminal alkynes.

In preliminary experiments, hydration of 1-octyne (**1b**) in aqueous ethanol in the presence of 5 mol% of $[RuCl_2(C_6H_6)(PPh_3)]$[8] as the catalyst precursor gave carbonyl products in 74% yield with an aldehyde/ketone ratio of 1/8 (Table 1, method D). Addition of PPh_3 to the initial reaction mixture inverted the aldehyde/ketone ratio to 5/1 but also lowered the efficiency of the reaction, so that the aldehyde was obtained in less than 10% yield. We investigated about 20 different phosphanes under various reaction conditions, two of which, $PPh_2(C_6F_5)$ and $P(3\text{-}C_6H_4SO_3Na)_3$, led to selective anti-Markovnikov addition of water and satisfactory yields of aldehydes.

The optimum conditions for the reaction with the fluorinated phosphane involve the addition of 10 mol% of $[RuCl_2(C_6H_6)\{PPh_2(C_6F_5)\}]$ and 30 mol% of $PPh_2(C_6F_5)$ to a solution of a 1-alkyne in aqueous 2-propanol (method A). Hydration of **1b** gave 1-octanal (**2b**) in 75% yield together with only 4.5% of methyl hexyl ketone, as determined by GLC analysis (Table 1). This method is applicable not only to other simple 1-alkynes (**1a**, **1c**), but also to substrates with a phenyl (**1f**), chloro (**1g**), or benzyl ether group (**1h**). The highest aldehyde selectivity, (aldehyde/ketone ratio of 67/1) was achieved with **1g**. In contrast, *tert*-butylacetylene (**1d**) and phenylacetylene (**1e**) gave only traces of aldehyde; this shows the steric limitations of this system. When $[RuCl_2(C_6H_6)\{PPh_2(C_6F_5)\}]$ and 3 equiv of $PPh_2(C_6F_5)$ were heated in 2-propanol to the reaction temperature (80 °C), the C_6H_6 ligand was liberated, as monitored by ^1H NMR spectroscopy. Hence, the initial active species in the catalytic cycle under the conditions of method A is probably of the type $[RuCl_2\{PPh_2(C_6F_5)\}_x]$.[9]

Table 1. Hydration of terminal alkynes **1a**–**h** under the conditions of methods A–D.

Substrate	Method[a]	T [°C]	t [h]	Yield [%][b] **2**	**3**	**4**	**2/3**
1a	A	65	12	71	3.0		24/1
1b	A	65	12	75	4.5		17/1
1b	B	100	40	45(41)	4.5	8.8	10/1
1b	C	100	40		6.1	61(58)	10/1[c]
1b	D	100	14	8.0	66		1/8
1c	A	80	7	51(50)	3.9		13/1
1c	B	100	36	40	4.4	1.2	9/1
1c	C	100	43		5.3	53(53)	10/1[c]
1d	A	80	18	0.9			1/0
1e	A	80	20	0.7	0.7		1/1
1e	D	100	24		41		0/1
1f	A	70	12	65	7.0	2.8	9/1
1f	C	80	42	2.2	6.3	59	9/1[c]
1f	D	80	22	4.3	58		1/13
1g	A	70	40	60	0.9		67/1
1h	A	80	12	67 (62)	7.2		9/1
1h	D	80	24	3.6	58 (56)		1/16

[a] Method A: $[RuCl_2(C_6H_6)\{PPh_2(C_6F_5)\}] + 3\,PPh_2(C_6F_5)$ in 2-propanol. Method B: $[RuCl_2(C_6H_6)]_2 + 8\,P(3\text{-}C_6H_4SO_3Na)_3$ in 2-methoxyethanol. Method C: $[RuCl_2(C_6H_6)]_2 + 8\,P(3\text{-}C_6H_4SO_3Na)_3$ in ethanol or 2-propanol. Method D: $[RuCl_2(C_6H_6)(PPh_3)]$ in ethanol or 2-propanol. [b] GLC yield; yield of isolated product in parentheses. [c] **4/3**.

The water-soluble ligand $P(3\text{-}C_6H_4SO_3Na)_3$ (TPPTS) is also a good auxiliary ligand. The use of $[RuCl_2(C_6H_6)]_2$ (5 mol%), TPPTS (40 mol%), and 2-methoxyethanol as the solvent (method B) gave aldehyde/ketone ratios of 9/1 to 10/1 and the hydrated products in 40–45% yield (Table 1). With ethanol or 2-propanol as solvent (method C), the aldehydes were reduced to primary alcohols, while ketones remained inert under these reaction conditions. Detection of acetaldehyde diethyl acetal in the reaction mixture indicates a Meerwein–Ponndorf–Verley type reduction mechanism. Use of the water-soluble phosphane has a practical advantage: The catalyst can easily be recovered after the reaction by using a two-phase system.[10]

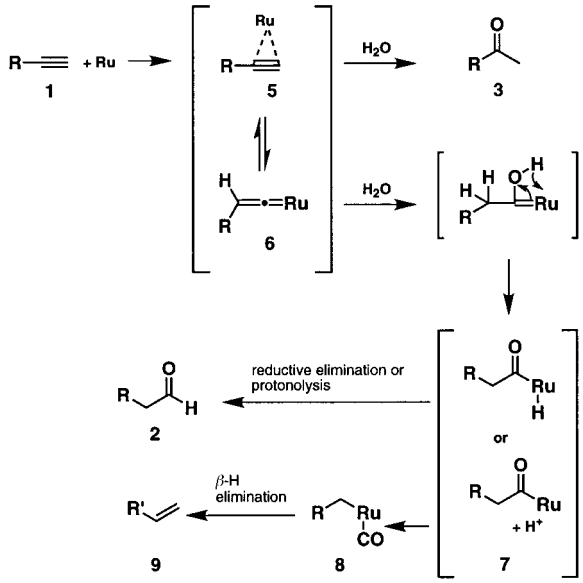
Although this reaction represents, to the best of our knowledge, the first example of the hydration of 1-alkynes to aldehydes, some related stoichiometric reactions are known in the coordination chemistry of vinylidenes, which are tautomers of 1-alkynes.[11] Bruce et al.[11b] observed that the reaction of the cationic phenylvinylideneruthenium complex $[Ru(C{=}CHPh)(PPh_3)(L)(\eta^5\text{-}C_5H_5)]^+$ with water gave the neutral phenylacetyl complex $[Ru(COCH_2Ph)(PPh_3)(L)(\eta^5\text{-}C_5H_5)]$ (L = CO) or the benzyl carbonyl complex $[Ru(CH_2Ph)(CO)(L)(\eta^5\text{-}C_5H_5)]$ (L = PPh_3). A similar reaction takes place in a related iron complex.[11a] The reaction mechanism was recently investigated in detail by Bianchini et al.[11g] Intramolecular attack of coordinated water on the vinylidene ligand gives a hydroxycarbene, which is deproto-

[*] Dr. Y. Wakatsuki, Dr. M. Tokunaga
The Institute of Physical and Chemical Research (RIKEN)
Wako-shi, Saitama, 351-0198 (Japan)
Fax: (+81) 48-462-4665
E-mail: waky@postman.riken.go.jp

 © WILEY-VCH Verlag GmbH, D-69451 Weinheim, 1998 1433-7851/98/3720-2867 $ 17.50+.50/0

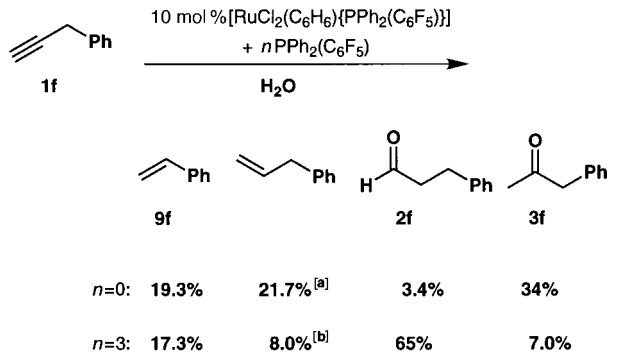
nated to a phenylacetylruthenium species, decarbonylation of which gives a benzylruthenium intermediate. Notably, they detected phentylacetaldehyde by GC/MS when the phenylvinylideneruthenium complex was hydrated under CO (30 atm). The highly electrophilic nature of vinylidene C_α atoms and their empty p orbital are well documented by reactions with nucleophiles[12] and by theoretical studies.[13]

It is therefore likely that the present ruthenium-catalyzed hydration of terminal alkynes involves the initial tautomerization of 1-alkyne complex **5** to the vinylidene complex **6** followed by the attack of the oxygen atom of water at the vinylidene C_α atom to form the hydroxycarbene intermediate and then the acyl intermediate **7** (Scheme 2). The formation of



Scheme 2. Proposed reaction path for Ru-catalyzed hydration.

ketones by metal-catalyzed hydration of alkynes, on the other hand, involves the nucleophilic attack of H_2O on a η^2-coordinated alkyne with Markovnikov regioselectivity (**5** → **3** in Scheme 2).[2, 4c, 5, 6b, 7b] The C–C bond cleavage or decarbonylation reaction **7** → **8** is expected to occur together with the main reaction, formation of aldehyde, since it is a highly facile reaction path in the stoichiometric systems of Bruce et al. and Bianchini et al. Indeed, olefins with one less carbon atom were always detected by GC in our catalytic system. Most evident in this respect was the hydration of **1f**, which gave up to 17% of styrene (**9f**) as the major by-product under the conditions of method A (Scheme 3). The amount of **9f** increased, albeit by only a few percent, when the reaction was carried out without additional phosphane; the major product was ketone **3f**. We confirmed further that aldehyde **2f**, once formed, is not decarbonylated: When the hydration of **1b** was carried out in the presence of **2f**, the aldehyde remained intact, and no styrene was formed. The ruthenium-containing solid recovered after the reaction showed IR absorption bands for coordinated CO ligands (1970–2070 cm^{-1}). All of these observations are in accord with the proposed reaction path of Scheme 2.



Scheme 3. Influence of the addition of phosphane on the yields of products in the hydration of **1f**. [a] Contains 6.2% β-methylstyrene. [b] Contains 2.1% β-methylstyrene.

We believe that the role of the added phosphane is to shift the equilibrium between **5** and **6** in favor of the vinylidene complex and to retard the decarbonylation of the intermediate **7**. A pronounced effect of the amount and type of added phosphane ligands was noted previously in a Ru^{II}-catalyzed dimerization of a terminal acetylene, in which tautomerization of the 1-alkyne to the corresponding vinylidene plays an important role, as in the present case.[14]

Experimental Section

All reactions were carried out under an atmosphere of argon. $[RuCl_2(C_6H_6)\{PPh_2(C_6F_5)\}]$ was synthesized by a procedure similar to that for $[RuCl_2(C_6H_6)(PPh_3)]$.[8] ^1H NMR (270 MHz, $CDCl_3$): $\delta = 5.55$ (s, 6H, C_6H_6), 7.34–7.50, 7.80–7.92 (m, 10H, $PPh_2(C_6F_5)$); ^{31}P NMR (162 MHz, $CDCl_3$): $\delta = 17.0$ (t, $J = 10.3$ Hz); elemental analysis calcd for $C_{24}H_{16}Cl_2F_5PRu$: C 47.85, H 2.68; found C 47.44, H 2.69.

Method A: 1-Octyne (110.2 mg, 1.0 mmol) was added to a mixture of $[RuCl_2(C_6H_6)\{PPh_2(C_6F_5)\}]$ (60.2 mg, 0.1 mmol) and $PPh_2(C_6F_5)$ (105.7 mg, 0.3 mmol) in 2-propanol/water (2.5/0.75 mL). The mixture was stirred for 12 h at 65 °C, then Et_2O (5 mL) was added, and the solution was dried with Na_2SO_4. Yields were determined by GC (nonane as internal standard).

Method C: $[RuCl_2(C_6H_6)]_2$ (25.0 mg, 0.05 mmol) and $P(3\text{-}C_6H_4SO_3Na)_3$ (227.4 mg, 0.4 mmol) were stirred for 3 min at 100 °C in water (1.25 mL), then 1-octyne (110.2 mg, 1.0 mmol) and ethanol (1.25 mL) were added, and the mixture was stirred for 40 h at 100 °C . Et_2O (5 mL) was added, and the organic layer was separated. The products were separated by column chromatography on silica gel (hexane/Et_2O 1/1) to give pure 1-octanol (75.5 mg, 58%).

All the organic products obtained in this study are known. Authentic samples were commercially available for all compounds except for **3f** and **2g** (both synthesized from the corresponding alcohols) and **2h** (characterized by GC/MS and ^1H and ^{13}C NMR spectroscopy; data are consistent with those reported in R. Baudouy, P. Prince *Tetrahedron* **1989**, *45*, 2067).

Received: May 18, 1998 [Z11874IE]
German version: *Angew. Chem.* **1998**, *110*, 3024–3027

Keywords: aldehydes · alkynes · homogeneous catalysis · hydration · ruthenium

[1] For example, see M. Tokunaga, J. F. Larrow, F. Kakiuchi, E. N. Jacobsen, *Science* **1997**, *277*, 936.
[2] R. C. Larock, W. W. Leong in *Comprehensive Organic Synthesis*, *Vol. 4* (Eds.: B. M. Trost, I. Flemming, M. F. Semmelhock), Pergamon Press, Oxford, **1991**, p. 269; J. March, *Advanced Organic Chemistry*, Wiley, New York, **1992**, p. 762.
[3] Y. Fukuda, K. Utimoto, *J. Org. Chem.* **1991**, *56*, 3729.

 © WILEY-VCH Verlag GmbH, D-69451 Weinheim, 1998 1433-7851/98/3720-2868 $ 17.50+.50/0

[4] a) J. Halpern, B. R. James, A. L. W. Kemp, *J. Am. Chem. Soc.* **1961**, *83*, 4097; b) J. Halpern, B. R. James, A. L. W. Kemp, *J. Am. Chem. Soc.* **1966**, *88*, 5142; c) M. M. Taqui Khan, S. B. Halligudi, S. Shukla, *J. Mol. Cat.* **1990**, *58*, 299.

[5] J. Blum, H. Huminer, H. Alper, *J. Mol. Catal.* **1992**, *75*, 153.

[6] a) W. Hiscox, P. W. Jennings, *Organometallics* **1990**, *9*, 1997; b) J. W. Hartman, W. C. Hiscox, P. W. Jennings, *J. Org. Chem.* **1993**, *58*, 7613.

[7] a) N. X. Hu, Y, Aso, T. Otsubo, F. Ogura, *Tetrahedron Lett.* **1986**, *27*, 6099; b) I. K. Meier, J. A. Marsella, *J. Mol. Catal.* **1993**, *78*, 31.

[8] M. A. Bennett, A. K. Smith, *J. Chem. Soc. Dalton Trans.* **1974**, 233.

[9] The complex $[RuCl_2(PPh_2(C_6F_5))_3]$ was prepared separately and showed similar catalytic activity without added phosphane. The catalytic activity, however, was lower than that of the catalyst system of method A.

[10] W. A. Herrmann, C. W. Kohlpaintner, *Angew. Chem.* **1993**, *105*, 1588; *Angew. Chem. Int. Ed. Engl.* **1993**, *32*, 1524.

[11] a) O. M. Abu Salah, M. I. Bruce, *J. Chem. Soc. Dalton Trans.* **1974**, 2302; b) M. I. Bruce, A. G. Swincer, *Aust. J. Chem.* **1980**, *33*, 1471; c) B. P. Sullivan, R. S. Smythe, E. M. Kober, T. J. Meyer, *J. Am. Chem. Soc.* **1982**, *104*, 4701; d) C. Mountassir, T. B. Hadda, H. L. Bozec, *J. Organomet. Chem.* **1990**, *388*, C13; e) S. G. Davies, J. P. Mcnally, A. J. Smallridge, *Adv. Organomet. Chem.* **1990**, *30*, 1; f) W. Knaup, H. Werner, *J. Organomet. Chem.* **1991**, *411*, 471; g) C. Bianchini, J. A. Casares, M. Peruzzini, A. Romerosa, F. Zanobini, *J. Am. Chem. Soc.* **1996**, *118*, 4585; h) G. Poignant, F. Martin, V. Guerchais, *Synlett* **1997**, 913.

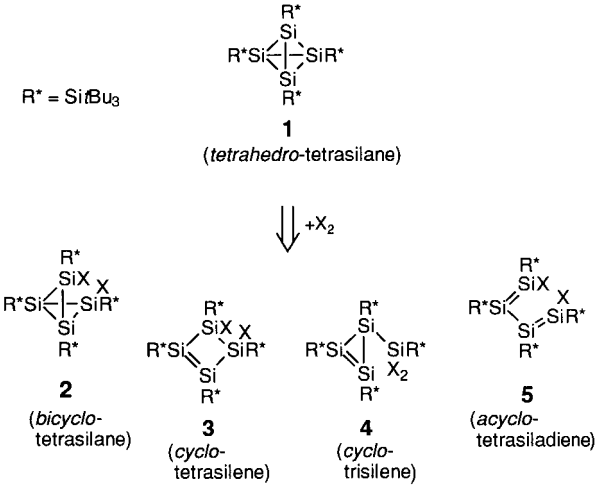
[12] M. I. Bruce, *Chem. Rev.* **1991**, *91*, 197; R. Mahé, Y. Sasaki, C. Bruneau, P. H. Dixneuf, *J. Org. Chem.* **1989**, *54*, 1518; B. M. Trost, G. Dyker, R. J. Kulawiec, *J. Am. Chem. Soc.* **1990**, *112*, 7809; C. A. Merlic, M. E. Pauly *J. Am. Chem. Soc.* **1996**, *118*, 11319.

[13] N. M. Kostić, R. F. Fenske, *Organometallics* **1982**, *1*, 974; Y. Wakatsuki, N. Koga, H. Yamazaki, K. Morokuma, *J. Am. Chem. Soc.* **1994**, *116*, 8105; Y. Wakatsuki, N. Koga, H. Werner, K. Morokuma, *J. Am. Chem. Soc.* **1997**, *119*, 360.

[14] Y. Wakatsuki, H. Yamazaki, N. Kumegawa, T. Satoh, J. Y. Satoh, *J. Am. Chem. Soc.* **1991**, *113*, 9604.

tions. Compound **1** turned out to be more susceptible towards oxidizing agents; initially, however, the tetrahedrane could only be oxidized to complex product mixtures. We have now found that upon reaction with iodine in equimolar amounts at room temperature, **1** quantitatively yields a compound with the molecular formula $R^*_4Si_4I_2$, whose structure, reactivity, and synthesis are described here.

As long as migrations of the supersilyl groups during the iodination of $R^*_4Si_4$ are excluded, the four isomeric structures **2**–**5** (X = I) are possible for $R^*_4Si_4I_2$ (Scheme 1). A *bicyclo*-tetrasilane of type **2** was first proven by Masamune et al. in the



Scheme 1. Possible structural isomers for the molecular formula $R^*_4Si_4X_2$.

Diiodotetrasupersilylcyclotetrasilene (tBu$_3$Si)$_4$Si$_4$I$_2$—A Molecule Containing an Unsaturated Si$_4$ Ring**

Nils Wiberg,* Harald Auer, Heinrich Nöth, Jörg Knizek, and Kurt Polborn

A few years ago we were able to synthesize the first molecular silicon compound containing a Si_4 tetrahedron, the orange tetrasupersilyl-*tetrahedro*-tetrasilane $R^*_4Si_4$ (**1**; R* = tri-*tert*-butylsilyl, SitBu$_3$, supersilyl).[1] We noted at the time that **1** is very stable towards water, air, light, and high temperatures and cannot be reduced by sodium even in the presence of [18]crown-6 in benzene under standard conditions. Compound **1** turned out to be more susceptible towards oxidizing agents; initially, however, the tetrahedrane could only be oxidized to complex product mixtures. We have now found that upon reaction with iodine in equimolar amounts at room temperature, **1** quantitatively yields a compound with the molecular formula $R^*_4Si_4I_2$, whose structure, reactivity, and synthesis are described here.

As long as migrations of the supersilyl groups during the iodination of $R^*_4Si_4$ are excluded, the four isomeric structures **2**–**5** (X = I) are possible for $R^*_4Si_4I_2$ (Scheme 1). A *bicyclo*-tetrasilane of type **2** was first proven by Masamune et al. in the form of the pale yellow species tBu$_2$(2,6-Et$_2$C$_6$H$_3$)$_4$Si$_4$ (the tBu groups are located on the central Si atoms of the "Si$_4$ butterfly").[2] We prepared a further species of type **2**, colorless $R^*_4H_2Si_4$ (X = H in **2**).[3] The deep orange, air-sensitive (tBuMe$_2$Si)$_6$Si$_4$ obtained by Kira et al. in low yields represents a *cyclo*-tetrasilene of type **3**.[4] Upon irradiation, it is supposed to rearrange to a red-brown *bicyclo*-tetrasilane isomer **2**, which in the dark slowly reverts to **3**. The red-brown species (2,4,6-iPr$_3$C$_6$H$_2$)$_6$Si$_4$, recently synthesized by Weidenbruch et al.,[5] represents a tetrasiladiene of type **5**. A *cyclo*-trisilene of type **4** has so far only been obtained as the homologous germanium compound $R^*_4Ge_3$ (Ge instead of Si and R* instead of SiX_2R^* in **4**).[6]

$R^*_4Si_4I_2$ crystallizes from benzene at room temperature in the form of red-orange, light- and moisture-sensitive platelets which are stable in air. They melt with decomposition at 128–130 °C. The structure of this compound is presented in Figure 1. It was obtained by an X-ray structure analysis of a crystal (monoclinic, space group $P2_1/c$) that also contained one molecule of benzene per molecule of $R^*_4Si_4I_2$.[7] According to the analysis, $R^*_4Si_4I_2$ exhibits the structure **3** (X = I) and can be termed 1,2-diiodo-1,2,3,4-tetrasupersilylcyclotetrasil-3-ene. The central structural element, which has not been observed before, is a bent unsaturated Si_4 ring with iodine substituents (angle between the planes Si1-Si2-Si3/Si3-Si4-Si1 27.8° and Si2-Si3-Si4/Si4-Si1-Si2 28.1°). The Si=Si distance is 2.257(2) Å and is therefore similar to that in the disilene (iPr$_3$Si)$_4$Si$_2$ (2.251(1) Å), which carries very bulky substitu-

[*] Prof. Dr. N. Wiberg, Dipl.-Chem. H. Auer, Prof. Dr. H. Nöth, Dipl.-Chem. J. Knizek, Dr. K. Polborn
Institut für Anorganische Chemie der Universität
Meiserstrasse 1, D-80333 München (Germany)
Fax: (+49)-89-5902-578

[**] Compounds of Silicon, Part 124. Unsaturated Compounds of Silicon and Its Homologues, Part 53. Sterically Overloaded Compounds of Silicon, Part 17. This research was supported by the Deutsche Forschungsgemeinschaft. Parts 123 and 52: N. Wiberg, S. Wagner, S.-K. Vasisht, *Chem. Eur. J.*, in press; part 16: N. Wiberg, K. Amelunxen, H.-W. Lerner, H. Nöth, J. Knizek, I. Krossing, *Z. Naturforsch. B.* **1998**, *53*, 333.

 © WILEY-VCH Verlag GmbH, D-69451 Weinheim, 1998 1433-7851/98/3720-2869 $ 17.50+.50/0

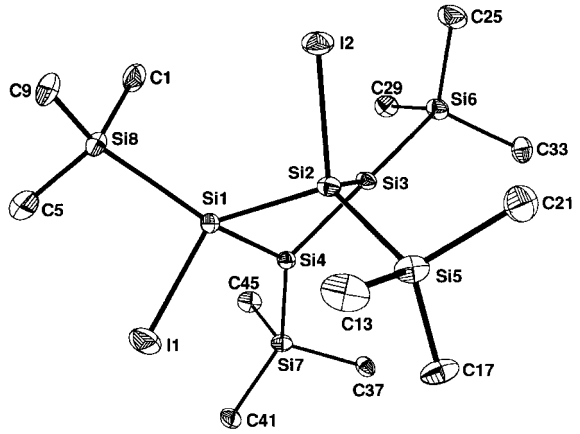
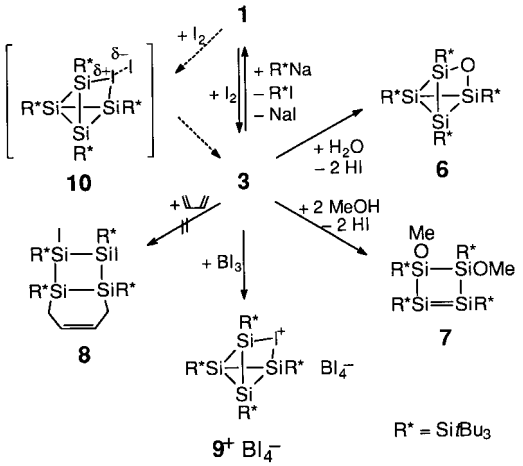


Figure 1. Crystal structure of $\mathbf{3}\cdot C_6H_6$ showing the atom labeling scheme (ORTEP plot, 25% thermal probability ellipsoids; for clarity, methyl groups are not shown). Selected interatomic distances [Å] and angles [°]: Si1–Si2 2.406(2), Si2–Si3 2.379(2), Si3–Si4 2.257(2), Si1–Si4 2.377(2), Si1–Si8 2.527(2), Si2–Si5 2.544(2), Si3–Si6 2.505(2), Si4–Si7 2.504(2), Si1–I1 2.544(2), Si2–I2 2.554(1), Si–C (av) 1.95; Si2-Si1-Si4 84.77(8), Si2-Si1-Si8 126.41(8), Si4-Si1-Si8 124.82(9), Si1-Si2-Si3 84.96(7), Si1-Si2-Si5 125.17(8), Si3-Si2-Si5 122.61(9), Si2-Si3-Si4 88.10(8), Si2-Si3-Si6 135.06(8), Si4-Si3-Si6 136.04(8), Si1-Si4-Si3 88.40(7), Si1-Si4-Si7 135.02(9), Si3-Si4-Si7 136.14(9), Si2-Si1-I1 108.63(7), Si4-Si1-I1 111.55(7), Si8-Si1-I1 100.26(7), Si1-Si2-I2 110.27(7), Si3-Si2-I2 111.64(6), Si5-Si2-I2 101.88(6), C-Si-C (av) 110.8; Si1-Si4-Si3-Si6 142.3, Si6-Si3-Si4-Si7 44.9, Si7-Si4-Si3-Si2 144.7, Si2-Si3-Si4-Si1 28.1, Si4-Si1-Si2-Si3 26.4, Si3-Si2-Si1-Si8 103.8, Si8-Si1-Si2-I2 7.5, I2-Si2-Si1-I1 111.4, I1-Si1-Si2-Si5 10.6, Si5-Si2-Si1-Si4 100.4, Si4-Si1-Si2-Si3 26.4. Crystal structure of $\mathbf{7}\cdot C_6D_6$ (not shown; OMe instead of I in Figure 1). Only the Si and O layers can be described with sufficient accuracy. Selected interatomic distances [Å] and angles [°]: Si1–Si2 2.427, Si1–Si4/Si2–Si3 2.387, Si3–Si4 2.258, Si1–Si8/Si2–Si5 2.465, Si3–Si6/Si4–Si7 2.473, Si1–01/Si2–O2 1.632; Si2-Si1-Si4/Si1-Si2-Si3 85.9, Si2-Si3-Si4/Si1-Si4-Si3 85.93, sum of angles for Si3/Si4 358.9.

ents.[8] The Si–Si single bonds (2.38–2.54 Å) are longer than expected (2.34 Å).[9] The ring atoms Si3 and Si4 are surrounded in an approximately planar fashion by one double-bonded and two single-bonded Si atoms (sum of angles around Si3 359.2, around Si4 359.6°; the planes Si2-Si3-Si6 and Si1-Si4-Si7 form an angle of 2.9 and 2.2°, respectively, with the line along Si3–Si4; for comparison: $(t\mathrm{BuMe_2Si})_6Si_4$:[4] 13.3 and 13.2°). The angle between the middle planes Si3-Si2-Si6-Si4 and Si4-Si1-Si7-Si3 (Si=Si torsion angle or Si–Si=Si–Si dihedral angle) is 30.8° (in fact, Si3 and Si4 are displaced by 0.87 and 0.12 Å, respectively, above the planes Si2-Si6-Si4 and Si1-Si7-Si3, respectively). The ring atoms Si1 and Si2 are each surrounded in a distorted tetrahedral fashion by one I and three Si atoms. The substituents on Si1 and Si2 are arranged in a staggered conformation, with the I atoms in a *gauche* position to each other (if the Si_4 ring were flattened, the I atoms would be in a *trans* configuration).

The cyclotetrasilene **3**, which can be prepared from **1** and I_2, can be converted back into **1** by reaction with supersilylsodium. The unsaturated Si atoms as well as the Si atoms bonded to iodine within the Si_4 ring of **3** act as reactive centers (Scheme 2). The unsaturated character of the Si–Si double bond, observed for other disilenes, is not strong owing to the steric shielding by the rather bulky substituents.[10] This can be seen, for example, in the fact that the compound is thermally stable up to over 100 °C. The double bond also reacts



Scheme 2. Reactivity and synthesis of $R^*_4Si_4X_2$.

relatively slowly with iodine, which can also be determined from the possibility of a synthesis of **3** (X = I) from **1** and I_2 (in fact, I_2 does react with **3**—albeit more slowly than with **1**—to form R*I and $R^*_3Si_4I_5$).[11] Contrary to expectations, water and methanol do not attack the disilene moiety, but rather substitute the silicon-bound iodine atom with formation of the light yellow species **6**, which exhibits the *bicyclo*-tetrasilane structure **2** (X/X = O; cf. Fig. 2), or the orange compound **7**, which has the *cyclo*-tetrasilene structure **3** (X/X = OMe/OMe; see Figure 1; Scheme 2). Finally, under standard conditions, **3** (X = I) is inert towards butadiene (the Diels–Alder adduct **8** is not formed) and oxygen. However, the rearrangement of the *cyclo*-tetrasilene framework into the *bicyclo*-tetrasilane structure, which is required for the hydrolysis of **3** to yield **6**, cannot take place without participation of the Si–Si double bond. This indicates that the double bond reacts slowly only in intermolecular, but not in intramolecular reactions (see the formation of $\mathbf{9}^+$ from **3**).

The fact that **3** converts comparatively readily at room temperature into **6** and **7** is surprising, as substitutions at Si centers usually proceed by associative activation (S_N2 mechanism) and are therefore drastically slowed down by bulky, nonreactive groups at the substitution site, such as in **3** (X = I).[9] As such bulky, nonreactive groups tend to facilitate substitutions proceeding by dissociative activation (S_N1 mechanism), one possible explanation for the rapid conversion of **3** into **6** and **7** is that the intermediate $\mathbf{9}^+$ is formed.[12] An observation in favor of this mechanism is that **3** (X = I) reacts with equimolar amounts of BI_3 in dichloromethane at room temperature to yield a colorless compound. Based on its ^{11}B NMR spectrum, this species contains only BI_4^- as a boron-containing group, and its ^1H, ^{13}C, and ^{29}Si NMR spectra are consistent with the structure of the cation $\mathbf{9}^+$ shown in Scheme 2 (see the Experimental Section). Furthermore, addition of H_2O or MeOH to a solution of this species results in the formation of **6** and **7**. The very small, colorless needles obtained from dichloromethane at –25 °C proved unsuitable for a crystal structure analysis.

It was, however, possible to determine the structure of **6**, which is isoelectronic (in terms of valence electrons) to $\mathbf{9}^+$ and which had been identified by mass spectrometry and NMR

 © WILEY-VCH Verlag GmbH, D-69451 Weinheim, 1998 1433-7851/98/3720-2870 $ 17.50+.50/0 *Angew. Chem. Int. Ed.* **1998**, *37*, No. 20

spectroscopy as $R^*_4Si_4O$. Crystals of the composition $R^*_4Si_4O \cdot 0.75\,C_6D_6$ were obtained and a X-ray crystal structure analysis was performed. There was a disorder in the position of the O atom which spans one the six edges in the $R^*_4Si_4$ tetrahedron in **6**; the O atom is disordered over all six possible positions. The crystallographic characterization can therefore only be taken as proof of the gross structure. The Si–Si distances range from 2.376(2) to 2.434(2) Å, and the Si–O distances from 1.67(3) to 1.73(3) Å. As expected, the longest Si–Si distance (Si1–Si4) is that where the oxygen atom exhibits the highest occupancy factor (0.404). Figure 2 depicts this structure of **6** (the sum of all occupancy factors is 1).[13]

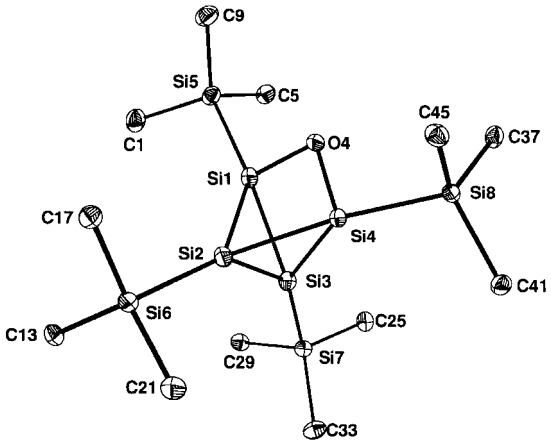


Figure 2. Crystal structure of $\mathbf{6} \cdot 0.75\,C_6D_6$ showing the atom labeling scheme (ORTEP plot, 25% thermal probability ellipsoids; for clarity, methyl groups are not shown). The O atom is disordered over the six edges of the tetrahedron formed by Si1-Si2-Si3-Si4, but it has the highest occupancy between Si1 and Si4 (0.4039; only the unit with this O position is shown). The interatomic distances [Å] and angles [°] found therefore only approximate the actual values: Si1–Si2 2.386(2), Si1–Si3 2.391(2), Si1–Si4 2.434(2), Si2–Si3 2.398(2), Si2–Si4 2.376(2), Si3–Si4 2.395(1), Si1–Si5 2.376(2), Si2–Si6 2.378(2), Si3–Si7 2.377(1), Si4–Si8 2.370(1); Si–O distances within the Si-O-Si bridges: Si1-O-Si2 1.73(3)/1.68(2), Si1-O-Si3 1.68(2)/1.69(2), Si1-O-Si4 1.676(6)/1.726(8), Si2-O-Si3 1.72(2)/1.74(2), Si2-O-Si4 1.70(3)/1.67(3), Si3-O-Si4 1.66(1)/1.70(1); Si-Si-Si angle in the Si1-Si2-Si3-Si4 tetrahedron: at Si1 60.25(4)/59.04(4)/59.51(4), at Si2 61.49(4)/60.23(4)/59.97(4), at Si3 61.15(4)/59.78(5)/59.43(4), at Si4 60.33(4)/59.46(5)/59.34(4); Si1-O-Si2 89(1), Si1-O-Si3 90(1), Si1-O-Si4 91.4(3), Si2-O-Si3 87.6(8), Si2-O-Si4 90(2), Si3-O-Si4 91.0(7). Structure of $2\,R^*_4Si_4O \cdot R^*_4Si_4O_2 \cdot 4.5\,C_6D_6$ in the mixed crystal (not shown). As for $\mathbf{6} \cdot 0.75\,C_6D_6$, the O atoms of the molecules are disordered over the six edges of the central Si_4 tetrahedron. The Si–Si distances range from 2.391(3) to 2.463(3) Å, and the Si–O distances from 1.61(3) to 1.70(3) Å. The longest Si–Si distance is found for those Si atoms above which the O atom position with the highest occupancy factor (0.444) is located (sum of all occupancy factors is 1.31).

The preparation of **3** by the action of I_2 on **1** in heptane at 0 °C in the dark leads initially to a heptane-insoluble black solid, which slowly converts into the red species **3** (X = I) when dissolved in benzene at room temperature. The black intermediate could be species **10**, which rearranges into the iodine-containing compound **3** by way of the dissociation products $\mathbf{9}^+$ and I^- (Scheme 2). This mechanism would also explain why the two iodine atoms in **3** are located on opposite sides of the Si_4 ring.

Experimental Section

3 (X = I): A solution of iodine (0.13 g, 0.51 mmol) in *n*-heptane (50 mL) is slowly added, under exclusion of light, to a solution of **1**[1] (0.45 g, 0.49 mmol) in *n*-heptane (50 mL) at 0 °C; a black suspension forms thereby. After all volatile components have been removed under an oil-pump vacuum, benzene (50 mL) is added to the remaining black residue. The residue dissolves within one hour, forming a red solution. NMR spectra of this solution show **3** (X = I) to be the sole product. The benzene is removed under an oil-pump vacuum. Recrystallization of the red residue in benzene (10 mL) at room temperature yields $\mathbf{3} \cdot C_6H_6$ (0.35 g, 0.30 mmol, 61%) in the form of red platelets which melt with decomposition at 128–130 °C; ^{1}H NMR (C_6D_6, TMS internal standard): $\delta = 1.39/1.61$ (s/s; 6*t*Bu/6*t*Bu); ^{13}C{^{1}H} NMR (C_6D_6, TMS internal standard): $\delta = 26.4/28.0$ (6*C*Me$_3$/6*C*Me$_3$), 33.7/33.9 (6C*Me$_3$*/6C*Me$_3$*); ^{29}Si NMR (C_6D_6, TMS external standard): $\delta = 38.2/49.2$ (2Si*t*Bu$_3$/2Si*t*Bu$_3$), −56.5 (2SiI), 164.4 (2 > Si=).

Preparation of **6** from **3**: An NMR tube is filled with **3** (X = I; 0.08 g, 0.07 mmol) and C_6D_6 (0.5 mL), then sealed, but not completely airtight, and left to stand for one week. The red solution slowly turns light yellow, and light yellow crystals of the composition $\mathbf{6} \cdot 0.75\,C_6D_6$ are formed (according to NMR spectra, the remaining solution only contains **6**); ^{1}H NMR (C_6D_6, TMS internal standard): $\delta = 1.33/1.42$ (s/s; 6*t*Bu/6*t*Bu); ^{13}C{^{1}H} NMR (C_6D_6, TMS internal standard): $\delta = 24.6$ (12*C*Me$_3$), 31.8/32.4 (6C*Me$_3$*/6C*Me$_3$*); ^{29}Si NMR (C_6D_6, TMS external standard): $\delta = 27.8/39.0$ (2Si*t*Bu$_3$/2Si*t*Bu$_3$), −106.4 (SiSi), −7.2 (SiOSi); MS: *m*/*z* (%): 924.8 (100) [M^+], 908.8 (0.7) [$M^+ - O$] (the correct isotopic pattern was observed in both cases; in addition, the product with the composition $2\,R^*_4SiO \cdot R^*_4SiO_2 \cdot 4.5\,C_6D_6$, which was obtained from **1** and excess water-containing I_2, showed a small signal at 940.8 [$M^+ + O$]).

7: A solution of **3** (X = I; 0.11 g, 0.09 mmol) in benzene (20 mL) is allowed to react for one hour at room temperature with degassed methanol (2 mL). After all volatile components have been removed under an oil-pump vacuum, the residue is dissolved in C_6D_6 (0.6 mL; heated to 60 °C). Upon cooling and concentration of the solution, 0.03 g (0.03 mmol, 33%) of orange platelets precipitate that exhibit the composition $\mathbf{7} \cdot C_6D_6$. They melt with decomposition at 160–161 °C; ^{1}H NMR (C_6D_6, TMS internal standard): $\delta = 1.38/1.44$ (s/s; 6*t*Bu/6*t*Bu), 3.55 (s, 2OCH$_3$); ^{13}C{^{1}H} NMR (C_6D_6, TMS internal standard): $\delta = 25.4/25.6$ (6*C*Me$_3$/6*C*Me$_3$), 33.1/33.3 (6C*Me$_3$*/6C*Me$_3$*), 54.9 (2OCH$_3$); ^{29}Si NMR (C_6D_6, INEPT, TMS external standard): $\delta = 29.9/44.0$ (2Si*t*Bu$_3$/2Si*t*Bu$_3$).

$\mathbf{9}^+BI_4^-$: Compound **3** (X = I; 0.031 g, 0.027 mmol) and BI_3 (0.011 g, 0.028 mmol) are dissolved in CD_2Cl_2 (0.6 mL). A new compound is formed exclusively, which, according to NMR spectra and other results, is $\mathbf{9}^+BI_4^-$. Thus far, only very small colorless needles have been obtained upon cooling, which have proven unsuitable for X-ray crystal structure analysis; ^{1}H NMR (CD_2Cl_2, TMS internal standard): $\delta = 1.34/1.36$ (br/s; 6*t*Bu/6*t*Bu); ^{13}C{^{1}H} NMR (CD_2Cl_2, TMS internal standard): $\delta = 25.5$ (12*C*Me$_3$), 32.4/32.7 (6C*Me$_3$*/6C*Me$_3$*); ^{29}Si NMR (CD_2Cl_2, TMS external standard): $\delta =$ 50.8/51.6 (2Si*t*Bu$_3$/2Si*t*Bu$_3$), −129.7 (two central Si atoms of the Si_4 butterfly; typical high-field signal for Si_3 rings), −29.9 (two outer Si atoms of the Si_4 butterfly; owing to the neighboring positive charge on the I atom these signals are shifted downfield compared to typical signals for Si_3 rings; Si shifts for Si cations or Si atoms in Si=Si groups are expected at δ values above +100[10, 14]); ^{11}B NMR (CD_2Cl_2, BF_3 internal standard): $\delta = -127$ (BI_4^-; this corresponds to the literature value for BI_4^-[15]).

Received: June 15, 1998 [Z11991IE]
German version: *Angew. Chem.* **1998**, *110*, 3030–3033

Keywords: cations · cyclotetrasilene · iodine · silicon · structure elucidation

[1] N. Wiberg, C. M. M. Finger, K. Polborn, *Angew. Chem.* **1993**, *105*, 1140; *Angew. Chem. Int. Ed. Engl.* **1993**, *32*, 923.
[2] S. Masamune, Y. Kabe, S. Collins, *J. Am. Chem. Soc.* **1985**, *107*, 5552; R. Jones, D. J. Williams, Y. Kabe, S. Masamune, *Angew. Chem.* **1986**, *98*, 176; *Angew. Chem. Int. Ed. Engl.* **1986**, *25*, 173.
[3] N. Wiberg, *Coord. Chem. Rev.* **1997**, *163*, 217.
[4] M. Kira, T. Iwamoto, C. Kabuto, *J. Am. Chem. Soc.* **1996**, *118*, 10303; T. Iwamoto, M. Kira, *Chem. Lett.* **1997**, 277.

[5] M. Weidenbruch, S. Willms, W. Saak, G. Henkel, *Angew. Chem.* **1997**, *109*, 2612; *Angew. Chem. Int. Ed. Engl.* **1997**, *36*, 2503.

[6] A. Sekiguchi, H. Yamazaki, C. Kabuto, H. Sakurai, S. Nagase, *J. Am. Chem. Soc.* **1995**, *117*, 8025.

[7] Crystal structure analysis of $R_4^*Si_4I_2 \cdot C_6H_6$: Siemens P4 diffractometer, $Mo_{K\alpha}$ radiation, graphite monochromator, CCD area detector, crystal dimensions $0.45 \times 0.35 \times 0.12$ mm^3, the crystal was mounted in perfluoro ether oil, $T = 183(3)$ K, $C_{54}H_{114}I_2Si_8$, $M_r = 1241.97$, red-orange platelets, monoclinic, $a = 17.9758(1)$, $b = 13.9928(1)$, $c = 26.7119(1)$ Å, $\beta = 96.709(1)^\circ$, $V = 6672.88(7)$ Å^3, $Z = 4$, space group $P2_1/c$, $\rho_{calcd} = 1.1236$ Mg m^{-3}, $\mu = 1.117$ mm^{-1}, $F(000) = 2624$. Data collection: 2θ from 2.28 to 58.08°, $-24 \le h \le 20$, $-17 \le k \le 17$, $-33 \le l \le 32$; of 36314 reflections, 10560 were independent and 8668 were considered observed ($F > 4\sigma(F)$); semi-empirical absorption correction (max./min. transmission 0.8754/0.6736), $R_1 = 0.0594$, $wR_2 = 0.1342$ ($F > 4(F)$), GOF(F^2) = 1.138; largest residual electron density 2.883 e Å^{-3}. The weighting factor was $w^{-1} = \sigma^2F_o^2 + (0.0487P)^2 + 30.7084P$ with $P = (F_o^2 + 2F_c^2)/3$.[16] The monoclinic unit cell dimensions of $R_4^*Si_4(OMe)_2 \cdot C_6D_6$: $a = 15.9308(1)$, $b = 12.8660(2)$, $c = 17.0268(1)$ Å, $\beta = 90.018(1)^\circ$, $Z = 2$, space group $P2$.[16]

[8] M. Kira, T. Maruyama, C. Kabuto, K. Ebata, H. Sakurai, *Angew. Chem.* **1994**, *106*, 1575; *Angew. Chem. Int. Ed. Engl.* **1994**, *33*, 1489.

[9] *Holleman-Wiberg*, *Lehrbuch der Anorganischen Chemie*, 101st ed., deGruyter, Berlin, **1995**.

[10] See G. Raabe, J. Michl in *The Chemistry of Organic Silicon Compounds*, *Part 2* (Eds.: S. Patai, Z. Rappoport), Wiley, Chichester, **1989**, p. 1015; T. Tsumuraya, S. A. Batcheller, S. Masamune, M. Weidenbruch, *Coord. Chem. Rev.* **1994**, *130*, 275; R. Okazaki, R. West in *Multiply Bonded Main Group Metals and Metalloids* (Eds.: R. West, F. G. A. Stone), Academic Press, San Diego, **1996**, p. 232.

[11] N. Wiberg, H. Auer, K. Polborn, M. Veith, V. Huch in *Organosilicon Chemistry* IV (Eds.: N. Auner, J. Weis), WILEY-VCH, Weinheim, **1999**, in press.

[12] A. R. Bassindale, P. G. Taylor in *The Chemistry of Organic Silicon Compounds*, *Part 1* (Eds.: S. Patai, Z. Rappoport), Wiley, Chichester, **1989**, p. 839.

[13] Crystal structure analysis of $R_4^*Si_4O \cdot 0.75\,C_6D_6$: Siemens P4 diffractometer, $Mo_{K\alpha}$ radiation, graphite monochromator, CCD area detector, crystal dimensions $0.3 \times 0.3 \times 0.2$ mm^3, the crystal was mounted within a capillary tube, $T = 173(3)$ K, $C_{52.50}H_{112.50}OSi_8$, $M_r = 984.65$, light yellow prism, monoclinic, $a = 13.3772(1)$, $b = 16.5350(2)$, $c = 30.1050(3)$ Å, $\beta = 91.202(1)^\circ$, $V = 6657.59(9)$ Å^3, $Z = 4$, space group $P2_1/c$, $\rho_{calcd} = 0.982$ Mg m^{-3}, $\mu = 0.191$ mm^{-1}, $F(000) = 2190$. Data collection: 2θ from 2.70 to 58.36°, $-17 \le h \le 17$, $-21 \le k \le 21$, $-38 \le l \le 38$; of 37866 reflections, 12890 were independent and 9598 were considered observed ($F > 4\sigma(F)$); absorption correction using the program SADABS, Sheldrick 1997 (max./min. transmission 0.9627 and 0.9448), $R_1 = 0.0753$, $wR_2 = 0.2134$ ($F > 4\sigma(F)$), GOF(F^2) = 1.128, largest residual electron density: 1.146 e Å^{-3}. The weighting factor was $w^{-1} = \sigma^2F_o^2 + (0.1119P)^2 + 9.8371P$ with $P = (F_o^2 + 2F_c^2)/3$.[16] The dimensions of the monoclinic unit cell of $2\,R_4^*Si_4O \cdot R_4^*Si_4O_2 \cdot 4.5\,C_6D_6$ resemble those of $R_4^*Si_4O \cdot 0.75\,C_6D_6$ ($a = 13.434(2)$, $b = 16.692(4)$, $c = 30.452(6)$ Å, $\beta = 91.17(2)^\circ$, $V = 6827(2)$ Å^3, $Z = 4$, space group $P2_1/c$).[16]

[14] J. B. Lambert, Y. Zhao, *Angew. Chem.* **1997**, *109*, 389; *Angew. Chem. Int. Ed. Engl.* **1997**, *36*, 400.

[15] H. Nöth, B. Wrackmeyer in *Basic Principles and Progress*, *Vol. 14* (Eds.: P. Diehl, F. Fluck, P. Kosfeld), Springer, Heidelberg, **1978**, p. 389.

[16] The structures were solved by direct methods (SHELXS-97, **1990**; for $R_4^*Si_4O_{1.31}$, SHELXS-86 was used). All non-hydrogen atoms were refined using anisotropic thermal parameters. Hydrogen atoms were included in calculated positions and refined using fixed isotropic U_i values and a riding model. Crystallographic data (excluding structure factors) for the structures reported in this paper have been deposited with the Cambridge Crystallographic Data Centre as supplementary publication no. CCDC-101877, -101800, and -101969 ($\mathbf{3} \cdot C_6H_6$, $\mathbf{6} \cdot 0.75\,C_6D_6$, and $\mathbf{6} \cdot 0.5\,R_4^*Si_4O_2 \cdot 2.25\,C_6D_6$, respectively). Copies of the data can be obtained free of charge on application to CCDC, 12 Union Road, Cambridge CB2 1EZ, UK (fax: (+44) 1223-336-033; e-mail: deposit@ccdc.cam.ac.uk).

Expanding the Potential of DNA for Binding and Catalysis: Highly Functionalized dUTP Derivatives That Are Substrates for Thermostable DNA Polymerases**

Kandasamy Sakthivel and Carlos F. Barbas III*

Nucleic acid libraries provide tremendous opportunities for the selection of novel ligands and catalysts since the polymerase chain reaction (PCR) allows for the synthesis and selection of libraries containing more than 10^{14} different molecules. There are now many examples of nucleic acids that have been selected to bind proteins and small molecules and to catalyze a limited set of reactions.[1–3] The catalytic and mechanistic scope of nucleic acids is limited since the natural nucleotide monomers possess minimal functionality relative to the repertoire available to nature's dominant catalytic biopolymers, proteins. In recognition of this shortcoming much attention has been focused on the development of functionalized nucleotides suitable for in vitro selection with the hope of increasing the potential of nucleic acids for binding and catalysis.[4] Functionalized nucleotide triphosphates have been shown to be substrates for RNA polymerases,[4d, h] and catalytic RNAs that are dependent on the modified base[5] for their activity have been selected. In a similar manner to RNA, DNA has also been selected to bind proteins and small molecules and more recently to catalyze reactions.[1–3] While DNA possesses enhanced stability relative to RNA, the lack of a 2′-hydroxyl group, which provides for the enhanced stability of this molecule, further reduces the potential for chemical functionalization. In contrast to the success achieved in identifying modified nucleotide triphosphates for RNA libraries, there is but a single example of a deoxynucleotide triphosphate, 5-(1-pentynyl)-2′deoxyuridine triphosphate, which is a good substrate for a thermostable DNA polymerase and has been utilized in an in vitro DNA selection study.[6] Indeed, difficulties in identifying modified deoxynucleotide triphophate substrates for the thermostable polymerases required for PCR have led recently to the development of novel strategies for in vitro selection without enzymatic amplification.[7] Therefore, the major impediment to the creation of novel functionally modified DNA catalysts and binding molecules is the determination of the structures of the substrate that are accepted by the thermostable polymerases. Herein, we provide a solution to this problem through the systematic synthesis and study of deoxyuridine triphosphate derivatives and disclose the discovery of a class

[*] Prof. C. F. Barbas III, Dr. K. Sakthivel
The Skaggs Institute for Chemical Biology
and the Department of Molecular Biology
The Scripps Research Institute
10550 North Torrey Pines Road, La Jolla, CA 92037 (USA)
Fax: (+1) 619-784-2583
E-mail: carlos@scripps.edu

[**] We thank R. Fuller and S. Gramatikova for technical assistance and the Skaggs Institute for Chemical Biology for support.

Supporting information for this article is available on the WWW under http://www.wiley-vch.de/home/angewandte/ or from the author.

 © WILEY-VCH Verlag GmbH, D-69451 Weinheim, 1998 1433-7851/98/3720-2872 $ 17.50+.50/0

of highly functionalized derivatives suitable for in vitro selections of modified DNAs.

Studies directed towards defining base modifications that are tolerated by thermostable polymerases began with the synthesis of 5-(3-aminopropenyl)-2′deoxyuridine triphosphate from the known compound **2** (Scheme 1). We found a palladium catalyzed route starting from commercially available 5-iododeoxyuridine preferable to the earlier synthesis[8] that started with 5-chloromercuri-2′-deoxyuridine, though both provided **2** in similar yields. Optimization of the synthesis of **2** and its conversion into the corresponding 5′-triphosphate by the methodology of Kovács and Ötvös[9] followed by deprotection of the amine provided **3**, which could be isolated on a 100-mg scale with analytical purity (Scheme 1).[10]

We studied the ability of **3** to act as a substrate in place of deoxythymidine triphosphate (dTTP) for thermostable DNA polymerases under typical PCR conditions. Commercially available thermostable DNA polymerases from four organisms were studied; Taq from *Thermus aquaticus*, Vent from *Thermococcus litoralis*, Pfu from *Pyrococcus furiosus*, and rTh from *Thermus thermophilus*. PCR assays with compound **3** demonstrated its incorporation[11] into the 519 base pair product only with rTh polymerase (Figure 1). Successful PCR with this template requires incorporation of 246 modified bases including a single stretch of eight contiguous thymidine groups. Despite this limited success we derivatized **3** with three different *N*-hydroxysuccinimide esters and produced **4a**–**c** (Scheme 2).

Compound **4a**, a 4-imidazole acrylic acid derivative, proved to be an excellent substrate for all the polymerases tested, and produced a similar amount of PCR product as that obtained with dTTP. Further study of substrates **4b** and **4c** with variation in the Mg^{2+} concentration (15 to 30 mM) and analogue concentration (200 to 800 μM) failed to define conditions that allowed for incorporation of these modified bases. To study the structural feature of **4a** that allowed for it to be recognized as a good substrate for the polymerases we synthesized **4d**, a reduced analogue of **4a**. No conditions could be defined with any of the polymerases that allowed for PCR with **4d**, which suggested that the rigid and extended α,β-unsaturated arm of the 4-imidazole acrylic acid provided for its activity. To test this structure–activity relationship we

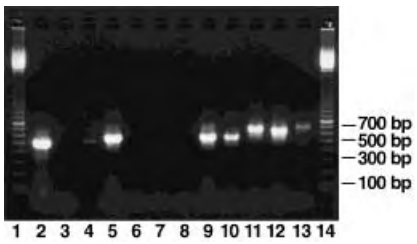
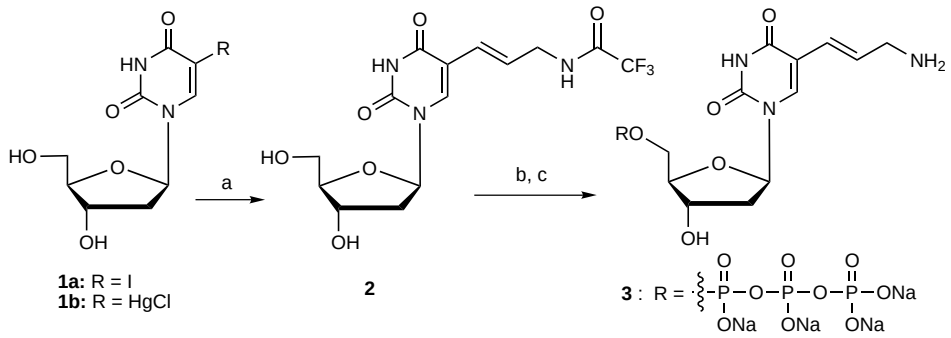


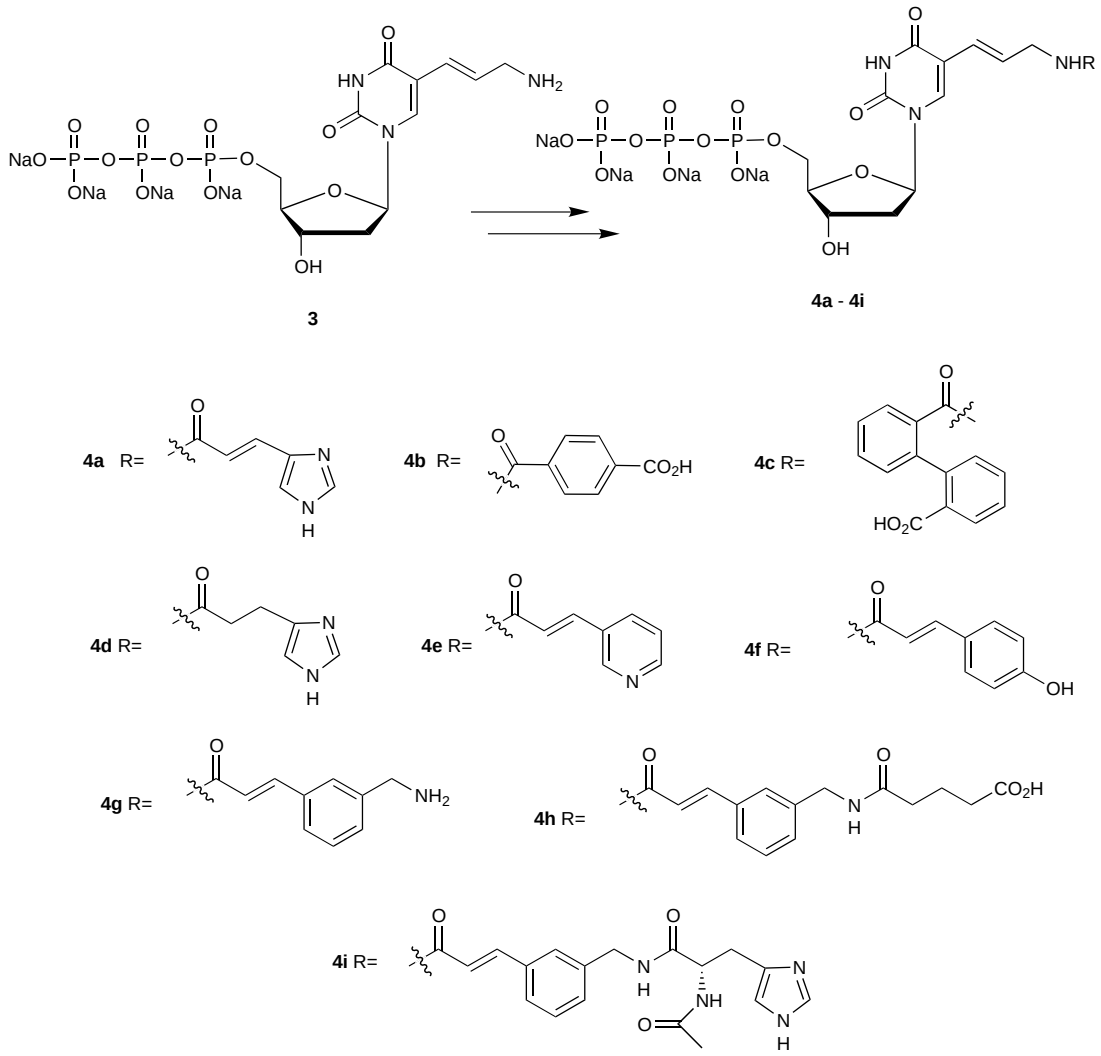
Figure 1. PCR assays of dUTP derivatives: total volume 100 μL, 1 μL (10 ng μL^{-1}) of DNA template pMal7CS2 (7030 bp), 1 μL (13 pmol) of each primer, Malseq B (GTA AAA CGA CGG CCA GTG CCA AGC) and Malseq F (GAC GCG CAG ACT AAT TCG AGC), 1 μL (5 U μL^{-1}) of Taq polymerase (AmpliTaq) (except lanes 4 and 13 where rTh polymerase was used), 8 μL of modified dNTP mix (2.5 mM of each nucleotide) or natural dNTPs (2.5 mM of each nucleotide). Conditions: 94 °C/30 s; 30 cycles of 94 °C/1 min, 56 °C/1 min, 74 °C/2 min; 74 °C/10 min. Aliquots of PCR products (10 μL each, except lane 4 where 20 μL was used) were analyzed by electrophoresis (1.5% agarose gel) and visualized by staining with ethidium bromide. Lanes 1 and 14: marker DNA (100 bp); lane 2: positive control (dTTP+dATP+dGTP+dCTP); lane 3: negative control (dATP+dGTP+dCTP); lane 4: **3**+dATP+dGTP+dCTP; lane 5: **4**+dATP+dGTP+dCTP; lane 6 : **4b**+dATP+dGTP+dCTP; lane 7: **4c**+dATP+dGTP+dCTP; lane 8: **4d**+dATP+dGTP+dCTP; lane 9: **4e**+dATP+dGTP+dCTP; lane 10: **4f**+dATP +dGTP+dCTP; lane 11: **4g**+dATP+dGTP+dCTP ; lane 12: **4h**+dATP+dGTP+dCTP; lane 13: **4i**+dATP+dGTP+dCTP.

synthesized **4e**–**4g** with the α,β-unsaturated linker arm common to **4a** maintained (Scheme 2). Compounds **4e**–**4g** were substrates for all the polymerases tested. Compound **4g** bears a free amino group suitable for further derivatization. We tested the possibility of **4g** to serve as a template for higher level modification by the synthesis and testing of **4h** and **4i**.

Analogue **4h** was a good substrate for all thermostable polymerases tested, while **4i** was a substrate only for rTh polymerase. Evidence that the modified dUTPs are indeed incorporated into the PCR products is provided by the substantial mobility shift that is obtained on electrophoresis for the modified DNA products, which is indicative of both the mass increase associated with the modified base as well as the charge of the DNA product (Figure 1). Note that DNA incorporating the analogue **4g** should possess a full positive charge at neutral pH and migrates slower than DNA incorporating **4h** that has an increased mass and negative charge at neutral pH (Figure 1). The role of the extended linker arm is apparent in comparison of the efficiency of incorporation of **3** with **4g**, where both carry a primary amine group. The larger derivative **4g** bears the extended linker arm and is a robust substrate for PCR relative to **3**. PCR products that incorporate modified bases were found to be resistant to cleavage by the restriction enzymes *Sac* I and *Xba* I that recognize the sequences GAGCTC and TCTAGA, respectively, and cleave the natural DNA product. PCR products obtained with modified dUTPs



Scheme 1. Synthesis of 5-(3-aminopropenyl)-2′-deoxyuridine triphosphate: a) *N*-allyltrifluroacetamide, $Na_2[PdCl_4]$ in sodium acetate (0.1M, pH 5.2), 24 h; b) 1. $POCl_3$ in trimethylphosphate, 1.8-bis(dimethylamino)naphthalene (proton sponge), tri-*n*-butylammonium pyrophosphate, tri-*n*-butylamine; 2. NH_3 (aq.); c) sodium perchlorate in acetone.



Scheme 2. Synthesis of highly functionalized dUTPS.

were cloned and sequenced.[12] The fidelity of the incorporation of the modified dUTPs was similar to that observed with dTTP incorporation in the control reactions. The key criteria for the use of a modified dNTP in an in vitro selection methodology is its ability to serve as a substrate for thermostable polymerases and the resulting product to serve as a template for multiple cycles of PCR amplification. These criteria are met with **3**, **4a**, and **4e**–**i**. Reverse transcriptases may also be utilized in conjunction with PCR for in vitro selection schemes of DNA enzymes. We tested the ability of **3** and **4**–**i** to act as substrates of a reverse transcriptase (Superscript II, Gibco/BRL) and determined that all but **4c** and **4h** were substrates in template directed synthesis assays (see supporting information). The specificity of this reverse transcriptase is broader and not predictive of the structural requirements of the thermostable polymerases. In our design of analogues we have attempted to provide functional groups that are lacking in DNA in order to expand its catalytic scope. The functional groups of the natural nucleic acids have pK_as far removed from neutral pH and are therefore not suited for general acid–base catalysis in this pH range.[13] The analogues described here address this limitation as well as provide potential for covalent binding, electrostatic interactions, and particularly metal ion catalysis. Analogues **4g** and **4h** provide the first examples of the incorporation of cationic and anionic nucleotide analogues into DNA by PCR, which dramatically alter its electrostatic properties. With the exception of **4e**, the analogues may be regarded as functional equivalents of the amino acids lysine: **3** and **4g**, histidine: **4** and **4i**, tyrosine: **4f**, and aspartic and glutamic acid: **4h**. The successful incorporation of L-histidine in analogue **4i** supports the possibility of incorporating other natural amino acids as well as small peptides. All the analogues provide new potential for hydrophobic binding interactions that are essential for folding and pocket formation in protein enzymes, as well as for pK_a perturbations of functional groups.[14]

In summary, we have defined a class of highly functionalized C5-substituted dUTP derivatives that are substrates for thermostable DNA polymerases and reverse transcriptase, and are suitable for in vitro selection studies and the enzymatic synthesis of combinatorial DNA libraries. While we have defined here only substrates that replace the natural DNA base thymidine, the tremendous breadth of substrate analogues accepted by the polymerases we have studied, provided certain structural guidelines are followed, suggests the likelihood that guanine, cytosine, and adenine analogues

 © WILEY-VCH Verlag GmbH, D-69451 Weinheim, 1998 1433-7851/98/3720-2874 $ 17.50+.50/0

could be identified, which would then allow four coded substitutions into modified DNA libraries. While this falls short of the 20 coded amino acids available in protein libraries, higher order coding of derivatives may be obtained by treating synthesized libraries with designed alkylating or acylating reagents to introduce additional functionality wherein the chemical reactivity of the targeted deoxynucleotide is encoded by its structural context. Given the size of the libraries accessible with nucleic acids and PCR, and the ease with which they may be evolved through many generations in the laboratory, we anticipate that modified DNA will make significant inroads into areas of catalysis that were previously believed to be the sole purview of protein catalysts.

Experimental Section

2: This compound was first synthesized by Cook and his co-workers[8] from 5-chloromercuri-2′-deoxyuridine **1b**. We synthesized **2** from commercially available 5-iodo-2′-deoxyuridine by a similar procedure: A suspension of 5-iodo-2′-deoxyuridine **1a** (3.5 g, 10 mmol) in sodium acetate buffer (0.1 M, pH 5.2) was treated with *N*-allyltrifluroacetylamide (13 g, 88 mmol) followed by a solution of sodium tetrachloropalladate (2.5 g in 5 mL water). The mixture was stirred at room temperature for 18 h and then filtered through celite. The filtrate was concentrated and extracted several times with ethyl acetate. The combined organic layers was dried over anhydrous magnesium sulfate. The solvent was evaporated to dryness and the product purified by column chromatography on silica gel with ethyl acetate as eluent to give **2** (1.7 g, 44 %). ^{1}H NMR (CD_3OD): $\delta = 8.11$ (s, br, 1H; C-6H), 6.45 (m, 1H) and 6.16 (m, 2H; H_{vinyl} and H-1′), 4.32 (m, 1H; H-3′), 3.8, (m, 3H; H_{allyl}, H-4′), 3.75 – 3.60 (m, 2H; H-5′, H-5″), 2.17 (m, 2H; H-2′, H-2″).

3:[9]: Compound **2** (126 mg, 0.33 mmol) was stirred in dry trimethylphosphate (0.75 mL) with 1,8-bis(dimethylamino)naphthalene (proton sponge, 100 mg, 0.47 mmol) at 0 °C. Phosphorous oxychloride (35 µl, 99.9 % Aldrich) was added and the mixture was stirred at 0 – 4 °C. After 2.5 h a solution of tri-*n*-butylammonium pyrophosphate in anhydrous DMF (0.5 M, 3 mL) and tri-*n*-butylamine (0.3 mL) was added quickly to the reaction mixture at 0 °C. After 1 min an aqueous solution of triethylammonium bicarbonate (0.2 M) was poured into the mixture. After evaporation the residue was treated with aqueous ammonia (2 mL), and stirred overnight at room temperature. After evaporation of the ammonia, the residue was purified by column chromatography on DEAE-Sephadex A-25 with triethylammonium bicarbonate buffer (0.2 – 0.5 M, pH 7.5). The final purification was achieved by reversed-phase HPLC with the gradient 0 – 3 % acetonitrile in 50 mM triethylammonium bicarbonate buffer over 30 min to give **3** (110 mg, 54 %). ^{1}H NMR (D_2O): $\delta = 8.17$ (s, br, 1H; C-6H), 6.58 – 6.54 (d, 1H), 6.48 – 6.40 (m, 1H), and 6.35 (t, 1H; H_{vinyl} and H-1′), 4.66 (m, 1H; H-3′), 4.26 – 4.2 (m, 3H; 5′, 5″, H-4′), 3.70 (d, 2H; H_{allyl}), 2.41 (m, 2H; H – 2′,2″); ^{13}C NMR (D_2O): $\delta = 166.67$, 153.35, 141.0, 128.74, 124.7, 114.00, 88.27, 87.90, 72.7, 67.66, 43.60, 41.98; ^{31}P NMR (D_2O): $\delta = -9.42$ (d), -10.73 (d), -21.38 (t); electrospray MS: *m/z*: 589 [M+H$^+$], 611 [M+Na$^+$], 633 [M+2Na$^+ -$ 2H$^+$]; elemental analysis calcd for $C_{12}H_{16}N_3Na_4O_{14}P_3$: C 23.58, H 2.64, N 6.88; found: C 23.75, H 2.81, N 7.00.

General synthesis of **4**, **4d**, **4e**, and **4f**: Compound **3** (30 mg, 50 µmol) was treated with a slight excess of the corresponding *N*-hydroxysuccinimide ester in 0.1 M sodium borate buffer/DMF (1/1) at room temperature and stirred for 10 – 20 h. After completion of the reaction (as monitored by TLC with ammonia/water/isopropanol, 2/1/1), the mixture was evaporated to dryness. The triphosphates were purified by reversed-phase HPLC. For complete physical data and synthetic procedures for all compounds see supporting information.

Received: May 29, 1998 [Z11913IE]
German version: *Angew. Chem.* **1998**, *110*, 2998 – 3002

Keywords: aptamers · combinatorial chemistry · DNA-enzymes · in vitro selection · nucleotides

[1] Ligand-binding nucleic acids: a) S. E. Osborne, A. D. Ellington, *Chem. Rev.* **1997**, *97*, 349 – 370; b) M. Famulok, J. W. Szostak, *Angew. Chem.* **1992**, *104*, 1001 – 11; *Angew. Chem. Int. Ed. Engl.* **1992**, *31*, 979 – 88; c) L. Gold, B. Polisky, O. Uhlenbeck, M. Yarus, *Annu. Rev. Biochem.* **1995**, *64*, 763 – 97.

[2] Catalytic nucleic acids: a) R. R. Breaker, *Chem. Rev.* **1997**, *97*, 371 – 390; b) R. R. Breaker, *Curr. Opin. Chem. Biol.* **1997**, *1*, 26 – 31; c) J. R. Lorsch, J. W. Szostak, *Acc. Chem. Res.* **1996**, *29*, 103 – 110.

[3] Catalytic DNA: a) R. R. Breaker, G. F. Joyce, *Chem. Biol.* **1994**, *1*, 223 – 9; b) B. Cuenoud, J. W. Szostak, *Nature* **1995**, *375*, 611 – 14; c) R. R. Breaker, G. F. Joyce, *Chem. Biol.* **1995**, *2*, 655 – 60; d) C. R. Geyer, D. Sen, *Chem. Biol.* **1997**, *4*, 579 – 593; e) S. W. Santoro, G. F. Joyce, *Proc. Natl. Acad. Sci. U.S.A.* **1997**, *94*, 4262 – 4266; f) P. Burgstaller, M. Famulok, *Angew. Chem.* **1995**, *107*, 1303 – 1306; *Angew. Chem. Int. Ed. Engl.* **1995**, *34*, 1189 – 1192; g) D. Faulhammer, M. Famulok, *Angew. Chem.* **1996**, *108*, 2984 – 88; *Angew. Chem. Int. Ed. Engl.* **1996**, *35*, 2837 – 2841; h) D. Faulhammer, M. Famulok, *J. Mol. Biol.* **1997**, *269*, 188 – 202; i) Y. Li, D. Sen, *Nat. Struct. Biol.* **1996**, *3*, 743 – 747; j) J. Burmeister, G. von Kiedrowski, A. D. Ellington, *Angew. Chem.* **1997**, *109*, 1379 – 81; *Angew. Chem. Int. Ed. Engl.* **1997**, *36*, 1321 – 1324; k) N. Carmi, L. A. Shultz, R. R. Breaker, *Chem. Biol.* **1996**, *3*, 1039 – 1046; l) N. Carmi, H. R. Balkhi, R. R. Breaker, *Proc. Natl. Acad. Sci. U.S.A.* **1998**, *95*, 2233 – 2237.

[4] a) B. E. Eaton, W. A. Pieken, *Annu. Rev. Biochem.* **1995**, *64*, 837 – 63; b) B. E. Eaton, *Curr. Opin. Chem. Biol.* **1997**, *1*, 10 – 16; c) G. J. Crouch, B. E. Eaton, *Nucleosides Nucleotides* **1994**, *13* 939 – 44; d) T. M. Dewey, A. Mundt, G. J. Crouch, M. C. Zyzniewski, B. E. Eaton, *J. Am. Chem. Soc.* **1995**, *117*, 8474 – 5; e) T. M. Dewey, M. C. Zyzniewski, B. E. Eaton, *Nucleosides Nucleotides* **1996**, *15*, 1611 – 1617; f) C. Tu, C. Keane, B. E. Eaton, *Nucleosides Nucleotides* **1995**, *14*, 1631 – 8; g) P. A. Limbach, P. F. Crain, J. A. McCloskey, *Nucleic Acids Res.* **1994**, *22*, 2183 – 96; h) H. Aurup, D. M. Williams, F. Eckstein, *Biochemistry* **1992**, *31*, 9636 – 41.

[5] a) T. W. Wiegand, R. C. Janssen, B. E. Eaton, *Chem. Biol.* **1997**, 4, 675 – 683; b) T. M. Tarasow, S. L. Tarasow, B. E. Eaton, *Nature* **1997**, *389*, 54 – 57.

[6] J. A. Latham, R. Johnson, J. J. Toole, *Nucleic Acids Res.* **1994**, *22*, 2817 – 22.

[7] J. Smith, E. V. Anslyn, *Angew. Chem.* **1997**, *109*, 1956 – 58; *Angew. Chem. Int. Ed. Engl.* **1997**, *36*, 1879 – 1881. These authors state that "when modified oligomers are incorporated, the selection procedure is terminated after just one round of amplification since polymerases will not tolerate most modified mononucleotides".

[8] A. F. Cook, E. Vuocolo, C. L. Brakel, *Nucleic Acids Res.* **1988**, *16*, 4077 – 95.

[9] T. Kovács, L. Ötvös, *Tetrahedron Lett.* **1988**, *29*, 4525 – 8.

[10] Compound **3** was synthesized previously from deoxyuridine triphosphate (dUTP), however, problems with by-products and the expense of dUTP as a starting material posed serious obstacles for this synthetic route. P. R. Langer, A. A. Waldrop, D. C. Ward, *Proc. Natl. Acad. Sci.U.S.A.* **1981**, *78*, 6633 – 7.

[11] Several derivatives of **3** have been shown to be substrates for *E. coli* DNA polymerase and useful in nick translation and random primed synthesis when they replace dTTP. Homogeneous incorporation of these derivatives in PCR is not possible because of chain termination, see ref. [11c] for a discussion of derivatives in PCR. a) M. Shimkus, J. Levy, T. Herman, *Proc. Natl. Acad. Sci. U.S.A.* **1985**, *82*, 2593 – 7; b) B. L. Iverson, P. B. Dervan, *J. Am. Chem. Soc.* **1987**, *109*, 1241 – 3. and ref. [10]; c) H. Yu, J. Chao, D. Patek, R. Mujumdar, A. S. Waggoner, *Nucleic Acids Res.* **1994**, *22*, 3226 – 32.

[12] PCR products with incorporated modified nucleotide analogues were cloned into the vector pCR2.1TOPO with the topoisomerase-activated vector provided from the manufacturer (Invitrogen).

[13] S. Nesbitt, L. A. Hegg, M. J. Fedor, *Chem. Biol.* **1997**, *4*, 619 – 630.

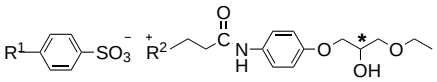
[14] Reviews of the structures of nucleic acids that were selected to bind ligands detail the differences between the ligand-binding pockets of nucleic acids and proteins, see a) K. A. Marshall, M. P. Robertson, A. D. Ellington, *Structure* **1997**, *5*, 729 – 734; b) M. Egli, *Angew. Chem.* **1997**, *109*, 494 – 497; *Angew. Chem. Int. Ed. Engl.* **1997**, *36*, 480 – 482; c) D. J. Patel, *Curr. Opin. Chem. Biol.* **1997**, *1*, 32 – 46; d) J. Feigon, T. Dieckmann, F. W. Smith, *Chem. Biol.* **1996**, *3*, 611 – 617.

 © WILEY-VCH Verlag GmbH, D-69451 Weinheim, 1998 1433-7851/98/3720-2875 $ 17.50+.50/0

Unusual Disordered Crystal Structure of a Racemate Exhibiting a Novel Enantiomeric Resolution: Preferential Enrichment**

Rui Tamura,* Hiroki Takahashi, Ken Hirotsu,* Yoshitaka Nakajima, Takanori Ushio, and Fumio Toda

Recently we reported the first case of enantiomeric resolution by simple recrystallization of a series of racemic compounds ((±)-ST,[1, 2] (±)-SC[3] and (±)-SN[4]), although in principle this type of enantiomeric resolution was believed to be impossible for more than a century since the mechanical resolution of enantiomeric conglomerates by Pasteur[5] and the discovery of the "preferential crystallization" technique by Gernetz.[6,7] We refer to this new phenomenon of enantiomeric resolution as "preferential enrichment" in the



ST, R^1=CH_3 R^2=Me_2S **SN**, R^1=NO_2 R^2=Me_2S
SC, R^1=Cl R^2=Me_2S **NC**, R^1= Cl R^2=Me_2NH

mother liquor. Preferential enrichment has the following features: 1) Repeated recrystallization of the racemate and each crop of deposited crystals results in a remarkable alternating enrichment of the two enantiomers up to 100% *ee* in the mother liquors (enantiomeric enrichment in the mother liquors). 2) When nonracemic crystals with low *ee* values are recrystallized, the resulting deposited crystals always have the opposite chirality (reversal of chirality in the deposited crystals)[1–4] (Figure 1). An X-ray crystallographic analysis of the racemic single crystals (0% *ee*) of ST and SC indicated that their stable crystalline forms are composed of a regular packing of the *R* and *S* enantiomers in the crystal lattice (space group $P\bar{1}$, $Z=2$).[1–3] In addition, it was shown that several related racemic (disordered) mixed crystals[8] in which the same sites are occupied by molecules of the *R* and *S* enantiomers in equal amounts do not exhibit preferential enrichment.[4] Here we report another new case

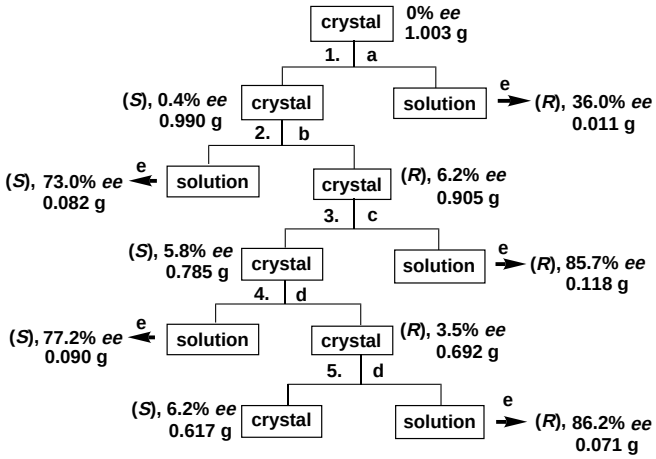


Figure 1. Preferential enrichment of NC. The crystals were dissolved in EtOH by heating. The saturated solution was cooled to 25 °C, stirred until crystallization began, and then allowed to stand for the stated period of time. Crystallization conditions: a) EtOH (10 mL), 25 °C, 17 d; b) EtOH (10 mL), 25 °C, 5 d; c) EtOH (10 mL), 25 °C, 3 d; d) EtOH (8 mL), 25 °C, 3 d; e) removal of the solvent by evaporation. The *ee* values of the mother liquors and crystals were determined by HPLC analysis on a chiral stationary phase (Chiralcel OD-H, 0.46 × 25 cm) and a mixture of hexane, EtOH, CF_3COOH, and Et_2NH (800/200/5/1) as the mobile phase.

of preferential enrichment in which the stable crystalline form of the racemate is the (disordered) mixed crystal, which, however, is composed of a weakly ordered arrangement of the two enantiomers and contains the centrosymmetric heterochiral cyclic dimer (*R*,*S*) as the major component (ca. 54%) in the crystal lattice.

Preferential enrichment of the ammonium analogue of (±)-SC, (±)-{2-[4-(3-ethoxy-2-hydroxypropoxy)phenylcarbamoyl]ethyl}dimethylammonium *p*-chlorobenzenesulfonate [(±)-NC], was effected by recrystallization from a fivefold supersaturated solution in ethanol or 2-propanol at 25 °C. Both the alternating enantiomeric enrichment in the mother liquors (up to 86% *ee*) and the reversal of chirality in the deposited crystals were observed (Figure 1). The X-ray powder diffraction pattern of the racemate was similar to but clearly different from that of the pure enantiomer. Furthermore, the melting point of the racemate (124.4–130.0 °C) determined by differential scanning calorimetry (DSC) is higher than that of the pure enantiomer (73.5–96.2 °C). From these results, we predicted that the stable crystalline form of the racemate of NC would be a racemic compound, as was observed for related compounds.[1–4]

Single crystals of the racemate and the *S*-enriched nonracemic material (ca. 40% *ee*) were obtained by crystallization without stirring from twofold supersaturated racemic and nonracemic (65% *ee*) solutions in 2-propanol at 25 °C, respectively, followed by very slow evaporation of the solvent, and were subjected to X-ray crystallographic analysis. The crystal structure of the racemate of NC was solved in the space group $P\bar{1}$, because the single crystals obtained were composed of almost the equal amounts of the two enantiomers with an *ee* value of less than 0.4% (HPLC analysis). The unique molecular arrangement of *R* and *S* enantiomers is shown in Figures 2 and 3. Contrary to our expectation, the stable

[*] Prof. R. Tamura
Graduate School of Human and Environmental Studies
Kyoto University
Kyoto 606-8501 (Japan)
Fax: (+81) 75-753-2957
E-mail: tamura@helios.jinkan.kyoto-u.ac.jp
Prof. K. Hirotsu, Y. Nakajima
Department of Chemistry, Graduate School of Science
Osaka City University, Osaka (Japan)
H. Takahashi
Division of Material Science
Graduate School of Environmental Earth Science
Hokkaido University, Sapporo (Japan)
Dr. T. Ushio
Taiho Pharmaceutical Co. Ltd., Saitama (Japan)
Prof. F. Toda
Department of Applied Chemistry, Faculty of Engineering
Ehime University, Matsuyama (Japan)

[**] This work was partly supported by the Grants-in-Aid for Scientific Research from the Ministry of Education, Science, Sports and Culture of Japan.

 © WILEY-VCH Verlag GmbH, D-69451 Weinheim, 1998 1433-7851/98/3720-2876 $ 17.50+.50/0

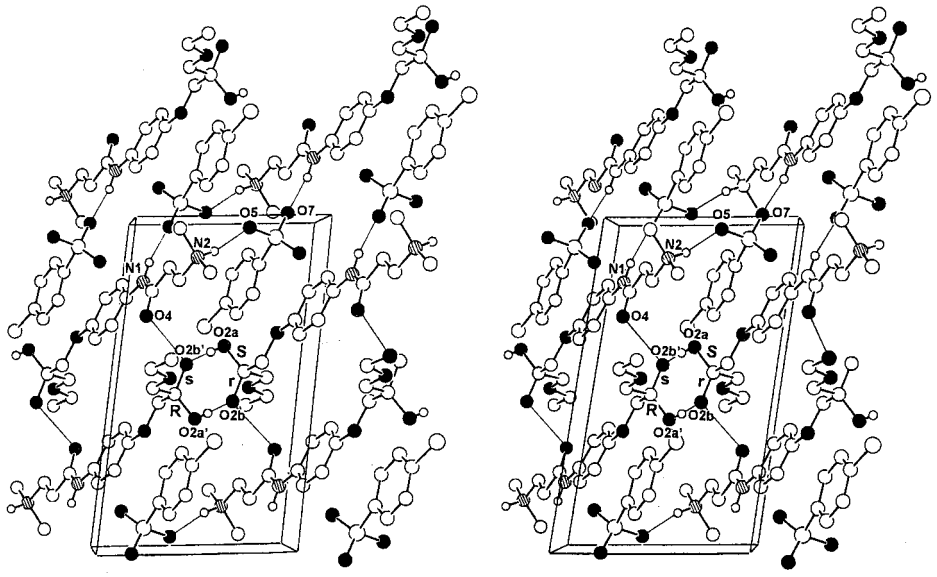


Figure 2. Crystal structure of (±)-NC viewed down the *a* axis (stereoview). The *b* axis is vertical, and the *c* axis is horizontal. The carbon, oxygen, and nitrogen atoms are represented by open, full, and hatched circles, respectively. Hydrogen atoms are omitted for clarity except for those of hydroxyl and amido groups. Hydrogen bonds are indicated by thin lines. **R** and **r** represent the more and less highly occupied sites of the *R* enantiomers, and **S** and **s** the corresponding sites of the *S* enantiomer.

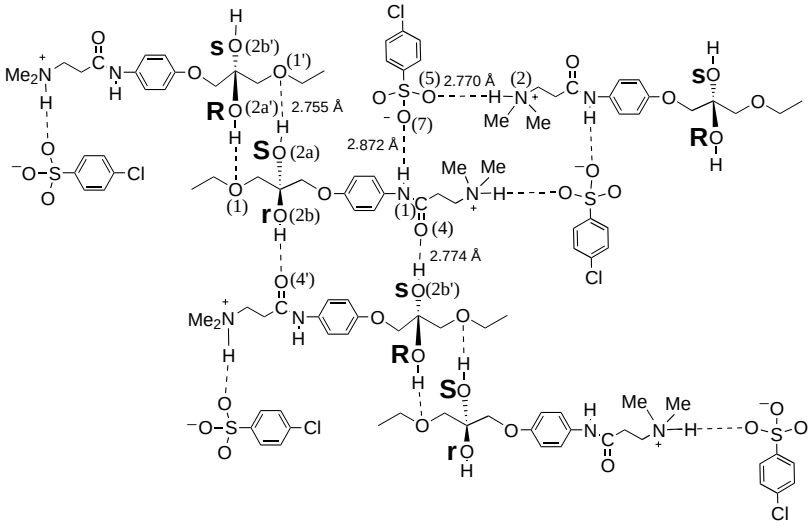


Figure 3. Schematic representation of the various types of intermolecular hydrogen bonds in the crystal of (±)-NC.

crystalline form of (±)-NC is not a racemic compound, but the racemic (disordered) mixed crystal. It is surprising that a racemate existing as a stable racemic (disordered) mixed crystal can exhibit preferential enrichment.[4] To gain an insight into this unexpected result, we investigated the crystal structure of (±)-NC in detail and compared it with that of the nonracemic crystal.

The crystal structure of (±)-NC is characterized by hydrogen bonds between the hydroxyl group and the oxygen atom of the ethoxy or amido group of the long-chain cation, and between the ammonium and amido NH groups of the long-chain cation and the sulfonate groups of the anion. Interestingly, the hydroxyl group on an asymmetric carbon atom (C4) is disordered over two positions. Constrained refinement of these two positions gave occupancy factors of 0.737 and 0.263 for O2a and O2b, respectively. Hence, either the *R* or the *S* enantiomer can be located at the same site in the crystal lattice. The occurrence of the racemic (disordered) mixed crystal is explained in terms of the presence of a site in the crystal lattice that can accomodate O2a and O2b and allow the interaction of both O2a and O2b with hydrogen-bond acceptors. The *R* and *S* enantiomers in the sites with higher occupancy factors are designated **R** and **S** (occupancy factor: 0.737 each), and those in sites with lower occupancy factors **r** and **s** (occupancy factor: 0.263 each) in Figures 2 and 3. The hydroxyl group of **R** (HO2a′) and **S** (HO2a) forms hydrogen bonds with the ethoxy oxygen atom (O1 or O1′) of the symmetry-related **S** and **R** molecules, respectively; this leads to the formation of a head-to-head cyclic dimer around a center of symmetry at ½, ½, ½ (probability: $0.737 \times 0.737 = 0.543$); the lengths of the hydrogen bonds are 2.755(3) Å for O2a′ – O1 and O2a – O1′. Similarly, the hydroxyl groups of **r** (HO2b) and **s** (HO2b′) form hydrogen bonds with the carbonyl oxygen atoms (O4′ and O4) of the symmetry related molecules to give a side-by-side cyclic dimer around a center of symmetry at 1, ½, 1 and 0, ½, 0 (probability: $0.263 \times 0.263 = 0.069$); the lengths of the hydrogen bonds are 2.774(8) Å for O2b ··· O4′ and O2b′ ··· O4. The major hydrogen-bonding mode between **R** and **S** molecules and the minor one between **r** and **s** molecules were observed in the related compounds (±)-SC[3] and (±)-ST,[1, 2] respectively. The rest of the crystal consists of equal amounts of *R* and *S* enantiomers that do not form cyclic dimers. The values of the occupancy factors were reproducible for the racemic crystals. For a crystal grown from a different batch, the occupancy factors were 0.747 for O2a and 0.253 for O2b.

Although the initial structure determination showed that the nonracemic crystal was isomorphous with that of (±)-NC, and *E* statistics and the $N(z)$ cumulative probability distribution[10a] were consistent with the existence of a center of symmetry, the crystal structure of *S*-enriched nonracemic NC was solved and refined in the space group *P*1, since the *ee* value of the crystals was about 40 % by HPLC analysis. The

Hamilton test indicated that the space group of the nonracemic crystal is *P*1 at the 99.5 % significance level.[10b] The crystal structure of the mixed crystal of *S*-enriched nonracemic NC was isomorphous with that of (±)-NC (Figure 2). The hydroxyl groups are disordered around a pseudo-center of symmetry, but the initial refinement showed that one of the two independent molecules is essentially ordered and has the *S* configuration. At this stage, the occupancy factor of the OH group (O2a in Figure 2) with *S* configuration was fixed at 1.0, and that with *R* configuration (O2b) was removed from the atom list. The occupancy factors of the hydroxyl groups belonging to the other of the two independent molecules were refined to 0.59 for the *R* configuration (O2a′) and to 0.41 for the *S* configuration (O2b′). An *ee* value of 41 % was calculated for this nonracemic crystal. The X-ray powder diffraction pattern of this nonracemate is intermediate between those of the racemate and the pure enantiomer. Therefore, it can be assumed that with increasing fraction of *S* enantiomers in the crystal, the occupation of the sites HO2a and HO2b′ increases and that of HO2a′ and HO2b decreases (Figures 2 and 3), so that the crystal structure of the pure *S* enantiomer is approached. Thus, the stable crystalline form of nonracemic NC is proved to be the (disordered) mixed crystal composed of different amounts of the two enantiomers.

The origin of these unique crystal structures of racemic and nonracemic NC might be accounted for, at least in part, by the third intermolecular hydrogen-bonding mode in the crystals. The tails of the long-chain cations interact strongly with the sulfonate groups of the anions through a hydrogen bond/salt bridge N2−H···O5−S (N2···O5 2.770(3), O5−S 1.452(2) Å) and the hydrogen bond N1−H···O7 (N1···O7 2.872(3), O7−S 1.436(2) Å) to give a cyclic dimer (Figures 2 and 3). These interactions should also play an important role in determining the arrangement of NC molecules in the crystal.

Although the stable crystalline form of racemic NC is a (disordered) mixed crystal of the two enantiomers, which was considered undesirable for the preferential enrichment, due to the weakly ordered arrangement of the two enantiomers with the centrosymmetric cyclic dimer structure (*R*,*S*) as the major component in the crystal lattice, preferential enrichment was obtained. This discovery could expand the range of applications of preferential enrichment.

Experimental Section

(±)-NC: A mixture of the precursor (±)-{2-[4-(3-ethoxy-2-hydroxypropoxy)phenylcarbamoyl]ethyl}dimethylamine (1.52 g, 4.90 mmol) and *p*-chlorobenzenesulfonic acid (1.20 g, 6.23 mmol) in acetone (20 mL) was stirred for 15 h at 55 °C, cooled to 25 °C and then 5 °C, and filtered. The residue was washed with a small amount of diethyl ether to give (±)-NC as a white solid (1.94 g, 79 % yield, 0 % *ee*). The *ee* value was determined by HPLC analysis. (*S*)-(+)-NC was similarly prepared from (*S*)-(+)-epichlorohydrin. The specific rotation $[\alpha]_D^{25}$ (2.03, MeOH) was +1.7° (standard deviation 0.2).

Received: March 3, 1998 [Z11548IE]
German version: *Angew. Chem.* **1998**, *110*, 3002 – 3005

Keywords: crystal growth · enantiomeric resolution · mixed crystals · preferential enrichment · racemic compounds

[1] T. Ushio, R. Tamura, H. Takahashi, N. Azuma, K. Yamamoto, *Angew. Chem.* **1996**, *108*, 2544 – 2546; *Angew. Chem. Int. Ed. Engl.* **1996**, *35*, 2372 – 2374.
[2] T. Ushio, R. Tamura, N. Azuma, K. Nakamura, F. Toda, K. Kobayashi, *Mol. Cryst. Liq. Cryst.* **1996**, *276*, 245 – 252.
[3] R. Tamura, T. Ushio, K. Nakamura, H. Takahashi, N. Azuma, F. Toda, *Enantiomer*, **1997**, *2*, 277 – 280.
[4] R. Tamura, T. Ushio, H. Takahashi, K. Nakamura, N. Azuma, F. Toda, K. Endo, *Chirality*, **1997**, *9,* 220 – 224.
[5] L. Pasteur, *Ann. Chim. Phy.* **1848**, *24*, 442.
[6] M. Gernez, *C. R. Hebd. Seances Acad. Sci.* **1866**, *63*, 843.
[7] a) A. Collet, M.-J. Brienne, A. Jacques, *Chem. Rev.* **1980**, *80*, 215 – 230; b) E. Eliel, S. H. Wilen, L. N. Mander, *Stereochemistry of Organic Compounds*, Wiley, New York, **1994**, pp. 297 – 322; c) A. Collet in *Comprehensive Supramolecular Chemistry, Vol. 10* (Ed.: D. N. Reinhoudt), Pergamon, Oxford, **1996**, pp. 113 – 149; d) K. Kinbara, Y. Hashimoto, M. Sukegawa, H. Nohira, K. Saigo, *J. Am. Chem. Soc.* **1996**, *118*, 3441 – 3449.
[8] J. Jacques, A. Collet, S. H. Wilen, *Enantiomers, Racemates and Resolutions*, W Krieger Publishing, Malabar, FL, **1994**, pp. 104 – 131.
[9] The X-ray data were collected on a Rigaku AFC7R four-circle diffractometer ($T = 296$ K). The structures were solved by direct methods (SHELX86) and subsequent Fourier recycling (DIRDIF94), and refined by full-matrix least-squares refinement against $|F|$, with all hydrogen atoms fixed at calculated positions. Empirical absorption corrections were applied. All calculations were performed with the crystallographic software package teXsan (Molecular Structure Corporation, **1985**, **1992**). Crystal data for (±)-NC: $C_{22}H_{31}O_7N_2SCl$, $M_r = 503.01$, triclinic, space group $P\bar{1}$, $a = 9.896(1)$, $b = 15.250(2)$, $c = 8.496(3)$ Å, $\alpha = 98.20(1)$, $\beta = 91.88(1)$, $\gamma = 71.15(1)°$, $V = 1200.9(4)$ Å^3, $Z = 2$, $\rho_{calcd} = 1.391$ g cm^{-3}, $Mo_{K\alpha}$ radiation ($\lambda = 0.71073$ Å), $\mu = 2.91$ cm^{-1}, $2\theta_{max} = 50°$, $R = 0.043$, $Rw = 0.070$, 4224 independent reflections, 3379 observed reflections ($I > 2.0\sigma(I)$), 303 refined parameters, maximum residual electron density 0.34 e Å^{-3}. The disordered O2a and O2b atoms were refined anisotropically and isotropically to give thermal factors of 3.4 Å^2 (B_{eq}) and 5.0 Å^2 (B_{iso}), respectively. The thermal ellipsoid of O2a is not anomalous. Crystal data for (*S*)-(+)-enriched nonracemic NC: $a = 9.917(2)$, $b = 15.248(2)$, $c = 8.502(1)$ Å, $\alpha = 98.26(1)$, $\beta = 92.27(1)$, $\gamma = 71.13(1)°$, $V = 1203.9(4)$ Å^3, triclinic, space group *P*1, $Z = 2$, $\rho_{calcd} = 1.387$ g cm^{-3}, $Cu_{K\alpha}$ radiation ($\lambda = 1.54178$ Å), $\mu = 26.07$ cm^{-1}, $2\theta_{max} = 120.1°$, $R = 0.039$, $Rw = 0.049$, 3571 independent reflections, 2761 observed reflections ($I > 2.0\sigma(I)$), 595 refined parameters, maximum residual electron density 0.32 e Å^{-3}. The disordered O2a′ and O2b′ atoms were refined isotropically to give thermal factors of 3.4 and 5.0 Å^2, respectively. Crystallographic data (excluding structure factors) for the structure reported in this paper have been deposited with the Cambridge Crystallographic Data Centre as supplementary publication no. CCDC-101 049. Copies of the data can be obtained free of charge on application to CCDC, 12 Union Road, Cambridge CB2 1EZ, UK (fax: (+44) 1223-336-033; e-mail: deposit@ccdc.cam.ac.uk).
[10] a) E. R. Howells, D. C. Phillips, D. Rogers, *Acta Crystallogr.* **1950**, *3*, 210 – 214; b) W. C. Hamilton, *Acta Crystallogr.* **1965**, *18*, 502 – 510.

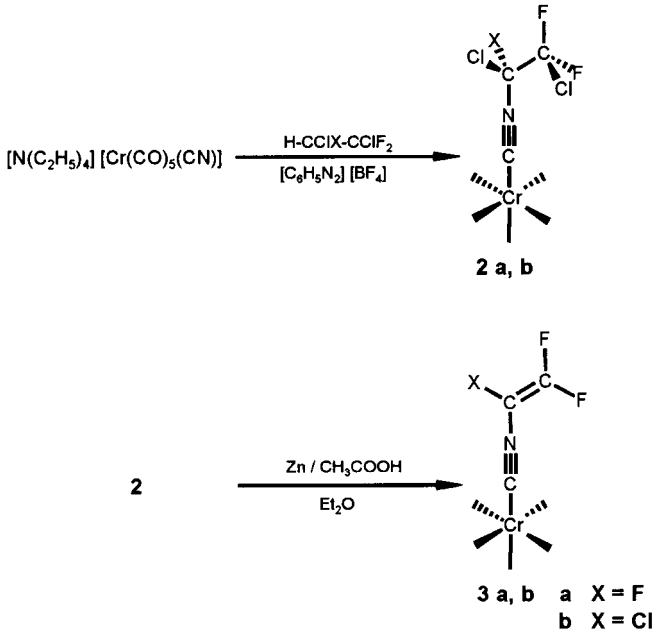
 © WILEY-VCH Verlag GmbH, D-69451 Weinheim, 1998 1433-7851/98/3720-2878 $ 17.50+.50/0

Cyanoisocyanoacetylene, N≡C–C≡C–N≡C**

Christoph Bartel, Peter Botschwina,* Hans Bürger,* Antonio Guarnieri,* Änne Heyl, Aiko Huckauf, Dieter Lentz,* Tatjana Merzliak, and El Bachir Mkadmi

More than 100 years after the synthesis of the first isocyanides, ethyl isocyanide by Gautier[1] and phenyl isocyanide by Hofmann,[2] we reported the synthesis, microwave study, and structure of the only known alkynyl isocyanide compound HC≡C–NC,[3] which was subsequently detected by Kawaguchi et al.[4] in the interstellar molecular cloud TMC1. Cyano- and isocyanopolyynes are of great interest due to their presence in interstellar space. Fehlhammer and Kunz[5] synthesized the alkynyl isocyanides as ligands on the metal complex fragment $[(CO)_5Cr(CN–C\equiv C–R)]$ (R = H, $SiMe_3$, C_6H_5). Ethynyl isocyanide (R = H) is the parent compound of the isocyanopolyynes, the isomers of cyanopolyynes that have been intensively studied by Kroto and et al.[6] The simplest cyanoisocyanopolyyne, $CN–(C\equiv C)_n–CN$ ($n = 1$), was obtained photochemically in an argon matrix at 16 K, and identified by IR spectroscopy[7] by comparison with the results from ab initio calculations.[8] However, a synthesis that would yield sufficient material for the measurement of rotation and high-resolution IR spectra was hitherto unavailable.

Our synthesis strategy for the preparation of CN–C≡C–CN (**1**) and $CN–(C\equiv C)_n–H$ ($n = 2$) begins with the 2,2-difluoro substituted ethenyl isocyanide complexes **3a**[9] and **3b**, which can be synthesized in good yields and whose substituents can be varied by nucleophilic substitution. The metal complex fragment fulfills several functions at once. First it enables the synthesis of the complex in two steps by radical alkylation of tetraethylammonium pentacarbonyl(cyano)chromate(0) to form the halogenated ethyl isocyanide complexes **2a** and **2b**, and subsequent dehalogenation with zinc in diethyl ether/acetic acid (Scheme 1). Second the $[(CO)_5Cr]$ fragment serves as a protecting group preventing the otherwise facile polymerization of the halogenated isocyanides.[10] Third the finely dispersed metal that is released during the vacuum pyrolysis is used to generate the C–C triple bond by dehalogenation, a reaction which appears to be particularly problematic due to the strength of the C–F bond.



Scheme 1. Synthesis of **2a**, **2b** and **3a**, **3b**.

Nucleophilic substitution of a β-fluorine atom proceeds under remarkably mild conditions with various nucleophiles. Reaction of **3a** and **3b** with potassium cyanide or the alkynyl Grignard reagents RC≡CMgBr (R = H, $SiMe_3$, C_6H_5) yields the complexes **4a** and **4b**, and **5a**–**e**, respectively. Isotope labeling to yield ^{13}CN-**4b** and C^{15}N-**4b**, which are important for spectroscopic investigations, can be readily performed (Scheme 2). Only the β-carbon atom is attacked by the nucleophile.

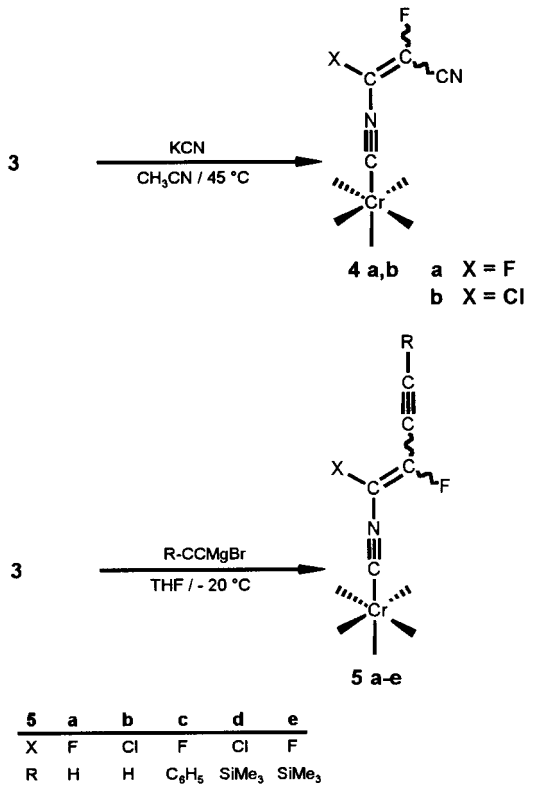
The pyrolysis of **4b** to yield cyanoisocyanoacetylene (3-isocyano-2-propyne nitrile) (**1**) proceeds in a far more complex fashion than the pyrolysis of $[(CO)_5Cr(CN–CCl=CClH)]$ to give HC≡C–NC (Scheme 3).[4] The pyrolysis products identified consist mainly of unconverted **4b**, carbon monoxide, 1-chloro-2-cyano-2-fluoroethenyl isocyanide (**6**), and **1**. The latter condenses during vacuum pyrolysis in a trap cooled to $-196\,^{\circ}C$ and can be separated from **6** by fractional condensation under vacuum. The unequivocal identification of the binary carbon–nitrogen compound **1** was confirmed experimentally by mass spectrometry, high-resolution IR spectroscopy in the frequency range 2000–2400 cm^{-1} and, above all, by millimeter (MMW) wave spectroscopy, which is particularly informative for linear molecules. In addition, MS, IR, and one- and two-dimensional

[*] Prof. P. Botschwina, Ä. Heyl, T. Merzliak
Institut für Physikalische Chemie der Universität
Tammannstrasse 6, D-37077 Göttingen (Germany)
Fax: (+49) 551-39-3144
E-mail: pbotsch@gwdg.de
Prof. H. Bürger, Dr. El B. Mkadmi
Anorganische Chemie der Universität
Gaussstrasse 20, D-42097 Wuppertal (Germany)
Fax: (+49) 202-4392901
E-mail: buerger1@uni-wuppertal.de
Prof. A. Guarnieri, A. Huckauf
Lehrstuhl für Hochfrequenztechnik
Technische Fakultät der Universität
Kaiserstrasse 2, D-24143 Kiel (Germany)
Fax: (+49) 431-77572-453
E-mail: ag@techfak.uni-kiel.de
Dr. D. Lentz, C. Bartel
Institut für Anorganische und Analytische Chemie
der Freien Universität
Fabeckstrasse 34–36, D-14195 Berlin (Germany)
Fax: (+49) 30-838-2424
E-mail: lentz@chemie.fu-berlin.de

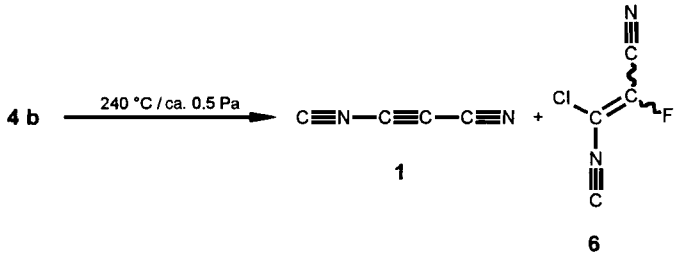
[**] This work was supported by the Fonds der Chemischen Industrie and by the Deutschen Forschungsgemeinschaft (DFG). According to IUPAC the title compound should be named 3-isocyano-2-propyne nitrile.

Supporting information for this article is available on the WWW under http://www.wiley-vch.de/home/angewandte/ or from the author.

 © WILEY-VCH Verlag GmbH, D-69451 Weinheim, 1998 1433-7851/98/3720-2879 $ 17.50+.50/0



Scheme 2. Synthesis of **4a**, **4b** and **5a–e**.



Scheme 3. Synthesis of **1** and **6**.

^{19}F and ^{13}C NMR spectroscopy enabled the identification of the two isomeric ethenyl isocyanide compounds **6**.

New ab initio calculations have been carried out with the CCSD(T) method[11] and Dunning's cc-pVTZ basis set,[12] the results of which have already been reported in part.[13] The CCSD(T) equilibrium structure is given in Figure 1a together with a recommended equilibrium structure (Figure 1b) which

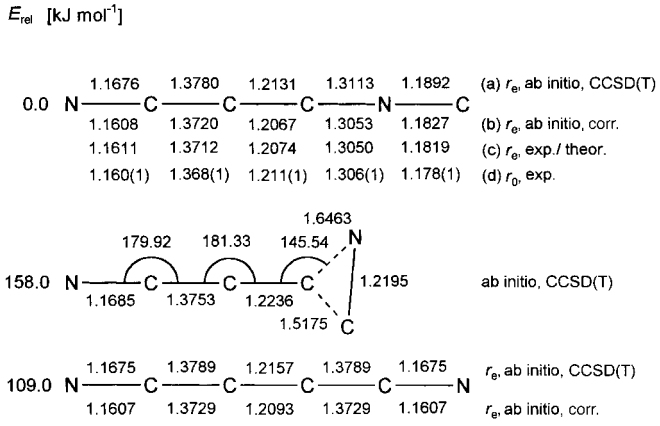


Figure 1. Structure data for **1** (top) and dicyanoacetylene (bottom), and for a planar transition structure that appears during isomerization and corresponds to a saddle point on the potential hypersurface (middle). Energies are given relative to **1** (left). The bond lengths [Å] and angles [°] were obtained by various methods (right). CCSD(T) = coupled cluster single, double and triple excitations.

involves corrections for systematic errors, taken over from HC_5N[14] and HC_2NC.[15] Structure (b) yields an equilibrium rotational constant B_e (NC_3NC) of 1408.58 MHz. Combining it with the CCSD(T) value for the difference $B_0 - B_e$ of 1.05 MHz as obtained from vibration–rotation coupling constants calculated by second-order perturbation theory in normal coordinate space,[16] we arrive at a B_0 prediction of 1409.63 MHz, which proved to be very useful in the search for the MMW spectrum of **1**.

A total of ten isotopomers, which originated from the complexes **4b** and C^{15}N-**4b**, were investigated by MMW spectroscopy. Accurate B_e values (Table 1) were obtained by combination of experimental ground-state values B_0 and theoretical values for the difference $B_e - B_0$. Therefrom, a numerically very stable equilibrium structure (Figure 1c) was obtained through least-squares fit. It agrees with the corrected CCSD(T) equilibrium structure within the joint estimated error bars (ca. 0.0005 Å). Besides C_5O,[17] **1** is the largest linear

Table 1. Rotation and centrifugal-distortion constants for different isotopomers of **1**.

Isotopomer	B_0 [MHz][a]	B_e [MHz][b]	D_0 [Hz][a]	D_e [Hz][c]	N	σ_{Fit} [kHz]
NCCCNC	1409.975270(26)[d]	1408.923	34.5472(37)[d]	31.8	46	6[d]
N^{13}CCCNC	1395.68724(30)	1394.655	34.20(12)	31.4	12	16
NC^{13}CCNC	1408.75194(19)	1407.729	34.483(79)	31.8	14	11
NCC^{13}CNC	1408.30202(19)	1407.262	34.320(86)	31.8	12	9
NCCCN^{13}C	1372.62445(20)	1371.575	32.432(73)	30.0	12	9
^{15}NCCCNC	1374.080484(75)	1373.047	32.805(31)	30.2	10	3
^{15}N^{13}CCCNC	1361.05560(56)	1360.042	31.93(23)	29.7	6	15
^{15}NC^{13}CCNC	1373.07526(38)	1372.070	32.85(16)	30.1	8	11
^{15}NCC^{13}CNC	1372.29168(41)	1371.271	32.27(16)	30.1	7	12
^{15}NCCCN^{13}C	1337.69348(25)	1336.663	31.262(97)	28.4	7	7

[a] Experimental values obtained from millimeter wave spectroscopy. [b] Calculated according to $B_e \approx B_0(\text{exp.}) + \sum_i \alpha_i(\text{theor.}) d_i/2$, where α_i is the vibration–rotation coupling constant and d_i is the degeneracy factor for vibration mode i (d_i: 1 for stretching vibrations, 2 for bending vibrations). [c] Calculated from the corrected equilibrium structure (see Figure 1) and the quadratic force constants for the stretching vibrations (CCSD(T)/cc-pVTZ). [d] The experimental constants for the main isotopomer in the table refer to an adjustment in which the sixth-order centrifugal distortion constant was included; the adjustment yielded $H_0 = 2.08 \times 10^{-6}$ Hz. H_0 could not be determined from the available data for the other isotopomers and was set to zero. N = number of common lines.

 © WILEY-VCH Verlag GmbH, D-69451 Weinheim, 1998 1433-7851/98/3720-2880 $ 17.50+.50/0

molecule for which an equilibrium structure could be determined by these joint experimental and theoretical methods. We also determined a r_0 structure of **1** (Figure 1 d) by least-squares fit to the B_0 values of all ten isotopomers investigated. Comparison with the structures of HCCNC[3] and HCCCN[18] shows that all triple bonds in **1** are somewhat elongated due to increased conjugation, whereas the single bonds are shortened.

The high-resolution IR spectra are very dense due to the presence of "hot" bands that have not yet been analyzed. However the three very intense vibrations ν_1, ν_2, and ν_3, which have estimated relative intensities of 1.5:1:2, were well resolved. The spectroscopic constants for **1** obtained by high-resolution IR spectroscopy are presented in Table 2. They are in excellent agreement with the predictions made from ab initio calculations.[8]

Table 2. Spectroscopic constants for **1**[a] obtained with high-resolution IR spectroscopy.

	$\tilde{\nu}_1$	$\tilde{\nu}_2$	$\tilde{\nu}_3$
$\tilde{\nu}_0$ [cm^{-1}][b]	2295.72337(9)	2209.62521(4)	2052.98160(7)
$(B''-B')\times 10^4$ [cm^{-1}][c]	1.7223(13)	1.16163(13)	0.8413(9)
$(D''-D')\times 10^{10}$ [cm^{-1}]	6.8(3)	0.115(8)	4.95(23)
J_{max}	67	145	66
number of data	110	233	126
$\sigma_{Fit}\times 10^4$ [cm^{-1}]	4.1	3.6	3.7

[a] Millimeter wave data (Table 1) was used to determine B'' and D''. The values in parentheses are the standard deviations. [b] Results from ab initio calculations with the CEPA-1-method: $\tilde{\nu}_1 = 2320.7$, $\tilde{\nu}_2 = 2231.1$, $\tilde{\nu}_3 = 2061.3$ cm^{-1}.[8] [c] Theoretical predictions: 1.69, 1.19, and 0.90×10^{-4} [cm^{-1}].[8]

The energy difference between the potential minima of the isomers N≡C−C≡C−N≡C and N≡C−C≡C−C≡N is 109.0 kJ mol^{-1} (Figure 1). This value is reduced to 107.6 kJ mol^{-1} after inclusion of the zero-point energy. The planar saddle point of the associated isomerization reaction lies 158.0 kJ mol^{-1} above the energy minimum of **1**. The triple bonds remain almost unchanged along the energetically most favorable isomerization pathway; only the N−C bond in the three-membered ring at the saddle point is slightly extended by 0.031 Å.[19]

Due to the modular construction of the precursor complexes from the easily synthesized starting compound **3**, it appears likely that it will be possible to synthesize further alkynyl isocyanides, which might also exist in interstellar space. These compounds might also be detectable by radio astronomy after extensive investigations with various spectroscopic methods. For the chemist, these multifunctional alkynyl and alkenyl isocyanide compounds could be interesting synthesis building blocks and complex ligands. However, extensive investigation of their chemical properties is limited by the fact that only small quantities can be synthesized.

Experimental Section

High-resolution IR spectroscopy: A high-resolution IR spectrum of **1** was recorded at room temperature between 1800 and 2400 cm^{-1} with a Bruker-120HR interferometer. This was equipped with a Globar IR light source, a KBr beam splitter, and an InSb detector cooled by liquid nitrogen. A band-pass filter was used, and the resolution (reciprocal maximum optical path difference) was set at 2.3×10^{-3} cm^{-1}. Peaks from OCS were used for calibration.[20] By using a 28 cm long IR gas cell at a pressure of about 200 Pa, a total of 320 single scans were coadded. Under these conditions, the strongest line had a transmission of about 75 %. The lines were assigned interactively with Loomis – Wood program.[21]

Millimeter wave spectroscopy: The rotation spectra were recorded according to the source double modulation procedure with the MMW spectrometer extensively described in ref. [21]. A Ku band backward wave oscillator (BWO) (HP-8695-A) and a klystron (OKI-20V10) (in combination with an active frequency multiplier) were used as the radiation source in the frequency range 40 to 120 GHz. The higher frequency range (240 to 315 GHz) was covered without further multiplication by a Russian BWO (Istok-OB-30). The measurements were carried out in a 2.40 m long, glass free-absorption cell at a temperature of 28 °C and a pressure of 1 Pa. A liquid-helium-cooled InSb bolometer (Putley detector) was used as the detector. The maximum errors for frequency measurements carried out in this way are about ±5 kHz.

In order to analyze the spectra, the measured absorption frequencies were adjusted according to the least squares method with the expression $\nu = 2B_0(J+1) - 4D_0(J+1)^3 + H_0(J+1)^3[(J+2)^3 - J^3]$ which is valid for a transition of the type $J+1 \leftarrow J$.

Ab initio calculations: The ab initio calculations were performed with the MOLPRO96 program.[23] The CCSD(T) implementation is described in ref. [24, 25].

The NMR spectroscopic investigations were performed with a 400 MHz (^{1}H) multinuclear NMR spectrometer at 22 °C. Unless otherwise stated, $CDCl_3$ was the solvent. The chemical shifts are relative to tetramethylsilane (^{1}H, ^{13}C) and trichlorofluoromethane (^{19}F).

2b: Tetraethylammonium pentacarbonyl(cyano)chromate(0) (5.37 g, 15.4 mmol) was suspended in 1,1,2-trichloro-2,2-difluoroethane (56 g) and the suspension cooled to −78 °C. Phenyldiazonium tetrafluoroborate (3.45 g, 18.0 mmol) was added whilst cooling under reflux (−5 °C) under an inert atmosphere, and the suspension was slowly warmed to 20 °C. After 4 h the solvent was removed at −20 °C and 0.1 Pa. The residue was extracted with pentane. The extract was purified over silica gel with pentane. The first fraction was sublimed on a cold finger (−25 °C) at 30 °C and 0.1 Pa. M.p. 62 °C; ^{13}C NMR: $\delta = 212.6$ (s, CO_{trans}), 212.1 (s, CO_{cis}), 202.8 (s, NC), 124.7 (t, $^1J(C,F) = 303$ Hz, $CClF_2$), 84.9 (t, $^2J(C,F) = 38$ Hz, CCl_2); ^{19}F NMR: $\delta = -65.07$ (s, $CClF_2$); IR (pentane): $\tilde{\nu} = 1986$ (vs), 1955 (m), 1899 (w) cm^{-1}; MS (80 eV): m/z: 385 [M^+], 329 [$M^+ - 2CO$], 301 [$M^+ - 3CO$], 273 [$M^+ - 4CO$], 245 [$M^+ - 5CO$], 210 [$M^+ - 5CO - Cl$], 175 [$M^+ - 5CO - 2Cl$], 78 [$CrCN^+$], 52 [Cr^+].

3b: Compound **2b** (3.8 g, 9.8 mmol) was dissolved in diethyl ether (50 mL) and treated with zinc powder (6.4 g, 98.0 mmol) and acetic acid (2 mL). After stirring for 12 h, the suspension was filtered. The filtrate was purified over silica gel with pentane. The product was isolated from the second fraction. A yellow solid (2.47 g, 7.8 mmol, 80 %) was obtained by sublimation at 35 °C and 0.1 Pa on a cold finger (−25 °C). M.p. 58 °C; ^{13}C NMR: $\delta = 214.6$ (s, CO_{trans}), 213.2 (s, CO_{cis}), 191.2 (s, NC), 156.8 (dd, $^1J(C,F) = 300$, $^1J(C,F) = 294$ Hz, CF_2), 86.3 (dd, $^2J(C,F) = 51$, $^2J(C,F) = 39$ Hz, CCl); ^{19}F NMR: $\delta = -80.64$ (d, $^2J(F,F) = 11.4$ Hz, 1 F, CF_2), −87.97 (d, $^2J(F,F) = 11.4$ Hz, 1 F, CF_2); IR (pentane): $\tilde{\nu} = 2116$ (w), 2029 (s), 1977 (vs), 1946 (m), 1902 (vw), 1731 (m) cm^{-1}; MS (70 eV): m/z: 315 [M^+], 287 [$M^+ - CO$], 259 [$M^+ - 2CO$], 231 [$M^+ - 3CO$], 203 [$M^+ - 4CO$], 175 [$M^+ - 5CO$], 78 [$CrCN^+$], 52 [Cr^+].

4b: Compound **3b** (966 mg, 3.1 mmol) was dissolved in anhydrous acetonitrile (20 mL) and the solution was warmed to 45 °C. Potassium cyanide (586 mg, 9.0 mmol) was added. After stirring for 45 min, the suspension was placed on a silica gel column and eluted with pentane. Two fractions were obtained. Unconverted **3b** was recovered from the first fraction, the second fraction contained the product. A yellow solid (706 mg, 71 %) was obtained by sublimation at 35 °C and 0.1 Pa on a cold finger (−25 °C). M.p. 64 °C; ^{13}C NMR: δ {2nd isomer} = 212.8 {212.6} (s, CO_{trans}), 212.0 (s, CO_{cis}), 203.8 {202.4} (d, $^4J(C,F) = 6$ {5} Hz, NC), 131.3 {131.9} (d, $^1J(C,F) = 259$ {256} Hz, CF), 115.2 {117.4} (d, $^2J(C,F) = 33$ {46} Hz, CCl), 109.4 {108.9} (d, $^2J(C,F) = 40$ {40} Hz, CN); ^{19}F NMR: δ {2nd isomer} = −122.06 {−129.99} (s, 1 F, CF); IR (pentane): $\tilde{\nu} = 1987$ (vs), 1977 (m), 1955

 © WILEY-VCH Verlag GmbH, D-69451 Weinheim, 1998 1433-7851/98/3720-2881 $ 17.50+.50/0

(w), 1900 (vw) cm^{-1}; MS (80 eV): *m/z*: 322 [M^+], 294 [$M^+ - CO$], 266 [$M^+ - 2CO$], 238 [$M^+ - 3CO$], 210 [$M^+ - 4CO$], 182 [$M^+ - 5CO$], 78 [$CrCN^+ - 5CO$], 52 [Cr^+].

^{15}N-**4b**: ^{15}N NMR ($CDCl_3$,CH_3NO_2 ext.): δ {2nd isomer} = −90.5 {−91.9} (s, CF-CN); ^{13}C NMR {2nd isomer}: ^1J(N,C) = 18 {17}, ^2J(N,C) = 3 {4} Hz; ^{13}C-**4b**: ^{13}C NMR {2nd isomer}: ^1J(C,C) = 116 {113}, ^2J(C,C) = 13 {11} Hz.

4a: Synthesis analogous to **4b**. M.p. 35 °C; ^{13}C NMR: δ (*E*{*Z*} isomer) = 211.6 {211.6} (s, CO_{trans}), 211.51 {211.58} (s, CO_{cis}), 209.2 (s, NC), 137.5 {135.8} (dd, ^1J(C,F) = 265 {278}, ^2J(C,F) = 44 {37} Hz, CN*C*F), 123.7 {121.3} (dd, ^1J(C,F) = 240 {251}, ^2J(C,F) = 62 {38} Hz, *C*FCN), 108.1 {109.0} (dd, ^2J(C,F) = 37 {36}, ^3J(C,F) = 10 {3} Hz, CN); ^{19}F NMR: δ (*E*{*Z*} isomer) = −114.8 {−90.0} (d, ^3J(F,F) = 128 {3} Hz, 1F, NCCF), −165.8 {−156.7} (d, ^3J(F,F) = 128 {3} Hz, 1F, CFCN); IR (hexane): $\tilde{\nu}$ = 2015 (w), 1999 (vw), 1986 (vs), 1964 (br) cm^{-1}; MS (70 eV): *m/z*: 306 [M^+], 278 [$M^+ - CO$], 250 [$M^+ - 2CO$], 222 [$M^+ - 3CO$], 194 [$M^+ - 4CO$], 166 [$M^+ - 5CO$], 78 [$CrCN^+$], 52 [Cr^+].

5a–e: General method: The Grignard reagents of the ethyne derivatives (2 equiv) were synthesized according to standard methods[26] in THF and then added to **2** (1 equiv). After 2 h, three times the amount of pentane was added and the suspension was filtered. The product was then purified by sublimation at 0.1 Pa on a cold finger (−20 °C).

5a: ^{1}H NMR: δ(*E*{*Z*} isomer) = 4.10 {3.92} (dd, ^4J(H,F) = 3 {3}, ^5J(H,F) = 1 {3} Hz, 1H, CCH); ^{19}F NMR: δ (*E*{*Z*} isomer) = −127.4 {−108.3} (d {s}, ^3J(F,F) = 127 Hz, 1F, CNCF), −147.5 {−137.8} (dd {d}, ^3J(F,F) = 127, ^4J(H,F) = 3 {3} Hz, 1F, CFCCH); MS (70 eV): *m/z*: 305 [M^+], 277 [$M^+ - CO$], 249 [$M^+ - 2CO$], 221 [$M^+ - 3CO$], 193 [$M^+ - 4CO$], 165 [$M^+ - 5CO$], 52 [Cr^+].

5b: M.p. 32 °C; ^{1}H NMR: δ {2nd isomer} = 4.00 {3.97} (d, ^4J(H,F) = 3 {4} Hz, 1H, CH); ^{13}C NMR: δ {2nd isomer} = 214.5 {214.6} (s, CO_{trans}), 213.2 {213.0} (s, CO_{cis}), 189.0 {193.8} (s, NC), 142.2 {140.4} (dd, ^1J(C,F) = 251 {254}, ^3J(C,H) = 5 {6} Hz, CF), 110.8 {109.9} (d, ^2J(C,F) = 52 {40} Hz, CCl), 93.2 {94.2} (dd, ^1J(C,H) = 261 {261}, ^3J(C,F) = 5 {5} Hz, *C*CH), 70.9 {71.3} (dd, ^2J(C,H) = 51 {51}, ^2J(C,F) = 27 {25} Hz, *C*CH); ^{19}F NMR: δ {2nd isomer} = −110.54 {−105.50} (d, ^4J(F,H) = 3 {4} Hz, 1F, CF).

5c: M.p. (*E*{*Z*} isomer}: 62 {105} °C; ^{19}F NMR: δ (*E*{*Z*} isomer} = −128.4 {−110.7} (d {s}, ^3J(F,F) = 127 Hz, CNCF), −143.4 {−133.6} (d {s}, ^3J(F,F) = 127 Hz, CFCC); MS (70 eV): *m/z*: 381 [M^+], 353 [$M^+ - CO$], 325 [$M^+ - 2CO$], 297 [$M^+ - 3CO$], 269 [$M^+ - 4CO$], 241 [$M^+ - 5CO$], 52 [Cr^+].

5d: M.p. (1st isomer) 83 °C; ^{1}H NMR: δ {2nd isomer} = 0.27 {0.27} (s, 9H, CH_3); ^{13}C{^{1}H} NMR (1st isomer): δ = 214.9 (CO_{trans}), 213.1 (CO_{cis}), 192.4 (NC), 140.7 (d, ^1J(C,F) = 254 Hz, CF), 115.2 (d, ^3J(C,F) = 4 Hz, *C*CSi), 108.8 (d, ^2J(C,F) = 43 Hz, CCl), 90.7 (d, ^2J(C,F) = 34 Hz, *C*CSi), −0.8 (s, CH_3); ^{13}C NMR (2nd isomer): δ = 214.8 (s, CO_{trans}), 213.3 (s, CO_{cis}), 186.9 (s, NC), 142.2 (d, ^1J(C,F) = 250 Hz, CF), 113.8 (m, *C*CSi), 109.5 (d, ^2J(C,F) = 56 Hz, CCl), 90.2 (d, ^2J(C,F) = 35 Hz, *C*CSi), −1.0 (^1J(C,H) = 122, ^3J(C,H) = 2 Hz, CH_3); ^{19}F NMR : δ {2nd isomer} = −109.63 {−104.99} (s); IR (pentane, 2nd isomer): $\tilde{\nu}$ = 2130 (vw), 2112 (w), 2020 (s), 1974 (vs), 1945 (s), 1843 (vw), 1652 (vw) cm^{-1}; MS (70 eV): *m/z*: 393 [M^+], 337 [$M^+ - 2CO$], 309 [$M^+ - 3CO$], 281 [$M^+ - 4CO$], 253 [$M^+ - 5CO$], 132 [$M^+ - Cr(CO)_5 - SiMe_3$], 52 [Cr^+].

5e: ^{1}H NMR: δ (*E* isomer) = 0.24 (s, 9H, CH_3); ^{13}C NMR: δ (*E* isomer) = 214.1 (s, CO_{trans}), 212.7 (s, CO_{cis}), 201.6 (d, ^3J(C,F) = 8 Hz, NC), 136.0 (dd, ^1J(C,F) = 254, ^2J(C,F) = 54 Hz, CNCF), 132.3 (dd, ^1J(C,H) = 237, ^2J(C,F) = 56 Hz, CFCC), 117.1 (m, *C*CSi), 88.5 (dd, ^2J(C,F) = 32, ^3J(C,F) = 10 Hz, *C*CSi), −0.9 (q, ^1J(C,H) = 121 Hz); ^{19}F NMR: δ (*E*{*Z*} isomer) = −128.24 {−110.13} (d {s}, ^3J(F,F) = 127 Hz, NCCF), −144.28 {−134.81} (d, ^3J(F,F) = 127 {3} Hz, CFCC); MS (70 eV): *m/z*: 377 [M^+], 321 [$M^+ - 2CO$], 293 [$M^+ - 3CO$], 265 [$M^+ - 4CO$], 237 [$M^+ - 5CO$], 52 [Cr^+].

1,6: Compound **4b** (526 mg) was pumped at 0.1 Pa through a 20 cm long pyrolysis zone heated to 240 °C. The pyrolysis gas was fed through a grease-free system of cold traps at −78 °C and −196 °C. During pyrolysis, finely dispersed chromium deposited in the heating zone. Five equivalents of carbon monoxide were released. The rate of pyrolysis was adjusted so that the apparatus was under a pressure of about 0.5 Pa.

Unconverted **4b** sublimed in the −78 °C cold trap. The pyrolysis gases condensed at −196 °C were purified by fractional condensation at 0.1 Pa and −100 °C in a −196 °C cold trap. The receiving flask contained essentially only **6**. ^{13}C NMR (CD_2Cl_2, −45 °C): δ {2nd isomer} = {181.1} (s, *C*NC), 133.2 {134.6} (d, ^1J(C,F) = 271 {261} Hz, CF), 109.1 {108.7} (d, ^2J(C,F) = 39 {39} Hz, CCl); ^{19}F NMR (CD_2Cl_2, −45 °C): δ {2. isomer} = −114.47 {−121.13} (s). Compound **1** was condensed at −196 °C together with a small amount of as-yet unidentified gases. IR (gas): $\tilde{\nu}_1$ = 2296, $\tilde{\nu}_2$ = 2210 and $\tilde{\nu}_3$ = 2053 cm^{-1}.

Received: May 28, 1998 [Z 11909 IE]
German version: *Angew. Chem.* **1998**, *110*, 3036–3040

Keywords: alkynes · chromium · isocyanides · nitriles · structure elucidation

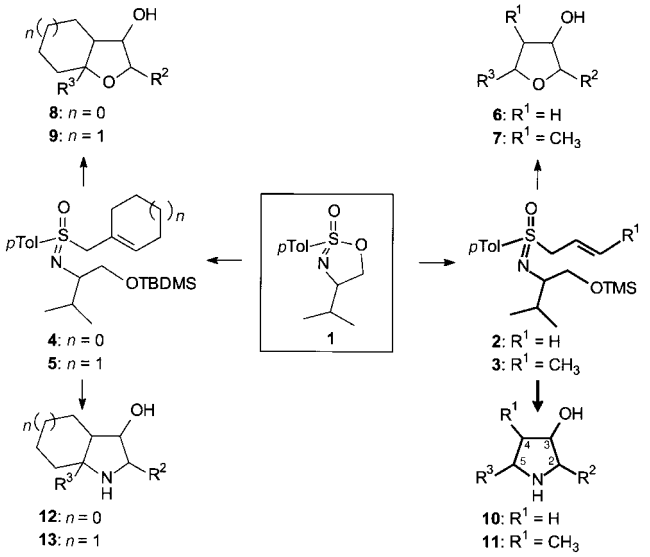
[1] A. Gautier, *Justus Liebigs Ann. Chem.* **1867**, *142*, 289; A. Gautier, *Justus Liebigs Ann. Chem.* **1868**, *146*, 124.
[2] A. W. Hofmann, *Justus Liebigs Ann. Chem.* **1867**, *144*, 114; A. W. Hofmann, *Justus Liebigs Ann. Chem.* **1868**, *146*, 107.
[3] M. Krüger, H. Dreizler, D. Preugschat, D. Lentz, *Angew. Chem.* **1991**, *113*, 1674; *Angew. Chem. Int. Ed. Engl.* **1991**, *30*, 1644.
[4] K. Kawaguchi, M. Ohishi, S.-I. Ishikawa, N. Kaifu, *Astrophys. J.* **1992**, *386*, L51.
[5] R. Kunz, W. P. Fehlhammer, *Angew. Chem.* **1994**, *106*, 331; *Angew. Chem. Int. Ed. Engl.* **1994**, *33*, 330.
[6] See for example: H. W. Kroto, *Angew. Chem.* **1992**, *104*, 113; *Angew. Chem. Int. Ed. Engl.* **1992**, *31*, 111; R. F. Curl, *Angew. Chem.* **1997**, *109*, 1636; *Angew. Chem. Int. Ed. Engl.* **1997**, *36*, 1566; H. W. Kroto, *Angew. Chem.* **1997**, *109*, 1649; *Angew. Chem. Int. Ed. Engl.* **1997**, *36*, 1578; R. E. Smalley, *Angew. Chem.* **1997**, *109*, 1667; *Angew. Chem. Int. Ed. Engl.* **1997**, *36*, 1594, and references therein.
[7] A. Smith, G. Schallmoser, A. Thoma, V. Bondybey, *J. Chem. Phys.* **1993**, *98*, 1776.
[8] P. Botschwina, M. Horn, J. Flügge, S. Seeger, *J. Chem. Soc. Faraday Trans.* **1993**, *89*, 2219; M. Horn, P. Botschwina, J. Flügge, *Theoret. Chim. Acta* **1994**, *88*, 1.
[9] D. Lentz, D. Preugschat, *J. Chem. Soc. Chem. Commun.* **1992**, 1523.
[10] D. Lentz, *Angew. Chem.* **1994**, *106*, 1377; *Angew. Chem. Int. Ed. Engl.* **1994**, *33*, 1315.
[11] K. Raghavachari, G. W. Trucks, J. A. Pople, M. Head-Gordon, *Chem. Phys. Lett.* **1989**, *157*, 479.
[12] T. H. Dunning, *J. Chem. Phys.* **1989**, *90*, 1007.
[13] P. Botschwina, Ä. Heyl, M. Horn, presented at the 15th Colloquium on High Resolution Molecular Spectroscopy, Glasgow, Great Britain, **1997** (Poster F17).
[14] P. Botschwina, Ä. Heyl, M. Oswald, T. Hirano, *Spectrochim. Acta A* **1997**, *53*, 1079.
[15] P. Botschwina, M. Horn, S. Seeger, J. Flügge, *Chem. Phys. Lett.* **1992**, *195*, 427, **1992**, *200*, 651.
[16] I. M. Mills in *Molecular Spectroscopy: Modern research* (Eds.: K. N. Rao, C. W. Matthews), Academic Press, New York, **1972**, pp. 115–140.
[17] P. Botschwina, J. Flügge, P. Sebald, *J. Phys. Chem.* **1995**, *99*, 9755.
[18] M. D. Harmony, V. W. Laurie, R. L. Kuezkowski, R. E. Schwendeman, D. A. Ramsay, F. J. Lovas, W. J. Lafferty, A. G. Maki, *J. Phys. Chem. Ref. Data* **1979**, *9*, 619.
[19] An extensive discussion of the potential hypersurface in the region of the saddle point and a comparison with results obtained from various other methods will be given elsewhere: P. Botschwina, V. Dyczmons, T. Merzliak, unpublished results.
[20] Wavenumber calibration tables from heterodyne frequency measurements: A. G. Maki, J. S. Wells, *NIST Spec. Publ.* **1991**, 821.
[21] J. Doose, A. Guarnieri, W. Neustock, R. Schwarz, F. Winther, F. Hegelund, *Z. Naturforsch. A* **1989**, *44*, 538.
[22] B. P. Winnewisser, J. Reinstädtler, K. M. T. Yamada, J. Behrend, *J. Mol. Spectrosc.* **1989**, *136*, 12.
[23] MOLPRO96 is an ab initio program package from H.-J. Werner and P. J. Knowles with contributions from J. Almlöf, R. D. Amos, M. J. O. Deegan, S. T. Elbert, C. Hampel, W. Meyer, K. A. Peterson, R. Pitzer, A. J. Stone, P. R. Taylor, R. Lindh, M. E. Mura, T. Thorsteinson.
[24] C. Hampel, K. Peterson, H.-J. Werner, *Chem. Phys. Lett.* **1992**, *190*, 1.
[25] M. J. O. Deegan, P. J. Knowles, *Chem. Phys. Lett.* **1994**, *227*, 321.
[26] L. Brandsma, *Preparative Acetylenic Chemistry*, 2nd ed., Elsevier, Amsterdam, **1988**.

 © WILEY-VCH Verlag GmbH, D-69451 Weinheim, 1998 1433-7851/98/3720-2882 $ 17.50+.50/0

Metalated 2-Alkenylsulfoximides in Asymmetric Synthesis: Diastereoselective Preparation of Highly Substituted Pyrrolidine Derivatives**

Michael Reggelin* and Timo Heinrich

Enantiomerically pure metalated 2-alkenylsulfoximides from cyclic sulfonimidates **1**[1] were introduced in 1994 and proved to be efficient asymmetric d^3-synthons.[2, 3] The isomerically pure, highly substituted tetrahydofuranes **6** and **7**[4] (derived from the open-chain precursors **2** and **3**) as well as the oxabicyclic systems **8** and **9**[3] (derived from **4** and **5**) could be synthesized efficiently by use of reagent **1** (Scheme 1).[2, 4]

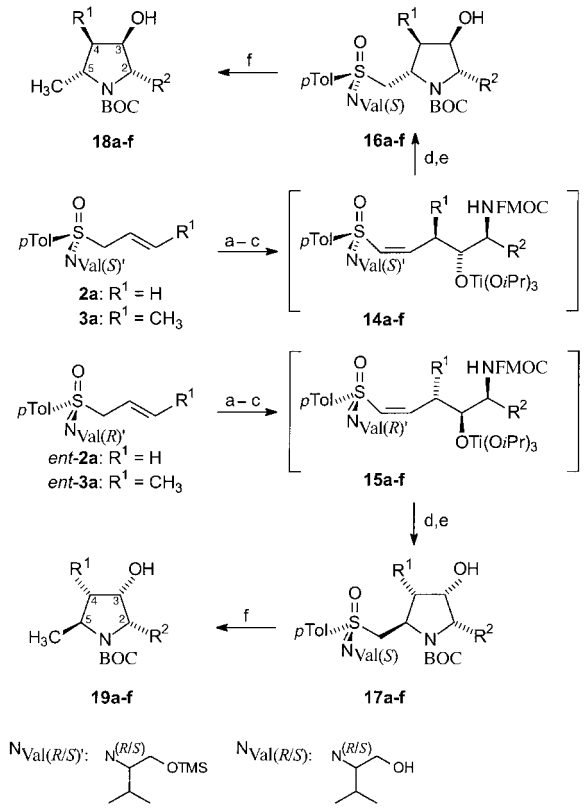


Scheme 1. Heterocyclic compounds available from the cyclic sulfonimidate **1**. R^2 = alkyl, alkaryl, alkheteroaryl; $R^3 = CH_2S(O)(p\text{Tol})N_{val}$, vinyl, methyl. TMS = trimethylsilyl, TBDMS = *tert*-butyldimethylsilyl.

Based on these results, the extension of our method to the synthesis of azamono- (**10** and **11**) and azabicycles (**12** and **13**) seems to be rather promising. Here we describe the stereoselective synthesis of enantiomerically pure, highly substituted pyrrolidine derivatives **10** and **11**. This structural element is found in various biologically active alkaloids[5] such as glycosidase inhibitors,[6] excitatoric aminoacid antagonists,[7] or ACE inhibitors (ACE = acetylcholinesterase).[8] Furthermore, pyrrolidine derivatives are important as catalysts in asymmetric synthesis, for example in the addition of dialkyltin compounds to aldehydes,[9] in the enantioselective reduction of ketones,[10] or in asymmetric Diels–Alder reactions.[11]

A number of methods are available for establishing the five-membered heterocyclic ring with two to four substituents.[12] Many of these possible entries are restricted in their constitutional and configurational versatility; these limits also hold for approaches from natural precursors.[13] The 1,3-dipolar cycloaddition of azomethine-ylides to olefins or acetylene dipolarophiles controlled by chiral auxiliaries[14] is a common way to obtain pyrrolidines. The electronic demands of the dipolarophile necessitate the formation of 2-alkoxycarbonyl-substituted derivatives. However, this method has been applied for the synthesis of combinatorial libraries, which suggests the importance of these substances for pharmaceutical purposes.[15]

Here we demonstrate that the addition of α-aminoaldehydes to titanated 2-alkenylsulfoximides offers a versatile approach to a multitude of highly substituted pyrrolidines in good yields (Scheme 2, Table 1). In contrast to the protocol



Scheme 2. Synthesis of pyrrolidines **18a–f** and **19a–f**, starting from open-chain 2-alkenylsulfoximides. a) *n*BuLi, −78 °C. b) Chlorotris(isopropoxy)-titanium, 0 °C. c) **21a–c**, −78 °C. d) Piperidine, 20 °C; $(NH_4)_2CO_3$, NH_4Cl. e) K_2CO_3, MeOH; BOC_2O, $NaHCO_3$. f) SmI_2. FMOC = (9H-fluoren-9-ylmethoxy)carbonyl.

described earlier,[2, 3] we used toluene instead of THF as solvent for the deprotonation and transmetalation of the allylsulfoximides **2a** and **3a** as well as their enantiomers (*ent*-**2a** and *ent*-**3a**). Only in this solvent are high yields and very high diastereoselectivities obtained ($ds \geq 96\%$, determined by NMR spectroscopy from the crude product). The FMOC-protected α-aminoaldehydes were generated without racemization by Dess–Martin oxidation[16] of the corresponding

[*] Priv.-Doz. Dr. M. Reggelin, T. Heinrich
Fachbereich Chemie der Universität
Marie-Curie-Strasse 11, D-60439 Frankfurt/Main (Germany)
Fax: (+49) 69-7982-9128
E-mail: re@krypton.org.chemie.uni-frankfurt.de

[**] This work was supported by the DFG (Re 1007/1–4) and Solvay Pharmaceuticals GmbH (Hannover, Germany). Continous support by Prof. Dr. C. Griesinger is gratefully acknowledged. We thank the Degussa AG for generous gifts of amino acids.

Table 1. Highly substituted pyrrolidines from metalated 2-alkenylsulfoximides.

Compd	R^1	R^2	Yield [%]	*ds* [%][a]	$[\alpha]_D^{20}$ [°][b]	M.p [°C]
18a	H	Bn	27	67	−37.71 (0.4)	108.5
18b	H	*i*Bu	23	65	+28.17 (0.6)	oil
18c	H	*t*BuOCH$_2$	21	68	+24.46 (0.8)	115.7
18d	CH$_3$	Bn	63	≥96	−37.29 (1.0)	127.8
18e	CH$_3$	*i*Bu	42	≥96	−19.99 (0.9)	96.9
18f	CH$_3$	*t*BuOCH$_2$	44	≥96	+14.80 (0.3)	oil
19a	H	Bn	33	59	+6.52 (1.4)	107.7
19b	H	*i*Bu	36	67	−37.29 (1.0)	oil
19c[c]	H	*t*BuOCH$_2$	31	54	+1.80 (0.3)	93.1
19d	CH$_3$	Bn	43	≥96	+26.70 (1.0)	91.0
19e	CH$_3$	*i*Bu	34	≥96	+66.20 (1.0)	97.3
19f[c]	CH$_3$	*t*BuOCH$_2$	30	≥96	−20.80 (0.3)	187.2

[a] Determined from the ^{1}H NMR spectra of the crude products. [b] *c* in dichloromethane. [c] Deprotected at nitrogen and isolated as the *p*-toluenesulfonate; optical rotation recorded in methanol.

amino alcohols, and were allowed to react without further purification.[17]

After deprotonation of the sulfoximides with *n*BuLi, transmetalation with chlorotris(isopropoxy)titanium (ClTIPT), and addition of the protected aldehydes, O-titanated 5-amino-4-hydoxyvinylsulfoximides **14a–f** and **15a–f** were formed but not isolated (Scheme 2). After one hour piperidine (10 equiv) was added at −78 °C to deprotect the nitrogen atom, which attacked the acceptor-substituted double bond of the vinylsulfoximide (Figure 1). After crystallization of the

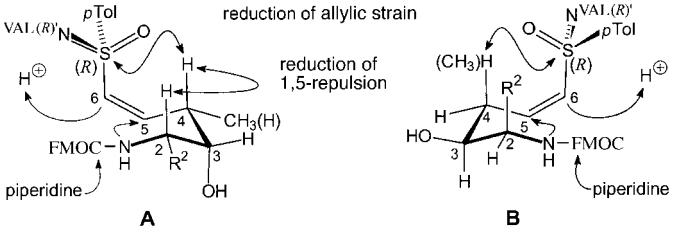


Figure 1. Stereochemical aspects of the cyclization. The topicity of the attack of the nitrogen atom on the 5-position is directed by two conformational aspects: reduction of allylic strain and 1,5-repulsion.

dibenzofulvene–piperidine adduct from methanol and column filtration, the silyl ether group in the auxiliary was cleaved by solvolysis and the pyrrolidine nitrogen atom was protected with a *tert*-butoxycarbamoyl group. The removal of the auxiliary from the resulting 5-sulfonimidoylmethyl-substituted heterocycles **16a–f** and **17a–f** was successful with samarium diiodide in methanol/THF (1/2). This way of desulfuration is described here for the first time and is superior to alternative methods described in the literature.[18] It is essential to manipulate the heteroatoms as described above. If the silyl ether is still present no reaction occurs,[19] and an open-chain homoallylamine is formed if the pyrrolidine nitrogen atom is deprotected.

After recording a ^{15}N–^{1}H HMBC spectrum[20] of **20**, the cyclization product of **14e**, we were able to verify the successful pyrrolidine synthesis (Figure 2). The pyrrolidine nitrogen atom resonates at $\delta = 56.6$ and shows two $^3J_{NH}$ correlations to the methylene group adjacent to the sulfur

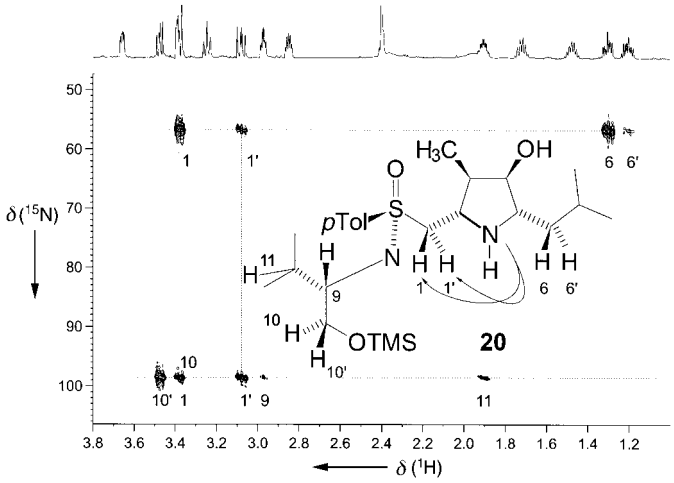


Figure 2. Part of the ^{15}N–^{1}H HMBC spectrum of **20**. Verification of the cyclization (thick bond) is provided by the correlation of the pyrrolidine nitrogen atom to the protons (1, 1′) of the sulfonimidoylmethyl group.

atom (H-1 and H-1′). This is possible only if the cyclization had taken place. The relative and absolute configuration of the pyrrolidines derived from the crotylsulfoximide **3a** (*S* configuration at sulfur) could be verified by X-ray structure analysis of the N-tosylated derivative prepared from **14d**.[21] As expected the absolute configurations of the pyrrolidine alcohol center
(C-3) and the neighboring C-4 atom resulted from a *Re*-side attack of the allyl moiety on the *Re* side of the α-aminoaldehyde (*lk* process).[2, 3] In agreement with our interpretation of the stereochemical outcome of the cyclization process, the sulfonimidoylmethyl fragment is always oriented *trans* to the hydroxyl functionality at C-3.[4] As expected, for the series of crotylsulfoximides obtained from *ent*-**3a** (*R* configuration at sulfur), the induced absolute configurations were the result of a *Si*,*Si* process. This was verified by X-ray structure analysis of the pyrrolidine **19d**.[22]

The total control of the absolute configurations at the newly formed stereogenic centers at C-3 and C-4 in the pyrrolidines **19a–f** merits comment. The addition of a 2-alkenylsulfoximide with the absolute configuration *R* at sulfur to a *S*-configurated α-aminoaldehyde represents an intermolecular "mismatched pair",[23] because the preferred topicity of the nucleophile (*Si*) does not correlate with the Cram side of the aldehyde (*Re*). In perfect agreement with our results with the lactaldehydes,[2, 3] the stereochemical bias excerted by the α-chiral aldehyde is totally overcompensated (reagent control).

The absence of the terminal methyl group in the parent systems (**2a** and *ent*-**2a**) results in a decrease in the stereocontrol at C-5, as already discussed for the THF derivatives (Figure 1).[4] The topicity of attack of the nitrogen nucleophile onto the 5-position is dominated by the attempt of the system to minimize allylic strain and 1,5-repulsion. For the vinylsulfoximides **3**, which lead to the 4-methyl-substituted pyrrolidines, there exists an optimal solution, conformation A. In contrast, derivatives **2**, which lead to the 4-unsubstituted pyrrolidines, can also react via conformation B. In this arrangement the absolute topicity of the attack on the 5-position is inverted. With respect to the 1,5-interaction, B

 © WILEY-VCH Verlag GmbH, D-69451 Weinheim, 1998 1433-7851/98/3720-2884 $ 17.50+.50/0 *Angew. Chem. Int. Ed.* **1998**, *37*, No. 20

is less stable than A. Within this model, the desired 3,5-*trans* product, the result of a cyclization via A, should be formed in slight excess, which is indeed the case (Table 1). Structural verification was again achieved by X-ray structure analysis of the minor compounds 5-*epi*-**19a** and 5-*epi*-**18a**, confirming the predicted 3,5-*cis* relative configuration.[24]

Our results can be summerized as follows:

1) The γ-hydroxyalkylation of the enantiomeric allyl- and crotylsulfoximides **2a**/**3a** and *ent*-**2a**/*ent*-**3a**, respectively, with α-aminoaldehydes results in the formation of isomerically pure vinylsulfoximides **14** and **15**, which can be transformed to highly substituted pyrrolidines **16** and **17** with piperidine as a deblocking agent.

2) The absolute configuration at the newly formed stereogenic centers C-3 and C-4 is controlled by the absolute configuration at sulfur (reagent control). The configuration at C-5 is the result of conformational preferences of the cyclization precursor. Therefore only 3-substituted derivatives allow total control of this stereogenic center.

3) Samarium diiodide was introducted as a superior desulfuration agent.

The expansion of this new strategy to synthesize isomerically pure, saturated nitrogen heterocycles such as substituted 1- and 2-azabi- and -tricyclic derivatives by proper combination of open-chain or cyclic 2-alkenylsulfoximides with open-chain or cyclic α-aminoaldehydes was already successful (e.g. **12**, **13**, Scheme 1) and will be published in due course. Furthermore, we found that with certain pharmacophoric substituents R^2 and after installation of such substituents at the free OH group (e.g. by benzylation), a number of biologically active substances are available.[25]

Experimental Section

18d: To a solution of **3a** (329 mg, 0.89 mmol) in toluene (2 mL) was added *n*BuLi (492 mg, 2.27 mmol g^{-1} in hexane) at $-78\,^{\circ}$C by syringe. After 15 min ClTIPT (487 mg, 2.50 mmol g^{-1}) was added, and the mixture was warmed to $0\,^{\circ}$C and stirred for 30 min. The mixture was again cooled to $-78\,^{\circ}$C, **21a** (754 mg, 1.79 mmol) dissolved in THF (3 mL) was added, and the mixture was stirred at $-78\,^{\circ}$C for 60 min. Piperidine (0.9 mL, 8.90 mmol) was added, and the temperature was raised to $0\,^{\circ}$C. After 10 h the reaction mixture was poured onto a well-mixed, saturated solution of $(NH_4)_2CO_3$ (25 mL) layered with ethyl acetate (4 mL). After 30 min two clear phases could be separated. The aqueous phase was extracted three times with ethyl acetate (10 mL), and the combined organic layers were extracted with a saturated solution of NH_4Cl. After the organic phase was dried over Na_2SO_4 and the solvent was evaporated in vacuo, the benzofulvene–piperidine adduct was crystallized from methanol. The resulting crude product was purified by column filtration (eluent: diethyl ether/hexane 1/1; ethyl acetate), and the obtained polar fraction was treated with K_2CO_3 (136 mg, 0.99 mmol) in methanol (3 mL). The pyrrolidine (desilylated **3a**) nitrogen atom was protected with di-*tert*-butoxycarbonate (BOC_2O, 350 mg, 1.60 mmol) and $NaHCO_3$ (100 mg, 1.2 mmol) in dioxane (4 mL) and water (8 mL). Then residual **3a** and unchanged BOC_2O were removed by flash chromatography.

To remove the chiral auxiliary samarium (545 mg, 3.63 mmol) was suspended in THF (12 mL), and diiodomethane (860 mg, 3.21 mmol) was added by syringe at $0\,^{\circ}$C. After 15 min the reaction was maintained at room temperature for 60 min, and the pyrrolidine was added in methanol (1.5 mL) and THF (3 mL). To quench the reaction, the mixture was poured into a saturated solution of NH_4Cl (20 mL), and 0.5 N HCl was added until two clear phases resulted. After the organic layer was extracted three times with diethyl ether (20 mL), and the pyrrolidine was purified by flash chromatography (diethyl ether/hexane 1/1) to yield 129 mg of **18d** (63 %). M.p. 127.8 °C; $[\alpha]_D^{20} = -37.29$ ($c = 1.00$ in dichloromethane); ^{1}H NMR (270 MHz, [D$_{10}$]xylol, 80 °C): $\delta = 0.849$ (d, $^3J = 6.9$ Hz, 3H; 4-CH$_3$), 1.230 (d, $^3J = 6.1$ Hz, 3H; 5-CH$_3$), 1.448 (s, 9H; C(CH$_3$)$_3$), 1.618 (dqq, $^3J = 8.8$, $^3J = 6.9$, $^3J = 6.1$ Hz, 1H; 4-H), 2.459 (dd, $^3J = 9.4$, $^2J = 13.6$ Hz, 1H; A-H), 2.988 (dd, $^3J = 4.6$, $^2J = 13.6$ Hz, 1H; B-H), 3.427 (dq, $^3J = 8.8$, $^3J = 6.1$ Hz, 1H; 5-H), 3.591 (br s, 1H; 3-H), 3.934 (ddd, $^3J = 9.4$, $^3J = 4.6$, $^3J = 5.7$ Hz, 1H; 2-H), 7.013–7.177 (m, 5H; arom.); ^{13}C NMR (67.9 MHz, [D$_{10}$]xylol, 80 °C): $\delta = 11.12$ (C-4′), 19.44 (C-5′), 28.88 (C(*C*H$_3$)), 40.97 (C-A/B), 44.62 (C-4), 59.33 (C-5), 69.46 (C-2), 75.73 (C-3), 79.00 (*C*(CH$_3$)), 126.71, 128.63, 129.23 (5C, arom.), 139.75 (*ipso*-arom.), 154.49 (C=O); IR (KBr): $\tilde{\nu} =$ 3430.1 (OH), 2973.0, 2930.6 (CH$_3$), 1672.4 (C=O) cm^{-1}; elemental analysis calcd for $C_{18}H_{27}NO_3$ (305.41): C 70.79, H 8.91, N 4.59; found: C 70.59, H 8.93, N 4.63.

Received: May 28, 1998 [Z11917IE]
German version: *Angew. Chem.* **1998**, *110*, 3005–3008

Keywords: asymmetric synthesis · heterocycles · pyrrolidines · samarium · sulfoximines

[1] a) M. Reggelin, H. Weinberger, *Tetrahedron Lett.* **1992**, *33*, 6959–6962; b) M. Reggelin, R. Welcker, *Tetrahedron Lett.* **1995**, *36*, 5885–5886.
[2] M. Reggelin, H. Weinberger, *Angew. Chem.* **1994**, *106*, 489–491; *Angew. Chem. Int. Ed. Engl.* **1994**, *33*, 444–446.
[3] a) M. Reggelin, H. Weinberger, M. Gerlach, R. Welcker, *J. Am. Chem. Soc.* **1996**, *118*, 4765–4777; b) M. Reggelin, M. Gerlach, M. Vogt, unpublished results.
[4] M. Reggelin, H. Weinberger, T. Heinrich, *Liebigs Ann.* **1997**, 1881–1886.
[5] W. H. Pearson in *Studies in Natural Product Chemistry*, *Vol. 1* (Ed.: Atta-Ur-Rahman), Elsevier, Amsterdam, 1988, pp. 323–358.
[6] a) G. W. Fleet, *Top. Med. Chem.* **1988**, *65*, 149–162; b) R. T. Schwarz, R. Datema, *Trends Biochem. Sci.* **1984**, *9*, 32–34; c) V. Wehner, V. Jäger, *Angew. Chem.* **1990**, *102*, 1180–1182; *Angew. Chem. Int. Ed. Engl.* **1990**, *29*, 1169–1171, and references therein.
[7] R. J. Bridges, F. E. Lovering, J. M. Humphrey, M. S. Stanley, T. N. Blakely, M. F. Cristopharo, A. R. Chamberlin, *Bioorg. Med. Chem. Lett.* **1993**, *3*, 115–121, and references therein.
[8] a) E. W. Petrillo, M. A. Ondetti, *Med. Res. Rev.* **1982**, *2*, 1–41; b) H. S. Cheung, D. W. Cushman, *Biochim. Biophys. Acta.* **1973**, *293*, 451–463.
[9] K. Soai, S. Niwa, *Chem. Rev.* **1992**, *92*, 833–856.
[10] E. J. Corey, R. K. Bakshi, S. J. Shibata, *J. Am. Chem. Soc.* **1987**, *105*, 5551–5553.
[11] S. Kobayashi, M. Murakami, T. Harada, T. Mukayama, *Chem. Lett.* **1991**, 1341–1344.
[12] M. Pichon, B. Figadère, *Tetrahedron: Asymmetry* **1996**, *7*, 927–964.
[13] a) R. H. Wightman, *Tetrahedron* **1993**, *49*, 3827–3840; b) F. Nicotra, *Tetrahedron Lett.* **1993**, *34*, 4555–4558; c) C. Kibayashi, *J. Org. Chem.* **1987**, *32*, 1956–1962; d) T. Livinghouse, *J. Am. Chem. Soc.* **1993**, *115*, 11458–11489.
[14] a) P. Deprez, J. Royer, H. P. Husson, *Tetrahedron: Asymmetry* **1991**, *2*, 1189–1192; b) P. Garner, W. B. Ho, *J. Org. Chem.* **1990**, *55*, 3973–3975; c) P. Garner, F. Arya, W. B. Ho, *J. Org. Chem.* **1990**, *55*, 412–414; d) R. M. Williams, W. Zhai, D. Aldous, S. C. Aldous, *J. Org. Chem.* **1992**, 57, 6527–6532, zit. Lit.; e) W. J. Lown in *1,3-Dipolar Cycloaddition Chemistry*, *Vol. 1* (Ed.: A. Padwa), Wiley, New York, **1984**.
[15] a) G. Liu, J. A. Ellman, *J. Org. Chem.* **1995**, *60*, 7712–7713. b) M. M. Murphy, J. R. Schullek, E. M. Gordon, M. A. Gallop, *J. Am. Chem. Soc.* **1995**, *117*, 7029–7030.
[16] a) D. B. Dess, J. C. Martin, *J. Am. Chem. Soc.* **1991**, *113*, 7277–7287; b) D. B. Dess, J. C. Martin, *J. Org. Chem.* **1983**, *48*, 4156–4158.
[17] After addition of 84 mol % of the chiral shift reagent Pr(hfc)$_3$, the enantiomeric excess of the aldehydes could be determined by integration of the ^{1}H NMR signal of the aldehyde protons: M. Reggelin, T. Heinrich, unpublished results.
[18] Raney Nickel requires a large excess (> 10 equiv) to provide satisfying results, and much of the pyrrolidine formed is absorbed. Lithium naphthalenide works fast, but ring-opened by-products are formed.

 © WILEY-VCH Verlag GmbH, D-69451 Weinheim, 1998 1433-7851/98/3720-2885 $ 17.50+.50/0

[19] Desilyation of the TMS-protected derivative occurs by solvolysis during the desulfuration. More stable silyl ethers must be previously cleaved in an extra step.
[20] $^{13}C-^{1}H$ HMBC: A. Bax, M. F. Summers, *J. Am. Chem. Soc.* **1986**, *108*, 2093 – 2094.
[21] M. Bolte, *Acta Crystallogr. Sect. C* **1997**, *C53*, *IUC 9700029*.
[22] J. Bats, T. Heinrich, M. Reggelin, *Acta Crystallogr. Sect. C*, submitted.
[23] S. Masamune, W. Choy, J. S. Petersen, L. R. Sita, *Angew. Chem.* **1985**, *97*, 1 – 31; *Angew. Chem. Int. Ed. Engl.* **1985**, *24*, 1 – 30.
[24] J. Bats, T. Heinrich, M. Reggelin, *Acta Crystallogr. Sect. C*, eingereicht.
[25] M. Reggelin, T. Heinrich, B. Junker, J. Antel, U. Preuschoff, DE-B 19821418.9, **1998**.

Synthesis and Properties of Lanthanum – Pyrene Complexes—Structure of $[(Cp^*La)_3(\mu\text{-}Cl)_3(thf)(\mu\text{-}\eta^2\text{:}\eta^6\text{-}C_{16}H_{10})]$, the First Complex with a Pyrene Trianion**

Karl-Heinz Thiele,* Sergio Bambirra, Joachim Sieler, and Svea Yelonek

The reduction of polyarenes with alkali metals in ethers leads to compounds in which ether-stabilized contact-ion pairs,[1] triples,[2] or even quintuples[3] occur. The known magnesium anthracene[4] and probably also some naphthalene complexes of europium, samarium, and ytterbium[5] are similarly built. Complexes of trivalent lanthanoids with naphthalene and anthracene have also been described in the last few years.[6] In this context, the reduction of benzanthracene, pyrene, and acenaphthylene with decamethylsamarocene to form dinuclear complexes is of particular interest.[7] In these compounds, η^2, η^3, η^4, and η^5 bonds are found between the metal atom and the arene.

Most organolanthanoid compounds examined so far contain $\{(C_5H_5)_2Ln\}$ and $\{(C_5Me_5)_2Ln\}$ units. Reactions of $[CpLnX_2]$ derivatives, for which diverse conversions with condensed aromatic hydrocarbons in the presence of alkali metals can be expected, have been far less extensively investigated. We report here on the synthesis, structure, and bonding of lanthanum – pyrene complexes with partly novel and completely unexpected coordination modes.

In the reaction of $[Cp^*LaCl](\mu\text{-}Cl)_2Li(thf)_2]$ (**1**) in toluene with pyrene and potassium under the strictest exclusion of air and moisture, a red-violet solution is obtained from which the pyrene complex $[(Cp^*LaCl)_3(C_{16}H_{10})]\cdot thf$ (**2**) was isolated in the form of red-violet, extremely air-sensitive crystals ($Cp^* = C_5Me_5$). Unusual bonding modes prevail in **2**, in which La atoms are coordinated in two different ways. According to the crystal-structure analysis,[8] La1 and La2 are positioned above opposite rings of the pyrene molecule in a η^6 coordination hitherto unknown in polyarene complexes of the lanthanoids, and the La – C bond lengths lie between 2.76 and 3.07 Å (Figure 1). La3 is η^2-bound to one of the middle rings of the pyrene molecule. The La3 – C4 and La3 – C5 distances of 2.82 and 2.84 Å, respectively, are almost identical. Thus, La3 is coordinatively unsaturated and sterically less shielded, which is compensated at least in part by the addition of a THF molecule. Therefore, La1 and La2 form the centers of distorted tetrahedrons and both have a coordination number (CN) of eight, whereas La3 with CN = 7 is arranged in a distorted trigonal bypramid. Pyrene, which is planar when uncoordinated, is slightly twisted in **2**. The atoms C9 and C14 lie 0.115(9) and 0.095(9) Å, respectively, above the plane determined for the $C_{16}H_{10}$ system, with C11 and C12 both lying 0.095(10) Å below it. As with the $\{La_3(pyrene)\}$system, the pyrene unit thus adopts trianionic character.[9] Compound **2** can also be understood as a trinuclear complex with a phenanthrene bridge to which a noncoordinated double bond is attached; this view is supported by the strongly differing bond lengths C4 – C5 and C11 – C12 of 1.41 and 1.35 Å, respectively. The angles of the perpendiculars of the Cp*La and LaC_6 fragments are 128.13° and 128.56°, respectively, for La1 and La2, and thus lie between those values for $[\{Cp_3La\}_n]$[10] and $\{Cp^*_2La\}$ systems.[11]

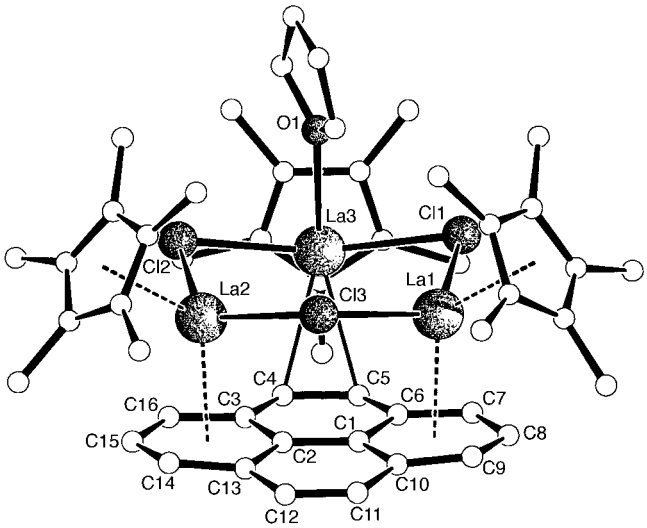


Figure 1. Structure of **2** in the crystal. Selected bond lengths [Å] and angles [°]: La1 – C1 3.047(9), La1 – C6 3.072(8), La1 – C7 2.951(8), La1 – C8 2.843(8), La1 – C9 2.766(8), La1 – C10 2.936(9), La2 – C2 3.014(8), La2 – C3 3.061(8), La2 – C16 2.951(9), La2 – C15 2.872(11), La2 – C14 2.903(10), La2 – C13 2.959(9), La3 – C4 2.823(9), La3 – C5 2.841(8), La – Cl 2.810(3) – 2.894(2), La3 – O1 2.694(7), C11 – C12 1.35(2), C4 – C5 1.417(13); La3-Cl1-La1 93.96(8), La3-Cl2-La2 94.04(6), La1-Cl3-La2 102.10(6)

These results indicate that the formation of **2**, a compound with different coordination modes for La atoms bound in the complex, can be described by Equation (1). The reaction of

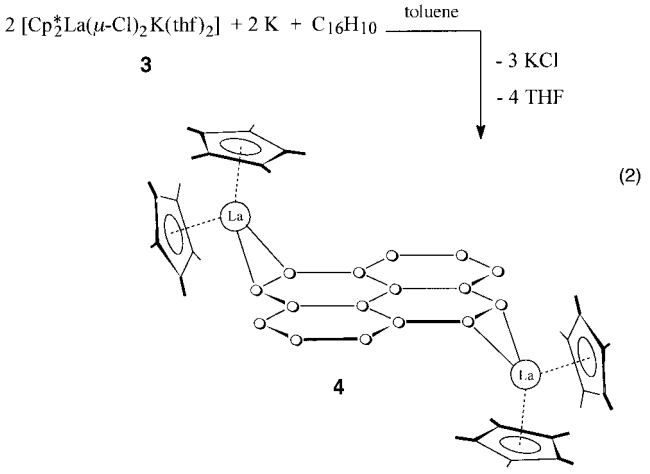
$$3\,\mathbf{1} + 3\,K + C_{16}H_{10} \xrightarrow[-5\,THF]{\text{toluene}} \mathbf{2} + 3\,LiCl + 3\,KCl \qquad (1)$$

[*] Prof. Dr. K.-H. Thiele, Dr. S. Bambirra
Institut für Anorganische Chemie der Universität Halle-Wittenberg
Kurt-Mothes-Strasse 2, D-06120 Halle (Germany)
Fax: (+49) 345-55-27028
Prof. Dr. J. Sieler, Dipl.-Chem. S. Yelonek
Institut für Anorganische Chemie der Universität Leipzig (Germany)

[**] This work was supported by the Deutsche Forschungsgemeinschaft and the Fonds der Chemischen Industrie.

 © WILEY-VCH Verlag GmbH, D-69451 Weinheim, 1998 1433-7851/98/3720-2886 $ 17.50+.50/0

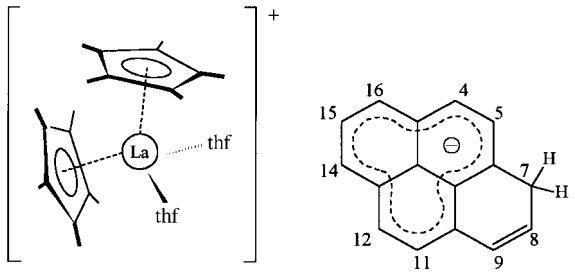
$[Cp^*_2La(\mu\text{-}Cl)_2Li(thf)_2]$ (**3**) with potassium and pyrene in a molar ratio of 2:2:1 in toluene [Eq. (2)] yields the dinuclear lanthanum–pyrene complex **4**, which was isolated from a



(2)

dark green solution in the form of green-black crystals. The ^{1}H NMR spectrum displays one signal for the H atoms H4, H5, H11, and H12, and a broad singlet at $\delta = 4.39$ (numbering of the atoms according to Figure 1). The atoms H7, H9, H14, and H16 give a doublet at $\delta = 4.25$, H8 and H9 a triplet at $\delta = 5.51$. The signals of the Cp* groups are included as two singlets of equal intensity at $\delta = 2.18$ and 1.87. The ^{13}C NMR spectrum also displays only one signal for the atoms C4, C5, C11, and C12 ($\delta = 101.9$). Therefore **4** is highly symmetrical, and free rotation of the Cp^*_2La units can be ruled out. Thus, **4** can be regarded as $[(Cp^*_2La)_2(\mu\text{-}\eta^2\text{:}\eta^2\text{-}C_{16}H_{10})]$, in accord with the formula given in Equation (2).

The reaction of **3** with dipotassium pyrenediide in THF does not lead to **4**. Instead the deep red reaction solutions gave red crystals of the mononuclear lanthanum–pyrene complex $[Cp_2Ln(thf)_2][C_{16}H_{11}]$ (**5**) in modest yields. The



5

^{1}H NMR spectrum displays ten split signals for the pyrene moiety (see Experimental Section). Of these, one doublet at $\delta = 4.12$ (H7) is twice as intense as the other signals. According to the results of single-beam experiments and the coupling constants, the pyrene unit is significantly less symmetrical, which can be explained with a protonation of C7. The formation of **5** is probably accompanied by ether cleavage, after which an H atom is transferred to the C7 atom of the pyrene framework, thereby forming a substituted phenalene anion. Due to the homogeneous distribution of the negative charge throughout this anion, a solvent-separated ion pair of the composition $[Cp^*_2La(thf)_2]^+[C_{16}H_{11}]^-$ (**5**) is evidently obtained instead of the concentration of a partial charge in one position. The course of the reaction and the properties of **5**, for example the strikingly low solubility in aromatic hydrocarbons, resemble those described by Müllen et al. for the alkali metal–hydropyrene salts also built from ion pairs.[12]

Experimental Section

2: Potassium (0.38 g, 10.0 mmol) and pyrene (0.40 g, 2.0 mmol) were added to a suspension of **1**[13] (1.8 g, 4.00 mmol) and toluene (150 mL). The reaction mixture was sonicated at 65 °C for about 20 h, after which the red-violet solution was filtered, the filtrate was evaporated to dryness and the residue extracted with *n*-pentane (100 mL). After the mixture was cooled to about −10 °C, red-violet crystals of **2** were isolated from the extract (yield: 1.11 g, 28 %). Recrystallization from *n*-pentane afforded red-violet, cuboid single crystals. Correct C,H,La analysis; ^{1}H NMR (300 MHz, C_6D_6, 20 °C): $\delta = 3.81$ (m; THF), 2.22 (br. s; C_5Me_5), 1.63 (m; THF).

4: Potassium (0.62 g, 16.00 mmol) and pyrene (1.61 g, 8.00 mmol) were added to a suspension of $[Cp^*_2La(\mu\text{-}Cl)_2K(thf)_2]$ (11.9 g, 16 mmol) and toluene (150 mL) at room temperature. The mixture was sonicated for 5–8 h at 55–60 °C, in the course of which the color changed from pale yellow to dark green. After filtration the solvent was drawn off and the black-green residue extracted from a circulation frit with *n*-pentane until the discharged solvent remained colorless. After the mixture had been cooled to −10 °C, black-green crystals of **4** were obtained from the dark green extract (yield 4.28 g, 26 %). ^{1}H NMR (300 MHz, C_6D_6, 25 °C): $\delta = 5.51$ (t, $J = 7.3$ Hz, 2H; $C_{16}H_{10}$), 4.39 (s, 4H; $C_{16}H_{10}$), 4.25 (d, $J = 7.0$ Hz, 4H; $C_{16}H_{10}$), 2.18 (s, 30H; Cp*), 1.87 (s, 30H; Cp*); ^{13}C NMR (300 MHz, C_6D_6, 25 °C): $\delta = 140.7$, 139.6, 126.0, 125.2 ($C_{16}H_{10}$), 120.2, 119.3 (Cp*), 101.9 ($C_{16}H_{10}$).

5: A solution of dipotassium pyrenediide $[K_2(C_{16}H_{10})]$ (5 mmol), prepared from pyrene ($C_{16}H_{10}$) (1.01 g, 5 mmol) and potassium (0.39 g, 10 mmol) in THF (100 mL), was added dropwise to a stirred and cooled (−50 °C) suspension of $[Cp^*_2La(\mu\text{-}Cl)_2K(dme)]$ (7.22 g, 10 mmol) and THF (100 mL), with concomitant color change to bright red (dme = 1,2-dimethoxyethane). After warming the mixture to room temperature and stirring for 12 h, the solvent was removed in vacuo, the residue was transferred to a circulation frit, then washed with *n*-pentane and finally extracted with diethyl ether (60 mL). Red crystals of **5**, which were obtained after the extract had been concentrated and cooled to −5 °C, were filtered off and dried in vacuo (yield 0.98 g, 13 %). ^{1}H NMR (300 MHz, [D$_8$]THF, 25 °C): $\delta = [5.87$ (t, $J = 7.4$ Hz), 5.69 (d, $J = 7.5$ Hz), 5.52 (d, $J = 7.8$ Hz), 5.50 (d, $J = 7.8$ Hz), 5.45 (d, $J = 9.7$ Hz), 5.25 (d, $J = 7.7$ Hz), 5.15 (d, $J = 7.4$ Hz), 4.90 (d, $J = 7.5$ Hz) 4.33 (dt, $J = 3.7$, 9.4 Hz), 4.12 (d, $J = 9.4$ Hz) ($C_{16}H_{11}$)], 1.97 (s, 30H; Cp*).

Received: October 23, 1997,
Revised version: July 1, 1998 [Z 11072 IE]
German version: *Angew. Chem.* **1998**, *110*, 3016–3018

Keywords: arene complexes · lanthanum · metallocenes · structure elucidation

[1] a) W. Jost, M. Adam, V. Enkelmann, K. Müllen, *Angew. Chem.* **1992**, *104*, 883–884; *Angew. Chem. Int. Ed. Engl.* **1992**, *31*, 878–879; b) H. Viebrock, U. Behrens, E. Weiss, *Chem. Ber.* **1994**, *127*, 1399–1400; c) C. Näther, H. Bock, R. F. C. Claridge, *Helv. Chim. Acta* **1996**, *79*, 84–91.

[2] a) W. E. Rhine, J. Davis, G. Stucky, *J. Am. Chem. Soc.* **1975**, *97*, 2079–2085; b) H. Bock, K. Ruppert, Z. Havlas, W. Bensch, W. Hönle, H. G. von Schnering, *Angew. Chem.* **1991**, *103*, 1197–1200; *Angew. Chem. Int. Ed. Engl.* **1991**, *30*, 1183–1186; c) H. Bock, C. Näther, Z. Havlas, *J. Am. Chem. Soc.* **1995**, *117*, 3869–3870.

[3] H. Bock, K. G.-Hubmann, C. Näther, N. Nagel, Z. Havlas, *Angew. Chem.* **1996**, *108*, 720–722; *Angew. Chem. Int. Ed. Engl.* **1996**, *30*, 631–632.

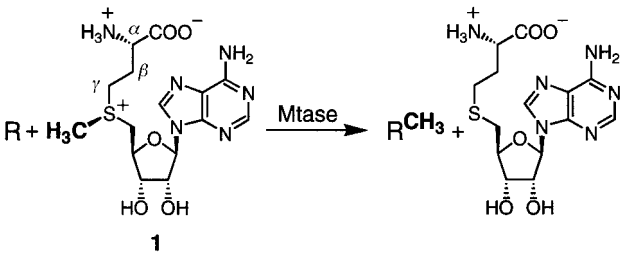
 © WILEY-VCH Verlag GmbH, D-69451 Weinheim, 1998 1433-7851/98/3720-2887 $ 17.50+.50/0

[4] a) B. Bogdanović, N. Janke, C. Krüger, R. Mynott, K. Schlichte, U. Westeppe, *Angew. Chem.* **1985**, *97*, 972 – 974; *Angew. Chem. Int. Ed. Engl.* **1985**, *24*, 972 – 973; b) L. M. Engelhardt, S. Harvey, C. L. Raston, A. H. White, *J. Organomet. Chem.* **1988**, *341*, 39 – 51.
[5] a) M. N. Bochkarev, A. A. Trivonov, E. A. Federova, N. S. Emelyanova, T. A. Basalgina, G. S. Kalinina, G. A. Razuvaev, *J. Organomet. Chem.* **1989**, *372*, 217 – 224; b) M. N. Bochkarev, I. L. Fedushkin, H. Schumann, J. Loebel, *J. Organomet. Chem.* **1991**, *410*, 321 – 326.
[6] a) D. M. Roitershtein, A. M. Ellen, M. Yu. Antipin, L. F. Rybakova, Yu. T. Struchkov, E. S. Petrov, *Mendeleev Commun*. **1992** 118 – 120; b) A. V. Protchenko, L. N. Zakharov, M. N. Bachkarev, Yu. T. Struchkov, *J. Organomet. Chem*. **1993**, *447*, 209 – 212; c) D. M. Roitershtein, L. F. Rybakova, E. S. Petrov, A. M. Elllen, M. Yu. Antipin, Yu. T. Struchkov, *J. Organomet. Chem*. **1993**, *460*, 39 – 45; d) I. L. Fedushkin, M. N. Bochkarev, H. Schumann, L. Esser, G. Kociok-Köhn, *J. Organomet. Chem*. **1995**, *489*, 145 – 151.
[7] W. J. Evans, S. L. Gonzales, J. W. Ziller, *J. Am. Chem. Soc.* **1994**, *116*, 2600 – 2608.
[8] Crystal structure determination: $C_{50}H_{63}Cl_3La_3O$ ($M_r = 1203.08$), $a = 12.299(3)$, $b = 18.734(3)$, $c = 23.954(5)$ Å, $\beta = 101.11(2)^\circ$, $V = 5416(2)$ Å^3 ($T = 220$ K), $\rho_{calcd} = 1.476$ g cm^{-1}, $F(000) = 2372$, $\lambda = 0.71073$ Å, monoclinic, $P2_1/n$, $Z = 4$, diffractometer: STOE-STADI 4, crystal dimensions: $0.30 \times 0.28 \times 0.22$ mm^3, ω-θ scans, 7409 measured reflections in the range $\theta = 1.69 - 25.02^\circ$, of which 7409 were independent and used for refinement. All C, O, Cl, and La layers were refined anisotropically, the H centers in calculated positions isotropically, *R* values: for [$F > 2\sigma(F)$] $R1 = 0.0397$, $wR2 = 0.1413$. Crystallographic data (excluding structure factors) for the structure reported in this paper have been deposited with the Cambridge Crystallographic Data Centre as supplementary publication no. CCDC-100445. Copies of the data can be obtained free of charge on application to CCDC, 12 Union Road, Cambridge CB21EZ, UK (fax: int. code + (44) 1223-336033; e-mail: deposit@ccdc.cam.ac.uk).
[9] H. Bock, Z. Havlas, D. Hess, C. Näther, *Angew. Chem.* **1998**, *110*, 518 – 520; *Angew. Chem. Int. Ed.* **1998**, *37*, 502 – 504.
[10] S. H. Eggers, J. Kopf, R. D. Fischer, *Organometallics* **1986**, *5*, 383.
[11] A. Scholz, A. Smola, J. Scholz, J. Loebel, H. Schumann, K.-H. Thiele, *Angew. Chem.* **1991**, *103*, 444 – 445; *Angew. Chem. Int. Ed. Engl.* **1991**, *30*, 435 – 436.
[12] C. Schnieders, K. Müllen, W. Huber, *Tetrahedron* **1984**, *40*, 1701 – 1711.
[13] M. Booiji, N. H. Kiers, H. J. Heeres, J. H. Teuben, *J. Organomet. Chem.* **1989**, *364*, 79 – 86.

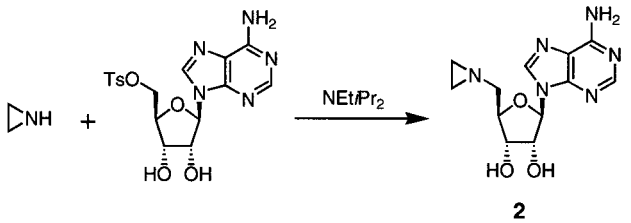
Coupling of a Nucleoside with DNA by a Methyltransferase**

Marc Pignot, Christoph Siethoff, Michael Linscheid, and Elmar Weinhold*

S-Adenosyl-L-methionine-dependent methyltransferases (Mtases) catalyse the transfer of the activated methyl group from the cofactor *S*-adenosyl-L-methionine (**1**) to sulfur, nitrogen, oxygen, and carbon acceptors (Scheme 1) of small molecules, phospholipids, proteins, RNA, and DNA with high specificty.[1] The transfer of larger chemical entities in a Mtase-catalyzed reaction has not been reported and thus represents an interesting challenge for bioorganic chemists. In principal, covalent linking of the activated methyl group with the γC atom of **1** would yield a three-membered thiiranium compound, which could lead to a coupling of the whole cofactor to the target substrate. Since thiiranium compounds are known to be unstable in nucleophilic solvents,[2] we concentrated on the more stable aziridine analogues, which can be activated as alkylating reagents upon protonation of their ring nitrogen atom.[3] *N*-Adenosylaziridine (**2**) was synthesized by nucleophilic substitution of the tosylate group of 5′-deoxy-5′-tosyladenosine (tosyl = Ts = toluene-4-sulfonyl) with aziridine (Scheme 2).



Scheme 1. Reaction catalyzed by *S*-adenosyl-L-methionine-dependent methyltransferases (Mtases). R = an acceptor with sulfur, nitrogen, oxygen, or carbon atoms to which the methyl groups become attached.



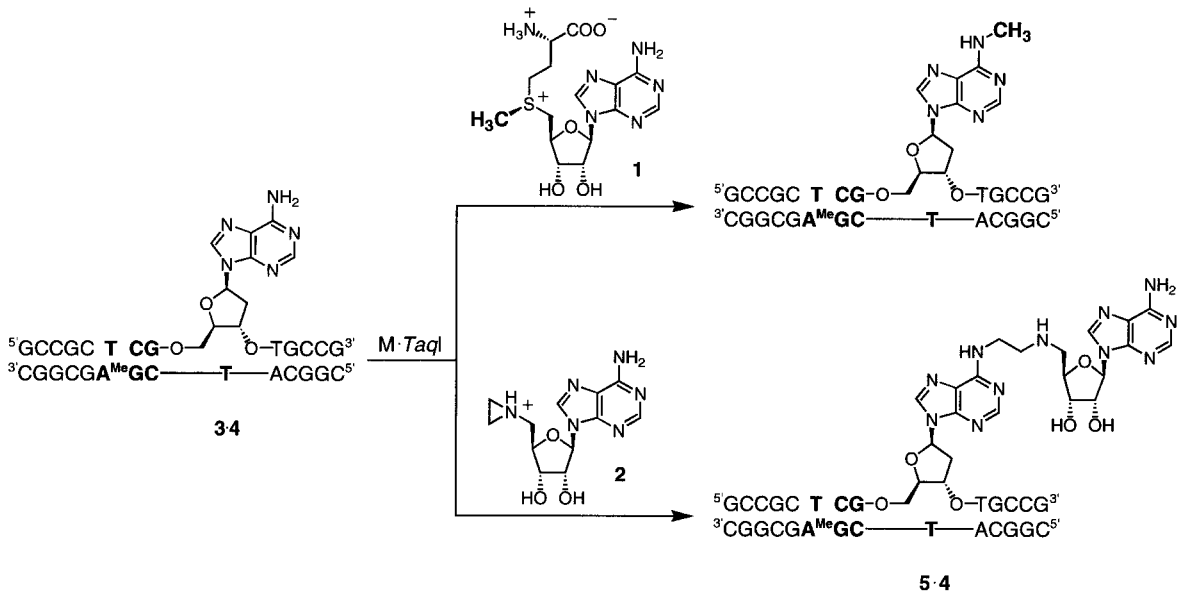
Scheme 2. Synthesis of *N*-adenosylaziridine (**2**).

To test whether the cofactor analogue **2** serves as a cofactor for a Mtase we used the DNA Mtase from *Thermus aquaticus* (M · *Taq*I). Naturally, M · *Taq*I catalyzes the transfer of the methyl group from the cofactor **1** to the exocyclic amino group of 2′-deoxyadenosine within the double-stranded 5′-TCGA-3′ DNA sequence (Scheme 3, top).[4] For our studies we used the short duplex oligodeoxynucleotide **3** · **4** (Scheme 3), in which strand **4** contains N^6-methyl-2′-deoxyadenosine (A^{Me}) at the target position, so that it cannot be further methylated by M · *Taq*I. The reaction of the cofactor analogue **2** with the duplex **3** · **4** was performed in the presence of a stoichiometric amount of M · *Taq*I and monitored by anion exchange chromatography. A new compound with a shorter retention time relative to **3** · **4** was formed during the reaction (Figure 1), and after 240 min the duplex **3** · **4** had reacted quantitatively. The shorter retention time of the product is consistent with the proposed structure **5** · **4** (Scheme 3, bottom), since **5** · **4** contains an additional aliphatic amino group that ought to be protonated under the conditions used to elute the reaction mixture (pH 7.6).

[*] Dr. E. Weinhold, Dipl.-Chem. M. Pignot
Max-Planck-Institut für molekulare Physiologie
Abteilung Physikalische Biochemie
Rheinlanddamm 201, D-44139 Dortmund (Germany)
Fax: (+49) 231-1206-229
E-mail: elmar.weinhold@mpi-dortmund.mpg.de
Dr. C. Siethoff, Priv.-Doz. Dr. M. Linscheid
ISAS Institut für Spektrochemie und Angewandte Spektroskopie
Bunsen-Kirchhoff-Strasse 11, D-44139 Dortmund (Germany)

[**] This work was supported by the Deutsche Forschungsgemeinschaft. We would also like to thank Prof. Roger S. Goody for his continuous support.

 © WILEY-VCH Verlag GmbH, D-69451 Weinheim, 1998 1433-7851/98/3720-2888 $ 17.50+.50/0



Scheme 3. Reactions catalyzed by the DNA methyltransferase M · *Taq*I. Top: Transfer of a methyl group by the natural cofactor *S*-adenosyl-L-methionine (**1**). Bottom: Coupling of protonated *N*-adenosylaziridine (**2**) to the duplex **3** · **4** ($A^{Me} = N^6$-methyl-2′-deoxyadenosine).

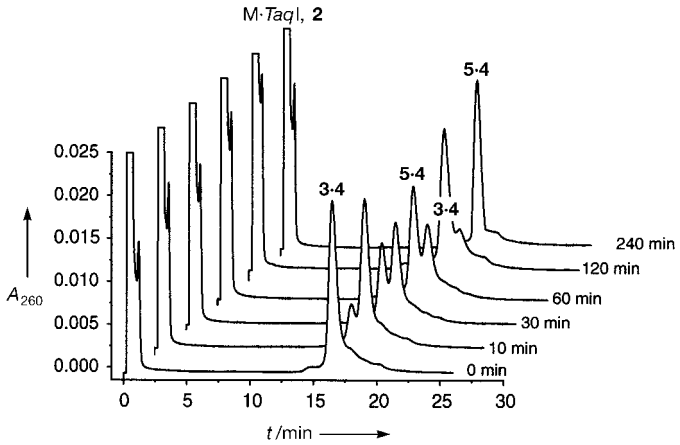


Figure 1. Analysis of the reaction between the duplex oligodeoxynucleotide **3** · **4** and the cofactor analogue **2** in the presence of M · *Taq*I by anion exchange chromatography. Aliquots (50 µL) of the reaction mixture were withdrawn after different incubation times, mixed with a urea solution (100 µL, 6 M) and injected onto an anion exchange column (Poros 10 HQ, 10 µm, 4.6 × 100 mm, PerSeptive Biosystems). Compounds were eluted with aqueous KCl (0.5 M for 5 min, followed by a linear gradient to 1 M in 30 min, 4 mL min^{-1}) in Tris-HCl buffer (10 mM, pH 7.6). A_{260} = absorption at 260 nm.

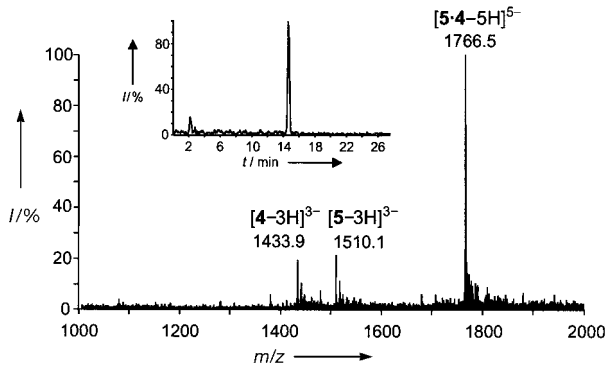


Figure 2. RP-HPLC/ESI mass spectrum of the product **5** · **4** performed with an ion-trap electrospray mass spectrometer (LCQ, Finnigan MAT) equipped with a micro HPLC system (M480 and M300, Gynkotek). Purified and desalted solutions of **5** · **4** were injected onto a capillary column (Hypersil-ODS, 3 µm, 0.3 × 150 mm, LC Packings) and eluted with a CH_3CN gradient (7–10% in 10 min, followed by 10–70% in 30 min, 150 µL min^{-1}) in triethylammonium acetate buffer (0.1 M, pH 7.0). The chromatogram obtained by observing the total ion current is given in the inset. *I* = relative intensity.

The reaction product **5** · **4** was isolated by anion exchange chromatography, and its structure was verified by reversed-phase HPLC-coupled electrospray ionisation mass spectrometry (RP-HPLC/ESI-MS). The duplex **5** · **4** eluted after 14.6 min and was detected as the fivefold negatively charged ion at *m/z* 1766.5 (Figure 2, Table 1). Some of the duplex **5** · **4** underwent dissociation in the mass spectrometer, and the single strands **4** and **5** were detected as their threefold negatively charged ions at *m/z* 1433.9 and 1510.1, respectively. No signal for a modification of strand **4** with *N*-adenosylaziridine was observed. The duplex **5** · **4** was further analyzed by ESI-MS with direct infusion (Table 1). In this case **5** · **4** was no longer detectable in its duplex form. The single strands **4** and **5** were detected as five-, six- (Figure 3), and sevenfold negatively charged ions. In addition, **4** and **5** were also detected as sodium, potassium, and copper adducts, which were not observed under the RP-HPLC/ESI-MS conditions. The sixfold negatively charged state of **5** is demonstrated directly by the mass differences of the isotope multiplet of the $[\mathbf{5} - 6\,H]^{6-}$ ion (expansion in Figure 3), and the derived monoisotopic relative molecular weight of 4530.9 is identical to the calculated value.

It is well known that aziridines react with the nucleobases of DNA. Several covalent adducts between antitumor drugs such as bis(2-chloroethyl)methylamine (nitrogen mustard),[5] 2,5-bis(1-aziridinyl)-1,4-benzoquinones,[6] mitomycin C,[7] and carzinophilin (azinomycin A)[8] and DNA have been charac-

Table 1. Characterization of oligodeoxynucleotides by negative-ion electrospray mass spectrometry.

Compd	Charge	$(m/z)_{expt}$	M_{expt}	M_{calcd}
RP-HPLC/ESI-MS[a]				
5·**4**[b]	5 –	1766.5	8837.5	8836.9
5[b]	3 –	1510.1	4533.3	4533.1
4[b]	3 –	1433.9	4304.7	4303.8
3·**4**[c]	5 –	1708.0	8545.0	8544.6
3[c]	3 –	1412.7	4241.1	4240.8
ESI-MS by direct infusion[d]				
5[c]	7 –	646.4	4531.9	4533.1
5[e]	6 –	754.5	4533.1	4533.1
5[c]	5 –	905.6	4533.0	4533.1
4[c]	7 –	613.7	4303.0	4303.8
4[e]	6 –	716.1	4302.7	4303.8
4[c]	5 –	859.9	4304.5	4303.8
3[c]	7 –	604.8	4240.6	4240.8
3[c]	6 –	705.7	4240.3	4240.8
3[c]	5 –	847.2	4241.0	4240.8

[a] See legend in Figure 2. [b] Data shown in Figure 2. [c] Data not shown in Figures 2 or 3. [d] See legend to Figure 3. [e] Data shown in Figure 3.

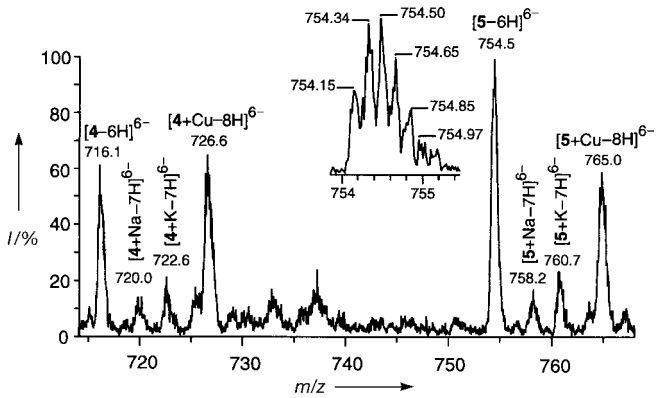


Figure 3. ESI mass spectrum of the product **5**·**4** obtained by direct infusion with a double focussing sector field mass spectrometer (MAT 90, Finnigan MAT) equipped with an electrospray ion source (ESI II). Desalted **5**·**4** (aqueous solution) and a liquid sheath flow (2-propanol) were delivered with a syringe pump (Harvard apparatus). The expansion shows the signal of the $[\mathbf{5}-6\mathrm{H}]^{6-}$ ion with isotopic resolution. I = relative intensity.

terized. However, no product of a nonenzymatic reaction was observed under the conditions used in this study. A covalent adduct between **2** and the duplex **3**·**4** was only formed in the presence of M·*Taq*I. In this adduct strand **3**, which contains an adenine at the target position within the recognition sequence of M·*Taq*I, is modified exclusively. Our observation that strand **4**, which contains N^6-methyladenine at the other target position and an adenine outside the recognition sequence, is not modified gives strong evidence that the base and sequence specificity of M·*Taq*I is not altered with the new cofactor **2**. This result also provides indirect structural evidence that the target adenine of strand **3** is the site of modification.[13]

This reaction represents the first example of a Mtase-catalyzed formation of a covalent bond between a group larger than a methyl group and the substrate for a Mtase. Since cofactor binding as observed in the three-dimensional structure of M·*Taq*I[9] is very similar to that of other DNA, RNA, protein, or small molecule Mtases,[10] **2** could also serve as a cofactor for other Mtases that act on a wide variety of substrates. In addition, it is conceivable that the new cofactor **2** in combination with M·*Taq*I could be used as a delivery system for fluorescent or other reporter groups. By the covalent attachment of such groups to the 8-position, which is directed towards the solvent in the crystal structure of M·*Taq*I in the complex with the natural cofactor **1**,[9] site-specific labeled DNA may be obtained. DNA fragments labeled in this way could find interesting applications in molecular biology.

Experimental Section

2: Dry aziridine[11] (360 µl, 7.2 mmol) was added slowly to a suspension of 5′-deoxy-5′-tosyladenosine (100 mg, 0.24 mmol, Aldrich) and NEt_iPr_2 (125 µL, 0.7 mmol) under argon, and the resulting solution was stirred at room temperature for three days. Any aziridine remaining was removed under reduced pressure, and the crude reaction product was dissolved in H_2O (1 mL) and neutralized with acetic acid. The solution (100 µL at a time) was injected onto a reversed-phase HPLC column (Hypersil-ODS, 5µm, 120 Å, 250 × 10 mm, Bischoff), and the product was eluted with a linear gradient of CH_3CN (7 → 10 % in 30 min, 2 mL min^{-1}) in triethylammonium hydrogencarbonate buffer (0.1M, pH 8.4). Fractions containing product (retention time 11.3 min) were combined, concentrated by lyophilization to 5.5 mL (10.5 mM with $\lambda = 260$, $\varepsilon = 15400$ of adenosine) and stored at −80 °C. Yield: 0.058 mmol (24 %). For characterization an aliquot was completely lyophilized to afford **2** as a white solid. ^{1}H NMR (500 MHz, D_2O): $\delta = 8.36$ (s, 1H; 2-H), 8.30 (s, 1H; 8-H), 6.13 (d, ^3J = 5.0 Hz, 1H; 1′-H), 4.84 (dd = t, ^3J = 5.3 Hz, 1H; 2′-H), 4.46 (dd = t, ^3J = 5.1 Hz, 1H; 3′-H), 4.35 (ddd = dt, ^3J = 4.6, 4.6, 6.7 Hz, 1H; 4′-H), 2.74 and 2.68 (AB part of ABX-spectrum, ^3J = 4.3, 6.6 Hz, ^2J = 13.3 Hz, 2H; 5′-Ha, 5′-Hb), 1.85 – 1.74 (m, 2H; aziridine-H), 1.49 – 1.40 (m, 2H; aziridine-H); FAB-MS (thioglycolic acid): *m/z* (%): 293 (100) $[M^+ + H]$, 250 (4) $[M^+ - C_2H_4N]$, 178 (11) $[B^+ + C_2H_4O]$, 167 (34), 165 (5), 164 (5) $[B^+ + CH_2O]$, 158 (36) $[M^+ - B]$, 149 (78), 136 (91) $[BH_2^+]$, 102 (23); B = deprotonated adenine.

Enzymatic reaction: Synthesis, purification, and annealing of oligodeoxynucleotides as well as preparation of M·*Taq*I were performed as descibed before.[12] The enzymatic reaction was carried out in a mixture (500 µL) of M·*Taq*I (10 µM), **3**·**4** (10 µM), **2** (1 mM) and Tris-OAc (20 mM, pH 6.0; Tris = tris(hydroxymethyl)aminomethane), KOAc (50 mM), $Mg(OAc)_2$ (10 mM) and Triton X-100 (0.01 %) at 37 °C.

Received: May 4, 1998 [Z11817IE]
German version: *Angew. Chem.* **1998**, *110*, 3050 – 3053

Keywords: aziridine · DNA modifications · enzyme catalysis · mass spectrometry · oligonucleotides

[1] E. C. Webb, *Enzyme Nomenclature*, Academic Press, San Diego, **1992**.
[2] W. A. Smit, M. Z. Krimer, E. A. Vorob'eva, *Tetrahedron Lett.* **1975**, 2451 – 2454.
[3] D. Tanner, *Angew. Chem.* **1994**, *106*, 625 – 646; *Angew. Chem. Int. Ed. Engl.* **1994**, *33*, 599 – 619.
[4] M. McClelland, *Nucleic Acids Res.* **1981**, *9*, 6795 – 6804.
[5] S. M. Rink, M. S. Solomon, M. J. Taylor, S. B. Rajur, L. W. McLaughlin, P. B. Hopkins, *J. Am. Chem. Soc.* **1993**, *115*, 2551 – 2557.
[6] S. C. Alley, K. A. Brameld, P. B. Hopkins, *J. Am. Chem. Soc.* **1994**, *116*, 2734 – 2741.
[7] M. Tomasz, *Chem. Biol.* **1995**, *2*, 575 – 579.
[8] R. W. Armstrong, M. E. Salvati, M. Nguyen, *J. Am. Chem. Soc.* **1992**, *114*, 3144 – 3145.
[9] J. Labahn, J. Granzin, G. Schluckebier, D. P. Robinson, W. E. Jack, I. Schildkraut, W. Saenger, *Proc. Natl. Acad. Sci. USA* **1994**, *91*, 10957 – 10961.
[10] a) G. Schluckebier, M. O'Gara, W. Saenger, X. Cheng, *J. Mol. Biol.* **1995**, *247*, 16 – 20; b) S. Djordjevic, A. M. Stock, *Structure* **1997**, *5*, 545 – 558; c) W. Gong, M. O'Gara, R. M. Blumenthal, X. Cheng, *Nucleic Acids Res.* **1997**, *25*, 2702 – 2715.

 © WILEY-VCH Verlag GmbH, D-69451 Weinheim, 1998 1433-7851/98/3720-2890 $ 17.50+.50/0

[11] a) S. Gabriel, *Chem. Ber.* **1888**, *21*, 2664–2669; b) S. Gabriel, R. Stelzner, *Chem. Ber.* **1895**, *28*, 2929–2938.
[12] B. Holz, S. Klimasauskas, S. Serva, E. Weinhold, *Nucleic Acids Res.* **1998**, *26*, 1076–1083.
[13] The site of modification was further proven by enzymatic fragmentation of the duplex **5**·**4** with phosphodiesterase from *Crotalus durissus*, phosphodiesterase from calf spleen, DNase I, and alkaline phosphatase. Reverse-phase HPLC analysis of the digest revealed besides dC, dG, T, dA, and dA^{Me} an additional compound. This was isolated and detected as positively charged ion at *m*/*z* 544.6 in an ESI-MS experiment. The observed mass is identical with the calculated molecular mass of a protonated 2′-deoxyadenosine modified with *N*-adenosylaziridine.

Metallosupramolecular Thin Polyelectrolyte Films**

Markus Schütte, Dirk G. Kurth,* Matthew R. Linford, Helmut Cölfen, and Helmut Möhwald

The manufacture and investigation of supramolecular devices is an active area of research in chemistry and materials science.[1] Supramolecular devices open new avenues to functional materials with potential applications in electronics, photonics, and catalysis.[2] The realization of such materials will depend on improving existing methods and finding new routes for integrating supramolecular units in ordered, structurally coherent macroscopic assemblies.

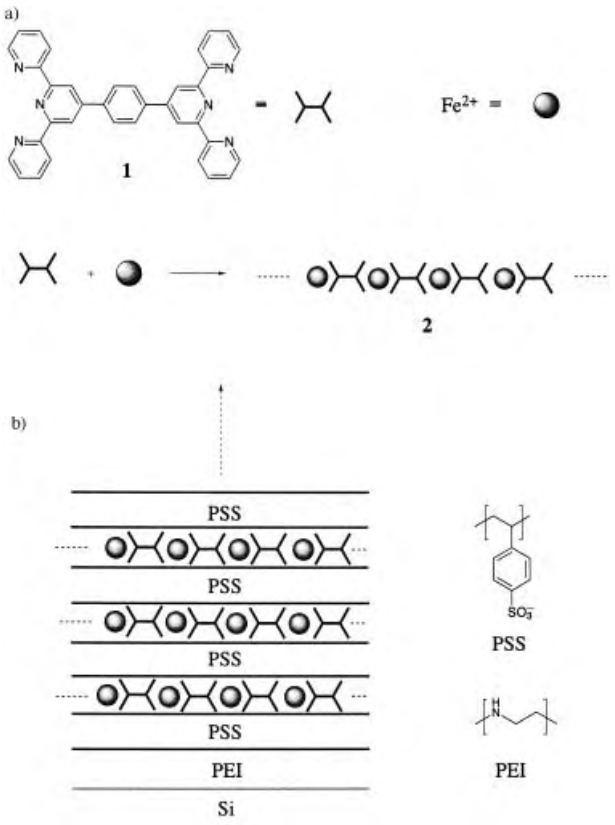
Molecular units can be integrated in ordered arrays in Langmuir–Blodgett films or in self-assembled monolayers.[3] Decher et al. developed a versatile approach to assembled multilayer structures by alternating adsorption of oppositely charged polyelectrolytes.[4] This method has been applied to a number of polyelectrolytes (colloids, enzymes, etc.). Mallouck et al. investigated lamellar inorganic structures based, for example, on zirconium phosphates.[5]

Here we present the first integration of metallosupramolecular functional units in structurally coherent, ultrathin polyelectrolyte interfaces.[6] We employed a two-step self-assembly process: first, metal ions react with polytopic ligands to form a charged metallosupramolecular coordination polyelectrolyte,[7] then alternating adsorption with negatively charged polyelectrolytes generates molecular films.[8]

The synthesis of coordination polyelectrolytes is shown in Scheme 1a. Reaction of 1,4-bis(2,2′,6′,2″-terpyrid-4′-yl)benzene (**1**) with metal ions in a 1:1 ratio in solution gives the coordination polyelectrolyte **2**. With most metal ions terpyridine (tpy) forms stereochemically defined octahedral complexes with D_{2d} symmetry.[9] It therefore seems reasonable to assume that **2** has a linear structure in which the positive charge lies along the molecular axis.

[*] Dr. D. G. Kurth, Dipl.-Chem. M. Schütte, Dr. M. R. Linford, Dr. H. Cölfen, Prof. Dr. H. Möhwald
Max-Planck-Institut für Kolloid- und Grenzflächenforschung
Rudower Chaussee 5
D-12489 Berlin-Adlershof (Germany)
Fax: (+49) 30-6392-3102
E-mail: kurth@mpikg.fta-berlin.de

[**] We thank Dr. P. Druska from the Institut für Angewandte Chemie in Berlin for the XPS measurements. M.R.L. thanks the Max-Planck-Gesellschaft for a Schlossmann stipendium.



Scheme 1. a) Ligand **1** and metal ions in a 1:1 ratio form the coordination polyelectrolyte **2**. The counterions are omitted for clarity. b) Assembly of multilayers by sequential deposition of oppositely charged polyelectrolytes. PEI = polyethyleneimine, PSS = poly(styrene sulfonate).

A comparison of the UV/Vis and ^{1}H NMR spectra of **2** and $[Fe(me\text{-}ph\text{-}tpy)_2]Br_2$ (**3**; me-ph-tpy = 4′-*p*-tolyl-2,2′,6′,2″-terpyridine) confirms the presence of a coordination compound. Formation of a metal complex results in a characteristic metal-to-ligand charge-transfer (MLCT) transition in the visible region and a downfield shift of the ^{1}H NMR signals. The polymeric nature of **2** leads to broadening of the ^{1}H NMR signals and a red shift of the MLCT band relative to that of **3**.[10]

The molecular mass and polydispersity of **2** in methanol were determined by analytical ultracentrifugation. The sedimentation coefficient ($s = 1.60$ S) and an estimated diffusion coefficient ($D \leq 5.259 \times 10^{-7}$ cm^2 s^{-1}) were determined from the sedimentation velocity at 25 °C. Since the polydispersity leads to additional broadening of the sedimentation profile, the value of the diffusion coefficient will be too large. From the Swedberg formula, the lower limit of the molecular mass is 14900. For a dissociated polyelectrolyte with a molecular mass per repeat unit of 596.5, this corresponds to 25 repeat units. The width at half height of the particle size distribution function is 40%, that is, coordination polyelectrolytes of different chain length are present in solution. The fragment $[Fe(\mathbf{1})_2]^{2+}$ was observed in the electrospray (ES) mass spectra; oligomeric structures were not detected. Investigations by time-of-flight MS with matrix-assisted laser-desorption ionization (MALDI-TOF-MS) gave no further indications for the molecular weight of **2**.

 © WILEY-VCH Verlag GmbH, D-69451 Weinheim, 1998 1433-7851/98/3720-2891 $ 17.50+.50/0

Solutions of **2** were used to fabricate multilayer structures (Scheme 1b). A suitable substrate (e.g. quartz, silicon) was treated with polyethyleneimine (PEI) and poly(styrene sulfonate) (PSS) to give a negatively charged interface. In the following steps, alternating adsorption of **2** and PSS generated metallosupramolecular superlattices.

Owing to the intense blue color of **2** and the strong UV absorption of PSS at 185 and 225 nm, the assembly of the multilayers on quartz substrates can be monitored by UV/Vis spectroscopy. Figure 1 shows the absorption spectra of **2** as a function of the number of layers. Since the characteristic

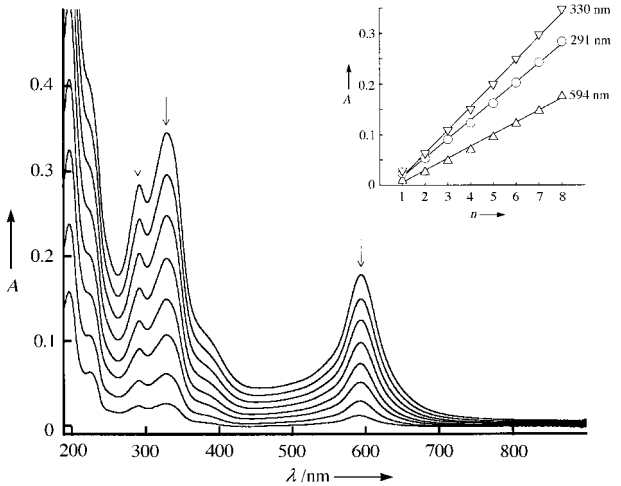


Figure 1. UV/Vis spectra of **2** on quartz glass as a function of the number of layers n. The MLCT band at 594 nm indicates the incorporation of **2** in the multilayer structure. The UV/Vis spectra of the PSS deposition cycle are omitted for clarity. The insert shows the absorption maxima at 291, 330, and 594 nm as a function of the number of layers. The linear increase indicates that equal amounts are deposited in each adsorption cycle.

bands of **2** are retained after deposition of PSS, the removal of **2** during deposition can be ruled out. The insert of Figure 1 shows a linear increase in the characteristic absorption maxima of **2** at 294, 330, and 594 nm. The MLCT transition at 594 nm is shifted by approximately 4 nm to lower energy; this could result from a change of polarity in the film.[11]

The assembly of multilayers was confirmed by X-ray reflectivity measurements. Figure 2 shows the interference curves of a PEI/(PSS/**2**)$_n$/(PSS)$_m$ ($n = 3,4$; $m = 0,1$) multilayer. The presence of fringes is consistent with a smooth, plano-parallel interface. An increase of the film thickness results in closer interference fringes. Curve fitting of the reflectivity data for a PEI/(PSS/**2**)$_3$/PSS film gives a total film thickness of 99 Å. Deposition of an additional layer of **2** increases the thickness by 17 Å to 116 Å; adsorption of PSS increases the thickness by 7 Å to 123 Å. The film thickness approximately corresponds to the molecular dimension of **2** perpendicular to the molecular axis. The roughness of the interfacial surface was determined from the XRR data to be less than 8 Å.

The elemental composition of the film was investigated by X-ray photoelectron spectroscopy (XPS). The XPS data confirm the presence of the expected elements. Quantitative analysis of the XPS bands gives an Fe:N atomic ratio of 0.96:6 (estimated error ± 10 %), which is in agreement with octahedrally coordinated Fe^{II}.

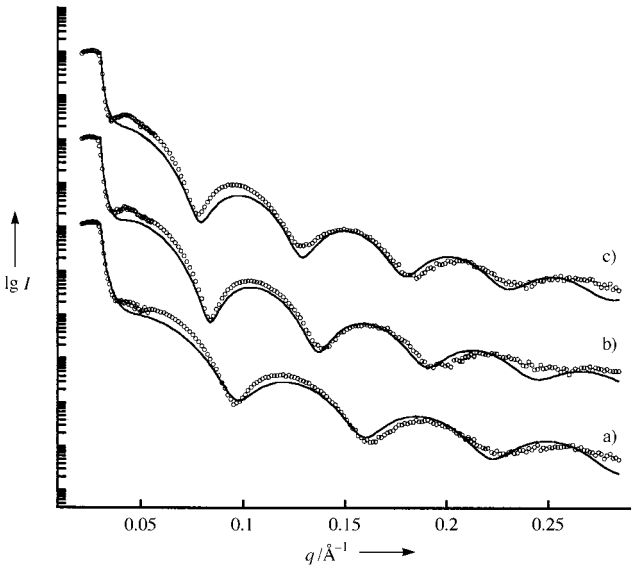


Figure 2. Experimental (dots) and calculated (lines) X-ray reflection interference curves for multilayers with the following compositions: a) PEI/(PSS/**2**)$_3$/PSS (thickness: 99 Å), b) PEI/(PSS/**2**)$_4$ (116 Å), c) PEI/(PSS/**2**)$_4$/PSS (123 Å). q = scattering vector.

Our results open a novel route for the integration of functional supramolecular units in ultrathin multilayers. The combination of two principles of supramolecular chemistry (molecular recognition by coordination of metal ions and electrostatic interactions) permits assembly of a wide variety of multilayered structures with intriguing properties.

Experimental Section

Ligand **1** was synthesized by literature procedures.[12]

2: A solution of Fe(OAc)$_2$ (16.5 mg, 0.092 mmol) in methanol (30 mL) was added to a solution of **1** (51.9 mg, 0.093 mmol) in refluxing toluene (100 mL) under an inert atmosphere. After 30 min the deep blue solution was concentrated under vacuum until **2** precipitated. The precipitate was washed with hot toluene and dried under vacuum (yield: 18 %). Compound **2** is soluble in methanol and ethanol. For the elemental analysis, **2** was isolated as the bromide by precipitation from aqueous solution. ^{1}H NMR (CD_3OD, room temperature): $\delta = 9.74$ (H3′), 8.95 (H3), 8.75 (HAr), 8.10 (H4), 7.44 (H6), 7.31(H5); UV/Vis (ethanol): MLCT band at 579 nm; IR (KBr): 1602, 1462, 1433, 1403, 1160, 831, 786, 731 cm^{-1}; elemental analysis calcd for $C_{36}H_{24}N_6FeBr_2 \cdot 6H_2O$: C 50.0, H 4.2, N 9.7, found: C 49.9, H 3.2, N 9.9.

Compound **3** was synthesized according to literature procedures.[13] ^{1}H NMR (CD_3OD, room temperature): $\delta = 9.43$ (H3′), 8.85 (H3), 8.32 (HAr), 7.96 (H4), 7.61 (HAr), 7.30 (H6), 7.18 (H5), 2.56 (HMe); UV/Vis (ethanol): MLCT band at 567 nm; IR (KBr): 3050, 3015, 2915, 1605, 1465, 1430, 1410, 1160, 820, 790, 730 cm^{-1}.

Multilayers were prepared by the method developed by Decher et al.[14] The following solutions were used: 10^{-2} M polyethylenimine in water, 10^{-3} M sodium poly(styrene sulfonate) in 1 M NaCl, $0.03 \cdot 10^{-3}$ M solution of **2** in water/methanol (90/10). The substrate for the UV/Vis spectroscopic investigations was quartz glass (Hellma Optik, Jena, Germany). For the XRR measurements, polished (100) silicon wafers (Silchem, Dresden, Germany) were employed. XRR measurements were made on a unit from the company STOE&CIE (Darmstadt, Germany); $U = 40$ kV, $I = 50$ mA, $\lambda = 1.54$ Å (CuK_α). The XRR data was analyzed according to a published procedure.[15]

The molecular mass was measured with a Beckman Optima XL-I ultracentrifuge (Beckman Instruments, Palo Alto, USA) with integrated UV/Vis absorption and Rayleigh interference optics. The samples were

 © WILEY-VCH Verlag GmbH, D-69451 Weinheim, 1998 1433-7851/98/3720-2892 $ 17.50+.50/0

measured in 0.1N KOAc/methanol and 1.0N NH_4OAc/methanol solutions at 25 °C and 60000 rpm; both protocols gave similar results. In pure methanol the sample sedimented very slowly as a result of electrostatic repulsion. The partial specific volume of 0.6305 $mL\,g^{-1}$ was used.[16]

Received: October 7, 1997
Revised version: June 29, 1998 [Z11007IE]
German version: *Angew. Chem.* **1998**, *110*, 3058–3061

Keywords: N ligands · polymers · supramolecular chemistry · thin films

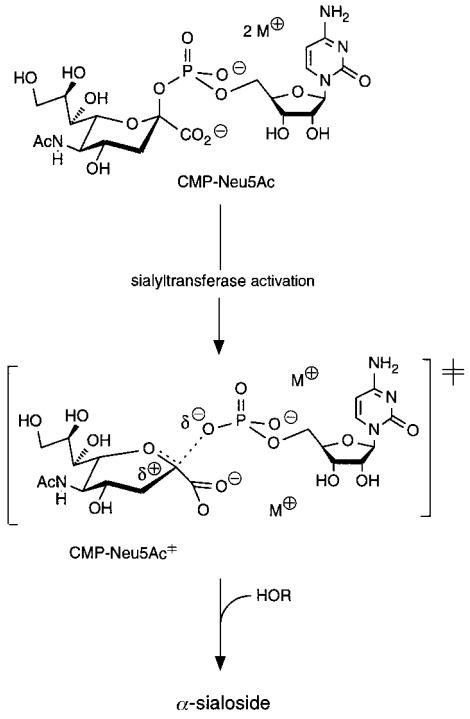
[1] a) J.-M. Lehn, *Supramolecular Chemistry*, VCH, Weinheim, **1995**; b) C. Floriani, A. E. Merbach in *Perspectives in Coordination Chemistry* (Ed.: A. F. Williams), VCH, Weinheim, **1992**.
[2] V. Balzani, F. Scandola, *Supramolecular Photochemistry*, Ellis Horwood, New York, **1991**.
[3] Reviews: a) A. Ulman, *An Introduction to Organic Thin Films—From Langmuir–Blodgett to Self-Assembly*, Academic Press, San Diego, CA, **1991**; b) J. D. Swalen, D. L. Allara, J. D. Andrade, E. A. Chandross, S. Garoff, J. Israelachvili, T. J. McCarthy, R. Murray, R. F. Pease, J. F. Rabolt, K. J. Wynne, H. Yu, *Langmuir* **1987**, *3*, 932–950; c) A. R. Bishop, R. G. Nuzzo, *Curr. Opin. Coll. Interf. Sci.* **1996**, *1*, 127–136; d) H. Kuhn, D. Möbius in *Investigations of Surfaces and Interfaces, Part B Methods of Chemistry Series*, *Vol. IXB* (Eds.: B. W. Rossiter, R. C. Baetzold), 2nd ed., Wiley, New York, **1993**, pp. 375–542.
[4] G. Decher in *Comprehensive Supramolecular Chemistry*, *Vol. 9* (Eds.: J. L. Atwood, J. E. D. Davies, D. D. MacNicol, F. Vögtle), Pergamon, Oxford, **1996**, pp. 507–528.
[5] T. E. Mallouck, H.-N. Kim, P. J. Ollivier, S. W. Keller in *Comprehensive Supramolecular Chemistry*, *Vol. 7* (Eds.: J. L. Atwood, J. E. D. Davies, D. D. MacNicol, F. Vögtle), Pergamon, Oxford, **1996**, pp. 189–217.
[6] a) E. C. Constable, A. M. W. Cargill Thompson, D. A. Tocher in *Supramolecular Chemistry* (Eds.: V. Balzani, L. De Cola), Kluwer, Dordrecht, **1992**, pp. 219–233; b) E. C. Constable, *Pure Appl. Chem.* **1996**, *68*, 253–260.
[7] Other examples of coordination polyelectrolytes: a) U. Velten, B. Lahn, M. Rehahn, *Macromol. Chem. Phys.* **1997**, *198*, 2789–2816; b) E. C. Constable, A. J. Edwards, D. Phillips, P. R. Raithby, *Supramol. Chem.* **1995**, *5*, 93–95.
[8] Examples of thin films containing metal ions: a) G. Caminati, D. Berti, G. Gabrielli, S. Leporatti, R. Rolandi, M. G. Ponzi-Bossi, B. Yang, *Thin Solid Films* **1996**, *284–285*, 181–186; b) H. Huesmann, C. A. Bignozzi, M. T. Indelli, L. Oavanin, M. A. Rampi, D. Möbius, *Thin Solid Films* **1996**, *285*, 62–65; c) T. R. Vierheller, M. D. Foster, A. Schmidt, K. Mathauer, W. Knoll, G. Wegner, S. Statija, C. F. Maijkrzak, *Langmuir* **1997**, *13*, 1712–1717; d) M. Maskus, H. D. Abruna, *Langmuir* **1996**, *12*, 4455–4462; e) Y. Liang, R. H. Schmehl, *J. Chem. Soc. Chem. Commun.* **1995**, 1007–1008.
[9] E. C. Constable, *Adv. Inorg. Chem. Radiochem.* **1986**, *30*, 69–121.
[10] a) G. D. Storrier, S. B. Colbran, D. C. Craig, *J. Chem. Soc. Dalton Trans.* **1997**, 3011–3028; b) E. C. Constable, A. M. W. C. Thompson, *J. Chem. Soc. Dalton Trans.* **1992**, 3467–3475.
[11] J. B. Lambert, H. F. Shurvell, D. A. Lightner, R. G. Cooks, *Introduction to Organic Spectroscopy*, Macmillan, New York, **1987**, pp. 249–268.
[12] E. C. Constable, A. M. W. Cargill Thompson, *J. Chem. Soc. Dalton Trans.* **1992**, 3467–3475.
[13] W. Spahni, G. Calzaferri, *Helv. Chim. Acta* **1984**, *67*, 450–454.
[14] a) G. Decher, Y. Lvov, J. Schmitt, *Thin Solid Films* **1994**, *244*, 772–777; b) G. Decher, J. D. Hong, J. Schmitt, *Thin Solid Films* **1992**, *210/211*, 831–835, c) Y. Lvov, F. Essler, G. Decher, *J. Phys. Chem.* **1993**, *97*, 13773–13777.
[15] a) A. Asmussen, H. Riegler, *J. Chem. Phys.* **1996**, *104*, 8159–8164; b) electron densities were taken from T. P. Russel, *Mater. Sci. Rep.* **1990,** *5*, 171–271.
[16] The density of $[Fe(tpy)_2]^{2+}$ was used in the calculations: A. T. Baker, H. A. Goodwin, *Aust. J. Chem.* **1985**, *38*, 207–214.

Efficient Sialyltransferase Inhibitors Based on Transition-State Analogues of the Sialyl Donor**

Bernd Müller, Christoph Schaub, and Richard R. Schmidt*

Sialic acid containing epitopes are involved in important biological processes, such as cell adhesion and inflammation.[1] There is also a correlation between the sialyl content of glycoconjugates and the malignancy of tumor cells.[2] Furthermore, differences in sialylation type between tumor cells and normal cells were found;[3, 4] for instance, although *N*-glycolylneuraminic acid has not been observed thus far on the surface of normal human cells, 30–50% of tumor cells of different origin contain this compound in small amounts.[3] Recently, an interesting correlation between α(2-6)-sialylation of *N*-acetyllactosamine and B lymphocyte activation and immune function was reported, which could find medicinal application.[5] Therefore, to study the influence of sialyl residues in biological systems it is highly desirable to develop efficient inhibitors for sialyltransferases.

The various sialyltransferases employ, independent of their source and their acceptor specificity, cytidine monophosphate *N*-acetylneuraminic acid (CMP-Neu5Ac, Scheme 1) as sialyl



Scheme 1. Mechanism of the sialylation.

[*] Prof. Dr. R. R. Schmidt, Dipl.-Chem. B. Müller, Dipl.-Chem. C. Schaub
Fakultät für Chemie der Universität, Fach M 725
D-78457 Konstanz (Germany)
Fax: (+49) 7531-88-3135

[**] This work was supported by the Deutsche Forschungsgemeinschaft and the Fonds der Chemischen Industrie. C.S. gratefully acknowledges a fellowship from the Fonds der Chemischen Industrie. We are grateful to Dr. A. Geyer for his help in the structural assignments by NMR experiments.

 © WILEY-VCH Verlag GmbH, D-69451 Weinheim, 1998 1433-7851/98/3720-2893 $ 17.50+.50/0

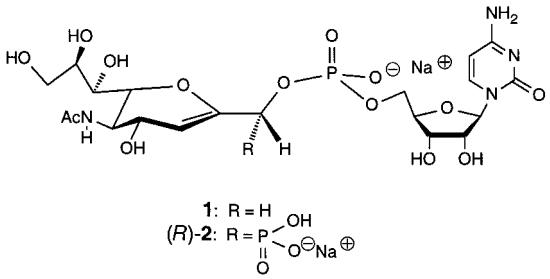
donor.[6] Analogues derived from the transition state of the proposed reaction course (CMP-Neu5Ac$^+$ in Scheme 1)[7, 8] could exhibit high enzyme affinity and thus lead to particularly efficient inhibitors. So far, only a few donor and acceptor analogues (=substrate analogues) which serve as sialyltransferase inhibitors have been reported;[7–13] however, their potency is only in the micromolar range and thus close to that of the substrate CMP-Neu5Ac, which binds to α(2-6)-sialyltransferase from rat liver (EC 2.4.99.1) with $K_M = 46$ μM (Table 1).[7] Therefore, we have initiated a program on the

Table 1. Affinity of CMP-Neu5Ac (K_M) to α(2-6)-sialyltransferase of rat liver and inhibition constants (K_i) of transition-state analogues (*R*)-**2**, **3h**, **3l**, **4h**, **4l**, (*R*)-**6**, (*S*)-**6**, (*R*)-**7**, (*S*)-**7**, (*E*)-**8**, and (*Z*)-**9**.[a]

	K_M [μM]	K_i [μM]	Ref.
CMP-Neu5Ac	46 ± 7	–	[7]
(*R*)-**2**	–	0.35 ± 0.05	[8]
3h	–	0.20 ± 0.05	–
3l	–	1.0 ± 0.2	–
4h	–	0.28 ± 0.06	–
4l	–	1.0 ± 0.3	–
(*R*)-**6**	–	10 ± 2	–
(*S*)-**6**	–	7 ± 2	–
(*R*)-**7**	–	15 ± 3	–
(*S*)-**7**	–	23 ± 5	–
(*E*)-**8**	–	6.0 ± 0.5	[8]
(*Z*)-**9**	–	0.04 ± 0.008	–

[a] For details see ref. [7a].

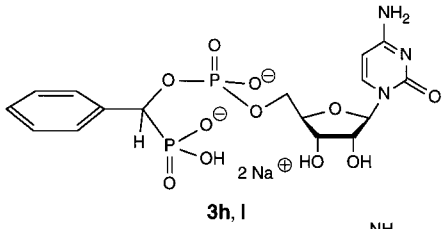
synthesis of transition-state analogues.[7, 14] Compounds **1** and **2** were derived from the transition-state model CMP-Neu5Ac$^+$ (Scheme 1), which is deduced from the recently supported S_N1-type mechanism;[7, 8, 15] they were considered as



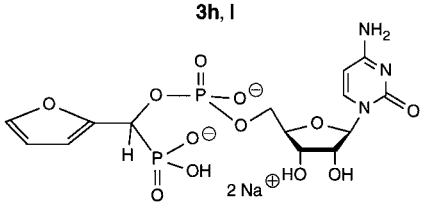
1: R = H
(*R*)-**2**: R = P(O)(OH)(O$^\ominus$Na$^\oplus$)

potential inhibitors because the distance between the anomeric center (C-2 of the Neu5Ac residue) and the leaving group (CMP) is increased, and thus similar to the distance in the transition-state model (CMP-Neu5Ac$^+$). In particular compound **2**[8] was of interest, because it contains two negative charges separated by five bonds, as in CMP-Neu5Ac. In addition, the anomeric center is trigonal planar, thus favoring a conformation assumed for a S_N1-type transition state. This concept turned out to be very fruitful, because (*R*)-**2** is a very potent inhibitor which binds in the nanomolar range to α(2-6)-sialyltransferase (Table 1).[8] This result led to two questions: 1) Is the neuraminyl residue as shown in (*R*)-**2** required at all or can it be replaced by a simple aryl, hetaryl, or related moiety, thus making these type of compounds readily accessible? 2) Will a different geometry of the substituents around the anomeric center increase the binding affinity?

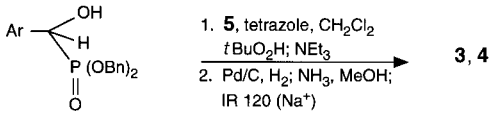
To investigate the first question, compounds **3** and **4** were prepared (Scheme 2). To this end, benzaldehyde and furfural were transformed with dibenzyl phosphonate into the corresponding α-hydroxyphosphonates[16] (racemic mixtures).

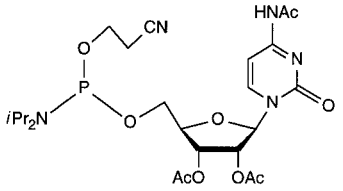


3h, l



4h, l





5

Scheme 2. Synthesis of **3** and **4**. Bn = benzyl.

Their condensation with cytidine-phosphitamide **5**[17] in the presence of tetrazole followed by oxidation with *tert*-butyl hydroperoxide and base-catalyzed cleavage of the cyanoethyl group afforded the target molecules **3h**, **3l** and **4h**, **4l** (Table 2) after hydrogenolytic debenzylation, deacylation, chromatography over RP-18 silica gel ($Et_3NH \cdot HCO_3$ buffer as eluent), and ion exchange with IR-120 (Na^+); the diastereoisomers were separated based on their different R_f values (*h*igh, *l*ow); the configuration of the new stereogenic center was not assigned. Compounds **6** and **7**, in which the phosphonate residue is replaced by a carboxylate group, can be readily obtained from methyl (*R*)- and (*S*)-mandelate and methyl (*R*)- and (*S*)-phenyllactate in a similar fashion (Scheme 3, Table 2).

As can be seen in Table 1, phenyl derivative **3h** exhibits an even higher binding affinity to α(2-6)-sialyltransferase than does neuraminyl derivative (*R*)-**2**, and furyl derivative **4h** is also a very good competitive inhibitor.[18] Apparently, the configuration at the carbon atom bearing the CMP moiety has no dramatic influence on inhibition (K_i values: **3h**:**3l** ≈ 1:5; **4h**:**4l** ≈ 1:4). Replacement of the phosphonate group by a carboxylate group as in (*R*)- and (*S*)-**6** and in (*R*)- and (*S*)-**7** decreases the binding affinity by about one order of magnitude; again the configuration at the carbon atom bearing the

 © WILEY-VCH Verlag GmbH, D-69451 Weinheim, 1998 1433-7851/98/3720-2894 $ 17.50+.50/0

Table 2. Selected physical data of **3h**, **3l**, **4h**, **4l**, (*R*)-**6**, (*S*)-**6**, (*R*)-**7**, (*S*)-**7**, and (*Z*)-**9**.[a]

3h: HPLC (2% CH_3CN, 10 mL min^{-1}): $t_R = 10.1$ min; $[\alpha]_D^{20} = -37.9$ ($c = 0.8$, H_2O); ^1H NMR: $\delta = 3.38$ (br d, 1H; 4′-H), 3.60 (m, 1H; 5a′-H), 3.81–3.95 (m, 3H; 2′-, 3′-, 5b′-H), 5.04 (dd, $^3J(1'',P) = 13.0$ Hz, $^2J(1'',P) = 11.0$ Hz, 1H; 1″-H); MS: $m/z = 494$ $[M - 3Na + 2H]^-$, 559.30 for $C_{16}H_{18}N_3Na_3O_{11}P_2$

3l: HPLC (2% CH_3CN, 10 mL min^{-1}): $t_R = 12.5$ min; $[\alpha]_D^{20} = +23.3$ ($c = 0.8$, H_2O); ^1H NMR: $\delta = 3.66–3.95$ (m, 5H; 2′-, 3′-, 4′-, 5a,b′-H), 5.02 (dd, $^3J(1'',P) = 14.0$ Hz, $^2J(1'',P) = 10.0$ Hz, 1H; 1″-H); MS: $m/z = 494$ $[M - 3Na + 2H]^-$, 559.30 for $C_{16}H_{18}N_3Na_3O_{11}P_2$

4h: HPLC (1% CH_3CN, 8 mL min^{-1}): $t_R = 15.7$ min; ^1H NMR: $\delta = 3.5–4.0$ (m, 5H; 2′-, 3′-, 4′-, 5a,b′-H), 5.04 (dd, $^3J(1'',P) = 15$ Hz, $^2J(1'',P) = 9.2$ Hz, 1H; 1″-H); ^{31}P NMR: $\delta = 0.73$ (d, $^3J(P,P) = 33.4$ Hz; phosphate), 12.56 (d; phosphonate); MS: $m/z = 486$ $[M - 2Na + H - H_2O]^-$, 504 $[M - 2Na + H]^-$, 525 $[M - Na]^-$, 549.2 for $C_{14}H_{16}N_3Na_3O_{12}P$

4l: HPLC (1% CH_3CN, 8 mL min^{-1}): $t_R = 19.9$ min; ^1H NMR: $\delta = 3.65–3.82$ (m, 2H; 5a,b′-H), 3.9–4.0 (m, 3H; 2′-, 3′-, 4′-H), 5.03 (dd, $^3J(1'',P) = 15.1$ Hz, $^2J(1'',P) = 9.5$ Hz, 1H; 1″-H); ^{31}P NMR: $\delta = 1.07$ (d, $^3J(P,P) = 33.4$ Hz; phosphate), 12.49 (d; phosphonate); MS: $m/z = 486$ $[M - 2Na + H - H_2O]^-$, 504 $[M - 2Na + H]^-$, 525 $[M - Na]^-$, 549.2 for $C_{14}H_{16}N_3Na_3O_{12}P$

(*R*)-**6**: HPLC (3% CH_3CN, 8 mL min^{-1}): $t_R = 13.67$ min; $[\alpha]_D^{20} = -41$ ($c = 1.09$, H_2O); ^1H NMR: $\delta = 3.55–3.64$ (m, 2H; 5a,b′-H), 3.80–3.92 (m, 3H; 2′-, 3″-, 4′-H), 5.19 (d, $^3J(1'',P) = 8.9$ Hz, 1H; 1″-H); ^{31}P NMR: $\delta = -0.13$ (s; phosphate); MS: $m/z = 455$ $[M - 2Na + H]^-$, 501.3 for $C_{17}H_{18}N_3Na_2O_{10}P$

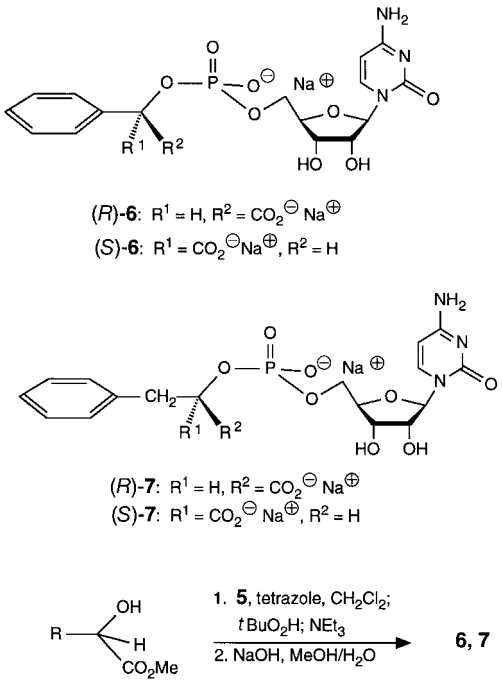
(*S*)-**6**: HPLC (3% CH_3CN, 8 mL min^{-1}): $t_R = 21.32$ min; $[\alpha]_D^{20} = +37.6$ ($c = 0.5$, H_2O); ^1H NMR: $\delta = 3.70–3.91$ (m, 5H; 2′-, 3′-, 4′- 5a,b′-H), 5.16 (d, $^3J(1'',P) = 9.1$ Hz, 1H; 1″-H); ^{31}P NMR: $\delta = 0.20$ (s; phosphate); MS: $m/z = 455$ $[M - 2Na + H]^-$, 501.3 for $C_{17}H_{18}N_3Na_2O_{10}P$

(*R*)-**7**: TLC: $R_f = 0.81$; $[\alpha]_D^{20} = +5.5$ ($c = 1$, H_2O); ^1H NMR: $\delta = 2.80–2.97$ (m, 2H; 2a,b″-H), 3.50–3.58 (m, 1H; 5a′-H), 3.80–3.94 (m, 4H; 2′-, 3′-, 4′-, 5b′-H), 4.38–4.48 (m, 1H; 1″-H); ^{31}P NMR: $\delta = 0.07$ (s; phosphate); MS: $m/z = 470$ $[M - 2Na + H]^-$, 515.07 for $C_{18}H_{20}N_3Na_2O_{10}P$

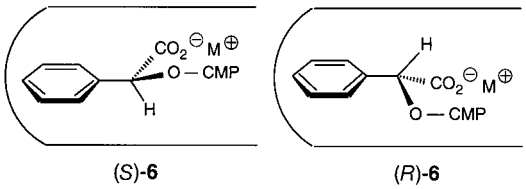
(*S*)-**7**: TLC: $R_f = 0.81$; $[\alpha]_D^{20} = -9.4$ ($c = 1$, H_2O); ^1H NMR: $\delta = 2.81$ (dd; $J(2a'',2b'') = 14.2$ Hz, $J(2a'',1'') = 7.0$ Hz, 1H; 2a″-H), 2.89 (dd, $J(2b'',1'') = 5.3$ Hz, 1H; 2b″-H), 3.60–3.74 (m, 2H; 5a,b′-H), 3.88–3.96 (m, 2H; 2′-,3′-H), 4.00 (dd, $J(4',3') = J(4',5a') = 4.5$ Hz, 1H; 4′-H), 4.38 (ddd, $J(1'',P) = 8.4$ Hz, 1H; 1″-H); ^{31}P NMR: $\delta = -0.04$ (s; phosphate); MS: $m/z = 470$ $[M - 2Na + H]^-$, 515.07 for $C_{18}H_{20}N_3Na_2O_{10}P$

(*Z*)-**9**: HPLC (2% CH_3CN, 10 mL min^{-1}): $t_R = 14.4$ min; ^1H NMR (600 MHz, D_2O): $\delta = 1.89$ (s, 3H; NHAc), 3.42 (dd, $J(7'',8'') = 9.1$ Hz, $J(7'',6'') = 1.9$ Hz, 1H; 7″-H), 3.51 (dd, $^2J(9a'',9b'') = 11.9$ Hz, $J(9a'',8'') = 7.0$ Hz, 1H; 9a″-H), 3.75 (dd, $J(9b'',8'') = 2.8$ Hz, 1H; 9″b-H), 3.84 (dd, $J(6'',5'') = 9.8$ Hz, 1H; 6″-H), 3.91 (m, 1H; 8″-H), 4.13 (m, 2H; 3′,4′-H), 4.15–4.20 (m, 3H; 2′-, 5a,b′-H), 4.73 (ddd, $J(5'',4'') = J(5'',3'') = 1.9$ Hz, 1H; 5″-H), 5.76 (ddd, $J(4'',3'') = 10.4$ Hz, $J(4'',P) = 2$ Hz, 1H; 4″-H), 5.85 (d, $J(1',2') = 4.2$ Hz, 1H; 1′-H), 6.50 (ddd, $J(3'',P) = 2.8$ Hz, 1H; 3″-H); ^{31}P NMR (242.5 MHz, D_2O): $\delta = -3.6$ (br s; phosphate), 3.6 (br s; phosphonate); MS: $m/z = 644$ $[M - 3Na + 2H]^-$, 710.42 for $C_{20}H_{27}N_4Na_3O_{16}P_2$

[a] ^1H NMR: 250 MHz, D_2O, unless indicated otherwise. ^{31}P NMR: 161.7 MHz, D_2O, unless indicated otherwise. MS: MALDI, negative mode, matrix ATT. HPLC: RP-18, 1–3% CH_3CN, 0.05 M $Et_3NH \cdot HCO_3$. TLC: ethyl acetate/methanol/1 M $CH_3CO_2NH_4$ 1/1/1.



Scheme 3. Synthesis of **6** and **7**.

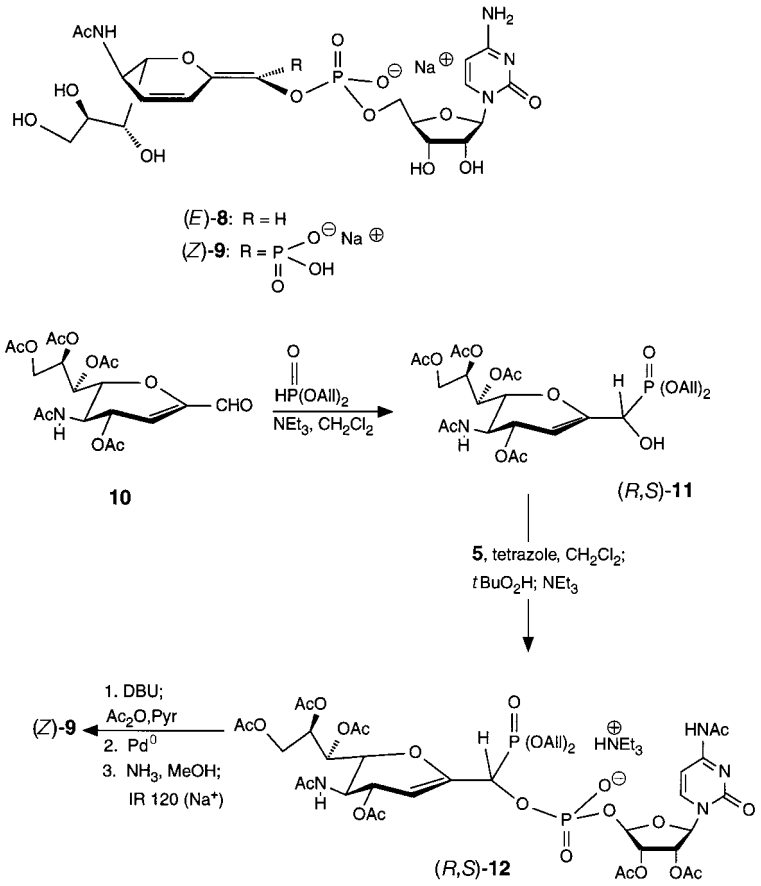


Scheme 4. Formation of **6** with accomodation of the configurational difference.

CMP moiety has no major influence on the K_i values. Thus, binding as depicted for the examples for (*R*)- and (*S*)-**6** in Scheme 4 is supported, which could accomodate the configurational difference.

The high affinity of **3h** (which contains a flat benzene ring), the minor influence of the carbon atom bearing the CMP group, and the unexpected high affinity of elimination product (*E*)-**8** (Scheme 5; obtained during the synthesis of (*R*)-**2** by deacetoxyphosphonylation)[8] led us to combine the positive effects of (*R*)-**2**, **3h** and (*E*)-**8** and to introduce a phosphonate residue at the methylene group of **8**. Thus, in the derived target compound (*Z*)-**9** the orientation of the two decisive moieties—the phosphonate and the CMP moiety—have the desired different geometry, and the pyran ring generated from the neuraminyl residue will be flatter than in (*R*)-**2** and thus more similar to the benzene ring in **3h**. The synthesis of (*Z*)-**9** could be readily accomplished (Scheme 5): Reaction of aldehyde **10**[8] with diallyl phosphonate[19] gave α-hydroxyphosphonate **11** (as a mixture of diastereomers (*R,S*)-**11**), which reacted by condensation with **5** as described above to diastereomers (*R,S*)-**12**. Base-supported (DBU) elimination of acetic acid followed by deallylation with $[Pd(PPh_3)_4]$ in the presence of dimedone and base-catalyzed deacylation afforded target molecule (*Z*)-**9** only (Table 2). This compound exhibited very potent competitive inhibition of α(2-6)-sialyltransferase ($K_i = 40$ nm, Table 1), and its affinity to α(2-6)-sialyltransferase[20] is three orders of magnitude higher than that of the natural substrate CMP-Neu5Ac; this supports the conceptual approach discussed here.

Potent sialyltransferase inhibition can be based on flat pyranosyl ring mimics which possess a methyl or a methylene carbon atom bearing a phosphonate and a CMP residue, as clearly exhibited for **1**, (*R*)-**2**, **3h**, (*E*)-**8**, and (*Z*)-**9**. Thus, further details of the transition-state geometry in the enzymatic sialyl transfer can be deduced, which provides leads for the extension of this research.



Scheme 5. Synthesis of (*Z*)-**9**. All = allyl, DBU = 1,8-diazabicyclo[5.4.0]undec-7-ene.

Experimental Section

A) Protocol for the synthesis of α-hydroxyphosphonates: The aldehyde (1 equiv) was dissolved in a small amount of CH_2Cl_2, and then the phosphonic acid diester (2 equiv) and a few drops of NEt_3 were added. The solution was stirred for 18 h, concentrated, and purified by chromatography on silica gel.

B) Protocol for the condensation with **5**: Compound **5** (1.5 equiv) and α-hydroxyphosphonate (1 equiv) were dissolved in CH_2Cl_2 and evaporated to dryness. The remaining foam was dissolved under nitrogen in dry CH_2Cl_2, and 1*H*-tetrazole (2 equiv) was added. After the reaction mixture had been stirred for 3 h, an anhydrous solution of *tert*-butyl hydroperoxide (1.5 equiv) was added, and after an additional hour NEt_3 (50 equiv) was added. After 18 h of stirring, the reaction mixture was concentrated at 20 °C and purified by chromatography on silica gel (ethyl acetate/methanol 5/1, 1 % NEt_3).

O-Debenzylation and/or O/N-deacetylation was performed as previously described[8] to afford **3h**, **3l**, **4h**, **4l**, (*R*)-**6**, (*S*)-**6**, (*R*)-**7**, and (*S*)-**7**.

C) Synthesis of (*Z*)-**9**: The synthesis of (*R,S*)-**11** and (*R,S*)-**12** followed protocols A and B, respectively. Compound (*R,S*)-**12** (180 mg, 0.16 mmol) and 1,8-diazabicyclo[5.4.0]undec-7-ene (DBU, 70 µL, 0.48 mmol) were dissolved in dry THF (2 mL) and heated to 60 °C; after 2 h additional DBU (50 µL, 0.33 mmol) was added, and stirring continued for 3 h. Then acetic anhydride (2 mL) and pyridine (4 mL) were added at room temperature, and after 15 h the reaction mixture was concentrated and purified by chromatography on silica gel (ethyl acetate/methanol 5/1, 1 % NEt_3) to give protected (*Z*)-**9** (120 mg, 70 %); $R_f = 0.10$ (ethyl acetate/methanol 4/1, 1 % NEt_3). For the removal of the protecting groups (*Z*)-**9** (40 mg) was dissolved in THF (2 mL) and treated with $[Pd(PPh_3)_4]$ (4.2 mg, 4 µmol) and dimedone (21 mg, 0.15 mmol), and the mixture stirred for 30 min in the dark. The reaction mixture was purified by chromatography on RP-18 silica gel (water/ethanol 3/1) and concentrated in vacuo. Then an aqueous ammonia solution (30 %, 3 mL) was added in order to remove the acetyl groups. The solution was concentrated under reduced pressure and then dissolved in water (1 mL) and stirred with IR-120 (Na^+). Filtration and subsequent addition of ethanol (8 mL) afforded (*Z*)-**9** (yield 24 mg, 80 %).

Received: May 29, 1998 [Z11914IE]
German version: *Angew. Chem.* **1998**, *110*, 3021 – 3024

Keywords: enzyme inhibitors · neuraminic acids · phosphonates · transition states

[1] a) A. Rosenberg, *Biology of Sialic Acids*, Plenum, New York, **1995**; b) F. Dall'Olio, N. Malagolini, F. Serafini-Cessi, *Int. J. Cancer* **1992**, *50*, 325 – 330; c) J. Morgenthaler, W. Kemmner, R. Brossmer, *Biochem. Biophys. Res. Commun.* **1990**, *171*, 860 – 866.

[2] a) R. J. Bernacki, *Science* **1977**, *195*, 557 – 580; b) Q. Zhou, S. Hakomori, K. Kitamura, Y. Igarashi, *J. Biol. Chem.* **1994**, *269*, 1959 – 1965; c) J. W. Dennis in *Cell Surface Carbohydrates and Cell Development* (Ed.: M. Fukuda), CRC, Boca Raton, FL, USA, **1991**, pp. 174 – 175; d) W. Kemmner, D. Kruck, P. M. Schlag, *Clin. Exp. Metastasis* **1994**, *12*, 245 – 254.

[3] a) T. Kawai, A. Kato, H. Higashi, S. Kato, M. Naiki, *Cancer Res.* **1991**, *51*, 1242 – 1246; b) F.-G. Hanisch, B. Witter, G. Crombach, W. Schänzer, G. Uhlenbruck, *Tumor-Associated Antigens*, *Oncogenes*, *Receptors*, *Cytokines in Tumor Diagnosis and Therapy at the Beginning of the Nineties. Cancer of the Breast-State and Trends in Diagnosis and Therapy* (Ed.: R. Klapder), Zuckerschwerdt, München, **1992**, pp. 367 – 370.

[4] a) E. Sjoberg, A. Manzi, K. Khoo, A. Varki, *J. Biol. Chem.* **1992**, *267*, 16200 – 16211; b) T. Kageshita, S. Hirai, T. Kimura, *Cancer Res.* **1995**, *55*, 1748 – 1751.

[5] T. Hennet, D. Chui, J. C. Paulson, J. D. Marth, *Proc. Natl. Acad. Sci. USA* **1998**, *95*, 4504 – 4509.

[6] A. Harduin-Lepers, A. Recchi, P. Delaunnoy, *Glycobiology* **1995**, *5*, 741 – 758.

[7] a) C. Schaub, B. Müller, R. R. Schmidt, *Glycoconjugate J.* **1998**, *15*, 345 – 354; b) C. Schaub, R. R. Schmidt, *Abstr. Pap. 2nd Eur. Conf. Carbohydr. Mimics* (La Garda, Italy), **1996**, p. C10.

[8] F. Amann, C. Schaub, B. Müller, R. R. Schmidt, *Chem. Eur. J.* **1998**, *4*, 1106 – 1115.

[9] B. Müller, T. J. Martin, C. Schaub, R. R. Schmidt, *Tetrahedron Lett.* **1998**, *39*, 509 – 512.

[10] a) W. Korytnyk, N. Angelino, W. Klohs, R. J. Bernacki, *Eur. J. Med. Chem.* **1980**, *15*, 77 – 84; b) I. Kijima-Suda, Y. Migamata, S. Toyoshima, M. Itoh, T. Osawa, *Cancer Res.* **1986**, *46*, 858 – 862; c) S. H. Khan, K. L. Matta in *Glycoconjugates*, *Composition*, *Structure*, *Function* (Eds.: H. J. Allen, E. C. Kisailus), Dekker, New York, **1992**, pp. 361 – 378, and references therein.

[11] a) H. Hashimoto, K. Sato, T. Wakabayashi, H. Kodama, Y. Kajihara, *Carbohydr. Res.* **1993**, *247*, 179 – 193; b) M. Imamoto, H. Hashimoto, *Tetrahedron Lett.* **1996**, *37*, 1451 – 1454.

[12] a) R. G. Kleineidam, T. Schmelter, R. T. Schwarz, R. Schauer, *Glycoconjugate J.* **1997**, *14*, 57 – 66; b) D. H. van den Eijnden, T. J. Martin, R. R. Schmidt, unpublished results; c) G. Dufner, Dissertation, Universität Konstanz, **1997**.

[13] Recently antisense technology has been investigated in order to decrease sialyltransferase expression: W. Kemmner, K. Hohaus, P. M. Schlag, *FEBS Lett.* **1997**, *409*, 347 – 350.

[14] Other examples of transition-state analogues of sugar nucleotides: UDP-Gal: a) K. Frische, Dissertation, Universität Konstanz, **1992**; b) K. Frische, R. R. Schmidt, *Bioorg. Med. Chem. Lett.* **1993**, *3*, 1747 – 1750; GDP-Fuc: c) S. Cai, M. R. Strond, S. Hakomori, T. Toyokuni, *J. Org. Chem.* **1992**, *57*, 6693 – 6696.

[15] B. A. Horenstein, M. Bruner, *J. Am. Chem. Soc.* **1996**, *118*, 10371 – 10379; b) B. A. Horenstein, M. Bruner, *Biochemistry* **1998**, *37*, 289 – 297, and references therein.

 © WILEY-VCH Verlag GmbH, D-69451 Weinheim, 1998 1433-7851/98/3720-2896 $ 17.50+.50/0

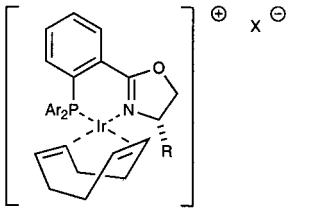
[16] M. Hoffmann, *Synthesis* **1988**, 62 – 64.
[17] a) Y. Kajihara, K. Koseki, T. Ebata, H. Kodama, H. Matsusita, H. Hashimoto, *Carbohydr. Res.* **1994**, *264*, C1 – C5; b) Y. Kajihara, K. Koseki, T. Ebata, H. Kodama, H. Matsusita, H. Hashimoto, *J. Org. Chem.* **1995**, *60*, 5732 – 5735.
[18] For details of the measurement of the K_i values, see ref. [7a].
[19] Commercially available from Aldrich.
[20] Investigation of inhibition with a recombinant rat liver α(2-3)-sialyltransferase led to similar results: C. Schaub, Dissertation, in preparation.

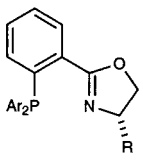
Enantioselective Hydrogenation of Olefins with Iridium – Phosphanodihydrooxazole Catalysts

Andrew Lightfoot, Patrick Schnider, and Andreas Pfaltz*

Enantioselective hydrogenation is one of the most powerful methods in asymmetric catalysis, with the most versatile catalysts being rhodium– and ruthenium – diphosphane complexes.[1] However, with a few exceptions, the range of substrates is still limited to certain classes of olefins bearing polar groups that can coordinate to the catalyst. Moreover, even in standard substrate categories derivatives can be found that give unsatisfactory enantioselectivities. There are only a few examples of highly enantioselective hydrogenations of unfunctionalized olefins.[2, 3] The most impressive results in this field have been obtained by Buchwald, who used Brintzinger's chiral titanocene complexes.[3] Although high *ee* values were obtained, the low catalyst activity required that a relatively high catalyst loading ($\geq$5 mol %) was used. Therefore, the search for new catalysts to fill these methodological gaps continues.

We recently reported enantioselective hydrogenation of imines catalyzed by iridium – phosphanodihydrooxazole complexes of the type **1** with PF_6^- as anion.[4] The coordination environment of the iridium center resembles that in Crabtree's catalyst, a cationic iridium complex with a monophosphane and pyridine as ligands.[5] Owing to the remarkable properties of Crabtree's catalyst—that is, the ability to hydrogenate tri- and tetrasubstituted olefins that do not react with rhodium– or ruthenium – phosphane catalysts—we decided to study complexes **1** as catalysts for the hydrogenation of unfunctionalized tri- and tetrasubstituted olefins.

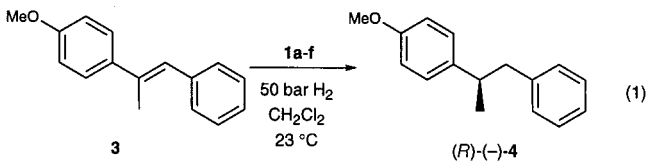




1a	Ar = Ph	R = *i*Pr	X = PF_6
1b	Ar = Ph	R = *t*Bu	X = PF_6
1c	Ar = *o*-Tol	R = *i*Pr	X = PF_6
1d	Ar = *o*-Tol	R = *t*Bu	X = PF_6
1e	Ar = Ph	R = *i*Pr	X = BARF
1f	Ar = *o*-Tol	R = *t*Bu	X = BARF
1g	Ar = Ph	R = CH_2tBu	X = BARF

2a	Ar = Ph	R = *i*Pr
2b	Ar = Ph	R = *t*Bu
2c	Ar = *o*-Tol	R = *i*Pr
2d	Ar = *o*-Tol	R = *t*Bu
2e	Ar = Ph	R = CH_2tBu

Initial experiments with complex **1a** led to encouraging results. Indeed, the hydrogenation of olefin **3** in CH_2Cl_2 with 4 mol % of **1a** [Eq. (1)] gave a good *ee* value of 75 %, albeit with moderate conversion (78 %, Table 1). Lower catalyst loadings led to decreased conversion. Preliminary kinetic data



(1)

with (*E*)-1,2-diphenyl-1-propene as substrate shows a large initial turnover frequency (TOF) of 41 min^{-1} (olefin: 0.31 M, catalyst: 0.003 M), but as the reaction proceeds the TOF decreases to essentially zero within one hour.[6] Deactivation has also been observed with Crabtree's catalyst, which is explained by the formation of inactive hydride-bridged trimers.[5] In our case the origin of deactivation is not known, but traces of water appear to enhance this undesired side reaction. Thus, the addition of molecular sieves to the above system gave an increased conversion. Alternatively, running the reaction under strictly anhydrous conditions, using freshly dried CH_2Cl_2 (distilled over CaH_2) and standard Schlenk techniques, allows full conversion to be obtained with 4 mol % of **1a** with the same *ee* value as before. Analytically pure product **4** was isolated in essentially quantitative yield by removal of the solvent and distillation.

Table 1. Enantioselective hydrogenation of **3** with use of catalysts **1a** – **f** [Eq. (1)].

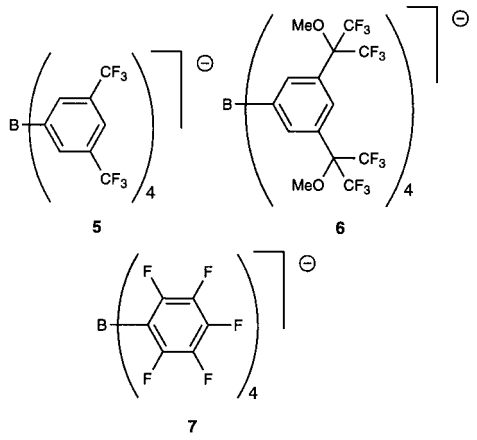
Entry	Cat. (mol %)	Conversion [%]	*ee* [%]
1	**1a** (4)	78	75
2	**1b** (4)	98	90
3	**1c** (4)	> 99	91
4	**1d** (4)	57	97
5	**1e** (0.3)	> 99	70
6	**1f** (0.3)	> 99	98

A systematic study of ligands **2a** – **d** led to a highly enantioselective catalyst for the hydrogenation of **3** (Table 1). Thus, replacement of the isopropyl group of ligand **2a** with a *tert*-butyl group (**2b**) increased the *ee* value to 90 %. Alternatively, replacement of the diphenylphosphanyl group of **2a** with a bis(*o*-tolyl)phosphanyl group (**2c**) increased the *ee* value to 91 %. The combined use of a *tert*-butyl group and a bis(*o*-tolyl)phosphanyl group (**2d**) led to the highest enantioselectivity (97 % *ee*, 57 % conversion with 4 mol % of **1d**). Attempts to further increase the conversion by varying the reaction conditions and introducing additives, such as iodide, were met with little success.[7] However, replacement of the PF_6^- anion with BARF (tetrakis[3,5-bis(trifluoromethyl)phe-

[*] Prof. Dr. A. Pfaltz, Dr. A. Lightfoot, Dr. P. Schnider
Max-Planck-Institut für Kohlenforschung
Kaiser-Wilhelm-Platz 1, D-45470 Mülheim an der Ruhr (Germany)
Fax: (+49) 208-306-2992
E-mail: pfaltz@mpi-muelheim.mpg.de

 © WILEY-VCH Verlag GmbH, D-69451 Weinheim, 1998 1433-7851/98/3720-2897 $ 17.50+.50/0

nyl]borate, **5**)[8] had a dramatic effect on the conversion and allowed a reduction in the catalyst loading to typically less than 1 mol%. For example, in a concentrated solution (4 M)



5 **6** **7**

(*E*)-1,2-diphenyl-1-propene was hydrogenated with 70% *ee* (>99% conversion) with 0.05 mol% of **1e**. Similar weakly coordinating anions such as **6**[9] (0.1 mol% of catatyst, 65% *ee*, >99% conversion) and **7**[10] (0.1 mol% of catalyst, 60% *ee*, 84% conversion) also gave active catalysts, whereas all other anions tested (SbF_6^-, BF_4^-, BPh_4^-, TfO^-, halides) resulted in much lower activity. Curiously, the catalysts with BARF as counterion appear to be tolerant of traces of moisture, and the reaction solutions can be prepared in the air without specially dried solvents. The initial TOF of the catalysts with BARF as counterion is even higher than that of the hexafluorophosphate complexes (70–135 min^{-1}, olefin **8**: 0.31 M, **1e**: 0.003 M).

The most efficient catalyst in this series proved to be **1f**, which gave high conversions and yields as well as good to excellent *ee* values for a number of trisubstituted olefins (Figure 1). Until now, unfunctionalized olefins of this type could not be hydrogenated with high enantioselectivity using other catalysts at such low loading (0.1–0.5 mol%). (*Z*)-1,2-Diarylolefins are unreactive towards this catalyst, whereas both (*E*)- and (*Z*)-2-(4-methoxyphenyl)-2-butene (**11** and **12**, respectively) gave high conversions but only moderate *ee* values. The major enantiomer derived from the *Z* isomer was found to be opposite to that obtained for the *E* isomer. The allylic acetate **13** was also hydrogenated with high *ee* value. Even the tetrasubstituted olefin **14** could be hydrogenated in high yield, and with remarkable enantioselectivity for this type of substrate, using complex **1g**, which was the best catalyst in this case. Allyl alcohols and α,β-unsaturated esters, on the other hand, gave only low conversion with the BARF complexes **1e** and **1f**. For these classes of substrates, the hexafluorophosphate complex **1d** proved to be a superior catalyst. Thus, **16** was hydrogenated efficiently with 1 mol% of **1d** (96% *ee*, 95% conversion), demonstrating that these complexes provide an alternative to the ruthenium/BINAP system.[11] The same catalyst was successfully employed in the enantioselective synthesis of the artificial fragrance lilial (Scheme 1).[12] The allyl alcohol **17**[13] was hydrogenated in the presence of 2 mol% of **1d** to give 95% of the corresponding alcohol with 94% *ee*. Oxidation with pyridinium chlorochromate (PCC) led to lilial in 56% yield.

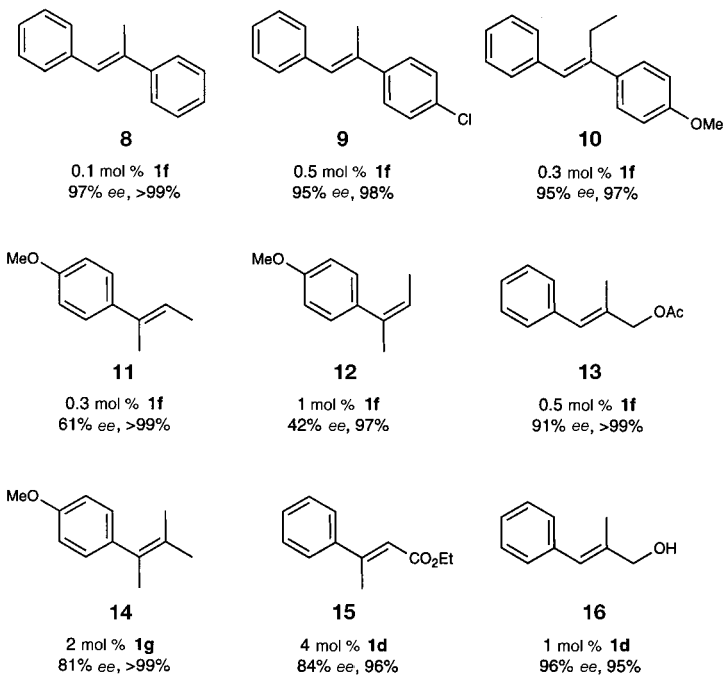
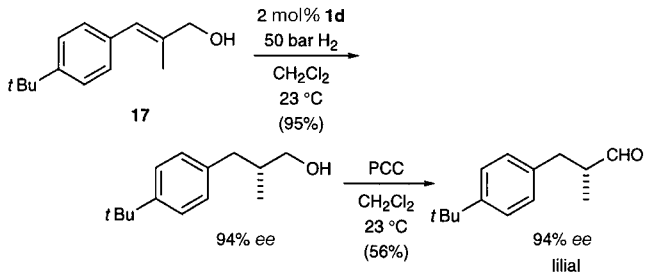


Figure 1. Substrates for hydrogenation with catalysts **1a**–**g** along with catalyst amounts, *ee* values, and conversions.



Scheme 1. Synthesis of lilial. PCC = pyridinium chlorochromate.

We have demonstrated that cationic iridium complexes with chiral phosphanodihydrooxazoles are efficient catalysts for the enantioselective hydrogenation of olefins. The complexes are air-stable and easy to handle. Depending on the counterion, BARF or hexafluorophosphate, certain unfunctionalized aryl-substituted olefins or allyl alcohols can be hydrogenated in high yields and with excellent enantioselectivities.

Experimental Section

1f: To a two-necked flask fitted with a condenser was added **2d**[14] (400 mg, 0.96 mmol), [{Ir(cod)Cl}$_2$] (324 mg, 0.48 mmol), and CH_2Cl_2 (10 mL). The deep red mixture was heated under Ar to reflux for 1 h, until thin layer chromatography (TLC; silica gel, CH_2Cl_2) indicated that **2d** had been consumed. After the mixture was cooled to room temperature, Na[BARF] (1.31 g, 1.5 mmol) was added followed by H_2O (10 mL), and the resulting two-phase mixture was stirred vigorously for 10 min. Counterion exchange from the chloride ($R_f = 0$) to BARF ($R_f = 0.95$) was indicated by TLC (silica gel, CH_2Cl_2). The layers were separated, and the aqueous layer was extracted with further portions of CH_2Cl_2 (2×10 mL). The combined organic extracts were washed with H_2O (10 mL) and evaporated. The residue was taken up in EtOH (10 mL) and crystallized by the slow addition of H_2O (1 mL) to give **1f** (935 mg, 62%) as a dark orange solid. Elemental analysis calcd for $C_{67}H_{54}BF_{24}IrNOP$: C 50.96, H 3.45, N 0.89;

 © WILEY-VCH Verlag GmbH, D-69451 Weinheim, 1998 1433-7851/98/3720-2898 $ 17.50+.50/0

found: C 51.11, H 3.46, N 0.92; m.p. 200–203 °C (decomp); $[\alpha]_{589} = -160$ ($CDCl_3$, $c = 0.2$, 23 °C); ^{1}H NMR (300 MHz, $CDCl_3$): $\delta = 0.46$ (br s, 9H; *t*Bu), 1.43 (m, 2H; CH_2 (COD)), 1.92 (m, 2H; CH_2 (COD)), 2.15–2.33 (m, 8H; 2Me, CH_2 (COD)), 2.99 (br s, 3H; CH, CH_2 (COD)), 3.37 (br s, 1H; CH (COD)), 3.85 (m, 1H; CH_2O), 4.21 (t, $J = 9.45$ Hz, 1H, CHN), 4.45 (m, 1H; CH_2O), 4.64 (m, 1H; CH (COD)), 4.75 (br s, 1H; CH (COD)), 6.37 (m, 1H; arom. H), 6.78 (m, 1H; arom. H), 6.96 (m, 1H; arom. H), 7.11–7.17 (m, 4H; arom. H), 7.24–7.37 (m, 4H; arom. H), 7.43 (s, 4H; BARF), 7.52 (m, 2H; arom. H), 7.63 (s, 8H; BARF), 8.13–8.08 (m, 1H; arom. CH); ^{31}P NMR (100 MHz, $CDCl_3$): $\delta = 11.0$.

Hydrogenation of **3**. To a 35-mL autoclave with magnetic stirrer was added **1f** (1.6 mg, 0.001 mmol, 0.3 mol %), **3** (74 mg, 0.33 mmol), and CH_2Cl_2 (0.3 mL). The autoclave was sealed and pressurized to 50 bar with H_2, and the mixture was stirred for 2 h. The CH_2Cl_2 solvent was removed and replaced with heptane (3 mL), and the solution passed through a short plug of silica (0.5 cm) to remove the metal salts. Analysis by gas chromatography (GC) indicated 99.8 % conversion into **4**. Kugelrohr distillation (130–140 °C/0.04 mbar) afforded **4** as a clear oil (75 mg, 99 %). The reaction of 4 mmol of **3** and 0.3 mol % of **1f** gave the same results. HPLC (Chiralcel OJ, *i*PrOH/heptane 5/95, 0.5 mL min^{-1}, 20 °C, 254 nm): t_R (*R*) = 15.6 min, t_R (*S*) = 20.3 min, 98 % *ee*; $[\alpha]_{589} = -94.4$ (CH_2Cl_2, $c = 2.93$, 23 °C); ^{1}H NMR (200 MHz, $CDCl_3$): $\delta = 1.21$ (d, 3H; $J = 8.3$ Hz, Me), 2.67–3.01 (m, 3H; CH, CH_2), 3.77 (s, 3H; OMe), 6.81 (d, 2H; $J = 8.8$ Hz, arom. H), 7.07–7.26 (m, 7H; arom. H); ^{13}C NMR (75 MHz, $CDCl_3$): $\delta = 21.0$ (Me), 40.7 (CH), 45.1 (CH_2), 55.5 (OMe), 113.9, 126.1, 128.2, 128.4, 129.5 (arom. CH), 139.5, 141.3, 158.3 (arom. C).

HPLC analysis of the hydrogenation products from **8**–**13** and **15**–**17** (0.5 mL min^{-1}, 20 °C, 254 nm): **8** (Chiralcel OJ, *i*PrOH/heptane 1/99): t_R = 12.6 min (major enantiomer), 20.6 min (minor enantiomer); **9** (Chiralcel OJ, *i*PrOH/heptane 1/99): 12.9/15.7 min; **10** (Chiralcel OJ, *i*PrOH/heptane 5/95): 12.1/17.3 min; **11** (Chiralcel OD-H, *i*PrOH/heptane 0.01/99.99): 15.3/13.9 min; **12** (Chiralcel OD-H, *i*PrOH/heptane 0.01/99.99): 14.1/16.0 min; **13** was hydrolyzed (MeOH/K_2CO_3), and the resulting alcohol was analyzed (Chiralcel OD-H, *i*PrOH/heptane 5/95, 40 °C): 17.4/15.1 min; **15** (Chiralcel OB-H, *i*PrOH/heptane 0.5/99.5): 18.4/21.4 min; **16** (Chiralcel OD-H, *i*PrOH/heptane 5/95, 50 °C), 16.4/14.6 min; **17** (Chiralcel OD-H, *i*PrOH/heptane 5/95, 40 °C): 18.0/15.6 min. Analysis by GC of the hydrogenation product from **14** (20 % *t*Bu β-CD, 80 % OV1701, 25 m, 0.5 bar H_2, 50–180 °C, 1° min^{-1}): t_R = 52.4 min (major enantiomer), 51.2 min (minor enantiomer).

Received: May 27, 1998 [Z11908IE]
German version: *Angew. Chem.* **1998**, *110*, 3047–3050

Keywords: asymmetric catalysis · dihydrooxazoles · hydrogenations · iridium · N ligands · P ligands

[1] R. Noyori, *Asymmetric Catalysis in Organic Synthesis*, Wiley, New York, **1994**, pp. 16–94; H. Tayaka, T. Ohta, R. Noyori in *Catalytic Asymmetric Synthesis* (Ed.: I. Ojima), VCH, New York, **1993**, pp. 1–39; A. Pfaltz, *Methods Org. Chem.* (*Houben-Weyl*), 4th ed., Vol. E21, **1995**, chap. 2.5.1.2.1/2, pp. 4334–4359.

[2] R. L. Halterman, K. P. C. Vollhardt, M. E. Welker, D. Bläser, R. Boese, *J. Am. Chem. Soc.* **1987**, *109*, 8105–8107; V. P. Conticello, L. Brard, M. A. Giardello, Y. Tsuji, M. Sabat, C. L. Stern, T. J. Marks, *J. Am. Chem. Soc.* **1992** *114*, 2761–2762; M. A. Giardello, V. P. Conticello, L. Brard, M. R. Gagné, T. J. Marks, *J. Am. Chem. Soc.* **1994**, *116*, 10241–10254.

[3] R. D. Broene, S. L. Buchwald, *J. Am. Chem. Soc.* **1993**, *115*, 12569–12570.

[4] P. Schnider, G. Koch, R. Prétôt, G. Wang, F. M. Bohnen, C. Krüger, A. Pfaltz, *Chem. Eur. J.* **1997**, *3*, 887–891.

[5] R. H. Crabtree, *Acc. Chem. Res.* **1979**, *12*, 331–338.

[6] D. Blackmond, T. Rosner, Max-Planck-Institut für Kohlenforschung, unpublished results.

[7] For the effect of additives upon iridium-catalyzed hydrogenation of imines, see Y. N. C. Chan, D. Meyer, J. A. Osborn, *J. Chem. Soc. Chem. Commun*. **1990**, 869–871; T. Morimoto, K. Achiwa, *Tetrahedron: Asymmetry* **1995**, *6*, 2661–1664; K. Tani, J.-I. Onouchi, T. Yamagata, Y. Kataoka, *Chem. Lett.* **1995**, 955–956; F. Spindler, B. Pugin, H.-P. Jalett, H.-P. Buser, U. Pittelkow, H.-U. Blaser, *Chem. Ind.* (*Dekker*) **1996**, *68*, 153–168.

[8] H. Nishida, N. Takada, M. Yoshimura, T. Sonoda, H. Kobayashi, *Bull. Chem. Soc. Jpn*. **1984**, *57*, 2600–2604.

[9] G. H. Zhang, T. Imato, Y. Asano, T. Sonoda, H. Kobayashi, N. Ishibashi, *Anal. Chem*. **1990**, *62*, 1644–1648.

[10] A. G. Massey, A. J. Park, *J. Organomet. Chem*. **1962**, *2*, 245–250.

[11] H. Takaya, T. Ohta, N. Sayo, H. Kumobayashi, S. Akutagawa, S. Inoue, I. Kasahara, R. Noyori, *J. Am. Chem. Soc.* **1987**, *109*, 1596–1597, 4129.

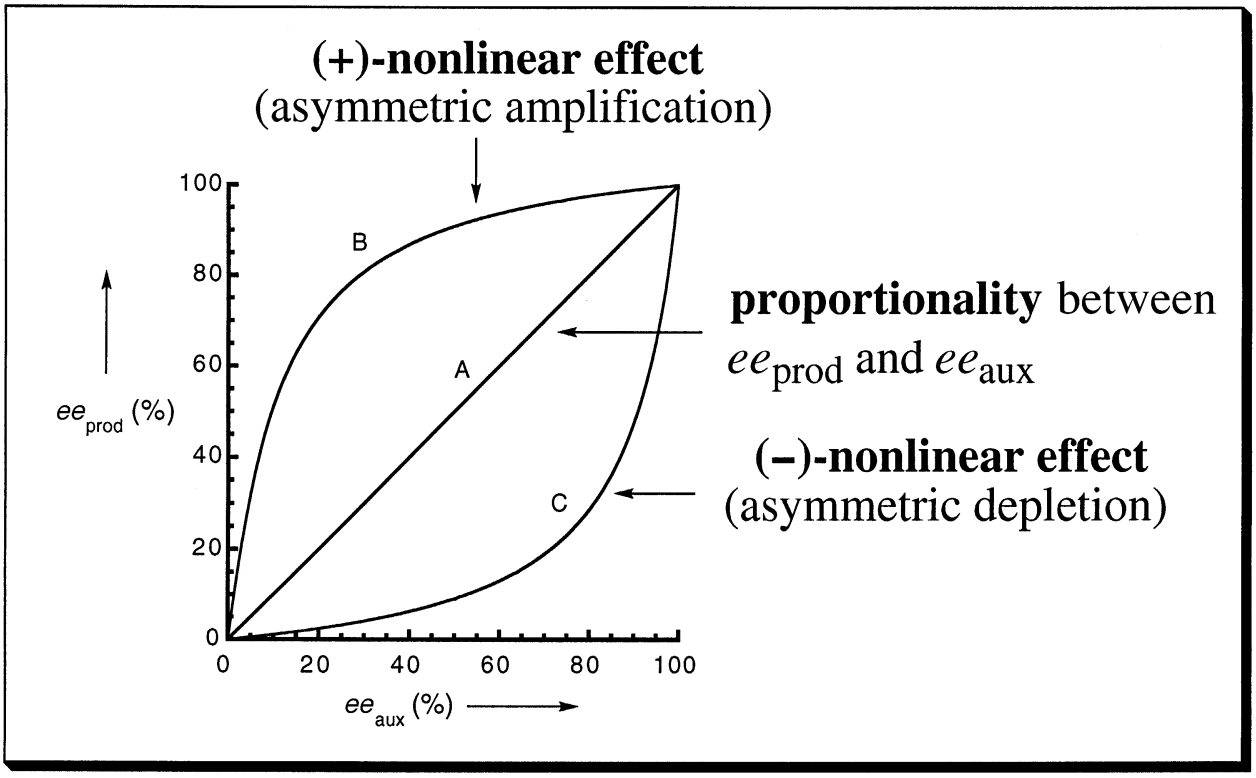
[12] "Flavours and Fragrances": K. Bauer, D. Garbe, H. Surberg in *Ullmann's Encyclopedia of Industrial Chemistry, Vol. A11*, VCH, Weinheim, **1988**, pp. 141–250; D. Enders, H. Dyker, *Liebigs Ann. Chem*. **1990**, 1107–1110.

[13] Prepared by stereoselective Horner–Wadsworth–Emmons olefination (I. Paterson, K.-S. Yeung, J. B. Smaill, *Synlett* **1993**, 774–776), followed by reduction of the α,β-unsaturated ester (E. J. Corey, H. A. Kirst, J. A. Katzenellenbogen, *J. Am. Chem. Soc*. **1970**, *92*, 6314–6319).

[14] Prepared by the directed ortho lithiation method: G. Koch, G. C. Lloyd-Jones, O. Loiseleur, A. Pfaltz, R. Prétôt, S. Schaffner, P. Schnider, P. von Matt, *Recl. Trav. Chim. Pays-Bas.* **1995**, *114*, 206–210.

 © WILEY-VCH Verlag GmbH, D-69451 Weinheim, 1998 1433-7851/98/3720-2899 $ 17.50+.50/0

Enantioselective catalysis with partially resolved chiral auxiliaries



In many enantioselective reactions ee_{prod} *is not always proportional* to ee_{aux}.

ANGEWANDTE CHEMIE ©WILEY-VCH

Nonlinear Effects in Asymmetric Synthesis and Stereoselective Reactions: Ten Years of Investigation

Christian Girard and Henri B. Kagan*

Dedicated to Professor Dieter Seebach on the occasion of his 60th birthday

The first preoccupation of organic chemists was to develop their ability to reproduce the organization of atoms in natural products. This incursion in nature's laboratory gave rise to numerous techniques to transform matter but led to the discovery of her subtle way of producing substances with chirality and the preference of one enantiomer over the other in the living matter gave a lesson in perfection. The development of asymmetric synthesis gave the opportunity to elaborate methods, reagents, and reactions in order to prepare enantiomerically pure compounds. But this journey is far from being over, and there is a lot of surprises left. No chemist would have thought that an enantiomerically impure chiral auxiliary or ligand could give a stereoselection higher than its own and even equivalent to the pure one. Molecules can behave in numerous ways in solution; aggregation or organization can occur depending on the nature of the molecule or its environment. These phenomena give rise to modification of the anticipated enantiomeric excess (*ee*) of the reaction product. The relation between the *ee* value of the auxiliary or ligand and the *ee* value of the product deviates from linearity to give what we now call nonlinear effects (NLEs). The nonlinear effects in asymmetric synthesis and stereoselective reactions reflect molecular interactions and complexity in reaction mechanisms. They can be used to generate products with high *ee*'s from an enantiomerically impure, and more economical to prepare, chiral auxiliary or ligand. Furthermore, the NLEs can also act as a probe to obtain information on the subtle mechanisms by which the enantioselectivity is generated.

Keywords: asymmetric amplification · asymmetric catalysis · asymmetric synthesis · autocatalysis · chiral auxiliaries

1. Introduction

In the early years of organic chemistry chemists became aware of the importance of chirality in nature. Differences between biological activities of two enantiomers were soon uncovered and the importance of producing mainly or exclusively one enantiomer was highlighted. From the study of enantiomeric mixtures, behavioral differences between racemic and enantiomerically pure compounds were discovered.

In 1848 Pasteur demonstrated that tartaric acid rotated the plane of polarized light, but in a different way depending on its origin.[1] This discovery triggered the use of polarimetry as the technique for gathering information on the enantiomeric purity of compounds, since enantiomers of opposite absolute configuration gave the same degree of deviation of the plane of light, but in opposite sign. Mixtures of enantiomers that differed from racemic composition were therefore analyzed in this fashion and the relative amounts of each constituents were deduced from the total rotation.[2]

However, exceptions to this method were found to be more than a few. Horeau's work on 1-ethyl-1-methylsuccinic acid showed that its specific rotation in chloroform was not strictly related to enantiomeric composition.[5] The phenomenon was explained on the basis of diastereomeric associations by hydrogen bonding that gave rise to a nonlinear relationship between the enantiomeric excess (*ee*) of the acid and its optical purity (*op*). When methanol was used as a solvent for recording this optical property a strictly linear interrelation ($ee = op$) was observed as a consequence of the solvent preventing the aggregation.

The general problem of diasteromeric interactions in a solution of a mixture of enantiomers was discussed in 1974 by Horeau and Guetté.[6] The physicochemical properties of such mixtures may be modified with a change of enantiomeric composition. For example the ^{1}H NMR spectrum (in solution)

[*] Prof. Dr. H. B. Kagan
Laboratoire des Réactions Organiques Sélectives
Institut de Chimie Moléculaire d'Orsay
Bâtiment 420, Université de Paris-Sud, F-91405 Orsay Cedex (France)
Fax: (+33) 169-15-46-80
E-mail: kagan@icmo.u-psud.fr
Dr. C. Girard
Laboratoire de Vectorisation Moléculaire et Cellulaire
Ecole Nationale Supérieure de Chimie de Paris
11, rue Pierre et Marie Curie, F-75231 Paris Cedex (France)
E-mail: cgirard@ext.jussieu.fr

 © WILEY-VCH Verlag GmbH, D-69451 Weinheim, 1998 1433-7851/98/3721-2923 $ 17.50+.50/0

of a racemic mixture or of an enantiopure compound may differ, as found for the first time by Uskokovic et al. in the case of dihydroquinine.[7] Recently the first example of fractionation by distillation of a non racemic mixture of enantiomers was discovered.[8] Isopropyl trifluorolacetate is highly associated by hydrogen bonding, it also shows variation in the infrared absorptions in the liquid (neat) phase. The enantiomeric composition of a non racemic mixture may also be modified significantly by chromatography with achiral stationary and mobile phases. There are several examples in the literature that were explained by diastereomeric associations in the mobile and (or) the stationary phases.[9–14] A mathematical simulation of this phenomenon has been performed.[15]

A nonideal behavior of a mixture of enantiomers may have some consequences on chemical reactions in solution. Wynberg and Feringa pointed out in 1976 that, based on symmetry considerations and free energy arguments, the surroundings of a given *R* enantiomer should be different if it is an enantiopure material or a racemic mixture.[16] In the latter *R/S* interactions may develop, which are absent in the enantiopure system. The authors proposed the following principle: *When a chiral substance undergoes a reaction, the reaction rate and the product ratio will depend—inter alia—upon the enantiomeric excess present in the starting material*. Wynberg and Feringa found some cases that are in agreement with the above principle. The diasteroselectivity of the $LiAlH_4$ reduction of camphor, the McMurry coupling of camphor, and the *ortho*-coupling of a phenol derivative were compared for the enantiopure and racemic systems. Significant differences could be observed. For example, the ratio of isoborneol to borneol was 90.2:9.8 or 88.7:11.3 for the reduction of (+)-camphor or racemic camphor, respectively. In the above publication there were no cases of reactions dealing with chiral substrates having an *ee* value different from 0 or 100%, nor discussion on the quantitative variation of the diastereoselectivity as a function of the *ee* of the substrate.

The chiral auxiliary that is needed in asymmetric synthesis is always of nonracemic composition, preferably of 100% *ee*. One may wonder if an enantiomeric excess lower than 100% will lower the enantiomeric excess of the product in a proportional manner, or if the *ee* of the product will have an unexpected value (as in the Wynberg and Feringa examples) because of a perturbation generated by the *ee* of the chiral auxiliary. This problem had almost never been questioned by the practitioners of asymmetric synthesis.[17] It was in 1986 that the quantitative aspects of the influence of the *ee* value of the chiral auxiliary on the corresponding *ee* value of the product were discussed and studied experimentally.[19] This review article will summarize the main results obtained in that area.[20] The cases of asymmetric catalysis, stoichiometric asymmetric synthesis, and diastereoselective reactions (with a chiral substrate) will be developed successively.

2. Asymmetric Catalysis

2.1. The First Examples—1986

In 1986 Kagan, Agami et al. considered the case of asymmetric synthesis with a chiral catalyst or auxiliary that was not enantiomerically pure.[19] The well accepted assump-

Henri B. Kagan was born in Boulogne-Billancourt (France) in 1930. He graduated from the Sorbonne and Ecole Nationale Supérieure de Chimie de Paris in 1954. He did his doctorate with Prof. J. Jacques, as his first student, and obtained his diploma for work on modified steroids. He then joined Prof. A. Horeau at the Collège de France in Paris in 1962 as a research associate and became involved in studies on stereochemistry and asymmetric synthesis. In 1965 he worked with Prof. T. Mabry at the University of Texas, Austin (USA). He was appointed assistant professor in 1968 at the Université de Paris-Sud, Orsay (France); where he became full professor in 1973. Kagan has been the recipient of several French and international awards and distinctions over the years. He was elected a member of the Académie des Sciences of the Institut de France in 1991 and is a member of the Institut Universìtaire de France.



H. B. Kagan



C. Girard

Christian Girard was born in Grandes-Bergeronnes (Québec, Canada) in 1966. After graduating from the François-Xavier Garneau College with an Health Sciences diploma in 1985, he studied chemistry at the Université Laval (Québec, Canada) where he obtained his B. Sc. (1988) and M. Sc. (1990) with Prof. P. Brassard for work on quinonoid compounds. He then moved to Université de Montréal (Canada) where he completed his Ph. D. in 1994 with Prof. S. Hanessian on the use of samarium(II) iodide in carbohydrate chemistry. The same year, having been granted a Chateaubriand Postdoctoral Fellowship, he then joined Prof. H. B. Kagan at Université de Paris-Sud, Orsay (France) where he became involved in the study of nonlinear effects in asymmetric synthesis. Since 1996, he has been working as a post-doctoral fellow with Prof. J.-P. Genêt at Ecole Nationale Supérieure de Chimie de Paris, Paris (France), where he has been recently appointed as Maitre de Conférence.

tion that the *ee* value of the product (ee_{prod}) of an asymmetric synthesis is linearly correlated to the *ee* value of the chiral auxiliary (ee_{aux}) was questioned. The usual procedure to get an approximation of the experimental *ee* value (ee_{prod}) by correction, knowing the maximum *ee* value of the product (ee_o) is reached with the enantiopure chiral catalyst or auxiliary, was to use Equation (1). This linear relationship is

$$ee_{prod} = ee_o\, ee_{aux} \quad (1)$$

represented for an $ee_o = 100\,\%$ as Curve A in Figure 1. Equation (1) takes into account only the highest enantioselectivity (ee_o) reached with the chiral auxiliary. This linearity

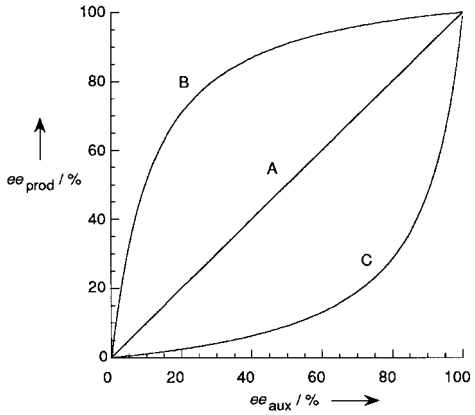


Figure 1. Typical curves for positive (B) and negative (C) nonlinear effects.

was theoretically not to be encountered in systems subjected to other influences, such as interaction between the catalytic species. If the linear relationship is not followed one can expect a plain curve above (curve B, positive nonlinear effect, abbreviated as (+)-NLE) or below (curve C, negative nonlinear effect or (−)-NLE) the straight line, respectively (Figure 1). By convention, all graphs of NLE will be presented as in Figure 1, whatever the absolute configuration of the chiral auxiliary and the product. We will not consider negative coordinates unless there is a special need.

The nonlinearities shown in Figure 1 may in principle arise by auto association or association around a matrix of the initial chiral species, which give diastereomeric perturbations. Those perturbations should then be added to Equation (1) as a multiplication factor to divert the relation between ee_{prod} and ee_{aux} from linearity. Equation (1) must then to be used with caution.

Three systems were studied in 1986 to test this hypothesis.[19] The results that emerged from the data collected provided clear indications that in several cases such nonlinear effects were to be encountered.[20] The first reaction studied was the asymmetric Robinson annulation (Hajos-Parrish-Wiechert reaction[25]) of the triketone **1** using (*S*)-proline as a catalyst (Figure 2). When the *ee* value of (*S*)-proline (ee_{aux}) was plotted against the *ee* value of the *cis*-ketol **2** (ee_{prod}) a slight (−)-NLE was observed, as depicted in Figure 2. Mechanistic investigations by Agami et al. suggested that the reaction proceeds through the formation of a chiral enamine followed by a complexation with a molecule of

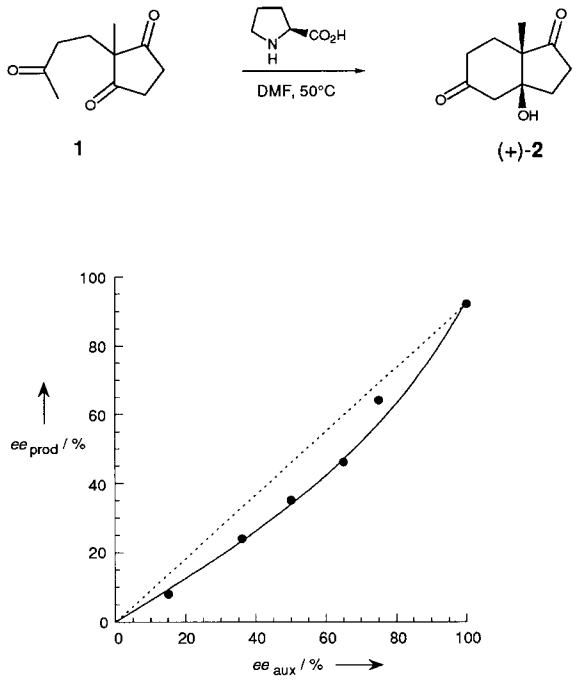


Figure 2. (−)-NLE in the Hajos-Parrish-Wiechert reaction of **1** to **2** catalyzed by (*S*)-proline (3 mol %).

catalyst. This was confirmed by a kinetic model based on a second-order reaction in respect to proline.[26] Furthermore, the (−)-NLE was explained by the fact that, by considering the complexes **3** as intermediates, the reaction involving heterochiral complexes proceed twice as fast as the one of homochiral complexes (Figure 3).

A different effect was however observed in the Sharpless epoxidation[27] of geraniol (**4**) during this investigation.[19] A positive nonlinear effect takes place in this reaction with (*R,R*)-(+)-diethyl tartrate ((*R,R*)-(+)-DET) of various *ee*'s

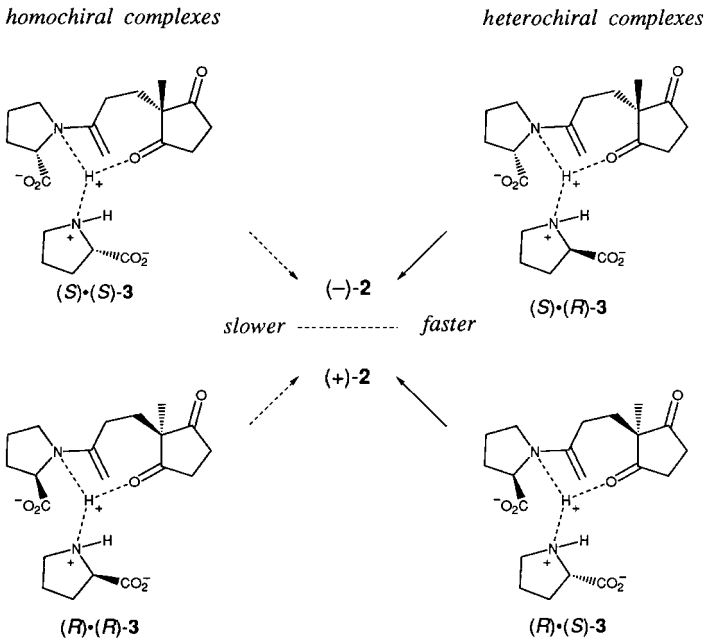


Figure 3. Intermediate complexes **3** in the asymmetric Robinson annulation of **1** to **2**.

(Figure 4). The enantiomeric excess of the produced epoxide **5** (ee_{prod}) when plotted as a function of the *ee* of (+)-DET (ee_{aux}) was indeed greater than expected. The use of a dimeric heterochiral species that is less reactive, and thus more stable,

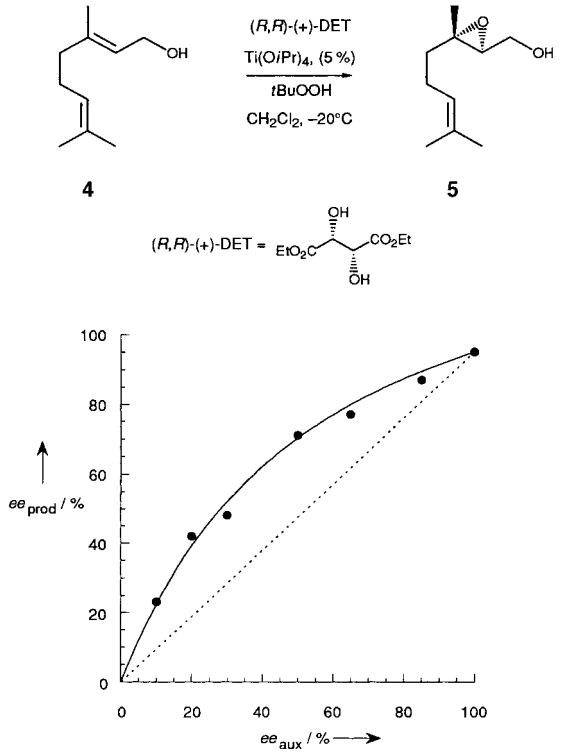


Figure 4. (+)-NLE in the Sharpless epoxidation of geraniol (**4**).

than its homochiral counterparts provides a way of understanding the (+)-NLE of the reaction, since some racemic DET will be retained in the inactive complex. This proposal is compatible with the Sharpless mechanism of asymmetric epoxidation, which indicates the intervention of a dimeric complex that introduces two tartrate units in the active species.[27b] The (+)-NLE discovered here for the first time has been found subsequently in many reactions and has been named "asymmetric amplification" by Oguni et al.[28]

A water-modified Sharpless reagent has been developed by Kagan et al. for the asymmetric oxidation of sulfides by hydroperoxides.[29] The oxidation of methyl-*p*-tolyl sulfide **6** to sulfoxide **7** is quite unexpected by comparison with the results previously discussed (Figure 5). The relation between the *ee*'s is clearly a (−)-NLE, but this effect affects the enantioselectivity until the value of 70% *ee* is reached for the diethyl tartrate. The linear relationship then prevails until enantiomerically pure DET is used. This perturbed behavior is indicative of a quite complicated structure for the water-modified reagent.[30]

These first experiments were a revelation in the behavior of mixtures of enantiomeric reagents or catalysts. They were an indication that some complex and subtle interactions were taking place in solutions with participation from a diastereomeric species. Furthermore, the analysis of the perturbations on the enantioselectivity of the reaction generated by mixing

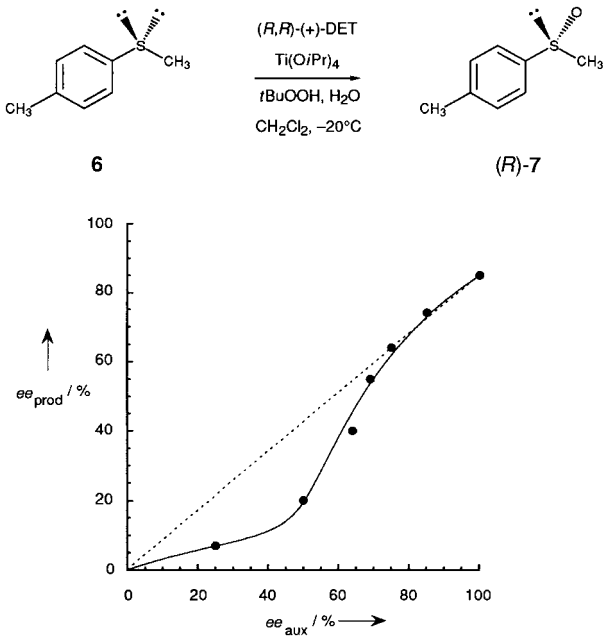


Figure 5. (−)-NLE in the asymmetric oxidation of sulfide **6** with a chiral titanium reagent.

various amounts of enantiomers also gave information about the reaction itself. It became clear that the search for nonlinear effects in a given system also becomes a probe for analyzing the nature of the catalytic species or the nonreacting species involved in an asymmetric synthesis.

2.2. Models and Principles

To get a better understanding and to have some insight into the behavior of catalysts during the course of a reaction that leads to a NLE, simplified mathematical models were developed by Kagan et al. in 1994.[31] These models were discussed in the cited article and will not be explained here in detail. The systems, equations, and the resulting curves will be presented in this section to demonstrate their usefulness.

2.2.1. The ML_2 System

The first model is based on a system in which a fast ligand exchange occurs at a metallic center (M) of a reactive species bearing two chiral ligands (L_R and L_S): the ML_2 system (Figure 6). The following discussion can easily be applied to $(ML)_2$ systems as well to reversible dimerization in the absence of the metal (e.g. association by hydrogen bonding). The model was based on the assumption of a steady state for the three expected complexes ML_RL_R, ML_SL_S, and ML_RL_S (in

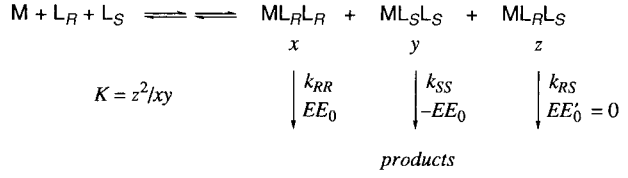


Figure 6. Illustration of the ML_2 system to explain NLEs.

the relative concentrations x, y, and z, respectively), a final irreversible step with pseudo-first order constants k_{RR}, k_{SS} ($=k_{RR}$), and k_{RS}, and a zero-order dependence with respect of the substrate. Furthermore, the *meso* catalyst (ML_RL_S) generated racemic product while the homochiral complexes gave enantiomeric products. It became easy to evaluate the *ee* of a product formed from this kind of system by obtaining the mathematical formula describing it. Equation (2) permits the

$$EE_{\text{prod}} = EE_0 \cdot ee_{\text{aux}} \frac{1+\beta}{1+g\beta} \tag{2}$$

ee value of the product (EE_{prod}) to be calculated for each value of ee_{aux} by knowing the maximum value reached with enantiopure catalyst (EE_0) and the parameters for the studied system. The new parameters introduced in this equation are β, the relative amounts of the complexes ($\beta = z/(x+y)$), and g, the relative reactivities of the hetero- over the homochiral catalysts ($g = k_{RS}/k_{RR}$).

If $\beta = 0$ (no *meso* catalyst) or $g = 1$ (identical reactivities of hetero- and homochiral species), then Equation (2) is simplified to Equation (1) and a linear relationship is observed. In other situations the correction factor $(1+\beta)/(1+g\beta) \neq 1$ is needed and a nonlinear relation takes place. When this factor is greater than one the system displays a (+)-NLE; the amplitude of which will depend on the size of the value of this factor. This will be the case of systems where g is less than one, in which a less reactive heterochiral complex exists. However, if g is greater than one the system will present a (−)-NLE as a consequence of a greater reactivity of the *meso* catalyst. In order to calculate curves from this model it was necessary to transform Equation (2) in terms of ee_{aux} and the relative amounts of the complexes by using the variable $K = z^2/(xy)$ (which is the equilibrium constant if these complexes are in fast interconversion during their formation). The ratio β of the hetero- and homochiral species then becomes available from Equation (3).

$$\beta = \frac{-Kee_{\text{aux}}^2 + \sqrt{-4\,Kee_{\text{aux}}^2 + K(4+ee_{\text{aux}}^2)}}{4+Kee_{\text{aux}}^2} \tag{3}$$

It was then possible to evaluate the EE_{prod} by using Equations (2) and (3) and to plot curves derived from this model. In Figure 7 the results for two cases in which $K = 9$ and 2500 are presented. The curves are generated for different values of g. In the particular case where the ligands are statistically distributed between the complexes a simplification occurs and K becomes equal to four. Furthermore, the term β is also simplified and, from Equation (3), is given by $\beta = (1-ee_{\text{aux}}^2)/(1+ee_{\text{aux}}^2)$. By introducing these new values and formula into Equation (2), EE_{prod} can be calculated from the resulting Equation (4).

$$EE_{\text{prod}} = EE_0\, ee_{\text{aux}} \frac{2}{1+g+(1-g)\,ee_{\text{aux}}^2} \tag{4}$$

The maximum (+)-NLE that can be encountered in this system will be obtained at $g = 0$, when none of the heterochiral species reacts. Linearity could be observed here as well for $g = 1$. At greater g values the NLE will be negative. The computer-calculated curves for this model are presented in Figure 8.

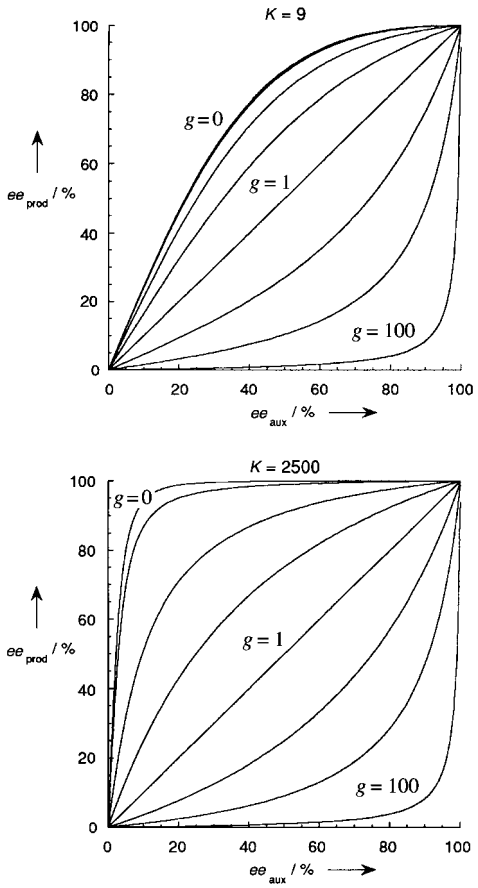


Figure 7. Computer-calculated curves for the ML_2 system for $K = 9$ and 2500.

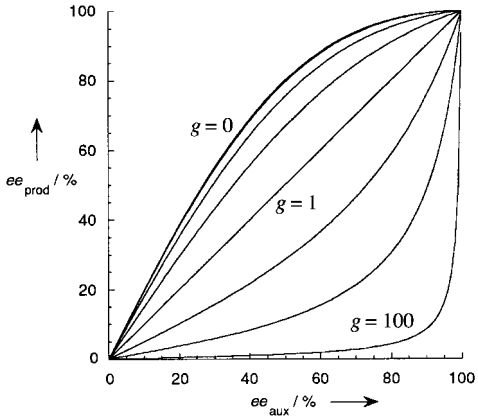


Figure 8. Computer-calculated curves for the ML_2 system with a statistical distribution of the ligands.

Good fits of experimental data can often be achieved from the nonstatistical distribution model, for example Equations (2) and (3).[30] For example, in the asymmetric epoxidation of geraniol (**4**) discussed in Section 2.1; the curve that corresponds well to the data is the one with $EE_0 = 95\,\%$, $K = 1000$, and $g = 0.35$ (Figure 4). These findings imply that the *meso* titanium complex is less reactive ($g = k_{RS}/k_{RR} \approx 1/3$) and much more abundant once the equilibrium is reached ($K = z^2/(xy) = 1000$). This example demonstrates that this model can be of some use in the study of NLEs and, furthermore,

provides some parameters for the discussion of the possible catalysts involved in enantioselective reactions.

A useful development to the ML_n model was reported recently by Blackmond.[20] The author showed that this model could be used to predict some relative reaction rates. These kinetic predictions may then be compared with the experimental data and provide an independent confirmation of the postulated model. For example, the calculations performed for the ML_2 model need to obtain the relative amounts (x, y, z) for the three complexes of Figure 6 as a function of ee_{aux} for a given K value. The overall rate may then be easily computed and compared to the rate for the homochiral complex ($ee_{aux} = 100\,\%$). The calculation has been carried out for the NLE of Figure 4 and showed a strong diminution of the reaction rate when ee_{aux} decreases. As often found in subsequent examples of this review a (+)-NLE usually comes at the cost of the rate of formation of the product.

2.2.2. M*L$_2$ System

A model, similar to the ML_2 system previously discussed, can be elaborated for the case in which the introduction of chiral ligands on M creates a center of chirality. In such a model, the *meso* complex ML_RL_S encountered in the preceding section becomes $M^*L_RL_S$. The stereochemistry on M is generated by the sequential introduction of the ligands, first producing the monoligated complexes M_RL_R, M_RL_S , M_SL_R, and M_SL_S. Subsequent reaction of those complexes with L_R and L_S finally gives the four pairs of enantiomers as illustrated in Figure 9. Here the heterochiral complexes such as $M_RL_RL_S$

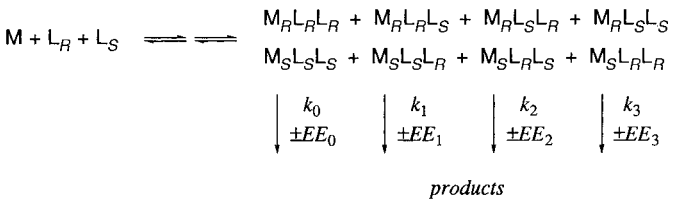


Figure 9. Another model for the NLEs: the M^*L_2 system.

and $M_SL_SL_R$ are enantiomers. Each stereoisomer in Figure 9 has its respective reactivity (k_i) and selectivity (EE_i) and will contribute to the final EE_{prod}. By using the same hypotheses as for the ML_2 system, the M^*L_2 model can be treated with Equations (2) and (3), the only difference being in the definition of the parameters K, g, and EE_o.

This model can be applied to reactions such as the asymmetric Robinson annulation (Section 2.1, Figure 2). The intermediates illustrated in Figure 3 are of the M^*L_2-type and for example, in a complex such as $M_RL_RL_S$, M_R symbolizes the creation of an asymmetric carbon atom with R configuration during the formation of the enamine with the first proline (L_R), and L_S is the second proline molecule involved in the formation of the complex. In this particular situation, where only four stereoisomers are formed, the system can be treated with a statistical distribution as with the ML_2 model. Equation (4) gave, with $EE_0 = 93\,\%$ and $g(=k_{RS}/k_{RR}) = 2$, a curve fitting the experimental results. The same value was found by Agami et al. in their kinetic analysis of the reaction ($k_{homo}/k_{hetero} = 0.5$).[26]

The equations found for the ML_2 systems can be applied to cases where ML_RL_R, ML_SL_S, and ML_RL_S complexes dissociate irreversibly to ML_R and ML_S, with or without the influence of the substrate, that are implicated in the final irreversible catalytic step. This approximation gives fair results but will not be discussed here.[31]

2.2.3. ML$_3$ System

A model in which species of the type ML_3 or $(ML)_3$ are active catalytic species can be proposed. At least four entities may be responsible for the catalysis: $ML_RL_RL_R$, $ML_SL_SL_S$, $ML_RL_RL_S$, and $ML_SL_SL_R$. The heterochiral complexes encountered here are always chiral and an enantiomerically enriched product is generated simultaneously from homo- and heterochiral species (Figure 10). Calculation of EE_{prod} as

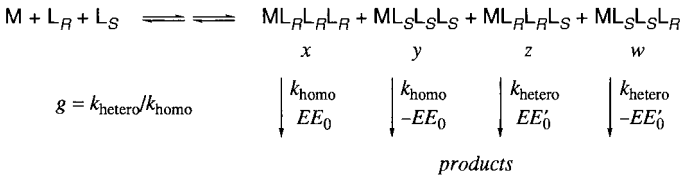


Figure 10. The more complex description of NLEs by the ML_3 system.

a function of ee_{aux} is much more complex in this case. However, the assumption of a statistical distribution of the chiral ligands between the four complexes gives a simplified function (Equation (5)). In this formula, EE_0 and EE'_0 are the

$$EE_{prod} = EE_0 ee_{aux} \frac{3 + 3g\,EE'_0/EE_0 + (1 - 3g\,EE'_0/EE_0)ee^2_{aux}}{1 + 3g + 3(1-g)ee^2_{aux}} \qquad (5)$$

enantiomeric excesses of the product from homochiral and heterochiral complexes (of 100 % *ee*). The parameter $g = k_{hetero}/k_{homo}$ is defined as for the ML_2 system. Figure 11 shows some curves selected for a case where homochiral complexes are more selective ($EE_0 = 100\,\%$) than their heterochiral counterparts ($EE'_0 = 50\,\%$).

From these curves one can observe that if the homochiral complexes are more reactive ($0 \le g < 1$) a (+)-NLE takes

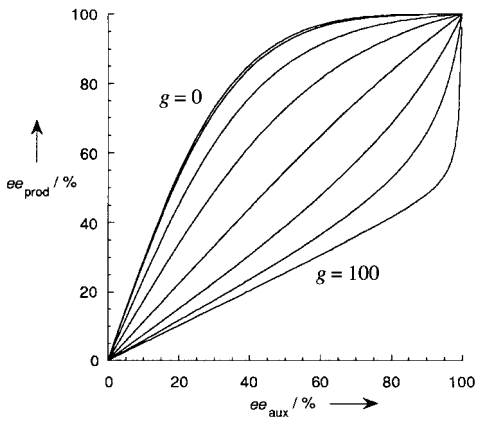


Figure 11. Computer-calculated curves for the ML_3 system with $EE_0 = 100\,\%$ and $EE'_0 = 50\,\%$.

place. If the less selective heterochiral complexes react faster ($g > 1$), a (−)-NLE will then be observed. If the heterochiral complexes are more enantioselective than the homochiral ones, the situation will be quite different. By selecting $EE_0 = 50\,\%$ and $EE'_0 = 100\,\%$, the curves produced by the use of Equation (5) were plotted for various values of g (Figure 12).

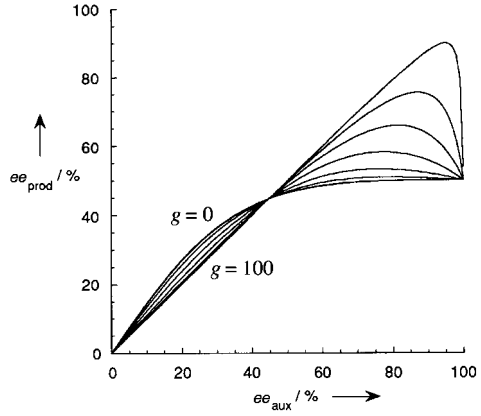


Figure 12. Computer-calculated curves for the ML_3 system for $EE_0 = 50\,\%$ and $EE'_0 = 100\,\%$.

For g values less than one, the curves display a similar behavior as in Figure 11. However, an interesting phenomenon occurs in this mathematical model for larger values of g. The EE_{prod} can be higher at lower ee_{aux} than at 100 % ee_{aux}; at which it drops to the EE_0 (= 50 %) value. If a system can fit this model, the chiral auxiliary will be much more efficient when partially resolved than when enantiomerically pure!

2.2.4. ML_4 System

In an even more complicated scenario the complex can bear up to four chiral ligands to become a ML_4 or $(ML)_4$ system. This will generate the five following complexes: $M(L_R)_4$, $M(L_S)_4$, $M(L_R)_3L_S$, $M(L_S)_3L_R$, and $M(L_R)_2(L_S)_2$. If the $M(L_R)_2(L_S)_2$ complex is assumed to be a *meso* complex (which gives a racemic product), that no additional stereoisomers involving the M center are present, and that, finally, the ligands are distributed on the center in statistical mode, the system is greatly simplified. By introducing the relative reactivities of the two heterochiral complexes (g and f) and taking into account the enantioselectivities of enantiopure homo- (EE_0) and heterochiral (EE'_0) complexes, Equation (6)

$$EE_{prod} = 8\,EE_0\,ee_{aux}\,\frac{1 + ee_{aux}^2 + 2\,g\,(1 - ee_{aux}^2)\,EE'_0/EE_0}{(1 + ee_{aux})^4 + (1 - ee_{aux})^4 + 8\,g\,(1 - ee_{aux}^4) + 6\,f\,(1 - ee_{aux}^2)^2} \quad (6)$$

is obtained. When there is no statistical distribution between the four complexes, two additional parameters are needed to define the relative contribution of the complexes[31]

The ML_4 model can efficiently describe the behavior of catalysts such as the one used in the asymmetric oxidation of methyl-*p*-tolyl sulfide (**6**, Figure 5). A calculated curve that fits the experimental data can thus be obtained. The parameters used mean that an active, but poorly, selective heterochiral species and a large predominance of a weakly active *meso* complex are involved. Quite complicated curves can be generated by the use of the ML_4 model. As an example, two triple-shaped curves are presented in Figure 13.[31]

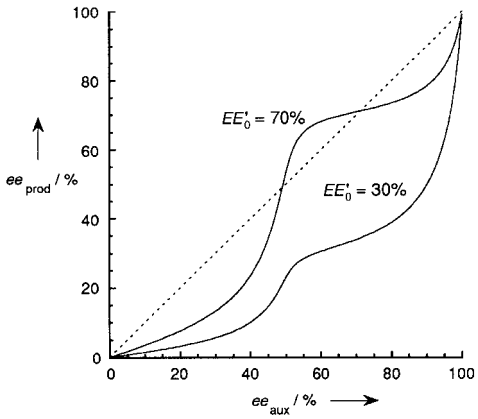


Figure 13. Computer-generated curves for the ML_4 system for $EE'_0 = 30\,\%$ or $EE'_0 = 70\,\%$, $K = 1000$, $K' = 1$, $g = 10$, and $f = 100$.

2.2.5. The Reservoir Effect

The use of a partially resolved chiral ligand in asymmetric catalysis can produce some perturbations generated by the formation of diasteromeric complexes, either within the catalytic cycle or at its periphery. Such perturbation in the cycle cannot be deduced from the sole behavior of the catalyst prepared from the enantiopure complexant. A more detailed analysis is needed and a model in which the active and inactive complexes are taken into account can better describe the system. The model presented here is based on the formation of those two types of catalysts (Figure 14).

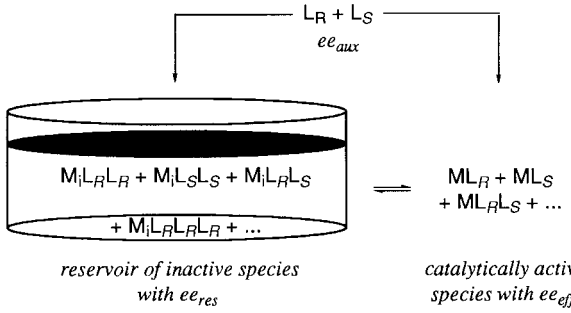


Figure 14. A large pool of unproductive complexes: the reservoir effect model. ee_{res} and ee_{eff} are for the ligands overall.

When a molar amount of ligand with a defined ee_{aux} reacts to form the different species, a part of this (α) can be diverted towards a reservoir; a pool of unproductive complexes with an ee_{res}. This storage will affect the resulting *ee* value of the active portion of the catalysts in such a way that a new value for the *ee* of the $1 - \alpha$ portion of the catalyst left will be attained and called the effective enantiomeric excess (ee_{eff}). This new value can be easily calculated from Equation (7). Such a reservoir

$$ee_{eff} = \frac{ee_{aux} - \alpha\,ee_{res}}{1 - \alpha} \quad (7)$$

can be created through several kind of processes. For example, aggregation can take place before, or in parallel with, the catalytic cycle reaching its steady state. The complexes can thus be stored in inactive oligomeric species, with the one with low aggregation numbers behaving as the catalyst or the catalyst precursor. A reservoir of racemic composition is more easily created by the formation of a heterodimer (*meso*), which is thermodynamically stable and catalytically inactive. Most of the reported (+)-NLEs presented in this review can be explained in such a way. In this simplified model ee_{eff} replaces ee_{aux} in Equation (1), and gives a fair approximation when used to draw curves that fit experimental data.[31]

The models presented in this section can be very useful in the understanding of the behaviors of catalysts. The mathematical expressions are in these cases utilized to extract quantitative parameters relative to the different oligomeric catalytic species that exist in solution. This approach is a mere mathematical interpretation of the experimental data recorded. The following Sections will present some of the results obtained by several groups in search of nonlinear effects in asymmetric synthesis.

2.3. Enantiomeric Catalysts

2.3.1. Addition of Organozincs to Aldehydes

One useful method of alkylating carbonyl compounds is the use of organozinc compounds coupled with a catalyst, which is needed for any reaction to be observed. During their work on the alkylation of benzaldehyde (**8**) by diethylzinc, Oguni et al. discovered in 1988 that a nonlinear effect was present when chiral β-amino alcohols were used as catalysts.[28] Figure 15 shows the results of alkylation in the presence of various chiral amino alcohols. All catalysts exhibited a (+)-NLE in this reaction (called asymmetric amplification by the authors). In Figure 15 (as in all the graphs of this article) positive values will be arbitrarily attributed to the ee_{prod}; such as here where (−)-PDB (or (−)-DDB) and (+)-P_yDB give alcohols of opposite absolute configuration. The (+)-NLE was explained by the authors by the formation of dimeric species in solution. This was confirmed by cryoscopic molecular weight measurements on catalysts generated by the treatment of diethylzinc on enantiomerically pure PDB and racemic PDB. Furthermore, kinetic experiments showed that the reaction with a catalyst prepared with 60% *ee* PDB was 5.5 times faster than the one from racemic PDB.

From these results one can assume that dimers, similar to those discussed in the preceding section, should participate in this amplification of the ee_{prod}. In this alkylation by diethylzinc, it is logical to conclude that if dimers are formed the heterochiral species that retains the minor enantiomer of the catalyst should be less implicated in the reaction; thus leaving the homochiral-enriched dimer free to operate as the active agent or its precursor. Oguni's system with PDB (Figure 15) may be described by the ML_2 model with $EE_0 = 94\%$, $K = 4000$ and $g = 0.015$ ($k_{RS}/k_{RR} \approx 1.5/100$), which shows again the lower reactivity and higher abundance of the heterochiral

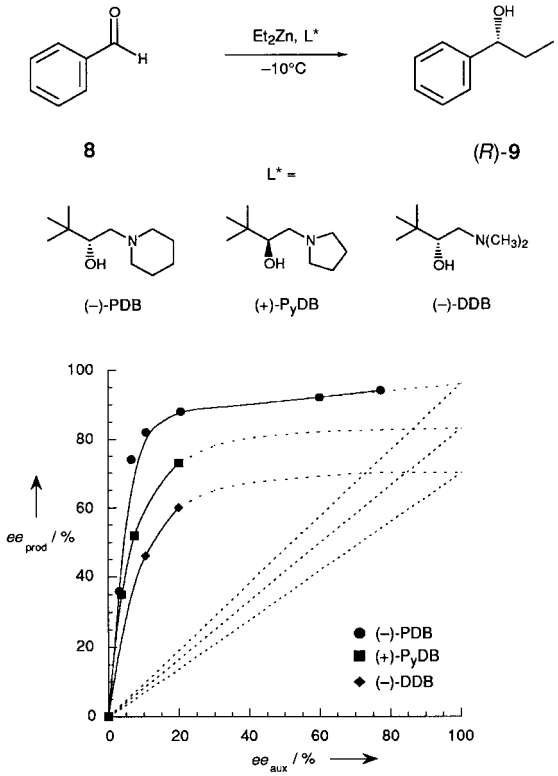


Figure 15. (+)-NLEs on addition of diethylzinc to benzaldehyde (**8**) in *n*-hexane catalyzed by aminoalcohol ligands L* (2 mol%).

catalytic species. If the reservoir effect model is used instead the results are fitted by the use of similar parameters ($EE_0 = 94\%$, $ee_{res} = 0\%$ and $\alpha = 0.87$).

In 1989 Noyori et al. published a mechanistic study on their system of catalyzed addition of organozinc complexes to aldehydes.[32] They also observed a strong (+)-NLE by using various *ee*'s of (−)-3-*exo*-(dimethylamino)isoborneol ((−)-DAIB) as a catalyst (Figure 16). This effect is even more important than the preceding one, with the maximum enantioselectivity of the reaction being reached at a very low *ee* of DAIB (curve ●). Thus, 1-phenylpropanol ((*S*)-**9**) can be prepared in high enantiomeric purity (95% *ee*) with a very impure catalyst (15% *ee*). A similar but less pronounced effect was also observed when dimethylzinc (curve ■) was used in the alkylation. Noyori et al. supposed that this strong (+)-NLE was a result of auto association of the chiral reagent generated by the reaction between (−)-DAIB and the organozinc compound. The organometallic DAIB–zinc complex formed undergoes dimerization as depicted in Figure 17. When a mixture of (−) and (+)-DAIB was used, two types of dimeric species were formed: homochiral ((−)·(−)-**10** and (+)·(+)-**10**) and heterochiral ((−)·(+)-**10**); the signs refer to the enantiomer of the chiral ligand included in the complex. The enantiomeric monomers DAIB–ZnR (R = Me or Et) are the active catalysts in this reaction and each one produces predominantly one enantiomer of alcohol **9**.

In a study on the influence of the amount of chiral catalyst on the outcome of the reaction, (−)-DAIB in 14% *ee* was used and the ee_{prod} of (*S*)-**9** was plotted as a function of the relative amount (mol%) of the catalyst (Figure 18). From

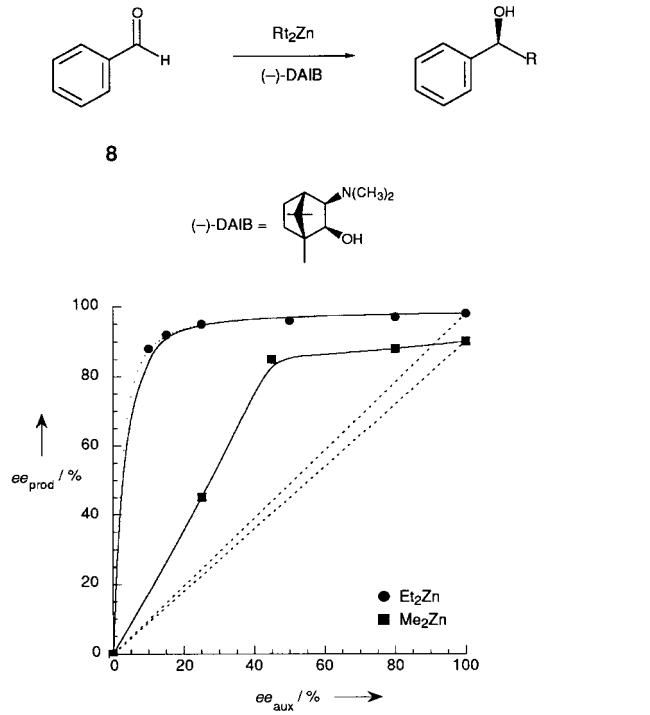


Figure 16. (+)-NLEs in the DAIB-catalyzed (8 mol%) addition of dialkylzinc compounds to benzaldehyde (**8**) in toluene.

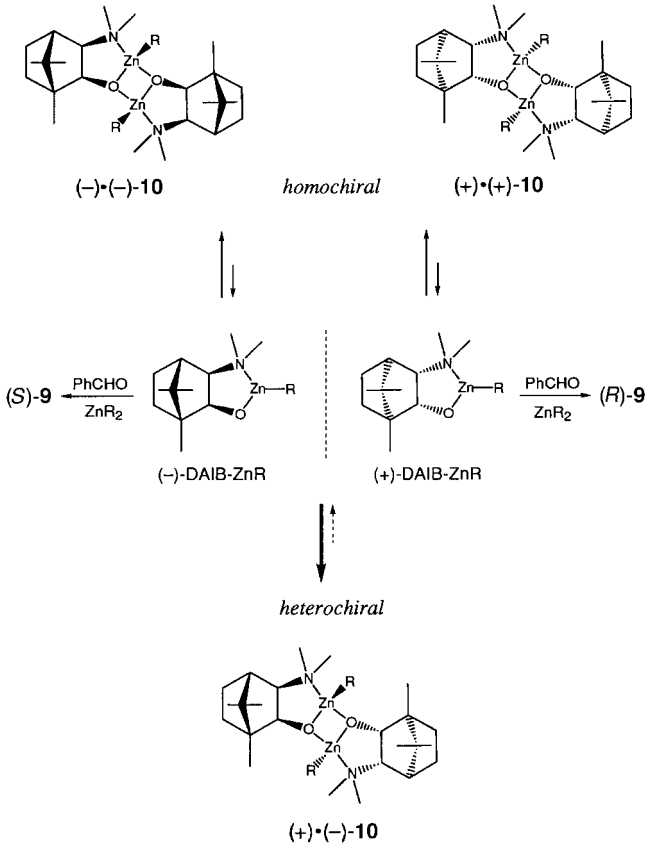


Figure 17. Homochiral and heterochiral dimers formed by the DAIB-alkylzinc reagent.

these results, the turnover efficiency of the homochiral precatalyst was estimated to be 1200 times greater than that of the heterochiral one.

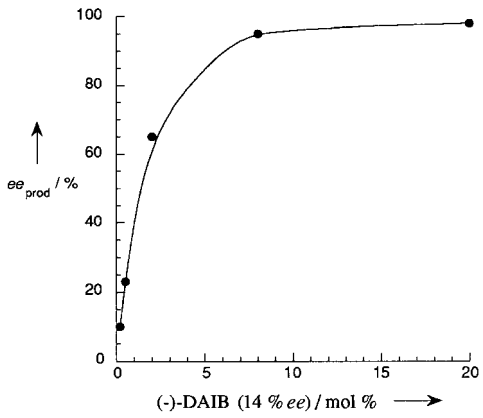


Figure 18. Variation in the ee_{prod} for (*S*)-**9** as a function of the amount of (−)-DAIB (14% *ee*) used in the addition of diethylzinc to benzaldehyde (**8**).

The existence and behavior of the dimeric species were well confirmed by numerous experiments. Cryoscopic molecular weight measurements demonstrated that DAIB – ZnR existed effectively as dimers in solution. NMR measurements of homochiral and heterochiral reagents gave insights as to the relative stability of the dimeric organozinc compounds. Noticeable changes were observed in the NMR spectrum of the homochiral dimer (−)·(−)-**10** upon addition of benzaldehyde, whereas the spectrum of the heterochiral complex (+)·(−)-**10** remained the same, thus revealing a greater stability.

The differences were understood by X-ray diffraction analysis of each of the dimers obtained by treatment of dimethylzinc with the chiral catalyst (Figure 19). The homo

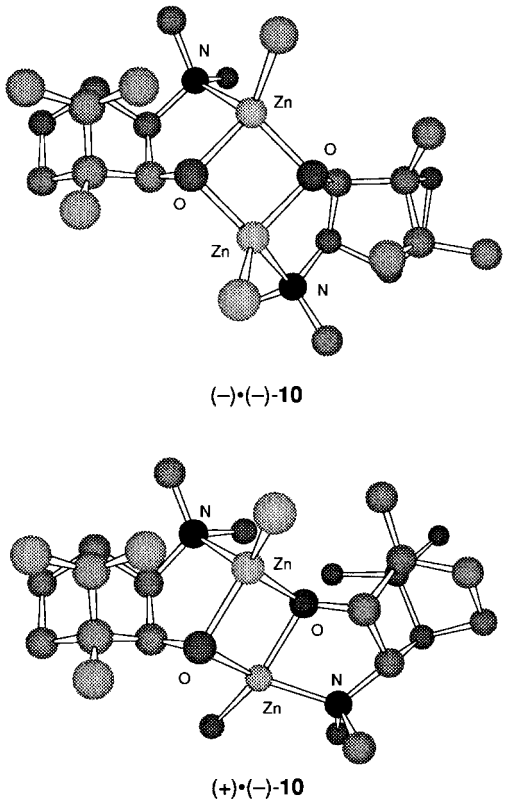


Figure 19. Three-dimensional models of the dimers of (−)-DAIB-methylzinc: (−)·(−)-**10** (homochiral) and (−)·(+)-**10** (heterochiral).

chiral species $(-)\cdot(-)$-**10** ($R = CH_3$) possesses a C_2 symmetry with a Zn_2O_2 four-membered ring with a *syn* relationship between the methyl groups on the zinc atoms. This ring is "*endo* fused" relative to the DAIB–Zn system. The heterochiral dimer $(+)\cdot(-)$-**10** ($R = CH_3$) also has a Zn_2O_2 cycle "*endo* fused" to the structure but the methyl groups on the metallic centers, as well as the DAIB fragments, are oriented in an *anti* fashion, which explains the greater thermodynamical stability of this dimer. This was later complemented by energetic calculations on simpler models by the same group.[32b]

If the ML_2 model is used for the reaction performed by Noyori et al. with their DAIB catalyst, the values of $EE_0 = 98\,\%$, $K = 5000$, and $g = 0.01$ ($k_{RS}/k_{RR} \approx 1/100$) give a curve that fits the experimental results. The results may also be analyzed using the reservoir effect model. Noyori's system approximates better to $EE_0 = 98\,\%$, $ee_{res} = 0\,\%$, and $\alpha = 0.88$. The values extracted hereby confirm a greater stability ($k_{RS}/k_{RR} \approx 1/100$) of the heterochiral complex, and its preponderance ($K = 5000$), in regard to the homochiral one.

Bolm et al. worked on this alkylation reaction as well but used a substituted pyridine alcohol as the chiral catalyst (Figure 20).[33] The ethylation of benzaldehyde (**8**) was very

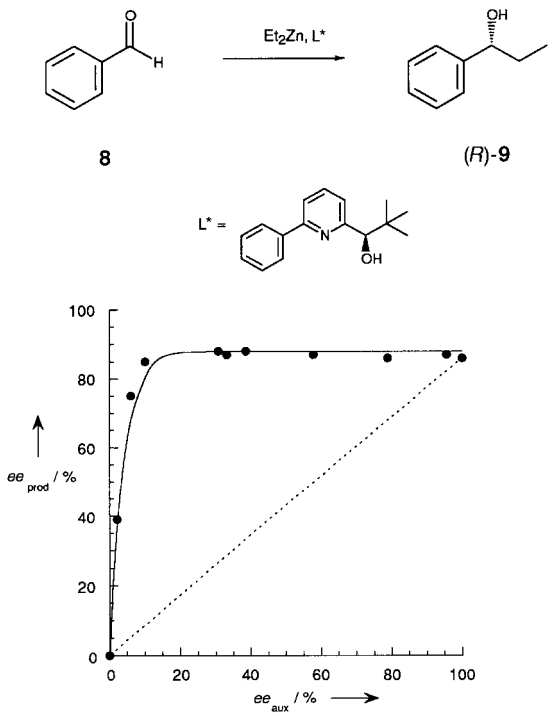


Figure 20. (+)-NLEs in the addition of diethylzinc to benzaldehyde (**8**) with a pyridine alcohol as the catalyst.

efficient with 5 mol% of the catalyst and Et_2Zn and gave access to (*R*)-1-phenylpropanol ((*R*)-**9**). By varying the *ee* value of the pyridine catalyst, they discovered that a (+)-NLE was taking place, as seen in Figure 20.

The (*R*)-cat-ZnEt and the (*S*)-cat-ZnEt can interact in solution to give the homochiral dimers $(R)\cdot(R)$-**11** and $(S)\cdot(S)$-**11** and the heterochiral species $(R)\cdot(S)$-**11** (Figure 21). If the heterochiral complex is favored over the homochiral ones,

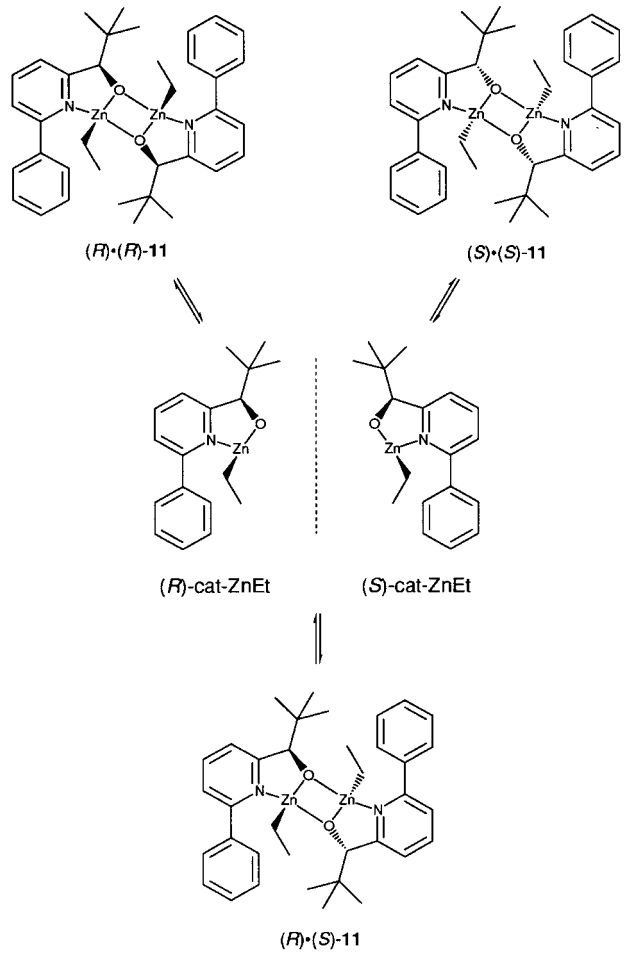


Figure 21. The different dimers formed in solution between the enantiomeric pyridine alcohol–ethylzinc reagents.

the effect of diverting the minor enantiomer from the reaction mixture will be a net increase in the *ee* value of the active catalyst, thus generating this strong (+)-NLE.

Bolm et al. observed the formation of a white precipitate when the pyridine alcohol was treated with an excess of diethylzinc. Starting with a (*R*)-catalyst in 50% *ee*, filtering off the resulting solid, and hydrolyzing both mother liquor and precipitate, two fractions of the ligand catalyst were obtained. The one from the crystalline material, and corresponding to 74% of the starting materials, had a value of 44% *ee*. However, the ligand recovered from the filtrate (26% yield) was of 84% *ee*. This was a clear indication of enrichment of the major enantiomer by predominant precipitation of the *meso* complex and suggested a possible greater stability of this species.

When the precipitation was conducted independently with the (*R*)-catalyst and its racemic form, the solid from the enantiopure pyridine alcohol was very unstable while the one from the racemic alcohol was stable enough to be isolated. The structure of the crystallized solid was determined by X-ray analysis and proved to be the one of a C_i-symmetric dinuclear zinc complex composed of each of the enantiomeric catalysts around a central Zn_2O_2 four-membered cycle; namely the heterochiral dimer $(R)\cdot(S)$-**11** (Figure 22). The ethyl and *tert*-butyl substituents on each subunit are *syn* to

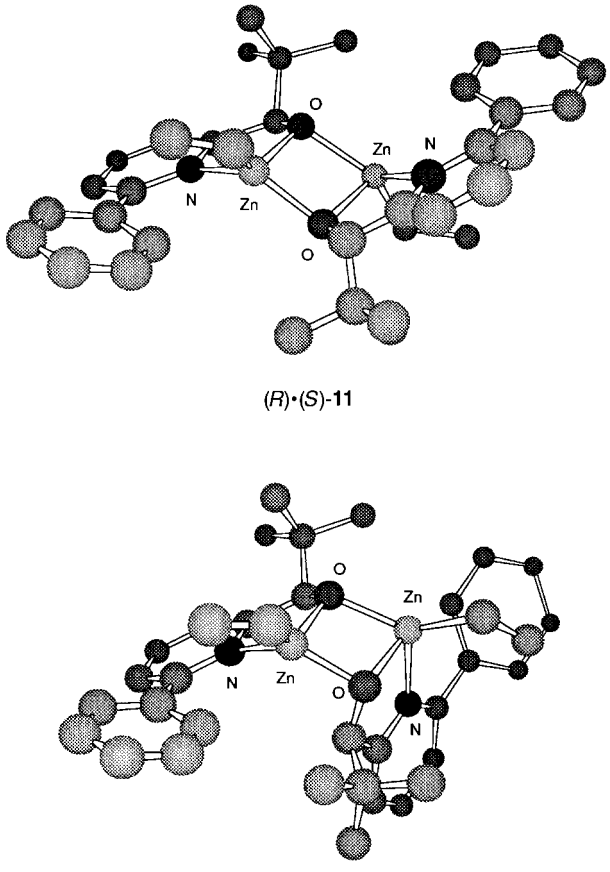


Figure 22. Structure of the dimeric species $(R)\cdot(S)$-**11** in the crystal and proposed structure of $(R)\cdot(R)$-**11**.

each other, but they end up *anti* to the substituents of the other unit in the global structure as a result of the overall symmetry. The speculated structure of the homochiral dimer is also presented in Figure 22. The $(R)\cdot(R)$-**11** complex has C_2 symmetry with the usual Zn_2O_2 cycle. The alkyl chains on the subunits are still *syn* to each other but the complex system presents a molecular cavity. The steric congestion generated by this geometry, in conjunction with the fact that the zinc atoms are relatively exposed on the convex surface of the dimer, can be an explanation of its lower stability and high reactivity towards air and moisture.

The dimeric structure was easily detected by mass spectrometry. However, the solid isolated from the (*R*)-catalyst showed no evidence of such dimeric species with the molecular ion peak in the mass spectrum being very weak in intensity. This indicates that, if the homodimer is formed, it possess a low stability. The exact structure was not elucidated, but NMR spectroscopy of homo- and hetero-dimeric zinc compounds were reported to be different.

Another example of nonlinear effects in this area is the work of Kellogg et al. on derivatives and analogues of ephedrine as catalysts.[34] The reactions were performed with 5 mol% of *N*-methylephedrine (NME), *N*-methylephedrine disulfide (NMED), and *N*-methylephedrinethiol chlorhydrate (NMET·HCl) as shown in Figure 23. The ethylation of benzaldehyde (**8**) under those conditions leads to the alcohol

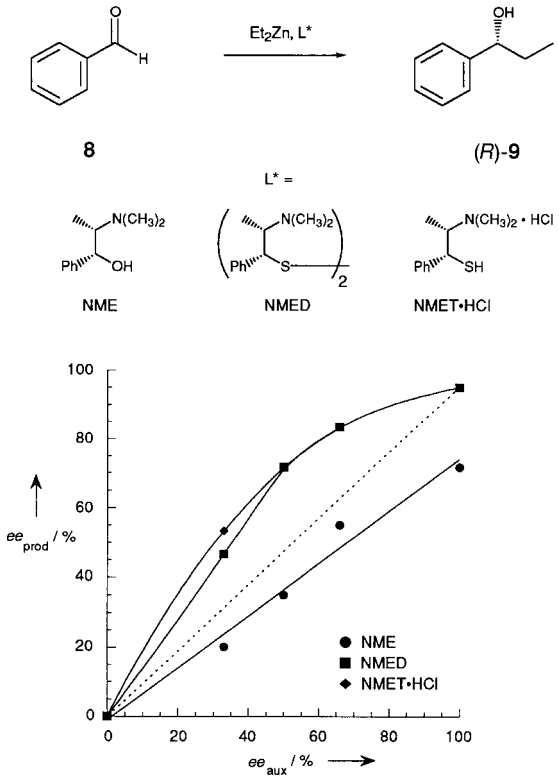


Figure 23. NLEs observed in the 1,2-addition of diethylzinc to benzaldehyde (**8**) catalyzed by derivatives and analogues of ephedrine (5 mol%, toluene, $-20\,^{\circ}C$).

(*R*)-**9** in all cases. The use of NME showed no particular irregularities in the linear relationship between its *ee* value and the *ee* value of (*R*)-**9** alcohol. However, when using NMED or NMET·HCl an evident (+)-NLE was observed, which was almost identical regardless of the catalyst used.

In order to understand the differences between the catalysts cryoscopic molecular weight measurements were done with NME and NMET·HCl after reaction with various amounts of Et_2Zn. With one equivalent of diethylzinc, oligomeric structures seem to exist in solution in both cases. NME was expected to give rise to an equal mixture of dimer and tetramer based on the results, while NMET·HCl only gave the molecular weight of a tetrameric complex. Addition of an extra equivalent of the dialkylzinc compound only resulted in a total breakdown of the oligomeric structures, with only monomers being detected with the two chiral compounds. It was then proposed by the authors that, in order to observe any NLE, heterochiral (*meso*) aggregates have to be stable to extra diethylzinc and generate an aggregation-induced enrichment of the major enantiomer of the catalyst.

2.3.2. 1,4-Addition of Organozinc Compounds

The use of alkylzinc compounds, far from being limited to the 1,2-addition reported in the preceding section, can also be extended to conjugated additions on α,β-unsaturated carbonyl compounds. This can be achieved by using nickel in catalytic amounts, the dialkylzinc compound, and a chiral catalyst in order to perform an asymmetric version of the reaction.

Bolm and his group studied this reaction with pyridine alcohol acting as the catalyst precursor (Figure 24).[35] The addition of diethylzinc to chalcone (**12**) in the presence of

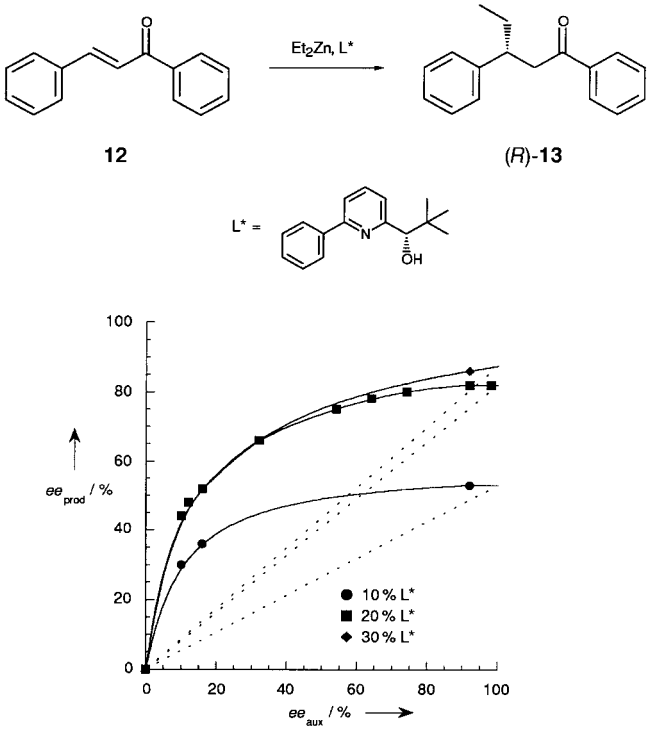


Figure 24. (+)-NLEs encountered in the pyridine alcohol (20 mol %) catalyzed asymmetric 1,4-addition of diethylzinc to chalcone (**12**) (1 mol % $[Ni(acac)_2]$, acetonitrile, $-30\,^{\circ}C$).

20 mol % of the catalyst and 1 mol % of $[Ni(acac)_2]$ gave efficient access to the ketone (*R*)-**13** (acac = acetylacetone acetate). When the catalyst was used in various enantiomeric excesses under these conditions, a strong (+)-NLE was observed. Moreover, the use of different quantities of the catalyst had an influence on the resulting curves. While 30 mol % gives essentially the same shape as with 20 mol % (curves ◆ and ■, respectively), a smaller amount of catalyst (10 mol %, curve ●) lowers the enantioselectivity and modifys the appearance of the curve.

The positive influence of the concentration of the catalyst was also confirmed by performing the reaction with the chiral pyridine ligand in 16 % *ee* at various mol %. The results are shown in Figure 25 a) and the plot against ee_{prod} clearly demonstrates the increased selectivity of larger amounts of the catalytic species, which reaches a maximum at 30–40 mol %. The asymmetric amplification was also tested against the time until the reaction was complete (Figure 25 b). When a 19 % *ee* catalyst was used in this reaction the ee_{prod} was shown to strongly decrease with the conversion. The use of the substituted pyridine with 89 % *ee* also demonstrated a time dependence of the ee_{prod}, but in a less pronounced fashion.

The (+)-NLE was initially explained on the basis of the results and studies done by this group during the course of their research on the 1,2-addition of organozinc compounds.[33] Formation of dimeric zinc catalysts (Figure 21) is sufficient to understand the phenomenon taking place. The stable heterochiral dimer, which acts as a trap for the minor enantiomer, increases the *ee* value of the major one (reservoir effect). The more reactive homochiral dimers left should then react with nickel(II) to form the active catalyst with an *ee* value greater than the one of the chiral pyridine introduced to the mixture. The concentration effect can be explained by a shift in the equilibrium between monomers and dimers. The more concentrated the catalyst becomes, the more dimers should form and thus increase the (+)-NLE.

However, the use of coordinating solvents such as acetonitrile, needed for the nickel catalysis, has deleterious effects on enantioselectivities in carbonyl alkylation reactions. This is possibly the result of the solvent preventing the dimerization of the catalyst–zinc species. Another explanation was thus necessary and was offered by Bolm et al. (Figure 26). A similar type of homo and heterochiral relationship between the two molecules of catalyst implicated can be found here, but the metal complexation is quite different. In this case, it has been postulated that the chiral pyridine first reacted with $[Ni(acac)_2]$ to form the two enantiomeric (*S*)- and (*R*)-**14**. These react further with another molecule of the pyridine with the same (homo) or the opposite (hetero) configuration. This leads to the formation of homochiral mononuclear complexes (*S*)·(*S*)-**15** and (*R*)·(*R*)-**15** and the heterochiral complexes (*S*)·(*R*)-**15**. The reaction of diethylzinc with these nickel complexes should proceed with the less stable ones and, from the (+)-NLE observed in this particular case, it has to be the homochiral (*S*)·(*S*)- and (*R*)·(*R*)-**15** dimers. A *meso*, or heterochiral species{(*S*)·(*R*)-**15**}, diverts the minor enantiomer from the catalytic pathway and generates this positive nonlinear effect.

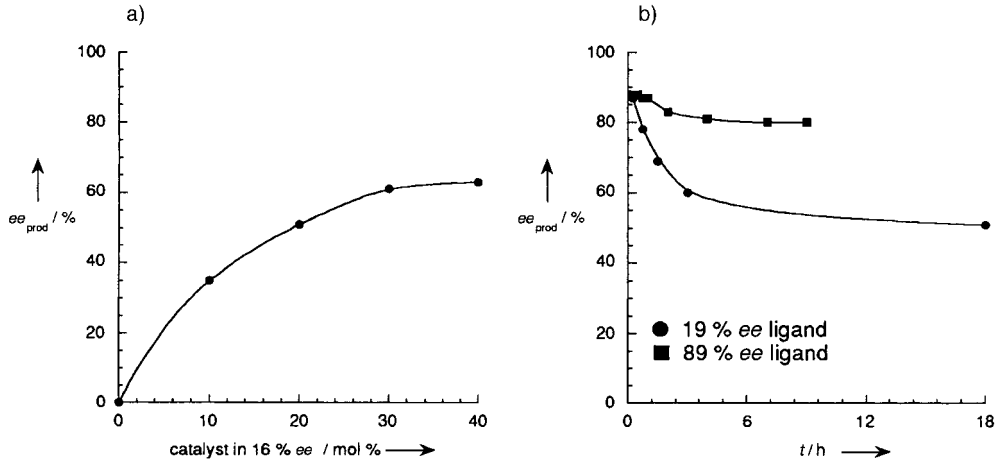


Figure 25. *ee* of product (*R*)-**13** as a function of a) the quantity of pyridine alcohol (16 % *ee*) and b) the reaction time with the ligand in 19 and 89 % *ee*.

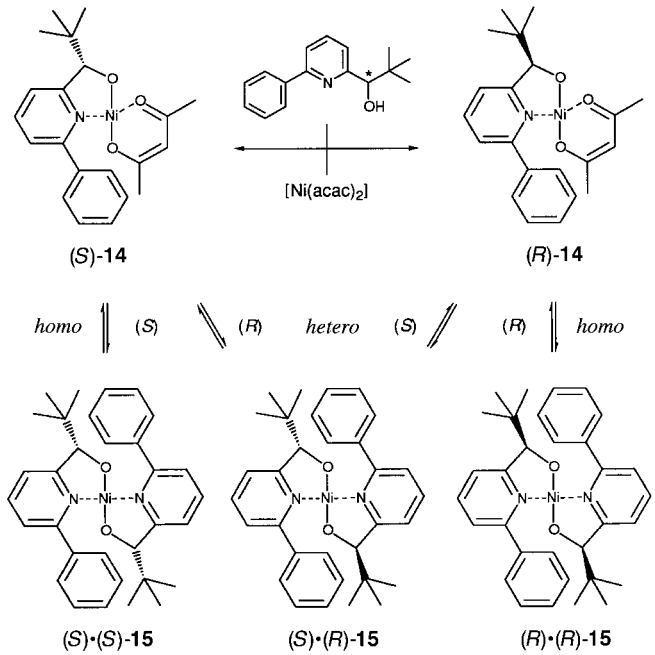


Figure 26. Proposed equilibrium between the monomers and dimers in the catalyzed addition of dialkylzinc compounds in the presence of nickel(II).

Since the formation of the heterochiral dimer reduces the total amount of active catalyst in solution, the decrease in the reaction rate on using a catalyst with a low *ee* value can be explained. One can see from the curves of Figure 25 that a reaction completed in 9 h with a 89% *ee* catalyst takes twice this time with a catalyst in 19% *ee*, because of the presence of a larger amount of the less reactive *meso* dimer. Even if the heterochiral complex is much more stable than the homochiral species longer reaction times seem to permit its dissociation, since ee_{prod} drops with conversion. The 89% *ee* catalyst, in which a lower amount of heterochiral dimeric structure is present, shows only a slight drop in the *ee* value while the one from 19% *ee* falls quite abruptly.

Bolm's 1,4-addition of diethylzinc to chalcone (Figure 24) displayed an $EE_0 = 82\%$, $K = 1000$, and $g = 0.1$ ($k_{RS}/k_{RR} \approx 1/10$) if one uses the ML_2 model to describe the system. These values and the experimental data are in accordance with the more stable *meso* complex hypothesis. The same reaction was studied by Feringa et al. but with (−)-DAIB as the chiral catalyst (Figure 27).[36] The 1,4-addition reaction to chalcone (**12**) was run with 16 mol% of DAIB. By varying its *ee* value and constructing a plot against the measured *ee* value of the resulting ethylated product (*R*)-**13** it was easy to visualize a (+)-NLE. This NLE was shown to be dependent on the concentration, as for Bolm's system, but in this case the influence of the amount of Ni^{II} salt was investigated. While the amount of DAIB was kept constant (16 mol%), the quantity of $[Ni(acac)_2]$ used for the reaction was of 1, 7, and 8 mol% (curves ●, ■, and ◆, respectively). The effect of increasing the nickel ratio was deleterious for both maximum enantioselectivity and the amplitude of the NLE.

It was suggested that two equivalents of DAIB reacted with $[Ni(acac)_2]$ as illustrated in Figure 28. Such an introduction of two molecules of the chiral auxiliary should give rise to three

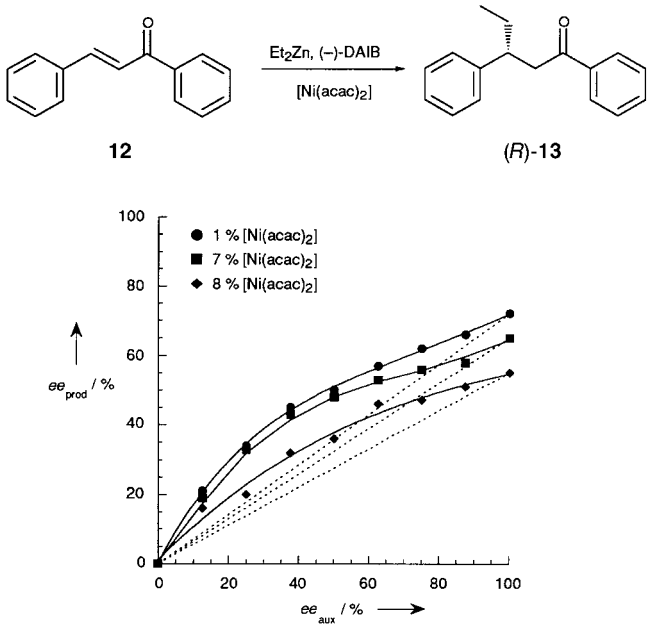


Figure 27. (+)-NLEs in DAIB-catalyzed (16 mol%) 1,4-addition of diethylzinc compounds to chalcone (**12**) (acetonitrile, −30 °C).

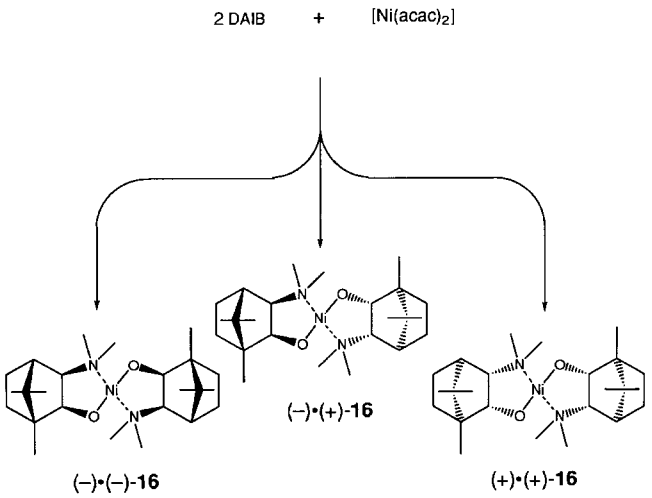


Figure 28. Intermediate dimeric species formed during the DAIB-catalyzed 1,4-addition.

possible complexes: homochiral (−)·(−)-**16** and (+)·(+)-**16** entities and the heterochiral complex (−)·(+)-**16**. The (+)-NLE taking place here implies, as it was seen before, a greater stability of the *meso* (−)·(+)-**16** species. The structures shown in Figure 29 can help to understand structural differences

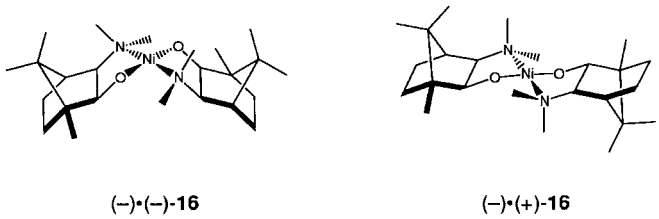


Figure 29. Perspective structural formulas of the DAIB – nickel complexes (−)·(−)-**16** and (−)·(+)-**16**.

between (−)·(−) and (−)·(+)-**16**. In the latter the two enantiomeric aminoisobornyloxy moieties are antiperiplanar, which assures lower steric interactions than its (−)·(−) analogue. The less stable homochiral structures should then be implicated more readily in the reaction than the heterochiral one, which keeps the minor enantiomer away in a thermodynamically-driven dimerization process.

2.3.3. 1,4-Addition of Cuprates

Nonlinear effects in 1,4-addition reactions are not restricted to the reagents discussed previously, but can also be encountered when cuprates are used. In 1994 Pfaltz and Zhou reported a (−)-NLE in the addition of isopropylcuprate to cycloheptenone (**17**, Figure 30).[37] The use of a chiral copper

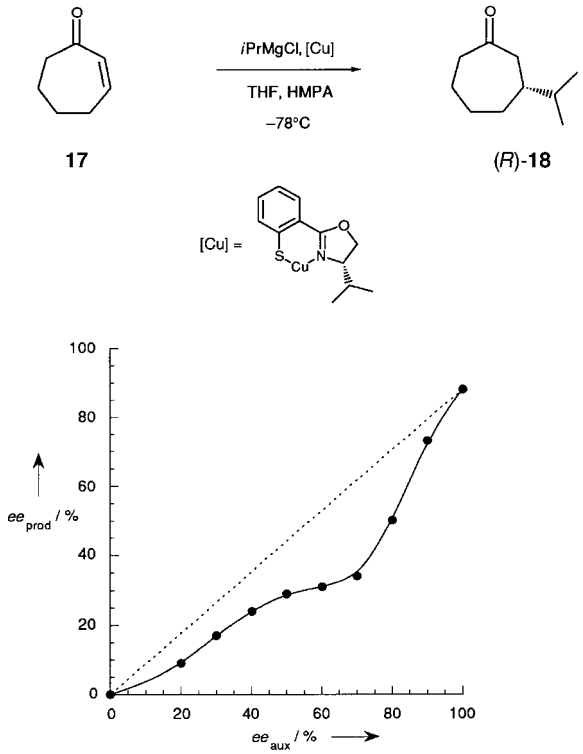


Figure 30. (−)-NLE observed in the copper catalyzed 1,4-addition of *i*PrMgCl to **17**.

oxazolinethiolate as the catalyst in this reaction gave access to the substituted suberone (*R*)-**18**. The *ee* value of this product was, for all ee_{aux}, lower than it should be, and thus generates the multishaped curve in Figure 30. This (−)-NLE is a clear indication of a different behavior of the copper catalyst when compared with the results of the 1,4-addition presented in the preceding section. Even if no explanation was given for this NLE, one can suggest that the aggregation of cuprates, which is usually more complex than with other organometallic reagents, is responsible for this effect. However, more information on the structure of the catalytic species involved is necessary to get a better understanding of this phenomenon.

This behavior seems to be a constant in cuprate addition reactions (at least with analogous catalysts); van Koten et al. discovered a multishaped NLE while working on the methylation of benzylideneacetone (**19**).[38] Thus, the chiral, aromatic copper aminothiolate (Figure 31) permits an effective alkylation and gives rise to the product (*S*)-**20**. A nonlinear effect that is just above the linear relation relation-

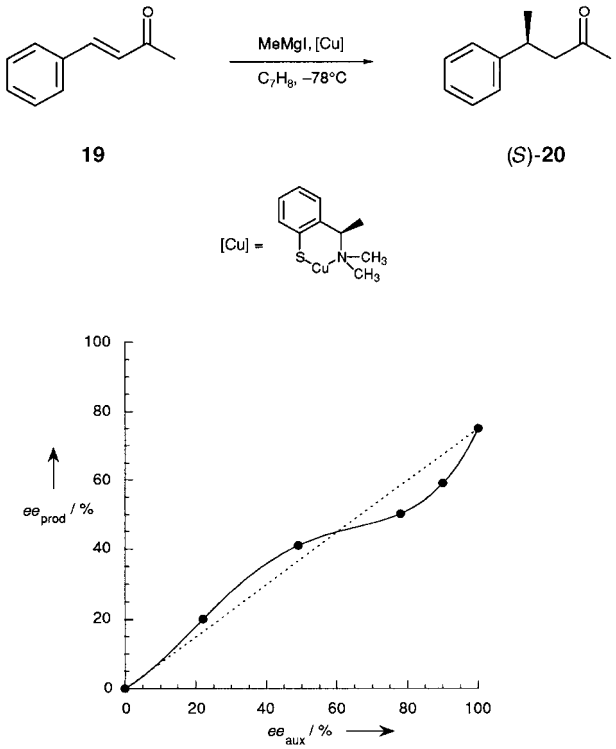


Figure 31. NLE in a copper-catalyzed 1,4-addition of MeMgI to benzylideneacetone (**19**).

ship between ee_{prod} and ee_{aux} was observed from 0 to 50% *ee*; at higher *ee* values, it becomes a moderate (−)-NLE. The intervention of multinuclear species as being responsible for this NLE has been invoked, but no exact explanation can be given here. The oligomeric structures should influence the *ee* value of the catalyst, and leave a mononuclear species with a modified enantiomeric excess. The curves of Figure 30 and 31 are reminiscent of those discussed for the ML_4 model.

2.3.4. Glyoxylate–Ene Reaction

One of the earliest and striking reports of nonlinear effects was published in 1990 by Mikami, Nakai et al.[39] In their study of the glyoxylate–ene reaction, mediated by chiral Lewis acid catalysts, they encountered a very strong (+)-NLE with the titanium catalyst derived from 1,1′-bi-2-naphthol (BINOL). Figure 32 depicts the reaction of α-methylstyrene (**21**) and methyl glyoxylate (**22**). The *ee* value of (*R*)-**23** was plotted against the one of (*R*)-BINOL (ee_{aux}). From the curves it can be observed that the effect is almost identical for catalysts prepared from (*R*)-BINOL and $(i\text{-PrO})_2TiBr_2$ (curve ●) or $[Ti(OiPr)_2Cl_2]$ (curve ○).

A series of studies were undertaken by this group and proved to be very helpful in understanding the exact nature of the catalyst in solution.[39c] The BINOL should react first with $[Ti(OiPr)_2X_2]$ (X = Cl, Br) to form, by alkoxy exchange, both

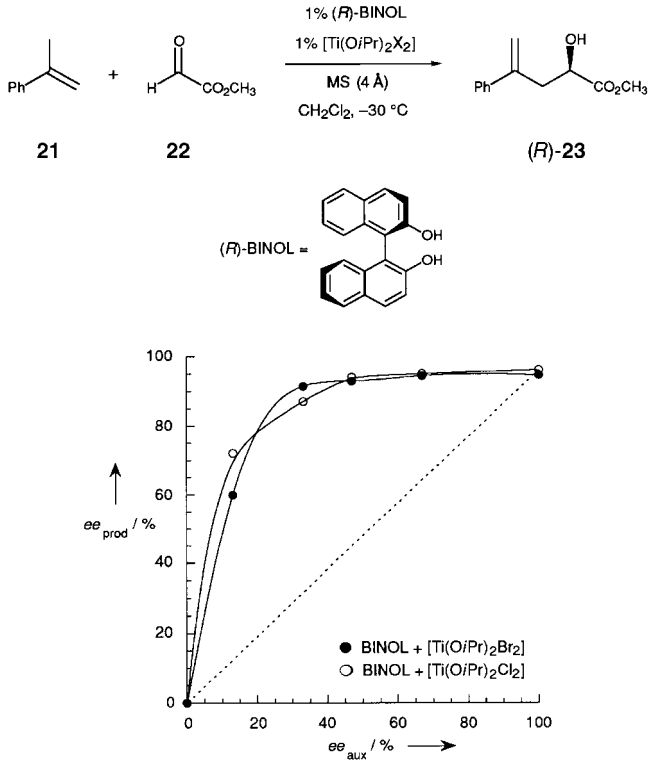


Figure 32. (+)-NLEs in the BINOL–titanium catalyzed ene reaction between **21** and **22**. MS = molecular sieve.

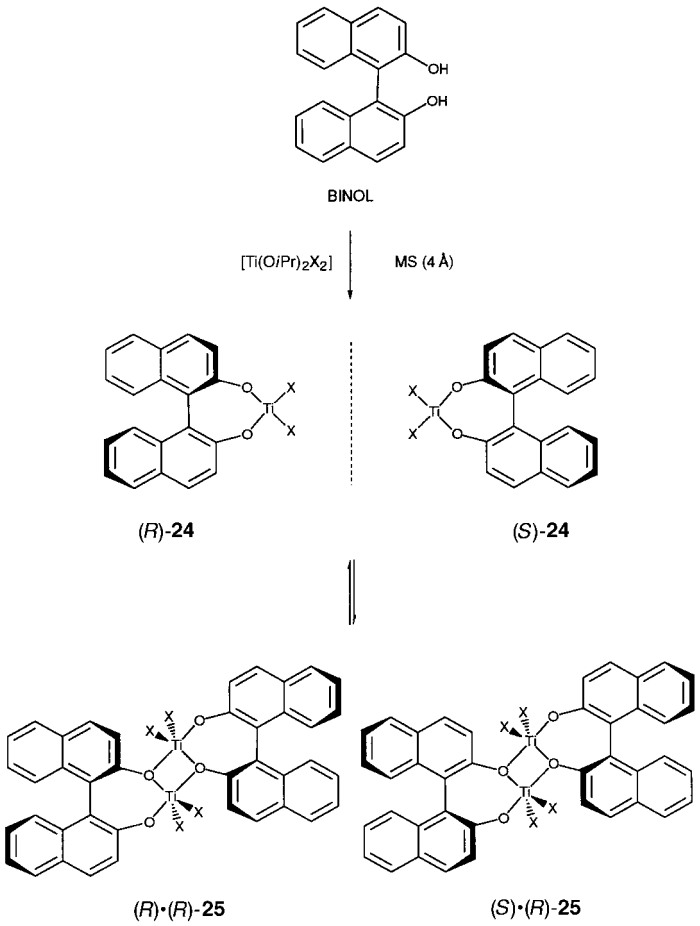


Figure 33. Homochiral ((*R*)·(*R*)-**25**) and heterochiral ((*S*)·(*R*)-**25**) dimers formed between the enantiomeric BINOL–titanium catalysts.

enantiomers of BINOL-TiX_2, (*R*)- and (*S*)-**24** (Figure 33). Those monomers then become implicated in an equilibrium with their dimers (*R*)·(*R*)-**25**, (*S*)·(*S*)-**25** (not shown here), and (*S*)·(*R*)-**25**. The same behavior discussed previously must be encountered to generate the (+)-NLE. Vapor pressure osmometry measurements showed that dimers are formed. Furthermore, the molecular weight of the complex prepared from enantiomerically pure (*R*)-BINOL (homochiral) was concentration dependent, whereas the one from *rac*-BINOL (heterochiral) does not change at all with dilution. This observation is an indication of a greater stability of the *meso* dimer. Kinetic measurements showed (*R*)·(*R*)-**25** to be 35 fold more active than (*S*)·(*R*)-**25**. Since the monomeric species are held responsible for the catalysis, these experiments clearly show that the homochiral dimeric structures dissociate more readily than the corresponding heterochiral ones.

Stability differences can be understood by simply looking at three-dimensional representations of the dimers proposed by the authors (Figure 34). Both structures possess a central four-membered Ti_2O_2 ring around which are organized the chiral

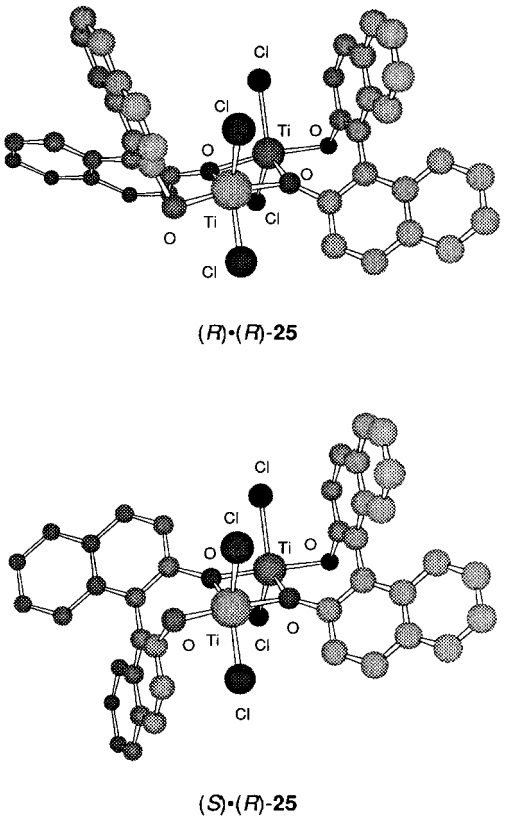


Figure 34. Structures of the dimeric species (*R*)·(*R*)-**25** and (*S*)·(*R*)-**25**.

units. Steric interactions are much more important in the C_2 symmetrical dimer (*R*)·(*R*)-**25**, since the binaphthyl moieties are *syn*-periplanar and close together. However, in the heterochiral complex (*S*)·(*R*)-**25**, which has a C_i symmetry and a coplanar instead of distorted Ti_2O_2 ring, the spatial orientation of the ligands (*anti*-periplanar) seems in fact to offer a greater stability.

The effect of the amount of catalyst on the NLE was also investigated. Various quantities of (*R*)-BINOL (31 % *ee*) ranging from 1 mol % to 100 mol % were introduced in the mixture and the ee_{prod} measured. Figure 35 shows that an

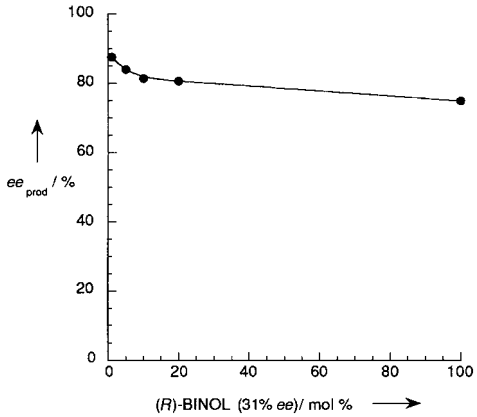


Figure 35. ee_{prod} of (*R*)-**23** as a function of the amount of (R)-BINOL (31 % *ee*).

increase in the amount of catalytic species, and thus its concentration, lowers the NLE. This observation is in total disagreement with the monomer/dimer equilibrium. This divergent behavior was, however, explained from molecular weight determinations on the catalyst prepared from 31 % *ee* BINOL by the appearance of a trimeric species at higher concentrations.[39c, d] The Mikami and Nakai ene-reaction with a BINOL-derived catalyst can however be described with the following parameters for the ML_2 system; $EE_0 = 98\,\%$, $K = 2300$ and $g = 0.005$ ($k_{RS}/k_{RR} \approx 1/200$), which give the best fit with the experimentally derived curve.

The glyoxylate – ene reaction can also be driven by another type of catalyst developed more recently. Mikami and Terada,[40] and later Nakai et al.,[41] reported the preparation of this new titanium catalyst **26** (Figure 36). Reaction of (*R*)-BINOL with either $[Ti(OiPr)_2X_2]$ (where X = Cl, Br) or

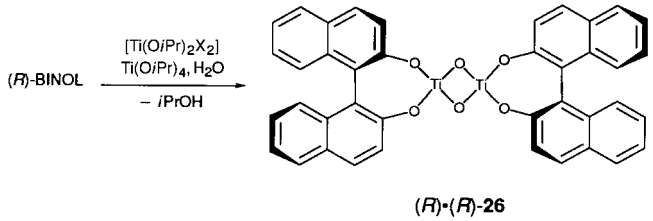


Figure 36. Synthesis of **26**.

$[Ti(OiPr)_4]$ and water, followed by heating and the azeotropic removal of isopropyl alcohol in refluxing toluene led to the formation of the μ-oxo titanium complex $(R)\cdot(R)$-**26**. The existence of such a μ-oxo dimeric species in solution was confirmed by molecular mass measurements by vapor pressure osmometry and infrared spectroscopy,[40] as well as by mass spectrometry and NMR spectrocopy.[41] Moreover, the μ-oxo complex mass has a different behavior depending on the *ee* value of the BINOL used to prepare it.[40] When enantiomerically pure (*R*)-BINOL was utilized the apparent molecular weight was shown to be concentration-dependent; while with the racemic BINOL it remained unchanged upon dilution. This indicates a greater stability of the μ-oxo dimer prepared from *rac*-BINOL in solution over the homochiral complex (see above). This was an indication of a possible nonlinear behavior with this new catalyst.

When the ee_{prod} was tested in the glyoxylate – ene reaction against the *ee* value of the BINOL used to prepare the catalyst **26** a strong (+)-NLE was observed (Figure 37). The amount of

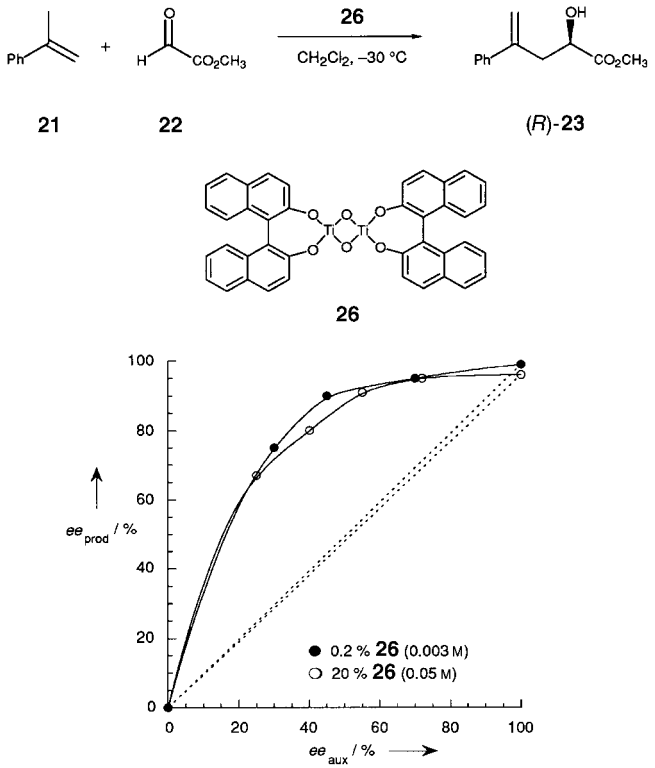


Figure 37. (+)-NLE observed in the ene reaction catalyzed by **26**.

the catalytic species had little effect on the amplifying phenomenon. The *meso* μ-oxo catalyst accounted for the increase of the *ee* value of the catalytic substance. In fact, the homochiral catalyst possessed a catalytic activity nine times superior to that of the heterochiral one. Furthermore, molecular modeling on the three-dimensional representations of the μ-oxo $(R)\cdot(R)$- and $(S)\cdot(R)$-**26** (Figure 38) showed the heterochiral $(S)\cdot(R)$-**26** to be 1.08 kcal mol^{-1} lower in energy.[40]

2.3.5. *Trimethylsilylcyanation of Carbonyl Compounds*

Oguni et al. investigated the asymmetric cyanation of carbonyl compounds with trimethylsilylcyanide (TMSCN), as illustrated in Figure 39.[42]. The catalyst is prepared by freeze-drying a solution of an equimolar mixture of (+)-diisopropyl tartrate {(+)-DIPT} and $[Ti(OiPr)_4]$. It is then used in the reaction in the presence of isopropyl alcohol. This reaction gives trimethylsilylated cyanohydrines in both good chemical yields and enantioselectivity. For example, benzaldehyde (**8**) gives the corresponding compound (*R*)-**27**. This

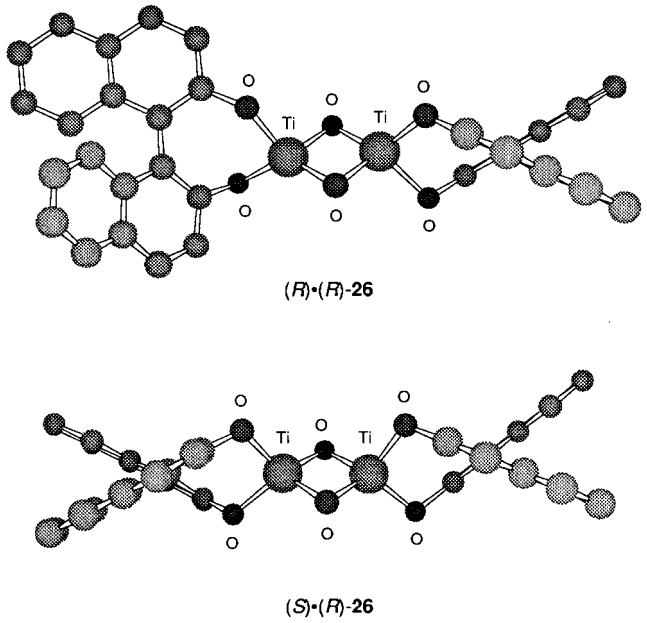


Figure 38. Three-dimensional representations of homo- and heterochiral μ-oxo-titanium complexes $(R)\cdot(R)$- and $(S)\cdot(R)$-**26**.

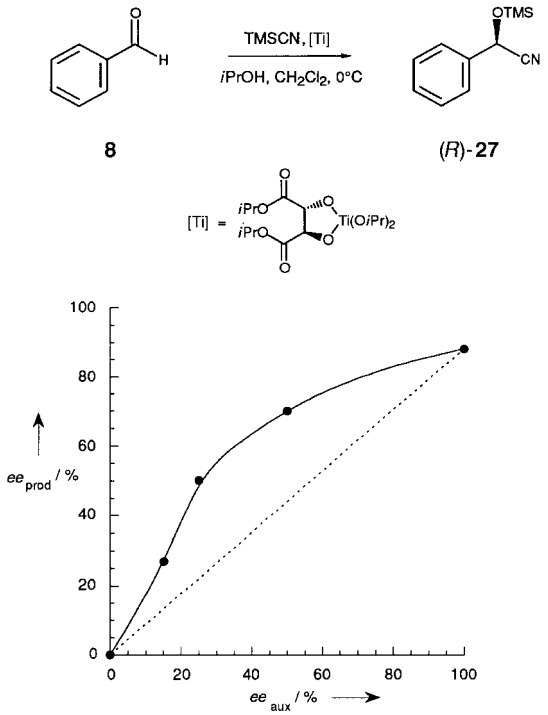
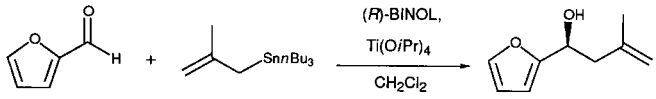


Figure 39. (+)-NLE in the trimethylsilylcyanation of benzaldehyde (**8**) with a chiral titanium catalyst (20–100 mol%).

asymmetric synthesis works well with 20 mol% of the catalyst, but selectivities are better with stoichiometric amounts. The authors tested the effect of the incorporation of partially resolved (+)-DIPT in the preparation of the catalyst. By using one equivalent of this species, the enantiomeric excesses of the product **27** were measured and a nonlinear effect observed (Figure 39). This effect was not explained because of the lack of information on the structure of the catalyst. However, the spectral analysis of the freeze-dried compound suggested an oligomeric structure of the type $[\{Ti(OiPr)_2(DIPT)\}_n]$, which breaks down to a simpler structure upon addition of the alcohol to the mixture.[42b] This NLE is reminiscent of the one encountered in the Sharpless epoxidation discussed in the Section 2.1.

2.3.6. Allylation and Aldol Condensation on Aldehydes

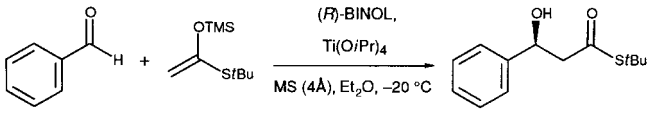
Keck et al. studied the asymmetric allylation and aldolization of aldehydes with a BINOL-derived titanium catalyst.[43] In their work they investigated the effect of using a chiral ligand that was not enantiomerically pure. In the allylation reaction furfural (**28**) was treated with tri-*n*-butylmethallylstannane (**29**) to give the product (*S*)-**30** (Scheme 1).[43a] When



Scheme 1. The asymmetric BINOL–titanium catalyzed allylation of furfural (**28**) with a dependence of a NLE on the presence of molecular sieves.

the catalyst was prepared by the reaction of an equimolar mixture of BINOL and $Ti(OiPr)_4$, in the presence of molecular sieves (4 Å), a positive nonlinear effect could be detected when the reaction was performed at $-20\,^{\circ}C$. The use of 50% *ee* or 100% *ee* BINOL gave **30** with an *ee* of 88 or 99%, respectively. By comparison, simple mixing of BINOL and $Ti(OiPr)_4$ (in a 2:1 ratio) at room temperature without molecular sieves led to a strictly linear relationship between ee_{aux} and ee_{prod}. The departure from linearity can be explained as a result of the formation of the usual, more stable heterochiral dimer. The molecular sieves play an important role in the formation and interaction of the complexes, since in its absence no NLE is observed. The nature of the catalyst in the latter case is however unknown and maybe quite different from the one discussed previously.

The same catalyst was then used in the aldol condensation of aldehydes.[43b] Reaction of benzaldehyde (**8**) with the ketene acetal **31** gives access to the thioester (*S*)-**32** when 20 mol% of the BINOL-titanium catalyst, prepared in the presence of molecular sieves, is employed (Scheme 2). In this



Scheme 2. Asymmetric aldol condensation of benzaldehyde (**8**) with **31**.

reaction the ee_{prod} varies nonlinearly with respect to different *ee*'s of the BINOL. A (+)-NLE takes place as expected for this type of catalyst, which is almost identical to the one presented in Scheme 1. The use of BINOL with 50% *ee* gave a product with an enantiomeric excess of 91% while the enantiopure diol gave the adduct with 97% *ee*.

Faller et al. and Tagliavini et al. were also interested in the allylation of aldehydes and reported a similar study of nonlinear effects in this reaction. A comparison was done between two types of BINOL-metal catalysts in the reaction of allyltributyltin (**34**) and aldehydes, as illustrated in Figure 40. Faller et al. prepared their catalyst by mixing (*R*)-BINOL with various *ee*'s with Ti(O*i*-Pr)$_4$ in the presence of

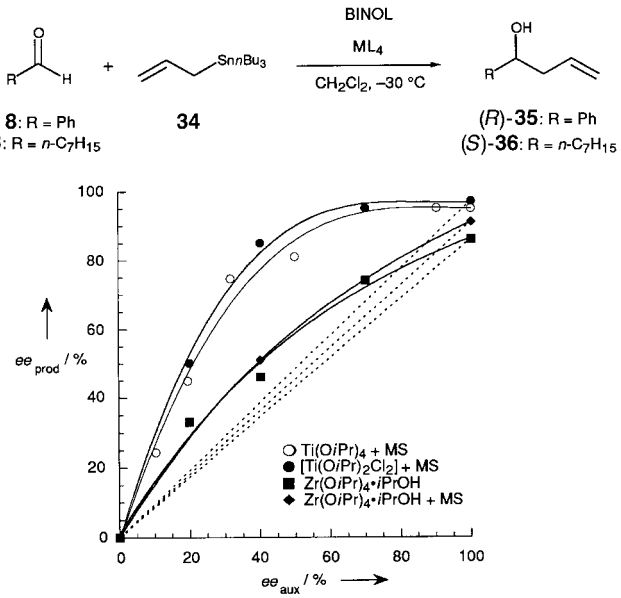


Figure 40. NLEs observed in the asymmetric allylation of aldehydes with various BINOL – metal catalysts (20 – 30 mol %).

4-Å molecular sieves.[44] The use 30 mol % of this catalyst in the allylation of benzaldehyde (**8**) gave rise to the usual (+)-NLE seen for BINOL catalysts (curve ○). Tagliavini et al. studied the reaction of octanal (**33**) catalyzed by 20 mol % of the complex that was prepared by reaction between (*S*)-BINOL and [Ti(O*i*Pr)$_2$Cl$_2$] in the presence of molecular sieves, and observed a pronounced (+)-NLE (curve ●).[45] A strong resemblance with the effect reported with the same catalyst in the ene reaction (Section 2.3.4.) is seen. In the allylation reaction the homochiral dimeric species was calculated to be 100 times more active than its heterochiral equivalent and, therefore, explains the NLE observed here.

When the chiral catalyst was prepared from Zr(O*i*Pr)$_4$ · *i*PrOH, with (curve ■) or without (curve ◆) the addition of molecular sieves, a moderate (+)-NLE could be recorded. The similarity of the results, for both methods of preparation, has been explained from the NMR analysis. While solutions of BINOL and [Ti(*i*PrO)$_2$Cl$_2$] remained unchanged if no molecular sieves are added, those of BINOL and Zr(O*i*Pr)$_4$ · *i*PrOH showed the formation of the catalyst [Zr(O*i*Pr)$_2$BINOL] with and without molecular sieves. Only a slight modification in the level of enantioselectivity takes place.

Kinetic experiments with the zirconium catalyst showed that the one prepared from pure (*S*)-BINOL needed four hours to complete the reaction, while the other catalyst derived from *rac*-BINOL was a little less active (10 h). The moderate deviation from the linear relationship was further explained by the activity of the homochiral zirconium complex being only two times greater. This value is quite small when compared to the activity difference in the case of the titanium catalysis. Tagliavini et al. found out, from the ML$_2$ model, that the BINOL – titanium catalyst possesses a $g = 0.01$ ($k_{RS}/k_{RR} = 1/100$), while the BINOL – zirconium one displays a $g = 0.6$ ($k_{RS}/k_{RR} \approx 1/1.7$).

Carreira et al. reported similar results from the allylation of pivalaldehyde with allyltrimethylsilane with a BINOL – Ti catalyst prepared from BINOL and TiF$_4$. In their case, the use of 50 % *ee* BINOL gave an allylic alcohol with 82 % *ee* while the enantiopure BINOL gave 95 % *ee* for the same alcohol.[46]

2.3.7. Asymmetric Epoxidation

In 1994 Kagan et al. reported an additional example of nonlinear effects during a Sharpless epoxidation (for geraniol epoxidation, see Section 2.1.) that involved the formation of the epoxide **38** from the allylic alcohol **37** (Figure 41).[31] A moderated amplification of the expected enantiomeric excess

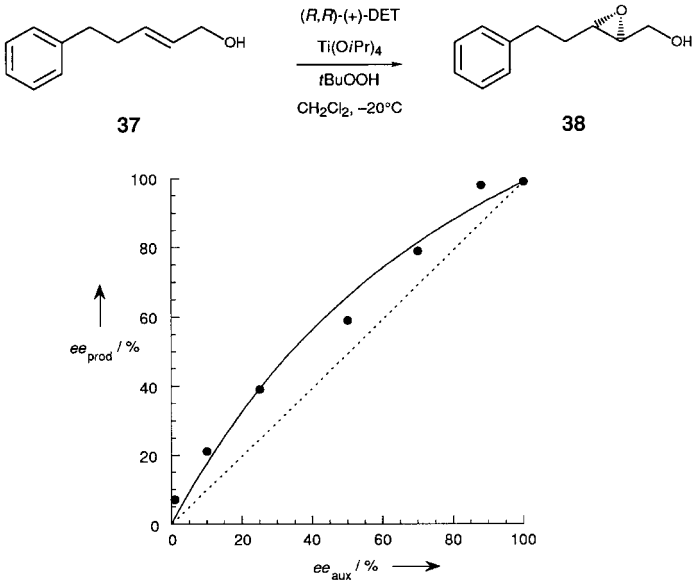


Figure 41. (+)-NLE in the Sharpless epoxidation of **37**.

was noted. Based on a model in which two chiral ligands are bound to the metallic center, this NLE was explained by the formation of the usual diasteroisomeric species. The heterochiral species was shown to possess half the catalytic activity of one of the homochiral complexes. On the basis of the ML$_2$ model, this asymmetric epoxidation of an allyl alcohol is described well by the parameters $EE_0 = 99\,\%$, $K = 1000$ and $g = 0.5$. The heterochiral species is slightly more stable ($k_{RS}/k_{RR} \approx 1/2$) and abundant ($K = 1000$).

2.3.8. Asymmetric Sulfoxidation

One of the first nonlinear effects was discovered by Kagan et al. during sulfide oxidation mediated by a chiral titanium complex.[19] The negative nonlinear effect resulting from this reaction was discussed in Section 2.1. Uemura et al. reported interesting results in their study of asymmetric oxidation of

sulfides promoted by a chiral BINOL–titanium catalyst.[47a] The method employs a reagent similar to Kagan's, but with BINOL as the chiral unit. This complex can be used at the catalytic level and sulfides such as **6** are efficiently transformed into sulfoxide (*R*)-**7** (Figure 42).

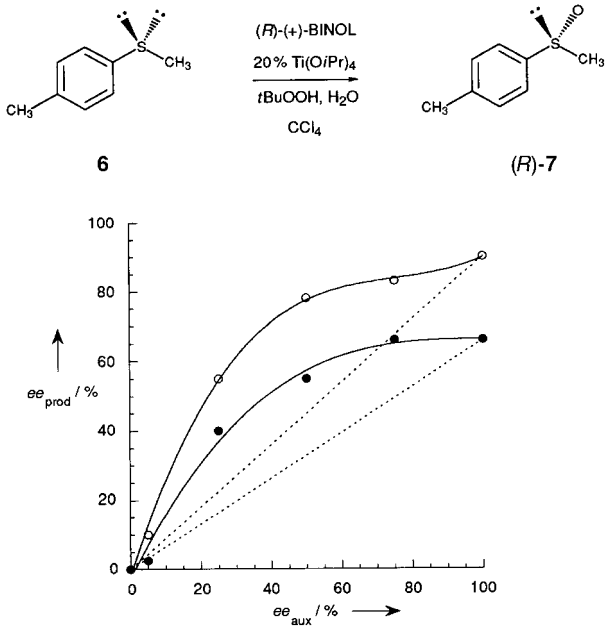


Figure 42. (+)-NLE in a BINOL–titanium catalyzed oxidation of sulfide **6** under various reaction conditions. Curve ●: Argon, −20 °C; curve ○: air, 0 °C.

The variation of the *ee* value of (*R*)-BINOL generated a (+)-NLE in the case of the two sets of experimental conditions, namely under argon at −20 °C (curve ●) and in air at 0 °C. When the reaction was performed under argon with a solution of *t*-BuOOH in toluene a moderate (+)-NLE was observed as well as a low selectivity at 100% *ee* of BINOL. The enantioselectivity of the transformation was however much better when the second method was employed; the use of 70% aqueous *t*-BuOOH at 0 °C with the reaction being carried out open to the atmosphere, generated higher levels of asymmetric induction as well as a stronger (+)-NLE (curve ○). The authors concluded that the existence of a (+)-NLE with this catalyst, in comparison with the negative effect observed with Kagan's reagent, was a result of a strong difference between the two catalysts. However, neither the NLE nor the structure of the catalyst itself was analyzed.

The presence of a NLE in this system can easily be understood if one takes into account the results already discussed with BINOL-metal catalysts (Sections 2.3.4 and 2.3.6). However, Uemura et al. discovered, by studying the evolution of the ee_{prod} over time, that a second reaction was also involved in the stereochemical outcome of the reaction.[47b] With the enantiopure BINOL, the *ee* value of the sulfoxide **7** was shown to increase considerably with the advancement of the reaction. This augmentation of the enantiomeric excess was accompanied by increased amounts of the overoxidation product, namely the corresponding sulfone. As the formation of the sulfone proceeds a process of kinetic resolution[48] takes place, which assures a better *ee* value of (*R*)-**7** over time. A study showed that racemic **7** indeed gave rise to a kinetic resolution in which there is some asymmetric amplification. The curves of Figure 42 are thus a complicated function of (+)-NLE for both the sulfoxidation and the subsequent kinetic resolution.[47b]

2.3.9. Allylic Oxidation

Feringa et al. reported that NLEs can be observed in the asymmetric allylic oxidation with copper salts and (*S*)-proline.[49] This NLE is however modified by the presence or absence of a catalytic amount of anthraquinone as seen in Figure 43. When proline of different enantiomeric excesses

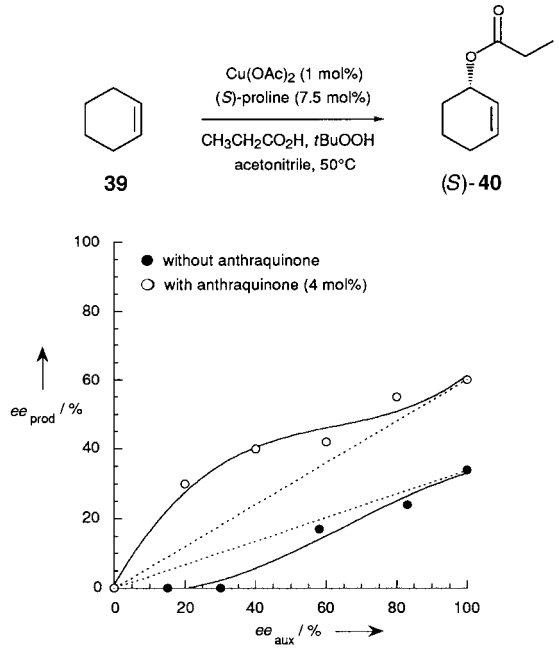


Figure 43. Modification of the NLE in an asymmetric allylic oxidation of **39** catalyzed by (**S**)-proline with the addition of anthraquinone.

was introduced alone into the reaction mixture a small (−)-NLE took place (curve ●) in this reaction of low enantioselectivity. When 4 mol% of anthraquinone was added to the mixture, an increase in the reaction selectivity as well as a moderate (+)-NLE were encountered. Both procedures transform cyclohexene (**39**) into (*S*)-2-cyclohexenyl propionate ((*S*)-**40**).

The authors stipulated that the generation of the (−)-NLE by the use of proline with copper(II) acetate was the result of more than one proline molecule being involved in the stereodiscriminating step, as was the case in the example from Agami (Section 2.1). It is also possible that dinuclear or oligonuclear catalytic complexes are implicated. The blue solution formed with the copper salt becomes more turbid when the *ee* value of proline is lowered. It was suggested that the precipitate was composed of the *meso*- or heterochiral complex (*R*)-prolinato-(*S*)-prolinato-copper(II). Moreover, the (*R*)·(*S*)-complex remaining in solution must be more

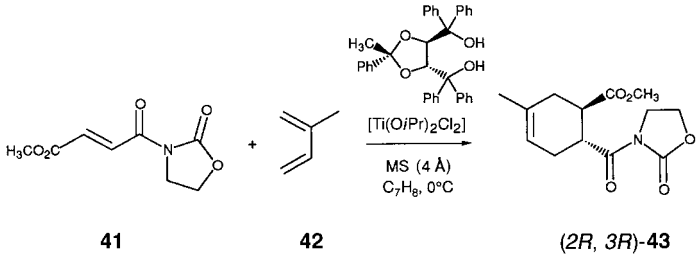
reactive than the homochiral ones, $(R)\cdot(R)$ and $(S)\cdot(S)$, in order to observe the negative effect.

Feringa et al. proposed that in the presence of anthraquinone a mechanistic or structural change occurred, which involved the interaction of the catalyst and quinone. The effect of anthraquinone cannot be ascertained, but since the reaction passes through a Cu^{III} intermediate, one can propose that it should play a role in the redox pathways of the reaction.

2.3.10. Diels–Alder Reaction

The Diels–Alder reaction, one of the most powerful methods for the synthesis of 6-membered rings, was studied in great detail and its asymmetric version developed with a certain success. Since chiral catalysts are utilized in the reaction, several groups tested the existence of nonlinear effects during its course.

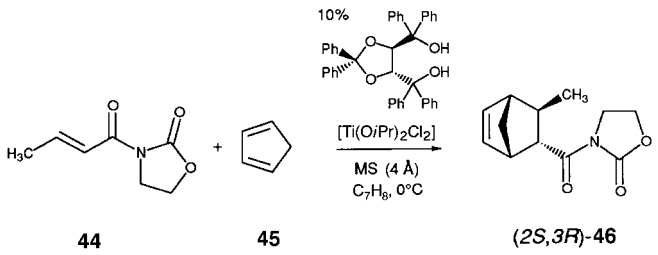
As early as 1989 Narasaka et al. observed a peculiar behavior of a TADDOL-type diol when used with titanium as a catalyst in the Diels–Alder reaction illustrated in Scheme 3 (TADDOL = tetraaryldioxolanedimethanol.[50] When the 3-acyl-1,3-oxazolidin-2-one **41** was allowed to react



Scheme 3. Asymmetric Diels–Alder reaction between **41** and **42** with a TADDOL–titanium catalyst.

with 2-methyl-1,3-butadiene (**42**), in the presence of the catalyst generated by using the diol and $[Ti(OiPr)_2Cl_2]$, the product *(2R,3R)*-**43** derived from the *endo* transition state was isolated. When the authors took a diol with 25% *ee* for preparing the catalyst, the product **43** was isolated with an *ee* of 83%. Furthermore, a precipitate was observed during the preparation of the catalytic species. This observation was an indication of interactions in solution that lead to a NLE-type of behavior for the catalyst. This was further proved by admixing the diol (25% *ee*) and $[Ti(OiPr)_2Cl_2]$, removal of the precipitate, and performing the reaction with the supernatant solution. Once again the product **43** was isolated with 83% *ee*. The filtrated solid was hydrolyzed to retrieve the diol, which was in this case racemic. This result suggested that the species formed was at least dimeric, and the 1:1 ratio of enantiomers was an indication that the precipitated compound was the heterochiral complex.

Irrure et al. reported some years later a more complete study of NLE in the Diels–Alder reaction by using a similar diol as the chiral unit of the titanium catalyst.[51] With 10 mol% of the catalytic species, the cycloaddition of the oxazolidinone **44** and the diene **45** gave the expected product **46** (Figure 44). By varying the *ee* value of the diol, a (+)-NLE was observed for the *ee* of the product. The greater stability of



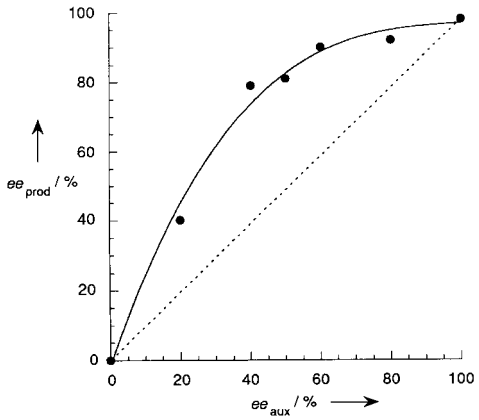


Figure 44. (+)-NLE in an asymmetric Diels–Alder reaction of **44** and **45** with a TADDOL–titanium catalyst.

the *meso*-dimeric species can be appreciated qualitatively by the formation of a precipitate when starting from the *rac*-diol, while enantiopure diol produced only a clear and limpid solution of the catalyst.

By keeping a constant amount of catalyst, and using the same reaction conditions, the influence of the enantiomeric purity of the diol on the chemical yield as well as the formation of the *endo* product **46** was evaluated (Figure 45). The racemic diol generates a poor catalytic system and, after 21 h at 0 °C, only 6% of **46** was obtained with a diastereoselectivity of 58% in favor of the *endo* isomer. This suggested that the very insoluble heterochiral dimer was very stable and thus, less easily implicated in a catalytic cycle. The enantiopure diol-derived catalyst is however much more efficient. Since it is constituted only of totally soluble homochiral dimeric species, it gave under the exact same conditions 68% of **46** at 87% *de* (diastereomeric excess). Figure 45 allows visualization of the effect of the variation of the *ee* value of the diol between 0 and 100% *ee* on the yield (a) and diastereoselectivity (b) in this reaction.

Mikami's group also studied an asymmetric Diels–Alder reaction but with their BINOL-titanium catalyst, and again obtained excellent results.[52] Condensation of the diene **47** with methacrolein (**48**) gave efficient access to the carbocycle **49**, as depicted in Figure 46. In this reaction, the (*R*)-BINOL/$TiCl_2$ catalyst ((*R*)-**24**) was prepared in the usual way (see Section 2.3.4.) and the molecular sieve filtered-off before using it for catalysis. To study NLEs in this reaction the authors decided to vary the *ee* value of the catalyst **24** using two methods: In the first, molecular sieve-free (*R*)-**24** and *rac*-**24**, prepared independently from enantiopure or racemic BINOL respectively, were admixed to reach the desired *ee*

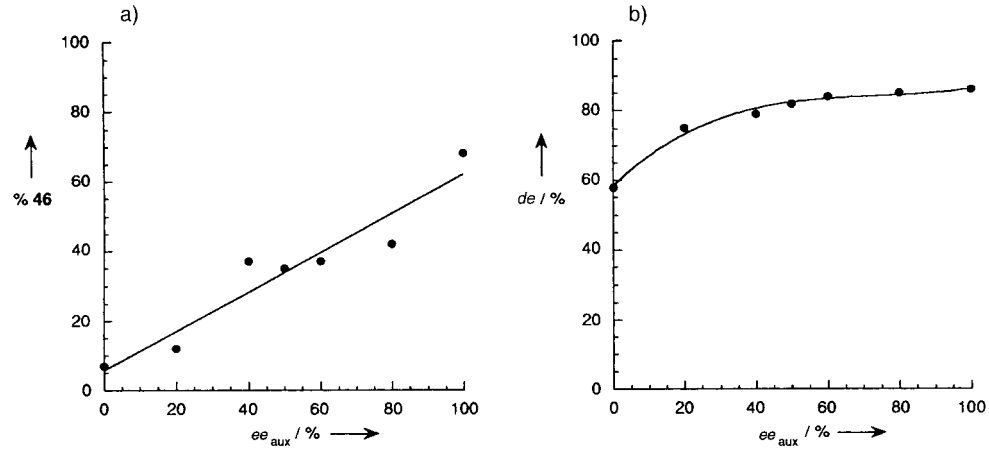
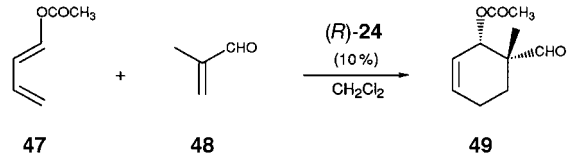
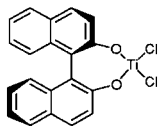


Figure 45. Yield and diasteromeric excess (*de*) of the product **46** with variation in the *ee* value of the diols.





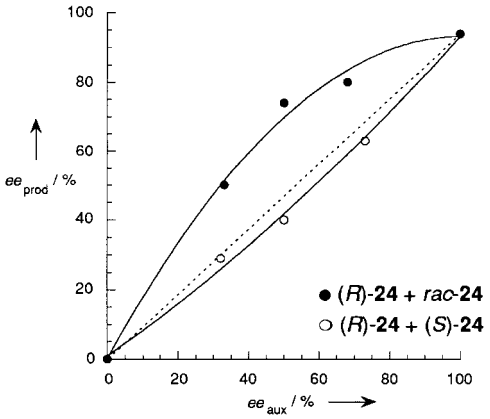


Figure 46. Variation of the NLE observed in a BINOL–titanium catalyzed Diels–Alder reaction with variation in the preparation of the catalyst.

value. The results of the asymmetric induction using this approach generated the curve ● of Figure 46, with a moderate (+)-NLE being observed.

In the second method, molecular sieve-free (*R*)-**24** and (*S*)-**24** were synthesized separately before using them to prepare the catalyst of various enantiomeric purities (curve ○). In this case, the relation was almost linear, which shows a strong difference with the preceding method of preparation and the results from Section 2.3.4. This result suggests that the presence of molecular sieves is important for establishing the equilibrium between the dimers. The fact that a mix of (*R*)-**24** and *rac*-**24** leads to a NLE, while (*R*)-**24** and (*S*)-**24** admixing gives a linear relationship, confirms that little exchange between the dimeric species takes place in the absence of molecular sieves. Thus in the first method catalyst *rac*-**24**, which exists as the more stable and less catalytically active heterochiral dimeric species, is mixed with the homochiral dimer generated from (*R*)-**24**. Since the exchange is almost nonexistent, the reaction will mainly be catalyzed by (*R*)-**24** that is readily liberated from the homochiral complex, with the *meso* complex acting mainly as a spectator. For the other technique homochiral dimers act independently in the reaction to give a product with an *ee* value reflecting the enantiomeric composition of the catalyst. It is intriguing that in this case the liberated monomeric (*R*)- and (*S*)-**24** seem to be implicated only in the catalysis and not in a heterochiral dimerization process. If the catalyst prepared from BINOL with 50% *ee*, followed by the filtration of molecular sieves, is used in this reaction, product **49** is isolated with an *ee* of 76%. This is the result of the formation of homo- and heterochiral species prior to removal of the molecular sieves.

The greater stability of the *meso* dimer was evaluated by kinetic experiments. The molecular sieve-free catalyst prepared from (*R*)-BINOL (curve ●) was shown to be five times catalytically more active than the one obtained from *rac*-BINOL (curve ○, Figure 47). The same group also

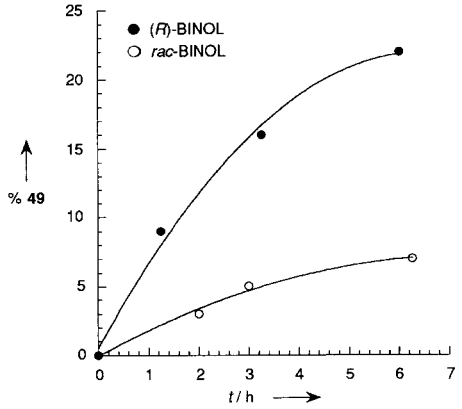


Figure 47. Yield of the product **49** as a function of reaction time for enantiomerically pure (*R*) and racemic BINOL.

observed a (+)-NLE of the same amplitude when using the catalyst prepared from (*R*)- and *rac*-**24** in an hetero-Diels–Alder reaction. The effect was examined in the reaction between the diene **50** and methyl glyoxylate (**22**) to afford the dihydropyrane **51** (Figure 48).

In their study of the asymmetric version of the Diels–Alder reaction Kobayashi et al. discovered various kinds of non-

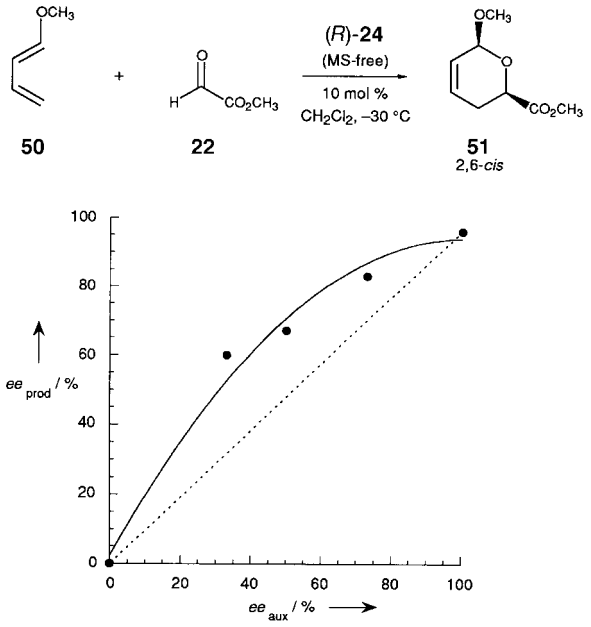


Figure 48. (+)-NLE in an asymmetric hetero-Diels–Alder reaction between **50** and **22** with a BINOL–titanium catalyst.

linear effects with some BINOL–lanthanide catalysts.[53] When (*R*)-BINOL was treated with scandium(III) triflate ($Sc(OTf)_3$) in the presence of *cis*-1,2,6-trimethylpiperidine (TMP) and molecular sieves, an efficient catalyst was prepared. The structure is the one of a simple chelate of the three constituents, namely $[Sc(tmp)_2((R)\text{-BINOL})]\cdot(OTf)_3$. When this catalyst was prepared from BINOL of various *ee* values, a (+)-NLE was observed for the *ee* value of the *endo* product **53** formed from the reaction between the acylated oxazolidinone **44** and cyclopentadiene (**52**), as seen in Figure 49 (curve ●).

The aging of the catalyst was proven to have deleterious effects on the selectivities of the reaction. While the scandium catalyst can be used as such in quick reactions, its ytterbium analogue needed stabilization in order to work properly. Furthermore, the additives used to stabilize the catalyst can even have a direct effect on the enantiofacial selectivity in this Diels–Alder reaction. When the Yb^{III} catalyst was prepared in the usual way, but with some 3-acetyl-1,3-oxazolidin-2-one (AOD) added as a stabilizer, the resulting nonlinear effect was much different from the preceding one. A (−)-NLE takes place with BINOL of to 60% *ee*, the value at which the linear relationship is observed for the enantiopure BINOL (curve ■). By changing the reaction temperature as well as the additive, in this case 3-phenylacetylacetone (PAA), a strong change was observed in the stereochemical outcome of this cycloaddition. Not only was the facial selectivity completely inverted, leading to (2*R*,3*S*)-**53** , but the NLE became strongly negative (curve □).

The differences between the scandium and ytterbium catalyst are the result of different levels of aggregation, especially when chelating additives are used. The perturbation created by the use of such compounds was shown to have a strong influence on the importance of the NLE.[53]

Seebach et al. studied the same reaction as Kobayashi's group, with the only difference being in the catalyst utilized.[54]

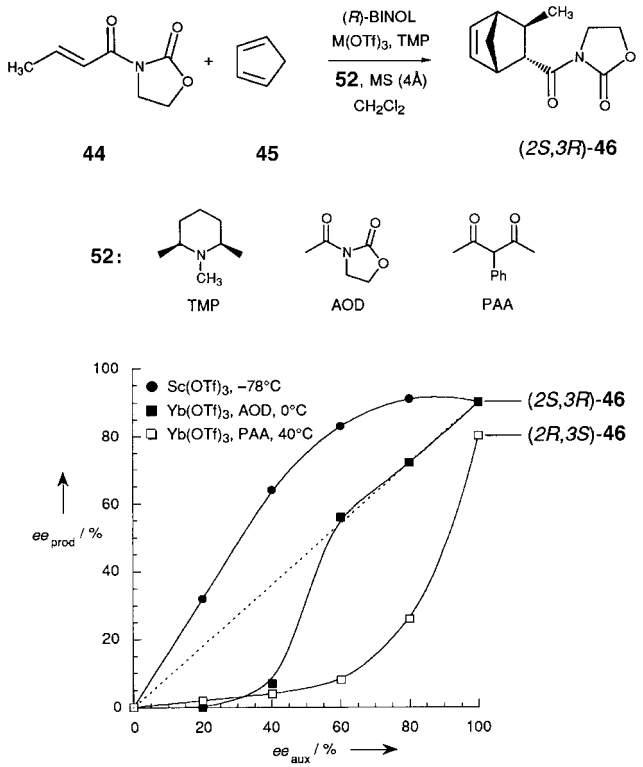


Figure 49. NLEs in a Diels–Alder reaction catalyzed by different BINOL–metal catalysts (20 mol%) in the presence of additives **52**.

The authors chose to use a highly hindered TADDOL-type diol to prepare the titanium catalyst needed to perform the Diels–Alder (Figure 50). When the diol of various *ee* values was allowed to react with $[Ti(OiPr)_2Cl_2]$ in order to form the

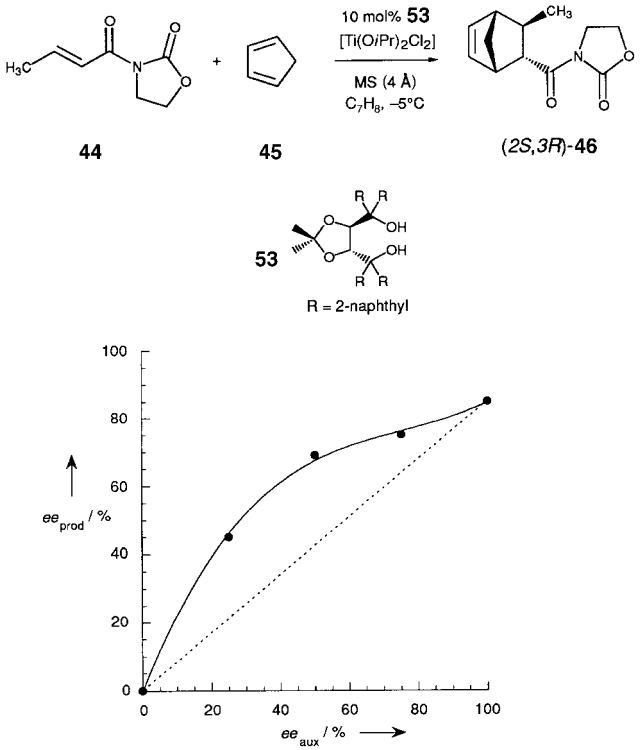
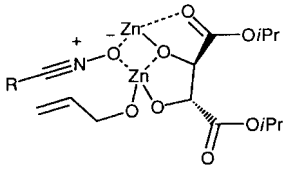


Figure 50. (+)-NLE in a titanium-catalyzed Diels–Alder reaction between **44** and **45**.

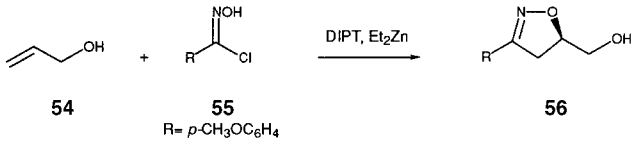
catalyst, which was then used in the reaction, a (+)-NLE was easy to observe. The same homo- and heterochiral species should be implicated here in the building of the amplification. However, unlike Narasaka's use of another TADDOL, there was no formation of a precipitate. The reaction mixture stayed homogeneous during the course of the transformation (except for the molecular sieves present in it) for all *ee*'s of the diol.

2.3.11. 1,3-Dipolar Cycloadditions

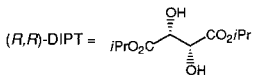
It has been found recently that Et_2Zn promotes the 1,3-dipolar cycloaddition of nitrile oxides to allyl alcohol in the presence of catalytic amounts of diisopropyl tartrate (DIPT).[55] From this method, 2-isoxazolines are obtained in good yields and up to 90% ee. A positive nonlinear effect has been observed during the reaction between allyl alcohol (**54**) and the nitrile oxide generated in situ from the hydroxymoyl chloride **55** to give the isoxazoline **56** (Figure 51). Presumably the (+)-NLE originates from soluble inactive zinc aggregates with DIPT. In this procedure, 1,4-dioxane is needed in order to avoid precipitation of highly aggregated complexes containing DIPT and zinc salts. The authors postulated that the key step of the cycloaddition involves the complex **57**.



57



54 **55** R= *p*-$CH_3OC_6H_4$ **56**



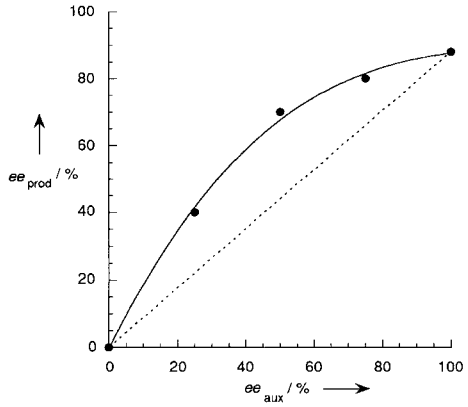
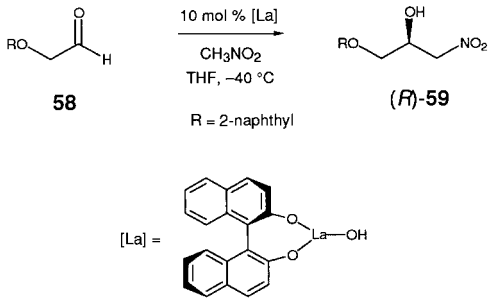


Figure 51. (+)-NLE in a 1,3-dipolar cycloaddition in the presence of DIPT (20 mol%) and Et_2Zn (dioxane, $CHCl_3$, 0 °C).

2.3.12. Nitroaldol Reaction

Shibasaki et al. reported that a BINOL–lanthanum complex is active in an asymmetric version of the Henry reaction (Scheme 4).[56] The nitroaldolization of α-naphthoxyacetaldehyde (**58**) in the presence of this enantiopure catalyst gave the nitroalcohol (*R*)-**59** in 87% *ee*. If the BINOL used to prepare the catalytic species was not enantiopure, in this case 56% *ee*, the enantiomeric excess of the product **59** was higher than expected (68% *ee*). This observation was an indication of an additional example of (+)-NLE for a BINOL-derived catalyst. The authors explained the NLE encountered with this lanthanum catalyst by its existence as an oligomer.

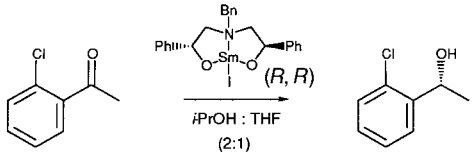


58 (*R*)-**59**

Scheme 4. Nitroaldolization of **58** with a BINOL–lanthanum catalyst.

2.3.13. Meerwein-Ponndorf-Verley Reduction

During the course of the elaboration of an asymmetric version of the MPV reaction, Evans et al. tested a chiral aminodiol-samarium(III) catalyst for NLEs (Scheme 5).[57]



60 (*R*)-**61**

Scheme 5. Meerwein-Ponndorf-Verley reaction with a chiral samarium catalyst (5 mol%) at room temperature.

They discovered that the use of an aminodiol of 80% *ee* in the preparation of the catalyst, and its subsequent use in the reduction of *o*-chloroacetophenone (**60**), gave the product (*R*)-**61** in a higher *ee* value than expected (95% *ee*). The use of an enantiopure catalyst gave the product with 97% *ee*. A more stable heterochiral dimer $(R,R)\cdot(S,S)$ was suggested as a trap for the minor enantiomer, which thus increased the *ee* value of the major one that is implicated both in the homodimer formation and catalysis.

2.3.14. Ring-Opening of meso-Epoxides

Jacobsen et al. described a catalytic system for the asymmetric nucleophilic ring-opening of *meso* epoxides (Figure 52).[58] In their investigation in to the nature of the catalytic system, the authors discovered that the chiral (salen)chromium(III) complex used in this reaction showed a nonlinear behavior when its *ee* value was modified. The reaction of cyclohexene oxide (**62**) with the trimethylsilylated azidoalcohol **63** showed a (+)-NLE. On the basis of kinetic considerations and measurements, the authors postulated the formation of a bimetallic species to account for the observed

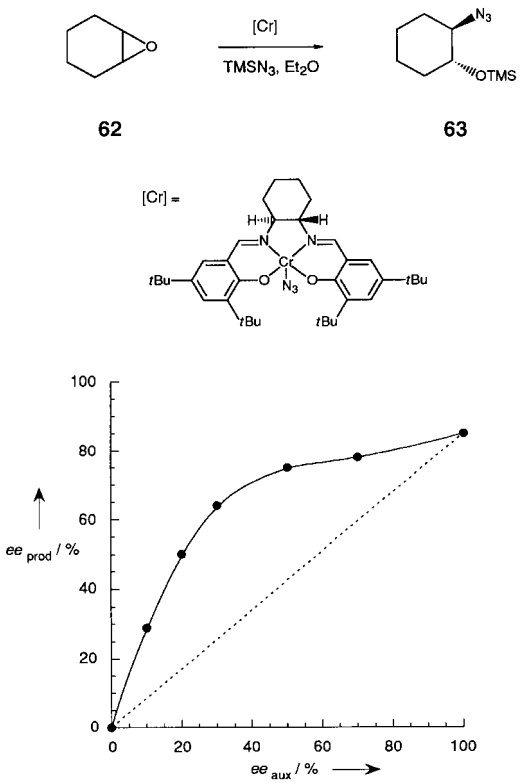


Figure 52. Ring-opening of *meso*-epoxide **62** catalyzed by a Salen–chromium catalyst (2 mol%).

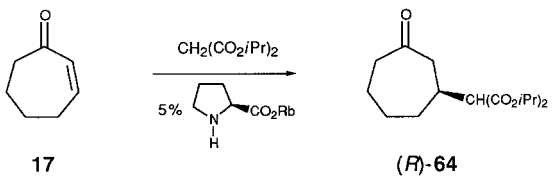
NLE. The epoxide is activated by one chiral salen–chromium unit, while the nucleophilic attack involves a second azido salen–chromium entity. The rate-determining step involves the prefered homochiral combination. Thus the evaluation of the nonlinear effects gave confirmation of the suggested mechanism that the catalyst is a bimetallic species that can act as both a nucleophile and an electrophile.

2.3.15. Nonlinear Effects as a Probe

The preceding Sections clearly demonstrated that the study of nonlinear effects in asymmetric catalysis could be more than useful in understanding and getting quantitative information about the species involved in the catalytic cycle and their behavior in solution. This Section will now describe the qualitative use of NLEs by a number of groups to ascertain the nature of the catalytic entity responsible for the enantioselective reaction.

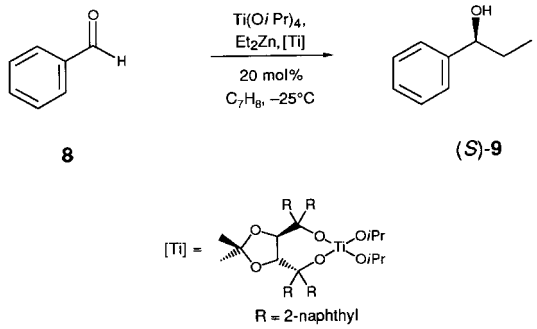
Yamaguchi et al. used NLE as a probe for the determination of the mechanism in asymmetric Michael additions with proline salts.[59] The 1,4-addition of diisopropyl malonate to cycloheptenone (**17**) by using a proline–rubidium salt gave them the opportunity to prepare the alkylated ketone (*R*)-**64** (Scheme 6). In contrast to the Hajos-Parrish-Wiechert reaction with proline presented in Section 2.1, the variation of the *ee* value of the proline salt resulted in a linear relationship with ee_{prod}. The authors concluded that the transition state of their reaction contained only one molecule of prolinate.

Seebach and Schmidt[60] used the NLE test to determine the nature of their catalytic species in diethylzinc addition on



Scheme 6. 1,4-Addition of a malonate to the enone **17** catalyzed by a proline–rubidium salt ($CHCl_3$, room temperature).

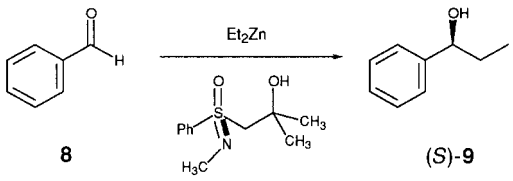
aldehydes. Their experiments regarding benzaldehyde (**8**) are included in Scheme 7. By variation of the enantiomeric purity of the TADDOL-type diol used to prepare the spirotitanate



Scheme 7. TADDOL-titanium catalyzed addition of diethylzinc to benzaldehyde (**8**).

catalyst, and by determination of the resulting *ee* value of the product, they discovered that no NLE was present. A strict linear relationship was obtained, which suggested that only one chiral unit was involved in the stereochemical rate-determining step of the stereoselective reaction. These results are in sharp contrast to those they obtained with the same catalyst in the Diels–Alder reaction (Section 2.3.10, Figure 50), where a moderate (+)-NLE was observed.

Bolm et al.,[61] were interested in getting a better understanding of the catalyst used in the enantioselective addition of diethylzinc to aldehydes catalyzed by β-hydroxysulfoximines. The use of the enantiomerically pure sulfoximine illustrated in Scheme 8 for the addition to benzaldehyde (**8**),



Scheme 8. Chiral sulfoximine (10 mol%) catalyzed 1,2-addition of diethylzinc to benzaldehyde (**8**).

gave the corresponding alcohol **9** with an *ee* of 85%. The nonmonomeric nature of the catalyst was proven by the authors by performing the same reaction with a sulfoximine of 23% *ee*, which gave rise to an alkylation product with an amplified *ee* of 70%.

The structure of the zinc species was later suggested to be dimeric in nature from NMR experiments.[61b] Furthermore, homochiral aggregates were estimated to react five times

faster than *meso* species, which explained the (+)-NLE observed in this case. The origin of the stability difference between the oligomers can be visualized by spatial representations of both *meso* and homochiral species (Figure 53). The

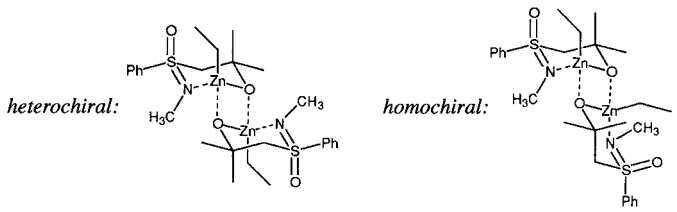
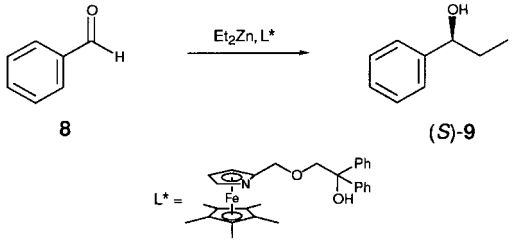


Figure 53. Dimers formed from the reaction shown in Scheme 8..

ethyl chains on the zinc atoms in the Zn–O four-membered cycle of the *meso* complex are *anti* to each other, whereas in the homochiral complex they end up *syn*, which has a destabilizing effect on the structure.

Another example of the addition of diethylzinc was performed by Fu and his group with a ferrocenyl chiral ligand (Scheme 9).[62] Despite several encounters with NLE in the



Scheme 9. Addition of diethylzinc to benzaldehyde (**8**) catalyzed by a chiral ligand (3 mol%, toluene, room temperature).

use of amino alcohols (Section 2.3.1.) the authors obtained a linear relationship in this case when their ligands with various *ee*'s were used.

During the course of the elaboration of a catalytic asymmetric epoxidation with a BINOL-derived catalyst, Shibasaki et al. tried to determine the exact structure of their catalyst.[63] Unfortunately, the spectroscopic analyses were unsatisfactory and the only conclusion was that the species were of oligomeric nature. In order to obtain more insights on the structure, the authors performed the NLE analysis. The chiral catalyst prepared from (*R*)-BINOL and Yb(O*i*Pr)$_3$ in the presence of molecular sieves was used in different *ee*'s in the epoxidation of benzylideneacetone (**19**) by *tert*-butylhydroperoxide (Figure 54). A (+)-NLE was observed in this case and the authors concluded that the oligomeric structure of the lanthanoid–BINOL complex should play a key role in their asymmetric epoxidation of enones. This type of NLE was not observed when chiral SALEN-type catalysts as reported by Schwenkreis and Berkessel were used, where perfect linearity is obtained.[64]

Bolm and Bienewald reported that in the asymmetric oxidation of sulfides the use of an imino alcohol chiral ligand with a vanadium salt and hydrogen peroxide oxidized methylphenyl sulfide (**66**) to sulfoxide **67** with a good

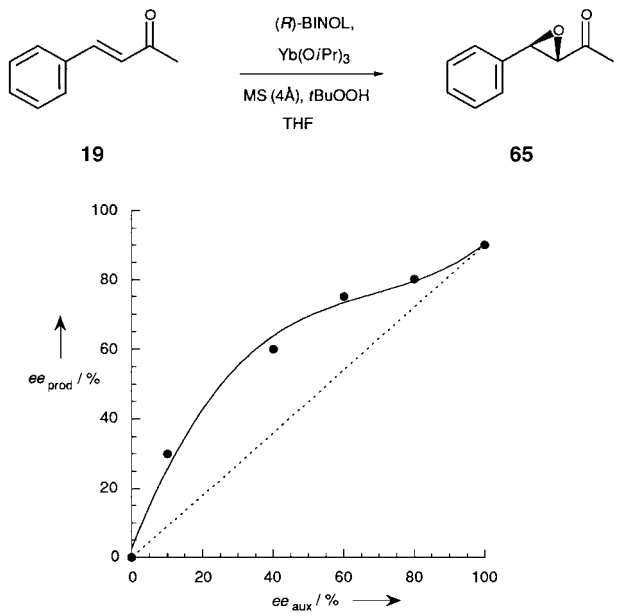
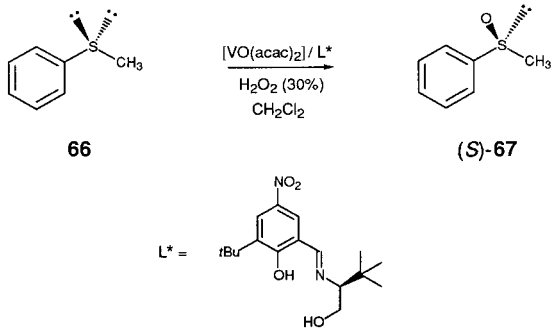


Figure 54. (+)-NLE in the asymmetric epoxidation of benzylideneacetone (**19**) catalyzed by a BINOL–ytterbium catalyst (5 mol%).

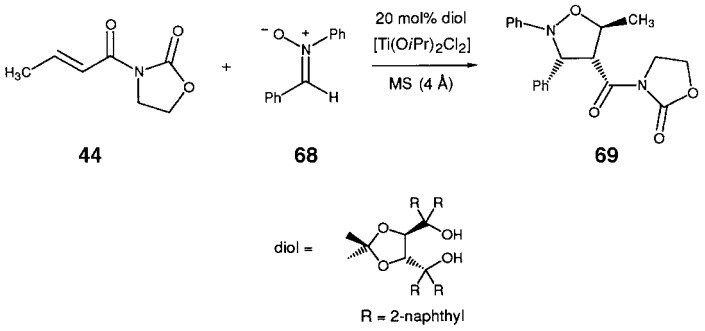
enantioselection (Scheme 10).[65] No NLEs were found in this system. The authors concluded that the catalyst contained only one molecule of chiral ligand.



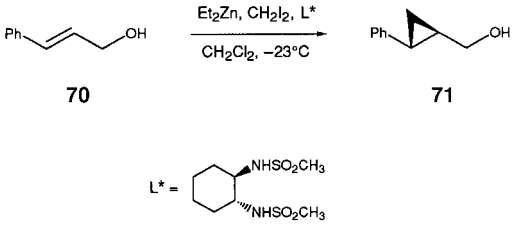
Scheme 10. Asymmetric oxidation of sulfide **66** with catalytic amounts (1 mol%) of a vanadium salt and a chiral iminoalcohol ligand.

Seebach et al., as part of their studies on the use of TADDOL-type ligands with titanium salts, were interested in probing the nature of the catalytic species that was involved in the [3+2] cycloaddition between **44** and the nitrone **68** to give **69** (Scheme 11).[66] The relationship between the *ee* value of the product and that of the chiral diol used to prepared the catalyst was strictly linear. This result was in sharp contrast with the (+)-NLE encountered with the same catalyst during a Diels–Alder reaction (Section 2.3.10, Figure 50).

Denmark and co-workers studied the cyclopropanation with a catalyst prepared from zinc salt and C_2-symmetrical disulfonamide (Scheme 12).[67] The use of this ligand in conjunction with bis(iodometyl)zinc permitted an enantioselective cyclopropanation of cinnamyl alcohol (**70**) to the corresponding carbocycle **71**. The relation between the *ee*'s of the ligand and the product was found to be perfectly linear. The authors interpreted these results as a consequence of only



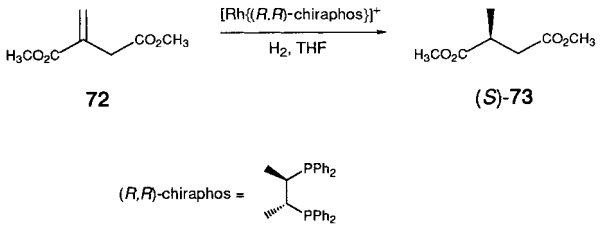
Scheme 11. [3+2] cycloaddition of **44** and **68** with a TADDOL–titanium catalyst (toluene, room temperature).



Scheme 12. Cyclopropanation of cinnamyl alcohol (**70**).

one molecule of ligand being present in the transition state responsible for the enantioselectivity, and that the stable species of all the ligand–zinc complexes is monomeric or dissociates with low activation energy.

Finally, Faller et al. reported the use of the NLE test to obtain information about the nature of the complexes implicated in some asymmetric hydrogenation reaction.[68a, 68b] The use of a cationic rhodium complex [Rh(norbornadiene)(chiraphos)]BF_4 in the hydrogenation of dimethyl itaconate (**72**) led to the corresponding methylsuccinate (*S*)-**73** in 98% *ee* (Scheme 13). When the chiraphos–rhodium complex



Scheme 13. Asymmetric hydrogenation of **72** with a rhodium catalyst (10 mol%).

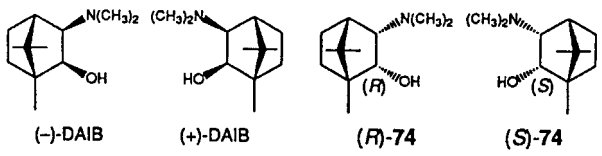
used had a 33% *ee*, the product **73** was obtained in 60% *ee*, which was indicative of a (+)-NLE. This effect was explained by the formation of dimeric species generated by the hydrogenation of [Rh(norbornadiene)(chiraphos)]BF_4 into $[\{Rh(chiraphos)\}_2]^{2+}$.[68c–e] Accordingly to this scenario, the use of enantiomerically impure chiraphos should generate homo and heterochiral dimeric species. The authors reported that ^{31}P NMR studies in nonpolar solvents showed that the heterochiral dimer was the more stable. The dissociation of the dimers to give the monomeric, catalytically active species in this case explained the positive nonlinear effect observed. Burgess and van der Donk found that the use of a chiral rhodium catalyst incorporating DIOP in hydroboration reactions led however to linearity (DIOP = 2,3-*O*-isopropylidene-2,3-dihydroxy-1,4-bis(diphenylphosphanyl)butane).[69]

The results presented in this Section demonstrate that the study of the presence or absence of NLE in a catalytic system can complete the usual analyses, and can even be used as the sole analysis when all the others fail to give some insights into the nature of the involved species. However, this was limited to catalysis on mixtures of enantiomers. The Sections to come will present the study of NLEs in different systems and the information that can be extracted by this method of analysis.

2.4. Diastereomeric Catalysts

One may assume that the phenomena that are at the origin of nonlinear effects when using a mixture of *enantiomers* of chiral auxiliary, will remain if the chiral auxiliary is now a mixture of *diastereomers*. This assumption means that some deviations are expected from the predictions of the *ee*'s of the product as a result of the diastereomeric composition.

Noyori et al. have studied the mechanism of asymmetric amplification with DAIB as the promoter of the chiral catalyst (Section 2.3.1).[32] They concluded that a quite stable *meso* dimer of DAIB–zinc alcoholate was at the origin of the strong (+)-NLE, because of the storage of some racemic DAIB (reservoir effect). Recently these authors studied the effect of various mixtures of (−)- or (+)-DAIB and the *endo* diastereomer (*R*)-**74** or (*S*)-**74**.[70] These two catalysts gave (*R*)- or (*S*)-alcohols **9** with 94% *ee* while (−)-DAIB provided (*S*)-alcohol with 98% *ee*. Noyori et al. also compared the



catalytic efficiency of these catalysts when enantiopure. Aminoalcohol **74** is 2.6 times more reactive as a promoter of the reaction than DAIB.

From the above data the authors computed the expected curves ee_{prod} as a function of the catalyst composition and initial rate v_0 as a function of the composition of the chiral auxiliary. They selected the mole equivalent amount (%) of one of the two components of the mixture as the chiral auxiliary composition. A curve and not a straight line was calculated for the relationship between ee_{prod} and the composition of the chiral auxiliary, but experimental data shows some significant departure to the calculated curve (Figure 55a).[71] The nonlinear effect is apparent for the mixture of (−)-DAIB with (*R*)-**74**, where the two individual catalysts generate alcohols of opposite absolute configuration. The catalysts prepared from (−)-DAIB or (*S*)-**74** gave alcohol (*S*)-**9** (see above) with similar rates of reaction. The mixture of these two catalysts showed almost perfect linearity for ee_{prod}. The formation of aggregates **10**, **76**, and **77**, with higher stability for the mixed dimer **76**, explains the above data (Figure 56). This was confirmed by measurements of the rates

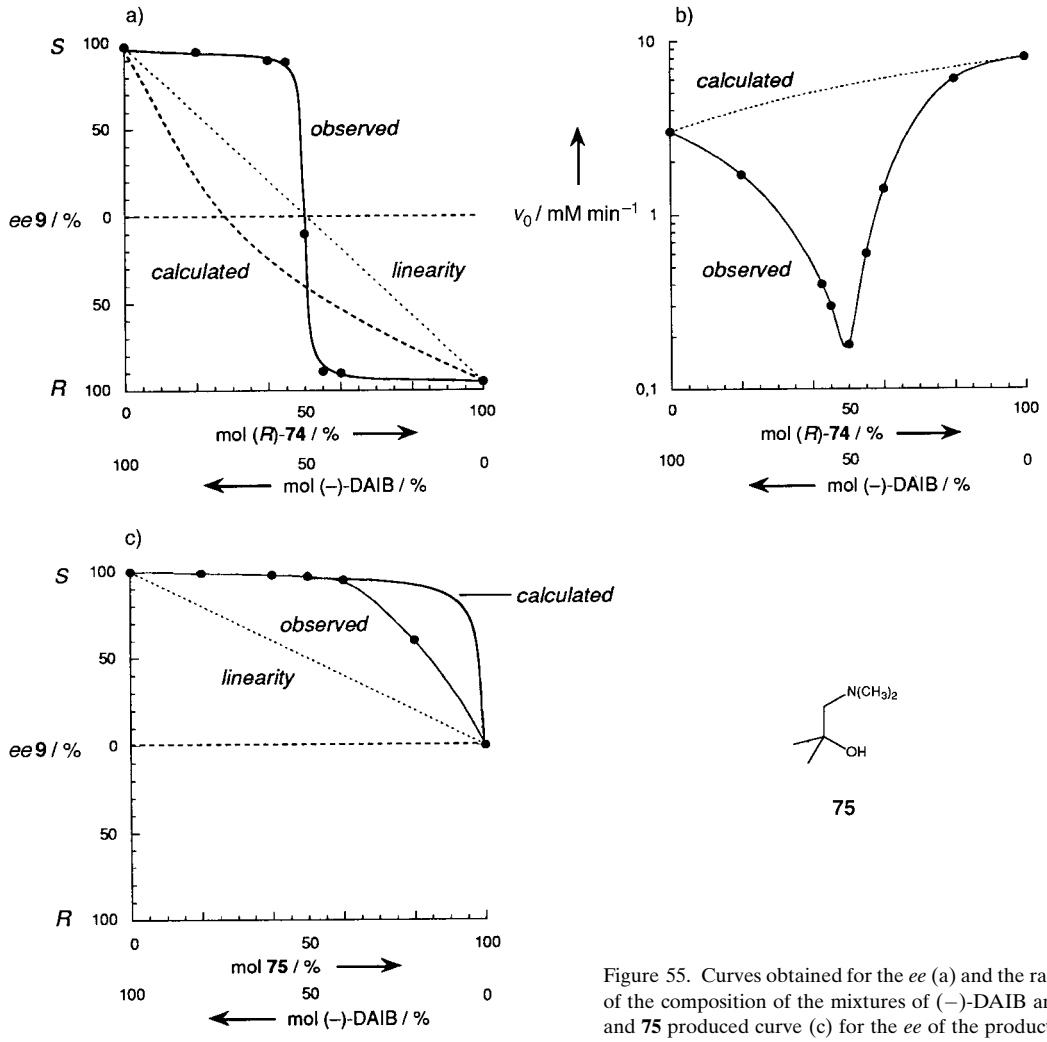


Figure 55. Curves obtained for the *ee* (a) and the rate of the reaction (b) as a function of the composition of the mixtures of (−)-DAIB and (*R*)-**74**. Mixtures of (−)-DAIB and **75** produced curve (c) for the *ee* of the product.

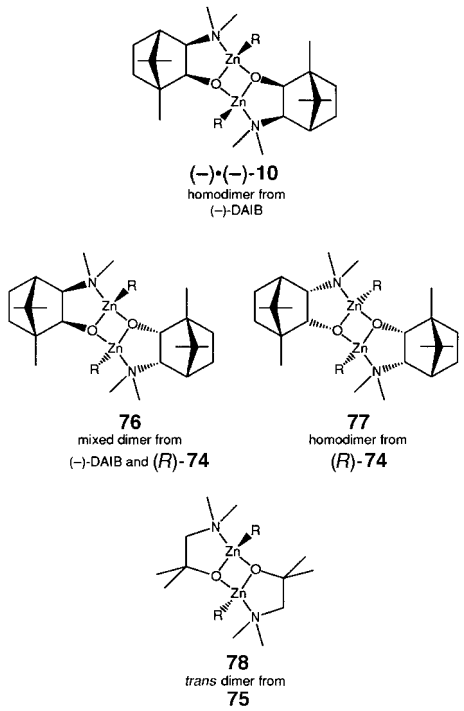


Figure 56. Some of the various dimers formed in the mixtures of DAIB and other aminoalcohols.

as a function of the catalyst composition. For example a mixture of (−)-DAIB and its diastereomer (*R*)-**74** showed a sharp minimum around a 1:1 composition, indicative of the preferred formation of heterodimer **76** of low reactivity (Figure 55b). In an additional experiment the enantioselectivity of (−)-DAIB in the presence of various amounts of the *achiral* β-aminoalcohol **75** was investigated (Figure 55c). The curve has been interpreted by the occurrence of *trans* dimer **78**, which is more stable than the *cis* dimer (not represented); which is itself more stable than homodimer **10**.

Kagan et al.[72] studied the Sharpless asymmetric dihydroxylation (AD)[73] of dibromostilbene (**79**) since several classes of diastereomeric ligands based on alkaloids are easily available. The *p*-chlorobenzoate of dihydroquinine (PCB–DHQ) gave (*S,S*)-diol **80** in 97% *ee*. The ligands of the second generation, namely phthalazine bisdihydroquinine (PHAL(DHQ)$_2$) and quinidine (PHAL(DHQD)$_2$) led to (*S,S*) and (*R,R*)-diols **80** in 98–99% *ee* in a faster reaction. Mixtures of PHAL(DHQ)$_2$ and PHAL(DHQD)$_2$ gave a curve very close to a straight line (Figure 57a), as expected from two pseudoenantiomeric ligands (similar reaction rates and similar enantioselectivities, but of opposite chirality). This experiment is in agreement with the reaction proceding through independent catalysts, and not through or involving a mixed

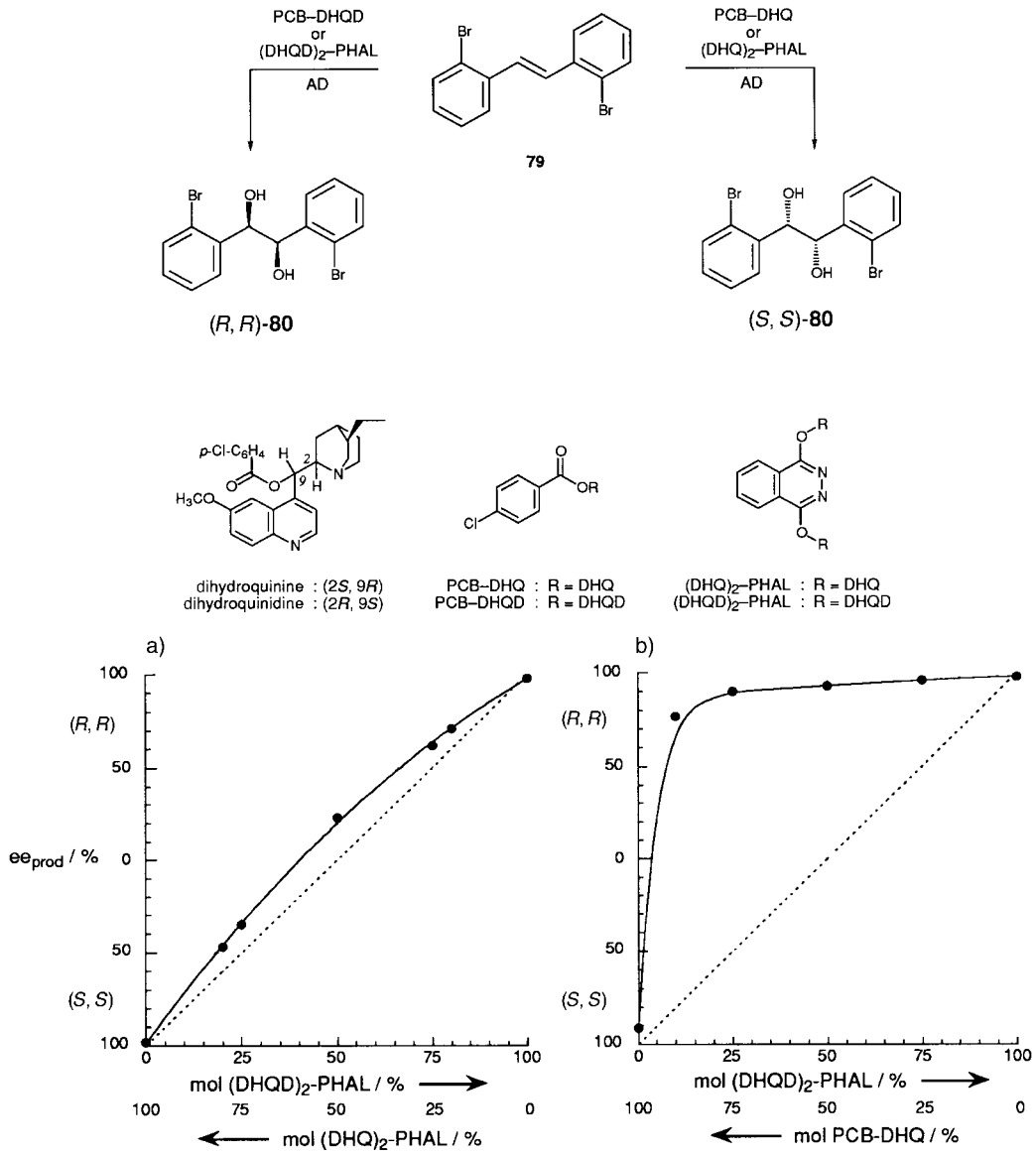
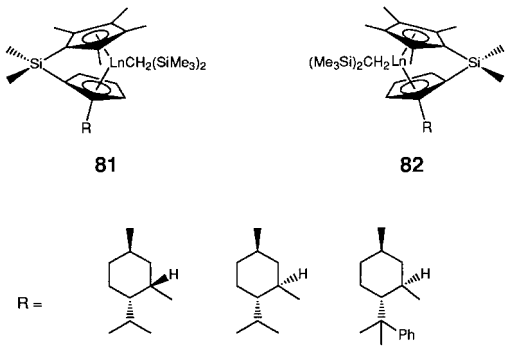


Figure 57. Curves of the *ee* of **80** obtained in the asymmetric dihydroxylation of **79** by mixing $(DHQD)_2PHAL$ with (a) $(DHQ)_2PHAL$ and (b) PCB–DHQ.

species. The mixture of PCB–DHQ and $PHAL(DHQD)_2$ gave a very strong nonlinear behavior (Figure 57b). This observation reflects the higher reactivity of the catalyst based on $PHAL(DHQD)_2$, presumably because of the larger affinity of this ligand (with respect to PCB–DHQ) towards OsO_4, as well as by the rate-acceleration given by the "chiral pocket mechanism" which has been established with the phthalazine ligands.[73]

Corey et al. evaluated the relative reactivities of some osmium catalysts, prepared from two different ligands derived from alkaloids, for AD.[74] They also used ligands (1:1 mixture) of opposite enantioselectivities in AD of styrene derivatives as a way to study these systems.

Marks et al. prepared diastereomeric chiral lanthanide complexes **81** and **82** as catalysts for the enantioselective hydrogenation of alkenes or hydroamination/cyclization of amino olefins.[75] Surprisingly the enantioselectivity in hydroamination reactions is insensitive to the metallocene chirality, since a 1:1 mixture of the two complexes gave the same ee_{prod} as diastereomerically pure **81**. This behavior has been



81 **82**

explained by epimerization around the lanthanide center (equilibrium of decomplexation and complexation during the reaction). In the hydrogenation of 2-phenyl-1-butene there is a significant difference between of **81** and **82**, in both rates and enantioselectivities. The 1:1 mixture of the two complexes gives rates and ee_{prod} that are very close to the calculated values. Obviously there are no NLE effects with these catalysts that act independently from each other.

2.5. Autocatalytic Systems

The reactions where a compound catalyzes its own formation were considered for a long time as important in prebiotic chemistry. They are of special interest in the generation and propagation of optical activity on earth.[76, 77] In the ideal case where a chiral compound (100% *ee*) replicates with 100% *ee* one may consider that the problem is solved. Actually the most efficient chiral catalysts presently known seldom reach enantioselectivities higher than 99.9% *ee* (enantiomer ratio: *er* = 1999). These spectacular levels of efficiency are however unsatisfactory for the large scale production of chiral compounds by asymmetric autocatalysis. This is easily demonstrated by considering a simplified description of an asymmetric catalysis (Figure 58) where the

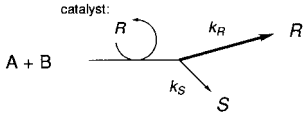


Figure 58. The asymmetric autocatalysis process.

two enantiomeric products *R* and *S* are derived from a chiral catalyst *R* (100% *ee*). A rough computation may be done by an iterative process.

If the rate ratio k_R/k_S is high (1999) 1 mol equivalent of the product (by respect to catalyst) will be considered to be formed after one catalytic cycle with *ee* = 99.9% (*er* = 1999). After mixing this product with 1 mole equivalent of the initial *R* catalyst (*ee* = 100%, *er* = ∞) one ends up with 2 mole equivalent (*ee* = 99.95%, *er* = 3999). The next catalytic cycle will provide 4 mole equivalents of catalyst (*ee* = 99.85%, *er* = 1337). There is an endless erosion of the enantiomeric excess of the product which ineluctably will accumulate in a large amount, but in racemic composition.

Kinetics models have been proposed to overcome the above inherent tendency of *ee* degradation in asymmetric autocatalysis. Frank[76] first described a simple model where each enantiomer catalyzes its own formation but is competitively deactivated by interaction with the enantiomer of opposite configuration (Figure 59). In this model complete

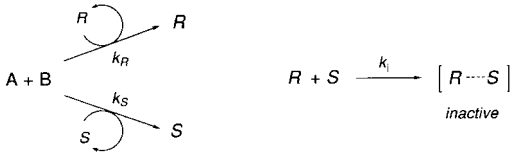
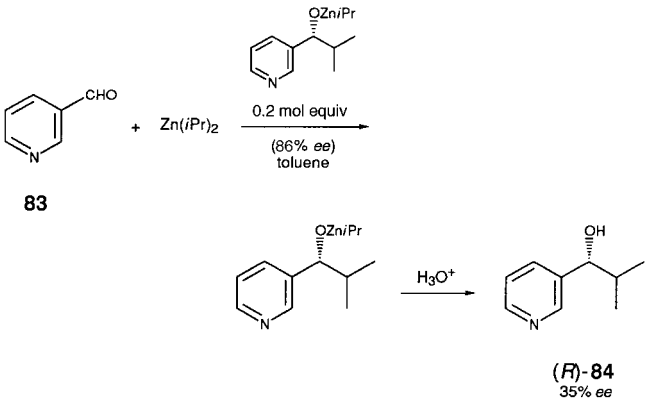


Figure 59. Frank's model with deactivation by dimerization.

enantioselectivity is assumed during the catalysis by the *R* or *S* enantiomer. The initial *R/S* enantiomeric ratio of the catalyst (close to 1) is amplified because of the autocatalysis (which ensures the growth of the amount of catalyst), which is combined to a continuous removal of a racemic material. In conclusion asymmetric autocatalysis from a small amount of enantiopure catalyst has no chance of propagating molecular chirality on a large scale unless it is sustained by additional reactions (such as the mutual inhibition of enantiomers in the Frank model). The situation is even worse if the initial catalyst is of low enantiomeric excess.

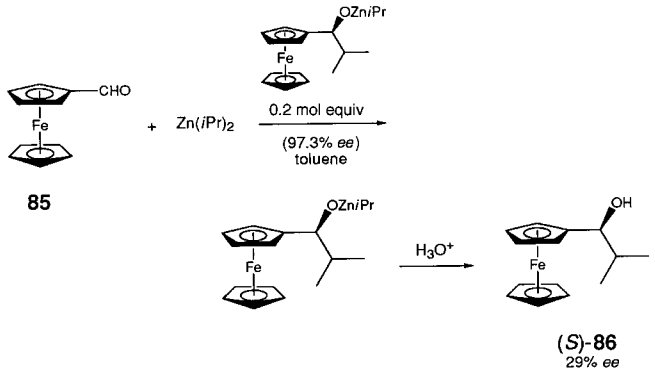
In that context a (+)-NLE superposed onto the autocatalytic reaction could be a convenient way to both amplify the initial *ee* value and to maintain it at a high level through the whole course of the autocatalytic reaction. There are quite a few identified asymmetric autocatalytic reactions.[78] Addition of a dialkylzinc compound to aromatic aminoaldehydes was the reaction pioneered by Soai et al. in the search of autocatalytic systems. In 1990 they discovered that pyridyl alcohol **84** is able to catalyze asymmetrically its own formation (Scheme 14).[80] The important point is that (*R*)-alcohol **84** (86% *ee*) catalyzes formation of (*R*)-**84**, although with a low enantioselectivity (35% *ee*, calculated by removal of the contribution of the initial catalyst).



Scheme 14. Autocatalysis in the addition of diisopropylzinc to pyridine-3-carbaldehyde (**83**).

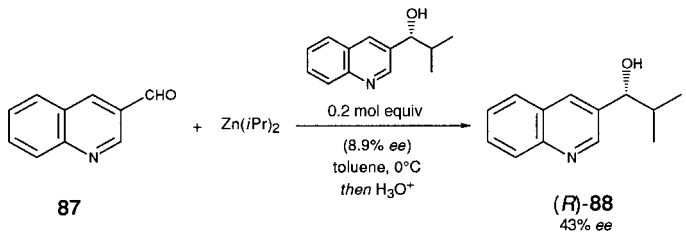
Subsequent investigations of Soai et al. on various types of aromatic aldehydes allowed the *ee* value of the product to be increased, which was also obtained with the same absolute configuration as the initiator. Ferrocene carboxaldehyde (**85**, Scheme 15) and diisopropylzinc in the presence of 0.2 mol equivalent of alcohol (*S*)-**86** (97.3% *ee*) gave 4.75 times more alcohol (*S*)-**86** (29% *ee*).[81]

A significant improvement was made recently in the reaction of quinoline-3-carboxaldehyde (**87**) with diisopropyl



Scheme 15. Autocatalysis in the addition of diisopropylzinc to ferrocene-carbaldehyde (**85**).

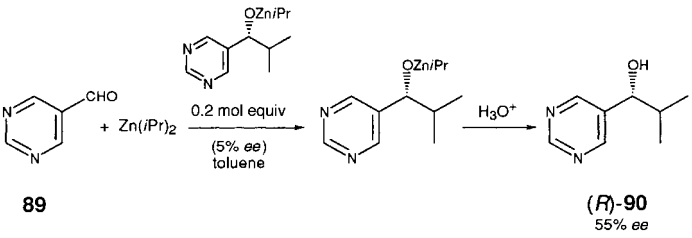
zinc catalyzed by alcohol (*R*)-**88** (Scheme 16).[82] By optimization of the experimental conditions (1.2 mol equivalent of $Zn(iPr)_2$ instead of 2 mol equiv, a proper dilution to give a



Scheme 16. Autocatalysis in the addition of diisopropylzinc to quinoline-3-carbaldehyde (**87**).

4 mM concentration of the initial catalyst) it was discovered that **88** (93.6 % *ee*) replicates 3.2 times into **88** (89.7 % *ee*).[83a] These experimental conditions were selected to study the influence of the initial *ee* value of **88** on the *ee* value of the additional **88** produced; in this particular case there is a strong (+)-NLE. For example 8.9 % *ee* of **88** generates 2.8 times more **88** (43.3 % *ee*).

A further investigation has been conducted by using 5-pyrimidyl carboxaldehyde (**89**) and the alcohol **90** (Scheme 17).[84] Even with an initial *ee* of 2 % for the **90**

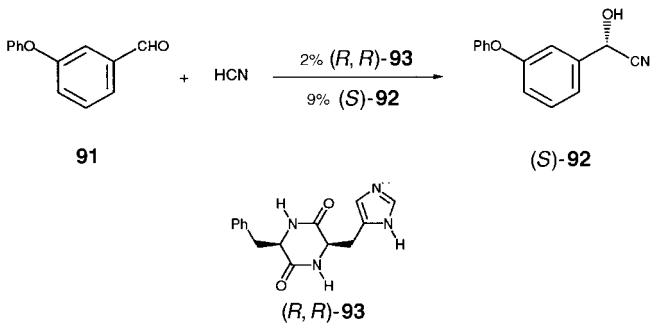


Scheme 17. Autocatalysis in the addition of diisopropylzinc to pyrimidyl-5-carbaldehyde (**89**).

formed, a plot of the *ee* value of newly formed **90** (ee_{prod}) versus the *ee* of the starting catalyst **90** (ee_{aux}) showed a typical (+)-NLE, with a strong amplification. The authors also made a correlation between their experimental data by taking the enantiomer ratios instead of the *ee*'s as parameters.[85] The above experiments have been performed by taking an initial catalyst of low *ee* and reusing the resulting product (with amplified *ee*) as a catalyst in a new reaction. By such a cycle of reactions the authors could use a sample of 2 % *ee* and reached a level of 88 % *ee* in five consecutive cycles. When the same procedure was applied to quinoline carboxaldehyde (**87**), by using the alcohol **88** with an initial 8.9 % *ee*, the enantiomeric excess obtained for (*R*)-**88** at the end of the cycle was 88 % as well (Scheme 16).[83a] A one-pot asymmetric autocatalytic reaction with a remarkable amplification (from 0.2 % *ee* to 90 % *ee*) was obtained recently in the formation of **90** by a special experimental procedure.[83b]

A catalytic enantioselective autoinductive reaction is a process that may be of interest to propagate high *ee*'s. This process is based on stereoselective reactions in which the products initially formed may influence the stereoselectivity of the proceding reaction (catalytic or stoichiometric). Albert and Wynberg coined the expression "enantioselective" autoinduction during their studies of a stoichiometric enantioselective reaction.[88]

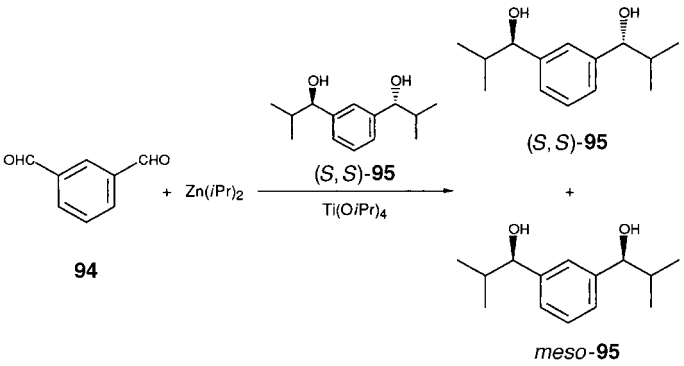
The first example of enantioselective autoinduction in a catalytic reaction seems to be the report of Danda et al.[89] on the formation of cyanhydrine in the presence of small amounts of cyclic dipeptide **93** (Scheme 18). The authors



Scheme 18. Autoinduction in cyanohydrine formation in the presence of a cyclic dipeptide (**93**) (toluene, 5 °C).

found that the initial catalyst **93** is replaced in situ by the combination of **93** with product **92**. This has been established by adding a small amount of (*S*)-**92** with high *ee* value to the cyclic dipeptide **93** (enantiopure or of small *ee* value) at the beginning of the reaction. It is the enantiomeric purity of (*S*)-**92** that is the stereocontrolling factor on the catalytic production of cyanohydrine (*S*)-**92**. For example, in a given set of experimental conditions 0.022 mol equivalent of catalyst (*R,R*)-**93** (2 % *ee*) gave product (*S*)-**92** (81.6 % *ee*) in 43 % yield from the corresponding aldehyde **91**. The initially added (*S*)-**92** acts as a chiral co-catalyst. Interestingly, the catalyst prepared from **93** (66.8 % *ee*) and (*S*)-**92** (92.0 % *ee*) was able to generate (*S*)-**92** in 89 % yield with 96.0 % *ee* (which is higher than the *ee* of both components of the catalyst). The mechanistic details of the reaction, which works in heterogeneous conditions as a gel are not well understood, several mechanisms have been proposed.[90]

Soai et al. recently studied a catalytic enantioselective reaction with autoinduction in the particular case of addition of diisopropylzinc on an aromatic dialdehyde **94** (Scheme 19).[91] The catalyst is a chiral titanium complex



Scheme 19. Autoinduction in the double addition of diisopropylzinc with **94**.

presumably with a 1:2 stoichiometry, formed from the combination of $Ti(OiPr)_4$ with the chiral diol **95**. This chiral catalyst is different from the chiral zinc alkoxide which is derived from **95**, hence the expression "autoinduction". Here again the absolute configuration of the product **95** is the same as for the initiator **95** engaged in the catalyst. Unfortunately the product is obtained in lower *ee* value (30% *ee*) than the initial *ee* value of **95** (>99% *ee*), together with a large amount of *meso* diol.[92]

In conclusion asymmetric autocatalysis seems to be a promising area of investigation, as stated earlier by Wynberg.[93] The possibility of asymmetric amplification has been well established recently[84] and seems a consequence of the intervention of positive nonlinear effects (most presumably by a reservoir effect, see Section 2.2).[94]

3. Stoichiometric Asymmetric Synthesis

3.1. Principles

A chiral reagent may be prepared by modification of an achiral reagent with a chiral auxiliary X_c that will be bound covalently (**96**) or not (**97**) to the reagent Y (Figure 60). A

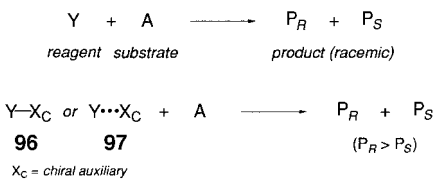


Figure 60. Formation of covalently bound (**96**) or associated (**97**) species in noncatalyzed asymmetric synthesis.

chiral silane R^*_3SiH (R^* = chiral group) or the combination *sec*-BuLi, sparteine (for asymmetric deprotonation) are examples of chiral reagents of type **96** ($Y{-}X_c$) or **97** ($Y\cdots X_c$).

Two basic situations are described in Figure 61. In the first case reagent $Y{-}X_c$ (**96**) is transformed into an inert by-

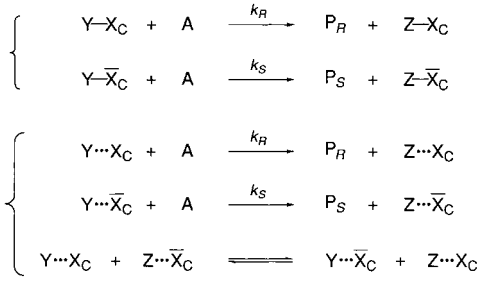


Figure 61. Two possible pathways in the noncatalyzed asymmetric synthesis. Xc and $\bar{X}_c$ = chiral intermediates of opposite configuration, Z = reagent that replaces Y.

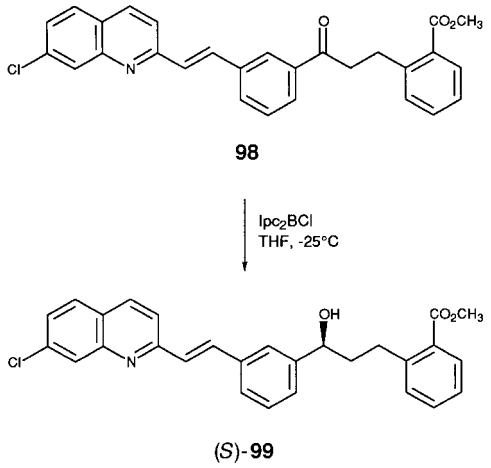
product $Z{-}X_c$, the auxiliary is then removed from the reaction simultaneously to the formation of the product. When reagent $Y\cdots X_c$ (**97**) is used it may behave as above if the by-products $Z\cdots X_c$ and $Z\cdots \bar{X}_c$ retain their structures and do not exchange the X_c and $\bar{X}_c$ fragments with the reagents. If there are some exchanges of these groups (for example, as chiral ligands of some organometallic compounds) one may end up in the situation of asymmetric catalysis where there is a fast exchange of ligands (see Section 2). The enantioselectivity of the reaction must be independent of the conversion, with or without NLE that arises from the the number of X_c groups around Y, and of the relative reactivities of the diastereomeric species. One expects the same general behavior and the same models as discussed in Section 2.

The covalent reagent **96** gives a different scenario. If it involves only one X_c group the initial enantiomer ratio will remain constant during the course of the reaction and no NLE will appear. If this reagent gives rise to some aggregation one finds again the general features discussed for catalytic reactions (Section 2), some diastereomeric aggregates may be unreactive and the reaction will proceed through a monomeric reagent or a given diastereomer. NLE will be produced by a reservoir effect or through the $(ML)_n$ model.[96] The nonlinear effect will depend on conversion because the enantiomeric composition of the reagent should change if diastereomeric aggregates are of different reactivities. For example, if an heterochiral dimer is less reactive, the reaction will start with a (+)-NLE and in the latter stages of the reaction it will very much slow down with the generation of the racemic product. A constant (+)-NLE is expected if a large excess of reagent (in respect to substrate) is used. A reactive heterodimer will provide a strong (−)-NLE, and an excess of reagent will enhance this trend.

A special case, which is worth mentioning, is the use of a chiral reagent obtained by the permanent linking of two chiral fragments X_c to the achiral reagent Y. If the enantiopure reagent $Y(X_c)_2$, or $Y(\bar{X}_c)_2$, or the mixture of these enantiomeric reagents can be used in asymmetric synthesis, one would expect perfect linearity (unless aggregation occurs). However if the chiral reagent is prepared by the reaction of a mixture of X_c and $\bar{X}_c$ with Y there is the possibility that some heterochiral reagent $Y(X_c)(\bar{X}_c)$ will be generated. We then have a mixture of diastereomeric reagents in which the more reactive diastereomer has a chance to operate during part of the reaction, and provide an invariant NLE.

3.2. Asymmetric Reaction of Boron Compounds

Until now there were very few experimental data on NLE in stoichiometric asymmetric synthesis. One of the first examples seems to be an asymmetric synthesis at Merck in 1994 of an alcohol, which is a useful intermediate in the synthesis of a LTD_4 antagonist.[98, 99] It was found that Ipc_2BCl, prepared from (−)-α-pinene and BH_2Cl, reduced the ketone **98** to give alcohol **99** in 97% *ee* or 95% *ee* with (+)-α-pinene of 98% *ee* or 70% *ee* (Figure 62). It was hypothesized that three reagents (two homochiral and one *meso*) are in statistical distribution, with the *meso* borane being very sluggish to react. More recently the authors studied in detail the relationships between the *ee* value of the alcohol **99** and the *ee* value of the α-pinene (Figure 62). There is a good agreement between the calculated curve and experimental data, when the hypothesis of a statistical distribution and an



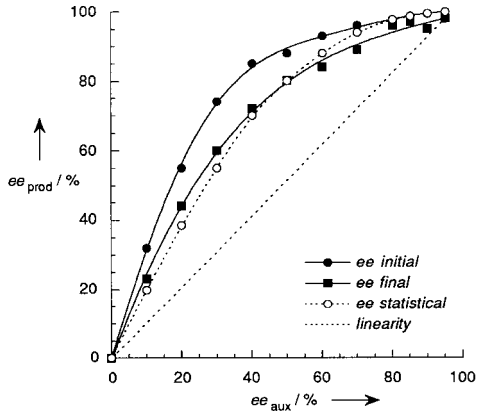
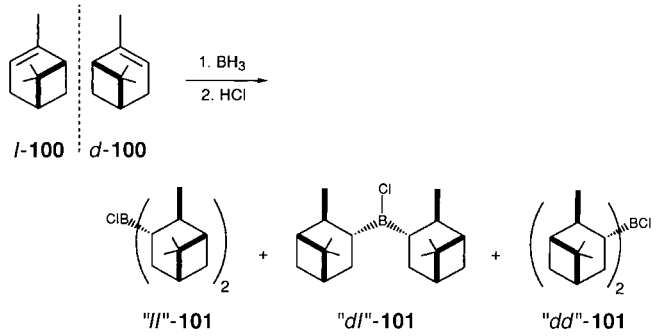


Figure 62. (+)-NLE in Ipc_2BCl reduction of the ketone **98**. Ipc = isopinocampheyl.

unreactive *meso* Ipc_2BCl is employed.[99] However, a quite large deviation has been observed at low conversion giving a higher *ee* value of **99** than after complete reduction.

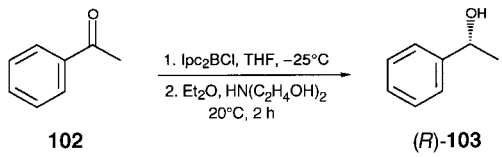
In 1995 Kagan and Girard studied the asymmetric reduction of acetophenone by Ipc_2BCl (4 equiv) by using a reagent derived from (−)-α-pinene (**100**).[100] Ipc_2BCl was prepared according to the procedure of Brown and Joshi.[101] The way the reagent was synthesized was very important for the outcome of the reduction of acetophenone (**102**, Scheme 20). The separate preparation of Ipc_2BCl (**101**) from enantiopure α-pinenes gave "*ll*"-**101** and "*dd*"-**101**, which were then mixed in various amounts to reach the desired ee_{aux}. The other procedure starts from a mixture of (−)- and (+)-α-pinene in the required *ee*'s



Scheme 20. Homochiral ("*ll*"- and "*dd*"-**101**) and heterochiral ("*dl*"-**101**) reagents generated during the formation of Ipc_2BCl (**101**).

(*l*- and *d*-**100**) to give rise to the formation of three boranes: "*ll*"-**101,** "*dd*"-**101** and "*dl*"-**101.** The first procedure gave perfect linearity between ee_{aux} and ee_{prod} (Figure 63a), while the second method generated a strong (+)-NLE, the asymmetric amplification being especially good above 30% *ee* for α-pinene (Figure 63b). The linear relationship indicates that each of the enantiomeric reagents acts independently in the reduction process. The (+)-NLE is in agreement with a very low reactivity of the *meso* reagent "*dl*"-**101**, which is presumably formed in quite a large amount.

As an added proof, the recent study by the Merck group demonstrated that the *ee* value of their reduction product was time-dependent.[102] The NLE was indeed more pronounced at lower conversion than after completion of the reaction. The curves however keep the same shape during the course of the reduction; which is close to the calculated curve based on a statistical distribution of the pinene on the boron atom. Kagan and Girard also presented another study where the stoichiometry of Ipc_2BCl (**101**) was varied from one to four equivalents.[103] The curves had the same shape, but the NLE increased with the amount of reductant used. These complementary results suggest that a higher *ee* value at the beginning



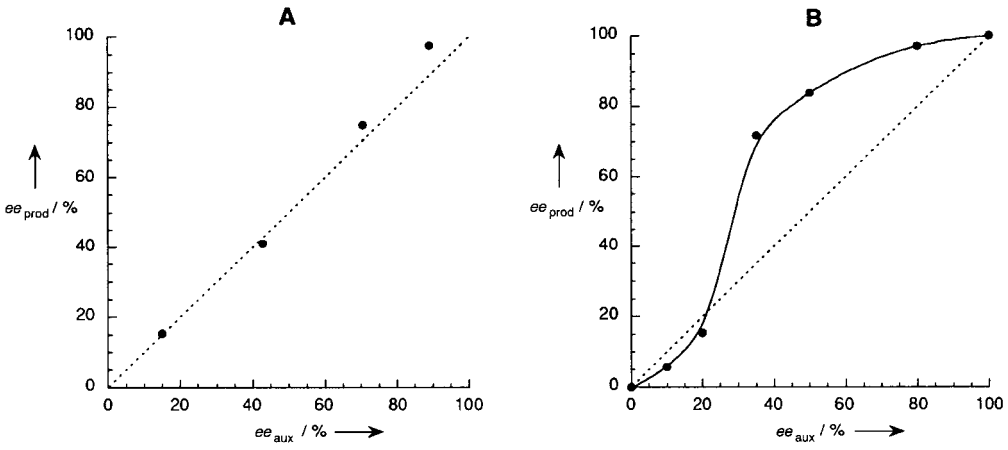


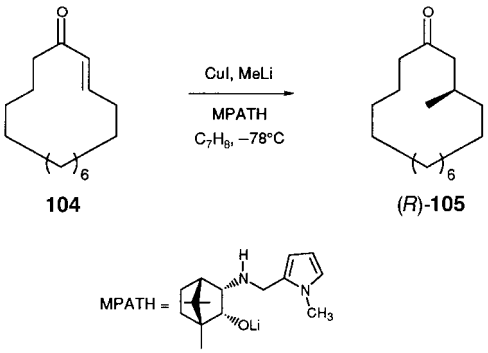
Figure 63. Variation in the *ee* value of (*R*)-**103** with the *ee* value of α-pinene (see text for further details).

of the reaction will be provided by the more reactive homochiral species or by the use of a larger quantity of reagent. But as soon as the amount of this species drops, with time or by using less reagent, the "unreacting" heterochiral borane becomes involved in the reduction, which lowers slightly the *ee* value of the product.

Apart from mechanistic interest, the possibility of creating a strong (+)-NLE in Ipc_2BCl reductions allows the expensive enantiopure α-pinene to be avoided, and instead cheaper α-pinene of *ee*'s lower than 90% can be used.[98, 99]

3.3. Cuprate Addition

Tanaka et al. studied an asymmetric synthesis of muscone **105** by the 1,4-addition of a methylcuprate complexed by the chiral bidentate ligand MPATH to the enone **104**.[104] An interesting NLE was observed, the data given in the paper allows to draw a two-shaped curve (Figure 64). The authors



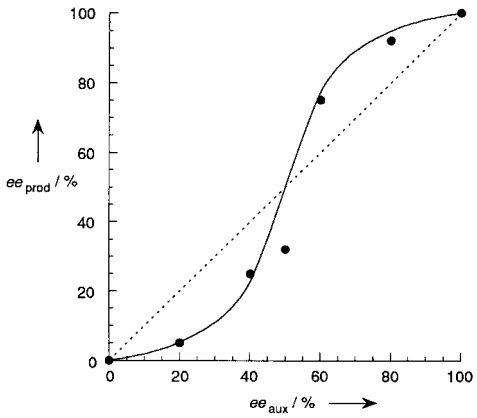
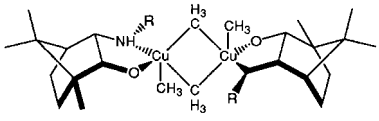


Figure 64. Two-shaped NLE curve observed in the synthesis of muscone (**105**) from **104**.

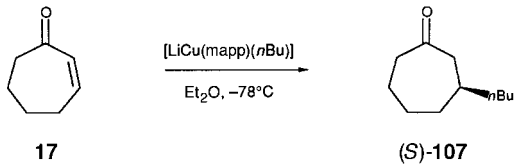
postulated the formation of dimeric species such as **106**. The curve was accurately reproduced by using the $(ML)_4$ model,



106

which could mean the involvement of an aggregation of dimers.[31]

Rossiter et al. observed a (+)-NLE in the asymmetric addition of a *n*-butylcuprate to 2-cycloheptenone (**17**) by using the lithium salt of an aminoalcohol chiral ligand, (*S*)-mapp (Figure 65).[105] The authors assumed a statistical



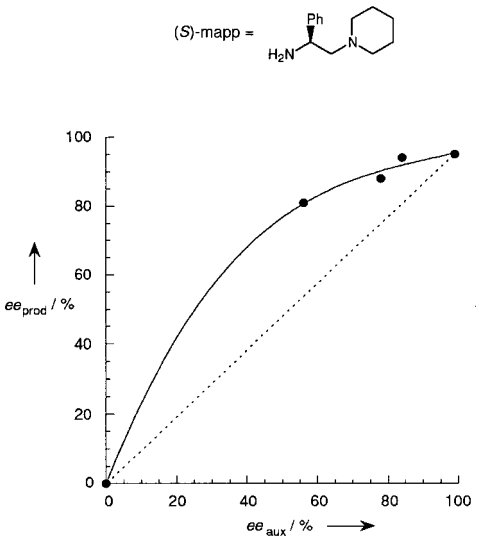
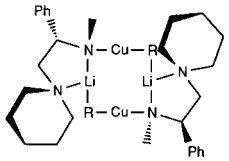


Figure 65. (+)-NLE observed in the mapp-catalyzed cuprate addition to **17**.

distribution of ligands into dimers such as the unreactive *meso* dimer **108**. Calculations are in good agreement with these hypotheses. For example, enantiopure ligand in this case gave 96% *ee* of product, while the (*S*)-MAPP at 56% *ee* provided a product with 81% *ee* (instead of 54% *ee* for linearity and 81.9% *ee* calculated with the above hypotheses). When the reaction was performed in diethyl ether with additives such as HMPA or solvents such as THF, which break the dimeric structure by lithium solvation, suppression of the enantioselectivity, presumably by generation of non-enantioselective monomers, was observed (HMPA = hexamethylphosphoramide). The cases of 1,4-additions of Grignard reagents in the presence of catalytic amounts of chiral copper complexes were discussed in Section 2.3.3.

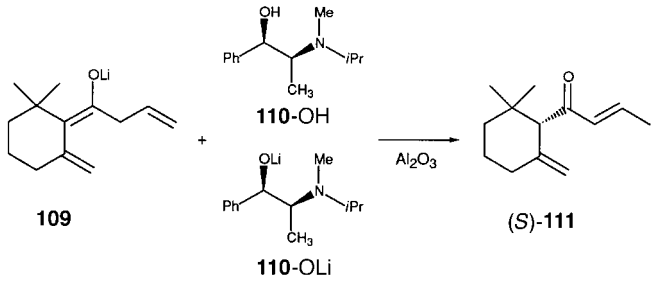


108

3.4. Asymmetric Protonation

A (+)-NLE has been observed in the asymmetric protonation of a lithium enolate **109** to (*S*)-γ-damascone ((*S*)-**111**)

by a 1:2 mixture of the amino alcohol **110**-OH and its corresponding lithium alkoxide **110**-OLi (Scheme 21).[106] The use of an enantiopure protonating agent (100% *ee*) gave the product **111** with 75% *ee*, while the use of 50% *ee* mixture of



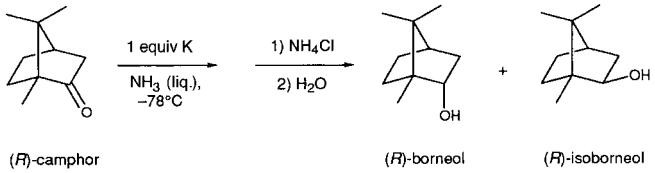
Scheme 21. Asymmetric protonation of **110** to (*S*)-γ-damascone (**111**).

110 gave the product with the same 50% enantiomeric excess. The chiral protonating agent was proposed to form a complicated and dimeric structure, which is in agreement with the observed nonlinear effect prevailing in the present case.

4. Diastereoselective Reactions

In this section the reactions of chiral substrates that give rise to isolable diastereomers are considered. The reactions may be realized with an achiral or a chiral reagent, or with a chiral catalyst. If during the course of the reaction some aggregation occurs it may generate perturbations, as observed in enantioselective reactions. These perturbations should be reflected by nonlinearities between the diastereomeric excess and the *ee* value of the substrate or the reagent. Until now there were very few reports in that area. Wynberg and Feringa discovered that the $LiAlH_4$ reduction of racemic or enantiopure camphor gave different values for the isoborneol/borneol ratio[16] (see Section 1) but there were no data with camphor of intermediate *ee*'s, and then no knowledge of the variation of *de* of the product with the *ee* of the camphor.

Rautenstrauch et al. carefully investigated the reduction of camphor by potassium in liquid ammonia (Scheme 22).[107] They looked at the diastereomeric composition of the resulting alcohols (*dc*, percentage of the major



Scheme 22. Reduction of (*R*)-camphor by potassium in liquid ammonia.

diastereomer) as a function of the enantiomeric composition (*ec*, percentage of the major enantiomer) of camphor. Surprisingly, borneol is the major product when one starts from racemic camphor, while borneol slightly predominates if enantiopure camphor is the starting material.

In Figure 66 the *dc* of the alcohol versus *ec* of the camphor is shown. It is easy to establish that the relationships $de_{product} = EE_0 ee_{substrate}$ and $dc_{product} = EC_0 ec_{Substrate}$ are equivalent (EE_0 and EC_0 are the enantiomeric excess or the enantiomeric composition of the major alcohol derived from reduction of an enantiopure substrate).[108] There is almost a linear behavior for the diastereoselectivity of the reaction (Figure 66a), while a strong nonlinear effect has been

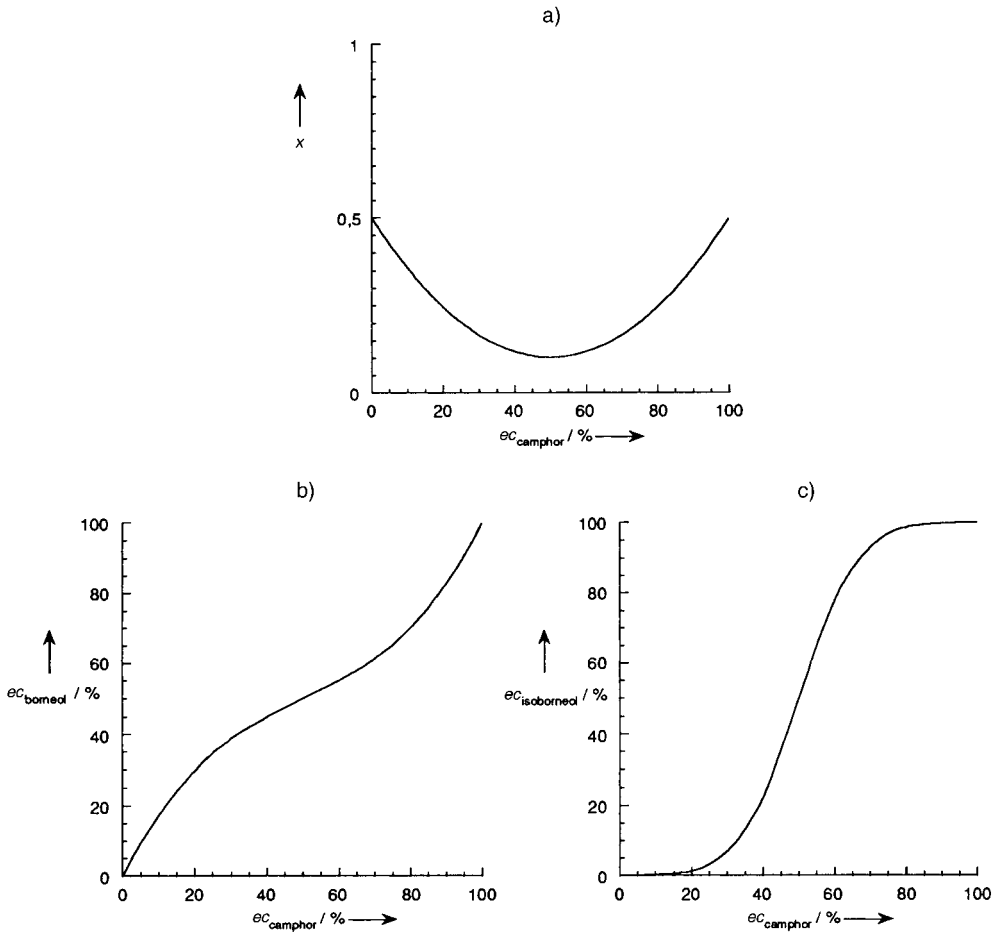
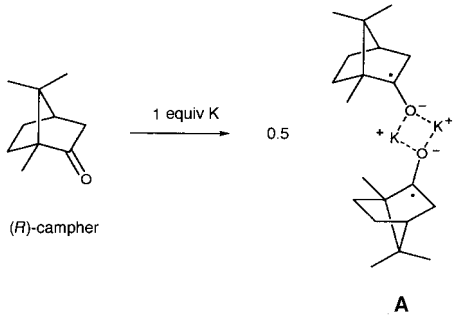


Figure 66. a) Mole fraction *x* of isoborneol and also the *ec* of b) borneol and c) isoborneol as functions of the enantiomeric composition of camphor.

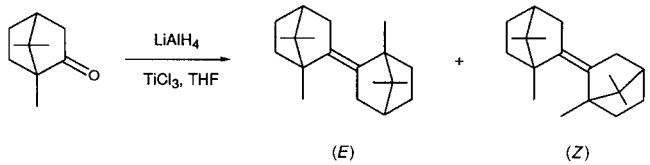
observed for the enantiomeric composition of borneol or isoborneol (Figures 6b, c). These observations have been explained by a mechanism that involves the initial formation of a ketyl anion radical (as a dimeric species). Experimental results have shown that hydrogen transfers between two dimers **A** provide (after hydrolysis) equimolar amounts of alcohols and camphor (Scheme 23). A kinetic analysis of the



Scheme 23. The dimeric diastereomeric species **A** formed during the reduction of camphor.

results is in agreement with the reaction being fourth order in camphor (second order in respect to the dimers **A**). This analysis highlights the importance of associations of lithio species for stereochemical controls. The key factor that explains the deviation from linearity is the formation of diastereomeric species **A**, which give rise to new routes in the subsequent disproportionations into products.

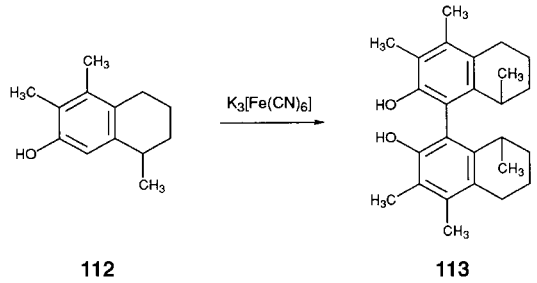
The self-coupling reaction may give different products if the reactant is enantiopure or a mixture of enantiomers (homochiral or a mixture of homochiral and heterochiral coupling products are formed, respectively). Moreover the coupling reaction may create a new stereochemical unit (*E*/*Z*, *R*/*S*, *P*/*M*). It is this situation that has been investigated by Wynberg and Feringa in the case of McMurry coupling of camphor and the *ortho*-coupling of phenols with an asymmetric center[16] (Scheme 24). These reactions were only



Scheme 24. McMurry coupling of camphor.

performed for 100% *ee* or 0% *ee*, and showed some stereochemical differences according to the initial *ee* value. For example, the McMurry coupling of enantiopure camphor gave homochiral dimers ($E/Z = 1.68$). McMurry coupling of racemic camphor provided homochiral dimers ($E/Z = 1.67$) and heterochiral dimers ($E/Z = 2.9$) in a ratio of 1.8:1

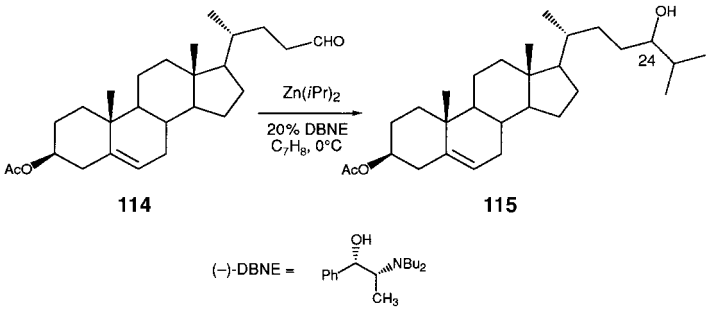
The oxidative coupling of enantiopure (*S*)-phenol **112** (Scheme 25) led to only one (>97.5%) configuration for the new atropoisomeric unit **113** (*P*), while the coupling of racemic **112** gave the following distribution of **113**: (*S*,*S*,*P*) + (*R*,*R*,*M*)/(*S*,*S*,*M*) + (*R*,*R*,*P*)/(*R*,*S*,*P*) + (*R*,*S*,*M*) in the relative



Scheme 25. Oxidative coupling of a phenol derivative **112**.

ratio of 66.0:7.9:26.1. In the above reactions, as well as in the reduction of camphor by $LiAlH_4$, it would be of interest to follow the various diastereoselectivities as a function of the enantiomeric excess of the substrate.

The condensation of a reagent (chiral or not) with a chiral substrate with the creation of an asymmetric center may also give rise to nonlinear effects if there is an external chiral auxiliary (in stoichiometric or catalytic amounts). A reagent control has been observed by Tanaka et al. in the catalyzed addition of diisopropylzinc on the steroid **114** (Scheme 26).[109]



Scheme 26. DBNE-catalyzed addition of diisopropylzinc to the steroid **114**.

The chiral catalyst (a β-aminoalcohol of various *ee*'s) controls the configuration at C_{24}. The diastereoselectivity of the reaction is not proportional to ee_{aux}. The catalyst (−)-DBNE (100% or 21% *ee*) gave a product **115** with 24-(*R*) configuration (97.0% *de* in both cases) while with (+)-DBNE (100%) the (*S*)-product **115** (87% *de*) was obtained. These data are indicative of a positive nonlinear effect (asymmetric amplification) under reagent control.[110]

5. Summary and Outlook

In only a ten year period nonlinear effects have established themselves as an ubiquitous phenomenon in asymmetric reactions, especially in enantioselective catalysis. It provides a simple and additional tool to detect and to discuss aggregation and self-assemblies that may arise in given reactions. The generation of diastereomeric species is the key feature that gives deviation from linearity. Asymmetric amplification characterizes a (+)-NLE and is a useful property for a reacting system since enantioselectivity is higher than expected, which allows the convenient use in some cases of

enantiomerically impure chiral auxiliaries. It also paves the way to the possibility to build some autocatalytic systems with autoinduction. These systems could be synthetically useful or could suggest additional models for prebiotic generation of optical activity on earth.

The presence or not of nonlinear effects may depend of the experimental conditions in the preparation of the chiral catalyst or reagent. This may also enlighten some aspects of the reaction. The basic concepts, which are the roots of the nonlinear effects in enantioselective reactions, should apply as well to kinetic resolution[47b, 111] and diastereoselective reactions, for example in the creation of a new asymmetric center in enantiopure substrates under the influence of a chiral catalyst. The diastereoselectivity of the reaction may be influenced by the enantiomeric excess of the catalyst with a deviation from linearity. The burgeoning of the reports on NLEs for a wide range of reactions show how useful this concept is, and how it provides a kind of specific signature to a given process. One may anticipate that new developments will continue to accumulate in the near future.

Funds provided by the Centre National de la Recherche Scientifique de France and Institut Universitaire de France are greatly acknowledged. C.G. wants to thank the Ministère des Affaires Étrangères de France and the Ambassade de France au Canada for the Chateaubriand fellowship, which made his post-doctoral stay possible.

The curves, schemes, and molecular structures presented here are redrawn as accurately as possible from the original papers cited in this article.

Received: July 18, 1997 [A 245 IE]
German version: *Angew. Chem.* **1998**, *110*, 3088 – 3127

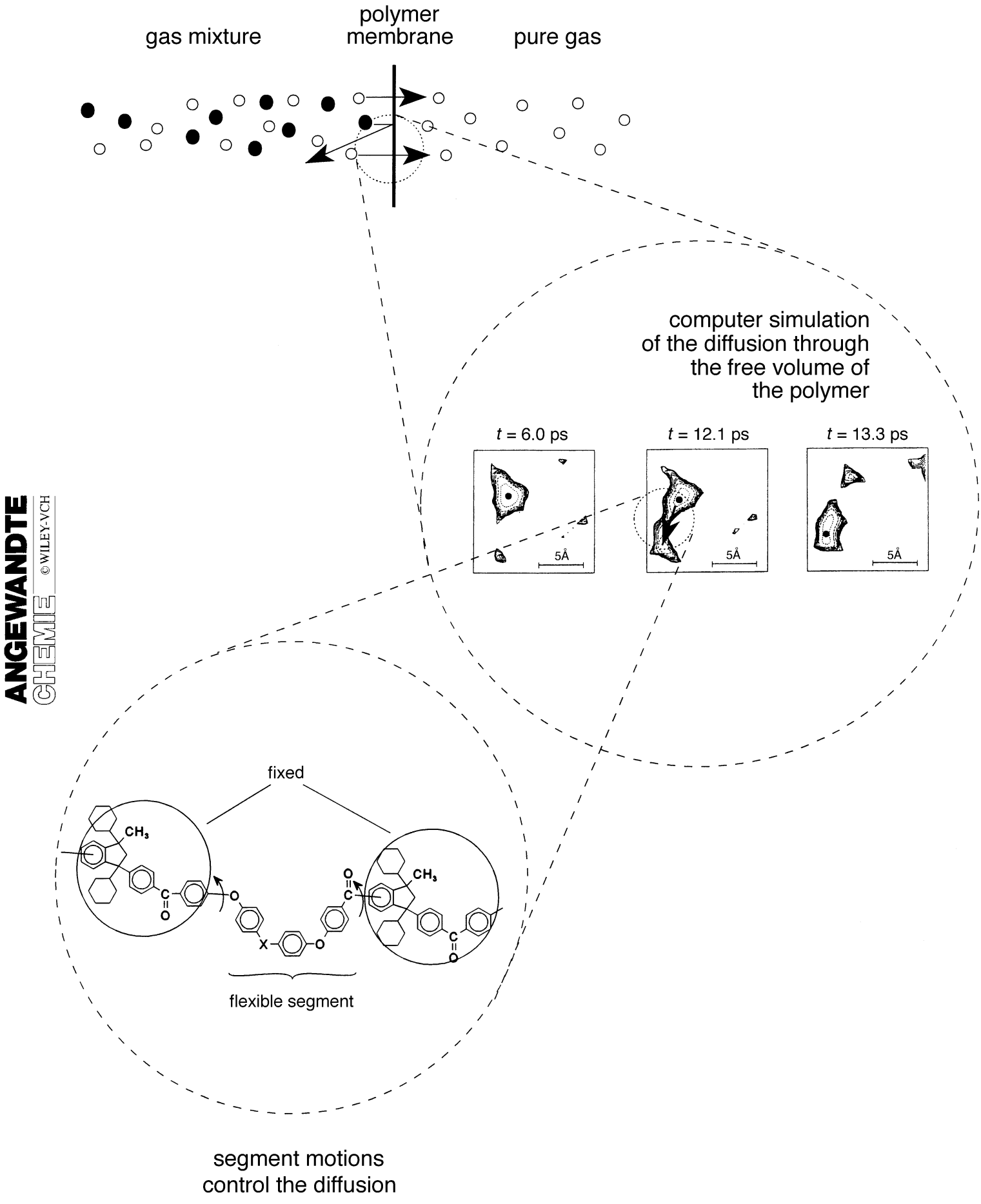
[1] L. Pasteur, *C. R. Acad. Sci. Paris* **1848**, *26*, 535.
[2] The optical purity (op) has been defined as the ratio of the observed specific rotation of the compound $[\alpha]^{D}_{obs}$ divided by the specific rotation of the enantiopure compound $[\alpha]^{D}_{max}$. It is easy to establish that $op(\%) = \frac{R-S}{R+S} \times 100$ (R = mole fraction of the major enantiomer), to give a way to calculate the relative amounts of the two enantiomers. Morrison and Mosher[3] proposed the use of the expression "enantiomeric" excess (*ee*) defined as $ee(\%) = \frac{R-S}{R+S} \times 100$. This definition has the advantage that *ee* coincides with op, even when the measurement is performed by nonpolarimetric methods. (See also ref. [4] for a discussion on that topic.)
[3] J. D. Morrison, H. S. Mosher, *Asymmetric Organic Reactions*, Prentice Hall, Englewood Cliffs, **1971**, p. 10.
[4] E. L. Eliel, S. H. Wilen, L. N. Mander, *Stereochemistry of Organic Compounds*, Wiley, New York, **1994**, p. 214.
[5] A. Horeau, *Tetrahedron Lett.* **1969**, 3121.
[6] A. Horeau, J. P. Guetté, *Tetrahedron* **1974**, *30*, 1923.
[7] T. Williams, R.G. Pitcher, P. Bommer, J. Gutzwiller, M. Uskokovic, *J. Am. Chem. Soc.* **1969**, *91*, 1871.
[8] T. Katagiri, C. Yoda, K. Furuhashi, K. Ueki, T. Kubota, *Chem. Lett.* **1996**, 115.
[9] a) K. C. Cundy, P. A. Crooks, *J. Chromatogr.* **1983**, *281*, 17; b) R. Charles, E. Gil-Av, *J. Chromatogr.* **1984**, *298*, 516.
[10] W.-L. Tsai, K. Hermann, E. Hug, B. Rohde, S. S. Dreiding, *Helv. Chim. Acta* **1985**, *68*, 2238.
[11] A. Dobashi, Y. Motoyama, K. Kinoshita, S. Hara, N. Fukasaku, *Anal. Chem.* **1987**, *59*, 2209.
[12] R. Matusch, C. Coors, *Angew. Chem.* **1989**, *101*, 624; *Angew. Chem. Int. Ed. Engl.* **1989**, *28*, 626.
[13] R. M. Carman, K. D. Klika, *Aust. J. Chem.* **1991**, *44*, 895.
[14] P. Diter, S. Taudien, O. Samuel, H. B. Kagan, *J. Org. Chem.* **1994**, *59*, 370.
[15] M. Jung, V. Schurig, *J. Chromatogr.* **1992**, *605*, 161.
[16] a) H. Wynberg, B. Feringa, *Tetrahedron* **1976**, *32*, 2831; b) H. Wynberg, *Chimia* **1976**, *30*, 445.
[17] However, Izumi and Tai pointed out that the measurement of the asymmetric induction in an asymmetric synthesis may not be necessarily correlated simply to the *ee* value of the chiral auxiliary, especially in asymmetric catalysis.[18]
[18] Y. Izumi, A. Tai, *Stereo-Differentiation Reactions*, Academic Press, New York, **1977**, p. 244.
[19] C. Puchot, O. Samuel, E. Duñach, S. Zhao, C. Agami, H. B. Kagan, *J. Am. Chem. Soc.* **1986**, *108*, 2353.
[20] There are a few review articles on some aspects of nonlinear effects.[21–24] For recent highlights and discussion on NLEs, see M. Avalos, R. Babiano, P. Cintas, J. L. Jiménez, J. C. Palacios, *Tetrahedron: Asymmetry* **1997**, *8*, 2997; M. Reggelin, *Nachr. Chem. Tech. Lab.* **1997**, *45*, 392, 622; D. G. Blackmond, *J. Am. Chem. Soc.* **1997**, *119*, 12934.
[21] R. Noyori, M. Kitamura, *Angew. Chem.* **1990**, *30*, 34; *Angew. Chem. Int. Ed. Engl.* **1990**, *30*, 49.
[22] R. Noyori, *Asymmetric Catalysis in Organic Synthesis*, Wiley, New York, **1994**, pp. 273 – 297.
[23] C. Bolm in *Advanced Asymmetric Synthesis* (Ed. G. R. Stephenson), Blackie Academic and Professional, New York, **1996**, pp. 9 – 26.
[24] H. B. Kagan, C. Girard, D. Guillaneux, D. Rainford, O. Samuel, S. Y. Zhang, S. H. Zhao, *Acta Chem. Scand.* **1996**, *50*, 345.
[25] a) U. Eder, G. Sauer, P. Wiechert, *Angew. Chem.* **1971**, *83*, 492; *Angew. Chem. Int. Ed. Engl.* **1971**, *10*, 496; b) Z. G. Hajos, D. Parrish, *J. Org. Chem.* **1974**, *39*, 1615.
[26] a) C. Agami, C. Puchot, *J. Mol. Cat.* **1986**, *38*, 341; b) C. Agami, *Bull. Soc. Chim. Fr.* **1988**, 499.
[27] a) K. Katsuki, K. B. Sharpless, *J. Am. Chem. Soc.* **1980**, *102*, 5974; b) M. G. Finn, K. B. Sharpless, *J. Am. Chem. Soc.* **1991**, *113*, 113.
[28] N. Oguni, Y. Matsuda, T. Kaneko, *J. Am. Chem. Soc.* **1988**, *110*, 7877.
[29] P. Pitchen, E. Duñach, M. N. Deshmukh, H. B. Kagan, *J. Am. Chem. Soc.* **1984**, *106*, 8188.
[30] For a simulation of the curve of Figure 5 under the assumption of a dimeric titanium species with four DET, see ref. [31].
[31] D. Guillaneux, S. H. Zhao, O. Samuel, D. Rainford, H. B. Kagan, *J. Am. Chem. Soc.* **1994**, *116*, 9430.
[32] a) M. Kitamura, S. Okada, R. Noyori, *J. Am. Chem. Soc.* **1989**, *111*, 4028; b) M. Yamakawa, R. Noyori, *J. Am. Chem. Soc.* **1995**, *117*, 6327; see also [21, 22].
[33] C. Bolm, G. Schlingloff, K. Harms, *Chem. Ber.* **1992**, *125*, 1191.
[34] K. Fitzpatrick, R. Hulst, R. M. Kellog, *Tetrahedron: Asymmetry* **1995**, *6*, 1861.
[35] a) C. Bolm, *Tetrahedron: Asymmetry* **1991**, *2*, 701; b) C. Bolm, M. Ewald, M. Felder, *Chem. Ber.* **1992**, *125*, 1205; c) C. Bolm, M. Felder, J. Müller, *Synlett* **1992**, 439.
[36] A. H. M. de Vries, J. F. G. A. Jansen, B. L. Feringa, *Tetrahedron* **1994**, *50*, 4479.
[37] Q.-L. Zhou, A. Pfaltz, *Tetrahedron* **1994**, *50*, 4467.
[38] G. van Koten, *Pure Appl. Chem.* **1994**, *66*, 1455.
[39] a) M. Terada, K. Mikami, T. Nakai, *J. Chem. Soc. Chem. Commun.* **1990**, 1623; b) K. Mikami, M. Terada, S. Narisawa, T. Nakai, *Synlett* **1992**, 255; c) K. Mikami, M. Terada, *Tetrahedron* **1992**, *48*, 5671; d) K. Mikami, *Adv. Asymmetric Synth.* **1995**, *1*, 1.
[40] M. Terada, K. Mikami, *J. Chem. Soc. Chem. Commun.* **1994**, 833.
[41] D. Kitamoto, H. Imma, T. Nakai, *Tetrahedron Lett.* **1995**, *36*, 1861.
[42] a) M. Hayashi, T. Matsuda, N. Oguni, *J. Chem. Soc. Chem. Commun.* **1990**, 1364; b) M. Hayashi, T. Matsuda, N. Oguni, *J. Chem. Soc. Perkin Trans.* **1992**, 3135.
[43] a) G. E. Keck, D. Krishnamurthy, M. C. Grier, *J. Org. Chem.* **1993**, *58*, 6543; b) G. E. Keck, D. Krishnamurthy, *J. Am. Chem. Soc.* **1995**, *117*, 2363.
[44] J. W. Faller, D. W. I. Sams, X. Liu, *J. Am. Chem. Soc.* **1996**, *118*, 1217.
[45] P. Bedeschi, S. Casolari, A. L. Costa, E. Tagliavini, A. Umani-Ronchi, *Tetrahedron Lett.* **1995**, *36*, 7897.

[46] D. R. Gauthier, Jr, E. M. Carreira, *Angew. Chem.* **1996**, *108*, 2521; *Angew. Chem. Int. Ed. Engl.* **1996**, *35*, 2363.
[47] a) N. Komatsu, M. Hashizume, T. Sugita, S. Uemura, *J. Org. Chem.* **1993**, *58*, 4529; b) N. Komatsu, M. Hashizume, T. Sugita, S. Uemura, *J. Org. Chem.* **1993**, *58*, 7624.
[48] H. B. Kagan, J.-C. Fiaud, *Top. Stereochem.* **1988**, *18*, 249.
[49] C. Zondervan, B. L. Feringa, *Tetrahedron: Asymmetry* **1996**, *7*, 1895.
[50] N. Iwasawa, Y. Hayashi, H. Sakurai, K. Narasaka, *Chem. Lett.* **1989**, 1581.
[51] J. Irurre, C. Alonso-Alija, A. Fernández-Serrat, *Afinidad* **1994**, *51*, 413.
[52] K. Mikami, Y. Motoyama, M. Terada, *J. Am. Chem. Soc.* **1994**, *116*, 2812.
[53] S. Kobayashi, H. Ishitani, M. Araki, I. Hachiya, *Tetrahedron Lett.* **1994**, *35*, 6325.
[54] D. Seebach, R. Dahinden, R. E. Marti, A. K. Beck, D. A. Plattner, F. N. M. Kühnle, *J. Org. Chem.* **1995**, *60*, 1788.
[55] M. Shimizu, Y. Ukaji, K. Inomata, *Chem. Lett.* **1996**, 455.
[56] H. Sasai, T. Susiki, N. Itoh, M. Shibasaki, *Tetrahedron Lett.* **1993**, *34*, 851.
[57] D. A. Evans, S. G. Nelson, M. R. Gagné, A. R. Muci, *J. Am. Chem. Soc.* **1993**, *115*, 9800.
[58] K. B. Hansen, J. L. Leighton, E. N. Jacobsen, *J. Am. Chem. Soc.* **1996**, *118*, 10924.
[59] M. Yamaguchi, T. Shiraishi, M. Hirama, *J. Org. Chem.* **1996**, *61*, 3520.
[60] B. Schmidt, D. Seebach, *Angew. Chem.* **1991**, *103*, 1383; *Angew. Chem. Int. Ed. Engl.* **1991**, *30*, 1321.
[61] a) C. Bolm, J. Müller, G. Schlingloff, M. Zehnder, M. Neuburger, *J. Chem. Soc. Chem. Commun.* **1993**, 182; b) C. Bolm, J. Müller, *Tetrahedron* **1994**, *50*, 4355.
[62] P. I. Dosa, J. C. Ruble, G. C. Fu, *J. Org. Chem.* **1997**, *62*, 444.
[63] M. Bougauchi, S. Watanabe, T. Arai, H. Sasai, M. Shibasaki, *J. Am. Chem. Soc.* **1997**, *119*, 2329.
[64] T. Schwenkreis, A. Berkessel, *Tetrahedron Lett.* **1993**, *34*, 4785.
[65] C. Bolm, F. Bienewald, *Angew. Chem.* **1995**, *107*, 2883; *Angew. Chem. Int. Ed. Engl.* **1995**, *34*, 2640.
[66] D. Seebach, R. E. Marti, T. Hintermann, *Helv. Chim. Acta* **1996**, *79*, 1710.
[67] S. E. Denmark, B. L. Christenson, S. P. O'Connor, *Tetrahedron Lett.* **1995**, *36*, 2219.
[68] a) J. W. Faller, J. Parr, *J. Am. Chem. Soc.* **1993**, *115*, 804; b) J. W. Faller, M. R. Mazzieri, J. T. Nguyen, J. Parr, M. Tokunaga, *Pure Appl. Chem.* **1994**, *66*, 1463; c) D. P. Fairlie, B. Bosnich, *Organometallics* **1988**, *7*, 936; e) D. P. Fairlie, B. Bosnich, *Organometallics* **1988**, *7*, 946; f) S. H. Bergens, P. Noheda, J. Whelan, B. Bosnich, *J. Am. Chem. Soc.* **1992**, *114*, 2121.
[69] K. Burgess, W. A. van der Donk, *Inorg. Chim. Acta* **1994**, *220*, 93.
[70] a) M. Kitamura, S. Suga, M. Niwa, R. Noyori, *J. Am. Chem. Soc.* **1995**, *117*, 4832; b) M. Kitamura, M. Yamakawa, H. Oka, S. Suga, M. Niwa, R. Noyori, *Chem. Eur. J.* **1997**, *2*, 1173.
[71] The authors used Equations (8) and (9) to draw the calculated curves: where v_0^A and v_0^B are the initial rates of pure cat_A- and cat_B-catalyzed reactions proceeding with enantioselectivities of ee_A and ee_B, respectively. The abscissa or the graphics are catalyst composition expressed as $100\,cat_A/([cat_A]+[cat_B])$ or $100\,cat_B/([cat_A]+[cat_B])$.

$$ee_{ber} = \frac{ee_A v_0^A [cat_A] + ee_B v_0^B [cat_B]}{[cat_A] + [cat_B]} \quad (8)$$

$$v_{0,ber} = \frac{v_0^A [cat_A] + v_0^B [cat_B]}{[cat_A] + [cat_B]} \quad (9)$$

[72] S. Y. Zhang, C. Girard, H. B. Kagan, *Tetrahedron: Asymmetry* **1995**, *6*, 2637.
[73] K. B. Sharpless, W. Amberg, Y. L. Bennani, G. A. Crispino, J. Hartung, K.-S. Jeong, H.-L. Kwong, K. Morikawa, Z.-M. Wang, X.-L. Zhang, *J. Org. Chem.* **1992**, *57*, 2768.
[74] E. J. Corey, M. C. Noe, *J. Am. Chem. Soc.* **1993**, *115*, 12579.
[75] a) M. A. Giardello, V. P. Conticello, L. Brard, M. R. Gagné, T. J. Marks, *J. Am. Chem. Soc.* **1994**, *116*, 10241; b) P.-F. Fu, L. Brard, Y. Li, T. J. Marks, *J. Am. Chem. Soc.* **1995**, *117*, 7157.
[76] F. C. Frank, *Biochim. Biophys. Acta* **1953**, *11*, 459.
[77] M. Calvin, *Chemical Evolution*, Clarendon, London, **1969**, Chap. 7.
[78] For a recent highlight on asymmetric autocatalysis with amplification of chirality, see ref. [79a]. For a possible asymmetric autocatalytic system (liquid phase autoxidation) see ref. [79b].
[79] a) C. Bolm, F. Bienewald, A. Seger, *Angew. Chem.* **1996**, *108*, 1767; *Angew. Chem. Int. Ed. Engl.* **1996**, *35*, 1657 and references therein; b) T. Buhse, D. Lavabre, J. C. Micheau, W. Thiemann, *Chirality* **1993**, *5*, 341.
[80] K. Soai, S. Niwa, H. Hori, *J. Chem. Soc. Chem. Commun.* **1990**, 983.
[81] K. Soai, T. Hayase, K. Takai, *Tetrahedron: Asymmetry* **1995**, *6*, 637.
[82] T. Shibata, K. Choji, T. Hayase, Y. Aizu, K. Soai, *Chem. Commun.* **1996**, 751.
[83] a) T. Shibata, K. Choji, T. Hayase, Y. Aizu, K. Soai, *Chem. Commun.* **1996**, 1235; b) T. Shibata, T. Hayase, J. Imamoto, K. Soai, *Tetrahedron: Asymmetry* **1997**, *8*, 1717.
[84] K. Soai, T. Shibata, H. Marioka, K. Choji, *Nature* **1995**, 767.
[85] For advantages or disadvantages of the use of the enantiomeric ratio (*er*) in stereochemical problems or Horeau amplification, see refs. [86, 87].
[86] H. B. Kagan, *Rec. Trav. Chim. Pays-Bas* **1995**, *114*, 203.
[87] V. Rautenstrauch, *Bull. Soc. Chim. Fr.* **1994**, *131*, 515.
[88] a) A. H. Alberts, H. Wynberg, *J. Am. Chem. Soc.* **1989**, *111*, 7265; b) A. H. Alberts, H. Wynberg, *J. Chem. Soc. Chem. Commun.* **1990**, 453.
[89] H. Danda, H. Nishikawa, K. Otaka, *J. Org. Chem.* **1991**, *56*, 6740.
[90] Y. Shvo, M. Gal, Y. Becker, A. Elgavi, *Tetrahedron Lett.* **1996**, *7*, 911, and references therein.
[91] K. Soai, Y. Inoue, T. Takahashi, T. Shibata, *Tetrahedron Asymmetry* **1996**, *7*, 13355.
[92] The interpretation of the reaction is complicated here by the possibility of a double asymmetric reaction.[87]
[93] H. Wynberg, *Chimia* **1989**, *43*, 150.
[94] A qualitative model for asymmetric autocatalytic processes has been proposed by Bailey.[95] It is based on the ML_2 model,[31] the reaction involving the formation of L. As discussed above it is possible to introduce a (+)-NLE, which makes this system useful for self-replication of chirality.
[95] P. D. Bailey, *J. Chem. Soc. Chem. Commun.* **1995**, 1707.
[96] Equations based on competitive reactions of Figure 60 have been developed to describe the various cases where stoichiometric asymmetric synthesis can give rise to NLE.[97]
[97] C. Girard, H. B. Kagan, manuscript in preparation.
[98] a) A. O. King, E. G. Corley, R. K. Anderson, R. D. Larsen, T. R. Verhoeven, P. J. Reider, Y. B. Xiang, M. Belley, Y. Leblanc, M. Labelle, P. Prasit, R. J. Zamboni, *J. Org. Chem.* **1993**, *58*, 3731; b) I. Shinkai, A. O. King, R. D. Larsen, *Pure Appl. Chem.* **1994**, *66*, 7551.
[99] Initial reports from Merck[98] indicated that NLE was observed for one value of *ee* of pinene. An excellent and complete study was published later.[102]
[100] C. Girard, H. B. Kagan, *Tetrahedron :Asymmetry* **1995**, *6*, 1881.
[101] H. C. Brown, N. N. Joshi, *J. Org. Chem.* **1988**, *53*, 4059.
[102] M. Zhao, A. O. King, R. D. Larsen, T. R. Verhoeven, P. J. Reider, *Tetrahedron Lett.* **1997**, *38*, 2641.
[103] C. Girard, H. B. Kagan, *Tetrahedron: Asymmetry* **1997**, *23*, 3851.
[104] K. Tanaka, J. Matsui, Y. Kawabata, H. Suzaki, A. Watanabe, *J. Chem. Soc. Chem. Commun.* **1991**, 1632.
[105] a) R. E. Rossiter, M. Eguchi, A. E. Hernandes, D. Vickers, J. Medich, J. Marr, D. Heninis, *Tetrahedron Lett.* **1991**, *32*, 3973; b) R. E. Rossiter, G. Miao, N. M. Swingle, M. Eguchi, A. E. Hernandez, R. G. Patterson, *Tetrahedron: Asymmetry* **1992**, *3*, 231.
[106] a) C. Fehr, J. Galindo, *J. Org. Chem.* **1988**, *53*, 1828; b) C. Fehr, J. Galindo, *Helv. Chem. Acta* **1995**, *78*, 539; c) C. Fehr, *Angew. Chem.* **1996**,*108*, 2726; *Angew. Chem. Int. Ed. Engl.* **1996**, *35*, 2567.
[107] V. Rautenstrauch, P. Mégard, B. Bourdin, A. Furrer, *J. Am. Chem. Soc.* **1992**, *114*, 1418.
[108] For the advantages and disadvantages of the use of *ee*, *ec*, or *er* in various problems, see ref. [86].
[109] M. Okamoto, M. Tabe, T. Fujii, T. Tanaka, *Tetrahedron: Asymmetry* **1995**, *6*, 767.
[110] S. Masamune, W. Choy, J. S. Petersen, L. R. Sita, *Angew. Chem.* **1985**,*97*, 1; *Angew. Chem. Int. Ed. Engl.* **1985**, *24*, 1.
[111] C. Girard, T. Luukas, H. B. Kagan, unpublished results.



ANGEWANDTE CHEMIE ©WILEY-VCH

Gas Separation with Polymer Membranes

Gerhard Maier*

The gas permeability of amorphous polymers has been long utilized industrially for the separation of gas mixtures. In spite of a large collection of data regarding permeability coefficients and selectivities of nearly all film-forming polymers, the relationship between the chemical structure of a polymer and its properties as a membrane for gas separation has only been insufficiently explored up to now. Modifications of the chemical structure of a polymer chain often lead to an improvement of the permeability coefficient at the cost of selectivity, or vice versa. The transport of gas molecules in amorphous, vitreous polymers occurs through the free volume, that is, through the gaps between the polymer chains. It is affected by the thermal motion of segments of the main polymer chain. To obtain materials with optimized transport properties, attempts are made to increase the chain stiffness by incorporating rigid and bulky groups into the polymer chain, which in turn, by affecting the packing density, increases the free volume. The goal is to increase simultaneously the selectivity and the permeability coefficients. This approach, however, has failed to succeed up to now, as the structural modifications have been limited—owing to necessary considerations for industrial applications—by the availability of starting materials and the preparative effort during the monomer synthesis. New impulses can come from the synthesis of special polymers, which contain very short, but relatively flexible segments between rigid and bulky structural elements. Such segments should retain limited mobility even in the vitreous state. It is crucial to limit this mobility to the actual flexible segments, as otherwise the selectivity will likely be negatively affected. The transport of the gas molecules should then be primarily controlled by the flexible segments, which should yield hints for further structural optimization, in terms of length and flexibility of these chain segments. Studies on two series of polyimides and one series of poly(ether ketone)s, all containing bulky indane groups as well as flexible phenyl ether segments in the repeat unit, have provided the first indications for such behavior. Relative to observations with known polymers, the polyimides did not exhibit unusual changes in permeability and selectivity when the polymer backbone was altered. The poly(ether ketone)s, however, when compared to polymers studied thus far, did show significant changes in the relationship between free volume and the permeability coefficient as well as in the dependence of the selectivity on the chemical structure of the polymer.

Keywords: gas separation · membranes · polymers

1. Introduction

Gases occupy a central position in the chemical feed stock industry. Six of the ten most important industrial feed stock chemicals are gases: oxygen, nitrogen, ammonia, chlorine, ethylene, and propylene.[1] Their proportions may vary in different industrialized countries, but the general picture remains the same. In 1994 the worldwide market volume for industrial gases was 26 billion US dollars, with an expected annual growth of 4 % in the industrialized countries and up to 14 % in Asia.[2]

[*] Priv.-Doz. Dr. G. Maier
Lehrstuhl für Makromolekulare Stoffe
der Technischen Universität München
D-85747 Garching (Germany)
Fax: (+49) 89-289-13562
E-mail: maier@makroserv.tech.chemie.tu-muenchen.de

Gases are primarily purified by cryogenic techniques or by adsorption and washing methods. The requirements for purity and, hence, for the purification method, depend heavily on the origin and the application of the gas in question. For nitrogen as inert gas for food packaging, for instance, a purity of 99 % is perfectly adequate. For medical purposes, pure oxygen is usually not required, but air enriched with oxygen to a level of 40 % is sufficient. If purity levels below 99.95 % are adequate, the purification of nitrogen in a membrane setup is usually the most economical procedure.[3]

In principle, all materials that form sufficiently thin films can be used to create membranes. This includes metals, glass, ceramics, and polymers as well as well-ordered monomolecular layers of surfactant molecules in liquid membranes. The thickness of these membranes varies from a few nanometers for Langmuir–Blodgett films (single or multiple layers of molecules which are deposited in a controlled fashion) up to

 © WILEY-VCH Verlag GmbH, D-69451 Weinheim, 1998 1433-7851/98/3721-2961 $ 17.50+.50/0

hundred micrometers for membranes with strong mechanical properties.

This review is concerned with the field of gas separation with polymers as membrane materials,[3–10] as nearly all commercial membranes for gas separation as well as the overwhelming majority of membranes studied in the laboratory for this purpose consist of polymer films. Polymer membranes operate according to the solution–diffusion mechanism.[3] Other separation mechanisms are found, for example, in metal membranes for the preparation of ultrapure hydrogen,[3, 11] which rely on the catalytic dissociation of hydrogen in palladium–silver alloys, as well as for certain ceramic membranes,[3, 12–15] which utilize a molecular-sieve effect.

2. Industrial Applications of Polymer Membranes for Gas Separation

Even though there are a large number of potential applications for gas separation with polymer membranes,[3–5, 7, 9, 10] only relatively few of them have become applied in practice. The commercial applications began only in 1979 with "prism separators" from Monsanto.[3, 9, 10] These were gas-separation devices with a modular design, which were used for the separation of hydrogen from the product stream of ammonia synthesis[3] and the oxo process.[3] The highlight of applications to date is probably the plant for the separation of air into its constituent gases from Praxair in Loenhout, Belgium, which began operation in 1996 and which can yield up to 19100 $Nm^3 h^{-1}$ (nearly 24 $t h^{-1}$) of pure nitrogen.[2] This plant is about five times larger than those built before, which could yield up to 3500 $Nm^3 h^{-1}$ of nitrogen.[2]

Other applications of membranes for gas separation and purification are quite well developed in some cases, but have so far not been successfully introduced into practical use.[3–5, 7, 9, 10] These include the removal of CO_2, H_2S, and H_2O from natural gas (to increase to fuel efficiency and decrease pipe corrosion), the recycling of hydrogen from the effluent streams of natural gas or crude oil desulfurization and other hydrogenation processes, the preparation of oxygen-enriched air (e.g., for medical purposes), the recycling of helium, the separation of olefins and alkanes (processing of cracking products), and the separation of SO_2 and NO_x from exhaust fumes.

Only integrated asymmetrical and composite membranes are currently used industrially for the separation of gases.[3, 9, 10, 32] These types of membranes are characterized by very thin nonporous layers which are gas-selective and are deposited onto highly porous carrier materials. As the material transport is inversely proportional to the membrane thickness, only such an arrangement yields sufficiently high throughputs. The porous carrier materials provide the necessary mechanical strength, but do not contribute to transport resistance.

3. Quantitative Description of Material Transport through Membranes

In 1866 Graham postulated the model concepts for the mechanism of gas permeation that are still valid today.[16] He observed that the rates at which gases passed through a membrane did not correlate with the well-known gas diffusion constants. From this, he concluded that the transport does not occur through pores (defects in the polymer films), at least not to a significant degree, but indeed through the membrane material itself. According to Graham's model, the passage of a gas through a nonporous polymer film occurs in three stages. Initially, the gas must be dissolved in the membrane material, then the gas particles must diffuse through the polymer, and finally the gas must be released. According to this model, the process is termed a "solution–diffusion mechanism".

In 1955 Fick studied the quantitative description of gas diffusion through nonporous membranes of cellulose nitrate.[17] The relationship between throughput, membrane area, membrane thickness, and driving force which was found by Fick for the stationary state became generally known as "Fick's 1st law" for material transport though boundary layers. According to this relationship, the quantity J_X of gas X which passes through the membrane per unit time and area is proportional to the difference in pressure between the input (p_1) and permeate sides (p_2) and inversely proportional to the



Gerhard Maier, born in 1960, studied chemistry at the Technische Universität München from 1980 to 1986. His diploma thesis (Synthesis of Partially Fluorinated Seven-Membered Heterocycles) was completed under the direction of Prof. K. Burger. His dissertation research was completed in 1989 under the direction of Prof. O. Nuyken at the Universität Bayreuth (Synthesis of Polymers by 1,3-Dipolar Cycloadditions). In 1992 he returned with Prof. Nuyken to the Technische Universität München, where he completed his habilitation in 1996, working on high-temperature polymers. During a one-year stay at the University of North Carolina in 1994, he worked with Prof. J. M. DeSimone on the synthesis of polyesters in supercritical CO_2. Currently he is Privatdozent at the Technische Universität München. His research projects concern high-temperature polymers as membranes for the separation of gases; the synthesis of telechelic polymers, block copolymers, and highly branched polymers by cycloaddition; and the development of polymer dielectrics for microelectronic applications and molecular imprinting.

membrane thickness d [Eq. (1)].[9, 10] In the case of gas permeation, the proportionality constant P_X is called the per-

$$J_X = P_X \frac{p_1 - p_2}{d} \quad (1)$$

$$P_X[\text{Barrer}] = 10^{-10} \frac{V\,[\text{cm}^3(\text{STP})]\,d\,[\text{cm}]}{A\,[\text{cm}^2]\,t\,[\text{s}]\,\Delta p\,[\text{Torr}]} \quad (2)$$

$$P_X = S_X D_X \quad (3)$$

meability coefficient of the given material for the gas X. Hence, it is a substance-specific quantity and characteristic for each membrane material. The permeability coefficient with the unit "Barrer" is defined by Equation (2); V is the permeate volume at standard pressure and temperature (STP), d the membrane thickness, A the membrane area, t the time, and Δp the pressure difference between input and permeate sides. Von Wroblewski showed that the permeability coefficient can be viewed as the product of the solubility coefficient S_X and the diffusion coefficient D_X [Eq. (3)].[18]

The ideal selectivity α of a membrane material for a pair of gases X and Y is defined as the ratio of the permeability coefficients for X and Y [Eq. (4)]. The ideal selectivity is

$$\alpha = \frac{P_X}{P_Y} \quad (4)$$

determined from separate measurements of the two gases X and Y. For real gas mixtures, the different partial pressures on the input and permeate sides must be taken into account. In addition, problems may arise from the different interactions of the gases with the polymer.[7, 9, 10] If, for example, one of the gases softens the polymer, this will not only affect the permeability coefficient of this particular gas, but also that of the other gas. Usually, this leads to a significant loss of selectivity. These types of effects overshadow the sought-after effects of the polymer structure. Therefore, laboratory studies nearly always employ ideal selectivities.

The permeability coefficients of different polymers for the same gas can vary by several orders of magnitude.[3, 7, 19–21] For oxygen, for instance, one finds $P(O_2)$ values from 5×10^{-4} Barrer (with Vectra, a liquid crystalline polyester) to 4×10^3 Barrer (with poly(trimethylsilylpropyne), PTMSP).[20] The selectivity (e.g., $\alpha(O_2/N_2)$) decreases from $\alpha = 15$ (Vectra) to $\alpha = 1.5$ (PTMSP).[20] If the application requires a high selectivity, polymers with $P(O_2)$ values greater than 1 Barrer and $\alpha(O_2/N_2)$ values greater than 5 are of interest. If high productivity is the main goal, it is possible to work with poly(dimethylsiloxane) membranes, which exhibit a selectivity of only $\alpha(O_2/N_2) = 1.5$, but a $P(O_2)$ of 1000 Barrer. Higher purity levels are then obtained using multiple-step plants. This is only economical, however, if the permeability coefficients are very large.

4. Transport Mechanisms and Model Concepts

Knudsen diffusion, the molecular-sieve effect, and the solution–diffusion mechanism are the three general principles that could govern gas separation by membranes.[3, 9] Knudsen diffusion relies on the separation based on the different molecular weights of the gases. The selectivity is proportional to the square root of the inverse ratio of the molecular weights.[3, 9] This means that the best achievable selectivity is too low for many applications: In the case of nitrogen/oxygen separation, $\alpha(N_2/O_2)$ is only 1.07.

To exploit the molecular sieve effect, membranes must be created containing pores with diameters that are in between those of the gas particles to be separated. This is, in principle, possible with glass membranes,[3, 15, 22, 23] for example. Apart from the lack of suitable mechanical properties and the difficulties in creating large membrane surfaces, however, fouling by condensable impurities in the gas stream that clog the pores turns out to be a significant problem.

The membranes that are currently commercially available and the majority of the membranes studied in the laboratory operate according to the solution–diffusion mechanism. Therefore, some related model concepts will now be discussed. In this particular mechanism, the material transport occurs in the three steps already mentioned, namely, absorption, diffusion, and release. The rate-determining parameter is the permeability coefficient, which can be viewed as the product of a solubility coefficient and a diffusion coefficient [Eq. (3)]. The question of which step is actually rate-determining—that is, poses the most resistance to the transport—cannot always be readily answered. Dayes et al. concluded, from measurements in the steady state as well as in the initial non-steady-state stage of material transport through polymer membranes, that in order to describe fully the gas permeation according to the solubility-diffusion mechanism it is necessary to know at least two of the three parameters P, D, and S.[24, 25] This viewpoint formed the basis for most of the studies described in this review.

The theoretical approaches for the description of gas diffusion in polymers and of gas permeation through polymers have been discussed in numerous reviews,[3, 7, 9, 10, 19] and will therefore not be presented here in detail. They are primarily based on the free volume of the polymer, statistical arguments, or energetic considerations. The parameters that are employed in these models to describe the polymer are not directly related to structural elements of the polymer chain. Therefore these models do not yield sufficiently concrete indications of how the chemical structure of a given class of polymers could be optimized.

Models which take the structure of the polymer chains into account, such as that of Pace and Datyner,[26] are more suitable. The first question that arises is the location of the gas atoms or molecules in the polymeric material. It must be realized that the macroscopic space which a polymer occupies is not completely filled by its chains. Gaps between the chains remain which cannot be filled due to conformational constraints (bond angles, steric bulk), especially in the case of amorphous polymers. A fraction of these gaps is large enough to accommodate gas particles.[27] The sum of these gaps is called the "free volume".[28] As the free volume of amorphous polymers is generally much larger than that of crystalline polymers, essentially only amorphous polymers are is used for gas separation.

According to the notions of Pace and Datyner,[26] the transport of gas particles occurs by leaps between these gaps.

These jumps occur when the thermal motions of certain segments of the polymer chain open up a sufficiently large channel to a neighboring gap. The gas particle can then diffuse through this channel. Once the channel closes afterwards, the jump has been successfully concluded. In this scenario, the selectivity of a membrane material depends on the control of these leap channels: Large openings—that is, substantial segment motions—permit the rather unrestricted passage of all present gas particles, whereas more limited motions permit the passage of smaller species much more frequently than of larger particles. A number of computer simulations[29–31] are based on these ideas, and the rapid increase in computing power as well as the constant refinement of programs, potentials, and parameters to describe amorphous polymers as solids promise important future advances in this field. A number of graphic depictions of these processes are shown in Figure 1.

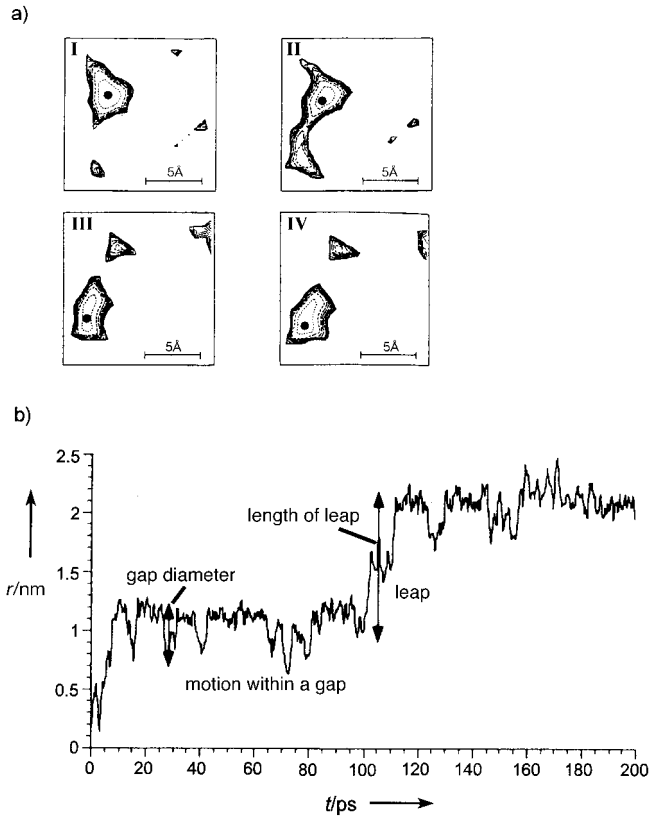


Figure 1. Computer simulation of transport leaps of single gas particles in a polymer. a) Movement of an O_2 molecule in a polymethylene matrix:[29] situation after 6 (I), 12.1 (II), 13.3 (III) and 16.1 ps (IV). b) Relative motion of a CO_2 molecule in a polyimide matrix.[30] r indicates the distance from the starting point of the particle in the computer simulation.

When these models are applied to the problem of determining the structure–property relationships of gas permeation through polymers, the question of which chain segments actually control the leap channels immediately arises. This is the starting point for the systematic variation of substructures within a class of polymers. By comparing permeability coefficients and selectivities for selected pairs of gases, one tries to identify the crucial chain segments. The results are verified by modifying the local chain flexibility at the corresponding critical points by introducing substituents, or by varying the length of the assumed critical segments by inserting or removing small partial structural elements within the repeat unit of the polymer. This leads to an accurate classification of segments of the polymer chain as important or unimportant for gas transport. This, in turn, allows the optimization of the polymer for a given separation task.

5. Conventional Membrane Polymers

The potential application of a polymer as a separation membrane depends upon the possible throughput and the purity of the product. This means that both the permeability coefficient for the gas that is transported more rapidly and the selectivity should be as large as possible. When the selectivity is plotted on a double logarithmic scale versus the permeability coefficient for the more rapidly permeating gas for many different polymers,[20, 21] one finds a relatively unstructured set of data points (Figure 2). It is characteristic that this

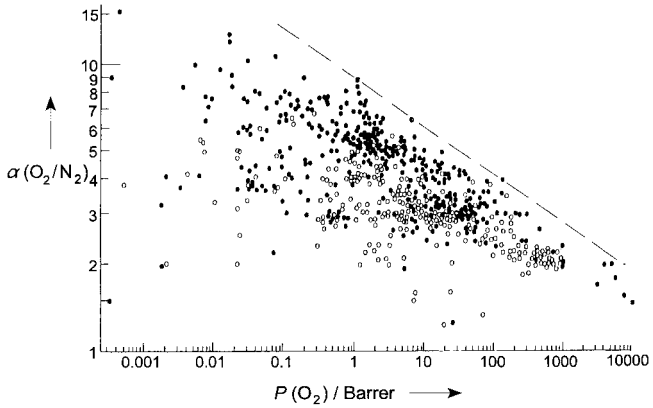


Figure 2. Relationship between the O_2/N_2 selectivity and the O_2 permeability coefficients for conventional polymers according to Robeson.[21] ●: vitreous polymers ($T_g < T_{measurement}$), ○: elastomeric polymers ($T_g > T_{measurement}$). The dashed line indicates the empirical upper bound line.

set of data points shows an apparently linear upper boundary where both P and α are large.[20, 21] It is thus possible to find polymers that exhibit high selectivity and low permeability, and vice versa, in addition to those that combine low selectivities with low permeabilities. There do not, however, appear to be any polymers that show the desired trend to large values for both P and α.

An even more important observation is that simple modifications in the polymer structure often lead only to a trade-off: One of the parameters is improved, while the other is simultaneously affected negatively.[3, 7, 20, 21] Therefore, such measures only shift the compromise between permeability coefficient and selectivity, but do not constitute a real improvement. Table 1 shows the data for three pairs of polymers selected as examples. In each case, only one structural element has been modified. In all three cases it is apparent that the increase in selectivity is accompanied by a lowering of the permeability coefficient.[19, 32]

Table 1. Apparent mutual dependence of selectivity and permeability coefficients.[19, 32]

Polymer	P[Barrer]			α		
	He	O_2	N_2	He/O_2	He/N_2	O_2/N_2
poly(methyl methacrylate)	8.4	0.14	0.02	60	420	7.0
poly(ethyl methacrylate)	23.8	1.9	0.33	12.5	72	5.8
PMDA-ODA[a]	8.0	0.61	0.1	13.1	80	6.1
PMDA-IPDA[b]	37.1	7.1	1.5	5.2	24.7	4.7
cellulose acetate	16.0	0.82	0.15	19.5	107.7	5.5
ethyl cellulose	39.8	12.4	3.4	3.2	11.7	3.6

[a] PMDA-ODA: polyimide from pyromellitic acid dianhydride and 4,4′-diaminodiphenyl ether. [b] PMDA-IPDA: polyimide from pyromellitic acid dianhydride and 2,2-bis(4′-aminophenyl)propane.

This unsatisfactory situation leads to the question of what the detailed relationships between the structure of a polymer and its properties regarding gas separation are. In particular, the connection between permeability and diffusion coefficients on one hand and other physical properties on the other is still unclear. The permeability and diffusion coefficients do not correlate with the density or the glass-transition temperature, as can be seen from published tables or review articles.[7–10, 19] There is, however, a relatively good correlation between the inverse of the fractional free volume in the polymer and the logarithm of the permeability coefficient.[9, 10, 33, 34] The fractional free volume V_f is obtained from the experimentally determined density and the volume that is actually occupied by the structural elements of the polymer chain.[35, 36] The latter is usually calculated by the increment method according to Bondi.[35] Using new data by Park and Paul,[33] which take into account that different fractional free volumes are accessible to gas atoms or molecules of different sizes, one usually finds a relatively good correlation (Figure 3).

This approach should directly allow predictions of the ideal selectivity for any given pair of gases, as the permeability coefficients can be calculated from the free volume. A detailed analysis shows, however, that the calculated value of P for gases such as He, O_2, N_2, and CO_2 can differ from the experimentally found value by a factor of 2 to 5. The prediction of the selectivity is also not yet sufficiently accurate. A series of chemically different polymers which showed experimentally determined selectivities of $\alpha(O_2/N_2) = 7$ yielded calculated values of between 5 and 8.5.[33] However, differences of these dimensions often determine whether an actual installation can be economically operated or not.

Upon detailed examination, it is also clear that the slope of the lines in the plot of $\lg P$ versus $1/V_f$ depends markedly on the polymer class. This observation, however, is often not sufficiently taken into account (Figure 4).

The approach to relate permeability and selectivity to the free volume has two major weaknesses. For one, it is reasonable to assume that not only the total free volume plays a role, but that the distribution of gap diameters is also important.[7] In addition, increment methods, such as the one used to calculate the free volume, can only incompletely reflect the chemical structure of a polymer. To take regioisomers into account, for example, the number of increments must be significantly increased. Bulky substituents in *ortho* positions to flexible groups such as ether or carbonate linkages will contribute much more to chain rigidity than those in the 2,2′ positions of a biphenylene unit, which is

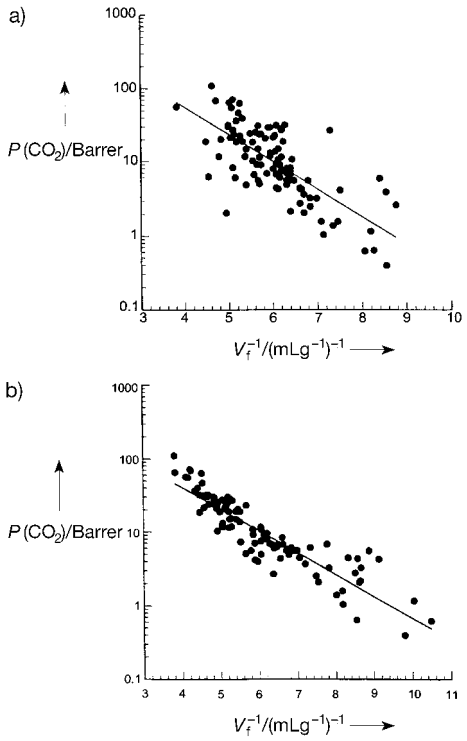


Figure 3. Correlation between the free volume V_f of a polymer and the permeability coefficient P for a specific gas (in this case CO_2). The V_f value was calculated with a) increments by Bondi and van Krevelen,[35] and b) a new set of increments according to Park and Paul.[33]

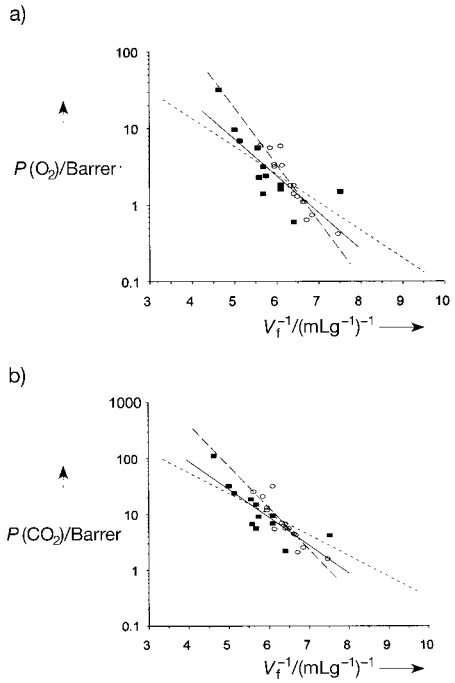


Figure 4. Relationship between permeability coefficient P and the fractional free volume V_f for different polymer classes and the resulting empirical limit. ■, ——: polycarbonates; ○, – – –: poly(ether sulfone)s; - - - -: best fit line from Figure 3b; a) for O_2; b) for CO_2.

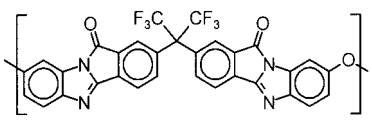
already rigid by itself. This behavior has been observed for a series of polycarbonates and discussed in detail.[3] It was found that the stiffening of the main polymer chain through structural modifications within the bisphenol moiety lead to the typical trade-off (high permeability → low selectivity, and vice versa), while stiffening that involved the carbonate group increased both P and α.

6. Strategy for Structure Optimization

The facts presented so far lead to the conclusion that significant improvements in permeability and selectivity of polymers can no longer be achieved by more or less random, readily performed structural variations of basic structures which are primarily chosen on the basis of availability. The typical and wide-spread trade-off behavior between selectivity and permeability coefficient,[20, 21] the correlation between fractional free volume and permeability coefficient,[9, 10, 33, 34] and the linear relationship between the slope of the empirical boundary line and the difference in diameters of a pair of gases to be separated can be interpreted to imply that the free volume of the conventional polymers studied thus far, or at least the distribution of gap diameters which make up the free volume, cannot be controlled. Instead, a relatively broad distribution develops. The observation of the different line slopes in the plots of $\lg P$ versus $1/V_f$ for different classes of polymers allows the conclusion that the distribution of gap diameters is different for different polymers.

A plausible suggestion for the further development of membrane polymers stems from Koros.[7] He recommended that the central point of this development should be the attempt to control the mean diameter and the distribution of diameters of the gaps between the polymer chains which make up the free volume. Probably more important, however, is the control over the extent and frequency of the segment motions, which, according to the model described earlier, control the leap channels. According to the suggestion from Koros,[7] a narrower distribution of gap diameters could be achieved with a certain type of polymer architecture. Polymer chains that consist of alternating bulky and flat units should be preferentially packed in such a manner that the bulky groups act as spacers and prevent a tight packing of the flat groups. This leaves gaps in the vicinity of the flat chain segments, and their dimensions can be determined directly from the size of the basic chain building blocks. The polypyrrolone 6FDA-TADPO (Scheme 1) has been suggested as an example of such a chain architecture.[3, 7] This polymer is indeed currently one of the best membrane materials for the separation of O_2 and N_2.[21]

The argument that the simple consideration of individual chain segments and their flexibility to explain changes in the permeability coefficients cannot appropriately take into account different solubilities and, hence, cannot provide a sufficient interpretation has some validity. It turns out, however, that in many cases, this is only of secondary importance. Equations (3) and (4) yield expression (5) for the selectivity α; S_X/S_Y is the solubility selectivity, and D_X/D_Y the diffusion selectivity.



Scheme 1. Structural formula of the polypyrrolone 6FDA-TADPO.

$$\alpha = \frac{P_X}{P_Y} = \frac{S_X}{S_Y}\frac{D_X}{D_Y} \quad (5)$$

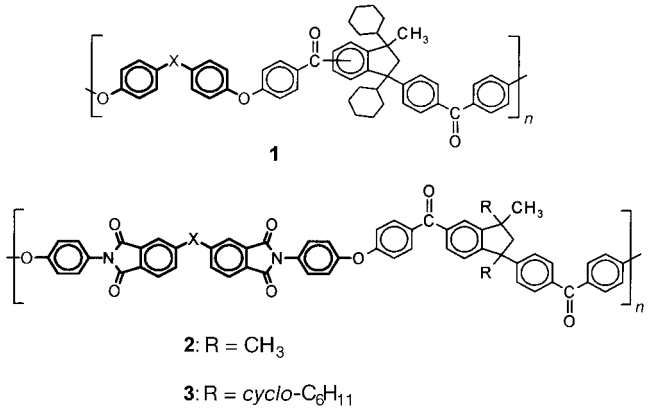
Especially for the frequently studied aromatic polycondensates such as polycarbonates, poly(ether sulfone)s and polyimides, the solubility selectivity for different pairs of gases is practically independent of the polymer structure. For a series of 18 polyimides,[37] the $S(O_2)/S(N_2)$ values were 1.31 ± 0.2, while $S(CO_2)/S(CH_4)$ values were 3.37 ± 0.5. The solubility selectivities of different polycarbonates (PC)[10] and poly(ether sulfone)s (PES)[10] are very similar for those two pairs of gases as well (PES: O_2/N_2: 1.4–1.7; CO_2/CH_4: 2.7–3.7; PC: O_2/N_2: 1.36–1.65; CO_2/CH_4: 2.58–3.62). However, the selectivities α varied from 4.6 to 8.1 (polyimides, O_2/N_2) and 26 to 65 (polyimides, CO_2/CH_4).[37] Similar results are found for polycarbonates and poly(ether sulfone)s.[10] This implies that, at least for these types of polymers, the selectivity is primarily determined by the diffusion selectivity, that is, the different mobility of the gas particles in the polymer matrix. This situation changes when gases are studied that either condense readily or that can undergo strong, specific interactions with functional groups in the polymer matrix, such as water vapor or larger hydrocarbons. If only simple gases such as the nobel gases, hydrogen, oxygen, nitrogen, carbon dioxide, and methane are considered, the effect of the solubility selectivity can be ignored, at least in the case of aromatic polycondensates with high glass-transition temperatures.

7. Polymers with Indane Groups in the Main Chain as Membranes for Gas Separation

7.1. Polymer Structures

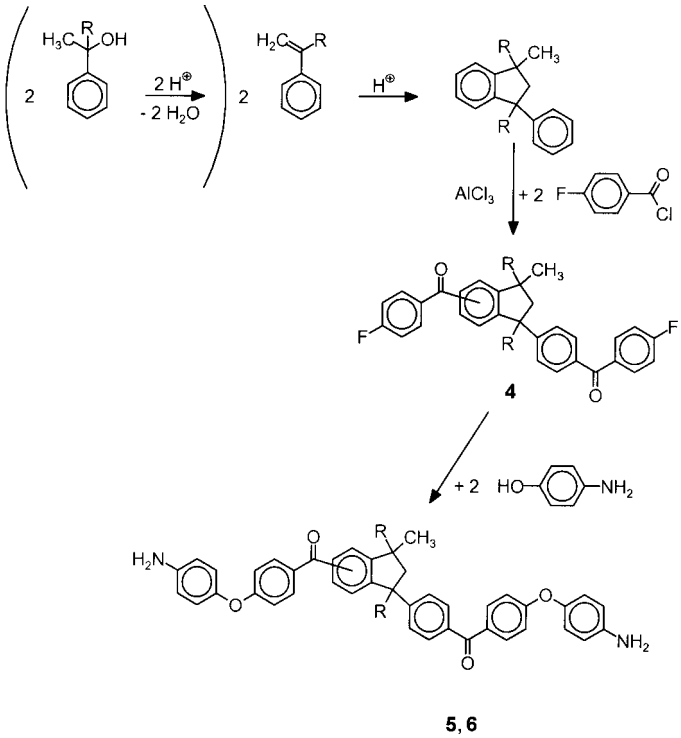
A series of polymers with 1,1,3-trialkyl-3-phenylindane groups in the main chain will now be used to demonstrate how polymers with alternating flexible, sterically undemanding and bulky, rigid segments can be prepared, and how such a chain architecture affects the gas permeabilities and selectivities. The use of an indane derivative as the bulky group has the advantage of easy accessibility. In addition, the bulkiness of this group can be adjusted by varying the alkyl substituents. Oxy-1,4-phenylene chains as linkages between the indane groups represent a good compromise between rigidity (to control the segment motions) and flexibility (to obtain the highest possible number of channels opening up per unit time). The flexibility and bulkiness of these segments can be varied over a wide range. Imide groups were introduced for comparison, as polyimides are empirically known to be good membrane materials for gas separation, and a large amount of

data for this class of polymers is available.[3, 7, 19–21, 37] Scheme 2 shows the polymer structures chosen for this study.



Scheme 2. General structures of poly(ether ketone)s **1** and poly(etherimide)s **2** and **3** with indane groups. For the bridging group X, see Tables 2 and 3.

The synthesis and characterization of these polymers have been described in detail[38–41] and will only be briefly summarized here (Scheme 3). The starting point for the



Scheme 3. Synthesis of the monomers **4**–**6**, the starting materials for the polymers **1**–**3**. **5**: R = methyl, **6**: R = cyclohexyl.

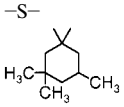
synthesis of methyl derivative **5** is the acid-catalyzed dimerization of α-methylstyrene, yielding 1,1,3-trimethyl-3-phenylindane. Subsequent Friedel–Crafts acylation with 4-fluorobenzyol chloride leads to the methyl derivative of monomer **4**. An approximately equimolar mixture of two isomers is obtained, as 1,1,3-trimethyl-3-phenylindane has more than one position in the phenyl rings that is activated for electrophilic substitution. This, however, has no effect on the properties of the resulting polymers, as was expected based on the asymmetric structure of the indane group. A further reaction with 4-aminophenol in the presence of a base leads to a nucleophilic substitution of the fluorine atoms in the 4-fluorobenzyol groups, yielding the diamino monomer **5**, which is used to prepare the polyimides **2**. The introduction of the cyclohexyl substituents in the indane system is achieved by directly employing the tertiary alcohol from the Grignard reaction between methylmagnesium bromide and cyclohexyl phenyl ketone as starting material for the acid-catalyzed cyclodimerization. In the presence of a strong acid, water is released, and the olefin formed cyclodimerizes to the indane derivative (Scheme 3). The further steps to monomer **6** are the same as for **5**.

7.2. Synthesis and Properties of Polymers with Indane Groups in the Main Chain

The polymer synthesis follows previously described methods.[42, 43] The difluoro monomer **4** (R = cyclohexyl) undergoes condensation with bisphenols in the presence of K_2CO_3 as base and toluene as azeotropic water remover in a dipolar aprotic solvent, resulting in the poly(ether ketone)s **1**. The polyimides **2** and **3** are prepared in two steps from the diamino monomers **5** and **6**, respectively, and aromatic tetracarboxylic acid anhydrides. The diamine and the dianhydride are initially stirred together for several hours in a dipolar aprotic solvent, which leads to the poly(amide acid).[39, 40] The resulting solution is poured into a film. The temperature is then raised in a stepwise manner up to 280 °C in a vacuum, which dries the film and leads to imidization by release of water. Tables 2 and 3 summarize some important data of these polymers.

The segment motions, which have their onset at the glass-transition temperature, are strongly cooperative and involve longer pieces of the main polymer chain (several repeat units). These segment motions can therefore be used as a measure of the global flexibility of the polymer chain, at least within a series of polymers with similar structures.[28] The data

Table 2. Physical properties of the poly(ether ketone)s **1**.[38, 41]

Polymer	X	T_g[a] [°C]	$\bar{M}_n$[b]	ρ[c]	V_f[d] (CO_2)	V_f[d] (O_2)
1a	–O–	232	16600	1.19	0.121	0.124
1b	$-C(CF_3)_2-$	235	17900	1.22	0.170	0.175
1c	–	255	13200	1.20	0.138	0.139
1d	$-C(CH_3)_2-$	234	12700	1.14	0.137	0.140
1e		236	8400	1.18	0.133	0.136
1f	–S–	218	15600	1.19	0.131	0.134
1g		255	14200	1.18	0.126	0.133
1h	–CO–	229	12700	1.19	0.126	0.130
1i	$-SO_2-$	251	17200	1.25	0.147	0.149

[a] DSC, 20 K min^{-1}. [b] In g mol^{-1}, determined by GPC in THF, polystyrene standard. [c] Density in g mL^{-1}, determined by the flotation method. [d] $V_f = (V_S - V_0)/V_S$; V_S: specific volume (from the density), V_0: specific volume at 0 K (from increments by Park and Paul[33]).

Table 3. Physical properties of the polyimides **2** and **3**.[39, 40]

Polymer	−X−	T_g[a] [°C]	$\bar{M}_n$[b]	ρ[c]	V_f[d] (CO_2)	V_f[d] (O_2)
2a	$-C(CF_3)_2-$	241	28000	1.286	0.159	0.161
2b	$-SO_2-$	251	20800	1.275	0.139	0.139
2c	−CO−	232	21300	1.245	0.133	0.132
2d	−O−	233	[e]	1.255	0.123	0.124
2e	–	246	31500	1.240	0.119	0.119
3a	$-C(CF_3)_2-$	269	30700	1.275	0.169	0.169
3b	$-SO_2-$	272	8100	1.235	0.147	0.144
3c	−CO−	261	[e]	1.220	0.139	0.135
3d	−O−	264	[e]	1.215	0.128	0.127
3e	–	274	25800	1.210	0.124	0.122

[a] DSC, 20 K min^{-1}. [b] In g mol^{-1}, determined by GPC in $CHCl_3$, polystyrene standard. [c] Density in g mL^{-1}, determined by the flotation method. [d] $V_f = (V_S - V_0)/V_S$; V_s: specific volume (from the density), V_0: specific volume at 0 K (from increments by Park and Paul[33]). [e] Insoluble in $CHCl_3$.

in Tables 2 and 3 show that the polymers containing indane groups in the main chain exhibit high glass-transition temperatures (T_g), which indicates a relatively rigid main chain. The T_g values of the poly(ether ketone)s **1**,[41] for example, are about 80 K higher than those of analogous polymers without the 1,3-biscyclohexyl-1-methyl-3-phenylindane structural element. A comparison of polyimides **2** and **3** shows that the replacement of the methyl groups by the two cyclohexyl moieties raises the glass-transition temperature by 30 K. Within each series of polymer, the glass-transition temperatures follow the expected trend, dependent on the bridging element X (see Scheme 2).[43, 44] Flexible groups such as ether or sulfide lead to relatively low values of T_g, while rigid or strongly polar groups, such as the biphenyl moiety or the sulfone group, result in the highest glass-transition temperatures.

The molecular masses were determined by gel permeation chromatography (GPC). This is a relative method, which requires calibration with standards having known molecular weights (usually polystyrene). Nevertheless, values within a class of polymers compare relatively well, and it has been our experience, at least for amorphous poly(aryl ether)s, that the average molecular masses determined by GPC measurements in THF or chloroform usually do not differ by more than 10% from the values found with absolute methods, such as membrane or vapor pressure osmometry.[38, 45] Corresponding to the values for $\bar{M}_n$ found in Table 2, the poly(ether ketone)s posses comparable molecular masses, perhaps with the exception of polymer **1e**. As it was possible, however, to cast this polymer into mechanically stable, flexible films as well, it can be assumed that it also falls into the range of molecular masses where the effect of the molecular mass on the physical properties is only of secondary importance.[28] The results for the members of this series of polymers should, hence, be readily comparable with each other.

Similar arguments apply to the polyimides, with the exception that the polyimides **2d**, **3c**, and **3d** in the fully imidized forms are completely insoluble at room temperatures, so that a molecular mass determination was not possible. All polyimides could be obtained as mechanically stable, flexible films.

The polymers **1**–**3** exhibit relatively low densities (see Tables 2 and 3).[3, 10, 37] These value are, however, not unusual when one takes into account the presence of the bulky indane group, which prevents a dense packing of the chains. The V_f values are also in the range expected for poly(arylethers) and polyimides.[3, 10, 37] The data for V_f in Tables 2 and 3 are based on the increment method by Park and Paul,[33] which takes into account that different fractions of V_f are accessible to different gases due to their different molecular diameters. As an example, fractional free volumes are given for CO_2 and O_2 in the Tables. However, these differences are relatively small, only about 2–5%. A comparison of the data for the polymers **2** and **3** is of interest, as it shows that the introduction of the two cyclohexyl substituents on the indane system causes an increase in V_f. This is because of the increased space requirements of this structural element.

7.3. Permeabilities and Selectivities of Polymers 1–3

For the measurement of the permeability coefficients, a cell was employed that was separated into two compartments by the membrane. Both compartments were initially evacuated. To begin the measurement, the input chamber was filled with the gas to be studied. The pressure p_1 in the input chamber was kept constant, while an increase in pressure Δp in the permeate chamber was measured. Once the stationary state was achieved, the increase in pressure was linear with time t. The volume of the measurement cell V, the membrane area A, the membrane thickness d, the temperature T, and the pressure p_1 on the input side are all known and constant, so that the permeability coefficient can be calculated according the Equation (6).

$$P_X = \frac{\Delta p}{\Delta t}\frac{V d}{A p_1}\frac{1}{RT} \quad (6)$$

The permeabilities of hydrogen, carbon dioxide, oxygen, and nitrogen were determined for all polymers **1**–**3**. The measurements were performed at 22 °C and 1.25 bar. The results are summarized in Tables 4 and 5 for poly(ether ketone)s **1**) and in Tables 6 and 7 for polyimides **2** and **3**.

7.3. Discussion of the Permeabilities

7.3.1. Poly(ether ketone)s 1

The measurements of the permeability coefficients for hydrogen, carbon dioxide, oxygen, and nitrogen (Table 4) yield data for six pairs of gases (Table 5). The interpretation of the data is best done with plots of the selectivity versus the permeability coefficient. The identification of general trends is of primary interest, whereas the discussion of specific results will initially be of secondary importance. The goal of our studies is primarily a deeper understanding of generally valid relationships between polymer structure and permeability/selectivity.

Table 4. Permeability coefficients of the poly(ether ketone)s **1** (in Barrer).

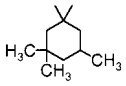
Polymer	X	$P(H_2)$	$P(CO_2)$	$P(O_2)$	$P(N_2)$
1a	−O−	11.6	4.18	1.08	0.21
1b	$-C(CF_3)_2-$	17.3	7.7	1.64	0.32
1c	–	14.9	6.45	1.47	0.42
1d	$-C(CH_3)_2-$	17.7	9.36	1.83	0.33
1e		16.7	7.39	1.57	0.29
1f	−S−	13.5	5.7	1.12	0.2
1g		36	18.9	3.58	0.64
1h	−CO−	12.5	5	1.03	0.16
1i	$-SO_2-$	14.5	7.2	1.32	0.23

Table 5. Selectivities of the poly(ether ketone)s **1**.

Polymer	$\alpha(O_2/N_2)$	$\alpha(H_2/N_2)$	$\alpha(CO_2/N_2)$	$\alpha(H_2/CO_2)$	$\alpha(CO_2/O_2)$	$\alpha(H_2/O_2)$
1a	5.1	55.2	19.9	2.8	3.9	10.7
1b	5.1	54.1	24.1	2.2	4.7	10.5
1c	3.5	35.5	15.4	2.3	4.4	10.1
1d	5.5	53.6	28.4	1.9	5.1	9.7
1e	5.4	57.6	25.5	2.3	4.7	10.6
1f	5.6	67.5	28.5	2.4	5.1	12.1
1g	5.6	56.2	29.5	1.9	5.3	10.1
1h	6.4	78.1	31.3	2.5	4.9	12.1
1i	5.7	63.0	31.3	2.0	5.5	11.0

The plot for O_2/N_2 (Figure 5a) shows that the selectivities of all poly(ether ketone)s **1** (with the exception of **1c**) are very similar. Within this series of polymers, the bridging unit X was the only structural element that was changed, but the differences in polarity, geometry, and steric bulk are considerable. The structural elements varied from small flexible ether or sulfide bridges over rigid biphenyl units or strongly polar sulfone groups to the sterically very demanding trimethylcyclohexylidene group. Nevertheless, the effects of these structural modifications on the selectivity are very small. The group X, however, does show a clear effect on the permeability coefficient. The sterically least demanding groups, such as ether, sulfide, or carbonyl moieties (**1a**, **1f**, **1h**) yield the lowest permeability coefficients, whereas the sterically most demanding species, the trimethylcyclohexylidene group (**1g**), leads to the largest permeability coefficient.

Very similar relationships for the selectivities and the permeability coefficients are found for the gas pairs H_2/N_2 (Figure 5b) and CO_2/N_2 (Figure 5c). Exceptions are polymer **1h**, which deviates for H_2/N_2 towards a larger selectivity, and polymer **1a**, which deviates towards a lower selectivity for CO_2/N_2.

The other pairs of gases (H_2/O_2, CO_2/O_2, and H_2/CO_2) do not exhibit these anomalies regarding the selectivities.

*7.3.1.1. Permeability Coefficients of **1***

At a first glance, the explanation for the relationship between permeability coefficients and the structure of bridging group X appears straightforward: Sterically more demanding groups reduce the packing density of the polymer chains, thereby increasing the free volume and the permeability coefficients. When examined more closely, however, the explanation cannot be that simple. Polymer **1g**, which always exhibits the highest permeability coefficients, definitely does not posses an unusually high free volume (see Table 2). In contrast, the V_f values for this polymer lie in the lower middle of the range found for poly(ether ketone)s. This observation clearly shows that one must not simply consider the total fractional free volume, but only that fraction that is actually accessible to the gas particles during the diffusion process.

Correspondingly, the relationship between permeability coefficients and fractional free volume is very different for the poly(ether ketone)s **1** than for the other polymers studied thus far. Figure 6 shows the plots for O_2 and CO_2 as examples for this behavior; the plots for H_2 and N_2 are very similar. The comparison with Figures 3b and 4 indicates that the best fit lines for poly(ether ketone)s **1** have a much smaller slope than the general best fit line or the best fit lines for the conventional poly(ether sulfone)s and polycarbonates. This implies that the permeability coefficients of the poly(ether ketone)s **1** are much less dependent on the total fractional free volume

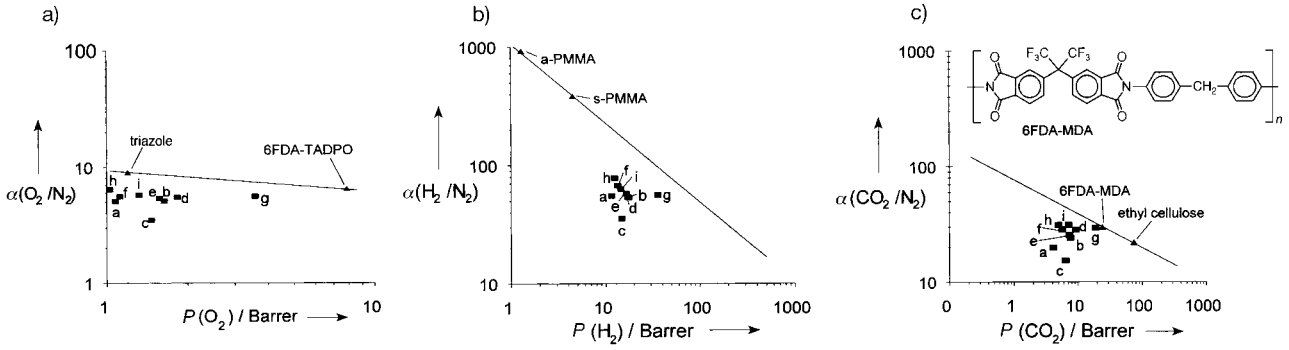


Figure 5. Plots of the selectivity α for the gas pairs a) H_2/N_2, b) CO_2/N_2, and c) O_2/N_2 versus the O_2, H_2, and CO_2 permeability coefficients of poly(ether ketone)s **1**. The graphs show the empirical limits as well as some data points from the literature (▲): triazole (poly(1-phenyl-1,3,4-triazole-2,5-diyl-1,4-phenylen)),[8] 6FDA-TADPO (see Scheme 1),[3] a-PMMA (atactic poly(methyl methacrylate)),[20] s-PMMA (syndiotactic poly(methyl methacrylate)),[20] 6FDA-MDA,[7] and ethyl cellulose.[19]

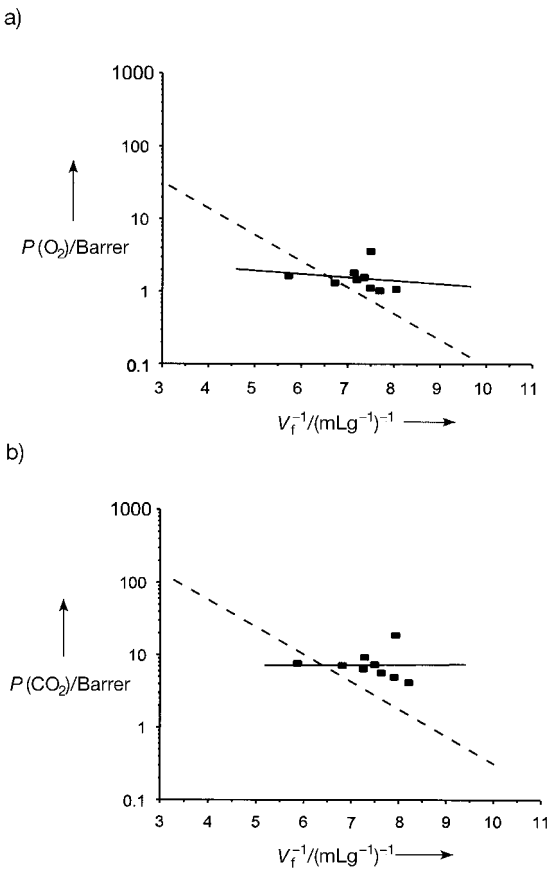


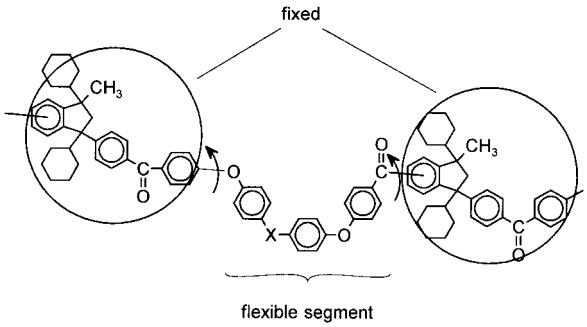
Figure 6. Relationship between permeability coefficient and free volume for poly(ether ketone)s **1** a) for O_2 and b) for CO_2. For clarity, the corresponding general best fit lines are indicated as well (– – –: compare with Figure 4).

than usual. We currently assume that the reason for this behavior can be found in the distribution of the diameters of the voids making up the free volume. The architecture of the poly(ether ketone)s **1** apparently controls these voids to some extent, and the group X resides at a critical position in the polymer chain. It is possible that the void diameters are strongly dependent on the length of the phenoxy segments between the bulky, rigid indane groups. In this case, the bridging unit X exerts significant control over the fractional free volume that is accessible to the gas particles (at least for H_2, CO_2, O_2, and N_2). Therefore, the permeability coefficients vary only very slightly with the total fractional free volume, but quite strongly with the steric demand of the groups X.

According to this scenario, the indane groups themselves do not significantly affect the gas-transport processes, but act as anchors for the flexible segments, which in turn control the gas transport. It is quite likely that not all polymer chains are packed in the manner that is necessary for this idealized situation. For poly(ether ketone)s **1**, it must be assumed, however, that the overwhelming majority of transport leaps and thus the gas transport through the membrane is indeed controlled by the described segments. Otherwise, one would not expect this behavior, which deviates so significantly from the norm.

*7.3.1.2. Selectivities of **1***

The interpretation presented in the previous section also leads directly to a plausible explanation for the different behavior of the selectivity of polymer **1c** (with a biphenyl unit). All polymers **1**, except for **1c**, are bent at the position X. If it is assumed that the segments between the indane groups control the gas transport through their motions, the situation depicted in Scheme 4 can be envisioned. The bend in the



Scheme 4. Chain segments of poly(ether ketone)s **1** which control the gas transport within the polymer (proposal).

polymer chain at the bridging group X could be crucial for the function of the phenoxy segments as controlling elements for gas transport. If X is replaced by a single bond as in polymer **1c**, the possibility of this conformation no longer exists. Instead, a distinctly more stretched arrangement must be assumed. This leads to a significant lengthening of the segment that must move in order to open up a leap channel. This in turn results in a widening of the channels, which reduces the ability to differentiate between gas particles of different sizes.

In the cases of the gas pairs H_2/O_2, CO_2/O_2, and H_2/CO_2, polymer **1c** does not show this deviating behavior. This is understandable when the kinetic diameters of the gas molecules are taken into account. These are 0.289 nm (H_2), 0.33 nm (CO_2), 0.346 nm (O_2), and 0.364 nm (N_2). Hence, nitrogen has the largest molecules of the gases studied. As the polymers **1** show relatively good O_2/N_2 selectivity, the critical segment motions must be capable of differentiating between these two gases. This means that oxygen can diffuse through the channels controlled by the crucial segments, and that diffusion must even be easier for carbon dioxide and hydrogen. This implies in turn that the selectivity between CO_2/O_2, H_2/O_2, and H_2/CO_2 is not necessarily controlled by exactly the same segment motions. In other words, effects which are critical for pairs of gases involving nitrogen do not inevitable influence separations involving gases with molecules smaller than nitrogen to the same degree. This is exactly what is observed for polymer **1c**. In this context, it is interesting that the selectivity of the polymers **1** for H_2 over CO_2 ($\alpha = 1.9-2.8$) is surprisingly low, even though the difference in diameters ($\Delta d = 0.41$ Å) is much larger than for CO_2/O_2, ($\alpha = 3.9-5.5$, $\Delta d = 0.16$ Å), O_2/N_2 ($\alpha = 3.5-6.4$, $\Delta d = 0.18$ Å), and CO_2/N_2 ($\alpha = 15.4-31.3$, $\Delta d = 0.34$ Å). This confirms the conclusion that while the segment discussed thus far, and sketched in Scheme 4, does control the selectivity of the

polymers **1** for smaller gas particles over nitrogen, it does not necessarily control the selectivities for the other gases which all have molecules smaller than nitrogen.

The functionally separated structure of the repeat unit into two segments is the most significant modification which distinguishes the poly(ether ketone)s **1** from conventional polymers, such as the polycarbonates, poly(ether sulfone)s, polyimides, and cellulose derivatives which have been commonly employed as gas-separation membranes. The indane moiety with its substituents serves as a more or less fixed group and acts as a hinge about which a flexible chain segment of defined length can perform its (limited) thermal motions. According to our idealized model, this construction has two important consequences. Firstly, the sequence of bulky indane groups and small, flexible segments leads to a narrower distribution of the gap diameters in the free volume. Secondly, the gas transport through the polymer is primarily controlled by the motions of the segments between the indane groups. The physical structure of the polymer, especially the length and flexibility of the segments between the indane groups, governs which gases can be differentiated and how well, thus determining the possible extent of a separation. Polymers with a conventional structure—such as bisphenol A-polycarbonate, poly(ether sulfone), and polysulfone—do not exhibit a comparable segmentation of the repeat unit. Therefore the hinges and the flexible segments are made up of the same structural elements in these polymers. This is bound to lead to a compromise, as the structural elements cannot be optimized separately for their specific tasks. In addition, all structural modifications, such as the introduction of substituents or the variation of bridging units, affect the hinges as well as the flexible segments. Hence, any simple modification can alter the behavior in an uncontrolled manner. This affects primarily the flexibility and length of the critical segments as well as the distribution of gap diameters in the free volume. It is apparent that for those polymers, it becomes more difficult to derive concrete structure–property relationships on a molecular level and to obtain "blueprints" for better membrane materials.

From the analysis of data obtained for **1**, a general guideline can be derived for the structure of polymers for the further study of the relationship between polymer structure and permeability/selectivity. The polymer chains should incorporate large, bulky structural elements which are linked by flexible segments. The dimensions of the bulky groups and the length of the flexible chain segments in between them should control the distribution of the gap diameters in the free volume. This would bring about the possibility of directly adjusting the fractional free volume that is accessible to gases with different molecular diameters. At the same time, the selectivity should primarily be determined by the length of the flexible segment and its architecture (bond angle, structure) as well as the degree of free rotation around those bonds that form the hinges between the flexible segments and the fixed, bulky groups.

Recently, a research group at Air Products & Chemicals presented an increment method for the calculation of the permeability coefficients of various aromatic polymers for helium, nitrogen, and oxygen.[46] The types of polymers to which this method can be applied include polyesters, poly(aryl ether)s, and polycarbonates. In contrast to the already mentioned approach of Park and Paul,[33] this new method is not based on the free volume of the polymers. Instead, increments were determined for the contributions to the permeability coefficients by various structural elements that are frequently found in polymers. The agreement between the thus calculated permeability coefficients and the actually measured ones is surprisingly good.[46]

There are currently no increments for the 1,1,3-trimethyl- or the 1,3-biscyclohexyl-1-methylindane groups, and so a comparison between the experimental data for the poly(ether ketone)s **1** and calculated values is not possible. There are, however, increments for the 3,3,3′,3′-tetramethylspirobis-1,1′-indane group.[46] By the method by Robeson, Smith, and Langsam, interesting permeability coefficients and, hence, selectivities for the gases O_2/N_2 can be calculated for a number of polymers that are analogous to the poly(ether ketone)s **1**, but contain the tetramethylspirobisindane group instead of the 1,3-biscyclohexyl-1-methylindane moiety. Just like the poly(ether ketone)s **1**, the hypothetical 3,3,3′,3′-tetramethylspirobis-1,1′-indane polymers all show a very similar O_2/N_2 selectivity of around $\alpha = 5$, which is very close to the value of $\alpha = 5.5$ found experimentally for the polymers **1** (see Table 5). The polymers with X = O, S, and CO show relatively low permeability coefficients as well. Unfortunately, there are no increments for the trimethylcyclohexylidene group, so that no similar comparison can be made. The increment method predicts an increase in $P(O_2)$ by a factor of 2 for the relatively bulky structural element 6F relative to the simple ether bridge. Experimentally, the polymers **1** exhibit an increase by a factor of 1.52.

All in all, the predictions of this increment method agree surprisingly well with the experimental data, except for one important point. While calculations for the polymer with the biphenyl unit (X = —) yield a selectivity that is lower than for most other polymers in this group, the difference is not comparable with that found experimentally for the poly(ether ketone)s **1**. This stems from a fundamental difference between the increment approach and our model. The increment method simply sums up the structural elements that are present without considering their relative positions. In our model, however, the position of a structural element plays a crucial role. With the increment method, a polymer that contains several rigid, bulky groups in a row followed by several flexible segments would yield the same permeability coefficients and selectivities as a polymer in which the same structural elements are present in a strictly alternating fashion. According to our model, the polymer with the "segmented" structure should behave very differently from the polymer with the strictly alternating structure, because of the inhomogeneous, sometimes very low, sometimes very large, chain flexibility in the former and the homogeneous local flexibility in the latter polymer. This should then lead to different permeability coefficients and selectivities. Future modifications of the poly(ether ketone)s **1** will show which approach is more useful. In particular, it is planned to introduce methyl groups in the *ortho* position relative to various bridging units between the phenyl rings. This will

show whether this modification has the same effect in all locations within the repeat unit or, as we expect, there are indeed positions where structural modifications have either a very strong effect or none at all.

7.3.2. *Polyimides 2 and 3*

The repeat unit of the polyimides **2** and **3** exhibits, relative to the structure of the poly(ether ketone)s, phthalimide groups that are introduced between the bridging group X and the benzene rings (see Scheme 2). Although the segment between the indane groups is thereby lengthened, its mobility is reduced by the intermolecular dipole–dipole interactions between the strongly polar imide groups. The results of the measurements are summarized in Tables 6 and 7.

Figure 7 shows the plots of selectivity for H_2/N_2, CO_2/N_2, and O_2/N_2 versus permeability coefficient for O_2, H_2, and CO_2, respectively. It is apparent that the behavior of the polyimides **2** and **3** is much less clear cut than what was observed for the poly(ether ketone)s **1**. Some trends are observed, but the relationship between the modifications of the polymer structure and the changes in the permeability data are not only not readily apparent, they are also not unambiguous.

Table 6. Permeability coefficients of the polyimides **2** and **3** (in Barrer).

Polymer	−X−	$P(H_2)$	$P(CO_2)$	$P(O_2)$	$P(N_2)$
2a	$-C(CF_3)_2-$	21.3	5.58	2.05	0.32
2b	$-SO_2-$	12.7	3.6	0.91	0.16
2c	−CO−	8.3	1.96	0.47	0.08
2d	−O−	10.5	3.05	0.68	0.09
2e	–	8.8	2.51	0.57	0.11
3a	$-C(CF_3)_2-$	23.1	9.64	1.92	0.33
3b	$-SO_2-$	10.2	3.2	0.75	0.16
3c	−CO−	9.2	1.68	0.91	0.22
3d	−O−	13.23	3.76	0.9	0.08
3e	–	13.3	5.68	1.11	0.28

Table 7. Selectivities of the polyimides **2** and **3**.

Polymer	$\alpha(O_2/N_2)$	$\alpha(H_2/N_2)$	$\alpha(CO_2/N_2)$	$\alpha(H_2/CO_2)$	$\alpha(CO_2/O_2)$	$\alpha(H_2/O_2)$
2a	6.4	66.6	17.4	3.8	2.7	10.4
2b	5.7	79.4	22.5	3.5	4.0	14.0
2c	5.9	103.7	24.5	4.2	4.2	17.7
2d	7.6	116.7	33.9	3.4	4.5	15.4
2e	5.2	80	22.8	3.5	4.4	15.4
3a	5.8	70	29.2	2.4	5.0	12.0
3b	4.7	63.7	20.6	3.1	4.4	13.6
3c	4.1	41.8	7.6	5.5	1.8	10.1
3d	11.2	165.4	47	3.5	4.2	14.7
3e	4.0	47.5	20.3	2.3	5.1	12.0

The polyimides with $X = C(CF_3)_2$ (**2a**, **3a**) show the highest permeability coefficients in their series (Table 6), while those with X = O (**2d**, **3d**) exhibit the highest selectivities (Table 7). The lowest permeability coefficients for cyclohexyl-substituted polyimides were found for **3b** and **3c**, and, in the case of methyl-substituted polyimides, for **2e** and **2c**. For most pairs of gases studied, the lowest selectivities were observed for **3c** and **2a**. In general, the selectivities of the methyl-substituted polyimides **2** vary less than those of the cyclohexyl-substituted analogues **3**.

As was observed for the poly(ether ketone)s **1**, the order of the permeability coefficients of the polyimides **2** and **3** does not simply follow the fractional free volume (see Table 3). It is possible that also here varying the bridging group X in the main polymer chain affects primarily the fraction of the free volume that is accessible to the gas molecules. This is in itself not surprising, as the architecture of the polyimides is very similar to that of the poly(ether ketone)s.

The effect of exchanging the methyl substituents on the indane system with cyclohexyl groups poses a problem, however. It had been observed earlier that cyclohexyl groups—probably owing to their conformational flexibility—do not lead to significantly improved permeability coefficients.[10] Upon comparison of the polyimides **2** and **3** one finds that the introduction of the cyclohexyl groups can have completely different effects. While with X = O (**d**) there is an improvement in both permeability coefficient and selectivity, with X = − (**e**) there is the typical trade-off, where increased permeability goes hand-in-hand with a lower selectivity. For $X = SO_2$ (**b**) or CO (**c**), one observes a loss of selectivity, which is usually also accompanied by a lower permeability coefficient.

The reasons for this behavior are not clear. The effect of the cyclohexyl substitution appears to be strongly connected to the nature of the bridging group X. Such correlations make the derivation of structure–property relationships much more difficult. It will be necessary to introduce substituents with a lower conformational flexibility than cyclohexyl rings, such as *tert*-butyl groups, to determine whether this observation is limited to the cyclohexyl moiety or represents a more general phenomenon.

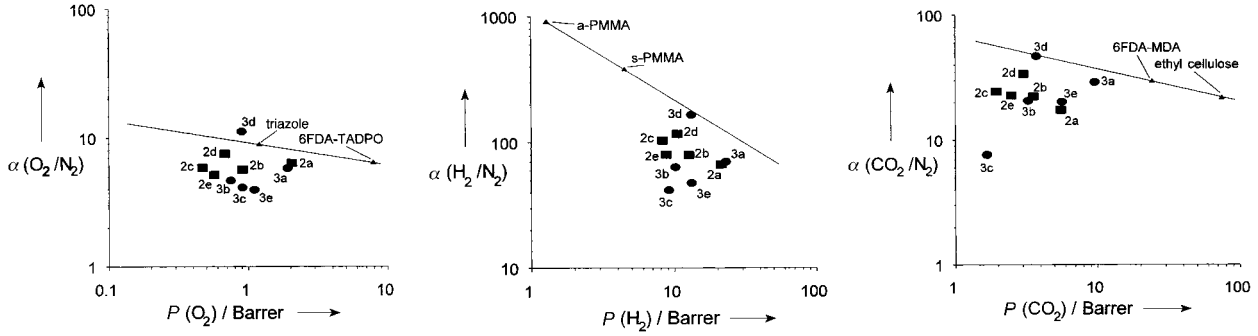


Figure 7. Plots of the selectivity α for the gas pairs a) O_2/N_2, b) H_2/N_2, and c) CO_2/N_2 versus the O_2, H_2, and CO_2 permeability coefficients of the polyimides **2** (■) and **3** (●). The graphs show the empirical limits as well as some data points (▲) from the literature (compare with Figure 5).

One conclusion, however, can be made based on the varying effects of the cyclohexyl groups: If the indane group as a whole participated in the segment motions that control the gas transport, one would expect a rather uniform effect, as the enlargement of the indane moiety due to the introduction of the cyclohexyl substituent should directly affect the mobility of this chain segment. If, however, the indane group itself does not participate in the motions of the critical chain segment, the changes introduced by the bulkiness of the substituent only act indirectly by changing the free volume, which in turn affects the conditions for the rest of the polymer chain. This also explains why the effect of the cyclohexyl substituents is strongly dependent on the nature of the bridging group X. This idea fits very well into the model discussed for the poly(ether ketone)s, namely, immobile indane groups separated by flexible segments.

It must also be considered, however, that very different values for permeability coefficients are reported, in particular for polyimide membranes, even for chemically identical structures. The reason appears to be that often the histories of the membranes are not strictly identical, in particular with respect to contact with solvents and the conditions for imidization. The insolubility of many polyimides requires working with the usually soluble poly(amic acid) precursors, with subsequent imidization in the film. One also finds a strong dependence on the imidization conditions for other macroscopic properties such as the glass-transition temperature, the elasticity module, or the impact strength. Within a given series of polyimides, usually essentially identical imidization conditions are employed, but the comparison between data sets from different laboratories is often difficult. Even though the literature offers the biggest data base for permeability coefficients for polyimides, crucial advances in the search for structure–property relationships are most likely easier and more reliably obtained using other classes of polymers.

To confirm the reliability of our permeability measurements, we had the polymers **2a** and **2d** tested in another laboratory as well.[47] The results differed only very little,[48] so that we consider our results reliable and reproducible in spite of the generally problematic situation for polyimides.

8. Conclusions and Outlook

Future systematic studies on series of polymers in which each member contains only one modified structural element can yield detailed information about the relationship between the structure of a polymer and its suitability as a membrane for gas separation. Whether this information can then also be utilized to create tailor-made membrane materials for any given separation problem depends critically upon the challenge of separating the influence of structural parameters on permeability and selectivity. If this separation is not successful, the further "development" of membrane materials will continue to be limited primarily to the selection of a material that represents an acceptable compromise between price, processing, selectivity, and permeability from a multitude of given polymers that were, in many cases, optimized for other applications (e.g., polysulfones, polycarbonates, cellulose acetate).

Most promising appears to be the proposal by Koros[7] to improve the selectivity without affecting the permeability coefficients negatively by better control of the distribution of the free volume. This approach is limited, however, by the difficulties in gaining experimental access to this distribution. While computer simulations yield plausible results,[27] it is the experimental verification that is crucial. The technique of positron annihilation spectroscopy represents a possible approach to this problem.[49–52] Simply speaking, the polymer sample is irradiated with positrons, and the radiation released by the mutual annihilation of positrons and electrons can yield information about the lifetime of the positrons in the polymer material, which in turn provides information about the free volume. For most polymers, the lifetime distributions of the positrons are made up of three components, the longest of which correlates with the free volume. For polymers with a very large fractional free volume, such as poly(trimethylsilylpropyne), however, a fourth component is observed.[53] At the same time, the contribution of the third component is reduced. This indicates a significant difference in the distribution of the free volume between the classic amorphous polymers and the "high free volume" polymers such as PTMSP. There is much to do in this area, however, until the exact relationships are explored.

The proposal of Koros does provide new ideas for polymer syntheses, which go far beyond the currently employed rule of thumb "bulky groups →large permeability coefficients; rigid polymer chains →high selectivity". Polymers with main chains consisting of alternating bulky, rigid structural elements and flexible segments represent an interesting approach in this context. It is possible to envision an idealized amorphous state in which the gaps between the polymer chains are strongly controlled by the molecular dimensions of the bulky group and the distance between these groups in the main polymer chain. A orderly arrangement of the polymer chains is not necessary in this case. Gas transport, controlled by local segment motions, occurs only through the free volume, actually only through a small fraction of the free volume, as most of it has subatomic dimensions. Therefore, only a small fraction of the chain segments actually influences the gas transport. It is necessary to identify these segments and to control their motions in terms of extent and frequency. The measurement of physical quantities that refer to longer segments or to average values for many polymer chains (T_g, elasticity module, interchain distances, persistence lengths, etc.) cannot yield useful information in this context. Consequently, one finds no correlation between these data and the permeability and selectivity of polymers, in spite of many attempts to find such correlations.

We attempt to use our polymers with indane groups in the main chain to obtain optimized "blueprints" for polymeric membrane materials for a given separation problem. This is done by varying the length of the flexible segments, the rotational barriers around the assumed hinges, the "internal" flexibility of these segments, and their steric bulk. Structural variations in the flexible and the rigid, bulky segments should lead to different effects on the permeability and selectivity of

a series of polymers. In this respect, our approach differs fundamentally from the increment methods that are commonly studied these days. According to these methods, certain structural elements make fixed contributions to the free volume or even directly to the permeability coefficients. These models therefore ignore regioisomerism. The position of a given structural element along the main polymer chain ought to be irrelevant according to these models. Further studies will show which approach corresponds more closely to reality. The indane moiety can very likely be replaced by other structural elements as the bulky, rigid group, and the same is valid for the phenyl ether sequences as the flexible segments. These replacements may even lead to improved results. This area will prove to be a fertile research field for the preparative polymer chemist.

Finally, it should be mentioned that our models only represents an attempt to overcome the often-discussed trade-off problem between general chain rigidity and the free volume. We are aware that our ideas may very well have to be amended after further studies. Compared to the current models, however, our ideas should facilitate the task of selecting structural modifications by kind and position in a more specific manner.

The polymers were prepared and characterized by Dr. Dazhong Yang (currently with Netzsch Gerätebau, Rep. Office Shanghai) and Dr. Martin Wolf (currently with Brückner Maschinenbau GmbH, Siegsdorf, Germany) during their diploma and dissertation studies. They are particularly acknowledged for their efforts regarding the often nontrivial monomer syntheses. The permeability measurements were performed by Dr. Z. Pientka from the Department of Polymer Membranes (Dr. M. Bleha) at the Institute of Macromolecular Chemistry, Prague (Czech Republic). Dr. C. D. Smith and Dr. M. Langsam of Air Products & Chemicals, Allentown, NY (USA) are acknowledged for their help with some of the measurements.

Received: October 29, 1997 [A259IE]
German version: *Angew. Chem.* **1998**, *110*, 3128 – 3143

[1] See, for example, E. Fitzer, W. Fritz, G. Emig, *Technische Chemie*, 4th ed., Springer, Berlin, **1995**, p. 12; *Taschenbuch der Chemie* (Ed.: K. Schwister), 2nd ed., Fachbuchverlag Leipzig, Carl Hanser Verlag, Leipzig, **1996**, p. 580.
[2] *CHEManager* **1996** (9), GIT Verlag. Nm^3 = norm cubic meter.
[3] W. J. Koros, G. K. Fleming, *J. Membr. Sci.* **1993**, *83*, 1 – 80.
[4] I. Cabasso in *Encyclopedia of Polymer Science and Engineering, Vol. 9*, 2nd ed., Wiley, New York, **1988**, pp. 509 – 579.
[5] H. Strathmann in *Ullmann's Encyclopedia of Industrial Chemistry*, *Vol. A16*, VCH, Weinheim, **1992**, pp. 187 – 263.
[6] W. Pusch, A. Walch, *Angew. Chem.* **1982**, *94*, 670 – 695; *Angew. Chem. Int. Ed. Engl.* **1982**, *21*, 660 – 685.
[7] S. A. Stern, *J. Membr. Sci.* **1994**, *94*, 1 – 65.
[8] E. R. Hensema, *Adv. Mater.* **1994**, *6*, 269 – 279.
[9] R. E. Kesting, A. K. Fritzsche, *Polymeric Gas Separation Membranes*, Wiley, New York, **1993**.
[10] *Polymeric Gas Separation Membranes* (Eds.: D. R. Paul, Yu. P. Yampol'skii), CRC Press, Boca Raton, FL, **1994**.
[11] R. Govind, D. Atnoor, *Ind. Eng. Chem. Res.* **1992**, *30*, 591 – 594.
[12] H. Suda, K. Haraya, *J. Chem. Soc. Chem. Commun.* **1995**, 1179 – 1180.
[13] M. B. Rao, S. Sircar, *J. Membr. Sci.* **1996**, *110*, 109 – 118.
[14] A. S. Damle, S. K. Gangwal, V. K. Venkataraman, *Gas Sep. Purif.* **1994**, *8*, 137 – 147.
[15] J. D. Way, D. L. Roberts, *Sep. Sci. Technol.* **1991**, *27*, 29 – 41.
[16] T. Graham, *Philos. Mag.* **1866**, *32*, 401 – 420.
[17] A. Fick, *Ann. Phys. Chem.* **1955**, *94*, 59.
[18] S. von Wroblewski, *Ann. Phys. Chem.* **1879**, *8*, 29.
[19] J. Brandrup, E. H. Immergut, *Polymer Handbook*, 3rd ed., Wiley, New York, **1989**, p. VI/435.
[20] L. M. Robeson, *J. Membr. Sci.* **1991**, *62*, 165 – 185.
[21] L. M. Robeson, W. F. Burgoyne, M. Langsam, A. C. Savoca, C. F. Tien, *Polymer* **1994**, *35*, 4970 – 4978.
[22] J. Koresh, A. Soffer, *Sep. Sci. Technol.* **1987**, *22*, 973 – 982.
[23] B. N. Nair, H. Suematsu, M. Aizawa, K. Keizer, S.-I. Nakao, *Polym. Mater. Sci. Eng.* **1997**, *77*, 325.
[24] G. A. Shakespear, H. A. Daynes, *Proc. R. Soc. London A* **1920**, *97*, 273 – 286.
[25] H. A. Daynes, *Proc. Roy. Soc. London A* **1920**, *97A*, 286.
[26] R. J. Pace, A. Datyner, *J. Polym. Sci. Polym. Phys. Ed.* **1979**, *17*, 437 – 451.
[27] V. M. Shah, S. A. Stern, P. J. Ludovice, *Macromolecules* **1989**, *22*, 4660 – 4662.
[28] See textbooks of polymer chemistry, for example, H.-G. Elias, *Makromoleküle*, 5th ed., Hüthig, Basel, **1990**; G. Odian, *Principles of Polymerization*, 3rd ed., Wiley, New York, **1991**.
[29] H. Takeuchi, *J. Chem. Phys.* **1990**, *93*, 2062 – 2067.
[30] E. Smit, M. H. V. Mulder, C. A. Smolders, H. Karrenbeld, J. van Eerden, D. Feil, *J. Membr. Sci.* **1992**, *73*, 247 – 257.
[31] F. Müller-Plathe, *J. Chem. Phys.* **1991**, *94*, 3192 – 3199.
[32] W. J. Koros, G. K. Fleming, S. M. Jordan, T. H. Kim, H. H. Hoehn, *Prog. Polym. Sci.* **1988**, *13*, 339 – 401.
[33] J. Y. Park, D. R. Paul, *J. Membr. Sci.* **1997**, *125*, 23 – 39.
[34] S. A. Stern, S. Trohalaki, *ACS Symp. Ser.* **1990**, *423*, 22.
[35] D. W. Van Krevelen, *Properties of Polymers*, 3rd ed., Elsevier, Amsterdam, **1990**, p. 71.
[36] R. N. Haward, *J. Macromol. Sci. Rev. Macromol. Chem.* **1970**, *C4*, 191 – 242.
[37] K. Tanaka, H. Kita, M. Okano, K. Okamoto, *Polymer* **1992**, *33*, 585 – 592.
[38] G. Maier, D. Yang, O. Nuyken, *Makromol. Chem.* **1993**, *194*, 1901 – 1914.
[39] G. Maier, D. Yang, M. Wolf, O. Nuyken, *High Perform. Polym.* **1994**, *6*, 335 – 346.
[40] G. Maier, M. Wolf, *Macromol. Chem. Phys.* **1996**, *197*, 781 – 796.
[41] G. Maier, M. Wolf, *Macromol. Chem. Phys.* **1997**, *198*, 2421 – - 2438.
[42] R. N. Johnson, A. G. Farnham, R. A. Clendinning, W. F. Hale, C. N. Merriam, *J. Polym. Sci. Part A-1,* **1967**, *5*, 2375 – 2398.
[43] P. A. Staniland in *Comprehensive Polymer Science, Vol. 5*, (Eds.: G. Allen, J. C. Bevington), Pergamon, Oxford, **1989**, pp. 483 – 497.
[44] H. R. Kricheldorf in *Handbook of Polymer Synthesis*, *Vol. A*, (Ed.: H. R. Kricheldorf), Marcel Dekker, New York, **1992**, p. 545.
[45] G. Maier, R. Hecht, O. Nuyken, K. Burger, B. Helmreich, *Macromolecules* **1993**, *26*, 2583 – 2591.
[46] L. M. Robeson, C. D. Smith, M. Langsam, *J. Membr. Sci.* **1997**, *132*, 33 – 54.
[47] C. D. Smith, M. Langsam, Air Products & Chemicals, Allentown, NY.
[48] Smith et al. found the following values for **2a**: $P(O_2) = 2.05$, $P(N_2) = 0.33$ (Table 6: 2.05 and 0.32); for **2d**: $P(O_2) = 0.65$, $P(N_2) = 0.097$ (Table 6: 0.68 and 0.09).
[49] V. V. Volkov, A. V. Goldanskii, S. G. Durgar'yan, V. A. Onishchuk, V. P. Shantarovich, Yu. P. Yampol'skii, *Vysokomol. Soedin.* **1987**, *29*, 192 – 197.
[50] K. Tanaka, K. Okamoto, H. Kita, Y. Ito, *Polym. J.* **1993**, *25*, 577 – 584.
[51] Y. Kobayashi, K. Haraya, S. Hattori, T. Saegusa, *Polymers* **1994**, *35*, 925 – 928.
[52] Y. C. Jean, J.-P. Yuan, J. Liu, Q. Deng, H. Yang, *J. Polym. Sci. Part B* **1995**, *33*, 2365 – 2371.
[53] Yu. P. Yampol'skii, V. P. Shantarovich, *Polym. Mater. Sci. Eng.* **1997**, *77*, 306.

[7] R. S. Varma, R. K. Saini, *Tetrahedron Lett.* **1997**, *38*, 4337 – 4338, and references therein.
[8] a) J. Hornke, R. Lipphardt, R. Meldt in *Produktionsintegrierter Umweltschutz in der chemischen Industrie* (Ed.: J. Wiesner) DECHEMA, Frankfurt/Main, **1990**, pp. 17 – 18; b) A. N. Thayer, *Chem. Eng. News* **1995**, *73*(37), 15 – 20.
[9] K. Komiya, S. Fukuoka, M. Aminaka, K. Hasegawa, H. Hachiya, H. Okamoto, T. Watanabe, H. Yoneda, J. Fukawa, T. Dozono in *Green Chemistry, Designing Chemistry for the Environment* (Eds.: P. T. Anastas, T. C. Williamson), American Chemical Society, Washington DC, **1996**, p. 20 – 32.
[10] a) J. O. Metzger, R. Mahler, *Angew. Chem.* **1995**, *107*, 1013 – 1015; *Angew. Chem. Int. Ed. Engl.* **1995**, *34*, 902 – 904; b) J. O. Metzger, R. Mahler, G. Francke, *Liebigs Ann.* **1997**, 2303 – 2313.
[11] a) Z.-Y. Yang, B. V. Nguyen, D. J. Burton, *Synlett* **1992**, 141 – 142; b) J. O. Metzger, R. Mahler, A. Schmidt, *Liebigs Ann.* **1996**, 693 – 696.
[12] K. Adelhorst, F. Björkling, S. E. Godtfredsen, O. Kirk, *Synthesis* **1990**, 112 – 115.
[13] K. S. Bisht, Y. Y. Svirkin, L. A. Henderson, R. A. Gross, D. L. Kaplan, G. Swift, *Macromolecules* **1997**, *30*, 7735 – 7742.
[14] K. S. Bisht, L. A. Henderson, R. A. Gross, D. L. Kaplan, G. Swift, *Macromolecules* **1997**, *30*, 2705 – 2711.
[15] K. S. Bisht, F. Deng, R. A. Gross, D. L. Kaplan, G. Swift, *J. Am. Chem. Soc.* **1998**, *120*, 1363 – 1367.
[16] K. Sato, M. Aoki, J. Takagi, R. Noyori, *J. Am. Chem. Soc.* **1997**, *119*, 12386 – 12387.
[17] a) K. Sato, M. Aoki, M. Ogawa, T. Hashimoto, R. Noyori, *J. Org. Chem.* **1996**, *61*, 8310 – 8311; b) K. Sato, M. Aoki, M. Ogawa, T. Hashimoto, D. Panyella, R. Noyori, *Bull. Chem. Soc. Jpn.* **1997**, *70*, 905 – 915.
[18] L. E. Martinez, J. L. Leighton, D. H. Carsten, E. N. Jacobsen, *J. Am. Chem. Soc.* **1995**, *117*, 5897 – 5898.
[19] D. Rajagopal, K. Rajagopalan, S. Swaminathan, *Tetrahedron: Asymmetry* **1996**, *7*, 2189 – 2190.
[20] E. Diez-Barra, A. de la Hoz, S. Merino, A. Rodriguez, P. Sanchez-Verdu, *Tetrahedron* **1998**, *54*, 1835 – 1844.
[21] G. Bram, G. Decodts, *Synthesis* **1985**, 543 – 545.
[22] a) J. Barry, G. Bram, G. Decodts, A. Loupy, P. Pigeon, J. Sansonlet, *J. Org. Chem.* **1984**, *49*, 1138 – 1140; b) P. Vinczer, S. Sztruhar, L. Novak, C. Szantay, *Org. Prep. Proced. Int.* **1992**, *24*, 540 – 543.
[23] T. K. Lindhorst, C. Kieburg, *Synthesis* **1995**, 1128 – 1130.

Amyloid Aggregates, Presenilins, and Alzheimer's Disease

Ralf Baumeister* and Stefan Eimer

Alzheimer's disease is today the most common cause of neurodegenerative death in the western world. The disease is characterized by two fundamental events, the accumulation of insoluble fibrillar aggregates of β-amyloid peptide (Aβ) and the degeneration and death of neurons in the brain regions that are concerned with learning and memory processes. Abnormal protein deposition is also a shared characteristic of other age-related neurodegenerative disesases, such as Parkinson's disease, Huntington's disease, and the Prion diseases. There is increasing evidence that the mechanism of this aggregation may be similar in each of these diseases.[1] Several recent studies have advanced our understanding considerably of the molecular and cellular mechanisms that cause the disease. The purpose of this article is to summarize recent results.

The Biochemistry of APP Processing and Amyloid Aggregation

The central role in the pathogenesis of Alzheimer's disease is played by a small, 40 – 42 amino acid long, four kDa peptide called Aβ. Aβ is derived from the 695 – 770 amino acid long amyloid precursor protein (APP) by various proteolytic steps that are thought to take place in several intracellular compartments[2] (Figure 1). The detailed mechanism of Aβ production from APP, the exact localization of the three proteases involved, and the functions of Aβ and APP are not yet understood (for review articles see refs. [3, 4]). The 40 amino acid peptide Aβ40 is the predominant form that is produced during the metabolism of APP. Under pathological conditions the production of a 42 amino acid variant (Aβ42), normally a minor product, is enhanced.

Aβ40 is kinetically inert for several days in solution. In the disease state it is converted into a fibrous form, which is relatively resistant to chemical denaturing or proteolytic digestion.[5] This conversion is mediated by a change in the three-dimensional structure of Aβ40 and results in an increase in the hydrophobicity of the peptide. The peptide then aggregates and forms an ordered fibrillar morphology. The structural properties of the Aβ aggregates suggest that, in contrast to amorphous precipitates, their formation is seeded and involves polymerization from a nucleus.[1, 6] This process is very slow because of the high entropy of intermolecular interactions.[6] For this reason, the sporadic forms of Alzheimer's disease, which comprise the fast majority of clinical cases, occur late in life (usually between the ages of 75 and 85), although Aβ can be detected much earlier. Another Aβ variant, Aβ42, is more hydrophobic and may produce the pathogenic seed in the development of the disease.[6] Aβ42 is highly aggregable and is the predominant form of Aβ in senile plaques.[2] Overexpression of APP increases the amount of Aβ40 and Aβ42 and results in faster aggregation.[7] It is in this context interesting to note that patients with Down's syndrome, who have an additional copy of chromosome 21 on which the APP gene is located, invariantly develop symptoms of Alzheimer's disease and develop them significantly earlier.[3]

[*] Dr. R. Baumeister, Dipl.-Biochem. S. Eimer
Genzentrum der Ludwigs-Maximillians-Universität
Feodor-Lynen-Strasse 25, D-81377 Munich (Germany)
Fax: (+49) 89-7401-7314
E-mail: bmeister@lmb.uni-muenchen.de

 © WILEY-VCH Verlag GmbH, D-69451 Weinheim, 1998 1433-7851/98/3721-2978 $ 17.50+.50/0

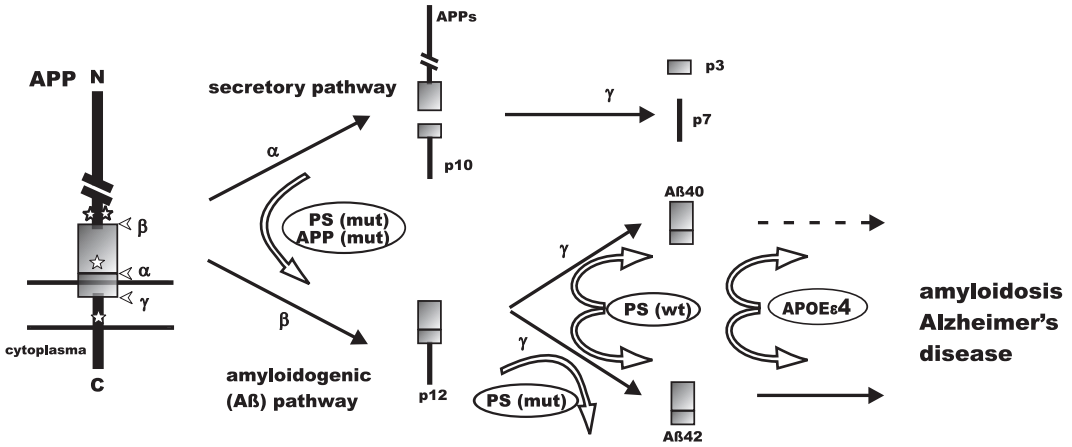


Figure 1. Flowchart of APP metabolism. The factors that affect the processing of APP and the onset of the disease are shown. Left: Schematic representation of APP with the relative positions of mutations indicated by asterisks. The position of the Aβ region is shown by a box. p3, p7, p10, p12 = APP cleavage products with molecular weights of 3, 7, 10, and 12 kDa size, respectively; α, β, γ = secretases involved in the cleavages; mut: mutation; wt = normal type.

Modulators of Aggregation

The first susceptibility gene identified for the common, sporadic form of Alzheimer's disease was the *apoe* gene, which encodes a protein involved in cholesterol transport.[8] People with a particular variant of the APOE protein (the ε4 isoform), have an increased risk of developing sporadic late-onset Alzheimer's disease.

Convincing evidence that the *apoe* gene directly affects Aβ deposition was provided by Paul's research group.[9] They crossed transgenic mice overexpressing a human APP variant, which exhibits strong Aβ and amyloid deposition, with *apoe*-knock-out mice. The progeny from this cross showed a dramatic reduction of Aβ deposits, which indicates that the main contribution of the APOE protein is to promote Aβ fibril formation. Another recent report suggests that other polymorphisms in the transcriptional regulatory region of the *apoe* gene might also be associated with an increased risk of Alzheimer dementia, even in the absence of the ε4 isoform.[10]

The APOE protein may be considered a modifier of Alzheimer's disease since APOE variants do not result in an earlier onset of the disease but promote the late stages of the disease. In contrast, mutations in the three identified loci on chromosomes 2, 14, and 21 cause an heritable form of the disease (FAD, familial Alzheimer's disease) that generally leads to an earlier onset and faster progression of the disease relative to the sporadic cases. All mutations have been shown to promote the seeding of amyloid aggregates. The first gene identified encodes APP itself.[2, 11] The various mutations affect the overproduction of Aβ42 or an overall increase in Aβ secretion. However, these mutations are rare and were found only in a small patient group worldwide. The vast majority of FAD cases correlate with two genes, which encode transmembrane proteins, which been designated presenilin-1 (PS1) and presenilin-2 (PS2). Mutations in PS1 and PS2 are responsible for the most aggressive clinical forms of Alzheimer's disease, with a mean age of onset of approximately 45 and 52 years, respectively. Recent research on the function of the presenilins provides an important clue to understanding the mechanism of the disease.

Presenilin Mutants and Amyloid Formation

PS1 and PS2 encode proteins of 467 and 448 amino acids, respectively, which are about 67 % identical in their primary sequence.[12] The presenilins are highly conserved in evolution, and have been identified in nematodes (*Caenorhabditis elegans*), fruit flies (*Drosophila*), clawed frogs (*Xenopus*), Zebrafish, and mammals.[13] Several research groups have recently analyzed the topology of PS1[14, 15] and its *C. elegans* homologue SEL-12.[16] The amino and carboxy termini of both proteins have a cytoplasmic localization and is followed by six transmembrane (TM) domains and a large, hydrophilic loop, which again protrudes into the cytoplasma of the cell (Figure 2). It is very likely that the other presenilins adopt similar structures based on the sequence conservation.

The phenotypes associated with mutations in the presenilin genes are most informative for understanding their function in the nervous system. To date, more than 35 mutations in the PS1 gene and two mutations in the PS2 gene have been isolated from FAD patients, which supports the key role of the presenilins in the mechanism of the disease.

With the noteworthy exception of PS1Δ10, a splice variant which eliminates exon 10 (but results in a mutation of a highly conserved serine to cysteine at the splice site in TM6), all mutations that have been isolated from patients are single amino substitutions. No mutations have so far been isolated from FAD patients that result in frameshifts or premature translational stops and cause truncations of the carboxy terminal. This suggests that severe structural or functional defects cannot be tolerated in the presenilins. The embryonic lethality of presenilin-knock-out mice supports this view. One plausible explanation would be that the FAD mutations cause subtle defects, since they do not have embryonic phenotypes. More than 80 % of the mutations occur in amino acids that are conserved in presenilins of different species.[17] The local-

 © WILEY-VCH Verlag GmbH, D-69451 Weinheim, 1998 1433-7851/98/3721-2979 $ 17.50+.50/0

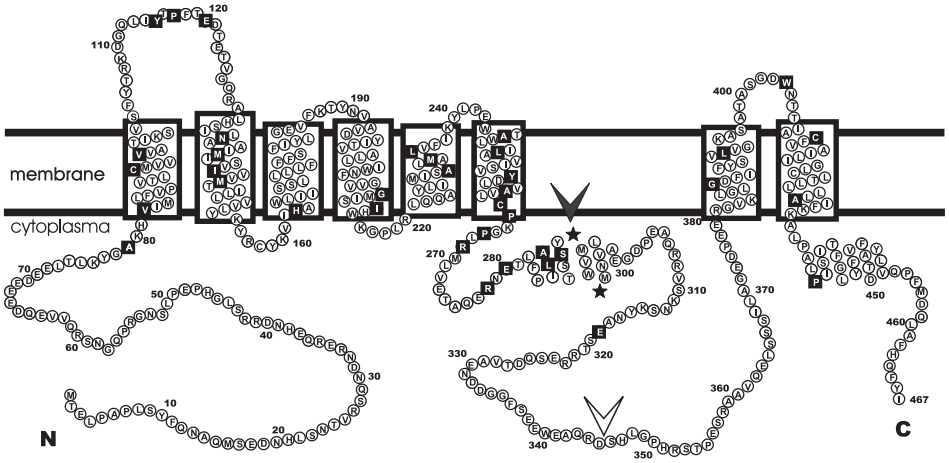


Figure 2. The structure of PS1. The eight transmembrane domain model of PS1 structure is depicted as suggested by Li et al.[16] Putative TM domains are boxed. Sites of proteolytic cleavage by presenilinase (black arrowhead, exact position: black asterisk) and caspase (white arrowhead) are indicated. Positions of FAD mutations in PS1 are boxed.

ization of these mutations suggests that TM2 and the two large hydrophilic loops are most critical for PS1 function.

Proteolytic Processing of Presenilins

Only a minor amount of the endogenous presenilin proteins can be isolated as full-length proteins. The most abundant fragments identified are an approximately 27–28 kDa amino-terminal fragment (NTF) and an approximately 18–20 kDa carboxy-terminal fragment (CTF).[12] PS2 is proteolytically cleaved into two stable cellular polypeptides of about 20 kDa and 34 kDa.[18] The cleavage in the large cytoplasmic loop is obviously tightly regulated, since overproduction of PS results in the accumulation of the full-length protein, but not of the proteolytic fragments. The resulting fragments are very stable and interact with one another. Since they are found in complexes with a higher molecular weight, they probably bind other currently unidentified proteins as well. Considerable effort was made to identify whether presenilinase cleavage is a functional requirement,[19] a stable degradation intermediate,[20, 21] or even a preparation artifact.[22] This question has not yet been fully resolved. Lack of cleavage is probably not a central feature of pathogenesis in FAD patients, since little, if any, full-length PS1 is observed in brain tissue of patients carrying PS1 mutations.[23]

The presenilins PS1 and PS2 are also proteolytically processed by proteases of the caspase superfamily (proteins that take part in programmed cell death, apoptosis).[18] This process generates a larger NTF and a smaller CTF if full-length presenilin is the substrate, or only a smaller CTF if the conventional CTF is the substrate (Figure 2). There was a lot of excitement last year when Tanzi's research group reported that the PS2 mutation N141I enhances the intracellular concentration of the alternative CTF derived by caspase-cleavage.[24] It was postulated that apoptosis-mediated cleavage may be required for the effect of mutant PS proteins on abnormal Aβ processing. Indeed, a functional involvement of PS in apoptosis had been reported before. However, a combined effort of three research groups showed recently that the inhibition of caspase cleavage does not affect Aβ generation. Moreover, mutation of the caspase cleavage site prevented the apoptotic proteolysis, but did not affect the biological activity of human PS1 and PS2 in *C. elegans*.[25]

Presenilins and the Metabolism of APP

Mutant presenilin proteins, like mutant APP itself, affect proteolytic processing of APP (Figure 1). Mutations in all three genes enhance the processing pathway that results in an increased production of the 42 amino acid variant Aβ42, whereas Aβ40 levels are not affected.[12] Since this variant aggregates much faster than Aβ40, these results strongly support the model of Aβ42 being the key component involved in the disease mechanism. All PS1 and PS2 mutations analyzed to date increase the Aβ42 levels significantly. These results strongly support the central role of Aβ formation and presenilin function in the disease mechanism.

How are the presenilins involved in the proteolytic processing of APP? It has long been thought that proteolysis of APP mostly occurs at or near the cytoplasmic membrane (the non-amyloidogenic or secretory pathway, upper part in Figure 1) or during reinternalization (Aβ generating pathway, lower part in Figure 1).[26] In contrast, the presenilins are located mostly in the membranes of the endoplasmic reticulum (ER) and the early Golgi apparatus. However, last year several research groups identified intracellular Aβ formation and showed that the ER is the first compartment where Aβ42 accumulates.[27–29] These results also suggest that the proteolytic cleavage at the carboxy terminus of Aβ40 and Aβ42 are accomplished by different enzymes and/or by a different intracellular localization of the enzyme(s) involved. These data provoked an exciting new model that explained how the presenilin can affect APP processing. The localization of the presenilin in the ER and Golgi membranes suggests that they are in a perfect position to control the transport and/or trafficking of APP. There is indeed support for such a role: the presenilin SPE-4 in the nematode *C. elegans* controls the sorting and protein trafficking in specialized organelles.[30] In addition, several recent publications report that there may be direct binding of PS1 and PS2 to the immature form of APP in

 © WILEY-VCH Verlag GmbH, D-69451 Weinheim, 1998 1433-7851/98/3721-2980 $ 17.50+.50/0 *Angew. Chem. Int. Ed.* **1998**, *37*, No. 21

the ER.[31, 32] Although these interactions, identified through co-immunoprecipitation studies and in the yeast-two-hybrid system, nicely fit into this model, attempts to reproduce these results in other research groups have failed.[33] Nevertheless, the generally observed increase in Aβ42 production in the presence of presenilin mutants indicates that APP and presenilins at least interfere functionally.[34] It came as a big surprise that in cells of PS1-knock-out mice the Aβ40 and Aβ42 levels dropped by 80%, whereas neurons in FAD patients have increased levels of Aβ42.[35] Although the subcellular localization of these fragments could not be determined, the most obvious interpretation is that the presenilins themselves have protease (γ-secretase, see Figure 1) activity or may regulate the activity of this protease. However, these results are also compatible with PS1 having a role in the intracellular compartmental transport of membrane proteins. In accordance with the latter model a lack of PS1 could redirect APP sorting and transport from the ER through compartments that lack γ-secretase activities. It is puzzling to see that both Aβ40 and Aβ42 are equally affected by PS mutants. Additional work is clearly required to solve these discrepancies, and eventually the presenilins might even serve as a therapeutic target for Alzheimer's disease. A significant decrease of presenilin activity, accomplished by either reducing the expression levels or by interfering with the processing, is suggested to reduce the Aβ production and, thus, the aggregation of plaque formation in the brain.

Biological Function of Presenilins

To fully understand the role of presenilins in Alzheimer's disease it is essential to know more about their biological function. The few data we have are derived from work carried out on the nematode *C. elegans* and in mice. The SEL-12 mutants *C. elegans* suggest that the presenilins play a role in the signal transduction of the Notch transmembrane receptor, a pathway through which adjacent cells communicate.[36] The human presenilins are also linked to the Notch pathway, since human PS1 and PS2 are functional in *C. elegans*[20, 21] and Notch activity is strongly reduced in PS1-knock-out mice.[37, 38] It is not clear, at this point, whether the PS proteins function in the signaling pathway or activity of Notch, or, at an earlier step, in the sorting and transport of Notch from the ER to the membrane. Since SEL-12 mutations seem to influence the function of other secreted transmembrane proteins as well,[39] which supports the latter model, we suggest that the PS proteins play a more general role in the cell.

Outlook

Significant progress has been made in the past couple of years to understand the molecular and genetic basis of Alzheimer's disease and FAD. The fundamental importance of Aβ42 and the presenilins as key players in the disease mechanism has been substantiated. Work in the following years will most likely concentrate on the identification of new genes and interactors to close the remaining gaps in the story. The nematode *C. elegans* model as a biological assay system to identify additional components required for presenilin function, and the availability of several mouse models for Aβ aggregation will provide additional clues and maybe targets for therapeutic intervention in the near future.

German version: *Angew. Chem.* **1998**, *110*, 3148 – 3152

Keywords: Alzheimer's disease · amyloids · presenilin · protein structures

[1] P. T. Lansbury, Jr., *Neuron* **1997**, *19*, 1151 – 1154.
[2] R. E. Tanzi, D. M. Kovacs, T. W. Kim, R. D. Moir, S. Y. Guenette, W. Wasco, *Neurobiol. Disease* **1996**, *3*, 159 – 168.
[3] D. J. Selkoe, *J. Biol. Chem.* **1996**, *271*, 18295 – 18298.
[4] D. J. Selkoe, *Science* **1997**, *275*, 630 – 631.
[5] J. T. Jarrett, E. P. Berger, P. T. Lansbury, Jr., *Ann. N.Y. Acad. Sci.* **1993**, *695*, 144 – 148.
[6] J. D. Harper, C. M. Lieber, P. T. Lansbury, Jr., *Chem. Biol.* **1997**, *4*, 951 – 959.
[7] K. Hsiao, P. Chapman, S. Nilsen, C. Eckman, Y. Harigaya, S. G. Younkin, F. Yang, G. Cole, *Science* **1996**, *274*, 99 – 102.
[8] W. J. Strittmatter, A. D. Roses, *Proc. Natl. Acad. Sci. USA* **1995**, *92*, 4725 – 4727.
[9] K. R. Bales, T. Verina, R. C. Dodel, Y. Du, L. Altstiel, M. Bender, P. Hyslop, E. M. Johnstone, S. P. Little, D. J. Cummins, P. Piccardo, B. Ghetti, S. M. Paul, *Nature Genet.* **1997**, *17*, 263 – 264.
[10] M. J. Bullido, M. J. Artiga, M. Recuero, I. Sastre, M. A. Garcia, J. Aldudo, C. Lendon, S. W. Han, J. C. Morris, A. Frank, J. Vazquez, A. Goate, F. Valdivieso, *Nature Genet.* **1998**, *18*, 69 – 71.
[11] A. Goate, M. C. Chartier-Harlin, M. Mullan, J. Brown, F. Crawford, L. Fidani, L. Giuffra, A. Haynes, N. Irving, L. James, R. Mant, P. Newton, K. Rooke, P. Roques. C. Talbot, M. Pericak-Vance, A. Roses, R. Williamson, M. Rossor, M. Owen, J. Hardy, *Nature* **1991**, *349*, 704 – 706.
[12] C. Haass, *Neuron* **1997**, *18*, 687 – 690.
[13] R. Baumeister, C. Haass in *The Molecular Biology of Alzheimer's Disease* (Ed.: C. Haass), Harwood Academic Publishers, Chur, **1998**, in print.
[14] A. Doan, G. Thinakaran, D. R. Borchelt, H. H. Slunt, T. Ratovitsky, M. Podlisny, D. J. Selkoe, M. Seeger, S. E. Gandy, D. L. Price, S. S. Sisodia, *Neuron* **1996**, *17*, 1023 – 1030.
[15] S. Lehmann, R. Chiesa, D. A. Harris, *J. Biol. Chem.* **1997**, *272*, 12047 – 12051.
[16] X. Li, I. Greenwald, *Neuron* **1996**, *17*, 1015 – 1021.
[17] R. E. Tanzi, D. M. Kovacs, T.-W. Kim, R. D. Moir, S. Y. Guenette, W. Wasco, *Alzheimer's Disease Review* **1996**, *1*, 90 – 98.
[18] T.-W. Kim, W. H. Pettingell, O. Hallmark, R. D. Moir, W. Wasco, R. E. Tanzi, *J. Biol. Chem.* **1997**, *272*, 11006 – 11010.
[19] G. Thinakaran, D. R. Borchelt, M. K. Lee, H. H. Slunt, L. Spitzer, G. Kim, T. Ratovitsky, F. Davenport, C. Norderstedt, M. Seeger, J. Hardy, A. I. Levey, S. E. Gandy, N. A. Jenkins, N. G. Copeland, D. L. Price, S. S. Sisodia, *Neuron* **1996**, *17*, 181 – 190.
[20] D. Levitan, T. G. Doyle, D. Brousseau, M. K. Lee, G. Thinakaran, H. H. Slunt, S. S. Sisodia, I. Greenwald, *Proc. Natl. Acad. Sci. USA* **1996**, *93*, 14940 – 14944.
[21] R. Baumeister, U. Leimer, I. Zweckbronner, C. Jakubek, J. Grünberg, C. Haass, *Genes Funct.* **1997**, *1*, 149 – 159.
[22] N. N. Dewji, C. Do, S. J. Singer, *Proc. Natl. Acad. Sci. USA* **1997**, *94*, 14031 – 14036.
[23] L. Hendriks, G. Thinakaran, C. L. Harris, C. D. Jonghe, J.-J. Martin, S. S. Sisodia, C. V. Broeckhoven, *NeuroReport* **1997**, *8*, 1717 – 1721.
[24] T. W. Kim, W. H. Pettingell, Y. K. Jung, D. M. Kovacs, R. E. Tanzi, *Science* **1997**, *277*, 373 – 376.
[25] M. Brockhaus, J. Grünberg, S. Röhrig, H. Loetscher, N. Wittenburg, R. Baumeister, H. Jacobsen, C. Haass, *NeuroReport* **1998**, *9*, 1481 – 1486.
[26] D. J. Selkoe, *Cold Spring Harbor Symp. Quant. Biol.* **1996**, *61*, 587 – 596.
[27] C. Wild-Bode, T. Yamazaki, A. Capell, U. Leimer, H. Steiner, Y. Ihara, C. Haass, *J. Biol. Chem.* **1997**, *272*, 16085 – 16088.
[28] T. Hartmann, S. C. Bieger, B. Bruhl, P. J. Tienari, N. Ida, D. Allsop, G. W. Roberts, C. L. Masters, C. G. Dotti, K. Unsicker, K. Beyreuther, *Nature Med.* **1997**, *3*, 1016 – 1020.

 © WILEY-VCH Verlag GmbH, D-69451 Weinheim, 1998 1433-7851/98/3721-2981 $ 17.50+.50/0

[29] D. G. Cook, M. S. Forman, J. C. Sung, S. Leight, D. L. Kolson, T. Iwatsubo, V. M. Lee, R. W. Doms, *Nature Med.* **1997**, *3*, 1021 – 1023.
[30] S. W. L. Hernault, G. M. Benian, R. B. Emmons, *Genetics* **1993**, *134*, 769 – 780.
[31] A. Weidemann, K. Paliga, U. Dürrwang, C. Czech, G. Evin, C. L. Masters, K. Beyreuther, *Nature Med.* **1997**, *3*, 328 – 332.
[32] W. Xia, J. Zhang, R. Perez, E. H. Koo, D. J. Selkoe, *Proc. Natl. Acad. Sci. USA* **1997**, *94*, 8208 – 8213.
[33] S. S. Sisodia, G. Thinakaran, H. H. Slunt, P. C. Wong, D. R. Borchelt, S. Naruse, H. Zheng, D. L. Price, *J. Neurochem.* **1998**, *70*, *Suppl. 1*, S3.
[34] L. Holcomb, M. N. Gordon, E. McGowan, X. Yu, S. Benkovic, P. Jantzen, K. Wright, I. Saad, R. Mueller, D. Morgan, S. Sanders, C. Zehr, K. O'Campo, J. Hardy, C. M. Prada, C. Eckman, S. Younkin, K. Hsiao, K. Duff, *Nature Med.* **1998**, *4*, 97 – 100.
[35] B. De Strooper, P. Saftig, K. Craessaerts, H. Vanderstichele, G. Guhde, W. Annaert, K. von Figura, F. Van Leuven, *Nature* **1998**, *391*, 387 – 390.
[36] D. Levitan, I. Greenwald, *Nature* **1995**, *377*, 351 – 354.
[37] J. Shen, R. T. Bronson, D. F. Chen, W. Xia, D. J. Selkoe, S. Tonegawa, *Cell* **1997**, *89*, 629 – 639.
[38] P. C. Wong, H. Zheng, H. Chen, M. W. Becher, D. J. S. Sirinathsinghji, M. E. Trumbauer, H. Y. Chen, D. L. Price, L. H. T. Van der Pleog, S. S. Sisodia, *Nature* **1997**, *387*, 288 – 292.
[39] R. Baumeister, unpublished results.

Deposition of Data from X-Ray Structure Analyses

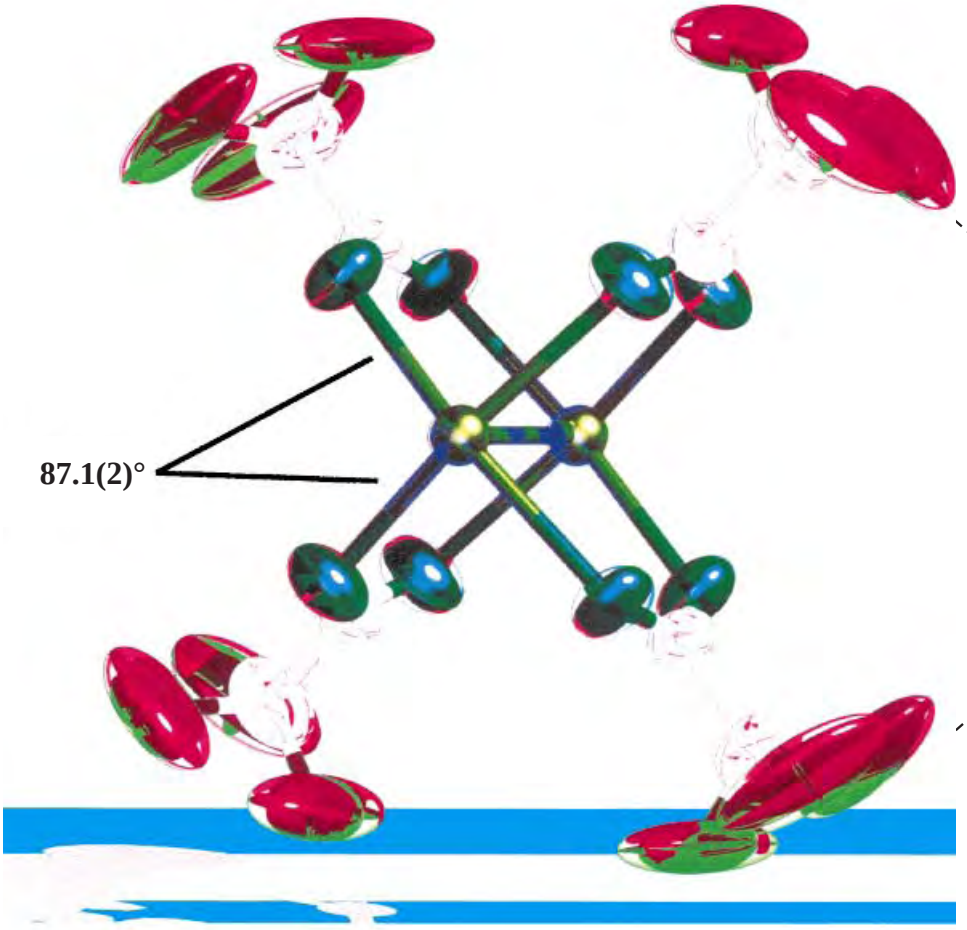
In order to make life easier for authors and referees the Cambridge Crystallographic Data Centre (CCDC) and the Fachinformationszentrum Karlsruhe (FIZ) have unified their procedures for the depostion of data from single-crystal X-ray structure analyses.

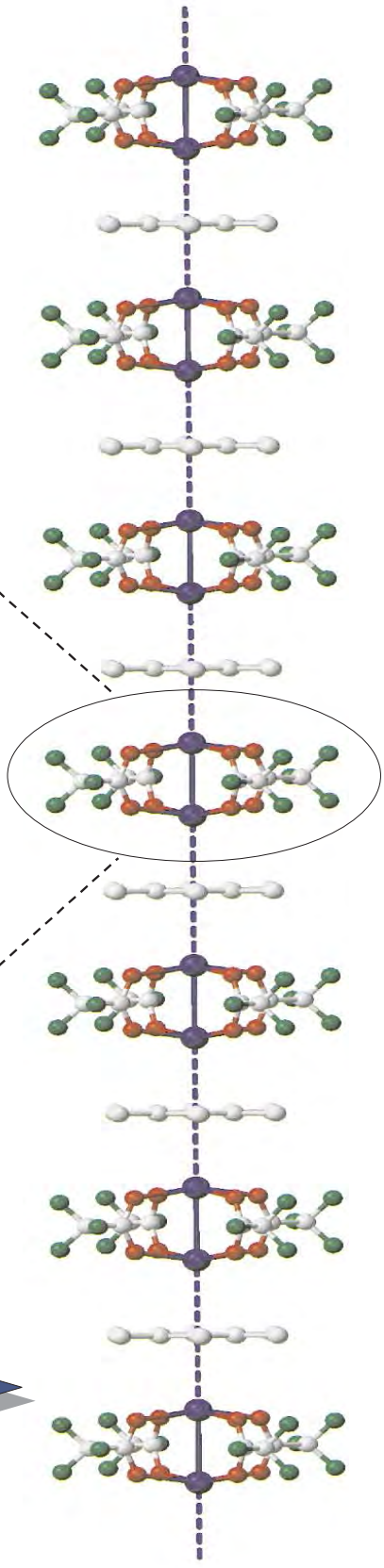
Prior to submitting a manuscript please deposit the data for your compound(s) **electronically** at the appropriate date base, that is, at the CCDC for organic and organometallic compounds and at the FIZ for inorganic compounds. Both data bases will be pleased to provide help (see our *Notice to Authors* in the first issue of this year). In general, you will receive a depository number from the data base within two working days after electronic deposition; please include this number with the appropriate standard text (see our Notice to Authors) in your manuscript. This will enable the referees to retrieve the structure data quickly and efficiently if they need this information to reach their decision.

This is now the uniform procedure for manuscripts submitted to the journals *Advanced Materials, Angewandte Chemie, Chemistry–A European Journal, the European Journal of Inorganic Chemistry, and the European Journal of Organic Chemistry.*

 © WILEY-VCH Verlag GmbH, D-69451 Weinheim, 1998 1433-7851/98/3721-2982 $ 17.50+.50/0

Coordination sphere of the dimetal unit in the bismuth(II) trifluoroacetate molecule: the packing forces on the indicated periphery lead to the given deviation from the ideal tetragonal-prismatic arrangement in the crystal.





$[Bi_2(O_2CCF_3)] \cdot C_{12}H_{18}$: a one-dimensional coordination copolymer of a main group element compound with hexamethylbenzene.

Further details on this arene adduct of the first reduced main group element carboxylate are discussed on the following pages.

 © WILEY-VCH Verlag GmbH, D-69451 Weinheim, 1998 1433-7851/98/3721-2983 $ 17.50+.50/0

$[Bi_2(O_2CCF_3)_4]\cdot C_6Me_6$—Arene Adduct of a Reduced Main Group Element Carboxylate with Paddle Wheel Structure**

Walter Frank,* Vera Reiland, and Guido J. Reiß

Dedicated to Professor Otto J. Scherer on the occasion of his 65th birthday

In the course of the development of bonding models for systems containing isolated metal–metal bonds, transition metal complexes with tetragonal-prismatic coordination and among these especially the transition metal carboxylates with "paddle wheel structure" have played an outstanding role.[1] Remarkably hitherto no corresponding main group element species within this class of compounds have been presented. On the whole very few examples of carboxylato groups functioning as bridging ligands at element–element bonds have been observed in the field of the representative elements: $B_3H_6(O_2CR)$,[2a] $Ga_2(CH(SiMe_3)_2)_2(O_2CR)_2$,[2b] and $Ph_4Sn_2(O_2CR)$.[2c] In our work on the chemistry and coordination chemistry of bismuth(III) trifluoroacetate and its π-arene complexes we isolated the title compound **1** which contains the first reduced main group element carboxylate as part of a one-dimensional coordination copolymer with hexamethylbenzene.

$[Bi_2(O_2CCF_3)_4]\cdot C_6Me_6$ **1**

Dark red crystals of **1** were obtained by an as yet unclarified route by thermolysis of bismuth(III) trifluoroacetate[3] in the presence of hexamethylbenzene in a sealed glass tube. The crystals, which are remarkably stable when exposed to air, were characterized by elemental analysis, mass spectrometry, and a crystal structure determination.[4] These crystals are negligibly soluble in arenes and in donor solvents. In the mass spectrum (electron impact) the peak corresponding to the highest mass observed is attributed to $[Bi_2(O_2CCF_3)_4]$. In addition the signals related to the members of the series $[Bi_2(O_2CCF_3)_n]^+$ with $n = 3-0$ are present. Although the Bi atoms of the complex are held together by both the Bi–Bi bond and the bridging ligands, signals related to the series $[Bi(O_2CCF_3)_n]^+$ with $n = 2-0$ are observed as well.

Under the conditions described here **1** crystallizes in the monoclinic space group *C*2/*m*. $Bi_2(O_2CCF_3)_4$ and C_6Me_6 molecules acting as η^6 bridging ligands on both sides build up chains along [010] (Figure 1).[5] Both components occupy special positions of crystallographic point group symmetry 2/*m*. The distance between the metal atom and the plane of the arene ligand (3.053(2) Å) is slightly shorter than in $[Me_6C_6(BiCl_3)_2]$[6a] (3.07 Å) and significantly longer than in the cationic complex $[Me_6C_6BiCl_2][AlCl_4]$ (2.62 Å).[6b] The

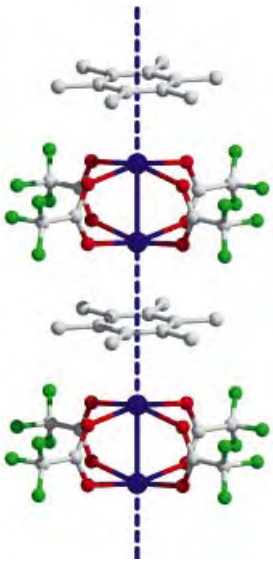


Figure 1. Segment of the one-dimensional coordination-polymeric arrangement of bismuth(II) trifluoroacetate and hexamethylbenzene molecules in the crystal of **1**; Bi atoms are shown blue, F atoms green, O atoms red, and C atoms gray. The distances Bi–Bi and Bi–$arene_{center}$ which are characteristic intercepts on the "supramolecular axis" are very similar (2.9466(11) and 3.053(2) Å, respectively). The distances between the Bi atom and the three crystallographically independent ring C atoms are 3.354(4), 3.357(4), and 3.358(3) Å.

Bi–Bi distance of 2.947(1) Å is significantly shorter in **1** than in $(Me_3Si)_4Bi_2$ (3.035(3) Å),[7a] 2,2′,5,5′-tetramethyldibismole (2.9905(5) Å),[7b] and the three structurally characterized modifications of Ph_4Bi_2 (2.984(2)–2.990(2) Å).[7c–e] It is just 5% longer than in Tbt_2Bi_2 (Tbt = 2,4,6-tris[bis(trimethylsilyl)methyl]phenyl)(2.8206(8) Å),[8] which recently was presented as a compound containing a Bi–Bi double bond. The Bi–O distances of 2.387(6) and 2.417(7) Å are comparable to the shorter ones in $Bi(O_2CCF_3)_3\cdot HO_2CCF_3$,[3b] which exhibits a Bi–O distance spectrum ranging from 2.26(3) to 2.91(3) Å. If the center of the arene is considered to be a coordination site, the Bi atoms are six-coordinate. The geometry of the coordination sphere reflects the insufficient span of the carboxylato ligands with respect to the length of a Bi–Bi bond. The coordination sphere (Figure 2) does not show any gap interpretable in the sense of a stereochemically active lone pair of electrons, an extremely rare situation in the coordination chemistry of bismuth(III) complexes with oxygen donor ligands.[9]

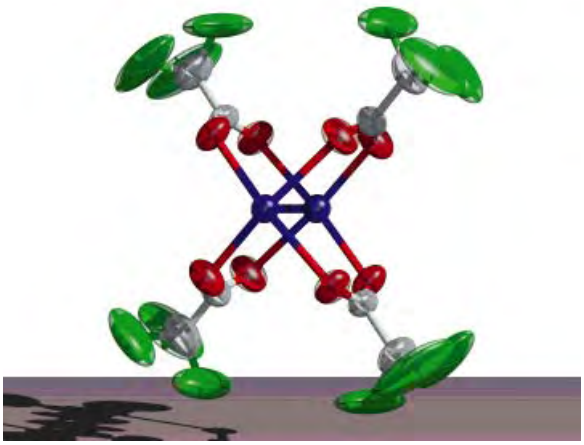


Figure 2. Structure of the $Bi_2(O_2CCF_3)_4$ molecule having C_{2h} point group symmetry in the crystal of **1**; anisotropic displacement ellipsoids are drawn at the 50% probability level; color coding as in Figure 1. The representation of the CF_3 groups indicates their high mobility.

[*] Prof. Dr. W. Frank, Dipl.-Chem. V. Reiland, Dr. G. J. Reiß
Fachbereich Chemie der Universität
Postfach 3049, D-67653 Kaiserslautern (Germany)
Fax: (+49) 631-205-2187
E-mail: wfrank@rhrk.uni-kl.de

[**] Heavy Metal π Complexes, Part 14. This research was supported by the Fonds der Chemischen Industrie. Part 13: W. Frank, V. Reiland, *Acta Crystallogr. Sect. C*, in press.

 © WILEY-VCH Verlag GmbH, D-69451 Weinheim, 1998 1433-7851/98/3721-2984 $ 17.50+.50/0

In addition to the red needles described we obtained small orange plates of another modification of **1** under different reaction conditions. Furthermore, the red phase slowly changes into a yellow one at low temperature. Thus investigations on the phase relations as well as efforts to solve the formation mechanism of **1** are in progress.

Experimental Section

catena-Poly{[tetrakis(μ-trifluoroacetato-$\kappa O,\kappa O'$)dibismuth($Bi-Bi$)]-μ-η^6-hexamethylbenzene} (**1**): A mixture of $Bi(O_2CCF_3)_3$[3b] (0.010 g, 0.18 mmol) and freshly sublimed hexamethylbenzene (0.020 g, 0.12 mmol) in a sealed Duran glass tube was heated to 100 °C in an aluminum block oven. Small light yellow plates of $Bi(O_2CCF_3)_3 \cdot 0.5\,C_{12}H_{18}$ which initially grew at the glass surface disappeared in the course of several weeks, while dark red needles of **1** grew (0.019 g, 20.5% isolated; a yellow-gray residue remained). Elemental analysis calcd for ($M_r = 1032.30$) (%): C 23.1, H 1.7; found: C 22.1, H 1.8; MS (EI, 70 eV, 1.0 mA, QT = 220 °C): *m/z* (%): 870 (9) [$(\mathbf{1}-C_{12}H_{18})^+$], 757 (24) [$(Bi_2(O_2CCF_3)_3)^+$], 644(7) [$(Bi_2(O_2CCF_3)_2)^+$], 531(6) [$(Bi_2(O_2CCF_3))^+$], 435 (8) [$(Bi(O_2CCF_3)_2)^+$], 418 (6) [$Bi_2^+$], 322(19) [$(Bi(O_2CCF_3))^+$], 209 (50) [$Bi^+$], 162 (57) [$C_{12}H_{18}^+$], 147 (100) [$C_{11}H_{15}^+$].

Received: June 22, 1998 [Z 12017 IE]
German version: *Angew. Chem.* **1998**, *110*, 3153 – 3155

Keywords: arene complexes · bismuth · carboxylato complexes · metal – metal interactions · stacking interactions

[1] a) F. A. Cotton, R. A. Walton, *Multiple Bonds Between Metal Atoms*, 2nd ed., Oxford University Press, Oxford, **1992**; b) F. A. Cotton, R. A. Walton, *Struct. Bonding* **1985**, *62*, 1; c) F. A. Cotton, M. H. Chisholm, *Chem. Eng. News* **1982**, *60*, 40; d) F. A. Cotton, *Chem. Soc. Rev.* **1983**, *12*, 35; e) M. H. Chisholm, I. P. Rothwell, *Progr. Inorg. Chem.* **1982**, *29*, 1.

[2] a) H. Binder, B. Brellochs, B. Frei, A. Simon, B. Hettich, C*hem. Ber.* **1989**, *122*, 1049; b) W. Uhl, I. Hahn, H. Reuter, *ibid.* **1996**, *129*, 1425; c) S. Adams, M. Dräger, B. Mathiasch, *J. Organomet. Chem.* **1987**, *326*, 186.

[3] a) P. V. Radheshwar, R. Dev, G. H. Cady, *J. Inorg. Nucl. Chem.* **1972**, *34*, 3913. b) G. J. Reiß, W. Frank, J. Schneider, *Main Group Metal Chem.* **1995**, *18*, 287.

[4] $C_{20}H_{18}Bi_2F_{12}O_8$, $M_r = 1032.30$; crystal dimensions: $0.02 \times 0.02 \times 0.1$ mm^3, monoclinic, space group $C2/m$, $a = 19.963(4)$, $b = 9.053(2)$, $c = 9.040(2)$ Å, $\beta = 109.22(3)^\circ$, $Z = 2$, $V = 1542.7(6)$ Å^3, $\rho_{calcd} = 2.222$ Mg m^{-3}, $T = -10 \pm 1$ °C, $2\theta_{max} = 52.1^\circ$, STOE-IPDS, $Mo_{K\alpha}$ radiation ($\lambda = 0.71073$ Å), 5558 measured, 1397 unique, and 1321 observed reflections with $I > 2\sigma(I)$, LP correction ($\mu = 11.50$ mm^{-1}), Patterson method and ΔF synthesis, minimization of $\Sigma w(F_o^2 - F_c^2)^2$ with $w = 1/[\sigma^2(F_o^2) + (0.0599\,P)^2]$ where $P = (F_o^2 + 2\,F_c^2)/3$, 114 refined paramters, $R_1 = 0.0367$, $wR_2 = 0.0850$; $\Delta\rho_{max}/\Delta\rho_{min} + 1.18/-1.37$ e Å^{-3}. Crystallographic data (excluding structure factors) for the structure reported in this paper have been deposited with the Cambridge Crystallographic Data Center as supplementary publication no. CCDC-102011. Copies of the data can be obtained free of charge on application to CCDC, 12 Union Road, Cambridge CB2 1EZ, UK (fax: (+44) 1223-336-033; e-mail: deposit@ccdc.cam.ac.uk).

[5] The figures in this paper were drawn on basis of ORTEX images (P. McArdle, *J. Appl. Cryst.* **1995**, *28*, 65) with RASTEP and RENDER (E. A. Merrit, D. J. Bacon, *Meth. Enzymol.* **1997**, *277*, 505).

[6] a) A. Schier, J. M. Wallis, G. Müller, H. Schmidbaur, *Angew. Chem.* **1986**, *98*, 742; *Angew. Chem. Int. Ed. Engl.* **1986**, *25*, 757; b) W. Frank, J. Weber, E. Fuchs, *Angew. Chem.* **1987**, *99*, 68; *Angew. Chem. Int. Ed. Engl.* **1987**, *26*, 74.

[7] a) O. Mundt, G. Becker, M. Rössler, C. Witthauer, *Z. Anorg. Allg. Chem.* **1983**, *506*, 42; b) A. J. Ashe, III, J. W. Kampf, D. B. Puranik, A. M. Al-Taweel, *Organometallics* **1992**, *11*, 2743; c) F. Calderazzo, A. Morvillo, G. Pelizzi, R. Poli, *J. Chem. Soc. Chem. Commun.* **1983**, 507; d) F. Calderazzo, R. Poli, G. Pelizzi, *J. Chem. Soc. Dalton Trans.* **1984**, 2365; e) K. H. Whitmire, J. M. Cassidy, *Acta Crystallogr. Sect. C* **1992**, *48*, 917.

[8] N. Tokitoh, Y. Arai, R. Okazaki, *Science* **1997**, *277*, 78.

[9] W. Frank, G. J. Reiß, J. Schneider, *Angew. Chem.* **1995**, *107*, 2572; *Angew. Chem. Int. Ed. Engl.* **1995**, *34*, 2416.

Cooperative Hydrogen Bonding and Enzyme Catalysis**

Hong Guo* and Dennis R. Salahub*

Understanding the structural basis for stabilization of transition states in enzyme-catalyzed reactions is of fundamental importance. Such knowledge would help to improve existing enzymes and to design new ones.[1, 2] High-resolution structures have revealed important features at enzyme active sites.[3, 4] However, identification of the key factors responsible for the catalysis has proven to be difficult[5, 6] owing to the complexity of interactions that obscure the underlying mechanisms. This is the case for stabilization of transition states involving α helices, for example. Although the ability of the helices to stabilize negatively charged reaction intermediates and transition states has been well established,[2, 3, 7] the origin of the charge stabilization is still uncertain.[3, 5]

Here we report results of density functional calculations which reveal a large cooperative effect induced by the interaction of an anion with a peptide hydrogen bond network, directly or through an imidazole (Im) molecule. The major contribution to this cooperativity consists of nonadditive, many-body effects that can not be reflected by the pair-wise interactions of the charged ligand with the individual peptide units involved, and that are closely associated with the presence of the hydrogen-bond network. The increase of the cooperative effect on going from a neutral to a negatively charged ligand is sufficiently large that it could make an important contribution to the catalysis by stabilizing the charge formation along the reaction pathway in the enzyme-catalyzed reactions. The mechanism proposed here, based on the enhancement of cooperative hydrogen bonding, provides a consistent interpretation for both the wide occurrence of helices at enzyme active sites[3] and phosphate (sulfate) binding sites[7] as well as their absence in some instances.[8–11]

[*] Dr. H. Guo, Prof. D. R. Salahub
Centre de Recherche en Calcul Appliqué
5160, boul. Décarie, bureau 400
Montréal, Québec, H3X 2H9 (Canada)
and
Département de chimie, Université de Montréal
C.P. 6128 Succursale centre-ville
Montréal, Québec, H3C 3J7 (Canada)
Fax: (+1) 514-343-2468
E-mail: dennis.salahub@umontreal.ca

[**] Support for parts of this work from Biosym Technologies and from Astra Research Centre, Montreal, is gratefully acknowledged.

 © WILEY-VCH Verlag GmbH, D-69451 Weinheim, 1998 1433-7851/98/3721-2985 $ 17.50+.50/0

Although the existence of a cooperative effect in peptide and imidazole hydrogen bonding is known[12] and differential cooperativities have been proposed for the interpretation of other phenomena,[12b] such large π cooperativity and many-body effects have not been detected and their role in enzyme catalysis has not been discussed previously. The results of quantum mechanical calculations also suggest that helices with an α_N-type distortion[13] at the N terminus may be even more effective in the charge stabilization. The relationship between the cooperative hydrogen bonding and low-barrier hydrogen bonds[4] in enzyme catalysis is also discussed.

The model systems for peptide hydrogen bond networks used in this study are given in Figure 1 a. They include

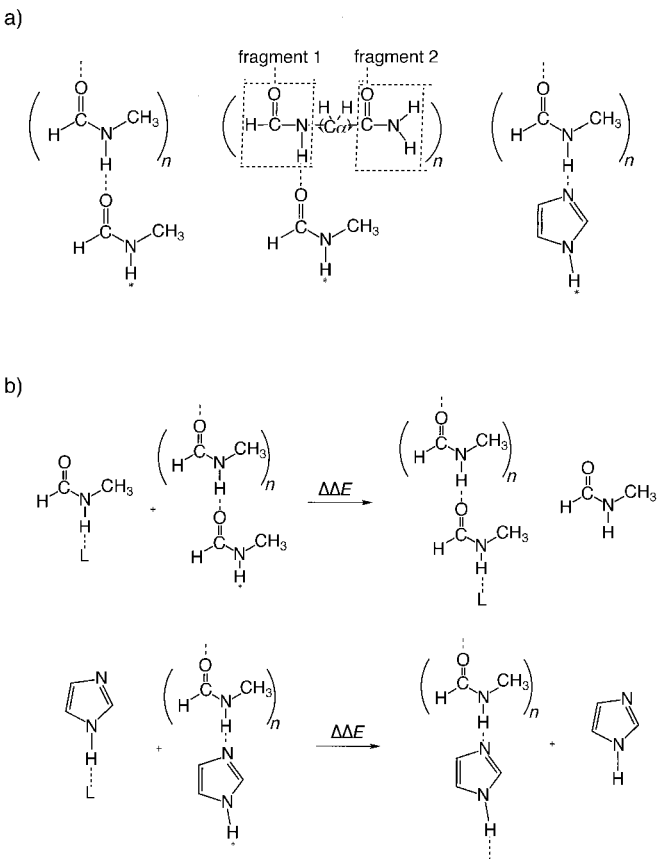


Figure 1. a) Model systems for peptide hydrogen bond networks used in this study. The star designates the binding site. From left to right: NMF$\cdots$(NMF)$_n$, NMF$\cdots$(GDA)$_n$, and Im$\cdots$(NMF)$_n$. (GDA)$_n$ contains two hydrogen-bonded peptide fragments, fragments 1 and 2, that are separated by the C_α carbon atoms. The initial structures of NMF$\cdots$(GDA)$_n$ for geometry optimizations were build from GDAs with $(\varphi,\psi)=(-60,-50^\circ)$. The final φ and ψ angles for NMF$\cdots$(GDA)$_n$ are (starting from the GDA next to NMF): for $n=2$, $(\varphi_1,\psi_1)=(-83,-20^\circ)$ and $(\varphi_2,\psi_2)=(-120,14^\circ)$; for $n=3$, $(\varphi_1,\psi_1)=(-80,-24^\circ)$, $(\varphi_2,\psi_2)=(-80,-24^\circ)$, and $(\varphi_3,\psi_3)=(-115,10^\circ)$. The φ and ψ angles for NMF$\cdots$(GDA$\cdot$2H$_2$O)$\cdots$GDA (see text) are: $(\varphi_1,\psi_1)=(-86,-16^\circ)$ and $(\varphi_2,\psi_2)=(-117,15^\circ)$. The geometry optimizations of NMF$\cdots$(GDA)$_n$ lead to stable conformations in which the carbonyl group of NMF forms only one hydrogen bond to the terminal NH group of fragment 1 of (GDA)$_n$. b) The processes used to determine the cooperative effects ($\Delta\Delta E_n$). Different definitions for the cooperativity have been used in the literature. The cooperative effect defined here also includes the two-body interactions of nonneighbors in addition to the many-body terms. Top: NMF$\cdots$(NMF)$_n$ is involved. Bottom: Im$\cdots$(NMF)$_n$ is involved. The process involving NMF$\cdots$(GDA)$_n$, NMF$\cdots$2(H$_2$O)$_6$, and NMF$\cdots$2(H$_2$O)$_8$ (not shown) are similar.

hydrogen-bonded *N*-methylformamide oligomers (NMF$\cdots$(NMF)$_n$, $n=1-4$) and NMF/GDA complexes (NMF$\cdots$(GDA)$_n$, $n=2$, 3), where GDA stands for a glycine dipeptide analogue.[14] We also use Im$\cdots$(NMF)$_n$ complexes for which the "N-terminal" NMF in NMF$\cdots$(NMF)$_n$ is replaced by imidazole.

We consider the exchange processes illustrated in Figure 1 b, where a neutral or anionic ligand (L) moves from the NMF or Im binding site to the binding site in the corresponding system with peptide hydrogen bond network(s). The energy changes for the processes are referred to as the cooperative effects ($\Delta\Delta E_n$)[15] that are induced by the ligand binding to the systems with the hydrogen-bonding network. The effectiveness of the peptide hydrogen bond networks in inducing cooperative effects is compared with those induced by two stable water hexamers or octamers (NMF$\cdots$2(H$_2$O)$_6$ and NMF$\cdot$2(H$_2$O)$_8$; see Figure 2 c).

The ball-and-stick representations for some of the systems are plotted in Figure 2. Different procedures may be used for the evaluation of the cooperative effects. The structures of all the systems involved in the process may be optimized, and the energies at these optimized geometries can then be used to determine the $\Delta\Delta E$ value. Alternatively, one can apply certain structural constraints to some of the systems. Two types of structural constraints have been considered in this work, in addition to the full geometry optimizations. In type A, the constraints are used only for the systems *with* a ligand (e.g., L$\cdots$NMF and L$\cdots$NMF$\cdots$(GDA)$_n$). Here geometry optimization was performed for the ligand and the N–H bond interacting with the ligand, whereas the rest of the structural parameters were fixed at the values found in the corresponding systems without the ligand (e.g., NMF and NMF$\cdots$(GDA)$_n$). In type B, the constraints are applied to the systems *without* a ligand (e.g., NMF and NMF$\cdots$(GDA)$_n$), for which only single-point calculations were performed at the structures found in the corresponding systems with a ligand (e.g., L$\cdots$NMF and L$\cdots$NMF$\cdots$(GDA)$_n$).

The $\Delta\Delta E_n$ values are listed in Table 1. The methods of density functional theory[16] have been used in this study with generalized gradient approximation functionals of the Becke–Perdew (BP) type. Three levels of calculation (BP/DZVP, BP/6-311++G** and BP/6-311++G**//BP/DZVP) have been performed, but only the BP/DZVP values are given here since the $\Delta\Delta E_n$ values are not very sensitive to the basis set and no new information was obtained. As is evident from Table 1, for neutral ligands $\Delta\Delta E_n$ is only about -1 to -2 kcal mol^{-1}, consistent with previous theoretical and experimental results.[12] In contrast, the cooperative effects are much larger (-7 to -35 kcal mol^{-1}) for the cases involving negatively charged groups, and they are not very sensitive to the nature of the anions involved. Thus, there is a large increase of $\Delta\Delta E_n$ in going from neutral to anionic ligands. Introducing solvent molecules on HCO_2^- reduces $\Delta\Delta E$ by only about 2–4 kcal mol^{-1}. The value of $\Delta\Delta E_n$ increases with increasing size of the system (n), and the replacement of the NMF interacting with the anions by Im leads to similar results; a large cooperative effect was also observed when the NMF molecule was replaced by CH_3OH. We will call such hydrogen-bonding networks with the Im and/or hydroxyl extension

 © WILEY-VCH Verlag GmbH, D-69451 Weinheim, 1998 1433-7851/98/3721-2986 $ 17.50+.50/0

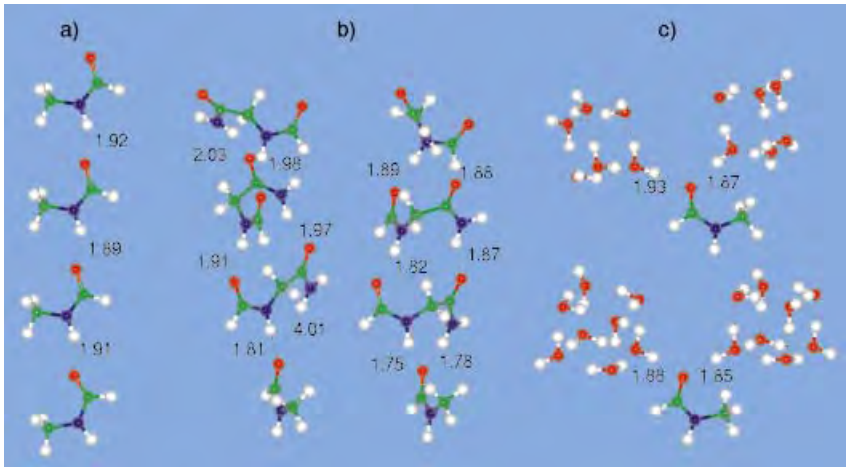


Figure 2. Ball-and-stick representations for some of the systems. Hydrogen bonds are designated by dashed lines. a) $NMF\cdots(NMF)_3$; b) $NMF\cdots(GDA)_3$; left: fully optimized structure; right: the structure with constraints of type B. c) $NMF\cdots2(H_2O)_{2n}$; top: $NMF\cdots2(H_2O)_6$; bottom: $NMF\cdots2(H_2O)_8$.

Table 1. Cooperative effects [kcal mol^{-1}] induced by the interactions of ligands with hydrogen-bond networks.[a]

Hydrogen-bond network	Ligand (L)	$\Delta\Delta E_n$			
		$n=1$	$n=2$	$n=3$	$n=4$
$NMF\cdots(NMF)_n$	H_2O	−1.1	−1.7	−1.8	−1.9
	HCO_2H	−1.3			
	Im	−1.8			
	HCO_2^-	−9.9	−13.8	−15.9	−17.2
	Im^-	−9.2			
	CH_3S^-	−9.0			
	$H_2PO_4^-$	−8.2			
	$2H_2O\cdots HCO_2^-$	−7.6	−10.7	−12.4	
	$H_2O\cdots H_2O\cdots HCO_2^-$	−6.8		−12.1	
$NMF\cdots(NMF)_n$[b]	HCO_2^-	−8.6	−12.7	−14.4	
$NMF\cdots(NMF)_n$[c]	HCO_2^-	−11.7	−16.9	−19.1	
$NMF\cdots(GDA)_n$	HCO_2^-		−22.4	−26.4	
$NMF\cdots(GDA)_n$[b]	HCO_2^-		−16.4	−20.3	
$NMF\cdots(GDA)_n$[c]	HCO_2^-		−29.2	−35.1	
$NMF\cdots(GDA\,2H_2O)\cdots GDA$[b]	HCO_2^-		−16.4		
$Im\cdots(NMF)_n$	H_2O	−1.1	−1.6		
	HCO_2^-	−10.1	−15.0		
	$2H_2O\cdots HCO_2^-$	−7.7	−11.7		
$NMF\cdots2(H_2O)_{2n}$	HCO_2^-			−16.3	−15.1

[a] BP/DZVP values. Except where otherwise noted, full geometry optimizations have been performed. For most of the cases involving formate, one of the orbitals *anti* to the C–H bond interacts with NMF or Im; the only exception is the case involving $H_2O\cdots H_2O\cdots HCO_2^-$, where one of the orbitals eclipsing the C–H bond is used. For $2H_2O\cdots HCO_2^-$, two water molecules interact, respectively, with the two orbitals of formate eclipsing the C–H bond. For $H_2O\cdots H_2O\cdots HCO_2^-$, one water donates two hydrogen bonds to the two orbitals *anti* to the C–H bond and another water donates one hydrogen bond to one of the orbitals eclipsing the C–H bond. [b] Constraints of type A applied (see text). [c] Constraints of type B applied.

augmented peptide hydrogen bond networks. Introducing two water molecules to the two carbonyl groups of the first GDA ($NMF\cdots(GDA\cdot2(H_2O)\cdots GDA$) has little effect on $\Delta\Delta E$.

The $\Delta\Delta E_n$ values obtained with the constraints of type B are greater than those obtained with the constraints of type A or with full geometry optimizations, as the systems of hydrogen-bonding networks are better adapted for the anion. This is especially true for the processes involving $NMF\cdots(GDA)_n$, where the cooperative effects obtained with the type B constraints are considerably larger, by as much as 7–15 kcal mol^{-1} (only 2–5 kcal mol^{-1} for the cases involving $NMF\cdots(NMF)_n$).

As can be seen from Figure 2b, the major structural difference for $NMF\cdots(GDA)_n$ is that with the constraints of type B the NMF molecule interacts with both NH groups from the next GDA, while it forms only one hydrogen bond to the NH group from fragment 1 in the optimized structure. Thus, the presence of HCO_2^- and the geometry optimization drive the NMF molecule to interact with the second NH group from fragment 2. To anticipate the formation of the second hydrogen bond with NMF, $(GDA)_n$ undergoes significant structural changes. Such structural changes are energetically unfavorable, as the energies of $NMF\cdots(GDA)_n$ become higher even with the compensation from the formation of the second hydrogen bond to fragment 2. Thus, the larger $\Delta\Delta E$ values are due to geometric relaxation which allows the formation of two peptide hydrogen bond networks connected to NMF, both of them being able to induce the cooperative effect. The implication of this finding to helix-charge interactions will be discussed later. As can be seen from Table 1, the two peptide hydrogen bond networks of $(GDA)_n$ are far more effective in inducing the cooperative effects than the two water clusters; the $\Delta\Delta E$ values are 6–10 kcal mol^{-1} larger than those obtained with two $(H_2O)_6$ or $(H_2O)_8$.

The energies of the pair interaction of HCO_2^- with its nonneighboring GDA or peptide units in some complexes are listed in Table 2; the fragment contributions are also given for the processes involving $NMF\cdots(GDA)_2$ using constraints of type A, that is, without anion-induced structural relaxation. The $\Delta\Delta E$ values of the fragments are additive in that the cooperative effect obtained with $(GDA)_2$ is basically the same as the sum of those from its two fragments. Fragment 1 of $(GDA)_2$ makes a major contribution (−12 kcal mol^{-1}) to the total $\Delta\Delta E$ value (−16.4 kcal mol^{-1}), while the contribution from fragment 2 is considerably smaller (−4.5 kcal mol^{-1}). Table 2 shows that the sums of the energies for pair interactions between nonneighbors are much smaller than the corresponding $\Delta\Delta E$ values in almost all cases; the only exception involves $NMF\cdots[(GDA)_2]^{frag2}$ (i.e., without a peptide hydrogen bond network connected to the anion). These analyses suggest that the many-body, nonadditive effects make a major contribution to the observed strong cooperativity and that the existence of peptide hydrogen bond networks is very important for a large energetic effect.

 © WILEY-VCH Verlag GmbH, D-69451 Weinheim, 1998 1433-7851/98/3721-2987 $ 17.50+.50/0

Table 2. Energies of pair interactions between HCO_2^- and its nonneighboring units as well as the fragment contributions of $(GDA)_2$ [kcal mol^{-1}].[a]

System	1,3	1,4	1,5	Total	$\Delta\Delta E_n$
$HCO_2^- \cdots NMF \cdots (GDA)_2$[b]	−7.6	−2.6		−10.2	−22.4
$HCO_2^- \cdots NMF \cdots (GDA)_2$	−5.5	−2.1		−7.6	−16.4
$HCO_2^- \cdots NMF \cdots [GDA)_2]^{frag1}$	−3.7	−1.3		−5.0	−12.0
$HCO_2^- \cdots NMF \cdots [GDA)_2]^{frag2}$	−2.0	−1.0		−3.0	−4.5
$HCO_2^- \cdots NMF \cdots (NMF)_2$	−3.9	−1.5		−5.4	−12.7
$HCO_2^- \cdots NMF \cdots (NMF)_3$[b]	−4.2	−1.6	−0.8	−6.6	−15.9
$HCO_2^- \cdots NMF \cdots (NMF)_3$	−3.9	−1.5	−0.8	−6.2	−14.4
$H_2O \cdots H_2O \cdots HCO_2^- NMF \cdots (NMF)_3$[b]	−2.1	−1.4	−0.7	−4.2	−12.1

[a] Except where otherwise noted, constraints of type A have been applied. $[(GDA)_2]^{frag1}$ designates that fragment 2 of the system is removed from $NMF \cdots (GDA)_2$ (Figure 1a) with the $C_\alpha H_2$ groups replaced by hydrogen atoms. The positions of the hydrogen atoms were optimized based on energy minimizations, whereas the rest of the structural parameters were fixed. Standard energy decomposition techniques were used for estimating the through-space pair interactions of the anion with its nonneighboring GDAs and peptide units. In this approach, the energies of the ligand (L) and each of its nonneighboring units are determined at their relaxed structures found in $HCO_2^- \cdots NMF \cdots (NMF)_n$, $HCO_2^- \cdots NMF \cdots (GDA)_2$, or $HCO_2^- \cdots NMF \cdots [(GDA)_2]^{frag1/frag2}$, and these energies are used as the reference energies for the interactions. The interaction energies are obtained for each pair of L and its nonneighboring unit fixed at their positions according to the geometries found in the complexes. [b] Full geometry optimization was performed for this complex. $H_2O \cdots H_2O \cdots HCO_2^-$ is considered as a single unit.

The results reported here suggest that peptide or augmented peptide hydrogen bond networks could make an important contribution to the charge stabilization through cooperative interactions. The large $\Delta\Delta E$ values will undoubtedly be moderated in the real environment of the protein and will depend on the mechanism of enzyme-catalyzed reactions so that the exact contribution of the hydrogen-bonding networks to the catalysis would have to be modified accordingly. Nevertheless, the identification of strong interactions between anions and hydrogen-bonded networks as an important factor for enzyme structure and function allows us to offer detailed insight into a number of structural features observed in the neighborhood of active sites that are prepared, during the folding process, for interactions with charged ligands or intermediates. In the following we will summarize several experimental results that can be attributed to such strong cooperativity.

As a major component of protein secondary structure, α helices provide a convenient way for arranging the peptide hydrogen bond networks. The mechanism proposed here can account for the observation that isolated peptide hydrogen bond networks occur at enzyme active sites as well as at phosphate (sulfate) binding sites even though no helix is present. Serine proteases represent a well-known case which suggests that the presence of a helix may not be a necessary condition for the charge stabilization. For subtilisin, there is an active-site helix, and, consistent with an earlier interpretation based on the helix macrodipole,[3] the catalytic serine residue (S221) is located at the N terminus of the helix with its amide group involved in the oxyanion hole interactions (Figure 3a).[17]

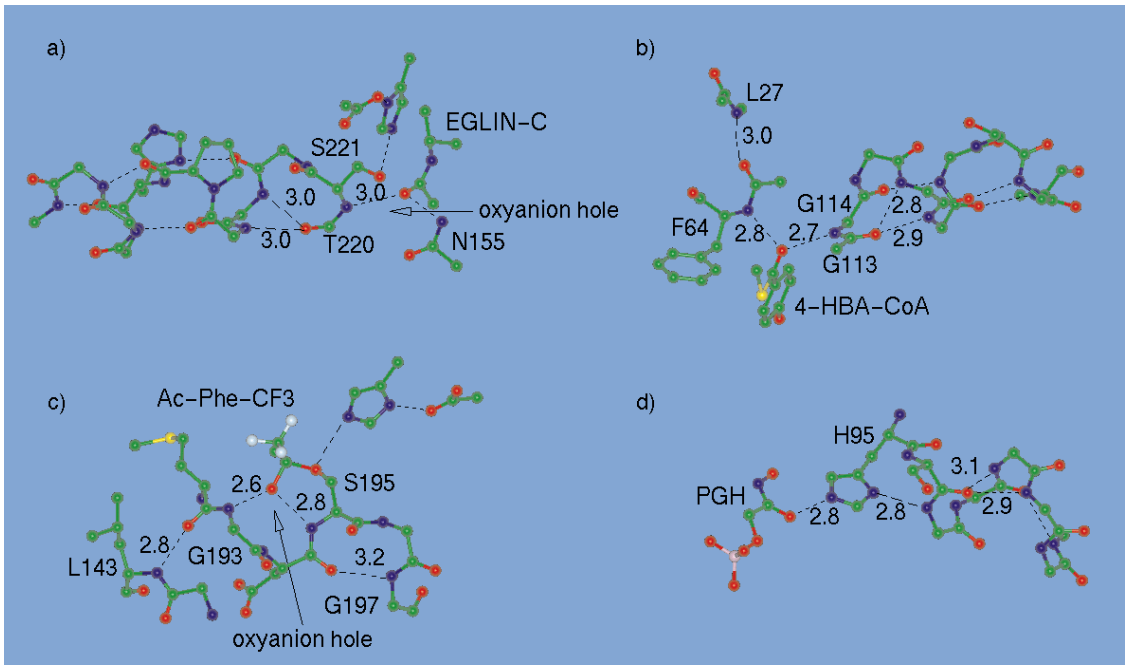


Figure 3. Examples of peptide hydrogen bond networks at enzyme active sites. Hydrogen bonds are designated by dashed lines. a) Subtilisin Carlsberg complexed with EGLIN-C.[17] The main-chain NH group of S221 interacts with EGLIN-C, and the carbonyl group of T220 is involved in a bifurcated 1–4 and 1–5 hydrogen bond in the active-site helix. b) 4-Hydroxybenzoyl-CoA (4-HBA-CoA) bound to 4-chlorobenzoyl-CoA dehalogenase.[8] An isolated peptide hydrogen bond network and an active-site helix are involved in the stabilization of the transition state. The main-chain NH group of G114 interacts with 4-HBA-CoA, and the carbonyl group of G113 is involved in a bifurcated 1–4 and 1–5 hydrogen bond in the helix. The isolated peptide hydrogen bond network involves the peptide linkage between G63 and F64 and that between A26 and L27; c) γ-Chymotrypsin complexed with Ac-Phe-CF_3.[9] Two isolated peptide hydrogen networks are involved in the stabilization of the transition state. One involves the peptide linkages between M192 and G193 and between G142 and L143, and the other involves the peptide linkages between D194 and S195 and between G196 and G197. d) Triosephosphate isomerase (TIM) complexed with phosphoglycolohydroxamate (PGH).[19] The main-chain NH group of E97 donates a hydrogen bond to H95, and the carbonyl group of S96 is involved in bifurcated 1–4 and 1–5 hydrogen bonds in an active-site helix.

 © WILEY-VCH Verlag GmbH, D-69451 Weinheim, 1998 1433-7851/98/3721-2988 $ 17.50+.50/0

Such an active-site helix, however, is not present in the chymotrypsin-related serine proteases. This difference can be understood by considering cooperative effects involving peptide hydrogen bond networks. Figure 3c shows the active site of a tetrahedral transition-state complex of chymotrypsin with a peptidyl trifluoromethyl ketone (Ac-Phe-CF_3).[9] Two peptide hydrogen bond networks are connected to the negatively charged oxygen atom of Ac-Phe-CF_3 and are involved in the oxyanion hole interactions. An isolated peptide hydrogen bond network also exists at the active site of the 4-chlorobenzoyl-CoA dehalogenase/4-HBA-CoA complex,[8] where the NH group of F64 interacts with the benzoyl moiety of 4-HBA-CoA; the carbonyl group within the same peptide linkage forms a hydrogen bond to the main-chain NH group of L27 (Figure 3b). This hydrogen-bond network as well as the one involving L143 in the chymotrypsin complex do not belong to an individual helix, turn, or sheet. A previous statistical survey[13] shows that this type of backbone hydrogen bond represents only 5% of the hydrogen bonds between main chains in proteins. Thus, the occurrence of these peptide hydrogen bond networks at the enzyme active sites might be considered as rather uncommon. These structural data support the results from the quantum mechanical calculations that suggest an important role of cooperative hydrogen-bond networks (as opposed to the helix macrodipole per se) in the charge stabilization. Isolated peptide hydrogen bond networks have also been observed to interact with phosphate (sulfate) moieties in phosphate-binding (sulfate-binding) proteins,[10, 11, 18] and a possible role of the hydrogen-bonding networks in the charge stabilization has been suggested.[11]

Triosephosphate isomerase (TIM)[2, 19] represents an interesting example where a "relay" of charge might be assisted by the cooperative effect. It uses a neutral histidine residue (H95) rather than the much more electrophilic imidazolium ring to interact with the carbonyl oxygen atom of the substrate; H95 is located at the N terminus of a short α helix (Figure 3d). As mentioned earlier, a neutral imidazole can participate in cooperative hydrogen bonding and thus serves as a simple extension of the peptide hydrogen-bond network(s) from the helix. This extension could enhance the cooperative effect, as suggested from the results on the model systems. Moreover, if a proton or a partial proton transfer from the histidine residue to the reaction intermediate or substrate is involved,[2, 4, 19] the charge formation on H95 could in turn be stabilized by a stronger cooperative effect induced by the interaction of H95 with the helix. A similar discussion can be made for citrate synthase (CS), where H274 located at the N terminus of an α helix plays a similar role. Such a strategy might also be used by other enzymes in which cooperative hydrogen-bond networks are well positioned to stabilize the charge formation along the reaction pathways through an enhancement of cooperative hydrogen bonding.

As discussed earlier, a larger cooperative effect can be induced if the carbonyl group of the peptide linkage interacting with an anion (NMF in our model systems) is involved in a bifurcated hydrogen bond with the amide groups of two peptide units or hydrogen-bonded networks. There is a frequent occurrence of α_N-type distortion at the N terminus of α helices[13a] in which the carbonyl oxygen atom of residue 1 is directed between the NH groups of residues 4 and 5 and therefore involved in a bifurcated 1-4 and 1-5 hydrogen bond. A survey[13a] of the crystal structures for twelve proteins shows that there are 16 examples of the α_N distortion among 50 α helices. Based on the mechanism of cooperative hydrogen bonding, it seems that the helices with the α_N distortion might be more effective in the charge stabilization, since two of the peptide hydrogen bond networks can be used to induce the cooperative effect. Such distortion exists widely in the active-site helices. This can be seen from Figure 3, where the α_N distortion exists in all three active-site helices. The suggestion proposed here also seems to be consistent with the appearance of phosphate groups at the end of 3_{10} helices even without well-aligned peptide dipoles.[7a]

It was recently proposed that low-barrier hydrogen bonds play an important role in enzyme catalysis,[4] but the energetic effects due to the formation of low-barrier hydrogen bonds have not been well established.[6] For many of the cases where a low-barrier hydrogen bond was suggested, there are actually cooperative hydrogen-bond networks involved. They include TIM, CS, and chymotrypsin, where H95, H274, and the NH groups of G193 and S195 were proposed to form low-barrier hydrogen bonds with the intermediates. Thus, it is possible that the energetic stabilization might come from the cooperative hydrogen bonding rather than the formation of low-barrier hydrogen bonds per se.

Received: February 24, 1998 [Z11513IE]
German version: *Angew. Chem.* **1998**, *110*, 3155 – 3160

Keywords: cooperative effects · density functional calculations · enzyme catalysis · hydrogen bonds · protein structures

[1] A. J. Kirby, *Angew. Chem.* **1996**, *108*, 770 – 790; *Angew. Chem. Int. Ed. Engl.* **1996**, *35*, 705 – 724.
[2] J. R. Knowles, *Nature* **1991**, *350*, 121 – 125.
[3] a) W. G. J. Hol, P. T. van Duijnen, H. J. C. Berendsen, *Nature* **1978**, *273*, 443 – 446; b) W. G. J. Hol, *Prog. Biophys. Mol. Biol.* **1984**, *45*, 149 – 195.
[4] a) J. A. Gerlt, P. G. Gassman, *Biochemistry* **1993**, *32*, 11943 – 11952; b) W. W. Cleland, M. M. Kreevoy, *Science* **1994**, *264*, 1887 – 1890; c) P. A. Frey, S. A. Whitt, J. B. Tobin, *Science* **1994**, *264*, 1927 – 1930; d) J. A. Gerlt, M. M. Kreevoy, W. W. Cleland, P. A. Frey, *Chem. Biol.* **1997**, *4*, 259 – 267, and references therein.
[5] a) J. Aqvist, H. Luecke, F. A. Quiocho, A. Warshel, *Proc. Natl. Acad. Sci. USA* **1991**, *88*, 2026 – 2030; b) B. Tidor, M. Karplus, *Biochemistry* **1991**, *30*, 3217 – 3228; c) B. Tidor, *Proteins* **1994**, *19*, 310 – 323.
[6] a) J. P. Guthrie, *Chem. Biol.* **1996**, *3*, 163 – 170, and references therein.; b) C. L. Perrin, J. B. Nielson, *Annu. Rev. Phys. Chem.* **1997**, *48*, 511—544, and references therein.; c) A. Warshel, A. Papazyan, P. Kollman, *Science* **1995**, *269*, 102 – 106.
[7] a) R. R. Copley, G. J. Barton, *J. Mol. Biol.* **1994**, *242*, 321 – 329; b) P. Chakrabarti, *J. Mol. Biol.* **1993**, *234*, 463 – 482.
[8] M. M. Benning, K. L. Taylor, R. Q. Liu, G. Yang, H. Xiang, G. Wesenberg, D. Dunaway-Mariano, H. M. Holden, *Biochemistry* **1996**, *35*, 8103 – 8109.
[9] K. Brady, A. Wei, D. Ringe, R. H. Abeles, *Biochemistry* **1990**, *29*, 7600 – 7607.
[10] H. Luecke, F. A. Quiocho, *Nature* **1990**, *347*, 402 – 406.
[11] F. A. Quiocho, J. S. Sack, W. K. Vyas, *Nature* **1987**, *329*, 561 – 564.
[12] a) G. A. Jeffrey, W. Saenger, *Hydrogen bonding in biological structures*, Springer, Berlin, **1991**; b) H. Guo, M. Karplus, *J. Phys. Chem.* **1994**, *98*, 7104—7105, and references therein.; c) H. Guo, M. Karplus, *J. Phys. Chem.* **1992**, *96*, 7273 – 7287; d) B. W. Gung, Z. Zhu,

 © WILEY-VCH Verlag GmbH, D-69451 Weinheim, 1998 1433-7851/98/3721-2989 $ 17.50+.50/0

Tetrahedron Lett. **1996**, *37*, 2189 – 2192; e) B. W. Gung, Z. Zhu, B. Everingham, *J. Org. Chem*. **1997**, *62*, 3436 – 3437; f) J. E. Del Bene, *J. Chem. Phys.* **1980**, *73*, 3423 – 3424.
[13] a) E. N. Baker, R. E. Hubbard, *Prog. Biophys. Mol. Biol*. **1984**, *44*, 97 – 179; b) D. Stickle, L. G. Presta, K. A. Dill, G. D. Rose, *J. Mol. Biol*. **1992**, *226*, 1143 – 1159.
[14] T. Head-Gordon, M. Head-Gordon, M. J. Frisch, C. Brooks III, J. A. Pople, *J. Am. Chem. Soc*. **1991**, *113*, 5989 – 5997.
[15] J. E. H. Koehler, W. Saenger, B. Lesyng, *J. Comput. Chem*. **1987**, *8*, 1090 – 1098.
[16] J. W. Andzelm, M. E. Casida, A. Koester, E. Proynov, A. St-Amant, D. R. Salahub, H. Duarte, N. Godbout, J. Guan, C. Jamorski, M. Leboeuf, V. Malkin, O. Malkina, F. Sim, A. Vela, *deMon Software*, University of Montreal, **1995**.
[17] W. Bode, E. Papamokos, D. Musil, U. Seemuller, H. Fritz, *EMBO J.* **1986**, *5*, 813 – 818.
[18] J. J. He, F. A. Quiocho, *Protein Sci*. **1993**, *2*, 1643 – 1647.
[19] R. C. Davenport, P. A. Bash, B. A. Seaton, M. Karplus, M. G. A. Petsko, D. Ringe, *Biochemistry* **1991**, *30*, 5821 – 5826.

New Protein Mimetics: The Zinc Finger Motif as a Locked-In Tertiary Fold

Gabriele Tuchscherer,* Christian Lehmann, and Marc Mathieu

Dedicated to Professor Murray Goodman on the occasion of his 70th birthday

De novo protein design aims to mimic some of the structural and functional properties of native proteins.[1–6] One of the most intriguing hurdles in this rapidly growing field is the complexity of the folding mechanism, that is, the pathway by which a linear polypeptide chain adopts its unique three-dimensional structure. To bypass this well-known protein-folding problem,[7–9] the concept of template assembled synthetic proteins (TASP) was introduced, in which topological template molecules direct the folding of covalently attached peptide blocks into a predetermined packing arrangement with a branched-chain architecture.[3, 10–12]

Recent progress in the synthetic methodology for assembling peptides allows us now to access the full potential of the TASP approach. For example, by conceptually separating the structural and functional domains of native proteins, we have recently proposed the use of topological templates as structure-supporting scaffolds for the assembly of receptor binding loops.[13] Here we extend the TASP concept of protein design to the construction of proteinlike packing topologies with multiply branched, oligocyclic chain architectures ("locked-in folds"). These synthetic macromolecules exhibit unique physicochemical and folding properties and serve as versatile scaffolds in protein design and mimicry.

[*] Dr. G. Tuchscherer, Dr. C. Lehmann, Dr. M. Mathieu
Institute of Organic Chemistry, University of Lausanne
BCH-Dorigny, CH-1015 Lausanne (Switzerland)
Fax: (+41) 21-692-3955
E-mail: gabriele.tuchscherer@ico.unil.ch

[**] This work was supported by the Swiss National Science Foundation.

As shown in Figure 1, the envisioned structural motif is based on the principles of a molecular kit, in which building blocks such as α helices, β sheets, and loops are assembled by means of templates or spacer molecules to give covalently cross-linked multiply bridged ("locked-in") tertiary folds. Folding into a predetermined three-dimensional structure is

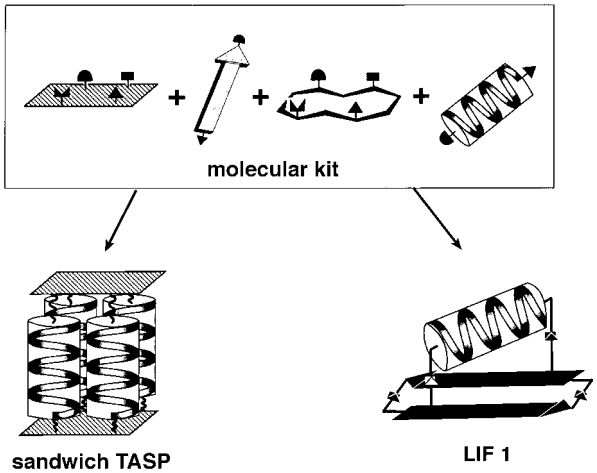


Figure 1. Molecular kit approach in de novo protein design: helices, β sheets, loops, and templates with chemoselectively addressable functional groups (e.g., aldehyde and aminooxy groups; depicted as solid symbols) are the constituents of a molecular kit. A variety of cheomoselective bond-forming methods allows the assembly of these building blocks into locked-in folds (LIF), and the folding problem of linear peptide chains can thus be bypassed.

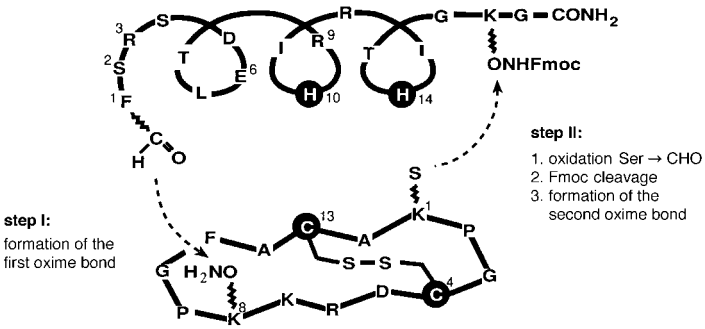
achieved by the enforced intramolecular association of secondary structure forming peptide blocks to give highly constrained tertiary folds of increased thermodynamic stability. Most importantly, the large number of alternative folding pathways and packing arrangements of linear polypeptide chains is drastically reduced due to the confined conformational space. The proposed concept relies strongly on new methodologies in synthetic peptide chemistry such as chemoselective ligation procedures[14–17] and orthogonal protecting group techniques,[12] which allow the specific assembly of unprotected peptide segments as building blocks according to a molecular kit approach.

Our first aim was to mimic some structural and functional features of a zinc finger motif (finger 1 of Zif268) by a locked-in fold with an overall topology similar to that of the native molecule. Zinc finger proteins contain one of the most interesting structural motifs for the separation of structural and functional domains[13] and for the modulation of DNA-binding specificities.[18, 19] The consensus sequence Xaa_2-Cys-Xaa_{2-4}-Cys-Xaa_{12}-His-Xaa_{2-4}-His-Xaa_4 (Xaa represents variable amino acids)[20, 21] folds in the presence of Zn^{II} ions into a $\beta\beta\alpha$ folded unit, which binds through its helical face to three base pairs of the DNA. Multimeric zinc finger proteins consisting of several zinc finger (Zif) modules play a key role in controlling gene expression.[18, 19]

On applying the general concept of locked-in folds, the $\beta\beta\alpha$ framework of the Zif motif immediately suggests the use of a strategy based on the principles of a molecular kit. The constituent elements are a cyclic β-sheet template that mimics

 © WILEY-VCH Verlag GmbH, D-69451 Weinheim, 1998 1433-7851/98/3721-2990 $ 17.50+.50/0

the β strand/turn/β strand motif (structural part) and a helical block (functional part). For the assembly of these building blocks into a locked-in fold (LIF1, Figure 1), the helix is covalently attached at both chain ends ("sticky ends") through nonpeptidic linker groups to a cyclic template consisting of 14 amino acids to result in a highly branched packing arrangement (Scheme 1). The binding site for the



Scheme 1. Selective oxime bond formation for the construction of LIF1.

complexation of Zn^{II} ions was introduced into the LIF1 molecule by incorporating two cysteine and two histidine residues in the template and the helix, respectively. The final zinc finger model was relaxed in the MAB force field.[22] The geometry of tetrahedrally coordinated Zn^{II} center was taken from the X-ray structure of a native zinc finger (1zaa.pdb) and kept constant during the entire optimization cycle. The geometry of the linker $HN(CO)HC{=}NOCH_2$ in the engineered molecule was initially chosen to be *trans*, on the basis of the geometries of a corresponding substructural fragment in a set of well-resolved crystal structures. Additional constraints included hydrogen bonds within the α-helical and the β-sheet regions.

Apart from the overall $\beta\beta\alpha$ topology, important features of a native zinc finger were also taken into account, for example the incorporation of a lypophilic pocket, which is created by the N-terminal phenylalanine residue of the helix. This increases the thermodynamic stability of LIF1, as shown by molecular dynamics studies,[23] and plays a crucial role in the folding and stability of linear zinc finger molecules.[6] Furthermore, a Thr-Gly moiety at the C terminus (Figure 2) was retained to favorably support the intrahelical hydrogen-bond network.

The synthesis of LIF1 (Scheme 1) began with the preparation of the individual building blocks, that is, the template molecule and the helical segment, by stepwise solid-phase synthesis.[24] After cleavage from the resin and reverse-phase HPLC purification, the side-chain deprotected peptides containing chemoselectively addressable groups as attachment sites were subjected in aqueous solution to a two-step condensation process in which the helical 18-mer peptide was attached to the cyclic template by selective oxime formation.[14, 15] After oxidation of the serine residue at the N terminus of the helical block, the resulting aldehyde readily formed an oxime bond with the aminooxyacetyl group of the template. The reaction was monitored by analytical HPLC (Figure 3a). In the second step, the serine residue attached to the ε-NH_2 group of lysine in the template was oxidized, the Fmoc protecting group of the aminooxy functionality at the C terminus of the helical fragment removed, and the second oxime bond formed. The final chemoselective reaction— the attachment of the C-terminal end of the helix to the underlying template—was very fast and proceeded in high yield.

As suggested by molecular modeling studies, LIF1 preserves essential structural features of the native Zif molecule. This is confirmed by the absorption and circular dichroism (CD) spectra and by the zinc-complexation properties. The CD spectrum (Figure 3b) indicates an increase in helicity upon complexation of Zn^{II} ions, but in contrast to the native linear polypeptide, LIF1 retains its secondary structural elements even in the absence of the zinc complex (Figure 3b). This reflects the onset of tertiary interactions in LIF1 enforced by C and N capping of the helical block on the template.

It is interesting to note that a Zn^{II}-independent folding was described for a Zif-derived linear $\beta\beta\alpha$ motif after iterative redesign of the native sequence.[6] In the case of LIF1, the trapped architecture results in stabilization of the helix and higher thermodynamic stability of the Zif folding motif, as indicated by the denaturation behavior (insert in Figure 3b). Molecular dynamics calculations and NMR studies showed[25] that this type of template preferentially adopts a β-sheet structure in which the side chains of the Zn^{II}-complexing site and the helix attachment sites are located on the same face of the template plane.

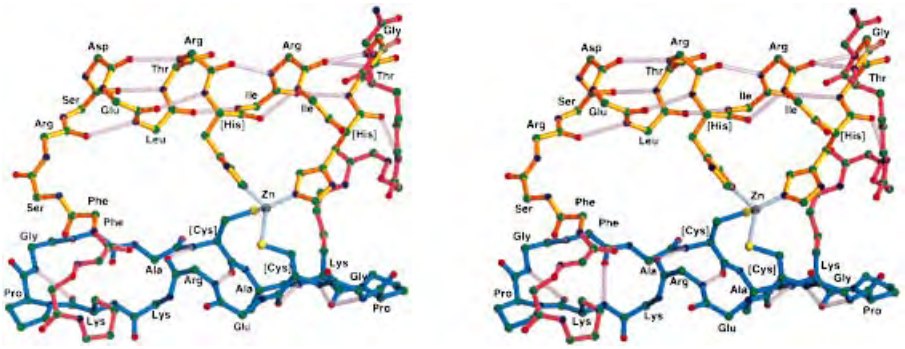


Figure 2. Stereoprojection of a strain-free, energy-minimized conformation of the locked-in fold LIF1 derived from the consensus sequence of finger 1 of Zif268. Covalent bonds between the ends of the helix (yellow) and the underlying template (blue) are shown in red. Only the side chains of the complex-forming amino acid residues are shown.

Cobalt(II) was used to investigate the metal-binding site of LIF1 due to its distinctive optical absorption spectra. The UV/Vis absorption spectrum (Figure 3c) indicates the formation of a Zif-like structure in the presence of Co^{II} ions. After reduction of the disulfide bond and addition of $CoCl_2$ the UV/Vis spectrum of LIF1 (Figure 3c) exhibits the characteristic absorption bands of a tetrahedral complex (as is present in native Zif modules) near 310 nm and 640 nm

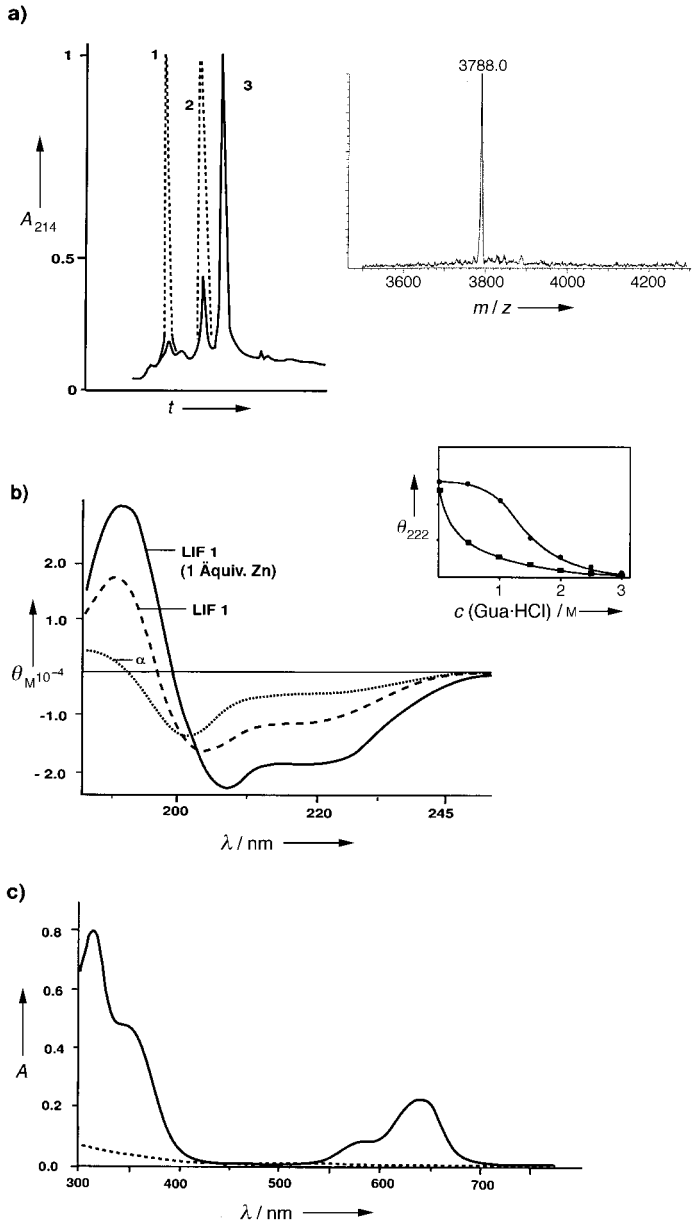


Figure 3. Characterization of LIF1. a) Left: RP-HPLC chromatogram after the first condensation step; the peaks of the starting materials (template (1), helix (2)) are dotted; peak 3 corresponds to the condensation product LIF1 after 18 h reaction time. Right: corresponding ESI-MS spectrum (m/z 3788.0). b) Circular dichroism (CD) spectra of LIF1 with the reduced disulfide bond in the absence of metal (– – –) and after the addition of stoichiometric amounts of Zn^{II} ions (——). The helicity increases moderately upon complexation of Zn; the spectrum of the completely unprotected helical block with an N-terminal serine residue (••••) reflects a predominantly unordered conformation. The spectra were recorded in 5 mM Tris buffer (pH 7) at a concentration of 10^{-5} M and normalized to the mean ellipticities per amino acid residue Θ_M. Insert: chemical denaturation (Gua · HCl) of LIF1 (●; $c = 0.25$ mg of peptide per mL; Θ_M at $\lambda = 222$ nm) and of the single helical block α (■; $c = 0.25$ mg mL^{-1}). c) UV/Vis spectra of LIF1 ($c = 150\,\mu$M) after addition of 150 μM $CoCl_2$ (——) and after addition of 150 μM $ZnCl_2$ (- - - -).

with a shoulder at 580 nm.[26, 27] Addition of one equivalent of a Zn^{II} salt to LIF1 readily displaces Co^{II} from the complex, even in the presence of a 50-fold excess of Co^{II}, with formation of the more stable Zn^{II} complex, which is indicated by the disappearence of the absorption maxima (Figure 3c). Titration curves with $CoCl_2$ and $Zn(BF_4)_2$ gave dissociation constants in the range of 10^{-6} M (Co^{II}) and 10^{-9} M (Zn^{II}),[28] which are comparable with those of natural zinc finger proteins such as transcription factor III A.[18, 26]

In the search for Zif mimetics with novel DNA-binding properties, the present approach offers some unique features:

1) The conformationally constrained template molecule serves as a stable scaffold that mimicks the β strand/turn/β strand motif of Zif.
2) The variable helical block is readily accessible by solid-phase peptide synthesis, and the incorporation of non-proteinogenic building blocks offers a wide range of structural and functional modifications.
3) The assembly of the constituent blocks to give tertiary locked-in folds by a single condensation step provides facile access to numerous analogues, including LIF libraries.
4) The chemical synthesis of multimeric locked-in folds with tailor-made DNA-binding specificities should become a powerful tool for studying protein DNA interactions.

In conclusion, the further elaboration of modern methodologies for peptide synthesis will rapidly expand the scope of the present approach and allow the construction of locked-in folds of even greater structural complexity. The concept elaborated here represents a chemical way to bypass the protein-folding problem in the design of synthetic proteins and opens interesting perspectives for the development of molecules of therapeutic relevance.

Experimental Section

The $\beta\beta\alpha$-Zif mimetic is based on the consensus sequence of finger 1 of Zif268.[29] The building blocks, helix and template, were synthesized according to standard procedures of solid-phase peptide synthesis[24] by the Fmoc strategy on Rink-MBHA (4-methylbenzhydrylamine)[30] or Sasrin (super acid sensitive resin).[31] The chemoselectively addressable sites were introduced as orthogonally protected aminooxy derivatives or serine residues.[13–15] After assembly of the linear template sequence Trt-K(Boc-S(*t*Bu))-P-G-C(Trt)-D(*t*Bu)-R(Pmc)-R(Pmc)-K(Dde)-P-G-F-A-C(Trt)-A (Trt: triphenylmethyl; Boc = *tert*-butoxycarbonyl; Pmc = 2,2,5,7,8-pentamethylchromane 6-sulfonyl; Dde = (4,4-dimethyl-2,6-dioxocyclohexylidene)ethyl) on a Sasrin resin, the peptide was cleaved with 1% trifluoroacetic acid (TFA) and cyclized with PyBOP (benzotriazole-1-yloxytrispyrrolidinophosphonium hexafluorophosphate) in dimethylformamide (DMF). After selective removal of the Dde protecting group with 10% $H_2NNH_2 \cdot H_2O$ in DMF (20 min), Boc-aminooxyacetic acid succinimide ester (Boc-$NHOCH_2COOSu$) was coupled to the ε-amino group of the lysine residue. Subsequently, all acid-labile protecting groups were removed with TFA/TIS/H_2O (95/2.5/2.5; TIS = triisopropylsilane), and the disulfide bridge was formed. The template molecule was purified by RP-HPLC (67% overall yield) and characterized by electrospray ionization mass spectrometry (ESI-MS: m/z: 1647).

The helical block Boc-S(*t*Bu)-F-S(*t*Bu)-R(Pmc)-S(*t*Bu)-D(O*t*Bu)-E(O*t*-Bu)-L-T(*t*Bu)-R(Pmc)-H(Trt)-I-R(Pmc)-I-H(Trt)-T(*t*Bu)-G-K(Dde) was synthesized on Rink-MBHA resin. The Dde protecting group was selectively removed with 10% H_2NNH_2 (20 min), and the liberated ε-NH_2 group of the C-terminal lysine residue was functionalized with Fmoc-$HNOCH_2COOSu$. After cleavage of the helix from the resin and simultaneous removal of all acid-labile protecting groups (95% TFA, 1.5 h), mild oxidation of the N-terminal serine residue with $NaIO_4$ (fivefold excess, 5 min) led to the aldehyde. The helical block was purified by RP-HPLC (53% overall yield) and characterized by ESI-MS (m/z: 2458).

To generate the first oxime bond between the N terminus of the helix and the aminooxy function of the lysine side chain in the template, 1.1 equiv of

 © WILEY-VCH Verlag GmbH, D-69451 Weinheim, 1998 1433-7851/98/3721-2992 $ 17.50+.50/0

the helix was dissolved in sodium acetate buffer (10 mM, pH 4) and added dropwise to a solution of the template in acetate buffer (pH 7.5). The condensation reaction was complete after 18 h, as monitored by analytical HPLC.

In the next step, the serine residue in the ε position of the lysine residue of the template was oxidized to the aldehyde (fivefold excess of $NaIO_4$, 5 min), and the peptide purified by RP-HPLC (56%). Subsequently, the Fmoc protecting group of the aminooxy group at the C-terminal lysine residue of the helix was removed with 20% piperidine in DMF. After precipitation with diethyl ether, the crude peptide was dissolved in 10 mM acetate buffer (pH 4); this resulted in immediate formation of the second oxime bond (>90%). The LIF 1 was purified by RP-HPLC and characterized by ESI-MS (*m*/*z*: 3788).

Optical absorption spectra of the Co^{II} peptide complex were recorded on a Beckmann spectrophotometer. Prior to complex formation, the internal disulfide bond of LIF 1 was reduced with 250 mM dithiothreitol (DTT) at room temperature for 10 h. After lyophilization, LIF 1 (150 μM) was suspended in Tris·HCl buffer (pH 7; degassed with helium) and 150 μM $CoCl_2$ added. The addition of an equimolar amount of $ZnCl_2$ to this solution readily displaces Co^{II} from the complex.

CD spectra were recorded on a Jobin Yvon Marck VI circular dichrometer in quartz cells (path length 0.1 cm). Prior to recording the spectra the internal disulfide bond in LIF 1 was reduced as described above, LIF 1 was taken up in Tris·HCl, and spectra were recorded before and after addition of equimolar amounts of $ZnCl_2$.

Received: April 14, 1998 [Z 11719 IE]
German version: *Angew. Chem.* **1998**, *110*, 3160 – 3164

Keywords: chemoselectivity · protein design · protein mimetics · proteins · zinc finger

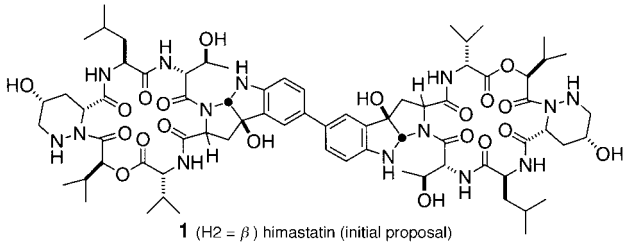
[1] J. S. Richardson, D. C. Richardson, *Trends Biochem. Sci*. **1989**, *14*, 304.
[2] J. W. Bryson, S. F. Betz, H. S. Lu, D. J. Suich, H. X. Zhou, K. T. O'Neil, W. F. DeGrado, *Science* **1995**, *270*, 935.
[3] a) S. Vuilleumier, M. Mutter, *Angew. Chem*. **1989**, *101*, 653; *Angew. Chem. Int. Ed. Engl*. **1989**, *28*, 535; b) M. Mutter, G. Tuchscherer, *Cell. Mol. Life Sci*. **1997**, *53*, 851.
[4] S. Kamtekar, J. M. Schiffer, H. Xiong, J. M. Babik, H. M. Hecht, *Science* **1993**, *262*, 1680.
[5] S. Olofsson, L. Baltzer, *Fold. Design* **1996**, *1*, 347.
[6] M. D. Struthers, R. P. Cheng, B. Imperiali, *Science* **1996**, *271*, 342.
[7] R. T. Sauer, *Fold. Design* **1996**, *1*, R27.
[8] B. Nolting, R. Golbik, A. R. Fersht, *Proc. Natl. Acad. Sci. USA* **1995**, *92*, 10668.
[9] E. Shakhnovich, V. Abkevich, O. Ptitsyn, *Nature* **1996**, *379*, 96.
[10] a) M. Mutter, G. Tuchscherer, *Makromol. Chem. Rapid Commun*. **1988**, *9*, 437; b) G. Tuchscherer, C. Servis, G. Corradin, U. Blum, J. Rivier, M. Mutter, *Protein Sci.* **1992**, *1*, 1377.
[11] a) M. Mutter, G. Tuchscherer, C. Miller, K.-H. Altmann, R. I. Carey, D. F. Wyss, A. M. Labhardt, J. E. Rivier, *J. Am. Chem. Soc*. **1992**, *114*, 1463; b) G. Tuchscherer, L. Scheibler, P. Dumy, M. Mutter, *Biopolym. Pept. Sci.* **1998**, *47*, 63.
[12] P. Dumy, I. M. Eggleston, S. E. Cervigni, U. Sila, X. Sun, M. Mutter, *Tetrahedron Lett*. **1995**, *36*, 1255.
[13] M. Mutter, P. Dumy, P. Garrouste, C. Lehmann, M. Mathieu, C. Peggion, S. Peluso, A. Razaname, G. Tuchscherer, *Angew. Chem*. **1996**, *108*, 1587; *Angew. Chem. Int. Ed. Engl*. **1996**, *35*, 1482.
[14] K. Rose, *J. Am. Chem. Soc*. **1994**, *116*, 30.
[15] a) G. Tuchscherer, *Tetrahedron Lett.* **1993**, *34*, 8419; O. Nyanguile, M. Mutter, G. Tuchscherer, *Lett. Pept. Sci.* **1994**, 1, 9.
[16] P. E. Dawson, S. B. H. Kent, *J. Am. Chem. Soc*. **1993**, *115*, 7263.
[17] C. F. Liu, J. P. Tam, *Proc. Natl. Acad. Sci. USA* **1994**, *91*, 6584.
[18] S. F. Michael, V. J. Kilfoil, M. H. Schmidt, B. T. Amann, J. M. Berg, *Proc. Natl. Acad. Sci. USA* **1992**, *89*, 4796.
[19] E. Rebar, C. O. Pabo, *Science* **1994**, *263*, 671.
[20] J. Miller, A. D. McLachlan, A. Klug, *EMBO J.* **1985**, *4*, 1609.
[21] R. S. Brown, C. Sanders, P. Argos, *FEBS Lett*. **1985**, *186*, 271.
[22] P. R. Gerber, K. Müller, *J. Comput. Aided Mol. Des.* **1995**, *9*, 251.
[23] D. Grell, C. Lehmann, M. Mathieu, G. Tuchscherer, unpublished results.
[24] J. M. Stewart, J. D. Young, Solid Phase Peptide Synthesis, Pierce Chemical, Rockford, IL, **1984**.
[25] a) P. Dumy, I. M. Eggleston, G. Esposito, S. Nicula, M. Mutter, *Biopolymers* **1996**, *39*, 297; b) G. V. Nikiforovich, C. Lehmann, M. Mutter, *Biopolymers*, in press.
[26] J. M. Berg, D. L. Merkle, *J. Am. Chem. Soc.* **1989**, *111*, 3759.
[27] I. Bertini, C. Luchinat, *Adv. Inorg. Biochem*. **1984**, *6*, 71.
[28] B. Rohwedder, PhD thesis, Lausanne, Switzerland, **1997**.
[29] N. P. Pavletich, C. O. Pabo, *Science* **1991**, *252*, 809.
[30] H. Rink, *Tetrahedron Lett.* **1987**, *28*, 3787.
[31] M. Mergler, *Tetrahedron Lett*. **1988**, *29*, 4005.

Studies in the Total Synthesis of Himastatin: A Revision of the Stereochemical Assignment**

Theodore M. Kamenecka and Samuel J. Danishefsky*

Dedicated to Professor E. J. Corey

The quest for new antibiotic and antitumor agents prompted scientists at Bristol Myers Squibb to investigate an actinomycete strain (ATCC 53653) from the state of Himachal Pradesh in India. In doing so, they encountered a new compound of formula $C_{72}H_{104}N_{14}O_2$, which they named himastatin.[1] After extensive optimization with the strain, himastatin could be obtained in scales adequate for sustaining chemical and biological investigation. While himastatin has not been developed to the point of clinical trials, its activity against gram-positive microorganisms and a variety of tumor probe systems is impressive. Based on spectroscopic investigations augmented by modest degradative studies, **1** was



1 (H2 = β) himastatin (initial proposal)
20 (H2 = α) himastatin (revised proposal)

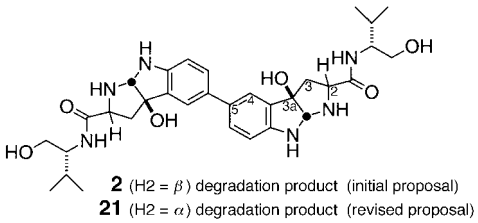
[*] Prof. S. J. Danishefsky,[+] T. M. Kamenecka
Laboratory for Bioorganic Chemistry
Sloan-Kettering Institute for Cancer Research
1275 York Avenue, Box 106, New York, NY 10021 (USA)
Fax: (+1) 212-772-8691
E-mail: c-kandell@ski.mskcc.org

[+] Further address:
Department of Chemistry, Columbia University
Havemeyer Hall, New York, NY 10027 (USA)

[**] This work was supported by the National Institutes of Health (grant nos. CA 28824 and HL 25848 (S.J.D) and CA-08748 (SKI Core Grant)). T.M.K. gratefully acknowledges the NIH for postdoctoral fellowship support (grant no. AI09355). We thank Bristol Myers Squibb for providing us with an authentic sample of himastatin. We thank Dr. George Sukenick and the NMR Core Facility Laboratory, Sloan-Kettering Institute for Cancer Research, for mass spectral and NMR analyses.

 © WILEY-VCH Verlag GmbH, D-69451 Weinheim, 1998 1433-7851/98/3721-2993 $ 17.50+.50/0

advanced as the structure of himastatin. A cleavage product of himastatin retaining only a D-valinol moiety from the peptidal domain was accordingly formulated as **2**.

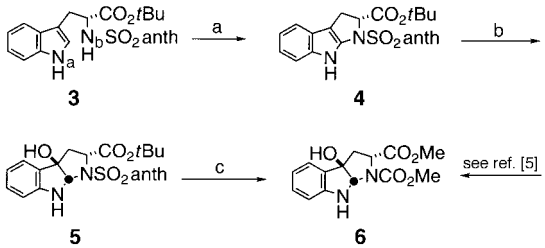


2 (H2 = β) degradation product (initial proposal)
21 (H2 = α) degradation product (revised proposal)

Our interest in himastatin first arose from the intrinsic challenge it posed to chemical synthesis. Solutions to problems of this scope often carry with them learning opportunities which transcend the confines of the particular problem under inquiry. Moreover, we had a focusing biological goal in mind. We hoped to evaluate representative "monomers" (see compound **17**) to ascertain whether the "dimeric" motif is constructed by the microorganism in response to an identifiable biological advantage.

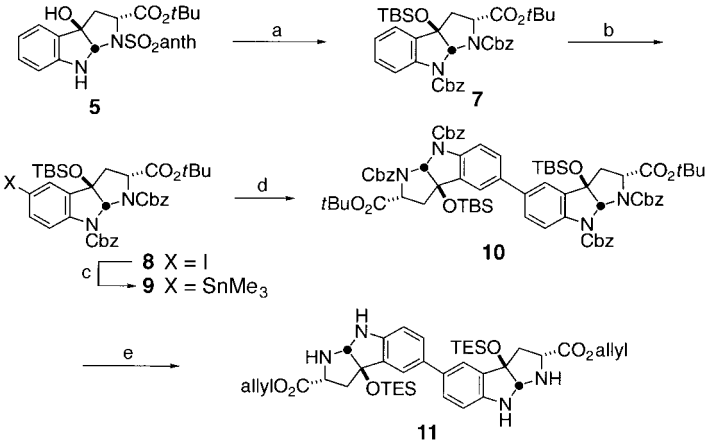
One of the many provocative structural features of **1** is the 2,3,3a,8a-hexahydropyrrolo[2,3-*b*]indole moiety bearing a potentially eliminable hydroxyl group in position 3a. Even if attention is confined to the system bearing a *cis* fusion of the five-membered rings, two possibilities for the relationship of the tryptophan carboxy equivalent at C2 to the junction present themselves. Given the structure **1** proposed for himastatin, we focused on the subtype with an *anti* relationship of this carboxy center.

The possibility, in principle, of oxidative cycloaromatization of various tryptophan derivatives (see compound **4**) had been known since the pioneering work of Witkop et al.[2] For the purpose of our synthesis, the use of an N_b-anthracenosulfonyl protecting group on the *tert*-butyl ester of tryptophan (**3**, Scheme 1)[3] proved to be of immense advantage.[4] Conversion of **3** into **4** was readily achieved, as was the conversion of **4** into **5**. For purposes of additional verification, the transformation of **5** to **6** was also accomplished. The latter correlates with a compound previously assigned to be in the *anti-cis* series.[5]



Scheme 1. Synthesis of **6**. a) NBS, TEA, CH_2Cl_2, 80%; b) 1. DMDO, CH_2Cl_2, $-78\,^{\circ}C$; 2. $NaBH_4$, MeOH, 75% (2 steps); c) 1. TFA; 2. CH_2N_2; 3. Al(Hg); 4. $ClCO_2Me$, pyridine, 50% (4 steps). anth = anthracen-9-yl, DMDO = 3,3-dimethyldioxirane, NBS = *N*-bromosuccinimide.

The use of a Stille coupling[6] was envisioned for joining the two indolyl moieties through a carbon–carbon bond. In practice compound **5** lent itself to conversion into **7** through a three-step sequence (Scheme 2). With the particular set of



Scheme 2. Synthesis of **11**. a) 1. Al(Hg), THF; 2. CbzCl, pyridine, CH_2Cl_2, 80%; 3. TBSCl, DBU, CH_3CN, $50\,^{\circ}C$, 90%; b) ICl, CH_2Cl_2, 2,6-di-*tert*-butylpyridine, 90%; c) Sn_2Me_6, THF, [$Pd(PPh_3)_4$], $60\,^{\circ}C$, 85%; d) [Pd_2dba_3], $AsPh_3$, **8**, $45\,^{\circ}C$, DMF, 50–70%; e) 1. TBAF; 2. TESCl, TEA; 3. H_2, Pd/C, EtOAc; 4. FMOC-HOSu, pyridine; 5. TESOTf, 2,6-lutidine; 6. allyl alcohol, EDCI, DMAP; 7. piperidine, CH_3CN, 30% (7 steps). Cbz = benzyloxycarbonyl, dba = 1,5-dibenzylideneacetone, DBU = 1,8-diazabicyclo[5.4.0]undec-7-ene, EDCI = 1-ethyl-3-(3-dimethylaminopropyl)carbodiimide, FMOC = (9*H*-fluoren-9-ylmethoxy)carbonyl, HOSu = *N*-hydroxysuccinimide, TBAF = tetrabutylammonium fluoride, TBS = *tert*-butyldimethylsilyl, TES = triethylsilyl, Tf = trifluoromethylsulfonyl.

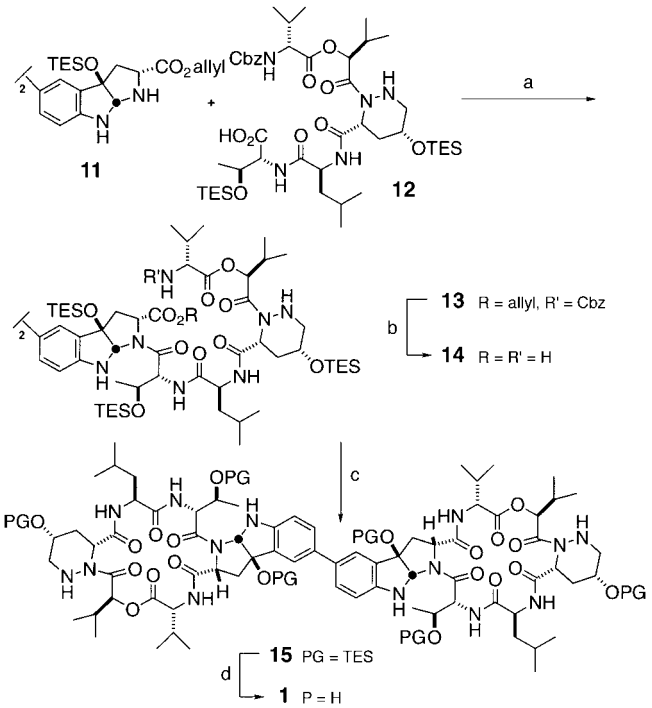
protecting groups chosen, iodination at C_5 of the indoline occurred with ICl (→**8**). The stannyl indole **9** was prepared from **8**. Palladium-mediated coupling of **8** and **9** gave rise to **10**. Following extensive trial and error probes, it was found that the arrangement of protecting groups in **11**, which was synthesized as shown, would allow us to advance toward **1** with viable prospects for eventual deprotection. We were attracted to the possibility of twofold leveraging of the subsequent interpolation by conducting it simultaneously in both sectors of the dimer.

In a parallel series of investigations, the ester tripeptide **12**, bearing a free carboxyl group in the terminal D-threonine residue, was synthesized (Scheme 3).[7] Coupling of **11** with **12** under the conditions shown gave rise to **13** after reprotection.[8] Cleavage of the carboxyl and amino protecting groups led to **14**, the substrate for the critical macroloactamization. Cyclization smoothly led to **15**, which on deprotection afforded fully synthetic **1**.

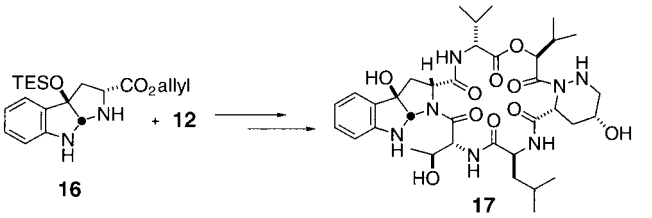
At this point it was clear that the ^1H NMR spectrum of **1** synthesized in our laboratory did not correspond with that recorded for naturally derived himastatin.[1c] Particularly striking were the two upfield signals at $\delta = 0.55$ and 0.35 for **1** corresponding to the valine isopropyl group. No such upfield resonances had been observed in the ^1H NMR spectrum of himastatin.

The strategy used to reach dimer **1** was applied to synthesize monomeric **17** (Scheme 4). For this goal, we utilized **16**, which is readily derived from **5**, and the previously described **12**. The synthesis proceeded in much the same manner as for **1**. Once again, the ^1H NMR spectrum of **17** contained upfield peaks at $\delta = 0.55$ and 0.35 having no counterpart in that of himastatin.[9] That this discrepancy was rooted in the pyrrolindoline sector of the molecule was shown when we obtained compounds **18** and **19**. The recorded chemical shifts of the

 © WILEY-VCH Verlag GmbH, D-69451 Weinheim, 1998 1433-7851/98/3721-2994 $ 17.50+.50/0

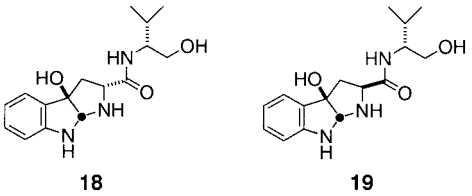


Scheme 3. Synthesis of "*epi-himastatin*" (**1**). a) 1. HATU, HOAt, collidine, CH_2Cl_2, $-10\,^{\circ}C \rightarrow RT$, 65%; 2. TESOTf, 2,6-lutidine, CH_2Cl_2, 63%; b) 1. $[Pd(PPh_3)_4]$, $PhSiH_3$, THF; 2. H_2, Pd/C, EtOAc, 40%; c) HOAt, HATU, $i Pr_2NEt$, DMF; d) TBAF, THF, HOAc, 25% (from **14**). HATU = *N*-[(dimethylamino)-1*H*-1,2,3-triazolo[4,5-*b*]pyridin-1-ylmethylene]-*N*-methylmethaneaminium hexafluorophosphate, HOAt = 1-hydroxy-7-aza-benzotriazole.



Scheme 4. Synthesis of the "*epi-himastatin*" monomer (**17**).

isopropyl methyl groups of the synthetic *syn-cis* monomer **19** ($\delta = 0.92$ and 0.88)[7] were in much closer harmony with the data ($\delta = 0.94$ and 0.89)[1c] of the degradation product of himastatin (hitherto formulated as **2**) than were those of the synthetic *anti-cis* structure **18** ($\delta = 0.78$ and 0.62).



Therefore, we postulated that the relationship of the *cis* junction and the C_2-carboxamido group in naturally occurring himastatin is *syn* rather than *anti*, as previously proposed. Given the chiroptical data accumulated in the Bristol Myers Squibbs investigation,[1c] we further favored a revision from a D-tryptophan matrix to the L-tryptophan series. Thus, the absolute stereochemistry of the pyrrolindoline junction remains unchanged from the previous assignment. However, the stereochemical assignment of the tricyclic carboxamido centers are reversed (*S*,*S* rather than *R*,*R*). The structure of himastatin is thus assigned as **20**, and that of its valinol degradation product as **21**. In the newly proposed structure of himastatin, the components in the depsipeptide domain are presented in alternating D and L configurations.[10] These various proposals were validated when a total synthesis of himastatin was realized.[11]

Received: June 5, 1998 [Z11949IE]
German version: *Angew. Chem.* **1998**, *110*, 3164–3166

Keywords: alkaloids · antibiotics · himastatin · structure elucidation · total synthesis

[1] a) K. S. Lam, G. A. Hesler, J. M. Mattel, S. W. Mamber, S. Forenza, *J. Antibiot.* **1990**, *43*, 956; b) J. E. Leet, D. R. Schroeder, B. S. Krishnan, J. A. Matson, *J. Antibiot.* **1990**, 961; c) J. E. Leet, D. R. Schroeder, J. Golik, J. A. Matson, T. W. Doyle, K. S. Lam, S. E. Hill, M. S. Lee, J. L. Whitney, B. S. Krishnan, *J. Antibiot.* **1996**, *49*, 299.

[2] M. Ohno, T. F. Spande, B. Witkop, *J. Am. Chem. Soc.* **1968**, *90*, 6521.

[3] Prepared from D-tryptophan: 1) $anthSO_2Cl$, TEA, THF, H_2O; 2) *N*,*N*′-diisopropyl-*O*-*tert*-butylisourea, CH_2Cl_2 (65% yield overall).

[4] a) The anthracene sulfonamide was readily cleaved with Al(Hg) at room temperature. b) The use of the *tert*-butyl ester afforded a much higher *anti*:*syn* stereoselectivity (>15:1) than the corresponding methyl ester (3:1).

[5] M. Nakagawa, S. Kato, S. Kataoka, S. Kodato, H. Watanabe, H. Okajima, T. Hino, B. Witkop, *Chem. Pharm. Bull.* **1981**, *29*, 1013.

[6] J. K. Stille, *Angew. Chem.* **1986**, *98*, 504; *Angew. Chem. Int. Ed. Engl.* **1986**, *25*, 508.

[7] Compound **12** was synthesized similarly to **20**, which is described in ref. [11].

[8] J. M. Humphrey, A. R. Chamberlin, *Chem. Rev.* **1997**, *97*, 2243.

[9] The ^1H NMR spectra of synthetic **1** and **17** are virtually identical upfield of 6.0 ppm.

[10] See M. R. Ghadiri, R. J. Granja, R. A. Milligan, D. E. McRee, N. Khazanovich, *Nature* **1993**, *366*, 324.

[11] T. M. Kamenecka, S. J. Danishefsky, *Angew. Chem.* **1998**, *110*, 3166–3168; *Angew. Chem. Int. Ed.* **1998**, *37*, 2995–2998.

Total Synthesis of Himastatin: Confirmation of the Revised Stereostructure**

Theodore M. Kamenecka and Samuel J. Danishefsky*

Dedicated to Professor E. J. Corey

In the preceding communication[1] we have provided the background of the himastatin problem and the findings that necessitated a revision in the assignment of the configuration

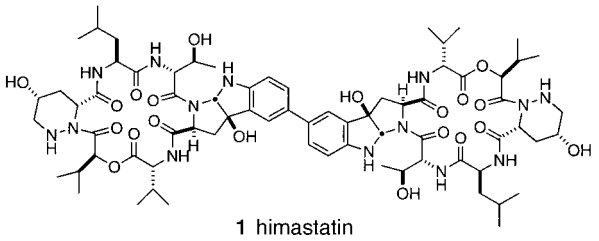
[*] Prof. S. J. Danishefsky,[+] T. M. Kamenecka
Laboratory for Bioorganic Chemistry
Sloan-Kettering Institute for Cancer Research
1275 York Avenue, Box 106, New York, NY 10021 (USA)
Fax: (+1) 212-772-8691
E-mail: c-kandell@ski.mskcc.org

[+] Further address:
Department of Chemistry, Columbia University
Havemeyer Hall, New York, NY 10027 (USA)

[**] This work was supported by the National Institutes of Health (grant nos. CA 28824 and HL 25848 (S.J.D) and CA-08748 (SKI Core Grant)). T.M.K. gratefully acknowledges the NIH for postdoctoral fellowship support (grant no. AI09355). We thank Bristol Myers Squibb for providing us with an authentic sample of himastatin. We thank Dr. George Sukenick and the NMR Core Facility Laboratory, Sloan-Kettering Institute for Cancer Research, for mass spectral and NMR analyses.

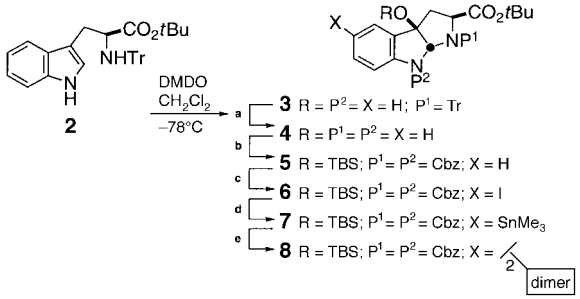
 © WILEY-VCH Verlag GmbH, D-69451 Weinheim, 1998 1433-7851/98/3721-2995 $ 17.50+.50/0

at the tryptophyl carboxyl stereogenic centers (C_2) in each of its two pyrroloindoline domains (see revised structure **1**). Here we describe the total synthesis of himastatin and confirm the structural arguments.



1 himastatin

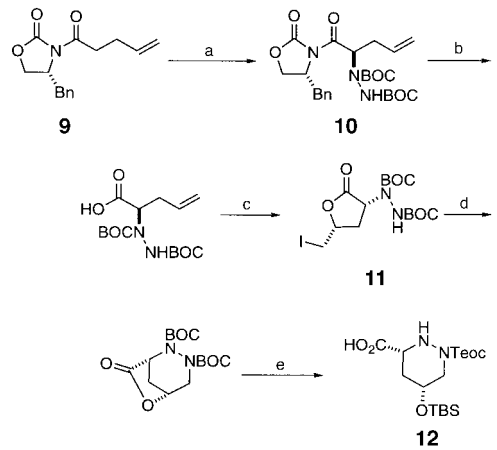
We first turned to the very important matter of gaining stereospecific access to the *syn-cis*-pyrrolo[2,3-*b*]indoline series.[2] Many tryptophan-derived congeners were screened as to their amenability for stereospecific oxidative cyclization in the desired mode. The *t*-butyl ester of N_b-trityl-L-tryptophan (**2**)[3] gave, upon oxidation with 2,2 dimethyldioxirane, **3** in 70% yield, apparently unaccompanied by the *anti-cis* diastereomer (Scheme 1). Following cleavage of the trityl



Scheme 1. Synthesis of **8**. a) HOAc, MeOH, CH_2Cl_2; b) 1. CbzCl, pyridine, CH_2Cl_2; 2. TBSCl, DBU, MeCN; c) ICl, 2,6-di-*tert*-butylpyridine, CH_2Cl_2, 75%; d) Me_6Sn_2, $[Pd(PPh_3)_4]$, THF, 86%; e) **6**, $[Pd_2dba_3]$, $AsPh_3$, DMF, 45°C, 79%. Cbz = benzyloxycarbonyl, dba = dibenzylideneacetone, DBU = 1,8-diazabicyclo[5.4.0]undec-7-ene, DMDO = 2,2-dimethyldioxirane, TBS = *tert*-butyldimethylsilyl, Tr = trityl = triphenylmethyl.

group, the two amino groups of **4** were protected as benzyloxycarbamate (N-Cbz) groups (→**5**). Upon reaction with ICl, an iodine atom was introduced at C_5 (→**6**). Part of iodo compound **6** was converted into arylstannane **7**. At this stage, we could take advantage of our ability (as demonstrated for the *anti-cis* series)[1] to join sophisticated pyrroloindolines through carbon–carbon bond formation by an extension of the Stille reaction. Under these conditions, **6** and **7** were coupled smoothly to produce **8**.

A stereoselective route to the 5-hydroxypiperazic acid started with the pentenoic acid derivative **9**.[4–6] Its sodium enolate reacted with bis(*tert*-butyl) azodicarboxylate to produce, stereospecifically, **10** (Scheme 2) Cleavage of the acyl–oxazolidinone bond was accomplished through the agency of lithium hydroperoxide in THF. Iodolactonization of the resultant acid under the influence of titanium isopropoxide gave the desired 2,4-*cis* compound **11** along with its *trans* counterpart in a 6:1 ratio. The iodine functionality was displaced upon deprotonation of the terminal Boc-protected



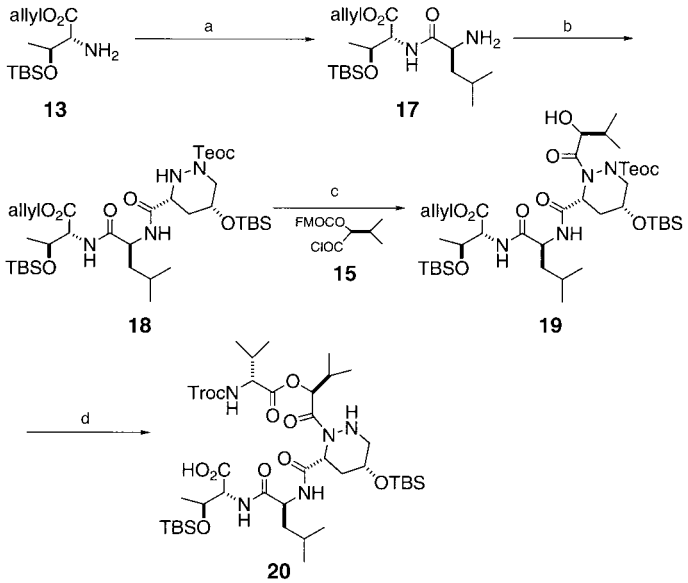
Scheme 2. Synthesis of **12**. a) NaHMDS, THF, −78°C, Boc–N=N–Boc, 80%; b) LiOOH, THF, 89%; c) NIS, $Ti(OiPr)_4$, 80%; d) NaH, DMF, 74%; e) 1. TFA, MeOH; 2. TeocCl, pyridine; 3. TBSOTf, 2,6-lutidine; 4. LiOH, 82%. Bn = benzyl, Boc = *tert*-butoxycarbonyl, HMDS = hexamethyldisilazane, NIS = *N*-iodosuccinimide, Teoc = 2-(trimethylsilyl)ethyloxycarbonyl, Tf = trifluoromethylsulfonyl, TFA = trifluoroacetic acid.

amino group, and an intramolecular N-alkylation took place to form a bicyclic intermediate. Cleavage of both Boc protecting groups and the lactone, acylation of the remote amino group with TEOCCl (TEOC = 2-(trimethylsilyl)ethyloxycarbonyl), protection of the alcohol functionality with a silyl group, and ester hydrolysis led to **12**.

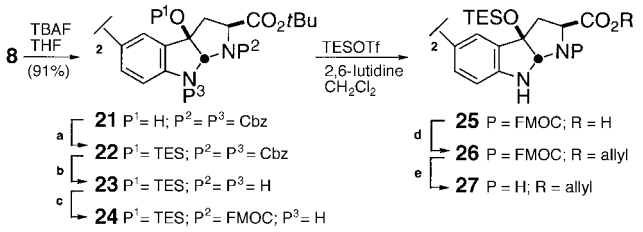
The other four fragments which were employed in building the peptidal domain were 1) the D-threonine derivative **13** (prepared from D-threonine), 2) FMOC-L-leucine (**14**, commercially available), 3) the hydroxyisovaleryl derivative **15** (prepared from commercially available *S*-hydroxyisovaleric acid), and 4) D-valine, as its TROC derivative **16** (Scheme 3). Coupling of **13** with **14** was followed by cleavage of the FMOC group to release the leucine amino functionality. Compound **17** was acylated with the piperazic acid (**12**) to provide **18**. The relatively unreactive N1 atom of the piperazic acid moiety in **18** was acylated by **15**. Following liberation of the hydroxyl functionality on the isovaleryl group (→**19**), acylation with **16**, and removal of the allyl ester and TEOC protecting groups, the required **20** was in hand.

We next turned to the bis(pyrroloindoline) system **8** (Scheme 4). Significant restructuring of this domain was necessary to render it suitable for initial attachment of the depsipeptide domain (to the pyrroloindoline) as well as for macrocyclization and deprotection. For instance, from parallel studies on a related series, it became clear that we would not be able to remove an angular *tert*-butyldimethylsilyl (TBS) protecting group at C3a when the full macrocycle was in place. Hence, the TBS blocking group was cleaved at the stage of **8** to provide **21**. Moreover, a triethylsilyl (TES) functionality could be introduced at this point through the agency of TESCl in the presence of DBU. The four Cbz functionalities in **22** were discharged, giving rise to **23**. Following protection in the form of FMOC derivative **24**, the *tert*-butyl ester was transformed into the triethylsilyl ester through the agency of triethylsilyl triflate and lutidine. Hydrolysis of this triethylsilyl ester gave rise to **25**, which

 © WILEY-VCH Verlag GmbH, D-69451 Weinheim, 1998 1433-7851/98/3721-2996 $ 17.50+.50/0 *Angew. Chem. Int. Ed.* **1998**, *37*, No. 21



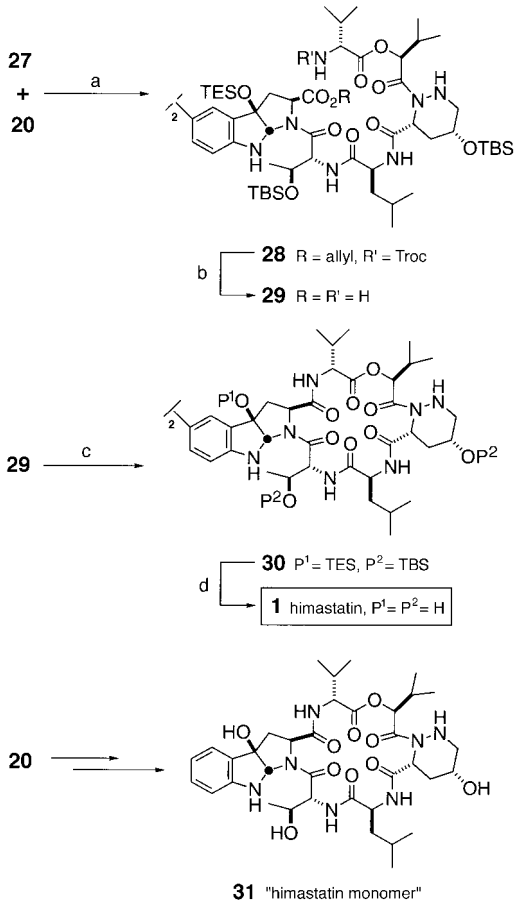
Scheme 3. Synthesis of **20**. a) FMOC-L-leucine (**14**), EDCI, DMAP, CH_2Cl_2; 2. piperidine, CH_3CN, 76%; b) piperazic acid (**12**), HATU, HOAt, collidine, CH_2Cl_2, 95%; c) 1. collidine, CH_2Cl_2, **15**; 2. piperidine, CH_3CN, 96%; d) 1, Troc-D-valine (**16**), IPCC, Et_3N, DMAP, CH_2Cl_2; 2. $ZnCl_2$, CH_3NO_2; 3. TBSOTf, 2,6-lutidine, CH_2Cl_2; 4. $[Pd(PPh_3)_4]$, $PhSiH_3$, THF, 72% (4 steps). DMAP = 4-(dimethylamino)pyridine, EDCI = 1-ethyl-3-(3-dimethylaminopropyl)carbodiimide, FMOC = (9*H*-fluoren-9-ylmethoxy)-carbonyl, HATU = *N*-[(dimethylamino)-1*H*-1,2,3-triazolo[4,5-*b*]pyridin-1-ylmethylene]-*N*-methylmethaneaminium hexafluorophosphate, HOAt = 1-hydroxy-7-aza-benzotriazole, IPCC = isopropenyl chloroformate, Troc = (2,2,2-trichloroethoxy)carbonyl.



Scheme 4. Synthesis of **27**. a) TESCl, DBU, DMF (92%); b) H_2, Pd/C, EtOAc (100%); c) FMOC-HOSu, pyridine, CH_2Cl_2 (95%); d) allyl alcohol, DBAD, PPh_3, THF (90% from **24**); e) piperidine, MeCN (74%). DBAD = di-*tert*-butyl azodicarboxylate, HOSu = *N*-hydroxysuccinimide, TBAF = tetrabutylammonium fluoride, TES = triethylsilyl.

was protected as its allyl ester derivative **26**. Finally, the FMOC functionalities were cleaved with piperidine, thereby providing **27**.

Based on pertinent model studies, we were confident that acylation would occur at N_b of the pyrroloindoline moiety of **27**. Indeed, coupling occurred smoothly at this center with the threonine-derived carboxylic acid **20** to provide **28** in 60% yield (Scheme 5). Following deprotection of the allyl ester and reductive cleavage of the TROC functionality, *seco* structure **29** was in hand. Fortunately, **29** underwent macrolactamization mediated by HATU[7] to give rise to the lactam ester **30**. In the last step of the synthesis the six silyl groups were cleaved to provide himastatin (**1**). The ^1H NMR spectrum of fully synthetic himastatin was identical with that published for the natural product. Furthermore, we independently meas-



Scheme 5. Synthesis of himastatin (**1**). a) HATU, HOAt, collidine, CH_2Cl_2, $-10\,^\circ C \rightarrow$ RT, 60%; b) 1. $[Pd(PPh_3)_4]$, $PhSiH_3$, THF; 2. Pb/Cd, NH_4OAc, THF, 56%; c) HOAt, HATU, iPr_2NEt, DMF; d) TBAF, THF, HOAc, 35% (from **29**).

ured the 500-MHz spectrum of a tiny reference sample of natural himastatin provided by the Bristol Myers Squibb corporation. It was clear by an overlay of the richly detailed spectra that the total synthesis of himastatin had at last been accomplished. This work establishes the correctness of the revised stereostructural formulation of himastatin. With related methodology **31**, containing the full depsipeptide domain on the monomeric parent pyrroloindoline system, has also been synthesized.

As a consequence of the himastatin program, we have learned how to synthesize the pyrroloindoline system in stereospecific form in either the *anti-cis* or *syn-cis* series. We have demonstrated for the first time the applicability of an extended Stille coupling to generate bis(pyrroloindoline) structures in rather delicate and complex settings. The parameters that allow for very subtle protection and deprotection operations of the pyrroloindoline structure have also been established. The biological evaluation of various monomeric and dimeric congeners of himastatin will now proceed in earnest.

Received: June 5, 1998 [Z11950IE]
German version: *Angew. Chem.* **1998**, *110*, 3166 – 3168

Keywords: alkaloids · antibiotics · himastatin · total synthesis

 © WILEY-VCH Verlag GmbH, D-69451 Weinheim, 1998 1433-7851/98/3721-2997 $ 17.50+.50/0

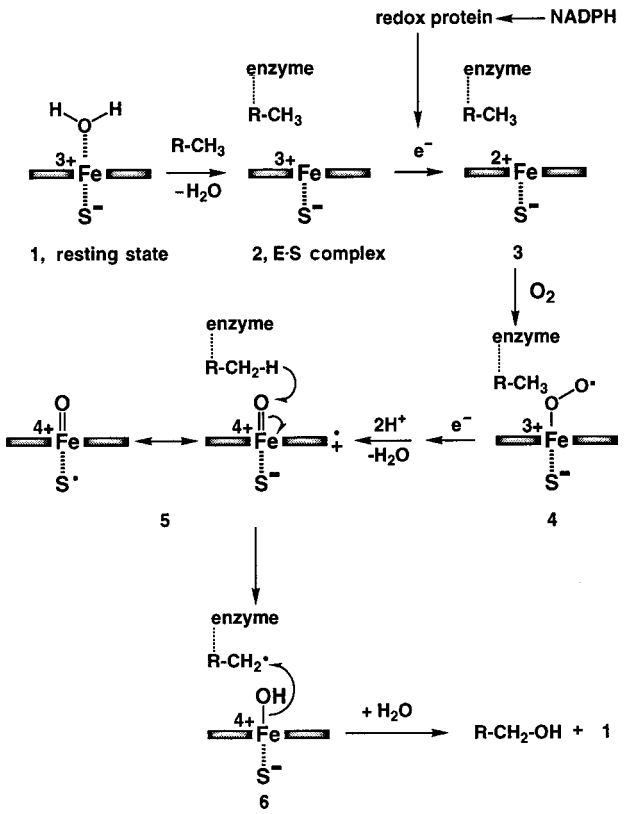
[1] T. M. Kamenecka, S. J. Danishefsky, *Angew. Chem.* **1998**, *110*, 3164–3166; *Angew. Chem. Int. Ed.* **1998**, *37*, 2993–2995.
[2] See inter alia a) W. E. Savige, *Aust. J. Chem.* **1975**, *28*, 2275; b) M. Nakagawa, S. Kato, S. Kataoka, S. Kodato, H. Watanabe, H. Okajima, T. Hino, B. Witkop, *Chem. Pharm. Bull.* **1981**, *29*, 1013; c) M. Somei, T. Kawasaki, Y. Fukui, F. Yamada, T. Kobayashi, H. Aoyama, D. Shinmyo, *Heterocycles* **1992**, *34*, 1877.
[3] Prepared from L-N_b-trityltryptophan and *N,N'*-diisopropyl-*O-tert*-butylisourea (CH_2Cl_2, RT): P. A. Hipskind, J. J. Howbert, S. Cho, J. S. Cronin, S. L. Fort, F. O. Ginah, G. J. Hansen, B. E. Huff, K. L. Lobb, M. J. Martinelli, A. R. Murray, J. A. Nixon, M. A. Staszak, J. D. Copp, *J. Org. Chem.* **1995**, *60*, 7033.
[4] D. Evans, T. C. Britton, R. L. Dorow, J. F. Dellaria, *J. Am. Chem. Soc.* **1986**, *108*, 6395.
[5] Compound **12** was more conveniently prepared in bulk by a non-stereospecific route starting with (*R*)-methyl 4,5-epoxypentanoate: P. T. Ho, N. Davies, *Synthesis* **1983**, 462.
[6] O. Kitagawa, T. Sato, T. Taguchi, *Chem. Lett.* **1991**, 177.
[7] J. M. Humphrey, A. R. Chamberlin, *Chem. Rev.* **1997**, *97*, 2243.

On the Origin of the Low-Spin Character of Cytochrome $P450_{cam}$ in the Resting State—Investigations of Enzyme Models with Pulse EPR and ENDOR Spectroscopy**

Hamed Aissaoui, Rainer Bachmann, Arthur Schweiger, and Wolf-Dietrich Woggon*

The cytochrome P450 enzymes, ubiquitous in nature, are heme–thiolate proteins which are important to the metabolism of endogenous compounds and xenobiotics.[1] The reactivity of these enzymes is associated with an iron(III)–protoporphyrin IX complex in the active site which is bound to the protein through hydrogen bridges of the two propionate side chains and through a thiolate ligand provided by a cysteine residue; the thiolate ligand is coordinated to the iron center from the proximal side of the porphyrin.

Our knowledge of various intermediates in the catalytic cycle of cytochromes P450 (Scheme 1) relies on X-ray structures of different forms of cytochrome $P450_{cam}$[2, 3] and numerous investigations on suitable model compounds.[4] Accordingly, the resting state of cytochrome $P450_{cam}$ (**1**) contains six water molecules in the substrate binding domain (one water molecule is coordinated to the iron center) which are all displaced when the natural substrate camphor is bound. It was recently suggested that Arg299, which according to the X-ray structure forms a salt bridge with one of the heme propionate



Scheme 1. Catalytic cycle of cytochrome P450.

groups, triggers the release of the active-site water cluster through a pathway other than the substrate access channel. On substrate binding, conformational changes of the propionate/Arg299 domain open a channel to a water cluster located close to the protein surface, on the proximal side of the heme.[5]

This change in the ligand sphere of iron is accompanied by a change in the spin-state equilibrium from greater than 96% low-spin Fe^{III} in the resting state **1** to predominantly high-spin Fe^{III} of the E·S complex **2**.[6] The redox potential of the heme–thiolate protein also shifts from −300 mV for **1** to −175 mV for **2**, rendering the latter capable of accepting an electron from NADPH through the redox protein putidaredoxin. Subsequently, the iron(II) complex **3** is formed, which binds oxygen to yield **4**. Reductive scission of the oxygen–oxygen bond furnishes the iron(IV) oxo intermediate **5**, which allows, for example, O insertion into nonactivated C–H bonds (see **6**).[4] Whether O insertion is in general a two-step process, as shown in Scheme 1, or whether it can also proceed in a concerted fashion is currently being disputed.[7]

Ever since the water cluster was discovered in **1**, the origin of the low-spin ground state has been a matter of debate, as it seems unlikely that thiolate and water, both weak ligands, would establish a low-spin iron(III) center. It was therefore suggested that ^-OH rather than water binds to iron or that the hydrogen-bonded water cluster induces a hydroxide-like character at the coordinated water molecule.[2b, 8] From ESEEM studies (ESEEM = electron spin echo envelope modulation) with ^{17}O-enriched water bound to $P450_{cam}$, however, it was concluded that one water molecule binds

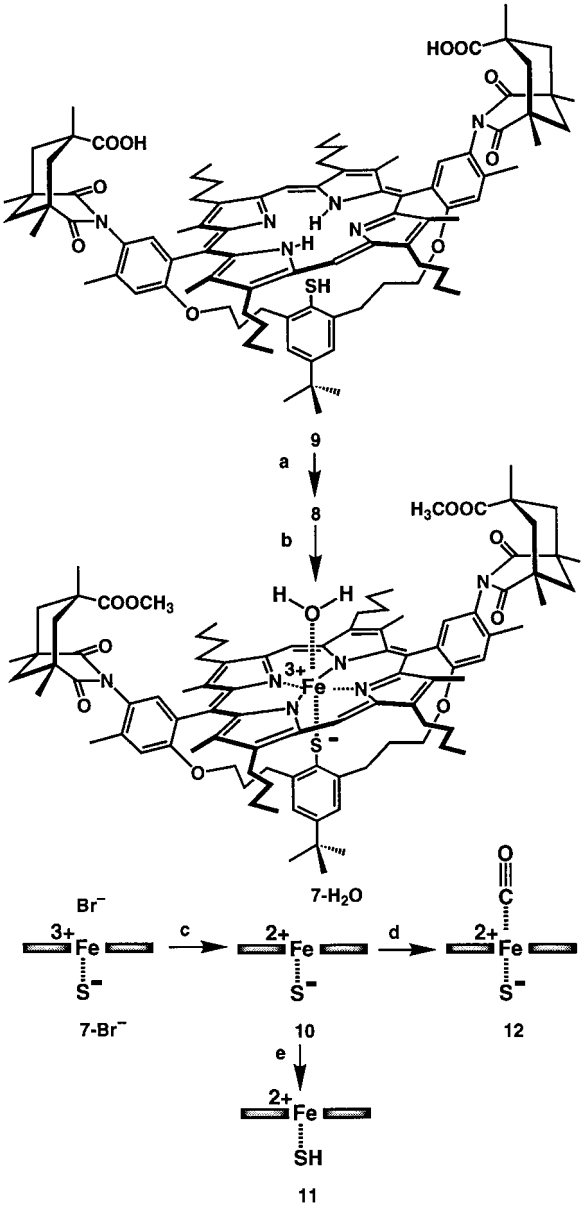
[*] Prof. Dr. W.-D. Woggon, Dipl.-Chem. H. Aissaoui
Institut für Organische Chemie der Universität
St.-Johanns-Ring 19, CH-4056 Basel (Switzerland)
Fax: (+41) 61-267-11-02
E-mail: woggon@wolfi.chemie.unibas.ch
Dr. R. Bachmann, Prof. Dr. A. Schweiger
Laboratorium für Physikalische Chemie
Eidgenössische Technische Hochschule
CH-8092 Zürich (Switzerland)

[**] This research was supported by the Swiss National Science Foundation. Gunnar Jeschke is gratefully acknowledged for stimulating discussions.

 © WILEY-VCH Verlag GmbH, D-69451 Weinheim, 1998 1433-7851/98/3721-2998 $ 17.50+.50/0

nonrandomly to iron; the presence of a hydroxide ion as the sixth ligand was excluded.[9] Since these investigations arrived at no conclusions whatsoever concerning the origin of the low-spin character of iron(III) in the given ligand field, we decided to prepare suitable enzyme models for the resting state of $P450_{cam}$ to investigate these complexes by CW EPR as well as pulse EPR and ENDOR techniques (CW = continuous wave, EPR = electron paramagnetic resonance, ENDOR = electron nuclear double resonance). Such studies should provide information on the possible structure and electronic nature of the first intermediate in the catalytic cycle of cytochrome $P450_{cam}$.

The P450 analogue **7** was prepared via **8** from the diacid **9**, a recently synthesized ligand for a P450 model with substrate recognition sites (Scheme 2).[10] After insertion of the iron center, the bromide **7**-Br^- was isolated ($\lambda_{max} = 400$ nm). Reduction of **7**-Br^- with KH in benzene/[18]crown-6 yielded the iron(II) complex **10** ($\lambda_{max} = 422$ nm), which was spectroscopically characterized in its protonated form **11**. Complex **10** binds CO to give **12**, which exhibits a shifted Soret band at 448 nm, characteristic of cytochrome P450. Furthermore, in catalytic amounts, **7** performes reactions common to P450 enzymes in the presence of "O" donors.[11] When **7**-Br^- was treated with water/toluene for 24 h the iron(III)–porphyrin **7**-H_2O was obtained; it was characterized by a Soret band at 408 nm. Electron spray ionization (ESI) mass spectrometry (m/z: 1623 [M^+]) indicated the coordination of one molecule of water to the iron center from the distal side. Accordingly, complex **7** qualifies as a good spectroscopic and chemical enzyme model for the resting state of cytochrome P450.



Scheme 2. Synthesis of **7**-H_2O, a spectroscopic and chemical enzyme model for the resting state of cytochrome $P450_{cam}$: a) CH_2N_2, CH_2Cl_2, 25 °C, 30 min; b) $FeBr_2$, 2,6-lutidine, toluene, reflux, 1 h; c) KH, [18]crown-6, benzene, 25 °C, 30 min; d) CO, toluene, 25 °C, 30 min; e) silica gel, [D_8]toluene.

In native $P450_{cam}$ the change from the state with hexacoordinated low-spin Fe^{III} in **1** to the state with pentacoordinated high-spin Fe^{III} in the enzyme–substrate complex **2** can be easily monitored by CW EPR spectroscopy. The low-spin state **1** shows an EPR spectrum with g values at 2.45, 2.26, and 1.91. The addition of camphor results in a conversion into a rhombically distorted high-spin form **2** with $g = 7.85$, 3.97, and 1.78.[12, 13] Figure 1a displays the CW EPR spectrum of the synthetic P450 analogue **7**-H_2O at 10 K. The almost axially symmetric EPR spectrum with $g_\perp = 5.67$ and $g_\parallel = 2.00$ is characteristic of high-spin iron(III) porphyrins without significant rhombic contributions from the ligand field. It is established that the $g_\parallel$ extremum is normal to the porphyrin plane and that of $g_\perp$ lies in the porphyrin plane.[14] Since the only indication of coordination of water to the iron center in **7**-H_2O came from the ESI mass spectrum, a more complete characterization of the iron(III) ligand sphere by pulse EPR and ENDOR techniques was required.

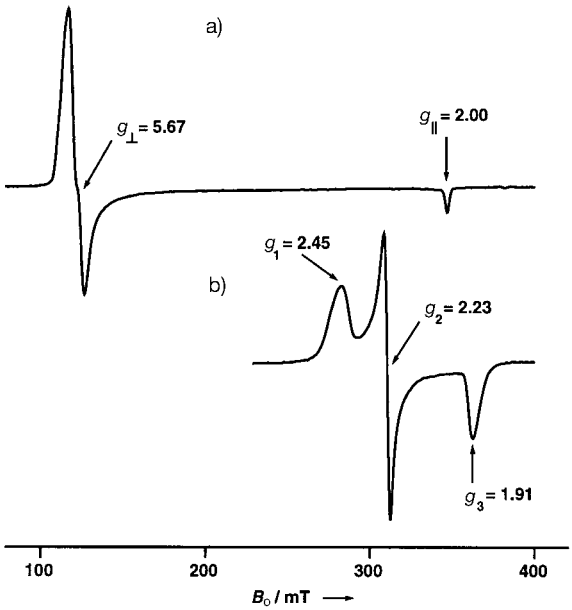
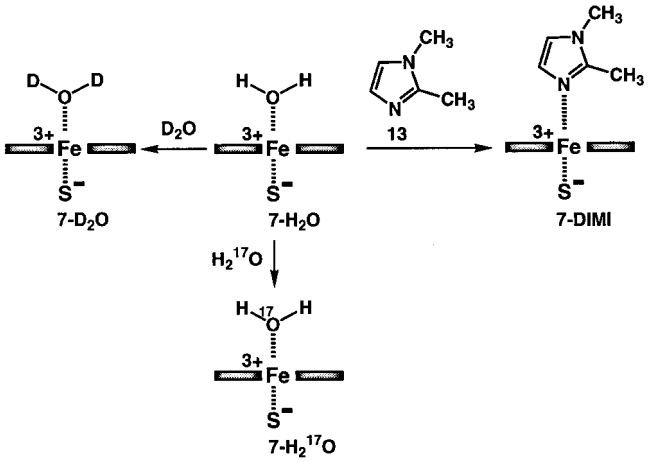


Figure 1. a) CW EPR spectrum of the high-spin state of **7**-H_2O (solvent: MTHF; $T = 10$ K). b) CW EPR spectrum of the low-spin state **7**-DIMI (solvent: MTHF; $T = 100$ K).

 © WILEY-VCH Verlag GmbH, D-69451 Weinheim, 1998 1433-7851/98/3721-2999 $ 17.50+.50/0

Replacement of the water ligand in **7**-H_2O by treatment with an excess of 1,2-dimethylimidazole (DIMI, **13**) induced a change to the low-spin complex **7**-DIMI (Scheme 3). It is important to note that the corresponding CW EPR spectrum



Scheme 3. Exchange reactions of the distal, sixth ligand of **7**-H_2O.

(Figure 1b) shows g values (2.45, 2.23, and 1.91) almost identical to those of the native $P450_{cam}$ in its low-spin state **1**. This additional spectroscopical conformity between the enzyme's resting state and its model system **7** lends further evidence to the suitability of the latter as an active-site analogue.

Concerning the coordination of water to Fe^{III}, the proton hyperfine couplings of several comparable native high- and low-spin heme systems are known from ENDOR studies.[15] In the high-spin case the expected proton hyperfine coupling along $g_{\|}$ ($a_{iso} + A(g_{\|})$) lies around 6 MHz and is predominantly dipolar in character.[16] The three-pulse ESEEM spectrum of **7**-H_2O shows no evidence of such a strong proton interaction (Figure 2a). Stirring **7**-H_2O in a mixture of 2-methyltetrahydrofuran (MTHF) and D_2O for 12 h provided the corresponding deuterated complex **7**-D_2O; its three-pulse ESEEM spectrum reveals an intensive deuterium signal pair centered at the nuclear Zeeman frequency of deuterium with a splitting of 1.04 MHz (Figure 2b).

The Fourier transformation of the ratio of the time domain signals of **7**-D_2O/**7**-H_2O includes only the deuterium modulation (Figure 2c), although, in principle, residual lines at frequencies corresponding to other nuclei and their combinations should be present. The intensities of these are, however, very small and can be neglected.[9a, 17]

From the deuterium interaction the expected proton coupling normal to the porphyrin plane can be calculated to 6.77 MHz ($g_H/g_D = 6.51$). A proton hyperfine coupling of exactly this value can be detected in the Davies ENDOR spectrum of **7**-H_2O (Figure 3a). The corresponding signal pair can be completely removed by exchange with D_2O; in contrast, all the other proton lines are not affected by the exchange reaction (Figure 3b).

In the Davies ENDOR spectrum the deuterium coupling is not detectable since this technique is not sensitive enough at low frequencies. On the other hand, the broad proton lines

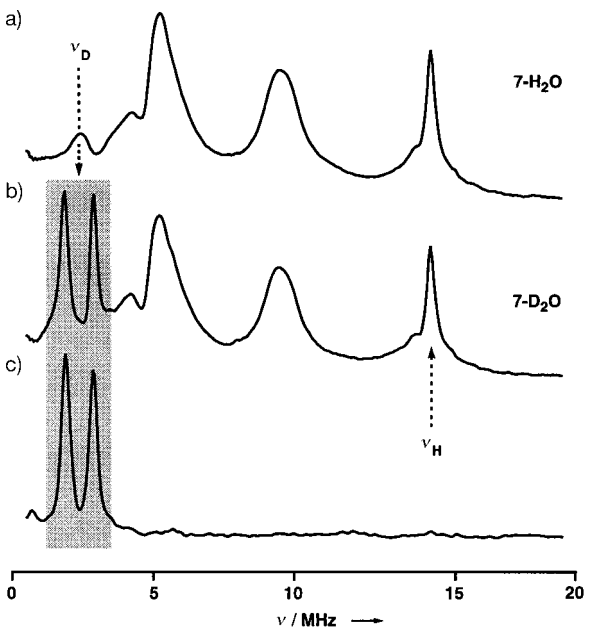


Figure 2. a), b) Three-pulse ESEEM spectra of **7**-H_2O and **7**-D_2O (solvent: MTHF; $T = 3.3$ K; orientation: $g_{\|}$; summation of 64 τ values. c) Fourier transform of the ratio of the time traces of **7**-H_2O and **7**-D_2O.

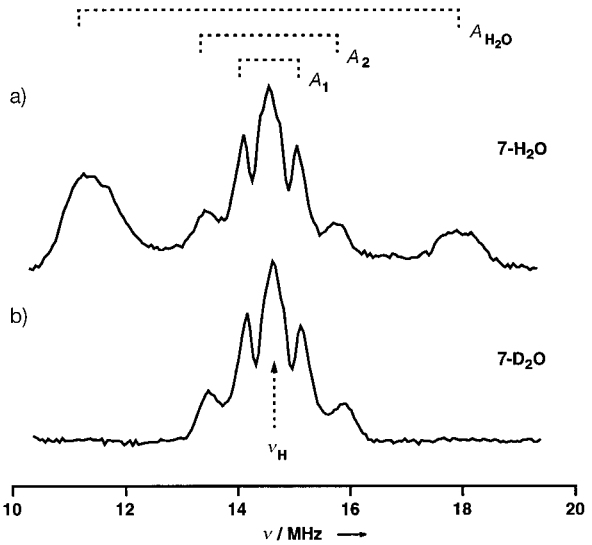


Figure 3. Davies ENDOR spectrum (proton region) of a) **7**-H_2O and b) **7**-D_2O (solvent: MTHF; $T = 3.3$ K; orientation: $g_{\|}$).

cannot be seen in the three-pulse ESEEM due to spectrometer dead time. Thus, Davies ENDOR and three-pulse ESEEM spectroscopy complement each other in an optimal fashion. The well-resolved small proton hyperfine couplings $A_1 = 0.95$ MHz and $A_2 = 2.30$ MHz (Figure 3) can tentatively be assigned to the *meso* protons of the porphyrin ligand and to the benzylic protons of the thiophenolate bridge spanning the porphyrin, respectively.

In further experiments the H_2O ligand of **7**-H_2O was exchanged for $H_2{}^{17}O$. The resulting complex **7**-$H_2{}^{17}O$ shows no line broadening in the CW EPR spectrum; the Davies ENDOR spectrum, however, is very informative (Figure 4). Subtraction of the ENDOR spectra of **7**-$H_2{}^{17}O$ and **7**-H_2O

 © WILEY-VCH Verlag GmbH, D-69451 Weinheim, 1998 1433-7851/98/3721-3000 $ 17.50+.50/0

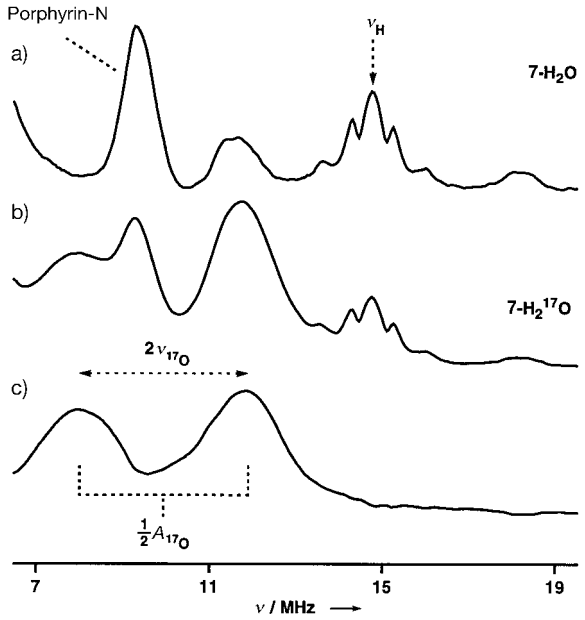


Figure 4. a), b) Davies ENDOR spectra of **7**-H_2O and **7**-$H_2{}^{17}O$ (not to scale; solvent: MTHF; $T = 3.3$ K; orientation: $g_{\|}$). c) Subtraction of the spectrum of **7**-H_2O from the spectrum of **7**-$H_2{}^{17}O$.

reveals two intense ^{17}O lines centered at $1/2\,A(^{17}O)$ ($A(^{17}O) = 19.83$ MHz); the splitting of the two signals corresponds to twice the nuclear Zeeman frequency of ^{17}O ($2\nu(^{17}O) = 3.98$ MHz), and the broadening is due to the nuclear quadrupole interaction of ^{17}O ($I = 5/2$). This hyperfine coupling is remarkably strong in comparison to the very weak Fe–^{17}O interaction in the low-spin state **1**, where the unpaired electron resides predominantly in the d_{yz} orbital of Fe^{III}.[9a]

Accordingly, it is unequivocally demonstrated that **7**-H_2O is a hexacoordinated iron(III) porphyrin in which a thiolate ligand and a water molecule coordinate to the iron center. In contrast to **1**, the resting state of $P450_{cam}$, the synthetic analogue **7**-H_2O is definitely in the high-spin state and changes only to a low-spin system if the water ligand is exchanged for a strong ligand, such as 1,2-dimethylimidazole (**13**). In view of the ESEEM studies of the enzyme $P450_{cam}$ discussed above,[9] water rather than a stronger ligand such as a hydroxide ion coordinates to the iron(III) center. Consequently, the coordination of water to iron in the active site of cytochrome P450 is not the single determining factor for establishing the low-spin character of the system. The results presented here provide the first experimental support for calculations reported recently.[18] The INDO/ROHF and molecular dynamics simulations of cytochrome $P450_{cam}$ suggested two cooperative factors favoring the low-spin state of **1**: The coordination of the water ligand to iron decreases the energy difference between the high-spin and low-spin states from 75.4 to 15.9 kJ mol^{-1}, and the electrostatic field from the protein can further stabilize the low-spin state by 7.5 kJ mol^{-1} below the high-spin state.

Regarding our enzyme model, a simple estimation revealed that a point charge 7 Å above the porphyrin plane of **7**-H_2O would be sufficient to establish an electrostatic potential of about 2 V. According to the calculations,[18] this would be enough to decrease the energy of the low-spin state of $P450_{cam}$ significantly below that of the high-spin state. Work is in progress to mimic the significance of the protein's electric field through attachment of positively charged substituents to the Kemp acids of **7**-H_2O.[19]

Experimental Section

8: To a solution of porphyrin **9**[10] (60 mg, 0.04 mmol) in CH_2Cl_2 (10 mL) was added dropwise a 0.23 M solution of CH_2N_2 (3 mL) in ether. The red solution was stirred for 30 min under argon at 25 °C. After evaporation of the solvent in vacuo the residue was purified by flash chromatography on silica gel (toluene/AcOEt 8/2) to give 52 mg (0.033 mmol, 83 %) of **8** as a red solid. TLC (toluene/AcOEt 8/2): $R_f = 0.85$; m.p. > 250 °C. UV/Vis (CH_2Cl_2): λ_{max} (%) = 416 (100), 510 (12), 574 (8), 588 (5), 654 nm (3); ^{1}H NMR (300 MHz, [D$_6$]acetone): $\delta = 10.15$ (s, 2H, *meso*-H), 8.35 (s, 2H, Ar-H), 7.17 (s, 2H, Ar-H), 6.26 (s, 2H, Ar-H), 4.05–4.01(m, 8H, pyrrole-CH_2), 3.71–3.69 (m, 4H, OCH_2), 3.35 (s, 6H, COOMe), 2.80–2.77 (s, 12H, pyrrole-CH_3 and m, 4H, H_{eq}), 2.39 (d, $J = 13.02$ Hz, 2H, H_{eq}), 2.30 (s, 6H, Ar-CH_3), 2.17–2.13 (m, 8H, pyrrole-CH_2CH_2), 1.82–1.77 (m, 8H, pyrrole-$(CH_2)_2CH_2$), 1.43 (s, 16H, 4Me), 1.29 (s, 6H, 2Me), 1.16 (m, 6H, H_{ax}), 1.09 (t, 12H, pyrrole-$(CH_2)_2CH_3$), 0.86 (s, 9H, *t*Bu), 0.85 (m, 4H, OCH_2CH_2), 0.62–0.50 (m, 4H, $O(CH_2)_2CH_2$), −2.10 (s, 1H, NH), −2.65(s, 1H, NH), −3.10 (s, 1H, SH); ESI-MS (CH_2Cl_2/MeOH 1/9): *m*/*z*: 1552 [M^+]; MALDI-TOF: *m*/*z*: 1551 [M^+] ($C_{96}H_{122}N_6O_{10}S$ (1550.89)).

7-Br^-: In a glove box, three drops of 2,6-lutidine and a spatula of $FeBr_2$ were added to a solution of **8** (50 mg, 0.032 mmol) in refluxing toluene (10 mL). The dark brown solution was stirred at reflux for 1 h. After evaporation of the solvent the residue was purified by flash chromatography on silica gel (toluene/AcOEt 8/2) to give 39 mg (0.024 mmol, 76 %) of **7**-Br^- as a brown solid. TLC (toluene/AcOEt 8/2): $R_f = 0.75$; m.p. > 250 °C; UV/Vis (toluene): λ_{max} (%) = 400 (100), 512 (8), 592 nm (5); ^{1}H NMR (250 MHz, $CDCl_3$): 78.9 (brs, 2H, *meso*-H), 40.5 (s, 12H, pyrrole-CH_3), 38.5 (s, 8H, pyrrole-CH_2), 12.8 (s, 2H, Ar-H), 9.5 (m, 4H, Ar-H), 5.3 (s, 6H, COOMe), 4.96 (m, 6H, OCH_2, $4H_{eq}$), 3.84 (m, 6H, OCH_2CH_2, $4H_{ax}$), 3.23 (s, 6H, Ar-CH_3), 2.99 (m, 8H, $2H_{ax} + 2H_{eq}$, pyrrole-CH_2CH_2), 2.69 (m, 8H, pyrrole-$(CH_2)_2CH_2$), 2.45 (s, 6H, 2Me), 1.77 (s, 12H, 4Me), 1.3 (m, 12H, pyrrole-$(CH_2)_3CH_3$), 0.91 (s, 9H, *t*Bu), 0.11 (s, 4H, $0(CH_2)_2CH_2$); ESI-MS (CH_2Cl_2/MeOH 1/9): *m*/*z*: 1606 [M^+]; MALDI-TOF: *m*/*z*: 1606 [M^+] ($C_{96}H_{119}N_6O_{10}FeS$ (1603.81)); both MS techniques display M^+ devoid of the Br^- counterion.

7-H_2O: To a solution of **7**-Br^- (10 mg, 6.23 μmol) in toluene (2 mL) was added water (0.5 mL). The mixture was stirred for 20 h at 25 °C under argon. The organic phase was separated and concentrated in vacuo to give a crude brown solid. Flash chromatography on silica gel (toluene/AcOEt 8/2) gave 7 mg (4.32 μmol, 69 %) of **7**-H_2O as a brown solid. UV/Vis (CH_2Cl_2): λ_{max} (%) = 408 (100), 519 (7), 595 nm (3); ESI-MS (CH_2Cl_2/MeOH 1/9): *m*/*z*: 1623 [M^+] ($C_{96}H_{121}N_6O_{11}FeS$ (1621.82)).

10 and **11**: In a glove box one small spatula of potassium hydride and three crystals of [18]crown-6 were added to a solution of **7**-Br^- (10 mg, 6.23 μmol) in [D$_6$]benzene (0.2 mL). The red solution was stirred at 25 °C for 30 min, and a small sample was removed to confirm the formation of **10**; UV/Vis (toluene): λ_{max} (%) = 422 (100), 565 (8), 655 nm (5). The mixture was then purified by flash chromatography on silica gel ([D$_8$]toluene) to give **11** as a red solid; UV/Vis (toluene): λ_{max} (%) = 418 (100), 486 (13), 510 (9), 564 (5), 622 (3), 648 nm (2); ^{1}H NMR (250 MHz, [D$_8$]toluene): $\delta = 39.96$ (s, 2H, *meso*-H), 7.1 (s, 4H, Ar-H), 6.96 (s, 2H, Ar-H), 4.50 (m, pyrrole-CH_2), 4.28 (m, 4H, OCH_2), 3.9–2.5 (m, 32H), 2.38 (s, 6H, Ar-CH_3), 2.11 (m, 2H), 1.65 (m, 8H, pyrrole-CH_2CH_2), 1.59 (m, 8H, pyrrole-$(CH_2)_2CH_2$), 1.32 (m, 12H, pyrrole-$(CH_2)_3CH_3$), 1.11 (m, 4H, OCH_2CH_2), 0.92 (s, 9H, *t*Bu), 0.37 (m, 4H, $O(CH_2)_2CH_2$), −42 (s, 1H, SH).

12: Carbon monoxide was bubbled through a solution of **10** in toluene for 3 h. A UV/Vis spectrum indicated the presence of the hexacoordinated CO complex **12**; UV/Vis (CH_2Cl_2): λ_{max} (%) = 416 (100), 448 (27), 510 (8), 574 (5), 654 nm (2).

7-DIMI: To a solution of **7**-Br^- (3 mg, 1.87 μmol) in MTHF (0.2 mL) was added **13** (18.4 mg, 0.191 mmol). The brown-red mixture was stirred at 25 °C under argon for 24 h. After removal of solvent in vacuo, toluene (3 mL) was added, and the mixture was filtered over celite to remove the

excess of **13**. Subsequent evaporation of the solvents gave a brown solid; UV/Vis (CH_2Cl_2): λ_{max} (%) = 402 (100), 512 (8), 592 nm (5).

7-D_2O and **7**-$H_2{}^{17}O$: To a 10 mM soution of **7**-H_2O (250 μL) in MTHF was added D_2O (100 μL; Cambridge Isotope Laboratories, enrichment of D 99.996%) or $H_2{}^{17}O$ (100 μL; Cambridge Isotope Laboratories, enrichment of ^{17}O 46%), and the mixture was stirred at 25 °C under argon for 12 h. After removal of the water phase the solution was directly used for the EPR experiments.

EPR and ENDOR sample preparation: The solutions of **7**-H_2O, **7**-D_2O, **7**-$H_2{}^{17}O$, and **7**-DIMI in MTHF (Fluka, purum), concentration 5-10 mM, were transferred to an EPR tube and degassed on a vacuum line by the freeze-pump-thaw method.

EPR and ENDOR equipment: The CW EPR spectra at 100 K were recorded on a Bruker ESP 300 spectrometer (microwave frequency 9.485 GHz) with use of a liquid nitrogen cryostat. The CW EPR spectra at 10 K and all pulse EPR and ENDOR spectra (3.3 K throughout) were recorded on a Bruker ESP 380 spectrometer (microwave frequency 9.717 GHz) with use of an Oxford liquid helium cryostat. The CW EPR spectra of frozen solutions were measured with a microwave power of 20 mW, a modulation amplitude of 0.5 mT, and a modulation frequency of 100 kHz. The magnetic field was measured with a Bruker NMR gaussmeter ER 035M. All pulse EPR and ENDOR measurements were conducted at a repetition rate of 1 kHz.

Three-pulse ESEEM spectra:[20] The experiments were carried out with the $\pi/2$-τ-$\pi/2$-t-$\pi/2$-τ-echo pulse sequence, and a pulse length of 16 ns. The echo intensity was measured as a function of time t, which was incremented from 16 to 8200 ns in steps of 8 ns. τ was varied between 88 and 592 ns in steps of 8 ns to avoid signal distortions due to blind spots. Four-step phase cycles were employed to eliminate unwanted echo contributions.[21]

Davies ENDOR spectra:[22] The spectra were recorded with the π-t-$\pi/2$-τ-π-τ-echo pulse sequence, and a pulse length of 48 and 96 ns for the $\pi/2$ and π pulses and a τ value of 104 ns. A selective radio frequency (RF) π pulse of variable frequency ν_{RF} was applied during the time interval t. The length of the RF pulse was 8504 ns, and the RF increment was set to 50 kHz.

Manipulation of EPR and ENDOR data: The data were processed with the program MATLAB 5.1. (The MathWorks, Inc., Natick, MA, USA). The time traces of the three-pulse ESEEM data were baseline corrected with a fifth-degree polynomial function and apodized with a Hamming window. Zero filling was performed prior to Fourier transformation. All frequency domain three-pulse ESEEM results represent absolute-value spectra. To remove blind spots, three-pulse ESEEM spectra measured at different τ values were added together.

Received: June 2, 1998 [Z11932IE]
German version: *Angew. Chem.* **1998**, *110*, 3191 – 3196

Keywords: cytochrome P450 · enzyme mimetics · EPR spectroscopy · porphyrinoids

[1] P. Ortiz de Montellano, *Cytochrome P450. Structure, Mechanism, and Biochemistry*, 1st ed., Plenum, New York, **1986**; 2nd ed., Plenum, New York, **1995**.
[2] a) T. L. Poulos, B. C. Finzel, I. C. Gunsalus, G. C. Wagner, J. Kraut, *J. Biol. Chem.* **1985**, *260*, 16122 – 16130; b) T. L. Poulos, B. C. Finzel, A. J. Howard, *Biochemistry* **1986**, *25*, 5314 – 5322.
[3] a) T. L. Poulos, B. C. Finzel, A. J. Howard, *J. Mol. Biol.* **1987**, *195*, 687 – 700; b) R. Raag, T. L. Poulos, *Biochemistry* **1989**, *28*, 916 – 922; c) R. Raag, T. L. Poulos, *Biochemistry* **1989**, *28*, 7586 – 7592.
[4] W.-D. Woggon, *Top. Curr. Chem.* **1996**, *184*, 39 – 96.
[5] T. I. Oprea, G. Hummer, A. E. Garcia, *Proc. Natl. Acad. Sci. USA* **1997**, *94*, 2133 – 2138.
[6] S. G. Sligar, *Biochemistry* **1976**, *15*, 5399 – 5406.
[7] a) S. Shaik, M. Filatov, D. Schröder, H. Schwarz, *Chem. Eur. J.* **1998**, *4*, 193 – 199; b) M. Newcomb, M.-H. Le Tadic, D. A. Putt, P. F. Hollenberg, *J. Am. Chem. Soc.* **1995**, *117*, 3312 – 3313; c) M. Newcomb, M.-H. Le Tadic-Biadatti, D. L. Chestney, E. S. Roberts, P. F. Hollenberg, *J. Am. Chem. Soc.* **1995**, *117*, 12085 – 12091.
[8] G. H. Loew, J. Collins, B. Luke, A. Waleh, A. Pudzianowski, *Enzyme* **1986**, *36*, 54 – 78.
[9] a) H. Thomann, M. Bernardo, D. Goldfarb, P. M. H. Kroneck, V. Ullrich, *J. Am. Chem. Soc.* **1995**, *117*, 8243 – 8251; b) D. Goldfarb, M. Bernardo, H. Thomann, P. M. H. Kroneck, V. Ullrich, *J. Am. Chem. Soc.* **1996**, *118*, 2686 – 2693.
[10] H. Aissaoui, S. Ghirlanda, C. Gmür, W.-D. Woggon, *J. Mol. Catal. A.* **1996**, *113*, 393 – 402.
[11] H. Aissaoui, W.-D. Woggon, unpublished results.
[12] R. Tsai, C. A. Yu, I. C. Gunsalus, J. Peisach, W. Blumberg, W. H. Orme-Johnson, H. Beinert, *Proc. Natl. Acad. Sci. USA* **1970**, *66*, 1157 – 1163.
[13] J. D. Lipscomb, *Biochemistry* **1980**, *19*, 3590 – 3599.
[14] C. P. Scholes, A. Lapidot, R. Mascarenhas, T. Inubushi, R. A. Isaacson, G. Feher, *J. Am. Chem. Soc.* **1982**, *104*, 2724 – 2735.
[15] a) R. Lobrutto, C. P. Scholes, G. C. Wagner, I. C. Gunsalus, P. G. Debrunner, *J. Am. Chem. Soc.* **1980**, *102*, 1167 – 1170; b) Y.-C. Fann, N. C. Gerber, P. A. Osmulski, L. P. Hager, S. G. Sligar, B. M. Hoffman, *J. Am. Chem. Soc.* **1994**, *116*, 5989 – 5990.
[16] C. F. Mulks, C. P. Scholes, L. C. Dickinson, A. Lapidot, *J. Am. Chem. Soc.* **1979**, *101*, 1645 – 1654.
[17] J. Peisach, W. B. Mims, J. L. Davis, *J. Biol. Chem.* **1984**, *259*, 2704 – 2706.
[18] D. Harris, G. H. Loew, *J. Am. Chem. Soc.* **1993**, *115*, 8775 – 8779.
[19] H. Aissaoui, R. Bachmann, A. Schweiger, W.-D. Woggon, unpublished results.
[20] a) A. Schweiger, *Angew. Chem.* **1991**, *103*, 223 – 250; *Angew. Chem. Int. Ed. Engl.* **1991**, *30*, 265 – 292; b) S. A. Dikanov, Y. D. Tsvetkov, *Electron Spin Echo Envelope Modulation (ESEEM) Spectroscopy*, CRC, Boca Raton, FL, **1992**.
[21] J.-M. Fauth, A. Schweiger, L. Braunschweiler, J. Forrer, R. R. Ernst, *J. Magn. Reson.* **1986**, *66*, 74 – 85.
[22] E. R. Davies, *Phys. Lett. A* **1974**, *47A*, 1 – 2; b) C. Gemperle, A. Schweiger, *Chem. Rev.* **1991**, *91*, 1481 – 1505.

Pyrrole Denitrogenation and Fragmentation of Tetramethylethylenediamine Promoted by a Nb^{II} Cluster**

Maryam Tayebani, Sandro Gambarotta,* and Glenn P. A. Yap

In memory of Lucio Senatore

Metal-promoted cleavage of the C – N bond of amines is a very rare but desirable transformation. So far, this is limited to the cleavage of C – N bonds of strained amines[1] or amidines.[2] Only by using highly reactive trivalent Group 5 metals (Nb and Ta) was it possible to rupture the C – N single bond of aniline[3] and to afford ring-opening of the pyridine aromatic ring.[4] These remarkable reactions are important for the perspectives and the possibilities offered in terms of industrial applications such as denitrogenation[5] of crude oil, catalytic degradation of heterocycles,[6] catalysis, and extrusion of nitrogen and ammonia from organic compounds.[7]

We have recently described the serendipitous preparation and characterization of a Nb^{II} cluster $[(tmeda)_2Nb_2Cl_5Li-$

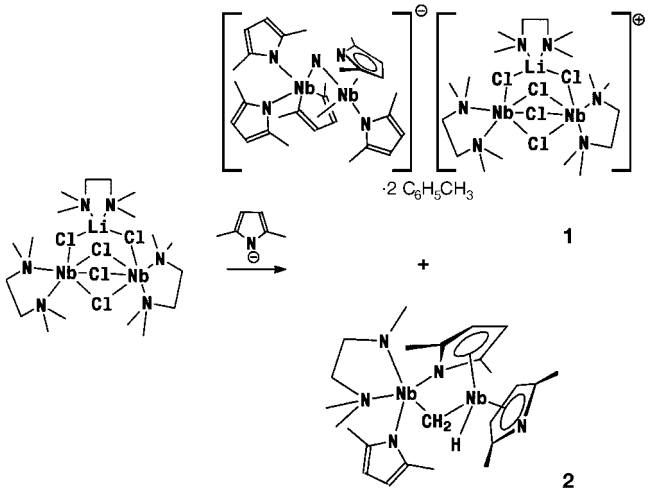
[*] Prof. Dr. S. Gambarotta, M. Tayebani, Prof. G. P. A. Yap
Department of Chemistry
University of Ottawa
Ottawa, Ontario, K1N 6N5 (Canada)
Fax: (+1) 613-5672-5170
E-mail: sgambaro @ oreo.chem.uottawa.ca

[**] This work was supported by the Natural Sciences and Engineering Council of Canada (NSERC) and by NATO (travel grant).

 © WILEY-VCH Verlag GmbH, D-69451 Weinheim, 1998 1433-7851/98/3721-3002 $ 17.50+.50/0

(tmeda)][8a] and reported how this species, upon ligand replacement by anionic amides, performs C–N, N–N, and C–H bond cleavage.[8] Herein we describe the first nitrogen atom abstraction from a pyrrole ring and fragmentation of a neutral tertiary amine.

In a complex redox reaction, the divalent complex $[(tmeda)_2Nb_2Cl_5Li(tmeda)]$[8a] reacts rapidly with the dimethylpyrrole lithium salt 2,5-$Me_2C_4H_2NLi$ in THF to afford a mixture of ionic **1** and neutral **2** (Scheme 1). Both compounds were isolated in analytically pure form by fractional crystallization and their structures were elucidated by X-ray diffraction.



Scheme 1. Synthesis of **1** and **2**.

The unit cell of **1** contains two units in the ratio 1:1. The cation $[(tmeda)_2Nb_2Cl_5Li(tmeda)]^+$, which contains both di- and trivalent niobium centers, displays isostructural connectivity with the divalent starting material $[(tmeda)_2Nb_2Cl_5Li(tmeda)]$ but with significantly different bond lengths and angles: the Nb–Nb distance (Nb(3)–Nb(4) 2.5211(6) Å) in **1** is considerably longer than in the neutral Nb^{II} starting complex (Nb–Nb 2.400(2) Å)[8a] and closely resembles that of the neutral mixed-valence ($Nb^{II}Nb^{III}$) complex $[(tmeda)_2Nb_2Cl_5]$ (Nb–Nb 2.545(1) Å) previously described.[8c] The anion of **1** is formed by two tetravalent niobium atoms (or one tri- and one pentavalent niobium atoms; Figure 1) linked together by one bridging nitride and one bridging dienediyl moiety, both of which arise from dimethylpyrrole denitrogenation. This moiety is σ-bonded to the Nb(1) metal center through the two terminal carbon atoms thus forming a planar niobacyclopentadiene ring, and is also symmetrically π-bonded to the second metal center.

The structural data clearly indicate that the cation of **1** is a mixed-valence $Nb^{II}Nb^{III}$ species, and is thus paramagnetic. Conversely, the anion is probably diamagnetic. The magnetic moment of **1** ($\mu_{eff} = 1.76\ \mu_B$ per formula) is indicative of the presence of only one unpaired electron per formula unit. Furthermore, the paramagnetic mixed-valence compound $[(tmeda)_2Nb_2Cl_5]$ was obtained as an insoluble, paramagnetic purple solid[8c] by treatment of crystalline **1** with THF. A diamagnetic solution remained whose NMR spectra were

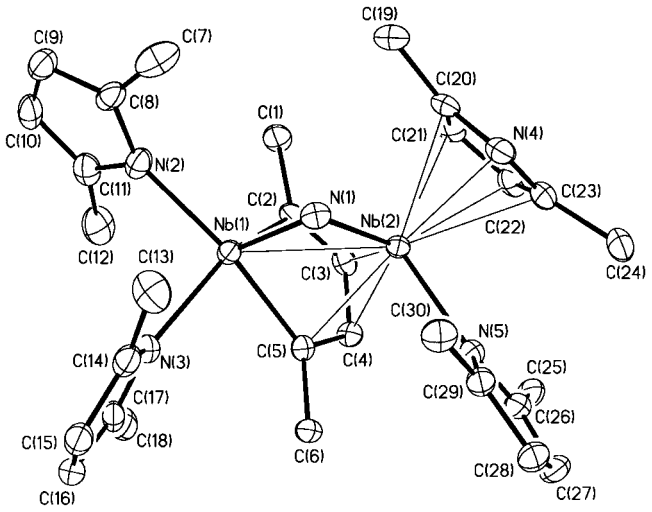


Figure 1. ORTEP drawing of the anion of **1**. Thermal ellipsoids are drawn at the 30% probability level. Selected bond lengths [Å] and torsion angles [°]: Nb(1)–N(1) 1.857(3), Nb(2)–N(1) 1.948(3), Nb(1)–C(2) 2.162(4), Nb(1)–C(5) 2.166(4), Nb(2)–C(2) 2.423(4), Nb(2)–C(3) 2.379(4), Nb(2)–C(4) 2.378(4), Nb(2)–C(5) 2.390(4), Nb(1)–N(2) 2.166(3), Nb(1)–N(3) 2.154(3), Nb(2)–N(4) 2.483(4), Nb(2)–C(20) 2.468(4), Nb(2)–C(21) 2.437(4), Nb(2)–C(23) 2.519(4); Nb(1)-C(2)-C(3)-C(4) 5.5(2), Nb(1)-C(5)-C(4)-C(3) 2.6(2), Nb(1)-N(2)-C(8)-C(9) 193.2(2).

consistent with the formulation $[\{(2,5\text{-}Me_2C_4H_2N)_2Nb\}\{(\eta^5\text{-}2,5\text{-}Me_2C_4H_2N)(2,5\text{-}Me_2C_4H_2N)Nb\}(\mu\text{-}N)(\mu,\eta':\eta':\eta^4\text{-}1,4\text{-}Me_2C_4H_2)][Li(tmeda)_2]$. The diamagnetism of this anion may be explained with the presence of a Nb–Nb single bond which is in agreement with the fairly short Nb–Nb distance (Nb(1)–Nb(2) 2.7872(7) Å).

The dinulcear complex **2** has two inequivalent niobium atoms. The Nb(2) center is π-bonded to two pyrrolyl rings forming a bent metallocene-like structure (Figure 2). One of the two pyrrolyl rings is also σ-bonded to the Nb(1) center

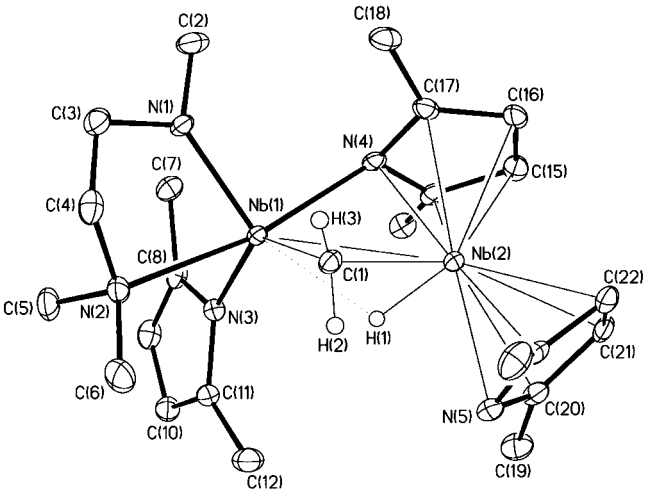


Figure 2. ORTEP drawing of **2**. Thermal ellipsoids are drawn at the 30% probability level. Selected bond lengths [Å] and angles [°]: Nb(2)–N(4) 2.201(3), Nb(2)–C(17) 2.319(4), Nb(2)–C(16) 2.417(4), Nb(2)–N(5) 2.341(3), Nb(2)–C(20) 2.355(4), Nb(2)–C(21) 2.442(4), Nb(1)–N(2) 2.404(4), Nb(1)–N(1) 2.004(3), Nb(1)–N(3) 2.172(3), Nb(1)–N(4) 2.201(3), Nb(1)–C(1) 2.098(4), Nb(2)–C(1) 2.272(4); Nb(1)-C(1)-Nb(2) 85.7(2), $C_4N_{centroid}$-Nb(2)-$C_4N_{centroid}$ 136.6(2).

 © WILEY-VCH Verlag GmbH, D-69451 Weinheim, 1998 1433-7851/98/3721-3003 $ 17.50+.50/0

which, in turn, is σ-bonded to another pyrrolyl ring and to one demethylated tmeda molecule. One bridging methylene group (Nb(1)–C(1) 2.098(4), Nb(2)–C(1) 2.272(4) Å) and one hydride atom (Nb(1)–H(1) 2.270(6), Nb(2)–H(1) 1.708(6) Å) are asymmetrically placed between the two metal centers and complete the structure. The crystal structure was of sufficient quality to locate and refine the hydride center and the methylene hydrogen atom positions.

Complex **2** is a paramagnetic mixed-valence $Nb^{III}Nb^{IV}$ species and its magnetic moment is consistent with the presence of one unpaired electron per formula unit ($\mu_{eff} = 1.77\ \mu_B$ per formula). In this case it was not possible to obtain satisfactory NMR data to support the proposed formulation. However, chemical degradation experiments carried out with anhydrous HCl in a closed vessel connected with a Toepler pump yielded 64% of the expected amount of H_2 and CH_4. The presence of a medium intensity resonance at 1637 cm^{-1} in the IR spectrum (Nb–H stretching) suggests that complex **2** should be regarded as a terminal rather than bridging hydride species. Unfortunately, isotope exchange experiments with D_2 failed due to the fact that the complex reacts in a destructive manner with hydrogen gas. In spite of the paramagnetism, reproducible ^1H NMR spectra show the resonances of two pyrrolyl rings as sharp, well resolved peaks. Also two rather broad features possibly account for the presence of the hydride ($\delta = 4.91$) and the methylene group ($\delta = 9.22$), as they have the correct integration. Conversely, no resonances were conclusively identified for the demethylated tmeda molecule. Perhaps, the partially resolved spectrum may be ascribed to either the 18 electron configuration of the niobium atom π-bonded to two pyrrolyl rings, or to possible dissociation of the dimeric structure in solution.

The formation of **1** and **2** arises from two different processes within the same reaction. Complex **1** is clearly the result of the cooperative attack of the two Nb^{II} centers on one pyrrolyl anion. The four electrons necessary to form the nitride and the dienyl dianion are obtained from the five electrons provided by the oxidation of the four Nb^{II} centers during the formation of **1**. The formation of **2** arises instead from the cleavage of one CH_3–N bond of the tmeda molecule and subsequent oxidative addition into the C–H bond of the cleaved CH_3 group. This process also requires four electrons. However, complex **2** is a mixed-valence $Nb^{III}Nb^{IV}$ complex and thus only three electrons were obtained from the two metal centers. Therefore, the formation of the two complexes appears to be interconnected in the sense that the total of eight electrons necessary for the pyrrole denitrogenation and tmeda fragmentation are provided by the formal oxidation of five niobium atoms leading to the formation of three Nb^{IV} and two Nb^{III} centers. A sixth Nb^{II} atom conserved the original divalent state and formed with one of the two Nb^{III} centers the mixed-valence Nb^{II}/Nb^{III} cation of **1**.

Experimental Section

Solid $[Nb_2Cl_5Li(tmeda)_3]$ (2.0 g, 2.8 mmol) was added to a solution of the lithium salt of 2,5-dimethylpyrrole (1.1 g, 11.0 mmol) in THF (100 mL) at room temperature. The mixture was evaporated to dryness and the residual solid was redissolved in toluene (70 mL). After filtration, diethyl ether (30 mL) was added, and the mixture was left to stand at −30 °C. This afforded dark crystals of **1** (0.2 g, 0.13 mmol, 14%). Elemental analysis (%) calcd for $C_{62}H_{105}N_{11}Nb_4LiCl_5$: C 47.72, H 6.78, N 9.87; found C 47.66, H 6.43, N 9.27; IR (Nujol mull): $\tilde{\nu} = 1495$ (w), 1376 (s), 1290 (w), 1255 (m), 1242 (m), 1233 (m), 1059 (s), 1036 (m), 1011 (m), 949 (m), 916 (w), 792 (s), 763 (m), 743 (m), 729 (s), 697 (w), 578 (m) cm^{-1}; magnetic moment: $\mu_{eff} = 1.76\ \mu_B$. ^1H NMR (500 MHz, C_6D_6, 23 °C, the tube was centrifuged to remove the purple insoluble $[Nb_2Cl_5(tmeda)_2]$: $\delta = 7.13$ (m, 10H, toluene), 5.88 (s, 2H, diene), 5.44 (s, 4H, pyrrole), 5.41 (s, 4H, pyrrole), 2.64 (s, 6H, Me-pyrrole), 2.49 (s, 6H, Me-pyrrole), 2.30 (s, 8H, CH_2-tmeda), 2.15 (s, 24H, Me-tmeda), 2.12 (s, 6H, toluene), 2.08 (br. s, 12H, Me-pyrrole), 0.88 (s, 6H, Me-diene); ^{13}C NMR (127.7 MHz, C_6D_6, 23 °C): $\delta = 139.2$(C_q-diene), 138.4, 135.3, 132.3 (C_q-pyrrole), 128.7, 128.9, 126.0 (toluene), 115.9 (CH-diene), 107.6, 107.0 (CH-pyrrole), 58.9 (CH_2-tmeda), 46.2 (Me-tmeda), 29.2 (Me-diene), 21.4, 18.5, 18.4, 17.5 (Me-pyrrole), 13.0 (Me-toluene).

The mother liquor of the above preparation was evaporated to dryness. The solid residue was redissolved in diethyl ether (100 mL), quickly filtered, and allowed to stand undisturbed at room temperature for a few hours. Dark green crystals of **2** separated (0.05 g, 0.08 mmol, 9%). Elemental analyis (%) calcd for $C_{24}H_{40}N_5Nb_2$: C 49.32, H 6.90, N 11.98; found C 48.94, H 6.71, N 11.83; IR (Nujol mull): $\tilde{\nu} = 1637$ (m), 1374 (s), 1341 (w), 1278 (w), 1260 (m), 1240 (s), 1195 (m), 1161 (w), 1103 (br. s), 1055 (s), 1053 (s), 1018 (s), 1015 (s), 949 (m), 871 (m), 836 (w), 822 (m), 801 (br. m), 790 (s), 730 (s), 670 (w), 641 (w) cm^{-1}; magnetic moment: $\mu_{eff} = 1.77\ \mu_B$; ^1H NMR (500 MHz, C_6D_6, 23 °C): $\delta = 9.2$ (br. s, 2H, bridging CH_2), 5.59 (s, 4H, CH-pyrrole), 4.91 (br. s, 1H, hydride), 1.85 (s, 12H, Me-pyrrole). .

Crystal structure analyses: **1**: $C_{62}H_{105}Cl_5N_{11}Nb_4Li$, $M_r = 1560.40$, triclinic $P\bar{1}$, $a = 12.295(3)$, $b = 14.916(3)$, $c = 20.818(5)$ Å, $\alpha = 96.763(4)$, $\beta = 91.542(4)$, $\gamma = 107.375(4)°$, $V = 3610(1)$ Å^3, $Z = 2$, $\rho_{calcd} = 1.435$ Mg m^{-3}, absorption coefficient 8.48 cm^{-1}, $F(000) = 1612$, reflections collected 10255, independent reflections 10228, GOF = 1.058, $R = 0.0385$, $wR^2 = 0.1061$. All non-hydrogen atoms were located and refined anisotropically. Hydrogen atoms were introduced at their idealized positions and refined with a riding mode. Two molecules of toluene per unit formula were located in the lattice. **2:** $C_{24}H_{40}N_5Nb_2$, $M_r = 584.43$, monoclinic *C2/c*, $a = 18.387(4)$, $b = 15.314(3)$, $c = 18.971(4)$ Å, $\beta = 110.377(3)°$, $V = 5007(2)$ Å^3, $Z = 4$, $\rho_{calcd} = 1.550$ Mg m^{-3} Absorption coefficient 9.36 cm^{-1}, $F(000) = 2408$, reflections collected 3571, independent reflections 3270, GOF = 1.192, $R = 0.0332$, $wR^2 = 0.0874$. All non-hydrogen atoms were located and refined anisotropically. The hydrogen atoms attached to C(1) as well as the hydride were located from the difference map. All the hydrogen atoms were refined with a riding model. Crystallographic data (excluding structure factors) for the structures reported in this paper have been deposited with the Cambridge Crystallographic Data Center as supplementary publication no. CCDC-101719 (**1**) and CCDC-101720 (**2**). Copies of the data can be obtained free of charge on application to CCDC, 12 Union Road, Cambridge CB2 1EZ, UK (fax: (+44) 1223-336-033; e-mail: deposit@ccdc.cam.ac.uk).

Received: May 25, 1998 [Z 11901 IE]
German version: *Angew. Chem.* **1998**, *110*, 3222–3225

Keywords: heterocycles · N ligands · niobium

[1] a) G . Proulx, R. G. Bergman, *J. Am. Chem. Soc.* **1994**, *116*, 7953; b) L. M. Atagi, D. E. Over, D. R. McAlister, J. M. Mayer, *J. Am. Chem. Soc.* **1991**, *113*, 870; c) C. C. Cummins, R. R. Schrock, W. M. Davis, *Inorg. Chem.* **1994**, *33*, 1448.

[2] a) F. A. Cotton, J. H. Matonic, C. A. Murillo, X. Wang, *Bull. Soc. Chim. Fr.* **1996**, *133*, 711; b) F. A. Cotton, L. M. Daniels, C. A. Murillo, X. Wang, *Inorg. Chem.* **1997**, *36*, 896; c) J. R. Agadorn, J. Arnold, *Organometallics* **1994**, *131*, 4670.

[3] a) J. B. Bonanno, T. P. Henry, D. R. Neithamer, P. T. Wolczanski, E. B. Lobkovski, *J. Am. Chem. Soc.* **1996**, *118*, 5132; b) M. H. Chisholm, K. Folting, J. C. Huffmann, J. Leonelli, N. S. Marchant, C. A. Smith, L. C. E. Taylor, *J. Am. Chem. Soc.* **1985**, *107*, 3722.

[4] a) T. S. Kleckley, J. L. Bennett, P. T. Wolczanski, E. B. Lobkowski, *J. Am. Chem. Soc.* **1997**, *119*, 247; b) S. D. Gray, K. J. Weller, M. A. Bruck, P. M. Briggs, D. E. Wigley, *J. Am. Chem. Soc.* **1995**, *117*, 10678.

 © WILEY-VCH Verlag GmbH, D-69451 Weinheim, 1998 1433-7851/98/3721-3004 $ 17.50+.50/0

[5] a) R. M. Laine, *Catal. Rev. Sci. Eng.* **1983**, *25*, 459; b) J. R. Katzer, R. C. Sivasubramanian, *Catal. Rev. Sci. Eng.* **1979**, *20*, 155; c) T. C. Ho, *Catal. Rev. Sci. Eng.* **1988**, 30, 117; d) Y. T. Shah, D. C. Cronauer, *Catal. Rev. Sci. Eng.* **1979**, *20*, 209.

[6] See for example: a) R. D. Adams, S. B. Falloon, J. L. Perrin, J. A. Queisser, J. H. Yamamoto, *Chem. Ber.* **1996,** *129,* 313; b) H. Imgartinger, A. Weber, *Tetrahedron Lett.* **1997**, *38,* 2075; c) M. H. Chisholm, S. T. Haubrich, J. C. Huffman, W. E. Streib, *J. Am. Chem. Soc.* **1997,** *119***,** 1634; d) A. R. Katritzky, E. S. Ignatchenko, S. M. Allin, R. A. Barcock, M. Siskin, C. W. Hudson, *Energy Fuels* **1997**, *11*, 160; e) A. J. Arce, A. Karam, Y. Desanctis, R. Machado, M. V. Capparelli, J. Manzur *Inorg. Chim. Acta*. **1997**, *254*, 119.

[7] a) J. L. Gary, G. E. Handwerk, *Petroleum Refining: Technology and Economics*, 3rd ed., Marcel Dekker, New York, **1993**; b) J. G. Speight, *The Chemistry and Technology of Petroleum*, Marcel Dekker, New York, **1983**; c) B. C. Gates, *Catalytic Chemistry*, Wiley, New York, **1992**; d) C. N. Satterfield, C. M. Smith, M. Ingalls, *Ind. Eng. Chem. Process Des. Dev.* **1985**, *24*, 1000; e) C. N. Satterfield, J. F. Cocchetto, *Ind. Eng. Chem. Process Des. Dev.* **1981**, *20*, 53; f) F. Gioia, V. Lee, *Ind. Eng. Chem. Process Des. Dev.* **1986**, *25*, 918; g) R. H. Fish in *Aspects of Homogeneous Catalysis* (Ed.: R. Ugo), Kluver, Dordrecht, **1990**, p. 342; h) R. J. Kinney, W. D. Jones, R. G. Bergman, *J. Am. Chem. Soc.* **1978**, *100*, 7902.

[8] a) M. Tayebani, A. Kasani, K. Feghali, S. Gambarotta, G. Yap, *Chem. Commun*. **1997**, *20*, 2001; b) M. Tayebani, K. Feghali, S. Gambarotta, C. Bensimon, G. Yap, *Organometallics* **1997**, *16*, 5084; c) M. Tayebani, K. Feghali, S. Gambarotta, G. Yap, *Organometallics*, in press; d) M. Tayebani, S. Gambarotta, G. Yap, *Organometallics*, in press; e) K. A. Hall, J. M. Mayer, *J. Am. Chem. Soc.* **1992**, *114*, 10402; f) R. R. Schrock, M. L. Listeman, L. G. Sturgeoff, *J. Am. Chem. Soc.* **1982**, *104*, 4291.

Valence Tautomerism in a *o*-Benzoquinone Adduct of a Tetraazamacrocycle Complex of Manganese**

Andrea Caneschi and Andrea Dei*

Among the molecular systems that exhibit electronic bistability, the *o*-benzoquinone–metal complexes, which are characterized by valence tautomerism, are a relatively new class of compounds.[1–3] Their main attractiveness resides in the formal equivalence of their physical behavior with that of the well-known spin-crossover metal complexes, whose reversible transformations can be utilized for creating addressable memories.[4, 5] To date valence tautomerism has been found only for a family of molecular *o*-benzoquinone complexes of general formula $[M(N{-}N)(diox)_2]$ (M = Co, Mn; N–N = diazine ligand; diox = catecholato, semiquinone anion); the transition temperatures T_c range from 100 to 350 K. We have now found a class of compounds of general formula [ML(diox)]Y (M = Mn, Co; L = tetraazamacrocyclic ancillary ligand) in which the valence tautomers are charged and thus allow the transition temperature to be tuned by using suitable counterions Y; the Mn system is reported here.

The reaction between $[Mn(cth)Cl_2]$ (cth = (±)*l*-5,7,7,12,14,14-hexamethyl-1,4,8,11-tetraazacyclotetradecane) and the 3,5-di-*tert*-butylcatecholate dianion (dtbcat) under inert atmosphere yields the complex [Mn(cth)(dtbcat)]. Upon exposure to air the $[Mn(cth)(diox)]^+$ cation is formed as the initial oxidation product. If this cation is precipitated as the tetraphenylborate salt, a yellow-brown product (**1**) is obtained, whereas green microcrystalline **2** precipitates with perchlorate. Analysis gave the general formulas [Mn(cth)(diox)]Y (Y = BPh_4, ClO_4). The two compounds have different physical properties in the solid state, but the spectroscopic properties of their solutions are identical.

Single crystals suitable for X-ray diffraction analysis were obtained only for **1**. The structure of the cation is shown in Figure 1.[6] The Mn center is six-coordinate, the macrocyclic ligand is bound in a folded configuration, and the benzoquinone acts as bidentate ligand. The features of the coordination

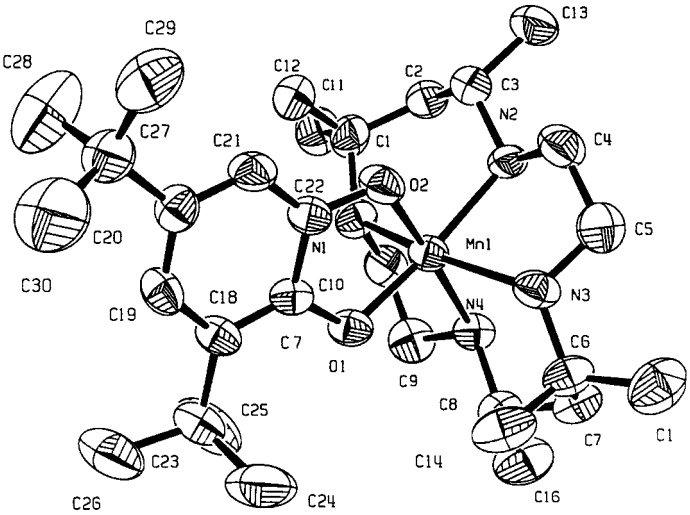


Figure 1. ORTEP plot of $[Mn(cth)(dtbcat)]^+$; the hydrogen atoms are omitted for clarity. Selected bond lengths [Å] and angles [°]: Mn–O1 1.881(4), Mn–O2 1.876(4), Mn–N1 2.311(5), Mn–N2 2.117(5), Mn–N3 2.313(5), Mn–N4 2.129(5), O1–C17 1.369(7), O2–C22 1.356(7), C17–C22 1.398(8); O1-Mn-O2 85.3(2), O1-Mn-N1 90.8(2), O1-Mn-N2 173.4(2), O1-Mn-N3 101.0(2), O1-Mn-N4 90.6(2), O2-Mn-N1 99.8(2), O2-Mn-N2 88.3(2), O2-Mn-N3 91.8(2), O2-Mn-N4 175.7(7).

polyhedron are fully consistent with the formulation of the cation as $[Mn^{III}(cth)(dtbcat)]^+$. The coordination geometry is strongly axially distorted, as expected for a high-spin d^4 electronic configuration. The M–N bond lengths are significantly longer for the apical nitrogen atoms than for the basal nitrogen atoms (2.31 and 2.12 Å, respectively) . The average Mn–O distance of 1.87 Å agrees well with those in other metal(III) catecholato derivatives.[7, 8] Finally, the structural parameters of the coordinated benzoquinone are typical of a catecholato dianion; the C–O and C–C bond lengths are similar to those observed for other dtbcat derivatives.[1]

The IR spectrum of **1** is virtually superimposable on those of the chromium, iron, and cobalt analogues, which can be

[*] Prof. A. Dei, Dr. A. Caneschi
Dipartimento di Chimica
Università di Firenze
Via Maragliano 75, I-50144 Firenze (Italy)
Fax: (+39) 55-354845
E-mail: adei@blu.chim1.unifi.it

[**] We are indebted to Professor D. Gatteschi for helpful criticism and discussion. The financial support of MURST, CNR, and 3MD of the EU network (contract no. ERB 4061 PL 97-0197) is gratefully acknowledged.

 © WILEY-VCH Verlag GmbH, D-69451 Weinheim, 1998 1433-7851/98/3721-3005 $ 17.50+.50/0

unambiguously described as containing catecholato adducts of the trivalent metal ions.[9] However, the physical properties of the green perchlorate salt **2** are consistent with semiquinonato (sq) character. Its IR spectrum is virtually superimposable on that of the nickel(II) and zinc(II) analogues, which can be unambiguously formulated as containing $[M^{II}(cth)(dtbsq)]^+$ cations (dtbsq = 3,5-di-*tert*-butyl-*o*-semiquinone anion),[10] and its reflectance spectrum indicates the presence of a semiquinonato chromophore.

The spectroscopic properties of both **1** and **2** are temperature-dependent. Heating solid **1** causes a reversible color change from yellow-brown to green, and cooling **2** in liquid nitrogen changes its color reversibly from green to yellow. Crystals of **1** are completely converted into the green form by heating for 1 h at 360 – 365 K under vacuum, and revert to the yellow-brown form after a few minutes at room temperature. The transition is noncooperative, as shown by the differential scanning calorimetry curve.

The electronic spectra of both compounds are strongly solvent-dependent (Figure 2). In highly polar solvents such as DMSO, the spectra of the yellow solutions are consistent with the presence of an $[Mn^{III}(cth)(dtbcat)]^+$ chromophore, whereas in weakly polar solvents such as toluene or acetone the spectra of the blue-green solutions are consistent with the presence of a $[Mn^{II}(cth)(dtbsq)]^+$ chromophore. In the latter solvents, both the energies and the intensities of the bands at 13000 and 25700 cm^{-1} are similar to those of $[Zn^{II}(cth)(dtbsq)]^+$.[10] The other bands can be reasonably attributed to metal-to-ligand charge transfer (19000 and 23300 cm^{-1}) and to d--d transitions involving some "trip multiplets" of the manganese(II) ion.[11, 12] The electronic spectra therefore suggest that this manganese – benzoquinone adduct may be described by the two charge distributions Mn^{III}–cat and Mn^{II} – sq, depending on the donor power of the solvent and the different solvation enthalpies of the two tautomers.[13, 14]

Complex **1** is has a χT value of 3.1 emu K mol^{-1} at 70 – 300 K, as expected for a d^4 metal ion in high-spin ground state (Figure 3). Below 70 K χT decreases and attains a value of 2.4 emu K mol^{-1} at 4.2 K. For **2**, χT decreases monotonically

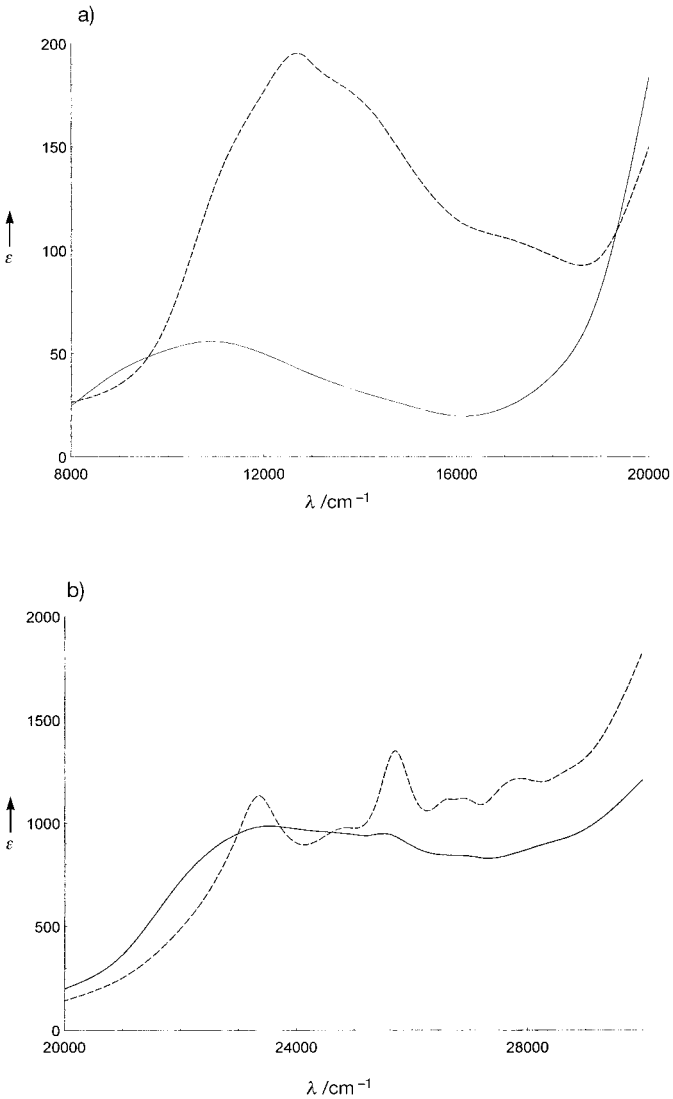


Figure 2. Electronic spectra of $[Mn(cth)(dtbcat)]BPh_4$ in acetone (----) and DMSO (——) in the range of 8000 – 20000 cm^{-1} (a) and 20000 – 30000 cm^{-1} (b).

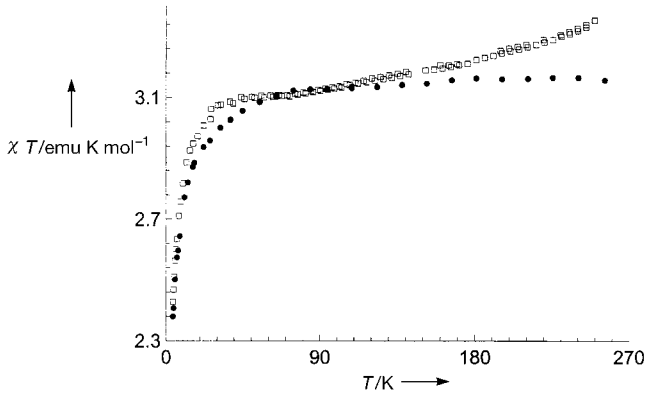


Figure 3. Change in χT as a function of temperature T for **1** (●) and **2** (□) in a magnetic field of 5000 G.

from 3.5 emu K mol^{-1} at 300 K to 3.1 emu K mol^{-1} at 90 K. Below 90 K the temperature dependence of **2** is similar to that of **1**, and a value of 2.4 emu K mol^{-1} is attained at 4.2 K. Since χT of **2** continues to increase at room temperature, at the high-temperature limit it greatly exceeds the value for a Mn^{III} ion. Therefore it can be suggested that at high temperature **2** is stable as Mn^{II}–sq. If the two paramagnetic species are not coupled, χT should be 4.75 emu K mol^{-1}. The decrease between 280 and 120 K might be due both to interconversion between the Mn^{II}–sq and Mn^{III}–cat forms and to antiferromagnetic coupling between the paramagnetic metal ion and the radical ligand.[7, 8, 15] If the former were dominant, the interconversion process should be of the noncooperative type. The X-band EPR spectra of **1** and **2** at low temperatures show several features which may be due to impurities. High-field EPR investigations are in progress.

The system reported here follows the general pattern of valence tautomerism,[1–3] in which an entropy-driven electron transfer process involves two species with nearly degenerate electronic states. The novelty of this system lies in the possibility of tuning the thermodynamics of the electron transfer process by varying the counterion.

 © WILEY-VCH Verlag GmbH, D-69451 Weinheim, 1998 1433-7851/98/3721-3006 $ 17.50+.50/0 *Angew. Chem. Int. Ed.* **1998**, *37*, No. 21

Experimental Section

$[Mn(cth)Cl_2]$ was prepared from $[(NEt_4)_2MnCl_4]$ (5 mmol) and cth (6 mmol) in acetonitrile (30 mL). The reaction between dtbcat (1 mmol) and $[Mn(cth)Cl_2]$ (1 equiv) in basic methanol (30 mL) under inert atmosphere gave [Mn(cth)(dtbcat)]. Crystals of **1** were obtained by adding an aereated solution of $NaBPh_4$ in methanol, and **2** by adding an aqueous solution of $NaClO_4$. The inert atmosphere was removed and the resulting suspensions were stirred for 1 h at room temperature. Complexes **1** and **2** were obtained in 80 and 70% yield, respectively.

Received: October 7, 1997
Revised version: June 17, 1998 [Z11008IE]
German version: *Angew. Chem.* **1998**, *110*, 3220–3222

Keywords: magnetic properties · manganese · O ligands · tautomerism

[1] C. G. Pierpont, C. W. Lange, *Progr. Coord. Chem.* **1993**, *41*, 381.
[2] P. Gütlich, A. Dei, *Angew. Chem.* **1997**, *109*, 2852; *Angew. Chem. Int. Ed. Engl.* **1997**, *36*, 2734.
[3] D. M. Adams, A. Dei, A. L. Rheingold, D. N. Hendrickson, *J. Am. Chem. Soc.* **1993**, *115*, 8221.
[4] P. Gütlich, A. Hauser, H. Spiering, *Angew. Chem.* **1994**, *106*, 2109; *Angew. Chem. Int. Ed. Eng.* **1994**, *33*, 2024.
[5] O. Kahn, C. Jay-Martinez, *Science* **1998**, *279*, 44.
[6] Crystal data for **1**: $MnBC_{55.5}H_{72}N_4O_{3.5}$, $M_r = 916.92$, $Mo_{K\alpha}$ radiation $\lambda = 0.71069$ Å, crystal dimensions $0.3 \times 0.2 \times 0.5$ mm, triclinic, space group $P\bar{1}$ (no. 2), $a = 11.225(2)$, $b = 11.545(1)$, $c = 21.800(2)$ Å, $\alpha = 83.64(1)$, $\beta = 77.78(1)$, $\gamma = 76.99(1)^\circ$, $Z = 2$, $V = 2684(2)$ Å^3, $\rho_{calcd} = 1.134$ g cm^{-3}. Of 5346 reflections collected at 293 K, 5021 were unique and observed. Final R values ($I > 2\sigma I$): $R1 = 0.0663$, $wR2 = 0.1715$. Hydrogen atoms were treated as fixed contributions in calculated positions with isotropic thermal parameters $B(H) = 1.2\ B_{eq}(C)$. An absorption correction based on a ψ scan was performed, and no decay was observed. Crystallographic data (excluding structure factors) for the structure reported in this paper have been deposited with the Cambridge Crystallographic Data Centre as supplementary publication no. CCDC-100691. Copies of the data can be obtained free of charge on application to CCDC, 12 Union Road, Cambridge CB2 1EZ, UK (fax: (+44) 1223-336-033; e-mail: deposit@ccdc.cam.ac.uk).
[7] A. S. Attia, C. G. Pierpont, *Inorg. Chem.* **1995**, *34*, 1172.
[8] A. S. Attia, C. G. Pierpont, *Inorg. Chem.* **1997**, *36*, 6184.
[9] C. Benelli, A. Dei, D. Gatteschi, L. Pardi, *Inorg. Chim. Acta* **1989**, *163*, 99.
[10] C. Benelli, A. Dei, D. Gatteschi, L. Pardi, *Inorg. Chem.* **1989**, *28*, 1476.
[11] A. B. P. Lever, *Inorganic Electronic Spectroscopy*, Elsevier, Amsterdam, **1984**.
[12] C. Benelli, A. Dei, D. Gatteschi, H. Gudel, L. Pardi, *Inorg. Chem.* **1989**, *28*, 3089.
[13] A. Dei, *Inorg. Chem.* **1993**, *32*, 5730.
[14] The reactivity of this complex towards dioxygen is markedly dependent on the solvent. Solutions in highly polar solvents, in which the catecholato species is predominant, are stable for days; however, in weakly polar solvents, in which the semiquinonato form is predominant, the complex is quickly oxidized ($t_{1/2} = 30$ min in acetonitrile). The reaction products are oxo dimers of the manganese tetraazamacrocycle complex and dtb-quinone (60%) as well as the extradiolic cleavage oxidation products 3,5-bis(1,2-dimethylethyl)-2*H*-pyranone (36%) and its isomer 4,6-bis(1,1 dimethylethyl)-2*H*-pyranone (4%).
[15] A. Dei, D. Gatteschi, *Inorg. Chim. Acta* **1992**, *198–200*, 813.

A Novel Beryllium Thiolate Resulting from N–Si Bond Cleavage: Liberation of Ammonia in the Reaction of $Be[N(SiMe_3)_2]_2$ with HSPh**

Scott Chadwick, Ulrich Englich, and Karin Ruhlandt-Senge*

In the course of our investigations into the synthesis and solid-state structures of alkaline earth metal thiolates, we have used the bis(trimethylsilyl)amides of beryllium, magnesium, and calcium as hydrocarbon-soluble metalating agents.[1] We anticipated clean metathesis reactions between the metal amide and arenethiols with formation of the amine $HN(SiMe_3)_2$. Here we present results that indicate competitive acid/base reactions between hexamethyldisilazane and unchanged thiol in the reaction of $[Be\{N(SiMe_3)_2\}_2]$ with stoichiometric amounts of HSPh in the presence of Lewis bases.

The chemistry of the beryllium–oxygen bond is by far the most extensively studied interaction between beryllium and another element.[2] In contrast, information on beryllium thiolates is scarce. In the only crystallographically characterized homoleptic beryllium thiolate, the sterically demanding SMes* ligand (SMes* = S-2,4,6-tBu$_3$C$_6$H$_2$) afforded the three-coordinate monomer $[Be(thf)(SMes^*)_2]$.[3] A three-coordinate monomeric structure was also identified in the mixed alkylberyllium thiolate $[Be(2,6\text{-}Mes_2C_6H_3)(SMes^*)(Et_2O)]$ (Mes = 2,4,6-$Me_3C_6H_2$), in which the metal center is also stabilized by bulky ligands.[4] A four-coordinate beryllium center was found in $[Be(S_2CN\textit{i}Pr_2)_2]$, in which both dithiocarbamato ligands chelate the cation through the two thiolato groups.[5] Finally, a small family of alkylberyllium thiolate compounds have been shown by ^{1}H NMR spectroscopy and cryoscopic measurements to exist as monomeric or oligomeric complexes, depending on the combination of ligands and donor, although detailed structural data are not available.[6] Here we report the synthesis and characterization of the novel, ammonia-coordinated, crown ether templated beryllium thiolate $[\{Be(SPh)_2(py)(NH_3)\}_2\{[18]crown\text{-}6\}] \cdot 2\,C_7H_8$ (**1**; py = pyridine), which is formed by a sequence of acid-promoted N–Si bond cleavage reactions and in situ trapping of the liberated ammonia.

The reaction of $[Be\{N(SiMe_3)_2\}_2]$[7] with two equivalents of HSPh in toluene in the presence of [18]crown-6 gave a thick, white suspension; addition of one equivalent of pyridine generated a homogenous solution,[8] from which **1** was obtained as colorless crystals, which were analyzed by single-crystal X-ray diffraction. The identity of **1** was also

[*] Prof. Dr. K. Ruhlandt-Senge, Dr. S. Chadwick, Dr. U. Englich
Department of Chemistry
1-014 Center for Science and Technology
Syracuse University
Syracuse NY 13244-4100 (USA)
Fax: (+1) 315-443-4070
E-mail: kruhland@syr.edu.

[**] This work was supported by the National Science Foundation (CHE-9409446 and CHE-9702246) and the Deutsche Forschungsgemeinschaft (postdoctoral stipendium for U.E.). Purchase of the X-Ray diffractometer was made possible by grants from the NSF (CHE-95–27898), the W. M. Keck Foundation, and Syracuse University.

 © WILEY-VCH Verlag GmbH, D-69451 Weinheim, 1998 1433-7851/98/3721-3007 $ 17.50+.50/0

confirmed by NMR and IR spectroscopy. The NH stretching frequency of 3302 cm^{-1} in the IR spectrum is similar to those of $[Be\{OC(CF_3)_3\}_2(NH_3)_2]$.[9] Compound **1** consists of two beryllium thiolate moieties that are associated with an [18]crown-6 molecule through ammonia molecules (Figure 1). The $\{Be(SPh)_2(py)(NH_3)\}$ units are located on opposite faces

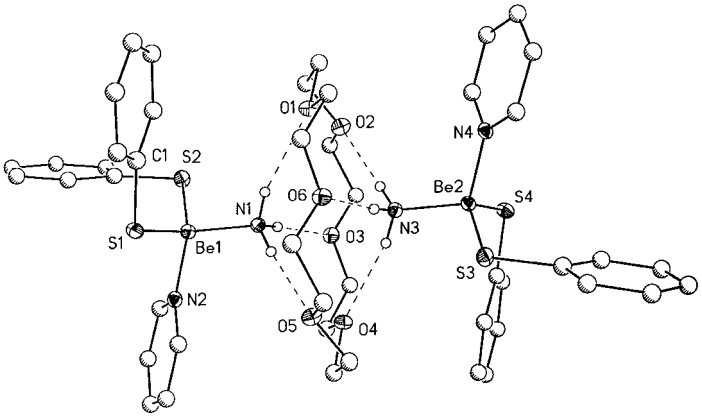


Figure 1. Structure of **1** (30% probability ellipsoids). For clarity, hydrogen atoms other than those of the two ammonia moieties have been omitted. Selected bond lengths [Å] and angles [°]: Be1–S1 2.103(3), Be1–S2 2.095(3), Be1–N1 1.724(4), Be1–N2 1.779(4), Be2–S3 2.086(3), Be2–S4 2.100(3), Be2–N3 1.731(4), Be2–N4 1.778(4), S1–C1 1.770(2), S2–C7 1.771(3), S3–C18 1.764(3), S4–C24 1.768(2); S1-Be1-S2 124.6(2), N1-Be1-N2 108.8(2), S3-Be2-S4 125.2(2), N3-Be2-N4 107.9(2).

of the crown ether, each with three N–H $\cdots$ O hydrogen bonds to alternate oxygen atoms. The H $\cdots$ O distances lie in the range of 2.20(1)–2.31(1) Å, in agreement with data for related transition metal complexes.[10] The coordination environment at each beryllium center is distorted tetrahedral with bond angles from 99.7(2) to 125.2(3)°. The Be–S distances range between 2.086(3) and 2.103(3) Å. These are somewhat longer than those at the three-coordinate Be centers in $[Be(thf)(SMes^*)_2]$ (1.987(8) and 1.991(7) Å), which can be attributed to the higher coordination number of Be in **1**. Regarding the Be–N distances, the cation–ammonia bonds (1.724(4) and 1.731(4) Å) are marginally shorter than the cation–pyridine interactions (1.779(4) and 1.778(4) Å).

Completely unexpected in the reaction of $[Be\{N(SiMe_3)_2\}_2]$ with two molar equivalents of HSPh was the formation and trapping of one NH_3 molecule per cationic center. The coordination of nascent donors has been observed in $[Zn\{Se\text{-}2,4,6\text{-}(CF_3)_3C_6H_2\}\{HN(SiMe_3)_2\}]$, $[Sr(\mu\text{-}SCEt_3)(NH_3)(py)]_\infty$, and $[Li_6(HNMe_2)_6\{Sb(PCy)_3\}_2]\cdot 2\,C_7H_8$ (Cy = cyclohexyl).[11–13] Here the in situ coordination of gaseous nitrogen compounds in the strontium thiolate (ammonia) and the lithium complex (dimethylamine) is noteworthy.

Protonolysis products, such as ammonia-coordinated lanthanides $[M\{OCH(CF_3)_2\}_3(NH_3)_2]$ (M = Sc, Pr)[14] were identified in metathesis reactions of lanthanide bis(trimethylsilyl)amide with a large excess of acid. In contrast, if stoichiometric amounts of reagents are utilized, protonolysis of the liberated amine with formation of NH_3 is generally not observed. In many cases, the NH_3 complexes were initially regarded as accidental hydrolysis products.[15] We now have conclusive evidence for a competitive protonolysis reaction that occurs when stoichiometric amounts of acid and base are combined and the initially formed $HN(SiMe_3)_2$ reacts competitively with remaining thiol (Scheme 1).

$$[Be\{N(SiMe_3)_2\}_2] + 6\ HSPh \longrightarrow [Be(SPh)_2] + 2\ NH_3 + 4\ PhSSiMe_3 \quad (a)$$

$$[Be\{N(SiMe_3)_2\}_2] + HSPh \longrightarrow [Be\{N(SiMe_3)_2\}(SPh)] + HN(SiMe_3)_2 \quad (b)$$

$$[Be\{N(SiMe_3)_2\}(SPh)] + HSPh \longrightarrow [Be(SPh)_2] + HN(SiMe_3)_2 \quad (c)$$

$$HN(SiMe_3)_2 + HSPh \longrightarrow H_2NSiMe_3 + Me_3SiSPh \quad (d)$$

$$H_2NSiMe_3 + HSPh \longrightarrow NH_3 + Me_3SiSPh \quad (e)$$

$$NH_3 + HSPh \longrightarrow NH_4SPh \quad (f)$$

Scheme 1. Reaction of $[Be\{N(SiMe_3)_2\}_2]$ with HSPh [Eq. (a)]. The individual reacions (b)–(f) emphasize the acid-promoted cleavage of the N–Si bond in $HN(SiMe_3)_2$.

In the first protonation step, $[Be\{N(SiMe_3)_2\}_2]$ and HSPh react to form the mixed beryllium amide thiolate $[Be\{N(SiMe_3)_2\}(SPh)]$. This intermediate can react with a second equivalent of thiol or disproportionate to produce the dithiolate $[Be(SPh)_2]$. The primary amine H_2NSiMe_3, NH_3, and the ammonium salt $[(NH_4)(SPh)]_\infty$ are thought to form by sequential protonation reactions between the initially liberated hexamethyldisilazane and thiol. Further evidence for this sequence is provided by the isolation of $[Be(SC_6F_5)_2(NH_3)(NH_2SiMe_3)]$ from the reaction of $[Be\{N(SiMe_3)_2\}_2]$ with two equivalents of HSC_6F_5 in toluene. Remarkably, two protonolysis products, H_2NSiMe_3 and NH_3 are coordinated to the beryllium center.[16] If an excess of thiol in pyridine is used, quantitative formation of the ammonium salt $[(NH_4)(SC_6F_5)py]_\infty$ is observed.[1c] We therefore assume that protonolysis competes with the desired metathesis reaction of beryllium bis(trimethylsilyl)amide and benzenethiol. It is noteworthy that **1** crystallizes reproducibly from the complex mixture of $[Be\{(SiMe_3)_2\}_2]$, $[Be\{N(SiMe_3)_2\}(SPh)]$, $[Be(SPh)_2]$, $PhSSiMe_3$, $HN(SiMe_3)_2$, H_2NSiMe_3, NH_3, and $[(NH_4)(SPh)]_\infty$.[17]

The identification of **1** provides evidence for acid-promoted N–Si bond cleavage in the reaction of $[Be\{N(SiMe_3)_2\}_2]$ with HSPh. In light of the widespread use of metal bis(trimethylsilyl)amides, this protonolysis is of general interest. For example, we have gathered preliminary evidence that a competitive protonolysis of the N–Si bond also occurs in the reaction of heavier alkaline earth metal bis(trimethylsilyl)-amides with arenethiols.

Experimental Section

All reactions were performed under a purified nitrogen atmosphere by modified Schlenk techniques or in a dry box (Braun Labmaster 150).

 © WILEY-VCH Verlag GmbH, D-69451 Weinheim, 1998 1433-7851/98/3721-3008 $ 17.50+.50/0 *Angew. Chem. Int. Ed.* **1998**, *37*, No. 21

Toluene was distilled from a Na/K alloy and degassed. $[Be\{N(SiMe_3)_2\}_2]$ was prepared according to a known procedure.[7] **Caution**: $[Be\{N(SiMe_3)_2\}_2]$ is a known carcinogen and should be handled only in a well-ventilated fume hood with proper precautions. Benzenethiol was dried over activated 4-Å molecular sieves. [18]Crown-6 was dissolved in hexane, and freshly cut potassium was added. The mixture was briefly heated to reflux, and the remaining potassium removed by filtration. The dried crown ether was isolated by crystallization from hexane.

1: HSPh (0.21 mL, 2.0 mmol) was added dropwise to $[Be\{N(SiMe_3)_2\}_2]$ (0.33 g, 1.0 mmol) and [18]crown-6 (0.26 g, 1.0 mmol) in toluene (20 mL) at room temperature. A heavy white precipitate formed after stirring for several minutes. Pyridine (0.1 mL, 1.2 mmol) was added dropwise, and a homogeneous light yellow solution was obtained. After the mixture had been stirred at room temperature for 30 min, it was filtered through a Celite-loaded frit and stored at 0 °C. Colorless plates gradually grew over several days, and 0.20 g (55 % yield) were collected from the first crystallization.[17] The white powder shrank slightly when heated above 80 °C and then irreversibly melted to a yellow oil in the range of 145 – 153 °C. ^{1}H NMR (300 MHz, 25 °C, [D$_8$]THF): $\delta = 8.54 - 6.71$ (broad overlapping signals, 40 H), 3.52 (s, 24 H), 2.31 (s, 6 H); IR (Nujol): $\tilde{\nu} = 3302$ m, 3197 m, 3043 w, 2926 s, 1643 m, 1610 m, 1576 s, 1463 s, 1377 m, 1352 m, 1317 s, 1286 m, 1216 m, 1137 m, 1105 s, 1070 m, 1050 m, 956 s, 837 m, 785 m, 743 s, 696 s, 648 w, 580 m, 478 cm^{-1} m.

Crystal structure data for **1**: $C_{60}H_{76}Be_2N_4O_6S_4$, $M_r = 1095.51$, triclinic, space group $P\bar{1}$, $a = 10.432(2)$, $b = 13.5950(3)$, $c = 22.0275(4)$ Å, $\alpha = 79.374(1)$, $\beta = 77.760(1)$, $\gamma = 87.160°$, $V = 3000.5(1)$ Å^3, $T = 150$ K, $Z = 2$, $\mu(Mo_{K\alpha}) = 0.210$, crystal dimensions $0.42 \times 0.20 \times 0.20$ mm. Of 12886 independent reflections collected ($2.56 \leq 2\theta \leq 56.00°$) on a Siemens SMART system with a three-circle goniometer and a CCD detector operating at -54 °C, 8176 were observed ($I > 2\sigma(I)$). Crystal decay was monitored by repeating a set of initial frames at the end of data collection and comparing the duplicate reflections; no decay was observed. An absorption correction was applied with the program SADABS.[18] The crystal structure was solved by direct methods with SHELXTL. Missing atoms were located in subsequent difference Fourier maps and included in the refinement. The structure of **1** was refined by full-matrix least-squares refinement on F^2.[19] Hydrogen atoms with the exception of the NH protons were placed geometrically and refined by using a riding model with U_{iso} constrained at 1.2 U_{eq} of the carrier C atom. All non-hydrogen atoms were refined anisotropically. NH_3 hydrogen atoms were located in difference maps and included in the refinement by using distance restraints. A center of symmetry, suspected in the center of the crown ether molecule could not be confirmed even after various symmetry checks and transformation of the suspected inversion center to the origin of the unit cell. The absence of significant correlations also confirms the correct symmetry. $R_1 = 0.0575$ for data with $I > 2\sigma(I)$, and $wR_2 = 0.1234$ for all data. Crystallographic data (excluding structure factors) for the structure reported in this paper have been deposited with the Cambridge Crystallographic Data Centre as supplementary publication no. CCDC-101292. Copies of the data can be obtained free of charge on application to CCDC, 12 Union Road, Cambridge CB2 1EZ, UK (fax: (+44) 1223-336-033; e-mail: deposit@ccdc.cam.ac.uk).

Received: March 31, 1998 [Z11664IE]
German version: *Angew. Chem.* **1998**, *110*, 3204 – 3206

Keywords: alkaline earth metals · amides · hydrogen bonds · protonations · S ligands

[1] a) K. Ruhlandt-Senge, *Inorg. Chem.* **1995**, *34*, 3499; b) K. Ruhlandt-Senge, *Comm. Inorg. Chem.* **1997**, *19*, 351; c) S. Chadwick, U. Englich, B. Noll, K. Ruhlandt-Senge, *Inorg. Chem.* **1998**, *37*, 4718.
[2] N. A. Bell in *Comprehensive Organometallic Chemistry*, *Vol. 1* (Eds.: G. Wilkinson, F. G. A. Stone, E. W. Abel), Pergamon, Oxford, **1995**, p. 35.
[3] K. Ruhlandt-Senge, R. A. Bartlett, M. M. Olmstead, P. P. Power, *Inorg. Chem.* **1993**, *32*, 1724.
[4] M. Niemeyer, P. P. Power, *Inorg. Chem.* **1997**, *36*, 4688.
[5] H. Nöth, D. Schlosser, *Chem. Ber.* **1988**, *121*, 1711.
[6] a) G. E. Coates, A. H. Fishwick, *J. Chem. Soc.* **1968**, 635; b) G. E. Coates, A. H. Fishwick, *J. Chem. Soc.* **1968**, 640.
[7] For the synthesis and solid-state structure of $[Be\{N(SiMe_3)_2\}_2]$, see a) H. Bürger, C. Forker, J. Goubeau, *Monatsh. Chem.* **1965**, *69*, 597; b) A. H. Clark, A. Haaland, *J. Chem. Soc. Chem. Commun.* **1969**, 912.
[8] Pyridine was used to obtain a family of soluble magnesium phenylthiolates: S. Chadwick, U. Englich, M. O. Senge, B. C. Noll, K. Ruhlandt-Senge, *Organometallics* **1998**, *17*, 3077.
[9] R. A. Anderson, G. E. Coates, *J. Chem. Soc. Dalton Trans.* **1975**, 1244.
[10] A. J. Amoroso, A. M. Arif, J. A. Gladysz, *Organometallics* **1997**, *16*, 6032, and references therein.
[11] D. Labahn, F. M. Bohnen, R. Herbst-Irmer, E. Pohl, D. Stalke, H. W. Roesky, *Z. Anorg. Allg. Chem.* **1994**, *620*, 41.
[12] A. P. Purdy, A. D. Berry, C. F. George, *Inorg. Chem.* **1997**, *36*, 3370.
[13] M. A. Beswick, J. M. Goodman, C. N. Harmer, A. D. Hopkins, M. A. Paver, P. R. Raithby, A. E. H. Wheatley, D. S. Wright, *Chem. Commun.* **1997**, 1879.
[14] D. C. Bradley, H. Chudzynska, M. E. Hammond, M. B. Hursthouse, M. Motevalli, W. Ruowen, *Polyhedron* **1992**, *11*, 375.
[15] C. Burns, personal communication.
[16] $[Be(SC_6F_5)_2(NH_3)(H_2NSiMe_3)]$ was synthesized by treatment of $[Be\{N(SiMe_3)_2\}_2]$ with two equivalents of HSC_6F_5 in toluene. The resulting colorless crystals were analyzed crystallographically. However, further spectroscopic analysis was not possible due to rapid decomposition of the sample. We were unable, even after several attempts, to trap the intermediate and obtain spectroscopic data. S. Chadwick, K. Ruhlandt-Senge, unpublished results.
[17] The maximum theoretical yield of this reaction is 66 % taking into account the 1:1 ratio of $[Be(SC_6H_5)_2]$ and NH_3 in the final product. Accordingly, the experimental yield was 55 %. Since the limiting reagent in this reaction is HSC_6H_5, the reaction was repeated with six equivalents of HSC_6H_5, as indicated in Scheme 1. Instead of isolating an increased amount of **1**, only $[(NH_4)(SC_6H_5)(py)]_\infty$ was identified in the solid state.
[18] G. M. Sheldrick, SADABS, Program for Absorption Correction Using Area Detector Data; Universität Göttingen, Germany, **1996**.
[19] G. M. Sheldrick, SHELXTL, Version 5. Siemens Analytical X-ray Instruments, Madison, WI, **1994**.

First Synthetic Carbohydrates with the Full Anticoagulant Properties of Heparin**

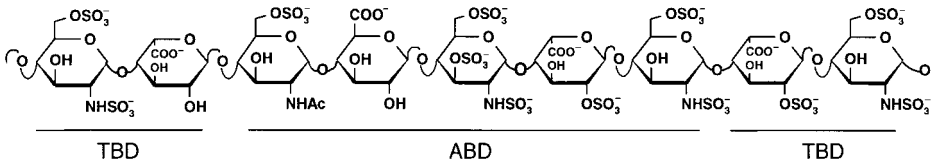
Maurice Petitou,* Philippe Duchaussoy, Pierre-A. Driguez, Guy Jaurand, Jean-P. Hérault, Jean-C. Lormeau, Constant A. A. van Boeckel, and Jean-M. Herbert

Heparin, a major drug for the prevention and treatment of cardiovascular diseases, exerts its activity through activation of the serine proteinase inhibitor antithrombin III (AT III), the main physiological inhibitor of blood coagulation.[1, 2] A unique pentasaccharide sequence[3] in the polysaccharide binds to the protein in a highly specific way, inducing a

[*] Dr. M. Petitou, Dr. P. Duchaussoy, Dr. P.-A. Driguez, Dr. G. Jaurand, Dr. J.-P. Hérault, Dr. J.-C. Lormeau, Dr. J.-M. Herbert
Sanofi Recherche
Haemobiology Research Department
195, route d'Espagne, F-31036 Toulouse Cedex (France)
Fax: (+33) 5-61-16-22-86
E-mail: maurice.petitou@sanofi.com
Prof. Dr. Constant A. A. van Boeckel
N.V. Organon, Oss (The Netherlands)

[**] This work is part of a collaborative project between N.V. Organon (The Netherlands) and Sanofi Recherche (France) on antithrombotic oligosaccharides.

 © WILEY-VCH Verlag GmbH, D-69451 Weinheim, 1998 1433-7851/98/3721-3009 $ 17.50+.50/0



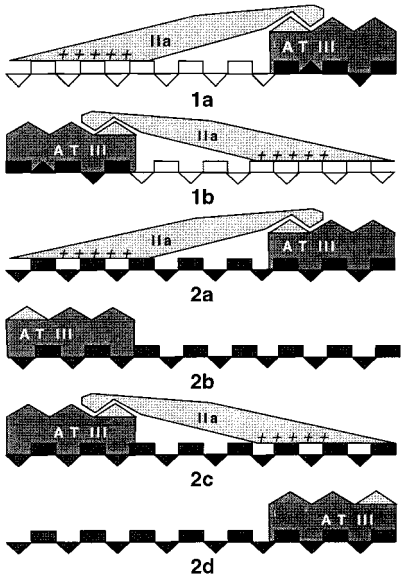
Scheme 1. An anticoagulant heparin molecule contains an antithrombin binding domain (ABD) prolonged at both ends by thrombin binding domains (TBDs). An ABD is a unique pentasaccharide sequence characterized by the presence of β-D-glucuronic acid linked to a *N*-sulfo-3,6-di-*O*-sulfo-α-D-glucosamine; TBDs mainly consist of repeated trisulfated disaccharides made of 2-*O*-sulfo-α-L-iduronic acid linked to *N*-sulfo-6-*O*-sulfo-α-D-glucosamine.

conformational change that allows adequate presentation of the inhibitory peptidic loop of AT III to the active sites of serine proteinases. The mere interaction with activated AT III is sufficient to inhibit coagulation factor Xa. This is at variance with thrombin inhibition, which requires the formation of a ternary complex involving heparin, AT III, and thrombin.[2] A longer heparin chain is then needed (Scheme 1) which contains the above-mentioned pentasaccharide that is prolonged at both ends by repeated trisulfated disaccharide units.[4] Thrombin is electrostatically attracted through its anion binding site exosite II,[5] and slides along the chain until it finally hooks itself on the inhibitory loop of activated AT III.

Thus, an oligosaccharide molecule containing both an AT III binding domain (ABD) and a thrombin binding domain (TBD) should be able to mimic the full anticoagulant activity of heparin. Various biochemical studies aimed at determining the size of such molecules pointed to tetradeca-, octadeca-, and eicosasaccharides.[6] It is noteworthy that when AT III is docked on its binding domain, thrombin, sliding along the heparin chain, must approach from the correct side to be inhibited. This implies that only one of the two possible ways of elongating the ABD with a TBD (reducing or nonreducing ends, Scheme 2) will allow thrombin inhibition.[7]

Synthesizing an oligosaccharide of this size, and reproducing the exact structure of the hypothetical heparin fragment, would be practically unfeasible.[9] In a first approach to overcome this difficulty, two saccharide molecules, an ABD and a TBD, were bridged by a non-carbohydrate linker.[8] The resulting conjugates displayed inhibition of thrombin and factor Xa, but in some assays the thrombin inhibitory potency was weaker than that of heparin. In the approach reported here we exploited the "non-glycosamino" glycan series of heparin analogues,[10] where *N*-sulfonato substituents are replaced by *O*-sulfonato groups and hydroxyl groups are alkylated. These structural modifications fully preserve the specific binding to AT III, yet they dramatically simplify the synthesis.

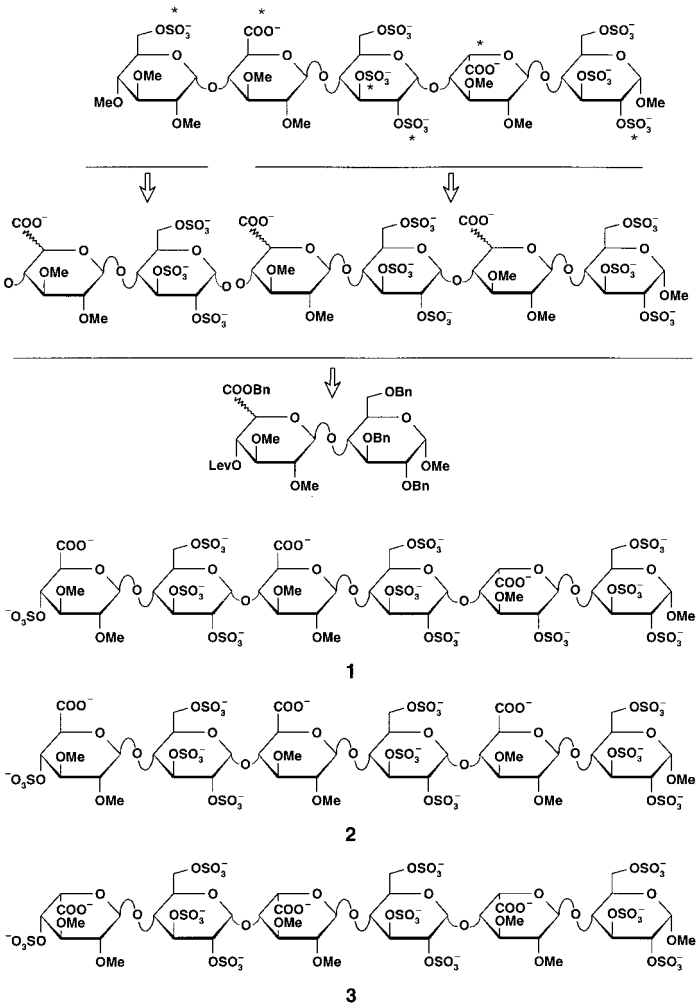
The structures of the target molecules stem from the following considerations: a) In contrast to the highly specific interaction between AT III and heparin, the interaction of thrombin with the polysaccharide merely results from an electrostatic attraction governed by the density of negative charges on the polysaccharide backbone.[4] Consequently the ABD, which contains at least six critical negative charges (Scheme 3), can also attract thrombin and serve as a TBD. b) A continuum of ABDs would necessarily display the correct relative position of ABD and TBD, since AT III can bind at either end of the molecule, and thrombin can be attracted by the rest of the chain (Scheme 2). c) For thrombin to efficiently compete with AT III for binding to a continuum of ABDs, the affinity of the AT III/ABD couple must preferably be in the same range of affinity as the thrombin/heparin couple—that is, in the micromolar range[11] and therefore two to three orders of magnitude lower than the highest affinity reached with some synthetic pentasaccharides. From this latter consideration it follows that we are, to a certain extent, allowed to adapt the structure of the ABD to our synthesis strategy (provided we preserve enough binding affinity). This is not a minor advantage for the synthesis of the targeted long saccharide fragments.



Scheme 2. Inhibition of thrombin by AT III and heparin. In an active anticoagulant molecule, AT III binds to heparin through the ABD pentasaccharide (see Scheme 1, symbolized in **1a**, **b** by black rectangles and triangles) and exposes its activated inhibitory loop (light grey triangle) to the catalytic site of thrombin (also called factor IIa). Thrombin, attracted by the negative charges of the TBD (white rectangles and triangles), slides along the chain until it hooks itself on the exposed loop of the inhibitor. Heparin and AT III dock themselves in a unique, unknown way (**1a** or **1b**), and thrombin apparently has to approach from the correct side to be inhibited. Among these two possible arrangements of ABD and TBD (both are present in a heparin molecule, see Scheme 1), the efficient one was unknown.[7] We therefore designed an hybrid molecule (dark grey rectangles and triangles) which is a continuum of ABDs. AT III can bind at either end of the molecule (**2a**–**d**), and, whatever the efficient arrangement (**2a** or **2b**), thrombin can be attracted and inhibited (**2a** or **IIc**) provided the saccharide chain is long enough to accommodate both proteins.

The structure of a pentasaccharide with high affinity for AT III[12] is shown in Scheme 3. The presence of two types of uronic acids having the D-*gluco* and the L-*ido* configurations is a structural features of high-affinity compounds. From this structure we reasoned that hexasaccharides consisting of a

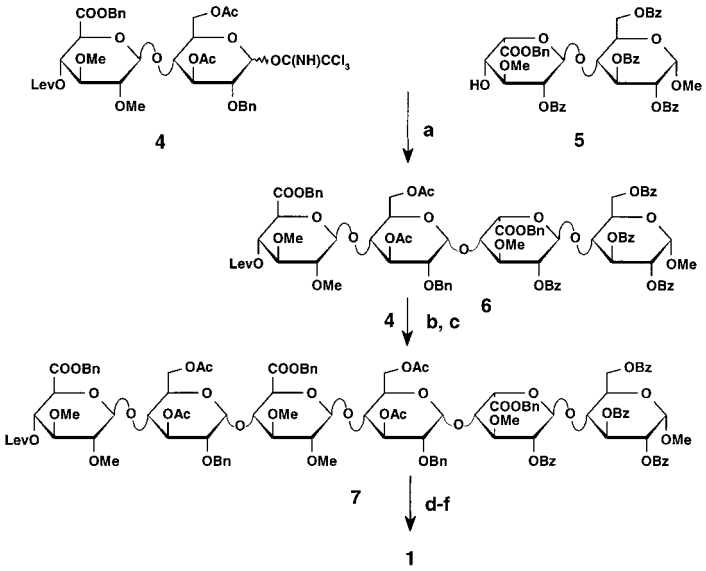
 © WILEY-VCH Verlag GmbH, D-69451 Weinheim, 1998 1433-7851/98/3721-3010 $ 17.50+.50/0



Scheme 3. Simplifying the structure of a high-affinity binding pentasaccharide sequence. The critical anionic groups involved in the interaction with AT III are labeled with an asterisk. The proposed changes (second line) introduce another sulfate group at position 3 of the third glucose unit and alter the configuration at C5 of the uronic acids. Such changes would allow synthesis from a single disaccharide building block (third line). Compounds **1**–**3** were synthesized to test these various possibilities: **1** contains a third trisulfated glucose residue, **2** contains only glucuronic acid, and **3** contains only iduronic acid (the latter was obtained from a single disaccharide building block).

single repeated disaccharide unit might display significant affinity for AT III, possibly in the desired micromolar range. Such hexasaccharides, obtainable from a single disaccharide synthon, meet our criteria for an easy synthesis of long fragments (the synthesis of the ultimate target longer saccharides would also be possible from the same basic synthon). To test this possibility we prepared the hexasaccharides **1**–**3** depicted in Scheme 3. Hexasaccharide **1** was synthesized to check the influence of adding one more trisulfated glucose unit, **2** to test whether the easily available D-glucuronic acid could substitute for L-iduronic acid, and **3** to obtain a compound in which L-iduronic acid is the only uronic acid present. The affinity of **1**–**3** for AT III was determined.

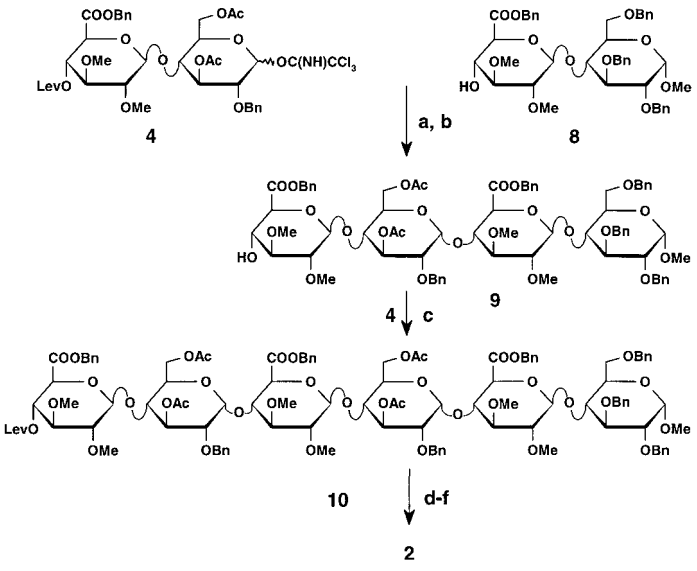
All three hexasaccharides were obtained using strategies (Scheme 4) where disaccharide building blocks were prepared first and then repeatedly condensed to each other by the imidate glycosylation procedure;[13] the final hexasaccharides



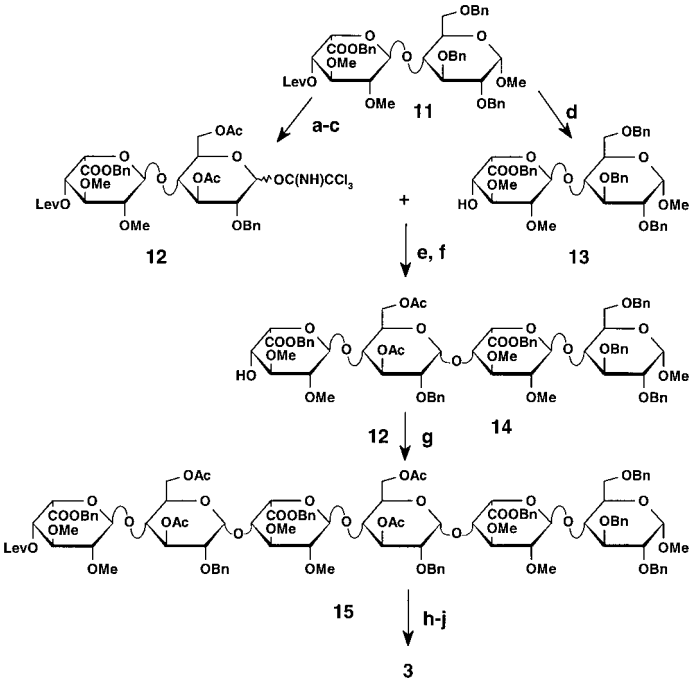
Scheme 4. a) $Me_3SiOSO_2CF_3$ (TMSOTf), toluene, 4-Å MS, $-20\,^{\circ}C$, 30 min, 62%; b) 1M NH_2NH_2/H_2O in pyridine/AcOH (3/2), 15 min, 87%; c) as for a), 48%; d) H_2, 10% Pd/C, MeOH, 24 h; e) 0.5M NaOH, 5 h (91% based on **7**); f) pyridine:SO_3, DMF, $55\,^{\circ}C$, 24 h, 98%.

were deprotected and sulfated. Thus, reaction of stoichiometric amounts of the known[14] glycosyl donor **4** and the acceptor **5** (prepared as reported for the methyl ester analogue[10a]) yielded the tetrasaccharide **6**[15] (62%, Scheme 4). Selective cleavage of the levulinic ester gave the corresponding glycosyl acceptor (87%), which was again condensed with **4** to afford the fully protected hexasaccharide **7** (a 5:1 mixture of the α and β anomers was formed, from which **7** was isolated in 39% yield after chromatography on silica gel). Catalytic hydrogenolysis of the benzyl groups was followed by saponification of the esters (91%). Complete removal of the protecting groups was monitored by high-field ^{1}H NMR spectroscopy. Subsequent sulfation and lyophilization gave **1** as a white powder (98%).[15] Compound **2**[15] was obtained in a similar manner (Scheme 5) from **4** and the acceptor **8**, which was prepared as reported for its methyl ester counterpart.[12] Finally, a similar series of reactions (Scheme 6) gave **3**.[15] The sequence started from **12** and **13**, which were both are derived from a common precursor, the disaccharide **11**, prepared as reported for its methyl ester counterpart.[12]

The affinity of **1**–**3** for AT III was determined by fluorescence spectroscopy[15] and compared to that of the pentasaccharide in Scheme 3 ($K_d = 1.4 \pm 0.2$ nM). The introduction of a third trisulfated glucose unit at the nonreducing end of the pentasaccharide sequence proved to be fully compatible with the recognition of AT III (K_d(**1**) $= 0.8 \pm 0.3$ nM). In contrast, substituting D-glucuronic acid for L-iduronic acid resulted in a dramatic loss of affinity (K_d(**2**) $= 3.4 \pm 0.3\,\mu$M). The opposite change (substituting L-iduronic acid for D-glucuronic acid), although it also decreased the affinity for AT III, nicely fitted our "relative affinity criterion" discussed above (c) since the affinity of **3** for AT III ($K_d = 0.35 \pm 0.01\,\mu$M) was very close to that reported[11] for thrombin and heparin (1 μM). We expected **3** (which like



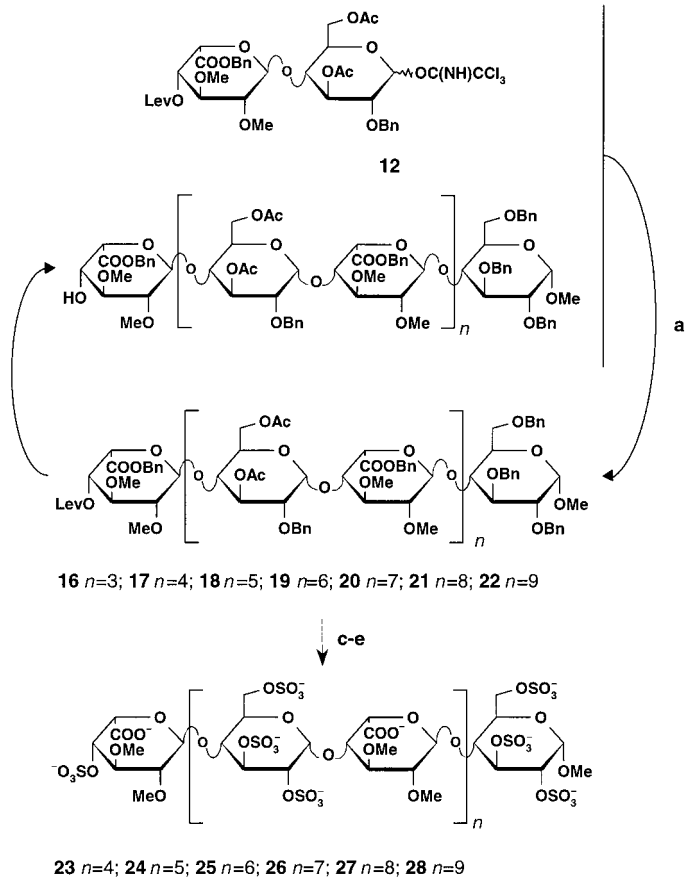
Scheme 5. a) TMSOTf, CH_2Cl_2, 4-Å MS, −20 °C, 30 min, 69 %; b) 1 M NH_2NH_2/H_2O in pyridine/AcOH (3/2), 15 min, 95 %; c) as for a), 63 %; d) H_2, 10 % Pd/C, MeOH, 24 h; e) 0.5 M NaOH, 5 h, 99 % (based on **10**); f) pyridine:SO_3, DMF, 55 °C, 24 h, 95 %.



Scheme 6. a) CF_3COOH/Ac_2O/AcOH, 60 °C, 4 h, 67 %; b) $HOCH_2$-CH_2NH_2, THF, RT, 74 %; c) CCl_3CN, K_2CO_3, CH_2Cl_2, RT, 1.5 h, 94 %; d) 1 M NH_2NH_2/H_2O in pyridine/AcOH (3/2), 15 min, 91 %; e) TBDM!SOTf, toluene, 4-Å MS, −20 °C, 30 min, 54 %; f) as for d), 99 %; g) as for e), 64 %; h) H_2, 10 % Pd/C, MeOH, 24 h; i) 0.5 M NaOH, 5 h; j) pyridine:SO_3, DMF, 55 °C, 24 h, 60 % (based on **15**).

heparin contains four negative charges per disaccharide unit) to have a similar affinity for thrombin. Interestingly, **3** also displays significant anti-factor Xa activity (325 units mg^{-1}). We were pleased that the synthesis of **3** involves repeated glycosylation at position 4 of a L-iduronic acid derivative, since in our experience such a glycosylation always afforded almost exclusively the desired α-coupled product when an imidate was used as the glycosyl donor.

Having identified an ABD that is easily obtainable from a single disaccharide building block (**11**), we attempted the synthesis of longer fragments consisting of a single repeating basic disaccharide unit. The strategy used to prepare **3** was further developed, as shown in Scheme 7. The imidate **12** was used as glycosyl donor to add disaccharide units to the new



Scheme 7. a) TMSOTf, toluene, 4-Å MS, −20 °C, 30 min; b) 1 M NH_2NH_2/H_2O in pyridine/AcOH (3/2), 15 min; c) H_2, 10 % Pd/C, MeOH, 24 h; d) 0.5 M NaOH, 5 h; e) pyridine:SO_3, DMF, 55 °C, 24 h.

glycosyl acceptor resulting from cleavage of the levulinoyl group of the oligosaccharide obtained at the preceding step.[17] The process was reiterated until an eicosamer was obtained. The structure of the fully protected intermediates (**16**–**22**) was ascertained by high-field ^1H NMR spectroscopy and mass spectrometry.[15] The yield of the successive coupling steps was about 60 % (not optimized), and no β-coupled product was detected. The large difference in size between the glycosyl donor disaccharide on the one hand, and the glycosyl acceptor and the product of the reaction on the other hand, made it very easy to recover, by gel permeation in dichloromethane/ethanol, a mixture containing exclusively the unchanged acceptor and the product. This mixture was occasionally submitted to another glycosylation reaction to improve the yield based on the expensive acceptors involved in the final steps of chain elongation. Deprotection and sulfation of the oligosaccharides (deca- to eicosamer) obtained at each step involved, as above for the preparation of hexasaccharides, hydrogenolysis, saponification, and sulfation. Complete re-

 © WILEY-VCH Verlag GmbH, D-69451 Weinheim, 1998 1433-7851/98/3721-3012 $ 17.50+.50/0 *Angew. Chem. Int. Ed.* **1998**, *37*, No. 21

Table 1. Properties of the sulfated iduronic acid containing oligosaccharides.

	3	**23**	**24**	**25**	**26**	**27**	**28**	heparin
saccharide units	6	10	12	14	16	18	20	10–50
molecular weight	2217	3606	4301	4995	5690	6384	7078	ca. 15000
factor Xa inhibition[a]	325 (±16)	405 (±32)	360 (±29)	310 (±16)	359 (±29)	270 (±23)	236 (±19)	180
thrombin inhibition[b]	>10	>10	>10	>10	130 (113–133)	23 (13–30)	6.7 (3–9)	3.3 (3–4)

[a] [units mg^{-1}] (standard deviation) ($n=3$). [b] IC_{50} [$ng\,mL^{-1}$] (95% confidence interval).

moval of the protecting groups was monitored before sulfation by high-field ^1H NMR spectroscopy. The desired sulfated oligomers **23**–**28** were obtained as white powders after lyophilization in yields of 49 to 86% over the three steps. Their purity was assessed by capillary electrophoresis, and their structure was clarified by ^1H NMR spectroscopy and electro spray ionization mass spectrometry (ESI-MS).[15]

These compounds were then submitted to biological tests to assess their ability to catalyze inhibition of factor Xa[18] and thrombin[19] by AT III (Table 1). All the compounds contain an ABD, which explains their ability to bind to AT III and their anti-factor Xa activity. The hexa-, deca-, dodeca-, and tetradecasaccharide were inactive in the thrombin inhibition assay, whereas the activity of the hexadeca-, octadeca-, and eicosasaccharide increased with size in this assay. The IC_{50} values show that the eicosamer is half as potent as standard heparin. Increasing the chain length would probably improve the thrombin inhibitory potency since the higher activity of the longer chains (compare **26**–**28**) reflects the well-known[2] greater ability of longer heparin fragments to electrostatically attract thrombin.

Using the imidate glycosylation procedure,[13] we have synthesized for the first time oligosaccharide molecules displaying the dual (anti-factor Xa and anti-thrombin) activity of heparin mediated by AT III. Regarding the long standing question[6] about the minimum size of heparin fragments able to catalyze thrombin inhibition, the present data restrict the choice to a pentadeca- or hexadecasaccharide.

Received: May 25, 1998 [Z11894IE]
German version: *Angew. Chem.* **1998**, *110*, 3186–3191

Keywords: drug research · enzyme inhibitors · heparin · oligosaccharides · serine proteinases

[1] *Heparin* (Eds.: D. A. Lane, U. Lindahl), Edward Arnold, London, **1989**.
[2] S. T. Olson, I. Björk, *Semin. Thromb. Hemost.* **1994**, *20*, 373–409.
[3] a) U. Lindahl, G. Bäckström, L. Thunberg, I. G. Leder, *Proc. Natl. Acad. Sci. USA* **1980**, *77*, 6551–6555; b) B. Casu, P. Oreste, G. Torri, G. Zoppetti, J. Choay, J.-C. Lormeau, M. Petitou, P. Sinaÿ, *Biochem. J.* **1981**, *197*, 599–609; c) J. Choay, J.-C. Lormeau, M. Petitou, P. Sinaÿ, J. Fareed, *Ann. N. Y. Acad. Sci.* **1981**, *370*, 644–649; d) L. Thunberg, G. Bäckström, U. Lindahl, *Carbohydr. Res.* **1982**, *100*, 393–410.
[4] B. Casu, *Adv. Carbohydr. Chem. Biochem.* **1985**, *43*, 51–134.
[5] Review: M. T. Stubbs, W. Bode, *Trends Biochem. Sci.* **1995**, *20*, 23–28.
[6] a) T. C. Laurent, A. Tengblad, L. Thunberg, M. Höök, U. Lindahl, *Biochem. J.* **1978**, *175*, 691–701; b) G. M. Oosta, W. T. Gardner, D. L. Beeler, R. D. Rosenberg, *Proc. Natl. Acad. Sci. USA* **1981**, *78, 829*–833; c) D. A. Lane, J. Denton, A. M. Flynn, L. Thunberg, U. Lindahl, *Biochem. J.* **1984**, *218*, 725–732; d) A. Danielsson, E. Raub, U. Lindahl, I. Björk, *J. Biol. Chem.* **1986**, *261*, 15467–15473.
[7] At the start of this project the correct relative position of the ABD and the TBD was not known. Molecular modeling studies then suggested that the ABD should be prolonged at the nonreducing end.[8a]
[8] a) P. D. J. Grootenhuis, P. Westerduin, D. Meuleman, M. Petitou, C. A. A. van Boeckel, *Nature Struct. Biol.* **1995**, *2*, 736–739; b) P. Westerduin, J. E. M. Basten, M. A. Broekhoven, V. de Kimpe, W. H. A. Kuijpers, C. A. A. van Boeckel, *Angew. Chem.* **1996**, *108*, 339–342; *Angew. Chem. Int. Ed. Engl.* **1996**, *35*, 331–333.
[9] Reviews on the synthesis of heparin fragments: a) M. Petitou, C. A. A. van Boeckel, *Prog. Chem. Org. Nat. Prod.* **1992**, *60*, 143–210; b) C. A. A. van Boeckel, M. Petitou, *Angew. Chem.* **1993**, *105*, 1741–1761; *Angew. Chem. Int. Ed. Engl.* **1993**, *32*, 1671–1690; c) M. Petitou, C. A. A. van Boeckel, *Pure Appl. Chem.* **1997**, *67*, 1839–1846.
[10] a) G. Jaurand, J. Basten, I. Lederman, C. A. A. van Boeckel, M. Petitou, *Bioorg. Med. Chem. Lett.* **1992**, *2*, 897–900; b) J. Basten, G. Jaurand, B. Olde-Hanter, M. Petitou, C. A. A. van Boeckel, *Bioorg. Med. Chem. Lett.* **1992**, *2*, 901–904; c) J. Basten, G. Jaurand, B. Olde-Hanter, P. Duchaussoy, M. Petitou, C. A. A. van Boeckel, *Bioorg. Med. Chem. Lett.* **1992**, *2*, 905–910.
[11] S. T. Olson, *J. Biol. Chem.* **1988**, *263*, 1698–1708.
[12] P. Westerduin, C. A. A. van Boeckel, J. E. M. Basten, M. A. Broekhoven, H. Lucas, A. Rood, H. van der Heijden, R. G. M. van Amsterdam, T. G. van Dinther, D. G. Meuleman, A. Visser, G. M. T. Vogel, J. B. L. Damm, G. T. Overklift, *Bioorg. Med. Chem.* **1994**, *2*, 1267–1280.
[13] R. R. Schmidt, W. Kinzy in *Adv. Carbohydr. Chem. Biochem., Vol. 50* (Ed.: D. Horton), Academic Press, London, **1994**, pp. 21–123.
[14] M. Petitou, P. Duchaussoy, G. Jaurand, F. Gourvenec, I. Lederman, J.-M. Strassel, T. Barzû, B. Crépon, J.-P. Hérault, J.-C. Lormeau, A. Bernat, J.-M. Herbert, *J. Med. Chem.* **1997**, *40*, 1600–1607.
[15] All new compounds were analyzed by ^1H NMR spectroscopy, by mass spectrometry, and occasionally by HPLC. Combustion analyses were systematically performed on disaccharidic building blocks only. Selected analytical data: ^1H NMR data were collected at 500 MHz in D_2O (external standard TSP; for polar compounds) or in $CDCl_3$ (internal standard TMS). The NMR data are given for anomeric protons of the nonreducing end (NR) to the reducing end (R) units. Mass spectrometry data were collected with liquid secondary ion mass spectrometry (LSI-MS) or ESI-MS. **1**: ^1H NMR: δ ($J_{1,2}$ [Hz]) = 4.64 (7.5; NR), 5.52 (3.7; NR-1), 4.63 (8.1; NR-2), 5.48 (3.5; R-2), 5.10 (6.5; R-1), 5.10 (3.5; R); LSI-MS: m/z: 2280.4 [$M-Na]^-$; $[\alpha]_D = +30$ ($c=1$ in H_2O). **2**: ^1H NMR: δ ($J_{1,2}$ [Hz]) = 4.66 (ca. 8; NR), 5.54 (3.7; NR-1), 4.64 (ca. 8; NR-2), 5.54 (3.7; R-2), 4.63 (ca. 8; R-1), 5.14 (3.6; R); LSI-MS: m/z: 2192.8 [$M-Na]^-$; $[\alpha]_D = +43$ ($c=0.7$ in H_2O). **3**: ^1H NMR: δ ($J_{1,2}$ [Hz]) = 5.10 (ca. 1; NR), 5.41 (ca. 3; NR-1), 5.06 (2.2; NR-2), 5.41 (ca. 3; R-2), 5.09 (ca. 1; R-1), 5.15 (3.7; R); LSI-MS: m/z: 2192.6 [$M-Na]^-$; $[\alpha]_D = +28$ ($c=1$ in H_2O). **7**: ^1H NMR: δ ($J_{1,2}$ [Hz]) = 4.16 (8; NR), 5.43 (3.5; NR-1), 4.03 (8; NR-2), 4.88 (ca. 3; R-2), 5.47 (6.1; R-1), 5.05 (ca. 3; R); $[\alpha]_D = +76$ ($c=0.3$ in CH_2Cl_2). **10**: ^1H NMR: δ ($J_{1,2}$ [Hz]) = 4.17 (ca. 8; NR), 5.39 (3.8; NR-1), 4.20 (ca. 8; NR-2), 5.33 (3.6; R-2), 4.14 (ca. 8; R-1), 4.56 (3.5; R); $[\alpha]_D = +86$ ($c=0.6$ in CH_2Cl_2). **15**: ^1H NMR: δ ($J_{1,2}$ [Hz]) = 4.90 (4.3; NR), 5.10 (3.9; NR-1), 5.23 (6.5; NR-2), 5.12 (3.9; R-2), 4.89 (6.8; R-1), 4.56 (ca. 3; R); $[\alpha]_D = +23$ ($c=0.5$, CH_2Cl_2). The ^1H NMR spectra of **16**–**22** were very similar in terms of chemical shifts, and, as expected, only the relative intensities of the signals varied between compounds. Resonances for the distinguishable anomeric protons: δ ($J_{1,2}$ [Hz]) = 4.92 (4–4.3;

 © WILEY-VCH Verlag GmbH, D-69451 Weinheim, 1998 1433-7851/98/3721-3013 $ 17.50+.50/0

NR), 5.10 (3.3–3.5; NR-1), 5.26 (6–7; R-1), 4.56 (3.5; R). Optical rotations of **16**–**22** were all in the range +20–22 ($c = 0.5–1$ in H_2O). Positive-mode LSI-MS (thioglycerol + NaCl/thioglycerol + KF): **16**: *m/z*: 2771/2787; **17**: *m/z*: 3402/3418; **18** (after cleavage of the levulinoyl group): *m/z*: 3934/3950; **19**: *m/z*: 4664/4680; **20**: *m/z*: not determined/5310; **21**: *m/z*: not determined/5940. The ^{1}H NMR spectra of **23**–**28** were very similar in terms of chemical shifts, and, as expected, only the relative intensities of the signals varied between compounds. Resonances for the distinguishable anomeric protons: δ ($J_{1,2}$ [Hz]) = 5.08–5.11 (1–2; NR), 5.38–5.41 (3–4; NR-1), 5.04–5.09 (1–2; CNR), 5.40–5.42 (3–4; CR), 5.05–5.09 (1–2; R-1), 5.10–5.15 (3.5; R). Optical rotations were all in the range +27–34 ($c = 0.4–0.6$ in H_2O); ESI-MS (monoisotopic mass/average mass/experimental mass ± standard deviation): **23**: *m/z*: 3603.5/3606.3/3605.13 ± 0.9; **24**: *m/z*: 4297.5/4300.7/4296.8 ± 0.9; **25**: *m/z*: 4991.4/4995.2/4993.0 ± 2.2; **26**: *m/z*: 5685.3/5689.6/5687.6 ± 2.3; **27**: *m/z*: 6379.2/6384.1/6381.4 ± 3.2; **28**: *m/z*: 7073.1/7078.5/7077.3 ± 3.2.

[16] D. H. Atha, J.-C. Lormeau, M. Petitou, R. D. Rosenberg, J. Choay, *Biochemistry* **1987**, *26*, 6454–6461

[17] Alternatively, a tetrasaccharide donor or a hexasaccharide donor obtained from the same basic disaccharide was used.

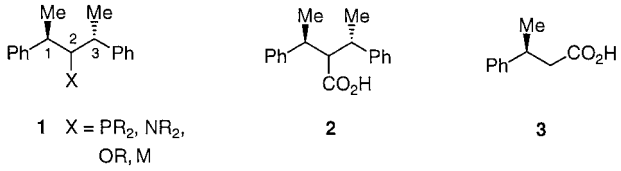
[18] A. N. Teien, M. Lie, *Thromb. Res.* **1977**, *10*, 399–410.

[19] J.-M. Herbert, J.-P. Hérault, A. Bernat, R. G. M. van Amsterdam, G. M. T. Vogel, J.-C. Lormeau, M. Petitou, D. G. Meuleman, *Circ. Res.* **1996**, *76*, 590–600.

New Chiral Ligands with Nonstereogenic Chirotopic Centers for Asymmetric Synthesis**

Claus-Dieter Graf, Christophe Malan, and Paul Knochel*

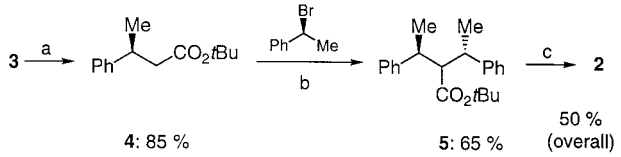
The design of new chiral ligands for asymmetric synthesis is an active field of research.[1] To obtain an efficient transfer of the stereochemistry the chiral information of the ligand should be as close as possible to the reaction center. This concept led to the development of *P*-chiral phosphanes[2] and to the ingenious design of "chiral pockets"[3] that give impressive enantioselectivities. Alternatively, ligands with chiral secondary organic groups linked to phosphorus or nitrogen atoms have also been used with excellent results in enantioselective reactions.[4] However, many of these ligands involve a challenging synthesis that requires the linkage of a sterically demanding secondary chiral carbon center to a heteroatom (P or N). Stimulated by the work of Mislow and Siegel on local chirality[5] we report the preparation of several new pseudo-C_2-symmetric ligands of type **1** and their utility in asymmetric synthesis. All these ligands avoid the difficulty of



1 X = PR_2, NR_2, OR, M **2** **3**

controlling the stereochemistry of the C(2) carbon center attached to the heteroatom (P or N).

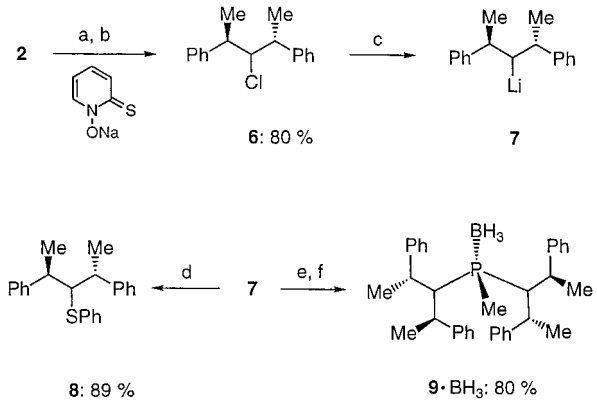
In accordance with the definition of Mislow and Siegel,[5] the center C(2) is not a chiral center, but rather a chirotopic center (a center in a chiral environment). This represents a great synthetic advantage since it avoids the necessity to control the stereochemistry at C(2). We chose the carboxylic acid **2** as the key intermediate for the preparation of ligands of type **1**. The esterification of commercially available (*S*)-3-phenylbutyric acid (**3**) with isobutene provides the *tert*-butyl ester **4**, which was alkylated in a clean S_N2-reaction with (*S*)-1-bromoethylbenzene (88% *ee*)[6] (Scheme 1). Simple recrystallization of (*S*,*S*)-*tert*-butyl ester **5** from pentane/acetone



Scheme 1. a) Isobutene, H_2SO_4 cat., CH_2Cl_2, −15→25 °C, 14 h, 85%; b) LDA, THF, −78 °C, 1.5 h, then HMPA (1.0 equiv), (*S*)-PhCH(Br)CH_3 (1.5 equiv), −20→25 °C, 65%; c) *p*-TosOH cat., toluene, 110 °C, 14 h, 95%. HMPA = hexamethyl phosphoramide; *p*-TsOH = *para*-toluenesulfonic acid.

removed the 10% contamination of the *meso* isomers, and provides the pure ester **5** (65% yield). The free carboxylic acid **2** is then obtained by the acid catalysed cleavage of the *tert*-butyl ester **5**. This simple reaction sequence has been performed on a 10-g scale with an overall yield of about 50%.

The carboxylic acid **2** was readily converted into the corresponding alkyl chloride **6** by a radical decarboxylation.[7] Thus, **2** was converted into its corresponding acid chloride followed by treatment with the sodium salt of 2-mercaptopyridine-*N*-oxide with simultaneous photolysis (Scheme 2).



Scheme 2. a) $SOCl_2$, 90 °C, 3 h; b) NaC_5H_4NOS, DMAP cat., CCl_4, 80 °C, *hv* (300 W), 2 h; c) lithium 4,4″-di-*tert*-butylbiphenylide, THF, −78 °C, 5 min; d) $(PhS)_2$, THF, −78→25 °C; e) $MePCl_2$, THF, −78→25 °C; f) $BH_3 \cdot SMe_2$. DMAP = 4-dimethylaminopyridine.

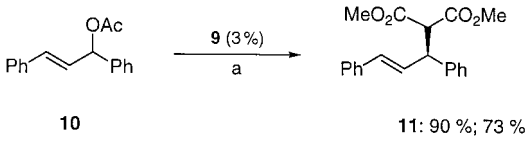
[*] Prof. Dr. P. Knochel, Dipl.-Ing. C.-D. Graf, Dr. C. Malan
Fachbereich Chemie der Universität
Hans-Meerwein-Strasse, D-35032 Marburg (Germany)
Fax: (+49) 6421-28-21-89
E-mail: knochel@ps1515.chemie.uni-marburg.de

[**] We thank the DFG (SFB 260, Leibniz-program) and the Fonds der Chemischen Industrie for generous support. We thank BASF, BAYER, Chemetall, and SIPSY (France) for the generous gift of chemicals.

 © WILEY-VCH Verlag GmbH, D-69451 Weinheim, 1998 1433-7851/98/3721-3014 $ 17.50+.50/0

The reductive lithiation of the alkyl chloride **6** forms the optically pure alkyllithium reagent **7** in approximately 90% yield. This compound was trapped with diphenyl disulfide to give the thioether **8** in 89% yield. Interestingly, the chiral organolithium **7** is indefinitely configurationally stable, since an epimerization of the anionic center is impossible for symmetry reasons.

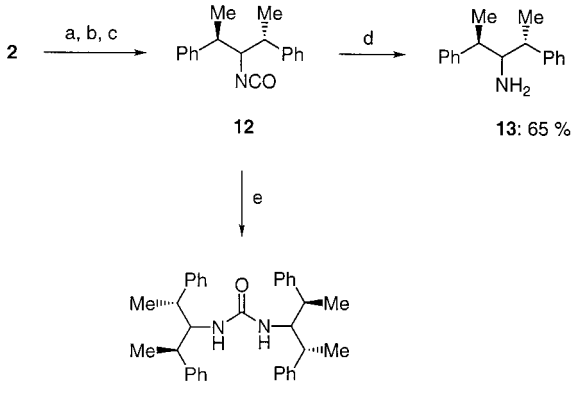
Treatment of **7** with methyldichlorophosphane (−78 °C to 25 °C, 2 h) afforded the chiral phosphane **9**, which was isolated and stored as its oxidation-stable BH_3-complex in 80% yield. After deprotection[8] this free phosphane catalyzed the enantioselective allylation[9] of dimethyl malonate with the allylic acetate **10** in the presence of $[\{Pd(\eta^3\text{-}C_3H_5)Cl\}_2]$ (1.4 mol%) in DMF. This reaction led to the malonate **11** in 90% yield and 73% *ee* under optimized conditions (Scheme 3).[10]



10 **11**: 90%; 73% *ee*

Scheme 3. Palladium catalyzed enantioselective allylation in the presence of **9**. a) $CH_2(CO_2Me)_2$ (3 equiv), *N,O*-bis(trimethylsilyl)acetamide (3 equiv), $[\{Pd(\eta^3\text{-}C_3H_5)Cl\}_2]$ (1.4 mol%), KOAc (5 mol%), DMF, 20 °C, 14 h.

Next, we turned our attention to the preparation of related chiral amines. The carboxylic acid **2** undergoes a straightforward Curtius rearrangement[11] to give the isocyanate **12**, which after purification by flash chromatography furnishes the primary amine **13** in 65% overall yield (Scheme 4). Interestingly, by stirring the isocyanate **12** with silica gel in

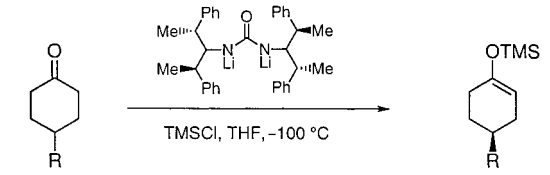


12 **13**: 65%

14: 67%

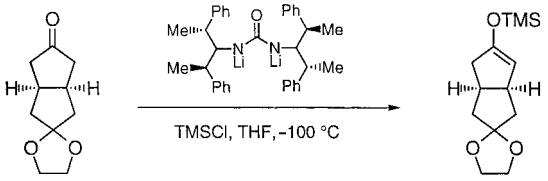
Scheme 4. a) $SOCl_2$, 90 °C, 3 h; b) NaN_3, nBu_4NBr cat., CH_2Cl_2/H_2O, 0 °C, 2 h; c) toluene, 110 °C, 1 h; d) flash chromatography on silica gel; e) stir with silica gel, pentane/diethyl ether, 25 °C, 14 h.

pentane/diethyl ether (25 °C, 14 h) the chiral urea **14** was obtained reproducibly in 67% yield. The double deprotonation of **14** with *n*BuLi provides a dianion that acts as an excellent base for the enantioselective deprotonation[12] of various prochiral cyclic ketones such as **15a**–**e** and **16**. These ketones can be transformed into the silylenol ethers **17a**–**e** and **18** with 83–88% *ee* by using Corey's protocol for in situ quenching[13] (Scheme 5).[14] The new chiral urea derivative **14** is also an excellent auxiliary for the enantioselective alkylation of ketones.[15] Thus, the treatment of α-tetralone **19** with



15a: R = *t*Bu
15b: R = Me
15c: R = *i*Pr
15d: R = Ph
15e: R = OTBS

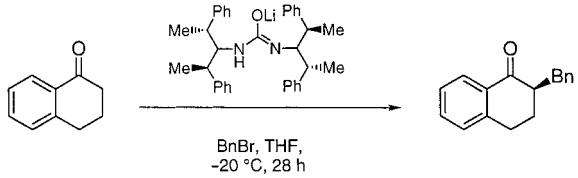
17a: R = *t*Bu : 85%; 87% *ee*
17b: R = Me : 87%; 84% *ee*
17c: R = *i*Pr : 84%; 87% *ee*
17d: R = Ph : 88%; 83% *ee*
17e: R = OTBS : 85%; 88% *ee*



16 **18**: 91%; 86% *ee*

Scheme 5. Enantioselective deprotonation mediated by the dianion of the chiral urea derivative **14**. TMS = trimethylsilyl; TBS = *tert*-butyldimethylsilyl.

the monoanion of **14** at −78 °C, followed by the addition of an excess of benzyl bromide affords the (*R*)-2-benzyltetralone **20** in 83% yield and 81% *ee* (Scheme 6).



19 **20**: 83%; 81% *ee*

Scheme 6. Enantioselective deprotonation mediated by the monoanion of the urea derivative **14**.

We have shown that chiral phosphorus or nitrogen ligands in which the chiral group is attached to the heteroatom by a nonstereogenic chirotopic center can be used for asymmetric synthesis. The new chiral urea derivative **14** proves to be useful in enantioselective deprotonations as well as in enantioselective alkylations. Extension of this concept to cyclic systems is currently underway.

Experimental Section

Typical procedure for the enantioselective allylation: Preparation of **11**: A two-necked flask under argon was charged with the phosphane **9** in CH_2Cl_2 (0.13 mL of a 0.14 M solution, 18 μmol). The solvent was evaporated and the phosphane dissolved in DMF (1.5 mL). After the addition of $[\{Pd(\eta^3\text{-}C_3H_5)Cl\}_2]$ (3.0 mg, 8 μmol), the reaction mixture was stirred for 0.5 h at room temperature to give a yellow solution. 1,3-Diphenyl-1-acetoxy-2-propene (150 mg, 0.60 mmol) was added, and after 0.5 h *N,O*-bis(trime-

thylsilyl)acetamide (366 mg, 1.80 mmol), dimethyl malonate (238 mg, 1.80 mmol), and KOAc (3.0 mg, 0.03 mmol) were added successively. The reaction mixture was stirred for 14 h and was worked up in the usual manner to afford the desired product **11** as a colorless oil (174 mg, 90% yield) after purification by flash chromatography (pentane/ethyl acetate 6/1). The enantiomeric excess (73% *ee*) was determined by HPLC (Daicel Chiralcel OD column, 0.4 mL min^{-1}, heptane/2-propanol 99/1, UV detection at 254 nm).

Typical procedure for the enantioselective deprotonation: Preparation of **17a**: A Schlenk-flask was charged with a solution of **14** (236 mg, 0.47 mmol) in dry THF (10 mL) under argon. The solution was cooled to $-78\,^{\circ}$C and *n*BuLi (1.60 M in hexane, 0.58 mL, 0.94 mmol) was added dropwise. The reaction mixture was allowed to warm to $0\,^{\circ}$C over 15 min, and was stirred for another 15 min at this temperature. The reaction mixture was rapidly cooled to $-100\,^{\circ}$C and chlorotrimethylsilane (0.24 mL, 1.89 mmol) was added dropwise. After the reaction mixture had stirred for 2 min at this temperature a solution of 4-*tert*-butylcyclohexanone (58 mg, 0.38 mmol) in dry THF (0.8 mL) was added dropwise over 5 min. After 50 min triethylamine (2 mL) was added, followed by a saturated solution of $NaHCO_3$ (2.5 mL). The reaction mixture was warmed to room temperature, extracted with diethyl ether, and the organic phase washed with water (3×15 mL). The combined aqueous phase was extracted with diethyl ether (20 mL), and the organic phase was dried over Na_2SO_4. The crude reaction mixture obtained after evaporation of the solvents was subjected to Kugelrohr distillation ($150\,^{\circ}$C, 10^{-3} bar). This afforded the desired product **17a** (90 mg, 85%) in 87% *ee* (GC analysis: Chirasil-DEX CB (Chrompak), carrier gas H_2 (100 kPa), $80\,^{\circ}$C (1 min) $\rightarrow 120\,^{\circ}$C, *T* gradient: $2\,^{\circ}$C min^{-1}: t_R = 20.5 (*S*), 20.8 (*R*) min). Any urea **14** (205 mg, 87%) recovered by distillation was reused in further reactions.

Typical procedure for the enantioselective alkylation: Preparation of **20**: A Schlenk flask was charged with a solution of **14** (505 mg, 1.00 mmol) in dry THF (7 mL) under argon. The solution was cooled to $-78\,^{\circ}$C and *n*BuLi (1.50 M in hexane, 0.67 mL, 1.00 mmol) was added dropwise. The reaction mixture was allowed to warm to $0\,^{\circ}$C over 15 min, and was stirred for another 15 min at this temperature. The reaction mixture was allowed to cool to $-40\,^{\circ}$C, and a solution of α-tetralone (120 µL, 0.90 mmol) in dry THF (2 mL) was added dropwise over 2 min. The reaction mixture was warmed to room temperature over 20 min and stirred for another 30 min. The reaction mixture was then cooled to $-78\,^{\circ}$C, and a solution of benzyl bromide (1.20 mL, 10.1 mmol) in dry THF (2 mL) was added dropwise over 15 min. The reaction mixture was allowed to warm to $-20\,^{\circ}$C and stirred for 28 h at this temperature. The reaction mixture was quenched with aqueous hydrochloric acid (1 M, 5 mL), and after warming to room temperature the reaction mixture was extracted with diethyl ether (80 mL) and the organic phase was washed successively with water (2×10 mL) and brine (10 mL). The combined aqueous phase was extracted with diethyl ether (10 mL) and the organic phase was dried (Na_2SO_4). Purification by flash chromatography (pentane/diethyl ether 3.5/1) afforded the desired product **20** as a colorless crystalline solid (180 mg, 83%, m.p. $54\,^{\circ}$C). The enantiomeric excess was determined by HPLC as 81% *ee* (Daicel Chiralcel OD column, 0.6 mL min^{-1}, heptane/2-propanol 99.5/0.5, UV detection at 254 nm).

Received: May 26, 1998 [Z 11905 IE]
German version: *Angew. Chem.* **1998**, *110*, 3215 – 3218

Keywords: alkylations · asymmetric synthesis · chiral auxillaries · chirotopicity · deprotonation

[1] R. Noyori, *Asymmetric Catalysis in Organic Synthesis*, Wiley, New York, **1994**.
[2] a) B. D. Vineyard, W. S. Knowles, M. J. Sabacky, G. L. Bachman, D. J. Weinkauff, *J. Am. Chem. Soc.* **1977**, *99*, 5946; b) F. Robin, F. Mercier, L. Ricard, F. Mathey, M. Spagnol, *Chem. Eur. J.* **1997**, *3*, 1365.
[3] (a) B. M. Trost, *Pure Appl. Chem.* **1996**, *68*, 779; b) B. M. Trost, D. E. Patterson, *J. Org. Chem.* **1998**, *63*, 1339; c) B. M. Trost, T. L. Calkins, C. Oertelt, J. Zambrano, *Tetrahedron Lett.* **1998**, *39*, 1713.
[4] a) M. D. Fryzuk, B. Bosnich, *J. Am. Chem. Soc.* **1977**, *99*, 6262; b) P. A. MacNeil , N. K. Roberts, B. Bosnich, *J. Am. Chem. Soc.* **1981**, *103*, 2273; c) M. J. Burk, J. E. Feaster, W. A. Nugent, R. L. Harlow, *J. Am. Chem. Soc.* **1993**, *115*, 10125; d) M. J. Burk, Y. M. Wang, J. R. Lee, *J. Am. Chem. Soc.* **1996**, *118*, 5142.
[5] K. Mislow, J. Siegel, *J. Am. Chem. Soc.* **1984**, *106*, 3319.
[6] (*S*)-1-phenylethylbromide was prepared from (*R*)-1-phenylethanol (PPh_3, Br_2, CH_3CN, $-30\,^{\circ}$C $\rightarrow -10\,^{\circ}$C, 1 h, 95% yield, 88% *ee*). The enantiomeric excess was determined directly by GC on a chiral stationary phase. See K. S. Y. Lau, P. K. Wong, J. K. Stille, *J. Am. Chem. Soc.* **1976**, *98*, 5832.
[7] D. H. R. Barton, D. Crich, W. B. Motherwell, *Tetrahedron* **1985**, *41*, 3901.
[8] L. McKinstry, T. Livinghouse, *Tetrahedron* **1995**, *51*, 7655.
[9] a) B. M. Trost, D. L. Van Vranken, *Chem. Rev.* **1996**, *96*, 395; b) P. von Matt, A. Pfaltz, *Angew. Chem.* **1993**, *105*, 614; *Angew. Chem. Int. Ed. Engl.* **1993**, *32*, 566; c) Z. Chen, Q. Jiang, G. Zhu, D. Xiao, P. Cao, C. Guo, X. Zhang, *J. Org. Chem.* **1997**, *62*, 4521.
[10] DMF is the optimum solvent for performing this reaction in; lower enantioselectivities are obtained in other solvents: THF (25% *ee*), toluene (43% *ee*), and CH_2Cl_2 (56% *ee*).
[11] J. R. Pfister, W. E. Wymann, *Synthesis* **1983**, 38.
[12] a) For excellent reviews, see D. M. Hodgson, A. R. Gibbs, G. P. Lee, *Tetrahedron* **1996**, *52*, 14361; b) P. J. Cox, N. S. Simpkins, *Tetrahedron: Asymmetry* **1991**, *2*, 1; c) B. J. Bunn, N. S. Simpkins, Z. Spavold, M. J. Crimmin, *J. Chem. Soc. Perkin Trans. 1* **1993**, 3113; d) R. Shirai, D. Sato, K. Aoki, M. Tanaka, H. Kawasaki, K. Koga, *Tetrahedron* **1997**, *53*, 5963.
[13] E. J. Corey, A. W. Gross, *Tetrahedron Lett.* **1984**, *25*, 495.
[14] Interestingly, the corresponding chiral urea derived from (*S*)-1-phenylethylamine affords the corresponding silylenol ether with only 40% *ee* (34% yield), which shows the importance of the pseudo-C_2-symmetric backbone.
[15] (a) M. Murakata, M. Nakajima, K. Koga, *J. Chem. Soc. Chem. Commun.* **1990**, 1657; b) Y. Hasegawa, H. Kawasaki, K. Koga, *Tetrahedron Lett.* **1993**, *34*, 1963; c) M. Imai, A. Hagihara, H. Kawasaki, K. Mamabe, K. Koga, *J. Am. Chem. Soc.* **1994**, *116*, 8829.

A New Strategy for the Destabilization of Double-Stranded Nucleic Acids by Phenylalkylamine Derivatives**

Anmar Ali, Martin Gasiorek, and Hans-Jörg Schneider*

The unwinding of double-stranded (ds) nucleic acids is an important process for the biological functions of DNA and RNA. Until now, most of the organic ligands studied stabilize the double-stranded form of nucleic acids,[1] which is characterized by an increase in the thermal denaturation temperature T_m. Only with high concentrations of organic solvents, copper salts,[2] and with some steroidal amines[3] has a decrease in the melting point been reported; stronger destabilization effects are accompanied by DNA precipitation.[4] Kimura et al. found that zinc complexes could desta-

[*] Prof. Dr. H.-J. Schneider, Dr. A. Ali, Dipl.-Chem. M. Gasiorek
FR 11.2 Organische Chemie der Universität des Saarlandes
D-66041 Saarbrücken
Fax: (+49) 691-302-4105
E-mail: ch12hs@rz.uni-sb.de

[**] Supramolecular Chemistry, Part 80. This work was supported by the Deutsche Forschungsgemeinschaft, Bonn, and the Fonds der Chemischen Industrie, Frankfurt. Support from A. Hauch with several measurements and syntheses is also acknowledged. Part 79: H.-J. Schneider; F. Hacket; V. Rüdiger; H. Ikeda, *Chem. Rev.* **1998,** *98*, in print.

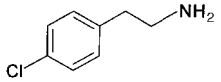
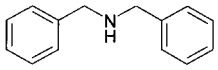
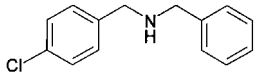
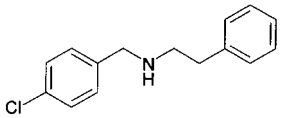
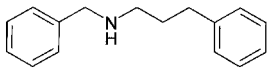
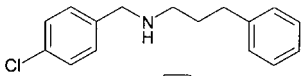
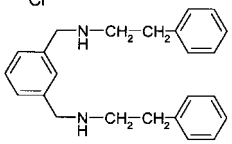
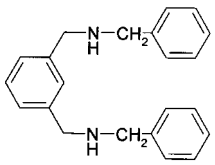
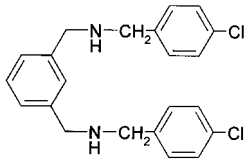
 © WILEY-VCH Verlag GmbH, D-69451 Weinheim, 1998 1433-7851/98/3721-3016 $ 17.50+.50/0

bilize ds poly(A:U), but could stabilize poly(dG:dC).[5] Less attention has been focused until now on the design of agents that can destabilize and unwind nucleic acid helices, although unpaired bases, particularly in RNA, are becoming an increasingly important target for new diagnostic and therapeutic strategies.[6] We describe here a new way to destabilize folded nucleic acid conformations by stabilizing unduplexed parts of the polymer, or single-stranded (ss) forms, which lead to destabilization effects of hitherto unknown magnitude with concentrations as low as 50 μM. The ligands chosen contain aromatic units that are not able to intercalate into ds nucleic acids, but are well suited for base stacking with ss nucleic acids. The new structural principles may interfere with replication and transcription and, therefore, may provide new lead compounds of medicinal interest.

Synthetic ligands that are designed to bind more strongly to ss than to ds nucleic acids should avoid large numbers of positive charges, as these bind and stabilize the duplex form. Moreover, they should contain aromatic units that can insert only between the flexible ss nucleic acid bases.[7] Since NMR spectroscopic measurements[8] have established that, in contrast to earlier assumptions,[9] the corresponding phenylalkylamines do not show the unwanted intercalation into ds forms, we have prepared ligands in which several phenyl rings are separated by spacers that allow bisintercalation-type binding into ss forms. Such compounds resemble building blocks of some proteins that bind to single-stranded nucleic acids.[10]

All compounds prepared with the strategy of having properly spaced phenyl rings and little positive charge indeed do cause destabilization of nucleic acid duplexes (Table 1), with a strong dependence on the spacers as well as on the substituents of the phenyl rings (Figure 1). The stacking interaction with a single phenyl ring is not sufficient to cause a significant reduction in the melting temperature, as seen with ligand **1**. The destabilization of the double strand becomes significant only if two phenyl rings are present, and only if

Table 1. Melting point changes ΔT_m [°C] of CT DNA complexed with various ligands.[a]

Compound		r[b] 0.26	0.52	0.78	1.3	2.6	3.9	6.5	13	26	39
1		–	–	–	–	–	–	–	+1	+1.3	+2
2		–	–	–	–	–	–	–	+1	+1	−0.3
3		–	–	–	–	–	–	–	−0.3	−0.3	−0.3
4		–	–	–	–	–	–	–	−0.4	−0.2	−21
5		–	–	–	–	–	–	–	−0.2	−0.8	−0.4
6		–	–	–	–	–	–	–	−0.5	−26	–[c]
7		–	–	–	+1	−17	−22	−28	−35		
8		–	–	–	–	–	–	−10	−17	−22	−24
9		+3	−18/+3	−28							

[a] Measurements with CT-DNA in MES buffer (MES = 2-(*N*-morpholino)ethanesulfonic acid) at pH 6.25; DNA base concentration 7.7×10^{-5} M. Absorption changes were followed at 260 nm as a function of temperature with a BioCary-1 spectrometer. The amines are fully protonated at the given pH. An average error of ΔT_m was determined as ±0.5 °C (duplicate runs). Values at other ligand concentrations could not be measured accurately as a result of the complex melting at too low a temperature or because of solubility problems. [b] Molar ratio of ligand to nucleic acid phosphate. [c] No deflection in the curve was detectable.

 © WILEY-VCH Verlag GmbH, D-69451 Weinheim, 1998 1433-7851/98/3721-3017 $ 17.50+.50/0

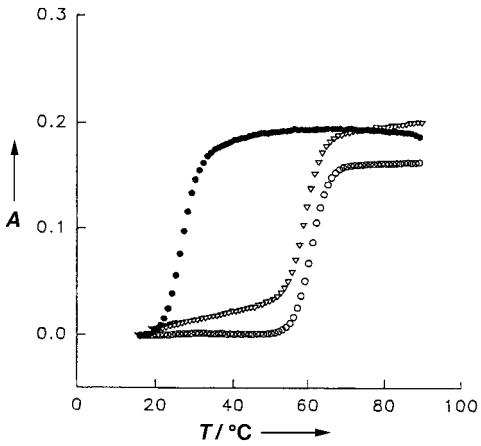


Figure 1. DNA melting curves of DNA alone (○), with **5** (▽), and with **6** (●); the molar ratio of ligand to nucleic acid phosphate is 1:26. The conditions are given in the footnote to Table 1.

they are arranged at a suitable distance by suitable spacers (Table 1). Higher ligand concentrations lead to complete denaturation of the nucleic acid duplex. The melting experiments suggest that the structure of the spacer between the phenyl rings must allow as far as possible strain-free insertion between neighboring nucleobases of single strands, or—in metastable, partially unfolded polymers—simultaneous insertion between two stacking base pairs. This will lead to substantial energies of complexation and, therefore, stabilization of unfolded nucleic acids. In line with this, short spacers as in structure **2** or **3** show less, or no melting point decrease. Remarkably, compound **4** with four atoms between the phenyl rings has a relatively large effect in contrast to the homologue **5** with a five atom spacer. However, introduction of chloro substituents has an even more dramatic influence on the destabilization of ds nucleic acids, as seen with ligand **6.** To enhance the affinity towards ss nucleic acids ligands **7** to **9** were designed with the help of computer-aided molecular modeling. These clamplike ligands provide a more convergent orientation of two phenyl rings toward a nucleobase of the single strand. Figure 2 demonstrates that compounds such as **9** indeed allow the stacking of a nucleobase without significant steric distortions. This ligand has by far a much stronger destabilizing effect than any other compound reported until now; a comparison of the results obtained with ligands **8** with **9** shows that this destabilization is clearly the result of the chlorine substituent.

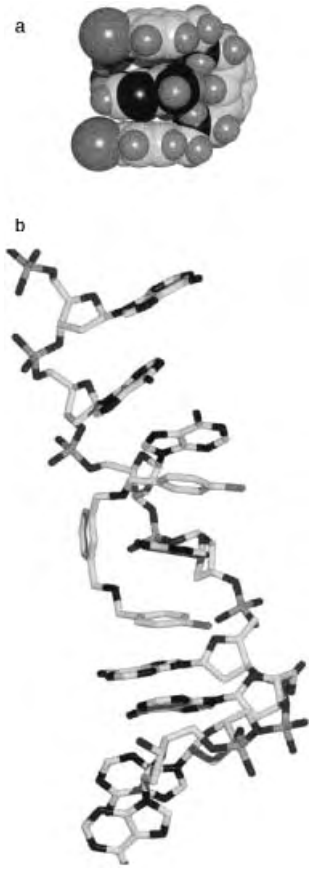


Figure 2. Computer-simulated (CHARMm energy minimization) stacked complex between ligand **9** and AMP (a) and of the intercalation of ligand **9** into a single-stranded poly(dA) strand (b).

Evidence for the mechanism of intercalation into single strands is provided not only by the dependence of T_m on the ligand structure. The NMR spectra of diphenylalkane compounds such as **6** with thermally denatured calf thymus DNA (CT-DNA) shows upfield shifts of the arene signals that are typical[8, 11] for exposure of the aryl protons to the anisotropy cone of the nucleobases (Figure 3). In contrast, the same

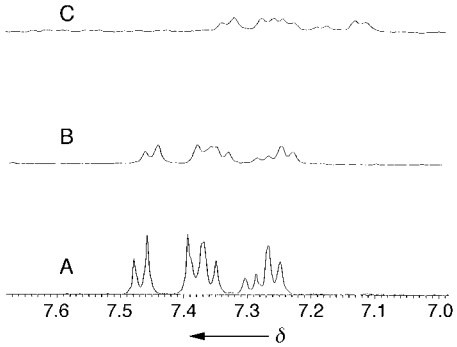


Figure 3. ^{1}H NMR spectra (400 MHz, 0.02 M sodium phosphate in D_2O, pD 7.4, sodium salt of trimethylsilylpropionic acid as an internal reference) of the aromatic region of ligand **6** (A), and its complexes with ds CT-DNA (B) and denatured CT-DNA (prepared by incubating CT-DNA at 80 °C for one hour followed by fast cooling) (C); the molar ratio of ligand to nucleic acid phosphate was 0.3:1.

derivative shows no appreciable shielding differences in a complex with ds DNA (Figure 3). This behavior differs considerably from the corresponding complexes with naphthylalkylamines, which are duplex intercalators and exhibit substantially larger line broadening.[9, 12] The shielding effects with ss DNA are, in comparison to those observed with duplexes, diminished by fast exchange of different protons. They are, however, noticeably larger for ligands that exhibit larger decreases in T_m, which again points to the insertion into single strands or unfolded parts of the nucleic acids as the driving force for the duplex destabilization.

Circular dichroism (CD) spectra of ds CT-DNA at 25 °C show a pronounced decrease in the intensity of the DNA band upon titration with compound **9** (Figure 4). Single stranded DNA is known to exhibit Cotton effects with ellipticities close to that of the duplex as a consequence of base stacking being preserved.[12] The observed decrease in the extinction coefficient $\Delta\varepsilon$ upon addition of the ligands indicates they bind to single strands with concommitant destruction of internucleobase stacking and loss of helicity. Similar observations were reported by Hélène et al for complexes of *p*-hydroxyphenylethylamine with ss DNA.[13] In accordance with their small effect on T_m ligands such as **3** have little influence on the CD spectra of ds DNA. However, a $\Delta\varepsilon$ reduction of approximately 50% is seen for **9** with both ds and ss DNA at concentrations of 5×10^{-5} M for the ligand and the DNA base pair. A corresponding affinity of $2 \times 10^4\,M^{-1}$ is in line also with the concentration of about 5×10^{-5} M of **9** that is needed to lower the melting point of ds DNA by approximately half of

 © WILEY-VCH Verlag GmbH, D-69451 Weinheim, 1998 1433-7851/98/3721-3018 $ 17.50+.50/0

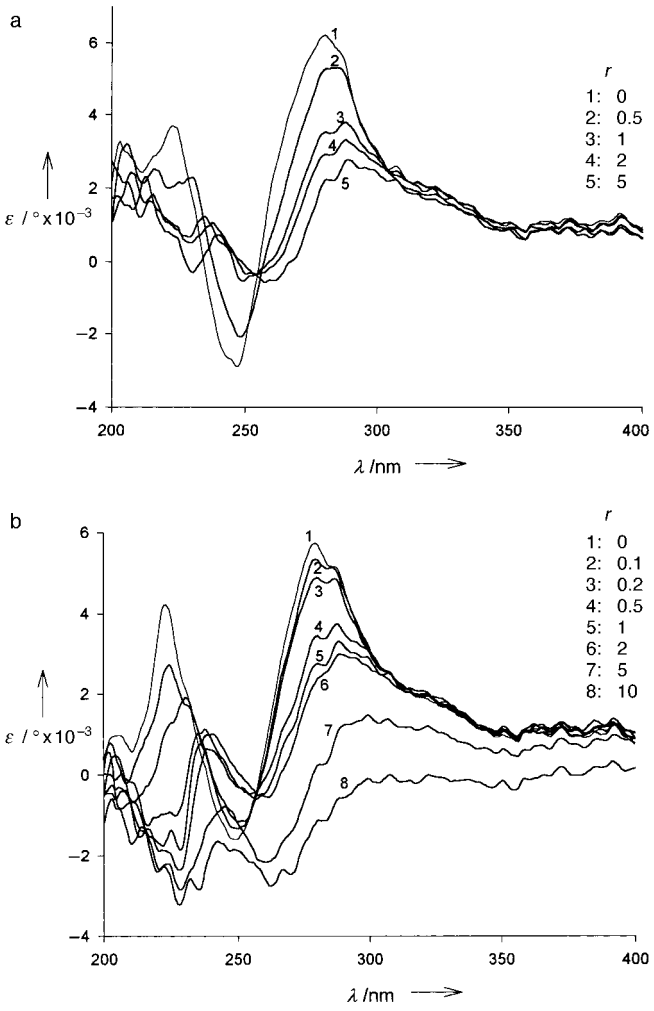


Figure 4. CD spectra of CT-DNA (see footnote to Table 1 for conditions); with ligand **9** at different ratios *r* to the nucleic acid phosphate (a) and thermaly denatured CT-DNA with ligand **9** at different ratios of ligand to nucleic acid phosphate (b). The CD spectra were obtained with a J-715 spectropolarimeter (JASCO) at 25 °C in cuvettes with a 1 cm path length. Curves presented are the average of three smothed scans. No Cotton effect was detected for the buffer.

the maximum value. An exact evaluation of the binding isotherms is difficult in view of the only approximately monophasic melting behavior and of solubility problems; with the latter also hampering NMR measurements.

The unpairing of double strands by base flipping is known to be involved in some protein–DNA interactions.[14] Only recently such a base flipping has also been achieved by a synthetic azoniacyclophane; on complexation with ds RNA the nucleobase becomes encapsulated in the cyclophane cavity.[15] In contrast to all these ligands the new phenylalkylamine derivatives are designed to interact preferentially with the ss form of nucleic acids and leave the duplex intact. The phenyl rings in the new ligands allow the introduction of a rich variety of substituents, which have a distinct influence on the observed duplex destabilization. Little is known about the dependence of the affinity towards single-stranded nucleic acids on the structure of the intercalating ligand. Studies with DNA duplexes do show appreciable variations in affinity upon substitution of the intercalating unit.[16, 17]

Agents that can unwind duplexes and bind selectively to unfolded nucleic acids can be the basis of potential antiviral and anticancer drugs. These compounds could disrupt RNA secondary structures such as hairpin stem–loop conformations, which are important recognition sites for gene regulatory proteins that control viral replication. Moreover, these compounds might be valuable in molecular biology methods such as sequencing or PCR (polymerase chain reaction), in which dissociation of folded nucleic acid parts is a necessary step.[18]

Received: May 25, 1998 [Z11897IE]
German version: *Angew. Chem.* **1998**, *110*, 3183–3186

Keywords: amines · intercalation · nucleic acids · stacking interactions · supramolecular chemistry

[1] a) W. D. Wilson in *Nucleic Acids in Chemistry and Biology* (Eds.: M. Blackburn, M. Gait), IRL, Oxford, chap. 8, **1989**; b) J. W. Lown, *Anti-Cancer Drug Des.* **1988,** *3*, 25; c) P. D. Dervan, *Science* **1986,** *232*, 464; d) S. Neidle, Z. Abraham, *CRC Crit. Rev. Biochem.* **1984**, *17*, 73; e) S. Neidle, T. Jenkins, *Mol. Des. Model. Part B* **1991**, *203*, 433; f) for interactions of RNA with small ligands, see "Design and Analysis of Molecular Motifs for Specific Recognition of RNA": K. Li, M. Fernandez-Saiz, C. T. Rigl, A. Kumar, K. G. Ragunathan, A. W. McConnaughie, D. W. Boykin, H.-J. Schneider, W. D. Wilson in *Bioorg. Med. Chem.* **1997**, Symposium Issue: *Strategies for RNA Recognition*, 1157.

[2] G. L. Eichhorn, *Nature* **1962**, *194*, 474.

[3] a) H.-P.Hsieh, J. G. Muller, C. J. Burrows, *J. Am. Chem. Soc.* **1994**, *116*, 1207; b) H. R. Mahler, R. Goutarel, Q. Khuong-Huu, *Biochemistry* **1968**, *7*, 1568.

[4] Double-strand destabilizations have also been reported with some intercalating reagents such as acridine orange, but with subsequent precipitations: J. Kapuscinsky, Z. Darzynkiewicz, *Nucleic Acids Res.* **1983**, *11*, 7555.

[5] E. Kimura, T. Ikeda, M. Shionoya, *Pure Appl. Chem.* **1997**, *69*, 2187.

[6] D. W. Wilson, L. Ratmeyer, M. T. Cegla, J. Spychala, D. Boykin, M. Demeunynck, J. Homme, G. Krishnan, D. Kennedy, R. Vinayak, G. Zon, *New J. Chem.* **1994**, *18*, 419.

[7] J.-L. Dimicoli, C. Hélène, *Biochemistry* **1974**, *13*, 724.

[8] J. Sartorius, H.-J. Schneider, *FEBS Lett.* **1995**, *374*, 387; H.-J. Schneider, J. Sartorius *in Physical Supramolecular Chemistry (NATO ASI Ser. Ser. C* **1996**, *485*), p. 11.

[9] L. Kapciak, E. J. Gabbay, *J. Am. Chem. Soc.* **1975**, *97*, 403; E. J. Gabbay, C. S. Baxter, *J. Am. Chem. Soc.* **1973**, *95*, 7850.

[10] D. L. Ollis, S. W. White, *Chem. Rev.* **1987**, *87*, 981.

[11] S. Chandrasekaran, S. Kusuma, D. W. Boykin, W. D. Wilson, *Magn. Res. Chem.* **1986**, *24*, 630; for similar shifts in self-associating nucleoside derivatives, see K. H. Scheller, H. Sigel, *J. Am. Chem. Soc.* **1983**, *105*, 5891; O. Yamauchi, A. Odani, H. Masuda, H. Sigel, *Met. Ions Biol. Syst.* **1996**, *32*, 207, and references therein.

[12] W. Curtis Johnson, Jr., *Circular Dichroism and the conformational analysis of biomolecules*, Plenum, New York, **1996**, pp. 433–468

[13] C. Hélène, T. Montenay-Garestier, J. L. Dimicoli, *Biochim. Biophys. Acta* **1971**, *254*, 349.

[14] R. J. Roberts, *Cell* **1995**, *82*, 9, and references therein.

[15] M. Fernandez-Saiz, H.-J. Schneider, J. Sartorius, W. D. Wilson, *J. Am. Chem. Soc.*, **1996**, *18*, 4739.

[16] L. Strekowski, J. L. Mokrosz, W. D. Wilson, M. J. Mokroz, A. Strekowski, *Biochemistry* **1992**, *31*, 10802; D. W. Wilson, L. Ratmeyer, M. T. Cegla, J. Spychala, D. Boykin, M. Demeunynck, J. Homme, G. Krishnan, D. Kennedy, R. Vinayak, G. Zon, *New J. Chem.* **1994**, *18*, 419.

[17] a) A. Korolkovas in *Essentials of Medicinal Chemistry*, Wiley, New York, **1988**; b) P. V. Scaria, J. C. Craig, R. H. Shafer, *Biopolymers* **1993**, *33*, 887; c) J. Sartorius , H.-J. Schneider, *J. Chem. Soc. Perkin Trans. 2* **1997**, 2319, and references therein.

[18] The synthesis of the new ligands will be reported elsewhere. All new compounds showed satisfactory analytical data.

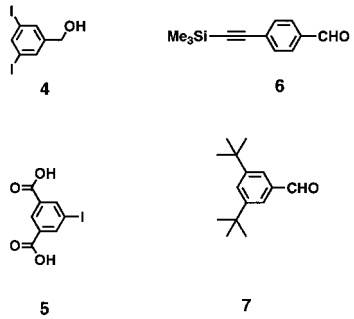
 © WILEY-VCH Verlag GmbH, D-69451 Weinheim, 1998 1433-7851/98/3721-3019 $ 17.50+.50/0

Metalloporphyrin Dendrimers with Folding Arms**

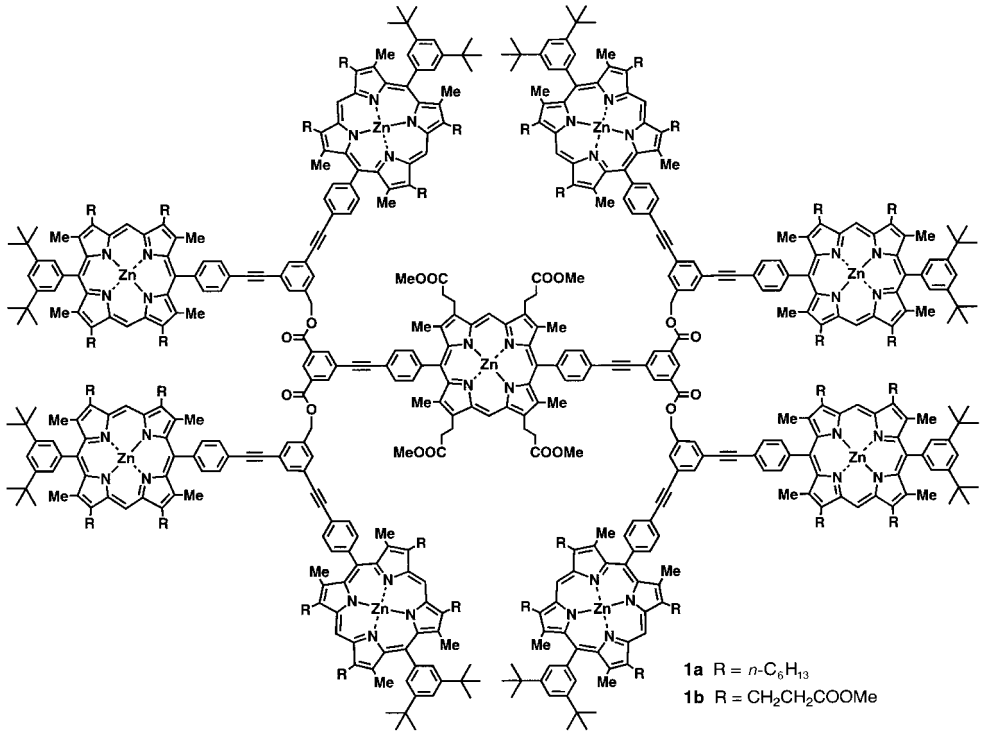
Chi Ching Mak, Nick Bampos, and Jeremy K. M. Sanders*

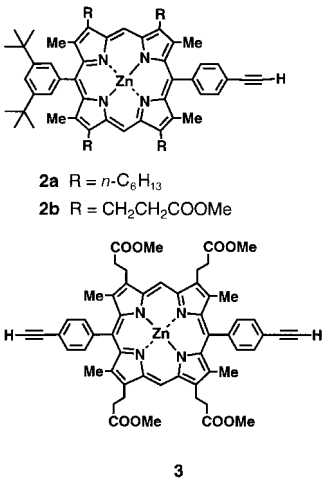
In memory of Ralph Raphael

We report here a new dendrimer system, **1**, possessing unusual features: It contains metalloporphyrins as the main building block both for the central core and the periphery,[1–3] and it has been constructed with a combination of rigid and flexible linkers in such a way that its four "arms" can fold in a cooperative and predetermined manner in response to the bifunctional ligand 1,4-diazabicyclo[2.2.2]octane (DABCO).



As high solubility of the dendrimer in a variety of solvents is essential for synthesis, characterization, and spectroscopic analysis, the main porphyrin building block is the unsymmetrical porphyrin **2** carrying two *tert*-butyl groups and either *n*-hexyl (**2a**) or methoxycarbonylethyl groups (**2b**) in the β positions; **2a** and **2b** were prepared on a gram scale by mixed condensation[7] of aldehydes **6**[8] and **7**[9] with dipyrromethane **8a** or **8b**[10] followed by metalation, desilylation, and separation from symmetrical analogues.[11] The yields given below, and the spectroscopic data in the Experimental Section, are generally for the **a** series; they are similar for the **b** series except where noted. The central porphyrin unit **3** was prepared as described previously.[8]





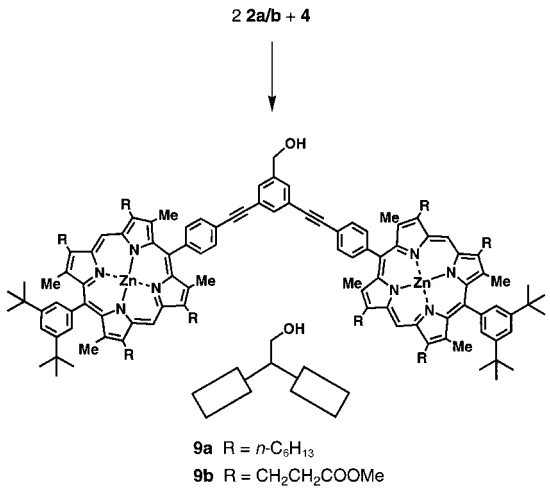
The efficient strategy applied for the synthesis of **1** has the potential to be generalized, for example, to light-harvesting model photosynthetic systems: It employs readily available unsymmetrical and symmetrical porphyrins **2** and **3** as the chromophore building blocks, and 3,5-diiodobenzyl alcohol (**4**) and 5-iodoisophthalic acid (**5**) as the branching units. The Pd-mediated[4] and Mitsunobu[5] coupling reactions avoid any activation or deprotection steps.[6]

The dendrimer was assembled as shown in Schemes 1 and 2 by Pd-mediated and Mitsunobu coupling reactions under mild and neutral to basic conditions in order to avoid acidic or forcing conditions that might cause demetalation and transmetalation, respectively. The rigid dendritic wedge **9a** was prepared in 90% yield, as shown in Scheme 1, under conditions which generate the Pd^0 reagent in situ and avoid the use of any copper cocatalysts that might lead to oxidative

[*] Prof. J. K. M. Sanders, Dr C. C. Mak, Dr. N. Bampos
Cambridge Centre for Molecular Recognition
University Chemical Laboratory
Lensfield Road, Cambridge, CB21EW (UK)
Fax: (+44) 1223-336-017
E-mail: jkms@cam.ac.uk

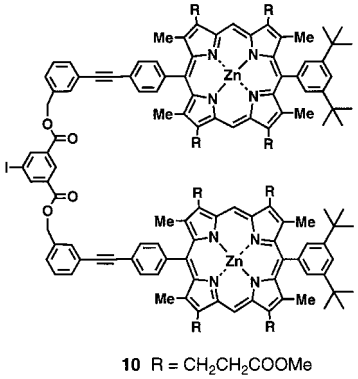
[**] We thank the Croucher Foundation and EPSRC for financial support, the EPSRC Mass Spectrometry Centre for FAB and electrospray mass spectra, and Tony Jackson (ICI) for MALDI-TOF mass spectra.

 © WILEY-VCH Verlag GmbH, D-69451 Weinheim, 1998 1433-7851/98/3721-3020 $ 17.50+.50/0

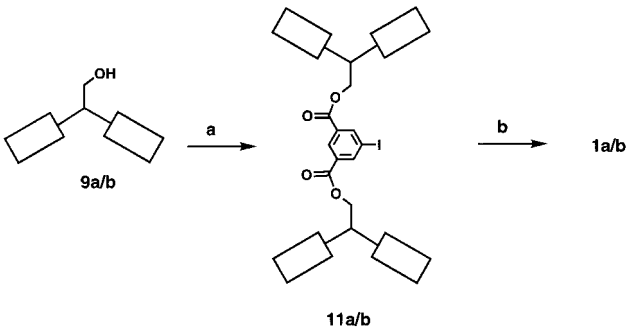


Scheme 1. Synthesis of rigid dendritic wedge **9**: cat. $[Pd_2(dba)_3]$, Ph_3As, Et_3N/CH_2Cl_2, room temperature (RT), 90% (for **9a**). dba = dibenzylideneacetone.

dimerization of the alkyne components.[4] As expected, the UV/Vis spectrum of **9a** was almost identical to that of **2a** as there can be little interaction between the porphyrins, but the fast atom bombardment (FAB) mass spectrum confirmed the successful formation of **9a** ($m/z = 2213$ $[M+H]^+$). For comparison of binding properties, the flexible dimer **10** was also prepared.



Mitsunobu condensation of **9a** with **5** afforded the four-porphyrin wedge **11a** in 85% yield (Scheme 2); its key structural features were confirmed by ^1H NMR spectroscopy and MALDI-TOF mass spectrometry (MALDI = matrix-assisted laser desorption ionization, TOF = time of flight).



Scheme 2. Synthesis of dendritic wedge **11** and dendrimer **1**: a) **5** (0.5 equiv), Ph_3P, DIAD, THF, RT, 85% (for **11a**); b) **3** (0.5 equiv), cat. $[Pd_2(dba)_3]$, Ph_3As, Et_3N/THF, RT, 60% (for **1a**). DIAD = diisopropyl azodicarboxylate.

Finally the nine-porphyrin dendrimer **1a** was prepared by Pd^0-catalyzed coupling of two molecules of **11a** with the central porphyrin core **3** (Scheme 2); the 60% yield of isolated product corresponds to about 78% per coupling step. It is important to note that the all-ester dendrimer **1b** was impossible to separate chromatographically from wedge **11b** and from the intermediate containing one four-porphyrin wedge coupled to **3**. Use of two different peripheral substitution patterns for the successive porphyrin layers in **1a** has no bearing on binding properties, but helps spectroscopic characterization and microanalytical differentiation, and gives great control over chromatographic mobility: Since the ester porphyrins are more polar, **1a** is distinctively more polar than **11a**, which facilitates the separation. Dendrimer **1a** is too large for successful FAB mass spectrometry, but its electrospray mass spectrum displayed weak peaks at $m/z =$ 2523, 2018, and 1685, consistent with multiply charged species $[M+4H]^{4+}$, $[M+5H]^{5+}$, and $[M+6H]^{6+}$, respectively. The MALDI-TOF mass spectrum showed a maximum at $m/z =$ 10087, consistent with the expected structure; the average molecular weight calculated for **1a** ($C_{660}H_{804}N_{36}O_{16}Zn_9$) is 10085.

A key feature of the design of **1** (and its component wedge **11**) is that each of the "arms" of the rigid porphyrin dimer is independent, but can be brought together with the other by cooperative binding of the two ends of DABCO as illustrated in Figure 1. Both ^1H NMR and UV/Vis spectra confirm that this occurs as expected: A DABCO molecule tightly bound to two Zn–porphyrin units gives a characteristic ^1H NMR signal at $\delta = -5$, while monomers or dimers that are incapable of intramolecular binding do not.[3b, 12] As expected, when 0.5 equivalents of DABCO per porphyrin unit are added, **10**, **11**, and **1a** give a sharp signal at $\delta = -5$, while the rigid **9** does not. On addition of excess DABCO the ligand resonance at $\delta = -5$ broadens and then disappears through exchange.[3b, 12]

At the porphyrin concentrations used for UV/Vis titrations (10^{-7} M), binding of DABCO to monomers (or to **9**) results in a shift of the Soret absorption from 412 to 426 nm. This is typical of a 1:1 porphyrin–DABCO complex;[12] analysis of the titration curves gives a binding constant (binding to monomer) of about $10^5\,M^{-1}$. By contrast, binding of DABCO to **10**, **11**, or **1a** leads through an isosbestic point to a Soret maximum at 420 nm (Figure 2); this blue shift of 6 nm is characteristic of a 2:1 porphyrin–DABCO complex[12] and is due to exciton coupling between the parallel porphyrin units.[13] It is difficult to extract precise binding constants from such complex systems: Each arm in **11** and **1a** will bind two DABCO molecules, and each DABCO molecule will have a first and second binding interaction. However, the fact that an exciton-coupled spectrum is obtained with a porphyrin concentration of 10^{-7} M implies that the second binding constant for the first DABCO molecule is at least $10^7\,M^{-1}$. Binding of the first DABCO molecule preorganizes the second binding site and leads to an exciton-coupled spectrum for that second site (as implied in Figure 1b).

The second DABCO molecule is likely to be bound even more strongly: The exciton-coupled spectrum persists even in the presence of 21000-fold excess DABCO for **11** and **1a**, and a fully sharp band at 426 nm is not achieved until almost

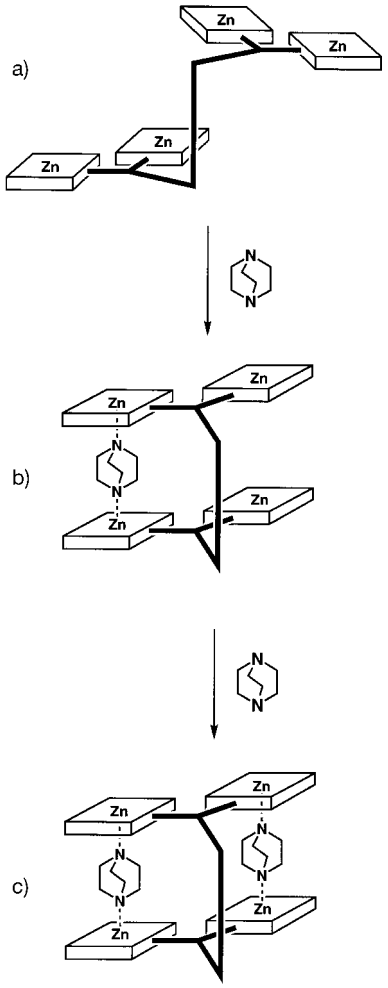


Figure 1. Cartoon representation of the DABCO-induced folding of **11** and **1**.

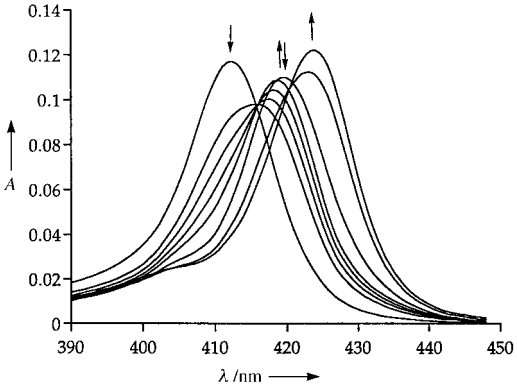


Figure 2. UV/Vis titration of **11a** with DABCO. Number of equivalents added per tetramer: 0, 0.6, 1.2, 3, 12, 7700, 250000, 900000.

10^6-fold excess is added. By contrast, **10** begins to lose exciton coupling after addition of only 7000-fold excess DABCO. The core porphyrin of **1a** is unable to bind DABCO in this 2:1 cooperative fashion, but (in the absence of a vast excess of DABCO) its single aborption around 426 nm is not readily detected in the presence of eight absorptions with $\lambda_{max} =$ 420 nm.

The convergent approach described here, which makes use of alternating coupling reactions,[6] gives easy access to dendrimers in general. Since any electron acceptor, electron donor, or metalloporphyrin could be chosen as the core for the present system, the electrochemical and photophysical properties of the resulting dendrimer can be fine-tuned. Finally, the conformational sensitivity of **1** to ligands may have profound effects on its viscosity, photophysics, and other properties; these are currently under investigation.

Experimental Section

9a: A solution of **2a** (250 mg, 0.24 mmol), **4** (40 mg, 0.11 mmol), $[Pd_2(dba)_3]$ (22 mg, 0.022 mmol), and $AsPh_3$ (40 mg, 0.13 mmol) in CH_2Cl_2/Et_3N (1/1, 10 mL) in a Schlenk tube was degassed twice (freeze-pump-thaw). The mixture was stirred at room temperature under argon for 15 h. After removal of the solvent, the reaction mixture was subjected to chromatography (silica, hexane/chloroform/ethyl acetate 10/1/1) to give **9a** (220 mg, 90%) as a purple solid. ^{1}H NMR (250 MHz, $CDCl_3$): $\delta = 0.93$ (t, $J = 7$ Hz, 12H), 0.94 (t, $J = 7$ Hz, 12H), 1.20–1.60 (m, 70H), 1.78 (quint, $J = 7$ Hz, 16H), 2.22 (quint, $J = 7$ Hz, 16H), 2.46 (s, 12H), 2.58 (s, 12H), 3.90–4.10 (m, 16H), 4.64 (s, 2H), 7.62–7.65 (m, 2H), 7.83 (t, $J = 2$ Hz, 2H), 7.95 (d, $J = 2$ Hz, 4H), 8.00 (d, $J = 8$ Hz, 4H), 8.17 (d, $J = 8$ Hz, 4H), 10.22 (s, 4H); ^{13}C NMR (62.9 MHz, $CDCl_3$): $\delta = 149.7$ (s), 148.0 (s), 147.4 (s), 146.5 (s), 146.4 (s), 144.6 (s), 143.7 (s), 143.4 (s), 142.5 (s), 140.7 (s), 138.6 (s), 137.7 (s), 133.8 (d), 133.6 (d), 130.8 (d), 129.5 (d), 128.0 (d), 123.8 (s), 122.7 (s), 121.0 (d), 120.9 (s), 118.2 (s), 97.7 (d), 90.6 (s), 89.2 (s), 63.5 (t), 35.2 (t), 33.4 (t), 32.0 (t), 31.7 (q), 30.1 (t), 29.7 (t), 26.9 (s), 22.8 (t), 15.7 (q), 14.9 (q), 14.2 (q); UV/Vis (CH_2Cl_2): λ_{max} (lgε) = 412 (5.71), 538 (4.37), 574 (4.04); elemental analysis calcd for $C_{147}H_{188}N_8OZn_2$: C 79.75, H 8.60, N 5.06; found: C 79.67, H 8.59, N 4.74.

11a: A solution of DIAD (42 mg, 0.21 mmol) in THF (2 mL) was added to a solution of **9a** (190 mg, 0.086 mmol), **5** (12 mg, 0.041 mmol), and PPh_3 (55 mg, 0.21 mmol) in THF (5 mL) at room temperature. After stirring of the mixture at room temperature for 4 h, solvent was removed and the residue was subjected to chromatography (silica, hexane/chloroform/ethyl acetate 20/1/1 →10/1/1) to give **11a** (163 mg, 85%) as a purple solid. ^{1}H NMR (250 MHz, $CDCl_3$): $\delta = 0.95$ (t, $J = 7$ Hz, 24H), 0.96 (t, $J = 7$ Hz, 24H), 1.25–1.70 (m, 136H), 1.78 (quint, $J = 7$ Hz, 32H), 2.10–2.35 (m, 32H), 2.51 (s, 24H), 2.52 (s, 24H), 3.84 (t, $J = 7$ Hz, 16H), 4.01 (t, $J = 7$ Hz, 16H), 5.61 (s, 4H), 7.89 (t, $J = 2$ Hz, 4H), 7.94 (d, $J = 2$ Hz, 4H), 8.03 (d, $J = 2$ Hz, 8H), 8.05–8.20 (m, 18H), 8.80 (d, $J = 1$ Hz, 2H), 8.98 (t, $J = 1$ Hz, 1H), 10.10 (s, 8H); ^{13}C NMR (62.9 MHz, $CDCl_3$): $\delta = 164.3$ (s), 149.7 (s), 148.0 (s), 147.3 (s), 146.5 (s), 146.2 (s), 144.6 (s), 143.5 (s), 143.4 (s), 143.0 (d), 142.5 (s), 138.6 (s), 137.5 (s), 136.4 (s), 134.9 (d), 133.5 (d), 132.2 (s), 131.7 (d), 130.8 (d), 130.6 (d), 128.0 (d), 124.6 (s), 122.5 (s), 121.0 (d), 120.9 (s), 118.0 (s), 97.6 (d), 91.3 (s), 89.0 (s), 66.8 (t), 35.2 (t), 33.3 (t), 32.0 (t), 31.7 (q), 30.0 (t), 29.7 (t), 26.8 (s), 26.6 (s), 22.8 (t), 15.6 (q), 14.9 (q), 14.2 (q); UV/Vis (CH_2Cl_2): λ_{max} (lgε) = 412 (6.29), 538 (4.96), 574 (4.57); MALDI-TOF-MS: m/z: 4684.4 $[M+H]^+$ (calcd 4684.6); elemental analysis calcd for $C_{302}H_{377}IN_{16}O_4Zn_4$: C 77.44, H 8.11, N 4.79; found: C 77.27, H 8.22, N 4.71.

1a: Following the same procedure as for **9a**, except with THF/Et_3N (1/1) as solvent mixture, **1a** was obtained from **3** and **11a** in 60% yield as a purple solid. ^{1}H NMR (250 MHz, $CDCl_3$): $\delta = 0.90$ (t, $J = 7$ Hz, 48H), 0.91 (t, $J = 7$ Hz, 48H), 1.25–1.85 (m, 336H), 2.00–2.30 (m, 64H), 2.35–2.60 (m, 108H), 2.77 (t, $J = 7$ Hz, 8H), 3.37 (s, 12H), 3.60–4.04 (m, 72H), 5.75 (s, 8H), 7.86 (t, $J = 2$ Hz, 8H), 7.95–8.20 (m, 68H), 8.85 (d, $J = 2$ Hz, 4H), 9.11 (d, $J = 2$ Hz, 2H), 9.56 (s, 2H), 10.00 (s, 16H); ^{13}C NMR (100.6 MHz, $CDCl_3$): $\delta = 173.2$ (s), 165.2 (s), 149.8 (s), 148.0 (s), 147.4 (s), 147.2 (s), 146.4 (s), 146.2 (s), 145.7 (s), 144.7 (s), 144.4 (s), 143.5 (s), 143.4 (s), 142.5 (s), 141.5 (s), 138.7 (s), 138.6 (s), 137.5 (s), 137.3 (d), 136.7 (s), 135.0 (d), 133.6 (d), 131.5 (d), 131.3 (s), 131.2 (d), 130.9 (d), 128.0 (d), 124.9 (s), 124.7 (s), 122.6 (s), 121.0 (d), 120.9 (s), 118.7 (s), 117.9 (s), 97.5 (d), 97.2 (d), 92.2 (s), 91.3 (s), 89.1 (s), 88.5 (s), 66.8 (t), 51.4 (q), 36.7 (t), 35.2 (t), 33.3 (t), 32.0 (t), 31.7 (q), 30.0 (t), 29.8 (t), 26.8 (s), 26.6 (s), 22.8 (t), 15.6 (q), 15.0 (q), 14.2 (q); UV/Vis (CH_2Cl_2): λ_{max} (lgε) = 412 (6.52), 540 (5.25), 574 (4.95); elemental analysis calcd for $C_{660}H_{804}N_{36}O_{16}Zn_9$: C 78.60, H 8.03, N 5.00; found: C 78.47, H 8.07, N 4.74.

Received: April 27, 1998 [Z 11781 IE]
German version: *Angew. Chem.* **1998**, *110*, 3169–3172

 © WILEY-VCH Verlag GmbH, D-69451 Weinheim, 1998 1433-7851/98/3721-3022 $ 17.50+.50/0

Keywords: cooperative effects · coordination modes · dendrimers · porphyrinoids

[1] For dendrimers with a single porphyrin core, see a) R.-H. Jin, T. Aida, S. Inoue, *J. Chem. Soc. Chem. Commun.* **1993**, 1260 – 1262; b) Y. Tomoyoce, D. Jiang, R. Jin, T. Aida, T. Yamashita, K. Horie, E. Yashima, Y. Okamoto, *Macromolecules* **1996**, *29*, 5236 – 5238; c) D.-L. Jiang, T. Aida, *Chem. Commun.* **1996**, 1523 – 1524; d) P. Bhyrappa, J. K. Young, J. S. Moore, K. S. Suslick, *J. Am. Chem. Soc.* **1996**, *118*, 5708 – 5711; e) P. J. Dandliker, F. Diederich, A. Zingg, J.-P. Gisselbrecht, M. Gross, A. Louati, E. Sanford, *Helv. Chim. Acta* **1997**, *80*, 1773 – 1801; f) J. P. Collman, L. Fu, A. Zingg, F. Diederich, *Chem. Commun.* **1997**, 193 – 194; g) K. W. Pollak, E. M. Sanford, J. M. J. Fréchet, *J. Mater. Chem.* **1998**, *8*, 519 – 527.

[2] For dendrimers with core and peripheral porphyrins, see a) D. L. Officer, A. K. Burrell, D. C. W. Reid, *Chem. Commun.* **1996**, 1657 – 1658; b) W. T. S. Huck, A. Rohrer, A. T. Anilkumar, R. H. Fokkens, N. M. M. Nibbering, F. C. J. M. van Veggel, D. N. Reinhoudt, *New J. Chem.* **1998**, *22*, 165 – 168.

[3] For related linear and star-shaped porphyrin oligomers, see a) T. Nagata, A. Osuka, K. Maruyama, *J. Am. Chem. Soc.* **1990**, *112*, 3054 – 3059; b) H. L. Anderson, *Inorg. Chem.* **1994**, *33*, 972 – 981; c) V. S.-Y. Lin, S. G. DiMagno, M. J. Therien, *Science* **1994**, *264*, 1105 – 1111; d) S. Anderson, H. L. Anderson, J. K. M. Sanders, *J. Chem. Soc. Perkin Trans. 1* **1995**, 2247 – 2254; e) O. Wennerström, H. Ericsson, I. Raston, S. Svensson, W. Pimlott, *Tetrahedron Lett.* **1989**, *30*, 1129 – 1132; f) R. W. Wagner, T. E. Johnson, J. S. Lindsey, *J. Am. Chem Soc.* **1996**, *118*, 11166 – 11180; g) P. N. Taylor, J. Huuskonen, G. Rumbles, R. T. Aplin, E. Williams, H. L. Anderson, *Chem. Commun.* **1998**, 909 – 910.

[4] R. W. Wagner, T. E. Johnson, F. Li, J. S. Lindsey, *J. Org. Chem.* **1995**, *60*, 5266 – 5273.

[5] a) O. Mitsunobu, *Synthesis* **1981**, 1 – 28; b) D. L. Hughes, *Org. React.* **1992**, *42*, 335 – 356.

[6] F. Zeng, S. C. Zimmerman, *J. Am. Chem. Soc.* **1996**, *118*, 5326 – 5327.

[7] a) A. Vidal-Ferran, N. Bampos, J. K. M. Sanders, *Inorg. Chem.* **1997**, *36*, 6117 – 6126; b) Z. Clyde-Watson, A. Vidal-Ferran, L. J. Twyman, C. J. Walter, D. W. J. McCallien, S. Fanni, N. Bampos, R. S. Wylie, J. K. M. Sanders, *New J. Chem.* **1998**, 493 – 502.

[8] N. Bampos, M. R. Prinsep, H. He, A. Vidal-Ferran, A. Bashall, M. McPartlin, H. Powell, J. K. M. Sanders, *J. Chem. Soc. Perkin Trans. 2* **1998**, 715 – 723.

[9] M. S. Newman, L. F. Lee, *J. Org. Chem.* **1972**, *26*, 4468 – 4469.

[10] The hexyl-substituted dipyrromethane **8a** and several porphyrins derived from it were first prepared in our laboratory by Dr. L. J. Twyman.

[11] Crystallographic data (excluding structure factors) for the structure (**2b**) reported in this paper have been deposited with the Cambridge Crystallographic Data Center as supplementary publication no. CCDC-101442. Copies of the data can be obtained free of charge on application to CCDC, 12 Union Road, Cambridge CB21EZ, UK (fax: (+44) 1223-336-033; e-mail: deposit@ccdc.cam.ac.uk).

[12] C. A. Hunter, M. N. Meah, J. K. M. Sanders, *J. Am. Chem. Soc.* **1990**, *112*, 5773 – 5780.

[13] C. A. Hunter, J. K. M. Sanders, A. J. Stone, *Chem. Phys.* **1989**, *133*, 395 – 404.

Windmill-Like Porphyrin Arrays as Potent Light-Harvesting Antenna Complexes**

Aiko Nakano, Atsuhiro Osuka,* Iwao Yamazaki, Tomoko Yamazaki, and Yoshinobu Nishimura

Photosynthetic organisms use light-harvesting complexes to capture weak sunlight. Upon photoexcitation, energy migration occurs between these pigments until a reaction center is encountered, where charge separation occurs. The energy migration is rapid and can involve hundreds of pigments.[1] A number of synthetic models have been developed in order to understand light-harvesting phenomena at the molecular level.[2] Ordered supramolecular arrays of porphyrins are also of interest for the design of molecular electronic devices.[3, 4] Here we report a novel one-pot synthesis of orthogonally arranged windmill-like porphyrin arrays involving a *meso*–*meso*-linked diporphyrin unit as an energy sink. This is an extension of our recent synthesis of *meso*–*meso*-linked porphyrin oligomers from a Zn^{II} 5,15-diarylporphyrin and Ag^{I} ions in $CHCl_3$.[5]

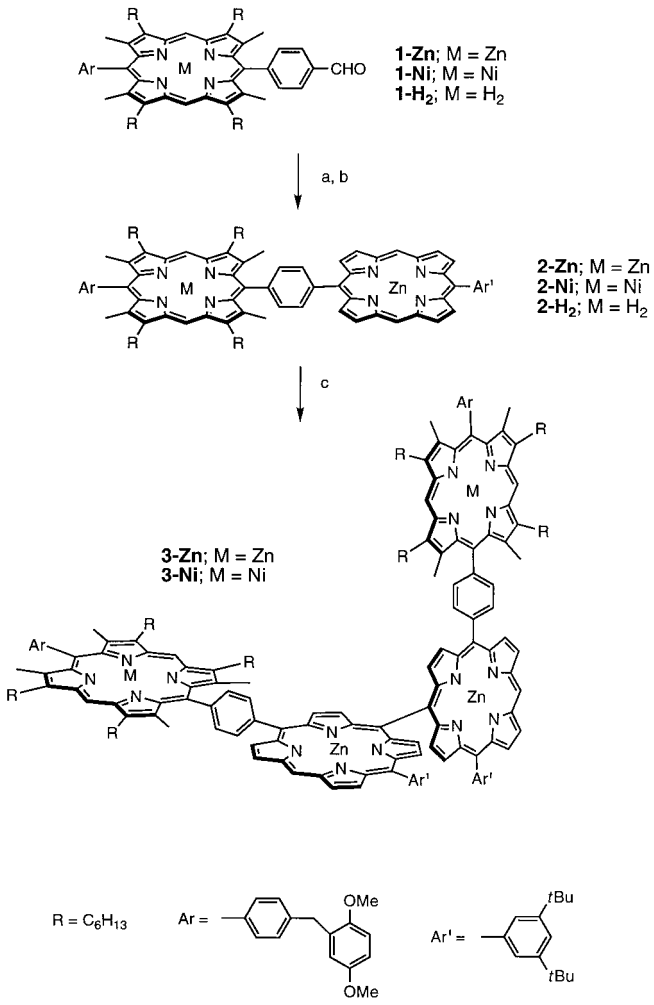
The synthetic route to porphyrin tetramers **3-Zn** and **3-Ni** is outlined in Scheme 1. Condensation of formyl-substituted **1-Zn** and 3,5-di-*tert*-butylbenzaldehyde with 2,2′-dipyrrylmethane under Lindsey conditions[4] afforded hybrid diporphyrin **2-Zn** in 31 % yield. Treatment of **2-Zn** with one equivalent of $AgPF_6$ at room temperature in $CHCl_3$ for 10 h followed by preparative size-exclusion chromatography (SEC) gave porphyrin tetramer **3-Zn** in 5 % yield (40 % of **2-Zn** was recovered). The fast atom bombardment (FAB) mass spectrum of **3-Zn** contains a parent ion peak at $m/z = 3254$ (calcd for $C_{206}H_{230}N_{16}O_4Zn_4$: $m/z = 3255$), and the ^{1}H NMR spectrum (500 MHz) showed signals for three *meso* protons at $\delta = 10.58$ (β-unsubstituted Zn^{II} porphyrin), 10.28, and 10.11 (Zn^{II} octaalkylporphyrin) as well as for eight β protons of the β-unsubstituted Zn^{II} porphyrin at $\delta = 9.78$, 9.69, 9.61, 9.28, 9.26, 8.86, 8.48, and 8.31 characteristic of the *meso*–*meso*-linked diporphyrins.[5]

The UV/Vis spectrum of **3-Zn** shows a broad Soret band at 413.5 nm with a shoulder at 447 nm (see Figure 2b). The latter can be assigned as a low-energy portion of split Soret bands characteristic of the *meso*–*meso*-linked diporphyrins.[5] Formation of the *meso*–*meso*-linked diporphyrin can be accounted for in terms of the initial one-electron oxidation of the zinc porphyrin with Ag^{I} followed by nucleophilic attack of

[*] Prof. A. Osuka, A. Nakano
Department of Chemistry, Graduate School of Science
Kyoto University
Sakyo-ku, Kyoto 606 – 8502 (Japan)
Fax: (+81) 75-753-3970
E-mail: osuka@kuchem.kyoto-u.ac.jp
Prof. I. Yamazaki, T. Yamazaki, Y. Nishimura
Department of Chemical Process Engineering, Graduate School of Engineering
Hokkaido University
Sapporo 060-8628 (Japan)

[**] This work was supported by Grant-in-Aids for Scientific Research (nos. 09440217 and 08874074) from the Ministry of Education, Science, Sports and Culture of Japan and by CREST (Core Research for Evolutional Science and Technology) of Japan Science and Technology Corporation (JST).

 © WILEY-VCH Verlag GmbH, D-69451 Weinheim, 1998 1433-7851/98/3721-3023 $ 17.50+.50/0

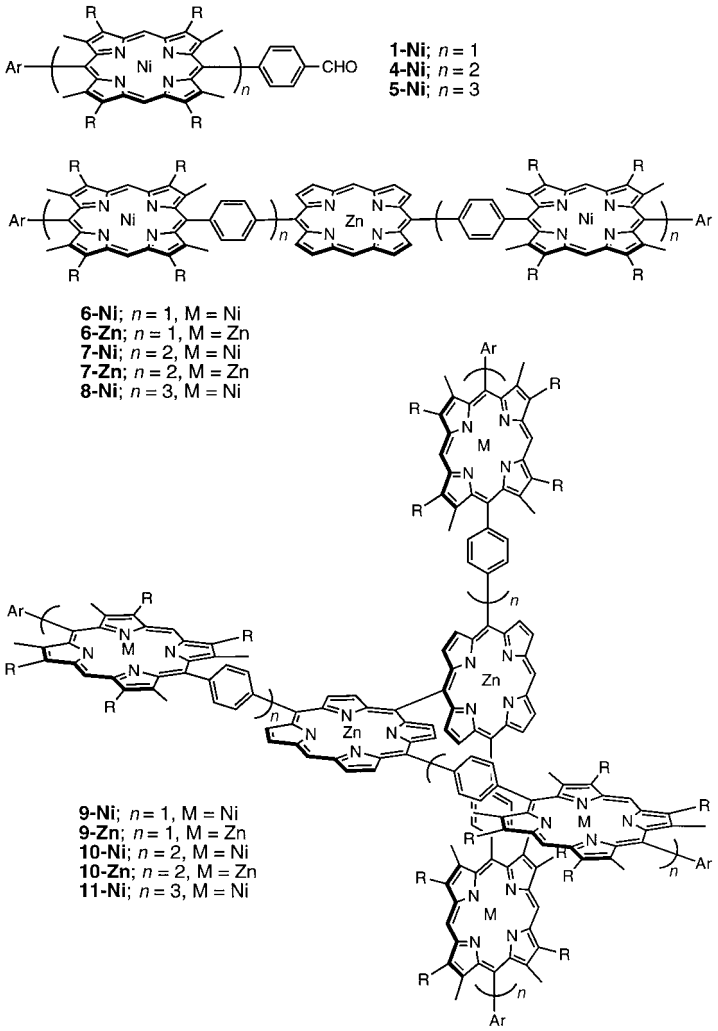


Scheme 1. Synthesis of the porphyrin tetramers **3**. a) 2,2′-Dipyrrylmethane, 3,5-di-*tert*-butylbenzaldehyde, trifluoroacetic acid (TFA), CH_2Cl_2; *p*-chloranil; b) $Zn(OAc)_2$, $MeOH/CH_2Cl_2$; c) $AgPF_6$/MeCN, $CHCl_3$.

a molecule of neutral zinc porphyrin. This mechanism is supported by the synthesis of the same diporphyrin by anodic electrochemical oxidation.[6] Since the potential for the one-electron oxidation of the Zn^{II} octaalkylporphyrin is 0.14 V lower than that of the reacting β-unsubstituted Zn^{II} porphyrin,[7] oxidation of the former should be easier, leading to preferential generation of the corresponding radical cation. However, this radical cation is probably unreactive due to severe steric hindrance, and instead the radical cation of the β-unsubstituted Zn^{II} porphyrin, which is slowly formed either by a bimolecular reaction with Ag^{I} ions or by intramolecular endothermic hole transfer from the radical cation of the Zn^{II} octaalkylporphyrin, reacts with a neutral β-unsubstituted Zn^{II} porphyrin.

The low yield of **3-Zn** suggested undesirable side reactions of the radical cation of the Zn^{II} octaalkylporphyrin. We therefore lowered the oxidation potential of the Zn^{II} octaalkylporphyrin by transmetalation ($Zn^{II} \rightarrow Ni^{II}$) or demetalation to the corresponding free porphyrin base.[7] The hybrid porphyrin dimer **2-Ni** was prepared in 21% yield from **1-Ni** under the same conditions, and **2-H$_2$** was obtained in 80% yield by reaction of **2-Zn** with 1N HCl. Upon treatment with 1.7 equivalents of $AgPF_6$ in $CHCl_3$, **2-Ni** gave porphyrin tetramer **3-Ni** in 30% yield (26% of **2-Ni** was recovered), but **2-H$_2$** gave only trace amounts of tetramer **3-H$_2$**. Based on these results, we decided to employ a Ni^{II} porphyrin as the "protecting group" for the β-octaalkylporphyrin.

We next prepared the symmetric, linear 1,4-phenylene-bridged porphyrin trimer **6-Ni** (51% yield), pentamer **7-Ni** (68%), and heptamer **8-Ni** (80%), again under Lindsey conditions,[4] from the formyl-substituted nickel porphyrin monomer **1-Ni**, dimer **4-Ni**, and trimer **5-Ni**, respectively (Scheme 2). The reaction of **6-Ni** with two equivalents of



Scheme 2. Synthesis of the higher porphyrin oligomers.

$AgPF_6$ produced porphyrin hexamer **9-Ni** along with porphyrin nonamer **12-Ni**, as monitored by analytical SEC (Figure 1); the retention times for **9-Ni** and **12-Ni** were 19.9 and 19.3 min, respectively. After 22 h **9-Ni** and **12-Ni** were separated by preparative SEC and isolated in 50 and 3% yields, respectively (47% of **6-Ni** was recovered). The molecular weights of these porphyrin arrays were determined by MALDI-TOF mass spectrometry (MALDI = matrix-assisted laser desorption ionization, TOF = time of flight): **6-Ni**: $m/z = 2494$ (calcd for $C_{158}H_{180}N_{12}Ni_2O_4Zn$: 2493), **9-Ni**: $m/z = 4985$ (calcd for $C_{316}H_{358}N_{24}Ni_4O_8Zn_2$: 4985), **12-Ni**: $m/z = 7476$

 © WILEY-VCH Verlag GmbH, D-69451 Weinheim, 1998 1433-7851/98/3721-3024 $ 17.50+.50/0 *Angew. Chem. Int. Ed.* **1998**, *37*, No. 21

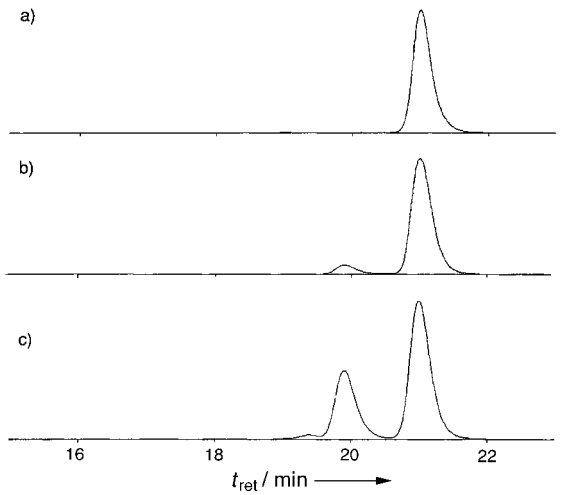


Figure 1. Analytical size-exclusion chromatograms obtained after the reaction of **6-Ni** with $AgPF_6$. a) Before reaction, b) after 4 h, c) after 12 h.

(calcd for $C_{474}H_{536}N_{36}Ni_6O_{12}Zn_3$: 7478).[8] The reaction of the linear porphyrin pentamer **7-Ni** with three equivalents of $AgPF_6$ for 25 h afforded porphyrin decamer **10-Ni** (MALDI-TOF-MS: $m/z = 8321$; calcd for $C_{532}H_{638}N_{40}Ni_8O_8Zn_2$: 8320) in 35% yield (15% of **7-Ni** was recovered). In this reaction we also obtained a fraction (15% yield) that probably contains the 15-mer, as judged by analytical SEC.[9] Finally, the reaction of the porphyrin heptamer **8-Ni** provided the 14-mer **11-Ni** (MALDI-TOF-MS: $m/z = 11640$; calcd for $C_{748}H_{918}N_{56}Ni_{12}O_8Zn_2$: 11656) in 14% yield. The regioselectiviy of this coupling reaction is quite high, and we could not detect any oligomers coupled at other positions.

To examine the photophysical properties of the windmill-like porphyrin arrays, the hexamer **9-Ni** and the decamer **10-Ni** were transformed into the corresponding Zn^{II} porphyrins **9-Zn** and **10-Zn** by demetalation with trifluoroacetic acid and 10% H_2SO_4 in refluxing toluene followed by insertion of Zn^{II} with $Zn(OAc)_2$. The UV/Vis spectra of **2-Zn**, **6-Zn**, and **7-Zn** in CH_2Cl_2 show split Soret bands that are characteristic of 1,4-phenylene-linked Zn^{II} porphyrin oligomers and relatively unperturbed Q bands; their fluorescence spectra are also similar (Figure 2a). On the other hand, the spectra of

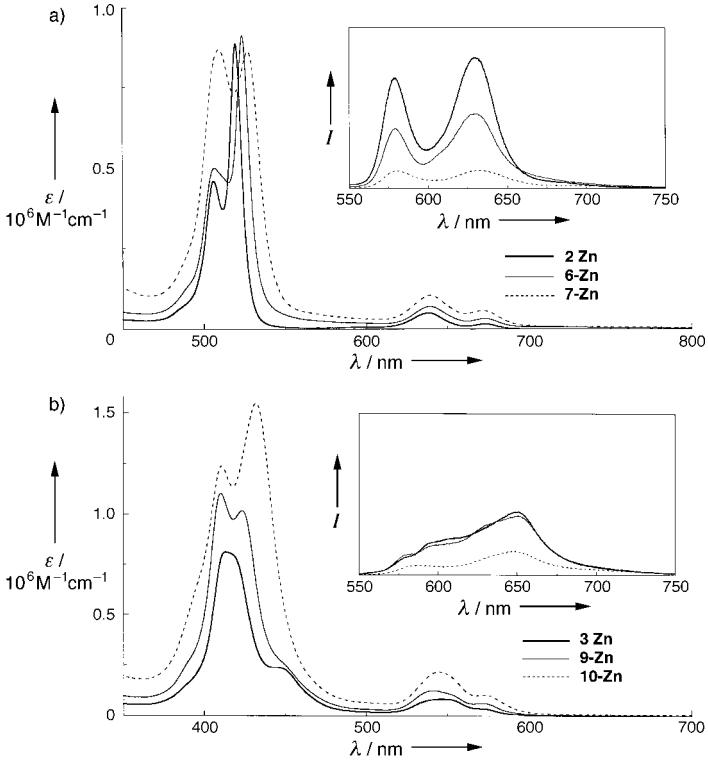
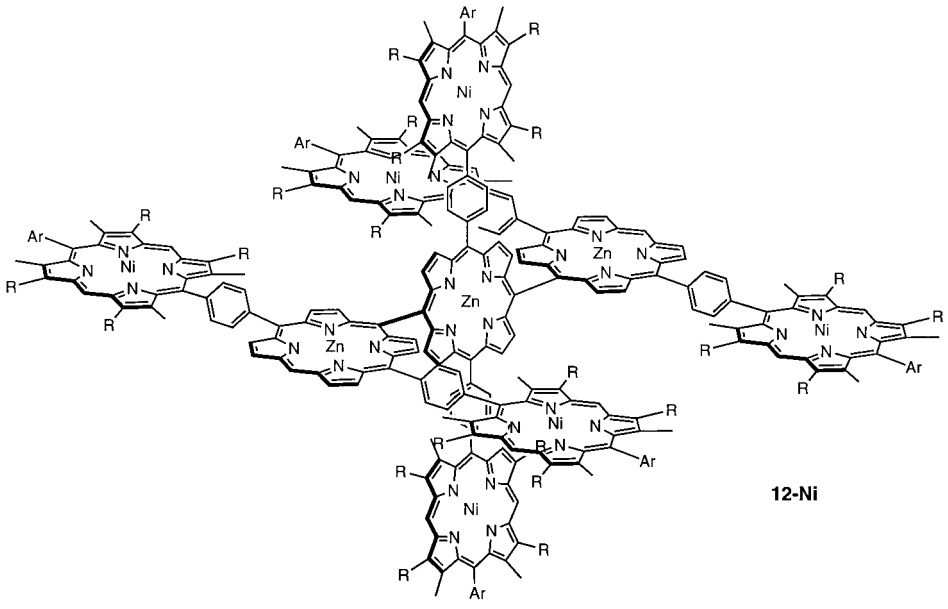


Figure 2. a) UV/Vis spectra of **2-Zn**, **6-Zn**, and **7-Zn** in CH_2Cl_2; the inset showes the steady-state fluorescence emission spectra taken for excitation at 540 nm of a solution with the absorbance at 540 nm adjusted at 0.10. b) Corresponding spectra of **3-Zn**, **9-Zn**, and **10-Zn** in CH_2Cl_2.

oligomers **3-Zn**, **9-Zn**, and **10-Zn** display broader Soret and Q bands (Figure 2b). As with the tetramer **3-Zn**, the spectrum of the hexamer **9-Zn** exhibits a shoulder at about 450 nm due to the low-energy portion of split Soret bands (see above),[5] but such a band is almost hidden in the spectrum of **10-Zn**. The steady-state fluorescence spectra of **3-Zn**, **9-Zn**, and **10-Zn** are all composed of dual emissions from the peripheral porphyrin rings ($\lambda_{max} = 580$ and 629 nm) and from the diporphyrin core ($\lambda_{max} = 651$ nm). The reduced fluorescence intensity of the peripheral porphyrin rings suggests a singlet–singlet energy transfer to the diporphyrin core. This is consistent with the slightly lower energy of the S_1 state of the diporphyrin (ca. 2.08 eV; for the peripheral porphyrin: 2.15 eV)[5]. The time-resolved picosecond fluorescence spectra of **3-Zn** (Figure 3) revealed that the emission from the peripheral porphyrin rings that predominated at an



12-Ni

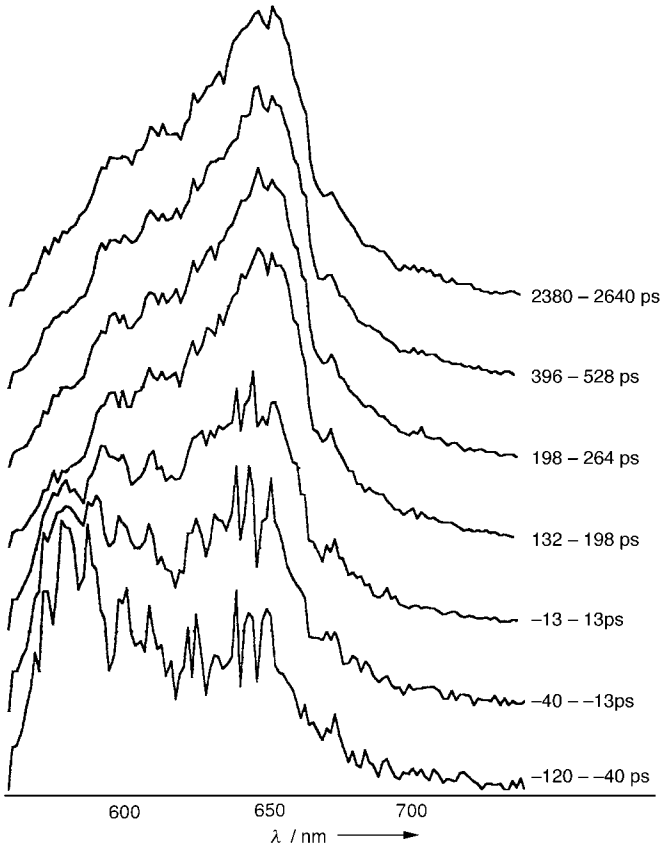


Figure 3. Time-resolved fluorescence emission spectra of **3-Zn** in CH_2Cl_2 taken after excitation at 532 nm. The times given correspond to the time difference from time at which the highest intensity was measured for the profile.

early stage decayed more rapidly than that from the diporphyrin core. The fluorescence decay at 580 nm can be analyzed as a double exponential function with time constants of 27 ps (72%) and 1.6 ns (28%). We have interpreted that the short-lived component mainly reflects the decay of the S_1 state of the peripheral porphyrin rings and that the longer lived component mainly reflects the decay of the S_1 state of the diporphyrin core.[10] Time-resolved fluorescence spectra of **9-Zn** and **10-Zn** are also similar to those of **3-Zn**, and indicate efficient flow of the excitation energy from the peripheral porphyrin rings to the diporphyrin core, even in larger arrays, while the singlet excited state lifetime of the *meso*–*meso* diporphyrin is not unaffected.

The coupling reaction described here enables a one-step construction of large, windmill-like porphyrin arrays with well-defined architectures that are soluble in common organic solvents. This fairly good solubility may arise from their orthogonal molecular arrangement, which may suppress porphyrin π–π stacking. Such orthogonal porphyrin arrays with a molecular length of more than 90 Å may be interesting in view of a concept for molecular electronic devices proposed by Aviram,[11] in which double-minimum potentials for a single electron has been suggested to serve as a fundamental unit of a molecular device. The coupling reaction is also of mechanistic interest. Considering that the oxidation potentials of the Ni^{II} octaalkylporphyrin and β-unsubstitued Zn^{II} porphyrin are almost the same and that the central β-unsubstitued Zn^{II} porphyrin is buried between the bulky peripheral Ni^{II} porphyrin rings, not only a direct oxidation of the Zn^{II} porphyrin with Ag^{I} ions but also an indirect oxidation pathway (oxidation of the Ni^{II} porphyrin with Ag^{I} ions and subsequent hole transfer) may generate the Zn^{II} porphyrin radical cation. The formation of the *meso*–*meso*-linked diporphyrin should thus be facilitated.

Experimental Section

A 50-mL round-bottom flask was charged with **6-Ni** (39 mg, 15.7 mmol) and $CHCl_3$ (10 mL) and then covered with foil. A solution of $AgPF_6$ (31 mmol) in acetonitrile was added all at once. The progess of the reaction was monitored by analytical size-exclusion HPLC (JAIGEL-2.5H, 3H-AF, and 4H-AF columns in series). The mixture was stirred for 22 h, diluted with water, and extracted with $CHCl_3$. The organic layer was separated, washed with water, and dried over anhydrous Na_2SO_4. A saturated solution of $Zn(OAc)_2$ in methanol was added, and the resulting solution was heated at reflux for 1 h, diluted with water, and extracted with $CHCl_3$. The organic layer was separated and dried over Na_2SO_4. The products were separated by preparative size-exclusion HPLC (Japan Analytical Industry Co. Ltd., recycling system with JAIGEL-1H, 2H, and 2.5H columns in series). Elution with $CHCl_3$ yielded three major fractions in the following order: materials of higher molecular weight containing a trace amount of the nonamer **12-Ni**, the hexamer **9-Ni** (19.4 mg, 50%), and the starting trimer **6-Ni** (18.5 mg, 47%). Isolation of the nonamer **12-Ni** and higher oligomers was difficult. The first fractions of several runs were combined and applied repeatedly to the same column, and **12-Ni** was isolated in an average yield of about 3%.

12-Ni: ^{1}H NMR (500 MHz, $CDCl_3$): $\delta = 10.71$ (s, 2H; *meso*-H), 9.82 (d, $J =$ 4.0 Hz, 4H; β-H), 9.64 (d, $J = 4.0$ Hz, 4H; β-H), 9.56 (br, 4H; *meso*-H), 9.41 (br, 4H; *meso*-H), 9.34 (d, $J = 4.0$ Hz, 4H; β-H), 9.33 (s, 4H; *meso*-H), 9.26 (d, $J = 4.0$ Hz, 4H; β-H), 8.76 (d, $J = 4.0$ Hz, 4H; β-H), 8.69 (d, $J = 8.5$ Hz, 8H; Ar), 8.65 (m, 8H; β-H and Ar), 8.32 (d, $J = 8.5$ Hz, 8H; Ar), 8.16 (d, $J = 8.0$ Hz, 4H; Ar), 7.75 (d, $J = 8.5$ Hz, 8H; Ar), 7.65 (d, $J = 8.5$ Hz, 4H; Ar), 7.44 (d, $J = 8.5$ Hz, 8H; Ar), 7.36 (d, $J = 8.5$ Hz, 4H; Ar), 6.90–6.76 (m, 18H; dimethoxy-Ar), 4.23 (s, 8H; ArCH_2Ar), 4.15 (s, 4H; ArCH_2Ar), 3.87 (s, 12H; OMe), 3.87–3.46 (m, 48H; β-hexyl), 3.81 (s, 12H; OMe), 3.75 (s, 6H; OMe), 3.46 (s, 6H; OMe), 3.00, 2.68, 2.58, 2.56 (2 × br, 2 × s, 72H; β-Me), 2.36–0.62 (m, 264H; β-hexyl); MALDI-TOF-MS: calcd av mass for $C_{474}H_{536}N_{36}Ni_6O_{12}Zn_3$: *m*/*z* 7478; found: 7476; UV/Vis (benzene): $\lambda_{max} =$ 418.5 (Soret), 474.5, 533.0, 564.5 nm.

10-Ni: ^{1}H NMR (500 MHz, $CDCl_3$): $\delta = 10.69$ (s, 2H; *meso*-H), 9.81 (d, $J =$ 4.5 Hz, 4H; β-H), 9.62 (d, $J = 4.5$ Hz, 4H; β-H), 9.56 (br, 8H; *meso*-H), 9.42 (br, 8H; *meso*-H), 9.22 (d, $J = 4.5$ Hz, 4H; β-H), 8.65 (d, $J = 8.0$ Hz, 8H; Ar), 8.55 (d, $J = 4.5$ Hz, 4H; β-H), 8.29 (d, $J = 8.0$ Hz, 8H; Ar), 8.12 (s, 16H; Ar), 7.74 (d, $J = 8.0$ Hz, 8H; Ar), 7.45 (d, $J = 8.0$ Hz, 8H; Ar), 6.90 (d, $J = 9.0$ Hz, 4H; dimethoxy-Ar), 6.86 (d, $J = 3.0$ Hz, 4H; dimethoxy-Ar), 6.81 (dd, $J = 9.0$, 3.0 Hz, 4H; dimethoxy-Ar), 4.23 (s, 8H; ArCH_2Ar), 3.88 (s, 12H; OMe), 3.81 (s, 12H; OMe), 3.88–3.50 (m, 64H; β-hexyl), 2.96 (br, 24H; β-Me), 2.74 (br, 24H; β-Me), 2.60 (br, 24H; β-Me), 2.25 (br, 24H; β-Me), 2.20–0.65 (m, 352H; β-hexyl); MALDI-TOF-MS: calcd av mass for $C_{532}H_{638}N_{40}Ni_8O_8Zn_2$: *m*/*z* 8320; found: 8321; UV/Vis (benzene): $\lambda_{max} =$ 410.0 (Soret), 430.0 (Soret), 534.0, 567.0 nm.

11-Ni: ^{1}H NMR (500 MHz, $CDCl_3$): $\delta = 10.69$ (s, 2H; *meso*-H), 9.81 (d, $J =$ 5.0 Hz, 4H; β-H), 9.62 (d, $J = 4.0$ Hz, 4H; β-H), 9.56, 9.46, 9.44 (br, 2 × s, 24H; *meso*-H), 9.22 (br, 4H; β-H), 8.67 (d, $J = 8.0$ Hz, 8H; Ar), 8.54 (br, 4H; β-H), 8.30 (d, $J = 8.0$ Hz, 8H; Ar), 8.15 (s, 16H; Ar), 8.14 (s, 16H; Ar), 7.76 (d, $J = 7.5$ Hz, 8H; Ar), 7.46 (d, $J = 7.5$ Hz, 8H; Ar), 6.91 (d, $J = 8.5$ Hz, 4H; dimethoxy-Ar), 6.87 (d, $J = 2.5$ Hz, 4H; dimethoxy-Ar), 6.82 (dd, $J =$ 8.5, 2.5 Hz, 4H; dimethoxy-Ar), 4.23 (s, 8H; ArCH_2Ar), 3.88 (s, 12H; OMe), 3.82 (s, 12H; OMe), 3.73, 3.66 (2 × br, 96H; β-hexyl), 2.99 (br, 12H; β-Me), 2.62 (br, 12H; β-Me), 2.76, 2.27 (2 × s, 120H; β-Me), 2.20–2.08 (br, 96H; β-hexyl), 2.00–1.26 (br, 288H; β-hexyl), 1.20–0.85 (br, 144H; β-hexyl-CH_3); MALDI-TOF-MS: calcd av mass for $C_{748}H_{918}N_{56}Ni_{12}O_8Zn_2$: *m*/*z* 11656; found: 11640; UV/Vis (benzene): $\lambda_{max} = 412.0$ (Soret), 434.0 (Soret), 535.5, 568.5 nm.

Received: April 27, 1998 [Z11783IE]
German version: *Angew. Chem.* **1998**, *110*, 3172–3176

 © WILEY-VCH Verlag GmbH, D-69451 Weinheim, 1998 1433-7851/98/3721-3026 $ 17.50+.50/0

Keywords: C–C coupling · donor–acceptor systems · photosynthesis · porphyrinoids · supramolecular chemistry

[1] T. Pullerits, V. Sundström, *Acc. Chem. Res.* **1996**, *29*, 381.
[2] M. R. Wasielewski, *Chem. Rev.* **1992**, *92*, 435. A. Osuka, K. Maruyama, *J. Am. Chem. Soc.* **1988**, *110*, 4454; T. Nagata, A. Osuka, K. Maruyama, *J. Am. Chem. Soc.* **1990**, *112*, 3054.
[3] J.-M. Lehn, *Supramolecular Chemistry—Concepts and Perspectives*, VCH, Weinheim, **1995**; C. M. Drain, J.-M. Lehn, *J. Chem. Soc. Chem. Commun.* **1994**, 2313; S. Prathapan, T. E. Johnson, J. S. Lindsey, *J. Am. Chem. Soc.* **1993**, *115*, 7519; R. W. Wagner, J. S. Lindsey, *J. Am. Chem. Soc.* **1994**, *116*, 9759; R. W. Wagner, J. S. Lindsey, J. Serth, V. Palaniappan, D. F. Bocian, *J. Am. Chem. Soc.* **1996**, *118*, 3996; K. Funatsu, A. Kimura, T. Imamura, Y. Sasaki, *Chem. Lett.* **1995**, 765. H. Higuchi, M. Takeuchi, J. Ojima, *Chem. Lett.* **1996**, 593; O. Mongin, A. Gossauer, *Tetrahedron* **1997**, *20*, 6835.
[4] L. S. Lindsey, I. C. Schreiman, H. C. Hsu, P. C. Kearney, A. M. Marguerettaz, *J. Org. Chem.* **1987**, *52*, 827; J. L. Sessler, V. L. Capuano, *Angew. Chem.* **1990**, *102,* 1162; *Angew. Chem. Int. Ed. Engl.* **1990**, *29*, 1134.
[5] A. Osuka, H. Shimidzu, *Angew. Chem.* **1997**, *109*, 93; *Angew. Chem. Int. Ed. Engl.* **1997**, *36*, 135; N. Yoshida, H. Shimidzu, A. Osuka, *Chem. Lett.* **1998**, 55; *meso–meso*-linked porphyrin dimers were prepared independently by other nondirect routes: K. Susumu, T. Shimizu, K. Tanaka, H. Segawa, *Tetrahedron Lett*. **1996**, *37*, 8399; R. G. Khoury, L. Jaquinod, K. M. Smith, *Chem. Commun*. **1997**, 1057.
[6] T. Ogawa, Y. Nishimoto, N. Yosida, N. Ono, A. Osuka, *Chem. Commun.* **1998**, 337.
[7] Potentials for the one-electron oxidation of **1-Zn**, **1-Ni**, **1-H_2**, and zinc 5,15-bis(3,5-di-*tert*-butyl-phenyl)porphyrin were measured by cyclic voltammetry in $CHCl_3$ to be 0.17, 0.32, 0.40, and 0.31 V, respectively, versus ferrocene/ferrocenium ion.
[8] All new porphyrin compounds reported here were fully characterized by ^{1}H NMR spectroscopy (500 MHz) as well as FAB and MALDI-TOF mass spectrometry.
[9] In the analytical SEC, **7-Ni** and **10-Ni** eluted after 20.1 and 18.9 min, respectively, while the porphyrin 15-mer eluted after 18.1 min. The reaction of **10-Ni** with excess $AgPF_6$ afforded the porphyrin 20-mer, as judged by SEC (retention time: 17.9 min) and MALDI-TOF-MS ($m/z = 16666$; calcd for $C_{1064}H_{1274}N_{80}Ni_{16}O_{16}Zn_4$: 16640), in 20–30% yield. However, the very broad signals in the ^{1}H NMR spectra of the 15-mer and 20-mer precluded their full characterization. These results may imply that not only the linear porphyrin arrays but also the windmill-like orthogonal porphyrin arrays are useful building blocks.
[10] Since the energy difference between the singlet excited state of the *meso–meso* diporphyrin and the peripheral porphyrin rings is small (0.07 eV), the energy transfer may be reversible and the dynamics of the photoexcited state of the windmill-like porphyrin arrays are very complicated.
[11] A. Aviram, *J. Am. Chem. Soc.* **1988**, *110*, 5687.

Supramolecular Assembly of Heterogeneous Multiporphyrin Arrays—Structures of $[\{Zn^{II}(tpp)\}_2(tpyp)]$ and the Coordination Polymer $[\{[Mn^{III}(tpp)]_2(tpyp)(ClO_4)_2\}_\infty]$**

R. Krishna Kumar and Israel Goldberg*

Multiporphyrin architectures have diverse potential for applications as biomimetic models or functional materials for the transport of energy, charge, molecules, and ions.[1, 2] The formulations of light-harvesting porphyrin arrays and new receptors for selective catalysis has relied mostly on covalent synthesis of oligomeric arrays.[3, 4] For many years the construction of stable multiporphyrin arrays by supramolecular aggregation has remained relatively unexplored, in spite of the diverse molecular recognition algorithm that can be incorporated into the porphyrin building blocks. Recent investigations have shown, however, that predictable architectures of oligomers and polymers from metallomacrocyclic building blocks can be rationally designed by selection of the coordination geometry of metals and the structure of multitopic ligands involved in the supramolecular synthesis.

Examples of successful attempts to assemble supramolecular porphyrin structures, in solution as well as in the solid state, include the generation of patterns stabilized by external metal centers[5] or multidentate bridging ligands,[6] and the construction of aggregates by self-coordination of suitably functionalized lateral substituents of a given porphyrin entity directly to the metal center of an adjacent unit.[7] In the latter context, we have described the assembly of one-, two-, and three-dimensional homogeneous coordination polymers consisting of the Zn^{II} tetra(4-pyridyl)porphyrin [Zn(tpyp)] or Zn^{II} tetra(4-cyanophenyl)porphyrin moieties.[8] Self-assembly of hydrogen-bonded arrays of porphyrin molecules that are peripherally substituted with molecular recognition groups has also been reported.[9]

The *meso*-tetrapyridylporphyrin free base is representative of square-shaped building blocks containing symmetrically disposed ligating sites. This is thus an excellent ligand for tetrametalloporphyrin assemblies[4b, 10] and a potentially excellent building block for the generation of heterogeneous supramolecular networks in combination with other metalloporphyrin units. We report here on the assembly and structural characterization of the supramolecular oligomer $[\{Zn^{II}(tpp)\}_2(tpyp)]$ (**1**) and the uniquely architectured coordination polymer $[\{[Mn^{III}(tpp)]_2(tpyp)(ClO_4)_2\}_\infty]$ (**2**; tpp = tetraphenylphorphyrin). To our knowledge, the latter represents the first example of a well-defined two-dimensional coordination polymer incorporating at least two different porphyrin entities.

[*] Prof. I. Goldberg, Dr. R. Krishna Kumar
School of Chemistry, Sackler Faculty of Exact Sciences
Tel-Aviv University
Ramat-Aviv, 69978 Tel-Aviv (Israel)
Fax: (+972) 3-6409293
E-mail: goldberg@post.tau.ac.il

[**] This research was supported in part by the United States–Israel Binational Science Foundation (BSF; grant no. 94-00344), Jerusalem, Israel.

The tpp and tpyp building blocks were synthesized from the corresponding aldehyde and pyrrole, and tpp was metalated with $Zn(OAc)_2$ or $Mn(OAc)_2$ by standard procedures.[8a, 11] The axial ligation of the metal ion inserted into the porphyrin center provides an important element in the construction of multiporphyrin assemblies. The Zn^{II} ion has a strong affinity for a five-coordinate environment, which favors axial ligation of only one ligand to the {Zn(tpp)} moiety. On the other hand, the paramagnetic Mn^{III} ion tends to adopt a six-coordinate structure.[12] This should facilitate the formation of coordination polymers with suitable multidentate ligands which might have significant potential as molecular magnetic materials.[2b, 6a–c] These preferences of the two metal ions are best illustrated by the different aggregation modes of $[Zn^{II}(tpp)]$ and $[Mn^{III}(tpp)]\cdot ClO_4$ with tpyp.

The reaction of $[Zn^{II}(tpp)]$ with tpyp in chloroform followed by recrystallization from nitrobenzene yields the 2:1 coordination oligomer **1**. Its structure consists of a tetrapyridyl unit which coordinates to, and effectively bridges, two centrosymmetrically related [Zn(tpp)] molecules (Figure 1). The zinc ions typically deviate inward from the porphyrin plane (by 0.27 Å) towards the axially coordinated pyridyl groups ($Zn\cdots N_{py}$ 2.197(7) Å). The three-porphyrin oligomer is capped from both sides by nitrobenzene molecules. The latter lie approximately parallel to the porphyrin frameworks at an average distance of 3.3 Å, which is indicative of significant $\pi-\pi$ interaction between the two aromatic systems. Formation in solution of similar supramolecular trimers consisting of one dipyridyldiphenylporphyrin and two {Zn(tpp)} moieties has been proposed earlier on the basis of NMR data.[7f] In accordance with the previous observations, ^{1}H NMR study of the dissolved crystals of **1** provides clear evidence that the coordination of [Zn(tpp)] to tpyp is present in this case as well. In chloroform, the signals of the 2,6-pyridyl (α to N), 3,5-pyridyl (β to N), and pyrrole N protons are shifted upfield by $\Delta\delta = 2.88$, 1.07, and 0.80, respectively in relation to those of uncoordinated tpyp (see the Experimental Section and related NMR data in references [4b] and [7f]). These values along with the broad nature of the signals and the absence of signals corresponding to uncoordinated pyridyl rings indicate that there is a rapid exchange of [Zn(tpp)] between the four pyridyl sites of tpyp. A solution of a 1:4 mixture of tpyp and [Zn(tpp)] in chloroform shows even higher upfield shifts of the tpyp protons, suggesting possible formation of a pentameric assembly $[\{Zn^{II}(tpp)\}_4(tpyp)]$ in which all pyridyl sites are involved in the coordination. No such complexes could be obtained as yet, however, in the crystalline form, which can be attributed to inefficient crystal packing of such pentameric porphyrin entities (in relation to the arrangement of the trimeric oligomers, which is more effective and of lower free energy).

The engineering of more extended heterogeneous arrays was made possible by the reaction of $[Mn^{III}(tpp)]\cdot ClO_4$ with neutral tpyp in chloroform. Detailed analysis of the resulting material reveals an unprecedented square-grid architecture of these assemblies (Figure 2). They represent heterogeneous coordination polymers made up of a single framework in which each tpyp unit is surrounded by, and coordinated to, four [Mn(tpp)] molecules and each [Mn(tpp)] molecule is coordinated to two neighboring tpyp units. Thus, the coordination potential of the two porphyrin building blocks involved in this structure is utilized to capacity in an exceptionally well-defined manner. In the two-dimensional polymers, which are roughly planar, the alternating metalloporphyrin and tetrapyridyl units are linked to each other by metal–ligand coordination; the $Mn\cdots N_{py}$ distances range from 2.34 to 2.37 Å. The polymeric layers are stacked in the crystal along the $b+2c$ direction (the average interlayer distance is about 10.2 Å) with an offset overlap to effectively accommodate the [Mn(tpp)] frameworks, which are aligned perpendicular to the polymeric networks and the tpyp molecules. This essentially docks one layer into the other, yielding a stable crystalline solid.

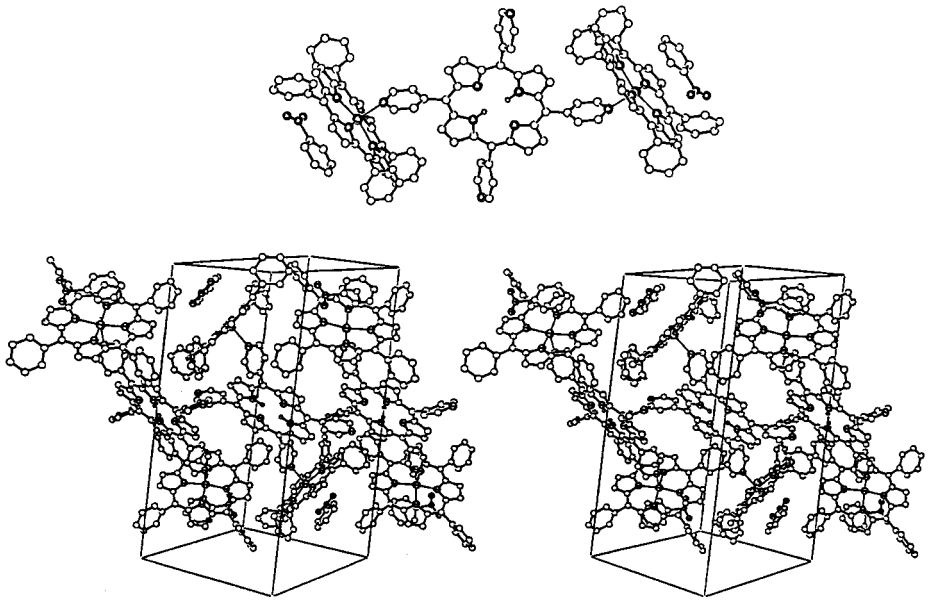


Figure 1. Structure of the trimeric $[\{Zn^{II}(tpp)\}_2(tpyp)]$ aggregate in **1** and stereoview of its crystal packing approximately along $b+c$ (the a axis is vertical). The tpyp molecules are located on centers of inversion. Noteworthy is the effective packing of the tpyp moieties along the direction of the noncoordinated pyridyl groups and the capping of the concave side of the [Zn(tpp)] unit by nitrobenzene.

Figure 3 shows the relative disposition of, and the packing interactions between, two adjacent layers in the crystal. The open nature of the polymeric layers gives rise to the formation of channels in the crystals which penetrate through the stacked layers. Thus, four small channels centered approximately at ¼,¼,z, ¼,¾,z, ¾,¼,z, and ¾,¾,z run along the c axis of the crystal. In addition, two wider channels centered at ¼,y,¾ and ¾,y,¼ propagate in the b direction; the smallest cross-section distance between van der Waals surfaces of the channels is about 4.5 Å. These tubularly

 © WILEY-VCH Verlag GmbH, D-69451 Weinheim, 1998 1433-7851/98/3721-3028 $ 17.50+.50/0

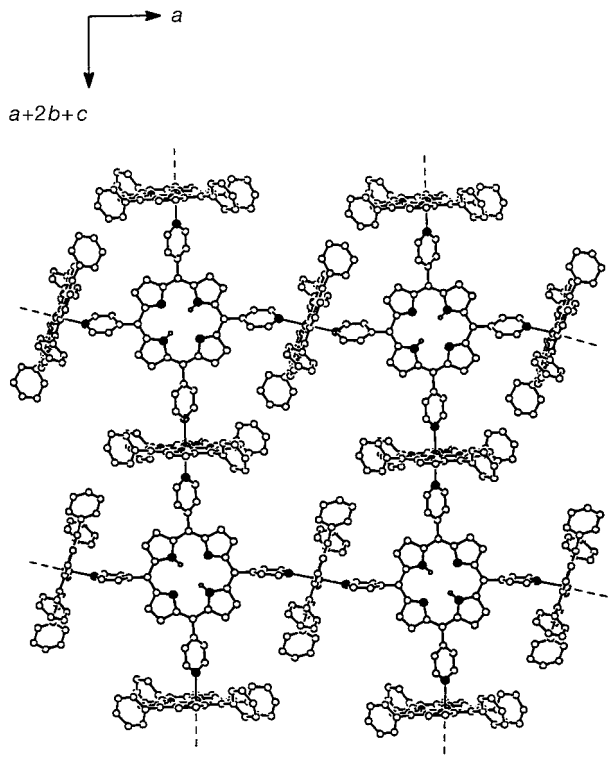


Figure 2. Structure of the heterogeneous coordination polymer in **2**. The Mn and N atoms are represented by partially darkened circles.

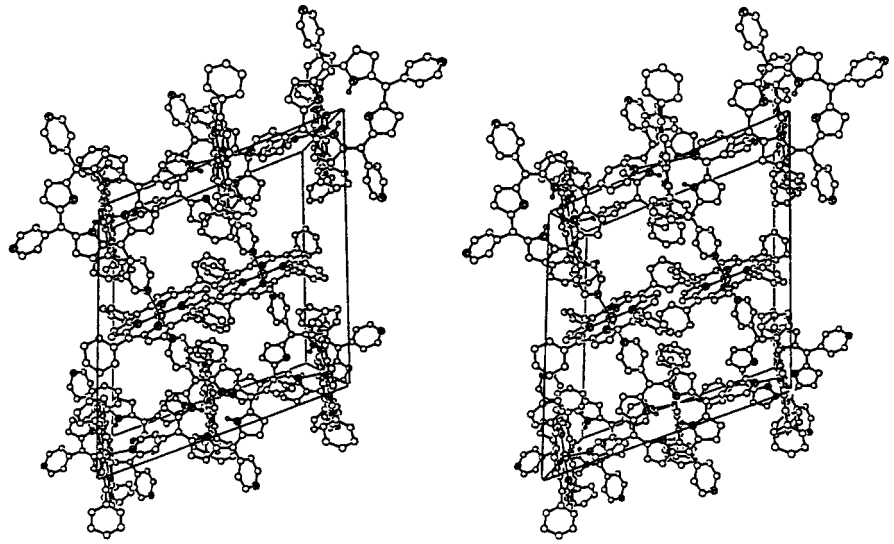


Figure 3. Stereoview of the crystal structure of **2** approximately along the *c* axis (*a* is nearly horizontal, and *b* is vertical). The relative displacement of, and steric fit between, two neighboring polymeric layers is depicted. Note the open channels which run through the polymeric layers along the *b* and *c* axes (see text). The perchlorate ions and nitrobenzene molecules which occupy these channels are omitted for clarity.

shaped voids that criss-cross the porphyrin structure are occupied by perchlorate counterions and nitrobenzene solvent molecules. Some of the latter access, and form $\pi-\pi$ interactions with, the open faces of the tpyp moieties. Various experimental results indicate that there are about twenty nitrobenzene molecules per unit cell, which occupy 46% (!) of the crystal volume. Their positions have all been determined reasonably well based on diffraction data. Thermogravimetric analysis (TGA) shows that the onset of solvent loss occurs in these crystals at 80 °C and is completed by 150 °C, and that no other phase transition of the solid occurs until 300 °C. The observed weight loss of about 32.5% of the nitrobenzene further confirms the high content of this solvent in the structure. It should be possible to fine-tune the solvent-accessible space within the lattice by introduction of small alkyl groups on the pyrrole rings of tpp and tpyp. These groups might also enhance the solubility of the material in organic solvents. Another variation involves utilizing negatively charged tpyp units, by incorporating neutral metal atoms into the porphyrin,[13] in order to balance the formal charge of the $[Mn^{III}(tpp)]$ moiety and maintain a lipophilic environment within the channels.

The ability to generate homogeneous as well as heterogeneous multiporphyrin coordination polymers of varying dimensionality by design provides a promising perspective for new molecular solids with interesting and useful properties. Their potential application in different areas of materials science, including formulation of new molecular magnetic materials and zeolite mimics, is also in sight.

Experimental Section

The analyzed materials were obtained by adding stoichiometric amounts of $[Zn^{II}(tpp)]$ or $[Mn^{III}(tpp)]\cdot ClO_4$ to a solution of tpyp in chloroform and stirring the resulting mixtures for 24 h. Single crystals of **1** and **2** suitable for X-ray diffraction analysis were obtained by dissolving the solids thus formed in hot nitrobenzene and allowing the solution to cool very slowly.

1 ($2\,C_{44}H_{28}N_4Zn\cdot C_{40}H_{26}N_8\cdot 2\,C_6H_5NO_2$): Elemental analysis: calcd: C 75.7, H 4.2, N 11.4; found: C 75.2, H 4.4, N 11.2; UV/Vis ($CHCl_3$): $\lambda_{max}=421$, 476, 513, 551, 591, 642 nm; ^1H NMR ($CDCl_3$, 360 MHz): $\delta=8.95$ (16H, s, β-pyrrole of [Zn(tpp)]), 8.25 (20H, m, *o*-phenyl of [Zn(tpp)] and *o*-nitrobenzene), 7.97 (8H, s, β-pyrrole of tpyp), 7.75 (26H, m, *m*- and *p*-phenyl of [Zn(tpp)], *p*-nitrobenzene), 7.54 (4H, t, *m*-nitrobenzene), 7.11 (8H, br d, β-H of tpyp), 6.16 (8H, br, α-H of tpyp), −3.7 (2H, s, N-pyrrole); IR (KBr): $\tilde{\nu}=1590$, 796 (tpyp), 1590, 1068, 1002, 992, 796, 752 ([Zn(tpp)]), 1523, 1343, 699 cm^{-1} (nitrobenzene).

2 ($2\,C_{44}H_{28}N_4Mn\cdot 2\,ClO_4\cdot C_{40}H_{26}N_8\cdot 10\,C_6H_5NO_2$): Elemental analysis: calcd: C 66.7, H 3.9, N 10.8; found: C 65.9, H 3.9, N 10.3; UV/Vis ($CHCl_3$): $\lambda_{max}=417$, 477, 513, 585, 614 nm; IR (KBr): $\tilde{\nu}=$ 1599, 803 (tpyp), 1599, 1012, 803, 755, 701 ($[Mn(tpp)]^+$), 1522, 1345, 703 (nitrobenzene), 1087 cm^{-1} (ClO_4^-).

Crystal structure analyses: Data for **1** and **2** were collected on a standard Enraf-Nonius CAD4 diffractometer with $Mo_{K\alpha}$ radiation ($\lambda=$ 0.7107 Å) and ω-2θ scans. In view of the very large unit cell of **2** and the high content of partially disordered solvent molecules, the measurements for this crystal were conducted at low temperature. The two crystals did not show significant diffraction beyond $2\theta=42.0°$. The crystal structures were solved by direct methods and Fourier techniques, and then refined by least squares employing the SHELXS and SHELXL program suite.[14] Crystallographic data (excluding structure factors) for the structures reported in this paper have been deposited with the Cambridge Crystallographic Data Centre as supplementary publication no. CCDC-101400. Copies of the data

can be obtained free of charge on application to CCDC, 12 Union Road, Cambridge CB2 1EZ, UK (fax: (+44) 1223-336-033; e-mail: deposit@ccdc.cam.ac.uk).

Crystal data for **1** (at ca. 298 K): $C_{44}H_{28}N_4Zn \cdot 0.5\,(C_{40}H_{26}N_8) \cdot C_6H_5NO_2$, $M_r = 1110.6$, monoclinic, space group $P2_1/c$, $a = 26.125(7)$, $b = 15.132(3)$, $c = 13.780(3)$ Å, $\beta = 98.57(2)^\circ$, $V = 5386.7$ Å^3, $Z = 4$, $\rho_{calcd} = 1.369$ g cm^{-3}, $F(000) = 2300$, $\mu(Mo_{K\alpha}) = 5.15$ cm^{-1}, crystal size $\approx 0.45 \times 0.40 \times 0.30$ mm, $2\theta_{max} = 42.0^\circ$, 5040 unique reflections, final $R1 = 0.069$ for 3541 reflections with $F > 4\sigma(F)$, $R1 = 0.101$, $wR2 = 0.187$, and GoF = 1.109 for all 5040 data. The noncoordinated nitro group of the solvent molecules exhibits a considerable "wagging" motion out of the plane of the aromatic ring. All non-hydrogen atoms (except for those of the disordered nitro group) were refined anisotropically, and hydrogen atoms were placed in calculated positions.

Crystal data for **2** (at ca. 150 K): $2\,(C_{44}H_{28}N_4Mn \cdot ClO_4) \cdot C_{40}H_{26}N_8 \cdot 10\,C_6H_5NO_2$, $M_r = 3384.0$, triclinic, space group $P\bar{1}$, $a = 19.944(8)$, $b = 20.615(8)$, $c = 21.334(6)$ Å, $\alpha = 97.33(3)$, $\beta = 98.59(3)$, $\gamma = 109.77(3)^\circ$, $V = 8011$ Å^3, $Z = 2$, $\rho_{calcd} = 1.403$ g cm^{-3}, $\rho_{obs.} = 1.39$ g cm^{-3}, $F(000) = 3500$, $\mu(Mo_{K\alpha}) = 2.76$ cm^{-1}, crystal size $\approx 0.30 \times 0.15 \times 0.10$ mm, $2\theta_{max} = 42.0^\circ$, 13749 unique reflections. The considerable crystallographic complexity of this structure can be appreciated from the size of the asymmetric unit: It contains one [Mn(tpp)] unit in a general position, two additional [Mn(tpp)] units on centers of inversion, two tpyp units on other centers of inversion, and two perchlorate anions as well as ten nitrobenzene molecules in general positions. Although the porphyrin lattice itself, which consists of centrosymmetric molecules, appears to have much simpler periodicity characteristics (Figure 2), lack of inversion in the tetrahedral perchlorate anions and somewhat random distribution of the numerous nitrobenzene molecules provide a plausible cause for the large unit cell identified from the diffraction data. Isotropic refinement (only the three Mn and two Cl atoms of the asymmetric unit were refined anisotropically) of the full structure with approximate positions of the ten partly disordered nitrobenzene molecules (of which at least six could not be modeled precisely) converged at final $R1 = 0.19$ for 7439 reflections with $F > 4\sigma(F)$ and 694 refined parameters, $R1 = 0.25$, $wR2 = 0.44$, and GoF = 1.99 for all 13749 data. The large size of the asymmetric unit (246 non-hydrogen atoms), the limited resolution of the diffraction data, and the partial disorder of the solvent molecules did not allow an anisotropic refinement of the full structure. Correspondingly, the correctness of the interporphyrin organization and interaction scheme was confirmed by further refinement calculations of the $[Mn(tpp)] \cdot ClO_4$ and tpyp fragments only by using the "bypass" technique in which the overall contribution of all the nitrobenzene solvent molecules (located in the channel-type voids of the lattice) to the diffraction pattern is substracted from the observed data.[15] The reduction in the number of atoms and the improved quality of the resulting ("noise-free") data allowed an anisotropic refinement of a much larger portion of the structure (only the phenyl carbon atoms of the [Mn(tpp)] residues and the oxygen atoms of the perchlorate anions remained isotropic), and led to considerably more precise results. This refinement converged smoothly at $R1 = 0.078$ for 6139 reflections with $F > 4\sigma(F)$ and 1128 refined parameters, $R1 = 0.117$ and $wR2 = 0.20$ for all 13749 data; min./max. residual electron density $0.614/-0.425$ e Å^{-3}. The residual electron density for the solvent molecules in the interporphyrin voids of the unit cell was assessed by the "bypass" method to be 1212 e, which is reasonably close to the calculated value of 1280 e for twenty nitrobenzene molecules. In all calculations, the hydrogen atoms were placed in calculated positions and added as fixed contributions to the structure factors.

Received: May 4, 1998 [Z11816IE]
German version: *Angew. Chem.* **1998**, *110*, 3176 – 3180

Keywords: coordination polymers · crystal engineering · pi interactions · porphyrinoids · supramolecular chemistry

[1] a) M. R. Wasielewski, *Chem. Rev.* **1992**, *92*, 435 – 461; b) V. S.-Y. Lin, S. G. DiMagno, M. J. Therien, *Science* **1994**, *264*, 1105 – 1111.

[2] a) R. W. Wagner, J. S. Lindsey, J. Seth, V. Palaniappan, D. F. Bocian, *J. Am. Chem. Soc.* **1996**, *118*, 3996 – 3997; b) J. S. Miller, A. J. Epstein, *Chem. Eng. News* **1995**, *73*(40), 30 – 41; c) T. J. Marks, *Angew. Chem.* **1990**, *102*, 886 – 908; *Angew. Chem. Int. Ed. Engl.* **1990**, *29*, 857 – 879.

[3] a) S. Prathapan, T. E. Johnson, J. S. Lindsey, *J. Am. Chem. Soc.* **1993**, *115*, 7519 – 7520; b) R. W. Wagner, J. S. Lindsey, *J. Am. Chem. Soc.* **1994**, *116*, 9759 – 9760.

[4] a) C. A. Hunter, R. K. Hyde, *Angew. Chem.* **1996**, *108*, 2064 – 2067; *Angew. Chem. Int. Ed. Engl.* **1996**, *35*, 1936 – 1938; b) S. Anderson, H. L. Anderson, A. Bashall, M. McPartlin, J. K. M. Sanders, *Angew. Chem.* **1995**, *107*, 1196 – 1200; *Angew. Chem. Int. Ed. Engl.* **1995**, *34*, 1096 – 1099; c) A. K. Burrell, D. L. Officer, D. C. W. Reid, *Angew. Chem.* **1995**, *107*, 986 – 988; *Angew. Chem. Int. Ed. Engl.* **1995**, *34*, 900 – 902; d) H. L. Anderson, A. Bashall, K. Henrick, M. McPartlin, J. K. M. Sanders, *Angew. Chem.* **1994**, *106*, 445 – 447; *Angew. Chem. Int. Ed. Engl.* **1994**, *33*, 429 – 431.

[5] a) C. M. Drain, J.-M. Lehn, *J. Chem. Soc. Chem. Commun.* **1994**, 2313 – 2315; b) B. F. Abrahams, B. F. Hoskins, D. M. Michail, R. Robson, *Nature* **1994**, *369*, 727 – 729.

[6] a) A. Böhm, C. Vazquez, R. S. McLean, J. C. Calabrese, S. E. Kalm, J. L. Manson, A. J. Epstein, J. S. Miller, *Inorg. Chem.* **1996**, *35*, 3083 – 3088; b) J. S. Miller, C. Vazquez, N. L. Jones, R. S. McLean, A. J. Epstein, *J. Mater. Chem.* **1995**, *5*, 707 – 711; c) J. S. Miller, J. C. Calabrese, R. S. McLean, A. J. Epstein, *Adv. Mater.* **1992**, *4*, 498 – 501; d) P. Turner, M. J. Gunter, T. W. Hambley, A. H. White, B. W. Skelton, *Inorg. Chem.* **1992**, *31*, 2297 – 2299;

[7] a) A. K. Burrell, D. L. Officer, D. C. W. Reid, K. Y. Wild, *Angew. Chem.* **1998**, *10*, 122 – 125; *Angew. Chem. Int. Ed.* **1998**, *37*, 114 – 116; b) R. T. Stibrany, J. Vasudevan, S. Knapp, J. A. Potenza, T. Emge, H. J. Schugar, *J. Am. Chem. Soc.* **1996**, *118*, 3980 – 3981; c) E. Alessio, M Macchi, S. Heath, L. G. Marzilli, *Chem. Commun.* **1996**, 1411 – 1412; d) M. O. Senge, K. M. Smith, *J. Chem. Soc. Chem. Commun.* **1994**, 923 – 924; e) Y. Kobuke, H. Miyaji, *J. Am. Chem. Soc.* **1994**, *116*, 4111 – 4112; f) E. B. Fleischer, A. M. Shachter, *Inorg. Chem.* **1991**, *30*, 3763 – 3769.

[8] a) R. Krishna Kumar, S. Balasubramanian, I. Goldberg, *Inorg. Chem.* **1998**, *37*, 541 – 552; b) H. Krupitsky, Z. Stein, I. Goldberg, C. E. Strouse, *J. Incl. Phenom.* **1994**, *18*, 177 – 192.

[9] a) K. Kobayashi, M. Koyanagi, K. Endo, H. Masuda, Y. Aoyama, *Chem. Eur. J.* **1998**, *4*, 417 – 424; b) P. Bhyrappa, S. R. Wilson, K. S. Suslick, *J. Am. Chem. Soc.* **1997**, *119*, 8492 – 8502. c) P. Dastidar, Z. Stein, I. Goldberg, C. E. Strouse, *Supramol. Chem.* **1996**, *7*, 257 – 270; d) I. Goldberg, H. Krupitsky, Z. Stein, Y. Hsiou, C. E. Strouse, *Supramol. Chem.* **1995**, *4*, 203 – 221; e) C. M. Drain, R. Fischer, E. G. Nolen, J.-M. Lehn, *J. Chem. Soc. Chem. Commun.* **1993**, 243 – 245.

[10] S. Anderson, H. L. Anderson, J. K. M. Sanders, *Acc. Chem. Res.* **1993**, *26*, 469 – 475.

[11] a) J. S. Lindsey, I. C. Schreiman, H. C. Hsu, P. C. Kearney, A. M. Marquerettez, *J. Org. Chem.* **1987**, *52*, 827 – 836; b) A. Bettelheim, B. A. White, S. A. Raybuck, R. W. Murray, *Inorg. Chem.* **1987**, *26*, 1009 – 1017.

[12] a) P. Turner, M. J. Gunter, B. W. Skelton, A. H. White, T. W. Hambley, *J. Chem. Res.* **1996**, *18*, 220 – 289; b) A. L. Balch, B. C. Noll, S. M. Reid, E. P. Zovinka, *Inorg. Chem.* **1993**, *32*, 2610 – 2611.

[13] S. Ciurli, S. Gambarotta, C. Floriani, A. Chiesi-Villa, C. Guastini, *Angew. Chem.* **1986**, *98*, 553 – 555; *Angew. Chem. Int. Ed. Engl.* **1986**, *25*, 553 – 554.

[14] a) G. M. Sheldrick, SHELXS-97. *Acta Crystallogr. Sect. A* **1990**, *46*, 467 – 473; b) G. M. Sheldrick, SHELXL-93 and SHELXL-97, Universität Göttingen, Germany, **1993** and **1997**.

[15] P. Van der Sluis, A. L. Spek, *Acta Crystallogr. Sect. A* **1990**, *46*, 194 – 201.

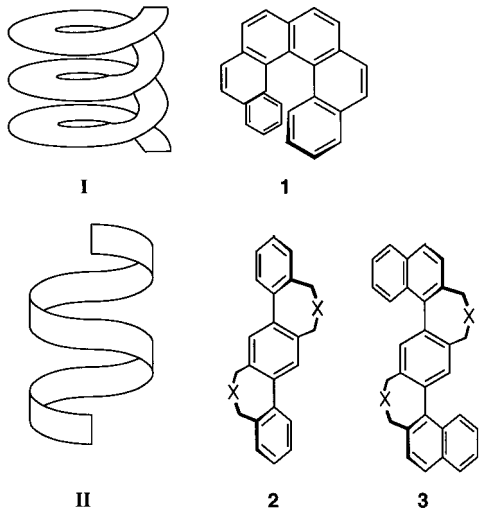
 © WILEY-VCH Verlag GmbH, D-69451 Weinheim, 1998 1433-7851/98/3721-3030 $ 17.50+.50/0

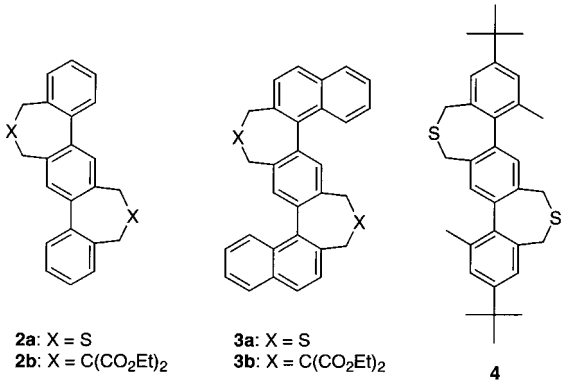
"Geländer" Helical Molecules**

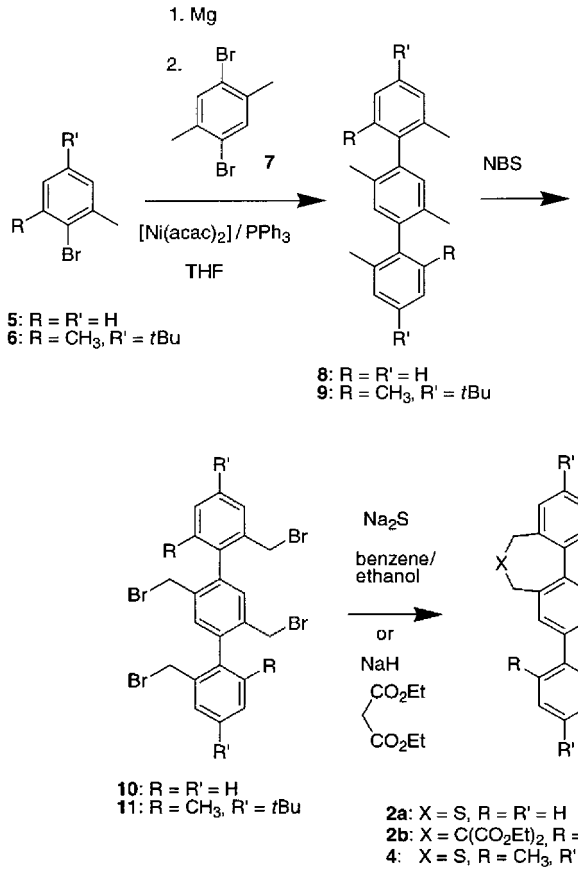
Bernd Kiupel, Christoph Niederalt, Martin Nieger, Stefan Grimme,* and Fritz Vögtle*

Asymmetric catalysis[1] with biphenyl and binaphthyl compounds as chiral ligands results in high enantiomeric excesses.[2] We here report on extended atropisomeric compounds which can serve as a basis for the development of new chiral inductors.

The doubly bridged *p*-terphenylophanes **2**–**4** offer a long type of screw-shaped molecule which had hitherto not been accessible: In contrast to helicenes, whose form is reminiscent of the shape taken by the steps of a spiral staircase (**I**),[3] *ortho*-bridged terphenyls resemble the banisters (German: "Geländer") of such a staircase, which are vertical to the steps (**II**). Owing to the elongated screw shape, **2**–**4** are expected to reveal high chirality like the helicenes.[4] The question arises whether the elongation of the screw (from biphenylo- to terphenylophanes) leads to an increased optical rotation as with the helicenes[3] and doubly helical oligoesters.[5] Clamping the terphenyls with suitable bridging elements should lead to stable conformers at room temperature. Substitution at the position *meta* to the bridges raises their stability on account of sterical hinderance.[6] Racemization barriers and the influence of substituents and bridges on these compounds have been well examined for biphenyls.[7] The solubility of the new helicenes has been increased with *tert*-butyl groups (**4**) and ester-containing bridges (**2b**, **3b**). The synthesis of **2**–**4** is described in Schemes 1 and 2; the fourfold functionalization with *N*-bromosuccinimide (NBS) is the key step.







Scheme 1. Synthesis of **2a**, **2b**, and **4**.

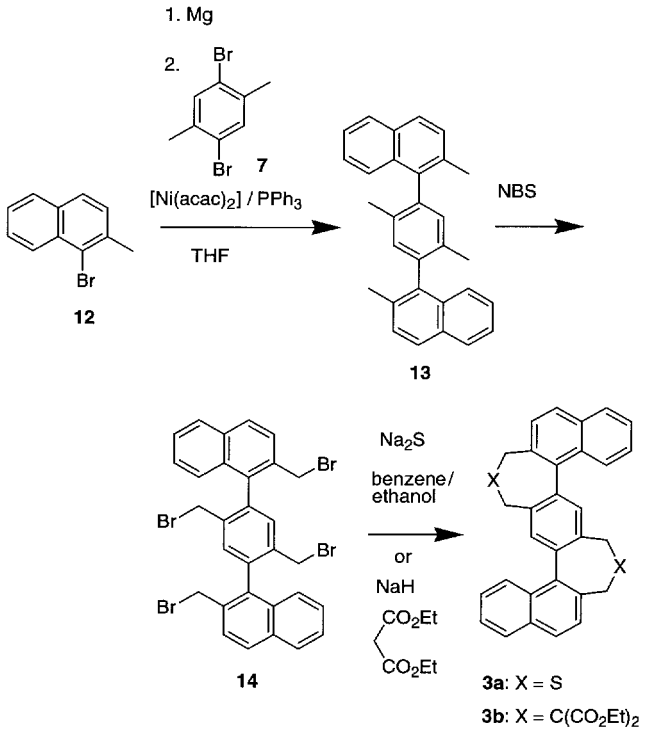
We provided the helical terphenylophane **4** with *tert*-butyl groups to improve the solubility and with methyl groups to raise the racemization barrier. For these geländer helices three stable conformations are possible (Scheme 3). Owing to the hindered rotation about the biphenyl axis and the resulting fixation of the bridges in **2**–**4**, the ^{1}H NMR spectra show geminal couplings of the methyl protons and thus AB systems. There and in the ^{13}C NMR spectra separate signals are observed for the *meso* as well as for the chiral conformers.

The intended sterical hindrance of the methyl groups in **4** or of the naphthalene units in **3a** and **4b** causes an increase in the racemization/inversion barrier relative to those of helices **2a** and **2b**. High-temperature ^{1}H NMR experiments in DMSO

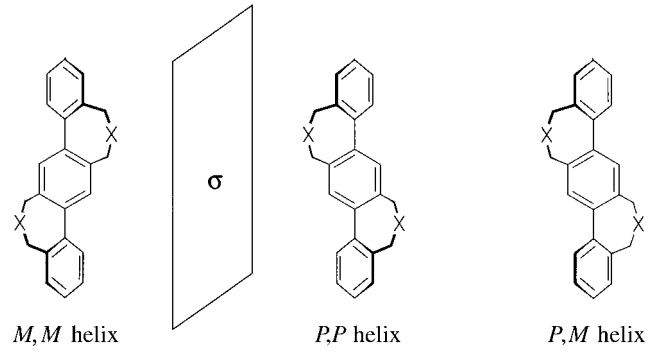
[*] Dr. S. Grimme, Dipl.-Chem. C. Niederalt
Institut für Physikalische und Theoretische Chemie der Universität
Wegeler Strasse 12, D-53115 Bonn (Germany)
E-mail: grimme@rs3.thch.uni-bonn.de
Prof. Dr. F. Vögtle, Dipl.-Chem. B. Kiupel
Kekulé-Institut für Organische Chemie und Biochemie der Universität
Gerhard-Domagk-Strasse 1, D-53121 Bonn
Fax: (+49) 228-73-56-62
E-mail: voegtle@uni-bonn.de
Dr. M. Nieger
Institut für Anorganische Chemie der Universität
Gerhard-Domagk-Strasse 1, D-53121 Bonn

[**] This work was supported by the Deutsche Forschungsgemeinschaft (SFB 334). "Geländer" is the German word for banister (see text).

 © WILEY-VCH Verlag GmbH, D-69451 Weinheim, 1998 1433-7851/98/3721-3031 $ 17.50+.50/0



Scheme 2. Synthesis of **3a** and **3b**.



Scheme 3. Twisted terphenylophanes form three different conformers: two chiral und one *meso* form with an inversion center.

provided $\Delta G^{\neq} > 95\ \mathrm{kJ\,mol^{-1}}$ for **3a** and **3b**. The influence of the sulfur atoms in **2a**, **3a**, and **4** and of the ester substituents in **2b** and **3b** on bond lengths and angles is reflected in the conformational flexibility of the aliphatic bridge. The ester groups increase the energy barrier for the arene–arene rotation in comparison to an unsubstituted propano bridge; this is known for the corresponding biphenyls.[8]

The helices **3a** and **3b** could be separated into their conformers on a chiral HPLC column (cellulose tris(3,5-dimethylphenylcarbamate) (CDMPC),[9] eluent *n*-hexane/2-propanol (200/1), flow rate 1.5 mL min^{-1}, $T = 0\,^{\circ}\mathrm{C}$); **3b** could only be enantiomerically enriched. The circular dichroism (CD) spectrum of the enantiomers of **3a** (Figure 1) shows intensive negative and positive Cotton effects. At 233 nm they are very intensive ($\Delta\varepsilon = +274$, $-265\ \mathrm{L\,mol^{-1}cm^{-1}}$; $g = 3.5 \times 10^{-2}$), the other three maxima ($\lambda = 251$ nm, $\Delta\varepsilon = \pm 7\ \mathrm{L\,mol^{-1}\,cm^{-1}}$, $g = 3.5 \times 10^{-3}$; $\lambda = 265$ nm, $\Delta\varepsilon = \pm 34\ \mathrm{L\,mol^{-1}cm^{-1}}$, $g = 2 \times 10^{-2}$; $\lambda = 308$ nm, $\Delta\varepsilon = 41$, $-43\ \mathrm{L\,mol^{-1}cm^{-1}}$, $g = 2.8 \times 10^{-2}$) have $\Delta\varepsilon$ values of less than ± 50. The specific rotation of the geländer helix **3a** is also quite large ($[\alpha]_{365}^{20} = +2608$, -2612 in CH_2Cl_2). Thus, this new helix type even surpasses some helicenes known for high rotatory strength (and molar rotation) or inherently chiral fullerenes[10] with regard to the $\Delta\varepsilon$ values.

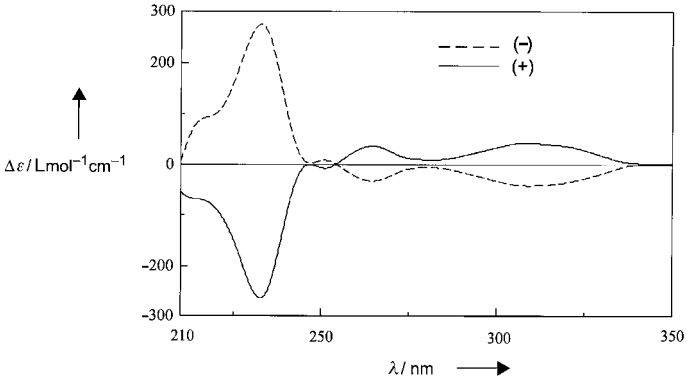


Figure 1. CD spectrum of **3a** (in CH_2Cl_2); CD spectrometer J-720, Jasco, Tokyo.

Colorless crystals of **3b** obtained from DMSO contained only the *meso* form, as the X-ray structure analyses showed (Figure 2a). The separation of the stereoisomers on the chiral HPLC column (see above) proved the *meso* conformer to be formed in excess relative to the enantiomeric forms. A single crystal of **3a** isolated from *n*-hexane/chloroform contained all three possible conformers *MM*, *PM*, and *PP* (Figure 2b).

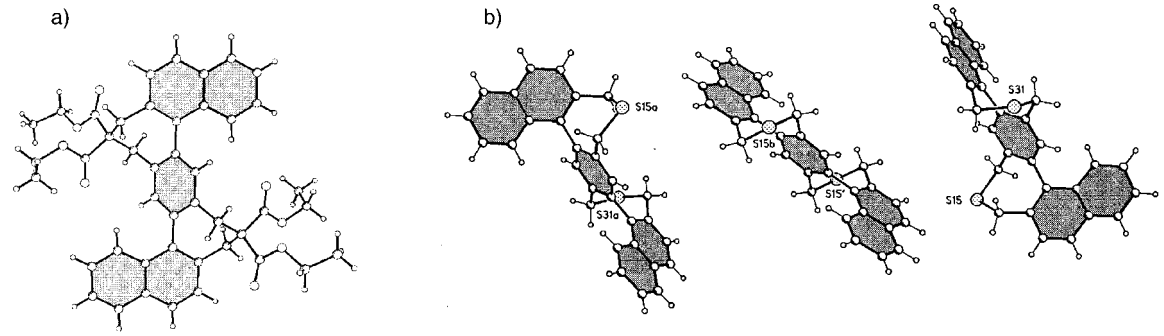


Figure 2. a) Crystal structure of (*P*,*M*)-**3b**; torsion angles 2-1-1′-2′: $-48.0(3)^{\circ}$; **3b** has C_i symmetry, and the angle between the two naphthyl rings is 180°. b) Crystal structure of **3a**, which contains all three conformers; the chiral forms have C_2 symmetry, and the angle between the two naphthyl rings is 73°. The *meso* conformer has the same symmetry as **3b**. Torsion angles for the achiral molecule in the middle: 2-1-1′-2′: $54.9(2)^{\circ}$; torsion angles for the chiral molecules: 2-1-1′-2′: $-52.6(2)^{\circ}$; 3′,4′,1″,2″: $-53.3(2)^{\circ}$.

 © WILEY-VCH Verlag GmbH, D-69451 Weinheim, 1998 1433-7851/98/3721-3032 $ 17.50+.50/0 *Angew. Chem. Int. Ed.* **1998**, *37*, No. 21

Remarkably, some of the crystals reveal optical activity. Solutions of these crystals gave distinct CD spectra, although the *n*-hexane/chloroform mother liquor was not optically active. Separation by HPLC under the conditions described above showed that the crystals contained different fractions of the stereoisomers.[11] A crystal whose solution shows a (+) rotation consists of approximately 20% of the *meso* form, 60% of the (+) enantiomer, and 20% of the (−) enantiomer (a different crystal with (−) rotation in solution is made up of 20% of the *meso* form, 30% of the (+) enantiomer, and 50% of the (−) enantiomer).

The CD spectrum of (*M*,*M*)-**3a** could be theoretically deduced.[12] Figure 3 shows the calculated spectrum, which is very similar to the experimental one (Figure 1) and which allows the determination of the absolute configuration.

As predicted, the elongation of biphenylo- to terphenylophanes results in high rotation values and distinct circular dichroisms. Thus, the geländer helices belong to the group of compounds with the highest $\Delta\varepsilon$ values. We now plan to investigate to what extent these compounds are suitable as ligands[13] in asymmetric catalysis.

Experimental Section

3a: Compound **14** (400 mg, 0.57 mmol) dissolved in benzene (200 mL) was slowly added through a precision dropping funnel to a suspension of sodium sulfide plates (60%; 410 mg, 3.15 mmol) in ethanol/benzene (500 mL, 1/1 v/v); the addition required 7 h. After the mixture was heated at reflux for another 12 h, the solvent was removed in vacuo. Purification of the residue by column chromatography on silica gel (elution with petroleum ether (40/60)/CH_2Cl_2, 3/1; $R_f = 0.18$) gave 139 mg (55% yield) of a colorless solid; m.p. 332 °C; ^{1}H NMR (400 MHz, $CDCl_3$, 25 °C, TMS): $\delta = 3.3-3.8$ (m, 8H), 7.4–7.6 (m, 8H), 7.9–8.1 (m, 6H); ^{13}C NMR (100.6 MHz, $CDCl_3$, 25 °C, TMS): $\delta = 31.70$, 31.80, 32.64, 32.68 (all CH_2S), 125.97, 126.05, 126.77, 126.83, 126.87, 127.10, 128.77, 128.81, 129.44, 129.48, 130.95, 131.03, 131.52, 133.06, 133.75, 133.78, 135.58, 135.85, 135.90, 138.39; MS (EI): *m/z* (%): 446.2 (100) [M^+ ($C_{30}H_{22}S_2$)], 367.2 (37), 353 (13); $[\alpha]_{365}^{20} = +2608, -2612$, $[\alpha]_{436}^{20} = +301, -308$ in CH_2Cl_2.

3b: Under an argon atmosphere sodium hydride (60%; 137 mg, 3.4 mmol) was washed with *n*-hexane by decanting. Then toluene (30 mL) and diethyl malonate (274 mg, 1.7 mmol) were added, and the mixture was heated under reflux for 2 h. Compound **14** (300 mg, 0.43 mmol) dissolved in toluene (20 mL) was added dropwise to the boiling suspension. After the mixture was heated for another 10 h, the solvent was removed in vacuo. The residue was purified by column chromatography on silca gel (elution with CH_2Cl_2/petroleum ether (40/60), 3/1; $R_f = 0.52$) to yield 70 mg (24%) of a colorless solid; m.p. 248 °C; ^{1}H NMR (400 MHz, C_6D_6, 25 °C, TMS): $\delta = 1.02$ (t, ^3J(H,H) = 7.1 Hz, 6H, CH_3), 1.10 (t, ^3J(H,H) = 7.1 Hz, 6H, CH_3), 3.35, 3.48 (d, ^2J(H,H) = 13.8 Hz, 4H, CH_2), 3.58, 3.76 (d, ^2J(H,H) = 13.8 Hz, 4H, CH_2), 3.99–4.16 (m, 4H, OCH_2), 4.23–4.35 (m, 4H, OCH_2), 7.43–7.49 (m, 2H), 7.65–7.72 (m, 4H), 7.74 (s, 2H), 7.78 (d, ^3J(H,H) = 8.4 Hz, 2H), 7.84 (d, ^3J(H,H) = 8.4 Hz, 2H), 8.72 (d, ^3J(H,H) = 8.4 Hz, 2H); ^{13}C NMR (250 MHz, $CDCl_3$, 25 °C, TMS): $\delta = 14.35$, 14.26 (all CH_3), 30.45 (C), 36.85, 37.67 (all CH_2), 61.71, 65.28 (all OCH_2), 125.46, 126.19, 126.41, 127.88, 128.27, 128.35, 131.32, 132.34, 133.24, 133.70, 134.90, 135.94, 136.94, 170.89 (CO_2); MS (FAB): *m/z* (%): 698.3 (100) [M^+ ($C_{44}H_{42}O_8$)], 625.3 (33) [$M^+ - C_3H_5O_2$]; elemental analysis calcd for $C_{44}H_{42}O_8 \cdot 0.13\,CH_2Cl_2$: C 74.68, H 6.00; found: C 74.67, H 6.21.

Crystal structure analyses: Single crystals of **3a** were obtained by slow evaporation of a solution of chloroform/hexane (1/1 v/v). Colorless single crystals of **3b** were obtained by cooling in DMSO. **3a** [**3b**] $C_{30}H_{22}S_2$ [$C_{44}H_{42}O_8$], Nonius Kappa-CCD [Nonius MACH 3], $Mo_{K\alpha}$ radiation (λ = 71.073 pm) [$Cu_{K\alpha}$ radiation (λ = 154.178 pm)], 123(2) [200] K, triclinic, $P\bar{1}$ (no. 2) [monoclinic, $P2_1/c$ (no. 14)]; $a = 1084.38(2)$ [1294.9(1)], $b = 1135.63(4)$ [1151.6(1)], $c = 1472.72(5)$ [1222.8(1)] pm, $\alpha = 73.222(2)°$, $\beta = 78.281(2)°$ [92.61(1)°], $\gamma = 74.078(2)°$, $V = 1.65458(9)$ [1.8216(3)] nm^3, $Z = 3$ [4], $\rho = 1.345$ [1.274] g cm^{-3}, crystal dimensions: $0.50 \times 0.48 \times 0.18$ [$0.43 \times 0.40 \times 0.20$] mm, range for data collection $2\theta_{max} = 56°$ [140°], refections collected 26002 [3971], independent reflections 6171 [3418] ($R_{int} = 0.024$ [0.029]). The structures were solved by direct methods; non-hydrogen atoms were refined anisotropically on F^2, and hydrogen atoms with a riding model. The final *R* value *wR*2 (F^2) was 1.072 [1.036] for 433 [235] parameters. *R*1 = 0.0323 [0.067] (for $I > 2\sigma(I)$), *wR*2 = 0.0907 [0.1883] (all data). For **3b** an absorption correction on the basis of Ψ scans was applied. Crystallographic data (excluding structure factors) for the structures reported in this paper have been deposited with the Cambridge Crystallographic Data Centre as supplementary publication no. CCDC-101385. Copies of the data can be obtained free of charge on application to CCDC, 12 Union Road, Cambridge CB2 1EZ, UK (fax: (+44) 1223-336-033; e-mail: deposit@ccdc.cam.ac.uk).

Received: May 8, 1998 [Z11831IE]
German version: *Angew. Chem.* **1998**, *110*, 3206–3209

Keywords: chirality · circular dichroism · enantiomeric resolution · helical structures · terphenyls

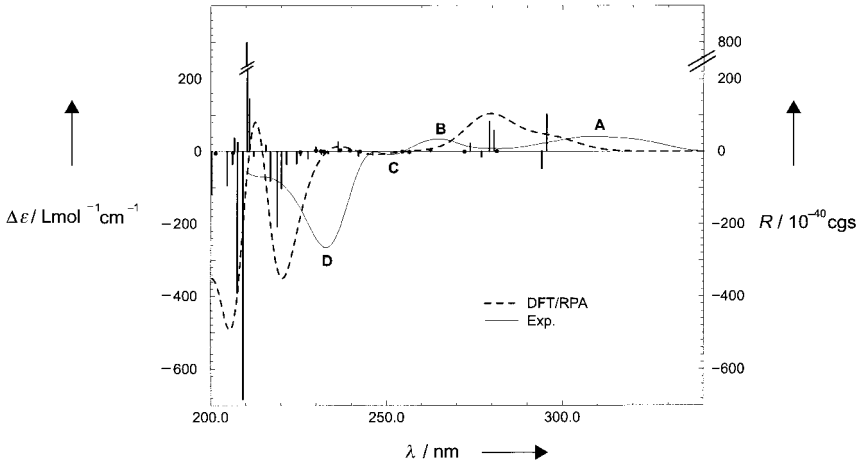


Figure 3. Calculated (DFT/RPA) and experimental CD spectrum for (*M*,*M*)-**3a**. *R* = rotational strength.

[1] Reviews: a) I. Ojima, *Catalytic Asymmetric Synthesis*, VCH, Weinheim, **1993**; b) E. L. Eliel, S. H. Wilen, *Stereochemistry of Organic Compounds*, Wiley, New York, **1994**; c) S. Hauptmann, G. Mann, *Stereochemie*, Spektrum, Heidelberg, **1996**, pp. 240–258; d) B. Cornils, W. A. Herrmann, *Applied Homogeneous Catalysis with Organometallic Compounds I, II*, VCH, Weinheim, **1996**; e) E. L. Eliel, S. H. Wilen, *Organische Stereochemie* (Eds.: H. Hopf, J. Mulzer), WILEY-VCH, Weinheim, **1998**, p. 549.

[2] a) R. Noyori, *Chem. Soc. Rev.* **1989**, *18*, 187–208; b) R. Noyori, *Tetrahedron* **1994**, *50*, 4259–4278.

[3] a) M. S. Newman, W. B. Lutz, D. Lednicer, *J. Am. Chem. Soc.* **1955**, *77*, 3420–3421; b) M. S. Newman, D. Lednicer, *J. Am. Chem. Soc.* **1956**, *78*, 4765–4770; c) R. H. Martin, *Angew. Chem.* **1974**, *86*, 727–738; *Angew. Chem. Int. Ed. Engl.* **1974**, *13*, 649–660; d) W. H. Laarhoven, W. J. Prinsen, *Top. Curr. Chem.* **1984**, *125*, 63; e) K. P. Meurer, F. Vögtle, *Top. Curr. Chem.* **1985**, *127*, 1; f) S. Grimme, J. Harren, A. Sobanski, F. Vögtle, *Eur. J. Org. Chem.* **1998**, 1491–1509.

[4] It is possible to arrange the chirality of closely related structures and to say "more" and "less" chiral with regard to the molecular structures as well as to the chiroptical properties. Further details: a) "An Epistemological Note on Chirality": K. Mislow, P. Bickart, *Isr. J. Chem.* **1976/1977**, *15*, 1–6; b) A. B. Buda, T. Auf der Heyde, K. Mislow, *Angew. Chem.* **1992**, *104*, 1012–1031; *Angew. Chem. Int. Ed. Engl.* **1992**, *31*, 989–1031; for a new method for the quantification of the chirality of molecules, see S. Grimme, *Chem. Phys. Lett.*, in press.

[5] K. Nozaki, T. Terakawa, H. Takaya, T. Hiyama, *Angew. Chem.* **1998**, *110*, 138 – 141; *Angew. Chem. Int. Ed.* **1998**, *37*, 131 – 133.
[6] a) W. E. Truce, D. D. Emrick, *J. Am. Chem. Soc.* **1956**, *78*, 6130 – 6137; b) K. Mislow, *Angew. Chem.* **1958**, 683 – 689; c) K. Mislow, H. B. Hopps, *J. Am. Chem. Soc.* **1962**, *84*, 3018 – 3020; d) K.Mislow, M. A. W. Glass, H. B. Hopps, E. Simon, G. H. Wahl, *J. Am. Chem. Soc.* **1964**, *86*, 1710 – 1733.
[7] a) K. Müllen, W. Heinz, F.-G. Klärner, W. R. Roth, I. Kindermann, O. Adamczak, M. Wette, J. Lex, *Chem. Ber.* **1990**, *123*, 2349 – 2371; b) C. Wolf, W. A. König, C. Roussel, *Liebigs Ann.* **1995**, 781 – 786.
[8] K. Mislow, M. A. W. Glass, R. E. O'Brien, P. Rutkin, D. H. Steinberg, J. Weiss, C. Djerassi, *J. Am. Chem. Soc.* **1962**, *84*, 1455 – 1478.
[9] a) Y. Okamoto, K. Hatano, R. Aburatani, K. Hatada, *Chem. Lett.* **1989**, 715 – 718; b) Y. Okamoto, E. Yashima, *Angew. Chem.* **1998**, 110, 1072 – 1095.
[10] Review: F. Diederich, C. Thilgen, A. Herrmann, *Nachr. Chem. Tech. Lab.* **1996**, *44*, 9 – 10, 12 – 14, 16.
[11] A. Collet, *Compr. Supramol. Chem.* **1996**, *10*, 113 – 149.
[12] Theoretical methods: The geometry was optimized in C_2 symmetry with the TURBOMOLE[12a] suite of programs at the Hartree – Fock – SCF level. A split-valence (SV) basis set[12b] was used, which was augmented with a polarization d function ($\alpha_d = 0.55$) at the sulfur atoms. The CD spectrum (exitation energies and rotatory strength) was caculated with a method[12c,d] combining the Kohn – Sham density functional theory (DFT) and the random phase approximation (RPA).[12e] The DFT calculations were performed with the TURBOMOLE suite of programs, whereby the B3-LYP exchange-correlation functional[12f] and a SV(P) basis set ($\alpha_d(C) = 0.8$, $\alpha_d(S) = 0.55$) were employed. In this case (and in usual) this method—containing only global empirical parameters, which are not adjusted to specific molecular systems—leads to errors in the excitation energies below 0.3 eV. A portion of the deviations from the experimental spectrum can possibly be explained by solvent effects. a) R. Ahlrichs, M. Bär, M. Häser, H. Horn, C. Kölmel, *Chem. Phys. Lett.* **1989**, *162*, 165 – 169; b) A. Schäfer, H. Horn, R. Ahlrichs, *J. Chem. Phys.* **1992**, *97*, 2571 – 2577; c) S. Grimme, *Chem. Phys. Lett.* **1996**, *259*, 128 – 137; d) S. Grimme, Habilitationsschrift, Universität Bonn, **1996**; e) T. H. Dunning, V. McKoy, *J. Chem. Phys.* **1967**, *47*, 1735 – 1747; f) A. D. Becke, *J. Chem. Phys.* **1993**, *98*, 5648 – 5652.
[13] We have already synthesized from **14** the tetrakis(diphenylphosphanyl oxide) compound, which can be reduced to tetraphosphane.

Modified, Amorphous Titania—A Hybrid Semiconductor for Detoxification and Current Generation by Visible Light**

Horst Kisch,* Ling Zang, Christian Lange, Wilhelm F. Maier, Christina Antonius, and Dieter Meissner

Although titania (titanium dioxide, TiO_2) absorbs only 2 – 3 % of the solar light reaching the surface of the earth, it is the best investigated semiconductor in the field of chemical conversion and storage of solar energy. While early work was predominantly concerned with photoelectrochemical conversion,[1–3] later investigations focused on chemical processes, especially on water cleavage.[4] More recently, detoxification of water has become the main topic since upon UV irradiation in the presence of oxygen titania is able to oxidize most organic and inorganic contaminants to harmless products such as carbon dioxide and mineral acids.[5, 6]

According to the proposed mechanism, the light-generated electron-hole pair in titania is trapped at surface sites at which interfacial electron transfer occurs from and to adsorbed substrates.[7] To obtain a more efficient utilization of solar light ($\lambda_{max} = 500$ nm), diverse efforts were made to shift the light sensitivity of titania ($E_{bg} = 3.2$ eV, $\lambda \leq 390$ nm) into the visible region. A classical example is the photosensitization of the photocurrent by dyes and transition metal complexes of the type $[RuL_3]^{2+}$ (L = a substituted 2,2′-bipyridyl ligand).[8, 9] Doping with ions of V, Cr, Mn, Fe, Co, Ni, and Cu results in a shift of light absorption into the visible range, but only in very few cases does it also enable generation of a current or a chemical reaction by visible light.[10] An example is the decomposition of NO_x, although it is unclear whether or not this process occurs through a semiconductor photocatalysis mechanism.[11] It was further reported that colloidal titania doped with 0.1 to 50 atom % of iron induces the degradation of dichloroacetate with visible light. However, concomitant cathodic dissolution of the iron(III) oxide occurs, which can be avoided only by addition of oxidizing agents like hydrogen peroxide.[12]

Typical for all mentioned investigations is that the crystalline modifications anatase and rutile were involved, while amorphous titania was reported to not be photoactive.[13] In connection with our work on the use of amorphous zinc and cadmium sulfide as photocatalysts for new chemical syntheses,[14] we have now found that amorphous, microporous titania (AMM-Ti) modified with transition metal salts induces a photocurrent and photocatalyzes the degradation of 4-chlorophenol with visible light.

The new hybrid photocatalysts were prepared by a sol – gel procedure through controlled hydrolysis of titanium alkoxides in the presence of disodium hexachloroplatinate, rhodium(III) chloride, and gold(III) chloride[15]. The obtained microporous powders display specific surface areas in the range of 160 – 200 $m^2 g^{-1}$ and a pore-size distribution with a maximum at 0.78 nm, and are amorphous according to X-ray diffraction. In agreement with the latter, no crystalline parts could be detected by high-resolution transmission electron micrography. The ESCA and EXAFS investigations (ESCA = electron spectroscopy for chemical analysis, EXAFS = extended X-ray absorption fine structure) of a sample of AMM-Ti doped with 1.1 % Pt^{IV} (**1**) revealed that platinum is present in the oxidation state IV and surrounded by four chloride ions. The EDX analyses (EDX = energy dispersive X-ray) with a lateral resolution of 1 – 2 nm do not give any evidence for the presence of discrete platinum particles. Therefore, it is assumed that platinum tetrachloride is homogeneously distributed in the matrix of amorphous titania.[16]

The diffuse reflectance spectrum of **1** resembles that of unmodified AMM-Ti, but exhibits an additional absorption in

[*] Prof. Dr. H. Kisch, Dr. L. Zang
Institut für Anorganische Chemie der Universität Erlangen-Nürnberg
Egerlandstrasse 1, D-91058 Erlangen (Germany)
Fax: (+49) 9131-858363
E-mail: kisch@anorganik.chemie.uni-erlangen.de
Dipl.-Chem. C. Lange, Prof. Dr. W. F. Maier
Max-Planck-Institut für Kohlenforschung, Mülheim an der Ruhr (Germany)
Dipl.-Chem. C. Antonius, Dr. D. Meissner
Institut für Energieverfahrenstechnik, Forschungszentrum Jülich (Germany)

[**] Heterogeneous Photocatalysis, part 18. This work was supported by the Fonds der Chemischen Industrie. L.Z. thanks the Alexander-von-Humboldt-Stiftung for a stipend. Part 17: P. Johne, H. Kisch, *J. Photobiol. Photochem. A Chem.* **1997**, *111*, 223.

 © WILEY-VCH Verlag GmbH, D-69451 Weinheim, 1998 1433-7851/98/3721-3034 $ 17.50+.50/0

the range of 400 – 550 nm, which is assigned to the platinum(IV) chloride centers (Figure 1).[17] When an electrode coated with **1** was irradiated at different wavelengths in a standard photoelectrochemical cell, a photocurrent was observed also in the visible region; that was not the case when unmodified titania was employed. It is evident from Figure 1 that the wavelength dependence of the photocurrent follows the absorption spectrum. The same result was

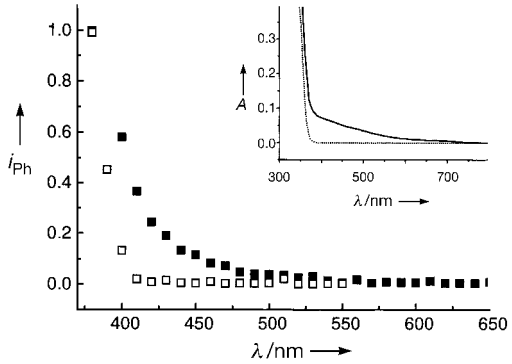


Figure 1. Photocurrent action spectrum for TiO_2 (Degussa P-25) (□) and **1** (■; in both cases the semiconductor powder was precipitated onto the ITO glass electrode (ITO = indium tin oxide) from an aqueous suspension. The photocurrent i_{ph} (arbitrary units) was measured in a conventional three-electrode arrangement (platinum and Ag/AgCl as counter and reference electrode, respectively, 0.1M NaOH as electrolyte), and a potential of 0.5 V (Ag/AgCl) was applied to the photoelectrode. The insert shows the diffuse reflectance spectra of TiO_2 (Degussa P-25, ••••) and **1** (——); the absorbance A is plotted as a Kubelka – Munk function.

obtained when the action spectrum was measured not potentiostatically but under short-circuit conditions to ensure careful exclusion of any external voltage.

To test the photocatalytic activity, the degradation of 4-chlorophenol, an ubiquitous contaminant in water, was investigated; it is well known that upon irradiation with UV light crystalline titania catalyzes complete mineralization to water, carbon dioxide, and hydrogen chloride.[5] Surprisingly, **1** enables this reaction to occur even with visible light ($\lambda \geq$ 455 nm, Figure 2), and the wavelength dependence of the apparent disappearance quantum yield is comparable with its

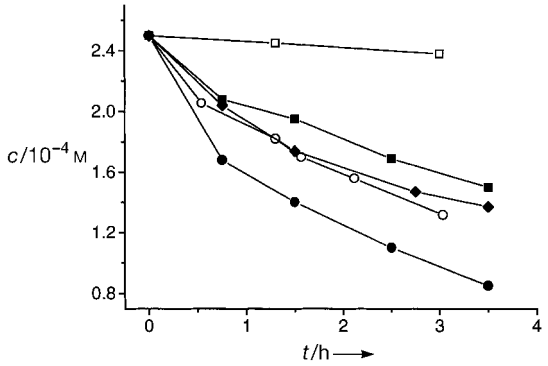


Figure 2. The decrease in 4-chlorophenol concentration ($c_0 = 2.5 \times 10^{-4}$M) upon irradiation of an aqueous suspension (0.5 gL^{-1}) of the semiconductor powder with visible light (Osram XBO 150-W xenon lamp, cut-off filter $\lambda \geq 455$ nm). □: TiO_2 (Degussa P-25); ■: 0.7% Pt^{IV}/AMM-Ti; ○: 1.1% Pt^{IV}/AMM-Ti, ●: 3.0% Pt^{IV}/AMM-Ti, ◆: 4.0% Pt^{IV}/AMM-Ti.

absorption spectrum (Figures 1, 3). Even after an irradiation time of 6 h the photocatalyst was deactivated only to a minor extent, since the degradation rate decreased only by 10% when the photocatalyst was employed in a second experiment. AMM-Ti powders modified with gold(III) choride and rhodium(III) chloride have similar photocatalytic properties.

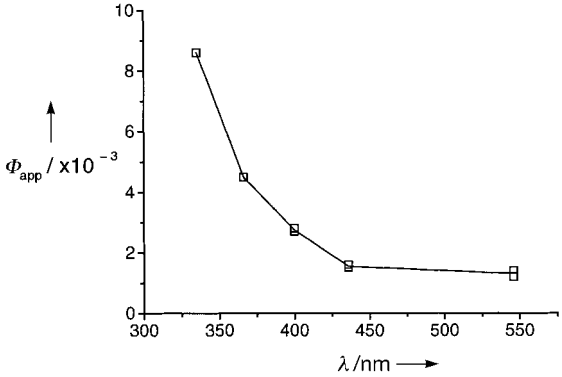
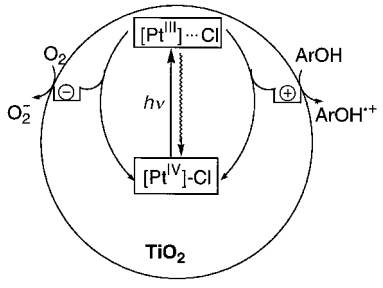


Figure 3. Wavelength dependence of the apparent disappearance quantum yield (Φ_{app}, uncorrected for light scattering) of the degradation of 4-chlorophenol photocatalyzed by **1**.

These results significantly differ from those for metal ion doped crystalline titania samples, which may absorb visible light but do not induce chemical transformations. The highest degradation rates were found when the platinum content in AMM-Ti was 3.0%. Formation of stoichiometric amounts of CO_2 and HCl was demonstrated by gravimetric and acidometric methods.[18] In the absence of air or upon reduction of Pt^{IV} to Pt^0, only negligible degradation was observed.[19] Platinum-free, white AMM-Ti exhibited only a very weak activity, irrespective of excitation in the UV or visible spectral region. The analogously prepared silica AMM-Si doped with 1.1% Pt^{IV} was inactive, while an aqueous solution of $PtCl_4$ induced a stoichiometric degradation.[20]

Both the photoelectrochemical and photochemical results suggest the presence of semiconductor photocatalysis, although a new mechanism of charge generation seems to operate. For a working hypothesis we propose that the titania matrix functions as a charge trap for the electronically excited platinum chloride component (Scheme 1).[21, 22] The thus formed surface redox centers (trapped charges) subsequently induce the multistep degradation of 4-chlorophenol by analogy with crystalline titania.[5, 23] In accordance with this



Scheme 1. Postulated mechanism of the photoinduced charge separation at amorphous, microporous **1**. Ar = 4-ClC_6H_4.

 © WILEY-VCH Verlag GmbH, D-69451 Weinheim, 1998 1433-7851/98/3721-3035 $ 17.50+.50/0

proposal the photocatalytic activity strongly depends on the electronic nature of the amorphous matrix.[20]

Received: April 21, 1998 [Z 11761 IE]
German version: *Angew. Chem.* **1998**, *110*, 3201 – 3203

Keywords: amorphous materials · photochemistry · sol – gel processes · titanium

[1] H. Gerischer, *Electrochim. Acta* **1990**, *35*, 1677.
[2] R. Memming, *Top. Curr. Chem*. **1988**, *143*, 79.
[3] A. J. Bard, *Science* **1980**, *207*, 139.
[4] a) K. Honda, A. Fujishima, *Nature* **1972**, *238*, 37; b) D. Meissner, R. Memming, B. Kastening, *Chem. Phys. Lett.* **1983**, *96*, 34.
[5] a) M. R. Hoffmann, S. T. Martin, W. Choi, D. W. Bahnemann, *Chem. Rev.* **1995**, *95*, 69, and references therein; b) D. W. Bahnemann, *Nachr. Chem. Tech. Lab.* **1994**, *42*, 378.
[6] N. Negishi, T. Iyoda, K. Hashimoto, A. Fujishima, *Chem. Lett*. **1995**, 841.
[7] A. L. Linsebigler, G. Lu, J. T. Yates, Jr., *Chem. Rev*. **1995**, *95*, 735; A. Meier, D. Meissner in *Nanoparticles in Solids and Solutions* (Eds.: J. H. Fendler, I. Dekany), Kluwer, Dordrecht, **1996**, pp. 421 – 449.
[8] P. V. Kamat, *Chem. Rev*. **1993**, *93*, 267.
[9] B. O'Regan, M. Grätzel, *Nature* **1991**, *353*, 737.
[10] K. Takahama, N. Nakagawa, K. Kishimoto, JP 09192496 A2, **1997**.
[11] Y. Ichihashi, H. Yamashita, M. Anpo, *Functional Materials* **1996**, *16*, 12.
[12] D. W. Bahnemann, D. Bockelmann, R. Goslich, M. Hilgendorff in *Aquatic and Surface Photochemistry* (Eds.: G. R. Helz, R. G. Zepp, D. G. Crosby), Lewis, Boca Raton, FL, **1994**, pp. 349 – 367.
[13] B. Ohtani, Y. Ogawa, S. Nishimoto, *J. Phys. Chem.* **1997**, *101*, 3746.
[14] H. Keck, W. Schindler, F. Knoch, H. Kisch, *Chem. Eur. J*. **1997**, *3*, 1638.
[15] W. F. Maier, I.-C. Tilgner, M. Wiedorn, H.-C. Ko, *Adv. Mater.* **1993**, *10*, 726; S. Klein, J. Martens, R. Parton, K. Vercuysse, P. A. Jacobs, W. F. Maier, *Catal. Lett*. **1996**,*38*, 209; W. F. Maier, DE 4303610.4, **1993**.
[16] L. Zang, Ch. Lange, W. F. Maier,I. Abraham, S. Storck, H. Kisch, *J. Phys. Chem.*, in press.
[17] By analogy to the spectrum in solution; L. E. Cox, D. G. Peters, E. L. Wehry, *Inorg. Nucl. Chem. Lett.* **1972**, *34*, 297.
[18] CO_2 as $BaCO_3$, HCl through measuring the pH value before (pH 7) and after irradiation (pH 2.7, after degradation of a 2.5×10^{-3} M solution of 4-chlorophenol).
[19] This is also a basic difference to crystalline TiO_2, the Pt^0 loading of which in general accelerates the rate of a photoreaction.
[20] W. Macyk, H. Kisch, unpublished results.
[21] The homolytic cleavage of the Pt–Cl bond is known from the photochemistry in homogeneous solution: P. C. Ford, D. Wink, J. Dibenedetto, *Prog. Inorg Chem.* **1983**, *30*, 213.
[22] From Figure 1 a threshold wavelength of about 500 nm (2.5 eV) is extracted. From that one can estimate that the reactive TiO_2 surface centers are located around 0.7 eV below the conduction and valence band edges, respectively. The potential of Cl/Cl^- is 2.6 V (normal hydrogen electrode): S. D. Malone. J. F. Endicott, *J. Phys. Chem.* **1972**, *76*, 2223.
[23] Superoxide is involved also in the secondary reactions of the radical cation, most likely through hydrogen abstraction by the HO_2 radical formed by its protonation.[5a]

Synthesis, Electrochemistry, and Spectroscopy of Blue Platinum(II) Polyynes and Diynes**

Muhammed Younus, Anna Köhler, Stephane Cron, Nazia Chawdhury, Muna R. A. Al-Mandhary, Muhammad S. Khan, Jack Lewis, Nicholas J. Long, Richard H. Friend, and Paul R. Raithby*

Conjugated polymers continue to attract great interest because of their potential use as organic semiconductors in optoelectronic devices such as light-emitting diodes,[1] lasers,[2] photocells,[3, 4] and field-effect transistors.[5] Organometallic conjugated polymers such as transition metal σ-acetylide polymers[6] provide information on the photophysical processes that occur in organic conjugated polymers.[7] Organometallic polymers of general formula **A** can be modified by

$$[-M(L)_n-C\equiv C-X-C\equiv C-]_\infty \qquad \mathbf{A}$$

(M = Fe, Ru, Os, Ni, Pd, Pt; L = phosphane or arsane, X = aromatic spacer)

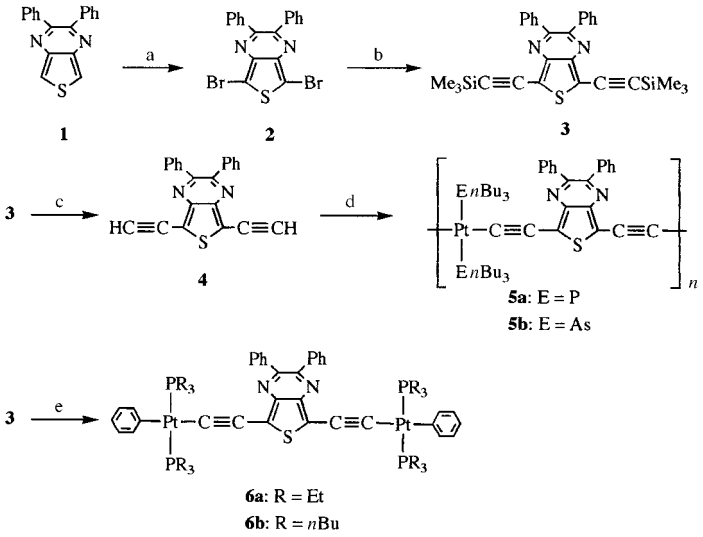
changing the metal, the auxiliary ligands, or the spacer.[8, 9] Most metal polyyne polymers characterized so far have large band gaps in the range of 2.4 – 3.2 eV,[8, 10, 11] which compare unfavorably with those of some new conjugated organic polymers (< 1 eV).[12, 13] These organic polymers were designed by using the concept[14] of alternating donor (electron-rich thiophene) and acceptor (electron-deficient thieno[3,4-*b*]pyrazine) units. With the aim of preparing a metal polyyne polymer with a band gap smaller than 2 eV, we synthesized a soluble donor – acceptor polymer in which an *n*-butylphosphane-substituted platinum(II) acetylene group acts as donor, and a thieno[3,4-*b*]pyrazine as acceptor.

The synthesis of the thieno[3,4-*b*]pyrazine ligand and of the platinum(II) polymer is summarized in Scheme 1. The compounds dibromo-5,7-diphenyl-2,3-thieno[3,4-*b*]pyrazine (**2**) and diphenyl-2,3-trimethylsilylethynyl-5,7-thieno[3,4-*b*]pyrazine (**3**) were prepared by literature methods.[15, 16] Treatment of **3** with four equivalents of K_2CO_3 afforded 2,3-ethynyl-5,7-thieno[3,4-*b*]pyrazine **4** as a brownish yellow, air- and light-sensitive solid in 75 % yield. The polymeric and dimeric

[*] Dr. P. R. Raithby, Dr. S. Cron, Prof. the Lord J. Lewis
University Chemical Laboratory
Lensfield Road, Cambridge, CB2 1EW (UK)
Fax: (+44) 1223-336362
E-mail: prr1@cam.ac.uk
Dr. M. Younus, Dr. N. J. Long
Department of Chemistry
Imperial College of Science, Technology and Medicine
South Kensington, London SW7 2AY (UK)
Dr. A. Köhler, N. Chawdhury, Prof. R. H. Friend
Cavendish Laboratory, University of Cambridge
Madingley Road, Cambridge, CB3 0HE (UK)
Dr. M. R. A. Al-Mandhary, Dr. M. S. Khan
College of Science, Sultan Qaboos University
PO Box 36, Al-Khod 123 (Sultanate of Oman)

[**] We wish to thank the French Foreign Office (Bourse Lavoisier; S.C.), Peterhouse (A.K.), the Cambridge Commonwealth Trust, and the ORS (M.Y.) for financial support and Johnson Matthey plc for a generous loan of platinum salts. We also thank Tuck-Mun Yong for molecular weight determinations and Dr. Malcolm Halcrow for helpful discussions. This work was supported by EPSRC.

 © WILEY-VCH Verlag GmbH, D-69451 Weinheim, 1998 1433-7851/98/3721-3036 $ 17.50+.50/0



Scheme 1. Synthesis of **4**–**6**: a) *N*-bromosuccinimide, CH_3COOH, $CHCl_3$; b) $Me_3SiC{\equiv}CH$, CuI, $Pd(OOCCH_3)_2$, PPh_3, iPr_2NH; c) K_2CO_3 (4 equiv), MeOH; d) *trans*-$[PtCl_2(PnBu_3)_2]$ or *trans*-$[PtCl_2(AsnBu_3)_2]$, CuI, iPr_2NH; e) e) 1) nBu_4NF, THF, 2) *trans*-$[PtCl(PR_3)_2(Ph)]$ (2 equiv), CuI, Et_2NH, CH_2Cl_2.

complexes of platinum were synthesized by classical condensation reactions between diterminal alkynes and platinum chlorides.[17] The reaction of freshly prepared diyne **4** with one equivalent of *trans*-$[PtCl_2(PnBu_3)_2]$ in the presence of CuI in diisopropylamine at 0 °C gave the deep blue polymer **5a** in 43 % yield. The average molecular weight of the polymer was determined by gel-permeation chromatography (GPC) to be 14006, which corresponds to an average value of $n = 15$. We were unable to prepare pure dimetallic complexes from **4** and two equivalents of *trans*-$[PtCl_2(PEt_3)_2]$, as the reaction gave a mixture of oligomers which could not be separated. Therefore, **4** was treated with two equivalents each of *trans*-$[PtCl(PEt_3)_2(Ph)]$ and *trans*-$[Pt(PnBu_3)_2Cl(Ph)]$, in which one coordination site is protected by a phenyl group, in CH_2Cl_2/Et_2NH in the presence of Cu^I at 20 °C to afford the pure platinum dimers **6a** and **6b** in about 70 % yield. The spectroscopic and analytical data are in accord with the proposed formulations of the new compounds. The metal complexes are all air-stable and soluble in common organic solvents. The reaction of one equivalent of *trans*-$[PtCl_2(AsnBu_3)_2]$ with **4** gave **5b** in 40 % yield. The average molecular weight of this polymer was $M = 17375$ ($n = 17$) according to GPC.

The electrochemical properties of the ligand **3** and of the metal complexes were studied by cyclic voltammetry (Table 1). The ligand showed a reversible reduction wave, as was observed for analogous organic polymers.[12, 13] We attribute this to the reduction of the thieno[3,4-*b*]pyrazine unit. The metal complexes **6a** and **6b** show one quasi-reversible and two irreversible oxidation waves for the stepwise two-electron oxidation at the platinum center [Eq. (1)]. The reference

$$Pt^{2+} \rightarrow Pt^{3+} + e^- \rightarrow Pt^{4+} + 2e^- \quad (1)$$

complex *trans*-$[Pt(C{\equiv}C\text{-}p\text{-}C_6H_4C{\equiv}CH)(PEt_3)_2(Ph)]$ also shows an irreversible oxidation wave (at +0.77 V), and Sato et al. reported an irreversible anodic wave at +0.61 V for *trans*-$[Pt(C_6H_4\text{-}p\text{-}CH_3)(C{\equiv}C\text{-}p\text{-}C_6H_5)(PPh_3)_2]$.[18]

Table 1. Absorption maxima λ_{max}, extiction coefficients ε, band gaps E_{gap}, and redox potentials of the ligand and platinum complexes.

Compd	λ_{max}[a] [nm] ($\lg\varepsilon$)	E_{gap} [eV][a] (in solid state)	$E_{1/2}$(ox)[b] [V]	$E_{1/2}$(red)[b] [V]
3	457 (3.91)	2.40 (2.36)	–	– 1.61
5a	627 (4.11)	1.77 (1.72)	+ 0.21,[c] + 1.03[c]	–
6a	583 (3.94)	1.83 (1.76)	+ 0.040 + 0.67,[c] + 0.92[c]	– 1.71[c]
6b	585 (3.71)	1.82	+ 0.003 + 0.65,[c] + 0.94[c]	–

[a] In CH_2Cl_2. [b] 0.1 M $[nBu_4N][BF_4]$ in CH_2Cl_2, Pt electrode, scan rate 100 $mV s^{-1}$, Ag wire reference electrode. [c] Irreversible process. All electrode potentials are relative to that of ferrocene in the same system.

The absorption spectra of **2**, **3**, **5a**, and **6a** are shown in Figure 1. The position of band I is lowered significantly (by 0.7 eV) when the metal is introduced—that is, on going from **3** to **5a**—in accordance with our expectations for a donor–acceptor compound.[14] In contrast to similar compounds,[7, 10] there is hardly any further shift on going from the monomer **6a** to the polymer **5a**. Hence, the lowest excited state is confined to a single repeat unit.

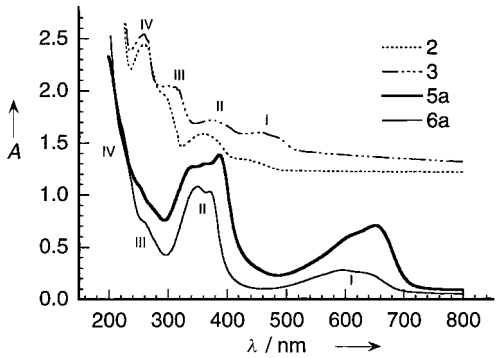


Figure 1. Absorption *A* of **2**, **3**, **5a**, and **6a**. The spectra have been scaled and shifted vertically for comparison and are not corrected for reflection. I–IV denote the different absorption bands.

The low band gap of **5a** allows the measurement of the photocurrent in a sandwich-type diode structure not only for excitation in absorption band I, but also for excitation in absorption bands II, III, and IV. We found that photoconductivity is associated with each of the higher energy absorption bands (Figure 2). In air, a photocurrent quantum yield of up to 1 % at 400 nm is attained, which is unusually high for single-layer sandwich diodes. This UV photoelectric behavior prompted analogous research on conjugated organic polymers.[19]

The photoluminescence spectra of **2**, **3**, and **5a** have very similar shapes, but the energetic position of the emission is

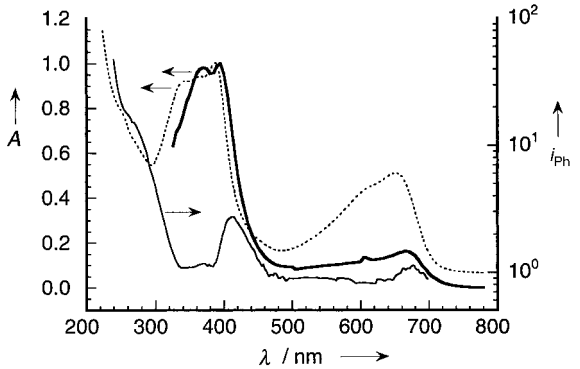


Figure 2. Absorption A of **5a** (dotted line) and photocurrent i_{Ph} (electrons per incident photon, corrected for the absorption of the electrode) of the Al/**5a**/indidum tin oxide photocell (thick line)and the Al/**5a**/Au photocell (thin line).

shifted (Figure 3). The peak at 695 nm in the emission spectrum of **3** disappears in dilute solution and can therefore be attributed to interchain interactions. From the similar form of the emission bands of ligand and polymer, we infer that the emission is mainly due to the $\pi-\pi^*$ transition of the conjugated ligand, although the energy levels of the orbitals involved are shifted by strong interaction with the metal center.

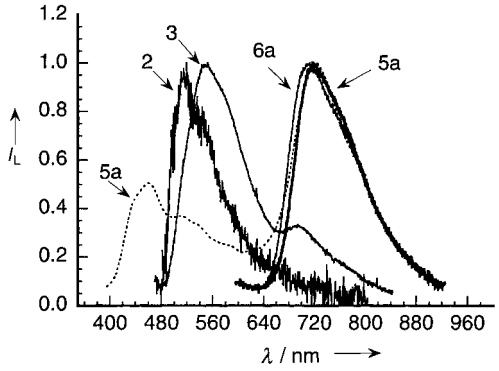


Figure 3. Photoluminescence spectra of **2**, **3**, **5a**, and **6a**, normalized to unity at the emission maxima. The excitation wavelength was 457 nm for **2** and **3**, 514 nm for **5a** (thick solid line) and **6a**, and 334–365 nm for **5a** (dotted line, smoothed data).

The low energy level of **5a** allows excitation in absorption band II. An additional high-energy emission at 460 nm is observed (Figure 3). Emission from higher excited states is unusual for most molecules, but well known for azulene and its derivatives.[20] For azulene, this is attributed to the large energy gap of about 1.5 eV between the S_2 and S_1 excited states.[20] Polymer **5a** also has a large S_2-S_1 gap of 1.3 eV and contains a similarly extended conjugated chromophore unit in the bridging ligand.

The low-energy emission of **5a** and **6a** at 715 nm is atypical for polymers of structure **A**. Polymers and monomers with other spacers X typically show a fine structure in the emission spectrum that is already evident at 20 °C[21] and particularly pronounced at low temperatures.[8–11, 22] In **5a** and **6a**, the only remnant of such a structure is very weak shoulder around 775 nm. Compounds with structure **A** also typically exhibit a strong emission from a triplet excited state due to strong spin–orbit coupling induced by the metal center.[9–11, 21] Such a triplet emission was not observed here.

Experimental Section

5a: To a solution of *trans*-[$PtCl_2(PnBu_3)_2$] (0.134 g, 2 mmol) in diisopropylamine (60 mL) at 0 °C were added CuI (3 mg) and freshly prepared **4** (0.67 g, 0.2 mmol). The solution was stirred for 3 h at 0 °C and then allowed to warm to 20 °C. Afterwards, it was stirred for a further 2 h at 20 °C. The color of the solution gradually changed from yellow to deep blue. The solvent was removed. The blue solid was dissolved in dichloromethane and passed through a short silica column first with dichloromethane and then with dichloromethane/ether (1/1). The first fraction (eluted with dichloromethane) was a mixture of polymer, oligomers, and platinum starting material which could not be separated. The second fraction was a solution of pure polymer. After removal of the solvent and washing with dry methanol, the blue polymer was obtained in 43% yield. Complex **5b** was prepared analogously from **4** and *trans*-[$PtCl_2(AsBu_3)_2$].

6a: To a solution of **3** (0.096 g, 0.2 mmol) in dichloromethane (10 mL) was added a 1M solution of nBu_4NF (0.4 mL, 0.4 mmol) in THF. The reaction mixture was stirred for 2 h. Desilylation of the acetylene was confirmed by IR spectroscopy and TLC (silica gel). To this solution were added diethylamine (10 mL), *trans*-[$PtCl(PEt_3)_2(Ph)$] (0.217 g, 0.4 mmol), and CuI (3 mg). The reaction mixture immediately changed from yellow to violet. It was stirred for another 4 h, in which time the color changed from violet to blue. The solvent was then removed, and the residue was purified by chromatography on a silica gel column with dichloromethane/hexane (2/1). The complex was obtained as blue solid (0.165 g, 61%) after washing with methanol.

6b was prepared by same the procedure as **6a** by using *trans*-[$PtCl(PnBu_3)_2(Ph)$]. The product was obtained as a blue oil which took months to crystallize.

Selected spectroscopic data. **3:** FAB-MS: m/z: 480.2 [M^+] (calcd 480.1); IR (CH_2Cl_2): $\tilde{\nu}=2138\ cm^{-1}$ (C≡C); ^1H NMR ($CDCl_3$, 250 Hz): $\delta=0.31$ (s, 18H, $(CH_3)_3Si$). **4:** FAB-MS: m/z: 333 [M^+] (calcd 336); IR (CH_2Cl_2): $\tilde{\nu}=2098\ cm^{-1}$ (C≡C), 3298 cm^{-1} (≡CH); ^1H NMR ($CDCl_3$, 250 Hz): $\delta=3.8$ (s, 2H, CCH). **5a:** IR (CH_2Cl_2): $\tilde{\nu}=2077\ cm^{-1}$(C≡C); $^{31}P\{^1H\}$ NMR ($CDCl_3$, 250 Hz): $\delta=-137.8$ (s, PBu_3), $J_{Pt,P}=2340$ Hz; elemental analysis calcd for $C_{46}H_{64}N_2P_2SPt$: C 59.16, H 6.91; found: C 58.65, H 6.85%. **5b**: IR (CH_2Cl_2): $\tilde{\nu}=2077\ cm^{-1}$ (C≡C); elemental analysis calcd for $C_{46}H_{64}N_2As_2SPt$: C 54.06, H 6.31; found: C 56.15, H 6.25. **6a:** FAB-MS: m/z: 1351.8 [M^+] (calcd 1351); IR (CH_2Cl_2): $\tilde{\nu}$ 2074 cm^{-1} (C≡C); $^{31}P\{^1H\}$ NMR ($CDCl_3$, 250 Hz): $\delta=-131.13$ (s, PBu_3), $J_{Pt,P}=2661$ Hz; elemental analysis calcd for $C_{58}H_{80}N_2P_4SPt_2$: C 51.55, H 5.92; found: C 51.68, H 5.44; **6b:** FAB-MS: m/z: 1483.5 [M^+] (calcd 1483.8); IR (CH_2Cl_2): $\tilde{\nu}=2084\ cm^{-1}$ (C≡C); $^{31}P\{^1H\}$ NMR ($CDCl_3$, 250 Hz) $\delta=-139.28$ (s, PBu_3), $J_{Pt,P}=2659$ Hz; elemental analysis calcd for $C_{82}H_{128}N_2P_4SPt_2$: C, 58.36, H, 7.59; found: C 58.50, H 7.62.

Films for optical measurements were spin-coated or drop-cast from solution onto quartz substrates. Film thicknesses were typically 100–200 nm. Optical absorption was measured with a Perkin-Elmer λ-9 spectrometer. Excitation for the photoluminescence measurements was provided by the 457 nm, 514 nm or UV (334–365 nm) lines of an Ar^+ laser. The samples were measured under nitrogen atmosphere. Photocurrent measurements were performed in air with zero external electric field applied on sandwich-type Al/**5a**/indium tin oxide (ITO) and Al/**5a**/Au photocells with excitation through the ITO or semitransparent Au electrode. Excitation was provided by a 100-W tungsten lamp or a 150-W xenon arc lamp, respectively, dispersed by appropriate monochromators. The spectra are corrected for the spectral curve of the illuminating system and for the absorption of the ITO or Au electrode.

Received: May 4, 1998 [Z11811IE]
German version: *Angew. Chem.* **1998**, *110*, 3180–3183

Keywords: diyne complexes · electrochemistry · platinum · polymers · UV/Vis spectroscopy

 © WILEY-VCH Verlag GmbH, D-69451 Weinheim, 1998 1433-7851/98/3721-3038 $ 17.50+.50/0

[1] J. H. Burroughes, D. D. C. Bradley, A. R. Brown, R. N. Marks, K. Mackay, R. H. Friend, P. L. Burn, A. B. Holmes, *Nature* **1990**, *347*, 539 – 541.
[2] N. Tessler, G. J. Denton, R. H. Friend, *Nature* **1996**, *382*, 695 – 697.
[3] J. J. M. Halls, C. A. Walsh, N. C. Greenham, E. A. Marseglia, R. H. Friend, S. C. Moratti, A. B. Holmes, *Nature* **1995**, *376*, 498 – 500.
[4] G. Yu, J. Gao, J. C. Hummelen, F. Wudl, A. J. Heeger, *Science* **1995**, *270*, 1789 – 1791.
[5] F. Garnier, R. Hajlaoui, A. Yassar, P. Srivastava, *Science* **1994**, *265*, 1684 – 1686.
[6] R. Nast, *Coord. Chem. Rev.* **1982**, *47*, 89 – 124.
[7] D. Beljonne, H. F. Wittmann, A. Kohler, S. Graham, M. Younus, J. Lewis, P. R. Raithby, M. S. Khan, R. H. Friend, J. L. Brédas, *J. Chem. Phys.* **1996**, *105*, 3868 – 3877.
[8] A. K. Kakkar, M. S. Khan, N. J. Long, J. Lewis, P. R. Raithby, P. Nguyen, T. B. Marder, F. Wittmann, R. H. Friend, *J. Mater. Chem.* **1994**, *4*, 1227 – 1232.
[9] H. F. Wittmann, R. H. Friend, M. S. Khan, J. Lewis, *J. Chem. Phys.* **1994**, *101*, 2693 – 2698.
[10] N. Chauwdhury, A. Köhler, R. H. Friend, M. Younus, N. J. Long, P. R. Raithby, J. Lewis, *Macromolecules* **1998**, *31*, 722 – 727.
[11] N. Chawdhury, A. Köhler, R. H. Friend, W.-Y. Wong, M. Younus, P. R. Raithby, J. Lewis, M. R. A. Al-Mandhury, T. C. Corcoran, M. S. Khan, *J. Chem. Phys.* **1998**, submitted.
[12] C. Kitamura, S. Tanaka, Y. Yamashita, *J. Chem. Soc. Chem. Commun.* **1994**, 1585 – 1586.
[13] M. Karikomi, C. Kitamura, S. Tanaka, Y. Yamashita, *J. Am. Chem. Soc.* **1995**, *117*, 6791 – 6792.
[14] E. E. Havinga, W. Tenhoeve, H. Wynberg, *Synth. Met.* **1993**, *55*, 299 – 306.
[15] R. M. Kellogg, A. P. Schaap, E. D. Harper, H. Wynberg, *J. Org. Chem.* **1968**, 2902 – 2905.
[16] H. Takashahi, K. Kuroyama, K. Sonogashira, N. Hagihara, *Synth. Commun.* **1980**, 625 – 629.
[17] S. Takashahi, M. Kariya, T. Yatake, K. Sonogashira, N. Hagihara, *Macromolecules* **1978**, *11*, 1063 – 1073.
[18] M. Sato, E. Mogi, M. Katada, *Organometallics* **1995**, *14*, 4837 – 4843.
[19] A. Köhler, D. A. d. Santos, D. Beljonne, Z. Shuai, J.-L. Brédas, R. H. Friend, A. B. Holmes, A. Kraus, K. Müllen, *Nature* **1998**, in press.
[20] N. J. Turro, *Modern Molecular Photochemistry*, Benjamins/Cummings, New York, **1991**.
[21] A. Köhler, H. F. Wittmann, R. H. Friend, M. S. Khan, J. Lewis, *Synth. Met.* **1996**, *77*, 147 – 150.
[22] J. Lewis, M. S. Khan, A. K. Kakkar, B. F. G. Johnson, T. B. Marder, H. B. Fyfe, F. Wittmann, R. H. Friend, A. E. Dray, *J. Organomet. Chem.* **1992**, *425*, 165 – 176.

Unprecedented Encapsulation of Carbonyl Guest with Designer Lewis Acid Receptor**

Takashi Ooi, Yuichiro Kondo, and Keiji Maruoka*

Physical inclusion of small molecules can be commonly effected with zeolites, cyclodextrins, and synthetic macrocycles as host molecules.[1–6] The self-assembly of cavity-forming smaller subunits serves as another strategy to encapsulate guest molecules.[7] We report here a new encapsulation of guest substrates with a bowl-shaped Lewis acid host, aluminum tris(2,6-diphenylphenoxide) (ATPH),[8] based on the Lewis acid – base complex formation. The resulting Lewis acid capsules persist over timescales that are sufficient to enable chemical processes to take place within them. Therefore, they serve a double function, as substrate protector and accelerator, in selective organic transformations (Figure 1).

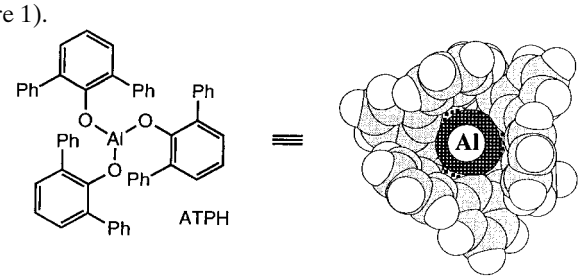


Figure 1. Space-filling model of aluminum tris(2,6-diphenylphenoxide) (ATPH) with an appropriate bowl-shaped cavity for guest molecules.

The Lewis acid receptor ATPH and its congeners self-assemble with a dicarbonyl guest molecule in organic solvents to form a dimeric capsule. The X-ray crystal structure of such a complex with 1,4-dimethylpiperazine-2,5-dione as a model guest is shown in Figure 2.[9, 10] Intermolecular coordinative

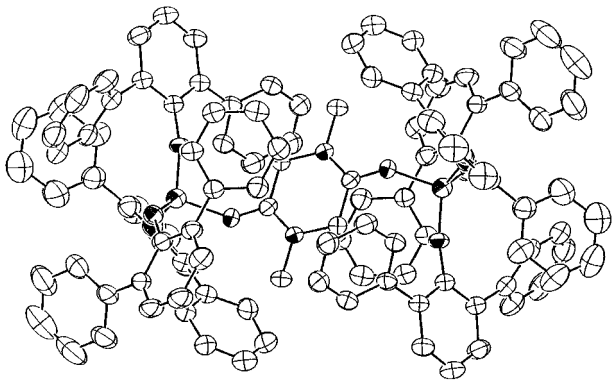


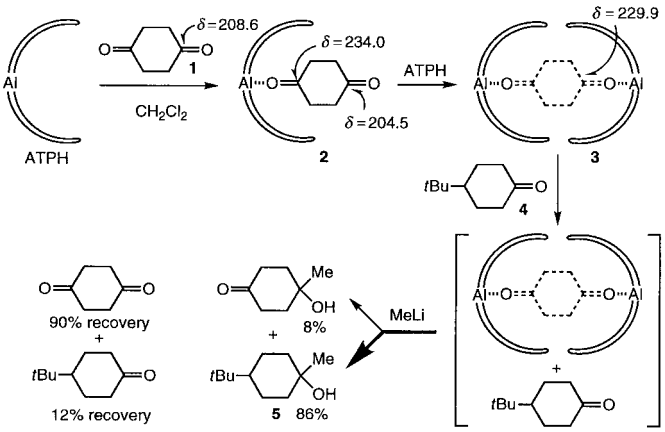
Figure 2. ORTEP diagram of the molecular capsule of ATPH and 1,4-dimethylpiperazine-2,5-dione through coordinative bonding. The solvent molecules (CH_2Cl_2) and all hydrogen atoms are omitted for clarity.

[*] Prof. K. Maruoka, Dr. T. Ooi, Y. Kondo
Department of Chemistry, Graduate School of Science
Hokkaido University, Sapporo, 060-0810 (Japan)
Fax: (+81) 11-746-2557
E-mail: maruoka@sci.hokudai.ac.jp

[**] We thank Ms. Akiko Nakano and Mr. Takayuki Miyajima (MAC Science Co. Ltd.) and Professor Tamotsu Inabe (Hokkaido University) for the single-crystal X-ray analysis of the 1,4-dimethylpiperazine-2,5-dione · 2 ATPH complex. This work was partially supported by a Grant-in-Aid for Scientific Research from the Ministry of Education, Science, Sports and Culture, Japan.

 © WILEY-VCH Verlag GmbH, D-69451 Weinheim, 1998 1433-7851/98/3721-3039 $ 17.50+.50/0

bonds between ATPH and carbonyl moiety hold the two subunits together. A similar capsule is formed with ATPH and 1,4-cyclohexanedione (**1**) (Scheme 1). In $CDCl_3$ the equilibrium shifts largely to the 2:1 ATPH complex **3**: ^{13}C NMR



Scheme 1. Stepwise encapsulation of 1,4-cyclohexanedione (**1**) with one and two equivalents of ATPH by complex formation through Lewis acid–base interactions, and its reaction with methyllithium in the presence of another carbonyl substrate.

measurements in $CDCl_3$ with 0.5 equivalents of ATPH and **1** at room temperature show the sharp and well-defined signals of the 1:1 ATPH/diketone complex **2** together with the peak of free **1** (Figure 3b). A considerable downfield shift is observed for the signal of the carbonyl group in **2** ($\delta = 234.0$; Figure 3b and c); and the signal for the uncomplexed carbonyl group appears at $\delta = 204.5$ (Figure 3b,c) which is shifted slightly upfield relative to that of the free 1,4-cyclohexanedione (**1**; $\delta = 208.6$, Figure 3a). After the addition of another

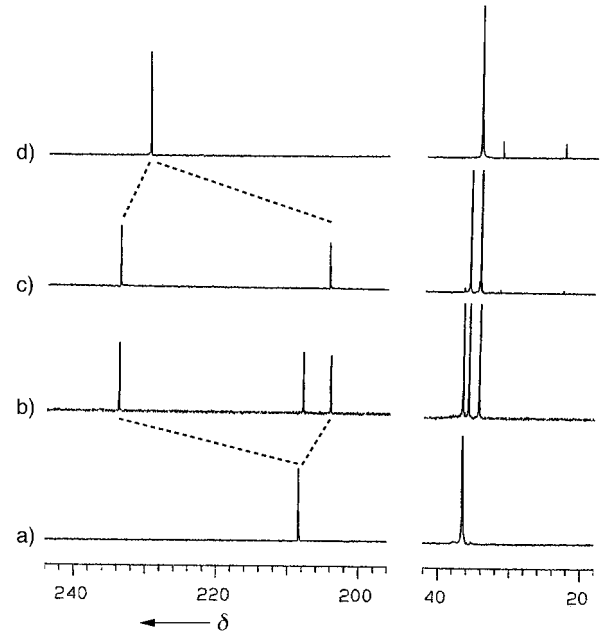
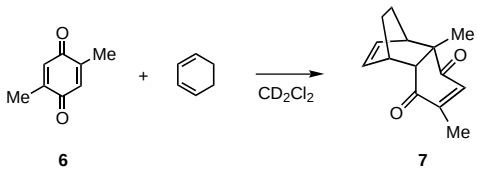


Figure 3. Signals of the carbonyl groups (left) and α-carbon atoms (right) in the ^{13}C NMR spectrum of 1,4-cyclohexanedione (**1**) and its complex with ATPH in $CDCl_3$. a) **1** alone; b) **1** with 0.5 equivalents of ATPH; c) **1** with one equivalent of ATPH; d) **1** with two equivalents of ATPH.

0.5 equivalents of ATPH, the carbonyl signal of free **1** completely disappeared (Figure 3c). Addition of one more equivalent of ATPH to this solution affords, under induction by the guest molecule **1**, the capsular form **3**, which is confirmed by the sharp single peak for the coordinated carbonyl group at $\delta = 229.9$ (Figure 3d). The capsule **3** was found to be stable in the presence of another carbonyl substrate. Indeed, addition of 4-*tert*-butylcyclohexanone (**4**) (1 equiv) to the dimeric complex **3** at $-78\,^{\circ}C$ and subsequent treatment with MeLi (1 equiv) at $-78\,^{\circ}C$ resulted in predominant formation of 4-*tert*-butyl-1-methylcyclohexanol (**5**) (86%) with 90% recovery of the diketone **1**.[11]

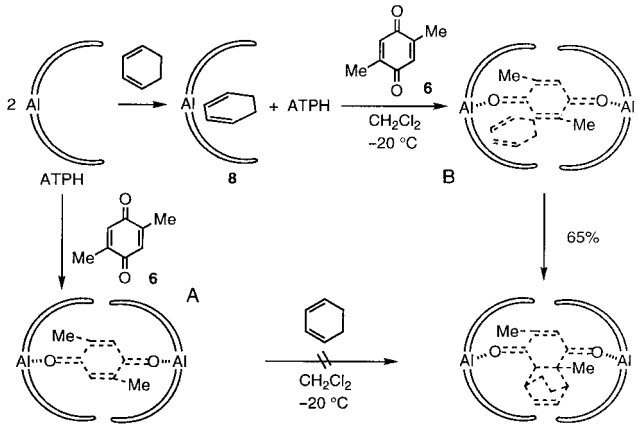
Simple addition of MeLi (1 equiv) to an equimolar mixture of **1** and **4** at $-78\,^{\circ}C$ gave 4-hydroxy-4-methylcyclohexanone and **5** in 49% and 47% yields, respectively. These results suggest the promising encapsulation of the diketone **1** in the presence of another carbonyl substrate, and two equivalents of ATPH can be utilized as an effective protector for the dicarbonyl compound **1** in the alkylation even with highly reactive organolithium nucleophiles.

With this information at hand, we studied the Diels–Alder reaction between 2,5-dimethyl-*p*-benzoquinone (**6**) and cyclohexa-1,3-diene. This cycloaddition proceeds very slowly at room temperature. In CD_2Cl_2 at molar concentrations of each component, no cycloadducts are detected by NMR spectroscopy after about two days [Eq. (1)]. Initial addition of 2,5-dimethyl-*p*-benzoquinone (**6**) (1 equiv) to ATPH (2.2 equiv)



(1)

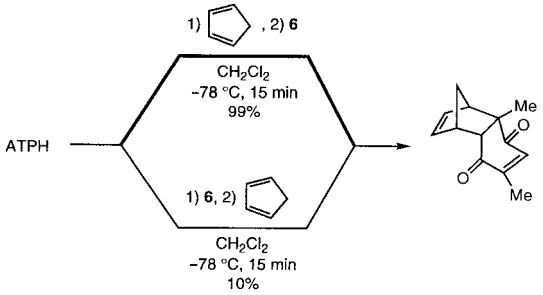
in CH_2Cl_2 at $-20\,^{\circ}C$ and subsequent treatment with cyclohexa-1,3-diene (1.1 equiv) resulted in only traces of the *endo*-cycloadduct **7**. This is due to the virtually complete protection against diene approach by the efficient encapsulation of quinone substrate (route A in Scheme 2).[11] In marked



Scheme 2. Encapsulation of 2,5-dimethyl-*p*-benzoquinone (**6**) and cyclohexa-1,3-diene with two equivalents of ATPH accelerates the Diels–Alder reaction. Cyclohexa-1,3-diene is selectively included by electronic interaction of the diene portion with the concave aromatic interior of ATPH.

 © WILEY-VCH Verlag GmbH, D-69451 Weinheim, 1998 1433-7851/98/3721-3040 $ 17.50+.50/0 *Angew. Chem. Int. Ed.* **1998**, *37*, No. 21

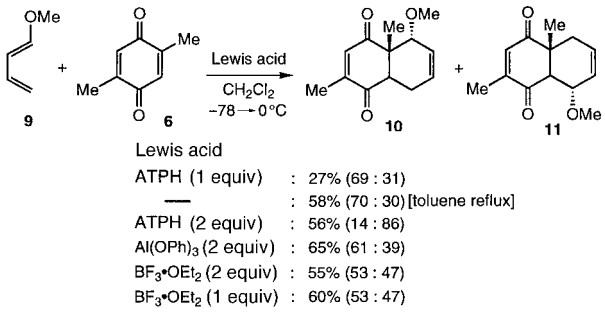
contrast, however, mixing of cyclohexa-1,3-diene (1.1 equiv) and ATPH (2.2 equiv) in CH_2Cl_2 at $-20\,^{\circ}C$ and subsequent addition of 2,5-dimethyl-*p*-benzoquinone (**6**) (1 equiv) under similar reaction conditions afforded the *endo*-cycloadduct **7** in 65% yield (route B in Scheme 2). This observation implies the effective inclusion of diene component by electronic interactions of the diene portion with the concave aromatic interior of the cavity of ATPH (**8** in Scheme 2). This facilitates the smooth cycloaddition on complexation and the capsule formation with a quinone substrate **6**.[12] A similar tendency is observed in the Diels–Alder reaction between 2,5-dimethyl-*p*-benzoquinone (**6**) and cyclopentadiene (Scheme 3).



Scheme 3. Rate acceleration of the Diels–Alder reaction of 2,5-dimethyl-*p*-benzoquinone (**6**) and cyclopentadiene by encapsulation.

In CD_2Cl_2, the Diels–Alder adduct **7** is readily encapsulated by ATPH, and a ^{13}C NMR signal unique to the encapsulated species can be observed. The original signals of the two carbonyl groups of the free compound **7** appeared at $\delta = 200.68$ and $\delta = 203.12$. Upon treatment with two equivalents of ATPH in CD_2Cl_2 at room temperature, these two signals significantly shifted downfield to $\delta = 211.56$ and $\delta = 216.38$, respectively, which supports the idea that the Diels–Alder adduct **7** is also a welcome guest. Therefore, the product can remain inside the capsule after the cycloaddition.

Another interesting feature of the present molecular assembly is the regio- and stereoselective Diels–Alder reactions of quinones and heterodienes that are capable of coordinating. The cycloaddition of quinone **6** with 1-methoxy-1,3-butadiene (**9**) (1 equiv) in the presence of ATPH (1 equiv) in CH_2Cl_2 at $-78 \rightarrow 0\,^{\circ}C$ for 1 h proceeded with complete *endo* preference to furnish the cycloadducts **10** and **11** in 27% combined yield in a ratio of 69:31 (Scheme 4); this result was



Scheme 4. Regioselective Diels–Alder reaction of **6** with methoxy diene **9** by means of the molecular assembly.

comparable with that of the thermal reaction in refluxing toluene for 15 h (58% yield; **10**:**11** = 70:30).[11] However, initial treatment of **9** with two equivalents of ATPH and subsequent addition of **6** (1 equiv) under similar reaction conditions afforded the cycloadducts **10** and **11** in 56% yield, and the regioselectivity was totally reversed (**10**:**11** = 14:86). This indicates that the preorganization of the heterodiene **9** and quinone **6** by complexation with ATPH prior to the capsule formation plays a crucial role in obtaining otherwise unattainable regioselectivity. The unusual regiochemical preference was lost when the cycloaddition was promoted by aluminum triphenoxide (2 equiv); commonly used Lewis acids such as $BF_3 \cdot OEt_2$ resulted in a total lack of selectivity regardless of the stoichiometry.

Received: May 18, 1998 [Z11872IE]
German version: *Angew. Chem.* **1998**, *110*, 3213–3215

Keywords: alkylations · aluminum · cage compounds · cycloadditions · Lewis acids

[1] D. J. Cram, *Nature* **1992**, *356*, 29.
[2] R. C. Helgeson, C. B. Knobler, D. J. Cram, *J. Am. Chem. Soc.* **1997**, *119*, 3229.
[3] J.-M. Lehn, *Angew. Chem.* **1988**, *100*, 92; *Angew. Chem. Int. Ed. Engl.* **1988**, *27*, 89.
[4] V. T. D'Souza, M. T. Bender, *Acc. Chem. Res.* **1987**, *20*, 146.
[5] R. Arad-Yellin, B. S. Green, *Nature* **1994**, *371*, 320.
[6] B.-H. Huisman, D. M. Rudkevich, F. C. J. M. van Veggel, D. N. Reinhoudt, *J. Am. Chem. Soc.* **1996**, *118*, 3523.
[7] R. M. Grotzfeld, N. Branda, J. Rebek, Jr., *Science* **1996**, 271, 487, and references therein.
[8] a) K. Maruoka, H. Imoto, S. Saito, H. Yamamoto, *J. Am. Chem. Soc.* **1994**, *116*, 4131; b) K. Maruoka, I. Shimada, H. Imoto, H. Yamamoto, *Synlett* **1994**, 519; c) K. Maruoka, M. Ito, H. Yamamoto, *J. Am. Chem. Soc.* **1995**, *117*, 9091; d) S. Saito, H. Yamamoto, *J. Org. Chem.* **1996**, *61*, 2928; e) T. Ooi, Y. Hokke, K. Maruoka, *Angew. Chem.* **1997**, *109*, 1230; *Angew. Chem. Int. Ed. Engl.* **1997**, *36*, 1181; f) T. Ooi, Y. Kondo, K. Maruoka, *Angew. Chem.* **1997**, *109*, 1231; *Angew. Chem. Int. Ed. Engl.* **1997**, *36*, 1183.
[9] Crystal data: $C_{116}H_{92}Al_2N_2O_8Cl_4$, $M_W = 1797.44$, monoclinic, space group $P2_1/n$, $T = 298$ K, $a = 16.897(4)$, $b = 14.626(3)$, $c = 19.586(4)$ Å, $\beta = 94.41(1)^{\circ}$, $V = 4826.0(1)$ Å^3, $Z = 2$, $\rho_{calcd} = 1.237$ g cm^{-1}, 3169 reflections obtained, $R = 0.065$, $R_w = 0.063$. Crystallographic data (excluding structure factors) for the structures reported in this paper have been deposited with the Cambridge Crystallographic Data Center as supplementary publication no. CCDC-103289. Copies of the data can be obtained free of charge on application to CCDC, 12 Union Road, Cambridge CB2 1EZ, UK (fax: (+44) 1223-336-033; e-mail: deposit@ccdc.cam.ac.uk).
[10] Although the relative binding strengths of the guests studied here have not been established precisely, it may be predicted based on our previous observation on the binding priority of various oxygen-containing substrates with a Lewis acidic bulky organoaluminum reagent (K. Maruoka, S. Nagahara, H. Yamamoto, *Tetrahedron Lett.* **1990**, *31*, 5475.)
[11] The concentration of the substrate was 0.0625 M in each case.
[12] For recent beautiful demonstration, see: J. Kang, J. Rebek, Jr., *Nature* **1997**, *385*, 50. See also: C. J. Walter, K. M. Sanders, *Angew. Chem.* **1995**, *107*, 223; *Angew. Chem. Int. Ed. Engl.* **1995**, *34*, 217; D. Philp, A. Robertson, *Chem. Commun.* **1998**, 879.

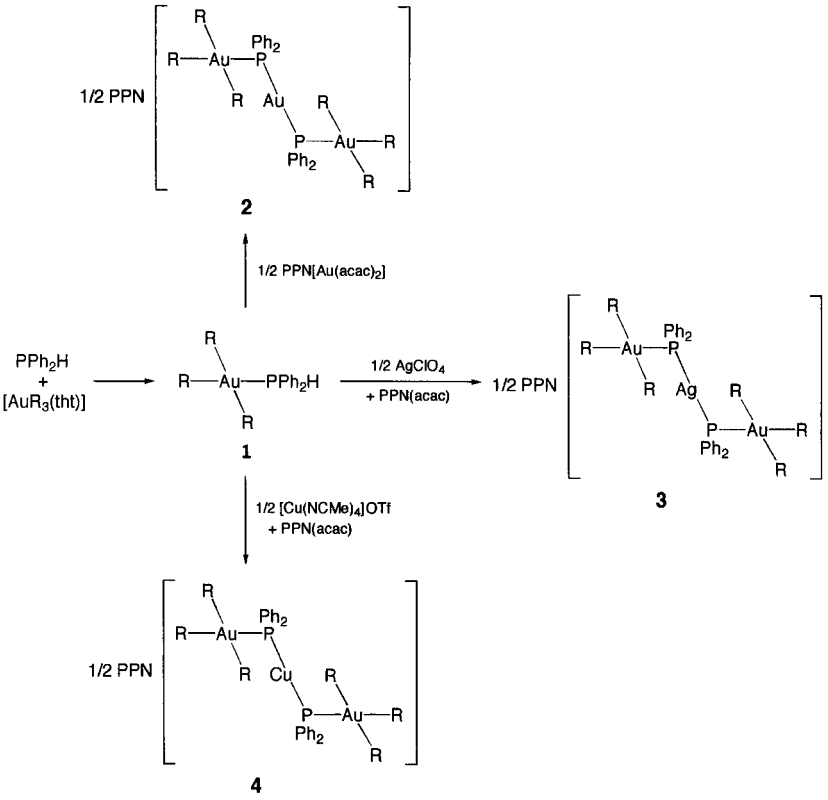
 © WILEY-VCH Verlag GmbH, D-69451 Weinheim, 1998 1433-7851/98/3721-3041 $ 17.50+.50/0

$[Au(C_6F_5)_3(PPh_2H)]$: A Precursor for the Synthesis of Gold(III) Phosphide Complexes**

M. Carmen Blanco, Eduardo J. Fernández, Peter G. Jones, Antonio Laguna,* José M. López-de-Luzuriaga, and M. Elena Olmos

Although a rich and fascinating chemistry of phosphido-bridged transition metal complexes has recently been developed for metals of Groups 9 and 10,[1] the corresponding gold chemistry has experienced little progress since Puddephatt and Thompson prepared $[AuPPh_2]_n$ in 1976;[2] only a few Au^I species containing PR_2H[3] or PR_2^- ligands[2–4] are known. The chemistry of Au^{III} is even more poorly represented, and only the dinuclear complex $[Au_2Me_4(\mu\text{-}PPh_2)_2]$ has been reported.[2] Attempts to prepare Au^{III} complexes with PPh_2H have led only to reduction of the Au^{III} centers.[3a]

We have succeeded in synthesizing a diphenylphosphanylgold(III) complex by exploiting the stabilizing effect of pentafluorophenyl groups. The starting material $[Au(C_6F_5)_3(tht)]$ (tht = tetrahydrothiophene) was treated with PPh_2H, giving $[Au(C_6F_5)_3(PPh_2H)]$ (**1**, Scheme 1). This is the first Au^{III} derivative containing a secondary phosphane.



Scheme 1. Synthesis of phosphane and phosphide derivatives.

Further reaction of **1** with suitable coinage metal species should furnish hitherto unknown phosphido-bridged Au^{III}–M species. As **1** can only be isolated in low yields as an oily material, freshly prepared solutions of **1** were used directly for further reactions. The reaction of $PPN[Au(acac)_2]$[5] (PPN = $[N(PPh_3)_2]^+$, acac = $CH(COCH_3)_2$) with such a solution (1:2) afforded the first mixed Au^{III}–M phosphido-bridged complex, $PPN[\{Au(C_6F_5)_3(\mu\text{-}PPh_2)\}_2Au]$ (**2**), which can be easily isolated as a solid in high yield. It behaves as a 1:1 electrolyte in acetone; its ^1H NMR spectrum displays only signals from the aromatic protons.

We wished to synthesize a set of isostructural complexes containing Au^I, Ag^I, or Cu^I centers, whose crystal structures would allow a comparison of the covalent radii of these three metals, a subject of recent discussion.[6] Reaction of **1** with $AgClO_4$ or $[Cu(NCMe)_4]TfO$ (TfO = CF_3SO_3) in the presence of PPN(acac) led to $PPN[\{Au(C_6F_5)_3(\mu\text{-}PPh_2)\}_2M]$ (M = Ag (**3**), Cu (**4**)). Both are air- and moisture-stable solids whose physical and spectroscopic data are in accordance with the proposed formulation.

Crystals of **2** and **3** suitable for X-ray diffraction studies were obtained from solutions in dichloromethane layered with hexane; unfortunately, we have not been able to obtain good crystals of **4**. Complexes **2** and **3**[7] are isotypic and thus allow a comparison of metal–ligand bond lengths (Figure 1).[6a] The M^I atom lies on an inversion center, so its

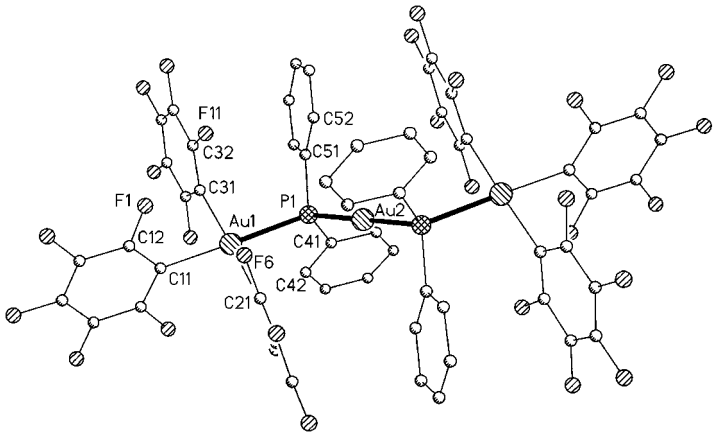


Figure 1. Structure of the inversion-symmetric anion of **2** in the crystal (the radii are arbitrary). Only the asymmetric unit is numbered. Complex **3** is isostructural; the central gold atom is replaced by silver.

[*] Prof. Dr. A. Laguna
Departamento de Química Inorgánica-ICMA
Universidad de Zaragoza-CSIC
E-50009 Zaragoza (Spain)
Fax: (+34) 976-761187
E-mail: alaguna@posta.unizar.es
M. C. Blanco, Dr. E. J. Fernández, Dr. J. M. López-de-Luzuriaga, Dr. M. E. Olmos
Departamento de Química, Universidad de La Rioja
Obispo Bustamante 3, E-26001 Logroño (Spain)
Prof. Dr. P. G. Jones
Institut für Anorganische und Analytische Chemie der Technischen Universität
Postfach 3329, D-38023 Braunschweig (Germany)

[**] This work was supported by the DGICYT. (PB94–0079), the University of La Rioja (API-98/B09), and the Fonds der Chemischen Industrie.

 © WILEY-VCH Verlag GmbH, D-69451 Weinheim, 1998 1433-7851/98/3721-3042 $ 17.50+.50/0

environment is exactly linear. The bond lengths and angles are almost identical in both structures (Table 1) except for the M^I-P distance, which is shorter by 0.07 Å in the gold complex. This confirms the results obtained by Schmidbaur et al., who compared the bond lengths in complexes

Table 1. Bond lengths [Å] and angles [°] for **2** and **3**.

	2 (M = Au)	**3** (M = Ag)
Au1–C31	2.052(5)	2.052(5)
Au1–C21	2.058(6)	2.068(5)
Au1–C11	2.073(6)	2.078(5)
Au1–P	2.365(2)	2.365(2)
M–P	2.319(2)	2.386(1)
P–C41	1.814(6)	1.804(5)
P–C51	1.818(7)	1.813(5)
C31-Au1-C21	176.4(2)	176.6(2)
C31-Au1-C11	87.6(2)	88.1(2)
C21-Au1-C11	89.5(2)	89.3(2)
C31-Au1-P	92.0(2)	91.9(1)
C21-Au1-P	90.9(2)	90.6(1)
C11-Au1-P	177.7(2)	178.0(1)
P-M-P′	180.0	180.0
C41-P-C51	101.4(3)	101.3(2)
C41-P-Au1	110.6(2)	110.9(2)
C51-P-Au1	110.7(2)	110.8(2)
C41-P-Au1	110.6(2)	110.9(2)
C41-P-M	111.9(2)	113.7(2)
C51-P-M	109.1(2)	108.2(2)
M-P-Au1	112.54(7)	111.48(5)

$[(Mes_3P)_2M]BF_4$ (M = Au, Ag).[6a] The Au^I-P bond distance in **2** is similar to those observed in $PPN[Mn(CO)_4\{(\mu\text{-}PPh_2)Au(C_6F_5)\}_2]$ (2.313(2) and 2.322(1) Å),[4b] but slightly shorter than those in $[\{Mn(CO)_4(\mu\text{-}PPh_2)_2Au\}_2]$ (2.332(3)–2.341(3) Å).[4b] The Au^{III} centers display the expected planar coordination, and the $Au^{III}-C$ bond lengths of 2.052(5)–2.078(5) Å are similar to those in other tris(pentafluorophenyl)gold(III) derivatives.[8] The $Au^{III}-P$ bond length of 2.365(2) Å is closely similar to that in $NBu_4[\{Au(C_6F_5)_3(Ph_2PCHPPh_2)\}_2Au]$ (2.367(2) Å).[8a]

Experimental Section

1: To a solution of $[Au(C_6F_5)_3(tht)]$ (0.236 g, 0.3 mmol) in diethyl ether was added PPh_2H (0.5 mL, 0.3 mmol). After 30 min the solvent was concentrated in vacuo, and cold hexane was added to afford **1** as a white solid (0.098 g, 37 %). ^{31}P NMR (300 MHz, $CDCl_3$, 25 °C, 83 % H_3PO_4): $\delta = -8.4$ (s, PPh_2H); ^1H NMR: $\delta = 7.57-7.43$ (m, 10H; Ph), ≈6.8 (d, $^1J(H,P) \approx 440$ Hz, 1H; PPh_2H).

2: To a freshly prepared solution of **1** (0.2 mmol) in dichloromethane was added $PPN[Au(acac)_2]$ (0.093 g, 0.1 mmol). After the reaction mixture was stirred for 1 h at room temperature, part of the solvent was evaporated, and hexane (20 mL) was added to afford **2** as a white solid (0.225 g, 90 %). ^{31}P NMR: $\delta = 30.9$ (s, PPh_2), 21.1 (s, PPN); ^1H NMR: $\delta = 7.60-7.17$ (m, Ph).

3: $AgClO_4$ (0.021 g, 0.1 mmol) and PPN(acac) (0.127 g, 0.2 mmol) were added to a solution of **1** (0.2 mmol) in diethyl ether. After 1 h a white precipitate ($PPNClO_4$) was removed by filtration, the solution was concentrated, and hexane was added to precipitate **3** as a white solid (0.159 g, 66 %). ^{31}P NMR: $\delta = 21.1$ (s, PPN), 4.5 (dd, $^1J(P,^{109}Ag) = 512.5$, $^1J(P,^{107}Ag) = 446.3$ Hz; PPh_2); ^1H NMR: $\delta = 7.63-7.14$ (m, Ph).

4: $[Cu(NCMe)_4]TfO$ (0.038 g, 0.1 mmol) and PPN(acac) (0.127 g, 0.2 mmol) were added to a solution of **1** (0.2 mmol) in dichloromethane. After 1 h the solvent was evaporated, and diethyl ether was added to precipitate $PPNClO_4$, which was removed by filtration. The solution was concentrated, and hexane was added to afford **4** as a pale yellow solid (0.121 g, 51 %). ^{31}P NMR: $\delta = 21.1$ (s, PPN), −7.0 (s, PPh_2); ^1H NMR: $\delta = 7.61-7.09$ (m, Ph).

Received: June 18, 1998 [Z12007IE]
German version: *Angew. Chem.* **1998**, *110*, 3199–3201

Keywords: copper · gold · P ligands · silver

[1] a) G. A. Acum, M. J. Mays, P. R. Raithby, H. R. Powel, G. A. Solan, *Chem. Commun.* **1997**, 3427–3434; b) K. Wang, T. J. Emge, A. S. Goldman, *Inorg. Chim. Acta* **1997**, *255*, 395–398; c) E. Alonso, J. Forniés, C. Fortuño, A. Martín, G. M. Rosair, A. J. Welch, *Inorg. Chem.* **1997**, *36*, 4426–4431.

[2] R. J. Puddephatt, P. J. Thompson, *J. Organomet. Chem.* **1976**, *117*, 395–403.

[3] a) R. G. Pritchard, D. B. Dyson, R. V. Parish, C. A. McAuliffe, B. Beagley, *J. Chem. Soc. Chem. Commun.* **1987**, 371–372; b) D. B. Dyson, R. V. Parish, C. A. McAuliffe, R. G. Pritchard, R. Fields, B. Beagley, *J. Chem. Soc. Dalton Trans.* **1989**, 907–914; c) H. Schmidbaur, A. A. M. Aly, *Z. Naturforsch. B* **1979**, *34*, 23–26; d) H. Schmidbaur, G. Weidenhiller, A. A. M. Aly, O. Steigelmann, G. Müller, *Z. Naturforsch. B* **1989**, *44*, 1503–1508.

[4] a) J. Vicente, M. T. Chicote, P. G. Jones, *Inorg. Chem.* **1993**, *32*, 4960–4964; b) G. A. Carriedo, V. Riera, M. L. Rodríguez, P. G. Jones, J. Lautner, *J. Chem. Soc. Dalton Trans.* **1989**, 639–643; c) F. S. Livotto, M. D. Vargas, D. Braga, F. Grepioni, *J. Chem. Soc. Dalton Trans.* **1992**, 577–584.

[5] a) E. J. Fernández, M. C. Gimeno, P. G. Jones, A. Laguna, M. Laguna, J. M. López-de-Luzuriaga, *J. Chem. Soc. Dalton Trans.* **1992** 3365–3370; b) J. Vicente, M. T. Chicote, I. Saura-Llamas, M. C. Lagunas, *J. Chem. Soc. Chem. Commun.* **1992** 915–916.

[6] a) A. Bayler, A. Schier, G. A. Bowmaker, H. Schmidbaur, *J. Am. Chem. Soc.* **1996**, *118*, 7006–7007; b) G. A. Bowmaker, H. Schmidbaur, S. Krüger, N. Rösch, *Inorg. Chem.* **1997**, *36*, 1754–1757.

[7] Structure analysis of **2**: $C_{96}H_{50}Au_3F_{30}NP_4$, rectangular block 0.25 × 0.22 × 0.20 mm³, monoclinic, *C*2/*c*, $a = 28.174(3)$, $b = 11.0751(9)$, $c = 30.202(3)$ Å, $\beta = 113.757(8)°$, $V = 8625.5(14)$ Å³, $Z = 4$, $\lambda(Mo_{K\alpha}) = 0.71073$ Å, $\mu = 5.28$ mm⁻¹, $\rho_{calcd} = 1.927$ Mg m⁻³, $T = -100$ °C. Of 9917 reflections collected to $2\theta = 50°$, 7559 were unique and used for all calculations. Absorption corrections were carried out by ψ scans with transmissions of 0.72–0.98. The structure was solved with Patterson methods, and refined anisotropically on F^2 (program SHELXL-93, G. M. Sheldrick, Universität Göttingen) with 580 restraints to *U* components of light atoms and local ring symmetry. Hydrogen atoms were included with a riding model. Final values: $wR2 = 0.051$, $R1 = 0.036$ for 606 parameters; $S = 0.79$, $\Delta\rho$ 0.89 e Å⁻³. Structure analysis of **3**: $C_{96}H_{50}AgAu_2F_{30}NP_4$, prism 0.5 × 0.4 × 0.4 mm³, monoclinic, C2/c, $a = 28.145(3)$, $b = 11.064(1)$, $c = 30.316(4)$ Å, $\beta = 114.08(8)°$, $V = 8619(2)$ Å³, $Z = 4$, $\mu = 3.81$ mm⁻¹, $\rho_{calcd} = 1.860$ Mg m⁻³, $T = -100$ °C. Of 10198 reflections collected to $2\theta = 50°$, 7514 were unique; transmissions of 0.57–0.76. Final values: $wR2 = 0.055$, $R1 = 0.033$; $S = 0.85$, $\Delta\rho$ 1.00 e Å⁻³. The structure was solved and refined as for **2**. Crystallographic data (excluding structure factors) for the structures reported in this paper have been deposited with the Cambridge Crystallographic Data Centre as supplementary publication no. CCDC-101732 (**2**) and CCDC-101733 (**3**). Copies of the data can be obtained free of charge on application to CCDC, 12 Union Road, Cambridge CB2 1EZ, UK (fax: (+44) 1223-336-033; e-mail: deposit@ccdc.cam.ac.uk).

[8] a) E. J. Fernández, M. C. Gimeno, P. G. Jones, A. Laguna, M. Laguna, J. M. López-de-Luzuriaga, *Organometallics* **1995**, *14*, 2918–2922; b) B. Alvarez, E. J. Fernández, M. C. Gimeno, P. G. Jones, A. Laguna, M. Laguna, J. M. López-de-Luzuriaga, *J. Organomet. Chem.* **1996**, *525*, 109–113; c) E. J. Fernández, M. C. Gimeno, P. G. Jones, A. Laguna, J. M. López-de-Luzuriaga, E. Olmos, *Chem. Ber.* **1997**, *130*, 1513–1517.

 © WILEY-VCH Verlag GmbH, D-69451 Weinheim, 1998 1433-7851/98/3721-3043 $ 17.50+.50/0

Crystallization of Calcite Spherules around Designer Nuclei**

Jörg Küther, Ram Seshadri, and Wolfgang Tremel*

Dedicated to Professor Bernt Krebs on the occasion of his 60th birthday

Living systems exercise considerable control over the crystallization of certain inorganic minerals.[1] This control extends to the nature and habit of the mineral polymorph and is usually guided towards a specific function. Sometimes this is achieved in seeming contradiction to thermodynamic expectation. An additional level of complexity is reached when living systems form composite structures that organize minerals in organic matrices.[2] The utility of organic–inorganic interfaces in mimicking these biomineralization processes have been exploited in the past. Langmuir monolayers,[3] protein-coated substrates,[4] polymer dispersions,[5] micellar media,[6] and self-assembled monolayers (SAMs)[7–9] have been used as templates or substrates for the crystallization of minerals such as calcium carbonate. We demonstrate here that standard SAM chemistry can be extended to produce controlled nanoscopic surfaces for the heterogeneous nucleation of inorganic minerals from aqueous solution. The seeds are about 5 nm large gold colloids coated with a *p*-sulfanylphenol SAM. An interesting aspect here is that while the nucleation is heterogeneous in the sense that it takes place at the liquid–solid interface, it commences from within a single homogeneous phase.

We have been interested in the crystallization of the carbonates of calcium and, to a lesser extent, strontium on self-assembled monolayers of long chain thiols, organized in two dimensions on gold-coated glass substrates.[8–11] Inspired in part by the kinds of processes taking place in living systems, we have examined how different substituents at the positions of the thiols can influence the nature and morphology of the calcium carbonate polymorph (calcite, aragonite, or vaterite) formed. In certain cases, we have also been able to establish a relationship between the specific 2D structure of the SAM and that of the growing crystal.[9] These studies complement existing work and have provided some insight into the templated crystallization of carbonate biominerals. Furthermore, they suggest mild routes to useful materials.

During the course of these studies, gold colloids attracted our attention. Their small size (in the range of 2–10 nm for the methods presented here) ensures that for a given quantity of gold a relatively large surface area is obtained. The self-assembly of thiols on gold colloids has in fact provided routes to preparing particles that are stabilized against aggregation and whose solubility in different solvents can be controlled through the size and functionality of the thiol molecules.[12, 13] Thiol-coated gold colloids can be purified by chromatography, evaporated, recondensed, precipitated, and redissolved; this is behavior that one usually associates with molecules.[12, 14, 15] Recently, we have been able to functionalize gold colloids with a Ru-containing polymerization catalyst to obtain a material that bridges homogeneous and heterogeneous catalytic behavior.[16] When coated with *p*-sulfanylphenol, the colloids are soluble in water at a pH value of about 12 or higher.[13] While solutions of these colloids are homogeneous in every sense, the colloids possess a surface capable of heterogeneous nucleation. These thiol-coated gold colloids can therefore be used to seed the crystallization of materials from saturated solutions. The different topologies of flat and spherical templates is to be noted. The use of gold colloids instead of flat gold surfaces should permit novel crystal or crystal-aggregate geometries to be obtained through templated crystallization.

Fritz et al.[17] have studied the formation of flat pearls on inorganic substrates inserted between the shell and mantle of the red abalone. They have determined that oriented calcite and template protein layers are initially formed. This is followed by the growth of stacks of aragonite along the pseudo-sixfold axis of the crystal. The proteins are generated within epithelial cells in the abalone mantle. Our approach is in contrast to this. We do not attempt to simulate natural pearls, but rather seek inspiration from the manner in which they are formed. The templating organic substance is the *p*-sulfanylphenol SAM. This is previously fixed to the substrate on which the crystallization is carried out rather than being in solution, which is the case in the formation of natural pearls.

The top right of Figure 1 shows schematically the thiol-coated particles used to nucleate the precipitation of calcium carbonate. At different seed concentrations ($10-100\ mg\,L^{-1}$) and temperatures ($4-45\,^{\circ}C$) the only polymorph we observe is calcite; a sample X-ray diffraction pattern is displayed in Figure 1.[18] The effect of the colloid seeds on the crystallization is observed in the scanning electron micrographs. Figure 2a shows rhombohedral crystals of calcite formed when crystallization was carried out at $22\,^{\circ}C$ in the absence of the colloid seed. This is the expected morphology. The presence of the colloids (here $100\ mg\,L^{-1}$) initially gives the solution a deep pink color. By the end of the crystallization, the solution is colorless and the scanning electron micrographs of the grey-black precipitate display a completely different morphology (Figure 2b). At higher magnification (Figure 2c), a typical crystallite assembly shows the individual spherules of Figure 2b to comprise a complex assembly of the calcite rhombohedra. The direction radiating out from the center is the direction connecting opposite edges of the calcite rhombohedra, that is, the crystallographic [001] direction.

Crystallization experiments carried out under identical conditions on flat *p*-sulfanylphenol SAM/gold surfaces (as opposed to colloidal seeds) do not suggest any sort of epitaxy between substrate and crystal. The crystallization on the flat surfaces is inhibited and results in rather ill-defined morphologies, perhaps because the phenolic OH groups are ionized at the high pH used. This does not seem to affect the efficiency

[*] Prof. Dr. W. Tremel, Dr. J. Küther, Dr. R. Seshadri
Institut für Anorganische Chemie
und Analytische Chemie der Universität
Johann-Joachim-Becher-Weg 24, D-55099 Mainz (Germany)
Fax: (+49) 6131-39-3922
E-mail: tremel@indigotrem1.chemie.uni-mainz.de

[**] We thank Degussa (Hanau, Germany) for a generous gift of gold and Dr. Gabriele Nelles for preliminary AFM measurements. Financial support from the Fonds der chemischen Industrie is gratefully acknowledged.

 © WILEY-VCH Verlag GmbH, D-69451 Weinheim, 1998 1433-7851/98/3721-3044 $ 17.50+.50/0

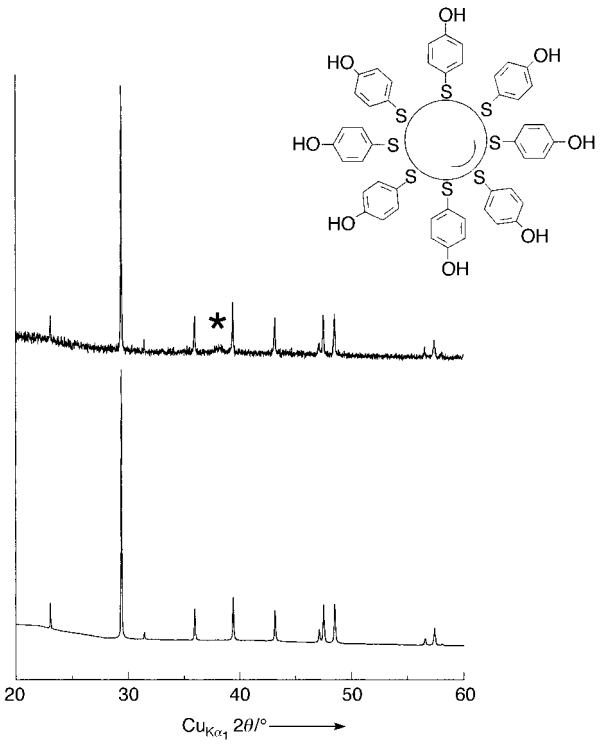


Figure 1. Measured and Rietveld-fitted X-ray diffraction profiles (transmission, $\theta-2\theta$) of $CaCO_3$ crystallized from solutions containing thiol-coated gold colloid seeds. The fit indicates pure calcite; the small hump marked by an asterisk is due to the (111) reflection of gold. The concentration of seeds used was 100 mg L^{-1} in solution, and the crystallization was carried out at 22 °C.

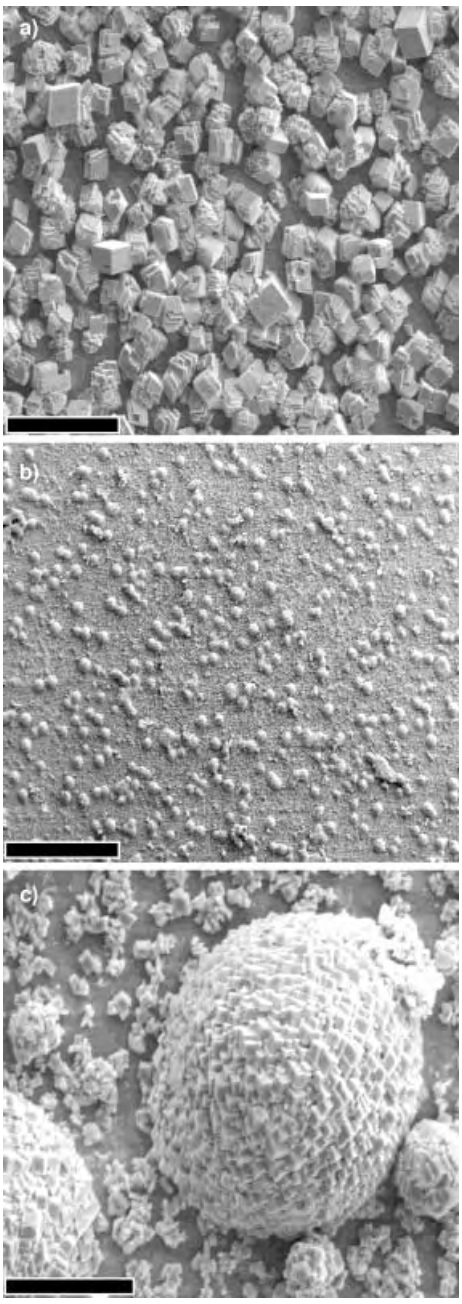


Figure 2. a) Scanning electron micrograph of the crystals formed by precipitation of $CaCO_3$ from solution at 22 °C. The rhombohedra are crystals of calcite displaying {104} faces. b) Scanning electron micrograph of the crystals formed on crystallization in the presence of the seeds (100 mg L^{-1} at 22 °C). A typical crystallite assembly seen at higher magnification is shown in c); the rhombohedra arrange spherically around some central point. The scale bars correspond to 50, 500, and 20 μm, respectively.

of the seeding, however. The organization of the calcite rhombohedra therefore arises from crystal–crystal interactions rather than crystal–substrate interactions, and from the fact that the crystals are obliged to pack around a sphere.[19] The manner in which the solution becomes clear after precipitation as well as the morphologies obtained in the presence of the colloid suggest that the colloids act as nuclei or seeds. We point out that the assemblies display a level of complexity that cannot be achieved with flat templates. The assemblies of the calcite rhombohedra are rather fragile. So far, attempts to fragment the spherules in order to better understand their structures have always resulted in the individual crystallites being damaged. It is possible that well-defined rhombohedra are found only near the outer surfaces of the spherules, and that within the spherules the morphology is quite different.

Figure 3a shows the precipitates obtained when the crystallization is carried out at about 4 °C instead of at 22 °C and fewer seed particles are used (30 mg L^{-1}). The morphology is still spheroidal, but at higher magnification (Figure 3b) it is seen to comprise spherulites rather than spherules, that is, needlelike crystals that radiate from a central point. Despite the changed morphology, X-ray diffraction experiments confirm that the samples are pure calcite.

The precipitates formed at 22 °C, unlike those formed at about 4 °C, comprise crystals with well-defined morphologies. Correspondingly, the X-ray diffraction profiles possess narrower linewidths. This is expected from considerations of the supersaturation ratios at the two temperatures. However, the dependence of the size of the precipitates on the amount of seed colloids used does not follow expectation. This could be because the distribution of sizes is not monomodal, as suggested from a closer analysis of the micrographs. Additionally, the number of seeds used are far in excess of the spherules that are formed. It is possible that some the seeds are incorporated into the spherules during the later stages of the crystallization. The spherelike nature of a large proportion

 © WILEY-VCH Verlag GmbH, D-69451 Weinheim, 1998 1433-7851/98/3721-3045 $ 17.50+.50/0

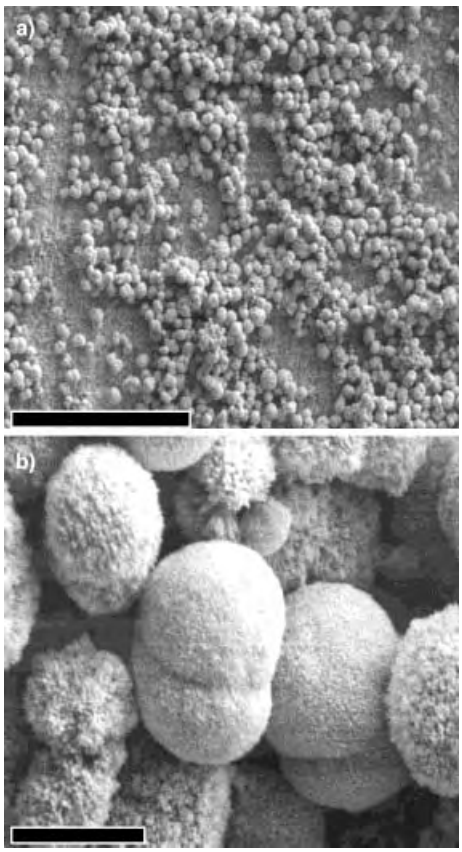


Figure 3. Scanning electron micrographs of precipitates obtained from crystallizations (30 mg L^{-1}) at about 4 °C. The spherelike morphology is retained (a), while at higher magnifications (b) differences become visible. The individual crystallites making up the assemblies are no longer rhombohedral, but fluffy and branched. Some bilobed structures are also observed. The scale bars correspond to 200 and 10 μm, respectively.

of the products also indicates that the spherules fall out of solution onto the witness glass slides only after nearly all the calcium in solution is depleted, as there is little or no growth of the assemblies after they settle.

The high initial pH value at which the crystallizations are carried out seems to favor the formation of calcite at the expense of aragonite. To simulate the formation of aragonite spherules, we crystallized $SrCO_3$, whose stable modification strontianite has the same structure. The different crystal structure (orthorhombic *Pmcn* for strontianite/aragonite, rhombohedral $R\bar{3}c$ for calcite) usually results in the phases precipitating from solution with completely different morphologies.[9] An attempt to make strontianite spherules is shown in Figure 4. The usual strontianite (or aragonite) morphology is needlelike. The use of the colloid seeds seems to induce the needles to cluster around a central point. This additionally demonstrates the utility of our designer nuclei.

Self-assembled monolayers of thiols on gold (or other) substrates can induce the controlled crystallization of inorganic materials, whereas gold colloids provide a novel way of looking at gold surfaces. The marriage of these concepts yields a method for controlled heterogeneous nucleation with the result that the crystallite assemblies so formed are very different from what one obtains (and what one can possibly obtain) with flat templates. The seeds are in solution and,

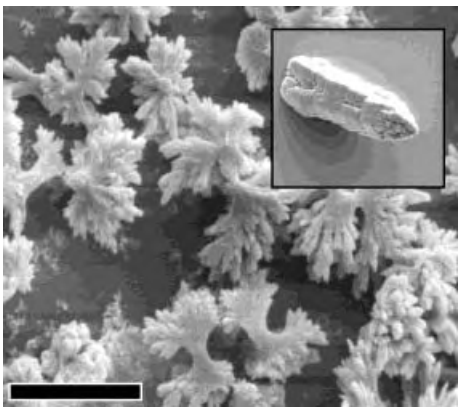


Figure 4. Scanning electron micrograph of $SrCO_3$ crystals precipitated from solutions containing the colloid seeds (30 mg L^{-1} at 4 °C). The scale bar corresponds to 10 μm. The inset shows a needle (ca. 15 μm long) of $SrCO_3$ in the strontianite modification obtained from precipitation in the absence of colloids. The needle grows along a pseudohexagonal [001] trilling axis.

hence, perfectly wetted. Classical theory predicts that they should act very much like homogeneous nuclei.[20] This is not observed in the micrographs. The examples outlined here testify to the ease with which nanoscopic seeds can be designed and used for controlled crystallizations.

Experimental Section

The gold colloids (diameters near 5 nm) were prepared in two-phase toluene–water systems by reported procedures.[11, 12] The organic phase was isolated and then mixed with a solution of *p*-sulfanylphenol in toluene, causing the colloids to precipitate. Surface plasmon spectroscopic measurements confirm that *p*-sulfanylphenol forms densely packed monolayers on gold surfaces. Attempts to obtain the 2D structure of the *p*-sulfanylphenol SAMs (on gold/mica) through atomic force microscopy failed due to the high acidity of phenolic OH group. Also the small size of the *p*-sulfanylphenol molecule might prevent its forming crystalline monolayers. The precipitate was washed and dried before being dissolved in 10 mM solutions of calcium or strontium chloride, whose initial pH value was raised to 12–13 with aqueous NaOH. The rather alkaline pH are necessary in order to take the colloids into homogeneous solution.[13] Precipitation of the carbonate was induced in closed desiccators through the slow diffusion of CO_2 from solid $(NH_4)_2CO_3$ placed within the desiccator. After 48 h the precipitates, which were collected on glass slides, were removed and fixed to aluminum stubs using conducting carbon glue. Before transferring to the microscope, gold was sputtered on to the glass slides.

Received: May 7, 1998 [Z11828IE]
German version: *Angew. Chem.* **1998**, *110*, 3196–3199

Keywords: biomineralization · calcium · colloids · crystal growth · monolayers

[1] *On Biomineralisation* (Eds.: H. A. Lowenstam, S. Weiner), Oxford University Press, New York, **1989**.
[2] S. Mann, *J. Mater. Chem.* **1995**, *5*, 935–946.
[3] B. R. Heywood, S. Mann, *Adv. Mater.* **1994**, *6*, 9–20.
[4] L. Addadi, S. Weiner, *Angew. Chem.* **1992**, *104*, 159–176; *Angew. Chem. Int. Ed. Engl.* **1992**, *31*, 153–170.
[5] P. A. Bianconi, J. Lin, A. R. Strzelecki, *Nature* **1991**, *349*, 315–317.
[6] D. Walsh, S. Mann, *Adv. Mater.* **1997**, *9*, 658–662.
[7] D. D. Archibald, S. B. Quadri, B. P. Gaber, *Langmuir* **1996**, *12*, 538–546.

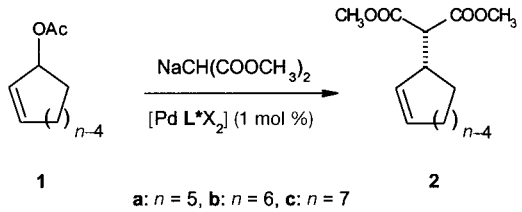
 © WILEY-VCH Verlag GmbH, D-69451 Weinheim, 1998 1433-7851/98/3721-3046 $ 17.50+.50/0

[8] J. Küther, R. Seshadri, W. Knoll, W. Tremel, *J. Mater. Chem.* **1998**, *8*, 641 – 650; J. Küther, W. Tremel, *Thin Solid Films*, in press.
[9] J. Küther, G. Nelles, R. Seshadri, M. Schaub, H.-J. Butt, W. Tremel, *Chem. Eur. J.* **1998**, *4*, 1834 – 1842.
[10] J. Küther, W. Tremel, *Chem. Commun.* **1997**, 2029 – 2030.
[11] J. Küther, R. Seshadri, G. Nelles, H.-J. Butt, W. Knoll, W. Tremel, *Adv. Mater.* **1998**, *10*, 401 – 404.
[12] M. Brust, M. Walker, D. Bethell, D. J. Schiffrin, R. Whymann, *J. Chem. Soc. Chem. Commun.* **1994**, 801 – 802.
[13] M. Brust, J. Fink, D. Bethell, D. J. Schiffrin, C. Kiely, *J. Chem. Soc. Chem. Commun.* **1995**, 1655 – 1656.
[14] R. L. Whetten, J. T. Khoury, M. M. Alvarez, S. Murthy, I. Vezmar, Z. L. Wang, P. W. Stephens, C. L. Cleveland, W. D. Luedtke, U. Landmann, *Adv. Mater.* **1996**, *8*, 428 – 433.
[15] A. L. Badia, S. Singh, L. Demers, L. Cuccia, G. R. Brown, R. B. Lennox, *Chem. Eur. J.* **1996**, *2*, 359 – 363.
[16] M. Bartz, J. Küther, R. Seshadri, W. Tremel, *Angew. Chem.* **1998**, *110*, 2658 – 2661; *Angew. Chem. Int. Ed.* **1998**, *37*, 2466 – 2468.
[17] M. Fritz, A. M. Belcher, M. Radmacher, D. A. Walters, P. K. Hansma, G. D. Stucky, D. E. Morse, S. Mann, *Nature* **1994**, *371*, 49 – 51.
[18] When the crystallizations are performed on *p*-sulfanylphenol SAMs on gold/glass substrates rather than on colloids, no modification other than calcite is observed. However, when the pH value is lowered to about 10.5, the aragonite:calcite ratio of crystals deposited on *p*-sulfanylphenol SAMs on gold/glass is about 40:60 at 22 °C and 85:15 at 45 °C, as determined from the Rietveld refinement of powder X-ray profiles. These are the highest aragonite weight fractions that we have been able to obtain at 22 °C on SAMs of simple thiols. We are now attempting to prepare colloids coated with thiols that permit dissolution of the colloids in water at neutral pH values in the hope of inducing aragonite.
[19] On the other hand, the use of (flat) SAM/gold templates with a well-defined hexagonal 2D crystal structure, such as SAMs of hexadecanethiol, result in calcite crystallizing with the [001] direction nearly always perpendicular to the substrate, suggesting the role of epitaxy.[9]
[20] B. Mutaftschiev, *Handbook of Crystal Growth*, *Vol. 1a* (Ed.: D. T. J. Hurle), North-Holland, Amsterdam, **1993**, pp. 187 – 247.

Enantioselective Allylic Substitution of Cyclic Substrates by Catalysis with Palladium Complexes of P,N-Chelate Ligands with a Cymantrene Unit**

Steffen Kudis and Günter Helmchen*

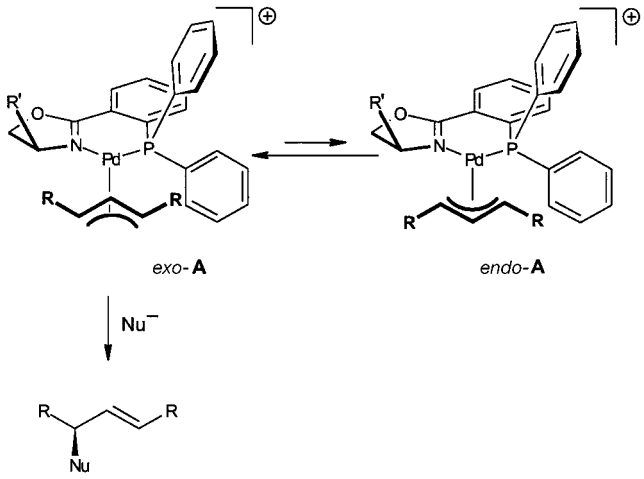
Palladium complex catalyzed asymmetric C–C bond forming reactions with allylic compounds are being investigated with great intensity.[1] As ligands, modular C_2 diphosphanes[2] and phosphanylcarboxylic acids[3] gave good results, particularly with small cyclic substrates. For acyclic substrates, chiral phosphanyldihydrooxazoles were successfully used as ligands,[4] and enantioselectivities of up to more than 99:1 were achieved. However, cyclic substrates **1** (Scheme 1) furnished



Scheme 1. Palladium complex catalyzed allylic substitution of cyclic allyl acetates.

low enantioselectivities with these ligands. Because of the favorable properties of phosphanyldihydrooxazoles, such as ease of synthesis and high turnover numbers in catalysis, it was of interest to develop ligands of this type that are suitable for cyclic substrates. We found such compounds on the basis of mechanistic considerations.

Key concepts of the reactions with dihydrooxazoles and other P,N ligands[5] are a) the assumption of preferred attack of the nucleophile at the carbon atom of the allyl group in the position *trans* to the phosphorus atom and b) the postulate that of the diastereomeric *exo*- and *endo*-π-allyl complexes **A** (Scheme 2), the *exo* isomer reacts faster. As the relative



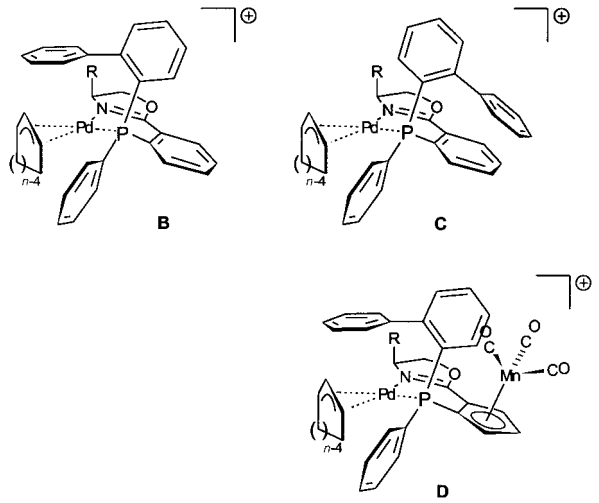
Scheme 2. The *exo* – *endo* isomerism of π-allylpalladium complexes with phosphanyldihydrooxazole ligands (R′ = *i*Pr, *t*Bu).

reactivities of these diastereomers are nearly equal, the ratio of their concentrations mainly determines the enantioselectivity of the substitution. The reason for the low selectivity with cyclic substrates is insufficient differentiation, that is, equal populations of *exo* and *endo* isomers.

With second-generation ligands, the enantioselectivity for cyclic substrates was increased significantly by substituting the pseudoaxial phenyl group by a 2-biphenylyl group;[6] *ee* values of 50 – 80 % were obtained. The higher enantioselectivity had been anticipated, since the crystal structure of complex **B** with R = *i*Pr and $n = 6$ displayed only the conformer in which the terminal phenyl group is directly above the allyl system. This conformer is the most favorable for achieving high selectivity. According to ^{1}H NMR NOE measurements,[7] conformer **B** is in equilibrium with conformer **C**, in which the 2-biphenylyl group is rotated away from the palladium center and does not interact with the allyl group. To restrict rotational freedom of

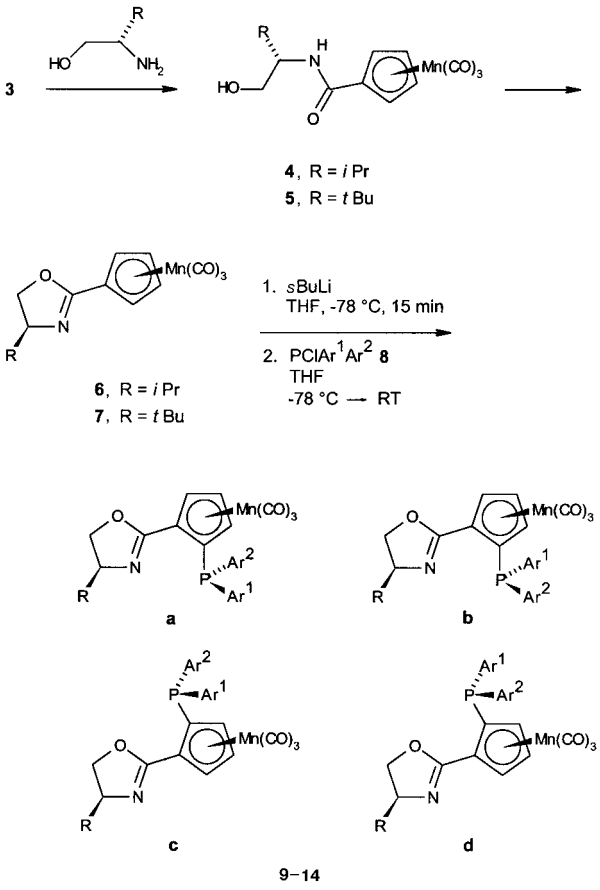
[*] Prof. Dr. G. Helmchen, Dipl.-Chem. S. Kudis
Organisch-chemisches Institut der Universität
Im Neuenheimer Feld 270, D-69120 Heidelberg (Germany)
Fax: (+49) 6221-54-4205
E-mail: en4@ix.urz.uni-heidelberg.de

[**] This work was supported by the Deutsche Forschungsgemeinschaft (SFB 247) and the Fonds der Chemischen Industrie. We thank Dr. F. Rominger and Dr. B. Nuber for crystal structure analyses.



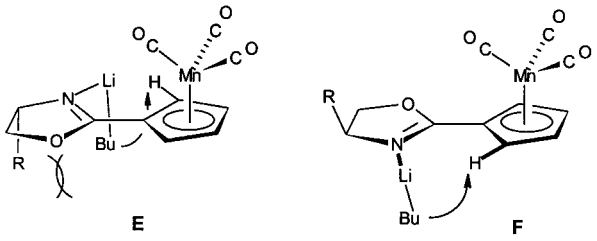
the 2-biphenylyl group, we replaced the "flat" benzene ring with a sterically demanding tricarbonylcyclopentadienylmanganese (cymantrene) unit (**D**).

To synthesize the new ligands, cymantrenecarbonyl chloride[8] (**3**) was treated with (*S*)-valinol and (*S*)-*tert*-leucinol to give the amides **4** (94%) and **5** (90%), which were transformed into the dihydrooxazoles **6** (81%) and **7** (80%) by established procedures[9] (Scheme 3). Like the analogous



Scheme 3. Synthesis of the cymantrene-containing phosphanyldihydrooxazoles **9**–**14**: **9a**, **9c**: R = *i*Pr, $Ar^1 = Ar^2 = Ph$; **10a**, **10c**: R = *t*Bu, $Ar^1 = Ar^2 = Ph$; **11a**, **11b**: R = *t*Bu, $Ar^1 = Ph$, Ar^2 = 2-Bp; **12a**, **12b**: R = *t*Bu, Ar^1 = 3,5-$(CH_3)_2C_6H_3$, Ar^2 = 2-Bp; **13a**, **13b**: R = *t*Bu, Ar^1 = 3,5-$(CF_3)_2C_6H_3$, Ar^2 = 2-Bp; **14a**: R = *t*Bu, $Ar^1 = Ar^2$ = 2-Bp (2-Bp = 2-biphenylyl).

ferrocene derivatives,[10] the new dihydrooxazoles can be diastereoselectively lithiated and then treated with chlorophosphanes. In contrast to the ferrocene derivatives, lithiocymantrenes slowly equilibrate, so that the time period between metalation and addition of the chlorophosphane should be kept as short as possible. For example, at −78 °C with 2 h between addition of *s*BuLi and chlorodiphenylphosphane, we obtained **9a** and **9c** (ratio 85:15) from **6**, and **10a** and **10c** (ratio 88:12) from **7**. The minor epimers **9c** and **10c** were not formed when an interval of 15 min was employed. The relative configurations of the new compounds were assigned by assuming reactions via the transition states **E** and **F** (preferred) in analogy to corresponding ferrocene derivatives.



Phosphorus was introduced as an additional stereogenic center by reaction of the lithio derivatives with (2-biphenylyl)(chloro)phenylphosphane. Epimers **11a** and **11b** were obtained in 64% yield in the ratio 6:5; **11c** and **11d** were not observed. Crystallization from *n*-hexane/ether gave **11b** with greater than 99.9% purity in 26% yield. The configuration was determined by X-ray structural analysis (see below). The pure epimer **11a** was obtained as an oil from the mother liquor in 31% yield by chromatography. Heating a mixture of the diastereomers to above 90 °C caused epimerization at the phosphorus atom and furnished **11a** with high selectivity (**11a**:**11b** = 9:1). The analogous phosphanes **12b** (32%), **13b** (31%), and **14a** (28%) were prepared in order to further assess electronic and steric effects.

The new ligands were tested in substitution reactions according to Scheme 1 (Table 1). Catalysts prepared in situ from these ligands were considerably more active than complexes of type **A** or **B** (approximate sixfold increase in reaction rate). As anticipated, the influence of the cymantrene unit was small for ligands **9a**, **9c**, and **10a** (entries 1–3). The touchstones for our concept are the diastereomeric ligands **11a** and **11b**. In analogy to **9** and **10**, **11a** induced only low (entry 4), but **11b** very high selectivity (entry 5), as expected for a complex of type **D**. By optimization of the reaction conditions, enantioselectivities of up to more than 99:1 were achieved with **11b** (entries 5–13). Comparatively low selectivities were obtained with the phosphanes **12b** and **13b**, containing substituents with differing electronic properties, and the particularly bulky phosphane **14a** (entries 14–16). Overall, **11b** induced higher reactivity and selectivity in this reaction than the previously known phosphanyldihydrooxazoles and other asymmetric ligands.

To test our hypothesis about the structure of complexes of type **D**, the allyl complex **16** was prepared by treatment of the known complex **15**[11] with the phosphane **11b** in dichloro-

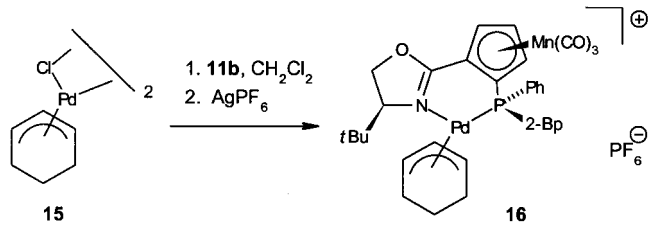
 © WILEY-VCH Verlag GmbH, D-69451 Weinheim, 1998 1433-7851/98/3721-3048 $ 17.50+.50/0

Table 1. Palladium complex catalyzed substitution of cyclic allyl acetates **1**[a] (Scheme 1).

Entry	Ligand	Substrate	*t* [min]	*T* [°C]	Solvent	Yield [%]	*ee*[b] [%]
1	**9a**	**1b**	10	20	THF	98	30
2	**9c**	**1b**	10	20	THF	98	20
3	**10a**	**1b**	10	20	THF	97	31
4	**11a**	**1b**	10	20	THF	91	31
5	**11b**	**1b**	10	20	THF	95	85
6	**11b**	**1a**	10	20	THF	86	80
7	**11b**	**1a**	120	−50	DMF	73	96
8	**11b**	**1b**	40	20	DMF	97	87
9	**11b**	**1b**	90	0	DMF	86	90
10	**11b**	**1b**	180	−20	DMF	62	93
11	**11b**	**1c**	5	20	THF	96	78
12	**11b**	**1c**	75	0	DMF	86	98
13	**11b**	**1c**	180	−20	DMF	32	> 99.9
14	**12b**	**1c**	75	0	DMF	71	87
15	**13b**	**1c**	120	0	DMF	79	92
16	**14a**	**1c**	120	0	DMF	82	44

[a] A solution of dimethyl malonate (198.0 mg, 1.5 mmol) in 2 mL of solvent was treated with NaH (33.6 mg, 1.4 mmol). The mixture was added to a solution of $[\{(\eta^3\text{-}C_3H_5)PdCl\}_2]$ (1.83 mg, 5.0 μmol), 11.0 μmol of the dihydrooxazole ligand (**9a**—**14a**) and 1.0 mmol of the cyclic allyl substrate (**1a**–**1c**) in the solvent given. The mixture was stirred for the stated period, treated with saturated NH_4Cl solution, and extracted three times with 20-mL portions of diethyl ether. The organic phase was dried with Na_2SO_4 and concentrated in vacuo. Products were purified by flash chromatography (silica, *n*-hexane/ethyl acetate 97/3). [b] In each case the product with *R* configuration was favored. Enantiomeric purities of **2b** and **2c** were determined by gas chromatography on a Chrompack CP Chirasil DEX CB column (25 m × 0.25 mm, 0.25 mm film thickness); **2b** (110 °C): t_R((−)-(*S*)-**2b**) = 37.7 min, t_R((+)-(*R*)-**2b**) = 38.2 min; **2c** (120 °C), t_R((−)-(*S*)-**2c**) = 36.9 min, t_R((+)-(*R*)-**2c**) = 37.8 min. The optical purity of **2a** was determined on the basis of the reference value (100 % *ee*) $[\alpha]_D^{20} = +98.7$ ($c = 2.3$ in $CHCl_3$). For control, a sample of **2** was saponified and decarboxylated to give 2-cyclopentenylacetic acid; this was transformed into the iodolactone, the enantiomers of which can be separated by gas chromatography (column as given above, 145 °C, t_R = 34.5 and 38.3 min).[6]

methane and subsequent replacment of the chloride counterion with hexafluorophosphate (Scheme 4). The X-ray crystal



Scheme 4. Preparation of the η^3-cyclohexenylpalladium complex **16**.

structure[12] (Figure 1) revealed a structure of type **D**. Only one species was observed by ^{31}P NMR spectroscopy for a solution of the complex in $[D_8]$THF at −78 °C. Isomerization was not observed on warming. Accordingly, it can be concluded that the products are formed from allyl complexes of type **D** by attack at the allyl terminus *trans* to the phosphorus atom. The bond lengths and angles are typical for (η^3-cyclohexenyl)palladium complexes with phosphanyldihydrooxazole ligands. An unusual feature of the structure are the positions of the *P*-aryl groups, the P–C bonds of which have an almost symmetrical arrangement with respect to the

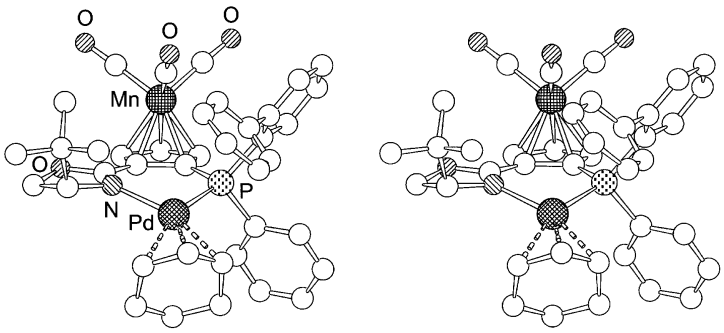


Figure 1. Stereoview of the crystal structure of the cation of complex **16**. Hydrogen atoms are omitted.

coordination plane (N-Pd-P). The reason for this is an interaction between the 2-biphenylyl group and the $Mn(CO)_3$ moiety, which precludes the usual pseudoaxial position of one *P*-aryl group.[13]

Received: March 25, 1998 [Z11638IE]
German version: *Angew. Chem.* **1998**, *110*, 3210–3212

Keywords: allyl complexes · asymmetric catalysis · ligand effects · N ligands · P ligands · palladium

[1] a) C. G. Frost, J. Howarth, J. M. J. Williams, *Tetrahedron: Asymmetry* **1992**, *3*, 1089–1122; b) T. Hayashi in *Catalytic Asymmetric Synthesis, Vol. 1* (Ed.: I. Ojima), VCH, New York, **1993**, p. 325; c) B. M. Trost, D. L. van Vranken, *Chem. Rev.* **1996**, *96*, 395–422.
[2] B. M. Trost, R. C. Bunt, *J. Am Chem. Soc.* **1994**, *116*, 4089–4090.
[3] G. Knühl, P. Sennhenn, G. Helmchen, *J. Chem. Soc. Chem. Commun.* **1995**, 1845.
[4] a) J. Sprinz, G. Helmchen, *Tetrahedron Lett.* **1993**, *34*, 1769–1772; b) J. Sprinz, M. Kiefer, G. Helmchen, M. Reggelin, G. Huttner, O. Walter, L. Zsolnai, *Tetrahedron Lett.* **1994**, *35*, 1523–1526; c) P. von Matt, A. Pfaltz, *Angew. Chem.* **1993**, *105*, 614–615; *Angew. Chem. Int. Ed. Engl.* **1993**, *32*, 566; d) G. Helmchen, S. Kudis, P. Sennhenn, H. Steinhagen, *Pure Appl. Chem.* **1997**, *69*, 513–518.
[5] a) H. Steinhagen, M. Reggelin, G. Helmchen, *Angew. Chem.* **1997**, *109*, 2199–2202; *Angew. Chem. Int. Ed. Engl.* **1997**, *36*, 2108–2110; b) A. Togni, U. Burckhardt, V. Gramlich, P. S. Pregosin, R. Salzmann, *J. Am. Chem. Soc.* **1996**, *118*, 1031–1037.
[6] P. Sennhenn, B. Gabler, G. Helmchen, *Tetrahedron Lett.* **1994**, *35*, 8595–8598.
[7] M. Reggelin, H. Steinhagen, unpublished results.
[8] a) E. Biehl, P. Reeves, *Synthesis* **1973**, 360–361; b) H. J. Lorkowski, R. Pannier, A. Wende, *J. Prakt. Chem.* **1967**, *35*, 149.
[9] M. Peer, J. C. deJong, M. Kiefer, Th. Langer, H. Rieck, H. Schell, P. Sennhenn, J. Sprinz, H. Steinhagen, B. Wiese, G. Helmchen, *Tetrahedron* **1996**, *51*, 7547–7583.
[10] a) Y. Nishibayashi, S. Uemura, *Synlett* **1995**, 79–81; b) T. Sammakia, H. A. Latham, *J. Org. Chem.* **1995**, *60*, 6002–6003; c) C. J. Richards, T. Damalidis, D. E. Hibbs, M. B. Hursthouse, *Synlett* **1995**, 74–76.
[11] B. M. Trost, P. E. Strege, L. Weber, T. F. Fullerton, T. J. Dietsche, *J. Am. Chem. Soc.* **1978**, *100*, 3407.
[12] Crystal data for **16**: $C_{39}H_{38}ClF_6MnO_4P_2Pd$, $M_r = 957.43$. Crystal dimensions 0.23 × 0.20 × 0.20 mm, triclinic, space group *P*1, $a = 11.2672(2)$, $b = 11.3084(2)$, $c = 18.6163(4)$ Å, $\alpha = 93.367(1)$, $\beta = 94.108(1)$, $\gamma = 104.114(1)°$, $V = 2287.33(8)$ Å^3, $Z = 2$, $\rho_{calcd} = 1.390$ g cm^{-3}; $\mu = 0.858$ mm^{-1}, $\theta_{max} = 25.56°$; 16586 reflections measured, 13304 unique reflections; $R_1 = 0.0678$, $wR_2 = 0.1495$. Siemens SMART CCD diffractometer (200 K, radiation $\lambda(Mo_{K\alpha}) = 0.71073$ Å). The structure was solved by direct methods and refined against F^2 for all observed reflexes; program used: SHELXTL (G. M. Sheldrick, Universität Göttingen). Crystallographic data (excluding structure factors) for the structure reported in this paper have been

 © WILEY-VCH Verlag GmbH, D-69451 Weinheim, 1998 1433-7851/98/3721-3049 $ 17.50+.50/0

deposited with the Cambridge Crystallographic Data Centre as supplementary publication no. CCDC-101206. Copies of the data can be obtained free of charge on application to CCDC, 12 Union Road, Cambridge CB2 1EZ, UK (fax: (+44) 1223-336-033; e-mail: deposit@ccdc.cam.ac.uk).

[13] The angle between the coordination plane and the ligand plane is only 28°. Other η^3-cyclohexenylpalladium complexes of phosphanyldihydrooxazoles have angles of around 50°: H. Steinhagen, P. Sennhenn, A. Pichota, G. Helmchen, unpublished results.

Catalytic Copolymerization of Ethene and Carbon Monoxide on Nickel Complexes**

Bernd Domhöver, Wolfgang Kläui,* Andreas Kremer-Aach, Ralf Bell, and Dietrich Mootz

Dedicated to Professor Peter Böttcher on the occasion of his 60th birthday

Polyketones from olefins and carbon monoxide, which were first industrially produced under the name "carilon" in 1996, are new plastics with interesting material properties. Among these are a strong rigidity and impact strength, good chemical resistance to acids, bases, and solvents as well as a high tracking resistance and stability against electrolytic corrosion—properties, which make polyketones superior to polyolefins, polyamides, and polyacetals.[1–3] Although copolymerization of ethene and carbon monoxide on tetracyanonickelate(II) at 100–200 °C was already described by Reppe in 1951 and by Shryne and Holler in 1976,[4, 5] the resulting polymers have never been prepared on an industrial scale. The breakthrough was achieved with a palladium–phosphane complex, which catalyzes the formation of a perfectly alternating 1:1 copolymer from ethene or propene and carbon monoxide under mild reaction conditions.[6, 7]

Can nickel replace the relatively expensive palladium, which is not recovered in the industrial production of plastics? So far only a few nickel(II) complexes are known that catalyze the alternating copolymerization of ethene and carbon monoxide under mild conditions: Klabunde et al. showed that polyketone formation is catalyzed by arylnickel(II) compounds with P,O chelate ligands of the same type that is used in SHOP procedures (SHOP = *S*hell *H*igher *O*lefins *P*rocess).[8, 9] Cavell et al. described similarly active arylnickel(II) compounds with N,O chelate ligands.[10] However, in both cases the polymerization must be initially started with ethene alone since carbon monoxide acts as a catalyst poison prior to the beginning of the reaction. This problem is circumvented by applying a catalyst for polyketone synthesis described by Keim et al. Apparently, this catalyst is formed in situ from thiolcarboxylic acids and nickel compounds.[11] We have now for the first time synthesized and structurally characterized an arylnickel(II) complex, which like the palladium–phosphane complexes catalyzes the polymerization of ethene and carbon monoxide already at above 20 °C and below 50 bar total pressure; a strictly alternating polyketone is formed exclusively. The reaction can be started without loss of activity by pressurizing with the carbon monoxide . Thus the aroyl complex is formed, which on addition of ethene initiates the formation of polyketone. The arylnickel(II) complex **1** was synthesized according to Equation (1).

$$[NiBr(o\text{-tolyl})(PPh_3)_2] + TlTp^{Ph} \longrightarrow [Ni(o\text{-tolyl})(PPh_3)(Tp^{Ph})]\ \mathbf{1} + TlBr + PPh_3 \quad (1)$$

As shown in Figure 1 the tripodal tris(pyrazolyl)borate ligand Tp^{Ph}[12] of **1** is coordinated as a bidentate chelate ligand to the nickel atom.[13] So far it could not be explained why this particular nickel complex catalyzes the polyketone formation. A priori one might expect that the presence of a third coordinating donor center rather impedes the formation of reversibly liberated coordination sites and thus suppresses the catalysis.[14] From investigations on the coordination chem-

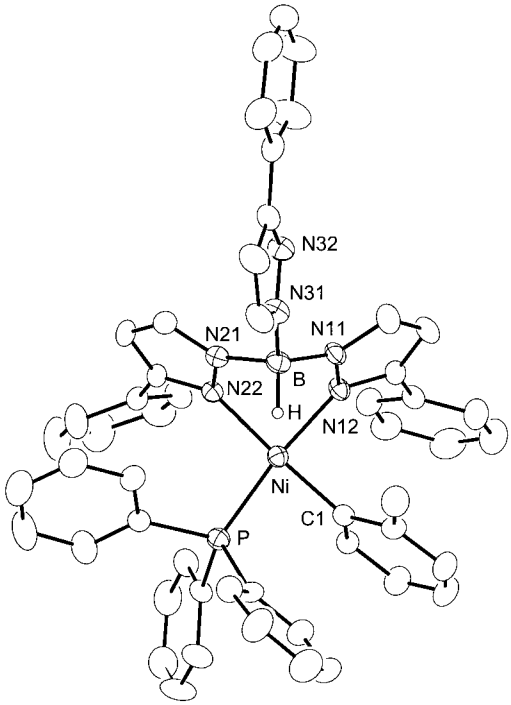


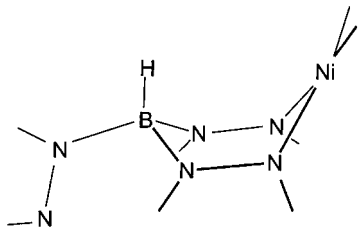
Figure 1. Structure of **1** in the crystal. Thermal ellipsoids for 25% probability, for C atoms without equators. The H atoms, with the exception of that at the B atom, are not shown for reasons of clarity. Selected bond lengths [Å], bond angles [°], and torsion angles [°]: Ni–N12 1.940(4), Ni–N22 1.961(4), Ni–C1 1.906(5), Ni–P 2.182(1), Ni···H 2.92(3), B–N11 1.544(6), B–N21 1.560(6), B–N31 1.517(5), B–H 1.20(3), N11–N12 1.384(4), N21–N22 1.369(4), N31–N32 1.371(5); N12-Ni-N22 87.0(2), N12-Ni-C1 90.4(2), N22-Ni-C1 174.9(2), P-Ni-C1 85.9(1), P-Ni-N12 164.3(1), P-Ni-N22 97.8(1), N11-B-N21 107.3(4), N11-B-N31 111.7(4), N21-B-N31 107.8(4), N11-B-H 112(2), N21-B-H 108(2), N31-B-H 110(2); N22-Ni-N12-N11 56.1(3), N12-Ni-N22-N21 −56.6(3).

[*] Prof. Dr. W. Kläui, Dr. B. Domhöver, Dr. A. Kremer-Aach, Dr. R. Bell, Prof. Dr. D. Mootz
Institut für Anorganische Chemie und Strukturchemie der Universität
Universitätsstrasse 1, D-40225 Düsseldorf (Germany)
Fax: (+49) 211-81-12287
E-mail: klaeui@uni-duesseldorf.de

[**] We thank Prof. Dr. W. Keim for helpful discussions and the BASF AG, Ludwigshafen, for the MALDI-TOF-MS-spectra.

 © WILEY-VCH Verlag GmbH, D-69451 Weinheim, 1998 1433-7851/98/3721-3050 $ 17.50+.50/0

istry of the Tp^{Ph} ligand we have recently shown that the flexibility of this ligand permits a facile alteration between bidentate and tridentate coordination.[15] Apparently the potential tridenticity is not a disadvantage. However, it is evidently of significance that the nitrogen centers as relatively hard Lewis bases and the high chelate effect of the Tp^{Ph} ligand can keep the nickel center at the oxidation state +II also in the presence of carbon monoxide. This is decisive for the lifetime of the catalyst since the catalysis terminates on the occurrence of a reduction with the formation of carbonyl–phosphane–Ni^0 complexes. The orientation of the noncoordinating third pyrazole ring observed in the solid state has the effect that the borane hydrogen atom lies in the vicinity of the nickel center. This was the reason why we assumed that an intermediary nickel hydride species might be responsible for initiating the catalysis cycle. To examine this assumption we attempted to prepare analogous arylnickel Tp complexes with other substituents. The reaction of [NiBr(*o*-tolyl)(PPh_3)$_2$] with TlTp or $TlTp^{Me,Me}$ according to Equation (1) gave the complexes [Ni(Tp)$_2$] and [Ni($Tp^{Me,Me}$)$_2$], respectively—catalytically inactive, octahedral nickel compounds, which lack the aryl group at the nickel center. The reaction with $TlTp^{p\text{-tolyl,Me}}$ only leads to decomposition products, and with the sterically even more demanding ligand Tp^{tBu} and dichloromethane as solvent the chloronickel complex [NiCl(Tp^{tBu})] is formed. Only when the ligand $Tp^{p\text{-tolyl}}$ is used were we able to prepare the arylnickel complex [Ni(*o*-tolyl)(PPh_3)($Tp^{p\text{-Tolyl}}$)] (**2**), which is analogous to **1**. Complex **2** is catalytically significantly less active than **1**, that is the accessibility and thus the catalytic activity of aryl nickel complexes with $Tp^{R,R'}$ ligands is highly dependent on the substituents R and R′. Whether the boron–hydrogen unit plays a role for the catalytic activity cannot be determined at present.



The presented catalyst opens a route to further nickel complexes which catalyze the formation of a strictly alternating polyketone under mild conditions. Only when some of them have been synthesized will we be able to search directly for ligands with optimal steric and electronic properties. Recently undertaken density functional and ab initio MO calculations on polyketone synthesis showed that the insertion of carbon monoxide and ethene occurs with a lower selectivity in the presence of nickel complexes than with palladium catalysts.[16] This finding is in accordance with the fact that when the nickel complexes described so far are used , the polymerization of ethene must be initiated before the 1:1 copolymerization of ethene and carbon monoxide occurs.

Experimental Section

Typical procedure for the catalysis: Compound **1** (0.10 g, 0.11 mmol) was dissolved in toluene (10 mL) and allowed to react with a mixture of ethene (0.3 mol, 4000 kPa) and carbon monoxide (350 kPa) in an autoclave under stirring at 60 °C for 16 h. The colorless precipitate was filtered, washed with THF, and the polyketone was dried in vacuo. Yield 1.15 g. M.p. 260–262 °C; IR (KBr): $\tilde{\nu} = 1690\ cm^{-1}$ (C=O); $^{13}C\{^1H\}$ NMR (50.3 MHz, $CDCl_3$): $\delta =$ 36.4 (s, CH_2), 212.7 (s, C=O); $M_w = 5770$, $M_w/M_n = 1.3$ (matrix-assisted laser desorption ionization time of flight mass spectrometry (MALDI-TOF-MS)). Elemental analysis: calcd for $(C_3H_4O)_n$: C 64.3, H 7.2; found: C 64.2, H 7.0.

1: Under an inert atmosphere [NiBr(*o*-tolyl)(PPh_3)$_2$] (2.0 g, 2.7 mmol) was dissolved in dichloromethane (25 mL), treated with thallium tris(3-phenylpyrazolyl)borate ($TlTp^{Ph}$) (1.7 g, 2.7 mmol), and stirred for 1 h. The precipitated TlBr was filtered off, hexane (10 mL) was added, and the solution was concentrated to half its volume. The resulting yellow solid was washed with hexane until the filtrate remained colorless. Consequently the complex was dissolved in a little toluene, once again filtered and the solution was concentrated after the addition of hexane. Yield 1.9 g (82%). Crystals suitable for X-ray structure analysis were obtained by recrystallization from diethyl ether. ^1H NMR (200 MHz, $CDCl_3$): $\delta = 1.60$ (s, 3H; CH_3-tolyl), 5.51 (dt, 1H; tolyl), 5.78 (d, $^3J_{HH} \approx 2.3$ Hz, 1H; pyrazolyl), 6.04 (d, $^3J_{HH} \approx 2.1$ Hz, 1H; pyrazolyl), 6.20 (m, 2H; tolyl), 6.52 (d, $J \approx 8.1$ Hz, 2H), 6.69 (m, 6H), 6.87 (d, $^3J_{HH} \approx 2.1$ Hz, 1H; pyrazolyl), 7.06 (m, 6H), 7.41 (m, 19H), 8.01 (d, $J \approx 7.2$ Hz, 2H), 8.28 (d, $^3J_{HH} \approx 2.2$ Hz, 1H; pyrazolyl); $^{13}C\{^1H\}$ NMR (50.3 MHz, $CDCl_3$): $\delta = 23.3$, 103.1, 106.3, 107.1, 119.8, 122.7, 126.7, 127.7 (d, $J_{PC} \approx 13.9$ Hz), 128.0, 128.2 (d, $J_{PC} \approx 9.7$ Hz), 128.5, 129.1, 129.3, 130.0, 130.1, 130.4, 130.7, 134.5 (d, $J_{PC} \approx 9.8$ Hz), 135.0, 135.1, 135.4, 135.7, 139.6, 140.1 (d, $J_{PC} \approx 5.2$ Hz), 146.3; $^{31}P\{^1H\}$ NMR (81 MHz, $CDCl_3$): $\delta = 18.4$ (s); IR (KBr): $\tilde{\nu} = 2382$ (w, BH), 1468 (w), 1438 (w), 1433 (w), 1371 (w), 1280 (w), 1207 (m), 530 cm^{-1} (m). Elemental analysis: calcd for $C_{52}H_{44}BN_6NiP \cdot C_4H_{10}O$: C 72.5, H 5.9, N 9.1; found: C 72.1, H 5.8, N 9.1

Received: May 20, 1998 [Z11885IE]
German version: *Angew. Chem.* **1998,** *110*, 3218–3220

Keywords: homogeneous catalysis · ketones · nickel · N ligands · polymerizations

[1] M. van Opstal, *Chem. Weekbl.* **1995**, (4/28. January).
[2] *Eur. Chem. News* **1996**, *66* (1727), 22.
[3] a) *Plastverarbeiter* **1997**, *48* (4), 104–5; b) C. E. Ash, *Int. J. Polym. Mater.* **1995**, *30*, 1–13.
[4] W. Reppe, US patent 2577208, **1951** [*Chem. Abstr.* **1952**, *46*, 6143b].
[5] T. M. Shryne, H. V. Holler (Shell), US patent 3984388, **1976** [*Chem. Abstr.* **1976**, *85*, 178219w].
[6] E. Drent, J. A. M. van Broekhoven, M. J. Doyle, *J. Organomet. Chem.* **1991**, *417*, 235–251.
[7] a) E. Drent, J. A. M. van Broekhoven, M. J. Doyle, P. K. Wong in *Ziegler Catalysts: Recent Innovations and Technological Improvements* (Eds.: G. Fink, R. Mülhaupt, H. H. Brintzinger), Springer, Berlin, **1995**, pp. 481–496; b) E. Drent, P. H. M. Budzelaar, *Chem. Rev.* **1996**, *96*, 663–681.
[8] U. Klabunde, T. H. Tulip, D. C. Roe, S. D. Ittel, *J. Organomet. Chem.* **1987**, *334*, 141–156.
[9] U. Klabunde, S. D. Ittel, *J. Mol. Catal.* **1987**, *41*, 123–134.
[10] S. Y. Desjardins, K. J. Cavell, J. L. Hoare, B. W. Skelton, A. N. Sobolev, A. H. White, W. Keim, *J. Organomet. Chem.* **1997**, *544*, 163–174.
[11] B. Driessen, M. J. Green, W. Keim (BP), US patent 5214126 **1993**, EP 470759 **1992** [*Chem. Abstr.* **1992**, *116*, 152623g].
[12] The abbreviation used here corresponds to the nomenclature introduced by Trofimenko: S. Trofimenko, *Chem. Rev.* **1993**, *93*, 943–980.
[13] Crystal structure analysis of **1** · Et_2O: monoclinic, space group $P2_1/c$, $Z = 4$, $a = 15.303(3)$, $b = 17.361(2)$, $c = 19.827(3)$ Å, $\beta = 109.60(1)°$, $V = 4962(1)$ Å^3, $\rho_{calcd} = 1.242\ g\,cm^{-3}$, $F(000) = 1952$, $T = 293$ K. The data was collected on a Syntex-Siemens-$P2_1$/P3 four-circle diffractometer (ω-2θ scan) with $Mo_{K\alpha}$ radiation ($\lambda = 0.71073$ Å) at room temperature. In total 9117 (8777 of which were independent) reflections were measured to an angle of $2\theta = 50°$. The structure was solved by direct methods and refined against F^2. One molecule of diethyl ether is contained per formula unit of the complex. All heavy atoms were refined anisotropically, the H atoms isotropically after localization in the difference Fourier map. (The H atoms of Et_2O were treated according to the riding model). The refinement of 733

 © WILEY-VCH Verlag GmbH, D-69451 Weinheim, 1998 1433-7851/98/3721-3051 $ 17.50+.50/0

parameters converged at $R = 0.044$ for 3122 observed reflections with $I > 2\sigma(I)$ and $wR2 = 0.096$ for all reflections. Min./max. residual electron density $-0.219/0.208\ e\,Å^{-3}$. The structure solution was carried out using SHELXS-86, the structure refinement with SHELXL-93. Crystallographic data (excluding structure factors) for the structure reported in this paper have been deposited with the Cambridge Crystallographic Data Centre as supplementary publication no. CCDC-101 494". Copies of the data can be obtained free of charge on application to CCDC, 12 Union Road, Cambridge CB2 1EZ (fax: (+44) 1223-336-033; e-mail: deposit@ccdc.cam.ac.uk).

[14] This was recently found from the catalytic hydrogenation with rhodium(i)complexes of tridentate phosphane ligands: J. Scherer, G. Huttner, H. Heidel, *J. Organomet. Chem.* **1997**, *539*, 67–76.

[15] A. Kremer-Aach, W. Kläui, R. Bell, A. Strerath, H. Wunderlich, D. Mootz, *Inorg. Chem.* **1997**, *36*, 1552–1563.

[16] K. Morokuma, Q. Cui, M. Svensson, D. G. Musaev, R. D. J. Froese, T. Matsubara, *Am. Chem. Soc., Div. Pet. Chem.* **1997**, *42* (1), 119–120.

How Does the Intrinsic Barrier of Intermolecular Proton Transfer Depend on Molecular Parameters?**

Martin Goez* und Rainer Heun

Especially with regard to biological systems, intermolecular proton transfer must be counted among the most important elementary chemical processes; its significance is comparable with that of electron transfer.[1] These two reaction types also have much in common conceptually, because the two lightest chemical particles are transferred and the overall structural changes are not very large. Yet, the difference in their theoretical understanding is considerable. Well established for both is that the relationship between thermodynamics and kinetics—that is, between the driving force of the reaction $-\Delta G^{\ominus}$ and the activation barrier $\Delta G^{\ddagger}$—can be expressed in terms of a single parameter, the intrinsic barrier $\Delta G^{\ddagger}_{\mathrm{int}}$, which is the activation barrier for the (often hypothetical) reaction with $\Delta G^{\ominus}$ equal to zero.[2] However, asking for the factors that govern the magnitude of the key quantity $\Delta G^{\ddagger}_{\mathrm{int}}$ reveals a fundamental gap in our knowledge. While $\Delta G^{\ddagger}_{\mathrm{int}}$ of electron transfer can be predicted numerically from molecular geometries, force constants, and charge densities,[3] much less is known about the dependence of $\Delta G^{\ddagger}_{\mathrm{int}}$ on molecular parameters in the case of proton transfer.[4–6] Here we explore the influence of electronic factors on $\Delta G^{\ddagger}_{\mathrm{int}}$ of proton transfer experimentally, and develop a valence bond configuration mixing (VBCM) model that is capable of explaining the results.

For the substrates we chose *para*-substituted *N,N*-dimethylanilines B, because these compounds lend themselves very well to a separation of electronic and steric effects: By changing the *para* substituent the electron density at the base center can be varied with negligible influence on the geometry of this site and the steric requirements for the reaction. Intermolecular proton transfer is often complicated by participation of the solvent (relay mechanism),[7] which causes the apparent (i.e., observed) activation barrier to be a compound quantity.[6] To avoid this, we carried out the experiments in water-free acetonitrile, which does not function as a hydrogen-bond donor and is a much weaker hydrogen-bond acceptor than is water.[8] The intrinsic barriers $\Delta G^{\ddagger}_{\mathrm{int}}$ were obtained directly from measurements of the rates of proton self-exchange [Eq. (1)] between the unprotonated and protonated forms B and BH^+ of our substrates by means of dynamic NMR spectroscopy.

$$BH^+ + B \rightleftharpoons B + BH^+ \qquad (\Delta G^{\ominus} = 0,\ \Delta G^{\ddagger} = \Delta G^{\ddagger}_{\mathrm{int}}) \tag{1}$$

Not only is this approach more economical than the usual one—namely, using the Marcus theory[2b] to calculate $\Delta G^{\ddagger}_{\mathrm{int}}$ from the activation barriers of a series of homologous cross reactions—it is also much more reliable because it circumvents the difficulties associated with the determination of $\Delta G^{\ominus}$, that is, the problem of acidities in a nonaqueous solvent.

All experimental details are given in a previous paper,[9] where the mechanism of these reactions was also cleared up in detail. As was shown there, thermally activated direct proton transfer between BH^+ and B is rate-determining; relayed proton transfer involving the solvent or residual water is absent, and formation of hydrogen bonds between BH^+ and B as well as tunnelling do not play a significant role. These findings mean that a unique and well-defined reaction mechanism is realized in these systems, which is an indispensible prerequisite for a study aiming to quantify the influence of molecular parameters on the intrinsic barrier of proton transfer.

As Figure 1 shows, there exists a good linear correlation between the values for $\Delta G^{\ddagger}_{\mathrm{int}}$ obtained in this way and the Hammett parameter σ^+. While σ^+ is not a molecular property of our substrates, it is nevertheless related to such: It is well known that σ^+ is a quantitative measure of the electron density at the nitrogen atom in these compounds, and basicity as well as ionization potential I_v of B are linear functions of σ^+.[10] This correspondence will play a key role for the theoretical interpretation that follows. We stress that Figure 1 differs in its implications from a usual Hammett plot: The latter is either a linear relationship between free energies or—when it is of the type $\lg k$ versus Hammett parameter—reflects the influence of the driving force of a reaction on its rate. However, for our self-exchange reactions $\Delta G^{\ominus}$ is zero, and the plot reveals how the *intrinsic* activation barrier $\Delta G^{\ddagger}_{\mathrm{int}}$ depends on an electronic parameter of the reactants. It is seen that the height of $\Delta G^{\ddagger}_{\mathrm{int}}$ is a linear function of the electron density at the nitrogen atom, and the higher the latter, the lower the intrinsic barrier. As a qualitative general trend, this behavior has been reported,[4] but to the best of our knowledge a linear relationship has not been observed before.

These findings can be explained by a VBCM model (Figure 2). Such models were introduced by Pross and Shaik,

[*] Prof. Dr. M. Goez, Dipl.-Chem. R. Heun
Fachbereich Chemie der Universität Halle-Wittenberg
Kurt-Mothes-Strasse 2, D-06120 Halle/Saale (Germany)
Fax: (+49) 345-55-27229
E-mail: goez@chemie.uni-halle.de

[**] This work was supported by the Deutsche Forschungsgemeinschaft and the Fonds der Chemischen Industrie.

 © WILEY-VCH Verlag GmbH, D-69451 Weinheim, 1998 1433-7851/98/3721-3052 $ 17.50+.50/0

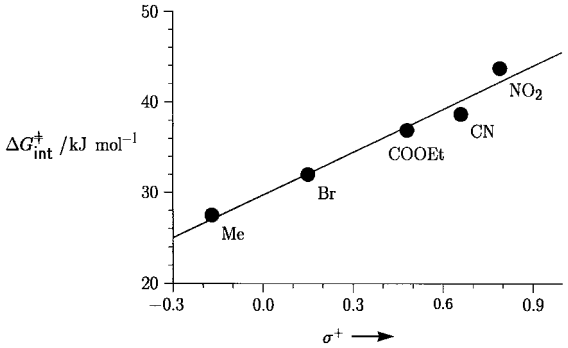


Figure 1. Proton self-exchange of *para*-substituted *N,N*-dimethylanilines in acetonitrile. The plot displays the intrinsic barrier $\Delta G^{\neq}_{int}$ as a function of the Hammett parameter σ^+. The labels at the data points denote the *para* substituent.

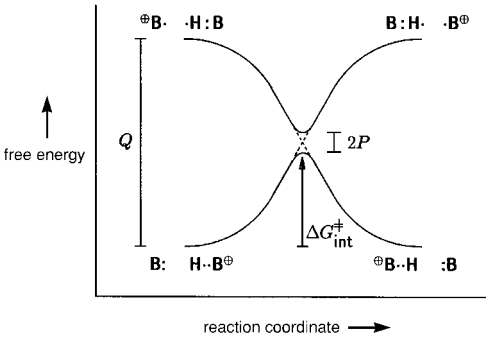


Figure 2. Valence bond configuration mixing (VBCM) model for proton self-exchange between a base B and its conjugated acid BH^+. For further explanation, see the text.

and have already been applied very successfully to many types of chemical reactions, for instance, nucleophilic aliphatic substitutions or cycloadditions.[11] The advantage of a valence bond (VB) description over a molecular orbital (MO) description is that VB configurations provide more chemical insight in the sense that they can be translated directly into a chemical picture and, above all, chemical notation (see below). On the other hand, in the limit of infinite basis sets and infinite configuration interaction, VB and MO models are completely equivalent.

The central idea of the VBCM approach is that the activation barrier of a chemical reaction arises from an avoided crossing of VB configurations. A minimum set of two configurations is very often sufficient: the reactant configuration, which provides the best VB description of the reacting sites in the reactants, and the product configuration, which is the analogue for the products. In our case, each configuration comprises the lone pair at the nitrogen atom in B and the N–H bond in BH^+; hence, the reactant configuration (lower left of Figure 2) is written as $B{:}\,H\cdot\cdot B^{\oplus}$, and the product configuration (lower right) as $^{\oplus}B\cdot\cdot H\,{:}B$. The free energies of these configurations are of course equal, which holds for every self-exchange reaction. The transfer of the proton in either direction is accompanied by an increase in the free energy of the respective starting configuration, because the N–H bond must be stretched and an unfavorable three-electron interaction arises between the lone pair and the approaching hydrogen atom. At the final geometry, the starting configuration is thus an excited configuration. The reactant configuration at the product geometry (upper right of Figure 2) can be represented as $B{:}\,H\cdot\cdot B^{\oplus}$, and the product configuration at the geometry of the reactants (upper left) as $^{\oplus}B\cdot\cdot H\,{:}B$. Owing to the symmetry of the reaction, both excitation energies are identical.

It is clear that the two configuration curves would cross during the reaction, as indicated by the dashed lines in Figure 2. However, around the crossing point they are degenerate or nearly degenerate in free energy, so any interaction between them—which is given by the matrix element $\langle\psi_p|\boldsymbol{H}|\psi_e\rangle$, where ψ_e and ψ_p are the configurations and $\boldsymbol{H}$ the Hamiltonian—causes a splitting of the levels. The amount of splitting $2P$ is determined by the ratio of $|\langle\psi_p|\boldsymbol{H}|\psi_e\rangle|$ to the difference $|G(\psi_p)-G(\psi_e)|$ calculated in the absence of an interaction between the configurations; it is, therefore, largest at the crossing point and decreases monotoneously when the system moves away from it. Owing to this mixing of configurations, the resulting curves (the solid lines in the center part of Figure 2) no longer connect the same configurations on both sides of the diagram. Instead, a change of configurations occurs in the vicinity of the avoided crossing.

The activated complex corresponds to the highest point on the lower curve in Figure 2. From simple geometric considerations,[11] the intrinsic barrier $\Delta G^{\neq}_{int}$ is given by Equation (2).

$$\Delta G^{\neq}_{int} = f\cdot Q - P \qquad (2)$$

The factor f takes into account the location of the transition state. Hence, f depends on the thermodynamics of the reaction (not applicable in our case) and on the functional form of the potential curves. Within a homologous series of substrates this form can hardly change, so f should be constant in our systems. The initial gap Q describes the separation of the configuration curves before the reaction (reactants *and* products at the geometry of the reactants); that is, Q is the free energy needed to excite the reactant configuration vertically. The splitting parameter P is predominantly determined by symmetry (for instance, P is directly responsible for the Woodward–Hoffmann rules),[11] so it should also be constant within our homologous series.

We point out that this VBCM model is essentially identical to the Marcus theory of electron transfer[2a,3a] despite the differences in notation: The Marcus expression for the intrinsic barrier of electron transfer is given by Equation (3),

$$\Delta G^{\neq}_{int} = \lambda/4 \qquad (3)$$

where the reorganization energy λ is the free energy needed to distort the geometry of the reactants (including that of the solvent shell) to that of the products, without transferring the electron. It is evident that λ is identical to the initial gap Q of the VBCM treatment. Furthermore, in the Marcus model nonadiabatic electron transfer (i.e., negligible P) and parabolic potential curves are assumed. Owing to the latter condition, f becomes equal to 1/4, so Equation (2) is transformed into Equation (3).

Reverting to the discussion of Equation (2), the dependence of $\Delta G^{\neq}_{int}$ on the electronic properties of our substrates

 © WILEY-VCH Verlag GmbH, D-69451 Weinheim, 1998 1433-7851/98/3721-3053 $ 17.50+.50/0

obviously arises through the quantity Q. The vertical transition from the VB configuration of the reactants to that of the products can be associated with a concrete chemical picture: The lone pair in B must be oxidized vertically, and the liberated electron must be accommodated by the antibonding orbital of the N–H bond in BH^+. This notion immediately leads to a linear relationship [Eq. (4)] with constants a and b.

$$\Delta G^{\neq}_{int} = a \cdot [I_v - E(\sigma^*_{NH})] + b \quad (4)$$

As the oxidation potential of B in solution is unavailable for most of our compounds, because they are irreversible redox systems,[10b] the (vertical) gasphase ionization potential I_v, which is known to be proportional to the former,[11c] has been used in Equation (4). AM1 calculations indicate that the preferred geometry of the N–H bond in BH^+ is in the plane of the aromatic ring. Because the electronic influence of the *para* substituent is transmitted predominantly through the π system, only a negligible interaction between this substituent and the N–H bond is possible, and the energy $E(\sigma^*_{NH})$ of the antibonding orbital of this bond is expected to be constant within our homologous series. This yields a linear relationship between $\Delta G^{\neq}_{int}$ and I_v [Eq. (5)] and explains, by virtue of the known fact that I_v and σ^+ are linear functions of one another,[10d] the experimentally observed dependence (Figure 1) of the intrinsic barrier on the Hammett parameter σ^+.

$$\Delta G^{\neq}_{int} = a' \cdot I_v + b' = a'' \cdot \sigma^+ + b'' \quad (5)$$

The intrinsic activation barriers of proton transfer have frequently been rationalized with the principle of nonperfect synchronization (PNS),[4,5] which states that the barrier arises because charge delocalization and above all solvation lag behind the motion of the proton. Ab initio calculations,[5c] however, indicate that the effect should also be pronounced in the gas phase, that is, in the absence of solvation. Hence, as in the case of electron transfer a significant inner-sphere contribution to the intrinsic barrier must exist, which is consistent with previous experimental results for our systems.[9] Although the present work is concerned with this inner-sphere term only, the VBCM model is expected to cover the solvent dependence of $\Delta G^{\neq}_{int}$ as well when I_v is measured in the medium used.

The PNS allows quantitative correlations between $\Delta G^{\neq}_{int}$, the slopes of Brønsted plots, and thermodynamics, but its potential for quantitative predictions of $\Delta G^{\neq}_{int}$ from molecular parameters of the reactants seems to be limited. It is our view that the VBCM approach is better suited for this task, while at the same time being just as intuitive and transparent as the PNS, and that for these reasons and because of its firm quantum mechanical basis the former should be preferred.

Received: April 29, 1998 [Z 11794 IE]
German version: *Angew. Chem.* **1998**, *110*, 3225 – 3228

Keywords: kinetics · NMR spectroscopy · protonations · valence bond methods

[1] a) R. P. Bell, *The Proton in Chemistry*, Chapman & Hall, London, **1973**; b) V. Gold, E. Caldin, *Proton-transfer Reactions*, Chapman & Hall, London, **1975**; c) C. H. Bamford, *Proton Transfer*, Elsevier, Amsterdam, **1978**; d) „Proton and Electron Transfer“: *Faraday Discuss. Chem. Soc.* **1982**, *74*; e) *Electron and Proton Transfer in Chemistry and Biology* (Eds.: A. Müller, H. Ratajczak, W. Junge, E. Diemann), Elsevier, Amsterdam, **1992**; f) „Hydrogen Transfer: Experiment and Theory“: *Ber. Bunsenges. Phys. Chem.* **1998**, *102*.

[2] a) R. A. Marcus, *J. Chem. Phys.* **1956**, *24*, 966 – 978; b) R. A. Marcus, *J. Phys. Chem.* **1968**, *72*, 891 – 899; c) F. Scandola, V. Balzani, *J. Am. Chem. Soc.* **1979**, *101*, 6140 – 6141.

[3] a) R. A. Marcus, *Annu. Rev. Phys. Chem.* **1964**, *15*, 155 – 196; b) M. Goez, *Z. Physik. Chem. Neue Folge* **1990**, *169*, 133 – 145.

[4] Recent reviews: a) C. F. Bernasconi, *Adv. Phys. Org. Chem.* **1992**, *27*, 119 – 238; b) C. F. Bernasconi, *Acc. Chem. Res.* **1992**, *25*, 9 – 16, and references therein.

[5] a) C. F. Bernasconi, P. J. Wenzel, *J. Am. Chem. Soc.* **1996**, *118*, 10949 – 10504; b) C. F. Bernasconi, P. J. Wenzel, *J. Am. Chem. Soc.* **1996**, *118*, 11446 – 11453; c) C. F. Bernasconi, P. J. Wenzel, J. R. Keeffe, S. Gronert, *J. Am. Chem. Soc.* **1997**, *119*, 4008 – 4020; d) C. F. Bernasconi, R. L. Montanez, *J. Org. Chem.* **1997**, *62*, 8162 – 8170.

[6] a) J. P. Guthrie, *J. Am. Chem. Soc.* **1996**, *118*, 12886 – 12890; b) J. P. Guthrie, *J. Am. Chem. Soc.* **1997**, *119*, 1151 – 1152.

[7] M. Eigen, *Angew. Chem.* **1963**, *75*, 489 – 508.

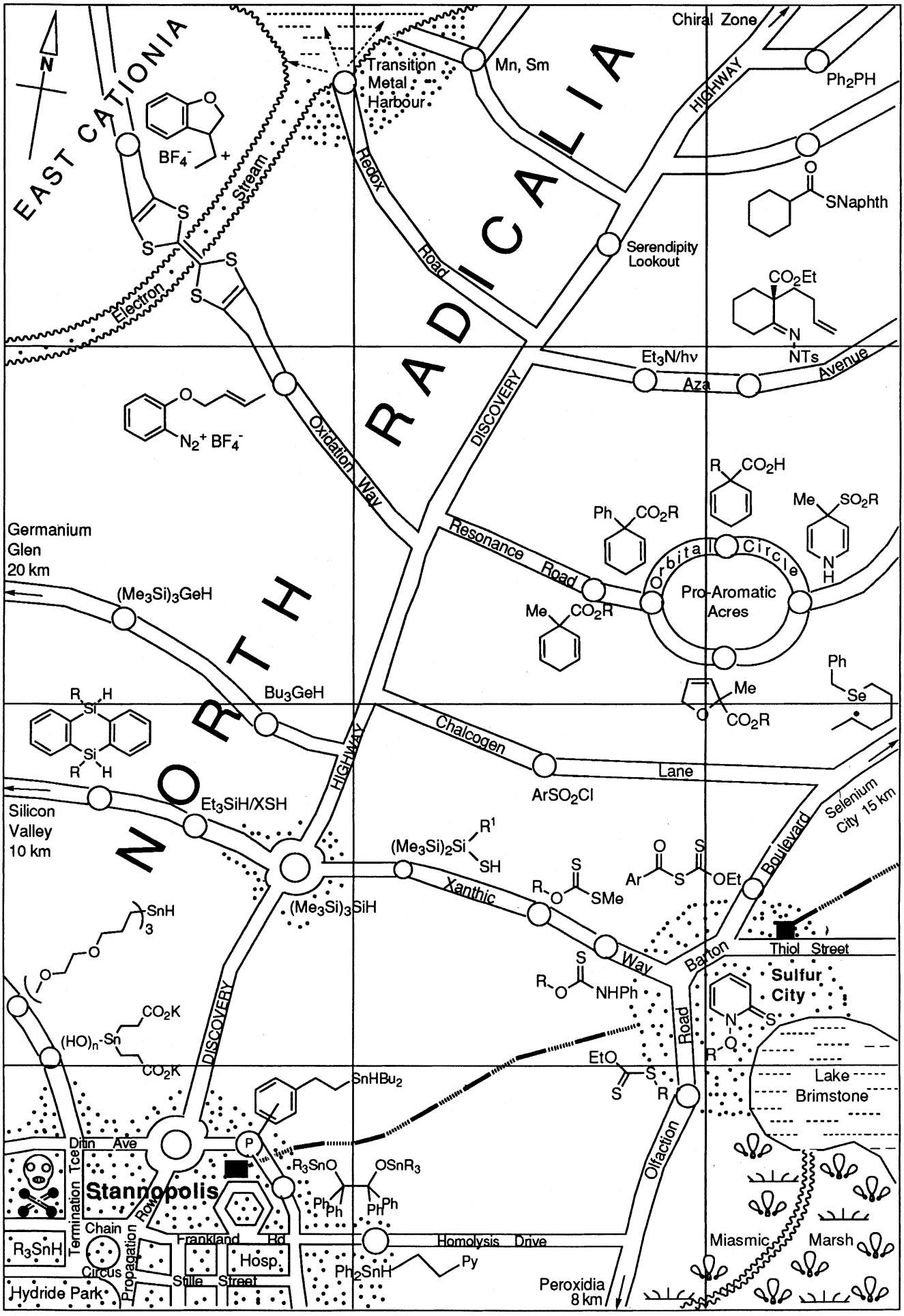
[8] J. F. Coetzee, *Prog. Phys. Org. Chem.* **1967**, *4*, 45 – 92.

[9] M. Goez, R. Heun, *Ber. Bunsenges. Phys. Chem.* **1998**, *102*, 560 – 566.

[10] a) H. K. Hall, Jr., *J. Phys. Chem.* **1956**, *60*, 63 – 70; b) B. M. Latta, R. W. Taft, *J. Am. Chem. Soc.* **1967**, *89*, 5172 – 5178; c) C. K. Mann, K. K. Barnes, *Electrochemical Reactions in Nonaqueous Systems*, Marcel Dekker, New York, **1970**; d) A. Buchs, *Helv. Chim. Acta* **1970**, *53*, 2026 – 2035.

[11] a) A. Pross, S. S. Shaik, *Acc. Chem. Res.* **1983**, *16*, 363 – 369; b) S. S. Shaik, H. B. Schlegel, S. Wolfe, *Theoretical Aspects of Physical Organic Chemistry. The S_N2 Mechanism*, Wiley Interscience, New York, **1992**; c) A. Pross, *Theoretical and Physical Principles of Organic Reactivity*, Wiley-Interscience, New York, **1995**.

 © WILEY-VCH Verlag GmbH, D-69451 Weinheim, 1998 1433-7851/98/3721-3054 $ 17.50+.50/0



ANGEWANDTE CHEMIE ©WILEY-VCH

Flight from the Tyranny of Tin: The Quest for Practical Radical Sources Free from Metal Encumbrances

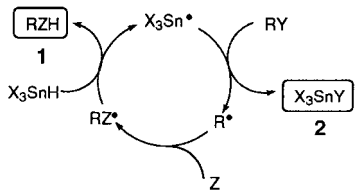
Paul A. Baguley and John C. Walton*

The versatility, predictability, and functional-group tolerance of free radical methodology has led to the gradual emergence of homolytic disconnections, which are steadily taking their place alongside more familiar ionic disconnections in the armory of synthetic chemistry. Currently, organotin reagents dominate the area and are the almost automatic choice for radical ring closures, ring expansions, cascade reactions, and the like. Organotin residues are notoriously difficult to remove from desired end products, and this, coupled with the fact that many organotin compounds are neurotoxins, makes techniques using tin inappropriate for syntheses of drugs, medicines, and other formulations intended for human consumption. Objections to tin apply with diminished but still significant force to other metals. These constraints have triggered quests for methods of nullifying the impact of tin, for new metal-free ways of generating free radicals, for new chain processes, for mediating efficient syntheses, and for all-organic single electron transfer agents. This review draws together the principal innovations in a fast-moving but scattered enterprise. Individual methods based around redesigned tin reagents, organosilyl substitutes, thiocarbonyl and related sulfur reagents, cyclohexadienes, tetrathiafulvalenes, and others are illustrated with synthetic examples. Brief descriptions of the strengths and weaknesses of individual reagents are supplied to enable dissatisfied synthetic chemists to make a rationally directed escape into tin-free comfort zones (such as that depicted in the frontispiece on the opposite page).

Keywords: radicals · silicon · synthetic methods · thiocarbonyl compounds · tin

1. Introduction

The burgeoning use of homolytic methodology in the field of organic synthesis owes much to the superlative flexibility of organotin reagents, which enables them to flourish with an exceptionally wide range of substrates and reaction conditions. Ever since the original discovery of radical generation by organotin hydrides (X_3SnH),[1] a spiral of applications has wound inexorably upward. At present tin reagents dominate free radical chemistry, and their influence is reaching continually deeper into the mainstream of synthetic science.[2] They have proved particularly serviceable for the substitution of hydrogen in place of halogen, hydroxyl, amino, nitro, thiol, selenide, carboxylate, and other functional groups.[3] Organotin hydrides also mediate radical additions to alkenes and alkynes (Z, Scheme 1) in reductive carbon–carbon bond formations,[4–6] although premature hydrogen transfer to the prior radical can be a problem. Allylstannanes have found considerable use as reagents for allylations,[6] as have propynylstannanes in the corresponding production of allenes.[7] Organotin-mediated one-carbon ring expansions of alicyclic, polycyclic, and heterocyclic β-keto esters take place in high yields for a variety of ring sizes.[8, 9]



Scheme 1. The basic organotin hydride mediated reaction chain.

Most importantly, however, tin-based methods exercise an autocratic influence in the domain of radical ring closures. A plethora of such annulations pervades the recent literature. Unsaturated alkyl, aryl, vinyl, acyl, aminyl, alkoxyl, and other heteroradicals propagate their cycles on chain gangs cease-

[*] Prof J. C. Walton
University of St. Andrews
School of Chemistry, St. Andrews
Fife KY16 9ST (UK)
Fax: (+44) 1334-463808
E-mail: jcw@st-and.ac.uk
Dr P. A. Baguley
Oxford Asymmetry International, Abingdon (UK)

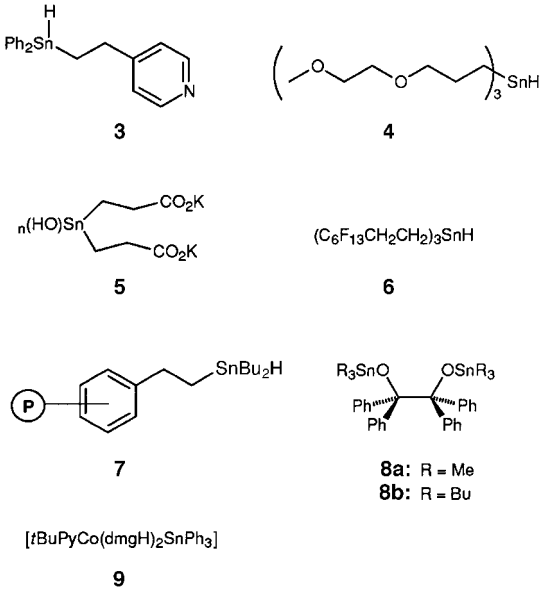
 © WILEY-VCH Verlag GmbH, D-69451 Weinheim, 1998 1433-7851/98/3722-3073 $ 17.50+.50/0

lessly disciplined by the vigilant agents of tin.[10–12] Five-membered rings with many different embellishments are a speciality, but larger rings, intricate polycycles, and a wide range of exotic heterocycles have all been hammered out on the anvils of tin. So pervasive is the method that even key steps in natural product syntheses have come to depend on organotin reagents.[13, 14] For example, the synthesis of (±)-morphine by Parker et al. incorporated a tin hydride mediated bicyclization of an aryl radical,[15] and the synthesis of prostaglandin $F_{2\alpha}$ by Stork et al. included an *exo*-cyclization of a cyclopentenyloxyalkyl iodide brought about by tin hydride generated in situ.[16] Also, Curran et al. have carried out several notable tin hydride assisted preparations of triquinane natural products, including silphiperfolene.[17] Cascade sequences are some of the most exquisite examples of the synthetic art, and organotin hydride promoted representatives are at the cutting edge.[18] Spectacular archetypes include the construction of a tetracyclic homosteroid by means of a quadruple *endo*-cyclization cascade starting from a tetraene selenoester[19] and the degradative triple β-scission cascades of bromomethylcubanes[20] and basketanes.[21]

The success of tin reagents has given them such prestige and notoriety that they practically monopolize the market place for homolytic synthetic and kinetic applications. It is small wonder that this dominance has been referred to as the "tyranny of tin". The tin hegemony has been established at no small price, and the main burdens under which the vassals of tin groan are the hazardous handling and disposal of toxic garbage (**2**) and the penchant of tin for prematurely zapping hydrogen onto immature structures. Medicines, drugs, and food additives contaminated with tin are unsafe for human consumption, hence there is an urgent need for new metal-free reagents to unlock the chemical doorway, liberate the vassals, and free-up radical methodology for use in the food and medicines industries. A great deal of attention has been directed recently to radical generation with reagents based on compounds of mercury, cobalt, manganese, or samarium, and some fascinating transformations have been achieved. However, these metals suffer toxic effects of their own and contamination by them of food or pharmaceuticals cannot be contemplated. This review focuses therefore on the search for metal-free methods of generating radicals, of propagating chain reactions, and of mediating alternative homolytic processes.

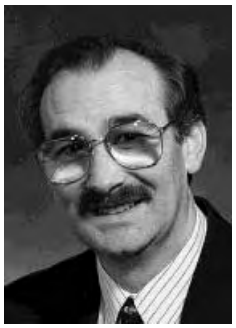
2. Viewing the Tyrant's New Clothes

A not inconsiderable enterprise of the tin federation has been the design and production of alternative tin compounds that will facilitate or minimize the disposal of tin garbage. Pyridylstannane **3**, prepared from 4-vinylpyridine, affords products in yields comparable to those obtained with tributyltin hydride.[22] The advantage of this reagent is that the organotin halide by-products have R_f values of approximately zero for elution with ethyl acetate/hexane, and this enables products to be isolated relatively easily (Scheme 2).



Scheme 2. New organotin reagents for homolytic transformations.

John Walton was born in St. Albans, UK, in 1941. He graduated from Sheffield University in 1963 and studied for his Ph.D. with Lord Tedder in Sheffield and Dundee. He moved to St. Andrews in 1970, where he is currently Professor of Reactive Chemistry. His research has focused on synthetic, mechanistic, and EPR spectroscopic aspects of free-radical chemistry, and he was awarded the Royal Society of Chemistry prize and silver medal for Organic Reaction Mechanisms in 1994. His current research interests include synthetic methods, cascade reactions, and organic conducting and magnetic polymers.



J. C. Walton



P. A. Baguley

Paul Baguley was born in Warrington, UK, in 1973, and studied chemistry at the University of Glasgow, graduating in 1994. He subsequently joined Professor Walton's group in St. Andrews, where his Ph.D. research was largely concerned with designing and testing alternative free radical sources. He was recently appointed as a Senior Scientist with Oxford Asymmetry International.

Converse techniques generate tin residues that are extremely nonpolar and elute before the product. One such method depends on treatment of the product mixture with an excess of sodium cyanoborohydride in *tert*-butyl alcohol, such that after completion the reaction mixture contains the desired product and regenerated organotin hydride.[23] Column chromatography allows separation of the product from the organotin hydride, which elutes from the column first and can be reused. An alternative chromatographic workup involves dilution of the reaction mixture with undried diethyl ether and addition of a slight excess of diazabicycloundecene (DBU) followed by dropwise addition of an ethereal solution of iodine until the iodine color just persists. The solution is filtered through a short column of silica gel with diethyl ether as eluent. Tin hydroxides and distannoxanes, together with DBU hydrohalides and excess DBU remain at the top of the column, and the product elutes virtually free of tin.[24]

The water-soluble tin hydride **4**[25] and hydroxide **5**[26] enable reductions and cyclizations to be carried out in environmentally friendly aqueous solutions. The polarity of **4** facilitates product isolation, though its synthesis is rather lengthy. Reagent **5** is heated with the substrate, $NaBH_4$, and the water-soluble initiator 4,4′-azobis(4-cyanovaleric acid) (ACVA) in a dilute aqueous alkali solution. The $NaBH_4$ reduces **5** to the corresponding hydride, which is utilized in situ to generate the corresponding tin radical.

A modest means of separating out tin compounds relies on the immiscibility of hexane and acetonitrile, and the extraction of organotin species into the hexane layer and of the organic product into the acetonitrile layer; however, this is limited by the partitioning of some organic products between both solvents.[27] An evolution of this approach employs fluorous reagent **6**, which can be prepared in a three-step synthesis.[28] Reactions are carried out in trifluoromethylbenzene, which is then evaporated and replaced by dichloromethane/perfluorocyclohexane. The fluorous tin by-products remain in the fluorocarbon layer, thus facilitating the clean isolation of the desired organic product. The method was also extended to the catalytic use of **6**, with sodium cyanoborohydride as reducing agent.

Polymer-supported tin hydrides are probably the most effective for isolating a desired organic compound free from tin by-products.[29–31] As the polymers are insoluble in the reaction solvent, an organic product can be isolated simply by filtering off the polymeric tin halides, which can usually be recycled to hydrides for further use. Polymers of type **7** have been reported to be of general use for reductions of halides and for ring closures,[29] although their preparation is not a trivial task.[29, 32]

The problem of premature reduction of intermediate radicals, which is so prevalent with tin hydrides, may be avoided by use of distannanes or by resort to other tin-based precursors. Use of bis(trimethylstannyl)benzopinacolate (**8a**) as a thermal source of trimethylstannyl radicals was advocated some time ago.[33] Recently, it has been demonstrated that alkyl radicals generated from halides and selenides, by use of **8a**, add to the carbon–nitrogen double bond of *O*-benzylformaldoxime.[34] Owing to the expense and toxicity of trimethylstannyl derivatives, the alternative tributyl reagent **8b**, which can be prepared in almost quantitative yield from benzopinacol and tributylstannyldimethylamine, has also been endorsed.[35] A disadvantage of these methods, however, is the troublesome removal of both tin residues and benzophenone.

Photolysis of (triphenyltin)cobaloxime **9** yields a triphenyltin radical which propagates cyclizations. An advantage is that the intermediate Co^{II} radical can oxidize the cyclized radical to yield an olefin.[36] Although some benefits may accrue from the use of these novel tin reagents, the fundamental problem of tin toxicity remains a constant menace. A significant number of radical chemists have therefore sought refuge with more clement relatives of tyrant tin.

3. Checking Silicon and Germanium: Sibling Imitators of the Tyrant

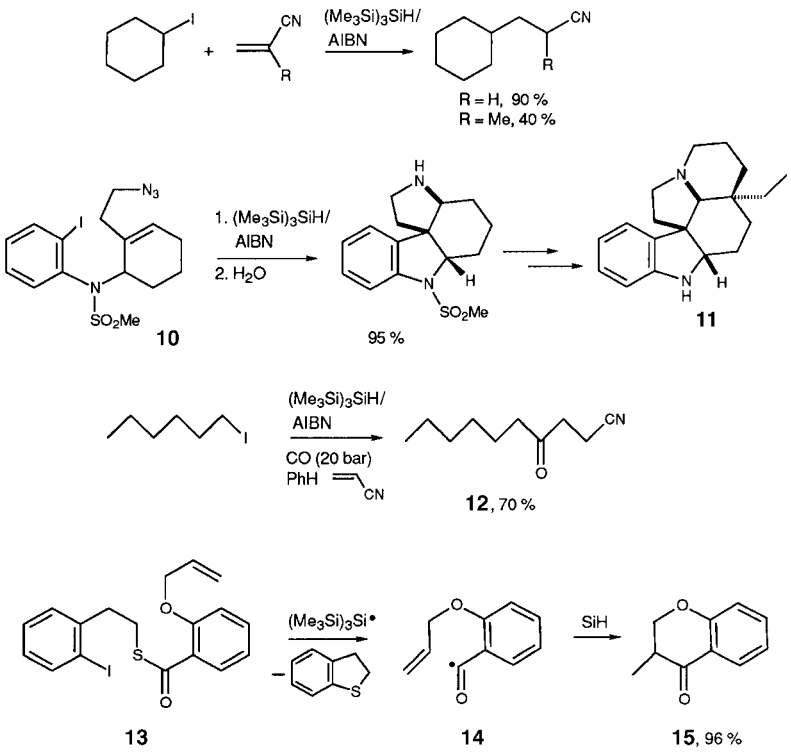
The silicon–hydrogen bond in simple triorganosilanes is too strong for ready hydrogen transfer, and therefore chain processes are difficult to maintain. Although triethylsilane[37–39] and diphenylsilane[40] have been advocated as alternatives to organotin hydrides, the range of amenable substrates is limited and the reaction temperature is often undesirably high (120–140 °C); it is unlikely that either will be a popular reagent. A shrewd remedy for this problem is to include a catalytic amount of an alkanethiol, such as *tert*-dodecanethiol (XSH), with the triethylsilane in the reaction mixture.[41] Nucleophilic alkyl radicals abstract hydrogen from thiols much more readily than from electron-rich trialkylsilanes, but the resulting electrophilic thiyl radicals abstract hydrogen from the silane more readily than the alkyl radicals. Thus, the thiol is regenerated along with the chain-carrying silyl radical, and yields of RH exceed 90%. This procedure, termed polarity-reversal catalysis, is also effective for hydrosilylation of alkenes using triethylsilane:[42]

$$R^{\cdot} + XSH \rightarrow RH + XS^{\cdot}$$

$$XS^{\cdot} + Et_3SiH \rightarrow XSH + Et_3Si^{\cdot}$$

$$Et_3Si^{\cdot} + RY \rightarrow R^{\cdot} + Et_3SiY$$

The most successful and widely used replacement for tin hydride is undoubtedly tris(trimethylsilyl)silane.[43, 44] Not only does this reagent pose little toxic threat, but it also produces fewer by-products of direct reduction because its Si–H bond is about 5 kcal mol^{-1} stronger than the Sn–H bond of tributyltin hydride. This has often enabled radical procedures to be accomplished with a stoichiometric amount of the silane in the initial reaction mixture, instead of the tedious slow-addition, high-dilution technique frequently essential with tin hydrides. Examples of intermolecular radical additions to acrylonitrile (R = H) and methacrylonitrile (R = CH_3),[44] an intramolecular double ring closure of an unsaturated aryl iodide **10**[45] in the synthesis of aspidospermidine (**11**), and an intermolecular tandem carbonylation–addition sequence yielding 3-oxonitrile **12**,[46] all mediated by $(Me_3Si)_3SiH$, are shown in Scheme 3. The aryl radical



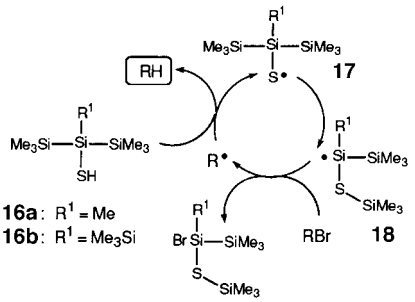
Scheme 3. Typical applications of tris(trimethylsilyl)silane.

obtained on treatment of thiol ester **13** with $(Me_3Si)_3SiH$ underwent an intramolecular homolytic substitution reaction (S_Hi) at sulfur to form dihydrobenzothiophene with displacement of acyl radical **14**, which underwent ring closure to yield cyclic ketone **15** after the final hydrogen-transfer step.

Variants of this reaction were also reported.[47] Alkylated heteroaromatic units have been prepared by use of $(Me_3Si)_3SiH$ (or $(Me_3Si)_4Si$) with an alkyl halide and a protonated quinoline or similar heterocycle.[48] $(Me_3Si)_4Si$ has also been used in place of $Me_3SnSnMe_3$ to mediate an efficient synthesis of the anticancer drug camptothecin.[49] The radical cascade reaction involved an intermolecular addition of an amidovinyl radical to phenylisonitrile to afford an imidoyl radical which underwent two intramolecular cyclizations. Similar routes were used to synthesize a range of derivatives.

$(Me_3Si)_3SiH$ is certainly a versatile reagent that can be used to accomplish a range of useful transformations. Its most serious drawback is the propensity of the $(Me_3Si)_3Si^{\bullet}$ radical to add to multiple bonds. In fact $(Me_3Si)_3SiH$ is an efficient reagent for hydrosilylating alkenes and alkynes.[50] Other disadvantages are the cost and the need to handle under argon; thus far it has barely dented the dominance of tin. One solution to the problem of high cost is to use the reagent in catalytic quantities, together with sodium borohydride to regenerate the reagent from the silicon–halogen by-products.[51] Good yields can be obtained with simple substrates, but this procedure undermines a general benefit of homolytic methodology, namely freedom from the need for protecting groups.

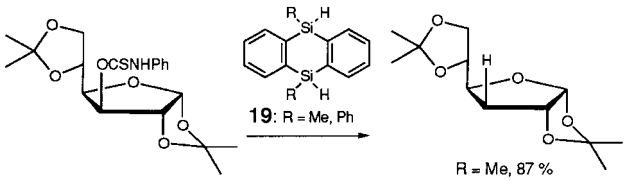
Several other silanes have emerged as challengers to the authority of tin. The electronegativity of sulfur, and the possibility of 3p–3p overlap between silicon and sulfur atoms, was expected to reduce the Si–H bond strength of tri(alkylthio)silanes below that of Et_3SiH. In some simple experiments with bromides, iodides, isocyanides, xanthate esters, and phenyl selenides, nearly quantitative yields of reduced products were obtained with $(Me_3Si)_3SiH$.[52] Heptamethyltrisilane-2-thiol[53] (**16a**) and tris(trimethylsilyl)silane-2-thiol[54] (**16b**) possess thiol groups which readily donate hydrogen atoms to C-centered radicals to afford thiyl radicals **17** (Scheme 4). These reagents then take advantage of the rapid



Scheme 4. Mode of action of trimethylsilylsilanethiols.

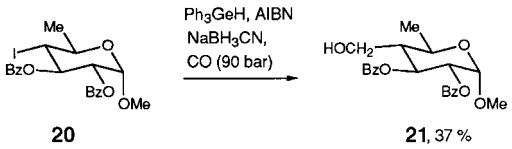
1,2-migration of a Me_3Si group from silicon to sulfur in **17**, thus unmasking silyl radical **18**. This selectively abstracts halogens, and hence reduction of a variety of organic halides is facilitated.

The synthetic range of (trimethylsilyl)silanethiol reagents is limited due to their thermal instability and the fast rate of hydrogen transfer by the thiol, which is approximately an order of magnitude greater than that of tributyltin hydride. Recently, 9,10-dihydro-9,10-disilaanthracenes **19** were shown to be effective for the reduction of alkyl halides and for the deoxygenation of alcohols, via *O*-thiocarbonyl derivatives, under mild conditions (Scheme 5).[55, 56] The ease of their preparation,[57] coupled with the good yields, are indicators of an auspicious future for these reagents.



Scheme 5. Use of 9,10-dihydro-9,10-disilaanthracenes for deoxygenation of alcohols.

Tributylgermanium hydride has a relatively strong Ge–H bond, and therefore direct substrate reduction is usually not significant.[58, 59] The advantage over tin hydrides that this bestows has been the basis of the rare applications of germanium hydrides. Thus, addition of C-centered radicals to alkenes can proceed with essentially equimolar amounts of the halide and alkene. The preparation of monosaccharide **21**, which was required for a mechanistic study of the complex natural product calicheamicin, exemplifies the use of germanium hydrides.[60] Attempts to replace the iodine atom of **20** (Scheme 6) with a hydroxymethyl substituent using ionic



Scheme 6. Use of triphenylgermanium hydride in a reductive carbonylation.

reagents were thwarted by elimination reactions. Attention was therefore turned towards generating the corresponding alkyl radical under an atmosphere of CO. The tin hydride method gave only the product of direct reduction, but use of catalytic quantities of Ph_3GeH with $NaBH_3CN$ resulted in the isolation of 37% of monosaccharide **21**. An additional advantage with the catalytic method was the in situ reduction of the carbonyl functionality to the hydroxyl group.

Simpler iodides, such as adamantyl iodide, underwent the same reaction in yields exceeding 60%.[60] However, the lower reactivity of Ge-centered radicals usually restricts reductions to iodides. Furthermore, tributylgermanium hydride is more prone to add to alkenes than its tin counterpart and is significantly more expensive.

Tris(trimethylsilyl)germane, $(Me_3Si)_3GeH$, reduces a variety of functional groups in high yields.[61] However, the rate of hydrogen abstraction from $(Me_3Si)_3GeH$ by a primary alkyl radical, measured with the hex-5-enyl radical clock, was found to be even faster than from tributyltin hydride,[61] and this will limit the reagent's usefulness.

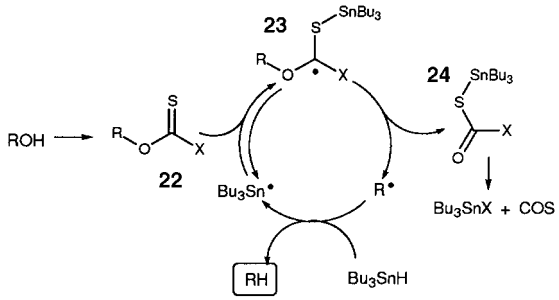
Highlights of the synthetic advantages of silicon and germanium reagents have been presented in this section. Many organic chemists have been beguiled into trying one or more of these reagents only to be disappointed by their cost, handling problems, and limited range of applicability and have returned to the thralldom of tin consoling themselves with the thought "better the devil you know".

4. Seeking Sanctuary in Sulfur's Odorous Realm

In the search for a complete break with harmful metal habits, the homolytic susceptibilities of numerous sulfur compounds have been explored. Promising results cluster around molecules containing the thiocarbonyl moiety.

4.1. On the Horns of the Thiocarbonyl Dilemma: To Collaborate or Not To Collaborate with Tin

The Barton–McCombie reaction of organotin hydrides with thiocarbonyl compounds **22** has been widely used as a means of generating radicals from primary and secondary alcohols and as a mild method for deoxygenating them.[62, 63] The reaction probably proceeds by reversible addition of the stannyl radical to the thiocarbonyl sulfur atom to generate C-centered radical **23**. This species undergoes β-scission to afford the corresponding carbonyl compound **24** and an alkyl radical, which abstracts hydrogen from the organotin hydride (Scheme 7).[64] The original procedure employed xanthates (**22**, X = SMe), thiobenzoates (**22**, X = Ph), or thiocarbonyl



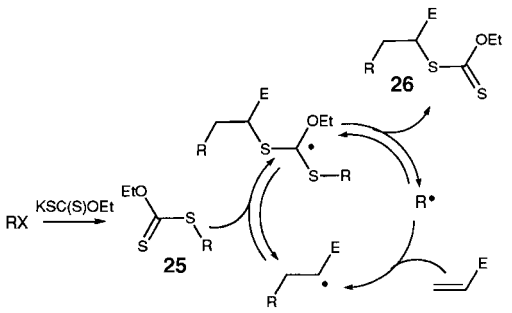
Scheme 7. Chain propagation of the Barton–McCombie deoxygenation of alcohols.

imidazoles (**22**, X = imidazole), but several other derivatives, notably thionocarbonates (**22**, X = OPh or OMe), are also satisfactory. Suitable procedures for the preparation of individual thiocarbonyls and applications of the method in the areas of steroids, carbohydrates, terpenoids, and nucleosides have been conveniently collated.[66]

The conspicuous catch with this procedure is the reappearance of obnoxious organotin hydride. Possible means of avoiding this are being sought. For example, *N*-phenylthioxocarbamates (**22**, X = NHPh) may be prepared in good yields by the reaction of the appropriate alcohol with phenyl isothiocyanate in the presence of sodium hydride.[67] Deoxygenations of alkanols, as well as sugars, proceed in yields of over 80% with these substrates, when $(Me_3Si)_3SiH$/AIBN is deployed in place of tin. Several phosphorus derivatives, including hypophosphorus acid and di-*n*-butylphosphane oxide, also function well as hydrogen donors. For example, *S*-methyl dithiocarbonates of tertiary and secondary alcohols were deoxygenated in high yields by use of the phosphane oxide in boiling dioxane; primary alcohols needed higher temperatures.[68] Methods that cut tin involvement to catalytic quantities have also been devised.[69, 70] A catalytic amount of $(Bu_3Sn)_2O$ may be combined with a stoichiometric amount of polymethylhydrosiloxane, TMSO{Si(HO)(Me)}$_n$TMS, as reducing agent. Thus, the organotin oxide is reduced in situ to tributyltin hydride, which induces the deoxygenation process. However, the reaction has to be performed in *n*-butyl alcohol to allow efficient reduction of the tin by-products. The advantages of this method include the use of very cheap reagents, diminished contamination problems, and the isolation of products in similar yields to the stoichiometric method.

4.2. Eluding Metal Overtures with the Aid of Xanthates

Dithiocarbonates (xanthates) and related compounds have been studied with particular thoroughness.[65] Following addition of a radical, ethoxyxanthates such as **25** (or the corresponding methoxy derivatives) do not fragment in the Barton–McCombie mode, but undergo C–S bond scission to generate R$^\cdot$ and a new xanthate **26**. Radical R$^\cdot$ can add to an alkene or, if unsaturated, cyclize before continuing the chain by addition to more starting xanthate **25** (Scheme 8). The additions of C-centered radicals to the xanthates are reversible, but by judicious choice of initial xanthates and reaction



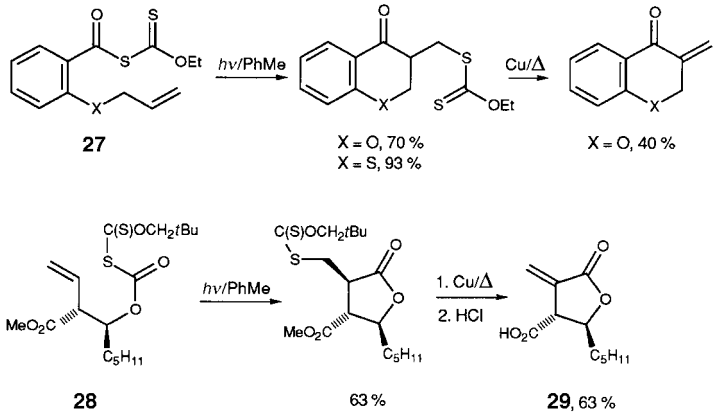
Scheme 8. Chain propagation steps for addition to alkenes of radicals generated from *O*-ethyl dithiocarbonates (xanthates).

conditions, good yields (> 60 %) of a wide variety of product xanthates **26** can be obtained.

Xanthates of type **25** are easily made by nucleophilic displacement from alkyl halides, tosylates, methylsulfonates, etc. by potassium *O*-ethyl xanthate, which is itself prepared from KOEt and CS_2 in ethanol. The chain reaction is initiated with catalytic quantities of peroxide and hence provides a metal-free route of considerable generality for homolytic inter-[71] and intramolecular syntheses[72, 73] which implement C–C bond formations and supply rings with various substitution patterns. The xanthate functionality can sometimes be removed by reduction with dilauroyl peroxide in propan-2-ol, or by treatment with DBU, or by heating with Cu powder.

The corresponding *S*-acyl xanthates (e.g. **27**) were convenient precursors of acyl radicals and were found to be useful reagents for additions and cyclizations.[65] Xanthic anhydrides ROC(S)SC(S)OR, derived from primary and secondary alcohols, extruded alkoxythiocarbonyl radicals on photolysis and hence, by rapid loss of COS, afforded R$^{\bullet}$.[74] More importantly, *S*-alkoxycarbonyl xanthates of the type ROC(O)SC(S)OCH$_2$*t*Bu functioned very satisfactorily as radical sources through loss of CO_2 from the intermediate alkoxycarbonyl radicals, and were thus transformed into ordinary xanthates (Scheme 9).[75]

The finding that appropriately unsaturated alkoxycarbonyl radicals (e.g. **28**) underwent ring closure before CO_2 loss was of special synthetic significance, because it supplied an auspicious route to lactones such as (±)-cinnamolide and the antibacterial agent (±)-methylenolactocin (**29**).[76, 77] Other members of the xanthate family such as thiocarbazones[78] and iminodithiocarbonates[79] were found to be good precursors for nitrogen-centered radicals, but catalytic or stoichiometric amounts of tin compounds were required for efficient chain propagation.

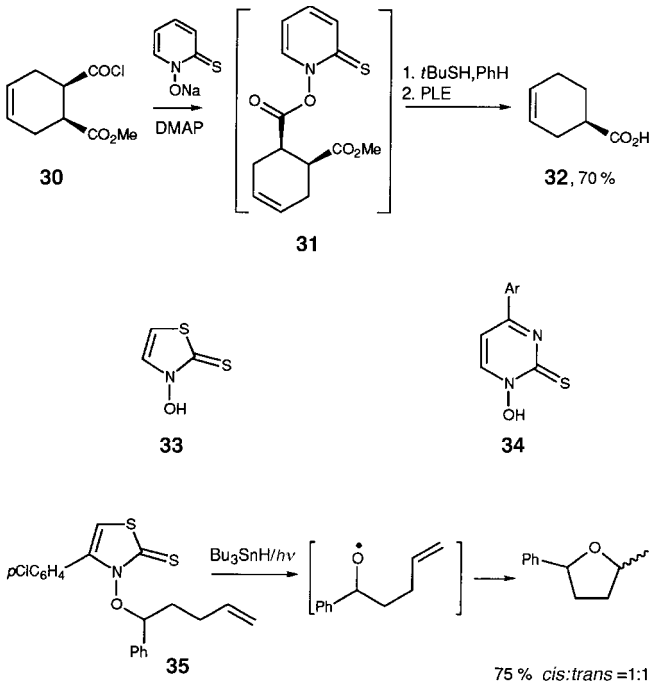


Scheme 9. Homolytic transformations of *S*-acyl xanthates and *S*-alkoxycarbonyl xanthates.

4.3. Weighing Thiohydroxamic Esters: Supple Partners for Tin and Sulfur

The now classic "Barton esters"—that is, *O*-acyl derivatives of the thionohydroxamic acid *N*-hydroxypyridine-2-thione, for example, **31**—have been widely applied for the mild decarboxylation of carboxylic acids.[3, 80] They may be used in concert with an organotin hydride, but the latter can often be replaced by a thiol (usually 2-methylpropane-2-thiol) with little if any loss of efficiency and easier removal of the resultant *tert*-butyl pyridyl disulfide by-product. The success of this methodology is due to the susceptibility of the thione functionality to addition of tin- and sulfur-centered radicals,[81] the weakness of the N–O bond, and the use of aromatization as a favorable thermodynamic driving force.

Since the introduction of Barton esters, numerous applications of this radical-based methodology have been reported, for example 1) the conversion of carboxylic acids into thiols,[82] cyanides[83] and isothiocyanides,[83] 2) the homologation of carboxylic acids either by two carbon atoms to yield amides[84] and α-keto acids[85] or by one carbon atom to give aldehydes,[86] and 3) the generation of oxygen-centered radicals.[87] The method is particularly popular for reductive decarboxylations. For example, (*R*)-3-cyclohexenecarboxylic acid (**32**) was required as the starting point for the synthesis of the natural product FK506 (Scheme 10).[88] Acid chloride **30**



Scheme 10. Examples of Barton esters and alternative thiohydroxamic esters as well as their synthetic applications. PLE = pig liver esterase.

was converted into the corresponding thiohydroxamic ester **31**, which underwent smooth decarboxylation with 2-methylpropane-2-thiol in benzene to give the required product after enzymic hydrolysis.

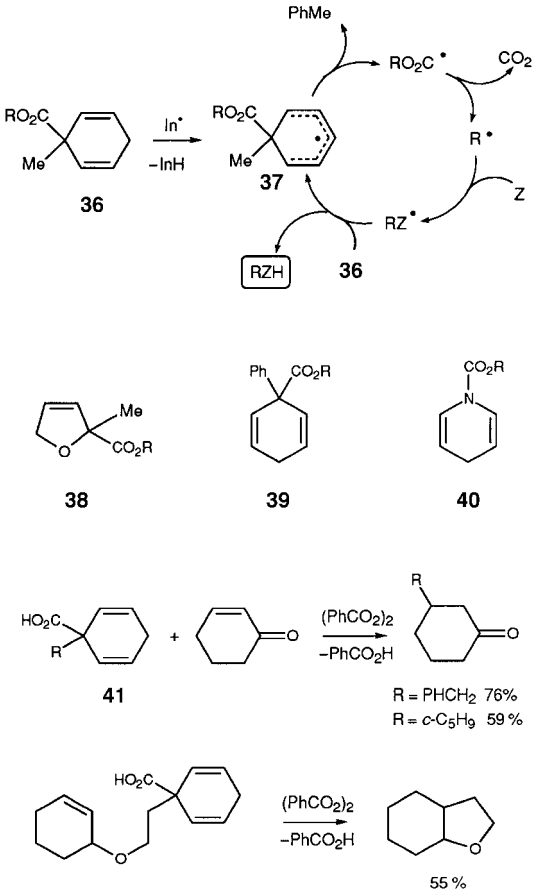
A range of alternative *N*-thiohydroxamic esters has been examined,[3, 89] including *O*-acyl derivatives of *N*-hydroxythiazole-2(3*H*)-thione (**33**) and *N*-hydroxy-2(1*H*)-pyrimidine-2-thione (**34**).[90] *N*-Alkoxy derivatives of 4-(*p*-chlorophenyl)-thiazole-2(3*H*)-thiones **35** yield alkoxyl radicals which, if appropriately functionalized, undergo ring closure to afford tetrahydrofuran derivatives in good yields.[91] Most of these alternatives need more vigorous conditions for use, or require organotin partners, so that the original type of esters **31** are generally best.

Although most of the sulfur-based reagents reach optimum performance in symbiotic relationships with organotin compounds, several practical metal-free systems have been discovered. The chief inconvenience of this chemistry lies in the fetid reek that accompanies the use of thiols and many other sulfur compounds. This miasma, which envelops products and personnel alike, evokes dire social and environmental repercussions.

5. Renouncing the Tin – Halogen – Chalcogen Carousel in Favor of "Proaromatic" Compounds

A potential means of avoiding tin depends on arranging hydrogen abstraction from a suitable reagent as the first stage of chain propagation, rather than halogen or chalcogen displacement. Because C-centered radicals are comparatively unselective in hydrogen abstractions, consequent problems with regioselectivity have inhibited design of suitable multipurpose reagents. However, several series of "proaromatic" esters deliver the required regioselectivity by means of allylic activation, simultaneously taking advantage of rearomatization as the driving force for generation of the desired radical.[92] 1-Methylcyclohexa-2,5-diene-1-carboxylic acid, which is easily made by Birch reduction and methylation of benzoic acid, acted as a prototype reagent and furnished a range of esters **36**. Their general mode of chain operation, for addition of the alcohol-derived radicals to alkenes (*Z*), is shown in Scheme 11; bromination/deoxygenation occurred in analogous fashion in the presence of excess NBS.[93] Good to moderate yields of adducts (or bromides) were obtained from **36** and the analogous 2-methyl-2,5-dihydrofuroic esters **38**, derived from secondary, tertiary, or benzylic alcohols.

Advantages of these reagents included the innocuous and volatile by-products, the success with use of metal-free initiators such as dibenzoyl peroxide and *tert*-butyl perbenzoate, and the comparatively slow rate of hydrogen donation by **36**, which repressed direct reduction of R·. However, the chains were short, so that comparatively large amounts of initiators had to be used. In addition, some β-scission of the intermediate cyclohexadienyl radicals **37** took place in the unwanted mode to generate Me· and yield aromatic esters $PhCO_2R$ as by-products. To evade this problem esters of 1-phenylcyclohexa-2,5-diene-1-carboxylic acid (**39**) and *N*-alkoxycarbonyl derivatives (**40**) of 1,4-dihydropyridine, both



Scheme 11. Use of 1-alkylcyclohexa-2,5-diene-1-carboxylic acids and esters and related compounds as proaromatic radical precursors.

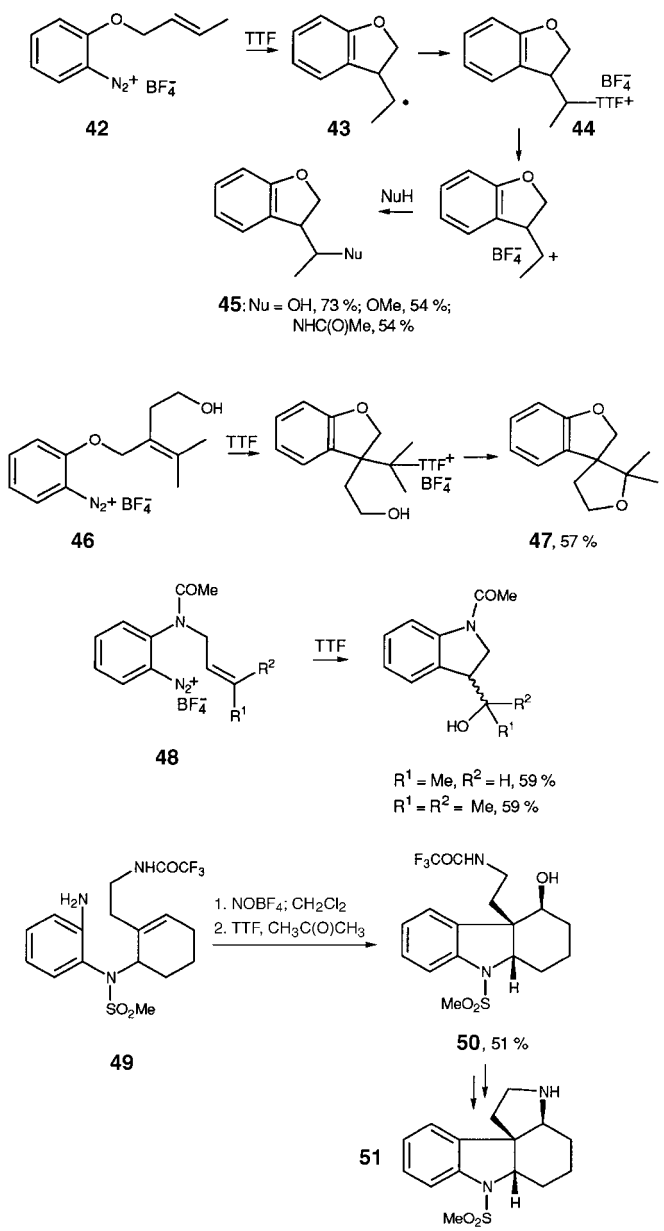
of which have only one viable fragmentation mode for the corresponding delocalized radicals, are currently under study.

Lateral thinking prompted the idea that 1-alkylcyclohexa-2,5-diene-1-carboxylic acids **41** could function in a similar way.[94] In this case fragmentation of the intermediate cyclohexadienyl radical yields mainly the desired radical together with benzoic acid, which is easily removed by an alkaline extraction. Examples of inter- and intramolecular additions are shown in Scheme 11. There was no problem with premature hydrogen donation, but loss of the hydroxyformyl radical, $\cdot CO_2H$, led to production of alkyl arenes RPh as by-products, particularly for primary radicals.

6. Metal Mimics: Crossing the Tetrathiafulvalene Bridge from Radicals to Cations

Production of aryl radicals by treatment of aryldiazonium salts with Cu^I has been in sporadic use ever since radicals were first recognized as reactive intermediates in solution. In a novel breakthrough, the metal is superseded as the electron donor by the all-organic tetrathiafulvalene (TTF).[95, 96] Treatment of aryldiazonium tetrafluoroborates **42** with TTF in acetone led to the formation of dihydrobenzofurans **45** in very respectable yields. Initial single electron transfer and nitrogen expulsion was followed by 5-*exo*-cyclization of the aryl radical to afford intermediate radical **43** plus the TTF radical cation,

which coupled together to produce the tetrathiafulvalenium salt **44**. Substitution of TTF in **44** occurred by S_N1 loss of the TTF group followed by trapping of the intermediate carbocation by an external nucleophile (Scheme 12).



Scheme 12. Stereocontrolled synthesis of polycycles by treatment of diazonium salts with TTF. Nu = nucleophile, DCM = CH_2Cl_2.

Suitably designed carbocations could be efficiently trapped by internal nucleophiles, thus opening new routes to a range of polycycles.[97] For example, diazonium salt **46** was prepared and allowed to react with TTF in situ to yield spirocyclic compound **47**. Similarly, functionalized indolines were synthesized by treating diazonium tetrafluoroborates such as **48** with TTF in moist acetone.[98] *N*-Benzoyl protection was not effective because competing cyclization onto the benzoyl group resulted in formation of a complex mixture of products. The method has also been successfully applied to the synthesis of the tetracycle **51**, which is a common subunit in alkaloid natural products such as aspidospermidine, strychnine, and vinblastine.[99, 100] One route involved preparation of aromatic amine **49**, which was diazotized and allowed to react with TTF in situ to afford hexahydrocarbazole **50** in a stereoselective manner, that is, with complete control of the stereochemistry at the three new stereocenters. Alcohol **50** was oxidized to the corresponding ketone, which on deprotection spontaneously gave the cyclic imine; this was reduced to **51** with excellent stereoselectivity.

The TTF-mediated radical-polar crossover methodology enables cascade sequences of radical and ionic reactions to be marshalled most effectively in the complete absence of metals. Attractive features of these reactions include the use of TTF in catalytic amounts and the ability to mediate cyclizations under mild conditions. The success of TTF as a reagent is due to its ability to act as an effective electron donor and its aptitude to trap radicals at a sufficiently slow rate to allow the aryl radical to cyclize before capture. Some control over the termination point of a cascade can be exercised by choosing functionalized diazadithiafulvalenes, because the rate of coupling of the radical with the fulvalene radical cation is sensitive to the steric environment around sulfur.[101] Currently the major limitation is the requirement for arenediazonium salts as starting materials.

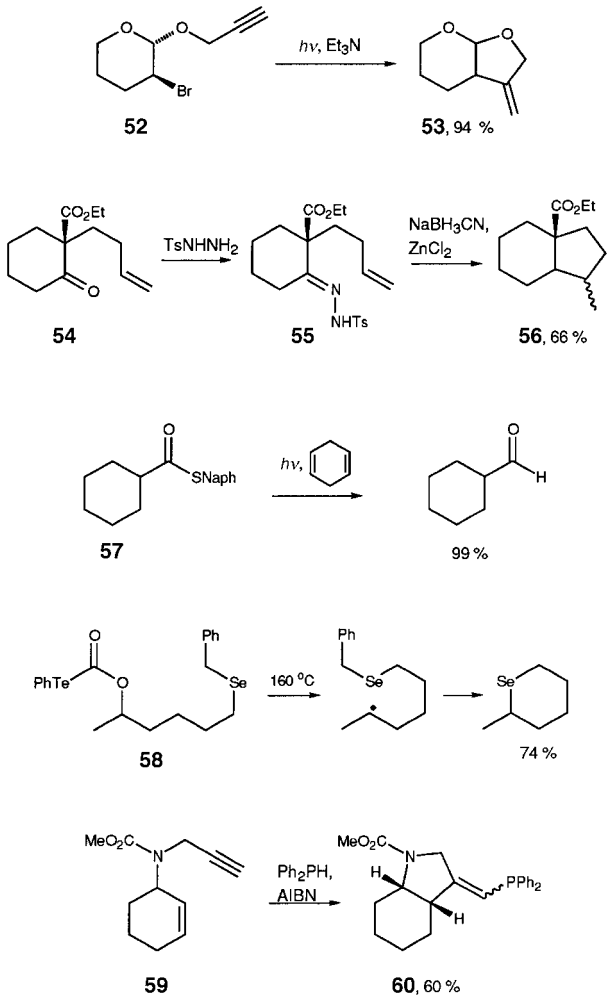
7. Assorted Allies on the March Away from Tin

Several new metal-free systems for generating radicals and managing homolytic sequences have been discovered recently. Alkyl bromides and iodides yield C-centered radicals simply on irradiation in the presence of an excess of triethylamine.[102] That this procedure was suitable for ring closures was demonstrated by the isolation of bicyclic ether **53** in almost quantitative yield on subjecting the bromotetrahydropyran derivative **52** to this operation (Scheme 13).

Reduction of tosyl hydrazone **55**, with $NaBH_3CN$ in the presence of $ZnCl_2$, yielded bicyclic ester **56** as a 3.5:1 mixture of diasteroisomers by a radical cyclization.[103] Thus, the ketone functional group in compound **54** could be regarded, in this reaction, as a synthetic equivalent to an alkyl radical. 2-Naphthyl thioesters have been introduced as new sources of acyl radicals.[104] For example, when a solution of thioester **57** in benzene was irradiated in the presence of the hydrogen donor cyclohexa-1,4-diene, cyclohexanal was formed in essentially quantitative yield.

Several tellurium compounds have been tested as sources of alkyl radicals in homolytic sequences. Aryltelluraformates (e.g. **58**), prepared by reaction of the corresponding chloroformates with diaryldditellurides and $NaBH_4$, generated alkyl radicals under thermal and photochemical conditions.[105] Thermolysis of **58** generated a C-centered radical, after decarboxylation, which cyclized by an intramolecular substitution reaction to yield 2-methylselenacyclohexane, which was isolated as the dibromide.

The P–H bond in diphenylphosphane is weak enough to sustain a radical chain process. For example, addition of $^{\bullet}PPh_2$ radicals to the alkyne group of unsaturated ester **59**, followed by ring closure, led to aza-bicycle **60** in 66% yield.[106] The scope, range of viability, and advantages of these processes have still to be properly mapped out.



Scheme 13. Synthetic applications of miscellaneous homolytic methods. Ts = tosyl = *p*-toluenesulfonyl, Naph = 2-naphthyl.

8. Summary and Outlook

The flight from tin is still proceeding at a rapid pace. None of the reagents developed so far has the flexibility or range of applicability possessed by organotin hydrides. However, selection from a range of positive measures for the avoidance of metal reagents and tin contamination is now a real option. Tris(trimethylsilyl)silane is usually a satisfactory replacement for stannanes in cyclizations and cascade reactions employing organohalide precursors. It is less successful with other precursors and in intermolecular reactions where silyl radical addition can compete. For those indifferent to odor, Barton ester/thiol methodology succeeds with a good range of carboxylic acid precursors. Likewise, xanthates show great promise for intra- and intermolecular transformations of alcohols. One of the most important challenges confronting homolytic chemistry in the next few years is the development of general protocols for control of stereochemistry. Proaromatic compounds based on cyclohexadienes are well adapted for inclusion of chiral substituents designed to promote chiral hydrogen transfer. The use of TTF, and related metal mimics, induces crossover from radical to cationic chemistry at an appropriate junction point. In this way, the well-established stereocontrol in radical bicyclizations may be successfully combined with proven ionic stereochemical know-how.

If none of these options are suitable, catalytic quantities of a tin reagent can be employed in conjunction with a reducing agent such as $NaBH_4$. This detracts from a general benefit of radical chemistry, namely tolerance of functional groups, because carbonyl and other moieties may be simultaneously reduced. Alternatively, contact with tin can be minimized by working with polymeric or water-soluble tin reagents.

Recent research has therefore opened up many promising avenues, and there is good hope that a large section of homolytic chemistry may eventually escape from the thraldom of tin.

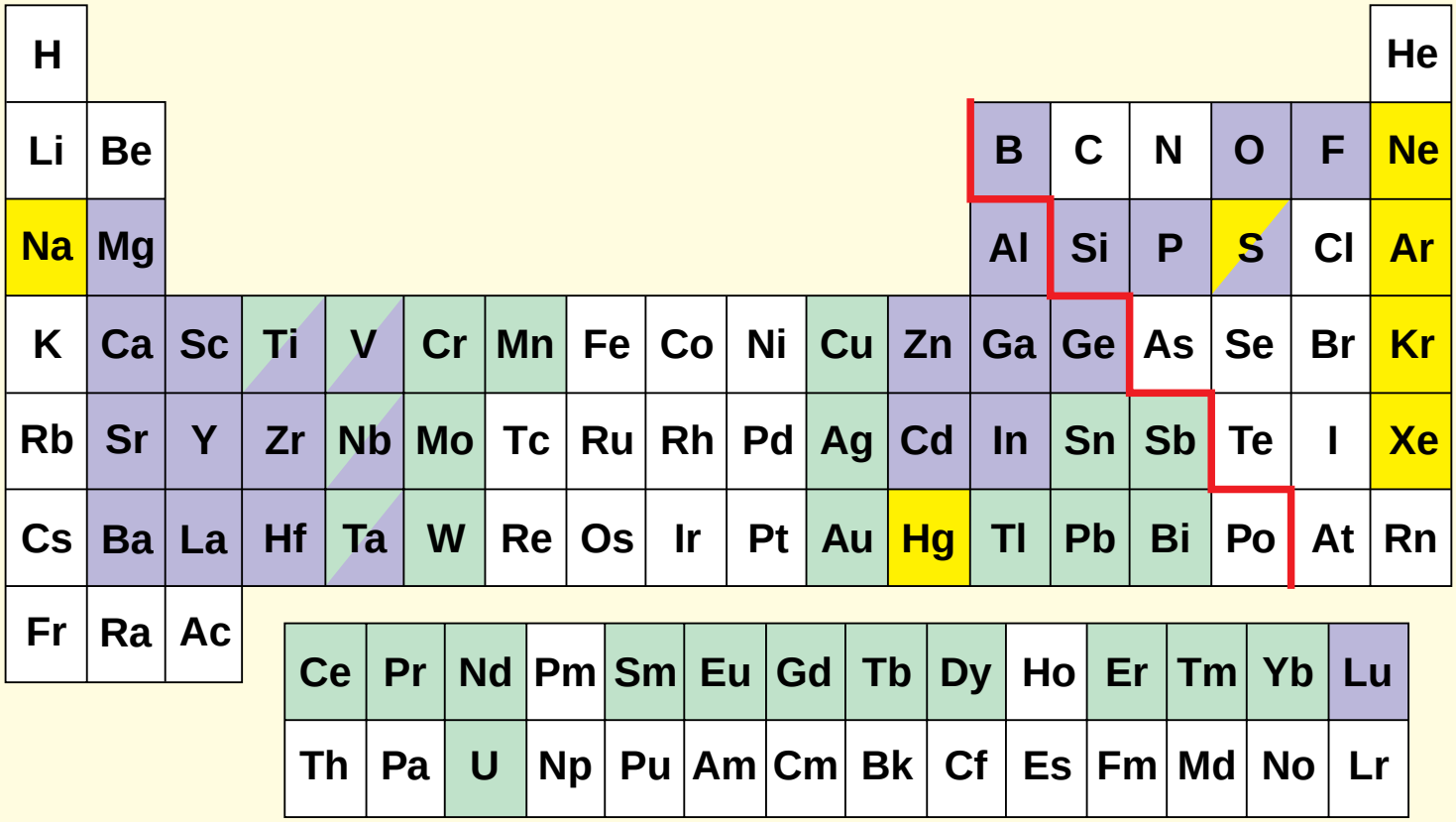
We thank the EPSRC for financial support of part of the research described in this review.

Received: December 15, 1997 [A265IE]
German version: *Angew. Chem.* **1998**, *110*, 3272 – 3283

[1] G. J. M. van der Kerk, J. G. Noltes, J. G. A. Luijten, *J. Appl. Chem.* **1957**, *7*, 356 – 365; H. G. Kuivila, *Acc. Chem. Res.* **1968**, *1*, 299 – 305.
[2] A. G. Davies, *Organotin Chemistry*, WILEY-VCH, Weinheim, **1997**.
[3] W. B. Motherwell, D. Crich, *Free Radical Chain Reactions in Organic Synthesis*, Academic, London, **1992**, chap. 3.
[4] S. D. Burke, W. B. Fobare, D. M. Armistead, *J. Org. Chem.* **1982**, *47*, 3348 – 3350.
[5] B. Giese, *Angew. Chem.* **1983**, *95*, 771 – 782; *Angew. Chem. Int. Ed. Engl.* **1983**, *22*, 753 – 764; A. Ghosez, B. Giese, H. Zipse, *Methoden Org. Chem.* (*Houben-Weyl*) *4th ed. 1952-*, Vol. E19b, **1989**, p. 834.
[6] G. E. Keck, J. B. Yates, *J. Am. Chem. Soc.* **1982**, *104*, 5829 – 5831.
[7] P. Renaud, T. Bourquard, *Tetrahedron Lett.* **1994**, *35*, 1707 – 1710.
[8] P. Dowd, W. Zhang, *Chem. Rev.* **1993**, *93*, 2091 – 2115.
[9] A. L. J. Beckwith, D. M. O'Shea, S. W. Westwood, *J. Am. Chem. Soc.* **1988**, *110*, 2565 – 2575.
[10] D. P. Curran, *Synthesis* **1988**, 417 – 439; D. P. Curran, *Synthesis* **1988**, 489 – 513.
[11] M. P. Sibi, J. Ji, *Prog. Heterocycl. Chem.* **1996**, *8*, 14 – 43.
[12] B. Giese, *Angew. Chem.* **1989**, *101*, 993 – 1004; *Angew. Chem. Int. Ed. Engl.* **1989**, *28*, 969 – 980.
[13] C. P. Jasperse, D. P. Curran, T. L. Fevig, *Chem. Rev.* **1991**, *91*, 1237 – 1286.
[14] U. Koert, *Angew. Chem.* **1996**, *108*, 441 – 443; *Angew. Chem. Int. Ed. Engl.* **1996**, *35*, 405 – 407.
[15] K. A. Parker, D. Fokas, *J. Am. Chem. Soc.* **1992**, *114*, 9688 – 9689.
[16] G. Stork, P. M. Sher, H.-L. Chen, *J. Am. Chem. Soc.* **1986**, *108*, 6384 – 6385.
[17] D. P. Curran, S.-C. Kuo, *Tetrahedron* **1987**, *43*, 5653 – 5661.
[18] R. A. Bunce, *Tetrahedron* **1995**, *51*, 13103 – 13159; L. F. Tietze, U. Beifuss, *Angew. Chem.* **1993**, *105*, 137 – 170; *Angew. Chem. Int. Ed. Engl.* **1993**, *32*, 131 – 163.
[19] L. Chen, G. B. Gill, G. Pattenden, *Tetrahedron Lett.* **1994**, *35*, 2593 – 2596; S. Handa, G. Pattenden, W.-S. Li, *Chem. Commun.* **1998**, 311 – 312; see also P. A. Zoretic, X. Weng, M. L. Caspar, D. G. Davis, *Tetrahedron Lett.* **1991**, *32*, 4819 – 4822.
[20] P. E. Eaton, Y. C. Yip, *J. Am. Chem. Soc.* **1991**, *113*, 7692 – 7697; E. W. Della, N. J. Head, P. Mallon, J. C. Walton, *J. Am. Chem. Soc.* **1992**, *114*, 10730 – 10738.
[21] G. T. Binmore, E. W. Della, G. M. Elsey, N. J. Head, J. C. Walton, *J. Am. Chem. Soc.* **1994**, *116*, 2759 – 2766.
[22] D. L. J. Clive, W. Yang, *J. Org. Chem.* **1995**, *60*, 2607 – 2609.
[23] D. Crich, S. Sun, *J. Org. Chem.* **1996**, *61*, 7200 – 7201.
[24] D. P. Curran, C.-T. Chang, *J. Org. Chem.* **1989**, *54*, 3140 – 3157.
[25] J. Light, R. Breslow, *Tetrahedron Lett.* **1990**, *31*, 2957 – 2958.
[26] R. Rai, D. B. Collum, *Tetrahedron Lett.* **1994**, *35*, 6221 – 6224.
[27] J. M. Berge, S. M. Roberts, *Synthesis* **1979**, 471 – 472.

[28] D. P. Curran, S. Hadida, *J. Am. Chem. Soc.* **1996**, *118*, 2531 – 2533; S. Hadida, M. S. Super, E. J. Beckman, D. P. Curran, *J. Am. Chem. Soc.* **1997**, *119*, 7406 – 7407; J. H. Horner, F. N. Martinez, M. Newcomb, S. Hadida, D. P. Curran, *Tetrahedron Lett.* **1997**, *38*, 2783 – 2786.
[29] U. Gerigke, M. Gerlach, W. P. Neumann, R. Vieler, V. Weintritt, *Synthesis* **1990**, 448 – 452.
[30] M. Gerlach, F. Jördens, H. Kuhn, W. P. Neumann, M. Peterseim, *J. Org. Chem.* **1991**, *56*, 5971 – 5972.
[31] G. Dumartin, G. Ruel, J. Kharboutli, B. Delmond, M.-F. Connil, B. Jousseaume, M. Pereyre, *Synlett* **1994**, 952 – 954.
[32] J. Junggebauer, W. P. Neumann, *Tetrahedron* **1997**, *53*, 1301 – 1310.
[33] H. Hillgärtner, W. P. Neumann, B. Schroeder, *Liebigs Ann. Chem.* **1975**, 586 – 599.
[34] D. J. Hart, F. L. Seely, *J. Am. Chem. Soc.* **1988**, *110*, 1631 – 1633.
[35] D. J. Hart, R. Krishnamurthy, L. M. Pook, F. L. Seely, *Tetrahedron Lett.* **1993**, *34*, 7819 – 7822.
[36] M. Tada, K. Kaneko, *J. Org. Chem.* **1995**, *60*, 6635 – 6636.
[37] K. Nishiyama, M. Oba, *Tetrahedron Lett.* **1993**, *34*, 3745 – 3748.
[38] D. H. R. Barton, D. O. Jang, J. Cs. Jaszberenyi, *Tetrahedron Lett.* **1991**, *32*, 7187 – 7190.
[39] C. Chatgilialoglu, C. Ferreri, M. Lucarini, *J. Org. Chem.* **1993**, *58*, 249 – 251.
[40] D. H. R. Barton, D. O. Jang, J. Cs. Jaszberenyi, *Tetrahedron* **1993**, *49*, 7193 – 7214.
[41] S. J. Cole, J. N. Kirwan, B. P. Roberts, C. R. Willis, *J. Chem. Soc. Perkin Trans. 1* **1991**, 103 – 112.
[42] H.-S. Dang, B. P. Roberts, *Tetrahedron Lett.* **1995**, *36*, 2875 – 2878.
[43] C. Chatgilialoglu, D. Griller, M. Lesage, *J. Org. Chem.* **1988**, *53*, 3641 – 3642; C. Chatgilialoglu, *Acc. Chem. Res.* **1992**, *25*, 188 – 194.
[44] B. Giese, B. Kopping, C. Chatgilialoglu, *Tetrahedron Lett.* **1989**, *30*, 681 – 684.
[45] M. Kizil, J. A. Murphy, *J. Chem. Soc. Chem. Commun.* **1995**, 1409 – 1410.
[46] I. Ryu, M. Hasegawa, A. Kurihara, A. Ogawa, S. Tsunoi, N. Sonoda, *Synlett* **1993**, 143 – 145.
[47] D. Crich, Q. Yao, *J. Org. Chem.* **1996**, *61*, 3566 – 3570; D. Crich, X. Hao, *J. Org. Chem.* **1997**, *62*, 5982 – 5988.
[48] H. Togo, K. Hayashi, M. Yokoyama, *Bull. Chem. Soc. Jpn.* **1994**, *67*, 2522 – 2527.
[49] H. Josien, S.-B. Ko, D. Bom, D. P. Curran, *Chem. Eur. J.* **1998**, *4*, 67 – 83.
[50] B. Kopping, C. Chatgilialoglu, M. Zehnder, B. Giese, *J. Org. Chem.* **1992**, *57*, 3994 – 4000.
[51] M. Lesage, C. Chatgilialoglu, D. Griller, *Tetrahedron Lett.* **1989**, *30*, 2733 – 2734.
[52] C. Chatgilialoglu, A. Guerrini, G. Seconi, *Synlett* **1990**, 219 – 220.
[53] J. Daroszewski, J. Lusztyk, M. Degueil, C. Navarro, B. Maillard, *J. Chem. Soc. Chem. Commun.* **1991**, 586 – 587.
[54] M. Ballestri, C. Chatgilialoglu, G. Seconi, *J. Organomet. Chem.* **1991**, *408*, C1 – C4.
[55] M. Oba, K. Nishiyama, *J. Chem. Soc. Chem. Commun.* **1994**, 1703 – 1704; M. Oba, Y. Kawahara, R. Yamada, H. Mizuta, K. Nishiyama, *J. Chem. Soc. Perkin Trans. 2* **1996**, 1843 – 1848.
[56] T. Gimisis, M. Ballestri, C. Ferreri, C. Chatgilialoglu, R. Boukherroub, G. Manuel, *Tetrahedron Lett.* **1995**, *36*, 3897 – 3900.
[57] W. Z. McCarthy, J. Y. Corey, E. R. Corey, *Organometallics* **1984**, *3*, 255 – 263.
[58] P. Pike, S. Hershberger, J. Hershberger, *Tetrahedron* **1988**, *44*, 6295 – 6304.
[59] P. Pike, S. Hershberger, J. Hershberger, *Tetrahedron Lett.* **1985**, *26*, 6289 – 6290.
[60] V. Gupta, D. Kahne, *Tetrahedron Lett.* **1993**, *34*, 591 – 594.
[61] C. Chatgilialoglu, M. Ballestri, *Organometallics* **1995**, *14*, 5017 – 5018.
[62] D. H. R. Barton, S. W. McCombie, *J. Chem. Soc. Perkin Trans. 1* **1975**, 1574 – 1585.
[63] D. Crich, L. Quintero, *Chem. Rev.* **1989**, *89*, 1413 – 1432.
[64] For a discussion of the mechanism and alternative possibilities, see reference [65].
[65] S. Z. Zard, *Angew. Chem.* **1997**, *109*, 724 – 737; *Angew. Chem. Int. Ed. Engl.* **1997**, *36*, 672 – 685.
[66] W. B. Motherwell, D. Crich, *Free Radical Chain Reactions in Organic Synthesis*, Academic, London, **1992**, pp. 37 – 47.
[67] M. Oba, K. Nishiyama, *Tetrahedron* **1994**, *50*, 10193 – 10200.
[68] D. O. Jang, D. H. Cho, D. H. R. Barton, *Synlett* **1998**, 39 – 40.
[69] R. M. Lopez, D. S. Hays, G. C. Fu, *J. Am. Chem. Soc.* **1997**, *119*, 6949 – 6950.
[70] D. S. Hays, G. C. Fu, *J. Org. Chem.* **1996**, *61*, 4 – 5.
[71] P. Delduc, C. Tailhan, S. Z. Zard, *J. Chem. Soc. Chem. Commun.* **1988**, 308 – 310.
[72] J. E. Forbes, C. Tailham, S. Z. Zard, *Tetrahedron Lett.* **1990**, *31*, 2565 – 2568.
[73] J. Axon, L. Boiteau, J. Boivin, J. E. Forbes, S. Z. Zard, *Tetrahedron Lett.* **1994**, *35*, 1719 – 1722.
[74] J. E. Forbes, S. Z. Zard, *Tetrahedron* **1993**, *49*, 8257 – 8266.
[75] J. E. Forbes, S. Z. Zard, *J. Am. Chem. Soc.* **1990**, *112*, 2034 – 2035.
[76] R. N. Saicic, S. Z. Zard, *J. Chem. Soc. Chem. Commun.* **1996**, 1631 – 1632.
[77] B. Quiclet-Sire, S. Z. Zard, *Pure Appl. Chem.* **1997**, *69*, 645 – 650.
[78] A.-C. Callier-Dublanchet, B. Quiclet-Sire, S. Z. Zard, *Tetrahedron Lett.* **1995**, *36*, 8791 – 8794.
[79] A.-C. Callier-Dublanchet, B. Quiclet-Sire, S. Z. Zard, *Tetrahedron Lett.* **1997**, *38*, 2463 – 2466.
[80] D. H. R. Barton, D. Crich, W. B. Motherwell, *J. Chem. Soc. Chem. Commun.* **1983**, 939 – 941; D. H. R. Barton, D. Crich, W. B. Motherwell, *Tetrahedron* **1985**, *41*, 3901 – 3924.
[81] D. H. R. Barton, P. Blundell, J. Cs. Jaszberenyi, *Tetrahedron Lett.* **1989**, *30*, 2341 – 2344.
[82] D. H. R. Barton, E. Castagnino, J. Cs. Jaszberenyi, *Tetrahedron Lett.* **1994**, *35*, 6057 – 6060.
[83] D. H. R. Barton, J. Cs. Jaszberenyi, E. A. Theodorakis, *Tetrahedron* **1992**, *48*, 2613 – 2626.
[84] D. H. R. Barton, W. S. Liu, *Tetrahedron Lett.* **1997**, *38*, 2431 – 2434.
[85] D. H. R. Barton, C.-Y. Chern, J. Cs. Jaszberenyi, *Tetrahedron Lett.* **1992**, *33*, 5017 – 5020.
[86] D. H. R. Barton, C.-Y. Chern, J. Cs. Jaszberenyi, T. Shinada, *Tetrahedron Lett.* **1993**, *34*, 6505 – 6508.
[87] D. H. R. Barton, J. Cs. Jaszberenyi, A. I. Morrell, *Tetrahedron Lett.* **1991**, *32*, 311 – 314.
[88] P. Kocienski, M. Stocks, D. Donald, M. Perry, *Synlett* **1990**, 38 – 39.
[89] D. H. R. Barton, P. Blundell, J. Cs. Jaszberenyi, *Tetrahedron* **1992**, *48*, 7121 – 7130.
[90] J. Liebscher, B. Riemer, J. Bendig, R. Stösser, *Tetrahedron Lett.* **1994**, *35*, 7009 – 7012.
[91] J. Hartung, M. Schwarz, *Synlett* **1997**, 848 – 850.
[92] G. Binmore, J. C. Walton, L. Cardellini, *J. Chem. Soc. Chem. Commun.* **1995**, 27 – 28.
[93] G. Binmore, L. Cardellini, J. C. Walton, *J. Chem. Soc. Perkin Trans. 2* **1997**, 757 – 762.
[94] P. A. Baguley, G. Binmore, A. Milne, J. C. Walton, *Chem. Commun.* **1996**, 2199 – 2200.
[95] C. Lampard, J. A. Murphy, N. Lewis, *J. Chem. Soc. Chem. Commun.* **1993**, 295 – 297.
[96] R. J. Fletcher, C. Lampard, J. A. Murphy, N. Lewis, *J. Chem. Soc. Perkin Trans. 1* **1995**, 623 – 633.
[97] J. A. Murphy, F. Rasheed, S. J. Roome, N. Lewis, *Chem. Commun.* **1996**, 737 – 738.
[98] J. A. Murphy, F. Rasheed, S. Gastaldi, T. Ravishanker, N. Lewis, *J. Chem. Soc. Perkin Trans. 1* **1997**, 1549 – 1558.
[99] M. Kizil, C. Lampard, J. A. Murphy, *Tetrahedron Lett.* **1996**, *37*, 2511 – 2514.
[100] R. J. Fletcher, D. E. Hibbs, M. Hursthouse, C. Lampard, J. A. Murphy, S. J. Roome, *Chem. Commun.* **1996**, 739 – 740.
[101] T. Koizumi, N. Bashir, J. A. Murphy, *Tetrahedron Lett.* **1997**, *38*, 7635 – 7638.
[102] J. Cossy, J.-L. Ranaivosata, V. Bellosta, *Tetrahedron Lett.* **1994**, *35*, 8161 – 8162; C.-K. Sha, K. C. Santhosh, C.-T. Tseng, C.-T. Lin, *Chem. Commun.* **1998**, 397 – 398.
[103] D. F. Taber, Y. Wang, S. J. Stachel, *Tetrahedron Lett.* **1993**, *34*, 6209 – 6210.
[104] J. H. Penn, F. Liu, *J. Org. Chem.* **1994**, *59*, 2608 – 2612.
[105] M. A. Luca, C. H. Schiesser, *J. Org. Chem.* **1996**, *61*, 5754 – 5761.
[106] J. E. Brumwell, N. S. Simpkins, N. K. Terrett, *Tetrahedron Lett.* **1993**, *34*, 1215 – 1218.

periodic table of the "lighting" elements



- activator elements
- plasma elements
- host lattice elements

ANGEWANDTE CHEMIE © WILEY-VCH

New Developments in the Field of Luminescent Materials for Lighting and Displays

Thomas Jüstel,* Hans Nikol,* and Cees Ronda*

While in the seventies and eighties the field of luminescent materials seemed to be fairly well covered, research in the nineties has been revitalized both in industry and academia. Improved performance of allegedly mature "classical" materials has demonstrated impressively the role of until then often neglected parameters such as surface and particle properties. In a business as developed as the lamp market new lamp features such as reduced mercury consumption can lead to a competitive edge and new phosphor research programs. Quantum cutter phosphors that generate two visible photons from one UV photon are the focus of research again, for example, for plasma display panels as huge flat and thin hang-on-the-wall TVs. Promising new developments such as electroluminescent full-color displays or the blue (laser) diode have created excitement and numerous research efforts in laboratories around the world. The direct conversion of electricity into light, common to both applications, challenges current concepts and might eventually revolutionize the way we illuminate rooms, car lights, or traffic signals, and how we display video information. A deep understanding of the interaction of light and matter together with advanced material chemistry is the key to both improved and new lighting and display products.

Keywords: displays · fluorescence · luminescence · materials science · rare-earth compounds

1. Introduction

Luminescent materials, also called phosphors, can be found in a broad range of every-day applications such as cathode ray tubes (CRTs[**]), projection televisions (PTVs), fluorescent tubes, and X-ray detectors, to name just the most important.[1, 2] Improvements over the last three decades have led to phosphor materials that operate close to their physical limits. It cannot be expected that properties such as quantum yield and spectral energy distribution will be significantly improved or that distinctly better materials will be found in the near future.

Although the phosphor selection for CRTs and fluorescent lamps was made long ago there is still considerable research activity to improve the chemical stability and to adapt the materials to the production technology of the respective application.[3, 4] Ongoing miniaturization, lifetime improvement, and spectral stability of fluorescent lamps on the one hand and brightness and contrast improvement in imaging systems on the other hand demand luminescent materials with very high stability that is invariable to operating conditions.

[*] Dr. T. Jüstel, H. Nikol, C. Ronda
Philips Research Laboratories
Weisshausstrasse 2, D-52066 Aachen (Germany)
Fax: (+49) 241-6003-483
E-mail: juestel@pfa.research.philips.com

[**] A list of the abbreviations used can be found in the Appendix.

The conditioning of the surface of the phosphor grains is a major research target these days to obtain luminescent materials with improved performance. This conditioning is achieved mainly by a chemical refining step after the synthesis or by an additional coating on the particle surface.[5, 6] Ideally, the chemical behavior is altered in such a way that a suspension of the phosphor material in water or an organic medium becomes more stable during the manufacturing process as well as under the harsh operating conditions in discharge lamps or TV tubes (i.e. electron and ion bombardment, respectively, as well as plasma interaction). Contrary to classical areas of application the search for new materials is most important for tomorrow's fields of light generation for displays and illumination. The research area is best organized by the excitation source. Luminescent materials in plasma display panels (PDP) and field emission displays (FED) use the high-energy side of the UV spectrum, that is vacuum ultraviolet (VUV) and even low voltage electrons, respectively. Phosphors on light emitting diodes (LED) and to some extent in fluorescent lamps for special applications are excited by near UV or blue light. Probably the most revolutionary is the direct excitation of semiconductors by electrical current in LEDs and of both organic and inorganic phosphor materials by organic and inorganic electroluminescence (EL), respectively. Consequently, the search for new materials is performed vigorously in industry and university laboratories. Thereby, classical doped solid-state materials are increasingly

 © WILEY-VCH Verlag GmbH, D-69451 Weinheim, 1998 1433-7851/98/3722-3085 $ 17.50+.50/0

giving way to new material classes such as doped zeolites, organic phosphors, and composite and nanosized materials.

After a brief introduction of the physical background of luminescent materials, the current situation for lighting applications and display technology is described in separate sections. New technologies and their impact on the research of luminescent materials follow together with a discussion of upcoming trends in this field of material research.

2. Basic Aspects of Luminescent Materials

Light of appropriate spectral distribution in discharge lamps or imaging systems is nowadays mostly generated with luminescent materials that act as the final partner in the energy transfer chain and emit photons in the visible, UV or IR spectral range (Figure 1). The photon emission of a material following energy supply is generally called luminescence. Several types of luminescence can be distinguished depending on the excitation source (Table 1).

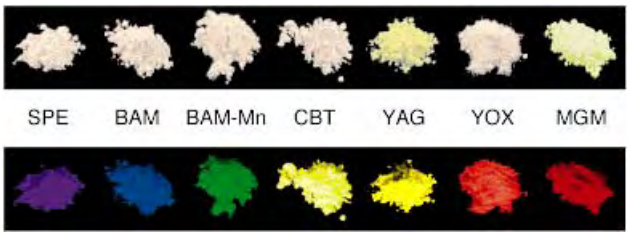


Figure 1. Commercial phosphor powders commonly applied in fluorescent lamps and displays. Top: under white light illumination; bottom: under irradiation with UV light (254 nm excitation wavelength). For an explanation of abbreviations and application areas: see Tables 2–4 and 6, and Section 3, respectively.

Table 1. Different forms of luminescence.

Luminescence type	Excitation source	Application
cathodoluminescence	electrons	TV sets, monitors
photoluminescence	(UV) photons	fluorescent lamps, plasma displays
X-ray luminescence	X-rays	X-ray amplifier
electroluminescence	electric field	LEDs, EL displays
sonoluminescence	ultrasound	
solvatoluminescence	photons	detectors, analytical devices
chemoluminescence	chemical reaction energy	analytical chemistry
bioluminescence	biochemical reaction energy	analytical chemistry
triboluminescence	mechanical energy	

While sono-,[7] solvato-, chemo-, bio, and triboluminescence are currently not used in lighting and display applications, quite a variety of materials has been developed for all other forms of luminescence. They can be divided into inorganic and organic phosphors; the former being mainly solid-state compounds that consist of crystals 1–10 μm in size, while the latter can either be polymers or low molecular weight materials applied as thin films or solid solutions.

"Classical" inorganic phosphors usually consist of a host lattice with activator ions doped into it in small concentrations, typically a few mole percent or less. The activator ions possess energy levels that can be populated by direct

Thomas Jüstel was born in Witten in 1968. He studied chemistry at the University of Bochum from 1987 to 1992. He received his Ph. D. in coordination chemistry in 1995 in the group of Prof. Dr. K. Wieghardt. After spending half a year as a postdoctoral fellow at the MPI Mühlheim für Strahlenchemie he entered the Philips Research Laboratory in Aachen in september 1995. He is currently working on luminescent materials for lamps and display applications.


T. Jüstel


H. Nikol


C. Ronda

Hans Nikol was born in 1966 and studied chemistry at the University of Regensburg from 1985 to 1990. He completed his Ph. D. in photochemistry in 1993 in the group of Prof. Dr. A. Vogler. The following two years he spent as a postdoctoral research fellow at the California Institute of Technology in the group of Prof. H. B. Gray. He joined the Philips Research Laboratory in Aachen in 1995 where he is working on luminescent materials for lamps and display applications.

Cees Ronda was born in Groningen, the Netherlands in 1959. He studied Solid State and Theoretical Chemistry at the State University of Groningen where he also obtained his doctorate degree. His thesis dealt with optical and electrical properties of layered metal chalcogenides and halides. In 1986 he joined Philips Research Laboratories in Eindhoven, the Netherlands. In 1989, he went to the Philips Research Laboratories in Aachen. Since joining Philips he has been studying luminescent materials for lamps and display applications.

excitation or indirectly by energy transfer, and are responsible for the luminescence. Generally, two types of activator ions can be distinguished. In the first type the energy levels of the activator ion involved in the emission process show only weak interactions with the host lattice. Typical examples are many of the lanthanide ions Ln^{3+}, where the optical transitions take place solely between 4f terms that are well shielded from their chemical environment by outer electrons. As a consequence characteristic line emission spectra can be observed.

The second type of activator ions strongly interact with the host lattice. This is the case when d electrons are involved, for example, in Mn^{2+}, Eu^{2+}, and Ce^{3+}, as well as for s^2 ions like Pb^{2+} or Sb^{3+}, or for complex anions such as MoO_4^{2-} or NbO_4^{3-}. The strong coupling of the electronic states with vibrational modes of the lattice mainly leads to more or less broad bands in the spectrum. Their half width FWHM is related to the Stokes shift S [Eqs (1a) and (1b)], that is the energy

$$\mathrm{FWHM} = \sqrt{8\ln 2}\sqrt{2kT}\sqrt{S}\,[\mathrm{eV}] \quad (1a)$$

$$S = S_e\hbar\omega_e + S_g\hbar\omega_g \quad (1b)$$

difference between absorption and emission maximum (harmonic approximation and high temperature limit; usually already valid at room temperature when the same excited state emits as is reached by absorption; S_e, S_g = Huang–Rhys parameter for the excited and ground state, respectively;[3f] Figure 2).

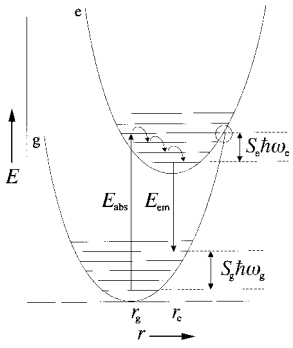


Figure 2. Potential energy curves illustrating an electronic transition from the ground to the excited state. The Stokes shift comprises of the terms $S_e\hbar\omega_e$ and $S_g\hbar\omega_g$.

Phosphors that show an emission with a large Stokes shift usually exhibit a low quenching-temperature, which is disadvantageous for many applications. Luminescent materials based on lanthanide ions circumvent this problem because the actual luminescent process is largely independent of its environment, a fact that makes them unique in the luminescence world. For example, for Eu^{3+} activated phosphors such as Y_2O_3:Eu^{3+} UV photons are absorbed through a charge-transfer state. In a consecutive step the energy is transferred to the f niveaux, which are deactivated and show the characteristic f–f emission line spectra ($^5D_J \rightarrow {}^7F_J$).

In general, the luminescent process can be divided into the steps of energy absorption, energy transfer, and emission. Energy absorption need not necessarily take place at the activator ion itself but can occur at a random place in the lattice. This implies that energy transfer of the absorbed energy to the luminescent center takes place before emission can occur. The migration of the energy absorbed by the lattice can take place through one of the following processes:

- migration of electric charge (electrons, holes),
- migration of excitons,
- resonance between atoms with sufficient overlap integrals,
- reabsorption of photons emitted by another activator ion or sensitizer.

The occurrence of energy transfer within a luminescent material has far-reaching consequences for its properties as a phosphor. On the one hand the absorbed energy can migrate to the crystal surface or to lattice defects where it is lost by radiationless deactivation. As a consequence the phosphor energy yield, that is the quotient of emitted light energy to initially absorbed energy, drops. Phosphors that emit UV, visible, or IR light upon UV excitation then show a decline in quantum yield QE [Eq. (2)]. Luminescent materials should be highly crystalline to achieve high light output, that is have as few lattice defects and impurities as possible. In addition, the surface area of the crystals has to be minimized, which means that their surface has to be clean and smooth.

$$\mathrm{QE} = \frac{n(\text{emitted photons})}{n(\text{absorbed photons})}\,[\%] \quad (2)$$

On the other hand the use of sensitizers with the potential to considerably increase the light output of a phosphor is only possible because of energy transfer. For example, all Tb^{3+}-activated phosphors currently used in fluorescent lamps are sensitized with Ce^{3+}.[2, 8] Tb^{3+} alone would absorb in most host lattices but at a wavelength shorter than 230 nm. UV photons with the main wavelength of 254 nm emitted by the mercury plasma in fluorescent lamps would therefore not be efficiently absorbed by the activator ion. Ce^{3+}, however, has a very high absorption coefficient between 250 and 350 nm and can effectively transfer the initially absorbed energy to Tb^{3+}.

Besides the quantum yield, the quality of a phosphor material is further characterized by its color point, the lumen equivalent, the reflection spectrum, and the emission lifetime under the given excitation conditions. The color point is derived from the spectral energy distribution of the emission and is defined according to the convention of the Commission Internationale d'Eclairage (CIE) [9] in a normalized two-dimensional coordinate system.

From the color coordinates in the color triangle (Figure 3) not only the color itself but also the color saturation can be derived. The latter is most important for display applications (see Section 3) because in order to display all colors of the visible spectrum by synthesizing them from the three primary colors their respective colors have to be as saturated as possible, that is the color coordinates have to be positioned close to the borders of the color triangle.

For lighting applications the color saturation of the phosphors is of less importance. In contrast, the luminescent materials should emit a spectrum with a high lumen equivalent. This value is calculated [9] by multiplication of the spectral power distribution $P(\lambda)$ of the phosphor emission, which integral has been normalized, with the spectral luminous efficiency for the human eye $V(\lambda)$ [Eq. (3), Figure 4].

$$\mathrm{LE} = \int_{380}^{780} V(\lambda)P(\lambda)d\lambda\,[\mathrm{lm\,W^{-1}}] \quad (3)$$

To obtain white light with a high lumen equivalent it is important that the phosphors applied in a mixture display very sharp emission spectra or, even better, emission lines

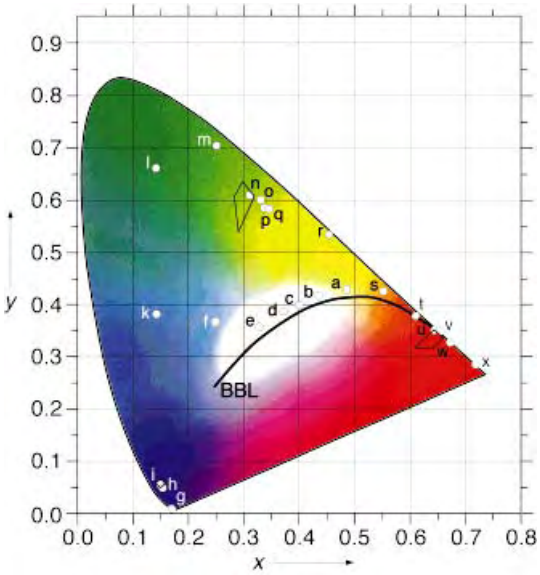


Figure 3. CIE color triangle showing the black body line (BBL) and the three EBU norm areas for cathode ray tube phosphors. The dots refer to the color points of the emission spectrum of the phosphor materials listed below. a)–e) Halophosphates with different color temperatures, f) blue emitting halophosphate, g) SPE, h) BAM, i) ZnS:Ag, k) SAE, l) BAM (green), m) ZSM, n) ZnS:Cu,Au,Al, o) CAT, p) LAP, q) CBT, r) YAG, s) SPS, t) CBTM, u) YOX, v) Y_2O_2S:Eu, w) YVE, x) MGM.

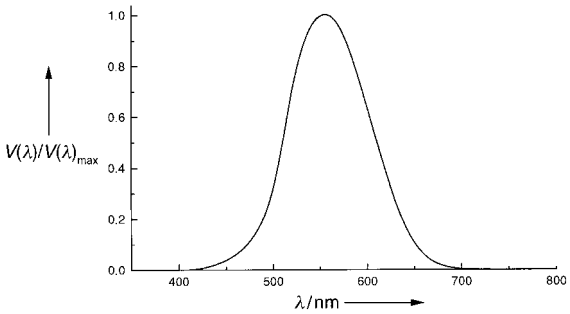


Figure 4. Normalized luminous efficiency for the human eye $V(\lambda)/V(\lambda)_{max}$ as a function of the wavelength.

rather than broad emission spectra, otherwise light is generated in spectral areas where the eye sensitivity is too low. Naturally, also the emission maximum of line-emitting phosphors should not be too far off the eye sensitivity curve maximum.

Besides the quantity there is also a quality performance of light sources, with one factor usually being a trade-off against the other. Light quality is mainly determined by the color rendering of the light source, which is the ability to display the colors of an irradiated object in a natural way. A qualitative measure is the color rendering index (CRI), which by definition can adopt values between 0 and 100.[9] This value is calculated by comparing the reflection spectra of selected test colors (either 8 or 14) obtained by irradiation with the light source under investigation with the reflection spectra when irradiated in the same way with a black body radiator. By definition a black body radiator like the sun or an incandescent lamp has a color rendering index of 100. In contrast, a line emitter with a single emission line at any part of the visible spectral region has a CRI of 0 because colors cannot be displayed under such an irradiation source. This is illustrated on a late car ride, for example, on a Belgium highway that is continuously lit up at night with mostly low pressure sodium discharge lamps. This lamp type solely emits yellow light consisting of the sodium atom emission lines centered at 589 nm. It does not allow the perception of colors and thus turns the colored world into gray.

Discharge lamps that use phosphors for light conversion have CRIs between 50 and 95. The CRI of fluorescent lamps strongly depends on the applied phosphors. While a combination of line emitters yields high light output but moderate color rendering, broad band emitters enable higher CRI values to be obtained. In addition, color rendering is very dependent on the spectral position of the emission maximum and thus on the spectral power distribution of the applied phosphors. A compromise has to be found between color rendering and high light output.

3. Luminescent Lighting

Of all the artificially generated photons on earth 90% originate from discharge lamps.[10] All of today's efficient lighting sources are based on either direct or indirect light emission from plasma discharges. Most widespread is the application of mercury plasma because of its high energy conversion efficiency of about 75%.[11] In general, the spectral energy distribution of a plasma discharge depends strongly on the vapor pressure of the plasma gas inside the lamp tube. In low-pressure mercury discharge lamps the vapor pressure amounts to just a few torr, which results in a line spectrum with the main emission lines at 185, 254, and 365 nm. Further weak emission lines appear in the blue and green spectral region, and result in a faint blue–greenish glow of the plasma. Upon increasing the Hg pressure the emission lines broaden and finally collapse to yield an almost continuous spectrum between 250 and 550 nm. The visible part of the emission is used in high pressure mercury lamps operating at some 1000 torr. In both discharge types luminescent materials are needed to obtain white light with sufficient color rendering and efficiency.

3.1. High Pressure Mercury Discharge Lamps

To apply the light of the high pressure Hg plasma for general lighting purposes a color correction is necessary because the blue–greenish plasma light completely lacks the red spectral region and results in a low CRI of about 25.[11] This tuning is achieved by introduction of a red emitting phosphor (Table 2) that has to absorb part of the UV and the

Table 2. Phosphors for the color correction in high-pressure Hg discharge lamps.

Phosphor	Abbreviation	$\lambda_{max.}$ (em.) [nm]	$\lambda_{max.}$ (ex.) [nm]	QE [%]	LE [lm W^{-1}]
$Mg_4GeO_{5.5}F$:Mn	MGM	655	280, 420	80	80
$(Sr,Mg)_3(PO_4)_2$:Sn	SPS	630	240	80	260
$Y_3Al_5O_{12}$:Ce	YAG	565	450	80	450
Y(V,B,P)O_4:Eu	YVE	615	255	85	225

blue–violet spectrum of the plasma. A further requirement on this phosphor material is a high emission-quenching temperature since the lamp tube can easily heat up to 300 °C. In the early 50s $Mg_4GeO_{5.5}F$:Mn was the first phosphor to be introduced[12] with a considerable increase in the CRI to 50. At the same time, the efficiency of the lamp decreased sharply for two reasons:

- The emission is located in the deep red spectral region where the eye sensitivity and, consequently, the lumen equivalent is very low.
- The phosphor absorbs both in the UV and blue spectral region, which takes away emission intensity in the useful spectral region.

This phosphor was later substituted by $(Sr,Mg)_3(PO_4)_2$:Sn with an emission maximum at 630 nm and therefore a higher lumen equivalent. Recently, $Y(V,B,P)O_4$:Eu has been introduced as a line emitter with a very high lumen equivalent and high stability (Table 2). A disadvantage is the insufficient absorption of the vanadate group between 340 and 400 nm, which means that the UV emission of the Hg plasma is not completely absorbed and converted. As an alternative, $Y_3Al_5O_{12}$:Ce with an intense 4f5d absorption at 460 nm might be used. However, its quantum yield is lower than in $Y(V,B,P)O_4$:Eu.

3.2. Low-pressure Mercury Discharge Lamps

Low-pressure mercury discharge lamps, better known as fluorescent or energy saving lamps, have penetrated the industrial and home lighting market to an impressive degree.[11] This is easily explained by their high efficacy of almost 100 lm W^{-1} (white light), which amounts to about a 30% energy conversion efficiency and is about eight times as high as that of an incandescent lamp. A further advantage is the almost exclusive UV-light output of the low-pressure mercury plasma, which makes it possible to produce lamps with a spectrum dependent only on the phosphor mixture. This possibility means that a decoupling of the desired optical lamp features of the principal lamp construction is necessary since the lamp spectrum, the efficiency, and hence the application area is only determined by the phosphor mixture applied on the inner tube wall (Figure 5). This was a crucial factor for the success of this lamp type. Conventional fluorescent lamps as well as more advanced lighting applications including for suntanning, photocopy machines, blacklight, advertising billboards, display backlights. have been developed. Triggered by the large variety of areas of application some 50 different phosphors are currently produced for fluorescent lighting.

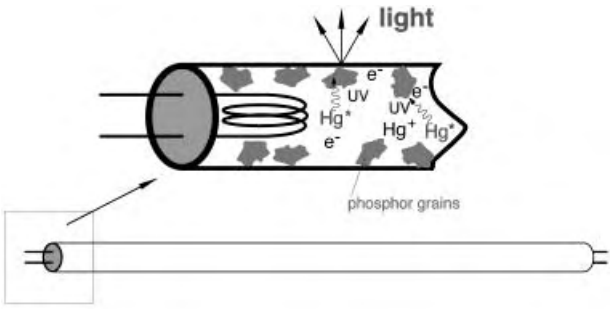


Figure 5. Schematic diagram of a fluorescent lamp illustrating the light generation process at the phosphor grains.

3.2.1. Halophosphate Lamps

To use low-pressure mercury discharge lamps for lighting applications, a phosphor had to be found to efficiently convert the UV light emitted from the plasma into white light. Since the early years of fluorescent lighting halophosphate materials with the composition $Ca_5(PO_4)_3(F,Cl)$:Sb,Mn (discovered in 1942) have been employed for this purpose.[13] They emit both in the blue (Sb^{3+}) as well in the orange (Mn^{2+}) spectral region, thus in addition yield white light. However, the color rendering CRI of these halophosphate lamps reaches only 60–65 at an efficiency of about 80 lm W^{-1}. Variation of the Mn^{2+} to Sb^{3+} ion ratio in the host lattice allows the free adjustment of the color temperature between 2700 and 6500 K. With the halophosphates a white emitting material had been found to produce fluorescent lamps with sufficient efficiency and various color temperatures at very low cost. Consequently, the search for alternative broad-band phosphors was soon abandoned. Halophosphate lamps still have a considerable market share and today's focus in development is on improving the lifetime and reducing the color point shift that occurs during lamp operation. Both are caused by phosphor degradation and can be improved by closed inorganic coatings.

3.2.2. Tricolor Concept—Color 80 Lamps

After the theoretical treatment by W. A. Thornton, Opstelten and Koedam demonstrated in the early 70s that fluorescent lamps with very high color rendering and efficiency can be obtained if three narrow band emitters with emission maxima at 450, 540, and 610 nm are employed.[14] These so-called tricolor lamps have color rendering CRI values of 80–85 at high efficiencies of 100 lm W^{-1}! Figure 6 shows the emission spectrum of a typical fluorescent lamp employing $BaMgAl_{10}O_{17}$:Eu, $(Ce,Gd,Tb)MgB_5O_{10}$ and Y_2O_3:Eu.

This new and clever concept triggered enormous research activities in both industry and universities in the field of

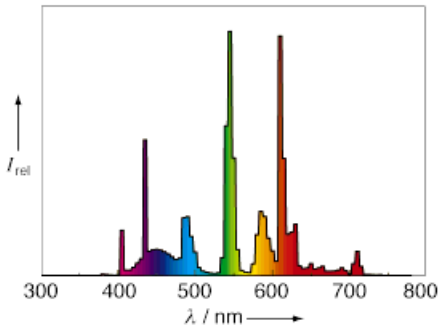


Figure 6. Emission spectrum of a tricolor fluorescent lamp.

lanthanide-activated phosphor materials. In particular Eu^{2+}-, Tb^{3+}-, and Eu^{3+}-doped host lattices were promising candidates because of their high quantum yields and spectral position of the emission, as described in numerous contributions.[2, 15] Nevertheless, the material selection was accomplished relatively soon and until today only a small number of phosphor materials is being applied in the so-called Color 80 lamps (Table 3).

Table 3. Phosphors currently applied in Color 80 lamps.

Phosphor	Abbreviation	$\lambda_{max.}$ (em.) [nm]	Absorption at 254 nm [%]	QE [%]	LE [lm W^{-1}]
$BaMgAl_{10}O_{17}$:Eu	BAM	450	90	90	90
(Ce,Tb)$MgAl_{11}O_{19}$	CAT	541	95	90	495
(Ce,Gd,Tb)MgB_5O_{10}	CBT	542	95	90	490
$LaPO_4$:Ce,Tb	LAP	545	95	93	500
Y_2O_3:Eu	YOX	611	75	90	280

The luminescent materials used in today's tricolor lamps have both excellent quantum yields and absorption properties, in addition to high luminous equivalents. Consequently, it cannot be expected that phosphors with distinctly higher light output can be found in the future. During the last few years research has therefore focused on price reduction of phosphor materials. In particular the green emitting phosphor and Y_2O_3:Eu are relatively expensive materials because of the high price of Tb, Eu, and Y minerals and the costly separation and purification of these lanthanides. The most effective price reduction in (Ce,Gd,Tb)MgB_5O_{10} would be achieved by lowering the Tb^{3+} dopant concentration, but this however at the same time effects the energy transfer from Ce^{3+} via Gd^{3+} to Tb^{3+}. Mn^{2+} activated materials like $Sr_3Gd_2Si_6O_{18}$:Pb,Mn [16] are discussed as cheap alternatives. Their drawback is a distinctly worse maintenance under lamp conditions than the Tb^{3+} phosphors $LaPO_4$:Ce,Tb, (Ce,Tb)$MgAl_{11}O_{19}$, or (Ce,Gd,Tb)MgB_5O_{10} (Table 3). In addition, Mn phosphors are band emitters that, depending on the position and halfwidth of their emission bands, have much lower lumen equivalents than rare earth phosphors. Similarly difficult is the situation for Y_2O_3:Eu. Neither could the Eu^{3+} concentration of currently about 5 mol % be lowered nor have better host lattices been found, although a variety of materials such as $BaGdB_9O_{16}$:Eu,[17] $BiSr_2V_3O_{11}$:Eu,[18] or $BaZrO_3$:Eu[19] show promising properties. However, no material so far was able to match "nature's gift", Y_2O_3:Eu. In this context, it will be exciting to watch the progress of combinatorial chemistry. Tens of thousands of combinations can be synthesized and evaluated on a single substrate wafer. A variety of often unusual phosphor materials has thus been identified by scanning libraries of even ternary systems.[20] Recently, (Y,Al,La)VO_4:Eu has been found to have an efficiency close to commercial red phosphors.[21]

Another approach for realizing cheap phosphor materials is the application of zeolites as host lattices.[22] Low-cost materials such as zeolite X can be modified such that they do not absorb at wavelength longer than 240 nm, which is important for lamp application. These zeolites can be loaded with Eu^{3+} or Tb^{3+} ions and indeed luminescing materials can be obtained, although only with low quantum yields and UV absorptions. The latter can be improved by employing organic sensitizers such as benzoate or inorganic transition metallates like MoO_4^{2-}.[5] However, Eu^{3+} and Tb^{3+} zeolites still haven't exceeded quantum yields of 7 and 50 %, respectively. One reason for these low values are the high frequency O–H vibrations of the zeolites hydroxyl groups at the binding sites of the rare-earth metal ion which effectively quench the metal ion emission, especially from Eu^{3+}. An elegant way around this problem is to use zeolites as precursors for Eu^{3+}- or Tb^{3+}-doped aluminosilicates. Recently, this method allowed the simple synthesis of a quaternary aluminosilicate, $EuMoAl_2Si_4O_{16}$, with a quantum yield of 40 %.[23]

3.2.3. *Tricolor Lamps with High Lumen Output*

Efficiency and color rendering of Color 80 lamps depend critically on the exact position of the emission maximum of the blue and red phosphor (Figure 7). Y_2O_3:Eu with its main emission line at 612 nm is ideally suited for high color rendering. However, the luminous efficacy of fluorescent

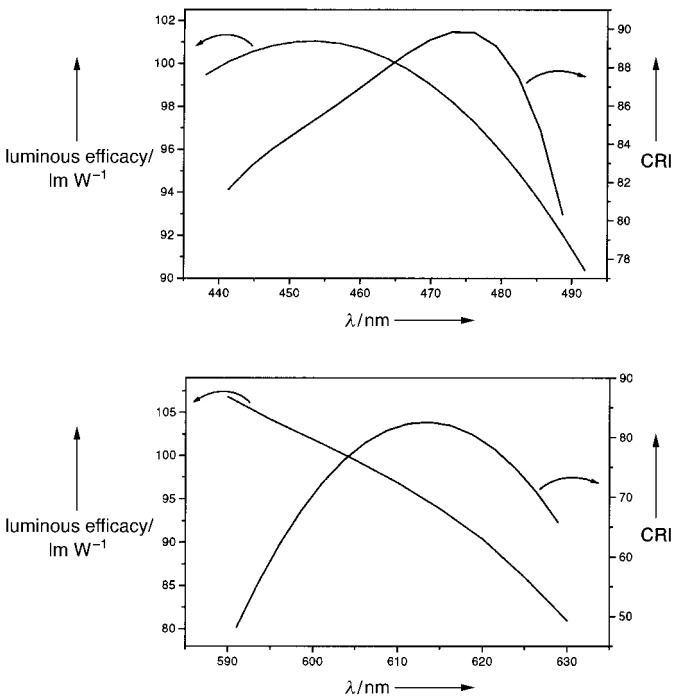


Figure 7. Luminous efficacy and color rendering index of a 36 W tricolor lamp as a function of the emission wavelength of the applied phosphor in the mixture. Top: Variation of the emission wavelength of the blue component. Bottom: Variation of the emission wavelength of the red component.

lamps can be further increased if the emission maximum of the red phosphor is shifted towards shorter wavelength and a decrease in color rendering is accepted. If the emission maximum of the red phosphor is shifted from 612 to 595 nm while leaving the green and blue phosphor unchanged, color rendering drops to 60–65 and the lumen efficiency increases by 12 % (Figure 7). This concept can be realized if Y_2O_3:Eu is

substituted by another line emitter at 595 nm. Such a phosphor can be obtained with Eu^{3+} as the dopant in different host lattices. The electronic transitions of Eu^{3+} doped into host lattices with a trivalent lattice site with inversion symmetry are electronic dipole forbidden. As a consequence, the phosphor emission is mostly restrained by the $^5D_0 - {}^7F_1$ transition at 595 nm. Host lattices with a local inversion symmetry (for example D_{3d}) are $InBO_3$, $ScBO_3$, $LuBO_3$ (calcite structure),[24] and $BaYB_9O_{16}$.[16]

Compared to the Y_2O_3:Eu "standard", these now orange phosphors show indeed a considerably increased lumen equivalent of between 340 and 360 lm W^{-1}. Their quantum yields, however, do not reach the almost theoretically maximal value of Y_2O_3:Eu, which in consequence would compensate for most of the lumen gain. Materials with a quantum yield close to the Y_2O_3:Eu benchmark have to be found in order to be successfully applied.

Recently, a new orange Eu^{3+} phosphor based on an $(In,Gd)BO_3$ host lattice with a quantum yield of 90% has been developed. Its main emission lines are at 591 and 597 nm, which result in a lumen equivalent of 350 lm W^{-1}.[25] In combination with $BaMgAl_{10}O_{17}$:Eu and $(Ce,Gd,Tb)MgB_5O_{10}$ (Table 3), a fluorescent lamp can be realized with about 7% more light output than with the classical tricolor mixture. The considerable emission intensity at 612 and 700 nm, which corresponds to the $^5D_0 \rightarrow {}^7F_{2,4}$ transitions, is responsible for the deviation from the calculated 12% gain. It is questionable whether a phosphor can be found where these long-wavelength transitions are completely suppressed.

3.2.4. Color 90 Lamps

The tricolor lamps mentioned above employ line emitters that generate light in discrete wavelength intervals. Colored objects that absorb outside these spectral regions appear with a slightly different body color when illuminated with these lamps rather than with a black-body radiator such as a light bulb. This is acceptable for most applications such as general indoor and outdoor lighting. Special lighting areas such as museums and bay windows of stores demand a very natural appearance of illuminated objects. For this purpose, Color 90 or Deluxe lamps have been developed.[8, 10]

Two measures serve to increase the color rendering of tricolor lamps. First, the emission maximum of the blue phosphor can be shifted towards longer wavelength (Figure 7). For example, substitution of $BaMgAl_{10}O_{17}$:Mn with $Sr_4Al_{14}O_{25}$:Eu yields lamps with a CRI of 90. Second, the red and green line emitters can be substituted by broad-band emitters covering the whole spectral range to yield even higher color rendering. For this concept, $(Ce,Gd,Tb)MgB_5O_{10}$:Mn has been developed as a red-band emitter; energy transfer from Ce^{3+} via Gd^{3+} to Mn^{2+} gives rise to an additional broad emission band at 630 nm.

Unfortunately, a green broad-band emitter with sufficient efficiency and stability is not yet known. However, an emission band in this region can be "simulated" by combining the green Tb line in $(Ce,Gd,Tb)MgB_5O_{10}$:Mn (Table 4) with the Mn^{2+} emission of $Ca_5(PO_4)_3(F,Cl)$:Sb,Mn. With a phosphor mixture of $Sr_4Al_{14}O_{25}$:Eu, $(Ce,Gd,Tb)MgB_5O_{10}$:Mn,[26] and $Ca_5(PO_4)_3(F,Cl)$:Sb,Mn a fluorescent lamp with a CRI of 95 can be obtained. As a trade-off, the emission intensity in the regions of low eye spectral response causes the lamp efficiency to drop to 65 lm W^{-1}.

Table 4. Phosphors for Color 90 lamps.

Phosphor	Abbreviation	$\lambda_{max.}$ (em.) [nm]	Absorption at 254 nm [%]	QE [%]	LE [lm W^{-1}]
$Sr_4Al_{14}O_{25}$:Eu	SAE	490	90	80	270
$(Ce,Gd,Tb)MgB_5O_{10}$:Mn	CBTM	630	90	80	215
$Y_3Al_5O_{12}$:Ce	YAG	565	45	80	450
$Ca_5(PO_4)_3(F,Cl)$:Sb,Mn	Halo	585	90	80	390
$(Ba,Sr,Ca)_2SiO_4$:Eu	BOSE	560	90	65	475

Color 90 lamps with a low color temperature ($T_c < 3000$ K) demand a reduction in the intensity of the blue emission lines (405, 435 nm) from the mercury plasma. Fluorescent lamps of this kind employ a fourth phosphor with a relatively long-wavelength absorption, $Y_3Al_5O_{12}$:Ce.[27] This material absorbs the blue–violet part of the spectrum very efficiently and converts it into a yellow emission at 565 nm.

$(Ba,Sr,Ca)_2SiO_4$:Eu has been developed as an alternative green-band emitter.[28] Depending on its exact composition, the phosphor emits between 550 and 580 nm with a high quantum yield. Unfortunately, the host lattice is not stable in water, which prevents its deposition on the lamp bulb from aqueous suspensions and, for environmental reasons more and more lamp producers use water as the suspending solvent in production instead of butyl acetate.

3.2.5. Suntanning Lamps

Suntanning lamps have been in production for more than 30 years. Besides high pressure mercury discharge lamps that operate without the application of phosphor materials low-pressure mercury lamps in combination with phosphors have become increasingly popular. The degree of freedom of designing the (UV) lamp spectrum by the phosphor mixture (see Section 2.2) becomes an important feature here. A sensitive parameter for cosmetic, attractive tanning is the ratio of persistent (indirect) to immediate (direct) pigmentation of the skin. While UV-A (320–400 nm) radiation mainly induces immediate pigmentation, which results in a fast tanning and grayish brown color of the skin, UV-B (280–320 nm) radiation promotes the long-lasting, reddish brown tanning of the skin (Figure 8).[10] Consequently, in the 70s the

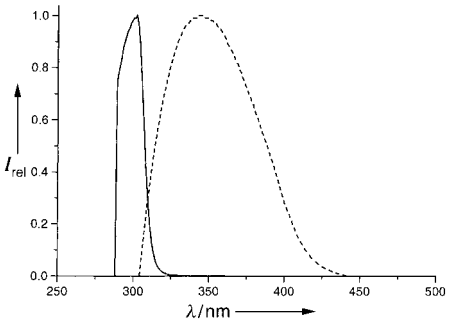


Figure 8. Persistent (solid line) and immediate pigmentation (dotted line) sensitivity of the skin in dependence on the wavelength of the incident UV light.

broad-band emitter (Sr,Zn)$MgSi_2O_7$:Pb (Table 5) was commonly used in suntanning lamps.[29] This phosphor, which has its emission maximum at 365 nm with a half width of 70 nm, enabled a balanced UV-A/UV-B ratio and resulted in fairly good tanning. The main drawback of this material is its low

Table 5. Phosphors for suntanning lamps.

Phosphor	Abbreviation	$\lambda_{max.}$ (em.) [nm]	Absorption at 254 nm [%]	QE [%]	FWHM [nm]
$SrAl_{12}O_{19}$:Ce	SAC	310	85	95	34
$BaSi_2O_5$:Pb	BSP	350	85	95	38
(Sr,Zn)$MgSi_2O_7$:Pb	SMS	365	88	85	70
SrB_4O_7:Eu	SBE	370	95	90	20

stability, which results in a low lamp maintenance. In addition, the large half width of the emission leads to considerable emission intensity beyond 400 nm where the skin sensitivity towards tanning and consequently the tanning effect is low (Figure 9).

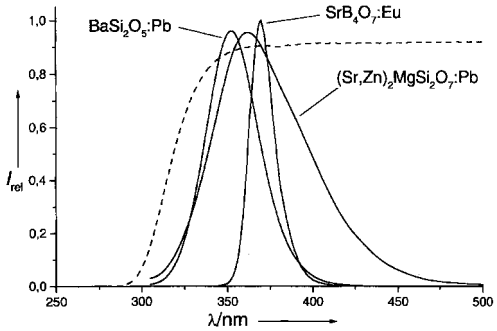


Figure 9. Emission spectra of the UV phosphors $BaSi_2O_5$:Pb, SrB_4O_7:Eu, $(Sr,Zn)_2MgSi_2O_7$:Pb applied in fluorescent tubes with a typical glass transmission (dashed line).

Besides these material-related shortcomings of (Sr,Zn)$MgSi_2O_7$:Pb, scientific evidence gained in the 70s showed that UV-B radiation is responsible for direct damage of DNA. Such damage was not found for UV-A radiation. As a consequence, $SrMgSi_2O_7$:Pb has been replaced by $BaSi_2O_5$:Pb which emits at 350 nm with a rather small FWHM of the emission band. The emission intensity is now concentrated in the UV-A region, which speeds up direct pigmentation. Also, the UV-B emission intensity accumulated on the skin is lowered. Unfortunately, the persistent pigmentation which is long lasting, is decreasing at the same time.

However, in the 80s the booming suntanning industry focused on UV lamps emitting mainly UV-A radiation. The lowering of the UV-B/UV-A ratio was achieved by two measures. First, the glass transmission in the UV-B region was reduced. In addition, some manufacturers applied a second UV-A phosphor, SrB_4O_7:Eu in a blend with $BaSi_2O_5$:Pb.[30] The enhancement of the UV-A radiation of suntanning lamps was driven by the belief that tanning with UV-A is safe.

Since the early 90s photobiological investigations have revealed that UV-A radiation might also be responsible for inducing serious skin cancer, namely malignant melanoma.[31] These considerations and the demand to enhance the long-lasting tanning have recently led to the development of UV lamps with larger UV-B/UV-A ratios. Today, $BaSi_2O_5$:Pb is typically used in combination with $SrAl_{12}O_{19}$:Ce.[32] The introduction of this UV-B phosphor with an emission at 350 nm allows the fine-tuning of the UV-B to UV-A ratio.

Triggered by the discussion about health risks of sun tanning, many lamp producers seek to further optimize the lamp spectrum. Positive effects of UV irradiation such as pigmentation, vitamin D production, epidermis thickening, and stimulation of the production of immunoglobulines can be enhanced by an accurate fine-tuning of the UV spectrum, while negative consequences such as photoceratitis, photoconjunctivitis, and photodimerization of pyrimidine bases should be lowered. Consequently, new phosphor combinations are tested as well as new phosphor materials that are developed to further improve the spectral power distribution of future suntanning lamps.

3.2.6. Specialties

Besides the discussed major application areas of low pressure mercury discharge lamps, a large variety of special lamps has been introduced into the market.[2, 10] The development of these specialties was possible because phosphor materials with any emission spectra can be designed, which determine the spectral power distribution of the fluorescent lamp. Specialty lamps used in photocopy machines, billboards, plant illumination, skin disease treatment,[33]for example, employ luminescent materials with emission spectra that serve the very special requirements of the respective application. Table 6 lists important applications together with the optical properties of the employed phosphors.

Table 6. Phosphors for specialty lamps.

Phosphor	Abbreviation	$\lambda_{max.}$ (em.) [nm]	Application area
(Gd,La)B_3O_6:Bi	GLBB	311	psoriasis lamps
$Sr_2P_2O_7$:Eu	SPE	420	photocopy lamps
$BaMgAl_{10}O_{17}$:Eu,Mn	BAM-Mn	520	neon lamps
$Mg_4GeO_{5.5}F$:Mn	MGM	655	neon lamps, butcher lamps

3.3. Maintenance Improvement

Generally, phosphors show a decrease in efficiency during lamp operation. The maintenance of a material is defined as the relation of efficiency after a certain operation time, for example 1000 h, to the initial brightness of the virgin tube. The following processes have been identified to contribute to degradation:

- adsorption of Hg,
- sputtering of the phosphor surface by the plasma,
- solarization (staining) of the phosphor.

It is quite obvious that the phosphor degradation during lamp operation depends strongly on the chemical nature of

the material, that is the composition of the host lattice and the nature of the activator ion. For illustration, special host lattices such as silicates (e.g. Zn_2SiO_4) show a strong affinity to Hg.[34] Adsorption of Hg onto the phosphor induces a complex chemistry that leads to surface defects of the phosphor grain or even the build-up of a Hg layer on the surface that consumes the mercury from the plasma. Redox-sensitive activator ions such as Mn^{2+} or Ce^{3+} easily undergo photochemical reactions such as photooxidation or -reduction. Solarization means the direct creation of defects in the phosphor grain by short wavelength UV light, which usually act as color centers that absorb UV- or visible light.

The loss of efficiency of a phosphor during lamp operation can be explained by the following processes:

- decrease of the UV absorption of the activator relative to the host lattice, that is, energy loss in the host lattice,
- drop of quantum yield because of energy transfer of the absorbed energy to so-called killer centers,
- increase of absorption of the emitted light in the single phosphor grain that leads to less light output of the phosphor (e.g. absorbing defects, photochemically generated absorbers),
- intrinsic quantum efficiency loss of the activator, for example by an oxidation or reduction process.

Phosphors with a good maintenance often consist of a host lattice with high chemical bond energies, for example Y_2O_3:Eu or aluminates. However, the actual application of a phosphor material in lamps is the result of a thorough evaluation of optical performance and price, which means that less stable materials are also applied. In many cases, the maintenance of phosphors can be considerably improved if the surface of the phosphor particle is "finished" with a coating.[4] The requirements of a coating material are stability and a high bandgap so that the incoming UV light is not already absorbed on the nonemissive coating surface. Typical materials are Al_2O_3, Y_2O_3,or La_2O_3, which are commonly applied by precipitation from soluble precursors in aqueous solutions[35] or by chemical vapor deposition (CVD).[36] While the former procedure is a rather cheap one, the latter one is capable of producing very dense and homogeneously closed coatings. A variety of luminescent materials has been considerably improved by coating technology (Table 7).

Table 7. Examples of currently coated phosphors.

Phosphor	Coating material	Process	Benefit
$BaMgAl_{10}O_{17}$:Eu	Y_2O_3 or Al_2O_3	homogeneous preciptation	improved maintenance
Zn_2SiO_4: Mn	Al_2O_3	CVD	improved maintenance
$BaSi_2O_5$:Pb	Al_2O_3	CVD	improved maintenance applicable in water suspension
YVO_4:Eu	Y_2O_3 or Al_2O_3	CVD	improved maintenance
Y_2O_3:Eu	Al_2O_3	CVD	applicable in water suspension
$Ca_5(PO_4)(F,Cl)$:Sb,Mn	Al_2O_3	CVD	reduced mercury consumption

Besides improved maintenance various other phosphor properties can be influenced positively. Lamp producers are increasingly applying phosphors from water-based suspensions (Section 2.2.3). Phosphors sensitive towards hydrolysis such as $BaSi_2O_5$:Pb and $Mg_4GeO_{5.5}F$:Mn could then not be applied. However, both materials can be coated quite well by CVD and thus be adapted to the new process technology. Coatings can also help to reduce the mercury consumption by the phosphor surface and the color point shifts of the phosphor during lamp operation.[37]

In summary, the maintenance improvement of luminescent materials is of increasing importance for phosphor producers. Particle coatings and the development of new coating processes improve both the applicability and stability of luminescent materials.

3.4. Alternative Discharge Types and Quantum Cutters

The overall efficiency of low pressure mercury discharge lamps ε_{lamp} is close to 30%. The value is mainly determined by the efficiency of the mercury plasma (75%), the energy loss from the conversion of UV light into visible radiation, and the quantum efficiency of the employed phosphors [Eq. (4)].

$$\varepsilon_{lamp} = \varepsilon_{discharge}[\lambda_{UV}/\lambda_{vis}]\,QE \quad (4)$$

Mainly for environmental reasons, alternative plasma discharges that could substitute the mercury plasma are widely investigated today. With regard to discharge efficiency, a xenon excimer plasma is the most promising candidate, with an efficiency of up to 65% reported recently.[38] A Xe discharge is also used in plasma display panels (PDPs) (Section 4.2.2). The main emissions are in the vacuum ultraviolet (VUV) at 147 (Xe fundamental line) and about 172 nm (Xe excimer band) and their ratio depends on the gas pressure in the discharge cell. Since they are at shorter wavelengths than the mercury plasma emission the overall efficiency of visible light generation is reduced because of the now much bigger energy gap between the excitation and emission levels. A scientifically quite exciting solution to this problem are phosphors that emit in a controlled way more than one visible photon per absorbed VUV photon. Such materials, so-called quantum cutters, were reported for the first time in the mid 70s independently by two research groups.[39] In the phosphors YF_3:Pr and $NaYF_4$:Pr the Pr^{3+} activator ion can be excited by a VUV photon into the very energy rich $^1S_0$ state. From there it can emit in a photon cascade emission (PCE) two visible photons of different energies. The initial absorption takes place in the host lattice at 185 nm via a 4f5d transition. It is important that the excited 4f5d state lies above the $^1S_0$ state so that energy transfer can lead to the excited $^1S_0$ state. Only if this condition is fulfilled can the two f-f states of Pr^{3+} be populated and emit with a combined quantum yield of about 140%. If the 5d state moves close to or below the $^1S_0$ state, as in $LiYF_4$:Pr or YPO_4:Pr, quantum cutting cannot be observed anymore. This is the case in host lattices with a strong crystal

field. Unfortunately, fluorides have pronounced disadvantages that have so far prevented their application. They are difficult to handle in production and show a poor maintenance in contact with plasma discharges. Consequently, research focuses now on alternative host lattices such as oxides, aluminates, or borates. Oxide anions create a stronger crystal field than fluorides, however, it can be weakened by a large coordination number. Recently, this concept has been realized successfully by Shrivastava et al. in several Pr^{3+}-doped host lattices with a coordination number of 10 or 12, for example $SrAl_{12}O_{19}$,[40] LaB_3O_6,[41] and $LaMgB_5O_{10}$.[42] Photon cascade emission has been observed; however, as a consequence of the very low transition probability in these hosts, the external quantum yield does not exceed 100%. Another drawback of Pr^{3+} quantum cutters is their emission spectra, which consists of two major emission lines at 610 and 410 nm, the latter of which is not very useful for fluorescent lamps because of low color rendering and efficiency (Section 3.2.3).

A few month ago Meijerink et al. presented a completely different quantum cutter concept based on the material $LiGdF_4$:Eu.[43] This system is particularly attractive because it yields solely "useful" Eu^{3+} emission at 612 nm with a demonstrated internal yield of 195%. A VUV photon is absorbed by the Gd^{3+} sensitizer and then transferred in two steps to a Eu^{3+} ion. In a first step the Eu^{3+} ion is excited by cross relaxation while in the second step another Eu^{3+} ion can be populated by energy transfer from Gd^{3+} to Eu^{3+} ions (Figure 10). Although again based on a fluoride host lattice,

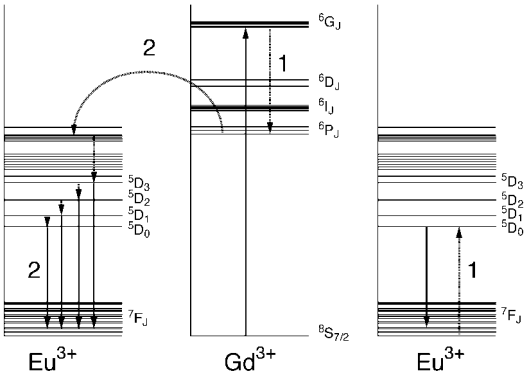


Figure 10. Energy level scheme of the quantum cutter $Li(Gd,Y)F_4$:Eu showing the transitions 1 and 2, which lead to emission of two photons.[43]

this material and the concept behind it might open new ways to realize quantum cutting with useful emission in novel lamp applications.

3.5. Light Emitting Diodes in Comparison and in Combination with Luminescent Materials

The invention of the blue-light emitting diode (LED) based on GaN can be regarded as a triumph of material chemistry. Electroluminescence based on III–V nitride semiconductors had already been abandoned when S. Nakamura picked up the topic again in the late 80s and developed it within only 5 years to an impressive level of maturity. Excellent reviews about the underlying semiconductor photophysics as well as the MOCVD technique used for LED chip production can be found elsewhere.[44, 45] External quantum yield, stability, and many other favorable properties of this material class allow even the construction of the blue laser diode, which will likely revolutionize the storage capacity of compact discs. Very recently, lifetimes exceeding 10000 h have been reported, which paves the way for a fast introduction of the blue laser into the market.[46] The blue diode itself however might already mark the beginning of a slow revolution of the lighting market. External efficiencies of close to 10% have already been achieved. Light outcoupling from the LED chip into the epoxy dome as well as the chip architecture still show considerable room for improvement, so much higher efficiencies seem possible. By varying the In content of the InGaN active layer the emission spectrum of GaN LEDs has successfully been extended into the green spectral region with still high efficiencies. As a consequence, for the first time it is possible to generate white light by direct conversion from electrical current in LEDs with an efficiency superior to halogen lamps. Two ways of generating white light appear likely. First, blue, green, and red diodes can be combined to yield white light. So-called cluster lamps consisting of blue, green, and red LEDs are already on the market. Second, in a very cheap way a single white LED can be obtained by combining a blue LED with green, yellow, and/or red emitting phosphor materials that absorb and convert part of the incident blue light. In comparison to the three LED device this causes a decrease in the overall efficiency because the quantum deficit of the light conversion from blue to yellow/red has to be taken into account. In the following paragraph this option will be discussed with regard to light quality and luminous efficiency.

In principle, it is possible to vary the emission wavelength of blue GaN-based LEDs between 370 nm, which marks the bandgap of pure GaN, and 470 nm by increasing the In content in InGaN devices. Assuming a conversion from the incident light by a phosphor material emitting at 555 nm (a spectral "mean value" for white light), the already mentioned quantum deficit decreases in the same direction from about 33% to 15%. The more favorable option is therefore a combination of a blue LED emitting at 470 nm and a broad-band phosphor that can be excited by that wavelength and reemits at about 550 nm to create white light composed of the blue and yellow–green emissions. Such a device has been realized by using $(Y_{1-x}Gd_x)_3(Al_{1-y}Ga_y)_5O_{12}$:Ce (YAG:Ce) as a broad-band yellow phosphor (Figure 11).[44] The variation of x and y causes a shift of the YAG:Ce emission between 510 and 580 nm. This allows the adjustment of white color temperatures from 8000 down to 3000 K. A color temperature of 6000 K has been chosen for commercialization in the Japanese market, which demands high color temperatures. As a consequence of the broad YAG:Ce emission the color rendering index (CRI) is high and reaches a value of 85. The luminous efficiency is 5 $lm\,W^{-1}$, which is already half of that of an incandescent lamp. This shows clearly the potential of the blue LED and its importance for the future lighting market. All low-power white-light sources that demand long lifetimes could possibly be replaced by white LEDs in the

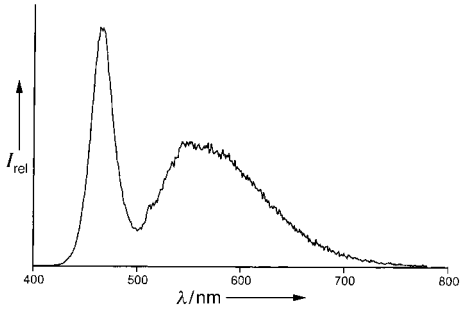


Figure 11. Emission spectrum of a white phosphor LED that consists of a blue LED that excites the YAG:Ce phosphor deposited as a thin layer on the LED chip.

medium term. However, it should be pointed out that about 80 such LEDs are still necessary to replace a 10 W light bulb, assuming a medium power operation of 50 mA at 5 V. The major drawback of this combination is the strongly decreasing overall efficiency upon lowering the color temperature. This is caused by the broad YAG:Ce emission, which shows less and less integral overlap with the eye sensitivity curve when shifted towards longer wavelengths (Figure 4) and hence decreases the luminous efficacy. Alternatively, pure organic perylene based materials (Lumogen dyes)[47] and light emitting polymers[48] can also be used for color conversion. Their advantage is the high absorption of the blue diode light. The white light energy yield achieved, however, is lower than for the YAG phosphor. An attractive alternative to the discussed broad-band phosphor systems would be the employment of line emitters in analogy to lamp phosphors (Section 2). The requirements can be concluded from the above discussions. The phosphor material has to have a sufficient absorption at the emission wavelength of the blue diode, the quantum yield should be high under UV/Vis excitation and the FWHM of the emission band should be as small as possible in order to achieve high luminous output. Selected rare-earth phosphors based on Eu^{3+} and Tb^{3+} fulfill the latter two options; however, there is a theoretical low energy limit for the maximum wavelength of the excitation peak. Even if tight sensitization schemes can be found, that is sensitizers with energy levels close to the ^5D terms of Eu^{3+} and Tb^{3+}, these ions cannot be excited with peak wavelengths longer than 420 and 370 nm, respectively. This is a result of the downward energy cascade that is necessary to effectively sensitize the rare-earth ion without back energy transfer.[49] GaN LEDs that emit at 370 nm (see above) could be used for excitation with the drawback of the larger quantum deficit.[50] Inorganic Eu^{3+} phosphors with high quantum efficiencies that absorb satisfactorily at 370 nm are Y_2O_2S:Eu and Y(V,P,B)O_4:Eu. Tb^{3+}-doped materials are hard to find; (Ce,Tb,Gd)MgB_5O_{10}, mainly used in tubular fluorescent lamps, absorbs only to about 10 % at 370 nm. Organic phosphors employing Eu^{3+} and Tb^{3+} coordinated to light-absorbing organic ligands can be designed to absorb efficiently at 370 – 400 nm.[51] However, stability and saturation issues have yet to be improved for these materials. Despite these difficulties and the higher quantum deficit, a LED emitting UV light at 370 nm covered with a rare-earth phosphor mixture would be an attractive option from a production point of view. In contrast to a phosphor deposited on a blue emitting LED chip at 470 nm, which only partly absorbs the blue light in order to generate white, a mixture of blue, green, and red phosphors on a UV LED absorbs all of the incident light emitted by the chip. The white light color coordinates are determined only by the phosphor portions in the mixture (see Section 3.2), which can be adjusted rather accurately. Consequently, white LEDs can be produced with color coordinates that vary only very little from LED to LED. This is considerably more difficult for a LED where white light is composed from incident blue emission from the diode and yellow/red light emitted by the phosphor. Deposition of a well-defined phosphor layer on the LED chip of some 1 mm^2 to achieve controlled absorption means a real manufacturing challenge. Further, the additional quantum deficit of about 15 % of a color conversion from 370 nm relative to 470 nm can be compensated for considerably by the very high lumen equivalents of Eu^{3+}- and Tb^{3+}-activated phosphors. By analogy to fluorescent lamps (see above), high color renderings can be obtained at the same time. The search for stable inorganic rare-earth phosphors with high absorptions in the near UV/blue spectral region is therefore an attractive research task.

4. Displays

4.1. Cathode Ray Tubes and Projection TV

The classical cathode ray tube (CRT) invented as the Brown tube more than 100 years ago has developed into a remarkably mature product considering the complexity of its manufacturing process. An illustrative example is the deposition of the phosphor material on an average-sized, warped (!) screen front: In three consecutive photolithographic steps more than one million phosphor dots less than 300 μm in diameter for each color have to be deposited, with not one final pixel missing. Today's mass production, which yields more than 100 million tubes per year, has caused the prices to drop to a level where it is hard for innovations to step in. On the other hand, it is this number that makes research on CRT phosphors still a respectable field as they contribute a total of only about 2 g (red, green, and blue, average tube size), which is only very little, to the product. The strong competition drives the research effort on luminescent materials into two directions, namely cheaper phosphors (especially red) and the addition of new features for superior performance. Basic requirements of display phosphors are stability (20000 hours operation) and emission color purity according to the standards set by the European Broadcasting Union (EBU).[2, 52] Color purity can be visualized in the chromaticity diagram as blue, red, and green regions, which the emission color coordinates of the luminescent material have to match (Figure 3). The blue and green phosphors are still the very cheap ZnS based materials, essentially the same ever since color TV was introduced in the 50s. The luminescence of both is based on donor – acceptor transitions in the ZnS host lattice that is doped with some 200 ppm Cl^- ions as donor and Ag^+ ions as acceptor for blue and Cu^+ ions, Au, Al for green.[53] Remarkably enough, these sulfidic lattices are quite stable

towards electron beam excitation of 30 keV where one electron can create up to 3000 visible photons in the phosphor grain. The energy density of this excitation source has been described very graphically by H. A. Klasens, a pioneer in luminescent materials: "ultraviolet excitation compares to striking one key of the piano, cathode-ray or X-ray excitation compares to throwing the piano down the stairs".[2] This stability is not a natural property as we can see for low-voltage excitation (see below). Originally, a ZnS based host lattice containing a certain amount of Cd doped with Ag^+ and Cl^- ions was used as the red phosphor. Intrinsic to a donor–acceptor transition, it displays a broad emission, in this case centered at 650 nm, which leads to a rather low lumen equivalent because a large fraction of the emission integral lies outside the eye sensitivity curve (see Section 2). For this and environmental reasons, it has been replaced by the much more expensive Y_2O_2S:Eu (a line emitter such as Y_2O_3:Eu) with main emission lines at 612 and 628 nm.

Key features of a modern CRT within a computer monitor or a TV set are brightness and contrast. The relation between the two is expressed by the luminance (L) contrast performance (LCP) gain [Eq. (5)], where R is the reflection of ambient light at the phosphor layer.

$$\mathrm{LCP} = L/\sqrt{R} \qquad (5)$$

From the equation two ways for improving LCP can be derived:

- increasing L, which is hardly possible anymore as all three phosphors are operating close to their physical limits, or
- reducing R, which is achieved by applying color filters and absorbing the ambient light while transmitting the light emitted by the phosphor.

Color filters can be applied by two means. Externally, as transparent layers on the screen glass or internally, as pigment on the phosphor surface. Pigmenting blue and red phosphors is the focus of CRT phosphor research these days. The phosphor grain is coated with nanosized pigments in the order of 100 Å such as α-Fe_2O_3 (red) and $CoAl_2O_4$ (blue) by a wet-chemical process. Figure 12 shows the absorption edges of the two pigments together with the emission bands of ZnS:Ag,Cl and Y_2O_2S:Eu. The green phosphor is not coated because calculations show that least LCP can be gained here and because no appropriate pigment can be found. It is easy to imagine that pigmentation changes the phosphor grain surface considerably and will consequently alter the phosphor suspension behavior in the industrial coating process. Also, pigment absorption can hamper the photolithographic deposition. The materials under development have to be adapted such that the industrial deposition techniques have to be changed as little as possible.

Projection TV (PTV) has a long history as well. Interestingly, the first color television developed in the 50s can be regarded as a projection TV. Requirements of projection TV phosphors are different.[2, 54] PTV is used for large screen sizes (>90 cm) or in special environments like planes. Three monochrome (red, green, and blue) images are projected and superimposed on a screen at a certain distance. The need for high light output and resolution causes higher excitation density at a smaller phosphor volume than in a conventional

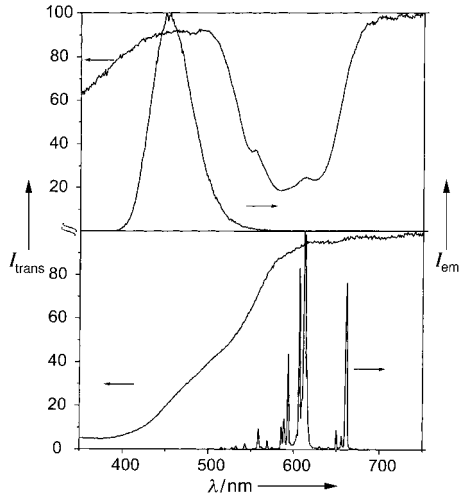


Figure 12. Color filter concept in cathode ray tubes. Emission and transmission spectra of the blue ZnS:Ag phosphor in combination with a $CoAl_2O_4$ filter (top) and the red Y_2O_2S:Eu phosphor in combination with a Fe_2O_3 color filter (bottom).

cathode ray tube. Most of the phosphor materials start to behave nonlinearly under these conditions, that is they don't increase light output L linearly upon increasing excitation density D [$J\,cm^{-2}pulse^{-1}$]. Saturation and heat-up of the phosphor grains up to 100 °C are the responsible factors. The former is the reason for switching from Y_2O_2S:Eu to the fluorescent lamp phosphor Y_2O_3:Eu, which is much less susceptible to saturation. As a green phosphor Y_2SiO_5:Tb is mostly used. The limiting phosphor and consequently research topic for a long time is the blue one. Introducing blue lighting phosphors (Section 3) does not work because all Eu^{2+} based materials suffer from severe degradation. Quite some effort, also in our lab, has been put into (La,Gd)OBr:Ce because of its good linear saturation behavior,[55] however, without reaching industrial maturity. Once again, ZnS:Ag,Cl is used as the blue phosphor, despite saturation at high excitation densities. However, the triumphant march of LCD technology might also displace phosphor screens. Newly developed, extremely powerful high-intensity discharge lamps can project images from three tiny, monochrome high-resolution LCD screens and superimpose them in analogy to images projected from phosphor screens.[56]

4.2. Flat Displays

The race for the flat screen has already begun. The big electronic companies are trying to enforce the ultimate display concepts for the respective application. For the smaller screen sizes up to 21″ (monitors) it will be most likely liquid crystal technology (LCD). As a nonemissive display, it will not be covered in the following sections; excellent reviews can be found elsewhere.[57] Various concepts exist for larger sizes up to 42″ and beyond (>1 m diagonal) for TV application. Besides the one screen principle, which also uses LCD technology and the so-called plasma-addressed liquid crystal (PALC) display, all of the methods create light from

luminescent materials and are presented below. Very new developments such as electroluminescence, both organic and inorganic, conclude this chapter.

4.2.1. Low Voltage Displays

Electrons accelerated by moderate voltages between some hundred volts and 8 kV (compared to about 30 kV for a CRT) are used for excitation in this display type. Most prominent are the flat CRT and field emission displays (FEDs). The flat cathode ray tube was a large research project within Philips, which had achieved an impressive maturity level.[58] It was aimed at medium to large sizes of screens to replace the bulky CRT by a hang-on-the-wall TV. Electrons are created at a flat cathode, the so-called backplate, and tunnel through a smart array of channels to arrive at a selection plate where they are distributed to address the phosphor pixels consisting of blue, green, and red phosphor dots.

The now very small distance between the back and front plate is filled with the channel plates and allows an acceleration voltage of only 4 – 6 kV in order to prevent shortcuts. Y_2O_2S, the red CRT phosphor, can be excited very well under these conditions. The green and blue ZnS phosphor, however, show a very fast degradation if excited this way. At a first glance, this seems rather surprising as less energy-rich electrons than in CRTs are used for excitation. The explanation is given in Figure 13. In contrast to high acceleration

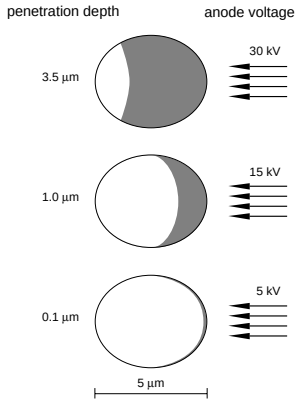


Figure 13. Dependence of the penetration depth of the electron beam in a phosphor grain of 5 µm diameter on the anode voltage of a cathode ray tube.

voltages, low-voltage electrons are not capable any more of penetrating the whole phosphor grain with an average diameter of about 5 µm. Instead, they create a high density surface excitation. This has physical and chemical consequences. The decreasing number of luminescent centers available for excitation at decreasing anode voltages results in severe phosphor efficiency saturation, even more as the energy density of excitation has to be increased in order to obtain a screen luminance comparable to a conventional CRT. Further, one of the main emission quenching pathways in a phosphor grain is formed by lattice defects that occur mostly at the surface. Low voltage surface excitation is therefore more strongly quenched than excitation taking place in the bulk phosphor grain. The saturation effect in the low-voltage excited region compares well to PTV excitation. For this reason, the green $Y_2SiO_5:Tb^{3+}$ phosphor used there (see above) has been successfully adapted and has replaced ZnS:Cu for low-voltage excitation.

In addition to these photophysical loss processes chemical degradation occurs in ZnS phosphors upon low-voltage excitation. Although the detailed reaction path is still not completely understood, the sum reaction is believed to be sulfur loss in the host lattice caused by oxidation of sulfide anions, which create new quenching centers at the surface.[59] Again, it is hard to find a more effective blue CRT phosphor than ZnS:Ag. As a consequence, efforts to develop a protective coating to prevent the fast degradation of ZnS:Ag under low voltage excitation have replaced the search for new materials. Inorganic coatings have been found, which form a completely closed, smooth, and only 20 nm thick layer on the surface. The so-called coulomb degradation is drastically reduced for coated ZnS:Ag. Most likely, the dense coating acts as a diffusion barrier and so maintains the sulfur balance within the host lattice.

Field emission display research is mainly conducted in the U.S. The display principle is similar to the flat CRT discussed above.[60] Instead of an electron transfer mechanism through channels, electrons in FEDs are created at micro-tips which act as tiny cathodes. Each cathode addresses a pixel on the front plate that is mounted at a certain distance from the tips on the backplate. The voltages in FEDs are typically somewhat lower than in the flat CRT, ranging from some 100 V to a few kV. The low voltage phosphors applied in the flat CRT can still be used in FEDs, however, it can easily be concluded from the above discussion that because of the lower voltages degradation problems become even more severe. Oxidic host lattices would be favorable, however, they lack efficiency. The phosphors commonly applied today can be seen in Table 8.

Table 8. Overview of currently applied FED phosphors.

Phosphor	Efficacy[a] [lm W^{-1}]	Color coordinates[a] x	y	Color
$SrTiO_3:Pr$	0.4	0.670	0.329	
$Y_2O_3:Eu$	0.7	0.603	0.371	red
$Y_2O_2S:Eu$	0.57	0.616	0.368	
$Zn(Ga,Al)_2O_4:Mn$	1.2	0.118	0.745	
$Y_3(Al,Ga)_5O_{12}:Tb$	0.7	0.354	0.553	green
$Y_2SiO_5:Tb$	1.1	0.333	0.582	
ZnS:Cu,Al	2.6	0.301	0.614	
$Y_2SiO_5:Ce$	0.4	0.159	0.118	
$ZnGa_2O_4$	0.15	0.175	0.186	blue
ZnS:Ag,Cl	0.75	0.145	0.081	

[a] At low-voltage excitation.

The white light generation efficiency is still well below 5 lm W^{-1}, which can already be achieved with LCDs. However, FEDs have other distinct advantages such as a very wide range of operational temperatures, they can operate under rugged conditions, and the emissive character results in a wide viewing angle. FEDs in the current status are mainly targeted towards military applications.[61] Recently, a display based on

an alternative cathode structure has been realized, a so-called surface-conduction electron emitter display (SCE).[62] This system consists of a structured PdO film that can easily be ink-jet printed. It operates at higher anode voltages (6 kV) and standard CRT phosphors were applied successfully. The performance of a 10″ prototype (luminance 690 cd m^{-2}; efficiency 5.3 lm W^{-1}) is well beyond that of "classical" FED concepts, not least because many phosphor problems have been overcome by the higher excitation energy.

4.2.2. Plasma Displays

Creating light from a plasma discharge ignited in the discrete display pixels is actually a rather old invention (the first laptop display was based on a plasma discharge). However, some years ago improved yields and refined production techniques have revitalized the principle. Today, all major electronic companies are conducting research on PDPs and mass production started about one year ago. The principle is sketched in Figure 14.[63] A discharge is ignited between two electrodes in each pixel cell at the front plate that are filled with a Xe gas mixture to lead to a Xe plasma. Excited Xe monomers and excimers are formed that emit at

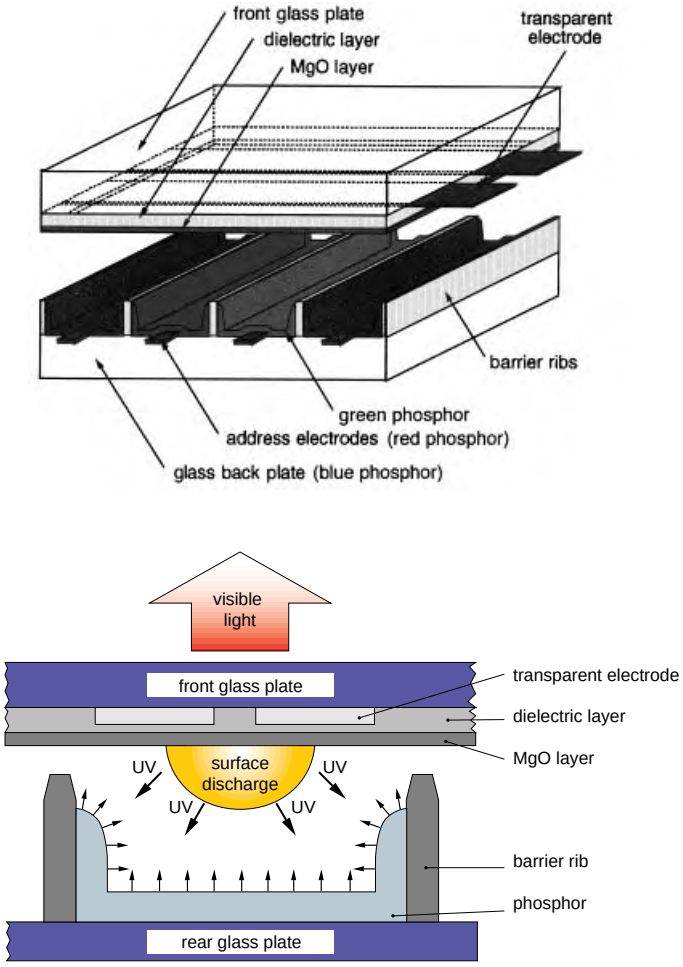


Figure 14. Top: schematic diagram of a plasma display panel. Bottom: cross-sectional view of a single plasma discharge cell illustrating the process of light generation

147 and 172 nm, respectively (Section 3.4). This light excites the phosphor layer on the wall of the discharge cell. As a consequence of the cell geometry, the discharge efficiency is rather low (about 6%), which is the major drawback of this display type. Currently, only about 1 lm W^{-1} screen efficacy (white light) is achieved compared to about 3 lm W^{-1} for a conventional CRT. This puts pressure on the phosphors for maximum performance.[64] For blue, $BaMgAl_{10}O_{17}$:Eu is mostly used because it can be excited very effectively. However, it shows degradation under VUV excitation, which might possibly be prevented by coatings. For green, the long known Zn_2SiO_4:Mn^{2+} phosphor (willemite) is used because its green emission color is very saturated (color coordinates: $x = 0.250$, $y = 0.704$; see Figure 3). However, the optical transition within the Mn dopant is of the d–d type and thus a strongly forbidden electric dipole transition. As a consequence, the decay time is rather long, typically tens of milliseconds. It would exclude this material from TV application because for fast moving pictures, for example during a soccer game, a green afterglow would always be blurring the displayed image. Interestingly, magnetic interactions between pairs of Mn^{2+} ions[65] can alter the transition probability. Thus, by increasing the concentration of the Mn^{2+} dopant the decay time starts to drop while the quantum efficiency is maintained.[66] But at rather high concentrations of the activator concentration quenching causes the quantum efficiency to drop. This unique effect could be exploited to obtain a material that can be applied in PDPs. As a red phosphor, (Y, Gd)BO_3:Eu is mostly applied today. Borates have much higher VUV absorptions than for example Y_2O_3:Eu does. However, because of the high symmetry of the trivalent site in the borate host lattice the $^5D_0 \rightarrow {}^7F_1$ transition of the Eu^{3+} ion at 595 nm becomes very pronounced. This leads to a too orange color point according to the CIE standards. Obviously, the introduction of a functioning red quantum cutter phosphor (Section 3.4) would boost the overall PDP performance considerably.

4.2.3. Electroluminescence

Analogous to LED light sources, electroluminescence (EL) displays means the direct transformation of electrical current into light. It can be cautiously stated that if at all, only EL is possible to challenge the very mature LCD technology omnipresent in today's notebooks and flat monitors. Inorganic and organic EL are very different. Inorganic EL has been studied for some 30 years and is already used, for example as information displays in the new ICE trains. Organic EL is a very recent discovery and will have to prove its potential yet.

Electroluminescent Inorganic Materials

In this section new developments in materials for thin film alternating current electroluminescence (ACTFEL) will be presented. Based on this principle, very thin full-color displays can be realized (with a thickness of a few centimeters, including the necessary electronics).[67] Full color ACTFEL displays are based on one of the two principles:

- Color by white: Here, white light is generated by a phosphor (a multilayer of ZnS:Mn/SrS:Ce). Color is

generated by the application of color filters. This principle has the advantage of a simple layer structure of the phosphor.

- Three color structure: In this principle, white light is generated by the application of three phosphors (emitting blue, green, and red, such as in a cathode ray tube). The phosphor layer structure and hence device fabrication is more difficult than in the color by white structure. In addition, for blue and red the color points of the emission spectrum are not fulfilling the EBU requirements. Therefore, also in this case, color filters are used. Nevertheless, these devices have a higher luminous efficacy than the ones based on the color by white structure (see below).

The following device structure is common to both principles:

glass substrate/electrodes/insulator/phosphor/insulator/electrodes/color filters.[68]

The luminescent materials applied are thin layers (in the order of 1 μm), generated by techniques like atomic or molecular beam epitaxy. The electroluminescent materials applied are sulfides, although oxides are under investigation as well. The ACTFEL materials are subjected to high fields and electrons are accelerated in these materials. The electrons excite the activator ions by impact excitation. At present, there is no general picture of the mechanism(s) underlying ACTFEL. One of the most important factors determining the success of ACTFEL is the device efficiency, an estimation of which[4] follows in brief below. The maximum efficiency η is given in Equation (6), where E_{em} is the photon energy of the emitted radiation, σ the cross-section for impact excitation, N the optimum concentration of luminescent centers, and F the electric field applied. $(\sigma N)^{-1}$ is the mean distance that an electron travels through the luminescent material between two excitation events.

$$\eta = E_{em}\sigma N/eF \quad (6)$$

The cross-section is not known a priori. In the case of ZnS:Mn (the most efficient ACTFEL material known) we approximate it by using atomic dimensions, that is $\sigma = 10^{-16}\,cm^2$ (the Mn^{2+} ion has the same charge as the Zn^{2+} ion). The other typical values are: $E_{em} = 2$ eV, $N = 10^{20}\,cm^{-3}$, and $F = 10^6\,V\,cm^{-1}$. It follows that the energy efficiency equals about 2%, which is in very good agreement with experiment. In this treatment, however, we have used a number of simplifications. We did not account for the Stokes shift. Moreover, we neglected light trapping effects in the thin layers. All these phenomena further reduce the energy efficiency. The energy efficiency is not likely to be improved significantly. This is mainly a consequence of the low value for the cross-section, because the value chosen for N cannot be too large in view of concentration quenching.

The mean energy the charge carrier has taken up from the electric field between two impact excitation events, neglecting any losses from phonon emission, equals $eF/\sigma N$. The minimum pathway L_{crit} that an electron has to travel to be able to excite an activator ion is $L_{crit} = E_{exc}/eF$, where E_{exc} is the energy needed for the excitation of the luminescence. Note that L_{crit} is dependent on the electric field strength. Incorporation of L_{crit} in Equation (6) yields Equation (7). In case of the excitation of luminescence through host–lattice states, the luminescence efficiency can be written very generally as Equation (8).

$$\eta = E_{em}/E_{exc}{}^*\sigma N^* L_{crit} \quad (7)$$

$$\eta = E_{em}/E_{exc}{}^*\eta_t{}^*\cdot\eta_{act}{}^*\cdot\eta_{esc} \quad (8)$$

In this expression η_t is the probability of energy transfer from the host lattice to the activator ions, η_{act} is the quantum efficiency of the activator, and finally η_{esc} is the escape probability, the ratio between the number of photons leaving the material and the number of photons generated in the material. By assuming η_{act} and η_{esc} to be unity, the maximum energy efficiency for the ACTFEL process is given by Equation (9).

$$\eta = E_{em}/E_{exc}{}^*\eta_t \quad (9)$$

Inspection of Equations (7) and (9) leads to the conclusion that N^*L_{crit} is the transfer efficiency. In the case of cathode ray excitation, this figure can be unity, as it is for efficient cathode ray phosphors. In the case of ZnS:Mn its optimal value is calculated to be about only 0.02. The low transfer efficiency of energy from the host lattice states to activator states is the main reason for the low energy efficiency of this material but still it is the most efficient one known!

The number of efficient ACTFEL materials known is rather small. In particular, an efficient blue emitting material is lacking, which is the reason that full color displays are not yet on the market. Recently, SrS:Cu has been presented as an efficient blue electroluminescent phosphor,[69] however, deposition as a thin film is a problem that has yet to be overcome. A general theory describing EL still needs to be developed, which is hampering a guided search for a blue emitter. The most important materials are summarized in Table 9. The EBU efficacy is the efficacy obtained after appropriate filtering to ensure that the emission spectrum complies with EBU standards.

Table 9. Overview of the most efficient EL phosphors.

Phosphor	Efficacy [lm W^{-1}]	EBU efficacy [lm W^{-1}]	Color
ZnS:Mn	5.0	1.1	red
ZnS:Tb	0.8	0.8 (no filter required)	green
SrS:Ce	1.6 [66]	0.07	blue
$CaGa_2S_4$:Ce	0.1 [67]	0.025	blue

From the figures in the table we can calculate, using a procedure not outlined here, a screen efficacy (for white light) of 0.44 lm W^{-1} for SrS:Ce as blue primary and 0.27 lm W^{-1} for the thiogallate as blue primary for electroluminescence displays complying with EBU standards with the three colour structure. Using the same procedure an efficacy of about 3 lm W^{-1} is calculated for CRTs (see Section 4.1).

In Table 10 efficacies are given for a white emitting SrS:Ce/ZnS:Mn multilayer after filtering to three primary colors, together with the resulting color coordinates. For green and blue, there are deviations from EBU (for green $0.28 < x < 0.315$ for $y = 0.61$, for blue $y < 0.072$ and $x > 0.143$). From these data, a screen efficacy of $0.18\ \mathrm{lm\,W^{-1}}$ is calculated for white light that results from additive mixing of the three primary colors.[68, 70, 71]

Table 10. Efficacy for the three primary colors obtained after filtering from a white emitting SrS:Ce/ZnS:Mn multilayer.

	Efficacy [lm W^{-1}]	CIE x-coordinate	CIE y-coordinate
no filter	2.0 [68]	0.39	0.48
red	0.11	0.65	0.34
green	0.26	0.20	0.61
blue	0.06	0.13	0.26

On judging the brightness figures for electroluminescence displays, however, one has to keep in mind that in electroluminescence displays contrast is higher than in CRTs with the same luminance as a result of the use of non-scattering thin films and color filters.

Electroluminescent Organic Materials

Activity in the field of organic EL increased dramatically in 1987 when C. W. Tang and coworkers presented an organic thin film device based on low molecular weight (LMW) materials. This device demonstrated for the first time that light can be generated efficiently by direct recombination of charge carriers in organic materials.[72] A typical organic LMW EL device structure is shown in Figure 15. A glass substrate is covered with a transparent conductor, in most cases indium tin oxide (ITO). In consecutive evaporation steps, a hole transport layer (HTL), optionally an emissive layer, an electron transport layer (ETL), and finally a cathode are stacked on each other. The chemical requirements on charge transport layers and the organic emitter are quite stringent. The materials have to be evaporable without decomposition, they must have a high glass transition temperature (T_g) to prevent crystallization at elevated temperatures, and they have to be extremely chemically stable. Hole transport materials are based on aromatic amines known for their low oxidation potential and high hole mobility.[73] In order to prevent crystallization the amine phenyl groups often carry sterically demanding substituents. A prominent representative that is extensively used as hole transport material in photocopy machines and laser printers is TPD (Figure 15).[72, 74] The most frequently used electron transport material is a complex of aluminum with 8-hydroxyquinoline (AlQ, Figure 15) because it has good morphological stability. This is important because usually very thin films of AlQ are applied to overcome the low electron mobility of the material. A device with only AlQ and a HTL already displays electroluminescence, however only with low efficiency. Stable organic fluorescent dyes doped in small amounts into the ETL (or sandwiched between the ETL and HTL) greatly enhance the electroluminescence efficiency and the device stability.[75] Similar to an inorganic phosphor, radiative transitions that follow energy transfer from the host to the dopant (see below) can be very effective when concentration quenching is avoided. Also, the choice of the fluorescent dye allows color tuning of the EL emission. Typical dopants are quinacridone (green), coumarin 6 (green), or rubrene (orange).[76] Blue EL has been achieved by perylene dopants in combination with a modified ETL;[77] in this context spiro compounds might be an interesting option as well.[78] Metals with a low working function such as Li, Ca, Mg, or alloys of them with Al or Ag are typically used as cathodes.[79]

The principle of EL in organic materials is explained in Figure 15.[80] A DC voltage, usually about 5 to 10 V is applied to the EL device between the ITO and metal cathode layer.

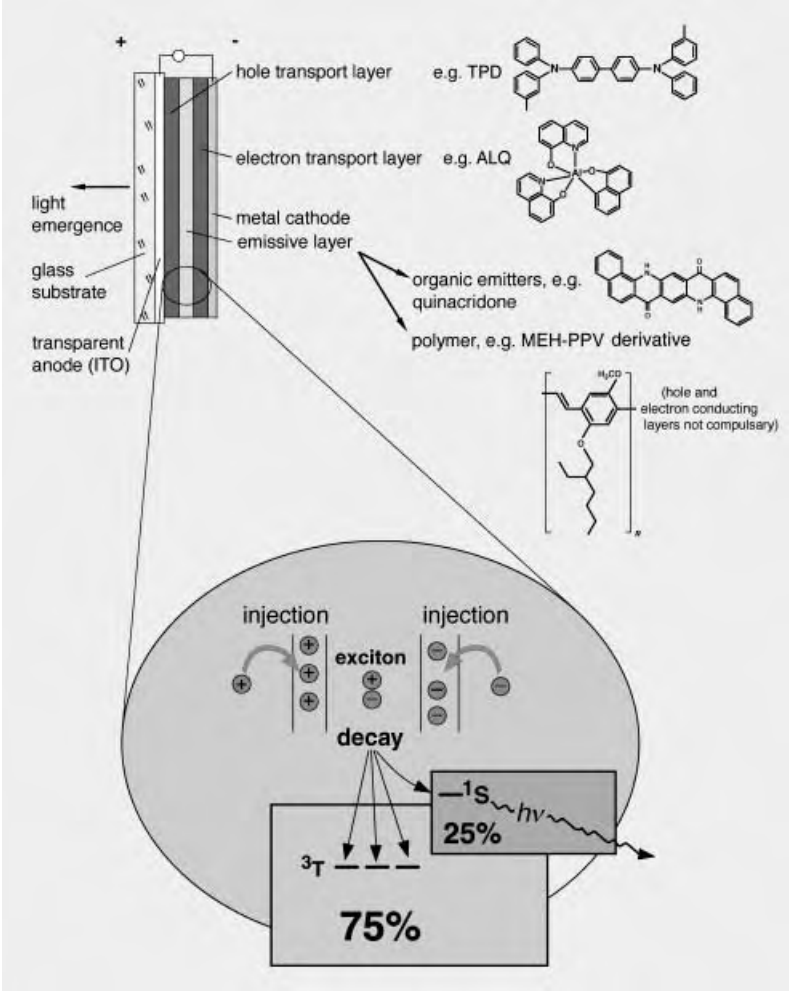


Figure 15. Top: Schematic diagram of an electroluminescent device showing the structural formulas of some commonly applied materials on the right. Bottom: Magnified illustration of the key processes of light generation in the device layers.

Positive charges are injected from the ITO into the HOMO of the HTL and electrons from the metal cathode into the LUMO of the ETL. For this step it is critical that the Fermi niveaus of the injecting layers and the accepting energy levels of the charge transport layers are adapted to each other in order to avoid injection barriers.[81] At the same time, the build-up of space charge has to be avoided, which is possible by applying ultra-thin films of the charge transport layers in the order of few thousand angstroms or less.[76] The HTLs are usually good electron blocking layers while the ETL can efficiently block positive charges. This means that the injected charges will be transported to the HTL–ETL interfacial region where the probability for recombination is maximized because of the potential barrier. Charge recombination leads to excitons, 25% of which have singlet and 75% triplet character on the basis of spin statistics.[82] In organic fluorescent dyes only the ^1S state of the fluorescent dye can be populated, which in principle consequently decays radiatively with the same quantum yield as measured for photoluminescence. The triplet excitons are lost in nonradiative transitions or even photochemical side reactions that can be potentially harmful for the device stability. This drawback of organic fluorescent dyes has triggered efforts to use rare-earth ions, such as Eu^{3+} or Tb^{3+} coordinated to organic ligands, as emitters in organic EL materials.[83] Here, the organic ligand acts as a sensitizer for the otherwise poorly absorbing rare-earth ion. In photoluminescence UV light is effectively absorbed by the organic ligand and leads to an excited singlet state. As a result of the close presence of the rare-earth metal ion intersystem crossing is effective in the compounds in which the ligand triplet state is populated. From there, the energy is efficiently transferred to the f levels of the lanthanide ion. In EL it appears likely that the ligand triplet levels can be populated directly after charge recombination. In theory, internal efficiencies of 100% should thus be possible. Another advantage of rare-earth organic EL materials is the color purity of the generated emission (see Section 2), that is pure green and pure red for Eu- and Tb-activated devices, respectively.

From the above discussion on device structure it can be concluded that stability is a serious issue in organic EL materials. First, the cathode is highly corrosive, which means that oxygen and water have to be strictly avoided during device assembly. Alloy compounds can provide some degree of stabilization, but the device handling should still be performed in a dry box under argon. Second, the distance of the cathode to the anode is in the order of some 100 nm, which means an electrical field strength in the order of $10^6\,V\,cm^{-1}$! Uneven substrates and impurities are a likely cause for short circuits. In industrial display development efforts concentrate on lowering the operation voltage and on sophisticated sealing techniques. A monochrome device basically consisting of TPD/AlQ doped with quinacridone has been realized with external efficiencies of up to 5% [84] and lifetimes of several thousand hours.

An alternative approach with a considerably simpler device structure is EL with polymer materials (PLEDs). Recently, certain polymers have been discovered that act at the same time as charge transport and emissive layer.[85] As shown in Figure 15, a typical PLED device consists of a polymer layer spin-coated or polymerized in-situ on a conducting substrate and an evaporated metal cathode. A variety of polymer materials has been synthesized spanning an EL color range from red to blue–green. The most prominent representative is poly(*p*-phenylenevinylene) PPV, and its derivatives, discovered by the group of R. H. Friend in 1990.[86] A challenge of this material class is purity, which is not as readily achieved as with LMW materials where the evaporation step means a purification step at the same time. Also, the photoluminescence quantum yield, usually indicative of EL efficiency, of EL polymers is still inferior to low molecular weight materials. However, polymer EL has advanced impressively within only six years and flexible displays[87] as well as polymer solid state lasers [88] are within the scope of the polymer EL community.

5. Summary and Outlook

The clever tricolor concept, introduced in fluorescent lamps almost 30 years ago, together with the unique properties of rare-earth metal ions has revolutionized the lighting market. Both efficiency and light quality have been improved considerably. As a rather impressive result of about 50 years of phosphor research the luminescent materials applied in today's lamps and displays operate close to their physical limits, and improvements will most likely not be of a principal nature. New applications such as plasma display panels, inorganic electroluminescence, field emission displays, or mercury-free fluorescent lamps can fall back upon already developed materials; however, the introduction of new phosphors still appears likely. The direct conversion of electrical power into light by semiconductor LEDs and organic electroluminescence, the latter still in a very early stage, might reshape dramatically light generation in lighting and display applications. Primary plasma generation efficiencies and the downward energy cascade limit classical phosphor-based light generation to about 50% maximum efficiency, while no principal limitations are foreseen for LEDs and organic electroluminescence. Although for these systems it is still a long way to go to compete with fluorescent lighting in price and efficiency, the already achieved performance with regard to lifetime and internal efficiency indicates clearly the future potential. Still indispensable for fine-tuning today's products and creating advanced products of tomorrow, classical phosphor development will likely give way to new, sophisticated forms of materials research. This work will be conducted increasingly under clean room conditions and many efforts will focus on thin film technologies. High-resolution full-color screens from laptop to home cinema size as well as much more efficient lighting sources than today's will be on the road ahead.

Abbreviations

ACTFEL	alternating current thin film electroluminescence
AlQ	aluminium-8-hydroxyquinolinate

CIE	Commission Internationale d'Eclairage
CRI	color rendering index
CRT	cathode ray tube
CVD	chemical vapor deposition
EBU	European Broadcasting Union
EL	electroluminescence
ETL	electron transport layer
FED	field emission display
FWHM	full width at half maximum
HTL	hole transport layer
ITO	indium tin oxide
LCD	liquid crystal display
LCP	luminance contrast performance
LE	lumen equivalent
LED	light emitting diode
MOCVD	metal-organic chemical vapor deposition
PALC	plasma addressed liquid crystal
PCE	photon cascade emission
PDP	plasma display panel
PLED	polymer light emitting diodes
PPV	poly(*p*-phenylenevinylene)
PTV	projection television
QE	quantum efficiency
TPD	triphenyldiamine
TV	television
VUV	vacuum ultraviolet

Received: December 15, 1997
Revised version: May 22, 1998 [A 264 IE]
German version: *Angew. Chem.* **1998**, *110*, 3250 – 3271

[1] G. Blasse, *J. Alloys Compd*. **1995**, *225*, 529.
[2] G. Blasse, B. C. Grabmeier, *Luminescent materials*, 1st ed., Springer, Berlin, **1994.**
[3] a) K. A. Franz, W. G. Kehr, A. Siggel, J. Wieczoreck, W. Adam in *Ullmanns Encyclopedia of Industrial Chemistry*, *Vol A15*, VCH, Weinheim, **1990**, p. 519; b) T. Welker, *J. Lumin.* **1991**, *48/49*, 49; c) G. Blasse, *J. Alloys Compd*. **1993**, *192*, 17; d) C. R. Ronda, *J. Alloys Compd*. **1995**, *225*, 534; e) C. R. Ronda, *J. Lumin.* **1997**, *72 – 74*, 49; f) C. R. Ronda, T. Jüstel, H. Nikol, *J. Alloys. Compd.*, in press.
[4] C. R. Ronda in *Spectroscopy and Dynamics of Collective Excitations in Solids*, *Vol 356*, Plenum, New York, **1997,** p. 339.
[5] M. Bredol, U. Kynast, C. Ronda, *Adv. Mater*. **1991**, *3*, 361.
[6] M. Bredol, U. Kynast, C. Ronda, *Chem. Unserer Zeit* **1994**, *28*, 36.
[7] *Advances in Sonochemistry*, *Vol 1 – 5* (Ed.: J. Mason), Jai Press, London, **1990 – 1998**.
[8] B. Smets in *Advances in Nonradiative Processes and Solids*, *Vol. 249* (Eds.: B. Di Bartolo, X. Chen), Plenum, New York, **1991**, p. 380.
[9] K. H. Butler, *Fluorescent Lamp Phosphors*, The Pennsylvania State University Press, University Park, PA, **1980**.
[10] W. J. van den Hoek, A. G. Jack in *Ullmanns Encyclopedia of Industrial Chemistry*, *Vol A15*, VCH, Weinheim, **1990**, p. 115.
[11] C. Meyer, H. Nienhuis, *Discharge Lamps*, Kluwer, Deventer, **1988**.
[12] L. Thorington, *J. Opt. Soc. Am.* **1950**, *40*, 579.
[13] a) A. H. McKeag, P. W. Ranby (General Electric Company), GB-B 578.192, **1942**; b) H. G. Jenkins, A. H. McKeag, P. W. Ranby, *J. Electrochem. Soc.* **1949**, *96*, 1.
[14] a) W. A. Thornton, *J. Opt. Soc. Am.* **1971**, *61*, 1155; b) M. Koedam, J. J. Opstelten, *Light. Res. Technol.* **1971**, *3*, 205; c) J. M. P. J. Verstegen, D. Radielovic, L. E. Vrenken, *J. Electrochem. Soc.* **1974**, *121*, 1627.
[15] a) D. van der Voort, G. Blasse, *Chem. Mater*. **1991**, *3*, 1041; b) A. Bril, W. L. Wanmaker, *J. Electrochem. Soc*. **1964**, *111*, 1363; c) G. Blasse, A. Bril, W. C. Nieuwpoort, *J. Phys. Chem. Solids* **1966**, *27*, 1587; d) G. Blasse, A. Bril, *Philips Res. Repts.* **1967**, *22*, 46.
[16] a) W. M. P. van Kemenade, H. C. G. Verhaar, *J. Mater. Chem. Phys.* **1992**, *31*, 213; b) R. Chapoulie, S. Dubernet, M. Schvoerer, *J. Mater. Chem. Phys.* **1991**, *30*, 47.
[17] F. Wen-Tian, C. Fouassier, P. Hagenmuller, *Mater. Res. Bull*. **1987**, *22*, 899.
[18] R. Jagannathan, *J. Lumin.* **1996**, *68*, 211.
[19] J. Alarcon, D. van der Voort, G. Blasse, *Mater. Res. Bull*. **1992**, *27*, 467.
[20] X.-D. Sun, C. Gao, J. Wang, X.-D. Xiang, *Appl. Phys. Lett*. **1997**, *70*, 3353.
[21] E. Danielson, J. H. Golden, E. W. McFarland, C. M. Reaves, W. H. Weinberg, X. D. Wu, *Nature* **1997**, *389*, 944.
[22] a) T. Arakawa, T. Takata, G.-Y. Adachi, J. Shiokawa, *J. Lumin.* **1979**, *20*, 325; b) O. A. Serra, E. J. Nassar, G. Zapparolli, I. L. V. Rosa, *J. Alloys. Compd*. **1995**, *225*, 63; c) S. B. Hong, J. S. Seo, C.-H. Pyun, C.-H. Kim, Y. S. Uh, *Catal. Lett*. **1995**, *30*, 87; d) G. Blasse, G. J. Dirksen, M. E. Brenchley, M. T. Weller, *Chem. Phys. Lett*. **1995**, *234*, 177.
[23] a) C. Borgmann, J. Sauer, T. Jüstel, F. Schüth, U. Kynast, unpublished results; b) C. Borgmann, T. Jüstel, F. Schüth (Philips N.V.), EP-B 972016653, **1997**.
[24] F. J. Avella, O. J. Sovers, C. S. Wiggins, *J. Electrochem. Soc.* **1967**, *114*, 613.
[25] T. Jüstel, C. Ronda (Philips N.V.), EP-B 96202416.2, **1996**.
[26] G. Blasse, M. Saakes, M. Leskela, *Mater. Res. Bull*. **1984**, *19*, 83.
[27] M. V. Hoffmann, *J. Illum. Eng. Soc*. **1977**, *17*, 89.
[28] a) M. Ouwerkerk, D. M. de Leeuw, C. A. Mutsaers, G. P. J. Geelen (Philips N.V.), EP-B 0550937 A2, **1993**; b) G. H. van der Linden, A. J. de Ridder, B. M. Smets (Philips N.V.) EP-B 0552513A1**, 1993**.
[29] E. C. Malarkey, M. R. Natale, J. W. Ogland (Westinghouse Electric Corporation), US-A 3,766,084, **1973**.
[30] R. Doeckel, F. A. S. Ligthart (Philips N.V.), DE-B 3544800 A1, **1987**.
[31] A. R. Young, *Eur. J. Dermatol*. **1996**, *6*, 225.
[32] L. Endres (Patent-Treuhand-Gesellschaft für elektrische Glühlampen mbH), DE-B 3729711 A1, **1989**.
[33] P. J. M. Willemsen, R. C. Peters, W. L. Konijndijk (Philips N.V.), DE-B 3024438 A1,**1981**.
[34] D. E. Harrison, *J. Electrochem. Soc*. **1960**, *107*, 210.
[35] S. Sakka, *Struct. Bonding (Berlin)* **1996**, *85*, 3.
[36] W. S. Rees, *CVD of Nonmetals*, Wiley-VCH, Weinheim, **1996**.
[37] C. R. Ronda, *Proc. 2nd Int. Display Workshops* (Hamamatsu, Japan) **1995**, 69.
[38] F. Vollkommer, L. Hitzschke (Patent-Treuhand-Gesellschaft für elektrische Glühlampen mbH), WO-A 94/23442, **1994**.
[39] a) W. W. Piper, J. A. DeLuca, F. S. Ham, *J. Lumin.* **1974**, *8*, 344; b) J. L. Sommerdijik, A. Bril, A. W. de Jager, *J. Lumin.* **1974**, *8*, 341.
[40] A. M. Srivastava, W. W. Beers, *J. Lumin.* **1997**, *71*, 285.
[41] A. M. Srivastava, D. A. Doughty, W. W. Beers, *J. Electrochem. Soc.* **1997**, *144*, L190.
[42] A. M. Srivastava, D. A. Doughty, W. W. Beers, *J. Electrochem. Soc.* **1996**, *143*, 4113.
[43] R. T. Wegh, H. Donker, A. Meijerink, *Abstr. Pap. 192. Meeting of the Electrochemical Society* (Paris) **1997**, p. 1766.
[44] a) S. Nakamura, G. Fasol, *The Blue Laser Diode*, Springer, Berlin, **1997**. b) S. Nakamura, *MRS Bulletin* **1997**, 29.
[45] a) A. Dodabalapur, *Solid State Commun.* **1997**, *102*, 259; b) W. Gebhardt, B. Hahn, H. Stanzl, M. Deufel, *J. Cryst. Growth* **1996**, *159*, 238; c) T. Matsuoka, *Adv. Mater.* **1996**, *8*, 469; d) S. Strite, in *Advances in Solid State*, *Festkörperprobleme Series* (Ed.: H-J. Queisser), Springer, Berlin, **1994**.
[46] Regularly updated news on GaN based LEDs and lasers can be found in the online *MRS Internet Journal of Nitride Semiconductor Research* under http://nsr.mij.mrs.org/.
[47] P. Schlotter, R. Schmidt, J. Schneider, *Appl. Phys.* **1997**, *A64*, 417.
[48] F. Hide, P. Kozodoy, S. P. Denbaars, A. J. Heeger, *Appl. Phys. Lett.* **1997**, *70*, 2664.
[49] V. Balzani, F. Scandola, *Supramolecular Chemistry*, Ellis Horwood, New York, **1991**.
[50] Y. Sato, N. Takahashi, S. Sato, *Jpn. J. Appl. Phys.* **1996**, *35*, L838.
[51] H. Boerner, T. Jüstel, H. Nikol, C. Ronda (Philips N.V.) DE-B 19708407.9, **1997**.
[52] T. Hase, T. Kano, E. Nakazawa, H. Yamamoto, *Adv. Electron. Electron Phys.* **1990**, *79*, 271.

[53] a) S. Shionoya in *Luminescence of Inorganic Solids* (Ed.: P. Goldberg), Academic Press, London, **1966**, p. 205; b) K. Era, S. Shionoya, Y. Washizawa, *J. Phys. Chem. Solids* **1968**, *29*, 1827; c) K. Era, S. Shionoya, Y. Washizawa, H. Ohmatsu, *J. Phys. Chem. Solids*. **1968**, *29*, 1843.

[54] H. Yamamoto, H. Matsukiyo, *J. Lumin.* **1991**, *48/49*, 43.

[55] a) C. R. Ronda, H. Bechtel, U. Kynast, T. Welker, *J. Appl. Phys.* **1994**, *75*, 4631; b) T. Welker, C. R. Ronda, K. J. B. M. Nieuwesteeg, *J. Electrochem. Soc.* **1991**, *138*, 602; c) C. R. Ronda, H. Bechtel, U. Kynast, T. Welker, *Eur. J. Solid State Inorg. Chem.* **1991**, *28* (suppl.), 545.

[56] P. C. Candry, *Proc. 15th Int. Display Res. Conf.* (Hamamatsu, Japan) **1995**, 75.

[57] a) M. Schadt, *Ann. R. Mater.* **1997**, *27*, 305; b) H. Katoh, *Proc. 15th Int. Display Res. Conf.* (Hamamatsu, Japan) **1995**, 689; c) for updated information see *Stanford Resources*, *Inc.* under http://www.webcom.-com/sr/main/homepage.html.

[58] H. Bechtel, W. Czarnojan, M. Haase, W. Mayr, H. Nikol, *Philips J. Res.* **1996**, *50*, 433.

[59] S. Itoh, T. Kimizuka, T. Tonegawa, *J. Electrochem. Soc.* **1989**, *136*, 1819.

[60] S. Itoh, T. Wanatabe, T. Yamaura, K. Yano, *Proc. 15th Int. Display Res. Conf.* (Hamamatsu, Japan) **1995**, 617.

[61] B. E. Gnade, *Abstr. Pap. 3rd Int. Conf. Sci. Technol. Display Phosphors* (Huntington Beach) **1997**, 1.

[62] E. Yamaguchi, K. Sakai, I. Nomura, T. Ono, M. Yamanobe, N. Abe, T. Hara, K. Hatanaka, Y. Osada, H. Yamamoto, T. Nakagiri, *J. SID* **1997**, *5/4*, 345.

[63] L. F. Weber, *Proc. 15th Int. Display Res. Conf.* (Hamamatsu, Japan) **1995**, 373.

[64] J. Koike, *Abstr. Pap. 3rd Int. Conf. Sci. Technol. Display Phosphors* (Huntington Beach) **1997**, 13.

[65] C. R. Ronda, T. Amrein, *J. Lumin.* **1996**, *69*, 245.

[66] C. Barthou, J. Benoit, P. Benalloul, A. Morell, *J. Electrochem. Soc.* **1994**, *141*, 524.

[67] a) Y. A. Ono, *Electroluminescent Displays*, World Scientific, Singapore, **1995**; b) A. Pakkala, *ITG-Fachbericht Display and Vacuum Electronics*, VDE, Berlin, **1998**, p. 85.

[68] a) R. H. Mauch, K. O. Velthaus, B. Hüttl, U. Troppenz, R. Herrmann, *SID'95 Int. Symp. Digest Technical Papers* (Orlando) **1995**, 720. b) K.-O. Velthaus, *ITG-Fachbericht Display and Vacuum Electronics*, VDE, Berlin, **1998**, p. 93.

[69] W. Park, T. C. Jones, W. Tong, B. K. Wagner, C. J. Summers, *Abstr. Pap. 3rd Int. Conf. Sci. Technol. Display Phosphors* (Huntington Beach) **1997**, 57.

[70] W. A. Barrow, R. C. Coovert, E. Dickey, C. N. King, C. Laakso, S. S. Sun, R. T. Tuenge. R. Wentross, J. Kane, *SID'93*, *Digest of Technical Papers* (Seattle) **1993**, 761.

[71] K. O. Velthaus, B. Hüttl, U. Troppenz, R. Herrmann, R. H. Mauch, *SID'97 Int. Symp. Digest Technical Papers* (Boston) **1997**, 411.

[72] C. W. Tang, S. A. Van Slyke, *Appl. Phys. Lett.* **1987**, *51*, 913.

[73] P. M. Borsenberger, J. J. Fitzgerald, *J. Phys. Chem.* **1993**, *97*, 4815.

[74] C. Adachi, S. Tokito, T. Tsutsui, S. Saito, *Jpn. J. Appl. Phys.* **1988**, *27*, L269.

[75] C. W. Tang, S. A. Van Slyke, C. H. Chen, *J. Appl. Phys.* **1989**, *65*, 3610.

[76] C. W. Tang, *J. SID* **1997**, *5/1*, 11.

[77] S. A. Van Slyke, P. S. Bryan, C. W. Tang in *Inorganic and organic electroluminescence/ EL 96 Berlin* (Eds.: R. H. Mauch, H.-E. Gumlich), W&T, Berlin, **1996**, p. 195.

[78] J. Salbeck in *Inorganic and organic electroluminescence/ EL 96 Berlin* (Eds.: R. H. Mauch, H.-E. Gumlich), W&T, Berlin, **1996**, p. 243.

[79] a) S. Saito, T. Tsutsui, M. Era, *Mol. Cryst. Liq. Cryst. Sci. Technol. Sect. A* **1994**, *253*, 417; b) T. Wakimoto, S. Kawami, K. Nayama, *Tech. Dig. Int. Symp. Inorg. Org. Electrolumin.* **1994**, 77.

[80] J. Schöbel, A. Böhler, S. Dirr, H.-H. Johannes, A. Rückmann, P. Urbach, S. Wiese, W. Kowalsky, *ITG-Fachbericht Display and Vacuum Electronics*, VDE, Berlin, **1998**, 99.

[81] M. Deußen, H. Bässler, *Chem. Unserer Zeit* **1997**, *31*, 76.

[82] M. Pope, C. E. Swenberg, *Electronic Processes in Organic Crystals*, Clarendon, Oxford, **1982**.

[83] a) J. Kido, W. Ikeda, M. Kimura, K. Nai, *Jpn. J. Appl. Phys.* **1996**, *35*, L394; b) J. Kido, H. Hayase, K. Hongawa, K. Nai, K. Okuyama, *Appl. Phys. Lett.* **1994**, *65*, 2124; c) J. Kido, K. Nai, Y. Okamoto, T. Skotheim, *Chem. Lett*. **1991**, 1267; d) J. Kido, K. Nagai, Y. Ohashi, *Chem. Lett*. **1990**, 657; e) H. Boerner, U. Kynast, W. Busselt, M. Haase (Philips N.V.) DE-B P4428450.0, **1994**; f) H. Boerner, W. Busselt, T. Jüstel, H. Nikol (Philips N.V.), DE-B 19726472.7, **1997**.

[84] Organic EL external quantum efficiency η is defined as $\eta = \eta$(charge recombination) $\times\ \eta$(energy transfer) $\times\ \Phi$(phosphor) $\times\ \eta$(light outcoupling); maximal values (approximation) are: 0.25 (only singlet exciton energy transfer) $\times\ 1 \times 1 \times 0.2$ (light guiding within the glass substrate).

[85] a) A. Kraft, A. C. Grimsdale, A. B. Holmes, *Angew. Chem.* **1998**, *110*, 416; *Angew. Chem. Int. Ed.* **1998**, *37*, 402; b) N. Yu, H. Schenk, H. Spreitzer, W. Kreuder, H. Becker, *ITG-Fachbericht Display and Vacuum Electronics*, VDE-Verlag GMBH, Berlin, **1998**, 79.

[86] J. H. Burroughes, D. D. C. Bradley, A. R. Brown, R. N. Marks, K. Mackay, R. H. Friend, P. L. Burn, A. B. Holmes, *Nature* **1990**, *347*, 539.

[87] See for example: D. Braun, A. R. Brown, E. Staring, E. W. Meijer, *Synth. Met*. **1994**, *65*, 85.

[88] N. Tessler, G. J. Denton, R. H. Friend, *Nature* **1996**, *382*, 695.

Directed Evolution of Enzymes

Uwe T. Bornscheuer*

Enzymes find increasing applications in organic synthesis.[1] Their high chemo-, regio-, and stereoselectivity under mild reaction conditions, combined with a steady increase in their commercial availability at acceptable prices, make biocatalysts an attractive alternative to chemical catalysts.

In nature, evolution has ensured a steady adaption of the organism and of the proteins involved in their biological function over billions of years. However, enzymes isolated from natural sources do not always fulfill the requirements of an efficient organic synthesis. For the targeted improvement of enzyme properties—such as activity, thermo- and solvent stability, and regio- or stereoselectivity—protein design is increasingly used. Several groups recently described directed evolution as a new and very elegant combinatorial approach for this purpose (Figure 1).[2]

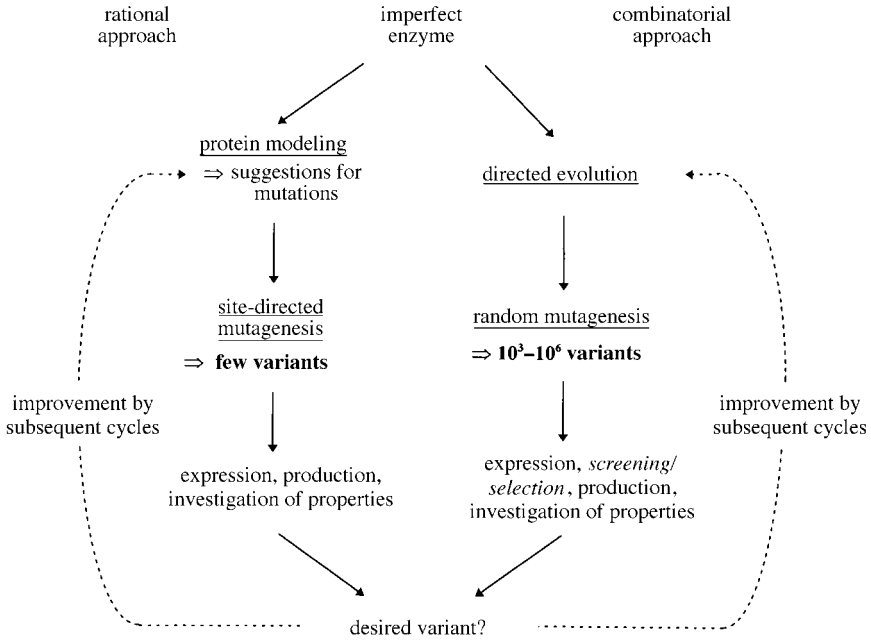


Figure 1. Comparison of the rational and the combinatorial approach for the mutagenesis of enzymes.

This method is based on the creation of enzyme libraries using modern techniques of molecular biology, which in combination with an efficient assay system allow the identification of improved biocatalysts. In contrast to the already employed rational approach of site-directed mutagenesis (Figure 1), no structural data of the enzyme and no knowledge of the relationship between amino acid sequence, structure, and mechanism of catalysis is required. Furthermore, site-directed mutagenesis is a time- and information-intensive method which allows the production of relatively few enzyme variants within reasonable lengths of time.

Prerequisites for a successful directed evolution are an effective mutation strategy for the improvement of the enzymes, the functional expression of the protein in a suitable microbial host, and a fast and reliable assay system for the identification of enzyme variants with desired properties out of a pool of 10^4 to more than 10^6 variants (Figure 1).[2c]

Two different strategies for the generation of improved enzyme variants, which are also named asexual and sexual evolution,[2d] have been described in the literature (Figure 2). In an asexual evolution, random mutagenesis is targeted preferentially towards the gene encoding one parent protein. An enzyme library is generated and then screened for improved properties. The best enzymes identified in the first generation can than be further optimized in subsequent cycles. However, this implies a step-by-step improvement of variants from the first generation by introduction of new and deletion of negative mutations (Figure 3).

In contrast, sexual evolution starts from a pool of homologous parent genes. These can originate from an asexual evolution, from related natural sequences, or from enzyme variants generated by rational design. The principle of this DNA or gene shuffling[3] is based on a partial DNase-I digestion of the gene followed by a recombination of fragments by a polymerase chain reaction (PCR). Again, an accumulation of positive and an elimination of negative

[*] Dr. U. T. Bornscheuer
Institut für Technische Biochemie der Universität
Allmandring 31, D-70569 Stuttgart (Germany)
Fax: (+49) 711-6853196
E-mail: itbubo@po.uni-stuttgart.de

 © WILEY-VCH Verlag GmbH, D-69451 Weinheim, 1998 1433-7851/98/3722-3105 $ 17.50+.50/0

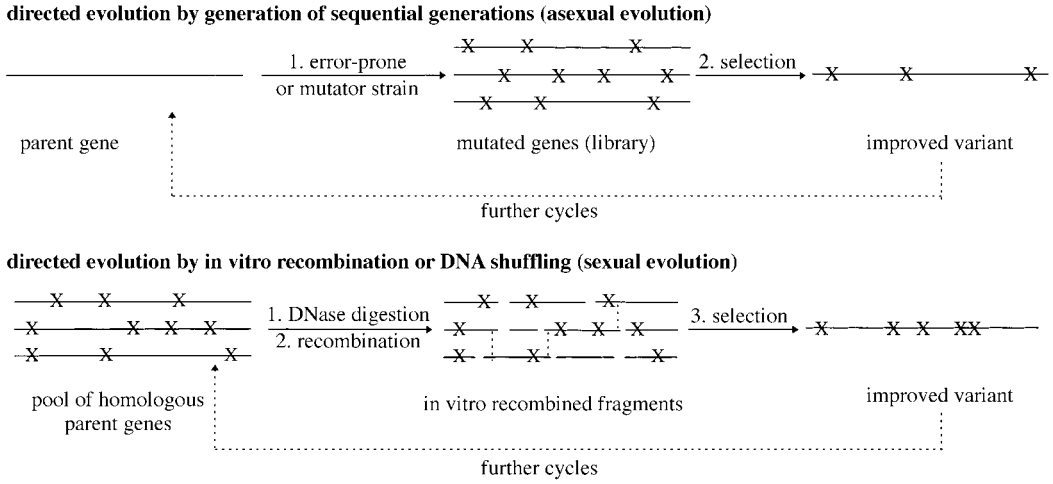


Figure 2. Methods for the directed evolution of enzymes. The asexual evolution of a starting gene through, for example, error-prone PCR or application of mutator strains introduces point mutations. The resulting enzyme library is then screened for improved enzyme variants. For sexual evolution, a pool of homologous genes is partially digested by DNAse-I and recombined by PCR in vitro to a library of enzyme variants differing in their mutation pattern. (Taken from ref. [2d, 3a] with modifications.)

mutations is desired (Figures 2 and 3). Disadvantages are that the homologous genes are not always available, the DNase digestion for the generation of fragments of suitable size is difficult to control, and there are problems with ligation efficiency during PCR. A further, recently described strategy for in vitro mutagenesis and recombination is based on a modified PCR protocol only. This staggered extension process (StEP) method allows the production of full-length genes which carry different sequence information. Beside the use of homologous parent genes, particularly short reaction times and the use of different templates during PCR are the basis of this StEP method.[4]

Probably the most important method for asexual evolution is the error-prone PCR.[5] When nonoptimal reaction conditions are used during PCR, the error rate, for example, for *Thermus aquaticus* (*Taq*) polymerase can be increased from 0.001 – 0.02 % under standard conditions to more than 1 % (Figure 2).[5b] This in vitro method is easy to perform, can be limited to the nucleotide sequence encoding the protein of interest and even shorter parts, and allows adjustment of the mutation rate. Disadvantages are the nonstatistical exchange of nucleotides and an often-observed low ligation efficiency during PCR. For the latter problem, modified PCR protocols have been developed.[5c, 6]

Alternatively, mutator strains with defects in their DNA-repair mechanisms can be used, which leads to the introduction of mutations during replication. The sequence which is subjected to mutations can be limited by locating the gene encoding the protein of interest on plasmids. The application of mutator strains which are, for example, commercially available as *Escherichia coli* variant *Epicurian coli* XL1-Red[7] (Stratagene, La Jolla, USA) is simpler than error-prone PCR, but the mutation rate cannot be adjusted. Furthermore, owing to a mutation of the entire plasmid—for example, in the promotor region—defects but also improvements can occur. Thus, while researchers can chose from a variety of methods to generate enzyme variants, it is still unclear which method is the best.

The number of enzyme variants which can be generated by directed evolution grows exponentially with the size of the enzymes and the number of simultaneously exchanged amino acids. Even for a small protein of 200 amino acids more than nine billion possible variants can theoretically be generated simply by introducing three substitutions at the same time.[2c] These cannot be analyzed with common tedious and time-consuming methods such as HPLC or gas chromatography. Therefore, according to the first law for directed mutagenesis proposed by F. Arnold, "you only get what you screen for", an efficient screening system is of extreme importance.[8] A selection can be based, for instance, on altered antibiotic resistance[9] or growth on media lacking components essential for growth.[10] Problems related to organic synthesis require assay systems which provide direct information about the enzyme properties. For example, the identification of a lipase variant with improved stereoselectivity is possible by measuring the ratio of the rates of hydrolysis of enantiomerically pure (*R*)- or (*S*)-*p*-nitrophenol esters.[11] Also fluorescence correlation spectroscopy[12] might allow the rapid identification of active enzyme variants in a library, because the change in fluorescence during the reaction can be followed for single molecules.

Often the enzyme library producing colonies cannot be assayed directly because the enzymes are, for example, produced intracellulary and a cell lysis is necessary. Additional prerequisites for the detection of all variants are correct processing and folding to ensure the production of active enzymes. Furthermore, all enzyme variants should exhibit high stability and activity under assay conditions.

The directed evolution of enzymes is a new area which is especially dominated by biochemistry. This might explain why so far only a few examples deal with the solution of problems related to organic chemistry. Some of them are presented at the end of this article. However, also for other problems, especially for the technical application of biocatalysts, directed evolution represents an attractive alternative to existing methods for protein design. For instance, enzyme often do not

 © WILEY-VCH Verlag GmbH, D-69451 Weinheim, 1998 1433-7851/98/3722-3106 $ 17.50+.50/0

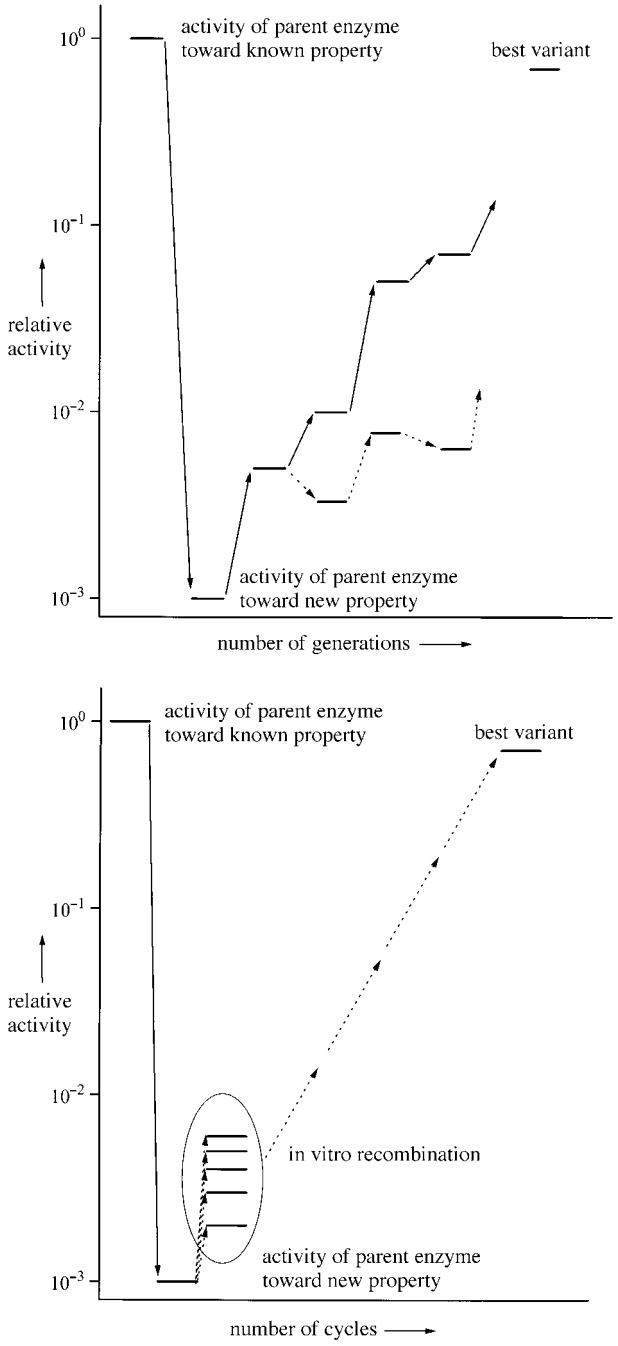


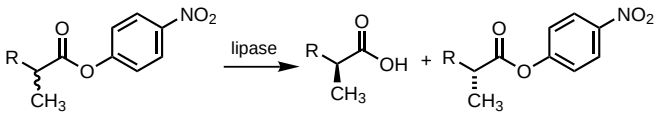
Figure 3. Strategies for improving a wild-type enzyme by production of sequential generations from one parent gene (asexual evolution, top) or by in-vitro recombination through DNA shuffling (sexual evolution, bottom). During asexual evolution a successive improvement (solid arrows) as well as a worsening (dashed arrows) can occur in higher generations. For sexual evolution, a pool of homologous variants from several parent genes (circle) is necessary before an in vitro recombination can be performed. (Taken from ref. [8] with modifications.)

exhibit sufficient stability under process conditions with respect to pH profile, temperature-dependent activity, and stability, and are not active in all solvents. These deficits are extremely difficult to overcome by site-directed mutagenesis. Here, directed evolution can contribute to the fast generation and identification of improved enzymes.

DNA shuffling as a method for sexual evolution led to the generation of a variant of the green-fluorescent protein (GFP) with a 45-fold increase in fluorescence.[13] The recombination of almost identical cephalosporinase genes by DNA shuffling increased the moxalactam resistance by a factor of 540.[9] In the case of cefotaxime resistance even a 16000 times greater resistance of a β-lactamase gene in *E. coli* could be achieved after three cycles of sexual evolution.[3b] The half-life of the protease subtilisin E at 65 °C was increased by 50 times through recombination of two subtilisin E variants by the StEP method.[4] A growth assay was used in the generation of a monomeric chorismate mutase (CM).[10b] This naturally dimeric enzyme catalyzes the conversion of chorismate into prephenate in the biosynthesis of L-tyrosine (L-Tyr) and L-phenylalanine (L-Phe). A combination of directed evolution with selection of variants on a media lacking L-Tyr and L-Phe allowed the identification of a 100-fold more active monomeric CM variant. This provided insight into the influence of the topology on structure, stability, and function of this protein. The generation of new antibiotics and other pharmacologically active substances should be possible through directed evolution of polyketide synthases (PKS). A number of PKS genes has been cloned already, and application of the methods described here for direction evolution has been proposed.[14] Further examples have been described in more detail in a number of recent reviews.[2]

For organic synthesis, the alteration of stereoselectivity and substrate specificity can be considered as being most important. Directed evolution might give access to a large number of optically pure compounds which are not or only insufficiently converted by wild-type enzymes.

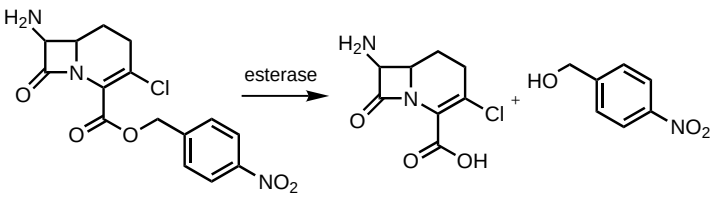
Based on the stereoselective photometrical assay with *p*-nitrophenol esters, the enantioselectivity of a lipase from *Pseudomonas aeruginosa* PAO1 for hydrolysis of racemic 2-methyl decanoate could be increased from 2% *ee* (wild-type) to 81% *ee* (variant) by error-prone PCR (Scheme 1).[11] A directed evolution of an esterase from



Scheme 1. Improvement of the stereoselectivity of a lipase from *Pseudomonas aeroginosa* PAO1 from 2% *ee* to 81% *ee* for hydrolysis of racemic 2-methyl decanoate by error-prone PCR.[11]

Pseudomonas fluorescens (PFE) with the mutator strain *Epicurian coli* XL1-Red produced a double mutant of this enzyme, which catalyzed the hydrolysis of a sterically hindered 3-hydroxy ester at a moderate rate and with moderate stereoselectivity.[10a] The 3-hydroxy ester can be used as a precursor in the synthesis of epothilones, and was not cleaved by 20 hydrolases including wild-type PFE. The screening of an esterase library was based on a combination of an indicator assay and a growth assay.[10a] A combination of error-prone PCR and DNA shuffling led to the generation of a more stable and active variant of an esterase from *Bacillus subtilis*.[15] This enzyme hydrolyzes the *p*-nitrobenzyl ester of loracarbef, a cephalosporin antibiotic, with 150 times higher activity compared to the wild-type enzyme in 15% dimethylformamide (Scheme 2).[8]

 © WILEY-VCH Verlag GmbH, D-69451 Weinheim, 1998 1433-7851/98/3722-3107 $ 17.50+.50/0



Scheme 2. A combination of error-prone PCR and DNA shuffling led to a variant of an esterase from *Bacillus subtilis* which exhibits 150-fold higher activity in 15% DMF compared to the wild-type enzyme for cleavage of the *p*-nitrobenzyl ester of loracarbef. For practical reasons, the assay was based on the hydrolysis of *p*-nitrophenol esters.[8, 15]

Despite the methods developed so far and the successful examples given above, several problems have to be solved to allow a broader application of directed evolution. This includes the further optimization of methods for the generation of mutations and enzyme libraries, and the development of molecular techniques which allow the use of directed evolution for other microbial expression systems. Of upmost importance are highly efficient assay systems, without which the generation of enzyme libraries does not make much sense. Here, equipment and protocols already developed for high-throughput screening in combinatorial chemistry might be used and optimized to allow the quick screening of large enzyme libraries. This might be achieved, for example, by the use of fusions proteins based on the easy detectable green-fluorescent protein.[16]

In general, directed evolution represents a promising extension to methods existing so far for protein design. It can be expected that it will largely contribute to the development of new or improved biocatalysts, but might also allow a better understanding of structure–activity relationships. Directed evolution might even become a biotechnological equivalent of combinatorial chemistry.

German version: *Angew. Chem.* **1998**, *110*, 3284–3288

Keywords: enzyme catalysis · molecular evolution · mutagenesis

[1] a) *Enzyme Catalysis in Organic Synthesis, Vol. 1 and 2* (Eds.: K. Drauz, H. Waldmann), 1. ed., VCH, Weinheim, **1995**; b) K. Faber, *Biotransformations in Organic Chemistry*, 3. ed., Springer, Berlin, **1997**; c) H. G. Davies, R. H. Green, D. R. Kelly, S. M. Roberts, *Biotransformations in Preparative Organic Chemistry: The Use of Isolated Enzymes and Whole Cell Systems in Synthesis*, 1. ed., Academic Press, London, **1989**; d) C.-H. Wong, G. M. Whitesides, *Enzymes in Synthetic Organic Chemistry*, 1. ed., Pergamon, Oxford, **1994**; e) *Biotechnology, Vol. 8: Biotransformations* (Eds.: H. J. Rehm, G. Reed, A. Pühler, P. J. W. Stadler), VCH, Weinheim, **1998**.

[2] a) W. P. C. Stemmer, *Bio/Technology* **1995**, *13*, 549–553; b) G. F. Joyce, *Sci. Am.* **1992**, *267*(6), 48–55; c) O. Kuchner, F. H. Arnold, *Trends Biotechnol.* **1997**, *15*, 523–530; d) F. H. Arnold, *Acc. Chem. Res.* **1998**, *31*, 125–131; e) A. Schwienhorst, *Biospektrum* **1998**, *4*, 44–47; f) S. Harayama, *Trends Biotechnol.* **1998**, *16*, 76–82.

[3] a) W. P. C. Stemmer, *Proc. Natl. Acad. Sci. USA* **1994**, *91*, 10747–10751; b) W. P. C. Stemmer, *Nature* **1994**, *370*, 389–391.

[4] H. Zhao, L. Giver, J. A. Affholter, F. H. Arnold, *Nature Biotechnol.* **1998**, *16*, 258–261.

[5] a) D. W. Leung, E. Chen, D. V. Goeddel, *Technique (Philadelphia)* **1989**, *1*, 11–15; b) R. C. Cadwell, G. F. Joyce, *PCR Meth. Appl.* **1992**, *2*, 28–33; c) J. H. Spee, W. M. de Vos, O. P. Kuipers, *Nucleic Acids Res.* **1993**, *21*, 777–778.

[6] J.-P. Vartanian, M. Henry, S. Wain-Hobson, *Nucleic Acids Res.* **1996**, *24*, 2627–2631.

[7] A. Greener, M. Callahan, B. Jerpseth, *Methods Mol. Biol.* **1996**, *57*, 375–385.

[8] F. H. Arnold, J. C. Moore, *Adv. Biochem. Eng. Biotechnol.* **1997**, *58*, 1–14.

[9] A. Crameri, S.-A. Raillard, E. Bermudez, W. P. C. Stemmer, *Nature* **1998**, *391*, 288–290.

[10] a) U. T. Bornscheuer, J. Altenbuchner, H. H. Meyer, *Biotechnol. Bioeng.* **1998**, *58*, 554–559; b) G. MacBeath, P. Kast, D. Hilvert, *Science* **1998**, *279*, 1958–1961.

[11] M. T. Reetz, A. Zonta, K. Schimossek, K. Liebeton, K.-E. Jaeger, *Angew. Chem.* **1997**, *109*, 2961–2963; *Angew. Chem. Int. Ed. Engl.* **1997**, *36*, 2830–2832.

[12] M. Eigen, R. Rigler, *Proc. Natl. Acad. Sci. USA* **1994**, *91*, 5740–5747.

[13] A. Crameri, E. A. Whitehorn, E. Tate, W. P. C. Stemmer, *Nature Biotechnol.* **1996**, *14*, 315–319.

[14] C. Khosla, R. Caren, C. M. Kao, R. McDaniel, S.-W. Wang, *Biotechnol. Bioeng.* **1996**, *52*, 122–128.

[15] J. C. Moore, F. H. Arnold, *Nature Biotechnol.* **1996**, *14*, 458–467.

[16] M. M. Enzelberger, F. Zocher, C. Schmidt-Dannert, U. T. Bornscheuer, R. D. Schmid, B. Hauer, H. Eipel, *BIOforum* **1998**, *4*, 192–194.

 © WILEY-VCH Verlag GmbH, D-69451 Weinheim, 1998 1433-7851/98/3722-3108 $ 17.50+.50/0

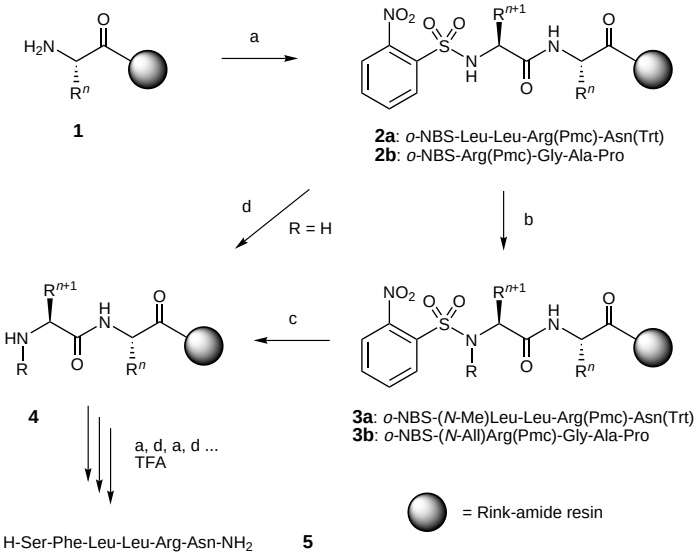
New Protecting Group Strategies for the Solid-Phase Synthesis and Modification of Peptides, Oligonucleotides, and Oligosaccharides

Oliver Seitz*

Merrifield's pioneering invention of solid-phase peptide synthesis[1] revolutionized the field of biological and medicinal chemistry. The solid-phase synthesis of peptides and oligonucleotides quickly reached a high level of maturity that allowed the repetative process to be automated. This enabled non-chemists to readily synthesize these complex biopolymers and allowed the first detailed investigations of the structure–affinity relationships of peptides and oligonucleotides. The efficiency of the automated process led many to the assumption that all problems had been solved and that new developments would be superfluous. However, the increasing pressure in pharmacological research to find more lead structures in even shorter periods of time has rejuvenated solid-phase methods, as demonstrated by the developments in combinatorial chemistry. Not only has this facilitated the preparation of peptides and oligonucleotides, it has also encouraged research into the solid-phase synthesis of highly complex oligosaccharides. Here new strategies for the solid-phase synthesis of these three classes of biopolymers are presented. The focus is on the use of activating protecting groups which increase both orthogonality and diversity.

Miller et al. utilized the acidifying effect of the *ortho*-nitrobenzenesulfonyl group (*o*-NBS) for the activation and selective N-alkylation of amido groups.[2] The incorporation of N-alkylated amino acids has often been used to probe the bioactive conformation of a peptide. To perform N-alkylations on a solid-phase, amino acids with N-*o*-NBS protecting groups were coupled to the unprotected amino group of a peptide **1** (Scheme 1).[3] Subsequently, the N-*o*-NBS peptide derivatives **2** were selectively alkylated at the acidic sulfonamide group. For example, reaction of the supported tetrapeptide **2a** with methyl 4-nitrobenzenesulfonate and the base 7-methyl-1,5,7-triazabicyclo[4.4.0]dec-5-ene (MTBD) gave **3a** in quantitative yield. The Pd^0-catalyzed N-allylation of **2b** succeeded with allylmethyl carbonate in a yield of 98%. The *o*-NBS group was cleaved by treating the tertiary sulfonamides **3** with sulfanylethanol and 1,8-diazabicyclo[5.4.0]undec-7-ene (DBU). Under these conditions, the unalkylated secondary sulfonamides remained intact.

The *o*-NBS group was also used as a general temporary protecting group in the solid-phase synthesis of unalkylated peptides. In the cleavage step, **2** was treated with 0.5 M potassium thiophenolate for 10 min; this liberated the amino group of **4** and a yellow chromophore. Thus, the course of the cleavage reaction can be conveniently monitored by photometry. The *o*-NBS and Fmoc (Fmoc = 9-fluorenylmethoxycarbonyl) strategies[4] were compared in the synthesis of the thrombine receptor agonist **5**. Purification of the crude products, which were obtained in 85% (*o*-NBS) and 91% (Fmoc) purity, by HPLC gave the pure peptide **5** in 50% (*o*-NBS) and 62% (Fmoc) overall yield.

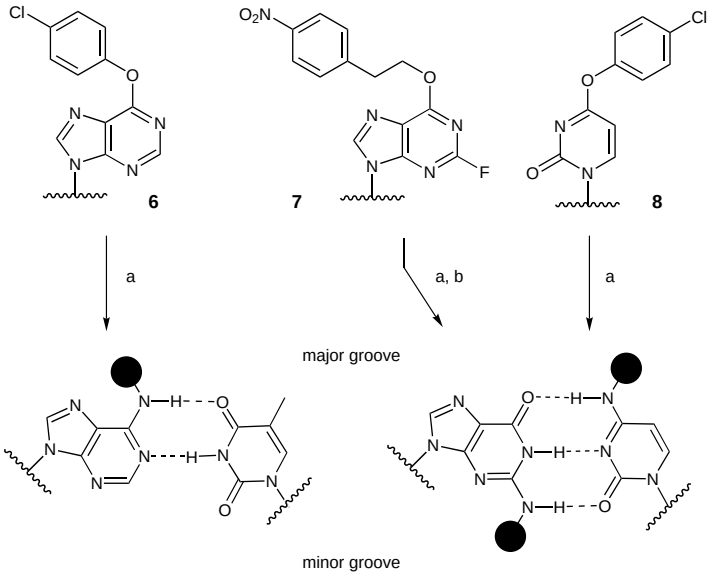


Scheme 1. a) 4 equiv *o*-NBS-NH(CHR^{n+1})COOH, 3.8 equiv HBTU, NMM, DMF, 20 min; b) R = Me: 4 equiv p-O_2NPhSO_3Me, 3 equiv MTBD, DMA, 30 min; R = All: 15 equiv AllOCOOMe, 10 mol% [Pd_2dba_3], $CHCl_3$, 80 mol% PPh_3, THF, 2 h; c) 10 equiv $HO(CH_2)_2SH$, 5 equiv DBU, DMF, 30 min; d) 0.5 M PhSH, 2 equiv K_2CO_3 per PhSH, DMF, 10 min. All = allyl, dba = dibenzylideneacetone, DBU = 1,8-diazabicyclo[5.4.0]undec-7-ene, DMA = *N*,*N*-dimethylacetamide, HBTU = 2-((1*H*)-benzotriazol-1-yl)-*N*,*N*,*N*′,*N*′-tetramethyluronium hexafluorophosphate, NMM = *N*-methylmorpholine, MTBD = 7-methyl-1,5,7-triazabicyclo[4.4.0]dec-5-ene, *o*-NBS = *ortho*-nitrobenzenesulfonyl, Pmc = 2,2,5,7,8-pentamethylchromane-6-sulfonyl, TFA = trifluoroacetic acid, Trt = trityl.

Protecting groups that allow the introduction of additional functional groups after a solid-phase synthesis are of particular interest for the construction of medically relevant DNA and RNA conjugates. In contrast to proteins, only a few functional groups of nucleic acids can be used for the conjugation of reporter groups or cross-links without compromising their biological function. In 1990, Verdine and MacMillan reported a method in which uridine derivatives were incorporated into oligonucleotides and subsequently modified.[5] This concept was recently extended to the synthesis of functionalized oligoribonucleotides.[6] The inosine base **6** and the uridine base **8** bear *para*-chlorophenyl groups at O6 and O4. Simple substitution with primary amines (RNH_2) resulted in the formation of the corresponding adenosine and cytidine derivatives (Scheme 2). Thus, the R group can be introduced into the major groove of a nucleic acid duplex. After substitution of the fluoride and cleavage of the nitrophenylethyl (NPE) protecting group, the fluoroinosine **7** forms a guanosine system, in which the the R group is located in the minor groove.

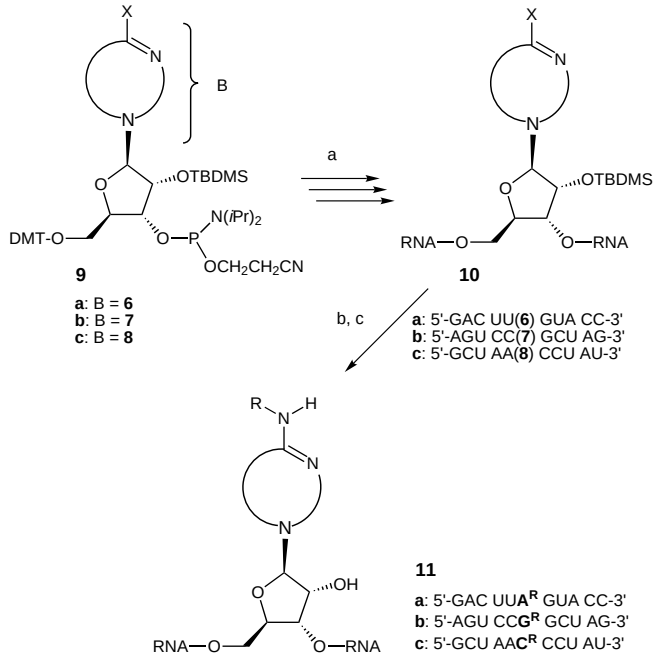
[*] Dr. O. Seitz
Institut für Organische Chemie der Universität
Richard-Willstätter-Allee 2, D-76128 Karlsruhe (Germany)
Fax: (+49) 721-608-4825
E-mail: seitz@ochhades.chemie.uni-karlsruhe.de

 © WILEY-VCH Verlag GmbH, D-69451 Weinheim, 1998 1433-7851/98/3722-3109 $ 17.50+.50/0



Scheme 2. Location of the R group in the duplex after reaction of the modifiable nucleosides **6**, **7**, and **8** with primary alkylamines a) RNH_2, MeOH; b) $NEt_3 \cdot 3HF$.

For the synthesis of the RNA-oligomers **10a–c** the phosphoamidites **9a–c** were incorporated by means of a slightly modified RNA synthesis protocol (Scheme 3). The



Scheme 3. Convergent modification of RNA. a) Solid-phase RNA synthesis by the phosphoamidite strategy; b) 2 M RNH_2 in MeOH (R = Me, 8 M CH_3NH_2 in MeOH); c) **10a**→**11a**, **10c**→**11c**: 1 M TBAF in THF; **10b**→**11b**: $NEt_3 \cdot 3HF$. DMT = 4,4′-dimethoxytrityl, TBDMS = *tert*-butyldimethylsilyl.

oligomers **10a–c** were functionalized with the amines listed in Table 1. Subsequent treatment with tetra-*n*-butylammonium fluoride (TBAF) or $NEt_3 \cdot HF$ removed the nitrophenylethyl (NPE) and *tert*-butyldimethylsilyl (TBDMS) protecting groups. The relative yields were evaluated after purifying

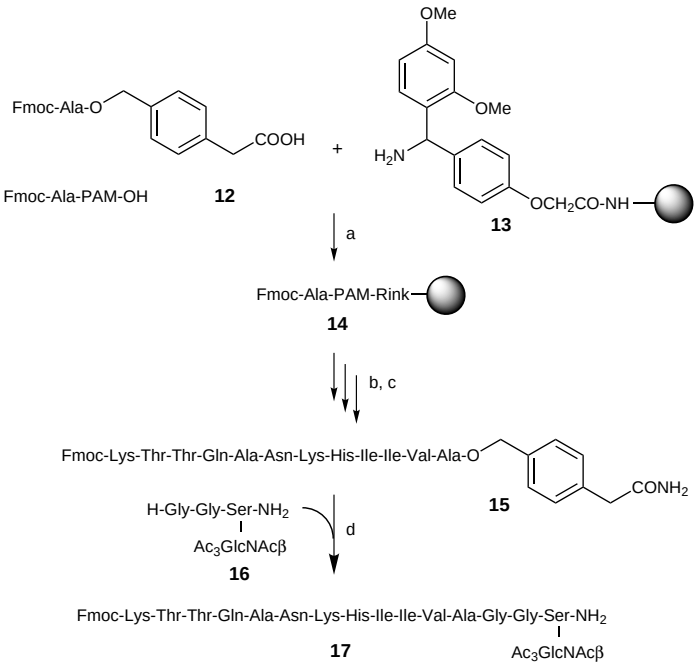
Table 1. Relative yields of substitutions of **10a–c** with RNH_2 to give **11a–c** (Scheme 3).

R	**a**[a]	**b**[b]	**c**[b]
H	0.24	1.0	1.0
CH_3	1.0	0.85	1.0
$H_2NCH_2CH_2$	1.0	0.9	0.96
$H_2N(CH_2)_4$	1.04	0.88	1.0
$HOCH_2CH_2$	1.1	1.0	1.04
$PhCH_2$	0.67	0.65	0.79

[a] Relative to the reaction with methylamine. [b] Relative to the reaction with ammonia.

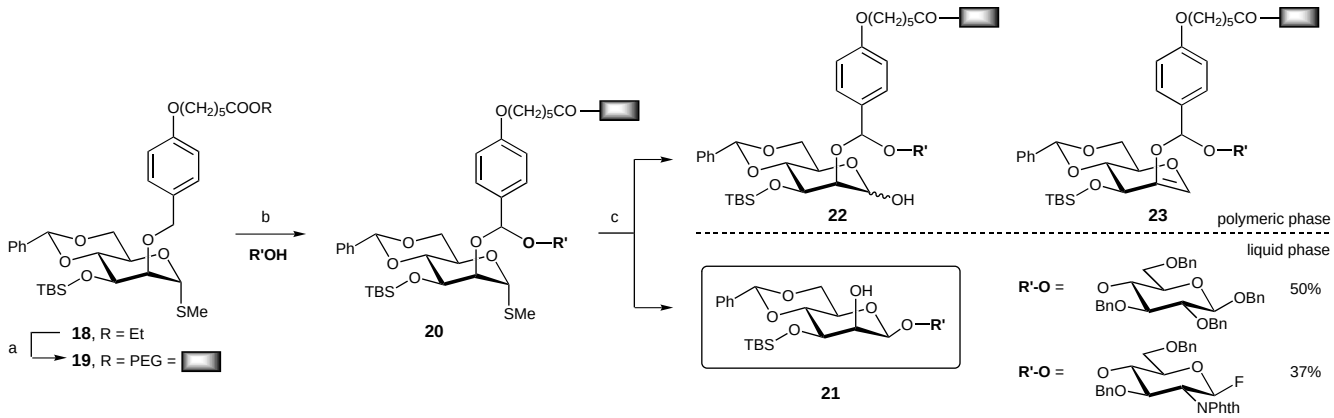
the products **11a–c** by denaturing polyacrylamide gel electrophoresis (PAGE) and enzymatic hydrolysis. Finally, the composition of the nucleic acid was determined by HPLC. All conversions proceeded in almost quantitative yield, with the exception of the reactions with benzylamine and of **10a** with ammonia.

The postsynthetic activation of a peptide ester was reported by Wong et al.[7] For the synthesis of a partial sequence of the C-terminal region of ribonuclease B, conjugate **12**, consisting of N-Fmoc-protected alanine and the acid- and base-stable phenylacetamidomethyl (PAM) linker, was coupled to the Rink amide resin **13** (Scheme 4). The elongation of **14** followed standard Fmoc protocols.[4] Standard TFA cleavage conditions removed all acid-labile protecting groups from the side chains and also detached the N-Fmoc-protected peptide–PAM ester **15** from the solid support. Since a benzhydrylamine-type linker was used, the peptide–PAM conjugate



Scheme 4. a) 1. HBTU, HOBt, NMM, DMF; 2. Ac_2O, py; b) 1. 20% piperidine/DMF; 2. Fmoc-AA-OH, HBTU, HOBt, NMM, DMF; 3. Ac_2O, py; c) TFA/Et_3SiH/H_2O (95/2.5/2.5), 89%; d) DMF/50 mM triethanolamine (9/1), subtilisin (8397 K 256 Y), 84%. $Ac_3GlcNAc$ = 2-acetamido-3,4,6-tri-*O*-acetyl-2-desoxyglucose, AA = amino acid, Fmoc = 9-fluorenylmethoxycarbonyl, HBTU = 2-((1*H*)-benzotriazol-1-yl)-*N*,*N*,*N*′,*N*′-tetramethyluronium hexafluorophosphate, HOBt = 1-hydroxybenzotriazole, NMM = *N*-methylmorpholine, TFA = trifluoroacetic acid.

 © WILEY-VCH Verlag GmbH, D-69451 Weinheim, 1998 1433-7851/98/3722-3110 $ 17.50+.50/0 *Angew. Chem. Int. Ed.* **1998**, *37*, No. 22



Scheme 5. a) 1. NaOH, *t*BuOH; 2. PEG monomethyl ether, $EtO_2CN{=}NCO_2Et$, PPh_3, CH_2Cl_2, THF, 80 %; b) DDQ, 4 Å molecular sieves, CH_2Cl_2, 3 h; c) MeOTf, MeSSMe, 2,6-di-*tert*-butyl-4-methylpyridine, $ClCH_2CH_2Cl$, 4 Å molecular sieves, 21 – 120 h. Bn = benzyl, DDQ = 2,3-dichloro-5,6-dicyano-1,4-benzoquinone, PEG = poly(ethylene glycol), Phth = phthaloyl, TBS = *tert*-butyldiphenylsilyl, Tf = triflate.

15 was liberated as a PAM amide. Such peptide esters with unprotected side chains can serve as acyl donors in enzyme-catalyzed peptide couplings. Accordingly, the segment condensation of **15** with the N-terminally unprotected glycotripeptide **16** was catalyzed by the protease subtilisin to give the glycopentadecapeptide **17** in 84 % yield. This synthetic strategy is a viable route for the preparation of acid- and base-stable peptide esters. Since these esters are converted to active esters by subtilisin, they can be used in enzymatic segment condensations, as an alternative to chemical processes.[8]

Recently, Ito and Ogawa demonstrated that polymer-bound protecting groups can stereospecifically direct the introduction of a reagent, as shown in the polymer-supported synthesis of β-mannoglycosides.[9] Because of the stereoelectronically unfavorable 1,2-*cis* configuration, the thermodynamically disfavored β-mannosidic bond in **21** (Scheme 5) presents a synthetic challenge. According to a strategy published in 1991 by Barresi and Hindsgaul, the axial 2-OH group can be utilized to direct the aglycon in the glycosylation reaction to the β face.[10] Ito and Ogawa introduced a *para*-alkoxybenzyl protecting group at this position. For the attachment to a polymeric support, the alkoxybenzyl group of the methyl sulfanylmannoside **18** carried a carboxyl group. Oxidation of the polymer-bound mannoside **19** with dichlorodicyanobenzoquinone (DDQ) in the presence of an alcohol yielded the acetal **20**. After activation of the thioglycoside with methyl triflate, **20** underwent intramolecular transacetalization to give the β-mannoside **21**. It is noteworthy that only the desired glycosylation products were liberated from the polymeric resin. Side products such as the hydrolysis product **22** or the elimination product **23** remained on the solid phase.

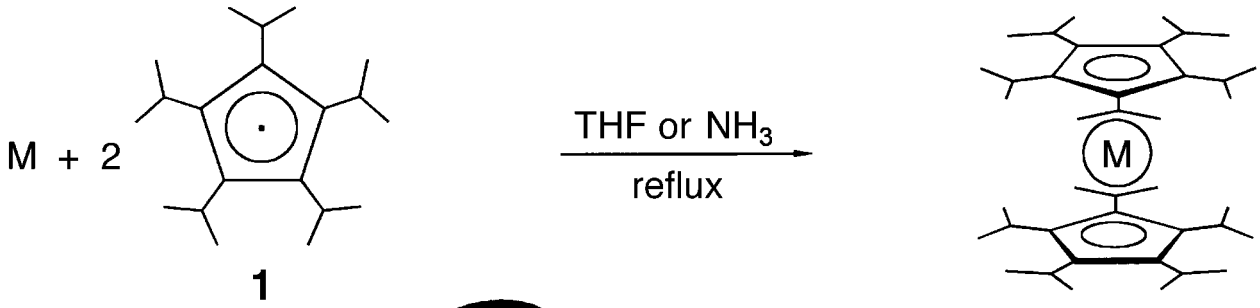
This example illustrates that protecting groups can be actively used in synthesis and achieve more than temporary blocking of a functional group. The activating effect of protecting groups such as *o*NBS, the PAM amide, and the chlorophenyl group allow subsequent selective reactions to be carried out, the products of which would normally be laborious to synthesize by other routes. The example of the polymer-supported synthesis of β-mannosides demonstrates how activatable protecting groups can initiate stereoselective reactions given a suitable orientation. The latter development is certainly attractive for future research. The polymeric resin could serve as a molecular gatekeeper, which in the final synthetic step liberates only the desired products. Thus, both the syntheses and the purification procedures, which are often time-consuming can be significantly simplified.

German version: *Angew. Chem.* **1998**, *110*, 3289 – 3291

Keywords: carbohydrates · nucleic acids · peptides · protecting groups · solid-phase synthesis

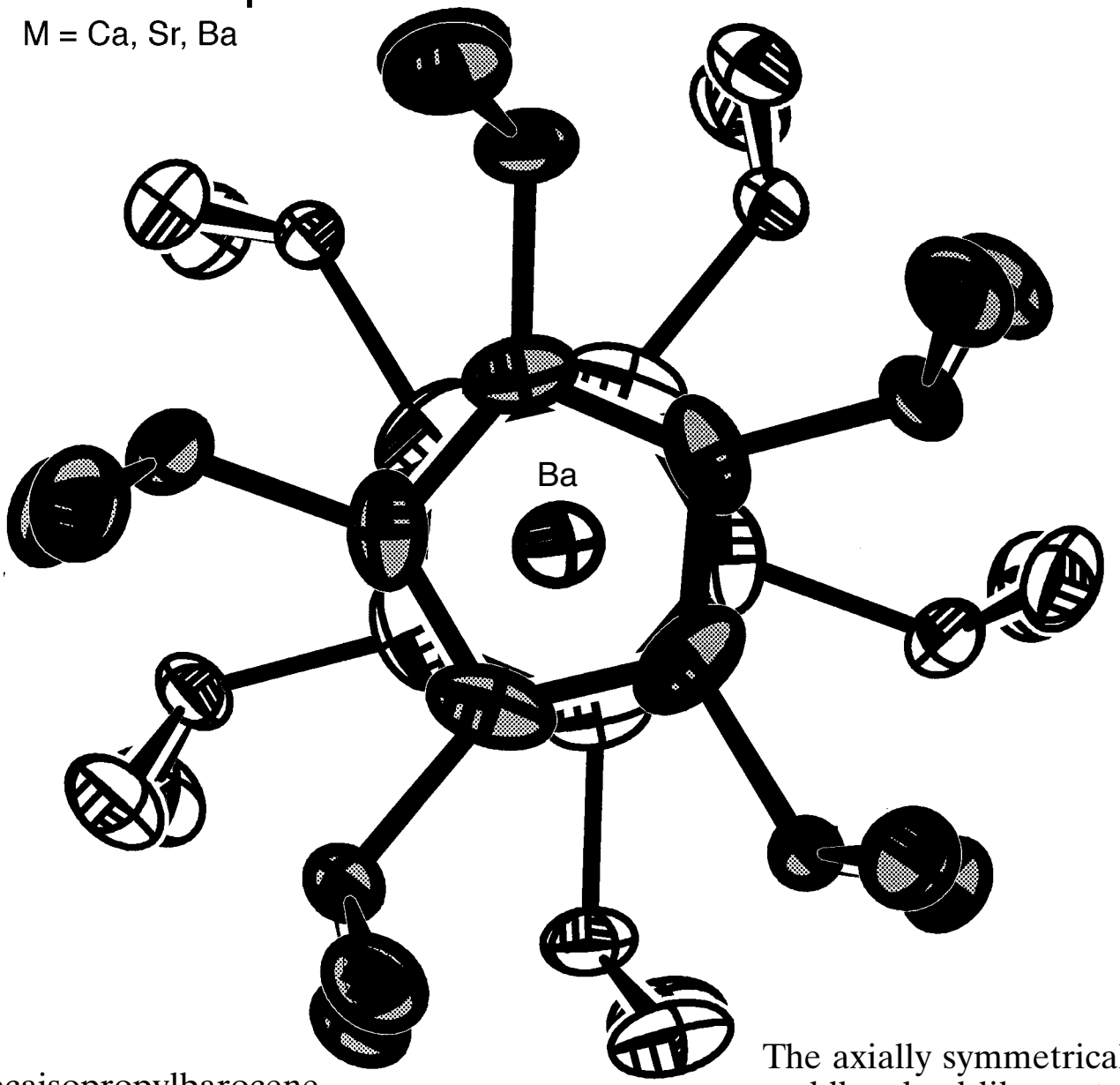
[1] R. B. Merrifield, *J. Am. Chem. Soc.* **1963**, *85*, 2149.
[2] S. C. Miller, T. S. Scanlan, *J. Am. Chem. Soc.* **1997**, *119*, 2301.
[3] S. C. Miller, T. S. Scanlan, *J. Am. Chem. Soc.* **1998**, *120*, 2690.
[4] E. Atherton, R. C. Sheppard, *Solid-Phase Peptide Synthesis: A Practical Approach*, IRL, Oxford, UK, **1989**.
[5] A. M. MacMillan, G. L. Verdine, *J. Org. Chem.* **1990**, *55*, 5931.
[6] C. R. Allerson, S. L. Chen, G. L. Verdine, *J. Am. Chem. Soc.* **1997**, *119*, 7423.
[7] K. Witte, O. Seitz, C.-H. Wong, *J. Am. Chem. Soc.* **1998**, *120*, 1979.
[8] The solid-phase synthesis of the more base-labile peptide-glycolate amide esters and their use in enzymic segment condensations: D. Y. Jackson, J. Burnier, C. Quan, M. Stanley, J. Tom, J. A. Wells *Science* **1994**, *266*, 243.
[9] Y. Ito, T. Ogawa, *J. Am. Chem. Soc.* **1997**, *119*, 5562.
[10] F. Barresi, O. Hindsgaul, *J. Am. Chem. Soc.* **1991**, *113*, 9376.

 © WILEY-VCH Verlag GmbH, D-69451 Weinheim, 1998 1433-7851/98/3722-3111 $ 17.50+.50/0



1

M = Ca, Sr, Ba



Decaisopropylbarocene was obtained from two equivalents of the cyclopentadienyl radical $[C_5R_5]^{\bullet}$ ($R = CHMe_2$) and elemental barium.

More details on the following pages.

The axially symmetrical paddle-wheel-like metallocene displays the largest distance between two neighboring parallel rings of a sandwich compound

 © WILEY-VCH Verlag GmbH, D-69451 Weinheim, 1998 1433-7851/98/3722-3113 $ 17.50+.50/0

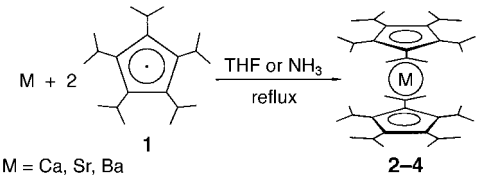
Synthesis of Symmetric Metallocenes from Metallic Calcium, Strontium, or Barium and Pentaisopropylcyclopentadienyl Radicals**

Helmut Sitzmann,* Thomas Dezember, and Michael Ruck

Dedicated to Professor Otto J. Scherer on the occasion of his 65th birthday

The bent sandwich geometry of the heavy alkaline earth metallocenes has been intensively investigated and is the subject of many review articles[1] and theoretical studies.[2] In order to achieve a symmetrical metallocene structure, the cyclopentadienyl ligand must possess axial symmetry and sufficient steric bulk. Since the pentaphenylcyclopentadienyl ring did not yield the desired decaphenylbarocene,[3] the pentaisopropylcyclopentadienyl ring appeared to be the only remaining candidate for the synthesis of symmetric calcium, strontium, or barium metallocenes. Furthermore, the availability of the stable pentaisopropylcyclopentadienyl radical (**1**)[4] as a starting material offered an unprecedented synthetic pathway to metallocene synthesis.

The reaction of metallic calcium, strontium, or barium with two equivalents of **1** proceeds smoothly in THF to form decaisopropylcalcocene (**2**), decaisopropylstrontocene (**3**), and decaisopropylbarocene (**4**) in good yields [Eq. (1)]. Sonication speeds up the reaction but is not essential.



(1)

Solutions of the heavy alkaline earth metals in liquid ammonia also react with **1** to form **2**–**4**. The solubility of all three metallocenes is, like decaisopropylstannocene[5] and -plumbocene,[6] low to moderate in pentane and toluene at room temperature, but can be increased by warming. When the solutions are cooled, the compounds crystallize readily in the form of colorless crystals. The crystalline calcocene and strontocene derivatives remain unchanged in air for several weeks. The barocene derivative develops a faint yellow tinge with time, which indicates very slow decomposition in air.

[*] Prof. Dr. H. Sitzmann, Dr. T. Dezember
FB Chemie der Universität
Erwin-Schrödinger-Strasse, D-67663 Kaiserslautern (Germany)
Fax: (+49) 631-205-2187
E-mail: sitzmann@rhrk.uni-kl.de
http://www.uni-kl.de/FB-Chemie/Sitzmann/index.html
Priv.-Doz. Dr. M. Ruck
Institut für Anorganische Chemie der Universität
(TH) Karlsruhe (Germany)

[**] Syntheses with free cyclopentadienyl radicals, Part 2. This work was supported by the Deutsche Forschungsgemeinschaft (Si 366/7-1). We are grateful to Prof. Dr. O. J. Scherer for his generous support, Dr. G. Hornung for the mass spectrometry measurements, and F. Weber for preparative assistance. Part 1: H. Sitzmann, G. Wolmershäuser, *Z. Naturforsch. B* **1995**, *50*, 750.

NMR spectra in the temperature range between 298 and 373 K indicate a gear-meshed conformation of the two pentaisopropylcyclopentadienyl rings, where the isopropyl groups have an equal or opposing orientation, thus giving rise to *rac* and *meso* isomers.[7] The isomers interconvert by isopropyl group rotation with Gibbs free activation enthalpy values of 71.8(1.5)/72.0(1.5) (**2**), 72.5(1.5)/72.8(1.5) (**3**), and 74.0(1.5)/74.6(1.5) kJ mol^{-1} (**4**). These values compare well with those found for the decaisopropylstannocene (74.8/75.5 kJ mol^{-1}) and -plumbocene isomers (73.0/73.7 kJ mol^{-1}), and with 71.3 kJ mol^{-1} found for the 1,2,3,4,5-pentaisopropylcobaltocenium cation.[8] The substantially larger rotational barrier found for the decaisopropylrhodocenium cation (85.5 kJ mol^{-1})[9] is presumably due to a relatively small interplanar distance with significant repulsive forces between adjacent rings.

The structure of **4** was determined by X-ray crystal structure analysis and is shown in Figure 1. Although the *meso* and *rac* isomers were distributed randomly throughout the crystal in a 1:1 ratio, the structure model could be refined very well.[10] The molecule was located on a center of symmetry with parallel and staggered arrangements of the pentaisopropylcyclopentadienyl rings. The inter-ring distance of 5.497(3) Å in barocene **4** is only 5.6% smaller than the value of 5.82 Å found for the free pentaisopropylcyclopentadienyl radical (**1**).[4] This is the largest interplanar distance yet reported for any sandwich compound to our knowledge.[11] The isopropyl methine carbon atoms connected to the five-membered ring are bent away from the central atom and are displaced out of the ring plane by an average of 0.139 Å. The distance between two adjacent pentaisopropylcyclopentadienyl rings of different molecules is 6.39 Å. This cannot be compared directly to the distance between rings in the free pentaisopropylcyclopentadienyl radical since the isopropyl groups are bent out of plane. The barocene molecules are stacked along the crystallographic *c* axis and are tilted towards this axis by approximately 11° (Figure 2). The Ba···Ba distance within a stack is 12.123(2) Å. Barocene **4** forms

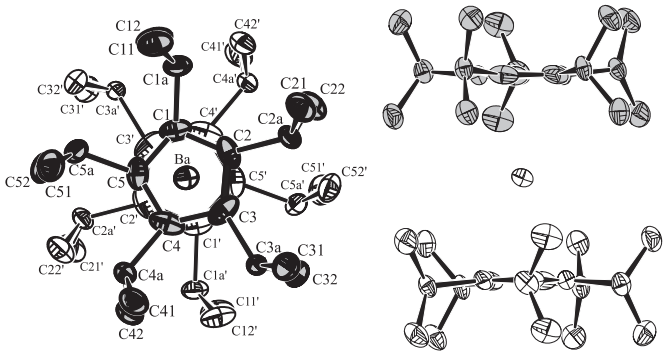


Figure 1. Molecular structure of **4** in the crystal (ellipsoids are drawn at the 50% probability level). Selected bond lengths [Å] and angles [°]: Ba–C1 2.981(2), Ba–C2 2.995(2), Ba–C3 3.014(2), Ba–C4 3.008(2), Ba–C5 2.989(2), C1–C2 1.402(3), C2–C3 1.407(3), C3–C4 1.413(3), C4–C5 1.401(3), C5–C1 1.405(3); Cp_{center}–Ba 2.748(2), Cp_{center}-Ba-Cp'_{center} 180. For clarity, only the *meso* isomer is shown.

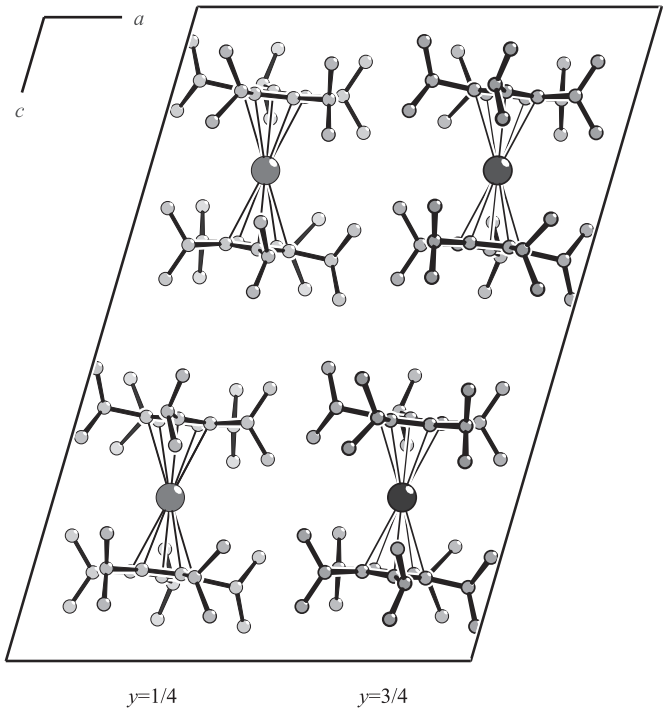


Figure 2. Stacking of **4** in the monoclinic unit cell.

near-hexagonal layers parallel to the *a*,*b* plane with Ba···Ba distances of 9.652(2) and 9.963(2) Å.

The only previous attempt known to us to use a cyclopentadienyl radical for metallocene synthesis was by Wilke et al.[12] who treated bis(1,5-cyclooctadiene)nickel(0) with Ziegler's pentaphenylcyclopentadienyl radical. From a formal point of view, the combination of a metal atom with two cyclopentadienyl radicals represents the simplest concept for metallocene synthesis. With the formation of **2**–**4,** this concept could be verified for the first time with the heavy alkaline earth metals calcium, strontium, and barium, and the pentaisopropylcyclopentadienyl radical $[C_5R_5]^{\cdot}$ ($R = CHMe_2$).

Experimental Section

1: Silver chloride (0.99 g, 6.96 mmol) was added to a solution of lithium pentaisopropylcyclopentadienide-diethyl ether adduct (2.48 g, 6.96 mmol) (prepared according to the published procedure[13]) in diethyl ether (50 mL) and the mixture was stirred for 48 h at room temperature. The silver precipitate was removed by centrifugation and the residue of the evaporated solution was recrystallized from petroleum ether at −30 °C to yield light green-yellow crystals of **1** (1.45 g, 5.27 mmol; 76 %). (For the characterization of **1** see ref. [4a].)

Synthesis of **4** (**2** and **3** were synthesized by the same procedure): Barium metal (380 mg, 2.76 mmol) was dissolved in liquid ammonia (150 mL) and a solution of **1** (1.52 g, 5.52 mmol) in diethyl ether (15 mL) was added dropwise within a few minutes. The mixture was stirred under reflux for 2 h. After removal of solvent, the residue was extracted with pentane (50 mL) at 0 °C and with toluene (50 mL) at 60–70 °C. The volatile products were sublimed off at 80 °C (0.1 mbar) from the residue of the pentane extract (340 mg). After sublimation, 170 mg of **4** was obtained and combined with the main fraction from the toluene extract. Yield: 1.51 g (2.23 mmol; 81 %). Recrystallization from hot toluene gave analytically pure crystalline **4**.

Alternative synthesis of **3** (**2** and **4** were synthesized by the same procedure): Strontium metal (131 mg, 1.50 mmol), **1** (827 mg, 3.00 mmol), and THF (15 mL) were sealed in a glass tube and sonicated in an ultrasonic bath for 12 h at 60 °C. The tube was opened in a glove box and the white suspension was collected, evaporated to dryness, extracted with toluene (40 mL) at 60–70 °C, filtered over celite and finally evaporated to ca. 5 mL residual volume. At −30 °C, the product precipitated as a microcrystalline, white solid which was washed with two 5 mL portions of pentane at 0 °C and dried in vacuo. Yield: 0.81 g (1.27 mmol; 84 %).

2: ^{1}H NMR (400 MHz, 313 K, C_6D_6): $\delta = 3.28$ (sept, 10H; C*H*Me$_2$), 1.56 (d, ^3J(H,H) = 7.0 Hz, 15H; inner CH$_3$ of one isomer), 1.54 (d, ^3J(H,H) = 7.0 Hz, 15H; inner CH$_3$ of other isomer), 1.24 (d, ^3J(H,H) = 6.6 Hz, 15H; outer CH$_3$ of both isomers); m.p. = 389 °C (decomp).

3: ^{1}H NMR (400 MHz, 313 K, C_6D_6): $\delta = 3.25$ (sept, 10H; C*H*Me$_2$), 1.46 (d, ^3J(H,H) = 7.2 Hz, 15H; inner CH$_3$ of one isomer), 1.44 (d, ^3J(H,H) = 7.2 Hz, 15H; inner CH$_3$ of other isomer), 1.29 (d, ^3J(H,H) = 6.8 Hz, 15H; outer CH$_3$ of both isomers); ^{13}C{^{1}H} NMR (100 MHz, 363 K, C_6D_6): $\delta = 125.6$ (s, 10C; ring C), 27.2 (s, 10C; *C*HMe$_2$), 24–26 (very broad, 20C; CH$_3$); CI-MS (isobutane, 120 eV): *m*/*z* (%): 638.1 (16) [M^+], 363.2 (6) [$M^+ - C_5(CHMe_2)_5$], 107.1 (100) [$C_5H_4(CHMe_2)^+$]. Compound **3** decomposed slowly above 400 °C without melting.

4: ^{1}H NMR (400 MHz, 313 K, C_7D_8): $\delta = 3.57$ (sept, 10H; C*H*Me$_2$), 1.58 (d, ^3J(H,H) = 7.1 Hz, 15H; inner CH$_3$ of one isomer), 1.56 (d, ^3J(H,H) = 6.7 Hz, 15H; inner CH$_3$ of other isomer), 1.47 (d, ^3J(H,H) = 7.1 Hz, 15H; outer CH$_3$ of both isomers); CI-MS (isobutane, 120 eV): *m*/*z* (%): 688.6 (2.4) [M^+], 413.3 (100) [$M^+ - C_5(CHMe_2)_5$], 275.4 (8.6) [$C_5(CHMe_2)_3^+$], 233.3 (2.9) [$C_5H(CHMe_2)_4^+$], 191.3 (11) [$C_5H_2(CHMe_2)_3^+$], 149.2 (45) [$C_5H_3(CHMe_2)_2^+$], 107.1 (95) [$C_5H_4(CHMe_2)^+$]. Compound **4** decomposed slowly above 400 °C without melting.

Received: July 23, 1998 [Z12196IE]
German version: *Angew. Chem.* **1998**, *110*, 3293–3296

Keywords: alkaline earth metals · barium · calcium · metallocenes · strontium

[1] Most recent review articles: P. Jutzi, N. Burford in *Metallocenes* (Eds.: A. Togni, R. Halterman), WILEY-VCH, **1998**, p. 28; M. L. Hays, T. P. Hanusa, *Adv. Organomet. Chem.* **1996**, *40*, 117.

[2] Theoretical studies: A. J. Bridgeman, *J. Chem. Soc. Dalton Trans.* **1997**, 2887; T. K. Hollis, J. K. Burdett, B. Bosnich, *Organometallics* **1993**, *12*, 3358; M. Kaupp, P. von R. Schleyer, M. Dolg, H. Stoll, *J. Am. Chem. Soc.* **1992**, *114*, 8202; R. Blom, K. Faegri, Jr., H. V. Volden, *Organometallics*, **1990**, *9*, 372.

[3] P. S. Tanner, T. P. Hanusa, *Polyhedron*, **1994**, *17*, 2417.

[4] H. Sitzmann, R. Boese, *Angew. Chem.* **1991**, *103*, 1027; *Angew. Chem. Int. Ed. Engl.* **1991**, *30*, 971; H. Sitzmann, H. Bock, T. Dezember, W. Kaim, M. Moscherosch, L. Zanathy, *J. Am. Chem. Soc.* **1993**, *115*, 12003.

[5] H. Sitzmann, R. Boese, P. Stellberg, *Z. Anorg. Allg. Chem.* **1995**, *622*, 751.

[6] H. Sitzmann, *Z. Anorg. Allg. Chem.* **1995**, *621*, 553.

[7] For more details see ref. [5].

[8] B. Gloaguen, D. Astruc, *J. Am. Chem. Soc.* **1990**, *112*, 4607.

[9] D. Buchholz, D. Astruc, *Angew. Chem.* **1994**, *106*, 1721; *Angew. Chem. Int. Ed. Engl.* **1994**, *33*, 1637.

[10] Crystal structure determination of **4**: STOE-IPDS diffractometer, $Mo_{K\alpha}$ radiation, $\lambda = 0.71073$ Å, $2\theta_{max} = 51.5°$, 320 images with $0° \le \phi \le 256°$ and $\Delta\phi = 0.8°$, $T = 200(2)$ K, crystal dimensions: $0.46 \times 0.36 \times 0.17$ mm^3, monoclinic, space group *I*12/*a*1 (no. 15), $a = 16.535(3)$, $b = 9.9626(11)$, $c = 24.245(4)$ Å, $\beta = 106.30(2)°$, $V = 3833$ Å^3, $Z = 4$, $\rho_{calcd} = 1.193$ g cm^{-1}, $\mu(Mo_{K\alpha}) = 11$ cm^{-1}, analytical absorption correction (ABSPSI), transmission factors 0.78–0.65, structure solution: direct methods (SIR97), full-matrix least-squares refinement based on F_o^2 (SHELXL-97), 13536 reflections, 3656 unique reflections, 252 parameters, $R1(2814\ F_o > 4\sigma(F_o)) = 0.022$, $wR2 = 0.053$, max./min. residual electron density 1.10/−0.35 e Å^{-3} (maximum 0.88 Å from Ba); the isopropyl groups are disordered, CH and CH$_3$ groups were refined as rigid groups with variable torsion angles (d(C–H) = 0.96 Å, C-C-H and H-C-H 109.5°). Graphical representation: DIAMOND, CORELDRAW. Further details of the crystal structure investigation can be obtained from the Fachinformationszentrum Karlsruhe,

D-76344 Eggenstein-Leopoldshafen (fax: (+49) 7247-808-666; e-mail: crysdata@fiz-karlsruhe.de) on quoting the depository number CSD-408943.

[11] 4.438 Å in [{η^6-$C_6H_3(CMe_3)_3$-2,4,6}$_2$Gd]: J. G. Brennan, F. G. N. Cloke, A. A. Sameh, A. Zalkin, *J. Chem. Soc. Chem. Commun.* **1987**, 1668; 4.80 Å in [Sn(C_5Ph_5)$_2$]: M. J. Heeg, C. Janiak, J. J. Zuckerman, *J. Am. Chem. Soc.* **1984**, *106*, 4259; 4.98 Å in [Sn(C_5R_5)$_2$] (R = $CHMe_2$): ref. [5]; 5.052 Å for two rings coordinated to both Er and K in [(η^8-C_8H_8)Er(μ,$\eta^{8:8}$-C_8H_8)K(μ,$\eta^{8:8}$-C_8H_8)Er(μ,$\eta^{8:8}$-C_8H_8)K(thf)$_4$]: J. Xia, Z. Jin, W. Chen, *J. Chem. Soc. Chem. Commun.* **1991**, 1214.

[12] A. Schott, H. Schott, G. Wilke, J. Brand, H. Hoberg, E. G. Hoffmann, *Justus Liebigs Ann. Chem.* **1973**, 508.

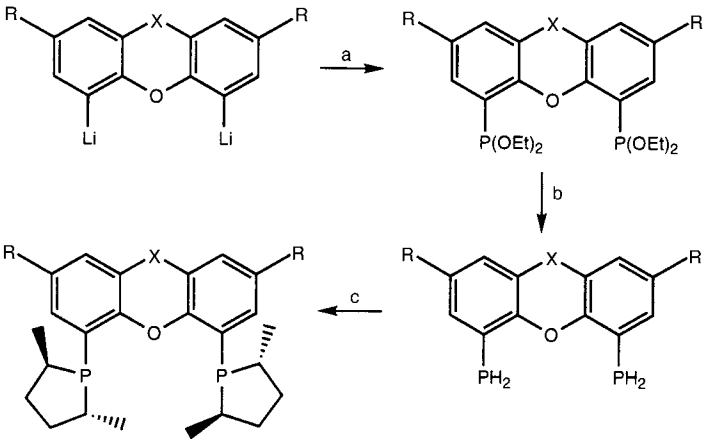
[13] T. Dezember, H. Sitzmann, *Z. Naturforsch. B* **1997**, *52*, 911.

Versatile Ligands for Palladium-Catalyzed Asymmetric Allylic Alkylation**

Peter Dierkes, Shailesh Ramdeehul, Laurent Barloy, Andre De Cian, Jean Fischer, Paul C. J. Kamer, Piet W. N. M van Leeuwen, and John A. Osborn*

The search for chiral ligands for asymmetric allylic substitution reactions with Pd complexes as catalysts continues apace.[1] High enantiomeric excesses (*ee*) were found for carbon-centered and other nucleophiles with *O*-acetyl-1,3-diphenyl-2-propen-3-ol as the model substrate. Much lower product *ee* values are generally observed for substrates with small substituents[1a] and with less sterically demanding cyclic substrates,[2] although for one family of diphosphane ligands the opposite appears to be true.[2b] The origin of enantioselectivity in these catalytic processes is still under debate, and several parameters are involved. It is generally accepted that in the attack of the nucleophile on the intermediate cationic (η^3-allyl)Pd^{II} complex, the repulsive interactions in the transition state[3] between the chiral ligand and the organic entity bound to the Pd center are an important factor which can largely determine the selectivity. To intensify these repulsive interactions at the Pd center, we synthesized rigid chelating chiral ligands with a large bite angle. Xanthene (dibenzo[*b*,*d*]pyran) and phenoxathiin (dibenzo-1,4-thioxin) were selected as rigid backbones, since 4,5 substitution of the former (older, nonsystematic numbering) and 4,6 substitution of the latter by phosphorus-containing groups leads to a large bite angle (>100°), as in Xantphos complexes.[4]

By attaching the chiral (2*R*,5*R*)-2,5-dimethylphospholano groups that were originally used in DUPHOS,[5] a family of several duxantphospholane-type chiral ligands are accessible. The new ligands were obtained in four steps by dilithiation of the backbone, reaction with diethyl chlorophosphonite, reduction with $LiAlH_4$, and treatment of the resulting phosphane with the cyclic sulfate of (2*S*,5*S*)-2,5-hexanediol. This is illustrated by the synthesis of the (*R*,*R*)-duthixantphospholane **A** (Scheme 1). The related chiral ligand, (*R*,*R*)-duxantphospholane **B**, in which the bridging S atom of **A** is formally replaced by a $C(CH_3)_2$ group, was prepared by the same method.[6]



A: R = CH_3, X = S
B: R = H, X = $C(CH_3)_2$

Scheme 1. Synthesis of the chiral P ligand **A**. a) $ClP(OEt)_2$; b) 1) 6 equiv $LiAlH_4$/TMSCl; 2) 30 equiv MeOH; c) 1) 2.0 equiv *n*BuLi; 2) cyclic sulfate of (2*S*,5*S*)-hexane-2,5-diol; 3) 2.2 equiv *n*BuLi. TMS = trimethylsilyl.

The effectiveness of such ligands in Pd-catalyzed allylation reactions was tested by employing dimethyl malonate as the nucleophile and three racemic allyl acetates possessing different steric properties: *O*-acetylcyclohex-2-enol (**1**), *O*-acetylpent-2-en-3-ol (**2**), and *O*-acetyl-1,3-diphenylprop-1-en-2-ol (**3**). Typically a 1 mol% solution of the catalyst was prepared



rac-**1** *rac*-**2** R = CH_3 *rac*-**3** R = C_6H_5

by the addition of one equivalent of **A** (or **B**) to 0.5 mol of [{Pd(η^3-C_3H_5)Cl}$_2$] and stirring under nitrogen for 15 min before adding the reactants (Table 1). The catalytic reactions are rapid with the less sterically hindered substrates **1** and **2**

[*] Prof. J. A. Osborn, S. Ramdeehul, Dr. L. Barloy
Laboratoire de Chimie des Métaux de Transition et de Catalyse
Université Louis Pasteur
Institut Le Bel, UMR 7513 CNRS
4 rue Blaise Pascal, F-67070 Strasbourg Cedex (France)
Fax: (+33) 388-416-171
E-mail: osborn@chimie.u-strasbg.fr

Prof. P. W. N. M van Leeuwen, Dr. P. Dierkes, Dr. P. C. J. Kamer
Universiteit van Amsterdam
Institute for Molecular Chemistry
van't Hoff Research Institute
Nieuwe Achtergracht 166
NL-1018 WV Amsterdam (The Netherlands)

Prof. J. Fischer, Dr. A. De Cian
Laboratoire de Cristallochimie et Chimie Structurale
Université Louis Pasteur
Institut Le Bel, UMR 7513 CNRS
4 rue Blaise Pascal, F-67070 Strasbourg Cedex (France)

[**] This work was supported by the Ministère de la Recherche et de l'Enseignement Supérieur (Ph.D. fellowship for S.R.), the Deutsche Forschungsgemeinschaft (Postdoctoral Fellowship for P.D.), the European Union (MMCOS network), and the CNRS (UMR 7513).

Supporting information for this article is available on the WWW under http://www/wiley-vch.de/home/angewandte/ or from the author.

 © WILEY-VCH Verlag GmbH, D-69451 Weinheim, 1998 1433-7851/98/3722-3116 $ 17.50+.50/0

Table 1. Results of alkylation reactions with different substrates.[a]

Entry	Ligand	Substrate	Solvent	Base	T [°C]	t	*ee* [%]
1	A	**1**	THF	NaH	20	5 min	87 (*S*)[b, d]
2	A	**1**	THF	NaH	20	30 min	81 (*S*)
3	A	**1**	THF	BSA	20	30 min	80 (*S*)
4	A	**1**	THF	BSA	0	2 h	87 (*S*)
5	A	**1**	THF	BSA	−20	4 h	93 (*S*)
6	A	**1**	CH_2Cl_2	BSA	20	50 min	82 (*S*)
7	B	**1**	THF	BSA	20	3 min	77 (*S*)
8	A	**2**	THF	BSA	20	< 1 min	24 (*S*)[b, d]
9	A	**2**	CH_2Cl_2	BSA	20	35 min	54 (*S*)
10	A	**2**	CH_2Cl_2	BSA	0	3 h	68 (*S*)
11	B	**2**	THF	BSA	20	30 min	66 (*S*)
12	B	**2**	THF	BSA	0	3 h	82 (*S*)
13	A	**3**	THF	BSA	0	16 h	83 (*R*)[c, d]
14	A	**3**	CH_2Cl_2	BSA	0	24 h	97 (*R*)

[a] The ratio of subtrate to catalyst was 100/1 in each case except entry 2 where it was 500/1. The yield (%) was determined by gas chromatography with a chiral column (*β*-cyclodextrin capillary column (30 m × 0.25 mm, SGE 25QCE2) by using dodecane as internal standard. [b] The enantiomeric excess was determined by 1H NMR spectroscopy ($CDCl_3$/0.1M solution of [Eu(hfc)$_3$]). [c] The % *ee* value was determined by HPLC with a chiral column (CHIRALPAK AD, Diacel, 250 × 4.6, flow rate 1 mL min^{-1}, *i*PrOH/*n*-hexane 9:1). [d] The configurations were assigned by comparing optical rotations with literature values.[7]

but slower for the more sterically demanding **3**. All reactions gave quantitative yields. With **A** as ligand, *rac*-**1** as substrate, and NaH as base in THF (entry 1), 100 turnovers are converted within 5 min at 20 °C with a product *ee* of 87% (*S*)[7]. Even 500 turnovers can be attained within 30 min with a small decrease in *ee* (entry 2). Similarly rapid reactions were observed with BSA[8] and KOAc (1 equiv) in THF (entry 3), which allows the reaction to be carried out conveniently at lower temperatures (entries 4 and 5) with 93% *ee* (*S*) in 4 h for 100 turnovers. The reaction is somewhat slower in CH_2Cl_2 (entry 6) but gives a similar *ee* value. With **B** as ligand, the reaction rates are even higher, but the *ee* values are somewhat lower (entry 7).

For substrate **2** with NaH/THF and ligand **A** (entry 8), the reaction is extremely rapid (complete conversion in less than 1 min) but gives a low *ee* value. With BSA/KOAc in CH_2Cl_2 (entry 9), the reaction is slower but the *ee* value increases, and at 0 °C (entry 10) after 3 h, the *S* product was obtained in 68% yield. With ligand **B**, the reactions rates were again higher, and the *ee* value increased from 66% at 20 °C to 82% at 0 °C (entries 11 and 12), which is one of the highest values achieved with this sterically undemanding substrate. The reactions of **3** (entries 13 and 14) with **A** as ligand gave the *R* product with 97% *ee*. Overall, these catalysts appear to be suitable for chiral synthesis with a range of structurally distinct substrates.

We isolated the complex $[Pd(\mathbf{A})(\eta^3\text{-}C_6H_9)]^+BF_4^-$ (C_6H_9 = cyclohexenyl) and characterized it by X-ray crystallography (Figure 1).[9] The bonding between the Pd center and the allyl group is essentially symmetric (Pd–C1 2.204(9), Pd–C3 2.200(8), Pd–P1 2.321(2), Pd–P2 2.312(2) Å). The P-Pd-P angle is 104.99(7)°. The closest intramolecular H–H interactions are between the CH_3 groups (C11 and C32) of the dimethylphospholane groups and the the allyl protons H1 (1.99 Å) and H3 (2.19 Å). The backbone of the ligand adopts

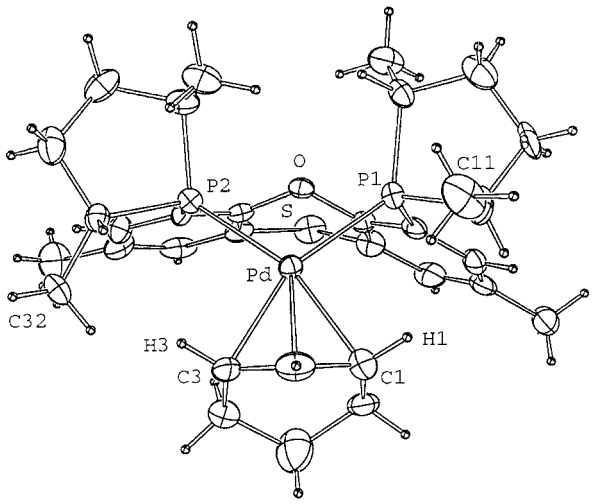


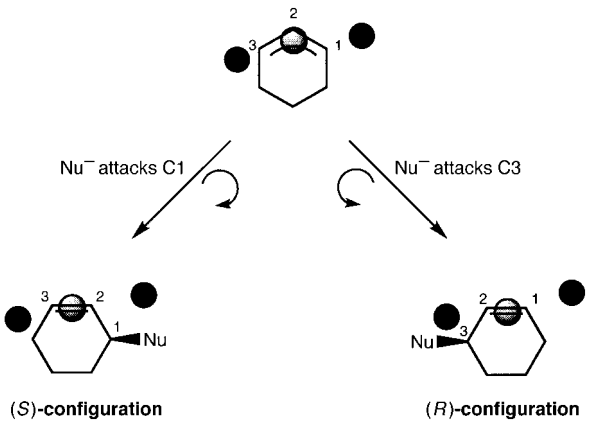
Figure 1. ORTEP view of the $[Pd(\mathbf{A})(C_6H_9)]^+$ ion. The BF_4^- ion is omitted for clarity.

an envelope conformation on the same side of the P-Pd-P plane as the boat-configured cyclohexenyl group and hence is *exo* to the η^3-allyl moiety. The $^{31}P\{^1H\}$ NMR spectrum of this complex in CD_3CN at 293 K shows an AB pattern with signals at $\delta = 35.9$ (P_A) and 35.4 (P_B) with $J_{P_A,P_B} = 43$ Hz. The $^{13}C\{^1H\}$ spectrum (CD_3CN, 293 K) shows two signals for C1 and C3 at $\delta = 92.9$ and 82.4, both of which are identically coupled to the *trans* P atom ($J_{C,P} = 25$ Hz). No changes are observed down to −40 °C.

These results show that although the C1 and C3 atoms are somewhat different electronically, steric interactions do not cause structural differentiation between these carbon centers in the cationic Pd(η^3-allyl) intermediate, and an early transition state for nucleophilic attack appears very improbable. A simple computer graphics model[10] in which the phospholane ligand is kept frozen, as in the structure of **A**, and the allyl group is replaced by cyclohexene shows that the most stable arrangement has the double bond in the P-Pd-P plane and Pd–C(vinylic) bonds of almost equal length (ca. 2.10 Å). There are notably close contacts between one of the allylic *endo*-CH_2 protons and a CH_3 group (a) of the phospholane (ca. 1.9 Å) and between a vinylic CH proton and the other proximal CH_3 group (b) of the ligand (ca. 2.2 Å); all other interactions are longer than 3 Å. We propose that the CH_3 group (a) will hinder all rotational processes of the organic moiety on Pd in which it would be traversed by an *endo* sp^3 C–H bond; no significant barrier is expected for the passage of sp^2 C–H bonds (Scheme 2).

The reaction of the nucleophile (Nu^-) with the (η^3-allyl)Pd cationic intermediate to form the Pd olefin complex must be accompanied by rotation,[11] and attack at C3 requires counterclockwise rotation. Hence, the *endo* sp^3 C3–H bond of the product must pass by the CH_3 group of the ligand, and this raises the barrier for the formation of the *R* product. No such steric interaction occurs in nucleophilic attack at C1, which involves clockwise rotation. Therefore, the *S* product should be favored, as is observed experimentally. Hence, a medium to late transition state is involved in the product-determining step. This preferential rotational (PR) concept allows us to understand how the nucleophile can discrimi-

 © WILEY-VCH Verlag GmbH, D-69451 Weinheim, 1998 1433-7851/98/3722-3117 $ 17.50+.50/0



Scheme 2. Preferential formation of the product with *S* configuration. The methyl groups at C11 and C32 are represented by black circles, and the Pd atom by a gray circle.

nated between C1 and C3, which otherwise differ little in their steric and electronic properties.

Received: March 5, 1998
Revised version: July 23, 1998 [Z11557IE]
German version: *Angew. Chem.* **1998**, *110*, 3299 – 3301

Keywords: alkylations · asymmetric catalysis · chiral ligands · homogeneous catalysis · palladium

[1] Reviews: a) B. M. Trost, D. L. van Vranken, *Chem. Rev.* **1996**, *96*, 395 – 422; b) T. Hayashi in *Catalytic Asymmetric Synthesis*, *Vol. 1* (Ed.: I. Ojima), VCH, New York, **1993**, pp. 325 – 365; c) C. G. Frost, J. Howarth, J. M. J. Williams, *Tetrahedron: Asymmetry* **1992**, *3*, 1089 – 1122; d) G. Consiglio, R. M. Waymouth, *Chem. Rev.* **1989**, *89*, 257 – 276.

[2] However, see a) G. Knühl, P. Sennhenn, G. Helmchen, *J. Chem. Soc. Chem. Commun*. **1995**, 1845 – 1846; b) B. M. Trost, A. C. Krueger, R. C. Bunt, J. Zambrano, *J. Am. Chem. Soc.* **1996**, *118*, 6520 – 6521.

[3] Both early and late transition states have been proposed. Early transition states: a) P. B. Mackenzie, J. Whelan, B. Bosnich, *J. Am. Chem. Soc.* **1985**, *107*, 2046 – 2054; b) J. Sprinz, M. Kiefer, G. Helmchen, M. Reggelin, G. Huttner, O. Walter, L. Zsolnai, *Tetrahedron Lett.* **1994**, *35*, 1523 – 1526; c) P. S. Pregosin, R. Salzmann, A. Togni, *Organometallics* **1995**, *14*, 842 – 847; d) A. Togni, U. Burckhardt, V. Gramlich, P. S. Pregosin, R. Salzmann, *J. Am. Chem. Soc.* **1996**, *118*, 1031 – 1037; late transition states: e) B. M. Trost, L. Weber, P. E. Strege, T. J. Fullerton, T. J. Dietsche, *J. Am. Chem. Soc.* **1978**, *100*, 3416 – 3426; f) J. M. Brown, D. I. Hulmes, P. J. Guiry, *Tetrahedron* **1994**, *50*, 4493 – 4506; g) P. von Matt, G. Lloyd-Jones, A. B. E. Minidis, A. Pfaltz, L. Macko, M. Neuburger, M. Zehnder, H. Rüegger, P. S. Pregosin, *Helv. Chim. Acta* **1995**, *78*, 265 – 284; h) H. Steinhagen, M. Reggelin, G. Helmchen, *Angew. Chem.* **1997**, *109*, 2199 – 2202; *Angew. Chem. Int. Ed. Engl.* **1997**, *36*, 2108 – 2110.

[4] a) M. Kranenburg, J. G. P. Delis, P. C. J. Kamer, P. W. N. M. van Leeuwen, K. Vrieze, N. Veldman, A. L. Spek, K. Goubitz, J. Fraanje, *J. Chem. Soc. Dalton Trans.* **1997**, 1839 – 1849; b) M. Kranenburg, Y. E. M. van der Burgt, P. C. J. Kamer, P. W. N. M. van Leeuwen, *Organometallics* **1995**, *14*, 3081 – 3089; c) M. Kranenburg, P. C. J. Kamer, P. W. N. M. van Leeuwen, *Eur. J. Inorg. Chem.* **1998**, 25 – 27.

[5] M. J. Burk, M. F. Gross, *Tetrahedron Lett.* **1994**, *35*, 9363 – 9366.

[6] A ligand derived from the xanthene backbone with chirality at phosphorus was recently reported: Y. Hamada, F. Matsuura, M. Oku, K. Hatano, T. Shioiri, *Tetrahedron Lett*. **1997**, *38*, 8961 – 8964.

[7] The configurations of the products were assigned by comparison of their optical rotations with literature data: a) P. Sennhenn, B. Gabler, G. Helmchen, *Tetrahedron Lett.* **1994**, *35*, 8595 – 8598; b) B. M. Trost, A. C. Krueger, R. C. Bunt, J. Zambrano, *J. Am. Chem. Soc.* **1996**, *118*, 6520 – 6521; c) P. von Matt, A. Pfaltz, *Angew. Chem.* **1993**, *105*, 614 – 616; *Angew. Chem. Int. Ed. Engl.* **1993**, *32*, 566 – 568.

[8] BSA = *N*,*O*-bis(trimethylsilyl)acetamide.

[9] a) Crystal data for $C_{32}H_{43}OP_2SPd \cdot BF_4$: $M_r = 730.92$, orthorhombic, space group $P2_12_12_1$, $a = 14.521(4)$, $b = 16.047(5)$, $c = 13.971(4)$ Å, $V = 3255(2)$ Å^3, $Z = 4$, $\rho_{calcd} = 1.49$ g cm^{-3}, $\mu(Cu_{K\alpha}) = 6.65$ mm^{-1}. Data were collected on a Philips PW1100/16 diffractometer with graphite-monochromated $Cu_{K\alpha}$ radiation ($\lambda = 1.5418$ Å) at $-100\,^{\circ}$C. A yellow crystal of dimensions $0.02 \times 0.30 \times 0.30$ mm was used, and a total of 2270 reflections were collected ($3 < \theta < 54^{\circ}$); 1931 reflections with $I > 3\sigma(I)$ were used for structure determination and refinement. The structure was solved by direct methods and refined against $|F|$. Hydrogen atoms were introduced as fixed contributors. Empirical absorption corrections, transmission factors: 0.53/1.00. For all computations the Nonius OpenMoleN package[9b] was used. The absolute structure was determined by refining the Flack x parameter: $x = 0.02(2)$. Final results: $R(F) = 0.032$, $Rw(F) = 0.045$, GOF = 1.051, maximum residual electron density 0.69 e Å^{-3}. Crystallographic data (excluding structure factors) for the structure reported in this paper have been deposited with the Cambridge Crystallographic Data Centre as supplementary publication no. CCDC-101072. Copies of the data can be obtained free of charge on application to CCDC, 12 Union Road, Cambridge CB2 1EZ, UK (fax: (+44) 1223-336-033; e-mail: deposit@ccdc.cam.ac.uk). b) C. K. Fair in MoleN. "An Interactive Intelligent System for Crystal Structure Analysis". Nonius, Delft, The Netherlands, 1990.

[10] A SPARTAN computer graphic programme was used, but in view of the approximate nature of these calculations, more detailed studies are in progress.

[11] The involvement of a rotational motion to explain, in part, the enantioselectivity of catalytic reactions with a P – N ligand was proposed by Brown et al.[3f] See also ref. [3d].

Mechanistic Implications of the Observation of Kinetic Resolution in a Palladium-Catalyzed Enantioselective Allylic Alkylation**

Shailesh Ramdeehul, Peter Dierkes, Rafael Aguado, Paul C. J. Kamer, Piet W. N. M van Leeuwen, and John A. Osborn*

The mechanism of Pd-catalyzed enantioselective allylic alkylation involves two steps which are of major importance in the catalytic cycle.[1] First, the allylic substrate, usually in the

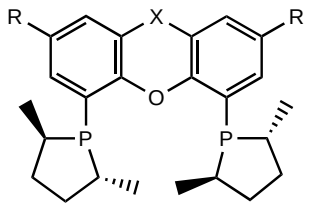
[*] Prof. J. A. Osborn, S. Ramdeehul, Dr. R. Aguado
Laboratoire de Chimie des Métaux de Transition et de Catalyse
Université Louis Pasteur
Institut Le Bel, UMR 7513 CNRS
4 rue Blaise Pascal, F-67070 Strasbourg Cedex (France)
Fax: (+33) 388-416-171
E-mail: osborn@chimie.u-strasbg.fr
Prof. P. W. N. M van Leeuwen, Dr. P. Dierkes, Dr. P. C. J. Kamer
Universiteit van Amsterdam
Institute for Molecular Chemistry
van't Hoff Research Institute
Nieuwe Achtergracht 166
NL-1018 WV Amsterdam (The Netherlands)

[**] This work was supported by the Ministère de la Recherche et de l'Enseignement Supérieur (Ph.D. fellowship for S.R.), the Deutsche Forschungsgemeinschaft (Postdoctoral Fellowship for P.D.), the European Commission (Marie Curie Research Fellowship, ERBFMBICT972198, for R.A.), the European Union (MMCOS network), and the CNRS (UMR 7513).

Supporting information for this article is available on the WWW under http://www/wiley-vch.de/home/angewandte/ or from the author.

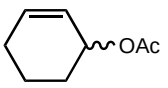
 © WILEY-VCH Verlag GmbH, D-69451 Weinheim, 1998 1433-7851/98/3722-3118 $ 17.50+.50/0

form of the acetate or carbonate, is activated by a Pd^0 complex with the probable formation of a (η^2-olefin)Pd^0 intermediate, which loses the anion to give a stable (η^3-allyl)Pd^{II} cationic intermediate. The second step involves the attack of the nucleophile on this cation to form the olefin product, which is bound η^2 to the Pd^0 center. The product is released in a subsequent step. Although the nature of the transition state in the second step and its role in determining the enantioselectivity of the overall process[2] have been extensively investigated, studies on the activation of the allylic substrate by Pd^0 are limited, since only one observation of enantioselective discrimination of the substrate (i.e., kinetic chiral resolution) by a Pd catalyst has been reported.[3] In most cases, rapid equilibration of the enantiomers apparently takes place and obscures any kinetic resolution process. It has even been proposed that this step is completely nonselective, which would be very surprising, since the reactions involved in the first step can be regarded as the reverse of those in the product-formation step, which can be highly enantioselective. We previously found that Pd catalysts containing the (*R*,*R*)-duxantphospholane ligands **A** and **B** give excellent product enantioselectivities[4] in the allylic alkylation reaction. We now report that kinetic resolution also occurs in the substrate-activation step and propose a mechanism that involves a favored rotational isomer.[4]

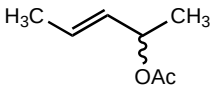


A: R = Me, X = S

B: R = H, X = $C(CH_3)_2$



rac-**1**



rac-**2**

We used *rac*-cyclohexenyl acetate (*rac*-**1**) and the *rac*-dimethylpropenyl acetate *rac*-**2** as substrates. In the reaction of dimethyl malonate with 0.5 equivalents of [{Pd(η^3-C_3H_5)Cl}$_2$], one equivalent of **A**, and 100 equivalents of *rac*-**1** in THF, (*S*)-**1** reacted much faster than (*R*)-**1** (Table 1). With BSA as base in THF, after 66% conversion to the (*S*)-malonate product with about 90% *ee*, the remaining acetate **1** had an *R*:*S* enantiomer ratio of 94:6 (88% *ee* (*R*), entry 1). We found that k_S/k_R had a constant value of 7 and was independent of the degree of conversion. The value of k_S/k_R does not change on increasing the quantity of **1** (400 equiv, entry 2), although the discrimination is somewhat temperature-dependent ($k_S/k_R \approx 8$ at 0 °C, entry 3). With NaH as base in THF (500 equiv **1**, entry 4) a slightly lower ratio ($k_S/k_R \approx 5$) is observed. However, for all reactions at 20 °C, the *ee* value of the malonate product remained almost unchanged at 82–87% (*S*). Furthermore, the *ee* of the product is the same at 50 and 100% conversion. Since (*S*)-**1** and (*R*)-**1** do not readily interconvert, the product enantioselectivity is not derived from the chirality of the substrate,[6] that is, no memory effect occurs.[5] Thus, the same *anti-anti*-(η^3-cyclohexenyl)Pd cation is formed from both (*S*)-**1** and (*R*)-**1**, and preferential attack[4] of the malonate on one of the allylic carbon atoms results in the observed enantioselectivity. Similar results were obtained with **B** as ligand. In CH_2Cl_2 with BSA/KOAc, both the reaction rate and k_S/k_R ratio of 2.4 (entry 5) were considerably lower, but the enantiomeric excess of the product remained unchanged.

High enantiodiscrimination and product enantioselectivity were also obtained with *rac*-**2**, for which in principle several (η^3-allyl)Pd cationic intermediates are possible. Figure 1 shows the composition of the reaction mixture as a function of time for the reaction of dimethyl malonate with *rac*-**2** (100 equiv), BSA/KOAc, and 1% **B** in THF at 20 °C. After 3 min 80% conversion to the malonate product has occurred, and the residual **2** has an *ee* of 92% (R), which corresponds to a k_S/k_R ratio of about 5. The decrease in concentraion of both (*S*)-**2** and (*R*)-**2** is first order with respect to substrate concentration. The half-lives of (*S*)-**2** and (*R*)-**2** in the first two to three half-lives of the reaction at 20 °C are approximately 30 s and 2 min, respectively. Similar values were obtained at 0 °C ($t_{1/2}$((*S*)-**2**) ≈ 7 min, $t_{1/2}$((*R*)-**2**) ≈ 1 h, $k_S/k_R \approx$ 6). As in the reaction of *rac*-**1**, the *ee* value of the malonate product from *rac*-**2** is the same at 50 and 100% conversion (*ee* = 82%). Therefore, the *S* and the *R* substrates must yield the same intermediate (η^3-allyl)Pd species, or if several

Table 1. Results of the kinetic chiral resolution.

Entry	Ligand	Substrate	Substrate/cat.	Solvent	Base	*T* [°C]	*t*	Conversion[b] [%]	*ee*[b] [%]	k_S/k_R[c]
1	A	*rac*-**1**	100	THF	BSA[a]	20	15 min	66	88	7.2
2	A	*rac*-**1**	400	THF	BSA	20	24 h	65	87	7.2
3	A	*rac*-**1**	100	THF	BSA	0	30 min	54	70	8.1
4	A	*rac*-**1**	500	THF	NaH	20	5 min	53	55	4.9
5	A	*rac*-**1**	100	CH_2Cl_2	BSA	20	35 min	87	77	2.4
6	B	*rac*-**2**	100	THF	BSA	20	3 min	80	92	4.3
7	B	*rac*-**2**	100	THF	BSA	0	45 min	66	82	5.8
8	A	*rac*-**2**	100	CH_2Cl_2	BSA	0	2 h	72	0	1.0

[a] BSA = *N*,*O*-bis(trimethylsily)acetamide. [b] Conversion and enantiomeric excess were determined by gas chromatography on a chiral stationary phase (β-cyclodextrin capillary column, 30 m × 0.25 mm, SGE 25QC2). For both substrates, the *R* enantiomer reacts more slowly, as was determined by comparing the optical rotations with literature values.[13, 14] [c] $k_S/k_R = \ln[(1 - C/100)(1 - ee/100)]/\ln[(1 - C/100)(1+ee/100)]$ (C = conversion; ee = enantiomeric excess of the recovered substrate).[3]

 © WILEY-VCH Verlag GmbH, D-69451 Weinheim, 1998 1433-7851/98/3722-3119 $ 17.50+.50/0

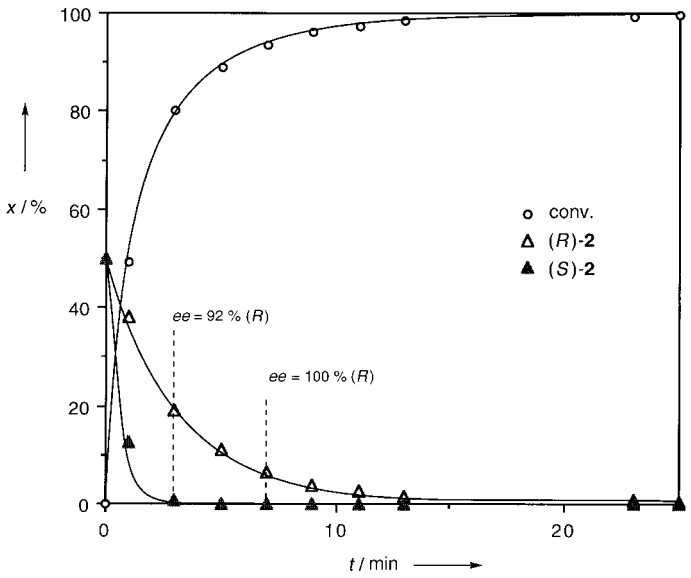


Figure 1. Fraction x of (R) and (S)-**2** in the Pd-catalyzed allylic alkylation (determined by gas chromatography on a β-cyclodextrin capillary column, 30 m × 0.25 mm, SGE 25QC2).

intermediates are involved, they must be equilibrated by fast exchange.

The cationic (η^3-dimethylpropenyl)Pd complex was isolated as the SbF_6^- salt after the reaction of **2** with the Pd catalyst with **B** as ligand. The ^1H, ^{13}C, and ^{31}P NOESY NMR data at 243 K in CD_2Cl_2 show the presence of an equilibrium mixture predominantly of the *exo* and *endo* forms of the *syn*,*anti*-(η^3-allyl)Pd diastereomers[7] in a ratio of about 6:1.

Our conclusions are illustrated in Scheme 1 for **2** as substrate.[7] The interacting methyl groups on the phospholane[8] ligand are depicted as "barriers **a** and **b**.

1) The initial complexation of **2** (R = Me) leads to four possible (η^2-olefin)Pd complexes.

2) The selective conversion of these complexes into the (η^3-allyl)Pd cations by oxidative addition results in the kinetic chiral resolution of **2**. Since interconversion of the (η^3-allyl)Pd cations is rapid under catalytic conditions, the reverse of this step must be sufficiently slow[6] in THF to allow kinetic resolution to occur.

3) If an antiperiplanar configuration[9] is assumed for oxidative addition and the preferential rotation (PR) model[4] with an early transition state is applied, we see that formation of two of the (η^3-allyl Pd) cations is disallowed, since clockwise rotation in the intermediates $\mathbf{O}_{S2}$ and $\mathbf{O}_{R2}$ is impeded by the the methyl group **a**.[8]

4) The kinetic resolution data show that the conversion of $\mathbf{O}_{S1}$ into the *syn*,*anti*-(η^3-dimethylpropenyl)Pd cation is more rapid than that of $\mathbf{O}_{R1}$ into the *syn*,*syn* form.

5) Since the *syn*,*anti*-(η^3-dimethylpropenyl)Pd cations are the most stable isomers and undergo rapid exchange under catalytic conditions the *syn*,*syn* form originating from $\mathbf{O}_{R1}$ would be expected to isomerize rapidly into these isomers.[10]

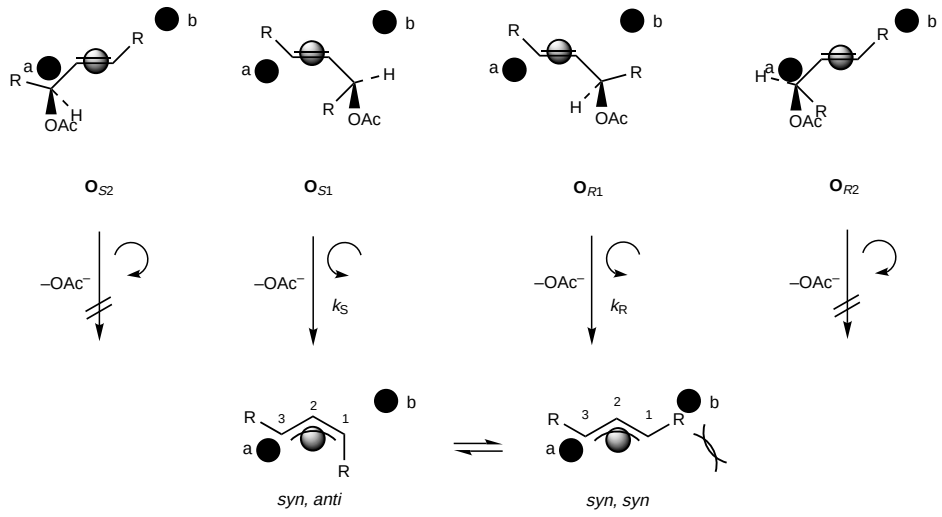
6) The first-order dependence of the rate of the overall reaction on the substrate concentration implies that the rate-determining step for the entire catalytic cycle under these conditions is either the coordination of the allyl acetate to the Pd^0 center or, more probably, the oxidative addition of the allylic substrate to Pd^0, which would necessitate that the complexation of allyl acetate to Pd^0 is weak and readily reversible.

7) The enantiomeric excess of the product results from two effects:

a) The dominance of the *syn*,*anti*-(η^3-allyl)Pd diastereomer in solution, which results from the spatial arrangement of barriers **a** and **b** in the ground state; the kinetic accessibility of this cation by isomerization of other allyl cations must be greater[11, 12] than the probability of the subsequent nucleophilic attack.

b) The selective attack of the nucleophile on the C1 atom of this cation, which is predicted to follow the PR mechanism with a late transition state[4] and avoids unfavorable rotational interactions with barrier **a**.

The PR model therefore plays a role in both the substrate-activation and product-formation steps. If the key and lock analogy is applied to this catalytic system, to obtain high enantioselectivity the key must not only be of the correct shape (7a) but will also be most effective if it can be turned only in one direction (7b).



Scheme 1. Mechanistic considerations for the kinetic chiral resolution in the Pd-catalyzed allylic alkylation of **2**. The methyl groups **a** and **b** of the chiral ligands are represented by black circles, and the Pd atom by a gray circle.

Received: March 5, 1998
Revised version: July 23, 1998 [Z11558IE]
German version: *Angew. Chem.* **1998**, *110*, 3302 – 3304

Keywords: alkylations · asymmetric catalysis · chiral resolution · palladium · P ligands

[1] Reviews: a) B. M. Trost, D. L. van Vranken, *Chem. Rev.* **1996**, *96*, 395 – 422; b) T. Hayashi in *Catalytic Asymmetric Synthesis*, *Vol. 1* (Ed.: I. Ojima), VCH, New York, **1993**, pp. 325 – 365; c) C. G. Frost, J. Howarth, J. M. J. Williams, *Tetrahedron:*

Asymmetry **1992**, *3*, 1089 – 1122; d) G. Consiglio, R. M. Waymouth, *Chem. Rev.* **1989**, *89*, 257 – 276.

[2] a) B. M. Trost, L. Weber, P. E. Strege, T. J. Fullerton, T. J. Dietsche, *J. Am. Chem. Soc.* **1978**, *100*, 3416 – 3426; b) P. B. Mackenzie, J. Whelan, B. Bosnich, *J. Am. Chem. Soc.* **1985**, *107*, 2046 – 2054; c) J. Sprinz, M. Kiefer, G. Helmchen, M. Reggelin, G. Huttner, O. Walter, L. Zsolnai, *Tetrahedron Lett.* **1994**, *35*, 1523 – 1526; d) J. M. Brown, D. I. Hulmes, P. J. Guiry, *Tetrahedron* **1994**, *50*, 4493 – 4505; e) P. S. Pregosin, R. Salzmann, A. Togni, *Organometallics* **1995**, *14*, 842 – 847; f) P. von Matt, G. Lloyd-Jones, A. B. E. Minidis, A. Pfaltz, L. Macko, M. Neuburger, M. Zehnder, H. Rüegger, P. S. Pregosin, *Helv. Chim. Acta* **1995**, *78*, 265 – 284; g) H. Steinhagen, M. Reggelin, G. Helmchen, *Angew. Chem.* **1997**, *109*, 2199 – 2202; *Angew. Chem. Int. Ed. Engl.* **1997**, *36*, 2108 – 2110.

[3] a) Kinetic chiral resolution in an allylic alkylation reaction: T. Hayashi, A. Yamamoto, Y. Ito, *J. Chem. Soc. Chem. Commun* **1986**, 1090 – 1091; b) reviews on kinetic chiral resolution: H. B. Kagan, J. C. Fiaud, *Top. Stereochem.* **1988**, *18*, 249 – 330.

[4] P. Dierkes, S. Ramdeehul, L. Barloy, A. DeCian, J. Fischer, P. C. J. Kamer, P. W. N. M. van Leeuwen, J. A. Osborn, *Angew. Chem.* **1998,** *110*, 3299 – 3301; *Angew. Chem. Int. Ed.* **1998**, *37*, 3116 – 3118.

[5] B. M. Trost, R. C. Bunt, *J. Am. Chem. Soc.* **1996**, *118*, 235 – 236.

[6] Note that the use of an excess of BSA to deliver a constant concentration of nucleophile rapidly removes acetate ion from the reaction. This will limit both the reverse of the oxidative addition step and the possible racemization of the substrate, which would obscure kinetic resolution, and pairing of the acetate ion with the Pd cation, which is proposed to be responsable for memory effects. However, we find that pure (*R*)-**1** is not detectably racemized by the catalyst over 1 h in THF, with or without an excess of OAc^-.

[7] Since the ligand adopts a rigid envelope conformation,[4] the η^3-allyl complexes exist in *exo* and *endo* forms. In the mechanistic discussion involving **2**, we depicted only the *exo* form; similar but not identical considerations also apply to the *endo* isomer. Selected NMR data for [Pd(**B**)(η^3-dimethylpropenyl)]$^+$: $^{31}P\{^1H\}$ NMR (121.5 MHz, CD_2Cl_2, 298 K): major isomer (85 %): $\delta = 32.3$ (d, $^2J_{P,P} = 35.6$ Hz), 36.9 (br d, $^2J_{P,P} = 35.6$ Hz); minor isomer (15 %): $\delta = 29.9$ (br), δ 34.2 (br); 2D ^1H NOESY spectrum (400 MHz, CD_2Cl_2, 243 K): η^3-dimethylpropenyl ligand (a = *anti*, s = *syn*, c = central): major isomer: $\delta = 5.41$ (m, H_s), 4.41 (dd, $^3J_{Hc\text{-}Ha} = 12.9$ Hz, $^3J_{Hs,Hc} = 7.5$ Hz, H_c), 4.34 (m, H_a); minor isomer**:** $\delta = 5.97$ (br m, H_s), 5.12 (dd, $^3J_{Hc,Ha} = 13.0$, $^3J_{Hs,Hc} = 8.0$ Hz, H_c), 4.20 (m, H_a)**.** Details of the *endo*/*exo* isomerization and the effects of chloride ions will be reported elsewhere.

[8] The X-ray structure of the *exo* isomer of [Pd(**A**)(η^3-cyclohexenyl)]$^+$ shows one methyl group of the ligand **A** in close proximity to the organic substrate.[4] This corresponds to barrrier **a** in Scheme 1. The methyl group barrier **b** is somewhat more distant and not related to **a** by a C_2 axis.

[9] J. C. Fiaud, L. Aribi-Zouioueche, *J. Chem. Soc. Chem. Commun.* **1986**, 390 – 392.

[10] For the relative stability of such allyl complexes, see B. Akermark, S. Hansson, A. Vitagliano, *J. Am. Chem. Soc.* **1990**, *112*, 4587 – 4588.

[11] U. Burckhardt, M. Baumann, A. Togni, *Tetrahedron Asymmetry* **1997**, *8*, 155 – 159.

[12] When large quantities of malonate anion are present (i.e., with the $NaH/CH_2(COOR)_2$ method), the overall rate of the reaction is faster, and the enantioselectivity of the product greatly reduced (*ee* = 33 % (S)). We believe that the malonate anion possibly increases the rate of the oxidative addition step by coordination[11] of the carbanion to Pd^0 and thus accelerates the product-forming step. Under these conditions the rate of isomerization of the intermediate Pd allyl cations is not sufficient to obtain high enantioselectivity.

[13] T. Fukazawa, Y. Shimoji, T. Hashimoto, *Tetrahedron*: *Asymmetry* **1996**, *7*, 1649 – 1658.

[14] J. C. McKew, M. J. Kurth, *J. Org. Chem.* **1993**, *58*, 4589 – 4595.

Catalytic Enantioselective Aza Diels – Alder Reactions of Imino Dienophiles

Sulan Yao, Mogens Johannsen,* Rita G. Hazell, and Karl Anker Jørgensen*

The asymmetric catalytic hetero Diels – Alder class of reactions has attracted considerable interest due to the importance of the products formed.[1] The asymmetric oxa Diels – Alder reactions of aldehydes[2] and ketones[3] catalyzed by chiral Lewis acid catalysts can be performed with a high degree of stereoselectivity, whereas methods are still lacking for the corresponding catalytic enantioselective aza Diels – Alder reaction.[4–6] The asymmetric aza Diels – Alder reaction provides an effective route to optically active piperidine and tetrahydroquinoline heterocycles, as well as other compounds of fundamental importance.[1]

Yamamoto et al. have recently developed an enantioselective aza Diels – Alder reaction of aldimines with Danishefsky's diene using a stoichiometric amount of a chiral boron complex.[4] To our knowledge, the first catalytic enantioselective aza Diels – Alder reaction with a chiral zirconium complex as the catalyst was elegantly achieved by Kobayashi et al. for reactions of aldimines derived from 1-naphthaldehyde and 2-aminophenol, for example.[5] The highest enantiomeric excess (*ee*) obtained was 93 % with 20 mol % of the chiral zirconium catalyst.

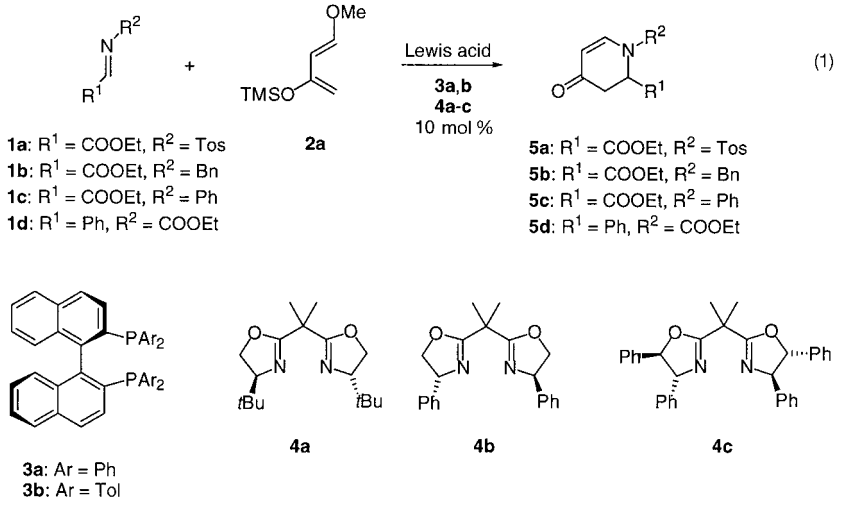
Here we present a catalytic enantioselective aza Diels – Alder reaction of imines derived from ethyl glyoxylate with activated dienes. The optically active aza Diels – Alder adducts formed contain an ester functionality in the α-position to the nitrogen atom in the ring and an α,β-unsaturated ketone fragment. These adducts make attractive precursors for a variety of synthetic targets, such as a straightforward and very efficient route to optically active, nonnatural α-amino acids of the piperidine type.

Recently highly enantioselective hetero Diels – Alder and ene reactions of α-carbonyl esters and α-dicarbonyl compounds have been developed.[2, 3] These results prompted us to investigate whether the corresponding α-imino carbonyl compounds could be substrates in an enantioselective aza Diels – Alder reaction. We anticipated that the imino nitrogen atom and the oxygen atom would coordinate to the chiral Lewis acid complex to form a fixed chiral environment around the aldimino group.

The potential of the α-imino carbonyl compounds **1a – d** as possible substrates for the aza Diels – Alder reaction with Danishefsky's diene (**2a**) [Eq. (1); $Tos = H_3CC_6H_4SO_2$; $TMS = Me_3Si$] was investigated. Different chiral ligands, such as the 2,2′-bis(diphenylphosphanyl)-1,1′-binaphthyl (BINAP) ligands **3a**, **b** and the bisoxazoline ligands **4a – c**, have, in combination with various Lewis acid complexes and under

[*] Prof. K. A. Jørgensen, M. Johannsen, S. Yao, R. G. Hazell
Center for Metal Catalyzed Reactions
Department of Chemistry, Aarhus University
DK-8000 Aarhus C (Denmark)
Fax: (+45) 861-961-99
E-mail: kaj@kemi.aau.dk

[**] This work was supported by the Danish National Science Foundation.

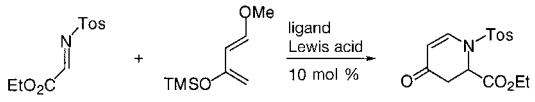


different reaction conditions, been tested as catalysts for the aza Diels–Alder reaction.

The α-imino carbonyl compounds **1a–d** all react smoothly with **2a** to generate the aza Diels–Alder adducts **5a–d** in good yield in the presence of various complexes derived from the chiral ligands **3a**, **b**, **4a–c** and Lewis acids such as $Zn(OTf)_2$, $Cu(OTf)_2$, CuOTf, $CuClO_4$, $AgSbF_6$, AgOTf, $AgClO_4$, $Pd(SbF_6)_2$, $Pd(ClO_4)_2$, $Pd(OTf)_2$, and $RuSbF_6$ (Tf = F_3CSO_2). However, under the present reaction conditions, only the α-imino ester **1a** reacted enantioselectively with **2a** to yield the product **5a**, when copper(I)–BINAP complexes were used as catalyst. Table 1 contains some representative results for the aza Diels–Alder reaction of **1a** with **2a** in the presence of **3a**, **b**, **4a–c** in combination with different metal salts. The combination of BINAP **3a** as the chiral ligand with $CuClO_4 \cdot 4MeCN$ or $2CuOTf \cdot C_6H_6$ as the metal salt results in a reasonable yield of the aza Diels–Alder adduct **5a** with an *ee* value of 64 or 61%, respectively (entries 1 and 2). Slow addition of **2a** improves the yield and the *ee* value of **5a** slightly (entry 3). Use of the 2,2′-bis(ditolylphosphanyl)-1,1′-binaphthyl (tol-BINAP) ligand **3b** with $CuClO_4 \cdot 4MeCN$ gives an even higher enantioselectivity of 80% *ee* (entry 4). $Cu(OTf)_2$ with **3b** in THF also results in a good *ee* value (entry 5). When CH_2Cl_2 is used as the solvent for the same reaction, however, the enantioselectivity is reduced to 40% (entry 6). If silver(I) and palladium(II) salts are used instead of copper(I), reasonable yields of **5a** are obtained but with low *ee* values (entries 9–14), while the use of ruthenium(I) leads to a racemic product (entry 15). The various combinations of bisoxazoline ligands **4a–c** with copper(I), copper(II), and zinc(II) salts as Lewis acid catalysts result in reasonable yields of **5a** but with very low *ee* values (entries 7, 8, 16, 17). In relation to the present aza Diels–Alder reaction, it should be noted that the combination of BINAP and late transition metals has recently been shown to be an effective catalyst for the enantioselective alkylation of imines by enol silanes and allyl stannane.[7]

The aza Diels–Alder reactions of the α-imino ester **1a** with the activated dienes **2a**, **b** catalyzed by different BINAP-$CuClO_4 \cdot 4MeCN$ catalysts under various reaction conditions are presented in Table 2. The reaction of α-imino ester **1a** with diene **2a** catalyzed by **3a**-$CuClO_4 \cdot 4MeCN$ (10 mol%) gives the aza Diels–Alder adduct **5a** in 78% yield with an *ee* value of 67% (Table 2, entry 1), while under similar reaction conditions **3b** gives a yield of only 68% but an improvement of the *ee* value to 80% (entry 2). The absolute stereochemistry of **5a** was assigned to be (*S*) at C1 on the basis of an X-ray structure analysis (Figure 1a). Use of the diene **2b** leads to a

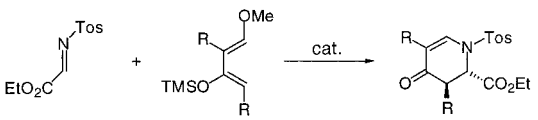
Table 1. The results for the aza Diels–Alder reaction of **1a** with **2a** in the presence of **3a**, **b**, and **4a–c** in combination with different Lewis acids (10 mol%) at −78 °C in THF, unless otherwise indicated.



Entry	Ligand	Lewis acid	Yield (**5a**)[a] [%]	*ee*[b] [%]
1	**3a**	$CuClO_4 \cdot 4MeCN$	65	64
2	**3a**	$2CuOTf \cdot C_6H_6$	60	61
3[c]	**3a**	$CuClO_4 \cdot 4MeCN$	78	67
4	**3b**	$CuClO_4 \cdot 4MeCN$	68	80
5	**3b**	$Cu(OTf)_2$	42	77
6[d]	**3b**	$Cu(OTf)_2$	72	40
7	**4a**	$2CuOTf \cdot C_6H_6$	74	12
8	**4a**	$Cu(OTf)_2$	60	10
9	**3a**	$AgSbF_6$	75	33
10	**3b**	AgOTf	85	30
11	**3b**	$AgClO_4$	90	34
12	**3b**	$Pd(SbF_6)_2$	76	30
13	**3b**	$Pd(ClO_4)_2$	68	11
14	**3b**	$Pd(OTf)_2$	88	11
15	**3b**	$RuSbF_6$	70	0
16	**4b**	$Zn(OTf)_2$	74	17
17	**4c**	$Zn(OTf)_2$	70	8

[a] Yield of isolated product. [b] Determined by HPLC with a Chiralpak-AD column. [c] Slow addition of **2a**. [d] Solvent: CH_2Cl_2.

Table 2. Results for the aza Diels–Alder reaction of **1a** with **2a**, **b** catalyzed by different $CuClO_4 \cdot 4MeCN$ complexes with the ligands **3a** and **b** at −78 °C in THF.



Entry	Catalyst	Load [mol%]	Alkene	Yield[a] [%]	*ee*[b] [%]
1	**3a**/$CuClO_4 \cdot 4MeCN$	10	**2a**	78	67
2	**3b**/$CuClO_4 \cdot 4MeCN$	10	**2a**	68	80
3	**3b**/$CuClO_4 \cdot 4MeCN$	10	**2b**	67	94
4	**3b**/$CuClO_4 \cdot 4MeCN$	5	**2b**	70[c]	94
5	**3b**/$CuClO_4 \cdot 4MeCN$	1	**2b**	70[c]	96
6[d]	**3b**/$CuClO_4 \cdot 4MeCN$	10	**2b**	70	81

[a] Total yield of isolated product. [b] Determined by HPLC with a Chiralpak-AD column. [c] Diastereoselective ratio = 10:1; [d] T = 20 °C.

 © WILEY-VCH Verlag GmbH, D-69451 Weinheim, 1998 1433-7851/98/3722-3122 $ 17.50+.50/0 *Angew. Chem. Int. Ed.* **1998**, *37*, No. 22

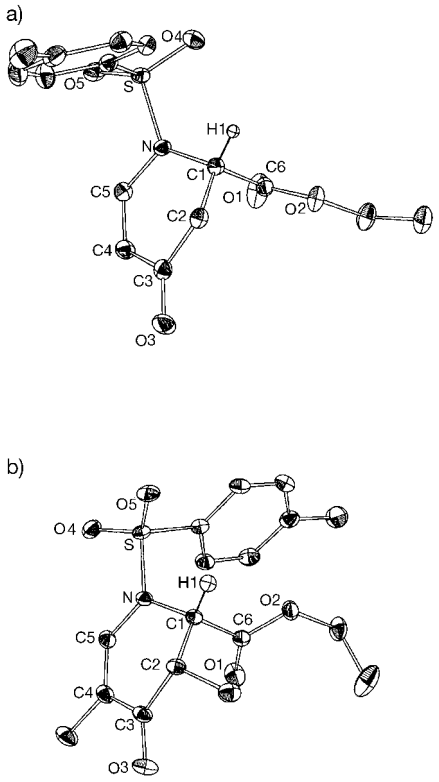


Figure 1. The X-ray crystal structure of **5a** shows the (*S*) configuration at C1 (a), while the X-ray crystal structure of *cis*-**6** shows the *cis* configuration at C1 and C2 (b).

significant improvement in the *ee* value of the major diastereomer *trans*-**6** of the aza Diels–Alder adduct (94% *ee*, diastereoselectivity ratio of 10:1; entry 3); while an *ee* value of 81% is obtained at room temperature (entry 6). The relative configuration of the minor diastereomer, *cis*-**6**, which corresponds to an *endo* approach of the diene, was also assigned by means of X-ray crystallography (Figure 1b). The major diastereomer, *trans*-**6**, is probably formed by *exo* attack of the diene. The aza Diels–Alder reaction can proceed with 5 mol% and, most importantly, 1 mol% of the catalyst **3b**-$CuClO_4 \cdot 4MeCN$ without adversely affecting the yield or the enantioselectivity (entries 4, 5). With a catalyst loading of 1 mol%, an *ee* value of 96% is obtained at $-78\,^{\circ}C$ (entry 5). The advantage of this aza Diels–Alder reaction is that it can be performed on the gram scale with a catalyst loading of only 1 mol% of **3b**-$CuClO_4 \cdot 4MeCN$. Under these conditions, the diastereomer *trans*-**6** can be isolated from the reaction of **1a** with **2b** in a yield of 90% with a diastereoselectivity ratio of 4:1 and an *ee* value of 93%, compared with 70% total yield of isolated product and stereoselectivity of 96% on a 0.2 mmol scale.

As evident from Table 1, the aza Diels–Alder reaction is almost independent of the counterion in the metal salt; the influence of metal, solvent, imine, and catalyst loading is, however, more pronounced. Generally, the diastereoselectivity decreased when the catalyst loading was reduced. The enantioselectivity of the minor diastereomer, the *endo* adduct *cis*-**6**, however, remained less than 30% even at low loading. An examination of the solvent effects in the reaction of **1a** with **2b** catalyzed by **3b**-$CuClO_4 \cdot 4MeCN$ at $-78\,^{\circ}C$ led to the conclusion that THF is the optimal solvent. In all other solvents not only did the diastereoselectivity decrease, but also the enantioselectivity of *trans*-**6** (Et_2O: 79% *ee*, CH_2Cl_2: 80% *ee*, toluene: 65% *ee*, DMF: 0% *ee*).

The potential of this new enantioselective aza Diels–Alder reaction of the α-imino ester **1a** with activated dienes is evident from the results in Table 2: highly valuable products in organic chemistry can be obtained with *ee* values of up to 96%. Furthermore, such enantiomeric excess is obtained in the presence of only 1 mol% of **3b**-$CuClO_4 \cdot 4MeCN$ catalyst, and the reaction can be performed on the gram scale with higher yields and the same high enantioselectivity.

Experimental Section

Ethyl 1-tosyl-3,5-dimethyl-4-oxo-1,2,3,4-tetrahydropyridine-2-carboxylate (*trans*-**6** and *cis*-**6**): (*R*)-tol-BINAP (30 mg, 0.044 mmol) and $CuClO_4 \cdot 4MeCN$ (13 mg, 0.04 mmol) were added to a flame-dried Schlenk tube under N_2. The mixture was dried under vacuum for 30 min, anhydrous THF (1 mL) was added and the resulting suspension was stirred for 1–2 h. The clear yellow catalyst solution was then cooled to $-78\,^{\circ}C$, and **1a** (105 mg, 0.4 mmol) was added, followed by **2b** (115 μL, 0.5 mmol). The reaction solution was stirred overnight, then trifluoroacetic acid (0.1 mL in 20 mL CH_2Cl_2) was added and the mixture stirred for 30 min at $0\,^{\circ}C$. Evaporation of the solvent gave the crude product which was purified by flash chromatography (15/85 ethyl acetate/pentane) to give a total yield of 67% with a diastereoselectivity ratio of 10:1, *trans*-**6** (83 mg, 94% *ee*; Chiralpak-AD column, hexane/*i*PrOH 85/15, 1.0 mL min^{-1}) and *cis*-**6** (8 mg) as a light yellow oil; *trans*-**6**: $[\alpha]_D^{20} = -91.9$ ($c = 0.67$ in $CHCl_3$); ^1H NMR (300 MHz, $CDCl_3$): $\delta = 7.76$ (d, $J = 8.3$ Hz, 2H; C_6H_4), 7.53 (t, $J = 1.1$ Hz, 1H; MeC=C*H*), 7.34 (d, $J = 7.6$ Hz, 2H; C_6H_4), 4.60 (m, 1H; COCHMeC*H*-CO_2Et), 3.98–4.10 (m, 2H; CO_2CH_2Me), 2.88 (dq, $J = 1.6$, 7.7 Hz, 1H; COC*H*MeCHCO$_2$Et), 2.45 (s, 3H; ArCH_3), 1.71 (d, $J = 1.1$ Hz, 3H; CH=CCH_3), 1.16 (t, $J = 7.1$ Hz, 3H; $CO_2CH_2CH_3$), 0.99 (d, $J = 7.7$ Hz, 3H; COCH_3CH); ^{13}C NMR (75 MHz, $CDCl_3$): $\delta = 193.93$, 168.16, 145.12, 137.46, 135.07, 130.04, 127.47, 113.10, 62.26, 62.23, 42.35, 21.66, 17.06, 13.91, 12.95; *cis*-**6**: ^1H NMR (300 MHz, $CDCl_3$): $\delta = 7.72$ (d, $J = 8.8$ Hz, 2H; C_6H_4), 7.47 (t, $J = 1.1$ Hz, 1H; MeC=C*H*), 7.34 (d, $J = 7.7$ Hz, 2H; C_6H_4), 4.77 (m, 1H; COCHMeC*H*CO_2Et), 3.77–3.91 (m, 2H; $CO_2CH_2CH_3$), 2.85 (q, $J = 7.1$ Hz, 1H; CHMeC*H*CO$_2$Et), 2.43 (s, 3H; ArCH_3), 1.73 (d, $J = 1.1$ Hz, 3H; =CCH_3), 1.13–1.04 (m, 6H; COCHCH_3CO$_2$CH$_2$CH_3); ^{13}C NMR (75 MHz, $CDCl_3$): $\delta = 192.59$, 167.08, 145.07, 136.79, 134.96, 130.04, 127.37, 114.51, 61.53, 61.31, 40.81, 21.64, 13.81, 12.95, 10.49.

Crystal structure analysis of **5a**: $C_{15}H_{17}NO_5S$, colorless platelets, $0.40 \times 0.34 \times 0.18$ mm^3, orthorhombic, space group $P2_12_12_1$, $a = 8.0821(3)$, $b = 11.8862(5)$, $c = 16.4544(7)$ Å, $V = 1580.7(1)$ Å^3, $Z = 4$, $\rho_{calcd} = 1.359$ Mg m^{-3}, $Mo_{K\alpha}$ radiation ($\lambda = 0.71073$ Å), $2\Theta_{max} = 58.6^{\circ}$, $T = 120$ K, $\mu = 0.227$ mm^{-1}, min./max. transmission 0.91/0.96. Area detector data collected on a Siemens SMART CCD diffractometer, nearly full sphere of reflections; data integration, correction for Lorentz, polarization, and absorption (by Gaussian integration) effects with SMART, SAINT, and XPREP software.[8] There were 21944 reflections measured, 3976 of which were independent, 3889 reflections with $I > \sigma(I)$ were used for refinement. Structure solved by direct methods (SIR97),[9] refined by full-matrix least-squares on $|F|^2$,[10] 269 parameters, hydrogen atoms refined with isotropic temperature parameters, all other atoms anisotropic, $R = 0.027$, w$R = 0.034$, max. residual electron density $\Delta\rho_{max} = 0.62(3)$ e Å^{-3}. The absolute configuration was determined by using the anomalous scattering from sulfur by refinement of the Rogers parameter.[11] The result was 0.93(9), which unambiguously established the chirality (Figure 1).[12] All hydrogen atoms, except the hydrogen atom at the chiral center, have been omitted for clarity.

Crystal structure analysis of *cis*-**6**: $C_{17}H_{21}NO_5S$, colorless hexagons, $0.40 \times 0.30 \times 0.12$ mm^3, triclinic, space group $P\bar{1}$, $a = 8.6699(4)$, $b = 9.6790(4)$, $c = 10.6235(5)$ Å, $\alpha = 77.436(1)$, $\beta = 89.189(1)$, $\gamma = 89.652(1)^{\circ}$, $V = 870.04(5)$ Å^3, $Z = 2$, $\rho_{calcd} = 1.341$ Mg m^{-3}, $Mo_{K\alpha}$ radiation ($\lambda = 0.71073$ Å), $2\Theta_{max} = 60^{\circ}$, $T = 120$ K, $\mu = 0.212$ mm^{-1}, min./max. transmission 0.934/0.975. There were 7952 reflections measured, 4374 of which were independent, 3948

reflections with $I > \sigma(I)$ were used in the refinement of 302 parameters. The procedure was the same as for **5a**.

Crystallographic data (excluding structure factors) for the structures reported in this paper have been deposited with the Cambridge Crystallographic Data Centre as supplementary publication no. CCDC-102362 and CCDC-102363. Copies of the data can be obtained free of charge on application to CCDC, 12 Union Road, Cambridge CB2 1EZ, UK (fax: (+44) 1223-336-033; e-mail: deposit@ccdc.cam.ac.uk).

Received: July 21, 1998 [Z12188IE]
German version: *Angew. Chem.* **1998**, *110*, 3318–3321

Keywords: asymmetric catalysis · copper · cycloadditions · Lewis acids · synthetic methods

[1] See for example: a) D. L. Boger, S. M. Weinreb, *Hetero Diels–Alder Methodology in Organic Synthesis*; Academic Press, New York, **1987**, chap. 2, 9; b) L. F. Tietze, G. Kettschau, *Stereoselective Heterocyclic Synthesis I*, *Vol. 189* (Ed.: P. Metz), Springer, Berlin, **1997**, p. 1; c) H. Waldmann, *Synthesis* **1994**, 535; d) *Organic Synthesis Highlights II* (Ed.: H. Waldmann), VCH, Weinheim, **1995**, p. 37; e) S. M. Weinreb in *Comprehensive Organic Synthesis, Vol. 5* (Eds.: B. M. Trost, I. Flemming, M. F. Semmelhack), Pergamon, Oxford, **1991**, p. 401.

[2] See for example: a) K. Maruoka, T. Itoh, T. Shirasaka, H. Yamamoto, *J. Am. Chem. Soc.* **1988**, *110*, 310; b) G. Keck, X.-Y. Li, D. Krishnamurthy, *J. Org. Chem.* **1995**, *60*, 5998; c) Q. Gao, K. Ishihara, T. Maruyama, M. Mouri, H. Yamamoto, *Tetrahedron*, **1994**, *50*, 979; d) Q. Gao, T. Maruyama, M. Mouri, H. Yamamoto, *J. Org. Chem.* **1992**, *57*, 1951; e) M. Bednarski, S. Danishefsky, *J. Am. Chem. Soc.* **1986**, *108*, 7060, and references therein; f) S. E. Schaus, J. Brånalt, E. N. Jacobsen, *J. Org. Chem.* **1998**, *63*, 403; g) M. Johannsen, K. A. Jørgensen, *J. Org. Chem.* **1995**, *60*, 5757; h) A. Graven, M. Johannsen, K. A. Jørgensen, *Chem. Commun*. **1996**, 2372.

[3] For reactions with a normal electron demand: a) M. Johannsen, S. Yao, K. A. Jørgensen, *Chem. Commun.* **1997**, 2169; b) S. Yao, M. Johannsen, H. Audrain, R. G. Hazell, K. A. Jørgensen, *J. Am. Chem. Soc.* **1998**, *120*, 8599. For reactions with an inverse electron demand: a) D. A. Evans, J. S. Johnson, *J. Am. Chem. Soc.* **1998**, *120*, 4895; b) J. Thorhauge, M. Johannsen, K. A. Jørgensen, *Angew. Chem.* **1998**, *110*, 2543; *Angew. Chem. Int. Ed.* **1998**, *37*, 2404.

[4] a) K. Hattori, H. Yamamoto, *J. Org. Chem.* **1992**, *57*, 3264; b) K. Hattori, H. Yamamoto, *Tetrahedron* **1993**, *49*, 1749; c) K. Ishihara, M. Miyata, K. Hattori, H. Yamamoto, *J. Am. Chem. Soc.* **1994**, *116*, 10520.

[5] a) H. Ishitani, S. Kobayashi, *Tetrahedron Lett.* **1996**, *37*, 7357; b) S. Kobayashi, S. Komiyama, H. Ishitani, *Angew. Chem.* **1998**, *110*, 1026; *Angew. Chem. Int. Ed.* **1998**, *37*, 979.

[6] See for example: a) P. Herczegh, I. Kovács, L. Szilágyi, M. Zsély, F. Sztaricskai, A. Berecibar, A. Olesker, G. Lukacs, *Tetrahedron Lett.* **1992**, *33*, 3133; b) R. Lock, H. Waldmann, *Tetrahedron Lett.* **1996**, *37*, 2753; c) P. N. Devine, M. Reilly, T. Oh, *Tetrahedron Lett.* **1993**, *34*, 5827; d) H. Waldmann, M. Braun, M. Dräger, *Angew. Chem.* **1990**, *102*, 1445; e) M. M. Midland, R. Koops, *J. Org. Chem.* **1992**, *57*, 1158; f) A. K. McFarlane, G. Thomas, A. Whiting, *J. Chem. Soc. Perkin Trans. 1* **1995**, 2803.

[7] a) D. Ferraris, B. Young, T. Dudding, T. Lectka *J. Am. Chem. Soc.* **1998**, *120*, 4548; b) H. Nakamura, K. Nakamura, Y. Yamamoto, *J. Am. Chem. Soc.* **1998**, *120*, 4242; c) E. Hagiwara, A. Fujii, M. Sodeoka, *J. Am. Chem. Soc.* **1998**, *120*, 2474.

[8] SMART, SAINT, and XPREP: Area Detector Control and Integration Software. Siemens Analytical X-ray Instruments Inc. Madison, WI (USA), **1995**.

[9] G. Cascarano, A. Altomare, C. Giacovazzo, A. Guagliardi, A. G. G. Moliterni, D. Siliqi, M. C. Burla, G. Polidori, M. Camalli, *Acta Crystallogr. Sect. A* **1996**, *52*, C50.

[10] a) W. T. Busing, K. O. Martin, H. A. Levy, *ORFLS*, *Report ORNL-TM-305*. Oak Ridge National Laboratory, TN (USA), **1962**; b) A. Hazell, KRYSTAL, An integrated system of crystallographic programs, Aarhus University (Denmark), **1995**.

[11] D. Rogers, *Acta Crystallogr. Sect. A* **1981**, *37*, 734.

[12] M. N. Burnett, C. K. Johnson, *ORTEP-III, Report ORNL-6895*. Oak Ridge National Laboratory, TN (USA), **1996**.

Mechanistic Insights into Cu-Catalyzed Asymmetric Aldol Reactions: Chemical and Spectroscopic Evidence for a Metalloenolate Intermediate**

Brian L. Pagenkopf, Jochen Krüger, Aleksandar Stojanovic, and Erick M. Carreira*

The aldol reaction ranks among the premier methods for carbon–carbon bond formation in chemical synthesis. Advances in both diastereoselective and enantioselective processes have produced remarkable achievements in the synthesis of stereochemically complex structures.[1] In contrast to the wealth of empirical and theoretical data available for diastereoselective aldol additions of metalloenolates to aldehydes,[2] mechanistic understanding of catalytic asymmetric processes with enol silanes is less advanced. Insight into the latter would be of considerable assistance in the design of newer, more efficient methods for asymmetric synthesis.[3]

We recently reported a catalytic aldol addition of the silyl dienolate **1** to a range of aldehydes in the presence of a bisphosphanyl-Cu^{II} fluoride complex which is generated in situ from (*S*)-Tol-BINAP,[4] $Cu(OTf)_2$, and $(Bu_4N)Ph_3SiF_2$ (Scheme 1).[5] Aromatic, heteroaromatic, and α,β-unsaturated



Scheme 1. Catalytic aldol addition of **1** to aldehydes.

aldehydes furnished aldol adducts with up to 95% *ee* and in 98% yield. Importantly, we postulated a metalloenolate as a key intermediate in the catalytic cycle.[6, 7] This role for a late transition metal catalyst contrasts the more conventional function of such metals as Lewis acids in related processes (Ag^{I},[8] Cu^{II},[9] Pd^{II},[6a–c] and Ni^{II}[10]). Here we report chemical and spectroscopic data that support the postulated catalytic cycle and the involvement of metalloenolate and metal aldolate intermediates.

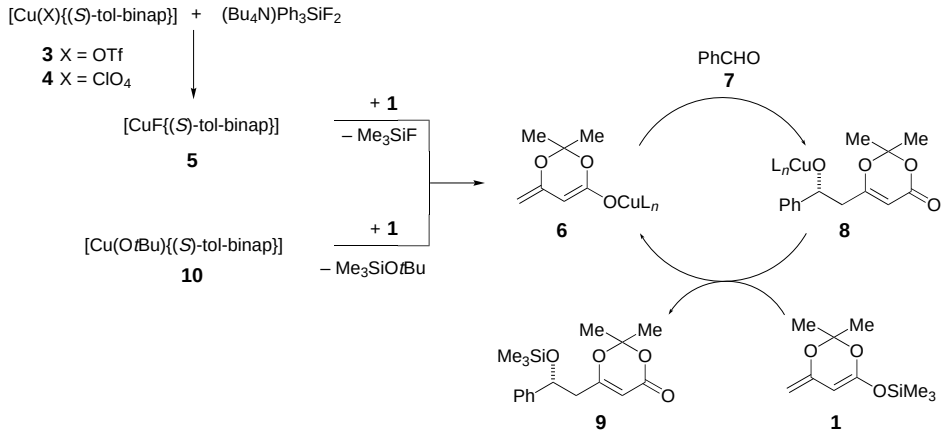
In mechanistic studies of the Cu-mediated reaction we observed that 5 mol% of the corresponding $Cu^{I}F$ complex (prepared in situ from (*S*)-Tol-BINAP, $[CuOTf \cdot C_6H_6]$, and $(Bu_4N)Ph_3SiF_2$) served equally well in the catalytic aldol reaction of **1** and benzaldehyde (**7**; 94% *ee* and 97% yield).

[*] Prof. Dr. E. M. Carreira, Dr. B. L. Pagenkopf, Dr. J. Krüger, Dr. A. Stojanovic
Arnold and Mabel Beckman Laboratory for Chemical Synthesis, California Institute of Technology
Pasadena, CA 91125 (USA)
Fax: (+1) 626-564-9297
E-mail: carreira@cco.caltech.edu

[**] B.L.P. thanks the National Institutes of Health (NIH), J.K. thanks the Deutsche Forschungsgemeinschaft, and A.S. is grateful to the Schweizerischer Nationalfonds for postdoctoral fellowships. Financial support was provided by the Packard Foundation, National Science Foundation (USA), NIH (USA), and generous funds from Eli Lilly, Merck, Novartis, Pfizer, Upjohn, and Zeneca.

 © WILEY-VCH Verlag GmbH, D-69451 Weinheim, 1998 1433-7851/98/3722-3124 $ 17.50+.50/0

This result, along with the known reduction of Cu^{II} to Cu^{I} by ketone-derived enol silanes,[11] suggested that a Cu^{I} complex functions as the catalytically relevant species. In the postulated catalytic cycle (Scheme 2), Cu^{I} complex **5** reacts with **1** to generate metallodienolate **6**,[12] which undergoes aldol addition to form the copper alkoxide **8**. Silylation by **1** converts **8** into the silylated adduct **9** with concomitant regeneration of metalloenolate **6**. This mechanistic pathway suggests that direct entry into the catalytic cycle may be possible with a Cu^{I} alkoxide. Accordingly, when the aldol reaction was conducted with 5 mol% of [Cu(O*t*Bu){(*S*)-tol-binap}] (**10**) (from (*S*)-Tol-BINAP + CuO*t*Bu[13]), aldol adducts were obtained for a range of aldehydes in yields and enantioselectivities identical to those that were obtained with the corresponding Cu^{I} or Cu^{II} fluoride complexes. These observations are not only consistent with the intermediacy of a Cu^{I} alkoxide species, but also underscore the ability of a metal alkoxide to participate in the catalytic cycle. For further in-depth spectroscopic studies, this more direct approach to the catalytic cycle was employed since it avoids salt formation and redox processes.



Scheme 2. Catalytic cycle with the metalloenolate **6** as central intermediate. OTf = trifluoromethanesulfonate.

The progress of the reaction of trimethylsilyl dienolate **1**, **7**, and 5 mol% of **10** at −78 °C in THF was monitored under an inert atmosphere by IR spectroscopy (ReactIR, Figure 1).[14] The IR spectrum of the starting dienolate **1** in THF displays a characteristic resonance at 1671 cm^{-1}, which was monitored throughout the progress of the reaction. When **7** (1710 cm^{-1}) and **10** were added, a time-dependent diminution in the intensity of the bands was observed for each reactant, with the emergence of a new absorption signal at 1729 cm^{-1}, which we assigned to the aldol adduct **9**.[15]

Additional insight into the process was obtained by examination of the reaction with stoichiometric amounts of complex **10**. Thus, treatment of **1** with one equivalent of **10** resulted in rapid disappearance of the dienolate signal at 1671 cm^{-1} and the emergence of two bands at 1690 and 1550 cm^{-1},

which we assigned to the copper enolate **6**. This species was stable at −78 °C, but subsequent addition of **7** resulted in replacement of the two bands by a new resonance at 1729 cm^{-1} for adduct **8**.[15]

Metalation experiments provided supporting evidence for assignment of the resonances at 1690 and 1550 cm^{-1} to an intermediate metalloenolate (Figure 2, Scheme 3). Reaction of **1** with $(Bu_4N)Ph_3SiF_2$ produced a new species (1625 cm^{-1}), which we assigned as the naked enolate **11**.[16] Addition of one equivalent of [Cu(ClO4){(*S*)-tol-binap}][17] resulted in the

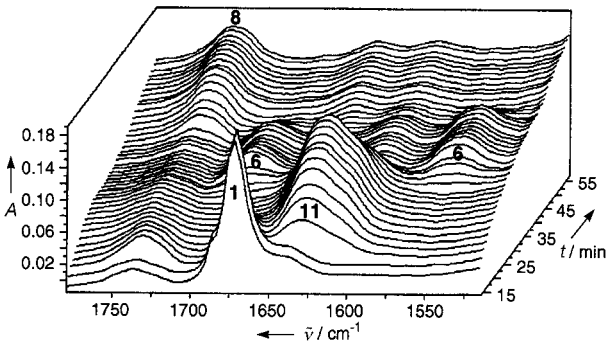


Figure 2. Metalation experiment depicted in Scheme 2 monitored by ReactIR.

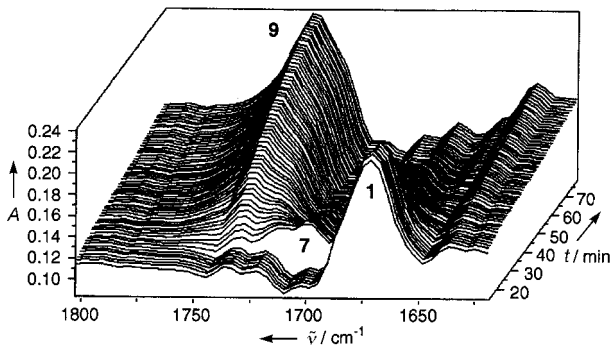
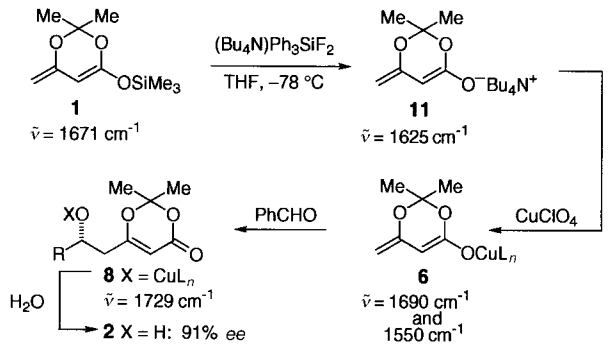


Figure 1. ReactIR of the reaction of **1**, **7**, and 5 mol% of **10**.



Scheme 3. IR absorption maxima of the participating species.

generation of the same two peaks (1690 and 1550 cm^{-1}) that were observed by direct metalation of **10** with **1**. These were also replaced by the signal corresponding to adduct **8** after the addition of **7**.[15]

In summary we have shown that tol-binap–copper(I) complexes are active catalysts for the asymmetric addition of dienolate **1** to aldehydes. Utilization of CuO*t*Bu for the preparation of the catalyst permits a more direct entry into the catalytic cycle, avoids the introduction of spectator salts, and circumvents redox chemistry. Successful initiation of the reaction by CuO*t*Bu suggests that a copper(I) alkoxide is recursively generated throughout the reaction process. Additionally, we document spectroscopic and chemical evidence for the existence of a copper enolate as a reactive species. Such a process provides a conceptual and practical alternative to the well-established Lewis acid promoted stereoselective aldol reactions. The development of asymmetric, catalytic carbonyl additions that proceed through metalloenolates offers considerable opportunities for the design of new catalysts in asymmetric organic synthesis.

Received: June 16, 1998 [Z11993IE]
German version: *Angew. Chem.* **1998**, *110*, 3312–3314

Keywords: aldol reactions · asymmetric catalysis · C–C coupling · IR spectroscopy

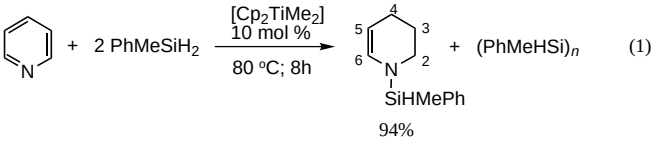
[1] For an extensive compilation of modern methods, see *Stereoselective Synthesis*, *Vol. 3* (Eds.: G. Helmchen, R. W. Hoffmann, J. Mulzer, E. Schaumann), Thieme, Stuttgart, **1996**.
[2] a) E. J. Corey, D. Barnes-Seeman, T. W. Lee, S. N. Goodman, *Tetrahedron Lett.* **1997**, *38*, 6513; b) D. A. Evans, M. J. Dart, J. L. Duffy, M. G. Yang, *J. Am. Chem. Soc.* **1996**, *118*, 4322; c) B. W. Gung, Z. Zhu, R. A. Fouch, *J. Org. Chem.* **1995**, *60*, 2860; d) S. E. Denmark, W. Lee, *J. Org. Chem.* **1994**, *59*, 707; e) A. Bernardi, A. Cassinari, A. Comotti, M. Gardner, C. Gennari, J. M. Goodman, I. Paterson, *Tetrahedron* **1992**, *48*, 4183; f) M. T. Reetz, B. Raguse, C. F. Marth, H. M. Hugel, T. Bach, D. N. A. Fox, *Tetrahedron* **1992**, *48*, 5731.
[3] a) W. W. Ellis, B. Bosnich, *Chem. Commun.* **1998**, 193; b) T. K. Hollis, B. Bosnich, *J. Am. Chem. Soc.* **1995**, *117*, 4570; c) E. M. Carreira, R. A. Singer, *Tetrahedron Lett.* **1994**, *35*, 4323; d) P. J. Pospisil, S. R. Wilson, E. N. Jacobsen, *J. Am. Chem. Soc.* **1992**, *114*, 7585.
[4] (*S*)-Tol-BINAP = (*S*)-(−)-2,2′-bis(di-*p*-tolylphosphanyl)-1,1′-binaphthyl, a commercially available bisphosphane.
[5] J. Krüger, E. M. Carreira, *J. Am. Chem. Soc.* **1998**, *120*, 837.
[6] Shibasaki has reported an aldol addition reaction of benzophenone-derived enol silanes, mediated by Pd·BINAP/H_2O/molecular sieves, which is proposed to proceed via a Pd enolate intermediate: a) M. Sodeoka, K. Ohrai, M. Shibasaki, *J. Org. Chem.* **1995**, *60*, 2648; b) Y. M. A. Yamada, N. Yoshikawa, H. Sasai, M. Shibasaki, *Angew. Chem.* **1997**, *109*, 1942; *Angew. Chem. Int. Ed. Engl.* **1997**, *36*, 1871; c) Pd enolates have also been recently postulated in imine additions: E. Hagiwara, A. Fujii, M. Sodeoka, *J. Am. Chem. Soc.* **1998**, *120*, 2474; d) E. R. Burkhardt, R. G. Bergman, C. H. Heathcock, *Organometallics* **1990**, *9*, 30; e) G. A. Slough, R. G. Bergman, C. H. Heathcock, *J. Am. Chem. Soc.* **1989**, *111*, 938.
[7] For related processes wherein alkaline earth or lanthanide enolates are generated by deprotonation, see a) D. A. Evans, S. G. Nelson, *J. Am. Chem. Soc.* **1997**, *119*, 6452; b) M. Shibasaki, H. Sasai, T. Arai, *Angew. Chem.* **1997**, *109*, 1290; *Angew. Chem. Int. Ed. Engl.* **1997**, *36*, 1237.
[8] A. Yanagisawa, Y. Matsumoto, H. Nakashima, K. Asakawa, H. Yamamoto, *J. Am. Chem. Soc.* **1997**, *119*, 9319.
[9] D. A. Evans, M. C. Kozlowski, C. S. Burgy, D. W. C. MacMillan, *J. Am. Chem. Soc.* **1997**, *119*, 7893.
[10] S. Kanemasa, Y. Oderaotoshi, S. Sakaguchi, H. Yamamoto, J. Tanaka, E. Wada, D. P. Curran, *J. Am. Chem. Soc.* **1998**, *120*, 3074.
[11] a) Y. Kobayashi, T. Taguchi, T. Morikawa, E. Tokuno, S. Sekiguchi, *Chem. Pharm. Bull.* **1980**, *28*, 262; b) F. H. Jardine, L. Rule, A. G. Vohra, *J. Chem. Soc. A* **1970**, 238.
[12] The depiction of **6** as an O-bound copper dienolate is not meant to suggest any detailed structural information regarding the nature of **6**.
[13] For the preparation of CuO*t*Bu, see T. Tsuda, T. Hashimoto, T. Saegusa, *J. Am. Chem. Soc.* **1972**, *94*, 658.
[14] The IR experiments were conducted with an ASI Applied Systems ReactIR 1000 spectrometer with a MCT detector (MCT = mercury cadmium telluride) and a DiComp probe.
[15] In these and all reactions the product was isolated in 91–94% *ee*, values which are similar to those we routinely obtain for this process under preparative conditions.
[16] In a control experiment, the quaternary ammonium dienolate was found to react rapidly with benzaldehyde at −78 °C to form racemic aldol adduct in 94% yield.
[17] $[Cu(CH_3CN)_4]ClO_4$ was prepared by the procedure described by Kubas: G. J. Kubas, *Inorg. Syn.* **1990**, *28*, 68.

Homogeneous Catalytic Hydrosilylation of Pyridines**

Leijun Hao, John F. Harrod,* Anne-Marie Lebuis, Ying Mu, Ronghua Shu, Edmond Samuel,* and Hee-Gweon Woo

Titanocene complexes are versatile catalysts for a large number of reactions.[1–11] The reaction of Me_3SiH with pyridine catalyzed by *heterogeneous* platinum-group catalysts was reported many years ago.[12] We now report the first examples of the hydrosilylation of pyridines with *homogeneous,* titanocene-based catalysts, and the first example of homogeneously catalyzed hydrosilylation of an aromatic substrate.

Typically, the reaction was carried out without solvent with a 2:1 molar ratio of silane to pyridine and 10 mol% of $[Cp_2TiMe_2]$ (based on pyridine) at 80 °C [Eq. (1)], but an inert



(1)

[*] Prof. Dr. J. F. Harrod, Dr. L. Hao, Dr. A.-M. Lebuis, Dr. Y. Mu, R. Shu, Dr. H.-G. Woo
Department of Chemistry, McGill University
Montreal, PQ H3A 2K6 (Canada)
Fax: (+1) 514-398-3797
E-mail: harrod@omc.lan.mcgill.ca
Dr. E. Samuel
Laboratoire de Chimie Organométallique de l'ENSCP
(URA 403 CNRS)
11 rue P. et M. Curie, 75005 Paris (France)
Fax: (+33) 1-4326-0061

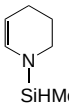
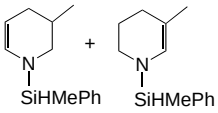
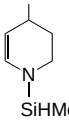
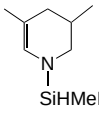
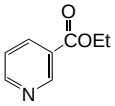
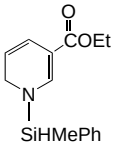
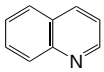
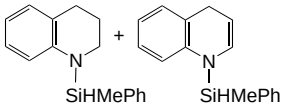
[**] This work was supported by the Natural Sciences and Engineering Research Council (Canada) and the Fonds FCAR du Quebec. We thank Dr. J. Britten for collecting the X-ray data set of **1b**.

 © WILEY-VCH Verlag GmbH, D-69451 Weinheim, 1998 1433-7851/98/3722-3126 $ 17.50+.50/0

hydrocarbon solvent, such as toluene, may be added if desired. The ^{1}H NMR spectrum of the crude products showed that the yields of hydrosilylated pyridines were in the range of 80–100%.

The results of the catalytic hydrosilylation of pyridine and several derivatives are summarized in Table 1. These show that 1) $[Cp_2TiMe_2]$ is an effective precatalyst for the hydrosilylation of pyridines and quinoline, with the formation of a

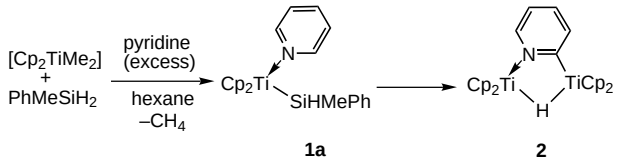
Table 1. Titanocene-catalyzed hydrosilylation/hydrogenation of pyridines.[a]

Entry	Pyridine	Product	Yield [%][b]
1			94
2			85 (3:2)
3			83
4			70
5			100
6			74 (3:1)

[a] All reactions were carried out neat at 80 °C with 10 mol% $[Cp_2TiMe_2]$ (relative to pyridine), the ratio of silane to pyridine was 2:1. [b] Based on the ^{29}Si NMR spectrum.

Si–N bond, 2) the reaction tolerates certain functional groups (entry 5), and 3) hydrogenation of the intermediate *N*-silyl-1,2-dihydropyridine sometimes occurs (entries 1–3) in a manner that is strongly dependent on the location of the substituents on the pyridine ring (entry 4). Substrates with methyl substituents in the 2- and/or 6-positions of the pyridine ring do not react under the conditions used.

Model stoichiometric reactions provide insight into the general pathway of the catalytic hydrosilylation reactions. Reaction of $[Cp_2TiMe_2]$ and $PhMeSiH_2$ (1:2 molar ratio) in the presence of excess pyridine in hexane/toluene (6/1) proceeded smoothly to give first the complex **1a**, as demonstrated by EPR spectroscopy and a color change of the solution from yellow to violet (Scheme 1). After one hour the violet solution had changed to dark brown, and brown-black,



1a **2**

Scheme 1. Illustration of the sequential formation of **1a** and **2**.

square-plate crystals of **2** precipitated when the solution was cooled to −20 °C for 24 h.

When Ph_2SiH_2 or $PhSiH_3$ replaced $PhMeSiH_2$ in the reaction, **1b** or **1c** was obtained, respectively. However, unlike **1a**, **1b** and **1c** did not undergo further reaction to **2**, and they are stable for several days at ambient temperatures in the presence of excess pyridine. These differences in thermal stability are reminiscent of the analogous silylphosphane complexes: $[Cp_2Ti(SiH_2Me)(PMe_3)]$ decomposes readily to give the hydride $[Cp_2TiH(PMe_3)]$, whereas compounds of the type $[Cp_2Ti(SiHR_2)(PMe_3)]$ ($R_2 = Ph_2$, PhH, H_2) are relatively stable under the same conditions.[13] Compounds **1b** and **1c** were isolated in good yield as dark violet crystals when the reaction was carried out in hexane.

$[Cp_2Ti(SiHMePh)(C_5H_5N)]$ **1a**

$[Cp_2Ti(SiHPh_2)(C_5H_5N)]$ **1b**

$[Cp_2Ti(SiH_2Ph)(C_5H_5N)]$ **1c**

$[Cp_2Ti(\mu\text{-H})(1\kappa N,2\kappa C\text{-pyridyl})TiCp_2]$ **2**

Complexes **1** exhibit characteristic EPR spectra. The spectrum of **1a** contains a pseudoquartet at $g = 1.9882$ due to the interaction of the unpaired electron with the ^{14}N nucleus ($a_N = 1.91$ G, $I = 1$) of the pyridine and the ^{1}H nucleus ($a_H = 2.16$ G, $I = 1/2$) of the silyl group, and well-resolved satellites due to the titanium nuclei ($a_{Ti} = 9.79$ G, ^{49}Ti, 7.75%, $I = 5/2$ and ^{47}Ti, 5.51%, $I = 7/2$). The spectrum of **1b** is, as expected, very similar to that of **1a** ($g = 1.9881$, $a_N = 1.92$ G, $a_H = 2.20$ G, $a_{Ti} = 9.75$ G), whereas the spectrum of **1c** contains a pseudoquintet at $g = 1.988$ with $a_N = 3.3$ G, $a_H = 2.30$ G, $a_{Ti} = 10.3$ G. Upon replacement of Si–H by Si–D, the spectra of **1** all simplify to a triplet (coupling to the ^{14}N nucleus) due to the much smaller (unresolved) superhyperfine coupling with D as opposed to H. The structure of **1b** was confirmed by X-ray crystallographic analysis (Figure 1).[14]

A single-crystal X-ray structure analysis of **2** revealed that it is a unique bimetallic titanocene(III) complex with one hydride and one pyridyl group as bridging ligands (Figure 2).[14] The Ti–Ti distance of 3.602(2) Å is too long for a metal–metal bond. The EPR spectrum of **2** in toluene displays a broad singlet ($g = 1.984$; $a_{Ti} = 12$ G; toluene, 250 K). The ^{1}H NMR spectrum of a saturated solution of **2** in toluene shows a very broad, paramagnetically shifted resonance at $\delta = 31.6$ ($\nu_{1/2} \approx 1080$ Hz), which is tentatively assigned to the Cp protons in **2**.

The formation of **2** can be rationalized according to Scheme 2. First, **1a** decomposes to generate the hydride **3**. Such a decomposition reaction has been seen in the analogous silylphosphane complexes.[13] The pyridine ligand of **3** then undergoes α-metalation and loss of H_2 to give **4**, which then

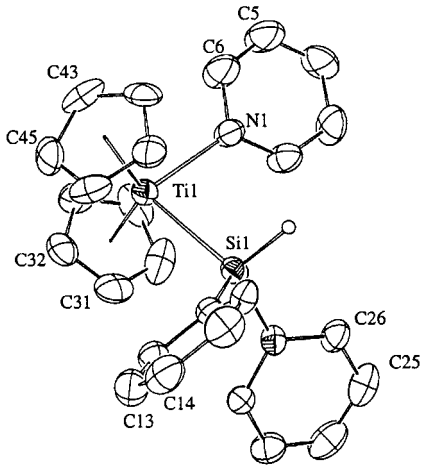


Figure 1. ORTEP drawing of the molecular structure of one of the two conformers of **1b** (thermal ellipsoids at the 30% probability level). Selected bond lengths [Å] and angles [°]: Ti1–N1 2.292(8), Ti1–Si1 2.678(3); Si1-Ti1-N1 87.2(2), Cp-Ti1-Cp 135.49(9), angle between the Si-Ti-N plane and plane of the pyridine ring 28.8(4).

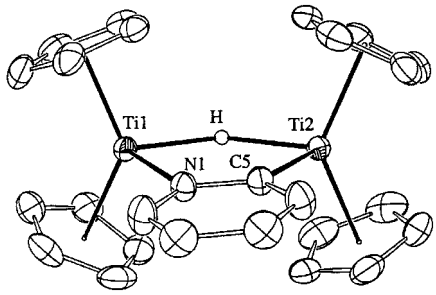
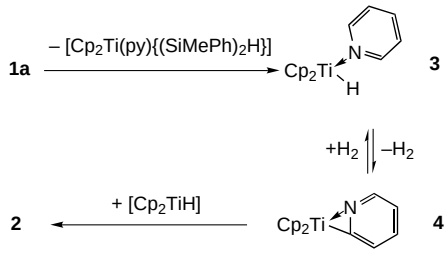


Figure 2. ORTEP drawing of the molecular structure of **2** (thermal ellipsoids at the 30% probability level). Selected bond lengths [Å] and angles [°]: Ti1–H 1.92(2), Ti2–H 1.91(2), Ti1–N1 2.202(2), Ti2–C5 2.205(2); H-Ti1-N1 79.2(9), H-Ti2-C5 79.1(9), Cp-Ti1-Cp 131.38(2), Cp-Ti2-Cp 132.25(2).

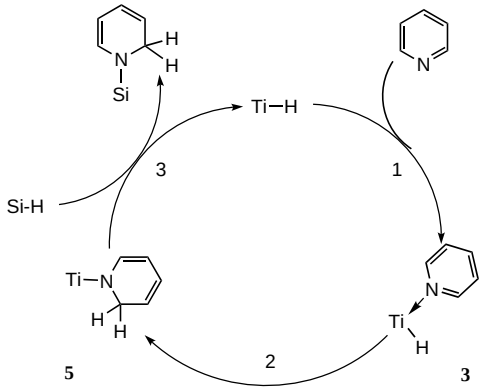


Scheme 2. Proposed mechanism for the formation of **2**.

reacts with another molecule of **3** to produce the pyridyl-bridged dimer **2**. A similar α-metalation process has also been reported for $[Cp_2Ti(alkyl)(py)]$ complexes.[15] *ortho*-Metalations of pyridine by other early transition metals have also been reported.[16–18] The hydride complex **3** was not observed directly in the hydrosilylation reactions, probably due to its high reactivity. A sample of **3**, generated from the reaction of $[\{Cp_2TiH\}_2]$[19] and pyridine at $-20\,^{\circ}C$, decomposes immediately upon warming to ambient temperatures to give **2** and a minor amount of **4** ($g = 1.9905$, which is close to the value of $g = 1.990$ for the analogous complex $[Cp_2Ti(\eta^2\text{-}N,C\text{-}2\text{-}MeC_5H_3N)]$).[15]

Experiments with $PhMeSiD_2$ and C_5H_5N, or $PhMeSiH_2$ and C_5D_5N gave products (entry 1, Table 1) in which H/D exchange was much more extensive at the 2- and 6-positions than at other positions of both the products and unchanged pyridine. Extensive H/D exchange also occurred at the 2- and 6-positions of pyridine when 1 atm of H_2 was applied to a solution containing 10 mol% of $[\{Cp_2TiH\}_2]$ in C_5D_5N.[19] Under 15 atm of H_2 complete exchange occurred at the 2- and 6-positions of the pyridine. These H/D exchange results support the mechanism depicted in Scheme 2, and can be easily rationalized by the reversibility between **3** and **4**.

These results show that the hydride **3** is, most likely, the key intermediate for the formation of **2**, H/D exchange, and hydrosilylation/hydrogenation reactions. The simplest mechanism for the hydrosilylation reaction, which conforms to all of the experimental data, is depicted in Scheme 3. In this



Scheme 3. Proposed mechanism of the catalytic hydrosilylation.

mechanism, formation of **3** (step 1) is followed by insertion of the N=C bond into the Ti–H bond (step 2) to give **5,** which then undergoes σ-bond metathesis with silane to regenerate Cp_2TiH with release of *N*-silyl-1,2-dihydropyridine. The further facile hydrogenation of the latter to the observed products in the presence of excess silane is expected, since it is well known that olefinic substrates (and in particular dienes) are very efficient hydrogen traps in silane dehydrocoupling reactions.[9] In hydrosilations where further reduction of another double bond occurs, 1,2-dimethyl-1,2-diphenyldisilane and higher oligosilanes are always observed in amounts commensurate with dehydrocoupling/cohydrogenation. If only one mole of silane is used per mole of pyridine, the products remain the same, but the conversion is reduced to less than 50%. In these cases, the hydrogenation step is more rapid than the hydrosilation step. Any absence of hydrogenation is explained by either steric hindrance (entry 4) or electronic deactivation (entry 5). When the reaction with 3,5-lutidine (entry 4) was carried out under 20 atm of H_2, and the reaction time extended to 8 days, diene and monoene were obtained in a ratio of 1:2.

In summary, we have demonstrated the unprecedented homogeneous catalytic hydrosilylation of an aromatic compound and followed several of the elementary steps of the reactions. Our homogeneous catalyst system has high selectivity towards the hydrosilylation of pyridines compared to

 © WILEY-VCH Verlag GmbH, D-69451 Weinheim, 1998 1433-7851/98/3722-3128 $ 17.50+.50/0

the previous heterogeneous system, and tolerates some substituents. Study of the catalyst intermediates suggests that the hydride [Cp_2TiH] is a key reactant in the catalytic cycle, as previously proposed for a number of other titanocene-catalyzed reactions.

Experimental Section

1b: [Cp_2TiMe_2] (50 mg, 0.24 mmol) was dissolved in a mixture *n*-hexane/toluene (4/1, 5 mL), pyridine (0.10 mL, 1.2 mmol), and phenylsilane (0.11 mL, 0.72 mmol). Over about one hour, the solution slowly changed color from orange to dark violet. This was accompanied by a slow gas evolution and the formation of violet, needle-shaped crystals of **1b**·$0.25\,C_5H_5N$. The crystals were separated, washed several times with cold hexane, and dried under vacuum (yield: 95 mg, 87%). Elemental analysis for $C_{27}H_{26}NSiTi$ (440.47): found (calcd): C 72.83 (73.62); H 5.99 (5.95); N 3.22 (3.18); Si 5.98 (6.37); Ti 10.26 (10.87). The deuterated form of **1b** was prepared with Ph_2SiD_2 instead of Ph_2SiH_2.

2: [Cp_2TiMe_2] (120 mg, 0.58 mmol) was added to a solution of phenylmethylsilane (0.24 mL, 1.73 mmol) and pyridine (1.0 mL, 12.4 mmol) in *n*-hexane/toluene (6/1; 7.0 mL). The solution turned deep violet after 2 hr without stirring, and dark brown after about a further 1 h. The solution was held at ambient temperatures for another 4 h and at $-20\,^\circ C$ for 24 h to yield dark brown plates suitable for X-ray chrystallographic analysis (yield: 83 mg, 56%). Elemental analysis for $C_{26}H_{26}Ti_2N$ (448.25): found (calcd): C 66.27 (68.98); H 5.12 (5.79); N 3.04 (3.22); Ti 22.33 (22.01).

General procedure for the catalytic hydrosilylation/hydrogenation: $PhMeSiH_2$ (1.20 mL, 8.75 mmol) and pyridine (0.35 mL, 4.34 mmol) were added to [Cp_2TiMe_2] (0.45 g, 0.43 mmol) in a Schlenk tube. After a short time at room temperature the solution turned blue-violet, and gas was evolved. The mixture was stirred at $80\,^\circ C$ for 8 h and then distilled under vacuum to give pure *N*-(phenylmethylsilyl)-1,2,3,4-tetrahydropyridine (entry 1) (b.p. $57\,^\circ C/0.12$ Torr; yield: 0.88 g, 50%). NMR analysis of the undistilled reaction mixture showed 94% conversion of pyridine. ^1H NMR (499.9 MHz, C_6D_6): $\delta = 0.28$ (d, 3H, $J = 3.3$ Hz, $SiCH_3$), 1.57 (m, 2H, C5-H), 2.00 (m, 2H, C4-H), 2.99 (m, 2H, C6-H), 4.62 (m, 1H, C3-H), 5.01 (q, 1H, $J = 3.3$ Hz, SiH), 6.28 (dt, 1H, $^3J = 7.8$ Hz, $^4J = 3.0$ Hz, C2-H), 7.20 (m, 3H, *m*,*p*-C_6H_5), 7.50 (m, 2H, *o*-C_6H_5); ^{13}C NMR (125.7 MHz, C_6D_6): $\delta = -0.50$ ($SiCH_3$), 22.16, 23.44, 43.79 (C2, C3, C4), 98.69, 123.49 (C5, C6), 128.18, 129.48, 130.13, 134.40 (Ph); ^{29}Si NMR (59.9 MHz, C_6D_6): $\delta = -9.10$; MS (70 eV): *m*/*z* (%): 203 (100) [M^+], 188 (18.5) [$M^+ - Me$], 121 (77) [$M^+ - C_5H_8N$].

Received: May, 25 1998 [Z11893IE]
German version: *Angew. Chem.* **1998**, *110*, 3314 – 3318

Keywords: homogeneous catalysis · hydrogenations · hydrosilylations · pyridines · titanium

[1] a) C. Aitken, J. F. Harrod, E. Samuel, *J. Organomet. Chem.* **1985**, *279*, C11; b) C. Aitken, J. F. Harrod, E. Samuel, *J. Am. Chem. Soc.* **1986**, *108*, 4059; c) L. S. Chang, E. R. Corey, *Organometallics* **1987**, *6*, 1595; d) L. S. Chang, J. Y. Corey, *Organometallics* **1989**, *8*, 1885; e) J. Y. Corey, X.-H. Zhu, T. C. Bedard, L. D. Lange, *Organometallics* **1991**, *10*, 924.

[2] C. Aitken, J. F. Harrod, A. Malek, E. Samuel, *J. Organomet. Chem.* **1988**, *349*, 285.

[3] H. Q. Liu, J. F. Harrod, *Organometallics* **1992**, *11*, 822.

[4] J. He, H. Liu, J. F. Harrod, R. Hynes, *Organometallics* **1994**, *13*, 336.

[5] H. Liu, J. F. Harrod, *Can. J. Chem.* **1990**, *68*, 1100.

[6] a) M. B. Carter, B. Schiott, A. Gutiérrez, S. L. Buchwald, *J. Am. Chem. Soc.* **1994**, *116*, 11670; b) S. Xin, J. F. Harrod, *J. Organomet. Chem.* **1995**, *499*, 181; c) S. Xin, J. F. Harrod, *Can. J. Chem.* **1995**, *73*, 999.

[7] R. D. Broene, S. L. Buchwald, *J. Am. Chem. Soc.* **1993**, *115*, 12659.

[8] C. A. Willoughby, S. L. Buchwald, *J. Am. Chem. Soc.* **1994**, *116*, 11631.

[9] J. F. Harrod, S. S. Yun, *Organometallics* **1987**, *6*, 1381.

[10] N. M. Kablaoui, S. L. Buchwald, *J. Am. Chem. Soc.* **1996**, *118*, 3182.

[11] T. Grasczyk, J. F. Harrod, *J. Polymer Sci. Part A* **1994**, *32*, 3183.

[12] N. C. Cook, J. E. Lyons, *J. Am. Chem. Soc.* **1965**, *87*, 3283; **1966**, *88*, 3396.

[13] L. Hao, A.-M. Lebuis, J. F. Harrod, *Chem. Commun*. **1998**, 1089.

[14] a) Crystal structure analysis of **1b**·$0.25\,C_5H_5N$: crystal dimensions $0.20 \times 0.11 \times 0.06$ mm^3, monoclinic, $P2_1/n$, $a = 18.991(1)$, $b = 8.356(1)$, $c = 31.381(2)$ Å, $\beta = 105.270(1)^\circ$, $V = 4804.3(4)$ Å^3, $T = 300(2)$ K, $Z = 8$ ($Z' = 2$), smart CCD P4 diffractometer (Siemens) $Mo_{K\alpha}$ radiation ($\lambda = 0.71073$ Å), 37192 measured reflections, 9317 independent and 3084 observed reflections [$I > 2\sigma(I)$], 573 refined parameters, $R_1 = 0.1327$, $wR_2 = 0.1446$.[14c] b) Crystal structure analysis of **2**·$0.5\,C_5H_5N$: crystal dimensions $0.75 \times 0.57 \times 0.21$ mm^3, monoclinic, $P2_1/n$, $a = 16.742(8)$, $b = 8.039(3)$, $c = 18.266(9)$ Å, $\beta = 114.03(1)^\circ$, $V = 2245(2)$ Å^3, $T = 220(2)$ K, $Z = 4$, CAD4 diffractometer (Enraf-Nonius), $Cu_{K\alpha}$ radiation ($\lambda = 1.54056$ Å), 18971 reflections measured, 4264 independent and 3876 observed reflections [$I > 2\sigma(I)$], 284 refined parameters, $R_1 = 0.0502$, w$R_2 = 0.1282$. The bridging hydrogen atom was located in the difference map.[14c] c) Crystallographic data (excluding structure factors) for the structures reported in this paper have been deposited with the Cambridge Crystallographic Data Centre as supplementary publication nos. CCDC-102515 (**2**) and CCDC-102516 (**1b**). Copies of the data can be obtained free of charge on application to CCDC, 12 Union Road, Cambridge CB21EZ, UK (fax: (+44) 1223-336-033; e-mail: deposit@ccdc.cam.ac.uk).

[15] a) E. Klei, J. H. Teuben, *J. Organomet. Chem.* **1981**, *214*, 53; b) E. Klei, J. H. Teuben, *J. Chem. Soc. Chem. Commun.* **1978**, 659.

[16] K. H. Den Haan, Y. Wielstra, J. H. Teuben, *Organometallics* **1987**, *6*, 2053.

[17] L. C. Francesconi, D. R. Corbin, D. N. Hendrickson, G. D. Stucky, *Inorg. Chem.* **1978**, *17*, 2078; L. C. Francesconi, D. R. Corbin, D. N. Hendrickson, G. D. Stucky, **1979**, *18*, 3074; L. C. Francesconi, D. R. Corbin, D. N. Hendrickson, G. D. Stucky, *Inorg. Chem.* **1981**, *20*, 2059.

[18] R. Jungst, D. Sekutiwski, J. David, M. Luly, G. D. Stucky, *Inorg. Chem.* **1977**, *16*, 1645.

[19] a) J. E. Bercaw, H. H. Brintzinger, *J. Am. Chem. Soc*. **1969**, *91*, 7301; b) R. H. Marvich, H. H. Brintzinger, *J. Am. Chem. Soc*. **1971**, *93*, 2046.

Synthesis of β-Mannosides via Prearranged Glycosides**

Thomas Ziegler* and Gregor Lemanski

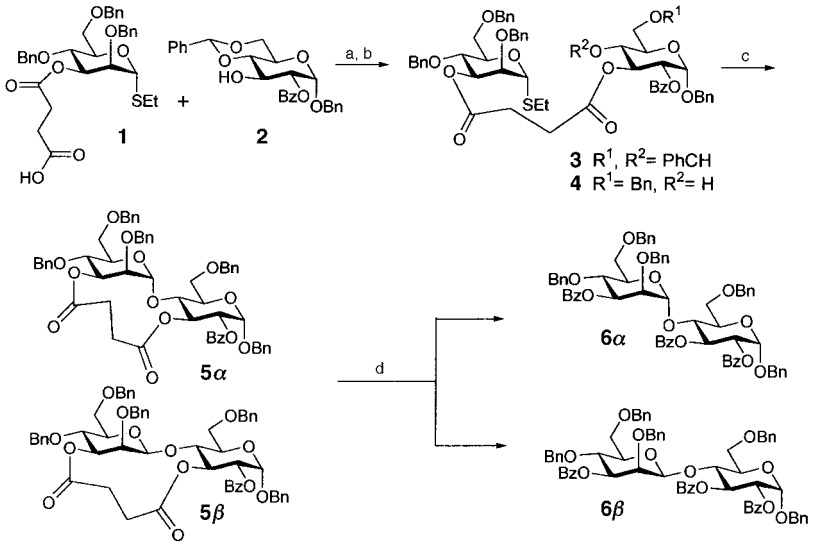
Although the chemical synthesis of oligosaccharides has reached a remarkable level several problematic cases of the diastereoselective formation of O-glycosidic bonds demand improvements. In particular, 1,2-*cis*-configurated O-glycosides are often realized solely with difficulties or with significant synthetic efforts. This is especially the case for saccharides that contain β-D-mannosidic and β-L-rhamnosidic linkages. Similarly, α-linked D-galactosyl and D-glucosyl residues are difficult to establish in some cases.

The Koenigs – Knorr reaction in combination with the silver silicate promotor developed by Paulsen et al. is still applied often to the synthesis of β-D-mannosidic and β-L-rhamnosidic linkages.[1] Since this glycosylation procedure and related

[*] Prof. Dr. T. Ziegler, Dipl.-Chem. G. Lemanski
Institut für Organische Chemie der Universität
Greinstrasse 4, D-50939 Köln (Germany)
Fax: (+49) 221-470-5057
E-mail: Thomas.Ziegler@Uni-Koeln.de

[**] Prearranged Glycosides, Part 7. Part 6: T. Ziegler, G. Lemanski, *Eur. J. Org. Chem.* **1998**, 163 – 170.

variants[2] are most often only applicable to reactive glycosyl donors and acceptors or to special cases[3] efficient alternatives have been developed in recent years that allow for the selective preparation of 1,2-*cis*-configurated glycosides. The latter are accessible from 2-ulosyl bromides as glycosyl donors by diastereoselective reduction of the carbonyl group.[4] Similarly, β-mannosides can be prepared from β-glucosides by Walden inversion of position 2 by S_N2 reactions.[5] Another method that has been investigated recently for the stereoselective synthesis of 1,2-*cis*-configurated O-glycosides is intramolecular glycosylation.[6] Here, the aglycon is linked first by a labile tether to the glycosyl donor. Next, the aglycon is "delivered" intramolecularly to the anomeric center during glycosylation. However, recent investigations of similar potential intramolecular glycosylations showed that an intermolecular mechanism may also be operative.[7] Furthermore, intramolecular glycosylations involving labile tethers are not suited in all instances to the formation of β-L-rhamnosidic linkages.[8]



Scheme 1. Reagents and conditions: a) **1** (1.0 equiv), **2** (1.0 equiv), DCC (1.2 equiv), CH_2Cl_2, RT, 23 h, 71 % **3**; b) **3** (1.0 equiv), $NaCNBH_3$ (12.5 equiv), HCl in Et_2O, THF, 0 °C, 5 min, 77 % **4**; c) **4** (1.0 equiv), *N*-iodosuccinimide (5.0 equiv), cat. trifluoromethanesulfonate, MeCN, −30 °C, 10 min, 66 % ***5α***; **4** (1.0 equiv), MeOTf (5.0 equiv), MeCN, RT, 3 h, 64 % ***5β***; d) ***5α*** (1.0 equiv), cat. NaOMe, MeOH, RT, 24 h, then BzCl (5.0 equiv), pyridine, RT, 24 h 77 % ***6α***; ***5β*** (1.0 equiv), cat. NaOMe, MeOH, RT, 24 h, then BzCl (5.0 equiv), pyridine, RT, 24 h 76 % ***6β***.

Recently we disclosed a "true" intramolecular glycosylation protocol in which a suitable glycosyl donor and a glycosyl acceptor were linked together by a stable bridge.[8, 9] The following intramolecular glycosylation step leaves the bridge intact and governs the anomeric outcome of the condensation.[10] The glycosylation variant via "prearranged glycosides" can be extended to regioselective glycosylations as well.[11] Although this variant is well suited for the construction of β-L-rhamnosidic, α-D-glucosidic, and α-D-galactosidic linkages it could not be extended yet to the synthesis of biologically important β-D-mannosides.[9] Herein we present methods for linking donor and acceptor that allow for the highly selective formation of β-mannosidic linkages via prearranged glycosides.

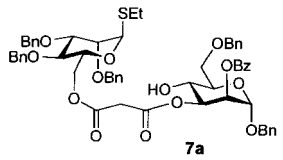
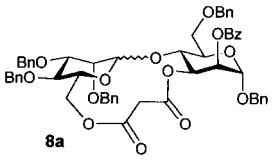
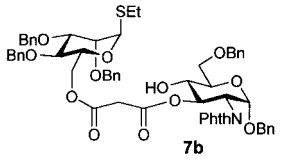
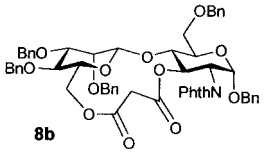
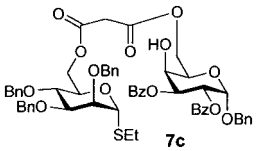
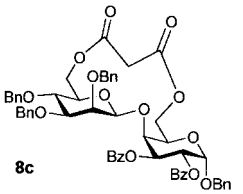
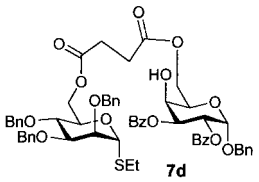
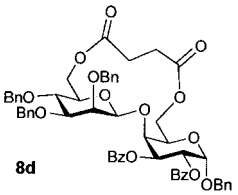
Previously, we used succinyl tethers for the construction of β-D-mannosidic linkages via prearranged glycosides. Similarly to the respective L-rhamnosyl donors, these tethers were used to link the mannosyl donor via its position 2 or 6 with a glycosyl acceptor. However, these mannosylations of appropriate glycosyl acceptors afforded an anomeric ratio α:β of 30:70 (for D-Man*p*-(1→4)-L-Glc*p*[10]), whereas the corresponding β-L-rhamnosides were formed in high yield.[9] Since during intramolecular glycosylation via prearranged glycosides a double diastereoselection influences the anomeric selectivity,[10] and furthermore, solely β-L-Rha*p*-(1→4)-D-Glc*p* disaccharides were obtained from L-rhamnosyl donors with a succinyl bridge at position 3,[9b] 3-O-succinyl-tethered mannosyl donors should afford the corresponding β-D-Man*p*-(1→4)-D-Glc*p* disaccharides.

Indeed, with activation by *N*-iodosuccinimide (NIS) in acetonitrile the intramolecular mannosylation of the prearranged glycoside **4** afforded solely the β-(1→4)-linked disaccharide ***5β***. The latter was characterized as ***6β*** after cleavage of all acyl groups and subsequent rebenzoylation (Scheme 1). In the ^{13}C NMR spectrum the CH coupling constant of $^1J = 158.5$ Hz at the anomeric center of the mannosyl residue in ***6β*** proves the β-configuration unambiguously.[12] Compound **4** is readily accessible from ethyl 1-thio-2,4,6-tri-*O*-benzyl-α-D-mannopyranoside via intermediates **1**–**3**, as described for the corresponding rhamnosylations.[9b] In contrast, activation of **4** with methyl trifluoromethanesulfonate (MeOTf) instead of NIS affords the corresponding α-(1→4)-linked disaccharide ***5α*** (once again characterized as ***6α*** showing a coupling constant of $^1J = 170.9$ Hz). The strong dependence of the anomeric selectivity of the intramolecular mannosylation on the activation procedure is surprising. However, a similar dependence was previously observed for comparable rhamnosylations in less pronounced form.[9b] Thus, α- or β-D-mannosidic linkages can now be established selectively from compound **4** by simple choice of the activator (NIS or MeOTf) for the glycosylation step.

Previous attempts toward intramolecular (1→4)-mannosylations of glycosyl acceptors via prearranged glycosides with a succinyl tether at postion 6 (mannosyl donor) and position 3 (glucosyl acceptor) resulted in low β-selectivities.[9c, 10] However, if the tether is shortened as realized in compound **7** (a malonyl instead of a succinyl tether), excellent selectivities are obtained for β-mannosyl saccharides **8** (Table 1). It is noteworthy that the anomeric selectivity of the intramolecular mannosylation of the glycoside **7** does not strongly depend on the activation procedure but on the glycosyl acceptor. For β-mannosylations (c.f. **7c** and **7d** in Table 1) even the length of the tether has no influence on the selectivity of the glycosylation. Solely the selectivity in case of the disaccharide β-D-Man-(1→4)-D-Man **8a** remains unsatisfactory and needs further optimization. Excellent β-selectivities are observed for the disaccharides β-D-Man-(1→4)-D-Glc ***5β***, β-D-Man-(1→4)-D-GlcN **8b**, and β-D-Man-(1→4)-D-Gal **8c** and **8d**,

 © WILEY-VCH Verlag GmbH, D-69451 Weinheim, 1998 1433-7851/98/3722-3130 $ 17.50+.50/0 *Angew. Chem. Int. Ed.* **1998**, *37*, No. 22

Table 1. Reaction of various prearranged glycosides **7** with *N*-iodosuccinimide (NIS) or methyl trifluoromethanesulfonate (MeOTf) to give the disaccharides **8**.[a]

Prearranged glycoside	Disaccharide	Activator	Yield	α:β
 **7a**	 **8a**	NIS	71 %	67:33
		MeOTf	72 %	50:50
 **7b**	 **8b**	NIS	51 %	0:100
		MeOTf	50 %	0:100
 **7c**	 **8c**	NIS	50 %	0:100
		MeOTf	55 %	0:100
 **7d**	 **8d**	MeOTf	53 %	0:100

[a] Reaction conditions are as described in Scheme 1 under c). Bn = benzyl, Bz = benzoyl, Phth = phthaloyl.

which all can now be applied to the synthesis of complex oligosaccharides.

Experimental Section

6α: 4 Å Molecular sieves (1.32 g) and **4c** (0.55 g, 0.53 mmol) were stirred under Ar for 10 min at 20 °C in MeCN (20 mL), and MeOTf (0.33 g, 2.65 mmol) was added. After stirring for 3 h the mixture was neutralized with Et_3N, diluted with CH_2Cl_2, and filtered through a layer of Celite. The filtrate was washed with water, dried, and concentrated. Chromatography of the residue toluene/ethyl acetate 20:1 on silica gel afforded **5α** (0.33 g, 64 %). Compound **5α** (0.21 g, 0.21 mmol) and a catalytic amount of NaOMe were stirred in MeOH/CH_2Cl_2 (1:2, 10 mL) for 24 h at 20 °C, neutralized by addition of Dowex H^+ ion exchange resin, filtered, and concentrated. The residue was dissolved in pyridine (5 mL), and benzoyl chloride (122 µL, 1.05 mmol) was added. After stirring for 24 h at 20 °C, the mixture was poured into ice-water, and extracted with CH_2Cl_2. The combined organic layers were subsequently washed with aqueous HCl and $NaHCO_3$ solution, dried, and concentrated. Chromatography of the residue in *n*-hexane/ethyl acetate 4:1 on silica gel afforded **6α** (0.15 g, 76 %). $[\alpha]_D^{20} = +43.6$ ($c = 1.8$ in $CHCl_3$); ^{1}H NMR ($CDCl_3$, 25 °C, 300 MHz, signals of benzoyl and benzyl groups are not given): $\delta = 6.10$ (dd, 1H, $J_{2,3} = 10.3$, $J_{3,4} = 9.2$ Hz; H-3), 5.60 (dd, 1H, $J_{2,3} = 3.0$, $J_{3,4} = 9.4$ Hz; H-3′), 5.33 (d, 1H, $J_{1,2} = 3.8$ Hz; H-1), 5.19 (dd, 1H; H-2), 5.14 (d, 1H, $J_{1,2} = 1.8$ Hz; H-1′), 4.40 (t, 1H, $J_{4,5} = 9.5$ Hz; H-4′), 4.13 (t, 1H, $J_{4,5} = 9.3$ Hz; H-4), 4.03 – 3.98 (m, 1H, $J_{5,6a} = 4.1$, $J_{5,6b} = 2.0$ Hz; H-5), 3.95 (dd, 1H, $J_{6a,6b} = -11.2$ Hz; H-6a), 3.86 – 3.80 (m, 2H, $J_{5,6b} = 3.1$, $J_{6a,6b} = -11.6$ Hz; H-5′,6a′), 3.84 (dd, 1H; H-2′), 3.73 (dd, 1H; H-6b), 3.74 (dd, 1H; H-6b′); ^{13}C NMR ($CDCl_3$, 25 °C, 75.46 MHz, signals of benzoyl and benzyl groups are not given): $\delta = 98.8$ ($J_{C\text{-}1,H\text{-}1} = 170.9$ Hz; C-1′), 95.1 (C-1), 77.7 (C-2′), 76.3 (C-4), 75.6 (C-4′), 73.9, 73.7, 73.5 (C-3,3′,5′), 72.4 (C-2), 70.2 (C-5), 68.8, 68.5 (C-6,6′); elemental analysis: calcd. for $C_{68}H_{64}O_{14}$: C 73.90, H 5.84; found.: C 74.05, H 5.93.

6β: 4 Å Molecular sieves (2 g), **4c** (0.94 g, 0.9 mmol), and NIS (1.01g, 4.5 mmol) were stirred under Ar for 20 min at 20 °C in MeCN (30 mL). The mixture was cooled to −30 °C and TMSOTf (41 µL, 0.25 mmol) was added. After stirring for 10 min, the mixture was neutralized with pyridine, diluted with CH_2Cl_2, and filtered through a layer of Celite. The filtrate was washed subsequently with aqueous $Na_2S_2O_3$ and $NaHCO_3$ solution, dried, and concentrated. Chromatography of the residue with toluene/ethyl acetate 20:1 on silica gel afforded **5β** (0.59 g, 66 %). The deacylation and rebenzoylation of **5β** (0.16 g, 0.16 mmol) as described for **6α** afforded **6β** (0.14 g, 76 %). $[\alpha]_D^{20} = -32.2$ ($c = 1.1$ in $CHCl_3$); ^{1}H NMR ($CDCl_3$, 25 °C, 300 MHz, signals of benzoyl and benzyl groups are not shown): $\delta = 6.10$ (t, 1H, $J_{2,3} = 10.2$, $J_{3,4} = 9.8$ Hz; H-3), 5.34 (d, 1H, $J_{1,2} = 3.8$ Hz; H-1), 5.21 (dd, 1H; H-2), 5.00 (dd, 1H, $J_{2,3} = 3.1$, $J_{3,4} = 9.8$ Hz; H-3′), 4.44 (s, 1H, $J_{1,2} < 1.0$ Hz; H-1′), 4.33 (t, 1H, $J_{4,5} = 9.8$ Hz; H-4), 4.00 (t, 1H, $J_{4,5} = 9.7$ Hz; H-4′), 4.05 – 3.99 (m, 1H, $J_{5,6a} = 2.8$, $J_{5,6b} = 1.8$ Hz; H-5), 3.89 (bd, 1H; H-2′), 3.74 (dd, 1H, $J_{6a,6b} = -11.2$ Hz; H-6a), 3.66 (dd, 1H, H-6b), 3.44 (dd, 1H, $J_{5,6a} = 4.5$, $J_{6a,6b} = -11.4$ Hz; H-6a′), 3.34 (dd, 1H, $J_{5,6b} = 1.8$ Hz; H-6b′), 3.26 – 3.21 (m, 1H, H-5′); ^{13}C NMR ($CDCl_3$, 25 °C, 75.46 MHz, signals of benzoyl and benzyl groups are not shown): $\delta = 100.6$ ($J_{C\text{-}1,H\text{-}1} = 158.5$ Hz; C-1′), 95.3 (C-1), 76.2, 76.0, 76.0 (C-2′,3′,5′), 74.9 (C-4), 73.0 (C-4′), 72.2 (C-2), 70.9, 70.2 (C-3,5), 68.8, (C-6′), 68.1 (C-6); elemental analysis: calcd. for $C_{68}H_{64}O_{14}$: C 73.90, H 5.84; found: C 74.10, H 5.90.

Received: June 15, 1998 [Z 11992 IE]
German version: *Angew. Chem.* **1998**, *110*, 3367 – 3369

Keywords: carbohydrates · cyclizations · glycosides · glycosylations · oligosaccharides

[1] a) H. Paulsen, O. Lockhoff, *Chem. Ber.* **1981**, *114*, 3102 – 3114; b) H. Paulsen, W. Kutschker, O. Lockhoff, *Chem. Ber.* **1981**, *114*, 3233 – 3241.

[2] a) W.-S. Kim, H. Sasai, M. Shibasaki, *Tetrahedron Lett.* **1996**, *37*, 7797 – 7800; b) K. Tatsuta, S. Yasuda, *Tetrahedron Lett.* **1996**, *37*, 2453 – 2456; c) D. Crich, S. Sun, *J. Org. Chem.* **1996**, *61*, 4506 – 4507; d) D. Crich, S. Sun, *J. Org. Chem.* **1997**, *62*, 1198 – 1199; e) G. Hodosi, P. Kovac, *J. Am. Chem. Soc.* **1997**, *119*, 2335 – 2336; f) Z.-W. Guo, Y. Nakahara, T. Ogawa, *Tetrahedron Lett.* **1997**, *38*, 4799 – 4802; g) D. Crich, S. Sun, *J. Am. Chem. Soc.* **1998**, *120*, 435 – 436.

[3] a) H. Ohtake, T. Iimori, S. Ikegami, *Tetrahedron Lett.* **1997**, *38*, 3413 – 3414; b) T. Iimori, H. Ohtake, S. Ikegami, *Tetrahedron Lett.* **1997**, *38*, 3415 – 3418.

[4] a) E. Kaji, F. W. Lichtenthaler, *Trends Glycosci. Glycotechnol.* **1993**, *5*, 121 – 142; b) F. W. Lichtenthaler, T. Schneider-Adams, *J. Org. Chem.* **1994**, *59*, 6728 – 6734; c) F. W. Lichtenthaler, T. Schneider-Adams, S. Immel, *J. Org. Chem.* **1994**, *59*, 6735 – 6738; d) F. W. Lichtenthaler, T. W. Metz, *Tetrahedron Lett.* **1997**, *38*, 5477 – 5480; e) F. W. Lichtenthaler, U. Kläres, Z. Szurmai, B. Werner, *Carbohydr. Res.* **1998**, *305*, 293 – 303.

[5] W. Günther, H. Kunz, *Carbohydr. Res.* **1992**, *228*, 217 – 241.

[6] a) F. Barresi, O. Hindsgaul, *Synlett* **1992**, 759 – 761; b) G. Stork, G. Kim, *J. Am. Chem. Soc.* **1992**, *114*, 1087 – 1088; c) M. Bols, *J. Chem. Soc. Chem. Commun.* **1992**, 913 – 914; d) F. Barresi, O. Hindsgaul, *Can. J. Chem.* **1994**, *72*, 1447 – 1465; e) Y. Ito, T. Ogawa, *Angew. Chem.*

1994, *106*, 1843 – 1845; *Angew. Chem. Int. Ed. Engl.* **1994**, *33*, 1765 – 1767; f) M. Bols, T. Skrydstrup, *Chem. Rev.* **1995**, *95*, 1253 – 1277; g) A. Dan, Y. Ito, T. Ogawa, *J. Org. Chem.* **1995**, *60*, 4680 – 4681.

[7] a) S. Inaba, M. Yamada, T. Yoshino, Y. Ishido, *J. Am. Chem. Soc.* **1973**, *95*, 2062 – 2063; b) M. E. Behrendt, R. R. Schmidt, *Tetrahedron Lett.* **1993**, *34*, 6733 – 6736; c) T. Iimori, T. Shibazaki, S. Ikegawa, *Tetrahedron Lett.* **1996**, *37*, 2267 – 2270; d) G. Scheffler, R. R. Schmidt, *Tetrahedron Lett.* **1997**, *38*, 2943 – 2946.

[8] G. Schüle, T. Ziegler, *Liebigs Ann.* **1996**, 1599 – 1607.

[9] a) T. Ziegler, R. Lau, *Tetrahedron Lett.* **1995**, *36*, 1417 – 1420; b) R. Lau, G. Schüle, U. Schwaneberg, T. Ziegler, *Liebigs Ann.* **1995**, 1745 – 1754; c) T. Ziegler, G. Lemanski, A. Rakoczy, *Tetrahedron Lett.* **1995**, *36*, 8973 – 8976; d) T. Ziegler, A. Ritter, J. Hürttlen, *Tetrahedron Lett.* **1997**, *38*, 3715 – 3718.

[10] T. Ziegler, G. Lemanski, *Eur. J. Org. Chem.* **1998**, 163 – 170.

[11] a) S. Valverde, A. M. Gómez A. Hernández, B. Herrandón, J. C. López, *J. Chem. Soc. Chem. Commun.* **1995**, 2005 – 2006; b) S. Valverde, A. M. Gómez, J. C. López, B. Herrandón, *Tetrahedron Lett.* **1996**, *37*, 1105 – 1108; c) H. Yamada, K. Imamura, T. Takahashi, *Tetrahedron Lett.* **1997**, *38*, 391 – 394.

[12] a) K. Bock, C. Pedersen, *J. Chem. Soc. Perkin Trans. 2*, **1974**, 293 – 297; b) K. Bock, C. Pedersen, *Acta Chem. Scand. Ser. B29*, **1975**, 258 – 262.

Layered Dendritic Block Copolymers**

Mikael Trollsås, Hans Claesson, Björn Atthoff, and James L. Hedrick*

Macromolecular engineering of complex molecular architectures through block copolymerization or the introduction of controlled branching has become a common theme of research in polymer science. The interest in these synthetic mesoscopic systems and nanostructures is driven by the possible unique mechanical, rheological, and solution properties. Block copolymers are simply two distinct homopolymers covalently bound at one point, and the molecular architecture, block lengths, and composition can be designed to produce materials with a wide range of properties and morphologies.[1] Furthermore, since the two dissimilar materials are covalently bound, miscibility is enhanced and phase separation is restricted to dimensions of 100 to 400 Å. Dendrimers provide the ultimate standard of a well-defined branched macromolecule, while hyperbranched polymers are less perfect elaborations of such three-dimensional structures.[2, 3] The combination of controlled branching with block copolymerization provides additional opportunities to devise new molecular architectures. For instance, dendrimers have often been used as cores for the preparation of star polymers with a well-defined number of arms.[4] Conversely, Fréchet et al.[5] terminated star polymers with dendrons at their focal point, and layered and segmented dendrimers have been reported by other groups.[6] In addition, Tomalia et al.,[7a] Möller and co-workers,[7b–d] and others have reported successive grafting of polymeric building blocks.[7] These "comb-burst" polymers, or arborescent graft polymers, utilize linear building blocks with narrow polydispersity in the construction of highly and randomly branched polymers. A new type of molecular architecture, denoted dendrimer-like star polymers, based on poly(ε-caprolactone) has been recently reported.[8] These highly branched dendrimer-like star polymers are different from comb-burst polymers because the branching is controlled and resembles that of traditional dendrimers. The use of living polymerization methods in combination with selective and quantitative organic transformations allows the design and preparation of classical polymers with molecular architectures similar to the most advanced dendrimers with layered and segmented block structures.

Here layered dendrimer-like star copolymers are reported. These novel polymers, characterized by a radial architecture, are constructed by alternating layers of high molecular weight polymer and dendrons emanating from a central core (Scheme 1). There are many possible routes to these novel geometries but this paper focuses on the possibility of using living polymerization techniques. These polymers contain multiple hydroxyl groups and are of interest in areas of surgery and medicinal chemistry as well as in nanotechnology. In addition, it is of interest to investigate whether these molecular structures display microphase-separated morphologies. The general synthetic strategy is shown in Scheme 1. A multifunctional core molecule is used as an initiator for the controlled ring opening polymerization of ε-caprolactone. The polymer obtained, G1(6OH), is the first generation of the final triblock copolymer. The chain ends of the six-arm star polymer are capped with functional dendrons of different sizes to produce diblock polymers with 12, 24, or 48 functional end groups. These macromolecules will serve as "macroinitiators" for the growth of an additional layer of poly(ε-caprolactone) or the third layer of the dendrimer-like triblock copolymers (Scheme 1).

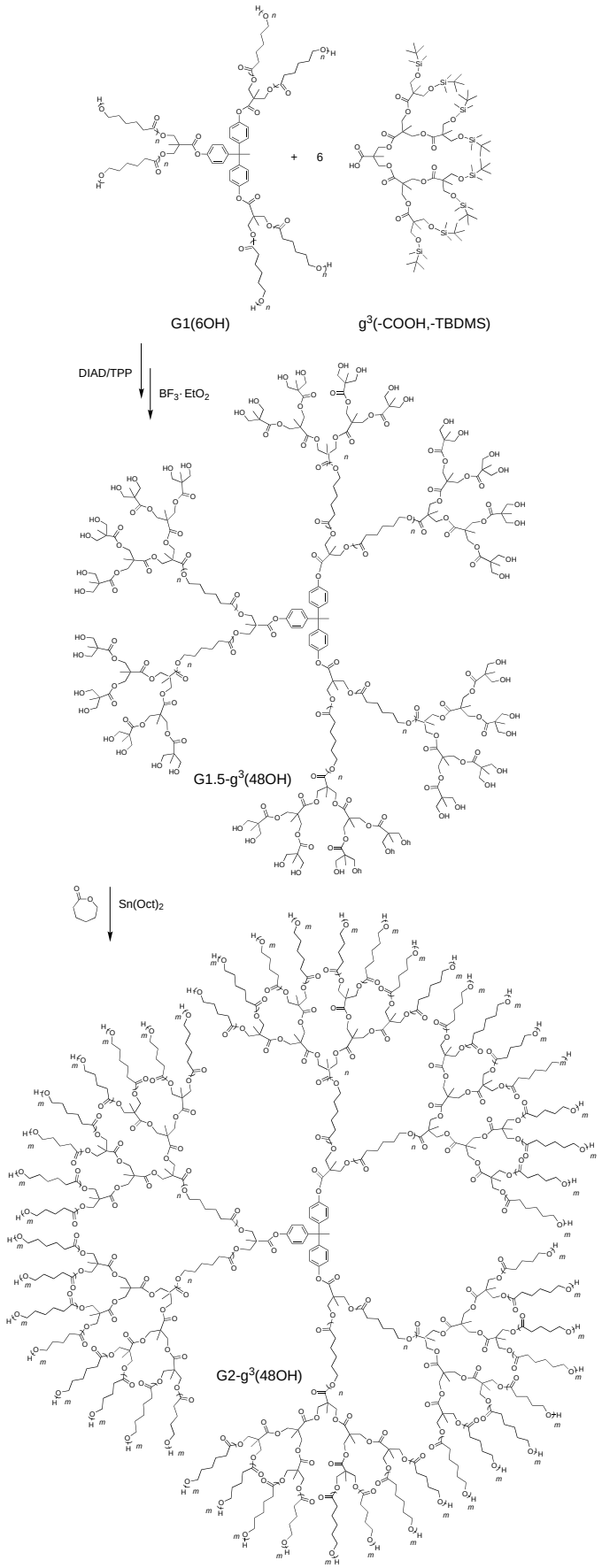
The six-arm star polymer G1(6OH) was synthesized by the reaction of one equivalent of a hexafunctional "initiator" and 120 equivalents of caprolactone in the presence of 1/400 equivalents of $Sn(Oct)_2$ under bulk conditions at 110 °C. The initiator is a first-generation hydroxyl-substituted dendrimer based on 2,2-bis(hydroxymethyl)proprionic acid (DMPA).[9] The target degree of polymerization (DP) was 20, and the DP obtained was calculated to be 20.6 by ^{1}H NMR spectroscopy. Protected DMPA or second- and third-generation dendrons derived from it were used to construct the second layer in the triblock dendrimer-like copolymer. The benzylidene-protected DMPA was synthesized in one step according to a procedure reported elsewhere,[10] while the

[*] Dr. J. L. Hedrick, M. Trollsås, H. Claesson, B. Atthoff
Center for Polymeric Interfaces and Macromolecular Assemblies (CPIMA)
IBM Research Division, Almaden Research Center
650 Harry Road, San Jose, CA 95120-6099 (USA)
Fax: (+1) 408-927-3310
E-mail: hedrick@almaden.ibm.com

[**] This work was supported by the NSF-funded MRSEC Center for Polymeric Interfaces and Macromolecular Assemblies CPIMA (NSF DMR-9400354). M.T. thanks the Swedish Foundation for International Cooperation in Research and Higher Education (STINT) for fellowship support.

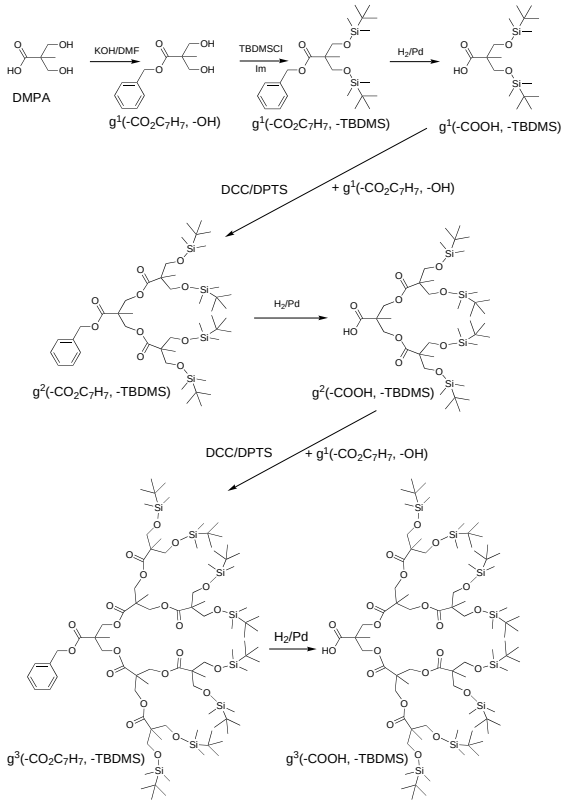
Supporting information for this article is available on the WWW under http://www.wiley-vch.de/home/angewandte/ or from the author.

 © WILEY-VCH Verlag GmbH, D-69451 Weinheim, 1998 1433-7851/98/3722-3132 $ 17.50+.50/0



Scheme 1. TBDMS = *tert*-butyldimethylsilyl, DIAD = diisopropyl azodicarboxylate, TPP = triphenylphosphane.

dendrons g^2(-COOH,-TBDMS) and g^3(-COOH,-TBDMS) were obtained by a convergent growth approach (Scheme 2). The hydroxyl groups of the benzyl ester g^1(-$CO_2C_7H_7$,-OH) were protected with *tert*-butyldimethylsilyl chloride (TBDMSCl) to give g^1(-$CO_2C_7H_7$,-TBDMS). The benzyl group could then be selectively removed by catalytic hydrogenolysis to give the free acid g^1(-COOH,-TBDMS), which



Scheme 2. Im = imidazole, DCC = dicyclohexylcarbodiimide, DPTS = 4-(dimethylamino)pyridinium *p*-toluenesulfonate.

was then coupled with g^1(-$CO_2C_7H_7$,-OH) to afford the second-generation dendron g^2(-$CO_2C_7H_7$,-TBDMS). This in turn could be readily hydrogenolysed to give g^2(-COOH,-TBDMS). The third-generation dendron g^3(-$CO_2C_7H_7$,-TBDMS) was synthesized by coupling of g^1(-$CO_2C_7H_7$,-OH) with g^2(-COOH,-TBDMS). Deprotection by hydrogenolysis gave the requisite dendron g^3(-COOH,-TBDMS). The structure of the dendrons was confirmed by ^{1}H and ^{13}C NMR spectroscopy. ^{13}C NMR spectroscopy was used to determine whether the DMPA derivatives were completely substituted or not.[8, 11] Figure 1 reveals that the synthesized dendrons only contain quaternary carbon atoms which originate from disubstituted DMPA, as shown in Scheme 2, without traces of contamination from mono substitution.

The acid-functional dendrons were coupled with the hydroxyl-substituted six-arm star poly(ε-caprolactone) under Mitsunobu conditions to produce diblock copolymers with 12, 24, or 48 hydroxyl groups.[8, 10] The extent of coupling was followed by ^{1}H and ^{13}C NMR spectroscopy and size-exclusion chromatography (SEC). Sections of the ^{13}C NMR spectra for the six-arm star and the copolymers with the third-generation

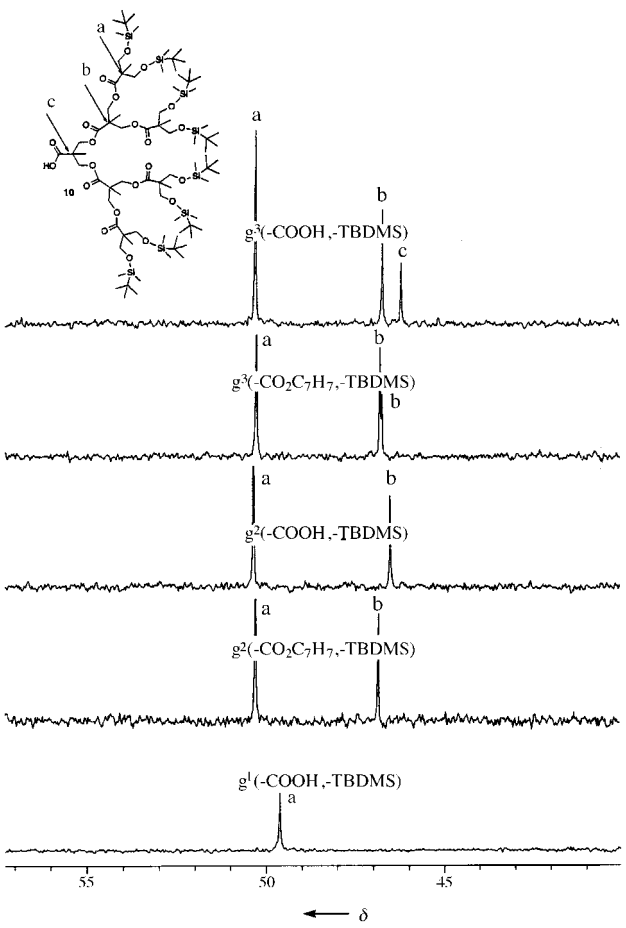


Figure 1. The quaternary carbon atom region in the ^{13}C NMR spectra of the dendrons.

dendron are shown in Figure 2. Quantitative functionalization is confirmed by the complete shift of the CH_2OH signal from $\delta = 62$ to 65 upon esterification of the hydroxyl groups.

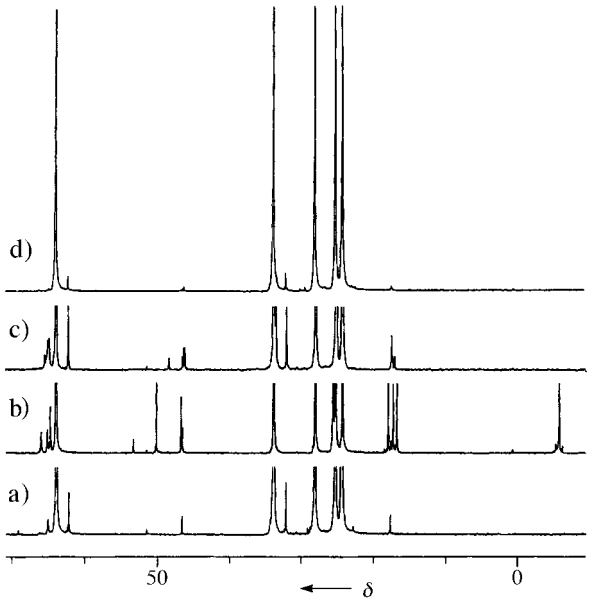


Figure 2. Part of the ^{13}C NMR spectra of a) G1(6OH), b) G1.5-g^3(TBDMS), c) G1.5-g^3(48OH), and d) G2-g^3(48OH).

Figure 3 shows an enlargement of the quaternary carbon atom region of the spectra. The diblock copolymer G1.5-g^3(TBDMS) displays five peaks in this region that are combined signals from the six-arm core and the third-generation dendron. The peak denoted c can be assigned to the outer generation of the dendron.

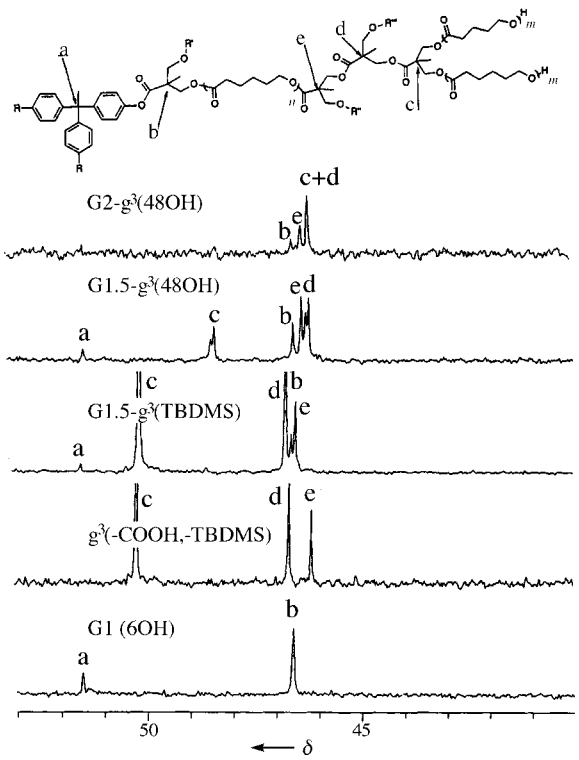


Figure 3. The quaternary carbon atom region in the ^{13}C NMR spectra of G2-g^3(48OH) and intermediates.

The benzylidene groups and the *tert*-butyldimethylsilyl protecting groups were then removed by hydrogenolysis and treatment of $BF_3 \cdot EtO_2$, respectively, to give the requisite 12, 24, and 48 hydroxyl groups along the periphery of the layered diblock polymers G1.5-g^1(12OH), G1.5-g^2(24OH), and G1.5-g^3(48OH) (Scheme 1). The ^{13}C NMR spectrum of G1.5-g^3(48OH) is free from peaks from the protecting group, which is consistent with quantitative deprotection (Figure 2). The transformation is also observed in the quantitative shift of the peak c derived from the quaternary carbon atom in the outer layer of the dendron (Figure 3).

The six-arm star diblock copolymers with 12, 24, and 48 hydroxyl groups at the periphery were used as "macroinitiators" for the growth of an additional layer of poly(ε-caprolactone). The diblock copolymers were soluble in ε-caprolactone, which allowed bulk polymerization. However, approximately 10 % toluene was added to reduce the viscosity of the melt. The polymerization mixtures became extremely viscous after 24 hours at 110 °C, and were then dissolved in THF and the products isolated by precipitation in methanol. It should be pointed out that the only purification needed after polymerization, functionalization, or deprotection was simple precipitation of the polymers into cold methanol. The structure of the 48-arm radial triblock copolymer G2-

 © WILEY-VCH Verlag GmbH, D-69451 Weinheim, 1998 1433-7851/98/3722-3134 $ 17.50+.50/0 *Angew. Chem. Int. Ed.* **1998**, *37*, No. 22

g^3(48OH) was confirmed by NMR spectroscopy. All peaks in the ^{1}H NMR spectra derived from the methylene protons of the outer layer of DMPA were shifted, which indicated that all hydroxyl groups initiated polymerization. This observation was confirmed by ^{13}C NMR spectroscopy (Figure 3). Complete initiation was observed from the quantitative shift of the quaternary carbon atom peak c into the disubstituted region. The experimental DP values, measured by ^{1}H NMR spectroscopy, correspond well with the target value (DP = 20) for G2-g^1(12OH) and for G2-g^2(24OH) (Table 1). However, the signals from the hydroxyl chain ends for G2-g^3(48OH) are much smaller than expected and may be a result of agglomeration.

Table 1. Characteristics of layered dendrimer-like star polymers.

Polymer	M_n[a]	M_n[b]	M_w/M_n[b]	DP[c]	T_m [°C] (ΔH [kJ mol^{-1}])
G1(6OH)	15000	23400	1.16	20.1[d]	53.1 (70.6)
G1.5-g^1(12OH)	15900	24000	1.14	20.1[d]	47.0 (61.5)
G1.5-g^2(24OH)	17000	26900	1.13	20.1[d]	48.8 (49.1)
G1.5-g^3(48OH)	20000	35300	1.09	20.1[d]	44.2 (46.8)
G2-g^1(12OH)	43100	58300	1.16	20.1[d], 21.3[e]	53.5 (60.8)
G2-g^2(24OH)	71800	91000	1.13	20.1[d], 24.7[e]	54.3 (85.6)
G2-g^3(48OH)	129300	221000	1.12	20.1[d, f]	57.1 (66.0)

[a] Theoretical. [b] Determined by SEC. [c] Degree of polymerization as determined by ^{1}H NMR spectroscopy. [d] First generation, [e] Second generation. [f] Second generation could not be measured.

The theoretical and the experimental number average molecular weights as measured by SEC are shown in Table 1. Also shown in Table 1 are the molecular weights and the molecular weight distributions as measured by SEC. The molecular weight distributions, as expected, are lowered when the six-arm stars are esterified with the monodisperse second blocks. The observed increase in molecular weight upon derivatization of the six-arm star with the dendrons, as well as the significant increase in molecular weight after the addition of the outer layer, are in the expected range for all three polymers. Figure 4 shows the size-exclusion chromatograms for each of the steps in the synthesis of the layered copolymers. The three distribution curves are monomodal and all polydispersities are below 1.20. Although these data are relative to a polystyrene standard and branched structures are known to have different hydrodynamic volumes than their linear analogues, the combined results from SEC and ^{13}C and ^{1}H NMR spectroscopy clearly suggest that all the prepared polymers have the requisite complex structures.

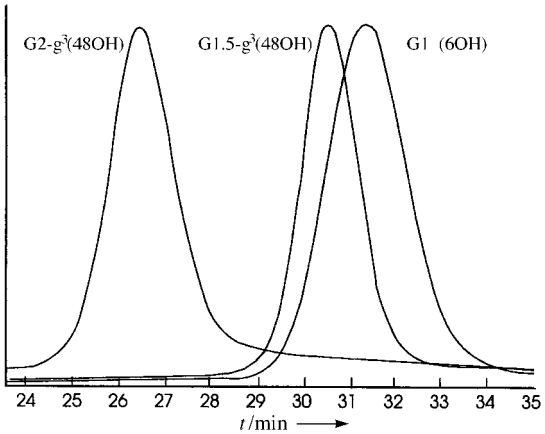


Figure 4. Sections of size-exclusion chromatograms of G2-g^3(48OH), G1.5-g^3(48OH), and G1(6OH).

All the diblock and triblock polymers are semicrystalline, as observed by differential scanning calorimetry (DSC) measurements (Table 1). In addition to the melting transition temperatures (T_m), glass-transition temperatures (T_g) of around $-50\,^\circ$C were observed for all polymers commensurate with the T_g observed for linear poly(ε-caprolactone). A second glass transition corresponding to the DMPA dendrons could not be detected by DSC since it was probably hidden beneath the melting endotherm of the ε-caprolactone block. Hult and co-workers have reported T_g values between -4 and $+57\,^\circ$C for dendrimers and hyperbranched polymers based on DMPA.[12] However, since the glass-transition temperatures are similar for the copolymers and the linear homopolymer, these data suggest that the different layers are partially phase-separated. If the layers were completely phase-mixed, a shift in T_g in accordance with the Fox equation would have been observed. Dielectric spectroscopy measurements indicate similar behavior. Films of the layered dendritic block copolymers were tough and ductile. A more thorough discussion of these results will be reported separately.

Experimental Section

The synthesis of the six-armed star poly(ε-caprolactone) and the benzylidene protected DMPA have been published elsewhere.[10, 11b] The synthesis of the second- and third-generation dendrons are available in the supporting information.

Synthesis of G1.5-g^2(TBDMS); a general procedure for esterification with DIAD: DIAD (1.30 g, 6.46 mmol) was slowly added to a stirred solution of G1(6OH) (8.00 g, 0.538 mmol), g^2(-COOH,-TBDMS) (3.98 g, 4.84 mmol), and TPP (1.69 g, 6.46 mmol) in THF (5 mL). After 12 h the mixture was poured into cold MeOH, and the precipitated product was filtered off to yield 10.56 g (99%) of a white crystalline powder. ^{1}H NMR ($CDCl_3$): $\delta =$ 0.00 (s, 144H; $Si(CH_3)_2$), 0.84 (s, 216H; $C(CH_3)_3$), 1.05 (s, 36H; CH_3), 1.20 (s, 18H; CH_3), 1.30–1.42 (m, poly; CH_2), 1.57–1.69 (m, poly; CH_2), 2.26–2.32 (t, poly; CH_2O), 3.57–3.72 (q, 48H; CH_2O), 4.01–4.07 (t, poly; CH_2CO), 4.10–4.26 (m, 24H; CH_2O), 4.33 (s, 12H; CH_2O), 6.91–7.09 (q, 12H; Ph); ^{13}C NMR ($CDCl_3$): $\delta = -5.59$, 17.00, 17.59, 18.18, 24.55, 25.50, 25.81, 28.33, 34.09, 46.77, 50.38, 64.11, 64.89, 65.27, 120.72, 129.70, 146.26, 148.65, 171.40, 172.61, 172.83, 173.50, 174.15.

Synthesis of G1.5-g^2(24OH); a general procedure for the removal of the TBDMS group: G1.5-g^2(TBDMS) (10.03 g, 0.52 mmol) was placed in a sealed flask. The flask was evacuated and flushed with nitrogen (3 ×). Dry dichloromethane (30 mL) and then $BF_3 \cdot Et_2O$ (0.37 g, 2.6 mmol) were added. The mixture was stirred for 12 h at 40 °C and then poured into cold MeOH. The precipitated product was filtered and dried to give 7.1 g (80%) of a white crystalline powder. ^{1}H NMR ($CDCl_3$): $\delta = 1.04$ (s, 36H; CH_3), 1.20 (s, 18H; CH_3), 1.32–1.42 (m, poly; CH_2), 1.57–1.69 (m, poly; CH_2CH_2), 2.26–2.32 (t, poly; CH_2O), 3.63–3.84 (m, 48H; CH_2O), 4.01–4.06 (t, poly; CH_2CO), 4.13–4.24 (t, 48H; CH_2OCO), 4.29–4.44 (m, 36H; CH_2CO), 6.91–7.09 (q, 12H; Ph); ^{13}C NMR ($CDCl_3$): $\delta = 17.03$, 17.71, 18.00, 24.47, 25.43, 28.24, 34.01, 46.29, 46.68, 49.82, 64.04, 64.79, 65.13, 66.84, 120.66, 129.62, 146.21, 148.59, 171.36, 172.77, 172.94, 173.45, 174.89.

Synthesis of G2-g^2(24OH); a general procedure for polymerization of ε-caprolactone: G1.5-g^2(24OH) (0.90 g, 0.05 mmol) was dried over $MgSO_4$ in warm THF, and filtered into a dried reaction flask, which was then sealed. The solvent was then evaporated under vacuum at 90 °C. Dry toluene

 © WILEY-VCH Verlag GmbH, D-69451 Weinheim, 1998 1433-7851/98/3722-3135 $ 17.50+.50/0

(2 mL) was added and evaporated to remove residual H_2O. This process was repeated three times. The reaction flask was then filled with nitrogen and dry toluene (2 mL) to dissolve the initiator. ε-Caprolactone (2.89 g, 25.3 mmol) was added, and the temperature was increased to 110 °C before a catalytic amount of $Sn(Oct)_2$ was added. The catalyst/initiator ratio was 1/400. The polymerization mixture was stirred for 24 h, diluted with THF, and poured into cold MeOH to precipitate a white crystalline powder. Yield: 3.7 g (98 %). ^{1}H NMR ($CDCl_3$): $\delta = 1.30-1.42$ (m, poly; CH_2), 1.55–1.69 (m, poly; CH_2), 2.26–2.32 (t, poly; CH_2O), 3.60–3.65 (t, 18H; CH_2OH), 4.01–4.07 (t, poly; CH_2CO), 4.33 (s, 12H; $CCH_3(CH_2O)_2$), 6.88–7.24 (m, 12H; Ph); ^{13}C NMR ($CDCl_3$): $\delta = 17.74$, 24.50, 25.45, 28.27, 32.20, 34.03, 46.69, 51.58, 62.38, 64.05, 65.07, 120.67, 129.64, 146.22, 148.60, 171.37, 172.78, 173.65.

Received: March 23, 1998
Revised version: June 29, 1998 [Z11629IE]
German version: *Angew. Chem.* **1998**, *110*, 3308–3312

Keywords: block copolymers · dendrimers · polymers · polymerizations

[1] a) G. Reiss, G. Hurtrez, P. Bahadur in *Encyclopedia of Polymer Science and Engineering* (Ed.: J. I. Korschwitz), Wiley, New York, **1985**; b) E. L. Thomas, D. M. Anderson, C. S. Henkee, D. Hoffman, *Nature* **1988**, *334*, 598; c) F. S. Bates, G. H. Fredrickson, *Annu. Rev. Phys. Chem.* **1990**, *41*, 525; d) F. S. Bates, *Science* **1991**, *251*, 898.

[2] a) D. A. Tomalia, H. Baker, J. Dewald, M. Hall, G. Kallos, R. Martin, J. Ryder, P. Smith, *Polym. J.* **1985**, *17*, 117; b) G. R. Newkome, Z. Yao, G. R. Baker, V. K. Gupta, *J. Org. Chem.* **1985**, *50*, 2003; c) C. J. Hawker, J. M. J. Fréchet, *J. Am. Chem. Soc.* **1990**, *112*, 7368; d) J. M. J. Fréchet, *Science* **1994**, *263*, 1710; e) J. F. Jansen, E. M. M. de Brabander van den Berg, E. W. Meijer, *Science* **1994**, *266*, 1226.

[3] a) Y. H. Kim, O. W. Webster, *Polym. Prepr.* **1988**, *29*, 310; b) Y. H. Kim, O. W. Webster, *Macromolecules* **1992**, *25*, 5561; c) C. Hawker, S. R. J. Turner, R. Lee, J. M. J. Fréchet, *J. Am. Chem. Soc.* **1991**, *113*, 4583; d) M. Johansson, E. Malmström, A. Hult, *J. Polym. Sci.* **1993**, *31*, 619; e) J. M. J. Fréchet, M. Henmi, I. Gitsov, S. Aoshima, M. Leduc, R. B. Grubbs, *Science* **1995**, *269*, 1080; f) K. Matyjaszewski, S. G. Gaynor, A. Kulfan, M. Podwika, *Macromolecules* **1997**, *30*, 5192.

[4] a) J. M. Warakomski, *Chem. Mater.* **1992**, *4*, 1000; b) J. Roovers, L.-L. Zhou, P. M. Toporowski, M. v. d. Zwan, H. Iatrou, N. Hadjichristidis, *Macromolecules* **1993**, *26*, 4324.

[5] a) I. Gitsov, K.-L. Wooley, J. M. J. Fréchet, *Angew. Chem.* **1992**, *104*, 1282; *Angew. Chem. Int. Ed. Engl.* **1992**, *31*, 1200; b) I. Gitsov, J. M. J. Fréchet, *J. Am. Chem. Soc.* **1996**, *118*, 3785.

[6] a) C. J. Hawker, J. M. J. Fréchet, *J. Am. Chem. Soc.* **1992**, *114*, 8405; b) D. Gudat, *Angew. Chem.* **1997**, *109*, 2039; *Angew. Chem. Int. Ed. Engl.* **1997**, *36*, 1951; c) H.-F. Chow, *J. Chem. Soc. Perkin Trans. 1* **1997**, 91.

[7] a) D. A. Tomalia, D. M. Hedstrand, M. S. Ferrito, *Macromolecules* **1991**, *24*, 1438; b) M. Gauthier, M. Möller, *Macromolecules* **1991**, *24*, 4548; c) S. S. Sheiko, M. Gauthier, M. Möller, *Macromolecules* **1997**, *30*, 2343; d) M. A. Hempenius, W. Michelberger, M. Möller, *Macromolecules* **1997**, *30*, 5602; e) J.-L. Six, Y. Gnanou, *Macromol. Symp.* **1995**, *95*, 137.

[8] M. Trollsås, J. L. Hedrick, *J. Am. Chem. Soc.* **1998**, *120*, 4644.

[9] H. Ihre, A. Hult, E. Söderlind, *J. Am. Chem. Soc.* **1996**, *118*, 6388.

[10] M. Trollsås, B. Atthoff, H. Claesson, J. L. Hedrick, *Macromolecules* **1998**, *31*, 3439.

[11] a) E. Malmström, M. Johansson, A. Hult, *Macromolecules* **1995**, *28*, 1698; b) M. Trollsås, J. L. Hedrick, D. Mecerreyes, P. Dubois, R. Jérôme, H. Ihre, A. Hult, *Macromolecules* **1997**, *30*, 8508.

[12] a) E. Malmström, M. Johansson, A. Hult, *Macromol. Chem. Phys.* **1996**, *197*, 3199; b) H. Ihre, A. Hult, J. M. J. Fréchet, I. Gitsov, *Macromolecules* **1998**, *31*, 4061–4068.

A Novel Domino Reaction: Cyclization of Alkynyl Sulfides by Reaction with IPy_2BF_4**

José Barluenga,* Gustavo P. Romanelli, Lorenzo J. Alvarez-García, Isidro Llorente, José M. González, Esther García-Rodríguez, and Santiago García-Granda

Synthetic methodologies relying on transition metal chemistry have opened unusual approaches to polycyclic structures.[1, 2] Intramolecular cyclizations of diynes mediated by organometallic complexes[3] often take place according to an *exo-exo* coupling mode,[4] whereas *endo-endo*[3] and *exo-endo*[5, 6] cyclizations have rarely been observed (Figure 1). Described here is a novel approach to accomplish the *exo-endo* cyclization of α,ω-diynes, and preliminary studies on a related intermolecular process.



Figure 1. Possible intramolecular cyclizations. The arrow shows the carbon–carbon bond formed in the metal-promoted intramolecular cyclization as a function of the diyne coupling mode.

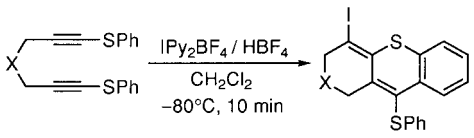
Bis(pyridyl)iodonium(I) tetrafluoroborate (IPy_2BF_4) can be efficiently used as a catalyst or a stoichiometric reagent for unconventional coupling reactions of 1-iodoalkynes[7] and 1-*t*BuMe_2Si-substituted alkynes.[8] These two processes were restricted to aryl-substituted alkynes. Now, we have found for the first time that upon activation by sulfur substituents aliphatic alkynes can enter in a carbocyclization process mediated by IPy_2BF_4. This provides a new entry to unusual *exo-endo* intramolecular cyclizations of α,ω-diynes, as depicted in Scheme 1 for the conversion of the acetylenic sulfide **1a**[9] derived from 1,6-heptadiyne.[10] The overall process comprises two different carbon–carbon bond forming reactions—namely, an alkyne–alkyne coupling and a novel Friedel–Crafts-like ring closure—and is thus a new domino reaction.[11] The process is very fast at low temperature and is completed within a few minutes; increasing the reaction time results in lower yields owing to significant side processes. The reaction takes place upon addition of the starting diynyl

[*] Prof. Dr. J. Barluenga, Dr. G. P. Romanelli, L. J. Alvarez-García, Dr. I. Llorente, Dr. J. M. González
Instituto Universitario de Química Organometálica "Enrique Moles"
Unidad Asociada al C.S.I.C, Universidad de Oviedo
E-33071 Oviedo (Spain)
Fax: (+34) 98-510-3450
E-mail: barluenga@sauron.quimica.uniovi.es
E. García-Rodríguez, Dr. S. García-Granda
Departamento de Química Física y Analítica
Universidad de Oviedo
E-33071 Oviedo (Spain)

[**] This research was supported by DGICYT (grants PB92-1005 and PB93-0330). G.P.R., L.J.A.-G., and I.L. thank CONICET, FICYT, and DGICYT, respectively, for fellowships.

Supporting information for this article is available on the WWW under http://www.wiley-vch.de/home/angewandte/ or from the author.

 © WILEY-VCH Verlag GmbH, D-69451 Weinheim, 1998 1433-7851/98/3722-3136 $ 17.50+.50/0



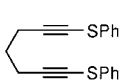
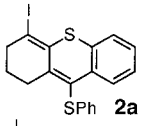
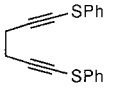
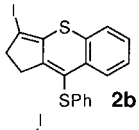
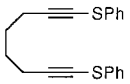
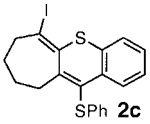
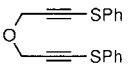
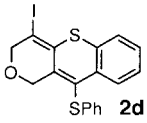
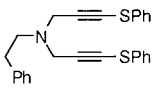
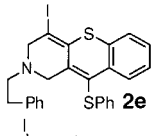
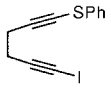
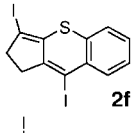
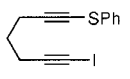
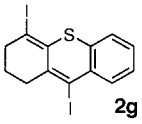
1a X: CH_2 (92%) **2a**
1d X: O (68%) **2d**

Scheme 1. Intramolecular cyclization of α,ω-diynyl sulfides **1** upon reaction with IPy_2BF_4/HBF_4.

sulfide **1** to a cooled solution of IPy_2BF_4 (0.1M in CH_2Cl_2) and HBF_4 (the acid activates the iodonium salt to furnish the reactive species;[12] molar ratio IPy_2BF_4:HBF_4 = 1:1, larger amounts of acid give poorer yields).

The scope of the reaction is indicated in Table 1.[13] Reactions 1, 4, and 5 show that the process can be used to form three linearly condensed six-membered rings from the corresponding 1,6-diynes. Moreover, it is compatible with the presence of different heteroatoms in the alkyl tethering chain. Spectroscopic data of the products are in agreement with the proposed structure, which was firmly established by an X-ray analysis of **2d**.[14] The use of phenyl sulfides derived from 1,5-hexadiyne allows the synthesis of a polycyclic structure **2b** containing five- and six-membered rings in a very rapid reaction (about two minutes).

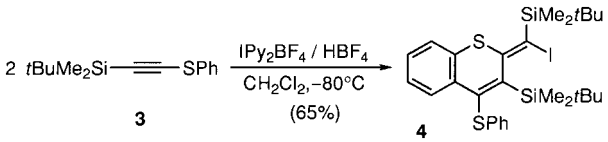
Table 1. Intramolecular *exo-endo* dimerization of α,ω-diynyl sulfides mediated by IPy_2BF_4.

Reaction	Substrate **1**	Product **2**	Yield [%][a]
1			92
2			69
3			71[b]
4			72
5			52
6			44
7			31

[a] Yield of isolated crystalline materials, based on the starting diyne. [b] Two equivalents of IPy_2BF_4/HBF_4 were used.

Interestingly, 1,7-diynes also react efficiently to furnish **2c**, a condensed structure featuring a medium-sized seven-membered ring, as proven by X-ray analysis.[14] This flexible synthesis of condensed thiin structures is efficient and starts from simple acyclic precursors. It takes advantage of the phenyl sulfide moiety to intramolecularly capture intermediate reactive species formed upon diyne dimerization. This step is very fast and, according to ^1H NMR spectroscopy, occurs even in the presence of external nucleophiles such as MeOH or *i*PrOH (as cosolvents) without addition of the alcohol to the reaction product. The activation of one triple bond by sulfur is essential for the first C–C bond forming step, but the second one might be replaced by a different substituent. Entries 6 and 7 show that mixed compounds substituted by sulfur and iodine cyclize in a related way, yielding interesting diiodinated structures. In contrast, no cyclization occurs with α,ω-diiododiynes.

We tested the reactivity of 1-hexynyl phenyl sulfide to explore a possible intermolecular coupling. Although the reaction proceeds in a similar way,[15] yields have so far been poor. Nevertheless, it shows that simple alkynes are compatible with this coupling. PhSC≡C$SiMe_2t$Bu (**3**) was a good model compound for the intermolecular coupling. Upon reaction of **3** with IPy_2BF_4/HBF_4 in CH_2Cl_2 (5×10^{-2}M) for 4 h, the temperature raised from $-80\,^\circ$C to $0\,^\circ$C, and **4** was obtained (Scheme 2).[13, 14] The transformation of **3** to **4** also

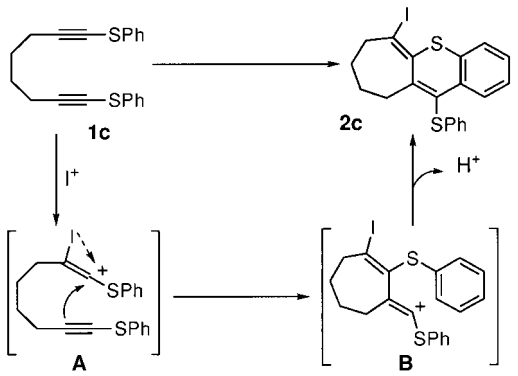


Scheme 2. Intermolecular coupling reaction of **3** upon reaction with IPy_2BF_4/HBF_4.

involves two different and sequential C–C bond forming reactions; the overall result is a regio- and stereoselective synthesis of a cyclic framework. The 1,3-diene moiety within the reaction product involves an interesting arrangement of five well-differentiated positions substituted with heteroatoms. Furthermore, the large torsional angle (74.1°) between the *exo*cyclic double bond and the C–Si bond (where C belongs to the cyclic frame) represents a remarkable structural motif, resulting in an unusual source of helical chirality.[16]

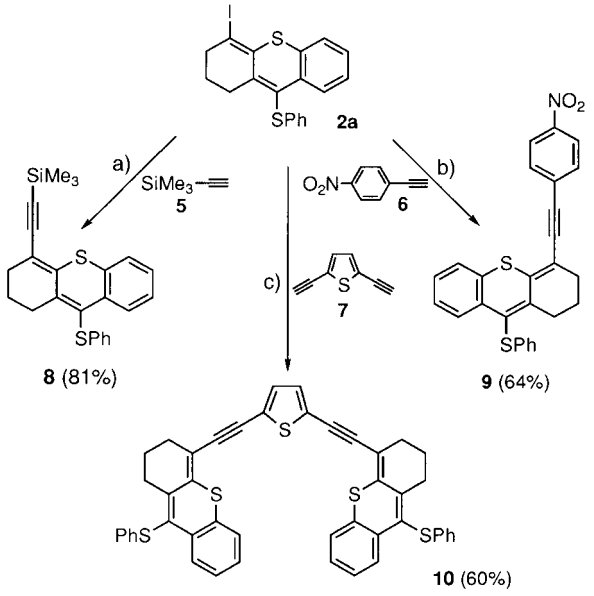
A tentative mechanism accommodating these results might involve an initial attack of the electrophilic iodine atom to a triple bond in **1c** to produce cation **A**,[17] a relatively stable vinyl cation substituted in the α position by sulfur (Scheme 3).[18, 19] Collapse of **A** by C–C bond formation would result in assembly of the first ring and creating of the new and reactive vinyl cation **B**.[20] The latter affords **2c** by subsequent ring closure involving participation of the phenyl group attached to sulfur.

A novel and synthetically valuable *exo-endo* intramolecular cyclization of α,ω-diynes has been developed, and the feasibility of the intermolecular coupling explored. An interesting feature is that the iodine promoting the reaction



Scheme 3. Proposed mechanism for the intramolecular cyclization of **1c** into **2c**.

can be exploited for further elaboration of the polycyclic frame, as for instance depicted in Scheme 4.[21] This fact, and the electronic tuning of the reactivity of the triple bond by other substituents in this type of reaction, might open new and unconventional synthetic pathways.



Scheme 4. Some synthetic transformations of the newly formed C–I bond in **2a**. Conditions for all reactions: reagent **5**, **6**, or **7**; $[PdCl_2(PPh_3)_2]$/CuI (cat.); Et_3N/THF; room temperature; 5 h (a), 30 h (b), or 17 h (c).

Experimental Section

All reactions were carried out under a positive pressure of nitrogen. Dichloromethane was dried by refluxing over P_2O_5 and distilled under a nitrogen atmosphere.

Reaction of diynes with IPy_2BF_4: IPy_2BF_4 (3.72 g, 10.0 mmol, 1.0 equiv) was dissolved in dry CH_2Cl_2 (100 mL) and stirred for 5 min. The solution was cooled to $-80\,^{\circ}C$, and tetrafluoroboric acid (1.36 mL, 54% solution in diethyl ether, 10.0 mmol, 1.0 equiv) was added by syringe. After 10 min a solution of the diyne (10.0 mmol, 1.0 equiv) in CH_2Cl_2 (2 mL) was added, and the reaction mixture was stirred. The reaction was quenched with a 10% aqueous solution of $Na_2S_2O_3$ (100 mL). The organic layer was washed with water (2×100 mL), dried over sodium sulfate, and concentrated. The products were purified by filtration through a short column of neutral aluminum oxide with hexane/ethyl acetate as eluent and recrystallization from mixtures of hexane and diethyl ether.

2a: Yellow solid, m.p. 102–103 °C; UV/Vis (CH_3OH): λ_{max} (ε) = 203 (40000), 263 (37500), 385 (8000), 484 nm (5500); IR (KBr): $\tilde{\nu}$ = 3057, 3052, 2996, 2976, 2953, 2928, 2907, 1580, 1535, 1470, 1437, 1427, 754, 743, 725, 689 cm^{-1}; ^1H NMR ($CDCl_3$): δ = 7.91 (d, J = 8.1 Hz, 1H), 6.95–7.30 (m, 8H), 3.12 (t, J = 6.0 Hz, 2H), 2.91 (t, J = 6.0 Hz, 2H), 1.84 (quint, J = 6.0 Hz, 2H); ^{13}C NMR ($CDCl_3$): δ = 141.1 (s), 136.4 (s), 133.0 (s), 132.0 (s), 130.4 (s), 129.0 (d), 128.6 (d), 127.7 (d), 125.9 (s), 125.8 (d), 125.6 (d), 125.0 (d), 124.4 (d), 98.0 (s), 42.4 (t), 31.0 (t), 24.2 (t); HR-MS (EI) calcd for $C_{19}H_{15}IS_2$: 433.9653; found: 433.9659; elemental analysis calcd for $C_{19}H_{15}IS_2$: C 52.54, H 3.48; found: C 52.65, H 3.53.

Received: April 20, 1998 [Z11747IE]
German version: *Angew. Chem.* **1998**, *110*, 3332–3334

Keywords: alkynes · cyclizations · domino reactions · heterocycles

[1] a) K. P. C. Vollhardt, *Angew. Chem.* **1984**, *96*, 525–541; *Angew. Chem. Int. Ed. Engl.* **1984**, *23*, 539–556; b) N. E. Schore, *Chem. Rev.* **1988**, *88*, 1081–1119.

[2] B. M. Trost, *Angew. Chem.* **1995**, *107*, 285–307; *Angew. Chem. Int. Ed. Engl.* **1995**, *34*, 259–281.

[3] The clasification as *exo-exo*, *exo-endo*, and *endo-endo* refers to the orientation of the acetylene units with respect to the ring formed: K. Tamao, S. Yamaguchi, M. Shiro, *J. Am. Chem. Soc.* **1994**, *116*, 11715–11722.

[4] Y. Ojima, M. Tzamarioudaki, Z. Li, R. J. Donovan, *Chem. Rev.* **1996**, *96*, 635–662.

[5] For examples of cyclization of macrocyclic diynes, see a) O. M. Behr, G. Eglinton, A. R. Galbraith, R. A. Raphael, *J. Chem. Soc.* **1960**, 3614–3625; b) J. D. Brandshaw, D. Solooki, C. A. Tessier,W. J. Youngs, *J. Am. Chem. Soc.* **1994**, *116*, 3177–3179; c) Q. Zhou, P. J. Carroll, T. M. Swager, *J. Org. Chem.* **1994**, *59*, 1294–1301; d) X.Gu, M. B. Sponsler, *Tetrahedron Lett.* **1996**, *37*, 1571–1574; e) H. Weigl, R. Gleiter, *Tetrahedron Lett.* **1997**, *38*, 1541–1542.

[6] For related examples from linear diynes, see a) N. Zhang, R. Wu, K. Li,C. O. Yoon, F. Wudl, *Chem. Mater.* **1993**, *5*, 1598–1599, and references therein; b) Y. Li, T. J. Marks, *J. Am. Chem. Soc.* **1996**, *118*, 707–708.

[7] J. Barluenga, J. M. González, I. Llorente, P. J. Campos, *Angew. Chem.* **1993**, *105*, 928–929; *Angew. Chem. Int. Ed. Engl.* **1993**, *32*, 893–894.

[8] J. Barluenga, I. Llorente, L. J. Alvarez-García, J. M. González, P. J. Campos, M. R. Díaz, S. García-Granda, *J. Am. Chem. Soc.* **1997**, *119*, 6933–6934.

[9] Acetylenic sulfides are useful compounds in organic synthesis: S. Y. Radchenko, A. A. Petrov, *Russ. Chem. Rev. (Engl. Transl.)* **1989**, *58*, 948–966; P. Nebois, N. Kann, A. E. Greene, *J. Org. Chem.* **1995**, *60*, 7690–7692; H. Ishitani, S. Nagayama, S. Kobayashi, *J. Org. Chem.* **1996**, *61*, 1902–1903.

[10] Alkynyl sulfides and iodides were prepared by conventional procedures and used immediately; see L. Brandsma, *Preparative Acetylenic Chemistry*, 2nd ed., Elsevier, Amsterdam, **1988**.

[11] Reviews on the concept and use of domino reactions in organic synthesis: a) L. F. Tietze, U. Beifuss, *Angew. Chem.* **1993**, *105*, 137–170; *Angew. Chem. Int. Ed. Engl.* **1993**, *32*, 131–163; b) L. F. Tietze, *Chem. Rev.* **1996**, *96*, 115–136.

[12] J. Barluenga, P. J. Campos, J. M. González, J. L. Suárez, G. Asensio, *J. Org. Chem.* **1991**, *56*, 2234–2237.

[13] All compounds **2** reported in Table 1 were fully characterized, and their spectroscopic and analytical data firmly support the proposed structures. For reaction conditions, a full list of ^{13}C and ^1H NMR data, representative UV/Vis, IR, and MS data and elemental analyses, see the supporting information.

[14] The structures of **2c**, **2d**, and **4** were determined by X-ray analysis. Crystallographic data (excluding structure factors) for the structures reported in this paper have been deposited with the Cambridge Crystallographic Data Centre as supplementary publication no. CCDC-102304 (**4**), CCDC-102305 (**2c**), and CCDC-102306 (**2d**). Copies of the data can be obtained free of charge on application to

 © WILEY-VCH Verlag GmbH, D-69451 Weinheim, 1998 1433-7851/98/3722-3138 $ 17.50+.50/0

CCDC, 12 Union Road, Cambridge CB2 1EZ, UK (fax: (+44) 1223-336-033; e-mail: deposit@ccdc.cam.ac.uk).
[15] Selected data for the dimer: HR-MS (EI) calcd for $C_{24}H_{27}IS_2$: 506.0599; found: 506.0603; ^{13}C NMR ($CDCl_3$): $\delta = 95.8$ (CI).
[16] Review: K. P. Meurer, F. Vögtle, *Top. Curr. Chem.* **1985**, *127*, 1–76; see also: A. Beck, R. Gompper, K. Polborn, H.-U. Wagner, *Angew. Chem.* **1993**, *105*, 1424–1427; *Angew. Chem. Int. Ed. Engl.* **1993**, *32*, 1352–1354; B. L. Feringa, N. P. M. Huck, A. M. Schoevaars, *Adv. Mater.* **1996**, *8*, 681–684.
[17] For addition reactions to alkynyl sulfides promoted by IPy_2BF_4, see J. Barluenga, P. J. Campos, F. López, I. Llorente, M. A. Rodríguez, *Tetrahedron Lett.* **1990**, *31*, 7375–7378.
[18] For the directive effect of sulfur on electrophilic addition to acetylene, see G. Modena, U. Tonellato, *Adv. Phys. Org. Chem.* **1971**, *9*, 185.
[19] Alternative radical pathways cannot be ruled out, but should occur in an *exo-exo* mode (according to S. Caddick, C. L. Shering, S. N. Wadman, *Chem. Commun.* **1997**, 171–172). No evidence for significant sulfur oxidation was found during the reaction. Moreover, the addition of BHT to the reaction mixture did not affect the cyclization.
[20] M. Hanack, *Angew. Chem.* **1978**, *90*, 346–354; *Angew. Chem. Int. Ed. Engl.* **1978**, *17*, 333–341.
[21] Compound **9** and related structures based on alkene linkers could be of interest for second-order nonlinear optics: S. R. Marder, J. W. Perry, *Adv. Mater.* **1993**, *5*, 804–815; M. S. Wong, C. Bosshard, F. Pan, P. Günter, *Adv. Mater.* **1996**, *8*, 677–680; M. S. Wong, C. Bosshard, P. Günter, *Adv. Mater.* **1997**, *9*, 837–842. Furthermore, **10**, or related compounds from the coupling of **7** with diiodides **2f** or **2g**, could be precursors for new poly(aryleneethynylene) (PAE) polymers containing 2,5-thienylene units: T. Yamamoto, K. Honda, N. Ooba, S. Tomaru, *Macromolecules* **1998**, *31*, 7–14.

Polycephalin B and C: Unusual Tetramic Acids from Plasmodia of the Slime Mold *Physarum polycephalum* (Myxomycetes)**

Alexander Nowak and Bert Steffan*

Light plays an important role during the life cycle of the myxomycete *Physarum polycephalum*.[1] Young plasmodia, which are of a remarkable yellow color, live inside decaying trees and move away from the light, while older plasmodia, which have stopped growing, move towards the light and sporulate. Photoreceptors in the UV-A or blue light range which contain maxima at 350 nm (UV-A) and 460 nm (blue light) in their action spectra are responsible[1b] for these phenomena.

Despite intensive efforts the nature of the photoreceptor concerning this "blue-light phenomenon" is as yet unknown. Different types of pigments such as pteridines,[2] phenols,[3] peptides, flavines, flavones, nitrogen-containing polyenes,[4] or phytochromes[5] were assumed to be involved in the signal cascade. Since not only the yellow plasmodia of wild-type *P. polycephalum* but also the white mutants are photosensitive, it was considered that the chromophore of the blue-light receptor may be a flavin or a pteridine and that the orange-yellow pigments occuring in the wild type have no function for the signal transduction.

We were able to prove that the yellow wild type as well as the white mutant LU 897 × LU 898[6] contain a very similar but only quantitatively different set of pigments of the polyene type absorbing in the range under consideration.[7] Taking into account that the UV maximum of a chromophore can be bathochromically shifted up to 80 nm by integration into a protein, as described for the photoreceptor of the halophilic purple bacterium *Ectothiorhodospira halophila*,[8] the yellow polyenes in *Physarum* plasmodia can be thought of as acting as antenna pigments within a protein or protein complex of this organism.

High-performance liquid chromatography (HPLC) of a myxomycete culture exposed to diffuse light after growing for five days under exclusion of light shows remarkable differences in the intensities of certain peaks in comparison to a myxomycete culture growing under exclusion of light only (Figure 1).[9] Apparently light stimulates the formation of two metabolites, which cause a striking increase in the intensities of peak 1 ($t_{ret} = 34.47$ min) and peak 2 ($t_{ret} = 32.74$ min). Here we report on the isolation and structure elucidation of these metabolites, which we have named polycephalin C (**1**) and B (**2**).

Because the compounds are very sensitive to light, all steps from incubation and extraction to chromatography were carried out under exclusion of light and at low temperature (4 °C). Plasmodia cultivated under axenic conditions[10] were first thoroughly extracted with a mixture of acetone, meth-

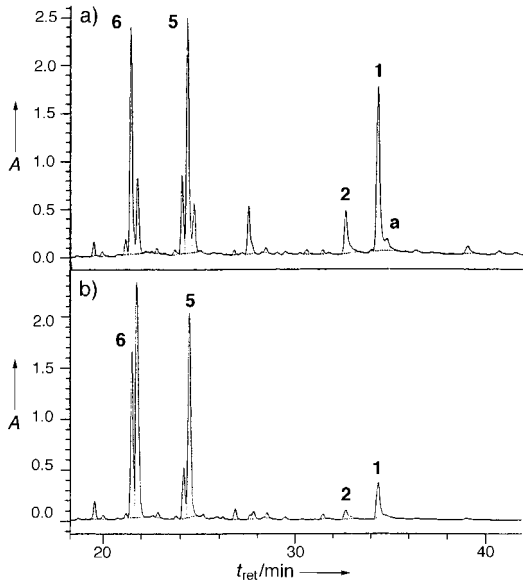


Figure 1. HPLD chromatograms for the chloroform extract of *P. polycephalum* cultures: a) growth for five days in the dark followed by two days under illumination; b) growth for seven days in the dark (control). Conditions for HPLC: column: Nucleosil 100–5 C_{18} (250 × 4 mm), mobile phase A: water/acetonitrile (9/1), 0.1% TFA, mobile phase B: acetonitrile, 0.1% TFA, linear gradient from A to B in 45 min, flow rate: 1.0 mL min^{-1}, photodiode array detection in the range of $\lambda = 200–800$ nm. A = absorbance, t_{ret} = retention time, TFA = trifluoroacetic acid.

[*] Dr. B. Steffan, Dr. A. Nowak
Institut für Organische Chemie der Universität
Karlstrasse 23, D-80333 München (Germany)
Fax: (+49) 89-5902-483
E-mail: bst@org.chemie.uni-muenchen.de

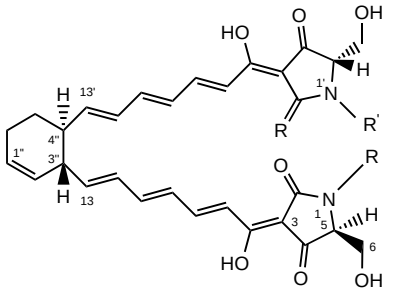
[**] This work was supported by the Deutsche Forschungsgemeinschaft (SFB 369). We wish to thank Dr. W. Spahl for recording the mass spectra.

 © WILEY-VCH Verlag GmbH, D-69451 Weinheim, 1998 1433-7851/98/3722-3139 $ 17.50+.50/0

anol, ethyl acetate, and chloroform (3/2/1/1). After the removal of lipophilic components by partitioning between *n*-hexane and methanol/water (9/1), the aqueous phase was concentrated, dissolved again in water, and extracted with chloroform. The organic phase was concentrated and separated by chromatography on Sephadex LH-20 with methanol as eluent. Further purification by partition between ethyl acetate and citrate/HCl buffer (100 mM, pH 3.0) or an aqueous solution of EDTA (50 mM, pH 4.75) provided polycephalin C (**1**) and B (**2**) as amorphous orange-red powders. Starting from 220 g of biomass 7.2 mg (0.003 %) of **1** and 11.8 mg (0.005 %) of **2** were obtained in pure form.

According to the high-resolution ESI mass spectrum, **1** has the molecular formula $C_{32}H_{36}N_2O_8$. The UV spectrum (methanol) shows absorption maxima at $\lambda = 253$ and 390 nm. Addition of dilute hydrochloric acid leads to a slight bathochromic shift of the long-wave absorption band (to $\lambda =$ 394 nm), which is displaced hypsochromically to $\lambda = 395$ nm after addition of a dilute solution of sodium hydroxide. This behavior is typical for tetramic acids.[11] The IR spectrum of **1** contains inter alia bands at $\tilde{\nu} = 1686$ (lactam), 1635, 1598 (polyene), and 2854 cm^{-1} (*N*-methyl).

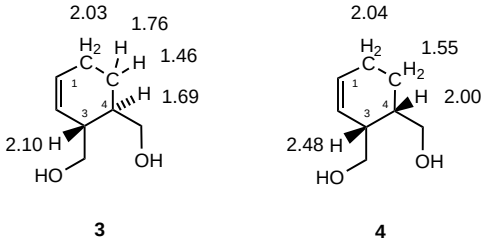
The ^1H NMR spectrum of **1** displays two overlapping groups of signals for triene moieties between $\delta = 7.51$ and 5.93, and signals for an AB_2 system at $\delta = 3.95$ ($2CH_2$) and 3.73 (2CH) for the two hydroxyethylidene groups. The aliphatic protons of the cyclohexene ring ($\delta = 1.56 - 2.80$) couple with those of both triene moieties. The ^{13}C NMR spectrum contains the signals for 14 olefinic CH, 4 aliphatic CH, 4 aliphatic CH_2, and 2 *N*-methyl groups as well as 8 quaternary carbon atoms. The HMBC and HMQC correlations connect each of the two hydroxyethylidene groups ($\delta = 59.29$, 69.35) with an *N*-methyltetramic acid ($\delta = 26.96$, 101.43, 173.31, 175.10, 194.34) that is linked with one of the triene chains, which are in turn leading vicinally into the cyclohexene ring. The above data indicate structure **1** for polycephalin C.[12]



1 R = R′ = CH_3
2 R = CH_3, R′ = H

The configuration at C-5 of the tetramic acid was established after hydration of **1** with hydrogen on Pd/C. The circular dichroism (CD) spectrum of the hydrated compound[13] shows a parallel lapse to that of decahydrophysarorubinic acid as well as that of the synthetically prepared 3-acetyl-5-hydroxymethyl-*N*-methyltetramic acid with 5*S* configuration.[7] Therefore, **1** should have *S* configuration at both C-5 and C-5′.

To confirm the structure of **1** and determine the relative stereochemistry at positions 3″ and 4″, the isomeric diols **3** and **4** were synthesized as model compounds. According to the method of Corey et al.,[14] 2,4-pentadienol and methyl acrylate were coupled by a Diels–Alder reaction, and the resulting species was reduced with $LiAlH_4$ to yield **3** and **4** (Figure 2).



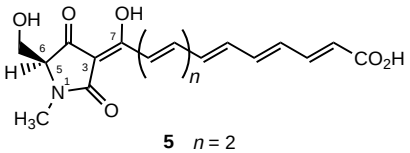
3 **4**

Figure 2. Structures and selected ^1H NMR data of *trans*- and *cis*-3,4-dihydroxymethylcyclohexene (**3** and **4**, respectively).

The coupling constant of the protons H-3 and H-4 is 5.3 Hz for the *cis* form **4**. The coupling constant of the *trans* compound **3** is 8.5 Hz, which is in accordance with the value found in **1** for the corresponding protons of the cyclohexene ring ($J = 8.8$ Hz). The protons at C-5 and C-6 of the *cis* isomer **4** appear as a coupled system of equivalent nuclei. In comparison, while the protons at position C-6 of the *trans* isomer **3** are isochronous, the protons of the methylene group at C-5 are not and appear at different shifts ($\delta = 1.46$ and 1.76). This is in exact agreement with the data obtained for **1**.

According to NMR spectroscopy and LC/APCI mass spectrometry (*m*/*z* 562, $C_{31}H_{34}N_2O_8$; APCI indicates chemical ionization at atmospheric pressure), peak 2 in the chromatogram in Figure 1) (polycephalin B) corresponds to an N-demethylated polycephalin C. The HMBC and HMQC correlations relate a hydroxyethylidene group ($\delta = 59.12$, 69.29) to an *N*-methyltetramic acid ($\delta = 26.95$, 101.44, 173.48, 174.81, 193.97). As in **1** the protons of the serine residue split into a doublet ($\delta = 3.96$, CH_2CH) and a triplet ($\delta = 3.76$, CH_2CH). The second hydroxyethylidene group ($\delta = 62.11$, 64.46) is connected to a tetramic acid without a substituent at N ($\delta =$ 101.44, 173.48, 174.81, 195.80). In this case the protons at position 6′ are not isochronous, and their signals split into a doublet of doublets. Thus, there are three signals at $\delta = 3.92$, 3.84, and 3.79 in the ^1H NMR spectrum of the serine residue. Which of the two tetramic acid moieties is N-methylated has not yet been determined. Considering these data polycephalin B is assigned structure **2**.[15]

Peak 5 in the chromatogram in Figure 1 corresponds to physarorubinic acid A (**5**), which we had isolated earlier.[7] Spectroscopic data reveal that peak 6 corresponds to a polyenetetramic acid which contains one less double bond.



5 *n* = 2
6 *n* = 1

 © WILEY-VCH Verlag GmbH, D-69451 Weinheim, 1998 1433-7851/98/3722-3140 $ 17.50+.50/0 *Angew. Chem. Int. Ed.* **1998**, *37*, No. 22

This compound, named physarorubinic acid B, has structure **6**.[16] Thus, two further polyene compounds which are responsible for the yellow color of the wild-type plasmodia of *Physarum polycephalum* have been isolated besides physarochrom A.[17]

Polycephalin C (**1**) is very sensitive to light and changes under specific illumination conditions to another compound corresponding to peak a (Figure 1). The structure elucidation of the compound corresponding to peak a will be reported in detail elsewhere together with the biosynthesis of **1**, which may contain the precursors **5** and **6**.

Received: September 26, 1997
Revised version: May 15, 1998 [Z10978IE]
German version: *Angew. Chem.* **1998**, *110*, 3341 – 3343

Keywords: natural products · phytochrome · polyenes · structure elucidation · UV/Vis spectroscopy

[1] a) L. Rakoczy in *The Blue Light Syndrome* (Ed.: H. Senger), Springer, Berlin, **1980**, pp. 570 – 583; b) T. Nakagaki, S. Umemura, Y. Kakiuchi, T. Ueda, *Photochem. Photobiol.* **1996**, *64*, 859 – 862.

[2] G. Werner-Felmayer, G. Golderer, E. R. Werner, P. Gröbner, H. Wachter, *Biochem. J.* **1994**, *304*, 105 – 111.

[3] P. Nair, G. G. Zabka, *Am. J. Bot.* **1966**, *53*, 887 – 92.

[4] L. Rakoczy, *Ber. Deutsch. Bot. Ges.* **1973**, *86*, 141 – 164, and references therein.

[5] C. Starostzik, W. Marwan, *FEBS Lett.* **1995**, *370*, 146 – 148.

[6] We wish to thank Dr. W. Marwan (Max-Planck-Institut für Biochemie, Martinsried, Germany) for a culture of the white mutant LU 897 × LU 898.

[7] A. Nowak, B. Steffan, *Liebigs Ann.* **1997**, 1817 – 1821.

[8] a) P. Galland in *Blue Light Responses, Vol. II* (Ed.: H. Senger), CRC Press, Boca Raton, FL, **1987**, pp. 37 – 52; b) R. Kort, H. Vonk, X. Xu, W. D. Hoff, W. Crielaard, K. J. Hellingwerf, *FEBS Lett.* **1996**, *382*, 73 – 78.

[9] The suspension culture of the myxomycete was grown for five days in the dark followed by two days under illumination. A control experiment was carried out in which the culture was incubated for seven days in the dark.

[10] J. W. Daniel, H. H. Baldwin in *Meth. Cell Physiol., Vol. 1* (Ed.: D. M. Prescott), Academic Press, London, **1964**, pp. 9 – 41.

[11] a) R. J. Cole, R. H. Cox, *Handbook of Toxic Fungal Metabolites*, Academic Press, London, **1981**, p. 688; b) F. A. MacKellar, M. F. Grostic, E. C. Olson, R. J. Wnuk, A. R. Branfman, K. L. Rinehart Jr., *J. Am. Chem. Soc.* **1971**, *93*, 4943 – 4945.

[12] **1**: TLC (silica gel 60 F_{254}, chloroform/methanol/water 60/40/9): R_f = 0.56; HPLC (for conditions see Figure 1): t_{ret} = 34.47 min; UV (c = 4.1427 μM, 3 mL of methanol): λ_{max} (lg ε) = 253 (4.15), 390 nm (4.74); UV (c = 3.94 μM, 3 mL of methanol + 50 μL of 3 M HCl): λ_{max} (lg ε) = 224 (4.22), 250 (4.20), 395 (4.93), 415 nm (sh, 4.92); UV (c = 3.7535 μM, 3 mL of methanol + 50 μL of 2 M NaOH): λ_{max} (lg ε) = 264 (4.29), 360 nm (4.70); CD (methanol): λ_{max} ($\Delta\varepsilon_{rel}$) = 213.5 (+1.42), 250.5 (−3.24), 271.5 (+0.57), 301 (+0.035), 363 (+5.73), 424 nm (−3.88); ^{1}H NMR ($CD_3OD/CDCl_3$ 1/1, 600.13 MHz): δ = 7.51 (dd, J = 15.5, 11.0 Hz, 2H; 9-H, 9′-H), 7.14 (d, J = 15.5 Hz, 2H; 8-H, 8′-H), 6.69 (dd, J = 15.4, 9.2 Hz, 1H; 11-H), 6.68 (dd, J = 15.4, 9.2 Hz, 1H; 11′-H), 6.42 (dd, J = 11.0, 15.4 Hz, 2H; 10-H, 10′-H), 6.27 (dd, J = 9.2, 15.1 Hz, 1H; 12′-H), 6.24 (dd, J = 9.2, 15.1 Hz, 1H; 12-H), 6.02 (dd, J = 15.1, 8.0 Hz, 1H; 13′-H), 5.93 (dd, J = 15.1, 7.9 Hz, 1H; 13-H), 5.83 (ddd, J = 10.1, 2.6, 3.4 Hz, 1H; 1″-H), 5.54 (ddd, J = 10.1, 2.5, 1.9 Hz, 1H; 2″-H), 3.95 (d, J = 3.3 Hz, 4H; 6-H_2, 6′-H_2), 3.73 (t, J = 3.3 Hz, 2H; 5-H, 5′-H), 3.05 (s, 6H; 2NCH_3), 2.80 (dm, J = 8.8 Hz, 1H; 3″-H), 2.25 (dddm, J = 8.0, 8.8, 2.8 Hz, 1H; 4″-H), 2.12 (br m, 2H; 6″-H_2), 1.84 (m, 1H; 5″-H_a), 1.56 (m, 1H; 5″-H_b); ^{13}C NMR ($CD_3OD/CDCl_3$ 1/1, 150.9 MHz): δ = 194.34 (s; C-4, C-4′), 175.10 (s; C-2, C-2′), 173.31 (s; C-7, C-7′), 145.50 (d; C-9, C-9′), 145.40 (d; C-13′), 144.54 (d; C-13), 144.24 (d; C-11′), 143.92 (d; C-11), 131.30 (d; C-12), 130.53 (d; C-12′), 130.22 (d; C-10, C-10′), 128.60 (d; C-1″, 128.03 (d; C-2″), 120.96 (d; C-8, C-8′), 101.43 (s; C-3, C-3′), 69.35 (d; C-5, C-5′), 59.29 (t; C-6, C-6′), 45.29 (d; C-3″), 43.88 (d; C-4″), 27.64 (t; C-5″), 26.96 (q; 2NCH_3), 24.41 (t; C-6″); IR (KBr): $\tilde{\nu}$ = 3418 (m), 3022 (w), 2925 (w), 2854 (w), 1686 (m), 1635 (s), 1598 (s), 1553 (s), 1480 (m), 1445 (m), 1407 (m), 1363 (w), 1287 (w), 1254 (w), 1132 (w), 1007 (m), 915 (w), 895 (w), 612 cm^{-1} (w); $[\alpha]_D$ = −73.2 (c = 0.0041 in methanol); ESI-MS: m/z: 577 $[M+H]^+$, 599 $[M+Na]^+$, 615 $[M-H+Ca]^+$, 1175 $[2M+Na]^+$; HR-MS (EI) calcd for $C_{32}H_{37}N_2O_8$ $[M+H]^+$: 577.25945, found: 577.25995.

[13] Hydrogenated polycephalin C: UV (methanol): λ_{max} = 240 (sh), 272, 280 nm (sh); CD (methanol): λ_{max} ($\Delta\varepsilon_{rel}$) = 203 (−4.99), 221, (+2.33), 239.5 (−1.04), 265.5 (+1.14), 290.5 (−2.68).

[14] E. J. Corey, M. Petrzilka, *Tetrahedron Lett.* **1975**, *30*, 2537 – 2540.

[15] **2**: TLC (silica gel 60 F_{254}, chloroform/methanol/water 60/40/9): R_f = 0.47; HPLC (for conditions see Figure 1): t_{ret} = 32.74 min; UV (c = 4.235 μM, 3 mL of methanol): λ_{max} (lg ε) = 247 (414), 386 (4.74), 406 nm (sh, 4.69); UV (c = 4.035 μM, 3 mL of methanol + 50 μL of 3 M HCl): λ_{max} = 220, 254, 388 nm; CD (methanol) λ_{max} ($\Delta\varepsilon_{rel}$) = 206 (+1.73), 250 (−1.54), 271 (+0.58), 297 (+0.25), 361 (+4.76), 415.5 (−4.51); ^{1}H NMR ($CD_3OD/CDCl_3$ 1/1, 600.13 MHz): δ = 7.54 (dd, J = 14.9, 11.4 Hz, 2H; 9-H, 9′-H), 7.17 (d, J = 14.9 Hz, 2H; 8-H, 8′-H), 6.73 (dd, J = 14.7, 10.6 Hz, 1H; 11′-H), 6.71 (dd, J = 14.7, 10.5 Hz, 1H; 11-H), 6.44 (dd, J = 11.4, 14.7 Hz, 2H; 10-H, 10′-H), 6.28 (dd, J = 10.6, 15.2 Hz, 1H; 12′-H), 6.26 (dd, J = 10.5, 15.1 Hz, 1H; 12-H), 6.04 (dd, J = 15.2, 8.2 Hz, 1H; 13′-H), 5.94 (dd, J = 15.1, 8.2 Hz, 1H; 13-H), 5.84 (ddd, J = 10.1, 6.3, 3.8 Hz, 1H; 1″-H), 5.54 (dd, J = 10.1, 2.2 Hz, 1H; 2″-H), 3.96 (d, J = 2.9 Hz, 2H; 6-H_2), 3.92 (dd, J = 3.2, 5.3 Hz, 1H; 5′-H), 3.84 (dd, J = 3.2, 11.6 Hz, 1H; 6′-H_a), 3.79 (dd, 5.3, 11.6 Hz, 1H; 6′-H_b), 3.76 (t, J = 2.9 Hz, 1H; 5-H), 3.06 (s, 6H; 2 NCH_3), 2.81 (m, 1H; 3″-H), 2.26 (dm, J = 8.2 Hz, 1H; 4″-H), 2.13 (br m, 2H; 6″-H_2), 1.85 (m, 1H; 5″-H_a), 1.57 (m, 1H; 5″-H_b); ^{13}C NMR ($CD_3OD/CDCl_3$ 1/1, 150.9 MHz): δ = 195.80 (s; C-4′), 193.97 (s; C-4), 174.81 (s; C-2, C-2′), 173.48 (s; C-7, C-7′), 145.68 (d; C-9, C-9′), 144.67 (d; C-13′), 144.62 (d; C-13), 144.11 (d; C-11, C-11′), 130.64 (d; C-10, C-10′), 130.44 (d; C-12), 130.25 (d; C-12′), 128.75 (d; C-1″), 128.06 (d; C-2″), 120.92 (d; C-8, C-8′), 101.44 (s; C-3, C-3′), 69.29 (d; C-5), 64.46 (d; C-5′), 62.11 (t; C-6′), 59.12 (t; C-6), 45.29 (d; C-3″), 43.91 (d; C-4″), 27.72 (t; C-5″), 26.95 (q; 2 NCH_3), 24.61 (t; C-6″); IR (KBr): $\tilde{\nu}$ = 3402 (s), 2924 (s), 2854 (m), 1686 (m), 1654 (s), 1636 (s), 1599 (s), 1554 (m), 1466 (w), 1438 (w), 1407 (w), 1288 (w), 1260 (w), 1008 (w), 915 (w), 896 (w), 611 cm^{-1} (w); LC-APCI-MS (negative mode): m/z: 562 $[M]^-$, 561 $[M-H]^-$, 544 $[M-H_2O]^-$, 543 $[M-H-H_2O]^-$; LC-APCI-MS (positive mode): m/z: 563 $[M+H]^+$, 545 ($[M+H-H_2O]^+$.

[16] **6**: TLC (silica gel 60 F_{254}, chloroform/methanol/water 60/40/9): R_f = 0.25; HPLC (for conditions see Figure 1): t_{ret} = 20.9 min; UV (methanol): λ_{max} (lg ε) = 247 (3.67), 286 (3.67), 393 (4.37), 409 nm (sh); UV (c = 17.3 μM, 1.5 mL of methanol + 25 μL of 3 M HCl): λ_{max} (lg ε) = 287 (3.67), 396 (4.43), 413 (4.46), 438 nm (sh); UV (c = 17.3 μM, 1.5 mL of methanol + 25 μL of 2 M NaOH): λ_{max} (lg ε) = 248 (3.80), 371 nm (4.35); CD (methanol): λ_{max} ($\Delta\varepsilon_{rel}$) = 207.0 (−2.06), 223.0 (+1.12), 260.0 nm (−0.63); ^{1}H NMR ($CD_3OD/CDCl_3$ 1/1, 600.15 MHz): δ = 7.54 (dd, J = 14.8, 12.0 Hz, 1H; 9-H), 7.36 (dd, J = 15.1, 11.5 Hz, 1H; 14-H), 7.31 (br, 1H; 8-H), 6.81 (dd, J = 13.6, 11.4 Hz, 1H; 11-H), 6.74 (dd, J = 13.9, 11.4 Hz, 1H; 12-H), 6.69 (dd, J = 13.6. 12.0 Hz, 1H; 10-H), 6.61 (dd, J = 13.9, 11.5 Hz, 1H; 13-H), 6.00 (d, J = 15.1 Hz, 1H; 15-H), 3.96 (br s, 2H; 6-H_2), 3.77 (br s, 1H; 5-H), 3.07 (s, 3H; NCH_3); ^{13}C-NMR ($CD_3OD/CDCl_3$ 1/1, 150.9 MHz): δ = 194 (br, C-4), 174.07 (C-2), 172.64 (C-7), 169.63 (C-16), 144.66 (C-9), 143.91 (C-14), 141.74 (C-11), 139.90 (C-12), 135.46 (C-10), 135.11 (C-13), 124.28 (C-15), 123.80 (C-8), 102.43 (C-3), 69.07 (C-5), 59.22 (C-6), 27.01 (NCH_3); IR (KBr):$\tilde{\nu}$ = 3418 (s), 2924 (s), 2853 (m), 1686 (s), 1618 (s), 1588 (s), 1549 (m), 1465 (m), 1406 (m), 1305 (m), 1260 (m), 1126 (m), 1081 (w), 1010 (m), 917 (w), 884 (w), 806 (w), 611 cm^{-1} (w); $[\alpha]_D$ = −146.8 (c = 0.019 in methanol); APCI-MS (positive mode): m/z: 320 $[M+H]^+$; HR-APCI-MS calcd for $C_{16}H_{18}NO_6$ $[M+H]^+$: 320.1134, found: 320.1148.

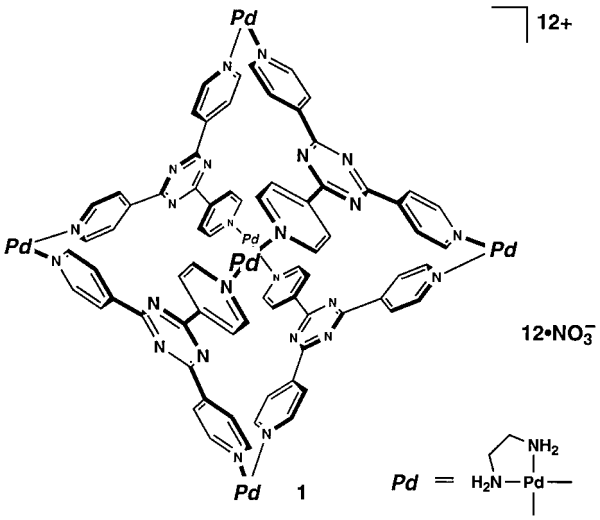
[17] B. Steffan, M. Praemassing, W. Steglich, *Tetrahedron Lett.* **1987**, *28*, 3667 – 3670.

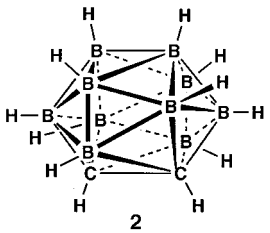
 © WILEY-VCH Verlag GmbH, D-69451 Weinheim, 1998 1433-7851/98/3722-3141 $ 17.50+.50/0

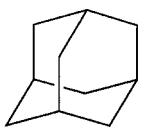
Encapsulation of Large, Neutral Molecules in a Self-Assembled Nanocage Incorporating Six Palladium(II) Ions**

Takahiro Kusukawa and Makoto Fujita*

Properties of molecules significantly change when they are encapsulated in cage compounds having functional groups in the interior space at fixed positions.[1–4] The cage compounds typically prepared by conventional covalent synthesis can encapsulate only one or two small molecules because the construction of larger cage frameworks is very difficult.[5–7] In contrast, noncovalent synthesis has been providing large cagelike structures quite efficiently. That is, hydrogen-bonded[8–11] and coordination-bonded[12] molecular capsules with large frameworks have been prepared by self-assembly. Recently, coordination cage **1** with a diameter of approximately 2 nm was constructed through transition metal mediated self-assembly from six metal ions and four ligands.[13, 14] We report herein on the remarkable ability of this complex to encapsulate large, neutral molecules.







[*] Prof. Dr. M. Fujita, Dr. T. Kusukawa
CREST, Japan Science and Technology Corporation (JST)
Coordination Chemistry Laboratories
Institute for Molecular Science
Myodaiji, Okazaki 444–8585 (Japan)
Fax: (+81) 564-555-245
E-mail: mfujita@ims.ac.jp

[**] This work was supported by the CREST (Core Research for Evolutional Science and Technology) project of the Japan Science and Technology Corporation.

We observed the remarkable ability of **1** to encapsulate large molecules in its inclusion of four molecules of *o*-carborane (**2**), an icosahedral carbon–boron cage molecule with a diameter of 8 Å.[15, 16] This large, neutral molecule is nonpolar and immiscible in water. However, when a hexane solution of **2** (10 mM, 5 mL) was stirred with a D_2O solution of **1** (5 mM, 1 mL, **2**:**1** = 10:1), four equivalents of **2** were rapidly transferred into the aqueous phase and the stoichiometric formation of $\mathbf{1}\cdot(\mathbf{2})_4$ complex was observed (Figure 1c). The

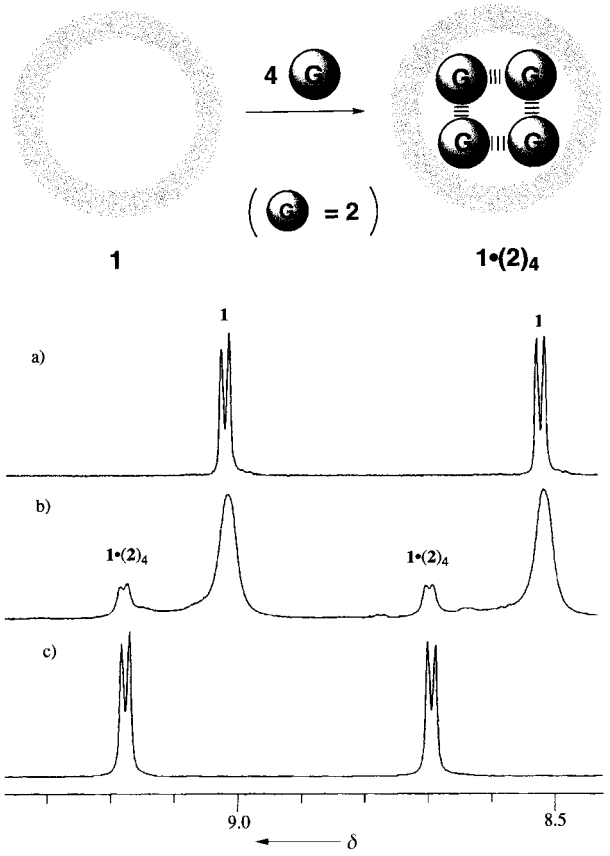


Figure 1. NMR observation of the encapsulation of *o*-carborane (**2**) in nanocage **1**. a) Empty **1**. b), c) A D_2O solution of **1** (5 mM, 1 mL) was treated with a hexane solution of **2** [10 mM; 0.5 mL (b), 5 mL (c)].

encapsulation of **2** in the cage of **1** was supported by the significant upfield shifting of δ_H signals of **2** appearing at $\delta =$ 1.3 to −0.3.[17] The 1:4 stoichiometry was confirmed by the integration ratio of signals of **1** and **2** in the ^1H NMR spectrum. Even when only one equivalent of **2** was employed (**2**: 10 mM, 0.5 mL; **1**: 5 mM, 1 mL), 82% of **2** was effectively transferred into the aqueous phase and complexed with **1** to give the $\mathbf{1}\cdot(\mathbf{2})_4$ complex in roughly 20% yield (or ca. 80% based on **2**, Figure 1b).[18] Surprisingly, a strong cooperative effect was observed in this complexation: that is, no intermediary complexes $\mathbf{1}\cdot(\mathbf{2})_n$ ($n = 1-3$) were observed.

Adamantane (**3**) was also encapsulated by **1** to form a 1:4 complex. Again, a D_2O solution of **1** (2 mM) was stirred with a saturated hexane solution of **3** at 60 °C. While the encapsulation of **2** by **1** was a rapid process, the transfer of **3** from hexane into water phase was slow (ca. 30 min until completion), and this process was clearly monitored by time-

 © WILEY-VCH Verlag GmbH, D-69451 Weinheim, 1998 1433-7851/98/3722-3142 $ 17.50+.50/0

dependent NMR measurement (Figure 2). The high upfield shift of ^{1}H NMR signals of **3** ($\Delta\delta = -0.4$ to -2.2) was consistent with the encapsulation in the cavity lined by

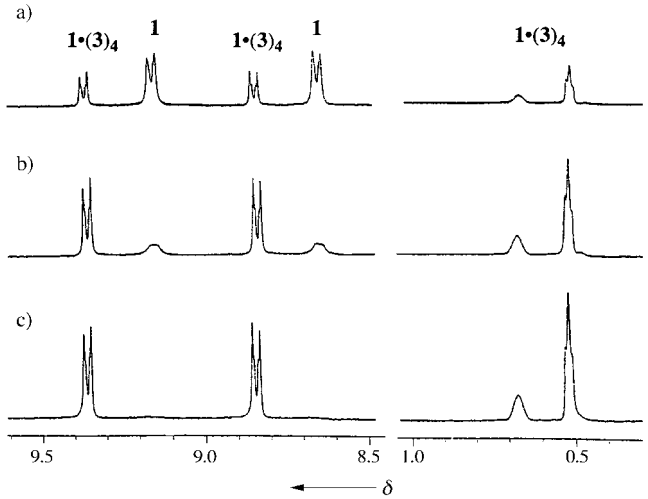


Figure 2. NMR observation of the formation of the $\mathbf{1}\cdot(\mathbf{3})_4$ complex from an aqueous solution of **1** and a saturated hexane solution of **3** at 60 °C after a) 1 min, b) 5 min, and c) 30 min.

aromatic rings. Again, intermediary complexes $\mathbf{1}\cdot(\mathbf{3})_n$ ($n = 1-3$) were not observed. More surprisingly, adamantane was transferred into the aqueous phase even in a solid–liquid two-phase system. Thus, the high-yield formation of $\mathbf{1}\cdot(\mathbf{3})_4$ (>95%) was observed when powdered **3** (excess amount) was suspended in a D_2O solution of **1** at 60 °C for four days.

The inclusion geometry of the guest molecules is particularly interesting. When 1- or 2-adamantanol (**4** or **5**, respectively) was employed as a guest, the formation of a stable 1:4 complex was again observed. Careful NMR analysis[19] of this complex showed that the signals of the hydrophobic moieties were shifted significantly upfield while those of the hydrophilic moiety were not (Figure 3). This result shows that the interior of host **1** is highly hydrophobic and the guest molecule is located in the cage such that the hydroxyl group is pointed outward.

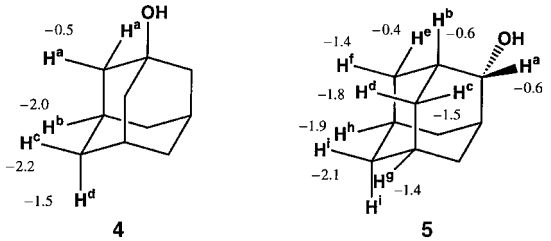
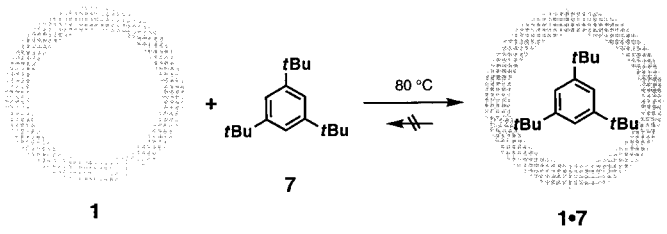


Figure 3. Change in the NMR chemical shifts of adamantanol guests **4** and **5** upon inclusion in **1**. Negative values indicate upfield shift values ($\Delta\delta$ in ppm).

Significant π-donor–acceptor interactions were observed when 1,3,5-trimethoxybenzene (**6**) was employed as a guest. Upon the addition of this aromatic guest, the solution turned yellow immediately and the 1:4 complex ($\mathbf{1}\cdot(\mathbf{6})_4$) formed quantitatively. The very large upfield shift ($\Delta\delta = -2.0$) of Ar*H* of **6** strongly supports an efficient aromatic stacking between guest **6** and the interior face of host **1**. Anisole behaved similarly as a guest, but addition of toluene, which is moderately electron-rich, did not lead to a significant color change although a 1:4 complex formed. In striking contrast, electron-deficient 1,4-dibromo-, 1,3,5-tribromo-, and perfluorobenzene were not complexed by **1** at all. These result clearly shows that the interior of the nanocage creates not only a hydrophobic but also an electrophilic microspace with properties quite different from those of the bulk phase.

It is also noteworthy that the complexation is much faster when the guest molecules are smaller. With such small guests as toluene or methoxy-substituted benzenes, the proton signals of both free **1** and the $\mathbf{1}\cdot(\mathbf{G})_4$ complex ($\mathbf{G}$ = guest) were completely averaged due to the rapid exchange on the NMR time scale.[20]

Particularly interesting is that tri-*tert*-butylbenzene (**7**), which is slightly larger than the portal of **1**,[21] is very slowly encapsulated by the cage through thermally induced slippage. Thus when a D_2O solution of **1** was stirred with a hexane



solution of **7** at 80 °C, the 1:1 complex **1**·**7** formed in approximately 40% yield after 2 h ($\Delta\delta = -1.5$ (*t*Bu), -2.5 (Ar*H*)). However, encapsulation and decapsulation become very slow at room temperature. Thus, once encapsulated, guest **7** did not escape from the cavity of **1** within two hours at room temperature even when the solution was treated with an organic solvent.

Experimental Section

Typical procedure: A hexane solution of *o*-carborane **2** (10.6 mM, 1 mL) was stirred with a D_2O solution of **1** (42.4 mM, 1 mL) for 3 h. The NMR spectrum of the aqueous phase showed the stoichiometric formation of the $\mathbf{1}\cdot(\mathbf{2})_4$ complex. $\mathbf{1}\cdot(\mathbf{2})_4$: ^{1}H NMR (500 MHz, D_2O): $\delta = 9.18$ (d, $J = 6.6$ Hz, 24H, Py Hα), 8.69 (d, $J = 6.6$ Hz, 24H, Py Hβ), 3.43 (s, 8H, carborane CH), 2.85 (s, 24H, -NCH_2CH_2N-), 1.3 to −0.3 (m, 40H, carborane BH); ^{13}C NMR (125 MHz, D_2O): $\delta = 170.1$ (Cq), 153.1 (CH), 145.6 (Cq), 126.6 (CH), 55.7 (carborane CH), 47.7 (CH_2).

$\mathbf{1}\cdot(\mathbf{3})_4$: ^{1}H NMR (500 MHz, D_2O): $\delta = 9.28$ (d, $J = 6.6$ Hz, 24H, Py Hα), 8.75 (d, $J = 6.6$ Hz, 24H, Py Hβ), 2.91 (s, 24H, -NCH_2CH_2N-), 0.59 (br s, 16H, adamantane CH) 0.44 (br s, 48H, adamantane CH_2); ^{13}C NMR (125 MHz, D_2O): $\delta = 170.0$ (Cq), 153.3 (CH), 145.3 (Cq), 126.0 (CH), 47.7 (CH_2), 37.3 (adamantane CH_2), 28.1 (adamantane CH).

$\mathbf{1}\cdot(\mathbf{4})_4$: ^{1}H NMR (500 MHz, D_2O): $\delta = 9.38$ (d, $J = 6.9$ Hz, 24H, Py Hα), 8.87 (d, $J = 6.9$ Hz, 24H, Py Hβ), 2.99 (s, 24H, -NCH_2CH_2N-), 1.24 (s, 24H, 1-adamantanol CH_2), 0.18 (s, 12H, 1-adamantanol CH), 0.12 (d, 12H, 1-adamantanol CH_2), −0.56 (d, 12H, 1-adamantanol CH_2); ^{13}C NMR (125 MHz, D_2O): $\delta = 170.2$ (Cq), 153.5 (CH), 145.2 (Cq), 126.1 (CH), 47.8 (CH_2), 44.5 (1-adamantanol CH_2), 35.8 (1-adamantanol CH_2), 30.5 (1-adamantanol CH).

$\mathbf{1}\cdot(\mathbf{5})_4$: ^{1}H NMR (500 MHz, D_2O): $\delta = 9.36$ (d, $J = 6.9$ Hz, 24H, Py Hα), 8.81 (d, $J = 6.9$ Hz, 24H, Py Hβ), 3.23 (s, 4H, 2-adamantanol CH), 2.99 (s, 24H, -NCH_2CH_2N-), 1.64 (d, 8H, $J = 12.5$ Hz, 2-adamantanol CH_2), 1.33 (s,

 © WILEY-VCH Verlag GmbH, D-69451 Weinheim, 1998 1433-7851/98/3722-3143 $ 17.50+.50/0

8H, 2-adamantanol CH), 0.45 (s, 4H, 2-adamantanol CH), 0.24 (d, 8H, J = 12.5 Hz, 2-adamantanol CH_2), 0.10 (d, 8H, J = 12.5 Hz, 2-adamantanol CH_2), 0.06 (d, 8H, J = 12.5 Hz, 2-adamantanol CH_2), −0.10 (s, 4H, 2-adamantanol CH), −0.43 (s, 8H, 2-adamantanol CH_2); ^{13}C NMR (125 MHz, D_2O): δ = 170.1 (Cq), 153.4 (CH), 145.2 (Cq), 126.0 (CH), 74.0 (2-adamantanol CH), 47.8 (CH_2), 37.2 (2-adamantanol CH_2), 36.1 (2-adamantanol CH_2), 31.0 (2-adamantanol CH_2), 27.3 (2-adamantanol CH), 26.8 (2-adamantanol CH).

1·(**6**)$_4$: ^{1}H NMR (500 MHz, D_2O): δ = 9.29 (d, J = 6.6 Hz, 24H, Py Hα), 8.65 (d, J = 6.6 Hz, 24H, Py Hβ), 4.09 (s, 12H, trimethoxybenzene CH), 2.98 (s, 24H, -NCH_2CH_2N-), 2.43 (br s, 36H, CH_3O); ^{13}C NMR (125 MHz, D_2O): δ = 169.9 (Cq), 160.6 (trimethoxybenzene Cq), 153.3 (CH) 145.9 (Cq), 126.2 (CH), 92.0 (trimethoxybenzene CH), 54.5 (CH_3O) 47.8 (-NCH_2CH_2N-).

1·**7**: ^{1}H NMR (500 MHz, D_2O): δ = 9.28 (br s, 24H, Py Hα), 8.72 (br s, 24H, Py Hβ), 4.8 (s, 3H, **7** Ar CH), 2.99 (s, 24H, -NCH_2CH_2N-), −0.12 (s, 27H, *t*Bu); ^{13}C NMR (125 MHz, D_2O): δ = 170.1 (Cq), 153.3 (CH) 149.0 (**7** Ar Cq), 146.3 (Cq), 126.0 (CH), 47.8 (-NCH_2CH_2N-), 33.8 (*t*Bu Cq), 30.4 (*t*Bu CH_3).

Received: June 2, 1998 [Z11936IE]
German version: *Angew. Chem.* **1998**, *110*, 3327 – 3329

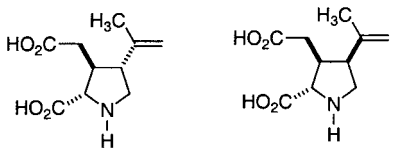
Keywords: adamantanes · boron · clusters · molecular recognition · palladium

[1] a) D. J. Cram, *Nature* **1992**, *356*, 29 – 36; b) D. J. Cram, M. T. Tanner, R. Thomas, *Angew. Chem.* **1991**, *103*, 1048 – 1051; *Angew. Chem. Int. Ed. Engl.* **1991**, *30*, 1024 – 1027.
[2] a) R. Warmuth, *Angew. Chem.* **1997**, *109*, 1406 – 1409; *Angew. Chem. Int. Ed. Engl.* **1997**, *36*, 1347 – 1350; b) R. Warmuth, *J. Chem. Soc. Chem. Commun.* **1995**, 59 – 60.
[3] J. Kang, J. Rebek, Jr., *Nature* **1997**, *385*, 50 – 52.
[4] S. Watanabe, K. Goto, T. Kawashima, R. Okazaki, *J. Am. Chem. Soc.* **1997**, *119*, 3195 – 3196.
[5] a) J. Yoon, D. J. Cram, *J. Am. Chem. Soc.* **1997**, *119*, 11796 – 11806; b) J. Yoon, D. J. Cram, *Chem. Commun.* **1997**, 497 – 498; c) J. Yoon, D. J. Cram, *Chem. Commun.* **1997**, 2065 – 2066; d) R. C. Helgeson, K. Paek, C. B. Knobler, E. F. Maverick, D. J. Cram, *J. Am. Chem. Soc.* **1993**, *115*, 10111 – 10116.
[6] a) P. Timmerman, W. Verboom, F. C. J. M. van Veggel, J. P. M. van Duynhoven, D. N. Reinhoudt, *Angew. Chem.* **1994**, *106*, 2437 – 2440; *Angew. Chem. Int. Ed. Engl.* **1994**, *33*, 2345 – 2348; b) B.-H. Huisman, D. M. Rudkevich, F. C. M. van Veggel, D. N. Reinhoudt, *J. Am. Chem. Soc.* **1996**, *118*, 3523 – 3524.
[7] J. R. Fraser, B. Borecka, J. Trotter, J. C. Sherman, *J. Org. Chem.* **1995**, *60*, 1207 – 1213.
[8] C. Sheu, K. N. Houk, *J. Am. Chem. Soc.* **1996**, *118*, 8056 – 8070.
[9] a) R. S. Meissner, J. Rebek, Jr., J. de Mendoza, *Science* **1995**, *270*, 1485 – 1488; b) N. Branda, R. Wyler, J. Rebek, Jr. *Science* **1994**, *263*, 1267 – 1268; c) R. Meissner, X. Garcias, S. Mecozzi, J. Rebek, Jr., *J. Am. Chem. Soc.* **1997**, *119*, 77 – 85; c) B. C. Hamann, K. D. Shimizu, J. Rebek, Jr., *Angew. Chem.* **1996**, *108*, 1425 – 1427; *Angew. Chem. Int. Ed. Engl.* **1996**, *35*, 1326 – 1329.
[10] L. R. MacGillivray, J. L. Atwood, *Nature* **1997**, *389*, 469 – 472.
[11] a) J. Scheerder, R. H. Vreekamp, J. F. Engbersen, W. Verboom, J. P. M. van Duynhoven, D. N. Reinhoudt, *J. Org. Chem.* **1996**, *61*, 3476 – 3481; b) R. H. Vreekamp, W. Verboom, D. N. Reinhoudt, *J. Org. Chem.* **1996**, *61*, 4282 – 4288.
[12] Self-assembled cage compounds containing metals: a) R. W. Saalfrank, A. Stark, K. Peters, H. G. von Schnering, *Angew. Chem.* **1988**, *100*, 878 – 880; *Angew. Chem. Int. Ed. Engl.* **1988**, *27*, 851 – 853; b) P. Baxter, J.-M. Lehn, A. DeCian, J. Fischer, *Angew. Chem.* **1993**, *105*, 92 – 95; *Angew. Chem. Int. Ed. Engl.* **1993**, *32*, 69 – 72; c) S. Mann, G. Huttner, L. Zsolnai, K. Heinze, *Angew. Chem.* **1996**, *108*, 2983 – 2984; *Angew. Chem. Int. Ed. Engl.* **1996**, *35*, 2808 – 2809; d) P. Jacopozzi, E. Dalcanale, *Angew. Chem.* **1997**, *109*, 665 – 667; *Angew. Chem. Int. Ed. Engl.* **1997**, *36*, 613 – 615; e) C. M. Hartshorn, P. J. Steel, *Chem. Commun.* **1997**, 541 – 542. f) T. Beissel, R. E. Powers, K. N. Raymond, *Angew. Chem.* **1996**, *108*, 1166 – 1168; *Angew. Chem. Int. Ed. Engl.* **1996**, *35*, 1084 – 1086. g) T. N. Parac, D. L. Caulder, K. N. Raymond, *J. Am. Chem. Soc.* **1998**, *120*, 8003 – 8004, and references therein.
[13] a) M. Fujita, D. Oguro, M. Miyazawa, H. Oka, K. Yamaguchi, K. Ogura, *Nature* **1995**, *378*, 469 – 471; b) A closely related complex: P. J. Stang, B. Olenyuk, D. C. Muddiman, R. D. Smith, *Organometallics* **1997**, *119*, 3094 – 3096.
[14] Guest-templated synthesis of a stable Pt^{II} derivative of **1**: F. Ibukuro, T. Kusukawa, M. Fujita, *J. Am. Chem. Soc.* **1998**, *120*, 8561 – 8562.
[15] *o*-Carborane – azacrown ether (1:1) complex has been reported: P. D. Godfrey, W. J. Grigsby, P. J. Nichols, C. L. Raston, *J. Am. Chem. Soc.* **1997**, *119*, 9283 – 9284.
[16] R. J. Blanch, M. W. Williams, G. D. Fallon, M. G. Gardiner, R. Kaddour, C. L. Raston, *Angew. Chem.* **1997**, *109*, 520 – 522; *Angew. Chem. Int. Ed. Engl.* **1997**, *36*, 504 – 505.
[17] In contrast, CH signal of carborane does not shift significantly implying the inclusion geometry with electronegative BH groups located inside and electropositive CH groups located outside. Four guest molecules are likely to reside in tetrahedral positions around the center of the cage, directed away from the octahedrally positioned Pd^{II} centers. See the X-ray structure of **1**·(**G**)$_4$ (**G** = adamantanecarboxylate) reported in ref.[13]
[18] The broadening of the signals is probably due to a slow exchange on the NMR time scale between the free and complexed host.
[19] The assignment of the signals was confirmed by H – H COSY, C – H COSY, NOESY, H – C HMBC.
[20] The 1:4 stoichiometry was estimated by the Job plot method.
[21] Force-field calculation clearly shows that tri-*tert*-butylbenzene is slightly larger than the portals of **1**.

Nickel and Palladium Catalysis in the Stereoselective Synthesis of Functionalized Pyrrolidines: Enantioselective Formal Synthesis of (+)-α-Allokainic Acid

Maxim V. Chevliakov and John Montgomery*

(+)-α-Allokainic acid and (−)-α-kainic acid are representative members of the kainoid family of neuroexcitatory amino acids whose biological activity has been attributed to their action as conformationally restricted analogues of glutamate (Scheme 1).[1] Extensive structure – activity studies have demonstrated that the C-4 isopropenyl substituent is the



(+)-α-allokainic acid (−)-α-kainic acid

Scheme 1. Kainoid natural products.

[*] Prof. J. Montgomery, M. V. Chevliakov
Department of Chemistry,
Wayne State University
Detroit, MI 48202-3489 (USA)
Fax: (+1) 313-577-1377
E-mail: jwm@chem.wayne.edu

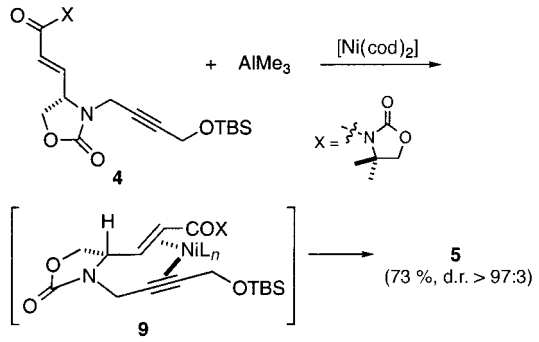
[**] This work was supported by the National Institutes of Health. J.M. acknowledges receipt of a National Science Foundation CAREER Award, a Camille Dreyfus Teacher-Scholar Award, and a 3M Pharmaceuticals New Faculty Award. M.V.C. acknowledges receipt of a Graduate Research Assistantship Award from Wayne State University. The authors thank Hélène Fain for helpful suggestions.

 © WILEY-VCH Verlag GmbH, D-69451 Weinheim, 1998 1433-7851/98/3722-3144 $ 17.50+.50/0

principal site at which structural variation is allowed without compromising neuroexcitatory activity.[2] Given the important role of these natural products in pharmacological investigations, we set out to develop a synthetic entry to this class of compounds that allows facile late-stage modification of the C-4 substituent and access to both the kainic acid and allokainic acid configurations.[3] Herein, we report our initial studies in this regard with a direct and highly stereoselective formal total synthesis of (+)-α-allokainic acid. The strategy involves the nickel-catalyzed cyclization of a D-serine-derived alkynyl enone with trimethyl aluminum followed by a palladium-catalyzed allylic carbonate reductive transposition (Scheme 2).

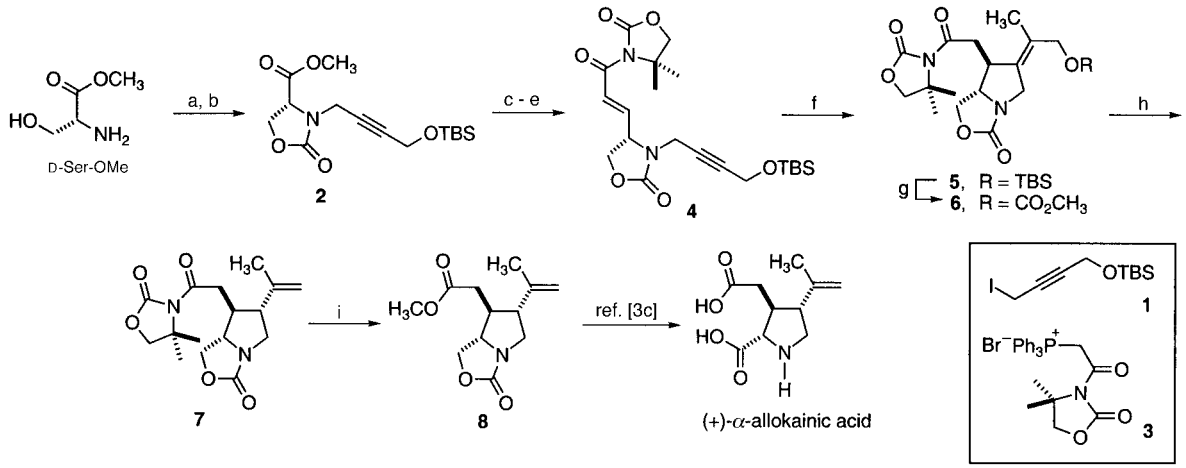
D-Serine methyl ester was efficiently converted to the central cyclization substrate **4** in straightforward fashion (Scheme 2). Condensation of D-serine methyl ester with triphosgene,[4] followed by N-propargylation with iodide **1** using KHMDS afforded **2** in 49% yield over two steps. Chemoselective ester reduction with $NaBH_4$,[5] oxidation under Swern conditions, and Wittig olefination with oxazolidinone **3**[6] gave substrate **4** in 74% overall yield from **2**.

Cyclization of **4** with MeLi/$ZnCl_2$ and 10 mol% $[Ni(cod)_2]$ by employing conditions previously reported[7–8] afforded high yields but moderate diastereoselectivities (ca. 3:1). Commercial trimethylaluminum or dimethylzinc, however, were found to be superior to MeLi/$ZnCl_2$ in achieving the desired *trans* stereochemical relationship of the C-2 and C-3 substituents. Cyclization of **4** with commercial trimethylaluminum and $[Ni(cod)_2]$ (10 mol%) in THF afforded a 73% yield of **5** with a diastereomeric ratio (d.r.) of >97:3 in favor of the desired *trans* isomer, and commercial dimethylzinc under identical conditions afforded a 67% yield of **5**, also with a >97:3 diastereomeric ratio. We believe that a parallel orientation of the two reactive π components in chelated structure **9** is responsible for the *trans* relationship of the two substituents in product **5** (Scheme 3).



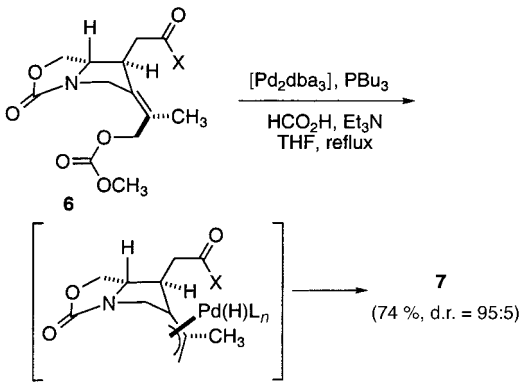
Scheme 3. Stereoselectivity of nickel-catalyzed alkylative cyclization.

A silyl to carbonate protecting group transposition was carried out in 73% yield to prepare substrate **6** for a palladium-catalyzed reduction with allylic transposition. Related systems were reported by Tsuji et al. to rearrange with palladium catalysis via intermediate π-allyl complexes to give the terminal alkene by hydride delivery to the more hindered allyl terminus.[9] The stereochemistry of oxidative addition ultimately sets the stereochemistry of the overall process, since decarboxylation and C–H bond reductive elimination both proceed with overall retention of configuration. Treatment of **6** with $[Pd_2(dba)_3]$/PBu_3 and HCO_2H/Et_3N cleanly produced **7** in 74% yield with a 95:5 diastereomeric ratio in favor of the all-*trans* stereochemical relationship of the three substituents at the pyrrolidine ring, as seen in allokainic acid. This result is consistent with *exo*-selective oxidative addition, *syn* to the adjacent side chain, to ultimately deliver hydride to the β-face of **6** (Scheme 4). The formal total synthesis of (+)-α-allokainic acid was then completed by converting the acyloxazolidinone unit to the corresponding methyl ester **8** upon treatment with CH_3OMgBr (Scheme 2).[10] Compound **8** was previously converted to (+)-α-allokainic acid by Hanessian et al.[3c]



Scheme 2. Formal synthesis of (+)-α-allokainic acid. a) Triphosgene, THF, 65 °C, 4 h; b) KHMDS (1.1 equiv), THF, 0 °C, 30 min; then **1** (3 equiv) in THF; 40 °C, 24 h, 49% (2 steps); c) $NaBH_4$, EtOH, 0–25 °C, 3 h, 91%; d) $(COCl)_2$ (1.5 equiv), DMSO (3 equiv), Et_3N (4 equiv), CH_2Cl_2, –78 °C; e) **3** (1.5 equiv), DMAP (3 equiv), CH_2Cl_2, –20 to 25 °C, 1.5 h, 81% (two steps); f) Me_3Al (3 equiv), 10 mol% $[Ni(cod)_2]$, THF, 0 °C, 40 min., 73% (97:3 diastereoisomeric ratio); g) HF·pyridine, THF, 0–25 °C, 24 h, 86%; then methylchloroformate (3 equiv), pyridine, CH_2Cl_2, 0–25 °C, 3 h, 83%; h) 10 mol% $[Pd_2(dba)_3]$, 40 mol% PBu_3, Et_3N (1.5 equiv), HCO_2H (1.5 equiv), THF, 65 °C, 74%, (95:5 diastereomeric ratio); i) MeOMgBr (3 equiv), 25 °C, 3 h, 54%. cod = cycloocta-1,5-diene, dba = 1,5-diphenylpenta-1,4-dien-3-one, DMAP = 4-dimethylaminopyridine, HMDS = hexamethyldisilazanide, TBS = *tert*-butydimethylsilyl.

 © WILEY-VCH Verlag GmbH, D-69451 Weinheim, 1998 1433-7851/98/3722-3145 $ 17.50+.50/0



Scheme 4. Palladium-catalyzed reductive transposition.

The above strategy should provide simple variation of the C-4 substituent of allokainic acid simply by selection of a more complex organoaluminum or organozinc reagent. In addition, the introduction of chirality in sequential operations provides the opportunity for modification of the above strategy to allow preparation of the epimeric series of kainoids typified by kainic acid itself through a late-stage common intermediate.[11]

Experimental Section

5: Trimethylaluminum (2.0 M in hexanes, 1.44 mmol) was added dropwise to a solution of $[Ni(cod)_2]$ (13.2 mg, 0.05 mmol) in THF (1.5 mL) at 0 °C. After 5 min, the mixture was transferred to a solution of **4** (210 mg, 0.48 mmol) at 0 °C in THF (3 mL) by cannula, and stirring was continued for 40 min at 0 °C. The reaction was quenched with NH_4Cl/NH_4OH pH 8 buffer, extracted with EtOAc (four times), dried over $MgSO_4$, filtered, and concentrated. Flash chromatography (EtOAc/hexanes 1/1) afforded **5** (160 mg, 0.35 mmol, 73 %) in a 97:3 diastereomeric ratio: $[\alpha]_D^{25} = -90.9$ ($c = 0.5$ in $CHCl_3$); ^{1}H NMR (500 MHz, $CDCl_3$): $\delta = 4.64$ (dd, $J = 4.5$, 3.5 Hz, 1H), 4.41–4.48 (m, 2H), 4.01–4.09 (m, 4H), 3.73 (dt, $J = 8.0$, 4.5 Hz, 1H), 3.59 (d, $J = 15$ Hz, 1H), 3.36 (d, $J = 16$ Hz, 1H), 2.91–3.02 (m, 2H), 1.68 (s, 3H), 1.58 (s, 3H), 1.55 (s, 3H), 0.89 (s, 9H), 0.06 (s, 3H), 0.05 (s, 3H); ^{13}C NMR (125 MHz, $CDCl_3$): $\delta = 173.0$, 161.1, 154.0, 132.8, 130.2, 75.4, 70.5, 65.1, 64.8, 60.5, 48.5, 44.2, 41.1, 25.9, 24.85, 24.81, 18.3, 16.3, −5.3, −5.4; IR (film): $\tilde{\nu} = 2928$, 1772, 1695, 1396, 1311; HRMS: *m/z*: calcd. for $C_{18}H_{27}N_2O_6Si$ 395.1639, found 395.1642 $[M - C(CH_3)_3^+]$.

7: Tributylphosphane (6.1 mg, 0.03 mmol) was added to a solution of $[Pd_2(dba)_3]$ (6.4 mg, 0.007 mmol) in THF (0.3 mL) at 0 °C. Formic acid (4.83 mg, 0.1 mmol) and triethylamine (10.6 mg, 0.1 mmol) were added neat, followed by carbonate **6** (25 mg, 0.06 mmol) in THF (0.3 mL), and the reaction mixture was refluxed (bath temperature 80–85 °C) for 3 h. The mixture was filtered through florisil, and the solvent was removed. Flash chromatography (EtOAc/hexanes 1/1) afforded **7** (15 mg, 0.05 mmol, 74 %) in a 95:5 diastereomeric ratio: $[\alpha]_D^{25} = -22.4$ ($c = 1.45$ in $CHCl_3$); ^{1}H NMR (500 MHz, $CDCl_3$): $\delta = 4.87$ (br. s,1H), 4.85 (t, $J = 1.5$ Hz, 1H), 4.45–4.49 (m, 2H), 4.02 (s, 2H), 3.74 (m, 1H), 3.47 (dd, $J = 8.5$, 11.0 Hz, 1H), 3.38 (dd, $J = 9.5$, 11.5 Hz, 1H), 3.20 (dd, $J = 17.0$, 4.0 Hz, 1H), 2.75 (m, 2H), 2.25 (dq, J = 9.5, 4.0 Hz, 1H), 1.70 (s, 3H), 1.54 (s, 6H); ^{13}C NMR (125 MHz, $CDCl_3$): $\delta = 172.4$, 160.7, 154.0, 141.6, 114.7, 75.3, 68.0, 64.8, 60.6, 54.9, 48.6, 42.9, 38.2, 24.7, 24.6, 18.2; IR (film): $\tilde{\nu} = 1774$, 1696, 1381, 1308; HRMS (EI): *m/z*: calcd for $C_{16}H_{22}N_2O_5$ 322.1529, found 322.1535 $[M^+]$.

Received: June 22, 1998 [Z 12026 IE]
German version: *Angew. Chem.* **1998**, *110*, 3346–3348

Keywords: cyclizations · neurotoxins · nickel · palladium · pyrrolidines

[1] a) S. Marukami, T. Takemoto, Z. Shimizu, *J. Pharm. Soc. Jpn.* **1953**, *73*, 1026–1028; b) A. F. Parsons, *Tetrahedron* **1996**, *52*, 4149–4174.
[2] R. Chamberlin, R. Bridges in *Drug Design for Neuroscience*, (Ed.: A. P. Kozikowski), Raven, New York, **1993**, pp. 231–259.
[3] a) For an overview of synthetic entries to kainic acid and allokainic acid, see reference [1b]; For representative syntheses, see: b) W. Oppolzer, K. Thirring, *J. Am. Chem. Soc.* **1982**, *104*, 4978–4979; c) S. Hanessian, S. Ninkovic, *J. Org. Chem.* **1996**, *61*, 5418–5424; d) S. Hatakeyama, K. Sugawara, S. Takano, *J. Chem. Soc. Chem. Commun.* **1993**, 125–127; e) C. Agami, M. Cases, F. Couty, *J. Org. Chem.* **1994**, *59*, 7937–7940; f) G. A. Kraus, J. O. Nagy, *Tetrahedron* **1985**, *41*, 3537–3545; g) H. H. Mooiweer, H. Hiemstra, W. N. Speckamp, *Tetrahedron* **1991**, *47*, 3451–3462; h) P. DeShong, D. A. Kell, *Tetrahedron Lett.* **1986**, *27*, 3979–3982.
[4] M. P. Doyle, A. B. Dyatkin, M. N. Protopopova, C. I. Yang, C. S. Miertschin, W. R. Winchester, S. H. Simonsen, V. Lynch, R. Ghosh, *Recl. Trav. Chim. Pays-Bas* **1995**, *114*, 163–170.
[5] M. P. Sibi, D. Rutherford, R. Sharma, *J. Chem. Soc. Perkin Trans 1* **1994**, 1675–1678.
[6] Reagent **3** was prepared in a fashion analogous to the reported procedure for a phenylalanine-derived reagent: D. A. Evans, W. C. Black, *J. Am. Chem. Soc.* **1993**, *115*, 4497–4513.
[7] a) J. Montgomery, A. V. Savchenko, *J. Am. Chem. Soc.* **1996**, *118*, 2099–2100; b) J. Montgomery, E. Oblinger, A. V. Savchenko, *J. Am. Chem. Soc.* **1997**, *119*, 4911–4920; c) application of the $[Ni(cod)_2]$/organozinc-mediated cyclization in the preparation of hetereocycles has been described: J. Montgomery, M. V. Chevliakov, H. L. Brielmann, *Tetrahedron* **1997**, *53*, 16449–16462; d) J. Montgomery; J. Seo; H. M. P. Chui, *Tetrahedron Lett.* **1996**, *37*, 6839–6842.
[8] For leading references to other classes of transition metal catalyzed carbocyclizations, see: I. Ojima, M. Tzamarioudaki, Z. Li, R. J. Donovan, *Chem. Rev.* **1996**, *96*, 635–662.
[9] a) T. Mandai, S. Suzuki, T. Murakami, M. Fujita, M. Kawada, J. Tsuji, *Tetrahedron Lett.* **1992**, *33*, 2987–2990; b) J. Tsuji, I. Shimizu, I. Minami, *Chem. Lett.* **1984**, 1017–1020; c) J. Tsuji, I. Minami, I. Shimizu, *Synthesis* **1986**, 623–627.
[10] D. A. Evans, M. M. Morrissey, R. L. Dorow, *J. Am. Chem. Soc.* **1985**, *107*, 4346–4348.
[11] For a conceptually related strategy involving intramolecular protodesilylations, see reference [3d].

Acrylate-Assisted Arene–Chromium Bond Cleavage: Generation of a $[Cr(CO)_2]$ Fragment under Mild Conditions*

E. Peter Kündig,* Mikhail Kondratenko, and Patrick Romanens

Ligand exchange is a key reaction in stoichiometric and catalytic applications of transition metal compounds. It is instrumental in the coordination of a substrate and, following metal-mediated reactions, in the release of the product. Therefore the rate of these processes often determines the efficiency of the overall transformation. Acceleration of ligand exchange and the increase in selectivity that results

[*] Prof. Dr. E. P. Kündig, Dr. M. Kondratenko, P. Romanens
Département de Chimie Organique, Université de Genève
30 Quai Ernest Ansermet, CH-1211 Genève 4 (Switzerland)
Fax: (+41) 22-328-7396
E-mail: peter.kundig@chiorg.unige.ch.

[**] We thank the Swiss National Science Foundation for support of this work (SNSF grants 20-045291.95 and 20-52478.97) and Dr. Allan Cunningham Jr., Ciba Specialty Chemicals for valuable discussions.

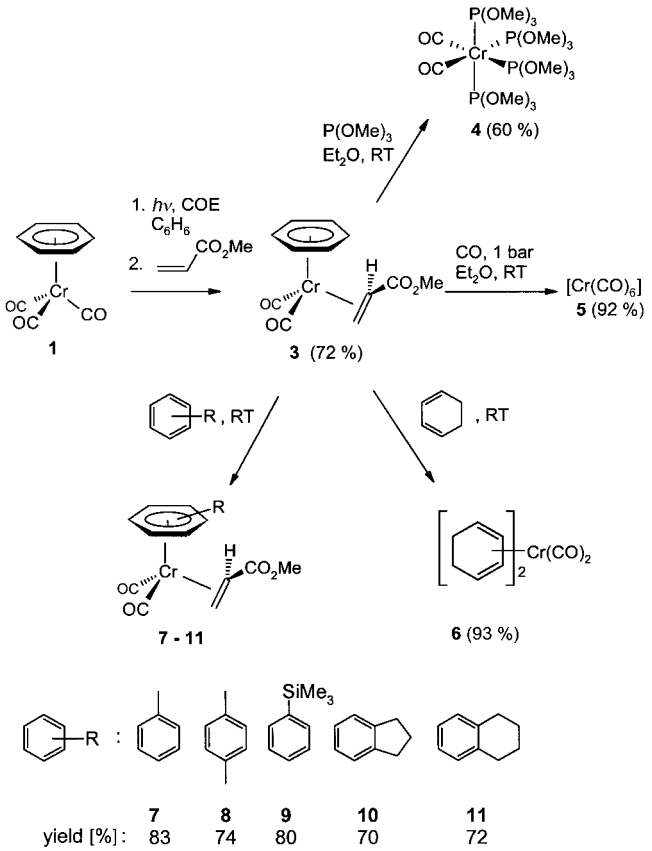
 © WILEY-VCH Verlag GmbH, D-69451 Weinheim, 1998 1433-7851/98/3722-3146 $ 17.50+.50/0

are prime objectives in the use of metals in synthesis.[1, 2] Herein we report the results of a study aimed at the labilization of a metal–benzene bond.

Thermal arene–metal bond cleavage in [(η^6-benzene)Cr(CO)$_3$] (**1**) requires quite harsh conditions (P*n*Bu$_3$: 135 °C, pyridine: reflux in neat pyridine, 2 h).[3, 4] Likewise, arene exchange reaction in **1** and analogous compounds is not a routinely useful method for the synthesis of functionalized arene complexes because of the high temperatures required (> 140 °C).[5, 6] [(η^6-naphthalene)Cr(CO)$_3$] (**2**) is an exception in this respect. Complex **2** is a convenient source of the Cr(CO)$_3$ fragment and has found application in catalysis and in the synthesis of functionalized [(arene)Cr(CO)$_3$] complexes.[5, 7, 8] Reasons for the faster ligand exchange in **2** compared to that in **1** are a weaker arene–metal bond and a lower energy pathway to arene displacement.[9] The arene–metal bond in **2** is labile because the haptotropic ring slippage ($\eta^6 \rightarrow \eta^4$) that is postulated to initiate arene displacement is far easier for naphthalene than for benzene.[3, 6b, 10]

We here show that facile slippage leading to arene displacement is not limited to Cr(CO)$_3$ complexes of condensed aromatic compounds but can be induced even in the normally rather inert benzene complex. The key to this is substitution of one of the three CO ligands in **1** for an acrylate ligand.

The η^2-methyl acrylate complex **3** was obtained by photolytic CO substitution for cyclooctene (COE) followed by alkene exchange.[11] Structural assignment of **3** is based on spectroscopic and analytical data and on comparison with literature data of η^2- and η^4-acrylate transition metal complexes.[12, 13] We next probed the propensity of **3** to undergo arene substitution and arene exchange reactions. The results are shown in Scheme 1.

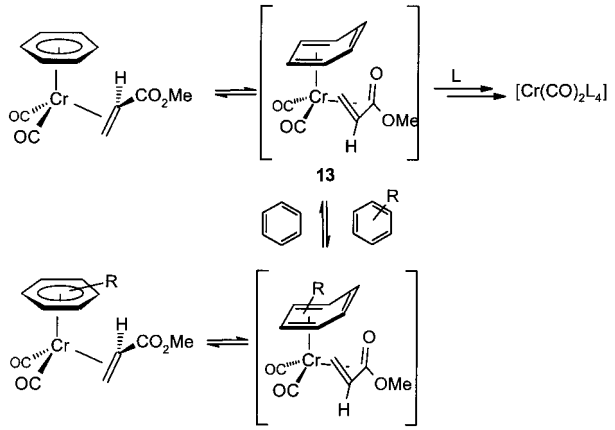


Scheme 1. Substitution and arene exchange reactions of complex **3** that occur at ambient temperature.

Treatment of **3** with P(OMe)$_3$ at ambient temperature led to the *cis*-dicarbonyl complex **4**.[14] Reaction of **3** with CO afforded a near quantitative yield of [Cr(CO)$_6$] (**5**), and dissolving **3** in cyclohexadiene presented a high-yield route to the recently reported complex bis(η^4-cyclohexadiene)dicarbonylchromium (**6**).[15] The reactions leading to **4**–**6** showed that both the arene–chromium and the acrylate–chromium bonds are labile. Surprisingly, the arene was displaced first. Had this not been the case, the products of the reactions with P(OMe)$_3$ and with CO would have been [Cr(benzene)(CO)$_2${P(OMe)$_3$}] (**12**) and [Cr(benzene)(CO)$_3$] (**1**), respectively. Neither **12** nor **1** undergo arene displacement reactions under the above conditions. Reaction of **3** with arenes resulted in arene exchange to give the arene complexes **7**–**11** in 70–83 % yield. The arene exchange reactions are reversible and to drive the reaction to a single product they are best carried out in neat arene; albeit in some cases (e.g. **8**) the yield was higher when ether was used as solvent. Generally, the analogous arenetricarbonylchromium complexes of **7**–**11** were secondary products formed in these reactions and were isolated in 10 to 20 % yield.

The ease of arene–chromium bond cleavage in **3** is not due to a weakening of the arene–metal bond. Other complexes with a Cr(CO)$_2$L fragment, where L is either a stronger electron acceptor (e.g. maleic anhydride (vide infra), CS) or a stronger electron donor (e.g. P(OMe)$_3$, PPh$_3$) than methyl acrylate, do not undergo these reactions. Scheme 2 shows a tentative rationalization for the observed reactivity and for the labilization effect of the methyl acrylate on the metal–arene bond. It is based on the ability of the acrylate ligand π system to coordinate in a η^2 or in a η^4 fashion to a transition metal. Haptotropic $\eta^2 \rightarrow \eta^4$ rearrangement of the acrylate in **3** would induce a $\eta^6 \rightarrow \eta^4$ rearrangement of the coordinated arene to give intermediate **13**.[16] Arene substitution and arene exchange in **13** would then follow low-activation energy pathways.

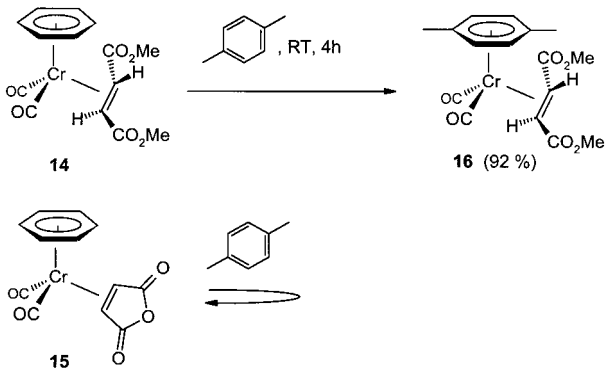
Preliminary experiments to test the above hypothesis have been carried out. By using the same route as for **3**, the



Scheme 2. Proposed mechanism for acrylate-assisted arene–metal bond cleavage.

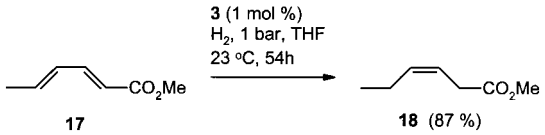
 © WILEY-VCH Verlag GmbH, D-69451 Weinheim, 1998 1433-7851/98/3722-3147 $ 17.50+.50/0

fumarate complex **14** and the maleic anhydride complex **15**[17] were obtained in 15 and 63 % yield, respectively. The low yield of **14** was due to competitive reduction of the dimethyl fumarate to give dimethyl succinate.[18] Remarkably, the fumarate complex **14** shows the same behavior as **3** but the maleic anhydride complex **15** does not. In **15**, rearrangement to a *cisoid* oxadiene is not possible and arene displacement cannot be triggered. (Scheme 3).



Scheme 3. The fumarate complex **14** exhibits reactivity analogous to that of **3** but the maleic anhydride complex **15** does not react under these conditions.

The *cisoid* conformation of the respective diene is also a key requirement in the use of [(η^6-arene)$Cr(CO)_3$] complexes in the catalytic hydrogenation of conjugated dienes to (*Z*)-alkenes and in the reduction of enones to ketones.[7] The arene complex is a precatalyst for the hydrogenation and the first step is arene dissociation. Reaction conditions therefore reflect the ease of this process. Benzene and substituted benzene complexes require temperatures in excess of 120 °C, whereas the naphthalene complex **2** already reacts at 25 °C. Our preliminary data show that complex **3** readily generates a catalyst at ambient temperature that hydrogenates methyl sorbate (**17**) to *cis*-methyl 3-hexenoate (**18**; Scheme 4).



Scheme 4. Hydrogenation of methyl sorbate (**17**) catalyzed by **3**.

In conclusion, a new mild arene displacement reaction has been discovered. The thermally stable complexes **3** and **16** are precursors to the highly unsaturated [$Cr(CO)_2$(alkene)] and [$Cr(CO)_2$] fragments.

Experimental Section

3: A solution of [Cr(η^6-benzene)(η^2-*cis*-cyclooctene)$(CO)_2$] was prepared by photolysis (Philips, HPK 125) of **1** (0.642 g, 3 mmol) in a mixture of benzene (200 mL) and cyclooctene (16 mL), according to the method given in reference [11]. After completion of the irradiation, methyl acrylate (270 μL, 3 mmol) was added to the reaction mixture. After 16 h the mixture was filtered over Celite and volatiles were removed in vacuo. The residue was taken up in hexane/benzene (20:1) and recrystallized at −40 °C to give red-orange crystals of **3** (0.586 g, 72 %); m.p.: 82–83 °C; ^{1}H NMR (C_6D_6, 200 MHz): δ = 4.35 (s, 6H, C_6H_6), 3.56 (s, 3H, OCH_3), 2.93 (dd, J = 11.3, 7.7 Hz, 1H, C=C*H*–CO_2Me), 2.76 (dd, J = 11.3, 0.8 Hz, 1H, CH_2=C), 2.37 (dd, J = 7.7, 0.8 Hz, 1H, CH_2=C); ^{13}C NMR (C_6D_6, 50 MHz): δ 246.6, 245.9, 177.2, 95.9, 50.1, 41.4, 38.6; IR (hexane): $\tilde{\nu}$ = 1948, 1896, 1704; MS (*m*/*z*): 272 ([M^+],0.4), 186(4), 158(7), 130(18), 78(100), 52(65); C,H analysis calcd for $C_{12}H_{12}CrO_4$ (272.22): C 52.95, H 4.44; found: C 52.72, H 4.36.

Received: July 13, 1998 [Z 12130 IE]
German version: *Angew. Chem.* **1998**, *110*, 3329–3332

Keywords: arene complexes · carbonyl complexes · chromium · ligand effects

[1] L. S. Hegedus, *Transition Metals in Organic Chemistry,* University Science Books, Mill Valley, CA, **1994**.
[2] For a review of ligand-accelerated catalysis, see: D. J. Berrisford, C. Bolm, K. B. Sharpless, *Angew. Chem.* **1995**, *107*, 1159; *Angew. Chem. Int. Ed. Engl.* **1995**, *34*, 1059.
[3] S. Zhang, J. K. Shen, F. Basolo, T. D. Ju, R. F. Lang, G. Kiss, C. D. Hoff, *Organometallics,* **1994**, *13*, 3692.
[4] a) G. Carganico, P. Del Buttero, S. Maiorana, G. Riccardi, *J. Chem. Soc. Chem. Commun*. **1978**, 989; b) A. Perez-Encabo, S. Perrio, A. M. Z. Slawin, S. E. Thomas, A. T. Wierzchleyski, D. J. Williams, *J. Chem. Soc. Perkin Trans.* **1994**, 629.
[5] For recent reviews of the use of [(arene)$Cr(CO)_3$] complexes see: a) M. F. Semmelhack in *Comprehensive Organometallic Chemistry II*, *Vol. 12* (Ed.: L. S. Hegedus), Pergamon, Oxford, **1995**, p. 979, 1017; b) S. G. Davies, T. D. McCarthy in *Comprehensive Organometallic Chemistry II* , *Vol. 12* (Ed.: L. S. Hegedus), Pergamon, Oxford, **1995**, p. 1039.
[6] a) E. L. Muetterties, J. R. Bleeke, A. C. Sievert, *J. Organomet. Chem*. **1979**, *178*, 197; b) E. L. Muetterties, J. R. Bleeke, E. J. Wucherer, T. A. Albright, *Chem. Rev.* **1982**, *82*, 499; c) M. Morris in *Comprehensive Organometallic Chemistry II*, *Vol. 5* (Eds. J. Labinger, M. J. Winter), Pergamon, Oxford, **1995**, pp. 394–450.
[7] For a review of catalysis with complex **2** see: M. Sodeoka, M. Shibasaki, *Synthesis* **1993**, 643.
[8] a) E. P. Kündig, C. Perret, S. Spichiger, G. Bernardinelli, *J. Organomet. Chem.* **1985**, *286*, 183; b) H.-G. Schmalz, B. Millies, J. W. Bats, G. Dürner *Angew. Chem.* **1992**, *104*, 640; *Angew. Chem. Int. Ed. Engl.* **1992**, *31*, 631; c) A. Alexakis, P. Mangeney, I. Marek, F. Rose-Munch, E. Rose, A. Semra, F. Robert, *J. Am. Chem. Soc.* **1992**, *114,* 8288; d) Y. Kondo, J. R. Green, J. Ho, *J. Org. Chem.* **1993**, *58*, 6182; e) M. Uemura, R. Miyake, K. Nakayama, M. Shiro, Y. Hayashi, *J. Org. Chem.* **1993**, *58*, 1238; f) E. P. Kündig, J. Leresche, L. Saudan, G. Bernardinelli, *Tetrahedron* **1996**, *52*, 7363; g) A. Fretzen, A. Ripa, R. Liu, G. Bernardinelli, E. P. Kündig, *Chem. Eur. J.* **1998**, *4*, 251.
[9] a) The value of E_{diss}(Cr–arene) in **1** is estimated to be 53 kcal mol^{-1}: S. L. Mukerjee, R. F. Lang, T. Ju, G. Kiss, C. D. Hoff, S. P. Nolan, *Inorg. Chem.* **1992**, *31*, 4885; b) Thermochemical data have been reported that indicate that the Cr–naphthalene bond in **2** is about 6 kcal mol^{-1} weaker than the Cr–benzene bond in **1**: ref. [3] and references therein.
[10] E. P. Kündig, V. Desobry, C. Grivet, B. Rudolph, S. Spichiger, *Organometallics* **1987**, *6*, 1173.
[11] I. S. Butler, A. M. English, K. R. Plowman, *Inorg. Synth.* **1982**, *XXI*, 2.
[12] η^2-Acrylate complexes: a) F. W. Grevels, M. Lindemann, R. Benn, R. Goddard, C. Krueger, *Z. Naturforsch. B* **1980**, *35*, 1298; b) U. Koemm, C. G. Kreiter, *J. Organomet. Chem.* **1982**, *240* , 27; c) W. A. Schenk, H. Mueller, *Chem. Ber.* **1982**, *115*, 3618; d) H. Berke, C. Sontag, *Z. Naturforsch. B* **1985**, *40*, 794; e) H. Berke, G. Huttner, C. Sontag, L. Zsolnai, *Z. Naturforsch. B* **1985**, *40*, 799; f) T. Aoshima, T. Tamura, Y. Mizobe, M. Hidai, *J. Organomet. Chem.* **1992**, *435*, 85; g) S. E. Kegley, K. A. Walter, D. T. Bergstrom, D. K. Macfarland, B. G. Young, A. L. Rheingold, *Organometallics* **1993,** *12*, 2339; h) E. Hauptman, S. Sabo-Etienne, D. S. White, M. Brookhart, J. M. Garner, P. J. Fagen, J. C. Calabrese, *J. Am. Chem. Soc.* **1994**, *116*, 8038.
[13] η^4-Acrylate complexes: a) T. Schmidt, R. Goddard, *J. Chem. Soc. Dalton Trans.* **1995**, 1563; b) T. Schmidt, *J. Organomet. Chem.* **1996**, *506*, 139.
[14] R. Mathieu, M. Lenzi, R. Poilblanc, *Inorg. Chem.* **1970**, *9*, 2030.
[15] S. Özkar, C. G. Kreiter, M. Kotzian *J. Organomet. Chem.* **1995**, *494*, 115.
[16] Alternatively, the second acrylate–chromium bond may involve a σ-O to Cr coordination bond (see ref. [13]).
[17] M. Herberhold, C. R. Jablonski, *Inorg. Chim. Acta* **1973**, *7*, 241.
[18] E. P. Kündig, M. Kondratenko, P. Romanens, unpublished results.

 © WILEY-VCH Verlag GmbH, D-69451 Weinheim, 1998 1433-7851/98/3722-3148 $ 17.50+.50/0

Synthesis of *p*-Phenylene Sulfide Molecular Asterisks**

Marc Gingras,* Alain Pinchart, and Carol Dallaire

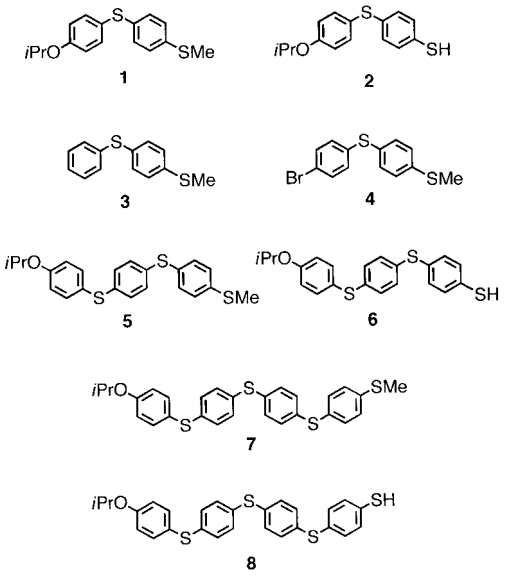
Research in supramolecular chemistry and nanotechnology has stimulated the synthesis of giant molecules with novel architectures, such as dendrimers[1] and various supramolecular systems.[2] We have developed an efficient synthesis of molecular asterisks; these lie at the interface between regular-sized molecules and macromolecules (see Scheme 1).[3] The preparations are simple and purification is relatively easy. Some molecular asterisks have a fluorescent core with interesting optical properties and are soluble in organic solvents such as $CHCl_3$, CH_2Cl_2, EtOAc, $PhCH_3$, and THF. These intriguing molecules—providing they can be appropriately functionalized—might find a variety of applications (multisite catalysis,[4] multivalent glycodendrimers,[5] fluorescent biosensors, new conductive materials,[6] etc.).

The strategy behind the synthesis of the molecular asterisks focused on three points:

1. A convergent approach was used to link the molecular wires to an aromatic core; this has facilitated the purification because the lack of one or more arms in the product led to considerable differences in the chemical properties.
2. The wires were attached to the core by a persulfuration of the arene unit, which is known as the MacNicol reaction.[7]
3. We needed wires of specific length. *p*-Phenylene sulfide oligomers were chosen because of their stability, solubility, and their conductivity after doping (important for the production of possible conductive asterisks).

Many methods are known for synthesizing poly(*p*-phenylene sulfide) polymers (PPS),[8] but PPS oligomers of definite length are rare.[9] Therefore, we developed practical syntheses of functionalized *p*-phenylene sulfide oligomers with chain lengths of two to six phenylene units, with a sulfanyl group at one end and another functional group at the other end.[10] We found that a combination of a methylsulfanyl and an isopropyloxy group was the best choice to enable the chemoselective nucleophilic deprotection of thiophenols in high yields.[10, 11]

Compound **1** was synthesized in 90% yield by the Pd-catalyzed coupling of 4-isopropyloxythiophenol to 4-bromothioanisole.[12] Demethylation of **1** with *i*PrSNa afforded the thiol **2** in 80% yield. The PPS chain with three phenylene



units was synthesized in a sequence starting with the Cu_2O-promoted coupling[13] of thiophenol and 4-bromothioanisole to afford **3** (99% yield). Bromination of **3** to **4**, followed by Pd-catalyzed coupling with 4-isopropyloxythiophenol gave **5** in 75% yield (recrystallized). Demethylation with *i*PrSNa afforded **6** as a thiol (75% yield). The protected wire **7** with four phenylene groups was obtained from a Cu_2O coupling of the bromide **4** with the thiol **2** (63% yield). Demethylation of **7** with *t*BuSNa provided the thiol **8** (99% yield). Most of the PPS molecular wires are white solids. Their relative stability to oxidation and their good solubility in common solvents (CH_2Cl_2, $CHCl_3$, and toluene) make them promising building blocks in supramolecular chemistry.

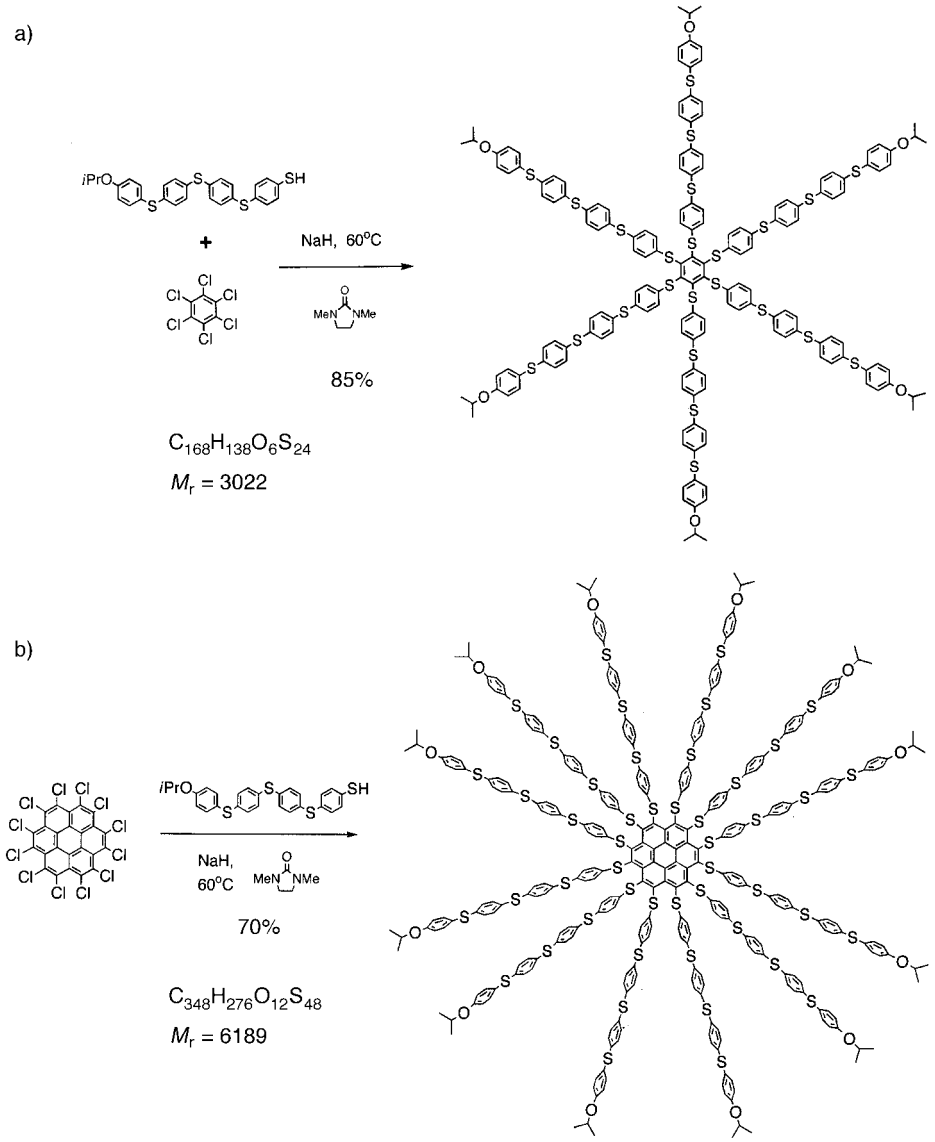
The molecular asterisks were synthesized by applying the MacNicol reaction[7] of hexachlorobenzene (or dodecachlorocoronene[14]) and the *p*-phenylene sulfide chains **2**, **6**, and **8**; in this way we obtained functionalized molecular asterisks of second, third, and fourth generation[3] with a central aromatic core (Scheme 1a). Although the MacNicol reaction was usually carried out with a twofold excess of a thiol at 20 °C, we found that the purification was not facilitated by such a large amount and the valued thiol was lost. We established that the reaction goes to completion by using a 1.5-fold excess of starting thiol relative to hexachlorobenzene at 50–60 °C. The purification was greatly facilitated by simple triturations and solubility differences of the components in the crude mixture. The use of smaller amounts of thiol gave incomplete reactions. The molecular asterisks were obtained in yields of 72% (second generation), 92% (third generation), and 85% (fourth generation). They are bright yellow fluorescent solids that are highly soluble in organic solvents. ^1H (250 or 600 MHz) and ^{13}C NMR spectroscopy and elemental analyses (C, H; fourth generation) confirmed the structures and are indicative of a good purity. Mass spectrometry using secon-

[*] Prof. Dr. M. Gingras, A. Pinchart, Dr. C. Dallaire
Laboratory of Supramolecular Chemistry and Catalysis
Faculty of Sciences
Université Libre de Bruxelles
C.P. 160–06, 50 Ave. F.D. Roosevelt,1050 Brussels (Belgium)
Fax: (+32) 2-650-2798
E-mail: mgingras@ulb.ac.be

[**] We thank the ULB Faculty of Sciences for generous funding and the staff responsible for mass spectrometry (ULB Organic Division) and NMR spectroscopy (ULB CIREM). C.D. warmly thanks the ULB Department of the International Relations for a scholarship. We are also grateful to Dr. P. N. W. Baxter (Université Louis-Pasteur) and Prof. R. Deltour (ULB) for interesting discussions. Dr. P. Thibault and D. Krajcarski from the National Research Council of Canada are thanked for MALDI-TOF MS. Prof. de Hoffmann and Dr. Rosenberg are thanked for DCI MS (Université Catholique de Louvain, Belgium).

Supporting information for this article is available on the WWW under http://www/wiley-vch.de/home/angewandte/ or from the author.

 © WILEY-VCH Verlag GmbH, D-69451 Weinheim, 1998 1433-7851/98/3722-3149 $ 17.50+.50/0



Scheme 1. a) Molecular asterisk with a benzene core; fourth generation (PPS-G4-[benzene]-O*i*Pr). b) Molecular asterisk with a coronene core—fourth generation (PPS-G4-[coronene]-O*i*Pr).

dary ion mass spectrometry (SIMS), desorption chemical ionization (DCI), and matrix-assisted laser desorption ionization time-of-flight (MALDI-TOF) techniques established their molecular weight from the isotope average molecular ions found at m/z values of 1724.8 (second generation), 2371 (third generation), and 3019 (fourth generation). The stepwise loss of many side arms was observed in the MALDI-TOF spectra.

Dodecachlorocoronene reacted under optimized conditions with a slight excess of thiol (1.1-fold excess of thiol per chloro ligand) at 60 °C in 1,3-dimethyl-2-imidazolidinone (DMI) and in the presence of NaH to afford the molecular asterisks with 12 functionalized arms in yields of 95 % (second generation), 89 % (third generation), and 70 % (fourth generation) (Scheme 1 b). All of the coronene derivatives were found to be relatively air-stable deep red solids under usual conditions and were soluble in many solvents. The structures and their purity were analyzed by ^{1}H (250 or 600 MHz) and ^{13}C NMR spectroscopy, and elemental analyses (C, H; fourth generation). MALDI-TOF spectrometry provided the corresponding average isotope molecular ions for each coronene derivatives at m/z values of 3593 (second generation), 4893 (third generation), and 6192 (fourth generation). Again, the fragmentation of the molecular ion showed signals corresponding to a regular loss of side arms.

Physical and spectroscopic data of the molecular asterisks are given in Table 1. The UV spectra of the molecular asterisks having a benzene core displayed a weak absorption band at 334 nm (λ shoulder) corresponding to the central persulfurated core and a large maximum absorption (λ_{max}) assigned to the *p*-phenylene sulfide wires at about 280 nm. Both the difference in the relative intensities of the two absorption bands and the extinction coefficient at 280 nm increase with the number of *p*-phenylene sulfide units. Excitation at 334 nm produced a maximum fluorescence emission at about 560 nm (λ_{max}), which was negatively affected by oxygen. The quantum yields were measured relative to 9,10-diphenylanthracene ($\Phi = 1.0$)[15a] and tris(2,2′-bipyridyl)ruthenium(II) chloride hexahydrate ($\Phi = 0.03$)[15b] under oxygen-free conditions.[15] Most molecular asterisks with a benzene core provided an approximate quantum yield (Φ) of 0.02. The UV spectra of the molecular asterisks with a coronene core displayed a maximum absorption band from the core at about 456 nm and an absorption band at 280 nm for the chains (λ_{max}). The extinction coefficients at 280 nm regularly increase with the generation number. No significant fluorescence was detected.

Table 1. Physical and spectroscopic data of the molecular asterisks.[a]

Core	Generation	M.p. [°C][b]	UV [λ_{max}][nm]	ε	Fluorescence [nm] [λ_{max}]	ϕ yield
benzene	2	145 – 146	286, 334	149000	560	–
benzene	3	119 – 120	278, 334	151000	517	0.02
benzene	4	90 (decomp)	280, 334	218000	525	0.02
coronene	2	151 – 152	288, 462	280000		
coronene	3	133 – 134	280, 450	285000		
coronene	4	85 – 86 (decomp)	278, 456	310000		

[a] All measurements were done in $CHCl_3$ at 22 °C, except for the ϕ measurements (in CH_2Cl_2). [b] Amorphous solids, not recrystallized. [c] λ(excitation) = 334 nm.

 © WILEY-VCH Verlag GmbH, D-69451 Weinheim, 1998 1433-7851/98/3722-3150 $ 17.50+.50/0

In summary, we have created soluble PPS molecular asterisks containing a polysulfurated benzene or a coronene core. In contrast to many supramolecules, some molecular asterisks possess an active flurorescent core. Preliminary tests indicated that deprotection by BCl_3 could provide molecular asterisks with phenolic groups ready for further functionalization. Applications toward multisite catalysis,[4] dendritic conductors,[6] glycodendrimers,[5] and fluorescent biosensors are in progress. The easy electroreduction of the first-generation molecular asterisks[16a] and some wires[16b] also suggests that they could have interesting electrochemical properties and further work is also in progress in that direction.

Experimental Section

PPS-G4-[benzene]-O*i*Pr**:** Hexachlorobenzene (15.0 mg, 0.0527 mmol) and thiol **8** (234 mg, 0.475 mmol) under N_2 were placed in a dry two-necked flask. DMI (0.80 mL, over molecular sieves 3 Å) was injected by syringe. Powdered NaH 95% (16 mg, 0.63 mmol) was weighed and placed in a lateral Gooch tube connected to the flask. Oxygen was removed by five freeze-thaw cycles with N_2. After the mixture had been cooled in an ice bath, NaH was added in small portions. The mixture turned bright yellow and stirring was continued for 30 min at 25 °C and then at 50–60 °C for two days. A solution of NaOH (3 M; 17 mL) was added while stirring vigorously for 10 min, followed by CH_2Cl_2 (28 mL). After separation of the organic phase, the latter was washed further with NaOH (1 M; 2 × 10 mL). After the organic phase had been dried over $MgSO_4$, filtration, followed by evaporation of the solvent gave a yellow oil. Thin-layer chromatography (EtOAc/*n*-hexane 1:4) indicated the expected yellow fluorescent product and a light impurity. Trituration in EtOH (2 × 15 mL) provided a yellow solid. This crude product was dissolved in a minimum amount of EtOAc (2–3 mL) and a white solid was removed by filtration. The yellow filtrate was evaporated to dryness. Repetitions of this procedure (4 or 5 times) with EtOAc ensured complete removal of the impurities. Afterwards, the yellow oil was triturared with EtOH (4 mL) to promote the precipitation of the compound PPS-G4-[benzene]-O*i*Pr as a yellow fluorescent solid (135 mg, 0.045 mmol; 85% yield). M.p. 90 °C (decomp); TLC (SiO_2; EtOAc/*n*-hexane 1:4): $R_f = 0.32$; UV/Vis ($CHCl_3$): λ_{max} (ε) = 280 (218 000), 334 nm ; fluorescence emission (λ_{max} (CH_2Cl_2) = 525 nm); ^{1}H NMR (600 MHz, $CDCl_3$, 25 °C, TMS): $\delta = 1.33$ (d, ^3J(H,H) = 6.0 Hz, 36 H; CH_3), 4.53 (sept, ^3J(H,H) = 6.0 Hz, 6 H; OCH), 6.79 (d, 12 H; J(H,H) = 8.4 Hz), 6.86 (d, 12 H, J(H,H) = 8.8 Hz), 7.03 (d, 12 H, J(H,H) = 8.4 Hz), 7.10 (d, 12 H, J(H,H) = 8.4 Hz), 7.13 (m, 24 H), 7.20 (d, 12 H, J(H,H) = 8.4 Hz), 7.37 (d, 12 H, J(H,H) = 6.4 Hz); ^{13}C NMR (62.8 MHz, $CDCl_3$, 20 °C, TMS): $\delta = 22.0$ (CH_3), 70.1 (OCH), 116.8 (CH), 122.9 (C), 128.4 (CH), 129.1 (CH), 130.6 (CH), 131.3 (CH), 131.6 (CH), 132.6 (CH), 133.7 (C), 134.2 (C), 135.8 (CH), 136.0 (C), 136.2 (C), 139.3 (C), 147.7 (C), 158.6 (C); MALDI-TOF MS (dithranol matrix, resolution ≈3500): m/z: 3019 [M^+]; elemental analyses: calcd: C 66.76, H 4.60; found: C 66.96, H 4.61.

PPS-G4-[coronene]-O*i*Pr: The same procedure as above was followed with dodecachlorocoronene (20.7 mg, 0.0290 mmol), thiol **8** (189 mg, 0.384 mmol), and NaH (95%; 13 mg; 0.51 mmol). After trituration with EtOH and purification, PPS-G4-[coronene]-O*i*Pr was obtained as a deep red solid (125 mg, 0.020 mmol; 70% yield). M.p. 85–86 °C (decomp); TLC (SiO_2; EtOAc/*n*-hexane 3:7): $R_f = 0.4$; UV/Vis ($CHCl_3$): λ_{max} (ε) = 278 (310 000), 456 nm ; ^{1}H NMR (600 MHz, $CDCl_3$, 30 °C, TMS): $\delta = 1.31$ (d, ^3J(H,H) = 6.0 Hz, 72 H), 4.51 (sept, 12 H, ^3J(H,H) = 6.0 Hz), 6.3 (m, 24 H); 7.0 (d, 24 H, J(H,H) = 8.4 Hz), 6.7–7.2 (m, 120 H), 7.33 (m, 24 H); ^{13}C NMR (62.8 MHz, $CDCl_3$, 20 °C, TMS): $\delta = 22.0$, 70.0, 116.8, 122.9, 127.2–127.7 (br.), 128.3, 130.4, 130.5–132.4 (br.), 132.5, 135.8, 136.1, 139.3, 158.6; MS MALDI-TOF (dithranol matrix, resolution ~3500): m/z: 6192 [M^+]; elemental analyses: calcd: C 67.54, H 4.49; found: C 67.48, H 4.30.

Received: December 1, 1997
Supplemented version: July 24 1998 [Z 11210 IE]
German version: *Angew. Chem.* **1998**, *110*, 3338–3341

Keywords: C–S coupling · dendrimers · materials science · supramolecular chemistry

[1] G. R. Newkome, C. N. Moorefield, F. Vögtle, *Dendritic Molecules*, VCH, Weinheim, **1996**.
[2] J.-M. Lehn, *Supramolecular Chemistry, Concepts and Perspectives*, VCH, Weinheim, **1995**.
[3] The size of the molecular asterisks are described here by generation, which is defined as the number of *p*-phenylene sulfide units growing from the core on a single arm. Generation zero is the persulfurated core.
[4] J. W. J. Knapen, A. W. van der Made, J. C. de Wilde, P. W. N. M. van Leeuwen, P. Wljkens, D. M. Grove, G. van Koten, *Nature* **1994**, *372*, 659–663.
[5] R. Roy, *Top. Curr. Chem.* **1997**, 187, 254–274; N. Jayaraman, S. A. Nepogodiev, J. F. Stoddart, *Chem. Eur. J.* **1997**, *3*, 1193–1199; R. Roy, D. Zanini, S. J. Meunier, A. Romanowska, *ACS Symp. Ser.* **1994**, *560*, 104–119.
[6] T. A. Skotheim in *Handbook of Conducting Polymers, Vol. 1* (Eds.: R. L. Elsenbaumer, L. W. Shacklette), Marcel Dekker, Basel, **1986**, pp. 239–254.
[7] Many researchers have described these reactions but most of the publications came from the MacNicol's group. Review: D. D. MacNicol in *Inclusion Compounds*, *Vol. 2* (Eds.: J. L. Atwood, J. E. Davies, D. D. MacNicol), Academic Press, London, **1984**, pp. 123–168.
[8] a) R. W. Lenz, C. E. Handlovits, H. A. Smith, *J. Polym. Sci.* **1962**, *58*, 351; b) J. T. Edmonds, Jr, H. W. Hill (Philips Petroleum Co.) USA 3354129, **1967** [*Chem. Abstr.* **1968**, *68*, 13598e]; c) M. Novi, G. Petrillo, M. L. Sartirana, *Tetrahedron Lett.* **1986**, *27*, 6129–6132; d) A. Fradet, *Bull. Soc. Chim. Belg.* **1989**, *98*, 635–641; e) D. R. Fahey, C. E. Ash, *Macromolecules* **1991**, *24*, 4242–4249; f) A. S. Hay, Y. Ding, *Macromolecules* **1997**, *30*, 1849–1850.
[9] PPS oligomers: a) E. Tsuchida, K. Yamamoto, K. Oyaizu, F. Suzuki, A. S. Hay, Z. Y. Wang, *Macromolecules* **1995**, *28*, 409–416; b) G. Petrillo, M. Novi, G. Garbarino, C. Dell'erba, *Tetrahedron* **1986**, *42*, 4007–4016; c) W. Koch, W. Heitz, *Makromol. Chem.* **1983**, *184*, 779–792; d) J. R. Campbell, *J. Org. Chem.* **1962**, *27*, 2207–2209; e) J. R. Campbell, *J. Org. Chem.* **1964**, *29*, 1830–1833; cyclic PPS: f) J. Franke, F. Vögtle, *Tetrahedron Lett.* **1984**, *25*, 3445–3448; g) M. L. Kaplan, W. D. Reents, Jr., *Tetrahedron Lett.* **1982**, *23*, 373–374.
[10] A. Pinchart, C. Dallaire, M. Gingras, *Tetrahedron Lett.* **1998**, *39*, 543–546.
[11] L. Testaferri, M. Tiecco, M. Tingoli, D. Chianelli, M. Montanucci, *Synthesis* **1983**, 751–755, and references therein.
[12] a) M. Kosugi, T. Shimizu, T. Migita, *Chem. Lett.* **1978**, 13–14; b) T. Migita, T. Shimizu, Y. Asami, J.-I. Shiobara, Y. Kato, M. Kosugi, *Bull. Chem. Soc. Jpn.* **1980**, *53*, 1385–1389.
[13] a) R. Adams, W. Reifschneider, M. D. Nair, *Croat. Chem. Acta* **1957**, 29, 277; b) R. Adams, A. Ferretti, *J. Am. Chem. Soc.* **1959**, *81*, 4927–4931.
[14] G. A. Downing, C. S. Frampton, D. D. MacNicol, P. R. Mallinson, *Angew. Chem.* **1994**, *106*, 1653; *Angew. Chem. Int. Ed. Engl.* **1994**, *33*, 1587–1589.
[15] a) J. B. Birks, *Photophysics of Aromatic Molecules*, 1st ed., Wiley-Interscience, **1970**, p. 121; b) K. Kalyanasundaram, *Photochemistry of Polypyridine and Porphyrin Complexes*, Academic Press, **1992**, p. 111.
[16] a) H. Brand, M. Gingras, J.-M. Lehn, J. H. R. Tucker, *J. Chem. Soc. Perkin Trans. 2* **1997**, 1303–1307; b) M. Mayor, J.-M. Lehn, K. M. Fromm, D. Fenske, *Angew. Chem.* **1997**, *109*, 2468–2471; *Angew. Chem. Int. Ed. Engl.* **1997**, *36*, 2370–2372.

 © WILEY-VCH Verlag GmbH, D-69451 Weinheim, 1998 1433-7851/98/3722-3151 $ 17.50+.50/0

Multiple Ga–Ga Bonding Character in $Na_2[Ga(GaTrip_2)_3]$, and a Comparison with Neutral $Ga(GaTrip_2)_3$ (Trip = 2,4,6-*i*$Pr_3C_6H_2$)**

Rudolf. J. Wehmschulte and Philip P. Power*

The syntheses and structures of the neutral digallane(4) **1** (Ga–Ga = 2.515(3) Å; Trip = 2,4,6-*i*$Pr_3C_6H_2$) and its singly reduced salt **2** (Ga–Ga = 2.343(2) Å) were reported in 1993.[1] The structural and spectroscopic data for the latter were consistent with the formation of a Ga–Ga π bond of formal order 0.5 as a result of the reduction.

$Trip_2GaGaTrip_2$ **1**

$[Li([12]crown\text{-}4)_2][Trip_2GaGaTrip_2]$ **2**

In effect, the added electron occupies a π-molecular orbital formed by overlap of a p orbital from each gallium atom. The attempted further reduction of **2** in diethyl ether to give the doubly reduced ion $[Trip_2GaGaTrip_2]^{2-}$, which should have a formal Ga–Ga π bond order of 1, was unsuccessful owing to apparent decomposition of the dianionic species.[1a] Detailed investigations by Uhl and co-workers[2] have shown that further reduction of the related radical anion species $[R_2AlAlR_2]^-$ (R = $CH(SiMe_3)_2$) in 1,2-dimethoxyethane leads to the formation of ether cleavage products with no Al–Al bonds. In view of the apparent reactivity of the aluminum and gallium dianions toward ethers, it was decided to attempt a double reduction of **1** by using a less reactive solvent such as triethylamine in order to synthesize a doubly reduced, multiply bonded species. We now report some findings of these investigations, which have resulted in the isolation of the novel dianion **3** and its neutral analogue **4**.

$Na_2[Ga(GaTrip_2)_3]$ **3**

$Ga(GaTrip_2)_3$ **4**

The dark red dianion **3** was synthesized by the treatment of **1** in triethylamine with a tenfold excess of sodium for about three days at room temperature. Large black crystals, suitable for X-ray crystallography, which correspond to the formula **3**·$3C_6H_6$ were grown from solutions in benzene. The X-ray crystal structure analysis[3] showed that molecules of **3** were composed of a central gallium atom (Ga(1)) bound to three $GaTrip_2$ moieties. The structure (Figure 1) is completed by two sodium ions which are sandwiched by Trip groups. Both Trip substituents attached to Ga(2) and one Trip substituent from Ga(3) and Ga(4) are involved in the complexation of the Na^+ ions. The coordination at all four gallium atoms is planar but there are significant distortions from idealized 120° angles. For example, at the central gallium atom, the Ga(3)-Ga(1)-Ga(4) angle of 107.66(4)° is at least 15° narrower than the other two angles. Furthermore, at the peripheral gallium

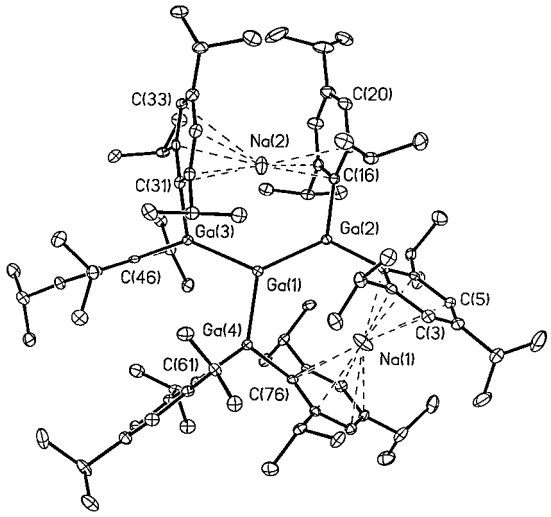


Figure 1. Molecular structure of **3** in the crystal (H atoms omitted). Selected bond lengths [Å] and angles [°]: Ga(1)–Ga(2) 2.3641(10), Ga(1)–Ga(3) 2.4062(10), Ga(1)–Ga(4) 2.3981(10), Ga(2)–C(1) 2.044(5), Ga(2)–C(16) 2.051(5), Ga(3)–C(31) 2.060(5), Ga(3)–C(46) 2.023(5), Ga(4)–C(61) 2.019(5), Ga(4)–C(76) 2.058(5); Ga(2)-Ga(1)-Ga(3) 128.96(3), Ga(2)-Ga(1)-Ga(4) 123.18(4), Ga(3)-Ga(1)-Ga(4) 107.66(4).

atoms the C-Ga-C angle is always narrowest, whereas at Ga(3) and Ga(4), the Ga(1)–Ga(3/4)-C(*ipso*) angle involving rings complexed to the Na^+ ions are 9 to 13° narrower than the Ga(1)-Ga(3/4)-C(*ipso*) angle involving uncomplexed rings. The Ga(1)–Ga(2) bond (2.364(1) Å) is about 0.04 Å shorter than the Ga(1)–Ga(3) (2.406(1) Å) or the Ga(1)–Ga(4) (2.398(1) Å) bonds. The shorter Ga(1)–Ga(2) distance corresponds to a lower torsion angle (17.7°) between the coordination planes at Ga(1) and Ga(2) than between the coordination planes Ga(1) and Ga(3) and Ga(1) and Ga(4) (angles 32.2° and 28.5°, respectively).

In spite of these distortions, which are attributable either to steric congestion or Na^+ ion complexation, the structural parameters are consistent with the formation of a two-electron π bond which is essentially delocalized over the Ga_4 array to afford a species with a formal Ga–Ga bond order of 1.33.[4] The average Ga–Ga distance in **3** (2.389(17) Å) is longer than that in the radical anion $[Trip_2GaGaTrip_2]^-$ (2.343(2) Å; formal Ga–Ga bond order = 1.5)[1a] but is shorter than those in the cyclic compounds $M_2[Ga(2,6\text{-}Mes_2C_6H_3)]_3$ (ca. 2.44 Å; formal Ga–Ga bond order = 1.33; M = Na or K; Mes = mesityl).[5] An additional feature of the structure of **3** is that all the Trip rings complexed to the Na^+ ions are bent towards the ion (Figure 1). The bending, which can be quantified by the deviation of the Ga–C(*ipso*) bonds from the planes of the aromatic rings, ranges between 9.6 and 14.3°, whereas for the two noncomplexed rings the deviation is only 2.4 and 3.4°. The apparently tight complexation of the Na^+ ions is consistent with the structural distortions described above. Moreover, the greater Ga(1)–Ga(2) bond shortening is in keeping with recent calculations on reduced organogallium complexes which suggest that Na^+ ion complexation can effect a significant contraction of Ga–Ga bond length.[6] However, the Na^+ ions are not bound equally strongly to the carbon atoms of the Trip rings (Na–C = 2.548(5) – 2.824(6) Å; Na – centroid 2.464 – 2.771 Å) but interact most strongly with

[*] Prof. P. P. Power, Dr. R. J. Wehmschulte
Department of Chemistry, University of California
Davis, CA 95616 (USA)
Fax: (+1) 530-752-8995
E-mail: pppower@ucdavis.edu

[**] This work was supported by the National Science Foundation.

 © WILEY-VCH Verlag GmbH, D-69451 Weinheim, 1998 1433-7851/98/3722-3152 $ 17.50+.50/0

the *ipso* carbon atoms. Also, the Na^+ ions deviate by 0.25 Å (Na(1)) and 0.55 Å (Na(2)) above and below the Ga_4 plane.

The neutral compound **4** was obtained as orange crystals by the reaction of **3** with one equivalent of dry O_2. The X-ray crystal structure analysis of **4** (Figure 2) shows that there are

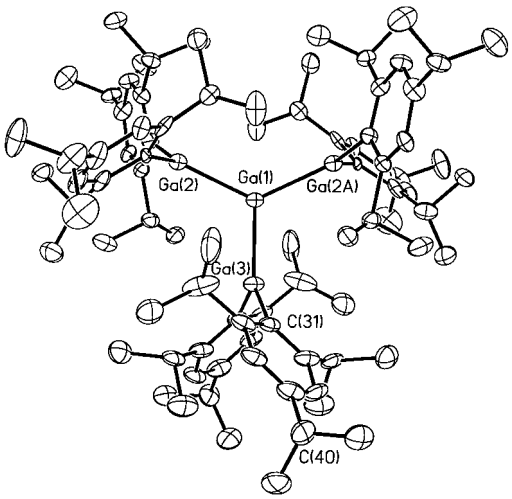


Figure 2. Molecular structure of one of the two molecules of **4** in the crystal (H atoms omitted). Selected bond lengths [Å] and angles [°] from both molecules: Ga(1)–Ga(2) 2.4813(17), Ga(1)–Ga(3) 2.465(3), Ga(2)–C(1) 1.961(13), Ga(2)–C(16) 1.992(11), Ga(3)–C(31) 1.987(12), Ga(4)–Ga(5) 2.4813(17), Ga(4)–Ga(6) 2.467(3), Ga(5)–C(46) 1.996(14), Ga(5)–C(61) 1.993(14), Ga(6)–C(76) 2.010(12); Ga(2)-Ga(1)-Ga(3) 116.17(5), Ga(2)-Ga(1)-Ga(2A) 127.65(10), Ga(5)-Ga(4)-Ga(6) 115.34(5), Ga(5)-Ga(4)-Ga(5A) 129.32(10).

two half molecules per asymmetric unit each of which has a crystallographically required twofold axis of symmetry along one of the Ga–Ga bonds. Essentially, the structure of **4** has a similar arrangement to **3** but without the presence of the Na^+ ions. The most interesting difference between **3** and **4** is that the Ga–Ga bonds are significantly lengthened (by ca. 0.08 Å) to an average value of 2.476(7) Å. This lengthening is consistent with a reduction of the overall gallium bond order to unity. This Ga–Ga distance is well within the known range for single bonds between three-coordinate gallium moieties.[7] Moreover, it is slightly shorter than that in **1** (2.515(3) Å). This is in agreement with the recently reported structure of $In(InTrip_2)_3$ which also has shorter In–In bonds (2.696(2) Å) than those in $Trip_2InInTrip_2$ (2.775(2) Å).[8] Another notable feature of the structure of **4** is that the torsion angles between the coordination planes at the peripheral gallium atoms Ga(2) and Ga(3) are increased to 81.4° and 72.9° which is consistent with the elimination of Ga–Ga π bonding in **4**. The lengthened Ga–Ga bonds make for a more sterically relaxed structure and this is reflected in the fact that the average C-Ga-C angle in **4** is significantly wider than that in **3**.

In summary, double reduction of $Trip_2GaGaTrip_2$ leads to $Na_2[Ga(GaTrip_2)_2]_3$ by an as yet unknown pathway. Clearly, the rearrangement involves cleavage of Ga–C bonds and a stoichiometric reaction may be written in accordance with Equation (1). The first step of this reaction may involve

$$4\,Na + 2\,Trip_2GaGaTrip_2 \longrightarrow Na_2[Ga(GaTrip_2)_2] + 2\,NaTrip \quad (1)$$

double reduction to give the doubly reduced $Na_2[Trip_2GaGaTrip_2]$ which may eliminate an equivalent of NaTrip to afford a species of formula $Na[TripGaGaTrip_2]$. Indeed, a neutral species with a related composition, $RGaGaR_2$ ($R = Si(tBu)_3$), has been reported recently by Wiberg and co-workers.[9] However, the subsequent steps in the reduction to give **3** remain unknown at present.

Attempts to measure the Ga–Ga π bond strength in **3** by using variable-temperature ^1H NMR spectroscopy have not yet led to conclusive results. Nonetheless, both **3** and **4** display dynamic NMR behavior.[10] For **3** two dynamic processes with barriers near 14 and 18 kcal mol^{-1} were observed, whereas **4** displayed an energy barrier near 18 kcal mol^{-1}. If it is assumed that the latter value is associated with ring flipping, it is possible that the 18 kcal mol^{-1} value for **3** represents the same phenomenon. The 14 kcal mol^{-1} process in **3** may be associated with rotation around the Ga–Ga bonds. Since this must also involve rupture of the Na^+ ring interactions, which may be quite strong,[11] it is probable that Ga–Ga π bond strength is significantly less than this value.

Experimental Section

All manipulations were carried out under anaerobic and anhydrous conditions.

3·3C_6H_6: Sodium (0.21 g, 9.1 mmol), cut into small pieces, was added to a solution of **1** (0.92 g, 0.96 mmol) in NEt_3 (40 mL) at room temperature. After about 20 h the solution had become a dark red-green color. After stirring the mixture for two more days, the solvent was removed under reduced pressure and the remaining dark brown, almost black, solid was extracted with *n*-hexane (ca. 80 mL). The dark red-green solution was then filtered through a sintered glass frit, concentrated to about 10 mL and cooled to −20 °C for one week to afford small black crystals. Recrystallization from benzene (3–4 mL) at 6 °C overnight gave 0.21 g of large (up to 6 mm) black crystals of **3**·3C_6H_6 based on the stoichiometry in Equation (1). Yield: 25 %. M.p. 190–200 °C. The compound loses some of the benzene of crystallization upon isolation and drying. UV/Vis (*n*-hexane): $\lambda(\varepsilon) = 850$ (9000), 422 nm (sh, 9000); ^1H NMR (C_7H_8, 60 °C): $\delta =$ 7.08 (br. s; *m*-H), 6.68 (br. s; *m*-H), 4.63 (br. s; *o*-CH), 3.19 (br. s; *o*-CH), 2.65 (sept, $^3J = 6.6$ Hz, *p*-CH) 1.63, 1.42, 1.27, 0.98, 0.79 (br. s; *o*-CH_3), 1.14 (d, $^3J = 6.6$ Hz; *p*-CH_3).

4: A solution of **3** (0.15 g, 0.1 mmol) in toluene (ca. 10 mL) was treated with dry air (11.0 mL, ca. 0.1 mmol 0_2) at 0 °C over a period of several hours in portions of 2 mL. The resulting red solution was concentrated to about 1–2 mL and cooled to −20 °C for three days to give small pale orange crystals of **4** which were washed with *n*-hexane (2 mL) and dried under reduced pressure. Yield: 50 mg (33 %). Crystals suitable for X-ray structure analysis were obtained from a saturated benzene solution at 6 °C. M.p. 210–212 °C (decomp; melts and becomes black); ^1H NMR (C_7D_8): $\delta = 7.04$ (s, *m*-H; 6 H), 6.95 (s, *m*-H; 6 H), 3.03 (sept, 6 H, $^3J = 6.6$ Hz; *o*-CH), 2.77 (sept, 12 H, $^3J = 6.6$ Hz; *o*- and *p*-CH), 1.48 (d, 18 H, $^3J = 6.6$ Hz; *o*-CH_3), 1.25 (d, 18 H, $^3J = 6.6$ Hz; *o*-CH_3), 1.23 (d, 36 H, $^3J = 6.6$ Hz; *p*-CH_3), 0.97 (d, 18 H, $^3J =$ 6.6 Hz; *o*-CH_3), 0.60 (d, 18 H, $^3J = 6.6$ Hz; *o*-CH_3). UV/Vis (*n*-hexane): λ (ε) = 348 nm (1200).

Received: June 30, 1998 [Z12073IE]
German version: *Angew. Chem.* **1998**, *110*, 3344–3346

Keywords: gallium · multiple bonds · pi interactions

[1] a) X. He, R. A. Bartlett, M. M. Olmstead, K. Ruhlandt-Senge, B. E. Sturgeon, P. P. Power, *Angew. Chem.* **1993**, *105*, 761; *Angew. Chem. Int. Ed. Engl.* **1993**, *32*, 717; b) similar reductions to give the anions $[R_2MMR_2]^-$ (R = -CH(SiMe$_3$)$_2$; M = Al or Ga) and $[TripAlAlTrip_2]^-$ were reported essentially simultaneously. see: Pluta, K.-R. Pörschke, C. Kruger, K. Hildenbrand. *Angew. Chem.* **1993**, *105*, 451; *Angew. Chem. Int. Ed. Engl.* **1993**, *32*, 388; c) W. Uhl, A. Vester, W. Kaim, J.

 © WILEY-VCH Verlag GmbH, D-69451 Weinheim, 1998 1433-7851/98/3722-3153 $ 17.50+.50/0

Poppe, *J. Organomet. Chem*. **1993**, *454*, 9; d) W. Uhl, U. Schutz, W. Kaim, E. Waldhör, *J. Organomet. Chem*. **1995**, *501*, 79; e) R. J. Wehmschulte, K. Ruhlandt-Senge, M. M. Olmstead, H. Hope, B. E. Sturgeon, P. P. Power, *Inorg. Chem*. **1993**, *32*, 2983.

[2] a) W. Uhl, A. Vester, D. Fenske, G. Baum. *J. Organomet. Chem*. **1994**, *464*, 23; b) W. Uhl, R. Gerding, A. Vester, *J. Organomet. Chem*. **1996**, *513*, 163; c) W. Uhl, *Coord. Chem. Rev*. **1997**, *163*, 132.

[3] Crystal data were obtained on a Syntex $P2_1$ ($\mathbf{3}\cdot 3\,C_6H_6$) diffractometer or a Siemens P4-RA (**4**) diffractometer at 130 K with $Cu_{K\alpha}$ ($\lambda =$ 1.54178 Å) radiation: $\mathbf{3}\cdot 3\,C_6H_6$: $C_{108}H_{156}Ga_4Na_2$, $M_r = 1779.2$, $a =$ 13.203(3), $b = 30.381(6)$, $c = 25.928(5)$ Å, $\beta = 103.26(3)^\circ$, $V =$ 10,123(3) Å^3, $Z = 4$, space group $P2_1/n$, $R1 = 0.057$ for 9826 ($I > 2\sigma(I)$) data; **4**, $C_{90}H_{138}Ga_4$, $M_r = 1498.9$, $a = 23.577(5)$, $b = 14.672(3)$, $c = 24.513(4)$ Å, $\beta = 91.09(2)^\circ$, $V = 8478(3)$ Å^3, $Z = 4$, space group $P2/c$, $R1 = 0.121$ for 7384 ($I > 2\sigma(I)$) data. Crystallographic data (excluding structure factors) for the structures reported in this paper have been deposited with the Cambridge Crystallographic Data Centre as supplementary publication nos. CCDC-102712, CCDC-102713. Copies of the data can be obtained free of charge on application to CCDC, 12 Union Road, Cambridge CB21EZ, UK (fax: (+44) 1223-336-033; e-mail: deposit@ccdc.cam.ac.uk).

[4] A simplified analysis of the π orbitals, assuming approximate D_3 point group symmetry for the Ga_4 array, affords two molecular orbitals (one bonding, one antibonding) of A_2 symmetry and two degenerate nonbonding orbitals of E symmetry. In **3** the bonding A_2 orbital is occupied by a pair of electrons, whereas in **4** it is unoccupied.

[5] X.-W. Li, W. T. Pennington, G. H. Robinson, *J. Am. Chem. Soc*. **1995**, *117*, 7578; X.-W. Li, Y. Xie, K. D. Gripper, R. C. Crittendon, C. F. Campana, H. F. Schaefer III, G. H. Robinson. *Organometallics* **1996**, *15*, 3798.

[6] F. A. Cotton, A. H. Cowley, X. Feng. *J. Am. Chem. Soc*. **1998**, *120*, 1795.

[7] P. J. Brothers, P. P. Power, *Adv. Organomet. Chem*. **1996**, *39*, 1.

[8] P. J. Brothers, K. Hübler, U. Hübler, B. C. Noll, M. M. Olmstead, P. P. Power, *Angew. Chem.* **1996**, *108*, 2528–2530; *Angew. Chem. Int. Ed. Engl*. **1996**, *35*, 2355.

[9] N. Wiberg, K. Amelunxen, H. Nöth, H. Schwenk, W. Kaim, A. Klein, T. Scheiring, *Angew. Chem.* **1997**, *109*, 1258–1261; *Angew. Chem. Int. Ed. Engl*. **1997**, *36*, 1213.

[10] D. Kost, E. H. Carlson, M. Raban, *J. Chem. Soc. Chem. Commun*. **1971**, 656.

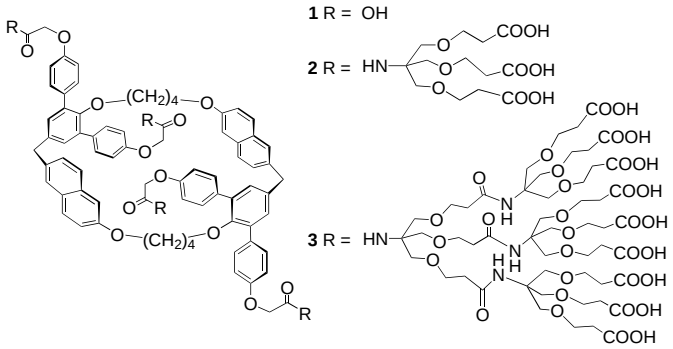
[11] Recent calculations on related Li–Ar π-interactions show that they can be as high as 21 kcal mol^{-1}. M. Tacke, *Eur. J. Inorg. Chem*. **1998**, 537.

Supramolecular Aggregates of Dendritic Cyclophanes (Dendrophanes) Threaded on Molecular Rods with Steroid Termini**

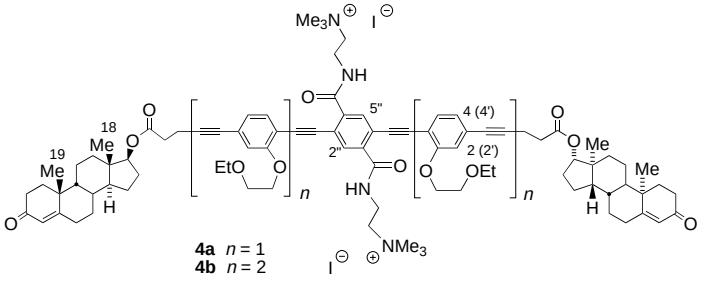
Benoît Kenda and François Diederich*

Noncovalent association of dendrimers[1] promises to provide a rapid, efficient way to construct higher molecular architectures with properties and functions[2] that are absent in the individual components. Whereas metal ion mediated assembly of dendritic branches (dendrons) to form higher generation compounds is well established,[1a, 3] the noncovalent networking[4a] of individual dendrimers to defined higher order structures in the absence of metal ions has only been achieved in a few cases.[4–7] A particularly intriguing example for dendritic self-association is the discrete hexameric assembly of dendritic wedges through directional COOH···COOH hydrogen-bonding interactions, which was reported by Zimmerman and co-workers.[6] Hydrophobic nonstoichiometric association of dendrimers in aqueous solution has been observed on several occasions,[5, 8] yet apolar bonding interactions and hydrophobic desolvation have not been previously employed to form structurally defined supramolecular aggregates containing two or more dendritic components. Here we report for the first time the formation of such assemblies in aqueous solution by hydrophobically driven threading of water-soluble dendrophanes (*dendr*itic cyclo*phanes*)[9] onto the testosterone termini of suitably designed molecular rods.

The initiator core cyclophane **1** (generation zero, G-0) and the two dendrophanes of the first (**2**, G-1; $M_r = 2486$) and second generation (**3**, G-2; $M_r = 6318$) had previously been shown to form stable 1:1 complexes (ΔG° at 298 K between -3.9 and -4.3 kcal mol^{-1}) with testosterone in borate-buffered D_2O (pD 10.5)/CD_3OD (1/1).[10] ^{1}H NMR investigation



of the bonding provided clear evidence that the steroid binds axially in the cyclophane cavity of **2** or **3** rather than in nonspecific fluctuating voids in the dendritic shells.[11] The molecular rods **4a** and **4b** consist of rigid oligo(phenylacetylene) spacers with terminal testosterone units for dendrophane complexation. Because of their different lengths, they



were expected to accommodate dendrophanes of different generation and size. Solubility of the rods in aqueous solutions represented a considerable challenge, which could be overcome with the attachment of both glycol ether groups and quaternary ammonium ions (to the central benzene ring). These ions were expected to undergo ion pairing with the

[*] Prof. Dr. F. Diederich, Dr. B. Kenda
Laboratorium für Organische Chemie, ETH-Zentrum
Universitätstrasse 16, CH-8092 Zürich (Switzerland)
Fax: (+41) 1-632-1109
E-mail: diederich@org.chem.ethz.ch

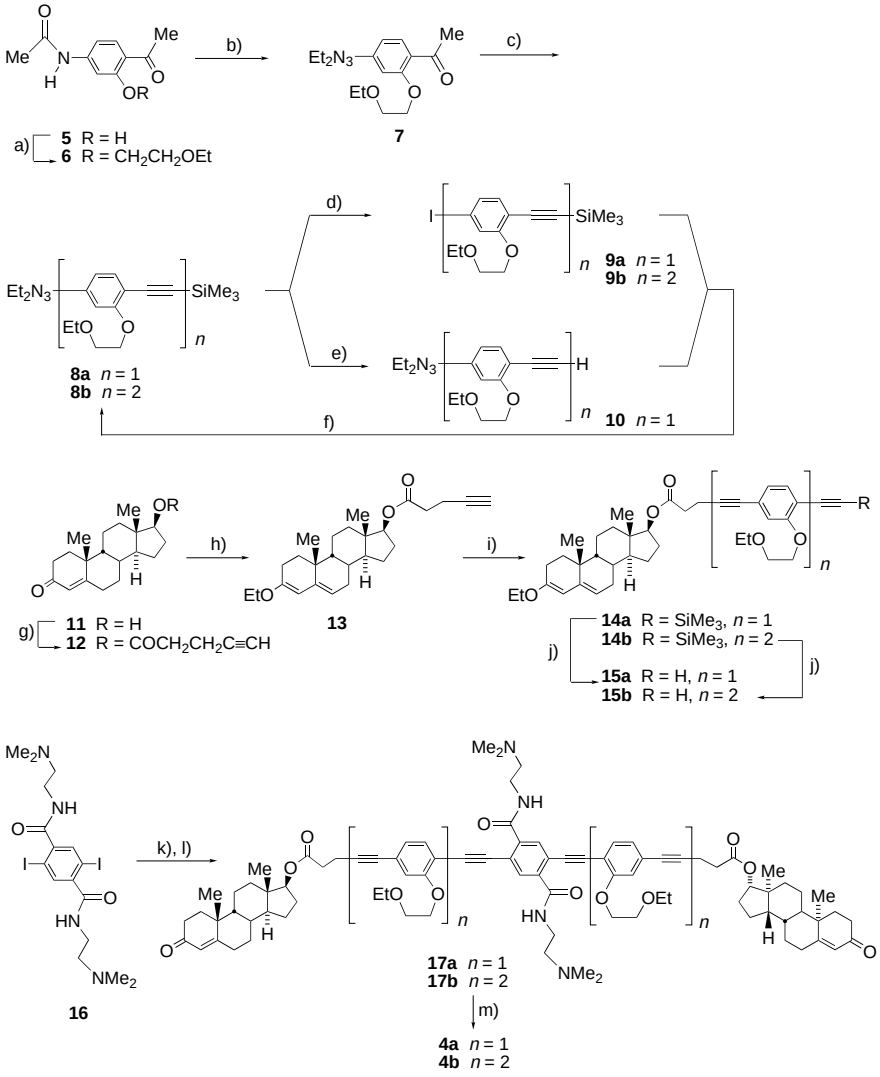
[**] This work was supported by the ETH Research Council and F. Hoffmann-LaRoche, Basel.

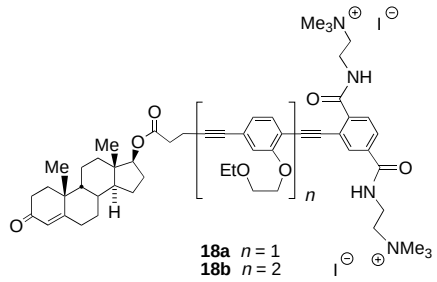
 © WILEY-VCH Verlag GmbH, D-69451 Weinheim, 1998 1433-7851/98/3722-3154 $ 17.50+.50/0

surface carboxylate residues in **1**–**3** and thus reduce the undesired electrostatic repulsion between two anionic dendrimers threaded onto one rod.

The synthesis of the novel molecular rods **4a** and **4b** utilizes in its key steps the elegant binomial strategy introduced by Moore and co-workers for the construction of oligo(phenylacetyene) sequences (Scheme 1).[1f, 12] The orthogonal doubly protected arylacetylene **8a**, which was obtained in three steps from **5**[13] via **6** and **7**, was transformed into iodide **9a** and the deprotected alkyne **10**.[14] Sonogashira cross-coupling between **9a** and **10** in pyrrolidine[15] yielded **8b**, which was converted into aryl iodide **9b**.

The attachment of testosterone (**11**) to **9a** and **9b** to yield **14a** and **14b**, respectively, was achieved by esterification with pent-4-ynoic acid (→**12**), protection of the steroid enone chromophore as dienol ether (→**13**),[16] and Sonogashira coupling. Deprotection of the alkyne group afforded **15a** and **15b**, which were coupled[17] to the 2,5-diiodoterephthalamide **16** (prepared in 30% yield by heating 2,5-diiodoterephthalic acid[18] with $SOCl_2$ to 100 °C for 4 h, followed by reaction with *N,N*-dimethyl-1,2-ethylenediamine in CH_2Cl_2 at 0°). Hydrolysis of the dienol ethers to give enones **17a** and **17b**, and quaternization of the tertiary amino groups led to the bis-steroid rods **4a** and **4b** (Table 1). Following a similar synthetic route, the mono-steroid rods **18a** and **18b** were prepared as controls.





Scheme 1. Synthesis of **4a** and **4b**. a) $EtO(CH_2)_2OTos$, K_2CO_3, DMF, 20 °C, 5 h, 75%; b) 10% aq HCl, 100 °C, 81%, then $NaNO_2$, 0 °C, 15 min, then Et_2NH, 0 °C, 15 min, 65%; c) lithium 2,2′,6,6′-tetramethylpiperidide (1.1 equiv), THF, −78 °C, 30 min, then $(EtO)_2POCl$, THF, −78 °C, then lithium 2,2′,6,6′-tetramethylpiperidide (2.2 equiv), THF, −78→20 °C, 1.5 h, then Me_3SiCl (2 equiv), THF, −78 °C, 64%; d) MeI, 130 °C, 17 h, 78% (**9a**), 97% (**9b**); e) K_2CO_3, MeOH, 20 °C, 1 h, 95%; f) $[Pd_2(dba)_3]$ (5 mol%), CuI (10 mol%), pyrrolidine, 20 °C, 97% (**8b**); g) pent-4-ynoic acid, *N,N′*-dicyclohexylcarbodiimide, 4-(dimethylamino)pyridine, CH_2Cl_2, 20 °C, 96%; h) $H(COEt)_3$, TosOH, EtOH, 20 °C, 1 h, 100%; i) **9a** or **9b**, $[PdCl_2(PPh_3)_2]$ (5 mol%), CuI (10 mol%), pyrrolidine, 20 °C; j) nBu_4NF, THF, 0 °C, 30 min; k) **15a** or **15b**, $[PdCl_2(PPh_3)_2]$ (5 mol%), CuI (10 mol%), PhMe/Et_3N 1/1, 110 °C, 6–17 h; l) 10% aq HCl/THF/MeOH 1/2/5, 0 °C, 2 h, then 20 °C, 1 h, 54% (**17a**) and 18% (**17b**) starting from **13**; m) MeI/CH_2Cl_2 1/1, $CaCO_3$ (traces), 20 °C, 2 h, 77% (**4a**), 95% (**4b**). Tos = *p*-toluenesulfonyl, dba = dibenzylideneacetone.

The bis-steroid rods **4a** and **4b** are light yellow solids (Table 1) that fluoresce strongly ($\lambda_{exc} = 370$ nm, $\lambda_{em} = 471$ (**4a**) and 482 nm (**4b**) in H_2O (0.15 M phosphate buffer, pH 6.9)/MeOH 1:1). Therefore, complexation by threading receptors **1**–**3** could not only be studied by ^1H NMR titrations in D_2O, but also by fluorescence titrations in H_2O; all data were evaluated by nonlinear least-squares curve-fitting analysis (Table 2).[19] Pure testosterone (**11**) forms 1:1 complexes with the G-0 receptor **1** ($\Delta G^\circ = -4.0$ kcal mol^{-1}) and the G-1 receptor **2** ($\Delta G^\circ = -4.4$ kcal mol^{-1}; entries 1 and 2 in Table 2).[10] Apolar bonding interactions and hydrophobic desolvation provide the driving force for formation of these complexes.[11] Much more stable 1:1 complexes are formed between **1**–**3** and the mono-steroid rods **18a** and **18b** (ΔG° between −5.9 and −6.4 kcal mol^{-1}; entries 3–8 in Table 2). Since the complexation-induced shifts (CIS) of the resonances for the steroid methyl groups in the ^1H NMR titrations adopt similar values in complexes of **11** with both **18a** and **18b**, the inclusion geometries must be similar. Thus, the steroid A–D rings of **18a** and **18b**, rather than the phenylacetylene moiety, are axially included in the cyclophane cavities. Therefore, the significantly

Table 1. Selected physical data for the molecular rods **4a** and **4b**.

4a: M.p. 171 °C; IR (KBr): $\tilde{\nu}$ = 3288, 1727, 1666 cm^{-1}; ^{1}H NMR (CD_3OD, 500 MHz): δ = 7.93 (s, 2H; H(2″), H(5″)), 7.50 (d, J = 8.0 Hz, 2H; H(5)), 7.13 (d, J = 1.6 Hz, 2H; H(2)), 7.06 (dd, J = 1.6, 8.0 Hz, 2H; H(4)), 5.74 (s, 2H; C=CHC=O), 4.74 (t, J = 8.1 Hz, 2H; CHOCO), 4.28 (t, J = 4.8 Hz, 4H; ArOCH_2), 3.95 (t, J = 6.5 Hz, 4H; N$^+$CH_2), 3.88 (t, J = 4.78 Hz, 4H; ArOCH$_2$CH_2O), 3.67 (q, J = 7.0 Hz, 4H; OCH_2CH$_3$), 3.63 (t, J = 6.8 Hz, 4H; NHCH_2), 3.24 (s, 18H; NCH$_3$), 2.78 (m, 4H; OOCCH$_2$), 2.66 (m, 4H; OOCCH$_2$CH_2), 2.05 – 2.55 (m, 12H; steroid), 1.30 – 1.95 (m, 20H; steroid), 1.25 (s, 6H; CH$_3$(19)), 1.23 (t, J = 7.0 Hz, 6H; CH_3CH$_2$O), 0.92 – 1.20 (m, 6H; steroid), 0.92 (s, 6H; CH$_3$(18)); ESI-MS (MeOH): m/z = 1573 (1%, $[M-I]^+$), 1431 (1%, $[M-Me-2I]^+$), 722 (100%, $[M]^{2+}$)

4b: M.p. 88 °C; IR (KBr): $\tilde{\nu}$ = 3288, 1727, 1655 cm^{-1}; ^{1}H NMR ($CDCl_3$, 500 MHz): δ = 8.50 (m, 2H; NH), 8.05 (s, 2H; H(2″)), 7.55 (d, J = 7.9 Hz, 2H; H(5′)), 7.38 (d, J = 7.9 Hz, 2H; H(5)), 7.18 (dd, J = 1.3, 7.9 Hz, 2H; H(4′)), 7.13 (d, J = 1.3 Hz, 2H; H(2′), 6.96 (d, J = 1.3, 7.9 Hz, 2H; H(4)), 6.93 (d, J = 1.3 Hz, 2H; H(2)), 5.71 (s, 2H; C=CHC=O), 4.67 (t, J = 8.1 Hz, 2H; CHOOC), 4.30 (m, 4H; ArOCH$_2$), 4.19 (t, J = 4.2 Hz, 4H; ArOCH$_2$), 3.98 – 4.03 (m, 8H; NHCH_2CH_2N$^+$), 3.86 (t, J = 4.2 Hz, 4H; ArOCH$_2$-CH_2O), 3.81 (t, J = 4.2 Hz, 4H; ArOCH$_2$CH_2O), 3.66 (q, J = 7.0 Hz, 4H; OCH_2CH$_3$), 3.55 (q, J = 7.0 Hz, 4H; OCH_2CH$_3$), 3.36 (s, 18H; NCH$_3$), 2.74 (t, J = 6.2 Hz, 4H; OOCCH$_2$), 2.64 (t, J = 6.2 Hz, 4H; OOCCH$_2$CH_2), 1.20 – 2.50 (m, 32H; steroid), 1.22 (t, J = 7.0 Hz, 6H; CH_3CH$_2$O), 1.17 (s, 6H; CH$_3$(19)), 1.11 (t, J = 7.0 Hz, 6H; CH_3CH$_2$O), 0.89 – 1.10 (m, 6H; steroid), 0.84 (s, 6H; CH$_3$(18)); ESI-MS (MeOH): m/z = 1949 (0.5%, $[M-I]^+$, 1807 (0.5%, $[M-Me-2I]^+$, 911 (100%, $[M]^{2+}$)

enhanced association strength ($\Delta(\Delta G^\circ)_{\mathbf{11}\rightarrow\mathbf{18a/18b}} \approx 2.0 \pm 0.2$ kcal mol^{-1}) measured for the complexes of **18a** and **18b**, as compared to complexes of pure testosterone (compare entries 1 and 2 with entries 3 – 8 in Table 2), is mainly a result of the additional ion pairing between the surface carboxylate residues of dendrophanes **1** – **3** and the quaternary ammonium ions of the mono-steroid rods. The extra stabilization of about 1 kcal mol^{-1} provided by each of the two salt bridges is in good agreement with results from previous studies.[20]

The binding of the G-0 derivative **1** to the bis-steroid rod **4a** was evaluated by fluorescence titrations, since precipitation of the formed complex occurred at the higher concentration ranges required for ^{1}H NMR titrations. An excellent fit of the titration data for a 2:1 binding model was obtained, with the threading of the two cyclophanes through **4a** occurring with nearly identical association strength ($\Delta G^\circ_{1:1} = -6.1$, $\Delta G^\circ_{2:1} = -5.9$ kcal mol^{-1}; entry 9 in Table 2). Clear evidence for the proposed 2:1 stoichiometry was also obtained by Job analysis.[21] Each cyclophane in the 2:1 complex (M_r = 4117) independently binds to one steroid terminus with similar association strength to that measured for the 1:1 complexation of **1** to the mono-steroid rod **18a**.

In contrast to these findings, significant differences in the driving force for the first and second binding event were measured when the G-1 derivative **2** was threaded onto the shorter bis-steroid rod **4a** (entries 10 and 11 in Table 2). Again, clear evidence for formation of a supramolecular complex with 2:1 stoichiometry was obtained.[21] In this case, however, the driving force for the second association step $\Delta G^\circ_{2:1}$ is between 2.1 (fluorescence) and 2.8 kcal mol^{-1} (^{1}H NMR) smaller than for the first association step, which with $\Delta G^\circ_{1:1} = -6.7$ kcal mol^{-1} has a driving force of similar magnitude to that for threading the G-0 derivative **1** on **4a**, **18a**, or **18b**. The two dendrophanes once again prefer inclusion of the tetracyclic steroid skeletons over the complexation of the phenylacetylene moieties of **4a**, as indicated by a comparison of the complexation-induced shifts of the ^{1}H NMR signals for steroid methyl groups CH$_3$(18) and CH$_3$(19). At saturation binding, these resonances in the 2:1 complex of **4a** with **2** (entry 10, Table 2) display strong upfield shifts similar to those observed in the 1:1 complexes of **11** (entry 2) and the mono-steroid rods **18a** and **18b** (entries 6 and 7). The considerable reduction in thermodynamic driving force for the second complexation step is undoubtedly a

Table 2. Association constants and binding free enthalpies for the complexes formed by dendrophanes **1** – **3** with testosterone (**11**) and the molecular rods **4a**/**4b** and **18a**/**18b** as well as complexation-induced shifts at saturation binding of signals monitored during ^{1}H NMR titrations.[a]

Entry	Titration method	Steroid substrate	Dendrophane	$K_{1:1}$ [L mol^{-1}]	$\Delta G^\circ_{1:1}$[b] [kcal mol^{-1}]	$K_{2:1}$ [L mol^{-1}]	$\Delta G^\circ_{2:1}$[b] [kcal mol^{-1}]	$\Delta\delta_{sat}$ [ppm] CH$_3$(18)	CH$_3$(19)	CH_3CH$_2$O
1	NMR[c]	**11**	G-0 (**1**)	900	– 4.0	–	–	–	–	–
2	NMR	**11**	G-1 (**2**)	1600	– 4.4	–	–	– 0.41	– 1.06	–
3	NMR	**18a**	G-0 (**1**)	21000	– 5.9	–	–	– 0.41	– 1.19	– 0.26
4	NMR	**18b**	G-0 (**1**)	30000	– 6.1	–	–	– 0.38	– 1.06[d]	– 0.27, – 0.28
5	fluor.[e]	**18b**	G-0 (**1**)	22000	– 5.9	–	–	–	–	–
6	NMR	**18a**	G-1 (**2**)	47000	– 6.4	–	–	– 0.31	– 1.50	– 0.21
7	NMR	**18b**	G-1 (**2**)	38000	– 6.2	–	–	– 0.38	– 1.02	– 0.14, – 0.20
8	fluor.[e]	**18b**	G-2 (**3**)	32000	– 6.1	–	–	–	–	–
9	fluor.[f]	**4a**	G-0 (**1**)	29000	– 6.1	23000	– 5.9	–	–	–
10	NMR	**4a**	G-1 (**2**)	79000	– 6.7	700	– 3.9	– 0.40	– 1.39	– 0.20
11	fluor.	**4a**	G-1 (**2**)	81000	– 6.7	2300	– 4.6	–	–	–
12	fluor.	**4b**	G-1 (**2**)	31000	– 6.1	30000	– 6.1	–	–	–
13	fluor.[g]	**4a**	G-2 (**3**)	15000	– 5.7	–	–	–	–	–
14	fluor.	**4b**	G-2 (**3**)	91000	– 6.8	4000	– 4.9	–	–	–

[a] The thermodynamic data were determined by 500-MHz ^{1}H NMR titration in D_2O (0.15 M phosphate buffer, pD 7.3)/CD_3OD 1/1 at 300 K and/or by fluorescence titrations in H_2O (0.15 M phosphate buffer, pH 8.7)/CH_3OH 1/1 at 298 K.[19] [b] Uncertainties: ± 0.1 kcal mol^{-1} for $\Delta G^\circ_{1:1}$ and ± 0.3 kcal mol^{-1} for $\Delta G^\circ_{2:1}$. [c] Titration at constant dendrophane concentration; a titration at a constant concentation of **11** in D_2O (0.1 M borate buffer, pD 10.5)/CD_3OD 1/1 gave K_a = 1350 L mol^{-1} as well as $\Delta\delta_{sat} = -0.24$ (CH$_3$(18)) and – 0.81 (CH$_3$(19)).[10] [d] Maximum shift. [e] The hypsochromic shift of the emission of **18b** at saturation binding was – 43 nm (entry 5) and – 40 nm (entry 8). [f] In H_2O (0.15 M phosphate buffer, pH 6.9)/CH_3OH 4/6 for solubility reasons. [g] Formation of a 1:1 complex with the given stability was also confirmed by ^{1}H NMR titrations at constant concentration of **4a** [$\Delta\delta_{sat}$: – 0.20 (CH$_3$(18)); – 0.16 (CH_3CH$_2$O)].

 © WILEY-VCH Verlag GmbH, D-69451 Weinheim, 1998 1433-7851/98/3722-3156 $ 17.50+.50/0 *Angew. Chem. Int. Ed.* **1998**, *37*, No. 22

consequence of the Coulombic repulsion between the surface carboxylate groups of the two threaded dendrophanes, which are positioned in too close proximity on the small rod.

Computer modeling[22] suggests that the distance between the junctions of the B and C rings of the two testosterone termini is approximately 41 Å. When the rod size is extended in **4b** to about 55 Å, the driving forces for threading the first and second dendrophane become identical again (entry 12 in Table 2). Fluorescence titrations yielded for both 1:1 and 2:1 complexation between **4b** and **2** a free enthalpy of formation of $\Delta G^\circ = -6.1$ kcal mol^{-1}, that is, nearly the same driving force as measured for the complexation of one dendrophane **2** by the mono-steroid rods **18a** and **18b**.[23] Thus, a highly stable supramolecular aggregate with a molecular mass of 6642 is formed in which the two dendrophanes, through inclusion of the testosterone termini, are placed at sufficient distance to avoid charge repulsion.

The bulky G-2 dendrophane **3** ($M_r = 6318$ D) only forms a 1:1 complex with the smaller rod **4a**, as evidenced by the curve fitting of fluorescence and ^{1}H NMR titration data and Job analysis; the fluorescence data gave a maximum at mole fraction $x(\mathbf{3}) = 0.5$ (entry 13 in Table 2). Formation of a stable 2:1 complex with a molecular mass of 14714 was, however, observed again by fluorescence titrations and Job analysis for the association between the longer rod **4b** and G-2 dendrophane **3** (entry 14 in Table 2). The threading of the first dendrophane is more favorable ($\Delta G^\circ = -6.8$ kcal mol^{-1}) than that of the second ($\Delta G^\circ = -4.9$ kcal mol^{-1}) owing to charge repulsion.[21, 23] Further extension of the phenylacetylenic sequence in the bis-steroid rod is currently under way to accommodate two G-2 dendrophanes with similar binding free enthalpy. The successful threading of two third-generation dendrophanes ($M_r = 17813$), which are already available,[10] to form 2:1 complexes with molecular weights approaching 40000 will require the construction of bis-steroid rods with even larger spacers.

We have demonstrated a novel, efficient dendrimer association process which takes advantage of apolar interactions, hydrophobic desolvation, and ion pairing to produce supramolecules of defined structures with molecular weights exceeding 14000. The experiments establish experimentally an optimal distance for threading two anionic dendrophanes in the thermodynamically most favorable way onto the steroid termini of molecular rods with rigid phenylacetylene spacers. For optimal binding, two G-0 dendrophanes **1** require an intramolecular steroid$\cdots$steroid distance of about 41 Å, whereas in the case of the G-1 dendrophanes **2** this distance is about 55 Å. From these data, the extensions of the complexed dendrophanes, which are hard to obtain otherwise, can be estimated. Thus, the bis-steroid rods **4a** and **4b** serve as rulers on the molecular scale.

Received: June 4, 1998 [Z11939IE]
German version: *Angew. Chem.* **1998**, *110*, 3357 – 3361

Keywords: cyclophanes · dendrimers · steroids · supramolecular chemistry

[1] a) G. R. Newkome, C. N. Moorefield, F. Vögtle, *Dendritic Molecules: Concepts, Syntheses, Perspectives,* VCH, Weinheim, **1996**; b) D. A. Tomalia, A. M. Naylor, W. A. Goddard III, *Angew. Chem.* **1990**, *102*, 119 – 157; *Angew. Chem. Int. Ed. Engl.* **1990**,*29*, 138 – 175; c) D. A. Tomalia, *Adv. Mater.* **1994**, *6*, 529 – 539; d) J. M. J. Fréchet, *Science* **1994**, *263*, 1710 – 1715; e) H. W. I. Peerlings, E. W. Meijer, *Chem. Eur. J.* **1997**, *3*, 1563 – 1570; f) J. S. Moore, *Acc. Chem. Res.* **1997**, *30*, 402 – 413; g) O. A. Matthews, A. N. Shipway, J. F. Stoddart, *Prog. Polym. Sci.* **1998**, *23*, 1 – 56; h) H. Frey, C. Lach, K. Lorenz, *Adv. Mater.* **1998**, *10*, 279 – 293.

[2] D. K. Smith, F. Diederich, *Chem. Eur. J.* **1998**, *4*, 1353 – 1361.

[3] a) V. Balzani, S. Campagna, G. Denti, A. Juris, S. Serroni, M. Venturi *Acc. Chem. Res.* **1998**, *31*, 26 – 34; b) C. Gorman, *Adv. Mater.* **1998**, *10*, 295 – 309; c) E. C. Constable, P. Harverson, *Chem. Commun.* **1996**, 33 – 34; d) R. J. Puddephatt, *Chem. Commun.* **1998**, 1055 – 1062; e) H.-F. Chow, I. Y.-K. Chan, D. T. W. Chan, R. W. M. Kwok, *Chem. Eur. J.* **1996**, *2*, 1085 – 1091; f) D. Tzalis, Y. Tor, *Tetrahedron Lett.* **1996**, *37*, 8293 – 8296.

[4] a) G. R. Newkome, R. Güther, C. N. Moorefield, F. Cardullo, L. Echegoyen, E. Pérez-Cordero, H. Luftmann, *Angew. Chem.* **1995**, *107*, 2159 – 2162; *Angew. Chem. Int. Ed. Engl.* **1995**, *34*, 2023 – 2026; b) Y. Tomoyose, D.-L. Jiang, R.-H. Jin, T. Aida, T. Yamashita, K. Horie, E. Yashima, Y. Okamoto, *Macromolecules* **1996**, *29*, 5236 – 5238.

[5] For a review on dendrimers in supramolecular chemistry, see F. Zeng, S. C. Zimmerman, *Chem. Rev.* **1997**, *97*, 1681 – 1712.

[6] a) S. C. Zimmerman, F. Zeng, D. E. C. Reichert, S. V. Kolotuchin, *Science* **1996**, *271*, 1095 – 1098; b) Y. Wang, F. Zeng, S. C. Zimmerman, *Tetrahedron Lett.* **1997**, *38*, 5459 – 5462.

[7] For recent examples of dendritic liquid crystalline phases, see a) S. D. Hudson, H.-T. Jung, V. Percec, W.-D. Cho, G. Johansson, G. Ungar, V. S. K. Balagurusamy, *Science* **1997**, *278*, 449 – 452; b) D. J. Pesak, J. S. Moore, *Angew. Chem.* **1997**, *109*, 1709 – 1712; *Angew. Chem. Int. Ed. Engl.* **1997**, *36*, 1636 – 1639.

[8] a) D. A. Tomalia in *Modular Chemistry*, Nato ASI Series, Vol. 499 (Ed.: J. Michl), Kluwer, Dordrecht, **1997**, pp. 183 – 191; b) J. C. M. van Hest, D. A. P. Delnoye, M. W. P. L. Baars, M. H. P van Genderen, E. W. Meijer, *Science* **1995**, *268*, 1592 – 1595; c) T. M. Chapman, G. L. Hillyer, E. J. Mahan, K. A. Shaffer, *J. Am. Chem. Soc.* **1994**, *116*, 11195 – 11196.

[9] S. Mattei, P. Seiler, F. Diederich, V. Gramlich, *Helv. Chim. Acta* **1995**, *78*, 1904 – 1912.

[10] a) S. Mattei, P. Wallimann, B. Kenda, W. Amrein, F. Diederich, *Helv. Chim. Acta* **1997**, *80*, 2391 – 2417; b) P. Wallimann, P. Seiler, F. Diederich, *Helv. Chim. Acta* **1996**, *79*, 779 – 788.

[11] For use of steroids in molecular recognition, see P. Wallimann, T. Marti, A. Fürer, F. Diederich, *Chem. Rev.* **1997**, *97*, 1567 – 1608.

[12] a) J. S. Zhang, J. S. Moore, Z. F. Xu, R. A. Aguirre, *J. Am. Chem. Soc.* **1992**, *114*, 2273 – 2274; b) J. S. Zhang, D. J. Pesak, J. L. Ludwick, J. S. Moore, *J. Am. Chem. Soc.* **1994**, *116*, 4227 – 4239; c) Z. F. Xu, M. Kahr, K. L. Walker, C. L. Wilkins, J. S. Moore, *J. Am. Chem. Soc.* **1994**, *116*, 4537 – 4550.

[13] M. Julia, M. Baillargé, *Bull. Soc. Chim. Fr.* **1952**, 639 – 642.

[14] All new compounds were fully characterized by ^{1}H NMR, ^{13}C NMR, and IR spectroscopy; EI, FAB, or MALDI-TOF mass spectrometry; and elemental analysis or high-resolution mass spectrometry. The rods **4a**/**4b** and **19a**/**19b** were additionally characterized by UV/VIS and fluorescence spectroscopy.

[15] a) M. Alami, F. Ferri, G. Linstrumelle, *Tetrahedron Lett.* **1993**, *34*, 6403 – 6406; b) K. Sonogashira in *Metal-catalyzed Cross-coupling reactions* (Eds.: F. Diederich, P. J. Stang), WILEY-VCH, Weinheim, **1998**, pp. 203 – 229.

[16] R. Gardi, A. Eridi in *Protecting Groups in Steroid Chemistry*, Vol. 1 (Eds.: R. Gardi, A. Eridi), Van Nostrand-Reinhold, New York, **1972**, pp. 388 – 390.

[17] Since **16** was only poorly soluble in the solvent mixture for the Sonogashira coupling (PhMe/Et_3N), long reaction times were applied and homocoupling of the terminal alkynes **15a** and **15b** became a competitive process.

[18] Q. Zhou, T. M. Swager, *J. Am. Chem. Soc.* **1995**, *117*, 12593 – 12602.

[19] For the evaluation of 1:1 complexes, the program Associate V. 1.6 (B. Peterson, Dissertation, University of California, Los Angeles, **1994**) was used. Complexes with higher stoichiometry (2:1) were analyzed

 © WILEY-VCH Verlag GmbH, D-69451 Weinheim, 1998 1433-7851/98/3722-3157 $ 17.50+.50/0

with the program SPECFIT V. 2.10 (R. A. Binstead, A. D. Hungerbühler, Spectrum Software Associates, Chapel Hill, NC, **1997**). This program performs global least-squares fits which, in fluorescence titrations, include the entire measured wavelength region (multiple wavelength analysis). In the ^{1}H NMR titrations at constant concentration of the molecular rod (c(rod) ≈ 0.1 – 0.2 mM, c(dendrophane) ≈ 0.05 – 1 mM), the complexation-induced shifts of the steroid CH_3(18) and CH_3(19) resonances and the CH_3CH_2O resonances were evaluated. In the fluorescence titrations at constant concentration of the molecular rod (c(rod) ≈ 0.01 – 0.02 mM, c(dendrophane) = 0.005 – 0.8 mM), the emission intensity of the rod decreased upon addition of dendrophane and the emission maxima of **4a**/**4b** at saturation binding shifted by 5 – 16 nm to higher energy.

[20] a) H.-J. Schneider, *Angew. Chem.* **1991**, *103*, 1419 – 1439; *Angew. Chem. Int. Ed. Engl.* **1991**, *30*, 1417 – 1436; b) H.-J. Schneider, T. Shiestel, P. Zimmermann, *J. Am. Chem. Soc.* **1992**, *114*, 7698 – 7703.

[21] Multiple evidence for 2:1 complexation by **4a**/**4b** was obtained: 1) An excellent fit of the fluorescence and/or ^{1}H NMR titration data to the 2:1 binding model was obtained. 2) Job plots of fluorescence data showed clear maxima at x(dendrophane) ≈ 0.66 (see D. V. Naik, W. L. Paul, R. M. Threatte, S. G. Schulman, *Anal. Chem.* **1975**, *47*, 267 – 270). 3) The complexation-induced shifts observed for the ^{1}H NMR signals for CH_3(18) and CH_3(19) of the steroids in solutions of **4a** and **2** are compatible with formation of a 2:1 complex; that is, they are of similar magnitude to those observed for these resonances in the 1:1 complexes formed by testosterone (**11**) or the mono-steroid rods **18a** and **18b**.

[22] Insight II program, V. 97.0, Molecular Simulations Inc., San Diego **1997**.

[23] Strong broadening of the resonances prevented the application of ^{1}H NMR titrations to determine stabilities of the complexes formed by **4b**.

Desolvation of a Novel Microporous Hydrogen-Bonded Framework: Characterization by In Situ Single-Crystal and Powder X-ray Diffraction**

Cameron J. Kepert, Dusan Hesek, Paul D. Beer,* and Matthew J. Rosseinsky*

Attention has recently focused on the use of the hydrogen bond,[1] and also the coordinate bond,[2] in the controlled assembly of porous molecular frameworks. Studies into the guest exchange and catalytic properties[3] of these materials have led to a growing recognition of molecular frameworks as zeolite analogues, many retaining their structural integrity with desolvation or solvent exchange. Aware of these developments, and of the importance of redox centers to heterogeneous catalysis[4] and molecular recognition by electrochemical sensing,[5] we have synthesized an electrochemically active organic species suitable for forming novel extended molecular frameworks. Here we show how hydrogen bonding and $\pi\cdots\pi$ nonbonding interactions can produce a microporous framework of this species linked to a transition metal complex. The material described displays remarkable flexibility, and undergoes significant structural rearrangements with desolvation to leave an empty-channel material that shows selectivity to guest sorption.

By making use of slow diffusion in aqueous silica gels, we have synthesized crystals incorporating the diprotonated, redox-active tetra(carboxyl)tetrathiafulvalene anion H_2(TC-TTF)$^{2-}$, hexaaquacobalt(II) cations, and solvent water molecules. $[Co^{II}(H_2O)_6]H_2(TC\text{-}TTF)\cdot 2H_2O$ (**A**) consists of a three-dimensional hydrogen-bonded network of $[Co(H_2O)_6]^{2+}$ and $H_2(TC\text{-}TTF)^{2-}$ ions (Figure 1).[6] Short

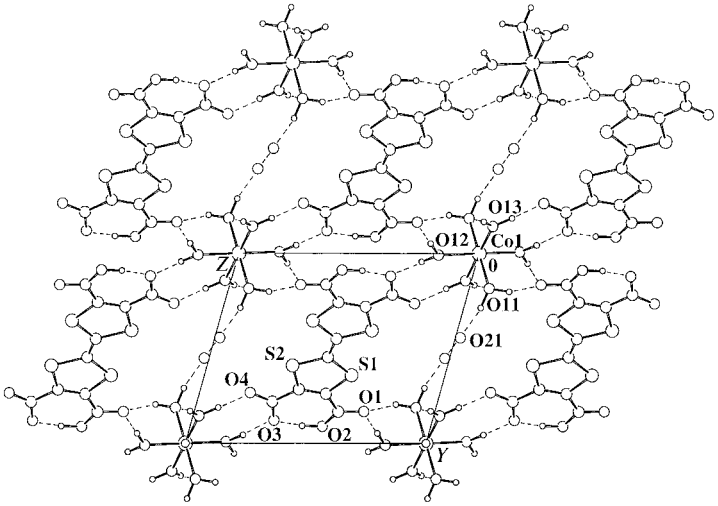


Figure 1. Projection of **A** down the *a* axis. For clarity, only one oxygen atom position of the disordered cavity water molecule is displayed. Selected bond lengths [Å] and angles [°] (a fixed value of 0.86 Å was used for O–H distances in the cation): O11 ··· O1* 2.715(4), O12 ··· O3* 2.773(4), O12 ··· O1* 2.802(4), O13 ··· O4* 2.685(4), O2 ··· O3 2.438(5), H2 ··· O3 1.47(8); O11–H11B ··· O1* 159(6), O12–H12B ··· O3* 173(8), O12–H12A ··· O1* 179(5), O13–H13A ··· O4* 174(6), O13–H13B ··· O11* 173(7), O3–H2 ··· O2 168(7).

hydrogen bonds exist between eight of the twelve protons in the hexaaquometal cation and six of the eight carboxyl oxygen atoms. The two protons of the doubly deprotonated acid form very short hydrogen bonds to neighboring carboxyl groups, giving this unit a rigid planarity. Running along the *a* axis, and lying parallel with slipped stacks of the TTF derivative and hydrogen-bonded chains of $[Co(H_2O)_6]^{2+}$ ions, are one-dimensional channels that are filled with zig-zag chains of disordered water molecules. The sites occupied by these molecules are defined by hydrogen bonding to the framework, primarily to a water molecule coordinated to Co^{2+} (O11) and to a lesser degree to O4 of the anion. Hydrogen bonding between solvent molecules occurs along the channels, the mean solvent separation being about 2.9 Å, compared with 2.8(1) Å for a typical hydrogen-bonded O ··· O distance.

[*] Dr. P. D. Beer, Dr. M. J. Rosseinsky, Dr. C. J. Kepert, Dr. D. Hesek
Inorganic Chemistry Laboratory, Department of Chemistry
University of Oxford
South Parks Road, Oxford, OX1 3QR (UK)
Fax: (+44) 1865-272-690
E-mail: cameron.kepert@chem.ox.ac.uk
paul.beer@chem.ox.ac.uk
matthew.rosseinsky@chem.ox.ac.uk

[**] C.J.K. thanks Christ Church, Oxford, for a Junior Research Fellowship. We thank Prof. C. K. Prout and Dr. D. J. Watkin for access to the X-ray diffractometer and for useful discussions.

Supporting information for this article is available on the WWW under http://www.wiley-vch.de/home/angewandte/ or from the author.

 © WILEY-VCH Verlag GmbH, D-69451 Weinheim, 1998 1433-7851/98/3722-3158 $ 17.50+.50/0

A slight mismatching of this distance and the channel periodicity is a likely contributor to the solvent disorder.

Thermogravimetry reveals that the water molecules in the channels of **A** are liberated at 50 °C to leave [Co-$(H_2O)_6$]H_2(TC-TTF) (**B**). Four further equivalents of water are lost at 80 °C to provide polycrystalline [$Co(H_2O)_2H_2$(TC-TTF)] (**C**),[7] in which the terminal carboxyl groups of the anion are thought to coordinate directly to the cobalt atom. Each of these desolvation steps leads to a considerable decrease in calculated density (see Table 1), with decreases in cell volume amounting to only about 8 Å^3 per liberated water molecule; the volume occupied by a typical solvent H_2O molecule is 40 Å^3.[8] The two remaining equivalents of water of **C** are lost above 120 °C, and decomposition occurs above 150 °C. The phases **A**–**C**, like other highly stable framework materials, are insoluble in a large range of common solvents (including water, alcohols, acetone, acetonitrile, carbon disulfide, and dichloromethane). Powder X-ray diffraction[7] indicates that **B** converts back into **A** upon rehydration at ambient temperature, whereas **C** transforms to a new crystalline form.

Remarkably, monocrystallinity is retained thoughout the transition from **A** to **B**, allowing structure determination of **B** by single-crystal X-ray diffraction (Figure 2).[6] To our knowledge, this is the first time that such a study has been

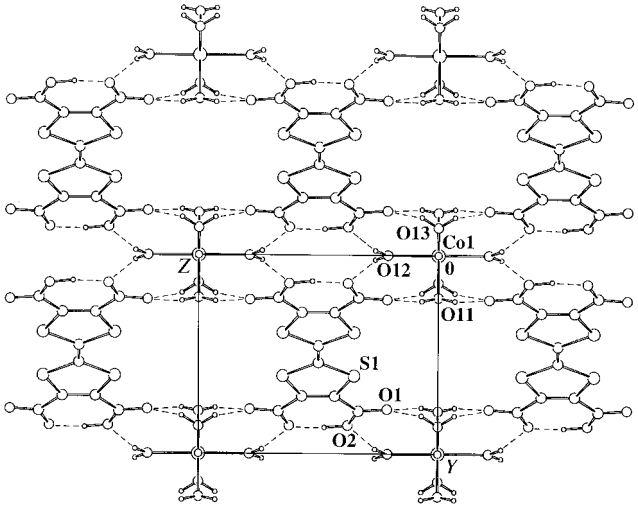


Figure 2. Projection of **B** (295 K) down the *a* axis. Note the retention of the one-dimensional channels from **A** upon desolvation. Selected lengths [Å]: O11 ··· O1* 2.897(14), O12 ··· O2* 2.812(11), O13 ··· O1* 2.727(12), O2 ··· O2* 2.421(17).

performed on an organic-based molecular framework material. Desolvation causes a considerable transformation of the unit cell, and an increase from triclinic to monoclinic symmetry (Table 1). Accordingly, the crystal morphology undergoes striking changes, in particular the adoption of a rectangular facet for the large (010) face and a considerable lengthening of the platelets. With the removal of the water molecules in the channel there are significant rotations of both cation and anion species, and both sites increase in symmetry from $\bar{1}$ to 2/*m*. The driving force of the rearrangement is the formation of new hydrogen bonds as both cationic and anionic components cross-link to form the new framework: In **B**, each hexaaquo cation makes twelve rather than ten framework-forming hydrogen bonds, with four new cation–anion bonds replacing the two cation–cation and the two cation–solvent bonds. The stacks of H_2(TC-TTF)$^{2-}$ undergo a considerable tilting from 45.1 to 33.3° with respect to the *a* axis, which is made possible by the presence of nonbonding $\pi \cdots \pi$ interactions between anions (Figure 3).

Table 1. Unit cell parameters, formula masses, and calculated densities of **A**, **A′**, **B′**, **B**, and **C** at 295(2) K. **A′** and **B′** are intermediate, partially hydrated phases observed in situ during the **B** → **A** resolvation.

	A[6, 7]	**A′**[7]	**B′**[7]	**B**[6, 7]	**C**[7]
a [Å]	5.239(1)	5.232(6)	6.426(2)	6.429(1)	6.956(4)
b [Å]	9.186(2)	9.134(17)	8.102(2)	8.079(2)	8.067(7)
c [Å]	11.749(3)	11.780(14)	9.915(4)	9.893(3)	9.063(8)
α [°]	74.158(11)	74.67(9)	90.0	90.0	80.51(3)
β [°]	76.737(12)	76.78(6)	90.0	90.0	104.92(6)
γ [°]	89.335(13)	89.29(10)	86.99(2)	86.76(2)	84.10(5)
V [Å^3]	528.7(2)	528.2(14)	515.3(3)	513.0(2)	479.0(6)
M [g mol^{-1}]	581.42	–	–	545.39	473.33
ρ_{calcd} [Mg m^{-3}]	1.826	–	–	1.765	1.641

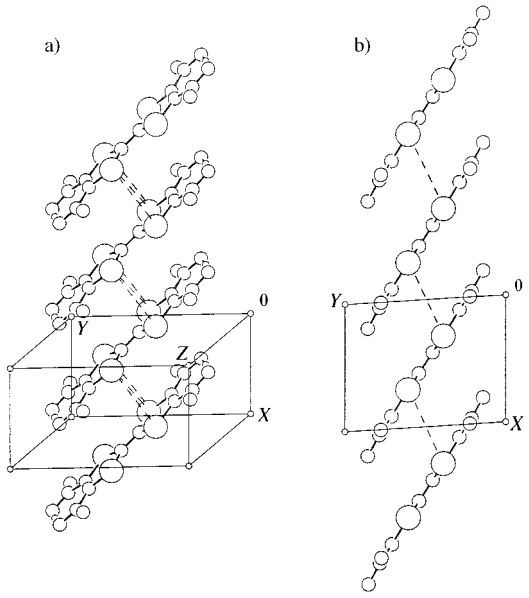


Figure 3. Projection of the one-dimensional stacks of H_2(TC-TTF)$^{2-}$ in **A** (a) and **B** (b), drawn perpendicular to the *a* axis and on the same scale. Selected bond lengths [Å] in **A**: S1 ··· S1* 3.824(3), S1 ··· S2* 3.737(2); in **B**: S1 ··· S1* 4.115(7), 4.374(6).

These changes accompany a reduction in cross-sectional dimensions of the pseudo-rectangular channels within the framework: The width decreases from about 9 to 8 Å, and the height from 7 to 5 Å. Accordingly, the channels diminish in volume from about 62 Å^3 (12% of the crystal volume) to about 41 Å^3 (8%) per unit cell,[8] despite lengthening by 23%.

In situ X-ray diffraction measurements[7] indicate that the resolvation transition **B** → **A** occurs homogeneously over a powdered sample, and involves a gradual expansion in volume towards a maximally hydrated phase of **B** (**B′**) followed by a structural transition to a minimally hydrated phase of **A** (**A′**; see Table 1). Further rehydration returns **A′** to **A**. The robustness of the crystals suggests these structural rearrangements follow a pathway of very low energy, with inhomogeneities in the distribution of channel water molecules

 © WILEY-VCH Verlag GmbH, D-69451 Weinheim, 1998 1433-7851/98/3722-3159 $ 17.50+.50/0

apparently causing insufficient strain to produce fracturing. The observation that the **B** phase is capable of both containing and transporting water molecules within its channels is in accord with calculations on the minimization of the energy of inclusion,[9] which suggest that water sites within **B** have similarly low energies to those within **A**. The **B′**→**A′** structural transition is therefore likely to be governed primarily by a balance of hydrogen-bond energies, high levels of channel hydration favoring the existence of cation–solvent bonds as seen in **A**, and low levels favoring the enhanced framework hydrogen bonding of **B**.

The empty channel structure of **B** shows a high degree of selectivity towards guest sorption. Powder X-ray diffraction shows that samples of **B** exposed to methanol vapor at room temperature convert into a new crystalline form, whereas samples exposed to ethanol, carbon disulfide, and acetonitrile vapor remain unchanged over periods exceeding one month. These observations suggest that small polar molecules may readily be included into the empty channels, whereas larger or less polar molecules are excluded.

Compound **A** consists of a three-dimensional framework of transition metal centers and redox-active tetrathiafulvalene species which houses one-dimensional channels occupied by exchangeable water molecules. The assembly of hydrogen-bonding components can interact in a switchable fashion both with each other and with guest species, allowing the framework topology to alter smoothly and reversibly in response to a guest. We attribute the remarkable flexibility and durability of this unique microporous framework material to the multitude of independent weak (hydrogen bond) or nonbonding ($\pi\cdots\pi$) intermolecular interactions present, meaning that bond breakage and formation energies are smaller than crystal fracturing energies. Importantly, the similarity in energies for interactions within the framework and between the framework and solvent molecules means that solvent inclusion may drastically affect the overall lattice energy, thereby providing a strong driving force for molecular rearrangement.

Experimental Section

Tetrathiafulvalenetetracarboxylic acid, H_4(TC-TTF), was synthesized according to literature methods.[10] Slow diffusion of H_4(TC-TTF) with 0, 2, and 4 parts of NaOH in aqueous silica gels afforded **A** on reaction with $[Co^{II}(NO_3)_2]\cdot 6H_2O$ (aq).

Cyclic voltammetry: H_4(TC-TTF) (aqueous, 0.5 mmol L^{-1}) undergoes a reversible one-electron oxidation at 0.58 V versus the standard mercury/calomel electrode (3.5 mol L^{-1} KCl).

Received: April 14, 1998
Revised version: August 3, 1998 [Z11721IE]
German version: *Angew. Chem.* **1998**, *110*, 3335–3337

Keywords: crystal engineering · hydrogen bonds · microporosity · redox chemistry · tetrathiafulvalene

[1] a) P. Brunet, M. Simard, J. D. Wuest, *J. Am. Chem. Soc.* **1997**, *119*, 2737–2738; b) K. Endo, T. Sawaki, M. Koyanagi, K. Kobayashi, H. Masuda, Y. Aoyama, *J. Am. Chem. Soc.* **1995**, *117*, 8341–8352; c) A. R. A. Palmans, J. A. J. M. Vekemans, H. Kooijman, A. L. Spek, E. W. Meijer, *Chem. Commun.* **1997**, 2247–2248; d) Y. Aoyama, K. Endo, T. Anzai, Y. Yamaguchi, T. Sawaki, K. Kobayashi, N. Kanehisa, H. Hashimoto, Y. Kai, H. Masuda, *J. Am. Chem. Soc.* **1996**, *118*, 5562–5571.

[2] a) C. J. Kepert, M. J. Rosseinsky, *Chem. Commun.* **1998**, 31–32; b) O. M. Yaghi, C. E. Davis, G. M. Li, H. L. Li, *J. Am. Chem. Soc.* **1997**, *119*, 2861–2868; c) M. J. Plater, A. J. Roberts, R. A. Howie, *Chem. Commun.* **1997**, 893–894; d) D. L. Lohse, S. C. Sevov, *Angew. Chem.* **1997**, *109*; 1692–1695; *Angew. Chem. Int. Ed. Engl.* **1997**, *36*, 1619–1621; e) S. O. H. Gutschke, M. Molinier, A. K. Powell, P. T. Wood, *Angew. Chem.* **1997**, *109*; 1028–1029; *Angew. Chem. Int. Ed. Engl.* **1997**, *36*, 991–992; f) G. B. Gardner, D. Venkataraman, J. S. Moore, S. Lee, *Nature* **1995**, *374*, 792–795; g) S. R. Batten, B. F. Hoskins, R. Robson, *J. Am. Chem. Soc.* **1995**, *117*, 5385–5386; h) O. M. Yaghi, G. M. Li, H. L. Li, *Nature* **1995**, *378*, 703–706; i) D. Venkataraman, G. B. Gardner, S. Lee, J. S. Moore, *J. Am. Chem. Soc.* **1995**, *117*, 11600–11601; j) B. F. Abrahams, B. F. Hoskins, D. M. Michail, R. Robson, *Nature* **1994**, *369*, 727–729; k) C. Robl, *Mat. Res. Bull.* **1992**, *27*, 99–107.

[3] a) K. Endo, T. Koike, T. Sawaki, O. Hayashida, H. Masuda, Y. Aoyama, *J. Am. Chem. Soc.* **1997**, *119*, 4117–4122; b) M. Fujita, Y. J. Kwon, S. Washizu, K. Ogura, *J. Am. Chem. Soc.* **1994**, *116*, 1151–1152.

[4] a) I. W. C. E. Arends, R. A. Sheldon, M. Wallau, U. Schuchardt, *Angew. Chem.* **1997**, *109*, 1190-1211; *Angew. Chem. Int. Ed. Engl.* **1997**, *36*, 1144–1163; b) J. A. Dumesic, W. S. Millman, *ACS Symposium Series* **1990**, *437*, 66–74.

[5] P. D. Beer, D. K. Smith, *Prog. Inorg. Chem.* **1997**, *46*, 1–96; C. Valerio, J. L. Fillaut, J. Ruiz, J. Guittard, J. C. Blais, D. Astruc, *J. Am. Chem. Soc.* **1997**, *119*, 2588–2589; P. D. Beer, *Chem. Commun.* **1996**, 689–696.

[6] Single crystals of **A** were placed in open-ended capillaries on an Enraf-Nonius DIP2000 diffractometer equipped with Eu/Ba image plates and a nitrogen cryostream. To form **B**, a crystal of **A** was heated at 10 K h^{-1} to 328(2) K, then cooled at 150 K h^{-1} to 295(2) K. Crystal data for **A**: $C_{10}H_{18}CoO_{16}S_4$, triclinic, space group $P\bar{1}$, $F(000)=297$, $\lambda(Mo_{K\alpha})=0.71073$ Å, $\mu(Mo_{K\alpha})=1.283$ mm^{-1}, crystal dimensions $0.45\times0.30\times0.08$ mm, $2\theta_{max}=53.26^\circ$, $T=295(2)$ K, mosaicity $=1.0^\circ$. Crystal data for **B** at $T=295(2)$ K and 328(2) K, respectively: $C_{10}H_{14}CoO_{14}S_4$, monoclinic, space group $P112/m$, $F(000)=277$, $\mu(Mo_{K\alpha})=1.309$ and 1.313 mm^{-1}, crystal dimension $0.50\times0.20\times0.04$ mm, $2\theta_{max}=53.44$ and 53.50°, mosaicity $=1.0^\circ$. Data reduction was carried out with the HKL suite of programs.[11] The structures were solved and refined with SHELXS-86 and SHELXL-93.[12] For **A**, **B** (295 K), and **B**(328 K), respectively, full-matrix least-squares refinement on F_o^2 for 2057, 1080, and 934 unique data (4011, 2889, and 1684 collected reflections; $R(\text{int})=0.034$, 0.101, and 0.109); 182, 87, and 86 parameters; and 16, 41, and 41 restraints converged to $wR2=0.1144$, 0.2988, and 0.3034 (all data); $R=0.0651$, 0.1686, and 0.1783 (1885, 954, and 779 data with $F_o>4\sigma F_o$); max./min. residual electron density 0.511/−0.385, 1.610/−1.146, and 0.807/−0.945 e $Å^{-3}$. Crystallographic data (excluding structure factors) for the structure(s) reported in this paper have been deposited with the Cambridge Crystallographic Data Centre as supplementary publication no. CCDC-101357. Copies of the data can be obtained free of charge on application to CCDC, 12 Union Road, Cambridge CB2 1EZ, UK (fax: (+44) 1223-336-033; e-mail: deposit@ccdc.cam.ac.uk).

[7] Ground samples were sealed in 0.5-mm capillaries on a Siemens D5000 X-ray powder diffractometer with monochromated $Cu_{K\alpha1}$ radiation and a linear position-sensitive detector (6°). Gradual rehydration of **B** was achieved over a period of five days through an open-ended capillary packed with glass wool; no peak broadening was observed.

[8] Channel volumes were calculated by summing voxels more than 1.2 Å from the van der Waals surface of the host: A. L. Spek, *Acta Crystallogr. Sect. A* **1990**, *46*, 194–201.

[9] Molecular docking using both CVFF and CFF91 atomic force fields: *Solids Docking 7.0, InsightII, Version 4.0.0*, Biosym Technologies, San Diego, CA, **1997**.

[10] S. Yoneda, T. Kawase, M. Inaba, Z. Yoshida, *J. Org. Chem.* **1978**, *43(4)*, 595–598.

[11] Z. Otwinowski, W. Minor in *Methods in Enzymology* (Eds.: C. W. Carter, R. M. Sweet), Academic Press, New York, **1996**, p. 276.

[12] G. M. Sheldrick, *SHELXS-86* and *SHELXL-93*, Universität Göttingen.

 © WILEY-VCH Verlag GmbH, D-69451 Weinheim, 1998 1433-7851/98/3722-3160 $ 17.50+.50/0

Two Coordination Modes of CO in Zeolites: A Temperature-Dependent Equilibrium

Carlos Otero Areán,* Alexey A. Tsyganenko, Estrella Escalona Platero, Edoardo Garrone, and Adriano Zecchina

Besides their wide application as solid acid catalysts in the petrochemical industry, zeolites are currently being investigated as catalysts for the manufacture of fine chemicals. New directions include the incorporation of redox metals and chiral centers either in the zeolite framework or as encaged extraframework species, which can lead to highly selective biomimetic solid catalysts.[1] Intrazeolite (catalytic) chemical processes are mediated, inter alia, by strong electrostatic fields acting inside the zeolite channels and by spatial restrictions imposed by the dimensions and topology of the intracrystalline void space. Electrostatic fields, created mainly by extraframework (exchangeable) cations, contribute to the formation of internal adducts with adsorbed molecules. The electron distributions of these molecules are thereby significantly modified, and this can lead ultimately to new reactivity patterns. Precise characterization of such intrazeolite species is a prime requirement to understanding chemical reactivity. Detailed knowledge of the interaction of CO with zeolites is also of considerable interest with regard to zeolite characterization, since CO is the most widely used probe molecule for IR spectroscopic investigations,[2] including determination of acidity and intrazeolite electrostatic fields. We report here on a variable-temperature (77 to 303 K) FT-IR study of CO adsorbed on Na-ZSM-5, which is a medium-pore zeolite having the MFI-type structure.[3] It is shown that CO can coordinate to Na^+ ions in two different modes: either through the C end or through the O end. Both adducts are in a temperature-dependent equilibrium which follows the van't Hoff relationship with a $\Delta H^{\ominus}$ value of 3.8 kJ mol^{-1}; the C-bonded adduct is the more stable species.

Interaction of CO at 77 K with extraframework alkali metal cations in zeolites is known to give rise to a main IR absorption band that is shifted to higher wavenumber with respect to the band for free CO (2143 cm^{-1}). In the case of M^+-ZSM-5 (M = Li, Na, K, Rb, Cs) this cation-specific high-frequency (HF) band appears at wavenumbers from 2188 cm^{-1} for Li^+ to 2157 cm^{-1} for Cs^+, and corresponds to the fundamental C–O stretching mode of CO perturbed by the electrostatic field created by cations in $M^+ \cdots$ CO species.[2, 4] A minor low-frequency (LF) band is also observed at 2108, 2113, 2117, 2119, and 2122 cm^{-1} for Li^+, Na^+, K^+, Rb^+, and Cs^+, respectively.[4, 5] Several authors have pointed out that this LF band could be assigned to the C–O stretching mode of $M^+ \cdots$ OC adducts.[6] It is clear that formation of such species would lead to a bathochromic shift of the C–O stretching frequency,[6, 7] but direct experimental proof of the correlation between HF and LF bands for adducts formed on the same cation was lacking so far. The question thus arises as to whether they reflect an isomerization equilibrium between C-bonded and O-bonded cation–CO adducts or whether they correspond to species formed on different sites. We show here that the first situation applies.

With an IR cell suitable for variable-temperature measurements, IR spectra of CO adsorbed on Na-ZSM-5 were taken between 77 K and room temperature; the IR cell was closed after dosing with CO. A selection of these spectra is depicted in Figure 1 a, b. All spectra show absorption bands at 2178

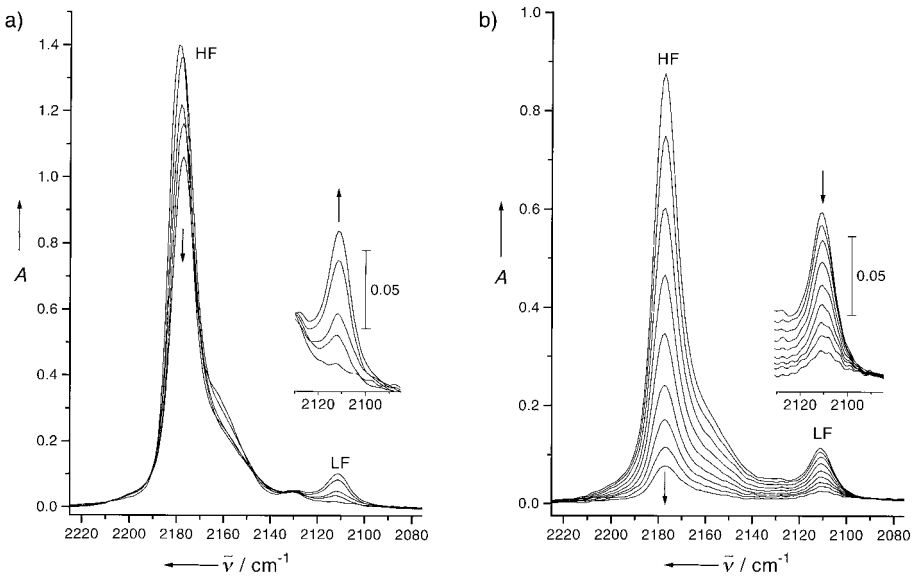


Figure 1. FTIR spectra of CO (ca. 0.8 Torr) adsorbed on Na-ZSM-5 at variable temperature. a) From top to bottom: 83, 133, 153, 183, and 203 K. b) From top to bottom: 223, 233, 243, 253, 263, 273, 283, 293, and 303 K. The inset shows an expanded view of the low-frequency bands.

(strong) and 2112 cm^{-1} (weak), which correspond to the aforementioned HF and LF bands, respectively. The small shoulder on the low-frequency side of the HF band is due mainly to a weak interaction of CO with silanol groups (and other spurious effects); its contribution was excluded when the integrated intensity was computed. A weaker feature centered at 2130 cm^{-1} is also observed in Figure 1 a, which corresponds to the ^{13}CO counterpart of the main band at 2178 cm^{-1}.

Correlation between the HF and LF bands is clearly shown in Figure 1 a: When the temperature is increased from 83 to

[*] Prof. C. Otero Areán, Dr. E. Escalona Platero
Departamento de Química
Universidad de las Islas Baleares
07071 Palma de Mallorca (Spain)
Fax: (+34) 971-173426
E-mail: dqueep0@ps.uib.es
Prof. A. A. Tsyganenko
Institute of Physics, St. Petersburg University (Russia)
Prof. E. Garrone, Prof. A. Zecchina
Dipartimento di Chimica Inorganica
Chimica Fisica e Chimica dei Materiali
Università di Torino (Italy)

 © WILEY-VCH Verlag GmbH, D-69451 Weinheim, 1998 1433-7851/98/3722-3161 $ 17.50+.50/0

203 K the intensity of the HF band decreases, whereas that of the LF band increases. At higher temperatures (Figure 1b) both bands decrease in intensity (because the net amount of adsorbed CO decreases), but the ratio of integrated intensities A_{LF}/A_{HF} increases over the whole temperature range. This behavior can only be explained in terms of an equilibrium between C-bonded and O-bonded species, as described by Equation (1); Z represents the zeolite framework. The intensity ratio A_{LF}/A_{HF} should be proportional to the equilibrium constant K through the corresponding ratio of extinction coefficients $\varepsilon_{LF}/\varepsilon_{HF}$. When the van't Hoff Equation (2) is applied for constant values of $\Delta H^{\ominus}$ and $\Delta S^{\ominus}$ [8] over the whole temperature range (83–303 K), an almost perfect linear plot of $\ln(A_{LF}/A_{HF})$ versus $1/T$ is obtained (Figure 2).

$$Z{-}Na^{+}\cdots CO \rightleftharpoons Z{-}Na^{+}\cdots OC \quad (1)$$

$$\ln K = -\Delta H^{\ominus}/RT + \Delta S^{\ominus}/R \quad (2)$$

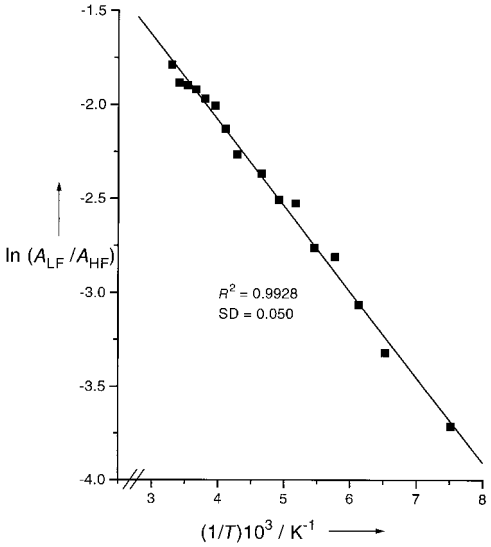


Figure 2. The van't Hoff plot of the natural logarithm of the intensity ratio of LF and HF bands versus the reciprocal of the temperature between 133 and 303 K.

From this linear plot, the resulting enthalpy change $\Delta H^{\ominus}$ for the process in Equation (1) is 3.8 kJ mol^{-1}. The enthalpy difference at 0 K between C-bonded and O-bonded species has been evaluated by means of quantum chemical calculations for adducts of CO containing both the bare Na^+ cation and the $[HAl(OH)_3]^-Na^+$ cluster;[6c, e] the values are 10.9 and 5.6 kJ mol^{-1}, respectively (the C-bonded species always shows the higher interaction energy). The experimental value reported here (3.8 kJ mol^{-1}) is even lower than that for the model cluster, thus showing that the zeolite framework reduces the difference in stability between C-bonded and O-bonded adducts.

The hypsochromic frequency shift of adsorbed CO with respect to the value for the free molecule (2143 cm^{-1}) gives a measure of the effective electric field near the Na^+ ion. If this shift is assigned to the vibrational Stark effect, a simple electrostatic model leads to $\Delta\tilde{\nu} = k_{ST}E$, where k_{ST} is the vibrational Stark constant for the CO molecule and E the electric field strength.[9] With $k_{ST} = 4.29 \times 10^{-9}$ cm^{-1} V^{-1} m,[10] the observed value $\Delta\tilde{\nu} = 35$ cm^{-1} (for the C-bonded adduct) yields $E = 8.2$ V nm^{-1}. More refined quantum chemical calculations lead to $E = 6.3$ V nm^{-1} for the same value of $\Delta\tilde{\nu}$.[6c, 11] In such a field, the estimated energy difference between the two orientations of the CO dipole (0.1098 D) is 2.8 to 3.6 kJ mol^{-1}, which is in fair agreement with the measured value of 3.8 kJ mol^{-1}.

Hydrogen-bonded $OC\cdots HF$ and $CO\cdots HF$ complexes similar to those described here have been obtained by UV photofragmentation of matrix-isolated formyl fluoride;[12] they showed C–O stretching bands at 2162 and 2129 cm^{-1}. The enthalpy difference at 20 K between these hydrogen-bonded isomers was estimated to be $\Delta H^{\ominus} = 0.3$ kJ mol^{-1}.[12] In a recent theoretical analysis, Lupinetti et al.[13] found a shortening of the C–O bond length (relative to that in free CO) in HCO^+ and a lengthening in COH^+. They ascribed these effects to a change in the polarization of the CO bonding orbitals induced by the positive charge of the proton. These variations in C–O bond length give rise to changes in vibration frequency.

The intercept of the straight line in Figure 2 with the vertical axis (at $1/T = 0$) is at -0.26. Since the computational estimate for $\Delta S^{\ominus}$ (in units of R) is two orders of magnitude smaller,[6c, e] we assume that $\Delta S^{\ominus}$ for the process in Equation (1) is negligible and ascribe the above intercept to the different values of ε_{LF} and ε_{HF}; it follows that $\varepsilon_{LF}/\varepsilon_{HF} = 0.8$. This is at variance with computational estimates, which suggest that coordination through the oxygen atom intensifies the fundamental C–O stretching mode, while the opposite applies to coordination through the carbon atom.[5]

Similar experiments carried out on other zeolite/CO systems have shown that equilibrium between C-bonded and O-bonded species occurs in all cases. For instance, in the case of CO adsorbed on faujasite-type Na-Y the HF and LF bands were found at 2170 and 2122 cm^{-1}, respectively, while for Ca-Y the corresponding values are 2198 and 2094 cm^{-1}. The different wavenumber values for Na-ZSM-5 and Na-Y show the influence of the zeolite framework. The full set of results (which is currently being analyzed) will be published shortly. Note that equilibrium between C-bonded and O-bonded species may have notable consequences on (catalytic) processes occurring in zeolites and involving CO, and it might also apply to other adsorbed species which could have their electron distribution modified in different ways depending on their interaction mode with cationic centers. We hope this work will encourage the investigation of similar amphipathic behavior of other heteroatomic molecules adsorbed (or encaged) in zeolites.

Experimental Section

The Na-ZSM-5 zeolite (Si/Al = 17) was synthesized following standard hydrothermal methods.[14] Powder X-ray diffraction showed good crystallinity and absence of any diffraction lines not assignable to the MFI-type structure. For IR studies, a thin self-supported wafer was prepared and activated in a dynamic vacuum (residual pressure less than 10^{-4} Torr) for 2 h at 680 K inside an IR cell which allowed in situ high-temperature activation, gas dosage, and variable-temperature measurements to be

 © WILEY-VCH Verlag GmbH, D-69451 Weinheim, 1998 1433-7851/98/3722-3162 $ 17.50+.50/0 *Angew. Chem. Int. Ed.* **1998**, *37*, No. 22

carried out. Details on the design and performance of this home-made IR cell are given elsewhere.[15] For better thermal contact between the zeolite wafer and the cooled environment, helium (about 0.5 Torr) was admitted into the sample compartment before the background spectrum was recorded at 77 K (liquid nitrogen). Then CO was dosed to an equilibrium pressure of about 0.8 Torr, and IR spectra were measured at 77 K and on gradual heating of the IR cell after evaporation of liquid nitrogen. Reversibility of the IR spectra was checked by cooling again after the spectrum at 303 K was taken, thus proving that the observed spectral changes are due solely to temperature variation and not to any (unexpected) alteration of the system upon heating. The temperature was measured by means of a platinum resistance thermometer; the accuracy was about ± 5 K. Transmission IR spectra were recorded at a resolution of 3 cm^{-1} with a Bruker IFS66 FTIR spectrometer. The spectrum of zeolite taken before dosage with CO was used as a background; this background spectrum was subtracted from all spectra shown in this work.

Received: May 6, 1998 [Z11825IE]
German version: *Angew. Chem.* **1998**, *110*, 3350 – 3353

Keywords: adsorption · carbon monoxide · heterogeneous catalysis · IR spectroscopy · zeolites

[1] See: J. M. Thomas, *Angew. Chem.* **1994**, *106*, 963 – 989; *Angew. Chem. Int. Ed. Engl.* **1994**, *33*, 913 – 937; P. B. Venuto, *Microporous Mater.* **1994**, *2*, 297 – 411; C. B. Dartt, M. E. Davis, *Catal. Today* **1994**, *19*, 151 – 186; I. W. C. E. Arends, R. A. Sheldon, M. Wallau, U. Schuchardt, *Angew. Chem.* **1997**, *109*, 1190 – 1211; *Angew. Chem. Int. Ed. Engl.* **1997**, *36*, 1144 – 1163.
[2] Review: A. Zecchina, C. Otero Areán, *Chem. Soc. Rev.* **1996**, *25*, 187 – 197.
[3] W. M. Meier, D. H. Olson, *Atlas of Zeolite Structure Types*, Butterworth-Heinemann, London, **1992**.
[4] A. Zecchina, S. Bordiga, C. Lamberti, G. Spoto, L. Carnelli, C. Otero Areán, *J. Phys. Chem.* **1994**, *98*, 9577 – 9582.
[5] P. Ugliengo, E. Garrone, A. M. Ferrari, A. Zecchina, C. Otero Areán, *J. Phys. Chem.*, submitted.
[6] a) H. Böse, H. Förster, *J. Mol. Struct.* **1990**, *218*, 393 – 398; b) M. Katoh, T. Yamazaki, S. Ozawa, *Bull. Chem. Soc. Jpn.* **1994**, *67*, 1246 – 1253; c) A. M. Ferrari, P. Ugliengo, E. Garrone, *J. Chem. Phys.* **1996**, *105*, 4129 – 4139; d) G. Turnes Palomino, C. Otero Areán, F. Geobaldo, G. Ricchiardi, S. Bordiga, A. Zecchina, *J. Chem. Soc. Faraday Trans.* **1997**, *93*, 189 – 191; e) A. M. Ferrari, K. M. Neyman, N. Rösch, *J. Phys. Chem.* **1997**, *101*, 9292 – 9298.
[7] N. S. Hush, M. L. Williams, *J. Mol. Spectrosc.* **1974**, *50*, 349 – 368.
[8] The results of computations on naked cations indicate that the difference in the specific heat between C-bonded and O-bonded adducts is negligible,[5, 6c] so that the assumption usually made leading to Equation (2) that $\Delta C_p^\circ = 0$ is fully justified.
[9] Yu. A. Tsyganenko, A. A. Tsyganenko, K. S. Smirnov, *Vib. Spectrosc.* **1993**, *6*, 15 – 23; Yu. A. Tsyganenko, V. A. Ermoshin, M. R. Keyser, K. S. Smirnov, A. A. Tsyganenko, *Vib. Spectrosc.* **1996**, *13*, 11 – 22.
[10] D. K. Lambert, *Solid State Commun.* **1984**, *51*, 297 – 300.
[11] G. Pacchioni, G. Cogliandro, P. S. Bagus, *Int. J. Quant. Chem.* **1992**, *42*, 1115 – 1139.
[12] G. Schatte, H. Willner, D. Hoge, E. Knözinger, O. Schrems, *J. Phys. Chem.* **1989**, *93*, 6025 – 6028.
[13] A. J. Lupinetti, S. Fau, G. Frenking, S. H. Strauss, *J. Phys. Chem. A* **1997**, *101*, 9551 – 9559.
[14] R. Szostak, *Molecular Sieves*, Van Nostrand Reinhold, New York, **1989**.
[15] M. A. Babaeva, D. S. Bystrov, A. Yu. Kovalgin, A. A. Tsyganenko, *J. Catal.* **1990**, *123*, 396 – 416.

Long-Range N → Si Interactions in Organosilicon Compounds with Hepta- and Octacoordinate Silicon Centers

Hans Bock,* Zdenek Havlas, and Volker Krenzel

Dedicated to Professor Corriu

Si centers in organosilicon compounds exhibit coordination numbers between 1 and 10,[1] and the resulting distances vary over wide ranges as exemplified by the interaction N → Si in 1-amino-8-silylnaphthalene derivatives[2, 3] (Figure 1). The

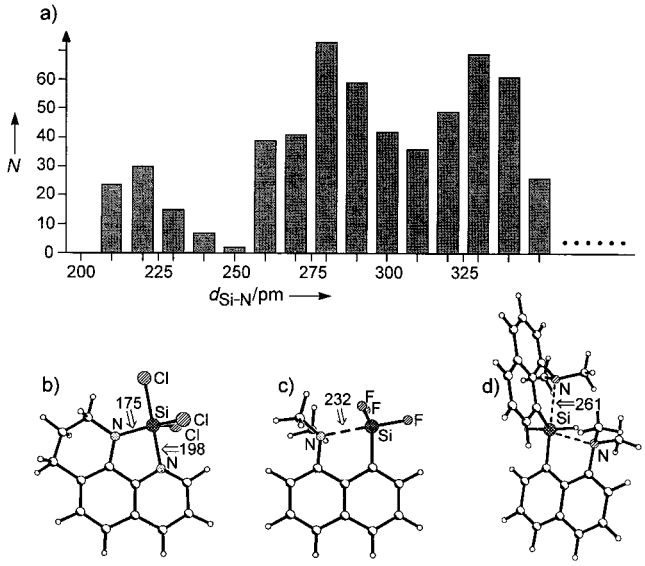


Figure 1. Differences in various Si – N bond lengths: a) histogram for the range between 200 and 350 pm, as revealed by a search in the Cambridge Structural Database, in which *N* is the number of hits within 10 pm ranges, and selected examples of Si – N interactions in 1-amino-8-silylnaphthalene derivatives (b, c), in which N ··· Si distances longer than 275 pm are also observed (d).

Cambridge Structural Database contains a total of 574 entries for d_{Si-N} distances greater than 200 pm (Figure 1a). The range of shorter interactions are assigned to so-called "SiN single bonds" such as in sitrol (Figure 1b). The compounds with SiN distances between 220 and 260 pm (Figure 1c and d)[3c,d] have repeatedly been defined as intramolecular donor – acceptor complexes. What type of interaction is, however, represented by the numerous distances Si ··· N exceeding 275 pm? Two selected structures with Si coordination numbers of 7[4] and 8[5]

[*] Prof. Dr. H. Bock, Dipl.-Chem. V. Krenzel
Institut für Anorganische Chemie der Universität
Marie-Curie-Straße 11, D-60439 Frankfurt am Main (Germany)
Fax: (+49) 69-798-29188
Dr. Z. Havlas,
Institute of Organic Chemistry and Biochemistry of the
Czech Academy of Sciences
Flemingovo nam 2, CZ-11610 Prague (Czech Republic)

[**] Molecular Interactions in Crystals, Part 145. This project was supported by the Hoechst AG, the Deutschen Forschungsgemeinschaft, the State of Hesse, the Fonds der Chemischen Industrie, and the Höchstleistungs-Rechenzentrum Stuttgart. Part 144: H. Bock, N. Nagel, *Z. Naturforsch. B.* **1998**, *53*, 805.

will be discussed here in detail, based on density functional theory (DFT) calculations.[6]

Tris[(2-dimethylaminomethyl)phenyl]silane, prepared by reaction of trichlorosilane with three equivalents of [(2-dimethylaminomethyl)phenyl]lithium, contains a formally sevenfold coordinated silicon center. Its structure determination[4] yields intramolecular Si–N distances of between 298.1(6) and 304.3(6) pm for both independent molecules in the crystal (Figure 2a). The energy of the Si–N interactions

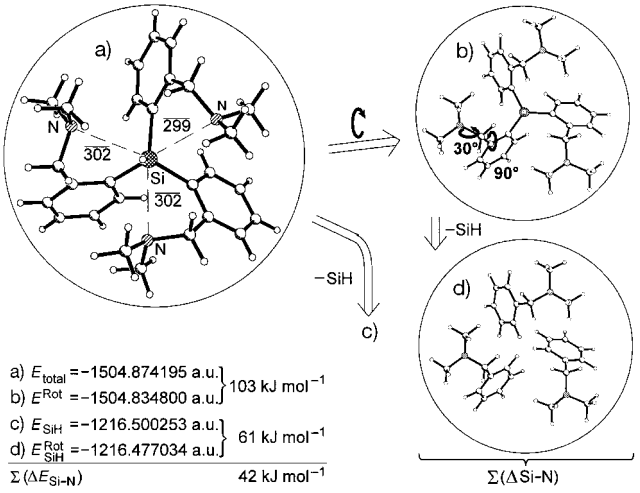


Figure 2. Density functional theory calculated[6] total energies for tris[(2-dimethylamino)methylphenyl]silane[4] a) based on its structural parameters, b) after twisting its three $H_4C_6-CH_2$ bonds by $\omega_1 = 90°$ as well as the H_2C-N bond by $\omega_2 = 30°$, and c) and d) after removal of the central SiH_2 subunit from the structures a) and b), respectively, accompanied by H saturation of the ruptured bonds of the phenyl substituents (see text).

can be approximated as follows:[6] The vector of each nitrogen electron pair, which deviates by 23° from its idealized SiN bond axis (Figure 2a), is twisted perpendicular to this axis under continuous structure control to avoid additional severe overlap of the substituents within the molecule (Figure 2b). The energy difference due to the inevitably varied van der Waals contacts in the periphery of the molecule is calculated after removal of the central SiH group accompanied by H saturation of the ruptured bond of each phenyl substituent (Figures 2c and d) to be about 60 kJ mol^{-1}. The sum of all DFT-calculated energy contributions for a rotation of the three N vectors out of their SiN axis positions between the Si centers that are at first seven- and finally four-coordinate amounts to $\Delta\Delta H_f(Si-N) = 42$ kJ mol^{-1} or to about 14 kJ mol^{-1} for a cooperation-free SiN interaction over a distance of about 300 pm (Figure 2).

Bis [2,6-bis(dimethylaminomethyl)phenyl]silane, the second selected "hypercoordinate" organosilicon compound, is prepared by treating 2,6-bis(dimethylaminomethyl)phenylsilane with an equimolar amount of 2,6-bis(dimethylaminomethyl)phenyllithium. Its structure determination[5] proves a formally eight-coordinate silicon center and exhibits intramolecular distances of 289.5(5) and 311.7(6) pm for the two different N→Si interactions between the two pairs of amino-N centers and the Si centers in the differently overcrowded halves (Figure 3a). The two types of N→Si interactions,

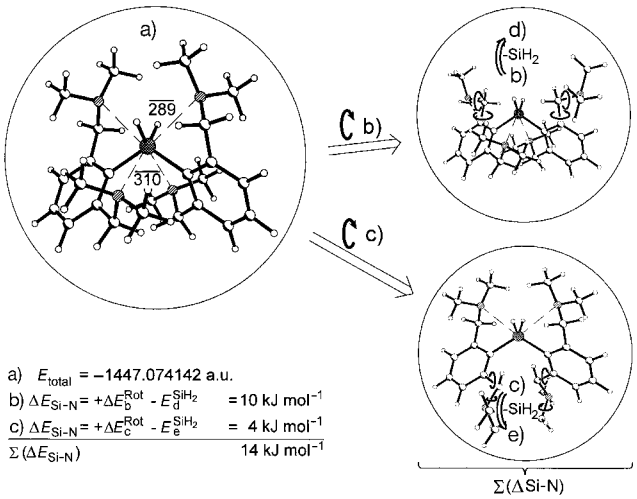
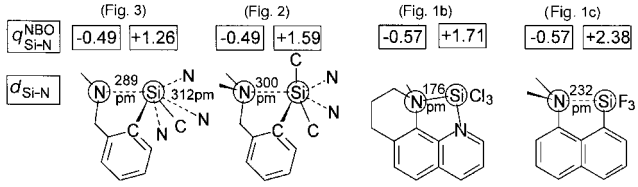


Figure 3. Density functional theory calculated[6] total energies for bis[2,6-bis(dimethylamino)methylphenyl]silane[5] a) based on its structural parameters, b) after twisting of the 289 pm distant or c) the 310 pm distant $(H_3C)_2N$ substituent groups by angles $\omega(H_3C_6-CH_2) = 120°$ as well as $\omega(H_2C-N(CH_3)_2) = 30°$, and d,e) after removal of the central SiH_2 unit accompanied by H saturation of the phenyl substituents starting from the structures in (b) and (c), respectively (see text).

which vary by 21 pm in length (Figure 3a) are approximated analogously to the ones in the seven-coordinate compound, but separately: altogether four rotations around the $H_3C_6-CH_2$ and $H_2C-N(CH_3)_2$ bonds (Figure 2b and c) turn the nitrogen electron pairs of the $(H_3C)_2N$ substituents perpendicular to the structurally characterized SiN connecting axes. The resulting van der Waals perturbations in the molecular periphery are approximated by two additional DFT calculations[6] after removal of the central SiH_2 group and H saturation of the phenyl substituents (Figures 2d and e). The energy contributions calculated for the interactions over the shorter and the longer SiN distances of $10 + 4 = 14$ kJ mol^{-1} (limit of deviation ± 2 kJ mol^{-1} [6]) differ predominantly because of the individual van der Waals wrapping of the two molecular halves.

Altogether three different long-range N→Si interactions in two organosilicon molecules containing seven- or eight-coordinate Si centers have been approximated by density functional theory calculations [6] (Schemes 1 and 2). The DFT charge densities q^{NBO}_{Si-N} resulting from "Natural Bond Orbital" analysis are complemented by those for 1-dimethylamino-8-trichlorosilylnaphthalene (sitrol, Figure 1b) and -trifluorosilylnaphthalene (Scheme 1). As can be seen from the data, the calculated DFT/NBO charge densities do not correlate with the experimental bond distances d_{Si-N}. Details such as the

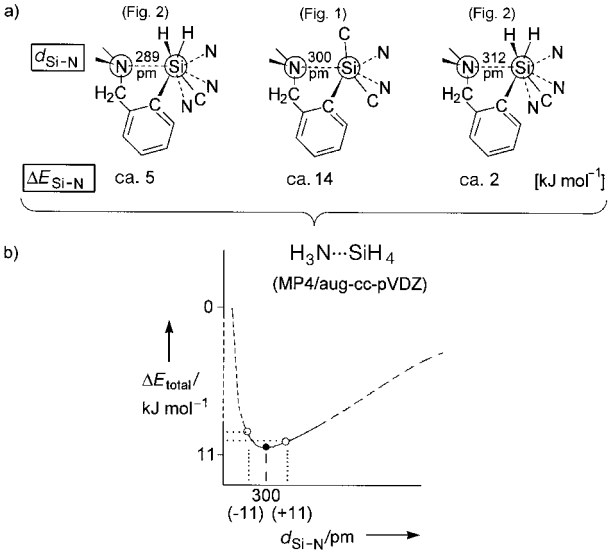


Scheme 1. DFT/NBO charge densities for N→Si interactions at distances of 176 and 300 pm in amino-organosilyl compounds with Si coordination numbers between 5 and 8.

 © WILEY-VCH Verlag GmbH, D-69451 Weinheim, 1998 1433-7851/98/3722-3164 $ 17.50+.50/0 *Angew. Chem. Int. Ed.* **1998**, *37*, No. 22

increase in positive charge at the Si center especially on substitution of F for Cl (Figure 1b and c) can be rationalized by the sequence of effective nuclear charges: Si < Cl < N < F. In the aminosilyl compounds with higher coordination numbers for Si (Figures 2 and 3), the charge density at the Si centers is lowered slightly as the number of SiN interactions increase, whereas that of the N centers remains constant.

The energy differences ΔE_{Si-N} estimated by DFT calculations (Figures 2 and 3) also cannot be correlated (directly) with the bond lengths d_{Si-N} (Scheme 2a). To test nonlinear



Scheme 2. Energies of N→Si interactions: a) DFT-estimated contributions based on the crystal structures of the amino.organosilyl compounds investigated with seven- and eight-coordinate Si centers; b) total energy potential curve for the model adduct $H_3N \rightarrow SiH_4$, calculated with basis sets aug-cc-pVDZ using MP2 correlation for the geometry optimization and MP4 correlation for all single point calculations.[7]

correlation and also to further support the relatively small DFT energy differences ΔE_{Si-N} (Scheme 2a), correlated calculations with large double-zeta basis sets at MP2 as well as MP4 levels have been performed for the simplest model adduct $H_3N \rightarrow SiH_4$.[7] The resulting geometry-optimized potential curve shows a minimum of -11 kJ mol^{-1} at 300 pm (Scheme 2b), which corresponds to the $\Delta E_{Si-N} \approx 14$ kJ mol^{-1} contribution estimated for the N→Si interaction at a distance of 300 pm (Scheme 2a). Remarkably, both the higher ($\Delta E_{Si-N} \approx 5$ kJ mol^{-1} for $d_{Si-N} = 289$ pm) as well as the lower value ($\Delta E_{Si-N} \approx 5$ kJ mol^{-1} for $d_{Si-N} = 312$ pm) follow the prediction of the potential curve: the first is shifted by 11 pm from the minimum towards the steeper slope (→repulsive interaction) and the other 11 pm towards the flatter part (→dissociative interaction) of the potential curve. The rather small DFT energy differences (estimated deviation limit ± 2 kJ mol^{-1})[6] are, therefore, convincingly confirmed by the nonlinear correlation (Scheme 2b).

The following comments on SiN bond lengths, discussed over a range of 312 − 176 = 126 pm (!), are based on additional assumptions: The shortest bond length of 176 pm in the trichlorosilyl compound sitrol (Figure 1b) might be favored for steric reasons by the undulated perhydropyridine ring, whereas for the longest bond lengths between 289 and 312 pm the minimum on the distance-dependent potential curve (Scheme 2b) can explain the DFT-calculated results for the experimentally determined structures. Again, however, we draw attention to the spatial overcrowding in the hypercoordinate aminosilyl compounds investigated (Figures 2 and 3), which causes numerous van der Waals contacts in the molecular periphery that are presumably bonding because of the considerable positive charge at their Si centers (Scheme 1). For a tentative answer concerning the possible origin of bonding in long range N···Si interactions, the pure electrostatic attraction between charges q_{Si} of +1.6 and q_N of −0.5 at 300 pm distance has been estimated to be about 60 kJ mol^{-1}. Accordingly, a proposal of Coulomb-dominated donor–acceptor bonding is forwarded for these special hypercoordinate N···Si compounds.

In conclusion the importance of long-range interactions for the chemist is emphasized—from the crystal growth[10, 11] to protein structures.[12] Therefore, an extension of the DFT calculations presented to other systems and especially those with Si···O interactions, which differ even more in their effective nuclear charges, is envisaged.

Received: February 13, 1998
Supplemented version: May 18, 1998 [Z11477IE]
German version: *Angew. Chem.* **1998**, *110*, 3305–3307

Keywords: density functional calculations · donor–acceptor systems · hypercoordinate compounds · silicon

[1] H. Bock, *Angew. Chem.* **1989**, *101*, 1659; *Angew. Chem. Int. Ed. Engl.* **1989**, *28*, 1627.
[2] See, for example, a) W. Sheldrick in *The Chemistry of Organosilicon Compounds* (Eds.: S. Patai, Z. Rappoport), Wiley, Chichester, **1989**, pp. 227–303; b) R. J. P. Corriu, J. C. Young in *The Chemistry of Organosilicon Compounds* (Eds.: S. Patai, Z. Rappoport), Wiley, Chichester, **1989**, pp. 1241 - 1288.
[3] a) Cambridge Structural Database (Version 5.10); b) G. Klebe, J. W. Bats, H. Fuess, *J. Am. Chem. Soc.* **1984**, *106*, 5202; c) F. Carré, R. J. P. Corriu, A. Kroton, M. Poirier, G. Royo, Y. C. Young, C. Belin, *J. Organomet. Chem.* **1994**, *470*, 43; d) C. Brelière, F. Carré, R. J. P. Corriu, G. Royo, M. W. C. Man, *Organometallics* **1994**, *13*, 307.
[4] N. Auner, R. Probst, F. Hahn, E. Herdtweck, *J. Organomet. Chem.* **1993**, *459*, 25, and references therein.
[5] F. Carré, C. Chuit, R. J. P. Corriu, A. Mehdi, C. Reyé, *Angew. Chem.* **1994**, *106*, 1152; *Angew. Chem. Int. Ed. Engl.* **1994**, *93*, 1097, and references therein.
[6] The density functional theory calculations have been performed based on the experimental structural data[4, 5] using the program Gaussian 94 (Revision E.2, authors: M. J. Frisch, G. W. Trucks, H. B. Schlegel, P. M. W. Gill, B. G. Johnson, M. A. Robb, J. R. Cheeseman, T. Keith, G. A. Petersson, J. A. Montgomery, K. Raghavachari, M. A. Al-Laham, V. G. Zakrzewski, J. V. Ortiz, J. B. Foresman, J. Cioslowski, B. B. Stefanov, A. Nanayakkara, M. Challacombe, C. Y. Peng, P. Y. Ayala, W. Chen, M. W. Wong, J. L. Andres, E. S. Replogle, R. Gomperts, R. L. Martin, D. J. Fox, J. S. Binkley, D. J. Defrees, J. Baker, J. P. Stewart, M. Head-Gordon, C. Gonzales, J. A. Pople, Gaussian Inc., Pittsburgh, PA, **1995**). For *Density Functional Theory B3LYP* see a) A. D. Becke, *J. Chem. Phys.* **1993**, *98*, 5648; b) C. Lee, W. Yang, R. G. Paar, *Phys. Ber. B* **1988**, *37*, 785; c) B. Miehlich, A. Sariu, H. Stoll, H. Preuss, *Chem. Phys. Lett.* **1989**, *157*, 200. The calculations with 6–31G* basis sets (W. J. Hehre, R. Ditchfield, J. A.

 © WILEY-VCH Verlag GmbH, D-69451 Weinheim, 1998 1433-7851/98/3722-3165 $ 17.50+.50/0

Pople, *J. Chem. Phys.* **1972**, *56*, 2257; M. S. Gordon, *Chem. Phys. Lett.* **1980**, *76*, 163) were carried out on the super-computer NEC-SX4 of the Höchstleistungs-Rechenzentrum Stuttgart. The starting point was the structure coordinates of the two compounds (Figure 1a and 2a), in which the vectors of the electron pairs on N were turned perpendicular to the connecting axes SiN while controlling the interatomic distances on-line to minimize additional structural changes (Figures 1b and 2b, c). Removal of the molecular Si centers (SiH or SiH_2) by H saturation of the ruptured bonds of the substituent groups (Figures 1c, d and 2d, e) allows an estimate of the van der Waals energy changes in the periphery of the molecule. After subtraction of the total energy from these estimations (Figures 1a and 2a), approximate sums of the energy contributions due to the long-range SiN interactions result. The accuracy of the B3LYP procedure has been statistically evaluated for relative energies to be about 0.4 kcal mol^{-1} (J. B. Foresmanm, A. Frisch in "Exploring Chemistry with Electronic Structure Methods", 2nd ed., GAUSSIAN Inc., Pittsburg, **1996**), and, therefore, deviations of only 1–2 kJ mol^{-1} are assumed for the basis sets used. In addition, substantial changes in the Si tetahedral geometry due to N→Si hyperconjugation can be excluded by comparison with the average bond angle $\varphi(CSiC) = 111^\circ$ in triphenylsilane (J. Allemand, R. Gerdi, *Cryst. Struct. Commun.* **1979**, *8*, 927): both the smaller average angle of 108° in the compound with the seven-coordinate Si center (Figure 2) as well as the larger one of 113° for eightfold coordination (Figure 3) can be straightforwardly rationalized by the different central SiH or SiH_2 units and the phenyl group substituents of considerably different bulk.

[7] The total energy potential curve for the model adduct chosen, H_3NA, has been calculated using fourth-order Møller-Plesset perturbation theory (MP4) and a correlation consistent basis set with polarized valence "double-zeta" functions(aug-cc-pVDZ) (D. E. Woon, T. H. Dunning, Jr., *J. Chem. Phys.* **1993**, *98*, 1358; R. A. Kendall, T. H. Dunning Jr., R. J. Harrison, *J. Chem. Phys.* **1992**, *96*, 6796). The same basis set also was employed in the geometry optimization at the MP2 level.

[8] a) A. Schäfer, M. Weidenbruch, K. Peters, H. G. von Schnering, *Angew. Chem.* **1984**, *96*, 311; *Angew. Chem. Int. Ed. Engl.* **1984**, *23*, 302; b) M. Weidenbruch, B. Flintjer, K. Peters, H. G. von Schnering, *Angew. Chem.* **1986**, *98*, 1090; *Angew. Chem. Int. Ed. Engl.* **1986**, *25*, 1129.

[9] H. Bock, J. Meuret, K. Ruppert, *Angew. Chem.* **1993**, *105*, 413; *Angew. Chem Int. Ed. Engl.* **1993**, *32*, 414; see also H. Bock, J. Meuret, C. Näther, K. Ruppert, *Organosilicon Chemistry – From Molecules to Materials*, VCH, Weinheim, **1994**, p. 11.

[10] "The Crystal as a Supramolecular Entity" in *Perspectives in Supramolecular Chemistry*, *Vol. 2* (Ed.: G. R. Desiraju), Wiley, Chichester, **1995**.

[11] H. Bock, Z. Havlas, A. Rauschenbach, C. Näther, M. Kleine, *Chem. Commun.* **1996**, 1529; see also: H. Bock, N. Nagel, A. Seibel, *Liebigs Ann.* **1997**, 2151.

[12] G. A. Jeffrey, W. Saenger, *Hydrogen Bonding in Biological Structures*, Springer, Berlin, **1991**.

[13] N. W. Mitzel, U. Losehand, *Angew. Chem.* **1997**, *109*, 2897; *Angew. Chem. Int. Ed. Engl.* **1997**, *36*, 2807.

Synthesis of Immobilized CMP-Sialic Acids and Their Enzymatic Transfer with Sialyltransferase**

Yasuhiro Kajihara,* Takashi Ebata, and Hisashi Kodama

The enzymatic synthesis of oligosaccharides and their analogues with glycosyltransferases (GTases) has progressed remarkably as a result of the ability to synthesize the donor substrates.[1] Sialyltransferase (STase)[2] and fucosyltransferase[3] reactions have also been used to study the structure and function of oligosaccharides on glycoproteins and on cell surfaces by use of modified sugar nucleotides. We have developed a concise synthetic method for the preparation of CMP-sialic acid (CMP-*N*-acetylneuraminic acid, CMP-NeuAc; CMP = cytidinmonophosphate) and its analogues.[4] Since then we have begun investigating possible applications of STase reactions with use of synthetic CMP-NeuAc analogues (Figure 1).

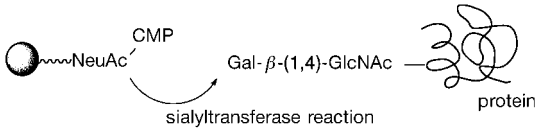


Figure 1. Schematic representation of the novel immobilization method for glycoproteins.

Many enzymes and lectins are glycoproteins containing N- or O-linked oligosaccharides. When these proteins have several oligosaccharides on their surfaces, this layer of oligosaccharides exhibits dynamic fluctuation.[5] Therefore, increasing the number of oligosaccharide chains also increases the surface area covered. With most immobilization methods[6] used for such glycoproteins, this carbohydrate layer hinders the approach to the amino or carboxyl groups on the surface of the protein. Unfortunately, if the reagent attaches to amino acids located close to the catalytic site, the immobilized enzyme may lose its activity. Therefore, we wanted to synthesize a CMP-NeuAc derivative in which the 9″-position is attached to the solid phase, and examine its sialyltransfer ability as part of a novel immobilization procedure. The nonreducing end of oligosaccharides are frequently galactosides which serve as acceptors in STase

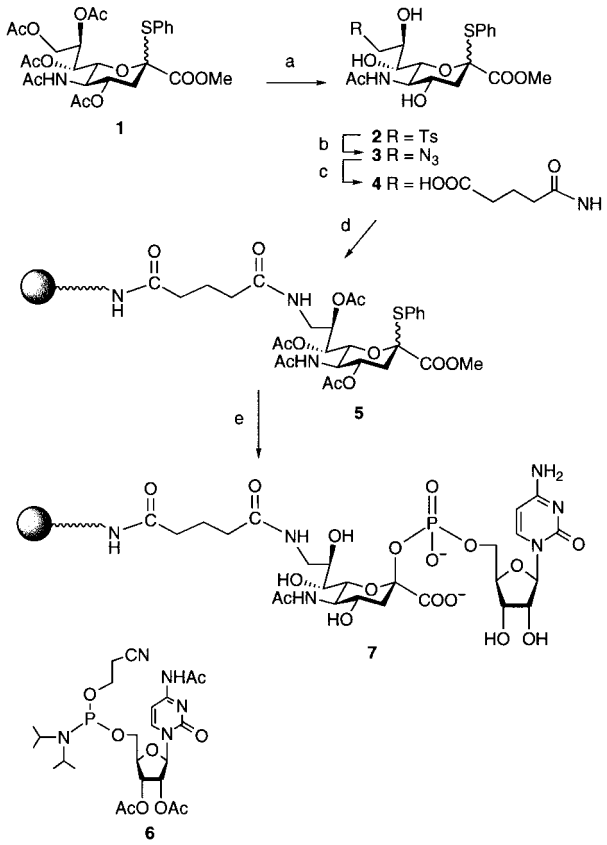
[*] Dr. Y. Kajihara
Department of System Function, Faculty of Science
Yokohama City University
22-2, Seto, Kanazawa-ku, Yokohama, 236-0027 (Japan)
Fax: (+81) 45-787-2370
E-mail: kajihara@yokohama-cu.ac.jp
Further address: Dr. Y. Kajihara, Dr. T. Ebata, Dr. H. Kodama
Life Science Research Laboratry
Japan Tobacco Inc.
6-2 Umegaoka, Aoba-ku, Yokohama 227-0052 (Japan)

[**] We are grateful to Dr. James C. Paulson (Cytel corporation) for a generous gift of α-(2→3)-sialyltransferase. We thank Dr. Hajime Matsushita and Dr. Koshi Koseki (Life Science Research Laboratory, Japan Tobacco Inc.) for helpful discussions and encouragement. We also thank Mr.Masayosi Kusama for the mass spectroscopic analyses (Japan Tobacco Inc.).

 © WILEY-VCH Verlag GmbH, D-69451 Weinheim, 1998 1433-7851/98/3722-3166 $ 17.50+.50/0

reactions. If STase successfully catalyzes the transfer of immobilized NeuAc to these terminal galactosides, a novel and mild immobilization method will have been discovered. Such a method would have two advantages. First, since the STase reaction generally occurs at the galactosides most remote from the protein, the immobilization reaction should smoothly occur in an area which avoids the steric hindrance of the carbohydrate layer. Second, since sialylation of galactosides at the nonreducing end of bioactive glycoproteins or enzymes may not depend on their activity in vitro,[7] sialoside can be used as a new type of linker between bioactive glycoproteins and the solid-phase support.

Here we report the solid-phase synthesis of CMP-NeuAc and its transfer reaction to both a corresponding oligosaccharide acceptor and an asialoglycoprotein (that is, a nonsialylated glycloprotein). The chemical synthesis of immobilized CMP-NeuAc is shown in Scheme 1. The NeuAc **4**,[8] which is modified in the 9-position and can be obtained by conventional methods from **1**,[9] was coupled with long-chain alkylamino controlled pore glass (CPG, Sigma).[10] The residual amino functionalities on the CPG were then capped by acetylation. Quantification by the periodate/resorcinol method[11] after O-deacetylation and saponification of **5** indicated 576 nmol of the immobilized NeuAc derivative per 1 g of CPG. By our previously developed method[4] the immobilized NeuAc **5** was converted into immobilized CMP-NeuAc **7**, which was identified by comparison of its ^{31}P NMR[12] spectrum with that of CMP-NeuAc (Figure 2).



Scheme 1. a) 1. NaOMe, MeOH, 25 °C; 2. TsCl, py, 25 °C, 48 % (2 steps); b) NaN_3, DMF, 80 °C, 92 %; c) 1. H_2S, py/NEt_3/H_2O (5/1/2), 25 °C; 2. glutaric anhydride, MeOH, 25 °C, 83 %, (2 steps); d) 1. CPG, 1-ethyl-3-(3-diaminopropyl)carbodiimide (HCl salt), NEt_3, DMF, 25 °C; 2. Ac_2O, py, DMAP, 25 °C, 3 – 5 % (estimated by the periodate/resorcinol method); e) 1. NBS, acetone/H_2O (10/1), 25 °C; 2. **6**, 1*H*-tetrazole, MeCN, 25 °C; 3. *t*BuOOH, MeCN, 25 °C; 4. DBU, THF, 25 °C; 5. NaOMe, MeOH/H_2O (2/1), 25 °C. Ts = *p*-toluenesulfonyl; py = pyridine; DMAP = 4-dimethylaminopyridine; NBS = *N*-bromosuccinimide; DBU = 1,8-diazabicyclo[5.4.0]undec-7-ene.

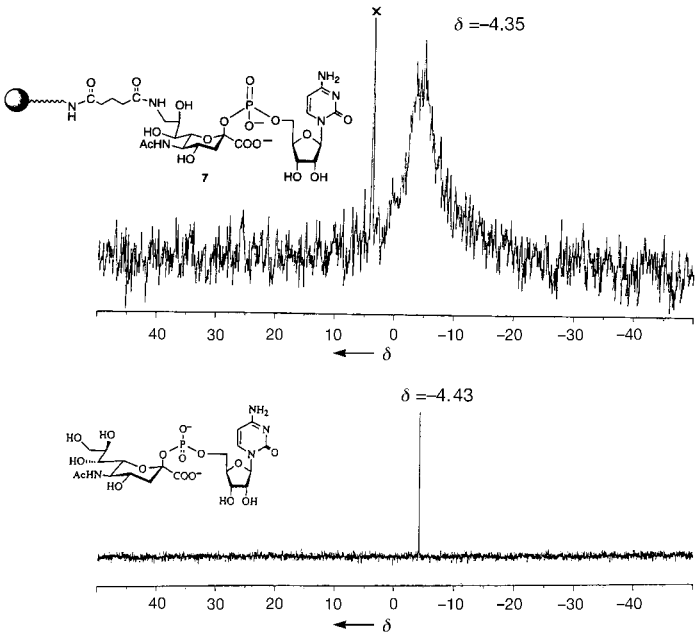


Figure 2. ^{31}P NMR spectra of immobilized CMP-NeuAc **7** (top) and CMP-NeuAc (bottom). X: impurity.

The transfer assay[13] was performed in a solution of HEPES buffer containing **7**, [U-^{14}C]-Gal-β-(1 →4)-GlcNAcβ-OMe([^{14}C]-LacNAc[14]), BSA (bovine serum albumin), and STase. If the immobilized NeuAc was transferred to [^{14}C]-LacNAc, sialyl-[^{14}C]-LacNAc formed on the surface of CPG. After incubation at 37 °C, isotope counts on CPG were measured with a liquid scintillation counter.[15] For the transfer reaction, we used both enzymes α-(2 →3)-STase (3STase, EC 2.4.99.6, Cytel) and α-(2 →6)-STase (6STase, EC 2.4.99.1, Boeringer-Mannheim). The results of the assays are presented in Figure 3 and Table 1 . Panel A (3STase) indicates that the transfer activity of NeuAc in the form of immobilized CMP-NeuAc **7** was elevated with increasing amounts of the enzyme. Transfer activities were also raised by increases in either the acceptor concentration or the incubation time (panels B and C, 3STase). In the case of 6STase (panels D – F), the reaction dynamics are similar to those of 3STase. When STase was first boiled under reflux for 5 min and then added to the reaction mixture, no transfer activity was observed (panel G). These results indicate that the immobilized CMP-NeuAc **7** can act as the sialyl donor. When the incubation time was extended to 24 h (panel B), the amount transferred at 500 mM [^{14}C]-LacNAc increased to 721 pmol. These data indicate that more than 721 pmol of CMP-NeuAc is immobilized on 1 mg of CPG. We also compared the relative transfer rates of CMP-NeuAc and **7**. The transfer rate for **7** was estimated to be 3 % of that for CMP-NeuAc.[16]

 © WILEY-VCH Verlag GmbH, D-69451 Weinheim, 1998 1433-7851/98/3722-3167 $ 17.50+.50/0

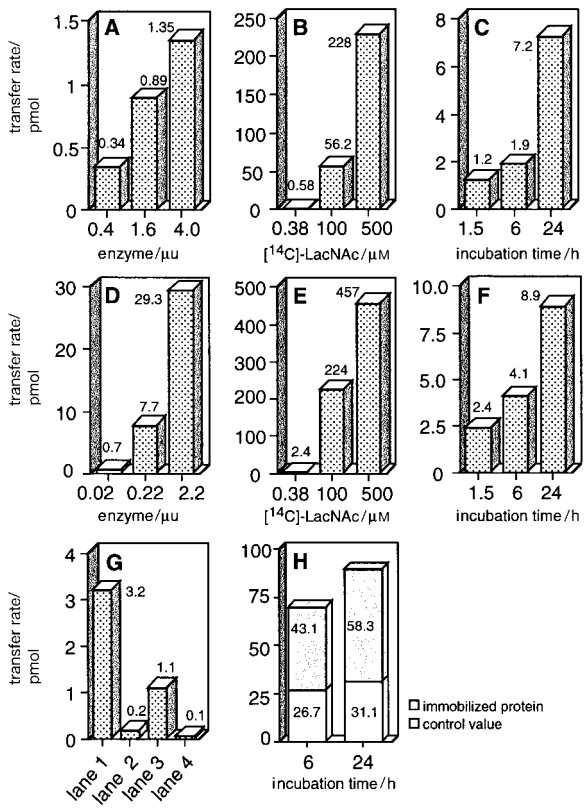


Figure 3. Amount [pmol] of immobilized CMP-NeuAc (**7**) transferred with α-(2→3)- and α-(2→6)-sialyltransferases. The assay conditions are given in Table 1.

Table 1. Assay conditions for the experiments presented in panels A – H of Figure 3.[a]

Panel	**7**	[^{14}C]-LacNAc	STase [μU]		Volume	Incubation time
	[mg]	[μg]	2,3	2,6	[μL]	[h]
A	2	0.4	[b]	–	32	5
B	1	[b]	0.8	–	32	3
C	1	1.0	0.8	–	35	[b]
D	2	3.8	–	[b]	32	4
E	1	[b]	–	2.2	32	3
F	1	1.0	–	2.0	34	[b]
G	2	0.7	[c]	[c]	34	3
H	1	[d]	0.8	–	27[e]	[b]

[a] Transfer assays with CMP-Neu5Ac (**7**) were carried out at 37 °C in 1.5-mL eppendorf tubes containing methyl *N*-acetyl-[1′-6′-^{14}C]-lactosaminide ([^{14}C]-LacNAc), ca 1.15 Kbq per 100 pmol to 1.15 KBq per 16 nmol by dilution with LacNAc, STase, HEPES buffer (0.1M, pH 7.0), and BSA (1 mg per 1 mL of assay mixture). All assays (except in G) were performed without enzyme system as control experiments. [b] Various amounts. [c] Enzyme quantities: lane 1 (6.6 μU of 6STase), lane 2 (6.6 μU of boiled 6STase), lane 3 (2.0 μU of 3STase), lane 4 (2.0 μU of boiled 3STase). [d] [^{14}C]-asialoglycoprotein, ca. 1.0 nmol. [e] The buffer solution contains 0.1 % nonidet P-40 and $MnCl_2$ (5 mM).

In addition, we examined whether **7** is active toward an asialoglycoprotein acceptor (α_1-acidic asialoglycoprotein containing [U-^{14}C]-gal[18]) by use of 3STase. As shown in panel H, the isotope counts for the asialoglycoprotein increased upon extention of the incubation time. However, isotope counts measured in the control assay (without enzyme) indicated as much as half the level of the actually immobilized glycoprotein. When [^{14}C]-LacNAc was used in the assays (panels A – F), the control values were less than 5 % of the value determined for the actually immobilized [^{14}C]-LacNAc. The control values for the assay in panel H are due to nonspecific binding of asialoglycoprotein to CPG. Therefore, the difference in control values between 6 h and 24 h is only 4.4 pmol. On the other hand, the difference in immobilized asialoglycoprotein between 6 h and 24 h is 15.2 pmol. Since the value for the immobilized protein increased independent of the control value upon simple extention of the incubation time, the data in panel H show that the immobilized CMP-NeuAc actively immobilizes asialoglycoprotein. In addition, the transfer activity is reproducible over several experiments. Since 58 pmol of α_1-acidic asialoglycoprotein was incorporated into CPG, about 10 % of the CMP-NeuAc was consumed during immobilization. Furthermore, these data also suggest that about 2.5 mg of the glycoprotein can be immobilized on 1 g of CPG. Since the α_1-acidic asialoglycoprotein used in this assay is estimated to have one equivalent of [U-^{14}C]-galactoside on its surface,[18] this glycoprotein may be a poor sialyl acceptor. Therefore, a glycoprotein containing several galactosides might be a good sialyl acceptor due to the multivalency effect, and, as a result, a practical quantity of glycoprotein might be immobilized.

Our methodology is currently limited to the immobilization of glycoproteins having galactosides at the nonreducing terminus. Other glycoproteins having fully sialylated oligosaccharides or high mannose-type oligosaccharides are more difficult to immobilize. In the former case, the immobilization can be performed after sialidase digestion. As shown in panel H, the overall efficiency[19] and yield[20] of immobilization are still not satisfactory. Work is in progress to solve the above difficulties in order to enable more efficient immobilization.

In conclusion, we have described a novel finding in which immobilized CMP-NeuAc reacts with sialyltransferase. This sialoside can be used as a new type of linker to covalently bond a labile biomolecule to a solid-phase support.

Received: April 6, 1998 [Z11690IE]
German version: *Angew. Chem.* **1998**, *110*, 3324 – 3326

Keywords: enzymes · glycoproteins · immobilization · sialic acids · solid-phase synthesis

[1] C. H. Wong, G. M. Whitesides, *Enzymes in Synthetic Organic Chemistry*, Pergamon, Oxford, **1994**.
[2] H. J. Gross, R. Brossmer, *Eur. J. Biochem.* **1988**, *177*, 583 – 589.
[3] G. Srivastava, K. J. Kaur, O. Hindsgaul, M. M. Palcic, *J. Biol. Chem.* **1992**, *267*, 22356 – 22361.
[4] Y. Kajihara, T. Ebata, K. Koseki, H. Kodama, H. Matsushita, H. Hashimoto, *J. Org. Chem.* **1995**, *60*, 5732 – 5735.
[5] R. A. Dwek, *Chem. Rev.* **1996**, *96*, 683 – 720.
[6] K. Mosbach, *Methods in Enzymology XLIV*, Academic Press, New York, **1976**, 134 – 148.
[7] A. Varki, *Glycobiology* **1993**, *3*, 97 – 130.
[8] The β isomer: ^{1}H NMR (300 MHz, CD_3OD; HOD: $\delta = 4.81$): $\delta =$ 7.49 – 7.24 (m, 5H; Ph), 5.28 – 5.21 (m, 2H; H-4,8), 4.60 (dd, $J = 2.3$, 10.3 Hz; H-7), 3.92 (dd, $J = 10.4$, 10.4 Hz, 1H; H-5), 3.61 (dd, $J = 3.2$, 14.5 Hz, 1H; H-9a), 3.51 (s, 3H; Me), 3.08 (dd, $J = 7.1$, 14.5 Hz, 1H;

 © WILEY-VCH Verlag GmbH, D-69451 Weinheim, 1998 1433-7851/98/3722-3168 $ 17.50+.50/0

H-9b), 2.51 (dd, $J = 4.8$, 13.8 Hz, 1H; H-3eq), 1.90, 1.88, 1.80, 1.77 (each s, 3H; Me); HR-FAB-MS: calcd for $C_{29}H_{38}N_2O_{13}SNa$ [M+Na$^+$]: 677.1993; found: 677.1997.

[9] A. Marra, P. Sinaÿ, *Carbohydr. Res.* **1989**, *187*, 35 – 42.

[10] The CPG was used for the solid-phase synthesis of glycopeptide: M. Schuster, P. Wang, J. C. Paulson, C. H. Wong, *J. Am. Chem. Soc.* **1994**, *116*, 1135 – 1136.

[11] G. W. Jourdian, L. Dean, S. Roseman, *J. Biol. Chem.* **1971**, *246*, 430 – 435.

[12] Immobilized CMP-NeuAc **7** was suspended in 0.5 mL of D_2O, and the ^{31}P NMR spectrum was measured in a conventional manner: W. L. Fitch, G. Detre, C. P. Holmes, *J. Org. Chem.* **1994**, *59*, 7955 – 7956.

[13] Prior to the assays, **7** was washed with BSA (2 mg of BSA in 1 mL of HEPES buffer) in a 1.5-mL eppendorf tube in order to prevent nonspecific absorption of STase or glycoprotein acceptor to the CPG. After centrifugation, the supernatant was removed. This treatment was repeated three times, and then **7** was washed with water. After lyophylization, CMP-Neu5Ac **7** was used for assays.

[14] S. Sabesan, S. Neira, F. Davidson, J. Ø. Duus, K. Bock, *J. Am. Chem. Soc.* **1994**, *116*, 1616 – 1634.

[15] After incubation (panels A – H) the mixture was filtered, and the CPG remaining on the filter paper was washed with water twice (3 mL). The filter paper and CPG were inserted into a scintillation vial for counting. The radioactivity on the CPG was measured by a liquid scintillation counter, and the amount of [^{14}C]-LacNAc incorporated on the CPG was estimated. The transfer rates after subtraction of control values are summarized in Figure 3 (panels A – F). The data given (panels A – H) are averages values.

[16] The transfer assays were performed by one of the following two methods. The assays of CMP-NeuAc were carried out at 37 °C with a solution of HEPES buffer (total 35 μL) containing CMP-[U-^{14}C]-NeuAc (12.1 KBq nmol^{-1}, 20 μM), LacNAc (1 μM), BSA, and 3STase (0.8 μU). The amounts that were transferred were estimated by the conventional method.[17] For immobilized CMP-NeuAc, a solution of HEPES buffer (total 35 μL) containing **7** (1 mg: the concentration of CMP-NeuAc corresponds to 20 μM based on 721 pmol of CMP-NeuAc on 1 mg of CPG), [^{14}C]-LacNAc (1 μM), BSA, and 3STase (0.8 μU) was incubated at 37 °C, and the transferred amount was estimated with the above method.[15]

[17] Y. Kajihara, H. Kodama, T. Wakabayashi, K.-I. Sato, H. Hashimoto, *Carbohydr. Res.* **1993**, *247*, 179 – 193.

[18] α_1-Acidic asialoglycoprotein with [U-^{14}C]-galactoside was prepared from α_1-acidic asialo-agalacto-glycoprotein by the action of UDP-[U-^{14}C]-galactose and β-(1 → 4)-galactosyltransferase: Y. Kajihara, T. Endo, H. Ogasawara, H. Kodama, H. Hashimoto, *Carbohydr. Res.* **1995**, *269*, 273 – 294.

[19] Immobilization of the STase as a side reaction of this method could not be detected in several self-immobilization assays of STase.

[20] Immobilization yields are estimated to be about 4.5% and 5.8% in the case of LacNAc and asialoglycoprotein, respectively, based on the sialylacceptors added.

Cationic Homoleptic Vanadium(II), (IV), and (V) Complexes Arising from Protonolysis of $[V(NEt_2)_4]$

Robert Choukroun,* Pierre Moumboko, Sandrine Chevalier, Michel Etienne, and Bruno Donnadieu

Although the chemistry of cations containing Group 4 metals is very well documented[1] and a subject of ongoing investigations, with regard to the modeling of the Ziegler – Natta polymerization, the chemistry of cationic vanadium complexes has not been as thoroughly studied as that of their neutral complexes.[2–4] The recent interest in complexes in which amido and imido groups are directly bound to a Group 4 or 5 metal atom has led to new catalysts in alkene polymerization.[5] Hydridotris(pyrazolyl)borate imidovanadium(V) in the presence of a methylaluminoxane (MAO) activator shows modest ethylene polymerization activity.[6] We reported that the protonolysis of $[Cp_2VMe_2]$ or $[Cp_2Zr(BH_4)_2]$ can lead to a disproportionation redox reaction resulting in cationic vanadium(III) or zirconium(III) complexes.[7,8] In this context we report here the formation of new cationic vanadium(II), (IV), and (V) species when $[V(NEt_2)_4]$ (**1**) is treated with the ammonium salt $[NHMe_2Ph][BR_4]$ (R = Ph, C_6F_5).

Treatment of **1** with one equivalent of $[NHMe_2Ph][BPh_4]$ in thf at room or low temperature (− 78 °C) causes precipitation of the unexpected air-sensitive, dicationic, heteroleptic dialkylamidovanadium(IV) complex **2** with one thf molecule of

$[V(NEt_2)_4]$ **1**

$[V(NEt_2)_2(thf)_4][BPh_4]_2 \cdot thf$ **2**

crystallization (yield: 26%). This crystalline red product was characterized by X-ray structure analysis (Figure 1).[9] The environment around the metal is octahedral and the V−N and V−O distances (2.054 and 2.11 Å (average), respectively) are comparable to those in other vanadium compounds containing the bis(trimethylsilyl)amide ligand and a coordinated thf molecule.[10] The sum of the angles about each N center is close to 360°, indicating that the amide ligands are probably acting as three-electron donors. We also observe that a small, nonquantifiable amount of an uncharacterized green precipitate is present among the crystals of **2**, providing evidence that the reaction is not simple.

Reconsidering the formation of **2**, we repeated our experiment with **1** and two equivalents of $[NHMe_2Ph][BR_4]$ (R = Ph or C_6F_5) in thf at room temperature. Compound **1** was treated with two equivalents of $[NHMe_2Ph][B(C_6F_5)_4]$ in thf, and pentane was allowed to diffuse slowly into the solution to give a mixture of crystalline, highly air-sensitive, red products.

[*] Dr. R. Choukroun, P. Moumboko, S. Chevalier, Dr. M. Etienne, B. Donnadieu
Laboratoire de Chimie de Coordination du CNRS
UPR 8241, 205 Route de Narbonne
F-31077 Toulouse Cedex 4 (France)
Fax: (+33) 561-5530-03
E-mail: choukrou@lcctoul.lcc-toulouse.fr

 © WILEY-VCH Verlag GmbH, D-69451 Weinheim, 1998 1433-7851/98/3722-3169 $ 17.50+.50/0

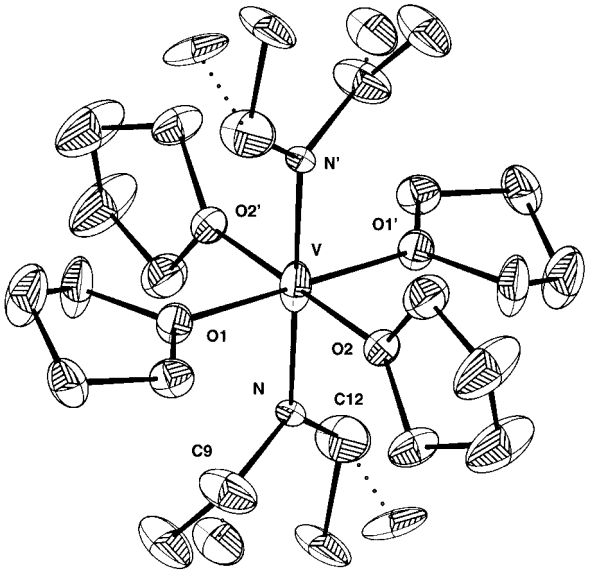


Figure 1. Molecular structure of the cation in **2** showing the labeling scheme; hydrogen atoms are omitted for clarity. The structure of the $[BPh_4]^-$ ion is normal. Selected bond lengths [Å] and angles [°]: V–O1 2.108(3), V–O2 2.121(3), V–N 2.050(3); O1-V-O2 89.4(1), O1-V-N 89.2(1), O2-V-N 89.8(1), V-N-C9 125.6(3), V-N-C11 126.6(3), C9-N-C11 107.7(4).

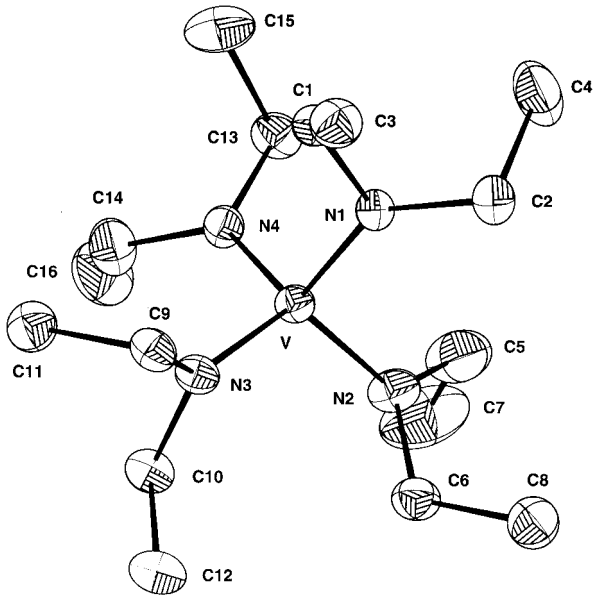


Figure 2. Molecular structure of the cation in **3** showing the labeling scheme; hydrogen atoms are omitted for clarity. The structure of the $[B(C_6F_5)_4]^-$ ion is normal. Selected bond lengths [Å] and angles [°]: V–N1 1.817(3), V–N2 1.826(3), V–N3 1.826(3), V–N4 1.847(3); N1-V-N2 104.1(1), N1-V-N3 111.8(1), N2-V-N3 114.5(1), N1-V-N4 107.6(1), N2-V-N4 109.0(1), N3-V-N4 109.5(1), V-N1-C1 115.7(2), V1-N1-C2 130.1(2), V1-N2-C5 122.9(3),V-N2-C6 122.0(3), V-N3-C9 131.4(2), V-N3-C10 114.1(2), V-N4-C13 120.6(2), V-N4-C14 125.0(2).

After careful and lengthy separation, we were able to elucidate their composition by X-ray crystal structure analysis.[9] Dark red crystals were identified as the unanticipated cationic homoleptic vanadium(v) complex **3** and bright red crystals as the dicationic vanadium(ii) species **4**, which crystallizes with two molecules of thf.

$[V(NEt_2)_4][B(C_6F_5)_4]$ **3**

$[V(thf)_6][B(C_6F_5)_4]_2 \cdot 2\,thf$ **4**

The crystal structure of **3** (Figure 2) shows that the complex has a tetrahedral core; the vanadium center is bound to four dialkylamido ligands. The sum of the angles around each nitrogen atom is nearly 360° and the V–N distances are in the expected range of 1.817 – 1.847 Å. These distances are shorter than those in **2** but consistent with the electronic contribution of the oxygen atom from the thf ligand in **3**. The angles of the four VNC_2 moieties in **3** are slightly different owing to the steric bulk of the ligand and the coordination number of the metal.

The X-ray structure of **4** (Figure 3) reveals an octahedral geometry in which the metal center is surrounded by six thf ligands, two $[B(C_6F_5)_4]$ counteranions, and two thf molecules. Similar $[VL_6]^{2+}$ compounds ($L = CH_3OH$, H_2O, CH_3CN)[11–14] have been characterized, but the thf analogue was described as $[V(thf)_4]^{2+}$.[12] The V–O distances are in the range of 2.13 – 2.15 Å, slightly longer than in **2**. In the compounds characterized by three X-ray crystallography the counteranions display the expected geometry.

The ^1H NMR spectrum of complex **3** exhibits the set of CH_2CH_3 resonances. The solution of **2** in CH_3CN gives a clearly resolved EPR spectrum ($g = 1.988$; $a(^{51}V) = 79.1$ G), indicating that the impurities observed with **2** are EPR-silent vanadium species. The ^1H NMR spectrum of **2** in CD_3CN shows free thf, which indicates that ligand exchange occurs between thf and CD_3CN to give presumably $[V(NEt_2)_2(CD_3CN)_4][BPh_4]_2$. Complex **4** was also characterized by EPR spectroscopy ($g = 1.979$; $a(^{51}V) = 91.0$ G).

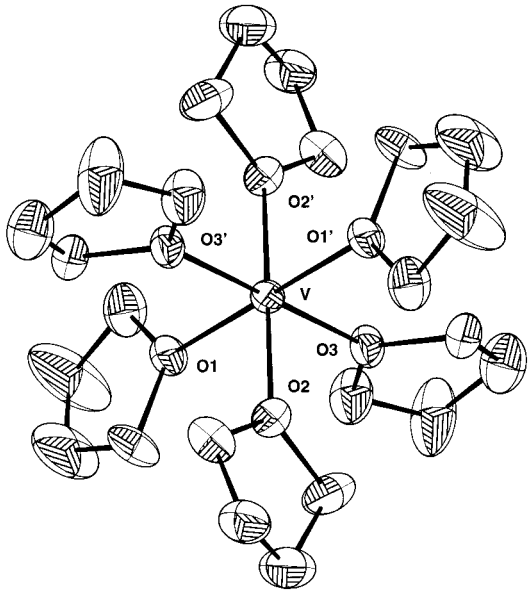


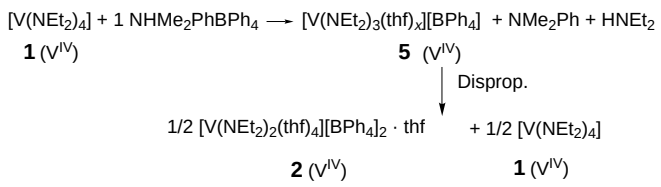
Figure 3. Molecular structure of the cation in **4** showing the labeling scheme; hydrogen atoms are omitted for clarity. The structure of the $[B(C_6F_5)_4]^-$ ion is normal. Selected bond lengths [Å] and angles [°]: V–O1 2.149(4), V–O2 2.146(4), V–O3 2.131(4); O1-V-O2 91.5(2), O1-V-O3 89.5(2), O2-V-O3 89.9(2), *trans* O-V-O 180.0 (av).

When **1** was treated with two equivalents of $[NHMe_2Ph][BPh_4]$ in thf, a red powder precipitated immediately, which we identified as **2** by its EPR spectrum; however,

 © WILEY-VCH Verlag GmbH, D-69451 Weinheim, 1998 1433-7851/98/3722-3170 $ 17.50+.50/0 *Angew. Chem. Int. Ed.* **1998**, *37*, No. 22

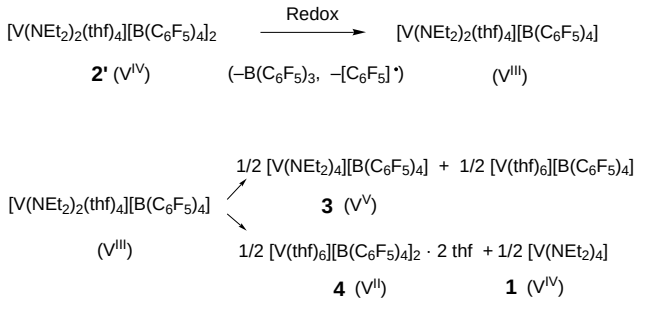
complete conversion into **2** was not possible (30–40% yield, in different experiments). The ^{11}B NMR spectrum of the filtrate shows a signal for $[BPh_4]^-$ at $\delta = -6.3$ and a broad resonance at $\delta = 2$, which we assign to a $BPh_3 \cdot NR_3$ adduct ($NR_3 = HNEt_2$) (an authentic sample of BPh_3 and HNR_2 was prepared). This indicates that a redox reaction probably occurs in the reaction with $[BPh_4]^-$, like that which we have already observed in the redox reaction of $[Cp_2V(CH_3)(thf)][BPh_4]$.[7] Addition of pentane to the green filtrate gave an oily product, which was then triturated with pentane to give a mixture of **3** and **4** (characterized by ^1H NMR and by EPR spectroscopy, respectively, but the yield was not quantified).

The formation of the moisture-sensitive compounds **2**–**4** is not a straightforward process, and different pathways seem to occur. First, the oxidation state of the vanadium center is preserved on going from **1** to **2**, whereas it loses two dialkylamido ligands. This reaction was monitored by EPR spectroscopy, and the characteristic signal of $[V(NEt_2)_4]$ ($g = 1.980$; $a(^{51}V) = 65.0$ G)[15] was continually observed together with that of a transient species **5** ($g = 1.977$; $a(^{51}V) = 72.0$ G). The red insoluble precipitate **2** was filtered off, and the EPR spectrum of the filtrate shows the sole presence of **1**, which is at roughly half of the concentration before its reaction with the ammonium salt. A disproportionation reaction is mainly responsible for the pathway (Scheme 1), and we tentatively suggest formula **5** ($x = 1$) for the intermediate species.



Scheme 1. Reaction of **1** with one equivalent of $[NHMe_2Ph][BPh_4]$ to give **2** by means of a disproportionation mechanism.

The reaction of **1** with two equivalents of the ammonium salt is more complicated, and we tentatively propose an idealized pathway involving redox and disproportionation reactions (Scheme 2). After monitoring the reaction with the tetraperfluoroborate ammonium salt by EPR spectroscopy for two days, we observed overlapping eight-line signals of different species. Compounds **1** and **4** were easily identified at the beginning and at the end of the reaction, respectively. Two



Scheme 2. Postulated mechanism deduced from the isolation of **3** and **4** from the reaction of **1** with two equivalents of $[NHMe_2Ph][B(C_6F_5)_4]$.

other species were also identified, **2′** and the presumed cation **5′** associated with the $[B(C_6F_5)_4]$ counteranion, based on the

$[V(NEt_2)_3(thf)]^+$ **5′**

similarity with the EPR spectra of the analogues **2** and **5**. Both appear as transient species (the EPR signal of **2′** was observed only during the first 30 min of the reaction until it overlapped with the signal of **4**; **5′** was seen for roughly 15 h). Peak positions and relative intensities of different spectra monitored during the course of the reaction validate these assumptions. After one week the diamagnetic species **3** had entirely precipitated and only **4** was observed by EPR spectroscopy (25–30% yield based on **1** (100%) in several experiments, with a small amount of an uncharacterized vanadium species).

The presence of **5′** can be explained on the basis of Scheme 1. We presume that the excess of the perfluoroborate ammonium salt serves either to trap **1**, which is formed in the disproportionation of **5′**,[16] or to convert **5′** directly into **2′**. Moreover, there is no evidence that the putative **5** (or **5′**) intermediate does not undergo a redox reaction with the neutral $[V(NEt_2)_3]$ being formed.[17] The vanadium atom in product **3** has increased its oxidation state from the starting state V^{IV} to V^V, whereas in **4** it has lowered its oxidation state to V^{II}. A competitive disproportionation reaction from $2\,V^{III}$ to V^V/V^I and V^{IV}/V^{II} is suggested. The mechanism involves the formation of the V^{III} species $[V(NEt_2)_2(thf)_4]^+$ from **2′** by means of a redox reaction with the $[B(C_6F_5)_4]^-$ ion[7,8] (the transfer of a C_6F_5 group from a $[B(C_6F_5)_4]^-$ ion to a metal is a recognized mechanism[18]). The reaction was analyzed by ^{11}B NMR spectroscopy. The spectrum shows the expected peak of the $[B(C_6F_5)_4]^-$ ion ($\delta = -16$) and a broad peak at $\delta = -2.5$ which may be due to the adduct $B(C_6F_5)_x(NEt_2)_{3-x} \cdot HNEt_2$ (by comparison with a sample prepared from $B(C_6F_5)_3$ and $HNEt_2$). However, the protonolysis of **1** was not further studied in detail due to its complexity.[19]

The mechanism for the formation of **2** is fully rationalized, but the pathways leading to **3** and **4** are not obvious and the mechanisms remain unknown. We do not yet have mechanistic details concerning these transformations owing to the propensity of the $[VNR_2]$ moiety to undergo amine elimination and redistribution/redox reaction in the presence of the ammonium salt. The different reactivity observed when the protonolysis of **1** is performed with the ammonium salt $[NHMe_2Ph]^+$ associated with the $[BPh_4]^-$ or the $[B(C_6F_5)_4]^-$ counterion is mainly due to the insolubility of **2**, which precipitates from the reaction mixture before it can react further, whereas the presence of the tetraperfluoroborate ion, leading to a more soluble complex **2′**, permits further degradation. Due to the tendency for the vanadium to assume different oxidation states, octahedral V^{II} and V^{IV} and tetrahedral V^V cationic complexes were obtained. The ability of the amido ligand to act as a three-electron ligand is worth underlining. The presence of different oxidation states in the cationic vanadium chemistry observed in this work further supports the recognized complexity of vanadium chemistry in Ziegler–Natta catalysis.[20] Procedures to convert species **2**–**4** into active cationic species for olefin polymerization[3b,5e] are in progress and will be reported elsewhere.

Experimental Section

2: Solid $[NHMe_2Ph][BPh_4]$ (344 mg, 0.78 mmol) was added to $[V(NEt_2)_4]$ (266 mg, 0.78 mmol) in thf (15 mL) at $-78\,^{\circ}C$. The resulting solution was stirred for 1 h and allowed to warm to room temperature. After 12 h red crystals of **2** were obtained and filtered, washed with thf, and dried in vacuo. Yield: 244 mg (26 %). Elemental analysis calcd for $C_{76}H_{100}B_2O_5N_2V$: C 76.45, H 8.38, V 4.27; found: C 75.82, H 7.92, V 4.40.

3, **4**: Solid $[NHMe_2Ph][B(C_6F_5)_4]$ (727 mg, 0.90 mmol) was added to $[V(NEt_2)_4]$ (154 mg, 0.45 mmol) in thf (15 mL) at room temperature. The resulting solution was stirred for 1 h, and pentane (20 mL) was slowly added to the solution. After slow diffusion of the pentane into the solution in thf, red-black **3** and bright red **4** crystals were obtained overnight, filtered, washed rapidly with thf (2×5 mL), and dried in vacuo (total mass: 304 mg). After careful and lengthy separation in the glove box, analytical analysis of **3** and **4** was attempted for characterization**,** but only **3** gave reproducible results. Elemental analysis calcd for $C_{40}H_{40}BF_{20}N_4V$: C 47.16, H 3.93, N 5.50; found: C 46.60, H 3.26, N 5.00; ^1H NMR (200 MHz, $[D_8]$thf): $\delta = 1.40$ (t, CH_3), 4.32 (q, CH_2); ^{11}B NMR (25.7 MHz, $[D_8]$thf): $\delta = -16.2$.

EPR experiments: In a typical experiment a solution of **1** in thf was prepared, and an aliquot of the solution was introduced into a standardized capillary tube for EPR measurements. This EPR spectrum served as a standard for the reaction. The solid ammonium salt was then added to the solution, and aliquots were removed by syringe periodically, introduced into the capillary tubes, and analyzed by EPR over one week. The acquisition parameters were kept constant for both the unknown and the standard sample measurements.

Received: April 6, 1998 [Z11689IE]
German version: *Angew. Chem.* **1998**, *110*, 3363 – 3367

Keywords: amides · EPR spectroscopy · redox chemistry · vanadium

[1] a) R. F. Jordan, *Adv. Organomet. Chem.* **1991**, *32*, 325; b) H. H. Brintzinger, D. Fischer, R. Mülhaupt, B. Rieger, R. Waymouth, *Angew. Chem.* **1995,** *107,* 1255 – 1283; *Angew.Chem. Int. Ed. Engl.* **1995**, *34*, 1143 – 1170; c) M. Bochmann, *J. Chem. Soc. Dalton Trans.* **1996**, 255 – 270.

[2] a) P. Berno, S. Gambarotta, D. Richeson in *Comprehensive Organometallic Chemistry II, Vol. 5* (Eds.: J. A. Labinger, M. J. Winter), Pergamon, Oxford, **1982 – 1994,** pp. 1 – 55; b) M. Moore, S. Gambarotta, G. Yap, L. M. Liable-Sands, A. L. Rheingold, *J. Chem. Soc. Chem. Commun.* **1997**, 643 – 644; c) H. Kawaguchi, K. Tatsumi, *Organometallics* **1995**, *14*, 4294 – 4299; d) V. J. Murphy, H. Turner, *Organometallics* **1997**, *16*, 2495 – 2497; e) P. T. Witte, A. Meetsma, B. Hessen, P. H. M. Budzelaar, *J. Am. Chem. Soc.* **1997**, *119*, 10561 – 10562; f) M. Moore, S. Gambarotta, C. Bensimon, *Organometallics* **1997**, *16*, 1086 – 1088.

[3] a) Y. Doi, N. Tokuhiro, M. Nunomura, H. Miyake, S. Suzuki, K. Soga in *Transition Metals and Organometallics as Catalysts for Olefin Polymerization* (Eds.: W. Kaminsky, H. Sinn), Proceedings of an International Symposium, Hamburg (Germany), **1987**, pp. 379 – 387 ; b) F. J. Karol, K. J. Cann, B. E. Wagner in *Transition Metals and Organometallics as Catalysts for Olefin Polymerization* (Eds.: W. Kaminsky, H. Sinn), Proceedings of an International Symposium, Hamburg (Germany), **1987**, pp. 149 – 161**.**

[4] H. J. De Liefde Meijer, G. J. M. van der Kerk, *Recl. Trav. Chim. Pays-Bas* **1966**, *85*, 1007 – 1017.

[5] a) C. Boisson, J.-C. Berthet, M. Ephritikhine, M. Lance, M. Nierlich, *J. Organomet. Chem.* **1997**, *531*, 115 – 119; b) P. T. Witte, A. Meetsma, B. Hessen, P. H. M. Budzelaar, *J. Am. Chem. Soc.* **1997**, *119,* 10561 – 10562; c) I. Kim, Y. Nishihara, R. F. Jordan, R. D. Rogers, A. Reingold, G. P. A. Yap, *Organometallics* **1997**, *16*, 3314 – 3323; d) N. A. H. Male, M. Thornton-Pett, M. Bochmann, *J. Chem. Soc. Dalton Trans.* **1997**, 2487 – 2494; e) I. Kim, R. F. Jordan, *Macromolecules* **1996**, *29*, 489 – 491.

[6] S. Scheuer, J. Fischer, J. Kress, *Organometallics* **1995**, *14*, 2627 – 2629.

[7] R. Choukroun, B. Douziech, C. Pan, F. Dahan, P. Cassoux, *Organometallics* **1995**, *14*, 4471 – 4473.

[8] R. Choukroun, B. Douziech, B. Donnadieu, *Organometallics* **1997**, *16*, 5517 – 5521.

[9] Crystal structure data of **2** [the data for **3**, **4** are given in square brackets]**:** Chemical formula $[V\{N(C_2H_5)_2\}_2(C_4H_8O)_4][B(C_6H_5)_4]\cdot C_4H_8O$ $[[\{V[N(C_2H_5)_2]_2\}_4][B(C_6F_5)_4]$, $[V(C_4H_8O)_6][B(C_6H_5)_4]_2\cdot 2\,C_4H_8O]$, $M_r = 1174.04$ [1018.4; 1981.84], monoclinic [triclinic, monoclinic], space group $P2_1/n$ [$P\bar{1}$, $P2_1/n$], $a = 11.9261(8)$ [11.095(2), 12.557(1)], $b = 13.2215(8)$ [11.181(2), 22.158(2)], $c = 21.126(2)$ [18.095(2), 15.648(2)] Å, $\alpha = 90$ [77.663(1), 90], $\beta = 92.527(7)$ [84.22(2), 106.368(8)], $\gamma = 90$ [89.13(1), 90], $V = 3327.8$ [2171, 4177] Å^3, $Z = 2$ [4,2], $\rho = 1.17$ [1.56, 1.58] g cm^{-1}, $\mu = 1.92$ [3.38, 2.50] cm^{-1}, $F(000) = 1033$ [1033, 1996], crystal size $0.32 \times 0.25 \times 0.05$ [$0.32 \times 0.25 \times 0.07$, $0.4 \times 0.2 \times 0.05$] mm^3, crystal form: platelet [plate, thin plate], crystal color: red [dark red, bright red], $Mo_{K\alpha}$ radiation, $\lambda = 0.71073$ Å, $T = 170$ [180, 180] K, number of measured reflections: 20817 [17214, 25545], number of independent reflections: 4508 [6422, 5741], $R_{av} = 0.09$ [0.05, 0.04], $R_a = 0.059$ [0.059, 0.056], $R_{wb} = 0.064$ [0.067; 0.063], weighting scheme Chebyshev, Ar coefficients: 3.67/ – 1.72/2.79/ – 0.081 [2.22/0.39/1.71, 2.75/ – 1.13/2.04/ – 0.336], GOF = 1.1 [1.1, 1.05], number of reflections used: 2174 [3033; 4870], observation criterion $I > \sigma(I)$ [$I > 1.5\sigma(I)$, $I > 3\sigma(I)$], number of parameters 402 [472, 596]. The selected crystal, sensitive to air and moisture, was protected in vaseline oil and placed in a capillary. The data were collected with a STOE IPDS diffractometer. Whole structures were solved by direct methods and refined by least-squares procedures on F_o. In **2** disorder was observed on one ethyl ligand; the electron density of CH_3 groups is statistically distributed over two sites with a 1:1 ratio. A similar situation has been observed for one molecule of the thf solvent molecule of **4** for which one C atom is also distributed over two positions. All non-hydrogen atoms were refined anisotropically except for the C atom of free thf molecule of **4**, which was only isotropically refined. Crystallographic data (excluding structure factors) for the structures reported in this paper have been deposited with the Cambridge Crystallographic Data Centre as supplementary publication no. CCDC-101352. Copies of the data can be obtained free of charge on application to CCDC, 12 Union Road, Cambridge CB2 1EZ, UK (fax: (+44) 1223-336-033; e-mail: deposit@ccdc.cam.ac.uk).

[10] C. P. Gerlach, J. Arnold, *Organometallics* **1996**, *15*, 5260 – 5262.

[11] F. A. Cotton, S. A. Duraj, L. E. Manzer, W. J. Roth, *J. Am. Chem. Soc.* **1985**, *107*, 3850 – 3855.

[12] P. Chandrasekhar, P. H. Bird, *Inorg. Chim. Acta* **1985**, *97*, L31 – L33.

[13] D. G. Holt, L. F. Larkworthy, D. C. Povey, G. W. Smith, G. J. Leigh, *Inorg. Chim. Acta* **1990**, *169*, 201 – 205.

[14] S. J. Anderson, F. J. Wells, G. Wilkinson, B. Hussain, M. B. Hursthouse, *Polyhedron* **1988**, *7*, 2615 – 2626.

[15] C. E. Holloway, F. E. Mabbs, W. R. Smail, *J. Chem. Soc. A* **1968**, 2980 – 2984.

[16] The following reactions were investigated as an alternative approach to provide assignable compounds. When **1** was treated with one equivalent of the perfluoborate ammonium salt, the same EPR spectra were observed (but we were unabled to isolate a vanadium complex). After complex **1** was treated with one or two equivalents of $B(C_6F_5)_3$ in thf at room temperature, the EPR spectrum of **5** was observed**;** the signals disappear after three days to again give the EPR signal of **1**. This is probably due to a disproportionation reaction, but we were unable, in both cases, to isolate any vanadium complex.

[17] This neutral V^{III} complex could react further with the ammonium salt to give the cationic V^{III} species leading to **3** and **4**. This possibility is under investigation.

[18] R. Gomez, M. L. H. Green, J. L. Haggit, *J. Chem. Soc. Dalton Trans.* **1996**, 939 – 946.

[19] We did not observe the formation of the perfluorinated biphenyl $(C_6F_5)_2$, whereas C_6F_5H was identified in the reaction mixture (by comparison with the ^{19}F NMR spectrum of an authentic sample and by a characteristic peak in its mass spectrum (m/z 168)). Nevertheless, the formation of C_6F_5H was also observed by ^{19}F NMR spectroscopy when $B(C_6F_5)_3$ and $HNEt_2$ were allowed to react. Therefore, a redox reaction could be inferred from the existence of C_6F_5H.

[20] Cucinella, A. Mazzei, *Chim. Ind.* **1971**, *53*, 653 – 661; 748 – 754; 934 – 938.

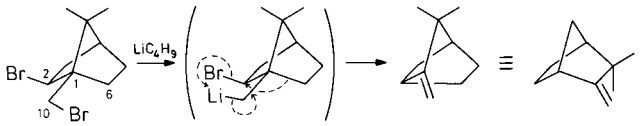
 © WILEY-VCH Verlag GmbH, D-69451 Weinheim, 1998 1433-7851/98/3722-3172 $ 17.50+.50/0

An Unprecedented Elimination-Driven Migration: The Reductive Dihalobornane–Camphene Rearrangement**

László Garamszegi and Manfred Schlosser*

The concept of the "variable transition state" of β-eliminations,[1] viewed as a mechanistic continuum stretching from E1(C^+) to E1cb, has fascinated generations of chemists and has profoundly shaped their reasoning. The fundamental idea, that not only ground states but also transition states can be conceived as resonance hybrids resulting from the superposition of two or more limiting structures, has later been extended with remarkable success to cycloaddition reactions,[2, 3] in particular for the rationalization of their ease and regioselectivity. Here we demonstrate that even complex elimination processes which involve the breaking and making of several bonds can be brought about in a highly concerted fashion under variable push–pull control. Similar conclusions have been previously drawn for fragmentation reactions on the basis of stereoelectronic criteria.[4]

In relation with recent work in the field of selective structural manipulations of monoterpenes,[5] we have observed the quantitative conversion of *exo*-2,10-dibromobornane into camphene upon treatment with butyllithium in tetrahydrofuran (or diethyl ether). This result can be plausibly explained by assuming that a halogen–metal exchange occurs at the 10- rather than the 2-position, thus generating the less basic *exo*-2-bromo-10-bornyllithium (**1a**; Scheme 1). This species would have to rearrange instantaneously under loss of lithium bromide to afford camphene.

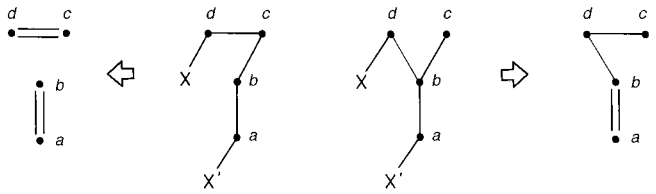


1a

Scheme 1. Conversion of *exo*-2,10-dibromobornane into camphene upon treatment with butyllithium by halogen–metal permutation.

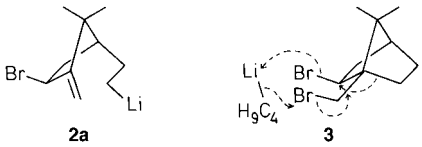
This migration–elimination mode differs from a classical heterolytic fragmentation[4] in essentially one respect. Since carbon atoms 2 and 6 (centers *d* and *c* in Scheme 2) are not yet connected at the stage of the intermediate **1a**, they will ultimately be linked by only a single rather than a double bond. The bond between carbon atoms 1 and 2 (centers *b* and *d*) is formally irrelevant since it does not directly participate in the reaction event, but just ensures the proximity of the crucial structural entities (in particular, centers *c* and *d*).

Other reaction patterns cannot be ruled out a priori, of course. Thus, a stepwise sequence consisting of the opening[6]



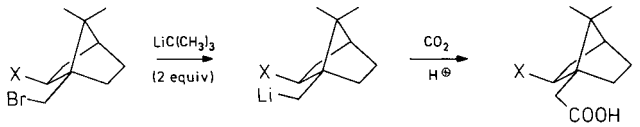
Scheme 2. Heterolytic fragmentation (left) and elimination–migration (right).

of the cyclopentylmethyllithium subunit to produce a 5-hexenyllithium intermediate (**2a**) immediately followed by intramolecular, ring-closing nucleophilic (S_N2-type) attack could be well envisioned. Alternatively, a hyperconcerted simultaneous removal of both bromine atoms under the action of butyllithium may take place (transition state **3**). In the second case, the initially postulated intermediate **1a** would be bypassed. Trapping experiments should hence allow one to proceed to a first mechanistic selection.



2a **3**

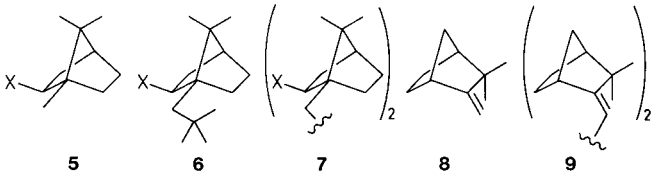
All attempts to characterize the presumptive intermediate **1a** by interception with dry ice or benzaldehyde failed, even at $-125\,^{\circ}C$. However, the corresponding chloro and fluoro analogues (**1b** and **1c**) could be trapped by carboxylation at $-125\,^{\circ}C$ and $-75\,^{\circ}C$, respectively, affording the acids **4b** and **4c** in 7% and 47% yield (Scheme 3). About 25 °C above the temperatures at which they had been generated, species **2b** and **2c** were converted into camphene (33% and 48%, respectively) by an elimination–migration process.



X = Br	**1a**	**4a** (0%)
X = Cl	**1b**	**4b** (7%)
X = F	**1c**	**4c** (47%)

Scheme 3. Evidence for intermediates **1** from trapping reactions.

In the chloro series, 2-chlorobornane (**5b**, ca. 30%), 2-chloro-7,7-dimethyl-1-(2,2-dimethylpropyl)bicyclo[2.2.1]-heptane (**6b**, ca. 15%), 2,2-dimethyl-3-methylidenebicyclo[2.2.1]heptane (**8**, ca. 5%), and 10,10′-biscamphenyl (**9**, ca. 5%) were identified as by-products. In the fluoro series, 2-fluoro-7,7-dimethyl-1-(2,2-dimethylpropyl)bicyclo[2.2.1]-heptane (**6c**, ca. 10%) and 10,10′-bis(2-fluorobornyl) (**7c**, ca. 30%) were detected.



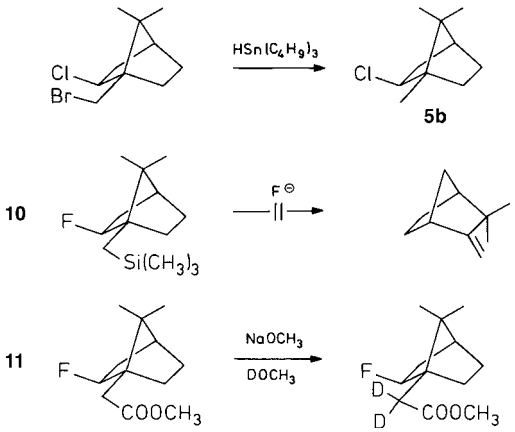
5 **6** **7** **8** **9**

[*] Prof. Dr. M. Schlosser, L. Garamszegi
Institut de Chimie Organique, Université Bâtiment de Chimie (BCh)
CH-1015 Lausanne (Switzerland)
Fax: (+41) 21-692-39-65

[**] This work was supported by the Schweizerische Nationalfonds zur Förderung der wissenschaftlichen Forschung (grants 20-41'887-94 and 20-49'307-96), Bern.

 © WILEY-VCH Verlag GmbH, D-69451 Weinheim, 1998 1433-7851/98/3722-3173 $ 17.50+.50/0

Further model reactions have been carried out to exclude remaining mechanistic options and thus, indirectly, to support the favored push – pull process. The rearrangement cannot be mediated by radicals since upon treatment of 10-bromo-2-chlorobornane with tributyltin hydride, 2-chlorobornane (**5b**) is obtained as the exclusive product (Scheme 4). It can neither

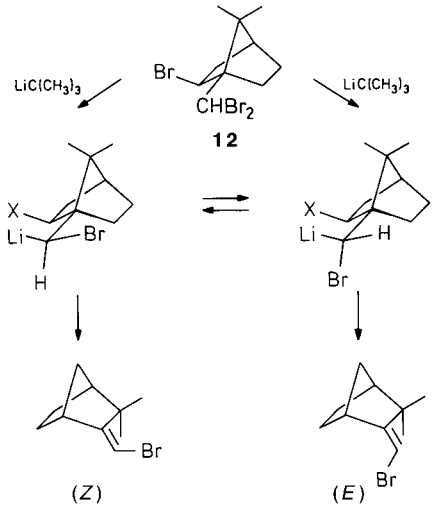


Scheme 4. Exclusion of possible reaction mechanisms with model reactions.

be cationic[7]—in other words, Wagner – Meerwein-like—since 2-bromo-, 2-chloro-, and 2-fluoronorbornane are perfectly inert towards butyllithium in the presence or absence of solubilized lithium bromide. Finally, it cannot even be anionic since no halide elimination accompanied by rearrangement occurs when 2-fluoro-10-(trimethylsilyl)bornane is desilylated with tris(dimethylamino)sulfonium difluorotrimethylsilicate (TASF) and methyl 2-fluoro-10-bornanecarboxylate is submitted to base-catalyzed hydrogen – deuterium exchange. The latter findings also argue against the intermediacy of ring-opened species such **2**, since the absence of a metal (lithium) should have no adverse effect on the rate of formation of the 2-halobornanide precursor (**1**, without metal) nor on the position of the equilibrium established between **1** and **2**.

The concerted push – pull elimination – migration process should be relatively insensitive to steric hindrance encountered in the final products. In accordance with this expectation, 2,10,10-tribromobornane (**12**) reacts with *tert*-butyllithium to give a *Z*/*E* mixture (2:3) of 10-bromocamphene in 69 % yield, from which the pure *Z* isomer, a versatile building block,[5] can be isolated after kinetic separation.[5] The tribromo compound **12** can be readily prepared by addition of bromine to the *E* isomer[5] of 10-bromocamphene (Scheme 5).

Numerous elimination-driven skeletal reorganizations are known, for example the Wagner – Meerwein, Fittig – Zincke (pinacolic), and Fritsch – Buttenberg – Wiechell rearrangements.[8] At first sight, they have mechanistically nothing in common with the present topic. In the same way, any coincidence between the 2,10-dihalobornane – camphene elimination – migration and the family of Lossen, Hofmann, and Curtius rearrangements[8] appears to be merely schematic, since all these latter reactions involve cationic intermediates. However, at least the solvolytic rearrangement of



Scheme 5. Insensitivity of the push – pull process to steric hindrance.

isoborneol esters must be supported by a push contribution, as it implies σ delocalization.[9, 10] Donor (e.g., trimethylstannylmethyl[11]) and acceptor substituents (e.g., cyano[12]) attached to the bridgehead C1 position indeed cause a pronounced rate enhancement or deceleration, respectively. Thus, we recognize the emerging of a new continuum of multibond reorganizing mechanisms. They simultaneously employ push (electrofugal) and pull (nucleofugal) actions in variable blends. Often one feature clearly predominates, but sometimes both are balanced in roughly equal proportions. The latter appears to be the case with the 2,10-dihalobornane – camphene rearrangement.

Received: May 29, 1998 [Z11919IE]
German version: *Angew. Chem.* **1998**, *110*, 3353 – 3355

Keywords: eliminations · fragmentations · intermediates · reaction mechanisms · rearrangements

[1] J. F. Bunnett, *Angew. Chem.* **1962**, *74*, 731 – 741; *Angew. Chem. Int. Ed. Engl.* **1962**, *1*, 225 – 235; J. Sicher, *Angew. Chem.* **1972**, *84*, 177 – 191; *Angew. Chem. Int. Ed. Engl.* **1972**, *11*, 200 – 214; M. Schlosser, *Methoden Org. Chem.* (*Houben-Weyl*) *4. ed. 1952-*, Vol. 5/1b, pp. 9 – 44.

[2] R. B. Woodward, R. Hoffmann, *Angew. Chem.* **1969**, *81*, 797 – 869; *Angew. Chem. Int. Ed. Engl.* **1969**, *8*, 781 – 853; M. J. S. Dewar, *Angew. Chem.* **1971**, *83*, 859 – 875; *Angew. Chem. Int. Ed. Engl.* **1971**, *10*, 761 – 775.

[3] J. Feuer, W. C. Herndon, L. H. Hall, *Tetrahedron* **1968**, *24*, 2575 – 2582; N. D. Epiotis, *J. Am. Chem. Soc.* **1973**, *95*, 5624 – 5632; K. N. Houk, *Acc. Chem. Res.* **1975**, *8*, 361 – 369; I. Fleming, *Frontier Orbitals and Organic Chemical Reactions*, Wiley, New York **1976**; I. Fleming, *Grenzorbitale und Reaktionen organischer Verbindungen*, VCH, Weinheim, **1990**; K. Fukui, *Angew. Chem.* **1982**, *94*, 852 – 861; *Angew. Chem. Int. Ed. Engl.* **1982**, *21*, 801 – 809.

[4] M. Geisel, C. A. Grob, R. A. Wohl, *Helv. Chim. Acta* **1969**, *52*, 2206 – 2215; C. A. Grob, P. W. Schiess, *Angew. Chem.* **1967**, *79*, 1 – 14; *Angew. Chem. Int. Ed. Engl.* **1967**, *6*, 1 – 15; C. A. Grob, *Angew. Chem.* **1969**, *81*, 543 – 554; *Angew. Chem. Int. Ed. Engl.* **1969**, *8*, 535 – 546.

[5] L. Garamszegi, M. Schlosser, *Chem. Ber.* **1997**, *130*, 77 – 82.

[6] For the reversibility of the ring closure of 5-hexenyl metal compounds to cyclopentylmethyl metal compounds, see A. Maercker, R. Geuss, *Chem. Ber.* **1973**, *106*, 773 – 797; see also M. Newcomb, M. T. Burchill,

 © WILEY-VCH Verlag GmbH, D-69451 Weinheim, 1998 1433-7851/98/3722-3174 $ 17.50+.50/0

Tetrahedron Lett. **1982**, *23*, 4867 – 4870; W. H. Bailey, L. M. J. Zarcone, *Tetrahedron Lett.* **1991**, *32*, 4425 – 4426.
[7] M. Schlosser in *Organometallics in Synthesis: A Manual* (Ed.: M. Schlosser), Wiley, Chichester, **1994**, pp. 28 – 29.
[8] *Molecular Rearrangements*, *Vol. 1* and *2* (Ed.: P. DeMayo), Wiley, New York, **1963** and **1964**; L. M. Harwood, *Polar Rearrangements*, University Press, Oxford, **1992**.
[9] R. Howe, E. C. Friedrich, S. Winstein, *J. Am. Chem. Soc.* **1965**, *87*, 378 – 381.
[10] J. A. Berson, *Angew. Chem.* **1968**, *80*, 765 – 777; *Angew. Chem. Int. Ed. Engl.* **1968**, *7*, 779 – 791; J. A. Berson, *Annu. Rev. Phys. Chem.* **1977**, *28*, 111 – 132.
[11] G. D. Hartmann, T. G. Traylor, *J. Am. Chem. Soc.* **1975**, *97*, 6147 – 6151.
[12] D. Lenoir, *Chem. Ber.* **1975**, *108*, 2055 – 2072.

The First Organobismuth Rings: $(RBi)_3$ and $(RBi)_4$, $R = (Me_3Si)_2CH$**

Hans Joachim Breunig,* Roland Rösler, and Enno Lork

Dedicated to Professor Bernt Krebs on the occasion of his 60th birthday

Monocyclic oligomers $(RE)_n$, R = organo group, $n = 3-6$, are only well known for the three central elements of the fifth main group (E = P, As, Sb). The existence of the corresponding organobismuth rings is questionable. Compounds such as $(PhBi)_x$,[1] and $(2,4,6\text{-}Ph_3C_6H_2Bi)_x$,[2] which are described in the literature are possibly rings but their structures have not been proven. The first fully characterized organobismuth(I) compound is a dibismuthene: $(RBi)_2$ $(R = 2,4,6\text{-}[(Me_3Si)_2CH]_3C_6H_2)$.[3]

Inorganic bismuth compounds have a tendency to form cyclic structures, for example, in the element bismuth, in polycyclic cations such as Bi_9^{5+}[4] and Bi_5^{3+},[5] and in bismutides such as Bi_4^{2-}.[6] Here we report the synthesis and the structure of the trimeric and tetrameric compounds **1** and **2,** the first organobismuth rings.

R_3Bi_3 R_4Bi_4 $(R = (Me_3Si)_2CH)$
1 **2**

Compounds **1** and **2** were synthesized by reduction of $RBiCl_2$[7] with magnesium filings in THF at $-35\,^\circ C$. In solution there is an equilibrium between the two organobismuth rings [Eq. (1)]. The equilibrium constant $K = [R_3Bi_3]^4/[R_4Bi_4]^3$ is $40 \pm 5\ mol\,L^{-1}$ in C_6D_6 at $23\,^\circ C$. As

$$4\,R_3Bi_3 \rightleftharpoons 3\,R_4Bi_4 \quad (1)$$

expected, the equilibrium is shifted in favor of the four-membered ring when the solution is cooled. Black crystals of **2** were grown from a solution in petroleum ether at low temperatures. When the crystals were dissolved in hydrocarbons fascinating color changes were observed: first the four-membered ring dissolved to give an intensive green solution. Within a few minutes the ring – ring equilibrium was established and the red color associated with the three-membered ring predominated in the solution. At low temperatures the fraction of **2** increased again and the solutions became first brown and then black on cooling. Both solutions of **1** and **2,** as well as the crystals of **2** are air-sensitive and thermolabile. In the absence of light and air, solutions in C_6D_6 decompose at ambient temperature with first-order kinetics to give R_3Bi[8] and bismuth. At $23\,^\circ C$ the concentrations of the rings decreased with half-life periods of 20.2 ± 2.0 h for **2** and 31.6 ± 2.7 h for **1**. At $-28\,^\circ C$ the crystals of **2** and the solutions of **1** and **2** are stable for several months.

The structure of **1** can be derived from the NMR spectra. It is a tribismirane with $(Me_3Si)_2CH$ groups in *cis – trans* positions. The ^1H NMR spectrum shows singlets for the methine protons, with an intensity ratio 1:2. As a consequence of the diastereotopy at the substituents in the *cis* positions there are three signals of equal intensity for the methyl protons. The ^{13}C NMR spectrum contains three signals for the carbon atoms of the methyl groups and two broad signals for the carbon atoms of the methine groups. The line broadening is a consequence of the interactions with the quadrupole moment of the bismuth nucleus. Similar signal patterns are also found in the NMR spectra of the antimony analogue of **1**, which was recently characterized by X-ray crystallography.[9] The ^1H and ^{13}C NMR spectra of **2** in C_6D_6 show two signals each, corresponding to an *all-trans* arrangement of the alkyl substituents. To date **1** and **2** could not be characterized by mass spectrometry; even with soft ionization techniques only signals of decomposition products (R_3Bi, R_4Bi_2) could be identified. A single-crystal X-ray structure analysis for **2** confirmed the *all-trans* configuration of the tetrabismethane in the solid state (Figure 1).[10]

The structure contains a folded four-membered bismuth ring. The bismuth – bismuth bond lengths lie between 297.0(5) and 304.4(2) pm. Similar Bi – Bi bond lengths were also measured for dibismuthanes Ph_4Bi_2 (299.0(2)[11]) and $(Me_3Si)_4Bi_2$ (303.5(3)[12]). The anionic ring Bi_4^{2-} has slightly shorter bonds (293.6(2), 294.1(2) pm).[6] The double bond in the dibismuthene $[\{2,4,6\text{-}[(Me_3Si)_2CH]_3C_6H_2Bi\}_2]$ (Bi – Bi 282.06(8) pm) is even shorter.[3] The Bi – C distances in **2** vary between 233(2) and 239(2) pm. They are a little longer on average than in R_3Bi ($R = (Me_3Si)_2CH$, Bi–C 230.6(13) – 234.7(13) pm).[8] The Bi-Bi-Bi bond angles in **2** lie between 78.97(8)and 79.93(6)°; in contrast the Bi-Bi-C angles are relative large (range between 93.9(6) and 109.5(5)°). The larger Bi–Bi distances and Bi-Bi-C angles may be related to repulsive interactions of the alkyl substituents in the mole-

[*] Prof. Dr. H. J. Breunig, R. Rösler, Dr. E. Lork
Institut für Anorganische und Physikalische Chemie (FB 02) der Universität
Postfach 330440, D-28334 Bremen (Germany)
Fax: (+49) 421-218-4042
E-mail: breunig@chemie.uni-bremen.de

[**] This work was supported by the Deutsche Forschungsgemeinschaft.

 © WILEY-VCH Verlag GmbH, D-69451 Weinheim, 1998 1433-7851/98/3722-3175 $ 17.50+.50/0

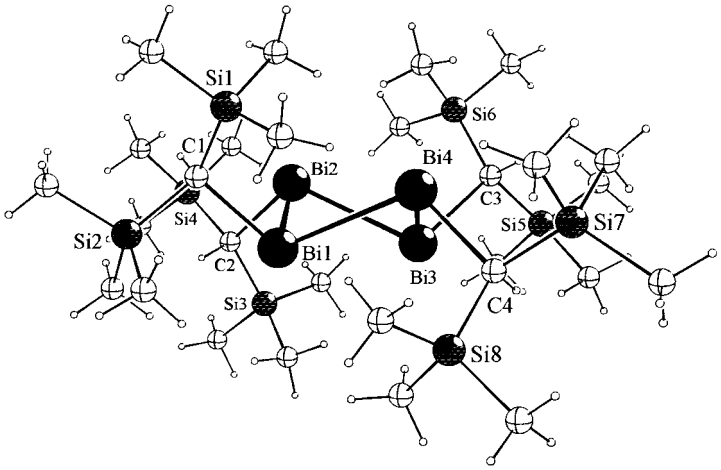


Figure 1. Structure of **2** in the crystal. Selected bond lengths [pm] and angles [°]: Bi(1)–Bi(2) 298.4(5), Bi(2)–Bi(3) 304.4(2), Bi(3)–Bi(4) 297.0(5), Bi(1)–Bi(4) 302.3(2), Bi(1)–C(1) 233(2), Bi(2)–C(2) 234.0(16), Bi(3)–C(3) 239.0(19), Bi(4)–C(4) 232(2), Bi(1)···Bi(3) 383.4, Bi(2)···Bi(4) 385.9; Bi(2)-Bi(1)-Bi(4) 79.93(6), Bi(1)-Bi(2)-Bi(3) 78.97(8), Bi(2)-Bi(3)-Bi(4) 79.82(8), Bi(1)-Bi(4)-Bi(3) 79.52(8), C(1)-Bi(1)-Bi(2) 93.9(6), C(1)-Bi(1)-Bi(4) 109.5(5), C(2)-Bi(2)-Bi(1) 97.9(5), C(2)-Bi(2)-Bi(3) 109.4(4), C(3)-Bi(3)-Bi(4) 97.1(5), C(3)-Bi(3)-Bi(2) 108.2(5), C(4)-Bi(4)-Bi(1) 107.5(5), C(4)-Bi(4)-Bi(3) 95.9(5); mean torsion angles Bi-Bi-Bi-Bi ± 46.12(8); mean fold angle between the Bi-Bi-Bi planes 112.7.

cules. As a consequence of the considerable folding of the four-membered ring, the Bi-Bi-Bi bond angles are surprisingly small for three-coordinate bismuth compounds. The fold angles are 112.6° and 112.9°. As in all four-membered rings $(RE)_n$ with *cis–trans* configuration the folding results from repulsive interactions of the substituents in 1,3-positions and from the tendency to avoid eclipsed conformations. The repulsive interactions should decrease with increasing bond lengths. Consequently, the folding decreases clearly from the phosphorus four-membered ring to the four-membered antimony ring (mean fold angles: $(RP)_4$ 109.8°,[13] $(RSb)_4$ 115.4°;[14] $R = (Me_3Si)_2CH$). An opposing effect is exerted by stabilising transannular E···E interactions.[15] The small increase of folding on the transition to the bismuth ring **2** may be related to transannular Bi···Bi contacts. The corresponding Bi–Bi distances are 383.4 and 385.9 pm. They clearly lie within the sum of the van der Waals radii of 480 pm.[16] For comparison with the analogous antimony ring $(RSb)_4$, the ratio E···E/E–E of the shortest E···E contact distance and the E–E bond length may be used.[12] The E···E/E–E ratio is 1.31 in $(RSb)_4$[14] but 1.29 in $(RBi)_4$ and displays the expected decrease for the heavier element. However, the difference from the corresponding antimony ring is minor and the prevailing impression is of a close relationship of the two structures.

Experimental Section

1 and **2**: All operations were carried out with careful exclusion of air in an argon atmosphere. At −80 °C a solution of $(Me_3Si)_2CHBiCl_2 \cdot 0.5\,Et_2O$ (1.48 g, 3.11 mmol) in THF (20 mL) was added dropwise with stirring to magnesium filings (0.25 g, 10.28 mmol) activated with 1,2-dibromoethane in THF (10 mL). Thereafter the mixture was warmed to −35 °C, stirred for 6 h at −35 °C and 1 h at −15 °C. The solvent was removed in vacuo and the residue was extracted with petroleum ether (250 mL). The dark brown solution was filtered at −10 °C through a frit and concentrated to dryness. After removal of the solvent a dark brown solid consisting of **1** and **2** remained. Yield 0.78 g, 68 %. Large black crystals of **2**, m.p. 89–91 °C, grew from a solution of the cyclobismuthane mixture in petroleum ether −28 °C in several weeks. Elemental analysis of $C_{28}H_{76}Bi_4Si_8$ (**2**): calcd. C 22.82, H 5.20; found: C 22.10, H 5.16; ^{1}H NMR (200 MHz, C_6D_6, 23 °C): **1**: $\delta = 0.25$ (s, $^2J(Si,H) = 6.4$ Hz, 18 H; *trans*-CH_3), 0.28 (s, $^2J(Si,H) = 6.2$ Hz, 18 H; *cis*-CH_3^a), 0.40 (s, $^2J(Si,H) = 6.3$ Hz, 18 H; *cis*-CH_3^b), 1.87 (s, $^2J(Si,H) = 7.7$ Hz, 1 H; *trans*-CH), 2.20 (s, $^2J(Si,H) = 7.5$ Hz, 2 H; *cis*-CH); **2**: $\delta = 0.33$ (s, $^2J(Si,H) = 6.3$ Hz, 18 H; CH_3), 2.31 (s, $^2J(Si,H) = 8.0$ Hz, 1 H; CH); ^{13}C NMR (50 MHz, C_6D_6, 23 °C): **1**: $\delta = -2.37$ (br, *cis*-CH), −0.70 (br, *trans*-CH), 4.53 (*cis*-CH_3^b), 5.50 (*trans*-CH_3), 6.02 (*cis*-CH_3^a); **2**: $\delta = 3.78$ (br, CH), 6.20 (CH_3). C,H correlation with HSQC and HMBC spectra; the indices a and b refer to the diastereotopic methyl groups. MS (CI+, NH_3): *m/z* (%): 1071 (5) $[[(Me_3Si)_2CH]_4Bi_2{+}NH_4^+]$, 918 (6), 1071 (5) $[[(Me_3Si)_2CH]_2Bi{+}NH_4^+]$, 687 (15) $[[(Me_3Si)_2CH]_3Bi^+]$, 671 (23) $[[(Me_3Si)_2CH]_3Bi^+ - CH_3]$, 627 (100) $[[(Me_3Si)_2CH]_2Bi^+]$.

The decomposition of a mixture of **1** and **2** (115 mg) in C_6D_6 (1 mL) at 23 °C was monitored by ^{1}H NMR spectroscopy, with 60 mmol L^{-1} TMS as reference. The equilibrium constant was determined from the ratio of intensities of the signals of **1** and **2**. The decomposition products are $[(Me_3Si)_2CH]_3Bi$[8] and elemental Bi. $[(Me_3Si)_2CH]_3Bi$: ^{1}H NMR (200 MHz, C_6D_6, 23 °C): $\delta = 0.29$ (s, $^2J(Si,H) = 6.2$ Hz, 18 H; CH_3), 1.37 (s, $^2J(Si,H) = 8.6$ Hz, 1 H; CH); ^{13}C NMR (50 MHz, C_6D_6, 23 °C): $[(Me_3Si)_2CH]_3Bi$ $\delta = 5.05$ (br; CH_3), 8.73 (br; CH).

Received: June 15, 1998 [Z11987IE]
German version: *Angew. Chem.* **1998**, *110*, 3361–3363

Keywords: bismuth · small ring systems · structure elucidation

[1] E. Wiberg, A. Mödritzer, *Z. Naturforsch. B* **1957**, *12*, 132–134.
[2] X.-W. Li, J. Lorberth, W. Massa, S. Wocadlo, *J. Organomet. Chem.* **1995**, *485*, 141–147.
[3] N. Tokitoh, Y. Arai, R. Okazaki, S. Nagase, *Science* **1997**, *277*, 78–80.
[4] R. M. Friedman, J. D. Corbett, *Inorg. Chem.* **1973**, *12*, 1134–1139.
[5] R. C. Burns, R. J. Gillespie, W.-C. Luk, *Inorg. Chem.* **1978**, *17*, 3596–3604.
[6] A. Cisar, J. D. Corbett, *Inorg. Chem.* **1977**, *16*, 2482–2487.
[7] H. Althaus, H. J. Breunig, R. Rösler, E. Lork, *Organometallics*, in press.
[8] B. Murray, J. Hvoslef, H. Hope, P. P. Power, *Inorg. Chem.* **1983**, *22*, 3421–3424.
[9] H. J. Breunig, R. Rösler, E. Lork, *Organometallics*, in press.
[10] X-ray structure analysis of **2** ($C_{28}H_{76}Bi_4Si_8$), $M_r = 1473.53$; crystal size $0.7 \times 0.6 \times 0.4$ mm^3; triclinic, space group $P\bar{1}$, $a = 1242(2)$, $b = 1307.1(7)$, $c = 1678.5(9)$ pm, $\alpha = 107.74(4)$, $\beta = 91.71(7)$, $\gamma = 102.56(6)°$, $V = 2.519(5)$ nm^3, $Z = 2$, $\rho_{calcd} = 1.943$ Mg m^{-3}, $\mu = 14.136$ mm^{-1}. A suitable single crystal was fixed with Kel-F oil on a glass fiber and measured on a Siemens P4 four-circle diffractometer at −100 °C. With graphite-monochromated $Mo_{K\alpha}$ radiation ($\lambda = 71.073$ pm) in $\omega/2\theta$ scan mode 7334 intensities were collected ($2.56° < \theta < 22.50°$); 6149 reflections ($R_{int} = 0.0549$) remained after averaging. After Lp correction the structure was solved by direct methods. The refinement converged after an absorption correction (DIFABS)[17] at $wR_2 = 0.1447$ (refinement against F^2) for all the 6149 reflections and 387 variables ($R1 = 0.0562$ for 4308 reflections with $I > 2\sigma(I)$). Heavy atoms obtained individual anisotropic displacement parameters. The hydrogen atoms were refined with a riding model and a common isotropic temperature factor. Max/min residual electron density: 1771/−1748 e nm^{-3}. The structure solution and refinement was carried out using SHELX-97.[18] For the figure the Diamond program was used.[19] Crystallographic data (excluding structure factors) for the structures reported in this paper have been deposited with the Cambridge Crystallographic Data Center as supplementary publication no. CCDC-101535. Copies of the data can be obtained free of charge on application to CCDC, 12 Union Road, Cambridge CB2 1EZ, UK (fax: (+44) 1223-336-033; e-mail: deposit@ccdc.cam.ac.uk).

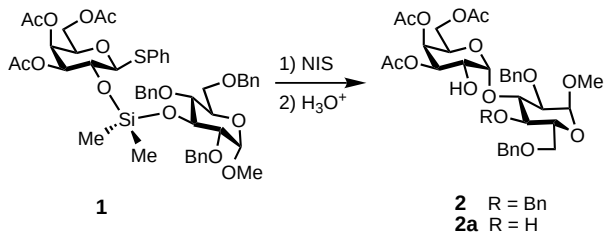
 © WILEY-VCH Verlag GmbH, D-69451 Weinheim, 1998 1433-7851/98/3722-3176 $ 17.50+.50/0

[11] F. Calderazzo, R. Poli, G. Pelizzi, *J. Chem. Soc. Dalton Trans.* **1984**, 2365 – 2369.
[12] O. Mundt, G. Becker, M. Rössler, C. Witthauer, *Z. Anorg. Allg. Chem.* **1983,** *506*, 42 – 58.
[13] R. Streubel, Dissertation, Bonn, **1990**.
[14] M. Ates, H. J. Breunig, K. Ebert, S. Gülec, R. Kaller, M. Dräger, *Organometallics* **1992**, *11*, 145 – 150.
[15] O. M. Kekia, R. L. Jones, Jr., A. L. Rheingold, *Organometallics* **1996**, *15*, 4104 – 4106.
[16] N. Wiberg, *Hollemann-Wiberg, Lehrbuch der Anorganischen Chemie*, Walter de Gruyter, Berlin, **1995**, p. 1838.
[17] N. Walker, D. Stuart, *Acta Crystallogr. Sect. A* **1983**, *39*, 158.
[18] G. M. Sheldrick, SHELX-97, Universität Göttingen, **1997**.
[19] DIAMOND - Visual Crystal Structure Information System, CRYSTAL IMPACT, Postfach 1251, D-53002 Bonn.

A New Intramolecular Reaction for the Regioselective Debenzylation or Protection of Alcohols**

Jacob Madsen and Mikael Bols*

In an earlier study of silicon-tethered intramolecular glycosidation reactions it was observed that treatment of compound **1** with *N*-iodosuccinimide (NIS) gave both the expected glycoside **2** and an unexpected debenzylated product **2a** (Scheme 1).[1] Originally we believed that this debenzylation reaction followed an intramolecular pathway involving silicon during the glycosidation procedure. We came to this conclusion for two reasons: The reaction was regioselective, and if the reaction mixture was not treated with acid after the glycosidation, a debenzylated, silicon-bridged product was isolated (Figure 1).[1a]



Scheme 1. Intramolecular glycosidation with formation of two products. Bn = benzyl.

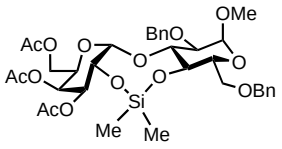


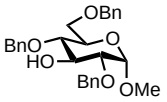
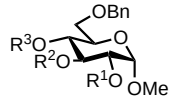
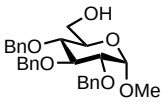
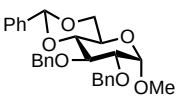
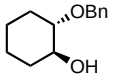
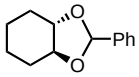
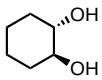
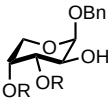
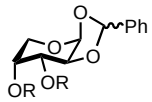
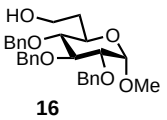
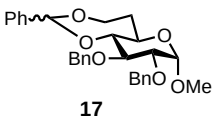
Figure 1. Compound isolated when the reaction mixture from Scheme 1 was not treated with acid.

[*] Dr. M. Bols, J. Madsen
Department of Chemistry
University of Aarhus
DK-8000 Aarhus (Denmark)
Fax: (+45) 86-196-199
E-mail: mb@kemi.aau.dk

[**] We thank the Danish National Research Council for financial support (grant no. 9502986).

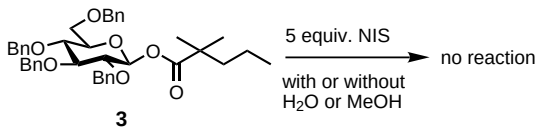
We have now reinvestigated the reaction (Scheme 1) and have come to the conclusion that the debenzylation apparently is not connected to the glycosidation process. In fact treatment of compound **2** with NIS in $MeNO_2$ gave compound **2a** (Table 1). This indicated an intermolecular reaction and indeed no participation by silicon. On the other hand the regioselectivity of the debenzylation suggested an intramolecular reaction and in that case the only possibility seemed to be participation of the free OH group at C-2 in the galactose unit.

Table 1. Reaction of benzylated compounds containing free OH groups with NIS.[11]

Reactant	Product	Solvent/Equiv. NIS	Yield [%]
2	**2a**	$MeNO_2$/2.5	36[a]
 **4**	 **5** R^1 = Bn, R^2 = R^3 = H **6** R^1 = R^2 = H, R^3 = Bn	$MeNO_2$/2.5[b]	80 (32) (48)
 **7**	 **8**	$MeNO_2$/5[c]	74
 **9**	 **10**	CH_2Cl_2/2.5[d]	49
9	 **11**	CH_2Cl_2/2.5[b, d]	66
 **12** R = H **14** R, R = CMe_2	 **13** R = H **15** R, R = CMe_2	CH_3CN/5	41 – 44
 **16**	 **17**	$MeNO_2$/5	84

[a] Not optimized. The crude product was a 2:1 mixture of **2** and **2a**, respectively, so the recovered yield was very high. [b] Treatment with TFA/H_2O 5/1. [c] Reaction with 20 equiv NIS gave **8** in 76% yield. [d] Reaction at room temperature.

The presence of the unprotected alcohol was found to be essential. When glucose derivative **3**[2] (Scheme 2) was treated with NIS (5 equiv), no reaction was observed even on addition of water or methanol. In contrast, when readily available alcohol **4**[3] was refluxed for 2 h in $MeNO_2$ with NIS (2.5 equiv) quantitative conversion to less polar products was observed (by thin-layer chromatography) with simultaneous formation of iodine (Table 1). These products could not be purified by chromatography due to their instability, but on



Scheme 2. Without an unprotected alcohol present in the molecule no reaction occurred.

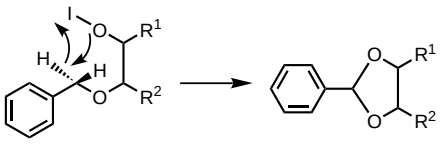
hydrolysis of the reaction products with TFA/H_2O 5/1 the two diols **5** and **6** were isolated in 32% and 48% yield, respectively (total yield: 80%). Compound **5** was identified by comparison with the known spectrum,[4] compound **6** by conversion to the diacetate.

The initially formed less polar products were assumed to be 1,2-*trans* benzylidene derivatives, which would account for the instability. To confirm the formation of a benzylidene derivative, compound **7**[5] was treated with NIS (5 equiv). This gave the anticipated product **8** in 74% yield.

We also investigated a compound of non-carbohydrate structure. Alcohol **9**[6] reacted with NIS (5 equiv) to give the new *trans*-benzylidene compound **10**[7] in 49% yield. ^{1}H and ^{13}C NMR and EI mass spectral data as well as the lower retention time of **10** than **9** on silica gel supported the proposed structure and configuration of **10**. Unlike the corresponding *cis*-benzylidene compound[8] the symmetry of **10** only allows formation of one stereoisomer at the benzylidene center; this exhibits different chemical shifts for all carbon and hydrogen atoms. The atoms H-1 and H-2 of **10** have slightly different chemical shifts but identical coupling constants. Furthermore these two H atoms display two large coupling constants, which were consistent with the protons being axial. The ^{1}H NMR spectra of **10** and its *cis* isomer[8] are very similar except that the signals of H-1 and H-2 lie between $\delta = 3.39 - 3.47$ in **10** and between $\delta = 3.99 - 4.3$ in the *cis* compound.[8] This also confirmed the axial position of H-1 and H-2 in **10**. The lower yield in this case was not a result of a low degree of debenzylation, but rather instability of **10** under the conditions of the reaction and isolation. Thus if in a similar experiment the reaction mixture was subjected to hydrolytic work-up diol **11** could be isolated in 66% yield.

Further examples of this new reaction, which appears to be generally applicable, are given in Table 1. Benzyl-β-D-arabinopyranoside **12**[9] and benzyl-3,4-isopropylidene-β-D-arabinopyranoside **14**[10] gave the expected acetals **13** and **15** in 44% and 41% yield, respectively. Again instability of the benzylidene compounds accounts for the diminished yields. Particularly noteworthy is the reaction of **12** because it is an example of a selective protection of a hydroxyl group vicinal to a benzyl ether. Interesting is also the conversion of compound **16**[10] to benzylidene derivative **17** in 84% yield as it results in the formation of a seven-membered ring.

The reaction occurs in a variety of solvents (MeCN, $MeNO_2$, CH_2Cl_2) with no large difference in rate. In general NIS is used in the reaction in stoichiometric amounts (2 equiv), but frequently several extra equivalents were necessary to ensure complete conversion. The mechanism of the reaction is probably ionic, as addition of 2,2′-azobisisobutronitrile (AIBN) did not favor the reaction; nor could NIS be substituted with *N*-bromosuccinimide. Since the reaction only occurs at benzyl groups vicinal to a hydroxyl group we suggest that the OH group participates in the reaction in the manner proposed in Scheme 3. Reaction between the hydroxyl group and NIS leads to formation of a hypoiodite that abstracts a proton from the neighboring benzyl group leading to a benzylidene group.



Scheme 3. Suggested mechanism for the formation of benzylidene derivatives.

Finally one may wonder why this reaction had not been detected previously as it would be expected to occur at least to some extent in NIS-promoted glycosidation of many benzylated glycosyl acceptors. In fact Hindsgaul et al. have observed the formation of **8** as a by-product in NIS-catalyzed tethered glycosidations which may well have been formed from **7**.[12]

In conclusion we have presented a new reaction that has considerable potential for selective reactions of polyfunctional alcohols or benzyl ethers and that should facilitate protection group chemistry. NIS very efficiently promotes debenzylation of monobenzylated 1,2-, 1,3-, and 1,4-diols and in many cases the intermediate benzylidene derivatives can be isolated.

Received: April 30, 1998 [Z11798IE]
German version: *Angew. Chem.* **1998**, *110*, 3348 – 3350

Keywords: acetals · carbohydrates · protecting groups

[1] a) M. Bols, *Tetrahedron* **1993**, *49*, 10049 – 10060; b) M. Bols, *J. Chem. Soc. Chem. Commun.* **1993**, 791 – 792.
[2] M. Bols, H. C. Hansen, B. I. Smith, *Acta Chem. Scand.* **1993**, *47*, 532 – 534.
[3] S. Koto, N. Morishima, M. Owa, S. Zen, *J. Carbohydr. Chem.* **1984**, *130*, 73 – 78.
[4] Q. Qin, T. Grindley, *J. Carbohydr. Chem.* **1994**, *13*, 475 – 490.
[5] K. Umemura, H. Matsuyama, M. Kobayshi, N. Kamigata, *Bull. Chem. Soc. Jpn.* **1989**, *62*, 3026 – 3028.
[6] D. Basavaiah, P. R. Krishna, *Tetrahedron* **1994**, *50*, 10521 – 10530.
[7] **10**: ^{1}H NMR (200 MHz, $CDCl_3$): $\delta = 7.6 - 7.2$ (m, 5H; arom. H), 6.05 (s, 1H; acetal), 3.47 (ddd, $J = 11.0$, 8.7, 3.7 Hz, 1H; H-1), 3.39 (ddd, $J = 11.0$, 8.7, 3.7 Hz, 1H; H-2), 2.2 (m, 2H), 1.85 (m, 2H), 1.6 – 1.2 (m, 4H); ^{13}C NMR (50 MHz, $CDCl_3$): 140.0, 130.2, 129.5, 128.9, 128.8 (arom. C), 104.1(C-7), 83.0, 80.6(C-1, C-2), 29.6, 29.2 24.2, 24.1 (C-3, C-4, C-5, C-6). MS (EI): *m*/*z*: 204 [M^+], 203 [$M^+ - H$].
[8] R. C. Cambie, P. S. Rutledge, P. A. Watson, P. D. Woodgate, *Aust. J. Chem.* **1989**, *42*, 1939 – 1949.
[9] R. E. Ireland, L. Courtney, B. J. Fitzsimmons, *J. Org. Chem.* **1983**, *48*, 5186 – 5198.
[10] W. Dong, T. M. Jespersen, T. Skrydstrup, M. Bols, M. R. Sierks, *Biochemistry* **1996**, *35*, 2788 – 2795.
[11] General reaction conditions: Compound (0.1 mmol) in solvent (10 mL) and NIS were refluxed for 2 – 4 h. Then EtOAc (75 mL) was added, and the mixture washed with 5% $Na_2S_2O_3$ solution (2 × 25 mL). The dried and evaporated organic phase was purified by flash chromatography (SiO_2).
[12] F. Barresi, O. Hindsgaul *Can. J. Chem.* **1994**, *113*, 1447 – 1465.

 © WILEY-VCH Verlag GmbH, D-69451 Weinheim, 1998 1433-7851/98/3722-3178 $ 17.50+.50/0

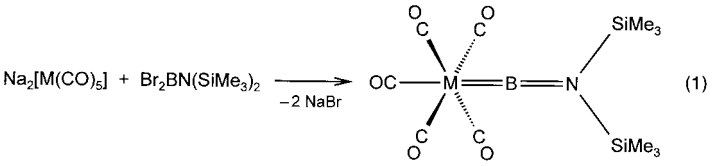
Synthesis and Structure of the First Terminal Borylene Complexes**

Holger Braunschweig,* Carsten Kollann, and Ulli Englert

Over the last years a new class of transition metal complexes displaying two-center two-electron (2c–2e) bonds between the metal center and a threefold-coordinated boron atom has been established.[1] These compounds include a large number of structurally characterized boryl complexes, mostly derived from catecholborane[2a–g] and nitrogen-substituted boranes,[3a–c] but there are only very few examples of complexes with bridging borylene ligands such as $[(\mu\text{-BR})\{(C_5H_5)Mn(CO)_2\}_2]$ and $[\{\mu\text{-BN(SiMe}_3)_2\}(\mu\text{-CO})\{(C_5H_5)\text{-Fe(CO)}\}_2]$.[4a–c, 3c] The coordination of the borylene BR ligand to a single metal center leads to formation of terminal borylene complexes with boron in coordination number two and a metal–boron double bond.[18]

An earlier report on such a compound describes the iron–borylene complex $[(CO)_4Fe(BNMe_2)]$, the structure of which was deduced from elemental analysis and IR and ^{11}B NMR spectroscopy.[5] The ^{11}B NMR shift at $\delta = -18$, however, strongly conflicts with the signals of the complexes described in the present paper, and also with the signal $\delta = 88.2$ for $[(CO)_4Fe\{BN(SiMe_3)_2\}]$.[6] Clearly, a structure needs to be ascribed to the reported iron complex which does not contain an iron–borylene unit.

The borylene complexes $[(CO)_5M\{BN(SiMe_3)_2\}]$ (M = Cr: **1a**; W: **1b**) were obtained according to Equation (1) in yields



(1)

1a, M = Cr
1b, M = W

of about 30% as light brown crystalline solids. Both products exhibit considerable stability: They show no sign of decomposition in solution at ambient temperature after several days, and in the crystalline state they can be handled in air for about one hour.

The structure of **1a** and **1b** in solution was deduced from the NMR and IR data. The ^1H NMR spectra show sharp singlets for the protons of the $SiMe_3$ groups, while the ^{13}C NMR spectra contain a signal for the methyl groups of the $N(SiMe_3)_2$ substituents along with two signals in a 1:4 ratio for the axial and equatorial carbonyl ligands. In comparison with amino-substituted boryl complexes, the borylene complexes exhibit considerably low field shifted ^{11}B NMR signals at $\delta =$ 92.3 (**1a**) and 86.6 (**1b**), which are close to the range observed for bridged aminoborylene complexes. As expected for these octahedral complexes, the IR spectra show three bands for the carbonyl groups which are considerably shifted to lower wavenumbers with respect to those for corresponding vinylidene complexes.[7]

The results of the X-ray structure analysis of **1b** (Figure 1) show that the molecule adopts C_1 symmetry in the crystal.[8] The $W(CO)_5$ moiety exhibits C-W-C angles of about 90° and

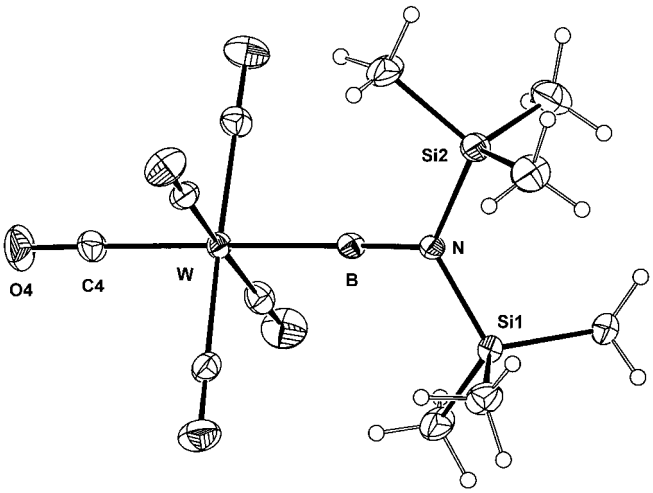


Figure 1. Structure of **1b** in the crystal (ellipsoids at the 30% probability level; the hydrogen atoms are shown with arbitrary radii).[17] Selected bond lengths [Å] and angles [°]: W–B 2.151(7), B–N 1.338(8); W-B-N 177.9(5).

very similar W–C and C–O distances, and thus displays approximately C_{4v} symmetry. The Si1-Si2-B plane is twisted by 37.2(2)° with respect to the C4-C2-C3 plane. The tungsten–boron bond together with the W-B-N angle are clearly the most interesting features of this structure: The bond length is 215.1(7) pm, and the three central atoms are arranged in an almost ideal linear way with an angle of 177.9(5)°. Compared to the metal–boron bond in $[(C_5H_5)(CO)_3W\{B(NMe_2)\text{-}BCl(NMe_2)\}]$, which is the only structurally characterized amino-substituted boryl complex of tungsten,[3a] the W–B bond of **1b** is shorter by about 22 pm, but still longer by 8 pm than that of the alkyl-substituted boryl complex $[(tpb')(CO)_2W\{BEt(CH_2\text{-}p\text{-}MeC_6H_4)\}]$ (tpb′ = tris(3,5-dimethylpyrazol-1-yl)hydroborate), which is stabilized by an agostic C–H interaction.[9]

The boron–nitrogen bond length of 133.8(8) pm is somewhat shorter than in the alkylidene(amino)borane $(Me_3Si)_2C{=}B{=}N\textit{i}Pr_2$ (136.3(4) pm), which also shows a double bond between a twofold-coordinated boron atom and a threefold-coordinated nitrogen atom.[10] The geometry of the axial CO group resembles those of the equatorial CO groups, thus indicating that there is no *trans* effect of the borylene ligand. These observations together with the IR data correspond to a description of the metal–boron double bond in terms of strong boron-to-metal σ donation and weaker π backbonding from the metal to boron. For aminoborylene complexes of first row transition metals this conclusion was predicted on the basis of ab initio calculations.[11]

[*] Dr. H. Braunschweig, C. Kollann, Dr. U. Englert Institut für Anorganische Chemie der Technischen Hochschule
Templergraben 55, D-52056 Aachen (Germany)
Fax: (+49) 241-888-8288
E-mail: holger.braunschweig@ac.rwth-aachen.de

[**] This work was supported by the Deutsche Forschungsgemeinschaft and the Fonds der Chemischen Industrie.

Experimental Section

1a: In analogy to the known synthesis of $Na_2[M(CO)_5]$ (M = Cr, W)[12] a solution of $[Me_3NCr(CO)_5]$ (1.21 g, 4.82 mmol) in THF (30 mL) was cooled to −78 °C, and a solution of $NaC_{10}H_8$ (57.8 mL, 0.20 M in THF were added dropwise over a period of 20 min. When the addition was complete all volatile materials were removed under high vacuum (0 °C/0.001 Torr). The remaining yellow solid was treated with Et_2O (50 mL) at 0 °C, filtered, and washed with Et_2O (2 × 10 mL). The light yellow product was dried briefly under high vacuum and subsequently suspended in toluene (30 mL) at 0 °C. $Br_2BN(SiMe_3)_2$[13] (1.36 g, 4.00 mmol) was added dropwise by a syringe, and the color of the suspension quickly turned from orange to dark brown. After the reation mixture was stirred for 30 min at 0 °C, it was warmed to ambient temperature and all volatile materials were removed under high vacuum. The dark brown residue was suspended in hexane (30 mL) and filtered, and the remaining solid was rinsed with hexane (10 mL). The filtrate was concentrated under vacuum to 20 mL and stored at −30 °C. After 72 h $[(Me_3Si)_2NBCr(CO)_5]$ (0.35 g, 36.7 %) was obtained as light brown crystals. All NMR spectra were recorded in in [D$_6$]benzene at 25 °C. ^{1}H NMR (500 MHz, TMS): $\delta = 0.14$ (s, $SiMe_3$); ^{11}B NMR (160 MHz, $Et_2O \cdot BF_3$): $\delta = 92.3$; ^{13}C NMR (126 MHz, TMS): $\delta = 2.6$ ($SiMe_3$), 217.6 (CO_{eq}), 218.0 (CO_{ax}); IR (toluene): $\tilde{\nu} = 2064$ (w), 1981 (m), 1942 (vs) cm^{-1} (CO); elemental analysis calcd for $C_{11}H_{18}CrNBO_5Si_2$: C 36.37, H 5.00, N 3.86; found: C 35.47, H 5.10, N 3.72.

1b: As described for **1a** $[Me_3NW(CO)_5]$[14] (0.85 g, 2.22 mmol) was treated with a solution of $NaC_{10}H_8$ (26.7 mL, 0.20 M) and then with $Br_2BN(SiMe_3)_2$ (0.68 g, 2.00 mmol). $[(Me_3Si)_2NBW(CO)_5]$ (0.24 g, 24.3 %) was obtained as light brown crystals. All NMR spectra were recorded in [D$_6$]benzene at 25 °C. ^{1}H NMR (500 MHz, TMS): $\delta = 0.12$ (s, $SiMe_3$); ^{11}B NMR (160 MHz, $Et_2O \cdot BF_3$): $\delta = 86.6$; ^{13}C NMR (126 MHz, TMS): $\delta = 2.9$ ($SiMe_3$), 196.5 (CO_{ax}), 197.2 (CO_{eq}); IR (toluene): $\tilde{\nu} = 2075$ (w), 1967 (m), 1941 (vs) cm^{-1} (CO); elemental analysis calcd for $C_{11}H_{18}NBO_5Si_2W$: C 26.68, H 3.66, N 2.83; found: C 26.29, H 3.59 N 2.72.

Received: June 9, 1998 [Z 11968 IE]
German version: *Angew. Chem.* **1998**, *110*, 3355 – 3357

Keywords: boron · chromium · transition metal complexes · tungsten

[1] H. Braunschweig, *Angew. Chem.* **1998**, *110*, 1882 – 1898; *Angew. Chem. Int. Ed.* **1998**, *37*, 1786 – 1801.
[2] a) J. R. Knorr, J. S. Merola, *Organometallics* **1990**, *9*, 3008 – 3012; b) S. A. Westcott, N. J. Taylor, T. B. Marder, R. T. Baker, N. J. Jones, J. C. Calabrese, *J. Chem. Soc. Chem. Commun.* **1991**, 304 – 305; c) J. F. Hartwig, S. Huber, *J. Am. Chem. Soc.* **1993**, *115*, 4908 – 4909; d) P. Nguyen, H. P. Blom, S. A. Westcott, N. J. Taylor, T. B. Marder, *J. Am. Chem. Soc.* **1993**, *115*, 9329 – 9330; e) J. F. Hartwig, S. R. de Gala, *J. Am. Chem. Soc.* **1994**, *116*, 3661 – 3662; f) D. R. Lantero, D. H. Motry, D. L. Ward, M. R. Smith, *J. Am. Chem. Soc.* **1994**, *116*, 10811 – 10812; g) C. Dai, G. Stringer, F. F. Corrigan, N. J. Taylor, T. B. Marder, N. C. Norman, *J. Organomet. Chem.* **1996**, *513*, 273 – 275.
[3] a) H. Braunschweig, B. Ganter, M. Koster, T. Wagner, *Chem. Ber.* **1996**, *129*, 1099 – 1101; b) H. Braunschweig, C. Kollann, M. Müller, *Eur. J. Inorg. Chem.* **1998**, 291 – 293; c) H. Braunschweig, C. Kollann, U. Englert, *Eur. J. Inorg. Chem.* **1998**, 465 – 468.
[4] a) H. Braunschweig, T. Wagner, *Angew. Chem.* **1995**, *107*, 904 – 905; *Angew. Chem. Int. Ed. Engl.* **1995**, *34*, 825 – 826; b) H. Braunschweig, B. Ganter, *J. Organomet. Chem.* **1997**, *545*, 163 – 167; c) H. Braunschweig, M. Müller, *Chem. Ber.* **1997**, *130*, 1295 – 1298.
[5] G. Schmid, W. Petz, H. Nöth, *Inorg. Chim. Acta* **1970**, *4*, 423 – 427.
[6] $[(CO)_4FeBN(SiMe_3)_2]$ was obtained in low yields by procedures similar to those for **1a,b**, and was characterized by NMR spectroscopy. H. Braunschweig, C. Kollann, unpublished results.
[7] A. Mayr, K. C. Schaefer, E. Y. Huang, *J. Am. Chem. Soc.* **1984**, *106*, 1517 – 1518.
[8] a) Crystal structure determination of **1b**: $C_{11}H_{18}BNO_5Si_2W$, Enraf-Nonius CAD4 diffractometer; MoK_α radiation ($\lambda = 0.7107$ Å, graphite monochromator); $T = 203$ K. Light brown rod, 0.16 × 0.12 × 0.08 mm^3, triclinic, space group $P\bar{1}$ (no. 2); $a = 9.250(1)$, $b = 9.302(1)$, $c = 12.109(2)$ Å, $\alpha = 109.53(1)$, $\beta = 98.54(1)$, $\gamma = 101.48(1)^\circ$, $V = 935.8(3)$ Å^3, $Z = 2$, $\rho_{calcd} = 1.74$ g cm^{-3}, $\mu(Mo_{K\alpha}) = 63.81$ cm^{-1}, $F(000) = 476$, 5222 measured reflections ($3 < \theta < 26^\circ$), $\omega - 2\theta$ scans. The empirical absorption correction on the basis of azimuthal scans provided transmission factors between 0.722 and 0.999.[15] The structure was solved by Patterson methods with use of the SDP program;[16] 3349 independent reflections with $I > \sigma(I)$, 190 variables. All non-hydrogen atoms were refined with anisotropic displacement parameters, all hydrogen atoms were included as riding (C–H = 98 pm, $U_{iso}(H) = 1.3\,U_{iso}(C)$). $R = 0.032$, $R_w = 0.034$, $w^{-1} = \sigma^2(F_o)$, GOF = 0.950. b) Crystallographic data (excluding structure factors) for the structure reported in this paper have been deposited with the Cambridge Crystallographic Data Centre as supplementary publication no. CCDC-101 812. Copies of the data can be obtained free of charge on application to CCDC, 12 Union Road, Cambridge CB2 1EZ, UK (fax: (+44) 1223-336-033; e-mail: deposit@ccdc.cam.ac.uk).
[9] H. Wadepohl, U. Arnold, H. Pritzkow, *Angew. Chem.* **1997**, *109*, 1009 – 1011; *Angew. Chem. Int. Ed. Engl.* **1997**, *36*, 974 – 976.
[10] R. Boese, P. Paetzold, A. Tapper, *Chem. Ber.* **1987**, *120*, 1295 – 1298.
[11] A. W. Ehlers, E. J. Baerends, F. M. Bickelhaupt, U. Radius, *Chem. Eur. J.* **1998**, *14*, 210 – 221.
[12] J. M. Maher, R. P. Beatty, N. J. Cooper, *Organometallics* **1985**, *4*, 1354 – 1361.
[13] W. Haubold, U. Kraatz, *Z. Anorg. Allg. Chem.* **1976**, *421*, 105 – 110.
[14] W. Strohmeyer, J. F. Guttenberger, H. Blumenthal, G. Albert, *Chem. Ber.* **1966**, *99*, 3419 – 3424.
[15] A. C. T. North, D. C. Phillips, F. S. Mathews, *Acta Crystallogr. Sect. A* **1968**, *24*, 351 – 359.
[16] B. A. Frenz, SDP, Version 5.0, Enraf-Nonius, Delft, **1989**.
[17] A. L. Spek, PLATON94, Utrecht, **1994**.
[18] Note added in proof (August 10, 1998): Recently the synthesis and structure of the borylene complex $[(\eta^5\text{-}Me_5C_5)BFe(CO)_4]$ was published. However, this compound shows a single bond between iron and a sixfold-coordinated boron atom. A. H. Cowley, V. Lomelí, A. Voigt, *J. Am. Chem. Soc.* **1998**, *120*, 6401 – 6402.

Remarkable Reaction of Hetero-S-Block-Metal Amides with Molecular Oxygen: Cationic $(NMNMg)_2$ Ring Products (M = Li or Na) with Anionic Oxo or Peroxo Cores

Alan R. Kennedy, Robert E. Mulvey,* and René B. Rowlings

Intensively studied since the early 1980s, the structural chemistry of lithium and sodium amides is based predominantly on $(NM)_n$ rings (M = Li or Na) which can remain discrete or self-associate by "ring-laddering".[1] Lithium 2,2,6,6-tetramethylpiperidide (LTMP) is representative of the former type as highlighted in a recent textbook:[2] two-coordinate Li centers bridge pairs of amide N centers in a tetrameric octagonal ring core. Considerably less work has been carried out on heterometallic amide systems where lithium or sodium is combined with a second metal. Recently

[*] Prof. R. E. Mulvey, Dr. A. R. Kennedy, R. B. Rowlings
Department of Pure and Applied Chemistry
University of Strathclyde
Glasgow, G1 1XL (UK)
Fax: (+45) 141-552-0876
E-mail: R.E.Mulvey@strath.ac.uk

[**] This research was supported by the UK Engineering and Physical Science Research Council.

 © WILEY-VCH Verlag GmbH, D-69451 Weinheim, 1998 1433-7851/98/3722-3180 $ 17.50+.50/0

we have turned our attention to synthesizing heterodimetallic Li–Mg and Na–Mg amides.[3] These mixed-metal compounds can be formally regarded as alkali metal amide derivatives in which a proportion of M^+ ions have been replaced by $[\{Mg(NR_2)\}^+]$ units. Such substitutions should encourage a modification in chemical structure, which, in turn, could translate into a modification in chemical reactivity. Hence the heterodimetallic system may exhibit a chemical behaviour distinct from that of the homometallic amide. The widespread use of lithium amide reagents throughout synthetic chemistry provides a major incentive for pursuing this interesting topic. Herein we report how this heterodimetallic approach can be used to create a truly remarkable new piece of chemistry. Thus, octagonal $(N\text{-}M\text{-}N\text{-}Mg)_2$ mixed-metal ring systems closely related to the LTMP original but with oxo or peroxo cores are readily preparable. The core atoms are introduced into the molecular frameworks by deliberately exposing reaction solutions to molecular oxygen—a manoeuvre normally unthinkable in s-block organometallic chemistry, where generally every effort is made to avoid hydrolytic and oxidative decomposition by working in an oxygen-free inert atmosphere.

We still use such an atmosphere (argon) in the initial stages of the preparations described here. Subsequently, however, the Schlenk tube is opened to the atmosphere, and a drying tube filled with fresh $CaCl_2$ is placed at the inlet. This allows atmospheric oxygen to enter, but not moisture. Alternatively, dry compressed oxygen can be directly passed through the liquid amine for several minutes immediately prior to carrying out the preparation. Both methods have proved successful, and reproducibly so, in the synthesis of the heterodimetallic oxo variant of the classic LTMP system **1**.

$[\{\overline{C(Me_2)CH_2CH_2CH_2C(Me_2)N}\}_4Li_2Mg_2(O)]$ **1**

Compound **1** is produced by mixing *n*-butyllithium with *n*,*s*-dibutylmagnesium in hydrocarbon solution, then adding enough amine to convert all the butyl groups to butane. X-ray crystallographic studies[4] reveal that the colorless, needle-shaped, single crystals of **1** are contaminated with some molecules of conventional LTMP, presumably as a consequence of the two octagonal ring systems having a similar, but not identical molecular shape (see below). Complete refinements on several different crystals show that the relative amount of LTMP contamination can be greatly reduced (e.g., from 39 to 7%) by increasing the Mg:Li stoichiometry used in the reaction from 1:1 to 2:1. Figure 1 shows the molecular structure of **1**. The core oxo atom occupies a square-planar site binding to all four metal atoms. Due to mutual substitution disorder the two Li and two Mg sites are indistinguishable. Their three-coordinate geometry is completed by two amido N atoms, which bridge to the metal atoms to produce the eight-membered ring. Though the disorder prejudices discussion of specific dimensions within the structure, it is still clear that the $(N_4Li_2Mg_2)$ ring takes on a star-shaped appearance with the N atoms located at the tips (evidenced by acute M-N-M bond angles of about 76°). This feature can be attributed to the additional pull on the metal atoms by the core oxo dianion, as it is not observed in the oxo-free structure of conventional LTMP, which has more open M-N-M bond angles of 101.5°.

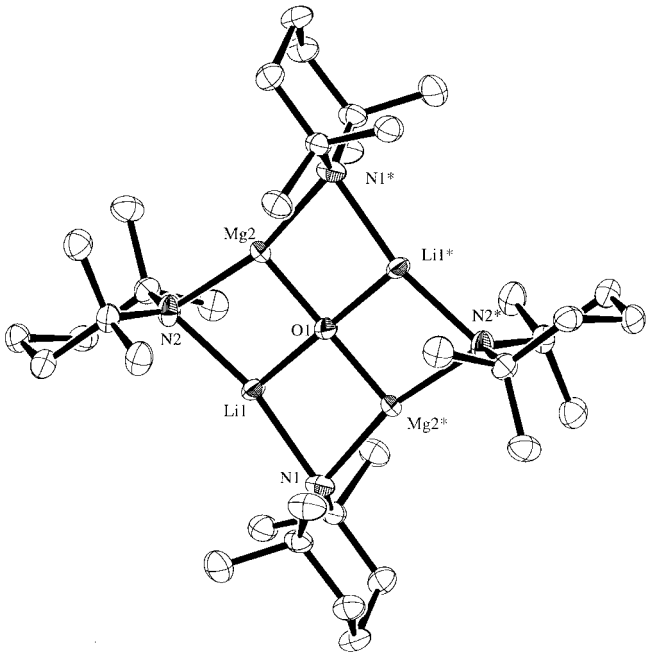


Figure 1. Molecular structure of **1** without hydrogen atoms and disorder component.

In an effort to circumvent the complication of Li/Mg substitutional disorder and to test the heterodimetallic strategy with a second amine, we tried the same reaction with *n*-butylsodium and 1,1,1,3,3,3-hexamethyldisilazane in place of *n*-butyllithium and tetramethylpiperidine, respectively. To our delight it proved successful and reproducible, yielding the desired complex **2**.

$[\{(Me_3Si)_2N\}_4Na_2Mg_2(O_2)_x(O)_y]$ **2**

The structure of **2** (Figure 2)[4] resembles that of **1**, though the octagonal ring has a more asymmetrical (but still planar) shape due to the significant size differential between Na and Mg atoms. For this reason there is no Na/Mg substitutional disorder in **2**; however, site disorder is found at the center of the structure, refined to 32% peroxide and 68% oxide for the specific crystal reported here. These appear to represent the kinetic and thermodynamic products, respectively, of the oxygen incorporation process. As such, a comparison can be made with reactions of alkyllithium compounds and molecular oxygen which produce alkoxides via unstable alkylperoxo intermediates.[5] Presumably steric shielding by the bulky amide ligand increases the stability of the peroxo component of **2**. Previously, we noted that the lithium analogue of **2** could be obtained as an unwanted by-product during the synthesis of mixed Li–Mg hexamethyldisilazide,[6] but at that time failed to recognize that it could be made by the rational method described here.

Oxygen incorporation in s-block compounds is not a new phenomenon. In 1964, the structure of the contaminated "Grignard reagent" $Mg_4Br_6(O)\cdot 4Et_2O$ was reported.[7] More recent examples include the tetradecalithium amide $[\{(c\text{-}C_5H_9)N(H)Li\}_{12}Li_2O]$[8] and the octadecalithium phos-

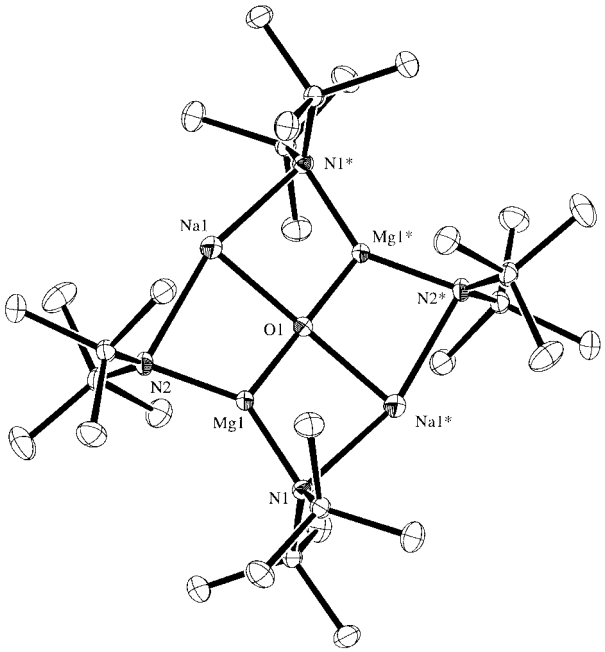
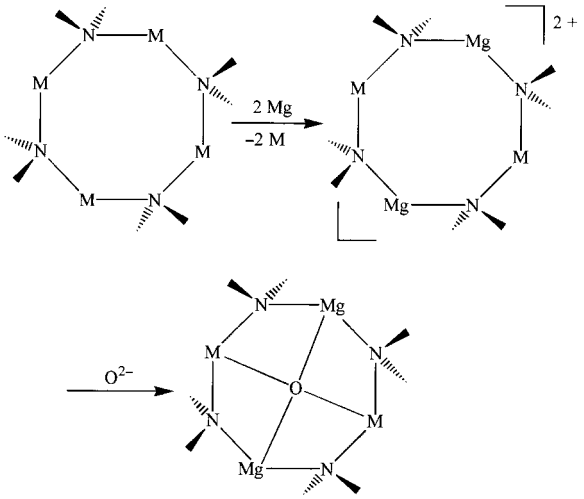


Figure 2. Molecular structure of **2** without hydrogen atoms and disorder component. Selected bond lengths [Å] and angles [°]: Mg1 ··· Na1 3.0099(7), Mg1 ··· Na1* 2.9459(8), Mg1–O1 1.8575(4), Na1–O1 2.3278(7), Mg1–N1 2.054(1), Mg1–N2 2.049(1), Na1–N1* 2.549(1), Na1–N2 2.595(1); N1-Mg-N2 141.60(5), N1*-Na1-N2 159.84(2), Mg-N1-Na1* 78.76(4), Mg1-N2-Na1 79.86(4). (*) = $-x, 1-y, 1-z$.

phanediide $[\{[i\mathrm{Pr}_2(\mathrm{Mes})\mathrm{Si}]\mathrm{P}\}_8\mathrm{Li}_{16}\cdot\mathrm{Li}_2\mathrm{O}]$.[9] However, such compositions are usually not planned, but obtained serendipitously, by reactions which cannot always be repeated. Furthermore, the source of the oxygen contamination is rarely, if ever, known with certainty, and is often vaguely attributed to Li_2O-containing butyllithium. Clearly by comparison, our rational, reproducible method, where oxygen is delivered into the system in a controlled, deliberate manner, represents a fundamental advance. In a *formal* sense, it can be regarded as a charge balance driven process (Scheme 1; though in reality it could be a one-step concerted mechanism): substituting two Mg^{2+} ions for two M^+ ions creates a cationic



Scheme 1. Formal course of the introduction of oxygen in the synthesis of **2**.

ring with a 2+ charge, the hole at the center of which is organized to capture small O^{2-} or O_2^{2-} ions to attain charge neutrality. Intriguingly this could be viewed, in effect, as the antithesis of a crown ether complex where a ring containing a series of oxygen atoms is used to capture a M^+ ion. While the principle of the methodology is all important, much work remains to be done to optimize the synthesis as present yields of **1** and **2** are modest (typically 5–12%), and to ascertain the fate of the amide anions formally displaced by the oxo ones (we suspect the other products of the redox reactions are hydrazines R_2NNR_2). But the key question our future research will address is "how widely applicable is this oxygen incorporation strategy?"

Experimental Section

1: A solution of *n*-butyllithium (5 mmol) in hexane was mixed with a solution of dibutylmagnesium (10 mmol) in heptane. (The possibility that the solutions contain a trace of moisture cannot be completely ruled out.) Oxygenated tetramethylpiperidine (25 mmol) was then introduced dropwise, resulting in an exothermic reaction. Turning orange in color, the solution deposited a precipitate which redissolved by adding oxygenated toluene and warming. This orange color deepened on standing. Allowing the solution to cool to ambient temperature on the bench afforded a crop of colorless needle crystals of **1**. M.p. 192–194 °C (decomp), c.f. 165–167 °C (decomp for LTMP).

2: *n*-Butylsodium (10 mmol) was placed in hexane (10 mL) and mixed in an ultrasonic bath until a fine suspension was obtained. The addition of dibutylmagnesium (10 mmol) in heptane resulted in a congealed brown mass. Oxygenated hexamethyldisilazane (30 mmol) was then introduced, causing the formation of a white precipitate which redissolved by adding oxygenated toluene and warming. On leaving the pale yellow solution to cool to ambient temperature, a batch of crystalline material was obtained. This was found to be a mixture of NaHMDS and **2**. Separation proved straightforward, since the former is significantly more soluble. Hence, several washings with hot toluene on a filter stick left pure **2**, which crystallized as distinctive colorless square-tipped needles. M.p. 224–226 °C (decomp) c.f. 175 °C for NaHMDS. Satisfactory C,H,Li,Mg,N,Na analyses for both compounds. Both readily hydrolyze in moist air, but remain crystalline under dry oxygen.

Received: May 19, 1998 [Z11881IE]
German version: *Angew. Chem.* **1998**, *110*, 3321–3323

Keywords: alkali metals · amides · heterodimetallic compounds · oxygenations · structure elucidation

[1] K. Gregory, P. von R. Schleyer, R. Snaith, *Adv. Inorg. Chem.* **1991**, *37*, 47.

[2] N. N. Greenwood, A. Earnshaw, *Chemistry of the Elements*, 2nd ed., Butterworth Heinemann, Oxford, **1997**, p. 101.

[3] W. Clegg, K. W. Henderson, R. E. Mulvey, P. A. O'Neil, *J. Chem. Soc. Chem. Commun.* **1994**, 769.

[4] Crystal structure analyses: All measurements were made at 123 K on a Rigaku AFC7S diffractometer using $Mo_{K\alpha}$ radiation ($\lambda = 0.71069$ Å), scan method $\omega/2\theta$. Intensities were corrected for Lp and, in the case of **1**, decay effects only. Structures were solved by direct methods[10] and refined using full-matrix least-squares. For **1**, $0.93\,C_{36}H_{72}Li_2Mg_2O \cdot 0.07\,C_{36}H_{72}Li_4$: ($0.7 \times 0.4 \times 0.3$ mm^3), monoclinic, *C*2/*c*, $a = 16.946(3)$, $b = 16.981(3)$, $c = 15.710(3)$ Å, $\beta = 118.925(10)^\circ$, $V = 3957(1)$ Å^3, $\rho_{calcd} = 1.073$ g cm^{-3}, $\mu = 0.091$ mm^{-1}; $2\theta_{max} = 55^\circ$, 4710 data measured, 4562 unique, $R_m = 0.0314$. H atoms were placed in calculated positions in a riding mode. All other atoms were treated anisotropically. Final refinement with all reflections was against F^2 with SHELXL-97[11]. $R = 0.049$, $Rw = 13.56$ (all reflections, F^2), GOF = 1.025, max./min. residual electron density = 0.341/ – 0.189. (isostructural structure with

 © WILEY-VCH Verlag GmbH, D-69451 Weinheim, 1998 1433-7851/98/3722-3182 $ 17.50+.50/0

0.61: 0.39 Mg_2Li_2:Li_4 ratio had unit cell dimensions, $a = 16.832(5)$, $b = 16.828(9)$, $c = 15.728(5)$ Å, $\beta = 118.45(2)^\circ$). For **2**, $C_{24}H_{72}Mg_2Na_2N_4O_{1.32}Si_8$; ($0.7 \times 0.4 \times 0.4$ mm^3), triclinic, $P\bar{1}$, $a = 10.778(2)$, $b = 12.695(4)$, $c = 8.8511(14)$ Å, $\alpha = 108.03(2)$, $\beta = 99.49(2)$, $\gamma = 95.21(2)^\circ$, $V = 1122.8$ (5) Å^3, $\rho_{calcd} = 1.120$ g cm^{-3}, $\mu = 0.310$ mm^{-1}; $2\theta_{max} = 58^\circ$, 6266 data measured, 5966 unique, $R_m = 0.020$. H atoms and the peroxide O were refined isotropically and all other atoms anisotropically. Final refinement with 5100 observations ($I > 2\sigma(I)$) on F with Texsan.[12] $R = 0.0295$, $R_w = 0.0426$, GOF = 1.573, max/min residual electron density = 0.457/ − 0.330. Crystallographic data (excluding structure factors) for the structures reported in this paper have been deposited with the Cambridge Crystallographic Data Centre, as supplementary publications no. CCDC-101597 and 101598. Copies of the data can be obtained free of charge on application to CCDC, 12 Union Road, Cambridge, CB2 1EZ. (fax: (+44) 1223-336-033; e-mail: deposit@ccdc.cam.ac.uk).

[5] T. G. Brilkina, V. A. Shushunov, *Reactions of Organometallic Compounds with Oxygen and Peroxides*, Iliffe Books, London, **1969**. For the first crystal structure of a ROOLi species see G.Boche, K. Möbus, K. Harms, J. C. W. Lohrenz, M. Marsch, *Chem. Eur. J.* **1996**, *2*, 604.

[6] A. R. Kennedy, R. E. Mulvey, R. B. Rowlings, *J. Am. Chem. Soc.* **1998**, *120*, 7816.

[7] G. D. Stucky, R. E. Rundle, *J. Am. Chem. Soc.* **1964**, *86*, 4821.

[8] W. Clegg, L. Horsburgh, P. R. Dennison, F. M. Mackenzie, R. E.Mulvey, *Chem. Commun*. **1996**, 1065.

[9] M. Driess, H. Pritzkow, S. Martin, S. Bell, D. Fenske, G. Baum, *Angew. Chem*. **1996**, *108*, 1064; A*ngew. Chem. Int. Ed. Engl*. **1996**, 35, 986.

[10] SIR program: M. C. Burla, M. Camalli, G. Cascarano, C. Giacovazzo, G. Polidori, R. Spagna, D. Viterbo, *J. Appl. Crystallogr.* **1989**, *22*, 389.

[11] SHELXL-97: G. M. Sheldrick, University of Göttingen, Germany, **1997**.

[12] TeXsan version 1.6: Molecular Structure Corporation, The Woodlands, Texas, USA, **1993**.

Novel Cyanide Coordination Models in Layer-Type Hydrated Double Salts of AgCN and AgF**

Guo-Cong Guo and Thomas C. W. Mak*

Dedicated to Professor James Trotter on the occasion of his 65th birthday

The chemistry of cyanide-bridged compounds has undergone quite spectacular advances in the last decade, especially in regard to one-, two-, and three-dimensional complexes that exhibit unusual magnetic and electrical properties.[1] Furthermore, the syntheses of oligonuclear cyanide-bridged complexes and investigation of the electronic interactions between their metal centers have been pursued by several research groups.[2] Recently another incentive to study bimetallic cyano complexes has emerged from finding that the enzyme cytochrome c oxidase is poisoned by cyanide.[3] During the course of our current study on the bonding interaction between the acetylenediide anion, C_2^{2-}, and silver(I) ions in various double salts of silver acetylide with other soluble silver salts,[4] we also explored the possibility of stabilizing the related isoelectronic diatomic species CN^- by coordination to multiple silver(I) sites in a crystalline environment. Herein we report two new double salts, $3\,AgCN \cdot 2\,AgF \cdot 3\,H_2O$ (**1**) and $AgCN \cdot 2\,AgF \cdot 3\,H_2O$ (**2**), which exhibit novel layer-type structures and bonding interaction between the cyanide anion and adjacent silver ions.

The coordination modes of the cyanide group in their metal complexes show considerable diversity (Figure 1). By far the two most commonly observed modes are the terminal

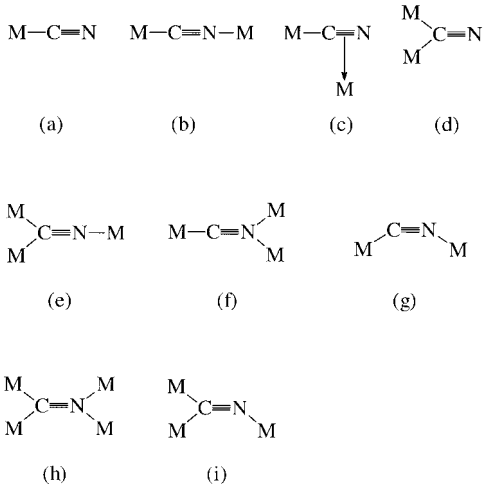


Figure 1. Coordination modes of the cyanide ion.

C-bound mode (a) and the linear-bridged arrangement (b), which are based on the well-known fact that the cyanide ion possesses a donor electron pair at both its C and N terminals.[5] Modes (c) – (g) are much less common,[6] and to our knowledge modes (h) and (i) are found for the first time in compound **1**.

The layer-type structure of **1** can be regarded as constructed from two basic building blocks, namely a nonlinear dimeric Ag_2F_2 unit and the first edge-bridged triangular silver(I) cluster core $[Ag_3(\mu\text{-}CN)_3(H_2O)_3]$ (Figure 2). The Ag – Ag distances, which range from 2.8110(8) to 2.9189(8) Å in the Ag_3 cluster, are comparable to the interatomic contact of 2.89 Å in silver metal,[7] and hence suggestive of the existence of weak interactions of the same order of magnitude. The Ag–Ag distance of 2.7484(9) Å in the Ag_2F_2 unit (Ag–F 2.316(4) – 2.422(4) Å) is significantly shorter than those in the Ag_3 cluster. To our knowledge the μ_4-$\eta^1\kappa C$:$\eta^1\kappa N$ and bent μ_3-$\eta^1\kappa C$:$\eta^1\kappa N$ coordination modes observed for the cyanide group, as well as their coexistence in the same complex, are both unprecedented. Each of the two independent μ_3-cyanide groups is symmetrically bridged to an edge of the Ag_3 triangle through its N terminal and also bonded to one Ag atom of an adjacent Ag_2F_2 unit through its C terminal. The μ_4-cyanide group bridges an edge of the Ag_3 triangle through its N

[*] Prof. T. C. W. Mak, G.-C. Guo
Department of Chemistry
The Chinese University of Hong Kong
Shatin, New Territories, Hong Kong (China)
Fax: (+359) 260-350-57
E-mail: tcwmak@cuhk.edu.hk

[**] This work was supported by Hong Kong Research Grants Council Earmarked Grant CUHK 4179/97P and Direct Grant A/C 2060129 of The Chinese University of Hong Kong.

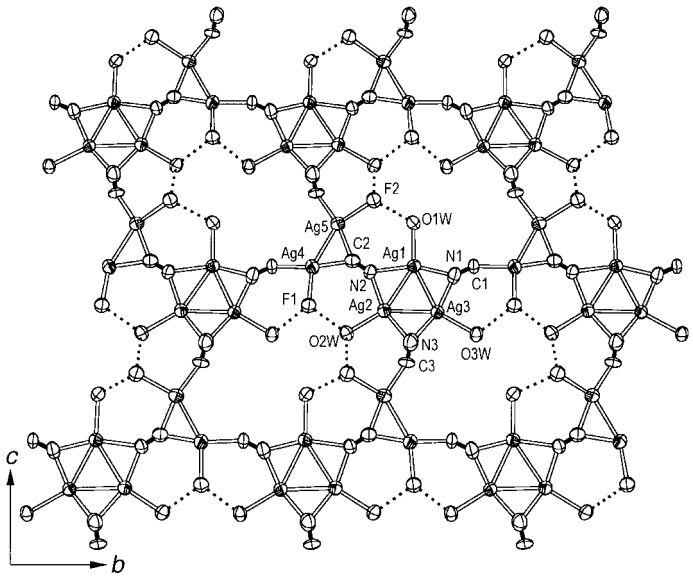


Figure 2. Layer structure of $3AgCN \cdot 2AgF \cdot 3H_2O$ viewed along the *a* direction. The thermal ellipsoids are drawn at the 50% probability level. The dotted lines represent hydrogen bonds in the layer. Selected bond lengths [Å] and angles [°]: Ag1–Ag3 2.8111(4), Ag1–Ag2 2.9195(4), Ag2–Ag3 2.8132(4), Ag1–N1 2.198(3), Ag1–N2 2.356(3), Ag1–O1W 2.384(2), Ag2–N3 2.236(3), Ag2–N2 2.256(2), Ag2–O2W 2.363(2), Ag3–N1 2.191(2), Ag3–N3 2.208(3), Ag3–O3W 2.389(2), Ag4–C1^{i} 2.161(3), Ag4–C2 2.173(4), Ag5–C3^{ii} 2.140(3), Ag5–C2 2.171(3), C1–N1 1.160(4), C2–N2 1.129(4), C3–N3 1.128(4); N1-C1-Ag4^{iii} 152.9(2), N2-C2-Ag5 143.2(3), N2-C2-Ag4 138.3(2), C2-N2-Ag2 140.9(2), C2-N2-Ag1 140.1(2), N3-C3-Ag5^{iv} 157.5(3). Symmetry codes: i: $x, y-1, z$; ii: $x-1, -y-1/2, z-1/2$; iii: $x, y+1, z$; iv: $x+1, -y-1/2, z+1/2$.

terminal in an asymmetrical manner, but is symmetrically bound to both metal atoms of the Ag_2F_2 unit through its C terminal. As seen from Figure 2, the $[Ag_3(\mu\text{-}CN)_3(H_2O)_3]$ clusters constitute a regular hexagonal array that is interconnected differently by the Ag_2F_2 units. It is worthy of note that all silver atoms, bridged cyanide groups, and terminal aqua ligands are nearly coplanar, resulting in a supraconjugated π system based on the frontier orbitals of Ag and O atoms and the cyanide groups. All fluoro ligands lie out of the mean plane of each layer on the same side, such that type F1 and F2 atoms are hydrogen-bonded to aqua ligands of type O1W and O3W, respectively, of an adjacent layer, thereby generating a double layer of thickness 3.16 Å (Figure 3). The separation between double layers is 2.53 Å.

The layer structure in **2** features a pseudo-cubane cluster with a void Ag position $[Ag_3F(H_2O)_3]$, which is unprecedented despite the fact that incomplete-cubane structures are commonly found in early transition metal chalcogenides.[8] The clusters are directly linked through corner silver(I) atoms of type Ag1 and Ag2 with a Ag – Ag distance of 2.7700(9) Å to generate zigzag chains at $y \approx 0$ running parallel to the *c* direction (Figure 4). Each μ_3-$\eta^1\kappa C$:$\eta^1\kappa N$-cyanide group is bound to the third Ag3 atom of a pseudo-cubane cluster through its N terminal and asymetrically bridges a Ag – Ag bond of an adjacent chain at $y \approx 1$ through its C terminal, resulting in the formation of a corrugated layer whose mean plane lies normal to the *b* axis. The crystal structure of **2** comprises a stack of layers, in which the aqua ligands form

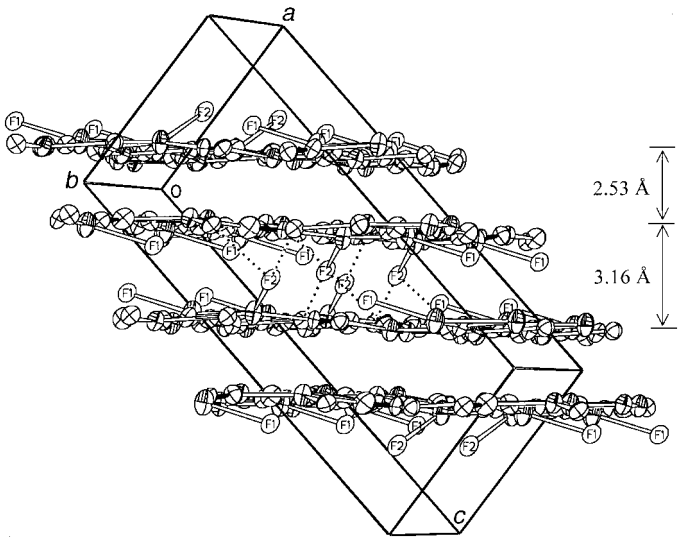


Figure 3. Crystal structure of $3AgCN \cdot 2AgF \cdot 3H_2O$. Hydrogen bonds between adjacent layers are represented by dotted lines.

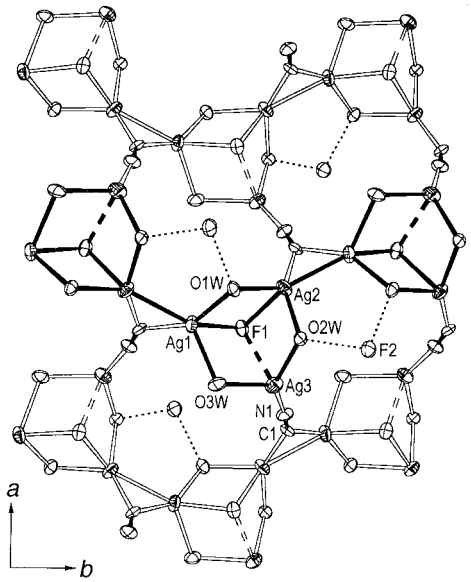


Figure 4. Layer structure of $AgCN \cdot 2AgF \cdot 3H_2O$ viewed along the *b* direction. The thermal ellipsoids are drawn at the 50% probability level. The cluster chains at $y \approx 0$ and $y \approx 1$ are differentiated by filled and open bond types. The broken lines represent the lengthened Ag–F distances, and the dotted lines represent hydrogen bonds. Selected bond lengths [Å] and angles [°]: Ag1–C1^{i} 2.226(6), Ag1–O1W 2.304(4), Ag1–O3W 2.462(4), Ag1–F1 2.471(3), Ag1–Ag2^{ii} 2.7700(9), Ag2–C1^{iii} 2.160(6), Ag2–O2W 2.318(4), Ag2–F1 2.443(4), Ag2–O1W 2.494(4), Ag2–Ag1^{iv} 2.7700(9), Ag3–N1 2.192(6), Ag3–O2W 2.349(4), Ag3–O3W 2.419(5), C1–N1 1.099(8); C1-N1-Ag3 173.6(5). Symmetry codes: i: $-x+1, -y+1, z-1/2$; ii: $-x+1/2, y, z-1/2$; iii: $x-1/2, -y+1, z$; iv: $-x+1/2, y, z+1/2$.

donor hydrogen bonds to the F atoms in adjacent layers, thus contributing to the stability of the solid-state structure.

Although compounds **1** and **2** were prepared under the same conditions, and crystal samples were obtained in different ways (see Experimental Section), there is no apparently simple mechanism for their structural interconversion. The cyanide group in transition metal cyanide compounds often exhibits head-to-tail disorder,[9] and O and F atoms are not easily differentiated in X-ray structure analysis. However, in **1**

 © WILEY-VCH Verlag GmbH, D-69451 Weinheim, 1998 1433-7851/98/3722-3184 $ 17.50+.50/0

and **2** an ordered arrangement of the cyanide groups can be assigned on the basis of refinement of their anisotropic thermal parameters, and the fluoro and aqua ligands can be identified by consideration of their thermal ellipsoids as well as the scheme of hydrogen bonding. The measured bond lengths of the μ_3-$\eta^1\kappa C$:$\eta^1\kappa N$ and μ_4-$\eta^1\kappa C$:$\eta^1\kappa N$ cyanide groups in **1** and **2** are comparable to those found in cyano complexes.[6] Thus the cyanide anion in **1** and **2** retains its triple-bond character inherited from its parent AgCN; this, is analogous to the case for double salts of Ag_2C_2 with soluble silver salts.[4]

Hitherto the shortest Ag – Ag distance reported for any silver dicyanide salt of known crystal structure is 3.11 Å, which was found in $Tl[Ag(CN)_2]$.[10] In the intertwined double $(-Ag-SR-)_n$ -strand chain structure of crystalline (3-methylpentane-3-thiolato)silver, the closest contact between strands is Ag–Ag = 2.886(4) Å, which is interpreted as nonbonding.[11] In contrast, the much shorter Ag–Ag distances of 2.748 – 2.811 Å in **1** and **2** provide supporting evidence for the significance of *argentophilicity* in polynuclear compounds of silver(I),[10] which is a complementary logical extension of the well-established concept of aurophilicity for gold(I) complexes.[12] It is worthy of note that the Raman spectra of **1** and **2** exhibit strong cyano stretching absorptions at 2078 and 2080 cm^{-1}, respectively, which are comparable to that of free CN^- in solution (2080 cm^{-1}), but significantly lower than those found in $Tl[Ag(CN)_2]$ (2107, 2250 cm^{-1})[10] and other silver cyano complexes.[13] Generally, $\tilde{\nu}$(C≡N) of a terminal M–C≡N group shifts to a higher frequency if it forms a bridge of the M–C≡N–M′ type derived from σ coordination of the weakly antibonding nitrogen lone pair to a second metal center M′. Thus the red shift of $\tilde{\nu}$(C≡N) in **1** and **2** attest to the existence of strong metal →cyanide π-backbonding in these compounds.

Experimental Section

AgCN was added to 2 mL of a concentrated aqueous solution of AgF (about 40%) in a plastic vessel with stirring until saturated. The excess amount of AgCN was filtered off, and the solution was divided into two equal parts. One part was placed in a desiccator charged with P_2O_5, and a good crop of colorless crystals of **1** was obtained after several days. The other part was put into a furnace kept at 50 °C, and a good crop of colorless crystals of **2** was obtained in the course of two days. Both compounds were obtained in satisfactory yields that normally exceed 50%. The crystals can be kept indefinitely when immersed in a concentrated aqueous solution of silver(I) ions, but are easily decomposed by common solvents such as water, methanol, and THF. After selecting a good sample of **2** for storage and X-ray analysis, the solution containing the remaining crystals was exposed to air, and the crystals redissolved in about two days. The solution was then transferred to a desiccator charged with P_2O_5, and crystals of **1** appeared after several days. Solid-state Raman absorption spectra (Renishaw System 2000 Raman Image Microscope): $\tilde{\nu}$ = 3622(m), 2078(s), 1329(w), 1061(m) cm^{-1} for **1** and 2080(s), 1334(vw), 1041(m), 888(vw) 811(vw) cm^{-1} for **2**.

Crystal structure data for **1**: Colorless plate, Rigaku RAXIS IIC diffractometer, $Mo_{K\alpha}$ radiation (λ = 0.71073 Å), 1968 unique reflections, 1657 of which with $I > 2\sigma(I)$ were considered as observed. $P2_1/c$ (No. 14), $Z = 4$, ρ_{calcd} = 4.122 g cm^{-3}, a = 6.944(1), b = 10.752(1), c = 15.638(1) Å, β = 101.69(1)°, V = 1143.3(2) $Å^3$, μ = 84.31 cm^{-1}, $R1$ = 0.0501, GOF = 1.069.

Crystal structure data for **2**: Colorless prism, Siemens P4/PC diffractometer, $Mo_{K\alpha}$ radiation (λ = 0.71073 Å), 1241 unique reflections, 732 of which with $I > 2\sigma(I)$ were considered as observed. $Pca2_1$ (No. 29), $Z = 4$, ρ_{calcd} = 3.925 g cm^{-3}, a = 13.946(3), b = 4.522(2), c = 11.853(3) Å, V = 747.5(4) $Å^3$, μ = 77.67 cm^{-1}, $R1$ = 0.0605, GOF = 1.121. The structures of **1** and **2** were solved by direct methods (SHELXS-86) and refined by full-matrix least squares on F^2 using the Siemens SHELXTL-93 (PC Version) package of crystallographic software. Further details of the crystal structure investigations may be obtained from the Fachinformationszentrum Karlsruhe, D-76344, Eggenstein-Leopoldshafen, Germany (fax: (+49) 7247-808-666; e-mail: crysdata@fiz-karlsruhe.de) on quoting the depository numbers CSD-408712 and CSD-408713.

Received: May 26, 1998 [Z11906IE]
German version: *Angew. Chem.* **1998**, *110*, 3296 – 3299

Keywords: clusters · coordination modes · cyanide · fluorine · silver

[1] a) O. Sato, T. Iyoda, A. Fujishima, K. Hashimoto, *Science* **1996**, *271*, 49 – 51; b) T. Mallah, S. Thiebaut, M. Verdaguer, P. Veillet, *Science* **1993**, *262*, 1554 – 1557; c) W. R. Entley, G. Girolami, *Science* **1995**, *268*, 397 – 402; d) C. A. Bignozzi, R. Argazzi, C. G. Garcia, F. Scandola, J. R. Schoonover, T. J. Meyer, *J. Am. Chem. Soc.* **1992**, *114*, 8727 – 8729; f) O. Kahn, *Molecular Magnetism*, VCH, Weinheim, **1993**; g) *Magnetic Molecular Materials* (Eds.: D. Gatteschi, O. Kahn, J. S. Miller, F. Palacio), Kluwer, Dordrecht, **1991**; h) J. S. Miller, A. J. Epstein, *Angew. Chem.* ***1994****, 106,* 399 – 432*; Angew. Chem. Int. Ed. Engl.* **1994**, *33*, 385 – 415; i) H. Miyasaka, N. Matsumoto, H. Okawa, N. Re, E. Gallo, C. Floriani, *J. Am. Chem. Soc.* **1996**, *118*, 981 – 994.

[2] a) Y. Obora, T. Ohta, C. L. Stern, T. J. Marks, *J. Am. Chem. Soc.* **1997**, *119*, 3745 – 3755; b) N. Zhu, H. Vahrenkamp, *Chem. Ber.* **1997**, *130*, 1241 – 1452; c) N. Zhu, H. Vahrenkamp, *Angew. Chem.* **1994***, 106,* 2166 – 2167*; Angew. Chem. Int. Ed. Engl.* **1994**, *33*, 2090 – 2091; d) F. L. Atkinson, N. C. Brown, N. G. Connelly, A. G. Orpen, A. L. Rieger, P. H. Rieger, G. M. Rosair, *J. Chem. Soc. Dalton Trans.* **1996**, 1959 – 1966; e) G. A. Carriedo, N. G. Connelly, M. C. Crespo, I. C. Quarmby, V. Riera, G. H. Worth, *J. Chem. Soc. Dalton Trans.* **1991**, 315 – 323; f) W. P. Fehlhammer, M. Fritz, *Chem. Rev.* **1993**, *93*, 1243 – 1280; g) V. O. Kennedy, C. L. Stern, D. F. Shriver, *Inorg. Chem.* **1994**, *33*, 5967 – 5969; h) C. A. Bignozzi, R. Argazzi, C. Chiorboli, S. Roffia, F. Scandola, *Coord. Chem. Rev.* **1991**, *111*, 261 – 266; i) F. Scandola, R. Argazzi, C. A. Bignozzi, C. Chiorboli, M. T. Indelli, M. A. Rampi, *Coord. Chem. Rev.* **1993**, *125*, 283 – 292; j) A. Burewicz, A. Haim, *Inorg. Chem.* **1988**, *27*, 1611 – 1614; k) H. Kunkely, V. Pawlowski, A. Vogler, *Inorg. Chim. Acta* **1994**, *225*, 327 – 330; l) W. M. Laidlaw, R. G. Denning, *Inorg. Chim. Acta* **1996**, *248*, 51 – 58.

[3] a) M. J. Scott, S. C. Lee, R. H. Holm, *Inorg. Chem.* **1994**, *33*, 4651 – 4662; b) D. J. Darrensbourg, J. C. Yoder, M. W. Holtcamp, K. K. Klausmeyer, J. H. Reibenspies, *Inorg. Chem.* **1996**, *35*, 4764 – 4769; c) S. C. Lee, M. J. Dcott, K. Kauffmann, E. Muenck, R. H. Holm, *J. Am. Chem. Soc.* **1994**, *116*, 401 – 402; d) M. T. Gardner, G. Deinum, Y. Kim, G. T. Babcock, M. J. Scott, R. H. Holm, *Inorg. Chem.* **1996**, *35*, 6878 – 6884.

[4] a) G.-C. Guo, Q.-G. Wang, G.-D. Zhou, T. C. W. Mak, *Chem. Commun.* **1998**, 339 – 340; b) G.-C. Guo, Q.-G. Wang, G.-D. Zhou, T. C. W. Mak, *Angew. Chem.* **1998**, 110, 652 – 654; *Angew. Chem. Int. Ed.* **1998**, 37(5), 630 – 632.

[5] D. F. Shriver, *Struct. Bonding (Berlin)* **1966**, *1*, 32 – 58.

[6] a) K. R. Dunbar, R. A. Heintz, *Prog. Inorg. Chem.*, **1997**, *45*, 283 – 391; b) A. M. Golub, H. K. H. Köhler, V. V. Skeopenko in *Chemistry of Pseudohalides* (Ed.: R. J. H. Clark), Elsevier, New York, **1986**, pp. 77 – 185.

[7] J. Emsley, *The Elements*, Clarendon Press, Oxford, **1989**, p. 174.

[8] a) G. Sakane, T. Shibahara, Characterization of Incomplete Cubane-Type and Cubane-Type Sulfur-Bridged Clusters, in *Transition Metal Sulfur Chemistry: Biological and Industrial Significance* (Eds.: E. I. Stiefel, K. Matsumoto), American Chemical Society, Washington, D.C., **1996**, pp. 225 – 239; b) T. Saito, Chalcogenide Cluster Complexes of the Early Transition Metals, in *Early Transition Metal Clusters with π-Donor Ligands* (Ed.: M. H. Chisolm), VCH, New York, **1995**, pp. 63 – 164.

 © WILEY-VCH Verlag GmbH, D-69451 Weinheim, 1998 1433-7851/98/3722-3185 $ 17.50+.50/0

[9] D. J. Williams, D. E. Partin, F. J. Lincoln, J. Kouvetakis, M. O'Keeffe, *J. Solid State Chem.* **1997**, *134*, 164 – 169.
[10] M. A. Omary, T. R. Webb, Z. Assefa, G. E. Shankle, H. H. Patterson, *Inorg. Chem.* **1998**, *37*, 1380 – 1386.
[11] I. G. Dance, L. J. Fitzpatrick, A. D. Rae, M. L. Scudder, *Inorg. Chem.* **1983**, *22*, 3785 – 3788.
[12] H. Schmidbaur, *Chem. Soc. Rev.* **1995**, 391 – 400.
[13] K. Nakamoto, *Infrared and Raman Spectra of Inorganic and Coordination Compounds*, 4th ed., Wiley, New York, **1986**, p. 272; I. G. Dance, L. J. Fitzpatrick, A. D. Rae, M. L. Scudder, *Inorg. Chem.* **1983**, *22*, 3785 – 3788.

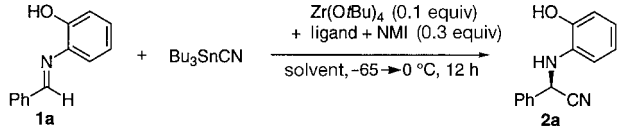
Catalytic, Enantioselective Synthesis of α-Aminonitriles with a Novel Zirconium Catalyst**

Haruro Ishitani, Susumu Komiyama, and Shū Kobayashi*

α-Aminonitriles are useful intermediates for the synthesis of amino acids[1] and nitrogen heterocycles such as thiadiazoles and imidazoles.[2] The Strecker reactions of aldimines with cyanides provide one of the most efficient methods for the preparation of α-aminonitriles,[3] and several diastereoselective approaches for the synthesis of optically active α-aminonitriles have been reported.[4] In 1996 Lipton et al. reported the first catalytic enantioselective Strecker-type reactions with use of a dipeptide ligand as catalyst.[5] Although efficient catalytic reactions provide α-aminonitriles derived from benzaldehyde derivatives in high enantioselectivities, low selectivities were observed in the reactions of aldimines derived from aliphatic and heterocyclic aldehydes.[6] Here we report chiral zirconium-catalyzed Strecker reactions of aldimines with tributyltin cyanide (Bu_3SnCN), which provide various types of α-aminonitriles in high yields and with high enantioselectivities.

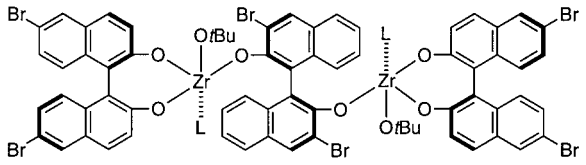
Recently, we reported the first catalytic enantioselective Mannich[7] and aza-Diels – Alder reactions[8] with a chiral zirconium catalyst. In these reactions, the zirconium catalyst effectively activates aldimines, which leads to efficient catalytic processes. We then used a zirconium catalyst in asymmetric Strecker reactions. In the presence of a zirconium catalyst (10 mol %) that was prepared from $Zr(OtBu)_4$, (*R*)-6,6′-dibromo-1,1′-bi-2-naphthol ((*R*)-6-Br-BINOL, 2 equiv),[9] and *N*-methylimidazole (NMI, 3 equiv), aldimine **1a** was treated with Bu_3SnCN[10] in dichloromethane at $-45\,^{\circ}C$. The reaction proceeded smoothly to afford the corresponding α-aminonitrile in 70 % yield with 55 % *ee*. After several reaction conditions were examined, the best results (92 % yield, 91 % *ee*) were obtained when the reaction was carried out in benzene/toluene (1/1) with use of a chiral zirconium catalyst prepared from $Zr(OtBu)_4$ (1 equiv), (*R*)-6-Br-BINOL (1 equiv), (*R*)-3,3′-dibromo-1,1′-bi-2-naphthol ((*R*)-3-Br-BINOL),[11] and NMI (3 equiv; Table 1). Use of other solvents resulted in a slight decrease in selectivity. The free hydroxyl group of the aldimine was important for obtaining both high yield and high selectivity.[7] When the aldimine prepared from aniline or 2-methoxyaniline was used under the same reaction conditions, the corresponding α-aminonitrile derivatives were obtained in much lower yields and with lower enantioselectivities (aniline: 29 % yield, 1 % *ee*; 2-methoxyaniline: 45 % yield, 5 % *ee*).

Table 1. Influence of ligands and solvents.



Ligand (equiv)	Solvent	Yield [%]	*ee* [%]
(*R*)-6-Br-BINOL (0.2)	CH_2Cl_2	70	55
(*R*)-6-Br-BINOL (0.2)	toluene/benzene (1/1)	72	69
(*R*)-6-Br-BINOL (0.1) + (*R*)-3-Br-BINOL (0.1)	toluene/benzene (1/1)	92	91
(*R*)-6-Br-BINOL (0.1) + (*R*)-3-Br-BINOL (0.1)	toluene	93	86
(*R*)-6-Br-BINOL (0.1) + (*R*)-3-Br-BINOL (0.1)	toluene/C_2H_5CN (1/1)	91	86
(*R*)-6-Br-BINOL (0.1) + (*R*)-3-Br-BINOL (0.1)	benzene/CH_2Cl_2 (1/1)	97	83
(*R*)-6-Br-BINOL (0.1) + (*R*)-3-Br-BINOL (0.1)	CH_2Cl_2	85	71

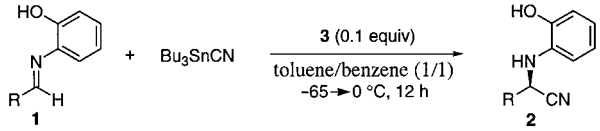
It was interesting that use of a mixture of (*R*)-6-Br-BINOL and (*R*)-3-Br-BINOL gave the best results. We then carefully examined the structure of the zirconium catalyst, and it was indicated from NMR studies that the zirconium binuclear complex **3** was formed under the reaction conditions (Scheme 1). Complex **3** consists of two zirconium centers, two (*R*)-6-Br-BINOL and two NMI units, and one (*R*)-3-Br-BINOL unit. The structure of this composition is very stable


Br
OtBu
Zr
L
O
Br
Br
Br

and is formed even with different molar ratios of $Zr(OtBu)_4$, (*R*)-6-Br-BINOL, (*R*)-3-Br-BINOL, and NMI; formation of **3** upon combination of 1 equiv of $Zr(OtBu)_4$, 1 equiv of (*R*)-6-Br-BINOL, 0.5–1 equiv of (*R*)-3-Br-BINOL, and 2–3 equiv of NMI was confirmed by ^1H and ^{13}C NMR spectroscopy.[12]

We then examined several different Strecker reactions (Table 2). Aldimines derived from aromatic aldehydes as well as aliphatic and heterocyclic aldehydes reacted with Bu_3SnCN smoothly to afford the corresponding α-aminonitrile derivatives in high yields and with high enantiomeric excesses. Since both enantiomers of the chiral ligands 6-Br-BINOL and 3-Br-BINOL are readily available, both enatiomers of α-aminonitrile derivatives can be easily prepared according to this protocol. In addition, it is noteworthy that Bu_3SnCN has been successfully used as a safe cyanide source. It is stable in water and does not react to produce HCN. This is in contrast to trimethylsilyl cyanide (TMSCN), which is easily hydrolyzed to form HCN even in the presence of a small amount of water.[13] After the reaction was completed, all tin sources were quantitatively recovered as bis(tributyltin) oxide, which can be converted into tributyltin chloride[14] and then into Bu_3SnCN.[9, 15]

Table 2. Catalytic, asymmetric Strecker reactions.

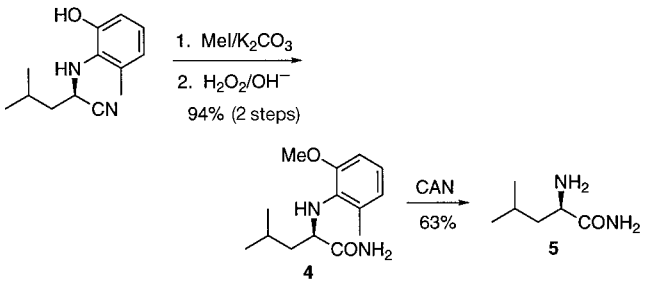


Entry	R	Yield [%]	ee [%]
1	1-Naphthyl	98	91
2	Ph	92	91
3	*p*-ClC_6H_4	90	88
4	*p*-$MeOC_6H_4$	97	76
5	*o*-MeC_6H_4	96	89[a]
6	*o*-MeC_6H_4	93	89 (*S*)[b]
7		85	87
8		89	80
9		89	92
10	$Ph(CH_2)_2$	55	83[c]
11	*i*Bu	79	83[c]
12	C_8H_{17}	72	74[c]

[a] When 0.05 equiv of **3** were used, a yield of 94% and 87% ee were obtained. [b] 0.1 equiv of *ent*-**3** were used. [c] The imine was prepared in situ from the corresponding aldehyde and 2-amino-3-methylphenol in the presence of 4-Å molecular sieves.

α-Aminonitrile **2b** was easily converted into leucinamide according to Scheme 2. Thus, after methylation of the phenolic OH group of **2b** with methyl iodide and potassium bicarbonate, the nitrile group was converted into an amide moiety.[16] Treatment of **4** with cerium ammonium nitrate (CAN)[17] gave leucinamide (**5**). The absolute configuration (*R*) was assigned by comparison of the configuration of the hydrochloride with that of an authentic sample.[18]

Catalytic enantioselective Strecker reactions of aldimines with Bu_3SnCN have been developed with use of a novel chiral zirconium binuclear catalyst. High enantioselectivities in the synthesis of α-aminonitrile derivatives with a wide range of substrates have been achieved.



Scheme 2. Synthesis of leucinamide (**5**).

Experimental Section

3: To a solution of $Zr(OtBu)_4$ (0.04 mmol) in toluene (0.25 mL) was added (*R*)-6-Br-BINOL (0.04 mmol) and (*R*)-3-Br-BINOL (0.04 mmol) in toluene (0.5 mL) and NMI (0.12 mmol) in toluene (0.25 mL) at room temperature. After the mixture was stirred for 1 h at the same temperature, solvent was removed and the residue was dried for 3 h at 50 °C in vacuo. ^1H NMR (CD_2Cl_2): $\delta = 1.22$ (s, *t*BuO), 2.60 (s, 3H, NMe), 5.59 (s, 1H, H4 or H5 of NMI), 5.65 (s, 1H, H4 or H5 of NMI), 6.02 (s, 1H, H_2 of NMI), 6.33 (d, 1H, $J = 8.5$ Hz), 6.41 (d, 1H, $J = 9.1$ Hz), 6.52 (d, 1H, $J = 9.1$ Hz), 6.55 (dd, 1H, $J = 7.0$, 8.5 Hz), 6.78 (d, 1H, $J = 9.1$ Hz), 6.82 (d, 1H, $J = 9.1$ Hz), 6.90 (dd, 1H, $J = 7.0$, 8.0 Hz), 7.33 (d, 1H, $J = 8.0$ Hz), 7.67 (d, 1H, $J = 8.9$ Hz), 7.69 (d, 1H, $J = 8.9$ Hz), 7.72 (s, 1H), 7.78 (s, 1H), 8.03 (s, 1H), 8.08 (d, 1H, $J = 8.9$ Hz), 8.20 (d, 1H, $J = 8.9$ Hz); ^{13}C NMR (CD_2Cl_2): $\delta = 30.6$ (*t*BuO), 34.0 (NMe), 114.2, 114.4, 117.6, 117.7, 118.7, 118.8, 119.1 (C4 and C5 of NMI), 122.0, 124.6, 124.7, 125.7, 126.1, 126.5, 126.6, 126.7, 126.8, 126.9, 127.0, 127.1, 127.2, 127.6, 128.86, 128.90, 128.93, 129.0, 130.5, 132.0, 132.9 (C2 of NMI), 155.5, 159.3, 159.9; other signals were assigned to free (*R*)-3-Br-BINOL.

Typical experimental procedure for the catalytic enantioselective Strecker reactions: To $Zr(OtBu)_4$ (0.04 mmol) in toluene (0.25 mL) was added (*R*)-6-Br-BINOL (0.04 mmol), (*R*)-3-Br-BINOL (0.04 mmol), and NMI (0.12 mmol) in toluene (0.75 mL) at room temperature. The mixture was stirred for 1 h at the same temperature, and then cooled to −65 °C. A solution of **1** (0.4 mmol) and Bu_3SnCN (0.44 mmol) in benzene (1.0 mL) was added. The mixture was stirred and warmed from −65 to 0 °C over 12 h, and a saturated aqueous solution of $NaHCO_3$ was then added to quench the reaction. The aqueous layer was extracted with dichloromethane. After a usual work up, the crude product was subjected to chromatography on silica gel to give the desired adduct. The optical purity was determined by HPLC analysis with a chiral column (see below). Since most of the adducts were unstable, they were characterized after methylation of the phenolic OH group as follows: The adduct was treated with a 20% MeI/acetone solution (5 mL) and K_2CO_3 (200 mg). After the mixture was stirred at room temperature for 6 h, saturated aqueous NH_4Cl was added to quench the reaction. After extraction of the aqueous layer with dichloromethane, the crude product was subjected to chromatography on silica gel to afford the corresponding methylated product quantitatively.

2-(2-Hydroxyphenyl)amino-2-phenylacetonitrile: HPLC (Daicel Chiralcel OD, hexane/*i*PrOH 9/1, flow rate 1.0 mL min^{-1}): $t_R = 40.0$ min (major product), 49.7 min (minor product).

2-(2-Methoxyphenyl)amino-2-phenylacetonitrile: ^1H NMR ($CDCl_3$): $\delta =$ 3.81 (s, 3H), 4.67 (d, 1H, $J = 8.3$ Hz), 5.43 (d, 1H, $J = 8.3$ Hz), 6.90–6.95 (m, 4H), 7.42–7.47 (m, 3H), 7.59–7.62 (m, 2H); ^{13}C NMR ($CDCl_3$): $\delta =$ 49.8, 55.4, 110.0, 111.6, 118.2, 119.6, 121.2, 127.2, 129.2, 129.4, 134.1, 134.5, 147.4; HR-MS calcd for $C_{15}H_{14}N_2O$ [M^+]: 238.1106, found: 238.1093.

4: The aminoamide **4** was synthesized according to the literature precedure.[16] The methylated adduct was prepared as described above, and the crude product (0.4 mmol) was dissolved in dichloromethane (1.0 mL). After the solution was cooled to 0 °C, a catalytic amount of Bu_4NHSO_4 (0.08 mmol), an excess amount of 30% aqueous hydrogen

 © WILEY-VCH Verlag GmbH, D-69451 Weinheim, 1998 1433-7851/98/3722-3187 $ 17.50+.50/0

peroxide, and 20% aqueous NaOH were added successively. The mixture was stirred for 1 h at the same temperature, and then warmed to room temperature. The reaction was monitored by thin-layer chromatography (TLC), and when there was no more starting material (ca. 2 h), ether was added, and the aqueous layer was extracted with dichloromethane. The pure N-protected leucinamide **4** was obtained in 94% yield from the cyanation product (two steps) after isolation by column chromatography on silica gel ($CHCl_3$/MeOH 19/1). ^{1}H NMR ($CDCl_3$): $\delta = 0.85$ (d, 3H, $J =$ 6.4 Hz), 0.95 (d, 3H, $J = 6.4$ Hz), 1.58–1.63 (m, 1H), 1.78–1.87 (m, 2H), 2.77 (s, 3H), 3.82 (s, 3H), 3.82 (br s, 1H), 6.71–6.82 (m, 3H), 6.88 (br s, 1H); ^{13}C NMR ($CDCl_3$): $\delta = 18.6$, 21.7, 23.35, 23.38, 24.9, 55.6, 60.0, 108.9, 120.8, 124.0, 127.3, 135.6, 149.8, 178.6.

5: The N-protected aminoamide **4** (0.38 mmol) was dissolved in 80% wet MeOH (5.0 mL). CAN (2.0 mmol) was added at 0 °C, and the mixture was stirred for 6 h at the same temperature. Water was added, and the acidic solution was washed with dichloromethane. The aqueous solution was made alkaline by adding 1N NaOH, and was then extracted with ethyl acetate. The combined organic layers were washed with brine and dried over Na_2SO_4. The solvent was removed, and the pure D-leucinamide **5** was obtained without further purification. ^{1}H NMR ($CDCl_3$): $\delta = 0.93$ (d, 3H, $J = 6.4$ Hz), 0.97 (d, 3H, $J = 6.4$ Hz), 1.39 (ddd, 1H, $J = 4.9$, 9.8, 13.8 Hz), 1.65 (ddd, 1H, $J = 4.3$, 4.9, 13.8 Hz), 1.55–1.80 (m, 3H), 3.76 (dd, 1H, $J =$ 4.3, 9.8 Hz), 6.37 (br s, 1H), 7.22 (br s, 1H); ^{13}C NMR ($CDCl_3$): $\delta = 21.0$, 23.1, 24.4, 43.7, 53.1, 178.8; HR-MS calcd for $C_6H_{14}N_2O$ [M^+]: 130.1107, found: 130.1091; (*R*)-leucinamide hydrochloride: $[\alpha]_D^{25} = -8.2$ ($c = 0.22$ in H_2O).[18]

Received: June 29, 1998 [Z 12067 IE]
German version: *Angew. Chem.* **1998**, *110*, 3369–3372

Keywords: amino acids · asymmetric catalysis · asymmetric synthesis · Lewis acids · zirconium

[1] Y. M. Shafran, V. A. Bakulev, V. S. Mokrushin, *Russ. Chem. Rev.* **1989**, *58*, 148–162.

[2] a) L. M. Weinstock, P. Davis, B. Handelsman, R. Tull, *J. Org. Chem.* **1967**, *32*, 2823–2829; b) W. L. Matier, D. A. Owens, W. T. Comer, D. Deitchman, H. C. Ferguson, R. J. Seidehamel, J. R. Young, *J. Med. Chem.* **1973**, *16*, 901–908.

[3] a) I. Ojima, S. Inaba, K. Nakatsugawa, *Chem. Lett.* **1975**, 331–334; b) K. Mai, G. Patil, *Tetrahedron Lett.* **1984**, *25*, 4583–4586; c) S. Kobayashi, H. Ishitani, M. Ueno, *Synlett* **1997**, 115–116.

[4] Reviews, a) R. M. Williams, *Synthesis of Optically Active α-Amino Acids*, Pergamon, Oxford, **1989**; b) R. M. Williams, J. A. Hendrix, *Chem. Rev.* **1992**, *92*, 889–917; c) R. O. Duthaler, *Tetrahedron* **1994**, *50*, 1539–1650; see also: d) H. Kunz, K. Rück, *Angew. Chem.* **1993**, *105*, 355–377; *Angew. Chem. Int. Ed. Engl.* **1993**, *32*, 336–358, and references therein; e) F. A. Davis, R. E. Reddy, P. S. Portonovo, *Tetrahedron Lett.* **1994**, *35*, 9351–9354; f) T. K. Chakraborty, K. A. Hussain, G. V. Reddy, *Tetrahedron* **1995**, *51*, 9179–9190.

[5] M. S. Iyer, K. M. Gigstad, N. D. Namdev, M. Lipton, *J. Am. Chem. Soc.* **1996**, *118*, 4910–4911.

[6] Quite recently, Jacobsen et al. reported elegant catalytic asymmetric Strecker reactions: a) M. S. Sigman, E. N. Jacobsen, *J. Am. Chem. Soc.* **1998**, *120*, 4901–4902; b) M. S. Sigman, E. N. Jacobsen, *J. Am. Chem. Soc.* **1998**, *120*, 5315–5316.

[7] a) H. Ishitani, M. Ueno, S. Kobayashi, *J. Am. Chem. Soc.* **1997**, *119*, 7153–7154; b) S. Kobayashi, H. Ishitani, M. Ueno, *J. Am. Chem. Soc.* **1998**, *120*, 431–432; see also c) H. Fujieda, M. Kanai, T. Kambara, A. Iida, K. Tomioka, *J. Am. Chem. Soc.* **1997**, *119*, 2060–2061.

[8] S. Kobayashi, S. Komiyama, H. Ishitani, *Angew. Chem.* **1998**, *110*, 1026–1028; *Angew. Chem. Int. Ed.* **1998**, 37, 979–981.

[9] For the use of 6,6′-dibromo-1,1′-bi-2-naphthol, see a) M. Terada, Y. Motoyama, K. Mikami, *Tetrahedron Lett.* **1994**, *35*, 6693–6696; b) H. Sasai, T. Tokunaga, S. Watanabe, T. Suzuki, N. Itoh, M. Shibasaki, *J. Org. Chem.* **1995**, *60*, 7388–7389.

[10] Bu_3SnCN is commercially available; a) J. G. A. Luijten, G. J. M. van der Kerk, *Investigations in the Field of Organotin Chemistry*, Tin Research Institute, Greenford, **1995**, p. 106; b) M. Tanaka, *Tetrahedron Lett.* **1980**, *21*, 2959–2962; c) S. Harusawa, R. Yoneda, Y. Omori, T. Kurihara, *Tetrahedron Lett.* **1987**, *28*, 4189–4190.

[11] P. J. Cox, W. Wang, V. Snieckus, *Tetrahedron Lett.* **1992**, *33*, 2253–2256.

[12] This could be partially due to the lower reactivity of (*R*)-3-Br-BINOL compared to (*R*)-6-Br-BINOL and equilibration of the coordination of NMI to the zirconium center. After careful examination, the best results and reproducibility were obtained when the catalyst was prepared by combining 1 equiv of $Zr(OtBu)_4$, 1 equiv of (*R*)-6-Br-BINOL, 1 equiv of (*R*)-3-Br-BINOL), and 3 equiv of NMI.

[13] When TMSCN was used in this system, moderate yields and moderate enantiomeric excesses were observed. The reaction of the aldimine prepared from 1-naphthaldehyde and 2-aminophenol with TMSCN led to the corresponding α-aminonitrile in 33% yield and with 63% *ee*; with triethylsilyl cyanide this product was obtained in 65% yield and with 63% *ee* (not optimized).

[14] a) J. M. Brown, A. C. Chapman, R. Harper, D. J. Mowthorpe, A. G. Davies, P. J. Smith, *J. Chem. Soc. Dalton Trans.* **1972**, 338–341; b) A. G. Davies, D. C. Kleinschmidt, P. R. Palan, S. C. Vasishtha, *J. Chem. Soc. C* **1971**, 3972–3976.

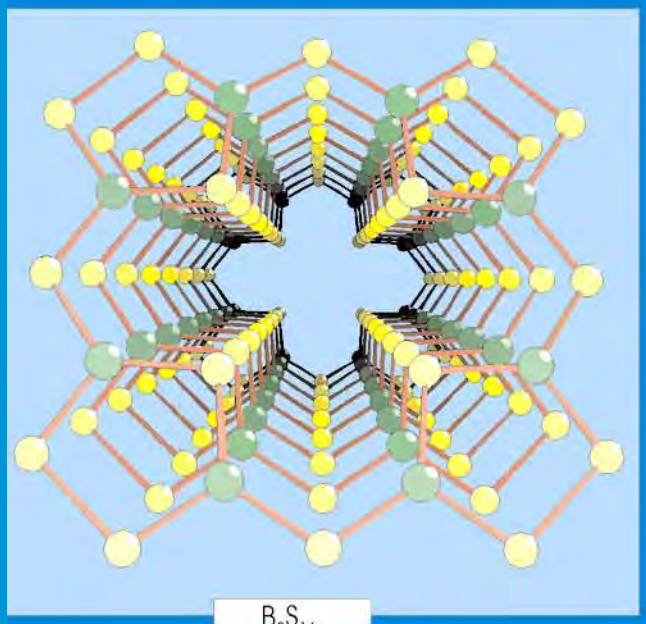
[15] Quite recently, we developed scandium triflate catalyzed Strecker reactions of aldehydes, amines, and Bu_3SnCN (achiral methods). In these reactions, the tin compounds were completely recovered by environmentally friendly chemical processes: S. Kobayashi, T. Busujima, S. Nagayama, *Chem. Commun.* **1998**, 981–982.

[16] S. Cacchi, D. Misiti, F. L. Torre, *Synthesis* **1980**, 243–244.

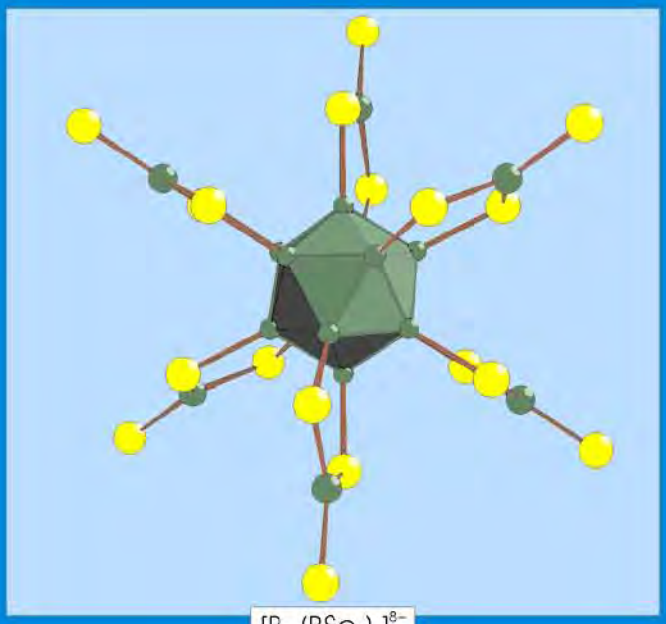
[17] D. R. Kronenthal, C. Y. Han, M. K. Taylor, *J. Org. Chem.* **1982**, *47*, 2765–2768.

[18] (*S*)-Leucinamide hydrochloride: $[\alpha]_D^{25} = +10$ ($c = 5$ in H_2O) (*Beilstein* **4** (3), 1414). (*S*)-Leucinamide hydrochloride is commercially available (Aldrich).

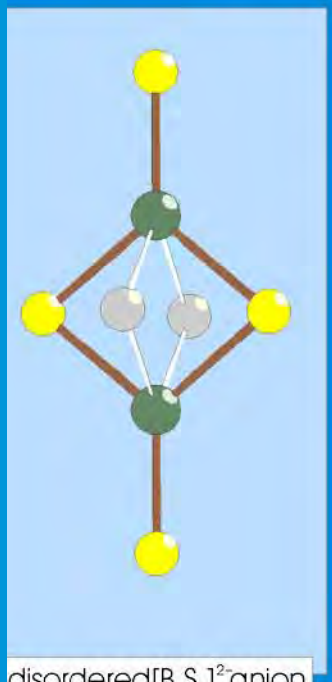
 © WILEY-VCH Verlag GmbH, D-69451 Weinheim, 1998 1433-7851/98/3722-3188 $ 17.50+.50/0



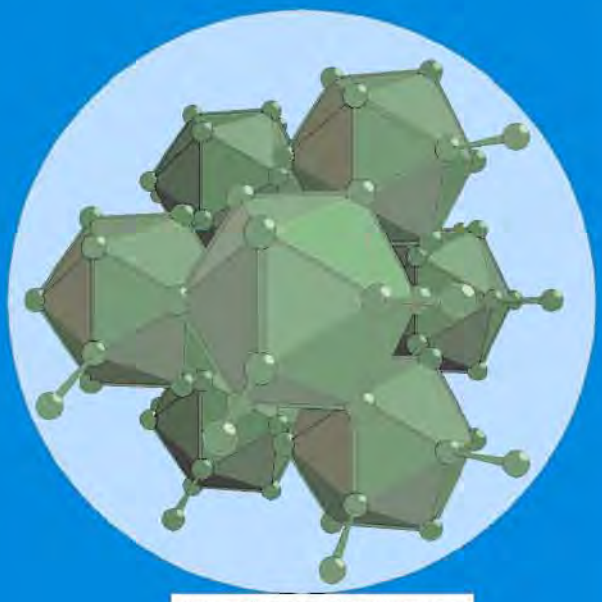
B_8S_{16}



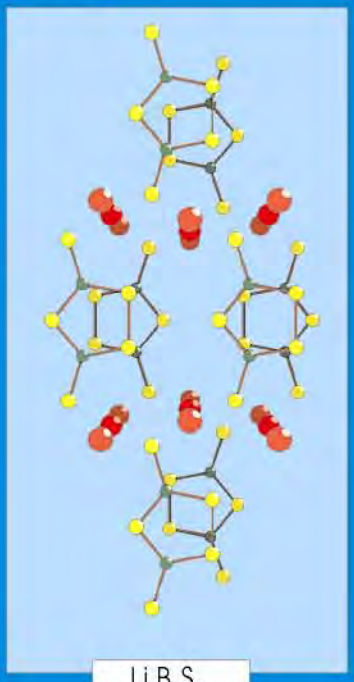
$[B_{12}(BSe_3)_6]^{8-}$



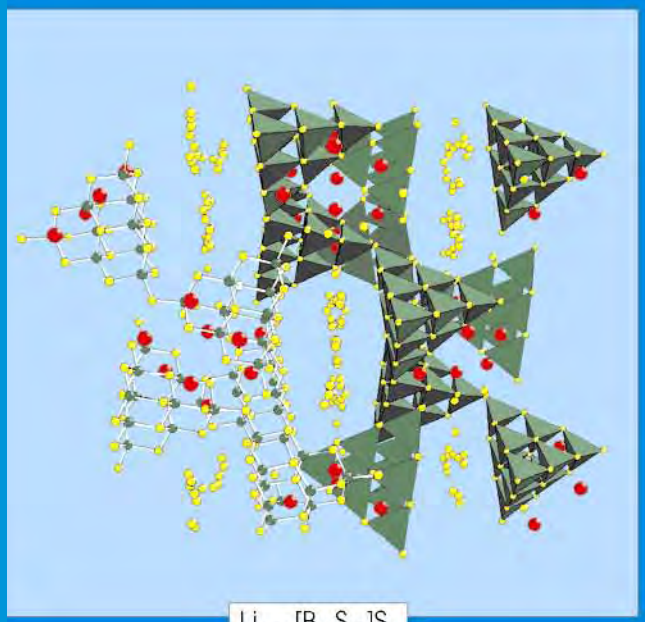
disordered $[B_2S_4]^{2-}$ anion



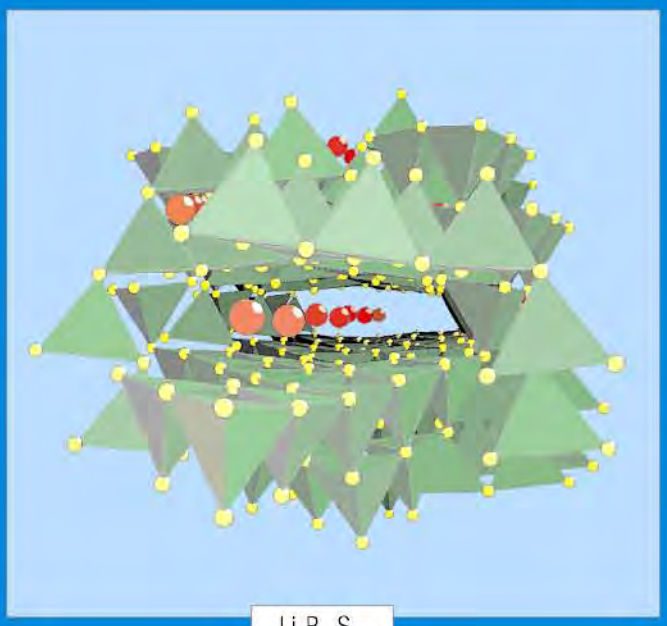
rhombohedral boron



$Li_2B_2S_5$



$Li_{6+2x}[B_{10}S_{18}]S_x$



$Li_9B_{19}S_{33}$

ANGEWANDTE CHEMIE ©WILEY-VCH

Boron – Sulfur and Boron – Selenium Compounds—From Unique Molecular Structural Principles to Novel Polymeric Materials

Olaf Conrad, Christoph Jansen, and Bernt Krebs*

Dedicated to Professor Dr. Walter Siebert

Boron is known to exhibit an unusual chemistry in all of its compounds. In addition, it shows a high tendency to form amorphous products over a wide range of temperatures. In the compounds with the heavier chalcogens, sulfur and selenium, both features are combined to open an intriguing field to the preparative chemist as well as to the crystallographer, the physicist, and the theoretician. In the past 15 years modern preparative methods have led to novel and often unexpected boron – sulfur and boron – selenium compounds, for example the persubstituted B_{12} icosahedron in the $[B_{12}(BSe_3)_6]^{8-}$ ionic molecule that features a planar B_3Se_2 ring at the chelating ligand, and the thioborate macromolecular anions that combine adamantanoid and superadamantanoid units in fascinating frameworks with a quasi-amorphous distribution of highly mobile lithium ions. An overwhelming number of different structures—not yet covered under one rule for all—has to be sorted and classified. Technical application of amorphous lithium thioborates call for an understanding of the mechanisms of ionic conduction in order to find rules for tailoring both crystalline and amorphous materials for intense physicochemical and theoretical examination. Preparation techniques have to be developed and refined to produce high-purity material in glassy, microcrystalline, and single crystalline aggregation at will.

Keywords: boron · selenium · solid-state structures · sulfur

1. Introduction

In medieval times amorphous alkaline oxoborates already played a significant role in daily life,[1] but the first preparation of elemental boron is attributed to the works of F. von Crell,[2] H. Davy,[3] and J. L. Gay-Lussac and L.-J. Thenard[4] in the early 19th century. In 1824 J. J. Berzelius[5] published the first reported boron chalcogenide,[6] "threefold sulfur boron" ("Dreifachschwefelbor"). Nevertheless, the knowledge about boron – sulfur and boron – selenium compounds remained very sparse for almost another 150 years. Problems of various kinds contributed to the reasons that made this class of compounds resist its examination:

- High-purity elemental boron was very difficult to get access to.
- The choice of reaction container material remained difficult for several years, because quartz glass is attacked by boron and results in a quantitative exchange of silicon with boron with formation of B_2O_3 and SiQ_2 (Q = S, Se), whereas the chalcogenophilicity of most metals excluded the common metal containers.
- The reaction products and often even the starting materials are readily oxidized and/or hydrolyzed by moist air.
- Chalcogenoborates tend to remain in an amorphous rather than a crystalline state.

Over the past 25 years the overcoming of these problems by improved high-temperature solid- and molten-state syntheses led to a better and deeper insight into the structural diversity, the chemistry, the bonding character, and some physical properties of binary, ternary, and quaternary chalcogenoborates. This review will give a comprehensive overview of the structurally characterized boron chalcogenides, molecular boron – chalcogen heterocycles, Lewis acid – base complexes of boron halides and chalcogenic electron donors, and thio- and selenoborates. This review will also cover their preparation, structural principles, and some of their physical properties.

[*] Prof. Dr. B. Krebs, Dr. O. Conrad, Dr. C. Jansen
Anorganisch-Chemisches Institut der Universität
Wilhelm-Klemm-Strasse 8, D-48149 Münster (Germany)
Fax: (+49) 251-833-8366
E-mail: krebs@uni-muenster.de

2. Synthetic Principles

The electron-deficient element boron is a more or less strong Lewis acid depending on its neighbors. In particular

 © WILEY-VCH Verlag GmbH, D-69451 Weinheim, 1998 1433-7851/98/3723-3209 $ 17.50+.50/0

boron with an empty or partially occupied p_z orbital, that is a sp^2-hybridized boron atom, is readily attacked by Lewis bases. Therefore any high-temperature solid-state or molten-state synthesis must be carried out in vacuo or in an inert gas atmosphere. The choice of container material is crucial for the success of the synthesis. Sealed, evacuated silica or quartz glass tubes with several layers of glassy carbon on the inner walls have proven best for daily use and for routine purposes. However, very long annealing periods at elevated temperatures ($t > 5$ d, $T > 750$ K) or reactions at very high temperatures ($T > 1100$ K) necessitate the use of tantalum pipe that is sealed under argon at atmospheric pressure and incorporated into an evacuated quartz glass ampoule. Alternatively, the use of graphite, boron nitride, or silicon-free aluminium oxide crucibles in stainless steel cylinders, and of evacuated quartz-glass tubes has also shown satisfactory results. Regular Schlenk techniques in dried aprotic solvents are sufficient for the synthesis of planar molecular boron–chalcogen ring compounds as well as for their further reactions.

3. Boron in Trigonal-planar Coordination

3.1. Binary Boron Chalcogenides

Aluminium shows coordination numbers not smaller than four in its binary chalcogenides, whereas in the case of boron chalcogenides the only exception to a trigonal-planar coordination is the metastable high-pressure phase B_2O_3-II which has boron distributed in the tetrahedral voids of a hexagonal close-packing arrangement of oxygen atoms.[7, 8] Although the ambient pressure modification B_2O_3-I exhibits boron along with trigonal-planar coordination, its three-dimensional interconnection differentiates the oxide from the sulfides and the selenide.[9] Despite a large number of publications on the existence of boron chalcogenides of different compositions[10–17] only B_2S_3,[18, 19] $(BS_2)_n$,[19, 20] B_8S_{16},[19, 20] and $(BSe_2)_n$[19, 20] have been characterized by means of single crystal X-ray structure determination (Figure 1). Suitable, but micro-twinned, colorless single crystals of B_2S_3 were prepared by controlled thermal decomposition of $Ag_6B_{10}S_{18}$ at about 1000 K. Colorless $(BS_2)_n$ and orange $(BSe_2)_n$ in amorphous and microcrystalline states can be prepared from the elements at temperatures of 1100 to 1300 K. Crystalline samples can be obtained by sublimation of the amorphous crude products in a temperature gradient of 670 to 400 K. Colorless B_8S_{16} is a by-product of the sublimation of $(BS_2)_n$ at the cooler end ($T <$ 373 K) of the sublimator in only a few milligrams yield. Any attempt to produce larger quantities of pure B_8S_{16}, though very much desired, has so far failed.

B_2S_3, the "normal" boron sulfide according to the valencies, has a layer structure. Sheets of interconnected B_3S_3 and B_2S_2 rings extend throughout the crystal. Each of the B_3S_3 rings is connected by sulfur bridges to two B_3S_3 rings and one B_2S_2 ring. In the structure exocyclic B–S bond lengths are longer than endocyclic ones. A closer look shows that the average value is 1.817 Å, whereas the average $B-S_{endo}$ bond length is 1.794 Å inside the six-membered ring and 1.811 Å in the

Olaf Conrad, born in 1967 in Berlin, Germany, studied chemistry at the University of Münster, where he received his Diplom in 1995. For his doctoral thesis he worked on the chemistry of aluminum chalcogenides and silver telluride and developed a further interest in the chemistry of thio- and selenoborates. He will spend a postdoctoral year in the group of Prof. Dr. R. S. Laitinen in Oulu/Finland, working on the chemistry of silicon sulfur and silicon selenium compounds.


O. Conrad


C. Jansen


B. Krebs

Christoph Jansen, born in 1964 in Billerbeck (Westfalen), Germany, started his career as a technician in chemistry (Chemielaborant) before he started his studies in 1988 at the University of Münster. He obtained his PhD in Chemistry in 1997 with a thesis on the synthesis and structures of thio- and selenoborates.

Bernt Krebs was born in 1938 in Gotha, Germany. He studied Chemistry at the University of Göttingen, Germany (1958–1963), and recieved his Ph D in 1965 for studies on the crystal structure and chemistry of trithiocarbonic acid under supervision of G. Gattow. Thereafter followed postdoctoral research at Brookhaven National Laboratory (X-ray and neutron diffraction on biological macromolecules), Habilitation in Inorganic Chemistry in Göttingen, and faculty positions in Kiel (1971), Bielefeld (1974), and Münster, where he has been a Full Professor since 1977. He received the Max Planck Research Award in 1992 and the Wilhelm Klemm Award of the GDCh in 1997. He is a member of the Academy of Sciences and Literature in Mainz, Germany. His primary research interests include chemical and structural studies on thio and seleno compounds, chalcogen halides, chalcogenide solid-state compounds, transition metal oxygen compounds, cis-platin-A analogues, and metalloproteins as well as model complexes for these metalloproteins.

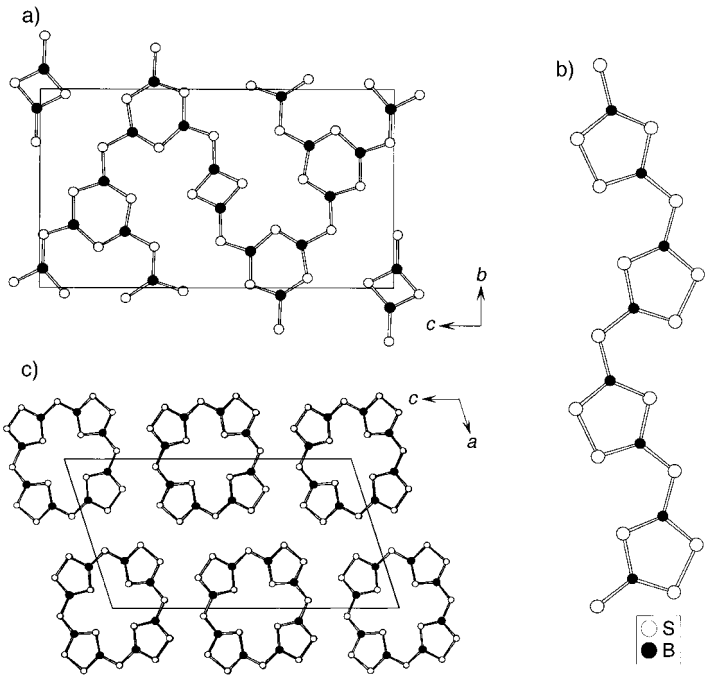


Figure 1. a) Crystal structure of B_2S_3; b) strand structure in $(BS_2)_n$ and $(BSe_2)_n$; c) crystal structure of B_8S_{16}.

strained four-membered ring. $(BQ_2)_n$ (Q = S, Se) exhibit layered structures, in which zigzag chains of interconnected 1,2,4-trithia(selena)-3,5-diborolane rings are oriented in a parallel manner within a plane and antiparallel to the strands of neighboring layers. In B_8S_{16} four of these B_2S_3 rings are connected to form a macrocycle that is topologically an analogue of porphin ($C_{20}H_{14}N_4$). The tetramers are stacked to form columns of parallel molecules. The plane vectors are tilted with respect to the columnar axis, which coincides with the crystallographic *b* axis. All rings are planar within experimental errors. The spacing between two layers is 3.48 Å in $(BS_2)_n$, which is significantly shorter than in B_2S_3 (3.81 Å) and the plane distance in B_8S_{16} (3.73 Å). The mean B – Q distance in the binary sulfides is 1.805 Å, in $(BSe_2)_n$ it is 1.934 Å. The transannular sulfur ··· sulfur distances of about 4.6 Å in B_8S_{16} suggest the capability of this molecule to incorporate Cu^{2+} ions in solutions. MO calculations indicate an energy gain comparable to that of cyclic thioether complexes of Cu^{2+} ions.[21]

3.2. Neutral Molecular Boron – Chalcogen Heterocycles

In 1955 E. Wiberg and W. Sturm found that $B_2S_3 \cdot BX_3$ (X = Cl, Br) in the early works of A. Stock at the beginning of the century[22] had to be rewritten as $(BSX)_3$,[23] a derivative of the hypothetical benzene analogue $H_3B_3S_3$. This initiated a broad research program on cyclic boron – chalcogen compounds in the following years. Four-membered 1.3.2.4-dithiadiboretanes,[24] five-membered 1.2.4.3.5-trithia(selena)diborolanes[25–27] and six-membered 1.3.5.2.4.6-trithia(selena)triborinanes[28–32] with several organic or halogen ligands were in most cases characterized by spectroscopic experiments. Structural information by electron diffraction experiments on gas phase molecules of $B_2S_3Cl_2$ and $B_2S_3(CH_3)_2$ proved these molecules to be exactly planar[33, 34] as was derived from the spectroscopic data and predicted from theoretical semiempirical calculations.[35] E. Wiberg and W. Sturm proposed the structure of $H_3B_3S_6$ to be a cyclic trimeric metathioboric acid,[29] which was proven in 1973 by single crystal X-ray structure determination.[36] The B_3S_6 entities deviate slightly from a perfectly planar arrangement. The average B – S distance is 1.803 Å. The proposed structure of $H_2B_2S_4$ by E. Wiberg and W. Sturm has not yet been verified, but J. A. Forstner and E. L. Muetterties reported the preparation of $B_2S_2(N(C_2H_5)_2)_2$,[24] the structure of which was verified later.[37] In 1974 W. Schwarz, H. D. Hausen, and H. Hess succeeded in the structure determination of $B_3S_3Br_3$.[38] The average B – S bond length of this planar molecule is 1.807 Å.

In recent years we were successful in several cases with systematic approaches to the preparation of suitable single crystals of molecular boron – chalcogen ring compounds, but a general method for this class of compounds is yet to be found. Selected data from the crystal structure determinations are shown in Table 1.[39, 40] In $B_3Q_3Ph_3$ (Q = S, Se) the six-membered heterocycle is planar within experimental errors.

Table 1. Structurally characterized molecular boron – chalcogen ring compounds and mean B – S(Se) distances [Å].

Compound	$\bar{d}$(B – Q)	Ref.	Compound	$\bar{d}$(B – Q)	Ref.
$B_2S_2[N(C_2H_5)_2]_2$	1.84	[37]	$B_3S_3Br_3$	1.807	[38]
$B_2S_3Cl_2$	1.794	[33, 34]	$B_3S_3Ph_3$	1.808	[39, 40]
$B_2S_3(CH_3)_2$	1.803	[33, 34]	$B_2Se_3I_2$	1.91	[39, 40]
$B_2S_3I_2$	1.795	[39, 40]	$B_2Se_3Ph_2$	1.93	[39, 40]
$B_2S_3Ph_2$	1.805	[39, 40]	$B_3Se_3Ph_3$	1.93	[39, 40]
$H_3B_3S_6$	1.803	[36]			

The B – Q bond lengths vary slightly and average to 1.808 and 1.93 Å for Q = S and Se, respectively. This is in excellent agreement to the bond lengths in the binary compounds and in $H_3B_3S_6$[36] and $B_3S_3Br_3$.[38] The three phenyl groups are rotated about the B – C bonds with different rotational angles. The B – C distances average to 1.55 Å in $B_3S_3Ph_3$ and 1.56 Å in $B_3Se_3Ph_3$, which are much longer than an average $C(sp^2)$ – $C(sp^2)$ bond length of about 1.42 Å. These data indicate that there is no, or very little, contribution of the π orbitals to the B – C bonds.

The five-membered ring in $B_2Q_3I_2$ (Q = S, Se) is planar within experimental error, whereas in $B_2S_3Ph_2$ and in $B_2Se_3Ph_2$ the bridging chalcogen atom is moved out of the plane. Figure 2 gives a representation of $B_2Se_3Ph_2$ and $B_2S_3I_2$. The angle between the normal vectors of planes B(1),Se(2),-Se(2a),B(1a) and B(1),Se(1),B(1a) is 7.40°. The average B – Q bond lengths are 1.795 Å in $B_2S_3I_2$, 1.805 Å in $B_2S_3Ph_2$, 1.91 Å in $B_2Se_3I_2$, and 1.93 Å in $B_2Se_3Ph_2$.

3.3. Ternary Chalcogenoborates

Early works report on a variety of chalcogenoborates, often in contradiction to each other. These include the

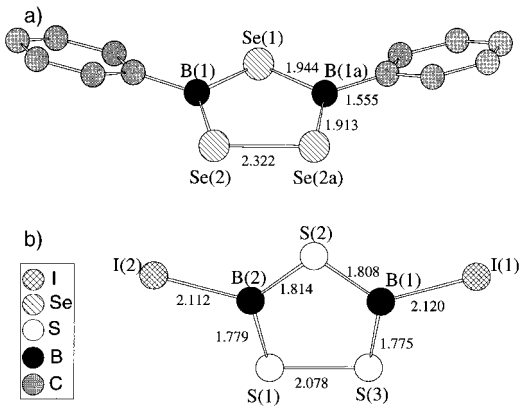


Figure 2. Crystal structures and bond lengths of a) $B_2Se_3Ph_2$ and b) $B_2S_3I_2$.

classes of compounds M^IBS,[41, 42] M^IBS_2,[41, 43–48] M^IBSe_2,[41] $M^{II}(BS_2)_2$,[49, 50] $M^I_4B_2S_5$,[45, 48] $M^{II}_2B_2S_5$,[50–53] $M^I_3BS_3$,[45, 47] $M^I_8B_2S_7$,[45, 48] $M^I_5BS_4$,[54] $M^I_4B_6S_{11}$,[47] M^IBS_3,[47, 55] and $M^I_2B_2S_5$.[55] By using the isotypic nature of the well-known structure of sodium trimetaoxoborate Chopin derived the structures of $Na_3B_3S_6$ and $K_3B_3S_6$ from X-ray diffraction powder patterns,[43, 46] but apart from an approximate model of $Pb_2B_2S_5$[52] structural data of chalcogenoborates was not published until the mid seventies.

Figure 3 shows the four types of thioborate anions with boron in solely trigonal planar coordination sites. It should be mentioned that Tl_3BSe_3 represents the only selenoborate of this type. $[BS_3]^{3-}$, $[B_2S_4]^{2-}$, and $[B_3S_6]^{3-}$ formally represent charged fragments of the B_2S_3 structure, while $[B_2S_5]^{2-}$ shows the motif of $(BS_2)_n$. They can be considered as deprotonated thioboric acids,

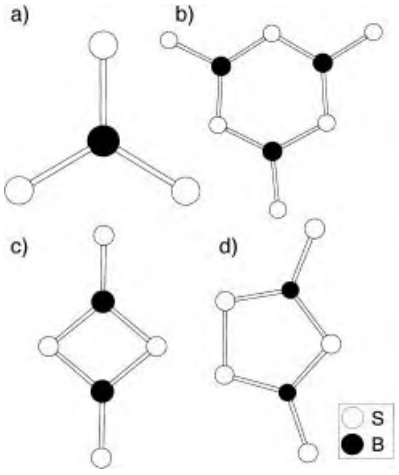


Figure 3. Types of thioborate anions with boron in trigonal-planar coordination, a) $[BS_3]^{3-}$, b) $[B_3S_6]^{3-}$, c) $[B_2S_4]^{2-}$, and d) $[B_2S_5]^{2-}$.

although H_3BS_3 and $H_2B_2S_5$ have not yet been reported. The structural nature of $H_2B_2S_4$ has not been determined by structure analysis but a cyclic structure was proposed.[23] Table 2 lists all thio- and selenoborates that are known today along with their degree of polymerization and some characteristic bond lenghts. The B – Q distances in BS_3^{3-} ions range

Table 2. Structurally characterized thio- and selenoborates and mean B – S(Se) distances [Å].

Compound	$\bar{d}(B_{tr}-S)$[a]	$\bar{d}(B_{tr}-S_{ex})$[b]	$\bar{d}(B_{tr}-S_{en})$[c]	$\bar{d}(B_{te}-S)$[d]	Ref.
Li_3BS_3	1.830				[56, 57]
Tl_3BS_3	1.833				[58]
$Sr_3[BS_3]_2$	1.826				[65]
$Ba_3[BS_3]_2$	1.814				[65]
Li_2CsBS_3	1.825				[60]
$LiSrBS_3$	1.824				[57]
$LiBaBS_3$	1.823				[59]
$KBa_4[BS_3]_3$	1.824				[61]
$K_4Ba_{11}[BS_3]_8S$	1.825				[60]
$Ba_{2.8}Sr_{4.2}[BS_3]_4S$	1.822				[60]
$Cs_2B_2S_4$	1.821	1.740	1.861		[62]
$Na_3B_3S_6$	1.805	1.768	1.824		[19, 64]
$K_3B_3S_6$	1.798	1.775	1.810		[19]
$Rb_3B_3S_6$	1.800	1.760	1.821		[65]
$Sr_3[B_3S_6]_2$	1.786	1.770	1.794		[65]
$LiSrB_3S_6$	1.804	1.778	1.817		[65]
$LiBaB_3S_6$	1.804	1.771	1.821		[59]
BaB_2S_4	1.808	1.786	1.821	1.926	[83]
SrB_2S_4				1.929	[69]
$TlBS_2$				1.930	[69, 70]
$Pb_4B_4S_{10}$				1.927	[19]
$Na_6B_{10}S_{18}$				1.922	[71]
$Ag_6B_{10}S_{18}$				1.915	[75]
$Li_{6+2x}[B_{10}S_{18}]S_x$	($x \approx 2$)			1.920	[74]
$Li_5B_7S_{13}$				1.922	[74, 76]
$Li_9B_{19}S_{33}$				1.925	[76]
$Li_{4-2x}Sr_{2+x}B_{10}S_{19}$	($x \approx 0.27$)			1.925	[71]
$Li_3Na_5B_{10}S_{19}$				1.925	[61]
Tl_3BSe_3	1.953				[58]

[a] Mean B – S(Se) distance with the boron center in a trigonal-planar coordination site; [b] mean exocyclic $B_{tr}-S$ distance; [c] mean endocyclic $B_{tr}-S$ distance; [d] mean B – S distance with the boron center in a tetrahedral coordination site.

from 1.814 to 1.830 Å and are remarkably unaffected by the nature of the counterion.[56–61] The average length of 1.823 Å is significantly longer than in the binary boron sulfides. This indicates less π interaction and is attributed to the high charge density of this small molecule. $Cs_2B_2S_4$ is the only known salt of the dimeric metathioboric acid.[62] It exhibits unusual bonding properties in the $B_2S_4^{2-}$ ion. The endocyclic B – S distances in this strained ring molecule are at 1.861 Å the longest reported for boron centers with trigonal planar coordination, the exocyclic distances are the shortest at 1.740 Å, whereas the average length of 1.821 Å corresponds to the BS_3^{3-} ions. The trigonal-planar coordination is highly distorted. The S_{endo}-B-S_{endo} angle in the ring is only 100.9°, the S_{endo}-B-S_{exo} angles are 129.5°. In addition, a nonbonding B ··· B distance of 2.37 Å is observed. This is, although very short, about 0.2 Å longer than in the four-membered ring of B_2S_3. This extreme situation can be attributed to repulsive forces between the boron atoms, which shift coplanarly from the center of the triangle towards the exocyclic sulfur atoms. The very short $B-S_{exo}$ distance indicates the exocyclic sulfur atoms to be the main carriers of the charge. This explanation is supported by the fact that the bonding situation is reversed in B_2S_3, where the $B-S_{endo}$ distance in the B_2S_2 ring averages to 1.801 Å and is shorter than the $B-S_{exo}$ distance (1.819 Å).

Alkali metal and alkaline earth salts of $H_3B_3S_6$ and thioborates with a $[B_2S_5]^{2-}$ ion exhibit a common structural feature: The average B – S distance of the anion ranges from

1.786 to 1.804 Å.[19, 43, 46, 63–65] Thus, the distance is about 0.02 Å shorter than in the other thioborates with boron in trigonal-planar coordination, and is close to the length of the B–S bonds in the binary compounds. Again, the bonding situation is reversed as compared to the binary sulfides. The $B-S_{exo}$ distances are shorter (ranging from 1.760 to 1.800 Å) than the $B-S_{endo}$ bond lengths (1.794 to 1.824 Å) in the thioborates. The B_3S_6 unit is crystallographically planar in $A_3B_3S_6$ (A = Na, K, Rb) but nonplanar in the cases of $Sr_3[B_3S_6]_2$ and $LiAB_3S_6$ (A = Sr, Ba), where the space group does not demand a planar molecule. The BS_3 subunits themselves are planar, so the distortion of the B_3S_6 entities is a consequence of packing forces in the crystal rather than coordinative interactions of p_z orbitals of boron to sulfur atoms of neighboring $[B_3S_6]^{3-}$ ions ($d(S\cdots S)_{min} = 3.590-3.793$ Å).

The $[B_2S_5]^{2-}$ ion is formally derived from $(BS_2)_n$ by thiolytic cleavage of the sulfur bridge. This anion has only been observed with the small alkali ions Li^+ and Na^+.[63] Because of the different coordination numbers of Li^+ (C.N. = 4) and Na^+ (C.N. = 8) these structures are not isotypic. The $B-S_{exo}$ distances of 1.768 Å are again significantly shorter than the $B-S_{endo}$ bond length of 1.818 Å in $Na_2B_2S_5$. But in the corresponding lithium salt they are at about the same length ($B-S_{exo}$ 1.800, $B-S_{endo}$ 1.807 Å). In both compounds the anions are crystallographically planar.

4. Boron with Tetrahedral Coordination

4.1. Coordinative Lewis Acid–Base Complexes

Trigonal-planarly coordinated boron close to sulfidic or disulfidic sulfur atoms may be subject to donor–acceptor complex formation. The strength of Lewis acidity and basicity can be modified by $p_\pi-p_\pi$ electron transfer from the sulfur to the boron in a B–S bond. Electron transfer can be increased by electron-withdrawing substituents (–I effect) on the boron atom or electron-donor substituents (+I-, +M effect) on the sulfur atom. It is known that the dihalogen(methylthio)boranes X_2BSCH_3 (X = Cl, Br) form cyclic trimers in the crystalline state.[66] This is an example of donor–acceptor complex formation. Boron is tetrahedrally coordinated, that is, it has been rehybridized from sp^2 to sp^3. The average $B(sp^3)-S$ bond length is 1.95 Å and is comparable to that found in chalcogenoborates with boron in a tetrahedral chalcogenic coordination. Table 3 summarizes the boron–sulfur donor–acceptor complexes with sp^3 boron centers. Crystal structure analyses of $(CH_3)_2Q\cdot BX_3$ and $(CH_2)_4S\cdot BX_3$ (Q = S, Se; X = Cl, Br, I)[67] showed the influence of the Lewis acidity on the strength of the complex formation. The molecules $(CH_3)_2S\cdot BX_3$ are shown in Figure 4. The S–B bond length decreases with increasing Lewis acidity of the boron trihalide ($BI_3 > BBr_3 > BCl_3$). An exception is $(CH_3)_2Se\cdot BI_3$ because intermolecular interaction of iodine and selenium (shortest Se···I distance: 4.112 Å) decreases the Lewis acidity of BI_3. The B–S bond length in these compounds ranges from 1.916 to 1.966 Å, while the B–Se bond length is between 2.065 and 2.101 Å. The products were synthesized from *n*-hexane (X = Cl) or CS_2 (X = Br, I).[68] Single crystals were grown by sublimation of the crude product in evacuated, sealed silica tubes in optimized temperature gradients. The crystals are colorless (X = Cl, Br) or pale yellow to pale red (X = I).

Table 3. B–S(Se) distances [Å] in donor–acceptor complexes of BX_3 and chalcogen donor ligands.[67]

Donor/acceptor	BCl_3	BBr_3	BI_3
$(CH_3)_2S$	1.963	1.934	1.923
thiophene	1.960	1.966	1.916
$(CH_3)_2Se$	2.101	2.065	2.079

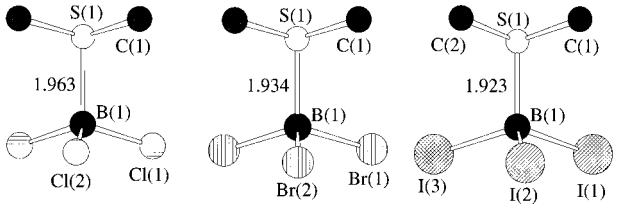


Figure 4. Crystal structure and B–S bond length [Å] of $(CH_3)_2S\cdot BX_3$ (X = Cl, Br, I).

4.2. Ternary and Quaternary Chalcogenoborates

The boron atoms in BS_3^{3-}, $B_2S_4^{2-}$ and $B_3S_6^{3-}$ are Lewis acidic. In the melt the sulfide, disulfide, and the sulfur atoms of the molecular anions are Lewis bases. In many thioborates and perchalcogenoborates that have been synthesized by high-temperature solid-state and molten-state techniques, anionic macromolecules and polymers are observed. This can be rationalized with the concept of donor–acceptor complex formation. The physical properties of the counterion seem to influence the strength of Lewis interaction. The counterions Li^+, Na^+, and Ag^+ favor extended, three-dimensional networks of macromolecular arrangements of adamantane- and "superadamantane"-type thioborate polymers.[51, 52, 69–77] On the other hand, isolated $[B_4S_{10}]^{8-}$ ions, or layered or chain-type polymers of BS_4 tetrahedra are found with soft ions like Pb^{2+}, Ba^{2+}, or Tl^+.[19, 51, 52, 69, 70] In planar boron–chalcogen ring compounds two cases of intermolecular Lewis-type interaction may be present:

- Interaction of exocyclic chalcogen atoms with boron atoms in a ring.
- Interaction of boron and chalcogen atoms between different rings.

In Figure 5 the formation of the polymeric $(BS_2)_n^{n-}$ ion in $TlBS_2$ is shown as interpreted on the basis of donor–acceptor complex formation between the exocyclic sulfur atoms and endocyclic boron atoms of $B_3S_6^{3-}$ units. In this case four-membered B_2S_2 rings are formed that, in contrast to B_2S_3, contain tetrahedrally coordinated boron centers. Consequently the formerly planar six-membered B_3S_3 ring is now in the chair conformation and is connected to three more B_3S_3 rings through B_2S_2 rings. A layered structure of polymerized B_3S_6 units is formed.[69, 70] A rehybridization of the boron center from sp^2 to sp^3 has taken place. Tetrahedral coordination enhances the flexibility of the boron atom to adjust to steric

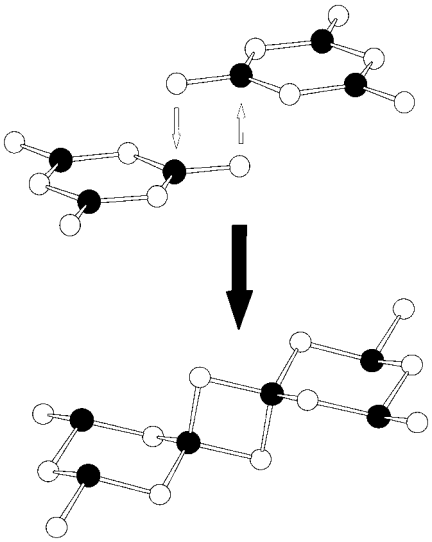


Figure 5. Donor–acceptor complex formation of $[BS_2]_n^{n-}$ in $TlBS_2$.

demands, as seen in the unusual bonding situation in the unfavoured four-membered ring: Two B–S bonds of 1.86 Å alternate with two contacts of 2.02 Å. The transannular B···B distance of 2.52 Å is larger than in $Cs_2B_2S_4$ (2.37 Å) as well as the transannular S···S distance of 2.930 Å ($Cs_2B_2S_4$: 2.871 Å). A similar donor–acceptor complex formation of $[B_3S_6]^{3-}$ and $[BS_2]^-$ fragments results in a layered arrangement of B_2S_2 and B_3S_3 rings in SrB_2S_4 (Figure 6).[69] The rather long B–S bond

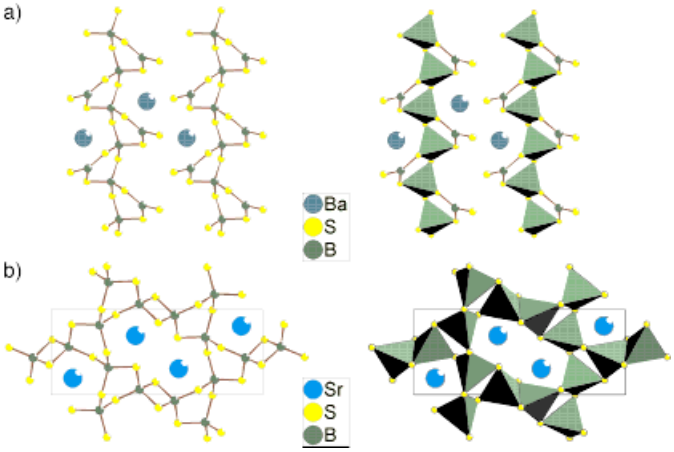


Figure 6. Crystal structures of a) BaB_2S_4 and b) SrB_2S_4.

length in the four-membered ring of 1.968 Å leads to transannular B···B contacts of 2.604 Å and S···S distances of 2.950 Å. The weak interaction between the chains of BS_4 tetrahedra, which arise from the formation of the four-membered ring, is totally avoided by the use of Ba^{2+} ions instead of the smaller Sr^{2+} ions. In BaB_2S_4 the chains of corner-sharing BS_4 tetrahedra are not connected through B_2S_2 rings (Figure 6). Instead, the boron atoms remain in a trigonal-planar coordination bridging only the BS_4 tetrahedra within the chain. This principle is also found in $AgBO_2$ and $TlBO_2$.[78, 79] Trigonal-planar and tetrahedral coordination of boron atoms in the same compound is common for oxoborates, but BaB_2S_4 is the only known example of this feature in thioborates.

Higher degrees of condensation to form even three-dimensional infinite networks of anionic macrotetrahedra is only found with small and medium-sized ions like Li^+, Na^+, Ag^+, and Sr^{2+}. In Figure 7 a possible interpretation of the formation of the adamantane-like $B_4S_{10}^{8-}$ ion is proposed. With just one

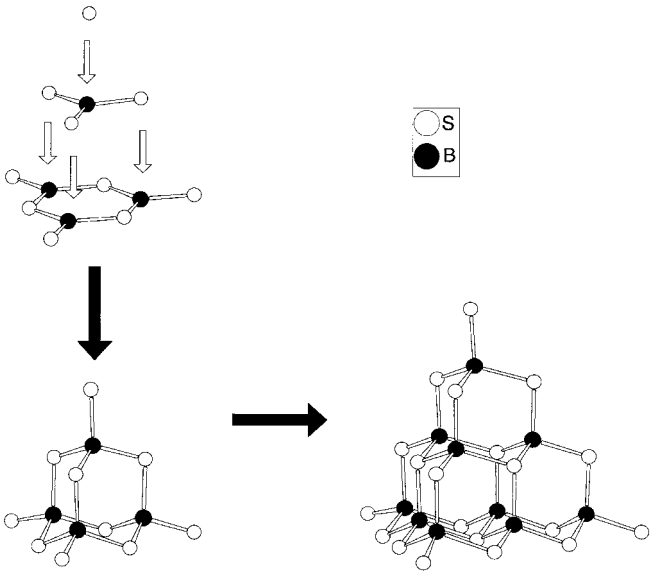


Figure 7. Donor–acceptor complex formation of adamantane- and "superadamantane"-type anionic fragments.

additional sulfide group this macrotetrahedron can be built starting from planar boron–sulfur units. Each sulfur atom of a planar BS_3^{3-} unit coordinates to one of the boron atoms in a B_3S_3 ring, which needs to be rehybridized to sp^3. A sulfur atom on top of the remaining boron atom completes the $B_4S_{10}^{8-}$ entity. The "superadamantane" $B_{10}S_{20}$ unit is built in a similar way. The relatively highly charged fragment $[B_4S_{10}]^{8-}$, which is isostructural to P_4O_{10}, P_4S_{10}, and the $[Ge_4S_{10}]^{4-}$ ion,[80] and isoelectronic to $[Ga_4S_{10}]^{8-}$ and $[In_4S_{10}]^{8-}$,[19] is found only in $Pb_4B_4S_{10}$.[19, 51, 52] Covalent interactions between lead and terminal sulfur atoms are discussed as partially compensating for the charges. On the other hand, a wide variety of polymerized macrotetrahedra characterizes the class of compounds with small cations. In $Li_3Na_5B_{10}S_{19}$[61] and $Li_{4-2x}Sr_{2+x}B_{10}S_{19}$ ($x \approx 0.27$)[71] chains of $B_{10}S_{18}S_{2/2}$ are present (Figure 8), while in $Na_6B_{10}S_{18}$,[71] $Li_{6+2x}[B_{10}S_{18}]S_x$ ($x \approx 2$),[72, 74] and $Ag_6B_{10}S_{18}$[75] all the corners of a $B_{10}S_{16}S_{4/2}$ macrotetrahedron are connected to neighboring units and two independent, interpenetrating infinite three-dimensional networks are formed (Figure 8). The smallest possible unit of this kind, a BS_4^{5-} ion, has never been observed on account of its high charge. In $Li_9B_{19}S_{33}$[76] two $B_{10}S_{16}S_{4/2}$ entities share a BS_4 subunit to again form two independent, interpenetrating infinite three-dimensional networks of corner-sharing $B_{19}S_{30}S_{6/2}$ units. (Figure 9). Another example of this kind is found in $Li_5B_7S_{13}$,[74, 76, 77] where an alternation of $B_4S_6S_{4/2}$ tetrahedra and $B_{10}S_{16}S_{4/2}$ supertetrahedra forms the networks (Figure 9). Compounds with infinite networks of macrotetrahedra form very rigid three-dimensional anionic frameworks with fairly large voids and channels. These spaces have similar energetic environments so movement of cations is not

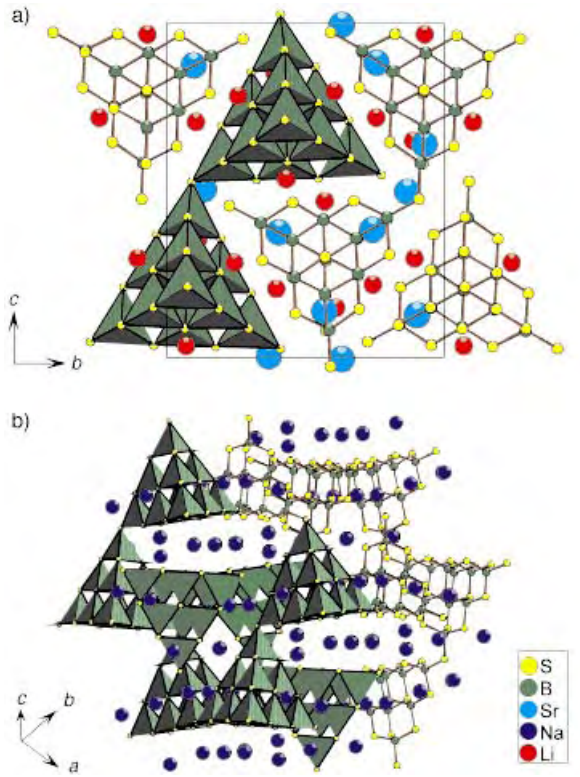


Figure 8. Crystal structure of a) $Li_{4-2x}Sr_{2+x}B_{10}S_{19}$ and b) $Na_6B_{10}S_{18}$.

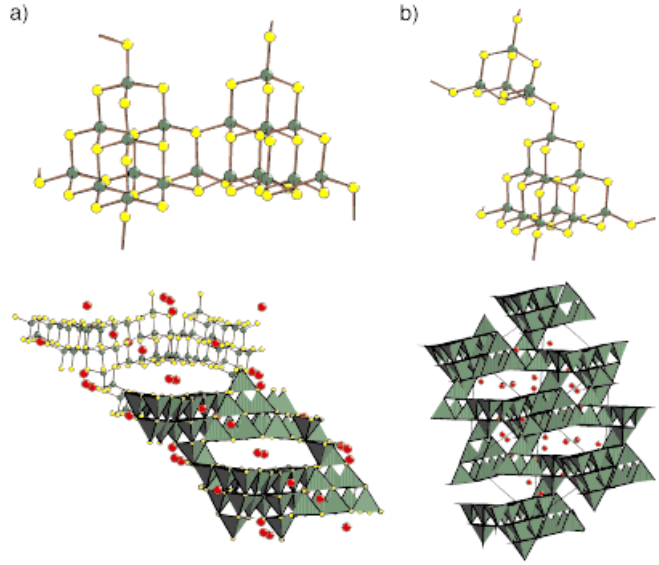


Figure 9. Crystal structure and building fragments of a) $Li_9B_{19}S_{33}$ and b) $Li_5B_7S_{13}$.

hindered. Solid-state NMR spectroscopy on ^7Li nuclei in $Li_5B_7S_{13}$, $Li_9B_{19}S_{33}$, $Li_{6+2x}[B_{10}S_{18}]S_x$, and $Li_{4-2x}Sr_{2+x}B_{10}S_{19}$ showed in some cases remarkable dynamics of the cations (see section 6).

4.3. Ternary and Quaternary Perchalcogenoborates

In recent times perthio- and perselenoborates have been the subject of intensive studies in our group. Their structures are dominated by chain-type polymeric anions that are based on the B_2Q_3 fragment (Q = S, Se) known from $(BQ_2)_n$. At least one example each of perthio- and perselenoborates has been synthesized with Li,[61, 63] Na,[63, 81] K,[81] Rb,[61, 82] Cs,[60] and monovalent Tl.[70, 82] Table 4 summarizes all known perchalcogenoborates. Only a small number of the thiobo-

Table 4. Structurally characterized perthio- and perselenoborates and mean B–S(Se) lengths [Å].

Compound	$\bar{d}$(B–S)	Ref.	Compound	$\bar{d}$(B–Se)	Ref.
$Li_2B_2S_5$	1.805	[63]	$Li_2B_2Se_7$	2.047	[61]
$Na_2B_2S_5$	1.802	[63]	$Na_2B_2Se_7$	2.044	[81]
$K_2B_2S_7$	1.919	[81]	$K_2B_2Se_7$	2.050	[81]
$RbBS_3$	1.927	[82]	$Rb_2B_2Se_7$	2.049	[61]
$CsBS_3$	1.930	[60]	$CsBSe_3$	2.064	[60]
$TlBS_3$	1.930	[70, 82]	$Cs_3B_3Se_{10}$	2.052	[60]
$Tl_3B_3S_{10}$	1.919	[70]	$TlBSe_3$	2.059	[83]

rates with boron atoms with tetrahedral coordination contain a disulfide bridge, whereas all known selenoborates with tetrahedrally coordinated boron atoms contain diselenide units. Only two of these perchalcogenoborates, $Li_2B_2S_5$ and $Na_2B_2S_5$, contain boron atoms with trigonal-planar coordination. They represent the only discrete perchalcogenoborate anions. In all other perchalcogenoborates the structural elements are $[BQ_3]_n^{n-}$, $[B_2Q_7]_n^{2n-}$, and $[B_3Q_{10}]_n^{3n-}$ polymers. They are displayed in Figure 10 a–c. Except for $Li_2B_2Se_7$ all of

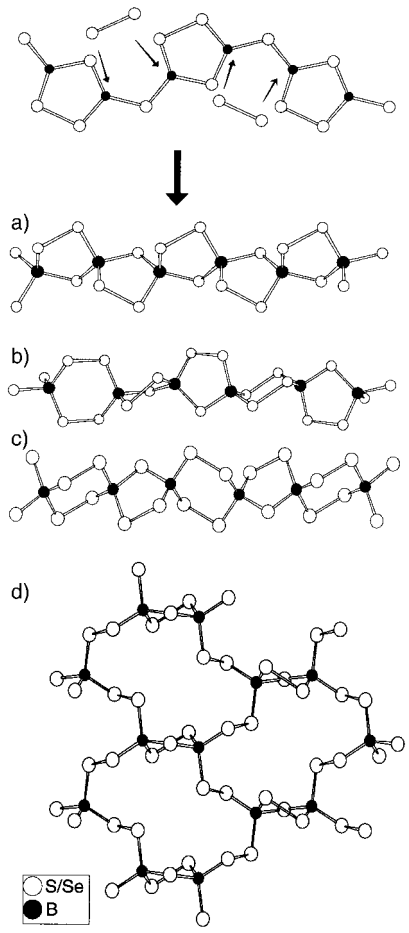


Figure 10. Donor–acceptor complex formation in perchalcogenoborates a) $[BQ_3]_n^{n-}$, b) $[B_3Q_{10}]_n^{3n-}$, c) $[B_2Q_7]_n^{2n-}$ and d) anion of $Li_2B_2Se_7$.

these are one-dimensional infinite polymers with a rising content of dichalcogenide in the order $[BQ_3]_n^{n-} < [B_3Q_{10}]_n^{3n-} < [B_2Q_7]_n^{2n-}$. The nucleophilic attack of diselenide to $(BSe_2)_n$ is also shown in Figure 10. As rehybridization of sp^2 to sp^3 is favored over oxidative cleavage of the B–Se bond, this again can be regarded as a donor–acceptor complex formation. This process results in an infinite chain of fused spirocyclic five-membered B_2Se_3 rings with boron centers in tetrahedral coordination. This motif is found in $RbBS_3$,[82] $CsBS_3$,[60] $TlBS_3$,[70, 82] $CsBSe_3$,[60] and $TlBSe_3$.[83] Insertion of a second diselenide bridge into every third ring results in the $[B_3Se_{10}]_n^{3n-}$ polymer, which is present in $Tl_3B_3S_{10}$[70] and $Cs_3B_3Se_{10}$.[60] A 1:1 ratio of spirocyclicly fused five-membered B_2Q_3 rings and six-membered B_2Q_4 rings is present in $[B_2Q_7]_n^{2n-}$ chains. These are found in $K_2B_2S_7$ and $A_2B_2Se_7$ (A = Na, K, Rb).[61, 81] In Figure 10d the anionic polymer in the compound $Li_2B_2Se_7$ is shown.[61] Here five-membered B_2Se_3 rings are connected by diselenide bridges into two dimensions. The four exocyclic diselenide bridges stretch out to four neighboring B_2Se_3 units to form a layered structure rather than to two entities to form a chain. In all perchalcogenoborates the B–Q bond lengths are within the range observed in other boron–chalcogen compounds. They range from 1.91 to 1.95 Å in perthioborates with sp^3 boron atoms and from 2.02 to 2.07 Å in perselenoborates.

5. Subvalent Chalcogenoborates

All syntheses of chalcogenoborates start from the corresponding metal chalcogenide, elemental chalcogen, and elemental boron. In the course of the reaction oxidation and fragmentation of the B_{12} icosahedra of elemental boron must occur to form the chalcogenoborates. The oxidant is clearly the chalcogen, but the steps of fragmentation of boron are as yet unknown. A hint, of course, could arise from crystallized intermediates, so a systematic search for subvalent chalcogenoborates must be undertaken. As the existence of $B_{12}S_{2-x}$[15] and $B_{12}SeB$[16] is proposed, a likely way of fragmentation proceeds via persubstitution of the B_{12} icosahedron. At the other end of the fragmentation path cyclic compounds with direct B–B contacts should be present. An example of this is found in B_4S_2 rings of 2.3.5.6-tetrakis(dimethylamino)1.4-dithiatetraborinane.[84]

The novel chalcogenoborate $Cs_8[B_{12}(BSe_3)_6]$[85] (Figure 11) contains the first B_{12} icosahedron completely saturated with chalcogen ligands. Six trigonal-planar selenoborate entities that function as bidentate ligands complete the B_{12} icosahedron to form a persubstituted *closo*-dodecaborate ion. This centrosymmetric molecule shows endocyclic B–Se bond lengths in the chelate-type B_3Se_2 ring of 1.952 to 2.011 Å, whereas the B–Se bonds to the exocyclic selenium atoms are significantly shorter (1.886 to 1.913 Å). This indicates that these atoms carry a large quantity of the charge of the $[B_{12}(BSe_3)_6]^{8-}$ ion. The *closo*-cluster contains 2n+2 binding electrons for the B_{12} unit and therefore obeys Wade's rules for cluster compounds. Six negative charges are located on the terminal selenium atoms, which leaves two negative charges on the central cluster. Additional interest for this compound

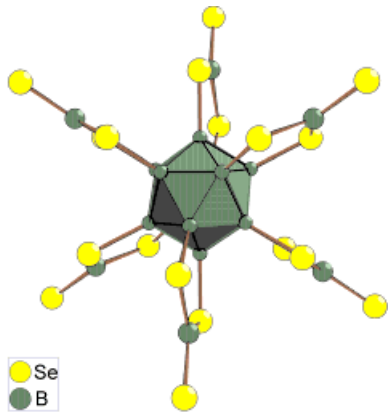


Figure 11. Structure of the $[B_{12}(BSe_3)_6]^{8-}$ ion in $Cs_8[B_{12}(BSe_3)_6]$

comes from its preparation: It has been synthesized by the high temperature reaction of a stoichiometric mixture of Cs_2Se, Se, and B at 973 K and subsequent annealing (10 h at 873 K, 24 h at 673 K, 120 h at 473 K). The B_{12} icosahedron was preserved under these rather severe reaction conditions.

6. Solid-State ^{7}Li NMR Studies on Thioborates

Superionic conducting materials, that is solid compounds with ionic conductivity of about 1 $S\,cm^{-1}$ with insignificant electronic conductivity, are of increasing interest for commercial applications like batteries, fuel cells, sensors, and electrochromic devices. As isotropic conductivity is wanted in most cases, amorphous materials are most commonly applied and therefore thoroughly investigated. But in the systematic search for new superionic conducting materials an understanding of the transport mechanisms of a charged mobile phase in an oppositely charged stationary phase is needed. Li^+- and Ag^+-containing thioborates with a rigid anionic framework are good candidates for high ionic conduction. In section 4.2. we presented the crystal structures of a number of these compounds that feature an anionic framework with a surplus of energetically similar sites along large voids and channels. The cations are distributed with high occupational disorder over a large number of these sites, which results in a quasi-amorphous distribution of the cations into a crystalline matrix. These compounds can serve as model systems for the study of transport mechanisms. In collaboration with the group of W. Müller-Warmuth ^{7}Li NMR spectroscopy experiments have been carried out with $Li_5B_7S_{13}$,[72] $Li_9B_{19}S_{33}$,[86] $Li_{4-2x}Sr_{2+x}B_{10}S_{19}$ ($x \approx 0.27$),[86] and $Li_{6+2x}[B_{10}S_{18}]S_x$ ($x \approx 2$).[72, 73] The spectra obtained are similar to those of glassy thioborates.[87–89] At low temperature (rigid lattice region), along with the dipolarly broadened central transition, an unstructured base of averaged quadrupole coupling signals is recorded, which can be attributed to the contribution of various energetically inequivalent lithium positions. Upon increased temperature a line narrowing caused by the motions of the lithium ions ("motional narrowing") is observed. An activation energy for the motion of about 20 to 30 $kJ\,mol^{-1}$ is estimated according to Waugh and Fedin[90] from the temperature at which motional narrowing starts. In contrast to glassy

lithium conductors, above a compound-specific temperature in crystalline thioborates one or two quadrupole coupling satellites evolve, which can be interpreted as anisotropic lithium motion over one or two energetically equivalent sites in the crystal lattice. From relaxation time measurements the double-exponential time dependency of the nuclear magnetization was extracted and interpreted on the basis of a contribution from the different mobilities of the ions in $Li_{6+2x}[B_{10}S_{18}]S_x$ as well as a contribution of different transport mechanisms in $Li_5B_7S_{13}$ and $Li_9B_{19}S_{33}$. In general, NMR studies on crystalline thioborates show good agreement to results from amorphous compounds and the same theory can be applied to describe the observations. Thus, as the structure is known from single-crystal analysis, structure–property relations can be examined and transferred to glassy ionic conductors.

7. Conclusions and Outlook

In the borderline field between molecular and solid-state chemistry the variable possibilities of preparative routes toward boron–sulfur and boron–selenium compounds have led to an ever growing number of different structural principles that are only in part fully understood and will definitely be the source of further surprise in future syntheses.

But tendencies can be named: Boron atoms in trigonal-planar coordination sites can be found mainly in sulfur reaction mixtures with a low boron sulfide content. If the ratio of M^I_2S (M^I = alkali metal, Ag, Tl):B_2S_3 is smaller than 1:1, the boron center is sp^3 hybridized, and the formation of three-dimensional networks of anionic macrotetrahedra is favored with smaller cations (Li^+, Na^+, Ag^+), whereas perthioborates are formed with K^+, Rb^+, Cs^+, and Tl^+. Perthioborates with Li^+ and Na^+ are known with a sp^2 hybridized boron center.

The size of selenium is incompatible to boron atoms to allow $\pi-\pi$ overlapping, so sp^2 hybridized boron centers cannot be stabilized. Perselenoborates with boron atoms with tetrahedral coordination are the by far most common boron–selenium compounds. Modifications in the selenium content as well as in the choice of counterions will be utilized to widen the range of possible interconnections of perselenoborate fragments. Much effort will be spent in the future on synthesizing macrotetrahedral networks in which sulfur is replaced by selenium, because there is no apparent reason why selenoborates shouldn't adopt this structural motif.

The discovery of $Cs_8[B_{12}(BSe_3)_6]$ opens the way to systematic research on subvalent chalcogenoborates. From this starting point the understanding of the steps involved in the reaction of boron with chalcogens will be a field of further very active research to try and bring light to the path from elemental boron at one end and the BQ_3^{3-} ion at the other.

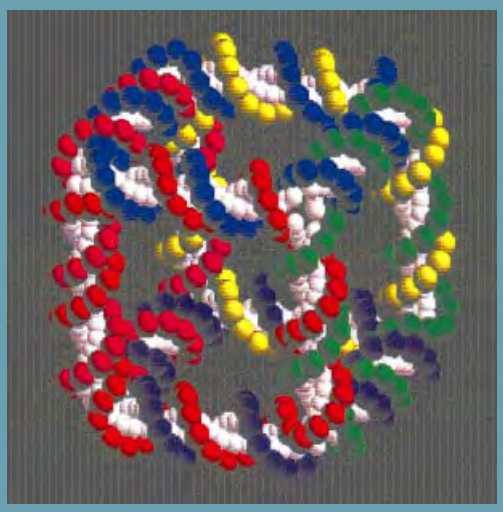
As the research on ionic conductors for the use in battery systems and fuel cells goes on, and more and more interest is focussed on the understanding of the dynamics in solids, the crystal structure determination of materials that are ionic conductors in the glassy state becomes crucial. Lithium oxo-, thio- and selenoborates have proved to be good candidates for further investigation.

The authors would like to thank the Deutsche Forschungsgemeinschaft and the Fonds der Chemischen Industrie for their generous support of our projects. We also thank Prof. Dr. W. Müller-Warmuth and his co-workers for their very valuable cooperations. Our special gratitude goes to all former and present co-workers that have contributed to these results with their enthusiasm and active cooperation.

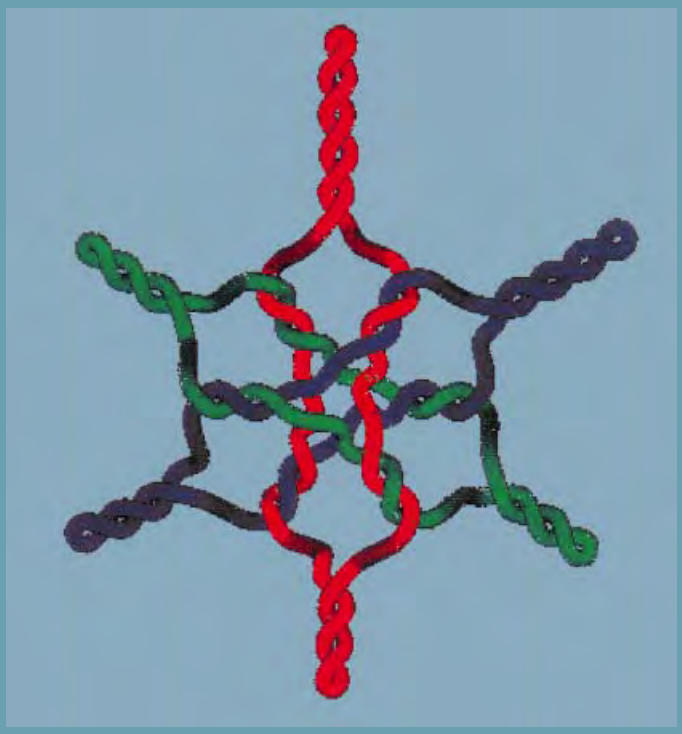
Received May 8, 1998 [A 281]
German version: *Angew. Chem.* **1998**, *110*, 3396–3407

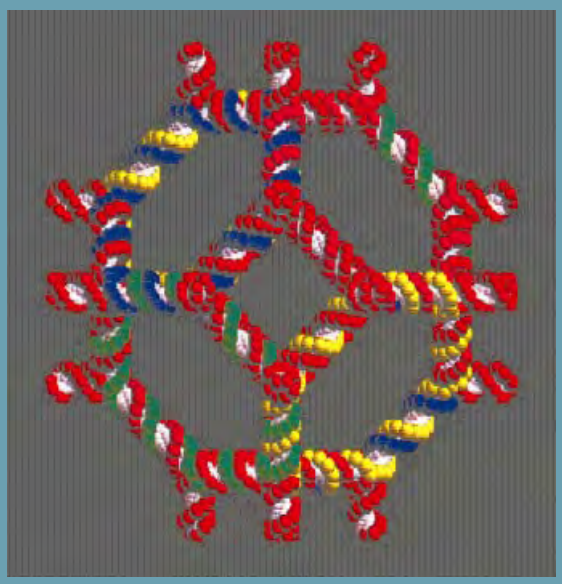
[1] Gmelin, *Handbuch der Anorganischen Chemie, Bor*, 8th ed., Springer, Berlin, **1926**, p. 1; and references therein.
[2] F. von Crell, *Ann. Chim.* **1800**, *35*, 202.
[3] H. Davy, *Gilb. Ann.* **1810**, *35*, 447.
[4] J. L. Gay-Lussac, L.-J. Thenard, *Rech. Phys.-Chim.*, **1811**, *1*, 277.
[5] J. J. Berzelius, *Ann. Phys. Chem.* **1824**, *2*, 113.
[6] In this review only sulfur and selenium are referred to as "chalcogen".
[7] S. L. Strong, R. Kaplow, *Acta Crystallogr. Sect. B* **1968**, *24*, 1032.
[8] G. E. Gurr, P. W. Montgomery, C. D. Knutson, B. T. Gorres, *Acta Crystallogr. Sect. B* **1970**, *26*, 906.
[9] C. T. Prewitt, R. D. Shannon, *Acta Crystallogr. Sect. B* **1968**, *24*, 869.
[10] A. Sommer, P. N. Walsh, D. White, *J. Chem. Phys.* **1960**, *33*, 296.
[11] P. Hagenmuller, F. Chopin, *C. R. Hebd. Seances Acad. Sci.* **1962**, *255*, 2259.
[12] a) Z. S. Medvedeva, A. Boryakova, Ya. Kh. Grinberg, E. G. Zhukov, *Zh. Neorg. Khim.* **1968**, *13*, 1440; b) Ya. Kh. Grinberg, E. G. Zhukov, V. A. Koryazhkin, Z. S. Medvedeva, *Zh. Neorg. Khim.* **1969**, *14*, 2583.
[13] a) F. T. Greene, P. W. Gilles, *J. Am. Chem. Soc.* **1962**, *84*, 3598; b) F. T. Greene, P. W. Gilles, *J. Am. Chem. Soc.* **1964**, *86*, 3964; c) H.-Y. Chen, P. W. Gilles, *J. Am. Chem. Soc.* **1970**, *92*, 2309; d) H.-Y. Chen, B. Conard, P. W. Gilles, *Inorg. Chem.* **1970**, *9*, 1776; e) H.-Y. Chen, P. W. Gilles, *J. Phys. Chem.* **1973**, *76*, 2035.
[14] D. Thomas, G. Tridot, *C. R. Hebd. Seances Acad. Sci.* **1964**, *259*, 3559.
[15] a) T. Lundström in *Boron-Rich Solids* (Eds.: D. Emin, T. Aselage, C. L. Beckel, I. A. Howard, C. Wood), American Institute of Physics, New York, **1991**, p. 186 *(AIP Conf. Proc. 231)*; b) T. Lundström, *J. Solid State Chem.* **1997**, *133*, 88.
[16] H. Bolmgren, T. Lundström, *J. Alloys Compd.* **1993**, *202*, 73.
[17] E. L. Muetterties, *The Chemistry of Boron and its Compounds*, Wiley, New York, **1967**, p. 647; and references therein.
[18] H. Diercks, B. Krebs, *Angew. Chem.* **1977**, *89*, 327; *Angew. Chem. Int. Ed. Engl.* **1977**, *16*, 313.
[19] B. Krebs, *Angew. Chem.* **1983**, *95*, 113; *Angew. Chem. Int. Ed. Engl.* **1983**, *22*, 113.
[20] B. Krebs, H. U. Hürter, *Angew. Chem.* **1980**, *92*, 479; *Angew. Chem. Int. Ed. Engl.* **1980**, *19*, 481.
[21] a) B. M. Gimarc, N. Trinajstic, *Inorg. Chem.* **1982**, *21*, 21; b) B. M. Gimarc, J.-K. Zhu, *Inorg. Chem.* **1983**, *22*, 479.
[22] A. Stock, F. Blix, *Ber. Dtsch. Chem. Ges.* **1901**, *34*, 3039.
[23] E. Wiberg, W. Sturm, *Angew. Chem.* **1955**, *67*, 483.
[24] J. A. Forstner, E. L. Muetterties, *Inorg. Chem.* **1966**, *5*, 164.
[25] a) M. Schmidt, W. Siebert, *Angew. Chem.* **1964**, *76*, 687; *Angew. Chem. Int. Ed. Engl.* **1964**, *3*, 637; b) M. Schmidt, W. Siebert, *Z. Anorg. Allg. Chem.* **1966**, *345*, 87; c) M. Schmidt, W. Siebert, *Chem. Ber.* **1969**, *102*, 2752; d) M. Schmidt, F. R. Rittig, *Z. Naturforsch.* B **1970**, *25*, 1062; e) M. Schmidt, W. Siebert, *Angew. Chem.* **1966**, *78*, 607; *Angew. Chem. Int. Ed. Engl.* **1966**, *5*, 597; f) M. Schmidt, W. Siebert, F. R. Rittig, *Chem. Ber.* **1968**, *101*, 281; g) M. Schmidt, F. R. Rittig, W. Siebert, *Z. Naturforsch. B* **1970**, *25*, 1344; h) M. Schmidt, F. R. Rittig, *Angew. Chem.* **1970**, *82*, 774; *Angew. Chem. Int. Ed. Engl.* **1970**, *9*, 738; i) M. Schmidt, W. Siebert, E. Gast, *Z. Naturforsch. B* **1967**, *22*, 557.
[26] W. Siebert, A. Ospici, *Chem. Ber.* **1972**, *105*, 464.
[27] W. Siebert, *Chem.-Ztg.* **1974**, *98*, 479.
[28] A. Stock, O. Poppenburg, *Ber. Dtsch. Chem. Ges.* **1901**, *34*, 399.
[29] a) E. Wiberg, W. Sturm, *Z. Naturforsch. B* **1955**, *10*, 112; b) E. Wiberg, W. Sturm, *Z. Naturforsch. B* **1955**, *10*, 113; c) E. Wiberg, W. Sturm, *Z. Naturforsch. B* **1955**, *10*, 114.

[30] R. H. Cragg, M. F. Lappert, B. P. Tilley, *J. Chem. Soc. A* **1967**, 947.
[31] A. B. Burg, R. J. Wagner, *J. Am. Chem. Soc.* **1954**, *76*, 3307.
[32] M. Schmidt, E. Kiewert, *Z. Naturforsch. B* **1971**, *26*, 613.
[33] A. Almenningen, H. M. Seip, P. Vassbotn, *Acta Chem. Scand.* **1973**, *27*, 14.
[34] H. M. Seip, R. Seip, W. Siebert, *Acta Chem. Scand.* **1973**, *27*, 21.
[35] O. Gropen, P. Vassbotn, *Acta Chem. Scand.* **1973**, *27*, 3079.
[36] W. Schwarz, H. D. Hausen, H. Hess, J. Mandt, W. Schmelzer, B. Krebs, *Acta Crystallogr. Sect. B* **1973**, *29*, 2029.
[37] G. W. Bushnell, G. A Rivett, *Can. J. Chem.* **1977**, *55*, 3294.
[38] W. Schwarz, H. D. Hausen, H. Hess, *Z. Naturforsch. B* **1974**, *29*, 596.
[39] R. Conrady-Pigorsch, W. Müller-Warmuth, G. Schwetlik, M. Wienkenhöver, B. Krebs, *Ber. Bunsen-Ges. Phys. Chem.* **1991**, *95*, 453.
[40] G. Schwetlik, B. Krebs, unpublished results.
[41] J. Kamsu Kom, *Ann. Chim. Paris* **1964**, *9*, 179.
[42] J. Flahaut, L. Domange, J. Kamsu Kom, *C. R. Hebd. Seances Acad. Sci.* **1962**, *254*, 299.
[43] F. Chopin, G. Turrell, *J. Mol. Struct.* **1969**, *3*, 57.
[44] J. Kamsu Kom, J. Flahaut, L. Domange, *C. R. Hebd. Seances Acad. Sci.* **1963**, *257*, 3919.
[45] P. Hagenmuller, F. Chopin, *C. R. Hebd. Seances Acad. Sci.* **1963**, *256*, 5578.
[46] F. Chopin, A. Hardy, *C. R. Hebd. Seances Acad. Sci.* **1965**, *261*, 142.
[47] F. Chopin, A. Richard, B. Castagna, *C. R. Seances Acad. Sci. Ser. C* **1969**, *269*, 921.
[48] V. V. Kirilenko, *Izv. Akad. Nauk. SSSR Neorg. Mater.* **1978**, *14*, 1992.
[49] D. Thomas, G. Tridot, *C. R. Hebd. Seances Acad. Sci.* **1964**, *258*, 2587.
[50] F. Chopin, B. Capdepuy, *Bull. Soc. Chim. Fr.* **1970**, 505.
[51] P. Hagenmuller, F. Chopin, B. Castagna, *C. R. Seances Acad. Sci. Ser. C* **1966**, *262*, 418.
[52] A. Hardy, *Bull. Soc. Fr. Minéral. Cristallogr.* **1968**, *91*, 111.
[53] J. C. Rosso, *C. R. Seances Acad. Sci. Ser. C* **1968**, *267*, 1609.
[54] D. Thomas, *C. R. Seances Acad. Sci. Ser. C* **1967**, *265*, 1325.
[55] F. Chopin, P. Hagenmuller, *Bull. Soc. Chim. Fr.* **1965**, 3031.
[56] P. Vinatier, P. Gravereau, M. Ménétrier, L. Trut, A. Levasseur, *Acta Crystallogr. Sect C* **1994**, *50*, 1180.
[57] F. Hiltmann, C. Jansen, B. Krebs, *Z. Anorg. Allg. Chem.* **1996**, *622*, 1508.
[58] a) B. Krebs, W. Hamann, *J. Less-Common Met.* **1988**, *137*, 143; b) B. Krebs, W. Hamann, *Acta Crystallogr. Sect. A* **1984**, *40*, C217.
[59] F. Hiltmann, B. Krebs, *Z. Anorg. Allg. Chem.* **1995**, *621*, 424.
[60] J. Küper, Dissertation, Universität Münster, **1996**.
[61] C. Jansen, Dissertation, Universität Münster, **1997**.
[62] A. Hammerschmidt, C. Jansen, J. Küper, C. Püttmann, B. Krebs, *Z. Anorg. Allg. Chem.* **1996**, *622*, 1330.
[63] C. Jansen, J. Küper, B. Krebs, *Z. Anorg. Allg. Chem.* **1995**, *621*, 1322.
[64] C. Püttmann, H. Diercks, B. Krebs, *Phosphorus, Sulfur Silicon* **1992**, *65*, 1.
[65] C. Püttmann, F. Hiltmann, B. Krebs, unpublished results.
[66] S. Pollitz, F. Zettler, D. Forst, H. Hess, *Z. Naturforsch. B* **1976**, *31*, 897.
[67] M. Wienkenhöver, Dissertation, Universität Münster, **1985**.
[68] M. Schmidt, H. D. Block, *Chem. Ber.* **1970**, *103*, 3705.
[69] C. Püttmann, W. Hamann, B. Krebs, *Eur. J. Solid State Chem.* **1992**, *29*, 857.
[70] B. Krebs, W. Hamann, *Z. Kristallogr.* **1983**, *162*, 149.
[71] A. Hammerschmidt, P. zum Hebel, F. Hiltmann, B. Krebs, *Z. Anorg. Allg. Chem.* **1996**, *622*, 76.
[72] M. Grüne, W. Müller-Warmuth, P. zum Hebel, B. Krebs, *Solid State Ionics* **1993**, *66*, 165.
[73] P. zum Hebel, B. Krebs, M. Grüne, W. Müller-Warmuth, *Solid State Ionics* **1990**, *43*, 133.
[74] C. Püttmann, P. zum Hebel, A. Hammerschmidt, B. Krebs, *Acta Crystallogr. Sect. A* **1990**, *46*, C279.
[75] B. Krebs, H. Diercks, *Z. Anorg. Allg. Chem.* **1984**, *518*, 101.
[76] F. Hiltmann, P. zum Hebel, A. Hammerschmidt, B. Krebs, *Z. Anorg. Allg. Chem.* **1993**, *619*, 293; corrected space group and unit cell: $a = 12.244(2)$, $c = 21.922(3)$ Å, space group $I4_1/a$ (No. 88); transformation matrix: 001,101,010; $R1 = 0.0470$, $wR2 = 0.0697$.
[77] M. Grüne, W. Müller-Warmuth, P. zum Hebel, B. Krebs, *Solid State Ionics* **1995**, *78*, 305.
[78] M. Trouboul, D. Amoussou, *Rev. Chim. Min.* **1978**, *15*, 223.
[79] G. Brachtel, M. Jansen, *Z. Anorg. Allg. Chem.* **1981**, *478*, 13.
[80] G. Eulenberger, *Z. Naturforsch. B* **1981**, *36*, 521.
[81] A. Hammerschmidt, J. Küper, L. Stork, B. Krebs, *Z. Anorg. Allg. Chem.* **1994**, *620*, 1898.
[82] C. Püttmann, F. Hiltmann, W. Hamann, C. Brendel, B. Krebs, *Z. Anorg. Allg. Chem.* **1993**, *619*, 109.
[83] W. Hamann, M. Wulff, B. Krebs, unpublished results.
[84] S. C. Malhotra, *Inorg. Chem.* **1964**, *3*, 862
[85] J. Küper, O. Conrad, B. Krebs, *Angew. Chem.* **1997**, *109*, 1995; *Angew. Chem. Int. Ed. Engl.* **1997**, *36*, 1903.
[86] R. Bertermann, W. Müller-Warmuth, C. Jansen, F. Hiltmann, B. Krebs, *Solid State Ionics*, submitted.
[87] M. Grüne, H. Meierkord, W. Müller-Warmuth, P. zum Hebel, B. Krebs, M. Wulff, *Ber. Bunsen-Ges. Physik. Chem.* **1989**, *93*, 1313.
[88] Z. Zhang, J. H. Kennedy, *Solid State Ionics* **1990**, *38*, 217.
[89] M. Ménétrier, A. Hojjaji, C. Estournes, A. Levasseur, *Solid State Ionics* **1991**, *48*, 325.
[90] J. S. Waugh , E. I. Fedin, *Sov. Phys. Solid State* **1963**, *4*, 1633.



Three aesthetically pleasing topological target structures resulting from DNA nanotechnology (from top to bottom): a cube, Borromean rings, and a truncated octahedron.





These molecules are constructed by applying the assembly methods of biotechnology to stable branched DNA molecules.

ANGEWANDTE CHEMIE ©WILEY-VCH

Nucleic Acid Nanostructures and Topology

Nadrian C. Seeman*

DNA is well known as the genetic material of all living organisms. However, the properties that allow it to serve so well in that role also can be exploited for chemical ends. Indeed, one of the most promising branches of nanotechnology is predicated on this genetic molecule. It is possible to make stable branched DNA molecules that can be combined through the specificity of cohesion of two ("sticky") ends with complementary overhangs to direct the construction of stick figures. Molecules whose edges consist of double-helical DNA have been constructed which show the connectivities of a cube and of a truncated octahedron. Two-dimensional arrays with programmed structural features have also been built. The topological properties of DNA have been exploited to produce specific knots and Borromean rings. In addition, DNA transitions can be used as the basis of nanomechanical devices. There is far more to DNA than a repository for genetic information!

Keywords: catenanes · DNA structures · mechanical bonds · nanostructures · topochemistry

1. Introduction

1.1. DNA Nanotechnology

The term "nanotechnology" has become a word encountered frequently in chemistry. There are many interpretations to this word, but the most visible goal of nanotechnology is to establish the same level of control over the manipulation and assembly of real molecules and molecular groupings that molecular graphics has over the manipulation and assembly of molecular models. There have been two key inspirations for this approach to very ambitious chemistry: The first was Feynman's famous talk, entitled "There's Plenty of Room at the Bottom".[1] He suggested that it would be possible to make machines that could make replicas of themselves on a somewhat smaller scale; the ultimate application of this procedure would be very tiny factories that could be packed densely. The second inspiration has been our growing knowledge of the ways that biological systems arrange their structural components, primarily by self-assembly on a supramolecular scale; hence, this second approach to nanotechnology is biomimetic. Feynman's approach has engendered the "top-down" methodology, best exemplified today by molecular assemblies that have been arranged by using scanning probe microscopes.[2] By contrast, biomimetic nanotechnology is "bottom-up", in that individual components are designed to assume particular tertiary structures, and ultimately to self-assemble into quaternary structures and arrays.

Top-down nanotechnology is characterized at this stage by elegance and by the ability to deal with substances of largely arbitrary composition. Its key limitation is its lack of parallelism; only small numbers of objects can be assembled at once. The bottom-up approach has a number of drawbacks, but it has the primary advantage of enormous parallelism; even chemistry done with a picomole of material results in more than 100 billion copies of the product species. Biomimetic nanotechnology cannot make use conveniently of intervention by the scanning probe microscopist; hence it has an additional burden, the design of molecules that fold correctly and reliably into their proper shapes. We understand this type of design best in those systems composed of biological macromolecules. This is a very restricted set of species, and their behavior is largely limited to aqueous systems. Nevertheless, we have better control over the folding of nucleic acids and, to a lesser extent, proteins than over most other polymers on the nanoscale. The design of a protein and accurate prediction of protein folding remain key challenges in the area, although striking progress is being made.[3] Nucleic acids are much simpler, and therefore we have a much better grasp of their folding. Here, we will dwell on nucleic acid nanotechnology, primarily DNA nanotechnology.

[*] N. C. Seeman
Department of Chemistry
New York University
New York, NY 10003 (USA)
Fax: (+1) 212-260-7905
E-mail: ned.seeman@nyu.edu

 © WILEY-VCH Verlag GmbH, D-69451 Weinheim, 1998 1433-7851/98/3723-3221 $ 17.50+.50/0

1.2. Key Targets for DNA Nanotechnology

There are many possible arrangements of matter that one might wish to assemble from DNA. The original motivation for this program was, from the point of view of crystallography, the desire to arrange DNA in a periodic array; the idea was to provide a scaffold on which to arrange other macromolecules that are intractable to conventional crystallization procedures.[4] A logical extension of this strategy is to use the same type of scaffolding to arrange molecular electronic components, thereby creating dense memories.[5] Neither of these goals has been achieved yet, but we will describe progress towards them.

When one thinks of chemical species derived from DNA, it is natural to ask whether they could be produced more economically by means of biologically based reproduction, either in vivo or by the polymerase chain reaction (PCR), which makes effective use of the cell's DNA replication enzymes.[6] Owing to topological considerations, these methods are likely to be applied most effectively to DNA knots. We will discuss work on DNA knots and other topological targets in Section 4.

Finally, DNA is a molecule that is known to undergo large structural transitions. These transitions present an opportunity to convert stable DNA species into nanomechanical devices. Two key transitions have been explored, and nanomechanical motion has been derived from each of them. These recent studies will be covered in Section 5.

2. DNA as a Construction Material

2.1. DNA as a Component for Molecular Design

DNA is well known as the genetic material of all living organisms. Indeed, its double-helical structure has become one of the cultural symbols of our civilization in much the same way that we associate previous societies with the Hanging Gardens of Babylon, the Colossus of Rhodes, or the Great Wall of China. The key feature that makes DNA so well suited to its biological role is the complementarity relationships that form hydrogen-bonded Watson – Crick base pairs:[7] Adenine (A) pairs with thymine (T), and guanine (G) pairs with cytosine (C). These classical interactions represent the acme in molecular recognition: From the standpoint of molecular design, DNA has the most predictable and readily programmed intermolecular interactions of any molecular species on its scale.

In general, it is very difficult to predict the preferred geometry by which two macromolecules will associate; extensive calculations are necessary to derive a set of potentially favorable interaction geometries between two molecules. However, in the case of DNA, these difficulties reduce to the base-pairing rules. Two complementary strands under appropriate conditions will form a double helix with Watson – Crick base pairs, in preference to any other possible interactions. This behavior of DNA has been exploited for a quarter of a century by biotechnologists. Two molecules with complementary overhanging sequences, called "sticky ends", will associate with each other preferentially. The sticky-ended association of DNA molecules by hydrogen bonding is illustrated in Figure 1. The local three-dimensional structure

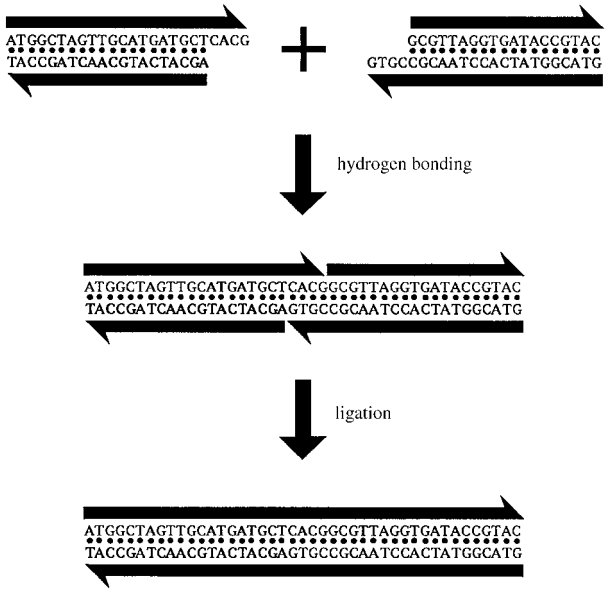


Figure 1. Sticky-ended cohesion and ligation. Top: two linear double-helical molecules of DNA. The antiparallel backbones are indicated by the black lines terminating in half-arrows. The half-arrows indicate the 5′ →3′ directions of the backbones. The right end of the left molecule and the left end of the right molecule have single-stranded extensions ("sticky ends") that are complementary to each other. Middle: under the proper conditions, the extensions bind to each other specifically by hydrogen bonding. Bottom: the extensions can be ligated to covalency by the proper enzymes and cofactors.



Nadrian C. Seeman was born in Chicago in 1945. Following a B.S. in biochemistry from the University of Chicago, he received his Ph.D. in biological crystallography from the University of Pittsburgh in 1970. His postdoctoral training, at Columbia University and the Massachusetts Institute of Technology, emphasized nucleic acid crystallography. He obtained his first independent position at the State University of New York in Albany, where his frustrations with the macromolecular crystallization experiment led him one day to the campus pub. There, he realized that the similarity between six-arm DNA branched junctions and the periodic array of flying fish in M. C. Escher's "Depth" might lead to a rational approach to crystallization and structural control on the nanometer scale. He has been trying to implement this form of DNA nanotechnology ever since, for the last ten years at New York University. Further information is available at http://seemanlab4.chem.nyu.edu in internet.

of the base-paired region is known to be B-DNA,[8] the familiar structure assumed by DNA in solution. Thus, not only can preferred affinity between DNA molecules be programmed and predicted, but so can the local structure of the intermolecular complex. Figure 1 also illustrates that it is possible to seal the two molecules together by using DNA ligase to catalyze the formation of phosphoester bonds in the backbone.[9]

In addition to the simplicity of directing its interactions, there are other advantages to DNA as a medium for nanoconstruction. The needs of biotechnology have resulted in extremely convenient automated phosphoramidite chemistry for the synthesis of arbitrary sequences.[10] In addition, many exotic phosphoramidites are commercially available to simplify the derivatization, detection, analysis, and purification of synthetic DNA molecules. It is also easy to manipulate DNA, because there is a large battery of commercially available DNA-modifying enzymes: These include restriction enzymes that cleave DNA at specific sequences, ligases that join ends, exonucleases that digest linear but not cyclic strands, and topoisomerases that catalyze operations in which strands are passed through each other (strand passage). DNA also has an external code[11] that can be read by proteins. Furthermore, as a polymer, DNA is both chemically stable[12] and relatively stiff, having a persistence length of roughly 500 Å under conventional conditions.[13] All of these advantages argue strongly for working with a DNA backbone, in contrast to nonstandard backbones,[14] which are not known to be substrates for modifying enzymes. The difficulties we experienced in a recent project involving RNA molecules[15] have reinforced our preference for DNA.

2.2. DNA Branched Junctions

At this point, the reader may be thinking that it is perhaps very convenient to tack DNA molecules together by programming sticky ends, but to what end? A long polymer of DNA has obvious biological utility, but what chemical targets does this open up? The answer is to be found in one of the subtle processes of biology, genetic recombination. The basic molecular feature of recombination is the interaction of two pieces of DNA to yield new genetic material. A key intermediate in recombination is the Holliday junction,[16] in which four connected double helices flank a branch point. The sequence that flanks the branch point of a Holliday junction is twofold symmetric; the symmetry enables the branch point to relocate within the region of symmetry by an isomerization known as branch migration.[17] Fortunately, it is possible to design synthetic sequences lacking this symmetry; thus, one can make branched molecules, termed junctions, with fixed branch points.[4]

The ability to direct DNA molecules to form branched structures adds a new geometrical element, the vertex, to DNA structural chemistry. The helix axes of linear DNA molecules are equivalent to line segments in geometry. By joining them as illustrated in Figure 1, one can make longer lines or circles, perhaps knots and catenanes. However, by including vertices among the components, objects and networks[18] become potential targets; these are often described as *N*-connected species,[18] where *N* refers to the number of edges that meet at a vertex. The objects will be stick figures, whose edges consist of double-helical DNA, and whose vertices correspond to the branch points of the junctions. This concept is illustrated in Figure 2, where four four-arm branched junctions are assembled into a quadrilateral. The junctions each contain four sticky ends, X and its complement X′, Y and its complement Y′. Each of the four junctions coheres with its neighbors by means of these sticky ends. In addition, there are sticky ends on the outside of the quadrilateral, so one could imagine extending this structure infinitely to tile the plane.

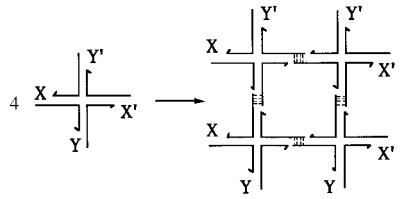


Figure 2. Formation of a two-dimensional lattice from an immobile junction with sticky ends. X and Y are sticky ends, and X′ and Y′ are their complements. DNA ligase can close the gaps.

How does one design DNA sequences to assemble into stable branched molecules? The fundamental assumption of the design is that under conventional conditions the most favorable structure for DNA is the linear double helix.[4, 19] Putting a branch into DNA costs free energy, relative to this favored structure.[20] However, a branch can form if double-helix formation covers the cost of branching. Our implementation of this concept is illustrated in Figure 3. First, to eliminate branch migration,[17] we ensure that the branch point is not flanked by a sequence with twofold symmetry. In

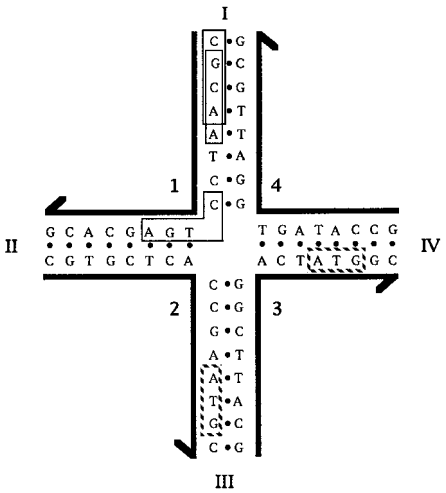


Figure 3. A stable DNA branched junction composed of four strands of DNA (1–4). The arms are labeled with I–IV. The 3′ end of each strand is indicated by a half-arrow. Each strand is paired with two other strands to form a double-helical arm. There is no homologous twofold sequence symmetry flanking the central branch point which stabilizes its position. Tetrameric elements are in solid boxes, and trimeric elements in dashed boxes.

addition, we divide the sequence of each strand into a series of overlapping elements. The elements shown are tetramers, so that each of the 16-mer strands is treated as a set of 13 overlapping tetramers. The first two tetramers on strand 1 are boxed: CGCA and GCAA. We insist that each of these tetrameric elements be unique. We also forbid the complement to any element that spans a bend: For example, there is no TCAG to complement the tetramer CTGA at the bend of strand 1. Using this approach, competition with the target duplex structures (octamers of base pairs in each arm) will come only from trimers, such as the ATG sequences in the dashed boxes. In principle these ATG sequences could pair with the wrong CAT, but in practice this type of problem is not seen; hence the algorithm is effective in producing target secondary structures.

Tetramers provide a vocabulary of 240 non-self-complementary sequences (4^4 less 16 self-complementary sequences), from which 52 elements can be selected to satisfy the conditions. If trimer elements were used, competition would only be from dimers, but there would be a vocabulary of only 64 elements (4^3) to supply the 56 trimers needed for the structure, which becomes difficult. It is clear that one must use longer elements (of length N) with larger structures. If the arms of the branched junctions do not get appreciably longer, then competition from $(N-1)$-mers may become significant, for example, pentamers if hexamer elements ($N=6$) are used. Although we have not done so, it may prove useful to check $(2N-1)$-mers for near-identity: With tetrameric elements, the algorithm would not be sensitive to the similarity between ATTCGCA and ATTAGCA (6 out of 7 nucleotides). In practice, one must often incorporate sequences into the target molecule that violate these rules: For example, restriction sites are frequently symmetric. We usually incorporate these sites first, and then design the rest of the sequence around them.

The number of arms in a branched DNA molecule is not limited to four. We have made junctions that contain three,[21] five, and six[22] arms; there is no clear limit to the number of arms that can flank a branch point.[23] However, the more arms that are incorporated, the longer the arms must be in order to stabilize the branch point;[22] the reason for this may be the accumulation of negative charge in the region of the branch point. The number of arms flanking a junction establishes the maximum connectivity of the objects or networks that can be constructed from it. For example, three-arm junctions can make a stick cube, but one needs four-arm junctions to make a stick octahedron, five-arm junctions for a stick icosahedron, and six-arm junctions for a simple cubic stick lattice.

2.3. Topology in DNA Constructions

The fact that DNA is a double helix, and not a double ladder, complicates thinking about the molecule, but it is not a serious impediment to working with it. In fact, the differences between helices and ladders open up a number of targets that otherwise would not be particularly suitable for DNA. Nevertheless, the consequences of the topology must be taken into account in experimental design. Figure 4 illustrates this point by showing two different designs for the assembly of the molecule in Figure 2. In Figure 4a, the branch points of the junctions are separated by exactly two turns of DNA. The resulting single strands are a series of cyclic molecules linked together to form molecular chain mail. Cyclic molecules held together by topological bonds are called catenanes. The array in Figure 4b is assembled by the same design, but here the vertices are separated by 1.5 turns of DNA. The resulting single strands form no circles, but correspond to a warp and weft interwoven network.

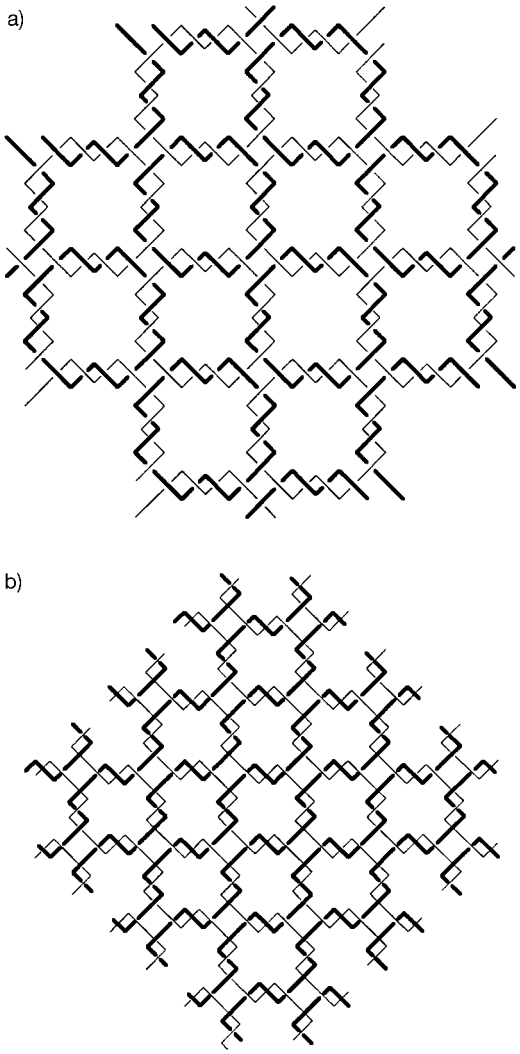


Figure 4. Topological consequences of ligating DNA molecules containing even and odd numbers of DNA half-turns in each edge. These diagrams represent the same ligation shown in Figure 2. However, they indicate the plectonemic (interwound) winding of the DNA, and its consequences. The DNA is drawn as a series of right-angled turns. a) Each edge of the square contains two turns of the DNA double helix. Paired strands are drawn with alternating thick and thin lines. b) Each edge of the square contains 1.5 turns of DNA.

The difference between the integral and half-integral separations of junctions arises repeatedly in the design of DNA objects. In a sense, the double-helical half-turn is the quantum of single-stranded DNA topology. It corresponds to

a crossing or node in a DNA catenane or knot.[*] Sometimes a node is called a "unit tangle".[24] We will see below that the equivalence between a double-helical half-turn and a unit tangle can be very useful in the construction of topological targets. It appears possible to design three-dimensional species whose vertices are separated by nonintegral numbers of half-turns.[25, 26]

2.4. Flexibility of DNA Branched Junctions

The assembly shown in Figure 2 is predicated on two assumptions, the cohesion between complementary sticky ends and the rigidity of the DNA branched junction. Figure 5 illustrates the fact that a variable angle between the arms could result in a different product: The same sticky ends are

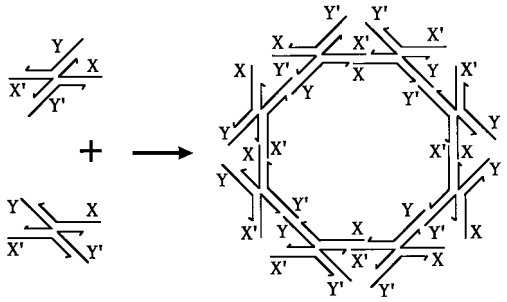


Figure 5. Consequences of variable angles between the arms. The same ligation is shown as in Figure 2, but the angles between the arms are variable. A cyclic complex corresponding to eight molecules is shown; any $4N$ complex could be cyclic in this system.

shown to adopt two conformations; when altered around the cycle, an octagonal figure results. Unfortunately, the angles between the arms of the junction are not fixed. We have investigated the rigidity of three-arm junctions,[21] four-arm junctions,[27] and three-arm bulged junctions[28] in ligation-closure experiments. A typical experiment involving three-arm junctions is illustrated in Figure 6. The junction contains two complementary sticky ends that have been phosphorylated, so that they can be ligated; the blunt end is excluded from the experiment, because it contains no phosphate group. The design of the experiment is important, because one must ensure that a "reporter strand" is available. This is a single strand whose fate reflects the fate of the complex; its size and linear or cyclic character can be ascertained readily by denaturing gel electrophoresis. In Figure 6, the reporter strand is shown labeled with a radioactive phosphate. If two or more junctions are ligated together, the length of the reporter strand increases proportionately. Similarly, if the complex cyclizes (Figure 6, right), then the reporter strand cyclizes. After ligation, the products are applied to a

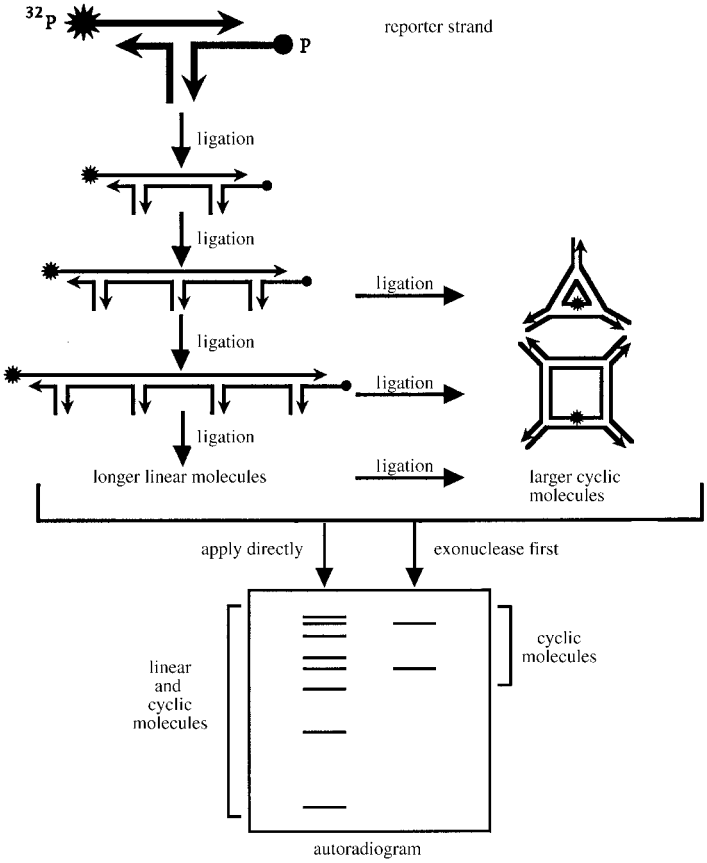


Figure 6. The experimental design used in the ligation assay. The three-arm junction employed in all of the experiments is indicated at the upper left. The 3′ ends of the strands are indicated by arrowheads. The 5′ end of the top strand contains a radioactive phosphate group (starburst), and the 5′ end of the strand below the first and to the right contains a nonradioactive phosphate group (filled circle). The third strand corresponds to the blunt end, and is not phosphorylated. Beneath this molecule are shown the earliest products of ligation, the linear dimer, the linear trimer, and the linear tetramer. The earliest cyclic products are shown on the right, the cyclic trimer and the cyclic tetramer. The blunt ends form the exocyclic arms of these cyclic molecules. Note that in each case the labeled strand has the same characteristics as the entire complex: It is an oligomer of the same multiplicity as the complex, and its state of cyclization is that of the complex; thus, it is a reporter strand. The analysis of the reactions products is shown in the lower part of the figure (see text for further details).

denaturing gel, and an autoradiogram is developed. The lane on the left, whose contents are applied directly to the gel, contains both linear and cyclic reporter strands. However, if the material is treated first with exonucleases (exo III and/or exo I; right lane), only cyclic products remain, because they are resistant to digestion by these enzymes. The unhappy result of these experiments is that all simple branched junctions tested result in a plethora of cyclic products, indicating that they contain variable angles. We will describe below a rigid DNA system, but the major stumbling block to controlling the assembly of DNA objects and lattices is the flexibility of the angles between the arms of branched junctions. This flexibility leads to only topological control over the products, rather than geometrical control; likewise, proofs of synthesis are topological proofs, rather than geometrical characterizations.

[*] A node (or unit tangle) is a crossing between two strands seen when the structure is projected onto a plane. A knot is a closed cyclic molecule that contains nodes that are unremovable (that is, they cannot be removed without breaking covalent bonds).

2.5. Characterization of Unusual DNA Motifs and Structures

The DNA branched junction is the first of several unusual DNA motifs that we will discuss in this article. It is important to mention the ways in which their structural features have been determined. Conventional physical techniques that are commonly used by chemists, for example NMR spectroscopy, have only recently yielded interesting data about these molecules,[29] and none of the species here has been crystallized yet. In general, we characterize a new motif first by means of non-denaturing gel electrophoresis, in order to establish whether the complex forms cleanly and with an appropriate molecular weight. On non-denaturing gels, hydrogen-bonded species migrate as a function of the molecular weight of the complex, as well as factors associated with the secondary structure such as the surface area. Bands appearing below the apparent monomer indicate instability,[22] and bands appearing above it indicate molecular strain, which can be relieved by making an oligomer.[30–32] Discrete bands indicate a closed complex (e.g., for a four-arm branched junction, molecule 1 forms hydrogen bonds to molecule 2, 2 to 3, 3 to 4, and 4 again to 1), but a smear of bands can indicate an open complex (1-2-3-4-1-2-3…), with no discrete closure. Stoichiometry is ascertained by titrating each strand against the others.[33] A Ferguson plot[34] is run in order to measure the friction constant of the complex, and to establish the dependence of mobility on gel concentration. Thermal denaturation profiles provide an estimate of the stability of the species.

The primary structural tool for analyzing these complexes is autofootprinting with $[Fe^{2+}EDTA]^{2-}$ (EDTA = ethylenediaminetetraacetate):[35] The pattern of chemical cleavage of the DNA by hydroxyl radicals generated by this reagent is monitored. The key to the analysis is that a radioactively labeled strand is complexed with its Watson–Crick linear duplex complement, and, in a separate experiment, with the other strands in the complex. Strands whose cleavage pattern is identical in both experiments are taken to be in a double-helical conformation; nucleotides that flank crossovers between helices exhibit a characteristic protection pattern. In addition to branched junctions, this type of analysis has been applied to antijunctions,[31, 32] mesojunctions,[31, 32] and double-crossover molecules.[30]

The more complex systems that are discussed here—a DNA cube, a DNA truncated octahedron, knots, and Borromean rings—are analyzed on denaturing gels. This is a system in which molecules of the same topology separate from each other as a function of their molecular weight; secondary structures are destroyed under denaturing conditions. Knotted molecules are compared with marker cyclic species in order to characterize their linking: The more tightly knotted a given strand is, the more rapidly it will migrate through a gel. All of these species contain restriction sites that are susceptible to restriction nucleases. In knots, lack of digestion is one of the demonstrations that a domain is in the Z conformation, and therefore contains positive nodes (see below). Catenated molecules are broken down to target catenanes or circles, for which markers can be prepared independently. Denaturing gel electrophoresis is very sensitive to topological differences: Two links differing only in their linking number will separate readily;[36] likewise, a linear catenane and a cyclic catenane of the same molecular weight are readily separated.[37]

3. Constructing DNA Objects and Arrays

3.1. Polyhedra and Solid-Support Synthesis

The flexibility of DNA branched junctions is a serious handicap if there is only a single complementary pair of sticky ends, as in Figure 6. However, a finite polygon or stick polyhedron can be made with a specific series of unique sticky ends. For example, to design a quadrilateral, a set of sticky ends {A, A′}, {B, B′}, {C, C′}, and {D, D′} will result in only of quadrilaterals or their multiples (octalaterals, dodecalaterals, and so on). As a practical matter, if the structure that has been designed is a favorable one, the cyclic tetramer will join to itself before larger cycles form in a solution of appropriate concentration. In our earliest attempt to produce a particular target molecule, we made a quadrilateral, which was purified readily from nontarget products.[38]

The first serious test of this system was the construction of a molecule whose helix axes have the connectivity of a cube;[37] its structure is illustrated in Figure 7. Each edge contains two turns of double-helical DNA; as with the square two-dimensional lattice, an integral number of turns per edge leads to cyclic strands. Each face corresponds to a cyclic strand linked twice to each of its four neighbors; hence, this object is a hexacatenane of DNA. Had we used an odd number of strands, the molecule would have been a tetracatenane corresponding to the projections down the body diagonals. To demonstrate synthesis, each edge contains a unique restriction site.

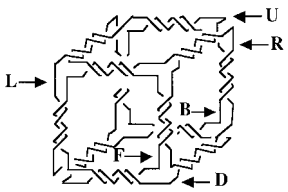


Figure 7. A DNA molecule whose helix axes have the connectivity of a cube. The molecule consists of six cyclic strands that have been catenated in this particular arrangement. They are labeled by the first letters of their positional designations: U: up; D: down; F: front; B: back; L: left; R: right. Each edge contains 20 nucleotide pairs of DNA, so we expect that their lengths will be about 68 Å. From model building, the axis-to-axis distance across a square face appears to be about 100 Å, with a volume (in a cubic configuration) of approximately 1760 nm^3 when the cube is folded as shown.

The synthesis is illustrated in Figure 8. Two squares were combined to form a ladderlike intermediate. One of the key lessons learned from this construction is that it is not possible to separate target molecules from by-products under non-denaturing conditions. Hence, we had to denature the complex, and then reconstitute it before a final round of ligation. The denatured intermediate was the linear triple catenane corresponding to the left (L), front (F), and right (R) faces of the cube. Among the most robust of our proofs of synthesis was the cleavage of the two edges contained in the L-F-R catenane to produce the linear triple catenane U-B-D, resulting from the up (U), back (B), and down (D) faces. Cleavage to release the U and D strands demonstrates that

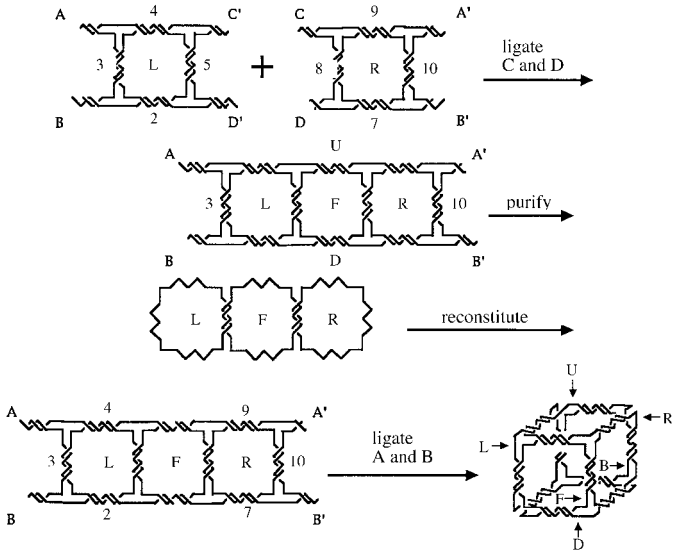


Figure 8. Synthesis of a DNA cube. The molecule is built from ten chemically synthesized strands, two 80-mers, and eight strands containing about 40 nucleotides. These are hybridized to form two quadrilaterals in the first step. Two ends (C and D) are ligated to form a beltlike molecule that must be denatured and reconstituted in order to purify it from side products. This molecule is then cyclized to form the cubelike molecule.

the target is the tetragonal prism, and not an octagonal or higher prism with $4N$ sides.

The synthesis of the cube was both a milestone and a disappointment. It was the first three-connected object synthesized from DNA, but the denaturation/reconstitution step clashed with the idea of forming specific edges through the specificity of DNA sticky ends. To restore the basic approach to this system we developed a solid-support methodology, patterned after the solid-support procedure used to synthesize oligonucleotides.[10]

The key advantage of the solid-support methodology[39] is that growing molecules can be isolated from one another on the support, so that the simplicity and specificity of sticky-ended ligation is not jeopardized by the presence of many copies of the same molecule in solution. In addition, the method permits the synthesis of individual edges at a time; control derives from the restriction of hairpin loops forming each side of the new edge. This corrects one of the major problems encountered in the cube construction, where a double ligation in the first step led to unwanted by-products. The strategy permits the separate execution of steps involving additions and cyclizations, which are optimized under different conditions. Each cycle of the procedure creates an object that is covalently closed and topologically bonded to itself, enabling some purification to take place on the support. As with other syntheses using solid supports, this methodology permits convenient removal of reagents and catalysts from the growing product.

Syntheses are designed so that the pair of restrictions that create a sticky end have different flanking sequences; hence the ultimate ligated edge contains a site for neither enzyme, and cannot be digested by it. For example, a typical pair of sites would be *Xho* I (C|**TCGA**G) and *Sal* I (G|**TCGA**C) (sticky ends in boldface); the ultimate sequence would be CTCGAC (paired with GTCGAG), immune to both enzymes that might be present in solution as contaminants, but sensitive to *Taq* I (TCGA), which is important for analytical purposes. It is possible to use symmetric sites for intramolecular ligations on the solid support, but it is unwise to use them in solution, because one cannot control whether the products will be intramolecular or intermolecular. In principle, the best enzymes to use for intermolecular ligations are those that produce asymmetric sticky ends. These can be produced by restriction enzymes that cleave at interrupted sites (e.g., *Bgl* I (GCCn**NNN**|nGGC)) or those that cut at positions distant from their recognition sequences (e.g., *Bbs* I, which leaves 5′ **NNNN**nnGTCTTC as a sticky end). Here, **N** represents any nucleotide that will be exposed as part of a sticky end, and n a nucleotide whose position is part of the enzyme's specificity, but its identity is not. However, as a practical matter, these enzymes are often less effective and more expensive than the more common enzymes with symmetric cleaving sequences.

Figure 9 illustrates a square synthesis: A three-arm branched junction with arms ending in hairpins is attached to the solid support, and one of its arms is restricted to expose a sticky end. This molecule is ligated to a second three-arm

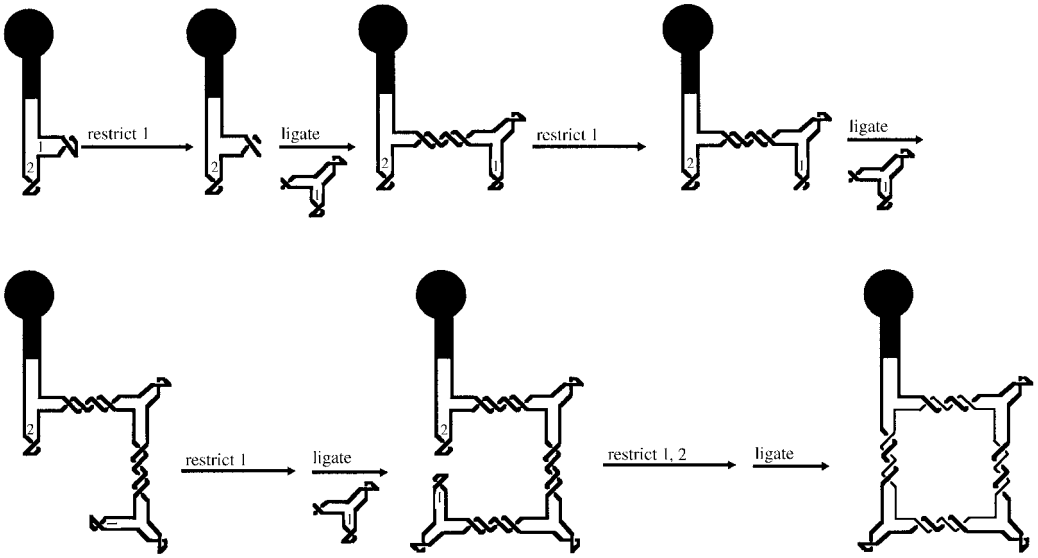


Figure 9. Synthesis of a quadrilateral. Beginning with the support containing a closed junction, alternate cycles of restriction and ligation are performed, always at position 1. Selection of the target product (triangle, quadrilateral, pentalateral…) is determined by the point at which one chooses to restrict at position 2, exposing a sticky end complementary to that exposed by restriction at position 1. This action corresponds to a strand switch (eliminating a zero node; see Figure 14). This is emphasized by the lines of different thickness with which the "square" catenane is drawn.

junction, consisting of two hairpins and an arm ending in the complementary sticky end. This process is repeated until the target precursor to a square is obtained. This is followed by a final round of double restriction and an intramolecular cyclization to produce the squarelike molecule; this species will be removed from the support and annealed shut by the addition of a hairpin.

To challenge and refine this methodology, we have constructed a truncated octahedron from DNA.[40] This Archimedean solid contains six squares flanking its fourfold symmetry axes, and eight hexagons that surround its threefold symmetry axes. As with the cube, there are two turns of DNA per edge, so each of the 14 faces corresponds to a single cyclic strand, and the final object is a [14]catenane. Each vertex of a truncated octahedron is bonded to three others (three-connected), but the molecule has been constructed from four-arm junctions; consequently, each vertex is associated with another arm that could be used to join the polyhedra, although this has not been done. The extra arms are hairpins extending from the strands that correspond to the square faces. The entire molecule contains 2550 nucleotides and has a molecular weight of about 790 kDa.

In this construction, the objects added to the support are squares and square groupings (Figure 10). The target has been made by carrying out two intermolecular additions to a square attached to the support. In the first addition, a tetrasquare complex is added, and in the second addition, the final square is added. The reason for adding the tetrasquare complex is that some restriction enzymes were found to be inefficient in the presence of the solid support. The structure on the lower left of Figure 10 is a heptacatenane complex of six squares. The square strands are already intact in this construct, and the hexagons all derive from the outer strand. The hexagons result from successive intramolecular closures of the sticky ends associated with the restriction enzyme site pairs S1-S1′ to S7-S7′. The final step involves releasing the structure from the support and annealing it with a hairpin. Proof is demonstrated in two stages: First, by showing that all six cyclic strands corresponding to the squares are in the heptacatenane, and second, by digesting the final product to the tetracatenanes that flank the squares. Once the ultimate goals of this program have been realized, it will be possible to characterize such targets by physical methods, particularly X-ray crystallography. However, characterization today is reminiscent of

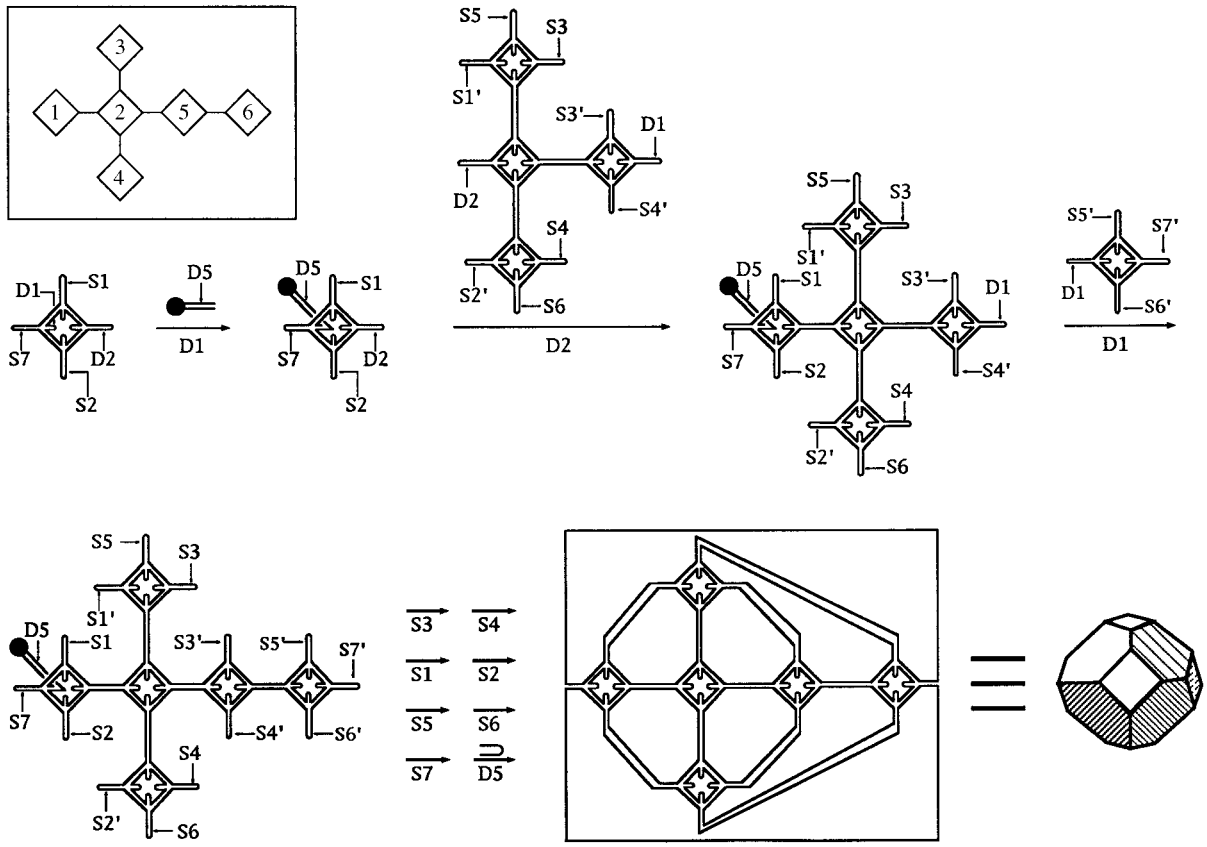


Figure 10. Synthesis of a truncated cctahedron on a solid support. The boxed diagram in the upper left corner indicates the numbering of the individual squares. Each square in the rest of the diagram is shown with its restriction sites indicated. Symmetrically cleaving restriction sites are indicated pairwise with S and S′; restriction sites that are cut distally by type II restriction enzymes are named D; restriction sites on the exocyclic arms are not indicated. The arms that will eventually be combined to form edges of the object are drawn on the outside of each square, and the exocyclic arms are drawn on the inside of the square. A reaction is indicated by an arrow above the name of a restriction site: This means that the restriction enzyme (or enzyme pair for those labeled S) is added, the protecting hairpins are removed, and then the two sticky ends are ligated together. The product is shown in two forms. On the left, the S1 – S6 closures are shown as triple edges to emphasize their origins; the two strands of the edge formed by the S7 closure are separated to maintain the symmetry of the picture. On the right, a rotated front view of a polyhedral representation of a truncated octahedron is shown without the exocyclic arms; the symmetry of the ideal object is evident from this view.

chemical proof before physical techniques came to the fore: We break molecules down to predictable fragments for which it is possible to make independent electrophoretic markers. As noted above, characterization, like synthetic control, is topological, rather than geometrical.

3.2. DNA Double-Crossover Molecules

Flexibility is the key shortcoming of DNA branched junctions as components for DNA nanostructure. We have demonstrated above that the control of topology in this system is strong, but this leads only to limited structural control. The variation of sticky ends can produce particular closed species in flexible systems, such as the cube and truncated octahedron. From the standpoint of sequence, these are low-symmetry structures, because all of the sticky ends are unique. However, the construction of periodic matter entails high-symmetry components, because the opposite faces of each unit cell are complementary. To address this problem, we have sought new DNA motifs to serve as rigid components. Initially, we were drawn to bulged branch junctions because of reports of their structural rigidity, which were borne out in preliminary experiments.[28] However, more rigorous testing showed that this motif was not sufficiently stiff for the purposes of DNA nanotechnology.[41] Fortunately, we have come across a system that appears to be much more rigid, the DNA double-crossover molecule (DX).[30, 42] This is a DNA structure that is an intermediate in the genetic process of meiosis.[43] It consists of two four-arm branches joined at two adjacent arms.

There are five isomers of DX molecules (Figure 11). Three of these isomers contain parallel (P) double-helical domains; this means that the dyad axis of backbone symmetry in DPE, DPOW, and DPON lies within the plane of the paper, parallel to the helix axes of the domains. The two other isomers DAE and DAO contain antiparallel helices, so that the dyad axis is perpendicular to the helix axes; in DAE it is perpendicular to the plane of the page and broken by the nick in the central strand, and in DAO it is horizontal within the plane of the page. The third descriptor of these isomers, E or O, signifies that the crossovers are separated by an even (E) or odd (O) number of double-helical half-turns. The DPO isomers are differentiated by whether the extra half-turn is a major groove (W for wide) separation or a minor groove (N for narrow) separation. Note that between the crossovers the strands of the two domains approach each other closely. There is electrostatic repulsion between these strands, because they are both negatively charged. Consequently, parallel isomers are not stable when the separations are very short, and they will not be discussed further here. Nevertheless, they have been used in analytical studies of recombination components,[36, 44] as have antiparallel DX molecules.[44, 45]

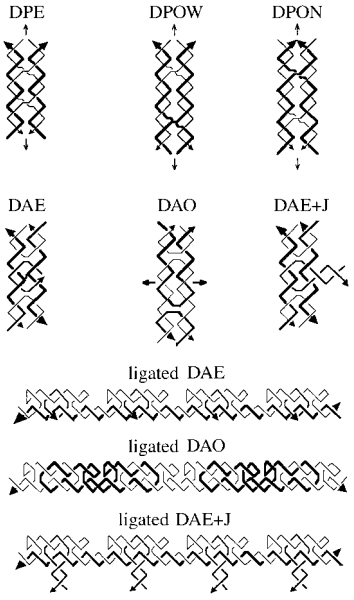


Figure 11. Double-crossover molecules and their ligation products. Arrowheads indicate 3′ ends of strands. Strands drawn with the same thickness are related by the vertical dyad axis indicated in the plane of the paper. In the case of DAO, strands of opposite thickness are related by symmetry. See text for further details.

The structure DAE + J on the right side of the middle row of Figure 11 is a variation on the DAE molecule. This molecule is created by replacing the nick of a conventional DAE (hard to seal when the separation is a single turn) with a bulged junction. It is also possible to produce molecules with multiple arms extending from the central portion of a double-crossover molecule: Winfree has constructed DAO + 2J molecules, and we have constructed DAE + 2J molecules;[48] in both cases, the extra helices are directed normal to the plane containing the helix axes.

The bottom portion of Figure 11 illustrates the topological consequences of oligomerizing one domain of these molecules. Oligomerization of DAE or DAE + J produces a reporter strand. However, oligomerization of DAO leads to a polycatenane. Owing to the difficulty of characterizing polycatenanes, we have explored the structural rigidities only of DAE and DAE + J.[42] In both cases, long reporter strands result; only minimal cyclization is observed with DAE + J, and there is no evidence for cyclization of DAE. The DAO molecules form closed structures more readily than DAE molecules, because they do not contain the cyclic central strand that is usually left unsealed in DAE molecules; we expect that DAO molecules are likely to be stiff, because they lack this nicked strand. Consequently, we conclude that antiparallel DX molecules represent a motif offering the needed rigidity in DNA construction.

3.3. DNA Arrays

The minimal requirements for a component to be used in the design of periodic matter are 1) predictable intermolecular interactions, 2) predictable local product structures, and 3) structural integrity.[28] Condition 1 is key, because the local affinities must be established under conditions of crystallization; condition 2 is needed to know how to design the lattice; and condition 3 is required if the system is to be translationally symmetric. In principle, one could imagine using many different sticky ends to create a pseudocrystal (same backbone, different sequences) held together with the same

specificity as the cube or the truncated octahedron. However, the preparation of those components would be prohibitively expensive; a conventional crystal is the cheapest way to assemble macroscopic materials whose structure is precise. We have seen above that the specificity of DNA is simple to design, and that the local structure at a sticky-ended overhang is B-DNA.[8] A known local structure is a subtle but key feature for the assembly of any specific geometrical species; for example, the structure of a sticky-ended cohesive join would be different if the overhangs assumed an exotic structure, such as parallel DNA.[46] In the last section, we introduced a DNA motif that satisfies the final criterion, molecular rigidity. Thus, in DNA, we have all the features necessary to form periodic matter.

How can we incorporate DNA antiparallel DX molecules into the self-assembly context described above? At least two routes seem promising. One way is to assemble arrays of DX molecules themselves. Winfree has identified four different topologies of antiparallel DX arrays.[47] These are illustrated in Figure 12. The arrays are made up of DAE or DAO

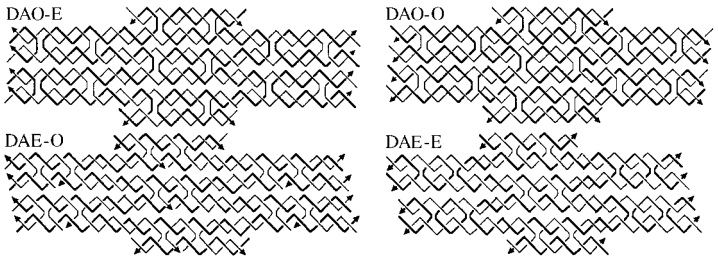


Figure 12. Topological structure of two-dimensional antiparallel DX arrays. Strand polarities are shown by the arrowheads on their 3′ ends. The strands are drawn with different thicknesses for clarity. See text for further details.

molecules, separated by even (DAE-E and DAO-E) or odd numbers (DAE-O and DAO-O) of double-helical half-turns. The topology of DAE-E is molecular chain mail. DAE-O produces two reporter strands in both the horizontal (straight) and vertical directions (zigzag). The DAO arrays lead to zigzag reporter strands in the vertical direction only. In our laboratory we have made DAE-O arrays, demonstrated by reporter strands, streptavidin gold labeling in the AFM, and DAE + 2J components; the 2J hairpins act as a topographic label. Winfree et al. have demonstrated[48] the assembly of DAO-E arrays by reporter strands and by means of DAO + 2J topographic labels in the AFM. We have shown that changing components leads to predictable alterations of AFM images.[48]

A second route to incorporating DX molecules into periodic matter is to have them serve as the edges of triangularly based species. This means using triangles in two dimensions and deltahedra (polyhedra whose faces are all triangles) in three dimensions. Triangles and convex deltahedra are rigid species, regardless of the flexibility of the angles between their edges.[49] Figure 13a illustrates a molecule we have made recently, a triangle with two sides composed of DAE molecules. Ligation in one dimension leads to a reporter strand that shows no evidence of cyclization on gels or by

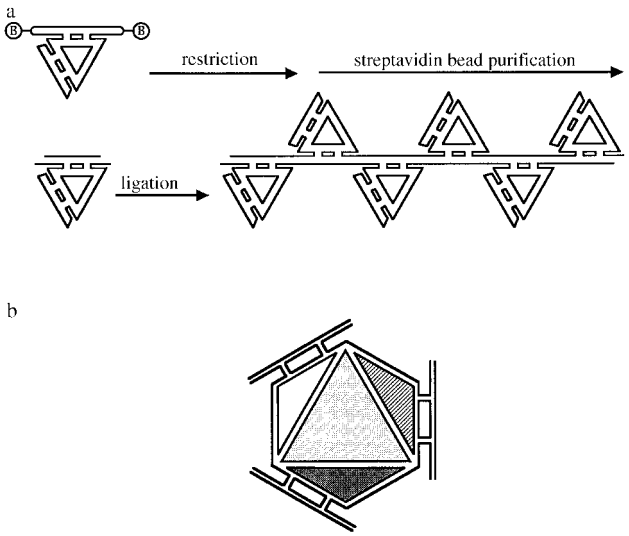


Figure 13. Structures containing double crossover. a) DX molecules incorporated in the edges of a triangle. Two edges of a triangle contain DAE molecules. Oligomerization will take place in the edge containing biotins (B) following restriction of those hairpins. b) An octahedron containing DX molecules. The top four faces of an octahedron are shown. Three edges that span a three-dimensional space contain DX molecules. The system would be ligated through the extra domains of the DX molecules.

AFM examination. Figure 13b shows a possible means of extending this system, with different components, to three dimensions: Three edges of an octahedron are shown to incorporate DX molecules. Despite their appearance in the drawing, these edges are not coplanar, but span three-dimensional space; sticky-ended cohesion along the outer domains would lead to a rhombohedral lattice. Note that the vertices of the octahedron are four-arm branched junctions, because the octahedron is a four-connected object. In a future scenario of polyhedral lattice construction in solution,[41] one can imagine building topologically closed complex objects (such as the octahedron) on solid supports, releasing them into solution, and annealing them to closure. They could then be purified under the denaturing conditions that work best for this purpose. Following purification, they could be restricted in solution, have their hairpins removed by streptavidin treatment, and be allowed to assemble.

4. Topological Construction

4.1. DNA and RNA Knots

The importance of topology in chemistry has been recognized at least since the work of Wasserman and Frisch,[50] and many investigators have made valuable experimental contributions in this area.[51] The investigators who have written the articles in reference [51] have synthesized a plethora of topological targets from small molecules, including a variety of knots and catenanes. All of their achievements required a great deal of chemical skill; by contrast, the production of deliberate single-stranded topological targets from DNA is relatively simple and straightforward.

There are three reasons why work on DNA geometrical objects has led to the construction of DNA (and RNA) topological targets: 1) Geometrical DNA objects are catenanes, and related closely to knots; 2) the nucleic acid double-helical half-turn is a ready-made unit tangle, the basic constituent of all knotted and catenated species; and 3) knots offer a potential route to the biological production of DNA polyhedra. Each of these points requires detailed explanation.

Figure 14a illustrates a transformation that interconverts knots and catenanes. At the left is a knot with five nodes, and the polarity of the strand is shown by the arrowhead (3′ end). In the middle molecule, one node has been destroyed. To see

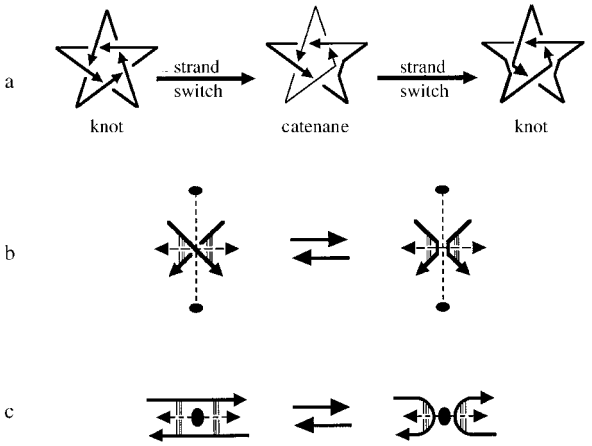


Figure 14. Zero-node operations. See text for details.

how this is done, divide each strand into a substrand before the node and a second substrand after the node, but maintain the polarity of each substrand. The node has been destroyed by switching the attachments of the substrands while maintaining their polarities. When this operation is performed, the knot is converted into a catenane. The drawing on the right indicates that the same operation applied to the catenane converts it into a knot. The operation shown is sometimes termed converting a positive or negative node into a zero node.[52]

It is useful to put this operation into the context of DNA.[53] This is shown in Figure 14b for a single node. The horizontal double-headed dashed line represents the DNA helix axis, and the vertical dashed line terminating in ellipses represents the DNA backbone dyad axis perpendicular to the helix axis. The strands are shown as arrows, which represent their polarities, and six nucleotide pairs connect the strands. Zero-node formation destroys the node, creating the structure on the right. Figure 14c illustrates this same operation in the same system, but the DNA is rotated by 90° about the helix axis, so that we are looking down the backbone dyad axis. In this view it is clear that the operation cleaves the two strands and creates two opposing hairpins. Note that in transforming this operation from topology to chemistry, we have replaced the right arrow with a pair of arrows indicating a reaction. The right arrow indicates the analytical operation devised by mathematicians to analyze knotted topology.[52] However, the arrow pointing left indicates a synthetic operation discussed in assembling DNA objects. Comparison of Figure 14c with the final step in Figure 9 shows that combining two intramolecular sticky ends, by the restriction/ligation operation, converts a knot (the trivial knot here, the circle) into a catenane; the two strands in Figure 9 are drawn with lines of different thickness to emphasize this point.

The fundamental unit of linking and knotting topology is the node or unit tangle.[24] Every knot or link is characterized by the number and relative positions of its nodes. Figure 15a illustrates that the double-helical half-turn can act as a unit tangle, thereby making the transition from topology to nucleic acid chemistry. A trefoil knot has been drawn with thick lines, and arrowheads indicating its trajectory. A half-turn of base paris is drawn between antiparallel strands, and the helix axes and dyad axes are shown. A dashed square has been drawn around each of its nodes, so that the strands of the knot act as its diagonals. The diagonals divide the square into four sections, two between parallel strands and two between antiparallel strands. The transition from topology to chemistry is made by drawing the six base pairs that flank a double-helical half-turn between the antiparallel strands. The rest of the knot can be made of unstructured oligodeoxythymidine (oligo-dT) units. Figure 15b indicates that nodes may possess either of two opposite chiralities. Negative (−) nodes are produced by right-handed B-DNA, the conventional structure of DNA. However, it is possible to produce positive (+) nodes by using left-handed Z-DNA (which has a zigzag nature).[54] Z-DNA is not geometrically enantiomorphic to B-DNA, but it is enantiomorphic in the topological sense.

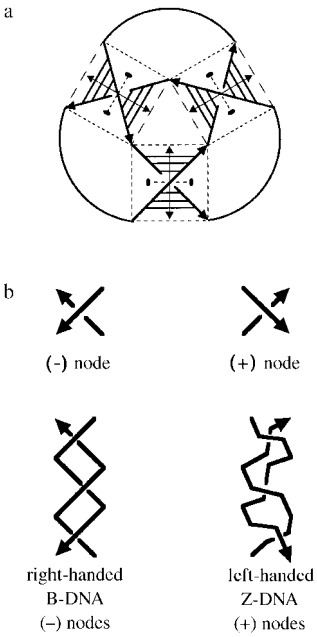


Figure 15. DNA topological methodology. The relationship between a half-turn and a node as well as the signs of the nodes is shown. See text for details.

By using the relationship between double-helical half-turns and nodes, we have constructed a variety of topological species. In each case, a complete DNA strand is synthesized, but the final ligation that circularizes the molecule is done enzymatically. We have made trefoil knots from two motifs of B-DNA,[55, 56] a figure-eight knot from a strand containing two negative nodes (B-DNA) and two positive nodes (Z-DNA),[57] and a trefoil knot containing positive nodes.[58] The figure-eight knot is a topological rubber glove,[59] that is, a structure whose molecular graph can be deformed to its mirror image, but cannot be deformed to a symmetry presentation.

Two conditions must be fulfilled for a segment of DNA to convert from B-DNA into Z-DNA: 1) The sequence must be

amenable to forming Z-DNA; and 2) the molecule must be in solution conditions that promote the B →Z transition, such as high ionic strength or in the presence of special cationic effectors, such as $[Co(NH_3)_6]^{3+}$.[54] Thus, the same strand can be used to create a variety of knots, depending on the conditions under which the final ligation takes place. For example, we have made a single strand adopt four different topologies by controlling ligation conditions, as shown in Figure 16. The regions X and X′ are complementary, as are the regions Y and Y′. Both regions can pair to form a single turn of DNA, and both regions can undergo the B →Z transition, although the Y-Y′ double helix has a greater propensity to form Z-DNA than the X-X′ double helix. Ligation at very low ionic strength results in only a circle. Increasing the ionic strength leads to the formation of a trefoil knot containing negative nodes, as both domains form B-DNA. Greater ionic strength converts the Y-Y′ domain into Z-DNA, producing a figure-eight knot. The addition of $[Co(NH_3)_6]Cl_3$ converts the X-X′ domain into Z-DNA as well, which generates the positive trefoil knot.

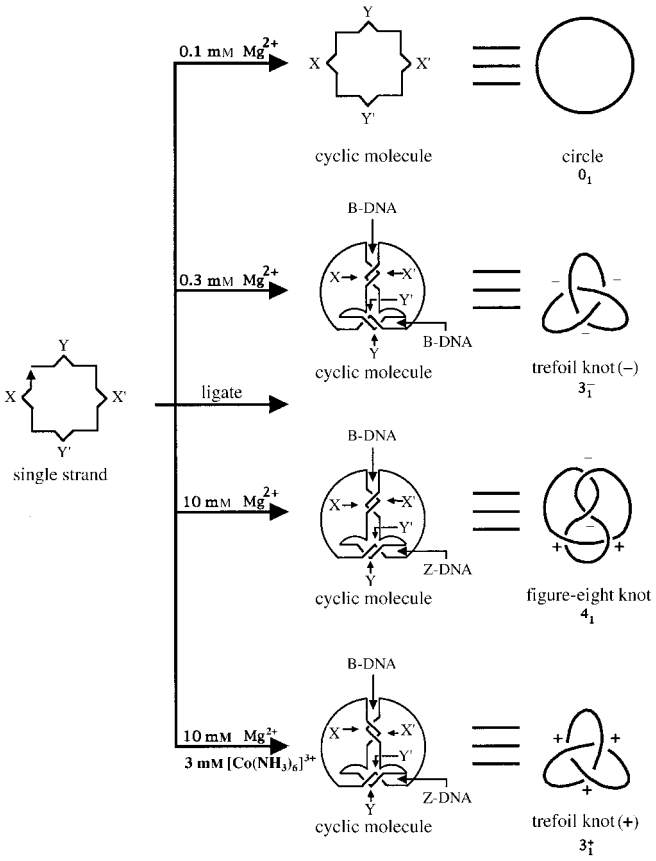


Figure 16. Synthesis of four different topologies from a single DNA strand. On the left is shown the molecule from which the target products are produced. The four pairing regions, X and its complement X′ and Y and its complement Y′, are indicated by the bulges from the square. The 3′ end of the molecule is denoted by the arrowhead. The four independent conditions used to generate the target products are shown to the right of the basic structure. The pairing and helical handedness expected in each case is shown to the right of these conditions, and the molecular topology of the products is shown on the far right of the figure. For an explanation of the topological sybols K_i, see Section 4.3.

We have shown that each of the species in Figure 16 can be interconverted through catalysis by DNA topoisomerase I or III from *E. coli*.[60] It is possible to ligate a knot under a certain set of conditions, and then to change the solution conditions to those favoring a different topological species. Even though a new species is favored, the covalent closure of the molecule prevents it from assuming that topology; for example, a figure-eight knot (containing a Z-DNA domain) removed from Z-promoting conditions cannot convert into a trefoil knot without the breakage of bonds. However, single-stranded (Type I) DNA topoisomerases can catalyze this conversion, because they facilitate strand-passage operations.

The efficient catalysis of strand passage in these knots by DNA topoisomerases suggested that knots might be a useful substrate to discover another biological activity, that of an RNA topoisomerase. In particular, we sought to determine whether the suggested activity of DNA topoisomerase III from *E. coli* as an RNA topoisomerase[61] could be established. We constructed a single-stranded RNA knot, and a circle of the same sequence. DNA topoisomerase III from *E. coli* was able to catalyze the interconversion of these species;[15] in addition, the enzyme catalyzed the catenation of a small amount of RNA. The instability of RNA, and the lack of effective modifying enzymes (no restriction enzymes, no exonucleases that lacked endonuclease contamination, and inefficient ligation by DNA ligases), converted a relatively straightforward experiment into a difficult technical project. Although related only indirectly to nucleic acid nanotechnology, the difficulties encountered in the discovery of the RNA topoisomerase have had a strong impact, reinforcing our inclination to work with standard DNA backbones.

DNA knots differ somewhat from DNA polyhedra: Polyhedra contain no unpaired nucleotides, but there are long single-stranded linker regions between pairing domains in knots. One has little control over the structures that can be assumed by single-stranded DNA. A possible solution to this problem is the temporary addition of single-stranded DNA complementary to the linker regions. Thus, their interactions are controlled during the ligation process; whereas these molecules are not topologically bonded to the target molecule, they can be removed readily upon purification of the product. This idea is illustrated for a catenane in Figure 17. We have shown that this procedure is quite effective when applied to catenanes of arbitrary sequence.[36] Ironically, even though topological protection was devised with knots in mind, it has proved singularly unsuccessful in that application. Indeed, attempts to apply topological protection have often resulted in larger amounts of undesired products.[56] We ascribe this failure to the oligo-dT sequences in the linkers; the complementary sequence, oligo-dA, is capable of forming triple helices, involving two linkers simultaneously, and leading to their linkage.

We suggested above that knots could offer a route to the biological production of DNA polyhedra. How could this be done? Figure 18a shows that replication of a stable branch by DNA polymerases is not possible: The heteroduplex region present in the first generation would be eliminated in the second generation if the DNA were replicated either intracellularly or by PCR. However, it may be possible to produce

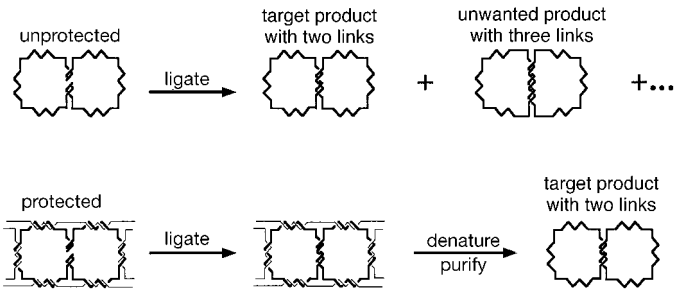


Figure 17. Topological protection of catenanes. This figure illustrates two catenation reactions: In the top reaction the two strands are ligated together in the absence of topological protecting groups, and in the bottom reaction topological protecting groups are present during ligation. The topological protecting groups are drawn as much thinner lines than the molecules to be linked together. In both cases, the final catenane has two turns of Watson – Crick complementarity, seen in the central duplex, where they are hybridized together. In the top reaction, the target doubly linked catenane is shown as a product, but another catenane is also drawn which contains an adventitious link. In the lower reaction, all the nucleotides of noncomplementary DNA were paired with their Watson – Crick complements, and were removed upon denaturation.

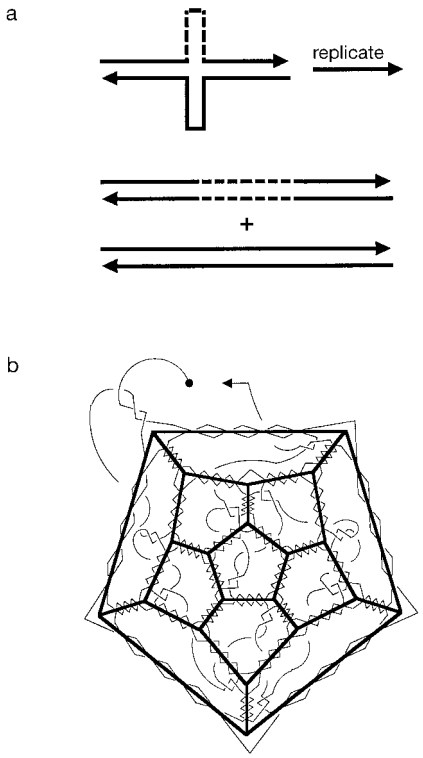


Figure 18. Cloning of branches. See text for details.

the molecules as a single long strand (Figure 18b).[62] A Schlegel diagram of a pentagonal dodecahedron is shown. Each edge is decorated with two turns of DNA; thus, each face corresponds to a cyclic strand. Each cycle has had an exocyclic arm added to it, and these exocyclic arms have been connected to form a single long strand. Biologically based production of this object might be accomplished by producing the strand, allowing it to fold (probably in the presence of Type I DNA topoisomerases), and then restricting the arms to remove the connecting strands. This protocol could lead to a polyhedron ready to connect to others through the sticky ends generated by restriction. Clearly the folding of the strand would need to be programmed very carefully, and then controlled closely, possibly by temperature.

4.2. DNA Borromean Rings

To challenge the level of topological control available with nucleic acids, we have used this system to construct Borromean rings.[63] These are a rich family of topological structures,[64] whose simplest member is a three-ring link (Figure 19, upper left) on the crest of the Borromeo family,

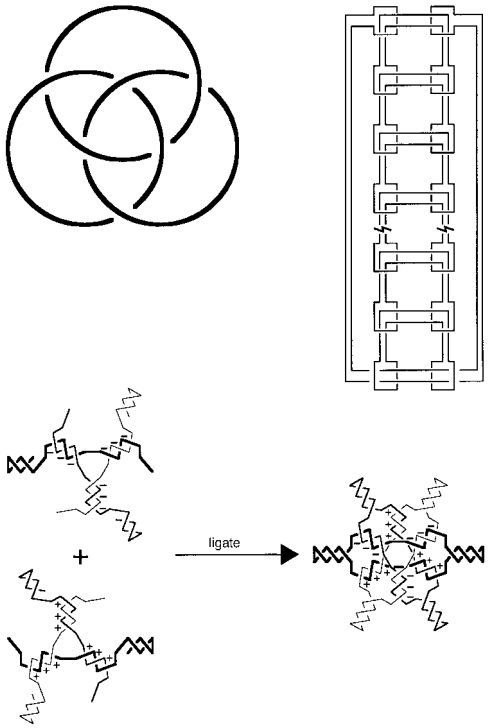


Figure 19. Borromean rings. Traditional Borromean rings are shown in the upper left corner; no two rings are linked. The diagram in the upper right illustrates the fact that an arbitrarily large number of rings can be linked in a Borromean arrangement, so that cleavage of any one of them results in the unlinking of the entire complex. The drawing at the bottom illustrates the synthesis of Borromean rings from DNA. A B-DNA branched junction (top) and a Z-DNA junction (bottom) are shown, each with 1.5 turns per arm; the signs of nodes are noted. The three strands are drawn with lines of different thickness. At the ends of each strand are partial hairpins (one almost complete, one that supplies the missing portion to another incomplete hairpin). When ligated under conditions that promote formation of the Z-helix, the Borromean arrangement on the right is formed.

prominent in the Italian Renaissance. The special property of Borromean rings is that cleavage of any member of the link results in separation of the other members of the link. This is evident in Figure 19, because no pair of rings are linked. The upper right portion of Figure 19 shows that there is no limit to the number of rings that can be joined while retaining the Borromean property.

In the three-ring link, the signs of the three outer nodes are opposite to those of the three inner nodes. Each of these nodes could be generated by utilizing a half-turn of double-

helical DNA. To simplify the construction, we replaced each of the half-turns of DNA with three half-turns of DNA, because that is a more stable structure. This is a topological structure, so it is possible to wrap it around a sphere. When this is done, the inner three helices correspond to a three-arm B-DNA branched junction flanking the north pole, and the outer three helices correspond to a three-arm Z-DNA branched junction flanking the south pole. We included hairpins on the "equator" to provide sites for ligation (Figure 19, bottom). These hairpins also contained restriction sites, so that the circles could be individually cleaved. Although not indicated in Figure 19, the hairpins were of slightly different lengths, so that the three circles could be separated conveniently on denaturing gels. Proof of synthesis consisted of cleaving each of the circles individually and showing that the products consisted only of the other circles and did not include any dicatenanes.

4.3. DNA Antijunctions and Mesojunctions

Working with knots has led to a generalization of the branched junction. If one designs a knot by the principle described in the last section, the arrangement of nodes leads to a series of substructures. For example, knot 9_{49} is shown in Figure 20a with every node written as a double-helical half-turn between antiparallel strands. (In the notation K_i for a knot, K refers to the number of nodes in a minimal plane representation of the knot, and i differentiates distinct knots with identical K values.[52]) The polarity of the knot is indicated by the direction of the arrow passing along it. Some of the enclosed regions contain other symbols that describe ways in which the double helices could be condensed: A solid triangle indicates that it is flanked by three double helices arranged like the arms of a three-arm branched junction, because their helix axes point towards the interior of the region. To its right are two helices connected by a curved double arrow, because these two half-turns could be condensed into a full turn of duplex DNA. To the left of the solid triangle is another area containing an unfilled square. Four half-turns flank this region, but they are not related like the arms of a branched junction, because their helix axes are circumferential, rather than pointing to its center. This is a new topology, termed an "antijunction".

The relationship between a junction and an antijunction is shown more clearly in Figure 20b. Here, the conventional four-arm branched junction is designated as 4_4 and the four-arm antijunction as 4_0, where the subscript indicates the number of arms pointing radially. The helix axes of the branched junction point towards the middle of the square, whereas the local dyad axes of the antijunction point towards the center. It is possible to switch the orientations of pairs of double helices without creating topological ambiguities, resulting in "mesojunctions". The two four-arm mesojunctions are designated as $^1\!4_2$ and $^2\!4_2$, where the subscript again indicates the number of radial helix axes, but the superscript is a serial number to distinguish the two species. Figure 20b also illustrates a three-arm branched junction (3_3) and the only possible three-arm mesojunction (3_1).

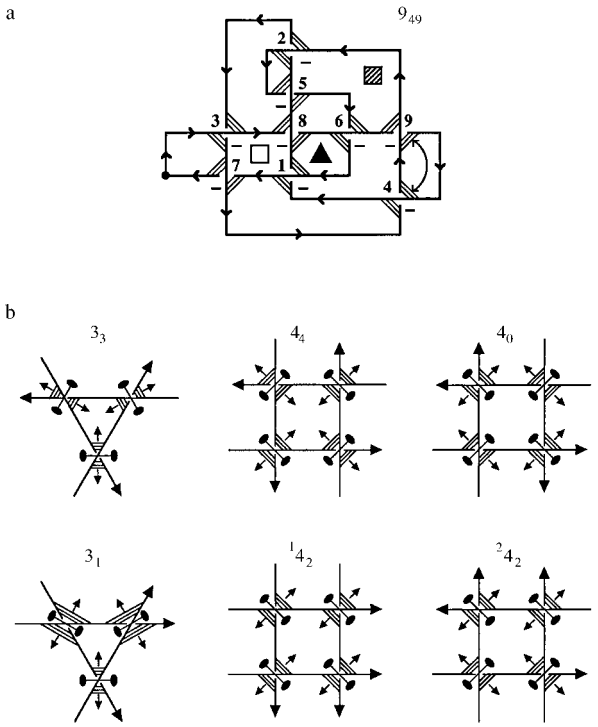


Figure 20. Antijunctions and mesojunctions. a) A 9_{49} knot drawn in the context of DNA. See text for details. b) Schematic drawings of three- and four-strand junctions, antijunctions, and mesojunctions. They are shown as helical arrangements that can flank a triangle or a square. Each polygon is formed from strands of DNA that extend beyond the vertices in each direction. The arrowheads indicate the 3′ ends of the strands. The vertices correspond to the nodes formed by a half-turn of double-helical DNA. Base pairs are represented by lines between antiparallel strands. Thus, the notation is similar to that used in (a), in that each set of six base pairs represents a half-turn of double-helical DNA. However, the half-turns are decorated more extensively: Thin arrows perpendicular to the base pairs, and pointing away from them, represent the axis of each helical half-turn; and the lines perpendicular to the helix axes terminating in ellipses represent the central dyad axes of the helical half-turns. The complexes 3_3 and 4_4 correspond to conventional branched junctions, whose helix axes (the arrows normal to the base pairs) point to the center of the triangle or the square. The complex 4_0 is a four-strand antijunction, whose helix axes are circumferential about the square, but whose dyad axes point towards the center of the square. The complexes on the bottom row are mesojunctions which contain a mix of the two orientations of helix axes.

We have constructed the antijunction and mesojunctions shown in Figure 20b. The stability of these species is a function of the number of half-turns in circumferential domains. We have attempted to construct these species with two and with three half-turns in each domain.[31, 32] These are not tractable species, and are much less stable than conventional branched junctions. Unless assembled at very low concentrations, mesojunctions form discrete closed oligomers of the target complex. Antijunctions often form open complexes (e.g., complexes like 1-2-3-4-1-2-3.., where the numbers refer to different molecules of a particular numbered strand); in contrast to closed complexes, there is no well-defined cyclic species found here.

Examination of antijunction and mesojunction molecules reinforces the notion that stacking may be the key element to consider in the design of DNA secondary structure. Structures that maximize base stacking appear to be favored in these systems, if they are compatible with the twists of the species

involved. Considering the origin of antijunctions and mesojunctions in nucleic acid knots, it is not surprising that they are related closely to pseudoknots seen in cellular RNA structures. In general, the intractability of antijunctions and mesojunctions militates for avoiding them in topological constructions. For example, it was possible to design Borromean rings as the sum of either two 3_1 mesojunctions or two 3_3 conventional junctions; the selection of the two conventional branched junctions was not a difficult decision to make.

5. Nanomechanical Devices

It is desirable to combine architectural properties of DNA with its dynamic properties in order to produce nanomechanical devices. There are two prominent transitions that can be utilized for this purpose. The first of these is branch migration[17] (Figure 21 a). In general, this transition can go in either direction; in a small system, the four-arm junction will resolve to two duplex molecules. However, the transition

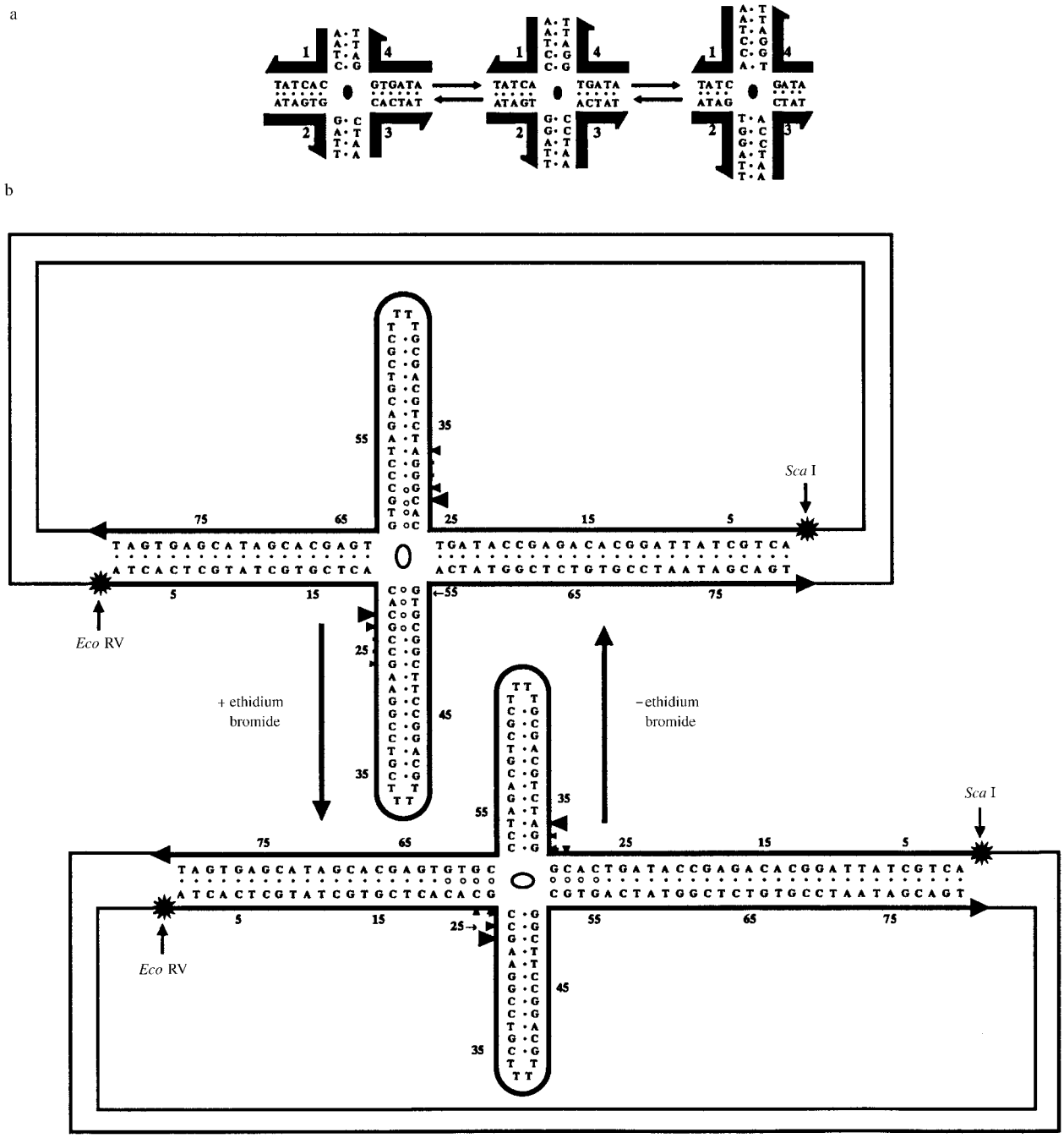


Figure 21. Control of branch migration. a) Branch migration. A four-arm branched junction is shown with twofold sequence symmetry about its branch point. The steps from left to right lead to the movement of base pairs from the horizontal arms to the vertical arms. b) A system to control branch migration. The molecule shown contains four mobile nucleotide pairs (joined by open circles, rather than filled circles, like the other base pairs), and its horizontal arms are linked to form a circle. In the top molecule they are in the vertical arms, indicated by the orientation of the ellipse at the branch point. In the bottom molecule, they have relocated to the horizontal arms by the positive supercoiling action of ethidium; the ellipse has rotated. Primary cleavage sites for endonuclease VII are indicated by the large and small arrowheads. Note that they move relative to the sequence, but not the branch point. Labeled restriction sites for analysis are indicated, as is numbering within the fragments.

can be controlled by putting torque on one pair of opposite arms:[65] If the horizontal arms are negatively supercoiled, then the vertical arms will be extruded; if the horizontal arms are positively supercoiled, then the extrusion will be reversed.

Figure 21b illustrates a system where this feature has been used.[66] The horizontal arms are connected by a circle, in order to apply directional torque. The central four nucleotide pairs are symmetric, but that is the extent of the possible excursion of the branch point. Torque is applied by adding ethidium to the system. When this occurs, the four nucleotide pairs in the vertical arms relocate to the horizontal arms. This relocation is demonstrated by cleavage with endonuclease-VII, which cleaves at the branch point, and then by restriction with *Sca*I and *Eco*RV to analyze the cleaved fragment.[66] This system works, but it is cumbersome.

A more promising system entails utilizing the B→Z transition to produce a rotation between two objects. We have connected two DAO molecules with an appropriate length of DNA that can undergo the B→Z transition (proto-Z-DNA; Figure 22). When the molecule is under conditions

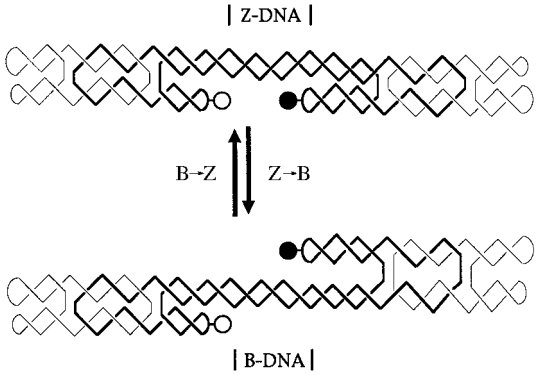


Figure 22. A nanomechanical device predicated on the B→Z transition. The molecule consists of two DAO molecules, connected by a segment containing proto-Z-DNA. The molecule consists of three cyclic strands, two on the ends drawn with a thin line, and one in the middle, drawn with a thick line. The molecule contains a pair of fluorescent dyes to confirm their separation by FRET. One is drawn as a filled circle, and the other as an empty circle. In the lower molecule, the proto-Z segment is in the B conformation, and the dyes are on opposite sides of the central double helix. In the top molecule, the proto-Z segment is in the Z conformation, and the dyes are on the same side of the central double helix. The length of the proto-Z-DNA and its conformation are indicated at top and bottom by the two vertical lines flanking the conformation descriptor.

that favor the B conformation, the unconnected domains of the DAO molecules are on opposite sides of the connecting domain. When the molecule is under conditions that favor the Z conformation, the unconnected domains are on the same side of the connecting domain. The transition is monitored by fluorescence resonance energy transfer (FRET) between two dye molecules. The system can be cycled between the two conditions, changing the structure of the molecules.[75] This is a relatively simple concept, but it has taken seven years to bring it to fruition, because the device requires rigid components to flank the proto-Z region. Only when the rigidity of DX molecules was established[42] was it possible to construct this device and demonstrate that it works.

6. Summary and Outlook

The aim of this review has been to demonstrate that the role of nucleic acids need not be limited to biological systems. The very properties that have allowed the process of natural selection to make such good use of the molecule as genetic material are the same ones that lead to a potentially valuable role in nanotechnology. The complementary relationship between the two opposite strands of DNA allows us to program its interactions to combine molecules in a desired fashion. This capability permits us to produce molecules with predictable topological properties. Thus, it has proved possible to build structures whose graphs have the connectivities of a cube or a truncated octahedron. Likewise, the linking topology of DNA is one of its most reliable properties; these geometrical constructions are precise catenanes of cyclic single strands of DNA. In the same manner, this topological control has enabled the construction of trefoil and figure-eight knots, along with the assembly of Borromean rings.

What is the future of this endeavor? There are several key issues that remain to be solved. The first of these is the construction of periodic matter. The recent assembly of two-dimensional arrays is an extremely encouraging development in this direction. Nevertheless, it remains to be shown that this success can be extended to three-dimensional systems. Furthermore, the currently successful assemblies are limited to simple DX molecules. Although we have successfully incorporated DX molecules into the edges of triangles, the triangles have not been assembled into periodic arrays yet. The greatest utility of this system is likely to be derived from arrays based on triangles or deltahedra; those arrays are most likely to accommodate large guest molecules within them, leading to the control of guest orientation within the host architecture.

The two-dimensional arrays that have been built do not have regular edges. Applications involving the use of such components to organize information will require the ability to address particular loci within an array. Well-defined edges are likely to be helpful to do this. Reif has suggested frames consisting of unique molecules in order to achieve this result.[67] Such assemblies are likely to be expensive, because each component of the frame must be unique.

Several of the goals outlined for DNA nanotechnology involve directing the spatial organization of other molecules by exploiting the architectural properties of DNA. It is easy to imagine chemical scenarios leading to this result, but little concrete progress has been made in this effort. Perhaps the most notable programmed attachment of a protein to DNA has been achieved by Smith et al., who placed specific cytosine methylases around a DNA molecule.[68] Further work must be done on the covalent attachment of organic molecules or polymers to DNA backbones.

Many research groups analyze the properties of DNA, and develop systems involving its hybridization and concatenation for bioanalytical purposes, but there has been little activity with structural objectives. Fortunately, this situation is changing. Recently, Mirkin et al. have attached DNA molecules to colloidal gold, with the goal of assembling nanoparticles into macroscopic materials[69] and with an eye toward diagnos-

tics.[70] Likewise, Alivisatos et al.[71] have used DNA to organize gold nanocrystals. Niemeyer et al.[72] had earlier used DNA specificity to generate protein arrays. In addition, Shi and Bergstrom[73] have attached DNA single strands to organic linkers. Nilsen, et al.[74] are working on another variation, DNA dendrimers.

DNA nanotechnology is a field poised for exploitation. The solid-support methodology appears to be a powerful means to assemble polyhedral objects from DNA. Likewise, DNA may be the most convenient system for the construction of topological targets. Although individual branched junctions are floppy, the DX molecule appears to be a DNA motif that has sufficient structural integrity that it can serve as the basis of periodic matter. Recent successes in the construction of two-dimensional periodic matter attest to this property. In addition, the use of DX molecules in a simple nanomechanical device supports the notion that this is the long-sought rigid component needed to exploit the properties of DNA as fully as they deserve. It is to be hoped that the advent of a rigid motif, linked with the useful properties exploited earlier will promote rapid progress in this field. Combined with the increase in activity from other laboratories, these developments suggest that DNA nanotechnology is likely to make major contributions in the twenty-first century.

This research has been supported by the Office of Naval Research (N00014-98-1-0093), the National Institutes of Health (GM-29554), the National Science Foundation (NSF-CCR-97-25021), and the Air Force Research Laboratory (F30602-98-C-0148). The experimental work reported here summarizes research performed in our laboratory at New York University by Junghuei Chen, Yuwen Zhang, John Mueller, Shouming Du, Hui Wang, Tsu-Ju Fu, Yinli Wang, Xiaojun Li, Xiaoping Yang, Jing Qi, Bing Liu, Hangxia Qiu, Furong Liu, Chengde Mao, Weiqiong Sun, Ruojie Sha, Lisa Wenzler, Zhiyong Shen, Hao Yan, Man Hoi Wong, Phiset Sa-Ardyen, and Siwei Zhang. I have also discussed research performed by Erik Winfree at the California Institute of Technology. I am grateful to all of these people for their collaboration in this work.

Received: January 2, 1998 [A 268 IE]
German version: *Angew. Chem.* **1998**, *110*, 3408 – 3428

[1] R. P. Feynman in *Miniaturization* (Ed: H. D. Gilbert), Reinhold Publishing, New York, **1961**, pp. 282 – 296.
[2] T. A. Jung, R. R. Schlittler, J. K. Gimzewski, H. Tang, C. Joachim, *Science* **1996**, *271*, 181 – 184.
[3] M. D. Struthers, R. P. Cheng, B. Imperiali, *Science* **1996**, *271*, 342 – 345.
[4] N. C. Seeman, *J. Theor. Biol.* **1982**, *99*, 237 – 247.
[5] B. H. Robinson, N. C. Seeman, *Protein Eng.* **1987**, *1*, 295 – 300.
[6] R. Saiki, T. L. Bugawan, G. T. Horn, K. B. Mullis, H. A. Ehrlich, *Nature* **1986**, *324*, 163 – 166.
[7] J. D. Watson, F. H. C. Crick, *Nature* **1953**, *171*, 737 – 738.
[8] H. Qiu, J. C. Dewan, N. C. Seeman, *J. Mol. Biol.* **1997**, *267*, 881 – 898.
[9] S. N. Cohen, A. C. Y. Chang, H. W. Boyer, R. B. Helling, *Proc. Natl. Acad. Sci. USA* **1973**, *70*, 3240 – 3244.
[10] M. H. Caruthers, *Science* **1985**, *230*, 281 – 285.
[11] N. C. Seeman, J. M. Rosenberg, A. Rich, *Proc. Natl. Acad. Sci. USA* **1976**, *73*, 804 – 808.
[12] T. Lindahl, *Nature* **1993**, *362*, 709 – 715.
[13] P. J. Hagerman, *Annu. Rev. Biophys. Biophys. Chem.* **1988**, *17*, 265 – 286.
[14] P. E. Neilsen, *Annu. Rev. Biophys. Biophys. Chem.* **1995**, *24*, 167 – 183.
[15] H. Wang, R. J. DiGate, N. C. Seeman, *Proc. Natl. Acad. Sci. USA* **1996**, *93*, 9477 – 9482.
[16] R. Holliday, *Genet. Res.* **1964**, *5*, 282 – 304.
[17] P. Hsieh, I. G. Panyutin in *Nucleic Acids and Molecular Biology*, *Vol. 9* (Eds.: F. Eckstein, D. M. J. Lilley), Springer, Berlin, **1995**, pp. 42 – 65.
[18] A. F. Wells, *Three-dimensional nets and polyhedra*, Wiley, New York, **1977**.
[19] N. C. Seeman, *J. Biomol. Struct. Dyn.* **1990**, *8*, 573 – 581.
[20] M. Lu, Q. Guo, L. A. Marky, N. C. Seeman, N. R. Kallenbach, *J. Mol. Biol.* **1992**, *223*, 781 – 789.
[21] R.-I. Ma, N. R. Kallenbach, R. D. Sheardy, M. L. Petrillo, N. C. Seeman, *Nucleic Acids Res.* **1986**, *14*, 9745 – 9753.
[22] Y. Wang, J. E. Mueller, B. Kemper, N. C. Seeman, *Biochemistry* **1991**, *30*, 5667 – 5674.
[23] N. C. Seeman, N. R. Kallenbach in *Molecular Structure: Chemical Reactivity and Biological Activity* (Eds.: J. J. Stezowski, J.-L. Huang, M.-C. Shao), Oxford University Press, Oxford, **1988**, pp. 189 – 194.
[24] D. W. Sumners, *Math. Intelligencer* **1990**, *12*, 71 – 80.
[25] N. C. Seeman, *J. Biomol. Struct. Dyn.* **1985**, *3*, 11 – 34.
[26] N. C. Seeman, *J. Mol. Graphics* **1985**, *3*, 34 – 39.
[27] M. L. Petrillo, C. J. Newton, R. P. Cunningham, R.-I. Ma, N. R. Kallenbach, N. C. Seeman, *Biopolymers* **1988**, *27*, 1337 – 1352.
[28] B. Liu, N. B. Leontis, N. C. Seeman, *Nanobiology* **1994**, *3*, 177 – 188.
[29] S. M. Miick, R. S. Fee, D. P. Millar, W. J. Chazin, *Proc. Natl. Acad. Sci. USA* **1997**, *94*, 9080 – 9084.
[30] T.-J. Fu, N. C. Seeman, *Biochemistry* **1993**, *32*, 3211 – 3220.
[31] S. M. Du, S. Zhang, N. C. Seeman, *Biochemistry* **1992**, *31*, 10955 – 10963.
[32] H. Wang, N. C. Seeman, *Biochemistry* **1995**, *34*, 920 – 929.
[33] N. R. Kallenbach, R.-I. Ma, N. C. Seeman, *Nature* **1983**, *305*, 829 – 831.
[34] D. Rodbard, A. Chrambach, *Anal. Biochem.* **1971**, *40*, 95 – 134.
[35] T. D. Tullius, B. Dombroski, *Science* **1985**, *230*, 679 – 681; M. E. A. Churchill, T. D. Tullius, N. R. Kallenbach, N. C. Seeman, *Proc. Natl. Acad. Sci. USA* **1988**, *85*, 4653 – 4656.
[36] T.-J. Fu, Y.-C. Tse-Dinh, N. C. Seeman, *J. Mol. Biol.* **1994**, *236*, 91 – 105.
[37] J. Chen, N. C. Seeman, *Nature* **1991**, *350*, 631 – 633; J. Chen, N. C. Seeman, *Electrophoresis* **1991**, *12*, 607 – 611.
[38] J.-H. Chen, N. R. Kallenbach, N. C. Seeman, *J. Am. Chem. Soc.* **1989**, *111*, 6402 – 6407.
[39] Y. Zhang, N. C. Seeman, *J. Am. Chem. Soc.* **1992**, *114*, 2656 – 2663.
[40] Y. Zhang, N. C. Seeman, *J. Am. Chem. Soc.* **1994**, *116*, 1661 – 1669.
[41] J. Qi, X. Li, X. Yang, N. C. Seeman, *J. Am. Chem. Soc.* **1996**, *118*, 6121 – 6130.
[42] X. Li, X. Yang, J. Qi, N. C. Seeman, *J. Am. Chem. Soc.* **1996**, *118*, 6131 – 6140.
[43] A. Schwacha, N. Kleckner, *Cell* **1995**, *83*, 783 – 791.
[44] T.-J. Fu, B. Kemper, N. C. Seeman, *Biochemistry* **1994**, *33*, 3896 – 3905.
[45] S. Zhang, T.-J. Fu, N. C. Seeman, *Biochemistry* **1993**, *32*, 8062 – 8067; S. Zhang, N. C. Seeman, *J. Mol. Biol.* **1994**, *238*, 658 – 668; X. Li, H. Wang, N. C. Seeman, *Biochemistry* **1997**, *36*, 4240 – 4247.
[46] E. M. Evertsz, K. Rippe, T. M. Jovin, *Nucleic Acids Res.* **1994**, *22*, 3293 – 3303.
[47] E. Winfree in *DNA Based Computing* (Eds.: E. J. Lipton, E. B. Baum), American Mathematical Society, Providence , RI, USA, **1996**, pp. 199 – 219.
[48] E. Winfree, F. Liu, L. A. Wenzler, N. C. Seeman, *Nature* **1998**, *394*, 539 – 544.
[49] J. Kappraff, *Connections*, McGraw-Hill, New York, **1990**, p. 273.
[50] H. L. Frisch, E. Wasserman, *J. Am. Chem. Soc.* **1961**, *83*, 3789 – 3795.
[51] J.-P. Sauvage, *Acc. Chem. Res.* **1990**, *23*, 319 – 327; D. M. Walba, *Tetrahedron* **1985**, *41*, 3161 – 3212; D. B. Amabilino, J. F. Stoddart, *Chem. Rev.* **1995**, *95*, 2725 – 2828; R. Jäger, F. Vögtle, *Angew. Chem.* **1997**, *109*, 966 – 980; *Angew. Chem. Int. Ed. Engl.* **1997**, *36*, 930 – 944; M. Fujita, F. Ibukuor, K. Yamaguchi, K. Ogura, *J. Am. Chem. Soc.* **1995**, *117*, 4175 – 4176; A. S. Lane, D. A. Leigh, A. Murphy, *J. Am. Chem. Soc.* **1997**, *119*, 11092 – 11093, and references therein.
[52] J. H. White, K. C. Millett, N. R. Cozzarelli, *J. Mol. Biol.* **1987**, *197*, 585 – 603.

[53] N. C. Seeman, J. Chen, S. M. Du, J. E. Mueller, Y. Zhang, T.-J. Fu, H. Wang, Y. Wang, S. Zhang, *New J. Chem.* **1993**, *17*, 739 – 755; N. C. Seeman, *Mol. Eng.* **1992**, *2*, 297 – 307.
[54] A. Rich, A. Nordheim, A. H.-J. Wang, *Annu. Rev. Biochem.* **1984**, *53*, 791 – 846.
[55] J. E. Mueller, S. M. Du, N. C. Seeman, *J. Am. Chem. Soc.* **1991**, *113*, 6306 – 6308.
[56] S. M. Du, N. C. Seeman, *Biopolymers* **1994**, *34*, 31 – 37.
[57] S. M. Du, N. C. Seeman, *J. Am. Chem. Soc.* **1992**, *114*, 9652 – 9655; H. Wang, S. M. Du, N. C. Seeman, *J. Biomol. Struct. Dyn.* **1993**, *10*, 853 – 863.
[58] S. M. Du, B. D. Stollar, N. C. Seeman, *J. Am. Chem. Soc.* **1995**, *117*, 1194 – 1200.
[59] E. Flapan, N. C. Seeman, *J. Chem. Soc. Chem. Commun.* **1995**, 2249 – 2250.
[60] S. M. Du, H. Wang, Y.-C. Tse-Dinh, N. C. Seeman, *Biochemistry* **1995**, *34*, 673 – 682.
[61] R. J. Di Gate, K. J. Marians, *J. Biol. Chem.* **1992**, *267*, 20532 – 20535.
[62] N. C. Seeman, *DNA Cell Biol.* **1991**, *10*, 475 – 486.
[63] C. Mao, W. Sun, N. C. Seeman, *Nature* **1997**, *386*, 137 – 138.
[64] C. Liang, K. Mislow, *J. Math. Chem.* **1994**, *16*, 27 – 35.
[65] M. K. Gellert, K. Mizuuchi, M. H. O'Dea, H. Ohmori, N. Tomizawa, *Cold Spring Harbor Symp. Quant. Biol.* **1978**, *43*, 33 – 40.
[66] X. Yang, A. V. Vologodskii, B. Liu, B. Kemper, N. C. Seeman, *Biopolymers* **1998**, *45*, 69 – 83.
[67] J. Reif, lecture at the Third Annual DIMACS Workshop on DNA Based Computers, University of Pennsylvania, Philadelphia, **1997**.
[68] S. S. Smith, L. Niu, D. J. Baker, J. A. Wendel, S. E. Kane, D. S. Joy, *Proc. Natl. Acad. Sci. USA* **1997**, *94*, 2162 – 2167.
[69] C. A. Mirkin, R. L. Letsinger, R. C. Mucic, J. J. Storhoff, *Nature* **1996**, *382*, 607 – 609.
[70] R. Elghanian, J. J. Storhoff, R. C. Mucic, R. L. Letsinger, C. A. Mirkin, *Science* **1997**, *277*, 1078 – 1081.
[71] A. P. Alivisatos, K. P. Johnsson, X. Peng, T. E. Wilson, C. J. Loweth, M. P. Bruchez, Jr., P. G. Schultz, *Nature* **1996**, *382*, 609 – 611.
[72] C. M. Niemeyer, T. Sano, C. L. Smith, C. R. Cantor, *Nucleic Acids Res.* **1994**, *22*, 5530 – 5539.
[73] J. Shi, D. E. Bergstrom, *Angew. Chem.* **1997**, *109*, 70 – 72; *Angew. Chem. Int. Ed. Engl.* **1997**, *36*, 111 – 113.
[74] T. W. Nilsen, J. Grayzel, W. Prensky, *J. Theor. Biol.* **1997**, *187*, 273 – 284.
[75] C. Mao, W. Sun, Z. Shen, N. C. Seeman, *Nature* **1998**, in press.

Resolution of Racemates: Did You Say "Classical"?

André Collet*

Discovered by Pasteur in 1853, the "classical resolution" method rests upon the combination of a racemate with one enantiomer of a chiral substance (resolving agent) to give a 1:1 mixture of (p,n)-diastereoisomeric salts, which are then separated by crystallization techniques. In spite of its somewhat ambiguous—and no longer justified—reputation of being more an art than a science, classical resolution is still essential in the preparation of a vast majority of the chiral active principles required in enantiopure form for the manufacture of pharmaceuticals and agrochemicals. To cite but a few examples, thousands of tonnes per year of (*S*)-naproxene,[1] D-phenyglycine, and D-4-hydroxyphenyglycine[2] are produced by separation of diastereoisomeric salts rather than by alternative processes based on asymmetric synthesis or bioresolutions. There are good reasons for this: in the context of large-scale enantiomer separations, crystallization techniques are often more straightforward and more economical than any other method. This is the fruit of the labor of academic and industrial researchers in the last decades to gain a better understanding of the physical chemistry concepts upon which separation of diastereoisomers by crystallization is based.[3, 4]

Utilizing phase diagrams generally speeds up the selection of a good resolving agent and the determination of the best crystallization conditions; industrial applications developed in less than six months are not the exception. Three basic types of phase diagrams exist for describing the solid–liquid equilibria for diastereoisomer mixtures. The simple eutectic, without terminal solid solutions, is the most interesting for separation purposes (Figure 1 a). Here the least soluble diastereoisomer (p) will be obtained in pure form after a single crystallization from the 1:1 (p,n) mixture of composition O. The expected yield is $Y = 100 \times (\mathrm{OE/Ep})/C_\mathrm{O}$, where C_O is the concentration of mixture O. This yield approaches its maximum value of 0.5 (or 50 %) when the eutectic E is close to the edges of the phase diagram. Such "good systems" probably represent less than 20 % of the cases. They lend themselves to very economical commercial applications (e.g. naproxen). Often eutectics are complicated by the presence of terminal solid solutions (Figure 1 b). Then several recrystallizations may be required to raise the enantiomeric purity to an acceptable level, and the final yield is less than that given by the above relationship. Terminal solid solutions in diastereoisomer phase diagrams are often major issues in industrial applications.

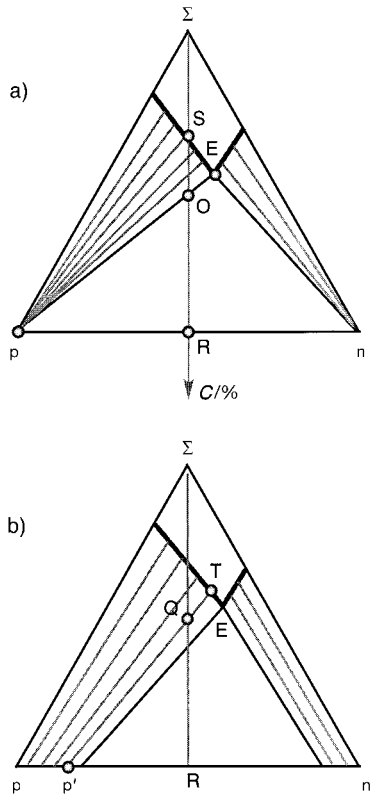


Figure 1. a) Ideal solubility isotherm for (p,n)-diastereoisomers forming an eutectic in solvent Σ. The less soluble diastereomer (p) can be obtained in pure state from solutions of composition between O and S. The maximum yield (Y) in p is obtained from solution O (see text). In the case shown, Y would be around 25 %, a figure which seems relatively common. b) Eutectic phase diagram with terminal solid solutions on both the p and n sides. On crystallization, a system of composition Q will give an impure solid (p′) in a liquid of composition T.

Cocrystallization of the two diastereoisomers to form a continuous series of solid solutions is also relatively common. Such systems are generally unsuitable for resolution, at least in the context of commercial processes.[5] The formation of 1:1 addition compounds (double salts) is also relatively frequent.

[*] Prof. Dr. A. Collet
École normale supérieure de Lyon
Stéréochimie et Interactions Moléculaires (UMR CNRS 117)
F-69364 Lyon Cedex 07 (France)
Fax: (+33) 472-72-84-83
E-mail: andre.collet@ens-lyon.fr

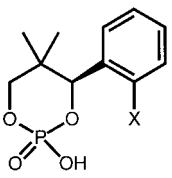
 © WILEY-VCH Verlag GmbH, D-69451 Weinheim, 1998 1433-7851/98/3723-3239 $ 17.50+.50/0

Here no separation of the diastereoisomers is possible by crystallization of their 1:1 mixture.

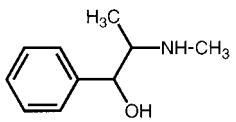
This is why the selection of a good resolving agent, in other words, one which will lead to a very dissymmetric eutectic phase diagram, if possible without terminal solid solutions, is of great importance. In general, this crucial selection is best made by trial and error. Even though such protocols can be made very systematic and efficient,[6] their success is not predictable. There are no established guidelines for predicting what will be the best resolving agent for a given substrate, except perhaps analogies, which may be valid within series of closely related substrates (for instance simple substituted mandelic acids are generally resolved with ephedrine). Although insolvable cases remain the exception (at least in my own experience), in many instances for which classical resolutions have been successfully devised the actual yield is not always close to the 50% limit, a circumstance that may be problematic in commercial applications. This is mostly due to the lack of time for screening enough resolving agents, and also to the limited number of commercially available resolving agents.

A recent paper by Vries et al.[7] conveys a new approach to this long-standing problem. The starting idea has something naively obvious: "It was reasonable to assume that the simultaneous addition of several resolving agents might materially shorten the time required for the hit-and-miss method of finding a resolving agent." Is this idea really as reasonable as it would seem? At first glance a combinatorial version of the usual protocol has little chance of success. The chance to get crystalline materials from such multicomponent mixtures must be very low, because the effective concentration of a given diastereoisomeric salt is reduced by a factor of 3 when a mixture of three resolving agents is used instead of a single one. Accordingly, only exceptionally insoluble salts can be selected by this method. In fact, the authors readily discovered that the use of random combinations of resolving agents did not work so well.

Things improved dramatically, however, when they started to utilize "mixes" consisting of several resolving agents of the same family (usually three). For example, the 1:1:1 mixture of three differently substituted phosphoric acids of the same configuration (**P** mix) constitutes such a family. Ten such



"P mix"
X = H, Cl, OCH_3



(±)-1
ephedrine (1*R*,2*S*)

ternary mixes are presented in the paper by Vries et al.[7] Some are acidic resolving agents, others are basic. In this context, the term "family" is very restrictive: the components of the mix are not only structurally and chemically related, but they are also almost isosteres.[8] For example, tartaric acid is not a member of the dibenzoyltartaric acid family.

According to the authors, when such a mix is added to a solution of a racemic substrate, a crystalline salt usually precipitates immediately. In most cases the substrate contained in the precipitated salt is resolved to about 90–98% *ee*. The important finding is that the salt always contains several resolving agents, which are present in a nonstoichiometric ratio. For instance, (±)-ephedrine ((±)-**1**) combined with the previously mentioned **P** mix in 2-propanol affords a salt having 98% *ee* in (+)-**1** and containing the three phosphoric acids of the **P** mix in a 1:1.2:1.1 ratio. In most cases the mixed salts retain a nonstoichiometric composition on repeated crystallizations. In this example the initial composition drifted to 1:14:55 after 20 crystallizations. This means that the mixed salts are not just mixtures of pure diastereoisomeric salts, but more likely consist of a single crystalline entity where the three resolving agents form a solid solution. The similarity of the structures of the components of the mix is in line with this hypothesis, which is also supported by the resolution of the crystal structure of a binary salt of (+)-ephedrine containing almost equimolecular amounts of two of the phosphoric acid components of **P** mix.

Despite the absence of any relevant phase diagrams or solubility data, I have the feeling that the solid-solution hypothesis provides a good key to a consistent interpretation of the phenomenon. Solid solutions often form between closely related chiral structures of like configuration.[8] This is one of the statements upon which Fredga's method is based.[9] This well-known method establishes the relative configurations of structurally related compounds from their melting point phase diagrams. For instance, *o*-chloro- and *o*-bromomandelic acids of the same configuration form such a solid solution. A solid solution may have a lower solubility and a greater density than the pure components. This is easy to understand: in a single-component crystal, the packing efficiency is restricted to a certain limit by the lattice symmetry requirements, while in a solid solution, even though the average crystal symmetry is maintained, the local symmetry is lowered due to the present of different species. This situation may allow a closer packing, hence a greater density. In turn, a closer packing should result in a better selectivity towards the configuration of the substrate. In other terms, terminal solid solutions between p and n salts (Figure 1b) would form less easily when a mix rather than a single resolving agent is utilized. This is perhaps the origin of the high *ee* values observed for the first precipitated mixed salts.

At this stage, it would be necessary to have more information on the physical properties of the various components of these complex systems and of their mixtures. Thanks to these discoveries, a new field of exploration is now wide open, which should consider various aspects of the question including phase equilibria, crystallization kinetics, the structures and dynamics of the solid and liquid phases, etc.

Whatever the physical chemical explanation, I tend to believe that the main practical interest in this "family approach" is perhaps not in the speeding up of the process of finding the best resolving agent, but rather in its ability to improve the quality of the diastereoisomeric salts, by allowing a sort of self-optimization of the crystal packing which takes advantage of the presence of several slightly different bricks

 © WILEY-VCH Verlag GmbH, D-69451 Weinheim, 1998 1433-7851/98/3723-3240 $ 17.50+.50/0

instead of a single one. DSM Andeno has used this method to resolve racemates on a scale of hundreds of kilograms.[10] Without a doubt "classical resolution" still has a great future, both on the fundamental and applied sides.

German version: *Angew. Chem.* **1998**, *110*, 3429 – 3431

Keywords: chirality · crystallization · diastereoisomers · enantiomeric resolution · resolving agents

[1] P. J. Harrington, E. Lodewijk, *Org. Process Res. Dev.* **1997**, *1*, 72.
[2] J. Kamphuis, W. H. J. Boesten, B. Kaptein, H. F. M. Hermes, T. Sonke, Q. B. Broxterman, W. J. J. van den Tweel, H. E. Schoemaker in *Chirality in Industry* (Eds.: A. N. Collins, G. N. Sheldrake, J. Crosby), Wiley, New York, **1994**, p. 189.
[3] J. Jacques, A. Collet, S. H. Wilen, *Enantiomers, Racemates, and Resolutions*, Wiley, New York, **1981**; J. Jacques, A. Collet, *Reissue with corrections*, Krieger, Malabar, FL, USA, **1994**.
[4] E. L. Eliel, S. H. Wilen, N. Mander, *Stereochemistry of Organic Compounds*, Wiley, New York, **1994**.
[5] J. Costante, N. Ehlinger, M. Perrin, A. Collet, *Enantiomer* **1996**, 1, 377 – 386.
[6] A. Collet in *Comprehensive Supramolecular Chemistry, Vol. 10* (Eds.: J. L. Atwood, J. E. D. Davies, D. D. MacNicol, D. N. Reinhoudt), Pergamon, Oxford, **1996**, pp. 113 – 149.
[7] T. Vries, H. Wynberg, E. van Echten, J. Koek, W. ten Hoeve, R. M. Kellogg, Q. B. Broxterman, A. Minnard, B. Kaptein, S. van der Sluis, L. Hulshof, J. Kooistra, *Angew. Chem.* **1998**, *110*, 2491; *Angew. Chem. Int. Ed.* **1998**, *37*, 2349.
[8] For a relevant discussion, see: A. Collet, L. Ziminski, C. Garcia, F. Vigné-Maeder in *Supramolecular Stereochemistry* (Ed.: J. S. Siegel), Kluwer, **1995**, pp. 91 – 110 (NATO ASI Series).
[9] A. Fredga, *Tetrahedron* **1960**, 8, 126.
[10] L. A. Hulshof, Q. B. Broxterman, T. R. Vries, H. Wijnberg, E. van Echten (DSM N.V.), EP-B 0 838 448 A1, **1997** [*Chem. Abstr.* **1998**, *129*, 4278].

In Vitro Evolution and Selection of Proteins: Ribosome Display for Larger Libraries**

Ulrich Hoffmüller and Jens Schneider-Mergener*

One of the most rapidly developing research areas since the beginning of the 90s is the generation and exploitation of molecular libraries (for a review see ref. [1]). The catchword is: combinatorial, paired with chemistry, biochemistry, or biology. Although the applied methods have hardly reached the text books, almost every researcher involved in the fields of chemistry and the biosciences is familiar with the term phage display, peptide, and nucleic acid libraries, or combinatorial chemistry. The common strategy as well as the goal of all chemical and biological approaches is always 1) to generate the largest and most comprehensive pool of molecules possible (the "library") and 2) to search through the library for individual substances with the desired properties such as, for example, for a starting substance (lead structure) for a drug or antibody for diagnostic purposes. Libraries are being used increasingly to identify interaction partners in signal transduction, cell – cell recognition, and immunological control processes. These kinds of approaches accelerate not only the handling of many problems, but also often provide the first possible means to solving them. Therefore, numerous chemists and biologists in industry and university labs have begun to develop novel methods that make it possible to create, analyze, and propagate libraries. The best-know procedure amongst the many described[1] is the so-called phage display method,[2, 3] where the peptide or protein library is expressed on the phage surface. The selection of the desired phage is achieved in vitro, whereas the amplification of the phages takes place in bacteria, that is, in vivo. Here lies a decisive problem with the use of this biologically generated repertoire. The size of the library, is limited by the first essential step of introducing the phage DNA, which contains the genes that code for the individual components of the library, into cells. This step is known as transfection or transformation and permits a repertoire size of between 10^7 and 10^9 different components.[4] In addition, the environment of the host cell imposes an additional selection pressure that may work against the desired variant.[5] A further "disadvantage" of phage display is the time consuming shuttling between in vitro and in vivo steps.

These problems could be avoided if the isolated protein synthesis machinery of the cell (ribosome) was used instead of intact cells for the production of peptide and protein libraries. This was successful first of all in the search for peptides with the desired properties by using the so-called polysome display.[6, 7] A polysome is a complex comprised of one mRNA and a number of ribosomes. A breakthrough was achieved by Hanes and Plückthun[8] who worked out a system for the general application of in vitro selection and evolution of proteins, which they called ribosome display. Selection and evolution systems are based on the following criteria: 1) generation of molecular diversity, 2) selection of molecules with

[*] Priv.-Doz. Dr. J. Schneider-Mergener, Dr. U. Hoffmüller
Institut für Medizinische Immunologie
Universitätsklinikum Charité, Humboldt-Universität
Schumannstrasse 20/21, D-10098 Berlin (Germany)
Fax: (+49) 30-2802-6460
E-mail: jsm@charite.de

[**] We would like to thank A. Warsinke and M. Paschke for critical reading of the manuscript. U.H. was supported by the DFG (INK 16A1-1).

 © WILEY-VCH Verlag GmbH, D-69451 Weinheim, 1998 1433-7851/98/3723-3241 $ 17.50+.50/0

desired properties, 3) amplification of the selected molecule, and 4) repetition of steps 2 and 3, or analysis of the selected molecule. If mutations are permitted during the amplification procedure, the system possesses an evolutionary character. The addition of nucleic acids facilitates problem-free, and very effective amplification of the required information. In step 2 it is possible to translate the information from the nucleic acids (genotype) into a protein, which can then be selected for according to its function (phenotype). The genotype and phenotype must be linked to each other and selected together so that the information (genotype) after selection can be amplified. Usually for such systems comprised of associated genotype and phenotype, such as phage display, time-consuming alternate in vitro and in vivo steps are required. However, the combination of genotype and phenotype with ribosome display functions without the aid of cells. Proteins are synthesized in vitro based on the coding by a mRNA, after which each mRNA molecule together with the translated protein remains attached to the ribosome. This complex can then be selected according to the phenotype of the protein.

The method functions according to the following principle (Figure 1): a DNA library encoding the desired protein is created. By using the polymerase chain reaction (PCR, for a review see ref. [9]) some regulatory elements, as clarified later, are attached to the DNA. By in vitro transcription the DNA is copied into a mRNA, which is translated in a prokaryotic in vitro system,[10] which gives rise to the ribosomal complex comprised of mRNA, ribosome, and translated protein. Various optimizing steps sustain the stability of the complex and permit correct folding of the protein. The complex is selected on the basis of the desired binding properties of the translated protein. During elution the complex dissociates and the mRNA is released. It is then isolated, converted by reverse transcriptase into cDNA (complementary DNA), and amplified by PCR. The resulting DNA can be introduced into the next selection cycle or analyzed by cloning and sequencing.

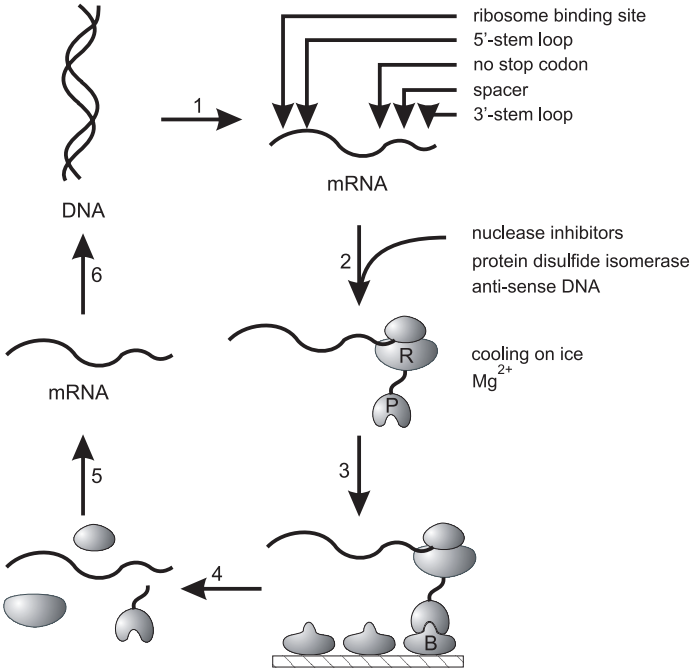


Figure 1. The principle of ribosome display. Step 1: a DNA library is amplified by PCR, which at the same time introduces the structural elements indicated, and then transcribed into RNA. Step 2: the mRNA is converted (translated) into a protein in an in vitro system. The addition of protein disulfide isomerase, nuclease inhibitors, and anti-sense DNA improves protein folding and protects the mRNA and protein. Step 3: the complex of ribosome (R), mRNA and protein (P) with the desired binding property is stabilized by cooling and addition of Mg^{2+}, and is selected with regard to its affinity for an immobilized binding partner (B). Unbound complexes are removed by washing. Step 4: elution of the bound ribosome complex. Step 5: isolation of the mRNA. Step 6: reverse transcription of RNA into DNA and amplification by PCR. The DNA is subjected to a further round of enrichment or can be analyzed by cloning and sequencing. Usually five cycles comprising these steps are carried out.

The ribosome display method was developed by using a single chain antibody (scFv) fragment as a model system and optimized and developed by numerous additions into a system for general application (Figure 1). These improvements protect the mRNA from enzymatic breakdown by nucleases, stabilize the ribosome complex, and facilitate the correct folding of the presented protein, and therefore increases significantly the overall efficiency of the method. As a measure of efficiency, the yields of the eluted mRNA that is isolated after the affinity selection with the antibody's binding partner (antigen), in this case a peptide, are compared. Here, the structure of the mRNA was found to play a significant role. A hairpin loop is introduced at both the 5′ and 3′ ends to protect the mRNA from exonucleases. The hairpin loop at the 3′ end is also responsible for the termination of translation since the mRNA contains no stop codon. If translation was to end at a stop codon this would lead to dissociation of the ribosome complex, which would then no longer be available for affinity selection. A spacer is introduced between the coding sequence for the antibody and the 3′-hairpin loop. This ensures that the actual polypeptide chain has already completely migrated out of the ribosome when transcription stops, and can fold up unhindered. Efficiency is further increased by the addition of nuclease inhibitors and protein disulfide isomerase, which catalyzes the formation of the correct disulfide bridges of scFv. A further, particularly noticeable, improvement relates to the inhibition of a protein degradation pathway: recently a peptide marking system was reported where proteins that derive from a mRNA without a stop codon are marked for degradation with a peptide coded for by a special RNA.[11] Indeed, through blocking of this RNA by the corresponding complementary (anti-sense) DNA the yields could be increased further.

Through the described structural changes in the mRNA and the reagents, which are added during the translation, the total yields were increased from 0.001 % to 0.2 %. Subsequently, a test experiment was carried our to assess how well a protein with a desired function can be enriched from a mixture of two proteins. Two mRNA constructs were created that were identical in the properties described above, one coding for an anti-hemagglutinin scFv[12] and the other for an anti-β-lactamase scFv.[13] These were mixed in a ratio of $1:10^8$ and selected in five cycles (Figure 1) on immobilized hemagglutinin peptide. At the end of the selection 90 % of the ribosome complexes contained the anti-hemagglutinin antibody fragment. Per cycle, therefore, the desired protein was enriched

 © WILEY-VCH Verlag GmbH, D-69451 Weinheim, 1998 1433-7851/98/3723-3242 $ 17.50+.50/0

100-fold. After the fifth round 20 clones were sequenced and of these 18 coded for the intended protein. Table 1 shows the clones arranged according to their relative binding strength and lists the mutations found. Two clones corresponded to the wild-type sequence, the rest showed one to four amino acid exchanges, which demonstrates the range of possible mutations that retained or even improved upon the original function.

Table 1. Mutations in the selected anti-hemagglutinin single chain antibody.[a]

Clone no.	Mutation V_L	V_H	linker	Binding strength
12	K45R	P41R		102
10		S30P		101
6				100
2				96
7		G16D		89
3	Y49H			86
9	E55G, E105G	A23V	S5P	86
1	T20A		G12E	80
18	N(27d)D	D10G, T50N		76
4	V13A, K28R	V12A		72
13	V58I	Y79C		65
16	L83R	I51V, K75E, A113V		63
14	K30E	D61G	S5P	43
17	F71S			18
8	E17G, K18E, K30E			14
5	L11P		G13D	9
11	S(27e)F, N90E	V48I		9
15	G64D, S77A	G15S		6

[a] For all the analyzed antibody clones the relative binding strength and the mutation(s) found in the three regions of the antibody (V_L = variable region of the light chain; V_H = variable region of the heavy chain; and the linker that connects both regions. The mutations are numbered according to Kabat et al.[18] Owing to the variable length of the complementary binding regions (CDRs), several positions are additionally labeled with lowercase letters.

This experiment from Hanes and Plückthun showed that ribosome display is suitable as a purely in vitro system for phenotypic selection following ligand binding. Also the correct folding and formation of disulfide bridges was feasible, which for a large proportion of proteins is essential. Therefore, ribosome display represents the first complete system that exists in vitro for the evolution and selection of folded native proteins. The transformation of DNA into cells is not required, and nothing more stands in the way of synthesizing and screening large protein libraries ($\gg 10^9$ single components). He and Taussig[14] recently succeeded in performing reverse transcription directly within the ribosomal complex with an analogous eukaryotic transcription/translation system, without previously purifying the mRNA. This could mean reduction in the time necessary for one cycle of ribosome display to 8 h. In addition, new methods such as "sexual PCR",[15] error-prone PCR,[16] or PCR with trinucleotide primers[17] could further increase the diversity of ribosome display. On the other hand, the error rate in ribosome display could be reduced by using polymerases with error correction or proofreading activity, if the method is to be used merely for searching through libraries.

Ribosome display has great potential to advance basic research in the areas of protein structure, folding, and evolution. At the same time the method greatly accelerates the process of searching for new lead compounds with interesting properties, as well as optimizing already known therapeutically relevant proteins. Furthermore, valuable insights into the exact location of active sites on protein surfaces may be gained, which will simplify the design of protein mimics and a new class of therapeutic substances.[3]

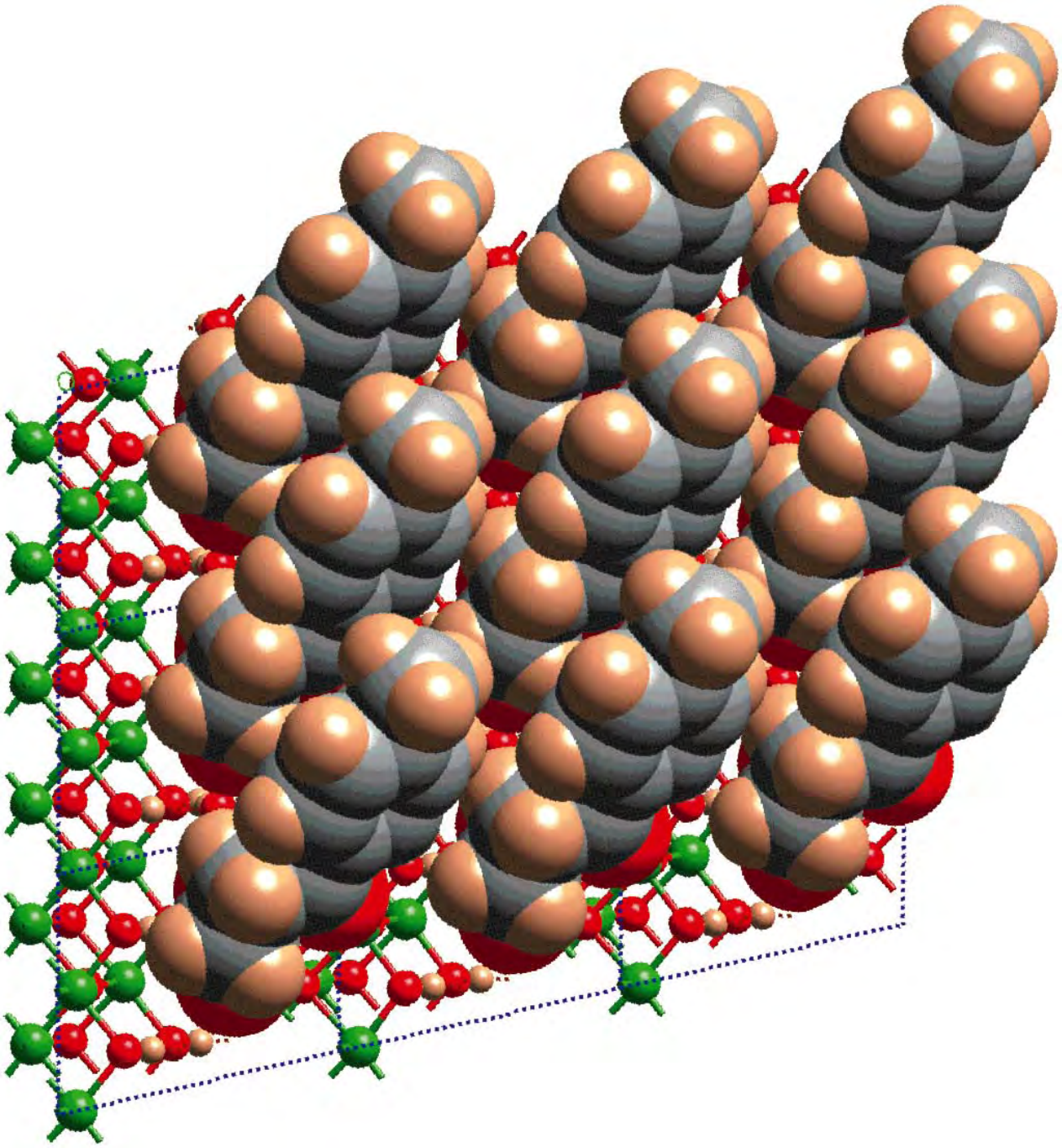
German version: *Angew. Chem.* **1998**, *110*, 3431 – 3434

Keywords: combinatorial chemistry · in vitro selection · nucleic acids · proteins · ribosome display

[1] D. R. Liu, P. G. Schultz, *Angew. Chemie* **1999**, *111*, No. 1; *Angew. Chem. Int. Ed.* **1999**, *38*, No. 1.
[2] G. P. Smith, J. K. Scott, *Methods Enzymol*. **1993**, 217, 228.
[3] U. Reineke, J. Schneider-Mergener, *Angew. Chem.* **1998,** *110*, 801; *Angew. Chem. Int. Ed* **1998**, *37*, 769.
[4] W. J. Dower, S. E. Cwirla, in *Guide to Electroporation and Electrofusion*, (Eds: D. C. Chang, B. M. Chassy, J. A. Saunders, A. E. Sowers), Academic Press, San Diego, **1992**, pp. 291 – 301.
[5] W. P. Yang, K. Green, S. Pinz-Sweeney, A. T. Briones, D. R. Burton, C. F. Barbas, *J. Mol. Biol*. **1995**, *254*, 392.
[6] H. Kawasaki, *PCT Int. Appl*. **1991**, WO 91/05058.
[7] L. C. Mattheakis, R. R. Bhatt, W. J. Dower, *Natl. Proc. Acad. Sci*. USA **1994**, *91*, 9022.
[8] J. Hanes, A. Plückthun, *Natl. Proc. Acad. Sci*. USA **1997**, *94*, 4937.
[9] H. A. Erlich, D. Gelfand, J. J. Sninsky, *Science* **1991**, *252*, 1643.
[10] I. D. Pokrovskaya, V. V. Gurevich, *Anal. Biochem.* **1994**, *220*, 420.
[11] K. C. Keiler, P. R. Waller, R. T. Sauer, *Science* **1996**, *271*, 990.
[12] U. Schulze-Gahmen, J. M. Rini, I. A. Wilson, *J. Mol. Biol*. **1993**, *234*, 1098.
[13] A. Krebber, S. Bornhauser, J. Burmester, A. Honegger, J. Willuda, H. R. Bosshard, A. Plückthun, *J. Immunol. Methods* **1997**, *201*, 35.
[14] M. He, M. J. Taussig, *Nucleic Acids Res.* **1997**, *25*, 5132.
[15] P. Stemmer, *Nature* **1994**,*370*, 389.
[16] R. C. Cadwell, G. F. Joyce, *PCR Methods Appl.* **1994**, *3*, 136.
[17] B. Virnekäs, L. Ge, A. Plückthun, K. C. Schneider, G. Wellnhofer, S. E. Moroney, *Nucleic Acids Res.* **1994**, *22*, 5600.
[18] E. A. Kabat, T. T. Wu, H. H. Perry, K. S. Gottesmann, C. Foeller in *Sequences of Proteins of Immunological Interest, Vol. 1* (Ed.: U.S. Department of Health and Human Services), 5th. ed., **1991**, pp. 151, 464.

 © WILEY-VCH Verlag GmbH, D-69451 Weinheim, 1998 1433-7851/98/3723-3243 $ 17.50+.50/0

The hydrophobic film displayed here as a space-filling model protects iron surfaces (ball-and-stick model) from corrosion. The protective coat is formed by an elegant multifunctional organic additive, and demonstrates how even simple molecules can perform technologically important tasks.



Find out more on the following pages.

 © WILEY-VCH Verlag GmbH, D-69451 Weinheim, 1998 1433-7851/98/3723-3245 $ 17.50+.50/0

Modeling Surface Engineering: Use of Polymetallic Iron Cages and Computer Graphics To Understand the Mode of Action of a Corrosion Inhibitor**

Marcus Frey, Steven G. Harris, Jeremy M. Holmes, David A. Nation, Simon Parsons, Peter A. Tasker,* Simon J. Teat, and Richard E. P. Winpenny*

The protection of metals from atmospheric corrosion is a major factor determining their usefulness, for example as construction materials.[1] As a consequence, most coatings for metals contain corrosion inhibitors as key constituents.[2] Chromates and other inorganic materials have proved effective in such a role, but their toxicity now restricts their use and more benign organic alternatives are being sought.[3] It can be envisaged that functionalized forms of such organic active species will allow surface engineering and could, for example, cross-link into polymer coatings to give improved adhesion. Despite the importance of organic surface modifiers, little attention has been paid to how they bind to oxidized metal surfaces, and why seemingly minor modifications in the structures of organic active compounds can have a profound effect on their efficacy. Here we illustrate a new approach, based on the synthesis of polymetallic complexes involving known organic active compounds, and the use of structural motifs found in such complexes to model relevant surface-active interactions, and hence understand the modes of action of known corrosion inhibitors.

The specific project chosen to demonstrate this approach involves a powerful corrosion inhibitor produced by Ciba Specialty Chemicals. The active ingredient, which is used in water-borne coatings for mild steel, is 3-(4-methylbenzoyl)-propionic acid (HL). It is thought to bind to oxidized iron surfaces in the deprotonated form to create a passivating film. Extensive testing of this compound and related derivatives as corrosion inhibitors in protective coatings[4] indicates that both the presence of the methyl group in the *para* position of the aromatic ring and the carbonyl group greatly increase the usefulness of the active compounds over organic molecules without the ketone functionality and with different types and positions of aromatic substituents.

Model iron complexes of L^- were made by procedures derived from work by Lippard and co-workers.[5, 6] Two structures are relevant.[7] Firstly, a decanuclear "ferric wheel" of formula $[\{Fe(OMe)_2(L)\}_{10}]$ (**1**), in which iron(III) centers are bridged by methoxide and L^- groups (Figure 1). Previous decanuclear iron(III) wheels have been reported with chloroacetate[5] and acetate ligands.[8] The second structure, the undecanuclear cage $[Fe_{11}(O)_6(OH)_6(L)_{15}]$ (**2**, Figure 2), is more complex and involves six iron centers (Fe3, Fe4, Fe6, Fe7, Fe9, Fe10) which describe a trigonal prism. This prism is then capped by two further iron atoms (Fe1, Fe2) on the triangular faces and three iron atoms (Fe5, Fe8, Fe11) on the rectangular faces. There are six μ_3-oxide oxygen atoms, which lie within the metal polyhedron, and six μ_3-hydroxide groups, which lie on the surface of the polyhedron. Carboxylate ligands complete the coordination spheres of each iron. A similar cage has been reported with benzoate.[6] Fe–O bond lengths in **1** are unremarkable; in **2** the Fe–O(oxide) bond distances are markedly shorter than Fe–O(hydroxide) dis-

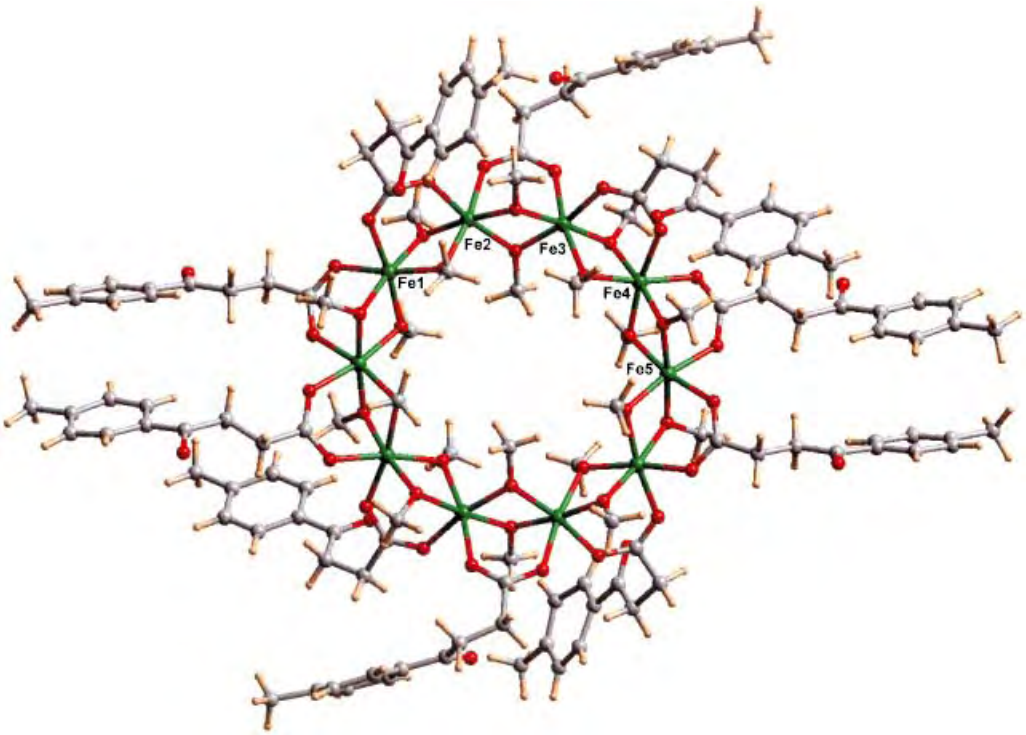


Figure 1. The structure of $[\{Fe(OMe)_2L\}_{10}]$ in the crystal, showing the bonding of the carboxylate head group to the Fe centers and that the ketone functionality of L is not involved (Fe: green, O: red, C: grey, H: light brown; these colors are also used in Figures 2–4). Bond lengths [Å]: Fe–O(methoxide) 1.962–2.000, Fe–O(L) 2.004–2.064 (esd 0.012); bond angles [°]: *cis* angle at Fe 77.3–99.9, *trans* angle at Fe 168.0–175.5 (esd 0.5).

[*] Prof. P. A. Tasker, Dr. R. E. P. Winpenny, S. G. Harris, Dr. J. M. Holmes, Dr. D. A. Nation, Dr. S. Parsons
Edinburgh Centre for Surface Coordination Chemistry
Department of Chemistry, The University of Edinburgh
West Mains Road, Edinburgh, EH9 3JJ (UK)
Fax: (+44) 131-650-4743
Dr. M. Frey
Ciba Specialties, Basel (Switzerland)
Dr. S. J. Teat
CCLRC Daresbury Laboratory,
Daresbury, Warrington, Cheshire, WA4 4AD (UK)

[**] This work was supported by Ciba Specialty Chemicals, the EPSRC (UK), the Royal Society of London, and Zeneca Specialties. We thank Prof. W. Clegg for help with the synchrotron X-radiation study.

 © WILEY-VCH Verlag GmbH, D-69451 Weinheim, 1998 1433-7851/98/3723-3246 $ 17.50+.50/0

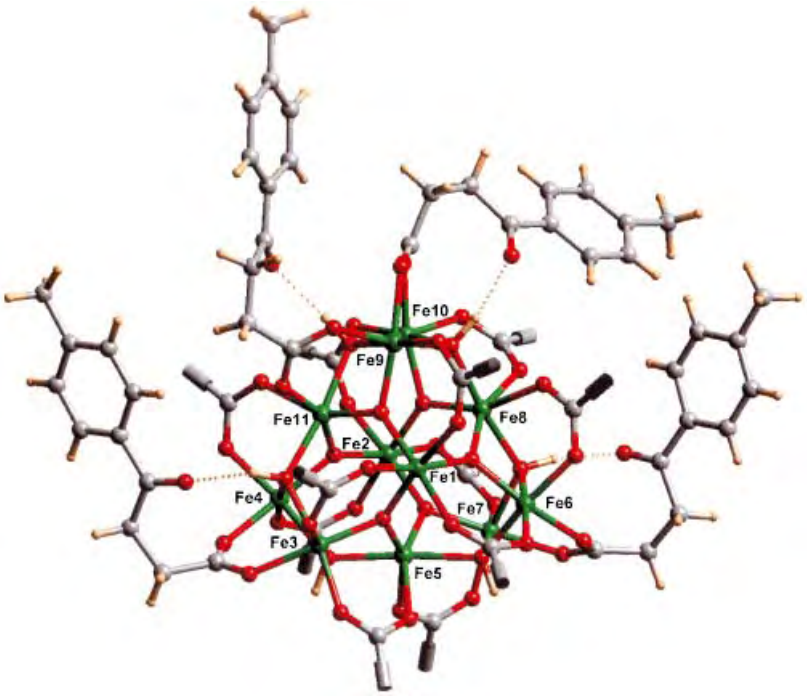


Figure 2. The structure of $[Fe_{11}(O)_6(OH)_6(L)_{15}]$ in the crystal, viewed along the trigonal axis of the metal polyhedron. The organic tail group of eleven of the L^- ligands is excluded for clarity. The four L ligands shown have hydrogen bonds, shown as dotted lines, to hydroxide groups bridging the metal core. Bond lengths [Å]: Fe–O(oxide) 1.878–1.941, Fe–O(hydroxide) 2.049–2.176, Fe–O(L) 1.936–2.158 (esd 0.008); bond angles [°]: *cis* angle at Fe 75.9–109.3, *trans* angle at Fe 154.6–177.4 (esd 0.3).

tances, which allows clear differentiation between these two ligand types. In both structures all Fe sites have approximately octahedral coordination geometries.

In both compounds L^- binds to the iron atoms exclusively through the carboxylate functionality, which spans metal–metal vectors in a 1,3-bridging mode. The ketone functionality does not bind to metal sites, and in **1** plays little part in the structure. In **2** the ligand again binds to the iron centers through the carboxylate group, but now the ketone plays a much more significant role. Four of the fifteen L^- ligands have hydrogen bonds between the ketone oxygen atom and a bridging hydroxide group of the cage (Figure 2). The structures of the model complexes suggest that the presence of the ketone in L^- enhances the performance of the corrosion inhibitor due to this ability to bind to hydroxide groups on a metal oxide hydroxide surface, while the carboxylate binds to the metals. This simple organic molecule is showing bifunctional recognition of the metal surface. To demonstrate that this ditopic binding mode is not a function of crystallization, **2** was also crystallized from EtOH and the structure analyzed.[7] Unfortunately the small crystals which resulted diffracted weakly and synchrotron radiation was required to obtain any data, which even then were of marginal quality. The metal cage in these crystals is identical to **2** when crystallized from MeCN; however, the paucity of observed data and severe disorder in the lattice solvent has prevented refinement of this structure reaching convergence, and we only report unit cell constants here together with the important conclusion that the cage structure is independent of crystallization solvent.

This proposed mode of action receives further support from computer modeling. Bravais–Friedel–Donnay–Harker theory[9] suggests that for lepidocrocite, which is the most common iron oxide hydroxide found on surfaces,[10] the {020}, {021}, and {110} Miller planes are responsible for 94% of the total surface area. Predicting the structures of corroded surfaces is difficult, and the assumptions involved in choosing this mineral seem as valid as any; similar results to those described below can be obtained for the (001) plane of magnetite or the (110) plane of goethite. These three phases—lepidocrocite, magnetite, and goethite—are those detected in rust samples.[10] Layers coplanar with the (021) plane contain iron(III) and hydroxide sites with very similar dispositions to those found in **2**. One molecule of L^- was attached to this (021) surface, using the bonding mode found in **2**, and the energy-minimized conformation for the organic molecule calculated (Figure 3).[11] This leads to the tolyl group of L^- lying at an angle of 48° to the metal oxide surface. When this orientation was used in a computer-generated monolayer, very good surface coverage is obtained (Figure 4) with efficient packing (ca. 50 $Å^2$ per L^-). Few gaps are found between L^- units, giving a

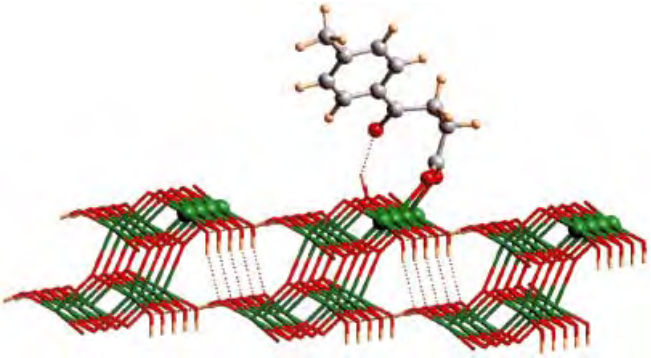


Figure 3. The bonding mode of a single molecule of L^-, derived from **2**, used to address the surface of lepidocrocite.

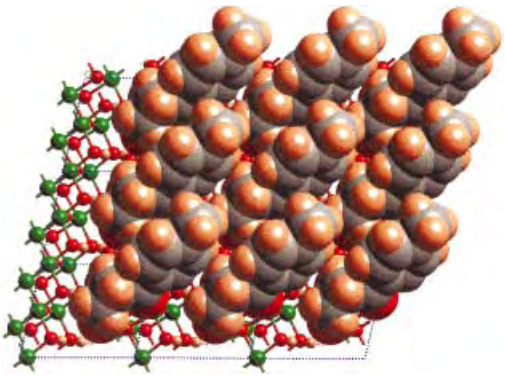


Figure 4. The packing of nine L^- ligands on the (021) surface of lepidocrocite based on the bonding mode found in the structure of $[Fe_{11}(O)_6(OH)_6(L)_{15}]$. For each L^- unit the carboxylate group is at the bottom left of the molecule as viewed, and the methyl group is at the top right.

 © WILEY-VCH Verlag GmbH, D-69451 Weinheim, 1998 1433-7851/98/3723-3247 $ 17.50+.50/0

surface which is hydrophobic and provides a barrier to ingress and egress of ionic species aiding corrosion. If the *para*-methyl group is absent from the tolyl ring the integrity of the barrier is diminished. Also, if the aromatic ring is substituted in different positions (e.g. *ortho* or *meta*) it is much more difficult to retain the bifunctional mode of attachment and close packing of ligands on the surface due to repulsion between the aromatic substituents of neighboring molecules.

Ligand L^- is therefore an extremely elegant multifunctional additive with three aspects to its utility: firstly, binding of the metal sites by the carboxylate head group; secondly, hydrogen bonding between the ketone and the hydroxide group on the metal oxide hydroxide surface; thirdly, the extremely efficient packing of the organic molecules above this surface, forming a well-integrated protective coat. While the first function is predictable based on known coordination chemistry of carboxylates, the other two functions could only be demonstrated by the combination of characterization of model complexes and computer modeling of the additive-surface interaction. The information gained from such studies will enable the design of further actives for modification of metal surfaces with a wide range of industrial applications.

Experimental Section

1: Hydrated ferric nitrate (0.93 g, 2.3 mmol) was allowed to react with Na(L) (0.49 g, 2.3 mmol) in MeOH (20 mL) to give a yellow powder in 85% yield, which was crystallized from DMF/MeOH to give a small quantity of yellow crystals. Elemental analysis calcd for $C_{130}H_{170}Fe_{10}O_{30}$: C 50.51, H 5.54; found: C 50.30, H 5.53.

2: Hydrated ferric nitrate (3.23 g, 8.0 mmol) was allowed to react with Na(L) (4.01 g, 18.7 mmol) in H_2O (100 mL) to give a light orange powder in 90% yield, which was analyzed to be the trinuclear species $[Fe_3(O)(L)_6(H_2O)_3]\cdot L$. Elemental analysis calcd for $C_{77}H_{83}Fe_3O_{25}$: C 58.68, H 5.31; found: C 59.69, H 5.23. The powder was redissolved in MeCN (20 mL), and, on allowing diethyl ether to diffuse into the solution, orange-brown crystals formed in the solution after several days. The compound could also be crystallized by being redissolved in EtOH (20 mL) followed by diffusion of diethyl ether into the solution.

Received: July 20, 1998 [Z12181IE]
German version: *Angew. Chem.* **1998**, *110*, 3435 – 3439

Keywords: clusters · corrosion · iron · surface chemistry

[1] T. W. Swaddle, *Inorganic Chemistry: An Industrial and Environmental Perspective*, Academic Press, London, **1997**.
[2] K. Doren, W. Freitag, D. Stoye, *Water-Borne Coatings: The Environmentally Friendly Alternative*, Hanser/Gardner, Cincinnati, **1994**.
[3] Yu. I. Kuznetsov, *Organic Inhibitors of Corrosion of Metals*, Plenum, New York, **1996**.
[4] Ciba Specialty Chemicals, unpublished results.
[5] K. L. Taft, C. D. Delfs, G. C. Papaefthymiou, S. Foner, D. Gatteschi, S. J. Lippard, *J. Am. Chem. Soc.* **1994**, *114*, 823.
[6] S. M. Gorun, G. C. Papaefthymiou, R. B. Frankel, S. J. Lippard, *J. Am. Chem. Soc.* **1987**, *109*, 3337.
[7] Crystal data for $\mathbf{1}\cdot$MeOH: $C_{131}H_{174}Fe_{10}O_{51}$, $M_r = 3123$, triclinic, $P\bar{1}$, $a = 10.537(4)$, $b = 18.856(6)$, $c = 19.392(7)$ Å, $\alpha = 101.23(2)$, $\beta = 105.36(2)$, $\gamma = 94.96(2)^\circ$, $V = 3605(2)$ Å^3, $Z = 1$ (the molecule lies on an inversion center), $T = 150.0(2)$ K, crystal size $0.49 \times 0.16 \times 0.16$ mm, $\mu(Mo_{K\alpha}) = 1.06$ mm^{-1}. Crystal data for **2**: $C_4H_6O\cdot 3C_2H_3N\cdot 0.5H_2O$: $C_{175}H_{191}Fe_{11}N_3O_{58.5}$, triclinic, $P\bar{1}$, orange-brown lath, $a = 19.534(8)$, $b = 21.320(11)$, $c = 22.821(14)$ Å, $\alpha = 83.71(4)$, $\beta = 74.13(4)$, $\gamma = 80.67(3)^\circ$, $V = 9000(8)$ Å^3, $Z = 2$, $T = 220.0(2)$ K, crystal size $0.39 \times 0.27 \times 0.12$ mm, $\mu(Mo_{K\alpha}) = 0.94$ mm^{-1}. Compound **2** was also crystallized from EtOH: crystal data for $\mathbf{2}\cdot 4.22\,EtOH\cdot 1.22\,Et_2O\cdot 3.0\,H_2O$; $C_{178.32}H_{214.52}Fe_{11}O_{65.44}$, $M_r = 4019$, triclinic, $P\bar{1}$, $a = 20.786(3)$, $b = 22.024(3)$, $c = 22.247(3)$ Å, $\alpha = 74.133(3)$, $\beta = 79.199(3)$, $\gamma = 80.096(3)^\circ$, $V = 9544(2)$ Å^3, $Z = 2$, $T = 160.0(2)$ K, crystal size $0.48 \times 0.10 \times 0.08$ mm, $\mu(Mo_{K\alpha}) = 0.89$ mm^{-1}. Data for **1** and $\mathbf{2}\cdot C_4H_6O\cdot 3C_2H_3N\cdot 0.5H_2O$ were collected with a Stoe Stadi-4 diffractometer equipped with an Oxford Cryosystems low-temperature device. Data for $\mathbf{2}\cdot 4.22\,EtOH\cdot 1.22\,Et_2O\cdot 3.0\,H_2O$ were collected with a Bruker AXS SMART three-circle diffractometer equipped with a CCD detector installed on Station 9.8 at the CCLRC Daresbury synchrotron radiation source. Absorption corrections were applied with ψ-scan data for **1** (min./max. transmission for **1**: 0.455/0.585). All structures were solved by direct methods (SIR92, A. Altomare, G. Cascarano, C. Giacovazzo and A. Guagliardi, *J. Appl. Cryst.* **1993**, *26*, 343) and completed by iterative cycles of ΔF syntheses and full-matrix, least-squares refinement against F^2 (SHELXTL, Brucker AXS). Hydrogen atoms were included in the first two structures in calculated positions, riding on parent carbon atoms, with $U(H) = 1.2\,U_{eq}(C)$ for aromatic hydrogen atoms and $U(H) = 1.5\,U_{eq}(C)$ for methyl hydrogen atoms. In the first two structures disordered and part-weight solvate molecules were found in the lattice, which were modeled as MeOH in **1**, and Et_2O, MeCN, and H_2O in **2**. All non-hydrogen atoms within the cages were refined with anisotropic displacement parameters: for **1**: 564 parameters, $wR2 = 0.3773$ for 9265 unique data ($2\theta \le 45^\circ$), $R1 = 0.1257$ for 3919 observed reflections with $F_o > 4\sigma(F)$, max./min. residual electron density 0.596/ – 0.589 e Å^3; for **2**: 2160 parameters, $wR2 = 0.2501$ for 19121 unique data ($2\theta \le 42^\circ$), $R1 = 0.0872$ for 10180 observed reflections with $F_o > 4\sigma(F)$, max./min. residual electron density 0.907/ – 0.627 e Å^3. Crystallographic data (excluding structure factors) for the structures reported in this paper have been deposited with the Cambridge Crystallographic Data Center as supplementary publication no. CCDC-102414, -102415, and -102416. Copies of the data can be obtained free of charge on application to CCDC, 12 Union Road, Cambridge CB2 1EZ, UK (fax: (+44) 1223-336-033; e-mail: deposit@ccdc.cam.ac.uk).
[8] C. Benelli, S. Parsons, G. A. Solan, R. E. P. Winpenny, *Angew. Chem.* **1996**, *108*, 1967; *Angew. Chem. Int. Ed. Engl.* **1996**, *35*, 1825.
[9] R. Docherty, K. J. Roberts, E. Dowty, *Comput. Phys. Commun.* **1988**, *51*, 423, and references therein.
[10] S. Music, D. Dragcevic, S. Popovic, I. Czako-Nagy, *Croat. Chem. Acta* **1995**, *68*, 315.
[11] All calculations were performed on a Silicon Graphics Indigo2 workstation equipped with the BIOSYM/MSI molecular modeling package Cerius2. Bravais – Friedel – Donnay – Harker calculations predicted that for a single crystal of lepidocrocite the surface would comprise four Miller planes: {010} (occupying 42.61% of total surface area), {021} (29.04%), {110} (22.83%), {111} (5.52%). No suitable carboxylate binding sites were found on the (010) plane, therefore calculations proceeded with the (021) plane. Simulated cleavage of a crystal parallel to the (021) plane results in a surface model with alternating parallel rows of μ_3-hydroxide anions and five-coordinate square-pyramidal metal sites. Ligand L^- was then attached to neighboring ferric sites, with the result that the carbonyl group came into hydrogen-bonding proximity of a nearby μ_3-hydroxide group. The energy-minimized conformation for L^- was calculated with a fixed O–H ··· O(ketone) distance of 2.9 Å. This conformation was then used to generate a surface layer of L^-, as shown in Figure 4. Ligand L^- occupies an area of 50 Å^2 for monolayer coverage.

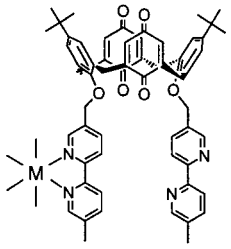
 © WILEY-VCH Verlag GmbH, D-69451 Weinheim, 1998 1433-7851/98/3723-3248 $ 17.50+.50/0

Electrostatic Control of Intramolecular Electron Transfer in Calix[4]diquinones Bearing an Appended Chromophore**

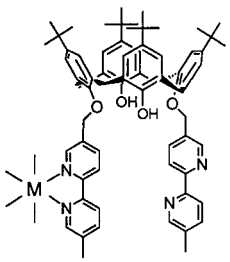
Muriel Hissler, Anthony Harriman,* Pierre Jost, Georges Wipff, and Raymond Ziessel*

Electron transfer is one of the few processes that can compete with deactivation of a short-lived excited state, and this facilitates construction of simple devices for use as chemiosensors, for signal recognition, or for information processing.[1–3] Numerous studies have shown that the rate of electron transfer increases as the reactants approach each other, reaching a maximum at orbital contact.[4] Thus, when the redox units are located at the terminals of a flexible hydrocarbon chain, the rate of light-induced electron transfer depends on the molecular conformation,[5–7] being slowest for fully extended conformers. This realization, in turn, can be exploited to design a reversible optoelectronic switch, provided the conformation can be modulated by external stimulation. We now describe an example of such artificial tropism in which cation binding elongates a flexible molecule and, because electron transfer occurs preferentially in the closed conformer, restores luminescence from the appended chromophore.

Construction of a suitable system requires the cooperation of three discrete components, namely, an electron-rich chromophore, an electron acceptor, and a chelator, joined together by a flexible superstructure in such a way as to maintain the chelator between the redox-active units. Compounds **1** and **2**, calix[4]diquinones functionalized with a pendant 2,2′-bipyridine (bpy) unit and, respectively, [Ru^{II}(bpy)$_3$] or *fac*-[$Re^{I}Cl(CO)_3$(bpy)] moieties, meet the essential requirements. These compounds, together with the appropriate reference complexes **3** and **4**, were prepared by heating of the relevant ligand[8, 9] at reflux with the precursor metallofragment followed by column chromatography.



1 M = [Ru(bpy)$_2$]$^{2+}$; 2 PF_6^-
2 M = *fac*-[ReCl(CO)$_3$]



3 M = [Ru(bpy)$_2$]$^{2+}$; 2 PF_6^-
4 M = *fac*-[ReCl(CO)$_3$]

The *tert*-butyl groups impose a *syn* conformation for the podand bpy functionalities, but ^{1}H NMR studies of **1** and **2** indicate that the quinoid walls of the macrocyclic receptor rotate through the calixarene annulus at ambient temperature, a common situation for calix[4]diquinones.[10] The ^{1}H NMR spectrum of **3**, in particular, exhibits a well-defined AB quartet for each bridging methylene group of the calixarene platform and a single AB quartet for the oxymethylene group next to the [Ru(bpy)$_3$] moiety, and the cone conformation is also apparent from ^{13}C NMR spectra[11] ($\delta =$ 34.0 and 33.9 for the bridging methylene C atoms). The phenolic compounds **3** and **4** contain the chromophores but lack the electron-affinic quinoid units, while compound **2** is a neutral analogue of **1**.

Illumination of **3** or **4** in deoxygenated acetonitrile gave rise to phosphorescence with a maximum ($\lambda_{lum.}$) around 600 nm (Table 1). The excited triplet states of these reference compounds decayed by first-order kinetics, allowing facile measurement of the triplet lifetime τ_T. The total emission quantum yield $\Phi_{lum.}$ was determined by integration of the corrected luminescence spectrum. Phosphorescence from the calix[4]-diquinone-derived species **1** and **2** was barely detectable, and these triplet states were considerably shorter lived than those of the corresponding phenolic compounds (Table 1). Luminescence quenching in **1** and **2** can be attributed to light-induced electron transfer from the triplet state of the metal complex to a nearby quinone unit. The thermodynamic driving forces (ΔG°) for these reactions can be estimated from cyclic voltammetry[12] and luminescence spectroscopy according to Equation (1); E_T is the triplet energy of the metal complex, ΔZ is the difference in electronic charge between radical pair and initial reactants, ε_S is the static dielectric constant of the solvent, and R is the distance separating the Ru^{II} or Re^{I} cation from the center of the quinone unit at the moment of electron transfer.

$$\Delta G^\circ = E_{ox} - E_{red} - E_T + \frac{\Delta Z e^2}{4\pi\varepsilon_0\varepsilon_S R} \quad (1)$$

Table 1. Photophysical and electrochemical properties of **1**–**4** in deoxygenated acetonitrile at 20 °C.

Compd	$\lambda_{lum.}$ [nm][a]	$\Phi_{lum.}$[b]	τ_T [ns][c]	E_{red}[d]	E_{ox}[e]	ΔG° [eV][f]
1	630	0.0004	6	−0.73 (72)	1.22 (72)	−0.26
1·Ba^{2+}	635	0.057	740	−0.59 (irr.)	–	−0.31
2	610	0.0004	5	−0.75 (89)	1.32 (irr.)	−0.28
2·Ba^{2+}	610	< 0.0001	0.085	−0.15 (irr.)	–	−0.78
3	625	0.085	1100	−1.43 (80)	1.35 (70)	> 0.6
4	615	0.0030	45	−1.35 (89)	1.36 (irr.)	> 0.6

[a] Phosphorescence maximum, ±5 nm. [b] Emission quantum yield, ±15%. [c] Triplet lifetime, ±5%. [d] Reduction potential [V vs. SCE], ±15 mV, measured with ferrocene as internal standard ($E_{red} = 0.32$ V vs. SCE, $\Delta E_p = 64$ mV). The splitting between anodic and cathodic peaks is given in parenthesis; irr. indicates irreversible. [e] Reduction potential for oxidation of the metal center [V vs. SCE], ±15 mV. [f] Thermodynamic driving force for light-induced electron transfer, ±0.05 eV.

[*] Prof. A. Harriman, Dr. R. Ziessel, M. Hissler
Laboratoire de Chimie, d'Electronique
et Photonique Moléculaires
Ecole Européenne de Chimie
Polymères et Matériaux (ECPM)
Université Louis Pasteur
1 rue Blaise Pascal, 67008 Strasbourg Cedex (France)
Fax: (+33) 388-41-68-25
E-mail: harriman@chimie.u-strasbg.fr
ziessel@chimie.u-strasbg.fr
Dr. P. Jost, Prof. G. Wipff
Laboratoire de Modélisation et Simulation Moléculaire
Institut Le Bel, Université Louis Pasteur, Strasbourg

[**] This work was supported by the ECPM, the CNRS, and the Royal Society of London. We thank Johnson Mathey PLC for their generous loan of precious metal salts.

 © WILEY-VCH Verlag GmbH, D-69451 Weinheim, 1998 1433-7851/98/3723-3249 $ 17.50+.50/0

For these calculations it is assumed that electron transfer takes place preferentially at orbital contact, so that R is assigned a tentative value of 8 Å. The terms E_{ox} and E_{red} refer to one-electron reduction potentials for the metal center and for the quinone unit, respectively (Table 1); where electrochemically irreversible couples were observed in the cyclic voltammograms, the peak potentials were used to estimate ΔG°. The derived ΔG° values are modest (Table 1) but, while not favoring rapid through-bond electron transfer between remote reactants, they are sufficient for fast electron transfer at orbital contact.[4]

Molecular dynamics (MD) simulations for **1** in acetonitrile indicate that the coordinated bpy ligands come into orbital contact with the quinoid walls of the macrocyclic receptor, the latter existing in a partial cone or 1,3-*alternate* conformation (Figure 1, top). Through-space electron transfer is favored over through-bond interactions by selective charge injection into the unsubstituted bpy units coordinated to the metal center at the triplet level and by the poor electronic properties of the connecting chain.[13] Furthermore, the MD simulations indicate the presence of conformations in which one of these parent bpy ligands lies almost cofacial and in very close proximity to a quinoid nucleus (Figure 1, top). Such structures are highly favorable for rapid (forward and reverse) electron transfer.[14] The electron-transfer pathway is less clear for **2**, where through-bond interactions might make some contribution to the overall process. Laser flash photolysis studies made for **1** and **2** with picosecond time resolution confirmed the short triplet lifetimes but could not resolve the anticipated redox products, indicating that the rate of charge recombination significantly exceeds that of charge separation.

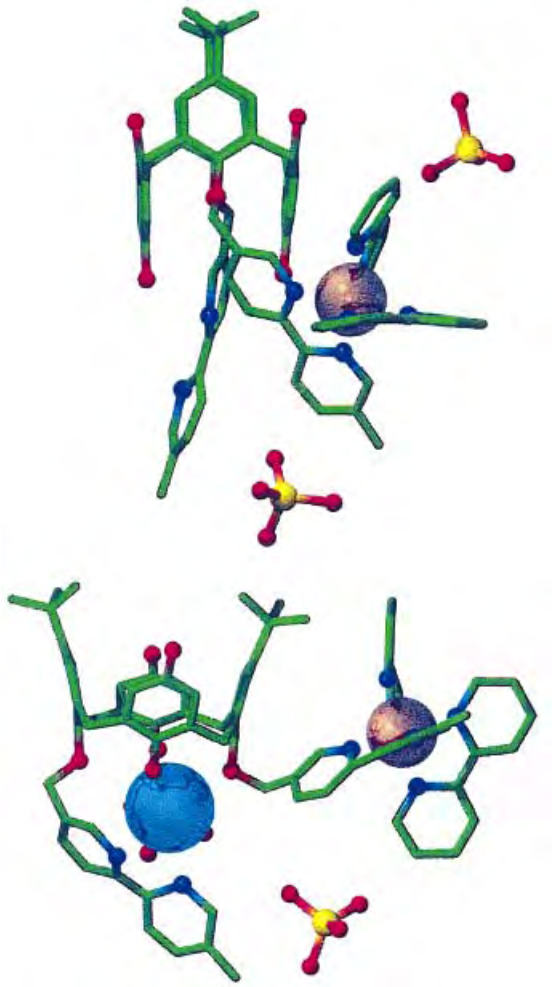


Figure 1. Energy-minimized conformations derived from molecular dynamics simulations for **1** (top) and **1**·Ba^{2+} (bottom) in a matrix of acetonitrile molecules. Many different conformers are predicted to exist in dynamic equilibrium in the absence of added Ba^{2+}, and the top structure corresponds to the conformation most favorable for rapid electron transfer.

Addition of a salt, such as $KClO_4$ or $Ba(ClO_4)_2$, to a solution of **3** or **4** in deoxygenated acetonitrile had no effect on the photophysical properties of the pendant metal complexes. For the rhenium(I) complex **2**, however, addition of salt caused extinction of residual phosphorescence, and in the presence of excess $Ba(ClO_4)_2$ the triplet lifetime was reduced to 85 ± 5 ps. Furthermore, transient absorption spectra recorded after laser excitation of **2** ($\lambda = 355$ nm, full width of half maximum height (FWHM) = 25 ps) in the presence of $Ba(ClO_4)_2$ (5 mM) showed that the initially formed triplet state of the rhenium(I) complex decayed with a lifetime of about 90 ps to form a radical ion pair, which itself decayed by first-order kinetics with a lifetime of 175 ± 25 ps to restore the ground state. Generation of the radical ion pair, by way of intramolecular electron transfer from the triplet state of the rhenium(I) complex to a quinone unit, is promoted by barium cations because of a substantial increase in ΔG°. This arises because E_{red} (-0.75 V vs. SCE) is rendered less negative[12] by about 600 mV upon complexation of $Ba(ClO_4)_2$ (Table 1). Consequencely, the rate of intramolecular electron transfer ($k_{ET} \approx 1.2 \times 10^{10}\ s^{-1}$) derived according to Equation (2), where τ_T^c and τ_T^0, respectively, refer to triplet lifetimes measured

$$k_{ET} = \frac{1}{\tau_T^c} - \frac{1}{\tau_T^0} \qquad (2)$$

for **2** in the presence of excess cation and for **4**, is increased 70-fold upon binding of the cation. Subsequent charge recombination ($k_{ET} \approx 5.7 \times 10^{9}\ s^{-1}$) occurs more slowly, suggesting that this process occurs within the Marcus inverted region[15] because of the large amount of energy ($\Delta G^{\circ} \approx -1.5$ eV) that must be dissipated among vibrational modes.

Remarkably, addition of a cation to a solution of **1** in deoxygenated acetonitrile (Figure 2) caused a progressive increase in phosphorescence yield L until a plateau value was attained, at which the final luminescence yield L_{∞} approached but never quite reached that measured for the phenol derivative (P°). Many different cations exhibit the same qualitative behavior (Table 2). In each case, the cation had little effect on the absorption spectrum of **1**, but the luminescence titration curve could be analyzed according to Equation (3); L_0 is the luminescence yield in the absence of cation, and K is the binding constant for formation of a 1:1 complex.

$$\frac{1}{L_0 - L} = \frac{1}{L_0 - L_{\infty}} + \frac{1}{K[\text{cation}](L_0 - L_{\infty})} \qquad (3)$$

Time-resolved luminescence studies showed the presence of a long-lived species following addition of a cation; the

 © WILEY-VCH Verlag GmbH, D-69451 Weinheim, 1998 1433-7851/98/3723-3250 $ 17.50+.50/0

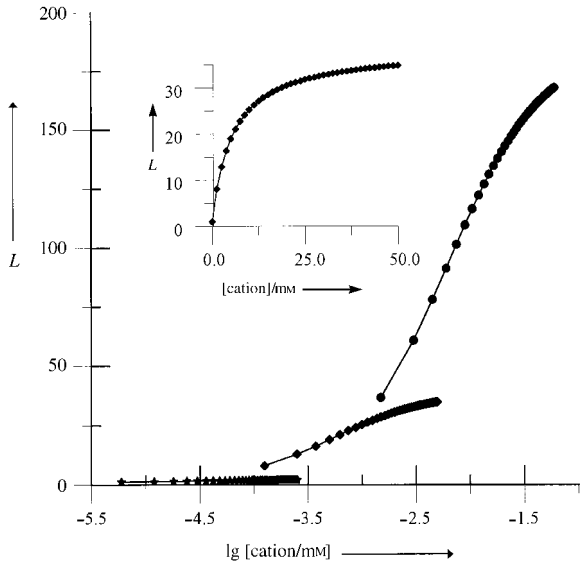


Figure 2. Effect of added $HClO_4$ (*), $KClO_4$ (◆), and $Ba(ClO_4)_2$ (●) on the phosphorescence yield L measured for **1** in deoxygenated acetonitrile containing 0.2 M Bu_4NClO_4 at 20 °C. The solid lines drawn through the data points correspond to nonlinear least-squares fits according to Equation (3) with the parameters listed in Table 2. The insert shows the titration curve recorded for addition of $KClO_4$ in a nonlogarithmic presentation to illustrate attainment of a plateau.

Table 2. Properties of the 1:1 complexes formed between **1** and a cation at 20 °C in deoxygenated acetonitrile containing 0.2 M Bu_4NClO_4.

Cation[a]	K [M^{-1}][b]	τ_T^c [ns][c]	L_∞/P°[d]	k_{ET} [10^6 s^{-1}][e]
–	–	6	0.003	250
H^+	15850	9	0.008	110
Li^+	420	160	0.16	5.3
Na^+	400	160	0.15	5.3
K^+	185	155	0.14	5.5
H_4NH^+	160	130	0.10	6.8
Me_4N^+	8	210	0.21	3.9
Ca^{2+}	22	680	0.62	0.56
Ba^{2+}	16	740	0.67	0.44
Sr^{2+}	12	725	0.65	0.47
Cd^{2+}	30	720	0.66	0.48

[a] Used as the perchlorate salt, in some cases with water of hydration present. [b] Stability constant for formation of a 1:1 complex measured by steady-state luminescence spectroscopy, ±7%. [c] Triplet lifetime for the cation complex, ±10%. [d] Ratio of steady-state luminescence quantum yields measured for the cation complex of **1** and **3**, ±10%. [e] Rate constant for intramolecular electron transfer in the cation complex, ±15%.

measured triplet lifetime (τ_T^0) of this species approached that of **3** (Table 2). Clearly, complexation of a cation causes amplification of luminescence from the appended [Ru^{II}-(bpy)$_3$] complex, in contradiction to the situation found for **2**. With $Ba(ClO_4)_2$ as the salt it was demonstrated that addition of excess [18]crown-6, a more avid cation complexer,[16] extinguished luminescence from $\mathbf{1}\cdot Ba^{2+}$ due to extraction of the cation.

The monocations are characterized by their relatively high binding constants and by their triplet lifetimes of about 150 ns, whereas the dications form less stable complexes with triplet lifetimes around 700 ns (Table 2). Protons bind avidly to the free bpy residue present in **1**, but have little effect on the photophysical properties (Figure 2). Cyclic voltammetry studies carried out with **1** in acetonitrile showed that E_{red} for the quinoid moiety[12] was raised by about 140 mV upon coordination of barium cations such that ΔG° is increased slightly (Table 1). Clearly, the observed amplification of phosphorescence upon cation binding is contrary to the behavior expected on the basis of simple thermodynamic considerations.

Detailed ^1H and ^{13}C NMR studies and MD simulations of the complex with $Ba(ClO_4)_2$ indicate that the cation binds to the lower rim of the calix[4]diquinone receptor,[17] where it is held in place by coordination to the four oxygen atoms and two nitrogen atoms provided by the free bpy ligand. The bound cation forces the macrocycle into a cone conformation and repells the appended [Ru^{II}(bpy)$_3$] moiety (Figure 1, bottom). This has the effect of both curtailing orbital contact between the reactants and preventing adoption of the closely spaced cofacial orientations believed to favor fast electron transfer. From the MD simulations we estimate that the maximum edge-to-edge separation between quinone and bpy functionalities is about 5 Å, so that one or more solvent molecules can fit between the reactants in the fully extended conformation (Figure 1). Given that the attenuation factor[4] for through-space electron tunnelling is around 1.2 $Å^{-1}$, elongation of the supermolecule would cause a 650-fold decrease in the rate of electron transfer. Allowing for the crudity of this estimation, together with the fact that ΔG° increases upon cation binding and that there are changes in orientation as well as separation, the observed decrease in k_{ET} appears to be of the expected magnitude for through-space electron tunneling.

Consequently, the dramatic drop in k_{ET} that accompanies cation binding to **1** can be attributed to an electrostatically driven conformational change that serves to separate the reactants and to force the calixarene into the cone conformation.[18–20] Amplification of emission depends only on the electronic charge of the cation, with k_{ET} remaining about 10-fold higher for a monocation than for a dication, although protons give an anomolously weak effect (Figure 2). The increase in luminescence is fully reversible, as illustrated in the top part of Figure 3 for the case of adding successive amounts of [18]crown-6 to the complex formed between **1** and $KClO_4$, with both complexation and decomplexation steps being fast. In fact, the bimolecular rate constant for complexation of Sr^{2+} by **1** in acetonitrile was measured by stopped-flow techniques to be around 2×10^5 $M^{-1}s^{-1}$, while subsequent decomplexation by [18]crown-6 occurred with a rate constant of about 1×10^5 $M^{-1}s^{-1}$ (Figure 3, bottom).

Experimental Section

The synthesis and characterization of complexes **1**–**4** will be described elsewhere. **1**: ES-MS (CH_3CN): m/z: 1487.6 [$M-PF_6$]$^+$, 671.1 [$M-2PF_6$]$^{2+}$; FT-IR (KBr): $\tilde{\nu}=1654$ cm^{-1} (s, CO); UV/Vis (CH_3CN): λ (ε) = 451 (14400), 288 (116500), 251 nm (81800); elemental analysis calcd for $C_{80}H_{72}F_{12}N_8O_6P_2Ru$ ($M_r=1632.51$): C 58.86, H 4.45, N 6.86; found: C 58.70, H 4.23, N 6.75.

Luminescence lifetimes were measured by time-correlated, single-photon counting methodology following laser excitation at 440 nm and with detection at 620 nm. Laser flash photolysis studies were made by pump-

 © WILEY-VCH Verlag GmbH, D-69451 Weinheim, 1998 1433-7851/98/3723-3251 $ 17.50+.50/0

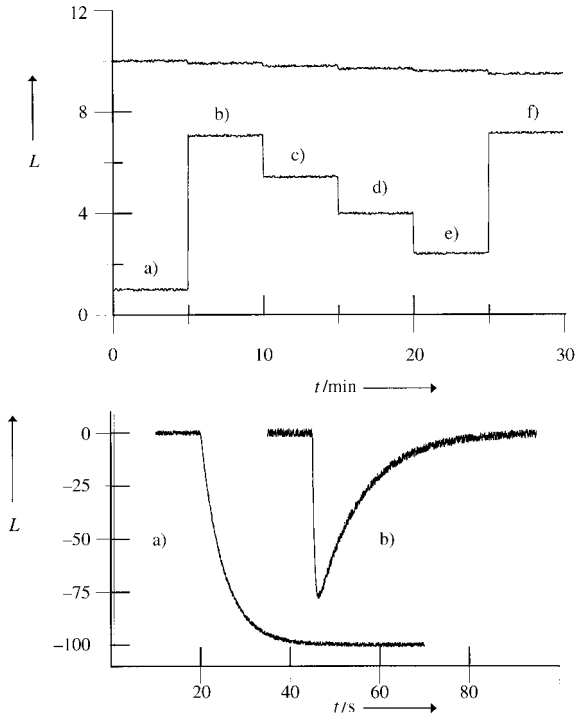


Figure 3. Top: The lower curve shows the phosphorescence intensity L recorded as a function of time t for 20 μM **1** in deoxygenated acetonitrile containing 0.1 M Bu_4NClO_4 a) before addition of a cation and b) upon addition of 1 mM $KClO_4$; c) – e) intensities after additions of 0.3, 0.3, and 0.4 mM [18]crown-6; f) intensity after addition of further 1 mM $KClO_4$ to the mixture. The upper curve shows the corresponding experiment made for **3** and is uncorrected for the (minor) effects of dilution. Top: Kinetic experiment showing a) the rate of appearance of phosphorescence upon rapid injection of 5 mM $Sr(ClO_4)_2$ into a solution of **1** (10 μM) in deoxygenated acetonitrile containing 0.1 M Bu_4NClO_4 and b) decomplexation caused by injection of 1 mM [18]crown-6 to the solution.

probe techniques following excitation at 355 or 440 nm with a 25-ps laser pulse. All studies were carried out with optically dilute solutions of the calix[4]arenes in deoxygenated acetonitrile. Binding constants were determined by monitoring absorption and/or luminescence spectral profiles as a function of cation concentration and using global analytical iterative routines provided by the SPECFIT commercial software. Rates of complexation and decomplexation were measured by stopped-flow techniques with luminescence detection at 20 °C under pseudo-first-order conditions for solutions of Bu_4NClO_4 (0.1 M) in acetonitrile. Molecular dynamics simulations were performed in acetonitrile with the AMBER4.0 software package for 500 ps. Interactions involving barium and ruthenium cations and all other nonbonding interactions are depicted by a 1-6-12 potential, where electrostatics are approximated by Coulombic forces, using atomic charges determined by ab initio calculation on the quinone, anisole, and $[Ru(bpy)_3]^{2+}$ molecular fragments. Reduction potentials were measured by cyclic voltammetry using Pt discs as working and counter electrodes and with an SCE reference calibrated versus ferrocene/ferrocium.

Received: June 8, 1998 [Z11956IE]
German version: *Angew. Chem.* **1998**, *110*, 3439 – 3443

Keywords: calixarenes · electron transfer · electrostatic interactions · luminescence · through-space interactions

[1] A. W. Czarnik in *Fluorescent Chemosensors for Ion and Molecule Recognition* (Ed.: A. W. Czarnik), *ACS Symp. Ser.* **1992**, *538*, 1.
[2] A. P. de Silva, H. Q. N. Gunaatne, T. Gunlaugsson, A. J. M. Huxley, C. P. McCoy, J. T. Rademacher, T. E. Rice, *Chem. Rev.* **1997**, *97*, 1515.
[3] P. D. Beer, *Acc. Chem. Res.* **1998**, *31*, 71.
[4] a) G. L. Closs, J. R. Miller, *Science* **1988**, *240*, 440; b) J. R. Miller, *Nouv. J. Chim*. **1987**, *11*, 83.
[5] A. Harriman, *Pure Appl. Chem.* **1990**, *62*, 1107.
[6] M. T. Indelli, C. A. Bignozzi, A. Harriman, J. R. Schoonover, F. Scandola, *J. Am. Chem. Soc.* **1994**, *116*, 3768.
[7] D. Goztola, B. Wang, M. R. Wasielewski, *J. Photochem. Photobiol. A* **1996**, *102*, 71.
[8] G. Ulrich, R. Ziessel, *Tetrahedron Lett*. **1994**, *35*, 6299.
[9] H. Cano-Yelo Bettega, J.-C. Moutet, G. Ulrich, R. Ziessel, *J. Electroanal. Chem.* **1996**, *406*, 247.
[10] A. Casnati, E. Cornelli, M. Fabbi, V. Bocchi, G. Mori, F. Ugozzoli, A. M. Manotti-Lanfredi, A. Pochini, R. Ungaro, *Recl. Trav. Chim. Pays-Bas* **1993**, *112*, 384.
[11] C. Jamie, J. de Mendoza, P. Prados, P. M. Nieto, C. Sànchez, *J. Org. Chem*. **1991**, *56*, 3372.
[12] Reduction of a calix[4]diquinone without an appended metal complex occurs by four successive one-electron steps, by which the two π radical anions are formed before the π dianions. The electrochemical inequivalence of the quinoid units arises from Coulombic effects. Addition of $Ba(ClO_4)_2$ removes the Coulombic effect, at least for formation of the π radical anions, and stabilizes the emergent negative charge by ion pairing. This stabilization amounts to about 490 meV and corresponds to the difference in stability constant for cation binding to the quinones and their π radical anions. In the presence of excess cation, the reductive process is electrochemically irreversible, whilst ion pairing might involve the bound cation or a second cation from solution. Similar behavior is found for **1** except that the shift in potential is decreased to around 140 meV. This latter finding suggests a much smaller change in the stability constant on going from the quinone to the π radical anion, presumably because the quinone O atoms are already involved in complexation and/or the dicationic donor inhibits secondary ion pairing. For **2**, stabilization of the π radical anions by $Ba(ClO_4)_2$ corresponds to about 600 m eV, suggesting that the dominant mode of ion pairing involves a second cation from the solution.
[13] A. C. Benniston, A. Harriman, V. Grosshenny, R. Ziessel, *New J. Chem*. **1997**, *21*, 405.
[14] B. Brocklehurst, *J. Phys. Chem*. **1979**, *83*, 536.
[15] R. A. Marcus, N. Sutin, *Biochim. Biophys. Acta* **1985**, *811*, 265.
[16] a) K. Ozutsumi, K. Kohyama, K. Ohtsu, T. Kawashima, *J. Chem. Soc. Dalton Trans.* **1995**, 3081; b) quantitative analysis of the fluorescence titration (a part is displayed in Figure 3a) gives $\lg K = 4.26$ for complexation of K^+ by [18]crown-6 under these conditions.
[17] P. D. Beer, P. A. Gale, Z. Chen, M. G. B. Drew, J. A. Heath, M. I. Ogden, H. R. Powell, *Inorg. Chem*. **1997**, *36*, 5880.
[18] S. Shinkai, S. Araki, M. Kubota, T. Arimura, T. Matsuda, *J. Org. Chem*. **1991**, *56*, 295.
[19] J. Blixit, C. Detellier, *J. Am. Chem. Soc*. **1995**, *117*, 8536.
[20] M. Gomez-Kaifer, P. A. Reddy, C. D. Gutsche, L. Echegoyen, *J. Am. Chem. Soc*. **1997**, *119*, 5222.

 © WILEY-VCH Verlag GmbH, D-69451 Weinheim, 1998 1433-7851/98/3723-3252 $ 17.50+.50/0

Surface Reconstitution of a De Novo Synthesized Hemoprotein for Bioelectronic Applications**

Eugenii Katz, Vered Heleg-Shabtai, Itamar Willner,* Harald K. Rau, and Wolfgang Haehnel*

Electrical contacting of redox proteins and electrode surfaces is of fundamental interest in the application of redox-active biomaterials in bioelectronic devices,[1] biosensors,[2] biofuel cells,[3] and optobioelectronic systems.[4] Modification of redox enzymes with electroactive relay groups[5] or immobilization of the biocatalysts in redox-functionalized polymers[6] provide means to establish electrical communication between the redox sites in the proteins and the electrode surfaces. Recently, reconstitution of an apo-flavoenzyme on an electrode functionalized with a relay-FAD monolayer was reported to yield an aligned biocatalyst exhibiting effective electron transfer with the electrode surface.[7] This concept was further broadened to organize enzyme electrodes by cross-linking cofactor–biocatalyst affinity complexes on the electrode surface. The resulting electrically contacted enzyme electrodes were then used as biosensors.[8]

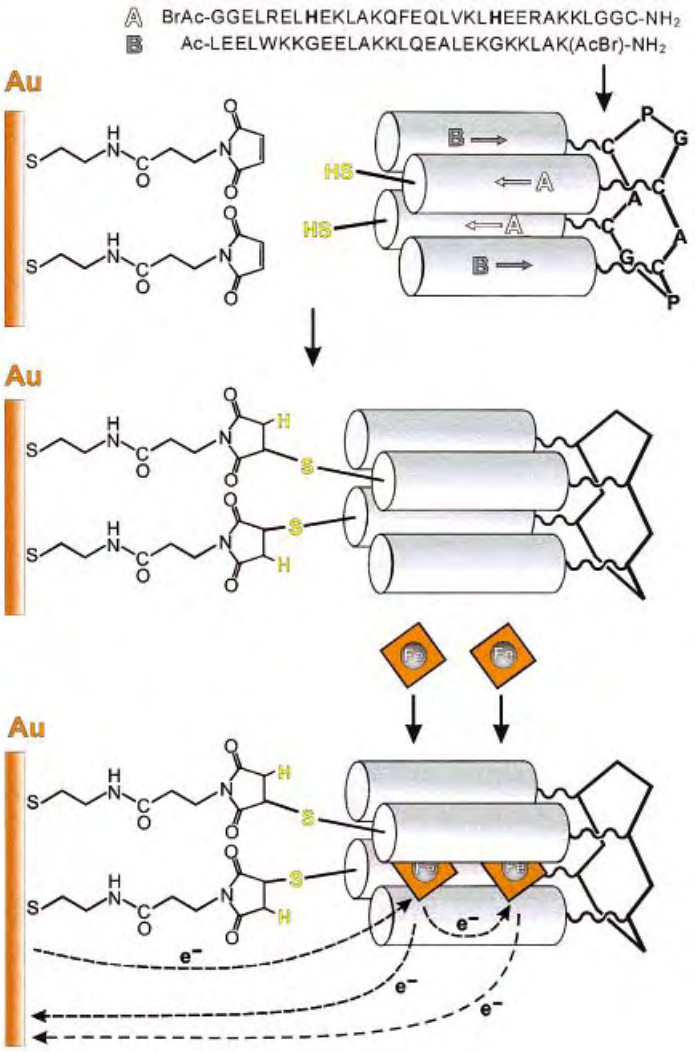
Extensive research efforts are directed to a de novo synthesis of proteins that provide wide variability in biomimetic chemistry.[9, 10] In particular, preparing synthetic proteins by antiparallel α-helix elements on a cyclic peptide is an efficient strategy for the synthesis of predetermined structures.[11] This method was successfully applied to tailor a synthetic cytochrome b analogue by the assembly of four antiparallel helices containing two heme binding sites in the hydrophobic interior.[12] The elucidation of catalytic properties and customized redox functions of these synthetic proteins remains a challenging perspective for future nanoscale bioelectronics.

Here we report on the assembly of a four-bundle synthetic protein as a monolayer on a Au electrode. We demonstrate the stepwise reconstitution of two Fe^{III}–protoporphyrin IX complexes into the synthetic protein. The resulting reconstituted protein reveals electrical contact with the electrode surface. Vectorial electron transfer proceeds in the aligned redox-active monolayer assembly, leading the synthetic hemoprotein to act as a rectifier. We also demonstrate that the synthetic hemoprotein functions as an electron transfer mediator for the native redox protein, nitrate reductase, and that the bioelectrocatalyzed reduction of nitrate is activated.

[*] Prof. I. Willner, Dr. E. Katz, V. Heleg-Shabtai
Institute of Chemistry
The Hebrew University of Jerusalem
Givat Ram, Jerusalem 91904 (Israel)
Fax: (+972) 2-6527715
E-mail: willnea@vms.huji.ac.il
Prof. W. Haehnel, H. K. Rau
Institute für Biologie II/Biochemie der Universität Freiburg
Schänzlestrasse 1, D-79104 Freiburg (Germany)
E-mail: haehnel@uni-freiburg.de

[**] This project was supported by the BMBF/Beo22 and by the Volkswagen Stiftung.

The structure of the synthetic de novo synthesized protein is shown in Scheme 1. The protein consists of 128 amino acids and has a mass of 14728 Da. It was prepared[12] from unprotected peptides (previously purified by HPLC) by the reaction of *N*ε-(bromoacetyl)lysine residues (of helix B) and



Scheme 1. Stepwise assembly of the monolayer of Fe^{III}-protoporphyrin reconstituted de novo synthetic protein on a Au electrode.

bromoacetyl glycine residues (of helix A) which were coupled to cysteine SH groups of the template. Flexible Gly-Gly-Cys units are part of the two helices A and provide a means for the covalent attachment of the de novo protein on an electrode surface. There are two histidine residues in each of the "A" helix bundles. The histidine units are positioned to allow axial ligation to the Fe^{III}–heme sites.

Scheme 1 also depicts the assembly of the synthetic protein as a monolayer on the Au surface. Coupling of a heterobifunctional reagent, *N*-succinimidyl-3-maleimidopropionate, to a cysteamine monolayer associated with a Au electrode was followed by covalent linkage of the terminal maleimide functionalities to the thiol groups of the protein.[13] The resulting monolayer was allowed to interact with Fe^{III}–protoporphyrin IX. The inset of Figure 1 A shows the cyclic

 © WILEY-VCH Verlag GmbH, D-69451 Weinheim, 1998 1433-7851/98/3723-3253 $ 17.50+.50/0

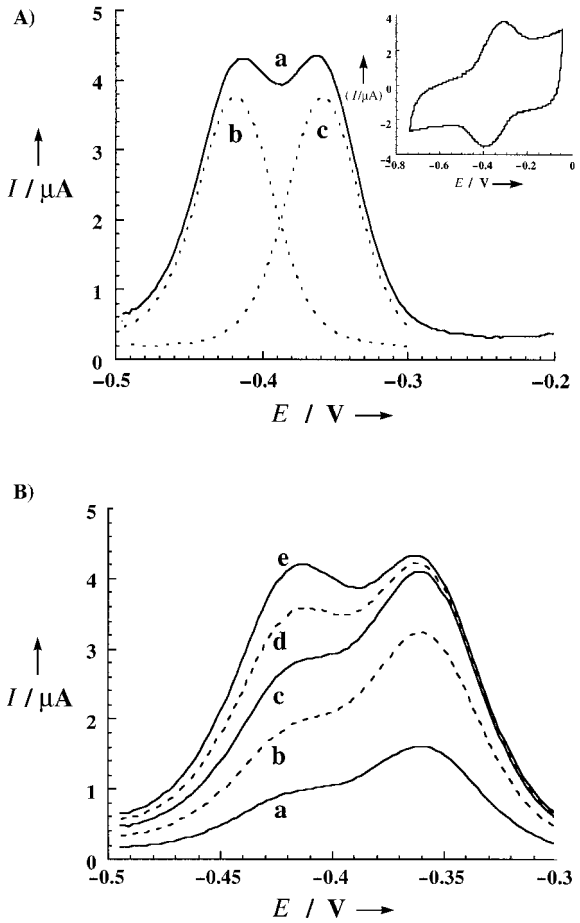


Figure 1. A) Differential pulse voltammogram (a) and deconvoluted voltammograms (b, c) of the monolayer of Fe^{III}–protoporphyrin IX reconstituted synthetic protein on the surface of the Au electrode. Inset: Cyclic voltammogram of the Fe^{III}-protoporphyrin reconstituted synthetic protein (scan rate 200 mV s^{-1}). B) Differential pulse voltammograms (scan rate 20 mV s^{-1}, pulse height 2 mV) of the synthetic proteins after reconstitution with Fe^{III}–protoporphyrin IX for 20 (a), 40 (b), 60 (c), 80 (d), and 100 min (e). Reconsitution was performed in DMSO with a Fe^{III}–protoporphyrin IX concentration of 1×10^{-4} M. The experiments were performed in 0.1 M phosphate buffer (pH 7.0) at 25 °C; electrode geometrical area 0.2 cm^2, roughness factor 1.3. I = current, E = potential vs. SCE.

voltammogram of the Fe^{III}–protoporphyrin IX reconstituted monolayer. A single redox wave is observed. Differential pulse voltammetry reveals that the electrical response of the heme consists of two overlapping redox waves (Figure 1 A). These waves were deconvoluted to two separate electrochemical processes: The reduction potential of one heme center is -0.423 V [versus the saturated calomel electrode (SCE)], and the reduction potential of the second heme center is shifted by about $+66$ mV to -0.357 V. These values are in agreement with those found for the soluble variant of the protein.

Coulometric analysis of the redox waves of the two heme sites reveals that the two Fe^{III}–protoporphyrin IX units occupy the protein bundle in a 1:1 ratio, and that the surface coverage of the heme-reconstituted synthetic protein is 2.5×10^{-11} mol cm^{-2}. Similar cyclic and differential pulse voltammograms were obtained by the coupling of a synthetic hemoprotein reconstituted with Fe^{III}-protoporphyrin IX in solution to the electrode. Assuming that the diameter of the base of the four-helix bundle is about 25 Å, the theoretical surface concentration of densely packed cylindrical four-helix bundles is around 2.7×10^{-11} mol cm^{-2}. Thus, we conclude that the resulting coverage by the four-helix bundles corresponds to an almost densely packed monolayer configuration.

Figure 1 B shows the differential pulse voltammetry waves of the monolayer upon interaction with Fe^{III}–protoporphyrin IX for different time intervals. It is evident that the heme site exhibiting the slightly more negative redox potential reconstitutes more slowly into the synthetic protein. The results indicate that the individual redox potentials of the heme sites can be tuned by the protein environment at the binding site.

Figure 2 A depicts the chronoamperometric response of the heme-reconstituted protein monolayer. For the two heme sites, positioned at different distances, a biexponential decay of the current is expected, where the fast electron transfer should occur to the heme positioned close to the electrode.[14]

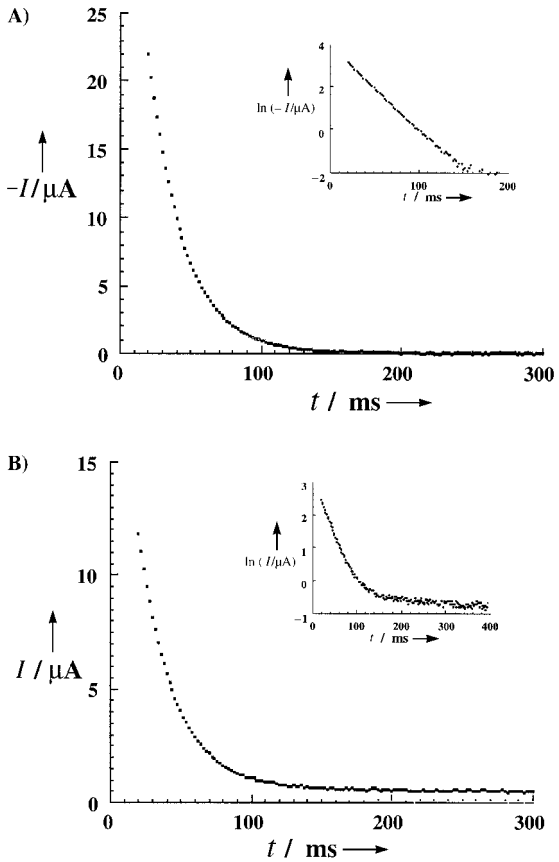
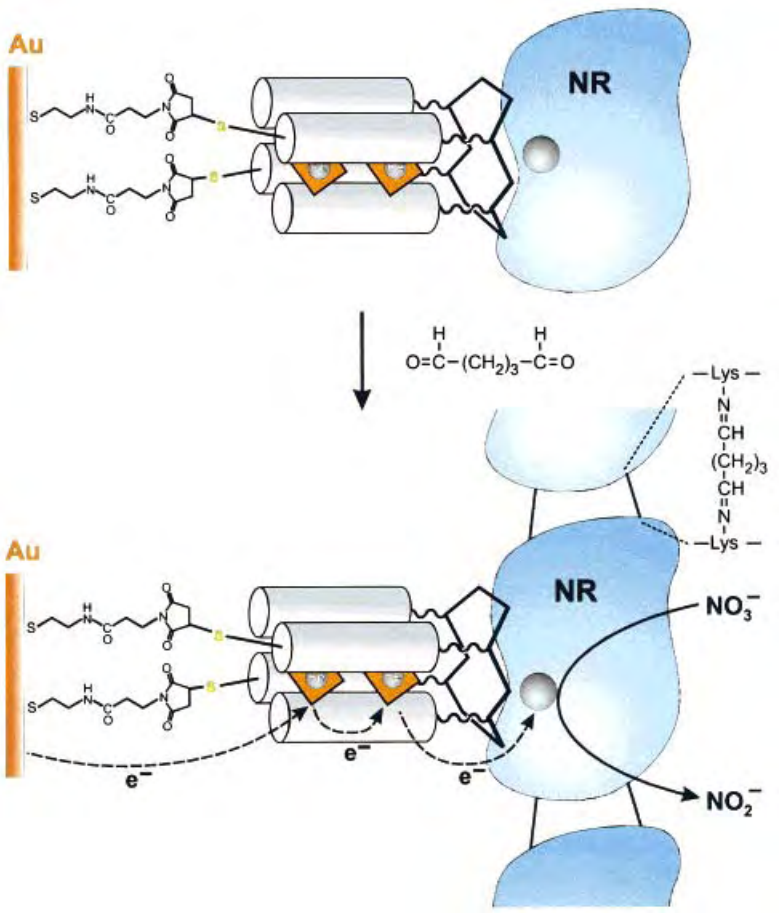


Figure 2. A) Chronoamperometric response upon reduction of the monolayer of the Fe^{III}–protoporphyrin IX reconstituted synthetic protein on the electrode (potential step from -0.2 to -0.5 V vs. SCE). Inset: semilogarithmic analysis of the decay of the current upon reduction. B) Chronoamperometric response upon oxidation of the monolayer of the Fe^{III}–protoporphyrin IX reconstituted synthetic protein on the electrode (potential step from -0.6 to -0.3 V vs. SCE). Inset: Semilogarithmic analysis of the decay of the current upon oxidation. All experiments were performed in 0.1 M phosphate buffer (pH 7.0) at 25 °C. I = current, E = potential vs. SCE.

 © WILEY-VCH Verlag GmbH, D-69451 Weinheim, 1998 1433-7851/98/3723-3254 $ 17.50+.50/0

The resulting transient current, however, follows a single-exponent electron transfer rate (inset of Figure 2A). This is attributed to a vectorial electron transfer in the bifunctional Fe^{III}–protoporphyrin IX array (Scheme 1). The rate constant for single electron transfer corresponds to the fast electron transfer to the heme site close to the electrode. Secondary, fast electron transfer to the second heme center that is mediated by the heme site close to the electrode competes with long-range direct electron transfer from the electrode to the second heme site. As a result, the rate of reduction of the bifunctional assembly is controlled by the rate of electron transfer to the heme center close to the electrode. These results imply that the heme center exhibiting the more negative potential is positioned close to the electrode, which results in the electron transfer cascade. Thus, the fact that the Fe^{III}–protoporphyrin unit exhibiting the more negative potential reconstitutes more slowly into the protein can be explained by the hindrance involved in the binding of the heme positioned close to the electrode surface. This conclusion, with regard to the vectorial electron transfer cascade in the synthetic hemoprotein, is supported by following the chronoamperometric response to the oxidation of the reduced assembly (Figure 2B). The oxidation involves a biexponential decay of the current with two components, one for a fast electron transfer ($k = 40\ s^{-1}$) and one for a slow electron transfer ($k = 1\ s^{-1}$; inset of the Figure 2B). The rate of the fast electron transfer is identical to that observed in the reduction, and hence corresponds to the oxidation of the Fe^{II}–heme site close to the electrode surface. The rate of the slow electron transfer is attributed to the oxidation of the remote Fe^{II} center. The slow electron transfer is detected, since the heme center close to the electrode cannot mediate the oxidation due to its more negative redox potential. Thus, the bifunctional heme–de novo protein assembly represents elements of a bioelectronic rectifier. Vectorial electron transfer proceeds effectively in the system due to appropriate ordering of the reduction potentials of the heme centers. The back electron transfer to the electrode is retarded since the primary heme site, close to the electrode, acts as a barrier for the oxidation process.



Scheme 2. Assembly of the integrated layered electrode composed of nitrate reductase (NR) and the Fe^{III}–protoporphyrin IX reconstituted synthetic protein.

The electrically contacted de novo hemoprotein monolayer associated with the electrode activates electron transfer to native redox proteins, and stimulates bioelectrocatalyzed transformations. Interaction of the synthetic bifunctional hemoprotein monolayer on the electrode with the native cytochrome-dependent nitrate reductase (NR; E.C. 1.9.6.1 from *E. coli*) results in the formation of an affinity complex (Scheme 2). Evidence for this was provided by microgravimetric quartz crystal microbalance studies. The association of nitrate reductase to the cyclic scaffold of the protein is supported by the fact that the de novo protein is in a densely packed configuration. The resulting affinity complex was cross-linked with glutaric dialdehyde to yield a stable and integrated bioelectrocatalytically active electrode.

Figure 3 shows the cyclic voltammogram of the resulting integrated enzyme electrode. The electrocatalytic cathodic current observed in the presence of added nitrate (NO_3^-) indicated the bioelectrocatalyzed reduction of NO_3^- at the potential characteristic of the synthetic hemoprotein. Control experiments revealed that no bioelectrocatalyzed reduction of NO_3^- occurs in the absence of NR, or upon direct coupling of the native biocatalyst (NR) to the base monolayer of maleimide on the electrode. Thus, the synthetic hemoprotein associated with the electrode stimulates electron transfer to NR, and the mediated electron transfer activates the bioelectrocatalyzed reduction of NO_3^-. The amperometric response of the integrated bioelectrocatalytic electrode is controlled by the concentration of nitrate (inset of Figure 3).

In conclusion, we have addressed the assembly of a bifunctional Fe^{III}–protoporphyrin de novo protein monolayer on a Au electrode, and demonstrated the electrical

 © WILEY-VCH Verlag GmbH, D-69451 Weinheim, 1998 1433-7851/98/3723-3255 $ 17.50+.50/0

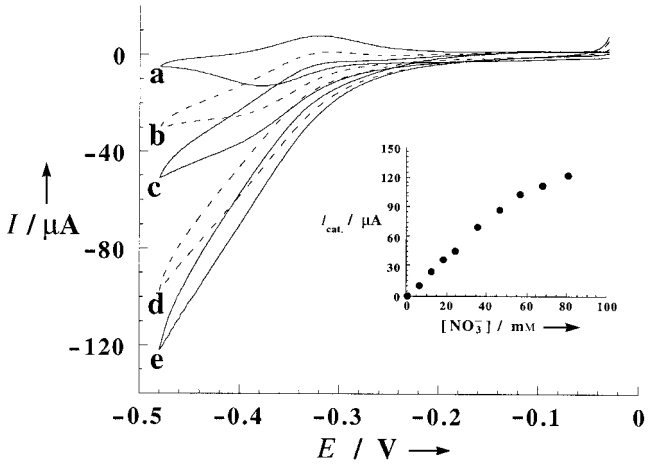


Figure 3. Cyclic voltammograms of the integrated layered electrode composed of cross-linked nitrate reductase and the Fe^{III}–protoporphyrin IX reconstituted de novo protein at NO_3^- concentrations of 0 (a), 12 (b), 24 (c), 46 (d), and 68 mM (e) (scan rate 5 mV s^{-1}). Inset: Calibration curve for the amperometric responses (at −480 mV vs. SCE) of the electrode at different NO_3^- concentrations. All experiments were performed in 0.1 M phosphate buffer (pH 7.0) at 25 °C; electrode geometrical area 0.2 cm^2, roughness factor ≈20. I = current, E = potential vs. SCE.

contacting of the synthetic redox protein with the conductive support. We presented the organization of the synthetic redox protein by the reconstitution of Fe^{III}–protoporphyrin IX into the protein, and discussed the use of this functionalized electrode for bioelectronic applications. Specifically, we demonstrated the activity of the electrically contacted bifunctional synthetic heme as a bioelectronic rectifier and as a base interface to organize integrated enzyme electrodes for biosensor applications. The potential perspectives of such reconstituted, electrically contacted de novo proteins seem to be very broad as the function of the de novo protein can be tuned and tailored within the synthetic protocol.

Received: June 8, 1998 [Z11957IE]
German version: *Angew. Chem.* **1998**, *110*, 3443–3447

Keywords: biosensors · electron transfer · enzyme catalysis · monolayers · proteins

[1] W. Göpel, *Biosens. Bioelectron.* **1995**, *10*, 35–59.
[2] a) P. N. Bartlett in *Biosensor Technology, Fundamentals and Applications* (Eds.: R. P. Buck, W. E. Hatfield, M. Umaña, E. F. Bowden), Marcel Dekker, New York, **1990**, chap. 7, pp. 95–115; b) A. Heller, *J. Phys. Chem.* **1992,** *96*, 3579–3587; c) I. Willner, E. Katz, B. Willner, *Electroanalysis* **1997,** *9*, 965–977; d) E. Katz, V. Heleg-Shabtai, B. Willner, I. Willner, A. F. Bückmann, *Bioelectrochem. Bioenerg.* **1997,** *42*, 95–104.
[3] a) I. Willner, G. Arad, E. Katz, *Bioelectrochem. Bioenerg.* **1998**, *44*, 209–214; b) I. Willner, E. Katz, F. Patolsky, A. F. Bückmann, *J. Chem. Soc. Perkin Trans. 2* **1998**, 1817–1822.
[4] a) I. Willner, *Acc. Chem. Res.* **1997**, *30*, 347–356; b) I. Willner, B. Willner, *Bioelectrochem. Bioenerg.* **1997**, *42*, 43–57; c) I. Willner, S. Rubin, *Angew. Chem.* **1996**, *108*, 419–439; *Angew. Chem. Int. Ed. Engl.* **1996**, *35*, 367–385; d) I. Willner, E. Katz, B. Willner, R. Blonder, V. Heleg-Shabtai, A. F. Bückmann, *Biosens. Bioelectron.* **1997**, *12*, 337–356.
[5] a) Y. Degani, A. Heller, *J. Am. Chem. Soc.* **1988**, *110*, 2615–2620; b) W. Schuhmann, *Biosens. Bioelectron.* **1995**, *10*, 181–193; c) I. Willner, N. Lapidot, A. Riklin, R. Kasher, E. Zahavy, E. Katz, *J. Am. Chem. Soc.* **1994**, *116*, 1428–1441.
[6] a) A. Heller, *Acc. Chem. Res.* **1990**, *23*, 128–134; b) I. Willner, E. Katz, N. Lapidot, P. Bäuerle, *Bioelectrochem. Bioenerg.* **1992**, *29*, 29–45.
[7] I. Willner, V. Heleg-Shabtai, R. Blonder, E. Katz, G. Tao, A. F. Bückmann, A. Heller, *J. Am. Chem. Soc.* **1996**, *118*, 10321–10322.
[8] a) A. Bardea, E. Katz, A. F. Bückmann, I. Willner, *J. Am. Chem. Soc.* **1997**, *119*, 9114–9119; b) V. Heleg-Shabtai, E. Katz, S. Levi, I. Willner, *J. Chem. Soc. Perkin Trans. 2* **1997**, 2645–2651; c) V. Heleg-Shabtai, E. Katz, I. Willner, *J. Am. Chem. Soc.* **1997**, *119*, 8121–8122.
[9] a) W. F. DeGrado, Z. R. Wassermann, J. D. Lear, *Science* **1989**, *243*, 622–628; b) M. Mutter, S. Vuilleumier, *Angew. Chem.* **1989**, *101*, 551–571; *Angew. Chem. Int. Ed. Engl.* **1989**, *28*, 535–554; c) J. W. Bryson, S. F. Betz, H. S. Lu, D. J. Suich, H. X. Zhou, K. T. O'Neil, W. F. DeGrado, *Science* **1995**, *270*, 935–941; d) R. B. Hill, W. F. DeGrado, *J. Am. Chem. Soc.* **1998**, *120*, 1138–1145; e) B. R. Gibney, S. E. Mulholland, F. Rabanal, P. L. Dutton, *Proc. Natl. Acad. Sci. USA* **1996**, *93*, 15041–15046.
[10] a) C. T. Choma, J. D. Lear, M. J. Nelson, P. L. Dutton, D. E. Robertson, W. F. DeGrado, *J. Am. Chem. Soc.* **1994**, *116*, 856–865; b) D. E. Robertson, R. S. Farid, C. C. Moser, J. L. Urbauer, S. E. Mulholland, R. Pidikiti, J. D. Lear, A. J. Wand, W. F. DeGrado, P. L. Dutton, *Nature* **1994,** *368*, 425–432; c) F. Rabanal, W. F. DeGrado, P. L. Dutton, *J. Am. Chem. Soc.* **1996**, *118*, 473–474; d) F. Arai, K. Kobata, H. Mihara, T. Fujimoto, N. Nishino, *Bull. Chem. Soc. Jpn.* **1995**, *68*, 1989–1998.
[11] M. Mutter, E. Altmann, K.-H. Altmann, R. Hersperger, P. Koziej, K. Nebel, G. Tuchscherer, S. Vuilleumier, H. U. Gremlich, K. Müller, *Helv. Chim. Acta* **1988**, *71*, 835–847.
[12] H. K. Rau, W. Haehnel, *J. Am. Chem. Soc.* **1998**, *120*, 468–476.
[13] From the surface coverage of the base monolayer of maleimide (4.8×10^{-11} mol cm^{-2}), we estimate an average intermolecular distance of 18 Å between the residues. This value is almost identical to the distance separating the two helices carrying the cysteine sites, and hence a bifunctional linkage of the de novo protein is assumed.
[14] E. Katz, I. Willner, *Langmuir* **1997**, *13*, 3364–3373.

 © WILEY-VCH Verlag GmbH, D-69451 Weinheim, 1998 1433-7851/98/3723-3256 $ 17.50+.50/0

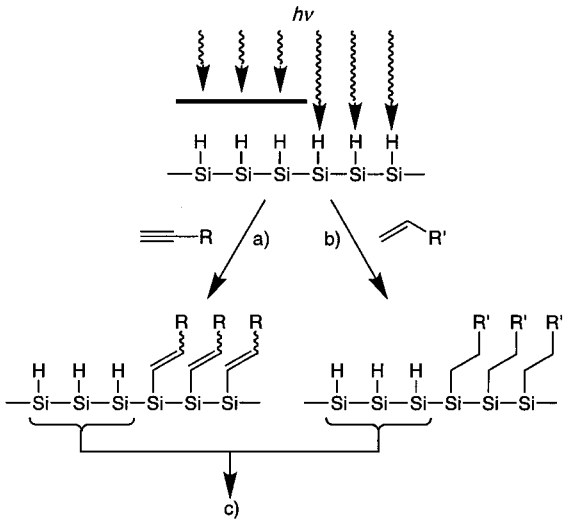
Photopatterned Hydrosilylation on Porous Silicon**

Michael P. Stewart and Jillian M. Buriak*

Porous silicon (por-Si) is a material produced by the anisotropic anodic or chemical corrosion of crystalline silicon by hydrofluoric acid.[1] The resulting hydride-passivated surface is populated with Si–H_x bonds ($x = 1, 2, 3$), exposed Si–Si bonds, and defects such as open valence, "dangling" Si atoms.[2] The por-Si material is composed of this surface, sublaminal nanocrystalline Si, and 55–95% empty space.[1] The report of visible photoluminescence (PL) in 1990[3] has attracted interest in the integration[4] of efficient[5] light-emitting por-Si devices into extant and future Si processing for high-speed, optoelectronic systems. We have been developing strategies for improved passivation of the por-Si surface and its effects on PL and chemical stability.

Recent developments in the functionalization of porous silicon have enabled Si–C bonds to be formed on the por-Si surface by attacking the weak Si–Si bonds of exposed nanocrystalline submaterial with Grignard[6] or alkyllithium[7] reagents. Grignard and alkyllithium transmetallation,[8] and the use of Lewis acid catalysis[9] have been used to exploit the large population of surface Si–H bonds. Thermal,[10] radical-mediated,[11] and UV photolytic[12, 13] alkene hydrosilylation is known on flat Si(100) and Si(111) hydride surfaces.

We now report that it is possible to achieve efficient functionalization of the por-Si surface through white light promoted hydrosilylation of unsaturated C–C bonds at 25 °C (Scheme 1). The light used for the functionalization is derived from an ordinary tungsten ELH light source of moderate intensity (0.22–44 mW cm^{-2}); a neat substrate is added to the surface under an inert atmosphere and the excess washed off after exposure times as short as 15 min. FT-IR transmission spectra of surfaces (Figure 1) prepared through hydrosilylation of 1-dodecene (surface **1**), 1-dodecyne (surface **2**), and styrene (surface **3**) are shown in Figure 2. The degree of incorporation of 1-dodecyne, determined at a constant exposure time (30 min), was dependent upon the light intensity at the sample (Figure 3). Low levels of substitution were observed for control experiments in the absence of light. Photoluminescence is largely retained after functionalization, which is essential for optoelectronic applications. Surfaces **1** and **2** show an average PL intensity of 97 ± 10% and 61% ± 10%,[14] respectively, relative to freshly prepared por-Si samples. A red shift of approximately 10 nm is observed in the maximum PL wavelength of functionalized samples as demonstrated in Figure 4 for surface **1**. Surfaces **1** and **2** are chemically stable to extended treatment (30 min) in boiling aerated, aqueous KOH (pH 10) solution. This is by far the simplest and most economical functionalization and stabilization strategy yet reported.



Scheme 1. White light promoted hydrosilylation on por-Si. By using a mask (black line) to protect part of the surface, the remaining surface can be functionalized with alkynes (a) or alkenes (b) before either dissolution of the unfunctionalized region in alkali or by hydrosilylation with a different substrate (c).

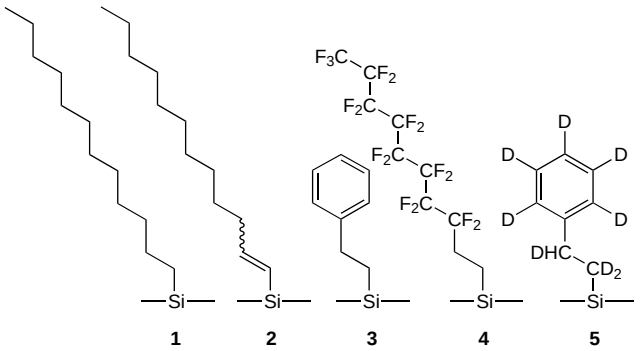


Figure 1. Surfaces prepared through white light promoted hydrosilylation on por-Si.

A very useful regiospecific application of the light-promoted hydrosilylation reaction involves alkyl substitution of the por-Si surface through photopatterning.[15] A white light pattern is focused on a por-Si sample to which neat liquid alkene or alkyne has been applied. After reaction times of 15 min or longer, alkyl incorporation in the illuminated areas can clearly be identified under PL conditions. Functionalized regions appear redshifted relative to nonfunctionalized regions as demonstrated by Figures 5a and 5b for the 1-dodecyne (surface **2**) and 1-dodecene (surface **1**) reacted surfaces, respectively. Photopatterning conducted with simple laboratory apparatus and a reducing lens (f/75) can achieve 40 μm resolution (25.0 lines mm^{-1}) between light and dark areas from a focused USAF 1951 resolution target.[16] Si lithography can be accomplished by treatment of the photopatterned sample in a boiling solution of alkaline KOH (pH 12, 15 s),

[*] Prof. Dr. J. M. Buriak, M. P. Stewart
Department of Chemistry
Purdue University
West Lafayette, IN 47907-1393 (USA)
Fax: (+1) 765-494-0239
E-mail: buriak@purdue.edu

[**] This work was supported by Purdue University, the Purdue Research Foundation, a Camille and Henry Dreyfus New Faculty Award (J.M.B.), and a pre-doctoral stipendium from the Link Foundation (M.P.S.). The groups of Professors Ben Amotz, Fenniri, and Lytle are thanked for optical and photographic assistance.

 © WILEY-VCH Verlag GmbH, D-69451 Weinheim, 1998 1433-7851/98/3723-3257 $ 17.50+.50/0

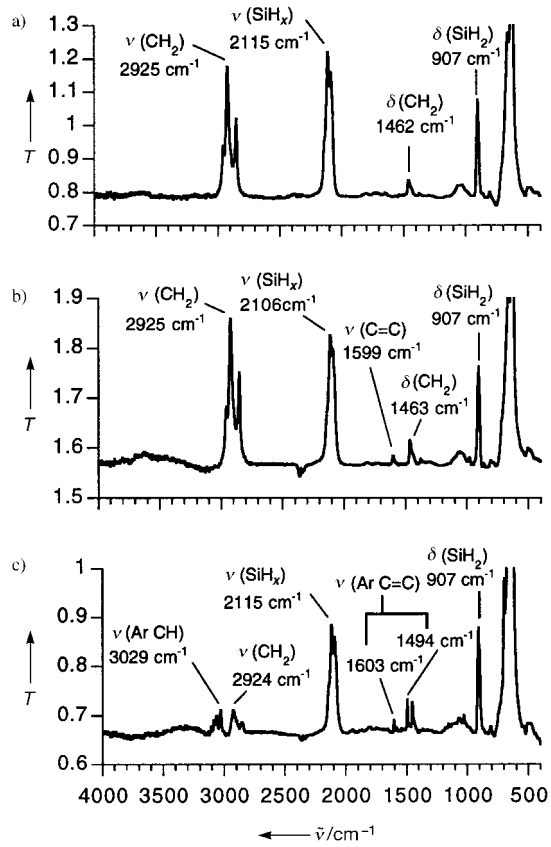


Figure 2. Transmission FT-IR spectra of surfaces **1** (a), **2** (b), and **3** (c), after 60 min at a light intensity of 22 mW cm^{-2}, 44 mW cm^{-2}, and 44 mW cm^{-2}, respectively. T = transmission.

which destroys normal por-Si[17] but leaves functionalized por-Si intact (Figures 5c, d). A por-Si sample was functionalized with two different types of substrates by illuminating half of a wafer while it was treated with neat styrene. After reaction excess styrene was washed off, the entire sample treated with 1-dodecene, and the second half exposed to light. FTIR spectra of the two sides showed almost exclusively phenethyl and dodecyl incorporation, respectively (Figure 6).

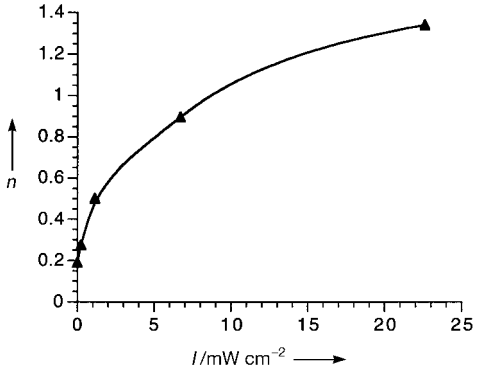


Figure 3. Relationship between incorporation and light intensity I for 1-dodecyne hydrosilylation on por-Si. The peak intensity of the $\nu_{as}(CH_2)$ vibration at 2925 cm^{-1} was used to determine the level of incorporation n. Because different samples were prepared for each data point, each was normalized with respect to the $\nu(Si{-}H_x)$ peak intensity at 2100 cm^{-1} before the hydrosilylation reaction so that absolute intensities of $\nu_{as}(CH_2)$ could be compared.

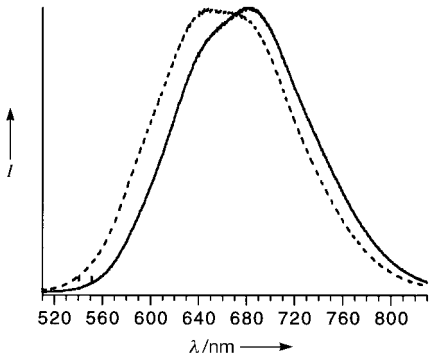


Figure 4. PL spectra of freshly etched por-Si (dotted line), and of por-Si after 60 min hydrosilylation with 1-dodecene and illumination with white light at an intensity of 22 mW cm^{-2} (surface **1**, solid line). I = intensity.

Preliminary mechanistic explorations suggest alkene and alkyne hydrosilylation on the surface of por-Si. By using [D_8]styrene as a substrate (surface **5**), a molecule with no C–H bonds, hydrosilylation was observed by the appearance of methylene vibrations at $\tilde{\nu}_{CD-H} = 2917$ and 2846 cm^{-1} in the IR spectrum,[18] which indicates the transfer of a surface hydride

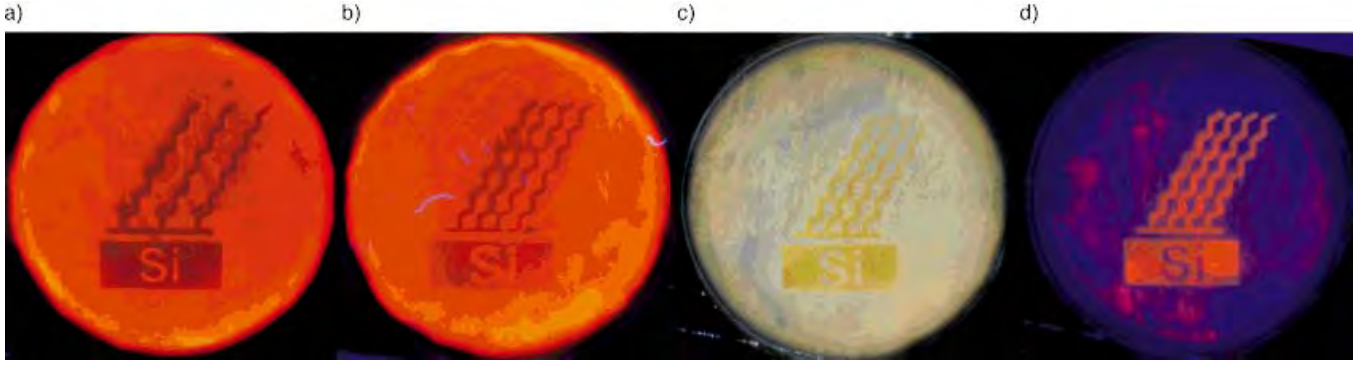


Figure 5. Photographs of por-Si samples (12 mm diameter) prepared through light-promoted hydrosilylation of 1-dodecyne (surface **2**) and 1-dodecene (surface **1**) through masking procedures. (a) The functionalized section of surface **2** appears as the darkened, red-shifted patterned area when illuminated with a 365 nm hand-held UV lamp. The other areas of the wafer are unfunctionalized (native Si–H termination). (b) Surface **1** (redshifted patterned area) upon illumination with 365 nm light. (c) Sample from (b) after boiling in aerated, aqueous KOH solution (pH 12) for 15 seconds. The unfunctionalized porous silicon (grey area) has dissolved, while the hydrosilylated surface (surface **1,** golden area) remains intact. (d) Illumination of the surface from (c) with a 365 nm hand-held UV lamp. The PL of the hydrosilylated area (surface **1**) remains intact while most of the unfunctionalized PL is destroyed.

 © WILEY-VCH Verlag GmbH, D-69451 Weinheim, 1998 1433-7851/98/3723-3258 $ 17.50+.50/0

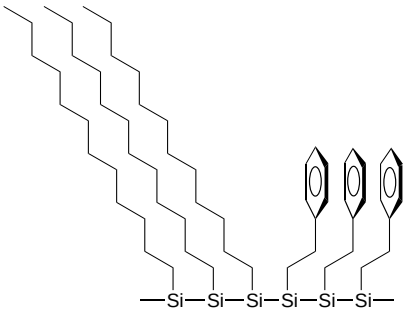


Figure 6. Two halves of a por-Si surface functionalized separately with 1-dodecene and styrene.

to the perdeuterated olefin. Difference transmission FT-IR spectra taken before and after hydrosilylation clearly indicate consumption of the Si–H groups. The role of the white light may be either to generate Si radicals by cleavage of weak Si–H bonds on the surface[13, 19] or to produce photogenerated holes on the surface that are subsequently attacked by alkyne or alkene nucleophiles.[20, 21] The observation that electron-deficient alkynes (phenylacetylene, 4-methylphenylacetylene and 4-chlorophenylacetylene) require longer reaction times (12 h) suggests a mechanism that involves nucleophilic attack. Dangling bonds present on freshly prepared porous silicon can also react with alkenes and alkynes, which accounts for the weak incorporation observed when the hydrosilylation reaction is allowed to proceed in the absence of light.[20] Monochromatic light promoted hydrosilylation of 1-dodecyne at 450, 550, and 650 nm (1 h, 1.8×10^{15} photons $cm^{-1} s^{-1}$) showed decreasing substitution with increasing wavelength.[22] The temperature of the silicon wafer during the photochemical reaction, monitored with a thermocouple, showed little change (maximum increase of 2 °C after 1 h at 22 mW cm^{-2}), which indicates that thermal activation is not an important factor. The nature of the solvent had no effect on the degree of incorporation as demonstrated by using solutions of 1-dodecyne (20%) in hexanes, toluene, CH_2Cl_2, and 0.1 M $N(n\mathrm{Bu})_4PF_6$ (in CH_2Cl_2).

If functionalized por-Si is to be involved in integratated circuit fabrication, minimal process interference would be advantageous. Photochemical activation of the por-Si surface to effect functionalization is a one-step reaction that avoids the costs and chemical hazards of using highly active organometallic reagents and, as the amount of heating is negligible, observes a minimal thermal budget.[23]

Experimental Section

FT-IR spectra were collected with a Perkin–Elmer 2000 spectrometer in transmission mode, typically at 4 cm^{-1} resolution with 16 to 32 scans collected. Reagents obtained from commercial sources were sparged with argon and filtered over anhydrous alumina in the glove box before use. Light intensities were measured with a hand-held radiometer (Metrologic).

Por-Si material was prepared from polished crystalline silicon wafers (n-type, P-doped, (100), 0.70 Ω cm; Transition Technology International). The etching was carried out in a solution of HF/H_2O (24/24/52) ethanol with either a 0.28 cm^2 or 1.1 cm^2 area exposed for 3 min at +71.4 mA cm^{-2} (0.28 cm^2) or +59.0 mA cm^{-2} (1.1 cm^2) and with white light illumination of ~25 mW cm^{-2} from a ELH W bulb (300 W; General Electric). After anodization the samples were washed with ethanol and blown dry under a nitrogen stream.

Hydrosilylation reactions: Typically, a 0.28 cm^2 etched wafer, still in the etching cell, was placed into the glove box. The substrate was added (100 μL) to the surface directly, followed if necessary by the solvent (400 μL). A ChemGlass window (borosilicate) was sealed with a Viton O-ring over the etching cell reservoir and clamped. The etching lamp was used as a light source with an intensity of 22.4 mW cm^{-2} at the sample. A thermocouple was assembled with the cell and mounted against the back of the wafer in experiments where the temperature was monitored. In wavelength-dependent studies, a single-grating monochromator (Bausch and Lomb) was used to isolate wavelengths to ~5 nm with transmittance of extraneous wavelengths at approximately 10^{-4}.

Photoluminescence (steady state) measurements: An Oriel 250 W mercury arc lamp and a Bausch and Lomb monochromator was set to 440 nm with a 450 nm SWP filter (CVI SPF450) as the excitation source, which gave an intensity of 0.2 mW cm^{-2} at the sample. Luminescence was passed through a 490 nm LWP filter (CVI LP490) into an Acton Research Spectra Pro 275 monochromator (0.275 m) and a Princeton Instruments CCD detector (model LN/CCD-1024-E/1) cooled with liquid nitrogen.

Photopatterning: Light from the W etching lamp was passed through a condenser lens onto a mirrored surface and was directed down toward a negative pattern approximately 30 cm from the light source. An achromatic lens (f/75) was positioned about 10 cm below the pattern and about 8 cm above the sample on the laboratory jack. The position of the second lens and the jack surface were manipulated to give the best focused pattern visible on the sample with a magnifying glass. All attempts were made to extinguish nonfocused light from the sample.

1H,1H,2H,2H-Perfluorodecyl terminated surface **4** IR: $\tilde{\nu}_{as}(CH_2) = 2921$, $\tilde{\nu}_{s}(CH_2) = 2854$, $\tilde{\nu}(SiH_2) = 2114$, $\tilde{\nu}(SiH) = 2082$, $\delta_{as}(CH_2) = 1439$, $\delta_{s}(CH_2) = 1353$, $\tilde{\nu}_{as}(CF_3) = 1241$, $\tilde{\nu}_{as}(CF_2) = 204$, $\tilde{\nu}_{s}(CF_2) = 1147$, $\tilde{\nu}(SiO) = 1061$, $\delta_{s}(SiH_2) = 904$, $\delta(SiH_2) = 657$, $\delta(SiH) = 628$ cm^{-1}.[24]

[D_8]Phenethyl terminated surface **5** IR: $\tilde{\nu}_{as}(CD\text{-}H) = 2917$, $\tilde{\nu}_{s}(CD\text{-}H) = 2846$, $\tilde{\nu}(ArD) = 2273$, $\tilde{\nu}(CD_2) = 2187$, $\tilde{\nu}(SiH_2) = 2114$, $\tilde{\nu}(SiH) = 2082$, $\tilde{\nu}(Ar\text{-}C{=}C) = 1569$, $\delta_{as}(CD{-}H) = 1450$, $\delta_{s}(CD{-}H) = 1323$, $\tilde{\nu}(SiO) = 1105$, $\delta_{s}(SiH_2) = 907$, $\delta(SiH_2) = 661$, $\delta(SiH) = 623$ cm^{-1}.

Received: June 16, 1998 [Z11997IE]
German version: *Angew. Chem.* **1998**, *110*, 3447–3450

Keywords: hydrosilylations · luminescence · optoelectronics · photolithography · silicon

[1] A. G. Cullis, L. T. Canham, P. D. J. Calcott, *J. Appl. Phys.* **1997**, *82*, 909–965.
[2] H. J. von Bardeleben, D. Stievenard, A. Grosman, C. Ortega, and J. Siejka, *Phys. Rev. B* **1993**, *47*, 10899–10902.
[3] L. T. Canham, *Appl. Phys. Lett.* **1990**, *57*, 1046–1048.
[4] K. D. Hirschman, L. Tsybeskov, S. P. Duttagupta, P. M. Fauchet, *Nature* **1996**, *384*, 338–341.
[5] X. Sheng, H. Koyama, N. Koshida, *J. Vac. Sci. Technol. B* **1998**, *16*, 793–795.
[6] N. Y. Kim, P. E. Laibinis, *J. Am. Chem. Soc.* **1998**, *120*, 4516–4517.
[7] J. H. Song, M. J. Sailor, *J. Am. Chem. Soc.* **1998**, *120*, 2376–2381.
[8] C. Viellard, M. Warntjes, F. Ozanam, J.-N. Chazalviel, *Proc. Electrochem. Soc.* **1996**, *95*, 250–258.
[9] J. M. Buriak, M. J. Allen, *J. Am. Chem. Soc.* **1998**, *120*, 1339–1340.
[10] A. B. Sieval, A. L. Demirel, J. W. M. Nissink, M. R. Linford, J. H. van der Maas, W. H. de Jeu, H. Zuilhof, E. J. R. Sudholter, *Langmuir* **1998**, *14*, 1759–1768.
[11] M. R. Linford, P. Fenter, P. M. Eisenberger, C. E. D. Chidsey, *J. Am. Chem. Soc.* **1995**, *117*, 3145–3155.
[12] a) J. Terry, M. R. Linford, C. Wigren, R. Y. Cao, P. Pianetta, C. E. D. Chidsey, *Appl. Phys. Lett.* **1997**, 71, 1056–1058; b) C. E. D. Chidsey, *Abstr. Pap.* 215th ACS National Meeting, Dallas, **1998**, ANYL 083.
[13] F. Effenberger, G. Götz, B. Bidlingmaier, M. Wezstein, *Angew. Chem.* **1998**, *110*, 2651–2654; *Angew. Chem. Int. Ed.* **1998**, *37*, 2462–2464.

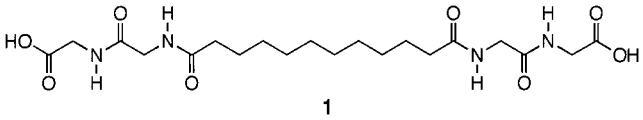
 © WILEY-VCH Verlag GmbH, D-69451 Weinheim, 1998 1433-7851/98/3723-3259 $ 17.50+.50/0

[14] Average of three samples for surface **1**, average of two samples for surface **2**.
[15] E. J. Lee, J. S. Ha, M. J. Sailor, *J. Am. Chem. Soc.* **1995**, *117*, 8295–8296.
[16] Resolution as observed through a microscope at 30 times magnification.
[17] T. Bischoff, G. Müller, W. Welser, F. Koch, *Sens. Actuators A* **1997**, *60*, 228–234.
[18] L. J. Bellamy, *The Infra-Red Spectra of Complex Molecules*, Methuen, New York, **1960**, p. 13.
[19] a) R. Walsh, *Acc. Chem. Res.* **1981**, *14*, 246–252; b) J. M. Kanabus-Kaminska, J. A. Hawari, D. Griller, C. Chatgilialoglu, *J. Am. Chem. Soc.* **1987**, *109*, 5267–5268; c) C. Chatgilialoglu, *Acc. Chem. Res.* **1992**, *25*, 188–194.
[20] J. L. Heinrich, A. Lee, M. J. Sailor, *Mater. Res. Soc. Symp. Proc.* **1995**, *358*, 605–610.
[21] O. Y. Okhlobystin, N. T. Berberova, *Dokl. Akad. Nauk. SSSR* **1993**, *332*, 599–600.
[22] The low incorporation observed at 650 nm is presumably almost exclusively a result of reaction with dangling bonds (ref. [20]) although migration of photogenerated excitons from the bulk into the porous layer may occur to a small extent: V. V. Doan, R. M. Penner, M. J. Sailor, *J. Phys. Chem.* **1993**, *97*, 4505–4508.
[23] R. P. S. Thakur, R. Singh, *Appl. Phys. Lett.* **1994**, *64*, 327–329.
[24] Y. H. Ogata, F. Kato, T. Tsuboi, T. Sakka, *J. Electrochem. Soc.* **1998**, *145*, 2439–2444.

Cross-Section Molecular Imaging of Supramolecular Microtubes with Contact Atomic Force Microscopy

Toshimi Shimizu,* Satomi Ohnishi, and Masaki Kogiso

Scanning probe microscopies, especially atomic force microscopy (AFM), are useful methods for obtaining molecularly resolved images of orientation and ordering in organic self-assemblies.[1, 2] In particular, AFM has been used to study two-dimensional, ordered organic molecules adsorbed on well-defined surfaces and at interfaces.[3] While there is an increasing number of studies on AFM imaging of biological macromolecules,[4–6] only a few reports[7–10] have described the morphologies and molecular orientation for synthetic supramolecular assemblies. However, no definitive information on these assemblies, especially along the molecular long axes, has been obtained at molecular resolution by AFM. Meanwhile, supramolecular self-organized fibers and their molecular arrangements have expertly been investigated with scanning and transmission electron microscopy.[11–13] We recently studied hydrogen bond directed self-assembly of chiral fibers[14] and microtubes[10, 15, 16] from synthetic sugar- and peptide-based bolaamphiphiles.[17] In light of the wide applicability of AFM, we explored vertical profiles along the molecular long axes within the microtube[15] made up of glycylglycine bolaamphiphile **1**. Here we report a molecularly resolved layered structure within the tube membranes that was observed by contact AFM in air.



1

Figure 1 a shows a nonfiltered AFM image (19 μm × 19 μm) of supramolecular vesicle-encapsulated microtubes made up of **1**. We can observe a clear image similar to that obtained with phase-contrast and dark-field light microscopies (Figure 1 b). Spherical, brighter portions (denoted by arrows in Figure 1 a) correspond to topographically higher regions, and

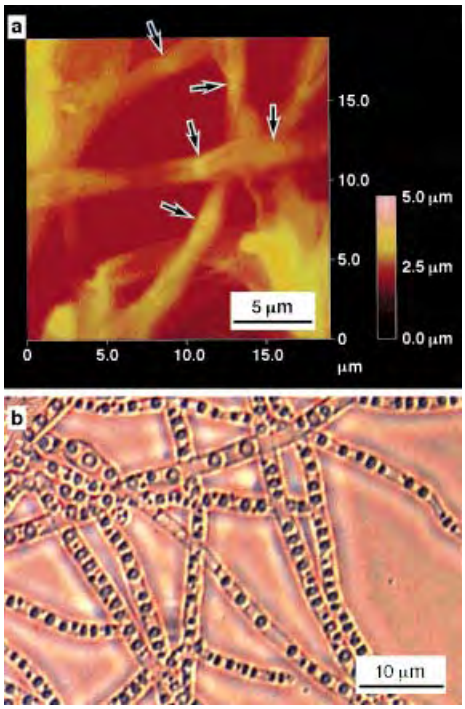


Figure 1. a) AFM height image (19 μm × 19 μm) of vesicle-encapsulated microtubes (denoted by arrows) made up of **1** and b) phase-contrast light micrograph of the microtubes (at 25 °C in water).

indicate the encapsulation of vesicular assemblies in the compartment.[15] Cross-section analysis of the portions with and without vesicle encapsulation provided information on the thickness of the tube membranes; the value of less than 100 nm corresponds to less than 30–40 molecular layers.[10] In addition, a high-resolution AFM image of the tube surfaces also revealed a distorted hexagonal arrangement of the peptide head groups.[10] These findings indicate that AFM is a very useful tool for studying the molecular packing as well as the morphological dimensions of supramolecular assemblies.

The surface morphology of one tube is shown in Figure 2. The AFM image (1.45 μm × 1.45 μm) revealed a crack in the tube membrane. One can see a number of domains arranging like scales of a fish on the top of the tube as well as rodlike

[*] Dr. T. Shimizu, Dr. S. Ohnishi, M. Kogiso
National Institute of Materials and Chemical Research
1–1 Higashi, Tsukuba, Ibaraki 305–8565 (Japan)
Fax: (+81) 298-54-4422
E-mail: tshmz@ccmail.nimc.go.jp

 © WILEY-VCH Verlag GmbH, D-69451 Weinheim, 1998 1433-7851/98/3723-3260 $ 17.50+.50/0

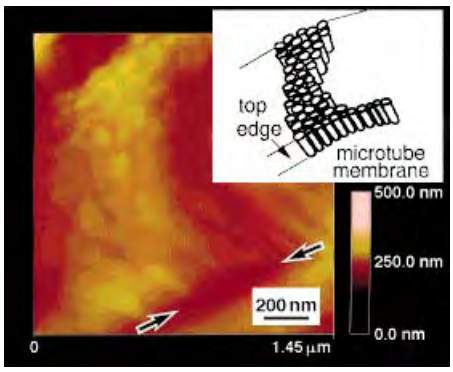


Figure 2. AFM height image (1.45 μm × 1.45 μm) of the microtube and the schematic illustration of the scalelike domains on the top and rodlike domains at the edge of the tube. A crack in the tube membrane is denoted by the arrows.

domains aligned parallel to the crack. The surfaces seem to have no homogeneous crystalline order on the micrometer scale. The diameters of the domains on the top of the tube are 20 – 100 nm, which agree well with the widths of the rodlike domains at the edge. This implies that columnar domains randomly assemble to construct the tube membranes (Figures 3a and 3b). Therefore, a high-resolution AFM image of the edge of the tube can be expected to directly provide

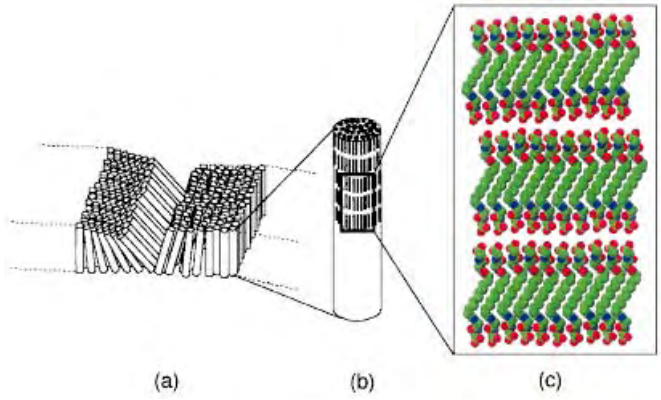


Figure 3. a) Microtube membrane composed of a number of columnar domains (b). c) A possible molecular alignment within a columnar domain.

information on the vertical molecular arrangement within the columnar domains. Such a crack in the tube membrane was frequently observed for this microtube. It occurs upon drying, not by deformation or damage due to interaction between the AFM tips and the tube membranes. The validity of this interpretation is supported by the AFM investigation in water. The dried microtubes swelled up again and exhibit no cracks when exposed to aqueous solution.

Figure 4 displays a high-resolution AFM image (friction mode, 8 nm × 8 nm) for the edge of the tube. The image revealed parallel rows with a spacing of approximately 0.44 – 0.50 nm. We always observed the same molecular orientation and alignment, regardless of the image position and scanning speed. One can see two brighter zones separated by a distance of 2.9 – 3.2 nm. Considering the bola structure of **1**, the layered brighter zone was assigned to a terminal peptide head groups.

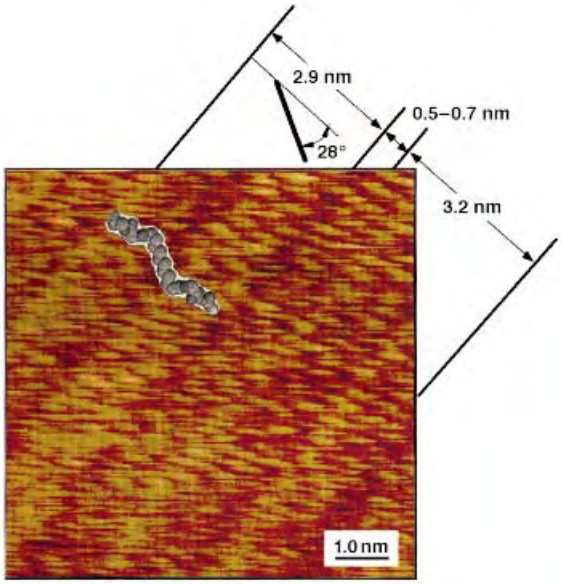


Figure 4. High-resolution AFM friction image (8.0 nm × 8.0 nm) of the edge of the tube.

In the AFM image, we can also find darker striations which correspond to the alkyl spacers. They align with their oligomethylene axes oriented at approximately 28° with respect to the normal of the layer plane. The image clearly shows that bolaamphiphilic molecules adopt a bent conformation at each end of the alkylene chain (Figure 3c). Relatively darker images at the middle of the molecules stem from smaller molecular volumes of the methylene group as compared with those of the peptide head groups. The observed features are in good accord with that in the crystal lattice (*ac* plane) of the same molecule.[18] Alternatively, we might be able to assign the layer zone to two sets of peptide head groups of neighboring layers adjacent to each other. The bolaamphiphilic molecules should then require crystalline dense packing through interlayer acid – acid hydrogen-bond formation. Furthermore, the evaluated molecular length (1.9 ± 0.1 nm) for this model is too short with respect to that obtained for the single crystal (2.72 nm). Therefore, the possibility of this molecular arrangement would be ruled out.

The distance between two head groups of neighboring layers varies from 0.5 to 0.7 nm. This finding implies that intralayer interactions rather than interlayer interactions determine the supramolecular tube structure. This also suggests the predominance of intralayer acid – anion hydrogen-bond networks in the microtube, as supported by FT-IR studies.[10, 15] Interlayer interactions between the head groups will enforce crystalline order to form a three-dimensional crystal.[16, 18] Only one single-crystal analysis has been so far reported for a long-chain carboxylate with a potassium cation.[19] The carboxylate groups of potassium palmitate face each other with a distance of approximately 0.3 nm. Therefore, the soap crystal sheet is extremely slippery due to the rejection of the charged carboxylate groups.[20] A similar situation can be imaged for the bolaamphiphile sheet within the supramolecular tube membranes by AFM. Actually, the monolayered sheets of **1** seems to be slightly distorted to form

 © WILEY-VCH Verlag GmbH, D-69451 Weinheim, 1998 1433-7851/98/3723-3261 $ 17.50+.50/0

a rippled structure. It has a good resemblance to the P_β phase observed for lecithin–water phases.[21]

In conclusion, by contact AFM we directly observed for the first time a hierarchical formation of structures (bent molecule–distorted layer–columnar domain) as a vertical profile of the microtube membranes.

Experimental Section

Supramolecular vesicle-encapsulated microtubes were prepared with a weak alkaline aqueous solution of glycylglycine bolaamphiphile **1** (10 mM, pH ≈ 8).[10] The formation of microtubes with uniform diameter (1.5–2.2 μm) was confirmed by phase-contrast and dark-field light microscopy (Figure 1b). Droplets (20–30 μL) of the solution containing the microtubes were placed with a pipette on to a clean glass substrate (Matsunami micro slide glass, precleaned, S-1111) and allowed to air-dry slowly (14 h) in an electric desiccator (Toyo Living auto dry, type FHO, humidity 15 ± 5 %). All AFM measurements were performed with a commercial atomic force microscope (Digital Instruments Inc., Santa Barbara, CA, Nanoscope IIIa) at room temperature in air. We used the contact-mode AFM with a microfabricated silicon nitride cantilever (spring constant 0.12 N m^{-1}). Images were recorded in the height or friction mode.

Received: May 5, 1998 [Z11821IE]
German version: *Angew. Chem.* **1998**, *110*, 3509–3511

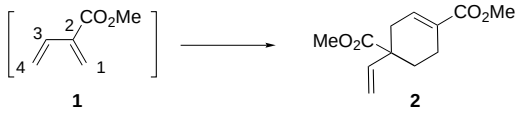
Keywords: amphiphiles · atomic force microscopy · hydrogen bonds · nanostructures · supramolecular chemistry

[1] H. G. Hansma, S. A. C. Gould, P. K. Hansma, *Langmuir* **1991**, *7*, 1051–1054.
[2] J. Y. Josefowicz, N. C. Maliszewskyi, S. H. J. Idziak, P. A. Heiney, J. J. P. McCauley, A. B. Smith III, *Science* **1993**, *260*, 323–326.
[3] S. Chiang in *Scanning Tunneling Microscopy I* (Eds.: R. Wiesendanger, H. J. Guntherodt), Springer, Berlin, **1991**, p. 181.
[4] S. M. Linsay in *Scanning Tunneling Microscope and Spectroscopy* (Ed.: D. A. Donned), VCH, New York, **1992**, p. 335.
[5] E. T. Kool, P. K. Hansma, M. Kashlev, S. Kasas, N. H. Thomson, B. L. Smith, H. G. Hansma, X. Zhu, M. Guthold, C. Bustamante, *Biochemistry* **1997**, *36*, 461–468.
[6] C. Bustamante, G. Zuccheri, S. H. Leuba, G. Yang, B. Samori, *Methods* **1997**, *12*, 73–83.
[7] I. Tuzov, K. Cramer, B. Pfannemuller, W. Kreutz, S. N. Magonov, *Adv. Mater.* **1995**, *7*, 656–659.
[8] K. Craemer, S. Demharter, R. Muelhaupt, H. Frey, S. N. Magonov, I. Tuzov, M.-H. Whangbo, *New. J. Chem.* **1996**, *20*, 5–11.
[9] K. Ariga, N. Yamada, M. Naito, E. Koyama, Y. Okahata, *Chem. Lett.* **1998**, 493–494.
[10] M. Kogiso, S. Ohnishi, K. Yase, M. Masuda, T. Shimizu, *Langmuir* **1998**, *14*, 4978–4986.
[11] J.-H. Fuhrhop, W. Helfrich, *Chem. Rev.* **1993**, *93*, 1565–1582.
[12] F. M. Menger, S. J. Lee, *J. Am. Chem. Soc.* **1994**, *116*, 5987–5988.
[13] C. F. v. Nostrum, R. J. M. Nolte, *Chem. Commun.* **1996**, 2385–2392.
[14] T. Shimizu, M. Masuda, *J. Am. Chem. Soc.* **1997**, *119*, 2812–2818.
[15] T. Shimizu, M. Kogiso, M. Masuda, *Nature* **1996**, *383*, 487–488.
[16] T. Shimizu, M. Kogiso, M. Masuda, *J. Am. Chem. Soc.* **1997**, *119*, 6209–6210.
[17] T. Shimizu, M. Masuda, M. Kogiso, M. Asakawa, *Kobunshi Ronbunsyu* **1997**, *54*, 815–828.
[18] M. Kogiso, M. Masuda, T. Shimizu, *Supramol. Chem.* **1998**, in press.
[19] J. H. Dumbleton, T. R. Lomer, *Acta. Crystallogr.* **1965**, *19*, 301–307.
[20] J.-H. Fuhrhop, J. Koening in *Membranes and Molecular Assemblies: The Synkinetic Approach,* The Royal Society of Chemistry, Cambridge, **1994**, p. 186.
[21] A. Tardieu, V. Luzzati, *J. Mol. Biol.* **1973**, *75*, 711–733.

A New Look at the Diels–Alder Transition State**

Claude Spino,* Marc Pesant, and Yves Dory*

In relation to the unexpectedly high reactivity of 2-carbomethoxy-1,3-butadiene (**1**) in Diels–Alder reactions (Scheme 1), we recently suggested the presence of a strong



1 **2**

Scheme 1. Dimerization of **1**. The reaction is fast at or below room temperature.

double-bond character between C2 and C3 in the transition state (TS).[1] To gain better insight into the mechanism of the Diels–Alder reaction, we reconstructed the whole butadiene–ethylene reaction pathway by means of the intrinsic reaction coordinate (IRC) approach.[2] Then, selected structures were extracted to obtain their orbitals, geometries, and energies. We were surprised to witness that the various orbital interactions do not occur simultaneously during the Diels–Alder reaction. The four-electron interaction of symmetric orbitals (Figure 1, green and red curves) begins well in advance at a distance of over 3.0 Å between the diene and dienophile.[3] By comparison the two-electron interaction between the antisymmetric orbitals (blue curve) commences at a distance near 2.4 Å! The reason behind this chronology is not yet clear. Remarkably though, many of the geometrical features observed in most (if not all) calculated concerted TS (Scheme 2) of the ethylene–butadiene reaction (and indeed of other systems) reflect perfectly this asynchronicity of molecular orbital interactions.[4] Shorter C2–C3 and longer C5–C6 bonds reflect an advanced $HOMO_{dienophile}-LUMO_{diene}$ interaction, while short C1–C2/C3–C4 and long forming σ bonds are indicative of an emerging $HOMO_{diene}-LUMO_{dienophile}$ interaction.[3] In effect, the long σ bonds reflect an early TS, while the well-developed C2–C3 π bond is reminiscent of a late TS, as we suggested earlier.[1]

Fukui's frontier molecular orbital (FMO) theory[5] has proved to be a valuable tool in predicting the rate and selectivity of organic reactions, in particular pericyclic reactions and cycloadditions.[6] This principle was used to predict

[*] Prof. C. Spino, Prof. Y. Dory, M. Pesant
Université de Sherbrooke
Département de Chimie
Sherbrooke, Qc, J1 K 2R1 (Canada)
Fax: (+1) 819-821-8017
E-mail: cspino@courrier.usherb.ca
ydory@aix1.si.usherb.ca

[**] We thank Prof. Jean Lessard for useful discussions. We acknowledge the Natural Sciences and Engineering Council of Canada for financial support. We thank Brett Bode for his great software MacMolPlt, which was used to display the orbital drawings of Figure 1.

Supporting information for this article is available on the WWW under http://www.wiley-vch.de/home/angewandte/ or from the author.

 © WILEY-VCH Verlag GmbH, D-69451 Weinheim, 1998 1433-7851/98/3723-3262 $ 17.50+.50/0

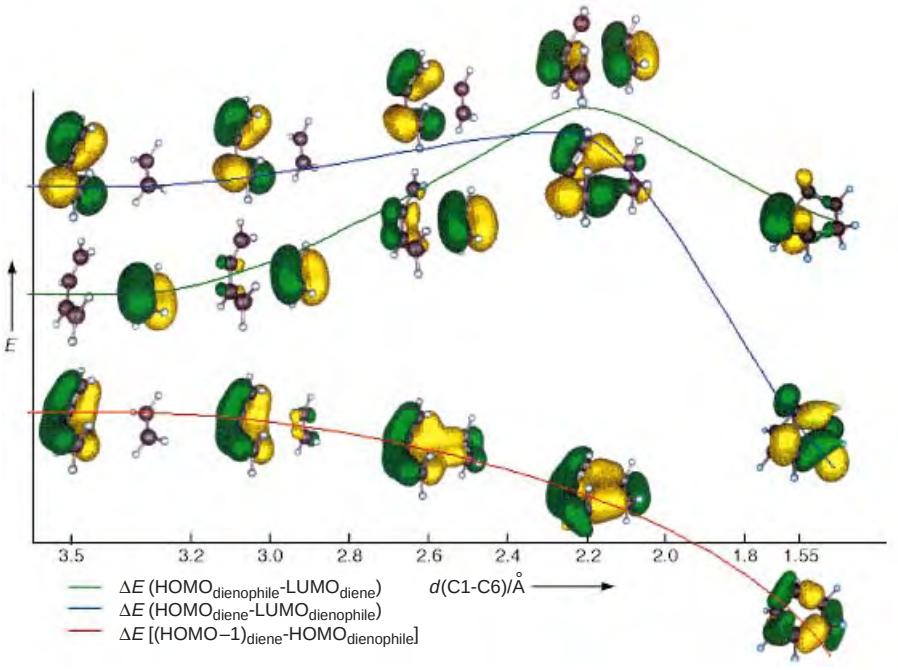
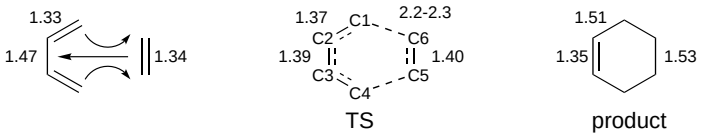


Figure 1. Energy profiles (approximately to scale) and chronology of orbital mixing for the three occupied π orbitals during the Diels–Alder reaction between butadiene and ethylene. For clarity, the total energy is not included.

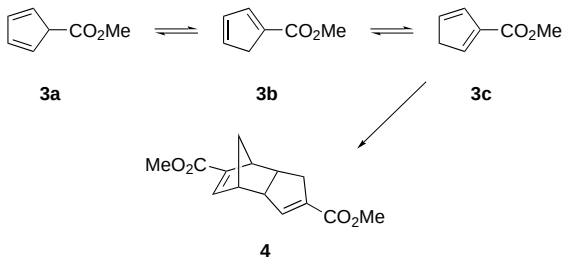


Scheme 2. Proposed formalism for the orbital interaction in Diels–Alder reactions (left) and typical bond lengths calculated for the transition state (TS) of the Diels–Alder reaction between ethylene and butadiene. On the right the bond lengths in the product are shown.

reactivity and selectivity issues in Diels–Alder reactions based on the strength of a single MO interaction, the "dominant" interaction. However, many reactions appear to disobey the FMO rules of regiochemistry[3] or reactivity,[7] including reactions of butadienes with conjugating substituents at C2 or C3.[1]

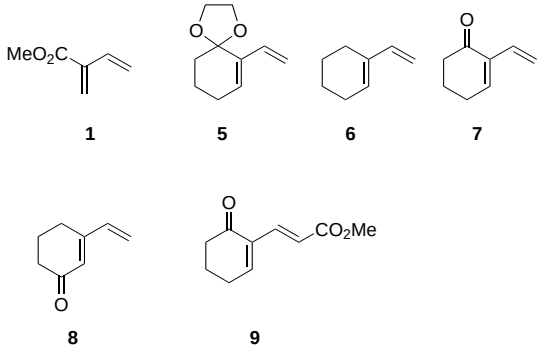
After examining Figure 1, we became convinced that the practice of taking only the dominant FMO interaction into account when assessing diene–dienophile reactivities is groundless in many cases. Our findings suggest two things: Firstly, the clearly well-developed C2–C3 π bond in the TS should allow conjugating substituents at C2 or C3 or aromatic systems (as in the *o*-quinodimethanes) to decrease the energy of the TS, supporting our earlier argument.[1] Secondly, predictions based on the energetic state of the initial HOMO$_{dienophile}$–LUMO$_{diene}$ interaction should be unreliable because this interaction is very different from that in the starting reagents. The drawing on the left of Scheme 2 expresses our perceptions of the orbital interactions in the Diels–Alder mechanism. We believe that this symbolism reflects the proper transfer of electrons in concerted [4+2] cycloadditions, especially those involving symmetrical partners.

The following three sets of experiments highlight some consequences of our findings in dealing with diene–dienophile reactivity. Earlier we had pointed out that the electron-deficient diene **1** is as or more reactive than electron-rich dienes (Scheme 1).[1] Many other dienes having conjugating substituents at C2 or C3—including cyano, sulfone, and ketone groups—are also highly reactive toward electron-deficient dienophiles.[8] Inukai and Kojima have reported that 2-cyanobutadiene is more reactive than isoprene, 2,3-dimethyl-1,3-butadiene, and 1,3-pentadiene in thermal Diels–Alder reactions with methyl acrylate.[9] This oddity is related to the well-known dimerization of methyl cyclopentadienylcarboxylate (**3**) to Thiele's ester (**4**, Scheme 3).[10] Diene **3a** should be more reactive, but only diene **3c** with the ester functionality in the 2-position gives an adduct with dienophile **3b**.



Scheme 3. Dimerization of **3**. The reaction is fast at or below room temperature.

Likewise, diene **7** was similar in reactivity to **5** or **6** with respect to various electron-poor dienophiles, while its analogue **8**, having the oxo group attached to C1, could not compete at all with any of the former dienes, including **7**. From



a FMO stand point, **7** and **8** should have displayed a similar reactivity.[6a] Moreover, dienes **8** and **9** competed for one equivalent of *N*-methylmaleimide to give a 45:55 mixture of

 © WILEY-VCH Verlag GmbH, D-69451 Weinheim, 1998 1433-7851/98/3723-3263 $ 17.50+.50/0

adducts favoring reaction with **9**. Dienes **7** and **9** are reactive because the conjugating ketone at the 2- or 3-position will decrease the overall energy of the TS through its capacity to stabilize the developing cycloadduct π bond.

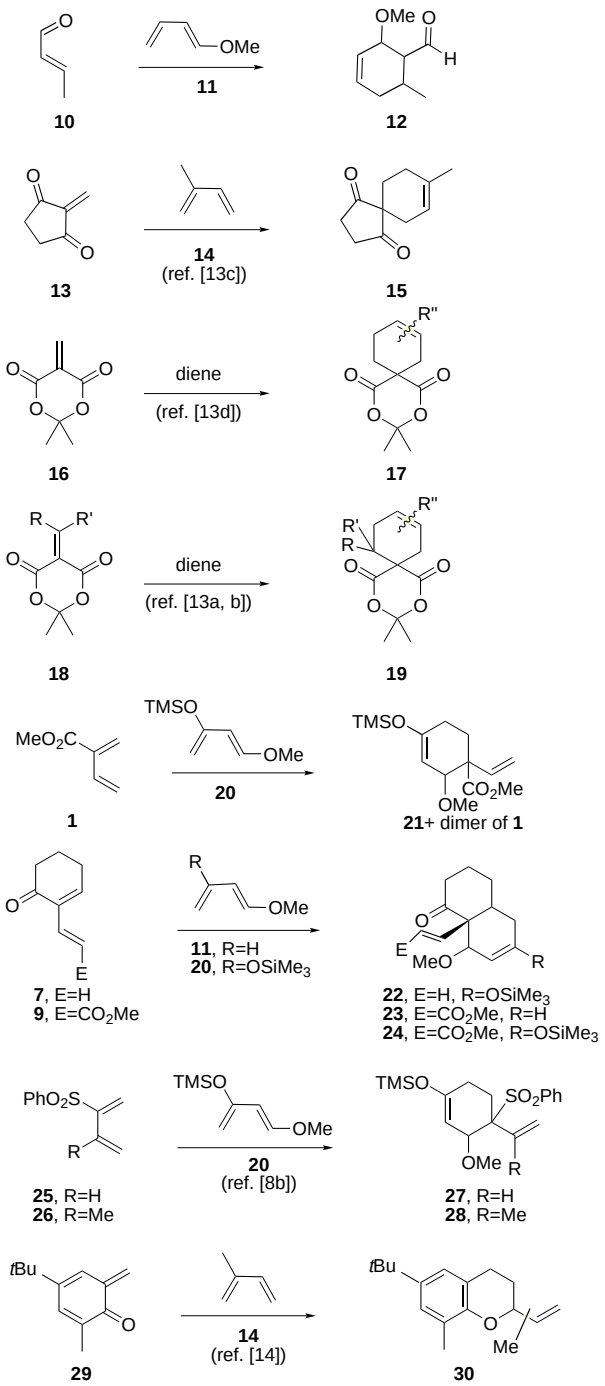
In the same vein, many electron-poor dienes reacted exclusively with electron-poor dienophiles even in the presence of electron-rich dienophiles. This has been previously demonstrated with diene **1**,[1, 11] but the trend held for many electron-poor dienes, for example **7**–**9**. In fact, for each of these three dienes, the reaction rate increased significantly with increasing electron deficiency of the dienophile (tetracyanoethylene > maleic anhydride > methyl vinyl ketone > ethyl vinyl ether).

The inability of the FMO theory to explain these cases may come from the fact that the dominant interaction is the $HOMO_{dienophile}-LUMO_{diene}$ interaction, leading to the cycloadduct π bond. As we said, predictive arguments based on the energetic state of the starting materials in this case is at least partly invalid. Therefore, the energy difference between the ground-state HOMOs of the electron-poor and the electron-rich dienophiles (ca. 2 eV)[6a] has a reduced significance in the TS. Still, why would electron-poor dienophiles be preferred? We suggest it is because electron-poor dienophiles provide an energetically lower lying LUMO (often by more than 3.0 eV).[6a] This results in a stronger $HOMO_{diene}-LUMO_{dienophile}$ interaction, which should be more influential for the energy of the TS than the $HOMO_{dienophile}-LUMO_{diene}$ interaction (despite its larger energy gap). This may also explain why Diels–Alder reactions with inverse electron demand are generally slower and more sluggish than normal Diels–Alder reactions.[12]

Lastly, and perhaps more convincingly, we have observed that electron-poor dienes react readily with electron-rich dienes in cross-Diels–Alder reactions to give exclusively the normal Diels–Alder cycloadducts. From unrelated examples in the literature, as well as our own work, we could find almost no exceptions to this rule (Scheme 4).[8b, 13] Reactions with **18** (R = Ar) or **9** constitute rather convincing examples, when one considers that the Diels–Alder cycloaddition is sensitive to sterically demanding groups on the dienophile. Also impressive are the examples with compounds **13**, **16**, and **18** in which the α,β-unsaturated ketone is held in a cisoid conformation and should have an advantage as a diene.[13a-c]

These cross-cycloaddition experiments offer unambiguous evidence since the dominant orbital interaction involves the same MOs in either electronic sense. However, in the normal reactions the dominant orbital interaction is $HOMO_{diene}-LUMO_{dienophile}$, while in the sense of inverse electron demand the same orbitals are involved in the $HOMO_{dienophile}-LUMO_{diene}$ interaction (Scheme 5). We conclude that the dienes will inherently prefer the cross-reaction path with the smaller $HOMO_{diene}-LUMO_{dienophile}$ energy gap, that is, the normal Diels–Alder pathway. Thus, the dienes minimize the energy of the TS by maximizing the strength of the interaction playing the predominant role in the relative rate of the reaction.

Finally, *o*-quinone methide (**29**) reacted with isoprene to give a product of a Diels–Alder reaction with inverse electron demand (Scheme 4).[14] The developing aromatic

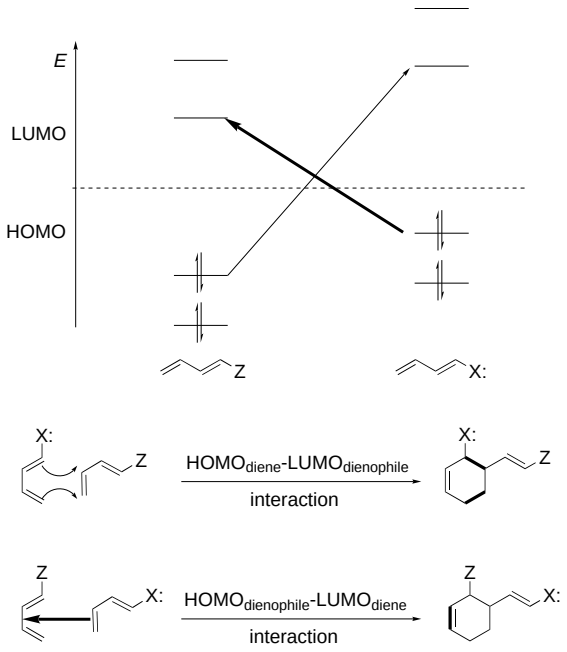


Scheme 4. Examples of cross-Diels–Alder reactions; in each case the cycloadduct shown is the exclusive product. TMS = Me_3Si.

character of the quinone methide ring caused by the strong double-bond character between C2 and C3 in the TS overpowers any stabilizing effect from MO interactions. The high reactivity of *o*-quinone dimethides with electron-poor, electron-rich, or even unactivated dienophiles must be due to that same phenomenon. This notion has never been formally proposed before because it conflicts with the accepted idea of an aromatic and "early" TS for the Diels–Alder reaction.

Our discovery changes and complements the current FMO treatment of the Diels–Alder reaction as pertaining to the reactivity of diene–dienophile partners. Our model should

 © WILEY-VCH Verlag GmbH, D-69451 Weinheim, 1998 1433-7851/98/3723-3264 $ 17.50+.50/0 *Angew. Chem. Int. Ed.* **1998**, *37*, No. 23



Scheme 5. The dominant interaction in cross-cycloaddition experiments leads to different orbitals in the final cycloadduct depending on the reaction path.

prove useful in predicting more accurately the reactivity of dienes and dienophiles. It will likely have repercussions on predictions of the regio- and stereoselectivity of the process as well.

Received: May 14, 1998
Revised version: August 24, 1998 [Z11857IE]
German version: *Angew. Chem.* **1998**, *110*, 3454 – 3457

Keywords: computer chemistry · cycloadditions · reaction mechanisms · transition states

[1] a) C. Spino, J. Crawford, M. Gugelchuk, Y. Cui, *J. Chem. Soc. Perkin Trans. 2* **1998**, 1499 – 1506; b) C. Spino, J. Crawford, *Can. J. Chem.* **1993**, *71*, 1094 – 1097.
[2] K. Fukui, *Acc. Chem. Res.* **1981**, *14*, 363 – 368.
[3] For a detailed description of the various orbital interactions in the Diels – Alder reaction of butadiene and ethylene, see R. D. Bach, J. J. W. McDouall, H. B. Schlegel, *J. Org. Chem.* **1989**, *54*, 2931 – 2935.
[4] a) K. N. Houk, Y. Li, J. D. Evanseck, *Angew. Chem.* **1992**, *104*, 711 – 739; *Angew. Chem. Int. Ed. Engl.* **1992**, *31*, 682 – 708; b) R. E. Townshend, G. Ramunni, L. E. Overmann, W. J. Hehre, L. Salem, *J. Am. Chem. Soc.* **1976**, *98*, 2190 – 2198; c) E. Goldstein, B. Beno, K. N. Houk, *J. Am. Chem. Soc.* **1996**, *118*, 6036 – 6043; d) K. N. Houk, *Pure Appl. Chem.* **1989**, *61*, 643 – 650; e) Y. Li, K. N. Houk, *J. Am. Chem. Soc.* **1993**, *115*, 7478 – 7485.
[5] a) K. Fukui, *Molecular Orbitals in Chemistry, Physics, and Biology*, Academic Press, New York, **1964**, p. 525; b) K. Fukui, *Acc. Chem. Res.* **1971**, *4*, 57 – 64.
[6] a) I. Fleming, *Frontier Orbitals and Organic Chemical Reactions*, Wiley, Chichester, **1976**, p. 249; b) T. N. Anh, *Orbitales frontières, manuel pratique*, InterEditions & CNRS Éditions, Paris, **1995**, p. 265.
[7] V. D. Kiselev, A. I. Konovalov, *Russ. Chem. Rev.* **1988**, *58*, 230 – 249, and references therein.
[8] a) P. G. Baraldi, A. Barco, S. Benetti, S. Manfredini, G. P. Pollini, D. Simoni, V. Zanirato, *Tetrahedron* **1988**, *44*, 6451 – 6454; b) T.-S. Chou, S.-C. Hung, *J. Org. Chem.* **1988**, *53*, 3020 – 3027; c) J. F. Honek, M. L. Mancini, B. Belleau, *Synthetic Comm.* **1984**, *14*, 483 – 491.
[9] T. Inukai, T. Kojima, *J. Org. Chem.* **1971**, *36*, 924 – 928.
[10] G. L. Dunn, J. K. Donohue, *Tetrahedron Lett.* **1968**, 3485 – 3487.
[11] J. M. McIntosh, R. A. Sieler, *J. Org. Chem.* **1978**, *43*, 4431 – 4433.
[12] D. L. Boger, S. M. Weinreb, *Hetero Diels – Alder Methodology in Organic Synthesis*, Academic Press, New York, **1987**, p. 366.
[13] a) G. A. K. Kraus, M. E., *J. Org. Chem.* **1986**, *51*, 3347 – 3350; b) G. A. Mock, A. B. Holmes, R. A. Raphael, *Tetrahedron Lett.* **1977**, 4539 – 4540; c) P. E. Eaton, W. H. Bunnelle, *Tetrahedron Lett.* **1984**, *25*, 23 – 26; d) J. F. Buzinkai, D. M. Hrubowchak, F. X. Smith, *Tetrahedron Lett.* **1985**, *26*, 3195 – 3198.
[14] D. A. Bolon, *J. Org. Chem.* **1970**, *35*, 3666 – 3670.

Kinetic and Thermodynamic Control in Self-Assembly: Sequential Formation of Linear and Circular Helicates

Bernold Hasenknopf, Jean-Marie Lehn,* Nedjia Boumediene, Emmanuelle Leize, and Alain Van Dorsselaer

The self-assembly of polynuclear metal coordination compounds has been very actively investigated in recent years, in particular that of complexes presenting a helical arrangement of ligand strands.[1–3] Whereas most of these helicates present linear axes, circular helical architectures have also been reported.[4–6] We recently described the self-assembly of circular helicates based on the octahedral coordination of three tris-bipyridine ligands such as **L** (see Figure 1) with iron(II) ions.[4, 5] On the other hand, with nickel(II) ions ligand **L** had earlier been found to lead to the formation of a complex presenting a triple-helicate structure.[7] Thus, the same ligand yields two different architectures with two metal ions that display the same coordination geometry. In view of these intriguing results we decided to follow more closely the self-assembly process, in order to gain insight into the structural, mechanistic, and physicochemical factors that may be at play.

In particular, whereas in the self-assembly of both synthetic and biological systems the thermodynamic product is usually formed (and should finally result in reversible equilibrium conditions), kinetic products may also be obtained if the shape of the energy hypersurface is such that the system becomes trapped in local minima. Indeed, self-assembly[1] is evidently a time-dependent process, and it may thus display kinetic control.

[*] Prof. J.-M. Lehn
Laboratoire de Chimie Supramoléculaire
ISIS, Université Louis Pasteur
4 rue Blaise Pascal, F-67000 Strasbourg (France)
Fax: (+33) 3-88411020
E-mail: lehn@chimie.u-strasbg.fr
Dr. B. Hasenknopf
Université Pierre et Marie Curie
Chimie Inorganique et Matériaux Moléculaires, Paris (France)
N. Boumediene, Dr. E. Leize, Prof. A. Van Dorsselaer
Laboratoire de Spectrométrie de Masse Bio-Organique,
Université Louis Pasteur, Strasbourg (France)

 © WILEY-VCH Verlag GmbH, D-69451 Weinheim, 1998 1433-7851/98/3723-3265 $ 17.50+.50/0

An equimolar mixture of ligand **L** (Figure 1) and $FeCl_2$ in ethylene glycol at a concentration of 10^{-3} M was heated to 170 °C for 50 min. Addition of aqueous NH_4PF_6 resulted in precipitation of a red solid, which was isolated by centrifugation. Thin layer chromatography (TLC) showed, beside a very small amount of $[5]^2$**cH**,[8] a single compound which was less polar than $[5]^2$**cH**; it was purified by several recrystallizations from acetonitrile/diethyl ether and analyzed. Its UV/Vis spectrum presents a band at 517 nm typical of the metal-to-ligand charge transfer (MLCT) band of a $[Fe(bipy)_3]$-type complex.[9] The ^{1}H NMR spectrum displays two singlets (of 2:1 relative intensity due to superposition of two singlets) and six doublet signals in the aromatic region, indicating that all the ligands in the complex are equivalent and that there is an axis of symmetry passing through the central C(2)–C(2′) bond. The CH_2CH_2 bridges give two AA′BB′ multiplets around $\delta = 2.1$ and 3.4. Electrospray mass spectrometry (ES-MS) indicates a complex $[Fe_3\mathbf{L}_3](PF_6)_6$; all the signals observed correspond to $[Fe_3\mathbf{L}_3]^{6+}$ with zero to four PF_6^- anions. Elemental analysis is also in agreement with the stoichiometry $[Fe_3\mathbf{L}_3](PF_6)_6$.

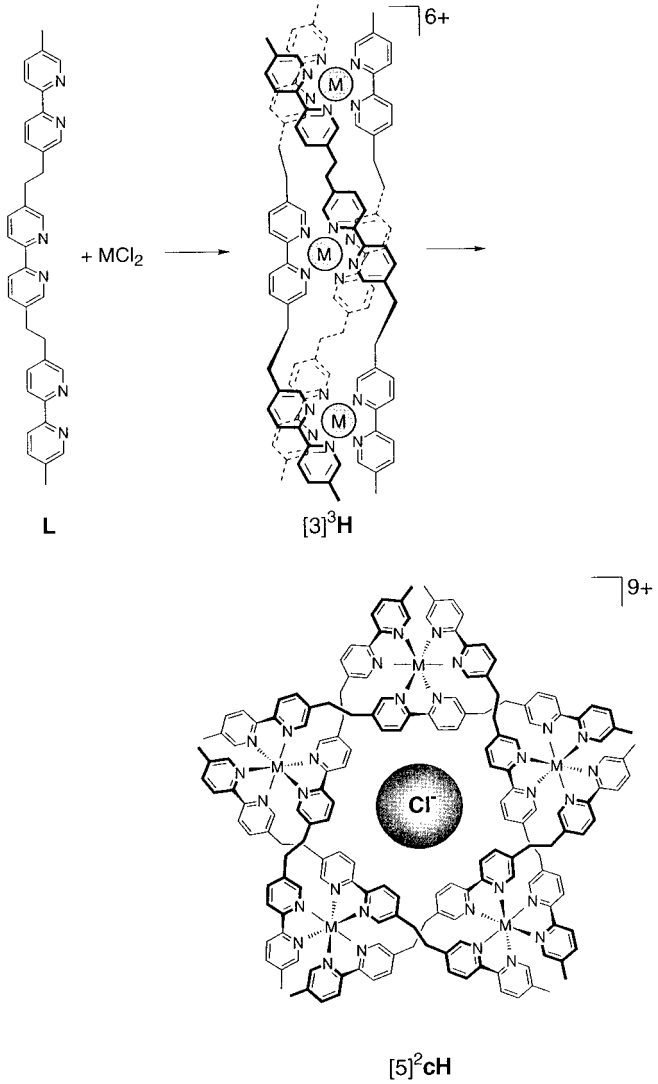


Figure 1. The chronological (but not necessarily mechanistic) sequence of self-assembly processes yielding first a triple helix $[3]^3$**H** and thereafter a circular double helix $[5]^2$**cH** as kinetic and thermodynamic products, respectively. M = Fe^{II} or Ni^{II}.

The cell parameters determined for a single crystal of this complex by X-ray diffraction were found to be identical to those reported for $[3]^3$**H**-Ni^{II},[7] and its structure was therefore not determined. One may conclude that the complex obtained is the iron(II) triple helicate $[3]^3$**H**, which is isostructural to the corresponding nickel(II) helicate.[7] The self-assembly of the ligand **L** and $FeCl_2$ thus yields the triple helicate $[3]^3$**H** after a relatively short reaction time, whereas the circular helicate $[5]^2$**cH** is obtained after prolonged heating.[4] We therefore decided to study the course of the reaction as a function of time.

An equimolar mixture of the ligand **L** with $FeCl_2$ in ethylene glycol ($c = 5 \times 10^{-3}$ M) was heated to 170 °C. At regular intervals, a sample of the solution was added to an aqueous solution of NH_4PF_6, and the red precipitate was isolated and analyzed by ^{1}H NMR spectroscopy and ES-MS.

Figure 2 shows the evolution of the aromatic part of the ^{1}H NMR spectra. The formation of $[3]^3$**H** is complete already after 1 min. Thereafter the signals of $[5]^2$**cH** appear, as well as signals belonging to minor intermediate species. After about 24 h all the complexes are converted into $[5]^2$**cH**. This experiment clearly indicates a chronological sequence of self-assembly processes. The initially formed trinuclear $[3]^3$**H** disassembles, at least partially, to allow generation of the pentanuclear $[5]^2$**cH**.

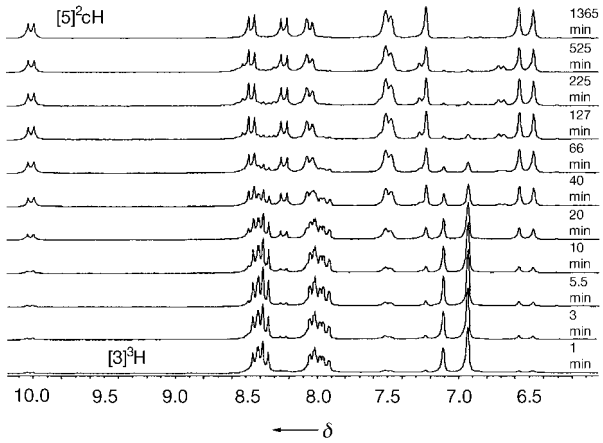


Figure 2. ^{1}H NMR spectra showing the formation of $[3]^3$**H**-Fe^{II} and its conversion into $[5]^2$**cH**-Fe^{II}. For further details, see the text.

The same samples were also analyzed with ES-MS. The first spectrum shows exclusively the triple helicate $[3]^3$**H**, and the last spectrum the circular helicate $[5]^2$**cH** (Figure 3). The intermediate spectra display the signals of both species. The relative intensities of the signals correlate well with the abundance of the complexes determined by NMR spectroscopy. The minor species observed by NMR spectroscopy correspond to complexes of the composition $[Fe_5\mathbf{L}_5]^{10+}$ and $[Fe_5\mathbf{L}_5(H_2O)_2]^{10+}$; they probably present a noncyclic arrangement as the ^{1}H NMR spectrum does not show the signal at $\delta = 9.0$, which is characteristic of the chloride-free cyclic

 © WILEY-VCH Verlag GmbH, D-69451 Weinheim, 1998 1433-7851/98/3723-3266 $ 17.50+.50/0 *Angew. Chem. Int. Ed.* **1998**, *37*, No. 23

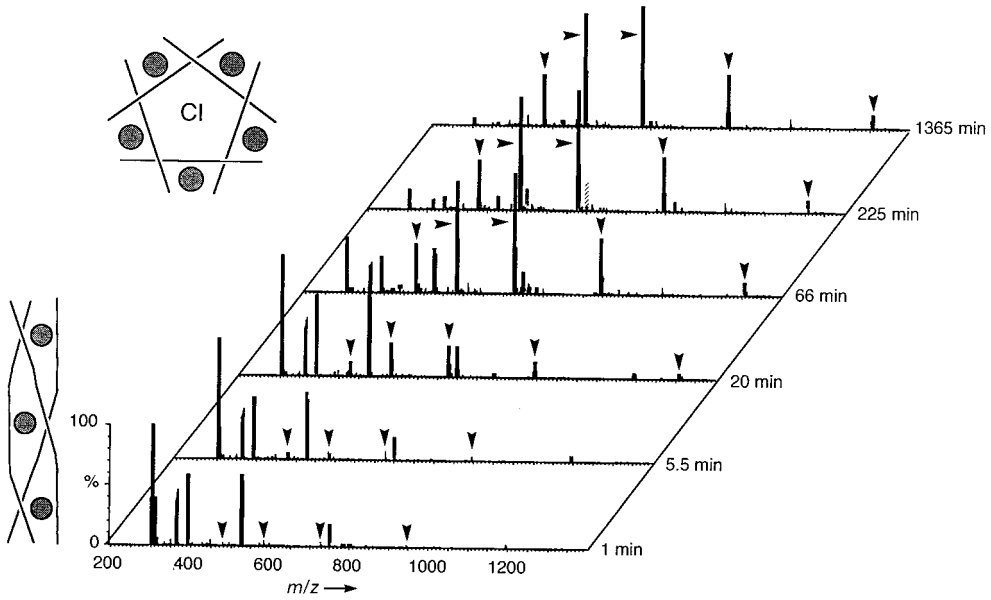


Figure 3. ES mass spectra showing the conversion of $[3]^3$**H**-Fe^{II} into $[5]^2$**cH**-Fe^{II}; the peaks of the latter are indicated by the arrowheads.

species $[5]^2$**cH** obtained by treating the chloride-containing species with a silver salt.

The self-assembly experiment was repeated at different concentrations, and the samples were analyzed by ES-MS. At 10^{-3} M, the formation of the triple helicate $[3]^3$**H** took about 25 min; it transformed slowly into $[5]^2$**cH**, but this conversion was not complete after 22 h. At a concentration of 10^{-2} M, the conversion of $[3]^3$**H** into $[5]^2$**cH** reached 80% already after 60 min, and was quantitative according to the NMR spectrum after 9 h. On the other hand, after 22 h all traces of $[3]^3$**H** had disappeared in the ES mass spectra. Thus, the rate of self-assembly of $[3]^3$**H** and $[5]^2$**cH** increases with concentration, as expected for a multicomponent process. More detailed study of the rate law may provide information about the mechanism of the assembly.

The present results indicate that the triple helicate is a kinetic product, formed reversibly from the components, which progressively converts into the thermodynamic product, the circular helicate $[5]^2$**cH**. The higher stability of $[5]^2$**cH** might be attributed to several factors, such as strain in the bound ligand and/or at the coordination centers, or electrostatic interaction with the included chloride anion. On the other hand, while these enthalpic contributions may drive the formation of the pentanuclear complex, it should be entropically less favorable than the trinuclear complex.

Since the Fe^{II} ions form initially the same triple helicate as Ni^{II}, it should in principle also be possible to form the circular pentanuclear architecture with nickel(II), as is the case with iron(II). To facilitate the conversion of $[3]^3$**H** into $[5]^2$**cH**, we searched for a way to accelerate the dissociation of the metal centers. It is known that lowering the pH by inducing protonation of the bipyridine nitrogen atoms increases the rates of decomplexation.[10, 11] An equimolar mixture of $NiCl_2$ and **L** in ethylene glycol was therefore heated to 190 °C in the presence of HCl. Following the initial formation of $[3]^3$**H**-Ni^{II}, ES-MS indicated the appearance of the circular helicate $[5]^2$**cH**-Ni^{II}, containing a single Cl^- ion like $[5]^2$**cH**-Fe^{II}. One may therefore consider that both complexes present an analogous structure. After a reaction time of four days, a 2:1 mixture of $[5]^2$**cH**-Ni^{II} and $[3]^3$**H**-Ni^{II} was obtained, as determined by ES-MS. Further transformation was not observed due to the slow decomposition of the ligand at the high reaction temperatures.

In conclusion, we have shown that both architectures $[3]^3$**H** and $[5]^2$**cH** can be obtained with either iron(II) or nickel(II) ions. The triple helicate is a kinetic product and is formed first and reversibly. It thereafter disassembles, and the system progressively transforms into the circular helicate. Although the formations of $[3]^3$**H** and $[5]^2$**cH** were observed successively, the triple helicate does not necessarily have to lie on the mechanistic pathway leading from the components $FeCl_2$ and **L** to $[5]^2$**cH**.[12] Preliminary kinetic studies show that the disappearance of $[3]^3$**H**-Fe^{II} follows a double-exponential decay. This indicates the possible existence of more than one mechanistic pathway from $[3]^3$**H** to $[5]^2$**cH**.

It is clear that in the self-assembly of complex architectures a number of kinetic products may appear before formation of the thermodynamic product(s). Indeed, self-assembly processes operate on energy hypersurfaces that may present both local and overall minima corresponding to kinetic and thermodynamic products, respectively. Depending on the heights of the related energy barriers a given process may display kinetic and/or thermodynamic control under a given set of conditions. In the present system, both the kinetic and thermodynamic products can be directly observed because of the slow rates of interconversion. Further studies are needed to establish the mechanistic pathways involved and the factors influencing this unique sequence of self-assembly processes. Finally, the intervention of kinetic control also points to extensions involving the role of nonequilibrium features in self-organization processes.[13]

Received: July 1, 1998 [Z12084IE]
German version: *Angew. Chem.* **1998**, *110*, 3458 – 3460

Keywords: helical structures · iron · nickel · N ligands · supramolecular chemistry

[1] J.-M. Lehn, *Supramolecular Chemistry: Concepts and Perspectives*, VCH, Weinheim, **1995**, chap. 9.
[2] C. Piguet, G. Bernardinelli, G. Hopfgartner, *Chem. Rev.* **1997**, *97*, 2005.
[3] A. Williams, *Chem. Eur. J.* **1997**, *3*, 15.
[4] B. Hasenknopf, J.-M. Lehn, G. Baum, B. O. Kneisel, D. Fenske, *Angew. Chem.* **1996**, *108*, 1987; *Angew. Chem. Int. Ed. Engl.* **1996**, *35*, 1838.

 © WILEY-VCH Verlag GmbH, D-69451 Weinheim, 1998 1433-7851/98/3723-3267 $ 17.50+.50/0

[5] B. Hasenknopf, J.-M. Lehn, N. Boumediene, A. Dupont-Gervais, A. Van Dorsselaer, B. Kneisel, D. Fenske, *J. Am. Chem. Soc.* **1997**, *119*, 10956.
[6] O. Mamula, A. von Zelewsky, G. Bernardinelli, *Angew. Chem.* **1998** *110*, 301; *Angew. Chem. Int. Ed.* **1998**, *37*, 289; C. Provent, S. Hewage, G. Brand, G. Bernardinelli, L. J. Charbonnière, A. F. Williams, *Angew. Chem.* **1997**, *109*, 1346; *Angew. Chem. Int. Ed. Engl.* **1997**, *36*, 1287.
[7] R. Krämer, J.-M. Lehn, A. De Cian, J. Fischer, *Angew. Chem.* **1993**, *105*, 764; *Angew. Chem. Int. Ed. Engl.* **1993**, *32*, 703.
[8] $[n]^m$**H** is used as a short notation for helicates (**H**) and circular helicates (**cH**). [*n*] indicates the number of metal ions, and *m* the helicity ($m = 2$ for a double helix, $m = 3$ for a triple helix).
[9] F. W. Cagle, Jr., G. F. Smith, *J. Am. Chem. Soc.* **1947**, *69*, 1860.
[10] J. H. Baxendale, P. George, *Trans. Faraday Soc.* **1950**, *46*, 736.
[11] F. Basolo, J. C. Hayes, H. M. Neumann, *J. Am. Chem. Soc.* **1953**, *75*, 5102.
[12] The interconversion of glucan polymers between linear triple helix and macrocycle forms was recently reported: T. M. McIntire, D. A. Brant, *J. Am. Chem. Soc.* **1998**, *120*, 6909.
[13] *Self-Organization. The Emergence of Order* (Ed.: F. E. Yates), Plenum, New York, **1987**.

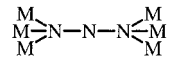
A μ-1,1,1,3,3,3 Azide Anion inside a Trigonal Prism of Silver Centers**

Guo-Cong Guo and Thomas C. W. Mak*

Dedicated to Professor George A. Jeffrey on the occasion of his 83rd birthday

Azide compounds have been known for more than a century and continue to attract much current interest.[1] The field has undergone quite spectacular advances in the last decade for three main reasons: 1) covalent inorganic azides are potentially better explosives than lead azide, which is used as a detonator;[2] 2) the μ-azido bridging ligand is undoubtedly one of the most versatile ingredients for the creation of new materials with different magnetic properties, leading to an intensive study of magnetostructural correlations in discrete complexes as well as in polymeric one-, two-, and three-dimensional systems;[3] 3) azido complexes can serve as precursors in preparative materials chemistry as a source of atomic nitrogen.[4] As a sequel to our study on the bonding interaction between silver(I) atoms and the acetylenediide anion, C_2^{2-},[5] we have turned our attention to the isoelectronic cyanide ion CN^-,[6] as well as the azide ion N_3^-, as these species have been well studied together with N_2 in comparative substrate binding to the FeMo cofactor of nitrogenase.[7]

Up to now the known coordination modes of the azido ligand in transition metal complexes are terminal monodentate or bridging bidentate (μ-1,1; μ-1,1,3), tridentate (μ-1,1,1; μ-1,1,3), and tetradentate (μ-1,1,3,3; μ-1,1,1,3).[8] Herein we report a novel compound $AgN_3 \cdot 2\,AgNO_3$ in which the azide unit exhibits an unprecedented bridging hexadentate (μ-1,1,1,3,3,3) coordination mode as an encapsulated species inside a trigonal prism (Scheme 1).



Scheme 1. Schematic representation of the μ-1,1,1,3,3,3 coordination mode of the azido ligand in the Ag_6 prisms of $AgN_3 \cdot 2\,AgNO_3$.

The layer-type framework in $AgN_3 \cdot 2\,AgNO_3$ can be regarded as constructed from a stacking of slant trigonal prisms each composed of silver atoms at its vertices with azide units imprisoned within half of them (Figure 1). The filled and hollow prisms are stacked on their trigonal faces to form a zigzag column extending along the *c* direction. Such prismatic columns share rectangular faces and edges alternately along the *a* direction to generate a grooved slab, with pendant η^1-nitrate anions attached to Ag1 atoms on both sides (Figure 2). In any filled trigonal prism, the Ag2 atoms and the encapsulated azide unit all lie on the same mirror plane. The azide unit in $AgN_3 \cdot 2\,AgNO_3$ is linear and asymmetrical (N1–N2 1.239(2), N2–N3 1.174(2) Å), which is consistent with its Raman spectrum. The terminal N atoms of the azide ligand are each asymmetrically bound to two Ag1 and one Ag2 atoms (Ag1–N1 2.503(1), Ag2–N1 2.278(2), Ag1–N3 2.409(1), Ag2–N3 2.351(2) Å), and the bond angles Ag-N1-N2 and Ag-N3-N2 lie in the range of 118.2 to 122.1°. It is

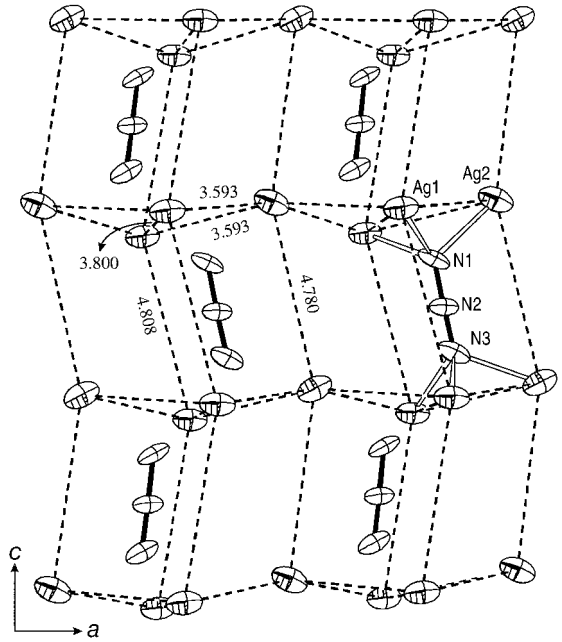


Figure 1. Layer-type framework in $AgN_3 \cdot 2\,AgNO_3$ built of filled and empty trigonal prisms viewed along the *b* direction. The lengths [Å] of the edges of a prism are shown. For clarity, the nitrate anions have been omitted, and Ag–N bonds are shown only for one of the encapsulated azide ions. Selected bond lengths [Å] and angles [°]: Ag1–N3^{i} 2.409(1), Ag1–N1 2.503(1), Ag2–N1 2.278(2), Ag2–N3^{ii} 2.351(2), N1–N2 1.239(2), N2–N3 1.174(2); N2-N1-Ag(2) 122.09(15), N2-N1-Ag1 118.21(8), N3-N2-N1 179.4(2), N2-N3-Ag2^{iii} 120.0(2), N2-N3-Ag1^{iv} 119.80(7). Symmetry codes: i: $-x, -y, z + 1/2$; ii: $-x - 1, -y, z + 1/2$; iii: $-x - 1, -y, z - 1/2$; iv: $-x, y, z - 1/2$.

[*] Prof. T. C. W. Mak, G.-C. Guo
Department of Chemistry, The Chinese University of Hong Kong
Shatin, New Territories, Hong Kong (China)
Fax: (+86) 852-260-35057
E-mail: tcwmak§cuhk.edu.hk

[**] This work was supported by Hong Kong Research Grants Council Earmarked Grant CUHK 4179/97P and Direct Grant A/C 2060129 of The Chinese University of Hong Kong.

 © WILEY-VCH Verlag GmbH, D-69451 Weinheim, 1998 1433-7851/98/3723-3268 $ 17.50+.50/0

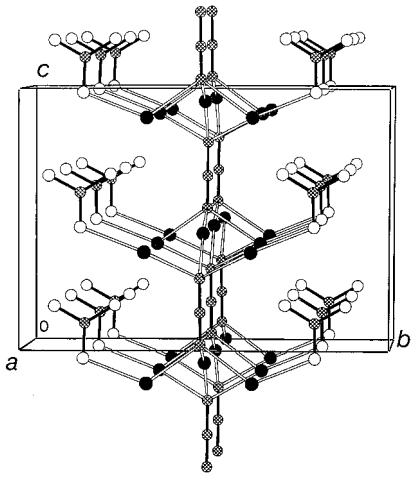


Figure 2. Crystal structure of $AgN_3 \cdot 2\,AgNO_3$ viewed along the *a* direction. The solid, cross-hatched and open circles represent Ag, N, and O atoms, respectively.

worthy of note that the Ag–N distances, especially those involving the Ag2 atom, are significantly shorter than that found in an early study of AgN_3 (2.56 Å).[9] The complete encapsulation of the azide species inside an Ag_6 polyhedron may be denoted as $N_3^-@Ag_6$, by analogy to $C_2^{2-}@Ag_6$,[5a] $C_2^{2-}@Ag_7$,[5c] $C_2^{2-}@Ag_8$,[10] and $C_2^{2-}@Ag_9$[5b] that are found in a series of complexes of silver acetylide with soluble silver salts. The coordination mode of the present N_3^- ion differs from those of other isoelectronic three-atom groups such as CN_2^{2-}, C_3^{4-}, BN_2^{3-}, and CBN^{4-}, which were found to exist in solid-state alkali and alkaline-earth compounds.[11]

It is interesting to compare the Raman spectra of NaN_3, AgN_3, and $AgN_3 \cdot 2\,AgNO_3$.[12] The azide unit of $AgN_3 \cdot 2\,AgNO_3$ exhibits both ν_s and ν_{as} stretching vibrations that are characteristic of a linear and asymmetrical structure. As expected, $\nu_{as}(N_3)$ in $AgN_3 \cdot 2\,AgNO_3$ shifts to a higher wavenumber in comparison with that in AgN_3, whereas a decrease of $\nu_s(N_3)$ in the sequence $NaN_3 > AgN_3 > AgN_3 \cdot 2\,AgNO_3$ may be reasonably rationalized in terms of increasing metal →ligand π-back bonding.

Two structural models have been considered for binding of dinitrogen to the FeMo cofactor of nitrogenase:[13] the substrate either binds externally to a Fe_4 rhombus face of a twisted form of the central Fe_6 trigonal prism,[14] or lies completely within the cavity.[15] The μ_6 coordination mode of dinitrogen in the latter model, denoted as $N_2@Fe_6$, is structurally analogous to the $N_3^-@Ag_6$ unit in $AgN_3 \cdot 2\,AgNO_3$, and also somewhat resembles the $[C_2^{2-}@Ag_n,\ n = 6-9]$ systems that exist in double salts of silver acetylide with soluble silver salts.[5, 10] The fact that acetylene is one of the longest established nitrogenase substrates and that C_2^{2-}, which has the same set of molecular orbitals as N_2, exhibits a strong tendency of being encaged inside an assembled silver polyhedron may be of relevance in understanding the binding and weakening of N_2 in the FeMo cofactor cavity.

Experimental Section

AgN_3 was prepared by mixing aqueous solutions of sodium azide and silver nitrate at room temperature.[16] The white precipitate was filtered, washed several times with de-ionized water, and temporarily stored in wet form in the dark. **Caution**: AgN_3 should never be dried or kept for a prolonged period, and only a small quantity should be used in any chemical reaction.

$AgN_3 \cdot 2\,AgNO_3$: Wet AgN_3 was added to a concentrated aqueous solution of $AgNO_3$ (2 mL; about 40 %) under stirring until saturated. The excess amount of AgN_3 was filtered off, and the solution was put into a desiccator charged with P_2O_5. In the course of two days colorless crystals of $AgN_3 \cdot 2\,AgNO_3$ were obtained in nearly quantitative yield. The compound is stable when immersed in its mother liquor; it is hygroscopic and slowly decomposes in air, and explodes violently when heated.

Crystal structure analysis: A colorless crystal of dimensions $0.15 \times 0.20 \times 0.10$ mm^3 mounted inside a 0.3 mm Lindemann glass capillary was used for data collection on a Rigaku RAXIS IIC imaging plate diffractometer using graphite-monochromated $Mo_{K\alpha}$ radiation ($\lambda = 0.71073$ Å, rotating-anode, 50 kV, 90 mA). Thirty-one oscillation frames were taken in the range of $\phi = 0-180^\circ$ with $\Delta\phi = 5.0^\circ$ and 8 min exposure per frame. Crystal data for $AgN_3 \cdot 2\,AgNO_3$: $M_r = 489.66$, orthorhombic, space group $Ccm2_1$ (No. 36), $a = 5.871(1)$, $b = 13.351(3)$, $c = 9.397(2)$ Å, $V = 736.6(3)$ Å^3, $T = 293$ K, $Z = 4$, $\rho_{calcd} = 4.416$ g cm^{-3}, $F(000) = 896$, $\mu(Mo_{K\alpha}) = 79.14$ cm^{-1}, absorption corrections applied using ABSCOR, relative transmission factors in the range 0.445–1.0. A total of 1178 reflections were collected in the 2θ range $4.0-52.0^\circ$ ($0 \le h \le 6$, $-15 \le k \le 16$, $-11 \le l \le 11$), yielding 653 unique reflections ($R_{int} = 0.0911$), 570 of which with $I > 2\sigma(I)$ were considered as observed, 71 parameters, $R(F^2) = 0.0733$, $R_w(F^2) = 0.1908$, and GOF(F^2) = 1.155. The structure was solved by direct methods (SHELXS-86) and refined by full-matrix anisotropic least squares on F^2 using the Siemens SHELXTL-93 (PC Version) package of crystallographic software. Data collected on another selected crystal did not lead to significantly improved precision of the crystal structure determination. Further details of the crystal structure investigation can be obtained from the Fachinformationszentrum Karlsruhe, D-76344 Eggenstein-Leopoldshafen, Germany (fax: (+49) 7247-808-666; e-mail: crysdata@fiz-karlsruhe.de), on quoting the depository number CSD-408802.

Received: June 15, 1998 [Z 11988 IE]
German version: *Angew. Chem.* **1998**, *110*, 3460–3462

Keywords: azides · clusters · coordination modes · N ligands · silver

[1] A. M. Golub, H. Kohler, V. V. Skopenko in *Chemistry of Pseudohalides* (Ed.: R. J. H. Clark), Elsevier, New York, **1986**, pp. 28–64, and references therein.

[2] a) I. C. Tornieporth-Oetting, T. M. Klapötke, *Angew. Chem.* **1995**, *107*, 559–568; *Angew. Chem. Int. Ed. Engl.* **1995**, *34*, 511–520, and references therein; b) K. O. Christe, W. W. Wilson, R. Bau, S. W. Bunte, *J. Am. Chem. Soc.* **1992**, *114*, 3411–3416; c) T. M. Klapötke, *Chem. Ber.* **1997**, *130*, 443–451; d) V. V. Zhdankin, A. P. Krasutsky, C. J. Kuehl, A. J. Simonsen, J. K. Woodward, B. Mismash, J. T. Bolz, *J. Am. Chem. Soc.* **1996**, *118*, 5192–5197

[3] a) J. Ribas, M. Monfort, I. Resino, X. Solans, P. Rabu, F. Maingot, M. Drillon, *Angew. Chem.* **1996**, *108*, 2671–2673; *Angew. Chem. Int. Ed. Engl.* **1996**, *35*, 2520–2522; b) A. Escuer, R. Vicente, M. A. S. Goher, F. A. Mautner, *Inorg. Chem.* **1998**, *37*, 782–787; c) G. Viau, M. G. Lombardi, G. De Munno, M. Julve, F. Lloret, J. Faus, A. Caneschi, J. M. Clemente-Juan, *Chem. Commun.* **1997**, 1195–1196; d) F. A. Mautner, R. Cortés, L. Lezama, T. Rojo, *Angew. Chem.* **1996**, *108*, 96–98; *Angew. Chem. Int. Ed. Engl.* **1996**, *35*, 78–80; e) R. Cortés, L. Lezama, F. A. Mautner, T. Rojo in *Molecule-Based Materials: Theory, Techniques, and Applications* (Eds.: M. M. Turnbull, T. Sugimoto, L. K. Thompson), American Chemical Society, Washington, DC, **1996**, pp. 187–200; f) P. D. Beer, M. G. B. Drew, P. B. Lesson, K. Lyssenko, M. I. Ogden, *J. Chem. Soc. Chem. Commun.* **1995**, 929–930; g) M. A. Halcrow, J. S. Sun, J. C. Huffman, G. Christou, *Inorg. Chem.* **1995**, *34*, 4167–4177.

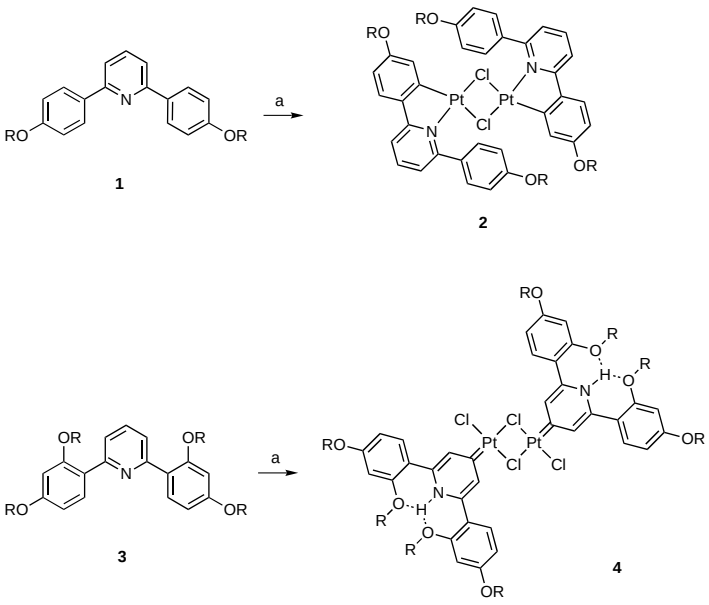
[4] a) D. Sellman, T. Gottschalk-Gaudig, F. W. Heinemann, *Inorg. Chim. Acta* **1998**, *269*, 63–72; b) D. A. Neumayer, A. H. Cowley, A. Decken, R. A. Jones, V. Lakhotia, J. G. Ekerdt, *J. Am. Chem. Soc.* **1995**, *117*, 5893–5894; c) R. A. Fischer, H. Sussek, A. Miehr, H. Pritzkow, E.

Herdtweck, *J. Organomet. Chem.* **1997**, *548*, 73 – 82; d) J. Kouvetakis, J. McMurran, P. Matsunaga, M. O'Keefe, J. L. Hubbard, *Inorg. Chem.* **1997**, *36*, 1792 – 1797.
[5] a) G.-C. Guo, Q.-G. Wang, G.-D. Zhou, T. C. W. Mak, *Chem. Commun.* **1998**, 339 – 340; b) G.-C. Guo, Q.-G. Wang, G.-D. Zhou, T. C. W. Mak, *Angew. Chem.* **1998**, *110*, 652 – 654; *Angew. Chem. Int. Ed.* **1998**, *37*, 630 – 632; c) G.-C. Guo, Q.-G. Wang, G.-D. Zhou, T. C. W. Mak, unpublished results.
[6] G.-C. Guo, T. C. W. Mak, *Angew. Chem.* **1998**, *110*, 3296 – 3299; *Angew. Chem. Int. Ed.* **1998**, *37*, 3183 – 3186.
[7] a) B. K. Burgess, D. J. Lowe, *Chem. Rev.* **1996**, *96*, 2983 – 3011; b) G. N. Schrauzer, G. W. Kiefer, P. A. Doemeny, H. Kirsh, *J. Am. Chem. Soc.* **1973**, *95*, 5582 – 5592.
[8] M. A. S. Goher, F. A. Nautner, *Polyhedron*, **1995**, *14*, 1439 – 1446, and references therein.
[9] a) J. I. Bryant, R. L. Brooks, *J. Chem. Phys.* **1971**, *54*, 5315 – 5323; b) C. D. West, *Z. Kristallogr.* **1936**, *85*, 421 – 425.
[10] a) G.-D. Zhou, *Acta Sinica Peking Univ.* **1963**, *9*, 389. [In Chinese]; b) X.-L. Jin, G.-D. Zhou, N.-Z. Wu, Y.-Q. Tang, H.-C. Huang, *Acta Chemica Sinica* **1990**, *48*, 232 – 236. [In Chinese].
[11] H.-J. Meyer, *Z. Anorg. Allg. Chem.* **1991**, *594*, 113 – 118, and references therein.
[12] Raman spectra of solid samples were measured on a Renishaw Raman Image Microscope System 2000: NaN_3: $\tilde{\nu}_s(N_3)$ 1361 cm^{-1}, $\tilde{\nu}_{as}(N_3)$ inactive; AgN_3: $\tilde{\nu}_s(N_3)$ 1338, $\tilde{\nu}_{as}(N_3)$ 2070 cm^{-1}; $AgN_3 \cdot 2\,AgNO_3$: $\nu_{as}(N_3)$ 2079, $\nu_s(N_3)$ 1330 cm^{-1}. The Raman spectrum of NaN_3 is consistent with $D_{\infty h}$ symmetry of the azide unit. However, the literature assignment of a linear and symmetrical structure for the azide unit in AgN_3[9] is at variance with the present data, which clearly indicate a linear and asymmetrical structure in both AgN_3 and $AgN_3 \cdot 2\,AgNO_3$.
[13] J. B. Howard, D. C. Rees, *Chem. Rev.* **1996**, *96*, 2965 – 2982.
[14] a) I. G. Dance, *Aust. J. Chem.* **1994**, *47*, 979 – 990; b) I. G. Dance, *Chem. Commun.* **1998**, 523 – 530.
[15] a) M. K. Chan, J. Kim, D. C. Rees, *Science (Washington)* **1993**, *260*, 792 – 794; b) K. K. Stavrev, M. C. Zerner, *Chem Eur. J.* **1996**, *2*, 83 – 87.
[16] N. R. Thompson in *Comprehensive Inorganic Chemistry Vol. 3* (Eds.: J. C. Bailar, H. J. Emeléus, R. Nyholm, A. F. Trotman-Dickenson), Pergamon, Oxford, **1973**, Chap. 2, Section 2.10, p. 101.

Inter- versus Intramolecular C–H Activation: Synthesis and Characterization of a Novel Platinum – Carbene Complex**

Gareth W. V. Cave, Andrew J. Hallett, William Errington, and Jonathan P. Rourke*

Cyclometalation is a reaction that has been both widely used[1, 2] and widely studied.[3, 4] Typically, the coordinating moiety within a ligand forms a bond to a metal center, and then intramolecular C–H activation takes place to yield a five- or six-membered chelate ring. In the course of our studies, we sought to synthesize a number of cycloplatinated species that would show novel mesogenic behavior. To this end, we have prepared a number of 2,6-disubstituted pyridines, such as **1** and **3** (Scheme 1), and allowed them to react



Scheme 1. Synthesis of **2** and **4**. a) $K_2[PtCl_4]$, acetic acid. $R = n\text{-}C_6H_{13}$.

with potassium tetrachloroplatinate under normal cycloplatination conditions.[5] When we used pyridine **1** we isolated the expected cycloplatinated product **2**, formed by coordination of the pyridine followed by intramolecular C–H activation, in high yield. However, when we used pyridine **3** we isolated a very different product. The only product isolated (indeed, the only product observed in the crude reaction mixture) was that which forms from the intermolecular activation of a C–H bond, that is, **4**. Complex **4** was isolated in reasonable yield and analyzed by ^1H and ^{13}C NMR spectroscopy and single-crystal X-ray diffraction.

The X-ray crystal structure of **4** shows a number of interesting features (Figure 1). A crystallographically imposed center of symmetry exists between the two platinum and two chlorine atoms (Cl1) to give a flat rectangle, with the other two chlorine atoms (Cl2) only 0.082(4) Å out of this plane. The nitrogen-containing ring is at an angle of 38.62(24)° to the plane defined by the Pt_2Cl_2 rectangle. Two extremes for the bonding of this organic fragment to this rectangle are illustrated in Scheme 2. The Pt–C bond length of 1.951(9) Å is very similar to the values observed for the Pt^0 – carbene complex derived from 1,3-dimesitylimidazol-2-ylidene (1.959(8) and 1.942(8) Å).[6] It is also similar to the length of 1.973(11) Å for the cationic Pt^{IV} – carbene complex $[PtCl_2\{C(NHMe)(NHC_6H_4Cl)\}(PEt_3)_2]ClO_4$,[7] and significantly shorter than that in the non-carbene cycloplatinated species $[\{PtCl(t\text{Bu}_2PCMe_2CH_2)\}_2]$ (2.062(6) Å)[8] or Pt^{II} – C_{aryl} single bond lengths of 1.98 – 2.02 Å in arylplatinum complexes.[9, 10] Two shorter Pt–C bonds have been reported: a bond length of 1.82(6) Å for the platinum – carbene complex $[\{PtCl(t\text{BuCH}_2CO i\text{Pr})\}_2]$[11] (though given the relatively large estimated standard deviations associated with this measurement, this value is not significantly different from ours), and a

[*] Dr. J. P. Rourke, G. W. V. Cave, A. J. Hallett, Dr. W. Errington
Department of Chemistry
Warwick University
Coventry CV4 7AL (UK)
Fax: (+44) 1203-524-112
E-mail: j.rourke@warwick.ac.uk

[**] This work was supported by the Engineering and Physical Sciences Research Council (UK). We thank Johnson Matthey for the loan of platinum salts.

 © WILEY-VCH Verlag GmbH, D-69451 Weinheim, 1998 1433-7851/98/3723-3270 $ 17.50+.50/0

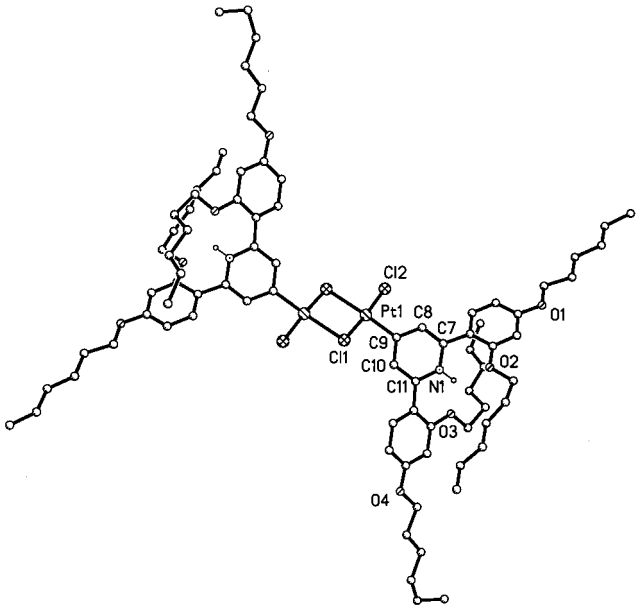
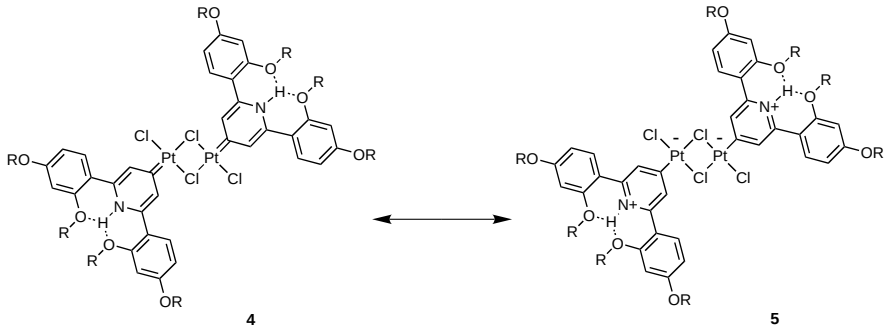


Figure 1. The crystal structure of **4**. Selected bond lengths [Å] and angles [°]: Pt1–C9 1.951(9), Pt1–Cl2 2.281(2), Pt1–Cl1 2.320(2), Pt1–Cl1′ 2.448(2), N1–C7 1.352(10), N1–C11 1.361(10), C7–C8 1.362(10), C8–C9 1.408(10), C9–C10 1.401(10), C10–C11 1.389(10); C9-Pt1-Cl2 91.2(3), C9-Pt1-Cl1 92.4(2), Cl2-Pt1-Cl1 175.86(8), C9-Pt1-Cl1′ 176.8(2), Cl2-Pt1-Cl1′ 91.56(7), Cl1-Pt1-Cl1′ 84.85(7), Pt1-Cl1-Pt1′ 95.155(7), C7-N1-C11 123.7(7), N1-C7-C8 119.0(8), C7-C8-C9 121.5(8), C10-C9-C8 116.6(7), C10-C9-Pt1 120.7(6), C8-C9-Pt1 122.6(6), C11-C10-C9 122.0(8), N1-C11-C10 117.1(8).



Scheme 2. The carbene **4** and the zwitterion **5** as possible formal structures. R = *n*-C_6H_{13}.

length of 1.90(1) Å for a sterically constrained Pt–C bond in an NCN tridentate donor.[12] Thus, the short C–Pt bond length would seem to suggest that a carbene structure—that is, **4**—is the correct representation of the structure. Further evidence for this form comes from the ^{13}C NMR spectrum, where a resonance at $\delta = 324.3$ indicates a carbene, and we can discount structure **5** as a possibility.

The proton attached to the nitrogen atom was inserted at a calculated position. The O3–N1 and O2–N1 distances are 2.622(9) and 2.720(8) Å, respectively. These distances are substantially shorter than the sum of the van der Waals radii of O and N (3.07 Å)[13] and thus confirm the presence of a hydrogen-bonding interaction. The O2–O3 distance, at 3.742(9) Å, is longer than the sum of the van der Waals radii, indicating no particular O–O interaction. One of the effects of this hydrogen bonding is to twist both of the phenyl rings to angles of 34.63(29)° (the ring to which O1 and O2 are attached) and 32.79(36)° (the ring to which O3 and O4 are attached) with respect to the nitrogen-containing ring, so that one oxygen atom is below the proton and one above. In the solution ^1H NMR spectrum this proton is very deshielded ($\delta = 12.77$). The positions of the two OR chains that are hydrogen bonded to this proton are locked in the solid state and remain locked in solution, as shown by the unusual proton resonances for these chains (for instance, the terminal methyl groups of these chains appear at $\delta = 0.69$ rather than at the more normal value of $\delta = 0.95$ for the other chains).

The solution ^1H NMR spectrum of **3** shows no unusual features (in particular, the resonances for the two different OR chains are identical), indicating that there are no unexpected steric restrictions on the conformations. Indeed, our own preliminary studies show that pyridine **3** exhibits a perfectly normal coordination chemistry.[14] On mixing **3** with $K_2[PtCl_4]$ in solution, one would expect that **3** would initially coordinate to the platinum center through the nitrogen atom. Such a coordinated species then has C–H bonds in close proximity that can be activated in an intramolecular fashion, giving rise to a cyclometalated species. All else being equal, the relative reactivity of intramolecular activation, compared with intermolecular activation, based upon the effective concentration, has been estimated at a factor of 10.[3] Thus the exclusive formation of the carbene species that we observe implies that this formation must be a very favorable process, which is presumably assisted by the stabilization offered by the hydrogen-bonded proton. One other feature of complex **4** is its remarkably stability: it melts in air at 246 °C with no decomposition.

Experimental Section

2: 2,6-bis(4-*n*-hexyloxyphenyl)pyridine (**1**; 103 mg, 0.239 mmol) was added to a solution of $K_2[PtCl_4]$ (99 mg, 0.239 mmol) in acetic acid (400 mL). The mixture was stirred at 70 °C for 60 h. The solvent was removed, and the product washed with water. The product was dissolved in chloroform, filtered, washed with hexane, and crystallized from ethyl acetate. Yield: 100 mg (63 %, 0.075 mmol). ^1H NMR (400 MHz, $CDCl_3$, 25 °C): $\delta = 7.71$ (4H, AA′XX′), 7.70 (2H, t, $^3J = 7.6$ Hz, pyridine), 7.36 (2H, dd, $^3J = 7.6$, $^4J = 1.2$ Hz, pyridine), 7.21 (2H, d, $^3J = 8.5$ Hz, cycloplatinated ring), 7.03 (2H, dd, $^3J = 7.6$, $^4J = 1.2$ Hz, pyridine ring), 6.91 (4H, AA′XX′), 6.60 (2H, dd, $^3J = 8.5$, $^4J = 2.3$ Hz, cycloplatinated ring), 6.46 (2H, d , $^4J = 2.3$ Hz, cycloplatinated ring), 3.97 (6H, t, $^3J = 6.7$ Hz, OCH_2), 3.86 (6H, t, $^3J = 6.7$ Hz, OCH_2), 1.79 (8H, m, CH_2), 1.44 (24H, m, CH_2), 0.95 (6H, t, $^3J = 7.0$ Hz, CH_3), 0.91 (6H, t, $^3J = 7.0$ Hz, CH_3); elemental analysis: found (calcd): C 52.6 (52.7), H 5.5 (5.5), N 2.2 (2.1).

4: 2,6-bis(2,4-di-*n*-hexyloxyphenyl)pyridine (**3**; 159 mg, 0.260 mmol) was added to a solution of $K_2[PtCl_4]$ (108 mg, 0.260 mmol) in acetic acid (400 mL). The mixture was stirred at 70 °C for 60 h. The solvent was removed, and the product washed with water. The product was dissolved in chloroform, filtered, washed with hexane, and crystallized from acetone. Yield: 84 mg (36 %, 0.047 mmol). ^1H NMR (400 MHz, $CDCl_3$, 25 °C): $\delta = 12.77$ (2H, t, $^4J = 2.1$ Hz, NH), 8.03 (4H, d, $^4J = 2.1$ Hz, pyridine ring), 7.78 (4H, d, $^3J = 8.9$ Hz), 6.64 (4H, dd, $^3J = 8.9$, $^4J = 2.4$ Hz), 6.52 (4H, d, $^4J = 2.4$ Hz), 4.00 (8H, t, $^3J = 6.4$ Hz, C4-OCH_2), 3.99 (8H, t, $^3J = 5.8$ Hz, C2-OCH_2), 1.80 (8H, m), 1.58 (8H, m), 1.44 (8H, m), 1.34 (24H, m), 1.15 (8H, m), 0.95 (20H, m, CH_2, CH_3 of the non-hydrogen-bonded chain), 0.69 (12H, t, CH_3 of the hydrogen-bonded chain); ^{13}C NMR (100.5 MHz, $CDCl_3$, 25 °C): $\delta = 324.3$ (C attached to Pt).

 © WILEY-VCH Verlag GmbH, D-69451 Weinheim, 1998 1433-7851/98/3723-3271 $ 17.50+.50/0

Crystal data for **4**: $C_{82}H_{122}Cl_4N_2O_8Pt_2 \cdot Me_2CO$, $M_r = 1853.93$, monoclinic, space group $C2/c$, $a = 32.261(2)$, $b = 15.7989(7)$, $c = 20.0825(9)$ Å, $\beta = 119.867(1)^\circ$, $V = 8876.4(7)$ Å^3, 180(2) K; final $R1$, w$R2$, and S values are 0.052, 0.084, and 1.013 for 454 parameters. Data were collected with a Siemens SMART CCD area-detector diffractometer. Refinement was by full-matrix least squares on F^2 for all data with SHELXL-96.[15] Crystallographic data (excluding structure factors) for the structure reported in this paper have been deposited with the Cambridge Crystallographic Data Centre as supplementary publication no. CCDC-101757. Copies of the data can be obtained free of charge on application to CCDC, 12 Union Road, Cambridge CB21EZ, UK (fax: (+44) 1223-336-033; e-mail: deposit@ccdc.cam.ac.uk).

Received: June 2, 1998 [Z11928IE]
German version: *Angew. Chem.* **1998**, *110*, 3466 – 3468

Keywords: carbene complexes · C–H activation · metalations · N ligands · platinum

[1] A. D. Ryabov, *Synthesis* **1985**, 233 – 252.
[2] M. Pfeffer, *Pure Appl. Chem.* **1992**, *64*, 335 – 342.
[3] A. D. Ryabov, *Chem. Rev.* **1990**, *90*, 403 – 424.
[4] P. Steenwinkel, R. A. Gossage, G. van Koten, *Chem. Eur. J.* **1998**, *4*, 759 – 762.
[5] R. M. Ceder, J. Sales, *J. Organomet. Chem.* **1985**, *294*, 389 – 396.
[6] A. J. Arduengo, S. F. Gamper, J. C. Calabrese, F. Davidson, *J. Am. Chem. Soc.* **1994**, *116*, 4391 – 4394.
[7] R. Walker, K. W. Muir, *J. Chem. Soc. Dalton Trans.* **1975**, 272 – 276.
[8] A. B. Goel, S. Goel, D. Vanderveer, *Inorg. Chim. Acta* **1981**, *54*, L267 – L269.
[9] L. W. Conzelman, J. D. Koola, U. Kunze, J. Strähle, *Inorg. Chim. Acta* **1984**, *89*, 147 – 149.
[10] L. Chassot, E. Muller, A. von Zelewsky, *Inorg. Chem.* **1984**, *23*, 429 – 434.
[11] Y. T. Struchkov, G. G. Aleksandrov, V. B. Pukhnarevich, S. P. Sushchinskaya, M. G. Voronkov, *J. Organomet.Chem.* **1979**, *172*, 269 – 272.
[12] J. Terheijden, G. van Koten, F. Muller, D. M. Grove, K. Vrieze, E. Nielsen, C. H. Stam, *J. Organomet. Chem.* **1986**, *315*, 401 – 417.
[13] A. Bondi, *J. Phys. Chem.* **1964**,*68*, 441 – 445.
[14] G. W. V. Cave, J. P. Rourke, unpublished results.
[15] G. M. Sheldrick, , Universität Göttingen, Germany 1996.

Solid-Phase Synthesis and Encoding Strategies for Olefin Polymerization Catalyst Libraries **

Thomas R. Boussie, Carla Coutard, Howard Turner, Vince Murphy,* and Timothy S. Powers*

Although the application of combinatorial methods in the pharmaceutical industry is fast becoming an industrial standard for the discovery and optimization of novel drug-based molecules,[1] similar methods aimed towards the identification of new materials and catalysts remain in their infancy.[2] Recent reports have appeared describing the synthesis and screening of libraries of organometallic catalysts for examining a number of transformations.[3] The application of combinatorial methods aimed toward the discovery and optimization of olefin polymerization catalysts is an area that promises to be of major importance especially to the chemical industry, which produces approximately 46 million metric tons of polyolefins annually.[4]

Since most commercial-scale polyolefin processes employ supports with high surface areas for immobilizing olefin polymerization catalysts, it is somewhat surprising that few reports have appeared examining the use of polystyrene as a catalyst support.[5] Fréchet and co-workers have recently shown that suitably modified cross-linked polystyrene can function as an efficient activator for catalysts based on Group 4 metallocenes.[6] Polystyrene with low cross-linking not only acts as a more chemically compatible support relative to silica, but also provides a "solutionlike" environment that more closely resembles the environment in which homogeneous metallocene catalysts function. In addition, a plethora of solid-phase synthetic methodologies have appeared in recent years, providing a broad knowledge base which should facilitate efforts in the field of olefin polymerization catalysis.[7]

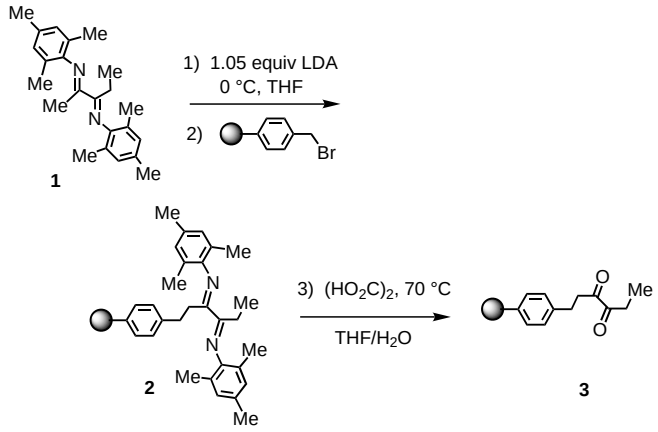
Recent reports have shown that certain catalysts based on complexes of late transition metals with diimines exhibit olefin polymerization activities comparable to those found for early transition metal single-site metallocene-based systems.[8] These systems offer advantages over their early transition metal counterparts in that they are easily synthesized and provide a broader range of functional-group compatabilities.[9] Herein we report the first example of a combinatorial approach to the parallel synthesis of a 1,2-diimine library complexed with Ni^{II} and Pd^{II} as olefin polymerization catalysts using 1 % cross-linked polystyrene as a solid support. Specifically, a general synthetic methodology has been developed that allows for the parallel synthesis and screening of ethylene polymerization catalyst libraries in a spatially addressable format.[10] Furthermore, we have discovered that it is possible to apply chemical encoding techniques to these catalysts and distinguish catalyst performance trends. Since steric bulk on the aryl rings has been shown to play a dramatic role on polymer yield and molecular weight (M_w) for these catalytic systems, we chose to synthesize aryl-substituted 1,2-diimine complexes of Ni^{II} and Pd^{II} on 1 % cross-linked polystyrene. In addition, we sought to examine how electronic perturbations may affect catalyst performance.

Our synthetic approach began with a regioselective alkylation of the unsymmetrical 1,2-diimine **1** with bromomethyl polystyrene (1.05 equiv of lithium diisopropylamide (LDA), 0 °C, THF) to give the polystyrene-grafted 1,2-diimine ligand **2** (Scheme 1).[11] To incorporate a variety of functionalized aryl-substituted 1,2-diimines, a divergent approach was explored starting from diketone resin **3**, which was obtained in high yield (> 95 % based on recovered 2,4,6-trimethylaniline) from the hydrolysis of 1,2-diimine resin **2** with oxalic acid in THF/H_2O (5/1 v/v) at 70 °C for 12 h. This transformation was monitored by single-bead FT-IR spectroscopy ($\tilde{\nu} = 1635$ (C=N), 1712 cm^{-1} (C=O)).

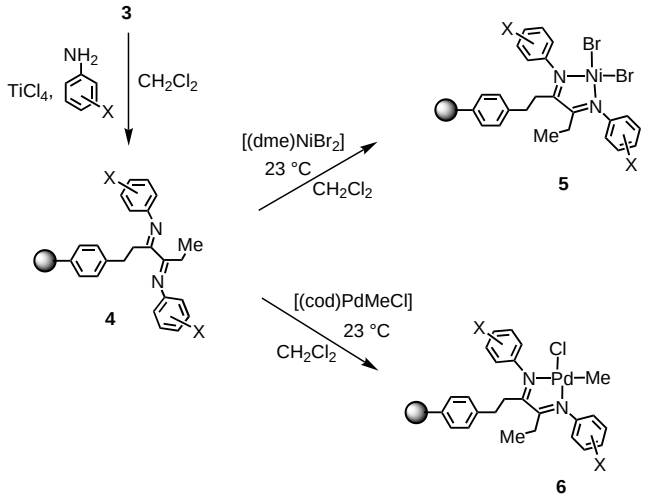
[*] V. Murphy, T. S. Powers, T. R. Boussie, C. Coutard, H. Turner
Symyx Technologies
3100 Central Expressway, Santa Clara, CA 95051 (USA)
Fax: (+1) 408-748-0175
E-mail: vmurphy@symyx.com
tpowers@symyx.com

[**] Financial support from Hoechst Research and Technology is acknowledged.

 © WILEY-VCH Verlag GmbH, D-69451 Weinheim, 1998 1433-7851/98/3723-3272 $ 17.50+.50/0



Scheme 1. Preparation of the solid-phase diketone resin **3**. The sphere represents 1% cross-linked polystyrene.



Scheme 2. Preparation of complexes **5** and **6**. dme = 1,2-dimethoxyethane, cod = 1,5-cyclooctadiene.

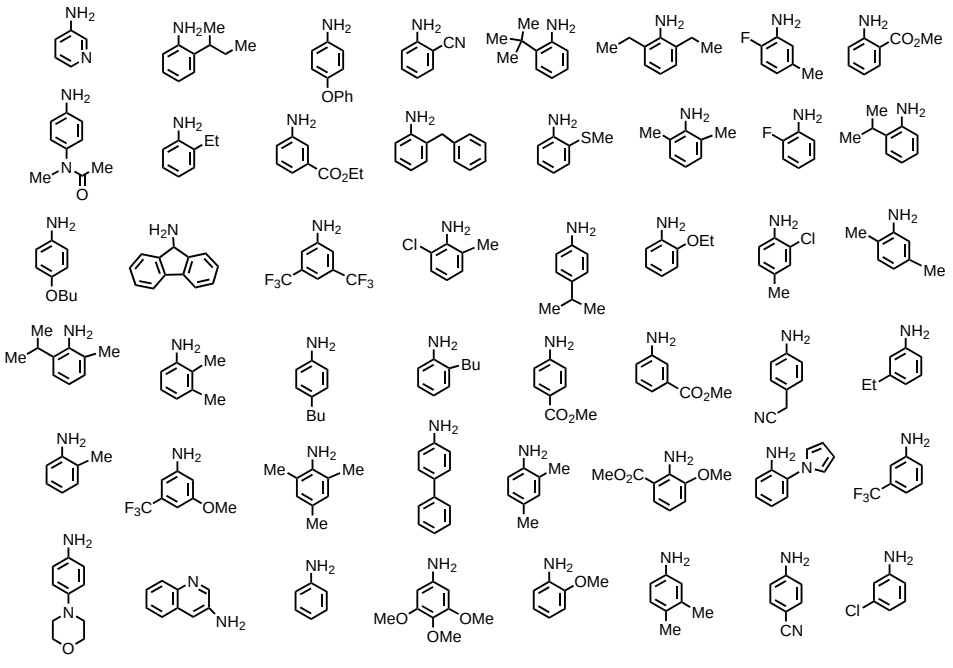
A total of 48 commercially available anilines with varying steric and electronic substituents (Table 1) was then used to prepare the corresponding 1,2-diimine resins. We obtained the best results when employing $TiCl_4$ as a Lewis acid (15 equiv) with the appropriate aniline (30 equiv) to effect 1,2-diimine formation (Scheme 2). A thorough washing protocol was implemented after this step to minimize excess aniline and titanium contamination of the library. These solid-supported 1,2-diimines were then split and converted into a 96-member solid-phase library consisting of Ni^{II} and Pd^{II} complexes **5** and **6**, respectively, in a parallel spatially addressable format.

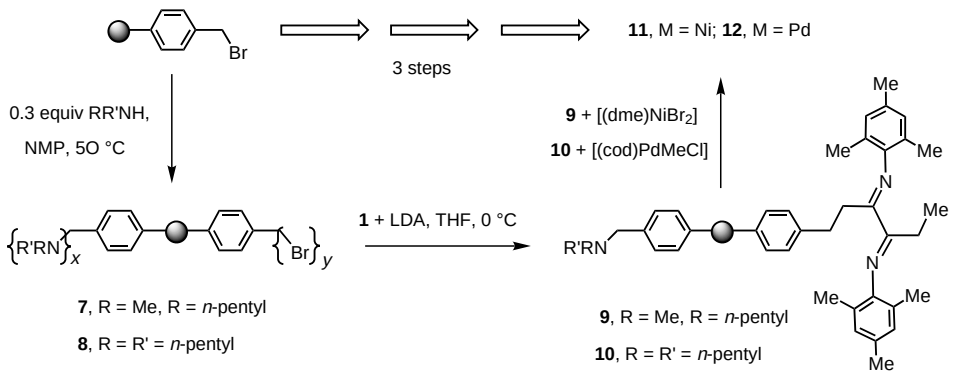
The active, cationic resin-bound Ni^{II} catalysts were generated in situ by the addition of methylalumoxane (MAO, 300 equiv) in toluene, whereas the resin-bound Pd^{II} catalysts were activated by the addition of sodium tetrakis(3,5-bistrifluoromethyl)phenyl borate (5 equiv) in dichloromethane. The beads were stirred at room temperature for 30 minutes before being exposed to ethylene in a high-pressure parallel polymerization reactor (60 psi) to ensure complete activation of the catalysts. Preliminary screening data from the library suggests that the solid-supported Ni^{II} catalysts display lower activities and produce polymers with lower molecular weight M_w relative to the corresponding solution-phase analogues which were synthesized by traditional methods and screened under identical conditions.

The polyethylene obtained from the supported catalyst, however, was isolated as discrete granules that had grown significantly in diameter (2–10 times) when compared to the initial polystyrene beads (diameter 70 μm). The polyethylene granules were isolated through a simple filtration step which allows for the convenient removal of excess MAO. In contrast to the solid-supported Ni^{II} catalysts, preliminary data suggest that the solid-supported Pd^{II} catalysts display higher activity than their solution-phase counterparts. Gel permeation chromatography (GPC) data also indicated that the molecular weights M_w and polydispersities (M_w/M_n) were nearly identical. Overall, the observed trends in relative activity and molecular weights obtained from the solid-supported catalysts were in agreement with related, previously reported systems prepared through traditional synthetic methods.[9]

To implement a chemical encoding strategy,[12, 13] substochiometric amounts of secondary amines were added as tags to (bromomethyl)polystyrene (0.3 equiv of RR′NH, *N*-methylpyrrolidone (NMP), 50 °C; **7**: R = Me, R′ = *n*-pentyl; **8**: R = R′ = *n*-pentyl) prior to attachment of the 1,2-diimine ligands (Scheme 3). The synthetic sequence shown herein was then used to prepare the tagged, polystyrene-supported Ni^{II} and Pd^{II}

Table 1. Commercially available anilines used to prepare 48 solid-phase 1,2-dimine ligands.





Scheme 3. Preparation of chemically tagged 1,2-diimine complexes of Ni^{II} (**11**) and Pd^{II} (**12**).

complexes **11** and **12**. The catalysts were pooled into a single reactor, activated with MAO, and exposed to 4.14 bar ethylene for 30 minutes. Upon workup, the product morphologies, when viewed under a microscope, indicated the presence of two distinct sizes of polymer products (Figure 1).

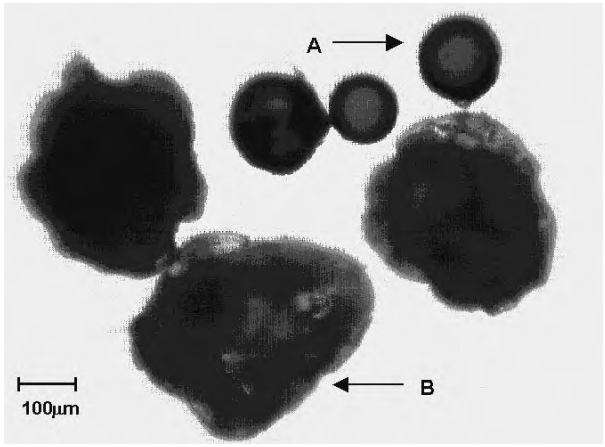


Figure 1. Microscope images of representative products obtained from a pooled polymerization. A: Product from the palladium catalyst, B: product from the nickel catalyst.

Five larger beads and five smaller beads were selected for decoding, which consisted of an amine cleavage procedure[14] coupled with HPLC and fluorescence detection (Figure 2).[12] Specifically, the beads were first treated with α-chloroethyl chloroformate, a reagent known to cleave N-benzyl-linked tertiary amines from solid supports. The cleaved secondary amines were then derivatized with dansyl chloride prior to detection by HPLC with fluorescence detection.[12] Importantly, the HPLC traces confirm a) the presence of the secondary amine tags, and b) that the larger polymer granules were prepared from the nickel catalyst, in accordance with the known relative performance trends of 1,2-diimine–Ni^{II} and 1,2-diimine–Pd^{II} olefin polymerization catalysts.[9,15] Thus, in these systems, olefin polymerization catalysts can be chemically encoded and pooled into a single reactor, and the resultant polymer granules can be decoded to deduce the synthetic history of the incipient polystyrene support.

The work described here demonstrates the feasibility of applying combinatorial techniques—including solid-support-ed synthesis, on-bead screening, and the potential for deconvoluting pooled libraries of catalysts—for the discovery and optimization of new catalysts. With these techniques now realized, work is currently underway to fully examine the library trends observed thus far and to expand the scope and utility of the techniques described herein to other olefin polymerization catalyst systems.

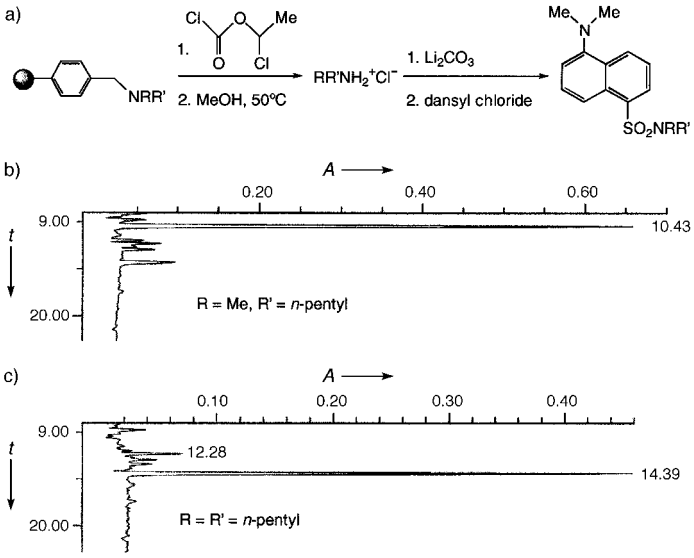


Figure 2. a) The decoding procedure. b, c) HPLC traces from the decoded products from five large beads and five small beads, respectively, formed with the nickel catalyst **11** and the palladium catalyst **12**.

Experimental Section

General procedure for the solid-phase synthesis of diketone **3**: To a cooled solution (0 °C) of 1,2-diimine **1** (0.50 g, 1.49 mmol) in dry THF (15 mL) under nitrogen was added LDA (1.09 mL, 1.49 mmol, 1.5 M in THF). After the mixture was stirred at 0 °C for 2 h, (bromomethyl)polystyrene (1.06 g, 0.75 mmol) was added, and the resulting suspension was stirred for 3 h at 0 °C and then 10 h at room temperature. The resin was filtered, washed with THF (2×10 mL), H_2O (2×20 mL), and CH_2Cl_2 (2×20 mL), and dried under high vacuum to afford 1.60 g of **2**. The loading capacity of this resin was calculated to be 0.40 mmol g^{-1} based on nitrogen analysis (1.21 % N). A strong absorbance at 1635 cm^{-1} (C=N) is observed by single-bead FT-IR spectroscopy. A stirred suspension of **2** (0.25 g, 0.09 mmol) and oxalic acid (42 mg, 0.47 mmol) in THF/H_2O (10 mL, 5/1 v/v) was heated to 70 °C for 12 h. After cooling to room temperature, the resin was filtered and washed with DMF (2×10 mL), H_2O (2×10 mL), and THF (2×10 mL) to yield 0.15 g of diketone resin **3**. A strong absorbance at 1712 cm^{-1} (C=O) is observed by single-bead FT-IR spectroscopy.

General procedure for the solid-phase synthesis of 1,2-diimine resins **4** and the corresponding complexes of Ni^{II} and Pd^{II}: The reactions were performed in glass tubes in a 48-cell parallel reactor. To a suspension of diketone resins **2** (0.10 g, 0.08 mmol) in dry CH_2Cl_2 (8 mL) was added the appropriate aniline (2.40 mmol) and $TiCl_4$ (1.20 mL, 1.20 mmol, 1.0 M in CH_2Cl_2) under nitrogen. The suspensions were shaken at room temperature for 24 h, after which the resins were filtered and washed extensively with CH_2Cl_2 (3×10 mL), $NaOCH_3$ in THF/MeOH (3×10 mL), and THF

 © WILEY-VCH Verlag GmbH, D-69451 Weinheim, 1998 1433-7851/98/3723-3274 $ 17.50+.50/0

(3×10 mL), and dried under high vacuum to yield the desired 1,2-diimine resins **4**. These resins were then split and converted into the corresponding complexes of Ni^{II} (**5**) and Pd^{II} (**6**) by the addition of [(dme)$NiBr_2$] (30 mg, 0.10 mmol) or [(cod)PdMeCl] (27 mg, 0.10 mmol) in CH_2Cl_2 (10 mL), and the reaction block was shaken for 12 h. The resins were then washed with CH_2Cl_2 (4×10 mL) and dried under high vacuum to afford the desired resin-bound complexes. Loading capacities for these resins were calculated to be approximately 0.30 mmol g^{-1} based on Ni and Pd analysis.

Received: June 22, 1998 [Z12025IE]
German version: *Angew. Chem.* **1998**, *110*, 3472 – 3475

Keywords: combinatorial chemistry · heterogeneous catalysis · polymers · solid-phase synthesis

[1] a) N. K. Terrett, M. Gardner, D. W. Gordon, R. J. Kobylecki, J. Steele, *Tetrahedron* **1995**, *30*, 8135 – 8173; b) E. M. Gordon, M. A. Gallop, D. V. Patel, *Acc. Chem. Res.* **1996**, *29*, 144 – 154.

[2] a) X.-D. Xiang, X. S. Sun, G. Briceño, Y. Lou, K.-A. Wang, H. Chang, W. G. Wallace-Freedman, S.-W. Chen, P. G. Schultz, *Science* **1995**, *268*, 1738 – 1740; b) G. Briceño, H. Chang, X. Sun, P. G. Schultz, S.-W. Chen, *Science* **1995**, *270*, 273 – 275; c) K. Burgess, D. Moye-Sherman, A. M. Porte in *Molecular Diversity Combinatorial Chemistry: Library Drug Discovery* (Eds.: I. M. Irwin, K. D. Janda), American Chemical Society, Washington, DC, **1996**, pp. 128 – 136; d) K. Burgess, A. M. Porte, *Adv. Catal. Processes* **1997**, *2*, 69 – 82; e) E. Danielson, J. H. Golden, E. McFarland, C. M. Reaves, W. H. Weinberg, X. D. Wu, *Nature* **1997**, *389*, 944 – 948; f) H. W. Weinberg, B. Jandeleit, K. Self, H. Turner, *Curr. Opin. Solid State Mater. Sci.* **1998**, *3*, 104 – 110.

[3] a) K. Burgess, H.-J. Lim, A. M. Porte, G. A. Sulikowski, *Angew. Chem.* **1996**, *108*, 192 – 194; *Angew. Chem. Int. Ed. Engl.* **1996**, *35*, 220 – 222; b) K. D. Shimuzu, B. M. Cole, C. A. Krueger, K. W. Kuntz, M. L. Snapper, A. H. Hoveyda, *Angew. Chem.* **1997**, *109*, 1784 – 1785; *Angew. Chem. Int. Ed. Engl.* **1997**, *36*, 1700 – 1702; c) S. R. Gilbertson, X. Wang, *Tetrahedron Lett.* **1996**, *37*, 6475 – 6478; d) G. Lui, J. A. Ellman, *J. Org. Chem.* **1995**, *60*, 7712 – 7713; e) M. S. Sigman, E. N. Jacobsen, *J. Am. Chem. Soc.* **1998**, *110*, 4901 – 4902; f) M. B. Francis, N. S. Finney, E. N. Jacobsen, *J. Am. Chem. Soc.* **1996**, *118*, 8983 – 8984.

[4] N. Kashiwa, J. Imuta, *Catal. Surv. Jpn.* **1997**, *1*, 125 – 142.

[5] a) L. Sun, A. Shariati, J. C. Hsu, D. W. Bacon, *Stud. Surf. Sci. Catal.* **1994**, *89*, 81 – 89; b) L. Sun, C. C. Hsu, D. W. Bacon, *J. Polym. Sci. Part A* **1994**, *32*, 2127 – 2134.

[6] S. B. Roscoe, J. M. Fréchet, J. F. Walzer, A. J. Dias, *Science* **1998**, *280*, 270 – 273.

[7] a) F. Balkenhohl, C. von dem Bussche-Hünnefeld, A. Lansky, C. Zechel, *Angew. Chem.* **1996**, *108*, 2436 – 2488; *Angew. Chem. Int. Ed. Engl.* **1996**, *35*, 2288 – 2337; b) J. S. Früchtel, G. Jung, *Angew. Chem.* **1996**, *108*, 19 – 46; *Angew. Chem. Int. Ed. Engl.* **1996**, *35*, 17 – 42; c) L. A. Thompson, J. Ellman, *Chem. Rev.* **1996**, *96*, 555 – 600; d) P. H. H. Hermkens, H. C. J. Ottenheijm, D. Rees, *Tetrahedron* **1996**, *52*, 4527 – 4554; e) S. J. Shuttleworth, S. M. Allin, P. K. Sharma, *Synthesis* **1997**, 1217 – 1239.

[8] a) L. K. Johnson, C. M. Killian, M. Brookhart, *J. Am. Chem. Soc.* **1995**, *117*, 6414 – 6415; b) C. M. Killian, L. K. Johnson, M. Brookhart, *Organometallics* **1997**, *16*, 2005 – 2007; c) B. L. Small, M. Brookhart, A. M. A. Bennett, *J. Am. Chem. Soc.* **1998**, *120*, 4049 – 4050; d) G. J. P. Britovsek, V. C. Gibson, B. S. Kimberly, P. J. Maddox, S. J. McTavish, G. A. Solan, A. J. P. White, D. J. Williams, *Chem. Commun.* **1998**, 849 – 850.

[9] L. K. Johnson, S. Mecking, M. Brookhart, *J. Am. Chem. Soc.* **1996**, *118*, 267 – 268.

[10] W. H. Weinberg, E. McFarland, I. Goldwasser, T. Bousie, H. Turner, J. A. M. van Beek, V. Murphy, T. Powers (Symyx Technologies), WO-A 98/03521, **1998**.

[11] N. DeKimpe, L. D'Hondt, E. Stanoeva, *Tetrahedron Lett.* **1991**, *32*, 3879 – 3882.

[12] a) D. Maclean, J. R. Schullek, M. M. Murphy, Z. J. Ni, E. M. Gordon, M. A. Gallop, *Proc. Natl. Acad. Sci. USA* **1997**, *94*, 2805 – 2810; b) Z. J. Ni, D. Maclean, C. P. Holmes, B. Ruhland, M. M. Murphy, J. W. Jacobs, E. M. Gordon, M. A. Gallop, *J. Med. Chem.* **1996**, *39*, 1601 – 1608.

[13] Review on encoding strategies: A. W. Czarnik, *Curr. Opin. Chem. Biol.* **1997**, *1*, 60 – 66, and references therein.

[14] The method employed was similar to that described in P. Conti, D. Demont, J. Cals, H. Ottenheijm, D. Leysen, *Tetrahedron Lett.* **1997**, *38*, 2915 – 2918.

[15] The tagged catalysts were also run separately to assess relative performance trends.

Dendritic Pseudorotaxanes**

Nori Yamaguchi, Lesley M. Hamilton, and Harry W. Gibson*

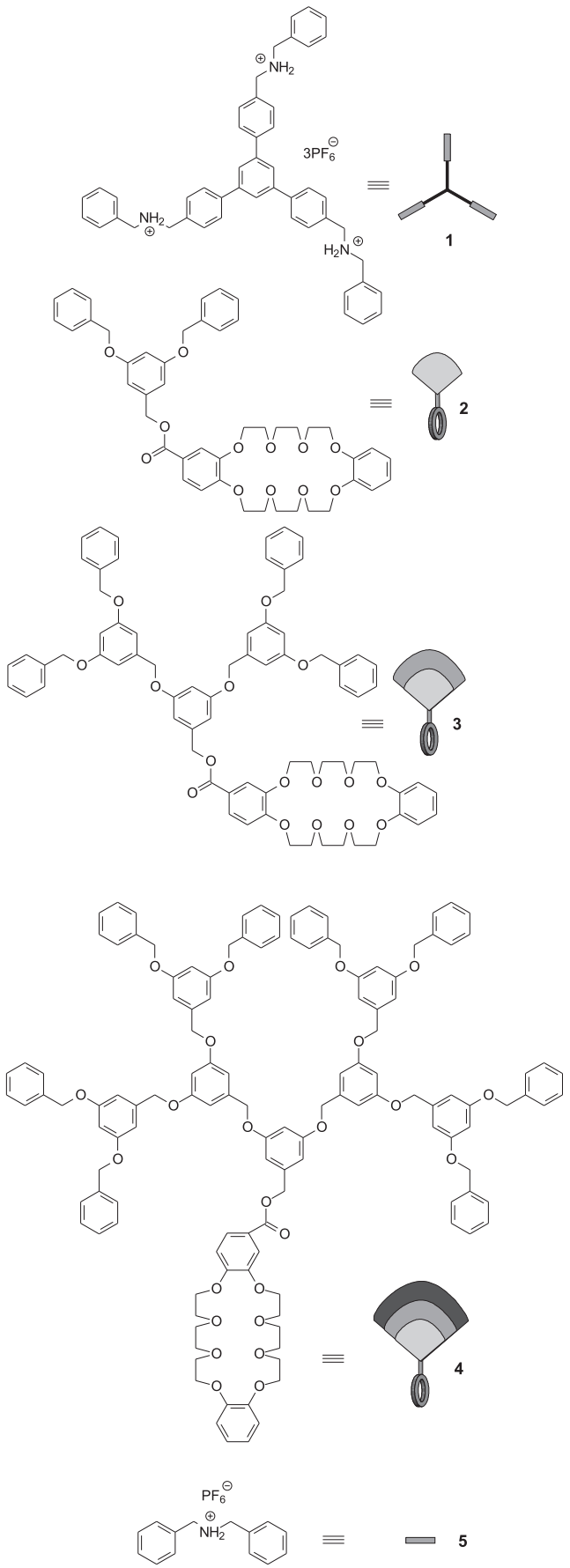
While dendrimers begin to find their potential applications in the fields of molecular electronics,[1] material science (high-performance polymers, catalysts, adhesives, etc.),[2] and membrane chemistry,[3] structural control[4] and synthetic efficiency still remain the major issues in dendrimer research. Three synthetic methods (convergent,[5] divergent,[6] and double-stage convergent[7]) are recognized, up to now, for the preparation of high molecular weight, monodisperse dendrimers. Recently, Zimmerman and Feng introduced a synthetic approach based on self-organization, which guarantees structural accuracy while eliminating steps from the conventional multistep approach.[8] In this case, six subunits were brought together by hydrogen bonding to construct supramolecular dendritic structures up to the fourth generation. Here, we report a concise self-organizing dendrimer synthesis in which 1:3 pseudorotaxane complexes between a triply charged ammonium salt (**1**)[9] (Scheme 1) and substituted dibenzo[24]crown-8 (DB24C8) units make up the core portions of the dendritic architectures. This is based on the finding of Stoddart et al. that DB24C8 forms pseudorotaxanes with secondary ammonium salts through noncovalent bonding.[10]

The cyclization reaction between tri(ethylene glycol) dichloride and methyl 3,4-dihydoxybenzoate at high dilution gave 4-methoxycarbonyldibenzo[24]crown-8 in 40% yield. The ester group was hydrolyzed and then esterified with a series of benzyl ether dendrons bearing primary alcohol moieties ([G1]-OH, [G2]-OH, and [G3]-OH)[5] using the redox system diethyl azodicarboxylate (DEAD) and triphenylphosphane (TPP)[11] to afford the corresponding dendrons with the macrocyclic unit at the focal points (**2** – **4**; Scheme 1). Our strategy to construct a series of self-organizing dendrimers is illustrated in Scheme 2.

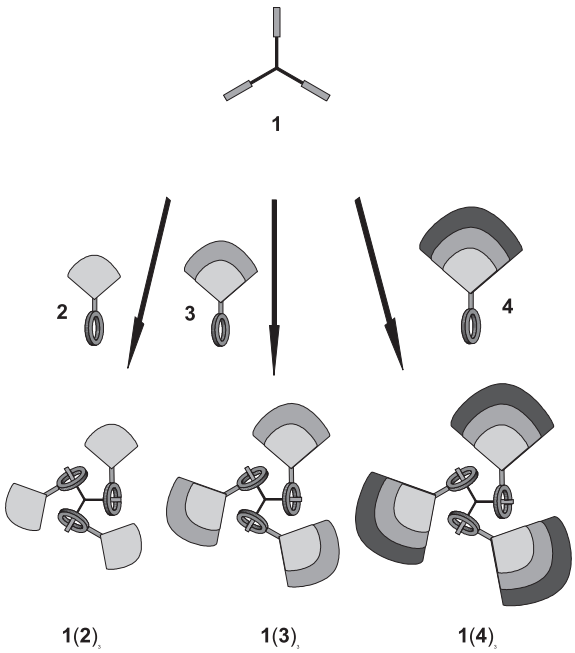
[*] Prof. H. W. Gibson, N. Yamaguchi, Dr. L. M. Hamilton
Department of Chemistry
Virginia Polytechnic Institute and State University
Blacksburg, Virginia, 24061 (USA)
Fax: (+1) 540-231-8517
E-mail: hwgibson@vt.edu

[**] This work was supported by the National Science Foundation (CHE95-21738). Mass spectra were provided by the Nebraska Center for Mass Spectrometry and the Washington University Mass Spectrometry Resource, an NIH Research Resource (grant no. P41RR0954).

 © WILEY-VCH Verlag GmbH, D-69451 Weinheim, 1998 1433-7851/98/3723-3275 $ 17.50+.50/0



Scheme 1. Cartoon representations of the tritopic salt **1**, [G1]-DB24C8 (**2**), [G2]-DB24C8 (**3**), and [G3]-DB24C8 (**4**), and the monotopic salt **5**.



Scheme 2. Schematic illustrations of the construction of a series of self-organizing dendritic pseudorotaxanes from complementary building blocks.

The first evidence of formation of the 1:3 dendritic pseudorotaxanes from **1** and the series of dendrons **2**–**4** in solution came from ^{1}H NMR spectrometry. In the case of the third-generation dendritic pseudorotaxane, when a 3.0×10^{-2} M solution of **4** in [D]chloroform was mixed with 1/3 mol equiv of solid **1**, the ^{1}H NMR spectrum of the mixture displayed signals associated with the complexed ammonium salt moiety of **1**, complexed **4**, and uncomplexed **4** on the basis of slow association and dissociation on the ^{1}H NMR time scale (Figure 1). A gradual dissolution of otherwise insoluble **1** with increasing mixing time was evidenced by the appearance of

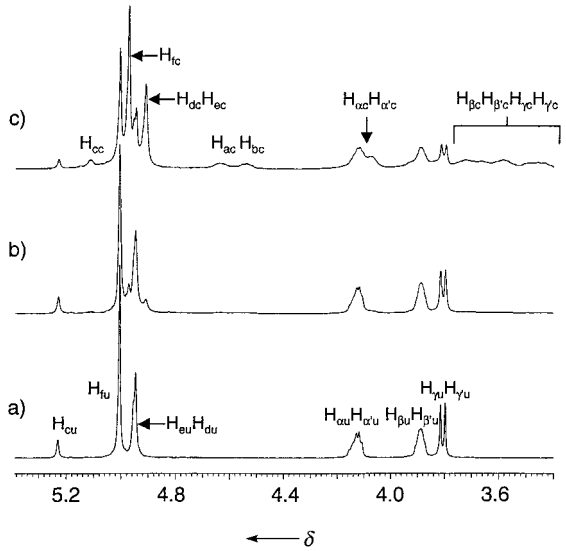
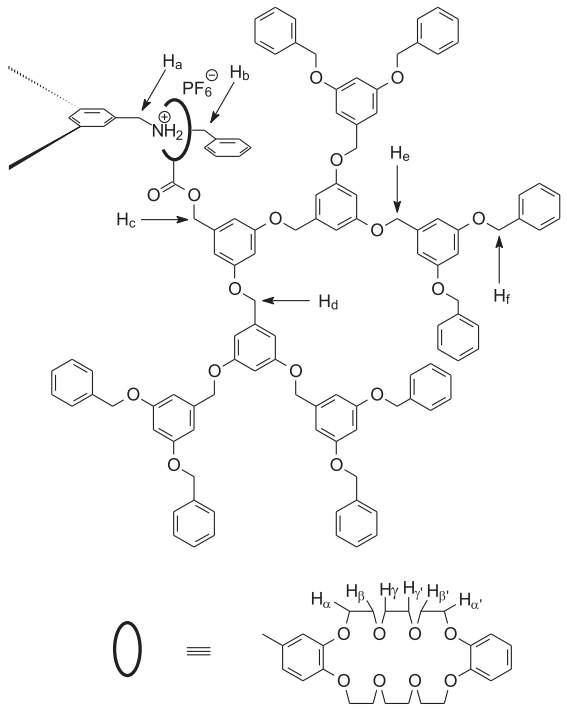


Figure 1. The aliphatic region of stacked ^{1}H NMR spectra (400 MHz, [D]chloroform, 21.8 °C) of a 3.0×10^{-2} M solution of **4** (a) and a 3.0×10^{-2} M solution of **4** mixed with 1/3 mol equiv of solid **1** recorded after 10 min (b) and 72 h (c).

 © WILEY-VCH Verlag GmbH, D-69451 Weinheim, 1998 1433-7851/98/3723-3276 $ 17.50+.50/0

the new signals for H_{ac} and H_{bc} of the complexed ammonium salt moiety of **1** (Scheme 3) and their gradual increase in intensity. The stoichiometry of the complex was determined to be 1:3 by simple integration of the signals for relevant protons since the signals for H_{au} and H_{bu} of the uncomplexed ammonium salt moiety of **1** were undetected, indicating the absence of the 1:1 and 1:2 complexes in chloroform. Ammonium salt **1** was taken into solution slowly (dissolution of 17, 57, and 59% after 10 min, 48 h, and 72 h, respectively), and the complexation process finally reached equilibrium after 72 h.

The slow formation of dendritic pseudorotaxane $\mathbf{1}(\mathbf{4})_3$ is presumably due to a combination of the poor solubility of **1** and steric hindrance experienced by neighboring dendron units in the 1:3 complex. The latter can be explained by the following two spectroscopic observations. 1) Significant upfield chemical shifts (Figure 1) were observed for the complexed benzylic protons H_{cc}, H_{dc}, H_{ec}, and H_{fc} of **4** in $\mathbf{1}(\mathbf{4})_3$ (see Scheme 3). By contrast, the ^{1}H NMR spectra of a 1.0×10^{-2} M solution of **4** in [D]chloroform mixed with 1 mol equiv of solid dibenzylammonium hexafluorophosphate (**5**), which were recorded periodically with increasing mixing time, were identical and showed that the signals for the benzylic protons



Scheme 3. The designation of the benzylic protons in **1** and **4** for the signal assignments in Figure 1.

of **4** in the 1:1 complex **4**(**5**) were not distinguishable from those of uncomplexed **4**.[12] 2) Similar ^{1}H NMR experiments for the formation of the dendritic pseudorotaxanes $\mathbf{1}(\mathbf{2})_3$ and $\mathbf{1}(\mathbf{3})_3$ in [D]chloroform revealed that complexation equilibrium was reached more quickly when the dendron units were less bulky (after 36 and 48 h, respectively).

Gel permeation chromatography (GPC) is routinely used for analyzing dendrimers, but accurate determination of molecular weight is difficult even with the principle of the universal calibration due to the low hydrodynamic volume of dendrimers.[5] In the present case in chloroform at 25 °C $\mathbf{1}(\mathbf{4})_3$ apparently dissociates in the column; only **4** elutes and salt **1** is retained in the column.

Mass spectrometry has been utilized increasingly in the characterization of dendrimers through the use of fast atom bombardment (FAB),[13] electron spray ionization (ESI),[14] and matrix-assisted laser desorption ionization time-of-flight (MALDI-TOF) techniques.[15] By these analytical methods mass accuracies are in the range of 0.0027 – 0.10%. The application of these techniques was thus extended to the self-organized dendritic pseudorotaxanes. The third-generation dendritic pseudorotaxane $\mathbf{1}(\mathbf{4})_3$ was characterized by MALDI-TOF-MS because of its high mass.[16] The spectrum (Figure 2) was dominated by three peaks which correspond to 1:3, 1:2, and 1:1 complexes.[17] The wholly complexed

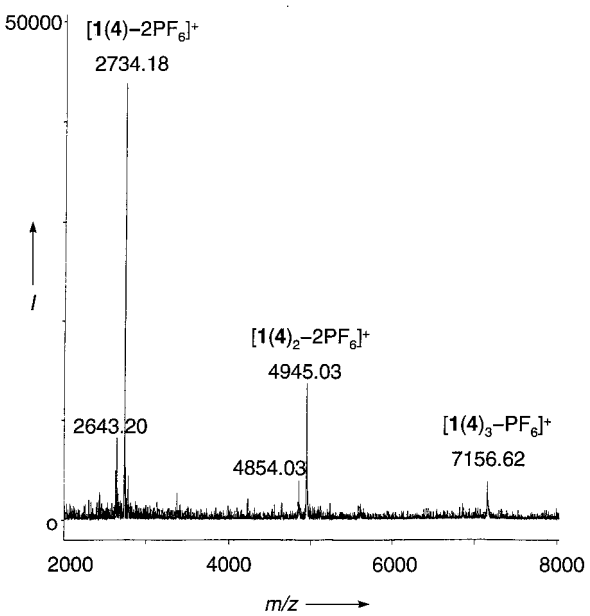


Figure 2. The MALDI-TOF mass spectrum of the third-generation dendritic pseudorotaxane $\mathbf{1}(\mathbf{4})_3$. The spectrum was measured in the positive-ion mode using 2,5-dihydroxybeznoic acid as the matrix and acetone as the solvent. I = signal intensity in counts.

dendritic pseudorotaxane $\mathbf{1}(\mathbf{4})_3$ was detected at m/z 7156.62 after loss of PF_6^-. The 1:2 and 1:1 complexes give rise to the peaks at m/z 4945.03 and 2734.18, respectively. The lower abundance side peaks at m/z 4854.03 and 2643.2 are found at regular intervals from $[\mathbf{1}(\mathbf{4})_2 - 2\,PF_6]^+$ and $[\mathbf{1}(\mathbf{4}) - 2\,PF_6]^+$ ($\Delta(m/z)$ 91.00 and 90.98, respectively), indicating loss of benzyl groups from the periphery of the dendrons. The calculated and observed masses (< 0.1% error) of the self-organized dendritic pseudorotaxanes $\mathbf{1}(\mathbf{2})_3$, $\mathbf{1}(\mathbf{3})_3$, and $\mathbf{1}(\mathbf{4})_3$ are summarized in Table 1.

We have designed and constructed various generations of self-organizing pseudorotaxane dendrimers concisely and efficiently. The ^{1}H NMR investigations in [D]chloroform indicated formation of the self-organizing dendritic pseudorotaxanes as a result of a simple recognition between the secondary ammonium salt moieties in **1** and dibenzo[24]-crown-8 units at the focal points of the dendron units. Mass

 © WILEY-VCH Verlag GmbH, D-69451 Weinheim, 1998 1433-7851/98/3723-3277 $ 17.50+.50/0

Table 1. Molecular formulae, calculated molecular masses, and observed (MS) mass/charge ratios of the supramolecular structures.

Structure	Molecular formula	Calcd mass	Obs m/z
$\mathbf{1}(\mathbf{2})_3 - PF_6$[a]	$C_{48}H_{48}N_3P_2F_{12}(C_{46}H_{50}O_{12})_3$	3339.3	3339.5
$\mathbf{1}(\mathbf{2})_2 - 2PF_6$[a]	$C_{48}H_{48}N_3PF_6(C_{46}H_{50}O_{12})_2$	2400.0	2400.2
$\mathbf{1}(\mathbf{2}) - 3PF_6$[a]	$C_{48}H_{48}N_3(C_{46}H_{50}O_{12})$	1460.7	1459.2
$\mathbf{1}(\mathbf{3})_3 - PF_6$[b]	$C_{48}H_{48}N_3P_2F_{12}(C_{74}H_{74}O_{16})_3$	4611.81	4611.06
$\mathbf{1}(\mathbf{3})_2 - 2PF_6$[b]	$C_{48}H_{48}N_3PF_6(C_{74}H_{74}O_{16})_2$	3248.34	3248.69
$\mathbf{1}(\mathbf{3}) - 2PF_6$[b]	$C_{48}H_{48}N_3PF_6(C_{74}H_{74}O_{16})$	1884.88	1884.90
$\mathbf{1}(\mathbf{4})_3 - PF_6$	$C_{48}H_{48}N_3P_2F_{12}(C_{130}H_{122}O_{24})_3$	7156.81	7156.62
$\mathbf{1}(\mathbf{4})_2 - 2PF_6$	$C_{48}H_{48}N_3PF_6(C_{130}H_{122}O_{24})_2$	4945.01	4945.03
$\mathbf{1}(\mathbf{4}) - 2PF_6$	$C_{48}H_{48}N_3PF_6(C_{130}H_{122}O_{24})$	2733.22	2734.18

[a] The FAB mass spectrum of the first-generation dendritic pseudorotaxanes was recorded in the positive-ion mode with 3-nitrobenzyl alcohol as the matrix and acetone as the solvent. [b] The FAB mass spectrum of the second-generation dendritic pseudorotaxanes was measured in the positive-ion mode with *trans*-3-indoleacrylic acid as the matrix and THF as the solvent.

spectrometry was also used to characterize the self-organized dendritic pseudorotaxanes. Space-filling (CPK) models of $\mathbf{1}(\mathbf{2})_3$, $\mathbf{1}(\mathbf{3})_3$, and $\mathbf{1}(\mathbf{4})_3$ show ball-shaped aggregates with diameters of approximately 8, 10, and 12 nm, respectively. This approach based on self-organization offers the possibility of generating even larger and more complex supramolecular dendrimers.

Experimental Section

4-Methoxycarbonyldibenzo[24]crown-8: To a 5-L three-necked, round-bottomed flask equipped with a mechanical stirrer, N_2 inlet, and a thermometer were added DMF (3.5 L), nBu$_4$NI (100 mg), and K_2CO_3 (80.60 g, 584 mmol), and the mixture was heated to 110 °C. A solution of *o*-bis(8-chloro-3,6-dioxooctyloxy)benzene (25.4 g, 61.8 mmol) and methyl 3,4-dihydroxybenzoate (10.4 g, 61.8 mmol) in DMF (120 mL) was added by syringe pump at the rate of 0.75 mL h^{-1}. After the addition was complete the reaction mixture was vigorously stirred for 3 d, cooled to 25 °C, and filtered through celite. The solvent was removed to give a brown viscous liquid. This was preabsorbed onto silica gel and the product was continuously extracted with Et_2O using a Soxhlet extraction apparatus. After the solvent was removed, the resulting yellow solid was recrystallized from EtOH to give a white powder (12.5 g, 39.8 % yield). M.p. 83 – 85 °C; ^{1}H NMR ($CDCl_3$): $\delta = 3.84$ (8H, m), 3.87 (3H, s), 3.93 (8H, m), 4.15 (4H, t, $J = 8.0$ Hz), 4.19 (4H, t, $J = 8.0$ Hz), 6.84 (1H, d, $J = 8.4$ Hz), 6.88 (4H, m), 7.52 (1H, d, $J = 2.0$ Hz), 7.64 (1H, dd, $J = 2.0$, 8.4 Hz); low-resolution (LR) FAB-MS: m/z: 506.2 $[M]^+$, 475.2 $[M - OCH_3]^+$; high-resolution (HR) FAB-MS: calcd for $[M]^+$ $C_{26}H_{34}O_{10}$: 506.2152; found: 506.2132; elemental analysis calcd for $C_{26}H_{34}O_{10}$: C 61.65, H 6.77; found: C 61.75, H 6.80.

4-Carboxydibenzo[24]crown-8: A 250-mL one-necked, round-bottomed flask was charged with 4-methoxycarbonyldibenzo[24]crown-8 (3.16 g, 6.24 mmol) and EtOH (100 mL). A solution of aqueous KOH (4 M, 10 mL) was added dropwise and the reaction mixture was heated at reflux for 12 h. Upon completion of the reaction the solvent was removed to give an off-white solid, which was redissolved in H_2O (100 mL) and neutralized with H_2SO_4. The solution was extracted with CH_2Cl_2 (2 × 100 mL), and the organic layers were combined, dried over $MgSO_4$, and concentrated to give a white solid, which was recrystallized from EtOH to give a white solid (2.73 g, 88.9 % yield). M.p. 182 – 183 °C; ^{1}H NMR ($CDCl_3$): $\delta = 3.84$ (8H, m), 3.93 (8H, m), 4.15 (4H, t, $J = 4.0$ Hz), 4.20 (4H, t, $J = 4.0$ Hz), 6.88 (5H, m), 7.56 (1H, d, $J = 1.6$ Hz), 7.71 (1H, dd, $J = 1.6$, 8.4 Hz); LR FAB-MS: m/z: 531.1 $[M + K]^+$, 492.2 $[M]^+$; HR FAB-MS: calcd for $[M]^+$ $C_{25}H_{32}O_{10}$: 492.1995; found: 492.1985; elemental analysis calcd for $C_{25}H_{32}O_{10}$: C 60.97, H 6.55; found: C 61.19, H 6.60.

General procedure for **2** – **4:** A 25-mL round-bottomed flask equipped with a magnetic stirrer was charged with the appropriate dendritic benzyl alcohol ([G1]-OH, [G2]-OH, or [G3]-OH)[5] (1.00 equiv), 4-carboxydibenzo[24]crown-8 (1.00 equiv), TPP (1.50 equiv), and THF. DEAD (1.50 equiv) was added dropwise by syringe, and the reaction mixture was stirred at 25 °C for 10 h. The solvent was evaporated to give a white solid (a yellow viscous liquid in the cases of **3** and **4**), which was passed through a short column of silica gel with EtOAc as the eluent. The resulting white solid (colorless viscous liquid in the cases of **3** and **4**) was redissolved in EtOAc and precipitated into MeOH to afford a white solid (a clear glass in the cases of **3** and **4**).

[G1]-DB24C8 (**2**): 84 % yield; m.p. 113 – 114 °C (MeOH); ^{1}H NMR ($CDCl_3$): $\delta = 3.84$ (8H, m), 3.93 (8H, m), 4.15 (4H, m), 4.20 (4H, m), 5.04 (4H, s), 5.26 (2H, s), 6.59 (1H, t, $J = 2.0$ Hz), 6.67 (2H, d, $J = 2.0$ Hz), 6.84 (1H, d, $J = 8.8$ Hz), 6.88 (4H, m), 7.30 – 7.43 (10H, m), 7.55 (1H, d, $J = 2.0$ Hz), 7.67 (1H, dd, $J = 2.0$, 8.8 Hz); LR FAB-MS: m/z: 794.4 $[M]^+$; HR FAB-MS: calcd for $[M]^+$ $C_{46}H_{50}O_{12}$ 794.3302; found: 794.3300: elemental analysis calcd for $C_{46}H_{50}O_{10}$: C 69.51, H 6.34; found: C 69.43, H 6.31.

[G2]-DB24C8 (**3**): 89 % yield, colorless glass; ^{1}H NMR ($CDCl_3$): $\delta = 3.82$ (8H, m), 3.91 (8H, m), 4.13 – 4.18 (8H, m), 4.97 (4H, s), 5.02 (8H, s), 5.25 (2H, s), 6.55 (1H, t, $J = 2.0$ Hz), 6.56 (2H, t, $J = 2.0$ Hz), 6.65 (2H, d, $J = 2.0$ Hz), 6.67 (4H, d, $J = 2.0$ Hz), 6.81 (1H, d, $J = 8.4$ Hz), 6.84 – 6.90 (4H, m), 7.31 – 7.41 (20H, m), 7.54 (1H, d, $J = 2.0$ Hz), 7.65 (1H, dd, $J = 2.0$, 8.4 Hz); LR FAB-MS: m/z: 1218.6 $[M]^+$; HR FAB-MS: calcd for $[M]^+$ $C_{74}H_{74}O_{16}$ 1218.4977; found: 1218.4943; elemental analysis calcd for $C_{74}H_{74}O_{16}$: C 72.89, H 6.12; found: C 72.82; H 6.10.

[G3]-DB24C8 (**4**): 93 % yield, colorless glass; ^{1}H NMR ($CDCl_3$): $\delta = 3.81$ (m, 8H), 3.89 (m, 8H), 4.13 (m, 8H), 4.95 (s, 12H), 5.01 (s, 16H), 5.23 (s, 2H), 6.53 (t, 2H, $J = 2.4$ Hz), 6.56 (t, 4H, $J = 2.4$ Hz), 6.58 (t, 1H, $J = 2.4$ Hz), 6.66 (m, 14H), 6.80 (d, 1H, $J = 8.4$ Hz), 6.87 (m, 4H), 7.28 – 7.41 (m, 40H), 7.54 (s, 1H), 7.64 (d, 2H, $J = 8.4$ Hz); LR FAB-MS: m/z: 2090.9 $[M + Na]^+$; HR FAB-MS: calcd for $[M + Na]^+$ $C_{130}H_{122}O_{24}Na$ 2090.8257; found: 2090.8227.

Received: May 25, 1998 [Z11898IE]
German version: *Angew. Chem.* **1998**, *110*, 3463 – 3466

Keywords: dendrimers · noncovalent bonding · pseudorotaxanes · supramolecular chemistry

[1] a) R. Sadamoto, N. Tomioka, T. Aida, *J. Am. Chem. Soc.* **1996**, *118*, 3978 – 3979; b) L. L. Miller, R. G. Duan, D. C. Tully, D. A. Tomalia, *J. Am. Chem. Soc.* **1997**, *119*, 1005 – 1010.

[2] a) J. C. M. van Hest, D. A. P. Delnoye, M. W. P. L. Baars, C. Elissen-Roman, M. H. P. van Genderen, E. W. Meijer, *Chem. Eur. J.* **1996**, *2*, 1616 – 1626; b) G. R. Newkome, C. N. Moorefield, F. Vögtle, *Dendritic Molecules: Concepts, Synthesis, Perspectives*, VCH, Weinheim, **1996**; c) R. Kopelman, M. Shortreed, Z. Y. Shi, W. Tan, Z. Xu, J. S. Moore, A. Bar-Haim, J. Klafter, *Phys. Rev. Lett.* **1997**, *78*, 1239 – 1242; d) M. Kawa, J. M. J. Fréchet, *Chem. Mater.* **1998**, *10*, 286 – 296.

[3] a) J. F. G. A. Jansen, E. M. M. de Brabander-van den Berg, E. W. Meijer, *Science* **1994**, *266*, 1226 – 1229; b) J. F. G. A. Jansen, E. W. Meijer, *J. Am. Chem. Soc.* **1995**, *117*, 4417 – 4417.

[4] J. S. Moore, *Acc. Chem. Res.* **1997**, *30*, 402 – 413.

[5] K. L. Wooley, C. J. Hawker, J. M. J. Fréchet, *J. Am. Chem. Soc.* **1991**, *113*, 4252 – 4261.

[6] a) G. R. Newkome, Z. Yao, G. R. Baker, V. K. Gupta, P. S. Russo, M. J. Sanders, *J. Am. Chem. Soc.* **1986**, *108*, 849 – 850; b) D. A. Tomalia, H. Baker, J. Dewald, M. Hall, G. Kallos, S. Martin, J. Roeck, J. Ryder, P. Smith, *Macromolecules* **1986**, *19*, 2466 – 2468.

[7] T. Kawaguchi, K. L. Walker, C. L. Wilkins, J. S. Moore, *J. Am. Chem. Soc.* **1995**, *117*, 2159 – 2165.

[8] F. Zeng, S. C. Zimmerman, *Chem. Rev.* **1997**, *97*, 1681 – 1712.

[9] Compound **1** has been previously reported: P. R. Ashton, A. N. Collins, M. C. T. Fyfe, P. T. Glink, S. Menzer, J. F. Stoddart, D. J. Williams, *Angew. Chem.* **1997**, 109, 59 – 62; *Angew. Chem. Int. Ed. Engl.* **1997**, *36*, 59 – 62.

[10] a) P. R. Ashton, P. J. Campbell, E. J. T. Chrystal, P. T. Glink, S. Menzer, D. Philp, N. Spencer, J. F. Stoddart, P. A. Tasker, D. J. Williams, *Angew. Chem.* **1995**, *107*, 1997 – 2001; *Angew. Chem. Int. Ed. Engl.* **1995**, *34*, 1865 – 1869; b) P. R. Ashton, E. J. T. Chrystal, P. T.

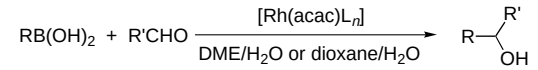
 © WILEY-VCH Verlag GmbH, D-69451 Weinheim, 1998 1433-7851/98/3723-3278 $ 17.50+.50/0

Glink, S. Menzer, C. Schiavo, N. Spencer, J. F. Stoddart, P. A. Tasker, A. J. P. White, D. J. Williams, *Chem. Eur. J.* **1996**, *2*, 709 – 728.
[11] a) O. Mitsunobu, *Synthesis* **1981**, *1*, 1 – 28; b) D. L. Hughes, *Org. Prep. Proced. Int.* **1996**, *28*, 127 – 164.
[12] The ^{1}H NMR spectra showed the existence of the 1:1 pseudorotaxane complex **4**(**5**) and uncomplexed **4** under conditions of slow exchange on the ^{1}H NMR time scale. The association constant for the 1:1 complex in chloroform was determined to be $7.9 \times 10^3\,\text{M}^{-1}$ (21.8 °C) from integration of the signals for the protons from complexed and uncomplexed **4** using the expression $K_a = [\mathbf{4}(\mathbf{5})]/[\mathbf{4}][\mathbf{5}]$. The K_a value for the 1:1 complex between the monotopic salt **5** and DB24C8 in [D]chloroform was estimated to be $2.7 \times 10^4\,\text{M}^{-1}$ (25 °C).[10] The lower association constant for 1:1 complex **4**(**5**) may be attributed to the reduced accessibility and flexibility of the macrocyclic moiety of **4** due to the bulky dendritic substituent.
[13] L. J. Twyman, A. E. Beezer, J. C. Mitchell, *J. Chem. Soc. Perkin Trans.* **1994**, *4*, 407 – 422.
[14] J. C. Hummelen, J. L. J. van Dongen, E. W. Meijer, *Chem. Eur. J.* **1997**, *3*, 1489 – 1493.
[15] a) Z. Xu, M. Kahr, K. L. Walker, C. L. Wilkins, J. S. Moore, *J. Am. Chem. Soc.* **1994**, *116*, 4537 – 4550; b) J. W. Leon, J. M. J. Fréchet, *Polym. Bull. Berlin* **1995**, *35*, 449 – 455.
[16] A solution of **4** (3.0×10^{-2} M) was mixed with 1/3 mol equiv of solid **1** for 3 d. The mixture was then filtered and the filtrate was concentrated to afford a white solid, which was submitted for MALDI-MS analysis.
[17] The apparent distribution of the complexes indicate partial dissociation of $\mathbf{1}(\mathbf{4})_3$ into subunits $\mathbf{1}(\mathbf{4})_2$ and **1**(**4**) during ionization. It is also noteworthy that MALDI-MS detectors are nonlinear with respect to molecular mass and thus do not give molar response. For a review on principles, instrumentation, and application of MALDI MS, see: F. Hillenkamp, M. Karas, R. C. Beavis, B. T. Chait, *Anal. Chem.* **1991**, *63*, 1193A – 1203A. ESI-MS has to date given similar results; we are currently investigating the use of low sample cone voltage (V_c) to minimize fragmentation. For reviews on characterization of hydrogen-bonded assemblies by ESI-MS, see: a) K. C. Russell, E. Leize, A. Van Dorsselaer, J.-M. Lehn, *Angew. Chem.* **1995**, *107*, 244 – 248; Angew. *Chem. Int. Ed. Engl.* **1995**, *34*, 209 – 213; b) X. Cheng, Q. Gao, R. D. Smith, E. E. Simanek, M. Mammen, G. M. Whitesides, *J. Org. Chem.* **1996**, *61*, 2204 – 2206.

Rhodium-Catalyzed Addition of Organoboronic Acids to Aldehydes

Masaaki Sakai, Masato Ueda, and Norio Miyaura*

The transmetalation between organo/main group metal reagents and transition metal compounds is of great importance for application in organic synthesis, since it allows the formation of new carbon – carbon bonds between various organometallic units and electrophiles. We previously demonstrated the efficiency of transmetalation between boron and palladium in the cross-coupling reaction of organoboron compounds with organic electrophiles[1] and the transmetalation between boron and rhodium in the catalytic 1,4-addition of aryl- or 1-alkenylboronic acids to enones.[2] An analogous addition reaction of organotin compounds to enones[3] and to aldehydes[4] has recently appeared. Here we report our first attempts to extend the protocol to the addition of aryl- and 1-alkenylboronic acids to aldehydes in an aqueous solution (Scheme 1). The insertion of carbonyl groups into transition metal – carbon bonds has not received much attention, but the use of transition metals as catalysts may allow addition of organometallics that are otherwise inert,[5] asymmetric addition using a chiral phosphane complex,[6] or reaction in an aqueous phase.



Scheme 1. Rhodium-catalyzed addition of organoboronic acids to aldehydes. R = aryl, 1-alkenyl; R′ = alkyl, aryl.

A combination of $[\text{Rh(acac)(CO)}_2]$ (acac = acetylacetonate) and a phosphane ligand in an aqueous solvent, conditions that gave good results for the 1,4-addition of organoboronic acids to enones,[2] was also effective for the addition to aldehydes (Table 1). The reaction was induced by phosphane complexes having a large P-Rh-P angle,[7a] which may affect the rate of carbonyl insertion into the Rh–C bond.[7b–d] Thus, monodentate phosphanes and dppe were totally ineffective ligands (entries 1 – 4), but the complexes derived from dppp, diop, and dppf exhibited high catalytic activity (entries 5, 7, and 8). However, the ligand dppb unexpectedly resulted in a low yield although it has a similar bite angle (entry 6). The reaction smoothly proceeded in aqueous 1,2-dimethoxyethane (DME), dioxane, and propanol at temperatures above 80 °C (entries 9 and 10), but it was very slow in the absence of water or at temperatures below 80 °C.

Table 1. Effect of ligand and solvent on the addition of phenylboronic acid to 4-methoxybenzaldehyde in the presence of $[\text{Rh(acac)(CO)}_2]$.[a]

Entry	Ligand	Solvent	Yield [%][b]
1	$3\,\text{Ph}_3\text{P}$	DME/H_2O	0
2	$3\,\text{Ph}_3\text{As}$	DME/H_2O	< 1
3	$3\,\text{Cy}_3\text{P}$	DME/H_2O	5
4	dppe[c]	DME/H_2O	0
5	dppp[d]	DME/H_2O	82 (79)
6	dppb[e]	DME/H_2O	17
7	diop[f]	DME/H_2O	66
8	dppf[g]	DME/H_2O	99 (83)
9	dppf[g]	dioxane/H_2O	72
10	dppf[g]	*n*PrOH/H_2O	84

[a] A mixture of $4\text{-MeOC}_6\text{H}_4\text{CHO}$ (1 mmol), PhB(OH)_2 (2 mmol) and $[\text{Rh(acac)(CO)}_2]$/ligand (3 mol %) was stirred at 80 °C for 16 h in solvent/H_2O (1/1) (6 mL). [b] GC yields based on the aldehyde and yields of the isolated product are given in the parentheses. [c] 1,2-Bis(diphenylphosphanyl)ethane. [d] 1,3-Bis(diphenylphosphanyl)propane. [e] 1,4-Bis(diphenylphosphanyl)butane. [f] 2,3-*O*-Isopropylidene-2,3-dihydroxy-1,4-bis(diphenylphosphanyl)butane. [g] 1,1′-Bis(diphenylphosphanyl)ferrocene.

Representative results are summarized in Table 2. The reaction is rather sensitive to electronic effects both in aldehydes and arylboronic acids, suggesting that the mechanism proceeds through the nucleophilic attack of the aryl group to the carbonyl. Thus, the reaction was facilitated in the

[*] Prof. Dr. N. Miyaura, M. Sakai, M. Ueda
Division of Molecular Chemistry
Graduate School of Engineering
Hokkaido University
Sapporo 060-8628 (Japan)
Fax: (+81) 11-706-6561 or 11-706-7882
E-mail: miyaura@org-mc.eng.hokudai.ac.jp

 © WILEY-VCH Verlag GmbH, D-69451 Weinheim, 1998 1433-7851/98/3723-3279 $ 17.50+.50/0

Table 2. Addition of arylboronic acids to aldehydes.[a]

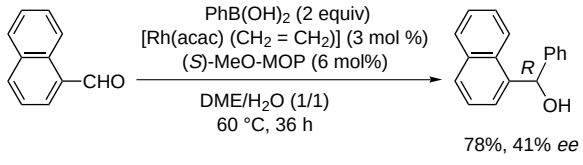
Entry	$ArB(OH)_2$	Aldehyde	Yield [%][b]
1	$PhB(OH)_2$	PhCHO	92
2	$PhB(OH)_2$	$4\text{-}CF_3C_6H_4CHO$	97
3	$PhB(OH)_2$	$4\text{-}NCC_6H_4CHO$	97
4	$PhB(OH)_2$	$4\text{-}MeCOC_6H_4CHO$	93
5	$PhB(OH)_2$	$4\text{-}NO_2C_6H_4CHO$	< 1[c]
6	$PhB(OH)_2$	$4\text{-}BrC_6H_4CHO$	88
7	$PhB(OH)_2$	$4\text{-}MeC_6H_4CHO$	48 (76)[d]
8	$4\text{-}MeOC_6H_4B(OH)_2$	$4\text{-}NCC_6H_4CHO$	84
9	$4\text{-}MeC_6H_4B(OH)_2$	$4\text{-}NCC_6H_4CHO$	99
10	$4\text{-}FC_6H_4B(OH)_2$	$4\text{-}NCC_6H_4CHO$	52
11	$4\text{-}MeCOC_6H_4B(OH)_2$	$4\text{-}NCC_6H_4CHO$	< 1[c]
12	$2\text{-}MeC_6H_4B(OH)_2$	$4\text{-}MeOC_6H_4CHO$	80 (86)[d]
13	$2,4,6\text{-}Me_3C_6H_2B(OH)_2$	$4\text{-}MeOC_6H_4CHO$	31 (43)[d]
14	$PhB(OH)_2$	2-furaldehyde	78
15	$PhB(OH)_2$	1-naphthaldehyde	91
16	$PhB(OH)_2$	$C_5H_{11}CHO$	69
17	$PhB(OH)_2$	$C_6H_{11}CHO$	45 (95)[d]
18	$(E)\text{-}C_4H_9CH{=}CHB(OH)_2$	$4\text{-}NCC_6H_4CHO$	76

[a] A mixture of $ArB(OH)_2$ (2 mmol), aldehyde (1 mmol), $[Rh(acac)(CO)_2]$ (3 mol %), and dppf (3 mol %) in DME/H_2O (1/1, 6 mL) was stirred at 80 °C for 16 h, unless otherwise noted. [b] Yields of products isolated by chromatography over silica gel. [c] The aldehyde were recovered unchanged. [d] The reactions were carried out at 95 °C for 16 h in dioxane/H_2O (1/1, 6 mL).

presence of an electron-withdrawing group in aromatic aldehydes (entries 1–7) and a donating group in arylboronic acids (entries 8–11). On the other hand, the addition to electron-rich aldehydes (entry 7) and the arylation with electron-deficient arylboronic acids (entries 10 and 11) were slow at 80 °C. In the one exceptional case 4-nitrobenzaldehyde remained intact during the reaction (entry 5).

The reaction is specific for aldehydes. Aromatic ketones, esters, nitriles, halides (Cl, Br) were unreactive, as evidenced by the recovery of these substrates. Steric hindrance around the boron atom retarded the reaction (entry 13), but the reactions of *ortho*-monosubstituted arylboronic acids proceeded smoothly at 80 °C (entry 12). The additions to aliphatic aldehydes such as hexanal and cyclohexanecarbaldehyde were very slow at 80 °C because their electrophilicity is lower than that of aromatic aldehydes, but the reaction at 95 °C in dioxane/H_2O gave the tertiary alcohols in high yields (entries 16 and 17). (*E*)-1-Hexenylboronic acid also participated in the catalytic reaction, and its stereochemistry was retained in the product (entry 18).

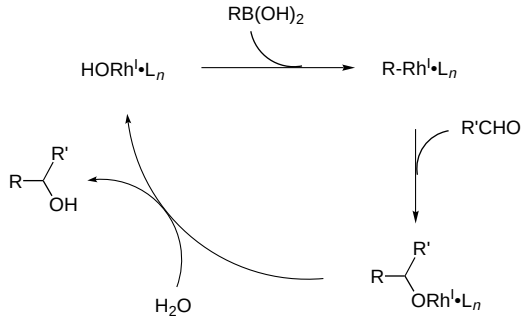
The facile addition of arylboronic acids to aldehydes encouraged us to examine the asymmetric version of this protocol (Scheme 2). The monodentate ligand 2-(diphenylphosphanyl)-2′-methoxy-1,1′-binaphthyl ((*S*)-MeO-MOP)[8] gave rise to a moderate asymmetric induction: (*R*)-(+)-(1-naphthyl)(phenyl)methanol was formed preferentially ($[\alpha]_D^{20} = +9.3$ ($c = 0.01$, EtOH), 41 % *ee*), though the chiral



Scheme 2. Asymmetric addition.

bidentate ligands such as diop and binap unfortunately resulted in the formation of racemic alcohols.

The reaction may involve the transmetalation between arylboronic acid and the RO–Rh species (RO = acac or OH) to give an $Ar{-}Rh^I$ complex and the insertion of an aldehyde into the Ar–Rh bond (Scheme 3).[4] The arylrhodium(I) complexes are unstable such as to preclude isolation in pure



Scheme 3. Proposed catalytic cycle.

form, but they have been reasonably speculated to be the key intermediates in various coupling reactions with organic halides[9] and the addition to alkenes and alkynes.[10] However, the insertion of aldehydes into the carbon–metal bond is very rare in transition metals except the allylic derivatives.[5, 11]

Experimental Section

Procedure for the reactions presented in Tables 1 and 2: $[Rh(acac)(CO)_2]$ (8 mg, 0.03 mmol, 3 mol %) and dppf (17 mg, 0.03 mmol, 3 mol %), $PhB(OH)_2$ (0.244 g, 2 mmol), and naphthaldehyde (0.156 g, 1.0 mmol) were dissolved in DME (3 mL) and water (3 mL) under nitrogen. After the mixture was stirred at 80 °C for 16 h, the product was extracted with benzene, dried over $MgSO_4$, and finally purified by chromatography on silica gel with hexane/ethyl acetate (20/1) to give (1-naphthyl)(phenyl)-methanol (0.213 g, 0.91 mmol, 91 %).

Asymmetric arylation (Scheme 2): $[Rh(acac)(CH_2{=}CH_2)_2]$ (8 mg, 0.03 mmol, 3 mol %) and (*S*)-MeO-MOP (28 mg, 0.06 mmol, 6 mol %), $PhB(OH)_2$ (0.243 g, 2 mmol), and naphthaldehyde (0.156 g, 1.0 mmol) were dissolved in DME (3 mL) and water (3 mL) under nitrogen. The mixture was stirred at 60 °C for 36 h and worked up. Chromatography on silica gel with hexane/ethyl acetate (10/1) gave the tertiary alcohol (0.181 g, 0.77 mmol, 77 %). The enantiomeric purity (41 % *ee*) and the absolute configuration (*R*) were established by high-pressure liquid chromatography (Daicel Chiracel OD-H, hexane/2-propanol 4/1) and by comparison with the reported optical rotation.[12]

Received: June 22, 1998 [Z12024IE]
German version: *Angew. Chem.* **1998**, *110*, 3475–3477

Keywords: aldehydes · boron · homogeneous catalysis · nucleophilic additions · rhodium

[1] N. Miyaura, A. Suzuki, *Chem. Rev*, **1995**, *95*, 2457–2483.
[2] M. Sakai, H. Hayashi, N. Miyaura, *Organometallics*, **1997**, *16*, 4229–4230; for an asymmetric 1,4-addition of aryl- or 1-alkenylboronic acids to enones, see Y. Takaya, M. Ogasawara, T. Hayashi, M. Sakai, N. Miyaura, *J. Am. Chem. Soc*. **1998**, *120*, 5579–5580.
[3] S. Oi, M. Moro, S. Ono, Y. Inoue, *Chem. Lett*. **1998**, 83–84.
[4] S. Oi, M. Moro, Y. Inoue, *J. Chem. Soc. Chem. Commun*. **1997**, 1621–1622.

 © WILEY-VCH Verlag GmbH, D-69451 Weinheim, 1998 1433-7851/98/3723-3280 $ 17.50+.50/0

[5] H. Nakamura, H. Iwama, Y. Yamamoto, *J. Am. Chem. Soc.* **1996**, *118*, 6641 – 6647.
[6] H. Nakamura, K. Nakamura, Y. Yamamoto, *J. Am. Chem. Soc.* **1998**, *120*, 4242 – 4243; J. M. Nuss, R. A. Rennels, *Chem. Lett.* **1993**, 197 – 200.
[7] The P-Rh-P angles increase in the order of dppe < dppp < dppb < dppf; see a) K. Angermund, W. Baumann, E. Dinjus, R. Fornika, H. Görls, M. Kessler, K. Krüger, W. Leitner, F. Lutz, *Chem. Eur. J.* **1997**, *3*, 755 – 764; for the effect on hydroformylation of alkenes, see b) C. P. Casey, G. T. Whiteker, M. G. Melville, L. M. Petrovich, J. A. Gavney Jr., D. R. Powell, *J. Am. Chem. Soc.* **1992**, *114*, 5535 – 5543; c) M. Kranenburg, Y. E. M. van der Burgt, P. C. J. Kamer, P. W. N. M. van Leeuwen, K. Goubitz, J. Fraanje, *Organometallics*, **1995**, *14*, 3081 – 3089; for the effect on hydrogenation of CO_2, see d) R. Fornika, H. Görls, B. Seemann, W. Leitner, *J. Chem. Soc. Chem. Commun.* **1995**, 1479 – 1481.
[8] Y. Uozumi, T. Hayashi, *J. Am. Chem. Soc.* **1991**, *113*, 9887 – 9888.
[9] L. S. Hegedus, P. M. Kendall, S. M. Lo, J. R. Sheats, *J. Am. Chem. Soc.* **1975**, *97*, 5448 – 5452; M. F. Semmelhack, L. Ryono. *Tetrahedron Lett.* **1973**, 2967 – 2970.
[10] M. Michman, M. Balog, *J. Organomet. Chem.* **1971**, *31*, 395.
[11] T. Kondo, H. Ono, N. Satake, T. Mitsudo, Y. Watanabe, *Organometallics*, **1995**, *14*, 1945.
[12] O. Cervinka, V. Suchan, B. Masar, *Collect. Czech. Chem. Commun.* **1965**, *30*, 1693 – 1699.

Highly Efficient Synthesis of Covalently Cross-Linked Peptide Helices by Ring-Closing Metathesis**

Helen E. Blackwell and Robert H. Grubbs*

Due to the frequency of helical secondary structures in peptides and proteins,[1] considerable effort has been directed toward the design of small-molecule helix mimetics and stabilized helix structures. Designed organic template molecules that initiate α-helix formation in peptide sequences have been reported.[2] Short α-helical peptides have also been stabilized by incorporation of naturally occurring capping motifs[3] and by stabilization of the intrinsic helix dipole.[4] Notably, significant progress has been made toward stabilizing synthetic α-helical peptides through the incorporation of covalent or noncovalent linkages between constituent amino acid side chains. Examples include salt bridges,[5] lactams,[6] disulfide bridges,[7] hydrophobic interactions,[8] and metal ligation between natural[9] and unnatural amino acids.[10] In several of these cases, it was found that substantial helix stabilization was achieved when the linkage was placed between the i and $i+4$ residues in the peptide backbone. Such a linkage encompasses approximately one turn of the helical peptide backbone and places the tethered side chains on the same side of the helix. Recently, the extraordinary functional group tolerance of olefin metathesis catalyst $[(PCy_3)_2Cl_2Ru{=}CHPh]$ (**1**)[11] has enabled the synthesis of cyclic amino acids[12] and peptides exhibiting β-turn[13] and β-sheet[14] secondary structure by ring-closing olefin metathesis (RCM).[15] This transformation effectively introduces non-native carbon – carbon bond constraints which may afford enhanced biostability. Here we present a concise synthesis and structural analysis of a series of cyclic helical peptides wherein RCM is used to incorporate a carbon – carbon tether between amino acid side chains.

We chose to study hydrophobic peptide model systems from the outset, because the use of apolar sequences permits characterization of conformation in poorly solvating organic solvents where folding is mainly controlled by intramolecular hydrogen bonding, nonbonding interactions, and electrostatic effects.[16] We became interested in a hydrophobic peptide (**2**) studied by Karle and Balaram et al.,[17] whose solubility in organic solvents would be compatible with alkylidene **1**.[18] Heptapeptide **2** contains two repeat units of valine – alanine – leucine (Val-Ala-Leu) separated by one α-aminoisobutyric acid residue (Aib), as shown schematically in Figure 1. The Aib residue is known to stabilize 3_{10}- and/or α-helical

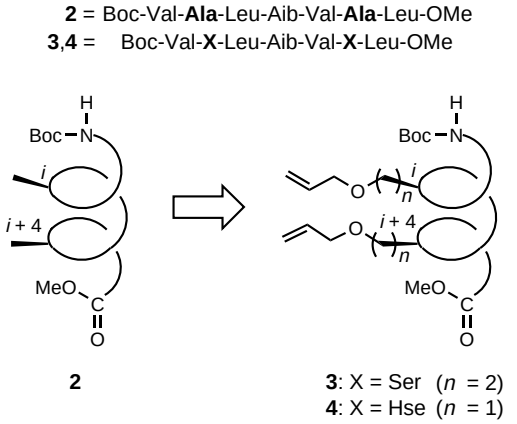


Figure 1. Karle and Balaram's heptapeptide **2**, and two dienic analogues **3** and **4**. Boc = *tert*-butoxycarbonyl.

conformations in apolar oligopeptides and is frequently found in peptides produced by microbial sources.[19] Examples of such Aib-rich peptides include the antibiotics alamethicin, zervamicin, and trichogin A IV, which are purported to adopt helical conformations within lipid bilayer membranes and aggregate therein to form ion channels. Heptapeptide **2** was shown to adopt an α-helical conformation in the solid state by X-ray crystallography and was found to adopt a similar helical conformation in $CDCl_3$ by solution-phase 2D NMR analyses.

[*] Prof. R. H. Grubbs, H. E. Blackwell
Arnold and Mabel Beckman Laboratories of Chemical Synthesis
Division of Chemistry and Chemical Engineering
California Institute of Technology
Pasadena, CA 91125 (USA)
Fax: (+1) 626-564-9297
E-mail: rhg@its.caltech.edu

[**] Financial support has been generously provided by the National Institutes of Health and Zeneca Pharmaceuticals. H. E. B. is grateful to the ACS Division of Organic Chemistry for a pre-doctoral fellowship (supported by Pfizer, Inc.). We thank Dr. Keith Russell (Zeneca) for instrumental discussions and Dr. Saeed Khan (UCLA) for X-ray crystallographic analyses. Dr. Isabella L. Karle, Prof. Barbara Imperiali, Prof. Scott J. Miller, and Prof. Daniel J. O'Leary are acknowledged for helpful discussions.

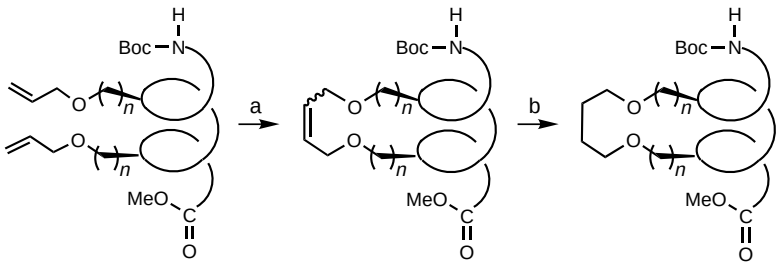
Supporting information for this article is available on the WWW under http://www.wiley-vch.de/home/angewandte/ or from the author.

 © WILEY-VCH Verlag GmbH, D-69451 Weinheim, 1998 1433-7851/98/3723-3281 $ 17.50+.50/0

Encouraged by these structural results, we endeavored to use heptapeptide **2** as a scaffold upon which to build acyclic peptide dienes. Furthermore, we were excited about the prospect of eventually applying RCM to the synthesis of constrained analogues of the previously mentioned peptide antibiotics in order to probe the requirements of a helical conformation on their ion channel forming activity.

Through analysis of the structure of **2** and molecular modeling, we predicted that replacement of the i and $i+4$ Ala residues of **2** with residues containing unbranched terminal olefin groups in the side chains would place the two olefins in proximity to one another, provided our dienic analogues also adopted a helical conformation and the derivatized side chains were of appropriate length. L-Serine (Ser) and L-homoserine (Hse) *O*-allyl ethers were selected as olefin-containing residues due to their ready availability and trivial derivatization as allyl ethers.[20] Acyclic peptide dienes **3** and **4**, shown schematically in Figure 1, were then prepared by standard solution-phase peptide chemistry.[21]

Dienes **3** and **4** were each treated with alkylidene **1** (20 mol% **1**, 5 mM in **3** or **4**, $CHCl_3$, 25 °C, 3–4 h) to yield 21- and 23-membered macrocyclic alkenes **5** and **6** in 85 and 90% yields, respectively (Scheme 1).[22] Each macrocycle was



Scheme 1. Synthesis of peptide macrocycles. a) 20 mol% of **1**, $CHCl_3$, 25 °C; b) cat. 10% Pd/C, 1 atm H_2, EtOH, 25 °C.

isolated as a mixture of olefin isomers (ca. 5:1 *E*/*Z*).[23] Catalytic hydrogenation (10% Pd/C, 1 atm H_2, EtOH, 25 °C, 2 h) then afforded the saturated species **7** and **8** in excellent yields.[24] The high yield and relatively fast rate of the RCM transformation suggested that the acyclic dienes were preorganized for ring closure in organic solvents. This prompted closer examination of the structures of acyclic peptides **3** and **4**, along with cyclic products **7** and **8**.

Far-UV circular dichroism (CD) spectra of solutions of peptides **3**, **4**, **7**, and **8** in trifluoroethanol (TFE) at 25 °C are shown in Figure 2. For peptides and proteins, TFE has been shown to be a strongly helix-promoting solvent comparable to $CHCl_3$,[25] and thus CD measurements in TFE can be correlated to the conformations accessed by the peptides during the RCM reaction. Two negative bands at approximately 203–205 (π-π*) and 218–222 nm (n-π*) are observed for all four compounds, transitions characteristic of largely helical conformations in short peptides. The n-π* absorptions are considerably weaker than those for π-π*, a trend that has been observed experimentally for numerous short 3_{10}-helical

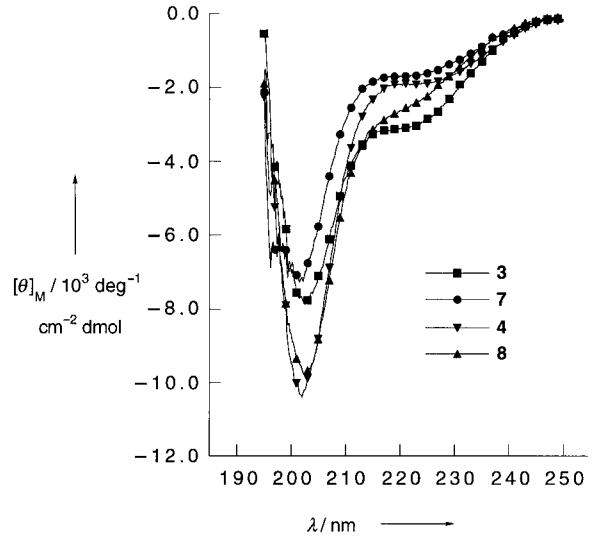


Figure 2. CD spectra (250–195 nm) of peptides **3**, **4**, **7**, and **8** (1 mM) in TFE at 25 °C. Total molar ellipticity values are given.

peptides[26] and reported recently to be the standard CD pattern for right-handed 3_{10}-helical peptides by Tonolio and co-workers.[27] Importantly, these data suggest that the peptide backbones of dienes **3** and **4** are *preorganized* in a helical conformation for RCM in organic solvents. Furthermore, the ellipticities for macrocycles **7** and **8** do not appear to differ noticeably from their acyclic precursors **3** and **4**, indicating that significant conformational change did not take place upon cyclization.[28]

Cyclic peptide **8** exhibited high crystallinity, enabling an X-ray crystal structure to be obtained (Figure 3).[29] When one views the peptide from the N to C terminus, it appears that the peptide backbone is helical for the first five residues and then the helix begins to fray for the last two (Hse 6 and Leu 7).[30] The average torsional angles ϕ (about N–C^{α}) and φ (about C^{α}–C′) for the first five residues are −57 and −34°, respectively, which approximate those for a right-handed 3_{10}-helix (−57 and −30°).[31] These torsional angles are marginally close to those for the average right-handed α-helix ($\phi = -63°$, $\varphi = -42°$), and therefore it is difficult to exclude the possibility of the peptide being α-helical or accessing a mixed $\alpha/3_{10}$-helix conformation. However, analysis of the amide N to carbonyl O distances (N···O) and respective angles (N···O=C) supports the presence of four consecutive 4→1 intramolecular hydrogen bonds (2.96–3.01 Å), involving N3–N6 and O2–O5, which are diagnostic of a 3_{10}-helix.[32] This iterative hydrogen-bonding pattern involves the carbonyl O and amide NH of amino acids that are two residues apart.[33, 34] We speculate that the Leu 3 carbonyl O5 could also be involved in a fifth extremely long 5→1 hydrogen bond with the Leu 7 amide N7 (N···O 3.50 Å), which may be lengthened due to the disorder of the helix at the C-terminus. Thereafter, the 4→1 hydrogen-bonding pattern is continued intermolecularly in a head-to-tail fashion, with the Val 5 carbonyl O7 hydrogen bonding to the Val 1 Boc amide N1 (N···O 2.91 Å) of the adjacent peptide molecule in

 © WILEY-VCH Verlag GmbH, D-69451 Weinheim, 1998 1433-7851/98/3723-3282 $ 17.50+.50/0

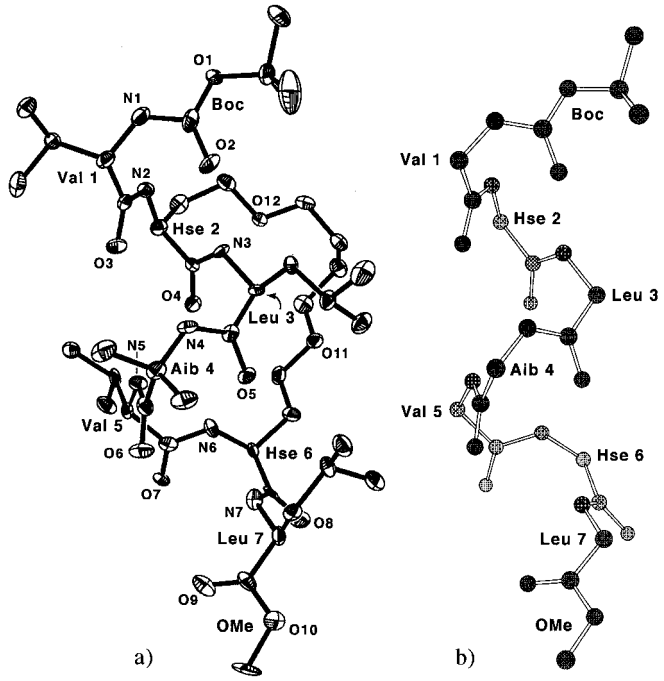


Figure 3. a) ORTEP diagram of the X-ray crystal structure of cyclic peptide **8**. Thermal ellipsoids represent 30% probability levels. Hydrogen atoms have been omitted for clarity. b) Chem 3D rendering of **8** without amino acid side chains.

the unit cell.[35] The evidence suggests that replacement of the two Ala residues in peptide **2** with tethered Hse residues in peptide **8** has induced the peptide backbone to transform from an α-helix to a predominantly 3_{10}-helix in the solid state. The constraint imposed by the side chain linkage in peptide **8** could be cause for this unique conformational shift.[36]

Acyclic dienes incorporated into a helical peptide scaffold have been treated with alkylidene **1** to afford macrocyclic peptide helices by a remarkably facile ring-closing metathesis reaction. The relative ease of introducing carbon–carbon bonds into peptide secondary structures by RCM and the predicted metabolic stability of these bonds renders olefin metathesis an exceptional methodology for the synthesis of rigidified peptide architectures. Specifically, we believe the macrocyclization of hydrophobic peptide helices is uniquely suited to RCM in organic solvents because helical conformations are frequently favored in apolar media. We are now applying RCM to the synthesis of cyclic/tethered analogues of naturally occurring helical peptide antibiotics (e.g. the trichogin family of lipopeptaibols) with the intent of exposing the requirements of a helical conformation on their activities.[37] Future work is also directed toward the syntheses of tethered peptide helix bundles and helix-turn-helix motifs by RCM, for potential use as peptide ligands for proteins and DNA. The recent advent of water-soluble olefin metathesis catalysts has accelerated our pursuit toward such complex, biologically relevant structures.[38]

Received: June 18, 1998 [Z12011IE]
German version: *Angew. Chem.* **1998**, *110*, 3469–3472

Keywords: carbene complexes · helical structures · macrocycles · metathesis · peptides

[1] The α-helical conformation is adopted by 40% of all residues in proteins. See: T. E. Creighton, *Proteins: Structures and Molecular Properties*, 2nd ed., Freeman, New York, **1984**, pp. 182–188.
[2] D. S. Kemp, T. P. Curran, J. G. Boyd, T. J. Allen, *J. Org. Chem.* **1991**, *56*, 6683–6697, and references therein.
[3] a) B. Forood, E. J. Feliciano, K. P. Nambiar, *Proc. Natl. Acad. Sci. USA* **1994**, *90*, 838–842; b) H. X. Zhou, P. C. Lyu, D. E. Wemmer, N. R. Kallenbach, *J. Am. Chem. Soc.* **1994**, *116*, 1139–1140.
[4] K. R. Schoemaker, P. S. Kim, E. J. York, J. M. Stewart, R. L. Baldwin, *Nature* **1987**, *326*, 563–567.
[5] J. M. Scholtz, H. Qian, V. H. Robbins, R. L. Baldwin, *Biochemistry* **1993**, *32*, 9668–9676, and references therein.
[6] J. C. Phelan, N. J. Skelton, A. C. Braisted, R. S. McDowell, *J. Am. Chem. Soc.* **1997**, *119*, 455–460, and references therein.
[7] D. Y. Jackson, D. S. King, J. Chmielewski, S. Singh, P. G. Schultz, *J. Am. Chem. Soc.* **1991**, *113*, 9391–9392.
[8] J. S. Albert, A. D. Hamilton, *J. Am. Chem. Soc.* **1995**, *34*, 984–990.
[9] a) R. J. Todd, M. E. Van Dam, D. Casimiro, B. L. Haymore, F. H. Arnold, *Proteins: Struct. Funct. Genet.* **1991**, *10*, 156–161; b) M. R. Ghadiri, A. K. Fernholz, *J. Am. Chem. Soc.* **1990**, *112*, 9633–9635.
[10] a) S. R. Gilbertson, X. Wang, *J. Org. Chem.* **1996**, *61*, 434–435; b) F. Ruan, Y. Chen, P. B. Hopkins, *J. Am. Chem. Soc.* **1990**, *112*, 9403–9404.
[11] PCy_3 = Tricyclohexylphosphane. For the synthesis of **1**, see: T. E. Wilhelm, T. R. Belderrain, S. N. Brown, R. H. Grubbs, *Organometallics* **1997**, *18*, 3867–3869, and references therein.
[12] a) F. P. J. T. Rutjes, H. E. Schoemaker, *Tetrahedron Lett.* **1997**, *48*, 677–680; b) S. J. Miller, R. H. Grubbs, *J. Am. Chem. Soc.* **1995**, *117*, 5855–5856.
[13] a) B. E. Fink, P. R. Kym, J. A. Katzenellenbogen, *J. Am. Chem. Soc.* **1998**, *120*, 4334–4344; b) J. Pernerstorfer, M. Schuster, S. Blechert, *Chem. Commun.* **1997**, 1949–1950; c) S. J. Miller, H. E. Blackwell, R. H. Grubbs, *J. Am. Chem. Soc.* **1996**, *118*, 9609–9614.
[14] T. D. Clark, M. R. Ghadiri, *J. Am. Chem. Soc.* **1995**, *117*, 12364–12365.
[15] For a recent review of olefin metathesis in organic synthesis, see: R. H. Grubbs, S. Chang, *Tetrahedron* **1998**, *54*, 4413–4450.
[16] I. L. Karle, P. Balaram, *Biochemistry* **1990**, *29*, 6747–6756.
[17] a) I. L. Karle, J. L. Flippen-Anderson, K. Uma, P. Balaram, *Biopolymers* **1993**, *33*, 827–837; b) I. L. Karle, J. L. Flippen-Anderson, K. Uma, P. Balaram, *Proteins: Struct. Funct. Genet.* **1990**, *7*, 62–73.
[18] Catalyst **1** is soluble and most active in CH_2Cl_2, $CHCl_3$, and C_6H_6.
[19] For general reviews on Aib-containing peptides, see: a) reference [16]; b) I. L. Karle, *Biopolymers* **1996**, *40*, 157–180; c) C. Toniolo, E. Benedetti, *Macromolecules* **1991**, *24*, 4004–4009.
[20] H. Sugano, M. Miyoshi, *J. Org. Chem.* **1976**, *41*, 2352–2353.
[21] All L-amino acids were used. See: M. Bodansky, *Peptide Chemistry*, Springer, New York, **1988**, pp. 55–146, and references therein.
[22] Both RCM reactions appeared quantitative by thin-layer chromatography. The yields are reduced only by the isolation procedure. Lower catalyst loadings (5–10 mol%) gave a reduced yield of macrocyclic products. This is often observed for RCM macrocyclizations and is believed to be rooted in the apparently accelerated decomposition of the ruthenium methylidene catalyst species at high dilution. For a review of macrocyclization by RCM, see reference [15].
[23] Each set of olefin isomers proved inseparable on silica gel. The ratio of olefin isomers was estimated by ^1H NMR integration.
[24] Full details of the RCM procedure and subsequent hydrogenation, along with complete spectral data for key compounds, is included in the supporting information.
[25] M. Goodman, I. Listowsky, Y. Masuda, F. Boardman, *Biopolymers* **1963**, *1*, 33–42. Details of our CD spectral analyses are given in the supporting information.
[26] For examples of small helical Aib-containing peptides exhibiting similar CD ellipticities in TFE, see: a) A. Banerjee, S. Raghothama, P. Balaram, *J. Chem. Soc. Perkin Trans. 2* **1997**, 2087–2094; b) I. L. Karle, A. Banerjee, S. Bhattachrjya, P. Balaram, *Biopolymers* **1996**, *38*, 515–526.
[27] The ratio $R = [\Theta]_{222}/[\Theta]_{208}$ has been determined to be approximately 0.4 for 3_{10}-helical peptides, while $R \approx 1$ for largely α-helical peptides.

 © WILEY-VCH Verlag GmbH, D-69451 Weinheim, 1998 1433-7851/98/3723-3283 $ 17.50+.50/0

The average R value for **3**, **4**, **7**, and **8** is 0.3. See: C. Toniolo, A. Polese, F. Formaggio, M. Crisma, J. Kamphuis, *J. Am. Chem. Soc.* **1996**, *118*, 2744 – 2745.

[28] From these data alone we cannot rule out the possibility of a conformational switch from an α- to a 3_{10}-helix (or vice versa) upon ring closure. See: G. Yoder, A. Polese, R. A. G. D. Silva, F. Formaggio, M. Crisma, Q. B. Broxterman, J. Kamphuis, C. Toniolo, T. A. Keiderling, *J. Am. Chem. Soc.* **1997**, *119*, 10278 – 10285.

[29] Colorless crystals of **8** were grown from CH_2Cl_2/hexane; crystal dimensions $0.3 \times 0.5 \times 0.5$ mm, orthorhombic, space group $P2_12_12_1$, $Z = 4$, $a = 19.30(1)$, $b = 24.73(2)$, $c = 12.134(7)$ Å, $V = 5791(6)$ Å^3, $\rho_{calcd} = 1.246$ g cm^{-3}; $2\theta = 1.6 - 50.0^\circ$ ($Mo_{K\alpha}$ radiation, $\lambda = 0.7107$ Å, graphite monochromator, 2θ-θ scan, $T = 156$ K); 4698 reflections measured, 2266 unique data used [$I > 3.0\sigma(I)$]; no absorption corrections were applied; direct methods (SHELXTL 86), refinement with full-matrix least squares, hydrogen atoms refined isotropically, all other atoms refined anisotropically; $R = 0.066$, $R_W = 0.077$; maximum residual electron density 0.80 e Å^{-3}; GOF = 2.28 for 633 variables. Crystallographic data (excluding structure factors) for the structure reported in this paper have been deposited with the Cambridge Crystallographic Data Center as supplementary publication no. CCDC-101810. Copies of the data can be obtained free of charge on application to CCDC, 12 Union Road, Cambridge CB2 1EZ, UK (fax: (+44) 1223-336-033; e-mail: deposit@ccdc.cam.ac.uk).

[30] Residues at the ends of peptide helices are often irregular in conformation. This effect is more pronounced at the C-terminus. See: C. Chothia, *Annu. Rev. Biochem.* **1984**, *53*, 537 – 572.

[31] C. Toniolo, E. Benedetti, *Trends Biochem. Sci.* **1991**, *16*, 350 – 353.

[32] The 4 → 1 N ··· O=C angles for these four hydrogen bonds range from 118 to 131°.

[33] The analogous hydrogen-bonding pattern in α-helices is 5 → 1, spanning three residues. See reference [30].

[34] ^{1}H NMR solvent titration experiments in $CDCl_3$/$(CD_3)_2SO$ mixtures (5 mM, 25 °C) suggest that **8** may exist as a 3_{10}-helix in $CDCl_3$. Full solution-phase 1D and 2D ^{1}H NMR analyses of peptides **3**, **4**, **7**, and **8** will be reported in a separate publication.

[35] All peptide helix axes are parallel in the unit cell of **8**. Head-to-tail hydrogen bonding is commonly observed in crystalline hydrophobic peptide helices. See reference [16].

[36] The different medium from which **2** and **8** were crystallized (CH_2Cl_2/hexane for **8**; methanol/H_2O for **2**) may contribute to the disparity in their crystal structures.

[37] a) C. Toniolo, M. Crisma, F. Formaggio, C. Peggion, V. Monaco, C. Goulard, S. Rebuffat, B. Bodo, *J. Am. Chem. Soc.* **1996**, *118*, 4952 – 4958; b) C. Toniolo, C. Peggion, M. Crisma, F. Formaggio, X. Q. Shui, D. S. Eggleston, *Nature Struct. Biol.* **1994**, *12*, 908 – 914; c) E. Benedetti, A. Bavoso, B. Di Blasio, V. Pavone, C. Pedone, C. Toniolo, G. M. Bonora, *Proc. Natl. Acad. Sci. USA* **1982**, *79*, 7951 – 7954.

[38] D. M. Lynn, B. Mohr, R. H. Grubbs, *J. Am. Chem. Soc.* **1998**, *120*, 1627 – 1628, and references therein.

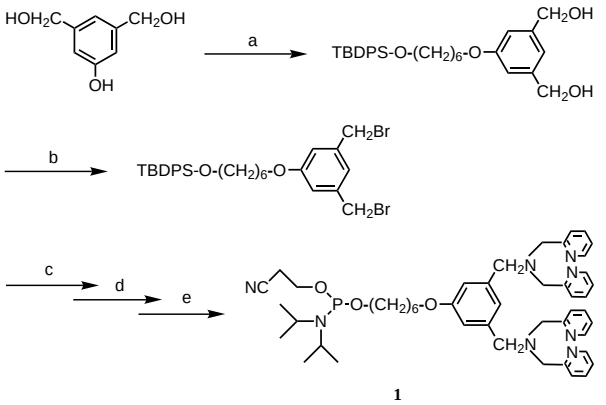
Conjugates of a Dinuclear Zinc(II) Complex and DNA Oligomers as Novel Sequence-Selective Artificial Ribonucleases**

Shigeo Matsuda, Akira Ishikubo, Akinori Kuzuya, Morio Yashiro, and Makoto Komiyama*

The sequence-selective scission of RNA has been attracting interest because of its potential applications, both in vivo and in vitro.[1] Artificial ribonucleases have been prepared by attaching catalytically active metal ions (mostly lanthanide ions) to DNA oligomers as sequence-recognizing moieties.[2–4] However, the following limitations remain: 1) divalent metal ions such as Zn^{II} and Mg^{II}, which are widely spread in vivo,[5] cannot be used, and 2) selective scission can be achieved only when free metal ions are absent in the reaction mixtures (otherwise, nonselective scission becomes dominant). Further progress is desirable.

It has previously been shown that dinuclear Zn^{II} complexes hydrolyze RNA under physiological conditions.[6, 7] Although the Zn^{II} ion itself is a rather poor candidate for RNA hydrolysis, a notable activity appears when two of them cooperate. Here we report that conjugates of a dinuclear Zn^{II} complex and DNA oligomers selectively hydrolyze RNA at the target site, even in the presence of a considerable amount of free Zn^{II} ions.

Phosphoramidite monomer **1** containing a *N*,*N*,*N*′,*N*′-tetrakis(2-pyridylmethyl)-3,5-bis(aminomethyl)benzene (TPBA) group was prepared according to Scheme 1. By use of **1** and



1

Scheme 1. a) K_2CO_3, [18]crown-6, THF, reflux, 26 h; b) CBr_4, PPh_3, THF, 0 °C, 1 min; c) *N*,*N*-bis(2-pyridylmethyl)amine, *N*,*N*-diisopropylethylamine, CH_3CN, room temperature (RT), 20 h; d) tetrabutylammonium fluoride, THF, RT, 1 h; e) $(iPr_2N)_2PO(CH_2)_2CN$, 1*H*-tetrazole, CH_3CN, RT, 90 min. TBDPS = *tert*-butyldiphenylsilyl.

[*] Prof. Dr. M. Komiyama, S. Matsuda, A. Ishikubo, A. Kuzuya, Prof. Dr. M. Yashiro
Department of Chemistry and Biotechnology
Graduate School of Engineering, The University of Tokyo
Hongo, Tokyo 113-8656 (Japan)
Fax: (+81) 3-5802-3340
E-mail: mkomi@chembio.t.u-tokyo.ac.jp

[**] This work was partially supported by a Grant-in-Aid for Scientific Research from the Ministry of Education, Science, and Culture, Japan.

Supporting information for this article is available on the WWW under http://www.wiley-vch.de/home/angewandte/ or from the author.

 © WILEY-VCH Verlag GmbH, D-69451 Weinheim, 1998 1433-7851/98/3723-3284 $ 17.50+.50/0

the conventional phosphoramidite monomers on an automated synthesizer, TPBA residues were tethered to the 5′ ends of DNA oligomers through a hexamethylene linker. The hydrolysis of RNA (labeled with ^{32}P at the 5′ end) by a mixture of the modified DNA (TPBA-DNA) and Zn^{II} ions was carried out at pH 7.0 and 37 °C, and analyzed by polyacrylamide gel electrophoresis.

Figure 1 shows the typical gel-electrophoresis patterns obtained. The DNA portion in TPBA-DNA is complementary to the U4-C23 part in the RNA substrate (Figure 2). When the feed ratio of Zn^{II} ions to TPBA-DNA is 2, a highly selective scission takes place at the 3′ side of C24 (Figure 1, lane 7; the arrow in Figure 2 shows the site). The band comigrates with the corresponding band for alkaline hydrolysis in lane 2. When the DNA in TPBA-DNA is complementary to the U2-A21 portion in the RNA (in place of the U4-C23 portion), selective scission occurs at the 3′ side of U22. When the DNA is complementary to the A1-G20 part in RNA, the 3′ sides of A21 and U22 are selectively hydrolyzed.

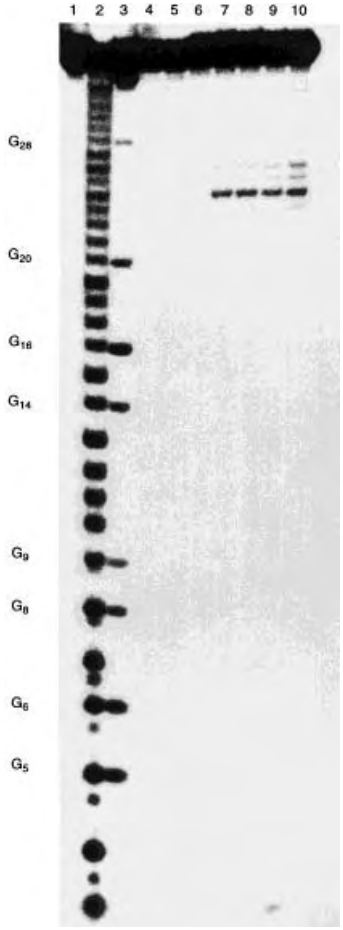


Figure 1. Autoradiographs for the sequence-selective hydrolysis of RNA (labeled with ^{32}P at the 5′ end) by the Zn^{II} complex of TPBA-DNA at pH 7.0 and 37 °C for 3 h: lane 1: no treatment; lane 2: alkaline hydrolysis; lane 3: hydrolysis by RNase T_1 (G-specific); lane 4: treatment with Zn^{II} only (5 μM); lane 5: treatment with a 2:1 mixture of Zn^{II} and TPBA which is not bound to DNA ($[Zn^{II}]_0 = 700$ μM); lanes 6–10: treatment with Zn^{II}/TPBA-DNA mixtures ($[Zn^{II}]_0/[TPBA\text{-}DNA]_0 = 1$, 2, 10, 50, and 100, respectively); $[RNA]_0 = 0.2$, $[TPBA\text{-}DNA]_0 = 5$ μM. The extent of RNA scission in lane 7 is around 5%.

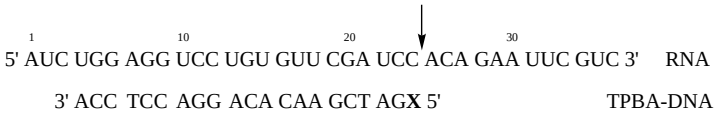


Figure 2. Sequences of the TPBA-DNA and substrate RNA used for the experiment in Figure 1. X is a residue carrying TPBA. The arrow indicates the site of selective scission.

Thus, sequence-selective ribonucleases employing Zn^{II} ions as catalytic centers have been prepared for the first time.

Quite importantly, the sequence selectivity for the scission is satisfactorily high, even when a large amount of free Zn^{II} ions exists in the reaction mixtures (see lanes 8–10 of Figure 1, where $[Zn^{II}]_0/[TPBA\text{-}DNA]_0 = 10$, 50, and 100, respectively; the subscripted 0 indicates initial concentration). The free Zn^{II} ions have no significant effect on the sequence-selective RNA scission.[8] It is also noteworthy that no measurable scission occurs when $[Zn^{II}]_0/[TPBA\text{-}DNA]_0 = 1$ (lane 6). The 2:1 Zn^{II}–TPBA complex in the artificial enzyme is responsible for the selective scission. This argument is further supported by the fact that the DNA conjugates with a *N*,*N*-bis(2-pyridylmethyl)amine residue, which forms a mononuclear Zn^{II} complex, are virtually inactive at pH 7.0 and 37 °C (see the supporting information).

When a TPBA molecule (not bound to DNA) is used in place of TPBA-DNA, no RNA hydrolysis is observed, even with $[Zn^{II}]_0 = 700$ μM (lane 5; $[TPBA]_0 = 350$ μM). Thus, selective RNA hydrolysis requires the formation of a heteroduplex, in which the Zn^{II}–TPBA complex is correctly placed near the target phosphodiester linkage (the selective reaction in lane 7 is achieved with $[Zn^{II}]_0 = 5$ μM). The free Zn^{II} ion shows no measurable RNA scission, at least under the conditions employed (lane 4).

The overwhelmingly important role of the 2:1 Zn^{II}–TPBA complex is further evidenced in the hydrolysis of adenylyl-(3′→5′)adenosine (ApA) by the combination of Zn^{II} and TPBA (which is not bound to DNA). There, $[Zn^{II}]_0$ is varied while $[TPBA]_0$ is kept constant at 2.5 mM. As expected, the rate of hydrolysis sigmoidally increases with increasing $[Zn^{II}]_0$, and attains a plateau at $[Zn^{II}]_0/[TPBA]_0 = 2$ (see the supporting information). Furthermore, the formation of a 2:1 complex has been confirmed by ^1H NMR spectroscopy.[9] The present artificial ribonucleases involving the dinuclear Zn^{II} complex as catalytic centers are promising for a variety of applications.

Experimental Section

The phosphoramidite monomer **1** and all of the reaction intermediates in Scheme 1 were characterized by ^1H and ^{31}P NMR spectroscopy. The sample of TPBA-DNA used for the experiment presented in Figure 1 was analyzed by matrix-assisted laser desorption ionization time-of-flight (MALDI-TOF) mass spectrometry: calcd: 6738.64; found: 6738.8. An HPLC analysis of the enzymatic digestion of TPBA-DNA was in fair agreement with the structure.

The RNA cleavage was carried out in 50 mM Tris-HCl buffer (pH 7.0; Tris = tris(hydroxymethyl)aminomethane) containing 0.2 μM RNA, 5 μM TPBA-DNA, 100 mM NaCl, and the required amount of $Zn(NO_3)_2$. The reaction mixture was heated to 85 °C for 1 min, and cooled to the reaction temperature (37 °C). After the reaction, the mixture was loaded onto a

15% denaturing polyacrylamide gel. The ApA hydrolysis by the 2:1 Zn^{II}–TPBA complex was followed by reverse-phase HPLC. The 2′,3′-cyclic monophosphate of adenosine as the intermediate was rapidly hydrolyzed to the 2′- and 3′-monophosphates; thus, not much intermediate accumulated.

Received: July 3, 1998 [Z12090IE]
German version: *Angew. Chem.* **1998**, *110*, 3477–3479

Keywords: cooperative effects · hydrolyses · phosphatases · RNA · zinc

[1] a) T. R. Cech, *Annu. Rev. Biochem.* **1990**, *59*, 543–568; b) A. D. Mesmaeker, R. Häner, P. Martin, H. E. Moser, *Acc. Chem. Res.* **1995**, *28*, 366–374; c) M. Komiyama, *J. Biochem.* **1995,** *118*, 665–670, and references therein.

[2] a) K. Matsumura, M. Endo, M. Komiyama, *J. Chem. Soc. Chem. Commun.* **1994**, 2019–2020; b) J. K. Bashkin, E. I. Frolova, U. Sampath, *J. Am. Chem. Soc.* **1994**, *116*, 5981–5982; c) D. Magda, R. A. Miller, J. L. Sessler, B. L. Iverson, *J. Am. Chem. Soc.* **1994**, *116*, 7439–7440; d) J. Hall, D. Hüsken, R. Häner, *Nucleic Acids Res.* **1996**, *24*, 3522–3526; e) J. K. Bashkin, J. Xie, A. T. Daniher, U. Sampath, J. L. Kao, *J. Org. Chem.* **1996**, *61*, 2314–2321; f) V. Duarte, S. Sixou, G. Favre, G. Pratviel, B. Meunier, *J. Chem. Soc. Dalton Trans.* **1997**, 4113–4118; g) D. Magda, S. Crofts, A. Lin, D. Miles, M. Wright, J. L. Sessler, *J. Am. Chem. Soc.* **1997**, *119*, 2293–2294; h) D. Magda, M. Wright, S. Crofts, A. Lin, J. L. Sessler, *J. Am. Chem. Soc.* **1997**, *119*, 6947–6948.

[3] Sequence-selective artificial ribonucleases involving organic "scissors" have also been prepared: a) M. Komiyama, T. Inokawa, K. Yoshinari, *J. Chem. Soc. Chem. Commun.* **1995**, 77–78; b) J. Hovinen, A. Guzaev, E. Azhayeva, A. Azhayev, H. Lönnberg, *J. Org. Chem.* **1995**, *60*, 2205–2209; c) M. A. Reynolds, T. A. Beck, P. B. Say, D. A. Schwartz, B. P. Dwyer, W. J. Daily, M. M. Vaghefi, M. D. Metzler, R. E. Klem, L. J. Arnold, Jr., *Nucleic Acids Res.* **1996**, *24*, 760–765; d) M. Endo, Y. Azuma, Y. Saga, A. Kuzuya, G. Kawai, M. Komiyama, *J. Org. Chem.* **1997**, *62*, 846–852.

[4] Conjugates of natural enzymes and DNA oligomers showed sequence-selective scission: R. N. Zuckermann, P. G. Schultz, *Proc. Natl. Acad. Sci. USA* **1989**, *86*, 1766–1770.

[5] S. J. Lippard, J. M. Berg, *Principles of Bioinorganic Chemistry*, University Science Books, Mill Valley, **1994**.

[6] M. Yashiro, A. Ishikubo, M. Komiyama, *J. Chem. Soc. Chem. Commun.* **1995**, 1793–1794.

[7] Dinuclear metal complexes for the hydrolysis of phosphoesters have been reported: a) D. R. Jones, L. F. Lindoy, A. M. Sargeson, M. R. Snow, *Inorg. Chem.* **1982**, *21*, 4155–4160; b) D. H. Vance, A. W. Czarnik, *J. Am. Chem. Soc.* **1993**, *115*, 12165–12166; c) D. Wahnon, A. M. Lebuis, J. Chin, *Angew. Chem.* **1995**, *107*, 2594–2597; *Angew. Chem. Int. Ed. Engl.* **1995**, *34*, 2412–2414; d) W. H. Chapman, Jr., R. Breslow, *J. Am. Chem. Soc.* **1995**, *117*, 5462–5469; e) A. Tsubouchi, T. C. Bruice, *J. Am. Chem. Soc.* **1995**, *117*, 7399–7411; f) B. K. Takasaki, J. Chin, *J. Am. Chem. Soc.* **1995**, *117*, 8582–8585; g) T. Koike, M. Inoue, E. Kimura, M. Shiro, *J. Am. Chem. Soc.* **1996**, *118*, 3091–3099; h) K. G. Ragunathan, H.-J. Schneider, *Angew. Chem.* **1996**, *108*, 1314–1316; *Angew. Chem. Int. Ed. Engl.* **1996**, *35*, 1219–1221; i) C. Bazzicalupi, A. Bencini, A. Bianchi, V. Fusi, C. Giorgi, P. Paoletti, B. Valtancoli, D. Zanchi, *Inorg. Chem.* **1997**, *36*, 2784–2790; j) P. Molenveld, S. Kapsabelis, F. J. Engbersen, D. N. Reinhoudt, *J. Am. Chem. Soc.* **1997**, *119*, 2948–2949.

[8] The weak bands in the 3′ side of the main scission site in lane 10 are tentatively ascribed to catalysis by zinc(II) hydroxide clusters formed at a high Zn^{II} concentration ($[Zn^{II}]_0 = 0.5$ mM).

[9] When $[Zn^{II}]_0 = [TPBA]_0 = 2.5$ mM in D_2O, TPBA gave one set of ^1H NMR signals which differed from those of the free ligand. Upon increasing the $[Zn^{II}]_0/[TPBA]_0$ ratio, another set of signals (corresponding to the 2:1 complex) gradually appeared. At a ratio of 2, only signals for the 2:1 complex were observed.

An STM Study of Chemically Deposited Silver Nanoclusters on Mixed Self-Assembled Monolayers**

Ulrich-Walter Grummt,* Matthias Geissler, Till Drechsler, Harald Fuchs, and Ralf Staub

Single electron tunneling (SET) processes in quantum-confined low-dimensional systems have gained increasing interest over recent years.[1, 2] Understanding of the mechanism of charge transport through single molecules is a prerequisite for the rational design of electronic devices based on single molecules.[3] A challenging problem is to establish metallic contacts in a stable and reproducible way to individual molecules. Mixed self-assembled monolayers (SAMs) containing a small number of the molecules to be studied as guests in a matrix of inert host molecules offer the possibility to address single molecules by the STM tip (STM = scanning tunneling microscopy). The basic idea of the present study is to generate silver clusters as small as Ag_4 in the immediate vicinity of a four-electron reducing agent which is incorporated in a monolayer of long-chain alkanethiols (Figure 1).[4] In connection with an STM tip the silver nanoclusters provide a vertical double tunnel junction, which should allow the observation of SET processes, even at room temperature if the cluster capacitance is sufficiently small ($e^2/2C \gg kT$). Chemical deposition of silver clusters on SAMs is a simple and more gentle alternative to deposition from a cluster beam[5] and evaporation techniques.[6]

A series of aromatic methyl sulfides were synthesized bearing two adjacent terminal hydroquinone units. For this study the compound BHQ1 (Figure 1) was selected to form mixed SAMs with an excess of *n*-decanethiol (nDT). On Au(111) nDT forms layers with a hexagonal $(\sqrt{3} \times \sqrt{3})R30^\circ$ structure.[7] Molecular resolution was achieved with pure nDT SAMs. All variants of superlattices described by Delamarche et al. could be observed.[8] The MM3 simulations of SAMs where one of 18 nDT molecules was replaced with BHQ1 predict that BHQ1 should protrude beyond the nDT surface. However, not unexpectedly, single molecules of BHQ1 could not be resolved. On the other hand, phase segregation of nDT and BHQ1 to form separate domains could be ruled out.

The treatment of the mixed SAMs with an aqueous ammonia-containing solution of silver nitrate (5 M $AgNO_3$ in water/ethanol 2/1, pH 10) results in the formation of silver

[*] Prof. Dr. U.-W. Grummt, Dipl.-Chem. M. Geissler
Institut für Physikalische Chemie der Universität
Lessingstrasse 10, D-07743 Jena (Germany)
Fax: (+49) 3641-948302
E-mail: cug@pc04.chemie.uni-jena.de
Dipl.-Phys. T. Drechsler, Prof. Dr. H. Fuchs
Physikalisches Institut der Universität Münster (Germany)
R. Staub
Institut für Angewandte Photophysik der Technischen Universität Dresden (Germany)

[**] U.-W.G. thanks the German Fonds der Chemischen Industrie for financial support. We thank Dr. W. Poppitz for performing the SIMS measurements and Dr. B. Schröter for the XPS experiments. We are also indepted to T. Schmitz-Hübsch, M. Törker, and Dr. F. Sellam for continuous support with the STM measurements.

 © WILEY-VCH Verlag GmbH, D-69451 Weinheim, 1998 1433-7851/98/3723-3286 $ 17.50+.50/0

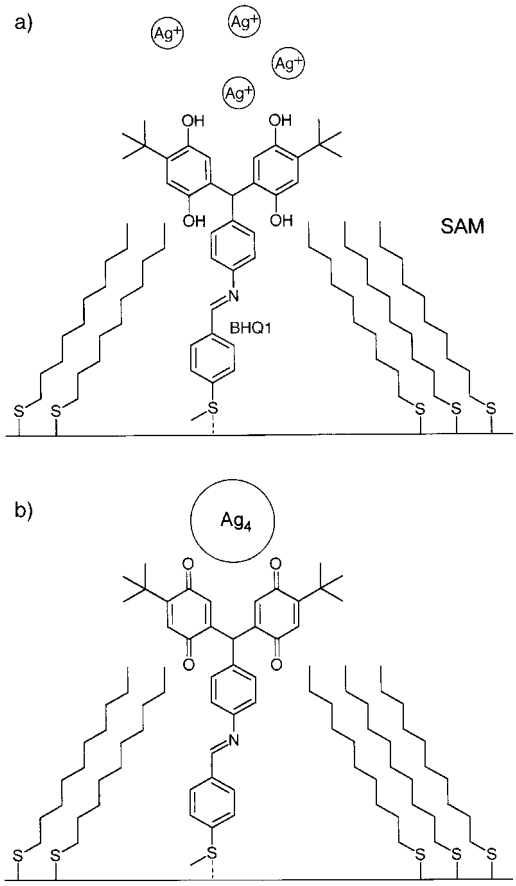


Figure 1. Contacting single molecules (BHQ1 with nDT on Au(111)). A solution of Ag^+ (pH 10) is added (a), and clusters such as Ag_4 form upon oxidation of the hydroquinone units of BHQ1 (b). See the text for further details.

nanoclusters. The presence of the clusters consisting of silver was proven by secondary ion mass spectrometry (SIMS) and X-ray photoelectron spectroscopy (XPS). The SIMS spectrum of a mixed SAM with silver clusters (Figure 2) shows the peaks of the isotopes ^{107}Ag and ^{109}Ag with the natural ratio of 51:49. The signals at m/z 129–136 are the Xe isotopes peaks. The following XPS signals were found: $Ag_{3d5/2}$: $E = 367.6$ eV ($\Delta E = -0.4$ eV), $Ag_{3d3/2}$: $E = 373.4$ eV ($\Delta E = -0.6$ eV),

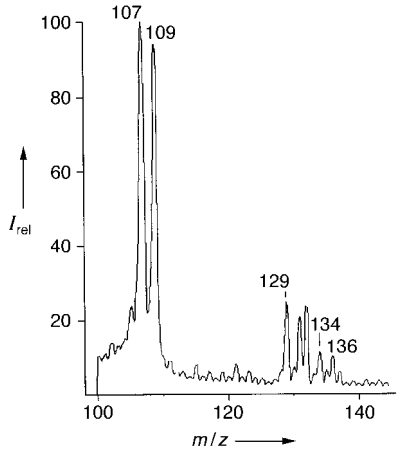


Figure 2. SIM spectrum of silver on a mixed SAM. I_{rel} = relative intensity.

$Ag_{3p3/2}$: $E = 572.6$ eV ($\Delta E = -0.4$ eV). The shifts ΔE are given relative to bulk silver; $Au_{4f7/2}$ was used as reference. The line positions agree reasonably well with literature data.[9] Most of the clusters are disklike with a height of 0.62 nm, corresponding to two atomic layers. Clusters containing 400–2000 atoms were observed by STM. A typical diameter is 5 nm, corresponding to about 510 atoms. An example is given in Figure 3.

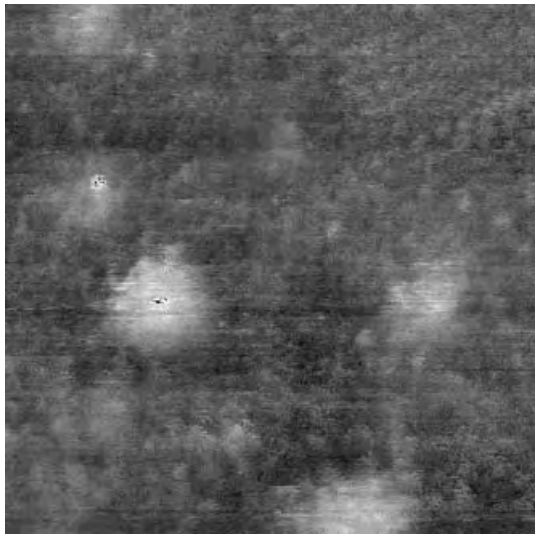


Figure 3. STM image of silver clusters generated on a mixed SAM of nDT/BHQ1 (3/1). The area is 20×20 nm^2. Constant-current mode, 0.19 nA, 1.19 V.

The resulting surface density of Ag atoms after the reduction process was obtained from statistical evaluations of the STM images (Figure 4). The straight line shows the surface density calculated with the assumption of a 1:1 replacement of nDT with BHQ1 under purely kinetic control

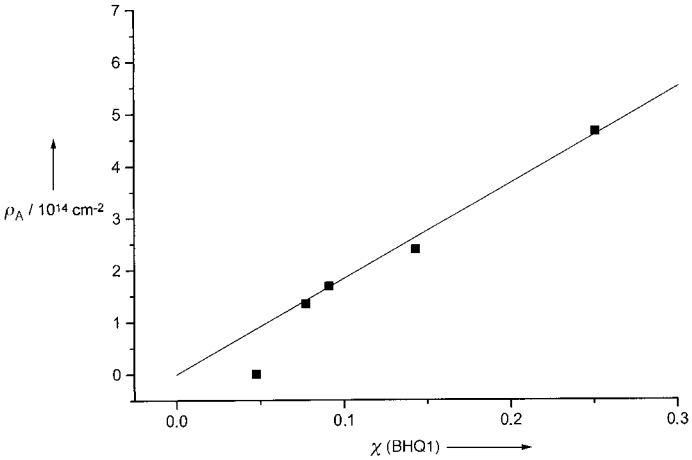


Figure 4. Surface density ρ_A of silver as a function of the mole fraction of BHQ1 in solution.

of the SAM formation. The experimental deviations at low BHQ1 admixtures might indicate that the assumption of kinetic control is not fully justified. The curvature of the experimental relationship has to be expected because the assumption of an 1:1 replacement must become invalid at

least with increasing admixtures of BHQ1. Since preformed BHQ1 aggregation is absent in the mixed SAM, we conclude that there is significant lateral surface diffusion of silver atoms or of very small clusters during the reduction process. The interaction of silver with terminal methyl groups of alkanethiol surfaces is very weak.[10] To reduce the surface mobility of silver, we also used 1-ω-sulfanyl alcohols as host matrices. However, the mean cluster size was insignificantly reduced.

Three types of current/voltage curves were observed, as shown in Figure 5. With the tip positioned above a cluster-free region of the SAM, sigmoid curves were obtained which never

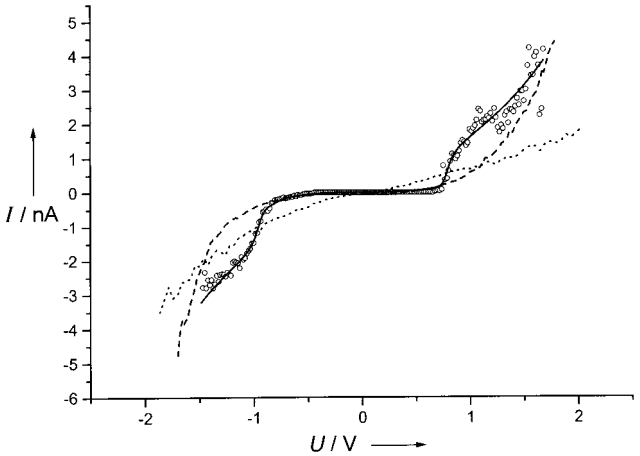


Figure 5. Current/voltage curves obtained from a cluster-free region of a SAM (– – –, $\times 10$) and of a silver cluster penetrating the SAM (- - - -, $\times 10$; both under ulta-high vacuum (UHV) and at room temperature) as well as of a silver cluster with the STM tip positioned above an isolated cluster (○, UHV, 100 K, $I = 40$ pA, $U = -1.0$ V).

showed a staircase shape. Most of the clusters give approximately linear curves with a more or less sigmoid distortion, indicating Ohmic behavior. As shown by Czanderna et al., silver deposited from a vacuum may rapidly penetrate through octadecanethiol SAMs.[11] It is also readily conceivable that upon heating the SAMs up to 150 °C the clusters come into direct Ohmic contact to the substrate due to desorption of organic molecules and diffusion of clusters to defect sites. Unequivocal observation of the typical XPS signals (S($2p_{3/2}$): $E = 162.1$ eV, S($2p_{1/2}$): $E = 163.7$ eV for thiolate SAMs and S($2p_{3/2}$): $E = 169.5$ eV for $RSCH_3$ SAMs[12]) proves that desorption of the organic material is at worst only partial. In particular, if clusters are sufficiently enlarged by physical development,[4] then Ohmic behavior becomes dominant. Apparently the probability of direct electric contact at some defect sites of the SAM increases with the cluster size.

On the other hand, we can unequivocally state that clusters do exist which are well isolated from the Au substrate. The observed staircase curve in Figure 5 is to be interpreted in terms of SET Coulomb blockades. The curve can be fitted using a semiclassical model of a two-junction system with the parameters C_i and R_i, the capacitance and resistance, respectively, of the ith junction, and a fractional charge Q_0 (Figure 6).[13] The parameter Q_0 originates from differences of the work functions of tip and sample. The least-squares fit of

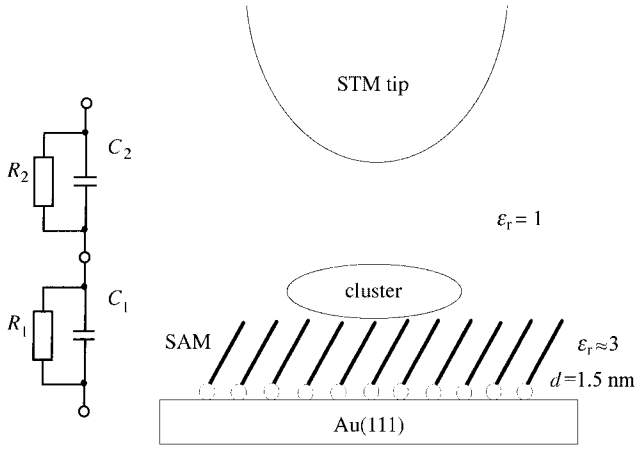


Figure 6. Geometrical model arrangement for estimating the electrical properties of the double junction.

the data yields $R_1 = 13.0\,M\Omega$, $C_1 = 1.01 \times 10^{-19}$ F, $R_2 = 643.5\,M\Omega$, $C_2 = 0.93 \times 10^{-19}$ F, and $Q_0/e = 0.051$. With the expression $C = 4\pi\varepsilon_r\varepsilon_0 r$ ($C \approx 1 \times 10^{-19}$ F, $\varepsilon_r = 3$) a cluster height of 0.6 nm could be estimated in a first approximation which agrees very well with the STM data.

Experimental Section

Characterization of BHQ1. Elemental analysis calcd for $C_{35}H_{39}NO_4S$ (M_r = 569.76): C 73.78, H 6.90, N 2.46, S 5.63; found: C 73.50, H 6.98, N 2.48, S 5.55; MS (DCI with H_2O): m/z (%): 93 (100), 404 (94.5), 343 (93.7), 570 (70.2), 153 (67.2), 228 (57.1), 253 (23.5), 325 (19.3), 285 (16.8), 514 (12.6); ^{1}H NMR (250 MHz, [D$_6$]DMSO): $\delta = 1.29$ (s, 18 H), 2.48 (s, 3 H), 5.83 (s, 1 H), 6.25 (s, 2 H), 6.61 (s, 2 H), 7.00 (d, $J = 8.38$ Hz, 2 H), 7.17 (d, $J = 8.38$ Hz, 2 H), 7.35 (d, $J = 8.47$ Hz, 2 H), 7.84 (d, $J = 8.46$ Hz, 2 H), 8.30 (s, 2 H), 8.40 (s, 2 H), 8.55 (s, 1 H); ^{13}C NMR (63 MHz, [D$_6$]DMSO): $\delta = 14.16$, 29.43, 33.91, 41.66, 113.37, 117.60, 120.54, 125.38, 127.83, 128.89, 129.73, 132.67, 133.07, 142.49, 142.60, 146.61, 147.54, 148.75, 158.79.

Sample preparation: For the majority of the experiments, Au(111) surfaces were prepared by high vacuum deposition of about 250 nm gold (99.99 %, Edelmetalle Freiberg, Germany) onto freshly cleaved mica at 300 °C.[14] Furthermore, Au(111) surfaces obtained by flame annealing of 200 nm Au/8 nm Cr on Tempax glass slides (SQ1 and BQ3, Sico Jena GmbH, Germany) were used as substrates.[15] The STM investigations show the expected hexagonal facet structure of atomically flat plateau areas with a step height of 0.24 nm. In most cases they also display the characteristic long-range $23 \times \sqrt{3}$ reconstruction. The SAMs were obtained by adsorption from 1 mM solutions of mixtures of nDT (Aldrich) with BHQ1 in ethanol for at least 10 h at room temperature. The samples were rinsed with ethanol and dried with nitrogen.

Apparatus: The STM images were recorded with a Nanoscope 2 (Digital Instruments) under ambient conditions using Pt/Ir tips. For low-temperature STS investigations a home-built beetle-type low-temperature STM under ultra-high vacuum (UHV; for detailed information see ref. [16]) was used. Current/voltage curves were taken with an Omicron combined AFM/STM after heating the sample for one hour at 150 °C in under UHV. Mass spectra were recorded on a SSQ-710 (Finnigen MAT). Elemental analyses were performed with a Leco CHNS-932 analyzer. The ^{1}H and ^{13}C NMR spectra were recorded with an AC-250 (Bruker). The XPS experiments were performed on a Specs EA 200 equipped with a multichannel hemispherical analyzer.

Received: May 29, 1998 [Z11915IE]
German version: *Angew. Chem.* **1998**, *110*, 3480 – 3482

Keywords: monolayers · nanostructures · scanning tunneling microscopy · silver

 © WILEY-VCH Verlag GmbH, D-69451 Weinheim, 1998 1433-7851/98/3723-3288 $ 17.50+.50/0

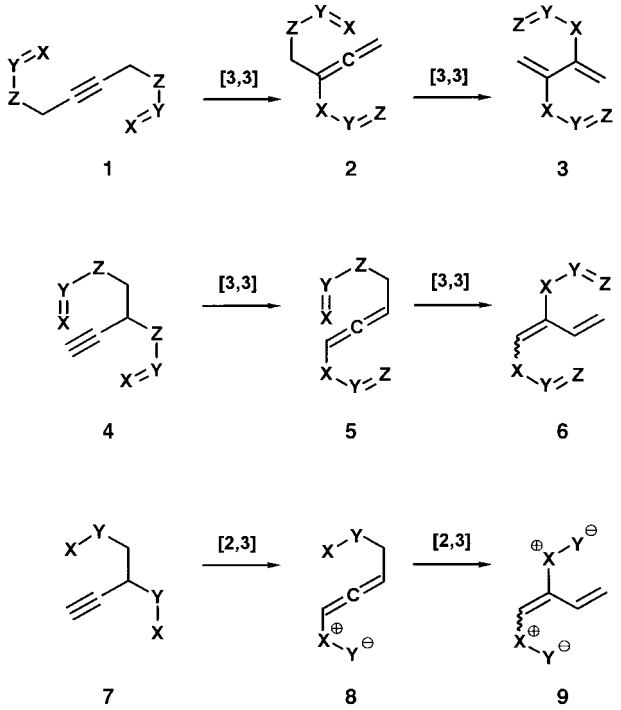
[1] K. Matsumoto, M. Ishi, K. Segawa, Y. Oka, B. J. Vartanian, J. S. Harris, *Appl. Phys. Lett.* **1996**, *68*, 34 – 36.
[2] M. Dilger, R. J. Haug, K. Eberl, K. von Klitzing, *Semicond. Sci. Technol.* **1996**, *11*, 1493 – 1497.
[3] A. Dhiorani, P.-H. Lin, P. Guyot-Sionnest, R. W. Zehner, L. R. Sita, *J. Chem. Phys.* **1997**, *106*, 5249 – 5253.
[4] U.-W. Grummt, M. Geissler, T. Schmitz-Hübsch, *Chem. Phys. Lett.* **1996**, *263*, 581 – 584.
[5] R. P. Andres, T. Bein, M. Dorogi, S. Feng, J. I. Henderson, C. P. Kubiak, W. Mahoney, R. G. Osifchin, R. Reifenberger, *Science* **1996**, *272*, 1323 – 1325.
[6] C. M. Fischer, M. Burghard, S. Roth, K. von Klitzing, *Appl. Phys. Lett.* **1995**, *66*, 3331 – 3333.
[7] C. A. Widrig, C. A. Alves, M. D. Porter, *J. Am. Chem. Soc.* **1991**, *113*, 2805 – 2810.
[8] E. Delamarche, B. Michel, H. A. Biebuyck, C. Gerber, *Adv. Mater.* **1996**, *8*, 719 – 729.
[9] G. Ertl, J. Küppers, *Low Energy Electrons and Surface Chemistry*, 2nd ed., VCH, Weinheim, **1985**, pp. 352 – 353.
[10] D. R. Jung, A. W. Czanderna, G. C. Herdt in *Polymer Surfaces and Interfaces: Characterization, Modification and Application* (Eds.: K. L. Mittal, K.-W. Lee), VSP, **1996**, pp. 189 – 221.
[11] G. C. Herdt, A. W. Czanderna, *J. Vac. Sci. Technol. A* **1994**, *12*, 2410 – 2414.
[12] M. Walczak, C. A. Alves, B. D. Lamp, M. D. Porter, *J. Electroanal. Chem.* **1995**, *396*, 103 – 114.
[13] A. E. Hanna, M. Tinkham, *Phys. Rev. B* **1991**, *44*, 5919 – 5922.
[14] J. A. DeRose, T. Thundat, L. A. Nagahara, S. M. Lindsay, *Surf. Sci.* **1991**, *256*, 102 – 108.
[15] H. Haiss, D. Lackey, J. K. Sass, K. H. Besocke, *J. Phys. Chem.* **1991**, *95*, 2193 – 2196.
[16] T. Drechsler, L. F. Chi, H. Fuchs, *Scanning* **1998**, *4*, 297 – 301.

Synthesis of 1,2-Difunctionalized 1,3-Butadienes through a Sequence of Sigmatropic Rearrangements**

Klaus Banert,* Wolfgang Fendel, and Jana Schlott

Dedicated to Professor Günter Marx on the occasion of his 60th birthday

Sequential [3,3] sigmatropic rearrangements such as the well-known reaction **1** → **2** → **3**, for example where XYZ = NCO,[1] NCS,[2] NCSe,[3] N_3,[4] $SCONMe_2$,[5] SCN,[6] C–CO_2R[7] (orthoester Claisen rearrangement), C–C=C[8] (Cope rearrangement), can be used to transform the 2-butyne-1,4-diyl precursors **1** into the 2,3-difunctionalized 1,3-butadienes **3** (Scheme 1). The synthesis of similar products proceeds analogously through two consecutive [2,3] sigmatropic isomerizations, for instance in the reaction of phosphinites to phosphane oxides,[9] phosphites to phosphonates,[10] sulfinates to sulfones,[11] or sulfenates to sulfoxides.[11, 12] To the best of our knowledge, however, sigmatropic rearrangements have not been employed to prepare 1,2-difunctionalized 1,3-butadienes. We describe here a sequence of sigmatropic isomerizations that provide a convenient approach to these target compounds. In this connection [3,3] migrations such as **4** → **5** → **6** as well as [2,3] shifts **7** → **8** → **9** are used to direct both functional groups into vinylic positions.

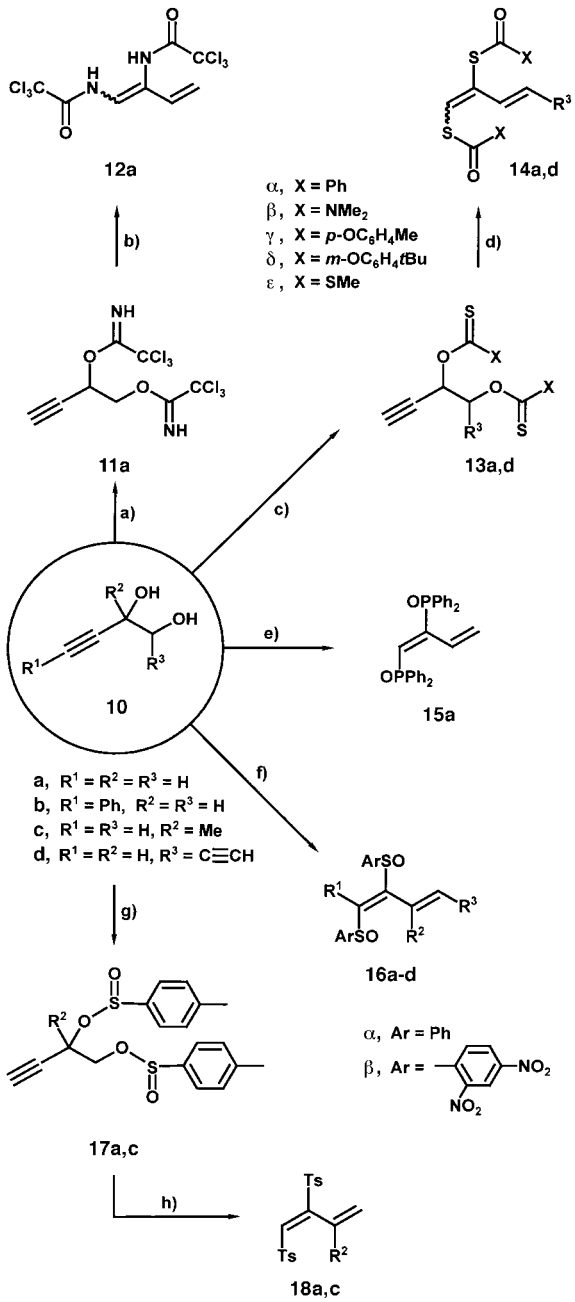


Scheme 1. Synthesis of doubly functionalized 1,3-butadienes by two consecutive sigmatropic rearrangements.

The hydroxyl groups of the readily available diols **10**[13] can be easily transformed into isomerizable functional groups (Scheme 2). The subsequent gas-phase thermolysis (flash vacuum pyrolysis)[14] of the imidate **11a** and the heating of the thiono carboxylates/carbamates/carbonates **13a,d** or sulfinates **17a,c** in solution lead to the 1,2-difunctionalized 1,3-butadienes **12a**, **14a,d**, and **18a,c**, respectively. The reactions of **10** to give **15a** or **16a – d** require no warming and succeed in one-pot procedures. The products **12a** and **14a**, which result from [3,3] sigmatropic rearrangements, are formed as mixtures of separable *E*/*Z* isomers. However, the [2,3] isomerizations afford the dienes **15a**, **16a – d**, and **18a,c** with exclusive *E* configuration. The sulfoxides **16a – d** are obtained as mixtures of *like*/*unlike* diastereomers as a consequence of the stereocenters at the sulfur atoms.[15] A subsequent isomerization of the C-C double bond is not observed on thermolysis in solution. For example, a constant ratio of 1:1 is detected for the distribution of products with *E* and *Z* configuration when the transformation **13a**γ → **14a**γ is investigated both immediately after low conversion and after very long reaction times (about 50 half-life periods of **13a**γ). In the case of **13d**β the sequences of [3,3] sigmatropic migrations prove to be stereospecific. Thus, *meso*-**13d**β furnishes nearly exclusively (*E*)-**14d**β, while *rac*-**13d**β leads almost solely to (*Z*)-**14d**β.

The bis(sulfenate) derived from *meso*-**10d** can give rise not only to **16d**α but also to a hexa-1,2,4,5-tetraene compound by

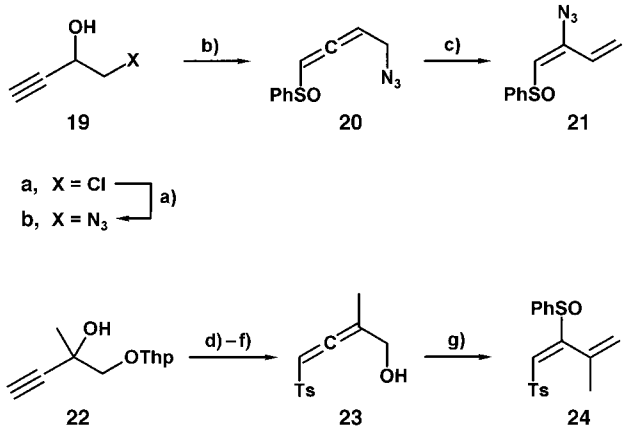
[*] Prof. Dr. K. Banert, Dr. W. Fendel, Dipl.-Chem. J. Schlott
Lehrstuhl für Organische Chemie der Technischen Universität
Strasse der Nationen 62, D-09111 Chemnitz (Germany)
Fax: (+49) 371-531-1839
E-mail: klaus.banert@chemie.tu-chemnitz.de
[**] Rearrangement Reactions, Part 7. This work was supported by the Deutsche Forschungsgemeinschaft and the Fonds der Chemischen Industrie. Part 6: K. Banert, *Liebigs Ann.* **1997**, 2005 – 2018.



Scheme 2. Transformation of the 3-butyne-1,2-diols **10** into the 1,2-difunctionalized 1,3-butadienes **12**, **14**, **15**, **16**, and **18**. a) DBU, CH_2Cl_2, Cl_3CCN, $-40 \rightarrow 20\,^{\circ}C$, 97%; b) gas-phase thermolysis at $400\,^{\circ}C/10^{-5}$ Torr, 40%, $E:Z = 1:4$; c) Py, THF, PhCSCl,[16] $0 \rightarrow 20\,^{\circ}C/5$ h, 69% **13a**α; NaH, THF, $0 \rightarrow 20\,^{\circ}C/16$ h, then Me_2NCSCl/THF, $-15\,^{\circ}C/1$ h $\rightarrow 20\,^{\circ}C/16$ h, 60% **13a**β; Py, THF, 4-MeC_6H_4CSCl, $-10\,^{\circ}C/1$ h $\rightarrow 20\,^{\circ}C/4$ h, 80% **13a**γ; Py, THF, 3-tBuC_6H_4CSCl, 69% **13a**δ; acetone, KOH, then CS_2, $-15\,^{\circ}C/35$ min, then MeI, $-15 \rightarrow 20\,^{\circ}C$, 32% **13a**$\varepsilon$; NaH, THF, $20 \rightarrow 35\,^{\circ}C/25$ h, then Me_2NCSCl/THF, $20\,^{\circ}C/6-16$ h, 62% *meso*-**13d**β; 71% *rac*-**13d**β; d) toluene, $110\,^{\circ}C/1.5-4$ h; approximately 100% **14a**α, $E:Z = 1:1$; 65% **14a**β, $E:Z = 1.4:1$; approximately 100% **14a**γ, $E:Z = 1:1$; 97% **14a**δ, $E:Z = 1.1:1$; 80% **14a**ε, $E:Z = 1.2:1$; 75% (*E*)-**14d**β (from *meso*-**13d**β); 75% (*Z*)-**14d**β (from *rac*-**13d**β); e) THF, BuLi, $-78\,^{\circ}C/45$ min, then addition to Ph_2PCl/THF, $-78\,^{\circ}C/1$ h $\rightarrow 20\,^{\circ}C$, 25%; f) THF, NEt_3, PhSCl,[17] approximately $-20 \rightarrow 0\,^{\circ}C$; 66% **16a**$\alpha$, diastereomers 1:1.2; 58% **16b**α, *like*:*unlike* = 1:1.5; 40% **16c**α, diastereomers 1:1.3; 65% **16d**α, diastereomers 1:1.3; THF, NEt_3, 2,4-$(O_2N)_2C_6H_3SCl$, $-25 \rightarrow 0\,^{\circ}C$, 46% **16a**$\beta$, diastereomers 1:1.4; g) 4-$MeC_6H_4S(O)Cl$,[18] NEt_3, THF or CH_2Cl_2, $0\,^{\circ}C/3$ h; h) PhCl, Li_2CO_3, $130\,^{\circ}C/27$ h, 55% **18a**, 40% **18c** (based on **10a** and **10c**, respectively). DBU = 1,8-diazabicyclo[5.4.0]undec-7-ene, Ts = *p*-toluenesulfonyl.

two independent [2,3] rearrangements. However, such a product has not been found. Evidently, the [2,3] migrations in the **7** $\rightarrow$ **8** $\rightarrow$ **9** direction are favored.

There are two methods to prepare 1,3-butadienes with two different functional groups in positions 1 and 2 by the aid of a sequence of sigmatropic isomerizations (Scheme 3): 1. The



Scheme 3. Synthesis of 1,3-butadienes with different functional groups at C-1 and C-2. a) NaN_3, H_2O, $60\,^{\circ}C/5$ h, 77%; b) CH_2Cl_2, NEt_3, PhSCl, $-15 \rightarrow 20\,^{\circ}C/24$ h; c) $CHCl_3$, $50\,^{\circ}C/17$ h, 48% based on **19b**; d) CH_2Cl_2, NEt_3, 4-$MeC_6H_4S(O)Cl$, $0\,^{\circ}C/3$ h; e) PhCl, Li_2CO_3, $130\,^{\circ}C/4$ h; f) MeOH, H_2SO_4, $20\,^{\circ}C/16$ h, 86% based on **22**; g) CH_2Cl_2, NEt_3, PhSCl, $0\,^{\circ}C/2$ h, 42%. Thp = tetrahydropyranyl.

two quite distinct, isomerizable groups, the azide[19] and the sulfenate function, are selectively introduced into the precursor **19a**[13a] so that regioisomer **21** results exclusively. The structure of this product is proved not only by spectroscopic data (Table 1), but also by its photochemical transformation into 3-ethenyl-2-phenylsulfinyl-2*H*-azirine. 2. Two relatively similar groups such as sulfinate and sulfenate functions are used selectively to synthesize the 1,3-butadiene **24** from the half-protected diol **22**[20] via **23**.[21]

Derivatives of the alcohol **25a**[22] can also be used as starting materials to prepare functionalized 1,3-butadienes on a sequence of sigmatropic isomerizations (Scheme 4). In this case, a Cope rearrangement is performed in the last step. The transformations **25a** $\rightarrow$ **25b** $\rightarrow$ **26**, **25a** $\rightarrow$ **27** $\rightarrow$ **28**, **25a** $\rightarrow$ **25c** $\rightarrow$ **29**, and **25a** $\rightarrow$ **25d** $\rightarrow$ **25e** $\rightarrow$ **30** $\rightarrow$ **31** lead to trichloroacetamides, thiocarbonates, sulfones, and isothiocyanates. Whereas flash vacuum pyrolysis of the thiocyanate **25e** at $400\,^{\circ}C$ generates (*E*)-**31** exclusively (80% yield), pyrolysis in the range of $320-260\,^{\circ}C$ gives a mixture of (*E*)-**31**/(*Z*)-**31** = 1.5:1 and allene **30** in 40–64% yield. A renewed thermolysis of this mixture at $400\,^{\circ}C$ gives the only product (*E*)-**31**. Apparently the Cope rearrangement **30** $\rightarrow$ **31** at least is reversible at higher temperatures.

Doubly functionalized dienes of type **6** and **9** may find use as synthetic building blocks. Preliminary investigations indicate that [4 + 2] cycloadducts are formed from tetracyanoethylene and **12a** (yield 63%), (*Z*)-**14a**α (28%), **14a**β (44%), (*Z*)-**14a**γ (64%), (*Z*)-**14a**δ (46%), (*Z*)-**14a**ε (71%), **26** (42%), (*E*)-**28** (60%), or (*E*)-**31** (57%). The sulfone **18a** is converted into **32** by regio- and stereoselective Diels–Alder reactions with electron-rich or electron-deficient dienophiles (Scheme 5). The nucleophilic substitution **18a** $\rightarrow$ **33** succeeds

 © WILEY-VCH Verlag GmbH, D-69451 Weinheim, 1998 1433-7851/98/3723-3290 $ 17.50+.50/0 *Angew. Chem. Int. Ed.* **1998**, *37*, No. 23

Table 1. Selected physical data of compounds (*Z*)-**12a**, **14aε**, **15a**, **16bα**, **18a**, **21**, **24**, and **31**.[a]

(*Z*)-**12a**: Colorless oil; ^{1}H NMR: $\delta = 5.26$ (d, $^3J = 10.9$, 1H; H-4), 5.27 (d, $^3J = 17.3$, 1H; H-4), 6.41 (dd, $^3J = 17.3$, 10.9, 1H; H-3), 6.74 (d, ^3J(NH,CH) = 9.4, 1H; H-1), 8.07 (br s, 1H; NH), 9.35 (br d, ^3J(NH,CH) = 9.4, 1H; NH); ^{13}C NMR: $\delta = 91.57$ (CCl_3), 91.75 (CCl_3), 113.94 (C-4), 118.76 (CH), 119.26 (C-2), 131.56 (CH), 159.38 (C=O), 160.68 (C=O).

(*E*)-**14aε**: Brown liquid; ^{1}H NMR: $\delta = 2.39$ (s, 3H; SMe), 2.51 (s, 3 H; SMe), 5.40 (d, $^3J = 10.5$, 1H; H-4), 5.70 (d, $^3J = 16.6$, 1H; H-4), 6.53 (dd, $^3J = 16.6$, $^3J = 10.5$, 1H; H-3), 7.42 (s, 1H; H-1); ^{13}C NMR: $\delta = 13.41$ (SMe), 13.49 (SMe), 120.18 (C-4), 124.67 (C-2), 130.65 (CH), 131.38 (CH), 184.44 (C=O), 188.64 (C=O); IR ($CDCl_3$): $\tilde{\nu} = 2933$, 1727 (C=O), 1652 (C=O), 1422, 1313, 1077, 971, 850, 802.

(*Z*)-**14aε**: ^{1}H NMR: $\delta = 2.41$ (s, 3H; SMe), 2.50 (s, 3H; SMe), 5.25 (d, $^3J = 10.5$, 1H; H-4), 5.54 (d, $^3J = 16.6$, 1H; H-4), 6.60 (dd, $^3J = 16.6$, $^3J = 10.5$, 1H; H-3), 7.65 (s, 1H; H-1); ^{13}C NMR: $\delta = 13.27$ (SMe), 13.38 (SMe), 116.97 (C-4), 125.93 (C-2), 134.83 (CH), 134.92 (CH), 185.48 (C=O), 185.80 (C=O).

15a: Colorless solid, m.p. 142–143 °C; ^{1}H NMR: $\delta = 5.43$ (d, $^3J = 11.4$, 1H; H-4), 5.73 (d, $^3J = 17.6$, 1H; H-4), 6.85 (t, J(P,H) = 23.0, 1H; H-1), ≈7.45 (m, 1H; H-3), 7.40–7.80 (m, 20H; 4 × Ph); ^{13}C NMR (the coupling constants correspond to ^{31}P,^{13}C coupling): $\delta = 126.54$ (dd, $^3J = 6$, $^4J = 1.5$; C-4), 128.64 (d, $^3J = 12.3$; Ph-*m*), 128.67 (d, $^3J = 12.3$; Ph-*m*), 130.53 (dd, $J = 9.5$, $J = 8.5$; C-3), 130.79 (d, $^2J = 9.9$; Ph-*o*), 130.80 (d, $^1J = 103$; Ph-*i*), 131.84 (d, $^3J = 9.9$; Ph-*o*), 131.97 (d, $^4J = 2.8$; Ph-*p*), 132.30 (d, $^4J = 2.8$; Ph-*p*), 132.78 (d, $^1J = 105$; Ph-*i*), 135.77 (dd, $^1J = 87$, $^2J = 6.3$; C-1), 151.98 (dd, $^1J = 81$, $^2J = 2$; C-2); ^{31}P NMR (external standard: 85% H_3PO_4): $\delta = 21.26$ (d, J(P,P) = 49.6), 30.22 (d, J(P,P) = 49.6); correct elemental analysis based on $C_{28}H_{24}O_2P_2$.

16bα (*unlike* isomer): Colorless solid, m.p. 155–157 °C (decomp); ^{1}H NMR: $\delta = 5.78$ (dd, $^3J = 11.6$, $^2J \approx 1.1$, 1H; H-4), 5.97 (dd, $^3J = 17.5$, $^2J \approx 1.1$, 1H; H-4), 6.55 (dd, $^3J = 17.5$, $^3J = 11.6$, 1H; H-3), 6.94 (br d, $J = 6.7$, 2H; Ph), 7.22–7.60 (m, 13H; Ph); ^{13}C NMR: $\delta = 123.91$, 124.59, 124.66, 127.50, 127.73, 127.88, 128.96, 129.10, 129.20, 130.89, 131.26, 131.40, 141.11, 141.83, 149.57, 151.56; (*like* isomer): ^{1}H NMR: $\delta = 5.77$ (d, $^3J = 11.5$, 1H; H-4), 5.82 (d, $^3J = 17.5$, 1H; H-4), 6.69 (dd, $^3J = 17.5$, $^3J = 11.5$, 1H; H-3), 6.83 (br d, $J \approx 6.7$, 2H; Ph), 7.22–7.60 (m, 13H; Ph); ^{13}C NMR: $\delta = 123.58$, 124.74, 127.57, 127.81, 128.02, 128.42, 129.15, 129.27, 129.79, 131.00, 131.14, 131.41, 142.09, 142.61, 148.98, 152.10; correct elemental analysis based on $C_{22}H_{18}O_2S_2$.

18a: Colorless solid, m.p. 95–97 °C; ^{1}H NMR: $\delta = 2.45$ (s, 3H; Me), 2.48 (s, 3H; Me), 5.69 (d, $^3J = 11.9$, 1H; H-4), 6.12 (d, $^3J = 17.9$, 1H; H-4), 7.00 (dd, $^3J = 17.9$, $^3J = 11.9$, 1H; H-3), 7.34 (2H; AA′BB′), 7.39 (2H; AA′BB′), 7.42 (s, 1H; H-1), 7.68 (2H; AA′BB′), 7.80 (2H; AA′BB′); ^{13}C NMR: $\delta = 21.66$ (Me), 21.70 (Me), 123.01 (C-3), 128.01 (CH), 128.37 (C-4), 128.55 (CH), 130.05 (CH), 130.25 (CH), 134.91, 135.51 (C-1), 136.71, 145.62, 145.87, 148.60; correct elemental analysis based on $C_{18}H_{18}O_4S_2$.

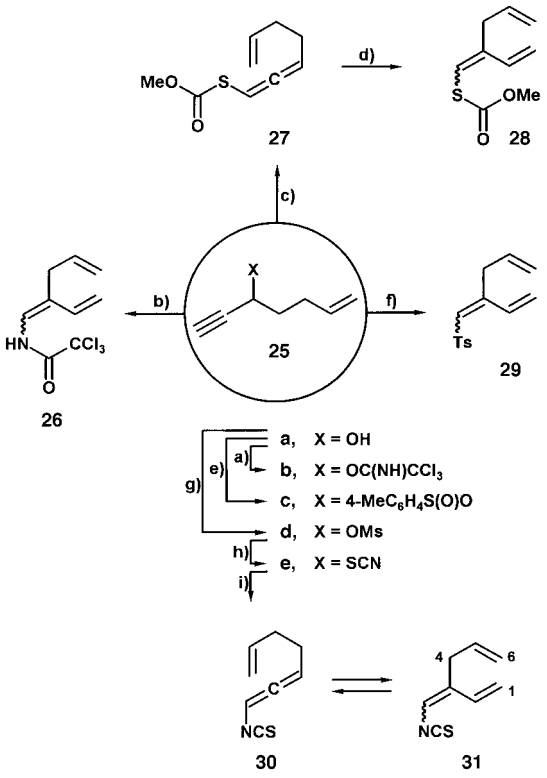
21: Colorless oil; ^{1}H NMR: $\delta = 5.60$ (br d, $^3J = 10.7$, 1H; H-4), 5.95 (d, $^3J = 16.7$, 1H; H-4), 6.00 (br s, 1H; H-1), 7.05 (dd, $^3J = 16.7$, $^3J = 10.7$, 1H; H-3), 7.49–7.67 (m, 5H; Ph); ^{13}C NMR: $\delta = 120.97$, 122.94, 123.87, 126.05, 129.32, 130.81, 144.02, 146.81; IR ($CDCl_3$): $\tilde{\nu} = 3061$, 2935, 2154, 2109, 1543, 1444, 1315, 1245, 1036.

24: Colorless solid, m.p. 119–121 °C; ^{1}H NMR: $\delta = 1.52$ (m, 3H; Me), 2.40 (s, 3H; Ar-Me), 4.83 (m, 1H; H-4), 5.22 (m, 1H; H-4), 6.95 (s, 1H; H-1), 7.31 (2H; AA′BB′), 7.40–7.58 (m, 5H; Ph), 7.75 (2H; AA′BB′); ^{13}C NMR: $\delta = 21.51$, 23.41, 120.10, 125.87, 127.08, 127.58, 129.14, 129.77, 132.16, 134.79, 137.29, 140.24, 144.90, 161.18; correct elemental analysis based on $C_{18}H_{18}O_3S_2$.

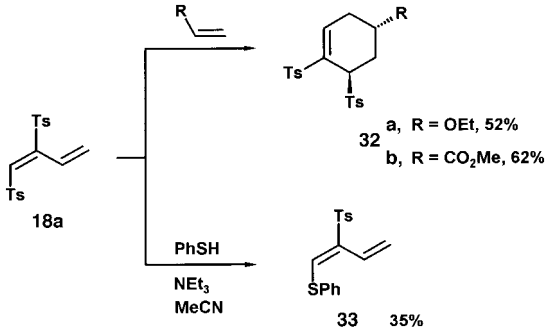
(*E*)-**31**: Colorless liquid; ^{1}H NMR: $\delta = 3.14$ (dt, $^3J = 6.3$, $^4J = 1.6$, 2H; H-4), 5.08 (dq, $^3J = 10.1$, $^2J = {}^4J = 1.6$, 1H; H-6), 5.13 (dq, $^3J = 17.3$, $^2J = {}^4J = 1.6$, 1H; H-6), 5.24 (dt, $^3J = 10.7$, $J \approx 0.6$, 1H; H-1), 5.43 (dt, $^3J = 17.3$, $J \approx 0.6$, 1H; H-1), 5.79 (ddt, $^3J = 17.1$, 10.1, 6.3, 1H; H-5), 6.04 (s, 1H; CHNCS), 6.26 (ddd, $^3J = 17.3$, $^3J = 10.7$, $J \approx 0.6$, 1H; H-2); ^{13}C NMR: $\delta = 30.77$ (C-4), 116.44 (CH–N), 116.61 (=CH_2), 117.23 (=CH_2), 133.90 (CH), 134.04 (CH), 135.61 (NCS), 139.80 (C-3); GC-MS: *m/z* (%): 151 (38) [M^+], 93 (100), 91 (63), 77 (91), 65 (40), 39 (91); IR ($CDCl_3$): $\tilde{\nu} = 2108$ (NCS).

(*Z*)-**31**: Colorless liquid; ^{1}H NMR: $\delta = 2.96$ (dq, $^3J = 6.6$, $^4J = 1.4$, 2H; H-4), 5.12 (dq, $^3J = 17.6$, $^2J = {}^4J = 1.4$, 1H; H-6), 5.12 (dq, $^3J = 10.0$, $^2J = {}^4J = 1.4$, 1H; H-6), 5.35 (d, $^3J = 11.0$, 1H; H-1), 5.46 (d, $^3J = 17.6$, 1H; H-1), 5.80 (ddt, $^3J = 17.6$, $^3J = 10.0$, $^3J = 6.6$, 1H; H-5), 5.89 (s, 1H; CHNCS), 6.81 (dd, $^3J = 17.6$, $^3J = 11.0$, 1H; H-2); ^{13}C NMR: $\delta = 33.65$ (C-4), 113.96 (CH), 117.47 (=CH_2), 118.01 (=CH_2), 130.52 (CH), 134.24 (CH), 136.23 (NCS), 137.77 (C-3).

[a] ^{1}H NMR: $CDCl_3$, 300 MHz, *J* in Hz; ^{13}C NMR: $CDCl_3$, 75 MHz, *J* in Hz, assignments of signals by DEPT experiments (DEPT = *d*istortionless *e*nhancement of *p*olarization *t*ransfer); MS: EI, 70 eV, IR: $\tilde{\nu}$ in cm^{-1}; elemental analysis: C, H, S.



Scheme 4. Synthesis of 2-allyl-1,3-butadienes with a functional group at C-1. a) DBU, Et_2O, Cl_3CCN, −40 °C/1 h → 20 °C/1 h, 97%; b) **25b**, gas-phase thermolysis 390 °C/10^{-3} Torr, 98%, *E*:*Z* = 1:2; c) **25a**, NaH, Et_2O, then dropwise addition to $CSCl_2/Et_2O$, 0 °C/1 h → 20 °C/24 h, then MeOH, 20 °C/16 h, 72%; d) gas-phase thermolysis at 400 °C/10^{-3} Torr, 83%, *E*:*Z* = 1:1.5; e) CH_2Cl_2, NEt_3, 4-$MeC_6H_4S(O)Cl$, 0 °C/3 h; f) **25c**, PhCl, 130 °C/15 h, 63% based on **25a**, *E*:*Z* = 1:1.6; g) $MeSO_2Cl$, NEt_3, 20 °C/24 h, 95%; h) NH_4SCN, MeOH, 60 °C/7 h, 75%; i) gas-phase thermolysis at 260–400 °C/10^{-3} Torr, 94–80% for **30**+**31**. Ms = methanesulfonyl.



Scheme 5. Bis(sulfone) **18a** as a synthetic building block.

with similar selectivity. Nucleophilic addition reactions are also possible.

Received: February 13, 1998 [Z11476IE]
German version: *Angew. Chem.* **1998**, *110*, 3488–3491

Keywords: alkynes · allenes · butadienes · pericyclic reactions · rearrangements

[1] K. Banert, S. Groth, *Angew. Chem.* **1992**, *104*, 865 – 867; *Angew. Chem. Int. Ed. Engl.* **1992**, *31*, 866 – 868.
[2] K. Banert, H. Hückstädt, K. Vrobel, *Angew. Chem.* **1992**, *104*, 72 – 74; *Angew. Chem. Int. Ed. Engl.* **1992**, *31*, 90 – 92; K. Banert, S. Groth, H. Hückstädt, K. Vrobel, *Phosphorus Sulfur Silicon Relat. Elem.* **1994**, *95 – 96*, 323 – 324.
[3] K. Banert, C. Toth, *Angew. Chem.* **1995**, *107*, 1776 – 1778; *Angew. Chem. Int. Ed. Engl.* **1995**, *34*, 1627 – 1629.
[4] H. Priebe, *Angew. Chem.* **1984**, *96*, 728 – 729; *Angew. Chem. Int. Ed. Engl.* **1984**, *23*, 736 – 737; K. Banert, *Tetrahedron Lett.* **1985**, *26*, 5261 – 5264; *Chem. Ber.* **1987**, *120*, 1891 – 1896; K. Banert, M. Hagedorn, *Angew. Chem.* **1989**, *101*, 1710 – 1711; *Angew. Chem. Int. Ed. Engl.* **1989**, *28*, 1675 – 1676.
[5] B. Müller, Diplomarbeit, Technische Universität Chemnitz, **1997**.
[6] A. Günther, Dissertation, Technische Universität Chemnitz, not yet published.
[7] Y. Ishino, I. Nishiguchi, M. Kim, T. Hirashima, *Synthesis* **1982**, 740 – 742; A. Srikrishna, S. Nagaraju, *J. Chem. Soc. Perkin Trans. 1* **1992**, 311 – 312.
[8] H. Hopf, R. Kirsch, *Tetrahedron Lett.* **1985**, *26*, 3327 – 3330.
[9] T. Pollok, H. Schmidbaur, *Tetrahedron Lett.* **1987**, *28*, 1085 – 1088; R. Y. Chen, B. Z. Cai, K. S. Feng, *Chin. Chem. Lett.* **1992**, *3*, 157 – 158.
[10] M. Huché, P. Cresson, *Bull. Soc. Chim. Fr.* **1975**, *3 – 4*, 800 – 804; M. Huché, P. Cresson, *Tetrahedron Lett.* **1973**, 4291 – 4292.
[11] G. Smith, C. J. M. Stirling, *J. Chem. Soc. C* **1971**, 1530 – 1535.
[12] S. Jeganathan, W. H. Okamura, *Tetrahedron Lett.* **1982**, *23*, 4763 – 4764.
[13] a) R. Lespieau, *Bull. Soc. Chim. Fr.* **1928**, *43*, 199 – 210; b) V. A. Engelhardt, J. E. Castle, *J. Am. Chem. Soc.* **1953**, *75*, 1734; c) D. Miller, *J. Chem. Soc. C* **1969**, 12 – 15; d) S. Holand, R. Epsztein, I. Marszak, *Bull. Soc. Chim. Fr.* **1969**, 3213 – 3218; e) H. P. Figeys, M. Gelbcke, *Tetrahedron Lett.* **1970**, 5139 – 5142; f) K. S. Jeong, P. Sjö, K. B. Sharpless, *Tetrahedron Lett.* **1992**, *33*, 3833 – 3836.
[14] For the conditions of the flash vacuum pyrolysis, see Scheme 2 and refs. [2, 3].
[15] The geometrical isomers are assigned on the basis of ^{1}H and ^{13}C NMR investigations (including homonuclear NOE difference spectra, studies with lanthanide shift reagents, $^{3}J(^{31}P,^{1}H)$ data, comparisons with ethene-1,2-diyl compounds analogously substituted). The configurations of the C – C double bonds can also be verified by comparison of the rates of the Diels – Alder reactions, with the rates being higher for (*Z*)-**12a**, (*Z*)-**14a*α* – *ε***, (*E*)-**26**, (*E*)-**28**, and (*E*)-**31**, respectively. The X-ray crystal structure analysis of the *unlike* isomer of **16b*α*** was performed. We thank Prof. Dr. H.-J. Deiseroth and Dr. L. Kienle, Universität-GH Siegen, for this investigation.
[16] H. Staudinger, J. Siegward, *Helv. Chim. Acta* **1920**, *3*, 824 – 833.
[17] A. G. M. Barrett, D. Dhanak, G. G. Graboski, S. J. Taylor, *Org. Synth. Coll. Vol.* **1993**, *8*, 550 – 553.
[18] F. Kurzer, *Org. Synth. Coll. Vol.* **1963**, *4*, 937 – 939.
[19] K. Banert, *Chem. Ber.* **1989**, *122*, 1963 – 1967.
[20] F. Sondheimer, N. Stjernström, D. Rosenthal, *J. Org. Chem.* **1959**, *24*, 1280 – 1284.
[21] Alternative preparation of **23**: T. G. Back, E. K. Y. Lai, K. R. Muralidharan, *J. Org. Chem.* **1990**, *55*, 4595 – 4602.
[22] Synthesis from ethynylmagnesium bromide and 4-pentenal, 59%; alternative preparation of **25a**: D. Seebach, A. K. Beck, B. Schmidt, Y. M. Wang, *Tetrahedron* **1994**, *50*, 4363 – 4384.

An Iron(III) – Catechol Complex as a Mushroom Pigment**

Franz von Nussbaum, Peter Spiteller, Matthias Rüth, Wolfgang Steglich,* Gerhard Wanner, Brandy Gamblin, Lorenzo Stievano, and Friedrich E. Wagner

Dedicated to Prof. Heinrich Nöth on the occasion of his 70th birthday

Cortinarius violaceus [(L.: Fr.) S. F. Gray][1] is a spectacular mushroom well known for its dark blue-violet color and its cedar-wood-like smell. Fries[2] described this type species of the genus *Cortinarius* as "species nobilissima, pulcherrima". Previous efforts to examine the chemical nature of the violet pigment failed because of its instability and polarity. The dark violet water extracts of fresh or freeze-dried fruit bodies became dark brown within minutes. We were able to suppress this decomposition by exhaustive extraction of the lyophilized mushrooms with methanol prior to the water extraction. After freeze-drying the resulting aqueous solution, the residue was purified by chromatography on a Sephadex LH-20 column with methanol/water (1/1). This procedure enabled us to enrich the highly sensitive pigment. The pigment's NMR spectra were inconclusive due to strong signal broadening by paramagnetic iron, which can be detected both in the extract and the mushrooms. Since the intensity of the violet color correlates with the concentration of iron, the presence of an iron complex as the coloring principle seems obvious.

Energy dispersive X-ray analysis[3] (EDX), atomic absorption spectroscopy[4] (AAS), and the thiocyanate test indicated that *C. violaceus* is capable of accumulating iron in a unique manner. The amount of iron in the mushroom is 4.5 – 7.5 mg g^{-1} (dry weight), which is about 100 times the average value of 0.06 mg g^{-1} determined for other basidiomycetes.[5, 6] The Mössbauer spectra[7] (Figures 1 and 2, Table 1) show that the iron in the pigment is trivalent, and the ESR spectra[8] indicate a high-spin Fe^{III} complex.[9] The spectra of the freeze-dried mushrooms and the water extracts are identical.

After addition of aqueous HCl to the enriched pigment (*R*)-*β*-dopa ((*R*)-**3**) can be identified as the complex ligand.[10] Chromatographic workup of the methanol extracts followed by recrystallization yields the analytically pure amino acid. The (*R*)-*β*-dopa amounts to 2% of the dry weight of the mushroom. *β*-Dopa is a new natural product that has been synthesized only as the racemate before.[11] We obtained

[*] Prof. Dr. W. Steglich, Dipl.-Chem. F. von Nussbaum, Dipl.-Chem. P. Spiteller, Dipl.-Chem. M. Rüth
Institut für Organische Chemie der Universität
Karlstrasse 23, D-80333 München (Germany)
Fax: (+49) 89-5902-604
E-mail: wos@org.chemie.uni-muenchen.de
Prof. Dr. G. Wanner
Botanisches Institut der Universität München (Germany)
B. Gamblin, Dipl.-Chem. Lorenzo Stievano, Prof. Dr. F. E. Wagner
Physik-Department E15 der Technischen Universität München, Garching (Germany)

[**] This work was supported by the Deutsche Forschungsgemeinschaft (SFB 369). We thank H. Hartl for the AAS measurements, G. Sturm for ESR spectra, and Prof. Dr. M. Spiteller for ESI-MS and APCI-MS investigations.

 © WILEY-VCH Verlag GmbH, D-69451 Weinheim, 1998 1433-7851/98/3723-3292 $ 17.50+.50/0

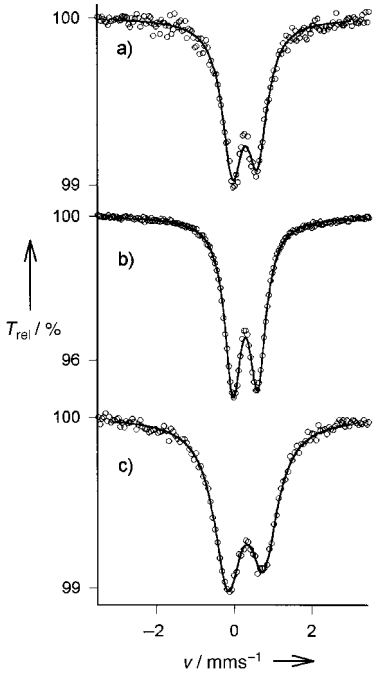


Figure 1. Mössbauer spectra at room temperature. a) Freeze-dried *C. violaceus*; b) water extract; c) synthetic 1:2 iron(III)–β-dopa complex at pH 6.2. T_{rel} = relative transmission.

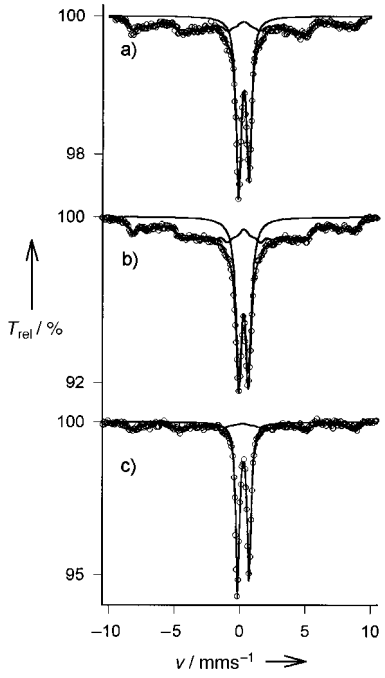


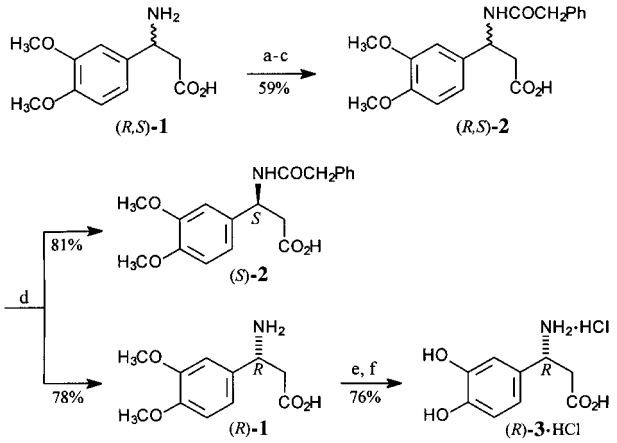
Figure 2. Mössbauer spectra at 4.2 K. a) Freeze-dried *C. violaceus*; b) water extract; c) synthetic 1:2 iron(III)–β-dopa complex at pH 6.2.

(*R*)-**3** from racemic (*R*,*S*)-3-amino-3-(3,4-dimethoxyphenyl)-propionic acid (**1**), which is easily accessible by Rodionov's procedure.[12] After conversion of (*R,S*)-**1** into the *N*-phenylacetyl derivative **2**, the action of penicillin acylase[13] yields optically pure (*R*)-**1**. Ether cleavage with 48% HBr affords (*R*)-β-dopa hydrobromide, which can be converted into the corresponding hydrochloride by ion exchange (Scheme 1).

Table 1. ^{57}Fe Mössbauer parameters[21] for the quadrupole doublets at room temperature and at 4.2 K. Quadrupole splitting *QS*; isomer shift *IS*; line width *LW*.

Sample	*T* [K]	QS [mm s^{-1}]	*IS*[a] [mm s^{-1}]	*LW* [mm s^{-1}]	Area[b] [%]
(a) freeze-dried	4.2	0.80(1)	0.38(1)	0.45(1)	50(1)
C. violaceus	294	0.64(1)	0.39(1)	0.62(2)	100
(b) water extract	4.2	0.74(1)	0.38(1)	0.53(1)	43(1)
	294	0.64(1)	0.40(1)	0.51(1)	100
(c) synthetic 1:2 Fe^{III}–	4.2	0.89(1)	0.40(1)	0.33(1)	70(1)
β-dopa complex (pH 6)	294	0.94(2)	0.41(1)	0.85(3)	100

[a] The isomer shifts refer to α-Fe. [b] The spectra recorded at 4.2 K show (in addition to the quadrupole doublet with the given fractional area) a magnetically split component with a distribution of hyperfine fields between 52.5(2) and 13.5(3) T, an effective quadrupole splitting of QS = 0.02(2) mm s^{-1} and an isomer shift of IS = 0.38(2) mm s^{-1}.



Scheme 1. Synthesis of (*R*)-**3**. a) MeOH, cat. HCl, reflux; b) $PhCH_2COCl$, CH_2Cl_2, NEt_3, cat. DMAP; c) LiOH, H_2O/MeOH (1/1); d) penicillin acylase, pH 7.5, phosphate buffer, 25 °C, 12 h; e) 48% HBr, 145 °C, 4 h; f) Dowex 50 WX8. DMAP = 4-dimethylaminopyridine.

Since comparison of the specific optical rotations of the natural and the synthetic products was ambiguous, the absolute configuration and optical purity of the natural ligand were determined by GC/MS.[14] For this purpose, natural β-dopa was O-methylated with diazomethane and subsequently acylated with Mosher's (*R*)-acid chloride.[15] The derivatives obtained from the natural and the synthetic amino acid were identical.[16] Within the scope of this method the natural product was enantiomerically pure.

The UV/Vis spectrum of the enriched pigment at pH 6.2, the physiological pH value of the mushroom, exhibited a ligand-to-metal charge-transfer (LMCT) absorption of λ_{max} = 571 nm, which is typical for iron(III)–catechol complexes. At pH 9.0 a hypsochromic shift to λ_{max} = 487 nm is observed. The blue-violet solution changes to bordeaux and decomposes quickly. Addition of KCN or ethylenediaminetetraacetic acid (EDTA) to the original solution causes discoloration.

The behavior of the pigment is consistent with that of other iron(III)–catechol complexes, in which the cation:ligand ratio depends on the pH value. An increase in the pH value leads to the typical color changes from green (pH 3, 1:1)[17] to blue-violet (pH 6, 1:2) and finally bordeaux (pH 9, 1:3; Figure 3). The UV/Vis data of iron(III)–dopamine[18] and iron(III)–

 © WILEY-VCH Verlag GmbH, D-69451 Weinheim, 1998 1433-7851/98/3723-3293 $ 17.50+.50/0

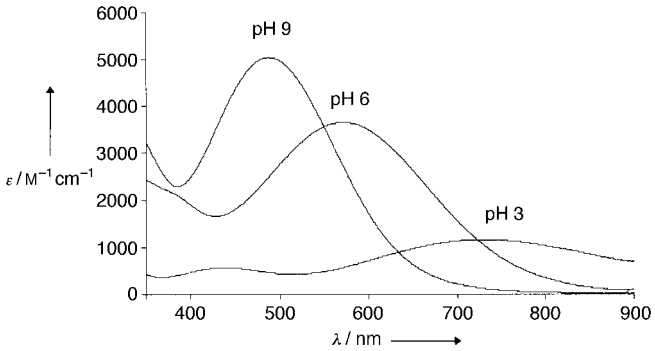
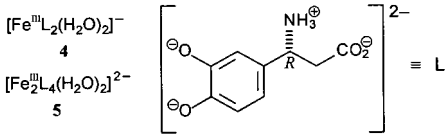


Figure 3. UV/Vis spectra of the synthetic iron(III)–β-dopa complex in water.

catechol complexes[19, 20] at various pH values are in close agreement with those of our pigment.

The experimental evidence indicates that the pigment from *C. violaceus* is an iron–ligand 1:2 complex; however, it cannot be determined if it is mono- or binuclear (**4** or **5**, Scheme 2).



Scheme 2. Proposals for the blue-violet 1:2 iron(III)–β-dopa complex species present in *C. violaceus* at pH 6.2.

The Mössbauer spectra[21] of the pigment are in good agreement with those of a binuclear 1:2 iron(III)–catechol complex,[22] whose structure has been established by X-ray analysis.[22] Neither mass spectroscopic methods nor chiroptical measurements led to a more detailed insight into the structure of the natural complex. The analogy of our pigment to an iron ink is clear. To the best of our knowledge, pigments of this type have not yet been discovered in nature.[23, 24]

Experimental Section

Isolation of (*R*)-**3**: Powdered, freeze-dried fruit bodies (12.7 g) of *C. violaceus* (collected in September 1996 in a spruce forest near Gilching, Oberbayern, Germany) were defatted with CH_2Cl_2 (200 mL) for 2 d and then extracted exhaustively with MeOH. After concentration of the extracts, the residue (5.1 g) was purified by chromatography on a Sephadex LH-20 column (40 × 8 cm) with MeOH. Fractional recrystallization of the crude material from dry MeOH removed sugar impurities and yielded analytically pure (*R*)-**3** (41 mg, 0.3 % of dry weight).

Isolation of (*R*)-**3**·HCl: The MeOH extracts (see the isolation of (*R*)-**3**) were purified by chromatography on a cation-exchange column (Dowex 50 WX8, H^+ form). After washing with water (300 mL) the ligand was eluted with 4 N HCl (100 mL). Further purification on Dowex 50 WX8 yielded (*R*)-**3**·HCl as a hygroscopic, beige foam (0.27 g, 2 % of dry weight).

Enrichment of the blue-violet pigment: After the treatment with MeOH, the mushroom residues were extracted with H_2O (200 mL) at 25 °C for 20 min under argon. The resulting deep blue-violet solution was freeze-dried and purified by chromatography repeatedly on Sephadex LH-20 (H_2O/MeOH/0.1 % KOH 25/25/1). Yield of pigment 15 mg, 0.1 % of dry weight.

Received: June 23, 1998 [Z 12032 IE]
German version: *Angew. Chem.* **1998**, *110*, 3483–3485

Keywords: amino acids · dyes · iron · Moessbauer spectroscopy · structure elucidation

[1] *Cortinarius violaceus* and *C. hercynicus* are synonymous; for the taxonomy of this widely distributed species, see for example T. E. Brandrud, *Nord. J. Bot.* **1983**, *3*, 577–592.
[2] E. Fries, *Monographia Hymenomycetum Suecicae*, Vol. II (Ed.: C. A. Leffler), Uppsala, **1863**, p. 46.
[3] EDX: Slices of freeze-dried fruit bodies were mounted on conductive carbon adhesive tabs (W. Plannet GmbH), coated with carbon, and examined in a field emission scanning electron microscope (Hitachi S-4100). The detection of the elements was carried out with an ultrathin window EDX detector (Noran Instruments) either in the spot or mapping mode.
[4] AAS: The amount of Fe was detected with a Perkin-Elmer 1100B instrument at 248.30 nm. A $FeCl_3$ solution (Titrisol, Merck) was used as standard.
[5] G. Tyler, *Trans. Br. Mycol. Soc.* **1980**, *74*, 41–49.
[6] The false chanterelle (*Hygrophoropsis aurantiaca*) and the bolete *Suillus variegatus* are also rich in iron (1–3 mg g^{-1} dry weight): M. Lupper, Dissertation, Universität Würzburg, **1988**.
[7] The ^{57}Fe Mössbauer spectra were recorded with a ^{57}Co source in Rh. Source and absorber were kept at the same temperature. The spectrometer, equipped with a Kr proportional counter to detect the 14.4-keV γ radiation used a sinusoidal velocity waveform.
[8] All ESR spectra were measured on solids and showed a characteristic signal at $g = 4.26$ ($\Delta h = 9.4$ mT); see also H. Oubrahim, J.-M. Richard, D. Cantin-Esnault, F. Seigle-Murandi, F. Trécourt, *J. Chromatogr. A* **1997**, *758*, 145–157.
[9] a) B. F. Anderson, D. A. Buckingham, G. B. Robertson, J. Webb, *Nature* **1976**, *262*, 722–724; b) L. Burlamacchi, A. Lai, M. Moduzzi, G. Saba, *J. Magn. Reson.* **1983**, *55*, 39–50.
[10] (*R*)-**3**: M.p. 194 °C; $[\alpha]_{589}^{23} = -12.1$ ($c = 0.5$ in 6 N HCl); R_f: 0.45 (*n*BuOH/EtOH/AcOH/H_2O 4/1/1/1); IR (KBr): $\tilde{\nu} = 3400$ (br), 3043 (s), 1608 (m), 1571 (s, CO_2^-), 1531 (s), 1466 (s), 1392 (s), 1361 (m), 1281 (m), 1250 (s), 1197 (w), 1173 (m), 1126 (m), 1042 (w), 986 (w), 948 (w), 929 (w), 868 (w), 818 (w), 792 (w), 775 (w), 696 (w), 650 (w), 595 (w), 573 (w), 460 cm^{-1} (w); ^{1}H NMR (600 MHz, [D$_6$]DMSO): $\delta = 2.30$ (dd, $J = 16.1$, 3.9 Hz, 1H; CH^{α}H$^{\beta}$), 2.41 (dd, $J = 16.0$, 10.0 Hz, 1H; CH$^{\alpha}H^{\beta}$), 4.14 (dd, $J = 9.6$, 3.8 Hz, 1H; ArCHN), 6.65 (dd, $J = 8.0$, 1.7 Hz, 1H; 6-H), 6.69 (d, $J = 8.0$ Hz, 1H; 5-H), 6.83 (s, 1H; 2-H); ^{13}C NMR (151 MHz, [D$_6$]DMSO): $\delta = 40.83$ (CH_2), 51.90 (ArCHN), 114.81 (C-2), 115.75 (C-5), 117.94 (C-6), 130.27 (C-1), 145.59 (C-4), 145.61 (C-3), 173.68 (CO_2H); EI-MS (decomposition, 70 eV): *m*/*z* (%): 180 (7) [$M - NH_3$]$^+$, 136 (100) [$M - NH_3 - CO_2$]$^+$; FAB-MS (glycerol): *m*/*z* (%): 198 (45) [M+H]$^+$, 181 (56), 171 (100), 153 (58), 136 (35); ESI-MS: *m*/*z* (%): 220 (8) [M+Na]$^+$, 198 (34) [M+H]$^+$, 181 (100), 171 (5), 163 (4), 139 (61); ESI-HR-MS: calcd for $C_9H_{12}NO_4$: 198.0766; found: 198.0767; elemental analysis calcd for $C_9H_{11}NO_4 \cdot \frac{1}{3}H_2O$: C 53.20, H 5.79, N 6.89; found: C 53.29, H 5.74, N 7.02. Tris(trimethylsilyl)-(*R*)-β-dopa: GC: $R_i = 2105$; GC/MS (70 eV): *m*/*z* (%): 413 (8) [M^+], 398 (2) [$M - CH_3$]$^+$, 396 (2) [$M - NH_3$]$^+$, 381 (1), 282 (100) [$M - CH_2CO_2Si(CH_3)_3$]$^+$, 268 (5), 210 (6), 194 (5), 167 (3), 147 (3), 117 (3), 75 (20) [$HOSi(CH_3)_2$]$^+$, 73 (49) [$Si(CH_3)_3$]$^+$; HR-GC/MS: calcd for $C_{18}H_{35}NSi_3O_4$: 413.1874, found: 413.1889.
[11] T. Posner, *Justus Liebigs Ann. Chem.* **1912**, *389*, 1–120.
[12] W. M. Rodionov, E. A. Postovskaja, *J. Am. Chem. Soc.* **1929**, *51*, 841–847.
[13] a) V. A. Soloshonok, N. A. Fokina, A. V. Rybakova, I. P. Shishkina, S. V. Galushko, A. E. Sorochinsky, V. P. Kukhar, M. V. Savchenko, V. K. Švedas, *Tetrahedron: Asymmetry* **1995**, *7*, 1601–1610; b) G. Cardillo, L. Gentilucci, A. Tolomelli, C. Tomasini, *J. Org. Chem.* **1998**, *63*, 2351–2353.
[14] For GC/MS a fused silica capillary column (DB-5ms, 30 m × 0.25 mm × 0.25 μm; J & W) was used. Injector temperature 280 °C. Temperature program: 3 min isothermic at 50 °C, 2 min at 100 °C, then heated to 300 °C with a rate of 3 K min^{-1}, and finally 10 min isothermic at 300 °C. An aliquot (0.5–1.5 μL) of a 1–2 % solution (m/v) was injected in every case. The Kováts indices were determined by co-injection of 0.2 μL of a mixture consisting of *n*-alkanes (C_{10}–C_{36}).

 © WILEY-VCH Verlag GmbH, D-69451 Weinheim, 1998 1433-7851/98/3723-3294 $ 17.50+.50/0

[15] A. J. Dale, H. S. Mosher, *J. Org. Chem.* **1969**, *34*, 2543 – 2549.
[16] Determination of the configuration by GC/MS: MeOH (1 mL) and a 5% solution of CH_2N_2 in diethyl ether (2 mL) were added to natural (*R*)-*β*-dopa (1 mg) at 25 °C. After 1 h the solvent was removed under argon, and Mosher's (*R*)-acid chloride (10 μL) was added to the residue. After an additional 12 h at 25 °C MeOH (50 μL) was added, and the GC/MS analysis was carried out. Methyl 3-(3,4-dimethoxyphenyl)-3-(3,3,3-trifluoro-2-methoxy-2-phenylpropionylamino)propionate: 2′*S*,3*R* derivative: GC: $R_i = 2684$; GC/EI-MS (70 eV): *m*/*z* (%): 455 (10) [M^+], 382 (8), 238 (45), 223 (83), 189 (38), 181 (100), 164 (33), 105 (23), 91 (13), 77 (19). 2′*S*,3*S* derivative: GC: $R_i = 2709$.
[17] U. El-Ayaan, E. Herlinger, R. F. Jameson, W. F. Linert, *J. Chem. Soc. Dalton Trans.* **1997**, 2813 – 2818.
[18] C. Gerard, H. Chehhal, R. P. Hugel, *Polyhedron* **1994**, *13*, 591 – 597.
[19] R. C. Hider, A. R. Mohd-Nor, J. Silver, I. E. G. Morrison, L. V. C. Rees, *J. Chem. Soc. Dalton Trans.* **1981**, 609 – 622.
[20] A. Avdeef, S. R. Sofen, T. L. Bregante, K. N. Raymond, *J. Am. Chem. Soc.* **1978**, *100*, 5362 – 5370.
[21] At 4.2 K the Mössbauer spectra of the natural samples show, in addition to the quadrupole doublet, a broad background caused by magnetic hyperfine splitting. The magnetic component is assigned to iron hydroxides, and it increases with the ageing of the mushrooms. The strongly broadened Mössbauer spectra observed at room temperature are caused by a superposition of the quadrupole doublet of the iron hydroxides, which do not show magnetic order yet, and the quadrupole doublet of the iron(III) – catechol complex. Differences in the line width and quadrupole splitting of the doublet observed at 4.2 K are attributable to badly crystallized iron hydroxides, which are not ordered even at 4.2 K. The higher Lamb – Mössbauer factor of the iron hydroxides causes an overrepresentation of the iron hydroxides in comparison to the iron(III) – catechol complex, especially at room temperature.
[22] V. A. Grillo, G. R. Hanson, D. Wang, T. W. Hambley, L. R. Gahan, K. S. Murray, B. Moubaraki, C. J. Hawkins, *Inorg. Chem.* **1996**, *35*, 3568 – 3576.
[23] A brown anthranoid – iron complex was isolated from lichens of the genus *Cladonia*: L. Alagna, T. Prosperi, A. A. G. Tomlinson, H. Kjøsen, F. Mo, *Biochim. Biophys. Acta* **1990**, *1036*, 71 – 77.
[24] a) *Iron transport and storage in microorganisms, plants and animals*: *Metal ions in biological systems*, *Vol. 35* (Eds.: A. Sigel, H. Sigel), Dekker, New York, **1998**; b) B. F. Matzanke, G. Müller-Matzanke, K. N. Raymond in *Iron Carriers and Iron Proteins*, *Physical Bioinorganic Chemistry Series*, *Vol. 5* (Ed.: T. M. Loehr), VCH, Weinheim, **1989**, pp. 1 – 122.

The First Coordinatively Saturated, Quadruply Stranded Helicate and Its Encapsulation of a Hexafluorophosphate Anion.**

David A. McMorran* and Peter J. Steel*

The use of metal ions to control the self-assembly of discrete supramolecular species has been an area of intense interest for some years,[1] with helicates having received particular attention.[2, 3] This interest has been driven, at least in part, by the potential use of helicates as functional components of molecular devices.[2] Although single-, double- and triple-stranded helicates have been well-documented,[2, 4] to our knowledge the only example of a quadruply stranded helicate is the recent report of pentanuclear metal complexes bridged by a pentadentate ligand.[5] These species contain metal – metal bonds with terminal ancillary ligands on octahedral metal centers and, as such, can be classified as unsaturated helicates.[2] It was predicted[2] that the synthesis of a saturated quadruply stranded helicate might be achieved by employing a combination of square-planar metal centers with oligomonodentate bridging ligands. We now report the successful realization of this challenge, with the synthesis and X-ray crystal structure of a quadruply stranded helicate that encapsulates a hexafluorophosphate anion.

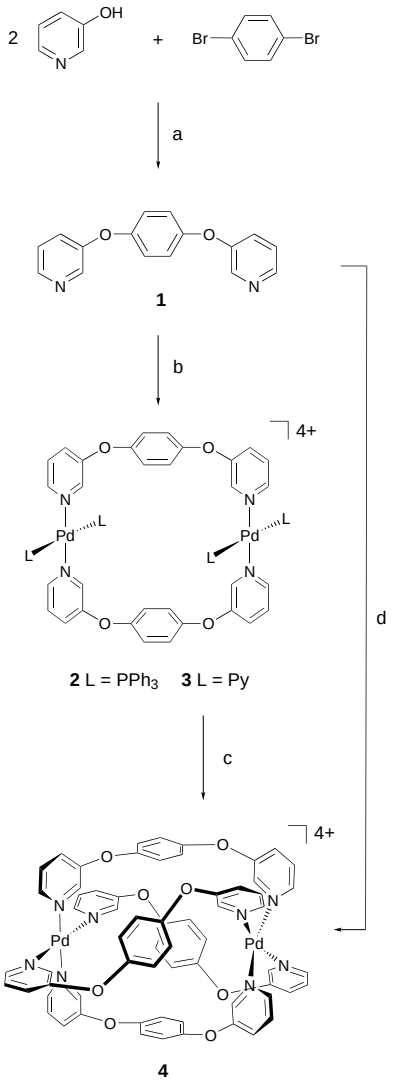
We have previously reported that reaction of 1,4-bis(2-pyridyloxy)benzene with silver nitrate results in the self-assembly of a M_2L_2 dimetalloparacyclophane with intimate $\pi - \pi$ stacking of the central benzene rings,[6] whilst replacement of the central *p*-phenylene ring with a 2,7-naphthylene spacer results in the formation of a M_2L_4 molecular box.[7] In order to change the topology of the ligand so as to enlarge the cavity within such metallosupramolecular species we have begun to examine the coordination chemistry of the 3-pyridyl analogues. Thus, the ligand 1,4-bis(3-pyridyloxy)benzene (**1**) was prepared (Scheme 1) by reaction of 3-hydroxypyridine with 1,4-dibromobenzene in the presence of potassium carbonate and copper bronze.[8] Reactions of **1** with $[PdCl_2(PPh_3)_2]$ and $[PdI_2(py)_2]$ (py = pyridine), in the presence of silver triflate, gave what we believe to be the dimeric complexes **2** and **3**, respectively, the formulations of which are supported by their elemental analyses, ^{1}H NMR and FAB mass spectra (see Experimental Section). Diffusion of diethyl ether into an acetonitrile solution of **3** containing ammonium hexafluorophosphate resulted in a reorganization of the components and the assembly of a M_2L_4 species (**4**), which deposited from the solution as a tetrakis(hexafluorophosphate) salt and as a bis(acetonitrile) solvate. This latter species was prepared more efficiently, in 70% yield, when the appropriate 2:1 ligand:metal stoichiometry was employed.

A single crystal X-ray structure determination was carried out to determine the structure of this compound unambiguously.[9] The compound crystallizes in the centrosymmetric space group $P2_1/n$, the asymmetric unit of which contains a full M_2L_4 helical cage (**4**) that has each square-planar palladium atom coordinated to the four bridging ligands and within which resides a well-ordered PF_6^- ion (Figure 1). External to the cage are three other PF_6^- anions (two of which are disordered) and two acetonitrile solvate molecules (not shown). The dimensions of the cage are defined by the Pd···Pd separation [8.8402(8) Å] and the distance between the centroids of the cofacial benzene rings [8.849(7) and 8.925(7) Å].

Figure 2 shows the cage viewed down the Pd – Pd axis, which serves to emphasize its approximate D_4 symmetry and the helical disposition of the ligands. The helical pitch is defined by the approximate 45° angle subtended by each ligand about the helical axis. The planes of the pyridine rings are all approximately orthogonal to the planes of the linking benzene rings. This cage can be classified as a saturated,

[*] Dr. D. A. McMorran, Dr. P. J. Steel
Department of Chemistry, University of Canterbury
Private Bag 4800, Christchurch (New Zealand)
Fax: (+64) 3-364-2110
E-mail: p.steel@chem.canterbury.ac.nz

[**] We thank the New Zealand Foundation for Research, Science, and Technology for funding this research through a postdoctoral fellowship to D.A.M.



Scheme 1. Preparations of **1**–**4**. a) K_2CO_3, Cu^0, dimethylacetamide, heat; b) **2**: $[PdCl_2(PPh_3)_2]$, AgOTf, CH_2Cl_2, **3**: $[PdI_2(Py)_2]$, AgOTf, acetone, NH_4PF_6; c) MeCN/Et_2O; d) 0.5 equiv $[PdI_2(Py)_2]$, AgOTf, MeCN, NH_4PF_6. OTf = Trifluoromethanesulfonate (triflate).

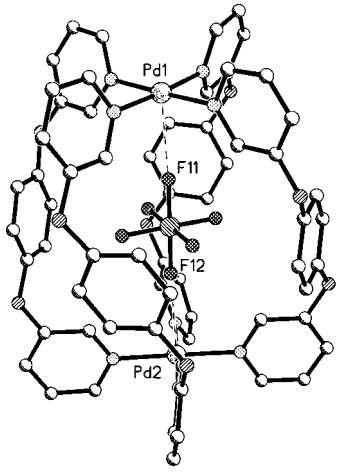


Figure 1. Perspective view of the helicate **4** and its encapsulated PF_6^- ion. Selected interatomic distances [Å] and angles [°]: Pd–N 2.008(6)–2.032(5), P1–F 1.565(5)–1.582(5), Pd1–F11 2.789(5), Pd2–F12 2.911(5); Pd1–Pd2 8.8402(8); N-Pd-N 87.1(2)–92.5(2)/176.4(2)–179.0(2), Pd1-F11-P1 176.4(4), Pd2-F12-P1 176.3(3).

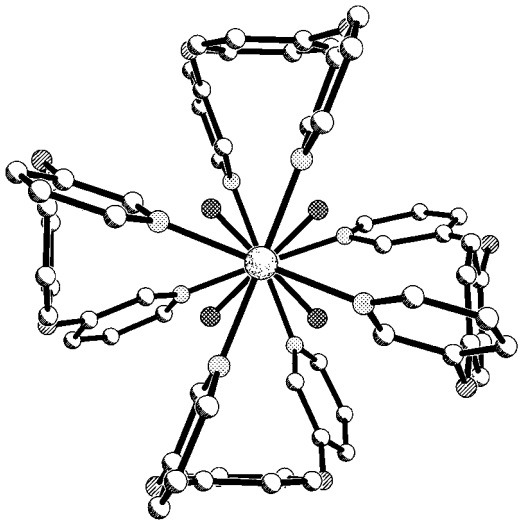


Figure 2. View of $[\mathbf{4}(PF_6)]^{3+}$ down the helical Pd–Pd axis.

homotopic, quadruply stranded helicate on the basis of the definitions of Piguet et al.,[2] and is the first such example.

A remarkable feature of the stucture is the encapsulation of the hexafluorophosphate anion. In contrast to the many molecular hosts capable of recognizing and complexing cationic guests, the search for similar species capable of complexing anionic guests has proved considerably more difficult.[10] Cryptates have long been known to encapsulate simple anions such as halide[11] and azide,[12] but only more recently have they been definitively shown to complex oxyanions and perfluoroanions.[13] Some metallosupramolecular species have been shown to act as hosts for neutral,[14] cationic,[15] and anionic[16] guests. Whereas cation encapsulation by triple helicates has been described,[15, 17] only one example of anion encapsulation by a helicate has been reported, this being a chloride ion enclosed by a circular double helicate.[18] Thus, the present example represents the first case of encapsulation of a polyatomic anion by a helicate and only the second crystallographically characterized example of encapsulation of a hexafluorophosphate anion by any species.[19]

Although PF_6^- ions normally act as noncoordinating anions,[20] the encapsulated anion within the cage **4** makes weak contacts with the palladium centers [Pd1–F11 = 2.789(5); Pd2–F12 = 2.911(5) Å], as indicated by the dashed lines in Figure 1. The four remaining fluorine atoms reside in the spaces between the faces of the four benzene rings. It is notable that this is the first crystallographically characterized example in which a hexafluorophosphate anion acts as a bridging ligand between two metal centers.[20]

Evidence for the fact that this structure is maintained in solution is provided by the observation that dissolution of the crystals in DMSO gives a solution that gives rise to a ^1H NMR spectrum consistent with the X-ray structure and, most importantly, a ^{19}F NMR spectrum that shows two doublets for the PF_6^- ions. This suggests that, on the timescale of the NMR experiment, the PF_6^- ion remains encapsulated within the helicate, but is tumbling within the cavity, rather than being locked in one orientation as in the solid state X-ray

 © WILEY-VCH Verlag GmbH, D-69451 Weinheim, 1998 1433-7851/98/3723-3296 $ 17.50+.50/0

structure. Experiments are underway to determine whether the PF_6^- ion can be exchanged for other anions and, therefore, how generally or selectively this molecular cage can act as a host for anions.

Experimental Section

2: $[PdCl_2(PPh_3)_2]$ (1 equiv) and AgOTf (2 equiv) were stirred in dichloromethane/acetonitrile (9/1) for 30 min. The AgCl was filtered off, the solvent removed, and the residue extracted with dichloromethane. This solution was filtered and stirred overnight with **1** (1 equiv). The solvent was then removed, the residue dissolved in chloroform (ca. 2 mL), and diethyl ether added. The resulting pale yellow solid was filtered off, washed with diethyl ether and dried in vacuo. Yield 84%; m.p. 182–184 °C (decomp); elemental analysis calcd for $C_{108}H_{84}P_4N_4O_{16}F_{12}S_4Pd_2 \cdot CHCl_3$: C 52.23, H 3.41, N, 2.23; found: C 52.99, H 3.64, N 2.65; ^{1}H NMR (300 MHz, $CDCl_3$): $\delta = 6.52$ (s, 8H, H2,3,5,6), 6.99 (m, 8H, H4′,5′), 7.41 (m, 36H, *m*, *p*-PPh_3), 7.68 (dd, 24H, *o*-PPh_3), 8.49 (s, 4H, H2′), 8.88 (d, 4H, H6′); FAB-MS: *m*/*z*: 1976 $[M-3(OTf)]^+$.

3: $[PdI_2(py)_2]$ (1 equiv) and AgOTf (2 equiv) were stirred in acetone for 30 min. The AgI was filtered off and the filtrate was stirred overnight with **1** (1 equiv). NH_4PF_6 (10 equiv) was added and the solvent was then removed. The residue was extracted with dichloromethane (ca. 2 mL), filtered, and diethyl ether added. The resulting pale yellow solid was filtered off, washed with diethyl ether and dried in vacuo. Yield 85%; m.p. > 210 °C (decomp); elemental analysis calcd for $C_{52}H_{44}N_8O_4P_4F_{24}Pd_2 \cdot CH_2Cl_2$: C 36.95, H 2.69, N 6.50; found: C 36.51, H 2.72, N 6.73; ^{1}H NMR (300 MHz, CD_3CN): $\delta =$ 7.00 (s, 8H, H2,3,5,6), 7.64 (t, 8H, py-H3,5), 7.77 (dd, 4H, H5′), 7.91 (d, 4H, H4′), 8.09 (t, 4H, py-H4), 8.62 (s, 4H, H2′), 8.85 (d, 8H, py-H2,6), 8.64 (d, 4H, H6′); FAB-MS: *m*/*z*: 1493 $[M-(PF_6)]^+$. Recrystallization of an acetonitrile solution of **3** by diethyl ether infusion gave cream crystals of $[\mathbf{4} \cdot (PF_6)_4 \cdot 2CH_3CN]$, suitable for X-ray diffraction.

4: $[PdI_2(py)_2]$ (1 equiv) and AgOTf (2 equiv) were stirred in dichloromethane/acetone (9/1) for 30 min. The AgI was filtered off, the solvent removed, and the residue extracted with dichloromethane. This solution was filtered and the solvent removed. The residue was then dissolved in acetonitrile and stirred overnight with **1** (2 equiv) and NH_4PF_6 (10 equiv). The solvent was then reduced to ca. 1 mL, chloroform (ca. 5 mL) and water (ca. 5 mL) were added and the off-white solid filtered off, washed with water, ethanol, and diethyl ether, and dried in vacuo. Yield 70%; m.p. > 250 °C (decomp); elemental analysis calcd for $C_{64}H_{48}N_8O_8P_4F_{24}Pd_2 \cdot 2H_2O$: C 40.75, H 2.78, N 5.94; found: C 40.65, H 2.57, N 6.41; ^{1}H NMR (300 MHz, [D$_6$]DMSO): $\delta = 6.93$ (s, 16H, H2,3,5,6), 7.85 (dd, 8H, H5′), 8.01 (d, 8H, H4′), 8.42 (s, 8H, H2′), 9.14 (d, 8H, H6′); FAB-MS: *m*/*z*: 1704.8 $[M-PF_6]^+$, 1559.8 $[M-2(PF_6)]^+$.

Received: May 20, 1998 [Z11888IE]
German version: *Angew. Chem.* **1998**, *110*, 3495–3497

Keywords: helical structures · host–guest chemistry · N ligands · palladium · supramolecular chemistry

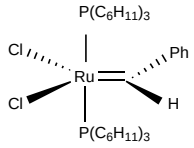
[1] P. J. Stang, B. Olenyuk, *Acc. Chem. Res.* **1997**, *30*, 502–518; M. Fujita in *Comprehensive Supramolecular Chemistry,* Vol. 9 (Eds.: J.-M. Lehn, J.-P. Sauvage, M. W. Hosseini), Pergamon, Oxford, **1996**, p. 253.
[2] C. Piguet, G. Bernardinelli, G. Hopfgartner, *Chem. Rev.* **1997**, *97*, 2005–2062.
[3] The term helicate was introduced by Lehn and co-workers: J.-M. Lehn, A. Rigault, J. Siegel, J. Harrowfield, B. Chevrier, D. Moras, *Proc. Natl. Acad. Sci. USA* **1987**, *84*, 2565–2569.
[4] E. C. Constable in *Comprehensive Supramolecular Chemistry,* Vol. 9 (Eds.: J.-M. Lehn, J.-P. Sauvage, M. W. Hosseini), Pergamon, Oxford, **1996**, p. 213; A. Williams, *Chem. Eur. J.* **1997**, *3*, 15–19; A. E. Rowan, R. J. M. Nolte, *Angew. Chem.* **1998**, *110*, 65–71; *Angew. Chem. Int. Ed.* **1998**, *37*, 63–68.
[5] S.-J. Shieh, C.-C. Chou, G.-H. Lee, C.-C. Wang, S.-M. Peng, *Angew. Chem.* **1997**, *109*, 57–59; *Angew. Chem. Int. Ed. Engl.* **1997**, *36*, 56–59.
[6] C. M. Hartshorn, P. J. Steel, *Inorg. Chem.* **1996**, *36*, 6902–6903.
[7] B. J. O'Keefe, P. J. Steel, *Inorg. Chem. Commun.* **1998**, *1*, 147–149.
[8] D. A. McMorran, P. J. Steel, *Acta Crystallogr. Sect. C* **1998**, *54*, 1132–1133.
[9] Crystal structure analysis of $\mathbf{4} \cdot (PF_6)_4 \cdot 2MeCN$ $[C_{68}H_{54}F_{24}N_{10}O_8P_4Pd_2]$: $M_r = 1931.9$, monoclinic, space group $P2_1/n$, $a = 16.8549(10)$, $b = 12.4869(6)$, $c = 35.834(2)$ Å, $\beta = 93.111(1)$, $V = 7530.7(7)$ Å^3, $F(000) = 3856$, ρ_{calcd} ($Z = 4$) $= 1.704$ g cm^{-1}, $\mu = 0.683$ mm^{-1}, approximate crystal dimensions $0.48 \times 0.27 \times 0.22$ mm^3, $2\theta_{max} = 48°$, radiation $Mo_{K\alpha}$ ($\lambda = 0.71073$ Å), $T = -123$ °C, 25288 measured data (Siemens CCD area detector), of which 11259 unique, 7018 observed with $I > 2\sigma(I)$. Lorentz and polarization correction, multi-scan absorption correction ($T_{max} = 0.864$, $T_{min} = 0.735$) were applied and the structute solved by direct methods (SHELXS), full-matrix least-squares refinement on F^2 with all data (SHELXL95), 1102 parameters. H atoms were placed in calculated positions with the conformational orientation of MeCN methyl hydrogen atoms deduced from circular Fourier syntheses, GOF = 0.964, $R = 0.065$, wR (all data) = 0.198. Crystallographic data (excluding structure factors) for the structure reported in this paper have been deposited with the Cambridge Crystallographic Data Centre as supplementary publication no. CCDC-101615. Copies of the data can be obtained free of charge on application to CCDC, 12 Union Road, Cambridge CB2 1EZ, UK (Fax: (+44) 1223-336-033; e-mail: deposit@ccdc.cam.ac.uk).
[10] P. D. Beer, D. K. Smith, *Prog. Inorg. Chem.* **1997**, *46*, 1–96; P. D. Beer, *Acc. Chem. Res.* **1998**, *31*, 71–80; F. P. Schmidtchen, M. Berger, *Chem. Rev.* **1997**, *97*, 1609–1646.
[11] J.-M. Lehn, *Pure Appl. Chem.* **1970**, *50*, 871–892.
[12] B. Dietrich, J. Guilhem, J.-M. Lehn, C. Pascard, E. Sonveaux, *Helv. Chim. Acta.* **1984**, *67*, 91–104.
[13] G. Morgan, V. McKee, J. Nelson, *J. Chem. Soc. Chem. Commun.* **1995**, 1648–1652.
[14] For example, see T. Beissel, R. E. Powers, K. N. Raymond, *Angew. Chem.* **1996**, *108*, 1166–1168; *Angew. Chem. Int. Ed. Engl.* **1996**, *35*, 1084–1086.
[15] R. W. Saalfrank, A. Dresel, V. Seitz, S. Trummer, F. Hampel, M. Teichert, D. Stalke, C. Stadler, J. Daub, V. Schunemann, A. X. Trautwein, *Chem. Eur. J.* **1997**, *3*, 2058–2062.
[16] P. Jacopozzi, E. Dalcanale, *Angew. Chem.* **1997**, *109*, 665–667; *Angew. Chem. Int. Ed. Engl.* **1997**, *36*, 613–615.
[17] M. Albrecht, H. Rottele, P. Burger, *Chem. Eur. J.* **1996**, *2*, 1264–1268.
[18] B. Hasenknopf, J.-M. Lehn, B. O. Kneisel, G. Baum, D. Fenske, *Angew. Chem.* **1996**, *108*, 1987–1990; *Angew. Chem. Int. Ed. Engl.* **1996**, *35*, 1838–1840.
[19] M. C. T. Fyfe, P. T. Glink, S. Menzer, J. F. Stoddart, A. J. P. White, D. J. Williams, *Angew. Chem.* **1997**, *109*, 2158–2160; *Angew. Chem. Int. Ed. Engl.* **1997**, *36*, 2068–2070.
[20] For an example of a PF_6^- ion strongly coordinated to tungsten, see R. V. Honeychuck, W. H. Hersh, *Inorg. Chem.* **1989**, *28*, 2869–2886. For examples of weaker coordination of a PF_6^- ion to silver, see Y. Yamamoto, K. Aoki, H. Yamazaki, *Inorg. Chim. Acta* **1983**, *68*, 75–78; M. Dartiguenave, Y. Dartiguenave, A. Mari, A. Guitard, M. J. Olivier, A. L. Beauchamp, *Can. J. Chem.* **1988**, *66*, 2386–2394. For examples of weak coordination of a PF_6^- ion to alkali metals, see J. M. Maud, J. F. Stoddart, H. M. Colquhoun, D. J. Williams, *Polyhedron* **1984**, *3*, 675–679; F. Weller, H. Borgholte, H. Stenger, S. Vogler, K. Dehnicke, *Z. Naturforsch. Teil B* **1989**, *44*, 1524–1530; P. D. Beer, H. Sikanyika, C. Blackburn, J. F. McAleer, M. G. B. Drew, *J. Chem. Soc. Dalton Trans.* **1990**, 3295–3300; D. S.Glueck, A. R.Brough, P.Mountford, M. L. H.Green, *Inorg. Chem.* **1993**, *32*, 1893–1902; S. P. Watton, M. I. Davis, L. E. Pence, J. Rebek, S. J. Lippard, *Inorg. Chim. Acta* **1995**, *235*, 195–204. In all of these examples the PF_6^- ion acts in a monodentate, chelating bidentate, or tripodal tridentate coordination mode; in no case does it act as a linear bridging ligand.

 © WILEY-VCH Verlag GmbH, D-69451 Weinheim, 1998 1433-7851/98/3723-3297 $ 17.50+.50/0

Ring-Closing Metathesis in Carbohydrate Annulation**

David J. Holt, William D. Barker, Paul R. Jenkins,*
David L. Davies, Shaun Garratt, John Fawcett,
David R. Russell, and Subtrata Ghosh

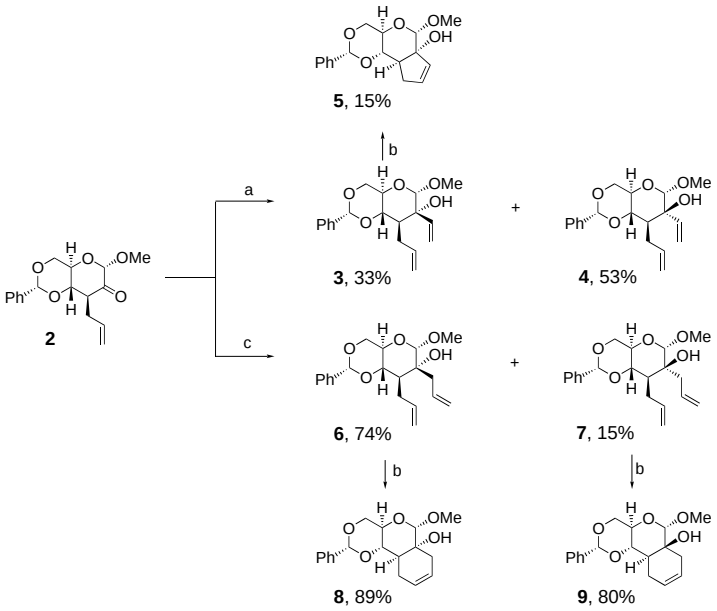
The Chiron Approach to the synthesis of chiral target molecules from carbohydrates is now a well established component in the armoury of organic chemistry.[1] A key element of this strategy is the range of methods available for the synthesis of cyclic compounds that include some or all of the carbon atoms of the original carbohydrate.[2] We have made several contributions to this area of carbohydrate annulation by using Robinson annulation,[3] aldol condensation,[4] radical cyclization,[5] and through the application of these ideas to the synthesis of a C-ring synthon of taxol.[6] In recent times there has been considerable interest in new applications of the ring-closing metathesis (RCM) reaction[7] by using the Grubbs catalyst **1**.[8] Carbohydrate substrates have been subjected to RCM to produce oxygen and nitrogen heterocyclic sugar derivatives.[9] The formation of macrocyclic lactones on sugar substrates in a RCM reaction was first reported by Descotes[10] using a tungsten catalyst. More recently lactonization using the Grubbs catalyst **1** has been reported,[11] along with applications in the synthesis of tricolorin A[12] and (+)-cyclitophellitol from xylose.[13]



1

As part of our continuing program on new methods for carbohydrate annulation we became interested in the application of RCM in the preparation of carbocyclic- and spiroannulated sugars to produce methods that could be applied in our synthetic route to taxoids[14] and other natural products. We report here our studies on the synthesis of five-, six-, and eight-membered annulated sugars along with spiro systems.

The starting material was the ketone **2** (Scheme 1), a derivative of methyl-α-D-glucopyranoside.[15] Reaction with vinylmagnesium chloride gave a mixture of allylic alcohols **3** (33%) and **4** (53%). RCM with the Grubbs ruthenium catalyst[8] was not successful on the diene **4**, probably because of the steric strain that would be produced in the *trans*-fused 5-6 ring system in the product. However, a 15% yield of **5** was obtained in the RCM reaction of **3**, along with 75% of recovered starting material. In addition to the usual spectroscopic characterization an X-ray crystal structure of **5** was obtained.[12]



Scheme 1. Reagents and conditions: a) $H_2C{=}CHMgCl$, THF, reflux, 2 h; b) $[RuCl_2(CHPh)\{P(C_6H_{11})_3\}_2]$ (**1**), benzene, 60 °C, 48 h for **5** and 17 h for **8** and **9**; c) $H_2C{=}CHCH_2MgCl$, THF, 2 h.

Addition of allylmagnesium chloride to ketone **2** furnished the *cis* diene **6** (74%) and the *trans* diene **7** (15%). Both **6** and **7** underwent ring-closing metathesis to produce the annulated sugar derivatives **8** and **9** in yields of 89 and 80%, respectively. An X-ray crystal structure of **8** was obtained.[16] Clearly there is no steric impediment to the formation of the *cis* and *trans* 6-6 ring systems in **8** and **9**, respectively.

While the addition of an allyl Grignard reagent to ketone **2** gives the β-alcohol **6** as the major product, the addition of the vinyl Grignard reagent gives the α-alcohol **4** as the major product. This strange reversal in the stereoselectivity deserves some comment. The major difference between vinyl and allyl Grignard reagents is that allylic rearrangement is possible during the addition of an allyl Grignard compound to a ketone. We believe that allylic rearrangement is best accommodated by an axial attack of allylmagnesium chloride on ketone **2** to afford the β-alcohol **6** as the major product. With vinylmagnesium chloride, however, there is a small preference in favor of α-attack to give the alcohol **4**.

A recent publication[17] has highlighted the difficulty of synthesizing eight-membered rings with the normal ring closure methods, and reported the use of the Claisen rearrangement in the conversion of D-glucose into an enantiomerically pure cyclooctenone. The synthesis of eight-membered carbocyclic and heterocyclic rings by RCM has been reported by Grubbs.[18a] Further examples have also appeared,[18b] and include the total synthesis of dactylol[18c] and the preparation of eight-membered ether rings in a sequence starting from glyceraldehydacetonide using a molybdenum catalyst for the RCM reaction.[18d] Scheme 2 illustrates the

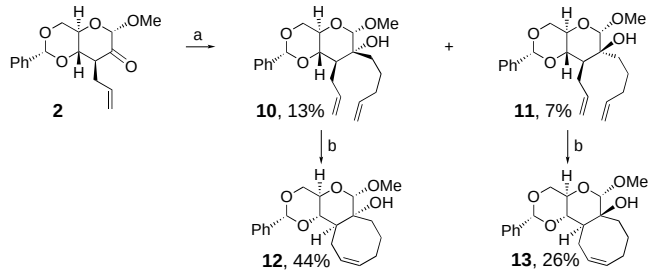
[*] Dr. P. R. Jenkins, D. J. Holt, W. D. Barker, Dr. D. L. Davies, S. Garratte, Dr J. Fawcett, Dr. D. R. Russell
Department of Chemistry, Leicester University
Leicester LE1 7RH (UK)
Fax: (+44) 116-252-3789
E-mail: kin@le.ac.uk

Prof. S. Ghosh
Indian Association for the Cultivation of Science
Department of Organic Chemistry
Calcutta 700032 (India)

[**] This work was supported by the Engineering and Physical Sciences Research Council, Pharmachemie BV, Haarlem, Holland, and the Indian National Science Academy – Royal Society study visit grant to S. Ghosh.

Supporting information for this article is available on the WWW under http://www.wiley-vch.de/home/angewandte/ or from the author.

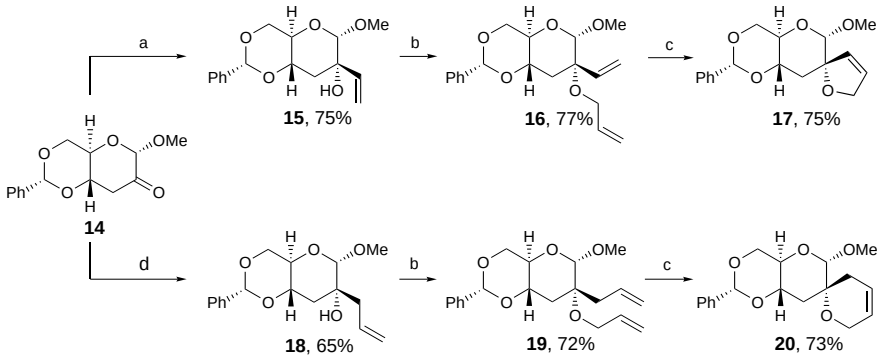
 © WILEY-VCH Verlag GmbH, D-69451 Weinheim, 1998 1433-7851/98/3723-3298 $ 17.50+.50/0



Scheme 2. Reagents and conditions: a) $H_2C{=}CH(CH_2)_3MgCl$, THF, reflux, 4 h; b) $[RuCl_2(CHPh)\{P(C_6H_{11})_3\}_2]$ (**1**), benzene, 31 h at 60 °C for **10**, and 17 h at 60 °C for **11**.

cyclooctaannulation of ketone **2** by RCM. The addition of the pentenyl Grignard reagent to the ketone **2** led to alcohols **10** and **11** in yields of 13 and 7%, respectively, along with a recovery of 37% starting material and 37% of a single alcohol that arises from reduction of the ketone **2**.[19] Dienes **10** and **11** were then treated with 9 mol% of catalyst **1** in benzene for 31 and 41 hours, respectively. This led to the cyclooctene derivatives **12** (44% yield with 32% recovered starting material) and **13** (26% yield with 48% recovered starting material). The assignment of structure **12** was confirmed by X-ray crystal structure analysis. The crystals were all weak diffractors, but the assignment of structure **12** was unambiguous.[16]

Methods for the synthesis of spiro-fused tetrahydrofuran or pyran ring systems are based on the addition of an appropriate reagent to a ketone, followed by spiroether formation,[20a] intramolecular radical addition,[20b] and intramolecular reaction of an oxonium ion on an allyl silane.[20c] The preparation of enantiomerically pure spiro products is achieved by starting from an enantiomerically pure ketone.[20d] We have applied RCM to the problem of spiroannulation (Scheme 3).[21] The starting point was the ketone **14**, a derivative of methyl-α-D-glucopyranoside.[22] Addition of vinylmagnesium chloride gave the allyl alcohol **15** in 75% yield. Deprotonation with sodium hydride, followed by allylation with allyl bromide furnished the ether **16** in 77% yield. Ring-closing metathesis of diene **16** gave the spiro-fused tricyclic compound **17** in 75% yield. The structure of **17** was confirmed by X-ray crystal structure analysis.[16] The equivalent reaction sequence with allylmagnesium chloride was also successful. Ketone **14** was converted into alcohol **18** in 65% yield, and subsequent conversion into the allyl ether **19** furnished the RCM substrate in 72% yield. This compound underwent RCM to give the spiro-fused dihydropyran system **20** in 73% yield. The structure of **20** was confirmed by X-ray crystal structure analysis.[16]



Scheme 3. Reagents and conditions: a) $H_2C{=}CHMgCl$, THF, reflux, 2 h; b) NaH, $CH_2{=}CHCH_2Br$, THF; c) $[RuCl_2(CHPh)\{P(C_6H_{11})_3\}_2]$ (**1**), benzene, 60 °C, 36 h; d) $CH_2{=}CHCH_2MgCl$, THF, 2 h.

In conclusion we have shown that ring-closing metathesis is an effective method for the annulation of glucose derivatives. Further studies are underway on the utilization of the enantiomerically pure annulated products in organic synthesis.

Experimental Section

All rections were performed under nitrogen. Solvents were dried by using standard methods. The yields reported refer to products purified by column chromatography.

Typical synthetic procedure for the ruthenium catalyzed RCM reaction: Nitrogen gas was bubbled for 2–3 minutes through a solution of the diolefin **7** (86 mg, 0.25 mmol) in benzene (10 mL). The catalyst **1** (4 mol%) was then added and the mixture heated at 60 °C for 17 h. The solvent was then removed under reduced pressure, and the crude reaction mixture purified by column chromatography (silica gel, petroleum ether (40–60 °C)/diethyl ether (3/1 → 2/1) to yield the cyclohexaannulated sugar derivative **9** as a colorless oil (63 mg, 80%).

Physical and spectroscopic data for **9**: $[\alpha]_D^{18} = +8.8$ ($c = 6.0$ in $CHCl_3$); $R_f =$ 0.13, petroleum ether (40–60 °C)/diethyl ether (1/1); ^{1}H NMR (250 MHz, $CDCl_3$): $\delta = 7.51-7.33$ (m, 5H, Ph), 5.76 (m, 1H, 9-H), 5.60 (m, 1H, 8-H), 5.53 (s, 1H, 11-H), 4.39 (s, 1H, 1-H), 4.25 (dd, $J = 3.6$, 9.0 Hz, 1H, 6 eq-H), 3.93–3.77 (t, $J = 9.0$ Hz, 1H, 6 ax-H; m, 1H, overlapping, 5-H), 3.65 (t, $J =$ 10.6 Hz, 1H, 4-H), 3.41 (s, 3H, OMe), 2.60 (m, 1H, C*H*H, 7-H), 2.47 (m, 1H, C*H*H, 10-H), 2.16 (dt, $J = 5.2$, 10.6 Hz, 1H, 3-H), 2.04 (s, 1H, O*H*), 2.02 (m, 1H, overlapping, CH*H*, 10-H), 1.86 (dd, $J = 4.4$, 18.2 Hz, 1H, CH*H*, 7-H); ^{13}C NMR (62.9 MHz, $CDCl_3$): $\delta = 138.2$ (C, Ph), 129.3 (CH, Ph), 128.6 (CH, Ph), 126.5 (CH, Ph), 126.1 (CH, C9), 123.5 (CH, C8), 103.3 (CH, C1), 102.3 (CH, C11), 80.2 (CH, C4), 71.9 (C, C2), 69.7 (CH_2, C6), 64.5 (CH, C5), 55.5 (CH_3, OMe), 37.6 (CH, C3), 34.3 (CH_2, C7), 24.4 (CH_2, C10); HR-MS (FAB): *m/z* (%): 319 (34) [*M*H$^+$]; calcd for $C_{18}H_{23}O_5$ [*M*H$^+$]: 319.1546; found: 319.1544.

Received: May 15, 1998 [Z11866IE]
German version: *Angew. Chem.* **1998**, *110*, 3486–3488

Keywords: annulation · carbohydrates · homogeneous catalysis · metathesis · ruthenium

[1] S. Hanessian, *Total Synthesis of Natural Products; The Chiron Approach*, Pergamon, Oxford, **1993**.
[2] R. J. Ferrier, S. Middleton, *Chem. Rev.* **1993**, *93*, 2779; J. C. Lopez, B. Fraser-Reid, *Chem. Commun*. **1997**, 2251.
[3] R. V. Bonnert, P. R. Jenkins, *J. Chem. Soc. Chem. Commun.* **1987**, 6; R. V. Bonnert, J. Howarth, P. R. Jenkins, N. J. Lawrence, *J. Chem. Soc. Perkin Trans. 1* **1991**, 1225.
[4] A. J. Wood, P. R. Jenkins, J. Fawcett, D. R. Russell, *J. Chem. Soc. Chem. Commun.* **1995**, 1567.
[5] R. V. Bonnert, M. J. Davies, J. Howarth, P. R. Jenkins, *J. Chem. Soc. Chem. Commun.* **1987**, 148; R. V. Bonnert, M. J. Davies, J. Howarth, P. R. Jenkins, N. J. Lawrence, *J. Chem. Soc. Perkin Trans. 1* **1992**, 27; A. J. Wood, P. R. Jenkins, *Tetrahedron Lett.*, **1997**, *38*, 1853.
[6] A. N. Boa, J. Clark, P. R. Jenkins, N. J. Lawrence, *J. Chem. Soc. Chem. Commun.* **1993**, 151.
[7] A. Fürstner, *Top. Catal*. **1997**, *4*, 285; S. Blechert, M. Schuster, *Angew. Chem.* **1997**,

109, 2124; *Angew. Chem. Int. Ed. Engl.* **1997**, *36*, 2036; R. H. Grubbs, S. Chang, *Tetrahedron* **1998**, *54*, 4413; S. K. Armstrong, *J. Chem. Soc. Perkin Trans 1* **1998**, 371.

[8] P. Schwab, M. B. France, J. W. Ziller, R. H. Grubbs, *Angew. Chem.* **1995**, *107*, 2179; *Angew. Chem. Int. Ed. Engl.* **1995**, *34*, 2039; P. Schwab, R. H. Grubbs, *J. Am. Chem. Soc.* **1996**, *118*, 100.

[9] H. S. Overkleeft, U. K. Pandit, *Tetrahedron Lett.* **1996**, *37*, 547; M. A. Leeuwenburgh, H. S. Overkleeft, G. A. van der Marel, J. H. van-Boom, *Synlett* **1997**, 1263; H. Ovaa, M. A. Leeuwenburgh, H. S. Overkleeft, G. A. van der Marel, J. H. van Boom, *Tetrahedron Lett.* **1998**, *39*, 3025; H. S. Overkleeft, P. Bruggeman, U. K. Pandit, *Tetrahedron Lett.* **1988**, *39*, 3869.

[10] G. Descotes, J. Ramza, J.-M. Basset, S. Pagano, E. Gentil, J. Banoub, *Tetrahedron* **1996**, *52*, 10903.

[11] H. E. Sukkari, J.-P. Gesson, B. Renoux, *Tetrahedron Lett.* **1998**, *39*, 4043.

[12] A. Fürstner, T. Muller, *J. Org. Chem*. **1998**, *63*, 424.

[13] F. E. Ziegler, Y. Wang, *J. Org. Chem.* **1998**, *63*, 426.

[14] P. R. Jenkins, *Pure Appl. Chem*. **1996**, *68*, 771.

[15] R. J. Ferrier, C.-K. Lee, T. A. Wood, *J. Chem. Soc. Chem Commun.* **1991**, 690.

[16] Crystallographic data (excluding structure factors) for the structures reported in this paper have been deposited with the Cambridge Crystallographic Data Centre as supplementary publication no. CCDC-101536, 101537, 101538, 101539, and 1015340. Copies of the data can be obtained free of charge on application to CCDC, 12 Union Road, Cambridge CB2 1EZ, UK (fax: (+44) 1223-336-033; e-mail: deposit@ccdc.cam.ac.uk).

[17] B. Werschkun, J. Thiem, *Angew. Chem.* **1997**, *109*, 2905; *Angew. Chem. Int. Ed. Engl*. **1997**, *36*, 2793.

[18] a) S. J. Miller, S.-H. Kim, Z.-R. Chen, R. H. Grubbs, *J. Am. Chem. Soc*. **1995**, *117*, 2108; b) M. S. Visser, N. M. Heron, M. T. Didiuk, J. F. Sagal, A. H. Hoveyda, *J. Am. Chem. Soc*. **1996**, *118*, 4291; c) A. Fürstner, K. Langemann, *J. Org. Chem*. **1996**, *61*, 8746; d) J. S. Clark, J. G. Kettle, *Tetrahedron Lett.* **1997**, *38*, 123; 127.

[19] Studies are underway aimed at improving these poor yields.

[20] a) D. D. Reynolds, W. O. Kenyon, *J. Am. Chem. Soc*. **1950**, *72*, 1593; P. Picard, D. Leclercq, J. Moulines, *Tetrahedron Lett*. **1975**, 2731; P. Canonne, G. B. Foscolos, D. Belanger, *J. Org. Chem.* **1980**, *45*, 1828; E. Piers, V. G. Ashvinikumar, *J. Org. Chem*. **1990**, *55*, 2380; b) D. S. Middleton, N. S. Simpkins, *Tetrahedron Lett.* **1988**, *29*, 1315; c) L. A. Paquette, J. Tae, *J. Org. Chem*. **1996**, *61*, 7860; d) L. A. Paquette, J. T. Negri, *J. Am. Chem. Soc*. **1991**, *113*, 5072.

[21] After submission of this paper a publication appeared on the spiroannulation of a different set of sugar derivatives by RCM: P. A. V. van Hooft, M. A. Leeuvwenburgh, H. S. Overkleeft, G. A. ven der Marel, C. A. A. van Boeckel, J. H. van Boom, *Tetrahedron Lett.* **1998**, *39*, 6061

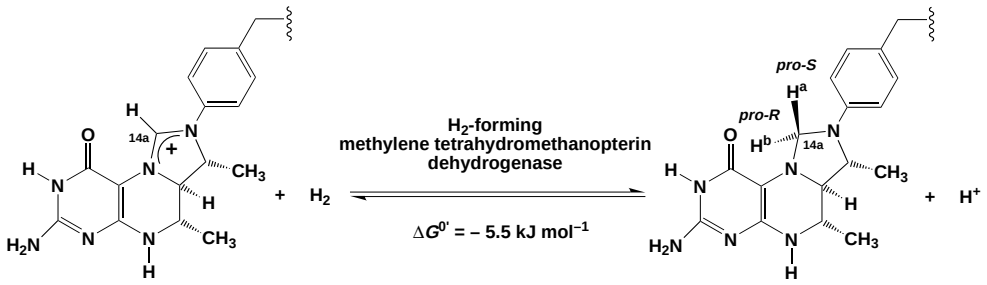
[22] A. Rosenthal, P. Catsoulacos, *Can. J. Chem*. **1969**, *47*, 2747.

Catalytic Mechanism of the Metal-Free Hydrogenase from Methanogenic Archaea: Reversed Stereospecificity of the Catalytic and Noncatalytic Reaction**

Bernhard H. Geierstanger, Thomas Prasch, Christian Griesinger,* Gudrun Hartmann, Gerrit Buurman, and Rolf K. Thauer*

Hydrogenases are enzymes that catalyze reactions with molecular hydrogen (H_2) either as substrate or as product.[1] They usually contain a redox-active nickel/iron or iron center that binds and activates H_2. Typically hydrogenases also contain several iron–sulfur clusters that transfer electrons to an electron acceptor.[2–4] In addition, most methanogenic archaea express a metal-free hydrogenase which, therefore, can neither activate H_2 nor catalyze electron transport.[5] All available evidence indicates that this enzyme activates the hydrogen acceptor, which then directly reacts with H_2.[6]

The metal-free hydrogenase catalyzes the reversible reduction of N^5,N^{10}-methenyl tetrahydromethanopterin (methenyl-H_4MPT, **1**) with H_2 to N^5,N^{10}-methylene tetrahydromethanopterin (methylene-H_4MPT, **2**; $\Delta G^{\circ\prime} = -5.5$ kJ mol^{-1}; Scheme 1).[7] This reaction is involved in the reduction of CO_2 with H_2 to form CH_4 in methanogenic archaea.[8, 9] The enzyme catalyzes a direct hydride transfer from H_2 into the *pro-R* position of **2**.[10] In addition, the enzyme catalyzes an exchange of the hydrogen atom in the *pro-R* position of **2** with the protons of water,[11] a methenyl-H_4MPT-dependent exchange of H_2 with the solvent,[12, 13] and a methenyl-H_4MPT-dependent *ortho/para* H_2 conversion.[14] These properties of metal-free hydrogenase are accounted for in the catalytic mechanism proposed in Scheme 2.[6] The mechanism is based



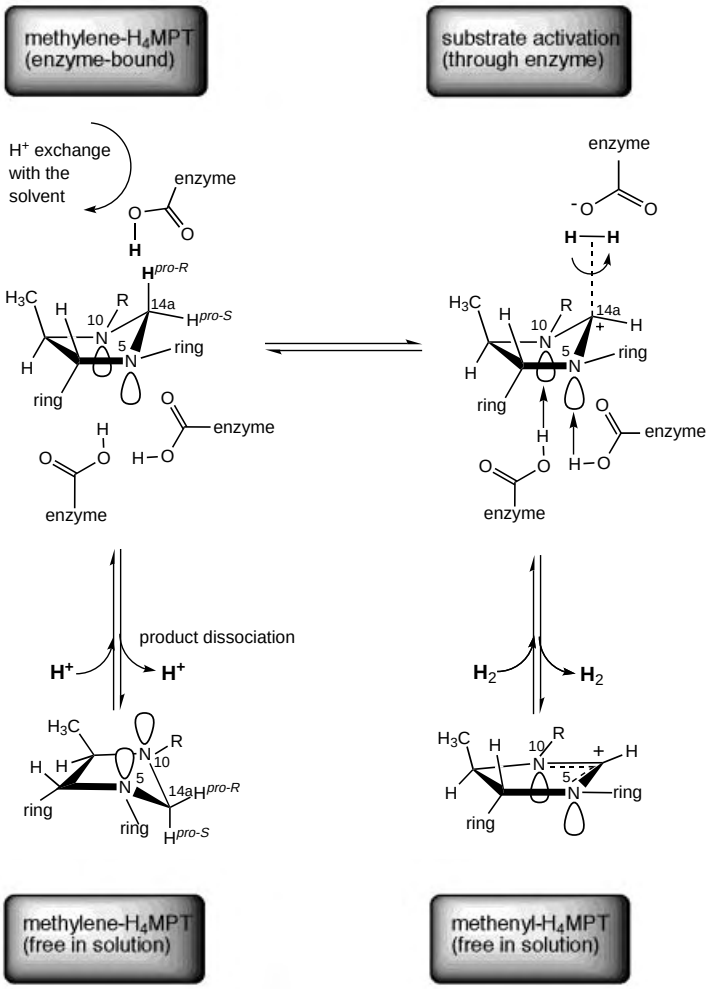
1 **2**

Scheme 1. The reaction catalyzed by the metal-free hydrogenase. For complete structures of **1** and **2** including sidechains, see references [5, 10].

[*] Prof. Dr. C. Griesinger, Dr. B. H. Geierstanger, Dr. T. Prasch
Institut für Organische Chemie der Universität
Marie-Curie-Strasse 11, D-60439 Frankfurt am Main (Germany)
Fax: (+49) 69-7982-9128
E-mail: cigr@org.chemie.uni-frankfurt.de
Prof. Dr. R. K. Thauer, Dr. G. Hartmann, G. Buurman
Max-Planck-Institut für terrestrische Mikrobiologie
Karl-von-Frisch-Strasse, D-35043 Marburg (Germany)
Fax: (+49) 6421-178209
E-mail: thauer@mailer.uni-marburg.de

[**] This work was supported by the Deutsche Forschungsgemeinschaft (SFB 472 P4).

 © WILEY-VCH Verlag GmbH, D-69451 Weinheim, 1998 1433-7851/98/3723-3300 $ 17.50+.50/0



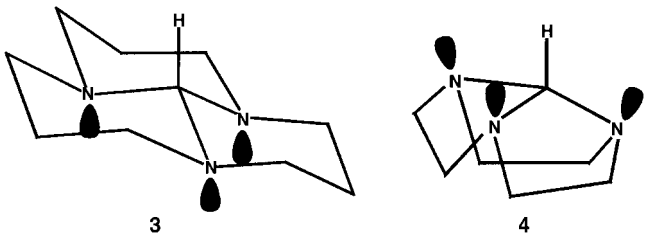
Scheme 2.

on the fact that in superacids carbocations can react directly with H_2 in the absence of other nucleophiles.[15]

In Scheme 2 it is assumed that **1** undergoes a conformational change upon binding to the enzyme. Thus, the conjugational stabilization is eliminated and a cationic center at C14a is created, which in its properties corresponds to a carbocation normally generated only under superacidic conditions. It can be predicted from the stereospecificity of the reaction that in a complex with the enzyme, **2** must be in a conformation in which the *pro-R* C–H bond is antiperiplanar to the free lone electron pairs of the flanking nitrogen atoms. Molecular orbital calculations of the transition state support this mechanism.[16–18]

In Scheme 2 it is further assumed that **2** in aqueous solution, when not bound to the enzyme, adopts a conformation in which the *pro-S* C–H bond is antiperiplanar to the lone electron pairs of the flanking nitrogen atoms. Thus, the conformation must change when the hydrogenation product dissociates from the enzyme. Whereas the conformation of **2** in aqueous solution could not be deduced from analysis of $^1H-^1H$ nuclear Overhauser effects (NOEs) and coupling constants,[19] we now provide evidence for this conformation based on the $^1J_{CH}$ coupling constants, the chemical shifts of the *pro-R* and *pro-S* protons, and the stereospecific deuteration of **1**.

Methylene-H_4MPT (**2**) should have similar properties as perhydro-3a,6a,9a-triazaphenalene (**3**),[6, 16] which reacts to the guanidinium salt and H_2 when equivalent amounts of aqueous HBF_4 are added at 110 °C.[20] The C–H bond of the



3 **4**

methine group of **3** is unusually reactive with respect to heterolysis to a carbocation and a hydride.[20–22] The high reactivity is caused by the interaction of the three lone electron pairs of the nitrogen atoms antiperiplanar to the C–H bond. This interaction manifests itself in an unusually low wavenumber for the C–H stretching band in the IR spectrum ($\tilde{\nu} = 2450\ cm^{-1}$;[21, 22] Bohlmann band),[23] a very small $^1J_{CH}$ coupling constant of 141 Hz,[24] and a NMR resonance shifted to high field ($\delta = 2.25 - 2.33$).[21, 22, 24] The latter two can be explained by the conjugation of the nitrogen n orbitals with the σ* orbital of the C–H fragment: The resulting weakening of the C–H bond should lead to a decrease in the coupling constant, and the negative partial charge should cause a high-field shift in the NMR spectrum.[20–22]

In contrast to **3**, the C–H bond of the methine group of perhydro-2a,4a,6a-triazacyclopenta[cd]pentalene (**4**) is much less reactive[20–22] because the methine proton of **4** is in the position *gauche* to the free lone electron pairs of the neighboring nitrogen atoms. A significantly bigger coupling constant $^1J_{CH}$ of 184 Hz,[24] a chemical shift of $\delta = 5.03$,[21, 24] and the absence of a Bohlmann IR band[22, 24] indicate that the C–H bond of the methine group of **4** is stronger. Thus, from these spectroscopic properties the relative orientation of the lone electron pairs to the C–H bond can be deduced.

Table 1 lists coupling constants $^1J_{CH}$ and chemical shifts of the *pro-R* and *pro-S* protons of methylene-H_4MPT (**2**) in aqueous solution. Comparing both parameters with those of **3** and **4** suggests that in aqueous solution **2** is in a conformation in which the *pro-S* proton is more reactive than the *pro-R* proton, and in which the *pro-S* C–H bond is therefore

Table 1. Coupling constants $^1J_{CH}$ and chemical shifts δ of the methylene groups of [^{13}C]methylene-H_4MPT and [^{13}C]methylene-H_4F.[a]

Compound	$^1J_{CH}$ [Hz]	δ
[^{13}C]methylene-H_4MPT		
pro-R	158.0	5.05
pro-S	150.0	4.10
pro-R (M)	157.5	4.98
pro-S (M)	145.5	3.67
[^{13}C]methylene-H_4F		
pro-R	157.0	4.93
pro-S	149.0	3.90

[a] The samples had a concentration of 4 mM and were dissolved in 20 mM formiate buffer (pH 3). (M) indicates samples that were measured in methanol/water (1/1).

 © WILEY-VCH Verlag GmbH, D-69451 Weinheim, 1998 1433-7851/98/3723-3301 $ 17.50+.50/0

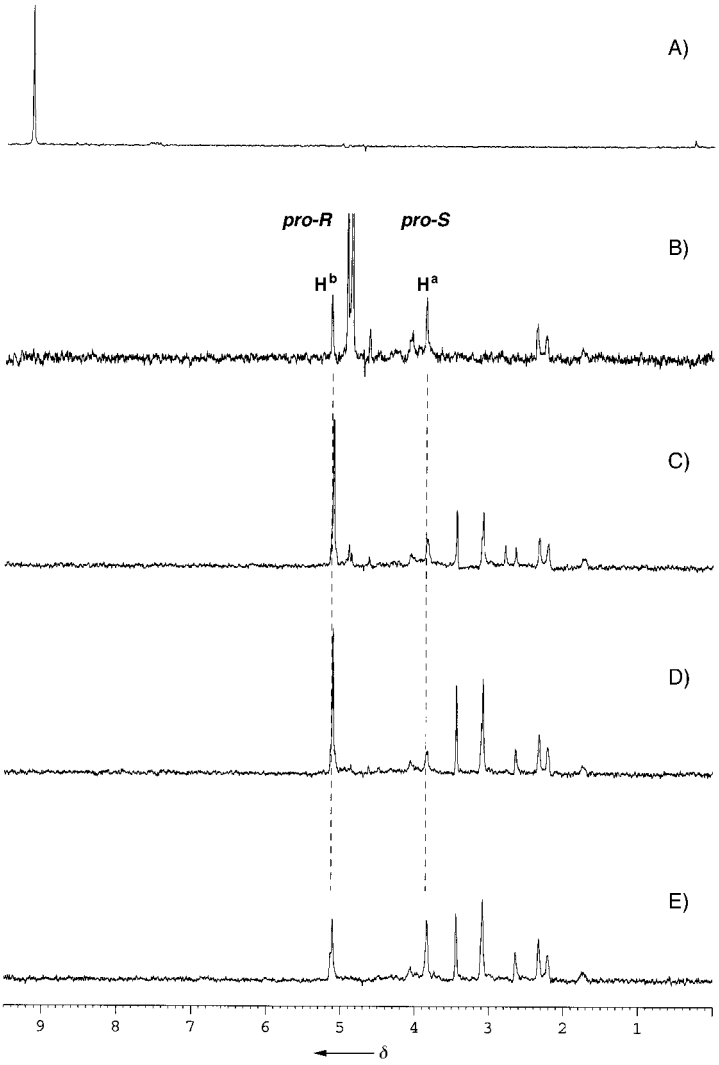


Figure 1. $^1H-^{13}C$ heteronuclear single quantum correlation (HSQC) NMR spectra to monitor the reduction of [14a-^{13}C]methenyl-H_4MPT[10] by $NaBD_4$ to [^{13}C]methylene-H_4MPT. A) Spectrum of a solution of [14a-^{13}C]methenyl-H_4MPT (ca. 2 mM) in 16 mM potassium phosphate (in D_2O, pH 6.0) and 20% acetonitrile. The ^{13}C frequency was set to $\delta = 170$ with $\Delta = 1/(4\,^1J_{CH}) = 1.19$ ms. B) Same sample as in A), but the spectrum was recorded at a ^{13}C frequency of $\delta = 70$. Small amounts of reduced [^{13}C]methylene-H_4MPT are present, as indicated by peaks at $\delta = 5.1$ for the *pro-R* proton H^b and at $\delta = 3.8$ for the *pro-S* proton H^a. C) Same sample as in A), but after addition of $NaBD_4$ (ca. 2 mg). Deuteration occurs selectively at the *pro-S* position, since only the signal intensity of the *pro-R* proton H^b increased. D) Reaction repeated under the same conditions. The acquisition of spectra C) and D) at a ^{13}C frequency of $\delta = 70$ was started approximately 15 min after addition of $NaBD_4$. E) Spectrum of sample from D) approximately 11 h after initiation of the reaction. The intensities of the signals for H^a and H^b have become equal because of epimerization at atom C14a. Experiments in pure water show the same effect. [14a-^{13}C]Methenyl-H_4MPT was produced as described.[19] All 1D $^1H-^{13}C$ HSQC NMR spectra[27–29] were acquired at a ^1H frequency of 600.14 MHz on an AMX600 spectrometer (Bruker) and processed with the program XWINNMR (Bruker) using an exponential window function with 3-Hz line broadening. After 16 dummy scans to allow for preequilibration 256 scans were signal averaged, except for spectrum B (64 scans). The recycle delay was 2 s. A total of 4096 real points were recorded over a spectral width of 6024.1 Hz. The ^{13}C decoupling was achieved by globally optimized alternating phase rectangular pulse (GARP) trains.[30] Spectra were scaled to allow for comparison of absolute peak intensities. All δ values were referenced to the signal for residual HDO in 1D ^1H presat spectra (not shown) at $\delta = 4.70$ and 303 K.

antiperiplanar to the lone electron pairs of the neighboring nitrogen atoms. As a consequence, a significant conformational change must occur when **2** dissociates from the metal-free hydrogenase (Scheme 2), because only the *pro-R* hydrogen atom reacts in the enzyme-catalyzed reaction.[10] In contrast, one would predict that the chemical reduction of methenyl-H_4MPT (**1**) in aqueous solution should lead to the incorporation of a hydrogen atom into the *pro-S* position of **2**, with the methenyl proton going into the *pro-R* position. Indeed, this is what was observed: When **1** was reduced with $NaBD_4$ in D_2O, the deuteride was incorporated into the *pro-S* position of **2** (Figure 1).

Table 1 also shows $^1J_{CH}$ coupling constants and chemical shifts of both methylene protons of N^5,N^{10}-methylene tetrahydrofolate (methylene-H_4F). The similarity between the measured NMR parameters of methylene-H_4F and **2** is evident. A low-field chemical shift correlates with a large $^1J_{CH}$ coupling constant, as does a small $^1J_{CH}$ coupling constant with a high-field chemical shift. It is striking that in this correlation the corresponding methylene protons of **2** and methylene-H_4F occupy almost the same positions (Figure 2). This suggests that the chemical reactivity of the methylene

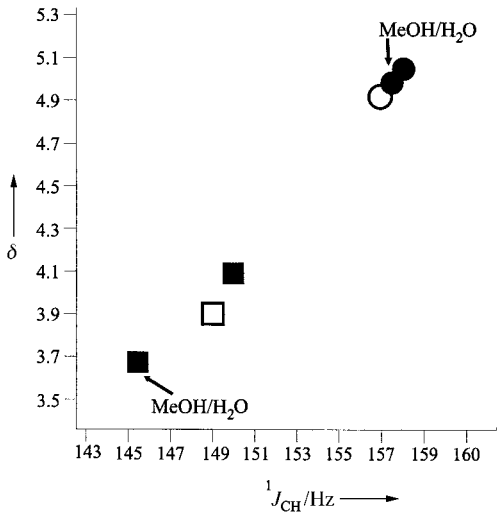


Figure 2. Correlation between chemical shifts δ and $^1J_{CH}$ coupling constants of the methylene protons of methylene-H_4F and methylene-H_4MPT; ■ = *pro-S* proton and ● = *pro-R* proton of methylene-H_4MPT, □ = *pro-S* proton and ○ = *pro-R* proton of methylene-H_4F. Data labeled with MeOH/H_2O were measured in methanol/water (1/1); all other data were recorded in 20 mM formiate buffer (pH 3). The data measured in MeOH/H_2O illustrate that chemical shift and coupling constant correlate regardless of the solvent.

protons is very similar in both compounds. Indeed, in the chemical reduction of N^5,N^{10}-methenyl tetrahydrofolate with $NaBH_4$, the hydride is incorporated into the *pro-S* position as well.[25] Interestingly the enzyme-catalyzed reduction of methenyl tetrahydrofolate with the reduced forms of nicotinamide adenine dinucleotide (NADH) or nicotinamide adenine dinucleotide phosphate (NADPH) to methylene-H_4F also proceeds with reversed stereospecificity.[25, 26]

In summary, the metal-free hydrogenase transfers molecular hydrogen to methenyl-H_4MPT (**1**) with a stereospecificity

 © WILEY-VCH Verlag GmbH, D-69451 Weinheim, 1998 1433-7851/98/3723-3302 $ 17.50+.50/0

that is reversed from that observed for the reduction of free substrate in solution. The same holds true for the enzyme-catalyzed reduction of methenyl-H_4F with NADH or NADPH as coenzyme. In both cases we can conclude from NMR spectroscopic data that the reactive conformation in the enzyme-catalyzed reaction does not match that in solution. In addition, in the enzyme-catalyzed reaction the product is formed in an energetically unfavorable conformation. This could possibly prevent product inhibition.

Received: July, 13, 1998 [Z 12128 IE]
German version: *Angew. Chem.* **1998**, *110*, 3491 – 3494

Keywords: carbocations · enzyme catalysis · hydrogenases · reductions · stereospecificity

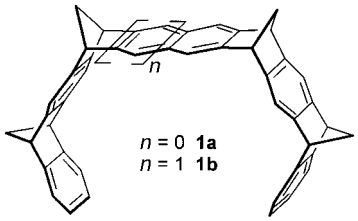
[1] S. P. J. Albracht, *Biochim. Biophys. Acta* **1994**, *1188*, 167 – 204.
[2] A. Volbeda, M.-H. Charon, C. Piras, E. C. Hatchikian, M. Frey, J. C. Fontecilla-Camps, *Nature* **1995**, *373*, 580 – 587.
[3] R. P. Happe, W. Roseboom, A. J. Pierik, S. P. J. Albracht, *Nature* **1997**, *385*, 126.
[4] Y. Higuchi, T. Yagi, N. Yasuoko, *Structure* **1997**, *5*, 1671 – 1680.
[5] R. K. Thauer, A. R. Klein, G. C. Hartmann, *Chem. Rev.* **1996**, *96*, 3031 – 3042.
[6] A. Berkessel, R. K. Thauer, *Angew. Chem.* **1995**, *107*, 2418 – 2421; *Angew. Chem. Int. Ed. Engl.* **1995**, *34*, 2247 – 2250.
[7] C. Zirngibl, R. Hedderich, R. K. Thauer, *FEBS Lett.* **1990**, *261*, 112 – 116.
[8] R. K. Thauer, *Antonie van Leeuwenhoek* **1997**, *71*, 21 – 32.
[9] C. Afting, A. Hochheimer, R. K. Thauer, *Arch. Microbiol.* **1998**, *169*, 206 – 210.
[10] J. Schleucher, C. Griesinger, B. Schwörer, R. K. Thauer, *Biochemistry* **1994**, *33*, 3986 – 3993.
[11] J. Schleucher, B. Schwörer, R. K. Thauer, C. Griesinger, *J. Am. Chem. Soc.* **1995**, *117*, 2941 – 2942.
[12] B. Schwörer, V. M. Fernández, C. Zirngibl, R. K. Thauer, *Eur. J. Biochem.* **1993**, *212*, 255 – 261.
[13] A. R. Klein, V. M. Fernández, R. K. Thauer, *FEBS Lett.* **1995**, *368*, 203 – 206.
[14] G. C. Hartmann, E. Santamaria, V. M. Fernández, R. K. Thauer, *J. Biol. Inorg. Chem.* **1996**, *1*, 446 – 450.
[15] G. A. Olah, N. Hartz, G. Rasul, G. K. S. Prakash, *J. Am. Chem. Soc.* **1995**, *117*, 1336 – 1343.
[16] J. Cioslowski, G. Boche, *Angew. Chem.* **1997**, *109*, 165 – 167; *Angew. Chem. Int. Ed. Engl.* **1997**, *36*, 107 – 109.
[17] J. H. Teles, S. Brode, A. Berkessel, *J. Am. Chem. Soc.* **1998**, *120*, 1345 – 1346.
[18] A. P. Scott, B. T. Golding, L. Radom, *New J. Chem.* **1998**, in press.
[19] J. Schleucher, B. Schwörer, C. Zirngibl, U. Koch, W. Weber, E. Egert, R. K. Thauer, C. Griesinger, *FEBS Lett.* **1992**, *314*, 440 – 444
[20] J. M. Erhardt, J. D. Wuest, *J. Am. Chem. Soc.* **1980**, *102*, 6363 – 6364.
[21] T. J. Atkins, *J. Am. Chem. Soc.* **1980**, *102*, 6364 – 6365.
[22] J. M. Erhardt, E. R. Grover, J. D. Wuest, *J. Am. Chem. Soc.* **1980**, *102*, 6365 – 6369.
[23] F. Bohlmann, *Angew. Chem.* **1957**, *69*, 641 – 642.
[24] G. R. Weisman, V. Johnson, R. E. Fiala, *Tetrahedron Lett.* **1980**, *21*, 3635 – 3638.
[25] L. J. Slieker, S. J. Benkovic, *J. Am. Chem. Soc.* **1984**, *106*, 1833 – 1838.
[26] A. R. Klein, R. K. Thauer, *Eur. J. Biochem.* **1995**, *227*, 169 – 174.
[27] G. Bodenhausen, D. J. Ruben, *Chem. Phys. Lett.* **1980**, *69*, 185 – 189.
[28] A. G. Palmer III, J. Cavanagh, P. E. Wright, M. Rance, *J. Magn. Reson.* **1991**, *93*, 151 – 170.
[29] L. E. Kay, P. Keifer, T. Saarinen, *J. Am. Chem. Soc.* **1992**, *114*, 10663 – 10665.
[30] A. J. Shaka, P. B. Barker, J. Keeler, *J. Magn. Reson.* **1985**, *64*, 547 – 552.

Modeling the Supramolecular Properties of Aliphatic-Aromatic Hydrocarbons with Convex – Concave Topology**

Markus Kamieth, Frank-Gerrit Klärner,* and François Diederich

Dedicated to Professor Emanuel Vogel on the occasion of his 70th birthday

In supramolecular and biological chemistry, for example in the case of molecular recognition, arenes make an important contribution to the formation of superstructures.[1] Their interactions with other arenes ($\pi-\pi$ or arene – arene interactions)[2] and with positively charged ions (cation – π interactions)[3] are particularly common and are used in the design of synthetic receptors. The properties of selective complexation[4] discovered for molecular tweezers of the type **1** and the results known from other receptors with concave – convex topology stimulated the theoretical model studies introduced here.



The molecular tweezers **1a** and **1b** serve as receptors for acceptor-substituted and cationic arenes as well as corresponding aliphatic substrates, whereas electron-rich arenes or anionic compounds are not complexed by them.[4] These experimental results, together with the established solvent dependence, indicate a substantial contribution of electrostatic interaction, as was already described in the electrostatic model for the attractive arene – arene interaction.[2] To find out the extent of electrostatic interaction in the molecular tweezers **1a** and **1b**, we calculated their electrostatic potential surfaces (EPSs) with the semiempirical AM1 method.[5] We thus found a potential which was surprisingly negative for pure hydrocarbons on the concave side of each molecule (most negative potentials: **1a**: -35.48, **1b**: -33.30 kcal mol^{-1}). In contrast, the potentials on the convex sides almost correspond to that of a tetraalkyl benzene such as durene (most negative potential: -25.60 kcal mol^{-1}; Figure 1, Table 1). When analogous calculations are performed for the potential substrates **2** – **6**, the complementary nature of their electrostatic potential surfaces to those of the cavity of the receptors **1a** and **1b** becomes evident.

[*] Prof. Dr. F.-G. Klärner, Dipl.-Chem. M. Kamieth
Institut für Organische Chemie der Universität
D-45117 Essen (Germany)
Fax: (+49) 201-183-3082
E-mail: klaerner@oc1.orgchem.uni-essen.de
Prof. Dr. F. Diederich
Laboratorium für Organische Chemie, ETH-Zentrum
Universitätstrasse 16, CH-8092 Zürich (Switzerland)

[**] This work was supported by the Deutsche Forschungsgemeinschaft and the Fonds der Chemischen Industrie.

 © WILEY-VCH Verlag GmbH, D-69451 Weinheim, 1998 1433-7851/98/3723-3303 $ 17.50+.50/0

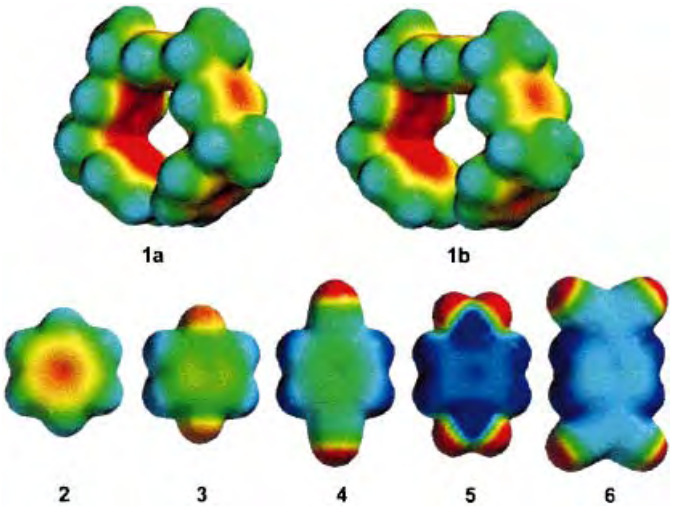


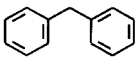
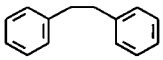
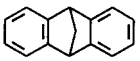
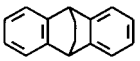
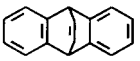
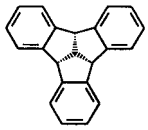
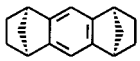
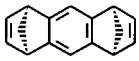
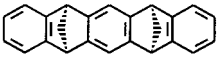
Figure 1. Semiempirically calculated (AM1) electrostatic potential surfaces of the molecular tweezers **1a** and **1b** (top) and the potential guest molecules benzene (**2**), *p*-difluorobenzene (**3**), *p*-dicyanobenzene (**4**), *p*-dinitrobenzene (**5**), and 7,7,8,8-tetracyanoquinodimethane (TCNQ, **6**). The color code spans from -25 (red) to 25 kcal mol^{-1} (blue).

Based on the semiempirically calculated EPSs of the potential guest molecules, a qualitative prediction of their binding affinity towards the receptor **1a** and **1b** also becomes possible:[6] Whereas benzene (**2**) and *p*-difluorobenzene (**3**) do not form detectable complexes with **1a** and **1b** in $CDCl_3$, the compounds with a more positive electrostatic potential, **4**–**6**, are suitable substrates (Figure 1).[4, 7] To establish whether this is a specific property of the molecular tweezers **1a** and **1b** or a universal principle for nonconjugated π-electron systems with concave–convex topology, corresponding calculations were performed on fragments of the molecular tweezers as well as on other molecular units used in synthetic receptors.

Table 1 lists, for some selected compounds, the AM1 values of the most negative electrostatic potentials on the electron density surfaces, which without exception are localized on the concave face of these molecules. The AM1 potentials on the convex sides of these molecules estimated by comparing the color scales are always less negative except in the case of **8**. It is important to note that absolute values are only comparable for molecules with identical substitution patterns, as each additional alkyl substituent decreases the electrostatic potential of the arene. Calculations with the semiempirical PM3 method[5] show the same trend as the AM1 calculations; the absolute values computed with PM3 are, however, smaller than the corresponding AM1 values. To test the semiempirical methods we also carried out ab initio calculations (RHF 6-31G**),[5] which are much more time-consuming, for the example of 9,10-dihydro-9,10-methanoanthracene (**7**), a fragment of **1**, as well as for model systems (Table 1, Figure 2). The results obtained with the different methods follow the same trend; therefore, the semiempirical methods are the methods of choice for EPS calculations, especially for the treatment of larger systems.

Compound **7** already shows a much more negative electrostatic potential on the concave side than on the convex face. The influence of neighboring π-electron systems on the EPS

Table 1. Semiempirically and ab initio calculated values [kcal mol^{-1}] of the most negative electrostatic potentials on the electron density surfaces.[a]

		AM1		PM3	(RHF 6-31G**)
		concave	convex	concave	concave
2		-20.65	–	-16.50	-20.21
		-22.11	–	-17.53	-21.63
11		-25.42	-22.1	-20.58	–
		-22.14	-22.1	-16.58	–
		-23.32	–	-18.77	-22.75
7		-29.70	-22.0	-24.60	-24.16
13		-29.24	-22.5	-24.05	–
12		-27.60	-24.5	-22.56	–
		-33.53	-22.0	-27.13	–
		-25.60	–	-21.11	-23.30
8		-26.51	-26.5	-22.05	-23.74
9		-29.42	-25.0	-24.32	-26.00
10		-31.07	-22.0	-26.64	–
1a		-35.48	-22.0	-29.70	–
1b		-33.30	-24.0	-27.76	–

[a] In all cases these potentials are localized on the concave side of the molecule. The potentials on the convex sides calculated with AM1 were estimated after comparison of the color scales.

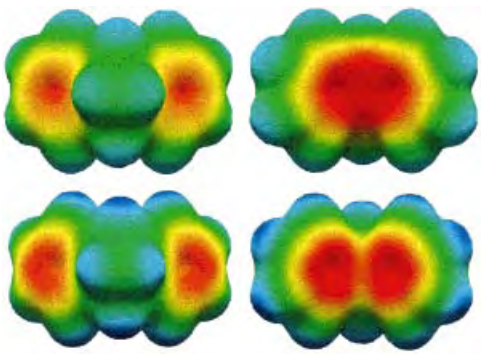


Figure 2. The semiempirically (AM1; top) and ab initio calculated (RHF 6-31G**; bottom) EPSs of 9,10-dihydro-9,10-methanoanthracene (**7**). The convex side of the molecule is shown on the left, and the concave side on the right. The color code spans from -25 (red) to 25 kcal mol^{-1} (blue).

 © WILEY-VCH Verlag GmbH, D-69451 Weinheim, 1998 1433-7851/98/3723-3304 $ 17.50+.50/0

of the concave side of the molecule becomes evident in the comparison of **8**–**10** (Figure 3): Whereas the electrostatic potentials on the convex and concave sides of the molecule hardly differ in **8** and are similar to that of durene (Table 1), the negative potential on the concave side increases at the

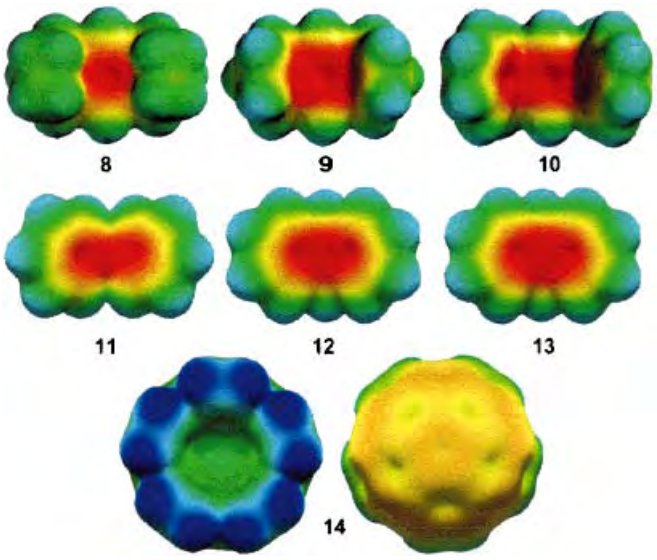


Figure 3. Semiempirically calculated EPSs (AM1) of the concave hydrocarbons **8**–**13** (see Table 1) and of $C_{30}H_{10}$ **14** (left: concave side, right: convex side). The color code spans from −25 (red) to 25 kcal mol^{-1} (blue).

central benzene ring due to the two additional nonconjugated double bonds in **9** and is due to the two additional terminal benzene rings in **10**. On the other hand, the values of the negative potentials on the convex sides of **8**–**10** decrease.

Also in the substructures **11**–**13**, which are present in many cyclophanes and other macrocyclic receptors[1] employed for the complexation of neutral and cationic substrates, a more negative electrostatic potential can be calculated for the concave side of the molecule (Figure 3). This also explains the "edge in angle" interaction[8] between guest molecules and the diphenylmethane units of the receptor often encountered in cyclophanes. The comparison of **12** and **13** is interesting: As **13** (most negative potential: −29.24 kcal mol^{-1}) has a more negative potential than **12** (most negative potential: −27.60 kcal mol^{-1}), the binding properties of the known receptors with the dibenzobarrelene unit[9] towards electron-deficient and positively charged substrates should improve upon hydrogenation of the C=C bond.[10]

The electrostatic potential at a certain site corresponds to the energy of interaction of a positive test charge with the nuclei and the wave functions of all the electrons of the investigated molecule and behaves inversely proportional to the distance from this test charge.[11] The observations made here can be illustrated with the "idealized" π atom of Hunter and Sanders,[2a] which assigns the negative charge (−0.5 on each side) to the π-electron system of an sp^2 C atom and the positive charge to the σ framework (Figure 4). If two "idealized" C atoms are in one plane and the distance between them is large enough, a positive test charge will not "feel" both isolated π-electron systems at the same time, and the electrostatic potential is not influenced by the introduc-

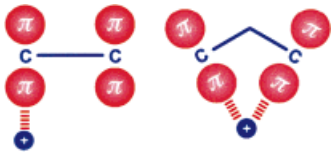


Figure 4. Schematic representation of the interaction of a positive test charge with nonconjugated "idealized" sp^2 C atoms[2] with linear (left) and concave geometry (right). The π-electron systems contain the negative, the σ framework the positive charges. The electrostatic potential is more negative in the concave case.

tion of the second π-electron system. If, on the other hand, the molecule is bent, the two π-electron systems approach on the concave side, and the potential will become more negative on this side at the same distance from the first π-electron system. The participating π molecular orbitals do not have to become significantly unsymmetrical with respect to the plane between the concave and convex sides of the molecule and do not have to undergo rehybridization.

The theoretical investigations presented here are in excellent agreement with experimental results and provide the reason for the new and surprising properties of the hydrocarbon tweezers **1a** and **1b** as synthetic receptors which selectively bind only acceptor-substituted and cationic substrates. In contrast to the nonconjugated aromatic systems examined here, the more negative potential lies on the convex side of bent conjugated molecules such as fullerene C_{60}[12a, b] as well as the fullerene fragments $C_{30}H_{10}$ (**14**) and corannulene.[12c] The reason for this is the rehybridization of the C atoms due to the nonplanarity of these concave–convex molecules.[12]

With quite simple semiempirical calculation methods the supramolecular properties of molecules based on electrostatic interactions can be visualized. The investigations described here make clear that, apart from the electronic structure, the topology of receptor molecules is of vital importance for the binding properties. The exact knowledge of cooperative effects of spatially separated molecule parts is necessary for the design and construction of new and efficient receptors as well as the self-organization of natural and nonnatural systems,[13] template-controlled syntheses,[14] crystal engineering,[15] and the production of new supramolecular materials.

Received: June 4, 1998 [Z11946IE]
German version: *Angew. Chem.* **1998**, *110*, 3497–3500

Keywords: electrostatic potential surfaces · host–guest chemistry · molecular tweezers · semiempirical calculations · supramolecular chemistry

[1] a) F. Vögtle, *Supramolekulare Chemie*, Teubner, Stuttgart, **1989**; b) J.-M. Lehn, *Supramolecular Chemistry. Concepts and Perspectives*, VCH, Weinheim, **1995**; c) C. D. Gutsche, *Calixarenes*, The Royal Society of Chemistry, Cambridge, **1989**; d) F. Diederich, *Cyclophanes*, The Royal Society of Chemistry, Cambridge, **1991**; e) D. J. Cram, *Container Molecules and Their Guests*, The Royal Society of Chemistry, Cambridge, **1994**; f) S. K. Burley, G. A. Petsko, *Science* **1985**, *229*, 23–28.

[2] a) C. A. Hunter, J. K. M. Sanders, *J. Am. Chem. Soc.* **1990**, *112*, 5525–5534; C. A. Hunter, *Chem. Soc. Rev.* **1994**, *23*, 101–109; b) P. Hobza, H. L. Selzle, E. W. Schlag, *J. Am. Chem. Soc.* **1994**, *116*, 3500–3506; c) W. L. Jorgensen, D. L. Severance, *J. Am. Chem. Soc.* **1990**, *112*, 4768–4777; d) M. Nishio, M. Hirota, Y. Umbezawa, Y. Takeushi, *Tetrahedron* **1995**, *51*, 8665–8701.

 © WILEY-VCH Verlag GmbH, D-69451 Weinheim, 1998 1433-7851/98/3723-3305 $ 17.50+.50/0

[3] a) D. A. Dougherty, *Science* **1996**, *271*, 163 – 168; b) J. C. Ma, D. A. Dougherty, *Chem. Rev.* **1997**, *97*, 1303 – 1324.
[4] a) J. Benkhoff, R. Boese, F.-G. Klärner, *Liebigs Ann./Recuil* **1997**, 501 – 516; b) F.-G. Klärner, J. Benkhoff, R. Boese, U. Burkert, M. Kamieth, U. Naatz, *Angew. Chem.* **1996**, *108*, 1195 – 1198; *Angew. Chem. Int. Ed. Engl.* **1996**, *35*, 1130 – 1133; c) F.-G. Klärner, U. Burkert, M. Kamieth, R. Boese, J. Benet-Buchholz, unpublished results.
[5] All methods of calculation used here are implemented in the program package SPARTAN 4.0, Wavefunction Inc., 18401 Von Karman, Suite 370, Irvine, CA 92715 (USA).
[6] For the use of semiempirically calculated EPSs for the qualitative prediction of the bond strength between aromatic molecules and cations, see also a) S. Mecozzi, A. P. West, D. A. Dougherty, *Proc. Natl. Acad. Sci. USA* **1996**, *93*, 10566 – 10571; b) S. Mecozzi, A. P. West, D. A. Dougherty, *J. Am. Chem. Soc.* **1996**, *118*, 2307 – 2308.
[7] The qualitative assessment of the EPSs for the prediction of bonding properties has also been successfully applied for other guest molecules not discussed here: F.-G. Klärner, U. Burkert, M. Kamieth, A. E. Wigger, unpublished results.
[8] a) C. Seel, F. Vögtle, *Angew. Chem.* **1992**, *104*, 542 – 563; *Angew. Chem. Int. Ed. Engl.* **1992**, *31*, 528 – 549; b) T. Z. Mondasini-Denti, W. F. VanGunsteren, F. Diederich, *J. Am. Chem. Soc.* **1996**, *118*, 6044 – 6051.
[9] a) D. A. Stauffer, R. E. Barrans, D. A. Dougherty, *Angew. Chem.* **1990**, *102*, 953 – 956; *Angew. Chem. Int. Ed. Engl.* **1990**, *29*, 915 – 918; b) A. McCurdy, L. Jimenez, D. A. Stauffer, D. A. Dougherty, *J. Am. Chem. Soc.* **1992**, *114*, 10314 – 10321; c) S. M. Ngola, D. A. Dougherty, *J. Org. Chem.* **1996**, *61*, 4355 – 4360.
[10] This is of course strictly true only for the gas phase, as different solvation of the receptor molecules could undoubtedly compensate for this effect.
[11] a) L. E. Chirlian, M. M. Francl, *J. Comput. Chem.* **1987**, *8*, 894 – 905; b) C. M. Breneman, K. B. Wiberg, *J. Comput. Chem.* **1990**, *11*, 361 – 373.
[12] a) R. C. Haddon, *Science* **1993**, *261*, 1545 – 1550; b) R. C. Haddon, *Acc. Chem. Res.* **1988**, *21*, 243 – 249; c) P. W. Rabideau, A. Sygula, *Acc. Chem. Res.* **1996**, *29*, 235 – 242.
[13] D. Philp, J. F. Stoddart, *Angew. Chem.* **1996**, *108*, 1242 – 1286; *Angew. Chem. Int. Ed. Engl.* **1996**, *35*, 1154 – 1196.
[14] P. L. Anelli, P. R. Ashton, R. Ballardini, T. T. Goodnow, A. E. Kaifer, D. Philip, M. Pietraszkiewicz, L. Prodi, M. V. Reddington, A. M. Z. Slawin, N. Spencer, J. F. Stoddart, C. Vincent, D. J. Williams, *J. Am. Chem. Soc.* **1992**, *114*, 193 – 218.
[15] G. R. Desiraju, *Angew. Chem.* **1995**, *107*, 2541 – 2558; *Angew. Chem. Int. Ed. Engl.* **1995**, *32*, 2328 – 2345.

Chemical Recycling of Plastics to Useful Organic Compounds by Oxidative Degradation**

Anne Pifer and Ayusman Sen*

With the production of polymeric materials on the rise and landfill space at a premium, it becomes increasingly important to develop new techniques for reducing the amount of material lost to the landfill. Approximately 20 % of landfill volume in the USA is consumed by plastics, and their lack of compatibility with the environment has generated much interest in increasing the amount of polymeric material that is reclaimed as structural material or chemically degraded to fuel or useful organic compounds.[1]

Chemical recycling, which has been increasingly applied in recent years, is defined as the breakdown of polymeric waste into materials that are reusable as fuel or chemicals, including monomers.[1a,c,d, 2] Most chemical recycling being done today focuses on the use of refinery technology and equipment to convert polymers into hydrocarbon feedstocks. Additionally, the depolymerization of condensation polymers, such as poly(ethylene terephthalate), to reusable monomeric material is currently practiced.[3] Of the 27 million tons of plastic material produced in the USA each year, 25 % is condensation polymers, while addition polymers constitute 75 % of this weight.[4] Addition polymers may be chemically recycled in refineries; however, the price of crude oil and hydrocarbon mixtures produced must compete with oil prices to be economically viable, and the risk to refinery equipment is high when postconsumer mixed plastics are used.[5, 2] Dufaud and Basset have reported a mild new procedure for the catalytic hydrogenolysis of polyolefins.[6] Here we describe a new oxidative degradation procedure that converts the most widely used (addition) polymers—such as polystyrene, polyethylene, and polypropylene—into useful organic compounds, including monomers for other polymerizations. The recycling of these polymers is currently problematical owing to the high costs of collection and sorting, the small difference in prices for virgin and recycled resins, and the reduction in polymer properties caused by the incompatibility of different plastics components.[7] These economic barriers could be overcome if the products generated from these polymers were more valuable and if mixed plastics could be processed together, eliminating sorting costs.

The oxidative degradation of the polymers involved reaction with nitrogen oxides and dioxygen at 170 °C. The results obtained are summarized in Table 1.

Polystyrene with average relative molecular weight of 280000 was converted into a mixture of benzoic acid, 4- and 3-nitrobenzoic acids, and gaseous oxides of carbon under the standard reaction conditions (170 °C, 16 h; partial pressures: 275 kPa NO, 690 kPa O_2, 3170 kPa N_2). No unchanged polymer was detected by ^{1}H NMR spectroscopy. The ratio of benzoic acid to nitrobenzoic acids varied significantly with NO and O_2 content in the reaction mixture; no reaction occurred without the presence of both gases. At a high partial pressure of NO (690 kPa), no benzoic acid was formed, 4-nitrobenzoic acid was the major product, and other nitro species were detected in trace amounts. On the other hand, at a low partial pressure of NO (175 kPa), benzoic acid and unchanged polystyrene predominated, and only trace amounts of nitrobenzoic acids were detected. In reactions where the partial pressure of NO was reduced (140 kPa) and that of O_2 increased (1035 kPa), all the polymer was converted, and the molar ratios of benzoic acid, 4-nitrobenzoic acid, and 3-nitrobenzoic acids were 7:1:1. In general, a O_2 partial pressure of 690 kPa or more was necessary for the reaction to proceed to completion. Benzoic acid, 4-nitrobenzoic acid, and 3-nitrobenzoic acid are easily separated by

[*] Prof. Dr. A. Sen, A. Pifer
Department of Chemistry
The Pennsylvania State University
University Park, PA 16802 (USA)
Fax: (+1) 814-863-8403
E-mail: asen@chem.psu.edu

[**] This research was supported by a grant from the US Department of Energy.

 © WILEY-VCH Verlag GmbH, D-69451 Weinheim, 1998 1433-7851/98/3723-3306 $ 17.50+.50/0

Table 1. Oxidative degradation of polymers by the NO_x/O_2 system.[a]

Polymer	Amount of starting material [g]	Amount of nonvolatile products [g]	Products	amount [g]
polystyrene ($M_w = 280000$)	0.26	0.19	benzoic acid	0.08
			4-nitrobenzoic acid	0.02
			3-nitrobenzoic acid	0.02
			3,5-dinitrobenzoic acid	traces
high-density polyethylene[b]	0.27	0.21	succinic acid	0.08
			glutaric acid	0.07
			adipic acid	0.02
			pimelic acid	0.03
			unknown organic compounds	traces
low-density polyethylene[b]	0.26	0.22	succinic acid	0.08
			glutaric acid	0.06
			adipic acid	0.02
			pimelic acid	0.01
			unknown organic compounds	traces
polypropylene[c] ($M_w = 250000$)	0.26	0.15	acetic acid	
			unknown organic compounds	
polymethyl methacrylate ($M_w = 96200$)	0.26	0.15	oligomers ($M_w = 985$)	
polyacrylic acid[d] ($M_w = 450000$)	0.25	0.10	oligomers	
nylon-6,6[e]	0.26	0.16	succinic acid	0.01
			glutaric acid	0.01
			adipic acid	0.06
			acetic acid	traces

[a] Standard conditions: 275 kPa NO, 690 kPa O_2, 3170 kPa N_2; 170°C; 16 h. [b] Reaction with 1035 kPa O_2. [c] Reaction with 480 kPa NO. [d] Reaction at 135°C

sublimation. While lab-grade polystyrene was employed in most experiments, similar results were also obtained starting with styrofoam cups and polystyrene packing material (Figure 1).



Figure 1. Polystyrene packing material before (left) and after reaction (right) under the standard conditions (170°C, 16 h; partial pressures: 275 kPa NO, 690 kPa O_2, 3170 kPa N_2). Part of the product mixture can be seen as a sublimate on the liner walls. No unchanged polymer remained.

It appears that the nitrobenzoic acids and benzoic acid arise from polystyrene through two independent parallel pathways. The former are generated by attack on the aromatic ring prior to cleavage of the polymer backbone. On the other hand, benzoic acid is generated by oxidation of the polymer backbone. After benzoic acid is formed, the carboxylic acid substituent deactivates the ring towards nitration. This mechanistic scenario is supported by the observation that under the same reaction conditions isopropyl benzene cleanly yielded benzoic acid.

When the standard reaction conditions were employed, both high-density polyethylene pellets ($d = 0.962$) and low-density polyethylene powder ($d = 0.915$) produced mixtures of short-chain α,ω-diacids (pimelic acid, adipic acid, glutaric acid, and succinic acid) in good yields (73 and 65%, respectively, by weight relative to the starting material) along with oxides of carbon. Only trace amounts of malonic acid were detected owing to its decomposition at temperatures above 135°C. No unchanged polymer was detected by ^{1}H NMR spectroscopy, and mass spectrometry indicated that oligomers with molecular weights of less than 350 were present in trace quantities. The formation of α,ω-diacids is noteworthy since these can be used as monomers in condensation polymerizations to yield commercially important polyamides and polyesters.[8]

When adipic acid was subjected to the standard reaction conditions, the product mixture consisted of unchanged adipic acid along with glutaric acid and succinic acid. This is consistent with a mechanism involving loss of carbon dioxide from a carboxyl radical followed by further oxidation of the resultant alkyl radical to the lower carboxylic acid. However, the good yield of α,ω-diacids precludes the possibility of products forming predominantly by successive decarboxylations starting with a long-chain carboxylic acid. Instead, the majority of the α,ω-diacids must arise through zip depolymerization via a series of cyclic transition states resulting from an attack of the carboxyl radical on the chain (backbiting mechanism). Such a series of steps has been postulated in the photooxidation of low-density polyethylene, although the latter reaction leads to a far more complex mixture of products.[9]

The reaction of isotactic polypropylene ($M_w = 250000$) under standard conditions resulted in a complex mixture of oligomeric and polymeric materials, as well as low molecular weight organic compounds. Upon increasing the partial pressure of NO to 480 kPa, the product mixture simplified to organic compounds with molecular weights below 155, as observed by mass spectrometry. No polymer remained, and the organic compounds were completely soluble in acetone (unlike the starting material or the products observed when 275 kPa NO was employed). The organic molecules formed consisted of ketones and carboxylic acids, including acetic acid. As with polyethylene, a backbiting radical mechanism is a possibility, as has been observed for the photooxidation of polypropylene.[10]

Nylon-6,6 was subjected to the standard reaction conditions (except at 135°C), and a mixture of α,ω-diacids was produced: adipic acid, glutaric acid, and succinic acid. When the reaction was conducted at 110°C, acetic acid, formic acid, and

 © WILEY-VCH Verlag GmbH, D-69451 Weinheim, 1998 1433-7851/98/3723-3307 $ 17.50+.50/0

ammonium ion were observed in trace quantities along with an insoluble black solid. These products were evidently formed by the oxidation of the diamine portion of the nylon-6,6 backbone since similar products were observed from the oxidation of hexamethylenediamine under the standard conditions.

Both polymethyl methacrylate and polyacrylic acid were oxidized under standard conditions to give oligomeric materials with drastically reduced molecular weights. For example, polymethyl methacrylate with $M_w = 96200$ and a polydispersity of 1.5 was oxidized to products with $M_w = 985$ and a polydispersity of 1.7, as observed by gel permeation chromatography in chloroform.

In conclusion, a wide variety of addition and condensation polymers can be oxidatively degraded under relatively mild conditions by a mixture of nitrogen oxides and dioxygen. In the particular cases of polystyrene, high- and low-density polyethylene, and perhaps polypropylene useful organic compounds are produced in moderate to good yields. The procedure is less useful for condensation polymers, such as nylon-6,6, since these can in principle be hydrolyzed back to the starting monomers.

Experimental Section

The reactions were carried out in 125-mL Parr pressure reactors with glass liners. Typically, the polymeric material (approx. 0.25 g) was added to a glass liner and then placed into the reactor, which was sealed. The reactor was purged with N_2, and then pressurized to 275 kPa with NO, to 3445 kPa with N_2, and finally to 4135 kPa with O_2. The reactor was heated to 170 °C for 16 h, following which it was cooled and the pressure released. The product mixture was then removed and analyzed by one or more of the following techniques: NMR spectroscopy, mass spectrometry, and gel permeation chromatography.

Received: May 22, 1998 [Z 11891 IE]
German version: *Angew. Chem.* **1998**, *110*, 3500 – 3502

Keywords: nitrogen oxides · oxidations · oxygen · polymers

[1] Reviews: a) C. P. Rader, S. D. Baldwin, D. D. Cornell, G. D. Sadler, R. F. Stockel, *Plastics, Rubber, and Paper Recycling*, American Chemical Society, Washington, **1995**; b) G. D. Andrews, P. M. Subramanian, *Emerging Technologies in Plastics Recycling*, American Chemical Society, Washington, **1992**; c) F. P. La Mantia, *Recycling of Plastic Materials*, ChemTec, Toronto-Scarborough, **1993**; d) R. D. Leaversuch, *Mod. Plast.* **1991**, *68*, 40 – 43; e) R. S. Stein, *Proc. Natl. Acad. Sci. USA* **1992**, *89*, 835 – 838.
[2] W. Kaminskiy, *J. Phys. IV* **1993**, *3*, 1543 – 1552.
[3] a) W. De Winter in ref. [1c], pp. 1 – 15; b) ref. [1d].
[4] G. Mackey in ref. [1a], pp. 161 – 169.
[5] M. W. Meszaros in ref. [1a], pp. 170 – 182.
[6] V. Dufaud, J.-M. Basset, *Angew. Chem.* **1998**, *110*, 848 – 852; *Angew. Chem. Int. Ed.* **1998**, *37*, 806 – 810.
[7] C. P. Rader, R. F. Stockel in ref. [1a], pp. 2 – 10.
[8] Review: H. R. Kricheldorf, *Handbook of Polymer Synthesis, Part A*, Marcel Dekker, New York, **1992**, chap. 11, 14.
[9] S. Karlsson, M. Hakkarainen, A.-C. Albertsson, *Macromolecules* **1997**, *30*, 7721 – 7728.
[10] S. Girois, L. Audouin, P. Delprat, J. Verdu, *Polym. Degrad. Stab.* **1996**, *51*, 133 – 141.

Investigation of the Molecular Recognition of Amino Acids by Cyclopeptides with Reflectometric Interference Spectroscopy**

Dietmar Leipert, Dirk Nopper, Marcus Bauser, Günter Gauglitz, and Günther Jung*

Molecular recognition plays a crucial part in many biological processes where guest molecules are bound very selectively and reversibly by their host. These mostly enantioselective recognition processes, in which chiral ligands interact with their receptors, can be imitated with synthetic molecules.[1] Synthetic receptors have various possible applications in the medical and pharmaceutical field, as new separation-phase material or sensitive coatings.[2] In fundamental research, important insights into the type of interaction in host – guest complexes are gained.[3] A multitude of different macrocyclic receptors such as crown ethers, cyclophanes, cyclodextrins, calixarenes, and cyclopeptides has already been synthesized.[4] With the cyclopeptides cyclo(Pro-Gly)$_3$ and cyclo(Pro-Gly)$_4$ the distinction between D and L amino acid salts in $CDCl_3$ became possible with NMR spectroscopic methods.[5] With macrocyclic peptides, chiral amines were distinguished,[6] and zwitterionic amino acids were complexed with chiral crown ethers.[7] These examinations of interactions between cyclopeptides and analyte were carried out with complicated methods.

We now report on novel sensor modules with surface-bound cyclopeptides as molecular receptors. In earlier work we were able to prove that cyclohexapeptide libraries can be used as chiral selectors in capillary electrophoresis.[8] With combinatorial solid-phase synthesis a host of such detector molecules can be produced.[9] Compared with singular procedures, as for calixarenes and cyclodextrins, our strategy shows a higher diversity by several orders of magnitude (virtual library: 10^{16} cyclohexapeptides from commercially available starting materials) and therefore a better chance of finding a receptor lead structure. Cyclohexapeptides are limited in their conformation,[10] and many basketlike structures can be synthesized by modifying the side chains. Based on these findings we immobilized the cyclopeptides **1** – **3** (Figure 1) on glass surfaces that function as transducers. The interaction between the cyclopeptide and the analyte is examined with reflectometric interference spectroscopy (RIfS).[11] In this optical method of detection, the reflection and the interference of light at phase boundaries are used for the time-resolved determination of changes in the optical film thickness (product of refractive index n and physical film thickness d) of thin transparent films from the resulting interference

[*] Prof. Dr. G. Jung, Dipl.-Chem. D. Leipert, Dipl.-Chem. M. Bauser
Institut für Organische Chemie der Universität
Auf der Morgenstelle 18, D-72076 Tübingen (Germany)
Fax: (+49) 7071-29-6925
E-mail: guenther.jung@uni-tuebingen.de
Dipl.-Chem. D. Nopper, Prof. Dr. G. Gauglitz
Institut für Physikalische Chemie der Universität Tübingen (Germany)

[**] We thank the Deutsche Forschungsgemeinschaft (project "Molecular pattern recognition with supramolecular structures and polymers") for financial support (GO 301/23-3).

 © WILEY-VCH Verlag GmbH, D-69451 Weinheim, 1998 1433-7851/98/3723-3308 $ 17.50+.50/0

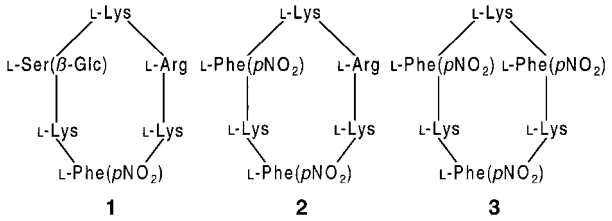


Figure 1. Amino acid sequences of the cyclohexapeptides **1**—**3** used as chemoreceptors.

pattern.[12] Adsorption or bonding processes on thin cyclopeptide layers can thus be registered directly, and a large amount of analytes and receptors can be examined in a short period of time.

To prepare our chemosensors, a monolayer of the cyclohexapeptides **1**–**3** was covalently bound to a glass support previously treated with epoxysilane through the amino functionalities of three lysine side chains (Figure 2). For this, the positions 1, 3, and 5 in the sequence were chosen as anchoring sites. L-Arginine, 4-nitro-L-phenylalanine and O-glycosidically modified serine were used in the positions 2, 4, and 6 of the sequence. L-arginine has proved itself as an important amino acid in cyclopeptide libraries. In the tricyclic peptide antibiotic vancomycin, used as chiral separatory phase material, sugar units and aromatic residues play an important part.[13] The properties of the cyclopeptides were modified as follows by means of sequence alterations: In the cyclopeptide **2**, the O-glycosidically modified serine of **1** is replaced by 4-nitro-L-phenylalanine. In addition, L-arginine is exchanged against 4-nitro-L-phenylalanine in the cyclopeptide **3**. To examine the amino acid/cyclopeptide interaction, solutions of different amino acids in neutral, buffer-free water were pumped over the sensitive layers, and the resulting optical film thickness was determined after a state of equilibrium was reached. Such a time-resolved course of the film thickness for different amino acids is shown in Figure 3; in this, the peak height is the signal utilized.

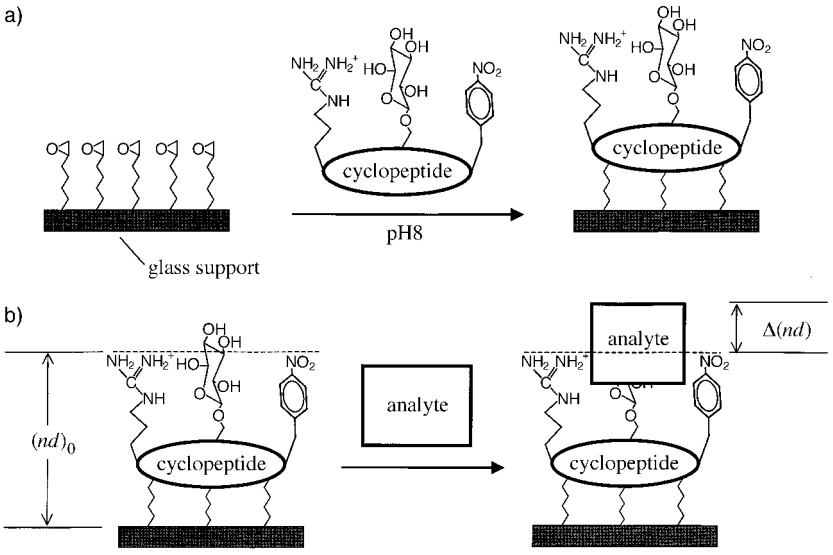


Figure 2. a) Linking of the cyclohexapeptides to the transducer surface. b) Change in optical film thickness ($\Delta(nd)$) after interaction with the analyte.

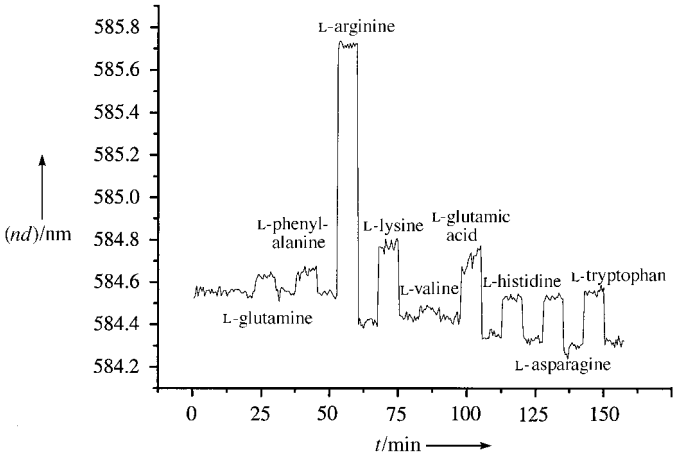


Figure 3. Course of the film thickness at the optical transducer for the interaction of **1** after the injection of different L-amino acids (1000 ppm each) in neutral, buffer-free water. The unit ppm corresponds to 1 mg amino acid per liter of water.

Furthermore, a test set of twelve L-amino acids with all three surface-bound cyclopeptides in neutral, buffer-free water was examined. The sensor signals thus obtained clearly show that all three cyclopeptides preferentially bind L-arginine but not L-lysine, which also contains two amino groups (Figure 4). For all amino acids, the RIfS signals are much more intense for the cyclopeptide **1** layer than for the coverage with **2** or **3**. Therefore the influence of the glucose group has to be considerable. The sensor signal for L-arginine is almost twice as high for cyclopeptide **1** as for the cyclopeptides **2** and **3**, which proves the selective interaction.

To examine a possible enantiomer recognition by the cyclohexapeptide layers, calibration measurements were carried out with L- and D-arginine in the concentration range from 0–880 mg L^{-1} (Figure 5). The two calibration graphs do not differ significantly; in the region of higher concentration a possible indication for the discrimination of enantiomers can be seen. For quantification purposes, a Langmuir adsorption curve was calculated from the experimental values using nonlinear regression according to Equation (1).[14]

$$Y = A + \frac{b\,c\,x}{1 + b\,x} \qquad (1)$$

Here, Y describes the measured signal, x the concentration, A the intercept, b the ratio of the constants for adsorption and desorption and c the saturation signal. With this function the detection limit for arginine can be determined if the tripled noise of the baseline for the film thickness is used as the Y value. The detection limits (x values) for L- and D-arginine thus obtained for all three chemoreceptors are summarized in Table 1. With the cyclopeptide **1**, a concentration of about 15 μmol L^{-1} arginine can be detected in neutral, buffer-free water.

A survey of the influence of different matrices on the interaction between cyclo-

 © WILEY-VCH Verlag GmbH, D-69451 Weinheim, 1998 1433-7851/98/3723-3309 $ 17.50+.50/0

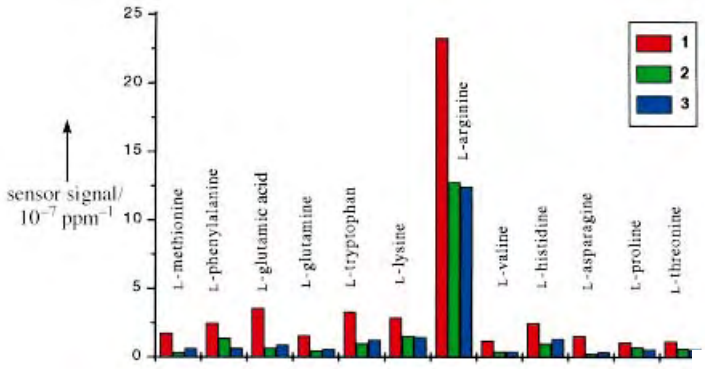


Figure 4. Comparison of the sensor signals of all three sensitive layers for different amino acids in water.

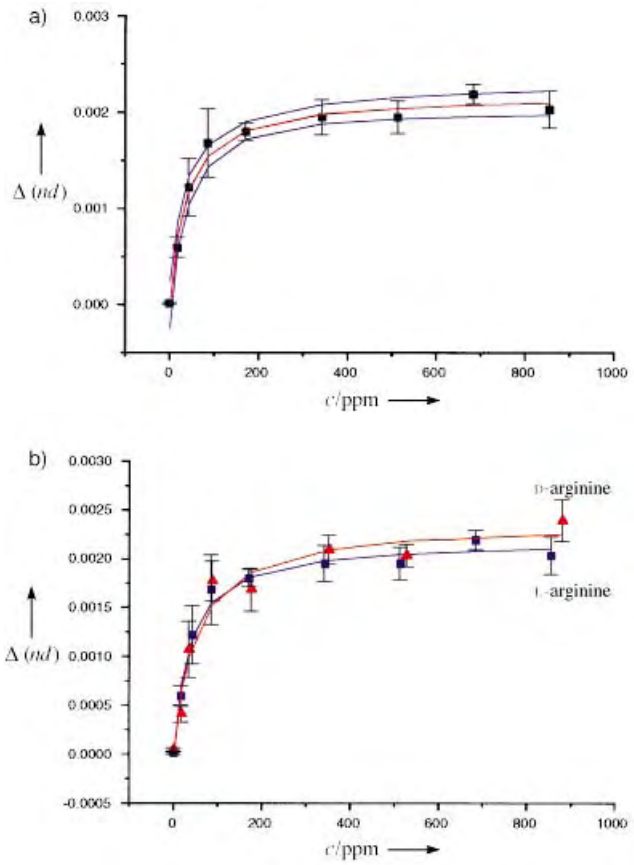


Figure 5. Calibration curves for both arginine enantiomers (▲: D-arginine, ■: L-arginine), determined for immobilized **1**. a) Progress of the calibration with L-arginine (layer **1**), course of the Langmuir function and confidence region of the calibration. b) Comparison of the calibrations for both isomers.

Table 1. Detection limits for L- and D-arginine.[a]

cyclohexapeptide	L-arginine [μmol L^{-1}]	D-arginine [μmol L^{-1}]
1	14.4	17.2
2	40.2	31.6
3	20.1	20.1

[a] For arginine, 1 μmol L^{-1} corresponds to 0.174 mg L^{-1}.

peptide and amino acid led to a different result when PBS buffer (*p*hosphate *b*uffered *s*aline, pH 7.4) was used as solvent. In PBS buffer the α-amino acids mainly are zwitterionic. The change in medium yields a completely different selectivity (Figure 6): From a test set of 14 amino acids, L-glutamine is now the most easily recognized one by all three sensors and is also distinguished from closely related L-asparagine. The signal-amplifying influence of the sugar unit again becomes apparent here. Although the two cyclopeptides **2** and **3** only differ in one recognition element, the signal height changes

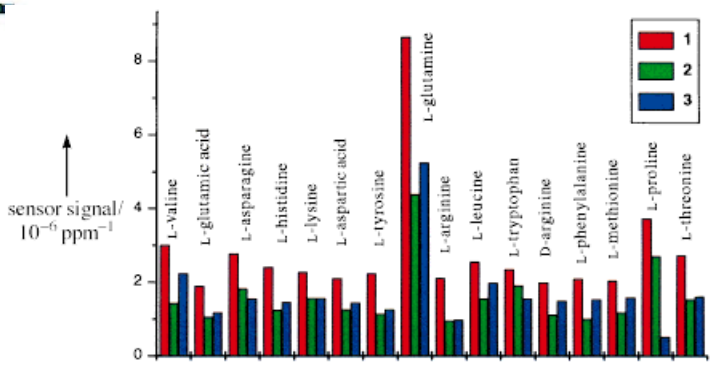


Figure 6. Signals of the three cyclopeptide sensors for different amino acids, measured in PBS buffer.

for different amino acids. This indicates that by varying the cyclopeptides and the constitution of the buffer solution further selectivities for other amino acids can specifically be researched.

In combination with reflectometric interference spectroscopy, optical transducers with surface-bound cyclohexapeptides allow the selective and fast detection of low concentrations of amino acids in aqueous solutions. The detection is possible without derivatization. With combinatorial solid-phase chemistry a multitude of new receptors can be synthesized. Not only single receptors, but also receptor libraries can be immobilized which can be deconvolutively adapted. At present we are selectively looking for receptors for certain analytes with sensor arrays. Owing to the narrow concentration range and the selectivity obtained, the use of the sensor is possible in a broad spectrum of biotechnological sensor applications and for medical diagnosis.

Experimental section

1–**3**: Multiple parallel peptide syntheses (15 μmol each) are carried out on a 2-chlorotritylchloride resin with 9-fluorenylmethoxycarbonyl (Fmoc) amino acids and diisopropylcarbodiimide activation. The hexapeptides, which are protected at the side chains, are cleaved with hexafluoro-2-propanol (30% in dichloromethane) and cyclized in solution (1 mM in DMF). The cyclization reagents are extracted, and the side-chain protecting groups are cleaved with trifluoroacetic acid/water/triisopropylsilane (95/2.5/2.5; 3 h). Then the peptides are precipitated with diethyl ether, centrifuged, dissolved in *tert*-butyl alcohol/water (4/1), and lyophilized. Peptide **1** is taken up in anhydrous methanol, and pH 10–11 is established by adding sodium methoxide (0.5 M in methanol). After 3 h the solution is neutralized with acetic acid and evaporated to dryness, and the residue is dissolved in *tert*-butyl alcohol/water (4/1) and lyophilized. **1**: ESI-MS: $[M+H]^+$: 979.0. **2**: ESI-MS: $[M+H]^+$: 925.5. **3**: ESI-MS: $[M+H]^+$: 962.0; HPLC purity >90% (RP-18, acetonitrile/H_2O, 214 nm).

 © WILEY-VCH Verlag GmbH, D-69451 Weinheim, 1998 1433-7851/98/3723-3310 $ 17.50+.50/0

Immobilization of **1**–**3** on the transducer surface: The surface of the glass is cleaned with a freshly prepared Piranha solution (H_2SO_4/H_2O 2/1) (1 h), washed with water, and dried at room temperature (RT). The silanization takes place with a solution of 3-glycidoxypropyltrimethoxysilane (20% in toluene; 4 h at 110 °C). To link the cyclopeptides to the surface, a solution of **1**, **2**, or **3** (0.1 mg mL^{-1}) in phosphate buffer (50 mM, pH 8) is added (24 h, RT). Then it is washed with brine (1M) and water. To characterize the cyclopeptide-functionalized glass supports, static contact-angle measurements were carried out with six different solvents and the polar (σ^P) and disperse share (σ^D) in the surface energy were determined. Immobilized cyclopeptide **1**: $\sigma^D = 23.51$ mN m^{-1}, $\sigma^P = 21.37$ mN m^{-1}. Immobilized cyclopeptide **2**: $\sigma^D = 23.18$ mN m^{-1}, $\sigma^P = 23.49$ mN m^{-1}. Immobilized cyclopeptide **3**: $\sigma^D = 23.27$ mN m^{-1}, $\sigma^P = 25.63$ mN m^{-1}.

Received: June 24, 1998 [Z 12041 IE]
German version: *Angew. Chem.* **1998**, *110*, 3503–3505

Keywords: chemosensors · cyclopeptides · interference spectroscopy · combinatorial chemistry · molecular recognition

[1] M. F. Cristofaro, A. R. Chamberlin, *J. Am. Chem. Soc.* **1994**, *116*, 5089–5098.
[2] X. X. Zhang, J. S. Bradshaw, R. M. Izatt, *Chem. Rev.* **1997**, *97*, 3313–3361.
[3] W. C. Still, *Acc. Chem. Res.* **1996**, *29*, 155–163.
[4] M. M. Conn, J. Rebek, Jr., *Chem. Rev.* **1997**, *97*, 1647–1668.
[5] C. M. Deber, E. R. Blout, *J. Am. Chem. Soc.* **1974**, *96*, 7566–7568.
[6] a) H. Miyake, Y. Kojima, *Coord. Chem. Rev.* **1996**, *148*, 301–314; b) H. Kataoka, T. Hanawa, T. Katagi, *Chem. Pharm. Bull.* **1992**, *40*, 570–574.
[7] F. Wudl, F. J. Gaeta, *J. Chem. Soc. Chem. Commun.* **1972**, 107.
[8] G. Jung, H. Hofstetter, S. Feiertag, D. Stoll, O. Hofstetter, K.-H. Wiesmüller, V. Schurig, *Angew. Chem.* **1996**, *108*, 2261–2262; *Angew. Chem. Int. Ed. Engl.* **1996**, *35*, 2148–2150.
[9] *Combinatorial Peptide and Nonpeptide Libraries* (Ed.: G. Jung), VCH, Weinheim, **1996**.
[10] H. Kessler, R. Gratias, G. Hessler, M. Gurrath, G. Müller, *Pure Appl. Chem.* **1996**, *68*, 1201–1205.
[11] G. Gauglitz, A. Brecht, G. Kraus, W. Nahm, *Sens. Actuators B* **1993**, *11*, 21–27.
[12] A. Brecht, J. Piehler, G. Lang, G. Gauglitz, *Anal. Chim. Acta* **1995**, *311*, 289–300.
[13] D. W. Armstrong, D. Rundlett, J.-R. Chen, *Chirality* **1994**, *6*, 496–509.
[14] *Comprehensive Polymer Science*, *Polymer Properties*, Pergamon, Oxford, **1989**.

FT-IR Mapping—A New Tool for Spatially Resolved Characterization of Polymer-Bound Combinatorial Compound Libraries with IR Microscopy**

Wolfgang J. Haap,* Tilmann B. Walk, and Günther Jung*

A decisive advantage of combinatorial organic solid-phase chemistry[1–5] for finding lead structures is its higher throughput compared to previous synthetic methods, as easily automated reactions are preferentially carried out on polymer resins.[6] Further improvement of the efficiency is directed to an increasing miniaturization of the synthesis as well as screening of the prepared compounds. Resin-bead analysis plays an important role in the development of such technologies. With the techniques that have now been established for analyzing single resin beads—such as NMR spectroscopy,[7, 8] matrix-assisted laser desorption ionization time-of-flight (MALDI-TOF) mass spectrometry, and FT-IR microscopy[9–11]—only polymer-bound single compounds could be analyzed so far. In combinatorial chemistry, however, techniques are needed with which a large number of compounds can be analyzed simultaneously.

Owing to its high sensitivity, the simplicity of the apparatus, and the high sample throughput, IR microscopy is suited for parallel analysis. The combination of a FT-IR microscope with a motor-driven *x*-*y* stage allows the automatic spectral mapping of surfaces and objects embedded in them. If single resin beads are embedded in a KBr window by pressing, they can be visualized with this measuring arrangement in the form of an IR map. The superpositioning of the visible video image of several resin beads with the corresponding IR map (Figure 1) shows the good correlation of both types of representations. In this case, for the IR reconstruction the typical polystyrene combination vibration at 1942 cm^{-1} was chosen.

Through mapping of larger areas, hundreds of embedded resin beads can be detected and the compounds bound to them identified. To exhibit the potential of this method, a model library of isoxazolidines[12] on Rink amide ARAM resin was synthesized by the split-and-combine method[13] (Scheme 1). The polymer-bound library obtained consists of a total of 18 compounds. If one considers the different building blocks of the synthesis, a nitro group or the carboxamidomethyl residue is found in 50% each of the

[*] Dr. W. J. Haap,[+] Prof. Dr. G. Jung, Dipl.-Chem. T. B. Walk
Institut für Organische Chemie der Universität
Auf der Morgenstelle 18, D-72076 Tübingen (Germany)
Fax: (+49) 7071-296925
E-mail: guenther.jung@uni-tuebingen.de
[+] New address:
Ciba Speciality Chemicals Inc., BS Antimicrobials
P.O. Box 1266, D-79630, Grenzach-Wyhlen (Germany)
E-mail: wolfgang.haap@cibasc.com

[**] This work was supported by the Bundesministerium für Bildung, Forschung und Technologie BMBF (FKZ 0311000; Librarian II, Teilprojekt "Kombinatorische Chemie und Synthesemonitoring"). We thank Dr. A. Rager (Bruker, Karlsruhe, Germany) for the technical assistance.

 © WILEY-VCH Verlag GmbH, D-69451 Weinheim, 1998 1433-7851/98/3723-3311 $ 17.50+.50/0

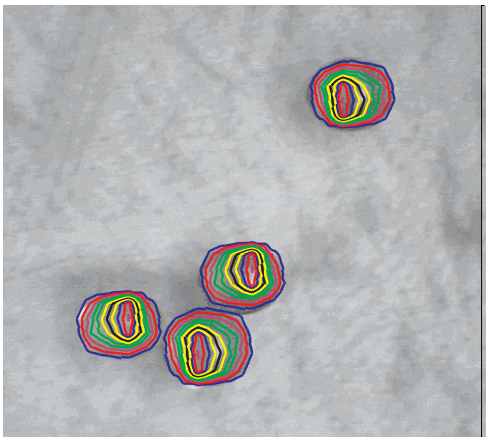
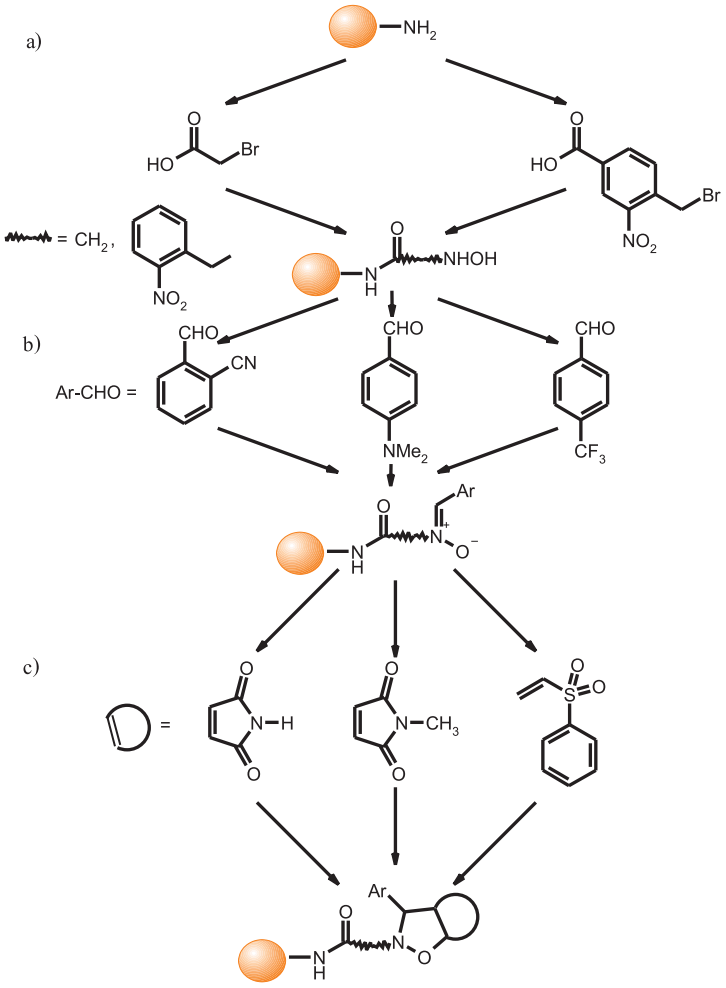


Figure 1. UV/Vis video image and IR reconstruction of four polystyrene resin beads with a diameter of about 80 μm. The IR map was obtained with a motor-driven *x*-*y* stage in combination with an IR microscope. For the reconstruction of the resin beads the integral of the polystyrene combination vibration at 1942 cm^{-1} was used.



Scheme 1. Solid-phase synthesis of isoxazolidines according to the split-and-combine method. a) Distribution of the resin into two equal portions, coupling of bromocarboxylic acids with *N*,*N*′-diisopropylcarbodiimide (DIC), combination of the resin, substitution with hydroxylamine; b) distribution of the resin into three equal portions, condensation with three different aromatic aldehydes to the corresponding nitrones, combination of the resin; c) distribution of the resin into three equal portions, cycloaddition with three different dipolarophiles to isoxazolidines, combination of the resin.

compounds; a cyano, *N*,*N*-dimethylamino, or trifluoromethyl group in 33 % each; and a succinimide, *N*-methylsuccinimide, or sulfone group in 33 % each. To verify that this library was successfully synthesized, a portion of the resin was removed, and the compounds were cleaved from the polymer with trifluoroacetic acid and analyzed with HPLC electrospray ionization mass spectrometry. All the compounds shown could be identified. Upon cycloaddition of the maleimides *endo/exo* isomers and, in the case of the vinylsulfones, regioisomers were obtained. This led to complex chromatograms of isomer compound mixtures; coelution occurred often. A quantification of the single compounds is not possible, and the peak area in the UV trace (detection at 214 nm) did not correlate with those of the total ion current chromatogram in the mass spectrum.

The isoxazolidine library prepared according to Scheme 1 was embedded in a KBr window by pressing. An area of $3 \times 3\ mm^2$ was automatically mapped. When the polystyrene absorption at 1942 cm^{-1} was used to visualize the IR map, all resin beads contained on the surface were detected (Figure 2).

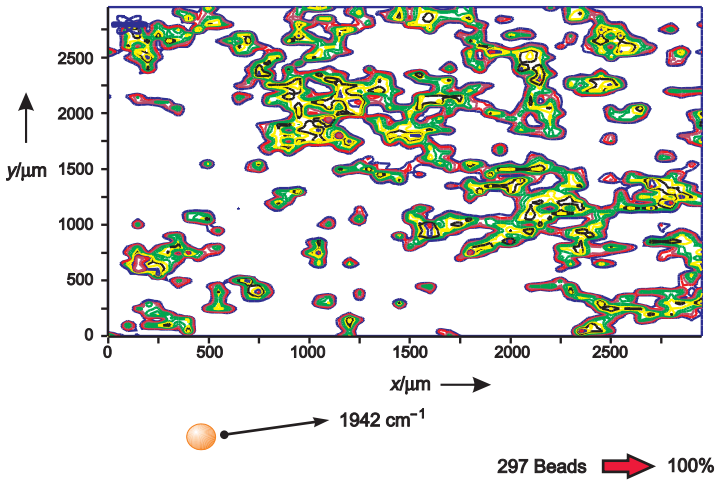


Figure 2. IR map of an area ($3 \times 3\ mm^2$) of a KBr window in which resin beads of the isoxazolidine library are embedded. By application of the polystyrene absorption at 1942 cm^{-1} all resin beads were detected. White region: KBr window; colored region: resin beads. There are a total of 297 resin beads in the scanned area.

Through choice of different absorption bands for visualization, those resin beads carrying a specific functional group can be selectively "fished out" from this library of 297 resin beads. For example, the resin beads with the *N*-methylsuccinimide group are extracted spectroscopically from the resin-bead mixture by visualization by means of the carbonyl absorption at 1715 cm^{-1}. In the scanned area there are a total of 112 resin beads (39.1 %) with this functional group (Figure 3). Analogous IR maps could be obtained for further functional groups (Figure 4).

The IR analysis of polymer-bound molecules is made difficult by the strong absorption of the polymer matrix itself. In the IR spectrum containing polymer and anchor absorptions, for example, signals for neither the *N*,*N*-dimethylamino nor the carboxamidomethyl groups can be recognized. However, as all further functional groups can be cleary differ-

 © WILEY-VCH Verlag GmbH, D-69451 Weinheim, 1998 1433-7851/98/3723-3312 $ 17.50+.50/0

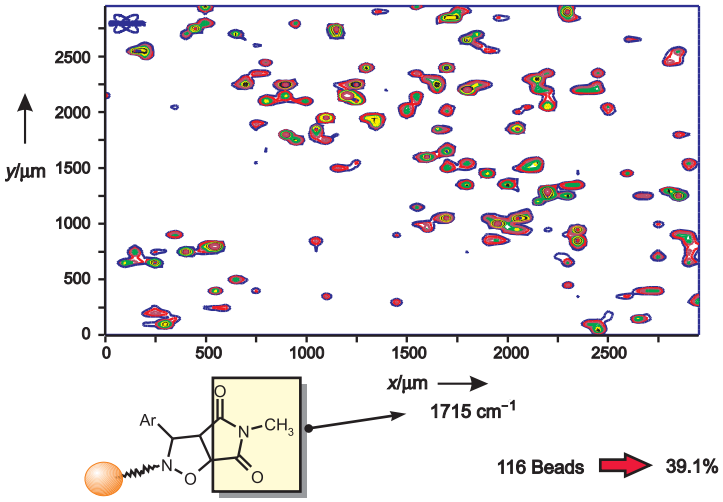


Figure 3. "*N*-Methylsuccinimide" resin beads extracted from the library by visualization over the carbonyl absorption at 1715 cm^{-1}.

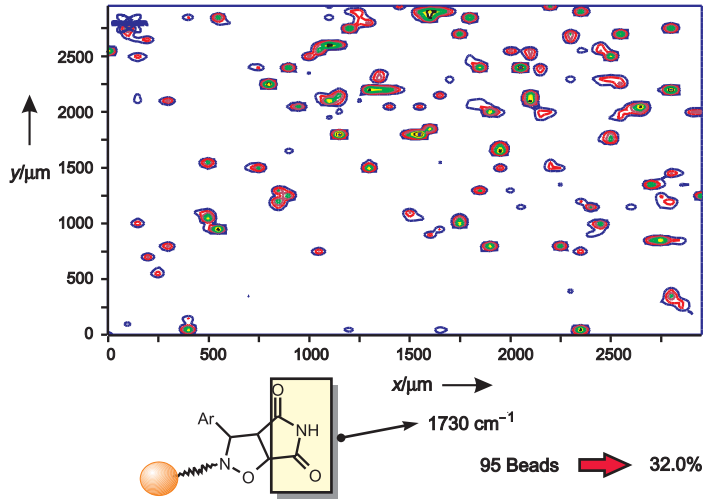


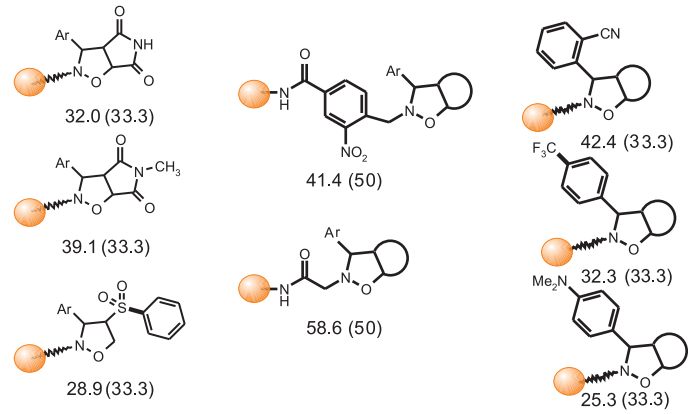
Figure 4. "Succinimide" resin beads extracted from the library by visualization over the carbonyl absorption at 1730 cm^{-1}.

entiated from one another, the number of resin beads carrying a specific group is given by the exclusion principle. If this method is applied to all resin beads, the distribution of all functional groups can be determined by single counting of the resin beads by data processing programs (Table 1).

Despite the relatively small amount of resin beads in the scanned regions, no significant deviations from the expected statistical distribution of the individual functional groups are observed. Although the carboxamidomethyl, cyano, and *N*-methylimide groups are somewhat overrepresented, their contributions are on the same order of magnitude. When applied together with a LC-MS analysis, IR mapping allows a statistical investigation and thus a rapid quality control of the library synthesized by the split-and-combine method.

The decisive advantage of this technique is that IR analysis, in contrast to mass spectrometry, can be carried out without destruction of the sample and with spatial resolution. Furthermore, a direct identification of resin-bound molecules is possible through superpositioning of the IR maps. If, for example, the maps of the imide (1730 cm^{-1}), nitro (1360 cm^{-1}), and cyano absorptions (2225 cm^{-1}) are placed on top of each other, the resin beads that carry exclusively compound **1** can be identified with spatial resolution in the overlapping regions (stars in Figure 5) of the functional groups. The FT-IR spectra of the individual resin beads extracted from the maps clearly confirm attachment of **1** to the resin bead (Figure 6).

Table 1. Statistical distribution [%] (the theoretical values are given in parentheses) of resin beads with specific functional groups.



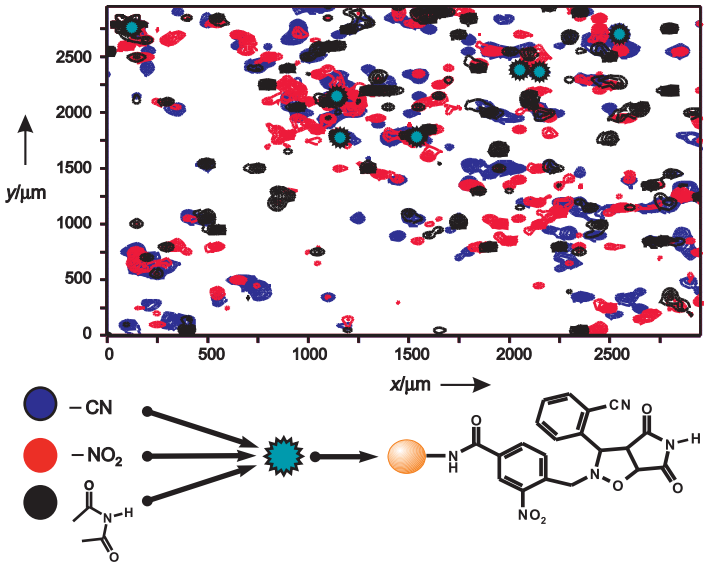


Figure 5. "FT-IR tagging" by superpositioning of the IR maps of imide (1730 cm^{-1}), nitro (1360 cm^{-1}), and cyano absorptions (2225 cm^{-1}). Resin beads on which **1** is immobilized were identified through overlapping regions of all IR maps.

In summary, a method has been developed that allows the spatially resolved and destruction-free characterization and quality control of polymer-bound compound libraries. Furthermore, by superpositioning of different IR maps, compounds immobilized on individual resin beads can be identified. Through improved embedding techniques, even larger areas with many resin beads can be mapped very quickly. This

 © WILEY-VCH Verlag GmbH, D-69451 Weinheim, 1998 1433-7851/98/3723-3313 $ 17.50+.50/0

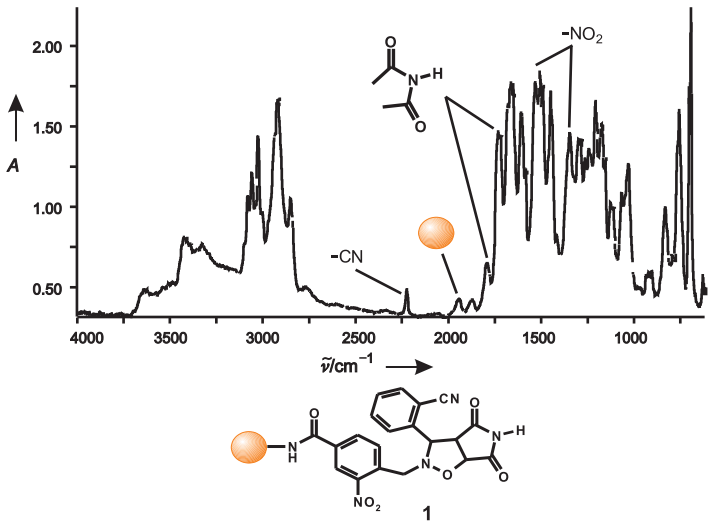


Figure 6. FT-IR spectrum of an individual resin bead on which **1** is immobilized.

method can thus provide a valuable contribution to the development of miniaturized syntheses on individual resin beads. The combination of IR mapping with MS and HPLC-MS analysis means that tagging concepts can be abandonned; technical procedures of automatic sorting of resin beads could even be developed.

Experimental Section

The FT-IR mapping was carried out with a Bruker IRScope II instrument. The resin beads modified according to Scheme 1 were embedded in a KBr window under a slight pressure. An area of 3×3 mm^2 was mapped with an IR microscope. With a step width of 50 μm 60 data points were measured in the x as well as the y direction, so that a total of 3600 IR spectra were registered for the IR mapping. For a resolution of 4 cm^{-1} and a summation of 4 scans per data point, the measurement time was 5 h.

Received: May 13, 1998 [Z11849IE]
German version: *Angew. Chem.* **1998**, *110*, 3506 – 3509

Keywords: combinatorial chemistry · IR spectroscopy · microscopy · solid-phase syntheses

[1] F. Balkenhohl, C. von dem Bussche-Hünnefeld, A. Lansky, C. Zechel, *Angew. Chem.* **1996**, *108*, 2436 – 2488; *Angew. Chem. Int. Ed. Engl.* **1996**, *35*, 2289 – 2337.
[2] J. S. Früchtel, G. Jung, *Angew. Chem.* **1996**, *108*, 19 – 46; *Angew. Chem. Int. Ed. Engl.* **1996**, *35*, 17 – 42.
[3] E. M. Gordon, M. A. Gallop, D. V. Patel, *Acc. Chem. Res.* **1996,** *29*, 144 – 154.
[4] *Combinatorial Peptide and Non-peptide Libraries* (Ed.: G. Jung), VCH, Weinheim, **1996**.
[5] L. A. Thompson, J. A. Ellmann, *Chem. Rev.* **1996**, *96*, 555 – 600.
[6] P. H. H. Hermkens, H. C. J. Ottenheijm, D. C. Rees, *Tetrahedron* **1997**, *53*, 5643 – 5678.
[7] M. Pursch, G. Schlotterbeck, L.-H. Tseng, K. Albert, W. Rapp, *Angew. Chem.* **1996**, *108*, 3043 – 3036; *Angew. Chem. Int. Ed. Engl.* **1996**, *35*, 2867 – 2869.
[8] S. K. Sarkar, R. Garigipati, J. L. Adams, P. A. Keifer, *J. Am. Chem. Soc.* **1996**, *118*, 2305 – 2306.
[9] a) B. Yan, G. Kumaravel, H. Anjaria, A. Wu, R. C. Petter, C. F. Jewell, Jr., J. R. Wareing, *J. Org. Chem* **1995**, *60*, 5736 – 5738; b) B. Yan, J. B. Fell, G. Kumaravel, *J. Org. Chem.* **1996**, *61*, 7467 – 7472.
[10] B. Yan, G. Kumaravel, *Tetrahedron* **1996**, *52*, 843.
[11] a) K. Russell, D. C. Cole, F. M. McLaren, D. E. Pivonka, *J. Am. Chem. Soc.* **1996**, *118*, 7941 – 7945; b) D. E. Pivonka, K. Russell, T. Giero, *Appl. Spectr.* **1996**, *50*, 1471.
[12] W. J. Haap, D. Kaiser, T. B. Walk, G. Jung, *Tetrahedron* **1998**, *54*, 3705 – 3724.
[13] A. Furka, F. Sebestyen, M. Asgedom, G. Dibo, *Int. J. Pept. Protein Res.* **1991**, *37*, 487 – 493.

Ba_3Ge_4: Polymerization of Zintl Anions in the Solid and Bond Stretching Isomerism**

Fabio Zürcher and Reinhard Nesper*

In memory of Jean Rouxel

In the fast-growing family of Zintl phases, an ever-increasing number of completely new bonding patterns of main group element clusters, Zintl anions, are being discovered. These oligo anions or polyanions often carry relatively high formal charges, which can be determined in accordance with the Zintl – Klemm concept.[1] In the solid, stabilization is achieved through a large number of surrounding cations. The transfer to solution has only been successful in a few cases until now, most of which were Zintl anions with low formal charges.[2] It has not yet proved possible to directly dissolve the smaller, highly charged oligomeric anions of Group 14 elements such as E_4^{4-},[3] E_4^{6-},[4] E_8^{16-},[5–7] E_{12}^{21-}[6–8] from the Zintl phase into solution. Apart from E_4 in the form of a tetrahedron[9] or a butterfly anion, none of these has even been synthesized as a molecular compound.

We investigated the different effects of cations on the Zintl anions in a series of experiments and were able to detect a strong relationship between the polyanion E_n^{m-} formed and the type of cation used. Small, polarizing cations, in particular Mg^{2+} and complex cations such as M_6X^{10+} (M = Ca, Sr, Ba; X = O) thus favor the formation of highly charged end groups or isolated E^{4-} ions. In contrast, large mononuclear cations preferentially stabilize E–E bonds, whereby the E atoms are less highly charged.[7] According to the Zintl – Klemm concept, semiconductor structures can only be formed in which the polyanions E_n^{m-} follow the $8-N$ rule or the cluster counting rules. There are often several structural solutions for a given composition and valence electron number, however, and then the factors mentioned above also play a part in determining the form of the Zintl anion formed. The influence of cation size in determining the structure of the polyanion type for a given electron number has been little investigated

[*] Prof. Dr. R. Nesper, Dr. F. Zürcher
Laboratorium für Anorganische Chemie, ETH Zurich
Universitätstrasse 6, CH-8092 Zurich (Switzerland)
Fax: +(41) 1-632-1149
E-mail: nesper@inorg.chem.ethz.ch
[**] This work was supported by the Schweizerischen Nationalfonds zur Förderung der wissenschaftlichen Forschung (project no. 20-43228.95).

 © WILEY-VCH Verlag GmbH, D-69451 Weinheim, 1998 1433-7851/98/3723-3314 $ 17.50+.50/0

until now. We have now found a borderline case with Ba_3Ge_4, which shows very clearly just this effect.

Of the binary Ba/Ge phases,[10] only the compounds Ba_2Ge,[11] BaGe,[12] and $BaGe_2$[13] have been characterized to date. Despite several indications for a phase with the composition Ba_3Ge_4,[14] this has not been described in more detail as yet. In contradiction to the published phase diagram,[10] we have now obtained Ba_3Ge_4 from a stoichiometric reaction of the elements between 1120 and 1360 K.[15]

There are two modifications of Ba_3Ge_4:[16] Above 630 K the β-Ba_3Ge_4 phase, isotypic with Ba_3Si_4, is stable, whereas the room-temperature phase α-Ba_3Ge_4 crystallizes in a new structural type.[16, 17] This is admittedly not isotypic with Ba_3Si_4, but it is related to it. According to the observed abrupt changes in volume and enthalpy the phase transition from the α to the β form cannot be second order and thus must be discontinuous. However, by careful warming of single crystals of α-Ba_3Ge_4 on the diffractometer these were converted into single crystals of β-Ba_3Ge_4, which were then measured. Slow cooling led to the reformation of the α form, but the single crystals were completely destroyed. Whereas Ba_3Si_4 contains exclusively isolated Si_4^{6-} butterfly anions (Figure 1a), in addition to the monomer the chainlike cross-linked polymer made up of butterfly anions of Ge_4^{6-} occurs in α-Ba_3Ge_4 (Figure 1b). We attribute this to the size of the Ba^{2+} ions being insufficient to separate the anions far enough from one another and thus stabilize the monomers. The anions are able to approach one another, leading to the polymerization of half of these groups with a simultaneous and considerable anisotropic reduction in volume of the unit cell. An orthorhombic distortion of the unit cell occurs, in which only the Zintl anions in the crystallographic a axis are linked (Figure 1b). The accompanying shortening in length is about 3%, whereas the other two axes remain almost unchanged.

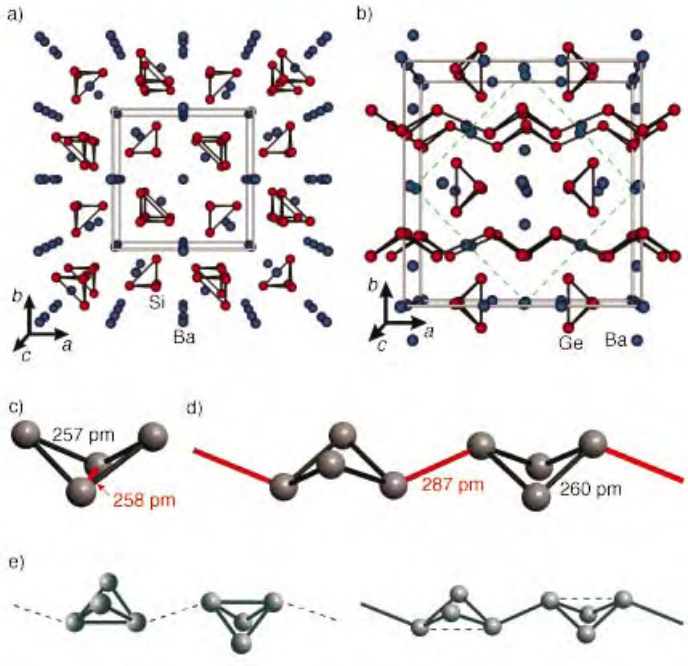


Figure 1. Structures of a) Ba_3Si_4 and b) α-Ba_3Ge_4. The position of the unit cell in (a) is indicated by green lines in (b). c) Isolated butterfly unit. d) Polymeric chain of butterfly anions. e) Geometric relationship between the arrangement of monomeric and polymeric butterfly anions.

The Zintl–Klemm concept is fulfilled by both modifications in different ways: $(Ba^{2+})_6[Ge_4^{6-}]$ $^1_\infty[Ge_4^{6-}]$ satisfies the $8-N$ rule just as does the $(Ba^{2+})_3[Ge_4^{6-}]$ modification made up entirely of monomers. The isolated butterfly anions E_4^{6-} contain two-valent and three-valent species $(2b)E^{2-}$ and $(3b)E^-$ with two or one free electron pair(s), respectively. In the polymer, the intermolecular linkage ($d(Ge{-}Ge)_{inter}$ = 287.4(2) pm) replaces the central intramolecular bond in the butterfly anion ($d(Ge{-}Ge)_{intra}$ = 327.4(3) pm; Figures 1c and 1d). Thus, neither the number of bonds, nor the charges are changed; the two-valent and three-valent germanium species $(2b)Ge^{2-}$ and $(3b)Ge^-$ are not swapped during the polymerization (Figures 1e).

According to experimental and theoretical studies on the neutral bicyclo[1.1.0] systems Si_4R_6 and $E_2C_2R_6$, this intramolecular bond possesses unusual properties even in the monomer. From structural investigations, both species with normal single bond lengths (d(Si–Si) = 237 pm) and those with very long central bonds (d(C–C = 178 pm) are known.[18–20] Results are available from quantum-mechanical calculations on Si_4H_6. Although these are of varying quality, they all confirm a double minimum potential with d_1(Si–Si) = 234 pm and d_2(Si–Si) = 273 pm.[18–20] The latter case is given as being somewhat more stable and corresponds to a singlet diradical, whereby the corresponding intramolecular interaction has significant π character. Because of the energetic proximity of the neighboring minima on the potential hypersurface, this system has been described as an example for bond stretching isomerism.[20, 21]

All E–E distances in the monomers in α-Ba_3Ge_4 and Ba_3Si_4 are approximately equal and correspond to single bonds (d(Si–Si) = 242 pm, $\bar{d}$(Ge–Ge) $\approx$ 259 pm). Longer bonds are found to occur in both modifications of Ba_3Ge_4, however. In the β form the central bond in the monomer (d(Ge–Ge) = 271.2(7) pm) and in the α form the linking bond in the polymer (d(Ge–Ge) = 287.4(2) pm). The latter is admittedly considerably longer than a single bond, but only slightly different from the long bond in the α form. It is also known from other studies on the somewhat shorter Si–Si single bonds that elongations in the distances of up to 280 pm can occur.[22] If the same should be true of the Ge–Ge bonds described here, as was calculated for the Si–Si bonds in the butterfly molecule, then these long bonds would lie in the expected range.

We determined the electronic structures using the extended Hückel (EH)[23] and the LMTO methods,[24] and calculated the electron localization function ELF.[25] The results are shown in Figures 2 and 3. Both methods lead to very similar densities of states with a small (EH, Figure 2a) or almost nonexistent band gap (LMTO, Figure 2b). This is in agreement with the experimental determination by the van der Pauw method (Figure 2c), although we are unable to distinguish between intrinsic and extrinsic conduction behavior. Comparison of the overlap populations (COOP[26]) for the monomers in the α and β phases as well as for the polymer shows that the bonds in question have a strong, a weak, and a very weak Ge(4s) contribution, respectively (Figures 2e–g).

 © WILEY-VCH Verlag GmbH, D-69451 Weinheim, 1998 1433-7851/98/3723-3315 $ 17.50+.50/0

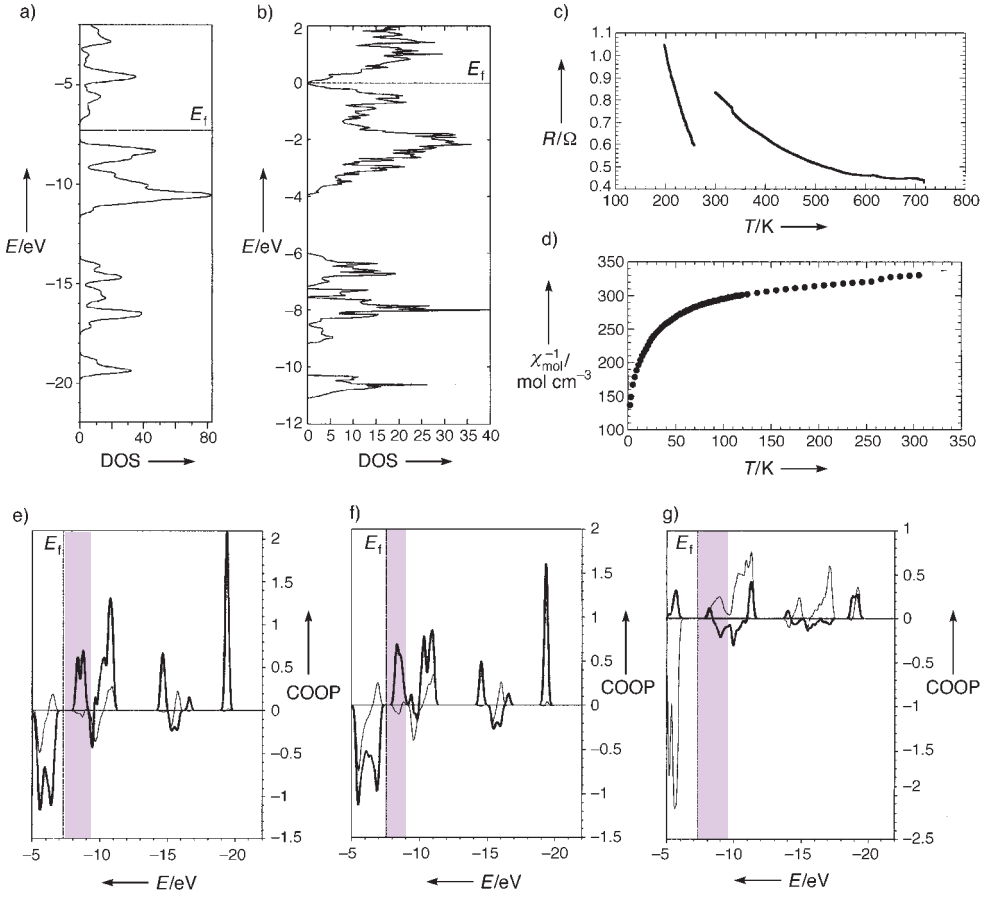


Figure 2. Electronic structure and physical properties of Ba_3Ge_4: a, b) calculated densities of states (DOS); EH (a) and LMTO (b). The DOSs are very similar; as expected, the DOS obtained by the EH calculation has a somewhat larger band gap. c) Temperature dependence of the electrical conductivity according to the four point van der Pauw method; the "band gap" is calculated to about 0.08 eV. The two curves correspond to measurements for two different samples. d) Temperature dependence of the magnetic susceptibility; there is no simple Curie–Weiss dependence. e–g) Overlap populations (COOP) of the intramolecular (thick lines) and intermolecular bonds (thin lines), calculated by the EH method: e) For the isolated anions in α-Ba_3Ge_4 with the relatively short intramolecular Ge–Ge bond (the strong Ge(4s) orbital contribution (population at about −20 eV) is typical for normal σ bonds, the intermolecular interaction is nonbonding). f) For the isolated anions in β-Ba_3Ge_4 with the relatively long intramolecular Ge–Ge bond (here too, the Ge(4s) orbital contribution is in the normal range for σ bonds (population at about −20 eV), the intermolecular interaction is also nonbonding). g) For the polymeric anions in α-Ba_3Ge_4 with the relatively long intermolecular Ge–Ge bond (the Ge(4s) orbital contribution is astonishingly low for σ bonds (population at about −19 eV), in this case the intramolecular interaction is unequivocally nonbonding). The states in the shaded regions were used to calculate the PDEN in Figure 3.

Isosurfaces of the electron localization function (ELF = 0.8) for the monomeric Ge_4^{6-} ions in α- and β-Ba_3Ge_4 are shown in Figures 3a and 3b with one short and one long intramolecular bond, respectively. The extended regions of the free electron pairs on the (2b)Ge atoms are conspicuous; their horse-shoe distributions almost give the impression of a linear part. We know from comparative studies of such highly charged anions that a clear tendency towards sp^2 hybridization occurs, the result of which is a p-type and an sp-type free electron pair. Situations like this have not been considered in the Nyholm–Gillespie rules as yet, and could lead to an extension of the VSEPR theory.[27] This is particularly apparent in the partial electron density (PDEN), which is calculated from the states highlighted in Figure 2e–g close to the Fermi level and shown in Figures 3d–f. The ELF sections through the intermolecular bond in the polymer indicate a weak interaction which results in a double maximum for the EH calculations (Figure 3c). The ELF values from the LMTO calculation are considerably weaker and less extended, partly because the cores can be reproduced better; only one maximum is indicated in this case (Figure 3h). At any rate, it is an interaction which, because of its distance and the strong p-orbital contribution, raises the supposition that a singlet diradical is present. If the ELF is calculated by the LMTO method with an artificially extended Ge–Ge bond of 300 pm, this method also leads to a double maximum on the line connecting the nuclei (Figure 3i). The spatial distribution of these two maxima can be clearly seen in the PDEN in Figure 3f.

We then carried out calculations on a LMTO basis under the assumption of spin polarization, in which in addition to the singlet diradical other radical situations were produced. Surprizingly, all calculations for 0 K converged to a diamagnetic ground state. As the magnetic measurements resulted in a distinct temperature-dependent paramagnetism (Figure 2d), the question still remains as to whether triplet states can occur at higher temperatures, or whether paramagnetic impurities (defects, Nb metal from the wall of the synthesis ampoule) are present. We conclude at any rate that the double maxima in the long bonds indicate an unusual form of the chemical bond and a transition to the diradical form.

Received: July 3, 1998 [Z12089IE]
German version: *Angew. Chem.* **1998**, *110*, 3451–3454

Keywords: electronic structure · electron localization function · solid-state chemistry · Zintl anions

[1] E. Zintl, *Angew. Chem.* **1939**, *52*, 1; E. Zintl, J. Goubeau, W. Dullenkopf, *Z. Phys. Chem. A* **1931**, *154*, 1; *Z. Phys. Chem. B* **1932**, *16*, 183; W. Klemm, *Proc. Chem. Soc. London* **1958**, 329; H. G. von Schnering, *Angew. Chem.* **1981**, *93*, 44; *Angew. Chem. Int. Ed. Engl.* **1981**, *20*, 33; R. Nesper, *Prog. Solid State Chem.* **1990**, *20*, 1.

 © WILEY-VCH Verlag GmbH, D-69451 Weinheim, 1998 1433-7851/98/3723-3316 $ 17.50+.50/0

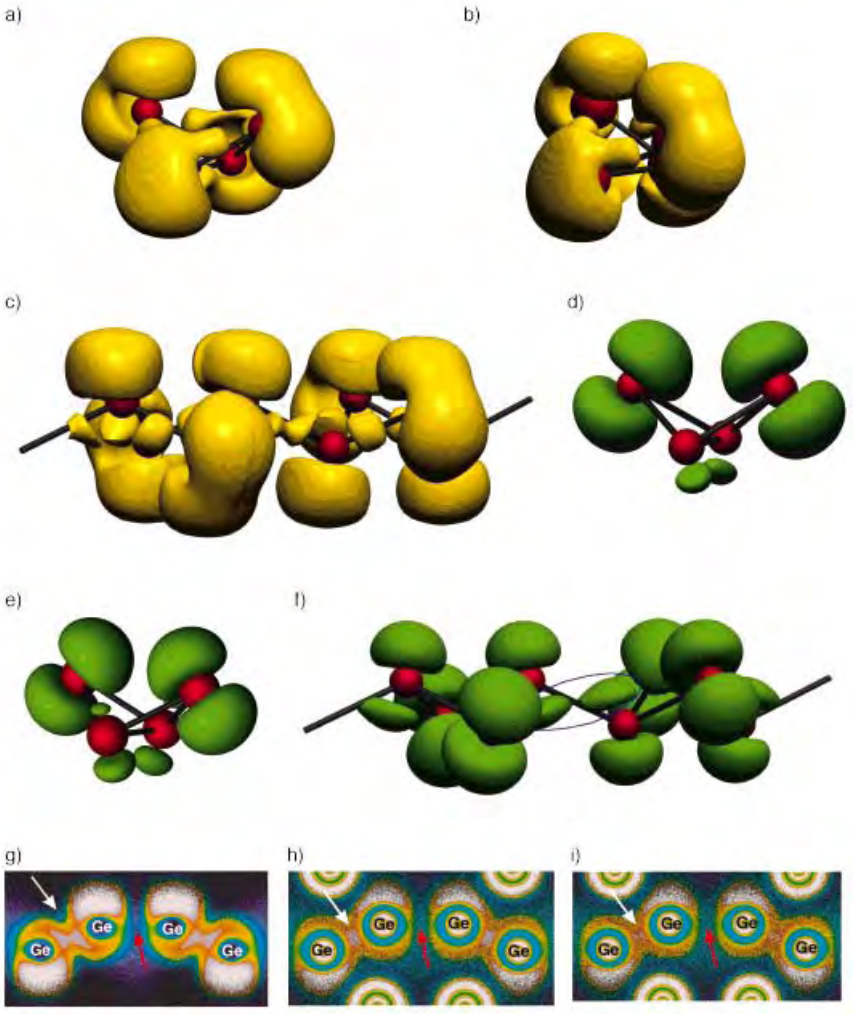


Figure 3. Depiction of the electron localization function ELF for Ba_3Ge_4: three-dimensional ELF isosurfaces (EH; ELF = 0.8): a) For the isolated Ge_4^{6-} in α-Ba_3Ge_4; the spatial requirement of the free electron pairs, with distinct p orbital character on the two-valent Ge atoms, is conspicuous. The central bond can be described as a bridge between the free electron pairs of the three-valent Ge atom. b) For the isolated Ge_4^{6-} in β-Ba_3Ge_4; the general ELF distribution is similar, but the long intramolecular bond is divided into two wedge-shaped pieces, which are attached to the free electron pairs of the three-valent Ge atoms. c) For the polymeric Ge_4^{6-} in α-Ba_3Ge_4; the general ELF distribution is again similar, but instead of the long intramolecular bond, a localization with two maxima between the three-valent Ge atoms occurs. d–f) The corresponding partial densities (PDEN[28]) for states near to the Fermi level for the structural parts in (a–c) show increasing p orbital contributions from (d) to (f) on the (3b) Ge atoms. g–i) Comparison of the ELF from EH and LMTO calculations in two-dimensional sections through the intramolecular (red arrow) and intermolecular bond (white arrow) in the polymer chain of β-Ba_3Ge_4. In all cases, no bonding localization occurs in the corresponding intramolecular region. Whereas the EH calculation (g) for the intermolecular bond clearly leads to two bright localization regions, for the LMTO calculation there is still no separation visible at 278 pm (h). At the extended distance of 300 pm this clearly does occur, however (i).

[2] H. G. von Schnering, *Rheinisch-Westfälische Akademie der Wissenschaften*, lecture N325, p. 7, Westdeutscher Verlag, Opladen **1984**; J. D. Corbett, *Struct. Bonding* **1997**, *87*, 157; H. G. von Schnering, W. Hönle, *Chem. Rev.* **1988**, *88*, 243; B. W. Eichhorn, R. C. Haushalter, *J. Chem. Soc. Chem. Commun.* **1990**, 937; T. F. Fässler, M. Hunziker, *Z. Anorg. Allg. Chem.* **1996**, *622*, 837.

[3] M. Schwarz, Dissertation, Universität Stuttgart, **1987**.

[4] B. Eisenmann, K. H. Janzon, H. Schäfer, A. Weiss, *Z. Naturforsch. B* **1969**, *24*, 457.

[5] A. Currao, J. Curda, R. Nesper, *Z. Anorg. Allg. Chem.* **1996**, *622*, 85.

[6] R. Nesper, A. Currao, S. Wengert in Organosilicon Chemistry II, From Molecules to Materials (Eds.: N. Auner, J. Weis), VCH, Weinheim, **1995**.

[7] S. Wengert, Dissertation no. 12070, ETH Zürich, **1996**.

[8] S. Wengert, A. Currao, R. Nesper, *Chem. Eur. J.* **1998**, *4*, 2244.

[9] N. Wiberg, C. M. Finger, K. Polborn, *Angew. Chem.* **1993**, *105*, 1140; *Angew. Chem. Int. Ed. Engl.* **1993**, *32*, 1054.

[10] T. B. Massalski, *Binary Alloy Phase Diagrams*, 2nd ed., ASM International, **1992**.

[11] K. Turban, H. Schäfer, *Z. Naturforsch. B* **1973**, *28*, 220.

[12] W. Rieger, E. Parthé, *Acta Crystallogr.* **1967**, *22*, 919.

[13] A. Betz, H. Schäfer, A. Weiss, R. Wulf, *Z. Naturforsch. B* **1968**, *23*, 878.

[14] J. Evers, Dissertation, Universität München, **1974**.

[15] Single-phase X-ray samples of α-Ba_3Ge_4 were prepared in a two-stage synthesis. A stoichiometric mixture of the pure elements were initially heated under inert gas in a sealed Nb ampoule for 24 h at 1120 K. The product obtained was finely ground under inert gas, heated for a further 24 h at 1360 K, and then cooled at a rate of 100–500 K h^{-1}. Metastable β-Ba_3Ge_4 at room temperature was not observed at this cooling rate. The compound was obtained in the form of gray, platelike, brittle crystals with a metallic sheen. They are extraordinarily sensitive to air and moisture and decompose in air within a few seconds to give an orange-red powder (presumably GeO). A biting smell was noted.

[16] F. Zürcher, Dissertation, no. 12546, ETH Zürich, **1998**.

[17] α-Ba_3Ge_4 crystallizes with a new structural type (*Cmmm*, $a = 1179.9(6)$, $b = 1221.0(6)$, $c = 1209.7(6)$ pm, $Z = 8$, $R(1083\,F^2(F^2 \geq \sigma(F^2))$, 46 parameters) = 0.031, $R_w(1083\,F^2(F^2 \geq \sigma(F^2))$, 46 parameters) = 0.067, β-Ba_3Ge_4 is stable above 350 °C with Ba_3Si_4 structure ($P4_2/mnm$, $a = 862.1(6)$, $b = 1203.1(8)$ pm, $Z = 4$, $R(310\,F^2(F^2 \geq \sigma(F^2))$, 24 parameters) = 0.054, $R_w(310\,F^2(F^2 \geq \sigma(F^2))$, 24 parameters) = 0.134. Further details on the crystal structure investigation may be obtained from the Fachinformationszentrum Karlsruhe, D-76344 Eggenstein-Leopoldshafen, Germany (fax: (+49) 7247-808-666; e-mail: crysdata@fiz-karlsruhe.de), on quoting the depository numbers CSD-391060 (α-Ba_3Ge_4) and CSD-391061 (β-Ba_3Ge_4).

[18] T. Dabisch, W. W. Schoeller, *J. Chem. Soc. Chem. Commun.* **1986**, 896; W. W. Schoeller, T. Dabisch, T. Busch, *Inorg. Chem.* **1987**, *26*, 4383.

[19] S. Collins, R. Dutler, A. Rauk, *J. Am. Chem. Soc.* **1987**, *109*, 2564.

[20] P. von R. Schleyer, A. F. Sax, J. Kalcher, R. J. Janoschek, *Angew. Chem.* **1987**, *99*, 374; *Angew. Chem. Int. Ed. Engl.* **1987**, *26*, 364.

[21] W.-D. Stohrer, R. Hoffmann, *J. Am. Chem. Soc.* **1972**, *94*, 779.

[22] H. Bock, T. Hauck, C. Näther, N. Rösch, M. Staufer, O. D. Häberlen, *Angew. Chem.* **1995**, *107*, 1439; *Angew. Chem. Int. Ed. Engl.* **1995**, *34*, 1353.

[23] The program EHMACC is based on a computer program by Hoffmann and Lipscomb: R. Hoffmann, W.N. Lipscomb, *J. Chem. Phys.* **1962**, *36*, 2179; M.-H. Whangbo, R. Hoffmann, R.B. Woodward, *Proc. R. Soc. London A* **1979**, *366*, 23; the extended Hückel calculation was carried out without prior charge iterations with the following atomic parameters on the basis of the structural data: Ba: $H_{ii}(6s) = -4.287$ eV, $\varsigma(6s) = 1.236$; $H_{ii}(6p) = -3.036$ eV, $\varsigma(6p) = 1.071$; Ge: $H_{ii}(4s) = -16.0$ eV, $\varsigma(4s) = 2.16$; $H_{ii}(3p) = -9.0$ eV, $\varsigma(3p) = 1.85$.

 © WILEY-VCH Verlag GmbH, D-69451 Weinheim, 1998 1433-7851/98/3723-3317 $ 17.50+.50/0

[24] Program TB-LMTO: M. van Schilfgaarde, T. A. Paxton, O. Jepsen, O. K. Andersen, Max-Planck-Institut für Festkörperforschung, Stuttgart, Germany, Version 4.6, **1994**.
[25] A. D. Becke, K. E. Edgecombe, *J. Chem. Phys.* **1990**, *992*, 5397; A. Savin, R. Nesper, S. Wengert, T. F. Fässler, *Angew. Chem.* **1997**, *109*, 1892; *Angew. Chem. Int. Ed. Engl.* **1997**, *36*, 1808.
[26] R. Hoffmann, *Solids and Surfaces, A Chemists View of Bonding in Extended Structures*, VCH, New York, **1988**.
[27] R. J. Gillespie, *Molecular Geometry*, Van Nostrand Reinhold, London, **1972**.
[28] T. F. Fässler, U. Häussermann, R. Nesper, *Chem. Eur. J.* **1995**, *1*, 625.

The Hydrogen-Bonded Framework of the First Anti-Zeotype: $[\{(H_2NEt_2)_2\}_2(CuCl_4)][AlCl_4]$**

James D. Martin* and Brian R. Leafblad

Zeolites are the archetypal class of porous framework materials whose host–guest interactions have been tailored to a variety of industrial processes such as catalysis and gas separation.[1] Zeolites are constructed from silicate and aluminate building blocks in which the tetrahedral cations are covalently linked by two-coordinate anions (oxygen) into a plethora of micro- and mesoporous frameworks.[2–4] In these systems the size and shape of the pore structure is controlled during synthesis by molecular or cationic templating species. By use of charge-matching techniques, numerous oxide-based framework materials analogous to zeolites have been reported, including frameworks rich in transition metals such as the recently reported cobalt phosphates.[5] We recently demonstrated an extension of such charge-matching techniques to include substitution of framework anions, as well as cations, in the preparation of halozeotypes $[Cu_nZn_{m-n}Cl_{2m}]^{n-}$, which are direct analogues of aluminosilicates.[6] The preparation of other non-oxide zeotype materials has recently been reviewed.[4] Here we describe the first example of an "inverse" charge-matching strategy, by which an anti-zeotype framework structure is constructed from the linkage of tetrahedral anions by two-coordinate cations.

The synthesis of open-framework materials based on principles of structural anti-types, in which the positions of the framework anions and cations are reversed (such as in fluorite, CaF_2, and anti-fluorite structures, Li_2O) has to our knowledge never been reported. Unlike classic zeotype frameworks, in which an anionic or neutral framework is templated by extra-framework cations or molecules, our anti-zeotype constructions, in which tetrahedral anions are linked by two-coordinate cations, can be utilized to prepare cationic frameworks templated by noncoordinating extra-framework anions. Such anion templating is expected to yield both novel open-framework structures and unique properties.[7]

Previously, several metal-organic cationic frameworks have been prepared in which neutral, bidentate ligands link cationic metal centers into covalent networks.[4, 8, 9] However, in these metal-organic frameworks, the cationic metal centers are coordinatively saturated by the two-coordinate linker ligands such that the internal surface of the framework cavity which surrounds the anionic template consists of the neutral ligands. By contrast, in our anti-zeotype constructions, the internal surface of the open-framework voids will be composed of two-coordinate cationic linking units. This cationic surface of the framework void may be exploitable to increase anion-binding affinities.

Because of the utility of hydrogen bonding for the construction of supramolecular assemblies, dialkylammonium cations were examined as potential two-coordinate cations to link $[MCl_4]^{n-}$ tetrahedral anions. In spite of the importance of hydrogen bonding between cations and anions for supramolecular assembly and molecular recognition in biological systems, to date only a small number of organic and metal-organic supramolecular hydrogen-bonded frameworks have been constructed using exclusively ionic components,[7, 10–12] compared with the number of hydrogen-bonded assemblies prepared using neutral molecules as donors and acceptors.[13–16] Nevertheless the strength of interionic hydrogen bonds of around 40–190 kJ mol^{-1}[10] make such ionic constructions attractive for the preparation of more robust framework structures. In this present work, we exploit the hydrogen-bonding ability of dialkylammonium cations to link $[CuCl_4]^{3-}$ tetrahedral anions into the novel anti-zeotype framework $[\{(H_2NEt_2)_2\}_2(CuCl_4)]^+$, in which $[AlCl_4]^-$ anions fill the framework void. This cationic partial structure is shown in Figure 1. Such hydrogen-bonded frameworks are not expected to provide the rigid structures found for covalent zeolite-type frameworks; however, Yaghi et. al. have recently demonstrated microporosity in a framework constructed from hydrogen-bonded metal-organic complexes.[15]

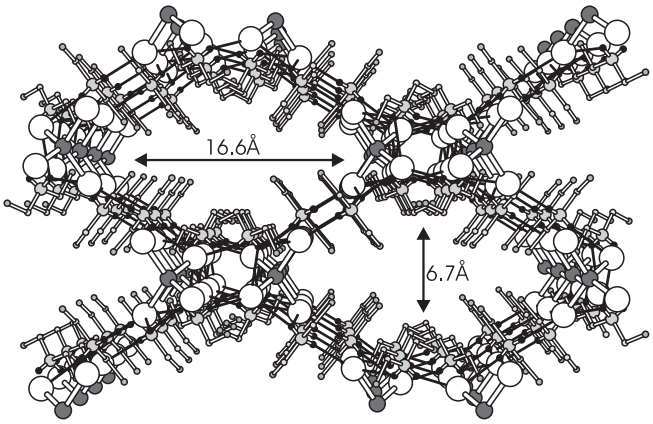


Figure 1. Cationic partial structure of **1**. The hydrogen-bonding contacts are indicated by solid lines. Cl: large open spheres, Cu: large black spheres, N: large gray spheres, C: small gray spheres, H: small black spheres.

[*] Prof. J. D. Martin, B. R. Leafblad
Department of Chemistry
North Carolina State University
Raleigh, NC 27695-8204 (USA)
Fax: (+1) 919-515-5079
E-mail: jdmartin@ncsu.edu

[**] This work was supported by the National Science Foundation, a CAREER award (DMR-9501370), and an instrumentation grant (CHE-9509532). J.D.M. is a Cottrell Scholar of the Research Corporation.

 © WILEY-VCH Verlag GmbH, D-69451 Weinheim, 1998 1433-7851/98/3723-3318 $ 17.50+.50/0

Slow cooling of a melt (250 °C) of CuCl, $AlCl_3$, and H_2NEt_2Cl yielded $[(H_2NEt_2)_4(CuCl_4)][AlCl_4]$ (**1**) as a single-phase, microcrystalline product, as confirmed by Guinier X-ray powder diffraction and elemental analysis. Single crystals suitable for X-ray diffraction studies were obtained from the reaction of CuCl, $AlCl_3$, and wet $HNEt_2$.[17] In the crystal structure, the $[AlCl_4]^-$ tetrahedra exhibit ideal tetrahedral geometry with Al–Cl bond lengths of 2.1322(8) Å, and four Cl-Al-Cl angles of 109.36(4)° and two of 109.69(4)°. The $[CuCl_4]^{3-}$ tetrahedra, however, exhibit a slight tetragonal elongation with a Cu–Cl bond length of 2.3761(7) Å, and two Cl-Cu-Cl angles of 104.82(2)° and four of 119.23(3)°. Interestingly the only short N–H···Cl contacts, indicative of hydrogen bonding, are to the $[CuCl_4]^{3-}$ tetrahedra with Cl···H distances of 2.43–2.61 Å (Cl–N 3.2–3.3 Å). The shortest contacts of the ammonium cations to the aluminum-bound chloride atoms are by the alkyl groups with distances of 3.9 Å between the aluminum-bound chloride and the methyl carbon atoms (Cl–N 4.5 Å). This is consistent with previous reports which indicate that the $[AlCl_4]^-$ ion is a poor hydrogen-bond acceptor due to the highly Lewis acidic Al^{III} center.[18] These same properties make $[AlCl_4]^-$ a noncoordinating anion that is well suited as a framework template.[19]

In the crystal structure of **1,** the dialkylammonium cations demonstrate a pairwise linkage between $[CuCl_4]^{3-}$ tetrahedra (Figure 2). Atom H(2) is hydrogen bonded to a single chloride ion at a distance of 2.43 Å, whereas H(1) is hydrogen bonded

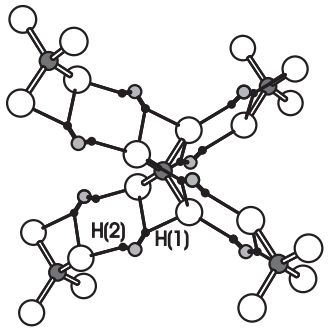


Figure 2. Representation of the $[\{(H_2NEt_2)_2\}_{4/2}(CuCl_4)]^+$ tetrahedral building blocks to highlight the hydrogen bonded connectivity. The ethyl groups have been removed for clarity.

to the edge of a neighboring $[CuCl_4]^{3-}$ tetrahedron with Cl–H distances of 2.54 and 2.61 Å. Nevertheless, each pair of inversion-related diethylammonium cations exclusively connects two tetrahedral anions. Four such pairwise linkages to nearest neighbor tetrahedra result in the $[\{(H_2NEt_2)_2\}_{4/2}(CuCl_4)]^+$ tetrahedral building blocks shown in Figure 2. These tetrahedral units are then assembled into a three-dimensional diamondoid network. For ease of visualization, each linking pair of ammonium cations is replaced by a sphere on the inversion center that relates them, and the $[CuCl_4]^{3-}$ anion is represented by a sphere at the tetrahedral center in Figure 3, so that the "A_2T" ($A = [(H_2NEt_2)_2]^{2+}$, $T = [CuCl_4]^{3-}$) anti-zeotype connectivity is readily apparent. A similar A_2T framework is observed for the structure of Cu_2O; however, in this case two such frameworks interpenetrate.[20]

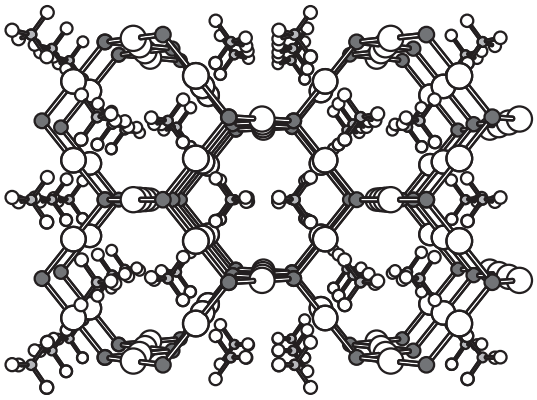


Figure 3. View of the diamondoid lattice of **1** in which the inversion-related pairs of $[H_2NEt_2]^+$ cations are represented as large open spheres and the $[CuCl_4]^{3-}$ anions are represented as dark spheres. The $[AlCl_4]^-$ anions template this hydrogen bonded network.

From this perspective it is clear that the cationic-framework partial structure of $[\{(H_2NEt_2)_2\}_2(CuCl_4)]^+$ adopts the cristobalite-related C9 structure,[21] where the T-A-T angle is required to be 180° because of the pairwise connectivity of the ammonium cations. By contrast, a collapsed C9 structure is observed for cristobalite with a T-O-T angle of approximately 137°. The resulting set of channels, which run through the framework along *a* and *b* exhibit C–C and Cu–Cu cross-channel contacts of 6.7 Å and 16.6 Å, respectively. In **1** the ethyl groups of the dialkylammonium cations, as well as the $[AlCl_4]^-$ anions, stuff and stabilize this expanded C9 structure type in the same fashion that $(t\mathrm{Bu})_2O$ stabilizes the expanded cristobalite-type framework of $Cd(CN)_2$.[22] Numerous other stuffed cristobalite structures are common such as $NaAlO_2$[23] and Na_2BeSiO_4,[24] which also exhibit ionic conductivity through the channel structure.

Experimental Section

All manipulations were performed under an atmosphere of dry nitrogen. $AlCl_3$ was purchased from Fluka and purified by literature procedures.[25] CuCl was prepared from Cu metal and $CuCl_2$ (Aldrich) according to literature methods.[26] H_2NEt_2Cl was dried overnight at 100 °C under vacuum. CuCl (44 mg, 0.447 mmol), $AlCl_3$ (60 mg, 0.447 mmol), and H_2NEt_2Cl (196 mg, 1.789 mmol) were mixed and added to a Pyrex ampoule, which was then evacuated and sealed. The reaction tube was heated to 250 °C for 12 h, and then cooled to room temperature at a rate of 10° h^{-1}. At room temperature a molten salt was produced which crystallized over a period of several days. Elemental analysis of the crystalline samples: calcd for $C_{16}H_{48}N_4AlCl_8Cu$: C 28.64, H 7.23, N 8.35; found: C 27.55, H 7.24, N 7.96.

Received: June 3, 1998 [Z11938IE]
German version: *Angew. Chem.* **1998**, *110*, 3511–3513

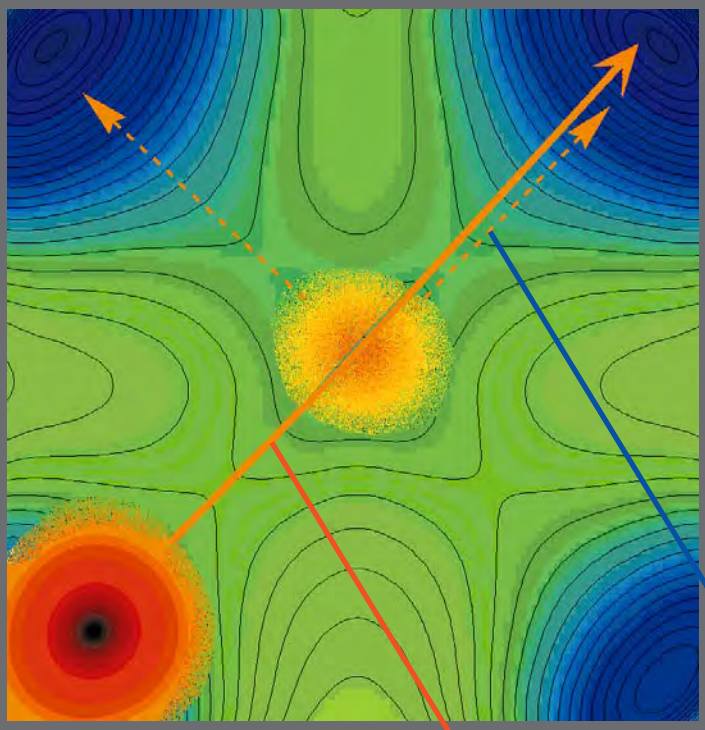
Keywords: clathrates · crystal engineering · hydrogen bonds · template synthesis · zeolite analogues

[1] D. W. Breck, *Zeolite Molecular Sieves*, Wiley, New York, **1974**.
[2] R. Szostak, *Handbook of Molecular Sieves*, Van Nostrand Reinhold, New York, **1992**.
[3] A. Corma, *Chem. Rev.* **1997**, *97*, 2373–2419.
[4] C. L. Bowes, G. A. Ozin, *Adv. Mater.* **1996**, *8*, 13–28.
[5] P. Feng, X. Bu, G. D. Stucky, *Nature* **1997**, *388*, 735–741.

 © WILEY-VCH Verlag GmbH, D-69451 Weinheim, 1998 1433-7851/98/3723-3319 $ 17.50+.50/0

[6] J. D. Martin, K. B. Greenwood, *Angew. Chem.* **1997**, *109*, 2162 – 2166; *Angew. Chem. Int. Ed. Engl.* **1997**, *36*, 2072 – 2075.
[7] J.-M. Lehn, *Supramolecular Chemistry: Concepts and Perspectives*, VCH, Weinheim, **1995**, pp. 31 – 35.
[8] B. B. Gardner, D. Venkataraman, J. S. Moore, S. Lee, *Nature* **1995**, *374*, 792 – 795.
[9] O. M. Yaghi, L. Hailian, T. L. Groy, *Inorg. Chem.* **1994**, *36*, 4292 – 4293.
[10] C. B. Aakeröy, K. R. Seddon, *Chem. Soc. Rev.* **1993**, 397 – 407.
[11] M. C. T. Fyfe, P. T. Glink, S. Menzer, J. F. Stoddart, A. J. P. White, D. J. Williams, *Angew. Chem.* **1997**, *109*, 2158 – 2160; *Angew. Chem. Int. Ed. Engl.* **1997**, *36*, 2068 – 2070.
[12] a) V. A. Russell, C. C. Evans, W. Li, M. D. Ward, *Science* **1997**, *276*, 575 – 579; b) V. A. Russell, M. D. Ward, *Acta Crystallogr. Sect. B* **1996**, *52*, 209 – 214.
[13] *Chem. Mater.* **1994**, *6* (special issue: *Structure and Chemistry of the Organic Solid State*).
[14] M. J. Zaworotko, *Chem. Soc. Rev.* **1994**, 283 – 288.
[15] O. M. Yaghi, H. Li, T. L. Groy, *J. Am. Chem. Soc.* **1996**, *118*, 9096 – 9101.
[16] S. B. Copp, K. T. Holman, J. O. S. Sangster, S. Subramanian, M. J. Zaworotko, *J. Chem. Soc. Dalton Trans.* **1995**, 2233 – 2243.
[17] Single crystal X-ray data of 1 ($C_{16}H_{48}AlCl_8CuN_4$) were collected at 298 K on an Enraf-Nonius CAD-4 diffractometer equipped with a $Mo_{K\alpha}$ source and a graphite monochrometer. The colorless crystals ($0.3 \times 0.3 \times 0.1$ mm) exhibited tetrahedral symmetry, space group $I4_1/a$ (no. 88), $a = 12.8059(4)$, $c = 20.434(2)$ Å, $V = 3351.0(3)$ Å^3, $Z = 4$, $\rho_{calcd} = 1.33\ g\,cm^{-1}$, $\mu(Mo_{K\alpha}) = 1.34\ cm^{-1}$. A total of 3929 unique intensities with $2\theta < 54^\circ$ were collected with a $\theta - 2\theta$ scan mode. Full-matrix least-squares calculations, based on F, of the 1284 observed unique reflections with $I_{net} > 1.0\sigma(I)$ and 117 variables were performed with the NRCVAX software package. All hydrogen atoms were located, and their positions refined. The structure was refined to a final model with $R = 0.039$ and $R_w = 0.046$. Crystallographic data (excluding structure factors) for the structure reported in this paper have been deposited with the Cambridge Crystallographic Data Centre as supplementary publication no. CCD-101662. Copies of the data can be obtained free of charge on application to CCDC, 12 Union Road, Cambridge CB2 1EZ, UK (fax: (+44) 1223-336-033; email: deposit@ccdc.cam.ac.uk).
[18] M. V. Gaudet, M. J. Zaworotko, P. S. White, *Inorg. Chem.* **1989**, *28*, 1191 – 1193.
[19] The $[AlCl_4]^-$ anion is reasonably considered a template for the structure of **1** since in its absence, $CuCl + 4(H_2NEt_2)Cl$ yields $[H_2NEt_2]Cu_2Cl_3 + 3(H_2NEt_2)Cl$; J. Yang, J. D. Martin, unpublished results.
[20] P. Niggli, *Z. Kristallogr.* **1922**, *57*, 2359.
[21] M. O'Keeffe, B. G. Hyde, *Acta Crystallogr. Sect B* **1976**, *32*, 2923 – 2936.
[22] T. Kitazawa, T. Kikuyama, M. Takeda, T. Iwamoto, *J. Chem. Soc. Dalton Trans.* **1995**, 3715 – 3720.
[23] J. A. Kaduk, S.-Y. Pei, *J. Solid State Chem.* **1995**, *115*, 126.
[24] S. Frostang, J. Grins, D. Loueer, P. E. Werner, *Solid State Ionics* **1988**, *31*, 131 – 138.
[25] a) J. S. Wilkes, J. A. Levisky, R. A. Wilson, C. L. Hussey, *Inorg. Chem.* **1982**, *21*, 1263 – 1267; b) R. J. Gale, R. A. Osteryoung in *Molten Salt Techniques* (Eds.: D. G. Lovering, R. J. Gale), Plenum, New York, **1983**, chap. 3.
[26] G. B. Kauffman, L. Y. Fang, *Inorg. Synth.* **1983**, *22*, 101.

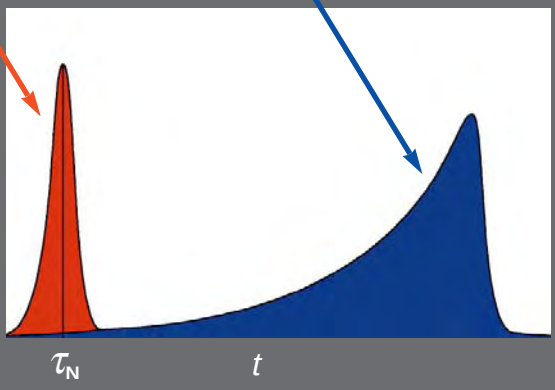
 © WILEY-VCH Verlag GmbH, D-69451 Weinheim, 1998 1433-7851/98/3723-3320 $ 17.50+.50/0



MD simulations suggest that thermally generated intermediates sometimes undergo rapid reactions along "direct" trajectories, which may pass through or near the intermediate region on the potential energy surface, but are not influenced by the symmetry of the underlying energy surface. Such reactions are wrongly assigned as concerted.

ANGEWANDTE CHEMIE © WILEY-VCH

The bimodal distribution of lifetimes t for the intermediate that will result when direct and statistical trajectories coexist can be probed by experiments conducted in supercritical fluids. Studies of this type can lead to experimental estimates for the lifetime τ_N of the nonstatistical population of intermediates, which can be compared directly with MD simulation results.



Dynamic Behavior of Organic Reactive Intermediates

Barry K. Carpenter*

Although organic chemists have traditionally relied on the so-called statistical models of kinetics, notably transition state theory (TST) and its microcanonical analogue, RRKM theory, to interpret their experiments, research conducted over the last few years has revealed that these models may be inadequate to describe the behavior of reactive intermediates generated in the course of normal, organic chemistry experiments. This review summarizes recent theoretical and experimental results, primarily from the author's laboratory, of studies that have concentrated on circumstances where the deviation from TST behavior is particularly marked. These are reactions involving high-potential energy intermediates that are capable of leading to more than one product.

Keywords: computer chemistry · diradicals · kinetics · molecular dynamics · supercritical fluids

1. Introduction

Research conducted over the last few years[1] has revealed that two of the statistical kinetic models intensively used—namely transition state theory[2] (TST) and its microcanonical analogue, RRKM theory[3]—by organic chemists to describe the behavior of reactive intermediates may be inadequate. It is a central feature of these models—indeed it is what makes them statistical models—that the redistribution of excess kinetic energy within molecules (principally vibrational energy) be assumed to occur much faster than chemical events, namely bond cleavage or formation. A corollorary to this assumption is that preparation of a set of molecules with a nonstatistical distribution of kinetic energy, say localized in a particular normal mode of vibration, should have no effect on the rate of reaction when compared to the reference rate for molecules with the same amount of energy statistically distributed. This is because the presumed fast redistribution would make the nonstatistical population into a statistical population before reaction could occur. The near universal failure of early experiments that were designed to divert the course of a thermal reaction by excitation of particular vibrational modes of the reactant with an infrared laser[4] led many people to the conclusion that the statistical approximation is a good one.

Researchers in the chemical physics community who are knowledgeable about the limitations of the statistical approximation might, if asked, have offered warnings about applying it to multistep reactions, especially those that involve intermediates with high potential energy. Nevertheless, most organic chemists have relied on kinetic models, TST or RRKM theory, that are based on the statistical approximation to analyze just such reactions. This review presents some reasons for thinking that incautious use of the statistical kinetic models might have led to a misinterpretation of some organic reaction mechanisms.

[*] Prof. B. K. Carpenter
Department of Chemistry, Baker Laboratory
Cornell University, Ithaca, NY 14853–1301 (USA)
Fax: (+1) 607-255-4137
E-mail: bkc1@cornell.edu

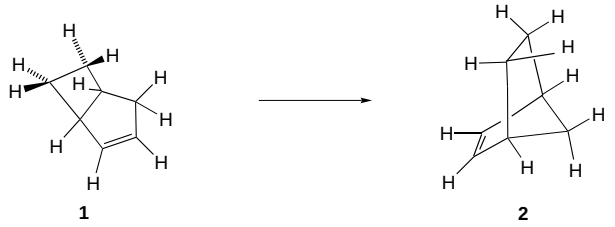
2. Direct Trajectories

A moment's thought can cause one to question the universal applicability of the statistical approximation. The physical mechanisms by which redistribution of vibrational energy and (unimolecular) chemical reaction occur are not very different. If a chemical event—bond cleavage or formation—were to take place within the period of a few molecular vibrations, it would necessarily occur on a timescale comparable to, or perhaps even faster than, redistribution of vibrational energy. The organic chemist's chemical intuition may lead him or her to conclude that for a reaction to be that fast it would either have to be essentially barrierless, or the reacting molecule would have to have excess energy far above the threshold value. However, such intuitive deductions merely serve to show how deeply entrenched the statistical models are in our thinking. Through association of the rates of reaction only with barrier heights and total energy content of the reacting molecules one has implicitly accepted the statistical approximation. Molecular dynamics simulations

 © WILEY-VCH Verlag GmbH, D-69451 Weinheim, 1998 1433-7851/98/3720-3341 $ 17.50+.50/0

suggest that molecules can undergo very fast reactions even when there is a significant energy barrier, and when the total energy is only slightly above the threshold for crossing that barrier.[5a]

A striking example of this behavior occurred in a simulation of the nominal [1,3] sigmatropic rearrangement that interconverted bicyclo[3.2.0]hept-2-ene (**1**) and bicyclo[2.2.1]hept-2-ene (norbornene, **2**).[5b,c] This reaction was studied by the so-called direct dynamics technique, in which the calculation of



1 **2**

the molecular potential energy, and the derivatives of that quantity with respect to all geometrical coordinates, are calculated "on the fly" for each trajectory as it evolves.[6] This technique has the great advantage of circumventing the extremely difficult procedure of mapping out the full potential energy surface (PES) for a reaction. Its biggest disadvantage is that it necessarily requires some relatively fast method for computing the potential energy and its derivatives. Typically, that means high-level ab initio calculations cannot be used, at least for molecules of a size of interest to organic chemists. In the present case of **1**→**2** the AM1[7] and PM3[8] semiempirical molecular orbital methods were employed.[9]

As revealed in the potential energy profile shown in Figure 1, the two models agree that the reaction occurs in a nonconcerted fashion via the biradical **3**, which is situated at a local minimum on the PES. However, the methods disagree about the depth of the potential-energy well that corresponds to **3**. At this point one must confront the fact that the fast semiempirical models, which make the direct dynamics simulation feasible, may not be giving accurate descriptions of the underlying PES. However, rather than enter the contentious debate about the reliability of semiempirical molecular orbital methods, I would prefer simply to ask "What if..?" What if the reaction did involve an intermediate

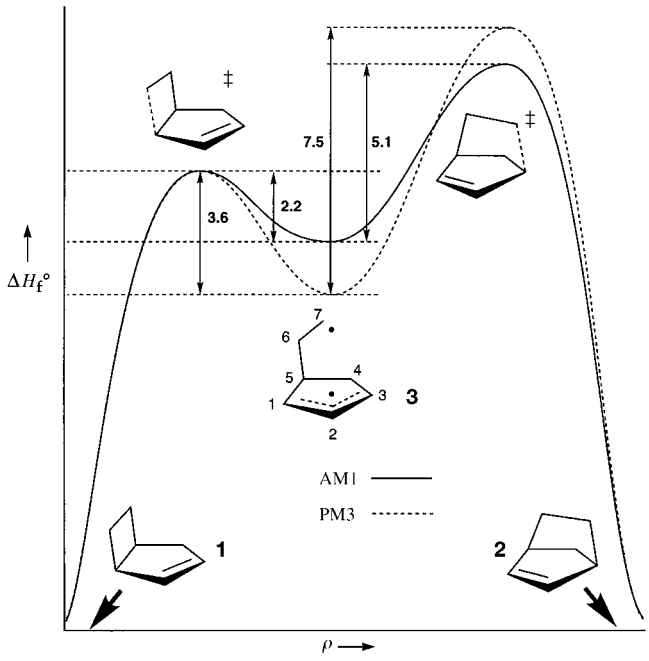


Figure 1. Variation in the enthalpy of the reaction Δ_f^0 in kcal mol^{-1} along the reaction coordinate ρ for the interconversion of **1** and **2**, according to AM1 and PM3 semiempirical molecular orbital calculations.

biradical; what evidence for its existence might one expect to see experimentally?

An answer might come from studying the stereochemistry of the reaction at the migrating carbon atom. If the barrier to internal rotation about the C6–C7 bond were smaller than the barrier to bond formation in the biradical (and both AM1 and PM3 claim that it is) then one might expect to see considerable loss of stereochemical integrity. If there were any stereoselectivity at all, one would expect it to correspond to retention of configuration, since, in a standard kinetic analysis, whatever stereoselectivity there may be could arise only from a failure of the biradicals to reach equilibrium among the rotamers prior to reaction. The experimental fact, first revealed in the classic experiments of Berson and Nelson[10] on an acetoxy derivative of **1**, is that there is a strong preference for inversion of configuration at the migrating carbon atom. Later studies with just deuterium labels revealed a somewhat lower stereoselectivity, but still with inversion preferred.[11] The latter experiments also



Barry K. Carpenter was born on February 13 1949 in Hastings, UK. He completed his B. Sc in Molecular Sciences at Warwick University (1970) before moving to the University College London where he completed his Ph D in organic chemistry in 1973. Between 1973–75 he was a NATO postdoctoral fellow with J. A. Berson at Yale University. Since 1975 he has been in the Department of Chemistry at Cornell University, first as an Assistant Professor (1975–1981), then as an Associate Professor (1981–1985), and since 1985 as Professor. Outside of research and teaching he has been a consultant to many companies, and has participated in many capacities in the organization of journals and conferences. He has received a number of awards which include: Elected Fellow of the American Association for Advancement of Science (1989), Alexander von Humboldt Senior Scientist Award (1990), ACS Cope Scholar Award (1997). His research interests are all in the field of reaction mechanisms.

revealed that the stereoselectivity appeared to exhibit a strange temperature dependence: 76:24 inversion:retention at 276 °C[11a] but 89:11 at 312 °C.[11b] Rarely do reactions show higher stereoselectivity at higher temperature. A possible explanation for this observation will be presented below.

Since the preference for inversion seems inexplicable by the biradical mechanism, and since inversion of configuration is exactly what the Woodward–Hoffmann rules predict for a concerted pericyclic mechanism,[12] there would appear to be persuasive evidence that, as feared, the semiempirical models are giving an incorrect description of the PES, and that the reaction is really a concerted process that involves no biradical intermediate at all.

Nevertheless, we decided to run molecular dynamics (MD) simulations on the AM1 and PM3 surfaces. The procedure involved starting the trajectories in the vicinity of the higher transition structure, allowing them to pass throught the region of the biradical, and then checking to see whether they crossed the lower barrier. This actually corresponds to running the reaction backwards from the way that it goes in reality, but microscopic reversibility allows one to draw useful conclusions anyway. Kinetic energy was supplied in a quantized fashion to the normal modes of the starting structures, with every mode having at least zero-point energy, and some (the lower frequency ones) having higher vibrational excitation. The distribution of energy was chosen to represent a sample from a population at a temperature of 300 °C. It was only feasible to run 100 trajectories on each surface because the calculations are very computationally intensive. This is not a large enough number to represent a statistically valid sample from which quantitative conclusions could be drawn. Nevertheless, the qualitative results were quite informative.

Four of the trajectories run on the PM3 surface passed through the region of the biradical intermediate and formed the closed-shell bicyclo[3.2.0]heptene in about 250–300 fs. The other 96 approached the geometry of the transition structure for C–C bond formation, but did not cross the barrier, and appeared instead to remained "trapped" in the region of the biradical. The feature that differentiated the molecules that reacted promptly from those that became trapped at the intermediate was not the total available energy—several of the "trapped" molecules actually had higher total energies than those that reacted promptly. The proportion of molecules that reacted rapidly was greater on the AM1 surface, with 10 of the 100 trajectories showing this behavior. Some of the trajectories of the trapped species were followed for 2 ps. On neither the AM1 nor the PM3 surface did any of them exit to a closed-shell product.

If one assumes that the "trapped" trajectories correspond to molecules for which the statistical approximation would work reasonably well then one can estimate their lifetimes in the region of the local minimum by RRKM calculation.[3] The results are summarized in Figure 2, where the lifetime of each trajectory in the region of the biradical is summarized in two histograms, one for the PM3 surface and one for the AM1 surface. On average, the molecules that reacted promptly underwent C–C bond formation about 300 times faster than the RRKM model estimates should have been possible.

But there was another feature of the rapidly reacting molecules that was at least as remarkable as their short sojourn in the region of the intermediate: all of them underwent C–C bond formation with a stereochemistry that corresponded to an inversion of configuration at the migating carbon atom. It seems reasonable to assume that the trapped trajectories would lose their "memory" of how they entered the region of the biradical and so would eventually exit to the products in a way that reflected the symmetry of the potential energy surface—that is, with a 50:50 probability of selecting the exits that corresponded to retention or inversion. However, this symmetry was apparently not "seen" by the promptly reacting molecules.

The claimed existence of the promptly reacting molecules, following what I will call from now on *direct trajectories*,[13] is clearly the feature of this dynamics simulation that distinguishes it from the predictions of any statistical model. The fact that the direct trajectories correspond to nonstatistical behavior is confirmed both by their brief duration and by their failure to conform to the symmetry of the underlying PES. But, these are symptoms of nonstatistical behavior; what is its cause?

If it is not total energy that distinguishes direct, nonstatistical trajectories from the trapped, statistical ones, it must be the distribution of the available energy among the

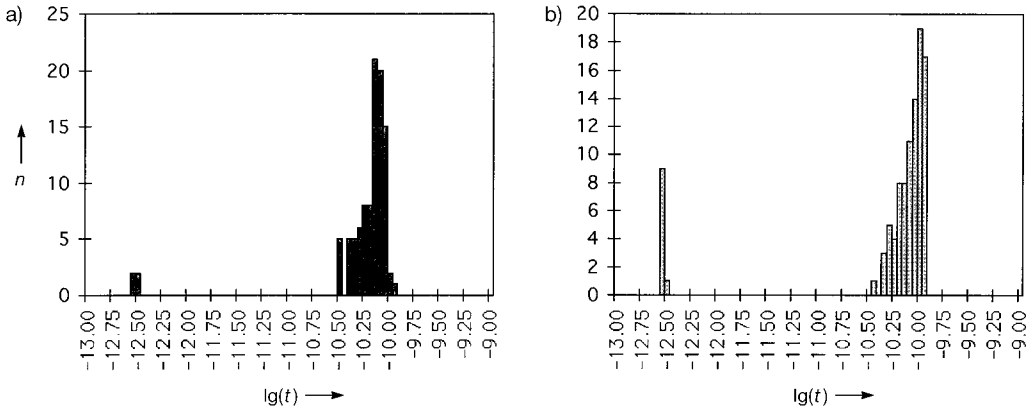


Figure 2. Lifetime (t, in seconds) distributions for the biradical **3** from a) PM3 and b) AM1 dynamic simulations. n = number of trajectories. See text for further discussion.

vibrational modes of the molecule. Indeed, inspection of the direct trajectories reveals that to be true. All of them had a distribution of vibrational energy that caused internal rotation about the C–C bond to the migrating carbon atom at about the same rate, and all with the same sense. Remarkably, the sense of this internal rotation had been deduced by Berson and Nelson from cleverly designed experiments back in 1970.[14] The promptly reacting molecules in our simulation behaved as if they had read the 1970 paper![*] In order to understand what these molecules are doing it is useful to remind ourselves of what would happen if the statistical approximation really were valid throughout the course of the reaction.

3. The Statistical Models

The RRKM picture of a thermal unimolecular reaction[3] is that molecules become energized by collisions, and that eventually a few will have enough total energy to cross the barrier to reaction. However, while possession of total energy above the threshold value is a necessary condition for reaction, it is not a sufficient one. The excess energy must be localized in the set of atomic motions that we call the reaction coordinate if chemical transformation is to occur. Thus, within the small set of molecules that possess sufficient total energy to react is an even smaller subset that has the energy localized in the right vibrational modes to cross the barrier. One could think of the transition–structure region on the potential energy surface as acting like a phase–space[15] filter that allows through only those few molecules that meet certain well-defined conditions. In the RRKM picture one can identify the conditions for passage through this filter and compute the fraction of molecules that meet the conditions by relatively straightforward statistical methods. For reactions in which the barrier height is much greater than kT, this model seems to work very well. However, it is not yet a complete description of what we are interested in. We have only considered crossing the first barrier. If we have defined our reaction to be one that involves an intermediate there must, by definition, be another barrier to be crossed before the reaction is complete. It is in the second step that dynamically interesting things can happen.

4. Dynamic Matching

At first sight there may be no obvious reason why crossing the second barrier would be any different from crossing the first. However, a little more thought allows one to recognize that the reactant molecules for this second step have rather different characteristics from those for the first step. Most importantly, they belong to the elite group that was allowed to pass through the first phase–space filter. In other words they must, at the moment they first attain the geometry of the intermediate, have a rather specialized distribution of their internal energy. Of course, if the statistical models were universally applicable, this special initial distribution of internal energy would have no consequence, because the information that it represented (essentially a history of formation of the intermediate) would be lost before the second reaction occurred. However, this is the point at which the statistical approximation can fail. For the original reactant molecules, which are energized far above their lowest vibrational states, the assumption of very rapid intramolecular redistribution of energy is probably a good one, because many of the vibrational modes will act quite anharmonically, and anharmonicity serves to transfer energy between vibrational modes. However, for a thermally generated intermediate of high potential energy most of the vibrational energy has been drained out of nonreactive modes in order to energize the reactant coordinate for its formation, and so the nonreactive modes can be expected to exhibit near harmonic behavior and consequent weak intermode coupling. Furthermore, the density of vibrational states of the nonreactive modes will typically be much lower than for a highly energized "normal" reactant, and this too can be expected to reduce the rates of energy redistribution.[3g]

If the statistical approximation did apply to the intermediate the small amount of excess vibrational energy that it possessed would become statistically scrambled among the accessible modes. One would then have to wait for sufficient kinetic energy to accumulate in the reaction coordinate for crossing the second barrier before the chemical transformation could be completed. This waiting period is the principal contributor to the lifetime of the intermediate, according to the statistical models. If, on the other hand, the statistical approximation did not apply one could conceive of a situation in which some of the newly created intermediates would find that they already possessed sufficient energy in the second reaction coordinate to sail right on over the second barrier. Those that satisfied this condition would exhibit lifetimes for the intermediate that would be much shorter than the statistical models could understand, since the reacting molecules would have bypassed the scrambling and relocalization of internal energy that such models assume to be necessary.

In order for the hypothesized nonstatistical behavior to occur it is clear that the reaction coordinate for crossing the first barrier must involve similar atomic motions to that for crossing the second. Under such circumstances there can exist efficient "dynamic matching"[5a] between the entrance and exit to the region of the local minimum in the PES that corresponds to the intermediate. In other words, reacting molecules can follow direct trajectories over the first barrier, through the region of the intermediate, and over the second barrier without experiencing the kind of redistribution of internal energy that unthinking application of the statistical kinetic models would seem to require. However, not all molecules can be expected to show such behavior in a thermal reaction. Although the first transition–structure region acts as a quite selective filter, it is not selective down to a single state. There may be molecules in many different states—which differ, for example, in the phase angles between the nonreactive modes—that would be granted entrance to the

[*] An animation of a direct and a trapped trajectory is found under http://www.chem.cornell.edu/~bkc1/dynamics.html.

intermediate. A mode that is effectively nonreactive for the first reaction coordinate may be of more importance for the second one, and so not all molecules admitted to the intermediate region may be allowed to exit on the first attempt. If the local minimum has any significant depth it is unlikely that those molecules that fail to make it out on the first try will succeed in doing so on the second. They will become the "trapped" species that the statistical models assumed should be representative of all reacting molecules. They will indeed have to redistribute their internal energy and wait for it to become localized in the second reaction coordinate.

The fraction of molecules that follow direct trajectories will be determined in large measure by the strength with which the dynamics for entrance to and exit from the region of the intermediate are coupled. In simple cases we have shown that the strength of coupling can be estimated by a vectorial analysis.[16] In more complex cases it has so far proven hard to make that estimate without doing a full dynamic simulation. However, one thing is clear: if there are several entrances to and exits from the region of the intermediate on the PES it is quite unlikely that a particular entrance will be dynamically coupled with equal strength to all exits, even when the symmetry properties of the PES would appear to make the exits equivalent. As shown in the simple contour plot of Figure 3 the vertical mirror plane that makes the two

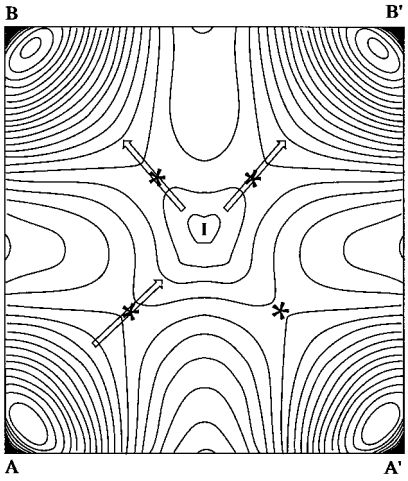


Figure 3. Contour plot of an arbitrary twofold-symmetric PES with a symmetrical intermediate. The reactants are **A** and **A′**, the products **B** and **B′**, and the transition structures are indicated by *. The arrow pointing towards the intermediate **I** symbolizes the reaction coordinate for its formation. The other two arrows symbolize the reaction coordinates for conversion of the intermediate into the products.

transition structures equivalent by symmetry for exit from the intermediate is not "seen" by direct trajectories that enter from just one reactant. If one thinks of the reaction coordinates for passage over each transition structure as simple vectors then it is apparent that the entrance vector makes very different angles with the two exit vectors. This is the reason why the direct trajectories in our simulation of the nominal [1,3] sigmatropic rearrangement did not lead to the two stereoisomeric products with equal probability. Only those trajectories that roll around the intermediate region for some time—the statistical trajectories—can be expected to take the two exits with equal probability.

It seems likely that the higher proportion of direct trajectories found on the AM1 surface for the [1,3] shift is related to the fact that the intermediate PE well is shallower on that surface than on the PM3 one. It is in the nature of the topology of smooth surfaces that shallower minima tend to have "wider" exit channels. This means that the second phase–space filter becomes looser in its acceptance criteria as the local minimum becomes shallower, and so there is a higher probability that molecules will be able to traverse entrance and exit barriers in a single pass.

While it could not be hoped that the MD simulations could reproduce quantitative experimental data—the semiempirical PE surfaces are too unreliable for that—one might be concerned that the small proportions of direct trajectories seen in the simulations do not seem even qualitatively consistent with the experimental stereoselectivities. However, there is an experimental fact about the rearrangement of compound **1** that has not yet been mentioned. Only about 1–2% of the product is **2**. The remaining 98–99% is cyclopentadiene plus DHC=CHD. Some of these products arise from retro-Diels–Alder decomposition of the product, but if the [1,3] rearrangement really did involve biradical **3** one could expect that some of the fragmentation products could come directly from it too. In fact, a recent femtosecond spectroscopy study has been interpreted as providing experimental evidence for just such a reaction of biradical **3**,[17] although it should be pointed out that the biradical in that case was generated photochemically and consequently had much higher excess internal energy than one would expect for the thermally generated intermediate.

No direct trajectories for fragmentation were seen in the simulations. While this negative result might be attributed to the small sample of trajectories and/or the poor quality of the molecular orbital methods employed, another explanation seems plausible. Fragmentation of **3** presumably requires excitation of modes with C5–C6 stretching components. There is no obvious reason why such modes should contribute significantly to the formation of **3** (in fact, Horn et al.[17] postulate that excitation of this stretch will lead to concerted retro-Diels–Alder fragmentation of norbornene, bypassing **3** altogether) and so dynamic matching between the formation of **3** and its fragmentation is expected to be weak; in other words there should be very few direct trajectories for such a reaction. In the biradical model of the reaction the only source of the rearrangement product with retention of configuration is the statistical population of **3**, and so reducing the contribution from this population, by bleeding it off in a fragmentation reaction, will increase the overall stereoselectivity. Furthermore, if the population of **3** that leads to fragmentation and to the component of **2** that has retained stereochemical configuration really is well described by statistical models, then one would be justified in using TST to analyze the temperature dependence of this competition. The fragmentation of **3** presumably would have a positive activation entropy, whereas the ring closure of **3** to **2** would presumably have a negative one. Consequently, raising the

temperature can be expected to increase the proportion of fragmentation, and hence increase the proportion of inversion in **2**. Perhaps this is the source of the unusual temperature dependence of the stereoselectivity that was cited earlier.

5. Stepwise and Concerted Reactions

For decades chemists, especially physical organic chemists, have concerned themselves with distinguishing stepwise from concerted reactions.[18] While there are undoubtedly some reactions that fall neatly into one category or the other, for many reactions the distinction is meaningless. In an earlier review[1] classes of PES were described for which it was not possible to determine whether a local minimum should or should not be called an intermediate in a particular reaction. Here the focus will be on another phenomenon that serves to make the mechanistic distinction moot.

Suppose for the moment that the results of the simulations on the [1,3] shift were qualitatively correct—the reaction really did occur with two dynamically distinct populations of a biradical intermediate. How would such a result be interpreted within the framework of a statistical kinetic model such as TST? The population that gave the two products with equal probability, and involved a relatively long-lived intermediate, would appear to be a "stepwise" component to the reaction. The population that gave just one product and involved something that, if it were an intermediate at all, lasted only for a few molecular vibrations, could well be assigned to the "concerted" category (an assignment bolstered in this case by the coincidental agreement of the observed major product with that predicted by the Woodward–Hoffmann rules[12]). However, concerted reactions are supposed to occur on a part of the PES where there is no local minimum that corresponds to an intermediate; the direct trajectories in the simulations all passed through exactly the same local minimum in which the statistical trajectories became trapped. Rather than there being two different mechanisms, stepwise and concerted, which occur on different parts of the PES, the simulation suggested that there are two different dynamic populations that occupy the same region of the PES.

This phenomenon, if generally applicable, would serve to resolve a long-standing problem. For many supposedly concerted reactions thermochemical estimates of the enthalpy barrier to the alternative stepwise reaction reveal little or no "energy benefit of concert."[19] This apparently coincidental equality of activation barriers for the two supposedly different mechanisms is revealed, in the present interpretation, not to be a coincidence at all, since the two "mechanisms" occur in the same region of the PES.

6. Dynamic Matching versus Barrier Height: Cyclopropane Stereomutation

One of the characteristics of molecules that follow direct trajectories is that they need not conform to the symmetry of the PES in the way that we have come to expect. Thus it is theoretically possible (and, perhaps, experimentally observed in reactions such as the vinylcyclopropane rearrangement[20]) for an optically active reactant to pass through an intermediate with an achiral minimum-energy structure and yet still give optically active products.

An even more stringent test would be to examine reactions for which the exit channel that experiences the best dynamic match to the entrance has a higher barrier to product formation than others that are only weakly dynamically coupled. TST on such a surface would make the clear prediction that the product corresponding to the lowest (free energy) barrier should be kinetically favored. Nonstatistical dynamics might give the preference to a higher barrier channel! It appears that cyclopropane stereomutation occurs on a PES for which such effects might come into play.

The stereomutation (interconversion of optical isomers and *cis*/*trans* isomers) of substituted cyclopropanes is an apparently simple reaction for which there are hidden mechanistic subtleties. Perhaps the feature that has commanded most attention over the many years of study of this reaction has been the prediction by Hoffmann[21] that the process for cyclopropane itself should occur by conrotatory ring opening to give a trimethylene biradical and, of course, conrotatory closure back to cyclopropane. Interestingly, the relative sense of the double methylene group rotation (conrotatory or disrotatory), which was really the essence of Hoffmann's prediction, has not yet been subjected to experimental scrutiny. Rather, the focus has been on the implicit prediction that correlated double rotation should be favored over single rotation of the terminal methylene groups of the trimethylene biradical. Had the trimethylene biradical sat in a relatively deep potential well on the PES one might have expected random rather than correlated rotations of the methylene groups.[22]

Experiments have been carried out on optically active [1,2-D_2]cyclopropane[23] and on optically active [^{13}C-1,2,3-D_3]cyclopropane.[24] In each case the kinetic studies afford two phenomenological rate constants: k_α, the rate constant for loss of optical activity, and k_i, the rate constant for approach to equilibrium of the geometrical isomers. The ratio k_i/k_α can be converted into a ratio of mechanistic rate constants for rotation of one or both methylene groups, k_1 and k_{12}, respectively. In the case of the doubly labeled cyclopropane the conversion requires an assumed value for a secondary H/D isotope effect; in the case of the quadruply labeled molecule it requires only the reasonable assumption that the ^{12}C/^{13}C isotope effect be negligible.

Sadly, these conceptually elegant and experimentally demanding investigations have come to conflicting conclusions. There is no plausible value of the H/D isotope effect that can make the results of the independent studies consistent, and hence no answer on which all researchers agree about whether double methylene group rotation really is favored over single rotation.

If one were willing to trust the predictions of modern electronic structure theory for a molecule as small as cyclopropane it would appear that a clear answer might come from that quarter. However, here too there are pitfalls for the incautious. All modern, high-level, ab initio calculations[25] agree that the lowest energy transition structure for cyclo-

propane stereomutation is that for conrotatory ring opening, just as Hoffmann had predicted from his extended Hückel calculations. However, the energy differences between conrotatory and disrotatory, or between conrotatory and monorotatory pathways are found in the modern calculations to be much smaller than the extended Hückel model had suggested—small enough that little selectivity between the pathways would be expected at the greater than 400 °C temperatures required for the reaction to occur at a reasonable rate.

Microscopic mechanisms exist for stereomutations that occur only via transition structures corresponding to correlated double rotation and yet wind up as net single-rotation events. These pathways apparently further reduce any preference for correlated double rotation. They are paths in which the trimethylene biradical is formed by disrotation and closes by conrotation, or vice versa.[25] Such reactions do not, as one might think, violate the principle of microscopic reversibility, since that principle tells one only about requirements for reactions that follow the lowest energy pathway. Molecules opening or closing the ring via a disrotatory transition structure would not be following the lowest energy pathway. Nevertheless, such paths might make significant contributions to the overall reaction if, as the modern calculations suggest, the energy differences between conrotatory and disrotatory transition structures were small.

In collaboration with the group of Professor W. T. Borden at the University of Washington we have recently completed a molecular dynamics study on the stereomutation of [1,2-D_2]cyclopropane.[26] The calculations involved fitting an analytical function to points from ab initio electronic structure calculations at the GVB/6-31G* and CASPT2N/6-31G* levels of theory. A projection of the resulting surface is shown in Figure 4. With the vicinities of the key stationary points (the

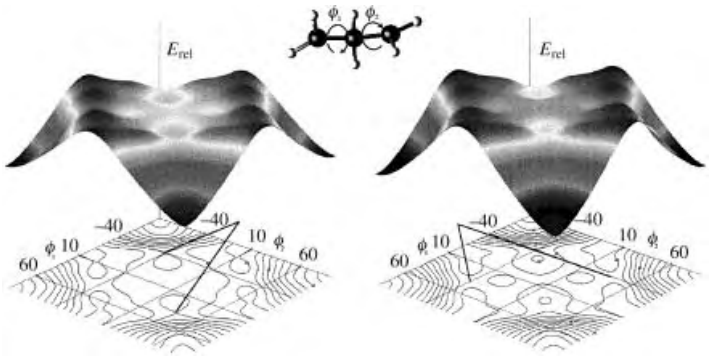


Figure 4. Projections of the analytical PES for the trimethylene biradical used in the MD simulation of cyclopropane stereomutation. The two geometrical coordinates in each graph are the dihedral angles for internal rotation of the terminal methylene groups. The graphs differ in the value of the C-C-C angle. The conrotation and disrotation transition states are shown on the left and right, respectively. E_{rel} is the relative potential energy.

conrotatory and disrotatory transition structures, and the monorotatory second-order stationary point) used as the starting points, 12000 trajectories were run on the surface. The ratio of double to net single rotations was computed, and compared with the predictions from TST. The difference was striking. As the qualitative analysis outlined above would lead one to expect, TST predicted a ratio of double to net single rotations of only 1.18. However the MD calculations on the same PES found a ratio of 4.73 ± 0.11 (with the uncertainty arising from sampling error).

The principal source of the difference is that the molecular dynamics reveal most of the trimethylenes formed by disrotation also reclose by disrotation, and not conrotation as the TST model would seem to imply. The reason is closely related to the phenomenon of conservation of angular momentum, which is applied in this case to the rotating methylene groups. Thus most of the trimethylenes formed by disrotation choose to return to cyclopropane by a path with a higher barrier than necessary. This constitutes a clear example of nonstatistical behavior, and hence a warning flag to those of us who have previously assumed TST-like kinetics for our reactive intermediates.

One must always wonder how sensitive the results of a MD simulation are to the assumptions involved—most particularly the approximation to the PES for the system. In the particular case of cyclopropane stereomutation there exists some information on that point. Concurrent with the simulation described above was one conducted by Doubleday, Bolton, and Hase using the direct dynamics technique.[27] Although their PES was somewhat different from ours, the results were similar. TST on their surface predicted double rotation to be favored over single rotation by 1.5:1, whereas their MD simulations gave a ratio between 2.9:1 to 3.5:1. Thus one can have some confidence that the difference between MD and TST models is not a result of some quirk in the calculations.

7. Experimental Evidence for Mechanistically Significant Direct Trajectories

The preceding discussion has had as a principal theme the claim that direct trajectories are of mechanistic significance because they can mimic behavior expected for a concerted reaction, that is a process occurring on a part of the PES where there is no local minimum that corresponds to an intermediate. In particular, the direct trajectories can lead to product ratios that fail to conform to the symmetry of the PES. It becomes important, therefore, to distinguish when a reaction really occurs by competitive mechanisms that explore different parts of the PES and when it occurs with coexistence of nonstatistical and statistical dynamic populations of a common "intermediate." We have recently developed an experimental technique that may allow such a distinction to be drawn.

The strategy behind the experiment is to try to intercept the putative direct trajectories by collision of the "intermediate" with a chemically unreactive partner. For a direct trajectory, redistribution of internal energy as a result of the collision would correspond to a deflection from the ballistic path to product, and might convert it into a trapped, presumably statistical, trajectory. This should result in a change in the product ratio. The situation can be modeled kinetically as shown in Figure 5b. In this scheme the PES is assumed to possess an effective symmetry element such that statistical trajectories will lead to the two products **P** and **Q** with equal probability. The direct trajectories are assumed to give only

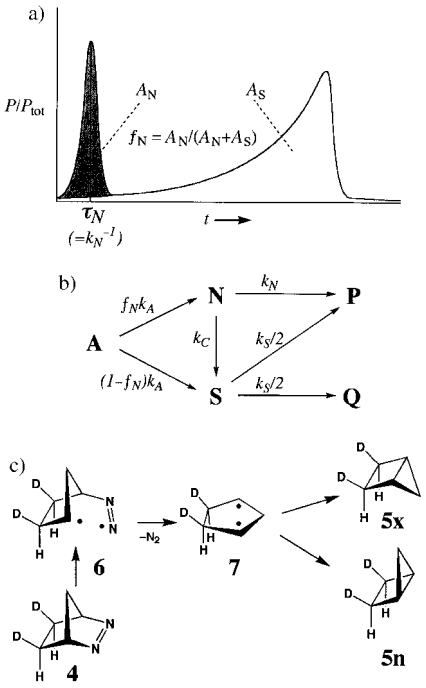


Figure 5. Kinetic representation of the supercrtical-fluid experiment described in the text. a) Schematic representation that generalizes the simulation results shown in Figure 2; P/P_{tot} = relative probability of the intermediate having a lifetime t, A_N/A_S = the proportion of the non-statistical/stastical population; b) the kinetic scheme; c) the particular reaction studied in the experiment.

one product (in this case **P**), for reasons discussed above. The phenomenological rate constants k_P and k_Q, for the formation of **P** and **Q**, respectively, from **A**, can be related to the microscopic rate constants of the mechanistic scheme by applying the usual steady-state approximation to the biradical populations **N** and **S** as shown in Equation (1). As expected,

$$\frac{k_P}{k_Q}=\frac{k_C+(1+f_N)k_N}{k_C+(1-f_N)k_N} \quad (1)$$

the ratio of phenomenological rate constants depends on the collision frequency k_C, on the fraction of trajectories that are nonstatistical f_N, and on the rate constant k_N, with which the nonstatistical population proceeds on to its product.

To intercept the direct trajectories it is clear that k_C has to be of similar magnitude to k_N. The simulations described earlier in this review have given values for the average lifetime of the nonstatistical populations of singlet biradicals ($\tau_N = k_N^{-1}$) in the range 100 to 300 fs.[5,26,27] That means one needs collision frequencies in the range of 10^{12} to 10^{13} s^{-1}. Such high collision frequencies are not easily attained in the gas phase, but are accessible in supercritical fluids.[28] In such a medium the density, and hence effective collision frequency, can be adjusted over a wide range by changing the pressure.[28,29] As shown by Equation (1) the dynamic model leads one to expect that the product ratio should approach unity as the pressure, and hence collision frequency, increases. This expectation stands in contrast to that from the competitive-mechanisms model, as illustrated by consideration of the specific reaction studied in the present work.

The azo compound **4** has long been known to give the stereoisomeric biyclopentanes **5x** and **5n** (Figure 5c) in a ratio that favors the *exo* isomer by about 3:1 in the gas phase.[30] Correction for the interconversion of the products during the reaction allows one to derive the intrinsic ratio (k_P/k_Q), which turns out to be constant at (4.7 ± 0.9):1 over a temperature range from 130 to 180 °C.[16] One mechanism for explaining the preferential formation of **5x** would be to invoke a concerted C–C bond formation and C–N bond cleavage from the biradical **6**, which is now generally agreed to be the first-formed intermediate.[31] If this concerted reaction occurred with inversion of configuration at the carbon center from which N_2 was departing, the result would indeed give **5x**.[30] In order to explain the source of **5n** one might invoke a competitive process in which C–N bond cleavage occurred prior to C–C bond formation to afford cyclopentane-1,3-diyl, which could give both stereoisomers of the bicyclopentane.

An alternative explanation for the stereochemistry has arisen from a combination of experiments[16] and molecular dynamics simulations[16,32] on the reaction. In this mechanism cleavage of the second C–N bond always precedes formation of the C–C bond. Some fraction (f_N) of the population of the resulting cyclopentane-1,3-diyl closes to product **5x** before it has had time to randomize its internal energy. The preference for formation of **5x** over **5n** in such a picture can be ascribed to better dynamic matching between the entrance channel to cyclopentane-1,3-diyl and the exit channel for inversion.[16]

As described above, the dynamic model leads one to expect that k_P/k_Q should decrease with increasing pressure if the reaction were run in a supercritical fluid. By contrast, one might expect from the competitive-mechanisms model that the product ratio would increase with increasing pressure. This expectation is because the only influence from a change in pressure that one might expect in the latter model would arise from differences in the activation volume for the two pathways. It is well known that activation volumes for uncharged systems are related to numbers of bonds being made and broken in the rate-limiting transition structure.[33,34] By this criterion, the activation volume for the putative concerted pathway should be smaller than that for the stepwise one, and so the former should be favored at higher pressure, and lead to an increase of k_P/k_Q (although it should be noted that the range of pressures explored here is smaller than that used in studies where such effects have been detected.[33]) This difference in expected outcomes from the two models is not specific to the reaction studied here. It is generally true that the dynamic model will lead to predictions of lower product ratios with increasing pressure whereas the competitive-mechanisms model will predict the opposite (at least for the common situation in which the mechanisms in competition are stepwise and concerted versions of the same transformation).

The experimental results are shown in Figure 6.[35] The lines through the data points correspond to best fits of an isolated-binary collision (IBC) model (solid line),[36] and of a Troe-type model (dashed line) in which the collision frequency in the supercritical propane is related to the inverse of the self-diffusion coefficient.[37] It is clear that the ratio of pheno-

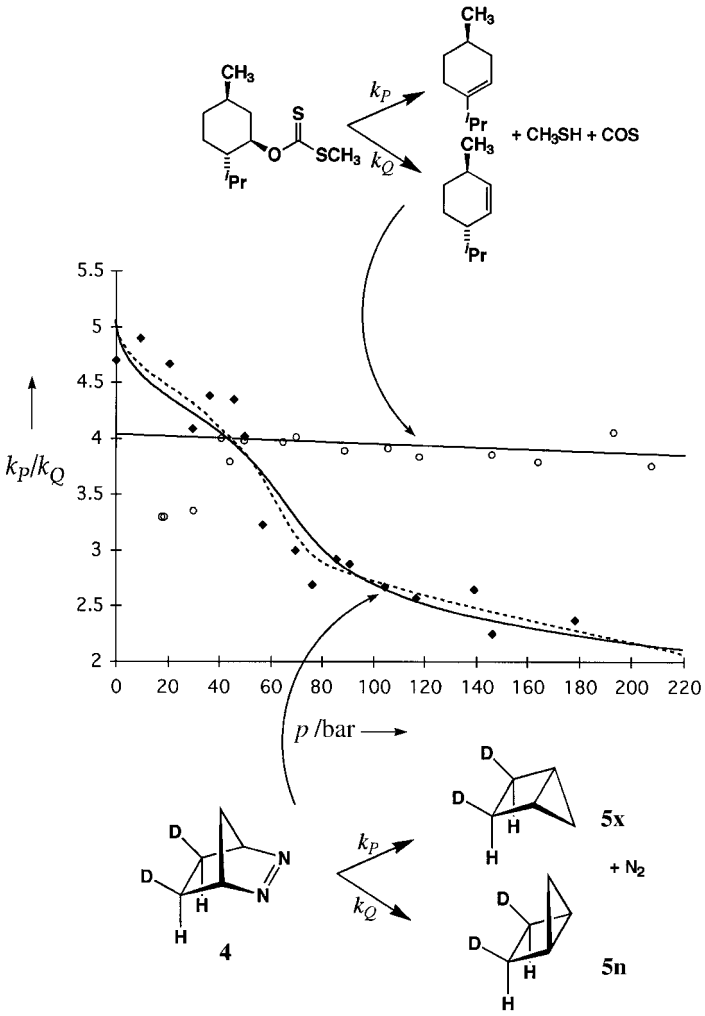


Figure 6. Experimental results for the ratio of phenomenological rate constants as a function of pressure in supercritical propane at 140 °C. The curves through the azo-compound data are from the IBC model (solid line) and the Troe model (dashed line).

menological rate constants decreases with increasing pressure, as expected for the dynamic model. The data smoothly interpolate between previously determined gas-phase and solution-phase values of k_P/k_Q.[16] Furthermore the best-fit values of the adjustable parameters for the IBC and Troe models seem physically reasonable.[35] Of special interest are the fraction (f_N) of reactions that occur via direct, nonstatistical trajectories, which turned out to be 0.67 for both models, and the lifetime ($\tau_N = k_N^{-1}$) of the nonstatistical population, which was found to be 130 ± 22 fs by the IBC model and 103 ± 13 fs by the Troe model.[35]

Also shown in Figure 6 (top) are results for a control reaction in which the products really do come from two competitive mechanisms. The competitive pathways for the control are both believed to be concerted reactions,[38] and in accord with that, one sees little dependence of product ratio on pressure in the region where the reactant is miscible with the supercritical fluid (above about 40 bar).[35] The azo compound can be shown to be miscible with the propane throughout the pressure range of the experiment.[35]

It appears that the study of reactions in supercritical media may be of general value for distinguishing dynamically controlled reactions from those that occur by genuinely different mechanisms. In the cases where the former appears to be the better description, such studies can also afford values for critical parameters that can be compared with simulation results.

8. Summary and Outlook

In this review the focus has been on the significant deviations from TST-like behavior that can be expected for some reactive intermediates. The work to date has concerned itself primarily with the behavior of singlet-state biradicals, but there is no obvious reason why other intermediates shouldn't show similar nonstatistical dynamics. In fact, the author's research group is examining, both experimentally and theoretically, reactions of radical pairs and singlet carbenes for which some preliminary results already suggest that similar behavior is being exhibited.

In a significant departure from the work to date we have also begun, in collaboration with Professor M. N. Paddon-Row at the University of New South Wales, to examine the role of molecular dynamics in intramolecular electron transfer. Here, attention is being paid to the role that molecular vibrations can have in promoting the electron-transfer event. This promises to provide an interesting complement to earlier studies that have sought to identify particular structural motifs that may facilitate the reaction.

As increasing computational power makes dynamic simulation of large molecules more feasible, it should be possible to expand the application of MD techniques to a wide range of organic transformations. The use of more accurate methods for computing the underlying PES is becoming feasible as computers become faster. Work along these lines is currently following three tracks. In one approach, semiempirical methods are recalibrated against the results of high-level ab initio models for specific reactions,[6] while in another, density functional theory with the local-density approximation is used to derive the potential energy and its derivatives.[39] In the third approach, hybrid quantum mechanical and molecular mechanics methods are employed.[40] All three methods have been used with good results.

If the work so far completed is any guide, such studies may reveal that the simple kinetic and structural models that we in the organic chemistry community have been forced to use in the past may not always have served us as well as we had hoped.

The experimental testing of the computational predictions is particularly challenging. The supercritical-fluid experiments described in this review promise to provide some useful insights, as well as quantitative data that can be compared with simulation results. However, there is certainly plenty of room for mechanistic chemists to devise other techniques that can probe the role of dynamics in reactions run under the conditions of the typical organic chemistry laboratory. This is a new kind of task for the physical organic chemist, and one that the author hopes some readers may choose to take on.

In the end, one probably doesn't want to be forced to carry out a full molecular dynamics simulation for every reaction in order to find out whether deviations from statistical behavior are to be expected. It is to be hoped that the community of organic chemists may be able to do for molecular dynamics what it did quite successfully for electronic structure theory, namely to derive simple, qualitative or semiquantitative rules that capture the essence of the full theory. We are currently rather far from that goal, and probably will remain so until enough full-scale simulations and experiments have been conducted for the community to begin to perceive the patterns of behavior of reactive intermediates.

The author would like to thank the National Science Foundation for support of the work described herein. He also owes a considerable debt of gratitude to the graduate students and postdoctoral associates who work on the experimental testing of the new theoretical models. The collaboration with Dr Borden's group and the congenial interaction with Drs Doubleday and Hase on the cyclopropane stereomutation calculations were much appreciated and are gratefully acknowledged. Finally, the author expresses his thanks for use of the facilities of the University of New South Wales, and for the kind hospitality of his host there, Prof. Michael Paddon-Row, during the sabbatical leave in which he wrote most of this review.

Received: January 20, 1997 [A270IE]
German version: *Angew. Chem.* **1998**, *110*, 3532 – 3543

[1] B. K. Carpenter, *Acc. Chem. Res.* **1992**, *25*, 520 – 528.
[2] a) H. Pelzer, E. Wigner, *Z. Phys. Chem. Abt. B* **1932**, *15*, 445 – 471; b) S. Glasstone, K. J. Laidler, H. Eyring, *Theory of Rate Processes*, McGraw-Hill, New York, **1940**.
[3] a) O. K. Rice, H. C. Ramsperger, *J. Am. Chem. Soc.* **1927**, *49*, 1617 – 1629; b) O. K. Rice, H. C. Ramsperger, *J. Am. Chem. Soc.* **1928**, *50*, 617 – 620; c) L. S. Kassel, *J. Phys. Chem.* **1928**, *32*, 225 – 242; d) L. S. Kassel, *J. Phys. Chem.* **1928**, *32*, 1065 – 1079; e) R. A. Marcus, O. K. Rice, *J. Phys. Colloid Chem.* **1951**, *55*, 894 – 907; f) R. A. Marcus, *J. Chem. Phys.* **1952**, *20*, 352 – 368; g) P. J. Robinson, K. A. Holbrook, *Unimolecular Reactions*, Wiley, New York, **1971**; h) W. Forst, *Unimolecular Reactions*, Academic Press, New York, **1973**.
[4] For an interesting discussion of this topic, see K. L. Kompa, R. D. Levine, *Acc. Chem. Res.* **1994**, *27*, 91 – 93.
[5] a) R. D. Kay, L. M. Raff, *J. Phys. Chem. A* **1997**, *101*, 1007 – 1017; b) B. K. Carpenter, *J. Am. Chem. Soc.* **1995**, *117*, 6336 – 6344; c) B. K. Carpenter, *J. Am. Chem. Soc.* **1996**, *118*, 10329 – 10330.
[6] For an example and key references, see Y.-P. Liu, D. Lu, A. Gonzalez-Lafont, D. G. Truhlar, B. C. Garrett, *J. Am. Chem. Soc.* **1993**, *115*, 7806 – 7817.
[7] M. J. S. Dewar, E. G. Zoebisch, E. F. Healy, J. J. P. Stewart, *J. Am. Chem. Soc.* **1985**, *107*, 3902 – 3909.
[8] J. J. P. Stewart, *J. Comput. Chem.* **1989**, *10*, 209 – 264.
[9] Calculations were carried out with Revision 2 of the MOPAC93 package (J. J. P. Stewart, Fujitsu Limited, Tokyo, Japan, **1993**).
[10] J. A. Berson, G. L. Nelson, *J. Am. Chem. Soc.* **1967**, *89*, 5503 – 5504.
[11] a) J. E. Baldwin, K. D. Belfield, *J. Am. Chem. Soc.* **1988**, *110*, 296 – 297; b) F.-G. Klärner, R. Drewes, D. Hasselman, *J. Am. Chem. Soc.* **1988**, *110*, 297 – 298.
[12] R. B. Woodward, R. Hoffmann, *The Conservation of Orbital Symmetry*, Verlag Chemie, Weinheim, **1970**.
[13] a) M. J. Davis, S. K. Gray, *J. Chem. Phys.* **1986**, *84*, 5389 – 5411; b) M. J. Davis, *J. Chem. Phys.* **1987**, *86*, 3978 – 4003; c) M. Simonson, K. S. Bradley, G. C. Schatz, *Chem. Phys. Lett.* **1995**, *244*, 19 – 26; d) A. A. C. C. Pais, A. I. Voronin, A. J. C. Varandas, *J. Phys. Chem.* **1996**, *100*, 7480 – 7487; e) S. R. Vande Linde, W. L. Hase, *J. Am. Chem. Soc.* **1989**, *111*, 2349 – 2351; f) W. L. Hase, *Science* **1994**, *266*, 998 – 1002.
[14] J. A. Berson, G. L. Nelson, *J. Am. Chem. Soc.* **1970**, *92*, 1096 – 1097.
[15] For a lucid review on the concept of phase space, see R. Q. Topper in *Reviews in Computational Chemistry*, *Vol. 10* (Eds.: K. B. Lipkowitz, D. B. Boyd), VCH, New York, **1997**.
[16] a) T. H. Peterson, B. K. Carpenter, *J. Am. Chem. Soc.* **1992**, *114*, 766 – 767; b) B. A. Lyons, J. Pfeifer, T. H. Peterson, B. K. Carpenter, *J. Am. Chem. Soc.* **1993**, *115*, 2427 – 2437.
[17] B. A. Horn, J. L. Herek, A. H. Zewail, *J. Am. Chem. Soc.* **1996**, *118*, 8755 – 8756.
[18] See, for example R. E. Lehr, A. P. Marchand in *Pericyclic Reactions*, *Vol. 1* (Eds.: A. P. Marchand, R. E. Lehr), Academic Press, New York, **1977**, chap. 1.
[19] W. von E. Doering, *Proc. Natl. Acad. Sci. USA* **1981**, *78*, 5279 – 5283.
[20] J. E. Baldwin, *J. Comput. Chem.* **1997**, *19*, 222 – 231, and references therein.
[21] R. Hoffmann, *J. Am. Chem. Soc.* **1968**, *90*, 1475 – 1485.
[22] S. W. Benson, H. O'Neal, *J. Phys. Chem.* **1968**, *72*, 1866 – 1887.
[23] a) L. D. Pedersen, J. A. Berson, *J. Am. Chem. Soc.* **1975**, *97*, 238 – 240; b) J. A. Berson, L. D. Pedersen, B. K. Carpenter, *J. Am. Chem. Soc.* **1976**, *98*, 122 – 143; c) S. J. Cianciosi, N. Ragunathan, T. R. Freedman, L. A. Nafie, J. E. Baldwin, *J. Am. Chem. Soc.* **1990**, *112*, 8204 – 8206.
[24] S. J. Cianciosi, N. Ragunathan, T. R. Freedman, L. A. Nafie, D. K. Lewis, D. A. Glenar, J. E. Baldwin, *J. Am. Chem. Soc.* **1991**, *113*, 1864 – 1866.
[25] a) S. J. Getty, E. R. Davidson, W. T. Borden, *J. Am. Chem. Soc.* **1992**, *114*, 2085 – 2093; b) J. E. Baldwin, Y. Yamaguchi, H. F. Schaefer III *J. Phys. Chem.* **1994**, *98*, 7513 – 7522; c) C. Doubleday, Jr. *J. Phys. Chem.* **1996**, *100*, 3520 – 3526.
[26] D. A. Hrovat, S. Fang, W. T. Borden, B. K. Carpenter, *J. Am. Chem. Soc.* **1997**, *119*, 5253 – 5254.
[27] C. Doubleday, Jr., K. Bolton, W. L. Hase, *J. Am. Chem. Soc.* **1997**, *119*, 5251 – 5252.
[28] T. W. Randolph, J. A. O'Brien, S. Ganapathy, *J. Phys. Chem.* **1994**, *98*, 4173 – 4179, and references therein.
[29] For an early experiment in which the influence of a similar phenomenon on the overall magnitude of the phenomenological rate constant was investigated, see M. L. Dutton, D. L. Bunker, H. H. Harris, *J. Phys. Chem.* **1972**, *76*, 2614 – 2617.
[30] a) W. R. Roth, M. Martin, *Justus Liebigs Ann. Chem.* **1967**, *702*, 1 – 7; b) W. R. Roth, M. Martin, *Tetrahedron Lett.* **1967**, 4695 – 4698; c) E. L. Allred, R. L. Smith, *J. Am. Chem. Soc.* **1967**, *89*, 7133 – 7134.
[31] a) C. J. S. M. Simpson, G. J. Wilson, W. Adam, *J. Am. Chem. Soc.* **1991**, *113*, 4728 – 4732; b) J. S. Adams, K. A. Burton, B. K. Andrews, R. B. Weisman, P. S. Engel, *J. Am. Chem. Soc.* **1986**, *108*, 7935 – 7938; c) J. S. Adams, R. B. Weisman, P. S. Engel, *J. Am. Chem. Soc.* **1990**, *112*, 9115 – 9121.
[32] D. C. Sorescu, D. L. Thompson, L. M. Raff, *J. Chem. Phys.* **1995**, *102*, 7910 – 7924.
[33] F.-G. Klärner, B. Krawczyk, V. Ruster, U. K. Deiters, *J. Am. Chem. Soc.* **1994**, *116*, 7646 – 7657.
[34] For lucid general descriptions of the physical basis for pressure effects on elementary reactions, including some cautionary notes on interpretation of activation volumes, see a) J. A. Montgomery, Jr., D. Chandler, B. J. Berne, *J. Chem. Phys.* **1979**, *70*, 4056 – 4066; b) J. Troe, *J. Phys. Chem.* **1986**, *90*, 357 – 365; c) W. L. Hase, *J. Phys. Chem.* **1986**, *90*, 365 – 374.
[35] M. B. Reyes, B. K. Carpenter, *J. Am. Chem. Soc.* **1998**, *120*, 1641 – 1642.
[36] K. E. Schultz, D. J. Russell, C. B. Harris, *J. Chem. Phys.* **1992**, *97*, 5431 – 5438.
[37] a) B. Otto, J. Schroeder, J. Troe, *J. Chem. Phys.* **1984**, *81*, 202 – 213; b) H. Hippler, V. Schubert, J. Troe, *J. Phys. Chem.* **1984**, *81*, 3931 – 3941; c) G. Maneke, J. Schroeder, J. Troe, F. Voss, *Ber. Bunsen-Ges Phys. Chem.* **1985**, *89*, 896 – 906.
[38] H. R. Nace, *Org. React. (N.Y.)* **1962**, *12*, 57 – 100.
[39] R. Car, M. Parrinello, *Phys. Rev. Lett.* **1985**, *55*, 2471 – 2474.
[40] F. Bernardi, M. Olivucci, M. A. Robb, *J. Am. Chem. Soc.* **1992**, *114*, 1606 – 1616.

High Yields of Methanol from Methane by C–H Bond Activation at Low Temperatures

Dorit Wolf*

Despite intensive research, until now no process for the direct selective conversion of methane into liquid chemicals such as methanol, formaldehyde, higher paraffins, and olefins exists which is satisfying from a technical and economical point of view.[1] The first step of methane conversion is the scission of a C–H bond. The high energy of dissociation (435 kJ mol^{-1}) aggravates a selective reaction. One reason for the comparatively low yields obtained upon thermal or radical activation of methane is the high activation energy for C–H bond scission, which requires high reaction temperatures. The desired products (oxygenates or olefins) are unstable intermediates, which in the presence of oxygen suffer fast consecutive reactions to carbon oxides at the high reaction temperatures.[2] Therefore, low reaction temperatures are desired for a potential catalytic process. In this respect, the following reaction steps have to be considered simultaneously, regardless of whether they are catalyzed homogeneously or heterogeneously: I) C–H bond scission, II) oxidation, and III) functionalization (when oxygenates are desired).

The reaction temperature required is determined by the highest activation energy of those steps. To ensure a stationary catalytic process, the structure of the catalyst (solid phase or metal–ligand complex in a homogeneous solution) may not be destroyed by changes in the oxidation state of the catalytically active sites during steps I–III. Against this background, heterogeneously and homogeneously catalyzed processes for the oxidative conversion of methane are summarized in Table 1.

The high yield of methanol obtained in the presence of Pt complexes in fuming sulfuric acid during the catalytica process (Periana et al.[13]) is remarkable [Eqs. (a)–(d)].

$$CH_4 + H_2SO_4 + SO_3 \longrightarrow CH_3OSO_3H + H_2O + SO_2 \quad (a)$$

$$CH_3OSO_3H + H_2O \longrightarrow CH_3OH + H_2SO_4 \quad (b)$$

$$SO_2 + \tfrac{1}{2}O_2 \longrightarrow SO_3 \quad (c)$$

$$\text{net reaction:} \quad CH_4 + \tfrac{1}{2}O_2 \longrightarrow CH_3OH \quad (d)$$

[*] Dr. D. Wolf
Institut für Angewandte Chemie Berlin-Adlershof
Rudower Chaussee 5, D-12484 Berlin (Germany)
Fax: (+49) 30-6392-4454
E-mail: dwolf@aca-berlin.de

Clearly this process, where methane is converted with 90% conversion and 81% selectivity into methyl bisulfate (methyl hydrogensulfate) in 102% sulfuric acid at 220 °C, fulfills the requirements of C–H bond scission, oxidation, and functionalization in the best way so far.

C–H Bond Activation

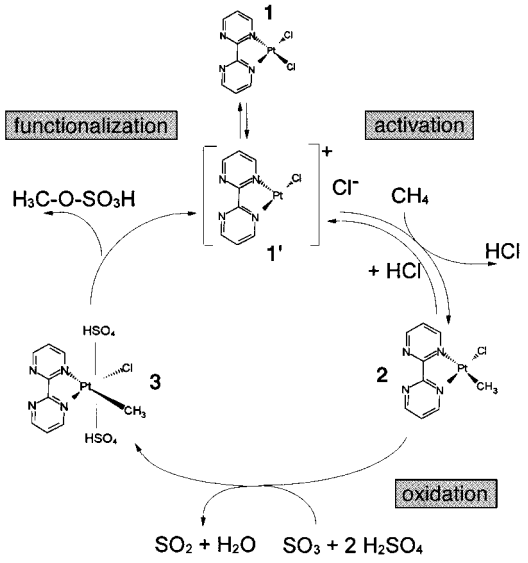
The strong C–H bond is activated by interaction of the methane with the (η^2-2,2′-bipyrimidyl)platinum(II) complex **1**, which is dissolved in the sulfuric acid (Scheme 1). The choice of appropriate ligands for the platium(II) complex determines the activity, selectivity, and stability of the catalyst in hot, strongly acidic and oxidizing environment of the fuming sulfuric acid. Ligands containing nitrogen atoms combine high thermal stability with high activity and selectivity. The bidiazine ligand in **1** proves to be well suited owing to its high affinity for the Pt^{II} center. The complex remains stable for over 50 hours at 200 °C in oleum.

It is very likely that the initial step of C–H bond activation includes interaction of the methane with the Pt^{II} center. Accordingly, when a nonoxidizing, acidic deuterated solvent (CF_3SO_3D) is applied, a H/D exchange is only observed in the presence of Pt^{II}, but not of Pt^{IV} or platinum black. Although catalytic activity of dissolved Pt^0 species cannot be ruled out, there have been no indications for the reduction of the Pt^{II} complex during the reaction. The expected key intermediate **2** (Scheme 1) is not observed at a reaction temperature of 180 °C. The reason for this is the low acid resistance of this complex, which immediately forms methane in stoichiometric amounts upon contact with sulfuric acid. Therefore, the back reaction of methane activation is fast, and under stationary conditions the concentration of the CH_3–Pt^{II} complex is probably low. At room temperature, decomposition of **2** is slow enough for the complex to be observed by ^{1}H NMR spectroscopy. At 180 °C methyl bisulfate is formed besides methane.

Concerning further improvement of the activity and selectivity of the catalyst, it is important to clarify whether the C–H bond activation is an oxidative addition with formation of a methylhydrido–Pt intermediate which loses one proton (as proposed by Shilov et al. for Pt^{II} centers[10a]), or whether it is an electrophilic substitution with formation of a

Table 1. Processes for direct oxidative conversion of methane.

	C–H bond activation	Oxidation	Functionalization	Maximum yield so far
heterogeneously catalyzed processes:				
oxidative coupling of methane on basic oxide catalysts[3, 4] $CH_4 + n\,O_2 \rightarrow C_2H_6, C_2H_4$ (600–900 °C)	substitution of the C–H bond by the weaker O–H bond at electrophilic oxygen centers of oxides; methyl radicals are formed as primary gas-phase products	reduction of the catalyst surface; catalyst regeneration proceeds by readsorption of oxygen	ethane is formed by recombination of radicals in the gas phase; ethylene and C_{2+} are formed by consecutive reactions	20–25 % ethane + ethylene
partial oxidation on transition metal oxides $CH_4 + n\,O_2 \rightarrow CH_3OH$, HCHO (250–600 °C)[5, 6]	substitution of C–H bonds by the weaker O–H bond at electrophilic oxygen centers of oxidic surfaces of solids	reduction of the catalyst surface; catalyst regeneration proceeds by readsorption of oxygen	functionalization by gas-phase reactions of methyl, methyl peroxo, and methoxy radicals	catalytic: < 4 % CH_3OH or HCHO (noncatalytic: up to 9 %)
oxidation with *tert*-butyl hydroperoxide and O_2 at 270 °C on Fe–phtalocyanine complexes encapsulated in zeolites[7]		mechanism not yet clarified		< 5 % CH_3OH + HCHO
homogeneously catalyzed processes:				
super acid catalyzed oxidation[8, 9]	protonation of methane to CH_5^+ and formation of CH_3^+ and H_2	oxidation with H_2O_2 or O_3	with H_2O_2 via $[HOOH_2]^+$ and formation of $[CH_3OH_2]^+$, with O_3 via $[OOOH]^+$ and formation of $[CH_3O]^+$	no information (selectivity towards CH_3OH + HCHO > 95 %)
electrophilic substitution and conversion with nucleophiles on Pt or Pd complexes[10, 11]	substitution of the C–H bond by the weaker Me–C bond	oxidation by reduction of the metal cations, no efficient oxidants are used which can be recycled	conversion with nucleophiles (here trifluoroacetates)	stoichiometric conversion
methane oxidation in fuming sulfuric acid on Hg^{II} salts[12] or Pt^{II} complexes[13] (150–220 °C)	substitution of the C–H bond by the weaker Me–C bond	oxidation by SO_3 reduction	formation of methyl bisulfate, which is protected from consecutive reactions and which can be converted into methanol by hydrolysis	Hg^{II} salt: 43 % CH_3OH Pt^{II} complex: 72 % CH_3OH



Scheme 1. Reaction mechanism for the oxidation of methane to methyl bisulfate on the Pt-complex catalyst **1** in fuming sulfuric acid.

methane–metal complex which loses a proton (as proposed for the Hg^{II} system[12]). So far there has not been enough evidence to prove this unambiguously. However, according to Periana et al.[13] it is a process with a cationic, highly electrophilic 14-electron complex (**1′**, Scheme 1). This thesis is supported by experiments on H/D exchange for a solution of **1′** in D_2SO_4. Introduction of deuterium only occurs with methane. When methyl bisulfate is used instead of methane, no H/D exchange with the deuterated sulfuric acid is observed. Therefore, it appears that the electron-withdrawing bisulfate group inhibits the electrophilic reaction between the metal complex and the C–H bond.

Oxidation

The oxidation of **2** in the strongly oxidizing fuming sulfuric acid is the rate-determining step of the catalytic cycle. There exists a direct correlation between the rate of oxidation of different Pt complexes (oxidation of Pt^{II} to Pt^{IV}) and the effective reaction rate of the formation of methyl bisulfate. However, complexes like $[(NH_3)PtCl_3]$, which can be oxidized at a high rate, also have short live times.

Functionalization

The functionalization can be investigated at 150 °C. At this temperature, only the C–H bond activation, but no oxidation of **2**, takes place. When Pt^{IV} is applied as $[H_2Pt(OH)_6]$ together with oleum, methyl bisulfate is formed. The amount of methyl bisulfate produced correlates with the amount of Pt^{IV} used. Therefore, the functionalization proceeds at the Pt^{IV}

 © WILEY-VCH Verlag GmbH, D-69451 Weinheim, 1998 1433-7851/98/3724-3352 $ 17.50+.50/0

centers. As explained above, the dissociation of the bond between the η^2-2,2′-bipyrimidyl ligand and the Pt^{II} center is reversible. The question may be raised whether the ligands are bonded to the Pt center during the transition state. As metal salts also catalyze the reaction—however, with lower activity and selectivity—the ligands must be relevant for the selectivity of the reaction.

How is the high selectivity of the process achieved? According to Periana et al., the rate constant of the oxidation step of CH_4 to methyl bisulfate is 100 times higher than that of the further oxidation of methyl bisulfate.[13] Methanol can be trapped by esterification and thus be protected from nonselective consecutive reactions. Therefore, only low amounts of CO_2 and traces of methyl chloride are formed. This appears to be the key towards high selectivities. A similar concept also enables high selectivities when methane is activated by super acids (Table 1): The selective products are trapped after protonation as $[CH_3OH_2]^+$ or $[CH_3O]^+$.[9] With catalyst **1**, space time yields of $10^{-6}\,mol\,cm^{-3}\,s^{-1}$ (ca. $0.1\,t\,m^{-3}\,h^{-1}$) are obtained. This makes the process interesting from a technical point of view. Whether such a process can be applied technically depends on the long-term stability of the catalyst. From the given turnover numbers and frequencies, a time span of 14 hours can be calculated during which the catalyst is completely deactivated. This shows that further improvement is necessary. Furthermore, when evaluating the process efficiency, the necessary workup steps—hydrolysis of the ester, destillation of methanol, oxidation of the formed SO_2 to SO_3 (space time yield $0.2-0.2\,t\,m^{-3}\,h^{-1}$) for regeneration of sulfuric acid as oxidizing agent—have to be taken into account.

German version: *Angew. Chem.* **1998**, *110*, 3545 – 3547

Keywords: homogeneous catalysis · methane · methanol · N ligands · platinum

[1] a) L. Guczi, R. A. van Santen, K. V. Sarma, *Catal. Rev. Sci. Eng.* **1996**, *13*, 356; b) *Catal. Today* **1997**, *37*(1) (Ed.: J. B. Moffat).
[2] C. Batiot, B. K. Hodnett, *Appl. Catal. A* **1996**, *137*, 179.
[3] a) M. Baerns, J. R. H. Ross in *Perspectives in Catalysis* (Eds.: J. A. Thomas, K. I. Zamaraev), Blackwell, **1992**; b) A. M. Maitra, *Appl. Catal. A* **1993**, *104*, 11.
[4] O. Forlani, S. Rossini, *Materials Chemistry and Physics* **1992**, *31*, 155.
[5] *Direct Methane conversion by Oxidative Processes* (Ed.: E. E. Wolf), von Nostrand Reinhold, New York, **1993**.
[6] O. V. Krylov, *Catal. Today* **1993**, *18*(3).
[7] R. Raja, P. Ratnasamy, *Appl. Catal. A* **1997**, *158*, L7.
[8] G. A. Olah, R. Renner, P. Schilling, Y. K. Mo, *J. Am. Chem. Soc.* **1973**, *95*, 4952.
[9] G. A. Olah, *Acc. Chem. Res.* **1987**, *20*, 422.
[10] a) L. A. Kushck,V. V. Lavrushko, Y. S. Misharin, A. P. Maravsky, A. E. Shilov, *New J. Chem.* **1987**, *7*, 8109; b) A. E. Shilov, *Activation of Saturated Hydrocarbons by Transition Metal Complexes*, Reidel, Dordrecht, **1984**.
[11] E. Getz, T. F. Oliver, A. Sen, *J. Am. Chem. Soc.* **1987**, *109*, 8109.
[12] a) R. A. Periana, D. J. Taube, E. R. Evitt, D. G. Loffler, P. R. Wentrcek, T. Masuda, *Science* **1993**, *259*, 340; b) R. A. Periana, E. R. Evitt, H. Taube (Catalytica Inc.), US patent 5,233,113, **1993**; c) R. A. Periana, D. J. Taube, H. Taube, E. R. Evitt (Catalytica Inc., US patent 5,306,855, **1994**.
[13] R. A. Periana, D. J. Taube, S. Gamble, H. Taube, T. Satoh, H. Fujii, *Science* **1998**, *280*, 560.

Large Molecules from the Virtual Bakery—Filling a Gap in Structure Research**

Peter Luger*

It is a common practice for preparative chemists to cook or bake their new compounds in hot ovens. By contrast, the determination of the structure of large molecules by "shake-and-bake" (or half-bake) in the gigabyte world of modern computers is a new, but very successful, method and fills a long-lamented gap in the otherwise very effective field of structure research by X-ray diffraction. When the Japanese group of Kondo et al.[1] solved the crystal structure of the deep-blue flower pigment commelinin six years ago, it caused such a sensation that this compound was featured on the cover of the first August issue of *Nature*. The group was also awarded the prize for the best poster contribution at the 16th International Crystallography Congress in Beijing in 1993.[2] The scientific community is used to the scientific literature being expanded through the addition of routine crystal structure solutions, so why was this particular one so special? One aspect may have been its aesthetic value, for the commelinin structure (Figure 1, top) is almost as beautiful as the flowers from which it is derived.

But there is more to its significance than just good looks. It contains 253 non-hydrogen atoms in the asymmetric unit and thus belongs to that group of middle-sized structures that were formidable tasks for crystallographers to solve in the early 1990s. The number of structures registered at the Cambridge Crystallographic Data Centre (CCDC) has increased almost exponentially for thirty years, with more than

[*] Prof. Dr. P. Luger
Institut für Kristallographie der Freien Universität
Takustrasse 6, D-14195 Berlin (Germany)
Fax: (+49) 30-838-3464
E-mail: luger@chemie.fu-berlin.de

[**] This work was supported by the Deutsche Forschungsgemeinschaft (SFB312, Vectorial Membrane Processes) and the Fonds der Chemischen Industrie.

 © WILEY-VCH Verlag GmbH, D-69451 Weinheim, 1998 1433-7851/98/3724-3353 $ 17.50+.50/0

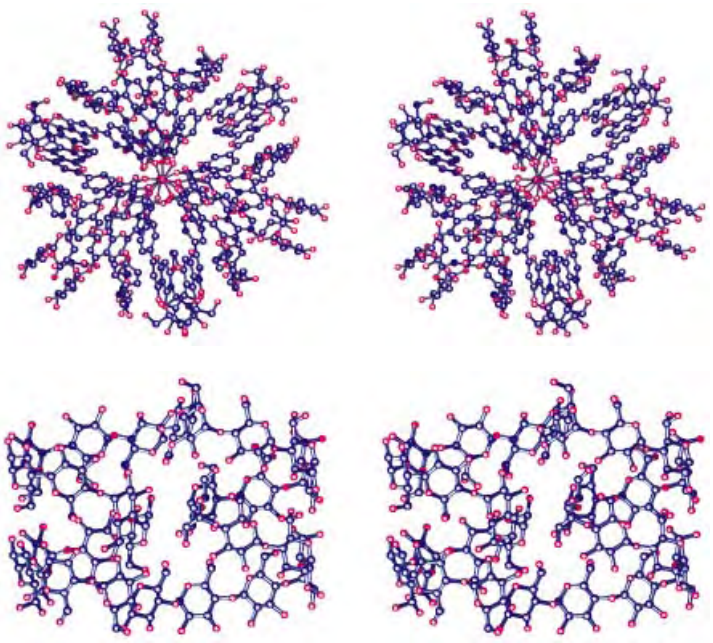


Figure 1. Top: Structure of the flower pigment commelinin[2] that was solved in the early 1990s by classical direct methods; bottom: structure of a cycloamylose[22] that consists of 26 glucose units and is one of the largest light-atom structures of atomic resolution solved by SHELXD. Both stereo figures are plotted with the program SCHAKAL.[30]

10000 new structures each year. The Brookhaven Protein Data Base has been through a similar development lately with about 1000 new structures each year (Figure 2). This progress

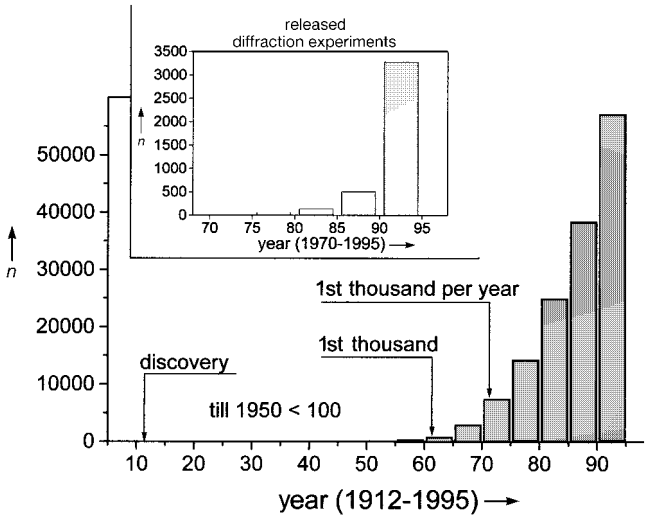


Figure 2. Number n of entries into the Cambridge Data File in the Cambridge Crystallographic Data Centre (CCDC) shown in five year intervals. The insert shows the corresponding entries into the Brookhaven Protein Data Bank (1970–1995).

has taken place with small structures, where the limit was first about 100 atoms and then increased to nearly 200 non-hydrogen atoms, and with protein structures of molecular weights in the kilodalton range. Structures with several hundred atoms in the asymmetric unit have remained difficult to solve. Among the purely organic structures stored in the Cambridge Data File fewer than 300 entries have more than 100 carbon atoms in the formula and only 16 entries have more than 200 carbon atoms.

In the April 1992 "Research News" article in Science[5] the author described the situation of the in-between molecules—those having between 200 and 500 atoms—in familiar terms: "In large families, the oldest child and the youngest often get most of their parents' attention, while the middle children seemingly get lost in the crowd". Actually, crystallographers cannot be called negligent parents. The reasons for their lack of attention have been serious. One problem is the difficulty with the crystallization of middle-sized compounds, because as the bulk increases the propensity to crystallize greatly diminishes. At the other end of the size spectrum, the very large structures, such as proteins, form less flexible and more globular molecules and tend to crystallize again better than the in-between ones. It also has to be added that a great deal of research effort, including trials in outer space, has been invested in the crystallization of macromolecules.[6]

A further problem is that the otherwise so effective "direct methods" for solving the crystallographic phase problem fail for the in-between molecules and that the methods usually employed for protein structures are not yet applicable. Thus, hardly any usable methods have been available for the determination of these middle structures. Hence, when one of them could be solved the success commanded a great deal of attention, as with the commelinin example.

Recently, two actinomycin structures were published by Sheldrick et al. [7] in *Angewandte Chemie* (actinomycin D and Z_3, with 314 and 307 atoms in the asymmetric unit, respectively), which indicates that the gap can now be closed if intensity data of atomic resolution (that is, down to about 1 Å) can be collected. However, methods with new strategies had to be developed. One source of such innovation was, once again, Herbert Hauptman, one of the fathers of direct methods, and the recipient of the 1985 Nobel Prize for chemistry, which he shared with Jerome Karle for their pioneering work in this area. In 1988 Hauptman introduced the minimal function $R(\varphi)$[8] in which a central role is played by the three- and four-phase structure invariants, the triplets $(\varphi_{hk} = \varphi_h + \varphi_k + \varphi_{-h-k})$ and quartets $(\varphi_{lmn} = \varphi_l + \varphi_m + \varphi_n + \varphi_{-l-m-n}$, where h,k,l... are reciprocal lattice vectors of Bragg reflections), which were known from classical direct methods. For the triplet and quartet relationships (more exactly, for $\cos\varphi_{hk}$ and $\cos\varphi_{lmn}$) the expectation values ε_T and ε_Q, respectively, can be calculated, and the minimal function $R(\varphi)$ is thus expressed by Equation (1).

$$R(\varphi) = \frac{\sum_{h,k} A_{hk}[\cos\varphi_{hk} - \varepsilon_T]^2 + \sum_{l,m,n} |B_{lmn}|[\cos\varphi_{lmn} - \varepsilon_Q]^2}{\sum_{h,k} A_{hk} + \sum_{l,m,n} |B_{lmn}|} \quad (1)$$

Hauptman also introduced the minimal principle,[9] which involves the minimization of $R(\varphi)$, and leads to a set of phases of the correct structure.[10]

The practical implementation of the minimal principle is the "shake-and-bake" algorithm and computer program.[11–13] It differs from the classical direct methods programs, which operate only in reciprocal space, in that during each of its cycles shake-and-bake carries out calculations alternately in reciprocal and direct space: This procedure automatically

 © WILEY-VCH Verlag GmbH, D-69451 Weinheim, 1998 1433-7851/98/3724-3354 $ 17.50+.50/0

takes account not only of the condition that the correct structure has positive electron density everywhere, but also of the fact that sharp local electron density maxima should appear that correspond to atomic positions. The atomicity of a chemical structure thereby enters the calculations directly.

Shake-and-bake is executed in several steps that alternate between direct and reciprocal space,[14] (Figure 3). First, a random test structure is generated in real space, whose Fourier transformation provides structure factors and hence

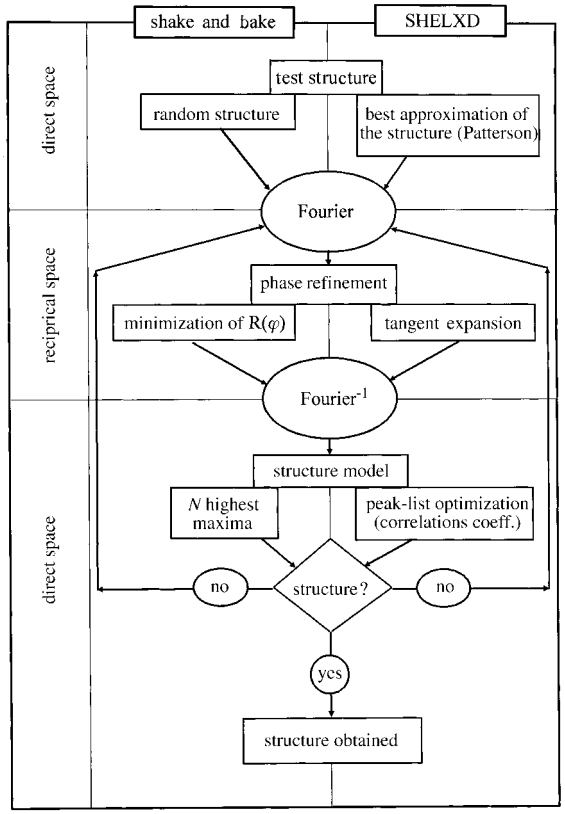


Figure 3. Schematic representation of the algorithms of shake-and-bake (left) and of SHELXD (right).

also starting phases in reciprocal space. This is the "shake step" of the procedure. Through phase refinement by iteration, the minimization of $R(\varphi)$ is attempted. After this cycle of minimization a new structure is "baked" by calculating an electron-density map in direct space with the now supposedly improved phases. The N highest maxima of this map is considered to be the new set of atoms, and the phases derived from them by another Fourier transformation, the next "shake step", give a new set of phases to be improved by phase refinement in reciprocal space.

This procedure usually has to go through several hundred shake-and-bake steps until it can be recognized from the trend of $R(\varphi)$ whether it converges to the correct structure. One test structure alone usually leads to a false minimum rather than to the desired result. Therefore, several thousand trials are carried out, each with another random starting set.

Inspired by shake-and-bake, George Sheldrick has developed SHELXD [15, 16] a program especially designed for the solution of structures in the 200–2000 atom range. The similarities and differences of the two methods can be seen in Figure 3. Sheldrick tries to dispense with the random starting structures. For instance, if a heavy atom is present in the structure he applies an ingenious Patterson interpretation[17, 18] routine at the outset. This approach makes the phases of the starting set more reliable than they are in a completely random structure. A conventional tangent phase-refinement is then applied, and an inverse Fourier transformation results in a new structure model. The highest N maxima are not selected automatically as input atoms for the further course of the process; instead a peak-list optimization[19] is initiated. Starting with the lowest peak the maxima are individually evaluated for their acceptability as atoms. This decision depends on whether the presence of a peak improves or worsens a correlation coefficient introduced by Fujinaga and Read in 1987.[20] A carefully screened atom list is thereby introduced into the next cycle.

By means of this peak-list optimization (and the possible Patterson evaluation at the beginning) SHELXD works with higher weight in direct space than shake-and-bake does. For some time Sheldrick himself called his method "half-baked",[19] but in view of the successes of the method, one could now call it "fully baked". In addition to the above-mentioned actinomycin structures, several others that were previously considered unsolvable, have been elucidated with SHELXD. Examples are vancomycin,[21] an important antibiotic with 313 independent (non-hydrogen) atoms in the asymmetric unit, and a cycloamylose consisting of 26 glucose units and having almost 650 atoms (two molecules in the asymmetric unit).[22] The latter long held the record as the largest light-atom structure determined with atomic resolution (Figure 1, bottom). This structure is surpassed by the present "world-record holder", the lantibiotic mersacidin,[23] whose size of 850 independent atoms corresponds to a protein with a 120 amino acid sequence. Somewhat outside this competition, since it was known before, is the triclinic structure of HEW-lysozyme (Figure 4), which was redetermined by the Sheldrick group, and exceeded the 1000-atom limit for the first time![24]

Given that several hundred cycles have to be calculated for one trial and several thousand trials have to be run for a structure determination, the computer time required for the methods discussed here may be expressed in VAX years.[19] Because VAX computers were the usual computing tools in chemical laboratories in the 1980s, neither shake-and-bake nor SHELXD would have been possible to run, even if these algorithms had already been worked out. Today's processors have increased the computing speed by two orders of magnitude, which reduces the computing time of VAX years to an acceptable number of hours or days. Because the new algorithms need data sets with atomic resolution, these methods could hardly have succeeded without the remarkable progress that has taken place in the experimental field in recent years, especially the new developments in crystallization techniques[25] and the improved possibilities for X-ray data collection. By using synchrotron radiation, possibly with the crystal samples kept at low temperatures, one can greatly improve the ratio of reflection intensity to background,

 © WILEY-VCH Verlag GmbH, D-69451 Weinheim, 1998 1433-7851/98/3724-3355 $ 17.50+.50/0

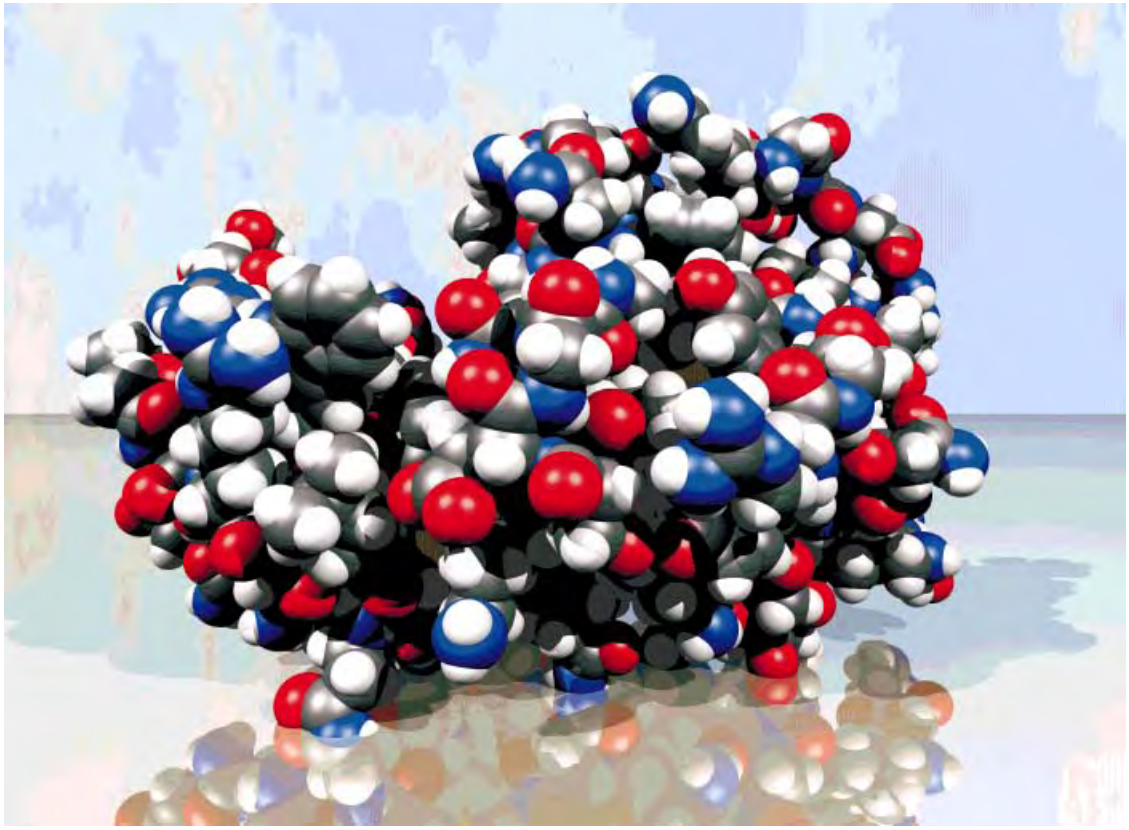


Figure 4. The 1001 independent atoms in the structure of the triclinic form of HEW-lysozyme.[24]

especially in high-angle ranges. If this radiation is combined with area detectors, such as the new CCD systems (for example the SMART-diffractometer,[26] which appeared on the market in April 1994), then not only the resolution increases, but also the speed of the data collection is enhanced by several orders of magnitude[27] relative to that of usual diffractometers with serial counters and conventional X-ray tubes, which is a very significant factor in the case of large structures. Through these developments—as in the 1960s—another great surge in innovations has taken place in crystal structure analysis, a leap propelled by concurrent breakthroughs in theory, experiment, and computer technology. It seems that the gap in the elucidation of molecules that contain several hundred atoms may close before the end of this century.

Modern chemistry offers numerous problems to solve. Only in the class of naturally occurring antibiotics or cytostatics, whose increasing importance has recently been emphasized in the highlight article by Lindel,[28] are there various molecules of several hundred atoms each. The solution of one of these has been until now, the exception,[29] but henceforth the chances of their successful X-ray structure determination are very good indeed.

German version: *Angew. Chem.* **1998**, *110*, 3548 – 3551

Keywords: computer chemistry · direct methods · structure elucidation · X-ray diffraction

[1] T. Kondo, K. Yoshida, A. Nakagawa, T. Kawai, H. Tamura, T. Goto, *Nature* **1992**, *358*, 515 – 518.
[2] A. Nakagawa, K. Yoshida, T. Kondo, T. Kawai, T. Goto, *Acta Crystallogr. Sect. A* **1993**, *49*, 201.
[3] F. H. Allen, O. Kennard, *Chem. Des. Autom. News* **1993**, *8*, 31 – 37.
[4] F. C. Bernstein, T. F. Koetzle, G. J. B. Williams, E. F. Meyer, Jr., M. D. Brice, J. R. Rodgers, O. Kennard, T. Shimanouchi, M. Tasumi, *J. Mol. Biol.* **1977**, *112*, 535 – 542.
[5] A. S. Moffat, *Science* **1992**, *256*, 309 – 310.
[6] F. Rosenberger, *Z. Kristallogr.* **1998**, *Suppl. 15*, 18.
[7] M. Schäfer, G. M. Sheldrick, I. Bahner, H. Lackner, *Angew. Chem.* **1998**, *110*, 2482 – 2485; *Angew. Chem. Int. Ed* **1998**, *37*, 2381 – 2384.
[8] H. A. Hauptman, *Proceedings of the ACA Meeting*, Philadelphia, USA **1988**, Abstract R4.
[9] H. A. Hauptman in *Crystallogr. Computing 5* (Eds.: D. Moras, A. D. Podjarny, J. C. Thierry), University Press, Oxford, **1991**, pp. 324 – 332.
[10] C. M. Weeks, G. T. DeTitta, R. Miller, H. A. Hauptman, *Acta Crystallogr. Sect. D* **1993**, *49*, 179 – 181.
[11] R. Miller, G. T. DeTitta, R. Jones, D. A. Langs, C. M. Weeks, H. A. Hauptman, *Science* **1993**, *259*, 1430 – 1433.
[12] G. T. DeTitta, C. M. Weeks, P. Thuman, R. Miller, H. A. Hauptman, *Acta Crystallogr. Sect. A* **1994**, *50*, 203 – 210.
[13] C. M. Weeks, G. T. DeTitta, H. A. Hauptman, P. Thuman, R. Miller, *Acta Crystallogr. Sect. A* **1994**, *50*, 210 – 220.
[14] R. Miller, S. M. Gallo, H. G. Khalak, C. M. Weeks, *J. Appl. Crystallogr.* **1994**, *27*, 613 – 621.
[15] G. M. Sheldrick, *SHELXD-CCP4 Workshop*, York, **1997**, 147 – 157.
[16] G. M. Sheldrick in *Direct Methods for Solving Macromol. Structures* (Ed.: S. Fortier), Kluwer Academic Publishers, Netherlands **1998**, pp. 401 – 411.
[17] G. M. Sheldrick in *Crystallogr. Computing 6* (Eds.: H. D. Flack, L. Parkanyi, L. Simon), University Press, Oxford, **1993**, 100 – 110.
[18] G. M. Sheldrick in *Direct Methods for Solving Macromol. Structures* (Ed.: S. Fortier), Kluwer Academic Publishers, Netherlands **1998**, pp. 131 – 141.

 © WILEY-VCH Verlag GmbH, D-69451 Weinheim, 1998 1433-7851/98/3724-3356 $ 17.50+.50/0

[19] G. M. Sheldrick, R. O. Gould, *Acta Crystallogr. Sect. B* **1995**, *51*, 423 – 431.
[20] M. Fujinaga, R. J. Read, *J. Appl. Crystallogr*. **1987**, *20*, 517 – 521.
[21] M. Schäfer, Th. R. Schneider, G. M. Sheldrick, *Structure* **1996**, *4*, 1509 – 1515.
[22] K. Geßler, I. Uson, T. Takaha, N. Krauss, S. Smith, G. M. Sheldrick, W. Saenger, *6. Jahrestagung Deutsche Gesellsch. f. Kristallogr.*, Karlsruhe, **1998**, *Abstract.*
[23] J. Kärcher, P. Lubini, E. Pohl, T. R. Schneider, G. M. Sheldrick, *6. Jahrestagung Deutsche Gesellsch. f. Kristallogr.*, Karlsruhe, **1998**, *Abstract.*
[24] G. M. Sheldrck **1998,** personal communication.
[25] J. Hulliger, *Angew. Chem*. **1994**, *106*, 151 – 171; *Angew. Chem*. *Int. Ed. Engl.* **1994**, *33*, 143 – 162.
[26] SMART, CCD-based structure determination system, Bruker-AXS Inc, Madison, WI, USA, **1994**.
[27] T. Koritsanszky, R. Flaig, D. Zobel, H.-G. Krane, W. Morgenroth, P. Luger, *Science* **1998**, *279*, 356 – 358.
[28] T. Lindel, *Angew. Chem*. **1998,** *110*, 806 – 808; *Angew. Chem*. *Int. Ed.* **1998**, *37*, 774 – 776.
[29] D. A. Langs, *Science* **1988**, *241*, 188 – 191.
[30] E. Keller, SCHAKAL88. User Manual, Univ. Freiburg, Germany, **1988**,
[31] The groups of A. Nakagawa (Sapporo/Japan), G. M. Sheldrick (Göttingen) and W. Saenger (Berlin) kindly contributed coordinates and picture material to Figures 1 and 4.

Deposition of Data from X-Ray Structure Analyses

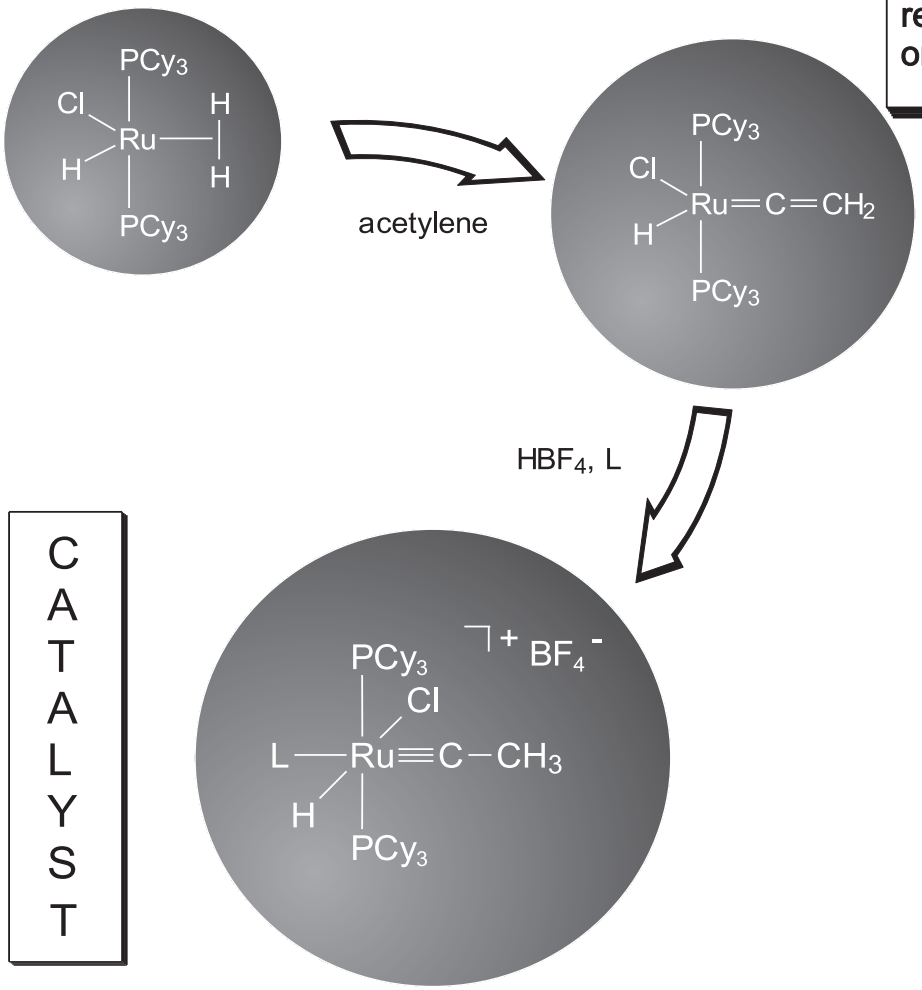
In order to make life easier for authors and referees the Cambridge Crystallographic Data Centre (CCDC) and the Fachinformationszentrum Karlsruhe (FIZ) have unified their procedures for the depostion of data from single-crystal X-ray structure analyses.

Prior to submitting a manuscript please deposit the data for your compound(s) **electronically** at the appropriate date base, that is, at the CCDC for organic and organometallic compounds and at the FIZ for inorganic compounds. Both data bases will be pleased to provide help (see our *Notice to Authors* in the first issue of this year). In general, you will receive a depository number from the data base within two working days after electronic deposition; please include this number with the appropriate standard text (see our Notice to Authors) in your manuscript. This will enable the referees to retrieve the structure data quickly and efficiently if they need this information to reach their decision.

This is now the uniform procedure for manuscripts submitted to the journals *Advanced Materials, Angewandte Chemie, Chemistry—A European Journal,* the *European Journal of Inorganic Chemistry,* and the *European Journal of Organic Chemistry.*

 © WILEY-VCH Verlag GmbH, D-69451 Weinheim, 1998 1433-7851/98/3724-3357 $ 17.50+.50/0

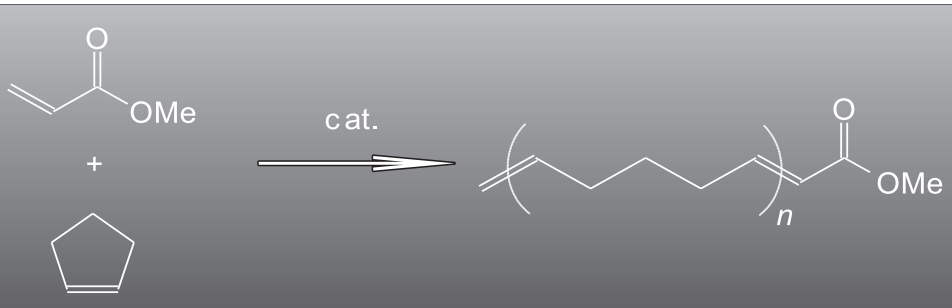
Werner and co-workers report more on this topic on pages 3421-3423.



CATALYST

In contrast to neutral carbeneruthenium compounds, cationic carbynehydridoruthenium complexes catalyze the cross-olefin metathesis of cyctopentene with methyl acrylate.

REACTION



 © WILEY-VCH Verlag GmbH, D-69451 Weinheim, 1998 1433-7851/98/3724-3359 $ 17.50+.50/0

Organizational Forms of Matter: An Inorganic Super Fullerene and Keplerate Based on Molybdenum Oxide

Achim Müller,* Erich Krickemeyer, Hartmut Bögge, Marc Schmidtmann, and Frank Peters

Dedicated to Professor Heinrich Nöth on the occasion of his 70th birthday

A knowledge of the linking rules of selected building blocks allows, in special cases, the generation of an enormous variety of structures, especially when a set of gradually differing building units is available that can be "tuned" in terms of linkage variability. Of utmost importance is that these basic units can be linked to larger fragments, which can again react in subsequent processes in different ways.[1] Of interest is certainly not only the production of mesoscopic (or nanostructured) and macroscopic objects with functional versatility, but also the aesthetic beauty of such assemblies. In this respect it should be mentioned that certain structures, such as spherical objects comprised of pentagons and hexagons, can be found repeatedly both on molecular and macroscopic levels, clearly because general organization principles are followed. Here we report on a relevant inorganic super fullerene or, in other words a giant molecular sphere with an integrated (inscribed) icosahedron, namely a Keplerate (see below) with more than 500 atoms and the highest Euclidean symmetry. The sphere consists of a total of 12 $\{Mo_{11}\}$-polyoxomolybdate fragments of fivefold symmetry. These fragments are generated from central pentagonal bipyramidal $\{MoO_7\}$ groups, which are abundant in several other giant polyoxomolybdate clusters.[2]

When an aqueous solution of ammonium molybdate is reduced to medium ratios of $[Mo^V]/[Mo^{VI}]$ at pH values at which the pentagonal bipyramidal $\{MoO_7\}$ groups are "generated" and discrete $\{Mo_2^VO_4(OOCCH_3)^+\}$, that is, $\{Mo_2^V\}$ groups, are stabilized by high concentrations of the bidentate acetate ligand, the spherical anion **1a** or the corresponding crystalline salt **1**, respectively, is formed. High $[Mo^V]/[Mo^{VI}]$ ratios inevitably result in the direct linking of the resulting $\{Mo_2^V\}$[3] groups whereas low ratios lead to the formation of molybdenum-blue species.[2, 4] (In the following text only the oxidation state of the Mo^V and not of the Mo^{VI} centers is given.)

$$(NH_4)_{42}[Mo_{72}^{VI}Mo_{60}^{V}O_{372}(CH_3COO)_{30}(H_2O)_{72}] \cdot ca.\ 300\,H_2O \cdot ca.\ 10\,CH_3COONH_4 \quad \mathbf{1}$$

The salt **1** was characterized by elemental analysis (including cerimetric titration to determine the number of Mo^V centers), thermogravimetry (for the determination of the crystal water content), bond valence sum (BVS) calculations[5] (to determine the positions of the H_2O ligands and to distinguish between Mo^{VI} and Mo^V centers), spectroscopic methods (IR, Raman, UV/Vis, and NIR spectroscopy), and single crystal X-ray structure analysis.[6]

[*] Prof. Dr. A. Müller, E. Krickemeyer, Dr. H. Bögge, M. Schmidtmann, Dipl.-Chem. F. Peters
Lehrstuhl für Anorganische Chemie I der Universität
Postfach 100131, D-33501 Bielefeld (Germany)
Fax: (+49) 521-106-6003
E-mail: a.mueller@uni-bielefeld.de

Compound **1** crystallizes in the cubic space group $Fm\bar{3}$.[6] The $\{Mo_{132}\}$-type cluster **1a** is built up of 12 $\{Mo_{11}\}$ fragments of the type $\{(Mo)Mo_5\}\{Mo_1^V\}_5$ (Figures 1 and 2) with central pentagonal bipyramidal $\{MoO_7\}$ groups, such that the fivefold symmetry axes are retained in the resulting spherical object, which shows an overall icosahedral symmetry, which includes the respective C_2 and C_3 symmetry axes (Figures 1 and 2). The central $\{MoO_7\}$ unit is linked to five $\{MoO_6\}$ octahedra through edges, with each Mo^V center of an $\{Mo_2^V\}$ group being linked to two adjacent $\{MoO_6\}$ octahedra. The basic spherical shape of **1a** is emphasized in Figure 2a, whereby the 12 corners of an icosahedron are spanned by the Mo centers of the pentagonal $\{MoO_7\}$ bipyramids of the $\{Mo/Mo_5\}$ pentagons. In all, the 12 $\{(Mo)Mo_5\}$ groups of the $\{Mo_{132}\}$-type cluster are linked by 30 $\{Mo_2^V\}$ groups, which are "stabilized"

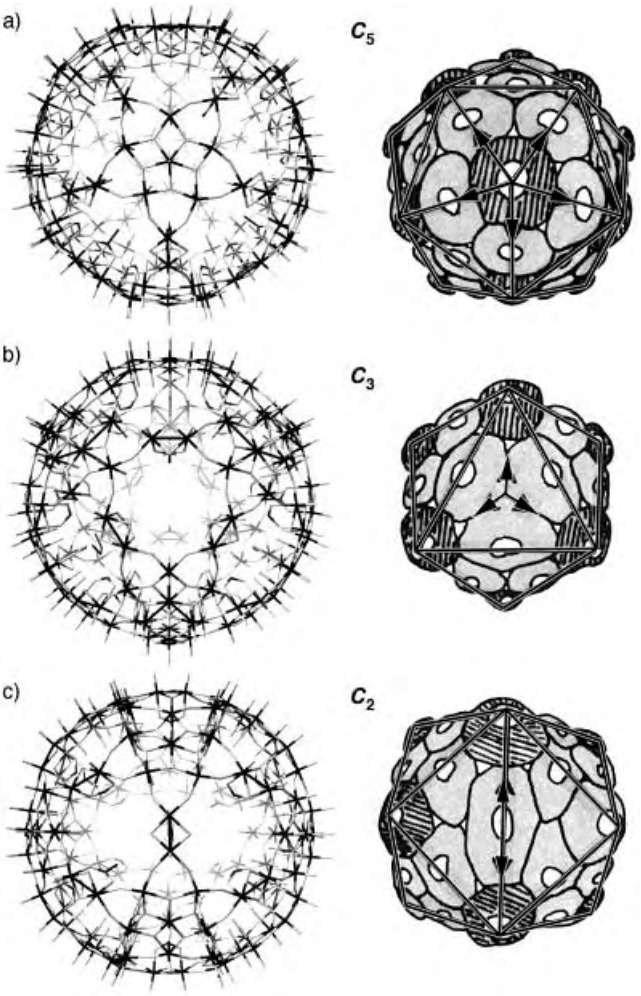


Figure 1. Illustration of the structure of **1a** with perspective views along a fivefold (a), a threefold (b), and a twofold (c) symmetry axis (because of the structural complexity of the spherical shape of **1a** in wireframe presentations). For the purpose of comparison the corresponding schematic representations of an icosahedral $T = 3$ virus capsid (see below) with 20 hexagonal and 12 pentagonal capsomers (morphology units) are presented. In both systems, the C_5 axes cross the centers of the pentagonal units (hatched) (a), the C_3 axes cross the midpoint between three units (b), and the C_2 axes cross the center of a unit (virus model figures are reproduced from reference [10c]). Whereas (a) refers to the centers of both the pentagonal $\{(Mo)Mo_5\}$ units and the pentagonal capsomers which are located at the 12 corners of an icosahedron (see Figure 2), (b) and (c) refer to the $\{Mo_2^V\}$ units of **1a** and the hexagonal capsomers, respectively.

 © WILEY-VCH Verlag GmbH, D-69451 Weinheim, 1998 1433-7851/98/3724-3360 $ 17.50+.50/0

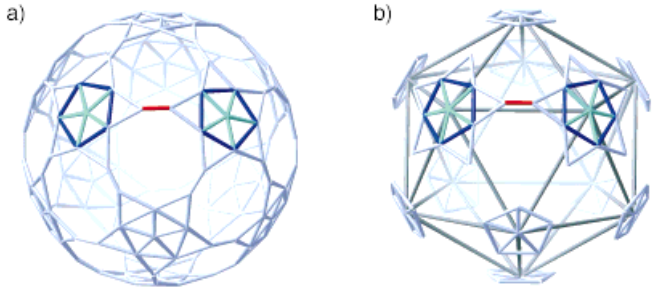


Figure 2. Schematic representation of the 132 molybdenum atom fragment of **1a** with the spherical nature highlighted (a) and the relation to the icosahedron spanned by the related {(Mo)Mo_5} subfragment located on the 12 corners (b). Two {Mo_{11}} units ({(Mo)Mo_5}{Mo^V}$_5$, blue, light blue) that are linked through a Mo^V–Mo^V bridge (red) are highlighted. The outer corners of an {Mo_{11}} unit are formed by the Mo centers of the {Mo^V–Mo^V} bridges.

by bidentate acetate ligands (Figure 2b). Therefore, **1a** can be formulated as $[\{Mo_2^VO_4(CH_3COO)\}_{30}\{(Mo)Mo_5O_{21}(H_2O)_6\}_{12}]^{42-}$. Interestingly, the 30 classical {Mo_2^V} dumb-bells (Mo–Mo: 2.6 Å) or 60 Mo^V atoms span a solid of icosahedral symmetry, which corresponds to that of the C_{60} fullerene (Figure 3),[7] in the present case a polyhedron with 12 regular pentagons and 20 trigonal hexagons. (It was possible to resolve several disordered H_2O molecules inside the sphere, a fact that is also interesting for related aspects of supramolecular chemistry.) Remarkable is that the anions **1a**, in which all O atoms of the 132 Mo–O_{term} groups lie on the outer-spherical surface and correspondingly the *trans*-positioned H_2O ligands of the 72 Mo^{VI} centers point to the center of the sphere, form a cubic close packing in the crystal (Figure 4).

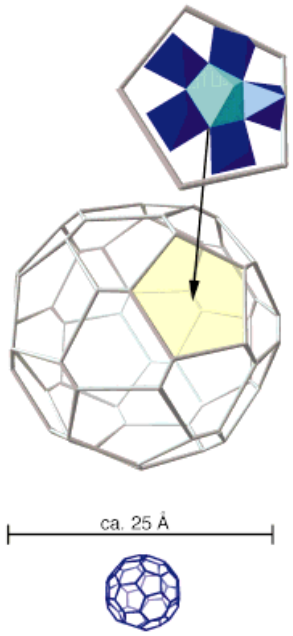


Figure 3. Structure of the icosahedral {Mo_2^V}$_{30}$ fragment with 12 regular pentagons and 20 trigonal hexagons as well as its coherence to the C_{60} fullerene, which is depicted on the same scale. A separated {(Mo)Mo_5} pentagon in a polyhedral representation is emphasized.

Furthermore, the anion **1a** belongs to the type I category within the Robin–Day classification for mixed-valence compounds,[8] which is evident from the red-brown color of the substance as well as the main absorption band at 450 nm, respectively, without any knowledge of the actual localization of the Mo^V and Mo^{VI} centers.

In the current context the recognizable topological coherence to the structures of the spherical viruses, which have icosahedral capsids, should be stressed. Corresponding virus capsids—similar to a fragment of the described cluster **1a**—consist of 60 (identical) structural motifs. Interestingly, a spherical shell/capsid of icosahedral symmetry is preferred even

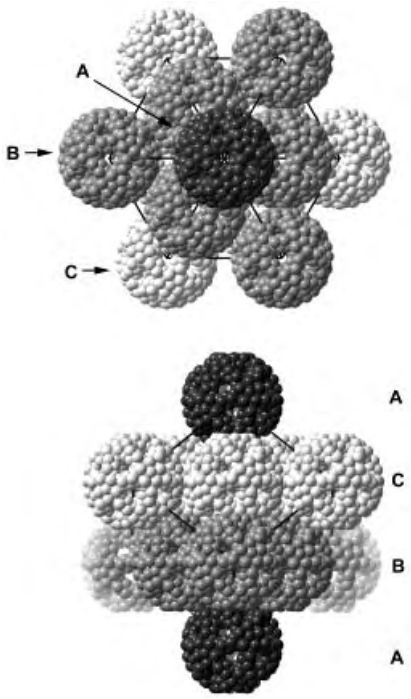


Figure 4. Representation of the packing of **1a** in the crystal lattice (space-filling model viewed along [111] (top) and perpendicular to [111] (bottom)). The spherical anions, the outer surface of which is formed by terminal oxygen atoms, are organized in a cubic–closest packing (sequence of layers ABCA…). Each edge of the additionally projected unit cell measures 46.06 Å.[15]

for viruses[7c, 9, 10] with more than 60 subunits (protein monomers), though there are only 20 equilateral triangles (and for each of these only three equivalent subunits), a situation which can be understood from the rules of Caspar and Klug, who were inspired by the designs of the geodesic domes of the architect Buckminster Fuller. In the present case the centers of 12 {(Mo)Mo_5} pentagons with the (12×5) MoO_6 subunits, which are analogous to the 12 pentagonal capsomers (morphology units) of the most simple virus with the (12×5) protein monomers span an icosahedron. The corresponding partial structure of **1a** can thus topologically be compared to that of the most simple satellite tobacco necrosis virus (STNV) with its (only) 60 monomeric protein subunits (Figure 5).[9, 10d, e] The crucial difference between the polyoxometalate **1a** and the satellite virus is that the structure **1a** is formed by covalent bonds. Of special interest for the inorganic chemist is of course the fact that the described cluster **1a** resembles icosahedral symmetry despite its large number of atoms.[11] This represents definitively an unprecedented event in chemistry. Plato and Kepler, but probably Heisenberg too, would have been pleased.

It can certainly be assumed that the variety of linking modes of molybdate fragments has not yet been exhausted and that it will be possible to obtain even macroscopic structures—that is, structures perceptive to our senses—in open systems. In this actual context the question arises as to whether limits exist for the molecular growth of very large assemblies formed by self-aggregation of subunits, especially in the case of objects of high, for example spherical, symmetry. In this respect, further studies not only on topological aspects

 © WILEY-VCH Verlag GmbH, D-69451 Weinheim, 1998 1433-7851/98/3724-3361 $ 17.50+.50/0

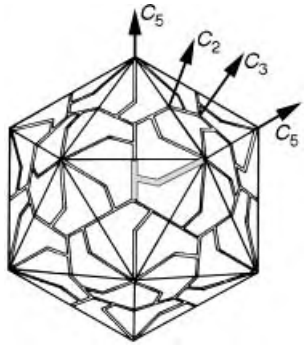


Figure 5. Representation of the packing of the 60 identical subunits of the $T = 1$ satellite tobacco necrosis virus, which are coded by only one gene.[10d] The linkage points lie on the five-, three- and twofold symmetry axes (see also Figure 1).

of carbon fullerenes[12] but also on Fuller cages in solid-state structures[13] would be stimulating. Here the comparison of **1a** with Kepler's early and famous model of the cosmos is certainly of interest. In his opus *Mysterium Cosmographicum*[14] Kepler described his vision of planetary motion, whereby distances between the orbits of the planets could be explained for him if the ratios between the successive orbits were designed to be equivalent to the spheres successively circumscribed around and inscribed within the five Platonic solids. In the case of **1a** the icosahedron inside the spherical shell of the 132 terminal oxygen atoms can be recognized. The 12 corners of the icosahedron are defined by the 12 central molybdenum atoms of the 12 {(Mo)Mo_5} pentagons (Figure 2b). Thus we suggest that the anion **1a** should be called a Keplerate since the systematic nomenclature would be far too unwieldy.

We are convinced that **1a**, based on its high stability in solution, its cage structure, and the possibility to take-up (or exchange) certain species in its cavity, and also the possibility to modify the shells (for example to integrate hetero atoms) or link them, will lead to the development of a Keplerate-type chemistry comparable to Keggin-type chemistry. Solid-state chemistry additionally may profit from the opportunity to study nucleation and structure-forming processes on rather large molecular spherical objects, for instance to understand principles of crystal growth, and also in the search for shell aufbau principles in solid-state structures that show condensed fullerene cages.[13] Last but not least, it can be expected that the planned synthesis of highly complex molecular objects with desired functionality on the basis of metal–oxygen fragments will be possible in the future.

Experimental Section

1:$N_2H_4 \cdot H_2SO_4$ (0.8 g, 6.1 mmol) was added to a solution of $(NH_4)_6Mo_7O_{24} \cdot 4H_2O$ (5.6 g, 4.5 mmol) and CH_3COONH_4 (12.5 g, 162.2 mmol) in H_2O (250 mL). The solution was then stirred for 10 min (color change to blue-green) and 50% CH_3COOH (83 mL) was subsequently added. The reaction solution, now green, was stored in an open 500-mL Erlenmeyer flask at 20°C without further stirring (fumehood; slow color change to dark brown). After 4 d the precipitated red-brown crystals of **1** were filtered off over a glass fritt (D2), washed with 90% ethanol, ethanol, and diethyl ether, and finally dried in air. Yield: 3.3 g (52% based on molybdate).

Characteristic IR bands of the basic cluster vibrations assignable to the irreducible representation F_{1u} (KBr pellet): $\tilde{\nu}$ [cm^{-1}]: 1626 (m, $\delta(H_2O)$), 1546 (m, $\tilde{\nu}_{as}$(COO)), 1440 (sh) and 1407 (m) ($\delta(CH_3)$, $\tilde{\nu}_s$(COO), ($\delta_{as}(NH_4^+)$)), 969 (m) and 936 (w–m) ($\tilde{\nu}$ (Mo=O)), 853 (m), 792 (s), 723 (s), 628 (w), 567 (s); characteristic Raman bands assignable to the irreducible representations A_{1g} (those with highest intensity) and H_g (KBr pellet; $\lambda_e = 1064$ nm; 1000–200 cm^{-1}): $\tilde{\nu}$ [cm^{-1}]: 953 (w), 935 (w) and 875 (s) ($\tilde{\nu}$(Mo=O)), ca. 845 (sh), 374 (m–s), 314 (m), 212 (w); Vis/NIR spectra (in H_2O/CH_3COOH; λ [nm]): 450, 260 (sh), 215 (KBr pellets gave basically the same spectrum).

Received: July 1, 1998 [Z12077IE]
German version: *Angew. Chem.* **1998**, *110*, 3567–3571

Keywords: cage compounds · clusters · fullerenes · polyoxometalates · supramolecular chemistry

[1] a) To our knowledge the following conditions and circumstances favor the generation of a variety of complex molecular structures in the present case (over several reaction steps) under one-pot conditions: 1) The presence of linkable groups, that is building units, with the general possibility to generate intermediates with high free enthalpy, which lead to high negative reaction enthalpies (for example, by formation of H_2O molecules); 2) the *possibility* of an easy structural change of the building units, of the uptake of hetero atoms, of the formation of larger and variably linkable fragments (especially with energetically low-lying unoccupied molecular orbitals), of a template-driven structure formation, of the generation of defects in reaction intermediates (with the consequence of different types of linking), of the localization and delocalization of valence electrons in different ways and the variation and control of the charge (for example by protonation, electron transfer reactions, and substitution of certain building units). b) In this context a novel *(polyoxometalate) nucleation growth* process has even been discovered inside a ring-shaped cluster compartment (A. Müller, S. Q. N. Shah, H. Bögge, M. Schmidtmann, *Nature*, in press). Aspects of related limited growth have been discussed: P. Ball, *Nature* **1998**, *395*, 745–748.

[2] See A. Müller, F. Peters, M. T. Pope, D. Gatteschi, *Chem. Rev.* **1998**, *98*, 239–271.

[3] A. Müller, J. Meyer, E. Krickemeyer, C. Beugholt, H. Bögge, F. Peters, M. Schmidtmann, P. Kögerler, M. J. Koop, *Chem. Eur. J.* **1998**, *4*, 1000–1006; A. Müller, S. Dillinger, E. Krickemeyer, H. Bögge, W. Plass, A. Stammler, R. C. Haushalter, *Z. Naturforsch. B* **1997**, *52*, 1301–1306; M. I. Khan, J. Zubieta, *Progr. Inorg. Chem.* **1995**, *43*, 1–149; H. K. Chae, W. G. Klemperer, T. A. Marquart, *Coord. Chem. Rev.* **1993**, *128*, 209–224.

[4] A. Müller, M. Koop, H. Bögge, M. Schmidtmann, C. Beugholt, *Chem. Commun.* **1998**, 1501–1502, and references therein.

[5] I. D. Brown in *Structure and Bonding in Crystals*, *Vol. II* (Eds.: M. O'Keeffe, A. Navrotsky), Academic Press, New York, **1981**, pp. 1–30.

[6] Space group $Fm\bar{3}$; $a = 46.0576(14)$ Å, $V = 97702(5)$ Å^3; $Z = 4$; the structure was solved with direct methods, $R = 0.0883$ for 3445 independent reflections ($F_0 > 4\sigma(F_0)$); Siemens-axs-SMART diffractometer (94920 reflections obtained at 158 K from 1271 frames each covering 0.3° in ω, $2\theta_{max} = 45°$). The crystals were taken directly from the reaction solution and measured immediately to prevent loss of crystal water. The measurement of several individual crystals led to the same results. An untypical coordination of an additional acetate group instead of H_2O ligands at the {(Mo)Mo_5} pentagons, observed in a similar compound, cannot be completely excluded because of the disorder present; but in any event this coordination is definitely not necessary for the structure formation. (There is no coordination of this type in the corresponding {Mo_{132}}-type cluster that contains formate instead of acetate ligands.) The structures were solved with the program SHELXS-96 and refined with the program SHELXL-93 (G. M. Sheldrick, University of Göttingen, **1996** and **1993**, respectively). Further details on the crystal structure investigation may be obtained from the Fachinformationszentrum Karlsruhe, D-76344 Eggenstein-Leopoldshafen, Germany (fax: (+49) 7247-808-666; e-mail: crysdata@fiz-karlsruhe.de), on quoting the depository number CSD-410097.

[7] a) H. W. Kroto, J. R. Heath, S. C. O'Brien, R. F. Curl, R. E. Smalley, *Nature* **1985,** *318*, 162–163; b) *Buckminsterfullerenes* (Eds.: W. E.

Billups, M. A. Ciufolini), VCH, Weinheim, **1993**; c) *Von Fuller bis zu Fullerenen*, *Beispiele einer interdisziplinären Forschung* (Eds.: W. Krätschmer, H. Schuster), Vieweg, Braunschweig, **1996**.

[8] M. B. Robin, P. Day, *Adv. Inorg. Chem. Radiochem.* **1967**, *10*, 247 – 422.

[9] Spherical viruses display a 60-fold identically packed fundamental structural motif that can formally be assigned to pentagonal and also hexagonal capsomers (morphology units or chemically definable oligomers of one or more viral proteins or subunits). The most simple example is presented by the satellite tobacco necrosis virus (Figure 5), in which only 12 pentagonal capsomers with a total of 60 identical viral proteins (subunits) coded by one gene only are placed at the 12 corners of an icosahedron. In the case of the larger spherical viruses—for example, those with $3 \times 60 = 180$ subunits—the motif that occurs 60 times shows (different) subunits organized in capsomers of five identically connected protein monomers (pentagons) centered at the corners and 20 additional capsomers (hexagons) built up by six protein monomers (see Figure 1). In accordance with Caspar and Klug[10a, h] the triangular faces of an icosahedron can be subdivided into an integral number of equilateral triangles. This procedure demonstrates that the "normal" spherical viruses, such as that of the TBSV (tomato bushy stunt virus) can have more than 60 subunits (which is also the case for **1a**). The resulting solid is an icosadeltahedron (a capped icosahedron is such a solid) with local symmetry elements that relate to its subunits in addition to the exact symmetry elements of the icosahedron. (Subunits that are distributed about each exact triangular vertex of a $T = 3$ icosadeltahedron are related by a local C_6 symmetry axis; corresponding adjacent subunits are only quasi-equivalent.) The number of subunits in an icosadeltahedron equals 60 T (where $T = h^2 + hk + k^2$ denotes the triangulation number, which is important for the architecture of viruses; h and k are integers[10a, d, h]). A virus structure with $T = 3$ (Figure 1) resembles 180 ($= 3 \times 60$) subunits (for $h = k = 1$) whereas the triangulation number $T = 1$ (with $h = 1$, $k = 0$) stands for the only 10 nm large satellite tobacco necrosis virus, and also for the fragment of **1a** with its 60 $\{MoO_6\}$ octahedral subunits of the 12 $\{(Mo)Mo_5\}$ pentagons. For a known, topologically comparable geodesic dome of Fuller $T = 36$[10a] (for extensive literature on this subject see reference [10]).

[10] a) See D. Voet, J. G.Voet, *Biochemie*, VCH, Weinheim, **1992**; see also A. Müller, C. Beugholt, *Nature* **1996**, *383*, 296 – 297; b) B. Alberts, D. Bray, J. Lewis, M. Raff, K. Roberts, J. D. Watson, *Molekularbiologie der Zelle*, VCH, Weinheim, **1990**; c) B. D. Davis, R. Dulbecco, H. N. Eisen, H. S. Ginsberg, *Microbiology*, Harper, Philadelphia, **1980**, p. 869; d) "The Structure of Satellite Tobacco Necrosis Virus": L. Liljas, B. Strandberg in *Biological Macromolecules and Assemblies*, *Vol. 1*, *Virus Structures* (Eds.: F. A. Jurnak, A. McPherson), Wiley, New York, **1984**, pp. 97 – 119; e) L. Liljas, T. Unge, T. A. Jones, K. Fridborg, S. Lövgren, U. Skoglund, B. Strandberg, *J. Mol. Biol.* **1982**, *159*, 93 – 108; f) S. C. Harrison, *Trends Biochem. Sci.* **1984**, 345 – 351; g) H. G. Schlegel, *Allgemeine Mikrobiologie*, Thieme, Stuttgart, **1992**; h) D. L. D. Caspar, A. Klug, *Cold Spring Harbor Symp. Quant. Biol.* **1962**, *27*, 1 – 24; i) M. Kemp, *Nature*, 1998, *396*, 123.

[11] This leads to the presence of the fivefold degenerate irreducible representation H_g (F. A. Cotton, *Chemical Applications of Group Theory*, 3rd ed., Wiley, New York, **1990**), for example with the consequence of only a few bands in the IR and Raman spectra.

[12] G. Brinkmann, A. W. M. Dress, *J. Algorithms* **1997**, *23*, 345 – 358.

[13] R. Nesper, *Angew. Chem.* **1994**, *106*, 891 – 894; *Angew. Chem. Int. Ed. Engl.* **1994**, *33*, 843 – 846.

[14] J. Kepler, *Mysterium Cosmographicum* **1596**; see also M. Kemp, *Nature* **1998**, *393*, 123.

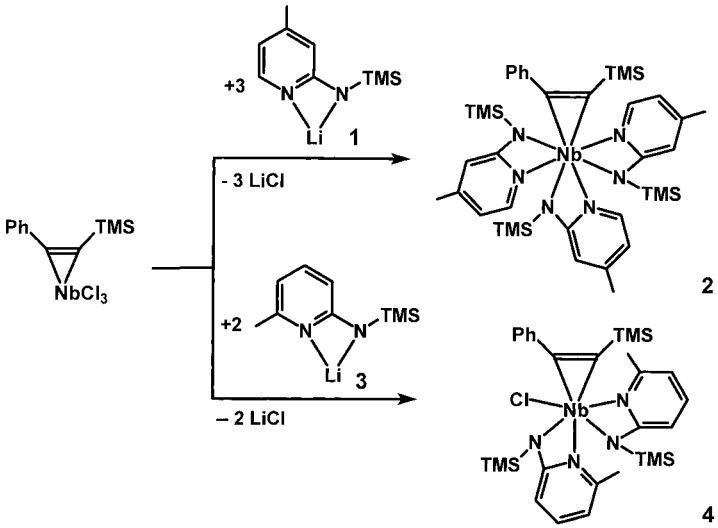
[15] There is also an additional, but marginal relationship to Kepler's conjectures of 1611 that no packing of spheres can be denser than in the face-centered-cubic lattice, observed for instance in crystals of **1**, a conjecture that could only now be confirmed (see N. J. A. Sloane, *Nature* **1998**, *395*, 435 – 436).

Novel Amidoniobium Complexes with a Functional Relationship to the $[Cp_2ZrR]^+$ Ion*

Anke Spannenberg, Hans Fuhrmann, Perdita Arndt, Wolfgang Baumann, and Rhett Kempe*

Niobium and tantalum compounds live in the shadow of metal complexes of Group 4. Possible reasons for this are the extremely interesting applications of the latter compounds in olefin polymerization[1] or in selective couplings of α-olefins for organic synthesis.[2] Hopes of catalysts with more versatility with regard to the functional groups of the olefins which are to be coupled have recently stimulated increased activity in the search for catalytically active species in Group 5;[3] for analogues of the known $[Cp_2MR]^+$ ions (M = Ti, Zr, Hf). Amido ligands might be useful in this respect.[4] Herein we report the first cationic amidoniobium compound, which can be used for selective coupling of α-olefins.

Treatment of $[NbCl_3(dme)(PhC{\equiv}CTMS)]$[5] (dme = dimethoxyethane, TMS = trimethylsilyl) with **1** (3 equiv) gave the orange-red alkyneniobium complex **2** (Scheme 1). The IR spectrum and the ^{13}C NMR data of **2** indicate that the alkyne



Scheme 1. Synthesis of **2** and **4**.

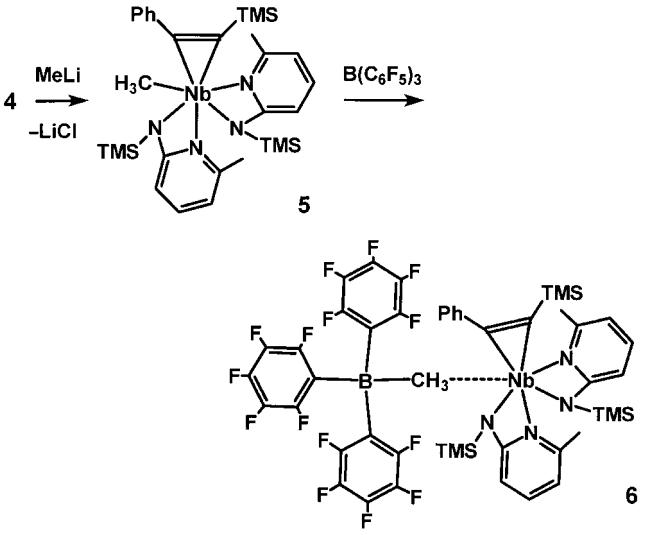
ligand functions as a 4e donor.[6] The niobacyclopropene ring in **2** is extremely stable and does not react with ketones, styrene oxide, alkynes, and olefins, as known for the metallocene alkyne complexes of the titanium triad.[7] Complexes with only two amido ligands are accessible by using the sterically more demanding aminopyridinato (Ap) ligands.

[*] Dr. R. Kempe, Dr. A. Spannenberg, Dr. H. Fuhrmann, Dr. P. Arndt, Dr. W. Baumann
Institut für Organische Katalyseforschung
an der Universität Rostock e.V.
Abt. Komplexkatalyse
Buchbinderstrasse 5 – 6, D-18055 Rostock (Germany)
Fax: (+49) 381-46693-74
E-mail: Rhett.Kempe@ifok.Uni-Rostock.de

[**] This work was supported by the Max-Planck-Gesellschaft and by the Fonds der Chemischen Industrie. We thank Prof. Rosenthal for his support of this work.

 © WILEY-VCH Verlag GmbH, D-69451 Weinheim, 1998 1433-7851/98/3724-3363 $ 17.50+.50/0

Thus, the otherwise analogous reaction of $[NbCl_3(dme)(PhC{\equiv}CTMS)]$ with **3** (2 equiv) led to **4**. Treatment of **4** with MeLi gave the alkyl complex **5** (Scheme 2). In this reaction



Scheme 2. Synthesis of **5** and **6**.

there are no indications of an attack at the coordinated alkyne or at the Ap ligands. The NMR spectra of **4** and **5** contain four sets of signals for the Ap ligands and two for the coordinated alkyne units. When the temperature is raised, two sets of Ap and one set of alkyne signals result in coalescence. Hence, two isomers exist in solution, which interconvert by ligand rotation on the NMR timescale. In addition, the two Ap ligands of the two isomers occur in chemically different environments and do not exchange within the temperature range examined. The X-ray structure analysis[8] of **5** reveals that two independent molecules are present in the asymmetric unit in the solid state; the alkyne ligands adopt different orientations with respect to the Ap–Nb fragment (Figure 1). Thus it is assumed that the two isomers observed in solution interconvert by alkyne rotation. Taking into consideration this assumption the activation barrier for rotation of the alkyne for **4** is $\Delta G^{\ddagger} = 80\ kJ\,mol^{-1}$.

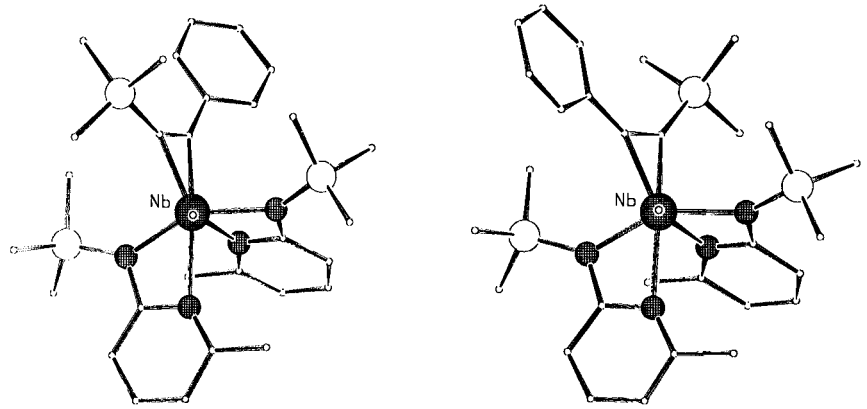


Figure 1. Molecular structures of both isomers of **5** in the crystal. View along the C(methyl)–Nb bond (the H atoms are omitted). Selected bond lengths [Å] (average values): Nb–C_{Me} 2.195(13), C–C(alkyne) 1.32(2).

The reaction of **5** with $B(C_6F_5)_3$ led to **6** (Scheme 2), whose NMR spectrum (C_6D_5Br) confirmed that an alkyne rotation also took place in this case. Compound **6** is the first X-ray structurally characterized[8] "zwitterionic" compound of a metal in Group 5, in which an apical alkyl ligand was partially abstracted by a borane (Figure 2). Similar compounds have

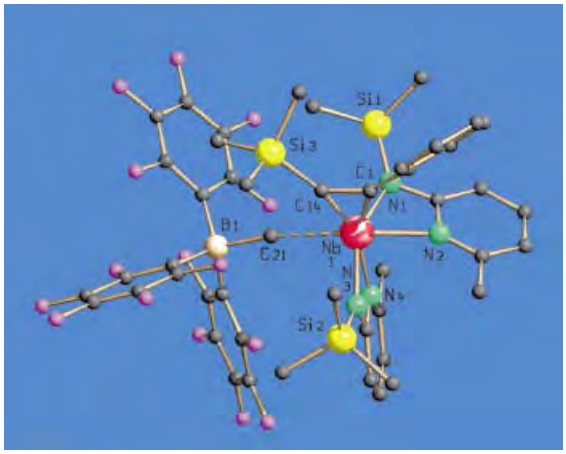


Figure 2. Molecular structure of **6** in the crystal. Selected bond lengths [Å] and angles [°]: C1–C14 1.313(6), C1–Nb1 2.081(4), C14–Nb1 2.117(4), C21–B1 1.671(6), C21–Nb1 2.611(5), N1–Nb1 2.105(4), N2–Nb1 2.218(3), N3–Nb1 2.058(3), N4–Nb1 2.353(4); C1-Nb1-C14 36.4(2), N1-Nb1-N2 62.24(14), N3-Nb1-N4 60.96(13), N3-Nb1-C21 96.23(14), N1-Nb1-C21 95.23(14), N4-Nb1-C21 78.16(13).

been described for metal complexes of the titanium triad[9] and are considered for comparison. The Nb–$C(Me_{bridge})$ distance of 2.611(5) Å resembles otherwise analogous Zr–C distances in zirconocenes (2.55–2.67 Å).[9] The same is true for the B–$C(Me_{bridge})$ distance. The C–C distance of the coordinated alkyne in **6** is 1.313(6) Å. This value is very similar to that of a $C(sp^2){=}C(sp^2)$ bond (1.321(13) Å)[10] and is expected for an alkyne functioning as a 4e donor . The compound **6** polymerizes ethene to polyethylene (PE) as a one-component system without addition of cocatalyst. However, the catalyst decomposes very rapidly under the reaction conditions ($t = 4$ h, $n_{cat.} = 0.5\ mmol\,L^{-1}$, $T = 80\,^{\circ}C$, $p_{ethene} = 6.5$ bar). This can be prevented by the addition of a little iBu$_3$Al as scavenger (activity: $4.4\ kg_{PE}\,mol_{Nb}^{-1}\,h^{-1}$).[11] The narrow mol mass distribution ($M_w/M_n = 1.8$) supports the presence of a uniform catalyst species. The average mol mass of $36\,000\ g\,mol^{-1}$ of the polymers obtained in the ethylene polymerization is low and illustrates the tendency for rapid chain breakage. 1-Butene can be selectively (98%) dimerized (TOF = $1200\ h^{-1}$) to give 2-ethylhexene with **6** at room temperature in the presence of methylalumoxane (MAO, 120 equiv). The reactivity of cationic aminopyridinatoniobium and -tantalum alkyne complexes such as **6** is currently under investigation.

 © WILEY-VCH Verlag GmbH, D-69451 Weinheim, 1998 1433-7851/98/3724-3364 $ 17.50+.50/0

Experimental Section

All experiments were carried out under argon with exclusion of oxygen and moisture.

2: 4-Methyl-2-trimethylsilylaminopyridine (638 μL, 3 mmol) in hexane (20 mL) was treated with 2.5 M *n*BuLi in hexane (1.2 mL, 3 mmol) at −78 °C, and stirred for 2 h at room temperature. The resulting solution was added to a suspension of [$NbCl_3$(dme)(PhC≡CTMS)] (464 mg, 1 mmol) in hexane (20 mL). This mixture was stirred for 16 h at room temperature, precipitated LiCl was filtered off, and the filtrate was concentrated under vacuum. Orange, crystalline **2** (435 mg, 54 %) was obtained at −30 °C; m.p.: 212 °C; elemental analysis ($C_{38}H_{59}N_6NbSi_4$, 805.18): calcd.: C 56.69, H 7.39, N 10.44; found: C 56.76, H 7.67, N 10.57; ^{1}H NMR (C_6D_6, 297 K): $\delta = 8.36$, 7.69, 6.94 (3 d, $J = 5.6$ Hz, each 1 H, H-6, Ap), 7.76, (d, 2 H, *o*-H, Ph), 7.24 (tr, 2 H, *m*-H, Ph), 7.04 (tr, 1 H, *p*-H, Ph), 6.22 (br., 2 H, H-3, Ap), 6.07, 5.98, 5.82 (3 d, each 1 H, H-5, Ap), 6.03 (s, 1 H, H-3, Ap), 1.96, 1.81, 1.75 (br., each 3 H, Me-Ap), 0.46, 0.28, 0.11, −0.15 (4 × s, each 9 H, $SiMe_3$); ^{13}C NMR (C_6D_6, 297 K): $\delta = 223.1$ (*C*$SiMe_3$), 209.1 (*C*Ph), 170.3, 169.8, 167.9 (C-2, Ap), 149.8, 147.7, 147.5 (C-4, Ap), 148.1, 145.5, 143.6 (C-6, Ap), 140.0 (*ipso*-C, Ph), 132.0, 128.4, 128.3 (*o*-, *m*-, *p*-C, Ph), 114.7, 113.6, 112.1, 111.6, 108.3, 107.4 (C-3, C-5, Ap), 21.6, 21.5, 21.4 (Me, Ap), 2.2, 1.6, 1.3, 1.3 ($SiMe_3$); IR (Nujol): $\tilde{\nu} = 1645$ cm^{-1} (C≡C, coordinated).

4: 6-Methyl-2-trimethylsilylaminopyridine (850 μL, 4 mmol) in hexane (20 mL) was treated with 2.5 M *n*BuLi in hexane (1.6 mL, 4 mmol) at −78 °C, and stirred for 2 h at room temperature. The resulting solution was added to a suspension of [$NbCl_3$(dme)(PhC≡CTMS)] (927 mg, 2 mmol) in hexane (20 mL). This mixture was stirred for 16 h at room temperature, precipitated LiCl was filtered off, and the filtrate was concentrated under vacuum. Compound **4** crystallized in the form of red prisms at −30 °C (1.044 g, 79 %); m.p.: 137 °C; elemental analysis ($C_{29}H_{44}N_4NbSi_3Cl$, 661.31): calcd.: C 52.67, H 6.71, N 8.47; found: C 52.71, H 6.55, N 8.63; ^{1}H NMR (C_6D_6, 297 K): $\delta = 8.52$ (dd, 2 H, Ap), 7.45 (dd, 2 H, Ap), 7.36 (tr, 2 H, Ap), 7.15 – 7.10 (m, 2 H, Ap + Ph), 6.9 – 6.7 (m, 2 H, Ap + Ph), 6.08 – 5.86 (m, 5 H, Ap + Ph), 2.33, 2.29, 2.09, 1.92 (4 s, each 3 H, Me-Ap), 0.76, 0.24, 0.29, 0.23, 0.13, 0.02 (6 s, each 9 H, $SiMe_3$); ^{13}C NMR (C_6D_6, 297 K): $\delta = 227.1$ (*C*$SiMe_3$), 163.9, 164.1, 162.7, 162.4 (C-2, Ap), 156.0, 155.6, 155.1, 154.9 (C-6, Ap), 142.0, 138.9 (*ipso*-C, Ph), 139.7, 139.6, 138.0, 137.9 (C-4, Ap), 133.2, 129.4, 128.9, 128.7, 128.5, 128.3 (*o*-, *m*-, *p*-C, Ph), 115.9, 115.7, 111.5, 111.2, 107.9, 107.6, 105.6, 105.4 (C-3, C-5, Ap), 23.5, 23.4, 21.4, 21.4 (Me, Ap), 2.1, 2.0, 1.9, 1.8, 0.08 ($SiMe_3$); the second quaternary C atom of the alkyne was not detected. Two isomers are present at room temperature in the ratio 1:1; IR (Nujol): $\tilde{\nu} = 1643$ cm^{-1} (C≡C, coordinated).

5: A solution of **4** (661 mg, 1 mmol) in hexane (10 mL) was treated with 1.6 M MeLi (625 μL, 1 mmol) at −40 °C, and stirred for 2 h at room temperature. The reaction solution was filtered and the filtrate was concentrated under vacuum. Red crystalline **5** (327 mg, 51 %) was obtained at −30 °C; m.p.: 168 °C; elemental analysis ($C_{30}H_{47}N_4NbSi_3$, 640.89): calcd.: C 56.22, H 7.39, N 8.74; found: C 56.24, H 7.44, N 9.18; ^{1}H NMR ([D_8]toluene, 230 K): $\delta = 8.01$, 7.52 (d, H-3, Ap), 7.32, 7.08, 6.87, 6.73, 5.95 – 5.86 (m, Ph + Ap), 5.81 (dd, H-5, Ap), 2.24, 2.22, 2.01, 1.88, 1.61, 1.58 (br., each 3 H, Me), 0.65, 0.27, 0.12, 0.08, 0.07, −0.03 (br., each 9 H, $SiMe_3$); ^{13}C NMR ([D_8]toluene, 230 K): $\delta = 235.3$, 235.1 (*C*$SiMe_3$), 165.0, 165.0, 164.9, 164 (C-2, Ap), 155.5, 155.2, 155.1, 155.0 (C-6, Ap), 142.0, 138.8 (*ipso*-C, Ph), 139.9, 139.8, 139.6, 137.9, 137.8, 137.6, 137.5 (C-4, Ap, *o*-, *m*-, *p*-C, Ph), 114.7, 114.5, 110.1, 109.9, 107.7, 107.5, 105.8, 105.6 (C-3, C-5, Ap), 23.5, 23.5, 23.4, 23.3 (Me), 2.1, 1.9, 1.4, 1.8, 1.7, 1.6 ($SiMe_3$); two isomers are present in solution at 230 K in the ratio 2:1; IR (Nujol): $\tilde{\nu} = 1622$ cm^{-1} (C≡C, coordinated).

6: A solution of **5** (641 mg, 1 mmol) in toluene (10 mL) was treated with $B(C_6F_5)_3$ (512 mg, 1 mmol) in toluene (10 mL). The mixture was stirred briefly, filtered, and the volume of the filtrate was concentrated to about half. Compound **6** was obtained as a red powder (1.083 mg, 94 %) at −30 °C. M.p.: 172 °C; elemental analysis ($C_{48}H_{47}N_4NbSi_3BF_{15}$, 1152.88): calcd.: C 50.01, H 4.11, N 4.86; found: C 49.90, H 4.32, N 4.86; ^{1}H NMR ([D_5]bromobenzene, 320 K): $\delta = 7.2 – 7.1$, 6.8 (m, 7 H, Ph, Ap), 5.95 (d, 2 H, Ap), 5.88 (d, 2 H, Ap), 1.44 (s, 6 H, Me), 0.96 (s, 3 H, Me), 0.14 (s, 9 H, $SiMe_3$), −0.07 (s, 18 H, $SiMe_3$); ^{19}F NMR ([D_5]bromobenzene, 297 K): $\delta =$ 182.9 (tr, *m*-F), 179.6 (tr, *p*-F), 147.1 (d, *o*-F); IR (Nujol): $\tilde{\nu} = 1641$ cm^{-1} (C≡C, coordinated).

Received: July 22, 1998 [Z 12191 IE]
German version: *Angew. Chem.* **1998**, *110*, 3565 – 3567

Keywords: homogeneous catalysis · niobium · N ligands · polymerizations

[1] a) W. Kaminsky, M. Arndt, *Adv. Polym. Sci.* **1997**, *127*, 144 – 187; b) M. Bochmann, *J. Chem. Soc. Dalton Trans.* **1996**, 255 – 270; c) R. H. Grubbs, G. W. Coates, *Acc. Chem. Res.* **1996**, *29*, 85 – 93; d) H. H. Brintzinger, D. Fischer, R. Mülhaupt, B. Rieger, R. M. Waymouth, *Angew. Chem.* **1995**, *107*, 1255 – 1282; *Angew. Chem. Int. Ed. Engl.* **1995**, *34*, 1143 – 1170.

[2] a) W. P. Kretschmer, S. I. Troyanov, A. Meetsma, B. Hessen, J. H. Teuben, *Organometallics* **1998**, *17*, 284 – 286; b) H. Vanderheijden, B. Hessen, A. G. Orpen, *J. Am. Chem. Soc.* **1998**, *120*, 1112 – 1113; c) S. Thiel, G. Erker, *Chem. Ber.* **1997**, *130*, 201 – 207; d) J. Christoffers, R. G. Bergmann, *J. Am. Chem. Soc.* **1996**, *118*, 4715 – 4716.

[3] a) J. Jaffart, C. Nayral, R. Choukroun, R. Mathieu, M. Etienne, *Eur. J. Inorg. Chem.* **1998**, 425 – 428; b) K. Hakala, B. Löfgren, M. Polamo, M. Leskelä, *Macromol. Rapid. Comm.* **1997**, *18*, 635 – 638; c) D. M. Antonelli, A. Leins, J. F. Stryker, *Organometallics* **1997**, *16*, 2500 – 2502; d) K. Mashima, S. Fujikawa, Y. Tanaka, H. Urata, T. Oshiki, E. Tanaka, A. Nakamura, *Organometallics* **1995**, *14*, 2633 – 2640; e) G. C. Bazan, S. J. Donnelly, G. Rodriguez, *J. Am. Chem. Soc.* **1995**, *117*, 2671 – 2672; f) S. Scheuer, J. Fischer, J. Kress, *Organometallics* **1995**, *14*, 2627 – 2629.

[4] a) D. Y. Dawson, J. Arnold, *Organometallics* **1997**, *16*, 1111 – 1113; b) D. Y. Dawson, H. Brandt, J. Arnold, *J. Am. Chem. Soc.* **1994**, *116*, 9797 – 9798.

[5] J. B. Hartung, S. F. Pedersen, *Organometallics* **1990**, *9*, 1414 – 1417.

[6] U. Rosenthal, C. Nauck, P. Arndt, S. Pulst, W. Baumann, V. V. Burlakov, H. Görls, *J. Organomet. Chem.* **1994**, *484*, 81 – 87.

[7] A. Ohff, S. Pulst, C. Lefeber, N. Peulecke, P. Arndt, V. V. Burlakov, U. Rosenthal, *Synlett* **1996**, 111 – 118.

[8] Structure analyses of **5** and **6**: STOE-IPDS diffractometer, graphite-monochromated $Mo_{K\alpha}$ radiation, $\lambda = 0.71069$ Å, structure solution with direct methods (SHELXS-86: G. M. Sheldrick, *Acta Crystallogr. Sect. A* **1990**, *46*, 467.), refinement with full-matrix least-squares methods against F^2 (SHELXL-93: G. M. Sheldrick, unpublished results), structure representation: XP (Siemens). **5**: Crystal dimensions $0.4 \times 0.3 \times 0.2$ mm^3, orange prisms, space group $P2_1$, monoclinic, $a = 18.500(2)$, $b = 11.376(1)$, $c = 18.905(2)$ Å, $\beta = 118.38(1)°$, $V =$ 3500.5(7) Å^3, $Z = 2$, $\rho_{calcd} = 1.216$ g cm^{-3}, 10535 measured, 10360 independent reflections, 6543 of which were considered as observed ($I \geq 2\sigma(I)$), $R = 0.046$, $wR^2 = 0.110$ (all data), 685 parameters. **6**: Crystal dimensions $0.5 \times 0.4 \times 0.2$ mm^3, red prisms, space group $P\bar{1}$, triclinic, $a = 12.420(2)$, $b = 16.994(2)$, $c = 17.934(3)$ Å, $\alpha = 77.12(1)$, $\beta = 74.72(1)$, $\gamma = 71.75(1)°$, $V = 3426.8(9)$ Å^3, $Z = 2$, $\rho_{calcd} =$ 1.385 g cm^{-3}, 10273 measured, 10273 symmetry-independent reflections, 8046 of which were considered as observed ($I \geq 2\sigma(I)$), $R =$ 0.054, $wR^2 = 0.174$ (all data), 785 parameters. Crystallographic data (excluding structure factors) for the structures reported in this paper have been deposited with the Cambridge Crystallographic Data Centre as supplementary publication nos. CCDC-101948 (**5**) and CCDC-101949 (**6**). Copies of the data can be obtained free of charge on application to CCDC, 12 Union Road, Cambridge CB21EZ (fax: (+44) 1223-336-033; e-mail: deposit@ccdc.cam.ac.uk).

[9] a) M. Bochmann, S. J. Lancaster, M. B. Hursthouse, K. M. Abdul Malik, *Organometallics* **1994**, *13*, 2235 – 2243; b) R. Gomez, M. L. H. Green, J. L. Haggitt, *J. Chem. Soc. Chem Commun.* **1994**, 2607 – 2608; c) R. Gomez, M. L. H. Green, J. L. Haggitt, *Chem Commun.* **1996**, 939 – 946; d) X. Yang, C. L. Stern, T. J. Marks, *J. Am. Chem. Soc.* **1991**, *113*, 3623 – 3626; e) X. Yang, C. L. Stern, T. J. Marks, *J. Am. Chem. Soc.* **1994**, *116*, 10015 – 10031; f) R. E. von H. Spence, J. D. Parks, W. E. Piers, M.-A. MacDonald, M. J. Zaworotko, S. J. Rettig, *Angew. Chem.* **1995**, *107*, 1337 – 1339; *Angew. Chem. Int. Ed. Engl.* **1995**, *34*, 1230 – 1232; g) R. Baumann, W. M. Davis, R. R. Schrock, *J. Am. Chem. Soc.* **1997**, *119*, 3830 – 3831.

[10] F. H. Allen, O. Kennard, D. G. Watson, L. Brammer, A. G. Orpen, R. Taylor, *J. Chem. Soc. Perkin Trans.* **1987**, S1 – S19.

[11] Compound **6**, for example, is stable in C_6D_5Br for 8 h at 80 °C without significant decomposition (NMR experiment).

 © WILEY-VCH Verlag GmbH, D-69451 Weinheim, 1998 1433-7851/98/3724-3365 $ 17.50+.50/0

Unique Formation of a Crystal Phase Containing Cyclic Oligomers and Helical Polymers of the Same Monomeric Fragment

Norberto Masciocchi,* G. Attilio Ardizzoia,* Girolamo LaMonica, Angelo Maspero, and Angelo Sironi*

Over the last years we have been actively working in the field of metal diazolates, with the aim of finding efficient and selective catalysts for oxidation.[1] In our studies, we tackled the problem of structurally characterizing binary species, precursors of the catalytic species, which are only obtained as fine, insoluble, powdered samples. An appropriate ab initio structure determination technique from X-ray powder diffraction (XRPD) data has been successfully developed,[2] which has led to the complete characterization of, among others, α-$[\{Cu(pz)\}_n]$, β-$[\{Cu(pz)\}_n]$, $[\{Ag(pz)\}_n]$, $[\{Ag(pz)\}_3]$, $[\{Ag(dmpz)\}_3]$, $[\{Cu(dmnpz)\}_3]$, $[\{Ag(imz)\}_n]$, and $[\{Ag(pymo)\}_6]$ (Hpz = pyrazole, Hdmpz = 3,5-dimethylpyrazole, Hdmnpz = 3,5-dimethyl-4-nitropyrazole, Himz = imidazole, Hpymo = 2-hydroxypyrimidine).[3, 4]

The many interesting features displayed by some of these compounds include the existence of different cyclic oligomers and polymeric species for the same monomeric unit and ready accessibility by selective synthetic routes. To our surprise, upon hydration/dehydration the $[\{Ag(pymo)\}_6]$ hexamer[4] reversibly transforms into the $[\{Ag(pymo)\}_n]\cdot 2H_2O$ polymer.[5] Here we report on the synthesis and XRPD structural characterization of the copper analogue.[6]

Treatment of a hot solution in ethanol of an equimolecular amount of $[Cu(CH_3CN)_4][BF_4]$ and Hpymo with NEt_3 causes the sudden precipitation of a yellow microcrystalline powder, which was analyzed to be [Cu(pymo)] (**1**). This very insoluble species could only be characterized by IR spectroscopy[7] and, thanks to its satisfactory degree of crystallinity, by the newly emerging technique of ab initio XRPD.[8] At variance with the spectrum observed for $[\{Ag(pymo)\}_6]$ ($\tilde{\nu}_{CO} = 1618\ cm^{-1}$),[4] the IR spectrum of **1** evidences at least two different CO environments ($\tilde{\nu}_{CO} = 1614$ and $1590\ cm^{-1}$), which suggests a more complex structure. Differential scanning calorimetry (DSC) and thermogravimetric analysis (TGA) of **1** under an N_2 atmosphere revealed no phase transitions nor solvent desorption up to about 350 °C, where decomposition to metallic copper occurred. We have tried to synthesize different crystal phases by changing the synthetic method or by applying heat or pressure (up to 1 GPa for 24 h), but we always observed the XRPD pattern of **1**. Solubilization of **1** was only possible by reaction with PPh_3 in CH_2Cl_2 to afford the monomeric complex $[Cu(PPh_3)_2(pymo)]$.[9]

The XRPD pattern, collected in the range $4 < 2\theta < 94°$ on an annealed sample of **1** (3 h at 200 °C under N_2), was fully indexed with TREOR[10] [monoclinic P, $a = 8.63$, $b = 13.81$, $c = 9.81$ Å, $\beta = 112.5°$, $V = 1080$ Å^3, $M(20)$[11] $= 19$, $F(20)$[12] $= 36$ (0.012, 43)]. Unfortunately, the 367 extracted intensities (with $2\theta < 64°$) did not afford any reasonable Patterson map, nor were direct methods successful in offering a suitable structural model in the "compatible" space groups. Only the search for higher symmetry metrics and supercells[13] evidenced a possible relationship between the available cell and a trigonal/hexagonal cell with a much larger (6×) cell volume (ca. 6500 Å^3). Suddenly, we recognized that our problem fell into one of the special cases studied by Mighell and Santoro.[14] They foresaw that different lattices with different reduced cell volumes may afford identical peak positions (in the monodimensional 2θ space), leading to ambiguous cell choices (clearly, such ambiguity does not exist in three-dimensional single-crystal diffractometry). Therefore, a new R-centered cell ($a = 27.58$, $c = 9.81$ Å) was used (with $Z = 54$!). However, owing to the 1-D projection of the reciprocal space inherent in powder experiments, the Laue group was still uncertain and a number of possible space groups, and therefore a multitude of structure-solution processes, had to be considered ($R\bar{3}m$ or one of its subgroups).

No matter which space group was chosen, the approximate locations of the metal atoms could be derived by Patterson and/or direct methods. This showed that the copper atoms were roughly arranged in columns running parallel to c, with interatomic distances of about $c/3$. After optimization of lattice parameters, background, and peak shape by the Le Bail technique,[15] refinement of the locations of the copper atoms in the space groups $R\bar{3}$, $R32$, $R3m$, and $R\bar{3}m$ versus the high-angle data ($2\theta > 30°$) clearly revealed $R\bar{3}$ as the best candidate (with three crystallographically independent copper atoms), while a refinement in $R3$ was found to be unstable. A significant asymmetrization of the initial Cu···Cu contacts was achieved; two interactions are markedly shorter than the third (ca. 3 versus ca. 4 Å).

These distances are much shorter than those expected for metals bridged by N,N'-pymo ligands (ca. 5.5–6.0 Å) and similar to those found for many unsupported Cu···Cu intermolecular interactions; therefore, the ligands must be roughly oriented in the ab plane. Analysis of the possible connectivity patterns (consistent with linearly bicoordinated metals) derived by joining metals which are about 5.7 Å apart in the space group $R\bar{3}$ revealed the existence of heterochiral helices (winding up about the 3_1 and 3_2 axes), leaving holes suitable for a cyclic hexamer of $\bar{3}$ crystallographic symmetry. Consistently, a difference Fourier map confirmed the presence of peaks near the positions expected for the nitrogen atoms from the above topological analysis. The remaining atoms were then determined by a combination of several difference Fourier maps and geometrically restrained Rietveld refinements. However, owing to the non-holoedric nature of the Laue group of **1**, the initial location of the C, N, and O atoms was of poor quality and the refinements were slow and rather unstable. Therefore, an

[*] Prof. A. Sironi, Dr. N. Masciocchi
Dipartimento di Chimica Strutturale e Stereochimica Inorganica
Università di Milano
via Venezian 21, I-20133 Milano (Italy)
Fax: (+39) 02-7063-5288
E-mail: angelo@csmtbo.mi.cnr.it

Dr. G. A. Ardizzoia, Prof. G. La Monica, Dr. A. Maspero
Dipartimento di Chimica Inorganica, Metallorganica e Analitica and Centro C.N.R.
Università di Milano
via Venezian 21, I-20133 Milano (Italy)
E-mail: attilio@csmtbo.mi.cnr.it

 © WILEY-VCH Verlag GmbH, D-69451 Weinheim, 1998 1433-7851/98/3724-3366 $ 17.50+.50/0

additional intermediate geometry optimization was performed (to minimize the overall (steric + packing) energy of the crystal) with the aid of a locally developed molecular mechanics program capable of dealing with, inter alia, polymers.[16] Our experience[17] has shown that the imperfect parametrization of the metal force field only marginally affects the geometry of the crystal packing once the positions of the metal atoms are fixed in their experimental locations. Indeed, feeding the optimized coordinates into the program GSAS[18] afforded an R_{wp} value as low as 0.09, which was a very good starting point for the final refinement against powder data only (with some intramolecular restraints for the pymo rings).

The crystal structure determination[19] surprisingly led to the formulation of **1** as a crystal phase containing separate hexamers (Figure 1a) and helical polymers (Figure 1b) in a 1:2 ratio. The digonal copper atoms are bound to

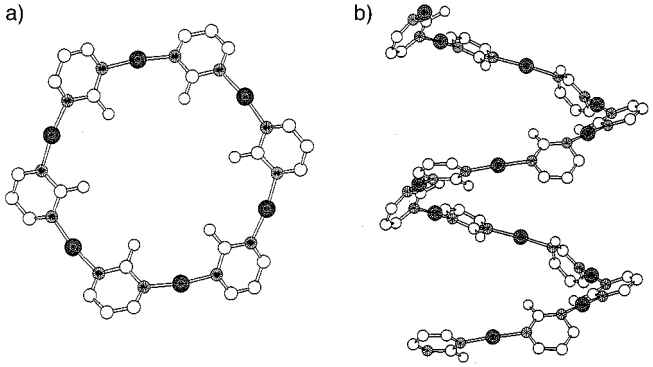


Figure 1. Molecular drawing of a) the $[\{Cu(pymo)\}_6]$ hexamer and b) a portion of the infinite helix of $[\{Cu_2(pymo)_2\}_n]$.

bidentate *N,N′*-pymo ligands (N7-Cu1-N8 177(1), N24-Cu13-N26 174(1), N25-Cu12-N27 175(1)°).[20] Therefore, **1** is better described as a $1/6[\{Cu(pymo)\}_6]\cdot 1/n[\{Cu_2(pymo)_2\}_n]$ adduct (stoichiometrically consistent with the original [Cu(pymo)] formulation). The helices contain six Cu(pymo) monomers per turn (with a pitch of 9.79 Å)—that is, they possess rare (noncrystallographic) 6_1 (or 6_5) character[21]—and are heavily compenetrated; each helix is trigonally surrounded by three helices of opposite chirality (Figure 2). This trigonal packing (hexagonality value $H = 1.73$), which is typical for heterochiral helices, is indeed favored by large compenetration.[22] It is noteworthy that adjacent helices are displaced by about one-third (and not one-half) of their pitch. In the space left by the packing of six adjacent helices, a closed cavity is formed (Figure 3) which perfectly matches the size and shape of $[\{Cu(pymo)\}_6]$.[23] Thus, once the hexamers fill this space, there are no other (solvent-accessible) holes in the packing of the helices in **1**. The helical nature of the polymeric portion of **1** closely ressembles that of poly(*m*-phenylene)[24] and the polyheterocyclic strand recently reported by Lehn et al.[25] Our observations thus confirm that *meta*-coordinated aromatic moieties (directly linked or connected by linear spacer(s) such as Cu^I atoms in **1**) favor helicity in their open oligomers and polymers.[26]

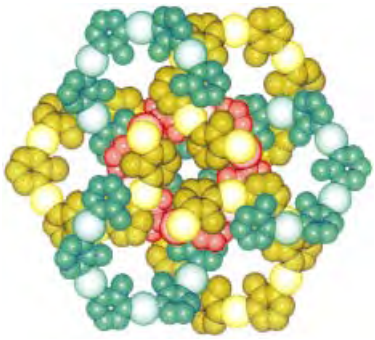


Figure 2. A packing diagram of compound **1**, viewed along [001]. Helices of different polarity are depicted by different colors (yellow and green). Within this trigonal packing of helices, the closed cavity about the origin hosts the $[Cu(pymo)]_6$ hexamer (red).

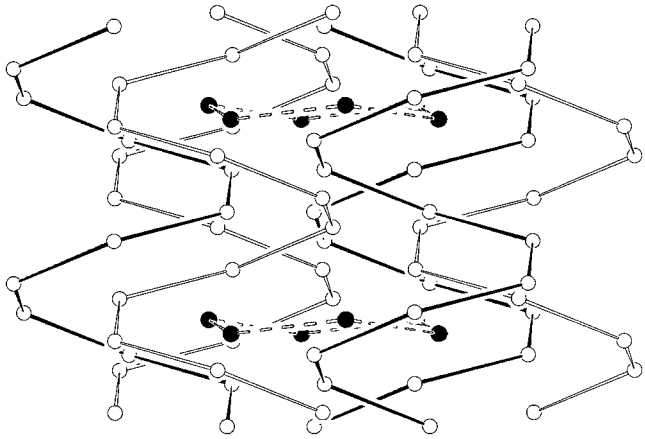


Figure 3. Schematic drawing of the *pseudo*-channel, defined by six adjacent helices, containing the $[Cu(pymo)]_6$ hexamers, viewed along [010] (the vertical axis is [001], black and white helices have opposite polarity). This channel periodically widens about the hexamers and shrinks above and below them.

Interestingly, all ligand-unsupported Cu···Cu contacts between adjacent helices (Cu12···Cu13 2.69(1) Å) are much shorter than those between helices and oligomers (Cu1···Cu13 2.96(1), Cu1···Cu12 4.36(1) Å), and fall well below the range observed in a number of related compounds.[3a] To our knowledge these contacts are the shortest ever observed in the absence of bridging ligands. This indicates either that the coupling of helices about these hinges might be the driving force for formation of the cavities or that the intrinsic size of the oligomers forces the helices to couple. This coupling offers evidences for a correlation between intermetallic distances and the color of the species: All analogues of general formulae $[\{CuL\}_n]$ (L = a monoanionic diazolate) are white and show longer (> 2.96 Å) distances.[3a] In contrast, **1** is yellow—like $[\{Cu(pz^*)\}_3]$ (Hpz* = 2-[3(5)-pyrazolyl]pyridine; 2.90 Å) and $[\{Cu(bmip)\}_2][ClO_4]_2$ (bmip = 2,6-bis(1-methylimidazol-2-yl)pyridine; 2.82 Å)[27]—while the $[\{Cu(dpad)\}_3]$ (dpad = 1,5-ditolyl-1,4-pentaazadien-3-ide) trimer is red even in solution due to the presence of very short intramolecular contacts (2.35 Å).[28]

With respect to metal diazolates, our structural study is novel in that 1) nondegenerate (i.e., non-2_1) helices were observed for the first time, and 2) the $[Cu(pymo)]_6$ unit has a

 © WILEY-VCH Verlag GmbH, D-69451 Weinheim, 1998 1433-7851/98/3724-3367 $ 17.50+.50/0

unique, high-symmetry (S_6) conformation.[4, 29] Above all, the fact that a polymer and one of its cyclic oligomers coexist in an ordered fashion in the same crystal lattice has never been reported before in any field.[30] Since such coordination polymers possessing labile metal–nitrogen bonds rarely dissolve without depolymerization, it is very unlikely that hexameric and polymeric molecules of **1** exist in solution. Thus, the rapid and unique formation of solid **1** can only be explained by a very selective self-recognition process at the crystal/solution interface promoting the actual crystal phase, but not the individual separate end members. This means that the nucleation process simultaneously controls the kinetics of the crystallization and the nature of the products. Hence, mixed phases similar to **1** may not be rare in the realm of "catenated" coordination compounds if a suitable nucleus is formed.[31]

Received: June 22, 1998 [Z12029IE]
German version: *Angew. Chem.* **1998**, *110*, 3561–3564

Keywords: copper · cyclooligomerizations · polymers · structure elucidation · X-ray powder diffraction

[1] G. LaMonica, G. A. Ardizzoia, *Prog. Inorg. Chem.* **1997**, *46*, 151–238, and references therein.
[2] N. Masciocchi, A. Sironi, *J. Chem. Soc. Dalton Trans.* **1997**, 4643–4650.
[3] N. Masciocchi, M. Moret, P. Cairati, A. Sironi, G. A. Ardizzoia, G. LaMonica, *J. Am. Chem. Soc.* **1994**, *116*, 7668–7676; N. Masciocchi, M. Moret, P. Cairati, A. Sironi, G. A. Ardizzoia, G. LaMonica, *J. Chem. Soc. Dalton Trans.* **1995**, 1671–1675; N. Masciocchi, P. Cairati, A. Sironi, *Powder Diffr.* **1998**, *13*, 35–40; G. A. Ardizzoia, S. Cenini, G. LaMonica, N. Masciocchi, A. Maspero, M. Moret, *Inorg. Chem.* **1998**, 4284–4292.
[4] N. Masciocchi, E. Corradi, M. Moret, G. A. Ardizzoia, A. Maspero, G. LaMonica, A. Sironi, *Inorg. Chem.* **1997**, *36*, 5648–5650.
[5] M. Quiros, *Acta Crystallogr. Sect. C* **1994**, *50*, 1236–1238.
[6] We have also prepared the "[Au(pymo)]" analogue, but, despite its evident polycrystalline nature, we were not able to determine its structure from the rather complex XRPD pattern. However, we can easily rule out its being isomorphous with [{Ag(pymo)}$_6$] or **1**.
[7] IR spectral data for **1** (nujol): $\tilde{\nu}$ = 1614 (s), 1590 (s), 1368 (s), 1356 (s), 1280 (s), 1268 (s), 1130 (m), 1089 (m), 1043 (m), 1002 (w), 973 (w), 798 (s), 771 (m), 764 cm^{-1} (m).
[8] A. K. Cheetham in *The Rietveld Method* (Ed.: R. A.Young), Oxford University Press, New York, **1993**; K. D. M. Harris, M. Tremayne, *Chem. Mater.* **1996**, *8*, 2554–2560; J. I. Langford, D. Louër, *Rep. Prog. Phys.* **1996**, *59*, 131–234; D. M. Poojary, A. Clearfield, *Acc. Chem. Res.* **1997**, *30*, 414–422.
[9] G. A. Ardizzoia, G. LaMonica, M. Moret, N. Masciocchi, unpublished results.
[10] P. E. Werner, L. Eriksson, M. Westdahl, *J. Appl. Crystallogr.* **1985**, *18*, 367–370.
[11] P. M. De Wolff, *J. Appl. Crystallogr.* **1968**, *1*, 108–113.
[12] G. S. Smith, R. L. Snyder, *J. Appl. Crystallogr.* **1979**, *12*, 60–65.
[13] Y. Le Page, *J. Appl. Crystallogr.* **1982**, *15*, 255–259; A. K. Spek, *J. Appl. Crystallogr.* **1988**, *21*, 578–579.
[14] A. D. Mighell, A. Santoro, *J. Appl. Crystallogr.* **1975**, *8*, 372–377.
[15] A. Le Bail, H. Duroy, J. L. Fourquet, *Mater. Res. Bull.* **1988**, *23*, 447–452.
[16] P. L. Mercandelli, M. Moret, A. Sironi, *Inorg. Chem.* **1998**, *37*, 2563–2569.
[17] E. Corradi, N. Masciocchi, G. Palyi, R. Ugo, A. Vizi-Orosz, C. Zucchi, A. Sironi, *J. Chem. Soc. Dalton Trans.* **1997**, 4651–4655; N. Masciocchi, F. Ragaini, S. Cenini, A. Sironi, *Organometallics* **1998**, *17*, 1052–1057.
[18] A. C. Larson, R. B. Von Dreele, LANSCE, MS-H805, Los Alamos National Laboratory, New Mexico, **1990**.
[19] a) Crystal data for **1**, $C_4H_3CuN_2O$: M_r = 158.62, trigonal, space group $R\bar{3}$, $a = b = 27.581(1)$, $c = 9.7870(6)$ Å, $V = 6447.8(5)$ Å^3, $Z = 54$, $\rho_{calcd} = 2.206$ g cm^{-3}, $\mu(Cu_{K\alpha}) = 53.61$ cm^{-1}, $F(000) = 4210$; $R_{wp} = 0.052$, $R_p = 0.032$, and $\chi 2 = 3.80$ for 107 parameters, 84 restraints, and 4051 data points collected in the range $8 < 2\theta < 89°$ (1173 reflections, $R_F = 0.067$) on a Rigaku D-III/MAX powder diffractometer equipped with Soller slits and a secondary beam graphite monochromator; optics used: DS/AS/RS 1.0/1.0/0.3°, θ:2θ step scan, $\Delta 2\theta = 0.02°$, $t = 12$ s step^{-1}. The structure was solved by Patterson methods, difference Fourier transformation, and geometrical modeling, and refined by GSAS.[18] The C–C (1.35 Å), C–N (1.35 Å), C–O (1.20 Å), and C–H bond distances (0.95 Å) and pymo ring angles (120°) were restrained at the values given. The refined isotropic thermal parameters (U_{iso}) for copper and the lighter atoms were 0.057(1) and 0.077(1) Å^2, respectively. The final Rietveld refinement plot is shown in Figure 4. b) Crystallographic data (excluding structure factors) for the structure reported in this paper have been deposited with the Cambridge Crystallographic Data Centre as supplementary publication no. CCDC-101957. Copies of the data can be obtained free of charge on application to CCDC, 12 Union Road, Cambridge CB2 1EZ, UK (fax: (+44) 1223-336-033; e-mail: deposit@ccdc.cam.ac.uk).

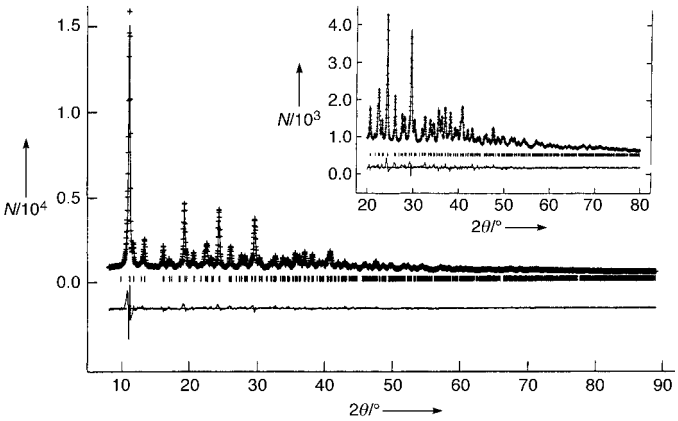


Figure 4. Rietveld refinement plot in the range $8 < 2\theta < 89°$ (λ = 1.5405 Å). The peak markers and the difference plot are given at the bottom. The insert shows an enlargement of the high-angle region. N = number of counts.

[20] The atom numbers refer to the atom sequence in the table of fractional atomic coordinates deposited with the Cambridge Crystallographic Data Centre.[19b]
[21] Recent examples: S. R. Batten, B. F. Hoskins, R. Robson, *Angew. Chem.* **1997**, *109*, 652–653; *Angew. Chem. Int. Ed. Engl.* **1997**, *36*, 636–637; M. A.Withersby, A. J. Blake, N. R. Champness, P. Hubberstey, W. S. Li, M. Schroeder, *Angew. Chem.* **1997**, *109*, 2421–2423; *Angew. Chem. Int. Ed. Engl.* **1997**, *36*, 2327–2329.
[22] S. V. Meille, G. Allegra, *Macromolecules* **1995**, *28*, 7764–7769.
[23] Heterochiral helices alone could pack in the same space group with no cavities but with a shorter pitch (ca. 6.50 Å) to ensure constancy of the crystal density.
[24] D. J. Williams, H. M. Colquhoun, C. A. O'Mahoney, *J. Chem. Soc. Chem. Commun.* **1994**, 1643–1644.
[25] G. S. Hanan, J. M. Lehn, N. Kyritsakas, J. Fischer, *J. Chem. Soc. Chem. Commun.* **1995**, 765–766.
[26] A. E. Rowan, R. J. M. Nolte, *Angew. Chem.* **1998**, *110*, 65–71; *Angew. Chem. Int. Ed. Engl.* **1998**, *37*, 63–68.
[27] K. Singh, J. R. Long, P. Stavropoulos, *J. Am. Chem. Soc.* **1997**, *119*, 2942–2943; R. F. Carina, G. Berardinelli, A. F. Williams, *Angew. Chem.* **1993**, *105*, 1483–1485; *Angew. Chem. Int. Ed. Engl.* **1993**, *32*, 1463–1465.
[28] J. Beck, J. Strähle, *Angew. Chem.* **1985**, *97*, 419–420; *Angew. Chem. Int. Ed. Engl.* **1985**, *24*, 409–410.

 © WILEY-VCH Verlag GmbH, D-69451 Weinheim, 1998 1433-7851/98/3724-3368 $ 17.50+.50/0

[29] R. G. Raptis, H. H. Murray III, J. P. Fackler, Jr., *J. Chem. Soc. Chem. Commun.* **1987**, 737–739; H. H. Murray III, R. G. Raptis, J. P. Fackler, Jr., *Inorg. Chem.* **1988**, *27*, 26–31.

[30] From a formal point of view, also $NaCD_3$ (E. Weiss, S. Corbelin, J. K. Cockroft, A. N. Fitch, *Angew. Chem.* **1990**, *102*, 728–729; *Angew. Chem. Int. Ed. Engl.* **1990**, *29*, 650–652; E. Weiss, S. Corbelin, J. K. Cockroft, A. N. Fitch, *Chem. Ber.* **1990**, *123*, 1629–1634) contains oligomers (in this case, tetramers) and polymeric chains. However, owing to a number of short intermolecular Na–C contacts between the two structural units, this distinction is not so evident.

[31] Indeed, a recent single-crystal structure determination performed in our laboratory on $[Ag(pyridazine)]NO_3$ has shown the copresence of dimers and 2_1-helical polymers: L. Carlucci, G. Ciani, D. M. Proserpio, A. Sironi, *Inorg. Chem.* **1998**, in press.

Combinatorial Material Libraries on the Microgram Scale with an Example of Hydrothermal Synthesis**

Jens Klein, Christian W. Lehmann, Hans-Werner Schmidt, and Wilhelm F. Maier*

Dedicated to Sir John Meurig Thomas on the occasion of his 65th birthday

As a consequence of the large number of possible polynary mixtures of oxidic materials, together with the potential use of many template molecules, it is attractive to apply combinatorial methods to hydrothermal synthesis.[1] While combinatorial methods are already established as important tools for the development of new lead structures in the areas of organic, biochemical, and pharmaceutical chemistry,[2] there are only a few examples known in the area of inorganic materials research or technical catalyst development. In particular the groups of P. G. Schultz and W. H. Weinberg have been actively involved since the mid 1990s in the development of combinatorial synthesis of new materials. These activities concentrated on the search of new compositions with superconducting,[3] magnetoresistant,[4] or luminescent[5] properties.

These applications are based on the deposition of the compounds as thin films through electron beam evaporation or RF sputtering. The library structure was obtained by the use of physical masks with lattice sizes between 100×100 and $200 \times 200\ \mu m^2$. Libraries with up to 25 000 different materials have been prepared and investigated by routine methods and new lead structures have already been "discovered".[3–5]

The most challenging problem is the analysis and characterization of the properties of interest. The amount of each sample is extremely small because of the miniaturized dimensions necessary for the generation of large libraries of materials. Akporiaye, Karlsson, and Wendelbo[6] published recently the application of combinatorial methods for hydrothermal synthesis. They developed an autoclave that allows 100 hydrothermal syntheses to be run in parallel at temperatures up to 200 °C. The phase diagram obtained in such a single experiment has been used to demonstrate the potential strengths of combinatorial approaches in the area of the synthesis of solid-state materials. In these experiments the reaction volumes were still in the range of 0.5 mL. The identification of the phases prepared still required manual removal of the solids from the reactors, followed by individual measurements with conventional X-ray diffraction techniques. The authors give no information on concentration and amounts of product actually achieved, but the amounts required were in the range of 1–10 mg. The sample handling after synthesis is still quite cumbersome. Every sample has to be prepared individually. Since we have been engaged for some time in the area of combinatorial methods for material synthesis, the above publication prompted us to present the results of our work.

The advantage of our reactor is the direct preparation of a library of materials, whose components can be identified automatically on the library substrate by X-ray microdiffraction. Another advantage is the reaction volume, which is smaller by a factor of 250 relative to that used in reference [6]. Figure 1 shows the construction with dimensions of the pressure reactor. For simplification the model shown has only 37 reaction chambers (each of diameter 1.4 mm and height 4 mm). There is no technical problem in reducing the size and



Figure 1. A cross-section of the multireactor autoclave (top) and a photograph of the individual reactor parts (bottom) with the orignial library on the Si wafer (second disk from the left).

[*] Prof. Dr. W. F. Maier, Dipl.-Chem. J. Klein, Dr. C. W. Lehmann, H.-W. Schmidt
Max-Planck-Institut für Kohlenforschung
Kaiser-Wilhelm Platz 1, D-45470 Mülheim an der Ruhr (Germany)
Fax: (+49) 208-306-2987
E-mail: maier@mpi-muelheim.mpg.de

[**] We thank the application laboratory of the Bruker AXS Company, Karlsruhe (Germany), especially A. Iberl for the use of their GADDS equipment and their support during the data collection. W.F.M. also thanks R. Boese for helpful discussions.

 © WILEY-VCH Verlag GmbH, D-69451 Weinheim, 1998 1433-7851/98/3724-3369 $ 17.50+.50/0

increasing the number of the drilled holes to provide about 100 chambers on an area of about 4 cm^2. The bottom of the reactor is a Si wafer, the reactor walls (teflon disk with drilled holes) are pressed onto the Si disk by the steel disk that contains the same drilling pattern as the teflon disk. The reaction mixtures are dosed in amounts of up to 2 μL by a microliter pipette or a robot. The theoretical amounts of material obtainable range between 50 and 150 μg, the concentration of the reaction solutions are around 1 $\mu mol\,\mu L^{-1}$. By proper dilution of the reaction solution it can be assumed that the dosing of such small volumes is not affected by the viscosity. Once filled the reactor is sealed by a teflon disk, whose pressure can be adjusted by the top steel disk. This multichamber microautoclave is then brought to the reaction temperature required for hydrothermal synthesis conditions. After completion of the reaction the autoclave is cooled to room temperature and the reaction solution is separated from the solids formed by using small porous rods, with the solids remaining on the surface of the Si wafer. This procedure does by no means lead to quantitative recovery of the solid on the Si wafer, since together with some of the liquid some crystals will stick to the porous rod as well as to the inner teflon and steel walls of the reactor. However, quantitation is not the subject of this technique, since only a few crystals are required to obtain the desired diffraction pattern for identification. The product is washed several times with distilled water directly in the microreactors. The open autoclave is then heated to 100 °C to remove the remaining moisture. Thereafter, the Si wafer with the dried-on crystals can be removed and calcined at the desired temperature. During calcination the products sinter onto the Si wafer and the wafer then represents the library. The identification of the individual products can be carried out directly with a GADDS microdiffractometer from Bruker AXS. The powder diffractrograms are recorded with a 500 μm collimator that illuminates the whole spot area. The X-ray beam can be focussed maintaining high X-ray intensity by means of bent Göbel mirrors[8] to a diameter of 50 μm, whereby individual μm-sized particles become accessible to X-ray analysis. The library is mounted on the xyz stage of the diffractometer and the diffractograms are obtained in the reflection mode after the step parameters have been specified and the points to be measured identified. Because of the short sampling time required for each sample a large number of diffractrograms of individual spots as well as individual particles can be recorded overnight.

The practical application of such a combinatorial material synthesis has been investigated under hydrothermal conditions. The recipe for the preparation mixture of the well-known titanium-containing silicalite TS-1[7] was selected as the reference solution and the template molecules and metal components varied. The only information expected was "crystalline or amorphous" with a qualitative indication of the class of materials that had been formed. Figure 2 shows the actual library with the associated distances and spot identification codes. Each microreactor was filled with 2 μL of the individual reaction solutions. Table 1 summarizes the molar compositions of the various reaction mixtures. The reactor was sealed and treated as described above. The

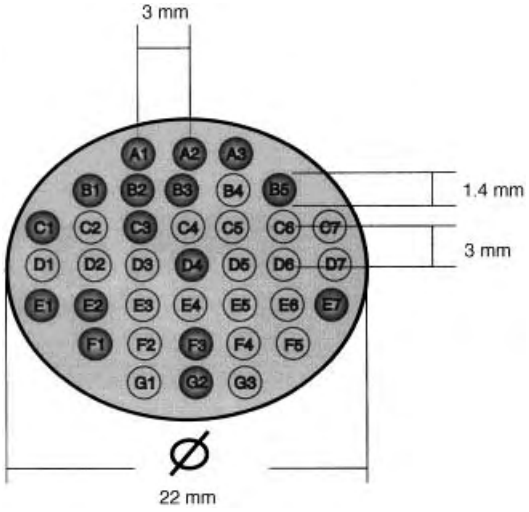


Figure 2. Identification plan of the library with the dimensions of the reactor chambers shown. The spots marked dark gray showed some crystallinity.

Table 1. Composition of the library shown in Figure 2.[a]

Chamber	Composition	Chamber	Composition
A1	Si:Ti:NPr_4OH 1:0.03:0.45	D5	Al:Ti:CTAB 1:0.05:0.1
A2	Si:Ti:NBu_4OH 1:0.03:0.45	D6	Al:Zr:NBu_4OH 1:0.2:0.4
A3	Si:Ti:NEt_4OH 1:0.03:0.45	D7	Al:Zr:NMe_4OH 1:0.2:0.4
B1	Si:Ti:NMe_4OH 1:0.03:0.45	E1	Al:Zr:NEt_4OH 1:0.2:1
B2	Si:Ti:C_4H_9N 1:0.03:0.45	E2	Al:Zr:CTAB 1:0.2:0.1
B3	Si:Ti:CTAB 1:0.03:0.045	E3	Ti:Zr:NBu_4OH 1:1:0.4
B4	Si:Ti:hexadecylamine 1:0.03:0.045	E4	Ti:Zr:NBu_4OH 1:1:0.4
B5	Si:Ti:hexadecylamine:NaOH 1:0.03:0.045:0.45	E5	Ti:Zr:NMe_4OH 1:1:0.4
C1	Si:Al:NPr_4OH 1:0.033:0.43	E6	Ti:Zr:NEt_4OH 1:1:1
C2	Si:Al:NPr_4OH 1:0.066:0.43	E7	Ti:Zr:CTAB 1:1:0.1
C3	Si:Zr:NPr_4OH 1:0.03:0.98	F1	Si:Ti:NPr_4OH 1:0.03:0.45
C4	Si:V:NPr_4OH 1:0.03:0.45	F2	Si:V:NPr_4OH 1:0.03:0.45
C5	Si:Zr:NBu_4OH 1:0.03:0.4	F3	Si:Ti:NEt_4OH 1:0.03:0.45
C6	Si:Zr:NMe_4OH 1:0.03:0.4	F4	Si:Zr:NPr_4OH 1:0.01:0.98
C7	Al:Ti:NBu_4OH 1:0.05:0.4	F5	Si:Al:NPr_4OH 1:0.1:0.43
D1	Al:Ti:NMe_4OH 1:0.05:0.4	G1	Si:Ti:NPr_4OH 1:0.03:0.45
D2	Al:Ti:NEt_4OH 1:0.05:1	G2	Al:Si:NPr_4OH 1:0.2:0.43
D3	Al:Ti:NEt_4OH 1:0.05:1	G3	Al:Si:NPr_4OH 1:0.1:0.43
D4	Al:Ti:CTAB 1:0.05:0.1		

[a] The molar ratio of the metal alkoxide (and also of the oxidized material in the product) and the templates are given under the composition. The sources for SiO_2, TiO_2, ZrO_2, and Al_2O_3 were tetraethoxysilane ($Si(OEt)_4$, TEOS), $Ti(OEt)_4$, $Ti(OiPr)_4$ or $Ti(OnPr)_4$, $Zr(OnPr)_4$ and $Al(OsBu)_3$. After removal of the alcohol from the externally prepared samples the reaction solutions were filled to 7.5 mL with distilled water, so that an excess of water was present for the hydrothermal synthesis of all samples (water:metal = 40:1).

 © WILEY-VCH Verlag GmbH, D-69451 Weinheim, 1998 1433-7851/98/3724-3370 $ 17.50+.50/0

crystals formed on the Si wafer were then automatically characterized by X-ray diffraction studies.[9]

The dark dots in Figure 2 identify those positions containing crystalline materials. Figure 3 shows the amplified picture of one individual spot on the library surface. This photograph gives a good impression of the morphology of the materials assembled on the surface of the Si wafer. In the center of the

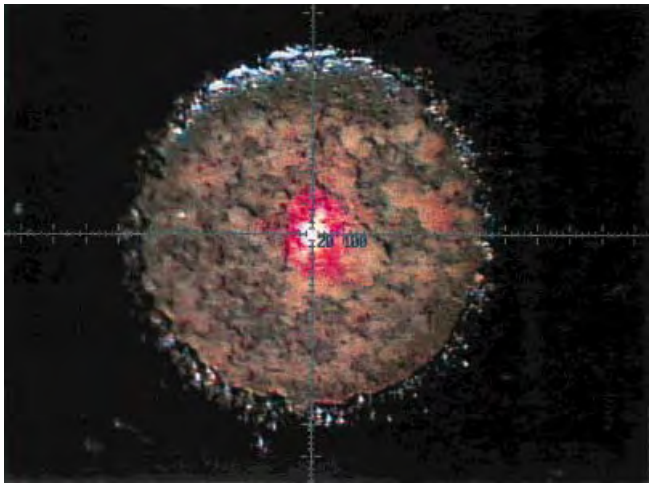


Figure 3. Photograph of the library spot B5 with the laser spot in the center (magnification 57).

cross-hairs a red laser spot can be identified, which is used to specify the position for the automated X-ray diffraction measurements. Figure 4 shows a typical X-ray image and the corresponding diffraction pattern obtained after integration,

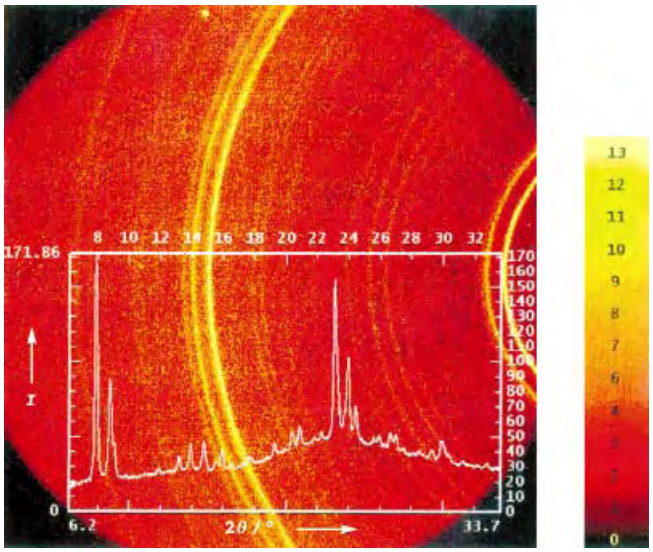


Figure 4. Typical diffraction pattern (number of faces) with the integrated reflection profile overlaid (point A1).

which is necessary to average particle and orientation effects that arise from the very small sample volume. Reflections from the library support were not brought into the diffracting position as a consequence of the selected measurement geometry.

Figure 5 shows the diffractograms of the two sample dots that contained the original synthesis solution for TS-1. Despite the small sample volume and the extremely small distances on the library an identical reproduction of the

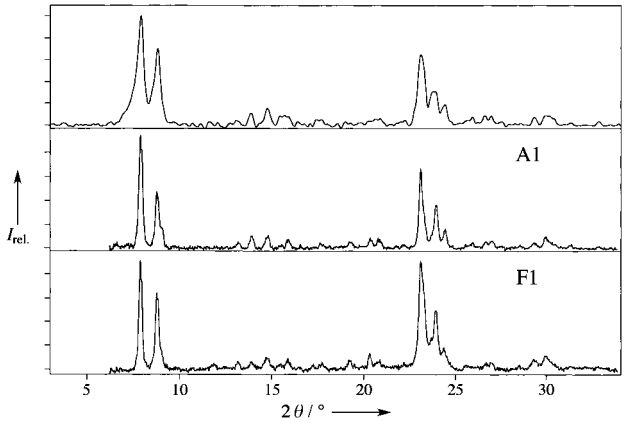


Figure 5. Comparison of the X-ray diffractogram from a conventionally obtained TS-1 sample (top) with the diffractograms from the library points A1 and F1 (middle and bottom, respectively).

original diffractogram[7] of TS-1 has been obtained, which confirms that zeolite synthesis on a microgram scale is possible and justified. Figure 6 displays selected diffractograms obtained from materials, which all show the MFI pattern typical for silicalites. This is not very surprising, since it is well-known that the identical structure of many Si-rich pentasil zeolites can be obtained with significantly different template molecules, such as diaminoalkanes, tetraalkylammonium, sols, or *n*-alkylamines.[10]

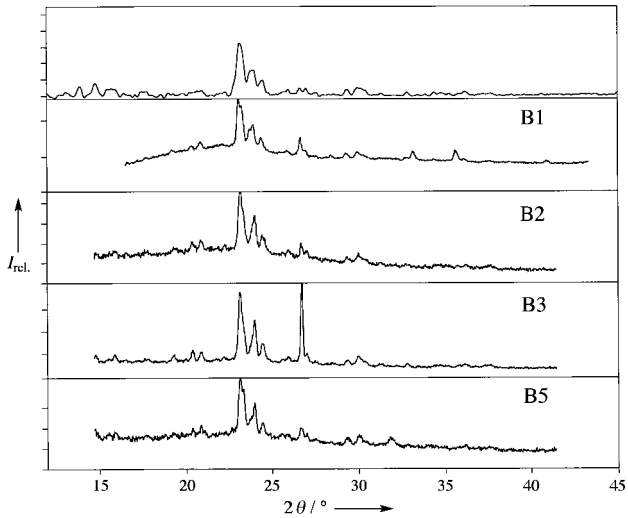


Figure 6. Diffractograms of the library points B1 – B5 showing the MFI structure typical for silicalites. The diffractogram of conventionally synthesized TS-1 is shown at the top.

Figures 3 – 6 show that by measurement over a larger 2θ area a complete phase identification is possible. Surprisingly, amorphous samples were also formed despite the pretreatment temperatures of 600 °C. The intensive powder line at

 © WILEY-VCH Verlag GmbH, D-69451 Weinheim, 1998 1433-7851/98/3724-3371 $ 17.50+.50/0

26.65° of sample B3 is also consistant with the (101) reflection of quartz, and also with a preferred orientation of silicalite crystals. Under the reaction conditions used an oxidation of the Si-library substrate can be excluded, which is supported by the lack of such a reflection in the rest of the library. Examination of the dot areas after the experiment by light microscopy shows no signs of attack of the single crystal–wafer surface after removal of the crystal layers. For detailed characterization of the individual materials formed the interesting reactions identified by X-ray diffraction would have to be repeated and investigated by conventional means in the laboratory.

Our reaction system combined with analyses has an enormous potential for increased efficiency in the development of new materials and the automatization of characterization of samples obtained by combinatorial methods, and it is certainly not limited to the synthesis under hydrothermal conditions. Currently, the lower limit of 50 μm for the focussing of the X-ray beam restricts the miniaturization of the diameter of the microreactors. The material selected for the reactor walls limits reaction temperatures up to 300 °C; much higher temperatures may become possible through the selection of different polymeric materials. An increase in the library dimension to 10 cm diameter as well as a decrease in the drilling distance can readily be realized without technical problems.

Minimization of the manual efforts for the preparation of starting solutions as well as for the filling of the microreactors can be achieved readily with commercially available pipetting robots. Even the direct synthesis in the reactor by the direct use of ultrasound for proper mixing of the tiny probe volumes is realizable. In general, every solid synthesis in liquid phase under pressure and temperature should be possible. Such a reactor should be ideal for the combinatorial screening of new microcrystalline or amorphous solids, especially since the reactor bottom can be exchanged and libraries can be prepared directly on the substrate of choice.

Experimental Section

Our standard experimental conditions for the preparation of this material library have been described in the original literature of Taramasso et al.[7] Since only very small amounts are necessary to fill of the microreactors, the reaction volumes were reduced by a factor of 200 and mixed in 10-mL flasks. The reaction mixtures have been modified as described in Table 1. A1 and F1 each contain the original recipe as described in the patent.

The reaction was carried out in a sealed autoclave at a temperature of 200 °C for 36 h. After reaction the mother liquor was separated from the microreactor and the remaining crystals in the microreactor were washed several times with 2 μL of destilled water. The removal of the liquid was achieved by the capillary forces of porous rods directly in the microreactors. The compounds were then dried in the open microreactors at 100 °C. After removal of the teflon and steel mask the Si wafer with the dried-on crystal products were calcined at 600 °C for 10 h.

Received: April 30, 1998 [Z11806IE]
German version: *Angew. Chem.* **1998**, *110*, 3557–3561

Keywords: · combinatorial chemistry · hydrothermal synthesis · materials science · X-ray powder diffraction

[1] E. P. Feijen, J. A. Martens, P. A. Jacobs in *Studies in Surface Science and Catalysis*, *Vol. 84*, **1994**, pp. 3–21; A. Corma, *Chem. Rev.* **1997**, *97*, 2373–2419
[2] a) "Combinatorial Chemistry" *Acc. Chem. Res.* **1996**, *29* (special issue); b) G. Lowe, *Chem. Soc. Rev.* **1995**, *24*, 309–317; c) S. R. Wilson, A. W. Czarnik, *Combinatorial Chemistry—Synthesis and Application*, Wiley, **1997**
[3] X.-D. Xiang, X. Sun, G. Briceno, Y. Lou, K.-A. Wang, H. Chang, W. G. Wallace-Freedman, S.-W. Chen, P. G. Schultz, *Science* **1995**, *268*, 1738–1740
[4] G. Briceno, H. Chang, X. Sun, P. G. Schultz, X.-D. Xiang, *Science* **1995**, *270*, 273–275)
[5] a) E. Danielson, J. H. Golden, E. W. McFarland, C. M. Reaves, W. H. Weinberg, X. D. Wu, *Nature* **1997**, *389*, 944–948; b) E. Danielson, M. Devenney, D. M. Giaquinta, J. H. Golden, R. C. Haushalter, E. W. McFarland, D. M. Poojary, C. M. Reaves, W. H. Weinberg, X. D. Wu, *Science* **1998**, *279*, 837–839
[6] a) D. E. Akporiaye, I. M. Dahl, A. Karlsson, R. Wendelbo, *Angew. Chem.* **1998**, 110, 629; *Angew. Chem. Int. Ed.* **1998**, *37*, 609; b) D. E. Akporiaye, I. M. Dahl, A. Karlsson, R. Wendelbo, patent pending, Norwegian application number 97.0788
[7] M. Taramasso, G. Perego, B. Notari (Snamprogetti), UK-GB, 2071071 B **1979**.
[8] M. Schuster, H. Göbel, *J. Phys. D* **1995**, *28*, A270–A275.
[9] All diffraction data were measured with $Cu_{K\alpha}$ radiation ($\lambda = 1.541$ Å). Data collection time varied from 5 to 80 min per spot. The distance between the sample and detector was 19.8 cm and the range between 6.2 and 33.2° (2θ). During data collection the sample oscillated by 2° and with an incident angle of the primary X-ray beam of 16°. The spatially corrected raw data have been integrated with a constant 2θ value (Laue cones).
[10] B. M. Lok, T. R. Cannan, C. A. Messina, *Zeolites* **1983**, *3*, 282–291.

Chiral C_2-Symmetric Cu^{II} Complexes as Catalysts for Enantioselective Hetero-Diels–Alder Reactions**

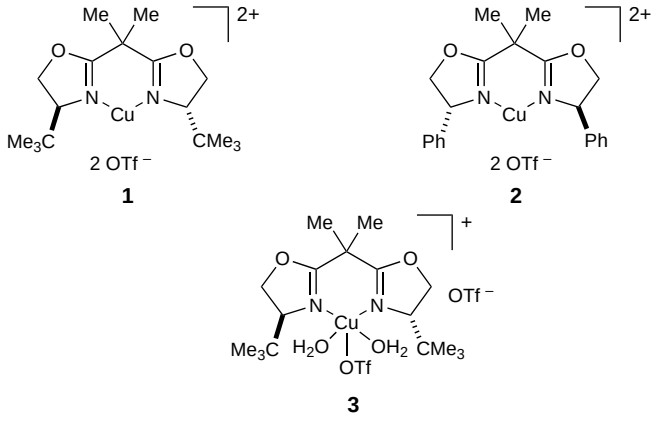
David A. Evans,* Edward J. Olhava, Jeffrey S. Johnson, and Jacob M. Janey

Previous reports from this laboratory have demonstrated that C_2-symmetric Cu^{II}–bis(oxazoline) complexes **1**–**3**[1] (Tf = trifluoromethanesulfanyl) are efficient chiral Lewis acid catalysts for Diels–Alder,[2] pyruvate aldol,[3] and glyoxylate–ene reactions.[4] Each of these processes exhibits behavior consistent with previously proposed chelation models for asymmetric induction. In a further extension of this methodology, we recently reported that α,β-unsaturated acyl phosphonates undergo enantioselective hetero-Diels–Alder

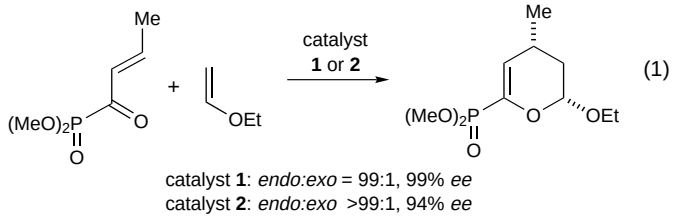
[*] Prof. D. A. Evans, E. J. Olhava, J. S. Johnson, J. M. Janey
Department of Chemistry & Chemical Biology
Harvard University
Cambridge, MA 02138 (USA)
Fax: (+1) 617-495-1460
E-mail: evans@chemistry.harvard.edu

[**] Financial support has been provided by the National Science Foundation. E.J.O. acknowledges a National Science Foundation Graduate Fellowship. J.S.J. acknowledges a Pharmacia and Upjohn Graduate Fellowship. The National Institutes of Health (BRS Shared Instrumentation Grant Program 1-S10-RR04870) and the NSF (CHE 88–14019) are acknowledged for providing NMR facilities.

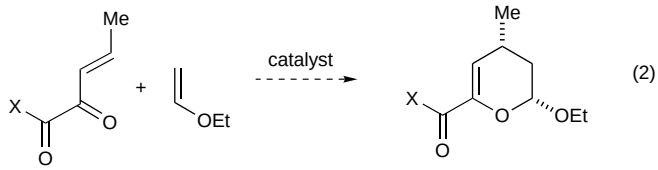
 © WILEY-VCH Verlag GmbH, D-69451 Weinheim, 1998 1433-7851/98/3724-3372 $ 17.50+.50/0



reactions[5] with enol ethers in the presence of chiral Cu^{II} complexes **1** and **2** [Eq. (1)].[6] We now disclose the analogous



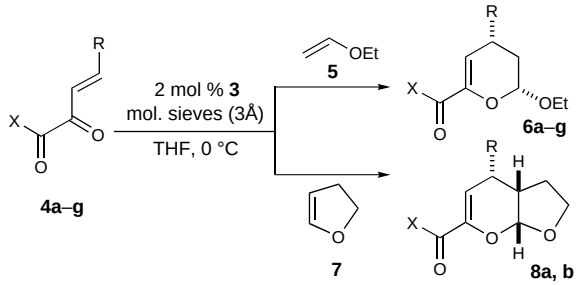
cycloaddition reactions of β,γ-unsaturated α-keto esters [Eq. (2)], reactions of established utility in the construction of enantiomerically enriched dihydropyrans.[7, 8] A similar



study has been recently reported by Jørgensen et al.[9] The present work expands the scope of this process providing significant operational simplifications including lower catalyst loadings, convenient reaction temperatures that facilitate short reaction times, and a catalyst recycling procedure. An X-ray crystallographic study is also provided in support of a proposed model for asymmetric induction.

Unsaturated keto esters **4a**–**4f** and keto amide **4g**[10] undergo highly enantioselective cycloaddition reactions with enol ethers in the presence of complexes **1** and **3** (Table 1). The reaction of ethyl vinyl ether with unsaturated keto ester **4a** in the presence of [Cu{(*S,S*)-*t*Bu-box}][OTf]$_2$ (**1**; 2 mol%, THF, 0 °C; box = bis(oxazoline)) provided cycloadduct **6a** in 93% yield, with an *endo*:*exo* selectivity of over 20:1, and with 97% *ee*. The same reaction in the presence of [Cu(OTf)-$(OH_2)_2$\{(*S,S*)-*t*Bu-box}][OTf] (**3**) and molecular sieves (3 Å) afforded identical results.[11] Complex **3**, a readily prepared blue powder that may be stored indefinitely without special precaution, is an attractive alternative to the hygroscopic anhydro complex **1**. While enantioselectivities of greater than 99% may be obtained for these cycloadditions at lower temperatures, we have found that these reactions may be

Table 1. Cycloaddition of heterodienes **4a**–**g** and enol ethers catalyzed by **3**.



Diene	X	R	Enol ether[a]	Product[b, c]	Yield [%][d]	*ee* [%][b]
4a	OEt	Ph	**5**	**6a** (>20:1)	93	97
4b	OEt	*i*Pr	**5**	**6b** (22:1)	95	96
4c	OEt	Me	**5**	**6c** (24:1)	87	97
4d	OEt	OMe	**5**	**6d** (59:1)	90	98
4e	OEt	OEt	**5**	**6e** (55:1)	98	98
4f	OEt	SBn	**5**	**6f** (>20:1)	97	99
4a	OEt	Ph	**7**	**8a** (16:1)	96	97
4b	OEt	*i*Pr	**7**	**8b** (16:1)	94	95
4g	N(OMe)Me	Me	**5**	**6g** (64:1)	99	99

[a] The reactions were conducted with 3 equiv of enol ether (relative to the diene). [b] Determined by capillary GLC or chiral HPLC. [c] The *endo*:*exo* ratio is given in parentheses. [d] Yield of isolated product. Bn = benzyl.

conveniently carried out at 0 °C with little loss in stereoselectivity (95–99% *ee*).

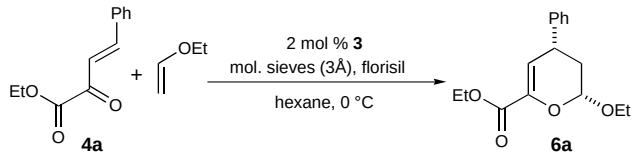
Consistent with previous observations,[2c, 3b, 5] complex **3** can be employed as an effective catalyst over a broad range of temperatures and solvents. Adduct **6a** was produced stereoselectively from unsaturated ester **4a** and ethyl vinyl ether in the presence of **3** at temperatures ranging from −40 °C to 25 °C.[12] An enantioselectivity/solvent profile with substrate **4c** and complex **3** (0 °C) demonstrates that excellent results may be obtained in a number of solvents (THF, *endo*:*exo* = 24:1, 97% *ee*; Et_2O, *endo*:*exo* = 24:1, 97% *ee*; toluene, *endo*:*exo* = 28:1, 98% *ee*; dioxane, *endo*:*exo* = 24:1, 93% *ee*; CH_2Cl_2, *endo*:*exo* = 19:1, 89% *ee*).

The reaction tolerates a broad range of substituents R at the unsaturated ester terminus. Alkyl (**4b**, **c**), aryl (**4a**), alkoxy (**4d**, **e**), and thiobenzyl substituents (**4f**) afford cycloadducts in excellent yields and stereoselectivities (Table 1). In addition, under identical reaction conditions, the Weinreb amide **4g** underwent a highly stereoselective reaction (*endo*:*exo* = 64:1, 99% *ee*) to yield **6g**. This adduct is particularly versatile in view of the malleability of the amide functionality.[13] To demonstrate the preparative utility of this reaction, 2 mol% of catalyst **3** was used to prepare 6.7 g (98%) of cycloadduct **6a** from 5.0 g of heterodiene **4a** (*endo*:*exo* > 99:1, 99% *ee*).[14] Cyclic enol ethers are also effective reaction partners. In the presence of **3** and molecular sieves (3 Å), 2,3-dihydrofuran reacted with the unsaturated esters **4a** and **4b** to provide bicyclic unsaturated esters **8a** and **8b** in good diastereo- and enantioselectivity (Table 1).

The cycloaddition to form **6c** was conducted with as little as 0.5 mol% of catalyst **3**; there was only a slight decrease in stereoselectivity (*endo*:*exo* = 19:1, 96% *ee*). Preliminary studies indicate that complex **3** can be reused in multiple reaction cycles (Table 2).[15] When the catalyzed cycloaddition is

 © WILEY-VCH Verlag GmbH, D-69451 Weinheim, 1998 1433-7851/98/3724-3373 $ 17.50+.50/0

Table 2. Enantioselective cycloaddition with catalyst recycling.

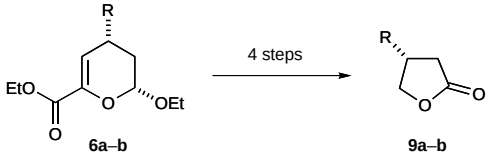


Cycle[a]	*endo*:*exo*	Yield [%]	*ee* [%]
1	> 99:1	89	96
2	> 99:1	98	96
3	> 99:1	91	96
4	> 99:1	98	93
5	> 99:1	92	95

[a] See text.

conducted in hexane in the presence of an adsorbent (florisil), conditions under which complex **3** is apparently insoluble, the product solution may be decanted at the end of the reaction and the catalyst reused. A series of five catalyst recycling experiments (Table 2) demonstrates that the catalyst/adsorbent mixture may be reused without significant diminution in yield or selectivity.[16]

The absolute configuration for structures **6a** and **6b** was unambiguously proven by chemical correlation with lactones **9a** and **9b** of known configuration [Eq. (3)].[17] The remaining



(3)

cycloadducts are assigned the indicated configuration by analogy.

The absolute configuration of the cycloadducts is consistent with our previously proposed model for asymmetric induction, in which the Cu^{II} complex and vicinal carbonyl functionalities form a well-defined reactive complex **11**. Stereoregular behavior has been observed with substrates which can engage in chelation with **1**, for example, *N*-acylimides,[2a] pyruvate and glyoxylate esters,[3b, 4] acyl phosphonates,[5] and now β,γ-unsaturated α-keto esters. In conjunction with the construction of a suitable catalyst – substrate model, the X-ray crystal structure of the bis(aquo) complex **3** was obtained (Figure 1). The crystallographic data for **3** reveal a distorted square pyramidal geometry, in which one of the triflate ligands is weakly bound to the metal center in the apical position (Cu–OTf 2.624 Å) while the other is fully dissociated (Cu–OTf 3.667 Å). The two water molecules occupy the equatorial positions and are distorted by approximately 26° out of the plane of the ligand. Replacement of the water molecules with the chelating substrate generates reactive complexes **10** and **11.** Semiempirical calculations (PM3) have been employed to model these catalyst – substrate complexes. For simplicity, the triflate counterions are omitted from the calculations. The cationic complexes [Cu(*t*Bu-box)(acyl phosphonate)]$^{2+}$ (**10**) and [Cu(*t*Bu-box)(β,γ-unsaturated α-keto ester)]$^{2+}$ (**11**) generated at the PM3 level are illustrated in Figure 1. In both cases, the heterodiene α-*Si* face of the heterodiene is blocked by the bulky *tert*-butyl substituent on the ligand, leaving the α-*Re* face accessible to the dienophile.

In summary, the stereoselective hetero-Diels – Alder reaction of β,γ-unsaturated α-keto esters and amides with enol ethers catalyzed by C_2-symmetric Cu^{II} – bis(oxazoline) complexes provides a general and practical entry into enantioenriched dihydropyrans. Application to complex target synthesis will be reported in due course.

Experimental Section

3: To an oven-dried round-bottom flask containing a magnetic stir bar was added, in an inert-atmosphere glove box, 2,2-bis{2-[4(*S*)-*tert*-butyl-1,3-oxazolinyl]}propane[1] (163 mg, 0.554 mmol) and copper(II) trifluoromethanesulfonate (200 mg, 0.554 mmol). The flask was fitted with a serum cap,

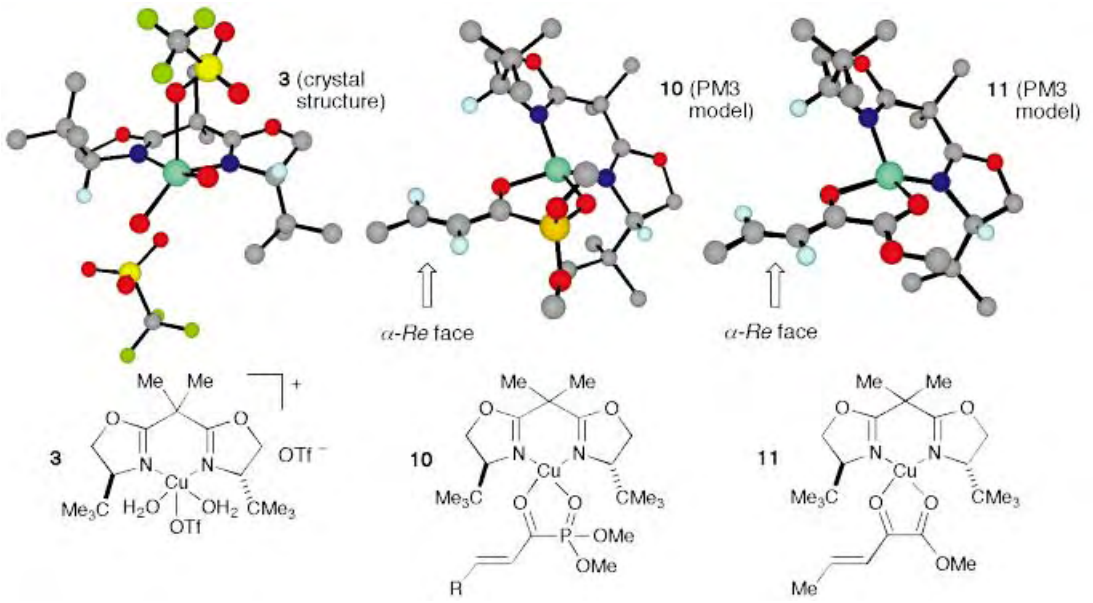


Figure 1. Crystal structure of bis(oxazoline) catalyst **3** and model structures calculated at the PM3 level for catalyst – substrate complexes **10** and **11**.

 © WILEY-VCH Verlag GmbH, D-69451 Weinheim, 1998 1433-7851/98/3724-3374 $ 17.50+.50/0

removed from the glove box, and charged with THF (20 mL). The reaction mixture was stirred under argon for 1 h, affording a clear green solution to which distilled water (20 mg, 1.11 mmol) was added. The resulting blue solution was concentrated in vacuo to afford a blue solid. Hexane (5 mL) was added, and the solvent was removed in vacuo to provide **3** as a light blue powder (372 mg, 0.538 mmol, 97 % yield). Elemental analysis calcd for $C_{19}H_{34}CuF_6N_2O_{10}S_2$: C 32.97, H 4.95, N 4.05; found: C 33.22, H 5.03, N 3.95.

6c: A dry round-bottom flask with magnetic stirrer was charged with **3** (4.8 mg, 0.007 mmol; 0.02 equiv) and powdered molecular sieves (3 Å; 25 mg). To this was added THF (1.75 mL) by syringe. The mixture was stirred for 1 h to produce a heterogeneous light green solution that was then cooled to 0 °C. The mixture was treated sequentially with ester **4c** (48 μL, 50 mg, 0.35 mmol) and freshly distilled ethyl vinyl ether (101 μL, 75.7 mg, 1.05 mmol). After 15 min the reaction solution was applied to a silica gel column and eluted with EtOAc/hexanes (15/85) to afford **6c** as a clear oil (65 mg, 0.30 mmol, 87 %). Analysis by GC (DB-1701, 110 °C for 10 min, then increased by 10 °C min^{-1}, 0.48 bar; t_r = 17.0 (minor product), 17.4 (major product) and HPLC (Chiralpak OD-H, EtOAc/hexanes (4/96), flow rate 1 mL min^{-1}, 254 nm; t_r = 7.9 (major product), 10.6 (minor product)) gave the isomeric composition of the product: d.r. 96:4, 97 % *ee*. Analytical data for **6c**: $[\alpha]_D = -77.3°$ (c = 0.44, $CHCl_3$); IR (KBR): $\tilde{\nu}$ = 2978, 2932, 2874, 1734, 1648, 1458, 1377, 1297, 1256, 1208, 1175, 1124, 1102, 1090, 1053, 1026, 982 cm^{-1}; ^{1}H NMR (400 MHz, $CDCl_3$): δ = 5.98 (d, J = 3.0 Hz, 1H, *H*C=CCO$_2$CH$_2$CH$_3$), 5.67 (dd, J = 6.9, 2.4 Hz, 1H, C*H*O$_2$), 4.27 (dq, J = 10.8, 7.1 Hz, 1H, CO$_2$C*H*HCH$_3$), 4.23 (dq, J = 10.8, 7.1 Hz, 1H, CO$_2$CH*H*CH$_3$), 3.97 (dq, J = 9.6, 7.1 Hz, 1H, CH$_3$C*H*HOCCHO), 3.60 (dq, J = 9.6, 7.1 Hz, 1H, CH$_3$CH*H*OCCHO), 2.50 (m, 1H, =CHC*H*CH$_3$), 2.03 (dddd, J = 13.5, 6.9, 2.4, 0.7 Hz, 1H, CH(CH$_3$)C*H*HCHO$_2$), 1.59 (m, 1H, CH(CH$_3$)CH*H*CHO$_2$), 1.32 (t, J = 7.1 Hz, 3H, CO$_2$CH$_2$C*H*$_3$), 1.24 (t, J = 7.1 Hz, 3H, CHOCH$_2$C*H*$_3$), 1.14 (d, J = 7.2 Hz, 3H, =CHCH$_2$C*H*$_3$); ^{13}C NMR (100 MHz, $CDCl_3$): δ = 163.0, 140.8, 117.0, 99.4, 64.5, 61.0, 34.8, 26.1, 20.6, 15.1, 14.2; TLC (hexanes/CH_2Cl_2 10/90): R_f = 0.27; HR-MS (CI, NH_3): m/z calcd for $C_{11}H_{22}NO_4$: 232.1549 $[M+NH_4]^+$, found: 232.1555; elemental analysis calcd for $C_{11}H_{18}O_4$: C 61.66, H 8.47; found: C 61.39, H 8.56.

Crystal data for **3** ($C_{19}H_{34}CuF_6N_2O_{10}S_2$): crystal dimensions 0.15 × 0.15 × 0.25 mm, orthorhombic, space group $P2_12_12_1$, a = 9.562(2), b = 12.166(2), c = 25.753(4) Å, β = 90°; V = 2996.0(9) Å^3, ρ_{calcd} = 1.535 mg mm^{-3}; Siemens SMART CCD diffractometer, $1.58 < \theta < 26.43°$, $Mo_{K\alpha}$ radiation (λ = 0.71073 Å), $\theta/2\theta$ scans, T = 213(2) K; of 14 840 measured reflections, 5889 were independent and 5005 were observed with $I > 2\sigma(I)$, $-11 \le h \le 6$, $-15 \le k \le 14$, $-27 \le l \le 22$; R = 0.0468, wR = 0.1253, GOF = 1.006 for 361 parameters, Flack parameter = −0.004(15), $\Delta\rho_{max}$ = 0.845 e Å^{-3}. The structure was solved by direct methods (SHELXTL Plus) and developed by least-squares refinement against $|F^2|$ (SHELXL93). Crystallographic data (excluding structure factors) for the structure reported in this paper have been deposited with the Cambridge Crystallographic Data Centre as supplementary publication no. CCDC-103312. Copies of the data can be obtained free of charge on application to CCDC, 12 Union Road, Cambridge CB2 1EZ, UK (fax: (+44) 1223-336-033; e-mail: deposit@ccdc.cam.ac.uk).

Received: October 6, 1998 [Z 12495 IE]
German version: *Angew. Chem.* **1998**, *110*, 3554 – 3557

Keywords: asymmetric catalysis · copper · cycloadditions · Lewis acids · synthetic methods

[1] For a practical synthesis of the (*S,S*)-*tert*-butyl-box ligand, see D. A. Evans, G. S. Peterson, J. S. Johnson, D. M. Barnes, K. R. Campos, K. A. Woerpel, *J. Org. Chem.* **1998**, *63*, 4541 – 4544.

[2] a) D. A. Evans, S. J. Miller, T. Lectka, *J. Am. Chem. Soc.* **1993**, *115*, 6460 – 6461; b) D. A. Evans, J. A. Murry, P. von Matt, R. D. Norcross, S. J. Miller, *Angew. Chem.* **1995**, *107*, 864 – 867; *Angew. Chem. Int. Ed. Engl.* **1995**, *34*, 798 – 800; c) D. A. Evans, M. C. Kozlowski, J. S. Tedrow, *Tetrahedron Lett.* **1996**, *37*, 7481 – 7484; d) D. A. Evans, D. M. Barnes, *Tetrahedron Lett.* **1997**, *38*, 57 – 58; e) D. A. Evans, J. S. Johnson, *J. Org. Chem.* **1997**, *62*, 786 – 787; f) D. A. Evans, E. A. Shaughnessy, D. M. Barnes, *Tetrahedron Lett.* **1997**, *38*, 3193 – 3194.

[3] a) D. A. Evans, J. A. Murry, M. C. Kozlowski, *J. Am. Chem. Soc.* **1996**, *118*, 5814 – 5815; b) D. A. Evans, M. C. Kozlowski, C. S. Burgey, D. W. C. MacMillan, *J. Am. Chem. Soc.* **1997**, *119*, 7893 – 7894.

[4] D. A. Evans, C. S. Burgey, N. A. Paras, T. Vojkovsky, S. W. Tregay, *J. Am. Chem. Soc.* **1998**, *120*, 5824 – 5825.

[5] D. A. Evans, J. S. Johnson, *J. Am. Chem. Soc.* **1998**, *120*, 4895 – 4896.

[6] Formal hetero-Diels – Alder reactions between electron-rich dienes and pyruvate have been reported with these complexes: a) M. Johannsen, K. A. Jørgensen, *Chem. Commun.* **1997**, *119*, 7893 – 7894; b) S. Yao, M. Johannsen, H. Audrain, R. G. Hazell, K. A. Jørgensen, *J. Am. Chem. Soc.* **1998**, *120*, 8599 – 8609.

[7] Auxilary- or catalyst-controlled asymmetric hetero-Diels – Alder reactions of α,β-unsaturated carbonyl compounds with enol ethers: a) G. Dujardin, S. Rossignol, E. Brown, *Synthesis* **1998**, 763 – 770; b) K. J. McRae, M. A. Rizzacasa, *J. Org. Chem.* **1997**, *62*, 1196 – 1197; c) E. Wada, W. Pei, H. Yasuoka, U. Chin, S. Kanemasa, *Tetrahedron* **1996**, *52*, 1205 – 1220, and references therein; d) L.-F. Tietze, C. Schneider, A. Grote, *Chem. Eur. J.* **1996**, *2*, 139 – 148, and references therein; e) L. D. Gaudenzi, S. Apparao, R. R. Schmidt, *Tetrahedron* **1990**, *46*, 277 – 290, and references therein.

[8] For general references on the hetero-Diels – Alder reaction, see a) D. L. Boger in *Comprehensive Organic Synthesis*, *Vol. 5* (Eds.: B. M. Trost, I. Fleming, L. A. Paquette), Pergamon Press, Oxford, **1991**, pp. 451 – 512; b) D. L. Boger, S. M. Weinreb, *Hetero Diels-Alder Methodology in Organic Synthesis*, Academic Press, San Diego, **1987**.

[9] J. Thorhauge, M. Johannsen, K. A. Jørgensen, *Angew. Chem.* **1998**, *110*, 2543 – 2546; *Angew. Chem. Int. Ed.* **1998**, *37*, 2404 – 2406. Absolute stereochemical assignments of the reaction products were not made in this investigation.

[10] Substrates **4a – c** were prepared by an aldol-elimination protocol: H. Sugimura, K. Yoshida, *Bull. Chem. Soc. Jpn.* **1992**, *65*, 3209 – 3211. Substrates **4d – e** were prepared by reaction of ethyl vinyl ether or methyl vinyl ether with ethyl chlorooxoacetate: L.-F. Tietze, H. Meier, E. Voss, *Synthesis* **1988**, 274 – 277. Substrate **4f** was prepared from **4e** and phenylmethanethiol in the presence of catalytic amounts of sodium bisulfate. Substrate **4g** was prepared by addition of 1-propenylmagnesium bromide to the bis(Weinreb amide) of oxalic acid: M. P. Sibi, M. Marvin, R. Sharma, *J. Org. Chem.* **1995**, *60*, 5016 – 5023. Details of the synthesis of these substrates will appear in a full account of this work.

[11] The use of bis(aquo) complex **3** without molecular sieves severely attenuated reactivity, indicating that the anhydrous complex **1** is generated in the presence of moleclar sieves (3 Å).

[12] At −40 °C: >99 % *ee*; at −20 °C: 98 % *ee*; at 0 °C: 97 % *ee*; at 25 °C: 94 % *ee*.

[13] For reviews on the synthetic utility of the Weinreb amide, see a) M. Mentzel, M. R. Hoffman, *J. Prakt. Chem.* **1997**, *339*, 517 – 524; b) M. P. Sibi, *Org. Prep. Proced. Int.* **1993**, *25*, 15 – 40.

[14] The ligand may also be recovered (50 %) by aqueous workup (3 M NH_4OH) and chromatographic separation of the adduct and ligand.

[15] For an example of catalyst recycling in an enantioselective reaction, see K. B. Hansen, J. L. Leighton, E. N. Jacobsen, *J. Am. Chem. Soc.* **1996**, *118*, 10924 – 10925.

[16] Catalyst activity is diminished slightly in subsequent runs. In the absence of florisil or in the presence of other adsorbents (SiO_2, Al_2O_3), lower enantioselectivity and/or reactivity is observed. Attempts to optimize this process and identify the role of the adsorbent are currently being actively studied.

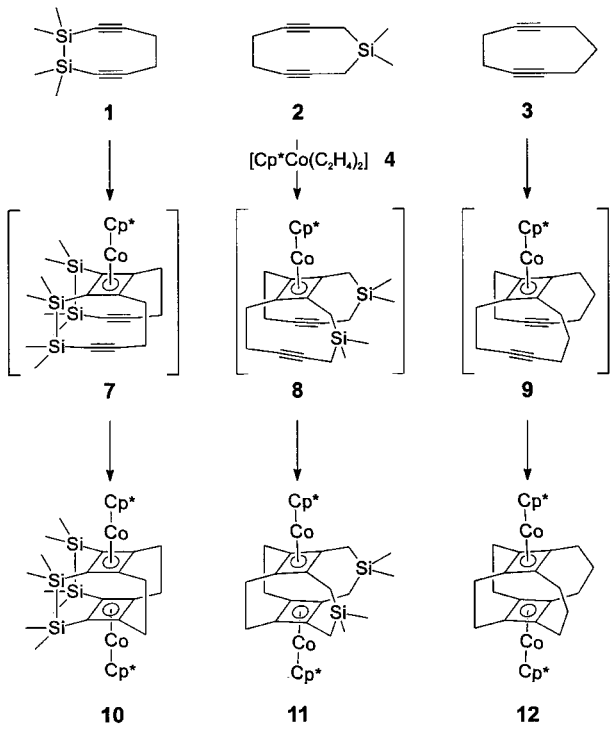
[17] The lactones were generated by the following procedure: a) O_3, MeOH/CH_2Cl_2 (1/1), −78 °C; $NaBH_4$, 25 °C; b) 1 M HCl (aq), THF, 65 °C; c) tetrapropylammonium perruthenate (TPAP; cat.), 4-methylmorpholine *N*-oxide (NMO), molecular sieves (4 Å), CH_2Cl_2, 25 °C. **9a** (3*S*): $[\alpha]_D = +38°$ (c = 0.34, MeOH) (lit.: $[\alpha]_D = +51°$; G. Helmchen, G. Nill, *Angew. Chem.* **1979**, *91*, 66 – 68; *Angew. Chem. Int. Ed. Engl.* **1979**, *18*, 65 – 66). **9b** (3*S*): $[\alpha]_D = -11°$ (c = 0.52, $CHCl_3$) (lit.: $[\alpha]_D = +14.7°$ (3*R*); C.-H. R. King, C. D. Poulter, *J. Am. Chem. Soc.* **1982**, *104*, 1413).

 © WILEY-VCH Verlag GmbH, D-69451 Weinheim, 1998 1433-7851/98/3724-3375 $ 17.50+.50/0

Threefold and Fourfold [2 + 2] Cycloadditions of Cyclic Diynes as a Consequence of Steric Effects: En Route to Polymers**

Gebhard Haberhauer, Frank Rominger, and Rolf Gleiter*

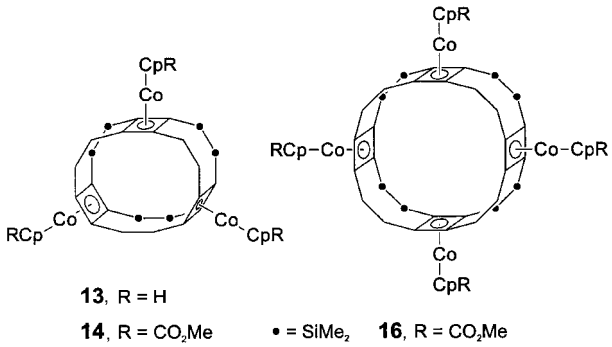
Cyclic diynes can react either in an intra- or intermolecular way with organometallic complexes. In the latter case defined oligomers or polymers may be formed. The polymers may consist of a ladder of metal-stabilized cyclobutadiene rings or a two-dimensional net of aromatic rings each of which are connected by hydrocarbon chains. It is important to know and understand the reaction mechanisms if the choice of the reaction pathway is to be controlled. A key intermediate in the reactions of two or more alkyne units with organometallic complexes is a metallacyclopentadiene species which has been proposed and substantiated by Yamazaki, Wakatsuki et al.[1] From this hypothesis we inferred for cyclic diynes two pathways: an intramolecular reaction path for large rings and an intermolecular route for smaller diynes.[2] In the latter case the degree of oligomerization was always two. When we used diynes which contained a disilyltetramethyl bridge on one side and a relatively long and flexible chain (C_4H_8, C_5H_{10}) on the other[3] the yield of superphanes was rather high. In our search for higher oligomers we reasoned that small chains on both sides or small chains on one side and a chain with bulky groups on the other might favor higher oligomers. In order to test these ideas we investigated the reaction of 1,1,2,2-tetramethyl-1,2-disilacycloocta-3,7-diyne (**1**),[4] 1,1-dimethyl-1-silacyclonona-3,7-diyne (**2**),[4] and cyclonona-1,5-diyne (**3**)[4] with bis(ethylene)(1,5-pentamethylcyclo-pentadienyl)cobalt (**4**), (η^4-cyclooctadiene-1,5)(η^5-cyclopentadienyl)cobalt (**5**), and (η^4-cyclooctadiene-1,5)(η^5-(methoxycarbonyl)(cyclopentadienyl)cobalt (**6**) (Scheme 1).



Scheme 1.

The reaction of **1**–**3** with **4** at 60 °C afforded the corresponding superphanes **10**–**12**. All three superphanes belong to the point group C_{2v}. The configurations of **10** and **12** have been confirmed by X-ray structural analyses.[5] The preference of the structures with C_{2v} symmetry can be rationalized by assuming that the rate-determining step is the formation of a tricyclic metallacycle.[1, 3] The yields of the superphanes **10**–**12** are relatively low (**10**: 12%, **11**: 10%, **12**: 3%)[6] if we compare them to those obtained by reaction of **4** with 1,1,2,2-tetramethyl-1,2-disilacycloundeca-3,10-diyne and 1,1,2,2-tetramethyl-1,2-disilacyclododeca-3,11-diyne (50–60%).[3] We ascribe the low yields to the fact that in the intermediate tricyclic systems (**7**–**9**) the short bridges tend to favor a conformation in which the triple bonds are nearly coplanar to the cyclobutadiene ring. Only the relatively large "cap" of the Cp* ring induces a conformation in which both alkyne units of **7**–**9** are forced in relatively close proximity in the half-space below the cyclobutadiene ring.

In order to detect higher oligomers we reduced the steric bulk of the ligand and replaced the Cp* cap by a Cp cap; that is we replaced **4** by **5** and **6**. Indeed, the reaction of **1** with **5** and **6** does not give detectable amounts of the corresponding superphanes but rather yields the trimers **13** (20%) and **14** (35%). In **13**[6] and **14**[6] formally three diynes have reacted with three CpCo fragments. The structural assignments of the resulting trimers are based on their spectroscopic data[5] and an X-ray structural analysis of **13** (Figure 1).[7, 8] This reveals that in the resulting trimer the silyl bridges lie on one side of the ring and the ethano bridges on the opposite side. Therefore the tube formed by the three units has a conical shape. The widest diameter in the tube is found to be 6.9 Å, the narrowest one is 4.5 Å. In the case of the reaction of **1** with **6** we were also able to isolate the tetramer **16** in 8–10% yield. The structural assignment of **16** is based on its spectroscopic data.[6] As in the case of **13** and **14** the NMR data suggest that the silyl and ethano bridges are on opposite sides of the ring.



[*] Prof. Dr. R. Gleiter, Dipl.-Chem. G. Haberhauer, Dr. F. Rominger
Organisch-chemisches Institut der Universität
Im Neuenheimer Feld 270, D-69120 Heidelberg (Germany)
Fax: (+49) 6221-54-4205

[**] Our work was supported by the Deutsche Forschungsgemeinschaft (SFB 247), the Fonds der Chemischen Industrie,and BASF Aktiengesellschaft, Ludwigshafen.

 © WILEY-VCH Verlag GmbH, D-69451 Weinheim, 1998 1433-7851/98/3724-3376 $ 17.50+.50/0

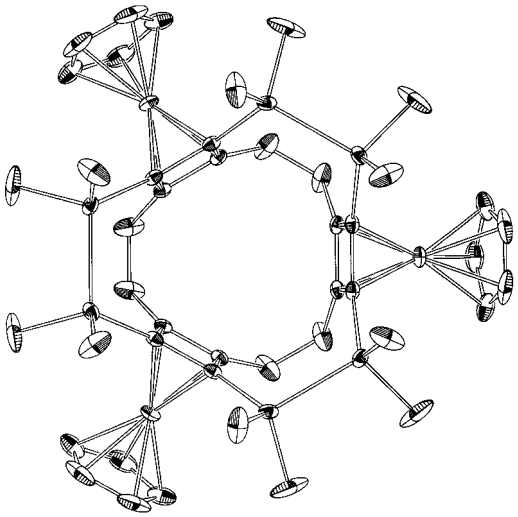


Figure 1. Molecular structure of **13**.

This gives rise to a conical shape of the ring for which we calculated (AM1[10]) the widest and narrowest diameter to be 8.4 Å and 5.5 Å, respectively. The species **13**, **14**, and **16** belong to the class of beltlike hydrocarbons[11] which have been investigated recently very intensively and for which several routes have been described.[11–14]

The reaction of **3** with $[Cp^*Co(C_2H_4)_2]$ at 60 °C also yields a species (**15**) which we assign to a trimer based on the high-resolution mass spectrum and ^{1}H NMR spectroscopic data.[6] The results obtained for **1** and **3** demonstrate that higher oligomers of cyclic diynes are amenable at elevated temperatures.

Received: June 24, 1998 [Z12043IE]
German version: *Angew. Chem.* **1998**, *110*, 3632–3634

Keywords: cobalt · cycloadditions · diynes · superphanes

[1] Y. Wakatsuki, H. Yamazaki, T. Kobayashi, Y. Sugawara, *Organometallics* **1987**, *6*, 1191; Y. Wakatsuki, O. Nomura, K. Kitaura, K. Morokuma, H. Yamazaki, *J. Am. Chem. Soc.* **1983**, *105*, 1907, and references therein.

[2] R. Gleiter, M. Merger, *Angew. Chem.* **1997**, *109*, 2532; *Angew. Chem. Int. Ed. Engl.* **1997**, *36*, 2420.

[3] R. Gleiter, H. Stahr, B. Nuber, *Tetrahedron Lett.* **1995**, *36*, 4607.

[4] G. Haberhauer, R. Roers, R. Gleiter, *Tetrahedron Lett.* **1997**, *38*, 8679.

[5] G. Haberhauer, F. Rominger, R. Gleiter, B. Nuber, unpublished results.

[6] Selected spectroscopic data of **10**–**16**. **10**: ^{1}H NMR (300 MHz, C_6D_6): $\delta = 0.35$ (s, 12H), 0.38 (s, 12H), 1.9 (m, 8H), 2.1 (s, 30H); ^{13}C NMR (125 MHz, C_6D_6): $\delta = -2.7$ (q), -1.5 (q), 11.8 (q), 23.6 (t), 65.0 (s), 86.6 (s), 88.6 (s); HR-MS (positive-ion FAB): *m*/*z*: calcd: 772.2593; found: 772.2629. **11**: ^{1}H NMR (300 MHz, C_6D_6): $\delta = 0.2$ (s, 12H), 1.29 (d, 4H), 1.34 (d, 4H), 1.9 (m, 8H), 2.0 (s, 30H); ^{13}C NMR (75 MHz, C_6D_6): $\delta = 0.6$ (q), 1.0 (q), 9.8 (q), 13.0 (t), 20.9 (t), 71.3 (s), 72.8 (s), 87.1 (s); HR-MS (Positiv-Ionen-FAB): *m*/*z*: calcd: 712.2741; found: 712.2733. **12**: ^{1}H NMR (500 MHz, C_6D_6): $\delta = 1.8$ (m, 20H), 1.9 (s, 30H); ^{13}C NMR (125 MHz, C_6D_6): $\delta = 11.1$ (q), 21.6 (t), 25.0 (t), 28.2 (t), 73.8 (s), 75.2 (s), 88.3 (s); HR-MS (positive-ion FAB): *m*/*z* calcd: 624.2576; found: 624.2587. **13**: ^{1}H NMR (300 MHz, C_6D_6, 60 °C): $\delta = 0.2$ (s, 18H), 0.4 (s, 18H), 2.1–2.3 (m, 12H), 4.7 (s, 15H); HR-MS (positive-ion FAB): *m*/*z*: calcd.: 948.1541; found: 948.1528. The low solubility of **13** in the usual solvents prevented the recording of a ^{13}C NMR spectrum. **14**: ^{1}H NMR (300 MHz, C_6D_6): $\delta = 0.2$ (s, 18H), 0.3 (s, 18H), 2.0–2.3 (m, 12H), 3.6 (s, 9H), 4.9 (t, 6H), 5.4 (t, 6H); ^{13}C NMR (75 MHz, C_6D_6): $\delta = -1.0$ (q), 2.8 (q), 27.0 (t), 51.5 (q), 69.5 (s), 83.0 (d), 83.1 (d), 86.4 (s), 92.7 (s), 167.9 (s); HR-MS (positive-ion FAB): *m*/*z*: calcd: 1122.1706; found: 1122.1708. **15**: ^{1}H NMR (500 MHz, C_6D_6): $\delta = 1.6–2.2$ (m, 30H), 1.8 (s, 45H); HR MS (positive-ion FAB): *m*/*z*: calcd: 936.3865; found: 936.3867. The small quantity of **15** prevented the recording of a ^{13}C NMR spectrum. **16**: ^{1}H NMR (300 MHz, C_6D_6): $\delta = 0.2$ (s, 24H), 0.4 (s, 24H), 2.2 (s, 16H), 3.6 (s, 12H), 5.0 (s, 8H), 5.5 (s, 8H); ^{13}C NMR (75 MHz, C_6D_6): $\delta = -0.1$ (q), 2.4 (q), 27.4 (t), 51.7 (q), 68.1 (s), 82.9 (d), 83.0 (d), 86.5 (s), 93.4 (s), 168.0 (s); HR-MS (positive-ion FAB): *m*/*z*: calcd.: 1496.2274; found: 1496.2233.

[7] About 30% of the silylene units in the single crystals of **13** are disordered. In this fraction the $Si_2(CH_3)_4$ groups adopt a δ and λ conformation, respectively, instead of a conformation with a plane of symmetry.

[8] X-ray structure of **13**: $C_{45}H_{63}Co_3Si_6$, $M_r = 949.28$, rhombohedral, space group *R*3*m*, crystal dimensions: $0.45 \times 0.09 \times 0.08$ mm^3, $a = 21.024(1)$, $c = 9.031(1)$ Å, hexagonal axes, $V = 3456.9(2)$ Å^3, $F(000) = 1494$, $Z = 3$, $\rho_{calcd} = 1.37$ g cm^{-3}, $\mu = 1.25$ mm^{-1}, $Mo_{K\alpha}$ radiation, $\lambda = 0.71073$ Å. X-ray data were collected with a Siemens CCD diffractometer at 200(2) K; 8557 reflections were collected. Of 1470 unique reflections measured, 1360 were observed with $I > 2\sigma(I)$. The structure was solved by direct methods by using the program SHELXTL.[9] Refinement of the non-hydrogen atoms was carried out anisotropically according to a full-matrix least-squares technique (F^2). $R1 = 0.035$, $wR2 = 0.081$. Crystallographic data (excluding structure factors) for the structures reported in this paper have been deposited with the Cambridge Crystallographic Data Center as supplementary publication no. CCDC-102941. Copies of the data can be obtained free of charge on application to CCDC, 12 Union Road, Cambridge CB2 1EZ, UK (fax: (+44) 1223-336-033; e-mail: deposit@ccdc.cam.ac.uk).

[9] Siemens SHELXTL 5.05, Siemens Analytical X-Ray, **1994**.

[10] M. J. S. Dewar, E. G. Zoebisch, E. F. Healy, J. J. P. Stewart, *J. Am. Chem. Soc.* **1985**, *107*, 3902.

[11] Review: A. Schröder, H.-B. Mechelburger, F. Vögtle, *Top. Curr. Chem.* **1994**, *172*, 180.

[12] S. Kammermeier, P. G. Jones, R. Herges, *Angew. Chem.* **1996**, *108*, 2834; *Angew. Chem. Int. Ed. Engl.* **1996**, *35*, 2669; *Angew. Chem.* **1997**, *109*, 2317; *Angew. Chem. Int. Ed. Engl.* **1997**, *36*, 2200.

[13] F. H. Kohnke, A. M. Z. Slawin, J. F. Stoddart, D. J. Williams, *Angew. Chem.* **1987**, *99*, 941; *Angew. Chem. Int. Ed. Engl.* **1987**, *26*, 892; P. R. Ashton, N. S. Isaacs, F. H. Kohnke, A. M. Z. Slawin, C. M. Spencer, J. F. Stoddart, D. J. Williams, *Angew. Chem.* **1988**, *100*, 981; *Angew. Chem. Int. Ed. Engl.* **1988**, *27*, 966.

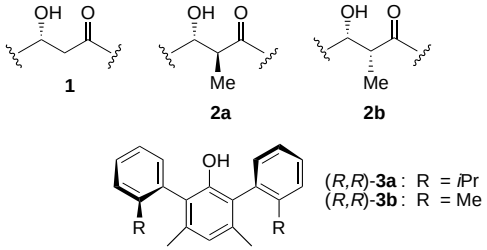
[14] W. Josten, S. Neumann, F. Vögtle, M. Nieger, K. Hägele, M. Przybylski, F. Beer, K. Müllen, *Chem. Ber.* **1994**, *127*, 2089.

 © WILEY-VCH Verlag GmbH, D-69451 Weinheim, 1998 1433-7851/98/3724-3377 $ 17.50+.50/0

Diastereoselective Aldol Reaction with an Acetate Enolate: 2,6-Bis(2-isopropylphenyl)-3,5-dimethylphenol as an Extremely Effective Chiral Auxiliary**

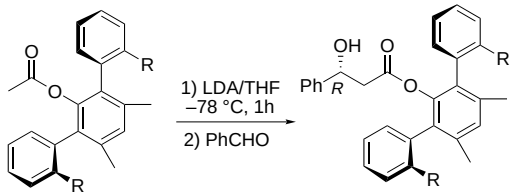
Susumu Saito, Keiko Hatanaka, Taichi Kano, and Hisashi Yamamoto*

The optically active 3-hydroxycarbonyl (**1**) and 3-hydroxy-2-methylcarbonyl units (**2**) are present in numerous natural products. When covalently bound by chiral auxiliaries, acetate and propionate enolates and their variants have found widespread use in the construction of **1** and **2**. Despite



thorough investigations and a variety of approaches to structural units **2**,[1] the aldol synthesis of unit **1**[2, 3] by use of a chiral auxiliary lacks general utility due to its inherent difficulties, as suggested by Braun and others.[2] The strategy of Braun et al. to use (*R*)- and (*S*)-(2-hydroxy-1,2,2-triphenylethyl)acetate (HYTRA) is widely recognized as the most practical and elegant approach, although extremely low temperatures (ca. −130 °C) are required for satisfactory diastereoselectivity.[3d, m] More recent efforts to develop procedures which are applicable to **1** have met with only limited success.[3e–i] Here we address the potential limitations of the aldolization to **1** by utilizing the sterically hindered 2,6-bis(2-isopropylphenyl)-3,5-dimethylphenol (**3a**)[4] as an effective chiral auxiliary for an acetate enolate.

The optically active, bulky phenols (*R*,*R*)- and (*S*,*S*)-**3** were readily accessible by the previously described method.[4] Chiral acetates **4** were prepared by sequential treatment of **3** with BuLi and acetyl chloride at 0 °C in THF. The procedure shown in Scheme 1 is representative of the aldol condensation of **4a** with aldehydes. Treatment of **4a** with lithium diisopropylamide (LDA, 1.1 equiv) at −78 °C for 1 h followed by addition of benzaldehyde (1.1 equiv) gave, after stirring for 1 h and subsequent purification by column chromatography on silica gel,[5] aldol adduct **5a** in 69% yield and with greater than 97% *de*. In comparison, the sterically less and more hindered analogues **4b** and **4c** gave **5b** and **5c** with



(*R*,*R*)-**4a**: R = *i*Pr
(*R*,*R*)-**4b**: R = Me

(*R*,*R*)-**5a**: R = *i*Pr
(*R*,*R*)-**5b**: R = Me

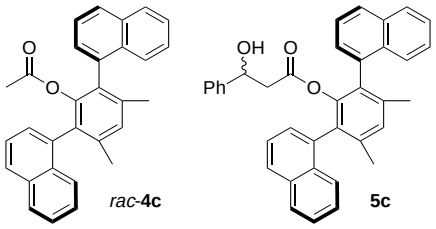
Scheme 1. Aldol reaction of chiral acetates **4a** and **4b** with benzaldehyde.

disappointingly lower *de* values of 76% and 78%, respectively (Table 1, entries 2 and 3). The effect of other solvents including Et_2O and dimethoxyethane (DME) also decreased

Table 1. Aldol reaction of chiral acetates with benzaldehyde under various reaction conditions.[a]

Entry	Chiral acetate	Base	Major product	Yield [%][b]	*de* [%][c]
1	**4a**	LDA	**5a**	69	97
2	**4b**	LDA	**5b**	58	76
3[d]	**4c**	LDA	**5c**	22	78
4[e]	**4a**	LDA	**5a**	49	81
5[f]	**4a**	LDA	**5a**	< 25	64
6	**4a**	Et_2NLi	**5a**	51	94
7	**4a**	$(CH_2)_4NLi$	**5a**	30	92
8	**4a**	LTMP[g]	**5a**	0	–
9	**4a**	LHMDS[h]	**5a**	0	–
10	**4a**	KHMDS[i]	**5a**	0	–

[a] Unless otherwise noted, the reactions were carried out with the acetate (1.0 equiv), base (1.1 equiv), and PhCHO (1.1 equiv) in THF at −78 °C. [b] Yield of isolated product. [c] In all the cases except for entry 3, the *de* value was determined by a chiral HPLC analysis (column: OB-H) after conversion of **5** into the corresponding diol. The absolute configuration at C3 of the major isomer was assigned to be *R* by comparison of the optical rotation of the diol with that reported in the literature; see T. H. Chan, K. T. Nwe, *J. Org. Chem.* **1992**, *57*, 6107. [d] Racemic **4c** was used. [e] Diethyl ether was used as solvent. [f] The reaction was performed at −50 °C with 1,2-dimethoxyethane (DME) as solvent. [g] LTMP = lithium 2,2,6,6-tetramethylpiperidide. [h] LHMDS = lithium hexamethyldisilazide. [i] KHMDS = potassium hexamethyldisilazide.



the degree of asymmetric induction (entries 4 and 5). An attempt to use less bulky bases such as Et_2NLi and $(CH_2)_4NLi$ led to high *de* values, but a decline in the yields of isolated products (entries 6 and 7). In contrast, more bulky bases gave no aldol adduct. However, about 96% of **4a** could be recovered, suggesting unsuccessful enolate generation (entries 8–10). The failure of the reaction could be attributed to the significant steric repulsion between the bulky bases and the auxiliary.

In light of the efficiency of the LDA-promoted system for **4a**, we further investigated this aldolization with a series of

[*] Prof. Dr. H. Yamamoto, Dr. S. Saito, K. Hatanaka, T. Kano
Graduate School of Engineering
Nagoya University, CREST
Japan Science and Technology Corporation (JST)
Furo-cho, Chikusa, Nagoya 464–8603 (Japan)
Fax: (+81) 52-789-3222
E-mail: j45988a@nucc.cc.nagoya-u.ac.jp.

[**] We thank the Japan Society for the Promotion of Science (JSPS) Research Fellowships for Young Scientists (to T.K.).

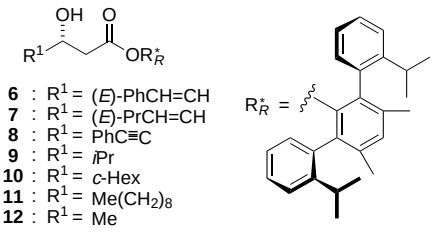
 © WILEY-VCH Verlag GmbH, D-69451 Weinheim, 1998 1433-7851/98/3724-3378 $ 17.50+.50/0

aldehydes; the results are summarized in Table 2. Excellent diastereoselectivity (94–99% *de*) was maintained for a range of alkyl-, alkenyl-, and alkynyl-substituted aldehydes. The

Table 2. Asymmetric aldol reaction of (*R*,*R*)-**4a** with various aldehydes.[a]

Entry	Aldehyde	Yield [%][b]	Product	*de* [%][c] (abs. config.)[d]
1	(*E*)-PhCH=CHCHO	77	**6**	> 99 (*R*)
2[e]	(*E*)-PrCH=CHCHO	90	**7**	95 (*R*)
3[e]	PhC≡CCHO	81	**8**	94 (*R*)
4	*i*PrCHO	62	**9**	> 99 (*R*)
5[f]	*c*-HexCHO	87	**10**	98 (*R*)
6	$Me(CH_2)_8CHO$	70	**11**	99 (*S*)
7	MeCHO	57	**12**	95 (*S*)

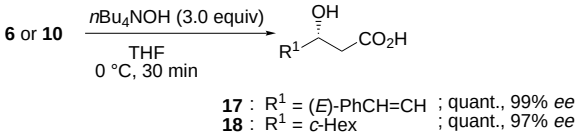
[a] Unless otherwise noted, the reactions were carried out with **4a** (1.0 equiv), LDA (1.1 equiv), and R^1CHO (1.1 equiv) in THF at −78 °C. [b] Yield of isolated product. [c] Determined by chiral HPLC or GC analyses. [d] The configuration at the carbon atom attached to the OH group was assigned by converting **6**–**12** into the corresponding products, whose optical rotations are known.[8] [e] The aldehyde was added at −100 °C. [f] Chiral acetate **4a** (1.8 equiv), LDA (1.8 equiv), and R^1CHO (1.0 equiv) were used.



diastereoselectivities and substrate generality that we observed match or exceed the best reported values with other chiral acetates or their analogues.[3d, i, m, q]

We were pleased to find reagent control,[6] in which the stereochemical preference of the chiral enolate governs the reaction stereochemistry (Table 3). For example, aldolization of a 1:1 mixture of (*S*)-**13a** and (*R*)-**13a** with (*R*,*R*)-**4a** at −78 °C gave *anti* (90% *ee*) and *syn* isomers (99% *ee*) of **14** in 49 and 41% yield, respectively.[7, 8] Thus, the absolute configuration of the emerging C_3 carbon atoms of *anti*- and *syn*-**14** are identical, and enantiofacial selectivity with respect to the aldehyde carbonyl group is consistent with all the results summarized in Table 2. When (*R*,*R*)-**4a** was replaced with (*S*,*S*)-**4a**, antipodes of **14** (*anti*- and *syn*-**15**) formed with equal effectiveness. The two major diastereomers out of four possible stereoisomers in each reaction were easily separated by chromatography. Similarly, 2-benzyloxypropanal (*rac*-**13b**) gave predominantly a 1:1 mixture[7] of *anti*- and *syn*-**16**, indicating again that chirality transfer occurred solely from (*R*,*R*)-**4a** and not from **13**.

The alkaline hydrolysis of adducts **6** and **10** proceeded smoothly with Bu_4NOH[9] in THF at 0 °C for 30 min to yield carboxylic acids **17** (99% *ee*) and **18** (97% *ee*) accompanied by a nearly quantitative amount of **3a**, which could be reused without loss of the optical purity (Scheme 2).[8] There was negligible stereoisomerization at the stereogenic centers due to a retro-aldol reaction.



Scheme 2. Alkaline hydrolysis of aldolates **6** and **10** derived from (*R*,*R*)-**4a**.

The X-ray crystal structure of (*R*,*R*)-**4a**[10] (Figure 1) revealed that the carbonyl plane is oriented perpendicular to the central phenyl plane of the auxiliary, thus minimizing the steric interaction with the two isopropylphenyl groups. In all the present cases, a large preference of the enolate of (*R*,*R*)-**4a** for attack on the *re* face of aldehydes was observed. We suggest two possible transition states—that is, twist boat[11] (A) and acylic models (B; Figure 2)—based on the X-ray

Table 3. Asymmetric aldol reaction of **4a** with racemic α-substituted propanal.[a]

Acetate	*rac*-Aldehyde	Conditions T [°C]	t [h]	Products[b, c]
(*R*,*R*)-**4a**	Me, CHO, Ph — *rac*-**13a**	−78	4	*anti*-**14** 49% (90% *ee*); *syn*-**14** 41% (99% *ee*)
(*S*,*S*)-**4a**	*rac*-**13a**	−100	0.5	*anti*-**15** 37% (95% *ee*); *syn*-**15** 27% (>99% *ee*)
(*S*,*S*)-**4a**	Me, CHO, OBn — *rac*-**13b**	−78	3	*anti*-**16** 39% (94% *ee*); *syn*-**16** 38% (98% *ee*)

[a] The reaction was carried out with the acetate (1.8 equiv), aldehyde (1 equiv), and LDA (1.7 equiv) in THF under the indicated conditions. [b] Yield of isolated, purified products. [c] Enantiomeric excess (*ee*) with respect to the two vicinal stereogenic carbon centers. The absolute and relative configurations were established by comparison with authentic materials; see reference [8].

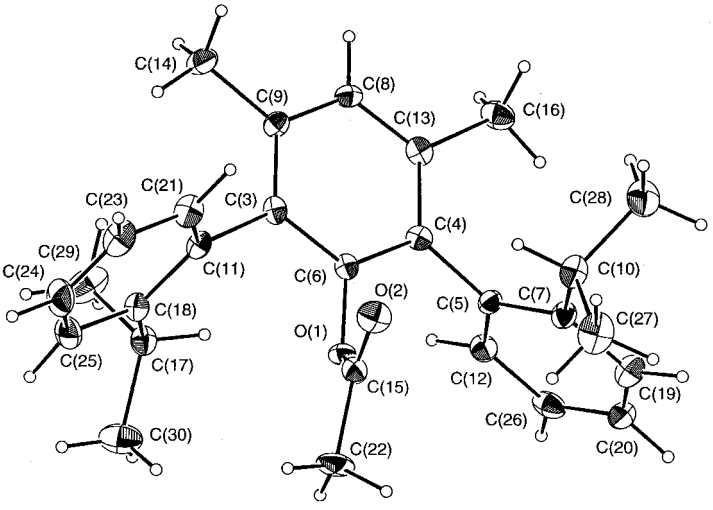


Figure 1. The X-ray crystal structure of (*R*,*R*)-**4a** (ellipsoids at the 15% probability level).

crystal structure and by taking into consideration the striking influence of the *i*Pr groups of (*R*,*R*)-**4a**. Whichever path is used, attack on the *re* face should be favored for the enolate addition.

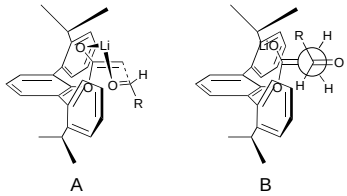


Figure 2. Proposed structure for the transition state of the aldolization: twist-boat (A) and acylic models (B).

In summary, we have successfully devised chiral auxiliary **3a** for the diastereoselective aldol reaction of an acetate with aldehydes. The present aldol system in which steric factors of **4a** predominate appears to have enhanced potential for providing high levels of diastereofacial selectivity. The ease of operation, mildness of the reaction conditions, the availability of both the enantiomers of the acetate, and substrate generality render this system advantageous and practical.

Experimental Section

The reaction of (*R*,*R*)-**4a** with benzaldehyde is representative. To a cooled (−78 °C) solution in THF of LDA—which was prepared by treatment of *i*Pr$_2$NH (77 μL, 0.55 mmol) in THF (1.0 mL) with a 1.59 M solution of *n*BuLi (0.35 mL, 0.55 mmol) in hexane at 0 °C for 30 min—was added a solution of (*R*,*R*)-**4a** (200 mg, 0.50 mmol) in THF (1.0 mL) under an argon atmosphere. After 1 h of stirring, benzaldehyde (56 μL, 0.55 mmol) was added, and the mixture was stirred at −78 °C for 1 h. The reaction mixture was quenched with H_2O at −78 °C and, after being allowed to stir at room temperature for 15 min, extracted with diethyl ether. The organic layer was dried over Na_2SO_4. Evaporation of the solvents and purification of the crude mixture by column chromatography on silica gel (diethyl ether/hexane 1/50 → 2/1) gave (*R*,*R*)-**5a** (175 mg, 69 % yield) as a colorless solid. (*R*,*R*)-**5a** (Table 1, entry 1): IR (KBr): $\tilde{\nu}$ = 3578, 2961, 1763, 1475 cm^{-1}; ^{1}H NMR (300 MHz, $CDCl_3$): δ = 7.39 – 7.03 (m, 14H), 4.49 – 4.46 (m, 1H), 2.72 (br, 2H), 2.09 (s, 6H), 2.45 – 1.92 (m, 2H), 1.75 (dd, 1H, J = 3.6, 2.0 Hz), 1.10 (br, 12H); ^{13}C NMR (75 MHz, $CDCl_3$): δ = 168.8, 147.5, 146.2, 141.9, 136.8, 134.4, 131.8, 130.3, 129.0, 128.2, 1218.1, 127.4, 125.5, 125.3, 125.1, 69.8, 43.5, 30.0, 24.2, 20.1; elemental analysis calcd for $C_{35}H_{38}O_3$: C 82.97, H 7.56; found: C 82.88, H 7.76; $[\alpha]_D$ = −5.3 (c = 1.00, $CHCl_3$).

Received: July 20, 1998 [Z 12172 IE]
German version: *Angew. Chem.* **1998**, *110*, 3579 – 3582

Keywords: aldol reactions · asymmetric synthesis · chiral auxiliaries · nucleophilic additions

[1] Examples of *syn*-selective aldolization with a chiral propionate: a) R. K. Boeckman, Jr., B. T. Connell, *J. Am. Chem. Soc.* **1995**, *117*, 12368, and references therein; examples of *anti*-selective aldolization with a chiral propionate: b) A. Abiko, J.-F. Liu, S. Masamune, *J. Am. Chem. Soc.* **1997**, *119*, 2586, and references therein; c) A. K. Ghosh, M. Onishi, *J. Am. Chem. Soc.* **1996**, *118*, 2527.

[2] General reviews of aldol reactions with chiral acetates: a) S. Masamune, W. Choy, J. S. Petersen, L. R. Sita, *Angew. Chem.* **1985**, *97*, 1; *Angew. Chem. Int. Ed. Engl.* **1985**, *24*, 1; b) M. Braun, *Angew. Chem.* **1987**, 99, 24; *Angew. Chem. Int. Ed. Engl.* **1987**, *26*, 24.

[3] Aldol reactions of acetates having chiral auxiliaries: a) M. Braun, R. Devant, *Tetrahedron Lett.* **1984**, *25*, 5031; b) G. Helmchen, U. Leikauf, I. Taufer-Knöpfgel, *Angew. Chem.* **1985**, *97*, 874; *Angew. Chem. Int. Ed. Engl.* **1985**, *24*, 874; c) Y. Nagao, Y. Hagiwara, T. Kumagai, M. Ochiai, T. Inoue, K. Hashimoto, E. Fujita, *J. Org. Chem.* **1986**, *51*, 2391; d) R. Devant, U. Mahler, M. Braun, *Chem. Ber.* **1988**, *121*, 397, and references therein; e) K. Prasad, K. Ming Chen, O. Repic, G. E. Hardtmann, *Tetrahedron: Asymmetry* **1990**, *1*, 703; f) T. Allmendinger, E. Felder, E. Hungerbühler, *Tetrahedron Lett.* **1990**, *31*, 7301; g) M. Nerz-Stormes, E. R. Thornton, *J. Org. Chem.* **1991**, *56*, 2489; h) T.-H. Yan, A.-W. Hung, H.-C. Lee, C.-S. Chang, *J. Org. Chem.* **1994**, *59*, 8187; i) T.-H. Yan, A.-W. Hung, H.-C. Lee, C.-S. Chang, W-H. Liu, *J. Org. Chem.* **1995**, *60*, 3301; j) S. Bond, P. Perlmutter, *J. Org. Chem.* **1997**, *62*, 6397; k) L. A. Paquette, D. Zuev, *Tetrahedron Lett.* **1997**, *38*, 5115; l) L. A. Paquette, A. Braun, *Tetrahedron Lett.* **1997**, *38*, 5119; m) M. Braun, S. Gräf, *Org. Synth. Col Vol. 72*, 38; for aldol reactions of enolates of acetates having chiral ligands on a metal center: n) S. Masamune, T. Sato, B.-M. Kim, T. A. Wollmann, *J. Am. Chem. Soc.* **1986**, *108*, 8279; o) R. O. Duthaler, P. Herold, W. Lottenbach, K. Oertle, M. Riediker, *Angew. Chem.* **1989**, *101*, 490; *Angew. Chem. Int. Ed. Engl.* **1989**, *28*, 495; p) F. Fringuelli, O. Piermatti, F. Pizzo, *J. Org. Chem.* **1995**, *60*, 7006; quite recently, camphor-based methyl ketone was exploited for a stereoselective "acetate" aldol reaction: q) C. Palomo, A. González, J. M. García, C. Landa, M. Oliarbide, S. Rodríguez, A. Linden, *Angew. Chem.* **1998**, *110*, 190; *Angew. Chem. Int. Ed.* **1998**, *37*, 180.

[4] S. Saito, T. Kano, K. Hatanaka, H. Yamamoto, *J. Org. Chem.* **1997**, *62*, 5651. A more efficient synthetic route to **3a** and **3b** will be published in due course.

[5] The crude samples of **5** – **12** and **14** – **16** were also subjected to HPLC analyses according to the procedures described in reference [8]. The *de* and *ee* values obtained were identical to those listed in Tables 1 – 3.

[6] Boron enolates having chiral ligands on the metal center control the stereoselectivity of the reaction; see a) C. Gennari, G. Pain, D. Moresca, *J. Org. Chem.* **1995**, *60*, 6248; b) M. T. Reetz, E. Rivadeneria, C. Niemeyer, *Tetrahedron Lett.* **1990**, *31*, 3863.

[7] The aldol reaction of the lithium enolates of acetates with α-substituted propionaldehyde generally leads to a 1:1 mixture of *syn* and *anti* products; see C. H. Heathcock in *Asymmetric Synthesis*, *Vol. 3* (Ed.: J. D. Morrison), Academic Press, San Diego, **1984**, chap. 2, p. 167, and references therein.

[8] The *ee* or *de* values of **6**, **8**, **10,** and **14** – **16** were determined by chiral HPLC analyses [HPLC column (Daicel, Ltd.): OB-H for **14** and **15**; OD-H for **6** (i.e., **17**), **8**, and **16**; AS for **10** (i.e. **18**)] after conversion into the corresponding methyl esters by hydrolysis with *n*Bu$_4$NOH/THF and subsequent methylation with $Me_3SiCH_2N_2$. The *de* values of **7** and **11** were established by HPLC analyses [HPLC column (Daicel, Ltd.): OD-H for **7**, doubly arrayed AD for **11**]. Authentic samples for **7** and **11** were synthesized as follows: 1) oxidation of **7** or **11** with Dess – Martin periodinane to give the corresponding β-oxoesters, 2) reduction of the ketone moiety with $NaBH_4$ to yield a diastereomixture (ca. 1:1) of the starting β-hydroxyesters. The *de* values of **9** and **12** were determined by chiral GC analyses of the corresponding diol of **9** and the bis(trifluoroacetate) of the corresponding diol of **12** [GC column (Astecs, Ltd.): γ-TA]. For the relative stereochemistry of **14** and **15**, see a) T. Matsumoto, I. Tanaka, K. Fukui, *Bull. Chem. Soc. Jpn.* **1971**, *44*, 3378; the absolute configurations of **14** and **15** were unambiguously established by comparison with authentic material, which was prepared by treatment of (*R*,*R*)-**4a** with (*S*)-**13a** (ca. 80 % *ee*); for **16**, see b) Z. Pakulski, A. Zamojski, *Tetrahedron* **1995**, *51*, 871; for **8** and **10**, see c) Y. Hiraga, W, Shi, D. I. Ito, S. Ohta, T. Suga, *J. Chem. Soc. Chem. Commun.* **1993**, 1367; for **9**, see: d) B. E. Rossiter, K. B. Sharpless, *J. Org. Chem.* **1984**, *49*, 3707; for **6** and **7**, see reference [3h]. The diol derived from **12** is commercially available.

[9] T. Hasegawa, H. Yamamoto, *Synlett* **1998**, 882; see also A. G. Myers, B. H. Yang, H. Chen, L. McKinstry, D. J. Kopecky, J. L. Gleason, *J. Am. Chem. Soc.* **1997**, *119*, 6496.

[10] The crystals of (*R*,*R*)-**4a** were grown from MeOH/H_2O at 20 °C. Crystal data: space group $P2_12_12_1$, a = 8.738(1), b = 12.727(1), c = 22.386(2) Å, $\alpha = \beta = \gamma = 90.00°$, V = 2489.6(3) Å^3, Z = 4, ρ_{calcd} = 1.065 g cm^{-3}, $\mu(Mo_{K\alpha})$ = 0.0652 mm^{-1}, 1079 reflections, $R1$ = 0.073, $wR2$ = 0.110, GOF = 3.691. The data were collected on a DIP-2030 (MacScience, Ltd.) imaging-plate diffractometer equipped with graphite-monochromated $Mo_{K\alpha}$ radiation (λ = 0.71073 Å). The struc-

 © WILEY-VCH Verlag GmbH, D-69451 Weinheim, 1998 1433-7851/98/3724-3380 $ 17.50+.50/0

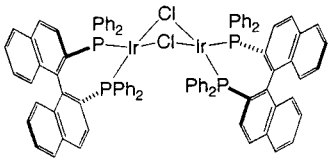
ture was solved by direct methods (maXus) and refined with all data by full-matrix least squares on *F*. All non-hydrogen atoms were refined anisotropically. Hydrogen atoms were added in idealized positions and included in the refinement. Crystallographic data (excluding structure factors) for the structure reported in this paper have been deposited with the Cambridge Crystallographic Data Center as supplementary publication no. CCDC-102228. Copies of the data can be obtained free of charge on application to CCDC, 12 Union Road, Cambridge CB21EZ, UK (fax: (+44) 1223-336-033; e-mail: deposit@ccdc.cam.ac.uk).

[11] It was proposed that the boron enolates of α-unsubstituted ketones favor the more stable U form over the W form by 1–2 kcal mol^{-1}. Similarly, it is conceivable that the bulky phenoxy group of the enolate of **4a** renders the U form most likely, and gives a twist-boat transition structure: a) C. Gennari, R. Todeschini, M. G. Beretta, G. Favini, C. Scolastico, *J. Org. Chem.* **1986**, *51*, 612; b) R. W. Hoffmann, K. Ditrich, S. Froech, *Tetrahedron* **1985**, *41*, 5517; see also reference [2b].

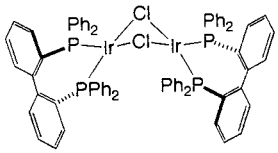
Facile Oxidative Addition of O–H Bonds of Methanol and Water to Ir^{I} Complexes Having Peraryldiphosphane Ligands**

Kazuhide Tani,* Aika Iseki, and Tsuneaki Yamagata

Studies on the oxidative addition of alcohol and water to transition metal complexes leading to the formation of hydrido(hydroxo) and hydrido(alkoxo) complexes, respectively, have received much attention for the past decade due to their potential relevance to catalysis.[1] In particular hydrido(alkoxo) complexes of late transition metals have often been postulated as intermediates or transition states in the catalytic hydrogenation of carbonyl compounds[1a] and catalytic hydrogen transfer reactions.[2] Isolation or detection of such complexes, however, is rare, and their chemistry remains relatively unexplored. About a decade ago we isolated and characterized a hydrido(alkoxo) complex of iridium as a model complex of the reaction intermediates for the rhodium-catalyzed hydrogenation of carbonyl compounds.[3] Milstein and his co-workers reported their efforts on the oxidative addition of hydrogen–heteroatom bonds to rhodium and iridium leading to hydrido(alkoxo) and hydrido(hydroxo) complexes, among others.[4] In addition the isolation of a few hydrido(alkoxo) complexes[5] and hydrido(hydroxo) complexes[1d, 5d] of late transition metals has also been reported. Almost all of these complexes, however, bear basic peralkylphosphane ligands or an electron-donating Cp* ligand (Cp* = C_5Me_5). We have found that dinuclear Ir^{I} complexes [IrCl(diphosphane)]$_2$ carrying even peraryldiphosphanes that are not so strongly electron donating (diphosphane = 2,2′-bis(diphenylphosphanyl)-1,1′-binaphthyl (binap), see **1a**, or 2,2′-bis(diphenylphosphanyl)-1,1′-biphenyl (bpbp), see **1b**)[6, 7] can easily activate protic molecules (MeOH or H_2O) at ambient temperature.

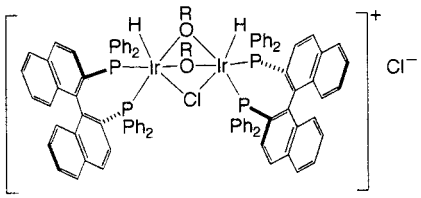


1a



1b

Upon treatment of a solution of the extremely air-sensitive complex **1a** in toluene with a large excess of methanol, the color changed immediately from deep red to pale yellow. After the reaction mixture had been stirred at room temperature for several hours, the solvents were removed in vacuo to give quantitatively the almost pure hydrido(methoxo) complex **2a** as air-stable and thermally stable pale yellow microcrystals. The formulation was supported by the elemental analyses (see Table 1 and the supporting information).



2a: R = Me
3a: R = H

The ^{31}P NMR spectrum of **2a** exhibits two doublets at $\delta = -15.2$ and -1.8 (^2J(P,P) = 19 Hz) in a 1:1 ratio, indicating the presence of two nonequivalent phosphorus atoms. The presence of terminal hydrido ligands was suggested by the IR ($\tilde{\nu}$(Ir–H) = 2270 cm^{-1}) and ^{1}H NMR spectra ($\delta = -23.10$ (dd, ^2J(H,P) = 18, 23 Hz)). The methoxy methyl protons appear at $\delta = 2.63$ as a triplet (^4J(H,P) = 3.4 Hz). The signal is more than 1 ppm upfield of the analogous signals of the mononuclear iridium complexes *mer-cis*-[Ir(Cl)(H)(OMe)(PEt$_3$)$_3$] ($\delta = 4.01$)[4d] and *cis*-[Ir(H)(OMe)(PMe$_3$)$_4$]$^+$PF$_6^-$ ($\delta = 3.637$)[4a] and appears at 0.55 ppm higher field than even that of the Ir^{I}-methoxo complex [Ir$_2$(μ-OMe)$_2$(cod)$_2$] ($\delta = 3.28$; cod = 1,5-cyclooctadiene).[8] This may be due to the diamagnetic shielding by a benzene ring of the diphenylphosphanyl moiety of the binap ligands (vide infra). Complex **2a** is much more thermally stable than these monomeric complexes. The ^{1}H NMR spectrum indicates the presence of a molecule of solvated methanol: a doublet at $\delta = 3.38$ ($J = 5.6$ Hz) for the methyl protons and a quartet at $\delta = 1.62$ for the OH proton. This may indicate strong hydrogen bonding between the chloro bridge and the solvated methanol even in solution (vide infra).[9] Exchange between the methoxo and the

[*] Prof. Dr. K. Tani, A. Iseki, Dr. T. Yamagata
Department of Chemistry, Graduate School of Engineering Science
Osaka University
Toyonaka, Osaka, 560–8531 (Japan)
Fax: (+81) 6-6850-6245
E-mail: tani@chem.es.osaka-u.ac.jp

[**] This work was partly supported by a Grant-in Aid for Scientific Research from the Ministry of Education, Science, Sports, and Culture of Japan.

Supporting information for this article is available on the WWW under http://www.wiley-vch.de/home/angewandte/ or from the author.

 © WILEY-VCH Verlag GmbH, D-69451 Weinheim, 1998 1433-7851/98/3724-3381 $ 17.50+.50/0

Table 1. Selected data for complexes **2a**, **b** and **3a**, **b**.

2a: M.p. > 108 °C (decomp in a capillary under vacuum); ^{1}H NMR (270 MHz, 35 °C, CD_2Cl_2): $\delta = -23.10$ (dd, ^2J(H,P) = 18, 23 Hz, 2H; Ir–H), 1.62 (q, J = 5.6 Hz, 1H; CH_3OH), 2.63 (t, ^4J(H,P) = 3.4 Hz, 6H; Ir–OCH_3), 3.38 (d, J = 5.6 Hz, 3H; CH_3OH), 6.14 – 8.02 (m, 64H; Ph + Naph); ^{31}P{^{1}H} NMR (109.25 MHz, 35 °C, CD_2Cl_2): $\delta = -1.8$ (d, ^2J(P,P) = 19 Hz), −15.2 (d, ^2J(P,P) = 19 Hz); IR (film): $\tilde{\nu} = 2270\ cm^{-1}$ (br m; Ir–H); $\Lambda_0 = 80.4\ S\,cm^2\,mol^{-1}$ (in dry MeOH, at 25 °C); the elemental analysis of **2a** obtained after the sample had been thoroughly dried in vacuo agreed well with the chemical formula without the solvate methanol; elemental analysis calcd for $C_{90}H_{72}Cl_2Ir_2O_2P_4$: C 61.25, H 4.11; found: C 61.05, H 4.27

2b: M.p. > 130 °C (decomp in capillary under vacuum); ^{1}H NMR (270 MHz, 35 °C, $CDCl_3$): $\delta = -23.25$ (dd, ^2J(H,P) = 18, 23 Hz, 2H; Ir–H), 2.77 (t, ^3J(H,P) = 3 Hz, 6H; Ir–OCH_3), 6.22 – 7.77 (m, 56H; ArH); ^{31}P{^{1}H} NMR (109.25 MHz, 35 °C, $CDCl_3$): $\delta = -3.3$ (d, ^2J(P,P) = 20 Hz), −13.3 (d, ^2J(P,P) = 20 Hz); IR (film): $\tilde{\nu} = 2261\ cm^{-1}$ (br m; Ir–H); elemental analysis calcd for $C_{74}H_{64}Cl_2Ir_2O_2P_4$: C 56.81, H 4.12; found: C 56.56, H 4.43

3a: M.p. > 110 °C (decomp in a capillary under vacuum); ^{1}H NMR (270 MHz, 35 °C, $CDCl_3$) $\delta = -22.14$ (dd, ^2J(H,P) = 16, 22 Hz, 2H; Ir–H), 1.49 (t, ^3J(H,P) = 3 Hz, 2H; Ir–OH), 6.43 – 7.86 (m, 64H; Ph + Naph); ^{31}P{^{1}H} NMR (109.25 MHz, 35 °C, $CDCl_3$): $\delta = -0.9$ (d, ^2J(P,P) = 20 Hz), −2.1 (d, ^2J(P,P) = 20 Hz); IR (film): $\tilde{\nu} = 3525$ (m, (O–H)), 2267 cm^{-1} (br m; Ir–H); $\Lambda_0 = 69.3\ S\,cm^2\,mol^{-1}$ (in THF/H_2O (1/1 v/v), at 25 °C); elemental analysis calcd for $C_{88}H_{68}Cl_2Ir_2O_2P_4$: C 60.86, H 3.95; found: C 60.96, H 4.35

3b: M.p. > 120 °C (decomp in a capillary under vacuum); ^{1}H NMR (270 MHz, 35 °C, $CDCl_3$): $\delta = -23.26$ (dd, ^2J(P,P) = 18, 22 Hz, 2H; Ir–H), 1.80 (br, 2H; Ir–OH), 6.10 – 7.82 (m, 56H; ArH); ^{31}P{^{1}H} NMR (109.25 MHz, 35 °C, $CDCl_3$): $\delta = -2.5$ (d, ^2J(P,P) = 20 Hz), −6.6 (d, ^2J(P,P) = 20 Hz); IR (film): $\tilde{\nu} = 3560$ (m; O–H), 2258 cm^{-1} (br m; Ir–H); elemental analysis calcd for $C_{72}H_{60}Cl_2Ir_2O_2P_4$: C 56.28, H 3.94; found: C 55.71, H 4.17

hydrido ligands with the solvated methanol was not detected below 40 °C in CD_2Cl_2 in ^{1}H NMR experiments.

The structure was confirmed by X-ray analysis. Single crystals of **2a** containing one molecule of solvated methanol suitable for X-ray analysis were grown from absolute methanol.[10] The molecular view in Figure 1 reveals the presence of a C_2 axis. The cationic part of **2a** has a dinuclear iridium structure. The coordination environment of each iridium atom can be described as a highly distorted octahedron with two phosphorus atoms, two bridging methoxo ligands, a chloro ligand, and a terminal hydrido ligand. The chloride counteranion is located near the solvate methanol, which is situated on a C_2 axis, as two disordered peaks and the hydrogen bond between the chloride and the methanol should be present (O2 ··· Cl2 2.62(2) Å). A terminal hydrido ligand should be present at the position *trans* to the μ-chloro ligand and *cis* to the methoxy groups. The methoxy methyl groups are situated just above the benzene rings of the diphenylphosphanyl moieties of the binap ligands. The complex has a bent $Ir_2(\mu\text{-}OMe)_2$ core with a hinge angle of 141.4(1)°, which deviates seriously from the expected value (109.5°) made by two fused face-sharing octahedrons. The dihedral angle between the pair of naphthyl planes is 81.4(1)°, the largest angle among binap complexes characterized to date.[6, 14] The Ir–Cl bond length (2.534(2) Å) is the longest of the Ir^{III}–μ-Cl distances reported so far.[15] These structural features agree well with the spectroscopic characteristics.

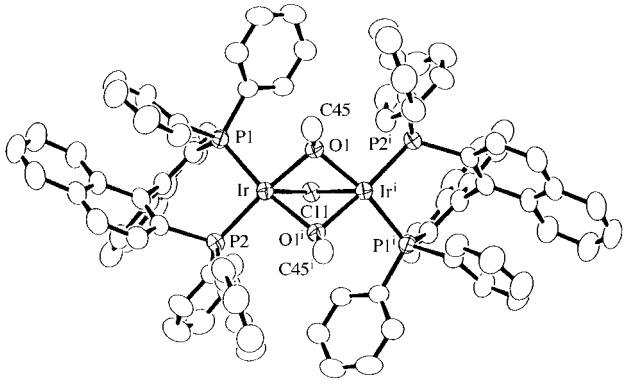
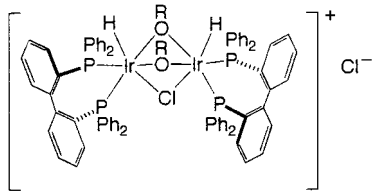


Figure 1. X-ray crystral structure showing the cationic part of **2a** (ORTEP view, ellipsoids at 50% probability). Selected interatomic distances [Å] and angles [°]: Ir–O1 2.106(4), Ir–O1^i 2.138(4), Ir–P1 2.2477(13), Ir–P2 2.2624(13), Ir–Cl1 2.534(2), Ir ··· Ir^i 3.1461(7); O1-Ir-O1^i 76.5(2), O1-Ir-P1 93.57(10), O1^i-Ir-P1 169.69(10), O1-Ir-P2 172.09(11), O1^i-Ir-P2 96.96(10), P1-Ir-P2 93.15(5), O1-Ir-Cl1 75.38(10), O1^i-Ir-Cl1 74.87(10), P1-Ir-Cl1 100.18(4), P2-Ir-Cl1 107.50(4), Ir-Cl1-Ir^i 76.75(5), Ir-O1-Ir^i 95.67(14), C45-O1-Ir 115.5(4), C45-O1-Ir^i 125.2(4). i: ($-x$, y, $-z$).

The analogous reaction of **1b** with methanol gave the corresponding hydrido(methoxo) complex **2b** as pale yellow crystals (see Table 1 and the supporting information). Complexes **1a** and **1b** can also activate water. Thus, the reaction of



2b: R = Me
3b: R = H

1a and **1b** with excess water in THF at ambient temperature gave hydrido(hydroxo) complexes **3a** and **3b**, respectively, as air-stable, pale yellow powders in almost quantitative yields (see Table 1). Based on the analogies in the ^{1}H NMR spectra of **2a** and **3a** [for the latter, Ir–H signal at $\delta = -22.14$ (dd, ^2J(H,P) = 16, 22 Hz), Ir–OH signal at $\delta = 1.49$ (t, ^3J(H,P) = 3 Hz)] and in the ^{31}P{^{1}H} NMR spectra [$\delta = -0.9$ (d, ^2J(P,P) = 20 Hz), −2.1 (d, ^2J(P,P) = 20 Hz)], complexes **3** are also considered to have similar triply bridged dinuclear structures with two μ_2-OH groups and a μ_2-Cl atom (vide supra). The ionic structure of **3a** has been confirmed by its limiting equivalent conductance, $\Lambda_0 = 69.3\ S\,cm^2\,mol^{-1}$ measured in THF/H_2O (1/1 v/v) at 25 °C.[16]

We have demonstrated that iridium – diphosphane complexes **1a** and **1b**, which have peraryldiphosphane ligands, easily activate methanol and water to give hydrido(methoxo) complexes **2** as well as hydrido(hydroxo) complexes **3** in good yield. The structures of these new complexes were characterized spectroscopically and by X-ray crystallographic analysis of **2a**. We are continuing to explore the catalytic application of these complexes.

Received: January 20, 1998
Revised version: August 20, 1998 [Z11386IE]
German version: *Angew. Chem.* **1998**, *110*, 3590 – 3592

Keywords: iridium · methanol · oxidative additions · P ligands · water

 © WILEY-VCH Verlag GmbH, D-69451 Weinheim, 1998 1433-7851/98/3724-3382 $ 17.50+.50/0

[1] a) H. E. Bryndza, W. Tam, *Chem. Rev.* **1988,** *88*, 1163 – 1188; b) T. Yoshida, Y. Ueda, S. Otsuka, *J. Am. Chem. Soc.* **1978**, *100*, 3941 – 3942; c) T. Yoshida, T. Okano, Y. Ueda, S. Otsuka, *J. Am. Chem. Soc.* **1981**, *103*, 3411 – 3422; d) T. Yoshida, T. Kitani, S. Otsuka, *J. Am. Chem. Soc.* **1979**, *101*, 2027 – 2038; e) T. Yoshida, T. Okano, T. Saito, S. Otsuka, *Inorg. Chim. Acta* **1980**, *44*, L135 – L135.

[2] R. A. W. Johnstone, A. H. Wilbi, I. D. Entwisth, *Chem. Rev.* **1985**, *85*, 129 – 170.

[3] K. Tani, E. Tanigawa, Y. Tatsuno, S. Otsuka, *J. Organomet. Chem.* **1985**, *279*, 87 – 101.

[4] a) D. Milstein, J. C. Calabrese, I. D. Williams, *J. Am. Chem. Soc.* **1986**, *108*, 6387 – 6389; b) D. Milstein, *J. Am. Chem. Soc.* **1986**, *108*, 3525 – 3526; c) A. L. Casalnuovo, J. C. Calabrese, D. Milstein, *Inorg. Chem.* **1987**, *26*, 971 – 973; d) O. Blum, D. Milstein, *Angew. Chem.* **1995**, *107,* 210 – 212; *Angew. Chem. Int. Ed. Engl.* **1995**, *34*, 229 – 231; e) O. Blum, D. Milstein, *J. Am. Chem. Soc.* **1995**, *117*, 4582 – 4594.

[5] a) R. S. Paonessa, A. L. Prignano, W. C. Trogler, *Organometallics* **1985**, *4*, 647 – 656; b) J. Fornies, M. Green, J. L. Spencer, F. G. A. Stone, *J. Chem. Soc. Dalton Trans.* **1977**, 1006 – 1009; c) D. Braga, P. Sabatino, C. Di Buugno, P. Leoni, M. Pasquali, *J. Organomet. Chem.* **1987**, *334,* C46 – C48; d) F. L. Ladipo, M. Kooti, J. S. Merola, *Inorg. Chem.* **1993**, *32*, 1681 – 1688; e) L. J. Newman, R. G. Bergman, *J. Am. Chem. Soc.* **1985**, *107*, 5314 – 5315; f) D. S. Glueck, L. J. N. Winslow, R. G. Bergman, *Organometallics* **1991**, *10*, 1462 – 1479; g) A. L. Seligson, R. L. Cowan, W. C. Trogler, *Inorg. Chem.* **1991**, *30*, 3371 – 3381; h) N. S. Akl, H. A. Tayim, *J. Organomet. Chem.* **1985**, *297*, 371 – 374; i) H. Werner, A. Michenfelder, M. Schulz, *Angew. Chem.* **1991**, *103,* 617; *Angew. Chem. Int. Ed. Engl.* **1991**, *30*, 596 – 598.

[6] T. Yamagata, A. Iseki, K. Tani, *Chem. Lett.* **1997**, 1215 – 1216.

[7] R. Dorta, P. Egli, F. Zücher, A. Togni, *J. Am. Chem. Soc.* **1997**, *119*, 10857 – 10858.

[8] R. Uson, L. A. Oro, J. A. Cabeza, *Inorg. Synth.* **1985**, *23*, 126 – 129.

[9] The NMR signal of a monomeric ROH proton appears at about $\delta = 0.5$; R. M. Silverstein, G. C. Bassler, T. C. Morrill, *Spectrometric Identification of Organic Compounds*, 4th ed., Wiley, New York, **1981**, Chap. 4.

[10] X-ray crystal structure determination of **2a**: $C_{90}H_{72}Cl_2Ir_2O_2P_4 \cdot CH_3OH$, $M_r = 1796.70$; crystal dimensions $0.43 \times 0.23 \times 0.13$ mm^3; monoclinic, space group $C2$, $a = 17.722(3)$, $b = 16.201(4)$, $c = 16.424(3)$ Å; $\beta = 113.604(12)^\circ$, $V = 4321.0(16)$ Å^3, $Z = 2$, $\rho_{calcd} = 1.381$ g cm^{-3}, $\mu = 3.258$ mm^{-1}. Single crystals suitable for X-ray measurements were obtained by repeated recrystallization of **2a** from anhydrous methanol under argon. Because the surface of the pale yellow crystals became rough immediately when isolated from the mother liquor, presumably as a consequence of loss of the solvate methanol, the crystals were coated with silicon grease and sealed in glass capillaries containing methanol. Cell constants and an orientation matrix for data collection were determined by the least-squares refinement, using the setting angles of 25 reflections in the range $23^\circ < 2\theta < 25^\circ$ on a Rigaku diffractometer (AFC-7R) equipped with a Rotaflex rotating anode X-ray generator (50 kV, 200 mA) with monochromated $Mo_{K\alpha}$ radiation. For the data collection, reflections in the range 0 to $+h$, 0 to $+k$, $-l$ to $+l$, and the corresponding Friedel pairs (matrix: $(-1\ 0\ 0)$, $(0\ -1\ 0)$, $(0\ 0\ -1)$) were measured by the $\omega - 2\theta$ scan technique (scan speed 16.0° min^{-1}, scan width $(1.57 + 0.30\tan\theta)^\circ$). Three standard reflections were monitored every 200 reflections and showed a 7.19% intensity decrease over the collection period. Intensity data were corrected for Lorentz and polarization effects. The absorption corrections ($T_{min} = 0.4874$, $T_{max} = 0.6545$) based on psi-scan data and a linear correction factor were applied for the raw data. A total of 10642 reflections ($3.0^\circ < 2\theta < 55.12^\circ$) were collected at 293(2) K, of which 9955 unique reflections ($R_{int} = 0.0171$) were used for the structure solution and refinement. The structure was solved by direct methods (SHELXS-86)[11] and weighted Fourier techniques[12] and refined on F^2 by full-matrix least-squares methods using SHELXL-93.[13] Non-hydrogen atoms of the cationic part were refined anisotropically. The chlorine atom of the anionic part and non-hydrogen atoms of methanol were refined isotropically. Hydrogen atoms of aromatic and methoxy groups were included in the refinement on calculated positions riding on their carrier atoms ($C{-}H_{sp^2} = 0.93$ Å, $C{-}H_{sp^3} = 0.96$ Å, $U_{iso}(H) = 1.2\,U_{eq}(C)$). The hydrogen atoms of the methyl group of the solvate methanol were located on a difference-Fourier map and fixed in the refinements. The OH hydrogen atoms of the methanol molecule were not included in the calculations. The function minimized was $[\Sigma w(F_o^2 - F_c^2)^2]$ ($w = 1/[\sigma^2(F_o^2) + (0.0534P)^2 + 1.6777P]$), where $P = (\max(F_o^2,0) + 2F_c^2)/3$ with $\sigma^2(F_o^2)$ from counting statistics. The functions $R1$ and $wR2$ were $(\Sigma\,||F_o| - |F_c||)/\Sigma\,|F_o|$ and $[\Sigma w(F_o^2 - F_c^2)^2/\Sigma(wF_o^4)]^{1/2}$, respectively; $R1 = 0.0290$ and $wR2 = 0.0838$ for 9226 reflections with $I > 2.0\sigma(I)$. Final R factors: $R1 = 0.0351$ and $wR2 = 0.0866$ for 9955 reflections (all data). The number of parameters is 455. Flack χ parameter shows $-0.018(7)$, and the absolute configuration of the binap ligand is R. GOF values are 1.153 for $I > 2.0\sigma(I)$ and 1.146 for all data. The maximum shift to esd ratio in the last full-matrix least-squares cycle was 0.000. The final difference Fourier map revealed a number of areas of residual electron density, the greatest of which corresponds to 1.109 e Å^{-3}. The minimum hole of the final difference Fourier map is -1.270 e Å^{-3}. For more details refer to the supporting information. Crystallographic data (excluding structure factors) for the structure reported in this paper have been deposited with the Cambridge Crystallographic Data Center as supplementary publication no. CCDC-101027. Copies of the data can be obtained free of charge on application to CCDC, 12 Union Road, Cambridge CB2 1EZ, UK (fax: (+44) 1223-336-033; e-mail: deposit@ccdc.cam.ac.uk). All calculations were carried out on Silicon Graphics SGI Power Challenge workstation at the Research Center for Protein Engineering, Institute for Protein Research, Osaka University.

[11] G. M. Sheldrick, SHELXS-86, Program for the Solution of Crystal Structures, University of Göttingen, Germany, **1985**.

[12] J. Karle, *J. Acta Crystallogr. Sect. B* **1968**, *24*, 182 – 186. The DIRDIF program system, Technical Report of the Crystallography Laboratory, University of Nijmegen, The Netherlands. teXsan: Single Crystal Structure Analysis Software, Version 1.6f, Molecular Structure Corporation, The Woodlands, TX 77381, USA, **1993**.

[13] G. M. Sheldrick, SHELXL-93 in Crystallographic Computing 6 (Eds.: P. Flack, P. Parknyi, K. Simon), University Press, Oxford, **1993**.

[14] R. Noyori, H. Takaya, *Acc. Chem. Res.* **1990**, *23*, 345 – 350, and references therein.

[15] A. G. Orpen, L. Brammer, F. G. Allen, O. Kennard, D. G. Watson, R. Taylar, *J. Chem. Soc. Dalton Trans.* **1989**, S1 – S83.

[16] Note added in proof (November 4, 1998): Recently, a facile oxidative addition of water to dinuclear ferrocenyldiphosphane-Ir^{I} complexes to give neutal hydrodido(hydroxo) complexes was reported: R. Dorta, A. Togni, *Organometallics* **1998**, *17*, 3423 – 3428.

Micro-Scale Frontal Affinity Chromatography with Mass Spectrometric Detection: A New Method for the Screening of Compound Libraries

David C. Schriemer, David R. Bundle, Liang Li, and Ole Hindsgaul*

The application of combinatorial chemistry to accelerated drug discovery has generated new problems in screening for potential therapeutics. Classical approaches of a one-compound, one-assay variety are often untenable because of time and resource constraints since the goal of combinatorial chemistry is to produce large libraries of compounds. These libraries are either generated on a solid phase (beads) or in solution.[1] A binding assay must be performed against a target at some point, and this usually means assaying either a large

[*] Prof. O. Hindsgaul, Dr. D. Schriemer, Prof. D. Bundle, Prof. L. Li
Department of Chemistry, University of Alberta
Edmonton, T6G 2G2 (Canada)
Fax: (+1) 403-492-7705
E-mail: ole.hindsgaul@ualberta.ca

 © WILEY-VCH Verlag GmbH, D-69451 Weinheim, 1998 1433-7851/98/3724-3383 $ 17.50+.50/0

number of beads or a mixture of compounds in solution. The identification and isolation of receptors has allowed for radioligand binding and ELISA-type assays as primary screening strategies for such mixtures.[2] Iterative synthesis and analysis are often required in the determination of structure – activity relationships. It would be ideal to examine an entire library (or sublibrary) to identify and rank the constituent ligands, and to ascertain the absolute binding constants for each in a single analysis. Current assays do not provide this level of analysis.

Mass spectrometry is emerging as an important tool for the interrogation of combinatorial libraries. It has been used to assess library quality[3, 4] and, when coupled with molecular recognition technologies, has allowed for some success in the isolation and characterization of active library compounds.[5] Most of the approaches to combining molecular recognition with mass spectrometry have incorporated a "capture and release" methodology, where compound mixtures are applied to immobilized receptors, washed, and the high-affinity ligands stripped with a denaturing solution and presented to the mass spectrometer.[6] As an alternative, we have investigated the direct coupling of frontal affinity chromatography (FAC) with mass spectrometry.

In FAC a receptor is immobilized on a suitable support material and packed in a column.[7] A mixture containing potential ligands is *continuously* infused through the column, rather than injected in the conventional "spike" form. Active ligands will bind to the column, but eventually the capacity of the column will be exceeded, which results in the ligands breaking through at their infusion concentration. All non-retained compounds will break through earlier in the void volume of the system. Traditionally, this technique has been used for the characterization of chromatographic stationary phases, and the determination of thermodynamic and kinetic binding data of individual compounds.[8] There are several advantages to miniaturizing FAC columns and coupling them to an electrospray mass spectrometer: The requirement for the precious receptor is greatly reduced and the demands on the amounts of ligand are proportionally decreased. Electrospray mass spectrometry allows for the sensitive detection of compounds that break through the column (less than 1 pmol μL^{-1}), but more importantly it provides an extra dimension to the analysis, namely the m/z ratio. Conventional FAC columns are most often interfaced with a single wavelength UV/Vis spectrophotometer. Such a detector is one-dimensional in the sense that all solution components contribute to the measured intensity at a given point in time. In this case, trace components would be indistinguishable from the background created by the excess of other compounds. By using a mass spectrometer as a detector the opportunity is provided for a two-dimensional analysis, where even a trace component can be identified provided it appears at a m/z value measurably distinct from the other solution components.

To illustrate the potential of FAC/MS for the screening of mixtures we prepared a microcolumn containing an immobilized monoclonal antibody and coupled it to an electrospray mass spectrometer (Figure 1). The carbohydrate-binding antibody recognizes the 3,6-dideoxy-D-xylohexose (abequose) epitope in *Salmonella paratyphi* B O-antigens.[9, 10] The affinity-purified antibody was biotinylated, and then incubated with beads bearing covalently-coupled avidin. The beads were then slurry-packed into a 11.5 cm long poly(ether ether ketone) (PEEK) column with an internal diameter of 500 μm (ca. 23 μL column volume). In this design a tee served a dual role as a column end-fitting and mixing chamber for the column eluent and organic make-up flow. The column was then directly connected to an electrospray mass spectrometer. For operation in frontal analysis chromatography mode, the column was first flushed with ammonium acetate buffer (NH_4OAc, 2 mM, pH 6.7). The flow was then switched to a second solution containing a mixture of six oligosaccharides (Scheme 1) in NH_4OAc buffer, each present at 1 μM . This solution was chosen to model a simple combinatorial "library" of compounds. Three of these oligosaccharides (**1**–**3**) have no specificity for the antibody. The remaining three (**4**–**6**) contain the minimal requirement for recognition (abequose) and span a range of affinity for the antibody. The K_d values for the active ligands were determined independently by titration microcalorimetry (Table 1).

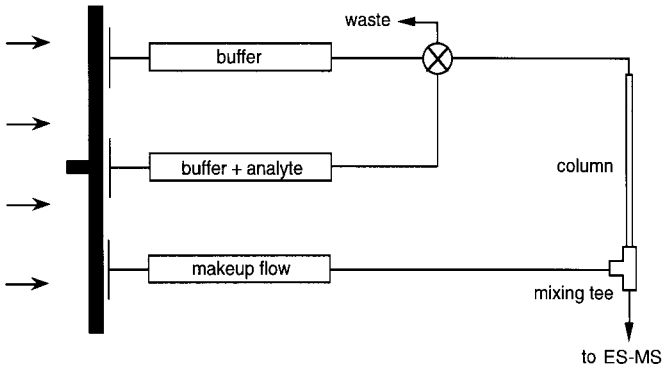


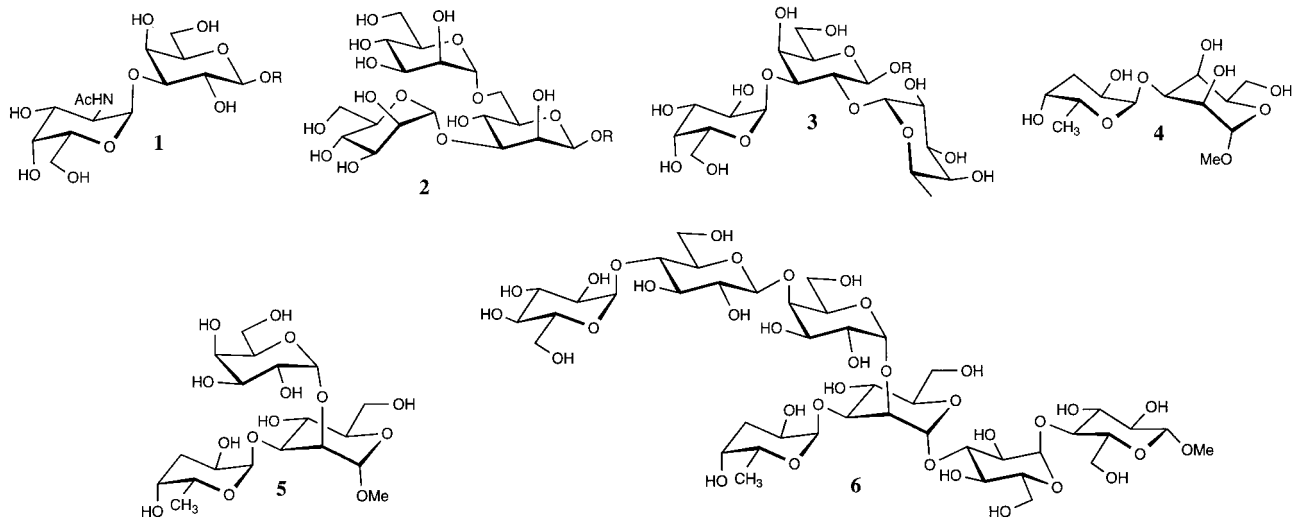
Figure 1. Schematic representation of the FAC/MS apparatus.

A total-ion chromatogram (TIC) was constructed from a 50 minute run time of this mixture through the column (Figure 2, top), which represents the consumption of only 400 pmol of each oligosaccharide. Peaks at specific m/z values could then be identified through the analysis of the mass spectra that give rise to the TIC, and selected ion chromatograms reconstructed from the TIC (Figure 2, middle). Mass spectra were generated from time-slices of the chromatogram and chart the progression of the various oligosaccharides through the column (Figure 2, bottom). Compounds **1**–**3** break through at the void volume (V_0), while compounds **4**–**6** break through later at volumes V_x, which relate to their concentrations and K_d values. The equation governing the breakthrough volume $V_x - V_0$ for the infusion of a single ligand can be determined by Equation (1), where B_t represents the dynamic binding capacity of the column and X the

$$V_x - V_0 = \frac{B_t}{[X]_0 + (K_d)_x} \quad (1)$$

compound with its corresponding dissociation constant K_d.[7] This simple equation indicates that once B_t and the concentration of the ligand are known, the dissociation constant can

 © WILEY-VCH Verlag GmbH, D-69451 Weinheim, 1998 1433-7851/98/3724-3384 $ 17.50+.50/0



Scheme 1. Structures of the oligosaccharides used ($R = O(CH_2)_8COOMe$).

Table 1. Molecular weight and dissociation constants of the oligosaccharides **1**–**6**.

Oligosaccharide ($R = O(CH_2)_8CO_2Me$)	m/z $[(MNa)]^{+}$[a]	$K_d \pm s$ [μM][b] microcalorimetry[c]	FAC/MS individual[d]	FAC/MS mixture[e]
αGalNAc(1→3)βGal-OR (**1**)	576.3	–	–	–
αGal(1→3)[αFuc(1→2)]βGal-OR (**2**)	681.3	–	–	–
αMan(1→3)[αMan(1→6)]βMan-OR (**3**)	697.3	–	–	–
αAbe(1→3)αTal-OMe (**4**)	347.0	190	185 ± 17	178 ± 23
αGal(1→2)[αAbe(1→3)]αMan-OMe (**5**)	509.2	6.3	12.6 ± 1.3	10.2 ± 1.1
αGlc(1→4)βGlc(1→4)αGal(1→2)[αAbe(1→3)]-αMan(1→3)αGlc(1→4)βGlc-OMe (**6**)	1157.4	0.88	1.79 ± 0.20	1.71 ± 0.16

[a] Monoisotopic molecular weight of the singly charged sodium adduct. [b] Dissociation constant with the corresponding standard deviation, calculated from Equation (1). All values are determined from triplicate experiments, with the exception of the first FAC/MS entry for **5** (determined from Figure 3). The standard deviations s include the uncertainty in B_t. [c] Unpublished data, as determined by methods discussed in ref. 9. [d] Values determined from infusion of individual ligand, with compounds **1**–**3**. [e] Values determined from the infusion of the six-compound mixture.

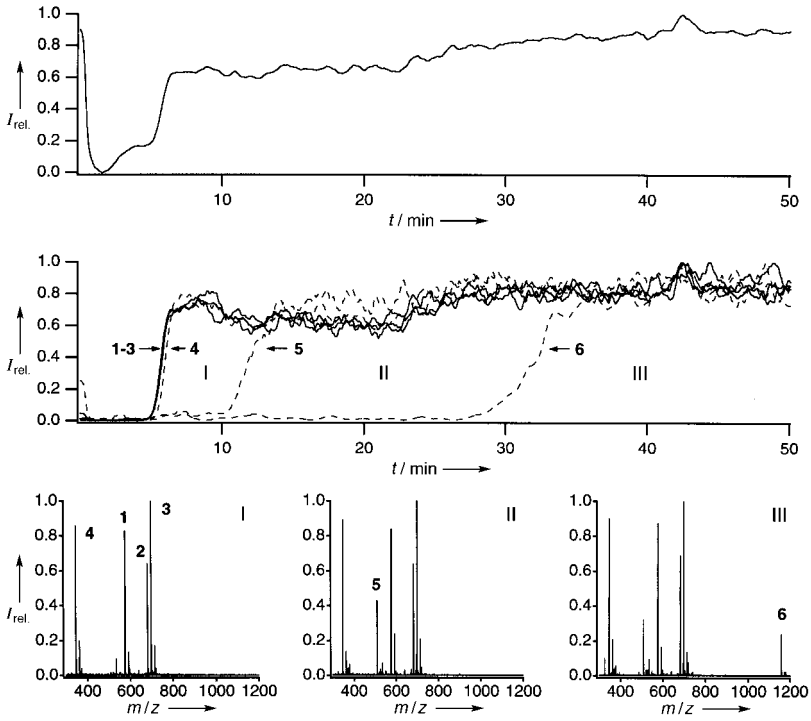


Figure 2. Extraction of data from a frontal chromatogram. Top: Total-ion chromatogram (TIC). Middle: Selected ion chromatograms of all six compounds. Compounds **1**–**3** break through simultaneously, as indicated by the solid line. Bottom: Spectra extracted from time-slices of the TIC. A spectrum representing the onset of break through of **4** is not shown.

be determined from a single measurement of its $V - V_0$. In order to determine B_t compound **5** was infused through the column at various concentrations and the corresponding $V - V_0$ values measured. A plot of $([\mathbf{5}](V - V_0))^{-1}$ versus $[\mathbf{5}]^{-1}$ was generated (Figure 3), where the reciprocal of the y intercept indicates a B_t of 554 pmol (analogous to a Lineweaver–Burk plot). Each antibody molecule contains two binding sites, therefore this corresponds to an active capacity of 277 pmol of protein (which represents ca. 100% of the total amount of protein bound). The negative reciprocal of the x intercept indicates a K_d of 12.6 μM for this compound, which is only a factor of two different from the value determined by microcalorimetry (Table 1).

Knowledge of the column capacity prior to the screening of a mixture, and control over the concentration of the mixture, allows the determination of dissociation constants for all ligands from a single frontal analysis chromatogram. For compounds with [X] much less than $(K_d)_x$, the K_d can be determined simply from Equation (1) even in the presence of stronger binders. For example, the K_d of

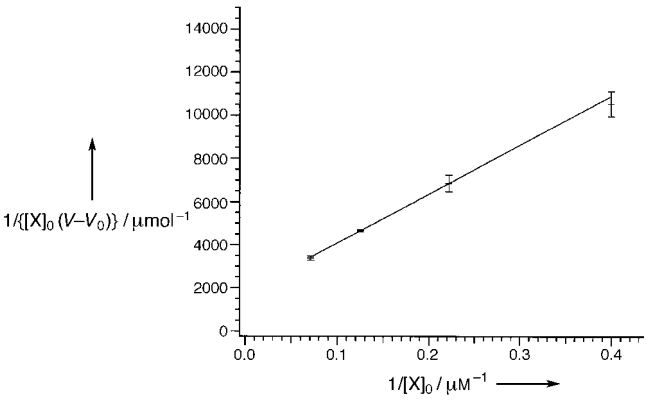


Figure 3. Determination of the column capacity and ligand binding affinity of **5** by FAC/MS, with a linear fit to the experimental data. Data points represent the average of three replicates, and the fit is weighted by the inverse of their standard deviations.

compound **4** as determined from the chromatogram of the multi-ligand mixture (Figure 2) is $178 \pm 23\,\mu M$, which is equivalent to the K_d determined individually ($185 \pm 17\,\mu M$, Table 1). The concentration of **5** was also sufficiently lower than its K_d ($12.6\,\mu M$) such that the equation can be used to calculate K_d from runs of the multi-ligand mixture. This value agrees with the one determined individually as well at the 95% confidence limit (Table 1). Furthermore, both compounds **4** and **5** are not present at concentrations high enough to compete with the binding of the strongest ligand (**6**), therefore its K_d could be determined from the mixture in a straightforward fashion from Equation (1). This is also verified by the equivalency between the values determined from the mixtures and individually (Table 1). It should be noted that if multi-ligand competition is expected the mixture can be diluted and re-run, such that conditions equivalent to this test case can usually be duplicated.

Of course, compounds that bind nonspecifically to column elements (walls, beads, or protein) would also demonstrate breakthrough volumes greater than the void volume of the system, and might give a false indication of activity. This can be easily ascertained. Library compounds that bind in a manner that affects the activity of the immobilized receptor will reduce the value of B_t. A known ligand that is flowed through the column, after the column has reached dynamic equilibrium with the mixture of library compounds, will generate a reduction in $V - V_0$ for this ligand, as it "sees" a lower B_t. The known ligand can be run through a fully active column to determine its expected $V - V_0$ value. Nonspecifically bound species would not give rise to a reduction in the $V - V_0$ value for this ligand, therefore an observed reduction indicates the presence of ligand(s) in the library.

The general FAC/MS approach is particularly advantageous in that a protein–ligand denaturing step is not required for the screening of the mixture or for the determination of dissociation constants. Column regeneration is achieved off-line by washing with a large volume of binding buffer, with or without a competitive ligand, thereby preserving the target receptor. The column used in this study was subjected to over 100 runs with no observable loss of activity and/or leaching of the antibody. Furthermore, not having to switch to a harsh denaturing buffer for compound elution has practical advantages for mass spectrometry. Electrospray detection only has to be optimized for one buffer system, rather than two or more.

This newly developed technique can also be used to accelerate the screening of compound libraries. Active components in mixtures can be both identified and ranked by their K_d value in a single chromatogram. An additional and very important advantage of this technique, relative to the traditional inhibition experiments, is that the molecular weight of the active compound is established, which effectively eliminates false positives that arise from reaction by-products or impurities. This approach should be widely applicable to other systems, and requires only the biotinylation of the receptor under investigation. The presence of isobaric compounds and/or discrimination between compounds in the generation of gas-phase ions[11] might limit the size of the library open to this approach; this will be investigated in future work.

Experimental Section

Affinity-purified antibody[10] (0.5 mg) was biotinylated with a biotin reagent containing a long chain spacer arm (NHS-LC-biotin, Pierce). The extent of biotin incorporation was monitored by matrix-assisted laser desorption/ionization, and the reaction was terminated at 14 biotins per immunoglobulin G (average).[12] The biotinylated antibody was then incubated with Ultralink immobilized avidin (25 μL; Pierce, cat. no. 53119) in bicarbonate buffer (pH 8.5) for 1 hour. The beads were thoroughly washed. A UV quantitation indicated that an immobilization of approximately 45 μg antibody per 25 μL beads was achieved.

All solutions were infused concurrently with a multi-syringe pump (PHD 2000, Harvard Apparatus) at a flow rate of $8\,\mu L\,min^{-1}$ per syringe (1-mL syringes). A Rheodyne valve (model 9725) was used for flow switching. The column eluent was combined with the make-up flow (10 vol% NH_4OAc buffer in acetonitrile) in the tee, to give a total flow rate of $16\,\mu L\,min^{-1}$ to the Hewlett–Packard series 1100 MSD electrospray single quadrupole mass spectrometer, operating in positive-ion mode. For the analysis the spectrometer was scanned from m/z 100–1500 in 2.5 seconds and the data stored in the standard peak maxima (condensed) mode. A chamber voltage of -4000 V with a grounded electrospray needle, N_2 drying gas flow rate of $4\,L\,min^{-1}$, and N_2 nebulizer pressure of 480 mbar were used. Breakthrough volumes were measured as midpoints in the selected ion chromatograms for each m/z value.

Received: July 1, 1998 [Z12085IE]
German version: *Angew. Chem.* **1998**, *110*, 3625–3628

Keywords: affinity chromatography · carbohydrates · combinatorial chemistry · mass spectrometry

[1] K. S. Lam, *Anti-Cancer Drug Des.* **1997**, *12*, 145–167.
[2] P. M. Sweetnam, C. H. Price, J. W. Ferkany in *Burger's Medicinal Chemistry and Drug Discovery*; (Ed.: M. E. Wolff), Wiley, New York, **1995**, pp. 697–731.
[3] R. H. Griffey, M. J. Greig, C. Guinosso, A. Kawasaki, H. Gaus, H. An, P. D. Cook in *Proceedings of the 45th ASMS Conference on Mass Spectrometry and Allied Topics*, Palm Springs, CA, **1997**, p. 400.
[4] L. Fang, M. Dreyer, Y. Chen, M. Plunkett, M. Hocker in *Proceedings of the 45th ASMS Conference on Mass Spectrometry and Allied Topics*, Palm Springs, CA, **1997**, p. 401.
[5] See, for example, a) Y.-H. Chu, Y. M. Dunayevskiy, D. P. Kirby, P. Vouros, B. L. Karger, *J. Am. Chem. Soc.* **1996**, *118*, 7827–7835; b) Y.-Z. Zhao, R. B. van Breemen, D. Nikolic, C.-R. Huang, C. P. Wood-

 © WILEY-VCH Verlag GmbH, D-69451 Weinheim, 1998 1433-7851/98/3724-3386 $ 17.50+.50/0

bury, A. Schilling, D. L. Venton, *J. Med. Chem.* **1997**, *40*, 4006 – 4012. c) Y. F. Hsieh, N. Gordon, F. Regnier, N. Afeyan, S. A. Martin, G. J. Vella, *Mol. Div.* **1996**, *2*, 189 – 196.
[6] See, for example, a) R. W. Nelson, J. R. Krone, A. L. Bieber, P. Williams, *Anal. Chem.* **1995**, *67*, 1153 – 1158; b) D. C. Schriemer, L. Li, *Anal. Chem.* **1996**, *68*, 3382 – 3387; c) R. Wieboldt, J. Zweigenbaum, J. Henion, *Anal. Chem.* **1997**, *69*, 1683 – 1691; d) R. B. van Breemen, C.-R. Huang, D. Nikolic, C. P. Woodbury, Y.-Z. Zhao, D. L. Venton, *Anal. Chem.* **1997**, *69*, 2159 – 2164.
[7] K.-I. Kasai, Y. J. Oda, *Chromatogr.* **1986**, *376*, 33 – 47.
[8] See, for example, a) H. Ibrahim, A. F. Aubry, *Anal. Biochem.* **1995**, *229*, 272 – 277; b) J. Renard, C. Vidal Madjar, C. Lapresle, *J. Colloid Interface Sci.* **1995**, *174*, 61 – 67; c) M. Bjorklund, M. T. W. Hearn, *J. Chromatogr. A.* **1996**, 145 – 162; d) S. Lin, L. R. Drake, G. D. Rayson, *Anal. Chem.* **1996**, *68*, 4087 – 4093, and references therein.
[9] D. R. Bundle, E. Eichler, M. A. J. Gidney, M. Meldal, A. Ragauskas, B. W. Sigurskjold, B. Sinnott, D. C. Watson, M. Yaguchi, N. M. Young, *Biochemistry* **1994**, *33*, 5172 – 5182.
[10] E. Altman, D. R. Bundle, *Meth. Enzymol.* **1994**, *242*, 243 – 253.
[11] U. Bahr, A. Pfenninger, M. Karas, B. Stahl, *Anal. Chem.* **1997**, *69*, 4530 – 4535.
[12] D. C. Schriemer, L. Li, *Anal. Chem.* **1996**, *68*, 3382 – 3387.

A Convenient and General Method for Pd-Catalyzed Suzuki Cross-Couplings of Aryl Chlorides and Arylboronic Acids**

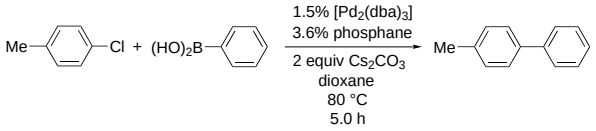
Adam F. Littke and Gregory C. Fu*

In memory of George Büchi

The Suzuki reaction has emerged as an extremely powerful method for the cross-coupling of aryl bromides, iodides, and triflates with arylboronic acids.[1] As compared with the Stille cross-coupling,[2] the Suzuki reaction possesses the practical advantages that the boron-containing by-products, unlike the tin-containing by-products of the Stille process, are nontoxic and are easily separated from the desired product.[3] One current limitation in the scope of the Suzuki reaction is its inefficiency when aryl chlorides are employed as substrates. Although there have been several accounts of Suzuki reactions of electron-poor aryl chlorides,[4–6] to the best of our knowledge there has been only one report of a coupling of an electron-neutral or an electron-rich aryl chloride (41% yield).[5i] In view of the increased availability and decreased expense of aryl chlorides relative to aryl bromides and iodides,[4a] this methodological gap becomes all the more significant. Herein we describe a solution to this problem: specifically, the development of conditions under which Suzuki cross-couplings of an array of electronically and sterically different aryl chlorides and arylboronic acids proceed in excellent yield with commercially available reagents (see Table 3).

In early experiments we established that 4-chlorotoluene and phenylboronic acid are efficiently cross-coupled in the presence of 1.5% $[Pd_2(dba)_3]$ (dba = dibenzylideneacetone), 3.6% P*t*Bu$_3$, and two equivalents of Cs_2CO_3 (dioxane, 80 °C; 86% yield by GC after 5.0 h; Table 1, entry 9). We observe little or no coupling in the absence of phosphane (entry 1) or in the presence of triarylphosphanes (entries 2 – 5) and chelating phosphanes (entries 6 and 7). Of the ligands that we have examined to date, only PCy_3 approaches P*t*Bu$_3$ in effectiveness (entries 8 and 9). , The use of a phosphane:Pd ratio between 1 and 1.5 appears to be optimal with P*t*Bu$_3$ as the ligand, an observation that suggests that the active palladium catalyst bears a single P*t*Bu$_3$ group. Thus, we believe that the steric bulk and the electron-richness of P*t*Bu$_3$ are critical for this unprecedented reactivity.[4, 7]

Table 1. Effect of phosphane on the palladium-catalyzed Suzuki cross-coupling of aryl chlorides.



Entry	Phosphane	Yield [%] (GC)
1	–	0
2	PPh_3	0
3	BINAP[a]	0
4	dppf[b]	0
5	P(*o*-tol)$_3$	10
6	$Ph_2P(CH_2)_3PPh_2$	0
7	$Cy_2P(CH_2)_2PCy_2$	0
8	PCy_3	75
9	P*t*Bu$_3$	86

[a] BINAP = 2,2′-bis(diphenylphosphanyl)-1,1′-binaphthyl. [b] dppf = 1,1-bis(diphenylphosphanyl)ferrocene.

Among the bases listed in Table 2, Cs_2CO_3 has proved to be the base of choice (entry 6).[8, 9] In the absence of base (entry 1) or in the presence of other bases commonly used in Suzuki reactions (entries 2 – 5), cross-coupling proceeds with diminished efficiency. In contrast to most Suzuki cross-couplings,[1] only one equivalent of base is required for our process (95% GC yield after five hours with 1.2 equiv Cs_2CO_3). We have found $[Pd_2(dba)_3]$ and dioxane to be best among the palladium sources (for example, $Pd(OAc)_2$) and solvents (for example, THF) that we have surveyed thus far.

A wide array of electronically and structurally diverse aryl chlorides and arylboronic acids can be cross-coupled very efficiently under these conditions (1.5% $[Pd_2(dba)_3]$, 3.6% P*t*Bu$_3$, 1.2 equiv Cs_2CO_3).[10] Thus, with respect to the aryl chloride, both electron-neutral 4-chlorotoluene and electron-

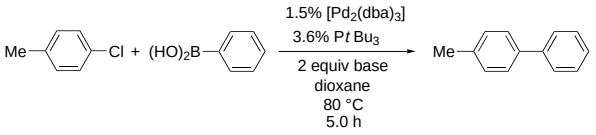
[*] Prof. Dr. G. C. Fu, A. F. Littke
Department of Chemistry
Massachusetts Institute of Technology
Cambridge, Massachusetts 02139 (USA)
Fax: (+1) 617-258-7500
E-mail: gcf@mit.edu

[**] Support has been provided by the Alfred P. Sloan Foundation, the American Cancer Society, Bristol – Myers Squibb, the Camille and Henry Dreyfus Foundation, Eli Lilly, Firmenich, Glaxo Wellcome, the National Science Foundation (Young Investigator Award, with funding from Merck, Pharmacia & Upjohn, DuPont, Bayer, and Novartis), the Natural Sciences and Engineering Research Council of Canada (predoctoral fellowship to A.F.L.), Pfizer, Procter & Gamble, and the Research Corporation.

Supporting information for this article is available on the WWW under http://www.wiley-vch.de/home/angewandte/ or from the author.

 © WILEY-VCH Verlag GmbH, D-69451 Weinheim, 1998 1433-7851/98/3724-3387 $ 17.50+.50/0

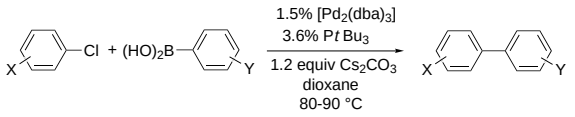
Table 2. Effect of base on the palladium-catalyzed Suzuki cross-coupling of aryl chlorides.



Entry	Base	Yield [%][a]	Entry	Base	Yield [%][a]
1	–	3	4	NEt_3	50
2	Na_2CO_3	23	5	K_3PO_4	83
3	K_2CO_3	29	6	Cs_2CO_3	86

[a] Determined by gas chromatography.

Table 3. Scope of the $[Pd_2(dba)_3]$/P*t*Bu_3/Cs_2CO_3-catalyzed Suzuki cross-coupling of aryl chlorides.



Entry	X	Y	Yield [%]
1	4-Me	H	87
2	4-MeCO	H	91
3	4-MeO	H	89
4	4-NH_2	H	92
5	4-Me	4-CF_3	86
6	4-Me	4-OMe	82
7	2-Me	H	90
8	2-Me	2-Me	87

poor 4-chloroacetophenone react with $PhB(OH)_2$ to provide the biaryl product in excellent yield (Table 3, entries 1 and 2). More remarkable is our observation that even extremely electron-rich aryl chlorides, including 4-chloroanisole and 4-chloroaniline, couple cleanly with $PhB(OH)_2$ in the presence of this catalyst system (entries 3 and 4).

The cross-coupling also proceeds smoothly regardless of the electronic character of the boronic acid component. More electron-rich boronic acids have been reported to be less reactive partners in other Suzuki reactions.[1] With our catalyst system, trifluoromethyl- and methoxy-substituted benzeneboronic acids couple with 4-chlorotoluene to produce the desired biaryls in excellent yields under comparable reaction conditions (Table 3, entry 5: 5 h at 80 °C; entry 6: 9 h at 80 °C).

Finally, this $[Pd_2(dba)_3]$/P*t*Bu_3-catalyzed cross-coupling is tolerant of *ortho* substitution in both the aryl halide and the arylboronic acid (Table 3, entries 7 and 8). For example, sterically hindered 2,2′-dimethyl-1,1′-biphenyl is formed in 87% yield after seven hours at 80 °C.

In summary, we have developed a general method for the Suzuki cross-coupling of aryl chlorides with arylboronic acids. Our catalyst system, which employs readily available components (1.5% $[Pd_2(dba)_3]$, 3.6% P*t*Bu_3, 1.2 equiv Cs_2CO_3), couples effectively a broad spectrum of substrates, to provide the desired biaryls in excellent yields. Because of the accessibility of aryl chlorides and the relatively innocuous nature of the boron-containing by-products of Suzuki reactions, we anticipate that this method is likely to find widespread use in synthetic organic chemistry. Future work will be directed at further optimization of this process and on the development of related coupling reactions.[11]

Received: August 18, 1998 [Z12301IE]
German version: *Angew. Chem.* **1998**, *110*, 3586 – 3587

Keywords: cross-coupling · homogeneous catalysis · palladium · Suzuki reaction

[1] For a review, see N. Miyaura, A. Suzuki, *Chem. Rev.* **1995**, *95*, 2457 – 2483.
[2] For a review, see V. Farina, V. Krishnamurthy, W. J. Scott, *Org. React.* **1997**, *50*, 1 – 652.
[3] For discussions of the toxicity of triorganotin compounds, see a) S. J. De Mora, *Tributyltin: Case Study of an Environmental Contaminant*, Cambridge University Press, Cambridge, **1996**, b) I. J. Boyer, *Toxicology* **1989**, *55*, 253 – 298.
[4] The low reactivity of aryl chlorides in cross-coupling reactions is generally ascribed to their reluctance to oxidatively add to Pd^0. Aryl halides that bear an electron-withdrawing group oxidatively add to Pd^0 more readily than do the corresponding unsubstituted aryl halides. For discussions, see a) V. V. Grushin, H. Alper, *Chem. Rev.* **1994**, *94*, 1047 – 1062; b) references [1, 2].
[5] a) S. Gronowitz, A.-B. Hörnfeldt, V. Kristjansson, T. Musil, *Chem. Scr.* **1986**, *26*, 305 – 309; b) W. J. Thompson, J. H. Jones, P. A. Lyle, J. E. Thies, *J. Org. Chem.* **1988**, *53*, 2052 – 2055; c) M. B. Mitchell, P. J. Wallbank, *Tetrahedron Lett.* **1991**, *32*, 2273 – 2276; d) M. Uemura, H. Nishimura, K. Kamikawa, K. Nakayama, Y. Hayashi, *Tetrahedron Lett.* **1994**, *35*, 1909 – 1912; e) M. Beller, H. Fischer, W. A. Herrmann, K. Ofele, C. Brossmer, *Angew. Chem.* **1995**, *107*, 1992 – 1993; *Angew. Chem. Int. Ed. Engl.* **1995**, *34*, 1848 – 1849; f) S. Saito, M. Sakai, N. Miyaura, *Tetrahedron Lett.* **1996**, *37*, 2993 – 2996; g) W. Shen, *Tetrahedron Lett.* **1997**, *38*, 5575 – 5578; h) W. A. Herrmann, C.-P. Reisinger, M. Spiegler, *J. Organomet. Chem.* **1998**, *557*, 93 – 96; i) F. Firooznia, C. Gude, K. Chan, Y. Satoh, *Tetrahedron Lett.* **1998**, *39*, 3985 – 3988.
[6] For nickel-catalyzed cross-couplings of aryl chlorides and arylboronic acids, see a) S. Saito, S. Oh-tani, N. Miyaura, *J. Org. Chem.* **1997**, *62*, 8024 – 8030; b) A. F. Indolese, *Tetrahedron Lett.* **1997**, *38*, 3513 – 3516; c) reference [5i].
[7] a) For reports of enhanced reactivity in palladium-catalyzed cross-couplings when P*t*Bu_3 is used as a ligand, see M. Nishiyama, T. Yamamoto, Y. Koie, *Tetrahedron Lett.* **1998**, *39*, 617 – 620; T. Yamamoto, M. Nishiyama, Y. Koie, *Tetrahedron Lett.* **1998**, *39*, 2367 – 2370; b) For other reports that deal with the use of electron-rich phosphanes in palladium-catalyzed cross-couplings, see M. Portnoy, D. Milstein, *Organometallics* **1993**, *12*, 1655 – 1664; M. Portnoy, D. Milstein, *Organometallics* **1993**, *12*, 1665 – 1673; M. Portnoy, Y. Ben-David, D. Milstein, *Organometallics* **1993**, *12*, 4734 – 4735; N. P. Reddy, M. Tanaka, *Tetrahedron Lett.* **1997**, *38*, 4807 – 4810; reference [4a].
[8] a) For reports of the use of Cs_2CO_3 in Suzuki reactions, see H. E. Katz, *J. Org. Chem.* **1987**, *52*, 3932 – 3934; C. R. Johnson, M. P. Braun, *J. Am. Chem. Soc.* **1993**, *115*, 11014 – 11015; b) For reports of the use of Cs_2CO_3 in other palladium-catalyzed cross-couplings, see J. P. Wolfe, S. L. Buchwald, *Tetrahedron Lett.* **1997**, *38*, 6359 – 6362; T. Satoh, Y. Kawamura, M. Miura, M. Nomura, *Angew. Chem.* **1997**, *109*, 1820 – 1822; *Angew. Chem. Int. Ed. Engl.* **1997**, *36*, 1740 – 1742.
[9] Very recently we have found that CsF is also an extremely effective base.
[10] General experimental conditions: A solution of aryl chloride (0.833 mmol; in dioxane (0.5 – 0.7 mL)) and a solution of P*t*Bu_3 (0.030 mmol; in dioxane (0.3 mL)) were added in turn to a Schlenk tube charged with $[Pd_2(dba)_3]$ (0.0125 mmol), boronic acid (0.875 mmol), Cs_2CO_3 (1.00 mmol), and a magnetic stir bar under an atmosphere of nitrogen. The Schlenk tube was stirred at 80 °C for five hours. The reaction mixture was then cooled to room temperature, diluted with Et_2O, filtered through a pad of Celite, concentrated, and purified by flash chromatography.
[11] Note added in proof (November 2, 1998): Buchwald et al. have reported a versatile method for Suzuki cross-coupling of aryl chlorides: D. W. Old, J. P. Wolfe, S. L. Buchwald, *J. Am. Chem. Soc.* **1998**, *120*, 9722 – 9723.

 © WILEY-VCH Verlag GmbH, D-69451 Weinheim, 1998 1433-7851/98/3724-3388 $ 17.50+.50/0

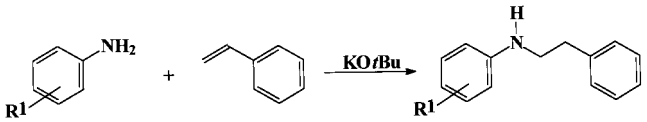
Base-Catalyzed Synthesis of *N*-(2-Arylethyl)anilines and Base-Promoted Domino Synthesis of 2,3-Dihydroindoles**

Matthias Beller,* Claudia Breindl, Thomas H. Riermeier, Martin Eichberger, and Harald Trauthwein

Dedicated to Professor Klaus Kühlein on the occasion of his 60th birthday

The hydroaminination of olefins to amines is in terms of atom economy the most efficient and most elegant method for the production of amines.[1] Hydroaminations of styrenes to 2-(arylethyl)amines are of particular interest, since this class of substances is of great importance as lead structures for psychodysleptics, strong analgesics, analeptics, antihistaminics, and anorectics.[2] Among the numerous pharmaceutical products that contain an $ArCH_2CH_2NR_2$ structual element are Fentanyl, Fenfluramin, Dimetinden, and Doxapram. Despite the fundamental advantages of hydroaminations—such as price, availabilitiy of the starting materials, and the avoidance of waste products—only a few base-catalyzed[3] and more recently metal-catalyzed aminations[4] of aromatic olefins are known. We have therefore investigated to what extent bases not used previously catalyze the hydroamination of styrene and functionalized styrenes. Furthermore, we were interested in the application of hydroaminations as part of new domino processes.[5]

Initially we were interested in the reaction of substituted anilines with styrene to give *N*-(2-phenethyl)anilines (Scheme 1), since the products could be converted comparatively easily into interesting heterocycles.[6] *N*-(2-Phenethyl)-anilines are also of current importance as pharmaceuticals—for example, Tromaril, which exhibits anti-inflammatory activity. Base-catalyzed reactions of aniline and styrene have been investigated previously by Wegeler and Pieper[3a] as well as by Schlott et al.[3c] Under "typical" reaction conditions (5–10 mol% *n*BuLi or lithium amide; THF, reflux) of base-catalyzed hydroaminations of styrene with aliphatic amines no reaction takes place, whereas a conversion of 70% of aniline is observed in the presence of 5–15 mol% sodium at 180–185 °C. With β-methylstyrene, under these reaction conditions the hydroamination product forms only in 10% yield.



Scheme 1. Base-catalyzed hydroaminations of styrene with substituted anilines.

As model system for the application of alternative base catalysts we investigated the reaction of styrene with aniline in more detail (Table 1). Here a 1:1 mixture of the starting materials in tetrahydrofuran as solvent in the presence of 10 mol% of a base catalyst was allowed to react in a pressure tube at 120 °C. After several hours the reaction mixture was allowed to cool to room temperature and terminated through the addition of water.

Table 1. Variation of the base catalyst in the reaction of styrene **2** with aniline **1**.[a]

Entry	Base	Cat. [mol %]	*T* [°C]	Amine: olefin	Yield[b] [%]
1	*n*BuLi	10	100	1:1	–
2	*n*BuLi/K_2CO_3	10/10	120	1:1	69
3	KO*t*Bu	10	120	1:1	85
4	LiO*t*Bu	10	100	1:1	–
5	NaO*t*Bu	10	100	1:1	–
6	K_2CO_3	10	100	1:1	–
7	KO*t*Bu	10	120	5:1	99
8	KO*t*Bu	5	120	2:1	96

[a] All reactions were carried out in Ace pressure tubes; reaction time 20 h; solvent THF. [b] Determined by GC analysis with hexadecane as internal standard.

In agreement with published results,[3c] no reaction of the starting materials occurred in the presence of 5–10 mol% *n*BuLi or lithium amide in THF under reflux. Even when the reaction was carried out at 120 °C under pressure no products were formed (Table 1, entry 1). It is assumed that the nucleophilicity of the lithium anilides which is lower than that of aliphatic amides, is no longer sufficient for an attack at the double bond of the styrene. Thus, we decided to prepare more ionic and therefore more reactive potassium anilides in situ, in order to increase the reactivity of the amide. Since the direct application of potassium anilides is not viable because of the sensitivity of the substances, we investigated to what extent an amination can be achieved by the addition of potassium salts to the above-mentioned reaction mixture. In fact styrene and aniline react in the presence of 10 mol% *n*BuLi and 10 mol% potassium carbonate regioselectively to give *N*-(2-phenethyl)aniline in 69% yield. We explain this finding by way of a side reaction in which the metal on the lithium anilides is exchanged to give trace amounts of the more reactive potassium anilides; the formation of mixed lithium–potassium anilides is likely.[7] Surprisingly, a subsequent screening of base catalysts showed that potassium *tert*-butylalcoholate is particularly suitable as catalyst for the hydroamination of styrene with aniline (Table 1). For instance, the corresponding *N*-(2-phenethyl)aniline **3** is obtained regioselectively in 85% yield together with traces of the doubly alkylated aniline (Table 1, entry 3) by using

[*] Prof. M. Beller, M. Eichberger[+]
Institut für Organische Katalyseforschung (IfOK)
an der Universität Rostock e.V.
Buchbinderstraße 5-6, D-18055 Rostock (Germany)
Fax: (+49) 381-4669324
E-mail: Matthias.Beller@ifok.uni-rostock.de
C. Breindl
Lehrstuhl für Anorganische Chemie
der Technische Universität München
Lichtenbergstrasse 4, D-85747 Garching (Germany)
Fax: (+49) 89-289-13473
Dr. T. H. Riermeier, Dr. H. Trauthwein
Aventis Research and Technologies
Industriepark Höchst G830, D-65926 Frankfurt (Germany)
[+] Deceased 1997.

[**] Anti-Markownikov Functionalizations of Unsaturated Compounds, Part 4. We thank Dr. J. Herwig (Celanese) for helpful discussions and advice. Part 3: M. Beller, C. Breindl, *Tetrahedron* **1998**, *54*, 6359.

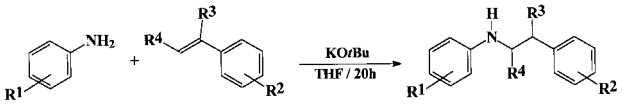
 © WILEY-VCH Verlag GmbH, D-69451 Weinheim, 1998 1433-7851/98/3724-3389 $ 17.50+.50/0

10 mol % KO*t*Bu in THF at 120 °C (> 99.9 % regioselectivity). If an excess of aniline is used (2 – 5 equivalents relative to styrene), **3** is formed in 96 – 99 % yield and with > 99 % selectivity (Table 1, entries 7, 8). The amount of catalyst can be reduced to 5 mol % without any adverse effects on the product yields. An important advantage of the new procedure compared to the classical nucleophilic substitution of phenethyl halides with primary amines is the excellent chemoselectivity with which the secondary amine product **3** is obtained. For instance, no tertiary amination product even in trace amounts is detected with five equivalents aniline (relative to styrene).

In order to investigate the practicability of potassium *tert*-butylalcoholate as hydroamination catalyst, the reaction of aniline with styrene was carried out on a 50-g scale without the use of pressure in a glass flask in toluene as solvent under reflux with a reaction time of 24 h. After distillation **3** was obtained without further optimization in 62 % yield (59 g).

The scope of application of the new base catalyst for hydroaminations is demonstrated in the reaction of substituted anilines with different styrenes that are functionalized at the ring and the double bond (Table 2).

Table 2. KO*t*Bu-catalyzed hydroamination of aryl olefins with substituted anilines.[a]

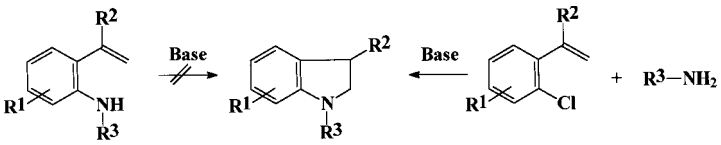


Entry	Amine	Olefin			Yield[b]	Product
	R^1	R^2	R^3	R^4	[%]	
1	H	H	H	H	85	**3**
2	4-F	H	H	H	75	**4**
3	2-OMe	H	H	H	85	**5**
4	H	4-Cl	H	H	72	**6**
5[c]	H	H	Me	H	34	**7**
6[c]	H	H	H	Me	50	**8**

[a] Reaction conditions: Amine (0.011 mol), olefin (0.011 mol), and 10 mol % KO*t*Bu (0.12 g) were heated in THF (10 mL) at 120 °C for 20 h in an Ace pressure tube. [b] Determined by GC analysis with hexadecane as internal standard. [c] Reaction temperature 160 °C.

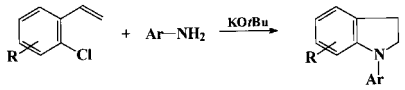
Aniline (Table 2, entry 1) and substituted anilines with electron-withdrawing or electron-donating substituents, even in the critical *ortho* position (Table 2, entries 2, 3) react in good yields (75 – 85 %) to give the desired products. Interestingly, hydroamination of α-methylstyrene and β-*trans*-methylstyrene (Table 2, entries 5, 6) can also be achieved, although the yields (34 and 50 %, respectively) are not optimized in this case.

In addition to the intermolecular base-catalyzed hydroamination, we have pursued the development of intramolecular variants of the method. As shown in Scheme 2, this has led to a new route to 2,3-dihydroindoles (indolines). The partial structure of the indole and of the indoline is found in numerous natural products and pharmacologically active substances such as Bufotenine or Lysergide.[2] Simple and viable synthesis routes to such substances are therefore of general interest.[8] Preliminary attempts at the realization of our concept as exemplified by the cyclization of 2-isopropenylaniline in the presence of different bases were however disapppointing, thus, we pursued an alternative route: By applying 2-halostyrenes a ring closure should be possible after hydroamination of the double bond by nucleophilic substitution of the suitably placed leaving group at the arene or by palladium-catalyzed C – N bond formation.[9] In fact the cyclization of 2-chlorostyrene with aniline (1.5 equiv) in the presence of three equivalents of potassium *tert*-butylalcoholate in toluene at 135 °C in the pressure tube gives *N*-phenyl-2,3-dihydroindole in 53 % yield! Under these reaction conditions, which have not been optimized, a series of substituted anilines can be converted (Table 3). Electron-withdrawing and electron-donating substituents on the aniline are tolerated without changing the yields. Structural variations are also possible on the styrene, for instance, *N*-(4-fluorophenyl)-4-chloro-2,3-dihydroindole is obtained by the reaction of commercially available 2,6-dichlorostyrene and 4-fluoroaniline in 50 % yield (isolated product, Table 3, entry 4). In order to minimize side reactions of the chloro substituents under the reaction conditions, the amount of amine in this reaction was reduced to 1.2 equivalents (relative to 2,6-dichlorostyrene) and that of the base to 1.5 equivalents (relative to 2,6-dichlorostyrene). In all domino reactions up to 10 % of the corresponding dehydrogenated reaction product (*N*-aryl indole) was clearly identified as a side product. The hydrogen acceptor necessary for this dehydrogenation appears to be the styrene used. The corresponding indoles are accessible in > 50 % yields by in situ dehydrogenation of the indolines with a suitable oxidation system.[10]



Scheme 2. Base-catalyzed and base-promoted cyclizations to give 2,3-dihydroindoles. R^2 = H, CH_3; R^3 = H, aryl.

Table 3. Domino hydroamination aryne cyclization reaction to give *N*-aryl indolines.



Entry	R	Ar	Yield [%]	Product
1	H	C_6H_5	53	**9**
2	H	4-FC_6H_4	54	**10**
3	H	2-$MeOC_6H_4$	58	**11**
4	6-Cl	4-FC_6H_4	50	**12**

With regard to the mechanism the new domino reaction proceeds by a base-catalyzed hydroamination and a subsequent intramolecular aryne reaction. Based on the comparison of the reactions of 2- and 3-chlorostyrene with aniline it could be shown that the cyclization indeed proceeds via an aryne intermediate. Both chlorostyrenes form the same aryne intermediate, thus *N*-phenyl-2,3-dihydroindole (**9**) is obtained

 © WILEY-VCH Verlag GmbH, D-69451 Weinheim, 1998 1433-7851/98/3724-3390 $ 17.50+.50/0 *Angew. Chem. Int. Ed.* **1998**, *37*, No. 24

in yields of between 50 and 55% regardless of the position of the halogen substituent.

A comparison of the new domino hydroamination aryne cyclization reaction with known cyclizations of 2-(2-chlorophenyl)ethylamines[11] clearly shows the superiority of the new method. The yields of the indoline products obtained are superior to the reported values by about a factor of 3.

KO*t*Bu-catalyzed hydroaminations of aromatic olefins with anilines make pharmacologically interesting *N*-(2-arylethyl)-anilines accessible with 100% atom economy and in a particularly viable manner in good to excellent yields. The excellent chemo- and regioselectivities are an important advantage over classical syntheses of N-substituted anilines. The use of 2- or 3-substituted halostyrenes as starting materials has enabled the synthesis of N-substituted indolines by a novel domino reaction. Very recent experiments indicate that this reaction is not limited to anilines, but that aliphatic amines also undergo analogous reactions.[12]

Experimental Section

Synthesis of *N*-phenyl-2,3-dihydroindole (**9**): In an Ace pressure tube (38 mL) 2-chlorostyrene (0.28 g, 2.0 mmol) and aniline (0.28 g, 3.0 mmol) were dissolved in toluene (10 mL) under argon. After addition of potassium *tert*-butylalcoholate (0.67 g, 6.0 mmol), the sealed reaction vessel was placed in an oil bath preheated to 135 °C and the reaction mixture was stirred vigorously. After 36 h the mixture was allowed to cool to room temperature and water (20 mL) was added with stirring. The aqueous phase was extracted three times with dichloromethane (10 mL). Subsequently the combined organic phases were dried over magnesium sulfate, and the solvent was removed under vacuum. The resulting crude product was separated by column chromatography with hexane as eluent. Compound **9** was obtained in 53% (0.21 g) yield. ^{1}H NMR (360 MHz, 25 °C, $CDCl_3$): $\delta = 7.32$ (dd, $^3J(H,H) = 8.0$, 7.1 Hz, 2H, *m*-Ph-H), 7.21 (d, $^3J(H,H) = 8.0$ Hz, 2H, *o*-Ph-H), 7.14 (d, $^3J(H,H) = 7.1$ Hz, 1H, Ar), 7.12 (d, $^3J(H,H) = 8.0$ Hz, 1H, Ar), 7.05 (dd, $^3J(H,H) = 8.0$, 7.5 Hz, 1H, Ar), 6.94 (t, $^3J(H,H) = 7.1$ Hz, 1H, *p*-Ph-H), 6.73 (dd, $^3J(H,H) = 7.5$, 7.1 Hz, 1H, Ar), 3.92 (t, $^3J(H,H) = 8.4$ Hz, 2H, NCH_2), 3.10 (t, $^3J(H,H) = 8.4$ Hz, 2H, CH_2); ^{13}C{^{1}H} NMR (90 MHz, 25 °C, $CDCl_3$): $\delta = 147.1$ (quart. Ph), 144.2 (quart. Ar-C-N), 131.2 (quart. Ar-C), 129.1 (*m*-Ph), 127.1 (Ar), 125.0 (Ar), 120.9 (Ar), 118.8 (Ar), 117.7 (*o*-Ph), 108.2 (*p*-Ph), 52.1 (NCH_2), 28.2 (CH_2); MS (70 eV): *m*/*z* (%): 195 (5) [M^+], 165 (70), 116, 91 (100), 77.

Received: May 12, 1998 [Z11845IE]
German version: *Angew. Chem.* **1998**, *110*, 3571 – 3573

Keywords: aminations · arynes · cyclizations · domino reactions · potassium

[1] Reviews: a) T. Müller, M. Beller, *Chem. Rev.* **1998**, *98*, 675; b) J.-J. Brunet, D. Neubecker, F. Niedercorn, *J. Mol. Catal.* **1989**, *49*, 235; c) D. M. Roundhill, *Chem. Rev.* **1992**, *92*, 1; d) D. Steinborn, R. Taube, *Z. Chem.* **1986**, *26*, 349.

[2] E. Mutschler, *Arzneimittelwirkungen,* 7th ed., Wissenschaftliche Verlagsgesellschaft, Stuttgart, **1996**.

[3] R. Wegler, G. Pieper, *Chem. Ber.* **1950**, *83*, 1; b) N. Imai, T. Narita, T. Tsuruta, *Tetrahedron Lett.* **1971**, *38*, 3517; c) R. J. Schlott, J. C. Falk, K. W. Narducy, *J. Org. Chem.* **1972**, *37*, 4243; d) T. Narita, T. Yamaguchi, T. Tsuruta, *Bull. Chem. Soc. Jpn.* **1973**, *46*, 3825; e) T. Narita, N. Imai, T. Tsuruta, *Bull. Chem. Soc. Jpn.* **1973**, *46*, 1242; f) T. Fujita, K. Suga, S. Watanabe, *Aust. J. Chem.* **1974**, *27*, 531.

[4] a) B. Åkermark, J. E. Bäckvall, L. S. Hegedus, K. Zetterberg, *J. Org. Chem.* **1974**, *72*, 127; b) L. S. Hegedus, J. M. McKearin, *J. Am. Chem. Soc.* **1982**, *104*, 2444; c) A. L. Casalnuovo, J. C. Calabrese, D. Milstein, *J. Am. Chem. Soc.* **1988**, *110*, 6738; d) M. Deeba, M. E. Ford, T. A. Johnson, D. W. in *Catalysis of Organic Reactions*, Marcel Dekker, New York, **1990**, p. 241; e) D. Selent, D. Scharfenberg-Pfeiffer, G. Reck, R. Taube, *J. Organomet. Chem.* **1991**, *415*, 417; f) M. R. Gagné, L. Brad, V. P. Conticello, M. A. Giardello, C. L. Stern, T. J. Marks, *Organometallics* **1992**, *11*, 2003; g) A. L. Seligson, W. C. Trogler, *Organometallics* **1993**, *12*, 744; h) Y. Li, T. J. Marks, *Organometallics* **1996**, *15*, 3770; i) R. C. Larock, T. R. Hightower, L. A. Hasvold, K. P. Peterson, *J. Org. Chem.* **1996**, *61*, 3584; j) R. Dorta, P. Egli, F. Zurcher, A. Togni, *J. Am. Chem. Soc.* **1997**, *119*, 10857.

[5] Selected reviews on domino reactions: L. F. Tietze, U. Beifuß, *Angew. Chem.* **1993**, *105*, 137; *Angew. Chem. Int. Ed. Engl.* **1993**, *32*, 131; b) L. F. Tietze, *Chem. Rev.* **1996**, *96*, 115.

[6] a) D. Lesieur, S. Yous, P. Depreux, J. Andrieux, G. Adam, D. H. Caignard, B. Guardiola (ADIR et Cie., France), EP-B 527687 A2, **1992** [*Chem. Abstr.* **1993**, *118*, 254750e]; b) Z. Budai, P. Benko, L. Pallos (Egyesult Gyogyszer, Hungary), HU-B 155783 [*Chem. Abstr.* **1969**, *71*, 21854n]; c) J. G. Berger, W. K. Chang, J. A. Kozlowski, G. Zhou (Schering Corp., USA), US-A 5530125 A, **1992** [*Chem. Abstr.* **1994**, *120*, 134315m].

[7] a) L. Lochmann, J. Trekoval, *J. Organomet. Chem.* **1979**, *179*, 123; b) P. G. Williard, G. J. MacEwan, *J. Am. Chem. Soc.* **1989**, *111*, 7671; c) F. M. Mackenzie, R. E. Mulvey, *J. Am. Chem. Soc.* **1996**, *118*, 4721.

[8] a) B. Robinson, *The Fischer Indole Synthesis*, Wiley-Interscience, New York **1982**; b) L. S. Hegedus, *Angew. Chem.* **1988**, *100*, 1147; *Angew. Chem. Int. Ed. Engl.* **1988**, *27*, 1113; c) G. W. Gribble, *Contemp. Org. Synth.* **1994**, *1*, 145; d) R. J. Sundberg, *Indoles*, Academic Press, San Diego, **1996**.

[9] a) F. Paul, J. Patt, J. F. Hartwig, *J. Am. Chem. Soc.* **1994**, *116*, 5969; b) J. F. Hartwig, S. Richards, D. Barañano, F. Paul, *J. Am. Chem. Soc.* **1996**, *118*, 3626; c) M. S. Driver, J. F. Hartwig, *J. Am. Chem. Soc.* **1996**, *118*, 7217; d) J. F. Hartwig, *J. Am. Chem. Soc.* **1996**, *118*, 7010; e) J. P. Wolfe, S. Wagaw, S. L. Buchwald, *J. Am. Chem. Soc.* **1996**, *118*, 7215; f) N. P. Reedy, M. Tanaka, *Tetrahedron Lett.* **1997**, *38*, 4807; g) M. Beller, T. H. Riermeier, C.-P. Reisinger, W. A. Herrmann, *Tetrahedron Lett.* **1997**, *38*, 2073; h) M. S. Driver, J. F. Hartwig, *Organometallics* **1997**, *16*, 5706; i) S. Wagaw, R. A. Rennels, S. L. Buchwald, *J. Am. Chem. Soc.* **1997**, *119*, 8451; j) M. Beller, T. H. Riermeier, A. Zapf, *Top. Catal.* **1997**, *4*, 301; k) R. A. Singer, J. P. Sadighi, S. L. Buchwald, *J. Am. Chem. Soc.* **1998**, *120*, 213; l) D. W. Old, J. P. Wolfe, S. L. Buchwald, *J. Am. Chem. Soc.* **1998**, *120*, 9722.

[10] a) K. Aoki, A. J. Peat, S. L. Buchwald, *J. Am. Chem. Soc.* **1998**, *120*, 3068; b) M. Beller, C. Breindl, T. H. Riermeier, unpublished results.

[11] a) R. Huisgen, H. König, *Chem. Ber.* **1959**, *92*, 203; b) R. Huisgen, H. König, N. Bleeker, *Chem. Ber.* **1959**, *92*, 424; c) H. König, R. Huisgen, *Chem. Ber.* **1959**, *92*, 429; d) H. Iida, S. Aoyagi, C. Kibayashi, *J. Chem. Soc. Perkin 1* **1975**, 2502.

[12] M. Beller, C. Breindl, unpublished results.

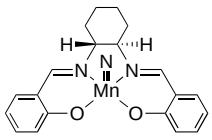
 © WILEY-VCH Verlag GmbH, D-69451 Weinheim, 1998 1433-7851/98/3724-3391 $ 17.50+.50/0

Novel Asymmetric and Stereospecific Aziridination of Alkenes with a Chiral Nitridomanganese Complex**

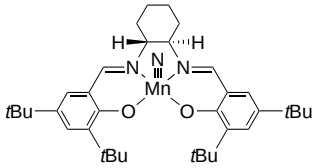
Satoshi Minakata, Takeya Ando, Masaaki Nishimura, Ilhyong Ryu, and Mitsuo Komatsu*

Optically active aziridines are useful building blocks for nitrogen-containing functional compounds.[1] They are also found in some natural and biologically active products such as mitomycins and azinomycins.[1, 2] Among the various routes that have been developed thus far to give chiral aziridines,[3] reagent-controlled asymmetric aziridinations of carbon–carbon double bonds are remarkable in terms of their simplicity and convenience as a synthetic procedure.[4] The chiral Cu^{I} or Mn^{III} complexes discovered by Evans,[4a,b] Jacobsen,[4c–e] and Katsuki[4f,g] represent efficient catalysts for such reactions when [*N*-(*p*-toluenesulfonyl)imino]phenyliodinane, PhI=NTs, is used as a nitrogen source. On the other hand, it is noteworthy that an approach for direct aziridination with nitrido(5,10,15,20-tetramesitylporphyrinato)manganese (TMPMnN) has been reported by Groves and Takahashi, but their study was restricted to the use of *cis*-cyclooctene as the alkene.[5] Recently this type of reaction was extended by Carreira and co-workers to the amination of silyl enol ethers and glycols with new types of nitridomanganese complexes.[6] An asymmetric version of this methodology, however, has not yet been achieved. This situation prompted us to investigate a novel chiral nitrido complex that would impart enantioselective aziridination. We report herein the first asymmetric and stereospecific aziridination of styrene derivatives by transfer of a nitrogen atom from a chiral nitridomanganese complex, wherein the additives play a key role in the performance of the reaction and its selectivity.

The chiral nitridomanganese complexes **1** and **2** were readily prepared from literature procedures,[7] including



1

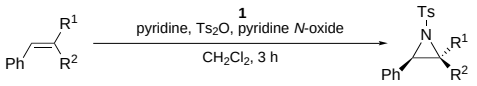


2

Carreira's method,[6a] by the treatment of chiral ligands with $Mn(OAc)_2$, NH_4OH, and NaOCl. An alternative procedure for the preparation of **1** was developed by us and consists of a reaction of a chiral Mn^{III} complex[8] with gaseous NH_3 and Chloramine-T as the oxidant in MeOH.[9]

Although trifluoroacetic anhydride (TFAA) was used by Groves as well as Carreira for the activation of their nitrido complexes, when we employed this reagent in the aziridination of unfunctionalized alkenes with the chiral nitridomanganese complex **1** no aziridine derivatives were obtained.[10] As a result we searched for another activating reagent and found *p*-toluenesulfonic anhydride (Ts_2O) to be effective for the aziridination of alkenes (Table 1). The reaction of the nitrido complex **1** with styrene (10 equiv) in methylene chloride at room temperature for 3 h in the presence of Ts_2O (1.2 equiv) and pyridine (1.5 equiv) gave the corresponding *N*-tosylaziridine in 49% yield based on **1**. The yield of aziridine increased up to 63% with a decrease in the amount of pyridine and with the enantiomeric excess (*ee*) of the product being 31%. The aziridination proceeded smoothly at 0 °C and retained both

Table 1. Asymmetric aziridination of styrene derivatives with the nitrido complex **1**[a]



Substrate R^1	Substrate R^2	Additive	T [°C]	Yield [%]	*ee* [%]
H	H	–	RT	63	31[b,c]
H	H	pyridine *N*-oxide	0	78	41[b,c]
Me	H	–	RT	60	73[d,e]
Me	H	pyridine *N*-oxide	0	72	85[d,e]
H	Me	–	RT	14	30[d,f]
H	Me	pyridine *N*-oxide	RT	34	25[d,f]
*n*Pr	H	pyridine *N*-oxide	0	66	90[b,f]
*i*Pr	H	pyridine *N*-oxide	0	53[g]	94[b,f]

[a] Reaction conditions: **1** (1 equiv), pyridine (0.5 equiv), Ts_2O (1.2 equiv), additive (1.2 equiv), alkene (10 equiv), 3 h, CH_2Cl_2. [b] The enantiomeric excess was determined by HPLC analysis on a Daicel Chiralcel OJ column. [c] The absolute configuration was determined as *R* by comparison of the measured optical rotations with the reported values.[4b] [d] The enantiomeric excess was determined by ^1H NMR analysis with $[Eu(hfc)_3]$. [e] The absolute configuration was determined as (2*R*,3*R*) by comparison of the measured optical rotations with the reported values.[4b] [f] The absolute configuration was not determined. [g] The reaction was run for 5 h.

the yield and enantioselectivity. In order to obtain better enantioselectivity, we examined the reaction in the presence of pyridine *N*-oxide.[11] The addition of pyridine *N*-oxide at 0 °C gave the best result (78%, 41% *ee*). The aziridination proceeded even at −20 °C with 40% *ee*. Thus, the use of pyridine *N*-oxide improved not only the enantioselectivity but also the yield of the product. These results represent the first example of the aziridination of styrene and, in addition, the first asymmetric synthesis with a chiral nitridomanganese complex. When complex **2**, which bears Jacobsen's ligand, was tested under the best conditions the yield was very low (9%) but the enantioselectivity of the aziridine was moderate (50%).

The pronounced effect of pyridine *N*-oxide was also observed in the aziridination of *trans*-β-methylstyrene. Although *trans*-β-methylstyrene was not aziridinated below

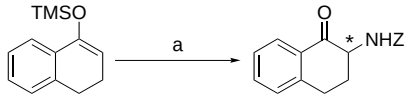
[*] Prof. Dr. M. Komatsu, Dr. S. Minakata, T. Ando, M. Nishimura, Dr. I. Ryu
Department of Applied Chemistry
Faculty of Engineering, Osaka University
Suita, Osaka 565-0871 (Japan)
Fax: (+81) 6-6879-7402
E-mail: komatsu@ap.chem.eng.osaka-u.ac.jp

[**] T. A. acknowledges the Ministry of Education, Science, Sports and Culture of Japan for a Grant-in-Aid for JSPS Research Fellowships for Young Scientists. We are grateful to Professor Dr. Erick M. Carreira for helpful discussions.

 © WILEY-VCH Verlag GmbH, D-69451 Weinheim, 1998 1433-7851/98/3724-3392 $ 17.50+.50/0

room temperature in the absence of pyridine *N*-oxide, the addition of the *N*-oxide to the reaction system resulted in a good yield and enantioselectivity (72%, 85% *ee*) even at 0 °C. In comparison, the aziridination of *cis*-β-methylstyrene was not observed at 0 °C in spite of the presence of pyridine *N*-oxide. In the absence of the *N*-oxide the desired *cis* aziridine was obtained in a poor yield and with a low *ee* value at room temperature. The addition of pyridine *N*-oxide improved the yield of aziridine, but a remarkable change in the *ee* value was not observed. The fact that the use of *trans*-β-methylstyrene resulted in high enantioselectivity encouraged us to investigate the asymmetric aziridination of other *trans*-disubstituted alkenes. The reaction of *trans*-1-phenyl-1-pentene with **1** under optimal conditions afforded the desired product in good yield (66%) and with high enantioselectivity (90% *ee*). Even better results were obtained when *trans*-3-methyl-1-phenyl-1-butene was utilized as the substrate. However, aziridination was not observed when a more bulky alkene, namely *trans* styrene with a *tert*-butyl substituent in the β position, was employed in the reaction. It is noteworthy that high stereospecificity was observed in all the aziridinations of *trans*- and *cis*-1,2-disubstituted alkenes, although such reactions in the presence of metal catalysts and PhI=NTs did not always show high streospecificity.[4] In addition, the allylic amination product was not produced in all the reactions.

The present reaction was applied with the aim of using the silyl enol ether to direct the asymmetric amination. The amination, which is presumed to take place via an aziridine intermediate,[6d, 12] proceeded smoothly to give the N-tosylated α-aminoketone in 76% yield and 48% *ee* (Scheme 1). When **1** was tested under Carreira's conditions[6a] the N-trifluoroacetylated α-aminoketone was obtained in moderate yield and *ee* (58%, 79% *ee*).[13] These results are of significance in that they suggest that additives such as Ts_2O and TFAA, which are used for the generation of the imido complex,[5a] might control the aziridination with **1**.



Z = Ts 76%, 48% *ee*
Z = CF_3CO 58%, 79% *ee*

Scheme 1. [a] Z = Ts: **1** (1 equiv), pyridine (0.5 equiv), Ts_2O (1.5 equiv), pyridine *N*-oxide (1.2 equiv), silyl enol ether (10 equiv), CH_2Cl_2, 0 °C, 6 h; Z = CF_3CO: **1** (2 equiv), pyridine (3 equiv), $(CF_3CO)_2O$ (2.4 equiv), silyl enol ether (1 equiv), CH_2Cl_2, −78 °C → RT, 3 h.

The aziridination of styrene derivatives proceeds with a chiral nitridomanganese complex **1** to give products in good yield and with excellent enantioselectivity. In addition, this methodology results in stereospecific aziridination. We also conclude that additives play an important role in the reaction; Ts_2O was the most effective reagent in the activation of **1**, and the use of pyridine *N*-oxide was necessary to obtain high enantioselectivity. Efforts to extend the scope of this process to other alkenes are currently in progress.

Experimental Section

General conditions for aziridination reactions: Pyridine (0.25 mmol), alkene (5.0 mmol), and a solution of *p*-toluenesulfonic anhydride (0.6 mmol) in CH_2Cl_2 (3 mL) were added to a solution of **1** (0.5 mmol) and pyridine *N*-oxide (0.6 mmol) in CH_2Cl_2 (2 mL) under nitrogen, and the mixture was stirred for 3 h. Pentane (15 mL), silica gel (400 mg), and celite (400 mg) were added and the mixture was stirred for 0.5 h. The reaction mixture was then passed through a 3-cm plug of silica gel with diethyl ether (5 × 15 mL) as eluent. The filtrate was concentrated in vacuo, and the residue purified by flash column chromatography on silica gel (EtOAc/hexane). Enantiomeric excesses of the aziridines were determined by chiral HPLC analysis (Daicel Chiralcel OJ) or by using the ^1H NMR chiral shift reagent [Eu(hfc)$_3$].

Received: July 10, 1998 [Z12126IE]
German version: *Angew. Chem.* **1998**, *110*, 3596 – 3598

Keywords: asymmetric synthesis · aziridinations · manganese · nitrides · N ligands

[1] a) J. A. Deyrup in *The Chemistry of Heterocyclic Compounds*, Vol. 42 (Ed.: A. Hassner), Wiley, New York, **1983**, pp. 1 – 214; b) A. Padwa, A. D. Woolhouse in *Comprehensive Heterocyclic Chemistry*, Vol. 7 (Ed.: W. Lwowski), Pergamon, Oxford, **1984**, pp. 47 – 93; c) W. H. Pearson, B. W. Lian, S. C. Bergmeier in *Comprehensive Heterocyclic Chemistry II*, *Vol. 1A* (Ed.: A. Padwa), Pergamon, Oxford, **1996**, pp. 1 – 60; d) K. M. L. Rai, A. Hassner in *Comprehensive Heterocyclic Chemistry II*, *Vol. 1A* (Ed.: A. Padwa), Pergamon, Oxford, **1996**, pp. 61 – 96.

[2] M. Kasai, M. Kono, *Synlett* **1992**, 778 – 790.

[3] a) D. Tanner, *Angew. Chem.* **1994**, *106*, 625 – 646; *Angew. Chem. Int. Ed. Engl.* **1994**, *33*, 599 – 619; b) H. M. I. Osborn, J. Sweeney, *Tetrahedron: Asymmetry* **1997**, *8*, 1693 – 1715; c) A.-H. Li, L.-X. Dai, V. K. Aggarwal, *Chem. Rev.* **1997**, *97*, 2341 – 2372.

[4] a) D. A. Evans, K. A. Woerpel, M. M. Hinman, M. M. Faul, *J. Am. Chem. Soc.* **1991**, *113*, 726 – 728; b) D. A. Evans, M. M. Faul, M. T. Bilodeau, B. A. Anderson, D. M. Barnes, *J. Am. Chem. Soc.* **1993**, *115*, 5328 – 5329; c) Z. Li, K. R. Conser, E. N. Jacobsen, *J. Am. Chem. Soc.* **1993**, *115*, 5326 – 5327; d) W. Zhang, N. H. Lee, E. N. Jacobsen, *J. Am. Chem. Soc.* **1994**, *116*, 425 – 426; e) Z. Li, R. W. Quan, E. N. Jacobsen, *J. Am. Chem. Soc.* **1995**, *117*, 5889 – 5890; f) K. Noda, N. Hosoya, R. Irie, Y. Ito, T. Katsuki, *Synlett* **1993**, 469 – 471; g) H. Nishikori, T. Katsuki, *Tetrahedron Lett.* **1996**, *37*, 9245 – 9248; h) R. E. Lowenthal, S. Masamune, *Tetrahedron Lett.* **1991**, *32*, 7373 – 7376; i) D. Tanner, P. G. Andersson, A. Harden, P. Somfai, *Tetrahedron Lett.* **1994**, *35*, 4631 – 4634; j) A. M. Harm, J. G. Knight, G. Stemp, *Synlett* **1996**, 677 – 678; k) T.-S. Lai, H.-L. Kwong, C.-M. Che, S.-M. Peng, *Chem. Commun.* **1997**, 2373 – 2374; l) M. J. Södergren, D. A. Alonso, P. G. Andersson, *Tetrahedron: Asymmetry* **1997**, *8*, 3563 – 3565; m) P. Müller, C. Baud, Y. Jacquier, M. Moran, I. Nägeri, *J. Phys. Org. Chem.* **1996**, *9*, 341 – 347; n) R. S. Atkinson, W. T. Gattrell, A. P. Ayscough, T. M. Raynham, *Chem. Commun.*, **1996**, 1935 – 1936.

[5] a) J. T. Groves, T. Takahashi, *J. Am. Chem. Soc.* **1983**, *105*, 2073 – 2074; b) J. T. Groves, T. Takahashi, W. M. Butlar, *Inorg. Chem.* **1983**, *22*, 884 – 887.

[6] a) J. D. Bois, J. Hong, E. M. Carreira, M. W. Day, *J. Am. Chem. Soc.* **1996**, *118*, 915 – 916; b) J. D. Bois, C. S. Tomooka, J. Hong, E. M. Carreira, *J. Am. Chem. Soc.* **1997**, *119*, 3179 – 3180; c) J. D. Bois, C. S. Tomooka, J. Hong, E. M. Carreira, M. W. Day, *Angew. Chem.* **1997**, *109*, 1722 – 1724; *Angew. Chem. Int. Ed. Engl.* **1997**, *36*, 1645 – 1647; d) J. D. Bois, C. S. Tomooka, J. Hong, E. M. Carreira, *Acc. Chem. Res.* **1997**, *30*, 364 – 372.

[7] a) J. W. Buchler, C. Dreher, K.-L. Lay, *Z. Naturforsch. B* **1982**, *37*, 1155 – 1162; b) J. W. Buchler, C. Dreher, K.-L. Lay, Y. J. A. Lee, W. R. Scheidt, *Inorg. Chem.* **1983**, *22*, 888 – 891; c) C. L. Hill, F. J. Hollander, *J. Am. Chem. Soc.* **1982**, *104*, 7318 – 7319.

[8] J. F. Larrow, E. N. Jacobsen, Y. Gao, Y. Hong, X. Nie, C. M. Zepp, *J. Org. Chem.* **1994**, *59*, 1939 – 1942.

 © WILEY-VCH Verlag GmbH, D-69451 Weinheim, 1998 1433-7851/98/3724-3393 $ 17.50+.50/0

[9] Treatment of the Mn^{III} complex[8] (35.6 mg, 0.09 mmol) with Chloramine-T (141 mg, 0.5 mmol) in MeOH (5 mL) at room temperature for 40 h afforded complex **1** in 84% yield.
[10] The use of trifluoromethanesulfonic anhydride or *p*-toluenesulfonyl chloride as an activator did not give good results relative to *p*-toluenesulfonic anhydride.
[11] Katsuki and his co-workers have reported that pyridine *N*-oxide is an effective additive for the asymmetric epoxidation catalyzed by salen–manganese(III) complexes, and they applied these findings to the asymmetric aziridination of alkenes with PhI=NTs: R. Irie, Y. Ito, T. Katsuki, *Synlett* **1991**, 265–266.
[12] a) D. A. Evans, M. M. Faul, M. T. Bilodeau, *J. Am. Chem. Soc.* **1994**, *116*, 2742–2753; b) A. Cipollone, M. A. Loreto, L. Pellacani, P. A. Tardella, *J. Org. Chem.* **1987**, *52*, 2584–2586; c) S. Lociuro, L. Pellacani, P. A. Tardella, *Tetrahedron Lett.* **1983**, *24*, 593–596.
[13] The chiral product could be purified to greater than 98% *ee* by recrystallization from benzene/hexane.

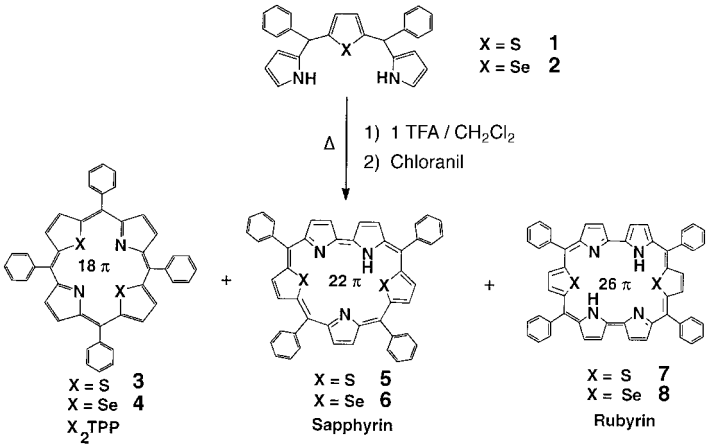
Sapphyrin Supramolecules through C–H···S and C–H···Se Hydrogen Bonds—First Structural Characterization of *meso*-Arylsapphyrins Bearing Heteroatoms**

Seenichamy Jeyaprakash Narayanan, Bashyam Sridevi, Tavarekere K. Chandrashekar,* Ashwani Vij,* and Raja Roy

Dedicated to Professors C. N. R. Rao and Jean'ne M. Shreeve on the occasion of their 65th birthdays

Controlling the assembly of macromolecules in the solid state through weak interactions such as hydrogen bonding and van der Waals forces is currently being explored for the synthesis of functional materials for molecular recognition and catalysis.[1] Many supramolecules held together by weak C–H···O and C–H···N hydrogen bonds are known.[2] In contrast, molecules held together by C–H···S and C–H···Se hydrogen bonds are very rare, and to the best of our knowledge there are only three reports to date on such interactions.[3] Here we describe the first structural characterization of two core-modified sapphyrins synthesized by an unprecedented coupling of a modified tripyrrane. Sapphyrins have been shown to self-assemble in the solid state to form a supramolecular ladder held together by weak C–H···S or C–H···Se and C–H···N hydrogen-bonding interactions.

Literature methods for the synthesis of sapphyrins include a traditional [3+2] acid-catalyzed MacDonald-type condensation between the appropriate precursors, reaction of diformylbipyrrole with benzaldehyde and pyrrole under Lindsey conditions,[4] and an acid-catalyzed condensation of *a,c*-biladienes with pyrrole-2-carbaldehydes.[5] Recently, a *meso*-substituted sapphyrin was isolated as a side product in 1% yield in the Rothemund reaction of benzaldehyde and pyrrole.[6] In all these reactions at least two precursors are required for the condensation under different conditions. However, our reaction of the modified tripyrranes **1** and **2** in dichloromethane containing an appropriate acid catalyst gave 18π, 22π, and 26π macrocycles in moderate yields (Scheme 1). The product distribution and the yields of isolated products were dependent on the nature of the acid catalyst and its concentration. For S- and Se-containing tripyrranes at lower concentrations of trifluoroacetic acid (TFA), the major product was rubyrin, while at higher concentrations of TFA, sapphyrin and rubyrin were isolated in moderately good yields in addition to small amounts of X_2TPP (X = S or Se; TPP = tetraphenylporphyrin). The formation of **5** and **6** requires partial acidolysis of tripyrranes under the reaction conditions. We have observed that both **1** and **2** undergo acidolysis, and the extent of acidolysis is dependent on the TFA concentration. The higher yields of **5** and **6** at higher concentrations of TFA is consistent with this observation. For the formation of **7** and **8** we suggest an acid-catalyzed self-condensation of two tripyrrane units through an oxidative coupling,[7] forming a rubyrinogen intermediate which on dehydrogenation gives rubyrin.[8] Attempts to isolate the corresponding rubyrinogen proved futile because it oxidizes readily to the corresponding aromatic congener. The sole formation of rubyrins at the lower concentrations of TFA (0.1 equiv) at which acidolysis is minimal suggests that the self-coupling is preferred at this concentration.



Scheme 1. Synthesis of various sapphyrins and rubyrins from **1** and **2**.

[*] Prof. Dr. T. K. Chandrashekar, S. J. Narayanan, B. Sridevi
Department of Chemistry, Indian Institute of Technology
Kanpur 208016 (India)
Fax: (+91) 512-590-007/597-436
E-mail: tkc@iitk.ac.in
Dr. A. Vij
Single-Crystal Diffraction Laboratory
University of Idaho, Moscow, ID 83834 (USA)
E-mail: Vij@uidaho.edu
Dr. R. Roy
NMR Division, Central Drug Research Institute
Lucknow (India)

[**] This work was supported by the Department of Science and Technology (DST; grant to T.K.C.) and by the Council of Scientific and Industrial Research (CSIR), Government of India, New Delhi (Senior Research Fellowship to S.J.N.). The single-crystal X-ray facility at the University of Idaho was established with the assistance of the NSF-Idaho EPSCoR program (NSF OSR-9350539) and the M. J. Murdock Charitable Trust, Vancouver, WA.

 © WILEY-VCH Verlag GmbH, D-69451 Weinheim, 1998 1433-7851/98/3724-3394 $ 17.50+.50/0

The composition of the new expanded porphyrins was established from the analytical data and FAB mass spectrometry, while their aromatic and porphyrinic nature were supported by ^{1}H NMR and UV/Vis spectral data (Table 1). The important feature of the ^{1}H NMR spectra is the revelation that the NH tautomerism of **5** is much more rapid than that of **6** at room temperature. Consequently, a broad signal appears for the inner NH protons of **6** while no corresponding signal is seen for **5.** However, when the solutions are cooled to $-90\,^\circ$C, sharp NH resonances are seen for both **5** and **6** at $\delta = -5.0$ and -5.35, respectively. Furthermore, two sets of equal-intensity resonances are seen for the pyrrole, thiophene, and selenophene rings, suggesting the existence of asymmetric tautomers in which the proton is located either on N3 or N2 of the bipyrrole unit. A similar observation was made by Latos-Grażyński and co-workers very recently for 26,28-dithiasapphyrin.[9] The rubyrins **7** and **8** did not show well-resolved resonances at room temperature. Only three broad resonances due to bipyrrole protons and *meso*-phenyl protons are observed, suggesting the rapid rotation of the selenophene rings in **8**. However, on cooling to $-50\,^\circ$C, sharp resonances were seen for the selenophene protons as well as inner-ring NH protons. Unlike **6**, no splitting of the bipyrrole protons is observed here, suggesting a symmetric tautomer in which each bipyrrole unit has one proton on either of the nitrogens. On protonation the rate of rotation slows down, and the chemical shifts and coupling constants reported in Table 1 for **8** were evaluated from the 2D COSY spectrum recorded at $-50\,^\circ$C.

Table 1. Selected physical data for the new compounds.

2: ^{1}H NMR (300 MHz, $CDCl_3$, 25 °C, TMS): $\delta = 5.96$ (s, 2H), 6.15 (q, 2H, $J = 8$ Hz), 6.69 (d, 2H, $J = 2$ Hz), 6.79 (d, 2H, $J = 3$ Hz), 7.29 (m, 10H), 7.92 (brs, 2H); MS (70 eV): m/z (%): 443 (100) [M^+ with ^{80}Se]

5: ^{1}H NMR (300 MHz, $CDCl_3$, 25 °C, TMS): $\delta = 7.85$ (m, 7H), 7.92 (m, 4H), 8.37 (m, 4H), 8.46 (m, 4H), 8.81 (s, 2H), 9.29 (d, 2H, $J = 3$ Hz), 9.93 (d, 2H, $J = 6$ Hz), 9.95 (d, 2H, $J = 6$ Hz), 10.06 (d, 2H, $J = 6$ Hz); ^{1}H NMR (300 MHz, $CDCl_3$/TFA, 25 °C, TMS): $\delta = -2.18$ (brs, 2H), -2.85 (s, 1H), 8.18 (m, 8H), 8.23 (m, 4H), 8.76 (m, 4H), 8.89 (m, 4H), 9.17 (s, 2H), 9.75 (d, 2H, $J = 6$ Hz), 10.12 (d, 2H, $J = 6$ Hz), 10.32 (d, 2H, $J = 6$ Hz), 10.33 (d, 2H, $J = 6$ Hz); UV/Vis (CH_2Cl_2): λ_{max} ($\varepsilon \times 10^{-4}$) = 470 (22.4), 584 (1.75), 623 (1.07), 730 (0.59), 820 nm (1.68); UV/Vis (CH_2Cl_2/TFA): λ_{max} ($\varepsilon \times 10^{-4}$) = 499 (12.3), 660sh (1.17), 727 (2.42), 826 nm (2.74); MS (FAB): m/z (%): 714 (100) [M^+]

6: ^{1}H NMR (300 MHz, $CDCl_3$, 25 °C, TMS): $\delta = -4.4$ (brs, 1H), 7.6 (m, 8H), 7.96 (m, 4H), 8.39 (m, 4H), 8.49 (m, 4H), 8.96 (s, 2H), 9.36 (d, 2H, $J = 6$ Hz), 10.01 (d, 2H, $J = 6$ Hz), 10.35 (d, 2H, $J = 6$ Hz), 10.47 (d, 2H, $J = 6$ Hz); UV/Vis (CH_2Cl_2): λ_{max} ($\varepsilon \times 10^{-4}$) = 475 (30.1), 517 (6.4), 592 (2.8), 631 (1.8), 736 (0.7), 823 nm (3.2); UV/Vis (CH_2Cl_2/TFA): λ_{max} ($\varepsilon \times 10^{-4}$) = 519 (19.8), 677 (0.96), 752 (1.83), 859 nm (2.9); MS (FAB): m/z (%): 810 (100) [M^+ with ^{80}Se]

7: ^{1}H NMR (300 MHz, $CDCl_3$/HCl, 25 °C, TMS): $\delta = -2.80$ (brs, 2H), -2.50 (brs, 2H), 8.04 (m, 12H), 7.92 (d, 4H), 8.82 (m, 8H), 9.71 (s, 4H), 10.49 (s, 4H); UV/Vis (CH_2Cl_2): λ_{max} ($\varepsilon \times 10^{-4}$) = 385 (0.16), 532 (14.2), 658 (1.12), 764 (0.9), 1017 nm (1.36); UV/Vis (CH_2Cl_2/TFA): λ_{max} ($\varepsilon \times 10^{-4}$) = 542 (19.4), 722 (0.82), 813 (1.8), 1004 nm (5.9); MS (FAB): m/z (%): 779 (100) [M^+]

8: ^{1}H NMR (300 MHz, $CDCl_3$, $-50\,^\circ$C, TMS): $\delta = 9.88$ (s, 4H), 9.66 (d, 4H, $J = 4.2$ Hz), 8.91 (d, 4H, $J = 4.2$ Hz), 8.64–8.66 (m, 8H), 7.94–8.10 (m, 8H), 7.68–7.81 (m, 4H), -0.06 (brs); ^{1}H NMR (300 MHz, $CDCl_3$/HCl, 25 °C, TMS): $\delta = -1.55$ (brs, 2H), -1.00 (brs, 2H), 7.98 (m, 20H), 8.87 (d, 4H, $J = 6$ Hz), 8.77 (d, 4H, $J = 6$ Hz), 9.58 (d, 2H, $J = 6$ Hz), 10.41 (d, 2H, $J = 6$ Hz); UV/Vis (CH_2Cl_2): λ_{max} ($\varepsilon \times 10^{-4}$) = 530 (13.4), 666 (1.09), 766 (0.62), 849 (0.77), 970 nm (1.34); UV/Vis (CH_2Cl_2/TFA): λ_{max} ($\varepsilon \times 10^{-4}$) = 546 (15.4), 728 (0.98), 814 (1.11), 1016 nm (5.07); MS (FAB): m/z (%): 875 (100) [M^+ with ^{80}Se]

The X-ray crystal structures of **5**[10] and **6** [11] (Figure 1) reveal that the replacement of the pyrrole NH group by S or Se changes the π-electron delocalization. The bond lengths in the macrocycle are altered compared to those of free thiophene or selenophene fragments, as was observed previously for the similar systems.[12] In both the cases the macrocycle is almost planar (deviations from the mean plane in **5** are 0.054, 0.027, and 0.028 Å for S1, S2, and N2 and -0.014 and -0.102 Å for N1 and N3, respectively). In both structures the imino H atom could not be assigned unequivocally to a specific nitrogen atom. This difficulty is most likely due to a statistical distribution of NH tautomers in the crystal or rapid interconversion of tautomers during the time required for measurement.[13] Our analysis suggests 70% probability of occupation on N3 and 30% probability on N1. It is pertinent to point out here that in the N5 *meso*-tetraphenylsapphyrin reported by Latos-Grażyński and coworkers the pyrrole ring opposite to bipyrrole is inverted in its free-base form.[6] However, in **5** and **6** such a ring inversion was not observed in either solid or solution state. The important feature of the structure is the presence of hydrogen-bonding interactions in the cavity between N1–H1···S1 (H1–S1 2.87 (8) Å) and N1–H1···S2 (H1–S2 2.55 (8) Å) in **5**. The corresponding distances for **6** are 2.63 (17) (H1–Se1) and 2.28 (17) Å (H1–Se2).

The packing diagram shown in Figure 2 reveals an interesting aspect of the structure. In **5** there are two short-range C23–H23···S1 hydrogen-bonding interactions (2.91 (4) Å, 136.3°) to form a dimeric structure. This dimer is further extended through the formation of the longer hydrogen bond between C19–H19···S2 (3.16 Å, 131.2°) and C20–H20···N1 (2.70 (5) Å, 156.3°) thus leading to a supramolecular assembly.[14] A similar assembly was formed in **6**, and the corresponding distances and angles for **6** are C23–H23···Se1 (2.98 (5) Å, 146°), C20–H20···Se2 (3.26 (5) Å, 129°), and C20–H20···N1 (2.74 (5), 155°). The C–H···S and the C–H···Se distances observed here compare well with the reported data (C–H···Se 2.94, 107°).[3a]

The protonation of pyrrole nitrogen atoms in sapphyrin and rubyrin leads to formation of dicationic species in which the positive charge is delocalized into the ring. Thus, the dications are anticipated to bind anions depending on the cavity size of the macrocycle and the size of the anion.[15] Preliminary binding studies reveal formation of stable complexes in solution. Specifically, 22π sapphyrins bind F^- and N_3^- ions strongly relative to the larger CO_3^{2-} and PO_4^{3-} ions, while the 26π rubyrins bind CO_3^{2-} and PO_4^{3-} ions with binding constants higher than those with F^- and N_3^- ions.

We have demonstrated the feasibility, by rational core modification of the porphyrin building blocks, of a controlled assembly of supramolecular multisapphyrin arrays through unusual C–H···Se and C–H···S and C–H···N hydrogen-bonding interactions. Furthermore, the synthesis presented here is not only elegant but also quite effective: 18π, 22π, and 26π macrocycles are prepared in one pot in moderately good

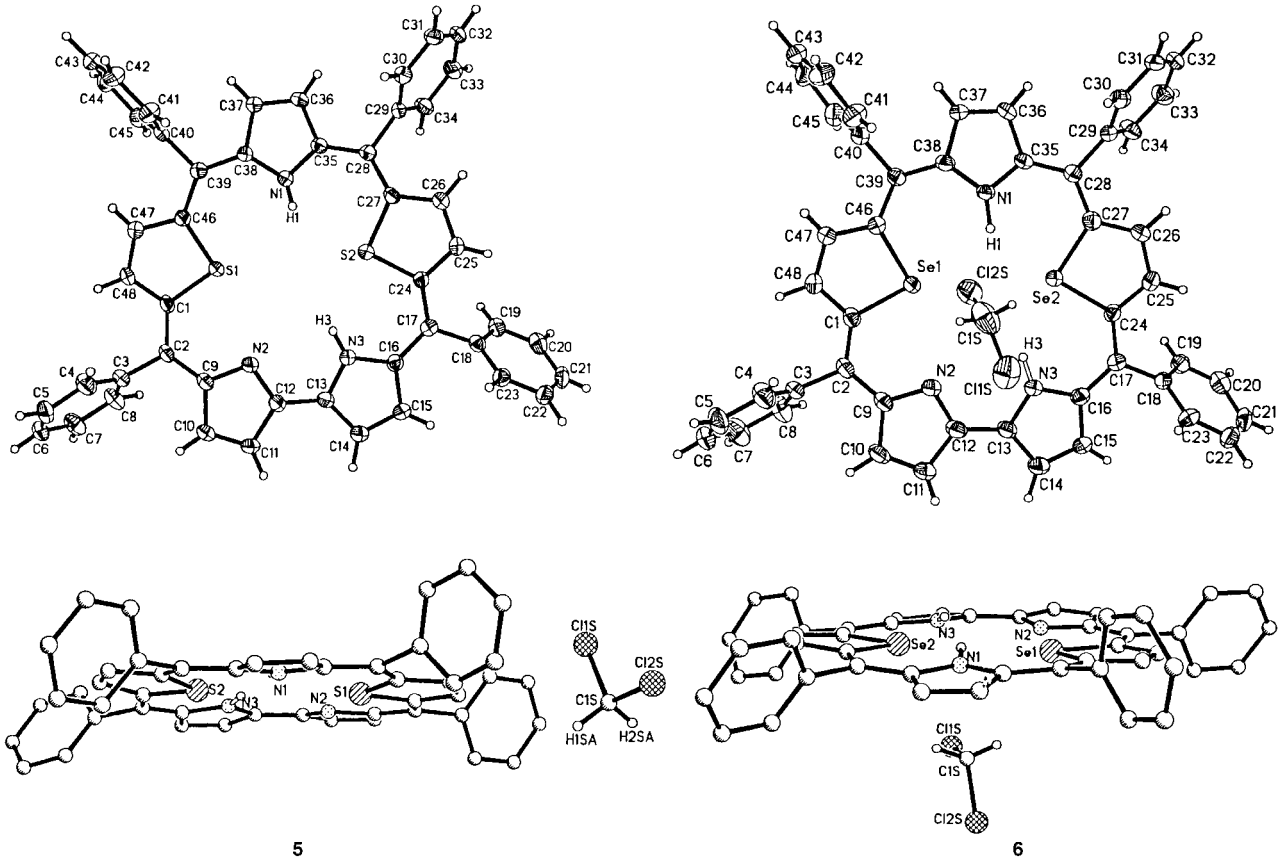


Figure 1. Crystal structures of **5** and **6** (in each case, top: plan view, bottom: side view). Selected distances in **5** [Å]: S1 ··· N2 2.911 (3), S1 ··· N1 3.244 (4), N2 ·· ·N3 2.835 (4), N3 ··· S2 3.058 (4), S2 ··· N1 3.122 (4), S1 ··· S2 4.346 (5). Selected distances in **6** [Å]: Se1 ··· N2 2.909 (4), Se1 ··· N1 3.226 (4), Se2 ·· ·N3 3.093 (4), Se2 ··· N1 3.035 (4), N2 ··· N3 2.820 (4), Se1 ··· Se2 3.9315 (8).

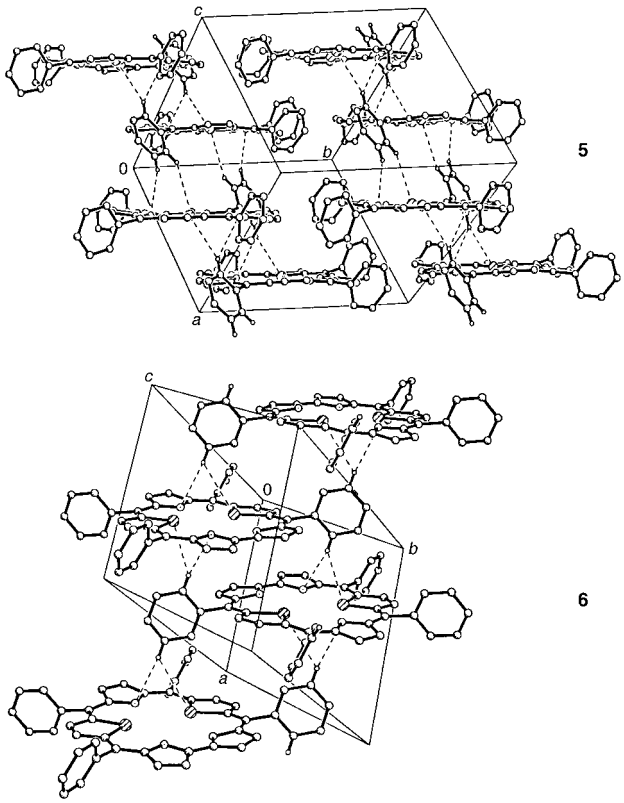


Figure 2. Molecular packing diagram of **5** and **6** showing two-dimensional ladder structures. Hydrogen-bonding interactions are represented by dotted lines.

yields. The fact that this methodology works smoothly for tripyrranes containing two different heteroatoms (S and Se) establishes the versatility of the method.

Experimental Section

Tripyrrane **1** (0.301 mmol) was dissolved in 150 mL of dichloromethane and stirred under a nitrogen atmosphere for 5 min. TFA (0.301 mmol) was added, and the stirring was continued for a further 90 min. Then chloranil (0.903 mmol) was added, and the reaction mixture heated at reflux for an additional 90 min. After removal of the solvent the residue was purified by chromatography on basic alumina (grade 3). The orange fraction, which eluted with petroleum ether/dichloromethane (4/1), was identified as **3** (2 mg, 1%); sapphyrin **5** (30 mg, 14%) eluted as a green band when the eluent was changed to EtOAc/CH_2Cl_2 (5/95); and the last pink band, which was eluted with EtOAc/CH_2Cl_2 (2/3), corresponded to rubyrin **7** (20 mg, 8.5%). The same procedure was followed for other reactions with appropriate modified tripyrranes and acid concentrations.

Received: April 20, 1998
Revised version: August 31, 1998 [Z11750IE]
German version: *Angew. Chem.* **1998**, *110*, 3582 – 3585

Keywords: hydrogen bonds · porphyrinoids · supramolecular chemistry

[1] a) J. Marfurt, C. Leumann, *Angew. Chem.* **1998**, *110*, 184 – 187; *Angew. Chem. Int. Ed.* **1998**, *37*, 175 – 177; b) F. H. Beijer, H. Kooijman, A. L. Spek, R. P. Sijbesma, E. W. Meijer, *Angew. Chem.* **1998**, *110*, 79 – 82; *Angew. Chem. Int. Ed.* **1998**, *37*, 75 – 78; c) R. K. Kumar, S. Balasubramanian, I. Goldberg, *Inorg. Chem.* **1998**, *37*, 541 – 552;

 © WILEY-VCH Verlag GmbH, D-69451 Weinheim, 1998 1433-7851/98/3724-3396 $ 17.50+.50/0

d) J. L. Sessler, A. Andrievsky, P. A. Gale, V. Lynch, *Angew. Chem.* **1996**, *108*, 2954 – 2957; *Angew. Chem. Int. Ed. Engl.* **1996**, *35*, 2782 – 2785; e) B. F. Abrahams, B. F. Hoskins, D. M. Michail, R. Robson, *Nature* **1994**, *369*, 727 – 729.

[2] a) G. R. Desiraju, *Acc. Chem. Res.* **1996**, *29*, 441 – 449; b) O. M. Yaghi, H. Li, T. L. Groy, *J. Am. Chem. Soc.* **1996**, *118*, 9096 – 9101; c) P. Bhyrappa, S. R. Wilson, K. S. Suslick, *J. Am. Chem. Soc.* **1997**, *119*, 8492 – 8502.

[3] a) M. Iwaoka, S. Tomoda, *J. Am. Chem. Soc.* **1994**, *116*, 4463 – 4464; b) J. J. Novoa, M. C. Rovira, C. Rovira, J. Veciana, J. Tarres, *Adv. Mater.* **1995**, *7*, 233. c) V. R. Pedireddi, S. Chatterjee, A. Ranganathan, C. N. R. Rao, *J. Am. Chem. Soc.* **1997**, *119*, 10867 – 10868.

[4] a) A. Jasat, D. Dolphin, *Chem. Rev.* **1997**, *97*, 2267 – 2340, and references therein; b)J. L. Sessler, M. C. Hoehner, A. Gebauer, A. Andrievsky, V. Lynch, *J. Org. Chem.* **1997**, *62*, 9251 – 9260.

[5] R. Paolesse, S. Licoccia, M. Spagnoli, T. Boschi, R. G. Khoury, K. M. Smith, *J. Org. Chem.* **1997**, *62*, 5133 – 5137.

[6] P. J. Chmielewski, L. Latos-Grażyński, K. Rachlewicz, *Chem. Eur. J.* **1995**, *1*, 68 – 73.

[7] H. A. Potts, G. F. Smith, *J. Chem. Soc.* **1957**, 4018 – 4020.

[8] Such an intermediate (sapphyrinogen) has been proposed by Latos-Grażyński for the formation of sapphyrins; see reference [6]. Experiments are in progress to monitor the formation of rubyrinogen by UV absorption spectroscopy.

[9] We would like to thank the referee who brought to our attention a recent paper by Latos-Grażyński and co-workers published after submission of this manuscript in which an asymmetric tautomer for 5,10,15,20-tetraphenyl-26,28-dithiasapphyrin was proposed. For details see: K. Rachlewicz, N. Sprutta, P. J. Chmielewski, L. Latos-Grażyński, *J. Chem. Soc. Perkin Trans. 2* **1998**, 969 – 975.

[10] a) Crystal structure data of **5**: $C_{48}H_{32}N_3S_2 \cdot CH_2Cl_2$, $M_r = 799.87$; crystals from CH_2Cl_2/CH_3OH (1/1); Crystal dimensions $0.50 \times 0.25 \times 0.20$ mm; triclinic, space group $P\bar{1}$, $a = 11.122$ (2), $b = 13.526$ (2), c = 15.109 (2) Å, $\alpha = 68.689$ (13), $\beta = 87.10$ (2), $\gamma = 66.785$ (11)°, $V = 1934.6$ (6) Å^3, $Z = 2$, $\rho_{calcd} = 1.373$ g cm^{-3}; F (000) = 830; μ ($Mo_{K\alpha} = 3.2$ cm^{-1}; 12202 measured reflections; 5833 observed reflections. ($F_o^2 > 2\sigma F_o^2$); $\theta_{max} = 28.3°$; $R = 0.0681$, $R_w = 0.1658$. b) The X-ray diffraction data were collected on a Siemens SMART3-circle diffractometer equipped with a CCD detector. The structure was solved by the direct method using the SHELX-904 program and refined by the least squares method on F^2 using SHELXTL Version 5.03.5. Crystallographic data (excluding structure factors) for the structures reported in this paper have been deposited with the Cambridge Crystallographic Data Center as supplementary publication no. CCDC-101360. Copies of the data can be obtained free of charge on application to CCDC, 12 Union Road, Cambridge CB2 1EZ, UK (fax: (+44) 1223-336-033; e-mail: deposit@ccdc.cam.ac.uk).

[11] Crystal structure data of **6**: $C_{48}H_{32}N_3Se_2 \cdot CH_2Cl_2$, $M_r = 891.60$; crystals from CH_2Cl_2/CH_3OH (1/1); crystal dimensions $0.10 \times 0.20 \times 0.35$ mm; triclinic, space group $P\bar{1}$, $a = 11.2565$ (14), $b = 13.689$ (2), $c = 15.116$ (2) Å, $\alpha = 67.911$ (7), $\beta = 86.897$ (9), $\gamma = 66.592$ (2)°, $V = 1968.1$ (5) Å^3, $Z = 2$, $\rho_{calcd} = 1.505$ g cm^{-3}; F (000) = 898; 11111 measure reflections; 7648 observed reflections. ($F_o^2 > 2\sigma F_o^2$); $\theta_{max} = 26.41°$; $R = 0.0510$, $R_w = 0.1099$.[10b]

[12] J. Lisowski, J. L. Sessler, V. Lynch, *Inorg. Chem.* **1995**, *34*, 3567 – 3572.

[13] E. Vogel, M. Kocher, H. Schmickler, J. Lex, *Angew. Chem.* **1986**, *98*, 262; *Angew. Chem. Int. Ed. Engl.* **1986**, *25*, 257 – 259.

[14] The ^{1}H NMR spectra of **6** which was recrystallized from dichloromethane and *n*-heptane showed sharp resonances (12.15 Hz), whereas the resonances were broad (20.1 Hz) for the sample recrystallized from a dichloromethane/methanol mixture. Furthermore, a titration of different concentrations of CD_3OD to a $CDCl_3$ solution of **6** resulted in gradual broadening of the signals, suggesting the existence of aggregates due to intermolecular interactions in solution.

[15] A. Srinivasan, M. V. Reddy, S. J. Narayanan, B. Sridevi, S. K. Pushpan, M. Ravikumar, T. K. Chandrashekar, *Angew. Chem.* **1997**, *109*, 2710 – 2713; *Angew. Chem. Int. Ed. Engl.* **1997**, *36*, 2598 – 2601.

A Functional Model of Cytochrome c Oxidase: Thermodynamic Implications**

James P. Collman,* Lei Fu, Paul C. Herrmann, Zhong Wang, Miroslav Rapta, Martin Bröring, Reinhold Schwenninger, and Bernard Boitrel

Cytochrome c oxidases (CcOs) are the terminal enzymes of the respiratory chains. These membrane bound assemblies catalyze the four-electron ($4e^-$), four-proton ($4H^+$) reduction of O_2 to H_2O, and couple this exergonic reaction to intramembrane proton translocation. The resulting energy is used to generate ATP as protons flow back through the membrane via ATP synthase.[1, 2] What makes this class of enzymes particularly well suited to the task is the fact that they do not release partially reduced intermediates, such as superoxide and peroxide, which would be devastating to the cell if released in large quantities.[3]

Recently, a plethora of research on CcO[4] has been stimulated by two X-ray crystal structures.[5–8] The fundamental question of how the enzymes convert O_2 into H_2O without releasing H_2O_2 remains unanswered, however. Attempts to prepare synthetic analogues of the O_2 binding/activating site in CcO have been reported over many years. Very few have mimicked the catalytic properties of CcO, however.[9]

Previously we reported the first functional CcO model that consisted of a Co^{II} – porphyrin with a Cu^{I}-coordinated distal superstructure and with a covalently attached imidazole group as the axial ligand.[10] We demonstrated that this complex catalyzes the $4e^-$ reduction of O_2 under physiological conditions without the release of H_2O_2. Our electrocatalytic studies also demonstrate that both the copper ion and the axial imidazole ligand are essential to achieve the reduction.

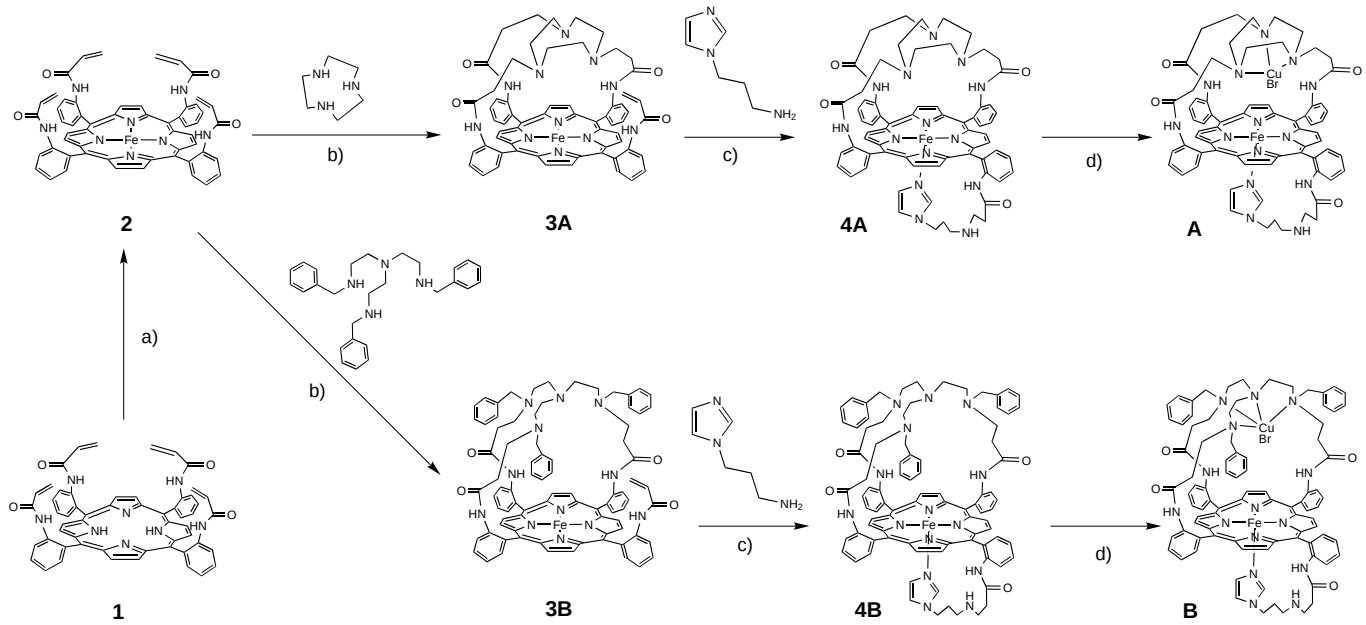
Herein we present the synthesis, characterization, and electrocatalytic chemistry of two Fe/Cu-containing synthetic analogues of the dioxygen activating site of CcO heme a_3 Cu_B. The only structural difference between these compounds is the nature of the distal superstructure in which the copper ion resides (Scheme 1). Compound **A** has a 1,4,7-triazacyclononane (TACN) distal cap whereas **B** features a *N*,*N*′,*N*″-tribenzyl-tris(aminoethyl)amine (TBTren) cap.

Compounds **A** and **B** both form stable 1:1 adducts with O_2 ($\mathbf{X_A}$ and $\mathbf{X_B}$, respectively) as demonstrated by UV/Vis spectroscopy after O_2-titration. The O_2 adduct of each compound features an apparently diamagnetic NMR spectrum[11] in contrast to the paramagnetic NMR spectrum observed with their O_2-free forms, **A** and **B**. This observation

[*] Prof. Dr. J. P. Collman, Dr. L. Fu, Dr. P. C. Herrmann, Dr. Z. Wang, Dr. M. Rapta, Dr. M. Bröring, Dr. R. Schwenninger, Dr. B. Boitrel
Department of Chemistry
Stanford University
Stanford, CA 94305 – 5080 (USA)
Fax: (+1) 650-725-0259
E-mail: jpc@chem.stanford.edu

[**] We thank the NIH (grant 1R01 GM-17880-28) and the NSF (grant CHE 9612725) for financial support. We also thank Drs. Henry Taube, Jean-Claude Marchon, and Steve Harford for helpful discussions.

Supporting information for this article is available on the WWW under http://www.wiley-vch.de/home/angewandte/ or from the author.



Scheme 1. Synthesis of the CcO model compounds **A** and **B**. a) $FeBr_2$, THF, △; b) methanol, △; c) methanol/toluene (1/5), △; d) CuBr, CH_3CN, △.

is consistent with the Fe^{III} and Cu^{II} centers being strongly antiferromagnetically coupled through a bridging peroxide group.

In both cases cobaltocene (Cp_2Co) can reduce the O_2 adduct to its deoxygenated form. Whereas complex $\mathbf{X_A}$ requires only two equivalents of Cp_2Co to regenerate **A**, $\mathbf{X_B}$ requires four equivalents to form the deoxygenated complex **B**. Both **A** and **B** were applied to a rotating ring-disk electrode (RRDE).[12] Compound **A** produced H_2O_2 from reduction of O_2 at pH 7, while **B** did not (Figure 1). Consequently we conclude that compound **A** predominately catalyzes the $2e^-$ reduction of O_2 to H_2O_2, while **B** catalyzes the $4e^-$ reduction of O_2 to H_2O under physiological conditions.

The different half-wave potentials measured by cyclic voltammetry demonstrate the effect of the distal superstructure on the Cu^I/Cu^{II} potential.[9] For the two different distal caps studied, not only are the absolute Cu^I/Cu^{II} potentials at different values, but the relation of the Fe – Cu potentials to each other differs as well. The TACN cap, which presents the copper ion with three nitrogen atoms, makes the Cu^{II} oxidation state less favorable than that of the TBTren cap that contains four nitrogen atoms. In the latter complex, the iron center should be reduced first, which possibly directs the binding of O_2 to the distal porphyrin locus.

To comprehend the thermodynamics of the $4e^-$ reduction, the electrochemical potential of the reaction is converted into ΔG.[13] The $4e^-$ reduction of O_2 catalyzed by the model catalyst (cat.) on the graphite disk can be written by Equations (1) to (3).

$$\text{cat.} + O_2 \rightleftharpoons \text{cat.}\cdot O_2^{2-} \qquad \Delta G_1^{\mathrm{B}} \qquad (1)$$

$$\text{cat.}\cdot O_2^{2-} + 4e^- + 4H^+ \rightleftharpoons 2H_2O + \text{cat.} \qquad \Delta G_2^{\mathrm{B}} \qquad (2)$$

$$O_2 + 4e^- + 4H^+ \rightleftharpoons 2H_2O \qquad \Delta G_{\mathrm{overall}}^{\mathrm{B}} \qquad (3)$$

Since step 1 [Eq. (1)] occurs spontaneously in solution only the second step [Eq. (2)] should require the input of electrons from the graphite disk. The potential recorded during the RRDE experiments (see Figure 1) represents the value of the second step (ΔG_2^{B}) alone. Thus, by subtracting this value from the overall reduction of O_2 ($\Delta G_{\mathrm{overall}}^{\mathrm{B}}$)[14] the lower limit of ΔG_1^{B} may be estimated. The calculated values are shown in Table 1 and illustrated graphically in Scheme 2.

It is significant that compound **B**, which catalyzes the $4e^-$ reduction of O_2 to H_2O, releases at least 47.4 kcal mol^{-1} of energy upon the addition of O_2 in the absence of a reducing agent (Table 1). The formation of this very stable intermediate ($\mathbf{X_B}$) results in the conversion of $\mathbf{X_B}$ into H_2O_2 being endergonic and thermodynamically unfavorable.[15] Therefore, the conversion of $\mathbf{X_B}$ into H_2O becomes a predominant pathway if it is kinetically possible (Scheme 2B).

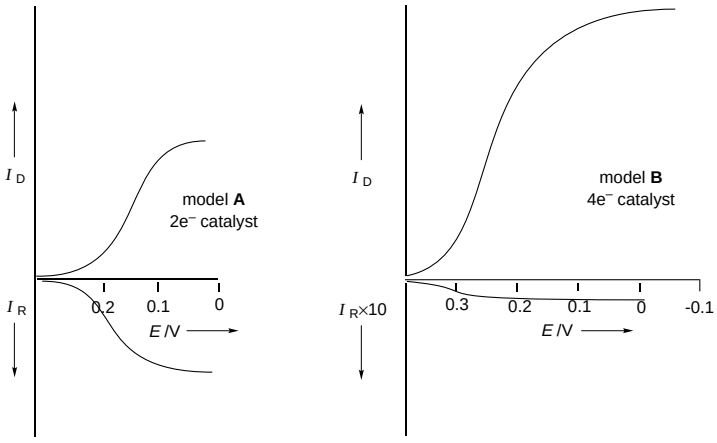


Figure 1. The RRDE experiment profiles (0.025 M phosphate buffer, pH 7; disk area 0.46 cm^2; scan rate 100 mV s^{-1}; collection efficiency 0.15; ring potential +1.1 V versus normal hydrogen electrode (NHE)). I_D = disk current; I_R = ring current.

 © WILEY-VCH Verlag GmbH, D-69451 Weinheim, 1998 1433-7851/98/3724-3398 $ 17.50+.50/0

Table 1. Thermodynamic data for the reduction of dioxygen.

Reaction	E [V] vs NHE (at pH 7)	ΔG [kcal mol^{-1}] ($= -nFE$)
$O_2 + 2e^- + 2H^+ \rightleftharpoons H_2O_2$ ($[H_2O_2] = 1$ M)	0.282[a]	−13.0
$O_2 + 2e^- + 2H^+ \rightleftharpoons H_2O_2$ ($[H_2O_2] = 10^{-6}$ M)		−16.6
$O_2 + 4e^- + 4H^+ \rightleftharpoons 2H_2O$	0.816[a]	−75.1
for model catalyst ***A***	0.20[b]	−9.2
$\mathbf{A}\cdot O_2 + 2e^- + 2H^+ \rightleftharpoons H_2O_2 + \mathbf{A}$		
$O_2 + \mathbf{A} \rightleftharpoons \mathbf{A}\cdot O_2$		−7.4[c]
for model catalyst ***B***	0.30[b]	−27.6
$\mathbf{B}\cdot O_2 + 4e^- + 4H^+ \rightleftharpoons 2H_2O + \mathbf{B}$		
$O_2 + \mathbf{B} \rightleftharpoons \mathbf{B}\cdot O_2$		−47.4
for cytochrome c oxidase		
$\mathbf{CcO}\cdot O_2 + 4e^- + 4H^+ \rightleftharpoons 2H_2O + \mathbf{CcO}$	0.245	−22.6
$\mathbf{CcO} + O_2 \rightleftharpoons \mathbf{CcO}\cdot O_2$		−52.5

[a] Taken from reference [32]. [b] Taken from the RRDE experiments (see Figure 1). [c] Based on the assumption that $[H_2O_2] = 10^{-6}$ M.

In contrast, compound **A**, which catalyzes the $2e^-$ reduction of O_2 to H_2O_2 at lower potential, releases far less energy upon binding O_2 under the same conditions. The paths from $\mathbf{X_A}$ to H_2O_2 and H_2O are both exergonic. Therefore, the catalytic stability of **A** to form H_2O_2 or H_2O probably depends on the rate of hydrolysis of the peroxide intermediate (Scheme 2C).

Our model can also be compared to the CcO enzyme family by making the assumption that cytochrome c behaves similarly to the graphite electrode. The published value of its redox potential (0.245 V)[4] permits the calculation of ΔG for the O_2-binding step of CcO under standard conditions. This analysis yields a value of -52 kcal mol^{-1}, which is comparable to that obtained for **B**.

In conclusion, we have demonstrated that the state of the bound peroxide is very sensitive to the nature of the distal superstructure. Ultimately, the copper ion can determine the fate of the catalyzed reaction, and it appears to be the deciding factor as to whether the reaction yields a $2e^-$ or $4e^-$ product. We propose that in the reactions catalyzed by compound **B** and the enzyme family CcO the initial reaction of the fully reduced catalyst with O_2 to yield the peroxide intermediate is exergonic enough that it thermodynamically traps the bound peroxide. This effectively blocks the release of the poisonous H_2O_2 since its production would be endergonic. Hence the CcO-catalyzed reaction can be limited by proton transfer even though there is a build up of peroxide intermediates. Since these intermediates are low enough in energy, relative to any toxic products, there is very little risk of dangerous compounds being released even though the concentration of the peroxide intermediate may be high.

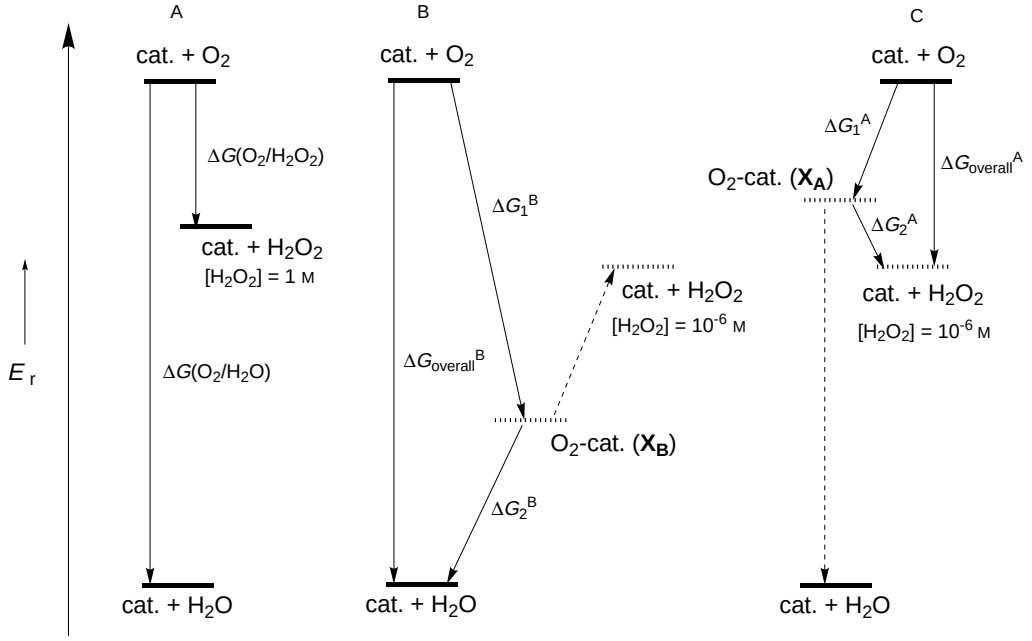
Experimental Section

The Michael acceptor **1** was metallated with $FeBr_2$ to yield **2**.[16] Compound **A** was prepared by capping **2** with 1,4,7-triazacyclononane (TACN), attaching a substituted imidazole tail in refluxing methanol/toluene, purifying, and metallating with CuBr in refluxing acetonitrile according to the reported method.[10, 17] The synthesis of compound **B** followed the same protocol except the metallated Michael acceptor **2** was capped with TBTren instead of TACN. All new compounds were fully characterized by spectroscopic methods (see the supporting information).

Received: June 16, 1998 [Z11998IE]
German version: *Angew. Chem.* **1998**, *110*, 3592 – 3595

Keywords: cytochrome c oxidase · electrochemistry · heme proteins · N ligands · O – O activation

[1] L. Stryer, *Biochemistry*, 4th ed, Freeman, New York, **1995**.
[2] M. Wikström, *Nature* **1977**, *266*, 271 – 273.
[3] M. A. J. Rodgers, E. L. Powers, *Oxygen and Oxy-Radicals in Chemistry and Biology,* Academic Press, New York, **1981**.
[4] S. Ferguson-Miller, G. T. Babcock, *Chem. Rev.* **1996**, *96*, 2889 – 2907.
[5] S. Iwata, C. Ostermeier, B. Ludwig, H. Michel, *Nature* **1995**, *376*, 660 – 669.
[6] T. Tsukihara, H. Aoyama, E. Yamashita, T. Tomizaki, H. Yamaguchi, K. Sinzawa-Itoh, R. Nakashima, R. Yaono, S. Yoshikawa, *Science* **1995**, *269*, 1069 – 1074.



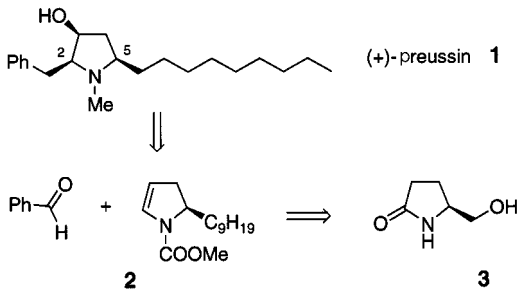
Scheme 2. Proposed energy diagram of dioxygen reduction. A) Thermodynamic data; B) the $4e^-$ reduction of O_2; C) the $2e^-$ reduction of O_2. E_r = relative energy.

[7] T. Tsukihara, H. Aoyama, E. Yamashita, T. Tomizaki, H. Yamaguchi, K. Shinzawa-Itoh, R. Nakashima, R. Yaono, S. Yoshikawa, *Science* **1996**, *272*, 1136 – 1144.
[8] S. Yoshikawa, K. Shinzawaitoh, R. Nakashima, R. Yaono, E. Yamashita, N. Inoue, M. Yao, M. J. Fei, C. P. Libeu, T. Mizushima, H. Yamaguchi, T. Tomizaki, T. Tsukihara, *Science* **1998**, *280*, 1723 – 1729.
[9] J. P. Collman, *Inorg. Chem.* **1997**, *36*, 5145 – 5155.
[10] J. P. Collman, L. Fu, P. C. Herrmann, X. Zhang, *Science* **1997**, *275*, 949 – 951.
[11] A more detailed discussion can be found in references [18 – 25].
[12] The RRDE consists of a graphite disk concentrically placed inside a platinum ring.[26, 27] During our experiment the assembly was submerged in an O_2-saturated, buffered (pH 7) solution, rotated at a constant rate, and then voltage was applied. The current produced at the platinum ring is correlated to the concentration of H_2O_2 produced.[28–31]
[13] The potential is converted into ΔG with the equation $\Delta G = -nFE$, where n is the number of electrons per mole, F is Faraday's constant, and E is the experimental reduction potential for the stated reaction.
[14] In the case of compound **B** the value of $\Delta G^{B}_{overall}$ can be compared to the standard ΔG value for the conversion of O_2 into H_2O since the concentrations of all pertinent species are known.
[15] The ΔG value for the O_2/H_2O_2 couple will be more negative if the activity of H_2O_2 is below 1.0 M in our experimental conditions.
[16] J. P. Collman, X. Zhang, P. C. Herrman, E. S. Uffelman, B. Boitrel, A. Straumanis, J. I. Brauman, *J. Am. Chem. Soc.* **1994**, *116*, 2681 – 2682.
[17] J. P. Collman, B. Boitrel, L. Fu, J. Galanter, A. Straumanis, M. Rapta, *J. Org. Chem.* **1997**, *2*, 193 – 194.
[18] G. N. La Mar, G. R. Eaton, R. H. Holm, F. A. Walker, *J. Am. Chem. Soc.* **1973**, *95*, 63 – 75.
[19] G. N. La Mar, F. A. Walker, *J. Am. Chem. Soc.* **1973**, *95*, 1782 – 1790.
[20] H. Goff, G. N. La Mar, C. A. Reed, *J. Am. Chem. Soc.* **1977**, *99*, 3641 – 3644.
[21] H. Goff, G. N. La Mar, *J. Am. Chem. Soc.* **1977**, *99*, 6599 – 6606.
[22] J. P. Collman, J. I. Brauman, K. M. Doxsee, T. R. Halbert, E. Bunnenberg, R. E. Linder, G. N. La Mar, J. Del Gaudio, G. Lang, K. Spartalian, *J. Am. Chem. Soc.* **1980**, *102*, 4182 – 4192.
[23] J. P. Collman, J. I. Brauman, T. J. Collins, B. L. Iverson, G. Lang, R. G. Pettman, J. L. Sessler, M. A. Walters, *J. Am. Chem. Soc.* **1983**, *105*, 3038 – 3052.
[24] J. P. Collman, P. C. Herrmann, B. Boitrel, X. Zhang, T. A. Eberspacher, L. Fu, *J. Am. Chem. Soc.* **1994**, *116*, 9783 – 9785.
[25] J. P. Collman, P. C. Herrmann, L. Fu, T. A. Eberspacher, M. Eubanks, B. Boitrel, P. Hayoz, X. Zhang, J. I. Brauman, *J. Am. Chem. Soc.* **1997**, *119*, 3481 – 3489.
[26] W. J. Albery, M. L. Hitchman, *Ring-Disc Electrodes,* Clarendon Press, Oxford, **1971**.
[27] T. Geiger, F. C. Anson, *J. Am. Chem. Soc.* **1981**, *103*, 7489 – 7496.
[28] V. G. Levich, *Physiochemical Hydrodynamics*, Prentice-Hall, Englewood Cliffs, NJ, **1962**.
[29] A. J. Bard, L. R. Faulkner, *Electrochemical Methods: Fundamentals and Applications*, Wiley, New York, **1980**.
[30] J. Koutecky, V. G. Levich, *Zh. Fiz. Khim.* **1956**, *32*, 1565 – 1575.
[31] J. P. Collman, P. S. Wagenknecht, J. Hutchison, *Angew. Chem.* **1994**, *106*, 1620 – 1639. *Angew. Chem. Int. Ed. Engl.* **1994**, *33*, 1537 – 1554.
[32] *Standard Potentials in Aqueous Solution* (Eds.: A. J. Bard, R. Parsons, J. Jordon), Marcel Dekker, New York, **1985**.

Unprecedented Facial Diastereoselectivity in the Paternò – Büchi Reaction of a Chiral Dihydropyrrole—A Short Total Synthesis of (+)-Preussin**

Thorsten Bach* and Harm Brummerhop

The Paternò – Büchi reaction[1] of aromatic aldehydes with enol and enamine derivatives gives 3-heteroatom-substituted 2-aryloxetanes in good yield.[2] Subsequent Pd-catalyzed hydrogenolysis of these compounds leads to a bond cleavage between the oxygen atom and the C2 atom of the oxetane and yields the products of a formal carbohydroxylation.[3] The carbohydroxylation of the N-acceptor-substituted 2,3-dihydropyrrole **2** appealed to us as an approach to the antifungal pyrrolidinol alkaloid (+)-preussin[4] (**1**). A straightforward synthesis[5] of this natural product appeared possible from the commercially available (*S*)-pyroglutaminol (**3**; Scheme 1).



Scheme 1. Retrosynthesis of (+)-preussin (**1**).

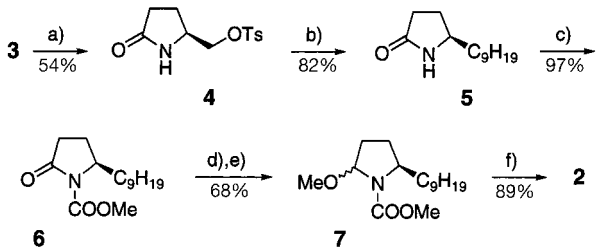
We now report on the realization of this goal in which the pivotal Paternò – Büchi reaction of **2** proceeded with a substrate-induced facial diastereoselectivity previously unobserved in photocycloaddition reactions. Indeed, a bulky substituent within a five-membered ring is known to direct the attack of a reactant to the opposite face (*anti* attack). Examples of this are found in Paternò – Büchi reactions[6] and in intermolecular [2+2] photocycloadditions.[7] The thermal addition of ketenes to dihydropyrroles, which are analogues of **2**, also proceeded with *anti* attack to the existent substituent.[8] The notion that made us hope for the *syn* attack shown in Scheme 1 was based on an observation by Beckwith and Chai[9] in which they showed that in radical reactions of N-acceptor-substituted five-membered rings that bear a stereogenic center in the C2 position the radical center in the C5 position is attacked from the same face as the large substituent at C2 points to. Since Paternò – Büchi reactions are known to occur via radical intermediates[1, 10] a selection at

[*] Prof. Dr. T. Bach, Dipl.-Chem. H. Brummerhop
Fachbereich Chemie der Philipps-Universität
Hans-Meerwein-Strasse, D-35032 Marburg (Germany)
Fax: (+49) 6421-288917
E-mail: bach@chemie.uni-marburg.de

[**] This project was supported by the Deutsche Forschungsgemeinschaft (Ba 1372-3/1 and -3/2) and by the Fonds der Chemischen Industrie. We thank Gregor Willanzheimer for skillful technical assistance. A gift of chemicals from Witco GmbH (Bergkamen) is gratefully acknowledged.

 © WILEY-VCH Verlag GmbH, D-69451 Weinheim, 1998 1433-7851/98/3724-3400 $ 17.50+.50/0

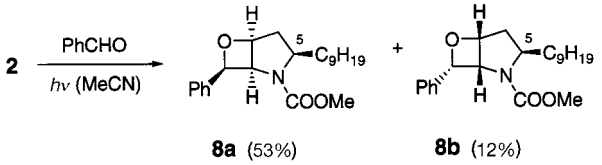
the triplet-1,4-biradical[11] stage was deemed to be likely and we turned to the synthesis of dihydropyrrole **2** (Scheme 2). The primary alcohol of (*S*)-pyroglutaminol[12] (**3**) was converted into the known tosylate **4**.[13] The nonyl side chain was then established by a nucleophilic substitution reaction with



Scheme 2. Synthesis of dihydropyrrole **2**. a) TsCl, pyridine, 25 °C, 5 h; b) $Li_2Cu(nC_8H_{17})_2CN$ in THF/hexane (2/1), −78 → 25 °C, 16 h; c) BuLi in THF/hexane (4/1), −78 °C, 1 h, then ClCOOMe, −78 → 0 °C, 3 h; d) $LiBEt_3H$ in THF, −78 → 0 °C, 3 h; e) $Me_2C(OMe)_2$, CSA in CH_2Cl_2, 0 °C, 0.5 h; f) TMSOTf, $EtNiPr_2$ in CH_2Cl_2, 0 °C, 0.5 h. CSA = camphorsulfonic acid, TMS = trimethylsilyl, Tf = trifluoromethanesulfonyl, Ts = toluene-4-sulfonyl.

a higher order dioctyl cuprate.[14] The endocyclic double bond was introduced in three steps after the pyrrolidinone **5** had been acylated with methyl chloroformiate. The pyrrolidinone **6** was reduced with $LiBEt_3H$ to the hemiaminal, which was transformed without isolation into the *N*,*O*-acetal **7** by treatment with dimethoxypropane. The subsequent elimination to the target compound **2** was conducted with $NiPr_2Et$/TMSOTf.[15]

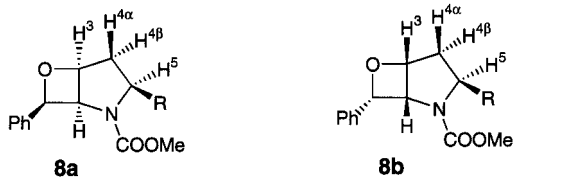
The Paternò–Büchi reaction of dihydropyrrole **2** with benzaldehyde proceeded smoothly and yielded three products (Scheme 3). One of the products was a 2-aminooxetane as determined by NMR spectroscopy, but because of its acid



Scheme 3. Paternò–Büchi Reaction of dihydropyrrole **2**.

lability it could not be isolated. The two other products were diastereoisomers of a 3-aminooxetane, and they were obtained in yields of 53 and 12%. NOESY NMR studies revealed that both products **8a** and **8b** exhibited an all-*cis* substitution pattern within the oxetane nucleus, which was to be expected from previous studies.[16] Consequently, the products differed from each other only in the relative configuration of the annelated four-membered ring and the nonyl substituent at the C5 position.

The structural proof of the products is based on the different ^1H NMR coupling patterns of the two diastereoisomers (Figure 1). The comparison with calculated coupling constants[17] facilitated an unambiguous correlation, which was confirmed by NOESY experiments. They clearly revealed that the attack of the photoexcited benzaldehyde on dihydropyrrole **2** had taken place on the face of the nonyl chain.

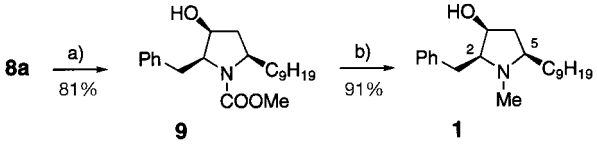


$J_{4\beta,5}$ = 9.1 (8.3), $J_{4\beta,3}$ = 5.2 (5.9) $J_{4\beta,5}$ = 6.2 (7.3), $J_{4\beta,3}$ = 2.2 (2.6)
$J_{4\alpha,5}$ = 1.9 (2.1), $J_{4\alpha,3}$ < 1 (1.7) $J_{4\alpha,5}$ = 7.2 (7.5), $J_{4\alpha,3}$ = 7.2 (6.8)

Figure 1. Measured (and calculated[17]) vicinal coupling constants [Hz] of the protons in the pyrrolidine ring of **8a** and **8b**.

The question why this is the case is currently being studied. On one hand, it is possible that a selection occurs in the intermediate 1,4-biradical as a consequence of the pyramidalization of the nitrogen atom.[18] On the other hand, hydrophobic interactions between the nonyl side chain and the phenyl nucleus may favor an approach from the *syn* face. Indeed force field calculations[17] revealed a clear preference for a conformation of the major diastereoisomer **8a** in which the alkyl chain and the phenyl group are oriented fully parallel to each other.

The synthesis of (+)-preussin was completed by hydrogenation of the major photocycloaddition product **8a** to the pyrrolidinol **9** (Scheme 4). The $LiAlH_4$ reduction of the methoxycarbonyl group to the methyl group was facile and we isolated (+)-preussin (**1**) as a yellowish oil. The optical rotation ($[\alpha]_D^{25} = +22.1$, $c = 1$ in $CHCl_3$) and the other analytical data are in accord with the literature data.[4]



Scheme 4. Completion of the synthesis of (+)-preussin (**1**). a) H_2, $Pd(OH)_2$/C in MeOH, 25 °C, 3.5 h; b) $LiAlH_4$ in THF, 66 °C, 2.5 h.

Overall the synthesis of **1** from (*S*)-pyroglutaminol (**3**) proceeded in a total yield of 10% over nine steps. In the chosen synthetic sequence the alkyl substituent in the C5 position can be varied at will by appropriate choice of the cuprate reagent. In previous studies[2, 19] it has already been shown that various aromatic aldehydes can be employed for the Paternò–Büchi reaction of heteroatom-substituted alkenes. Consequently, the arylmethyl substituent in the C2 positon can also be varied over a broad range.

Received: July 16, 1998 [Z12156IE]
German version: *Angew. Chem.* **1998**, *110*, 3577–3579

Keywords: asymmetric synthesis · cycloadditions · heterocycles · oxetanes · photochemistry

[1] For recent reviews on the Paternò–Büchi reaction, see a) J. Mattay, R. Conrads, R. Hoffmann, *Methoden Org. Chem. (Houben-Weyl) 4th ed.*, 1952–, Vol. E21c, **1995**, 3133–3178; b) J. A. Porco, S. L. Schreiber in *Comprehensive Organic Synthesis, Vol. 5* (Ed.: B. Trost), Pergamon, Oxford, **1991**, 151–192; c) T. Bach, *Synthesis* **1998**, 683–703.

[2] For a review, see T. Bach, *Liebigs Ann.* **1997**, 1627 – 1634.
[3] a) T. Bach, *Tetrahedron Lett.* **1994**, *35*, 1855 – 1858; b) T. Bach, *Liebigs Ann.* **1995**, 1045 – 1053; c) T. Bach, K. Jödicke, K. Kather, R. Fröhlich, *J. Am. Chem. Soc.* **1997**, *119*, 2437 – 2445.
[4] a) R. E. Schwartz, J. Liesch, O. Hensens, L. Zitano, S. Honeycutt, G. Garrity, R. A. Fromtling, J. Onishi, R. Monaghan, *J. Antibiot.* **1988**, *41*, 1774 – 1779; b) J. H. Johnson, D. W. Phillipson, A. D. Kahle, *J. Antibiot.* **1989**, *42*, 1184 – 1185.
[5] For previous syntheses of preussin, see A. Kanazawa, S. Gillet, P. Delair, A. E. Greene, *J. Org. Chem.* **1998**, *63*, 4660 – 4663, and references therein.
[6] For examples, see a) C. Rivas, R. A. Bolivar, *J. Heterocyclic Chem.* **1976**, *13*, 1037 – 1040; b) D. R. Morton, R. A. Morge, *J. Org. Chem.* **1978**, *43*, 2093 – 2101; c) S. R. Thopate, M. G. Kulkarni, V. G. Puranik, *Angew. Chem.* **1998**, *110*, 1144 – 1147; *Angew. Chem. Int. Ed.* **1998**, *37*, 1110 – 1112.
[7] For examples, see a) J. D. White, D. N. Gupta, *J. Am. Chem. Soc.* **1968**, *90*, 6171 – 6177; b) J. J. Partridge, N. K. Chadha, M. R. Uskokovic, *J. Am. Chem. Soc.* **1973**, *95*, 532 – 540; c) S. W. Baldwin, M. T. Crimmins, *J. Am. Chem. Soc.* **1980**, *102*, 1198 – 1201; d) T. Hansson, B. Wickberg, *J. Org. Chem.* **1992**, *57*, 5370 – 5376; e) A. B. Smith III, G. A. Sulikowski, M. M. Sulikowski, K. Fujimoto, *J. Am. Chem. Soc.* **1992**, *114*, 2567 – 2576.
[8] M. J. S. Carpes, P. C. M. L. Miranda, C. R. D. Correia, *Tetrahedron Lett.* **1997**, *38*, 1869 – 1872.
[9] A. L. J. Beckwith, C. L. L. Chai, *J. Chem.* Soc *Chem. Commun.* **1990**, 1087 – 1088.
[10] a) S. C. Freilich, K. S. Peters, *J. Am. Chem. Soc.* **1981**, *103*, 6255 – 6257; b) S. C. Freilich, K. S. Peters, *J. Am. Chem. Soc.* **1985**, *107*, 3819 – 3822.
[11] For a review, see H. Buschmann, H.-D. Scharf, N. Hoffmann, P. Esser, *Angew. Chem.* **1991**, *103*, 480 – 518; *Angew. Chem. Int. Ed. Engl.* **1991**, *30*, 477 – 515.
[12] S. Saijo, M. Wada, J. Himizu, A. Ishida, *Chem. Pharm. Bull.* **1980**, *28*, 1449 – 1458.
[13] E. Hardegger, H. Ott, *Helv. Chim. Acta* **1955**, *38*, 312 – 320.
[14] J. Ackermann, M. Matthes, C. Tamm, *Helv. Chim. Acta* **1990**, *73*, 122 – 132.
[15] P. G. Gassman, S. J. Burns, *J. Org. Chem.* **1988**, *53*, 5574 – 5578.
[16] T. Bach, *Angew. Chem.* **1996**, *108*, 976 – 977; *Angew. Chem. Int. Ed. Engl.* **1996**, *35*, 884 – 886.
[17] The force field calculations (MM3*) were conducted with Macromodel 4.5 (G. Chang, W. C. Guida, W. C. Still, *J. Am. Chem. Soc.* **1989**, *111*, 4379 – 4386). The coupling constants were calculated by an extended Karplus function. The ratio of the various conformers was deduced from a Boltzmann distribution at 373 K. As a simplification a butyl side chain at C5 was assumed instead of a nonyl group. We thank Dipl.-Chem. Thomas Trieselmann (research group of Prof. Hoffmann) and Dr. Ruth Gschwind cordially for their help in the course of the structure elucidation.
[18] D. P. Curran, N. A. Porter, B. Giese, *Stereochemistry of Radical Reactions*, VCH, Weinheim, **1995**, pp. 120 – 121.
[19] T. Bach, *Liebigs Ann.* **1995**, 855 – 866.

Ethenedithione (S=C=C=S): Does It Obey Hund's Rule?**

Ngai Ling Ma and Ming Wah Wong*

One of the fundamental rules governing the electronic structure of molecules is Hund's rule of maximum multiplicity. In order to minimize Coulombic repulsion, two electrons in a pair of degenerate orbitals prefer to be unpaired. Thus, for a molecule like O_2, the stability of the three lowest electronic states is in the order $^3\Sigma_g^- > {}^1\Delta_g > {}^1\Sigma_g^+$.

For the linear cumulated carbon oxides and carbon sulfides, XC_nX (X = O and S; n is even), such species have two electrons in the degenerate π HOMO, and hence are expected to have a triplet ground state. However, for the smallest member of the cumulated carbon sulfides, ethenedithione (S=C=C=S), the nature of its ground state remains controversial. C_2S_2 was first predicted by Schaefer et al. to be an experimentally accessible species in the gas phase that should have a triplet ground state.[1] The existence of this transient molecule has been demonstrated by mass spectrometry[2–4] and matrix isolation IR[3, 5] and UV[3, 5, 6] spectroscopy. Based on the unusual thermodynamic stability and extreme intermolecular activity, Wentrup et al. suggested that C_2S_2 is a triplet species.[3] On the other hand, Maier et al. observed a very weak signal in the ESR spectrum of C_2S_2, which indicated that it could possess a singlet ground state. In addition, they performed complete active space (CAS) SCF and CISD calculations and found that the ground state of C_2S_2 is $^1\Delta_g$, with a singlet – triplet (S – T) gap estimated to be 3 and 9 kJ mol^{-1}, respectively. Hence, C_2S_2 was suggested by Maier et al. to be one of the first examples for the "violation of Hund's rule in an equilibrium structure".[5]

Given that the reported S – T gap is rather small using moderate levels of theory, whether C_2S_2 is exists as a singlet or triplet remains uncertain. Herein we report ab initio calculations that are at a significantly higher level of theory than those reported previously in order to establish definitively the nature of the ground electronic state for ethenedithione.

First, we examined the energy difference of the three lowest states of C_2S_2, namely $^3\Sigma_g^-$, $^1\Delta_g$, and $^1\Sigma_g^+$, using various single-determinant methods (Table 1). The $^3\Sigma_g^-$ and $^1\Delta_g$ states were obtained by using an unrestricted Hartree – Fock (UHF) starting point. At the HF/6-31G* level, the $^1\Delta_g$ and $^1\Sigma_g^+$ states lie 31 and 98 kJ mol^{-1}, respectively, above the $^3\Sigma_g^-$ state. Inclusion of electron correlation at the MP2 level significantly lowers the energy gap by 15 and 61 kJ mol^{-1}, respectively. It is important to note that the $\langle S^2 \rangle$ values of the UHF wavefunctions of the $^3\Sigma_g^-$ (2.10) and $^1\Delta_g$ (1.07) states are significantly different from that of the corresponding pure spin states. In particular, the $^1\Delta_g$ state is severely spin contaminated

[*] Prof. Dr. M. W. Wong, Dr. N. L. Ma
Department of Chemistry,
National University of Singapore
Kent Ridge, Singapore 119260 (Singapore)
Fax: (+65) 7791691
E-mail: chmwmw@nus.edu.sg

[**] M.W.W. would like to thank the National University of Singapore for financial support (grant no. 970620).

 © WILEY-VCH Verlag GmbH, D-69451 Weinheim, 1998 1433-7851/98/3724-3402 $ 17.50+.50/0

Table 1. Calculated energies of the three lowest states of C_2S_2 by using various single-determinant methods.

Level[a,b]	E ($^3\Sigma_g^-$)[c]	ΔE($^1\Delta_g$)[d]	ΔE($^1\Sigma_g^+$)[d]
HF/6-31G*[e]	− 870.69070	31.1	98.4
B3-LYP/6-31G*[e]	− 872.52277	15.2	62.3
MP2/6-31G*[e]	− 871.16455	15.9	37.2
MP3/6-31G*	− 871.18191	16.8	40.0
MP4/6-31G*	− 871.21973	10.9	27.9
MP5/6-31G*	− 871.21033	14.0	37.3
PMP4/6-31G*	− 871.22323	20.0	37.1
RCISD/6-31G*[e, f]	− 871.11441	38.4	87.5
CISD/6-31G*[e]	− 871.11956	21.7	60.5
CCSD/6-31G*[e]	− 871.18955	16.3	39.8
QCISD/6-31G*	− 871.19249	16.2	40.1
QCISD(T)/6-31G*	− 871.21790	12.7	33.9
QCISD(TQ)/6-31G*	− 871.21670	12.7	34.3
QCISD(T)/6-311G*	− 871.30014	13.2	35.0
QCISD(T)/6-311 + G(2d)	− 871.35673	13.5	35.8
QCISD(T)/6-311 + G(2df)	− 871.44071	13.1	35.3

[a] Based on QCISD/6-31G*-optimized geometries (r(C=C) = 1.281, 1.283, and 1.287 Å, respectively, for $^3\Sigma_g^-$, $^1\Delta_g$, and $^1\Sigma_g^+$; r(C=S) = 1.580, 1.581, and 1.585 Å, respectively, for $^3\Sigma_g^-$, $^1\Delta_g$, and $^1\Sigma_g^+$), unless otherwise noted. [b] Frozen-core approximation for all correlated calculations. [c] Total energy [Hartree]. [d] Energy [kJ mol^{-1}] relative to the $^3\Sigma_g^-$ state. [e] Fully optimized at the level specified. [f] Based on a restricted Hartree–Fock (RHF) starting point.

by the triplet state. Thus, we would expect the stability of the $^1\Delta_g$ state to be overestimated by the UMP methods. This is readily indicated by the fact that the projected MP4 (PMP4)[7] relative energy is 9 kJ mol^{-1} higher than the UMP4 values (Table 1).

Maier et al. reported RCISD/6-31G* calculations with an active space of 9 occupied and 21 virtual orbitals, and they found that the $^1\Delta_g$ state is 9 kJ mol^{-1} more stable than the $^3\Sigma_g^-$ state. However, since the detail of the calculations was not reported, we have not been able to repeat their calculations. Instead, we have carried out full-valence RCISD calculations but the result is in distinct contrast to that reported previously.[5] The calculated relative stabilities of the $^3\Sigma_g^-$, $^1\Delta_g$, and $^1\Sigma_g^+$ states are 0, 38, and 88 kJ mol^{-1}, respectively. Both QCISD[8] and CCSD[9] methods predict similar relative energies for the $^1\Delta_g$ (16 kJ mol^{-1}) and $^1\Sigma_g^+$ (40 kJ mol^{-1}) states. Inclusion of triple excitations (QCISD(T)) reduces the relative energies by 4–6 kJ mol^{-1}, while further inclusion of quadruple excitations (QCISD(TQ)) has virtually no effect on the relative energies. Table 1 shows that the effect of basis set on the calculated relative energies is rather small. The relative energies computed with the 6-31G* basis set lie within 1 kJ mol^{-1} of the 6-311 + G(2df) values. Thus, based on single-determinant methods, our best estimate of the energy difference between the $^1\Delta_g$ and $^3\Sigma_g^-$ states is 13 kJ mol^{-1}, in favor of the triplet state. In summary, all the single-determinant methods predict the stability of the three lowest states of C_2S_2 is in the order of $^3\Sigma_g^- > {}^1\Delta_g > {}^1\Sigma_g^+$, and there is no evidence for the Hund's rule being violated.

Next, we examined the relative stability of the three states of C_2S_2 using the multiconfiguration (MC) SCF approach, which was expected to provide a proper description of the degeneracy problem involved. We have carried out a series of CASSCF[10] calculations with active space systematically expanded from the two-electron, two-orbital CAS (CASSCF(2,2)) to the twelve-electron, ten-orbital CAS (CASSCF(12,10)). The active orbitals involved are given in Table 2. For all the CASSCF calculations, we found that molecular orbitals lower than and including $7\sigma_g$ are always doubly occupied. The dominant configuration of the three states is identical to that of the HF reference state with coefficient > 0.7. Other dominant configurations with coefficients > 0.1 arise only from the excitation of the π electrons, $2\pi_u$, $2\pi_g$, and $3\pi_u$. Hence, we would expect an active space including all π orbitals, for example CASSCF(10, 8), to yield a reliable result. In fact, further expansion of the active space beyond CASSCF(10, 8) leads to small changes in the relative energies (Table 2). For our largest CASSCF calculation, CASSCF(12,10), the $^1\Delta_g$ and $^1\Sigma_g^+$ states lie 17 and 31 kJ mol^{-1}, respectively, above the $^3\Sigma_g^-$ ground state. As for the CISD calculation, we have not been able to reproduce the CASSCF(6,6) result of Maier et al.,[5] which suggests that the $^1\Delta_g$ state is more stable than the $^3\Sigma_g^-$ state.

Dynamic electron correlation effects were included by carrying out third-order multireference perturbation (CASPT3)[11] or multiconfiguration reference configuration interaction (MRCI)[12] single-point energy calculations at the CASSCF-optimized geometries. As with the single-determinant methods, inclusion of dynamic electron correlation stabilizes the singlet states. However, the $^3\Sigma_g^-$ state is still significantly more stable than the $^1\Delta_g$ state. Our best estimate of the relative energies of the $^1\Delta_g$ and $^1\Sigma_g^+$ states, based on MRCI-CASSCF(10,8) calculations with a significantly larger cc-pVQZ basis set, are 24 and 45 kJ mol^{-1}, respectively.

In conclusion, based on the various sophisticated single-determinant and multiconfiguration methods, we found no evidence that C_2S_2 violates Hund's rule. We hope that our theoretical prediction will stimulate further experimental

Table 2. Calculated energies[a] of the three lowest states of C_2S_2 by using various multiconfiguration methods, with the 6-31G* basis set.

CAS[b]	Active orbital	$^3\Sigma_g^-$[c]			$^1\Delta_g$[d]			$^1\Sigma_g^+$[d]		
		CASSCF	CASPT3	MRCI	CASSCF	CASPT3	MRCI	CASSCF	CASPT3	MRCI
(2,2)	$3\pi_u^2$	− 870.67221	− 871.16825	− 871.10762	49.9	30.7	37.9	99.5	50.4	69.5
(2,4)	$3\pi_u^2\ 3\pi_g^0$	− 870.67990	− 871.17004	− 871.11128	40.9	28.1	34.9	79.9	47.7	64.2
(6,4)	$2\pi_g^4\ 3\pi_u^2$	− 870.68239	− 871.17430	− 871.11295	32.5	28.6	30.1	59.4	53.6	56.4
(10,6)	$2\pi_u^4\ 2\pi_g^4\ 3\pi_u^2$	− 870.68574	− 871.17578	− 871.11421	30.8	25.8	27.5	57.5	45.8	50.6
(6,6)	$2\pi_g^4\ 3\pi_u^2\ 3\pi_g^0$	− 870.71394	− 871.18116	− 871.12876	44.9	30.9	33.3	83.0	52.7	57.8
(10,8)	$2\pi_u^4\ 2\pi_g^4\ 3\pi_u^2\ 3\pi_g^0$	− 870.75973	− 871.19034	− 871.14457	19.3	24.7	23.7	36.1	43.3	41.8
(12,10)	$7\sigma_g^2\ 2\pi_u^4\ 2\pi_g^4\ 3\pi_u^2\ 3\pi_g^0\ 7\sigma_u^0$	− 870.78861	− 871.18989	− 871.15226	16.6	24.9	23.0	31.2	43.0	40.3

[a] Based on the CASSCF optimized geometry. [b] Number electrons and number of orbitals in the active space. Note that full-valence CAS corresponds to CAS(20,16). [c] Total energy [Hartree]. [d] Energy [kJ mol^{-1}] relative to the $^3\Sigma_g^-$ state.

 © WILEY-VCH Verlag GmbH, D-69451 Weinheim, 1998 1433-7851/98/3724-3403 $ 17.50+.50/0

studies on this elusive molecule. To assist future characterization of the ground-state of C_2S_2, the predicted geometry, vibrational spectrum, rotational constants, heat of formation, ionization energy, and proton affinity are summarized in Table 3.

Table 3. Calculated properties for the C_2S_2 ground state ($^3\Sigma_g^-$).

Property	Value
geometry[a]	r(C=C) = 1.277 Å, r(C=S) = 1.579 Å
rotational constant[a]	$B_e = 1.5587$
IR spectrum[b]	2036 (0), 1198 (244), 561 (0), 364 (0), 175 cm^{-1} (0 $km\,mol^{-1}$)
heat of formation	380.1 (ΔH°_{f0}), 383.1 $kJ\,mol^{-1}$ (ΔH°_{f298})
ionization energy[c]	8.3 (adiabatic), 8.4 eV (vertical)
proton affinity[c, d]	731.8 $kJ\,mol^{-1}$
dissociation energy[c]	$C_2S_2 \rightarrow CS(^1\Sigma_g^+) + CS(^1\Sigma_g^+)$: $\Delta E = 138.6$ $kJ\,mol^{-1}$
	$C_2S_2 \rightarrow CS(^1\Sigma_g^+) + CS(^3\Pi)$: $\Delta E = 589.8$ $kJ\,mol^{-1}$

[a] QCISD/6-311 + G(2d)-optimized geometry. [b] QCISD/6-31G* values. Intensity values are given in parentheses. [c] G2//QCI[13] value. [d] The protonated C_2S_2 ion (SCC(H)S^+) has a singlet ground state. Proton affinity of SCCS ($^3\Sigma_g^-$) + $H^+ \rightarrow$ SCC(H)S^+ ($^1A'$) = 812.1 $kJ\,mol^{-1}$.

Received: June 30, 1998 [Z 12074 IE]
German version: *Angew. Chem.* **1998**, *110*, 3587 – 3589

Keywords: ab initio calculations · cumulenes · electronic structure · ethenedithione

[1] G. P. Raine, H. F. Schaefer, R. C. Haddon, *J. Am. Chem. Soc.* **1983**, *105*, 194 – 198.
[2] D. Sülzle, H. Schwarz, *Angew. Chem.* **1988**, *100*, 1384 – 1386; *Angew. Chem. Int. Ed. Engl.* **1988**, *27*, 1337 – 1339.
[3] C. Wentrup, P. Kambouris, R. A. Evans, D. Owen, G. Macfarlane, J. Chuche. J. C. Pommelet, A. Ben Cheikh, M. Plisnier, R. Flammang, *J. Am. Chem. Soc.* **1991**, *113*, 3130 – 3135.
[4] M. W. Wong, C. Wentrup, R. Flammang, *J. Phys. Chem.* **1995**, *99*, 16849 – 16856.
[5] G. Maier, H. P. Reisenauer, J. Schrot, R. Janoschek, *Angew. Chem.* **1990**, *102*, 1475 – 1477; *Angew. Chem. Int. Ed. Engl.* **1990**, *29*, 1464 – 1466.
[6] R. B. Bohn, Y. Hannachi, L. Andrews, *J. Am. Chem. Soc.* **1992**, *114*, 6452 – 6459.
[7] H. B. Schlegel, *J. Chem. Phys.* **1986**, *84*, 4530 – 4534.
[8] J. A. Pople, M. Head-Gordon, K. Raghavachari, *J. Chem. Phys.* **1987**, *87*, 5968 – 5975.
[9] A. C. Scheiner, G. E. Scuseria, J. E. Rice, T. J. Lee, H. F. Schaefer, *J. Chem. Phys.* **1987**, *87*, 5361 – 5373.
[10] B. O. Roos, *Adv. Chem. Phys.* **1987**, *69*, 399 – 446.
[11] H.-J. Werner, *Mol. Phys.* **1996**, *89*, 645 – 661.
[12] H.-J. Werner, P. J. Knowles, *J. Chem. Phys.* **1988**, *89*, 5803 – 5817.
[13] L. A. Curtiss, K. Raghavachari, J. A. Pople, *J. Chem. Phys.* **1995**, *103*, 4192 – 4200.

Closure of the Cavity in Permethylated Cyclodextrins through Glucose Inversion, Flipping, and Kinking**

Thomas Steiner* and Wolfram Saenger*

Dedicated to Professor Bernt Krebs on the occasion of his 60th birthday

Cyclodextrins (CDs) or cycloamyloses (CA) are macrocyclic oligosaccharides produced by enzymatic degradation of amylose; they can contain up to 100 or more $\alpha(1-4)$-linked glucose units.[1, 2] The well known smallest members with six to eight glucose residues called α-, β-, and γ-cyclodextrin are annular in shape (doughnut-form) reminiscent of a hollow, truncated cone. Their narrower side are formed by primary O6 hydroxyl groups and the wider side by secondary O2 and O3 hydroxyl groups. All the glucose residues are found exclusively in the $^4C_1$ chair form and are oriented *syn* about the glycosidic link so that all O2 and O3 hydroxyl groups are on the same side and connected by intramolecular $O2(n)\cdots O3(n-1)$ hydrogen bonds that stabilize the macrocyclic structures. The *anti* form with the O2 and O3 hydroxyl groups of adjacent glucose units on opposite sides has not yet been observed in any of the crystal structures of the common CDs.

Surprisingly, the solubility of the cyclodextrins in water increases manyfold if only O2 and O6 or all three of the hydroxyl groups of the glucose residues are methylated. Furthermore, the temperature coefficient of the solubility becomes negative, that is their solubility in water is lower at elevated temperatures and crystals can be grown by heating the solutions.[3] To shed light on these peculiar properties several partially and fully methylated CDs (that have practical importance as bioorganic host molecules) were crystallized from hot and cold water and analyzed by X-ray crystallography.[4–8]

Of particular structural interest are the fully methylated α-, β-, and γ-cyclodextrins hexakis-(2,3,6-tri-*O*-methyl)-α-, β-, and γ-CD (TRIMEA, TRIMEB, and TRIMEG, respectively) because intramolecular $O2(n)\cdots O3(n-1)$ hydrogen bonds cannot form. Crystals that have been grown from hot water include anhydrous TRIMEA,[6] TRIMEB monohydrate,[4] and TRIMEG dihydrate.[9] In all three cases the CD molecules adopt conformations characterized by greatly reduced cavity volumes. The remaining shallow cavities are only filled by O6 methyl groups of adjacent molecules and not by water, which occupies interstices in the crystal lattices of the hydrate forms. It is remarkable that the cavities are closed by three completely different structural mechanisms, which are discussed below. Because the molecular structure of

[*] Prof. Dr. W. Saenger, Dr. T. Steiner
Institut für Kristallographie der Freien Universität
Takustrasse 6, D-14195 Berlin (Germany)
Fax: (+49) 30-838-6702
E-mail: saenger@chemie.fu-berlin.de

[**] Topography of Cyclodextrin Inclusion Complexes, Part 43. This work was supported by the Deutsche Forschungsgemeinschaft (Sa 196/25-1) and Fonds der Chemischen Industrie. For Part 42, see T. Aree, J. Jacob, W. Saenger, H. Hoier, *Carbohyd. Res.* **1998**, *307*, 191 – 197.

 © WILEY-VCH Verlag GmbH, D-69451 Weinheim, 1998 1433-7851/98/3724-3404 $ 17.50+.50/0

TRIMEB monohydrate as reported by Caira et al.[4] is singular in the structural chemistry of CDs, we have repeated the study and fully verified the published results;[10, 11] this structure is discussed below only in points going beyond the original paper.

The molecular structures of anhydrous TRIMEA,[6] TRIMEB · H_2O,[10] and TRIMEG · 2 H_2O[9] are shown in Figure 1 (since the water molecules do not occupy the CD cavities they are not shown), and selected geometric parameters that define the molecular conformations are listed in Table 1. In anhydrous TRIMEA (Figure 1a) the molecule is in a distorted "round" conformation and all the glucoses residues are *syn* oriented. The C6 sides of two diametrically opposed glucose residues are tilted inward so that the primary methoxy groups can form contacts across the cavity opening and hence close it.[6] The molecule is, therefore, not doughnut but bowl shaped.

Because of the larger ring size a more dramatic structural change is required to close the molecular cavity in TRIMEB monohydrate, (Figure 1b). The glucose residues are still *syn* oriented relative to each other. One of them is inverted from the normal $^4C_1$ to the $^1C_4$ chair conformation,[4] which as yet has not been observed in any other cyclodextrin crystal structure. The consequences of this chair inversion are illustrated in Figure 2. The left half shows glucose units in the $^4C_1$ conformation: four of the five pyranose ring substituents are equatorial and one is in an axial orientation so that steric conflicts are minimized. Of the glycosidic oxygen

Table 1. Selection of geometric parameters for anhydrous TRIMEA,[6] TRIMEB monohydrate, and TRIMEG dihydrate (standard deviations are $< 0.5^\circ$. Flip sites are characterized by ψ angles of approximately -60°).

	Glucose residue							
	1	2	3	4	5	6	7	8
φ = C4(n)-O4(n)-C1($n-1$)-O5($n-1$)								
TRIMEA	91.6	115.7	97.7	94.8	110.9	97.7		
TRIMEB · H_2O	100.0	94.5	80.6	100.2	103.2	102.2	68.9	
TRIMEG · 2 H_2O	82.2	87.4	90.6	55.7	94.9	94.4	93.1	57.0
ψ = C3(n)-C4(n)-O4(n)-C1($n-1$)								
TRIMEA	109.7	151.2	137.1	117.2	140.8	145.0		
TRIMEB · H_2O	151.5	175.5	109.9	125.6	141.5	144.8	85.5	
TRIMEG · 2 H_2O	−63.0	91.7	134.5	77.0	−56.5	89.4	112.3	80.2
O4($n+1$) ··· O4(n) ··· O4($n-1$)								
TRIMEA	117.6	122.8	117.4	116.1	122.0	116.1		
TRIMEB · H_2O	119.0	92.0	161.5	118.3	116.1	120.1	144.6	
TRIMEG · 2 H_2O	129.7	141.8	111.4	134.3	146.0	131.9	118.9	135.9

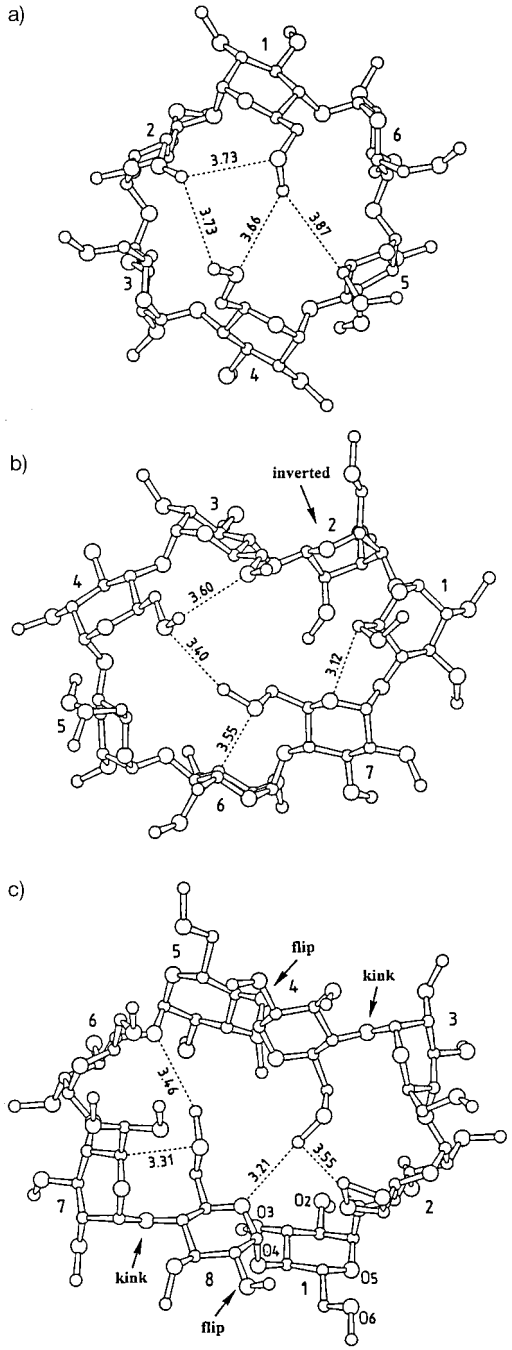


Figure 1. Molecular structures of permethylated cyclodextrins TRIMEA (a),[6] TRIMEB (b), and TRIMEG (c). Projection is on the least-squares plane through the O4 atoms. The short C ··· O contacts [Å] are indicative of C–H ··· O hydrogen bonding.

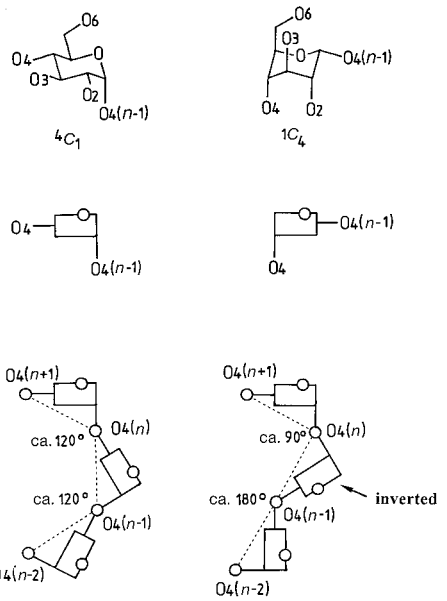


Figure 2. The consequence of the $^4C_1 - {}^1C_4$ chair inversion in a chain of α(1-4)-linked glucose residues.

 © WILEY-VCH Verlag GmbH, D-69451 Weinheim, 1998 1433-7851/98/3724-3405 $ 17.50+.50/0

atoms that link the residues O4(n) is equatorial while O4($n-1$), which belongs to the previous residue in the macrocycle, is axial. If glucose residues of this kind form a chain with the primary and secondary hydroxyl groups of neighboring residues in a *syn* arrangement a curved arrangement results with O4($n+1$)-O4(n)-O4($n-1$) angles of approximately 120°,[12] which can close to a cycle (as in the CDs) or form a helix (as in amylose). The right half of Figure 2 shows the effects of chair inversion to the $^1C_4$ conformation: four of the ring substituents are axial, which leads to severe steric conflits: in residue 2 of TRIMEB · H_2O, atoms O2 and O4 are 2.948(7) Å, apart and O3 and C6 3.27(1) Å. The glycosidic oxygen atom O4(n) is now axial, whereas O4($n-1$) is equatorial, that is, in a reversed situation as for "normal" $^4C_1$ glucose residues. If an inverted glucose unit is flanked by "normal" glucose molecules this leads to deviations from the regular curvature of the chain: O4(n) is now axial at both glucose residues to which it is bonded, which leads to a reduction of the O4($n+1$)-O4(n)-O4($n-1$) angle to about 90° (92.0(1)° in TRIMEB · H_2O). On the other hand, O4($n-1$) is now equatorial at both glucose residues to which it is bonded so that the O4(n)-O4($n-1$)-O4($n-2$) angle is opened to nearly 180° (161.5(1)° in TRIMEB · H_2O). Chair inversion of a single glucose residue in a cyclodextrin therefore leads to disruption of the "round" annular structure, and an "irregular" roughly elliptical shape is formed with partial closure of the molecular cavity. In addition, the axial O2 substituent of the inverted glucose residue is directed into the cavity and further reduces its volume (Figure 1b).

In the crystal structure of TRIMEG · $2H_2O$ the molecular cavity is also closed as shown in Figure 3, but the associated structural changes are different compared to TRIMEA and

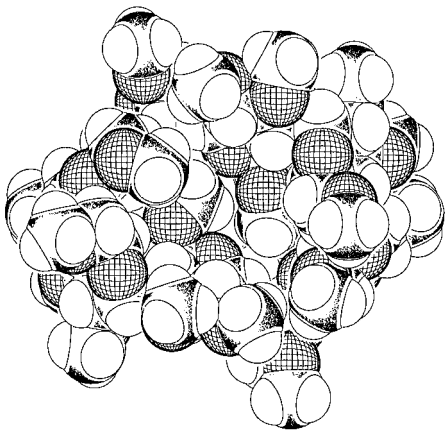


Figure 3. Space filling model of the TRIMEG molecule, drawn with the program PLUTON (A. L. Spek, *Acta Crystallogr. Sect. A* **1990**, *46*, C34).

TRIMEB. At two positions, diametrically opposed in the macrocycle adjacent glucose units are rotated by about 180° ("flip") and adopt *anti* orientations. Adjacent glucose residues are rotated by about 90° with respect to each other at the position preceding the flip site to form a "kink". The remaining glucose residues are in a *syn* arrangement (Figure 4) where the mutual orientation is drawn for all pairs of adjacent

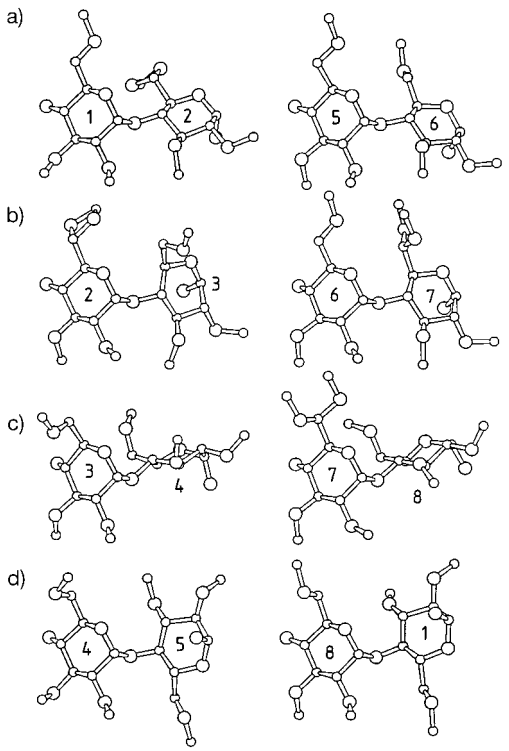


Figure 4. All pairs of adjacent glucoses in TRIMEG dihydrate, drawn in a common projection with respect to the left residue. a), b) regular orientation, c) kinks, d) flips. The primary methoxy groups of glucose units 2 and 7 are twofold disordered. The "regular" orientations are similar to those in anhydrous TRIMEA, or in crystalline complexes of TRIMEA and TRIMEB.

glucose residues. It should be noted that the flip is not local and does not involve one single glucose only; the amylose chain linked to it is also rotated, and hence the designation "chain-flip".[13] These structural features are reminiscent of the large crystalline cycloamyloses with 10 and 14 residues (CA10, CA14) where chain-flips and kinks also occur to relieve steric strain,[13] but they have never been observed before for a "normal" cyclodextrin with less than ten residues. As a consequence of such kink-flip sequences the "round" shape of a cyclodextrin becomes elliptical and the molecular cavity is narrowed. The glucose units of TRIMEG that are involved in the kink-flip sequence are strongly tilted, and their primary O6 methyl groups form van der Waals contacts across the molecular cavity, and thereby close it. These contacts are possibly associated with weak C–H···O hydrogen bonds that are formed by the terminal methyl groups, as is indicated by short C···O separations (Figure 1c).[14]

In the unmodified cyclodextrins O2(n)···O3($n-1$) hydrogen bonding between glucose units stabilizes the macrocyclic conformation. They adopt the "round" structure for α-, β-, and γ-CD; the next larger δ-CD is significantly distorted and from ε-CD (CA10) on, chain-flips and kinks are introduced and the macrocycles become elliptical.[13] In the permethylated series the chain-flips and kinks are already found for TRIMEG, probably because there is no hydrogen bonding to stabilize the relative orientations of adjacent glucose residues. We assume that the mechanism of chain-flipping is associated with glucose units in the $^1C_4$ conformation similar to that

 © WILEY-VCH Verlag GmbH, D-69451 Weinheim, 1998 1433-7851/98/3724-3406 $ 17.50+.50/0

found in TRIMEB. The $^1C_4$ form may be considered as a reaction intermediate because the O4(2)-O4(3)-O4(4) angle is 161.5° (Table 1)—instead of the average 128° in β-CD—and leads to an elliptical distortion of the macrocycle. Only a further slight rotation of the $^1C_4$ inverted glucose unit and revertion to the "normal" $^4C_1$ form would be required to complete the flip.

Thus far, the common property of all partially and fully methylated CDs crystallized from hot water is that water is not located in their molecular cavities. It seems that the expulsion of water molecules from the cavity is a major driving force for crystallization of these substances. "Empty" cavities can only be obtained if the cavity volumes are either greatly reduced or if the cavities are totally blocked. This principle requires different structural changes for CDs of different sizes, and is always associated with the inward rotation of two or three O6-methyl groups to close the cavities. Since the three permethylated CDs are of different size this closure requires different structural changes, and ranges from a simple tilting of glucose units to inversion of the chair form, and flipping by about 180°. As shown by a number of X-ray structure analyses this does not occur if a guest molecule is added that can fill the cavity.[15]

Received: March 2, 1998 [Z11536IE]
German version: *Angew. Chem.* **1998**, *110*, 3628 – 3632

Keywords: conformation analysis · cyclodextrins · structure elucidation

[1] W. Saenger, *Angew. Chem.* **1980**, *92*, 343 – 361; *Angew. Chem. Int. Ed. Engl.*, **1980**, *19*, 344 – 362.
[2] T. Takaha, M. Yanase, S. Takata, S. Okada, S. M. Smith, *J. Biol. Chem.* **1996**, *271*, 2902.
[3] J. Szejtli, *Cyclodextrin Technology*, Kluwer, Dordrecht, **1988**.
[4] M. R. Caira, V. J. Griffith, L. R. Nassimbeni, B. van Oudtshoorn, *J. Chem. Soc. Perkin Trans. 2*, **1994**, 2071 – 2072.
[5] T. Steiner, W. Saenger, *Carbohydr. Res.* **1995**, *275*, 73 – 82.
[6] T. Steiner, W. Saenger, *Carbohydr. Res.* **1996**, *282*, 53 – 63.
[7] T. Steiner, F. Hirayama, W. Saenger, *Carbohydr. Res.* **1996**, *296*, 69 – 82.
[8] K. Harata, *Supramolec. Chem.* **1995**, *5*, 231 – 236.
[9] Crystal structure of TRIMEG (Cyclolab, Budapest; crystallized as the dihydrate from water at approximately 80 °C, stable at ambient conditions). X-ray data were measured at room temperature on a Turbo-CAD4 diffractometer (Enraf – Nonius) with a FR571 rotating anode X-ray generator ($Cu_{K\alpha}$ radiation, $\lambda = 1.54176$ Å); $C_{72}H_{128}O_{40} \cdot 2H_2O$, $M_r = 1678.8$, crystal dimensions $0.75 \times 0.55 \times 0.20$ mm^3, orthorhombic, pace group $P2_12_12_1$ with $a = 16.730(13)$, $b = 16.875(8)$, $c = 32.172(14)$ Å, $V = 9083(9)$ Å^3, $Z = 4$, $\rho_{calcd} = 1.228$ g cm^{-1}, 7404 reflections measured, of which 7368 unique, 4494 observed with $I > 2\sigma(I)$. The structure was solved with SIR 92 (A. Altomare, G. Cascarano, G. Giacovazzo, A. Guagliardi, *J. Appl. Crystallogr.* **1994**, *27*, 435) and refined with SHELXL 93 (G. M. Sheldrick, *Program for crystal structure refinement*. University of Göttingen, Germany, **1993**). Hydrogen atoms were treated in the standard riding model with the methyl groups allowed to rotate. Two primary methoxy groups (at glucose residues 2 and 7) are twofold disordered. Four partially occupied water sites were located with a sum of occupancies of 2.01, water hydrogen atoms could not be located. $R = 0.081$, $R_w = 0.215$.[11]
[10] Crystal structure of TRIMEB (Cyclolab, Budapest; crystallized as the monohydrate at approximately 40 °C): Data collection and structure analysis were as for TRIMEG dihydrate. $C_{63}H_{112}O_{35} \cdot H_2O$, $M_r = 1445.5$, crystal dimensions $0.50 \times 0.25 \times 0.25$ mm^3, orthorhombic, space group $P2_12_12_1$ with $a = 14.823(5)$, $b = 19.382(3)$, $c = 26.534(5)$ Å, $V = 7623(3)$ Å^3, $Z = 4$, $\rho_{calcd} = 1.259$ g cm^{-3}, 6225 unique reflections measured, 6214 observed with $I > 2\sigma(I)$. Methoxy groups are ordered. Water hydrogen atoms could not be located. $R = 0.053$, $R_w = 0.126$.[11]
[11] Crystallographic data (excluding structure factors) for the structures reported in this paper have been deposited with the Cambridge Crystallographic Data Centre as supplementary publication no. CCDC-101208. Copies of the data can be obtained free of charge on application to CCDC, 12 Union Road, Cambridge CB2 1EZ, UK (fax: (+44) 1223-336-033; e-mail: deposit@ccdc.cam.ac.uk).
[12] The angle O4($n+1$)-O4(n)-O4($n-1$) between the O4 atoms of consecutive glucose units is flexible, and allows some opening and closing. In α-CD the average angle is 120°, in β-CD it is 128°, and in γ-CD it is 135°.
[13] J. Jacob, K. Gessler, D. Hoffmann, H. Sanbe, K. Koizumi, S. M. Smith, T. Takaha, W. Saenger, *Angew. Chem.* **1998**, *110*, 626 – 629; *Angew. Chem. Int. Ed* **1998**, *37*, 606 – 609.
[14] T. Steiner, *Chem. Commun.* **1997**, 727 – 734.
[15] K. Harata in *Comprehensive Supramolecular Chemistry*, *Vol. 3* (Eds. J. L. Atwood, J. E. D. Davies, D. D. MacNicol, F. Vögtle), Pergamon; Oxford, **1996**, Chapter 9.

$Ca_5Cl_3(C_2)(CBC)$: A Compound with a Layer Structure and an Unusual Anion Combination**

Olaf Reckeweg and Hans-Jürgen Meyer*

Reports concerning "calcium monochloride"[1] inspired us some years ago to investigate reactions in and with melts of calcium chloride. The colorless "calcium monochloride" was found to be CaHCl,[2] the red one turned out to be $Ca_3Cl_2C_3$.[3] The synthetic potential of calcium chloride melts as a solvent for graphite or calcium metal is well known. When CaC_2 is dissolved in a melt of $CaCl_2$ the compound $Ca_3Cl_2C_3$ with the C_3^{4-} ion is formed. Reactions of calcium with certain combinations of the elements B, C, and N in calcium chloride melts yield compounds such as Ca_3Cl_2CBN with CBN^{4-} ions,[4] Ca_2ClBN_2,[5] and $Sr_3(BN_2)_2$[6] with BN_2^{3-} ions or the title compound $Ca_5Cl_3(C_2)(CBC)$.[7]

In attempts to synthesize "$Ca_4Cl_3BC_2$" with the help of a melt of calcium chloride, the new compound $Ca_5Cl_3(C_2)$-(CBC) has been obtained which contains acetylide and dicarbidoborate ions. A characteristic feature of the structure of $Ca_5Cl_3(C_2)(CBC)$ is the puckered layers with the sequence Cl-Ca-Ca. The layered structure is reflected in the habitus of the crystals which occur as thin aggregates that are very often grown together. The C_2^{2-} and CBC^{5-} ions are sandwiched between double layers of calcium ions (Figure 1). The C_2^{2-} ions are coordinated by a distorted octahedron of Ca^{2+} ions.

[*] Prof. Dr. H.-J. Meyer, Dr. O. Reckeweg
Institut für Anorganische Chemie der Universität
Auf der Morgenstelle 18, D-72076 Tübingen (Germany)
Fax: (+49) 7071-295702
E-mail: juergen.meyer@uni-tuebingen.de

[**] This work was supported by the DFG. We are indebted to Dipl.-Chem. A. Baumann and Priv.-Doz. Dr. H. Mayer (University of Tübingen) for the ^{13}C MAS NMR spectra and Dr. F. Meyer and Prof. Dr. G. Thiele (University of Freiburg) for the Raman measurements.

 © WILEY-VCH Verlag GmbH, D-69451 Weinheim, 1998 1433-7851/98/3724-3407 $ 17.50+.50/0

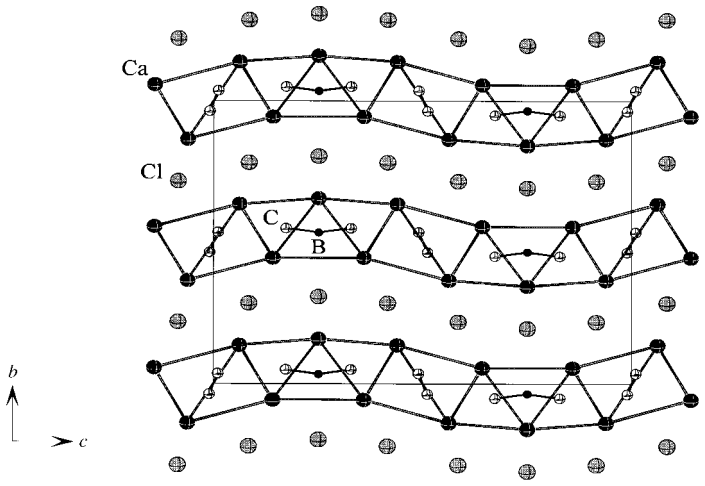


Figure 1. Projection of the structure of $Ca_5Cl_3(C_2)(CBC)$. The calcium ions are connected with lines to emphasize the double layers.

The initial results from the X-ray structure analysis reveal that the C_2^{2-} ion resides at the special position $8f$ (sited in the mirror plane at $x = 0$) and has an extremely short C–C bond length of 108 pm. A similar short C–C bond length of 109.5 pm has been reported for $Ca_{15}(CBN)_6(C_2)_2O$.[8] In this case the short C–C bond length is explained by virtual shortening due to thermal motion or statistical displacement. One could think that for the observed shortening of the acetylide in $Ca_5Cl_3(C_2)(CBC)$ the same was true. The refinement of a split position (50% occupation of the general position $16h$) results in a C–C bond length of 119(2) pm. This distance is in the range of the expected value for a C≡C triple bond (C–C bond length in CaC_2: 119(1) pm[9]). Therefore the virtual position of the C_{2-}^{2} ion in the mirror plane (1) is a superposition of the split position (2) (Figure 2).

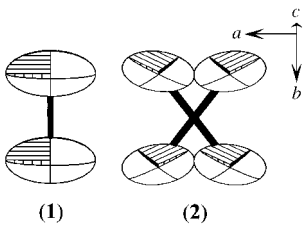


Figure 2. Virtual (1) and real position (2, split position) of the C_2^{2-} ion in $Ca_5Cl_3(C_2)(CBC)$.

Each BC_2^{5-} ion is surrounded by a bicapped trigonal prism of calcium ions. The boron atom is sited nearly in the middle of the prism. Each of the two carbon atoms of the BC_2 unit lie above a rectangular prismatic face that is capped by another calcium ion. Thus, the carbon atoms are coordinated by a nearly square pyramid of calcium ions. The double layers built up by calcium ions are interconnected by two crystallographically independent chloride ions. The Cl(1) ion is surrounded by a distorted tetrahedron of calcium ions ($\bar{d} = 281.4$ pm) and the Cl(2) ion is coordinated by a strongly distorted octahedron of calcium ions ($\bar{d} = 308.4$ pm).

A saltlike charge assignment leads to $(Ca^{2+})_5(Cl^-)_3(C_2^{2-})(BC_2^{5-})$. An indication for the saltlike character of this compound is the transparency of the orange-brown crystals, which are very sensitive to hydrolysis. The deviation of the C-B-C angle of the BC_2^{5-} unit (164.0(7)°) from linearity is very unusual. A linear arrangement would generally be expected for CO_2-like (isoelectronic) ions with 16 electrons, such as C_3^{4-}, CBN^{4-}, BN_2^{3-}, and BC_2^{5-}. The observed bent arrangement of such ions could be caused either by packing effects or by electronic effects.[10] The change of the energy levels and of the molecular orbitals of an isolated CBC fragment have been investigated as a function of the C-B-C angle.[11] The two extreme cases correspond formally to the linear arrangement of the atoms of a CO_2 molecule with 16 and of a bent SO_2 molecule (119°) with 18 valence electrons.

In compounds that contain triatomic anions the bond angle correlates with their charge. The change of the energy levels of an isolated (CBC) ion is shown as a function of its angle in the Walsh diagram in Figure 3. The degeneracy of the π levels

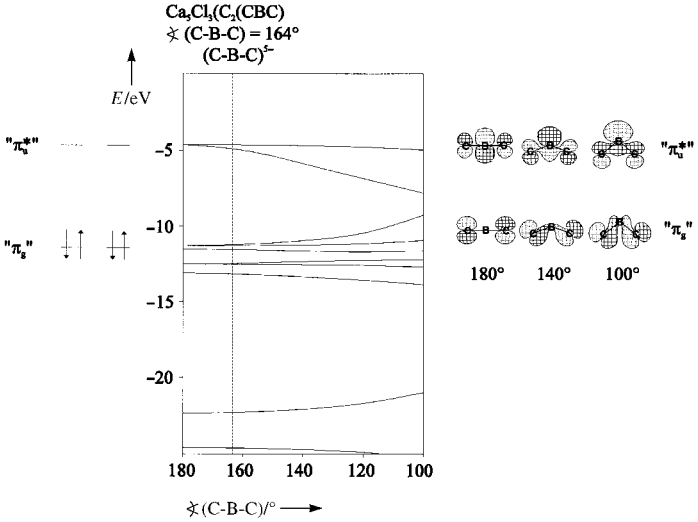


Figure 3. The change of the MO energy levels for an isolated (CBC) unit is shown from a linear (CBC) unit to a bent one (B–C bond length: 144 pm). For a CBC^{5-} ion the "π_g" orbitals and for a CBC^{7-} ion the "π_u^*" orbitals are occupied with two electrons each. Orbital combinations for the C-B-C angles 180°, 140°, and 100° are displayed. The order of the energy levels is given in reference [10].

vanishes for bent C-B-C arrangements. The change of the "π_g" (HOMO for BC_2^{5-}) and "π_u^*" energy levels (LUMO for BC_2^{5-}) becomes notable when the C-B-C angle deviates from 180°. As the bond angle decreases one of the "π_g" levels becomes more and more antibonding, while one of the other "π_u^*" levels becomes more and more bonding, which basically allows a transition from a 16-electron anion (BC_2^{5-}) to an 18-electron anion (BC_2^{7-}). An evident decrease of the HOMO–LUMO gap of an isolated BC_2^{5-} is observed when the C-B-C angle is smaller than about 160°.

Covalent d-p(π*) interactions have to be considered, however, in compounds of d or f metals with (CBC) ions. The simultaneous occupation of d-"π_u*" orbital combinations is sometimes regarded as "π* →d backbonding".[12] An analogous bonding behavior with d-p(π*) interactions is known from metal acetylides $Ln^{(3+)}C_2$ of the trivalent lanthanoids (=Ln). In alkaline earth metal acetylides (e.g. CaC_2) the "π*" orbitals are unoccupied which is the reason for the shorter C–C bond lengths compared to $Ln^{(3+)}C_2$.

When d-p(π*) interactions are present in compounds containing d and f metals, ionic charges can hardly be

 © WILEY-VCH Verlag GmbH, D-69451 Weinheim, 1998 1433-7851/98/3724-3408 $ 17.50+.50/0 *Angew. Chem. Int. Ed.* **1998**, *37*, No. 24

addressed to the di- or triatomic anions. The compound Sc_2BC_2 with linear $(CBC)^{5-}$ ions has been assigned as $(Sc^{3+})_2(BC_2^{5-})(e^-)$.[13] In $La_9Br_6(CBC)_3$ the C-B-C bond angle is 148° and the charges have formally been assigned as $(La^{3+})_9(Br^-)_6(CBC^{7-})_3$.[14] So the bent CBC^{7-} ions are isoelectronic to SO_2 with respect to the valence shell.

The example of $Ca_5Cl_3(C_2)(CBC)$ demonstrates very clearly that the observed C-B-C bond angle of the CBC ion (164.0(7)°, Table 1) is not a reliable proof for its ionic charge. The compound is saltlike (transparent, orange-brown crystal plates) and can be considered as $(Ca^{2+})_5(Cl^-)_3(C_2^{2-})(CBC^{5-})$. A bent C_3^{4-} ion (bond angle: 169°), which is isoelectronic with CBC^{5-}, has already been characterized in the compound $Ca_3Cl_2C_3$. Although the degeneracy of the π levels is broken up by the nonlinearity of such triatomic anions, there is no real change in energy for these levels at bond angles between 180 and 160° (Figure 3). Therefore the nonlinearity of triatomic anions in these saltlike compounds may not be viewed as a consequence of an electronic stabilization but from the dense packed matrix of the ions in the structure.

Table 1. Comparison of compounds containing BC_2 anions.

Compound	∢(C-B-C) [°]	*d*(B-C) [pm]	Formal charge	Ref.
$(Ca^{2+})_5(Cl^-)_3(C_2^{2-})(BC_2^{5-})$	164.0(7)	143.7(6)	−5	
$(Al^{3+})_3(C^{4-})(BC_2^{5-})$	180	144	−5	[15]
$(Sc^{3+})_2(BC_2^{5-})(e^-)$	180	148.4	−5	[13]
$(La^{3+})_9(Br^-)_6(BC_2^{7-})_3$	148	149	−7	[14]
$(La^{3+})_9(Br^-)_5(BC_2^{7-})_3(e^-)$	141(3) 151(3)	152(2)/154(2) 151(2)	−7	[16]

As expected the B–C bond lengths of CBC^{5-} ions in the saltlike compounds $Al_3C(CBC)$[14] and $Ca_5Cl_3(C_2)(CBC)$ are in good agreement (Table 1). For all compounds with partially occupied "π_u^*" orbitals longer B–C distances have been reported (Table 1).

^{13}C MAS NMR investigations on samples of $Ca_5Cl_3(C_2)(CBC)$ gave two signals with isotropic chemical shifts of $\delta = 185(1)$ and 199(1) (integration ratio: 1:1.04). The isotropic chemical shift could be assigned based on ^{13}C MAS NMR measurements on MC_2 (M = Ca, Sr, Ba, Table 2). Another indication supporting the assignment is the broadening of the signal base observed at $\delta = 185$. This broadening is due to the B–C coupling.

Raman spectra of single crystals and of powdered samples of $Ca_5Cl_3(C_2)(CBC)$ showed signals at 1885 cm^{-1} and at 1495 cm^{-1}. The first signal was assigned to the symmetric C–C stretching vibration (Table 2).

Table 2. Spectroscopic data of alkaline earth metal carbides.

Compound	$\delta(^{13}C)$[a] [ppm]	$\tilde{\nu}_{sym}$[b] [cm^{-1}]
CaC_2	200(5),[17] 206.2,[18] 199(1)[c]	1870[c]
SrC_2	212(3),[17] 213(1)[c]	1847,[18] 1850[c]
BaC_2	229(2),[17] 232,[18] 229(1)[c]	1831[18]
$Ca_5Cl_3(C_2)(CBC)$	185(1) (BC_2^{5-}), 199(1) (C_2^{2-})[c]	1495 (not assigned), 1885 (C_2^{2-})[c]

[a] NMR measurements have been performed with a Bruker MS200 or a Bruker ASX300 at a rotation frequency of 10 kHz. [b] Raman measurements have been performed with a Bruker FT-IR spectrometer IFS66V (FT-Raman module RFA106, Raman microscope, primary light source: 1064 Nd-YAG-Laser, (Adlas)). [c] Own measurements.

Experimentals Section

All manipulations were performed under the strict exclusion of oxygen and moisture in an argon-filled glove-box (M. Braun, Garching).

In an experiment to synthesize "$Ca_4Cl_3BC_2$" a few thin, orange-brown, transparent, rectangular platelets of the title compounds were found in the product mixture. $Ca_5Cl_3(C_2)(CBC)$ can be synthesized in quantitative yield by the reaction of stoichiometric amounts of Ca, $CaCl_2$, B, and graphite. The pure compound was synthesized from Ca (280.6 mg, 7 mmol; ABCR, 99.99%), B (21.7 mg, 2 mmol; ABCR, 99.7%), graphite (96.1 mg, 8 mmol; Merck, "Reinst", degased for 4 h at 670 K under vacuum conditions) and $CaCl_2$ (333 mg, 3 mmol; Strem, 99.99%, dried 4 h at 670 K under flowing HCl). The starting materials were heated in arc-welded, silica-jacketed tantalum ampoules at a heating rate of 10 K h^{-1} to 1170 K and kept for at least four days at this temperature. The oven was cooled down to room temperature at a cooling rate of 10 K h^{-1} (the obtained products were pure with respect to X-ray powder diffraction, but with ^{13}C MAS NMR and Raman spectroscopy traces of $Ca_3Cl_2C_3$ were detected). A single crystal obtained by the described method was chosen under a microscope in a glove-box and sealed in a Mark capillary.

A sample of $Ca_5Cl_3(C_2)(CBC)$ for the ^{13}C MAS NMR spectroscopy was synthesized by the same route, but approximately 10% of the employed graphite was substituted by ^{13}C (99%, amorphous, Chemotrade).

Received: May 14, 1998 [Z11856IE]
German version: *Angew. Chem.* **1998**, *110*, 3619–3621

Keywords: boron · calcium · carbides · solid-state chemistry

[1] a) W. Borchers, L. Stockem, *Z. Elektrochem.* **1902**, *8*, 757–758; b) L. Wöhler, G. Rodewald, *Z. Anorg. Allg. Chem.* **1909**, *61*, 54–90.
[2] P. Ehrlich, B. Alt, L. Gentsch, *Z. Anorg. Allg. Chem.* **1956**, *283*, 58–73.
[3] H.-J. Meyer, *Z. Anorg. Allg. Chem.* **1991**, *593*, 185–192.
[4] H.-J. Meyer, *Z. Anorg. Allg. Chem.* **1991**, *594*, 113–118.
[5] a) O. Reckeweg, H.-J. Meyer, *Z. Naturforsch. B* **1997**, *52*, 340–344; b) F. E. Rohrer, R. Nesper, *J. Solid State Chem.* **1998**, *135*, 194–200.
[6] H. Womelsdorf, H.-J. Meyer, *Z. Anorg. Allg. Chem.* **1994**, *620*, 262–265.
[7] Crystal structure analysis of $Ca_5Cl_3(C_2)(CBC)$: orange-brown, transparent plate, $0.18 \times 0.15 \times 0.04$ mm^3, space group: *Cmcm* (no. 63), $a = 389.24(7)$, $b = 1389.1(7)$, $c = 1859.1(13)$ pm; $V = 1005.2(9) \times 10^6$ pm^3, Ca(1): 0, 0.1573(1), ¼; Ca(2): 0, 0.3643(1), 0.5618(1); Ca(3): 0, 0.9446(1), 0.3586(1); Cl(1): 0, 0.8062(1), ¼; Cl(2): 0, 0.2836(1), 0.4153(1); B: 0, 0.5355(5), ¼; C(1): 0, 0.4501(4), 0.6735(3); C(2): −0.0629(36), 0.9635(4), 0.5106(4); temperature: $T = 293(2)$ K, $Mo_{K\alpha}$ radiation ($\lambda = 71.073$ pm), Enraf-Nonius-CAD4 diffractometer, graphite monochromator, ω scan, $6.26° < 2\theta < 53.84°$, LP correction, no other absorption correction applied, structure solution by direct methods with SHELXS-86,[19] structure refinement: full-matrix least-squares method with SHELXL-97 against $|F^2|$,[20] 46 parameters refined, all atoms refined anisotropically, $R1 = 0.041/0.065$; $wR2 = 0.090/0.096$; GooF = 1.089/1.089 (504 independent reflections $I > 4\sigma(I)$, all 642 independent reflections), residual electron density: $0.52/-0.97$ e 10^{-6} pm^{-3}). Further details of the crystal structure

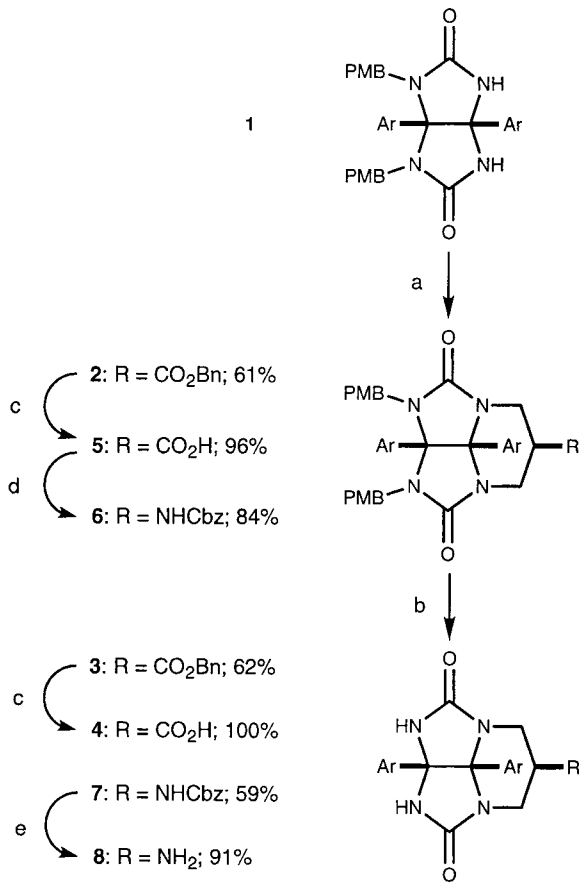
investigations can be obtained from the Fachinformationszentrum Karlsruhe, D-76344 Eggenstein-Leopoldshafen, Germany (fax: (+49) 7247-808-666; e-mail: crysdata@fiz-karlsruhe.de), on quoting the depository number CSD-406847.
[8] M. Wörle, H.-J. Muhr, H. Meyer zu Altenschildesche, R. Nesper, *J. Alloys Comp.* **1997**, *260*, 80–87.
[9] M. Atoji, *J. Chem. Phys.* **1961**, *35*, 1950–1960.
[10] R. Hoffmann, H.-J. Meyer, *Z. Anorg. Allg. Chem.* **1992**, *607*, 57–71.
[11] "CACAO": C. Mealli, D. Proserpio, *J. Chem. Ed.* **1990**, *67*, 399–402.
[12] A. Simon, H. Mattausch, R. Eger, R. E. Kremer, *Angew. Chem.* **1991**, *103*, 1210–1211; *Angew. Chem. Int. Ed. Engl.* **1991**, *30*, 1188–1189.
[13] J.-F. Halet, J.-Y. Saillard, J. Bauer, *J. Less-Comm. Met.* **1990**, *158*, 239–250.
[14] H. Mattausch, A. Simon, *Angew. Chem.* **1995**, *107*, 1764–1766; *Angew. Chem. Int. Ed. Engl.* **1995**, *34*, 1633–1635.
[15] H. Hillebrecht, F. D. Meyer, *Angew. Chem.* **1996**, *108*, 2655–2657; *Angew. Chem. Int. Ed. Engl.* **1996**, *35*, 2499–2500.
[16] H. Mattausch, A. Simon, C. Felser, R. Dronskowski, *Angew. Chem.* **1996**, *108*, 1805–1807; *Angew. Chem. Int. Ed. Engl.* **1996**, *35*, 1685–1687.
[17] T. M. Duncan, *Inorg. Chem.* **1989**, *28*, 2663–2668.
[18] B. Wrackmeyer, K. Horchler, A. Sebald, L. H. Merwein, C. Ross II, *Angew. Chem.* **1990**, *102*, 821–823; *Angew. Chem. Int. Ed. Engl.* **1990**, *29*, 807–809.
[19] G. M. Sheldrick, SHELXS-86, Göttingen, **1990**; G. M. Sheldrick, *Acta Crystallogr. Sect. A* **1990**, *46*, 467–473.
[20] G. M. Sheldrick, SHELX-97, Göttingen, **1997**.

Self-Assembling Sieves**

Tomas Szabo, Brendan M. O'Leary, and Julius Rebek, Jr.*

"Molecule within molecule"[1] complexes have been useful in stabilizing reactive intermediates,[2] defining new forms of stereoisomerism,[3] and accelerating Diels–Alder reactions.[4] Other applications await the availability of diverse sizes and shapes for selective and reversible encapsulation. We describe here a modular approach that gives access to some of the largest hydrogen-bonded capsules ($\approx 0.5\ nm^3$) reported to date. These modules promise versatility in the assembly of many new structures using diverse molecular scaffolds.

The modules are based on the glycoluril system, a structure that provides both molecular curvature and a richness of hydrogen-bonding sites (Scheme 1). Alkylation of the unprotected face of **1**[5] with benzyl 2-(bromomethyl)acrylate[6] gives the tricyclic structure **2** featuring the equatorial ester as the major product. The fused six-membered ring contributes to the overall rigidity of the glycoluril unit and offers an attachment point for coupling to appropriate spacer units. Two deprotection steps then yield acid module **4**, suitable for condensation with amine- or alcohol-bearing spacers. Alternatively, subjecting acid **5** to a modified Curtius rearrangement[7] followed by deprotection affords amine module **8** for use with spacers containing carboxylic or sulfonic acids.



Scheme 1. Synthesis of glycoluril building blocks **4** and **8**. a) Benzyl 2-(bromomethyl)acrylate, Cs_2CO_3, MeCN, reflux, 3 h; b) CAN, MeCN/H_2O (5/1), RT, 24 h; c) H_2, Pd/C, EtOH, 3 h; d) DPPA, PhMe, RT, 30 min; then BnOH, reflux, 2 h; e) H_2, Pd/C, EtOH/EtOAc/AcOH (49/49/2), 3 h. Ar = 4-*n*-heptylphenyl, PMB = 4-methoxybenzyl, Cbz = phenylmethoxycarbonyl; CAN = ceric ammonium nitrate, DPPA = diphenylphosphoryl azide.

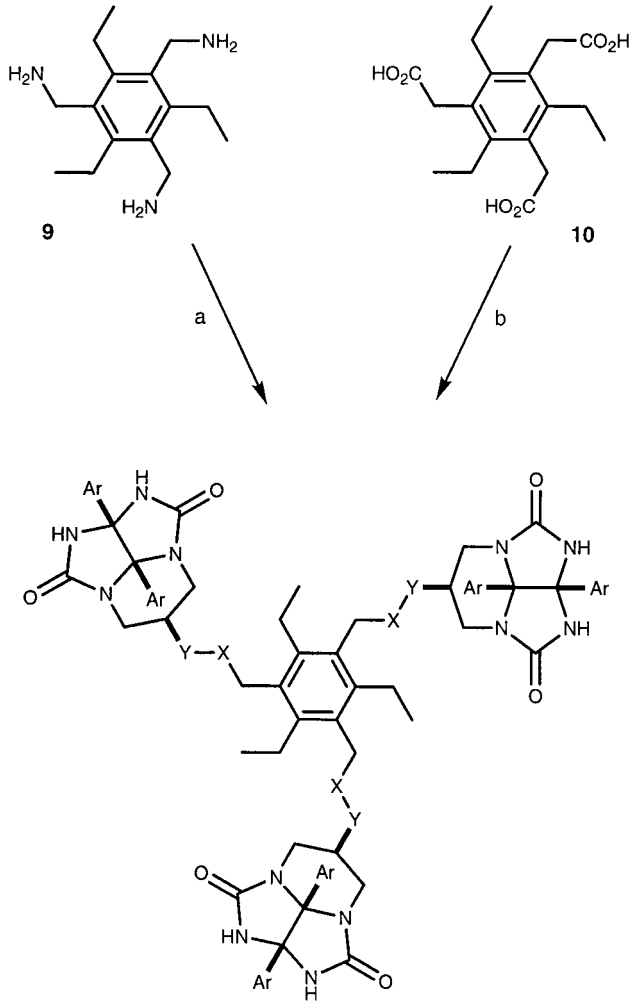
Our initial efforts focused on D_{3d}-symmetric capsules assembled through a seam of twelve hydrogen bonds. The hexa-substituted spacers **9**[8] and **10**[9] (Scheme 2) were expected to provide a geared arrangement[10] of substituents around the benzene ring and present all three modules on one side of the spacer. Condensation of triamine **9** with acid module **4** gave monomer **11** in 68% yield, while coupling triacid **10** with amine module **8** gave a 49% yield of monomer **12**, differing from **11** only by the "direction" of the amide linkage.[11]

Both systems gave tell-tale signs of exclusive dimerization as indicated by far downfield shifts for the glycoluril N–H resonances and sharp, first-order signals for the remaining

[*] Prof. J. Rebek, Jr., Dr. T. Szabo
The Skaggs Institute for Chemical Biology
The Scripps Research Institute
10550 North Torrey Pines Road, La Jolla, California 92037 (USA)
Fax: (+1) 619-7842876
E-mail: jrebek@scripps.edu
B. M. O'Leary
Department of Chemistry
Massachusetts Institute of Technology (USA)

[**] We are grateful to the Skaggs Research Foundation and the National Institutes of Health for financial support. T.S. is pleased to acknowledge a fellowship from the Knut and Alice Wallenberg Foundation. We also thank Prof. Eric Anslyn and Paul Thompson for advice on the synthesis of **9** and Dr. Sandro Mecozzi for advice on our computational methods.

 © WILEY-VCH Verlag GmbH, D-69451 Weinheim, 1998 1433-7851/98/3724-3410 $ 17.50+.50/0



Scheme 2. Synthesis of **11** and **12**. a) **4**, EDC, HOBt, Et_3N, DMF, RT, 6 h; b) **8**, EDC, HOBt, Et_3N, DMF, RT, 6 h. EDC = 1-(3-dimethylaminopropyl)-3-ethylcarbodiimide hydrochloride, HOBt = 1-hydroxybenzotriazole.

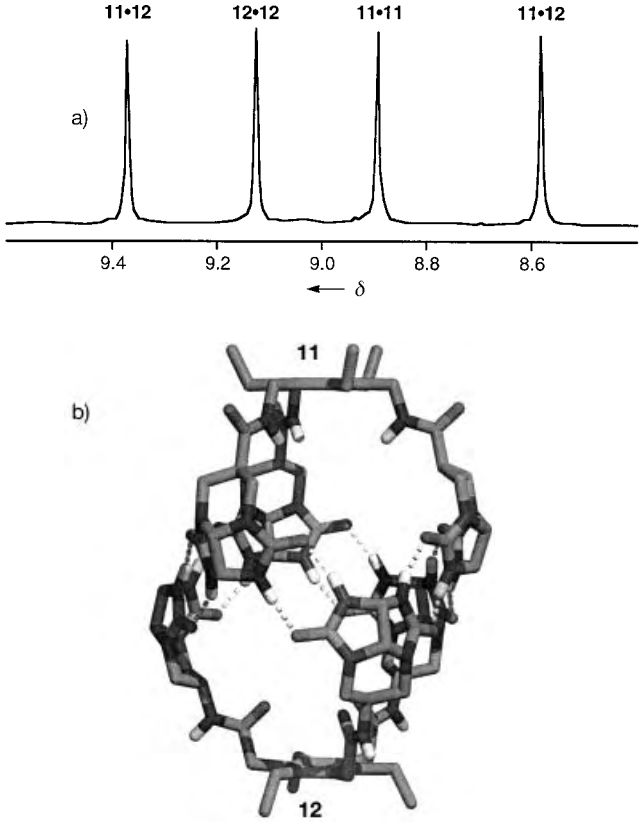


Figure 1. a) ^{1}H NMR spectrum showing glycoluril N–H resonances for a 1:1 mixture of **11** and **12**. The heterodimer **11**·**12** has two different glycoluril N–H resonances. b) Energy-minimized structure of **11**·**12** (some groups omitted).

protons in ^{1}H NMR spectra in $CDCl_3$.[12] Furthermore, no concentration dependence was observed for any shifts in solvents used for this study.[12] These indicators of large dimerization constants were supported by mass spectrometric (MALDI) detection of dimer **11**·**11**. Other proof of dimeric assemblies came from heterodimer formation upon mixing **11** and **12** (Figure 1 a), whose close structural resemblance led to a nearly statistical distribution of dimeric species. Finally, as described below, the dimers were found to encapsulate a variety of guests.

In contrast to the above indications of dimerization, mixtures of deuterated solvents failed to show the expected formation of at least two distinct complexes for hosts **11**·**11** and **12**·**12**.[13] This suggests that those solvent molecules rapidly move between the capsule interior and exterior resulting in an averaging of complexes on the NMR time scale. The mechanism of this exchange probably depends upon the breathing dynamics of these flexible capsules. Too fast to measure by NMR spectroscopy, these motions might increase the pore sizes enough to permit easy passage of solvent molecules through the dimer, akin to the flow of water through a sieve.

Previous studies identified solvent release as a significant driving force for encapsulation,[14] but the large holes in these sieve-like molecules led us to doubt their utility as hosts. If solvents could enter and depart at will, entropic gains from guest encapsulation might be too small to make the process favorable. Indeed, this idea was supported by the fact that **11**·**11** had little or no affinity for a variety of guests while dissolved in $CDCl_3$. However, dimer **12**·**12** showed remarkable binding affinity [Eqs. (1) and (2)] for several guests in this solvent (Table 1).

$$\text{host}\cdot(\text{solvent})_n + \text{guest} \rightleftharpoons \text{host}\cdot\text{guest} + n\,\text{solvent} \quad (1)$$

$$K_a = \frac{[\text{host}\cdot\text{guest}]}{[\text{host}\cdot(\text{solvent})_n]\,[\text{guest}]} \quad (2)$$

How can this discrepancy be explained? One possible answer rests with size and shape differences between the two cavities. In a recent report from our lab discussing size complementarity in liquid state host–guest systems, an ideal packing coefficient (PC) was proposed.[15] For the dimers described here, binding affinities can be understood through evaluating ideal PCs (0.59 ± 0.09) and shape congruence between cavity and guest.

 © WILEY-VCH Verlag GmbH, D-69451 Weinheim, 1998 1433-7851/98/3724-3411 $ 17.50+.50/0

Table 1. Apparent binding constants K_a in M^{-1} for **11**·**11** and **12**·**12** in the solvents $CDCl_3$ (71 Å^3) and [D_{12}]mesitylene (124 Å).

Guest (volume, Å^3)	**11**·**11**	**12**·**12**
$CDCl_3$		
[2.2]paracyclophane (195)	0	0.51
ferrocene (146)	0	2.7
1,1′-dimethylferrocene (178)	0	5.8
ferrocenemethanol (170)	[a]	$\gg 25$[b]
1,1′-ferrocenedimethanol (191)	[d]	24
ferrocenecarboxylic acid (170)	0	8.6
(1*S*)-(−)-camphor (159)	0	0.55
1-adamantaneethanol (184)	1.4×10^{-3}	1.5
[D_{12}]mesitylene		
[2.2]paracyclophane (195)	2.0×10^{-3}	[c]
ferrocene (146)	0	[c]
1,1′-ferrocenedimethanol (191)	$\gg 25$[b]	[c]
(1*S*)-(−)-camphor (159)	9.2×10^{-2}	[c]
1-adamantaneethanol (184)	4.6×10^{-3}	[c]

[a] Not evaluated. [b] Too large to measure accurately. [c] Insoluble host. [d] This guest appeared to break up the dimer **11**·**11** in this solvent.

Computer modeling of complex **11**·**11**, with pores blocked, reveals a rugby-ball shaped cavity measuring approximately 490 Å^3.[16] All six of the amide carbonyls point outward, while the amide NH groups point into the cavity. Dimer **12**·**12** has a related structure, but features a smaller, more spherical cavity (434 Å^3) because the six carbonyls point into the cavity. Figure 1b shows the calculated representation of the heterodimer **11**·**12** whose halves allude to the structures of the respective homodimers.

Dimer **12**·**12** readily encapsulates ferrocene as indicated by a ^{1}H NMR spectrum showing a new set of host peaks and a new peak for encapsulated ferrocene downfield of the "free" guest.[17] These characteristics indicate that ferrocene is too large to move freely through the dimer and is trapped in the sieve (slow exchange). Integration of these peaks reveals one ferrocene molecule per new host molecule corresponding to a PC of only 0.34.[18] This small PC suggests an unfavorable complex due to insufficient "solvation" of the cavity. However, co-inclusion of one or two chloroform molecules on average (fast exchange) with each ferrocene would increase the PC to a more comfortable 0.50 or 0.66, respectively. While still speculative, this scenario appears feasible by molecular modeling.

In contrast, dimer **11**·**11** does not encapsulate ferrocene even at large exterior concentrations of this compound. Encapsulation of two chloroform molecules and one ferrocene molecule produces a favorable PC of 0.59, but an ideal PC does not automatically translate into a good fit. Shape is a major consideration, that is a square peg may have the same volume as a round hole, but the different shapes preclude a good fit. The rugby-ball shaped cavity of **11**·**11** is presumably filled on average with four molecules of chloroform (PC = 0.58). These solvent molecules can be thought of as small spheres. Replacing two of these with a larger sphere (like free-tumbling ferrocene) may not be favorable because this new guest may not be able to "solvate" the tapered ends of the cavity as well as chloroform.

While almost every prospective guest shunned the cavity of **11**·**11** in $CDCl_3$, the story changed upon switching to the largest deuterated solvent available, [D_{12}]mesitylene (Table 1).[19] Calculation of PCs showed that the included guests plus one mesitylene gave values in the upper end of the ideal range. Unsurprisingly, the better binders tended to be more complementary in shape and possessed functionality capable of hydrogen bonding to polar surfaces within the cavity. In short, **11**·**11** preferred these guests to the poorer solvation offered by large, disc-shaped mesitylenes.[20] However, as indicated in Table 1, none of these guests could compete as well against chloroform solvation of the interior.

What is the mechanism of encapsulation? A clue is given by the heterodimerization of the two capsules. The disproportionation of **11**·**11** and **12**·**12** to the heterodimer requires the complete dissociation of a dimeric capsule by the eventual disruption of 12 hydrogen bonds. This process reaches equilibrium in chloroform over the course of hours. The common finding that encapsulation equilibrium is reached within minutes for all viable guests suggests a mechanism of guest uptake not dependent upon complete dissociation. Instead, modeling shows that opening one glycoluril "flap" by breaking four hydrogen bonds creates a pore large enough to accommodate the passage of most guests.[21]

In summary, large capsular assemblies are made readily available by modular syntheses. Studies with these porous capsules suggest that the encapsulation of large guests is not dependent on entropically favorable release of trapped solvent molecules and, instead, appears to be an enthalpy-driven process. Further reports detailing the unique host properties of these and other large systems will be forthcoming.

Received: April 28, 1998 [Z11793IE]
German version: *Angew. Chem.* **1998**, *110*, 3606 – 3609

Keywords: host – guest chemistry · hydrogen bonds · self-assembly · supramolecular chemistry

[1] This phrase first appeared as the title of a lecture by D. J. Cram at the C. David Gutsche Symposium, Washington University, St. Louis, Missouri, May 5, **1990**.
[2] D. J. Cram, M. E. Tanner, R. Thomas, *Angew. Chem.* **1991**, *103*, 1048 – 1051; *Angew. Chem. Int. Ed. Engl.* **1991**, *30*, 1024 – 1027.
[3] A. M. A. van Wageningen, P. Timmerman, J. P. M. van Duynhoven, W. Verboom, F. C. J. M. van Veggel, D. N. Reinhoudt, *Chem. Eur. J.* **1997**, *3*, 639 – 654; b) P. Timmerman, W. Verboom, F. C. J. M. van Veggel, J. P. M. van Duynhoven, D. N. Reinhoudt, *Angew. Chem.* **1994**, *106*, 2437 – 2440; *Angew. Chem. Int. Ed. Engl.* **1994**, *33*, 2345 – 2348.
[4] J. Kang, J. Rebek, Jr., *Nature* **1997**, *385*, 50 – 52.
[5] J. M. Rivera, T. Martin, J. Rebek, Jr., *J. Am. Chem. Soc.* **1998**, *120*, 819 – 820.
[6] Prepared analogously to the corresponding ethyl ester, see: J. Villieras, M. Rambaud, *Synthesis* **1982**, 924 – 926.
[7] T. Shioiri, K. Ninomiya, S. Yamada, *J. Am. Chem. Soc.* **1972**, *94*, 6203 – 6205.
[8] A. Metzger, V. M. Lynch, E. V. Anslyn, *Angew. Chem.* **1997**, *109*, 911 – 914; *Angew. Chem. Int. Ed. Engl.* **1997**, *36*, 862 – 865.
[9] Obtained by acidic hydrolysis of 1,3,5-tris(cyanomethyl)-2,4,6-triethylbenzene. see: C. Walsdorff, W. Saak, S. Pohl, *J. Chem. Res. (S)* **1996**, 282 – 283.
[10] D. J. Iverson, G. Hunter, J. F. Blount, J. R. Damewood, Jr., K. Mislow, *J. Am. Chem. Soc.* **1981**, *103*, 6073 – 6083; A. Metzger, E. V. Anslyn,

 © WILEY-VCH Verlag GmbH, D-69451 Weinheim, 1998 1433-7851/98/3724-3412 $ 17.50+.50/0

Angew. Chem. **1998**, *110*, 682 – 684; *Angew. Chem. Int. Ed.* **1998**, *37*, 649 – 652.
[11] All new compounds were characterized by high-resolution NMR spectroscopy and mass spectrometry.
[12] J. Rebek, Jr., *Chem. Soc. Rev.* **1996**, 255 – 264. All spectra recorded on a 600 MHz Bruker DRX spectrometer.
[13] See reference [16]. Mixtures employed: $CDCl_3/C_6D_6$, $CDCl_3/[D_{12}]$mesitylene, $[D_{10}]$*p*-xylene/$[D_{12}]$mesitylene, and $[D_{10}]$*p*-xylene/C_6D_6.
[14] a) J. Kang, J. Rebek, Jr., *Nature* **1996**, *382*, 239 – 241; b) R. Meissner, X. Garcias, S. Mecozzi, J. Rebek, Jr., *J. Am. Chem. Soc.* **1997**, *119*, 77 – 85.
[15] S. Mecozzi, J. Rebek, Jr., *Chem. Eur. J.* **1998**, *4*, 1016 – 1022. Cavity volumes likely are underestimated due to the necessary hole-blocking method used in calculations. Therefore, PCs will appear larger than the reported ideal. The best binders in this study gave an apparent average PC = 0.59 ± 0.09. [PC = volume of guest(s)/volume of cavity].
[16] Modeling was performed by using a Macromodel v5.5, Amber* forcefield. Pore blocking was necessary to define a cavity. This involved replacing the equatorial hydrogen atoms on each module's six-membered ring with a cyclopropyl group. Volumes are based upon a static structure and calculated as described in reference [15].
[17] The twelve phenyl groups of the glycolurils present their edges to the cavity which accounts for the downfield shifts of guests' signals from their "free" positions.
[18] Ferrocene derivatives were modeled by using MacSpartan Plus and their volumes were calculated by using MacroModel.
[19] Dimer **12**·**12** displayed poor solubility and dimer **11**·**11** was only moderately soluble in $[D_{12}]$mesitylene. This probably results from the poor shape complementarity of two encapsulated mesitylenes (PCs = 0.57 and 0.51, respectively) with the cavities.
[20] K. T. Chapman, W. C. Still, *J. Am. Chem. Soc.* **1989**, *111*, 3075 – 3077.
[21] T. Szabo, G. Hilmersson, J. Rebek, Jr., *J. Am. Chem. Soc.* **1998**, *120*, 6193 – 6194.

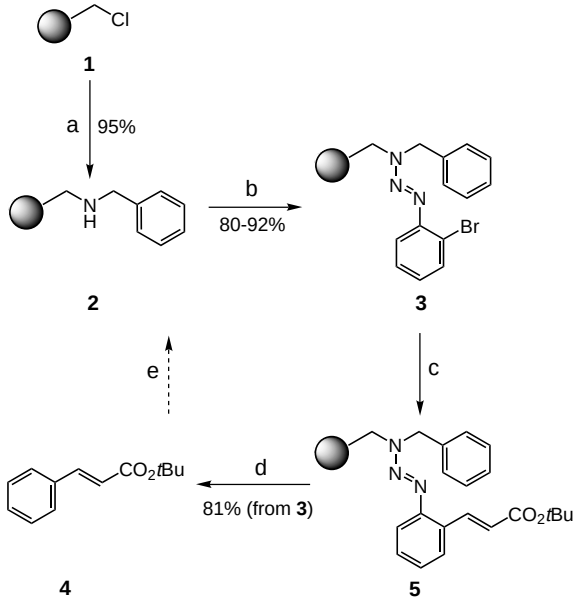
A Surprising Solid-Phase Effect: Development of a Recyclable "Traceless" Linker System for Reactions on Solid Support**

Stefan Bräse,* Dieter Enders, Johannes Köbberling, and Frank Avemaria

The development of high-throughput screening (HTS) processes and the associated demand for large substance libraries has recently led to an expansion of new synthetic strategies, often described as "combinatorial chemistry".[1] In connection with these developments was a renaissance in solid-phase synthesis. While mixtures of substances were synthesized initially, more recently parallel solid-phase synthesis of single compounds has been given a great deal of attention, because of the advantages of its ease of automation and unambiguous test results in HTS. The associated strategies for the construction of organic molecules and their functionalization are often limited by the nature of the linker.[2] Since most linkers are derived from protecting groups linked to the solid support the seceding molecules generated upon cleavage always contain a functional group that has to be present at the beginning of the synthesis and on which transformations cannot be carried out. To overcome this disadvantage the attached synthetic building block has to be connected to the resin in such a manner that only a C – H bond remains on the target molecule after cleavage ("traceless" cleavage). Only a few solutions exist for this particular problem, none of which are general.[3–5] During our work towards the synthesis of functionalized arenes by organometallic methods we were challenged by the problem of attachment and traceless removal of functionalized arenes. The published strategies of Ellman et al., Veber et al. and others.[3] that use the recently commercialized "silyl linker" suffer from the length of the synthesis and the sensitivity. Herein we report a new "traceless linker" system without these disadvantages, which in contrast, possesses the advantage that the resin can be regenerated.

One possible method by which functionalized arenes can be converted into the corresponding hydrocarbons is the reduction of diazonium compounds. Since they react with amines to yield triazenes,[6] which can be transformed under mildly acidic conditions back to diazonium compounds, the use of triazenes as "linkers" seemed to be very promising. The attachment of triazenes to a solid support is an immobilization method that is rarely used.[7]

Commercially available Merrifield resin (**1**; 1% divinylbenzene, 200 – 400 mesh, 0.72 mmol g^{-1} Cl) could be treated with benzylamine to yield **2** (Scheme 1) or with piperazine to give the corresponding resin (90 – 97%).[8] Coupling was



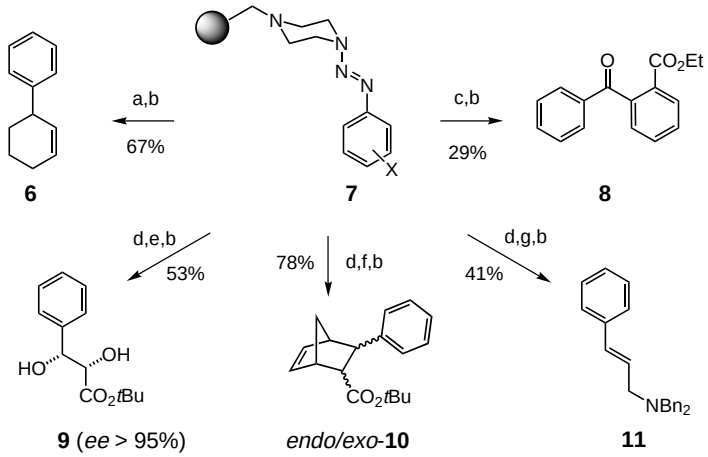
Scheme 1. Synthesis of **3** and Heck reaction. a) $BnNH_2$, DMF, 48 h, 60 °C; b) ArN_2^+, THF, 0 → 25 °C; c) $H_2C{=}CHCO_2tBu$, $Pd(OAc)_2$, PPh_3, NEt_3, DMF, 24 h, 80 °C, ultrasound; d) HCl/THF or H_3PO_2/Cl_2HCCO_2H; e) regeneration.

[*] Dr. S. Bräse, Prof. Dr. D. Enders, Dipl.-Chem. J. Köbberling, F. Avemaria
Institut für Organische Chemie der Technischen Hochschule
Professor-Pirlet-Strasse 1, D-52074 Aachen (Germany)
Fax: (+49) 241-8888127
E-mail: braese@oc.rwth-aachen.de

[**] This work was supported by the Deutsche Forschungsgemeinschaft (Leibniz price to D.E., Sonderforschungsbereich 380, and Transferbereich 11) and the Fonds der Chemischen Industrie (Liebig stipend to S.B.) We thank the companies Degussa AG, BASF AG, Hoechst AG, Bayer AG, and Wacker Chemie for donations of chemicals.

subsequently conducted with various diazonium salts. These salts were prepared from primary aromatic amines under non-aqueous conditions ($BF_3 \cdot OEt_2$, *t*BuONO). A multiple repetition (three times) of the coupling step was necessary to achieve good yields (> 80 % loading). Therefore, the resins **2** and the analogous piperazine resin were respectively swollen in THF, treated at room temperature with 1.0 – 1.5 equivalents of the diazonium salts, and agitated for 15 min. After washing the resin twice with THF/Et_3N (2/1) the coupling step was repeated. The resins **3** and **7** are air and water stable [9] and can be stored for long periods without loss of activity.

The halogenated resins **3** and **7** were used in Heck reactions[10] (12 – 24 h) with a variety of olefins (styrene, acrylate, dihydrofuran, cyclohexene). The expected products **4** (Scheme 1) and **6** (Scheme 2) were obtained after cleavage (see below) from the modified resins (such as **5**) in modest to good yields (42 – 81 %) and excellent purities (> 90 %, NMR). The solid-bound triazenes are thermally stable. A thermal Diels – Alder reaction of the polymer-bound cinnamic ester proceeded cleanly at 100 °C within 24 h[11] and yielded the expected mixture of *exo* and *endo* cycloadducts **10** after cleavage (Scheme 2). Remarkable is the fact that because of the ease of removal of the diene the reaction can be carried out in pure cyclopentadiene. Asymmetric functionalization of the polymer-bound cinnamic ester proceeded cleanly by dihydroxylation[12] and afforded the dihydroxy ester **9** (53 %, *ee* 95 %). A sequence that started from a Heck reaction of **7** (X = *p*-I) with *tert*-butyl acrylate, DIBAL-H reduction, esterification of the cinnamyl alcohol with acetic anhydride and subsequent palladium-catalyzed allylic substitution[13] with dibenzyl amine furnished the allyl amine **11** in satisfactory yields (41 %) after cleavage. Metal – halogen exchange (*n*Bu-Li, − 78 °C) on resin **7** (X = *p*-I) yielded, after reaction with diethyl phthalate and cleavage, the benzophenone derivative **8** in a nonoptimized yield of 29 %.



Scheme 2. Reactions on the triazene resin **7** (X = *p*-I). a) Cyclohexene, $Pd(OAc)_2$, PPh_3, NEt_3, DMF, 24 h, 80 °C, ultrasound; b) THF/conc. HCl (10/1), 5 min, 50 °C, ultrasound; c) *n*BuLi (3 equiv), − 78 °C, 30 min, then diethyl phthalate, 25 °C; d) $H_2C{=}CHCO_2tBu$, $Pd(OAc)_2$, PPh_3, NEt_3, DMF, 24 h, 80 °C, ultrasound; e) AD-mix β, acetone/H_2O (10/1), methanesulfonamide, 72 h; f) cyclopentadiene, 100 °C, 24 h; g) 1. DIBAL-H, CH_2Cl_2, − 78 °C, 1 h; 2. Ac_2O, NEt_3, CH_2Cl_2; 3. $[Pd(dba)_2]$, PPh_3, Bn_2NH, THF, 24 h. DIBAL-H = diisobutylaluminum hydride, dba = dibenzylideneacetone.

A variety of conditions could be used to achieve the cleavage of the functionalized arenes from the resins. The resins underwent reductive deamination with H_3PO_2[14] in dichloroacetic acid after 8 h to give the products in satisfactory total yields. In the search for a more efficient cleavage method investigations in the liquid phase were conducted on the corresponding triazenes parallel to experiments on the solid phase. Here, a surprising solid-phase effect was observed. While in the liquid phase triazenes were transformed cleanly with hydrogen halides into the corresponding halides, in the solid phase the triazenes react with HCl to give solely the hydrocarbons.[15] The use of HCl in THF furnished the desired products with high purity after five minutes of ultrasound, with side products being undetected or formed in only trace amounts (< 5 %).[16] Yields of between 29 and 81 %[17] were obtained from the triazene resins **3** or **7**. Acid-sensitive groups such as *tert*-butyl ester, secondary hydroxyl groups, or alkenes were found to be stable under these conditions. The resins could be reused directly for another diazotation with only a slight loss in activity (< 10 %). In addition, the intermediately regenerated diazonium salts (after cleavage with HBF_4 or TFA at 0 °C) can also be converted into a variety of functionalized arenes[18] (aryl halides,[7, 19] phenols,[6b] cross-coupling products).[10] These new cleavage products could potentially be used for further chemistry.

In conclusion, the triazene system presents a linker system that can be cleaved by "traceless" methods or by introduction of new functionalities. It is distinct from the existing alternatives by its accessibility, robustness, and ability to regenerate the resin. The reactions conducted at the resin can only be seen as examples. The broadness of applications in a number of organic reactions can be anticipated.

Received: May 5, 1998 [Z11818IE]
German version: *Angew. Chem.* **1998**, *110*, 3614 – 3616

Keywords: arenes · asymmetric synthesis · C – C coupling · solid-phase synthesis · triazenes

[1] a) E. M. Gordon, R. W. Barrett, W. J. Dower, S. P. Fodor, M. A. Gallop, *J. Med. Chem.* **1994**, *37*, 1385 – 1401; b) L. A. Thompson, J. A. Ellman, *Chem. Rev.* **1996**, *96*, 555 – 600; c) J. S. Früchtel, G. Jung, *Angew. Chem.* **1996**, *108*, 19 – 46; *Angew. Chem. Int. Ed. Engl.* **1996**, *35*, 17 – 42; d) F. Balkenhohl, C. von dem Bussche-Hünnefeld, A. Lansky, C. Zechel, *Angew. Chem.* **1996**, *108*, 2437 – 2487; *Angew. Chem. Int. Ed. Engl.* **1996**, *35*, 2288 – 2337; e) P. H. H. Hermkens, H. C. J. Ottenheijm, D. Rees, *Tetrahedron* **1997**, *53*, 5643 – 5678; f) *Combinatorial Peptide and Nonpeptide Libraries* (Ed.: G. Jung), VCH, Weinheim, **1996**; g) *Combinatorial Chemistry* (Eds.: S. R. Wilson, A. W. Czarnik), Wiley-Interscience, New York, **1997**, and references therein.

[2] B. J. Backes, J. A. Ellman, *Curr. Opin. Chem. Biol.* **1997**, *1*, 86 – 93.

[3] a) M. J. Plunkett, J. A. Ellman, *J. Org. Chem.* **1995**, *60*, 6006 – 6007; b) M. J. Plunkett, J. A. Ellman, *J. Org. Chem.* **1997**, *62*, 2885 – 2893; c) B. Chenera, J. A. Finkelstein, D. F. Veber, *J. Am. Chem. Soc.* **1995**, *117*, 11999 – 12000; d) T. L. Boehm, H. D. Showalter, *J. Org. Chem.* **1996**, *61*, 6498 – 6499; e) A. Routledge, H. T. Stock, S. L. Flitsch, N. J. Turner, *Tetrahedron Lett.* **1997**, *38*, 8237 – 8290; f) M. Schuster, N. Lucas, S. Blechert, *Chem. Commun.* **1997**, 823 – 824.

[4] For a Pd-catalyzed "traceless" cleavage, see S. Jin, D. P. Holub, D. J. Wustrow, *Tetrahedron Lett.* **1998**, *39*, 3651.

 © WILEY-VCH Verlag GmbH, D-69451 Weinheim, 1998 1433-7851/98/3724-3414 $ 17.50+.50/0

[5] a) For a "traceless linker" for isoquinolines, see B. A. Lorsbach, J. T. Bagdanoff, R. B. Miller, M. J. Kurth, *J. Org. Chem*. **1998**, *63*, 2244 – 2250; b) for a "linker" for amines, see X. Ouyang, R. W. Armstrong, M. M. Murphy, *J. Org. Chem*. **1998**, *63*, 1027 – 1032; c) for a photolabile benzyl sulfide linker, see F. W. Forman, I. Sucholeiki, *J. Org. Chem*. **1995**, *60*, 523 – 528; d) for a "traceless linker" for carboxylic acids, see P. Garibay, J. Nielsen, T. Hoeg-Jensen, *Tetrahedron Lett.* **1998**, *39*, 2207 – 2210; e) P. Conti, D. Demont, J. Cals, H. C. J. Ottenheijm, D. Leysen, *Tetrahedron Lett.* **1997**, *38*, 2915 – 2918; f) C. R. Johnson, B. Zhang, *Tetrahedron Lett.* **1995**, *36*, 9253 – 9256; g) for the use of sulfones as linkers, see L. M. Gayo, M. J. Suto, *Tetrahedron Lett.* **1997**, *38*, 211 – 214; h) for the use of an aliphatic C-H "traceless" linker, see X. Zhao, K. W. Jung, K. D. Janda, *Tetrahedron Lett.* **1997**, *38*, 977 – 980; *Tetrahedron Lett.* **1997**, *38*, 6645 – 6652; K. W. Jung, X. Zhao, K. D. Janda, *Tetrahedron Lett.* **1996**, *37*, 6491 – 6494; i) for further linkers, see I**.** Hughes, *Tetrahedron Lett.* **1996**, *37*, 7595 – 7598; j) R. Brown, D. C. Rees, Z. Rankovic, J. R. Morphy, *J. Am. Chem. Soc*. **1997**, *119*, 3288 – 3295; k) X. Zhao, K. D. Janda, *Tetrahedron Lett*. **1997**, *38*, 5437 – 5440; l) S. W. Kim, S. Y. Ahn, J. S. Koh, J. H. Lee, S. R. Ro, H. Y. Cho, *Tetrahedron Lett.* **1997**, *38*, 4603 – 4606; m) A. K. Szardenings, T. Burkoth, H. H. Lu, D. W. Tien, D. A. Campbell, *Tetrahedron* **1997**, *53*, 6573 – 6593; n) M. R. Gowravaram, M. A. Gallop, *Tetrahedron Lett*. **1997**, *38*, 6973 – 6976; o) A. D. Piscopio, J. F. Miller, K. Koch, *Tetrahedron Lett.* **1997**, *38*, 7143 – 7146; p) F. E. K. Kroll, R. Morphy, D. Rees, D. Gani, *Tetrahedron Lett.* **1997**, *38*, 8573 – 8576; q) for cleavage by metathesis, see J. U. Peters, S. Blechert, *Synlett* **1997**, 348 – 350; r) for an enzyme-labile linker, see B. Sauerbrei, V. Jungmann, H. Waldmann, *Angew. Chem*. **1998**, *110*, 1187 – 1190. *Angew. Chem. Int. Ed.* **1998**, *37*, 1143 – 1146.

[6] a) A. Engel in *Methoden Org. Chem. (Houben-Weyl*), 4th ed. 1952 – , Vol. E 16a, **1990**, pp. 1182 – 1226; b) K. C. Nicolaou, C. N. C. Boddy, S. Natarajan, T.-Y. Yue, H. Li, S. Bräse, J. M. Ramanjulu, *J. Am. Chem. Soc*. **1997**, *119*, 3412 – 3422, and references therein; c) S. Bräse, J. Köbberling, D. Enders, R. Lazny, J. Poplawski, *Tetrahedron Lett.*, submitted; d) S. Bräse, J. Köbberling, D. Enders, M. Wang, R. Lazny, *Tetrahedron Lett.*, submitted.

[7] a) P. J. Das, S. Khound, *Tetrahedron* **1994**, *50*, 9107 – 9112; b) J. C. Nelson, J. K. Young, J. S. Moore, *J. Org. Chem*. **1996**, *61*, 8160 – 8168.

[8] The modified resins were characterized by C,H,N analysis.

[9] The resins prepared, with the exception of the examples that contain iodine, are stable against light.

[10] S. Bräse, A. de Meijere in *Metal-catalyzed Cross-Coupling Reactions* (Eds.: F. Diederich, P. J. Stang), WILEY-VCH, Weinheim, **1998**, 99 – 167, and references therein.

[11] a) For examples on a solid support, see V. Yedida, C. C. Leznoff, *Can. J. Chem*. **1980**, *58*, 1144 – 1150; b) L. F. Tietze, T. Hippe, A. Steinmetz, *Synlett* **1996**, 1043 – 1044; c) thermal Diels – Alder reactions on a cinnamonic acid derivative need higher temperature.

[12] a) H. C. Kolb, M. S. VanNieuwenhze, K. B. Sharpless, *Chem. Rev.* **1994**, *94*, 2483 – 2547; b) H. Han, K. D. Janda, *Angew. Chem*. **1997**, *109*, 1835 – 1837; *Angew. Chem. Int. Ed. Engl.* **1997**, *36*, 1731 – 1733.

[13] L. F. Tietze, T. Hippe, A. Steinmetz, *Chem. Commun*. **1998**, 793 – 794, and references therein.

[14] a) N. Kornblum, *Org. React*. **1944**, *2*, 262; b) N. Kornblum, A. E. Kelly, G. D. Cooper, *J. Am. Chem. Soc*. **1952**, *74*, 3074 – 3076, and references therein.

[15] This kind of effect in which solid-phase chemistry is different to the corresponding reactions in the liquid phase is known.[1] Therefore, observations in either system are not always transferable. In this case a Meerwein reduction of the regenerated diazonium salt seems to be favored on the solid phase since the resin might enhance a radical mechanism relative to an ionic pathway.

[16] After longer reaction times (> 10 min) or higher reaction temperatures (> 50 °C) polymers of the solvent could be detected, which were removed by solid-phase extraction. Literature known compounds are identified by their spectroscopic data and by comparison with authentic samples. All new compounds gave correct spectroscopic data (IR, MS, NMR).

[17] The purity of the products are reproducibly excellent. In the case of lower yields, repetitive cleavage results in more material.

[18] S. Bräse, D. Enders, J. Köbberling, unpublished results.

[19] N. Satyamurthy, J. R. Barrio, *J. Org. Chem*. **1983**, *48*, 4394 – 4396.

Quantitative Monitoring of Solid-Phase Synthesis Using Gated Decoupling ^{13}C NMR Spectroscopy with a ^{13}C-Enriched Protecting Group and an Internal Standard in the Synthesis of Sialyl Lewis^x Tetrasaccharide**

Takuya Kanemitsu, Osamu Kanie,* and Chi-Huey Wong*

Polymer-supported organic synthesis is gaining increasing attention in connection to combinatorial chemistry. Despite the recent success of polymer-supported oligosaccharide synthesis, methods for the the qualitative and quantitative nondestructive monitoring of the reaction have not yet been developed. Among such monitoring approaches, those based on NMR spectroscopy[1] are perhaps the most useful. We are particularly interested in using ^{13}C NMR spectroscopy in this context since it can be performed with conventional high-field NMR spectrometers.[2] The ordinary method is, however, not realistic due to the low signal intensities and the lack of quantitative information, especially when small amounts of compounds are being synthesized for screening purposes. To overcome this problem, Look et al. reported the use of ^{13}C-enriched synthetic blocks in polymer-supported organic synthesis as a potential application to combinatorial chemistry.[2d] This method is indeed important; however, the incorporation of ^{13}C nuclei into a synthon will determine the practicality of the approach. The nuclear Overhauser effect (NOE) from directly attached proton(s) may also affect the integration. To demonstrate a successful application of the method to oligosaccharide synthesis, we have used a ^{13}C-enriched protecting group for the glycosylation reagents together with a ^{13}C-enriched internal standard. Also, the gated decoupling ^{13}C NMR spectroscopy[3] is performed in the presence of a relaxation agent to avoid complications arising from NOEs in the quantitative monitoring of the reaction. Hence the reaction progress can be monitored by integration of the ^{13}C NMR signal of the protecting group and comparing with that of the internal integral standard. Using this strategy, we report herein the first chemical solid-phase synthesis of sialyl Lewis^x tetrasaccharide (sLe^x), which is a ligand of selectins involved in inflammatory reactions.[4, 5]

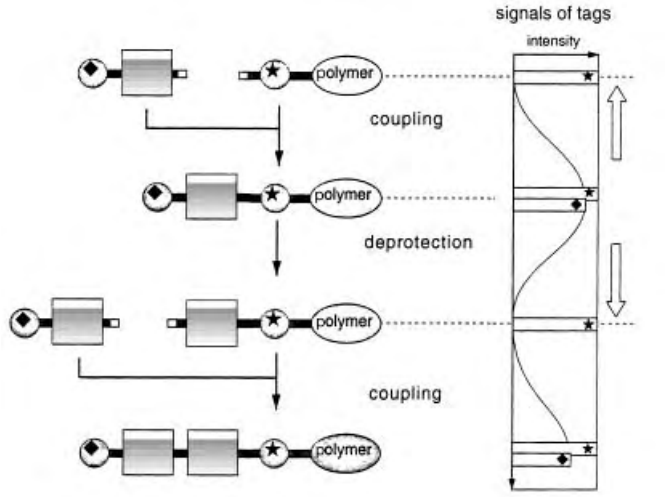
[*] Dr. O. Kanie, Prof. Dr. C.-H. Wong,[+] Dr. T. Kanemitsu
Frontier Research Program (FRP)
The Institute of Physical and Chemical Research (RIKEN)
2-1 Hirosawa, Wako-shi, Saitama 351-01 (Japan)
Fax: (+81) 48-467-3620
E-mail: kokanee@postman.riken.go.jp

[+] Permanent address:
Department of Chemistry, The Scripps Research Institute
10550 North Torrey Pines Road, La Jolla, CA 92037 (USA)
Fax: (+1) 619-784-2409
E-mail: wong@scripps.edu

[**] We thank Dr. Jun Uzawa (RIKEN) for valuable suggestions and discussions on NMR studies. We are also grateful to Dr. Yoshitaka Nagai and Dr. Tomoya Ogawa (RIKEN) for their continued support and encouragement. This research was supported by the Science and Technology Agency of the Japanese Government through the Special Postdoctoral Researchers Program (T.K.) and the FRP.

 © WILEY-VCH Verlag GmbH, D-69451 Weinheim, 1998 1433-7851/98/3724-3415 $ 17.50+.50/0

Our strategy is illustrated in Scheme 1. A ^{13}C-enriched linker (∗) is incorporated in the support as a satellite to a ^{13}C-enriched protecting group of the growing molecule (◆). The signal of the protecting group on the growing terminus during



Scheme 1. A strategy designed for quantitatively monitoring the progress of solid-phase oligosaccharide synthesis using gated decoupling ^{13}C NMR spectroscopy with ^{13}C-enriched protecting groups (◆) and an internal ^{13}C standard (∗) in the presence of a relaxation agent.

the coupling reaction can thus be compared to the one from the satellite to determine the completeness of the reaction.

To examine the feasibility of this strategy, we made several decisions prior to the synthesis: 1) At least three glycosylation reactions are carried out on the solid support to give a minimum of tetrasaccharide, which would cover the size of important carbohydrate moieties involved in recognition events. 2) Only two protecting groups—namely, benzyl as "permanent" and ^{13}C-enriched acetyl (◆) as "temporary" protecting groups—are used to avoid any complications. Only the sugar unit added last has other protecting groups. 3) The stereospecificity is controlled by means of solvent effects or by neighboring group participation. 4) ^{13}C-enriched glycine (∗), which is incorporated as a part of the linker, serves as the internal integration standard. 5) All of the donors are given as the thioglycosides.

We started the synthesis with incorporation of [1-^{13}C]glycine **1** into an amine on a Tentagel support (0.26 mmol g^{-1} polymer; **A** →**B**; Scheme 2).[2, 6] The second step, after the Fmoc group had been removed, was to introduce linker **2**, a hydroxyhexanoic acid derivative in which the hydroxyl group was protected with a *1*-^{13}C-labeled acetyl group (◆Ac), to give **D**. The yield was evident from the integration of ^{13}C NMR signals (97.2% yield; see Figure 1). We could have incorporated the first sugar residue as a glycoside of the linker; however, to illustrate the potential of the synthetic strategy and to keep the glycosylation reagents (glycosyl donors) universal, we decided to add the linker first. Removal of the ◆Ac group by treatment of the polymer with MeONa in MeOH/DMF resulted in complete disappearance of the corresponding ^{13}C NMR signal, indicating a quantitative deprotection. Next, the first glycosylation reaction was carried

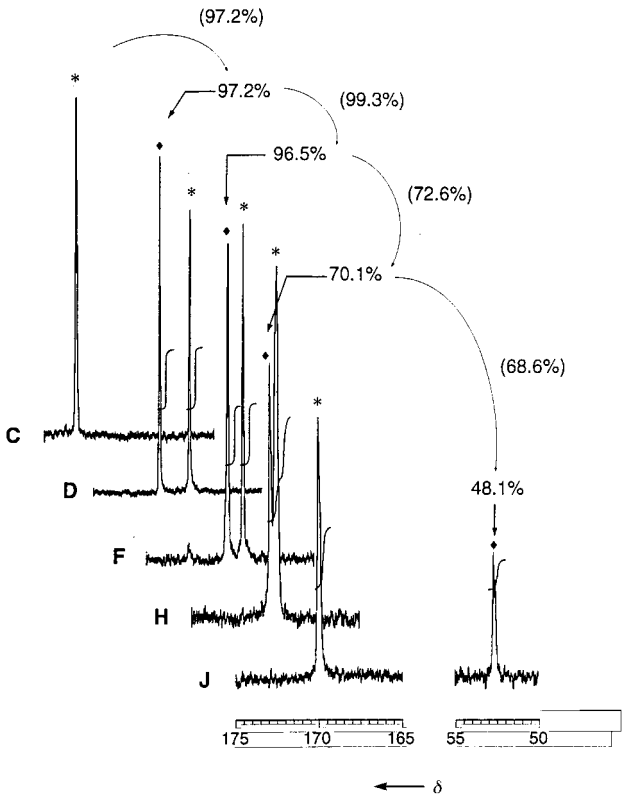
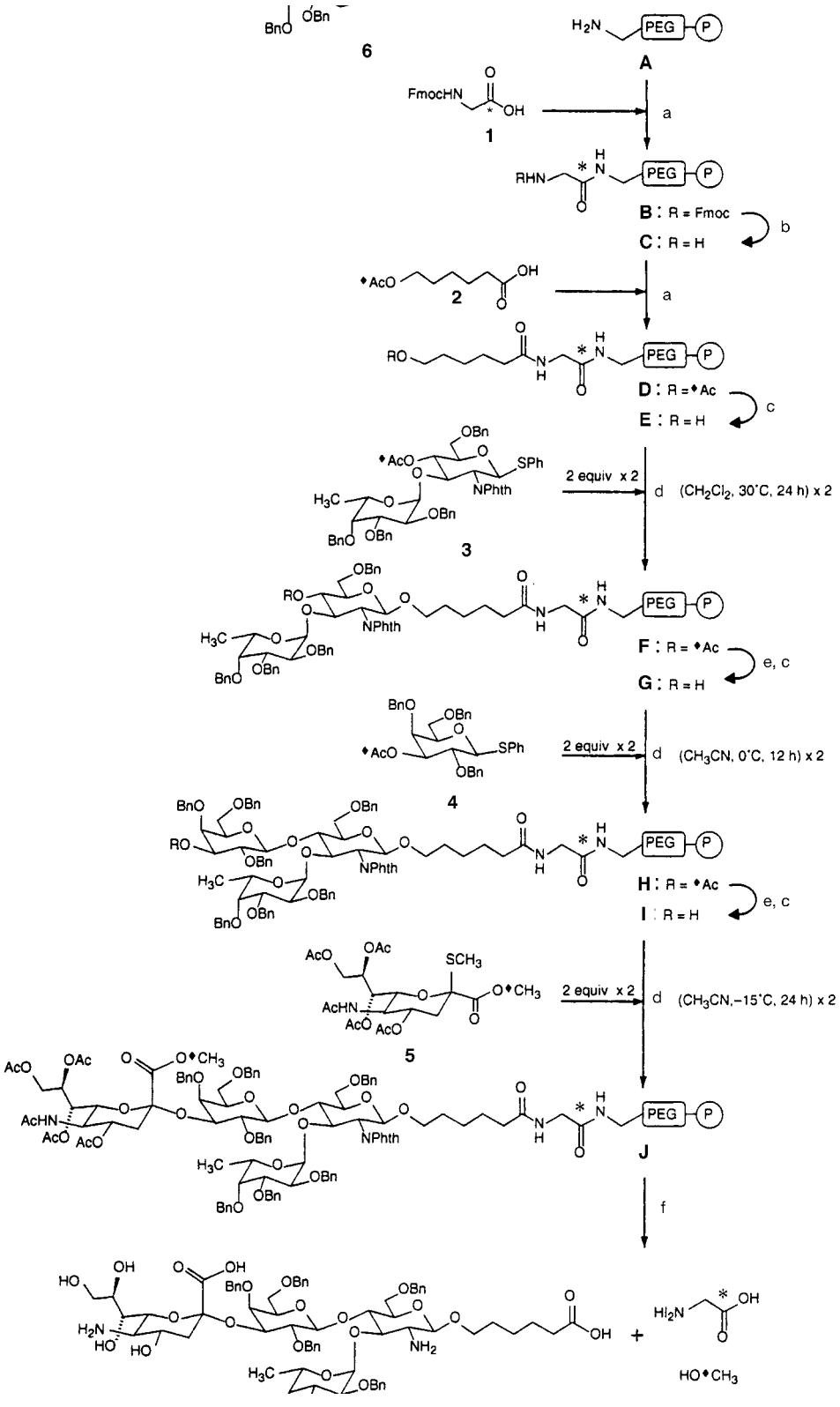


Figure 1. ^{13}C NMR spectra of polymers **C**, **D**, **F**, **H**, and **J**. Only selected areas are shown together with the yields calculated from the integrations. Each reaction yield is shown in brackets. ∗: Signal of the linker (^{13}C-labeled glycine C=O), ◆: signal of the ^{13}C-labeled protecting group in the growing molecule. The height of the signal ∗ in **D** appears lower due to the broadening of the signal.

out with donor **3**,[7] the 4-OH group of which was protected by ◆Ac. The reaction was carried out twice in the presence of DMTST[8] in CH_2Cl_2 at 30 °C to yield **F** (99.3%; see legend of Scheme 2 for abbreviations). To avoid the formation of incomplete sequence, the unreacted hydroxyl group was capped with a TBDMS group. After removal of the ◆Ac group (→**G**), the galactosyl donor **4**[9] was coupled under similar glycosylation conditions and again capped to give the Lewis^x trisaccharide **H** in 72.6%. Deprotection followed by sialylation using donor **5**,[10] the carboxylic acid function of which was protected as a ^{13}C methyl ester, in CH_3CN[11] gave the tetrasaccharide on the solid support (**J**) in 68.4% (overall yield 48.1%).

We have used ^{13}C-enriched carbonyl carbon atoms (◆Ac and ∗glycine) throughout the synthesis except for the terminal sialic acid. This raises a question about the reliability of the integration because the signal of the methyl carbon might be affected by the NOE from the directly attached protons. We finally treated the resin containing **J** with aqueous NaOH to release the tetrasaccharide as well as the ^{13}C-labeled methanol and glycine in a sealed vessel. The released materials were analyzed directly in solution by ^{13}C NMR spectroscopy. The integration of the MeOH signal was found to be 45% (ca. 6% error to gel-phase NMR data shown above) of that of the glycine signal, indicating the usefulness of the gated decoupling method in quantitative solid-phase monitoring. Con-

 © WILEY-VCH Verlag GmbH, D-69451 Weinheim, 1998 1433-7851/98/3724-3416 $ 17.50+.50/0 *Angew. Chem. Int. Ed.* **1998**, *37*, No. 24



Scheme 2. Solid-phase synthesis of tetrasaccharide **6**. Reagents and conditions: a) HBTU (3 equiv), HOBt (0.2 equiv)/CH_2Cl_2, 25 °C, 3 h: b) 50% piperidine/DMF, 25 C, 3 h; c) 0.05 M NaOMe in MeOH/DMF (1/1 v/v), 25 °C, 24 h; d) DMTST (8 equiv), 3-Å molecular sieves; temperatures, solvents, and reaction times are noted on the scheme; e) TBDMSCl, imidazole, CH_2Cl_2, 25 C, 24 h; f) 1N NaOH in EtOH/H_2O (1/1), 100 °C, 12 h. Bn = benzyl, DMF = dimethylformamide, DMTST = (dimethylthio)methylsulfonium triflate, Fmoc = 9-fluorenylmethoxycarbonyl, HBTU = 2-(1-*H*-benzotriazol-1-yl)-1,1,3,3-tetramethyluronium hexafluorophosphate, HOBt = 1-hydroxy-1*H*-benzotriazole, PEG = poly(ethylene glycol), Ⓟ = Tentagel support, Phth = phthaloyl, TBDMS = *tert*-butyldimethylsilyl.

firmation of the synthesized tetrasaccharide by MALDI TOF mass spectrometric analysis of the released mixture showed the presence of partially protected sialyl Le^x structure **6** (*m*/*z* 1481.8 $[M+H]^+$).

We have used two ^{13}C-enriched markers as an internal standard and as a protecting group on the growing molecule for the simple, nondestructive, and quantitative monitoring of solid-phase chemical oligosaccharide synthesis. Because the two markers are not directly incorporated in the molecule to be synthesized, one may use other tags instead of ^{13}C nuclei for the monitoring. In principle, different ^{13}C-labeled protecting groups can also be used in different orthogonal strategies. Though the anomeric purity of each glycosidic linkage remains to be determined, the strategy should be applicable to the small-scale solid-phase synthesis of oligosaccharides, and perhaps of other molecules, in a combinatorial manner.

Experimental Section

Typical coupling reaction: A suspension of the resin carrying hydroxyl groups (ca. 0.25 mmol g^{-1} resin, 500 mg), phenylthioglycoside (0.25 mmol), and 3 Å molecular sieves (500 mg) in dry CH_2Cl_2 (10 mL) was stirred at 25 °C for 12 h. To this mixture was added DMTST (1 mmol) below the temperature designated in Scheme 2. The reaction mixture was shaken with a vortex mixer at the designated temperature for 24 h. To monitor the course of the reaction, an aliquot of resin was taken from the reaction mixture at this stage. The resin used for the monitoring could be put back to the reaction mixture after it had been washed with $CHCl_3$. After successive washing of the resin with $CHCl_3$, MeOH, water, DMF, and $CHCl_3$, the glycosylation reaction was repeated once more under the same conditions. In order to cap the unreacted hydroxyl group, the resin was treated with *t*$BuMe_2SiCl$ and imidazole at 25 °C for 24 h after washing.

Gated decoupling ^{13}C NMR measurement: The dried resin (ca. 60 mg) was slurried in $CDCl_3$, and the sample was prepared with a relaxation agent,

 © WILEY-VCH Verlag GmbH, D-69451 Weinheim, 1998 1433-7851/98/3724-3417 $ 17.50+.50/0

chromium(III) 2,4-pentanedionate ([Cr(acac)$_3$], 0.1M] in an ordinary 5-mm ϕ NMR tube. The ^{13}C NMR spectrum was measured on a JEOL EX-270 spectrometer at 68 MHz and operated with 9-s relaxation delay and gated decoupling without NOE (160 transients, 0.6 s acquisition time). The spectra were referred to the resonance for TMS. ^{13}C NMR spin-lattice relaxation times (T_1) were measured by using the inversion recovery method at 298 K (16 data points, 16 scans per point). The T_1 values for methyl and carbonyl groups attached to the resin were shorter than 1 s in the presence of [Cr(acac)$_3$] and 12 s and 29 s in the absence of the relaxation agent.

Received: June 26, 1998 [Z12062IE]
German version: *Angew. Chem.* **1998**, *110*, 3574 – 3577

Keywords: analytical methods · glycosylations · NMR spectroscopy · oligosaccharides · solid-phase synthesis

[1] a) S. P. Douglas, D. M. Whitfield, J. J. Krepinsky, *J. Am. Chem. Soc.* **1991**, *113*, 5095 – 5097; b) R. Rodebaugh, S. Joshi, B. Fraser-Reid, H. M. Geysen, *J. Org. Chem.* **1997**, *62*, 5660 – 5661; c) P. H. Seeberger, X. Beebe, G. D. Sukenick, S. Pochapsky, S. J. Danishefsky, *Angew. Chem.* **1997**, *109*, 507 – 510; *Angew. Chem. Int. Ed. Engl.* **1997**, *36*, 491 – 493.

[2] a) E. Giralt, J. Rizo, E. Pedroso, *Tetrahedron* **1984**, *40*, 4141 – 4152; b) A. G. Ludwick, L. W. Jelinski, D. Live, A. Kintanar, J. Dumais, *J. Am. Chem. Soc.* **1986**, *108*, 6493 – 6496; c) F. A. Albericio, M. Pons, E. Pedroso, E. Giralt, *J. Org. Chem.* **1989**, *54*, 360 – 366; d) G. C. Look, C. P. Holmes, J. P. Chinn, M. A. Gallop, *J. Org. Chem.* **1994**, *59*, 7588 – 7590; e) J. Blumel, *J. Am. Chem. Soc.* **1995**, *117*, 2112 – 2113; f) J. M. Brown, J. Ramsden, *Chem. Commun.* **1996**, 2117 – 2118.

[3] J. N. Shoolery, *Prog. Nucl. Magn. Reson. Spectrosc.* **1977**, *11*, 79 – 93.

[4] a) M. L. Phillips, E. Nudelman, F. C. A. Gaeta, M. Perez, A. K. Singhal, S. Hakomori, J. C. Paulson, *Science* **1990**, *250*, 1130 – 1132; b) G. Walz, A. Aruffo, W. Kolanus, M. Berilacqua, B. Seed, *Science* **1990**, *250*, 1332 – 1335; c) J. B. Lowe, L. M. Stoolman, R. P. Nair, R. D. Larsen, T. L. Berhend, R. M. Marks, *Cell* **1990**, *63*, 475 – 484.

[5] Solid-phase syntheses of sialyl Lewis^x tetrasaccharide were achieved by enzyme reactions: a) M. Schuster, P. Wang, J. C. Paulson, C.-H. Wong, *J. Am. Chem. Soc.* **1994**, *116*, 1135 – 1136; b) O. Blixt, T. Norberg, *J. Org. Chem.* **1998**, *63*, 2705 – 2710.

[6] a) E. Bayer, K. Albert, H. Willisch, W. Rapp, B. Hemmasi, *Macromolecules* **1990**, *23*, 1937 – 1940; b) K. Nokihara, W. Rapp, *Shimadzu Rev.* **1993**, *50*, 25 – 31.

[7] Compound **3** was synthesized through coupling of phenylthioglycosides of tribenzyl L-fucose and *N*-phthaloyl-4,6-benzylidene-D-glucosamine derivative as donor and acceptor, respectively. The synthesis will be reported in due course.

[8] a) P. Fügedi, P. J. Garegg, *Carbohydr. Res.* **1986**, *149*, C9-C12; b) M. Ravenscroft, R. M. G. Roberts, J. G. Tillett, *J. Chem. Soc. Perkin Trans.* **1982**, *2*, 1569 – 1572.

[9] Compound **4** was synthesized according to a literature method: O. Kanie, Y. Ito, T. Ogawa, *Tetrahedron Lett.* **1996**, *37*, 4551 – 4554.

[10] a) O. Kanie, M. Kiso, A. Hasegawa, *J. Carbohydr. Chem.* **1988**, *7*, 501 – 506; b) A. Hasegawa, H. Ohki, T. Nagahama, H. Ishida, M. Kiso, *Carbohydr. Res.* **1991**, *212*, 277 – 281.

[11] A. Hasegawa, T. Nagahama, H. Ohki, K. Hotta, H. Ishida, M. Kiso, *J. Carbohydr. Chem.* **1991**, *10*, 493 – 498.

Single-Step Construction of a Nine-Membered Carbocycle by a New [4+4+1] Cycloaddition**

Masahiro Murakami,* Kenichiro Itami, and Yoshihiko Ito*

There is much interest in medium-sized, that is, eight- to eleven-membered, carbocycles because they are often an important structural feature of biologically active compounds. From the synthetic point of view, however, construction of medium-sized ring systems is a formidable objective due to unfavorable entropy factors as well as energy barriers inherent to cyclization (generally ascribed to arising angle strain, bond opposition (Pitzer) strain, and transannular interactions).[1, 2] Especially scarce are methods for the preparation of nine-membered carbocycles,[3] the development of which remains an important challenge in organic chemistry.

Vinylallene has been described to act as a versatile four-carbon unit in metal-catalyzed [4+1][4] and [4+2] cycloaddition[5] reactions. We expected that the use of an appropriate metal catalyst capable of simultaneous multiple coordination of vinylallene would make it possible to incorporate two or more molecules of vinylallene in the resulting skeleton in a single operation. Here we report a palladium-catalyzed [4+4+1] cycloaddition reaction which provides a new route to nine-membered carbocycles. To the best of our knowledge, this is the first example of a [4+4+1] cycloaddition.[6] While our approach presently requires certain substitution in the substrate, we believe that this new reaction may eventually lead to a useful strategy for the construction of nine-membered rings.

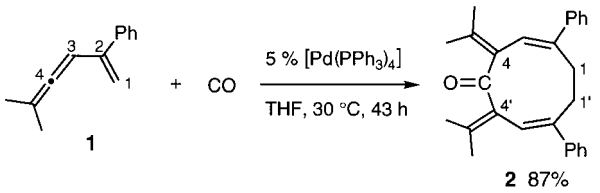
A solution of vinylallene **1** in THF was stirred under an atmosphere of carbon monoxide in the presence of 5 mol% palladium(0) catalyst at 30 °C. The reaction mixture was stirred for 43 hours, and vinylallene **1** was consumed to afford a sole product. From the spectroscopic data the structure was concluded to be the symmetrical nine-membered ketone **2**, as depicted in Scheme 1. The cyclic compound **2**, isolated in 87% yield, was assembled from two molecules of vinylallene **1** and one molecule of carbon monoxide. Vinylallene **1** coupled at the 1-position in a head-to-head manner, providing the two four-carbon units. Cheletropic incorporation of carbon monoxide between the 4-positions furnished the nine-membered ketone **2** as a [4+4+1] cycloadduct.

Vinylallene **3** also underwent an analogous [4+4+1] cycloaddition reaction to afford **4** as a solid in 61% yield (Scheme 2). Although the ketone gradually decomposed on exposure to light, careful recrystallization from ether/hexane generated single crystals suitable for X-ray crystallography,[7]

[*] Assoc. Prof. M. Murakami, Dr. K. Itami, Prof. Y. Ito
Department of Synthetic Chemistry and Biological Chemistry
Kyoto University, Yoshida, Kyoto 606-8501 (Japan)
Fax: (+81) 75-753-5668
E-mail: murakami@sbchem.kyoto-u.ac.jp

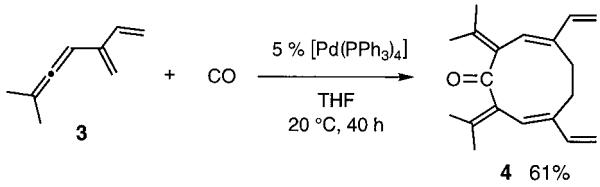
[**] Support from Monbusho (Grant-in-Aid for Scientific Research on Priority Areas, No. 283: Innovative Synthetic Reactions) is gratefully acknowledged. K.I. thanks the Japan Society for the Promotion of Science for a predoctoral fellowship.

 © WILEY-VCH Verlag GmbH, D-69451 Weinheim, 1998 1433-7851/98/3724-3418 $ 17.50+.50/0



1 2 87%

Scheme 1. Palladium-catalyzed [4+4+1] cycloaddition of **1** and carbon monoxide.



3 4 61%

Scheme 2. Synthesis of the nine-membered cyclic ketone **4**.

which unambiguously established the nine-membered-ring structure (Figure 1). Whereas the NMR data of **4** conformed to the symmetrical structure, significant deformation was

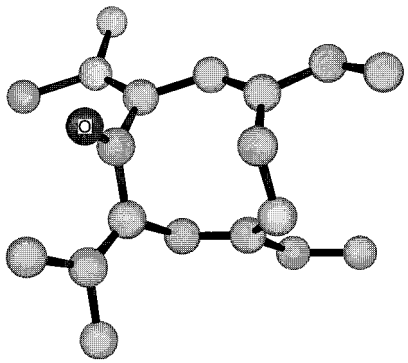
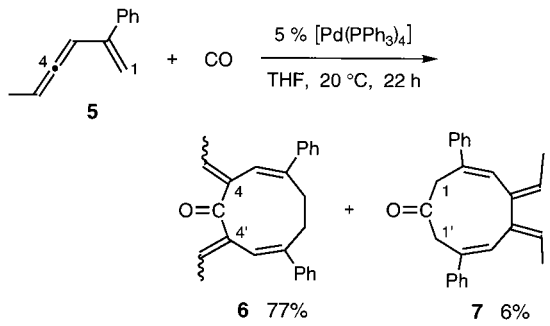


Figure 1. Molecular structure of **4** in the crystal (hydrogen atoms omitted for clarity).

observed in the solid state. On one side of the carbonyl group (the top half in Figure 1) the triene skeleton fits on a plane and is in full conjugation, but the triene unit severely deviates from the carbonyl plane. On the other side (the bottom half in Figure 1) the triene skeleton is divided into the exocyclic α,β-unsaturated carbonyl system and the remaining 1,3-diene system in terms of conjugation. Presumably the deformation reduces the steric congestion around the carbonyl group.

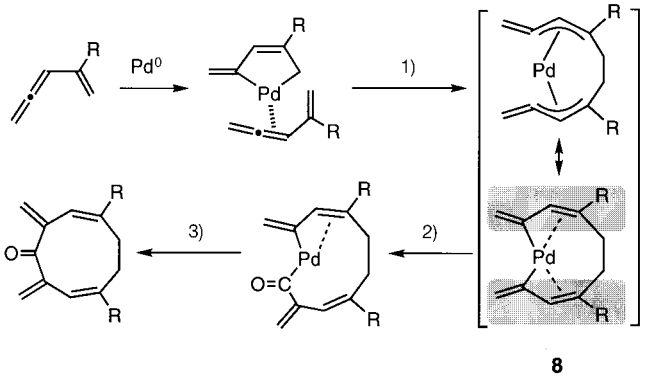
In the case of vinylallene **5** (Scheme 3), the [4+4+1] cycloadducts were obtained as a mixture of regio- and stereoisomers. In the dominant regioisomer (**6**), isolated in 77% yield, carbon monoxide was inserted between the sp^2 carbon atoms (4-positions), as is the case with **2** and **4**. The major regioisomer consisted of three stereoisomers with respect to the orientation of the two methyl groups of the exocyclic double bonds (outward–outward:outward–inward:inward–inward = 5:92:3).[8] Besides the major regioisomer (**6**), **7** was obtained as the minor regioisomer (6% yield), in which carbon monoxide was inserted between the sp^3 carbon atoms (1-positions). Interestingly, both of the methyl groups of **7** face outward, probably for steric reasons.



5 6 77% 7 6%

Scheme 3. Synthesis of the nine-membered cyclic ketones **6** and **7**.

A plausible mechanism to explain the formation of the nine-membered cyclic ketones **2**, **4**, and **6** is given in Scheme 4. A five-membered palladacycle is initially formed by the



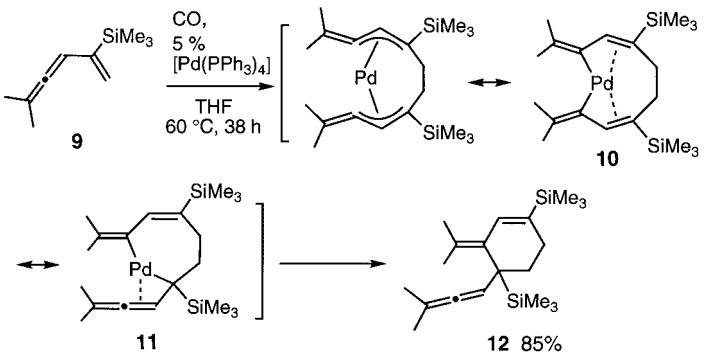
8

Scheme 4. Plausible mechanism of the [4+4+1] cycloaddition (substituents at the allenyl terminus omitted for clarity). 1) C–C bond formation, 2) CO insertion, 3) reductive elimination. Sections in the shaded boxes are conjugated.

reaction of a molecule of vinylallene with the palladium(0) catalyst. Another molecule of vinylallene binds to the palladium center at the allene site. A carbon–carbon bond is formed between the 1-positions producing a bis(π-allyl)-palladium intermediate.[5a] Among its resonance contributors, the σ-di(alkenyl)palladium form **8** would be of greater importance because it gains stabilization by the extended conjugation from the exocyclic C–C double bond through the endocyclic C–C double bond to the pendant unsaturated R (phenyl or vinyl) substituent. Insertion of carbon monoxide into the Pd–C_{sp^2} bond and subsequent reductive elimination would afford a nine-membered cyclic ketone.

For comparison, an analogous reaction was carried out with vinylallene **9**, which has a trimethylsilyl group as the pendant R substituent, and hence, no extended conjugation could be expected. With **9**, not a nine-membered carbocycle but the six-membered [4+2] cycloadduct **12** was formed exclusively (Scheme 5).[5a] In this case the σ-di(alkenyl)palladium form **10** might be less predominant due to the lack of stabilization by conjugation, and the other contributor (**11**) is liable to direct reductive elimination affording an easy-to-form, six-membered ring prior to insertion of carbon monoxide. This result, standing in marked contrast to the reactions with the vinylallenes **1**, **3**, and **5**, lends support to the mechanistic

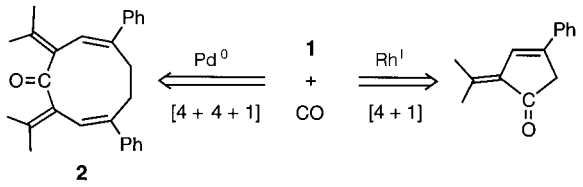
 © WILEY-VCH Verlag GmbH, D-69451 Weinheim, 1998 1433-7851/98/3724-3419 $ 17.50+.50/0



Scheme 5. Palladium-catalyzed [4+2] cycloaddition of **9** and CO. The reaction from **11** to **12** proceeds with reductive elimination.

interpretation that the extended conjugation with the pendant R substituent is crucial for the formation of the nine-membered carbocycle.

An unprecedented [4+4+1] cycloaddition is realized by a palladium(0)-catalyzed carbonylation with vinylallenes lacking coordinative heteroatom functionalities. Palladium(0) serves as a template to set three components in an array for a cycloaddition otherwise impossible to achieve. The usefulness of this new reaction is validated by the fact that nine-membered carbocycles that are normally difficult to form are constructed in a single chemical operation with good atom economy,[9] a concept which has gained in interest in organic synthesis. Although the full potential of the new cycloaddition reported here awaits exploration, it is clearly demonstrated that [4+4+1] is a viable mode. Finally, it should be noted that the present reaction with the palladium(0) catalyst provides a remarkable contrast to that with rhodium(I):[4d,e] palladium(0) drives the [4+4+1] cycloaddition to give a nine-membered adduct, whereas rhodium(I) promotes [4+1] cycloaddition producing a five-membered adduct from the same vinylallene and carbon monoxide (Scheme 6).



Scheme 6. Contrast in the assembly modes of cycloadditions mediated by Pd^0 and Rh^I catalysts.

Experimental Section

2: A mixture of $[Pd(PPh_3)_4]$ (54 mg, 47 μmol) and 5-methyl-2-phenyl-1,3,4-hexatriene (**1**, 160 mg, 940 μmol) in THF (3 mL) was stirred under an atmosphere of carbon monoxide at 30 °C for 43 h. The reaction mixture was passed through a pad of Florisil to remove the insoluble materials. The eluent was concentrated to dryness under vacuum, and the residue was subjected to column chromatography (silica gel, ether/hexane (1/10)) to afford **2** (150 mg, 87 %) as a white solid. ^{1}H NMR ($CDCl_3$, 200 MHz): $\delta =$ 1.88 (s, 6H), 2.04 (s, 6H), 2.80 (s, 4H), 6.47 (s, 2H), 7.15 – 7.30 (m, 10H); ^{13}C{^{1}H} NMR ($CDCl_3$, 50 MHz): $\delta =$ 22.4, 22.5, 30.2, 126.6, 127.0, 128.3, 136.3, 141.1, 141.3, 144.5, 203.1; IR (neat): $\tilde{\nu} =$ 1670, 1590 cm^{-1}; HRMS *m/z* calcd for $C_{27}H_{28}O$: 368.2140; found: 368.2121; elemental analysis calcd for $C_{27}H_{28}O$: C 88.00, H 7.66; found: C 87.74, H 7.71.

Received: July 6, 1998 [Z12096IE]
German version: *Angew. Chem.* **1998**, *110*, 3616 – 3619

Keywords: carbonylations · cycloadditions · palladium · synthetic methods · vinylallenes

[1] M. B. Smith in *Organic Synthesis*, McGraw-Hill, New York, **1994**, pp. 52 – 58.
[2] E. L. Eliel, S. H. Wilen in *Stereochemistry of Organic Compounds*, Wiley, New York, **1994**, pp. 675 – 685.
[3] a) B. M. Trost, T. R. Verhoeven, *J. Am. Chem. Soc.* **1979**, *101*, 1595; b) T. Onuma, N. Hata, N. Miyachi, T. Wakamatsu, Y. Ban, *Tetrahedron Lett.* **1986**, *27*, 219; c) B. M. Trost, P. R. Seoane, *J. Am. Chem. Soc.* **1987**, *109*, 615; d) P. A. Wender, M. Harmata, D. Jeffrey, C. Mukai, J. Suffert, *Tetrahedron Lett.* **1988**, *29*, 909; e) P. A. Wender, J. A. McKinny, C. Mukai, *J. Am. Chem. Soc.* **1990**, *112*, 5369; f) C. G. Kreiter, K. Lehr, M. Leyendecker, W. S. Sheldrick, R. Exner, *Chem. Ber.* **1991**, *124*, 3; g) T. V. Lee, J. R. Porter, F. S. Roden, *Tetrahedron* **1991**, *47*, 139; h) T. Doi, T. Takahashi, *J. Org. Chem.* **1991**, *56*, 3465; i) K. Iida, M. Hirama, *J. Am. Chem. Soc.* **1994**, *116*, 10310; j) S. Ma, E. Negishi, *J. Am. Chem. Soc.* **1995**, *117*, 6345; k) C.-J. Li, D.-L. Chen, Y.-Q. Lu, J. X. Haberman, J. T. Mague, *J. Am. Chem. Soc.* **1996**, *118*, 4216; l) J. H. Rigby, K. R. Fales, *Tetrahedron Lett.* **1998**, *39*, 1525; m) F. Matsuda, T. Sakai, N. Okada, M. Miyashita, *Tetrahedron Lett.* **1998**, *39*, 863.
[4] a) M. S. Sigman, B. E. Eaton, *J. Am. Chem. Soc.* **1996**, *118*, 11783; b) T. Mandai, J. Tsuji, Y. Tsujiguchi, *J. Am. Chem. Soc.* **1993**, *115*, 5865; c) C. Darcel, C. Bruneau, P. H. Dixneuf, *Synlett* **1996**, 218; d) M. Murakami, K. Itami, Y. Ito, *Angew. Chem.* **1995**, *107*, 2943; *Angew. Chem. Int. Ed. Engl.* **1995**, *34*, 2691; e) M. Murakami, K. Itami, Y. Ito, *J. Am. Chem. Soc.* **1997**, *119*, 2950.
[5] a) H. Siegel, H. Hopf, A. Germer, P. Binger, *Chem. Ber.* **1978**, *111*, 3112; b) T. Mandai, S. Suzuki, A. Ikawa, T. Murakami, M. Kawada, J. Tsuji, *Tetrahedron Lett.* **1991**, *32*, 7687; c) M. Murakami, K. Itami, Y. Ito, *J. Am. Chem. Soc.* **1997**, *119*, 7163; d) M. Murakami, M. Ubukata, K. Itami, Y. Ito, *Angew. Chem.* **1998**, *110*, 2362; *Angew. Chem. Int. Ed.* **1998**, *37*, 2248.
[6] For a review of transition metal mediated cycloaddition reactions, see: M. Lautens, W. Klute, W. Tam, *Chem. Rev.* **1996**, *96*, 49.
[7] **4**: $C_{19}H_{24}O$, $M_r = 268.4$, monoclinic, space group $P2_1/a$, $a = 11.295(7)$, $b = 15.972(8)$, $c = 10.006(6)$ Å, $\beta = 113.72(3)^\circ$, $V = 1652.7(5)$ Å^3, $Z = 4$, $\rho_{calcd} = 1.08$ g cm^{-3}, $\mu = 0.601$ cm^{-1}. Intensity data were collected on a Mac Science DIP2000 diffractometer with graphite-monochromated $Mo_{K\alpha}$ radiation ($\lambda = 71.069$ pm), using an imaging plate area detector with an oscillation mode. From a total of 16928 observations, 2796 unique reflections were processed by a MAC-DENZO program. The structure was solved by direct methods and refined by full-matrix least squares to $R = 0.066$ ($R_w = 0.073$) for 1169 reflections [$I > 3.0\sigma(I)$], using the Crystan GM program package. The non-hydrogen atoms were refined anisotropically. Hydrogen atoms were observed or calculated and refined isotropically with a fixed C–H distance of 0.96 Å. Crystallographic data (excluding structure factors) have been deposited with the Cambridge Crystallographic Data Centre as supplementary publication no. CCDC-102096. Copies of the data can be obtained free of charge on application to CCDC, 12 Union Road, Cambridge CB2 1EZ, UK (Fax: (+44)1223-336-033; e-mail: deposit@ccdc.cam.ac.uk).
[8] The three stereoisomers were separated by HPLC, and the stereochemistries were assigned based on ^{1}H NMR NOE experiments.
[9] B. M. Trost, *Science* **1991**, *254*, 1471.

 © WILEY-VCH Verlag GmbH, D-69451 Weinheim, 1998 1433-7851/98/3724-3420 $ 17.50+.50/0

Carbynehydridoruthenium Complexes as Catalysts for the Selective, Ring-Opening Metathesis of Cyclopentene with Methyl Acrylate**

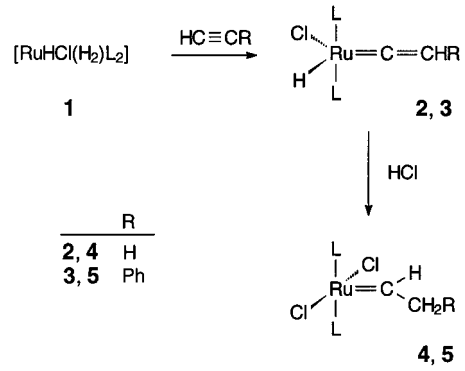
Wolfram Stüer, Justin Wolf, Helmut Werner,*
Peter Schwab, and Michael Schulz

Dedicated to Professor Ernst-Otto Fischer on the occasion of his 80th birthday

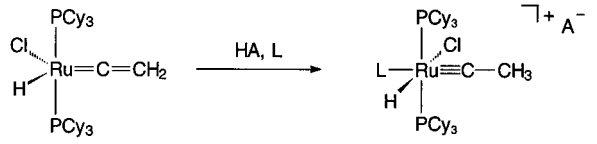
Carbeneruthenium complexes of the type $[RuCl_2(=CHR)(PR'_3)_2]$, which were first prepared by Grubbs and co-workers, are not only highly efficient catalysts for olefin metathesis,[1] but are also increasingly used in organic synthesis.[2] In contrast to related catalytically active compounds of molybdenum and tungsten, the ruthenium complexes have the advantage of tolerating substrates containing polar functional groups.[3] The disadvantage, however, is the low activity in the metathesis of electron-poor olefins such as acrylic acid and derivatives thereof. We are particularly interested in the selective ring-opening metathesis (ROM) of cyclopentene with various acyclic olefins as chain transfer reagents (CTA); the desired products are not telechelic polymers as in previous work,[4] but linear functionalized olefins with a chain length of up to 20 carbon atoms. Owing to the work by Blechert, Crowe and co-workers it is known that the Grubbs-type catalysts are unsuitable for metathesis with electron-poor acyclic olefins as CTA, whereas the catalytically active carbene complexes of the Schrock-type can be applied to some extent.[5] Here we describe the first catalysts based on ruthenium which are able to catalyze the selective ROM of cyclopentene with methyl acrylate as an electron-poor olefin, thereby leading to the formation of long-chain functionalized olefins as the main products.[6]

Recently, we reported an efficient one-pot synthesis of the carbeneruthenium complexes $[RuCl_2(=CHCH_2R)(PCy_3)_2]$ (R = H (**4**), Ph (**5**); Cy = cyclohexyl) from $RuCl_3$, Mg, PCy_3, H_2, HC≡CR, and H_2O.[7] For establishing this synthesis it was important to recognize that upon treatment of **1**[8] with 1-alkynes initially the hydridovinylidene compounds **2** and **3**[9] are formed, which then react with HCl or a synthetic equivalent thereof to afford the desired carbene complexes **4** and **5**, respectively (L = PCy_3).

Following this observation, we were interested to find out whether the reaction of the hydridovinylidene compounds **2** and **3** with acids HA, containing an anion that does *not* coordinate to a metal center, would lead to the formation of



cationic carbene complexes of the general composition $[RuCl(=CHCH_2R)(PCy_3)_2]^+$ (with A^- as anion). These 14-electron species could be the counterparts of the compound $[Ru(Ph)(CO)(PtBu_2Me)_2]^+$, which was recently described by Caulton et al.[10] Therefore, when a solution of complex **2** in CH_2Cl_2/Et_2O was treated with an excess of a solution of HBF_4 in Et_2O at −80 °C and then worked-up in an appropriate way, a yellow solid was obtained. This compound is not the anticipated cationic ethylidene derivative $[RuCl(=CHCH_3)(PCy_3)_2]BF_4$ but, in agreement with the NMR spectra, the carbynehydrido complex **6**. The ^1H spectrum displays no signal in the low-field region, which would be expected for the α-hydrogen atom of an ethylidene ligand, but a triplet resonance at $\delta = -6.91$ ($^2J(P,H) = 15$ Hz), assigned to a metal-bonded hydride. In the ^{13}C NMR spectrum of **6** the signal of the α-carbon atom of the carbyne ligand appears as a triplet at $\delta = 316.1$ ($^2J(C,P) = 9$ Hz), and that of the β-carbon atom as a singlet at $\delta = 41.4$. Moreover, some resonances are observed which are assigned to an Et_2O ligand. This ligand is, however, only weakly coordinated and easily displaced by H_2O to give **7**. Analogous to the formation of **6**, compound **2** also reacts with $[HNMe_2Ph][B(C_6F_5)_4]$ and $[H(OEt_2)_2][B\{C_6H_3(CF_3)_2\}_4]$[11] to afford the corresponding carbyne complexes **8** and **9**, which differ in the counterion and the donor ligand L. In addition to the spectroscopic data, the composition of **6**–**9** is supported by their reactivity towards soluble chloride sources. Instead of the neutral carbynehydrido complex $[RuHCl_2(≡CCH_3)(PCy_3)_2]$ the isomeric carbene complex **4** is formed in quantitative yield.



2

	A	L
6	BF_4	OEt_2
7	BF_4	OH_2
8	$B(C_6F_5)_4$	NMe_2Ph
9	$B\{C_6H_3(CF_3)_2\}_4$	OEt_2

To the best of our knowledge, compounds **6**–**9** are the first cationic carbynehydrido complexes of ruthenium. With respect to the characteristic ^1H and ^{13}C NMR spectroscopic data, they are related to the compound $[OsHCl(≡CCH_2Ph)(OH_2)(PiPr_3)_2]BF_4$, the only carbynehydridoosmium complex

[*] Prof. Dr. H. Werner, Dipl.-Chem. W. Stüer, Dr. J. Wolf
Institut für Anorganische Chemie der Universität
Am Hubland, D-97074 Würzburg (Germany)
Fax: (+49) 931-8884605
E-mail: helmut.werner@mail.uni-wuerzburg.de
Dr. P. Schwab, Dr. M. Schulz
BASF Aktiengesellschaft, Ammoniaklaboratorium
D-67056 Ludwigshafen (Germany)

[**] This work was supported by the Deutsche Forschungsgemeinschaft (SFB 347) and the BASF AG. W.S. thanks the Fonds der Chemischen Industrie for a Kekulé scholarship. We are grateful to Dr. A. Schäfer and Dr. M. Schäfer for helpful discussions, and to Dr. W. Buchner for recording the ^2H NMR spectra.

 © WILEY-VCH Verlag GmbH, D-69451 Weinheim, 1998 1433-7851/98/3724-3421 $ 17.50+.50/0

reported as yet.[12a] Some uncharged compounds of the general composition $[OsHCl_2(\equiv CCH_2R)(P\mathit{i}Pr_3)_2]$ are also known.[12b, c] Since for the corresponding osmium complex with R = Ph the *cis* disposition of the hydrido and carbyne ligands has been confirmed by a single-crystal X-ray structure analysis,[12b] we assume that for **6**–**9** a similar configuration exists. Density functional theory (DFT) calculations for **6** are in agreement with the proposed *cis* arrangement of the hydrido and carbyne ligands.[13]

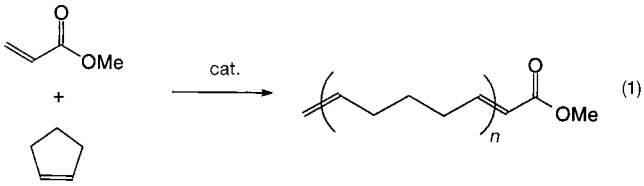
With regard to the mechanism of formation of compounds **6**–**9**, two possibilities are conceivable. The protonation of **2** either takes place at the β-carbon atom of the vinylidene ligand, or the attack of the proton is initially directed to the metal leading to the formation of the intermediate $[RuH_2Cl(=C=CH_2)(PCy_3)_2]^+$, which subsequently isomerizes to the respective carbynehydrido complex by a 1,3-hydrogen shift. A labeling experiment, based on the reaction of **2** with $[DNMe_2Ph][B(C_6F_5)_4]$, clearly confirms that the protonation follows the first pathway. As the ^2H NMR spectrum reveals, the deuterated compound $[RuHCl(\equiv CCH_2D)(NMe_2Ph)(PCy_3)_2][B(C_6F_5)_4]$ ([D$_1$]**8**) is exclusively formed, while an isotopomer with the deuterium bonded to the metal center cannot be detected.

Compounds **6**–**9** are yellow air-sensitive solids which in solution at room temperature completely decompose within 20–30 min. The stability depends only slightly on the counterion A^-, but is strongly influenced by the donor ligand L. Thus, the analogue of **6** with L = THF is significantly more labile in solution than the adduct with Et_2O. In this respect, it is important to note that the stability of the carbynehydrido derivatives increases considerably (up to several hours) upon addition of excess of L or HA to the solution. We therefore believe that the decomposition of **6**–**9** in solution is initiated both by the dissociation of L as well as by deprotonation.

The aforementioned lability of **6**–**9** possibly explains why these compounds are not accessible by halide abstraction from **4** with silver or thallium salts. At low temperature, no reaction between **4** and AgX or TlX occurs, and at room temperature unidentified mixtures of products are formed. However, if **4** is treated with a large excess (ca. 100-fold) of HBF_4 in Et_2O the carbynehydrido complex **6** is surprisingly generated in about 20% yield. As a by-product the phosphonium salt $[HPCy_3]BF_4$ (**10**) has been isolated.

Compounds **6**–**9** are highly efficient catalysts for olefin metathesis. We investigated in particular the catalytic activity of complex **6**, which catalyzes the ring opening metathesis polymerization (ROMP) of cyclic olefins such as cyclopentene, cyclooctene, cyclooctadiene, dicyclopentadiene, and oxanorbornene derivatives even more effectively than the Grubbs compound $[RuCl_2(=CHPh)(PCy_3)_2]$ (**11**).[14] A comparison experiment reveals that ROMP of cyclooctene (room temperature, $c_{cat.} = 10^{-3}$ M, time: 3 min, yield 90%) with **6** as catalyst is about 20 times faster than with **11**. The molecular-weight distribution and the polydispersity index of the polymer (amount of *trans* olefin 76%) is presently under investigation. From some preliminary experiments it can be concluded that the activity of **7**–**9** is comparable to that of **6**.

However, the carbynehydrido complexes **6**–**9** also catalyze the cross-olefin metathesis of cyclopentene with methyl acrylate [Eq. (1)]. Hereby a mixture of the first members of the homologous series of multiply unsaturated esters



(1)

$C_7H_{11}CO_2CH_3$, $C_{12}H_{19}CO_2CH_3$, and $C_{17}C_{27}CO_2CH_3$ are formed with a selectivity of 50, 40, and 10%. Compounds **4** and **11** are catalytically inactive in this process.

The cationic carbynehydrido complexes reported here are the first ruthenium compounds which are able to catalyze the metathesis of electron-poor olefins. Further applications of **6**–**9**, for example, for the cross-metathesis of alkynes,[15] are now being studied in our laboratory. Weiss[16a] as well as Fürstner[16b] and co-workers have recently shown that the carbynetungsten complex $[W(\equiv CCMe_3)(OCMe_3)_3]$ is a highly active catalyst both for the metathesis of acyclic diynes (ADIMET) and for the ring-closing reaction of diynes to cycloalkynes. For the neutral carbyneruthenium compounds $[RuCl(\equiv CR)(CO)(PPh_3)_2]$, which have been prepared by Roper et al. from $[RuCl_2(=CCl_2)(CO)(PPh_3)_2]$ and LiR,[17] a similar catalytic activity is unknown. Besides **6**–**9**, most recently also *cationic* allyl- and allenylideneruthenium complexes were described which partly catalyze olefin metathesis upon activation with diazoalkanes.[18]

Since the lifetime of the catalysts **6**–**9** is still lower than that of **4** or **11**, we are currently attempting to improve the stability by modifying the phosphane as well as the coordinated anionic ligand. The use of isocyanate or phenolate instead of chloride seems to be promising.

Experimental Section

6: Compound **2** (102 mg, 0.14 mmol) was dissolved in a mixture of CH_2Cl_2 (5 mL) and Et_2O (5 mL). The red-brown solution was then treated at −80 °C with an excess of HBF_4 in Et_2O (ca. 0.1 mL of a 1.6 M solution of HBF_4 in Et_2O). The reaction mixture was slowly warmed to 0 °C, the solvent was removed in vacuo, and Et_2O (5 mL) was added to the brown residue. After a few minutes a yellow solid precipitated, which was filtered and washed with Et_2O (5 mL). Yield: 90 mg (72%). Equivalent conductivity in CH_2Cl_2: 47 $cm^2\,\Omega^{-1}mol^{-1}$. The NMR spectra were measured in the presence of a small amount of Et_2O and $[HPCy_3]BF_4$ at room temperature (see text). ^1H NMR (400 MHz, CD_2Cl_2): $\delta = 4.77$ (q, $^3J(H,H) = 7.0$ Hz, 4H, $RuOCH_2CH_3$), 2.52–2.46 and 2.01–1.30 (both m, 75H, PCy_3, $RuOCH_2CH_3$ and $RuCCH_3$), −6.91 (t, $^2J(P,H) = 15$ Hz, 1H, RuH); ^{31}P NMR (162 MHz, CD_2Cl_2): $\delta = 55.5$ (s); ^{19}F NMR (376.4 MHz, CD_2Cl_2): $\delta = -151.1$ (s); ^{13}C NMR (100.6 MHz, CD_2Cl_2): $\delta = 316.1$ (t, $^2J(C,P) = 9$ Hz, $RuCCH_3$), 84.6 (s, $RuOCH_2CH_3$), 41.4 (s, $RuCCH_3$), 35.7 (vt, $N = 22$ Hz, C_1 of PCy_3), 31.6, 30.4 (both s, PCy_3), 27.6, 27.3 (both vt, $N = 10$ Hz, C_2 of PCy_3), 26.2 (s, PCy_3), 12.7 (s, $RuOCH_2CH_3$).

7: A solution of **6** (80 mg, 0.09 mmol) in CH_2Cl_2 (5 mL) was shaken with degassed H_2O (3 mL) for 1 min. The organic phase was separated, and the solvent was removed in vacuo to provide a yellow solid. Yield: 61 mg (81%). ^1H NMR (400 MHz, CD_2Cl_2, −60 °C): $\delta = 2.49$–2.39 and 2.00–1.09 (both m, 71H, PCy_3, OH_2, CH_3), −6.48 (br t, $^2J(P,H) = 12$ Hz, 1H, RuH); ^{31}P NMR (162 MHz, CD_2Cl_2, −60 °C): $\delta = 56.2$ (s); ^{13}C NMR (100.6 MHz, CD_2Cl_2, −60 °C): $\delta = 314$ (br s, $RuCCH_3$), 40.8 (s, $RuCCH_3$), 34.1 (vt, $N = 22$ Hz, C_1 of PCy_3), 30.6, 29.0, 26.8, 26.5, and 25.4 (all s, PCy_3).

 © WILEY-VCH Verlag GmbH, D-69451 Weinheim, 1998 1433-7851/98/3724-3422 $ 17.50+.50/0 *Angew. Chem. Int. Ed.* **1998**, *37*, No. 24

8: A solid sample of **2** (72 mg, 0.10 mmol) was mixed with $[HNMe_2Ph][B(C_6F_5)_4]$ (80 mg, 0.10 mmol) and treated at $-80\,^{\circ}C$ with of CD_2Cl_2 (2 mL). According to the NMR spectra, the generated yellow solution contained exclusively complex **8**. ^1H NMR (200 MHz, CD_2Cl_2, $-60\,^{\circ}C$): $\delta = 7.32-6.97$ (m, 5H, Ph-H), 3.0 (br s, 6H, NCH_3), 2.39–1.24 (m, 69H, PCy_3 and $RuCCH_3$), -6.33 (t, $^2J(P,H) = 15$ Hz, 1H, RuH); ^{31}P NMR (162 MHz, CD_2Cl_2, $-70\,^{\circ}C$): $\delta = 56.6$ (s); ^{13}C NMR (100.6 MHz, CD_2Cl_2, $-70\,^{\circ}C$): $\delta = 311.9$ (br s, Ru*C*CH_3), 147.4 (d, $^1J(C,F) = 239$ Hz, C_6F_5), 137.7 (d, $^1J(C,F) = 245$ Hz, C_6F_5), 135.7 (d, $^1J(C,F) = 247$ Hz, C_6F_5), 129.0 (s, NPh), 123.2, 118.1 and 113.4 (all br s, NPh), 41.5 (br s, NCH_3), 40.2 (s, Ru*C*CH_3), 34.0 (vt, $N = 23$ Hz, C_1 of PCy_3), 30.6, 28.9, 26.7, 26.4, and 25.3 (all s, PCy_3).

9: Analogous to the synthesis of **8**, compound **9** was prepared in quantitative yield from **2** (20 mg, 0.028 mmol) and $[H(OEt_2)_2][B\{C_6H_3(CF_3)_2\}_4]$ (28 mg, 0.028 mmol) in CD_2Cl_2 and characterized spectroscopically at room temperature. ^1H NMR (200 MHz, CD_2Cl_2): $\delta = 7.75$, 7.59 (both m, 12H, $B\{C_6H_3(CF_3)_2\}_4$), 3.36 (q, $^3J(H,H) = 6.6$ Hz, 8H, OCH_2CH_3), 2.7–1.2 (m, 69H, PCy_3 and $RuCCH_3$), 1.19 (t, $^3J(H,H) = 6.6$ Hz, 12H, OCH_2CH_3), -6.57 (t, $^2J(P,H) = 15$ Hz, 1H, RuH); ^{31}P NMR (81 MHz, CD_2Cl_2): $\delta = 57.2$ (s).

Selective ROM of cyclopentene with methyl acrylate: A solution of **2** (56 mg, 0.077 mmol) in a mixture of CH_2Cl_2 (2 mL), Et_2O (2 mL), and 0.5 mL of a 1.6 M solution of HBF_4 in Et_2O was added to a mixture of methyl acrylate (50 mL, 0.552 mol) and cyclopentene (4 mL, 0.045 mol) at room temperature. After the solution was stirred for 2 h at room temperature, the solvent and excess of substrate were distilled off at normal pressure, the remaining residue was treated with pentane (10 mL), and upon addition of Et_2O (60 mL) the solution was filtered through aluminum oxide (neutral, activity grade III). After removal of the solvent, a colorless liquid (2.5 g) was obtained, the composition of which was investigated by GC/MS. The liquid contained the first members of a homologous series of long-chain multiply unsaturated esters $C_7H_{11}CO_2CH_3$, $C_{12}H_{19}CO_2CH_3$, and $C_{17}C_{27}CO_2CH_3$ in ratios of 50, 40, and 10%.

Received: July 10, 1998 [Z12124IE]
German version: *Angew. Chem.* **1998**, *110*, 3603–3606
Keywords: carbyne complexes · metathesis · ruthenium · vinylidene complexes

[1] a) S. T. Nguyen, L. K. Johnson, R. H. Grubbs, *J. Am. Chem. Soc.* **1992**, *114*, 3974–3975; b) G. C. Fu, S. T. Nguyen, R. H. Grubbs, *J. Am. Chem. Soc.* **1993**, *115*, 9856–9857; c) S. T. Nguyen, R. H. Grubbs, J. W. Ziller, *J. Am. Chem. Soc.* **1993**, *115*, 9858–9859; d) P. Schwab, M. B. France, J. W. Ziller, R. H. Grubbs, *Angew. Chem.* **1995**, *107*, 2179–2181; *Angew. Chem. Int. Ed. Engl.* **1995**, *34*, 2039–2041; e) P. Schwab, R. H. Grubbs, J. W. Ziller, *J. Am. Chem. Soc.* **1996**, *118*, 100–110.

[2] Reviews: a) M. Schuster, S. Blechert, *Angew. Chem.* **1997**, *109*, 2124–2144; *Angew. Chem. Int. Ed. Engl.* **1997**, *36*, 2036–2055; b) A. S. K. Hashmi, *J. Prakt. Chem.* **1997**, *339*, 195–199; c) A. Fürstner, *Top. Catal.* **1997**, *4*, 285–299.

[3] Representative examples: a) R. R. Schrock, *Pure Appl. Chem.* **1994**, *66*, 1447–1454; b) J. H. Oskam, R. R. Schrock, *J. Am. Chem. Soc.* **1993**, *115*, 11831–11845; c) R. R. Schrock, *Acc. Chem. Res.* **1990**, *23*, 158–165.

[4] a) M. B. France, R. H. Grubbs, D. V. McGrath, R. A. Paciello, *Macromolecules* **1993**, *26*, 4742–4747; b) M. A. Hillmyer, S. T. Nguyen, R. H. Grubbs, *Macromolecules* **1996**, *30*, 718–721; c) J. C. Marmo, K. B. Wagener, *Macromolecules* **1995**, *28*, 2602–2606.

[5] a) M. F. Schneider, N. L. Lucas, J. Velder, S. Blechert, *Angew. Chem.* **1997**, *109*, 257–259; *Angew. Chem. Int. Ed. Engl.* **1997**, *36*, 257–259; b) W. E. Crowe, Z. J. Zhang, *J. Am. Chem. Soc.* **1993**, *115*, 10998–10999; c) W. E. Crowe, D. R. Goldberg, *J. Am. Chem. Soc.* **1995**, *117*, 5162–5163; d) W. E. Crowe, D. R. Goldberg, Z. J. Zhang, *Tetrahedron Lett.* **1996**, *37*, 2117–2120; e) P. O. Nubel, H. B. Yokelson, R. B. Moreland, V. Bagheri, S. A. Cohen, W. G. Bouslog, R. T. Behrends, J. P. Nelson (Amoco Corp.), EP-B 626402, **1994** [*Chem. Abstr.* **1995**, *123*, 10201p].

[6] *Kationische Rutheniumkomplexe, Verfahren zu ihrer Herstellung und ihre Verwendung*, BASF AG, NAE19980187.

[7] a) J. Wolf, W. Stüer, C. Grünwald, H. Werner, P. Schwab, M. Schulz, *Angew. Chem.* **1998**, *110*, 1165–1167; *Angew. Chem. Int. Ed.* **1998**, *37*, 1124–1126; b) *Verfahren zur Herstellung von Rutheniumkomplexen*, BASF AG, O.Z. 0050/48279.

[8] M. L. Christ, S. Sabo-Etienne, B. Chaudret, *Organometallics* **1994**, *13*, 3800–3804.

[9] M. Oliván, O. Eisenstein, K. G. Caulton, *Organometallics* **1997**, *16*, 2227–2229.

[10] D. Huang, W. E. Streib, O. Eisenstein, K. G. Caulton, *Angew. Chem.* **1997**, *109*, 2096–2098; *Angew. Chem. Int. Ed. Engl.* **1997**, *36*, 2004–2006.

[11] M. Brookhart, B. Grant, A. F. Volpe, *Organometallics* **1992**, *11*, 3920–3922.

[12] a) M. Bourgault, A. Castillo, M. A. Esteruelas, E. Oñate, N. Ruiz, *Organometallics* **1997**, *16*, 636–645; b) J. Espuelas, M. A. Esteruelas, F. J. Lahoz, L. A. Oro, N. Ruiz, *J. Am. Chem. Soc.* **1993**, *115*, 4683–4689; c) G. J. Spivak, J. N. Coalter, M. Oliván, O. Eisenstein, K. G. Caulton, *Organometallics* **1998**, *17*, 999–1001.

[13] Dr. A. Schäfer, BASF AG, unpublished results.

[14] W. Stüer, Dissertation, Universität Würzburg, to be submitted, **1998**.

[15] Some examples of alkyne metathesis reactions with a carbyne- or alkylidynemetal complex as catalyst are known: a) R. R. Schrock, *Acc. Chem. Res.* **1986**, *19*, 342–348; b) R. R. Schrock, *Polyhedron* **1995**, *14*, 3177–3195; c) K. Weiss in *Carbyne Complexes* (Eds.: H. Fischer, P. Hofmann, F. R. Kreissl, R. R. Schrock, U. Schubert, K. Weiss), VCH, Weinheim, **1988**, pp. 205–228.

[16] a) K. Weiss, A. Michel, E.-M. Auth, U. H. F. Bunz, T. Mangel, K. Müllen, *Angew. Chem.* **1997**, *109*, 522–525; *Angew. Chem. Int. Ed. Engl.* **1997**, *36*, 506–509; b) A. Fürstner, G. Seidel, *Angew. Chem.* **1998**, *110*, 1758–1760; *Angew. Chem. Int. Ed.* **1998**, *37*, 1734–1736.

[17] M. A. Gallop, W. R. Roper, *Adv. Organomet. Chem.* **1986**, *25*, 121–198.

[18] a) W. A. Herrmann, W. C. Schattenmann, O. Nuyken, S. C. Glander, *Angew. Chem.* **1996**, *108*, 1169–1170; *Angew. Chem. Int. Ed. Engl.* **1996**, *35*, 1087–1088; b) A. Fürstner, M. Picquet, C. Bruneau, P. H. Dixneuf, *Chem. Commun.* **1998**, 1315–1316.

Rapid Assembly of Oligosaccharides: Total Synthesis of a Glycosylphosphatidylinositol Anchor of *Trypanosoma brucei***

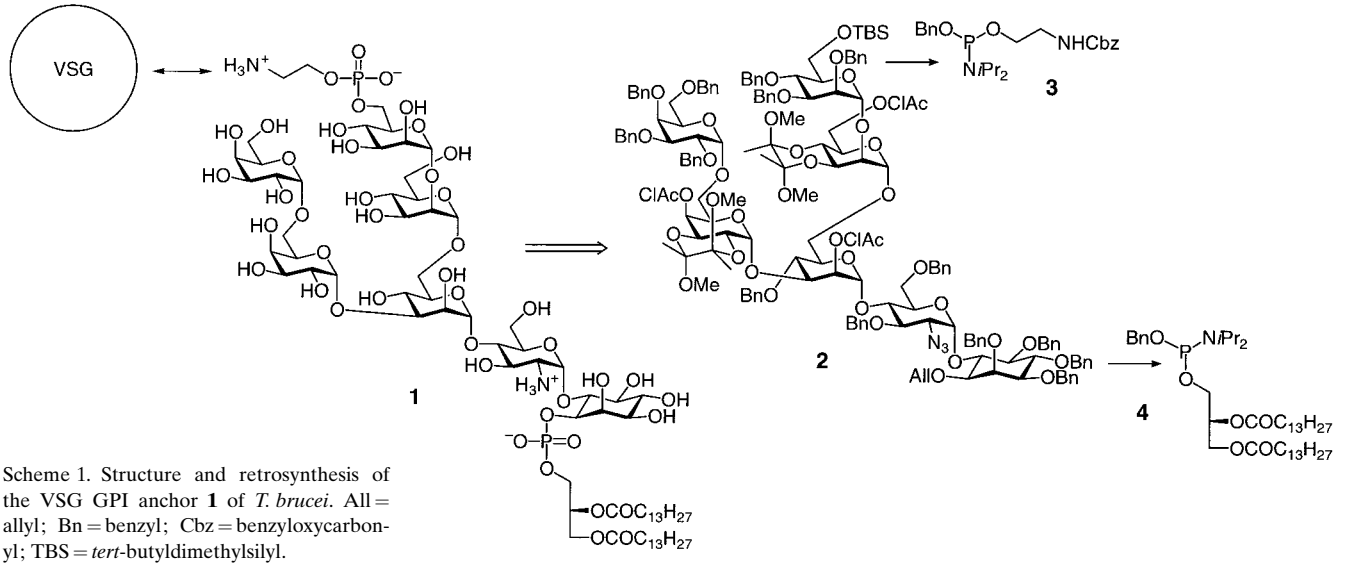
Daniel K. Baeschlin, André R. Chaperon, Virginie Charbonneau, Luke G. Green, Steven V. Ley,* Ulrich Lücking, and Eric Walther

Glycoproteins and glycolipids are major components of the outer surface of eukaryotic cells and play a vital role in fundamental biological processes such as viral, bacterial, and parasitic infections, immune defence, and inflammation.[1] Intensive research into the biological role of carbohydrates has led to an increased need for the synthesis of natural and modified glycoconjugates. Although remarkable progress has been made in the field of oligosaccharide synthesis,[2] further innovations are still required since the synthesis of complex oligosaccharides remains a highly specialized and time con-

[*] Prof. Dr. S. V. Ley, D. K. Baeschlin, Dr. A. R. Chaperon, V. Charbonneau, Dr. L. G. Green, U. Lücking, Dr. E. Walther
Department of Chemistry, University of Cambridge
Lensfield Road, Cambridge CB2 1EW (UK)
Fax: (+44) 1223-336442
E-mail: svl1000@cam.ac.uk

[**] This work was supported by a BP Endowment, a Novartis Research Fellowship, the Zeneca Strategic Research Fund, the Glaxo-Welcome Research Fund (S.V.L.), the Swiss National Science Foundation (D.K.B., A.C., and E.W.), and the EU (U.L.).

 © WILEY-VCH Verlag GmbH, D-69451 Weinheim, 1998 1433-7851/98/3724-3423 $ 17.50+.50/0



Scheme 1. Structure and retrosynthesis of the VSG GPI anchor **1** of *T. brucei*. All = allyl; Bn = benzyl; Cbz = benzyloxycarbonyl; TBS = *tert*-butyldimethylsilyl.

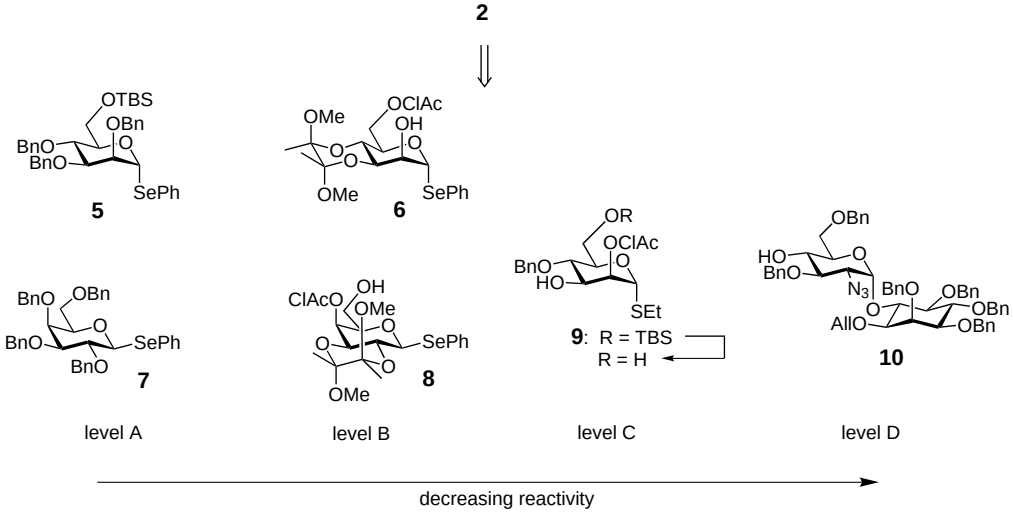
suming task relative to the synthesis of peptides or oligonucleotides. The 1,2-diacetal methodology recently developed in our laboratory can in many cases greatly simplify the assembly of oligosaccharides by considerably reducing the number of steps required.[3]

The African parasite *Trypanosoma brucei* is the cause of human sleeping sickness and a similar disease in domestic animals. As such it represents a serious problem in the tropical areas of Africa.[4] The parasite is able to survive in the host's bloodstream by virtue of a dense cell-surface coat that consists of variant surface glycoproteins (VSG) anchored to glycosylphosphatidylinositol (GPI) groups.[5] GPI anchors not only exist in *T. brucei* but are ubiquitous in eukaryotic cells. Their principal function is to attach proteins to the plasma membrane. Various proteins have been found to be GPI anchored and their role in biological recognition processes has attracted a great deal of attention.[6]

The structures of VSG GPI anchors of *T. brucei* were elucidated in 1988 (Scheme 1).[7] Since then the structures of other protein GPI anchors have been determined and the trimannose-glucoseamine-inositol backbone has been shown to be conserved in every known case. The biosynthetic pathways of GPI anchors have partly been elucidated and have given rise to some potential targets for chemotherapeutic agents.[8] Rapid synthetic access to VSG GPI anchors of *T. brucei*, other GPI anchors, and derivatives would aid investigations into the biosynthetic pathways of these molecules and into their role as protein anchors. Three total syntheses of GPI anchors have previously been reported[9] along with the syntheses of various partial structures.[10]

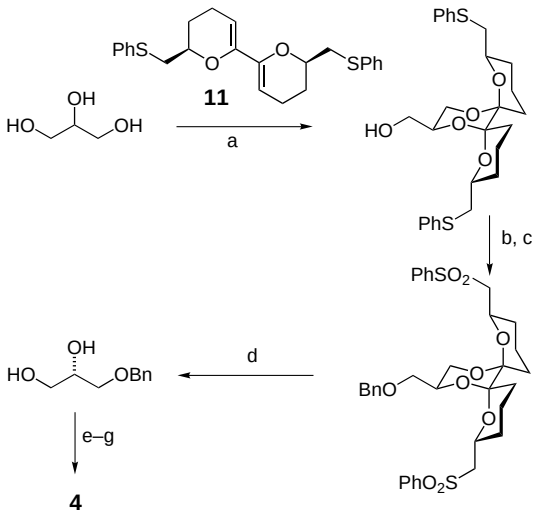
We report here a highly efficient and versatile synthesis of GPI anchor **1** by employing methods developed by our group.

A highly convergent strategy was chosen to allow the synthesis of various derivatives and to minimize the number of manipulations on the growing oligosaccharide. The GPI anchor **1** arises from the carbohydrate core **2** and the two phosphate linkers **3** and **4** (Scheme 1). The core **2** may be derived from six building blocks **5**–**10** (Scheme 2). We anticipated that the reactivity of the glycosyl donors **5**–**9** could be tuned by the use of 2,3-butanediacetal (BDA) protecting groups[11] and appropriate anomeric leaving groups to give four levels of descending reactivity (A, B, C, and D). This would allow assembly of the carbohydrate core in only six steps. The phosphoramidites **3** and **4** are easily accessible: **3** is available from literature methods,[9a] while **4** can be prepared by a desymmetrization of glycerol with chiral bis(dihyropyran) **11**, which was recently reported by our group (Scheme 3).[12] The pseudodisaccharide **10** should be accessible from suitably protected monomers: a glycosyl donor and a D-*myo*-inositol.



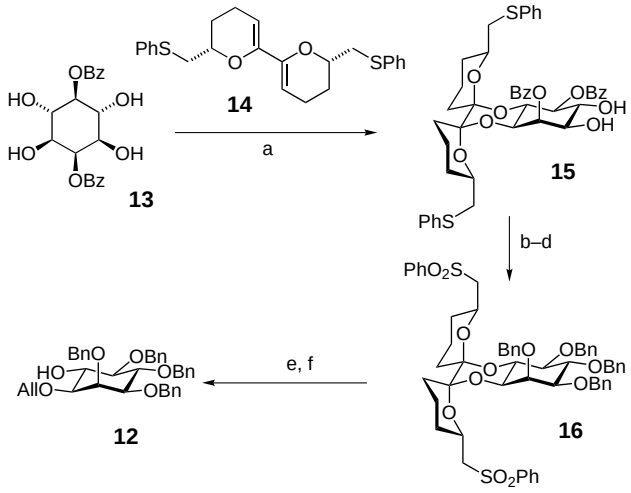
Scheme 2. Disconnection of **2** to building blocks **5**–**10**, which are grouped in four levels of reactivity. Level A: most reactive glycosyl donor; level B: the diacetal ring reduces donor reactivity; level C: change of Se to S reduces reactivity; level D: inert.

 © WILEY-VCH Verlag GmbH, D-69451 Weinheim, 1998 1433-7851/98/3724-3424 $ 17.50+.50/0



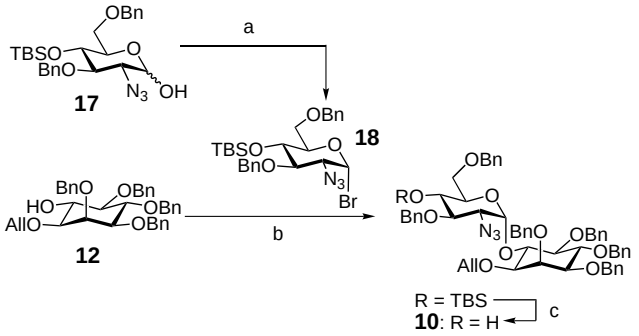
Scheme 3. Desymmetrization of glycerol. a) **11**, (±)-camphorsulfonic acid (CSA), $CHCl_3$, △, 88% (*ee* ≥ 98%); b) BnBr, NaH, DMF, 90%; c) mCPBA, CH_2Cl_2, 98%; d) $LiN(TMS)_2$, THF, 0 °C, 93%; v) $CH_3(CH_2)_{12}COCl$, pyridine, 84%; e) 10% Pd/C, H_2, EtOAc, 80%; f) $BnOP(NiPr_2)_2$, tetrazole, CH_2Cl_2, 85%. mCPBA = *meta*-chloroperbenzoic acid; TMS = trimethylsilyl.

The desymmetrization of *myo*-inositol has remained a problem despite the tremendous interest in the biological role of inositolphosphates as secondary messengers.[13] Most syntheses of *myo*-inositols include a chiral resolution or a low-yielding desymmetrization step.[14] We have reported a route to chiral L-*myo*-inositols that employs a chiral bis(dihydropyran).[12] The same strategy was used here to provide access to D-*myo*-inositol **12** (Scheme 4). One of the two enantiotopic



Scheme 4. Desymmetrization of *myo*-inositol **13**. a) **14**, $PPh_3 \cdot HBr$, $CHCl_3$, △, 71% (*ee* ≥ 98%); b) K_2CO_3 (aq), MeOH; c) NaH, BnBr, DMF, 56% over two steps; d) mCPBA, CH_2Cl_2, 93%; e) $LiN(TMS)_2$, THF, 0 °C, 93%; f) $Bu_2Sn(OMe)_2$, toluene, △, then allylbromide, tetrabutylammonium iodide (TBAI), 65%.

diol pairs in **13**[15] was selectively protected with chiral bis(dihyrdopyran) **14**[16] to give exclusively the dispiroketal **15** in 71% yield (*ee* ≥ 98%). Debenzoylation, per-O-benzylation, and oxidation led to sulfone **16**. Removal of the dispiroketal moiety with lithium hexamethyldisilazide (LHMDS) proceeded in excellent yield (93%). Selective allylation *via* the tin acetal furnished the desired alcohol **12** along with a minor amount of the undesired 6-O-allyl protected isomer, which could be isolated and recycled. The known glucose azide **17**[10c] was converted into the bromide **18** with thionylbromide and imidazole (Scheme 5).[17] Crude **18** was then coupled to inositol **12** using Leumieux's inversion protocol[18] to give the desired α-linked product with excellent selectivity.[19] Desilylation with tetrabutylammonium fluoride (TBAF) furnished pseudodisaccharide **10**.

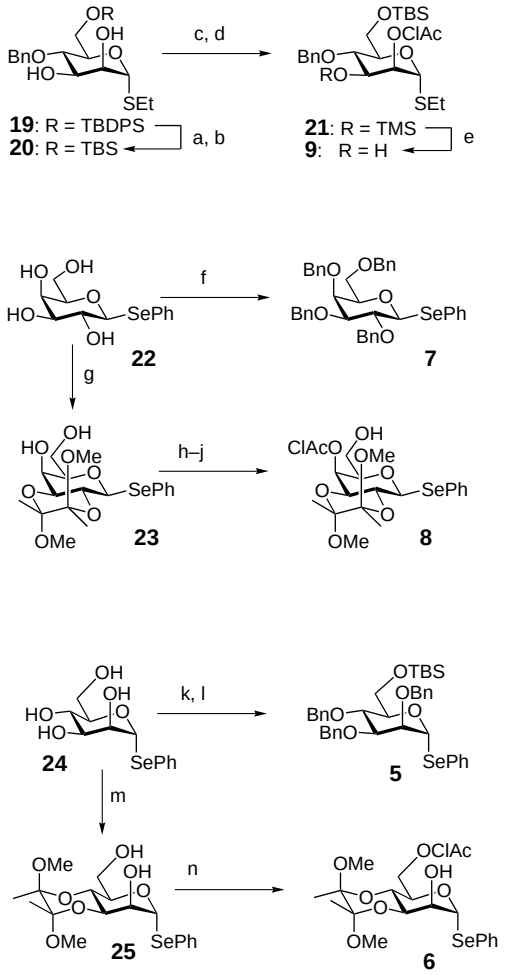


Scheme 5. Synthesis of pseudodisaccharide **10**. a) $SOBr_2$, imidazole, THF; b) **18** (1.5 equiv), TBAI, CH_2Cl_2, molecular sieves (4 Å), 3 d, 65%; c) TBAF, THF, 95%.

The central building block **9** was synthesized from the known mannoside **19**[10c] (Scheme 6). Treatment of **20** with trimethylsilyl chloride (TMSCl) and triethylamine (TEA) in CH_2Cl_2 led to selective silylation of the equatorial alcohol and was followed by acylation to give the fully protected mannoside **21** in 79% yield. Other attempts to distinguish between the 2 and 3-hydroxyl groups in **20**, such as by acylation under phase-transfer conditions, failed. The trimethylsilyl group was removed with one equivalent of aqueous HF to give acceptor **9**.[20]

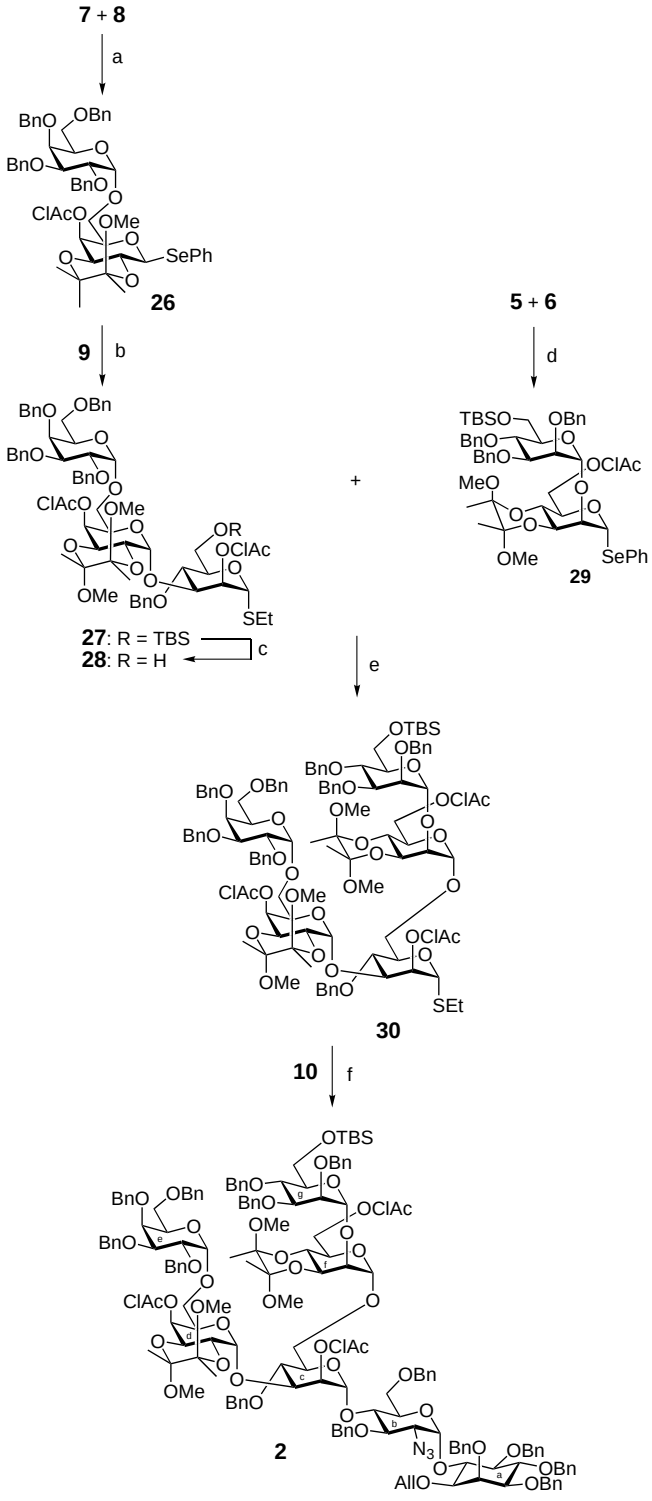
The galactosides **7** and **8** were synthesized from the common, readily available starting material **22**[21] (Scheme 6). The *trans*-diol of **22** was protected in one step to give diacetal **23** in 67% yield, subsequent selective silylation, acylation, and desilylation furnished acceptor **8**. Per-O-benzylation of **22** gave donor **7**. The mannosides **5** and **6** were accessible in a similar fashion from the common readily available selenide **24**.[3c] Selective protection of the *trans*-diol in **24** afforded the diacetal **25** in 80% yield. Acylation of the primary alcohol *via* the tin acetal furnished the desired acceptor **6**. Silylation of the primary hydroxyl group in **24** followed by per-O-benzylation yielded the required donor **5**.

With all the building blocks in hand the carbohydrate core **2** was assembled (Scheme 7). Galactosyl donor **7** was activated with *N*-iodosuccinimide (NIS) and catalytic amounts of triflic acid (TfOH) or trimethylsilyltriflate (TMSOTf)[22] in the presence of acceptor **8** to furnish the desired α-linked digalactoside **26** in 75% yield along with a minor amount of the separable β-linked isomer (14%). The deactivating effect of the BDA and the chloroacetate in acceptor **8** allowed selective activation of donor **7** and prevented any homocoupling. Digalactoside **26** was then used as a donor, by activation with methyl triflate (MeOTf),[23] and treated with the manno-



Scheme 6. Synthesis of building blocks **5**–**9**. a) TBAF, THF; b) TBSCl, imidazole, THF, 91% over two steps; c) TMSCl, TEA, CH_2Cl_2; d) $(ClAc)_2O$, pyridine, CH_2Cl_2, 0°C, 79% over two steps; e) 48% HF (aq), CH_3CN, 95%; f) BnBr, NaH, DMF, 75%; g) butanedione, $HC(OCH_3)_3$, CSA, MeOH, △, 67%; h) TBSCl, imidazole, THF; i) $(ClAc)_2O$, pyridine, CH_2Cl_2, 0°C, 80% over two steps; j) 48% HF (aq), CH_3CN, 95%; k) TBSCl, imidazole, THF, 91%; l) BnBr, NaH, DMF, 82%; m) butanedione, $HC(OCH_3)_3$, CSA, MeOH, △, 80%; n) $(Bu_3Sn)_2O$, toluene, △, then $(ClAc)_2O$, CH_2Cl_2, O°C, 95%. TBDPS = *tert*-butyldiphenylsilyl; TEA = triethylamine.

side **9** to afford trisaccharide **27** in 75% yield. In this case it is the higher reactivity of the selenophenyl leaving group in **26** that allows selective activation in the presence of the thioethyl group of acceptor **9**. The silyl ether was then removed with HF to allow for further glycosidation on alcohol **28**. Dimannoside **29** was obtained from building blocks **5** and **6** as a single anomer in excellent yield upon NIS/TMSOTf activation. As in the above galactoside case, the BDA and chloroacetate group tuned the reactivity of acceptor **6** and prevented homocoupling. The trisaccharide **28** was 6-O-glycosidated with selenophenyl donor **29** under MeOTf conditions to produce the pentasaccharide **30** in 75% yield. An excess of donor **29** (four equivalents), which was fully recovered, was used to supress formation of the anhydrosugar of **28**, which arises from intramolecular glycosidation of the 6-hydroxyl group in **28**. Activation of the thioethyl donor **30** with NIS/TfOH led to glycosidation of the inositol fragment **10** and furnished the heptasaccharide core **2** in 51% yield.

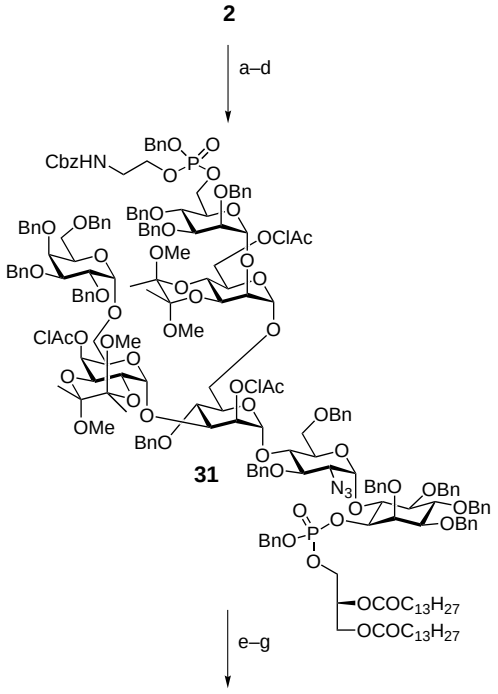


Scheme 7. Assembly of the carbohydrate core **2**. a) NIS (1 equiv), TMSOTf (cat.), Et_2O/CH_2Cl_2 (6/1), molecular sieves (4 Å), 75%; b) **9** (1 equiv), TfOMe (5 equiv), Et_2O, molecular sieves (4 Å), 75%; c) 48% HF (aq), CH_3CN, 89%; d) NIS (1 equiv), TMSOTf (cat.), Et_2O/CH_2Cl_2 (1/1), molecular sieves (4 Å), 87%; e) **29** (5 equiv), MeOTf (5 equiv), CH_2Cl_2, molecular sieves (4 Å), 12 h, 75%; f) **30** (1.4 equiv), NIS, TfOH (cat.), Et_2O/CH_2Cl_2 (3/1), molecular sieves (4 Å), 51%.

The carbohydrate core **2** was elaborated to the fully protected GPI anchor by well established phosphoramidite chemistry, which had been successfully applied in other GPI

 © WILEY-VCH Verlag GmbH, D-69451 Weinheim, 1998 1433-7851/98/3724-3426 $ 17.50+.50/0

syntheses (Scheme 8).[9] The ethanolamine linker was introduced after desilylation by phosphorylation with phosphoramidite **3** followed by oxidation with chloroperbenzoic acid (*m*CPBA). Deallylation with $PdCl_2$[24] followed by phosphorylation with **4** and oxidation furnished the fully protected GPI anchor **31**.



Scheme 8. Phosphorylations and deprotection. a) 48% HF (aq), CH_3CN, 75%; b) **3** (10 equiv), tetrazole (20 equiv), CH_3CN/CH_2Cl_2 (1/1), then mCPBA (−40→25 °C), 85%; c) $PdCl_2$, NaOAc, HOAc/H_2O (19/1), 66% (81% based on recovered starting material); d) **4** (10 equiv), tetrazole (20 equiv), CH_3CN/CH_2Cl_2 (1/1), then mCPBA (−40→25 °C), 81%; e) Pd/C, H_2, $CHCl_3$/MeOH/H_2O (3/3/1); f) $H_2NNHC(S)SH$, 2,6-lutidine/AcOH (3/1); g) TFA/H_2O (9/1), 2 min, 90% over three steps.

A final deprotection sequence involving hydrogenation, deacylation, and deacetalisation was planned. Studies on the deprotection of diacetals had shown that the hydrolysis of BDA groups gave better results if performed after debenzylation. Hydrogenation of **31** with Pd/C removed the benzyl ethers, the benzyloxycarbonyl (Cbz) group, and transformed the azide into the amine. Treatment with hydrazinedithiocarbonate[25] allowed the selective deacylation of the chloroacetates, whilst leaving the alkyl esters intact. Final rapid hydrolysis of the BDAs with aqueous trifluoroacetic acid (TFA) gave the GPI anchor **1** in 90% yield over the three steps. Selected physical data for **1**, **2**, and **31** are listed in Table 1.

In summary we have reported a highly convergent and efficient synthesis of GPI anchor **1**. The diacetal protection protocols have allowed us to desymmetrize *myo*-inositol and glycerol, as well as to conveniently protect monomers and tune the reactivity of the resulting glycosyl donors. This strategy is clearly adaptable to other syntheses of GPI anchors and their derivatives.

Received: August 14, 1998 [Z12287IE]
German version: *Angew. Chem.* **1998**, *110*, 3609–3614

Table 1. Selected physical data for compounds **1**, **2**, and **31**.[a]

1: ^{1}H NMR (600 MHz, [D$_6$]DMSO/D$_2$O (50/1), 60 °C): $\delta = 4.67$(s, 1H; 1Man-H), 4.83(s, 1H; 1Man-H), 4.87(d, ^3J(H,H) = 3.4 Hz, 1H; 1Gal-H), 4.91(d, ^3J(H,H) = 3.5 Hz, 1H; 1Gal-H), 4.94(s, 1H; 1Man-H), 5.35(s, 1H; 1Glu-H); ^{31}P NMR (243 MHz, CD_3CN/D_2O (3/1), 50 °C): $\delta = 9.24, 1.36$; matrix-assisted laser desorption/ionization time-of-flight (MALDI-TOF) MS (matrix: trihydroxyacetophenone, negative-ion mode): *m/z*(%): 1864 (100) [M^- − H].

2: ^{1}H NMR (600 MHz): $\delta = 4.58$(s, 1H; 1f-H), 4.85(s, 1H; 1e-H), 5.19(s, 1H; 1d-H), 5.27(s, 1H; 1g-H), 5.42(s, 1H; 1c-H), 5.70(d, ^3J(H,H) = 3.7 Hz, 1H; 1b-H); FAB-MS *m/z*(%): 3062 (95) [M^++Na], 2947.6 (100).

31 (as two separable pairs of diastereoisomers): **31a**: ^{31}P NMR (262 MHz): $\delta = 7.82, 7.79, -0.02, -0.12$; **31b**: ^{31}P NMR (243 MHz): $\delta = 6.89, 6.88, 0.00, -0.12$; FAB-MS *m/z*(%): 3913 (45) [M^++H], 3800 (100) [M^+ − Cbz+H].

[a] ^{1}H and ^{31}P NMR spectra were recorded in $CDCl_3$ at 26 °C, and FAB-MS with acidified 3-nitrobenzyl alcohol matrix in positive-ion mode unless otherwise indicated.

Keywords: acetals · glycosylations · inositolphosphates · oligosaccharides · protecting groups

[1] a) R. A. Dwek, *Chem. Rev.* **1996**, *96*, 683–720; b) A. Varki, *Glycobiology* **1993**, *3*, 97–130.
[2] a) H. Paulsen, *Angew. Chem.* **1995**, *107*, 1562–1564; *Angew. Chem. Int. Ed. Engl.* **1995**, *34*, 1432–1433; b) K. Toshima, K. Tatsuta, *Chem. Rev.* **1993**, *93*, 1503–1531, and references therein.
[3] a) L. Green, B. Hinzen, S. J. Ince, P. Langer, S. V. Ley, S. L. Warriner, *Synlett* **1998**, 440–442; b) N. L. Douglas, S. V. Ley, U. Lücking, S. L. Warriner, *J. Chem. Soc. Perkin Trans. 1* **1998**, 51–65; c) P. Grice, S. V. Ley, J. Pietruszka, H. M. I. Osborn, H. W. M. Priepke, S. L. Warriner, *Chem. Eur. J.* **1997**, *3*, 431–440, and references therein.
[4] I. Roditi in *Modern Synthetic Methods* (Eds.: B. Ernst, C. Leumann), Helvetica Chimica Acta, Basel, **1995**, pp. 259–279.
[5] a) M. A. J. Ferguson, *Philos. Trans. R. Soc. London B* **1997**, *352*, 1295–1303; b) M. J. McConville, M. A. J. Ferguson, *Biochem. J.* **1993**, *294*, 305–324.
[6] S. Udenfriend, K. Kodukula, *Annu. Rev. Biochem.* **1995**, *64*, 563–591.
[7] M. A. J. Ferguson, S. W. Homans, R. A. Dwek, T. W. Rademacher, *Science* **1988**, *239*, 753–759.
[8] a) T. Kinoshita, K. Ohishi, J. Takeda, *J. Biochem.* **1997**, *122*, 251–257; b) M. A. J. Ferguson, *Parasitology Today* **1994**, *10*, 48–52, and references therein.
[9] a) A. S. Campbell, B. Fraser-Reid, *J. Am. Chem. Soc.* **1995**, *117*, 10387–10388; b) T. G. Mayer, B. Kratzer, R. R. Schmidt, *Angew. Chem.* **1994**, *106*, 2289; *Angew. Chem. Int. Ed. Engl.* **1994**, *33*, 2177–2181; c) C. Murakata, T. Ogawa, *Carbohydr. Res.* **1992**, *235*, 95–114; for corrections see d) T. Ogawa, *Chem. Soc. Rev.* **1994**, *23*, 397–407.
[10] a) P. J. Garegg, P. Konradsson, S. Oscarson, K. Ruda, *Tetrahedron* **1997**, *53*, 17727–17734; b) A. Crossman, J. S. Brimacombe, M. A. J. Ferguson, *J. Chem. Soc. Perkin Trans. 1* **1997**, 2769–2774; c) G. J. Boons, P. Grice, R. Leslie, S. V. Ley, L. L. Yeung, *Tetrahedron Lett.* **1993**, *34*, 8523–8526, and references therein.
[11] a) N. L. Douglas, S. V. Ley, H. M. I. Osborn, D. R. Owen, H. W. M. Priepke, S. L. Warriner, *Synlett* **1996**, 793–795; b) J.-L. Montchamp, F. Tian, M. E. Hart, J. W. Frost, *J. Org. Chem.* **1996**, *61*, 3897–3899; c) U. Berens, D. Leckel, S. C. Oepen, *J. Org. Chem.* **1995**, *60*, 8204–8208.
[12] S. V. Ley, S. Mio, B. Meseguer, *Synlett* **1996**, 791–792.
[13] B. V. L. Potter, D. Lampe, *Angew. Chem.* **1995**, *107*, 2085–2125; *Angew. Chem. Int. Ed. Engl.* **1995**, *34*, 1933–1972.
[14] a) D. C. Billington, *Chem. Soc. Rev.* **1989**, *18*, 83–122; b) Y. Watanabe, M. Nakatomi, *Tetrahedron Lett.* **1998**, *39*, 1583–1586; c) B. Kratzer, T. G. Mayer, R. R. Schmidt, *Tetrahedron Lett.* **1993**, *34*, 6881–6884.
[15] Y. Watanabe, M. Mitani, T. Morita, S. Ozaki, *J. Chem. Soc. Chem. Commun.* **1989**, 482–483.
[16] S. V. Ley, S. Mio, B. Meseguer, *Synlett* **1996**, 787–788.
[17] Modified Darzen's procedure: *The Merck Index, 9th ed.*, Merck, Rahway, NJ, **1976**, p. ONR-22.

 © WILEY-VCH Verlag GmbH, D-69451 Weinheim, 1998 1433-7851/98/3724-3427 $ 17.50+.50/0

[18] R. U. Lemieux, K. B. Hendriks, R. V. Stick, K. James, *J. Am. Chem. Soc.* **1975**, *97*, 4056 – 4062.
[19] Trace amounts of the β-linked product were easily separated after the next step.
[20] This building block was always freshly prepared because migration of the chloroacetate to the 3-hydroxyl group was observed upon prolonged standing even at $-20\,^{\circ}C$.
[21] A. Mallet, J.-M. Mallet, P. Sinaÿ, *Tetrahedron: Asymmetry* **1994**, *5*, 2593 – 2608.
[22] a) P. Konradsson, U. E. Udodong, B. Fraser-Reid, *Tetrahedron Lett.* **1990**, *31*, 4313 – 4316; b) G. H. Veeneman, S. H. van Leeuwen, J. H. van Boom, *Tetrahedron Lett.* **1990**, *31*, 1331 – 1334.
[23] H. Lönn, *Carbohydr. Res.* **1985**, *139*, 105 – 113.
[24] T. Ogawa, H. Yamamoto, *Carbohydr. Res.* **1985**, *137*, 79 – 88.
[25] C. A. A. van Boeckel, T. Beetz, *Tetrahedron Lett.* **1983**, *24*, 3775 – 3778.

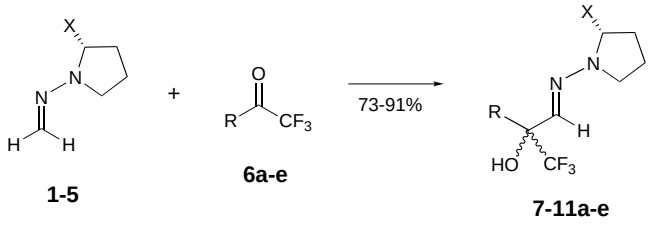
Synthesis of Enantiopure α-Alkoxy-α-Trifluoromethyl Aldehydes and Carboxylic Acids from Trifluoromethyl Ketones**

Rosario Fernández, Eloísa Martín-Zamora, Carmen Pareja, Juan Vázquez, Elena Díez, Angeles Monge, and José M. Lassaletta*

The unique properties conferred to organic compounds by the introduction of one or more fluorine atoms have recently found many applications in a variety of fields including pharmaceuticals, material science, and agrochemistry.[1] This fact, combined with the lack of appropriate fluorinated building blocks from natural sources, has evoked in the last few years the development of new synthetic methods for such compounds; the synthesis of enantiomerically enriched trifluoromethyl-containing building blocks is of particular significance in medicinal chemistry[2] and material science.[3] In this context, easily available trifluoromethyl ketones[4] appear as appropriate starting materials, but their reactions with d^1 reagents for the synthesis of interesting α-hydroxy-α-trifluoromethyl carbonyl compounds have been scarcely investigated.[5]

We have recently reported on the use of formaldehyde dialkylhydrazones as a new class of neutral formyl anion and cyanide equivalents, and this new methodology has been successfully applied to the formylation of several electrophilic substrates, including conjugated nitroalkenes,[6] α,β-unsaturated ketones,[7] and aldehydes.[8] As a natural extension of the method, we now report the nucleophilic 1,2-addition of these compounds to trifluoromethyl ketones, which provides a straightforward, short route to both racemic or enantiomerically pure α-alkoxy-α-trifluoromethyl aldehydes and carboxylic acids.

All tested couples of formaldehyde hydrazones **1** – **5** and a variety of trifluoromethyl ketones (**6a** – **e**) easily reacted in the absence of any catalyst or promoter, giving rise to the expected α-hydroxy-α-trifluoromethylhydrazones **7** – **11** in excellent yields, even when less reactive aromatic trifluoromethyl ketones (**6c**, **e**) were used as substrates (Scheme 1; selected results are collected in Table 1). Racemic adducts were best synthesized with the more reactive pyrrolidine-containing hydrazone **1**,[8] as this reagent led to the corresponding adducts **7a** – **e** in better yields and shorter reaction times than the simple formaldehyde dimethylhydrazone. Concerning the asymmetric version of the reaction, we found that use of the chiral formaldehyde SAMP-hydrazone **2**[6c] (SAMP = (*S*)-1-amino-2-(methoxymethyl)pyrrolidine) resulted in very low inductions under all tested reaction conditions; the selectivity of these additions was only slightly or not at all affected by temperature. Under the assumption that the origin of selectivity should be steric in nature, hydrazones **3** – **5**, in which the modified chiral auxiliaries are more sterically demanding than SAMP units, were synthesized. The influence by the tuned auxiliaries was analyzed from the results of the addition to compound **6b** (Table 1, entries 4 – 7). These experiments indicated a direct correlation between size and selectivity: The benzhydryl-containing reagent **3** gave slightly better results (d.r. 64:36) than **2**, while the asymmetric inductions effected by **4** and **5**, having bigger (quaternary) groups on position 2 of the pyrrolidine ring, were higher (d.r. 71:29 and 81:19, respectively). Nevertheless, crystalline derivative **5** proved to be the reagent of choice for practical



	1,7	2,8	3,9	4,10	5,11
X	H	CH_2OMe	$CHPh_2$	CEt_2OMe	CPh_2OMe

6-15	a	b	c	d	e
R	Me	Bn	Ph	n-C_7H_{15}	

Scheme 1. Synthesis of α-hydroxyhydrazones **7** – **11**.

[*] Dr. J. M. Lassaletta
Instituto de Investigaciones Químicas, CSIC-USe
c/Americo Vespuccio s/n
Isla de la Cartuja, E-41092 Seville (Spain)
Fax: (+34) 95-4460-565
E-mail: jmlassa@cica.es
Dr. R. Fernández, Dr. E. Martín-Zamora, C. Pareja, J. Vázquez, E. Diez
Departamento de Química Orgánica, Universidad de Sevilla
Dr. A. Monge
Instituto de Ciencia de Materiales de Madrid, CSIC, Madrid (Spain)

[**] We thank the Dirección General de Investigación Científica y Técnica for financial support (grant no. PB 94/1429). We also thank the Ministerio de Educación y Ciencia for a doctoral fellowship to E.D. and a postdoctoral fellowship to E.M.-Z.

 © WILEY-VCH Verlag GmbH, D-69451 Weinheim, 1998 1433-7851/98/3724-3428 $ 17.50+.50/0

Table 1. Synthesis of α-hydroxy-α-trifluoromethylhydrazones **7**–**11**.

Entry	Ketone **6**	Hydrazone	Adducts **7**–**11**, yield [%]	d.r.[a]	Pure adducts **11**,[b] yield [%]	$[\alpha]_D^{22}$ ($c = 1$, $CHCl_3$)
1	**6a**	**5**	*rac*-**7a**, 90			
2	**6a**	**6**	**13a**, 90	70:30	(*S*,*S*)-**11a**, 63	−170.2
					(*R*,*S*)-**11a**, 27	−163.4
3	**6b**	**1**	*rac*-**7b**, 81			
4	**6b**	**2**	**8b**, 84	54:46[c]		
5	**6b**	**3**	**9b**, 70	64:36[c]		
6	**6b**	**4**	**10b**, 70	71:29[c]		
7	**6b**	**5**	**11b**, 91[d]	81:19	(*S*,*S*)-**11b**, 74	−38.6
					(*R*,*S*)-**11b**, 17	−198.3
8	**6c**	**1**	*rac*-**7c**, 87			
9	**6c**	**5**	**11c**, 90	58:42	(*S*,*S*)-**11c**, 52	−152.7
					(*R*,*S*)-**11c**, 37	−154.4
10	**6d**	**1**	*rac*-**7d**, 80			
11	**6d**	**5**	**11d**, 85[d]	62:38	(*S*,*S*)-**11d**, 49	−175.1
					(*R*,*S*)-**11d**, 36	−119.2
12	**6e**	**1**	*rac*-**7e**, 73			
13	**6e**	**5**	**11e**, 82	51:49	(*S*,*S*)-**11e**, 42[e]	−172.1
					(*R*,*S*)-**11e**, 40[e]	−152.8

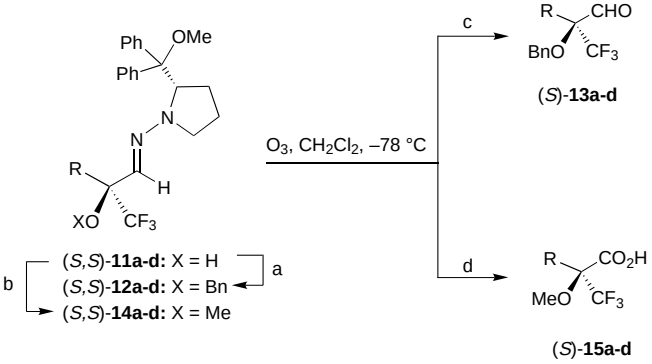
[a] Determined by ^{13}C and ^1H NMR spectroscopy of unpurified reaction mixtures. [b] After flash chromatography, $de \geq 96\%$. [c] Inseparable mixture of diasteromers. [d] 5% of Et_3N was added to the reaction mixture. [e] Configuration assigned tentatively.

The absolute configuration of the newly created quaternary center of the minor isomer (*R*,*S*)-**11a** was unequivocally determined by X-ray diffraction analysis[9] (Figure 1), while that of (*S*)-**15c** was assigned by comparison of its optical rotation with that of commercial Mosher's acid [(*S*)-MPTA]. The absolute configuration of compounds in the series **b** and **d** was assigned by analogy. Of course, use of *ent*-**5** (available from D-proline) would led to products with the opposite configuration.

To summarize, appropriate formaldehyde hydrazones, acting as neutral d^1 synthons, readily add to trifluoromethyl ketones. This reaction, combined with standard hydrazone cleavage, constitutes the first general method for the asymmetric synthesis of enantiomerically pure quaternary trifluoromethyl-substituted α-alkoxy carbonyl compounds.

reasons: With this reagent, both diastereoisomers (*S*,*S*)- and (*R*,*S*)-**11b** could be easily separated by simple flash chromatography. The interesting properties as resolving agent exhibited by the (*S*)-1-amino-2-(methoxydiphenylmethyl)pyrrolidine auxiliary proved to be a general characteristic, and led to the easy chromatographic separation of all diastereomeric mixtures obtained from **5** (see Table 1).

Adducts (*S*,*S*)-**11** were transformed in their O-benzyl derivatives (*S*,*S*)-**12** (Scheme 2); subsequent hydrazone cleavage by ozone afforded the corresponding aldehydes



Scheme 2. Synthesis of compounds (*S*,*S*)-**12**/(*S*,*S*)-**14** and (*S*)-**13**/(*S*)-**15**. a) BnBr, NaH, DMF; b) MeI, NaH, THF; c) Me_2S; d) $NaClO_2$, *t*BuOH, isobutene.

(*S*)-**13** in good yields. Alternatively, compounds (*S*,*S*)-**11** were transformed into carboxylic acids (*S*)-**15** by successive methylation [→(*S*,*S*)-**14**], ozonolysis, and in situ oxidation of the crude aldehydes. The (*S*)-2-methoxydiphenylmethyl-1-nitrosopyrrolidine obtained as by-product during the ozonolysis to **13** or **15** was recycled to the reagent **5** by reduction ($LiAlH_4$) and condensation with trioxane (79–86% overall yield). The results for the syntheses of compounds (*S*)-**12**–(*S*)-**15** are summarized in Table 2.

Table 2. Synthesis of compounds (*S*)-**12**–(*S*)-**15**.

Hydrazone (*S*,*S*)-**11**	R	(*S*,*S*)-**12**, yield [%]	(*S*)-**13**, yield [%]	$[\alpha]_D^{22}$[a]	(*S*,*S*)-**14**, yield [%]	(*S*)-**15**, yield [%]	$[\alpha]_D^{22}$[a]
a	Me	87	66	−38.5	85	90	−1.1
b	Bn	89	84	+43.1	87	72	+24.6
c	Ph	82	77	−39.8	73	74	−71.6[b]
d	*n*-C_7H_{15}	72	74	−24.1	83	80	−8.4

[a] $c = 1$, $CHCl_3$. [b] $c = 2$, MeOH; commercially available (*S*)-MPTA (Aldrich) has a $[\alpha]_D^{20}$ value of −73 under these conditions.

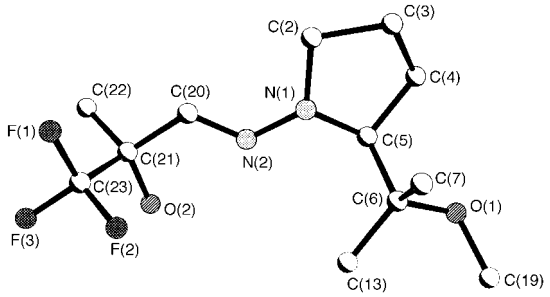


Figure 1. Crystal structure of (*R*,*S*)-**11a**. Phenyl groups have been omitted for clarity.

Experimental Section

Chiral auxiliary: Compound **3** was prepared from (*S*)-[3.3.0]-2-oxo-4,4-diphenyl-1-aza-3-oxa-bicyclooctane[11] by hydrogenolysis (Pd/C, H_2), nitrosation (*t*$BuNO_2$), reduction ($LiAlH_4$, THF), and condensation with trioxane (51% overall yield). Compounds **4** and **5** were prepared from their corresponding hydrazines[12] by reaction with trioxane, and purified by distillation and flash chromatography, respectively.

Adducts **7a**,**b**–**11a**,**b**: To a solution of the hydrazone **1**–**5** (3 mmol) in toluene (**a**, 2 mL) or cyclohexane (**b**, 5 mL) was added the ketone **6a** (6 mmol) or **6b** (12 mmol), and the mixture was stirred until thin-layer chromatography (TLC) indicated total consumption of the starting hydrazone. The mixture was then concentrated and purified by flash chromatography.

Adducts **7c–e** and **11c–e**: Hydrazone **1** or **5** was solved in excess (about 5 equiv) of ketone (**6c–e**), and the mixture was stirred until consumption of the former (TLC). Unchanged ketone was recovered (75–85%) by bulb-to-bulb distillation, and the residue was purified by flash chromatography.

Compounds **12** and **14** were synthesized from **11** under standard conditions.

Aldehydes **13**: Ozone was bubbled through a solution of **12** (1 mmol) in dry CH_2Cl_2 (5 mL) at $-78\,^{\circ}C$ until appearance of a permanent blue color (5–10 min). Me_2S (5 mmol) was added. The mixture was allowed to warm to room temperature and concentrated, and the residue purified by column chromatography.

Carboxylic acids **15**: Ozonolysis was carried out from **14** as described above, but only 1 mmol of Me_2S was added. To the resulting solution was added *t*BuOH (12 mL) and isobutene (10 mL). After the mixture was cooled to $0\,^{\circ}C$, a solution of $NaClO_2$ (10 mmol) and KH_2PO_4 (9 mmol) in H_2O (12 mL) was added dropwise and the mixture was stirred for 16 h. The solvent was removed, and the residue was treated with 1M NaOH and extracted with Et_2O (2×10 mL). The aqueous layer was acidified to pH 1 (HCl) and extracted with ethyl acetate (10×5 mL). The combined organic layers were then concentrated and purified by flash chromatography.

Received: June 19, 1998 [Z12015IE]
German version: *Angew. Chem.* **1998**, *110*, 3598–3600

Keywords: asymmetric synthesis · chiral auxiliaries · fluorine · hydrazones · nucleophilic additions

[1] a) J. T. Welch, S. Eswarakrishnan, *Fluorine in Bioorganic Chemistry*, Wiley, New York, **1991**; b) *Organofluorine Chemistry, Principles and Commercial Applications* (Eds.: R. E. Banks, B. E. Smart, J. C. Tatlow), Plenum, New York, **1994.**

[2] a) T. Ido, K. Fukushi, T. Irie in *Biomedicinal Aspects of Fluorine Chemistry* (Eds.: R. Filler, Y. Kobayashi), Kodansha, Tokio, and Elsevier, Amsterdam, **1982**; b) *Organofluorine Compounds in Medicinal Chemistry and Biomedical Applications* (Eds.: R. Filler, Y. Kobayashi, L. M. Yagupolskii), Elsevier, Amsterdam, **1993**.

[3] a) S. Arakawa, K. Nito, J. Seto, *J. Mol. Cryst. Liq.* **1991**, *204*, 15; b) R. Buchecker, S. M. Kelly, J. Fünfschilling, *Liq. Cryst.* **1990**, *8*, 217; c) T. R. Doyle, O. Vogol, *J. Am. Chem. Soc.* **1989**, *111*, 8510; d) Y. Suzuki, T. Hagiwara, I. Kawamura, N. Okamura, T. Kitazume, M. Kakimoto, Y. Imai, Y. Ouchi, H. Takezoe, A. Fukuda, *Liq. Cryst.* **1989**, *6*, 167.

[4] J. Wiedemann, T. Heiner, G. Mloston, G. K. Surya Prakash, G. Olah, *Angew. Chem.* **1998**, *110*, 880–881; *Angew. Chem. Int. Ed.* **1998**, *37*, 820–821, and references therein.

[5] a) P. Bravo, M. Frigerio, G. Resnati, *J. Org. Chem.* **1990**, *55*, 4216–4218; b) A. Dondoni, A. Boscarato, P. Formaglio, J.-P. Bégué, F. Benayoud, *Synthesis* **1995**, 654–658.

[6] a) J. M. Lassaletta, R. Fernández, *Tetrahedron Lett.* **1992**, *33*, 3691–3694; b) R. Fernández, C. Gasch, J. M. Lassaletta, J. M. Llera, *Tetrahedron Lett.* **1994**, *35*, 471–472; c) D. Enders, R. Syrig, G. Raabe, R. Fernández, C. Gasch, J. M. Lassaletta, J. M. Llera, *Synthesis* **1996**, 48–52; d) J. M. Lassaletta, R. Fernández, C. Gasch, J. Vazquez, *Tetrahedron* **1996**, *52*, 9143–9160.

[7] J. M. Lassaletta, R. Fernández, E. Martín-Zamora, E. Díez, *J. Am. Chem. Soc.* **1996**, *118*, 7002–7003; b) E. Díez, F. Fernández, C. Gasch, J. M. Lassaletta, J. M. Llera, E. Martín-Zamora, J. Vázquez, *J. Org. Chem.* **1997**, *62*, 5144–5155.

[8] J. M. Lassaletta, R. Fernández, E. Martín-Zamora, C. Pareja, *Tetrahedron Lett.* **1996**, *37*, 5787–5790.

[9] Suitable crystals were obtained from light petroleum ether at room temperature. $C_{22}H_{25}F_3N_2O_2$, $M_r = 406.44$, crystal size $0.1 \times 0.4 \times 0.4$ mm, crystal system orthorombic, space group $P2_12_12_1$, $a = 7.4267(10)$, $b = 14.081(2)$, $c = 20.344(3)$ Å, $V = 2127.5(5)$ Å^3, $Z = 4$, $\rho_{calcd} = 1.269$ g cm^{-3}, $1.76 < \Theta < 23.32^{\circ}$, $Mo_{K\alpha}$ radiation ($\lambda = 0.71073$ Å), $T = 296(2)$ K; of 4500 reflections collected, 2830 were independent [$I > 2\sigma(I)$]; 362 parameters, $R = 0.0682$ ($wR = 0.1100$). The crystal was coated with resin epoxy and mounted in a CCD diffractometer. The intensities were corrected for Lorentz and polarization effects. No absorption correction. The structure was solved by Patterson and Fourier methods, and a final mixed refinement was undertaken. Hydrogen atoms were located in a difference synthesis, and their coordinates and isotropic thermal parameters refined, except for H2 whose thermal parameter was fixed. Refinement on F^2 for all reflections. Weighted factors (wR) and all GOFs are based on F^2; conventional R factors are based on F. The configuration of C(5) is based on that known for the auxiliary. Crystallographic data (excluding structure factors) for the structure reported in this paper have been deposited with the Cambridge Crystallographic Data Center as supplementary publication no. CCDC-102999. Copies of the data can be obtained free of charge on application to CCDC, 12 Union Road, Cambridge CB21EZ, UK (fax: (+44) 1223-336-033; e-mail: deposit@ccdc.cam.ac.uk).

[10] D. J. Bailey, D. O'Hagan, M. Tavasli, *Tetrahedron: Asymmetry* **1997**, *8*, 149–153.

[11] D. Enders, H. Kipphardt, P. Gerdes, L. J. Breña-Valle, V. Buhshan, *Bull. Soc. Chim. Belg.* **1988**, *97*, 691–704.

Detection of Specific Noncovalent Zinc Finger Peptide–Oligodeoxynucleotide Complexes by Matrix-Assisted Laser Desorption/Ionization Mass Spectrometry**

Edda Lehmann and Renato Zenobi*

All retroviruses, including the human immunodeficiency virus type 1 (HIV-1), encode a gag precursor polyprotein which contains zinc binding domains of the type CCHC (CCHC = Cys-X_2-Cys-X_4-His-X_4-Cys, X = variable amino acid).[1] These zinc-coordinated motifs play an important role in the recognition of viral ribonucleic acid and replication of the virus. The interaction between peptides containing such motifs and single-stranded nucleic acids has been extensively studied,[2, 3] mainly in view of developing antiviral agents for the treatment of the acquired immunodeficiency syndrome (AIDS).[4] The methods used for these investigations are rather time-consuming and expensive. Here we report that matrix-assisted laser desorption/ionization mass spectrometry (MALDI-MS) is suitable for detecting specific noncovalent complexes, and that it is a potential method for rapidly screening antiviral agents. The use of MALDI-MS is now well known for the analysis of high molecular weight biopolymers.[5] However, its ability to detect specific noncovalent complexes is just starting to be explored.[6] Complexes that are stable under physiological conditions in solution may not survive laser desorption and ionization processes. Using carefully designed controls, we were able to establish a correlation between the existence of a specific noncovalent triple complex in solution and in the MALDI mass spectra.

[*] Prof. Dr. R. Zenobi, E. Lehmann
Laboratorium für Organische Chemie, ETH Zentrum
Universitätstrasse 16, CH-8092 Zürich (Switzerland)
Fax: (+41) 1-632-1292
E-mail: zenobi@org.chem.ethz.ch

[**] We thank Stefan Vetter for many fruitful discussions, Dr. Christophe Masselon for taking FTICR mass spectra, and the Kommission für Technologie und Innovation (KTI, project 3165,1) for financial support. E.L. gratefully acknowledges a Kekulé doctoral stipend from the Fonds der Chemischen Industrie.

 © WILEY-VCH Verlag GmbH, D-69451 Weinheim, 1998 1433-7851/98/3724-3430 $ 17.50+.50/0

The peptide selected for the investigation is an 18-residue peptide of the type CCHC with the amino acid sequence acVK**C**FN**C**GKEG**H**IARN**C**RA-OH. This sequence corresponds to the first zinc finger domain from the gag protein p55 of HIV-1, called p55F1. The peptide has no defined secondary structure in the absence of metal ions. Metal-ion binding induces peptide folding, which is required for the interaction with nucleic acids.[2, 7] Peptides of the type CCHC bind Zn^{2+} very tightly, whereas complexes with other transition metal ions are weaker.[8] In the Zn – p55F1 complex, Zn^{2+} is tetrahedrally coordinated by the three cysteine and the histidine residues.[9] A preliminary MALDI-MS study of the complexation between p55F1 and various metal ions was performed in our laboratory.[10] We found that the Zn – p55F1 complex detected is specific, and that the complex formation observed qualitatively correlates with that in solution (see also reference [11]).

We now investigated the triple complex Zn – p55F1 – d(TTGTT) with MALDI-MS, because it is known from solution experiments that d(TTGTT) binds to Zn – p55F1.[3] The oligodeoxynucleotide binds within a hydrophobic cleft on the peptide surface. For reasons of sample stability, it is common practice to use single-stranded oligodeoxynucleotides as structural probes for ribonucleic acid binding CCHC zinc fingers.[3]

All MALDI mass spectra were taken in the positive-ion mode on a linear time-of-flight instrument that has been described in detail before.[11] Figure 1 A shows the MALDI mass spectrum of a mixture of d(TTGTT) and p55F1. The signals for the protonated molecular ions of p55F1 ($[P+H]^+$) and d(TTGTT) ($[O+H]^+$) are observed besides weak peaks for an oligodeoxynucleotide fragment (*m*/*z* 1399) and a nonspecific adduct of both components. The latter is probably a result of electrostatic interactions. Upon addition of Zn^{2+}, the signal for the specific triple complex of p55F1, Zn^{2+}, and d(TTGTT) is observed (Figure 1 B, *m*/*z* 3598). Less intense signals for p55F1 – d(TTGTT) adducts without Zn^{2+} and with two Zn^{2+} ions are also observed. All signals correspond to singly charged species. The excess charge of Zn^{2+} is compensated by deprotonation of the peptide or the oligodeoxynucleotide, as confirmed by high-resolution Fourier transform ion cyclotron resonance (FTICR) mass spectrometry. Adduct peaks at higher mass were of negligible intensity.

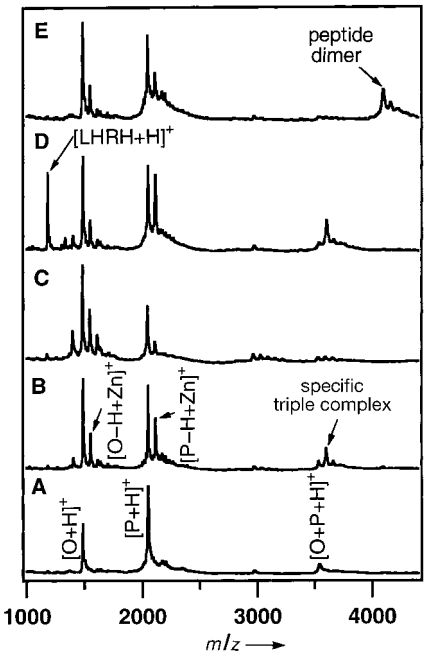


Figure 1. MALDI mass spectra (AMNP matrix) of p55F1 and d(TTGTT) in a 33:1 molar ratio A) without addition of Zn^{2+} at pH 6.5 – 7, B) with addition of Zn^{2+} (molar ratio Zn^{2+}:p55F1 = 5:1) at pH 6.5 – 7, C) same as (B) at pH 5 – 5.5, D) same as (B) with addition of LHRH at pH 7, E) same as (B) with addition of Cu^{2+} in the same molar amount as Zn^{2+}. The metal ion adducts to p55F1 (*m*/*z* 2113) and to its dimer (*m*/*z* 4262) stem from a nonspecific gas-phase reaction.

The signals of both the triple complex and the Zn – p55F1 complex are less intense than those of the individual components. The reasons in the case of Zn – p55F1 have already been discussed.[10] Similar arguments can also be made for the triple complex: Variations in desorption, ionization, and detection efficiencies among the triple complex, the Zn – p55F1 complex, the peptide (present in excess), and d(TTGTT) as well as partial peptide oxidation or partial dissociation of the complex ions upon crystallization or during the MALDI process may all contribute to the triple complex signal being less intense than that of the components. From this, it is clear that absolute abundances of the species in solution (the complex and its components) and peak intensities in the MALDI mass spectra cannot be directly compared.[10]

Furthermore, conclusions concerning complex specificity cannot be drawn purely on signal intensities. Carefully designed control experiments have to be performed, such as the variation of the pH or competition experiments. Such controls have already been done to prove the specificity of Zn – p55F1.[10] Similar controls for Zn – p55F1 – d(TTGTT) are described below.

The investigation of Zn – p55F1 with circular dichroism (CD) spectroscopy in solution showed that this complex is only stable above pH 6.[10] This is what we also expect for the triple complex, since the oligodeoxynucleotide only binds to the zinc-complexed p55F1. If MALDI mass spectra reflect solution-phase behavior, then decreasing the pH to a value below 6 should lead to a significant decrease in the MALDI signal of the specific triple complex. This is exactly what is observed experimentally (Figure 1 C): Besides a strong decrease of the Zn – p55F1 signal compared to that of p55F1, the triple complex signal is absent. Instead, weak signals of a nonspecific distribution of Zn^{2+} adducts to p55F1-d(TTGTT) and to the oligonucleotide dimer are observed. We assume that the negatively charged phosphodiester backbone of the oligonucleotide forms nonspecific adducts with the overall positively charged p55F1 and with Zn^{2+} ions. This assumption fits well with the observation of multiple Zn^{2+} adducts to the oligonucleotide in the mass spectrum in Figure 1 C.

To confirm whether the triple complex observed in Figure 1 B is indeed specific, another peptide (luteinizing hormone releasing hormone, LHRH, *m*/*z* 1182) was added to the sample (Figure 1 D). The peptide LHRH contains a histidine residue in its sequence and thus potentially binds to

Zn^{2+} ions. It also contains arginine with a positively charged side chain, which may bind through electrostatic forces to the phosphodiester groups of the oligodeoxynucleotide backbone. Both interactions would be nonspecific. The spectrum shows that neither a Zn^{2+} adduct to this peptide (expected at m/z 1246) nor a triple complex with Zn^{2+} and d(TTGTT) (expected at m/z 2730) is detected. However, the corresponding complex signals of p55F1 are as intense as in the absence of LHRH (Figure 1 B). They are even more intense because of a slightly higher pH value. This experiment supports the interpretation that the complex formation of Zn^{2+} with p55F1 and d(TTGTT) observed with MALDI-MS is specific.

The study of p55F1 with different metal ions showed that an excess of Cu^{2+} with respect to p55F1 oxidizes the peptide's thiol functionalities to an intramolecular disulfide bond with simultaneous reduction of Cu^{2+} to Cu^{+}.[10] The Cu^{2+} ion mimics the action of an antiviral agent in the sense that it chemically modifies the cysteine residues. Modified p55F1 forms complexes neither with Zn^{2+} nor with oligodeoxynucleotides. This is also reflected in the MALDI mass spectrum: If Cu^{2+} is added to the sample, the cysteine residues are oxidized and the signal of the triple complex disappears (Figure 1 E). A strong signal for the p55F1 dimer is detected instead, because peptide oxidation can lead to intermolecular disulfide bonds involving the third thiol group.

Besides d(TTGTT), the complexation of Zn – p55F1 with other sequences such as d(TTATT) and d(ACGCC) has also been investigated. Our MALDI experiments with d(TTATT) instead of d(TTGTT) support the findings of Lam et al.[2] and Gorelick et al.,[12] who report that Zn – p55F1 is not sequence-specific in solution. We found that the complex of d(TTATT) with Zn-p55F1 gave signals of about the same intensity as with d(TTGTT). MALDI experiments with oligodeoxynucleotide sequences lacking thymidine are, unfortunately, not very informative. If d(ACGCC) was used as the binding partner hardly any MALDI signal could be seen at all, although the corresponding triple complex should be stable in solution.[3] It is common knowledge that oligodeoxynucleotides that do not contain thymidines are much less stable, more prone to fragmentation, and thus much more difficult to detect under the same experimental MALDI conditions than those containing mostly thymidine residues.[13]

In summary, the present MALDI study demonstrates that specific, noncovalent complexes between Zn^{2+}, the zinc finger peptide p55F1, and different oligodeoxynucleotides can be detected with MALDI-MS. Moreover, this methods allows effects of pH and of chemical modifications of the zinc finger peptide on the formation of the triple complex to be studied. Therefore, MALDI-MS is a potential method for rapidly sceening antiviral agents. More generally, this work not only demonstrates the potential of MALDI-MS to rapidly and directly analyze noncovalent complexes, but also shows that the mass spectral data can, under carefully chosen conditions, reflect solution-phase chemistry.

Experimental Section

P55F1 (m/z 2049) was synthesized on TentaGel S resin from Fmoc-protected amino acid derivatives (Fmoc = (9*H*-fluoren-9-ylmethoxy)carbonyl), and purified on a reverse-phase high-performance liquid chromatography C18 column. As the thiol groups of the three cysteine residues in the CCHC motif are sensitive to oxidation, p55F1 was lyophilized, stored under an argon or nitrogen atmosphere, and handled rapidly during the experiments to minimize oxidation. The oligodeoxynucleotides d(TTGTT) (m/z 1484), d(TTATT), and d(ACGCC) were purchased in the desalted form from Microsynth, Balgach, Switzerland. Further desalination by the Millipore "drop dialysis method"[10] yielded MALDI mass spectra showing only the protonated molecular ion peak of the oligodeoxynucleotide and hardly any alkali ion adducts. 2-Amino-4-methyl-5-nitropyridine (AMNP) was used as a MALDI matrix for the analysis of the Zn – p55F1 – oligodeoxynucleotide complexes. This nonacidic matrix is optimized for MALDI-MS of oligodeoxynucleotides,[14] but allowed the simultaneous detection of both p55F1 and oligodeoxynucleotide at the physiological pH of the sample solution. For sample preparation, the aqueous peptide solution (10 μL, 5×10^{-4} M) was mixed with an aqueous solution of $ZnCl_2$ (2.5 μL, 10^{-2} M) and an aqueous oligodeoxynucleotide solution (2.5 μL, 6.1×10^{-5} M). The concentration of $ZnCl_2$ is unusually high for MALDI experiments, but was found to work well. The pH value was adjusted to 6.5 – 7 by addition of NH_4HCO_3. An aliquot (3.5 μL) of this mixture was mixed with a saturated, aqueous AMNP solution (10 μL). A portion (2 – 4 μL) of the resulting solution was deposited on the probe tip and dried in a cold stream of air.

Received: July 7, 1997 [Z 12106 IE]
German version: *Angew. Chem.* **1998**, *110*, 3600 – 3603

Keywords: mass spectrometry · oligonucleotides · peptides · zinc finger peptides

[1] L. E. Henderson, T. D. Copeland, R. C. Sowder II, G. W. Smythers, S. Oroszlan, *J. Biol. Chem.* **1981**, *256,* 8400-8406.
[2] W.-C. Lam, A. H. Maki, J. R. Casas-Finet, J. W. Erickson, B. P. Kane, R. C. Sowder II, L. E. Henderson, *Biochemistry* **1994**, *33,* 10693 – 10700.
[3] T. L. South, M. F. Summers, *Protein Sci.* **1993**, *2,* 3 – 19.
[4] a) W. G. Rice, J. G. Supko, L. Malspeis, R. W. Buckheit, Jr., D. Clanton, M. Bu, L. Graham, C. A. Schaeffer, J. A. Turpin, J. Domagala, R. Gogliotti, J. P. Bader, S. M. Halliday, L. Coren, R. C. Sowder II, L. O. Arthur, L. E. Henderson, *Science* **1995**, *270,* 1194 – 1196; b) N. B. McDonnell, R. N. De Guzman, W. G. Rice, J. A. Turpin, M. F. Summers, *J. Med. Chem.* **1997**, *40,* 1969 – 1976.
[5] F. Hillenkamp, M. Karas, R. C. Beavis, B. T. Chait, *Anal. Chem.* **1991**, *63,* 1193 A – 1203 A.
[6] a) I. Gruic-Sovulj, H.-C. Lüdemann, F. Hillenkamp, I. Weygand-Durasevic, Z. Kucan, J. Peter-Katalinic, *J. Biol. Chem.* **1997**, *272,* 32084 – 32091; b) L. R. H. Cohen, K. Strupat, F. Hillenkamp, *J. Am. Soc. Mass Spectrom.* **1997**, *8,* 1046 – 1052; c) M. O. Glocker, S. H. J. Bauer, J. Kast, J. Volz, M. Przybylski, *J. Mass Spectrom.* **1996**, *31,* 1221 – 1227; d) A. S. Woods, J. C. Buchsbaum, T. A. Worrall, J. M. Berg, R. J. Cotter, *Anal. Chem.* **1995**, *67,* 4462 – 4465.
[7] M. D. Delahunty, T. L. South, M. F. Summers, R. K. Karpel, *Biochemistry* **1992**, *31,* 6461 – 6469.
[8] a) L. M. Green, J. M. Berg, *Proc. Natl. Acad. Sci. USA* **1989**, *86,* 4047 – 4051; b) L. M. Green, J. M. Berg, *Proc. Natl. Acad. Sci. USA* **1990**, *87,* 6403 – 6407.
[9] M. F. Summers, T. L. South, B. Kim, D. R. Hare, *Biochemistry* **1990**, *29,* 329 – 340.
[10] E. Lehmann, R. Zenobi, S. Vetter, *J. Am. Soc. Mass Spectrom*. **1999**, *10*, in press.
[11] E. Lehmann, R. Knochenmuss, R. Zenobi, *Rapid Commun. Mass Spectrom.* **1997**, *11,* 1483 – 1492.
[12] R. J. Gorelick, D. J. Chabot, A. Rein, L. E. Henderson, L. O. Arthur, *J. Virol.* **1993**, *67,* 4207 – 4036.
[13] K. Schneider, B. T. Chait, *Org. Mass Spectrom.* **1993**, *28,* 1353 – 1361.
[14] M. C. Fitzgerald, G. R. Parr, L. M. Smith, *Anal. Chem.* **1993**, *65,* 3204 – 3211.

 © WILEY-VCH Verlag GmbH, D-69451 Weinheim, 1998 1433-7851/98/3724-3432 $ 17.50+.50/0

Digitonin as a Chemical Trigger for the Selective Transformation of Giant Vesicles**

Fredric M. Menger* and Jason S. Keiper

In memory of Craig West

The remarkable and enigmatic properties of lipid membranes have attracted the interest of many biologically inclined chemists. New challenges are constantly emerging as membrane behavior is defined. Among these is the need to evaluate bilayer interactions with natural and synthetic compounds. Giant vesicles,[1–4] enclosed spherical lipid bilayer assemblies with diameters of 5–200 μm, are ideal vehicles for such studies, as they offer the capabilities for membrane isolation, manipulation, and direct observation under the light microscope.[5] Herein we describe the effects of digitonin on giant vesicles. Digitonin (Figure 1), a member of the saponin family, is a steroid–pentasaccharide conjugate isolated from the european foxglove (*Digitalis purpurea*), which is known to induce lysis in erythrocytes and other cells that contain cholesterol. As will be shown, digitonin acts as a selective chemical "trigger" for membrane layering.[6]

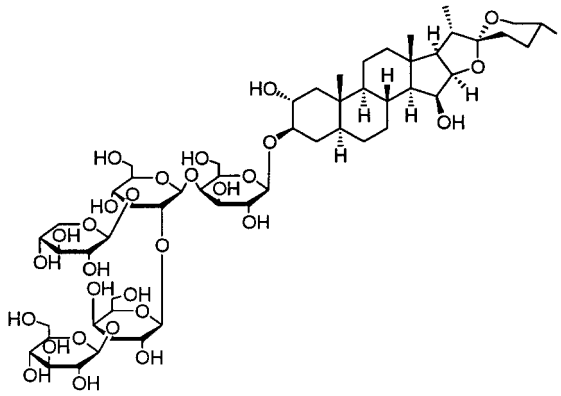


Figure 1. Structure of the steroid–saponin digitonin from *Digitalis purpurea*.

Saponins such as digitonin have wide application as foaming agents, detergents, sweeteners, and adjuvants,[7, 8] but they are perhaps most intriguing because of their ability to enter lipid membranes and form 1:1 complexes with cholesterol.[9–11] Complexation, the exact nature of which is unknown, is believed to be responsible for the lytic activity on cells that contain cholesterol. Although solutions of small vesicles (approximately 100 nm in diameter) have been used previously to study saponin-induced disruption,[12–20] we have taken advantage of the microscopic visibility of giant vesicles to evaluate digitonin's effect upon phospholipid membranes that contain cholesterol.

In the absence of membrane-bound sterols giant vesicles composed of phosphocholine (that is, 1-stearoyl-2-oleoyl-*sn*-glycero-3-phosphocholine (SOPC) or 1-palmitoyl-2-oleoyl-*sn*-glycero-3-phosphocholine (POPC)) experienced no observable morphological changes when exposed to over 100 injections (2.7 ± 0.5 pL each) of digitonin solution ($2.5\ mg\,mL^{-1}$). In contrast, inclusion of a sterol such as cholesterol or ergosterol led to reproducible digitonin-induced disruption of the vesicles. For example, a single external 2.7 pL microinjection of a $2.5\ mg\,mL^{-1}$ digitonin solution within 5 μm of a giant vesicle composed of SOPC/50% cholesterol completely destroyed the structure in 1.5 s. Only a mass of precipitate and amorphous lipid material remained.

Intermediate morphologies could be observed by using even lower concentrations of injected digitonin or lower percentages of membrane-bound cholesterol. For example, the exposure of a giant vesicle of POPC/33% cholesterol to 2.7 pL of a $1.25\ mg\,mL^{-1}$ solution of digitonin created transitional "nanocup" structures[21] as seen in Figure 2. The solid complex observed at the lip of the wound likely inhibits reclosure of the sphere. In fact, it required 30 s for the vesicle to erode totally as the circular gap expanded. Interestingly, the intact portion of the vesicle always retained its spherical shape throughout.

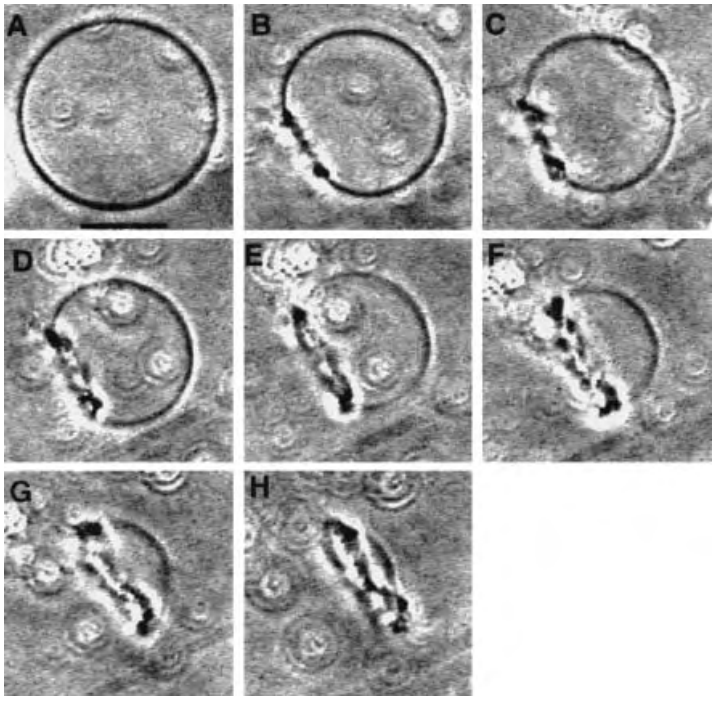


Figure 2. Rupture and gradual disintegration of a 67 μm POPC/33% cholesterol vesicle upon exposure to a single injection of digitonin solution (2.7 pL; $1.25\ mg\,mL^{-1}$). The intermediate "nanocup" morphologies (micrographs D–F) are also shown. Bar = 25 μm; time = 30 s.

In roughly 25% of the experiments, 3–10 μm long fibrous threads were visible at the periphery of the vesicles (Figure 3). Since fibers (believed to consist only of a saponin–sterol complex) have also been detected in submicroscopic vesicles by electron microscopy,[17–19] the behavior of small and giant vesicles overlap here despite their vastly different curvatures. In the giant vesicles' case, however, the fibers are transient and persist for no more than 10 s before they retract onto the

[*] Prof. Dr. F. M. Menger, J. S. Keiper
Department of Chemistry, Emory University
Atlanta, GA 30322 (USA)
Fax: (+1) 404-727-6586

[**] This work was supported by the U.S. National Institutes of Health.

 © WILEY-VCH Verlag GmbH, D-69451 Weinheim, 1998 1433-7851/98/3724-3433 $ 17.50+.50/0

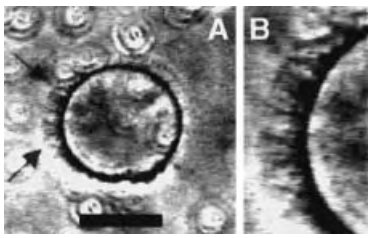


Figure 3. A) Fibrous tubules extend from the surface of a ruptured SOPC/10% cholesterol vesicle exposed to four injections of 2.5 mg mL^{-1} digitonin solution (each 2.7 pL) over a period of 16 s. The tubules retracted back to the surface of the structure 10 s after initial formation. B) Expanded view of the fibrous structures. Bar = 25 μm.

vesicle surface. Visualization of such dynamic processes constitutes a major advantage of light microscopy over electron microscopy.

Figure 4 depicts the molecular ratio of digitonin/cholesterol needed to disrupt SOPC/cholesterol giant vesicles. Data points are based on the minimal amounts of injected digitonin required to induce a rupture event in an isolated giant vesicle. Two conclusions can be deduced from the graph: a) vesicle size is not a critical factor within a 30–70 μm diameter range, with both 10% cholesterol (top plot) and 50% cholesterol (bottom plot); b) cholesterol clearly heightens the sensitivity of SOPC bilayers to digitonin-induced disruption since the digitonin/cholesterol ratio diminishes from about 3 for 10% cholesterol to about 0.15 for 50% cholesterol. Normally, cholesterol is believed to enhance the resistance of membranes to stress-induced ruptures.[1, 23] Formation of an insoluble digitonin/cholesterol complex within the membrane[13, 19, 20] must, therefore, supersede any stabilizing effect of cholesterol.

With the preliminary results in hand we were able to selectively trigger the rupture of giant vesicles within a group

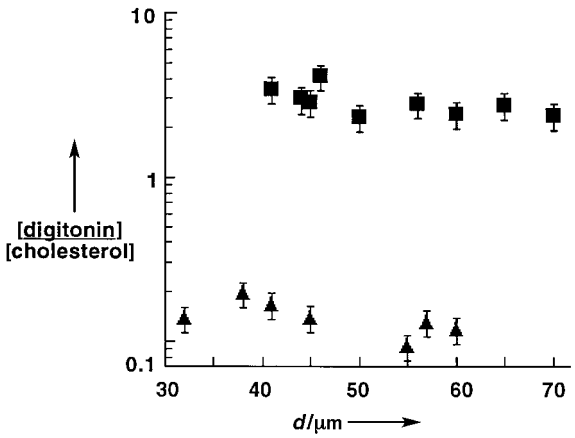


Figure 4. Digitonin/cholesterol molecular ratio for microinjection experiments on SOPC/cholesterol vesicles, based on the minimal amount of injected digitonin solution required to induce rupture of giant vesicles of a given size and composition. (■) SOPC/ 10% cholesterol vesicles; (▲) SOPC/ 50% cholesterol vesicles. Error bars are ±19%, based on the standard deviation of the injection volume. Cholesterol molecules/vesicle values were estimated from area/molecule values determined by Needham and Nunn at 15 °C.[22]

of two or more (the selectivity being based on the cholesterol content of the vesicles). Figure 5 A shows two oppositely charged vesicles that have electrostatically "snapped together" as described previously.[6] The upper cationic vesicle contained POPC/didodecyldimethylammonium bromide/cholesterol in a ratio of 78/2/20 mol%. The lower anionic vesicle contained POPC plus 1-palmitoyl-2-oleoyl-phosphoglycerol (POPG) in a ratio of 98/2 mol% but in the absence of cholesterol. With only 2% cationic and anionic lipid in the respective vesicles, they adhered without change for over 2 h. When the system was exposed to a single injection of a 2.5 mg mL^{-1} solution of digitonin, however, the cationic vesicle with 20 mol% cholesterol burst (Figure 5B) and collapsed upon the stable anionic vesicle (Figure 5C, D). Partial deposition on the anionic vesicle was confirmed by an image profile analysis (Figure 5E, F), which showed a coated membrane in region 2. This selective phenomenon was readily reproducible. When the cholesterol was switched to the anionic vesicle it was now the anionic vesicle that ruptured and collapsed upon its neighbor.

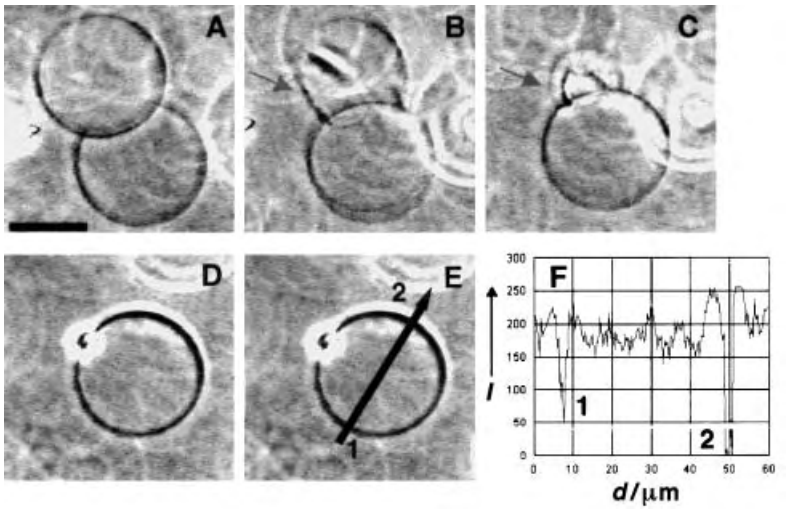


Figure 5. Selective rupture of a 34 μm cholesterol-containing vesicle (POPC/DDAB/cholesterol, 78/2/20 mol%) while adhered to a 40 μm cholesterol-free vesicle (POPC/POPG, 98/2 mol%). Micrographs A–C show the progressive breakdown of the vesicle upon a single 2.7 pL injection of a 2.5 mg mL^{-1} solution of digitonin ($t \sim 2$ s). Micrograph D shows the surviving vesicle, whose partial coating is confirmed with an intensity profile (E,F). The bright spot on the vesicle was precipitate or an anomalous lipid cluster. Bar = 25 μm.

The coating process was also visualized with epi-fluorescence microscopy. Figure 6A shows two adhered vesicles, with the upper one containing both 12 mol% cholesterol and 4-(4-dihexadecylamino)styryl)-*N*-methylpyridinium iodide (DiA; a membrane-soluble fluorescent dye). Since the lower vesicle possessed neither of these components only the upper vesicle with the dye fluoresced (Figure 6B). The upper vesicle burst upon exposure to digitonin and collapsed upon the lower one, to create a partial coating that was observable by fluorescence (Figure 6C).

This work opens new possibilities for selective delivery: A controllable percentile of a disparate giant vesicle population can now be chemically induced to release its contents while the remainder of the population survives intact.[24]

 © WILEY-VCH Verlag GmbH, D-69451 Weinheim, 1998 1433-7851/98/3724-3434 $ 17.50+.50/0

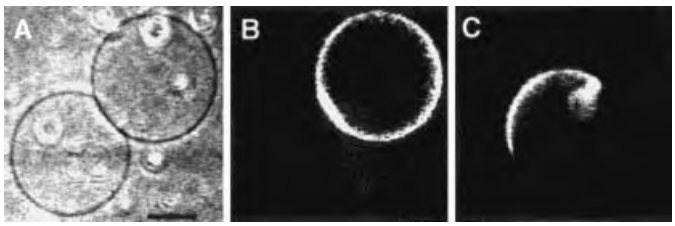


Figure 6. A) Phase-contrast and B) epi-fluorescence visualization of a 70 μm cholesterol-containing, fluorescently-labeled vesicle (POPC/DDAB/DiA/cholesterol, 85/2.5/0.5/12 mol%; upper right hand corner) adhered to a 67 μm POPC/POPG vesicle (98/2 mol%). C) Epi-fluorescence view of a static vesicle with layered lipid from the fluorescently-labeled vesicle, after collapse from exposure to digitonin (2.7 pL; 2.5 mg mL^{-1}). Bar = 25 μm.

Experimental Section

Digitonin (Boehringer Mannheim) was purified (45%) by the method of Kun et al.[25] (Elemental analysis: calcd for $C_{56}H_{92}O_{29}$: C 54.71, H 7.54; found: C 54.24, H 7.69%.) Particle sizing (Coulter N4 Plus) of dispersions of purified digitonin in Milli-Q water contained 3–8 nm structures at concentrations of 0.5–2.5 mg mL^{-1}, which indicated the presence of micellar or premicellar aggregates. DiA was purchased from Molecular Probes (USA). Vesicles were formed by the electroformation method developed by Angelova et al.[26] The typical procedure, which varied slightly with different compositions, was as follows: Droplets (1 μL) of lipid or lipid mixture solutions (0.25–1.0 mg mL^{-1} in diethyl ether/methanol (9/1) was placed on two parallel Pt wires (0.5 mm diameter) of the apparatus. After the film had dried under a stream of nitrogen for 45 minutes the apparatus was connected to an alternating current (initial $\nu = 10$ Hz; $V = 0.1$ V) from a function generator (Hewlett Packard, 33120A) coupled to an oscilloscope (Hewlett Packard 54600B), and the chamber filled with Milli-Q water (about 1.5 mL). The voltage (reading on the oscilloscope) was increased to 3 V as the frequency was progressively lowered to 0.5 Hz over a span of 2–5 hours. Giant spherical vesicles (presumably unilamellar or of only a few bilayers)[27] with diameters of 10–100 μm were formed upon removing the current. All electroformation and subsequent experiments were conducted at 20 °C.

Holding and injection pipettes were prepared from Narishige G-1 capillary tubes using a Sutter P-97 horizontal pipette puller. The holding pipettes were further polished with a Narishige MF-9 microforge. The vesicles were manipulated with Narishige micromanipulation gear connected to a Nikon PLT-188 picoinjector. The vesicles were grasped with holding pipettes and released near the bottom of the chamber to: a) reduce the influence of adventitious air currents that circulated the water and b) rupture the vesicle–wire lipid tether.[27] The tether, which is inherent in vesicles produced by electroformation, allows for water escape, which means that the tethered vesicles are not completely closed spheres. The absence of a tether in vesicles isolated with our method was confirmed by both epi-fluorescence microscopy and the fact that the vesicles did not "rebound" to the wire when released (as connected vesicles do). Microinjections of digitonin solution were performed at a pressure of 3.0 psi, a time of 50 ms, and a balancing pressure (to alleviate capillary action) of 0.042–0.055 bar. The injection volume, as determined by optical microscopy evaluation of pipette clearance,[28] averaged 2.7 ± 0.5 pL. External microinjections were performed 5–10 μm from the vesicle surfaces.

The samples were examined by phase-contrast microscopy with a Nikon Diaphot TMD microscope in tandem with a Dage-MTI CCD-72 solid-state camera, Panasonic AG-1960 SVHS VCR, Hamamatsu Argus-10 image processor, and a Sony black-and-white monitor. This system was connected to a Micron Millenia 166 PC workstation equipped with Image-Pro Plus image processing software, and images were printed on a Tektronix Phaser 440 color printer. Epi-fluorescence microscopy was achieved with the identical setup except for replacement of the CCD camera with a Dage-MTI VE 1000SIT low-light camera and application of either Nikon V-2A ($\lambda_{excitation} = 380–425$ nm; $\lambda_{barrier} = 450$ nm) or B-2A ($\lambda_{excitation} = 450–490$ nm; $\lambda_{barrier} = 520$ nm) filter combinations.

Received: July 16, 1998 [Z12159IE]
German version: *Angew. Chem.* **1998**, *110*, 3621–3624

Keywords: cytomimetic chemistry · membranes · phospholipids · saponins · vesicles

[1] E. Evans, D. Needham, *J. Phys. Chem.* **1987**, *91*, 4219.
[2] D. Needham in *Permeability and Stability of Lipid Bilayers* (Eds: E. DiSalvo, S. Simon), CRC Press, Boca Raton, FL, **1995**, pp. 49–76.
[3] H.-G. Döbereiner, E. Evans, M. Kraus, U. Seifert, M. Wortis, *Phys. Rev. E.* **1997**, *55*, 4458.
[4] F. M. Menger, K. D. Gabrielson, *Angew. Chem.* **1995**, *107*, 2260; *Angew. Chem. Int. Ed. Engl.* **1995**, *34*, 2091.
[5] F. M. Menger, J. S. Keiper, *Adv. Mater.* **1998**, *10*, 888.
[6] F. M. Menger, J. S. Keiper, *Angew Chem.* **1997**, *109*, 2602; *Angew. Chem. Int. Ed. Engl.* **1997**, *36*, 2489.
[7] K. Hostettmann, A. Marston, *Saponins*, Cambridge University Press, Cambridge, **1995**.
[8] D. C. Van Setten, G. van de Werken in *Saponins Used in Traditional and Modern Medicine* (Eds: G. R. Waller, K. Yamasaki) Plenum Press, New York, **1996**, pp. 185–193.
[9] A. M. Glauert, J. T.Dingle, J. A. Lucy, *Nature* **1962**, *196*, 953.
[10] S. Takagi, H. Otsuka, T. Akiyama, U. Sankawa, *Chem. Pharm. Bull.* **1982**, *30*, 3485.
[11] P. Muhr, W. Likussar, M. Schubert-Zsilavecz, *Magn. Reson. Chem.* **1996**, *34*, 137.
[12] R. Segal, I. Milo-Goldzweig, *Biochim. Biophys. Acta* **1978**, *512*, 223.
[13] T. Akiyama, S. Takagi, U.Sankawa, S. Inari, H. Saitô, *Biochemistry* **1980**, *19*, 1904.
[14] M. Nishikawa, S. Nojima, T. Akiyama, U. Sankawa, K. Inoue, *J. Biochem.* **1984**, *96*, 1231.
[15] M. Hu, K.Konoki, K. Tachibana, *Biochim. Biophys. Acta* **1996**, *1299*, 252.
[16] E. A. J. Keukens, T. de Vrije, H. de Boer, C. H. J. P. Fabrie, R. A. Demel, W. M. F. Jongen, B. de Kruijff, *Biochim. Biophys. Acta* **1992**, *1110*, 127.
[17] R. G. Miller, *Biochim. Biophys. Acta* **1984**, *774*, 151.
[18] P. M. Elias, J. Goerke, D. S. Friend, *J. Cell. Biol.* **1978**, *78*, 577.
[19] E. A. J. Keukens, T. de Vrije, C. van den Boom, P. de Waard, H. H. Plasman, F. Thiel, V. Chupin, W. M. F. Jongen, B. de Kruijff, *Biochim. Biophys. Acta* **1995,** *1240*, 216.
[20] E. A. J. Keukens, T. de Vrije, L. A. M. Jansen, H. de Boer, M. Janssen, A. I. P. M. de Kroon, W. M. F. Jongen, B. de Kruijff, *Biochim. Biophys. Acta* **1996**, *1279*, 243.
[21] F. M. Menger, S. J. Lee, *Langmuir* **1995**, *11*, 3685.
[22] D. Needham, R. S. Nunn, *Biophys. J.* **1990**, *58*, 997.
[23] E. Evans, D. Needham, *Faraday Discuss. Chem. Soc.* **1986**, *81*, 267.
[24] Progress along these lines with submicroscopic vesicles has been reported in Y. Nagawa, S. L. Regen, *J. Am. Chem. Soc.* **1991**, *113*, 7237.
[25] E. Kun, E. Kirsten, W. N. Piper, *Methods Enzymol.* **1979**, *55*, 115.
[26] M. I. Angelova, D. S. Dimitrov, *Faraday Discuss. Chem. Soc.* **1986**, *81*, 303.
[27] L. Mathivet, S. Cribier, P. F. Devaux, *Biophys. J.* **1996**, *70*, 1112.
[28] S. J. Lee, PhD thesis, Emory University (USA), **1996**.

 © WILEY-VCH Verlag GmbH, D-69451 Weinheim, 1998 1433-7851/98/3724-3435 $ 17.50+.50/0

An Access to Glycoconjugate Libraries through Multicomponent Reactions

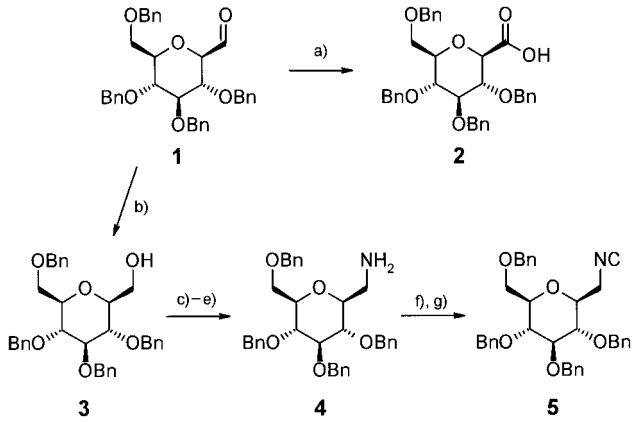
Oswald Lockhoff*

A new approach to the identification of lead structures for drug development is the combinatorial synthesis of compound libraries and their investigation in high-throughput screening (HTS) systems. In this way libraries of peptides,[1] oligonucleotides,[2] and other low molecular weight compounds[3] were built-up and studied. In contrast, and despite their biological importance,[4] libraries of oligosaccharides could not be investigated in HTS systems. Today's methods of glycoside and oligosaccharide syntheses[5] are compatible with demands for automatic syntheses only to a very limited extend. However, several new approaches presented recently[6] are very encouraging and will bring new solutions in the near future.

For drug design it is of particular interest that only substructures of oligosaccharides are involved in most carbohydrate–protein interactions. Several studies have shown that individual arrays of functional groups possibly located on different monosaccharide moieties are recognized by complementary receptors.[7] This is the rational basis for the design of glycomimetics which carry their essential functional groups in a matching spatial arrangement.[8] This further implies that the individual carbohydrate moieties do not have to be linked through glycosidic linkages which are difficult to couple. Instead, they can be linked through other bond types as long as the presentation of the essential functional groups is not restricted.

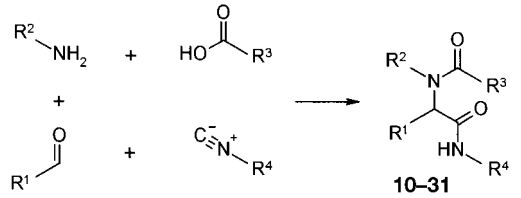
A suitable method for the generation of libraries of low molecular weight compounds in solution is the application of multicomponent condensations (MCC).[9] Combinatorial reactions such as the Ugi reaction[10] should also be suitable for producing glycoconjugate libraries if appropriate carbohydrate derivatives having aldehyde, amino, carboxylic acid, and isocyanide groups are used. This should open an effective access to libraries of glycomimetics and glycoconjugates. Here we report on our efforts to develop a MCC-based combinatorial synthesis of glycoconjugate libraries.[11] Meanwhile, solid-phase Ugi reactions with C-glycosyl aldehydes have been presented.[12]

In exploratory studies per-O-benzylated carbohydrate building blocks with *β*-D-*gluco* configuration were chosen (Scheme 1). The starting compound was glycosyl aldehyde **1**, which was obtained in good yields from tetra-*O*-benzyl-D-gluconolactone by addition of dithiane.[13] The oxidation of **1** under Masamune conditions[14] yielded the glycosylcarboxylic acid **2**. The reductive amination of **1** did not afford the glycosylmethylamine **4**[15] selectively, but rather led to **4** and the alcohol **3**. Therefore **1** was reduced to **3**, which was transformed into **4** by classical tosylation, azide substitution, and selective reduction. N-Formylation of **4** and dehydration



Scheme 1. Synthesis of C-glycoside building blocks **1**, **2**, **4**, and **5** for the four-component reactions. a) $KMnO_4$, *t*BuOH, H_2O, NaH_2PO_4, pH 4.5, 81%; b) $LiBH_4$, THF, 95%; c) TsCl, pyridine; d) NaN_3, DMF; e) $NaBH_4$, $NiCl_2$, EtOH, dioxane, 71% (over three steps); f) HCO_2Me, 40 °C, 87%; g) $(Cl_3CO)_2CO$, DABCO, CH_2Cl_2, 60%. Bn = benzyl, DABCO = 1,4-diazabicyclo[2.2.2]octane, Ts = toluenesulfonyl.

afforded the isocyanide **5**. The C-glycosides **1**, **2**, **4**, and **5** represent the desired carbohydrate prototypes for the Ugi condensation. It was now planned to investigate their synthetic suitability in a model reaction (Scheme 2). One



Scheme 2. The Ugi reactions by which four components react to provide a diamide; for R^1–R^4, see Table 1.

such reaction is that of benzaldehyde (**6**), *p*-methoxybenzylamine (**7**), acetic acid (**8**), and cyclohexylisocyanide (**9**) leading to **10**[16] by stepwise substitution of one or more non-carbohydrate components (Table 1). The condensation of the glycosyl aldehyde **1** with **7**–**9** afforded the diastereomers **11h** and **11l**,[17] which could be separated by column chromatography. Condensation of the glycosylmethylamine **4** led to diasteromers **12**, which could not be separated. The carboxylic acid **2** gave the amides **13h** and **13l**. The yields of these reaction were between 70 and 85%. Both diasteromers were formed in equal amounts. Glycosylisocyanide **5**, however, did not show conversion into condensation product **14** under these conditions even after several days. Amide **14** was produced only in moderate yields after addition of zinc chloride. Apparently the primary isocyanide **5** is only of low nucleophilicity. Nevertheless it should be emphasized that all components reacted as expected and should therefore be suitable for an assembly of glycoconjugate libraries.

We next addressed the combination of two or more carbohydrate building blocks in Ugi reactions to afford higher glycosylated amino acid derivatives. The synthesis of the six possible diglycosylated compounds **15**–**20** was studied first. Glycosyl aldehyde **1** and amine **4** together with **8** and **9** gave

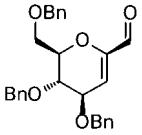
[*] Dr. O. Lockhoff
Bayer AG, Central Research, ZF-WF Q18
D-51368 Leverkusen (Germany)
Fax: (+49) 214-3050070
E-mail: oswald.lockhoff.ol@bayer-ag.de

 © WILEY-VCH Verlag GmbH, D-69451 Weinheim, 1998 1433-7851/98/3724-3436 $ 17.50+.50/0

Table 1. Condensation products of the Ugi reactions with carbohydrate building blocks. A = 2,3,4,6-tetra-*O*-benzyl-β-D-glucopyranosyl, B = 2,3,4,6-tetra-*O*-benzyl-β-D-glucopyranosyloxymethyl, PMB = 4-methoxybenzyl, **h**,**l** = diastereomers separated by chromatography into the higher (**h**) and lower (**l**) running stereoisomers, n.d. = not determined.

Aldehyde	Amine	Acid	Isocyanide	Product	R^1	R^2	R^3	R^4	Molecular formula	M_r	MS [*m*/*z*]	^{13}C NMR [δ] NCH,R^1CO	yield [%]
6	**7**	**8**	**9**	**10**	C_6H_5	PMB	CH_3	C_6H_{11}	$C_{24}H_{30}N_2O_3$	394.52	CI: 395 [*M* + H]	63.0	74
1	**7**	**8**	**9**	**11h,l**	A	PMB	CH_3	C_6H_{11}	$C_{52}H_{60}N_2O_8$	841.07	CI: 841 [*M* + H]	62.0, 62.1	41 + 37
6	**4**	**8**	**9**	**12**	C_6H_5	A–CH_2	CH_3	C_6H_{11}	$C_{51}H_{58}N_2O_7$	811.04	CI: 811 [*M* + H]	64.4, 64.2	74
6	**7**	**2**	**9**	**13h,l**	C_6H_5	PMB	A	C_6H_{11}	$C_{57}H_{62}N_2O_8$	903.14	CI: 903 [*M* + H]	63.6, 63.9	36 + 33
6	**7**	**8**	**5**	**14**	C_6H_5	PMB	CH_3	A–CH_2	$C_{53}H_{56}N_2O_8$	849.05	CI: 849 [*M* + H]	63.2	23
1	**4**	**8**	**9**	**15h,l**	A	A–CH_2	CH_3	C_6H_{11}	$C_{79}H_{88}N_2O_{12}$	1257.59	CI: 1257 [*M* + H]	62.3, 62.3	33 + 30
1	**7**	**2**	**9**	**16h,l**	A	PMB	A	C_6H_{11}	$C_{85}H_{92}N_2O_{13}$	1349.69	CI: 1349 [*M* + H]	62.2, 62.4	46 + 41
1	**7**	**8**	**5**	**17**	A	PMB	CH_3	A–CH_2	$C_{81}H_{86}N_2O_{13}$	1295.59	FAB: 1317 [*M* + Na]	n.d.	8
6	**4**	**2**	**9**	**18**	C_6H_5	A–CH_2	A	C_6H_{11}	$C_{84}H_{90}N_2O_{12}$	1319.66	CI: 1319 [*M* + H]	63.8, 63.1	72
6	**4**	**8**	**5**	**19**	C_6H_5	A–CH_2	CH_3	A–CH_2	$C_{80}H_{84}N_2O_{12}$	1265.57	FAB: 1287 [*M* + Na]	n.d.	11
6	**7**	**2**	**5**	**20**	C_6H_5	PMB	A	A–CH_2	$C_{86}H_{88}N_2O_{13}$	1357.67	FAB: 1379 [*M* + Na]	n.d.	18
1	**4**	**2**	**9**	**21**	A	A–CH_2	A	C_6H_{11}	$C_{112}H_{120}N_2O_{17}$	1766.21	FAB: 1787 [*M* + Na]	n.d.	61
1	**4**	**8**	**5**	**22**	A	A–CH_2	CH_3	A–CH_2	$C_{108}H_{114}N_2O_{17}$	1712.12	ESI: 1735 [*M* + Na]	n.d.	Spur
1	**7**	**2**	**5**	**23**	A	PMB	A	A–CH_2	$C_{114}H_{118}N_2O_{18}$	1804.21	ESI: 1827 [*M* + Na]	n.d.	Spur
6	**4**	**2**	**5**	**24**	C_6H_5	A–CH_2	A	A–CH_2	$C_{113}H_{116}N_2O_{17}$	1774.19	ESI: 1797 [*M* + Na]	n.d.	3
1	**4**	**2**	**5**	**25**	A	A–CH_2	A	A–CH_2	$C_{141}H_{146}N_2O_{22}$	2220.74	n.d.	n.d.	0
34	**4**	**2**	**5**	**26**	B	A–CH_2	A	A–CH_2	$C_{142}H_{148}N_2O_{23}$	2250.76	ESI: 2274 [*M* + Na]	n.d.	61
34	**7**	**8**	**9**	**27**	B	PMB	CH_3	C_6H_{11}	$C_{53}H_{62}N_2O_9$	871.09	CI: 871 [*M* + H]	59.3; 57.8	75
6	**37**	**8**	**9**	**28**	C_6H_5	B–CH_2	CH_3	C_6H_{11}	$C_{52}H_{60}N_2O_8$	841.07	CI: 841 [*M* + H]	62.3, 61.7	71
6	**7**	**36**	**9**	**29**	C_6H_5	PMB	B	C_6H_{11}	$C_{58}H_{64}N_2O_9$	933.16	CI: 933 [*M* + H]	63.9; 63.7	74
6	**7**	**8**	**39**	**30**	C_6H_5	PMB	CH_3	B–CH_2	$C_{54}H_{58}N_2O_9$	879.07	CI: 879 [*M* + H]	62.6, 62.1	78
34	**37**	**36**	**39**	**31**	B	B–CH_2	B	B–CH_2	$C_{145}H_{154}N_2O_{26}$	2340.84	MALDI: 2361 [*M* + Na]	n.d.	72

the desired diasteromers **15h** and **15l**. The unsaturated aldehyde **32** was identified as a by-product formed from **1** by α,β-elimination. The reaction of **1** and glycosylcarboxylic acid **2** together with **7** and **9** afforded **16h** and **16l** after chromatography. Diastereomers **18** obtained in comparable yields from glycosyl building blocks **4** and **2** could not be separated.

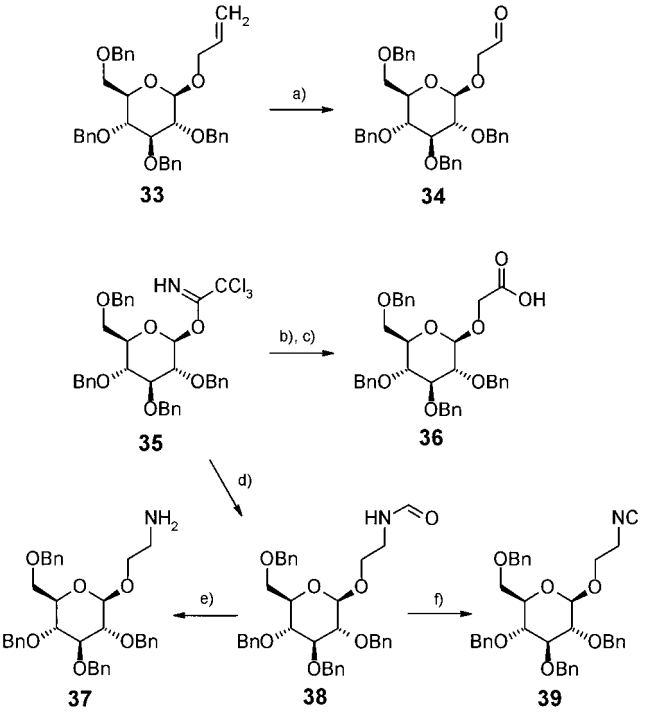


32

The three following reactions of the isocyanide **5** again reflected its low nucleophilicity. Combination of **1** and **5** after addition of zinc chloride afforded only 8% of the desired condensation product **17**; the main product was **32**. Diastereomers **19** were formed in a disappointing 11% total yield, **20** in only 18% yield.

The synthesis of the triply glycosylated amino acid derivative **21** from **1**, **4**, and **2** as well as **9** took its expected course in satisfactory yield. The next reactions, however, in which **1** and **5** were combined provided the target products **22** or **23**, respectively, in minute amounts detectable only by mass spectrometry. The main product was **32**. The fourth triply glycosylated amino acid derivative **24** was isolated in very low yields. As expected the synthesis of the fourfold-glycosylated amino acid **25** did not occur. The only isolated product resulting from the combination of the four glycosyl building blocks **1**, **2**, **4**, and **5** was the well-known aldehyde **32**. These results confirm previous findings that a wide application of the Ugi reaction is favored by a high nucleophilicity of the isocyanide component.[10]

Side reactions of the aldehyde component leading to elimination products were expected to be prevented if aldehydes were employed which cannot eliminate. Therefore, glycosyl aldehyde **34** was used, which was obtained from allyl glycoside **33**[18] by ozonolysis (Scheme 3). Indeed, **34** reacted with the glycosyl units **2**, **4**, and **5** in the presence of zinc chloride to provide the fourfold-glycosylated amino acid derivative **26** in more than 60% yield.

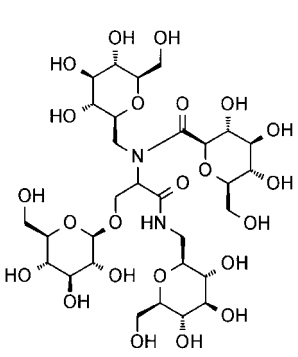


Scheme 3. Synthesis of O-glycosidic building blocks **34**, **36**, **37**, and **39** for the four-component reactions. a) O_3, CH_2Cl_2, Me_2S, −20 °C, 77%; b) $HOCH_2CO_2Et$, $BF_3 \cdot Et_2O$, THF, 82%; c) NaOH, MeOH, THF, 72%; d) $HOCH_2CH_2NHCHO$, $BF_3 \cdot Et_2O$, THF, 68%; e) NaOH, MeOH, THF, 66%; f) $(Cl_3CO)_2CO$, DABCO, CH_2Cl_2, 52%.

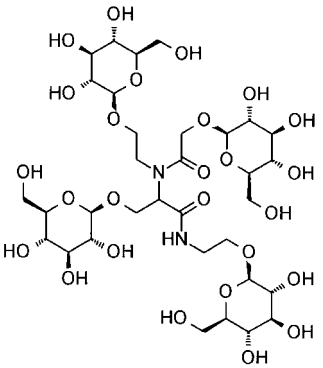
A second set of condensation reactions was designed using **34** as well as other O-glycosidic units in order to expand the diversity of the glycoconjugate libraries. The carboxylic acid **36** was obtained by O-glycosylation of ethyl hydroxyacetate with **35**[19] followed by saponification. The corresponding glycosylation of *N*-(2-hydroxyethyl)formamide with **35** afforded **38**. Saponification of **38** provided the amine **37**. Treatment of **38** with triphosgene gave the crystalline isocyanide **39**.

All four model Ugi reactions of these glycosylated building blocks with nonglycoslated partners provided the monoglycosylated amino acid derivatives **27**–**30** in good yields. Side reactions were not observed. Individual diasteromers could be detected with thin-layer chromatography or HPLC, but could not be resolved by preparative column chromatography. They were isolated as 1:1 mixtures. Finally, the condensation of **34**, **36**, **37**, and **39** furnished the desired fourfold-glycosylated amino acid derivate **31**.

The above-mentioned aldehyde, acid, and isocyanide building blocks also reacted smoothly in related Passerini reactions to give singly to triply glycosylated hydroxyacetic acid derivatives. According to further preliminary investigations, analogous reactions using unprotected building blocks provided the condensation products only in significantly lower amounts due to competitive reactions leading to acetals or aminals. O-Acetylated components gave rise to partial N-acetylation of the amine components. The hydrogenolysis of various perbenzylated condensation products in the presence of palladium on charcoal proceeded smoothly and afforded the completely deblocked glycosylated amino or hydroxy acid derivatives, for example **40** and **41**.[20] All products gave mass spectra in accordance with their molecular formula.



40



41

These reactions have opened a broad access to libraries of diverse glycoconjugate libraries. The combination of various carbohydrate components (with different configurations; C-, O-, or N-glycosidic bonds; different linkers between sugar moiety and functional groups; non-anomeric coupling of the functional groups) carrying aldehyde, acid, amino, and isocyanide groups should offer a huge variety of different branched glycoconjugates as tri- or tetrasaccharide mimetics. But also the mono- or diglycosyl compounds carrying further non-carbohydrate residues, reflecting the vast diversity of organic substituents, are highly important for HTS systems. As these prototype reactions have disclosed, various carbohydrate units can be assembled under similar conditions, thereby enabling automatization of the reactions which have been realized manually until now. It can be predicted that the biological investigation of these saccharide libraries will be of considerable interest.

Experimental Section

Aldehyde (0.05 mmol), amine (0.05 mmol), carboxylic acid (0.05 mmol), and isocyanide (0.05 mmol) were disolved in ethanol (1 mL) and tetrahydrofuran (1 mL) and stirred overnight. The mixture was treated with 1N hydrochloric acid (0.1 mL), stirred for 30 min, and evaporated. The residue was taken up in dichloromethane (5 mL), washed with water (2 mL), dried, evaporated, and purified by column chromatography over silica gel (hexane/ethyl acetate, 7/1 →3/1).

Received: June 25, 1998 [Z12050IE]
German version: *Angew. Chem.* **1998**, *110*, 3634–3637

Keywords: carbohydrates · combinatorial chemistry · glycoconjugates · glycomimetics · multicomponent reactions

[1] a) M. A. Gallop, R. W. Barrett, W. J. Dower, S. P. A. Fodor, E. M. Gordon, *J. Med. Chem.* **1994**, *37*, 1233–1251; b) G. Jung, A. G. Beck-Sickinger, *Angew. Chem.* **1992**, *104*, 375–391; *Angew. Chem. Int. Ed. Engl.* **1992**, *31*, 367–383.

[2] L. Gold, B. Polisky, O. Uhlenbeck, M. Yarus, *Annu. Rev. Biochem.* **1995**, *64*, 763–797.

[3] a) N. K. Terrett, M. Gardner, D. W. Gordon, R. J. Kobylecki, J. Steele, *Tetrahedron* **1995**, *51*, 8135–8173; b) L. A. Thompson, J. A. Ellman, *Chem. Rev.* **1996**, *96*, 555–600.

[4] a) J. C. Paulson, *Trends Biochem. Sci.* **1989**, *14*, 272–276; b) K. A. Karlsson, *Trends Pharmacol. Sci.* **1991**, *12*, 265–272; c) A. Varki, *Glycobiology* **1993**, *3*, 97–130; d) J. B. Lowe in *Molecular Glycobiology* (Eds.: M. Fukuda, O. Hindsgaul), IRL Press, Oxford, **1994**, pp. 163–205; e) R. A. Dwek, *Chem. Rev.* **1996**, *96*, 683–720.

[5] a) O. Lockhoff, *Methoden Org. Chemie (Houben-Weyl) 4th ed. 1952–*, Vol. E14a/3, pp. 621–1077; b) K. Toshima, K. Tatsuta, *Chem. Rev.* **1993**, *93*, 1503–1531; c) F. Barresi, O. Hindsgaul, *Mod. Synth. Methods* **1995**, *7*, 283–230; d) H. J. M. Gijsen, L. Qiao, W. Fitz, C.-H. Wong, *Chem. Rev.* **1996**, *96*, 443–473; e) G.-J. Boons, *Tetrahedron* **1996**, *52*, 1095–1121.

[6] a) P. Arya, R. N. Ben, *Angew. Chem.* **1997**, *109*, 1335–1337; *Angew. Chem. Int. Ed. Engl.* **1997**, *36*, 1280–1282; b) D. Kahne, *Curr. Op. Chem. Biol.* **1997**, *1*, 130–135; c) M. J. Sofia, *Mol. Diversity* **1998**, *3*, 75–94.

[7] a) D. Tyrrell, P. James, N. Rao, C. Foxall, S. Abbas, F. Dasgupta, M. Nashed, A. Hasegawa, M. Kiso, D. Asa, J. Kidd, B. K. Brandley, *Proc. Natl. Acad. Sci. USA* **1991**, *88*, 10372–10376; b) K. Scheffler, B. Ernst, A. Katapodis, J. L. Magnani, W. T. Wang, R. Weisemann, T. Peters, *Angew. Chem.* **1995**, *107*, 2034–2037; *Angew. Chem. Int. Ed. Engl.* **1995**, *34*, 1841–1844.

[8] a) A. Giannis, *Angew. Chem.* **1994**, *106*, 188–191; *Angew. Chem. Int. Ed. Engl.* **1994**, *33*, 178–180; b) J. H. Musser, M. B. Anderson, P. Fügedi, *Pharm. News* **1996**, *3*, 11–17; c) H. C. Kolb, B. Ernst, *Pure Appl. Chem.* **1997**, *69*, 1879–1884.

[9] a) I. Ugi, *J. Prakt. Chem./Chem.-Ztg.* **1997**, *339*, 499–516; b) A. Domling, *Comb. Chem. High Throughput Screening* **1998**, *1*, 1–22.

[10] a) I. Ugi, *Angew. Chem.* **1982**, *94*, 826–835; *Angew. Chem. Int. Ed. Engl.* **1982**, *21*, 810–819; b) G. Gokel, G. Lüdke, I. Ugi in *Isonitrile Chemistry* (Ed.: I. Ugi), Academic Press, New York, **1971**, pp. 145–199.

 © WILEY-VCH Verlag GmbH, D-69451 Weinheim, 1998 1433-7851/98/3724-3438 $ 17.50+.50/0

[11] O. Lockhoff (Bayer AG), *Ger. Offen*. DE 19636538, **1996** [*Chem. Abstr*. **1998**, *128*, 230687].
[12] D. P. Sutherlin, T. M. Stark, R. Hughes, R. W. Armstrong, *J. Org. Chem*. **1996**, *61*, 8350–8354.
[13] M. E. Lasterra Sanchez, V. Michelet, I. Besnier, J. P. Genet, *Synlett* **1994**, 705–708.
[14] A. Abiko, J. C. Roberts, T. Takemasa, S. Masamune, *Tetrahedron Lett.* **1986**, *27*, 4537–4540.
[15] M. T. Garcia Lopez, F. G. de las Heras, A. San Felix, *J. Carbohydr. Chem.* **1987**, *6*, 273–279.
[16] The C atoms from components **6**–**9** gave rise to characteristic ^{13}C NMR signals of condensation products that partially do not exist for glycosylated products. **10**: ^{13}C NMR ($CDCl_3$, 100.6 MHz): $\delta =$ 172.5 (N*C*OMe), 168.7 (*C*ONHC$_6$H$_{11}$), 158.6 (C4 of PMB), 135.4 (C1 of Ph), 130.4–127.4 (arom. *C*H), 113.8 (C3, C5 of PMB), 63.0 (NCH,PhCO), 55.2 (OCH_3), 50.5 (CH_2 of PMB), 48.5 (C1 of C_6H_{11}), 32.8 (C2, C6 of C_6H_{11}), 25.5 (C4 of C_6H_{11}), 24.7 (C3, C5 of C_6H_{11}), 22.5 (CO*C*H$_3$). The ^{13}C NMR signals of glycosyl residues and O-benzyl groups in glycosylated condensation products were detected between $\delta = 87.5$ and 68.0.
[17] The letters **h** and **l** indicate the higher or lower moving diastereomers in thin-layer chromatography. The absolute stereochemistry was not assigned.
[18] R. Lakhmiri, P. Lhoste, D. Sinou, *Tetrahedron Lett.* **1989**, *30*, 4669–4672.
[19] R. R. Schmidt, J. Michel, *Angew. Chem.* **1980**, *92*, 763–764; *Angew. Chem. Int. Ed. Engl.* **1980**, *19*, 731–732.
[20] **40**: ESI-HR-MS: *m*/*z* calcd for $C_{30}H_{52}N_2O_{23}Na$: 831.2859 $[M+Na]^+$, found: 831.2889. **41**: ESI-HR-MS: *m*/*z* calcd for $C_{33}H_{58}N_2O_{26}Na$: 921.3176 $[M+Na]^+$, found: 921.3199.

 © WILEY-VCH Verlag GmbH, D-69451 Weinheim, 1998 1433-7851/98/3724-3439 $ 17.50+.50/0